Acta Chemica Scandinavica A 32 (1978) 1 – 5

Hydrogen Bond Studies. 126. A ^2H NMR Study of $LiClO_4.3D_2O$ at 25 and −71 °C

BO BERGLUND and JÖRGEN TEGENFELDT

Institute of Chemistry, University of Uppsala, Box 531, S-751 21 Uppsala, Sweden

A deuteron magnetic resonance study of a single crystal of $LiClO_4 \cdot 3D_2O$ at 25 and −71 °C is reported. The determination of the electric field gradient tensors was based on quadrupole splittings from only one rotation axis.

At 25 °C the observed electric field gradient tensor corresponds to a rapidly flipping water molecule. The quadrupole coupling constant (e^2qQ/h) and asymmetry parameter (η) at the deuteron position were found to be 131.4(2) kHz and 0.758(2), respectively. The principal axis corresponding to the largest eigenvalue deviates by 4.0(6)° from the normal to the water molecule plane.

At −71 °C the spectra correspond to the slow-flipping limit. The quadrupole coupling constant and asymmetry parameter were found to be 245.2(1) kHz and 0.107(1), respectively. The principal axis corresponding to the largest eigenvalue deviates 1.8(6)° from the O−H direction. The angular displacement is out of the water molecule plane.

The results are consistent with the earlier neutron diffraction and infrared spectroscopic studies.

In hydrated perchlorates, relatively high stretching vibrations of isotopically dilute HDO molecules have been observed,[1,2] corresponding to rather weak hydrogen bonds between the water molecules and the perchlorate ion. $NaClO_4.H_2O$ serves as a good example. Very long O···O hydrogen bond distances have been observed [3.034(2),* 3.093(2) and 3.156(2) Å][3] as well as very high O−D stretching frequencies (2641 and 2610 cm^{-1}).[1] A deuteron magnetic resonance study has recently been performed on $NaClO_4.D_2O$.[4] It was shown that the hydrogen atoms are dynamically disordered, causing unexpectedly small quadrupole coupling constants [226.7(6) and 231.5(6) kHz], and complicating the interpretation of these coupling constants in terms of hydrogen-bond properties. Another perchlorate salt resently studied both by neutron diffraction[5] and IR-spectroscopy[1,6] is $LiClO_4.3H_2O$.

In $LiClO_4.3H_2O$ there is only one crystallographically independent O−H group with corresponding O···O hydrogen bond distance 2.989(2) Å and O−D stretching frequency 2619 cm^{-1}. As we are interested in studying the variation of the quadrupole coupling constants in different solid hydrates, and since $LiClO_4.3H_2O$ contains relatively weak hydrogen bonds, we decided to perform a ^2H NMR study on this hydrate. As $LiClO_4.3H_2O$ belongs to a highly symmetric space group ($P6_3mc$, hexagonal), it will also serve as a good example to show some of the advantages of the procedure used at this laboratory[7] for the determination of the electric field gradient (EFG) tensors instead of the method more commonly used elsewhere, as advanced by Volkoff *et al.*[8]

$LiClO_4.3H_2O$ has recently also been studied by proton wide line NMR as well as relaxation time measurements.[9] An activation energy for a hindered rotation of the water molecule (flip motion) was calculated from T_1 and T_{1D} relaxation measurements, and found to be 10 kcal/mol. It will be shown that this result is in good agreement with our ^2H NMR data.

In discussing structural data in this paper, we neglect any differencies that might exist between the structures of normal and deuterated $LiClO_4.3H_2O$ as well as temperature effects on the structure.

* Numbers in parenthesis here and throughout this paper are estimated standard deviations.

EXPERIMENTAL DETAILS

Preparation. $LiClO_4.3H_2O$ was synthesized from commercial Li_2CO_3 and perchloric acid ($HClO_4$) dissolved in water. Deuterated $LiClO_4.3H_2O$ was prepared by dissolving anhydrous $LiClO_4$ in heavy water (99.99 % D_2O). A single crystal of $LiClO_4.3D_2O$ was grown in a desiccator employing dried P_2O_5 as a desiccant. After a few weeks a well shaped flat crystal was obtained. The crystal was cut to an approximate size of $4 \times 3 \times 10$ mm^3 and sealed into a glass tube to prevent decomposition. The degree of deuteration in the crystal was calculated from the relative intensities of the O–H and O–D stretching bands in an infrared spectrum, using the intensity weighting factors 1.0 and 2.0, respectively. The degree of deuteration was found to be 94 %.

^2H NMR spectra. The single crystal of $LiClO_4.3D_2O$ was mounted on a goniometer head in such a way that the axis of rotation was tilted a few degrees away from the *c*-axis. The rotation axis was then determined on a 4-circle X-ray diffractometer and found to be $-0.0276a + 0.0170b + 0.1748c$, where *a*, *b* and *c* are the unit cell axes.

The crystal was then transferred to a modified Varian wide-line NMR spectrometer without changing its orientation relative to the goniometer head. The crystal was rotated systematically in the magnetic field through an angle ϕ in steps of 5° from 0 to 180° about the goniometer head axis. The precision in the setting of the angle ϕ was $\pm 0.05°$.

Deuteron magnetic resonance spectra were recorded at a crystal stabilized frequency of 7.0 MHz. The magnetic field was swept with a Varian Fieldial unit and the sweep rate was 5 and 10 mT/min. The field sweep was calibrated regularly by recording the position of the deuteron signals from a water sample (D_2O) at various frequencies, and measuring these frequencies with a frequency counter. The reproducibility of the sweep rate was 0.1 % over the whole data collection. The linearity of the utilized portion of the sweep was better than 0.3 % of the total sweep.

In order to improve the signal-to-noise ratios, all spectra were time-averaged using an IBM 1800 computer. The rf amplitude was kept low enough to avoid saturation effects.

One data set was collected at room-temperature (25 °C) where the water molecules reorient rapidly enough around their two-fold pseudosymmetry axes (flipping motion) to produce ^2H NMR signals from an averaged EFG tensor. The signals were unexpectedly broad, however. This was probably due to the water molecules not having reached a sufficiently high flip rate to produce the high temperature limiting spectrum containing narrow lines. It is well known that the ^2H NMR signals will be considerably broadened in the temperature range corresponding to the transition from the high temperature spectrum from rapidly flipping water molecules to the low temperature spectrum from "static" water molecules. This has been discussed in detail in Ref. 10. However, the spectra observed at 25 °C were judged to be sufficiently close to the high temperature limiting shape to allow a determination of the motionally averaged EFG tensor. No attempts were therefore made to produce narrower lines by increasing the temperature.

A second data set was collected at −71 °C where very narrow lines were observed from "static" water molecules. The temperature region for the line shape transition is correlated to the activation energy of the hindered rotation of the water molecule.[11,12] In Ref. 12 the following expression is given for the activation energy, E_a, in terms of the centre temperature, T, of the line shape transition region:

$$E_a = \frac{0.0374T}{1 - 0.00137T}$$

For the case of $LiClO_4.3D_2O$ a lower limit of T is −71 °C providing an estimate of the lower limit for the activation energy of 10.4 kcal/mol. This is consistent with the value of 10 kcal/mol obtained from relaxation measurements.[9]

The low temperature was obtained by using a cold nitrogen gas stream and measured with a copper-constantan thermocouple.

RESULTS AND DISCUSSION

The crystal structure of $LiClO_4 . 3H_2O$, shown in Fig. 1, belongs to the hexagonal space group $P6_3mc$ [$a = 7.719(2)$, $c = 5.455(2)$ Å],[5] with twelve asymmetric units in the unit cell. There is only one crystallographically independent O–H group, as the water oxygen is situated on a mirror plane, perpendicular to the molecular plane. On the other hand, all twelve EFG tensors at the deuteron positions in the unit cell are magnetically non-equivalent for a general orientation of the crystal relative the magnetic field. Hence, a maximum of twelve pairs of lines will appear at low temperatures when the water molecules flip sufficiently slowly, and six pairs at high temperatures, when the water molecules flip more rapidly. For the latter case, two of the EFG eigenvectors are in the mirror plane.

The ^2H NMR spectra were analyzed by using the least-squares program QSPL3 [7] in a procedure that has been described elsewhere.[13] The most widely used method to calculate the EFG tensors is the

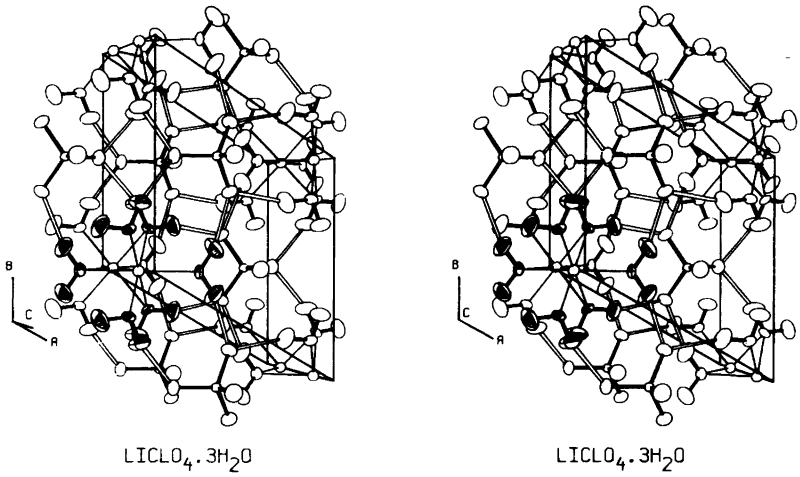

Fig. 1. A stereoscopic illustration of the crystal structure of $LiClO_4.3H_2O$, as given in Ref. 5. The six water molecules which are non-equivalent with respect to the external magnetic field are shaded.

method of Volkoff *et al.*[8] This method necessitates that the crystal be rotated in a magnetic field about three mutually orthogonal axes; the most common choice for these uses the crystallographic axes (*e.g.*, *a*, *b* and *c** for a monoclinic case). The disadvantages of this method are: (1) it fails to make explicit use of the information contained in the crystal symmetry; (2) ambiguities arise in the derived EFG tensors for certain choices of rotation axes; and (3) there can be difficulties in aligning the crystals along three orthogonal axes. The last point can be a severe problem when the crystal faces are poorly developed and optical alignment is used.

A method to calculate the EFG tensors has recently been proposed by El Saffar[14] for making use of the information from symmetry related EFG tensors. The method is based on observations of DMR splittings from only one rotation axis, provided that the observed rotation patterns are not related by a mirror plane. The method is applicable to all crystal classes except triclinic, and uses some of the information in the symmetry related splittings, but not all.

It can be shown that, for all symmetry classes except triclinic, it is also possible to extract at least partial information about the crystal orientation relative the magnetic field from the symmetry related DMR splittings. For symmetries higher than monoclinic the rotation axes and EFG tensors can, in fact, be simultaneously determined from the NMR data. One can therefore make use of crystal symmetry to correct for misalignments of the crystal, a problem that has often been discussed in the literature. It can also be shown that, for monoclinic and triclinic crystal classes, it is possible to determine some of the rotation axes (*e.g.* if one rotation axis of three is unknown, this axis may be derived from the NMR data). A procedure has been developed in this laboratory which makes full use of all crystal symmetry in the determination of EFG tensors and, where possible, also allows a simultaneous determination of the crystal orientation to be made. The procedure has been implemented in the computer program QSPL3, and the determination of the EFG tensors in $LiClO_4.3D_2O$ serves as a good example of the possibilities which this procedure offers.

The EFG tensors at 25 and −71 °C were calculated as follows: the orientation of the EFG tensors were estimated from the structural data,[5] and the quadrupole coupling constants from the hydrogen-bond distances. Putting the asymmetry parameters equal to 0.1 at −71 °C and 0.9 at 25 °C, rotation patterns were generated for both the high and low temperature cases for the rotation axis given above. These rotation patterns agreed very well with those obtained experimentally, and it was possible to assign all the rotation patterns to the appropriate symmetry operations.

All data (in all 620 observations) at both 25 and −71 °C were then used simultaneously in the refinement of the two EFG tensors, the rotation axis and the angle, θ, between the rotation axis and the

Table 1. Calculated eigenvalues and eigenvectors of the EFG tensors at 25 and −71 °C, and rotation axis for $LiClO_4.3D_2O$. The components of the vectors are given in the coordinate system defined by the unit cell axes.

Eigenvalues	Eigenvectors		
25 °C			
− 15.9(1)	−0.07477(1)	0.07477(1)	0.00430(39)
−115.5(2)	0.12955	0.12955	0
131.4(2)	−0.00175(16)	0.00175(16)	−0.18327(1)
$\eta = 0.758(2)$			
−71 °C			
−109.5(1)	−0.01704(5)	−0.13721(2)	−0.00264(149)
−135.7(1)	−0.00349(16)	0.00048(111)	−0.18324(2)
245.2(1)	0.14858(1)	0.05958(3)	−0.00461(10)
$\eta = 0.107(1)$			
Rotation axis			
0.02689(20)	−0.01699(20)	0.17511(7)	

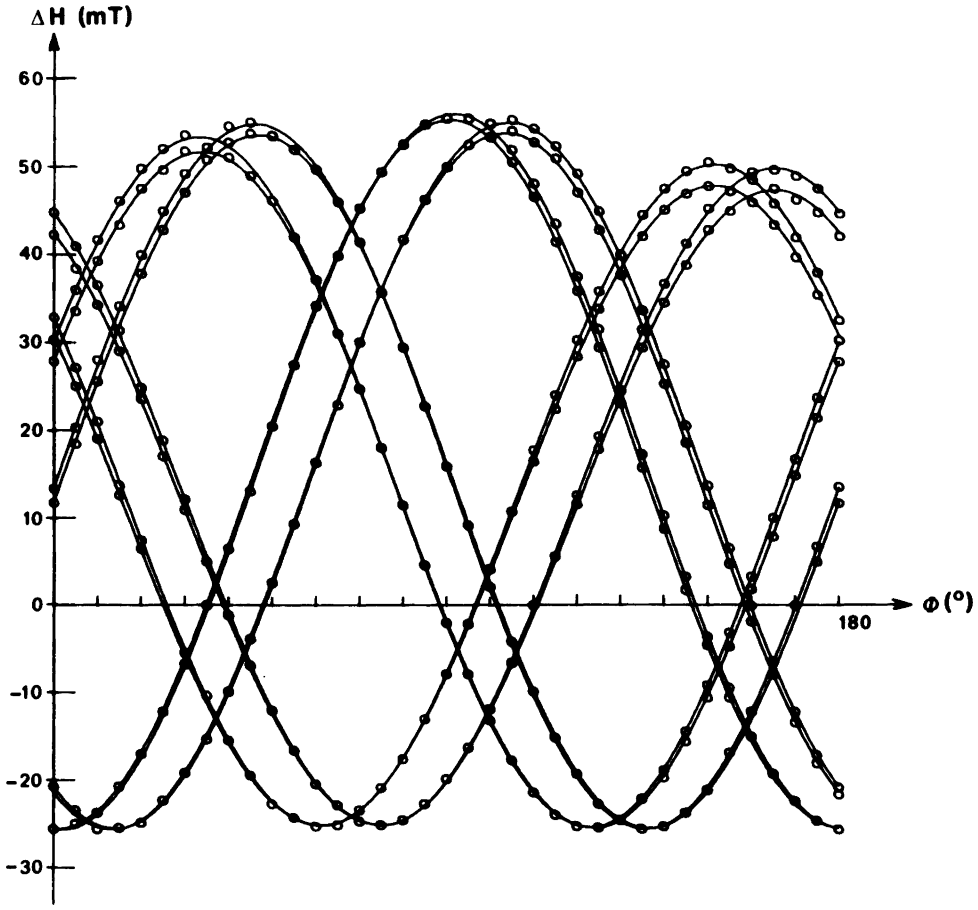

Fig. 2. Rotation patterns based on parameters given in Table 1 at −71 °C. The circles are experimental ^2H NMR-splittings.

Table 2. Some structural quantities related to the EFG tensor at −71 °C at the deuterium nuclei. α_1, α_2 and α_3 are the angles between the *z*-principal axis and the O−H, H···O and O···O vectors. β is the angle between the *y*-principal axis and the normal to the plane of the water molecule. Structural data are taken from Ref. 5.

Hydrogen bond angle O−H···O (°)	163.6(8)
O−H (Å)	0.972(7)
H···O (Å)	2.044(7)
O···O (Å)	2.989(2)
e^2qQ/h (kHz)	245.2(1)
η	0.107(1)
α_1 (°)	1.8(6)
α_2 (°)	10.1(5)
α_3 (°)	8.2(1)
β (°)	3.8(4)

external magnetic field. The estimated EFG tensors were used as start parameters in this procedure. The angle θ did not deviate significantly from 90°. The calculated EFG tensors and the rotation axis are given in Table 1. The refined rotation axis deviates by less than 0.4° from the one obtained from the diffractometer data. The rotation patterns based on the parameters in Table 1 at −71 °C are given in Fig. 2, together with the experimental ^{2}H NMR splittings. The overlap of some of the curves is due to the small angle (1.4°) between the *z*-principal axis and the $(2\bar{1}0)$ glide plane.

The root-mean-square deviation between observed and calculated splittings was 0.29 mT for the 620 observations. The single EFG tensor associated with one water molecule at 25 °C is very close to the average of the two symmetry related tensors of the same water molecule at −71 °C. The deviations are probably caused by differences in the vibrational motions at the two temperatures. The *z*-principal axis at 25 °C forms an angle of 4.0(6)° with the normal to the water molecule plane, and the *y*-principal axis is along the (110) direction as a consequence of the crystal symmetry. This is exactly along the D···D direction in the water molecule.

The *z*-principal axis at —71 °C forms an angle 1.8(6)° with the O−H direction. The angular displacement is out of the water molecule plane. In Table 2, the EFG tensor and some structural quantities are compared. The results are in good agreement with earlier results reported for other hydrates. The deuteron quadrupole coupling constant is one of the largest reported so far for a water molecule in a solid hydrate. This is in excellent agreement with the very long hydrogen bonds and the high value of O−D stretching frequency. The correlation between these quantities is discussed more extensively in Ref. 15.

Acknowledgements. The authors wish to thank Professor Ivar Olovsson for the facilities he has placed at their disposal. We also thank Mr. H. Karlsson for his invaluable technical assistance. This work has been supported by grants from the Swedish Natural Science Research Council which are hereby gratefully acknowledged.

REFERENCES

1. Brink, G. and Falk, M. *Can. J. Chem. 48* (1970) 2096.
2. Brink, G. and Falk, M. *Can. J. Chem. 48* (1970) 3019.
3. Berglund, B., Thomas, J. O. and Tellgren, R. *Acta Crystallogr. B 31* (1975) 1842.
4. Berglund, B. and Tegenfeldt, J. *Z. Naturforsch. Teil A 32* (1977) 134.
5. Sequeira, A., Bernal, I., Brown, I. D. and Faggiani, R. *Acta Crystallogr. B 31* (1975) 1735.
6. Berglund, B., Lindgren, J. and Tegenfeldt, J. *J. Mol. Struct. 45* (1978). *In press.*
7. Tegenfeldt, J. *UUIC-B13-6*, Institute of Chemistry, University of Uppsala, Sweden 1973.
8. Volkoff, G. M., Petch, H. E. and Smellie, D. W. L. *Can. J. Phys. 30* (1952) 270
9. Scheller, D. and Lippold, B. *Z. Phys. Chem. Leipzig 253* (1973) 105.
10. Berglund, B. and Tegenfeldt, J. *J. Magn. Reson. 28* (1977) 315.
11. Soda, G. and Chiba, T. *J. Chem. Phys. 50* (1969) 439.
12. Slotfeldt-Ellingsen, D. and Pedersen, B. *J. Phys. Chem. Solids 38* (1977) 65.
13. Berglund, B., Lindgren, J. and Tegenfeldt, J. *J. Mol. Struct. 21* (1974) 135.
14. El Saffar, Z. M. *J. Magn. Reson. 19* (1975) 233.
15. Berglund, B., Lindgren, J. and Tegenfeldt, J. *J. Mol. Struct. 45* (1978). *In press.*

Received July 19, 1977.

Acta Chemica Scandinavica A 32 (1978) 7 – 14

Solvent Extraction Studies on the Complex Formation between Methylmercury(II) and Bromide, Chloride and Nitrate Ions

MOHAMMAD JAWAID,[a] FOLKE INGMAN,[a] D. HAY LIEM[b] and TOM WALLIN[b]

[a] Department of Analytical Chemistry and [b] Department of Inorganic Chemistry, The Royal Institute of Technology (KTH), S-100 44 Stockholm 70, Sweden

Complex formation between $CH_3Hg(II)$ and Cl^-, Br^- and NO_3^- ions in the two-phase system *o*-xylene/*Y* M (Na,H)(Br,Cl,NO_3)(aq), $Y=1.0$ or 2.5, has been studied at 25 °C by radiometric measurement of the distribution of $CH_3{}^{203}Hg$ between the two phases as a function of the chloride, bromide and nitrate concentration. The distribution data, which have been analyzed using the computer program LETAGROP-DISTR, may be explained by the formation of the methylmercury(II) species CH_3HgCl, CH_3HgBr in both phases and additional formation of $CH_3HgBr_2^-$ in the aqueous phase and CH_3HgNO_3 in the organic phase. The values of the equilibrium constants are:

	$Y=1.0$	$Y=2.5$
	log $(K\pm3\sigma)$	log $(K\pm3\sigma)$
$CH_3Hg^+ + Br^- \rightleftharpoons CH_3HgBr(aq)$	6.37 ± 0.02	6.60 ± 0.25
$CH_3Hg^+ + Br^- \rightleftharpoons CH_3HgBr(org)$	8.06 ± 0.13	8.30 ± 0.20
$CH_3Hg^+ + NO_3^- \rightleftharpoons CH_3HgNO_3(org)$	-0.98 ± 0.09	-1.21 ± 0.04
$CH_3Hg^+ + 2Br^- \rightleftharpoons CH_3HgBr_2^-(aq)$	6.09 ± 0.14	5.98 ± 0.09
$CH_3Hg^+ + Cl^- \rightleftharpoons CH_3HgCl(aq)$		5.50 ± 0.01
$CH_3Hg^+ + Cl^- \rightleftharpoons CH_3HgCl(org)$		6.59 ± 0.01

The coordination chemistry of organomercurial ions, *e.g.* CH_3Hg^+ ions, with ligands in natural waters, *e.g.* the halogenides, OH^- and NO_3^- ions, is of great interest for a deeper understanding of their polluting effects on the environment. Organic mercury compounds enter natural waters in different ways.[1-3] In such forms mercury is easily absorbed by living organisms and the deletarious effects on the health of man and animals have been established.[4,5]

In natural waters, organomercurial ions are usually found in trace concentrations complexed with ligands present in the system. Studies of the chemical state of these compounds under similar conditions are of interest for understanding their distribution in nature. In this work, we report the results of liquid-liquid extraction studies on complex formation between methylmercury(II) and Cl^-, Br^- and NO_3^- ions in the system *o*-xylene/1.0 M (H,Na)(Br,Cl,NO_3)(aq) and *o*-xylene/2.5 M (H,Na)(Br,Cl,NO_3)(aq). Studies on the complex formation of MeHg(II) with Cl^- in the two-phase system *o*-xylene/1.0 M (H,Na)(Cl,ClO_4) and its hydrolysis and complex formation with phosphate ions in *o*-xylene/1.0 M (H,Na)(Cl,PO_4,NO_3) have been reported previously.[6,7] Preliminary results from this work have been reported elsewhere.[8]

Previous work

A potentiometric method of studying the complex formation between methylmercury(II) and Br^- ions has been used by Waugh *et al.*,[9] Schwarzenbach and Schellenberg,[10,11] and Zanella *et al.*[12] These authors reported the formation of CH_3HgBr species. Simpson[13] assumed the formation of CH_3HgBr in the aqueous and toluene phase and calculated from a

single experimental point the distribution constant $K_D = 45$. The kinetics of the formation of the species CH_3HgX^{1-n} from CH_3HgOH for $X^{n-} = Cl^-$, Br^-, I^-, SCN^- and SO_3^{2-}, have been studied by Eigen *et al.*[14] The complex formation between methylmercury(II) and Br^-, Cl^-, NO_3^- and OH^- ions studied by different methods are summarized in Table 3.

EXPERIMENTAL

Reagents. NaCl, *p.a.* (Merck), NaBr, AnalaR (Mallinckrodt) or Ultrapur quality were dried at 110–120 °C and used without further purification. The chloride content in the NaBr sample was determined mass spectrometrically. Typical results were 0.32 % NaCl in NaBr (*p.a.*) and 0.05 % in NaBr (Ultrapur). These values were used to correct the initial total concentration of chloride in the system. The purity of the non-radioactive methylmercuric hydroxide (Alfa Inorganics, Ventron) was checked by titration with standard acid and by an atomic absorption technique.[15] It was found to be better than 97 %. The radioactive $CH_3{}^{203}Hg$ was purchased in the form of CH_3HgCl (Radiochemical Centre, Amersham, England) and freed from inorganic ^{203}Hg as described previously.[6] For the distribution experiments, a stock solution of 1.6×10^{-6} M $CH_3{}^{203}HgCl$ in *o*-xylene was used. All the *o*-xylene (Merck *p.a.*) was purified as described previously.[7]

Distribution experiments

Manual method. Equal volumes (10–15 ml) of aqueous phase (with composition Y M (Na,H,MeHg)(Br,Cl,NO_3), $Y = 1.0$ or 2.5) and organic phase (MeHgCl–*o*-xylene) were equilibrated and the distribution of $CH_3Hg(II)$ between the phases measured radiometrically as described previously.[7]

Automatic method. Some of the distribution experiments were carried out using a computer-controlled AKUFVE apparatus. The method is based on the use of PDP-11/10 computer as the controlling unit using BASIC as the program language. A detailed description of the system will be published elsewhere.[16] AKUFVE is an apparatus for continous liquid-liquid extraction experiments constructed by Rydberg *et al.*[17]

All experiments were carried out in thermostated rooms at 25 °C.

SYMBOLS AND EQUILIBRIUM CONSTANTS

$[\ ], [\ ]_{org}$ = equilibrium concentration in the aqueous phase and the organic phase

C_X = the initial total concentration of the species X referred to the aqueous phase. $X = CH_3Hg(II)$, Cl^-, Br^- or NO_3^-

K_{pq}^{org} = formation constant of the complex $(MeHg^+)_p(X^-)_q(org)$ (*cf.* eqn. 1)

K_{rs}^{aq} = formation constant of the complex $(MeHg^+)_r(X^-)_s(aq)$ (*cf.* eqn. 2)

I_{org}, I_{aq} = radioactivity of $CH_3{}^{203}Hg$ in the organic and aqueous phase in counts per unit time and unit volume and corrected for background and deadtime

D = $\Sigma[MeHg]_{org}/\Sigma[MeHg]_{aq} = I_{org}/I_{aq}$, net distribution ratio of $CH_3Hg(II)$

D_{exp}, D_{calc} = experimental and calculated distribution ratio of $CH_3Hg(II)$

U_{min} = the minimized error-square sum, *e.g.* for $val = 1$ one minimizes $U = \sum_1^{Np}(\log D_{calc} - \log D_{exp})^2$, where Np is the number of experimental points (*cf.* Ref. 18)

BASIC ASSUMPTIONS AND CHEMICAL MODEL

In our treatment of the data we assumed the formation of the set of species $(H^+)_p(MeHg^+)_q(Cl^-)_r(Br^-)_s(NO_3^-)_t(org)$ and $(H^+)_k(MeHg^+)_l(Cl^-)_m(Br^-)_n(NO_3^-)_o(aq)$ (*cf.* Refs. 7, 18)

However, as no evidence for any mixed complexes has been found, we will in this paper for simplicity describe these sets of species as $(MeHg^+)_p(X^-)_q(org)$ and $(MeHg^+)_r(X^-)_s(aq)$, where $X^- = Cl^-$, Br^-, NO_3^- or OH^-, with the formation constants

$$K_{pq}^{org} = [(MeHg^+)_p(X^-)_q]_{org}[MeHg^+]^{-p}[X^-]^{-q} \quad (1)$$

and

$$K_{rs}^{aq} = [(MeHg^+)_r(X^-)_s][MeHg^+]^{-r}[X^-]^{-s} \quad (2)$$

It is assumed that in the organic phase, only uncharged complexes are formed and that the activity coefficient of the species is kept constant by maintaining a constant ionic strength (= 1 or 2.5 M). The distribution ratio of MeHg(II) may be expressed by

$$D_{calc} = \frac{\Sigma p K_{pq}^{org}[MeHg^+]^p[X^-]^q}{\Sigma r K_{rs}^{aq}[MeHg^+]^r[X^-]^s} \quad (3)$$

From (3) D_{calc} may be calculated for a given point, if C_{MeHg}, C_{Cl^-}, C_{Br^-}, $C_{NO_3^-}$, log $[H^+]$ and K_{pq}^{org} and K_{rs}^{aq} for the set of species are given.

The distribution data were analyzed using the computer program LETAGROP-DISTR.[18] In this analysis all points were given equal weights.

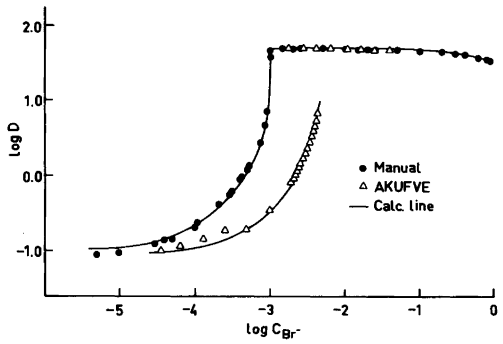

Fig. 1. The distribution of MeHg(II) between *o*-xylene and 1.0 M (Na,H)(Br,Cl,NO_3) aqueous phase as a function of initial total concentration of bromide and for two different levels of C_{MeHg}, 1.0×10^{-3} M and 4.9×10^{-4} M.

The full-drawn lines have been calculated using the equilibrium constants given in Table 2, Model No. V, for the formation of the species MeHgCl, MeHgBr and $MeHgBr_2^-$ in the aqueous phase and MeHgCl, MeHgBr and $MeHgNO_3$ in the organic phase.

RESULTS

The primary data from the distribution experiments are available from one of the authors (D.H.L.) on request.

The system o-xylene/1.0 M (Na,H)(Br,Cl,NO_3). The results are illustrated in Fig. 1. Log $[H^+] = -2.00$ and log C_{Cl^-} was varied from -2.08 to -8.06. As shown previously,[10,6] no hydrolyzed MeHg(II) species are formed at log $[H^+] = -2$. Fig. 1 shows that at low values of C_{Br^-} (less than 0.1 mM), log D levels off with decreasing C_{Br^-}. This indicates the extraction of MeHgCl as found previously, and other MeHg(II) species which do not contain Br^- ions. As will be shown, the data indicate the extraction of $MeHgNO_3$. The distribution curves form straight lines with increasing C_{Br^-} and level off to a horizontal line at $C_{Br^-} > 1$ mM. This may be explained by the formation of MeHgBr(org) and MeHgBr(aq). In addition, at $C_{Br^-} > 0.1$ M, log D decreases with increasing C_{Br^-} indicating the formation of $MeHgBr_2^-$(aq).

The results of the computer analysis for five models are summarized in Table 1. Previous studies[6] showed the formation of MeHgCl in the aqueous and *o*-xylene phases. The formation constants found, *i.e.* $K = 10^{6.39}$ M^{-1} for MeHgCl(org), and $K = 10^{5.32}$ M^{-1} for MeHgCl(aq), were used and not varied in the computer calculations. Minimizing the error-square sum ($Np = 72$ points) model V, in which the formation of MeHgCl(org), MeHgBr(org), $MeHgNO_3$(org), and MeHgCl(aq), MeHgBr(aq) and $MeHgBr_2^-$(aq) species is assumed, gives the best fit. For this model the minimized error-square sum $U_{min} = 0.118$ and $\sigma(\log D) = 0.04$.

Table 1. Equilibrium constants[a] log K for the formation of methylmercury(II) species in the system MeHg(II)–*o*-xylene/1.0 M (Na,H)(Br,Cl,NO_3) for various assumptions of MeHg(II) complexes that minimize the error-square sum, $U = \sum_1^{72} (\log D_{calc} - \log D_{exp})^2$.

Model	MeHg(II) species in the aqueous phase[b]		MeHg(II) species in the organic phase[c]		U_{min}	$\sigma(\log D)$
	MeHgBr	$MeHgBr_2^-$	MeHgBr	$MeHgNO_3$		
I	–	–	–	–	628	–
II	$K = 0$	–	–	–	628	2.97
III	6.43 max 6.98[d]	–	8.11 max 8.64[d]	–	6.63	0.31
IV	6.36(6)	–	8.03(7)	−0.99(8)	0.191	0.06
V[e]	6.37(2)	6.09(14)	8.06(13)	−0.98(9)	0.118	0.04

[a] The limits given correspond approximately to log $(K \pm 3\sigma)$. [b] For MeHgCl log $K = 5.32$. The value was kept constant during the course of computer calculations. [c] For MeHgCl log $K = 6.39$. The value was kept constant during the course of computer calculations. [d] If $\sigma(K) > 0.2K$, the maximum value = log $[K + 3\sigma(K)]$ is given. [e] The best model assumed.

Table 2. Comparison of formation constants for the species in model V (Table 1) in the two-phase system MeHg(II) – *o*-xylene/1.0 M (Na,H)(Br,Cl,NO_3) which minimizes the three types of error-square sum $U_1=\sum_1^{72}[\log (D_{calc}D_{exp}^{-1})]^2$, $U_2=\sum_1^{72}(D_{calc}D_{exp}^{-1}-1)^2$ and $U_3=\sum_1^{72}(D_{exp}D_{calc}^{-1}-1)^2$ respectively.

Type of error minimized	Species in the aqueous phase	$\log(K\pm3\sigma)$	Species in the organic phase	$\log(K\pm3\sigma)$	U_{min}	$\sigma(\log D)$
U_1	MeHgBr	6.37(2)	MeHgBr	8.06(13)	0.118	0.04
	$MeHgBr_2^-$	6.09(14)	$MeHgNO_3$	−0.98(9)		
U_2	MeHgBr	6.36(8)	MeHgBr	8.06(8)	0.626	0.09
	$MeHgBr_2^-$	6.13(24)	$MeHgNO_3$	−0.95(4)		
U_3	MeHgBr	6.36(10)	MeHgBr	8.06(10)	0.598	0.09
	$MeHgBr_2^-$	6.12 max 6.32[a]	$MeHgNO_3$	−1.00(4)		

[a] If $\sigma(K)>0.2$ *K*, the maximum value $\log[K+3\sigma(K)]$ is given.

Model IV, in which the species $MeHgBr_2^-$ is not considered, gives $U_{min}=0.191$ and $\sigma(\log D)=0.06$, which may also be considered as an acceptable fit to the data. However, the distribution at $C_{Br}>0.1$ M, *cf.* Fig. 1, indicates a systematic deviation due to the formation of $MeHgBr_n^{1-n}$, with $n>1$. These effects indicating the formation of $MeHgBr_2^-$ were found to be more pronounced in the two-phase system *o*-xylene/2.5 M (Na,H)(Br,Cl,NO_3), *cf.* Fig. 4. In Table 2, we compare the results obtained when other types of error-square sums are minimized. If the formation of the MeHg(II) species given in model V (Table 1) is assumed, practically the same values for the equilibrium constants are obtained for the three types of error-square sums. This supports the view that the data may be given equal weight. We conclude that the supposition of formation of the following methylmercury(II) species gives a good description of the distribution of MeHg(II) between the two phases.

	$\log(K\pm3\sigma)$	
$MeHg^+ + Br^- \rightleftharpoons MeHgBr(aq)$	6.37 ± 0.02	(4)
$MeHg^+ + 2Br^- \rightleftharpoons MeHgBr_2^-(aq)$	6.09 ± 0.14	(5)
$MeHg^+ + Cl^- \rightleftharpoons MeHgCl(aq)$	5.32 ± 0.09	(6)
	(*cf.* Ref. 10)	
$MeHg^+ + Br^- \rightleftharpoons MeHgBr(org)$	8.06 ± 0.13	(7)
$MeHg^+ + NO_3^- \rightleftharpoons MeHgNO_3(org)$	-0.98 ± 0.09	(8)
$MeHg^+ + Cl^- \rightleftharpoons MeHgCl(org)$	6.39 ± 0.09	(9)
	(*cf.* Ref. 10)	

Using eqns. (4), (5) and (6), we obtain the equilibrium constant for the exchange reaction:

$$MeHgCl(aq)+Br^- \rightleftharpoons MeHgBr(aq)+Cl^-;\quad \log(K\pm3\sigma)=1.05\pm0.09 \qquad (10)$$

$$MeHgCl(aq)+2Br^- \rightleftharpoons MeHgBr_2^-(aq)+Cl^-;\quad \log(K+3\sigma)=0.77\pm0.17 \qquad (11)$$

From eqns. (4) and (7), we obtain the distribution constant for MeHgBr:

$$MeHgBr(aq) \rightleftharpoons MeHgBr(org);\quad \log(K_D\pm3\sigma)=1.69\pm0.13 \qquad (12)$$

In Fig. 2, log *D* is plotted *versus* log $[Br^-]$. All the experimental points for different C_{MeHg} are seen to fall on the same line. This strongly indicates that only mononuclear methylmercury(II) species are formed.

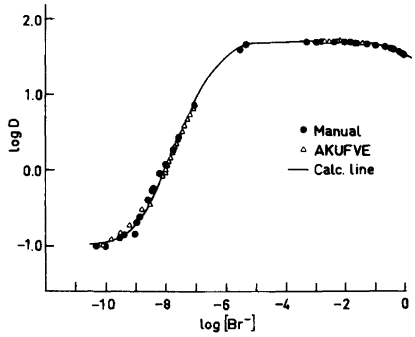

Fig. 2. The distribution of MeHg(II) between *o*-xylene and 1.0 M (Na,H)(Br,Cl,NO_3) as a function of the equilibrium concentration of bromide ions in the aqueous phase $[Br^-]$ M, and for the different initial total concentrations of methylmercury(II).

The full-drawn lines have been calculated using equilibrium constants given in Table 1, Model No. V.

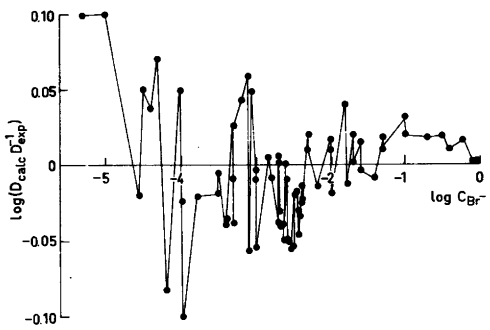

Fig. 3. The error log ($D_{calc}D_{exp}^{-1}$) as a function of log C_{Br^-} for the two-phase system MeHg(II)–*o*-xylene/1.0 M (Na,H)(Br,Cl,NO_3) assuming the species with the equilibrium constants given in Table 1, Model No. V.

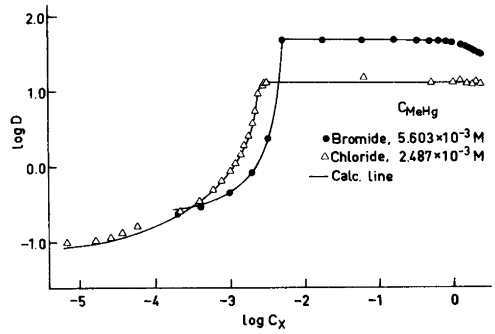

Fig. 4. The distribution of MeHg(II) in the two-phase system *o*-xylene/2.5 M (Na,H)(Br,Cl,NO_3) as a function of the total initial concentration of bromide at $C_{MeHg}=5.603\times10^{-3}$ M (●) and of chloride for $C_{MeHg}=2.487\times10^{-3}$ M (△). C_X represents C_{Br^-} or C_{Cl^-}.

The full-drawn lines have been calculated using the equilibrium constants given in Table 3 for the formation of the different MeHg(II) species.

In Fig. 3, the function log ($D_{calc}D_{exp}^{-1}$) is plotted *versus* log C_{Br^-} assuming model V in Table 1. The distribution of the points is seen to show no systematic deviations.

In Fig. 5, the mol % distribution of the MeHg(II) species is shown as a function of log [Br^-] at constant $C_{MeHg}=1.0\times10^{-3}$ M, $C_{Cl^-}=1.0\times10^{-5}$ M, $C_{NO_3^-}=1.0$ M and log [H^+] = −2.0. In Fig. 6, the distribution of the dominating species is plotted as a function of log [H^+] at constant $C_{MeHg}=1.0\times10^{-4}$ M, $C_{Br^-}=1.0\times10^{-4}$ M, $C_{Cl^-}=1.0\times10^{-3}$ M and $C_{NO_3^-}=1.0$ M. These curves were calculated using the HALTAFALL program,[23] assuming MeHg(II) species and equilibrium constants according to model V in Table 1. For MeHgOH the equilibrium constants determined previously[22] were used. The concentrations of the MeHg(II) species not repre-

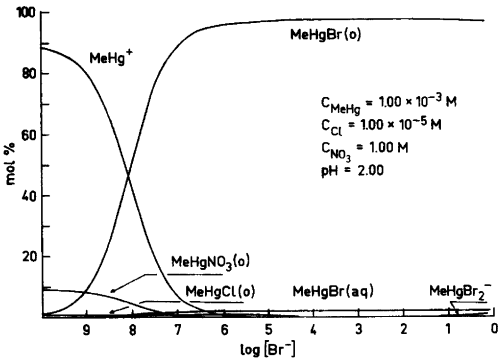

Fig. 5. The mol % distribution of different MeHg(II) species in the two-phase system *o*-xylene/1 M (Na,H)(Br,Cl,NO_3) as a function of log [Br^-] for constant values of $C_{MeHg}=1.00\times10^{-3}$ M, $C_{Cl^-}=1.00\times10^{-5}$ M, $C_{NO_3^-}=1.00$ M and [H^+] = 1.00×10^{-2} M.

The curves have been calculated assuming the species and equilibrium constants according to Model No. V in Table 1.

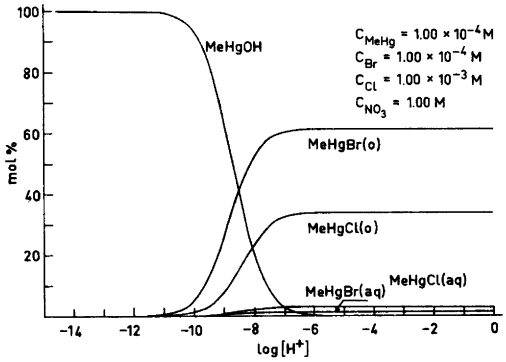

Fig. 6. The mol % distribution of the predominant MeHg(II) species in the two-phase system *o*-xylene/1 M (Na,H)(Br,Cl,NO_3) as a function of log [H^+] at constant $C_{MeHg}=1.0\times10^{-4}$ M, $C_{Br^-}=1.0\times10^{-4}$ M, $C_{Cl^-}=1.0\times10^{-3}$ M and $C_{NO_3^-}=1.0$ M. The MeHg(II) species not represented in the figure were found to be negligible under the extraction conditions studied.

sented in these figures were found to be negligible under the extraction conditions studied.

The system o-xylene/2.5 M (Na,H)(Br,Cl,NO_3). In Fig. 4, the distribution of MeHg(II) in the two-phase system *o*-xylene/2.5 M (Na,H)(Cl,NO_3) is illustrated for $C_{MeHg}=2.487\times10^{-3}$ M, log $[H^+]=-2.0$ and varying chloride concentration. In agreement with the previous conclusions,[6] the distribution curve indicates the formation of the species MeHgCl(aq) and MeHgCl(org). LETAGROP analysis of the data ($Np=23$ points) shows that these can be explained ($U_{min}=0.462$, $\sigma(\log D)=0.0145$) by assuming the following set of MeHg(II) species and equilibrium constants:

	log $(K\pm3\sigma)$	
$MeHg^+ + Cl^- \rightleftharpoons MeHgCl(aq)$	5.50 ± 0.01	(13)
$MeHg^+ + Cl^- \rightleftharpoons MeHgCl(org)$	6.59 ± 0.01	(14)
$MeHg^+ + NO_3^- \rightleftharpoons MeHgNO_3(org)$	-1.21 ± 0.04	(15)

The distribution constant of MeHgCl may thus be calculated from (13) and (14):

$MeHgCl(aq) \rightleftharpoons MeHgCl(org)$;
$\log(K_D\pm3\sigma)=1.09\pm0.01$ (16)

Fig. 4 also illustrates log D *versus* log C_{Br^-} for the system *o*-xylene/2.5 M (Na,H)(Br,Cl,NO_3). Comparing Fig. 4 and Fig. 1, we see not only the similarity of the curves but also the more pronounced effects on D, due to the formation of $MeHgBr_n^{1-n}$ species with $n>1$ at $C_{Br^-}>0.1$ M. Computer analyses of the data assuming the set of methylmercury(II) species found previously (Model V, Table 1), gives $U_{min}=0.018$ and $\sigma(\log D)=0.032$ for $Np=20$ points and the following values of the equilibrium constants:

	log $(K\pm3\sigma)$	
$MeHg^+ + Br^- \rightleftharpoons MeHgBr(aq)$	6.60 ± 0.25	(17)
$MeHg^+ + Br^- \rightleftharpoons MeHgBr(org)$	8.30 ± 0.20	(18)
$MeHg^+ + 2Br^- \rightleftharpoons MeHgBr_2^-(aq)$	5.98 ± 0.09	(19)

The values of K for the formation of MeHgCl(aq), MeHgCl(org) and $MeHgNO_3$(org) given in (13), (14) and (15) were not varied during the computer calculations. From (17) and (18) we obtain the distribution constant of MeHgBr:

$MeHgBr(aq) \rightleftharpoons MeHgBr(org)$
$\log(K_D\pm3\sigma)=1.69\pm0.31$

Table 3. Equilibrium constant for formation of methylmercury(II) species in various systems. The temperature is 25 °C, if not otherwise stated.

System	Equilibrium reaction	log K[a]	Method	Ref.
Water/toluene	$MeHgCl(aq) \rightleftharpoons MeHgCl(org)$	1.0[b]	DISTR	13
0–7 mM Cl^-	$MeHg^+ + Cl^- \rightleftharpoons MeHgCl(aq)$	5.45	EMF	9
Water	$MeHg^+ + Cl^- \rightleftharpoons MeHgCl(s)$	7.16	SOL	9
0.1 M KCl	$MeHg^+ + Cl^- \rightleftharpoons MeHgCl(aq)$	5.25	EMF	10, 11
0.1 M KNO_3	$MeHg^+ + Cl^- \rightleftharpoons MeHgCl(aq)$	4.90[c]	EMF	12
o-Xylene/1.0 M (Na,H)ClO_4	$MeHg^+ + Cl^- \rightleftharpoons MeHgCl(aq)$	5.32(9)	DISTR	6
	$MeHg^+ + Cl^- \rightleftharpoons MeHgCl(org)$	6.39(9)		
o-Xylene/2.5 M (Na,H)NO_3	$MeHg^+ + Cl^- \rightleftharpoons MeHgCl(aq)$	5.64(1)	DISTR	This
	$MeHg^+ + Cl^- \rightleftharpoons MeHgCl(org)$	6.73(1)		work
	$MeHg^+ + NO_3^- \rightleftharpoons MeHgNO_3(org)$	−1.21(4)		
Water/toluene	$MeHgBr(aq) \rightleftharpoons MeHgBr(org)$	1.7[b]	DISTR	13
0–7 mM	$MeHg^+ + Br^- \rightleftharpoons MeHgBr(aq)$	6.70	EMF	9
	$MeHg^+ + Br^- \rightleftharpoons MeHgBr(s)$	8.92	SOL	9
0.1 M (K,H)NO_3	$MeHg^+ + Br^- \rightleftharpoons MeHgBr(aq)$	6.62	EMF	10, 11
0.1 M KNO_3	$MeHg^+ + Br^- \rightleftharpoons MeHgBr(aq)$	5.98[c]	EMF	12
o-Xylene/1.0 M (Na,H)NO_3	$MeHg^+ + Br^- \rightleftharpoons MeHgBr(org)$	8.06(13)	DISTR	This work
o-Xylene/1.0 M (Na,H)NO_3	$MeHg^+ + Br^- \rightleftharpoons MeHgBr(aq)$	6.37(2)	DISTR	This
	$MeHg^+ + 2Br^- \rightleftharpoons MeHgBr_2^-(aq)$	6.09(14)		work
	$MeHg^+ + NO_3^- \rightleftharpoons MeHgNO_3(org)$	−0.98(9)		
Water	$MeHg^+ + OH^- \rightleftharpoons MeHgOH(s)$	13.66	SOL	22

[a] The limits given correspond approximately to log $[K\pm3\sigma(K)]$. [b] Calculated from one single experimental point available. [c] At 20 °C.

DISCUSSION

Equilibrium constants for the formation of the species between methylmercury(II) and Cl^-, Br^- and NO_3^- ions in different systems are summarized in Table 3. The present work shows that in the aqueous as well as in the organic phase, MeHg(II) and Cl^- ions form only the 1:1 complex, MeHgCl, up to C_{Cl^-} around 2.5 M. However, with Br^- ions and $C_{Br^-} > 0.1$ M, the formation of 1:2 species, $MeHgBr_2^-$ is also indicated.

Barbieri and Bjerrum[19] reported solubility measurements in 1 M $Na(X,ClO_4)$ indicating the formation of negatively charged complexes $RHgX_n^{1-n}$ (R = ethyl and 2-butyl, $n = 1, 2, 3$) for X = SCN and I. Rizzardi *et al.*[20] explained their ion exchange data by assuming the formation of C_2H_5HgCl at $C_{Cl^-} \leq 1$ M and the formation of $C_2H_5HgCl_2^-$ species at high chloride concentrations ($C_{Cl^-} = 1-10$ M). In the present work, however, no negatively charged methylmercury(II) chloride complexes have been found for $C_{Cl^-} \leq 2.5$ M.

The results of the computer analysis show that the constants for the formation of the species MeHgBr(aq) and MeHgBr(org) have smaller standard deviations from data of 1.0 M compared with those of 2.5 M ionic medium. This may be explained statistically by the greater number of data available for the case of 1.0 M ionic medium ($Np = 72$ points) compared with that of 2.5 M medium ($Np = 23$ points). For the formation of $MeHgBr_2^-$(aq) species, however, a smaller value of $\sigma(K)$ was found in the case of 2.5 M ionic medium compared with that of 1.0 M, which is understandable since according to the mass-action law the formation of $MeHgBr_2^-$ is expected to be more predominant at higher bromide concentrations.

The decrease of the constant for the formation of $MeHgNO_3$(org) found for 1.0 M ionic medium compared with that of 2.5 M medium may, in part, be due to the formation of $MeHgNO_3$(aq) which is expected to increase at higher nitrate concentrations in the aqueous medium. However, from the available data no definite conclusions on this matter can be made.

Mercury(II) is a typically soft acceptor. Since the methyl group must be regarded as an extremely soft donor, it is to be expected that the character of the methylmercury(II) ion will be pronouncedly harder than that of Hg(II). Comparison of the stabilities of the halide complexes of Hg(II) and MeHg(II) seems to support this hypothesis. The methylmercury ion is still soft, as indicated by the fact that the bromide complex of MeHg(II) is more stable than the chloride complex, but the difference is much less pronounced than for the corresponding first Hg(II) complexes.

Table 4. Stability constants for the halides MeHgX and HgX^+ (*cf.* Refs. 11, 24).

X	log K_{MeHgX}	log K_{HgX^+}
F^-	1.5	1.0
Cl^-	5.2	6.7
Br^-	6.6	9.0
I^-	8.6	12.9

Comparison of the other halide complexes also supports the hypothesis. This can be seen from Table 4, which illustrates for similar media, obtained by Schellenberg ($MeHg^+$)[11] and Paul (Hg^{2+}).[24]

The difference in charge between Hg^{2+} and CH_3Hg^+ is expected to affect the stability of a given methyl halide complex, which thus makes a direct comparison between the two types of metal complexes rather difficult. However, the effect of the metal group in CH_3Hg(II) on the stability of a halide complex may in part be seen by comparing the stability constants of MeHgX for different X, with that found in the case for the formation of HgX^+ (Table 4).

The distribution constants, K_D, for MeHgCl and MeHgBr, respectively, prove to be practically independent of the ionic strength. Thus, we find for $MeHgCl(aq) \rightleftharpoons MeHgCl(org)$, $K_D = 10^{1.07}$ at ionic strength 1.0 M (*cf.* Ref. 6) and $K_D = 10^{1.09}$ at 2.5 M. For MeHgBr, K_D is found to be $10^{1.69}$ at both these

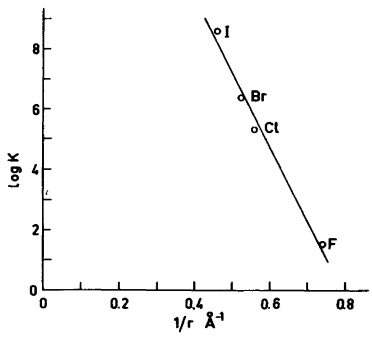

Fig. 7. The equilibrium constant for the formation of MeHgX, (X = F^-, Cl^-, Br^-, I^-) as a function of $1/r$, were r is the ionic radius of X taken from Ref. 27.

levels of ionic strength. This result is in agreement with the assumption that only uncharged species are involved in the relevant distribution equilibrium.

In Fig. 7 the value of log K for the formation of MeHgX is plotted as a function of the inverted value of the ionic radius. The points fall practically on a straight line indicating the formation of predominantly ionic bonds. A theoretical explanation for this has been given previously by Dyrssen.[25] A similar relation was shown by Dyrssen and Liem[26] to exist for complex formation between lanthanides, actinides and dialkylphosphoric acid.

Table 2 illustrates the results of minimizing different types of error-square sums. Practically the same values were found for the equilibrium constants for the formation of the methylmercury(II) species. This means that giving the same weight to the points, as was done during the computer analysis, is justified.

The extraction of methylmercury as methylmercury chloride in an organic phase has found application in analytical separation and assay of methylmercury.[21] The higher distribution constant of MeHgBr compared with MeHgCl ($\Delta \log K_D = 0.62$) indicates that the extraction efficiency will be increased considerably if bromide is substituted for chloride.

Acknowledgements. This work has been financially supported by the Swedish Natural Science Research Council and the Swedish Board for Technical Development. The authors are much obliged to Professor Ingmar Grenthe for his keen interest in the work and to Kjell Gustavsson for his help with the mass spectrometric analyses. Dr. Derek Lewis has revised the English of the manuscript.

REFERENCES

1. a. Lindström, O. *Trans. R. Inst. Technol. Stockholm* 1968; b. Torgeson, D. C. *Fungicides, Academic*, N. Y. 1967, Vol. I.
2. Jensen, S. and Jernelöv, A. *Nature 223* (1969) 753.
3. Wood, J. M., Kennedy, F. S. and Rosen, C. G. *Nature 220* (1968) 173.
4. Irukayama, K. *Adv. Water Pollut. Res. 3* (1967) 153.
5. Borg, K., Wanntorp, H., Ferne, K. and Hanko, E. *J. Appl. Ecol. 3* (1966) 171.
6. Budevsky, O., Ingman, F. and Liem, D. H. *Acta Chem. Scand. 27* (1973) 1277.
7. Ingman, F. and Liem, D. H. *Acta Chem. Scand. A 28* (1974) 947.
8. Jawaid, M., Ingman, F., Liem, D. H. and Wallin, T. *Proc. Conf. on the Effect of Toxic Metals on Man and Environment*, Luleå 1976, Sweden.
9. Waugh, T. D., Harold, F. W. and Laswick, J. A. *J. Phys. Chem. 59* (1955) 395.
10. Schellenberg, M. *Diss.*, ETH, Zürich 1963.
11. a. Schellenberg, M. and Schwarzenbach, G. *Proc. 7th Int. Conf. Coord. Chem.* Stockholm 1962, p. 157; b. *Helv. Chim. Acta 48* (1965) 28.
12. Zanella, P., Plazzogna, G. and Tagliavini, G. *Inorg. Chim. Acta 2(3)* (1968) 340.
13. Simpson, R. B. *J. Am. Chem. Soc. 83* (1961) 4711.
14. Eigen, M., Geser, G. and Kruse, W. *Experientia 9* (1954) 164.
15. Matsunaga, K., Ishida, T. and Oda, T. *Anal. Chem. 48* (9) (1976) 1421.
16. Wallin, T., Liem, D. H. and Högberg, K. *Proc. Int. Conf. Solvent Extraction Chem.* (ISEC 77), Toronto 1977. *In press.*
17. a. Rydberg, J. *Acta Chem. Scand. 23* (1969) 647; b. Reinhardt, H. and Rydberg, J. *Ibid. 23* (1969) 2781.
18. a. Liem, D. H. *Acta Chem. Scand. 25* (1971) 1521; b. Ingri, N. and Sillén, L. G. *Ark. Kemi 23* (1964) 97; c. Sillén, L. G. and Warnqvist, B. *Ibid. 31* (1969) 341; d. Arnek, R., Sillén, L. G. and Wahlberg, O. *Ibid. 31* (1969) 353.
19. Barbieri, R. and Bjerrum, J. *Acta Chem. Scand. 19* (1965) 469.
20. Rizzardi, G., Pietropaolo, R. and Barbini, R. *Gazz. Chim. Ital. 96* (1965) 1371.
21. Östlund, K. *Acta Pharmacol. Toxicol. 27* (1969) 1.
22. Jawaid, M., Ingman, F. and Liem, D. H. *Acta Chem. Scand. In press.*
23. Ingri, N., Kakolowicz, W., Sillén, L. G. and Warnqvist, B. *Talanta 14* (1967) 1221.
24. Paul, A. D. *Thesis*, Univ. Calif., Berkeley 1955.
25. Dyrssen, D. Diss., *Sven. Kem. Tidskr. 68* (1956) 212.
26. Dyrssen, D. and Liem, D. H. *Acta Chem. Scand. 14* (1960) 1100.
27. Pauling, L. *Nature of the Chemical Bond*, Cornell University Press, New York 1960.

Received July 11, 1977.

Acta Chemica Scandinavica A 32 (1978) 15–17

Equilibrium Constants in the Ammonium Carbonate–Carbaminate System. The Acid Dissociation Constant of Carbamic Acid

FINN CHRISTENSSON, HANS C. S. KOEFOED, ALLAN C. PETERSEN and KAJ RASMUSSEN

Chemistry Department, Royal Veterinary and Agricultural University, 40 Thorvaldsensvej, DK-1871 Copenhagen V, Denmark

The equilibrium constant for the reaction

$$NH_3 + HCO_3^- \rightleftharpoons NH_2COO^- + H_2O$$

the acid dissociation constant of carbamic acid, and the acid dissociation constant of the hydrogen carbonate ion, at the ionic strength 0.5 M and temperatures from 25 to 70 °C, have been determined from carbaminate contents in equilibrated mixtures of ammonium chloride and sodium carbonate.

The formalism of the carbamic acid, ammonia, carbon dioxide equilibrium is well known and frequently given in textbooks. Despite its widespread occurrence and its simple formalism, the thermodynamics and kinetics of carbaminate formation have not been studied since the early work of Faurholt in 1921–1924.[1-2]

Faurholt estimated the equilibrium constant K_1 of

$$NH_3 + HCO_3^- \rightleftharpoons NH_2COO^- + H_2O$$

to be $10^{0.36}$ M^{-1} at 18 °C and zero concentration from measurements in various NH_4^+/NH_3 buffered solutions. The temperature dependence of K_1 was found to be small. An upper limit of 10^{-6} M^{-1} for the dissociation constant K_2 of carbamic acid at 0 °C was estimated from colorimetric measurements. The constants necessary for the calculation of K_1 and K_2 were estimated at the existing ionic strength by means of the cube root activity coefficient law.[3]

In the present work K_1 and K_2 and the acid dissociation constant K_3 of the hydrogen carbonate ion were measured indirectly from analytic determinations of the carbaminate contents in equilibrated mixtures of aqueous solutions of ammonium chloride and sodium carbonate. The ionic strength was kept constant at 0.5 M. The temperature was kept constant at different values from 25 to 70 °C. The constants are based on concentrations, and no corrections for activity coefficients have been made.

METHOD

The equilibrium constants in aqueous mixtures of NH_4Cl and Na_2CO_3 are defined as follows

$$K_1 = [NH_2COO^-]/([NH_3][HCO_3^-]) \quad (1)$$

$$K_2 = [H^+][NH_2COO^-]/[NH_2COOH] \quad (2)$$

$$K_3 = [H^+][CO_3^{2-}]/[HCO_3^-] \quad (3)$$

$$K_4 = [H^+][NH_3]/[NH_4^+] \quad (4)$$

$$K_5 = [H^+][HCO_3^-]/[CO_2] \quad (5)$$

$$K_6 = [H^+][OH^-] \quad (6)$$

In eqn. (5) and in the following, $[CO_2]$ means $[CO_2]+[H_2CO_3]$. The remaining equations connecting concentrations are

$$C_{NH_4Cl} = [NH_4^+]+[NH_3]+[NH_2COOH]+[NH_2COO^-] \quad (7)$$

$$C_{Na_2CO_3} = [CO_3^{2-}]+[HCO_3^-]+[CO_2]+[NH_2COOH]+[NH_2COO^-] \quad (8)$$

$$C_{carbam.} = [NH_2COOH]+[NH_2COO^-] \quad (9)$$

$$[Na^+]+[H^+]+[NH_4^+] = [Cl^-]+2[CO_3^{2-}]+[HCO_3^-]+[NH_2COO^-] \quad (10)$$

Eqns. (7), (8) and (9) are trivial and eqn. (10) is obtained from the principle of electroneutrality. In all the mixtures $C_{NH_4Cl}=[Cl^-]$ and $C_{Na_2CO_3}=\frac{1}{2}[Na^+]$ are known from preparation. C_{carbam} is determined as described below.

On the basis of the ten equations, where K_4, K_5, and K_6 are known, and under the assumption of constants independent of anything but ionic strength and temperature, it follows that K_1, K_2, and K_3 can be found from C_{NH_4Cl}, $C_{Na_2CO_3}$ and C_{carbam} in three different mixtures of ammonium chloride and sodium carbonate, if they have equal ionic strength and temperature. The equations are solved iteratively since no explicit expression for the calculation can be made.

The three mixtures were prepared with a choice of C_{NH_4Cl} and $C_{Na_2CO_3}$ so as (1) to make the result nearly independent of K_5 and K_6, (2) to minimize the error on K_2, and (3) to obtain an ionic strength $I=0.5$ M. However, such a choice can be made only if all equilibrium constants are known in advance. The first three mixtures were therefore chosen on the basis of estimated values of K_1, K_2, and K_3. The new values of K_1, K_2, and K_3 obtained from these mixtures were used for the next choice of mixtures and so forth. Generally three consecutive choices of mixtures (nine different solutions) were necessary at each temperature to obtain the constants in solutions with ionic strength calculated to be 0.50 M.

K_4 is the only constant needed with higher accuracy in advance and during the calculation. The assumption of constants independent of anything but ionic strength holds inside two decimal places for the literature values of pK_4.[4-6] Therefore we assume that the literature values of pK_4 estimated for 0.5 M $NaNO_3$ or $NaClO_4$ are applicable here with an error less than 0.01.

EXPERIMENTAL

The mixtures were prepared from stock solutions of NH_4Cl (B.D.H. analytical reagent) and Na_2CO_3 (Merck analytical). A small content (about 2 %) of $NaHCO_3$ in the stock solutions of Na_2CO_3 was determined by a combination of acidimetric and gravimetric ($BaCO_3$) determinations.

The slow conversion of carbaminate to carbonate in cold alkaline solution makes it possible to determine C_{carbam}.

The aqueous solutions of NH_4Cl and Na_2CO_3 were equilibrated at constant temperature in 100 ml closed bottles (24–72 h). Further standing did not change the result. The equilibrated mixtures were poured into an excess of cold 0.2 M NaOH in order to fix the total carbaminate content. The temperature after mixing should never exceed 20 °C, therefore in some experiments it was necessary to supercool the NaOH solution to about −6 °C. 1 M $BaCl_2$ was then added in excess to total added Na_2CO_3, and $BaCO_3$ was filtered off by suction. The filtrate was heated in a closed bottle to about 90 °C for 3 h, cooled and filtered again. The last precipitated $BaCO_3$, which is equivalent to C_{carbam}, was determined acidimetrically. 0.01 M $BaCl_2$ was used at all quantitative transfers and washings of solid $BaCO_3$.

As shown in Table 1, the analysis has been carried out with high accuracy. All measured volumina have been taken from modern piston burettes with a reproducibility of 0.002 ml or better (which was checked). All measurements were repeated at least six times and C_{carbam} in Table 1 are averages.

RESULTS

The result appears from Tables 1 and 2. The variations of K_1 and K_2 with temperature correspond to the enthalpy changes of −10 (1) and 11 (2) kJ mol^{-1}, respectively. In Table 2, the standard deviations of the constants K_1, K_2 and K_3 illustrate the reproducibility of the analytical results and some supposed

Table 1. Final experimental data.

Temp. °C	C_{NH_4Cl} M	$C_{Na_2CO_3}+C_{NaHCO_3}$ (2.3 mol % $NaHCO_3$) M	C_{carbam}[a] M × 10^3
25	0.0493	0.1817	3.623(3)
25	0.1755	0.1849	18.759(5)
25	0.4340	0.0596	5.461(6)
35	0.0496	0.1826	3.599(9)
35	0.1801	0.1896	20.334(7)
35	0.4355	0.0597	5.277(8)
50	0.0500	0.1842	3.179(11)
50	0.1881	0.1981	21.049(10)
50	0.4378	0.0601	4.602(11)
70	0.0505	0.1858	2.849(11)
70	0.2006	0.2113	24.016(13)
70	0.4411	0.0555	4.254(9)

[a] Standard deviations on C_{carbam} are based on mean of six measurements.

Table 2. Equilibrium constants in aqueous mixtures of NH_4Cl and Na_2CO_3 at ionic strength 0.5 M.

Temp. °C	pK_1	pK_2	pK_3	pK_4 [a]	pK_5 [b]	pK_6 [b]
25	−0.328(4)	6.76(5)	9.58(1)	9.30(1)	6.0(2)	13.7(5)
35	−0.288(4)	6.61(7)	9.43(1)	9.00(1)	6.0(2)	13.4(5)
50	−0.182(6)	6.56(5)	9.26(2)	8.59(1)	6.0(2)	13.0(5)
70	−0.079(11)	6.49(2)	9.18(2)	8.10(0)	5.9(2)	12.5(5)

[a] Interpolated to $I = 0.5$ M from Refs. 4–6. [b] Interpolated to $I = 0.5$ M from Ref. 8.
Estimated errors on pK_4, pK_5, and pK_6 are the assumed uncertainties of literature values, used for the calculation of errors on pK_1, pK_2, and pK_3.

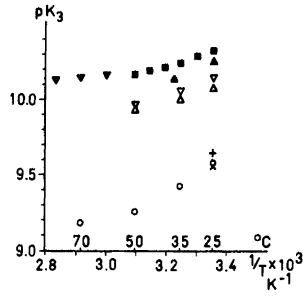

Fig. 1. The acid dissociation constant of HCO_3^-.

Symbol	Ionic strength	Medium	Method	Ref.
■	0	–	H/AgCl	8
▼	0	–	glass	9
▽	0.08	NaCl	H/AgCl	8
△	0.16	NaCl	H/AgCl	8
▲	0	–	H/H	10
+	0.5	NaCl	H/H	11
×	1.0	$NaClO_4$	glass	12
○	0.5	Na_2CO_3/ NH_4Cl	conc.	This work

errors on K_4, K_5, and K_6. We have no check on the assumption of constants independent of anything but ionic strength and temperature, and therefore these standard deviations do not reflect the true error. However, as the values of K_3 are near the values expected from literature (Fig. 1), we suppose that K_1 and K_2 are close to the true ones.

REFERENCES

1. Faurholt, C. *K. Dan. Vidensk. Selsk., Mat.-Fys. Medd. 3* (1921) 20.
2. Faurholt, C. *K. Vet.-Landbohøjsk., Årsskr.* (1924) 1.
3. Bjerrum, N. *Z. Elektrochem. 24* (1918) 321.
4. Bjerrum, J. *Metal ammine formation in aqueous solution*, Copenhagen 1941, reprinted 1957, pp. 122, 179.
5. Everett, D. H. and Wynne Jones, W. F. K. *Proc. R. Soc. London 169* (1938) 190.
6. Spike, C. G. *Thesis*, Univ. of Michigan 1953, quoted in *Stability Constants of Metal-Ion Complexes*, The Chemical Society, London 1964.
7. *Stability Constants of Metal-Ion Complexes*, The Chemical Society, London 1964.
8. Harned, H. S. and Scholes, S. R., Jr., *J. Am. Chem. Soc. 63* (1941) 1706.
9. Čuta, F. and Štafelda, F. *Collect. Czech. Chem. Commun. 48* (1954) 1308, quoted in *Stability Constants of Metal-Ion Complexes*, The Chemical Society, London 1964.
10. Kauko, Y. and Airola, A. *Z. Phys. Chem. Leipzig 179* (1937) 307.
11. Näsänen, R. *Suom. Kemistil. B 19* (1946) 90.
12. Frydman, N., Nilsson, G., Rengemo, T. and Sillén, L. G. *Acta Chem. Scand. 12* (1958) 878.

Received July 11, 1977.

Acta Chemica Scandinavica A 32 (1978) 19 – 24

Reaction Rate Studies of the Acid Hydrolysis of Some Chromium(III) Complexes. VIII. The Acid Hydrolysis and Isomerization of *cis*- and *trans*-Tetraaquadichloridochromium(III) Ions in Aqueous Perchloric Acid

L. MØNSTED and O. MØNSTED

Chemistry Department I, Inorganic Chemistry, The H. C. Ørsted Institute, University of Copenhagen, DK-2100 Copenhagen, Denmark

The acid hydrolysis and isomerization of the *cis*- and *trans*-tetraaquadichloridochromium(III) cations in acid perchlorate solution has been investigated. The experiments were carried out in the temperature and hydrogen ion concentration ranges 20 – 50 °C and 0.25 – 1.00 M, respectively, and the ionic strength was adjusted to 1.00 M by the addition of sodium perchlorate.

The following reaction rate constants at 25 °C and activation energies were found:
For the hydrolysis reactions:
(*cis*): $(1.53 \pm 0.15) \times 10^{-5}$ s^{-1}, 103 ± 5 kJ mol^{-1}
(*trans*): $(4.53 \pm 0.11) \times 10^{-5}$ s^{-1}, 98.2 ± 1.3 kJ mol^{-1}
and for the isomerization reactions:
(*cis* → *trans*): $(1.5 \pm 0.3) \times 10^{-5}$ s^{-1}, 111 ± 7 kJ mol^{-1}
(*trans* → *cis*): $(1.97 \pm 0.14) \times 10^{-5}$ s^{-1}, 117 ± 4 kJ mol^{-1}

In an appendix the application of nonlinear regression analysis to the parametrization of kinetic data, within reaction schemes composed of an arbitrary number of first and second order reactions, is described in some detail.

Reactions of the isomeric tetraaquadichloridochromium(III) complexes have been the subject of a number of publications during the past twenty years, but it was not until ten years ago that the importance of the isomerization reactions was fully realized.[1] Examples of isomerization reactions of chromium(III) complexes are not numerous, and in most of the cases so far discovered they constitute only minor contributions to the total reactivity of the complexes. As a result accurate characterization of such processes is usually lacking. However, for the isomeric tetraaquadichloridochromium(III) species isomerization competes favourably with aquation at 35 °C,[1] and it should therefore be possible to obtain well defined activation parameters for the isomerization reactions of these two complexes. The system was originally investigated by ion exchange chromatography of quenched reaction mixtures, but this is a tedious method if many kinetic experiments have to be carried out. Recently multi-wavelength absorption spectroscopy has been successfully applied to the far more complicated series of reactions involved in the hydrolysis of hexaamminechromium(III) to yield ultimately hexaaquachromium(III).[2] A brief description of the numerical background for this method has been given previously,[3] but in view of the advantages and the potential of such modern numerical methods it was thought worthwhile to publish the method in somewhat greater detail and also to demonstrate its application to a system which has already been investigated in a more traditional manner.

EXPERIMENTAL

Chemicals. *trans*-$[CrCl_2(OH_2)_4]Cl.2H_2O$ (Riedel de Haën AG) was recrystallized,[4] and $(NH_4)_2[CrCl_5(OH_2)]$ was prepared[5] according to literature methods. The source of the other chemicals

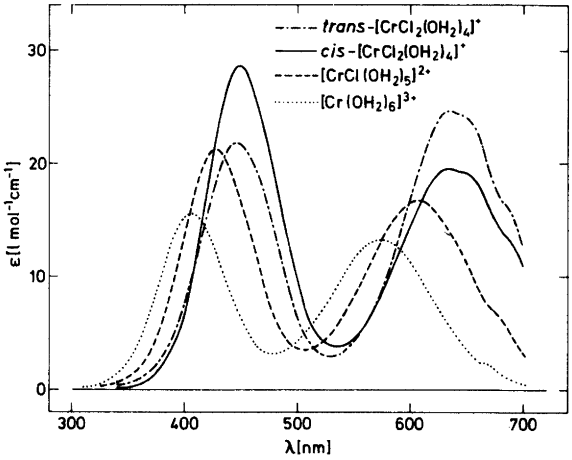

Fig. 1. Visible absorption spectra of complexes prepared and purified as described in the text, *cf.* Table 1.

employed has been described earlier.[3]

Preparation of solutions. *trans*-$[CrCl_2(OH_2)_4]$-$Cl.2H_2O$ dissolved in water, $(NH_4)_2[CrCl_5(OH_2)]$ aged in water solution at room temperature for 5 min and *trans*-$[CrCl_2(OH_2)_4]Cl.2H_2O$ aged in acidified water solution at 25 °C for 1½ h were used as the initial materials for the preparation of the *trans*-$[CrCl_2(OH_2)_4]^+$, *cis*-$[CrCl_2(OH_2)_4]^+$ and $[CrCl(OH_2)_5]^{2+}$ ions, respectively, in solution.

Purification of solutions obtained in this way was carried out by ion exchange chromatography as follows: A volume of solution containing about 0.25 mequiv. of chromium(III) was charged on to a 1 x 10 cm column packed with Sephadex SP C-25 cation exchange resin. The column was operated at 0 °C, and anionic and neutral species were first removed by elution with water. Next the monopositive tetraaquadichloridochromium(III) species were displaced with 0.05 M sodium perchlorate solution acidified with perchloric acid to pH ~3. Spectrophotometric monitoring of the eluate showed that fresh solutions of recrystallized green chromic chloride contained the *trans* isomer exclusively. In an analogous fashion aged solutions of aquapentachloridochromate(III) ions were found to contain both the *cis* and the *trans* isomer. Usually, however, the *trans* isomer comprised less than about 10 % of the monopositive species in such solutions, and the pure *cis* isomer was therefore readily obtained in solution by the chromatographic technique described above. After removal of monopositive species the dipositive pentaaquachloridochromium(III) ion could be eluted free from other species with acidified, pH ~3, 0.35 M sodium perchlorate solution.

Visible absorption spectra of solutions prepared in this way are given in Fig. 1 and Table 1.

Kinetic measurements, and the *Methods of analysis* were essentially as described previously,[3] except for the use of a modified Cary 118C spectrophotometer.

Method of calculation. The numerical treatment of the experimental material was conveniently divided into a number of distinct steps. The initial step is characteristic of the type and the mode of operation of the spectrophotometer employed and will consequently not be described. The results of these calculations are mean values and variances of absorptivities of the quenched reaction mixtures and of the pure components which constitute these reaction mixtures at a series of wavelengths. Absorp-

Table 1. Spectral characteristics of solutions of complexes prepared and purified as described in the text and diluted with perchloric acid to yield a 0.5 M perchloric acid solution.

Complex	λ_1 max [nm]	ε_1 max [l mol^{-1} cm^{-1}]	λ_2 max [nm]	ε_2 max [l mol^{-1} cm^{-1}]	ε_1 max/ ε_2 max
cis-$[CrCl_2(OH_2)_4]^+$	635	19.4	450	28.7	0.675
trans-$[CrCl_2(OH_2)_4]^+$	635	24.8	448	21.8	1.134
$[CrCl(OH_2)_5]^{2+}$	608	16.7	430	21.2	0.793

tion spectra in the range 290–700 nm measured at 10 nm intervals were employed in this work.

The next three steps of the calculations were all carried out within the framework of nonlinear regression analysis. This technique is excellently described in a number of textbooks on statistical methods and will therefore not be described here.

In the first step the absorption spectrum of a quenched reaction mixture, $A=A(\lambda)$, was expressed as a linear combination of the absorption spectra of the components in the reaction mixture, $\varepsilon=\varepsilon(\lambda)$. This was performed by minimization of:

$$s_1^2 = \sum_{\lambda}[(A_\lambda - \mathbf{c}^T\boldsymbol{\varepsilon}_\lambda)^2/(V(A_\lambda) + \mathbf{c}^T\mathbf{V}(\boldsymbol{\varepsilon}_\lambda)\mathbf{c})]$$

where A_λ is the mean value of the absorptivity of the reaction mixture at wavelength λ and $V(A_\lambda)$ is the variance of this mean value. $\boldsymbol{\varepsilon}_\lambda$ is the column vector of mean values of the molar absorptivities of the pure components and $\mathbf{V}(\boldsymbol{\varepsilon}_\lambda)$ is the matrix of variances of these mean values. Finally, $\mathbf{c}$, the result of the computation, is the column vector of mean values of component concentrations in the reaction mixture, and $\mathbf{V}(\mathbf{c})$, which is obtained simultaneously, is the matrix of variances of and covariances between these concentration mean values.

In the second step of the calculations, rate constants for the individual kinetic experiments were computed by minimization of:

$$s_2^2 = \sum_{t}[(\mathbf{c}_t - \mathbf{c}(t,\mathbf{c}_0,\mathbf{k}))^T\{\mathbf{V}(\mathbf{c}_t)\}^{-1}(\mathbf{c}_t - \mathbf{c}(t,\mathbf{c}_0,\mathbf{k}))]$$

where $\mathbf{c}_t$ and $\mathbf{V}(\mathbf{c}_t)$ are the quantities determined in the previous step of the calculations, now supplemented with an index to distinguish different reaction times. $\mathbf{c}(t,\mathbf{c}_0,\mathbf{k})$ is the column vector of calculated concentrations at time t as function of the column vectors of initial concentrations, $\mathbf{c}_0$, and rate constants, $\mathbf{k}$, obtained as described in the appendix. An example of the agreement found between calculated, $\mathbf{c}(t,\mathbf{c}_0,\mathbf{k})$, and observed concentrations, $\mathbf{c}_t$, is shown in Fig. 2.

In the third step of the calculations all sets of mean values of reaction rate constants were assembled to yield activation parameters by minimization of:

$$s_3^2 = \sum_{T,[H^+]}[(\mathbf{k} - \mathbf{k}([H^+],T))^T\{\mathbf{V}(\mathbf{k})\}^{-1}(\mathbf{k} - \mathbf{k}([H^+],T))]$$

where $\mathbf{V}(\mathbf{k})$ is the matrix of variances of and covariances between the reaction rate constants. For the present system, and within the range of hydrogen ion concentrations investigated, the hydrogen ion concentration dependence of the calculated rate constants is given by:

$$\mathbf{k}([H^+],T) = \mathbf{k}_0(T) + \frac{1}{[H^+]}\mathbf{k}_1(T)$$

For each term in the above two column vectors of calculated rate constants the temperature dependence is assumed to follow an expression of the form:

$$k(T) = \frac{RT}{Nh}\exp\{\Delta S^{\ddagger}/R - \Delta H^{\ddagger}/RT\}$$

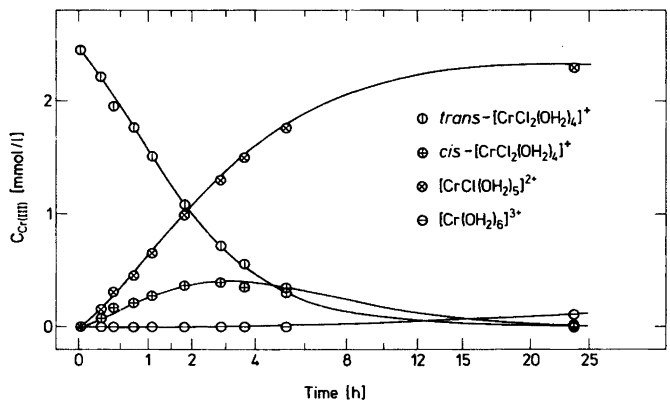

Fig. 2. Reaction kinetic experiment at 30.0 °C with $[H^+]=0.992$ M, started from *trans*-tetraaquadichlorodochromium(III). Experimental points are calculated from measured visible absorption spectra of a series of quenched reaction mixtures, and the solid curves are calculated from the parameters of Table 2. The improvement in the agreement between experimental points and calculated curves, which is obtained if rate constants calculated for this particular kinetic experiment are used, is too small to be seen clearly on the figure.

The parameters thus computed are characterized by very strong correlation between activation enthalpies and entropies associated with the same reaction. Consequently it is frequently desirable to represent the reduced data in a form characterized by less strong correlation between parameters of temperature dependent and independent terms. The smallest possible correlation is obtained by choosing parameters, k',E, according to:

$$k(T) = k' \exp\{-E(1/RT - 1/RT_0)\},$$

where T_0 is the average temperature of all the kinetic experiments considered.

RESULTS AND DISCUSSION

It was early shown that green crystalline chromium(III) chloride contains a tetraaquadichloridochromium(III) species.[7] Various pieces of indirect evidence concerning the detailed geometry of this ion were subsequently presented until the question was finally answered by two crystal structure analyses[8,9] which showed the species to be the *trans* isomer. The corresponding *cis* isomer has so far only been obtained in solution from products formed by heating green chromium(III) chloride. In this work a somewhat different method is used, but as can be seen from a comparison between Table 1 and Ref. 6 an identical species is obtained.

The first kinetic investigations of the reactions of the isomeric tetraaquadichloridochromium(III) species were all carried out with the implicit assumption that isomerization reactions were unimportant for the kinetics of the system. This hypothesis was finally shown to be incorrect[1] and evidence in favour of the reaction scheme shown in Fig. 3, with

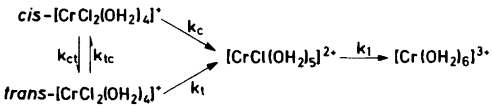

Fig. 3. Reaction scheme for isomerization and aquation of the isomeric tetraaquadichloridochromium(III) ions.

rate constants for the direct isomerization reactions comparable to those for the chloride ligand hydrolysis reactions and absence of isomerization *via* trichloridochromium(III) species, was presented.

In order to characterize the acid-independent paths of these reactions further, a number of kinetic experiments employing a 1.00 M perchlorate medium covering the hydrogen ion concentration and temperature ranges 0.25 – 1.00 M and 20 – 50 °C, respectively, were carried out. The final results obtained are shown in Table 2 and are compared in Table 3 with the earlier investigation which was carried out at 34.8 °C in 0.203 M perchloric acid.

As is usual with kinetic investigations of complicated reactions, the dominating reaction in the system, *i.e.* the hydrolysis of the *trans*-tetraaquadichloridochromium(III) ion, is well characterized, whereas the remaining reactions in the system are necessarily less well defined. Therefore conclusions about the reactions of the *cis* isomer are less certain than those which may be reached for the *trans* isomer, for which it is evident that the isomerization reaction must proceed *via* a transition state which differs from that for the chloride ligand hydrolysis reaction, since the activation energy for the latter process is significantly lower than that for the former.

Table 2. Rate constants at 35 °C and activation energies, mean values ± standard deviations upon the mean values, and correlation coefficients for the acid independent reactions of *cis* and *trans*-tetraaquadichloridochromium(III) ions in aqueous 1.00 M perchlorate solution. *Cf.* Fig. 3.

Parameter symbol	Parameter values	Correlation coefficients							
k_{tc}	$(9.1 \pm 0.4) \times 10^{-5}$ s^{-1}	–							
k_t	$(16.4 \pm 0.4) \times 10^{-5}$ s^{-1}	+.55	–						
k_{ct}	$(6.4 \pm 1.1) \times 10^{-5}$ s^{-1}	+.42	+.50	–					
k_c	$(5.8 \pm 0.6) \times 10^{-5}$ s^{-1}	−.19	−.61	−.81	–				
E_{tc}	(117 ± 4) kJ mol^{-1}	−.03	−.06	−.06	+.10	–			
E_t	(98.2 ± 1.3) kJ mol^{-1}	+.01	+.21	+.11	−.19	+.50	–		
E_{ct}	(111 ± 7) kJ mol^{-1}	+.03	+.25	+.29	−.44	+.26	+.42	–	
E_c	(103 ± 5) kJ mol^{-1}	−.03	−.03	−.34	+.52	−.04	−.46	−.78	–

Table 3. Comparison with literature values of rate constants at 34.8 °C and $[H^+]=0.203$ M.

Reaction (*cf.* Fig. 3)	Ref. 1 $10^5 \times (k_{obs})$ $[s^{-1}]$	This work $10^5 \times (k_0+k_1/0.203)$ $[s^{-1}]$
k_{tc}	7.8	7.4
k_t	18.0	16.7
k_{ct}	6.2	8.5
k_c	8.3	7.0

In Table 4 data for the reactions of the tetraaqua complexes investigated here have been compared with literature data for the corresponding tetraammine complexes. The most noteworthy feature is the absence of detectable isomerization for the latter two species. The explanation for this may be the same as that proposed to rationalize the differences in behaviour with respect to racemization of the *cis*-diaquabis(1,2-ethanediamine)-chromium(III) ion and the tris(1,2-ethanediamine)chromium(III) ion,[12] namely that changes in configuration are facilitated by exchange reactions of coordinated solvent molecules. Direct verification of this hypothesis is still lacking for the chromium(III) complexes cited here, but was obtained long ago for the isomerization of the *trans*-diaquabis(1,2-ethanediamine)cobalt(III) ion.[13]

Comparisons between the hydrolysis reactions of the tetraaqua- and tetraammine complexes reveal the trend normally associated with chromium(III) aquation reactions. For the pair of *cis* complexes the reactivity difference is dominated by the greater *trans* effect of coordinated ammonia than that of coordinated water. The pair of *trans* complexes is seen to react at roughly equal rates at 25 °C, but inspection of the activation parameters shows that this is accidental. The reaction of the tetraammine complex is described by significantly lower values of both activation enthalpy and activation entropy. Additional experimental data would evidently be of value for further elucidation, and the reactions of the remaining *trans*-dichlorido chromium(III) complexes of the general formula *trans*-$[CrCl_2(NH_3)_x(OH_2)_{4-x}]^+$ ($x=3$, "*trans*"-2, "*cis*"-2, and 1) are therefore currently being studied.

Acknowledgement. The authors wish to thank Dr. Martin Hancock for revising the English manuscript.

APPENDIX

The coupled first order differential equations which may be used to describe the transformations occurring between p species in kinetic systems in solution, where both first and second order reactions take place, may be written:

$$\frac{d\xi_j(t)}{dt} = \sum_{r=1}^{p} [\gamma_{jr} + \sum_{s=r}^{p} \{\psi_{jrs}\xi_s(t)\}]\xi_r(t) \qquad (A.1)$$

Table 4. Kinetic parameters for chloride ligand hydrolysis and isomerization of some *cis*- and *trans*-dichlorido chromium(III) complexes.[c]

Complex	10^5k (25 °C) $[s^{-1}]$	$\Delta H^{\neq}$ $[kJ\ mol^{-1}]$	$\Delta S^{\neq}$ $[J\ K^{-1}\ mol^{-1}]$	Ref.
Hydrolysis				
cis-$[Cr(NH_3)_4Cl_2]^+$	33.0 ±0.15	84±2	−25±6	10
cis-$[Cr(OH_2)_4Cl_2]^+$	1.53±0.15	101±5	+1±17	[a]
trans-$[Cr(NH_3)_4Cl_2]^+$	4.9 ±0.2	87.9±1.3	−33±4	11 [b]
trans-$[Cr(OH_2)_4Cl_2]^+$	4.53±0.11	95.7±1.4	−7±4	[a]
Isomerization				
cis-$[Cr(NH_3)_4Cl_2]^+$	Unobserved	–	–	10
cis-$[Cr(OH_2)_4Cl_2]^+$	1.5 ±0.3	108±7	+25±25	[a]
trans-$[Cr(NH_3)_4Cl_2]^+$	Unobserved	–	–	11
trans-$[Cr(OH_2)_4Cl_2]^+$	1.97±0.15	114±4	+50±13	[a]

[a] This work. [b] The values given here are calculated from k (45 °C) and the activation energy. [c] Numerical data are quoted as mean values ± standard deviations upon the mean values.

In this expression $\xi_i(t)$ $(i=1,2,\ldots,p)$ are the time dependent concentrations of the species, and γ_{ij} and ψ_{ijk} are quantities which are easily related to reaction rate constants.

The numerical integration of these coupled differential equations may be performed by expressing $\xi_i(t)$ as a power series in $(t-t_0)$:

$$\xi_j(t) = \sum_{i=0}^{\infty} \mu_{ij}(t_0)\,(t-t_0)^i \qquad \text{(A.2)}$$

For this series expansion it is readily verified that the coefficients $\mu_{ij}(t_0)$ may be obtained from:

$$\mu_{0j}(t_0)=\xi_j(t_0) \qquad (i=0)$$

$$\mu_{ij}(t_0)=\frac{1}{i}\sum_{r=1}^{p}\left[\gamma_{jr}\mu_{i-1,r}(t_0)+\right.$$

$$\left.\sum_{s=r}^{p}\psi_{jrs}\left\{\sum_{u=0}^{i-1}\mu_{i-1-u,r}(t_0)\;\mu_{us}(t_0)\right\}\right] \qquad (i>0)$$

This provides a convenient numerical method for the integration of the differential equations given by eqns. A.1, but in order to carry out a regression analysis differentials of $\xi_i(t)$ with respect to all desired parameters, in particular γ_{ij} and ψ_{ijk}, are also necessary. To simplify the notation the subsequent derivations have been restricted to reaction schemes in which only first order reactions take place, *i.e.* for which $\psi_{ijk}=0$. In this case eqns. A.1 reduce to:

$$\frac{\mathrm{d}\xi_j(t)}{\mathrm{d}t} = \sum_{r=1}^{p}\gamma_{jr}\,\xi_r(t)$$

Eqns. A.2 may be differentiated to yield:

$$\frac{\partial\xi_j(t)}{\partial\gamma_{rs}} = \sum_{i=0}^{\infty}\frac{\partial\mu_{ij}(t_0)}{\partial\gamma_{rs}}(t-t_0)^i \qquad \text{(A.3)}$$

and the μ-differentials may be computed from:

$$\frac{\partial\mu_{0j}(0)}{\partial\gamma_{rs}} = 0$$

$$\frac{\partial\mu_{0j}(t_0)}{\partial\gamma_{rs}} = \frac{\partial\xi_j(t_0)}{\partial\gamma_{rs}}$$

$$\frac{\partial\mu_{ij}(t_0)}{\partial\gamma_{rs}} = \frac{1}{i}\left[\delta_{rj}\,\mu_{i-1,s}(t_0) + \sum_{k=1}^{p}\gamma_{jk}\frac{\partial\mu_{i-1,k}(t_0)}{\partial\gamma_{rs}}\right]$$

where δ_{rj} is equal to 1 for $r=j$ and equal to 0 otherwise.

Differentials with respect to other parameters may be evaluated analogously although at the present time only the inclusion of initial concentrations of one or more reactant species has been carried out.

In numerical calculations the summations in eqns. A.1 and A.3 must be restricted to a finite number of terms. In cases where comparisons with analytical solutions of the differential equations could be made it was found that a polynomial of degree 10 reproduced the analytical solution satisfactorily when combined with an adjustment of the step-length, $t-t_0$, so as to make the last term in the series expansion insignificant relative to those already summed.

The general equations given in this appendix may easily be applied to actual systems, and computer programs which handle suitably written reaction schemes are readily constructed. Such programs have provided a very flexible tool for the interpretation of the kinetics in a number of complicated multicomponent systems.[2,14]

REFERENCES

1. Salzman, J. D. and King, E. L. *Inorg. Chem. 6* (1967) 426.
2. Mønsted, L. and Mønsted, O. *Acta Chem. Scand. A 28* (1974) 569.
3. Mønsted, L. and Mønsted, O. *Acta Chem. Scand. 27* (1973) 2121.
4. Bjerrum, N. *K. Dan. Vidensk. Selsk. Skr. Naturvidensk. Math. Afd. IV.1* (1907) 8.
5. Neumann, G. *Justus Liebigs Ann. Chem. 244* (1888) 329.
6. King, E. L., Woods, Sr., M. J. M. P. O. and Gates, H. S. *J. Am. Chem. Soc. 80* (1958) 5015.
7. Werner, A. and Gubser. A, *Ber. Deut. Chem. Ges. 34* (1901) 1579.
8. Dance, I. G. and Freeman, H. C. *Inorg. Chem. 4* (1965) 1555.
9. Morosin, B. *Acta Crystallogr. 21* (1966) 280.
10. Jackson, W. G., Vowles, P. D. and Fee, W. W. *Inorg. Chim. Acta 19* (1976) 221.
11. Hoppenjans, D. W., Hunt, J. B. and Gregoire, C. R. *Inorg. Chem. 7* (1968) 2506.
12. Mønsted, L. and Mønsted, O. *Acta Chem. Scand. A 29* (1975) 29.
13. Kruse, W. and Taube, H. *J. Am. Chem. Soc. 83* (1961) 1280.
14. Mønsted, L. *Acta Chem. Scand. A 30* (1976) 599.

Received July 19, 1977.

Acta Chemica Scandinavica A 32 (1978) 25–30

Conformational Spectroscopic Studies of Halogenated Cyclohexanes in Thiourea Clathrates

JORUNN E. GUSTAVSEN, PETER KLÆBOE and HILDA KVILA

Department of Chemistry, University of Oslo, Oslo 3, Norway

The IR spectra of the monosubstituted compounds: chloro-, bromo-, iodo-, cyano- and isocyanatocyclohexane and the disubstituted compounds: *trans*-1,2-dichloro- and *trans*-1,2-dibromocyclohexane; *trans*-1,4-dichloro- and *trans*-1,4-dibromocyclohexane as thiourea clathrates were recorded as Nujol mulls between 1500 and 400 cm^{-1}. Raman spectra of the solid clathrates were also obtained.

From earlier assignments of these cyclohexane spectra it was clear that the conformational equilibrium was shifted towards the axial (diaxial) conformer compared to the liquid (dissolved) state in all the cyclohexanes. Semiquantitative calculations of the shift in conformational equilibrium were carried out, independently based upon IR bands situated around 1000 and 850 cm^{-1}. In iodocyclohexane and isocyanatocyclohexane considerable amounts of the equatorial conformer were present in the thiourea clathrate, for the other cyclohexanes negligible concentrations of this conformer were found.

Some reassignments of the previous work regarding equatorial and axial bands were carried out.

It was reported by Nishikawa from IR spectroscopy long time ago that certain halogenated cyclohexanes probably existed in the axial conformer when occluded in a thiourea adduct.[1] Very recently two independent studies were published; Allen *et al.*[2] studied the thiourea clathrates of chloro-, bromo- and iodocyclohexane by Raman spectroscopy, while Fukushima[3] extended the IR spectra of the chlorocyclohexane clathrate to the low frequency region. Both groups confirmed the earlier results[1] regarding the preference for the axial conformers in the clathrate.

It is well-known[4,5] that the conformational equilibrium in monosubstituted cyclohexanes is displaced towards the equatorial conformer in the vapour, in the liquid and in solution. Moreover, they crystallize in the equatorial conformer, including fluorocyclohexane,[6] at low temperature[7–9] as well as under high pressure.[8] Therefore, the predominance of the axial conformer in the thiourea clathrates[1–3] is quite unexpected and is probably related to the steric dimensions within the cavity of the host lattice.

We have studied the conformational equilibria of various mono- and dihalogenated (and pseudohalogenated) cyclohexanes for some time, and felt it would be of interest to investigate the clathrates of these compounds. In particular, we wanted to establish possible conformational preferences for these cyclohexanes in the thiourea clathrates. Better understanding of the host-guest interactions and the apparent preference for the axial conformers should be achieved when more cyclohexane derivatives have been investigated. In the present study we shall report our data for five monosubstituted cyclohexanes (including the three halocyclohexanes reported previously[1–3]), two *trans*-1,2-dihalo- and two *trans*-1,4-dihalocyclohexanes. Additional data for fluorocyclohexane,[6] other *trans*-1,4-dihalocyclohexanes and methylcyclohexanes will be given in a forthcoming paper.

EXPERIMENTAL

The monosubstituted cyclohexanes (chloro-, bromo-, iodo-, cyano- and isocyanatocyclohexane) as well as *trans*-1,4-dichlorocyclohexane were all commercial products; their supplier and methods of purification have been described in earlier papers. *trans*-1,2-Dichloro- and dibromocyclohexane[10] and *trans*-1,4-dibromocyclohexane[11] were purified sam-

ples from our earlier investigations. Thiourea was *puriss.* grade from Fluka AG., used without purification.

The thiourea clathrates of the liquid cyclohexanes were prepared[3] by adding the cyclohexane to a saturated methanol solution of thiourea, filtering and drying the precipitate. The *trans*-1,4-dihalocyclohexanes which are crystalline solids at room temperature, were dissolved in methanol and added to the methanolic thiourea solution and cooled. Excess of cyclohexane on the "outside" of the solid clathrate was removed by subsequent washing with carbon tetrachloride.

The clathrates were investigated as thick nujol mulls between KBr-plates in the region 1500–400 cm^{-1} with a Perkin-Elmer model 225 spectrometer. The Raman spectra were recorded with a Cary 81 spectrometer, modified[12] for 90° illumination, using the 5145 Å argon line for excitation.

RESULTS

The IR spectrum of solid thiourea (orthorhombic) has a number of intense bands below 1500 cm^{-1},[13] which are considerably perturbed in the clathrates (rhombohedral). Several bands are shifted (Table 1), some are enhanced and, *e.g.*, the broad band at 630 cm^{-1} in thiourea is split into a sharp doublet at 654 and 615 cm^{-1} in the occlusion compounds. In the present series of clathrates the thiourea bands seemed practically identical for the various cyclohexane guest molecules.

The cyclohexane bands were negligibly displaced from their positions in the liquid (or solutions). Therefore, we have reported the same wave numbers in the clathrates as those previously observed for the free cyclohexane derivative.

The IR (and Raman) bands of the cyclohexane have generally lower intensities than those of the polar thiourea, and there are at least three times as many host molecules as guests in the clathrates. Therefore, only certain spectral regions are suitable for these studies. While Fukushima[3] focussed his attention on the far-IR region below 650 cm^{-1}, we preferred the region between the thiourea bands at 1058 and 761 cm^{-1}. For *trans*-1,2-dihalocyclohexanes many bands below 700 cm^{-1} were also useful for identification. Fairly complete lists of vibrational bands belonging to the equatorial, axial or both conformers are known for the present cyclohexanes from previous experimental work. We feel that it is highly preferable to base our present

Table 1. Infrared spectral data for thiourea and thiourea in cyclohexane clathrates (1500–400 cm^{-1}).

Thiourea (orthorhombic)	Thiourea clathrates (rhombohedral)
	1491 vs[a]
1412 s	1402 vs
1378 s	1378 vs
1200 m, br	1210 m, br
1082 vs	1086 vs
	1058 m
	955 vw
	888 w[b]
765 vw	761 s
731 s	723 s
630 s	654 s
	615 s
488 m, br	478 m
460 m, br	418 m
412 m	408 vw

[a] Abbreviations: s, strong; m, medium; w, weak; v, very; br, broad.
[b] Apparent in the spectra of the *trans*-1,4-dihalocyclohexanes only.

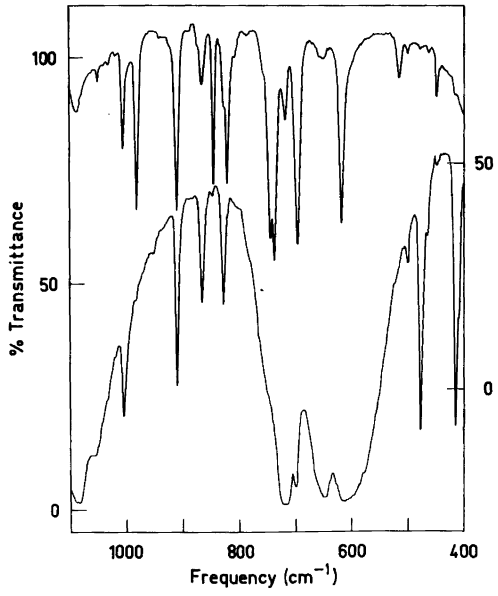

Fig. 1. Infrared spectra of liquid *trans*-1,2-dichlorocyclohexane (top, right ordinate axis) and crystalline thiourea clathrate (bottom, left ordinate axis) in the region 1100–400 cm^{-1}.

Table 2. Infrared spectral data for monosubstituted cyclohexane-thiourea clathrates (1400 – 400 cm^{-1}).

Cl[a]	Br[a]	I[a]	CN[b]	NCO[b]
1259 s	1252 s			1321 m,a
1214 vw	1191 m		1123 w,a	1262 w
1014 m,a	1010 m,a,	1006 m,a	1013 w,a	1020 w,a
993 vw,e	988 vw,e	988 m,e	935 m	1010 w,e
	919 m	920 w	920 w	928 w
				905 w
889 w,e[c]	885 w,e[c]	883 w,e[c]	892 vw,e	893 s,e
868 w,a	864 m,a	862 m,a	862 s,a	881 w,e
858 m	852 s[d]	848 s[d]		863 m,a
852 vw,e[c]			840 vw,e	839 m,e
817 w,e	810 vw,e			815 m,a
807 w,a	804 m,a	806 w,e		780 w,e
731 vw,e				759 w,a
684 m,a				
558 m,a	513 m,a	493 w,a	496 m,a	523 vw,e
472 m,a	458 m,a	445 s,a		

[a] For wavenumbers and conformers, see Ref. 8. [b] For wavenumbers and conformers, see Ref. 17. [c] For conformers, see Ref. 9. [d] Assigned as *e* in Ref. 9.

work upon experimental evidence, instead of on normal coordinate analyses.[3] Various such analyses have been performed on the monohalocyclohexanes,[3,14-16] but it seems unreliable to assign the vibrational bands to the conformers from these calculations alone.

The observed IR bands which were attributed to the guest molecules are listed in Tables 2 (halo and pseudohalo cyclohexanes), 3 (*trans*-1,2-dihalocyclohexane) and 4 (*trans*-1,4-dihalocyclohexanes). As examples, the infrared curves between 1100 and 400 cm^{-1} of the thiourea clathrates of *trans*-1,2-dichlorocyclohexane (Fig. 1) and iodocyclohexane (Fig. 2) are given with the corresponding liquid cyclohexane spectra.

We found the Raman spectra of the present clathrates to be generally less informative than the IR-spectra. Since the Raman spectra of the three halocyclohexane clathrates have recently been

Table 3. Infrared spectral data for *trans*-1,2-dihalocyclohexane – thiourea clathrates (1400 – 200 cm^{-1}).

ClCl[a]	BrBr[a]
	1255 w,aa
1214 m,aa	1195 w,aa
	1178 s,aa
1140 w,aa	1160 w,ee
	1032 w,aa
1005 s,aa	999 s,aa
980 vvw,ee	972 vw,ee
909 s[b]	903 s
865 s,aa	861 s,aa
845 vw,ee	840 vw,ee
826 s,aa	812 m,aa
	803 vw,aa
698 m,aa	685 vw,ee
498 m,aa	664 m,aa
462 w,aa	540 vs,aa
361 m,aa	
209 m,aa	

[a] For wavenumbers and conformers, see Ref. 10. [b] Assigned as ee in Ref. 10.

Table 4. Infrared spectral data for *trans*-1,4-dihalocyclohexane – thiourea clathrates (1400 – 400 cm^{-1}).

ClCl[a]	BrBr[a]
1363 vw,aa	
1270 m,aa	1245 m,aa
1006 m,aa	1003 m,aa
995 vw,ee	988 vw,ee
890 vw,ee	886 vw,ee
874 m,aa	869 m,aa
860 vw,aa	861 vw,aa
558 m,aa	495 m,aa

[a] For wavenumbers and conformers, see Ref. 11.

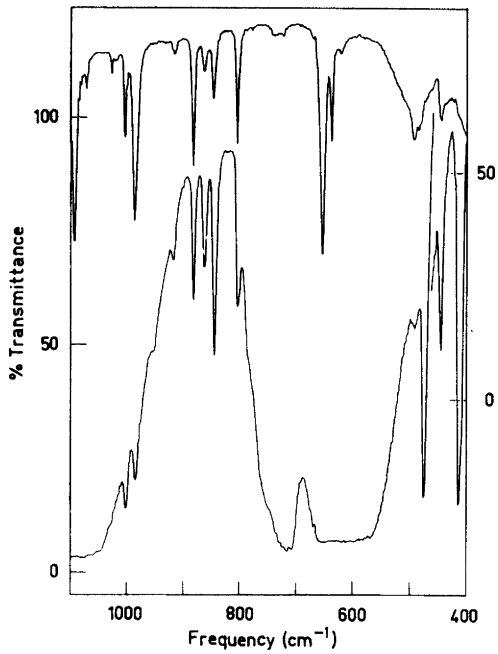

Fig. 2. Infrared spectra of liquid iodocyclohexane (top, right ordinate axis) and crystalline thiourea clathrate (bottom, left ordinate axis) in the region 1100–400 cm^{-1}.

reported,[2] our corresponding data will not be given. However, the Raman spectra of the clathrates served as a supplement to our IR values and confirmed in all the cases the conclusions drawn.

The data of Tables 2–4 clearly reveal that for all the present compounds except iodo- and isocyanatocyclohexane, the intense bands all belong to the *a* (*aa*) conformer or are common to both conformers, whereas the *e*-bands are missing or have very low intensities.

For iodo- and isocyanatocyclohexane the equatorial conformers were still present in the clathrates, although with less abundance than in the liquid state. Preliminary results on fluorocyclohexane,[6] *trans*-1,4-diiodo- and the unsymmetrical *trans*-1,4-dihalocyclohexanes suggest considerable amounts of the equatorial conformers present in their thiourea clathrates as well.

Conformational displacement. The shift of the conformational equilibria between the liquid (or dissolved) cyclohexane and the clathrate was estimated from the infrared band intensities. For this purpose we selected the characteristic pair of bands[10,17] around 1000 cm^{-1} which are intense in IR and well suited for quantitative studies. Also, the intense IR-bands in the region 900–800 cm^{-1}, discussed previously[17] were employed, but for the *trans*-1,4-dihalocyclohexanes a host lattice band around 890 cm^{-1} apparently interfered. The intense C–halogen stretching bands which have been the subject of several detailed studies[18] were completely covered by the host bands (Figs. 1 and 2) and therefore not useful for this purpose.

The ratio between the absorbances (A_a) of the *a* and the neighbouring *e* conformer bands (A_e) was calculated independently for both the 1000 and 850 cm^{-1} bands whenever feasible. These values are given for the liquids (A_a^l/A_e^l) and for the clathrates (A_a^c/A_e^c) in Table 5. Applying the Lambert-Beer's law for the liquid (I)

$$A_a^l/A_e^l = (\varepsilon_a/\varepsilon_e)C_a^l/C_e^l \quad \text{(I)}$$

$$A_a^c/A_e^c = (\varepsilon_a/\varepsilon_e)C_a^c/C_e^c \quad \text{(II)}$$

and the clathrate (II) we obtain eqn. (III), assuming that the molar absorbance indexes (ε_a and ε_e) are the same in the liquid and in the clathrate. (C_a and C_e)

$$\frac{A_a^c/A_e^c}{A_a^l/A_e^l} = \frac{C_a^c/C_e^c}{C_a^l/C_e^l} = \frac{K_c}{K_l} = f \quad \text{(III)}$$

are the concentrations of axial and equatorial conformer, respectively, $K_c = C_a^c/C_e^c$ and $K_l = C_a^l/C_e^l$). Values for f readily available from the IR-absorbance values, are listed in Table 5, and they represent the ratio between the equilibrium constants in the clathrate (K_c) and the liquid (K_l). The value of K_c (or K_l) cannot be derived from this simple arithmetic since the values of the absorbance indexes (ε_a and ε_e) are not known.

The independent values for f listed in Table 5 agree satisfactorily considering the low intensities of some of the IR-bands involved and the rather coarse approximation of constant $\varepsilon_a/\varepsilon_e$ in the liquid and clathrate.

Spectral interpretations. The vibrational bands of the present cyclohexanes were previously attributed to the respective conformers from various criteria, of which the most important was the spectral simplification upon crystallization. Most of the present cyclohexanes crystallize in the equatorial conformer at low temperature and high pressure (*vide infra*). For these compounds the axial bands

Table 5. Displacement of conformational equilibrium from liquid to thiourea clathrate of substituted cyclohexanes.

Substituent	IR bands	A_a/A_e [a]		$f=\frac{K_{clath.}}{K_{liq.}}$ [b]	IR bands	A_a/A_e [a]		$f=\frac{K_{clath.}}{K_{liq.}}$
		Liquid (solution)	Clathrate			Liquid (solution)	Clathrate	
	1014 *a*				868 a			
Cl		0.17	2.22	13		0.13	1.25	10
	993 *e*				889 e			
	1010 *a*				864 a			
Br		0.26	3.47	13		0.15	2.40	16
	988 *e*				885 e			
	1006 *a*				862 a			
I		0.40	0.90	2		0.16	0.74	5
	988 *e*				883 e			
	1013 *a*				862 a			
CN		0.95	10.85	11		0.53	6.17	12
	1042 *e*				892 e			
	1020 *a*				863 a			
NCO		0.48	0.81	2		0.20	0.54	3
	1010 *e*				839 e			
	1005 *aa*				865 aa			
1,2-*trans*-Cl_2		0.51	22.50	45		0.27	16.37	60
	980 ee				845 ee			
	999 *aa*				861 aa			
1,2-*trans*-Br_2		2.40	13.82	6		4.04	24.62	6
	972 *ee*				840 ee			
	1006 *aa*							
1,4-*trans*-Cl_2		0.85	28.00	33				
	995 *ee*							
	1003 *aa*							
1,4-*trans*-Br_2		1.21	8.24	7				
	988 *ee*							

[a] A_a (A_e) absorbance of axial (equatorial) band. [b] $K_{clath.}$ and $K_{liq.}$ are equilibrium constants C_a/C_e in clathrate and liquid cyclohexane, respectively.

can be attributed with certainty while the distinction between equatorial bands and bands common to both conformers is uncertain. Obviously, the predominantly axial conformer observed in most of the clathrates gives added spectral information. Thus, the weak bands at 889, 885 and 883 cm^{-1} for chloro-, bromo- and iodocyclohexane, respectively, (Table 2) are probably equatorial[9] and not common to both conformers.[8] The strong bands at 852 (bromo-) and 848 cm^{-1} (iodocyclohexane) must be common to both conformers[8] and not equatorial,[9,17] whereas the 852 cm^{-1} band in chlorocyclohexane should be equatorial.[9] For isocyanatocyclohexane the equatorial and axial conformers were detected[17] in the low temperature and high pressure crystals, respectively, and no further results were obtained from the clathrate.

In *trans*-1,2-dichlorocyclohexane (Table 3) the intense 909 cm^{-1} band must be common to both conformers (as is the 903 cm^{-1} band in *trans*-1,2-dibromocyclohexane) and not diequatorial as reported.[10] In *trans*-1,2-dibromocyclohexane the crystals consist of molecules in the *aa*-conformer[10] and no further information was extracted from the present clathrate spectra. Finally, in the *trans*-1,4-dichloro- and dibromocyclohexane spectra the attributions to diequatorial and diaxial conformers are based upon very thorough data[11] and the agreement with the clathrate spectra (Table 4) is excellent.

DISCUSSION

The urea and thiourea molecules in the clathrates are linked together by hydrogen bonding,[19] leaving long channels[20] of hexagonal cross-sections in which the guest molecules are located.[19-22]

With the possible exception of cyano- and isocyanatocyclohexane, the present cyclohexanes are not hydrogen-bond acceptors and specific host-guest interactions are impossible. The preferred cross-sectional dimensions of adducts in thiourea are *ca.* 5.8–6.8 Å,[23] and parent cyclohexane falls well within these values. Therefore cyclohexane molecules can be stacked with the three-fold axis centred along the thiourea channel axis. In substituted cyclohexanes an equatorial substituent like, *e.g.*, chlorine, will increase the cyclohexane diameter to *ca.* 7 Å. An axial substituent, however, is ideally parallel to the cyclohexane three-fold axis and will therefore not increase the cyclohexane diameter significantly. The axially substituted cyclohexanes can therefore be stacked with the substituents directed parallel to the channels. Moreover, the axial conformers of mono- and 1,4-dihalocyclohexanes have smaller volumes than the equatorial conformers[24] which might independently favour the axial conformer in the clathrates.

Equatorial substituents can, if parallel or oblique to the channels, also be accomodated in the host lattice. The three-fold axis of the cyclohexane ring should then be oriented roughly perpendicular to the channels. Such packing of the guest molecules should be much less efficient than what is possible for the axially substituted cyclohexanes. Structure determinations by X-ray crystallography are needed to determine the guest molecule orientation.

The linear cyanogroup in cyanocyclohexane would also follow this pattern. Isocyanatocyclohexane has a non-linear side chain which apparently makes the axial conformer less favourable. The present and former[2] results for iodocyclohexane as well as preliminary[6] data for fluorocyclohexane clathrates indicate that the axial conformer is less preferable for these than for the chloro and bromo compounds. Hopefully, we shall be able to clarify the effects of the halogen size when the thiourea clathrates of more cyclohexanes have been investigated.

Acknowledgement. We are grateful to K. Ruzicka for preparing and purifying the cyclohexanes. Financial support from the Norwegian Research Council for Science and the Humanities is acknowledged.

REFERENCES

1. Nishikawa, M. *Chem. Pharm. Bull. 11* (1963) 977.
2. Allen, A., Fawcett, V. and Long, D. A. *J. Raman Spectrosc. 4* (1976) 285.
3. Fukushima, K. *J. Mol. Struct. 34* (1976) 67.
4. Eliel, E. L., Allinger, N. L., Angyal, S. J. and Morrison, G. A. *Conformational Analysis*, Interscience, New York 1966.
5. Hirsch, J. A. In Allinger, N. L. and Eliel, E. L., Eds., *Topics in Stereochemistry*, Interscience, New York 1967, Vol. 1 , p. 199.
6. Christian, S. D., Grundnes, J. and Klæboe, P. *To be published.*
7. Klæboe, P., Lothe, J. J. and Lunde, K. *Acta Chem. Scand. 10* (1956) 1465.
8. Klæboe, P. *Acta Chem. Scand. 23* (1969) 2641.
9. Rey-Lafon, M., Rouffi, C., Camiade, M. and Forel, M. T. *J. Chim. Phys. Phys. Chim. Biol. 67* (1970) 2030.
10. Klæboe, P. *Acta Chem. Scand. 25* (1971) 695; Horntvedt, H. T. and Klæboe, P. *Ibid. 26* (1972) 3797.
11. Ellestad, O. H. and Klæboe, P. *J. Mol. Struct. 26* (1975) 25.
12. Gilbert, B. and Duyckaerts, G. *Spectrochim. Acta A 26* (1970) 2197.
13. Stewart, J. E. *J. Chem. Phys. 26* (1957) 248.
14. Opaskar, C. G. and Krimm, X. *Spectrochim. Acta A 23* (1967) 2261.
15. Remizov, A. B. and Sverdlov, L. M. *Izv. Vyssh. Uchebn. Zaved. Fiz. 11* (1968) 150.
16. Rey-Lafon, M. and Forel, M. T. *J. Mol. Struct. 29* (1975) 193.
17. Horntvedt, H. T. and Klæboe, P. *Acta Chem. Scand. A 29* (1975) 528.
18. Altona, C., Hageman, H. J. and Havinga, E. *Spectrochim. Acta A 24* (1968) 633.
19. For a review see Bhatnagar, V. M. *Zh. Strukt. Khim. 8* (1967) 568.
20. Fetterly, L. C. In Mandelcorn, L., Ed., *Non-Stoichiometric Compounds*, Academic, New York 1964.
21. Fawcett, V. and Long, D. A. *J. Raman Spectrosc. 3* (1975) 263.
22. Clement, R., Claude, R. and Mazieres, C. *Chem. Commun.* (1974) 654.
23. Schiessler, R. W. and Flitter, D. *J. Am. Chem. Soc. 74* (1952) 1720.
24. Christian, S. D., Grundnes, J. and Klæboe, P. *J. Am. Chem. Soc. 97* (1975) 3864; *Appl. Spectrosc. 30* (1976) 227.

Received August 26, 1977.

Acta Chemica Scandinavica A 32 (1978) 31 – 39

NMR-Studies of the Interaction of Metal Ions with Poly-(1,4-hexuronates). V. Quantitative Separation of Contact and Dipolar Contributions to Lanthanide Induced Shifts in ^{1}H NMR Spectra of Methyl α-D-Gulo- and Methyl β-D-Hamamelo-pyranosides, 1,6-Anhydro-β-D-manno-, 1,6-Anhydro-β-D-talo- and 1,6-Anhydro-β-D-allo-pyranoses and Epi-inositol

HANS GRASDALEN,[a] THORLEIF ANTHONSEN,[b] OLE HARBITZ,[a] BJØRN LARSEN[a] and OLAV SMIDSRØD[a]

[a] Institute of Marine Biochemistry, The University of Trondheim and [b] Institute of Organic Chemistry, The Norwegian Institute of Technology, N-7034 Trondheim-NTH, Norway

Some 1:1 complexes between epi-inositol and various lanthanide ions were analysed according to a mirror symmetric structure in solution where an *ax-eq-ax* sequence of three hydroxy groups formed the binding site. It was assumed that in the substrate three of the protons (H6, H2, H4) showed only dipolar lanthanide induced shifts (LIS) in the case of Pr^{3+}. The McConnel-Robertson equation was found to account for the dipolar part of the LIS for all Ln ions when compared with data given by Bleaney. The remaining LIS corresponded relatively well with theoretical contact LIS from Ce^{3+} to Tb^{3+}. Most of the heavier Ln ions gave bad agreement. It was concluded that separation of LIS by using theoretical shift patterns should be limited, at present, to the lighter lanthanides.

Such analysis was carried out for a series of glycopyranosides containing a similar binding site as epi-inositol. The analysis showed that whereas the contact LIS in epi-inositol was large only when bond connecting the proton and the cation formed a planar zig-zag arrangement, the introduction of a ring oxygen altered this pattern leading to a considerable contact interaction also at other protons.

The McConnel-Robertson equation was used in an attempt to locate the Ln-ion bound to methyl α-D-gulopyranoside.

Numerous attemps have been made recently in applying LIS in NMR spectra for obtaining structural informations of molecules and their metal complexes in solution.[1] One limitation in the method is that two different mechanisms operate in LIS: Fermi contact and dipolar interaction, and that only the dipolar LIS which is geometry dependent, has the potential for quantitative structure determination. Reliable methods are therefore required to dissect the two shift contributions before the technique can become generally applicable. The object of the present paper is to investigate the utility and limitation of such methods for a certain type of compounds containing a high affinity binding site for Ln-ions, consisting of three consecutive hydroxy groups with an *ax-eq-ax* arrangement.

Many recent studies of LIS provide evidence for significant contact interactions at ^{1}H nuclei close to the complexing site.[2-4] In epi-inositol, Fig. 1, the contact interaction is found to be stereospecific,[2] *i.e.* it is greatest when the bonds connecting the proton and the cation form a planar zig-zag arrangement. As pointed out by Angyal,[2] the contact interaction may then be detectable over several intervening bonds. We have used the LIS-data of Angyal[4] for epi-inositol and utilized the mirror symmetry of the complex, and the resulting sym-

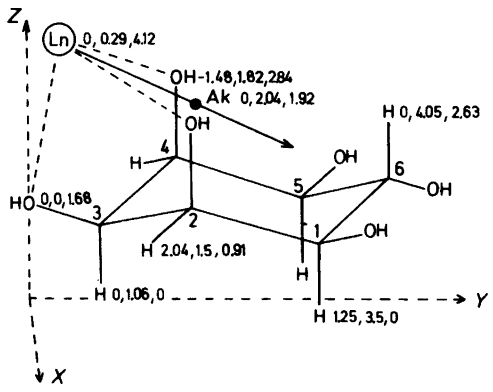

Fig. 1. The proposed Ln–epi-inositol complex located in cartesian coordinates as discussed in the text. The complex has a mirror symmetry through Ln, O3, H3, and H6 in the *yz*-plane. The coordinates (*x*, *y*, *z*) are given in units of Å.

metry of the LIS, to separate between the contact and dipolar contributions to the shifts. By this quantitative method we are able to confirm the conclusions which Angyal[3] arrived at based upon qualitative arguments. In addition the results suggest that the general structure independent method[5] for separation of contact and dipolar shifts based upon theoretical values[6,7] for different Ln ions, in the present case should be limited to the lighter Ln-ions.

In our earlier study[8] of methyl α-D-gulopyranoside (*1*) the shift ratio for Eu^{3+} and Pr^{3+} at the H2 proton was found to be significantly different from the nearly equal ratios observed at the other protons. In view of the results for epi-inositol it is reasonable to suggest that the planar zig-zag arrangement of Ln–O2–C2–H2 in *1* may cause a considerable contact shift contribution at proton H2 also in this case. In order to clarify this point we have remeasured LIS for *1* with several of the lighter Ln ions, and used the general structure independent method[5] to dissect the shifts. This method was also applied to recently reported LIS data[9] for methyl, β-D-hamameloside (*2*), 1,6-anhydro-β-D-manno- (*3*), talo- (*4*) and allopyranoses (*5*).

The set of dipolar shifts obtained for the Ln complex of methyl α-D-gulopyranoside has been used with the computer search program described earlier,[10] to obtain information of the structure of the complex. The results obtained have been compared to those reported previously.[8]

RESULTS

Dissection of LIS for complexes with mirror symmetry. The Ln-epi-inositol complex, Fig. 1, has a mirror symmetry through O3, H3, H6 and the

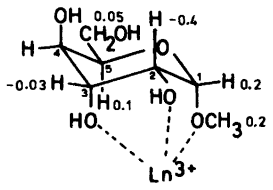

1

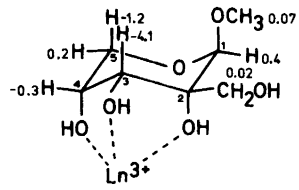

2

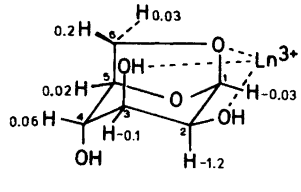

3

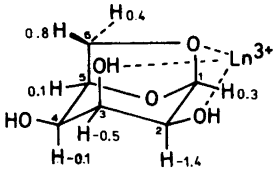

4

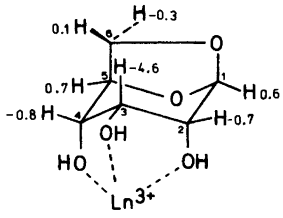

5

Table 1. Comparison of theoretical and estimated dipolar and contact shifts induced by lanthanides in epi-inositol.[4] Positive values indicate downfield shifts.

	Rel. theor. shifts dipolar contact		Lanthanide induced shifts (ppm) in epi-inositol											
			H1,5			H2,4			H3			H6		
	Bleaney[2]	Golding[3]	$\Delta\nu_{obs}$ [a]	$\Delta\nu_{dip}$ [b]	$\Delta\nu_{cont}$	$\Delta\nu_{obs}$	$\Delta\nu_{dip}$	$\Delta\nu_{cont}$	$\Delta\nu_{obs}$	$\Delta\nu_{dip}$	$\Delta\nu_{cont}$	$\Delta\nu_{obs}$	$\Delta\nu_{dip}$	$\Delta\nu_{cont}$
La^{3+}	0	0	0.17	0	0	0.27	0	0	0.55	0	0	0.07	0	0
Ce^{3+}	−6.3	0.98	−0.4	−0.6	0.03	−0.7	−0.73	−0.24	0.8	−0.8	1.05	−1.05	−1.12	0
Pr^{3+}	−11	3	−1.05	−1.92	0.70	−2.05	−2.32	0 [c]	2.05	−2.56	4.06	−3.5	−3.57	0
Nd^{3+}	−4.2	4.5	0.3	−0.93	1.06	−1.10	−1.12	−0.25	6.1	−1.23	6.8	−1.65	−1.72	0
Sm^{3+}	−0.7	−0.06	−0.05	−0.2	−0.02	0.15	−0.24	0.12	0.3	−0.26	0.01	−0.3	−0.37	0
Eu^{3+}	4	−10.7	−0.35	0.85	−1.37	1.6	1.03	0.30	−7.2	1.13	−8.9	1.65	1.58	0
Tb^{3+}	−86	−31.8	−18	−10.2	−7.93	−19	−12.4	−6.9	−35	−13.6	−22	−19	−19	0
Dy^{3+}	−100	−28.5	−21	−14	−7.2	−21	−16.9	−4.4	−24	−18.6	−5.95	−26	−26	0
Ho^{3+}	−39	−22.6	−8	−8.1	−0.07	−5	−9.8	4.53	−12	−10.7	−1.85	−15	−15	0
Er^{3+}	33	−15.4	0.5	1.96	−1.63	2.1	2.36	−0.53	−3.4	2.6	−6.6	3.7	3.63	0
Tm^{3+}	53	−8.2	−4.5	3.0	−7.7	−10	3.67	−13.9	−16	4.03	−20.5	5.7	5.63	0
Yb^{3+}	22	−2.6	−0.25	2.4	−2.82	−2.05	2.85	−5.5	−4.8	3.14	−8.5	4.45	4.38	0
Lu^{3+}	0	0	0.16	0	0	0.23	0	0	0.50	0	0	0.06	0	0

[a] $\Delta\nu_{obs} = \Delta\nu_{obs}(La^{3+}) + \Delta\nu_{dip} + \Delta\nu_{cont}$. [b] $\Delta\nu_{dip}$ was calculated according to $\Delta\nu = C(3\cos^2\theta - 1)/r^3$ by use of appropriate coordinates given in Fig. 1. The constant C was adjusted to give only dipolar shift at proton H6. [c] $\Delta\nu_{cont}$ was assumed to be zero at H2,4 for Pr^{2+} in order to determine the location of the symmetry axis.

Ln^{3+} ion, which is demonstrated by equally large LIS observed at protons H2,4 and H1,5, as shown in Table 1. This means that the principal magnetic symmetry axis must be located in the mirror plane, corresponding to the *yz*-plane in Fig. 1. The Ln^{3+}-oxygen distance used, ~2.46 Å, was estimated as a mean value of reported solid state crystal values.[11-14] Space coordinates for the hydrogens of epi-inositol were obtained by using conformational angles and bond lengths given in a crystal structure[15] and assuming a C–H distance of 1.09 Å. As pointed out by Angyal,[3] the observed LIS for protons H6 and H2,4 can be accounted for by an approximately pure dipolar mechanism. This is demonstrated in Fig. 2 where the measured LIS at H6 is shown to match the theoretical dipolar LIS[6] through the Ln series quite closely. The same finding prevails for measured LIS at H2,4 except for Tm^{3+} and Yb^{3+}. Since the contact interaction caused by Pr^{3+} is small,[7] it may therefore be a good approximation to use the total Pr^{3+} induced shifts at protons H6 and H2,4 in determining the orientation of the principal magnetic symmetry axis in the presumed axially symmetric complex by using the space coordinates defined in Fig. 1 and the McConnel-Robertson equation[16]

$$\Delta\nu/\nu = C(3\cos^2\theta - 1)/r^3 \qquad (1)$$

Here r is the length of the vector joining the Ln ion and the proton and θ is the angle between this vector and the symmetry axis.

Calculations on this rigid substrate molecule is thus simple. The axis was found to go through the point Ak as indicated in Fig. 1. By assuming the same structure for the homologous Ln complexes, the relative dipolar LIS for all protons are given by eqn. (1). The absolute dipolar LIS values were found by adjusting the constant C in eqn. (1) according to pure dipolar shift at proton H6 throughout the Ln series. The relationship between the LIS contributions is given by

$$\Delta\nu_{obs} = \Delta\nu_{obs}(La^{3+}) + \Delta\nu_{dip} + \Delta\nu_{cont} \qquad (2)$$

Hence, the numerical values for the contact LIS, $\Delta\nu_{cont}$, are found as the difference between the observed LIS, $\Delta\nu_{obs}$, corrected for La-induced diamagnetic shifts, $\Delta\nu_{obs}(La^{3+})$, and the calculated dipolar LIS, $\Delta\nu_{dip}$. The resulting dipolar and contact LIS values are listed in Table 1. As shown in Fig. 2 the estimated relative contact LIS at H3 and H1,2

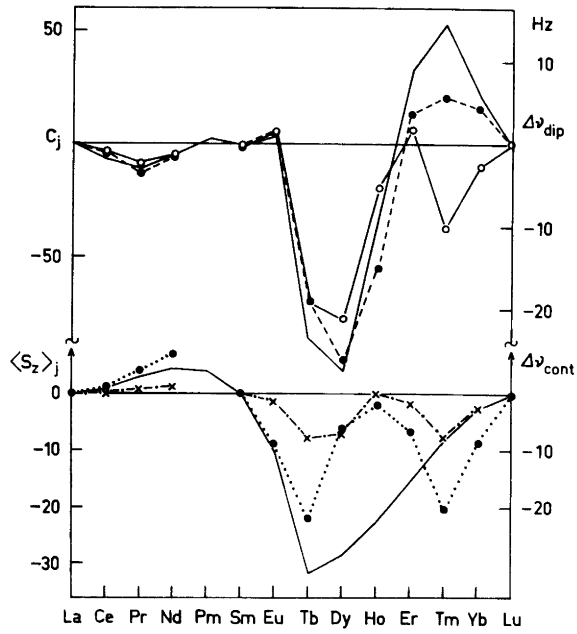

Fig. 2. Variation of the theoretical relative dipolar, C_j, and contact, $\langle S_z \rangle_j$, LIS (—) through the lanthanide series. Measured LIS: H6 (●---●), H2,4 (○——○). Estimated contact LIS: H1,2 (×-·-×), H3 (●···●). (All protons of epi-inositol).

both agree with theory down to Tb^{3+}. However, a substantial discrepancy occurs for the heavier lanthanides.

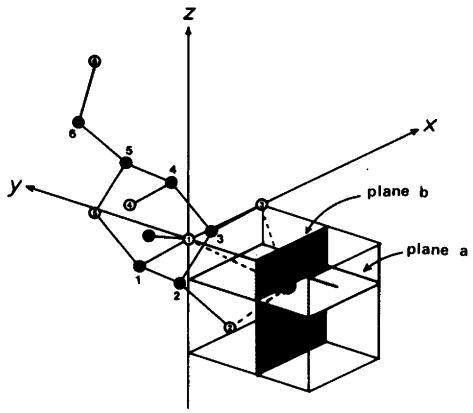

Fig. 3. Location of the cube used for calculation of the Ln^{3+} – methyl α-D-gulopyranoside complex. The coordinates for the lanthanide ion were found to be $x = 1.1$ Å, $y = -1.5$ Å and $z = -0.8$ Å. The magnetic axis has been omitted from the figure in sake of clarity.

Dissection of LIS by the general structure-independent method.[5] The methyl α-D-gulopyranoside (*1*), Fig. 3, is a neutral sugar derivative containing an ax-eq-ax sequence of two hydroxy groups and one OCH_3 group, which most probably constitute the Ln^{3+} binding site as reported recently. Due to the ring oxygen and the OCH_3 group, this substrate lacks the symmetry found in epi-inositol which enabled us to deduce the structure of its Ln complex in a straightforward manner. In the case of (*1*) we used a structure-indepdendent method, outlined and tested by Reilly *et al.*,[5] where advantage is taken of the fact that dipolar and contact LIS vary in a characteristic but different way with Ln ions. It is essential for using this method that the structure of the complexes stay constant throughout the lanthanide series employed, and that they have axial symmetry around their Ln cations. Our results for epi-inositol support this assumption in case of the lighter lanthanides. The contact hyperfine coupling constant and the ligand field should then remain invariant with changing the Ln ion. The contact shift is proportional to the expectation value of the z component of the total electron spin, $\langle S_z \rangle$, whereas

Table 2. Measured LIS values[a] (ppm) at 0.24 M substrate and 0.24 M lanthanide, $\Delta\nu_{obs}$, for methyl α-D-gulopyranoside and the corresponding computed values for contact, $\Delta\nu_{cont}$, and dipolar, $\Delta\nu_{dip}$, contributions.

	LIS	Pr^{3+}	Nd^{3+}	Eu^{3+}	Tb^{3+}	G_i	F_i	AF
H1	$\Delta\nu_{obs}$	−0.60	−0.32	0.35	−3.16			
	$\Delta\nu_{dip}$	−0.51	−0.20	0.19	−4.02	0.047	−0.019	0.082
	$\Delta\nu_{cont}$	−0.06	−0.08	0.20	0.60			
H2	$\Delta\nu_{obs}$	0.20	0.35	−0.44	−0.40			
	$\Delta\nu_{dip}$	0.11	0.04	−0.04	0.88	−0.010	0.041	0.190
	$\Delta\nu_{cont}$	0.12	0.18	−0.44	−1.31			
H3	$\Delta\nu_{obs}$	0.41	0.20	−0.15	2.80			
	$\Delta\nu_{dip}$	0.39	0.15	−0.14	3.03	−0.035	0.003	0.051
	$\Delta\nu_{cont}$	0.01	0.01	−0.03	−0.10			
H5	$\Delta\nu_{obs}$	−0.60	−0.32	0.28	−3.40			
	$\Delta\nu_{dip}$	−0.53	−0.20	0.19	−4.13	0.048	−0.013	0.094
	$\Delta\nu_{cont}$	−0.04	−0.06	0.14	0.41			
H6	$\Delta\nu_{obs}$	−0.16	−0.08	0.07	−0.60			
	$\Delta\nu_{dip}$	−0.12	−0.05	0.04	−0.93	0.011	−0.004	0.311
	$\Delta\nu_{cont}$	−0.01	−0.02	0.05	0.14			
OCH_3	$\Delta\nu_{obs}$	−0.61	−0.32	0.28	−3.24			
	$\Delta\nu_{dip}$	−0.52	−0.20	0.19	−4.08	0.047	−0.014	0.124
	$\Delta\nu_{cont}$	−0.04	−0.06	0.15	0.44			

[a] NMR spectra were measured with a Varian XL-100-12 NMR spectrometer at 100 MHz in D_2O solutions at 30 °C. Positive values indicate downfield shifts. The diamagnetic La^{3+} induced LIS could not be measured and $\Delta\nu_{par}$ was approximated by $\Delta\nu_{obs}$ in the calculations.

the dipolar shift is proportional to the constant C in eqn. (1). These terms are dependent only upon the Ln ion employed. Under these conditions the sum of the two paramagnetic LIS contributions, $\Delta\nu_{par}$, at proton i induced by the Ln ion j may be written

$$\Delta\nu_{par,ij} = \Delta\nu_{cont,ij} + \Delta\nu_{dip,ij} = F_i\langle S_z\rangle_j + G_iC_j \quad (3)$$

where F_i and G_i are related to the structure and depend only upon the proton i being observed. The factor F_i reflects the effectivity of contact interaction at proton i while the G_i value includes the geometric factor of that proton in eqn. (1). By measuring the LIS for Pr^{3+}, Nd^{3+}, Eu^{3+} and Tb^{3+} (varying indices j), Table 2, an appropriate number of simultaneous equations was set up, eqn. (3), using theoretical values for $\langle S_z\rangle_j$ and C_j given by Golding[7] and Bleaney,[6] respectively. In order to obtain the weighted average least squares values for F_i and G_i in Table 2, the observed predominant shift for Tb^{3+} and the values of $\langle S_z\rangle$ and C for this ion were scaled down by a factor of 8 before solving the equations. In the calculated agreement factors

$$AF = [\Sigma_i(\Delta\nu_{par,i}^{(obs)} - \Delta\nu_{par,i}^{(cal)})^2/\Sigma_i(\Delta\nu_{par,i}^{(obs)})^2]^{\frac{1}{2}} \quad (4)$$

also listed in Table 2, the full observed paramagnetic LIS, $\Delta\nu_{par}^{(obs)}$, and calculated LIS, $\Delta\nu_{par}^{(cal)}$, were used. The resulting dipolar and contact shift values are listed in Table 2. Here $\Delta\nu_{par}$, approximated by $\Delta\nu_{obs}$, is not perfectly equal to the sum of $\Delta\nu_{dip}$ and $\Delta\nu_{cont}$ because these values found via a least square approach deviated from a perfect fit *i.e.* the agreement factor $AF > 0$.

This method was also used to analyse reported LIS data[9] for the complexes *2*, *3*, *4* and *5*. The dipolar and contact LIS contributions are given in Table 3. The contact shifts (ppm) for Eu^{3+} in these complexes are indicated in the figures. The LIS data for *1*−*5* were measured at about the same

Table 3. Measured LIS values,[9] $\Delta\nu_{par}=\Delta\nu_{obs}-\Delta\nu(La^{3+})$ at 0.25 M substrate and 0.25 equiv. of lanthanide, in ^{1}H NMR spectra, and the corresponding computed values for contact, $\Delta\nu_{cont}$, and dipolar, $\Delta\nu_{dip}$, contributions. Positive values indicate downfield shifts.

Cation	$\Delta\nu_{par}$	$\Delta\nu_{dip}$	$\Delta\nu_{cont}$	$\Delta\nu_{par}$	$\Delta\nu_{dip}$	$\Delta\nu_{cont}$	$\Delta\nu_{par}$	$\Delta\nu_{dip}$	$\Delta\nu_{cont}$	$\Delta\nu_{par}$	$\Delta\nu_{dip}$	$\Delta\nu_{cont}$	$\Delta\nu_{par}$	$\Delta\nu_{dip}$	$\Delta\nu_{cont}$	$\Delta\nu_{par}$	$\Delta\nu_{dip}$	$\Delta\nu_{cont}$
	1,6-Anhydromannose																	
	H1			H2			H3			H4			H5			H6 *endo*			H6 *exo*		
Pr^{3+}	−1.67	−1.68	0.01	0.87	0.62	0.35	0.96	0.91	0.04	−0.81	−0.82	−0.02	−1.03	−1.07	−0.01	−4.04	−4.11	−0.06	−2.07	−2.11	−0.01
Nd^{3+}	−0.65	−0.64	0.01	1.12	0.24	0.51	0.34	0.35	0.06	−0.46	−0.31	−0.03	−0.58	−0.41	−0.01	−2.19	−1.57	−0.10	−0.99	−0.81	−0.01
Eu^{3+}	0.58	0.62	−0.03	−1.33	−0.23	−1.23	−0.49	−0.33	−0.14	0.32	0.30	0.06	0.35	0.39	0.02	1.54	1.49	0.23	0.73	0.77	0.03
	1,6-Anhydrotalose																				
Pr^{3+}	−1.62	−1.55	−0.08	0.52	0.12	0.40	0.77	0.63	0.14	−0.34	−0.37	0.03	−0.91	−0.88	−0.03	−3.63	−3.40	−0.23	−1.75	−1.63	−0.12
Eu^{3+}	0.83	0.56	0.27	−1.47	−0.04	−1.43	−0.72	−0.23	−0.49	0.02	0.14	−0.12	0.43	0.32	0.11	2.07	1.24	0.84	1.02	0.59	0.43
	1,6-Anhydroallose																				
Pr^{3+}	−1.88	−1.71	−0.17	−0.38	−0.57	0.19	1.05	−0.25	1.30	−0.45	−0.67	0.22	−1.71	−1.52	−0.19	−0.75	−0.71	−0.04	−0.69	−0.77	0.08
Eu^{3+}	1.24	0.62	0.62	−0.48	0.21	−0.69	−4.55	0.09	−4.64	−0.55	0.25	−0.80	1.24	0.55	0.69	0.40	0.26	0.14	~0	0.28	−0.28
	Methyl β-D-hamamelopyranoside																				
	H1			H3			H4			H5*eq*			H5*ax*			CH_2			Me		
Pr^{3+}	−1.60	−1.48	−0.12	1.31	0.15	1.16	1.38	1.29	0.09	0.13	0.18	−0.05	0.23	−0.10	0.33	−1.09	−1.09	~0	−0.38	−0.36	−0.02
Eu^{3+}	0.98	0.54	0.44	−4.19	−0.06	−4.14	−0.79	−0.47	−0.32	0.11	−0.07	0.18	−1.14	0.04	−1.18	0.41	0.40	0.02	0.2	0.13	0.07

conditions and allow an approximate comparison of the LIS values in these compounds. The LIS values for epi-inositol are reported as limiting shifts and are not directly comparable as far as absolute shifts are concerned.

Evaluation of the Ln ion binding site. For methyl α-D-gulopyranoside the existence of a single, best-fit site in the vicinity of the three oxygen functions O1, O2 and O3 was investigated by computer calculation of an agreement factor for space points equally spaced within a cube. The cube was located with one corner in O1, one corner in O3, and with O2 lying in the plane of the side O1 – O3 as shown in Fig. 3. The edge of the cube is thus equal to the distance O1 – O3 (2.6 Å). No other atoms in the carbohydrate structure will be located inside this cube. The agreement factor is given by a formula similar to eqn. (7) in which the dipolar LIS is used, and where $\Delta\nu_{dip,i}^{(obs)}$ was taken as the value relative to the dipolar shift for H1. The resulting value was divided by six to give the average square-root deviation per proton signal observed.

Starting at the far end of the cube with respect to the oxygen atoms, the agreement factor was calculated for all points constituting a cube-grid of 0.2 Å. The calculation is equivalent to placing the Ln ion in a grid position, calculating the theoretical shifts and the agreement factor and minimizing the latter with respect to the direction of the magnetic axis through a search procedure. The minimum value for the agreement factor is thus obtained for all the grid points. A smaller part of the cube was also investigated using a grid size of 0.1 Å. These calculations gave a contour plot for the AF values consistent with only one minimum within the cube, thus demonstrating that there exists only one best-fit site for the Ln ion within the part of space around the sugar molecule which is physically and chemically reasonable. Fig. 4 shows contour plots in two perpendicular planes a and b through the best-fit position. In three dimensional space the inner contours form a cigarshaped cavity. The equidistance corresponds to 0.0003, and the minimum value of the agreement factor is 0.0024 (grid size 0.1 Å, angular accuracy for magnetic axis 0.1°). The distances from the three oxygen functions O1, O2, and O3 are 2.0, 2.2 and 2.3 Å, respectively. The direction of the magnetic axis is defined by the angle $\alpha=62.8°$ with the x-axis and $\beta=62.8°$ with the z-axis (intersection with the xz-plane in 0.20, 0.00, 0.10).

The evaluated binding site was checked by using

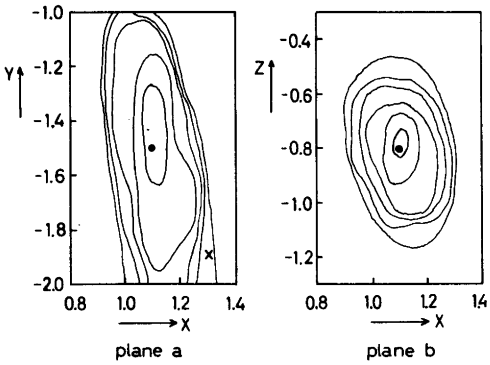

Fig. 4. Contour plot of two perpendicular planes through the best-fit position according to the agreement factor between observed and calculated dipolar LIS for methyl α-D-gulopyranoside. The average position from crystal structures lies in plane *a*, and is marked with a cross.

relaxation reagent. After addition of $Pr(NO_3)_3$ to separate overlapping resonances, $Gd(NO_3)_3$ was added and its relaxation effects on the separated resonances were measured. Appropriate corrections for outer sphere effects were made by subtracting the observed relaxation rate for internal dioxane. The proton relaxivity in dioxane induced by Gd^{3+} was very low indicating that dioxane did not bind significantly to Ln^{3+} ions in D_2O solutions. The net effects of the Gd^{3+} in the binding site were of the order: H1 ≈ H2 ≈ H3 ≈ H5 ≈ OMe > H4 > H6. This is in accordance with an r^{-6} dependence valid for a dipolar paramagnetic relaxation mechanism where r is the distance from the substrate proton to the evaluated Ln binding site.

DISCUSSION

Here we have dealt with complexes consisting of six-membered rings, cyclitols and neutral sugar derivatives, possessing three neighbouring hydroxy groups in an *ax-eq-ax* sequence which are known to form an active site of rather high affinity for calcium and lanthanide ions.[3] Our estimates of contact, and dipolar shift contributions to proton LIS data clearly demonstrate some geometrical relationships which strongly influence the effects of contact interaction in these lanthanide complexes.

The contact shifts are caused by either or both of two mechanisms: (a) Direct delocalization of unpaired electron spin density from the paramagnetic cation leading to[17] upfield shifts for all protons with Eu^{3+} and (b) spin polarization giving alternating shifts in pairs along the bonds.[18] The fact that alternating upfield and downfield contact shifts occur indicates clearly that spin polarization plays an important role in these systems. Evidently the total effect of contact interaction is increased by a planar zig-zag path which is most clearly demonstrated by the LIS data for epi-inositol,[4] Table 1. Here the upfield contact shift for Eu^{3+} at proton H3 is suprisingly large, ~8.9 ppm. The bonds connecting H1,5 to the cation are in a plane, those of H2,4 are not. These two proton pairs show contact shift in opposite direction which is about a factor of 4 greater at H1,5 even though these protons are one bond further away from the cation. A similar type of stereospecificity of contact interaction is found in all the investigated complexes. The pyranose rings show a more complex LIS pattern than the cyclohexane ring.

The validity of our analysis is strongly supported by the internal consistency of the results obtained for epi-inositol bound to lighter lanthanides. In dissecting the LIS data for these complexes, no assumptions conserning values of theoretical shifts were utilized. We stress that for lanthanides lighter than Tb^{3+}, both the calculated dipolar and contact LIS show a remarkably good overall agreement with theoretical values given by Bleaney[6] and Golding,[7] respectively. These values have earlier been reported to be consistent with experimental data.[19] Possible errors in our analysis of epi-inositol arising from structure faults are probably small and play a minor role because no protons possess position close to the magic angle (54.7°) position in eqn. (1). The reason why the contact LIS for the heavier lanthanides showed bad agreement may probably be due to some alterations in the metal-substrate bond and/or small conformational changes. Reported works[20] indicate that although the bonding may be predominantly of pure electrostatic nature in all Ln complexes, the possibility of $f\pi - p\pi$ bonding may be important in complexes of the heavier Ln ions. The ionic radius decreases slightly along the Ln series, being largest for Ce^{3+} (1.034 Å), and this may cause some structural changes for the heavier lanthanides. The hydration number of the Ln ions has also been reported to decrease from 9 for La^{3+} to 8 for Yb^{3+} somewhere in the middle of the Ln series.[21]

Except for methyl α-D-gulopyranoside, the LIS

data have been corrected for the small downfield diamagnetic shift contributions caused by the charge of the cation as measured by adding La^{3+}. For methyl α-D-gulopyranoside (*1*) the NMR spectral lines were so heavily overlapping that no La^{3+} induced shifts could be measured. This is also the reason why the shift values at proton H4 are absent in Table 2. Only small shifts comparable to diamagnetic shifts were observed at this proton.

We have used the dipolar shifts in Table 2 to determine the Ln binding site on *1*. The consistent results for epi-inositol suggest that the dipolar shifts in this tridentate system can be accounted for by use of the McConnel-Robertson equation. This equation requires the complex to have an axial symmetry. Provided this is the case, the calculations strongly suggest that there exists only one site within a reasonable distance from the three oxygen functions O1, O2 and O3. It should be mentioned here that it is very important to use a sufficiently small angular step (less than 2°) in the search procedure for the axis direction giving the minimum *AF*-value, otherwise apparent local minima may develop.

The site defined by the minimum in *AF* has Ln–O distances of 2.0, 2.2 and 2.3 Å to O1, O2 and O3, respectively. The shortest Ln–O distance in our "best fit" site, 2.0 Å is somewhat outside the range of Ln–O distances in crystals 2.46 ± 0.3 Å.[11-14] The error in our calculated position depends mainly upon uncertainties in dissecting the LIS which in turn relies on relative theoretical values given by Bleaney[6] and Golding.[7] We have carried out Monte-Carlo calculations to study the effect of a randomly distributed error inside $\pm 10\,\%$ in all the shifts, and compared calculated *AF* values for our "best fit" site and the "average" site from crystal data letting the computer in all cases find the minimum in *AF* by varying the orientation of the magnetic axis. Our "best fit" site yielded *AF* values from 0.8 to 5.2×10^{-3}. For the "average" site the *AF* values ranged from 1.0 to 6.5×10^{-3}. Therefore, if we assume an error of $\pm 10\,\%$ in our dipolar LIS data, the heavy overlap between the two sets of *AF*-values shows that we are not able to discriminate between these sites which are *ca.* 0.5 Å apart.

However, even though substantial uncertainties in this type of structure elucidation still exist, important conclusions concerning the localization of ions in complexes may still be drawn, particularly when one has the choise between different sites as is often the case in many large or macromolecular substrates.

In a previous paper[8] we demonstrated that the complex formed between Eu^{3+} and methyl α-D-gulopyranoside had a 1:1 stoichiometry. An attempt was made to explain the LIS as being due to a complex of rhombic symmetry. The site arrived at after applying a correction for the asymmetry gave the following distances between the Ln ion and the oxygen atoms O1, O2, and O3, respectively: 1.7, 1.85, and 3.0 Å. The distance to O3 was larger than expected for a complex where this oxygen plays a significant role. The too short distances to the other two oxygens, and the resulting unsymmetric position of the cation relative to the binding oxygens also seemed questionable.

The more reasonable position found in this paper indicates that the LIS for methyl α-D-gulopyranoside is due to both contact and dipolar shift mechanisms, and that these contributions may be effectively separated provided measurements have been carried out with a set of Ln ions.

REFERENCES

1. Dobson, C. M. and Levine, B. A. In Pain, R. H. and Smith, B. E., Eds., *New Techniques in Cell Biology and Biophysics*, Wiley, New York 1976, Vol. 3, Chapter 2.
2. Angyal, S. J., Greeves, D. and Pickles, V. A. *Chem. Commun.* (1974) 589.
3. Angyal, S. J. *Tetrahedron 30* (1974) 1695.
4. Angyal, S. J. and Greeves, D. *Aust. J. Chem. 29* (1976) 1223.
5. Reilley, C. N. and Good, B. W. *Anal. Chem. 47* (1975) 2110.
6. Bleaney, B., Dobson, C. M., Levine, B. A., Martin, R. B., Williams, R. J. P. and Xavier, A. V. *Chem. Commun.* (1972) 791.
7. Golding, R. M. and Halton, M. P. *Aust. J. Chem. 25* (1972) 2577.
8. Grasdalen, H., Anthonsen, T., Larsen, B. and Smidsrød, O. *Acta Chem. Scand. B 29* (1975) 17.
9. Angyal, S. J., Greeves, D., Littlemore, L. and Pickles, V. A. *Aust. J. Chem. 29* (1976) 1231.
10. Grasdalen, H., Anthonsen, T., Larsen, B. and Smidsrød, O. *Acta Chem. Scand. B 29* (1975) 99.
11. Erasmus, C. S. and Boeyens, J. C. A. *J. Cryst. Mol. Struct. 1* (1971) 83.
12. Hoard, J. L., Lee, B. and Lind, M. D. *J. Am. Chem. Soc. 87* (1965) 1611.
13. Cunningham, J. A., Sands, D. E., Wagner, W. F. and Richardson, U. F. *Inorg. Chem. 8* (1969) 22.
14. Dyer, D. S., Cunningham, J. A., Brooks, J. J., Sievers, R. E. and Rondeou, R. E. In Sievers, R. E., Ed., *Nuclear Magnetic Resonance, Shift Reagents*, Academic, London 1973, p. 21.

15. Jeffrey, G. A. and Kim, H. S. *Carbohydr. Res.* *15* (1970) 310.
16. McConnel, H. M. and Robertson, R. E. *J. Chem. Phys. 29* (1958) 1361.
17. Tori, K., Yoshimura, Y., Kainosho, M. and Ajisaka, K. *Tetrahedron Lett.* (1973) 1573.
18. Yonezawa, T., Morishima, I. and Ohmori, Y. *J. Am. Chem. Soc. 92* (1970) 1267.
19. Reuben, J. *J. Magn. Reson. 11* (1973) 103.
20. Kanekar, C. R., Thakur, N. V. and Jogdeo, S. M. *Bull. Chem. Soc. Jpn. 41* (1968) 759.
21. Spedding, F. H., Pikal, M. J. and Ayers, B. O. *J. Phys. Chem. 70* (1966) 2440.

Received July 11, 1977.

Acta Chemica Scandinavica A 32 (1978) 41 – 45

The Tris [(±)-*trans*-1,2-cyclohexanediamine]chromium(III) System

SVEN E. HARNUNG and TROELS LAIER

Chemistry Department I (Inorganic Chemistry), University of Copenhagen, The H. C. Ørsted Institute, Universitetsparken 5, DK-2100 Copenhagen Ø, Denmark

The eight isomers of $[Cr((\pm)chxn)_3]^{3+}$ (chxn = *trans*-1,2-cyclohexanediamine) have been isolated. Absorption and circular dichroism spectra are presented of aqueous solutions at *ca.* 300 K in the visible and UV spectral region, and of ethanol/methanol solutions at *ca.* 110 K in the range 610–680 nm of the spin-forbidden transitions.

1. INTRODUCTION

The purpose of this work is an experimental investigation of the electronic transitions of a series of chromium complexes whose geometries resemble the conformations of the tris(ethylenediamine)-chromium(III) ion.

The stereochemistry of the compounds with the formula tris[(±)-*trans*-1,2-cyclohexanediamine]-chromium(III) chloride, $[Cr((\pm)chxn)_3]Cl_3$, has been thoroughly discussed in the work [1] on the analogous cobalt(III) complexes. The number of isomers is determined [2] by the conformation, δ or λ, of each of the five-membered chelate rings and by the configuration, Δ or Λ, around the central metal ion. This gives rise to four racemic pairs of complexes:

$$\begin{array}{ll}
\Delta\text{-}[Cr((-)chxn)_3, \lambda\lambda\lambda]^{3+} & \Delta lel_3 \\
\Lambda\text{-}[Cr((+)chxn)_3, \delta\delta\delta]^{3+} & \Lambda lel_3 \\
 & \\
\Delta\text{-}[Cr((-)chxn)_2((+)chxn), \lambda\lambda\delta]^{3+} & \Delta lel_2ob \\
\Lambda\text{-}[Cr((+)chxn)_2((-)chxn), \delta\delta\lambda]^{3+} & \Lambda lel_2ob \\
 & \\
\Delta\text{-}[Cr((+)chxn)_2((-)chxn), \delta\delta\lambda]^{3+} & \Delta ob_2lel \\
\Lambda\text{-}[Cr((-)chxn)_2((+)chxn), \lambda\lambda\delta]^{3+} & \Lambda ob_2lel \\
 & \\
\Delta\text{-}[Cr((+)chxn)_3, \delta\delta\delta]^{3+} & \Delta ob_3 \\
\Lambda\text{-}[Cr((-)chxn)_3, \lambda\lambda\lambda]^{3+} & \Lambda ob_3
\end{array} \qquad (1)$$

Here the symbols lel and ob (para*llel* and *ob*lique) refer to the direction of the bond between the carbon atoms of the chelate ring relative to the threefold axis defined by the three edges of the octahedron which are spanned by the ligands. Thus, the complexes may be classified as lel_3, lel_2ob, ob_2lel, and ob_3, each class comprising a Δ and a Λ isomer.

The eight isomers, eqn. (1), can be separated and isolated, as is also the case for the similar complexes of cobalt(III),[1] rhodium(III),[3] and iridium(III).[4] For the analogous tris(ethylenediamine)metal(III) complexes all the isomers of a given configuration are in equilibrium in solution. Accordingly, it is of interest to observe the absorption spectra (ABS) and the circular dichroism spectra (CD) of each of the isomers, and the experimental results are recorded in the present paper.

2. EXPERIMENTAL

Preparation and separation of the isomers. $[Cr(chxn)_3]Cl_3$ was prepared according to E. Pedersen [5] by use of optically active [3] or racemic chxn. Ion-exchange separations [1] were carried out at 5 °C in darkness on columns packed with Sephadex Cation Exchanger SP-C25.

Inspection of eqn. (1) shows that in a preparation of $[Cr((—)chxn)_3]Cl_3$ only the isomers Δlel_3 and Λob_3 can be obtained. They were formed in the ratio $\Delta lel_3 - \Lambda ob_3 = 99:1$. The more abundant isomer was partially removed by repeated precipitation (four times) from a mixture of ethanol–water = 6:1 at −17 °C till the ratio $\Delta lel_3 - \Lambda ob_3 = 2:1$ was obtained. The isomers were then separated on a column using 0.1 M trisodium phosphate as eluent. From 39 g of crude $[Cr((-)chxn)_3]Cl_3$ we obtained after recrys-

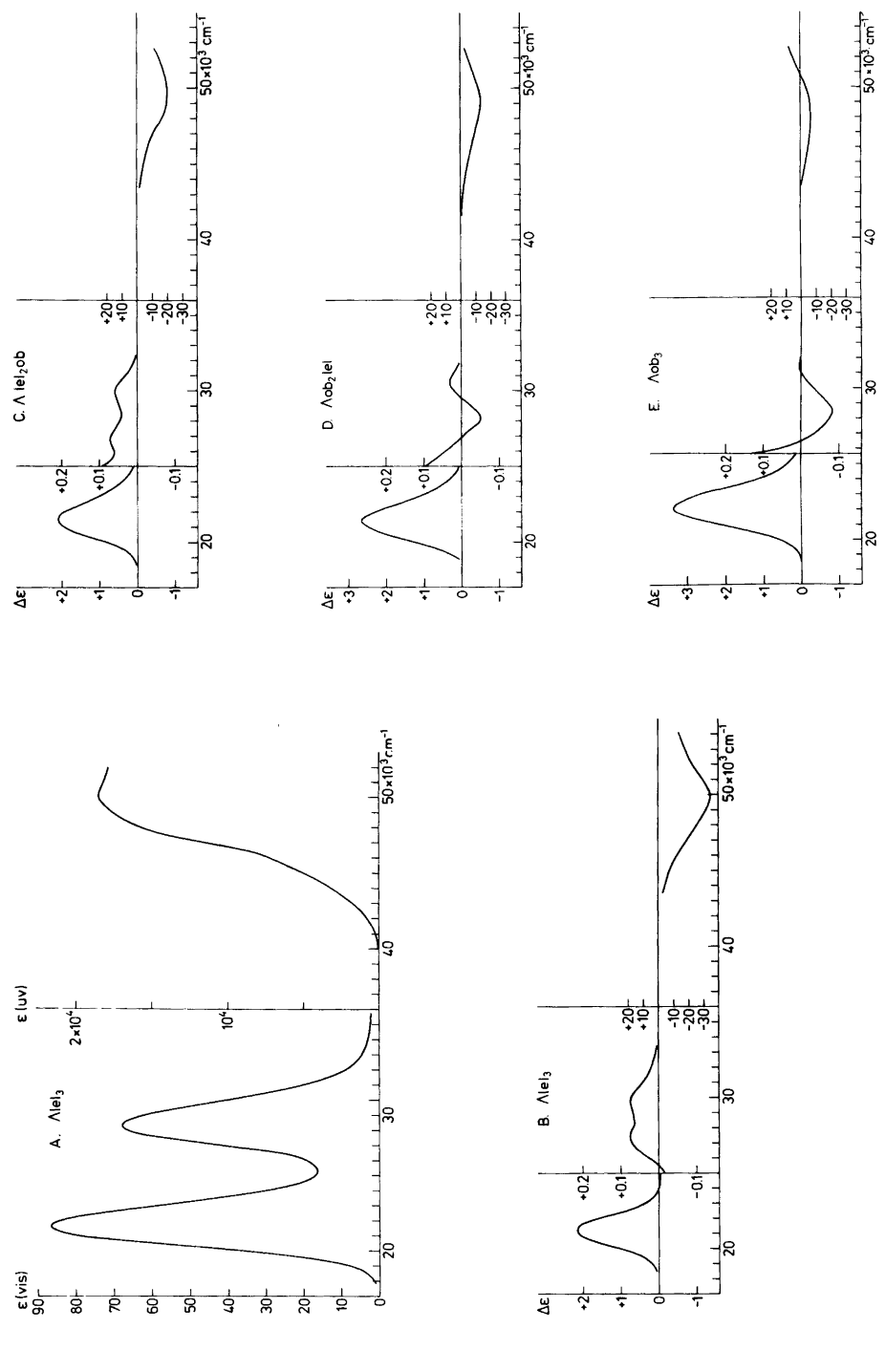

Fig. 1. Absorption and circular dichroism spectra of the spin-allowed transitions of aqueous solutions of the Λ-$[Cr(chxn)_3]Cl_3$ series at *ca.* 300 K. The concentrations in the visible spectral region were: A, ABS. and B, CD of Λ-$[Cr((+)chxn)_3,\delta\delta\delta]Cl_3$ (0.97×10^{-2} M); C, CD of Λ-$[Cr((+)chxn)_2((-)chxn),\delta\delta\lambda]Cl_3$ (1.37×10^{-2} M); D, CD of Λ-$[Cr((-)chxn)_2((+)chxn),\lambda\lambda\delta]Cl_3$ (1.17×10^{-2} M); E, CD of Λ-$[Cr((-)chxn)_3,\lambda\lambda\lambda]Cl_3$ (0.95×10^{-2} M). For the UV spectra the solutions were diluted 20-fold for CD and 200-fold for ABS.

Table 1. Spectral data of Λ-[Cr(chxn)$_3$]Cl$_3$ at *ca.* 300 K. The measurements were carried out on Δlel$_3$, Λlel$_2$ob, Λlelob$_2$, and Λob$_3$ in concentrations as stated in the legend to Fig. 1. The molar absorptivity, ε, is given for the maximum of the ABS-spectra and $\Delta\varepsilon = \varepsilon_l - \varepsilon_r$ is given for the extrema of the CD spectra. Unit for $\bar{\nu}$ is 10^3 cm^{-1}.

Λlel$_3$				Λlel$_2$ob				Λlelob$_2$				Λob$_3$			
ABS		CD		ABS		CD		ABS		CD		ABS		CD	
$\bar{\nu}$	(ε)	$\bar{\nu}$	(Δε)	$\bar{\nu}$	(ε)	$\bar{\nu}$	(Δε)	$\bar{\nu}$	(ε)	$\bar{\nu}$	(Δε)	$\bar{\nu}$	(ε)	$\bar{\nu}$	(Δε)
21.69	(87)	21.22	(+2.17)	21.72	(83)	21.58	(+2.10)	21.74	(82)	21.83	(+2.69)	21.83	(80)	22.00	(+3.40)
		24.5	(−0.03)			26.3	(+0.06)								
28.37	(68)	27.3	(+0.08)	28.37	(68)	26.8	(+0.07)	28.37	(68)			28.37	(65)		
		28.3	(+0.06)			28.3	(+0.04)			28.2	(−0.05)			28.3	(−0.08)
		29.8	(+0.08)			29.9	(+0.05)			30.5	(+0.03)			31.5	(+0.01)
50.3	(1.85 × 10^4)	49.5	(−34)	50.3	(1.95 × 10^4)	49.5	(−20)	50.3	(1.91 × 10^4)	49.3	(−14)	50.3	(1.85 × 10^4)	48.5	(−7)

tallization from water 30 g of Δlel$_3$ and 0.30 g of Λob$_3$.

When [Cr((±)chxn)$_3$]Cl$_3$ was prepared from racemic chxn, three racemic pairs of isomers were formed in the ratio lel$_3$ − lel$_2$ob − ob$_2$lel = 20:4:1, and the pair of ob$_3$-isomers was not detected. Around 40 % of the lel$_3$-pair was precipitated from a mixture of ethanol − water = 1:1 at −17 °C. Then the racemic pairs were separated on a column using 0.1 M trisodium phosphate as eluent, and finally each pair was resolved into optically active components by use of 0.2 M disodium tartrate as eluent. All column separations[6,2] were quite analogous to those previously described.[1] From 26 g of crude [Cr(±)chxn)$_3$]Cl$_3$ the yields of recrystallized isomers were: 3 g of each of Δlel$_2$ob and Λlel$_2$ob, and 0.25 g of each of Δob$_2$lel and Λob$_2$lel.

Identification of the isomers. The absolute configuration of the Δ-[Cr((−)chxn)$_3$]$^{3+}$ ion has been determined as Δlel$_3$ through the X-ray powder spectra[7] of the active racemate of this compound and Λ-[Co((+)chxn)$_3$]$^{3+}$ whose absolute configuration[8] was known. An analogous investigation of the solubility and the X-ray powder spectrum of the active racemate of the chloride of Δ-[Cr((−)chxn)$_2$((+)chxn)]$^{3+}$ and Λ-[Co((+)chxn)$_2$((−)chxn)]$^{3+}$, whose absolute configuration[9] is known, reveals that the chromium compound is Δlel$_2$ob. The absolute configuration of Λ-[Cr((−)chxn)$_3$]$^{3+}$ follows from the method of preparation and the identification of the Δ-[Cr((−)chxn)$_3$]$^{3+}$ isomer. Then the identification of the ob$_2$lel isomers follows from the method of preparation and the CD spectra.

Absorption and circular dichroism spectra. The room temperature spectra were measured on aqueous solutions using a Cary 14 Spectrophotometer and a Jouan Dichrographe 2B. The data are recorded in Table 1 and the spectra are shown in Fig. 1. Molar absorptivities were determined through analyses of the chromium concentrations by means of a Perkin Elmer Atomic Absorption Spectrophotometer 403.

The low temperature glass spectra of the spin-forbidden transitions between 610 and 680 nm, Fig. 2, were measured at *ca.* 110 K on alcoholic solution ethanol − methanol = 5:1. In order to obtain suitable concentrations, the compounds lel$_3$ acetate, ob$_2$lel trifluoroacetate, and ob$_3$ trifluoroacetate were made by metatheses. The solutions were placed in a cryostat cell whose windows were assembled using indium-washers.[10] The CD spectra were recorded on a Roussel Jouan Dichrographe and it was checked that a blank alcoholic solution did not

Table 2. Positions (10^3 cm^{-1}) of the peaks (p) and shoulders (sh) of the ABS and CD around 22×10^3 cm^{-1} of the Λ[Cr(chxn)$_3$]$^{3+}$ series (~10^{-2} M in ethanol − methanol = 5:1) at *ca.* 100 K.

Λlel$_3$		Λlel$_2$ob		Λlelob$_2$		Λob$_3$	
ABS	CD	ABS	CD	ABS	CD	ABS	CD
			21.6 (sh)				
21.91 (sh)	21.44 (p)	21.79 (sh)	21.83 (p)	21.79 (sh)	21.93 (p)	21.74 (sh)	22.0 (sh)
22.22 (p)	22.0 (sh)	22.25 (p)	22.4 (sh)	22.25 (p)	22.4 (sh)	22.27 (p)	22.42 (p)
							22.7 (sh)

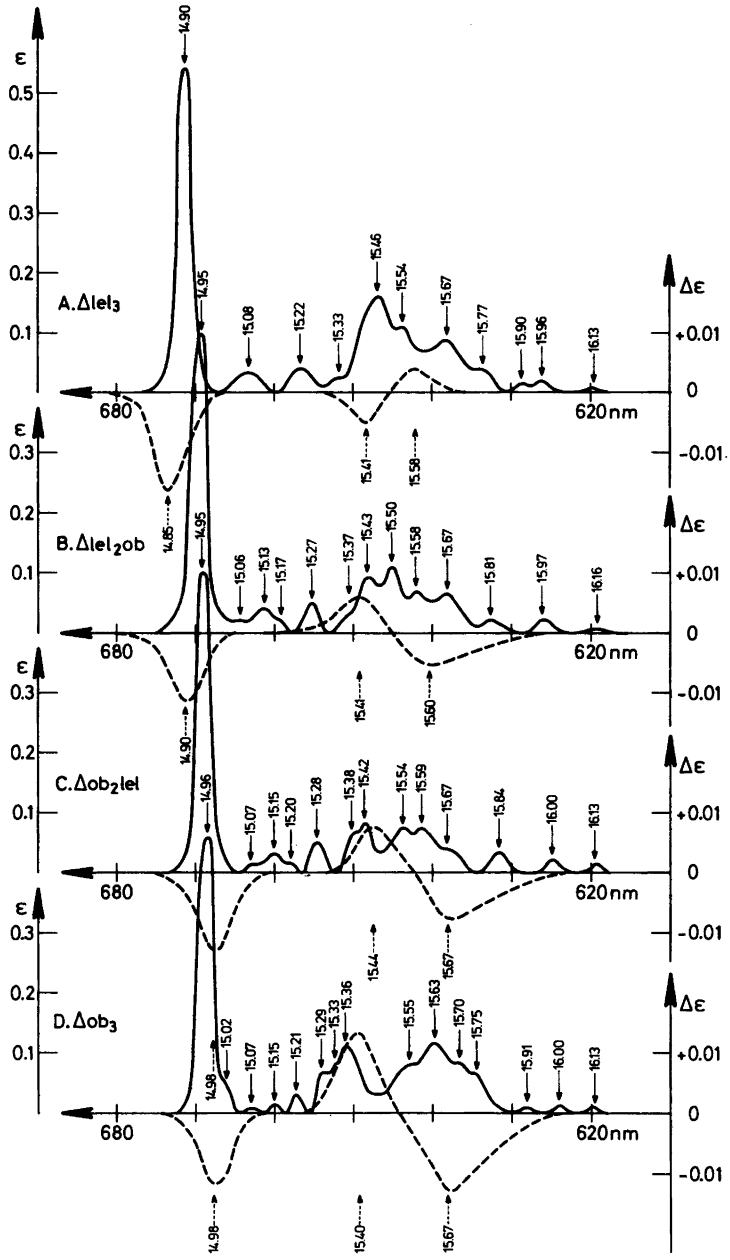

Fig. 2. Absorption spectra (———) and circular dichroism spectra (– – –) of the spin-forbidden transitions of alcoholic solutions (ethanol:methanol = 5:1) of the Δ-$[Cr(chxn)_3]^{3+}$ series at *ca.* 110 K. The spectra are drawn in a wavelength scale, whereas the positions of the peaks are given in units of 10^3 cm^{-1}. The absolute values of ε and Δε have not been determined. A, Δ[Cr((−)chxn)$_3$, λλλ]$(CH_3COO)_3$ (5×10^{-2} M); B, Δ[Cr((−)chxn)$_2$((+)chxn), λλδ]Cl_3 (5×10^{-2} M); C, Δ[Cr((+)chxn)$_2$((−)chxn), δδλ]$(CF_3COO)_3$ (4×10^{-2} M); D, Δ[Cr((+)chxn)$_3$, δδδ]$(CF_3COO)_3$ (4×10^{-2} M).

show any birefringence.

The temperature dependence of the spectra. By cooling off the solutions to *ca.* 110 K the ABS and CD around 22 kK (1 $K = 1\ cm^{-1}$) develop a fine-structure near the peaks. Since the solutions contract considerably, we have in Table 2 only given the positions of the peaks and the shoulders. For all the isomers, the ABS around 28 kK shifts *ca.* 0.16 kK towards higher energies.

The ABS in the region 610–680 nm changes for all the isomers on cooling. Thus, two small peaks on the low-energy side of the peak at 14.9 kK disappear and the more detailed structure shown in Fig. 2 develops. The temperature dependence of the CD of the lel_3-isomers is different from that of the other ones: At 300 K the CD of Δlel_3 in the region 630–665 nm is slightly negative, having a minimum at 15.6 kK; at 110 K the spectrum is as shown in Fig. 2. The CD of the three other Δ-isomers does not change much upon cooling.

3. DISCUSSION

The optical transitions between 14 kK and 36 kK can be assigned in the same way as in the $[Cr(en)_3]^{3+}$ ion (en = ethylenediamine).[11] For all the $[Cr(chxn)_3]^{3+}$ isomers, the transitions can be described in terms of the octahedral parentages as follows:

$$\begin{aligned} {}^2E &\leftarrow {}^4A_2 && \text{at } ca.\ 15\ kK \\ {}^2T_1 &\leftarrow {}^4A_2 && \text{at } ca.\ 15.5\ kK \\ {}^2T_2, {}^4T_2 &\leftarrow {}^4A_2 && \text{at } ca.\ 22\ kK \\ {}^4T_1 &\leftarrow {}^4A_2 && \text{at } ca.\ 28\ kK \end{aligned} \qquad (2)$$

The spin-forbidden transitions in the region 14.7–16.4 kK (680–610 nm) are particularly interesting. Firstly, the great similarity between the ABS of the lel_3 at 110 K and the polarized spectra[12] of $[Cr(en)_3]^{3+}$ at 20 K is noted. Secondly, with reference to a recent discussion of the satelite lines that have been observed in the vicinity of the ${}^2E \leftarrow {}^4A_2$ transition in a crystal of $2[Cr(en)_3]Cl_3.KCl.6H_2O$ at 1.6 K,[12] the uniform shift of this absorption towards higher energies through the series lel_3 to ob_3 should be recognized. Therefore, the low-energy satelite lines can hardly be due to ob conformations of some of the chelate rings as proposed. Finally, the CD of the ${}^2T_1 \leftarrow {}^4A_2$ transition deserves some comments. The spectra of optically active $[Cr(en)_3]^{3+}$ at room temperature have been published recently.[13,14] For the Δ-isomer in a solution of ethanediol–water = 2:1 the CD-peaks are[14]

$$\begin{aligned} &14.94\ kK, && \Delta\varepsilon = -0.016 \\ &15.25\ kK, && \Delta\varepsilon = +0.007 \\ &15.55\ kK, && \Delta\varepsilon = -0.007 \end{aligned} \qquad (3)$$

By comparison of the spectra in Fig. 2, taking into account the temperature dependence of the lel_3 spectrum, and the data of eqn. (3), one can infer that a minor part of $[Cr(en)_3]^{3+}$ in solution is the lel_3 conformer.

The trigonal components of the ${}^2T_1$ level in $[Cr(en)_3,lel_3]^{3+}$ have been assigned on the basis of the polarized crystal spectra.[12] Since the Δlel_3-isomer has the same symmetry, D_3, we propose that the CD at 15.41 kK is due to the transition ${}^2E({}^2T_1) \leftarrow {}^4A_2$ and that the CD at 15.58 kK is due to ${}^2A_2({}^2T_1) \leftarrow {}^4A_2$. On this basis and the CD of the ob_3-isomer we assign the CD at 15.40 kK of this isomer as due to the transition ${}^2A_2({}^2T_1) \leftarrow {}^4A_2$ and 15.67 kK as due to ${}^2E({}^2T_1) \leftarrow {}^4A_2$. Apparently, the magnitude of the splitting increases from lel_2ob through ob_2lel to ob_3.

REFERENCES

1. Harnung, S. E., Sørensen, B. S., Creaser, I., Maegaard, H., Pfenninger, U. and Schäffer, C. E. *Inorg. Chem. 15* (1976) 2123.
2. Harnung, S. E., Kallesøe, S., Sargeson, A. and Schäffer, C. E. *Acta Chem. Scand. A 28* (1974) 285.
3. Galsbøl, F., Steenbøl, P. and Sørensen, B. S. *Acta Chem. Scand. 26* (1972) 3605.
4. Galsbøl, F. *To be published.*
5. Pedersen, E. *Acta Chem. Scand. 24* (1970) 3362.
6. Yoshikawa, Y. and Yamasaki, K. *Inorg. Nucl. Chem. Lett. 6* (1970) 523.
7. Andersen, P., Galsbøl, F., Harnung, S. E. and Laier, T. *Acta Chem. Scand. 27* (1973) 3973.
8. Marumo, F., Utsumi, Y. and Saito, Y. *Acta Crystallogr. B 26* (1970) 1492.
9. Sato, S. and Saito, Y. *Acta Crystallogr. B 33* (1977) 860.
10. Smith, F. J., Smith, J. K. and McGlynn, S. P. *Rev. Sci. Instrum. 33* (1962) 1367.
11. Griffith, J. S. *The Theory of Transition-Metal Ions*, Cambridge University Press, Cambridge 1961.
12. McCarthy, P. J. and Vala, M. T. *Mol. Phys. 25* (1973) 17.
13. Kaizaki, S., Hidaka, J. and Shimura, Y. *Inorg. Chem. 12* (1973) 142.
14. Hilmes, G. L., Brittain, H. G. and Richardson, F. S. *Inorg. Chem. 16* (1977) 528.

Received August 18, 1977.

Acta Chemica Scandinavica A 32 (1978) 47 – 50

The Crystal Structure of Hexakis(phenyl isocyanide)chromium(0), $Cr(CNC_6H_5)_6$

EVERT LJUNGSTRÖM

Department of Inorganic Chemistry, University of Göteborg and Chalmers University of Technology, P.O.Box, S-402 20 Göteborg 5, Sweden

The crystal structure of hexakis(phenyl isocyanide)-chromium(0), $Cr(CNC_6H_5)_6$ has been determined by single crystal X-ray methods. The compound crystallizes in space group $R\bar{3}$ with $a = 10.574(7)$ Å and $\alpha = 111.41(5)°$, $Z = 1$. A final R value of 0.044 was obtained for 1030 independent reflexions. The isocyanide groups have an almost octahedral arrangement around the chromium atom with Cr – C and C – N bond lengths of 1.938(3) and 1.176(4) Å, respectively. The Cr – C – N angle is 173.7(2)° and the C – N – C angle is 172.9(3)°.

The nature of the metal-ligand bond in transition metal isocyanide complexes has been the subject of much interest in recent years. Evidence for considerable π-bonding, especially in complexes with a formally zerovalent metal atom has come from spectroscopical studies [1,2] and a few X-ray structure determinations.[3-6] Some semi-empirical molecular orbital calculations have also been performed, the results of which are in good agreement with available experimental data.[4,7,8] The X-ray studies and the MO calculations have dealt mainly with alkylisocyanide complexes.

Strong similarities can be expected between transition metal hexaisocyanide complexes and the corresponding hexacyanide complexes. In connection with an investigation on bonding in transition metal hexacyanides, in progress at this department, M(II) – C(N) bond distances have been found to be shorter than their M(III) – C(N) counterparts, indicating an increase in the π-contribution to the M – C bond with decreasing formal oxidation state of the metal ion. Crystal structure studies on transition metal hexaisocyanide complexes have now been started in order to extend the investigation to metal ions with a low formal charge.

EXPERIMENTAL

The compound was prepared by the method due to Malatesta *et al.*, in which an alcoholic suspension of chromium(II) acetate is treated with an excess of phenyl isocyanide.[9] Phenyl isocyanide was prepared according to Malatesta and purified by vacuum distillation immediately before use.[10] Red rhombohedric crystals suitable for X-ray work were obtained from a benzene solution of the compound into which light petroleum vapor (b.p. 60 – 80 °C) was allowed to diffuse.

A crystal of dimensions 0.11 × 0.18 × 0.19 mm was chosen for the data collection. Intensities were collected for $\sin\theta/\lambda \leq 0.76$ with a SYNTEX $P2_1$ automatic four-circle diffractometer using graphite monochromatized Mo radiation. The $\omega - 2\theta$ scan method was used and the 2θ scan speed was allowed to vary between 2 and 10° min^{-1}, depending on the intensity of the measured reflexion. Preliminary investigations showed the thermal motion of the atoms to be considerable and the crystal was therefore cooled to −105 °C using the SYNTEX LT 1 low temperature device. Cell parameters were determined from a least squares fit of the refined diffractometer setting angles for 15 reflexions.

No separate measurements of background were made during data collection. A profile analysis based on the Larsen-Lehmann method was instead applied to the 96 step profile collected for each reflexion.[11] Correction was made for Lorentz and polarization effects and from the 2130 measured independent reflexions 1030 with $F_o^2 \geq 3\sigma(F_o^2)$ were considered as being observed and were used in the subsequent calculations.

CRYSTAL DATA

Hexakis(phenyl isocyanide)chromium, $Cr(CNC_6H_5)_6$; M = 670.7 trigonal, space group $R\bar{3}$

with $a = 10.574(7)$ Å and $\alpha = 111.41(5)°$ at -105 °C [$a = 10.658(7)$ Å and $\alpha = 111.22(5)°$ at 22 °C] $U = 838.5$ Å^3. $Z = 1$, $D_x = 1.328$ g cm^{-1}, $D_m = 1.33$ g cm^{-1}, μ(Mo) = 3.0 cm^{-1}. The compound crystallizes as bright red rhombohedric crystals.

STRUCTURE DETERMINATION

The positions of all the non-hydrogen atoms were found from a Patterson map and subsequent electron density calculations (DRF).[12] Refinement of an overall scale factor, atomic coordinates and anisotropic thermal parameters, using the block diagonal approximation, converged at an R-value of 0.065 (BLOCK)[12] ($R = \Sigma \| F_o | - | F_c \| / \Sigma | F_o |$). Due to the chromium atom being on a site of symmetry $\bar{3}$ its thermal parameters U_{22}, U_{33}, U_{13} and U_{23} were not included in the refinement but after each cycle the shift on U_{11} was applied to U_{22} and U_{33} and the shift on U_{12} was applied to U_{13} and U_{23}. A difference synthesis calculated with the parameters obtained in the block refinement revealed the hydrogen atoms as the five highest peaks in the map (DRF).[12] Introducing these atoms with isotropic thermal motion and using full matrix least squares refinement an R-value of 0.044 was obtained for the 95 parameters (LALS).[12] The weighting scheme used was that of Cruickshank [$w = (a + F_o + cF_o^2 + dF_o^3)^{-1}$] with $a = 12.0$, $c = 0.04$ and $d = 0$.[13] The atomic scattering factors for Cr(0), C and N were those due to Doyle and Turner[14] while those for H were taken from Stewart, Davidson and Simpson.[15] A final difference synthesis showed no peaks higher than 0.35 e Å^{-3}.

RESULTS AND DISCUSSION

The final atomic coordinates and thermal parameters are given in Tables 1 and 2, respectively. Distances and angles within the molecule are listed in Table 3. The values in Table 3 are calculated using the low temperature cell parameters. Fig. 1 shows a stereoscopic projection of part of the structure (ORTEP).[12] The chromium atom is approximately octahedrally coordinated by the six isocyanide ligands, the deviation from the ideal 90° C–Cr–C angle being 4.1°. A plane defined by the phenyl groups of one centrosymmetrically related pair of ligands approximately contains the isocyanide C and N atoms of one of the two remaining pairs while the CN groups of the last pair are nearly perpendicular to this plane (Fig. 1). The maximum deviation from a least squares plane through the ring carbon atoms is 0.006 Å for the ring carbon atoms and 0.04 Å for the hydrogen atoms. The molecules pack with the planes of neighbouring phenyl groups practically parallel. The shortest C–C distance between two such rings is 3.13 Å.

Table 1. Atomic coordinates with their standard deviations. C(2)–C(7) belong to the phenyl ring. The hydrogen atoms are numbered according to the carbon atom to which they are bonded.

Atom	x/a	y/a	z/a
Cr	0	0	0
C(1)	0.0797(3)	0.2263(3)	0.0709(3)
N(1)	0.1400(3)	0.3683(3)	0.1277(3)
C(2)	0.1913(3)	0.5304(3)	0.1841(3)
C(3)	0.1892(3)	0.5809(3)	0.0786(3)
C(4)	0.2328(3)	0.7401(3)	0.1313(4)
C(5)	0.2787(3)	0.8494(3)	0.2880(4)
C(6)	0.2828(4)	0.7997(4)	0.3937(4)
C(7)	0.2382(4)	0.6402(4)	0.3421(4)
H(3)	0.505(4)	−0.031(4)	0.161(4)
H(4)	0.773(4)	0.061(4)	0.227(4)
H(5)	0.955(5)	0.321(5)	0.308(5)
H(6)	0.877(5)	0.498(5)	0.312(5)
H(7)	0.615(5)	0.418(5)	0.246(5)

Table 2. Thermal parameters ($\times 10^3$ for the non hydrogen atoms) and their standard deviations. The anisotropic temperature factor has the form $\exp[-2\pi^2(a^{*2}h^2U_{11} + b^{*2}k^2U_{22} + c^{*2}l^2U_{33} + a^*b^*hkU_{12} + a^*c^*hlU_{13} + b^*c^*klU_{23})]$. The isotropic temperature factor is $\exp\{-B[(\sin\theta)/\lambda]^2\}$.

Atom	U_{11} or B	U_{22}	U_{33}	U_{12}	U_{13}	U_{23}
Cr	20.9(4)	20.9	20.9	29(1)	29	29
C(1)	27(1)	28(1)	27(1)	35(2)	33(2)	38(2)
N(1)	35(1)	27(1)	46(1)	35(2)	41(2)	46(2)
C(2)	22(1)	22(1)	34(1)	22(2)	29(2)	33(2)
C(3)	29(1)	29(1)	30(1)	32(2)	38(2)	33(2)
C(4)	27(1)	29(1)	37(1)	29(2)	39(2)	45(2)
C(5)	34(1)	24(1)	42(1)	32(2)	45(2)	34(2)
C(6)	44(2)	34(2)	33(2)	41(3)	46(3)	31(3)
C(7)	34(1)	34(1)	30(1)	33(3)	32(2)	40(3)
H(3)	1.1(7)					
H(4)	0.7(6)					
H(5)	2.0(8)					
H(6)	2.2(8)					
H(7)	2.0(8)					

Table 3. Distances (Å) and angles (°) in $Cr(CNC_6H_5)_6$ at −105 °C with their standard deviations. The atoms C(2)−C(7) belong to the phenyl ring and the hydrogen atoms are numbered according to the carbon atom to which they are bonded.

Cr−C(1)	1.938(3)	C(4)−C(5)	1.386(5)
C(1)−N(1)	1.176(4)	C(5)−C(6)	1.392(4)
N(1)−C(2)	1.388(4)	C(6)−C(7)	1.387(4)
C(2)−C(3)	1.398(4)	C(7)−C(2)	1.394(4)
C(3)−C(4)	1.385(4)	C(3)−H(3)	0.99(3)
C(4)−H(4)	0.93(3)	C(5)−H(5)	0.93(4)
C(6)−H(6)	0.94(4)	C(7)−H(7)	0.92(4)
C(1)−Cr−C(1)′	85.9(2)	Cr−C(1)−N(1)	173.7(2)
C(1)−N(1)−C(2)	172.9(3)	N(1)−C(2)−C(3)	119.4(3)
N(1)−C(2)−C(7)	120.4(3)	C(3)−C(2)−C(7)	120.2(2)
C(4)−C(3)−C(2)	119.7(3)	C(5)−C(4)−C(3)	120.3(3)
C(6)−C(5)−C(4)	119.9(3)	C(7)−C(6)−C(5)	120.4(3)
C(2)−C(7)−C(6)	119.5(3)		

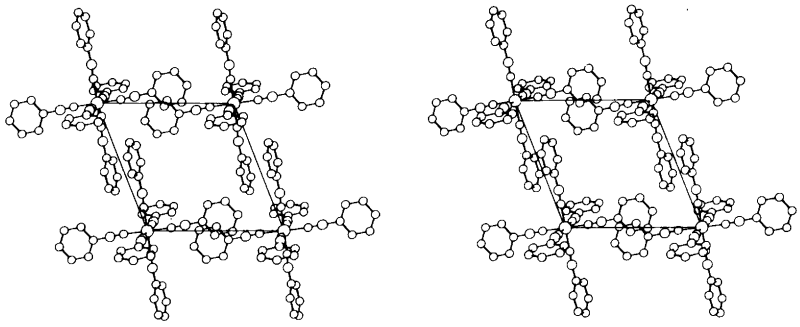

Fig. 1. Stereoscopic projection of $Cr(CNC_6H_5)_6$ perpendicular to the *ab* plane.

The metal-ligand bonding in the hexakis(phenyl isocyanide)chromium(0) molecule has been discussed in Refs. 1 and 2. The lowering of the infrared C−N stretch frequency from 2130 cm^{-1} in the free ligand to two peaks at 2012 and 1965 cm^{-1} in the complex has been interpreted in terms of a weakening of the C−N bond due to partial filling of the π^*_{C-N} orbitals. The short Cr(0)−C bond of 1.938(3) Å found in this investigation indeed indicates that extensive d-π^* back donation takes place. The Cr(0)−C bond is significantly shorter than the Cr(II)−C bond of 2.053(4) Å found in $Na_4[Cr(CN)_6].10H_2O$ [16] and the Cr(III)−C bond of 2.077(5) Å in $K_3[Cr(CN)_6]$.[17] The difference in formal charge on the central atom alone should have an effect opposite to that observed. The tendency in this series confirms the theory that a low formal charge on the metal atom enhances the π-contribution to the metal-ligand bond.

Although several hexaaryl isocyanide Cr(0) complexes have been prepared,[2,9] no hexaalkyl isocyanide Cr(0) complex is known. It would appear that the aromatic part of the ligand stabilizes the complex. The orientation of the rings relative to the rest of the molecule in the present compound is favourable for interaction between part of the C−N π system and the π system of the ring. Delocalization of the backdonated electrons over the whole ligand should make an aryl isocyanide ligand a better π-acceptor than an alkyl isocyanide. Such a delocalization ought, in principle, to be detectable in the C−C bond lengths of the benzene ring. The C−C bond lengths in hexakis(phenyl isocyanide)chromium(0) do not, however, deviate significantly from the normal phenyl C−C value.

Acknowledgements. The author wishes to thank Professor N.-G. Vannerberg for valuable discussions and Dr. S. Jagner for revising the English text. The work has been supported financially by the Swedish Natural Science Research Council (NFR 2286-026).

REFERENCES

1. Mann, K. R., Cimolino, M., Geoffroy, G. L., Hammond, G. S., Orio, A. A., Albertin, G. and Gray, H. B. *Inorg. Chim. Acta 16* (1976) 97.
2. Cotton, F. A. and Zingales, F. *J. Am. Chem. Soc. 83* (1961) 351.
3. Cotton, F. A., Dunne, T. G. and Wood, J. S. *Inorg. Chem. 4* (1965) 318.
4. Sarapu, A. C. and Fenske, R. F. *Inorg. Chem. 11* (1972) 3021.
5. Cotton, F. A., Dunne, T. G. and Wood, J. S. *Inorg. Chem. 3* (1964) 1495.
6. Joshi, K. K., Mills, O. S., Paulson, P. L., Shaw, B. W. and Stubbs, W. H. *Chem. Commun.* (1965) 181.
7. Sarapu, A. C. and Fenske, R. F. *Inorg. Chem. 14* (1975) 247.
8. Fantucci, P., Naldini, L., Cariati, F., Valenti, V. and Bussetto, C. *J. Organomet. Chem. 64* (1974) 109.
9. Malatesta, L., Sacco, A. and Ghielmi, S. *Gazz. Chim. Ital. 82* (1952) 516.
10. Malatesta, L. *Gazz. Chim. Ital. 77* (1947) 238.
11. Lehmann, M. S. and Larsen, F. K. *Acta Crystallog. A 30* (1974) 580.
12. Program library of Department of Inorganic Chemistry, University of Göteborg and Chalmers University of Technology: DRF written by Zalkin, A., BLOCK by Lindgren, O., LALS by Gantzel, P., Sparks, R. and Trueblood, T. and ORTEP by Johnson, C. K.
13. Cruickshank, D. W. J. In *Crystallographic Computing*, Munksgaard, Copenhagen 1970, p. 195.
14. Doyle, P. A. and Turner, P. S. *Acta Crystallogr. A 24* (1968) 390.
15. Stewart, R. F., Davidson, E. R. and Simpson, W. T. *J. Chem. Phys. 42* (1965) 3175.
16. Ljungström, E. *Acta Chem. Scand. A 31* (1977) 104.
17. Jagner, S., Ljungström, E. and Vannerberg, N.-G. *Acta Chem. Scand. A 28* (1974) 623.

Received July 21, 1977.

Acta Chemica Scandinavica A 32 (1978) 51 – 56

A Conformational Study of Some 1,2-Disubstituted Ethanes by an *ab initio* Method

KARI KVESETH

Department of Chemistry, University of Oslo, Blindern, Oslo 3, Norway

The conformational energy differences in 1,2-difluoro-, 1,2-dichloro- and 1,2-dicyano-ethane have been estimated from *ab initio* calculations with Gaussian type basis functions and a limited geometry variation. The *anti* conformer is found to have the lowest energy for all three molecules, revealing a discrepancy in the relative energy up to 2 kcal mol^{-1} when compared to the experimental values (1 kcal = 4.184 kJ). It is suggested that an incomplete cancelling of the correlation energy, possibly due to dispersion forces between the *gauche* halogens, may explain the apparent discrepancy for the dihaloethanes.

It has been extensively reported in the literature[1-3] that standard SCF-LCAO-MO procedures usually are able to reproduce torsional potentials in reasonably good agreement with available experimental data. Especially if care is taken in applying an adequately chosen basis set and optimizing, at least partially, the geometry during the internal rotation, the calculated conformational energy differences agree reasonably well with experimental results.

1,2-disubstituted ethanes have two conformers, *gauche* and *anti*. Usually *anti* is the most stable, but with substituents that can have some kind of favourable interactions, *gauche* has the lowest energy. Also 1,2-difluoroethane is most stable in *gauche*.[4-9,42] The relative stability of *gauche* to *anti* cannot be rationalized simply on the basis of steric effects. It has therefore been proposed that interactions between lone pairs or between unsaturated bonds can be attractive. Provided this effect is due to a bond established between the two substituents it should be detectable within the Hartree-Fock limit of calculations *ab initio*. However, if the stabilization of *gauche* is due to dispersion forces (arising from the interpair correlated electron motions) it should not be detectable with this method.

In a similar study of 1,2-difluoroethane Pople *et al.*[3] estimated the energy difference between *gauche* and *anti* to be +1.0 kcal mol^{-1}. This result is in obvious disagreement with the experimental data,[4-9,42] which give a *gauche* contribution of about 90 % at room temperature. In Ref. 3 standard geometry parameters were used,[10] only optimizing the torsional angle. Polarization functions are not included in the 4–31 G[11] basis set used. These could be the reasons for the apparent discrepancy. In a recent *ab initio* study of 1,2-difluoroethene Binkley and Pople[12] found, in agreement with experiments, the *cis* configuration to be the most stable one, provided the basis set applied was large enough (6–311 G*)[12] and polarization functions were included for both carbon and fluorine.

The scope of this work is to evaluate further these effects on the conformational predictions as obtained from *ab initio* calculations, as part of a conformational study of some disubstituted ethanes.[13-15] Thereby it is hoped to get some understanding of the factors determining the torsional potentials and the conformational mixtures in the gas phase. The *gauche-anti* energy differences in these molecules are rather small, and a careful analysis of the calculated energy differences is of importance, since, in these cases, even small contributions to the total energy might affect rather strongly the equilibrium parameters.

METHOD

The program MOLECULE,[16] which solves the Roothaan-Hall equations for a Gaussian type basis

set, was used in the calculations, carried out with (7,3) primitive basis[17] for C, N and F, and (10,6) for Cl. For hydrogen a 4 s primitive basis[18,19] was used. A double zeta contraction was employed for all atoms.

The polarization effects in the carbon–halogen bonds were studied in a limited number of runs by including *d*-orbitals in the basis set of the halogens, with exponents equal to 1.0[20] for F and 0.68[21] for Cl. The torsional angle in *gauche* was varied in all cases to minimum energy with rigid, experimental geometry[4,5,13–15] (Tables 1 and 4). Keeping this angle at the optimized value, the other most important structural parameters were optimized for both conformers (Table 5–7). Finally, energy differences between conformers with optimal geometry were calculated, and these are compared to the experimental values in Table 8.

Table 1. Structural parameters (distances in Å, angles in °) as determined from electron diffraction (ED), reported standard deviations in parentheses, and optimal values from *ab initio* calculations.

	ED	*ab initio*	
		anti	*gauche*
$C_2H_4F_2$[4,5]			
C–C	1.505(10)[a]	1.513	1.504
C–F	1.389(7)	1.404	1.404
C–H	1.095(10)	–	–
∠CCF	110.3 (20)	107.4	109.6
∠CCH	110.6 (30)	–	–
ϕ	69.4 (70)[a]	180.0	75.0
$C_2H_4Cl_2$[13,14]			
C–C	1.531(3)	–	–
C–Cl	1.790(2)	1.815	1.811
C–H	1.112(5)	–	–
∠CCCl	109.0 (2)	–	–
∠CCH	113.2 (13)	–	–
ϕ	75.3(9)	180.0	70.5
$C_2H_4(CN)_2$[15]			
C–C	1.534(3)	1.554	1.550
C–CN	1.471(1)	1.464	1.465
C≡N	1.156(1)	–	–
C–H	1.110(4)	–	–
∠CCC	111.8 (2)	111.0	111.9
∠CCH	109.5 (11)	–	–
ϕ	70 (–)	180.0	67.0

[a] Mijlhoff[6] reports C–C = 1.535 Å and ϕ_g = 74.5°, and Butcher[31] ϕ_g = 73°, when C–C = 1.51 Å.

All calculations have been carried out on the CYBER 74 computer at the University of Oslo.

RESULTS

Equilibrium structure. An inspection of Table 1 reveals a general good agreement between the calculated and experimental geometries, most of the deviations being smaller than 0.02 Å and 1.0°. Compared with the C–C distance in ethane (1.538

Table 2. Atomic net charge.[36]

		anti	*gauche*
$C_2H_4F_2$	C	−0.004	+0.002
	F	−0.409	−0.404
	H	+0.207	+0.189
	H′	+0.207	+0.213
$C_2H_4Cl_2$	C	−0.390	−0.394
	Cl	−0.142	−0.128
	H	+0.266	+0.252
	H′	+0.266	+0.269
$C_2H_4(CN)_2$	C	−0.297	−0.306
	C(N)	−0.027	−0.009
	N	−0.258	−0.261
	H	+0.291	+0.284
	H′	+0.291	+0.292

Table 3. Estimated force constants (stretch in mdyn Å^{-1}, bend and torsion in mdyn Å rad^{-2}) as obtained from normal coordinate analysis (Exp) and minimizing the *ab initio* energy as a function of the geometry (Calc).

		Exp.	Calc.
$C_2H_4F_2$	f_{C-C}	4.0[9]	4.62
	f_{C-F}	5.15	7.11
	f_{CCF}	1.21	a:1.82
			g:1.57
	f_{CCH}	0.70	a:1.57
			g:1.48
	$f_{\tau,g}$	0.13	0.12
$C_2H_4Cl_2$	f_{C-Cl}	3.18[35]	a:2.35
			g:4.70
	$f_{\tau,g}$	0.253[13]	0.17
$C_2H_4(CN)_2$	f_{C-C}	4.62[15]	4.79
	f_{C-CN}	5.47	5.27
	f_{CCC}	1.09	1.72
	$f_{\tau,g}$	0.12	0.17

Å[22]) the experimentally observed trend is reproduced in these calculations, giving a shorter C–C bond upon fluorination, a longer upon substitution with larger groups (*e.g.* CN).

Because of the large number of basis functions used for dichloroethane, only the C–Cl distance has been varied in addition to the torsional angle (ϕ_g). The optimal geometries have been obtained from the minima in the assumed parabolic potential surfaces (Tables 5–7). The energies were recalculated for these optimized sets to confirm the minima.

Comparison between the parameters in *anti* and *gauche* reveals no important structural changes, although a slight shortening in the C–C distance together with an opening of the CCF angle when going from *anti* to *gauche* is seen for difluoroethane.

Also the atomic net charges (Table 2) show only minor changes between the conformers, although there is a small flow of electrons to the hydrogen opposing the substituent as going from *anti* to *gauche*, most prominently in difluoroethane.

The obtained force constants are given in Table 3. Except for f_{C-F} the agreement with those obtained from normal coordinate analysis is remarkable, especially when considering the rather limited geometry optimization that has been done.

1,2-Difluoroethane. Inclusion of *d*-orbitals (Tables 4 and 8) leads to an even larger discrepancy between calculated and observed conformational energy difference (*i.e.* favouring *anti* even more). Only a (7,3) primitive set has been used, and *d*-orbitals have only been added for fluorine, since previous experience[23–26] indicates that an enlargement of the primitive set does not change the results significantly, and that polarization functions are of importance mainly for atoms with lone pairs.

This is in contradiction of the results for 1,2-difluoroethene, which may be explained by a superposition error in the basis set used by Binkley and

Table 4. Energies (kcal mol^{-1}) for different torsional angles ϕ (°), given relatively to *anti* ($\phi = 180°$), rigid rotation. Parameters as given in Table 1, ED.

	E_{anti} (a.u.)						
$C_2H_4F_2$		ϕ_g	60	65	69.4	75	90
	−276.51045	E	1.27	0.92	0.75	0.69	1.32
	−276.55289	E[d]				0.95	
$C_2H_4Cl_2$		ϕ_g	70	71.8	70.5[d]	75.5	80
	−996.56618	E	2.40	2.38		2.44	2.65
	−996.62067	E[d]	2.32		2.31	2.41	2.66
$C_2H_4(CN)_2$		ϕ_g	60	65	67	70	80
	−262.35204	E	0.64	0.48	0.47	0.50	1.00

[d] including *d*-orbitals on halogen.

Table 5. $C_2H_4F_2$. Energies (kcal mol^{-1}) given relatively to the energy of the corresponding experimental model (Table 1) in *anti* and *gauche* respectively, $\phi_g = 75.0°$.

C–C/∠CCF	E_{anti}	E_{gauche}	C–F	E_{anti}	E_{gauche}	∠CCH	E_{anti}	E_{gauche}
1.465/110.3	0.671	0.445	1.349	2.698	2.900	106.6	1.951	1.405
1.505/110.3	0	0	1.389	0	0	110.6	0	0
1.545/110.3	0.439	0.621	1.429	0.577	0.370	114.6	2.459	2.748
1.505/106.0	−0.514							
1.505/114.0	2.811							
1.545/106.0	−0.238							
1.505/106.3		0.696						
1.505/114.3		1.500						
1.465/106.3		1.430						

Table 6. $C_2H_4Cl_2$. Energies (kcal mol^{-1}) given relatively to the energy of the corresponding experimental model (Table 1) in *anti* and *gauche* respectively, $\phi_g = 70.5°$.

C–Cl	E_{anti}	E_{gauche}
1.79	0	0
1.83	−0.122	−0.038
1.813	−0.199	
1.811		−0.286

Pople.[12] The superposition error in the present investigation has been estimated. HF and F^- have been used as test molecules, adding an empty basis set identical to that of fluorine, but with no charge on the nucleus, at an F···F distance corresponding to that in *gauche* and *anti* difluoroethane, respectively. The *gauche*-like form was favoured with 0.08 and 0.2 kcal mol^{-1}, respectively. This indicates that with the basis used here, the superposition effect is negligible. The effect may, however, be of greater importance when the core electrons are less well described, and may therefore explain why Binkley and Pople[12] obtained a result for difluoroethene in better agreement with the experiment.

The reasons for the apparent discrepancies have therefore to be sought in the Hartree-Fock theory itself. As experienced by Roos[27,28] and others the neglect of correlation energy in different isomers may introduce an error in the calculated energy difference of as much as 3 kcal mol^{-1}, disfavouring the form where correlated electron motion (*i.e.* dispersion forces) seems to be of some importance. Although in general the correlation energy is believed to cancel out when conformational energy differences are calculated,[29,30] in the case of difluoroethane *gauche* seems to be favoured by ~2 kcal mol^{-1} due to this difference (see Table 8). This is the same amount that Roos *et al.*[27] found stabilized the $F-H_2O^-$ system, which may be considered as an upper limit.

The calculated torsional angle $\phi_g = 75.0°$ is somewhat larger than the observed values, and may also indicate that the repulsion between the F atoms in *gauche* is overemphasized.

1,2-Dichloroethane. Even for this more electron-rich compound inclusion of *d*-orbitals only leads to a minor shift in the estimated torsional angle (Table 4) and the energy difference remains essentially unchanged.

A graphical plot of the calculated energies as a function of ϕ_g, indicates that inclusion of *d*-orbitals makes the potential curve sharper, but does not change the minimum position. It was felt appropriate, therefore, to include *d*-orbitals on the Cl

Table 7. $C_2H_4(CN)_2$. Energies (kcal mol^{-1}) given relatively to the energy of the corresponding experimental model (Table 1) in *anti* and *gauche* respectively, $\phi_g = 67.0°$.

C–C/∠CCC	E_{anti}	E_{gauche}	C–CN	E_{anti}	E_{gauche}
1.491/111.0	1.157	1.162	1.434	0.618	0.683
1.531/111.0	0	0	1.474		0
1.571/111.0	−0.053	−0.042	1.514		1.746
1.531/107.0	1.241	1.769			
1.531/115.0	1.168	0.601			
1.571/115.0	1.428	0.920			

Table 8. Conformational energy differences $\Delta E = E_g - E_a$ (kcal mol^{-1}), optimal geometries as given in Table 1, calculated and observed dipole moments, μ(D), and bond moments, μ_{C-X}(D).

	E_{anti}	ϕ_g	ΔE	$\Delta E^{exp\,b}$	μ_g	$\mu^{exp\,c}$	μ_{C-X}	μ_{C-X}^{exp}
$C_2H_4F_2$	−276.51187	75.0	1.32	−0.59 − 1.42	3.35	2.67[32]	2.24	1.86[34]
$C_2H_4Cl_2$	−996.62099	70.5	2.32[a]	1.05	3.14	1.18[33]	2.03	2.03[33]
$C_2H_4(CN)_2$	−262.35246	67.0	0.48	~2.5	5.77	3.48[33]	3.73	4.03[33]

[a] With *d*-orbitals on Cl. [b] The difference in zero point vibrational energy between the two conformers is approximately 0.2 kcal mol^{-1}, therefore $\Delta E \approx \Delta E^{exp}$. [c] Given at appropriate temperatures, that is 25(?), 35 and 170 °C, respectively.

atoms in the remaining calculations.

Table 8 reveals a discrepancy between the observed and calculated conformational energy differences, the *ab initio* method again favouring *anti* too much. If contributed to the difference in correlation energy, it means that this difference must be ~ 1.3 kcal mol^{-1} in favour of *gauche*.

The calculated torsional angle $\phi_g = 70.5°$ is somewhat smaller than the observed value.

1,2-Dicyanoethane. These calculations agree with the energy difference and torsional angle estimated from the previously reported torsional potential.[43] The energy difference between *gauche* and *anti* remains unchanged when essential parts of the geometry are optimized (Tables 4 and 8). But, contrary to the results for difluoro and dichloroethane the calculated energy difference is too small. The experimental value is very uncertain, but is definitely not smaller than 1.5 kcal mol^{-1}.[15] Although *d*-orbitals have not been included in this case, the previous results of this investigation indicate that inclusion of polarization functions may improve the results by about 0.3 kcal mol^{-1}.

DISCUSSION

Although a general trend is hard to find, the present calculations on 1,2-disubstituted ethanes seem consistent with the assumption that the neglect of correlation energy may cause errors in calculated conformational energy differences, especially when the substituents are easily polarizable, so that dispersion forces may be established between the substituents. This attractive force must be in the order of 1 kcal mol^{-1} for dihaloethanes. Such attractions between halogens fit the earlier observations on 2,2'-dihalobiphenyls,[5,38,39] and 1,3-dihalopropanes,[40,41] and were also proposed earlier by Abraham for 1,2-difluoroethane.[7]

Why the discrepancy appears larger in difluoroethane than in dichloroethane, and why the energy difference is too small in dicyanoethane is not easily understood, but may be connected with the estimate of the dipole moments, and thereby with the set of basis functions applied. The discrepancies between the experimental and calculated C–X bond vectors are consistent with an error in the calculated energy differences of about -0.4 kcal mol^{-1} for difluoroethane and 0.2 kcal mol^{-1} for dicyanoethane due to dipole/dipole repulsions.[37]

This is also consistent with the somewhat too large calculated ϕ_g for difluoroethane. Although the effect is too small to account for the error in ΔE for dicyanoethane, it seems reasonable that the apparent difference in correlation energy between difluoro- and dichloro-ethane, is due to a somewhat too large estimate of the calculated C–F bond vector.

The difference in correlation energy seems negligible in dicyanoethane. While each halogen has three lone pairs, which may interact in *gauche*, the electrons on C(N) are mainly localized on the "backside", in the triple bond to nitrogen, and therefore not so easily polarized by the other $-C\equiv N$ group in *gauche*. The lone pairs on N are too far apart to get in van der Waals' contact with each other.

If one expands the torsional potential as a Fourier series, terminated after the third term $[V(\phi) = \frac{1}{2}\sum_{n=1}^{3} V_n(1+\cos n\phi)]$, one can associate the steric and electrostatic repulsions with the V_1 term, the electronegativity with the V_2 term and bond/bond repulsion with the V_3 term.[2] The relative size of V_1 to V_2 determines whether *gauche* or *anti* is the most stable form. In the case of difluoroethane, where the steric effect is relatively small,[7] the correlation energy makes V_1 sufficiently small, and the most stable conformer is *gauche*. For dichloroethane the steric and electrostatic repulsions dominate. Even though approximately the same correlation effect is found, V_1 is dominating and *anti* is the most stable conformer.

Acknowledgement. The author wish to acknowledge Dr. Jan Almlöf for his interest and many valuable discussions, as well as for his helpful comments on the manuscript. I am also indebted to cand.real. Harald Jensen and Dr. Hans Martin Seip for their contributions in the initial stage of this investigation.

REFERENCES

1. Lowe, J. P. *Prog. Phys. Org. Chem. 6* (1968) 1.
2. Radom, L., Hehre, W. J. and Pople, J. A. *J. Am. Chem. Soc. 94* (1972) 2371.
3. Radom, L., Lathan, W. A., Hehre, W. J. and Pople, J. A. *J. Am. Chem. Soc. 95* (1973) 693.
4. Brunvoll, J. *Thesis*, Trondheim 1962.
5. Bastiansen, O., Seip, H. M. and Boggs, J. E. *Perspectives in Structural Chemistry 4* (1971) 97.
6. van Schaick, E. J. M., Geise, H. J., Mijlhoff, F. C. and Renes, G. *J. Mol. Struct. 16* (1973) 23.
7. Abraham, R. J. and Parry, K. *J. Chem. Soc. B* (1970) 539.
8. Abraham, R. J. and Kemp, R. H. *J. Chem. Soc. B* (1971) 1240.

9. Klæboe, P., Nielsen, C. J., Torgrimsen, T. and Nicolaisen, T. *To be published.*
10. Pople, J. A. and Gordon, M. S. *J. Am. Chem. Soc. 89* (1967) 4253.
11. Ditchfield, R., Hehre, W. J. and Pople, J. A. *J. Chem. Phys. 54* (1971) 724.
12. Binkley, J. S. and Pople, J. A. *Chem. Phys. Lett. 45* (1977) 197.
13. Kveseth, K. *Acta Chem. Scand. A 28* (1974) 482.
14. Kveseth, K. *Acta Chem. Scand. A 29* (1975) 307.
15. Fernholt, L. and Kveseth, K. *To be published.*
16. Almlöf, J. *USIP Report 74-29, University of Stockholm* (1974).
17. Roos, B. and Siegbahn, P. *Theor. Chim. Acta 17* (1970) 209.
18. Huzinaga, S. *J. Chem. Phys. 42* (1965) 1293.
19. Dunning, T. H. *J. Chem. Phys. 53* (1970) 2823; the exponents in Ref. 18 were scaled by a factor 1.44.
20. Jensen, H. *Private communication.*
21. Roos, B. and Siegbahn, P. *Theor. Chim. Acta 17* (1970) 199.
22. Newton, M. D., Lathan, W. A., Hehre, W. J. and Pople, J. A. *J. Chem. Phys. 52* (1970) 4064.
23. Skancke, P. N. and Sæbø, S. *J. Mol. Struct. 28* (1975) 279.
24. Dunning, T. H. *J. Chem. Phys. 63* (1975) 1847.
25. Veillard, A. In Orville-Thomas, W. J., Ed., *Internal Rotation in Molecules*, Wiley, London 1974, p. 385.
26. Veillard, A. In Pullman, B., Ed., *Quantum Mechanics of Molecular Conformations*, Wiley, London 1976, p. 1.
27. Diercksen, G. H. F., Kraemer, W. P. and Roos, B. O. *Theor. Chim. Acta 36* (1975) 249.
28. Roos, B. O., Kraemer, W. P. and Diercksen, G. H. F. *Theor. Chim. Acta 42* (1976) 77.
29. Ahlrichs, R., Driessler, F., Lischka, H., Staemmler, V. and Kutznelnigg, W. *J. Chem. Phys. 62* (1975) 1235.
30. Freed, K. F. *Chem. Phys. Lett. 2* (1968) 255.
31. Butcher, S. S., Cohen, R. A. and Rounds, T. C. *J. Chem. Phys. 54* (1971) 4123.
32. McClellan, A. L. *Tables of Experimental Dipole Moments, II*, Rahara Enterprises, El Cerrito, Cal. 1974.
33. Bloom, G. I. M. and Sutton, L. E. *J. Chem. Soc.* (1941) 727.
34. Larkin, M. and Gordy, W. *J. Chem. Phys. 38* (1963) 2329.
35. Schachtschneider, J. H. and Snyder, R. G. *Vibrational Analysis of Polyatomic Molecules IV*, Shell Div. Company, Tech. Report No. 122-63.
36. Mulliken, R. S. *J. Chem. Phys. 23* (1955) 1833.
37. Lehn, J.-M. and Ourisson, G. *Mem. présentés a la Soc. Chim.* (1963) 1113.
38. Bastiansen, O. and Smedvik, L. *Acta Chem. Scand. 8* (1954) 1593.
39. Bastiansen, O. *Acta Chem. Scand. 4* (1950) 926.
40. Stølevik, R. *Acta Chem. Scand. A 31* (1977) 359.
41. Grindheim, S. and Stølevik, R. *Acta Chem. Scand. A 30* (1976) 625.
42. Hanis, W. C., Holtzclaw, J. R. and Kalasinsky, V. F. *J. Chem. Phys. 67* (1977) 3330.
43. Radom, L. and Stiles, P. J. *Chem. Commun.* (1974) 190.

Received August 9, 1977.

Acta Chemica Scandinavica A 32 (1978) 57–61

The Crystal and Molecular Structure of Bis(chloroacetato)-(*N*,*N*,*N*′,*N*′-tetramethylethylenediamine)copper(II), $Cu(C_6H_{16}N_2)(ClC_2H_2O_2)_2$

MARKKU AHLGRÉN, REIJO HÄMÄLÄINEN and URHO TURPEINEN

Department of Inorganic Chemistry, University of Helsinki, SF-00100 Helsinki 10, Finland

The crystal and molecular structure of the title compound has been determined from three-dimensional X-ray data. The blue crystals belong to the monoclinic space group $P2_1$ with $a=7.266(3)$ Å, $b=14.846(7)$ Å, $c=7.260(2)$ Å, $\beta=103.41(3)°$ and $Z=2$. The structure was solved by direct and Fourier methods and refined by block-diagonal least-squares procedures to an R value of 0.022 for 1981 independent reflections having $I>3\sigma(I)$. The structure is built-up from discrete $Cu(C_6H_{16}N_2)(ClC_2H_2O_2)_2$ molecules and the copper(II) ion is surrounded by four atoms in a distorted square-planar arrangement with two Cu–N bonds, 2.039(3) and 2.037(3) Å, from the diamine ligand and two Cu–O bonds, 1.977(3) and 1.975(3) Å, from the chloroacetate groups. The two remaining oxygen atoms of the chloroacetate groups are at distances of 2.627(3) and 2.624(3) Å from the Cu atom. The angles between the "out-of-plane" Cu···O directions and the normal to the "square-plane" are 25.7 and 25.6°, respectively, with the O···Cu···O angle 140.3(1)°.

Nickel(II) salts of simple aliphatic monocarboxylic acids form 1:1 complexes with *N*,*N*,*N*′,*N*′-tetramethylethylenediamine.[1] These complexes are dimeric, with nickel(II) atoms joined by one water molecule and two carboxylate ions. The bridging carboxylate ligands have a *syn-syn* configuration as in most binuclear copper(II) carboxylate complexes, but the Ni–Ni distances are much longer (~3.55 Å) than in copper(II) complexes (~2.62 Å)[2] indicating that no metal-metal bonding occurs. The present work was undertaken in order to elucidate the structural changes that occur when copper(II) replaces nickel(II) in the system.

EXPERIMENTAL

Preparation and analyses. The compound was prepared by adding 0.05 mol of *N*,*N*,*N*′,*N*′-tetramethylethylenediamine (Fluka AG) to a methanol solution containing 0.05 mol of copper(II) chloroacetate, which was prepared from copper(II) carbonate (J. T. Baker) and chloroacetic acid (BDH). Propanol was added and the solution was allowed to evaporate at room temperature. After several days the product crystallized in the form of blue plates.

Copper was analyzed electrolytically. Calc. for $Cu(C_6H_{16}N_2)(ClC_2H_2O_2)_2$: Cu 17.33 %. Found: Cu 17.24 %. A density of 1.607 g/cm^3 was determined by the flotation method using carbon tetrachloride and methyl iodide. The calculated value with $Z=2$ is 1.599 g/cm^3.

Space group, unit cell and intensity data. Preliminary rotation and Weissenberg photographs taken with Cu$K\alpha$ radiation showed that the crystals belong to the monoclinic system, and systematic absences were recognized for the reflections $0k0$, when k odd. This indicated that the space group is $P2_1$ (No. 4) or $P2_1/m$ (No. 11). The centrosymmetric space group $P2_1/m$ could be excluded because in that space group the copper(II) ions would be in a special position, introducing too high symmetry requirements for the complex molecule.

Lattice parameters $a=7.266(3)$ Å, $b=14.846(7)$ Å, $c=7.260(2)$ Å and $\beta=103.41(3)°$ were obtained from a least-squares refinement of twelve well-centered reflections on a Syntex $P2_1$ automatic diffractometer using graphite-monochromatized Mo$K\alpha$ radiation ($\lambda=0.71069$ Å). The crystal selected for X-ray intensity measurement was approximately $0.40\times0.45\times0.50$ mm^3. Intensity data were collected ($5°<2\theta<60°$) at room temperature using the ω-scan technique and the scan rate varying from 2.02 to

29.3° min^{-1} depending upon the peak intensity. The intensity of one standard reflection, recorded after every 99 measurements to monitor the crystal stability, remained essentially constant throughout the data collection. Out of 2320 measured intensities 1981 were observed on the basis of $I > 3\sigma(I)$. The data were corrected for Lorentz and polarization factors and for absorption (μ(Mo$K\alpha$) = 18.5 cm^{-1}) from ϕ-scan data.

STRUCTURE DETERMINATION AND REFINEMENT

The MULTAN program system[3] was used to calculate phases for the 250 greatest $|E|$'s. Eight reflections were used in the starting set. The phase set with the highest combined figure of merit yielded an E-map from which the coordination sphere of the copper(II) ion could be found. The other non-hydrogen atoms were located by three-dimensional Fourier synthesis using the X-RAY 76 program system.[4]

Block-diagonal least-squares refinement was carried out on F. The function minimized was $\Sigma w(|F_o| - |F_c|)^2$ with the weighting scheme $w = 1/(45.0 + |F_o| + 0.005|F_o|^2)$. Scattering factors for Cu, Cl, O, N, and C were those tabulated by Cromer and Mann[5] and for H atoms those of Stewart, Davidson and Simpson.[6] The effect of anomalous dispersion was taken into account in the structure factor calculation, using the values of $\Delta f'$ and $\Delta f''$ for Cu and Cl given in International Tables for X-Ray Crystallography.[7] Refinement of a model including all non-hydrogen atoms with individual isotropic thermal parameters led to an R value of 0.073 ($R = \Sigma\|F_o| - |F_c\|/\Sigma|F_o|$). Further refinement with anisotropic thermal parameters reduced the R factor to 0.038. At this point all of the hydrogen atoms were located from a difference Fourier map. Five more least-squares cycles were then computed, in which non-hydrogen atoms were assigned anisotropic and hydrogen atoms isotropic thermal parameters. After the last cycle the final R value was 0.022 for the 1981 observed reflections.

The final atomic coordinates and thermal parameters together with their estimated standard deviations are given for non-hydrogen atoms in Table 1 and for hydrogen atoms in Table 2. A list of observed and calculated structure factors is obtainable on request from the authors.

Table 1. Fractional atomic coordinates ($\times 10^4$) and anisotropic thermal parameters[a] ($\times 10^3$) for non-hydrogen atoms. Estimated standard deviations are given in parentheses.

	x	y	z	U_{11}	U_{22}	U_{33}	U_{12}	U_{13}	U_{23}
Cu	1030(1)	4743(1)	−1030(1)	26(0.1)	24(0.1)	26(0.1)	2(0.2)	8(0.1)	2(0.2)
N1	−1693(4)	4363(2)	−1156(4)	25(1)	30(1)	27(1)	2(1)	5(1)	−1(1)
C1	−2195(4)	4783(4)	524(4)	27(1)	44(2)	33(1)	2(2)	11(1)	−2(2)
C2	−523(4)	4705(4)	2194(4)	35(1)	43(2)	27(1)	−4(2)	11(1)	1(2)
C3	−1953(6)	3375(3)	−1126(6)	43(2)	32(2)	49(2)	−7(1)	11(2)	−3(2)
C4	−2904(4)	4731(4)	−2919(4)	37(1)	51(2)	35(1)	3(2)	0(1)	−3(2)
C5	2922(4)	4756(5)	2903(4)	36(1)	53(2)	37(1)	−2(2)	−1(1)	7(2)
C6	1113(6)	6112(3)	1956(5)	51(2)	32(2)	42(2)	−4(2)	14(2)	−8(1)
N2	1161(4)	5124(2)	1693(4)	29(1)	29(1)	26(1)	−3(1)	6(1)	1(1)
O1	1172(4)	4006(2)	−3261(3)	47(1)	31(1)	34(1)	10(1)	15(1)	1(1)
C7	2133(5)	3312(2)	−2558(4)	35(2)	31(2)	32(2)	6(1)	13(1)	0(1)
C8	2380(5)	2650(2)	−4088(5)	50(2)	32(2)	37(2)	11(1)	16(1)	0(1)
Cl1	3670(1)	1664(1)	−3162(2)	48(1)	35(1)	62(1)	13(1)	16(1)	4(1)
O2	2774(4)	3185(2)	−858(4)	64(2)	58(2)	32(1)	21(2)	5(1)	−1(1)
O3	3258(3)	5478(2)	−1172(4)	34(1)	32(1)	46(1)	1(1)	15(1)	10(1)
C9	2557(4)	6173(2)	−2125(5)	32(1)	31(2)	33(1)	−1(1)	13(1)	3(1)
C10	4079(5)	6838(3)	−2387(5)	40(2)	34(2)	45(2)	2(1)	15(1)	11(1)
C12	3160(2)	7820(1)	−3671(1)	64(1)	33(1)	48(1)	3(1)	17(1)	12(1)
O4	856(4)	6303(2)	−2761(4)	34(1)	56(2)	63(2)	−1(1)	6(1)	20(2)

[a] The anisotropic thermal parameters are of the form $\exp[-2\pi^2(h^2a^{*2}U_{11} + \cdots 2hka^*b^*U_{12} + \cdots)]$.

Table 2. Fractional atomic coordinates ($\times 10^3$) and isotropic temperature factors ($\times 10^2$) for hydrogen atoms. Estimated standard deviations are given in parentheses.

	x	y	z	U		x	y	z	U
H1	−339(6)	444(3)	083(6)	4(1)	H11	310(6)	415(3)	274(6)	5(1)
H2	−262(6)	540(3)	021(6)	5(1)	H12	299(6)	488(5)	426(6)	7(1)
H3	−017(6)	407(3)	260(6)	6(1)	H13	405(6)	510(3)	254(6)	5(1)
H4	−087(5)	501(3)	334(5)	4(1)	H14	−001(8)	648(4)	115(8)	10(2)
H5	−150(7)	315(3)	−219(6)	6(1)	H15	099(6)	625(3)	316(6)	5(1)
H6	−329(7)	327(4)	−103(7)	7(1)	H16	226(6)	641(3)	171(6)	5(1)
H7	−112(6)	314(3)	−017(6)	5(1)	H17	116(7)	242(3)	−493(6)	5(1)
H8	−242(6)	440(3)	−398(6)	5(1)	H18	313(8)	297(4)	−491(7)	8(2)
H9	−426(6)	458(3)	−301(6)	5(1)	H19	491(6)	655(3)	−301(6)	5(1)
H10	−270(6)	532(3)	−305(6)	4(1)	H20	481(6)	706(3)	−125(6)	4(1)

Table 3. Interatomic distances (Å) and angles (°).

The Copper(II) environment					
Cu−N1	2.039(3)	N1−Cu−N2	86.9(1)	N1−Cu−O2	102.2(1)
Cu−N2	2.037(3)	N1−Cu−O1	92.6(1)	N1−Cu−O4	106.5(1)
Cu−O1	1.977(3)	N2−Cu−O3	92.5(1)	N2−Cu−O2	106.5(1)
Cu−O3	1.975(3)	O1−Cu−O3	93.7(1)	N2−Cu−O4	101.9(1)
Cu−O2	2.627(3)	N1−Cu−O3	161.7(1)	O1−Cu−O2	55.6(1)
Cu−O4	2.624(3)	N2−Cu−O1	161.6(1)	O1−Cu−O4	95.8(1)
		O2−Cu−O4	140.3(1)	O3−Cu−O2	95.6(1)
				O3−Cu−O4	55.7(1)
The diamine ligand					
N1−C1	1.488(5)	Cu−N1−C1	105.5(2)	Cu−N2−C2	105.4(2)
N1−C3	1.480(5)	Cu−N1−C3	113.5(2)	Cu−N2−C5	108.2(2)
N1−C4	1.480(4)	Cu−N1−C4	108.2(2)	Cu−N2−C6	113.8(2)
C1−C2	1.509(4)	C1−N1−C3	110.3(3)	C2−N2−C5	110.3(3)
N2−C2	1.490(5)	C1−N1−C4	110.2(3)	C2−N2−C6	109.7(3)
N2−C5	1.479(4)	C3−N1−C4	109.0(3)	C5−N2−C6	109.4(3)
N2−C6	1.481(5)	N1−C1−C2	108.8(3)	N2−C2−C1	109.0(3)
The chloroacetate ligands					
O1−C7	1.282(4)	Cu−O1−C7	104.2(2)	O1−C7−C8	111.9(3)
O2−C7	1.229(4)	Cu−O2−C7	75.5(2)	O2−C7−C8	123.5(3)
C7−C8	1.525(5)	O1−C7−O2	124.6(3)	C7−C8−Cl1	113.2(2)
C8−Cl1	1.784(4)				
O3−C9	1.280(4)	Cu−O3−C9	104.2(2)	O3−C9−C10	112.3(3)
O4−C9	1.230(4)	Cu−O4−C9	75.5(2)	O4−C9−C10	123.1(3)
C9−C10	1.527(5)	O3−C9−O4	124.6(3)	C9−C10−C12	113.6(2)
C10−C12	1.775(4)				

RESULTS AND DISCUSSION

The interatomic distances and angles together with their estimated standard deviations are given in Table 3. The structure of the molecule, as shown in Fig. 1, is monomeric with one diamine and two chloroacetate ligands coordinating to a copper(II) ion. The molecules have pseudo C_2 symmetry and are held in the crystal lattice by van der Waals' forces. With the exception of the contacts $O1\cdots C2^{I}$ 3.405(4), $O3\cdots C1^{II}$ 3.408(4) and $C3\cdots C6^{III}$ 3.491(6) Å, all intermolecular distances between non-hydrogen atoms are greater than 3.5 Å. I, II and III refer to the equivalent positions $(x,y,z-1)$, $(1+x,y,z)$ and $(-x,y-1/2,-z)$, respectively.

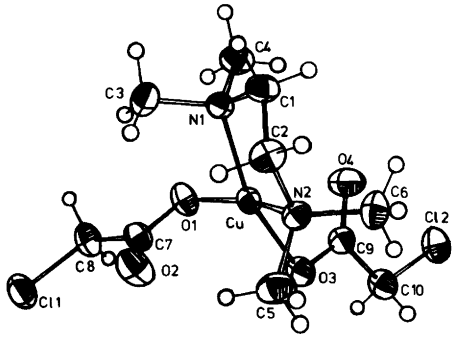

Fig. 1. A view of the complex molecule. Thermal ellipsoids are scaled to enclose 50 % probability.

The copper(II) ion is surrounded by four atoms in a distorted square-planar arrangement forming two Cu – O bonds of lengths 1.977(3) and 1.975(3) Å, and two Cu – N bonds of lengths 2.039(3) and 2.037(3) Å. The distortion is tetrahedral with N1 and O3 0.319 and 0.310 Å above the least-squares plane through N1, N2, O1 and O3, and with N2 and O1 0.319 and 0.309 Å below this plane, *cf.* Table 4. The degree of distortion is more clearly expressed by the dihedral angle of 25.6° between the Cu, N1, N2 and Cu, O1, O3 planes; the ideal value for square-planar arrangement is 0° and for tetrahedral arrangement 90°. The two remaining oxygen atoms O2 and O4 of the chloroacetate groups are at Cu – O distances of 2.627(3) and 2.624(3) Å, respectively. If the normal to the N1, N2, O1, O3 plane is considered as the "tetragonal axis" of the complex, the angles between the "out-of-plane" Cu···O directions and the "tetragonal axis" are 25.7 and 25.6°, respectively; the O2 – Cu – O4 angle is 140.3(1)°.

The stereochemistry of the copper(II) complex may be considered as distorted square-planar or tetragonally distorted octahedral, depending upon whether or not the "out-of-plane" oxygen atoms are considered to be bonded to Cu. Since the "in-plane" copper-ligand distances are not as short as those generally found for square-planar copper(II) complexes,[8] some interaction between the copper(II) and the "out-of-plane" oxygen atoms may exist, so that the environment of the copper(II) ion is best described as extremely tetragonally distorted octahedral, like that in $Cu(ClCH_2COO)_2(\alpha\text{-picoline})_2$.[9]

The dimensions and angles of the diamine ligand are as expected. The diamine chelate ring is practically in symmetric *gauche* configuration. The ring carbon atoms lie 0.356 and 0.355 Å above and below the plane defined by Cu, N1, N2. In substituted ethylenediamine ligands the largest deviations are found in the ring carbon-carbon bond length. In this compound the C1 – C2 length of 1.509(4) Å agrees quite well with those of 1.523(14) and 1.497(9) Å found in $Cu(CH_3CHOHCOO)_2(tmen)$[10] and $Ni(CH_3CHOHCOO)_2(tmen)$[11] but is somewhat shorter than the normal carbon – carbon single bond distance of 1.54 Å.[12] One possible explanation for this difference from the carbon – carbon single bond value is to be found in Maslen and Waters' suggestion that the ring C – C bond length in complexes ethylenediamine is somewhat flexible and responsive to the demands of the chemical system in which it finds itself.[13]

The C – H distances lie in the range 0.88 – 1.07 Å, with estimated standard deviations of about 0.05 Å. The acetate groups are planar and the copper(II) ion is only slightly displaced from these planes, as are the chlorine atoms, *cf.* Table 4. The dihedral angles between planes C, C, O, O and C, C, Cl are 1.0 and 0.8°. The O – C – O angles of 124.6(3)° agree well with the previously reported values of 123.8 – 125.4° found in $Cu(ClCH_2COO)_2(\alpha\text{-picoline})_2$,[9] $NH_4H(ClCH_2COO)_2$,[14] and two forms of $ClCH_2COOH$,[15,16] but seem to be slightly smaller than those of 126.6 – 129.0° in $[Cu(ClCH_2COO)_2(\alpha\text{-picoline})]_2$[17] and $[Ni_2(ClCH_2COO)_4(tmen)_2$-

Table 4. Deviations (Å) of atoms from least-squares planes.

Plane I:		N1, N2, O1, O3									
N1	0.319	N2	−0.319	O1	−0.309	O3	0.310		0.000		
Plane II:		O1, O2, C7, C8									
O1	−0.001	O2	−0.001	C7	0.002	C8	−0.001	Cu	−0.013	Cl1	−0.031
Plane III:		O3, O4, C9, C10									
O3	0.001	O4	0.001	C9	−0.001	C10	0.000	Cu	0.007	Cl2	0.025

The angles between the planes: I, II = 85.9°; I, III = 86.1°; III = 86.2°

H_2O].[1a] The C–O bond lengths of 1.229–1.230(4) and 1.282–1.280(4) Å are significantly different, as are the C–C–O angles of 111.9–112.3(3)° and 123.5–123.1(3)°, *cf.* Table 3. From a chemical point of view the longer C–O bond length of each chloroacetate group would be expected to belong to the oxygen atom that is more strongly coordinated to the copper(II) ion and this is consistent with the observed Cu–O distances. These facts indicate that the carboxyl groups in the present compound are neither fully ionized or neutral in character.

REFERENCES

1. a. Turpeinen, U. *Finn. Chem. Lett.* (1976) 173; b. *Ibid.* (1977) 36; c. *Ibid.* (1977) 123; d. Turpeinen, U., Ahlgrén, M. and Hämäläinen, R. *Ibid.* (1977) 246.
2. Doedens, R. J. *Prog. Inorg. Chem. 21* (1976) 227.
3. Main, P., Woolfson, M. M., Lessinger, L., Germain, G. and Declercq, J.-P. *MULTAN 74, A System of Computer Programmes for the Automatic Solution of Crystal Structures from X-Ray Diffraction Data.*
4. Stewart, J. M., Ed., *The X-Ray System, Version of 1976*, Technical Report TR-446, Computer Science Center, University of Maryland, College Park.
5. Cromer, D. and Mann, J. B. *Acta Crystallogr. A 24* (1968) 321.
6. Stewart, R. F., Davidson, E. R. and Simpson, W. T. *J. Chem. Phys. 42* (1965) 3175.
7. *International Tables for X-Ray Crystallography*, Kynoch Press, Birmingham 1974, Vol. IV, p. 149.
8. Hathaway, B. J. and Billing, D. E. *Coord. Chem. Rev. 5* (1970) 143.
9. Davey, G. and Stephens, F. S. *J. Chem. Soc. A* (1971) 1917.
10. Ahlgrén, M., Hämäläinen, R. and Pajunen, A. *Finn. Chem. Lett.* (1977) 3.
11. Ahlgrén, M. and Turpeinen, U. *Finn. Chem. Lett.* (1977) 129.
12. Pauling, L. *The Nature of the Chemical Bond*, 3rd. Ed., Cornell University Press, Ithaca 1960, p. 222.
13. Maslen, H. S. and Waters, T. N. *Coord. Chem. Rev. 17* (1975) 158.
14. Ichikawa, M. *Acta Crystallogr. B 28* (1972) 755.
15. Kanters, J. A. and Roelofsen, G. *Acta Crystallogr. B 32* (1976) 3328.
16. Kanters, J. A., Roelofsen, G. and Feenstra, T. *Acta Crystallogr. B 32* (1976) 3331.
17. Davey, G. and Stephens, F. S. *J. Chem. Soc. A* (1970) 2803.

Received September 5, 1977.

Acta Chemica Scandinavica A 32 (1978) 63 – 70

Conformational Analysis. The Temperature Effect on the Structure and Composition of the Rotational Conformers of 1,2-Dibromoethane as Studied by Gas Electron Diffraction

LIV FERNHOLT and KARI KVESETH

Department of Chemistry, University of Oslo, Blindern, Oslo 3, Norway

Gaseous 1,2-dibromoethane has been studied by electron diffraction at 25, 36, 85, 140 and 200 °C. The most stable conformer is *anti*, which contributes with 95 % at 25 °C decreasing to 82 % at 200 °C in the vapour. From the temperature dependency of the *gauche/anti* ratio thermodynamic differences for the conformational equilibrium, $\Delta E = E_g - E_a$ and $\Delta S = S_g - S_a$, were determined. Assuming the differences to be constant in the actual temperature range, gave $\Delta E = 2.20$ (14) kcal mol^{-1} and $\Delta S = 1.67(30)$ cal mol^{-1} deg^{-1}. The structure remained almost constant with respect to the temperature variations, and the main average parameters (r_a and $\angle_a$) are C – C = 1.506, C – Br = 1.950, C – H = 1.108(Å), ∠CCBr = 109.5, ∠CCH = 110.0 and $\phi_g = 73.0$ (°).

1,2-Disubstituted ethanes consist of a mixture of two conformers,[1-3] *anti* and *gauche*. Due to the difference in energy between the two conformers, the amount of each will vary with the temperature.

The *gauche/anti* ratio (K) may be studied by the gas electron diffraction method, considering K as one of the structural parameters in addition to the geometric and vibrational ones.

In previous studies of this kind,[4-6] the thermodynamic differences deduced from the temperature variations in K proved to give reasonable results. The main scope of this study of 1,2-dibromoethane is to confirm the accuracy of this method and to give a more detailed discussion of the temperature dependency of the thermodynamic quantities ΔE and ΔS.

EXPERIMENTAL

The sample of 1,2-dibromoethane, obtained from Koch-Light Laboratories, (>99 %) was used without further purification. Electron diffraction photographs were obtained with the Balzers Eldigraph KDG-2 unit.[7,8] The experimental conditions are summarized in Table 1. The optical densities at points in a rectangular array covering the plate were measured by a Joyce-Loebl densitometer. For each point in the array the scattering parameter s was calculated, and the final density value obtained by averaging the density for points of very similar s-values.* For this particular molecule it was found necessary to use $\Delta s = 0.125$ Å^{-1} also for the shorter nozzle-to-plate distances.

These data were corrected in the usual way,[9] giving an intensity curve for each photographic plate. The intensities were modified with the function $s/|f_{Br}|^2$.

The background was subtracted separately from each intensity curve. The average for each set of plates was calculated, and composites made at 36 and 200 °C, by scaling a corresponding pair of curves and averaging the intensities in the overlap region. These molecular intensities are given in Fig. 1.

The amount of the two conformers, as well as the structural parameters, are determined by conventional least-squares refinements.

The theoretical molecular intensities were cal-

* In the standard routines applied in this laboratory, the densities were averaged at very similar radii and then converted into densities on the s-scale. These two-step interpolations were smoothing the data too much. This was probably connected with the rapidly oscillating and strongly contributing Br···Br$_a$ distance ($r = 4.6$ Å, $u = 0.072$ Å at 25 °C), and the way it is superposed on the contributions from the other distances.

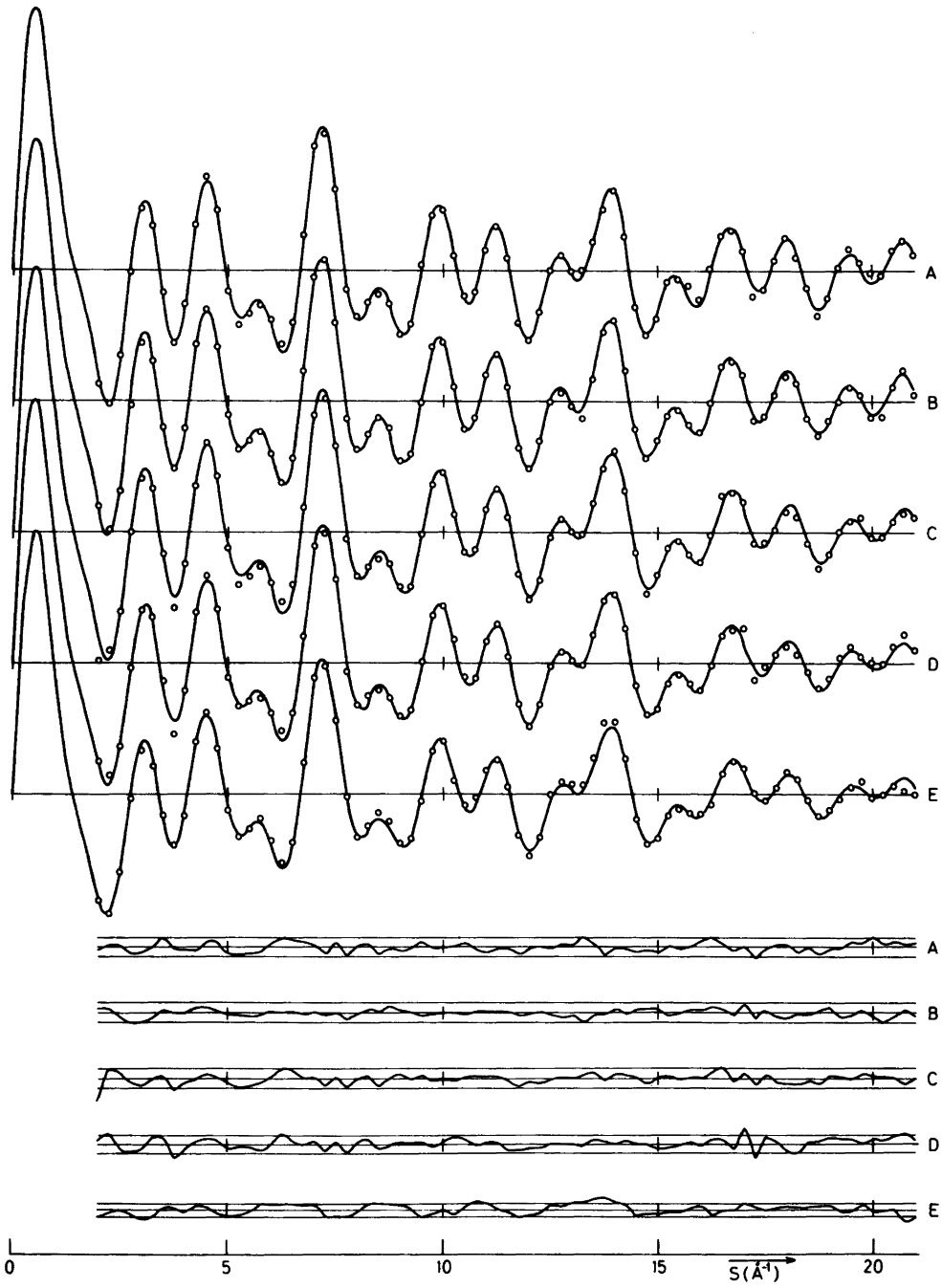

Fig. 1. Intensity and difference curves. The solid curves are theoretical, calculated from the parameters in Table 4, O are experimental values, the difference is experimental minus theoretical and the limits are 3σ, σ being the experimental standard deviation in the observations.
A: 25, B: 36, C: 85, D: 140 and E: 200 °C.

Table 1. Experimental conditions and photographic plate data.

Temperature (°C)	25	36		85	140	200	
Nozzle-to-plate distance (mm)	329.27	578.74	329.27	329.27	329.27	578.91	249.47
Electron wave length (Å)[a]	0.058510	0.058535	0.058510	0.058510	0.058510	0.058524	0.058530
Range of data (s)[b]	2.0–21.0	1.0–13.375	2.0–21.0	2.0–21.0	2.0–21.0	1.0–13.375	2.0–21.0
Data interval (Δs)	0.125	0.125	0.125	0.125	0.125	0.125	0.125
Number of plates used	6	5	6	7	6	6	6
Corresponding curves in Figs.							
Figs. 1 and 2	A	B		C	D	E	

[a] Determined from ZnO diagrams, systematically 0.1 % too low as compared with benzene.
[b] $s=4\pi/\lambda \sin\theta$ (Å^{-1}), 2θ is the scattering angle.

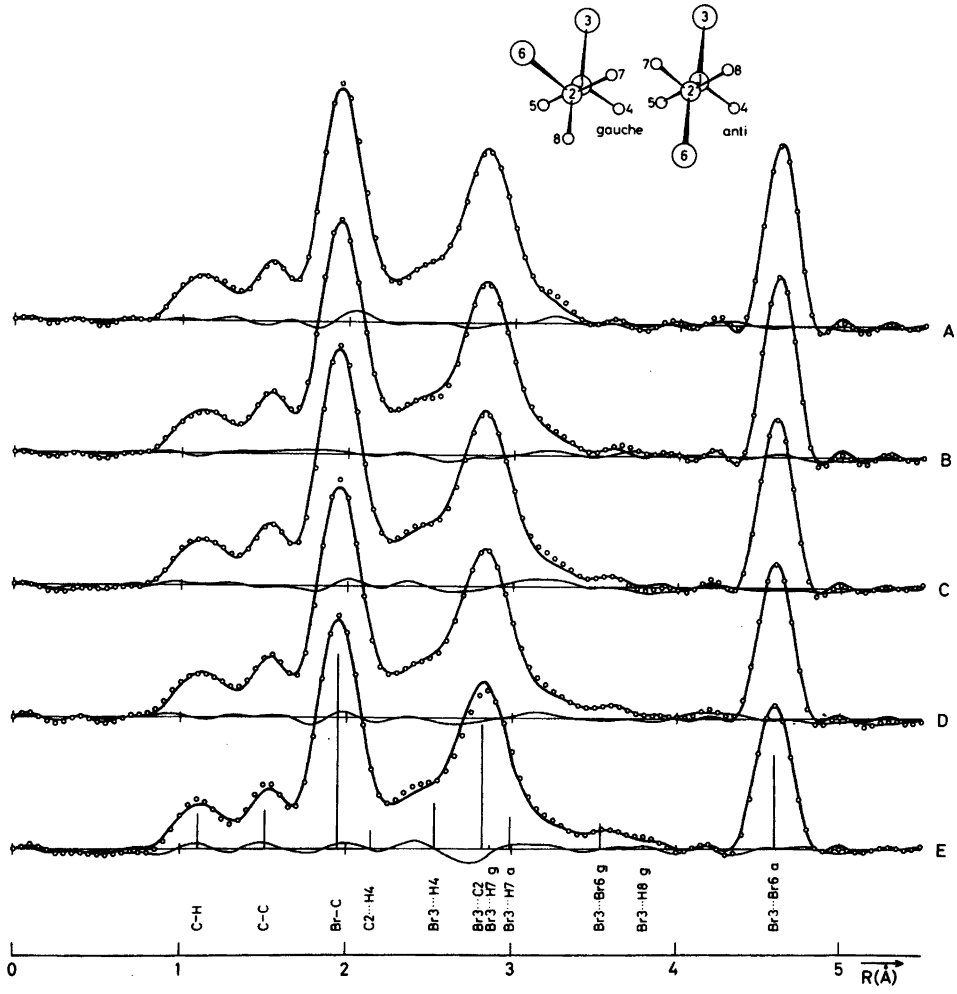

Fig. 2. Radial distribution curves and differences ($B=0.0015$ Å^2).

culated according to eqn. 11 of Ref. 9. The scattering amplitudes and phase shifts[9,10] were calculated analytically by a program originally written by Yates,[11] using Hartree-Fock-Slater potentials[12] for C and Br, and molecular bonded potential[13] for H.

Due to extraneous scattering from the bromine atoms, reproducable intensities were obtained in a more limited s-range than normally achieved, and intensities up to $s=21$ Å^{-1} are used in this study.

STRUCTURE ANALYSIS AND REFINEMENT

Radial distribution curves (RD-curves), calculated from the molecular intensities by a Fourier transformation,[9] are shown in Fig. 2. The bond distances contribute to the first three peaks, together with the short $r(H_4\cdots H_5)$. The peak complex between 2.5 and 4.0 Å corresponds to all the nonbonded distances, except the torsional dependent $r(Br_3\cdots Br_6)$ in *anti*, which gives rise to an isolated peak at 4.60 Å, the area of which varies directly with the amount present.

In addition to the torsional angle, ϕ, the three bond distances, r(C−C), r(C−Br) and r(C−H), and the angles ∠CCBr and ∠CCH, were chosen as independent geometric parameters. ϕ is defined as 180° an *anti*. Since the H-positions are not very well-defined, C_3-symmetry with respect to the angles was assumed in the $CBrH_2$ groups.

The molecular structure was calculated in the geometric consistent r_α-picture, the torsional independent part assumed to be identical in both conformers.[14] The bond distances were transformed by the eqn. $r_\alpha=r_a+u^2/r-k=r_a+D$, where k is the perpendicular amplitude correction coefficient[14,15] and r_a the operative electron diffraction parameter. The dependent structural parameters were then calculated from the geometric restraints, and transformed back to the corresponding r_a-values before the structure was refined. The reported angles correspond to the r_α-structure.

Vibrationally different distances in the two conformers were given different correction terms (D's). The differences are rather small, however, and the composition in the vapour phase is mainly determined from the torsional dependent distances, the

Table 2. The difference, $D=u^2/r-k$ (Å), between r_α and r_a, as calculated from the valence force field established by Schachtschneider and Snyder,[17] with torsional force constants from this work, $f_{\tau,g}=0.360$ and $f_{\tau,a}=0.234$ (mdyn Å rad^{-2}).

The suffix a and g refers to *anti* and *gauche* respectively, the first indicates the conformer, and in the double suffix, the second gives the type of distances considered.

Temp (°C)		25	36	85	140	200
r(C−C)	(1.50)	0	0	0	0	0
r(C−Br)	(1.94)	−0.0046	−0.0047	−0.0055	−0.0064	−0.0073
r(C−H)	(1.12)	−0.0107	−0.0108	−0.0113	−0.0120	−0.0128
$r(Br_3\cdots H_4)$	(2.51)	−0.0064	−0.0066	−0.0076	−0.0087	−0.0100
$r(H_4\cdots H_5)$	(1.79)	−0.0106	−0.0108	−0.0116	−0.0126	−0.0137
$r(C_2\cdots Br_3)$a	(2.83)	−0.0031	−0.0032	−0.0038	−0.0043	−0.0050
$r(C_2\cdots H_4)$a	(2.18)	−0.0020	−0.0020	−0.0022	−0.0025	−0.0028
$r(Br_3\cdots Br_6)$a	(4.60)	0.0011	0.0012	0.0013	0.0015	0.0017
$r(Br_3\cdots H_7)$a,g	(3.03)	0.0008	0.0008	0.0007	0.0007	0.0006
$r(H_4\cdots H_7)$a,a	(3.12)	−0.0028	−0.0028	−0.0030	−0.0031	−0.0034
$r(H_4\cdots H_8)$a,g	(2.56)	0.0011	0.0011	0.0009	0.0008	0.0006
$r(C_2\cdots Br_3)$g	(2.83)	−0.0003	−0.0003	−0.0004	−0.0004	−0.0005
$r(C_2\cdots H_4)$g	(2.18)	−0.0062	−0.0064	−0.0072	−0.0081	−0.0091
$r(Br_3\cdots Br_6)$g	(3.47)	0.0081	0.0084	0.0097	0.0112	0.0128
$r(Br_3\cdots H_7)$g,g	(2.96)	0.0026	0.0026	0.0028	0.0030	0.0033
$r(Br_3\cdots H_8)$g,a	(3.84)	−0.0025	−0.0025	−0.0027	−0.0030	−0.0033
$r(H_4\cdots H_7)$g,g	(2.61)	−0.0044	−0.0046	−0.0055	−0.0064	−0.0075
$r(H_4\cdots H_8)$g,g	(2.52)	−0.0060	−0.0062	−0.0073	−0.0084	−0.0097
$r(H_5\cdots H_7)$g,a	(3.12)	−0.0090	−0.0092	−0.0102	−0.0112	−0.0125

Table 3. The vibrational amplitudes, u(Å) as calculated from valence force field.

Temp (°C)		25	36	85	140	200
$u(C-C)$	(1.50)	0.0506	0.0506	0.0510	0.0515	0.0522
$u(C-Br)$	(1.94)	0.0534	0.0538	0.0554	0.0574	0.0597
$u(C-H)$	(1.12)	0.0780	0.0780	0.0780	0.0780	0.0780
$u(Br_3\cdots H_4)$	(2.51)	0.1112	0.1114	0.1125	0.1141	0.1161
$u(H_4\cdots H_5)$	(1.79)	0.1263	0.1263	0.1264	0.1267	0.1272
$u(C_2\cdots Br_3)$	(2.83)	0.0745	0.0754	0.0794	0.0838	0.0885
$u(C_2\cdots H_4)$a	(2.18)	0.1074	0.1075	0.1082	0.1091	0.1103
$u(Br_3\cdots Br_6)$a	(4.60)	0.0718	0.0730	0.0779	0.0832	0.0887
$u(Br_3\cdots H_7)$a,g	(3.03)	0.1656	0.1670	0.1737	0.1812	0.1893
$u(H_4\cdots H_7)$a,a	(3.12)	0.1267	0.1268	0.1271	0.1276	0.1283
$u(H_4\cdots H_8)$a,g	(2.56)	0.1708	0.1712	0.1731	0.1758	0.1793
$u(C_2\cdots Br_3)$g	(2.83)	0.0745	0.0754	0.0794	0.0838	0.0885
$u(C_2\cdots H_4)$g	(2.18)	0.1074	0.1075	0.1082	0.1091	0.1103
$u(Br_3\cdots Br_6)$g	(3.47)	0.1645	0.1674	0.1799	0.1930	0.2064
$u(Br_2\cdots H_7)$g,g	(2.96)	0.1597	0.1609	0.1665	0.1730	0.1802
$u(Br_3\cdots H_8)$g,a	(3.84)	0.1028	0.1032	0.1053	0.1078	0.1106
$u(H_4\cdots H_7)$g,g	(2.61)	0.1674	0.1678	0.1695	0.1719	0.1750
$u(H_4\cdots H_8)$g,g	(2.52)	0.1666	0.1669	0.1688	0.1713	0.1744
$u(H_5\cdots H_7)$g,a	(3.12)	0.1266	0.1267	0.1270	0.1274	0.1282

Br···Br distance in *gauche* (3.5 Å) and *anti* (4.6 Å) being most important.

D-Values and root-mean-square amplitudes (u-values) as calculated[15,16] from the established valence force field[17] and the cartesian displacement coordinates are given in Table 2 and 3, respectively. The torsional force constants were varied to reproduce the observed frequencies at 80 cm^{-1} in *gauche* (observed at 91 cm^{-1} in liquid[18,19]) and 118 cm^{-1} in *anti*. The values obtained are similar to those previously obtained for 1,2,3-tribromopropane.[20] The torsional force constant in *anti* was found to be slightly smaller than in *gauche*, similar to the difference previously found for 1,2-dichloroethane.

The absolute magnitude of all the calculated *D*-values is somewhat larger than found for 1,2-dichloroethane.[4,5] The estimated u-values are somewhat smaller than the corresponding ones in 1,2-dichloro- and 1,1,2,2-tetrafluoroethane,[21] whereas the others, which involve halogens generally are increasing in going from F to Br.

The vibrational amplitudes that did not refine, were given the calculated values, although refinements at the different temperatures of $u(C-Br)$, $u(C_2\cdots Br_3)$ and $u(Br_3\cdots Br_6)_a$ gave slightly lower values. Since the refined u-values were somewhat dependent of the subtracted experimental background, we chose to let the average refined values determine the level of these u-values, and estimated a new set assuming the same temperature slope as obtained from the force field calculations.

It was also quite obvious from the preliminary refinements that the shrinkage corrections based upon the harmonic force field calculations, were much too small for Br···Br *anti* distance, and it was decided to refine this distance as an independent parameter as well.

Repeated least-squares refinements revealed a slight dependency of some of the geometry parameters on the experimental background, whereas $r(C-Br)$, $\angle CCBr$ and $r(Br_3\cdots Br_6)_a$ were practically invariant, and almost identical at the different temperatures. Inspection of Tables 2 and 3 shows that of the parameters refined only the u-values for the long non-bonded distances and the *gauche/anti* ratio vary significantly with the temperature, in accordance with general experiences.

It was therefore felt appropriate in this case to determine an average geometry from the best fit at all temperatures. The final backgrounds were adjusted to the intensity differences obtained with this mean structural model, and the quality was judged by the smoothness of particularly the inner part of

Table 4. Molecular parameters, distances (r_a) and vibrational amplitudes (u) in Å, angles ($\angle_a$) in degrees, and estimated correlation coefficients larger than 0.5 (ρ). Standard deviation (1σ) in parentheses.

Temp (°C)	Average [a]	25	36	85	140	200
r(C−C)	1.506	(7)	(6)	(7)	(7)	(7)
r(C−Br)	1.950	(3)	(2)	(3)	(3)	(3)
r(C−H)	1.108	(8)	(7)	(8)	(8)	(8)
$r(Br_3\cdots Br_6)_a$		4.611(5) *	4.612(5) *	4.600(5) *	4.605(2) *	4.603(5) *
∠CCBr	109.5	(4)	(3)	(4)	(4)	(4)
∠CCH	110.0	(11)	(9)	(11)	(12)	(13)
ϕ_g	73.0	(46)	(32)	(27)	(22)	(20)
u(C−Br)	0.0534	0.049(3)	0.050(3)	0.051(4)	0.053(4)	0.056(4)
$u(C_2\cdots Br_3)$	0.0745	0.065(4)	0.066(4)	0.070(5)	0.075(6)	0.079(7)
$u(Br_3\cdots Br_6)_a$	0.0718	0.064(2)	0.065(2)	0.070(2)	0.075(2)	0.081(2)
n_a (%)		95.1(18) *	93.7(16) *	89.9(19) *	86.2(19) *	82.5(30) *
R_2 (%) [b]		10.3	8.9	11.0	11.4	12.3
$\rho(r$(C−C),∠CCBr)		−0.88	−0.88	−0.87	−0.87	−0.86
$\rho(\gamma$,∠CCH)		0.63	0.63	0.63	0.64	0.64
$\rho[\gamma,u$(C−Br)]		0.67	0.67	0.68	0.68	0.68
$\rho[\gamma,u(C_2\cdots Br_3)]$		0.50	0.53	0.60	0.65	0.68
$\rho(\gamma,n_a)$		−0.78	−0.78	−0.77	−0.76	−0.75
$\rho[n_a,u(C_2\cdots Br_3)]$		−0.54	−0.53	−0.54	−0.54	−0.54
$\rho[n_a,u(C_2\cdots Br_3)]$		−0.49	−0.53	−0.64	−0.71	−0.77

[a] See text, calculated u-values at 25 °C. 0.1 % r is added to the refined values to account for the systematic error in the wavelength. [b] $R_2=(\Sigma w\Delta^2/\Sigma wI^2)^{\frac{1}{2}}\times 100$.

the final RD-curves.

To get some information about the uncertainty introduced by fixing the structure to a mean, all the estimated values were refined one cycle, and corresponding standard deviations and correlation coefficients were calculated. These are given in Table 4, together with the mean structural parameters, the refined $r(Br_3\cdots Br_6)_a$ and the percentage of *anti* (n_a). The standard deviations are those obtained from diagonal[22,23] least-squares refinements, corrected for a uncertainty of 0.1 % in the wavelength. Refinements with fixed mean structure are marked.* Previous experience[4] seems to indicate that this estimate of σ_{n_a} probably is negligibly smaller than one would have obtained from a full individual structural refinement.

RESULTS AND DISCUSSION

The structural parameters (Table 4) are quite normal and agree very well with previously reported results,[20,24,25] except that u(C−Br) and $u(C_2\cdots Br_3)$ as estimated by Brunvoll[24] are definitely too large. Because of the relatively small *gauche* contribution, the torsional angle (ϕ_g) was difficult to determine. Several refinements, especially at the higher temperature recordings, indicated that 73° was a reasonably good values, as also is indicated by the relatively normal standard deviations in the first cycle refinements. This value is also identical to the angle previously reported by Brunvoll.[24] Although larger than the corresponding angle in 1,2,3-tribromopropane[20] (where 65.3° must be considered as a compromise between the Br/Br repulsions in the 1,2 and 1,3-positions) it agrees reasonably well with the torsional angle in 1,2-dichloroethane[4,5] [$\bar{\phi}_g=75.3(9)°$].

The measurements of the *gauche/anti* ratio as a function of the temperature have been used in a thermodynamic study of the conformational equilibrium. If we consider the conformational equilibrium *anti* ⇌ *gauche*, the difference in energy, $\Delta E=E_g-E_a$, and the difference in entropy, $\Delta S=S_g-S_a$, between the two conformers, may be obtained from the temperature variation of the *gauche/anti* ratio K[4,5,26], by use of the formula

$$K=\frac{n_g}{n_a}=e^{-(\Delta E-T\Delta S)/RT}=\frac{2\,Q_g}{Q_a}e^{-\Delta E^0/RT} \qquad (1)$$

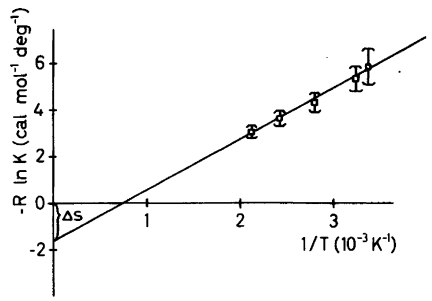

Fig. 3. $-R \ln K$ as a function of $1/T$. The standard deviations marked at each point by vertical lines, are calculated from σ_{n_a}.

n is the percentage of the conformers *gauche* (g) and *anti* (a). Q is the vibrational/rotational partition function and $\Delta E°$ is the energy difference between *gauche* and *anti* at the absolute zero point. The factor 2 is the statistical weight for the two identical *gauche* forms, and is included in ΔS. Thus $\Delta S = R \ln 2 + \Delta S_c$, where ΔS_c may be considered as the difference in conformational entropy.

These differences may be obtained in two ways. Firstly, if ΔE and ΔS are assumed to be temperature independent, they may be determined from the slope and intersection, respectively, of the straight line fitted to the observed $(-R \ln K, 1/T)$ points (see Fig. 3). Secondly, if the appropriate vibrational-rotational partition functions, as calculated from the valence force field, are combined with the observed K-values an average estimate of ΔE and ΔS may be calculated. As in the earlier papers[4-6] both approaches were used in this investigation, and the results are given in Table 5.

Columns A demonstrate that both ΔE and ΔS are practically constant in the actual temperature interval, indicating that the assumed linearity of $-R \ln K$ as a function of $1/T$ is valid. The constancy of ΔS is obviously due to the opposite temperature effect of the $R \ln Q_g/Q_a$ and $RT\,\partial/\partial T \ln Q_g/Q_a$ functions. The table also reveals, as previously found for 1,2-dihaloethanes,[5,18] that the deviation of ΔS from $R \ln 2$ is rather small (insignificant compared with the estimated standard deviation, 0.3 cal mol^{-1} deg^{-1}), but that both $R \ln Q_g/Q_a$ and $RT\,\partial/\partial T \ln Q_g/Q_a$ have to be included if more accurate calculations are to be made.

The discrepancy between the estimates of ΔS may be connected with the assumption that the internal rotation also is a harmonic motion as well as with the uncertainty in the assigned torsional frequencies: Shimanouchi[19] gives 91(l) and 118 (g) cm^{-1} in *gauche* and *anti* respectively, whereas Tanabe *et al.*[18] give ~70(l) and 126(l), the latter in much better agreement with the "pure" electron diffraction results (column B). In 1,2-dichloroethane[5] the conformational entropy was estimated to be less than zero ($\Delta S_C = \Delta S - R \ln 2 = -0.48$ cal mol^{-1} deg^{-1}). In 1,2-dibromoethane we obtain $\Delta S_C = 0.29$

Table 5. Thermodynamic terms, (A) calculated from estimated mol fractions ($K = n_g/n_a$) and partition functions (Q),[a] (B) from a least-squares fitted straight line to the observed $(-R \ln K, 1/T)$ points. Standard deviation (1σ) in parentheses.

Temp (°C)	A						B
	25	36	85	140	200	Average	
n_a (%)	95.1(18)	93.7(16)	89.9(19)	86.2(19)	82.5(20)		
$R \ln (Q_g/Q_a)$ (cal mol^{-1} deg^{-1})	0.072	0.056	−0.009	−0.067	−0.118	−0.013	0.71
$RT\,\partial/\partial T \ln (Q_g/Q_a)$ (cal mol^{-1} deg^{-1})	−0.457	−0.450	−0.422	−0.394	−0.362	−0.417	−0.42
$\Delta E°$ (kcal mol^{-1})	2.19(23)[b]	2.10(8)	2.05(15)	2.05(13)	2.05(13)	2.09(3)[c]	
ΔE (kcal mol^{-1})[d]	1.95	1.95	1.94	1.93	1.92	1.94	2.20(14)
ΔS (cal mol^{-1} deg^{-1})[e]	0.99	0.98	0.95	0.92	0.90	0.95	1.67(30)[f]

[a] Calculated from the valence force field[17] [$\nu_{\tau,g} = 80$ and $\nu_{\tau,a} = 118$ (cm^{-1})] and the products of the principal moments of intertia ($(I_A I_B I_C)_g = 2.056762 \times 10^7$ and $(I_A I_B I_C)_a = 1.335220 \times 10^7$ (a.w.Å^2)). Q is the rotational/vibrational partition function. [b] Standard deviations calculated according to $\sigma_{\Delta E°} = \partial/\partial n_a \Delta E° \sigma_{n_a}$. [c] Standard deviations calculated from the squared deviations from the mean. [d] $\Delta E = \Delta E° + RT^2 \partial/\partial T \ln (Q_g/Q_a)$,[26] the mean value, $\Delta E° = 2.09$, is used. [e] $\Delta S = R \ln 2 + R \ln (Q_g/Q_a) + RT\partial/\partial T \ln (Q_g/Q_a)$. [f] This ΔS corresponds to $\nu_{\tau,g}/\nu_{\tau,a} = 0.45$, giving $\nu_{\tau,g} = 53$ cm^{-1} if $\nu_{\tau,a} = 118$ cm^{-1} is assumed to be correct. The standard deviations are obtained from the least squares fitting.

cal mol^{-1} deg^{-1} from the straight line fit (column B, Table 5), whereas the estimated partition functions give $\Delta S_C = -0.42$ cal mol^{-1} deg^{-1} (column A, Table 5). Although these values are not significantly different from zero, the reasons for a positive value for ΔS_C in 1,2-dibromoethane may be that increased halogen/halogen interactions lead to a relatively broader minimum in *gauche* 1,2-dibromoethane than in *gauche* 1,2-dichloroethane. We therefore believe that the estimate by the straight line fit is the most reliable in this case.

The two estimates of ΔE are slightly, although not significantly, different, but definitely higher than previous estimates (*e.g.* 1.6 [ED(*g*)],[24] 1.5 [IR(*g*)],[29] 0.9 [IR,R(*l*)],[18] 0.75 [R(*l*)] estimated 1.6 (*g*),[27] 0.9 [R(*l*)][28] [kcal mol^{-1}]).

Because of the stabilization of the more polar form (*i.e., gauche*) in the liquid state, it is generally expected that ΔE in the liquid state should be smaller than the vapour phase value.[3] The difference in the case of 1,2-dibromoethane, approximated from dielectric constants and dipole moments to 0.9 kcal mol^{-1},[27] and from experiment[29] to 0.8 kcal mol^{-1}, is reducing the apparent discrepancy, but the straight line estimate (column B, Table 5) is still the highest observed value for this conformational energy difference.

The estimated standard deviation ($1\sigma = 0.14$ kcal mol^{-1}) is rather small, but covers, of course, only random errors in ΔE. The critical point in this type of thermodynamic study is the assumption that the nozzle temperature is identical to the gas temperature[30,31] at the scattering point. Previous experiences[4,5,32] seem to indicate that this assumption is sufficiently accurate at the present level of accuracy of the electron diffraction method. However, applying the formula $T_{sample} = 0.8\ T_{nozzle}$[33] reduces the estimate in this case to $\Delta E' = 1.76$ kcal mol^{-1}, which is significantly lower. This suggests that for larger ΔE the uncertainty in the temperature may be of greater importance, provided Bauer's formula gives the correct temperature, and that the equilibrium was established at this temperature.

Acknowledgement. We are indebted to siv.ing. R. Seip for recording the electron diffraction data, and to Mrs. S. Gundersen for technical assistance.

REFERENCES

1. Bastiansen, O., Seip, H. M. and Boggs, J. E. *Perspect. Struct. Chem. 4* (1971) 60.
2. Orville-Thomas, W. J., Ed., *Internal Rotation in Molecules*, Wiley, London 1974.
3. Wyn-Jones, E. and Pethrick, R. A. *Top. Stereochem. 5* (1970) 205.
4. Kveseth, K. *Acta Chem. Scand. A 28* (1974) 482.
5. Kveseth, K. *Acta Chem. Scand. A 29* (1975) 307.
6. Almenningen, A., Fernholt, L. and Kveseth, K. *Acta Chem. Scand. A 31* (1977) 297.
7. Zeil, W., Haase, J. and Wegmann, L. *Z. Instrumentenkd. 74* (1966) 84.
8. Bastiansen, O., Graber, R. and Wegmann, L. *Balzers High Vacuum Report 25* (1969) 1.
9. Andersen, B., Seip, H. M., Strand, T. G. and Stølevik, R. *Acta Chem. Scand. 23* (1969) 3224.
10. Strand, T. G. and Bonham, R. A. *J. Chem. Phys. 40* (1964) 1686.
11. Yates, A. C. *Computer Physics Commun. 2* (1971) 175.
12. Liberman, D., Walser, J. J. and Cromer, D. *Phys. Rev. 137* (1965) 1727.
13. Stewart, R. F., Davidson, E. R. and Simpson, W. T. *J. Chem. Phys. 42* (1965) 3175.
14. Kuchitsu, K. *Bull. Chem. Soc. Jpn 44* (1971) 96.
15. Stølevik, R., Seip, H. M. and Cyvin, S. J. *Chem. Phys. Lett. 15* (1972) 263.
16. Gwinn, W. D. *J. Chem. Phys. 55* (1971) 477.
17. Schachtschneider, J. H. and Snyder, R. G. *Vibr. Analysis of Polyatomic Molecules IV*, Shell Div. Company, Tech. Report No. 122–63.
18. Tanabe, K., Hiraishi, J. and Tamura, T. *J. Mol. Sruct. 33* (1976) 19.
19. Shimanouchi, T. *Tables of Molecular Vibrational Frequencies*, NSRDS-NBS 39, VH *1* (1972) 99.
20. Stølevik, R. *Acta Chem. Scand. A 28* (1974) 299.
21. Brown, D. E. and Beagley, B. *J. Mol. Struct. 38* (1977) 167.
22. Seip, H. M., Strand, T. G. and Stølevik, R. *Chem. Phys. Lett. 3* (1969) 617.
23. Seip, H. M. and Stølevik, R. In Cyvin, S. I., Ed., *Molecular Structure and Vibrations*, Elsevier, Amsterdam 1972.
24. Brunvoll, J. *Thesis*, Trondheim 1962.
25. Farup, R. E. and Stølevik, R. *Acta Chem. Scand. A 28* (1974) 680.
26. Glasstone, S. *Theoretical Chemistry*, van Nostrand, New York 1964, p. 396.
27. Fujiyama, T. and Kakimoto, M. *Bull. Chem. Soc. Jpn. 9* (1976) 2346.
28. Hiraishi, J. and Shinoda, T. *Bull. Chem. Soc. Jpn. 8* (1975) 2385.
29. Sheppard, N. *Adv. Spectrosc. 1* (1959) 288.
30. Almenningen, A., Arnesen, S. P., Seip, H. M. and Seip, R. *Chem. Phys. Lett. 1* (1968) 569.
31. Ryan, R. R. and Hedberg, K. *J. Chem. Phys. 50* (1969) 4986.
32. Hedberg, K. *Private communication* on NO_2/N_2O_4.
33. Gallaher, K. L. and Bauer, S. H. *J. Phys. Chem. 78* (1974) 2380.

Received August 26, 1977.

Acta Chemica Scandinavica A 32 (1978) 71 – 77

Conformation and Vibrational Spectra of 1,1,2-Trichloro-2,3,3-trifluorocyclobutane

DAVID L. POWELL* and P. KLÆBOE

Department of Chemistry, University of Oslo, Oslo 3, Norway

Infrared spectra in vapour, liquid, and crystalline states and Raman spectra in the liquid and crystalline states have been obtained for 1,1,2-trichloro-2,3,3-trifluorocyclobutane. Based on the disappearance upon crystallization of a total of 22 different bands, the results are interpreted in terms of two conformers being present in the vapour and liquid but only one in the crystal.

When the ring in a cyclobutane is non-planar, one substituent on each carbon atom can be described as axial and the second as equatorial in a way completely analogous to the notation used in cyclohexanes.[1] Earlier work has shown that the more stable configuration for a compound with a single halogen substituent on a cyclobutane ring is that in which the halogen assumes the equatorial position.[1]

Several years ago Rothschild claimed, on the evidence of the disappearance upon crystallization of one band each in the spectra of cyclobutyl chloride and cyclobutyl bromide, the presence of two conformers in each of these compounds.[2] Durig *et al.* in their further study of these compounds and various deuterated derivatives treated this interpretation with some skepticism but eventually concluded that their results supported this interpretation.[3,4] In the case of the bromo compound this is somewhat surprising since the results of a far infrared investigation indicated that that compound possessed only a single minimum in the puckering potential and hence only a single conformer.[5] Only the conformer with the chlorine equatorial was found in a microwave investigation of cyclobutyl chloride, but it must be noted that this study was carried out at −70 °C.[6]

In *trans*-1,3-bromochlorocyclobutane, in which both halogen substitutents cannot simultaneously assume the equatorial position, the electron diffraction data for the vapour have been interpreted in terms of a nearly 50:50 mixture of the two conformers.[7]

Several 1,1-difluorocyclobutanes have been studied by ^{19}F NMR[8,9] and in some cases the spectra have been interpreted in terms of an equilibrium between two conformers. In the only one of these compounds in which all substituents are monatomic and in which a definite conclusion was reached, 1,1-difluoro-2,2,3-trichlorocyclobutane, the ratio between the two conformers at room temperature was approximately 3:1.[8] In a separate study, the title compound among others was investigated, but no conclusions about conformation were reached.[10]

EXPERIMENTAL

The sample used was purchased from PCR, Inc. and purified by distillation before use. Its identity was confirmed by mass spectrometry.

Infrared spectra were recorded of the vapour, liquid, and solid on a Perkin-Elmer Model 225 Infrared Spectrophotometer. For the solid, spectra were taken both of the unannealed material and of the crystal after prolonged annealing. Even after careful annealing, approximately 5 % amorphous material remained.

Far infrared spectra of the pure liquid were recorded on a Bruker Model 114C Fourier transform spectrometer over the range 400 – 40 cm^{-1} using 6, 12, and 23 μm beamsplitters.

* On leave from the College of Wooster, Wooster, Ohio 44691 (USA) 1976 – 1977.

Raman spectra were run on a Cary Model 81 Raman spectrometer, modified for 90° illumination and equipped with a CRL model 52G argon ion laser, for the liquid and for the solid deposited on a cold copper block cooled with liquid nitrogen. Even the first spectrum taken immediately after deposition of the solid showed a weakening of those bands eventually shown to be due to the non-dominant conformer. Disappearance of the minor conformer, as shown by the complete disappearance of several bands, occurred spontaneously, and only very minor changes were then observed during several annealings. For the liquid, polarization measurements were made and proved useful as a means of resolving several bands. Even though without symmetry all bands are polarized, the bands of course may be polarized in varying degrees.

RESULTS

The experimental results obtained are shown in Table 1. Infrared spectra of the unannealed and annealed solid and Raman spectra of the liquid and crystalline solid are shown in Figs. 1–4.

In Table 1 it can be seen that, in general, bands marked as disappearing in the infrared spectrum of the crystal were still weakly present indicating that all material was not crystalline. In contrast, completely crystalline material was obtained in the Raman cryostat.

DISCUSSION

A cyclobutane of this sort can be expected to possess a non-planar cyclobutane ring.[11] For three of the carbon atoms in this compound, where the

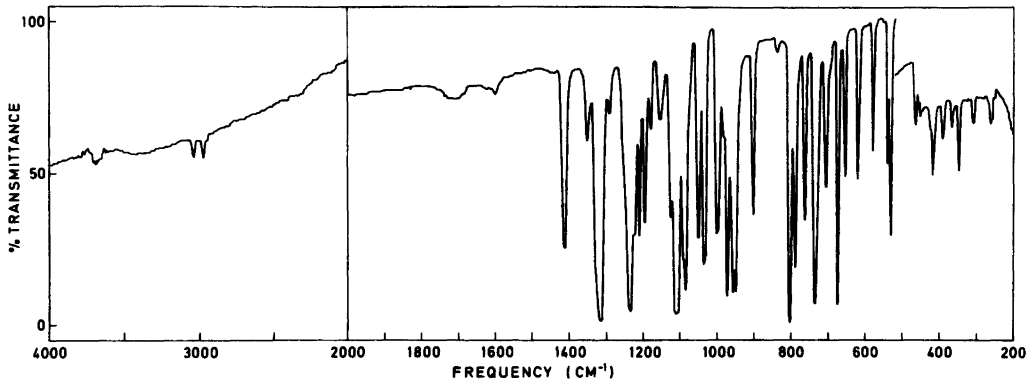

Fig. 1. The infrared spectrum of liquid 1,1,2-trichloro-2,3,3-trifluorocyclobutane (4000–200 cm^{-1}).

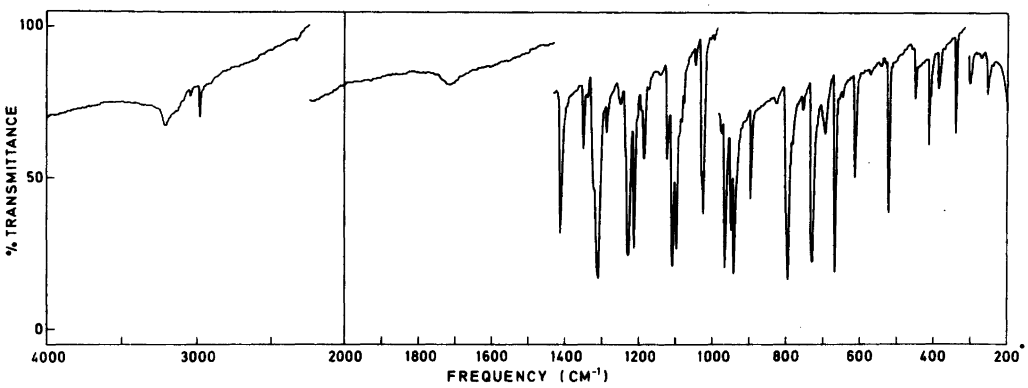

Fig. 2. The infrared spectrum of crystalline 1,1,2-trichloro-2,3,3-trifluorocyclobutane (4000–200 cm^{-1}) at −185 °C.

Table 1. Vibrational spectral data for 1,1,2-trichloro-2,3,3-trifluorocyclobutane.

Infrared[a]				Raman[a]			Interpretation	
Vapour	Liquid	Unannealed Solid	Crystal	Liquid	Unannealed Solid	Crystal	Conformer	Approx. motion
	3048 w[b]	3041 w	3036 w	3039 m	3037 m	3036 m	*a,e*[c]	CH_2 str
	2975 w	2974 m	2975 m	2975 s	2971 s	2970 s	*a,e*	CH_2 str
					1429 vw	*?[d]		
		~1420 vw	*?					
1424 w								
1421 m	1414 s	1410 m	1415 m	1413 w	1409 w	1414 w	*a,e*	CH_2 def
1417 w								
~1352 vw	1350 w	1350 w	1353 w					
		1343 vw	1343 vw					
		1327 w	1325 w					
1319 s	1314 vs	1314 s	1313 s	1315 vw	1316 w	1316 w	*e*	CF str
~1290 vw	1290 vw	1290 vw	1291 vw					
					1275 vw	1276 vvw		
			1255 w					
		1250 vw	*		1250 vw	*	*a*	CH_2 def
			1241 vw					
1248 m								
1242 s	1236 vs	1235 s	1232 s	1235 vw			*e*	CF str
					1225 vw	1224 vw		
		1222 m	1217 m					
1214 w								
1210 m	1208 s	1209 m	*	1210 vw		*	*a*	CF str
1205 w								
1197 vw			1199 vw					
	1193 m	1194 m	1191 mw	1194 vw	1192 vw	1189 vw	*e*	CH_2 def
	1178 w	1178 w	1178 w					
1169 mw								
		1153 w	*				*a*	CH_2 def
	1146 vw		1145 vw					
	1122 w	1125 m	1128 m	1122 w	1122 vw	1122 w		
1117 s	1111 vs	1112 s	1112 s	1112 w	1108 w	1109 w	*e*	CF str
	1104 m	1104 s	1102 s		1102 mw	1101 mw		
			1093 vw					
	1090 m	1092 w	1088 w					
1095 s	1084 vs	1084 s	1081 w (*)				*a*	CF str
1054 m	1047 s	1050 m	1052 w (*)	1050 vw	1050 vw	*	*a*	CF str
		1034 s	1035 w					
1036 ms	1031 m	1030 ms	1033 m	1030 vw	1032 vw	1030 vw	*e*	
1032 ms			1029 ms				*e*	
			1011 vvw					
1003 m	996 s	1000 m	*	1001 vw		*	*a*	
998 mw		995 mw	*	993 vw		*	*a*	
		980 vw	980 vw		380 vw	980 vw		
	968 s	970 s	970 s		970 mw	968 mw	*e*	CH_2 def
			963 vw	965 vw				
				955 w	958 w	*	*a*	CC str
960 s								
955 s	953 s	953 s	953 ms				*e*	
	947 w	947 s	946 s				*e*	
904 mw	900 m	901 m	900 m	903 w	901 w	900 w	*e*	
840 w	830 vw	840 w	832 vvw(*)				*a*	

Table 1. Continued.

806 ms 796 ms 790 ms	800 s	800 s	797 s	~800 vw	800 vw	804 vw	*e*	CCl str
	787 s	786 ms	786 vvw (*)	785 vw		*	*a*	CCl str
765 mw	760 s	760 ms	759 vw (*)	762 vw	764 vw	*	*a*	CCl str
738 m	734 s	732 s	732 s	734 w	733 w	732 mw	*e*	CCl str
713 w 709 m	703 vw	703 m	*				*a*	
	688 vw	~695 w	697 w					
672 mw	671 s	672 s	672 s	672 s	674 s	672 s	*e*	CCl str
	667 m	667 w	667 w					
653 w	653 m	652 m	650 vw (*)	654 s	654 mw	*	*a*	CCl str
619 w *e*	616 m	617 ms	616 m	615 w	617 mw	615 mw	*e*	
				610 vw				
					590 w	*	*a*	
577 mw	576 m	577 m	576 vw (*)	578 s	578 s	*	*a*	
		547 vw	547 vw			~550 vw?		
540 vw 536 mw	534 m	535 m	533 vw (*)	537 w		*	*a*	
531 mw 527 mw 520 vw	527 m	527 ms	524 ms	530 s	527 s	525 s	*e*	ring def
				~505 w	~500 vw	*	*a*	
458 w	457 m	461 mw	461 vvw(*)	460 s	463 s	*	*a*	
	452 m	452 w	453 w		454 mw	453 mw	*e*	
		~385 vw	~385 vw					
	364 w	363 w	*	366 m	365 w	*	*a*	
	343 m	344 m	345 m	347 m	346 m	346 m	*e*	
	327 vw			329 m	328 w	*	*a*	
	306 w	306 w	306 w	308 m	307 m	308 m	*e*	CF_2
		302 w	302 w					CCl_2
	278 vw	275 vw	277 vw	280 w	~280 vw	281 w	*e*	def
	268 w	~265 vw	*	268 vw	269 w	*	*a*	
	258 w	259 mw	259 mv	260 w	261 w	260 mw	*e*	
	235 vw			239 m		*	*a*	
	230 w			226 mw	225 mw	226 mw	*e*	
	205 vw	205 vw	204 vw	208 w	207 vw	207 w	*e*	
	180 vvw			180 w	185 vw	184 w	*e*	
	~167 vw			167 w	164 vw	164 w	*e*	
	160 w							
	149 vw			146 m				
					136 vw	136 vw		

[a] Weak bands in the regions above 3100 cm^{-1} and between 2800 and 1500 cm^{-1} have been omitted. [b] Abbreviations: s, strong; m, medium; w, weak; v, very; C, C type contour. [c] *a* refers to the conformer which disappears upon crystallization; *e* in most cases refers to the stable conformer or both conformers. Bands denoted, *e*, *a* or *e,a* are considered as fundamentals. [d] An asterisk signifies that the band vanishes in the spectrum of the crystalline solid.

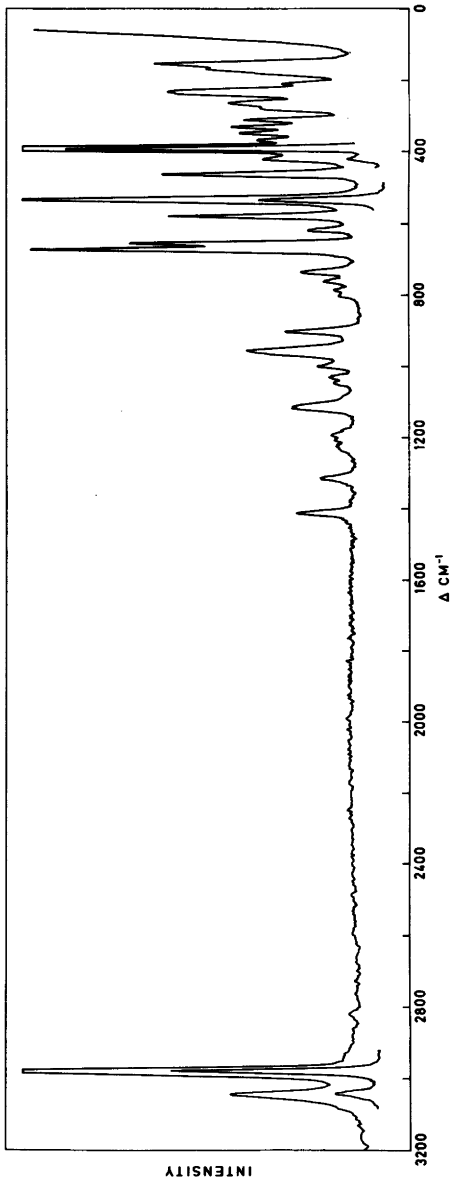

Fig. 3. The Raman spectrum of liquid 1,1,2-trichloro-2,3,3-trifluorocyclobutane.

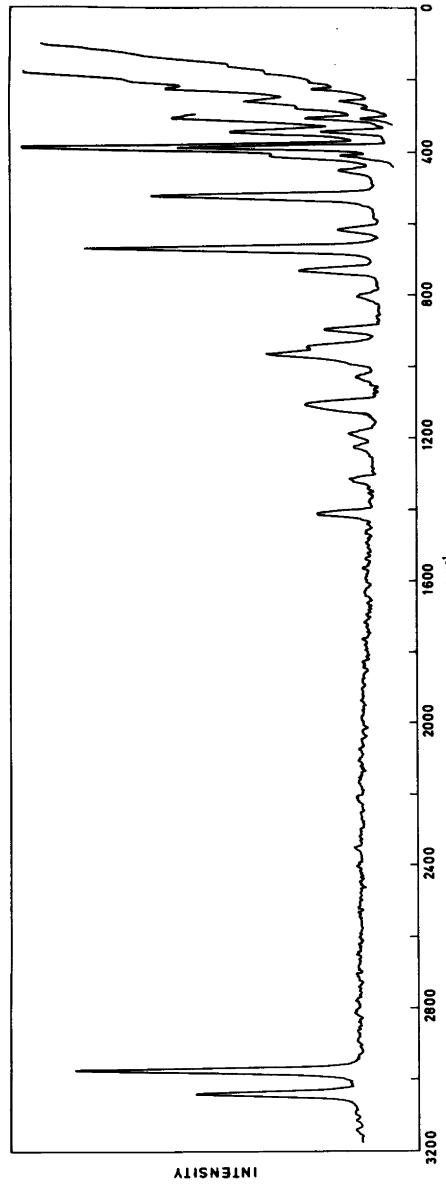

Fig. 4. The Raman spectrum of crystalline 1,1,2-trichloro-2,3,3-trifluorocyclobutane at −185 °C.

substituents are identical, this does not lead to different species. On the fourth, though, clearly the fluorine atom must be axial and the chlorine equatorial in one conformer – or *vice versa* in the other.

In 1,1,2-trichloro-2,3,3-trifluorocyclobutane there is in effect a competition between the chlorine and fluorine atoms for the favoured equatorial position. Since the effectiveness of each in minimizing the energy of the system in the equatorial position will be roughly the same, substantial amounts of each conformer should be present in the liquid.

Our conclusion is that this expectation is borne out by the experimental results. Upon crystallization four infrared bands, five Raman bands, and 13 bands common to both effects may definitely be classed as disappearing, or a total of 22 different bands. The spectra of the crystal which remains can well be interpreted in terms of a single conformer; those bands which disappear are quite reasonable for a second conformer. To our knowledge, this study is the first in which a cyclobutane, existing in more than one conformer in the vapour and liquid, is shown conclusively to exist in only one conformer in the crystalline solid.

In order to obtain some approximate idea of the relative abundance of the two conformers in the liquid phase, we can note that, very roughly, each disappearing band is about half as intense as some near-lying counterpart, or that the ratio of abundance must be somewhere near 1:2, with the conformer present in the crystal being the more stable.

For each conformer of this 12 atom compound a total of 30 normal modes is expected, all but three lying below 1400 cm^{-1}, and all potentially active in both the infrared and Raman. In the spectra of the crystalline solid, a total of about 30 bands which are strong in one or both effects is readily found. Those which we think are fundamentals in the dominant conformer appear in Table 1 labelled with an *e* (or with *a,e* if we think they are common to both), and those we think are fundamentals in the other conformer are labelled with an *a*. Because no possible conformer in this compound, even the unlikely one with the ring planar, possesses any symmetry at all, the normal modes should be highly mixed and the atomic motions suggested in Table 1 should be considered highly approximate.

A few general observations can be made, though. As in 1,1,2,2-tetrafluorocyclobutane[12] and 1-chloro-2,2,3,3-tetrafluorocyclobutane,[13] introduction of fluorine atoms leads to higher than normal CH_2 stretching frequencies. As is usual, modes with a high degree of CF stretching character give strong infrared and very weak or invisible Raman bands, *e.g.* those bands at 1319, 1246, and 1117 cm^{-1} of the dominant conformer and 1210, 1095, and 1054 cm^{-1} of the disappearing conformer.

Often, but not always, the symmetric stretching of a ring gives rise to a strong Raman band, near 1000 cm^{-1} in the case of cyclobutane rings. Such a band is not obvious here; perhaps the many electronegative atoms tend to withdraw electrons from the ring and so weaken the band. In C_4Cl_8, for example, a band which was not especially strong was assigned to this motion.[14]

Several bands of appreciable intensity in both infrared and Raman can be noted which are probably associated with C–Cl stretching. In the dominant conformer these bands occur at 796, 738, and 672 cm^{-1} and in the other conformer at 787, 765, and 653 cm^{-1}.

We located no band which we could ascribe to the ring puckering mode.

However, the most interesting question is which form is which. Placing the compound in solvents of varying polarity would not give useful information as both conformers should have nearly the same dipole moment.

Correlations have been suggested between conformation and carbon-halogen stretching frequency[15] except for fluorine where the conclusion was that such correlation does not exist.[16] The situation would be complicated here, in utilizing the C–Cl frequencies, by the three chlorine atoms in the molecule. Thus each conformer should give rise to 3 C–Cl stretching frequencies, in the one case two axial and one equatorial and in the other one axial and two equatorial. Further complications, even if modes richest in C–Cl stretching character could be unequivocally identified, result from the question of whether such correlations can be extended to the case of a cyclobutane and from their known shortcomings in the case of compounds containing several chlorine atoms, *e.g.* 1,2,3-trichloropropane.[17,18]

Lacking at the present time any experimental evidence one way or the other, we are still willing to hazard the guess that the more stable form is that in which the more bulky atom, in this case the chlorine, occupies the equatorial position (*cf.* for example Ref. 8 and references cited therein). Thus we feel those bands marked with *e* in Table 1 belong

to the conformer with two chlorine atoms in equatorial positions.

The implications of this work on the simpler cyclobutyl chloride and cyclobutyl bromide must also be explored. The comments of Durig *et al.* with reference to the two conformer interpretation are reminiscent of the principle that when all which is impossible has been eliminated, then whatever remains, however unlikely, must be the truth.[19]

If a total of 22 bands disappear in our compound, then obviously some of these must be associated with modes other than carbon-halogen stretching frequencies. In the related monohalocyclohexanes, at least 10 bands per compound show substantial conformation dependence.[20] It then seems extremely unlikely than only the C−Cl or C−Br stretches should be conformation-sensitive in the cyclobutyl halides. At the very least, the two C−X bending frequencies and probably also some of the ring modes should depend upon conformation. Thus, somewhat paradoxically, in showing what we think is a clear case of conformations in a cyclobutane, we feel that we have cast doubt on an earlier report of the same effect.

Acknowledgement. We wish to thank Jorunn Gustavsen who recorded some of the spectra and K. Ruzicka who purified the compound. Financial support from the Norwegian Research Council for Science and the Humanities was received.

REFERENCES

1. Eliel, E. L., Allinger, N. L., Angyal, S. J. and Morrison, G. A. *Conformational Analysis*, Inscience, New York 1966.
2. Rotschild, W. G. *J. Chem. Phys. 45* (1967) 1214, 3599.
3. Durig, J. R. and Morrissey, A. C. *J. Chem. Phys. 46* (1967) 4854.
4. Durig, J. R. and Green, W. H. *J. Chem. Phys. 47* (1967) 673.
5. Blackwell, C. S., Carreira, L. A., Durig, J. R., Karriker, J. M. and Lord, R. C. *J. Chem. Phys. 56* (1972) 1706.
6. Kim, H. and Gwinn, W. D. *J. Chem. Phys. 44* (1966) 865.
7. Almenningen, A., Bastiansen, O. and Walløe, L. In Andersen, P., Bastiansen, O. and Furberg, S., Eds., *Selected Topics in Structure Chemistry*, Universitetsforlaget, Oslo 1967, pp. 91−104.
8. Lambert, J. D. and Roberts, J. D. *J. Am. Chem. Soc. 87* (1965) 3884.
9. Hopkins, R. C. *J. Mol. Spectrosc. 27* (1968) 499.
10. Ernst, R. R. *Mol. Phys. 16* (1969) 241.
11. Cotton, F. A. and Frenz, B. A. *Tetrahedron 30* (1974) 1587.
12. Durig, J. R. and Harris, W. C. *Spectrochim. Acta A 27* (1971) 649.
13. Harris, W. C. and Yang, D. B. *J. Mol. Struct. 18* (1973) 257.
14. Miller, F. A. and Capwell, R. J. *Spectrochim. Acta A 27* (1971) 1113.
15. Altona, C. *Tetrahedron. Lett. 19* (1968) 2325.
16. Crowder, G. A. and Mao, H. K. *J. Mol. Struct. 16* (1973) 165.
17. Thorbjørnsrud, J., Ellestad, O. H., Klæboe, P. and Torgrimsen, T. *J. Mol. Struct. 17* (1973) 5.
18. Chenery, D. H., Dempster, A. B., Price, K. and Sheppard, N. *J. Mol. Struct. 26* (1975) 189.
19. Holmes, S. as quoted by Watson, J. H. In Doyle, A.C., Ed., *The Bruce-Partington Plans, The Strand Magazine*, London 1907.
20. Klæboe, P. *Acta Chem. Scand. 23* (1969) 2641.

Received August 26, 1977.

Acta Chemica Scandinavica A 32 (1978) 79–83

Stability Constants of Copper(II), Zinc, Manganese(II), Calcium, and Magnesium Complexes of *N*-(Phosphonomethyl)glycine (Glyphosate)

H. E. LUNDAGER MADSEN, H. H. CHRISTENSEN and C. GOTTLIEB-PETERSEN

Chemistry Department, Royal Veterinary and Agricultural University, Thorvaldsensvej 40, DK-1871 Copenhagen V, Denmark

The stability constants of several 1:1 metal complexes of *N*-(phosphonomethyl)glycine (glyphosate) at $I=0.1$ (KNO_3) and 25 °C have been determined by potentiometric pH titration. The following values for log K_{ML} were found: Cu(II) 11.92, Zn 8.4, Mn(II) 5.53, Ca 3.25, and Mg 3.25. The pK values of glyphosate are: $pK_1=2.27\pm0.02$, $pK_2=5.57\pm0.004$, and $pK_3=10.25\pm0.02$; these are mixed constants, valid for $I=0.1$ (KNO_3).

A large number of important chelating agents belong to the group of aminopolyacids; two of the best known are nitrilotriacetic acid and ethylenediaminetetraacetic acid, and others contain methylphosphonic instead of one or more of the acetic acid groups. Numerous determinations of stability constants of metal complexes with these ligands have been carried out;[1] one interesting exception, for which no data are available, is *N*-(phosphonomethyl)glycine (trivial name: glyphosate), $^-HO_3PCH_2NH_2^+CH_2COOH$, marketed since 1971 as a herbicide.[2] A study of the chelating properties of this substance is justified not only by its chemical interest, but also because this information is essential for understanding the behaviour of the herbicide in soil and plants.

In order to ensure consistent results, we have determined the dissociation constants of glyphosate at $I=0.1$ (KNO_3), the medium used for the determinations of stability constants of the metal complexes.

EXPERIMENTAL

Apparatus. pH was measured at 25 °C with a Radiometer digital pH meter model 64 using a combined glass/calomel electrode type C.

Materials. All solutions were prepared with boiled demineralized water. Standard buffers for calibration were prepared from analytical grade chemicals. Potassium hydroxide, 0.05 M, was prepared from May and Baker concentrated volumetric solution. Metal nitrate stock solutions, 0.1 M, were standardized by complexometric titration with EDTA, using standard methods.[5]

Glyphosate was prepared from the commercial product Roundup® by ion-exchange chromatography on Dowex 1. Formic acid, 2 M, was used for elution, and the crude product was recrystallized three times from water/ethanol.

All solutions, except standard buffers, were adjusted to an ionic strength of 0.1 with KNO_3.

pH calibrations. Three standard buffers were used for calibrations: phthalate (pH = 4.008), phosphate (pH = 7.413), and borax (pH = 9.180). Calibration was rechecked after each run of a titration curve; no deviation ever exceeded 0.005 pH units.

In order to be able to calculate $[H^+]$ and $[OH^-]$ from pH readings, we measured pH in a series of HNO_3 solutions from 1 mM to 10 mM and in a series of KOH solutions from 0.25 mM to 1.25 mM. We found $pH+\log[H^+]=0.067\pm0.005$ and $pH-\log[OH^-]=13.76\pm0.06$.

Recording a titration curve. The initial volume of the titrand solution was 30.0 cm^3, and it was 2.67 mM with respect to glyphosate. Metal concentration was equal to ligand concentration. A total of 5 cm^3 0.05 M KOH was added, and about 50 points of the titration curve were recorded. Stirring was stopped at each reading, to avoid a streaming potential at the reference electrode.

CALCULATIONS

Titration curves without metal. The degree of neutralization, n, is given by

$$n = \frac{B - A + [H^+] - [OH^-]}{C_L} \quad (1)$$

where C_L is the total molar concentration of glyphosate, A is the excess of strong acid added prior to titration ($A=0$ in the actual case), and B is the amount of strong base added, in equiv./dm^3. $[H^+]$ and $[OH^-]$ were calculated from measured pH values and the results of measurements on dilute nitric acid and potassium hydroxide.

Preliminary measurements showed that, although glyphosate should be able to take up a proton to form a positive ion, the corresponding pK value is negative. Hence we disregard this possibility in the sequel.

As the pK values are widely spaced, they can be calculated simply as

$$pK_1 = pH + \log\frac{1-n}{n} \qquad 0<n<1 \quad (2)$$

$$pK_2 = pH + \log\frac{2-n}{n-1} \qquad 1<n<2 \quad (3)$$

$$pK_3 = pH + \log\frac{3-n}{n-2} \qquad 2<n<3 \quad (4)$$

These values are so-called mixed constants (hydrogen ion activity, but concentration of acid and base).

Titration curves with metal. The method of Chaberek and Martell[6] had to be modified to take into account the acid-base properties of the complex. The calculations were carried out as follows:

The total concentrations of metal (M) and of ligand (L) are given by

$$C_M = [M^{2+}] + [ML^-] + [MLH] + [MLOH^{2-}] \quad (5)$$

$$C_L = [L^{3-}] + [HL^{2-}] + [H_2L^-] + [H_3L] + [ML^-] + [MLH] + [MLOH^{2-}] \quad (6)$$

where $MLOH^{2-}$ denotes a complex ion, where a proton has been removed from one of the coordinated water molecules. As in all experiments $C_M = C_L$, we have from (5) and (6)

$$[L^{3-}] + [HL^{2-}] + [H_2L^-] + [H_3L] = [M^{2+}]$$
$$[L^{3-}]\alpha_{L(H)} = [M^{2+}] \quad (7)$$

with the side-reaction coefficient $\alpha_{L(H)}$ given by

$$\alpha_{L(H)} = 1 + a(H^+)/K_3 + a(H^+)^2/K_2K_3 + a(H^+)^3/K_1K_2K_3 \quad (8)$$

where $a(H^+)$ is defined as 10^{-pH}. A further equation is the proton-balance equation, which yields

$$B + [H^+] - [OH^-] = [H_2L^-] + 2[HL^{2-}] + 3[L^{3-}] + 3[ML^-] + 2[MLH] + 4[MLOH^{2-}] \quad (9)$$

If we multiply (6) by 3 and subtract (9), we find

$$[L^{3-}] = \frac{3C_L - B - [H^+] + [OH^-] - [MLH] + [MLOH^{2-}]}{a(H^+)\alpha'_{L(H)}} \quad (10)$$

where

$$\alpha'_{L(H)} = 1/K_3 + 2a(H^+)/K_2K_3 + 3a(H^+)^2/K_1K_2K_3 \quad (11)$$

$[L^{3-}]$ may be calculated directly from (10) when $[MLH] - [MLOH^{2-}]$ is negligible; otherwise, we have

$$\frac{[ML^-]}{[M^{2+}][L^{3-}]} = K_{ML} \quad (12)$$

$$\frac{[MLH]}{a(H^+)[ML^-]} = K_{H(ML)} \quad (13)$$

$$\frac{[MLOH^{2-}]}{a(OH^-)[ML^-]} = K_{OH(ML)} \quad (14)$$

which yields, using (7)

$$[MLH] - [MLOH^{2-}] = K_{ML}\alpha_{L(H)}\alpha'_{ML(H)}a(H^+)[L^{3-}]^2 \quad (15)$$

where

$$\alpha'_{ML(H)} = K_{H(ML)} - K_{OH(ML)}Kw/a(H^+)^2 \quad (16)$$

$[Kw = a(H^+)a(OH^-)]$.

When (15) is inserted in (10), the following quadratic equation for $[L^{3-}]$ results:

$$K_{ML}\alpha_{L(H)}\alpha'_{ML(H)}a(H^+)[L^{3-}]^2+a(H^+)\alpha'_{L(H)}[L^{3-}] -3C_L+B+[H^+]-[OH^-]=0 \quad (17)$$

As the coefficient of $[L^{3-}]^2$ is given in terms of the unknown stability constants, the solution must be found by iteration.

When $[L^{3-}]$ has been found, $[M^{2+}]$ is calculated from (7) and $[ML^-]$ from

$$[ML^-]=(C_M-[M^{2+}])/\alpha_{ML(H)} \quad (18)$$

where

$$\alpha_{ML(H)}=1+K_{H(ML)}a(H^+)+K_{OH(ML)}a(OH^-) \quad (19)$$

is the side-reaction coefficient of the complex.

Finally, K_{ML} is calculated, and its logarithm plotted against pH. Different values of $K_{H(ML)}$ and $K_{OH(ML)}$ are tried, in order to find those giving the least possible variation of log K_{ML} with pH.

In the pH interval where nearly all the ligand is bound in complex, it is sometimes possible to calculate $K_{H(ML)}$ and $K_{OH(ML)}$ in the same manner as for the free ligand [eqns. (1–4)]. In this case, we may obtain $[L^{3-}]$, and hence K_{ML}, directly.

RESULTS

Five titration curves were recorded for the free ligand and two for each of the metal complexes (three for Mg). The shapes of the curves are shown in Fig. 1, the calculated dissociation constants are given in Table 1, and the stability constants of metal complexes are given in Table 2.

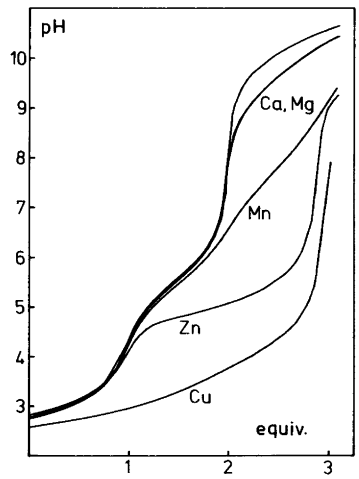

Fig. 1. Titration curves of glyphosate (upper curve) and of five solutions with metal. The abscissa is the number of equivalents of KOH added per mol of glyphosate.

Table 1. Dissociation constants of glyphosate at $I=0.1$ (KNO_3) and 25 °C.

Expt. No.	pK_1	pK_2	pK_3
1	2.22	5.56	–
2	2.26	5.58	10.29
3	2.27	5.58	10.28
4	2.29	5.58	10.21
5	2.31	5.58	10.22
Mean	2.27(2)	5.576(4)	10.25(2)

The numbers in parentheses give the standard deviation on the last digit shown.

DISCUSSION

The results for the three dissociation constants of glyphosate agree qualitatively with previously reported values.[3,4] In order to test the quantitative agreement with Wauchope's results,[4] we may calculate the thermodynamic dissociation constants with the aid of the Debye-Hückel equation for activity coefficients:

$$\log \gamma_i = -\frac{Az_i^2\sqrt{I}}{1+Ba\sqrt{I}} \quad (20)$$

Wauchope takes $a=5.5$ Å for H_2L^-, 6.0 Å for HL^{2-}, and 6.5 Å for L^{3-}. With these values, we have for the thermodynamic constants:

	I	pK_1	pK_2	pK_3
Wauchope[4]	~0.05	2.32	5.86	10.86
Present study	0.1	2.37	5.872	10.72

The agreement is satisfactory in view of the experimental uncertainty in glass electrode measurements at low and high pH values and the limitations of the Debye-Hückel law.

The values of the stability constants of the metal complexes place the metals in the order to be expected from a knowledge of the stabilities of complexes with related ligands.[1] It is particularly interesting to compare the chelating power of glyphosate with that of iminodiacetic (IDA) acid

Table 2. Stability constants K_{ML}, $K_{H(ML)}$, and $K_{OH(ML)}$ of the metal complexes of glyphosate at $I=0.1$ (KNO_3) and 25 °C.

Metal	Expt. No.	log K_{ML}	log $K_{H(ML)}$	log $K_{OH(ML)}$
Cu	1	11.93	4.05	–
	2	11.91	4.05	–
	Mean	11.92	4.05	–
Cu	1	11.71	4.33	–
(2nd method)	2	11.71	4.36	–
	Mean	11.71	4.35	–
Zn	1	8.4	–	–
	2	8.4	–	–
	Mean	8.4	–	–
Mn	1	5.55	6.93	4.37
	2	5.52	6.91	4.23
	Mean	5.53	6.92	4.30
Ca	1	3.25	–	2.7
	2	3.25	–	2.9
	Mean	3.25	–	2.8
Mg	1	3.25	–	2.7
	2	3.24	–	2.9
	3	3.25	–	2.9
	Mean	3.25	–	2.8

Table 3. Stability constants (log K_{ML}) of metal complexes of iminodiacetic acid and glyphosate at $I=0.1$ (KNO_3) and 25 °C.

	Cu	Zn	Mn	Ca	Mg
IDA	10.55[6]	7.0[6]	–	2.59[a]	2.94[a]
Glyphosate	11.92	8.4	5.53	3.25	3.25

[a] 20 °C.[1]

(Table 3). We see that the substitution of a phosphonic for a carboxylic group increases the chelating power. This effect does not, however, appear to represent a general trend for the aminopolyacids.[7]

Glyphosate is probably a tridentate ligand. At present, no precise statements can be made with respect to the detailed structure of the complexes or to the interpretation of the values of $K_{H(ML)}$ and $K_{OH(ML)}$.

The pH interval useful for calculation of stability constants from pH titration curves is the one in which the concentrations of free and complexed metal are comparable. This interval should not include any of the pK values of the ligand, because of the strong buffering action of the ligand around this value, nor should it lie above the highest pK value of the ligand, as in this region pH will hardly be affected by complexing.

Fig. 2 shows the variation of the fraction of metal complexed as a function of pH. We see that the conditions for a precise determination of stability

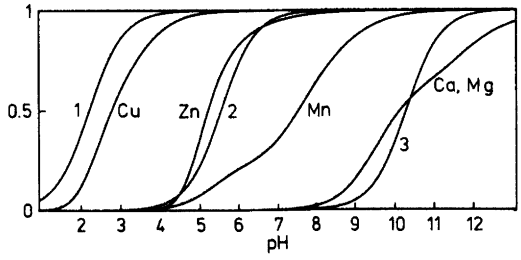

Fig. 2. Fractions of metal complexed as functions of pH at $C_M=C_L=0.0025$ M and $I=0.1$ (KNO_3). The curves marked 1, 2, and 3 represent the base fractions at the three dissociation steps of glyphosate.

constants are fulfilled for Cu and Mn, but not for Zn, Ca, and Mg. Indeed, this was what we experienced when performing the calculations. Hence, the situation calls for a check of the results by other methods, even for Cu due to the discrepancy between results of the two methods of calculation. Experiments with ion-selective electrodes, polarography, and gel chromatography are in progress at our laboratory.

REFERENCES

1. Sillén, L. G. and Martell, A. E. Stability Constants, *Chem. Soc. Spec. Publ. Nos. 17* (1964) and *25* (1971).
2. Franz, J. E. (to Monsanto Co.) *Ger. Patent* 2152826 (1972).
3. Sprankle, P., Meggitt, W. F. and Penner, D. *Weed Sci. 23* (1975) 229.
4. Wauchope, D. *J. Agric. Food Chem. 24* (1976) 717.
5. Schwarzenbach, G. *Die komplexometrische Titration*, Enke, Stuttgart 1956.
6. Chaberek, S. and Martell, A. E. *J. Am. Chem. Soc. 74* (1952) 6228.
7. Ockerbloom, N. and Martell, A. E. *J. Am. Chem. Soc. 80* (1958) 2351.

Received August 22, 1977.

Acta Chemica Scandinavica A 32 (1978) 85 – 93

Short Communications

On the Extraction with Long-chain Amines. XXVIII. The System TLA – $CHCl_3$ – HCl and Aqueous 1.00 M LiCl at 25 °C

STEFAN POTURAJ * and ERIK HÖGFELDT

Department of Inorganic Chemistry, The Royal Institute of Technology,
S-100 44 Stockholm 70, Sweden

In all solvents studied so far by the Stockholm group, the salts of trilaurylamine (=TLA) have been found to be associated.[1] In the hope of finding a nonaggregating system, it was decided to use chloroform as solvent. The experiments were performed as emf titrations[2] at 25.0±0.05 °C, and chloroform and LiCl were purified as described elsewhere.[3,4] The amine concentrations used were: 7.9, 17.0, 17.6, 72.9 and 147.3 mM.

In Fig. 1 Z is plotted against lg h, where Z is defined by

$$Z=[HCl]_{org}/[TLA]_{tot,org}=H/B \quad (1)$$

and $h=[H^+]_{aq}$, the hydrogen ion concentration as measured by a glass electrode calibrated in terms of hydrogen ion concentration.[2] Since $[Cl^-]_{aq}=1.00$ the product $h[Cl^-]$ is equal to h [*cf.* reaction (2)].

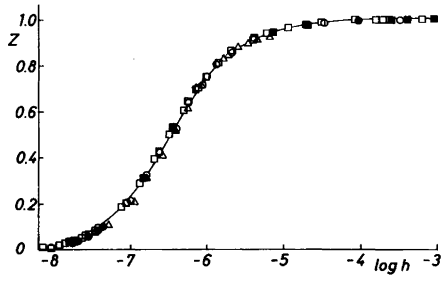

Fig. 1. Z plotted against lg h for: ○, 7.9 mM TLA; ●, 17.0 mM TLA; □, 17.6 mM TLA; ■, 72.9 mM TLA; △,147.3 mM TLA. The curve has been computed from the eqn $Z=10^{6.48}h(1+10^{6.48}h)^{-1}$.

In Fig. 1 practically all data fall on a single curve, with the exception of the highest amine concentration. However, the shift is in the wrong direction for association to occur and this must be due to some systematic error in the titration. It can thus be concluded that the association is practically negligible in chloroform. By using the well-known method of normalized curves[5] the equilibrium constant of the reaction

$$TLA(org)+H^+(aq)+Cl^-(aq)\rightleftharpoons TLAHCl(org) \quad (2)$$

was found to be

$$\lg k_{1,1}=6.48$$

Using the least-squares minimizing program LETAGROP[6] the following value was obtained

$$\lg k_{1,1}=6.475\pm0.014$$

When taking systematic errors into account (a possible reason for the shift of the curve $Z(\lg h)$ for the highest amine concentration) the following value was obtained

$$\lg k_{1,1}=6.510\pm0.015$$

Since we did not further investigate possible systematic errors we prefer to give

$$\lg k_{1,1}=6.48\pm0.03 \quad (3)$$

Table 1. VPO-data for TLA and TLAHCl at 25 °C. Concentrations in M (mol l^{-1}).

TLA		TLAHCl		
B (M)	$\Delta R/B$ (ohm M^{-1})	B (M)	ΔR (ohm)	$\bar{n}$
0.0174	367	0.0135	5.02	0.998
0.0281	373	0.0242	8.93	1.005
0.0616	369	0.0465	17.11	1.008
0.0800	368	0.0717	26.89	0.989
0.1084	374	0.0990	36.33	1.010
0.1527	377	0.1500	59.10	0.942
Average: 371±4			Average: 0.992±0.026	

* Present address: AB Atomenergi, S-611 01 Nyköping, Sweden.

When comparing experimental and calculated Z-values all data with the exception of 3–4 experimental points fall within ± 0.02 in Z, which can be regarded as an acceptable fit. Anyone interested in the primary experimental data and the comparison of the calculated and experimental Z-values can write to Erik Högfeldt.

That TLAHCl is monomeric in chloroform receives further independent support from some vapor phase osmometry (VPO) data. The first two columns in Table 1 give the stoichiometric concentration (B) in mol l^{-1} of TLA in chloroform at 25 °C together with $\Delta R/B$. ΔR is the measured unbalance of the resistance bridge in the Mechrolab Vapor Phase Osmometer (model 301 A) used. Using the calibration constant obtained from these data the true concentration of TLAHCl (B') can be computed from the measured ΔR in solutions of TLAHCl in chloroform. That TLA is a suitable calibration substance is due to the fact that it is monomeric in organic solvents.[7] The average degree of association ($\bar{n}$) is now computed from B/B'. As seen from the last column in Table 1 all data cluster around $\bar{n}=1$, the average being 0.992 ± 0.026 and no association was found for TLAHCl in chloroform.

Acknowledgement. The work presented in this paper is part of a program financially supported by the Swedish Natural Science Research Council (NFR).

1. Högfeldt, E. In Kertes, A. S. and Marcus, Y., Eds., *Solvent Extraction Research*, Wiley-Interscience, New York 1969, p. 157.
2. Högfeldt, E. and Fredlund, F. *Trans. R. Inst. Technol. Stockholm* (1964) No. 226.
3. Warnqvist, B. *Acta Chem. Scand. 21* (1967) 1353.
4. Muhammed, M., Szabon, J. and Högfeldt, E. *Chem. Scr. 6* (1974) 61.
5. Rossotti, F. J. C. and Rossotti, H. *The Determination of Stability Constants*, McGraw, New York 1961, Chapter 5.
6. Ingri, N. and Sillén, L. G. *Ark. Kemi 23* (1965) 97.
7. Duyckaerts, G., Fuger, J. and Müller, W. EUR 426f, Liège 1963.

Received October 10, 1977.

Hydrogen Bonds of γ-FeOOH

HENRIK CHRISTENSEN and
A. NØRLUND CHRISTENSEN

Department of Inorganic Chemistry,
Aarhus University, DK-8000 Aarhus C, Denmark

The crystal structure of Lepidocrocite, γ-FeOOH, was determined by Ewing[1] using X-ray diffraction methods. The compound has a layer crystal structure where close-packed FeO_6-octahedra are held together by 2.70 Å hydrogen bonds. Olés, Szytula and Wanic[2] reinvestigated the structure using neutron diffraction powder methods and found that the hydrogen atom was centered in the hydrogen bond, and that the diffraction pattern had a magnetic contribution of the (020) reflection at 4.2 K.

In the previously accepted space group for the structure of γ-FeOOH,[1,2] *Cmcm* (No. 63) a centered O−H−O bond has the hydrogen atom in site 4*a*. Another possibility for the position of the hydrogen atom would be in site 8*f* with ½H in this site. The hydrogen bond is rather long for a centered hydrogen bond (the hydrogen atom placed in the centre of the O−H−O bond), and a more likely structure would be the above suggested statistical arrangement with ½H atom in site 8*f* of space group *Cmcm*, or a structure described in the non-centrosymmetric space group $Cmc2_1$ (No. 36). This paper describes a reinvestigation of the crystal structure of γ-FeOOH using neutron powder diffraction methods. Two samples of γ-FeOOH were investigated, a mineral from Glendon, Pa., U.S.A., supplied by Petersen[3] and a synthetic sample supplied by Janes.[4] The powder patterns were measured at Risø using neutrons with wave length $\lambda = 0.998$ Å.

γ-FeOOH (mineral). The diagram was measured in the 2θ interval 5.0−56.0° in steps of 0.2°. The diagram showed that the specimen contained α-FeOOH (goethite) as a major impurity. Some of the reflections of γ-FeOOH overlapped with reflections of α-FeOOH and the diagram could thus not be used in a profile refinement procedure.[5,6]

γ-FeOOH (synthetic). Data I. The diagram was measured at 300 K in the 2θ interval 2.0−91.0° in steps of 0.2°. The diagram had 16 resolved peaks with contributions from 108 reflections (see Fig. 1).

Table 1. Results of the refinement of the structure of γ-FeOOH in space group $Cmc2_1$. $a = 3.08(1)$ Å, $b = 12.50(1)$ Å, $c = 3.87(1)$ Å.

Atom	*x*	*y*	*z*	*B*(Å²)
Data I, 108 reflections. $R = 13.24\ \%$ [c]				
Fe	0	−0.323(1)	0.25	0.8(2)
O1	0	0.295(1)	0.266(19)	0.7(4)
O2	0	0.072(1)	0.250[a]	0.6(3)
H	0.5	0.525(3)	0.452(12)	0.8(6)
Data II. 54 reflections. $R = 8.51\ \%$				[b]
Fe	0	−0.322(1)	0.25	0.2(1)
O1	0	0.294(1)	0.264(11)	0.2(1)
O2	0	0.074(1)	0.282(9)	0.2(1)
H	0.5	0.523(2)	0.458(11)	0.2(1)

[a] Coordinate due to oscillation in refinement.
[b] Overall temperature factor. [c] *R* (profile) for definition, see Ref. 6.

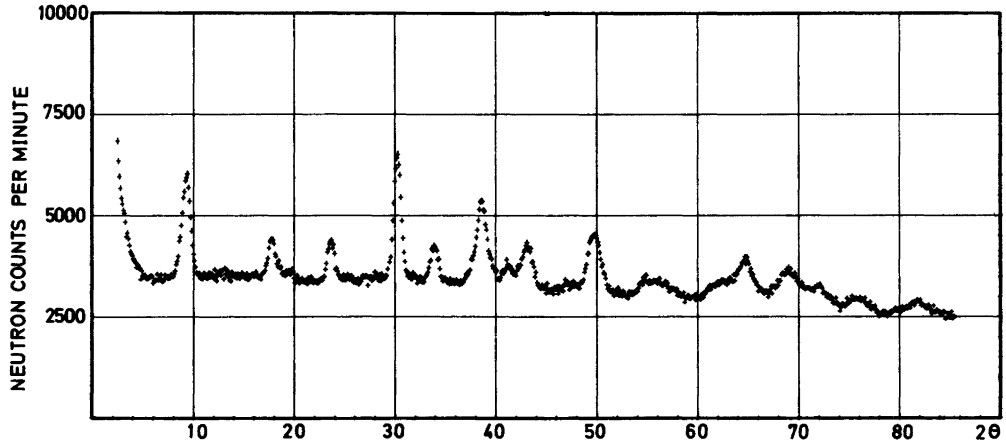

Fig. 1. Neutron diffraction powder patterns of γ-FeOOH, Data I. $\lambda = 0.998$ Å of incident neutrons.

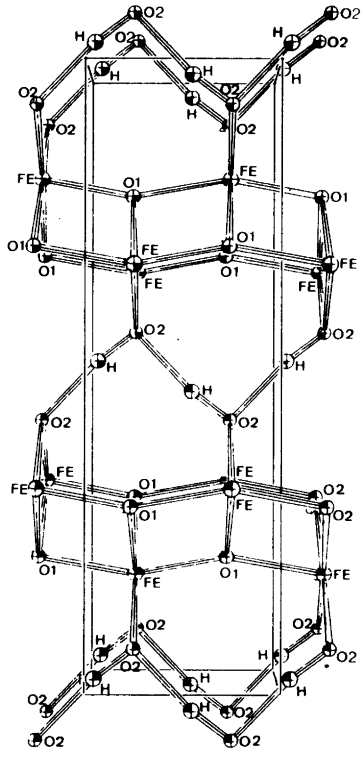

Fig. 2. Projection of the structure of γ-FeOOH along the 100-direction.

γ-FeOOH (synthetic). Data II. The diagram was measured at 7.5 K in the 2θ interval 7.5–62.0° in steps of 0.1°. The diagram had 12 resolved peaks with contributions from 54 reflections. None of the observed peaks in this diagram had scattering contributions from magnetic reflections.

The structure of γ-FeOOH was refined in the space groups *Cmcm* and $Cmc2_1$, using the Rietveld refinement programme for powder intensities.[5,6] The scattering lengths used were (in 10^{-12} cm): $b_{Fe}=0.951$, $b_O=0.580$, and $b_H=-0.374$.[7] The best agreement between observed and calculated intensities was obtained when the structure was refined in space group $Cmc2_1$ (see Table 1). In the space group *Cmcm* the agreement factor R was 16.15 % (Data I), when the hydrogen atom was placed in site 4*a* and the Debye-Waller factor for the hydrogen atom was 4.41 Å^2. With half-hydrogen atoms placed in site 8*f* the agreement factor was $R=13.71$ % and the Debye-Waller factor became negative (−2.19 Å^2). It is thus only the space group $Cmc2_1$ that gives a physically meaningful model for the structure of γ-FeOOH.

For Data II an R-value of 8.51 % was obtained. In order to restrict the number of parameters, an overall isotropic temperature factor parameter was used in this refinement. Fig. 2 is a projection of the structure along the 100 direction. It shows the hydrogen bonds placed between the oxygen atoms named O2. This oxygen atom is tetrahedrally coordinated with two Fe atoms and one H atom and has thus a vacant sp^3 hybride orbital for hydrogen bonds. The hydrogen bond is non-centered and the distances in it are O–H···O: 2.68(2) Å, O–H: 0.93(2) Å, and H···O: 1.75(2) Å, in acceptable agreement with hydrogen bond distances found for other oxide hydroxides.[8] The present investigation gave no indication of a magnetic structure of γ-FeOOH a 7.5 K.

Acknowledgements. We are indebted to Dr. O. V. Petersen and Dr. D. L. Janes for the specimens of γ-FeOOH. Mrs. B. Lebech, Department of Physics, Risø, is acknowledged for assistance in measuring the neutron diffraction powder patterns.

1. Ewing, E. J. *J. Chem. Phys. 3* (1935) 420.
2. Olés, A., Szytula, A. and Wanic, A. *Phys. Status. Solidi 41* (1970) 173.
3. Petersen, O. V. Mineralgisk Museum, Østre Voldgade 5–7, DK-1350 København K., Lepidocrocite, M. M., No. 1970.11 from Glendon, South Easton, Pennsylvania, U.S.A.
4. Janes, D. L. Minnesota Mining and Manufacturing Company, Saint Paul, Minnesota 55101, U.S.A.
5. Rietveld, H. M. *Program F418-Fortran IV Version*, Reactor Centrum Nederland, Petten (N.H.), The Netherlands.
6. Rietveld, H. M. *J. Appl. Crystallogr. 2* (1969) 65.
7. Bacon, G. E. *Acta Crystallogr. A 28* (1972) 357.
8. Hamilton, W. C. and Ibers, J. A. *Hydrogen Bonding in Solids*, W. A. Benjamin, New York 1968.

Received September 26, 1977.

The Temperature Factor Parameters of Some Transition Metal Carbides and Nitrides by Single Crystal X-Ray and Neutron Diffraction

A. NØRLUND CHRISTENSEN

Department of Inorganic Chemistry, Aarhus University, DK-8000 Aarhus C, Denmark

The transition metal carbides and nitrides have been the subject of intensive investigations because of their unusual combination of physical properties. They have metallic conductivity, high melting points, great hardness and brittleness, and some of them show superconductivity. The hardness may be correlated with the temperature factor parameters of the atoms in the crystal lattice. As single crystals of some of these hard materials became available, it was decided to compare the temperature factor parameter of the atoms in these hard materials with the temperature factor parameters of the sodium and the chlorine atoms in the softer compound sodium chloride.

Single crystals were made by zone melting, zone annealing, and annealing crystal growth methods of the compounds TiC, $TiN_{0.90}$, δ-$NbN_{0.90}$, and $Nb_{0.83}Ti_{0.17}N_{0.77}C_{0.05}$.[1,2] All four compounds have the sodium chloride structure, space group *Fm3m*, No. 225, with the metal atoms in site 4*a* and the non-metal atoms in site 4*b*. Further pertinent crystallographic data for the compounds are listed in Table 1. The present communication describes the determination of the temperature factor parameters for the compounds using single crystal X-ray diffraction for TiC, and single crystal neutron diffraction techniques for the other three compounds.

A single crystal of TiC was made from a thin blade obtained when a large specimen was fractured. The blade was placed on a microscope slide on the microscope table and could be cleaved with the edge of another microscope slide. The crystal surfaces were all cleavage planes belonging to class {100}. A total of 76 independent *hkl* reflections with $I > 3\sigma(I)$ were measured on a Picker four circle diffractometer using monochromatic Ag$K\alpha$ radiation ($\lambda = 0.5608$ Å). The $\omega - 2\theta$ scan technique was used. The monochromator was a graphite crystal and the counter was a scintillation counter in conjunction with a pulse height analyzer. Lorentz-polarization corrections were applied and a correction was made for absorption using Well's method.[3]

Single crystals for the neutron diffraction measurements (Table 1) were cut from larger specimens using a diamond cut off wheel. The neutron diffraction data were measured on a four circle diffractometer at DR3, Risø, using 1.07 Å neutrons, and the standard $\omega - 2\theta$ scan technique.[4] The data were reduced using a standard procedure[5] and Lorentz-polarization and absorption corrections were made.

Observed and calculated structure factors were compared using the least-squares program *LINUS*.[6] For TiC the form factors for Ti and C reported by Fukamachi[7] were used in the calculations. The neutron scattering amplitudes used for Nb, Ti, C, and N were 0.711, −0.335, 0.6648, 0.940, respectively, all in units of 10^{-12} cm.[8] The results of the calculations with the values of the refined parameters are listed in Table 2. The corresponding lists of observed and calculated structure factors can be obtained from the author on request.

The result of the investigation shows that the compounds have low values for the isotropic temperature factor parameters, in agreement with the hardness of these materials. Sodium chloride has much higher values for the isotropic temperature factor parameters at 300 K, but at 4.2 K the values of the parameters are comparable with the isotropic temperature factor parameters for TiC at 300 K (see Table 2). This thus reflects the great hardness of titanium carbide. The Debye-temperatures obtained from the temperature factor parameters using the harmonic approximation[11] are listed in Table 2 together with values for θ_B obtained from low temperature specific heat measurements[9]

Table 1. Crystallographic data for compounds with space group *Fm3m*.

Compound	Unit cell parameter in Å	Linear absorption coefficient in cm^{-1}	Volume of specimen in mm^3	Number of reflections	
				Total	Independent
TiC	4.328(2)	34.5[a]	5×10^{-4}	2497	76
$TiN_{0.90}$	4.239(1)	0.42	124	294	19
δ-$NbN_{0.90}$	4.377(1)	0.14	19	225	20
$Nb_{0.83}Ti_{0.17}N_{0.77}C_{0.05}$	4.346(1)	0.55	27	204	19

[a] for X-rays Ag$K\alpha$.

Table 2. Results X-ray (TiC) and neutron diffraction. Standard deviations in parenthesis.

Compound	R %	Scale Factor	Extinction Parameter	Temperature Factor Parameter B(Å^2)		Debye Temperature θ_DK	
				M	X	This work	Ref. 9
TiC	1.6	5.40(3)	0.421(8)	0.26(1)	0.44(3)	604(24)	614–676
$TiN_{0.90}$	3.6	2044(39)	1.4(6)	1.06(17)	1.07(10)	332(17)	636
δ-$NbN_{0.90}$	3.8	487(19)	0.11(2)	0.66(10)	0.64(9)	320(25)	307
$Nb_{0.83}Ti_{0.17}N_{0.77}C_{0.05}$	3.2	632(20)	0.15(2)	0.60(8)	0.70(7)	337(15)	323[a]
NaCl, 295 K, Ref. 10				1.70(10)	1.44(3)		
NaCl, 4.2 K, Ref. 10				0.35(8)	0.27(4)		

[a] For the compound $NbN_{0.81}C_{0.09}$.

and are in acceptable agreement with these values for the Debye-temperatures. Surprisingly, it is found that $TiN_{0.90}$ has higher values for the temperature factor parameters than the three other compounds, and the calculated Debye-temperature is thus correspondingly lower. It is obvious, judged from the hardness of $TiN_{0.90}$ that is comparable with the hardness of TiC, that the isotropic temperature factor parameters arrived at here are too high. It is well-known that systematic errors in the diffraction data or in the calculations can be accummulated in the isotropic temperature factor parameters giving these physically meaningless values. This must be the case for $TiN_{0.90}$. It is observed (see Table 2) that the extinction parameter for $TiN_{0.90}$ is rather large which supports this hypothesis. The data have not been corrected for thermal diffuse scattering. This is a possible error source. An incorrect value for the scattering length of titanium would also have the observed effect on the extinction parameter and the isotropic temperature factor parameters. The Debye-temperature of $TiN_{0.95}$ has recently been determined from Raman scattering experiments[12] as 518 K in acceptable agreement with a Debye-temperature of 485 K obtained for $TiN_{0.99}$ from heat capacity measurements.[13] An average isotropic temperature factor parameter for Ti and N corresponding to the value 518 K would be 0.45 Å^2.

1. Christensen, A. N. *Acta Chem. Scand. A 29* (1975) 563.
2. Christensen, A. N. and Fregerslev, S. *Acta Chem. Scand. A 31* (1977) 861.
3. Wells, M. J. *Acta Crystallogr. 13* (1960) 722.
4. Lehmann, M. S., Larsen, F. K., Poulsen, F. R., Christensen, A. N. and Rasmussen, S. E. *Acta Chem. Scand. 24* (1970) 1662.
5. Lehmann, M. S. and Larsen, F. K. *Acta Crystallogr. A 30* (1974) 580.
6. Busing, W. R., Martin, K. O. and Levy, H. A. *ORFLS, A Fortran Crystallographic Least Squares Program*, Report ORNL-TM-305, Oak Ridge National Laboratory, Oak Ridge 1962; *LINUS* is a 1971 version of *ORFLS*.
7. Fukamachi, T. *Mean X-ray scattering factors calculated from analytical Roothaan-Hartree-Fock wave functions by Clementi*, Technical Report of ISSP, Series B, No. 12, Tokyo 1971, The Institute of Solid State Physics, The University of Tokyo, Japan.
8. Bacon, G. E. *Acta Crystallogr. A 28* (1972) 357.
9. Toth, L. E. *Transition Metal Carbides and Nitrides*, Academic, New York and London 1971.
10. Butt, N. M., Cheetham, A. K. and Willis, B. T. M. *Acta Crystallogr. A 29* (1973) 727.
11. MacGillavry, C. H., Rieck, G. D. and Lonsdale, K. *International Tables for X-Ray Crystallography, Physical and Chemical Tables*, Kynoch Press, Birmingham 1962, Vol. III.
12. Spengler, W., Kaiser, R., Christensen, A. N. and Müller-Vogt, G. *Phys. Rev. B* (1977). *Submitted.*
13. Roedhammer, P., Weber, W., Gmelin, E. and Reider, K. H. *J. Chem. Phys. 64* (1976) 581.

Received September 26, 1977.

Crystal Conformation of 1,4,8,11-Tetraoxacyclotetradecane at −150 °C

P. GROTH

Department of Chemistry, University of Oslo, Oslo 3, Norway

As part of a study of conformational problems in tetraoxacyclodecanes the 1,4,8,11-tetraoxacyclotetradecane, $C_{10}H_{20}O_4$, has been synthesized.[1] No definite conclusions about the ring conformation could be drawn on basis of NMR-data, and the crystal structure is now reported.

The crystals belong to the monoclinic system with space group $P2_1/n$, cell dimensions $a=8.026(1)$ Å, $b=9.033(1)$ Å, $c=15.711(2)$ Å, $\beta=102.64(1)°$, and $Z=4$ ($D_m=1.20$ g cm^{-3}, $D_x=1.22$ g cm^{-3}).

With $2\theta_{max}=50°$ and Mo$K\alpha$-radiation 1966 independent reflections were measured on an automatic fourcircle diffractometer at −150 °C. Using an observed-unobserved cutoff at 2.5 (I) 1683 reflections were recorded as observed. No corrections for absorption or secondary extinction were applied (crystal size $0.45\times0.60\times0.25$ mm^3).

The structure was solved by direct methods[2] and refined by full-matrix least-squares technique.[3,*] Hydrogen atom positions were calculated. Anisotropic temperature factors were introduced for O and C atoms and weights in least-squares were calculated from the standard deviations in intensities, $\sigma(I)$, taken as

$$\sigma(I)=[C_T+(0.02C_N)^2]^{\frac{1}{2}}$$

where C_T is the total number of counts and C_N the net count. The form factors used were those of Hanson *et al.*[4] except for hydrogen.[5] The final R-value was 2.9 % (weighted value $R_w=3.4$ %) for 1683 observed reflections.

Final fractional coordinates together with the thermal parameters are listed in Table 1. The principal thermal vibration ellipsoids for oxygen

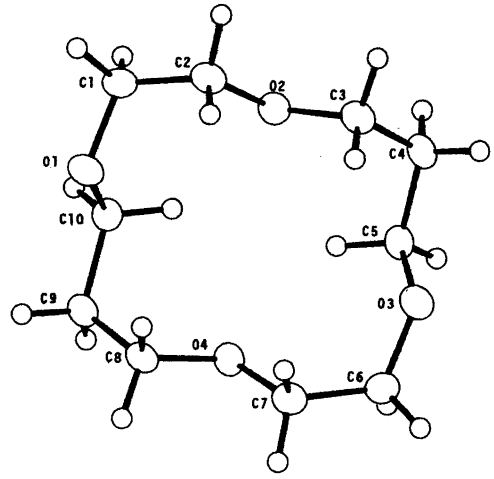

Fig. 1. Schematic drawing of the molecule.

* All programs used (except those for phase determination) are included in this reference.

Table 1. Final fractional coordinates and thermal parameters with estimated standard deviations. The expression for anisotropic vibration is $\exp[-2\pi^2(h^2a^{*2}U11+\cdots+2klb^*c^*U23)]$. Atom Hmn is bonded to Cm.

ATOM	X	Y	Z	U11	U22	U33	U12	U13	U23
O1	.0431B(10)	.07688(10)	.09268(6)	.0223(5)	.0278(5)	.0314(5)	.0025(4)	.0083(4)	-.0071(4)
O2	-.1644B(10)	.07760(9)	.13807(5)	.0254(5)	.0229(5)	.0249(5)	.0011(4)	.0042(4)	-.0013(4)
O3	.1308A(11)	.64027(10)	.09131(5)	.0264(5)	.0271(5)	.0207(5)	-.0000(4)	.0031(4)	.0056(4)
O4	.3198B(10)	.56032(9)	.17589(5)	.0240(5)	.0264(5)	.0222(5)	-.0035(4)	.0034(3)	-.0005(4)
C1	-.1339B(16)	.78935(16)	.09186(9)	.0217(7)	.0335(8)	.0299(7)	.0048(6)	.0049(6)	-.0059(6)
C2	-.1781B(17)	.78396(15)	.00394(9)	.0226(7)	.0249(7)	.0313(7)	.0025(6)	.0022(5)	-.0005(6)
C3	-.1795B(17)	.74368(15)	.68466(8)	.0255(7)	.0249(7)	.0290(7)	.0043(6)	.0032(6)	.0040(6)
C4	-.1089B(17)	.62171(15)	.69834(8)	.0260(7)	.0267(7)	.0215(7)	.0001(6)	-.0004(5)	.0037(6)
C8	.0841(16)	.54699(14)	.61089(8)	.0268(7)	.0224(7)	.0286(7)	-.0009(5)	.0035(5)	.0015(5)
C6	.3981(17)	.59822(16)	.68328(9)	.0243(7)	.0323(8)	.0288(8)	.0005(6)	.0003(6)	.0022(6)
C7	.3709B(17)	.64388(16)	.71476(9)	.0230(7)	.0285(8)	.0301(7)	-.0033(6)	.0050(5)	.0033(6)
C8	.3884A(16)	.81703(15)	.66201(8)	.0192(7)	.0288(8)	.0261(7)	-.0010(5)	.0000(5)	-.0043(6)
C9	.2881(B(16)	.88842(15)	.99178(9)	.0243(7)	.0247(7)	.0223(7)	.0020(5)	.0003(5)	-.0010(6)
C10	.0881(7(16)	.88999(14)	.90838(8)	.0255(7)	.0222(7)	.0223(7)	-.0007(5)	.0047(5)	-.0025(5)

ATOM	X	Y	Z	B	ATOM	X	Y	Z	B
H11	-.1663(17)	.7708(16)	.9348(9)	2.1(3)	H12	-.2837(18)	.8174(16)	.0899(8)	2.2(3)
H81	-.0888(17)	.8622(15)	.0815(8)	1.7(3)	H22	-.2876(18)	.8315(15)	.7931(9)	2.2(3)
H31	-.0881(16)	.8147(14)	.6867(8)	1.9(3)	H32	-.2868(19)	.7992(16)	.6369(9)	2.4(3)
H41	-.1884(16)	.6629(15)	.6326(9)	1.8(3)	H42	-.2861(18)	.5484(16)	.5911(8)	2.1(3)
H81	-.0812(15)	.4488(14)	.5726(8)	1.3(2)	H52	.0351(15)	.5188(14)	.6726(8)	1.2(2)
H61	.3898(17)	.6379(15)	.8044(9)	1.9(3)	H62	.3899(16)	.4638(16)	.6188(8)	1.9(3)
H71	.3466(16)	.7528(16)	.7212(8)	1.7(3)	H72	.5018(19)	.6329(15)	.7247(9)	2.2(3)
H81	.3868(16)	.7211(15)	.9638(8)	1.6(3)	H82	.4883(18)	.6128(14)	.8884(8)	1.9(3)
H91	.3840(17)	.8594(15)	.9826(9)	1.8(3)	H92	.3156(16)	.4175(15)	.9188(8)	1.7(3)
H101	.0373(16)	.4533(15)	.9342(8)	1.6(3)	H102	.0431(14)	.5185(13)	.8368(8)	1.1(2)

Table 2. Bond distances, bond angles, and dihedral angles with estimated standard deviations.

DISTANCE	(Å)	DISTANCE	(Å)
O1 - C1	1.426(1)	O1 - C10	1.434(1)
O2 - C2	1.428(1)	O2 - C3	1.425(1)
O3 - C5	1.433(1)	O3 - C6	1.426(2)
O4 - C7	1.422(2)	O4 - C8	1.425(1)
C1 - C2	1.503(2)	C3 - C4	1.509(2)
C4 - C5	1.514(2)	C6 - C7	1.506(2)
C8 - C9	1.508(2)	C9 - C10	1.514(2)

ANGLE	(°)	ANGLE	(°)
O1 - C1 - C2	112.9(1)	C1 - O1 - C10	113.7(1)
O1 - C10 - C9	107.7(1)	O2 - C2 - C1	109.5(1)
C2 - O2 - C3	112.4(1)	O2 - C3 - C4	108.8(1)
O3 - C5 - C4	107.4(1)	C5 - O3 - C6	114.2(1)
O3 - C6 - C7	113.2(1)	O4 - C7 - C6	110.1(1)
C7 - O4 - C8	111.8(1)	O4 - C8 - C9	108.7(1)
C8 - C9 - C10	113.8(1)	C8 - C9 - C10	112.6(1)

DIHEDRAL ANGLE	(°)
C10 - O1 - C1 - C2	-92.7(1)
O1 - C2 - C1 - O1	75.9(1)
C3 - O2 - C2 - C1	-172.8(1)
C4 - C3 - O2 - C2	179.8(1)
O2 - C3 - C4 - C5	-64.8(1)
C3 - C4 - C5 - O3	-78.6(1)
C6 - O3 - C5 - C4	167.8(1)
C7 - C6 - O3 - C5	-89.1(1)
O4 - C7 - C6 - O3	77.1(1)
C8 - O4 - C7 - C6	-172.2(1)
C9 - C8 - O4 - C7	176.9(1)
O4 - C8 - C9 - C10	-64.7(1)
C8 - C9 - C10 - O1	-89.3(1)
C9 - C10 - O1 - C1	169.4(1)

and carbon atoms were calculated from the thermal parameters of this table, and the maximum r.m.s. amplitudes range from 0.16 to 0.20 Å.

Bond distances, bond angles and dihedral angles may be found in Table 2. The standard deviations, given in parentheses, are estimated from the correlation matrix of the final least-squares refinement cycle.

Fig. 1 is a schematic drawing of the molecule, indicating the numbering of atoms.

For cyclotetradecane itself, the "rectangular" diamond-lattice conformation has the lowest calculated enthalphy[6] as well as being the observed one in liquid and solution.[7] Recently it has been shown that it also is the experimental crystal conformation.[8] Furthermore, this centrosymmetric "rectangular" conformation is indeed the preferred one in the crystals of 1,3,8,10-tetraoxacyclotetradecane.[9]

However, it turned out that the ring skeleton of the present compound has a conformation with approximate two-fold rotational symmetry (Fig. 1).

From Table 2 it may be seen that the distances O1–C10 [1.434(1) Å] and O3–C5 [1.433(1) Å] seem to be somewhat longer than the other six (mean value 1.424 Å). The same effect, but less pronounced, is seen for C9–C10 [1.514(2) Å] and C4–C5 [1.514(2) Å] compared to the average value of the other four (1.506 Å).

Bond distances and angles agree within error limits with corresponding values for 1,3,8,10-tetraoxacyclotetradecane,[9] and also with those of 1,5,9,13-tetraoxacyclohexadecane.[10] In 1,3,8,10-tetraoxacyclotetradecane the shortest intra-molecular nonbonded H···H contact is 2.19 Å, while in the present compound no such contacts shorter than 2.4 Å occur. No short inter-molecular distances are observed.

Acknowledgement. The author thanks Dr. G. Borgen for preparing the crystals.

1. Borgen, G. and Dale, J. *To be published.*
2. Germain, G., Main, P. and Woolfson, M. M. *Acta Crystallogr. A 27* (1971) 368.
3. Groth, P. *Acta Chem. Scand. 27* (1973) 1837.
4. Hanson, H. P., Herman, F., Lea, J. D. and Skillman, S. *Acta Crystallogr. 17* (1964) 1040.
5. Stewart, R. F., Davidson, E. R. and Simpson, W. T. *J. Chem. Phys. 42* (1965) 3175.
6. Dale, J. *Acta Chem. Scand. 27* (1973) 1115.
7. Borgen, G. and Dale, J. *Chem. Commun.* (1970) 1340.
8. Groth, P. *Acta Chem. Scand. A 30* (1976) 155.
9. Bassi, W. I., Scordamaglia, R. and Fiore, L. *J. Chem. Soc. Perkin Trans. 2* (1972) 1726.
10. Groth, P. *Acta Chem. Scand. 25* (1971) 725.

Received October 10, 1977.

Furfuryl Alcohol. Part 2. Dielectric Behaviour of Furfuryl Alcohol and Carbon Tetrachloride Mixtures

LIISA STRANDMAN

Department of Physical Chemistry, University of Helsinki, Meritullinkatu 1, SF-00170 Helsinki 17, Finland

Self-association of furfuryl alcohol (FOH) in carbon tetrachloride solutions was previously studied by a near-infrared spectrometric method.[1] In an attempt to determine the structures of the associated FOH species, dielectric data are here analysed in terms of the Kirkwood-Fröhlich correlation parameter g, which is a measure of the short-range intermolecular forces that lead to specific dipole-dipole orientations.

Experimental. The samples were purified as in the preceding work.[1] The observed refractive indices were: furfuryl alcohol 1.4842 and carbon tetrachloride 1.4561 at 25 °C. The refractive indices were measured with an Abbe refractometer (Model G, Carl Zeiss, Jena) at the wavelength of the sodium D-line. The dielectric constants were measured by the heterodyne beat method at 2 MHz with a Dipolmeter DM 01 (Wissenschaftlich-Technische Werkstätten, Weilheim, West-Germany) and cells MFL 1/S and MFL 2/S. The values of dielectric constants were read from large-scale calibration curves. The densities were measured with an Ostwald-Sprengler pycnometer having a volume of 10. 4733 cm^3. The temperature was maintained at 25 °C within 0.1 °C. All weighings were corrected to vacuum.

Calculations and results. The dipole moment of FOH, $\mu_0 = 1.95$ D, was computed by the method of Hedestrand[2] from the measured values of dielectric constants ε and densities d of very dilute solutions. Both ε and d are within experimental error linear functions of X_1, the mol fraction of FOH in CCl_4, for $X_1 < 0.04$. The estimated uncertainty in the dipole moment is ± 0.02 D.

The Kirkwood-Fröhlich parameters g[3,4] were calculated from the relations presented in Refs. 5 and 6 for the pure dipolar compound and for binary mixtures of polar liquid and nonpolar solvent. The results are given in Table 1. In general the g values for pure alcohols range from 2.5 to 3.1.[5,6] When the alcohol concentration decreases ($X_1 \rightarrow 0.1$) g decreases to a minimum value, often considerably less than one. With further dilution, g increases towards unity. A value of g less than one indicates that a considerable amount of cyclic alcohol complexes are formed owing to an antiparallel alignment of near neighbour dipoles.[3-7] Because the measured correlation parameter represents the overall average of the different sizes and structures of complexes formed, the reason for the somewhat low value 1.87 of pure FOH might be an equilibrium between open and cyclic associates, or more probably the association ratio is low owing to the steric hindrance against the formation of large multimers.[5] The g values of FOH in dilute solutions give a minimum of 0.95 at $X_1 = 0.085$. The minimum g value of FOH remains closer to unity than that of most other alcohols studied.[5,6,8] Accordingly, one can conclude that furfuryl alcohol has a relatively weak tendency to form cyclic dimers and/or trimers and open associates prevail.

Table 1. Values of the density, the dielectric constant and the correlation parameter at different mol fractions, X_1, of FOH in CCl_4 at 25 °C. The uncertainty in the correlation parameter is about 2%.

X_1	d (g cm^{-3})	ε	g
0.0000	1.5847	2.241	1.000
0.0395	1.5679	2.425	0.998
0.0620	1.5586	2.533	0.963
0.0851	1.5490	2.647	0.946
0.108	1.5396	2.788	0.976
0.165	1.5159	3.177	1.036
0.340	1.4409	4.934	1.268
0.489	1.3753	7.095	1.471
0.503	1.3693	7.319	1.485
0.660	1.2968	9.975	1.631
0.813	1.2230	13.00	1.765
1.000	1.1286	16.85	1.874

1. Strandman, L. *Acta Chem. Scand. A 29* (1975) 632.
2. Hedestrand, G. *Z. Phys. Chem. B 2* (1929) 428.
3. Kirkwood, J. G. *J. Chem. Phys. 7* (1939) 911.
4. Fröhlich, H. *Theory of Dielectrics*, Clarendon Press, Oxford 1950, pp. 36–53.
5. Gold, P. I. and Perrine, R. L. *J. Phys. Chem. 71* (1967) 4218.
6. Gold, P. I. and Perrine, R. L. *J. Chem. Eng. Data 12* (1967) 4.
7. Dannhauser, W. *J. Chem. Phys. 48* (1968) 1911.
8. Singh, B. and Vij, J. K. *Bull. Chem. Soc. Jpn. 49* (1976) 1824.

Received September 30, 1977.

Acta Chemica Scandinavica A 32 (1978) 95 – 100

Crystal and Molecular Structure of Hexakis(dimethylsulfoxide)-mercury(II) Perchlorate, $[Hg((CH_3)_2SO)_6](ClO_4)_2$

MAGNUS SANDSTRÖM[a] and INGMAR PERSSON[b]

[a] Department of Inorganic Chemistry, Royal Institute of Technology, S-100 44 Stockholm 70, Sweden and [b] Inorganic Chemistry 1, Chemical Center, University of Lund, P.O.B. 740, S-220 07 Lund 7, Sweden

The compound $[Hg(DMSO)_6](ClO_4)_2$ crystallizes in the triclinic space group $P\bar{1}$ (No. 2) with $a = 7.418(2)$, $b = 10.831(6)$, $c = 11.241(4)$ Å, $\alpha = 118.37(4)$, $\beta = 93.10(3)$, $\gamma = 92.60(3)°$ and $Z = 1$. The X-ray investigation was based on 2001 independent reflections collected with a computer-controlled Syntex $P2_1$ four-circle diffractometer using Mo$K\alpha$ radiation. The structural parameters were refined by least-squares methods to a conventional R value of 0.035.

The structure is built up from discrete hexakis-(dimethylsulfoxide)mercury(II) complex ions and perchlorate ions. The mercury atom is coordinated to six DMSO molecules through the oxygen atoms in an almost regular octahedron. The average Hg – O bond length is 2.34 Å. The perchlorate group is disordered and performs large librational movements in the absence of hydrogen bonds.

The most common configuration of hexa-coordinated mercury is that of a distorted octahedron, with two short linear bonds.[1] Discrete complexes with regular octahedral coordination seem to be rare, but an example has been found in the compound $[Hg(C_5H_5NO)_6](ClO_4)_2$ with an Hg – O bond length of 2.35(2) Å.[2] Moreover, X-ray diffraction[3,4] and Raman[4] measurements on DMSO and aqueous solutions are consistent with a regular coordination of six solvent molecules to the Hg^{2+} ion. The average Hg – O bond lengths are 2.393(5) and 2.41(1) Å,[4] respectively. For a comparison with the structures found for the solvated ions in solution the crystal structures of the solvates $[Hg(H_2O)_6](ClO_4)_2$,[5] $Hg(ClO_4)_2.4DMSO$,[6] and $[Hg((CH_3)_2SO)_6](ClO_4)_2$ in the present paper, were determined.

EXPERIMENTAL

Preparation of crystals. Saturated DMSO solutions, 0.94 M at 25 °C, were prepared by dissolving the compound $Hg(ClO_4)_2.4DMSO$ in pure DMSO.[4] By slow evaporation or by cooling, colourless prismatic crystals of the composition $Hg(ClO_4)_2.6DMSO$ were formed. The crystals were filtered off and washed with cold acetone. Methods and results of analyses of the crystals are given elsewhere.[4]

The crystals were very hygroscopic and decomposed rapidly in air. Even when stored in a closed tube they decomposed slowly losing DMSO. After two months the average number of DMSO molecules per mercury atom was found to be 5.4(1).

X-Ray data collection. The intensity data were collected at 25 ± 2 °C by a computer-controlled four-circle diffractometer of type Syntex $P2_1$, equipped with a scintillation counter. Graphite-monochromatized Mo$K\alpha$-radiation ($\lambda = 0.71069$ Å) was used.

A prismatic crystal with maximum dimensions of about 0.1 mm, contained in a capillary, was aligned optically. Approximate positions of 20 reflections were obtained from an oscillation photograph on the diffractometer. These reflections were automatically centred and used in an auto-indexing routine to determine the lattice constants, which were refined using least-squares methods. The unit cell was found to be triclinic with the crystal data: $a = 7.418(2)$, $b = 10.831(6)$, $c = 11.241(4)$ Å, $\alpha = 118.37(4)°$, $\beta = 93.10(3)°$, $\gamma = 92.60(3)°$, $V = 790.9(6)$ Å^3, $D_m = 1.76(3)$ and $D_x = 1.82$ g cm^{-3} for $Z = 1$.

The $\theta - 2\theta$ scan mode was used for the intensity data collection with different scan speeds, the minimum scan speed being 2° min^{-1}. Stationary background measurements were made on each side of a peak. The total background counting time was equal to the scan time.

The intensity, I, of each reflection was calculated by subtracting the total background count, BG, from the total scan count, SC. The standard deviation, $\sigma(I)$, was obtained from $\sigma(I)=(SC+BG)^{1/2}$. The values obtained were then multiplied with the scan rate to compensate for the different scan speeds. All intensities were corrected for Lorentz and polarization effects and converted to scaled $|F_o|$ values by means of a data reduction program. Of the 2064 possible independent reflections for $2\theta<45°$, 2001 had intensities larger than 1.96 $\sigma(I)$ and were considered observed.

After every 50th reflection three check reflections were measured. Their intensities varied within ± 15 % during the data collection. They first increased and then slowly decreased, probably due to extinction changes during a gradual decomposition of the crystal. No correction for this was applied.

The absorption coefficient $\mu(\mathrm{Mo}K\alpha)$ is 55.7 cm^{-1}. A semi-empirical absorption correction method was used.[7] The intensities of selected reflections, which had χ values close to 90° and 2θ values evenly distributed over the 2θ range used, were measured for a full flat-cone rotation around the diffraction vector in steps of 10°. The relative intensity variations obtained were used to correct the intensities of all measured reflections in appropriate 2θ-intervals. The largest measured relative reduction in intensity was from 1.00 to 0.63.

Computer programs. The program system supplied by Syntex (XTL version 2)[8] for a NOVA 24K computer with a disk memory unit, was used for the calculations. In addition, the thermal-ellipsoid plot program for crystal structure illustrations, ORTEP 2, was used.[9]

STRUCTURE DETERMINATION AND REFINEMENTS

Determination of the structure. From a three-dimensional Patterson peak listing one Hg–Cl, three Hg–S and three Hg–O vectors, all with a multiplicity of two, could be identified. The space-group was therefore assumed to be the centrosymmetrical $P\bar{1}$ (No. 2), and the corresponding atomic parameters, with Hg at the origin of the unit cell, were refined by least-squares methods. The positions of the C atoms were found from a subsequent Fourier difference synthesis. Full-matrix least-squares refinements gave $R=0.070$ ($R_w=0.096$) with Hg anisotropic.

The conventional R-value is defined as $R=\Sigma\|F_o|-|F_c\|/\Sigma|F_o|$, and the weighted as $R_w=(\Sigma w\|F_o|-|F_c\|^2/\Sigma w|F_o|^2)^{1/2}$.

A three-dimensional Fourier difference map was calculated and showed regions of increased electron density at about 1.4 Å from the chlorine atoms. Seven more or less distinct peaks with heights between 1.1 and 2.4 e $\mathrm{Å}^{-3}$ were found. Their locations and relative sizes corresponded approximately to two alternative positions of the ClO_4^- group, obtained by rotating it ~60° around an axis through the Cl and the highest of the oxygen peaks. This oxygen, O4, was then given a fixed occupancy number 1.0 and the remaining six positions 0.5. After new refinements another Fourier difference synthesis revealed peaks around the C atoms with heights of 0.4 to 0.8 e $\mathrm{Å}^{-3}$, which could be ascribed to the 18 H atom positions.

Full-matrix least-squares refinements with all non-H atoms anisotropic and with a fixed B-value of 5 $\mathrm{Å}^2$ for the H atoms gave $R=0.036$ ($R_w=0.048$). Finally, also the occupancy numbers of the perchlorate oxygens were allowed to vary, which gave $R=0.035$ ($R_w=0.047$).

Test of the absorption correction. Similar final refinements were also performed for data without the semi-empirical absorption correction described above, and gave $R=0.036$ ($R_w=0.047$).

The main effect of this absorption correction was to decrease the largest remaining peaks in the final difference Fourier synthesis, which were located around Hg, from 1.4 to 0.9 e $\mathrm{Å}^{-3}$. The refined parameters were not significantly affected except for the oxygen atoms coordinated to Hg, where the average Hg–O bond distance increased by 0.01 Å. The data set with the absorption correction was considered to be the better one and was used for all other calculations reported here.

This semi-empirical absorption correction has, in some cases, been found to give almost identical results as those obtained using a Gaussian integration method, for some highly absorbing compounds.[10]

Test of non-centrosymmetry. In order to check if deviations from centrosymmetry would occur for the neighbouring atoms of the perchlorate groups, and if the perchlorate positions could be described in a better way, calculations were also performed in the non-centrosymmetric space-group $P1$ (No. 1). However, the R_w values obtained were not, according to statistical tests,[11] significantly lower than the corresponding values for $P\bar{1}$. Moreover, some of the anisotropic temperature coefficients, B_{ii}, of the DMSO oxygens became negative, which is physically meaningless.

Scattering factors and refinement conditions. The scattering factors used for all non-H atoms were calculated from analytical expressions for the neutral atoms.[11] For the H atoms the spherical form factors proposed by Stewart *et al.* were used.[12] Anomalous dispersion corrections were included for Hg, Cl and S.[11]

The least-squares refinements were based on the minimization of $\Sigma w \| F_o | - | F_c \|^2$ and 2001 reflections with $F_o > 3.92\ \sigma(F_o)$ were used. The weighting scheme used was $w = 1/[\sigma^2(F_o) + (0.04\ F_o)^2]$ which, according to a weight analysis, gave a satisfactory error distribution.

A total of 251 parameters, including one scale factor, was varied in the final refinements. The ratios of the shifts in the last cycle to the standard deviation were less than 0.1 in $P\bar{1}$, except for the thermal parameters of the perchlorate oxygens, where the largest ratio was 0.4.

The final refined parameter values are given in Tables 1 and 2.

Table 1. Final fractional atomic positional parameters with estimated standard deviations in parentheses. The *G* values are the refined occupancy factors.

Atom	*x*	*y*	*z*	*G*
Hg	0.0	0.0	0.0	
Cl	0.7029(3)	0.6945(3)	0.3486(3)	
S1	0.2146(3)	0.3271(2)	0.1231(2)	
S2	0.3437(3)	−0.0243(3)	0.2147(2)	
S3	−0.1518(3)	0.1841(2)	0.3012(2)	
O1	0.0299(8)	0.2451(5)	0.0709(6)	
O2	0.2391(8)	0.0613(6)	0.1647(6)	
O3	−0.2016(8)	0.0540(6)	0.1651(6)	
O4	0.683(6)	0.661(3)	0.448(3)	0.74(7)
O5	0.747(8)	0.833(3)	0.441(5)	0.61(8)
O6	0.567(5)	0.690(9)	0.386(9)	0.53(10)
O7	0.848(5)	0.628(5)	0.321(5)	0.73(10)
O8	0.640(5)	0.573(3)	0.233(3)	0.74(6)
O9	0.834(6)	0.750(7)	0.312(5)	0.63(10)
O10	0.591(8)	0.758(6)	0.306(6)	0.57(8)
C1	0.2116(7)	0.4286(12)	0.3026(11)	
C2	0.2056(23)	0.4656(16)	0.0841(16)	
C3	0.4053(19)	−0.1725(17)	0.0698(16)	
C4	0.1796(21)	−0.1149(16)	0.2602(15)	
C5	−0.2192(18)	0.1400(15)	0.4258(12)	
C6	−0.3233(24)	0.3007(16)	0.3195(14)	
H1	0.219(12)	0.364(10)	0.345(9)	
H2	0.289(13)	0.496(10)	0.322(10)	
H3	0.108(13)	0.484(10)	0.313(10)	
H4	0.197(15)	0.431(11)	0.011(11)	
H5	0.104(13)	0.527(10)	0.144(10)	
H6	0.318(13)	0.522(10)	0.131(10)	
H7	0.298(13)	−0.221(10)	−0.002(10)	
H8	0.477(15)	−0.150(13)	0.060(13)	
H9	0.488(12)	−0.204(9)	0.144(10)	
H10	0.169(12)	−0.030(10)	0.359(10)	
H11	0.095(13)	−0.166(10)	0.184(10)	
H12	0.266(12)	−0.167(10)	0.288(10)	
H13	−0.130(14)	0.098(10)	0.440(10)	
H14	−0.140(12)	0.233(10)	0.526(10)	
H15	−0.311(14)	0.119(11)	0.414(11)	
H16	−0.311(12)	0.368(10)	0.410(10)	
H17	−0.472(12)	0.235(10)	0.264(10)	
H18	−0.284(14)	0.320(11)	0.277(11)	

Table 2. Final anisotropic thermal parameters (Å^2) with estimated standard deviations in parentheses. The expression used is $\exp[-1/4(B_{11}h^2a^{*2}+\ldots+2B_{12}hka^*b^*+\ldots)]$.

Atom	B_{11}	B_{22}	B_{22}	B_{12}	B_{13}	B_{23}
Hg	4.00(2)	2.79(2)	2.51(2)	0.21(1)	0.31(1)	0.92(1)
Cl	4.51(12)	5.33(12)	6.11(13)	−0.20(10)	0.30(10)	3.21(11)
S1	3.74(9)	3.54(9)	4.41(10)	0.19(7)	0.37(7)	1.69(8)
S2	4.89(10)	5.11(11)	4.16(10)	0.60(8)	−0.53(8)	2.26(9)
S3	4.97(10)	4.87(11)	3.09(9)	−0.63(8)	0.63(8)	1.22(8)
O1	4.7(3)	2.7(2)	3.9(3)	−0.15(19)	−0.51(21)	0.60(20)
O2	5.7(3)	4.0(3)	4.5(3)	−0.02(23)	−1.68(24)	1.90(24)
O3	5.2(3)	4.6(3)	3.5(3)	−0.89(22)	1.13(22)	0.97(23)
O4	30.2(42)	19.6(24)	12.5(17)	3.2(24)	2.8(20)	13.1(17)
O5	28.4(50)	7.1(14)	18.1(37)	−4.3(18)	3.6(33)	−0.9(15)
O6	7.4(23)	37.2(94)	32.4(90)	−3.5(28)	11.6(34)	−4.8(60)
O7	12.7(23)	17.6(32)	39.4(61)	7.8(21)	9.8(29)	14.6(35)
O8	20.5(30)	15.5(22)	13.2(19)	−7.1(18)	−4.2(16)	7.2(16)
O9	13.2(27)	20.8(57)	23.7(45)	−6.8(28)	4.0(21)	11.1(39)
O10	25.2(57)	24.2(53)	28.0(54)	7.6(39)	−6.3(40)	19.8(47)
C1	6.2(6)	4.2(5)	4.8(5)	−1.2(4)	0.0(4)	1.2(4)
C2	8.8(8)	6.4(7)	7.4(7)	−2.1(6)	−1.2(7)	4.3(7)
C3	6.0(7)	8.2(8)	6.1(6)	1.8(6)	1.4(6)	2.9(6)
C4	8.7(8)	7.9(7)	5.9(7)	1.5(6)	1.7(6)	4.4(6)
C5	5.7(5)	8.7(8)	4.9(5)	0.7(6)	0.9(5)	4.2(6)
C6	11.0(10)	6.5(7)	4.9(6)	1.6(7)	1.4(6)	2.7(5)

DESCRIPTION AND DISCUSSION OF THE STRUCTURE

The crystal structure is composed of discrete $Hg(DMSO)_6^{2+}$ cations and ClO_4^- anions. Stereoscopic views of the molecular geometry of these ions are given in Figs. 1 and 2, and a unit cell view is shown in Fig. 3. Some intramolecular distances and angles are given in Table 3.

The $Hg(DMSO)_6^{2+}$ complex. Each Hg atom coordinates six DMSO molecules through the oxygen atoms. The resulting coordination polyhedron around the mercury(II) ion is a slightly distorted octahedron with an average Hg−O bond length

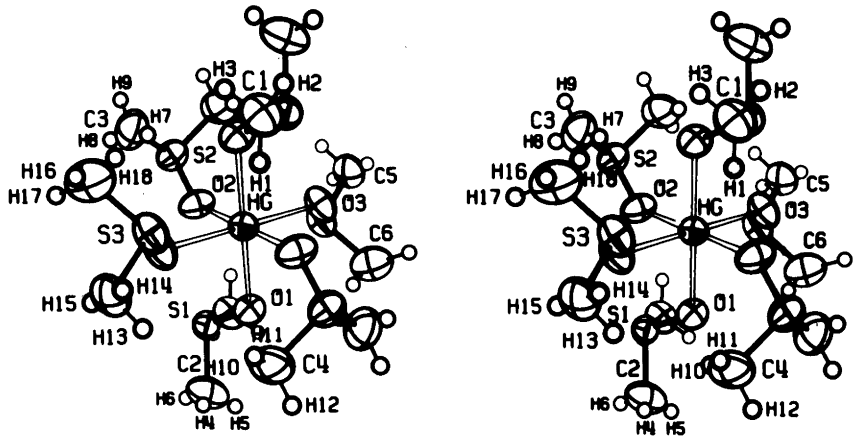

Fig. 1. A stereoscopic view of the centrosymmetrical $Hg(DMSO)_6^{2+}$ cation. All non-H atoms are represented by 50 % probability thermal ellipsoids. The H atoms have for clarity been given a *B*-value of 1 Å^2 in the figure.

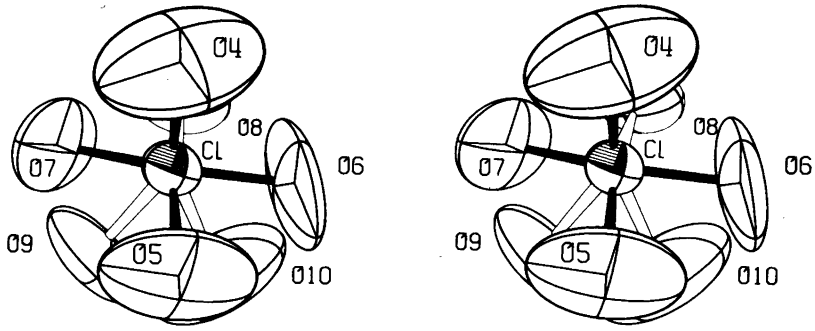

Fig. 2. A stereoscopic view of the disordered perchlorate ion. The thermal ellipsoids enclose 30 % probability. The alternative oxygen positions are those with unfilled bonds.

of 2.34 Å. The sulfur atoms also form a somewhat irregular octahedron around mercury, with an average Hg – S distance of 3.41 Å.

The average S – O and S – C distances within the pyramidal DMSO molecules are 1.52 and 1.77 Å, respectively, which are in good agreement with distances found for other compounds with oxygen-coordinated DMSO ligands.[13,14]

The C – H distances lie in the range 0.6 to 1.3 Å, the average value being 0.95 Å, close to values found by other X-ray diffraction determinations.[15,12]

The ClO_4^- ion. The seven oxygen positions O4 to O10 (Table 1) all belong to the perchlorate group (Fig. 2). The refined Cl – O distances are between 1.29 and 1.38 Å, except for Cl – O6 which is 1.12(5) Å. However, the corresponding distances for the oxygen peaks found from the Fourier difference map were all between 1.32 and 1.45 Å (Cl – O6 1.39 Å). The expected average Cl – O bond length should be 1.42 – 1.43 Å.[16] The large deviations from expected values found for bond lengths and angles in the least-squares refinements are probably caused by the inadequate way of representing the librational

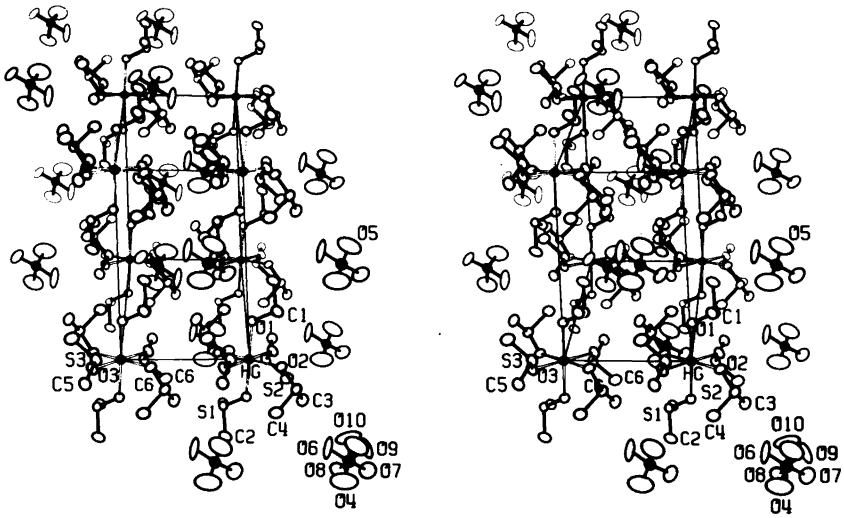

Fig. 3. A stereoscopic view along c^* of the triclinic unit cell. The a axis is horizontal in the figure. The thermal ellipsoids are drawn to enclose 30 % probability. For clarity, the H atoms are omitted and only four of the seven oxygen positions are shown but for one of the disordered perchlorate groups.

Table 3. Some intramolecular atomic distances (Å) and angles (degrees) of interest. Estimated standard deviations are given in parentheses.

Hg–O1	2.376(6)	Cl–O4	1.34(3)
Hg–O2	2.320(6)	Cl–O5	1.37(4)
Hg–O3	2.317(6)	Cl–O6	1.12(5)
		Cl–O7	1.29(4)
Hg–S1	3.404(2)	Cl–O8	1.38(3)
Hg–S2	3.520(2)	Cl–O9	1.31(6)
Hg–S3	3.302(2)	Cl–O10	1.31(7)
Hg–C1	4.40(1)	O1–Hg–O2	82.4(2)
Hg–C2	4.82(2)	O1–Hg–O3	86.3(2)
Hg–C3	3.85(2)	O2–Hg–O3	89.6(2)
Hg–C4	3.88(2)	S1–Hg–S2	81.41(6)
Hg–C5	4.69(1)	S1–Hg–S3	75.71(6)
Hg–C6	4.45(2)	S2–Hg–S3	78.33(6)
		Hg–O1–S1	120.1(3)
S1–O1	1.522(6)	Hg–O2–S2	132.2(4)
S2–O2	1.513(7)	Hg–O3–S3	117.3(4)
S3–O3	1.518(7)	O1–S1–C1	106.2(5)
		O1–S1–C2	105.1(6)
S1–C1	1.78(1)	C1–S1–C2	97.9(7)
S1–C2	1.76(2)	O2–S2–C3	106.8(6)
S2–C3	1.76(2)	O2–S2–C4	106.0(6)
S2–C4	1.77(2)	C3–S2–C4	96.8(8)
S3–C5	1.77(2)	O3–S3–C5	106.2(6)
S3–C6	1.79(2)	O3–S3–C6	105.6(6)
		C5–S3–C6	96.7(7)

movements of the perchlorate oxygens by the ellipsoidal approximation. The thermal ellipsoids obtained for these oxygen atoms are also very large (Fig. 2). The distances were not corrected for thermal motion.

However, the residual electron density in the vicinity of the ClO_4^- group is between 0.5 and −0.4 e $Å^{-3}$ from a Fourier difference map. The sum of the refined occupancy factors of the seven oxygen positions is 4.55(23). This would mean that the refined model still accounts for the electron density of the perchlorate group to a fairly good extent.

The closest intermolecular approaches are O10–H9 2.16(12) and O5–H10 2.28(12) Å. In the absence of hydrogen bonds these intermolecular interactions will hardly cause any serious restraints on the librational movements of the perchlorate group.

Disordered perchlorate ions are also found in the structures of $Ag(DMSO)_2ClO_4$[14] and $[Cd(DMSO)_6](ClO_4)_2$.[17] A survey of different types of disordered perchlorate ions is given in Ref. 14.

Acknowledgements. The authors wish to thank Dr. Georg Johansson and Prof. Sten Ahrland for valuable advice and interest in this work. The work has been financially supported by the Swedish Natural Science Research Council. A generous donation from the foundation Knut och Alice Wallenbergs Stiftelse to the departments of chemistry at the Royal Institute of Technology has made it possible to obtain the computer-controlled four-circle diffractometer with a complete program system for structure determinations.

REFERENCES

1. Gradenic, D. *Angew. Chem. Int. Ed. Engl. 12* (1973) 435; Wells, A. F. *Structural Inorganic Chemistry*, Clarendon Press, Oxford 1975.
2. Kepert, D. L., Taylor, D. and White, A. H. *J. Chem. Soc. Dalton Trans.* (1973) 670.
3. Johansson, G. *Acta Chem. Scand. 25* (1971) 2787.
4. Sandström, M., Persson, I. and Ahrland, S. *Acta Chem. Scand. A 32* (1978). *In press.*
5. Johansson, G. and Sandström, M. *Acta Chem. Scand. A 32* (1978) 109.
6. Sandström, M. *Acta Chem. Scand. A 32* (1978). *In press.*
7. Kopfmann, G. and Huber, R. *Acta Crystallogr. A 24* (1968) 348; North, A. C. T., Phillips, D. C. and Scott Mathews, F. *Ibid.* 351.
8. *Syntex Analytical Instruments*, Inc., 10040 Bubb Road, Cupertino, California 95014, USA.
9. Johnson, C. K. *A FORTRAN Thermal-Ellipsoid Plot Program for Crystal Structure Illustrations*, ORNL-5138, Oak Ridge National Laboratory, Oak Ridge 1976.
10. Åberg, M. *Acta Chem. Scand. A 32* (1978) 101; Sundvall, B. *To be published.*
11. *International Tables for X-Ray Crystallography*, Kynoch Press, Birmingham 1974, Vol. 4.
12. Stewart, R. F., Davidson, E. R. and Simpson, W. T. *J. Chem. Phys. 42* (1965) 3175.
13. Biscarina, P., Fusina, L., Nivellini, G. D., Mangia, A. and Pelizzi, G. *J. Chem. Soc. Dalton Trans.* (1974) 1846.
14. Björk, N.-O. and Cassel, A. *Acta Chem. Scand. A 30* (1976) 235.
15. Kvick, Å. *Aspects of Hydrogen Bonding in Biological Model Compounds, Acta Universitatis Upsaliensis*, Abstracts of Uppsala Dissertations from the Faculty of Science *322*, Almqvist & Wiksell, Stockholm 1974.
16. Berglund, B., Thomas, J. O. and Tellgren, R. *Acta Crystallogr. B 31* (1975) 1842.
17. Sandström, M. *Acta Chem. Scand. A 32* (1978). *In press.*

Received August 26, 1977.

Acta Chemica Scandinavica A 32 (1978) 101 – 107

The Crystal Structure of Hexaaqua-tri-μ-hydroxo-μ_3-oxo-triuranyl(VI) Nitrate Tetrahydrate, $[(UO_2)_3O(OH)_3(H_2O)_6]NO_3.4H_2O$

MÄRTHA ÅBERG

Department of Inorganic Chemistry, Royal Institute of Technology, S-100 44 Stockholm 70, Sweden

The title compound crystallizes in the triclinic space group $P\bar{1}$ (No. 2) with $a=8.026(2)$ Å, $b=11.276(2)$ Å, $c=12.346(4)$ Å, $\alpha=109.65(2)°$, $\beta=99.39(2)°$, $\gamma=88.62(2)°$, and $Z=2$. The crystal structure determination was based on 2513 independent reflections collected with a computer-controlled Syntex $P2_1$ four-circle diffractometer. The structural parameters were refined by least squares methods to a conventional R value of 0.074.

The structure is built up from hexaaqua-tri-hydroxo-oxo-triuranyl(VI) ions, nitrate ions, and water molecules of crystallization. The three U atoms form an equilateral triangle with an average U – U distance of 3.809 Å. They are linked through double bridges containing one O atom and one HO group. Each uranyl group is surrounded by five O atoms at the corners of an irregular planar pentagon. The mean bond lengths are: U – O (uranyl) = 1.78 Å, U – O(oxo) = 2.21 Å, and U – O (aqua or hydroxo) = 2.44 Å.

Polynuclear complexes are formed when aqueous uranyl(VI) salt solutions are hydrolyzed.[1] According to, *e.g.*, emf data, a dinuclear complex is predominant in all ionic media, but tri- and tetranuclear complexes are also of importance, at least in more strongly hydrolyzed solutions.[1] X-Ray diffraction investigations of concentrated hydrolyzed and acidic uranyl(VI) chloride solutions indicate that dinuclear and triangular trinuclear complexes are the predominant species.[2] From the hydrolyzed solutions two different solid phases have been crystallized. One of these phases is built up from dinuclear[3] and the second phase from tetranuclear uranyl(VI) complexes.[4] On studying the system $UO_3 - HCl - H_2O$ at 25 °C Prins and Cordfunke[5] found a third metastable hydrolyzed solid phase, of which it has not been possible to obtain crystals by evaporation at room temperature. In the system $UO_2(NO_3)_2 - UO_3 - H_2O$ at 25 °C one hydrolyzed phase, $UO_2(NO_3)_2.5UO_3.25H_2O$, has been found.[6] This compound is metastable, but crystals can easily be prepared. As n_{HO} (bound HO/U) = 5/3 for this solid as compared to 1 for the dinuclear and 3/2 for the tetranuclear hydrolyzed complex in the $UO_3 - HCl - H_2O$ system, a crystal structure determination has been carried out.

EXPERIMENTAL

Preparation of crystals. According to the phase diagram[6] the hydrolyzed solid nitrate is in equilibrium with a solution with the mol ratio $1.4 < NO_3^-/UO_2^{2+} < 1.5$. Amorphous ("active") UO_3[7] was dissolved in an aqueous solution of $UO_2(NO_3)_2.6H_2O$ (*p.a.*) until $NO_3^-/UO_2^{2+} = 1.45$. From this solution prismatic crystals were obtained by evaporation at room temperature.

Analysis. A powder photograph was taken in a Guinier focusing camera using Cu$K\alpha_1$ radiation ($\lambda = 1.54051$ Å). The diffraction pattern was found to be identical to that reported by Woodhead *et al.*[8] for a polynuclear uranyl(VI) nitrate with the suggested formula $[(UO_2)_6(OH)_{12}(H_2O)_{12}H_2](NO_3)_2.6H_2O$. Obviously the empirical formula is the same as that found by Cordfunke for the hydrolyzed nitrate in the $UO_2(NO_3)_2 - UO_3 - H_2O$ system.[6]

The density of the crystals was determined by benzene displacement to 3.50(4) g cm^{-3}. Woodhead *et al.*[8] obtained a value of 3.65 g cm^{-3}. The calculated density is 3.64 g cm^{-3} for $[(UO_2)_3O(OH)_3(H_2O)_6]NO_3.5H_2O$ and 3.58 g cm^{-3} for the tetrahydrate. The present density determination does not

give any clear indication whether there are five or four water molecules of crystallization. But when the crystal structure was solved only four were found.

X-Ray data collection. The intensity data were collected with a computer-controlled Syntex $P2_1$ four-circle diffractometer using graphite-monochromatized Mo$K\alpha$ radiation ($\lambda = 0.71069$ Å). The lattice parameters and the orientation matrix were determined as described previously using 16 reflections from an oscillation photograph.[9]

Crystal data for $[(UO_2)_3O(OH)_3(H_2O)_6]NO_3 \cdot 4H_2O$ are:

$a = 8.026(2)$ Å	$V = 1037.6(5)$ Å^3
$b = 11.276(2)$ Å	$Z = 2$
$c = 12.346(4)$ Å	$D_m = 3.50(4)$ g cm^{-3}
$\alpha = 109.65(2)°$	$D_x = 3.58$ g cm^{-3}
$\beta = 99.39(2)°$	μ(Mo$K\alpha$) = 222.2 cm^{-1}
$\gamma = 88.62(2)°$	Space group $P\bar{1}$ (No. 2)

The ω scan mode was used for the intensity data collection. The scan speed was variable, but most reflections were so weak that they were measured with the minimum scan speed of 2° min^{-1}. Background counts were taken at half the scan time on either side of the peak. The intensity, I, and its standard deviation, $\sigma(I)$, were calculated as previously.[9] 3640 reflections with $2\theta < 50°$ were processed in total. 2513 of these had intensities greater than $1.96\sigma(I)$ and were used in the data treatment. The intensities of four check reflections were measured after every 62th reflection. They remained constant to within ±6 %.

The intensity data were corrected for the Lorentz and polarization factors and for absorption. The crystal used was prismatic a with dimensions 0.123 mm × 0.068 mm × 0.052 mm along a, b, and $[01\bar{1}]$ and had seven boundary planes. The transmission factors varied between 0.133 and 0.321. A semi-empirical absorption correction method was also tried for comparison.[9,10] The maximum measured intensity variation ratio was then 1.000 to 0.313.

Computer programs. The computer program system supplied by Syntex (XTL version 2)[11] for a NOVA 24K computer with a disk memory unit was used for the calculations. In addition the program DATAPU was used for the absorption correction using the Gaussian integration method and the plot program ORTEP 2 for the crystal structure illustrations. The originally written programs[12] have been modified for IBM 360/75 in Stockholm.

STRUCTURE DETERMINATION

A three-dimensional Patterson map was calculated. From the peak listing six U–U vectors with a multiplicity of two and three with a multiplicity of one could be identified. Therefore the space group was assumed to be the centrosymmetrical $P\bar{1}$ (No. 2).

The positions of the three U atoms in the asymmetric unit were determined. These parameters in addition to individual isotropic temperature factors and a scale factor were refined using the block-diagonal least squares method to a conventional R value of 0.139.

The positions of all light atoms were found from subsequent difference Fourier maps. Block-diagonal followed by full-matrix least squares refinements with U anisotropic gave an R value of 0.074 (0.078 with the semi-empirical absorption corrections). The weighted R value according to Hamilton[13] was then 0.102 (0.105). In the last cycle of the refinements no parameter shifts were greater than 0.5 % of the calculated standard deviations. The weighting scheme was based on the counter statistics, $1/w = \sigma^2(F_o) + 0.0016F_o^2$. The function minimized was $\Sigma w(|F_o| - k|F_c|)^2$. Final difference Fourier maps revealed an essentially smooth background of 2–3 electrons Å^{-3}. All of the residual peaks were too close to the atoms already found to be interpreted as the O atom in a fifth water of crystallization.

When no absorption corrections were applied to the intensity data the final conventional R value was 0.100 and the weighted R value 0.128. The difference Fourier map then showed sharp peaks of 5–7 electrons Å^{-3} within 1 Å from the U atoms in addition to the essentially smooth background of 2–3 electrons Å^{-3}. The structural parameters were not changed significantly on introducing the absorption corrections but the standard deviations were slightly reduced.

The final parameter values are given in Tables 1 and 2. A listing of the observed and calculated structure factors is available from the author on request. All these values are based on data where the Gaussian integration absorption correction method has been applied.

An attempt to introduce anisotropic thermal parameters for the light atoms was not successful. One of the U(ii) elements for three of the O atoms came out slightly negative. The remaining errors in the data are thus too large to make such refinements physically meaningful.

As a test, refinements were also performed in the space group $P1$ (No. 1). Then the R value only decreased by 0.001 to 0.073 and some of the O atoms obtained negative U values.

Table 1. Final positional and isotropic thermal parameters (Å^2) in the form exp $[-8\pi^2 U(\sin^2\theta/\lambda^2)]$. The positional parameters of U(1) to O(16) are referred to atoms in the same trinuclear complex and those of N(1) to O(3N) to atoms in the same nitrate ion. O(N)=nitrate O atoms, O(W)=O atoms in water molecules of crystallization.

Atom	*x*	*y*	*z*	*U*
U(1)	0.42446(17)	0.24136(13)	0.48431(14)	
U(2)	0.30968(17)	0.04145(13)	0.16582(14)	
U(3)	0.09907(17)	0.35650(13)	0.28310(14)	
O(1)	0.2558(42)	0.1585(31)	0.5078(31)	0.049(9)
O(2)	0.6040(30)	0.3211(23)	0.4682(23)	0.021(6)
O(3)	0.1456(32)	−0.0410(24)	0.2005(24)	0.025(6)
O(4)	0.4833(34)	0.1129(25)	0.1204(25)	0.030(7)
O(5)	−0.0526(42)	0.2870(30)	0.3240(31)	0.048(9)
O(6)	0.2407(34)	0.4384(25)	0.2388(25)	0.028(6)
O(7)	0.2955(32)	0.2227(24)	0.3103(24)	0.026(6)
O(8)	0.4862(33)	0.0450(25)	0.3450(25)	0.027(6)
O(9)	0.2407(31)	0.4174(23)	0.4843(23)	0.022(6)
O(10)	0.0948(39)	0.1706(29)	0.1097(29)	0.043(8)
O(11)	0.6215(32)	0.1463(23)	0.5979(24)	0.023(6)
O(12)	0.4595(36)	0.3762(26)	0.6925(27)	0.035(7)
O(13)	0.4549(32)	−0.1514(24)	0.1105(24)	0.026(6)
O(14)	0.1993(32)	−0.0638(23)	−0.0462(24)	0.023(6)
O(15)	−0.0197(43)	0.5609(32)	0.3811(32)	0.052(9)
O(16)	−0.1154(41)	0.3930(30)	0.1316(30)	0.047(9)
N(1)	0.2121(44)	0.3379(32)	0.9260(32)	0.030(8)
O(1N)	0.2157(47)	0.2268(36)	0.9137(35)	0.062(10)
O(2N)	0.0714(61)	0.3788(44)	0.8945(45)	0.092(15)
O(3N)	0.3355(48)	0.4018(35)	0.9723(35)	0.062(10)
O(1W)	0.2966(35)	0.6468(26)	0.1303(26)	0.032(7)
O(2W)	0.0332(52)	0.8026(38)	0.3652(39)	0.076(12)
O(3W)	0.8296(48)	0.0375(36)	0.3195(36)	0.065(11)
O(4W)	0.5851(52)	0.3628(38)	0.2111(38)	0.076(12)

Table 2. Final anisotropic thermal parameters (Å^2) in the form exp $[-2\pi^2(h^2a^{*2}U(11)+ \ldots+2hka^*b^*U(12)+\ldots)]$.

Atom	*U*(11)	*U*(22)	*U*(33)	*U*(12)	*U*(13)	*U*(23)
U(1)	0.0161(7)	0.0185(7)	0.0212(9)	−0.0003(6)	0.0014(6)	0.0071(7)
U(2)	0.0170(7)	0.0165(7)	0.0221(9)	0.0013(6)	0.0038(6)	0.0042(7)
U(3)	0.0154(7)	0.0199(7)	0.0212(9)	0.0032(6)	0.0046(6)	0.0073(7)

The scattering factors used were those given in the International Tables, Vol. IV,[14] for neutral atoms. Corrections for anomalous dispersion for U were applied.

DESCRIPTION OF THE STRUCTURE

The structure is shown in Fig. 1. It is built up from discrete charged triangular trinuclear complexes, nitrate ions, and water molecules of crystallization. One trinuclear complex is drawn separately in Fig. 2. Some important distances and angles are given in Table 3.

Each U atom in a trinuclear complex is surrounded by seven O atoms. The coordination polyhedron is a distorted pentagonal bipyramid. Two of these seven O atoms are the uranyl O atoms. The corresponding U−O bond lengths vary from 1.69

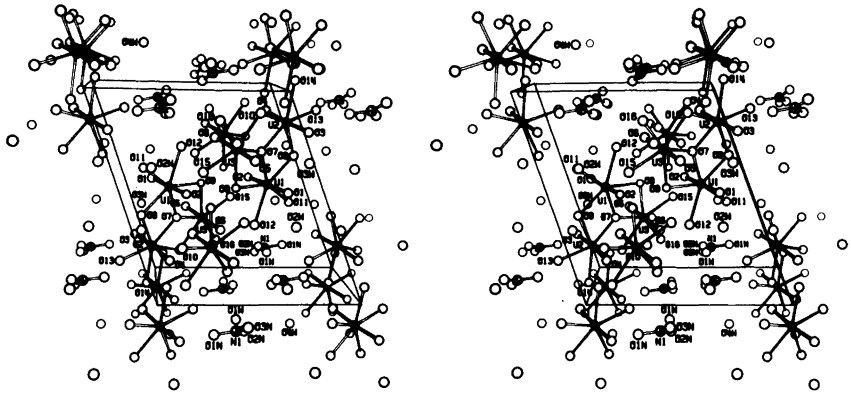

Fig. 1. A stereogram showing the unit-cell contents of $[(UO_2)_3O(OH)_3(H_2O)_6]NO_3.4H_2O$. The view is parallel to the a^* axis.

to 1.88 Å with an average value of 1.78 Å. One O atom, O(7), is shared between all three U atoms and is probably an O^{2-} oxygen atom. The corresponding U–O bond lengths are 2.17, 2.22 and 2.23 Å, the average value being 2.21 Å. Two O atoms within each pentagonal bipyramid are shared between two U atoms and are probably HO^- oxygens. The remaining two O atoms are coordinated to only one U atom and they are probably water O atoms. There are no significant differences in the U–O bond lengths for the HO^- and the water O atoms. The average value is 2.44 Å and the variation is from 2.39 to 2.50 Å. The formula of the complex ion can thus be written as $[(UO_2)_3O(OH)_3(H_2O)_6]^+$.

The U atoms are joined through double bridges containing one O atom and one HO group. The U–U distances are 3.788, 3.816 and 3.824 Å. The three U atoms in a trinuclear complex are at the corners of an equilateral triangle with an average edge length of 3.809 Å.

As the pentagons around the uranyl groups are roughly planar, least squares planes have been calculated through: (1) all three pentagons U(1), U(2), U(3), (2) the U(1) pentagon, (3) the U(2) pentagon, (4) the U(3) pentagon, (5) the uranyl groups of U(1) and U(2), (6) the uranyl groups of U(1) and U(3), (7) the uranyl groups of U(2) and U(3). A least squares plane through the nitrate group has also been calculated (8). The results are shown in Table 4. The deviations of atoms from the

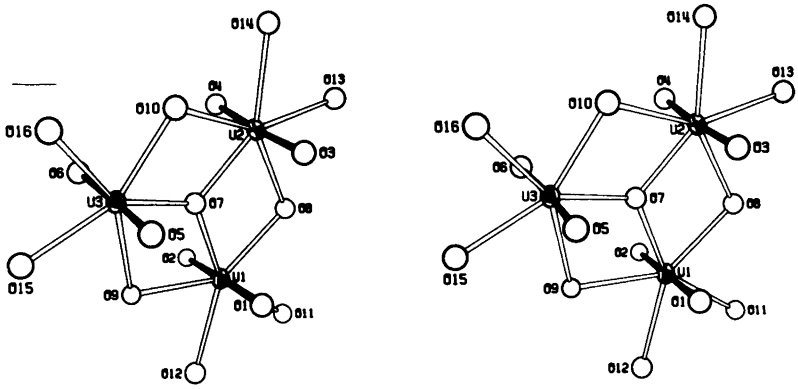

Fig. 2. A stereoscopic pair of perspective projections showing one trinuclear complex $[(UO_2)_3O(OH)_3(H_2O)_6]^+$. The thermal ellipsoids for U(1), U(2), U(3), O(2), O(3), O(9), O(11), and O(14) are scaled to include 50 % probability. For the other atoms U has been reduced to 0.025 $Å^2$ for clarity.

Table 3. Some important interatomic distances (Å) and angles (°).

U(1)–U(2)	3.788(2)						
U(1)–U(3)	3.816(2)	U(2)–U(3)	3.824(2)				
U(1)–O(1)	1.78(3)	U(2)–O(3)	1.81(3)	U(3)–O(5)	1.69(3)		
U(1)–O(2)	1.79(3)	U(2)–O(4)	1.88(3)	U(3)–O(6)	1.74(3)		
U(1)–O(7)	2.17(3)	U(2)–O(7)	2.23(3)	U(3)–O(7)	2.22(3)		
U(1)–O(8)	2.40(3)	U(2)–O(8)	2.41(3)	U(3)–O(9)	2.43(3)		
U(1)–O(9)	2.44(3)	U(2)–O(10)	2.40(3)	U(3)–O(10)	2.44(3)	O(7)–O(8)	2.60(4)
U(1)–O(11)	2.41(3)	U(2)–O(13)	2.39(3)	U(3)–O(15)	2.46(4)	O(7)–O(9)	2.59(4)
U(1)–O(12)	2.48(3)	U(2)–O(14)	2.50(3)	U(3)–O(16)	2.46(3)	O(7)–O(10)	2.61(4)

O(7)–U(1)–O(8)	69.1(10)	O(7)–U(2)–O(8)	68.0(10)	O(7)–U(3)–O(9)	67.6(9)
O(8)–U(1)–O(11)	76.0(9)	O(8)–U(2)–O(13)	76.5(9)	O(9)–U(3)–O(15)	75.4(10)
O(11)–U(1)–O(12)	71.0(9)	O(13)–U(2)–O(14)	74.0(9)	O(15)–U(3)–O(16)	75.2(12)
O(12)–U(1)–O(9)	76.0(9)	O(14)–U(2)–O(10)	72.5(10)	O(16)–U(3)–O(10)	74.0(11)
O(9)–U(1)–O(7)	68.0(10)	O(10)–U(2)–O(7)	68.7(11)	O(10)–U(3)–O(7)	68.1(11)
O(1)–U(1)–O(2)	175.9(14)	O(3)–U(2)–O(4)	174.9(12)	O(5)–U(3)–O(6)	174.4(15)
U(1)–O(7)–U(2)	118.8(12)	U(1)–O(7)–U(3)	120.7(13)	U(2)–O(7)–U(3)	118.5(12)
U(1)–O(8)–U(2)	103.7(11)	U(1)–O(9)–U(3)	103.1(10)	U(2)–O(10)–U(3)	104.6(12)
N(1)–O(1N)	1.21(6)			O(1N)–N(1)–O(2N)	117(4)
N(1)–O(2N)	1.26(6)			O(2N)–N(1)–O(3N)	124(4)
N(1)–O(3N)	1.18(5)			O(3N)–N(1)–O(1N)	119(4)

Table 4. Deviations (Å) of atoms from the calculated least squares planes.

Plane 1: U(1) 0.001(1), U(2) 0.000(1), U(3) 0.000(1), O(7) 0.18(3), O(8) −0.01(3), O(9) 0.00(2), O(10) −0.14(3), O(11) −0.11(3), O(12) −0.22(3), O(13) 0.00(3), O(14) −0.03(3), O(15) −0.03(3), O(16) −0.14(3)
Plane 2: U(1) 0.000(1), O(7) 0.02(3), O(8) −0.10(3), O(9) −0.04(2), O(11) 0.02(3), O(12) −0.07(3)
Plane 3: U(2) 0.000(1), O(7) 0.12(3), O(8) −0.07(3), O(10) −0.13(3), O(13) 0.02(3), O(14) 0.04(3)
Plane 4: U(3) 0.000(1), O(7) 0.08(3), O(9) −0.09(2), O(10) −0.13(3), O(15) 0.02(3), O(16) −0.01(3)
Plane 5: U(1) 0.000(1), U(2) 0.000(1), O(1) −0.02(3), O(2) −0.08(3), O(3) −0.08(3), O(4) −0.01(3)
Plane 6: U(1) 0.000(1), U(3) 0.000(1), O(1) 0.06(3), O(2) −0.06(3), O(5) −0.11(3), O(6) 0.04(3)
Plane 7: U(2) 0.000(1), U(3) 0.000(1), O(3) 0.07(3), O(4) −0.01(3), O(5) −0.01(3), O(6) 0.10(3)
Plane 8: N(1) 0.02(3), O(1N) −0.01(4), O(2N) −0.01(5), O(3N) −0.01(4)

planes are of the same magnitude as or smaller than those obtained for the tetranuclear complex $[(UO_2)_4Cl_2O_2(OH)_2(H_2O)_6].4H_2O$.[4] The maximum deviation of the dihedral angles from the ideal values 0 and 90° is 7° (between plane 2 and 4 and between plane 2 and 7).

As there are 23 H atoms in the asymmetric unit, hydrogen bonds are most probably holding the different complexes in the structure together. Table 5 gives a survey of the suggested hydrogen bond system.

DISCUSSION

According to statistical tests,[14] the absorption corrections based on the Gaussian integration method only marginally improved the intensity data in comparison with the semi-empirical absorption corrections. They are thus nearly equally good. The rather high final R value of 0.074 (0.078 with the semi-empirical absorption corrections) indicates that there are still systematic errors in the data. One reason for this is that there are very few strong reflections but many weak ones which were measured using the comparatively high minimum scan speed of 2° min^{-1}. Therefore it is not meaning-

Table 5. Intermolecular O–O distances (Å) for the suggested hydrogen bond system. The symmetry codes are:

(*a*)	$1-x,1-y,1-z$	(*g*)	$-x,1-y,1-z$
(*b*)	$x,y,-1+z$	(*h*)	$-1+x,y,z$
(*c*)	$1-x,-y,1-z$	(*i*)	$-1+x,1+y,z$
(*d*)	$x,-1+y,z$	(*j*)	$1+x,y,z$
(*e*)	$1-x,-y,-z$		
(*f*)	$-x,-y,-z$		

O(8)–O(3W)	2.82(5)	O(1W)–O(2N*g*)	2.93(6)
O(9)–O(2*a*)	3.06(4)	O(1W)–O(3N*b*)	2.84(5)
O(10)–O(1N*b*)	3.00(5)	O(2W)–O(1*g*)	2.95(5)
O(11)–O(8*c*)	2.68(4)	O(2W)–O(3W*i*)	3.24(6)
O(11)–O(2W*a*)	2.78(5)	O(3W)–O(3*j*)	3.10(5)
O(12)–O(1W*a*)	2.76(4)	O(3W)–O(5*j*)	2.97(6)
O(12)–O(4W*a*)	2.82(5)	O(4W)–O(4)	2.75(5)
O(13)–O(1N*c*)	2.79(5)	O(4W)–O(6)	2.91(5)
O(13)–O(1W*d*)	2.73(4)		
O(14)–O(4*e*)	2.83(4)		
O(14)–O(10*f*)	2.56(4)		
O(15)–O(9*g*)	2.58(4)		
O(15)–O(2W)	2.84(6)		
O(16)–O(2N*g*)	2.74(6)		
O(16)–O(4W*h*)	2.81(5)		

ful to discuss the hydrogen bond system in full detail.

The most remarkable aspect of the present structure as compared to those of other solids containing UO_2^{2+} and NO_3^- groups is that the nitrate ion is not coordinated to the U atom neither as a monodentate nor as a bidentate ligand. In $[UO_2(NO_3)_2(H_2O)_2].4H_2O$[15,16] and $[UO_2(NO_3)_2(H_2O)_2]$[17] each uranyl group is surrounded by two nitrate ions acting as bidentate ligands and by two water molecules. In $Rb[UO_2(NO_3)_3]$[18] and the isomorphous $Cs[UO_2(NO_3)_3]$[19] UO_2^{2+} is bidentately coordinated by three nitrate ions. In $M_2[UO_2(NO_3)_4]$ ($M=NH_4^+$, Rb^+, Cs^+)[20] the uranyl group is also hexa-coordinated. In these compounds, however, two nitrate ions act as monodentate and the other two as bidentate ligands.

Recently the crystal structure of $[(UO_2)_2(NO_3)_2(OH)_2(H_2O)_3].H_2O$ has been reported.[21] This phase was not found by Cordfunke during the investigation of the system $UO_2(NO_3)_2-UO_3-H_2O$ at 25 °C.[6] It is built up from dinuclear complexes. The two U atoms are joined through a double HO bridge. The nitrate ions are bidentately coordinated to the same U atom. Three of the water molecules are coordinated to the second U atom. The structure of $[(UO_2)_2(NO_3)_2(OH)_2(H_2O)_3].H_2O$ ($n_{HO}=1$) is thus different from that of the more hydrolyzed $[(UO_2)_3O(OH)_3(H_2O)_6]NO_3.4H_2O$ ($n_{HO}=5/3$). Furthermore it is different from that of $[(UO_2)_2Cl_2(OH)_2(H_2O)_4]$ ($n_{HO}=1$), which is also built up from dinuclear complexes with double HO bridges, but the Cl atoms are here coordinated to different U atoms.[3]

The U–O bond lengths obtained in the present investigation are in good agreement with those in the tetranuclear complex.[4] The shortest U–U distance, 3.788 Å, is nearly identical to the corresponding distance in the tetranuclear complex, *i.e.* the U–U distance within the HO/O bridge. The other two U–U distances, 3.816 and 3.824 Å, are significantly longer if only the standard deviations are considered. But because of the systematic errors, these differences may not be real. There might, however, be a chemical reason why the U(1)–U(3) and U(2)–U(3) distances are longer than the U(1)–U(2) distance. The HO^- oxygen atoms O(9) and O(10) bonded to U(3) seem to be more strongly hydrogen-bonded (2.58 and 2.56 Å, respectively) than the HO^- oxygen atom O(8) joining U(1) and U(2) (Table 5).

The nitrate ion is planar but slightly distorted. This distorsion may be only apparent, but as O(2N) seems to be the most strongly hydrogen-bonded of

the three nitrogen-coordinated O atoms, it is reasonable that the N(1)–O(2N) bond is longer than the other two N–O bonds.

CONCLUSION

In the $UO_2^{2+}-HO^--Cl^-$ as well as in the $UO_2^{2+}-HO^--NO_3^-$ system discrete polynuclear hydrolyzed complexes are formed as solids. The dinuclear complex $(UO_2)_2(OH)_2^{2+}$ has been isolated in both systems. Two anions and a number of water molecules are also coordinated. The structure of $[(UO_2)_2Cl_2(OH)_2(H_2O)_4]^3$ is, however, different from that of $[(UO_2)_2(NO_3)_2(OH)_2(H_2O)_3]$.[21] The trinuclear complex $(UO_2)_3O(OH)_3^+$ has been found in the nitrate system only. It does not coordinate any anions, only six water molecules. The tetranuclear complex $(UO_2)_4O_2(OH)_2^{2+}$ seems to be formed only in the presence of Cl^- ions, which act as bridges between the U atoms. Two Cl^- ions and six water molecules are coordinated.[4]

In hydrolyzed and acidic uranyl chloride solutions Cl^- ions are coordinated to U.[2] No X-ray diffraction investigations of uranyl nitrate solutions have been performed. Unfortunately, the system $UO_2(NO_3)_2-UO_3-H_2O$ is less favourable for such measurements than the corresponding Cl^- system. From the phase diagram[6] it can be estimated that $n_{HO}\approx 0.5$ for the region of highest solubility. The maximum value of n_{HO} is only about 0.7 and then the solubility is probably too low for an X-ray diffraction investigation. For the system $UO_3-HCl-H_2O$ the maximum n_{HO} obtainable was 1.11 when the solubility was about 3.1 M.[2]

Acknowledgements. I wish to thank Dr. Georg Johansson for his interest in this work and for valuable advice and Prof. Ingmar Grenthe for criticism of the manuscript. The work has been financially supported by the Swedish Natural Science Research Council. Through a generous grant from the "Knut and Alice Wallenberg's Foundation" it has been possible to buy the computer-controlled four-circle diffractometer with a complete program system for crystal structure determinations.

REFERENCES

1. Sillén, L. G. and Martell, A. (compilers) *Stability Constants of Metal-Ion Complexes*, Chem. Soc. Spec. Publ. No. 17 (1964); Suppl. No. 1, Spec. Publ. No. 25 (1971).
2. Åberg, M. *Acta Chem. Scand. 24* (1970) 2901.
3. Åberg, M. *Acta Chem. Scand. 23* (1969) 791.
4. Åberg, M. *Acta Chem. Scand. A 30* (1976) 507.
5. Prins, G. and Cordfunke, E. H. P. *J. Inorg. Nucl. Chem. 37* (1975) 119.
6. Cordfunke, E. H. P. *J. Inorg. Nucl. Chem. 34* (1972) 531.
7. Gibson, G. and Katz, J. J. *J. Am. Chem. Soc. 73* (1951) 5436.
8. Woodhead, J. L., Deane, A. M., Fox, A. C. and Fletcher, J. M. *J. Inorg. Nucl. Chem. 28* (1966) 2175.
9. Sandström, M. and Persson, I. *Acta Chem. Scand. A 32* (1978) 95.
10. Kopfmann, G. and Huber, R. *Acta Crystallogr. A 24* (1968) 348; North, A. C. T., Phillips, D. C. and Scott Mathews, F. *Ibid.* 351.
11. *Syntex Analytical Instruments, Inc.* 100 40 Bubb Road, Cupertino, California 95014, USA.
12. DATAPU, originally written by Coppens, P., Leiserowitz, L. and Rabinovich, D. *Acta Crystallogr. 18* (1965) 1035; Johnson, C. K. *ORTEP 2: A Fortran Thermal-Ellipsoid Plot Program for Crystal Structure Illustrations*, Report ORNL-5138, Oak Ridge National Laboratory, Oak Ridge 1976.
13. Hamilton, W. C. *Acta Crystallogr. 18* (1965) 502.
14. *International Tables for X-Ray Crystallography*, Kynoch Press, Birmingham 1974, Vol. IV.
15. Hall, D., Rae, A. D. and Waters, T. N. *Acta Crystallogr. 19* (1965) 389.
16. Taylor, J. C. and Mueller, M. H. *Acta Crystallogr. 19* (1965) 536.
17. Kent Dalley, N., Mueller, M. H. and Simonsen, S. H. *Inorg. Chem. 10* (1971) 323.
18. Barclay, G. A., Sabine, T. M. and Taylor, J. C. *Acta Crystallogr. 19* (1965) 205.
19. Živadinovic', M. S. *Bull. Boris Kidric Inst. Nucl. Sci., Phys. 18* (1967) 1.
20. Kapshukov, I. I., Volkov, Yu, F., Moskvichev, E. P., Lebedev, I. A. and Yakovlev, G. N. *Zh. Strukt. Khim. 12* (1971) 94.
21. Perrin, A. *Acta Crystallogr. B 32* (1976) 1658.

Received August 30, 1977.

Acta Chemica Scandinavica A 32 (1978) 109 – 113

The Crystal Structure of Hexaaquamercury(II) Perchlorate, $[Hg(H_2O)_6](ClO_4)_2$

GEORG JOHANSSON and MAGNUS SANDSTRÖM

Department of Inorganic Chemistry, Royal Institute of Technology, S-100 44 Stockholm 70, Sweden

The crystal structure of the hexahydrate of mercury(II) perchlorate has been determined from three-dimensional single-crystal X-ray diffraction data collected at room temperature on an automatic Syntex $P2_1$ four-circle diffractometer. The unit cell, which is trigonal with $a=b=8.005(4)$ Å and $c=5.344(2)$ Å, contains one formula unit. The space group is No. 164: $P\bar{3}m1$. The structure, refined to a final conventional R value of 0.035, is built-up from discrete octahedral $Hg(H_2O)_6^{2+}$ units and perchlorate ions. The six Hg – O bonds are equivalent with bond lengths of 2.341(6) Å. The complexes are held together by weak hydrogen bonds.

Mercury(II) frequently forms an irregular octahedral coordination with two short collinear bonds. Only for the compound $[Hg(C_6H_5NO)_6](ClO_4)_2$ has a regular octahedral oxygen coordination been reported with an Hg – O bond length of 2.35(2) Å.[1] Measurements of X-ray scattering and Raman spectra from aqueous[2,3] and dimethyl sulfoxide[3] (DMSO) solutions of mercury(II) perchlorate have been found to be consistent with a regular octahedral coordination around the mercury(II) ion, with the lengths of the Hg – O bonds close to 2.40 Å. In view of these results it seemed of interest to determine the crystal structures of the corresponding solid solvates for a comparison of the coordination around the mercury(II) ion with that found in solution.

The present paper reports the crystal structure of $[Hg(H_2O)_6](ClO_4)_2$. The crystal structures of $[Hg(DMSO)_6](ClO_4)_2$ and $Hg(ClO_4)_2.4DMSO$ will be reported in separate papers.[4,5]

EXPERIMENTAL

Preparation of crystals. Yellow mercury(II) oxide was dissolved in sufficient perchloric acid to avoid the formation of basic salts. Solutions with mol ratios $HClO_4 - HgO \geq 2$ were used. On slow evaporation over sulfuric acid in a desiccator, large, prismatic, colourless crystals of the hexahydrate were formed. They were found to be extremely soluble and were not stable outside the mother liquor.

Analyses. For the analyses excess solvent was centrifuged off and the crystals were quickly dissolved in water and weighed. Mercury was determined by a complexometric titration procedure using EDTA.[6] Perchlorate was determined by ion exchange on an H^+ saturated Dowex 50 cation exchange resin.

Values found were: 40.7 % Hg, 40.3 % ClO_4 and, by difference, 19.0 % H_2O. Calculated values for $Hg(ClO_4)_2.6H_2O$ are: 39.5 % Hg, 39.2 % ClO_4 and 21.3 % H_2O.

X-Ray data. A crystal, enclosed in a capillary and having the shape of a slightly elongated ellipsoid with a maximum dimension of about 0.2 mm, was used for the collection of the diffraction data.

The unit cell parameters were determined by the standard procedure on the computer controlled Syntex $P2_1$ four-circle diffractometer.[4] The angular coordinates of 15 centred reflections were used in a least-squares refinement of the lattice constants. The dimensions found for the trigonal unit cell were $a=b=8.005(4)$, $c=5.344(2)$ Å. The previously reported density[7] $D_m=2.791$ g cm^{-3} gave $Z=1$ and $D_x=2.84$ g cm^{-3}.

The ω scan technique with different scan speeds from 0.5° min^{-1} upwards was used. Four check reflections were measured regularly at intervals of 50 reflections. All 442 hkl and $hk\bar{l}$ reflections up to $2\theta=50°$ were measured (Mo$K\alpha$ radiation, $\lambda=0.7107$ Å). In addition, $h\bar{k}l$ and $h\bar{k}\bar{l}$ reflections were recorded,

but during this collection the intensities of the two strong low-angle check reflections $1\bar{1}0$ and $1\bar{2}0$, which had been slowly and continuously increasing, started to decrease rapidly. Therefore, only the first 265 of these reflections were used in the following data treatment. The maximum intensity variation for these two low-angle check reflections were within ± 16 % for the data range used. The other two, $3\bar{2}1$ and $2\bar{2}2$ at medium angles, remained fairly constant during the data collection.

A semi-empirical absorption correction, obtained by measuring intensity variations for selected reflections when rotating around the diffraction vector, was applied to the data.[8,4] The largest relative reduction in intensity measured for any of the reflections was from 1 to 0.36. The linear absorption coefficient is $\mu(\mathrm{Mo}K\alpha) = 138\ \mathrm{cm}^{-1}$.

Equivalent reflections were averaged giving a total number of 223 independent reflections, none of which had an observed intensity $< 7\sigma(I)$.

The data were corrected for Lorentz and polarization effects and approximate values for the temperature and scale factors were obtained by Wilson's method. All calculations were carried out by means of the *Syntex* XTL Crystallographic Program System.[9]

STRUCTURE DETERMINATION AND REFINEMENT

Space-group determination. The diffraction symmetry indicated the Laue group to be $\bar{3}m$. Since no systematic absences were observed, six space groups are possible, *viz.* *P*312, *P*321, *P*3*m*1, *P*31*m*, *P*$\bar{3}$1*m*, and *P*$\bar{3}$*m*1.[10]

With only one formula weight in the unit cell the single Hg atom and the two Cl atoms must occupy special positions on three-fold axes according to any of these symmetries. Some of the possible space groups would not lead to reasonable arrangements of oxygen atoms around the Hg and Cl atoms and could be eliminated on that ground. A three-dimensional Patterson function was consistent with a centrosymmetric structure having atomic positions according to the space group of highest symmetry, *P*$\bar{3}$*m*1 (No. 164), which, therefore, was assumed to be the correct one.

Least-squares refinements. With the atomic positions derived from the Patterson function as the starting point a full-matrix least-squares refinement was carried out. The function minimized was $\Sigma w \| F_o | - | F_c \|^2$ with the weighting function $w = 1/\{\sigma^2(F_o) + (0.04F_o)^2\}$ which, according to a statistical analysis of the error distribution, leads to a satisfactory weighting scheme.

The scattering factors used were calculated from analytical expressions for the neutral atoms.[10] Anomalous dispersion corrections were included for Hg and Cl.[10]

With isotropic temperature factors for all atoms, the final conventional R value ($R = \Sigma \| F_o | - | F_c \| / \Sigma | F_o |$) was 0.082 and $R_w = (\Sigma w \| F_o | - | F_c \|^2 / \Sigma w | F_o |^2)^{\frac{1}{2}}$ was 0.133. With anisotropic temperature factors for Hg only, the values were $R = 0.045$ and $R_w = 0.055$. In the final refinement anisotropic temperature factors were introduced for all atoms and a total of 20 parameters were refined, giving $R = 0.035$ ($R_w = 0.045$).

A similar refinement using data to which absorption corrections had not been applied, resulted in final R values about twice as large as those obtained for the corrected data.

The parameter shifts in the final refinement cycle were all less than 1 % of the corresponding standard deviation. A difference map calculated from the final parameter values showed some spurious peaks, the highest of which was 0.58 e/Å^3. None of these peaks seemed possible to relate to hydrogen atom positions.

The final parameter values are given in Tables 1 and 2.

Table 1. Final fractional atomic positional parameters. For the independently refined parameters estimated standard deviations are given in parenthesis.

Atom	Position	x	y	z
Hg	1(a)	0	0	0
Cl	2(d)	1/3	2/3	0.2043(7)
O1	6(i)	0.1327(5)	−0.1327	−0.2711(14)
O2	6(i)	0.4291(9)	−0.4291	0.2827(30)
O3	2(d)	1/3	2/3	−0.0715(44)

Table 2. Final anisotropic thermal parameters in $Å^2$ with estimated standard deviations within parenthesis. The temperature factor expression used is $\exp[-1/4(B_{11}h^2a^{*2}+\cdots+2B_{12}hka^*b^*+\cdots)]$.

Atom	$B_{11}=B_{22}$	B_{33}	B_{12}	$B_{13}=-B_{23}$
Hg	4.53(4)	2.97(4)	$=\frac{1}{2}B_{11}$	0
Cl	3.25(8)	4.07(15)	$=\frac{1}{2}B_{11}$	0
O1	5.6(3)	4.5(3)	3.7(3)	0.33(16)
O2	9.7(6)	10.9(8)	7.1(7)	−0.67(26)
O3	9.9(10)	6.7(11)	$=\frac{1}{2}B_{11}$	0

Table 3. Interatomic distances (Å) and angles (°) with estimated standard deviations in parenthesis. Assigned H bonds are denoted by dots.

Within an $Hg(H_2O)_6^{2+}$ octahedron			
Hg–O1	2.341(6)	O1–Hg–O1	85.81(18)
O1–O1	3.188(6)		94.19(18)
	3.430(9)		
Within a ClO_4^- tetrahedron			
Cl–O2	1.394(9)	O2–Cl–O2	111.4(6)
Cl–O3	1.472(24)	O2–Cl–O3	107.5(7)
O2–O2	2.302(6)		
O2–O3	2.311(24)		
Remaining distances < 3.6 Å and bond angles			
O1···O1	3.059(9)	Hg–O1···O3	120.9(3)
O1–O2	3.073(6)	Hg–O1···O1	104.9(2)
	3.390(14)	Cl–O3···O1	110.9(7)
O1···O3	2.981(10)	O1···O3···O1	108.0(4)
O2–O2	3.041(18)	O3···O1···O1	124.5(3)
O2–O3	3.483(11)		

DISCUSSION OF THE STRUCTURE

General. The atomic arrangement is illustrated in Figs. 1 and 2. Some interatomic distances and angles are given in Table 3.

The structure is built up of discrete HgO_6 octahedra and ClO_4 tetrahedra having no oxygen atoms in common. Both the mercury atom and the two chlorine atoms in the unit cell occupy positions on the three-fold axes.

The $Hg(H_2O)_6^{2+}$ complex ion. The $Hg(H_2O)_6$ octahedra are stacked on top of each other along the three-fold inversion axis with triangular faces

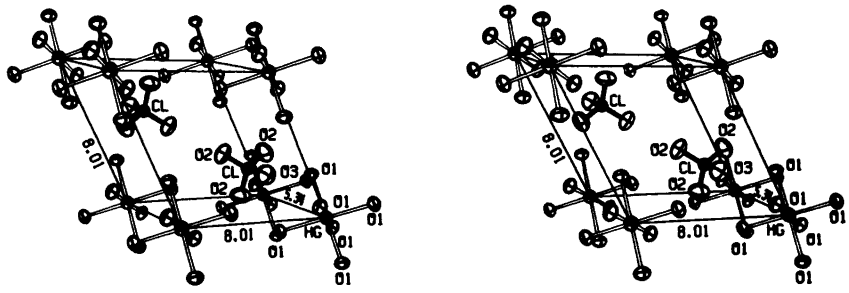

Fig. 1. A stereoscopic view of the trigonal unit cell. The lengths of the unit cell edges are given in Å. The *a* edge is horizontal in the picture. The ellipsoids are drawn to enclose 30 % probability.

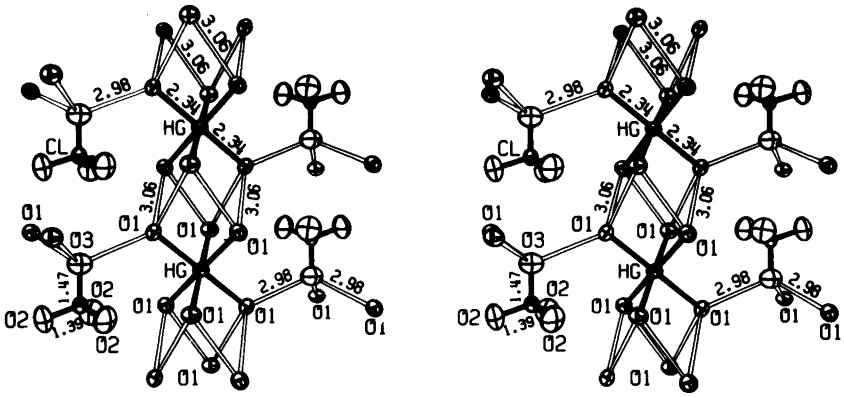

Fig. 2. A stereoscopic view showing a string of $Hg(H_2O)_6^{2+}$ octahedra along the *z* axis (vertical in the picture). Two of the six surrounding parallel columns of perchlorate ions are also shown. The assigned H bonds are illustrated by the unfilled bonds. The six equivalent H bond directions possible between the O1 water molecules in two adjacent $Hg(H_2O)_6^{2+}$ octahedra (see text) are indicated. Distances are given in Å. The thermal ellipsoids enclose 30 % probability.

parallel (Fig. 2). A string of octahedra of O1 atoms along the *z* axis is thus formed, every second of which contains an Hg atom. The distances between oxygen atoms in the triangular faces perpendicular to the three-fold axis are 3.19 Å. Since the *z* parameter of the O1 atom is slightly larger than 1/4 (Table 1), the octahedra containing the Hg atoms are slightly elongated along the *z* axis, resulting in a longer distance, 3.43 Å, for the remaining O1 – O1 distances within the HgO_6 octahedron. The empty octahedra are correspondingly compressed, leading to O1 – O1 distances of 3.06 Å, which are therefore the shortest distances between water molecules belonging to different $Hg(H_2O)_6$ octahedra. This deviation from a regular octahedral coordination around the Hg atom is the only one allowed by the space group symmetry. All the Hg – O1 bond lengths will still be equal and are found to be 2.341(6) Å which, for a regular octahedron, would correspond to an O – O distance of 3.31 Å.

The perchlorate ion. The tetrahedral ClO_4^- group is slightly elongated along the three-fold rotation axis (Fig. 2). The Cl – O3 bond, 1.472(24) Å, coinciding with this axis, is significantly longer than the three equivalent Cl – O2 bonds of 1.394(9) Å. The average Cl – O bond distance, 1.41_4 Å, does not differ significantly from values found for other weakly H bonded perchlorates, *e.g.* 1.42_6 Å for $NaClO_4.H_2O$ and $LiClO_4.3H_2O$.[11]

Hydrogen bonds. The distorsion of the $Hg(H_2O)_6^{2+}$ octahedron and the comparatively short O1 – O1 distance, 3.06 Å, between the water molecules in adjacent octahedra, can probably be related to a formation of hydrogen bonds. The arrangement of other oxygens around an O1 atom seems to suggest that one of the protons associated with O1 is involved in a bond of length 3.06 Å to one of the two equidistant O1 atoms belonging to a different $Hg(H_2O)_6$ octahedron.

With the assumed space group symmetry there are two equivalent alternatives for O1 to accept the H-bond. Since the refinement of the structure indicated no deviations from the symmetry $P\bar{3}m1$, a statistical distribution of the proton between the two possible positions seems likely. Of the six equivalent H bond directions between two different $Hg(H_2O)_6^{2+}$ octahedra, which are indicated in Fig. 2, only three would then be occupied simultaneously. Moreover, it seems probable that each O1 water molecule is the acceptor of only one of the H bonds at the same time. A bifurcated H bond seems less probable since this would lead to less favorable acceptor angles[12] than those given in Table 3.

The second proton of the O1 water molecule probably forms an H bond, of length 2.98(1) Å, to the O3 oxygen atom belonging to a perchlorate group. The arrangements around the atoms O1 and O3 are illustrated in Fig. 2, where the H bond lengths are given. Corresponding angles are found in Table 3.

Two more perchlorate oxygens, O2, occur within possible H bonding distances, 3.073(6) Å, from the

O1 water molecule. However, the corresponding angles (O3–O1–O2 70.2(3)°, O2–O1–O2 136.5(3)°, C1–O2–O1 125.8(6)°) deviate considerably from the tetrahedral value, which therefore makes an H bond formation between O1 and O2 less likely.

According to the proposed H bonding scheme, the O1 water molecule thus forms two weak H bonds to surrounding atoms and, on the average, accepts one bond. The O3 atom is the acceptor of three symmetrically arranged H bonds, with almost tetrahedral acceptor angles (Table 3). This assignment of H bonds is supported by the long Cl–O3 bond distance, 1.472(24) Å. Similar lengthenings of Cl–O bond distances, where the oxygen atom is engaged in H bonding, have been reported for other perchlorates.[13,14]

CONCLUSIONS

This crystal structure determination confirms the conclusions from previous X-ray scattering measurements on solutions,[2,3] that the mercury(II) ion can be octahedrally coordinated to oxygen atoms, forming six equivalent Hg–O bonds. The Hg–O bond lengths found for the solid compounds $[Hg(H_2O)_6](ClO_4)_2$(2.341(6) Å), and $[Hg(DMSO)_6](ClO_4)_2$ (2.317(6), 2.320(6) and 2.376(6) Å), are, however, significantly shorter than the corresponding Hg–O bond lengths found for solutions, 2.41(1) Å in aqueous solution[2,3] and 2.393(5) Å in DMSO solution.[3]

The compound $[Cd(H_2O)_6](ClO_4)_2$ seems to be isostructural with $[Hg(H_2O)_6](ClO_4)_2$. A slightly smaller trigonal unit cell with $a=b=7.96$, $c=5.30$ Å, $D_m=2.368$ g cm^{-3} and $Z=1$ has been reported.[7]

Acknowledgements. The authors wish to thank Mr. E. Hansen for skilful technical assistance. The Swedish Natural Science Research Council and the foundation "Knut och Alice Wallenbergs Stiftelse" are thanked for their support.

REFERENCES

1. Kepert, D. L., Taylor, D. and White, A. H. *J. Chem. Soc. Dalton Trans.* (1973) 670.
2. Johansson, G. *Acta Chem. Scand. 25* (1971) 2787.
3. Sandström, M., Persson, I. and Ahrland, S. *Acta Chem. Scand. A 32* (1978). *In press.*
4. Sandström, M. and Persson, I. *Acta Chem. Scand. A 32* (1978) 95.
5. Sandström, M. *Acta Chem. Scand. A 32* (1978). *In press.*
6. Schwarzenbach, G. *Complexometric Titrations*, Methuen, London 1957.
7. West, C. D. *Z. Kristallogr. 91 A* (1935) 480.
8. Kopfmann, G. and Huber, R. *Acta Crystallogr. A 24* (1968) 348; North, A. C. T., Phillips, D. C. and Scott Mathews, F. *Ibid.* 351.
9. *Syntex Analytical Instruments, Inc.*, 10040 Bubb Road, Cupertino, California 95014, U.S.A.
10. *International Tables for X-Ray Crystallography*, Kynoch Press, Birmingham 1969 and 1974, Vols. 1 and 4, respectively.
11. Berglund, B., Thomas, J. O. and Tellgren, R. *Acta Crystallogr. B 31* (1975) 1842.
12. Hamilton, W. C. and Ibers, J. A. *Hydrogen Bonding in Solids*, Benjamin, New York 1968, p. 212.
13. Almlöf, J. *Acta Crystallogr. B 28* (1972) 481.
14. Olovsson, I. *J. Chem. Phys. 49* (1968) 1063.

Received September 21, 1977.

Acta Chemica Scandinavica A 32 (1978) 115–119

The Molecular Structure and Conformation of Dichloromethyl Methyl Ether, $Cl_2HC—O—CH_3$, in the Gas Phase

E. E. ASTRUP

Department of Chemistry, University of Oslo, Oslo 3, Norway

The molecular structure and conformation of dichloromethyl methyl ether have been investigated in the gas phase by the electron-diffraction method. As expected, a shortening of the C–O bond compared to the corresponding bond in unsubstituted ethers and a lengthening of the C–Cl bond compared to chlorine-substituted alkanes are observed for this compound. From the analysis of dichloromethyl methyl ether the conclusion may be drawn that the *gauche-gauche* conformation, where the two dihedral angles δ(ClCOC) are (+)*gauche* and (−)-*gauche*, ($\pm 60.6°$), is strongly preferred.

The following parameters have been determined: $r(C-O)_{CH_3} = 1.405(9)$ Å, $r(C-O)_{CHCl_2} = 1.383(9)$ Å, $r(C-H) = 1.161(12)$ Å, $r(C-Cl) = 1.798(3)$ Å, $\angle COC = 118.6(2.1)°$, $\angle OCCl = 111.8(1.5)°$, $\angle OCH_{CH_3} = 112.5°$, $\delta ClC(2)OC(1) = 60.6(1.6)°$, $\delta H(1)C(1)OC(2) = 30.3(6.3)°$.

The molecular conformation of chloromethyl methyl ether and bis(chloromethyl) ether have already been investigated by different methods, *i.e.* dipole moments,[1–3] Raman,[4] infrared,[5–7] and microwave spectroscopy[8] and electron diffraction.[9,10] The conclusion obtained by all but one[6] of these investigations is that there is a preference for the chlorine atoms to be in *gauche* relation to the COC chain. Charles *et al.*[7] also report small amounts of molecules with *anti* dihedral angles δClCOC to be present for bis(chloromethyl) ether, while Chiba[1] suggests from his data the existence of slightly different conformers among which the *gauche* conformation has the lowest energy.

It was therefore of interest to investigate the molecular structure and conformation of dichloromethyl methyl ether (Fig. 1) in the gas phase by the electron diffraction method in order to see whether the chlorine atoms both prefer the *gauche* position (g^+g^-) or if the *anti* conformer (*ag*) is also present.

EXPERIMENTAL

The sample of dichloromethyl methyl ether used in this investigation was obtained from Fluka and was purified by GLC. The electron diffraction diagrams were taken on a Balzers Eldigraph KD G2. The pressure in the apparatus during the exposure was approximately 5×10^{-5} Torr. The sample temperature was kept at about 23 °C. The diffraction diagrams were recorded at two different nozzle-to-plate distances, *i.e.* 25.00 and 50.00 cm. The accelerating voltage of the electrons was approximately 42 kV, corresponding to a wavelength of the electrons of 0.05845 and 0.05848 Å, respectively. Four selected plates from each nozzle-to-plate distance were used in the analysis. The intensities were modified by $s/|f_C'||f_O'|$, where $|f'|$ is the scattering amplitude[11,12] for carbon and oxygen.

The experimental data were analysed in the usual way.[13] The experimental data obtained cover scattering angles corresponding to an s-range of 1.5–29.75 $Å^{-1}$. The molecular intensity curve is shown in Fig. 2.

The calculations have been carried out on CDC 3300 and CDC 7400(CYBER) computers.[13]

STRUCTURE ANALYSIS

Approximate values for the molecular parameters were estimated from the experimental radial distribution (RD) curve (Fig. 3) and refined by the least-squares procedure.

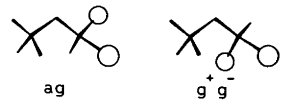

Fig. 1. Dichloromethyl methyl ether. The two distinguishable staggered conformations: *anti-gauche* (*ag*) and *gauche*(+)-*gauche*(−) (g^+g^-).

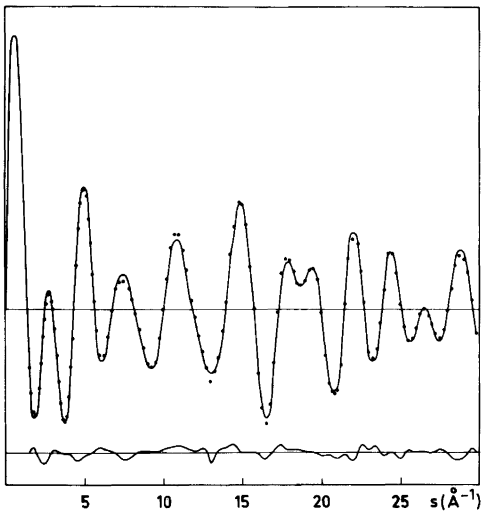

Fig. 2. Dichloromethyl methyl ether. Theoretical molecular intensity curve. The dots show the experimental values. The lower curve shows the difference between the experimental and the theoretical values.

The first peak at about 1.4 Å in the RD curve shows a shoulder at 1.16 Å, corresponding to the four C–H bond distances. Any possible difference in the C–H bond length in the methyl and dichloromethyl groups cannot be determined by this method. All the C–H distances are therefore assumed to be equal. The main peak at 1.4 Å contains the two C–O bond distances. As it has earlier been found that chlorine substitution on carbon atoms in α-position to an ether oxygen atom results in a decrease of the C–O bond length,[9,10] the two C–O bonds in dichloromethyl methyl ether were expected to be of different lengths. Due to the large correlation between the two C–O bonds and the corresponding vibrational amplitudes, the refinement of the parameters is only possible when some of the parameters are kept at fixed values during the refinement. It then seems fairly reasonable to assume the vibrational amplitudes (u-values) for the two C–O distances to be equal and of the same magnitude as the corresponding u-values in $ClCH_2-O-CH_2Cl$,[10] where the two C–O bonds are equal and therefore determined with larger accuracy. In the further refinement of the parameters these u-values were kept at fixed values (0.043 Å). The refinement of the carbon oxygen bond distances then results in a shorter length of 1.383 Å for the dichloromethoxy group and a length of 1.410 Å for the methoxy group. The well-resolved peak at 1.8 Å corresponds to the two Cl–C bond distances.

The C···C and Cl···H distances over one angle are found in the small peak at 2.4 Å, while the peak at 2.6 Å is mainly due to the two Cl···O distances. The Cl···Cl distance appears with large weight in the RD curve at 2.9 Å.

The conformation of the Cl–C–O–C skeleton may be determined from the non-bonded C···Cl distances [C(1)···Cl(1) and C(1)···Cl(2)]. As there are no pronounced peaks in the RD curve outside the shoulder at about 3.1 Å, the two C···Cl distances must come in this region. From Fig. 3 this is seen to give a good agreement between experimental and

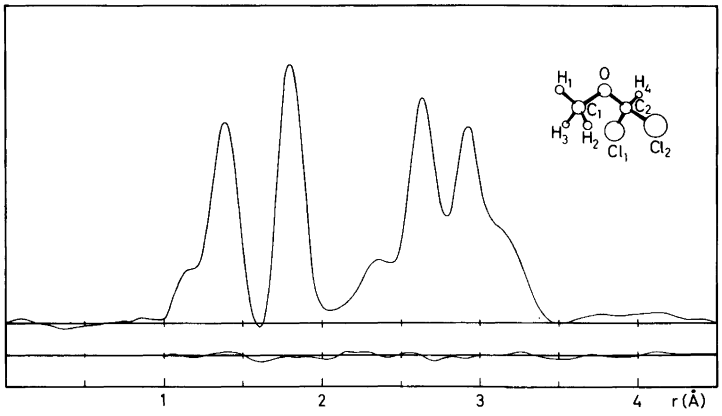

Fig. 3. Dichloromethyl methyl ether. Experimental radial distribution curve. The lower curve shows the difference between the experimental and the theoretical values. Artifical damping constant $k=0.0020$ Å.

theoretical data. Within the standard deviation the two Cl−C−O−C dihedral angles are found to be equal. In the final refinement the two dihedral angles ClC(2)OC(1) and Cl(2)C(2)OC(1) have therefore been assumed to be of the same magnitude with one chlorine atom on each side of the molecular plane.

By twisting the $CHCl_2$ group from a g^+g^- to an *ag* conformation one C···Cl distance is shifted from about 3.1 Å to about 4.0 Å. Refinements including both a g^+g^- and an *ag* conformation in mixture result in a contribution of approximately 4 % of the *ag* conformer. As, however, the standard deviation is larger than the determined percentage, the presence of the *ag* conformer is doubtful.

The poor scattering of electrons by hydrogen atoms makes the determination of hydrogen atom positions difficult by electron diffraction. As a consequence of this, it is not possible to obtain convergency in the least-squares refinement of the OCH angle. This angle, therefore, has been determined by trial and error.

When the three O···H distances from oxygen to methyl hydrogen atoms are of equal lengths, this will result in a disagreement between the experimental and theoretical RD curves at about 2.1 Å. An apparently better correspondance in this region is obtained by tilting the methyl group in such a way that the three-fold axis of the methyl group makes an angle with the $O-CH_3$ axis. However, as the error of square residuals is not decreased by introduction of the tilt parameter, and as the standard deviation of the tilt angle is very large, the tilt is not included.

The only information of any significance about the methyl hydrogen atom positions is given by the non-bonded Cl···H distances, and, unfortunately, even these distances appear with fairly small weight

Table 1. Structure parameters for dichloromethyl methyl ether. Distances (r_a-values) and mean amplitudes of vibration (*u*-values) are given in Å, angles in degrees. The standard deviations have been corrected to take into account data correlation. The uncertainty arising from error in the electron wavelength is included. (For numbering of the atoms see Fig. 3.)

No.	Parameter	r_a	*u*
1	C(1)−O	1.405(9)	0.043[a]
2	C(2)−O	1.383(9)	
3	C−H	1.161(12)	0.078
4	C−Cl	1.798(3)	0.042
5	Cl···Cl	2.909(5)	0.064(7)
6	Cl···O	2.644(3)	0.051(6)
7	Cl···C	3.114(12)	0.105(16)
8	C···C	2.397(14)	0.085(30)
9	Cl···H(4)	2.378(17)	0.085
10	Cl(2)···H(3)	3.970(85)	
11	Cl(2)···H(2)	2.661(66)	
12	Cl(2)···H(1)	3.887(71)	0.16−0.20
13	Cl(1)···H(3)	3.096(89)	
14	Cl(1)···H(2)	3.183(99)	
15	Cl(1)···H(1)	4.268(37)	
16	O···H(1)	2.068(60)	0.14
17	O···H(4)	2.149(71)	
18	∠COC	118.6(2.1)	
19	∠OCH(1)	112.5	
20	∠OCCl	111.8(1.5)	
21	∠OCH(4)	115.0	
22	∠ClCCl	108.0	
23	δClC(2)O	60.6(1.6)	
24	δH(4)C(2)OC(1)	180.0	
25	δH(2)C(1)OC(2)	30.3(6.3)	

[a] Fixed during refinement.

Table 2. Elements of the correlation matrix (× 100). Only elements [ρ(i,j)] of absolute values larger than 0.5 are given. The number associated with the distances, *r*; angles, ∠; and *u*-values, *u*, refer to those given in the parameter list, Table 1.

ρ(r1/r2)	−85	ρ(r1/∠18)	−64	ρ(r1/∠20)	78	ρ(r1/∠23)	64
ρ(r2/∠18)	63	ρ(r2/∠20)	−92	ρ(r2/∠23)	−76	ρ(r2/u6)	68
ρ(r3/u6)	−65	ρ(r3/u7)	82				
ρ(∠18/∠20)	−72	ρ(∠18/∠23)	−69	ρ(∠18/∠25)	85		
ρ(∠20/∠23)	91						
ρ(∠23/∠25)	63						
ρ(u7/u5)	82						

in the curves. The best agreement between experimental and theoretical curves is obtained for a dihedral angle δ H(2)C(1)OC(2) of 30.3° (6.3°).

As the peak at about 3.7−4.4 Å, containing mainly Cl···H distances, is not very pronounced, and as the Cl···H lengths are not very sensitive to small changes in the twist angle, the standard deviation for this angle is seen to be large.

In order to obtain convergency in the least-squares refinement it was necessary to keep not only the OCH angle and the *u*(C−O) at fixed values during the refinement, but also the *u*-values for non-bonded Cl···H, O···H, C···H and H···H distances. Keeping some parameters at fixed values during the refinement results in too small standard deviations for some of the parameters. To compensate for this the approach proposed by Seip[14] has been applied to some of the more important parameters. The final parameters are shown in Table 1 and elements from the correlation matrix in Table 2.

DISCUSSION

From the electron diffraction investigation of $Cl_2HC-O-CH_3$ it may be concluded that the only conformer present in the gas phase is the (+)*gauche*-(−)*gauche* conformer, where both chlorine atoms are in *gauche* positions relative to the COC chain on each side of the molecular plane. This result further supports the preference for a *gauche* conformation for the ClCOC skeleton, which has also been found for $ClH_2C-O-CH_3$[9] and $ClH_2C-O-CH_2Cl$.[10]

For comparison and in contrast to this it can be mentioned that halosubstituted alkanes usually exist as conformational mixtures.[15,16] This strong preference for *gauche* conformations when CH_2 groups in alkanes are replaced by the isoelectronic ether oxygen atom most probably is related to the oxygen lone pair electrons. A qualitative model may explain this: a repulsive interaction between lone pair electrons on oxygen and on α-substituted halogen will favour a conformation where the negative charges are further apart. The preferred conformation for the chlorine atom in α-halogeno-ethers will therefore be the *gauche* conformation, when other effects influencing the conformation are negligible. However, by exchange of the electronegative oxygen atom by a CH_2 group such repulsive interactions will not be present and therefore *anti* conformation for the halogen−C−CH_2−C dihedral angles may be present.

The two C−O bond distances in dichloromethyl methyl ether have been found to be of different lengths, *i.e.* 1.383 and 1.405 Å. In agreement with the C−O bond lengths determined for $ClH_2C-O-CH_2Cl$[10] (1.393 Å) and $ClH_2C-O-CH_3$[9] (1.368 and 1.410 Å), a shortening of the C−O bond in the chloro-methoxy group as compared to unsubstituted ethers has been observed. Simultaneously, a lengthening of the C−Cl distance [1.798(3) Å] as compared to chloro-alkanes [Ref. 20: 1.774(4) Å] has been found. These changes in the bond lengths due to chlorine substitution in ethers were first explained by Lucken[17] in 1959 and further supported by Williams in 1961[18] and 1962,[19] as a partial double bond due to charge migration from the reactive oxygen lone pair electron orbital to the antibonding σ*-orbital of the C−Cl bond. Consequently the shortening of the C−O bond must be accompanied by a lengthening of the C−Cl bond.

However, large uncertainties in the values of the C−O bonds are found for both $Cl_2HC-O-CH_3$ and $ClH_2C-O-CH_3$, because the two different C−O distances are present in the same unresolved peak in the RD curve and are strongly correlated (Table 2).

The dihedral angle Cl−C−O−C of 60.6° (1.6°) found in this investigation of dichloromethyl methyl ether is somewhat smaller than the corresponding dihedral angles found for bis(chloromethyl) ether[10] and chloromethyl methyl ether[9] (69.6 and 74.3°, respectively). However, the angle Cl−C−Cl in this molecule (108.0°) is in good agreement with the Cl−C−Cl angles determined for 1,1-dichloro-substituted propanes.[20,21]

Acknowledgement. The author is grateful to Siv. ing. R. Seip for recording the photographic plates.

REFERENCES

1. Chiba, T. *Bull. Chem. Soc. Jpn 28* (1955) 295.
2. Morino, Y., Shiio, H. and Miyagawa, I. *Rep. Radiat. Chem. Res. Inst. Tokyo Univ. 5* (1950) 6.
3. Borovikov, Yu. Ya., Topchii, V. A., Mester, B. S. and Tarasenko, V. S. *Zh. Org. Khim. 12* (1976) 280 (Eng.).
4. Katayama, M. and Morino, Y. *Rep. Radiat. Chem. Res. Inst. Tokyo Univ. 4* (1949) 1.
5. Mizushima, S., Shimanouchi, T., Miyazawa, T. and Hayashi, M. *Unpublished.*
6. Jones, R. G. and Orville-Thomas, W. J. *J. Chem. Soc.* (1964) 692.
7. Charles, S. W., Cullen, F. C. and Owen, N. L. *Spectrochim. Acta A 32* (1976) 1171.
8. Ikeda, T., Curl, Jr., F. R. and Karlsson, H. *J. Mol. Spectrosc. 53* (1974) 101.
9. Planje, M. C., Toneman, L. H. and Dallinga, G. *Recl. Trav. Chim. Pays-Bas 84* (1965) 232.
10. Astrup, E. E. and Aomar, A. M. *Acta Chem. Scand. A 30* (1976) 289.
11. Peacher, J. and Wills, J. C. *J. Chem. Phys. 46* (1967) 4809.
12. Strand, T. G. and Bonham, R. A. *J. Chem. Phys. 40* (1964) 1686.
13. Andersen, B., Seip, H. M., Strand, T. G. and Stølevik, R. *Acta Chem. Scand. 23* (1969) 3224.
14. Seip, H. M. *A Specialist Periodical Report: Molecular Structure by Diffraction Methods*, The Chemical Society, London 1973, Vol. 1, p. 53.
15. Farup, P. E. and Stølevik, R. *Acta Chem. Scand. A 28* (1974) 680.
16. Morino, Y. and Kuchitsu, K. *J. Chem. Phys. 28* (1958) 175.
17. Lucken, E. A. C. *J. Chem. Soc.* (1959) 2954.
18. Williams, J. F. A. *Trans. Faraday Soc. 57* (1961) 2989.
19. Williams, J. F. A. *Tetrahedron 18* (1962) 1477.
20. Johnsen, J. P. and Stølevik, R. *Acta Chem. Scand. A 29* (1975) 457.
21. Fernholt, L. and Stølevik, R. *Acta Chem. Scand. A 29* (1975) 651.

Received September 9, 1977.

Acta Chemica Scandinavica A 32 (1978) 121 – 125

A Mononuclear Copper(II) Complex with an Aminoalcohol. The Crystal and Molecular Structure of Bis(2-amino-2-methyl-1-propanol)copper(II) Dibenzoate

HEIKKI MUHONEN and REIJO HÄMÄLÄINEN

Department of Inorganic Chemistry, University of Helsinki, SF-00100 Helsinki 10, Finland

The crystal structure of $[Cu(C_4H_{11}NO)_2](C_7H_5O_2)_2$ has been determined from three-dimensional X-ray diffraction data collected by counter methods. The compound crystallizes in the space group $P2_1/c$, with $Z=2$ and the cell dimensions $a=5.654(2)$ Å, $b=22.974(11)$ Å, $c=9.166(4)$ Å and $\beta=101.66(3)°$. The structure was solved by heavy-atom Patterson and Fourier methods and refined by full-matrix least-squares techniques. The final R-value, based on 1394 reflections, was 0.063.

The structure consists of discrete $[Cu(C_4H_{11}NO)_2]^{2+}$-cations and $C_7H_5O_2^-$-anions. Cu(II) has a square-planar coordination with Cu – O and Cu – N distances of 1.933(5) and 1.972(5) Å, respectively. The N – Cu – O angle is 84.7(2)°. The benzoate ions connect the cations by means of hydrogen bond contacts in the direction of the a-axis.

The transition metal complexes of aminoalcohols have received considerable attention lately as a result of the current interest in the magnetic properties of polynuclear complexes. Uhlig and Staiger studied copper(II) complexes of the type Cu(AO)X, where AOH = aminoalcohol and X = halide ligand, and divided them into three categories on the basis of their room temperature magnetic moments.[1,2] Later Nishida and Kida measured the temperature dependence of magnetic susceptibilities of copper(II) complexes of the type $Cu(R_2AO)X$, where R_2AOH = *N*,*N*-dialkylaminoalcohol and $X=Cl^-$, Br^- or NCS^-, and proposed a new criterion for the classification of polynuclear copper(II) aminoalcohol complexes.[3,4] Other investigators too have studied the magnetic properties,[5,6] and several structures have been determined by X-ray diffraction to support the magnetic classifications and to explicate further the mechanisms of metal-metal interaction in alkoxo-bridged copper(II) complexes.[6-13] We know only one copper(II) aminoalcohol complex in which the benzoate group has been used as a ligand, and a dimeric structure has been proposed for this complex.[14]

The crystal and molecular structure of $[Cu(C_4H_{11}NO)_2](C_7H_5O_2)_2$ which we describe here is exceptional in that the alkoxo oxygen does not form a bridge between the metal atoms. It is the first structure reported for a complex with this aminoalcohol. Work is also in progress on additional (2-amino-2-methyl-1-propanol)copper(II) complexes.

EXPERIMENTAL

Crystal preparation. Copper(II) benzoate was prepared by the method described elsewhere for the preparation of copper *m*-bromobenzoate[15] and was used without prior analysis. $[Cu(C_4H_{11}NO)_2](C_7H_5O_2)_2$ was then prepared according to the method of Hein *et al.*,[14] with commercially obtained 2-amino-2-methyl-1-propanol (Merck). Violet crystals formed within a few days. After purification from coprecipitates under a microscope, the crystals were suitable for X-ray measurement. IR-spectra indicated the presence of aminoalcohol in the crystals.

Crystal data and space group. Oscillation and equi-inclination Weissenberg photographs revealed the crystals to be monoclinic. The space group, from systematic absences, is $P2_1/c$. The cell parameters were refined by the least-squares method, using data obtained from a powder photograph taken

with a camera of Guinier-Hägg type. Cu$K\alpha$ radiation ($\lambda = 1.5418$ Å) was employed and calcium fluoride ($a = 5.4630$ Å) was the internal standard. The calculated density of 1.378 g cm^{-3}, based on two formula units in the cell, is in agreement with that of 1.38 g cm^{-3} obtained by the flotation method in a mixture of carbon tetrachloride and dioxan. Crystal data for $[Cu(C_4H_{11}NO)_2]$-$(C_7H_5O_2)_2$ are:

$a = 5.654(2)$ Å	$V = 1166.1$ Å^3
$b = 22.974(11)$ Å	FW = 484.04
$c = 9.166(4)$ Å	$Z = 2$
$\beta = 101.66(3)°$	Space group $P2_1/c$

Intensity data. A crystal of dimensions 0.17 × 0.29 × 0.20 mm was mounted along the *a*-axis. Intensity data from levels $0kl - 5kl$ were collected with a Stoe-Güttinger diffractometer equipped with a scintillation counter and a pulse height analyser and using Ni-filtered Cu radiation (Cu$K\alpha$, $\lambda = 1.5418$ Å). The ω-scan, background–peak–background, technique was applied. The scan range was 3.0°, the scan speed 1°/min, and the scanning times were 30, 180 and 30 s. Of the 2130 recorded reflections, 1394 with $I > 3\sigma(I)$ were used for the structure analysis. The data were corrected for Lorentz and polarization factors but not for absorption [μ(Cu$K\alpha$) = 16.8 cm^{-1}].

Structure determination and refinement. From a three-dimensional Patterson vector map the special positions (0,0,0) and $(0,\frac{1}{2},\frac{1}{2})$ were found for the copper atoms. The approximate positions of the four aminoalcohol atoms which form the ring with the copper atom were also determined from this vector map. Subsequent Fourier syntheses based on these atoms gave the positions of the other non-hydrogen atoms of the complex.

The structure was refined by full-matrix least-squares techniques. Initially the refinement was carried out with isotropic thermal parameters to the *R*-value of 0.132 and continued then with anisotropic thermal parameters to the *R*-value of 0.080. At this stage a difference electron density map was calculated and the probable positions of the hydrogen atoms were found. When their atomic positional and isotropic thermal factors were included as parameters, the refinement, after two cycles, gave a final *R*-value of 0.063 ($R = \Sigma \| F_o| - |F_c \| / \Sigma |F_o|$). In the last cycle the average shift/error was 18 %. The weights were calculated according to the scheme $w = 1/(35 + |F_o|)$. The scattering factors for Cu^{2+} were taken from International Tables for X-Ray Crystallography,[16] those for O, N and C were from Cromer and Mann,[17] and those used for hydrogen atoms from Stewart *et al.*[18]

Calculations were carried out on a Univac 1108 computer using programs of the X-Ray systems.[19] The final parameters are given in Tables 1a and b. A list of the observed and calculated structure factors is obtainable on request from the authors.

Table 1a. Atomic positional and thermal parameters[a] multiplied by 10^4. Standard deviations are given in parentheses.

	x	*y*	*z*	U_{11}	U_{22}	U_{33}	U_{12}	U_{13}	U_{23}
Cu	0000	0000	0000	506(8)	378(6)	344(6)	91(7)	−22(5)	−48(7)
N(1)	3086(10)	260(3)	1238(6)	338(34)	286(29)	276(29)	82(26)	33(23)	−19(24)
O(1)	−1319(8)	688(2)	751(5)	319(25)	259(22)	332(24)	70(19)	−25(19)	−35(19)
O(2)	3344(10)	738(2)	−1718(6)	577(36)	505(33)	637(37)	46(27)	31(29)	292(29)
O(3)	6433(11)	1340(2)	−1116(6)	640(38)	459(32)	604(36)	107(28)	−239(30)	125(27)
C(1)	523(12)	1031(3)	1657(8)	363(40)	283(34)	420(38)	31(29)	50(30)	−102(31)
C(2)	2505(11)	638(3)	2451(7)	315(37)	346(33)	295(33)	−27(28)	28(27)	−43(27)
C(3)	1652(21)	248(5)	3560(10)	481(59)	652(57)	333(43)	−120(51)	6(39)	117(42)
C(4)	4643(16)	998(4)	3204(10)	374(49)	561(53)	426(48)	−97(40)	50(38)	−127(42)
C(5)	4389(14)	1197(3)	−1858(7)	507(48)	349(38)	330(36)	174(32)	62(33)	5(29)
C(6)	3206(12)	1634(3)	−3021(7)	405(40)	277(31)	287(31)	112(28)	71(28)	12(26)
C(7)	4484(15)	2103(3)	−3377(9)	348(46)	386(39)	500(44)	11(31)	−48(34)	47(34)
C(8)	3469(16)	2494(4)	−4451(9)	629(56)	384(40)	515(45)	−55(39)	90(40)	93(34)
C(9)	1132(16)	2423(4)	−5172(8)	590(52)	487(45)	369(41)	108(39)	−4(36)	137(36)
C(10)	−176(16)	1964(3)	−4807(9)	319(43)	553(44)	405(45)	38(40)	−47(33)	−51(37)
C(11)	858(13)	1566(3)	−3753(8)	430(44)	341(36)	377(37)	−17(32)	94(31)	−6(31)

[a] The anisotropic thermal parameters are of the form exp $[-2\pi^2(h^2a^{*2}U_{11} + \cdots + 2hka^*b^*U_{12} + \cdots)]$.

Table 1b. Atomic positional ($\times 10^3$) and thermal ($\times 10^2$) parameters for the hydrogen atoms. Standard deviations are given in parentheses.

	x	*y*	*z*	*U*
H(1)	−218(17)	94(4)	30(10)	8(3)
H(2)	105(14)	133(4)	115(9)	6(2)
H(3)	−6(9)	125(2)	226(6)	1(1)
H(4)	42(14)	12(3)	321(8)	2(2)
H(5)	249(17)	5(4)	391(10)	5(3)
H(6)	145(12)	51(3)	434(8)	4(2)
H(7)	579(16)	78(4)	356(10)	6(3)
H(8)	414(17)	138(4)	383(11)	9(3)
H(9)	492(12)	114(3)	253(8)	3(2)
H(10)	356(13)	58(3)	37(9)	6(2)
H(11)	388(9)	3(3)	154(6)	1(1)
H(12)	573(13)	214(3)	−299(8)	3(2)
H(13)	423(19)	272(4)	−445(11)	8(4)
H(14)	50(16)	273(4)	−577(10)	7(3)
H(15)	−164(12)	195(3)	−525(7)	3(2)
H(16)	−4(12)	131(3)	−346(8)	3(2)

DESCRIPTION AND DISCUSSION OF THE STRUCTURE

The structure consists of discrete $[Cu(C_4H_{11}NO)_2]^{2+}$-cations and $C_7H_5O_2^-$-anions. The $C_7H_5O_2^-$-ions connect the cations by means of hydrogen bonds in the direction of the *a*-axis as shown in Fig. 1.

The aminoalcohol ligand and coordination around Cu(II). Cu(II) has a square-planar coordination with Cu−O and Cu−N distances of 1.933(5) and 1.972(5) Å, respectively. The Cu−O distance agrees with those found in polynuclear aminoalcohol complexes but the Cu−N distance is a little shorter than normal. Commonly the Cu−N distances in polynuclear cases vary in the range 2.02−2.09 Å,[6-14] though shorter distances are not unknown.[20] Both the N−Cu−O angle of 84.7(2)° and the C−O distance of 1.431(8) Å agree with established values of polynuclear complexes. The mean aminoalcohol C−C distance is 1.509 Å and the three C−C distances are nearly equal (Table 2). The large benzoate anion has probably acted as a steric hindrance for the alkoxo-bridge formation between the metal atoms.

The ring has unsymmetrical *gauche* conformation, so that the ring carbon atoms C(1) and C(2) deviate 0.100 Å and −0.579 Å from the N−Cu−O plane, respectively. The dihedral angle between the planes O(1)−C(1)−C(2) and N(1)−C(2)−C(1) is 50.0°. The coordination around Cu(II) is shown in Fig. 2.

The benzoate anion and the hydrogen bond contacts. The Cu−O(2) distance is 3.184(6) Å and the

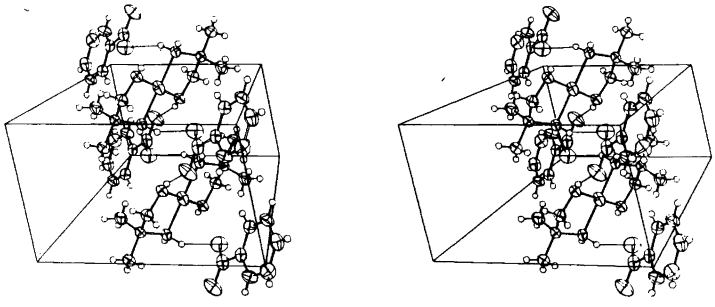

Fig. 1. A stereoscopic packing view of two complex units. The view direction is approximately along *b*; *c* is horizontal and *a* is approximately vertical.

Table 2. Interatomic distances (Å) and angles (°). Standard deviations are given in parentheses. Distances involving hydrogen atoms vary between 0.67 and 1.16 Å.

Cation			
Cu – N(1)	1.972(5)	N(1) – Cu – O(1)	84.7(2)
Cu – O(1)	1.933(5)	Cu – N(1) – C(2)	107.5(4)
C(1) – O(1)	1.431(8)	Cu – O(1) – C(1)	111.7(4)
C(1) – C(2)	1.508(9)	O(1) – C(1) – C(2)	109.4(5)
C(2) – N(1)	1.497(9)	N(1) – C(2) – C(1)	104.0(5)
C(2) – C(3)	1.506(13)	N(1) – C(2) – C(3)	107.8(6)
C(2) – C(4)	1.512(11)	N(1) – C(2) – C(4)	112.4(6)
		C(1) – C(2) – C(3)	112.0(7)
		C(1) – C(2) – C(4)	109.8(6)
		C(3) – C(2) – C(4)	110.7(6)
Anion			
C(5) – O(2)	1.227(9)	O(2) – C(5) – O(3)	125.2(6)
C(5) – O(3)	1.261(9)	O(2) – C(5) – C(6)	119.3(6)
C(5) – C(6)	1.519(9)	O(3) – C(5) – C(6)	115.5(6)
C(6) – C(7)	1.373(10)	C(5) – C(6) – C(7)	120.5(6)
C(6) – C(11)	1.370(9)	C(5) – C(6) – C(11)	120.9(6)
C(7) – C(8)	1.369(11)	C(11) – C(6) – C(7)	118.6(6)
C(8) – C(9)	1.363(12)	C(6) – C(7) – C(8)	121.4(7)
C(9) – C(10)	1.368(12)	C(7) – C(8) – C(9)	119.7(8)
C(10) – C(11)	1.372(10)	C(8) – C(9) – C(10)	119.5(7)
		C(9) – C(10) – C(11)	120.7(7)
		C(10) – C(11) – C(6)	120.1(7)

Table 3. Hydrogen bond contacts (Å). Roman numerals refer to the following equivalent positions: I, x,y,z; II, $1-x,-y,-z$; III, $x-1,y,z$.

X – H···Y	X – H	H···Y	X···Y	∠(X – H···Y)
N(1) – H(10)···O(2)^{I}	1.16(8)	1.93(8)	2.954(8)	146
N(1) – H(11)···O(2)^{II}	0.72(5)	2.34(6)	3.029(8)	161
O(1) – H(1)···O(3)^{III}	0.81(9)	1.66(9)	2.431(7)	160

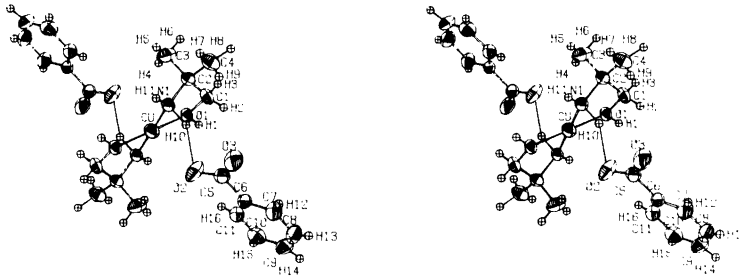

Fig. 2. A stereoscopic view of the complex unit.

line joining the atoms makes an angle of 64.4° with the Cu – N(1) – O(1) plane. In Cu(II) complexes formed by 1,3-propanediamine with benzoate and different substituted benzoates this distance is about 2.5 Å.[21-24] The mean values of the ring C – C bonds and C – C – C angles are 1.369 Å and 120.0°,

respectively. The greatest deviation of a ring C atom from the least-squares plane of the benzene ring is 0.011 Å. The angle between the benzene ring and the carboxylate group is 10.5° and between the benzene ring and the Cu – N(1) – O(1) plane, 65.7°. Each benzoate anion forms three hydrogen bonds and these are listed in Table 3. It is noteworthy that both of the amine hydrogen atoms have taken part in hydrogen bond formation and this may have had the effect of increasing the stability of the complex.

REFERENCES

1. Uhlig, E. and Staiger, K. *Z. Anorg. Allg. Chem. 346* (1966) 21.
2. Uhlig, E. and Staiger, K. *Z. Anorg. Allg. Chem. 360* (1968) 39.
3. Nishida, Y., Numata, F. and Kida, S. *Inorg. Chim. Acta 11* (1974) 189.
4. Nishida, Y. and Kida, S. *J. Inorg. Nucl. Chem. 38* (1976) 451.
5. Merz, L., Haase, W. and Keller, G. *Ber. Bunsenges. Phys. Chem. 80* (1976) 305.
6. Näsäkkälä, M. *Ann. Acad. Sci. Fenn. Ser. A 2* (1977) No. 181.
7. Pajunen, A. and Lehtonen, M. *Suom. Kemistil. B 44* (1971) 200.
8. Pajunen, A. and Smolander, K. *Finn. Chem. Lett.* (1974) 99.
9. Smolander, K. *Finn. Chem. Lett.* (1974) 199.
10. Estes, E. D. and Hodgson, D. J. *Inorg. Chem. 14* (1975) 334.
11. Mergehenn, R., Haase, W. and Allmann, R. *Acta Crystallogr. B 31* (1975) 1847.
12. Mergehenn, R., Merz, L. and Haase, W. *Z. Naturforsch. Teil B 30* (1975) 14.
13. Mergehenn, R. and Haase, W. *Z. Naturforsch. Teil B 30* (1975) 155.
14. Hein, F. and Ludwig, W. *Z. Anorg. Allg. Chem. 338* (1965) 63.
15. Orama, O., Huttner, G., Lorenz, H., Marsili, M. and Frank, A. *Finn. Chem. Lett.* (1976) 137.
16. *International Tables for X-Ray Crystallography*, Kynoch Press, Birmingham 1962, Vol. III.
17. Cromer, D. T. and Mann, J. B. *Acta Crystallogr. A 24* (1968) 321.
18. Stewart, R. F., Davidson, E. R. and Simpson, W. T. *J. Chem. Phys. 42* (1965) 3175.
19. *The X-Ray System, Version of June 1972.* Technical Report TR-192 of the Computer Science Center, University of Maryland, June 1972; *The X-Ray System, Version of 1976, X-Ray76.* Technical Report TR-446 of the Computer Science Center, University of Maryland 1976.
20. Näsäkkälä, M. *Ann. Acad. Sci. Fenn. Ser. A 2* (1977) No. 181, p. 39.
21. Uggla, R. and Klinga, M. *Suom. Kemistil. B 45* (1972) 10.
22. Orama, O. *Ann. Acad. Sci. Fenn. Ser. A 2* (1976) No. 180.
23. Klinga, M. *Finn. Chem. Lett.* (1976) 71.
24. Klinga, M. *Finn. Chem. Lett.* (1976) 179.

Received September 23, 1977.

Acta Chemica Scandinavica A 32 (1978) 127 – 131

The Crystal and Molecular Structure of 1,2-Dimethyl-1,2-diformylhydrazine at 110 K

TOR OTTERSEN

Department of Chemistry, University of Oslo, Oslo 3, Norway

The crystal and molecular structure of the title compound, $C_4H_8N_2O_2$, has been determined using 2546 observed reflections collected at 110 K. The crystals are monoclinic, space group $P2_1/c$ with cell dimensions $a=7.470(2)$ Å, $b=8.936(2)$ Å, $c=11.239(2)$ Å, $\beta=131.70°(1)$. The structure model was refined to an R of 0.076. In order to reduce the influence of valence electron asphericity on the structural parameters low-angle data were excluded from the final refinement.s The heavy atom parameters converged to their final values for a minimum sin θ/λ cutoff of 0.75 Å^{-1}, leaving 957 reflections, the R is 0.061. The molecule has C_2 symmetry and the torsional angle around the N – N bond is $-91.2°(2)$, with the angle between the planes of the two N – C = O fragments being 90.0°, whereas 1,2-diformylhydrazine is planar. Compared with 1,2-diformylhydrazine the loss of hydrogen bonding leads to a lengthening of the C – N bond by about 0.026 Å and a shortening of the C = O bond by about 0.021 Å, in agreement with earlier results.

The structure determination of 1,2-dimethyl-1,2-diformylhydrazine is part of a series of structure investigations of 3,6-pyridazinediones and related compounds, of which part of the purpose is to study the effect of hydrogen bonding on the N – C = O fragment. The experimental results have been complemented by a series of theoretical studies using hydrogen-bonded complexes of formamide as model systems (for a review see Ref. 1).

1,2-Diformylhydrazine is planar[2] and in the crystal the molecules are bound together by N – H···O hydrogen bonds such that each N – C = O fragment participates in two intermolecular hydrogen bonds. The structure of 1,2-diformylhydrazine has recently been reinvestigated using an extensive data set in order to study the deformation electron densities and obtain accurate hydrogen positions.[3] Recent structure investigations of hexahydro-1,2-dimethyl-3,6-pyridazinedione[4] and hexahydro-3,6-pyridazinedione[5,6] which have a hydrogen bonding corresponding to that in 1,2-diformylhydrazine, implied that the formation of the N – H···O bonds leads to a shortening of the C – N bonds by about 0.02 Å and a lengthening of the C = O bonds by about 0.02 Å. In order to get further quantitative results on the effect of hydrogen bonding on the N – C = O fragment, it was of interest to study 1,2-dimethyl-1,2-diformylhydrazine. The results from a series of structure determinations of some simple amides in the gaseous state[7-10] indicate that introduction of a methyl group at the nitrogen atom has little or no effect on the C – N bond, whereas a small lengthening (~0.005 Å) of the C = O bond is indicated.

The results for the hexahydro-3,6-pyridazinedione and hexahydro-1,2-dimethyl-3,6-pyridazinedione further show that the introduction of methyl groups leads to an increase in the torsional angles around the N – N bond and a larger degree of sp^3-hybridization for the nitrogen atoms. A similar introduction of methyl groups in 1,2-diformylhydrazine may give a nonplanar diformylhydrazine, as is found for tetraformylhydrazine[11] where the torsional angles around the N – N bond are 90°.

EXPERIMENTAL

Oscillation and Weissenberg photographs indicated monoclinic symmetry and the systematic absences were those characteristic of the space group $P2_1/c$. The density indicated four molecules in the unit cell.

An approximately cube-shaped crystal with edges of about 0.5 mm was used in the collection of intensity data. A computer-controlled Syntex $P\bar{1}$ four-circle diffractometer with graphite-monochromatized Mo$K\alpha$ radiation and equipped with a modified Enraf-Nonius liquid nitrogen cooling device was utilized in the determination of unit cell parameters and the recording of intensity data. Cell constants were determined by a least-squares treatment of the angular coordinates of fifteen reflections with 2θ-values between 50 and 54°. The temperature at crystal site was 110 K.

Three-dimensional intensity data were recorded using the $\omega-2\theta$ scanning mode with scan speed variable from 2.0 to 6.0° min^{-1}, depending on the peak intensity of the reflection. Background counting time was equal to 0.7 × scan time and the scan area was from $2\theta(\alpha_1)-0.8°$ to $2\theta(\alpha_2)+0.8°$. All reflections with 2θ-values less than 50° were recorded, whereas for reflections above this limit only those which had intensities larger than 5 cps determined in a 2 s scan were recorded. There was some accumulation of ice on the crystal during the data collection. However, the intensities of three standard reflections which were remeasured after every sixty reflections were essentially constant throughout the recording run.

The estimated standard deviations were taken as the square-root of the total counts with a 2 % addition for experimental uncertainties. Of the 3033 reflections measured ($2\theta_{max}=80°$), the 2546 which had intensities larger than twice their standard deviations were used in the refinements. The intensities were corrected for Lorentz and polarization effects. The computer program used, as well as programs subsequently employed, is part of a local assembly of computer programs which is described in Ref. 12.

The atomic scattering factors used were those calculated by Doyle and Turner[13] for oxygen, nitrogen and carbon, and of Stewart *et al.*[14] for hydrogen.

CRYSTAL DATA

1,2-Dimethyl-1,2-diformylhydrazine, $C_4H_8N_2O_2$, $M=116.12$ amu. Space group $P2_1/c$, cell dimensions at 110 K: $a=7.470(2)$ Å, $b=8.936(2)$ Å, $c=11.239(2)$ Å, $\beta=131.70°(1)$, $V=560.2(2)$ Å^3. D_{obs} (flotation, 19 °C)$=1.36$ g cm^{-3}, $Z=4$, $D_{calc}=1.376$ g cm^{-3}, $F(000)=248$.

STRUCTURE DETERMINATION AND REFINEMENTS

The phase problem was solved by the MULTAN program assembly.[15] The heavy atom structure model was refined with anisotropic temperature factors to a conventional R of 0.10. The eight hydrogen atoms were found among the ten largest peaks in a difference Fourier synthesis calculated using this structure model. These were included in the refinement with isotropic thermal parameters. Full-matrix least-squares refinement of all positional and thermal parameters converged to an R of 0.076 and an R_W of 0.096. The "goodness of fit", $\{[\Sigma w(F_o-|F_c|)^2]/(m-s)\}^{\frac{1}{2}}$, ($G$) is 4.73.

In order to remove the influence of the valence electron asphericity on the heavy atom parameters the minimum sin θ/λ cutoff value for data used in the refinements was increased systematically. The heavy atom parameters converged to their final values for a minimum sin θ/λ cutoff of 0.75 Å^{-1}, in agreement with earlier structure refinements.[3,16] The hydrogen parameters were not refined. The refinement using the 957 F_o's with sin θ/λ-values larger than 0.75 Å^{-1} converged to an R of 0.061, an R_w of 0.075 and a G of 2.31. These relatively large R-factors may be caused both by the accumulation of ice on the crystal during the data collection and the relatively large crystal size. Although this did not affect the intensities of the check reflection, it may have caused errors in other reflections, and part of the large crystal may have moved outside the homogenous part of the X-ray beam for certain diffractometer settings. A final difference Fourier synthesis showed only spurious peaks of maximum density 0.3 e Å^{-3} apart from the accumulation of density in bond and lone-pair regions. The final heavy atom parameters are listed in Table 1, together with the hydrogen parameters obtained in the refinement using all data. A list of observed and calculated structure factors is available from the author upon request. Standard deviations in molecular parameters were calculated from the correlation matrix.

DISCUSSION

Mean bond lengths and bond angles are listed in Fig. 1 where also the numbering of the atoms is indicated. The values of corresponding bonds and angles in the two N-methylformamide fragments are equal, the maximum deviations being 0.003(4) Å

Table 1. Fractional atomic coordinates and thermal parameters with estimated standard deviations. The anisotropic temperature factor is given by: $\exp\{-2\pi^2[U_{11}(a^*h)^2+\ldots+2U_{23}(b^*c^*kl)]\}$. The parameters given for nonhydrogen atoms are those obtained in the refinement using only data with $\sin\theta/\lambda>0.75$ Å^{-1}.

Atom	x	y	z	U_{11}	U_{22}	U_{33}	U_{12}	U_{13}	U_{23}
O1	.1307(4)	.4555(2)	.9166(3)	.0237(7)	.0137(6)	.0312(8)	−.0047(4)	.0176(6)	−.0042(4)
C2	.2136(3)	.5728(2)	.9906(2)	.0181(7)	.0133(6)	.0222(7)	−.0016(4)	.0139(6)	−.0003(4)
N3	.2871(3)	.6868(2)	.9524(2)	.0182(6)	.0120(5)	.0184(6)	−.0028(3)	.0130(5)	−.0025(4)
N4	.3828(2)	.8132(2)	1.0481(2)	.0138(6)	.0126(5)	.0167(6)	−.0008(3)	.0090(5)	−.0027(4)
C5	.2327(3)	.9272(2)	1.0098(2)	.0184(7)	.0142(6)	.0209(7)	.0009(4)	.0134(6)	−.0003(4)
O6	.2985(4)	1.0445(2)	1.0846(3)	.0299(8)	.0137(6)	.0305(8)	−.0007(4)	.0222(7)	−.0041(4)
C7	.2876(3)	.6787(2)	.8229(2)	.0208(7)	.0201(7)	.0189(7)	−.0008(5)	.0141(5)	−.0019(5)
C8	.6423(3)	.8213(2)	1.1779(2)	.0152(6)	.0201(7)	.0175(6)	−.0013(4)	.0091(5)	−.0015(4)

Atom	x	y	z	B	Atom	x	y	z	B
H2	.243(6)	.588(3)	1.089(4)	3.4(6)	H5	.075(4)	.911(3)	.917(3)	1.5(4)
H71	.429(6)	.709(3)	.859(4)	2.9(6)	H72	.148(5)	.723(3)	.732(3)	2.7(6)
H73	.270(5)	.577(3)	.783(3)	2.2(5)	H81	.717(5)	.780(3)	1.141(3)	1.9(5)
H82	.685(5)	.767(3)	1.265(3)	2.8(6)	H83	.697(5)	.928(3)	1.218(3)	2.3(6)

Table 2. Torsional angles (°), the angles are positive in a right-hand screw.

Angle		Angle	
O1−C2−N3−N4	−178.7(2)	O6−C5−N4−N3	−178.9(2)
O1−C2−N3−C7	−3.5(3)	O6−C5−N4−C8	−3.6(3)
C7−N3−N4−C5	93.4(2)	C2−N3−N4−C8	93.3(2)
C2−N3−N4−C5	−91.2(2)	C7−N3−N4−C8	−82.1(2)

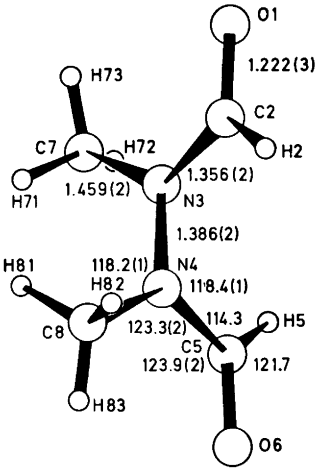

Fig. 1. Mean bond lengths (Å) and bond angles (°). The C−H lengths are in the range 0.89−1.02 Å.

between the two C=O bonds and 0.2°(2) between the angles C2−N3−N4 and C5−N4−N3.

The molecule has very close to C_2 symmetry with the twofold axis passing through the midpoint of the N−N bond (see Fig. 1). The *N*-methylformamide fragments are essentially planar, the mean deviations from least-squares planes through the two O=C−N fragments being: N4/N3 −0.026 Å, C7/C8 −0.076 H2/H5 −0.059 Å, respectively. This implies that the nitrogen atoms are sp^2-hybridized in agreement with the results found for amides.[17] The dihedral angle between these two planes are 90.0°, as was found for tetraformylhydrazine,[11] and the torsional angle C2−N3−N4−C5 is −91.2°(2). (Torsional angles are listed in Table 2.) 1,2-Diformylhydrazine was found to be planar,[2,3] and the large twist around the N−N bond in 1,2-dimethyl-1,2-diformylhydrazine must be caused by the introduction of the two bulky methyl groups and the decreased participation of the two nitrogen lone pairs in the conjugation over the N−C=O fragment caused

by the lack of hydrogen bonding. Evidence for the influence of the methyl groups on the twist around the N – N bond is found in hexahydro-1,2-dimethyl-3,6-pyridazinedione where this twist is restrained by the ring formation and the two methyl groups are bent out of the planes of the O = C – N fragments by −0.78 Å and 1.05 Å, respectively. On the other hand the torsional angle C7 – N3 – N4 – C8 is only −82.1°(2), and the more localized (than in 1,2-diformylhydrazine) nitrogen lone pairs must also have an influence on the twist around the N – N bond. Theoretical calculations[1] imply that the formation of N – H···O hydrogen bonds as found in 1,2-diformylhydrazine leads to a loss of σ-electron density from the oxygen *via* the hydrogen bond.[1] This is countered by a larger increase in the π-electron population on the oxygen, which in turn leads to a larger participation of the nitrogen lone pair in the conjugation over the N – C = O fragment, *i.e.* delocalized lone pairs. This leads to a planar 1,2-diformylhydrazine molecule.

The decreased participation of the nitrogen lone pairs in the conjugation caused by the lack of hydrogen bonding in 1,2-dimethyl-1,2-diformylhydrazine is evident in the C = O and C – N bond lengths when compared with those found in 1,2-diformylhydrazine[3] [1.2380(2) and 1.3316(2) Å, respectively]. Taking into consideration the lengthening of about 0.005 Å of the C = O bond induced by the introduction of a methyl group at the nitrogen atom (see Ref. 1 for a discussion of this), the formation of one intermolecular N – H···O. hydrogen bond such that both the nitrogen and oxygen atom in the N – C = O fragment participates in the hydrogen bonding, leads to a lengthening of the C = O bond by about 0.021 Å and a shortening of the C – N bond by about 0.026 Å. These values are in good agreement with those found for the hexahydro-3,6-pyridazinediones[4,6] (0.019 and 0.020 Å, respectively) and for the unreduced 3,6-pyridazinediones[1] (0.015 and 0.025 Å, respectively).

The introduction of methyl groups and the lack of hydrogen bonding leads to a lengthening of the N – N bond from 1.3797(2) Å in 1,2-diformylhydrazine to 1.386(2) Å in 1,2-dimethyl-1,2-diformylhydrazine. A similar difference was found for the two hexahydro-3,6-pyridazinediones [1.398(1) and 1.406(1) Å, respectively]. The N – C_{Me} bond lengths found in the present structure are equal to those found in hexahydro-1,2-dimethyl-3,6-pyridazinedione[4] and in the gas phase structure investigation of *N*-methylformamide.[10]

A comparison of the structures obtained for 1,2-dimethyl-1,2-diformylhydrazine and hexahydro-1,2-dimethyl-3,6-pyridazinedione,[4] and 1,2-diformylhydrazine[3] and hexahydro-3,6-pyridazinedione[6] reveals that the introduction of $-CH_2-$ groups at the carbon atoms leads to significant lengthenings of the bonds. The increases are about: C = O 0.008 Å, C – N 0.012 Å and N – N 0.019 Å. The changes in the C = O and C – N bonds are the same as those found between formamide[9] and acetamide,[7] and between *N*-methylformamide[10] and *N*-methylacetamide[8] in the gas phase. These results imply that restraints induced by the ring formation in the hexahydro-3,6-pyridazinediones have no effect, and that these lengthenings of the bonds are coupled to the inductive effect of the methyl groups. Theoretical calculations on formamide and acetamide[17] show that the overlap populations are significantly larger in acetamide than in formamide, although the gross population of the central carbon atom has decreased.

The shortest intermolecular contacts in the present structure are consistent with normal van der Waals-type contacts.

Acknowledgement. The author wants to thank Miss Ulla Sørensen and Dr. Carsten Cristophersen for supplying the crystals.

REFERENCES

1. Ottersen, T. *Adv. Mol. Relaxation Processes 9* (1976) 105.
2. Ottersen, T. *Acta Chem. Scand. A 28* (1974) 1145.
3. Hope, H. and Ottersen, T. *To be published.*
4. Ottersen, T. and Sørensen, U. *Acta Chem. Scand. A 31* (1977) 808.
5. Ottersen, T. *Acta Chem. Scand. A 29* (1975) 690.
6. Ottersen, T. and Almlöf, J. *To be published.*
7. Kitano, M. and Kuchitsu, K. *Bull. Chem. Soc. Jpn. 46* (1973) 3048.
8. Kitano, M., Fukuyama, T. and Kuchitsu, K. *Bull. Chem. Soc. Jpn. 46* (1973) 348.
9. Kitano, M. and Kuchitsu, K. *Bull. Chem. Soc. Jpn. 47* (1974) 67.
10. Kitano, M. and Kuchitsu, K. *Bull. Chem. Soc. Jpn. 47* (1974) 631.
11. Hinderer, A. and Hess, H. *Chem. Ber. 107* (1974) 492.
12. Groth, P. *Acta Chem. Scand. 27* (1973) 1837.
13. Doyle, P. A. and Turner, P. S. *Acta Crystallogr. A 24* (1968) 390.
14. Stewart, R. F., Davidson, E. R. and Simpson, W. T. *J. Chem. Phys. 42* (1965) 3175.

15. Germain, G., Main, P. and Woolfson, M. M. *Acta Crystallogr. A 27* (1971) 368.
16. Ottersen, T. and Hope, H. *To be published.*
17. Ottersen, T. *Acta Chem. Scand. A 29* (1975) 939.

Received August 30, 1977.

Acta Chemica Scandinavica A 32 (1978) 133 – 139

Reactions of 2-Substituted 1-Phenylethanones. 1. Nucleophilicity, Leaving Group Ability and Carbon Basicity of Cl^-, Br^-, SCN^- and $SeCN^-$ in Acetonitrile

TORE THORSTENSON and JON SONGSTAD

Department of Chemistry, University of Bergen, N-5014 Bergen-Univ., Norway

The reactions between some 2-substituted 1-phenylethanones (phenacyl compounds, ω-substituted acetophenones), $PhC(O)CH_2X$, and various ionic nucleophiles, Y^-, (X and Y = Cl, Br, SCN and SeCN) have been examined in acetonitrile. At 25.0 °C and for relatively short reaction times all the reactions proceed exclusively through nucleophilic attack at the methylene carbon atom and no formation of 2-isothiocyanato(2-isoselenocyanato)-substituted products could be observed.

For equal concentrations of reactants none of the reactions go to completion and equilibria are established. From the equilibrium constants it can be concluded that the carbon basicity order is $NCSe^- \geq NCS^- > Cl^- \gg Br^-$ toward the methylene carbon atom.

The reactions have been the subject of a kinetic study at 25.0 °C and all the reactions studied have been found to follow second order kinetics, first order in each of the reactants. The chloride ion, the bromide ion and the selenocyanate ion are approximately of the same nucleophilic strength and these ions are generally ten times more reactive than the thiocyanate ion toward the various substrates. The rates of reaction of the substrates suggest that the leaving group ability order is $Br^- \gg Cl^- > NCSe^- > NCS^-$.

As part of a program to study the effect of substituents upon the reactivity of alkyl halides toward nucleophilic species,[1] a kinetic study of 2-halo-1-phenylethanones (phenacyl halides, ω-haloacetophenones), $PhC(O)CH_2X$, was started. In this paper we want to report the results from a part of this study in which the thiocyanate ion, NCS^-, and the selenocyanate ion, $NCSe^-$, were used as the nucleophiles; eqn. 1.

$$PhC(O)CH_2X + Y^- \xrightarrow[25\ °C]{MeCN} PhC(O)CH_2Y + X^- \quad (1)$$

X = Cl and Br, Y = SCN and SeCN.

The reactions depicted by eqn. 1 were found to be clean substitution reactions toward the aliphatic carbon atom and no trace of isothiocyanato(isoselenocyanato)-substituted products could be detected. Some yellow coloration of the reaction mixtures could be observed only after 1 to 2 weeks at room temperature.

However, complications arose from the fact that none of the reactions studied were found to go to completion and the following equilibria were established, eqn. 2.

$$PhC(O)CH_2X + Y^- \underset{k_r}{\overset{k_f}{\rightleftharpoons}} PhC(O)CH_2Y + X^- \quad (2)$$

By suitable choice of the reactant concentrations both the forward and the reverse second-order rate constants, k_f and k_r, could be determined by following the rate of appearance or disappearance of the pseudohalide ions employing IR liquid cells.[2] The equilibrium constants, K, could be determined by the equilibrium concentrations of the reacting species and also by the ratio of the rate constants, k_f/k_r. The equilibrium constants could also be determined by NMR from more concentrated runs since the methylene protons in the various 2-substituted 1-phenylethanones are well-separated.

The purity of the reactions clearly indicated that 1-phenyl-2-thiocyanatoethanone, $PhC(O)CH_2SCN$, and 1-phenyl-2-selenocyanatoethanone, $PhC(O)CH_2SeCN$, could only yield the anticipated substi-

tution products in the presence of thiocyanate and selenocyanate ions. By employing ^{13}C-pseudohalide ions and the IR technique,[2] the following reactions could also be examined kinetically, eqns. 3–5.

$$PhC(O)CH_2SCN + NCS^- \xrightarrow{k_f} PhC(O)CH_2SCN + NCS^- \quad (3)$$

$$PhC(O)CH_2SCN + NCSe^- \underset{k_r}{\overset{k_f}{\rightleftharpoons}} PhC(O)CH_2SeCN + NCS^- \quad (4)$$

$$PhC(O)CH_2SeCN + NCSe^- \xrightarrow{k_f} PhC(O)CH_2SeCN + NCSe^- \quad (5)$$

From the equilibrium constant for the reaction depicted by eqn. 4, the relative carbon basicity of the thiocyanate ion and the selenocyanate ion could be determined.

EXPERIMENTAL

Materials. Acetonitrile, Baker Analyzed Reagent, was purified as previously described[1] and flushed with dry nitrogen prior to use. Diethyl ether, petroleum ether and cyclohexane were dried with metallic sodium.

2-Chloro-1-phenylethanone and 2-bromo-1-phenylethanone were commercially available and were crystallized from ethanol, acetonitrile, diethyl ether and finally from light petroleum (40–60 °C) prior to use.

1-Phenyl-2-thiocyanatoethanone was prepared as described by Dykerhoff[3] and crystallized from ethanol and finally from cyclohexane. M.p. 76 °C (74 °C[3]).

1-Phenyl-2-selenocyanatoethanone was prepared from the corresponding bromo compound and 10 % excess of potassium selenocyanate, KSeCN, in ethanol at room temperature.[4] As soon as a yellow colour started to appear, the reaction mixture was poured into a large volume of water and the mixture set aside for 1 h in the refrigerator. The product was filtered off and crystallized several times from diethyl ether/light petroleum (40–60 °C) and finally from cyclohexane. M.p. 88 °C (85 °C[4]). Ethanol as suggested by Hofmann[4] as a crystallization agent was found to give a somewhat sticky product.

Tetraphenylarsonium, Ph_4As^+, tetraphenylphosphonium, Ph_4P^+, and bis(triphenylphosphine)iminium, $[(Ph_3P)_2N]^+$, salts were used as the source of the nucleophiles. These salts were prepared and purified as previously described.[2,5] Only $[(Ph_3P)_2N]^+$-salts, abbreviated $[PNP]^+$-salts, were used as the source of the ^{13}C-pseudohalide ions. These compounds were prepared from potassium ^{13}C-cyanide,[5] 90.5 % enriched, used as received from British Oxygen Co. Ltd..

Determination of rate and equilibrium constants. In Table 1 are listed some IR, UV and NMR data for the 2-substituted 1-phenylethanones, RX, and the pseudohalide ions, X^-, employed in the present study. These data, except the IR data in the 1700 cm^{-1} region, column 3 in Table 1, formed the basis for the analytical methods applied in the present study for the determination of rate and equilibrium constants.

Table 1. IR, UV and NMR data for 1-phenyl-2-X-ethanones, ($PhC(O)CH_2X$), RX, and some anions, X^-, in acetonitrile.

RX,X^-	$\nu_{NCX}(cm^{-1})$[a]	$\nu_{CO}(cm^{-1})$[a]	$\lambda_{max}(>300\,nm)$	δ_{CH_2} (Rel. TMS)[b]
RCl		1708(s), 1690(m)	~324(ε= 68)	4.95
RBr		1688(s), 1706(m)	324(ε=121)	4.65
RS^{12}CN	2159(m)[c]	1689(s), 1702(m)		4.85
S^{12}CN$^-$	2059(s)[d]			
RS^{13}CN	2116(m)			
S^{13}CN$^-$	2012(s)			
RSe^{12}CN	2161(m)[e]	1675(s), 1695(m)		4.90
Se^{12}CN$^-$	2068(s)[f]			
RSe^{13}CN	2111(m)			
Se^{13}CN$^-$	2023(s)			

[a] ±2 cm^{-1}. [b] ±0.01 ppm. [c] Peak height of RSCN in MeCN is 15 % of peak height due to NCS^-. [d] $A = 4.1 \times 10^4$ $M^{-1}\,cm^{-2}$, $\Delta\nu_{\frac{1}{2}} = 12\,cm^{-1}$.[2] [e] Peak height of RSeCN is 11 % of peak height due to $NCSe^-$. [f] $A = 2.2 \times 10^4$ $M^{-1}\,cm^{-2}$, $\Delta\nu_{\frac{1}{2}} = 10\,cm^{-1}$.[2]

The rate of the reaction between ionic chloride, Cl^-, and 2-bromo-1-phenylethanone, RBr, was determined by UV by following the rate of decrease in absorption at 324 nm. The rate of the reverse reaction, $RCl+Br^-$, could not be determined experimentally due to the low carbon basicity of the bromide ion. This rate constant, k_r, was therefore calculated from the equilibrium constant, K, determined independently by NMR, and the forward rate constant, k_f, by $k_r=k_f/K$. For reactions involving the bromide ion as nucleophile, this procedure was generally applied.

All the remaining rate constants were determined by the IR technique employing liquid cells by following the rate of appearance or/and disappearance of the pseudohalide ions in the 2000–2200 cm^{-1} region. For the reaction depicted by eqn. 4, the reaction between RSCN and ionic selenocyanate, $NCSe^-$, and for the reverse reaction, RSeCN+NCS^-, ^{13}C-pseudohalide ions had to be employed since $N^{12}CS^-$ and $N^{12}CSe^-$ absorb at 2059 and 2068 cm^{-1}, respectively, which are not sufficiently apart for accurate studies. Due to the low extinction coefficients of RSCN and RSeCN in the 2000–2200 cm^{-1} region the peaks due to these compounds did not interfere with the measurements in the concentration ranges used.

The concentration of the ionic nucleophiles was usually in the $(2-7)\times10^{-3}$ M range, but for the slowest reactions, notably the reactions of RSCN, concentrations up to 2×10^{-2} M had to be used to avoid prolonged reaction times (see below). For some of the reactions both the effect of the cation, Ph_4As^+, Ph_4P^+ or $[PNP]^+$, and the concentration of the nucleophiles were examined and no dependence of rate constants upon cation or upon concentration was observed up to the maximum concentration employed, 2×10^{-2} M.

The rate constants were calculated from kinetic runs performed under both pseudo first-order and second-order conditions when experimentally possible, depending upon rate and equilibrium constants. When the pseudo first-order technique was used, the organic substrate and not the ionic nucleophile was the one in excess to avoid the concentration of the latter exceeding 2×10^{-2} M. (Examples: RSCN+$N^{13}CS^-$ and RSCN+Cl^-).

The linearity of the rate plots was generally satisfactory for several half-lives suggesting the reactions to be clean second-order reactions, first-order in each of the reactants. The only reactions deviating significantly from clean second-order kinetics when the reactions were followed for more than two half-lives were the slow reactions of 1-phenyl-2-thiocyanatoethanone, RSCN. For prolonged reaction times the reaction mixture turned slowly yellow and more thiocyanate ions were formed than calculated from the amount of consumed nucleophiles. The rate constants for the reactions of this substrate were therefore calculated from kinetic runs followed for only one to two half-lives. The equilibrium constants for reactions involving the thiocyanate ion were therefore calculated from more concentrated runs by the NMR technique or by IR after dilution.

The determination of equilibrium constants by NMR was performed on equilibrated solutions by comparison of peak heights due to the methylene protons. Concentrations up to 2×10^{-1} M were necessary to obtain reproducible results for equilibrium constants far from unity. (Reactions involving the bromide ion). In order to obtain sufficiently concentrated solutions of the anions only $[PNP]^+$-salts could be employed. In the calculations of the equilibrium constants the activity coefficients of the two competing anions were assumed to be the same.

Calculations. The reactions studied can be described with the following general equation, eqn. 6:

$$RA+B^- \underset{k_r}{\overset{k_f}{\rightleftharpoons}} RB+A^- \qquad (6)$$

where k_f and k_r are the second-order rate constants for the forward and the reverse reaction, respectively. For equal start concentration of the reactants, a, the integrated rate equation is:

$$(2aK_r^{\frac{1}{2}})^{-1} \ln \frac{a-x(1-K_r^{\frac{1}{2}})}{a-x(1+K_r^{\frac{1}{2}})} = k_f t \qquad (7)$$

where $K_r=k_r/k_f$ and x is the concentration of product at time t. For reactions where k_r is negligible compared with k_f, $K_r \ll 1$, the usual second-order rate equation can be applied, eqn. 8:

$$\frac{x}{a(a-x)} = k_f t \qquad (8)$$

When $[RA]_0=a$ and $[B^-]_0=b$ and $a\neq b$, the following rate equation is valid, eqn. 9:

$$M^{-1} \ln \frac{2ab-x(a+b-M)}{2ab-x(a+b+M)} = k_f t \qquad (9)$$

where $M=[(a-b)^2+4K_r]^{\frac{1}{2}}$ and $K_r=k_r/k_f$ as in eqn. 7.

For pseudo first-order reactions, $a \gg b$, eqn. 9 is reduced to:

$$Z^{-1} \ln \frac{2ab-x(a-Z)}{2ab-x(a+Z)} = k_f t \qquad (10)$$

where $Z=(a^2+4abK_r)^{\frac{1}{2}}$.

For pseudo first-order reactions where the reactions are monitored by the rate of disappearance of the minor reactant, b, the rate equation is:

$$Z^{-1} \ln \frac{b(a+Z)+(b-x)(a-Z)}{b(a-Z)+(b-x)(a+Z)} = k_f t \qquad (11)$$

where Z is as given above, eqn. 10, and $(b-x)$ is the concentration of the minor reactant at time t.

For the isotope exchange reactions, the reactions depicted by eqn. 3 and 5, $[RA]_0=[B^-]_0+[A^-]_0=a$ for equal concentrations of reactants, eqn. 6. When the isotope purity of the applied ^{13}C-pseudohalide ions is 90.5 %, $[B^-]_0=0.905\ a$. Since K is necessarily unity, the following rate equation is obtained:

$$(2a)^{-1} \ln \frac{0.778a}{a-2.22x} = k_f t \qquad (12)$$

where x denotes the concentration of products at time t.

When the progress of the reaction is followed by the rate of disappearance of the ^{13}C-pseudohalide ion, $(b-x)$, the integrated rate equation is:

$$(2a)^{-1} \ln \frac{0.778a}{2.22(b-x)-a} = k_f t \qquad (13)$$

Instrumental. The UV measurements were performed with a Varian-Techtron UV-VIS Spectrofotometer, Model 635, employing matched 1 cm quartz cells. The IR measurements were performed with a Unicam SP 200 Infrared Spectrophotometer. IR liquid cells of 0.1 cm path-length were employed.

The reaction solutions were kept in a thermostated oil-bath at 25.0±0.1 °C. 4 to 8 aliquots were withdrawn periodically for each kinetic run.

The NMR measurements were performed at ≈27 °C on a JEOL NMR C-60 H Spectrometer. A Spin-decoupler JNM-SO 30 Counter was used to determine the resonance positions.

RESULTS

In Table 2 are listed the second-order rate constants, k_f, and the equilibrium constants, K, determined in the present study. The values for k_f and K are the average values from measurements performed at least in duplicate with varying concentrations of reactants. In column 4 in Table 2 are listed the calculated relative rate constants, k_f(rel), for each nucleophile reacting with the various substrates; the rate constant for the least reactive compound, RSCN, is unity.

As indicated in Table 2, several of the rate constants and especially some of the equilibrium constants have limited accuracy. Even though most of the equilibrium constants were determined in

Table 2. Second-order rate constants, k_f, relative rate constants, k_{rel}, (rate constants for RSCN reacting with each nucleophile are unity) and equilibrium constants, K, for the reactions between 2-substituted 1-phenylethanones, ($PhC(O)CH_2X$), RX, and various nucleophiles, Y^-, in acetonitrile at 25.0 °C.

RX	Y^-	$k_f/M^{-1}s^{-1}$	k_{rel}	K
RBr	$NCSe^-$	4.7±0.9	1.3×10^4	$(6\pm3)\times10^{2\,a}$
RCl	$NCSe^-$	$(2.2\pm0.2)\times10^{-2}$	60	10 ± 2^b
RSeCN	$N^{13}CSe^-$	$(6.3\pm0.3)\times10^{-3}$	18	1
RSCN	$N^{13}CSe^-$	$(3.7\pm0.3)\times10^{-4}$	1	1.2±0.1
RCl	Br^-	$\sim8\times10^{-2\,c}$	~100	$(1.0\pm0.2)\times10^{-2\,b}$
RSeCN	Br^-	$(6\pm3)\times10^{-3}$	9	$(1.8\pm0.9)\times10^{-3}$
RSCN	Br^-	$(7\pm2)\times10^{-4\,c}$	1	$(1.1\pm0.3)\times10^{-3}$
RBr	Cl^-	~8	$\sim2.5\times10^4$	$(1.0\pm0.2)\times10^{2\,a}$
RSeCN	Cl^-	$(2.6\pm0.2)\times10^{-3}$	8	0.13±0.01
RSCN	Cl^-	$(3.3\pm0.5)\times10^{-4}$	1	0.2±0.02
RBr	NCS^-	$(6.2\pm0.4)\pm10^{-1}$	2.5×10^4	$(9\pm3)\times10^{2\,a}$
RCl	NCS^-	$(1.9\pm0.2)\times10^{-3}$	75	5 ± 1^b
RSeCN	$N^{13}CS^-$	$(3.1\pm0.3)\times10^{-4}$	12	0.84±0.1
RSCN	$N^{13}CS^-$	$(2.5\pm0.2)\times10^{-5}$	1	1

[a] Calculated from K for the reverse reaction. [b] Determined only by NMR at 27 °C. [c] Calculated from K and k_r.

three independent ways; NMR, IR and, when possible, by the ratio of k_f and k_r, the experimental uncertainty was considerable for the equilibrium constants far from unity, *i.e.* for reactions involving the bromide ion. The equilibrium constants between 10 and 10^{-1}, however, are probably well within 20 %.

With the exception of the reactions of 2-bromo-1-phenylethanone, RBr, and the isotope exchange reactions, eqns. 3 and 5, all rate constants had to be calculated from rate equations in which the equilibrium constants were parameters, eqns. 7, 9, 10 and 11. The uncertainty in the equilibrium constants thus influenced the accuracy by which the rate constants could be determined. For the reactions of RBr, the simple second-order rate equation, eqn. 8, could be used with negligible error due to the low carbon basicity of the leaving group, the bromide ion. However, all reactions of this substrate were too rapid for both the UV and the IR techniques to allow the rate constants to be determined with high accuracy. (Half-lives from 30 to 300 s).

In none of the reactions studied, even after very long reaction times, could any formation of 2-isothiocyanato- and 2-isoselenocyanato-substituted products, $PhC(O)CH_2NCS$ and $PhC(O)CH_2NCSe$, respectively, be observed. Due to the large extinction coefficients of this class of compounds in the 2000–2200 cm^{-1} region,[6] it should have been possible to detect only trace amounts. No formation of elemental selenium or sulfur could be observed in any of the reactions.

All the 2-substituted 1-phenylethanones in the present study exhibited two strong absorptions in the 1700 cm^{-1} region. (Column 3 in Table 1). Due to the proximity of these peaks, they could not be used for the determination of rate and equilibrium constants. In the case of the chloro-substituted compound, the peak at the higher wavenumber has the highest intensity while the opposite is the case for the remaining three compounds. Apparently, the chloro-substituted compound exists predominantly in the *cis*-conformation while the 2-bromo-, 2-thiocyanato- and the 2-selenocyanato-1-phenylethanones prefer the *gauche*-conformation in acetonitrile. As has been pointed out by Jones and Spinner,[7] the *cis-gauche* equilibrium in 2-substituted 1-phenylethanones appears to be due to a complex interplay of electron-withdrawing effects and steric demands of the substituents.

DISCUSSION

2-Halo-1-phenylethanones, $PhC(O)CH_2X$ (X = Cl, Br and I), have long been known to be highly reactive toward nucleophilic species.[8-10] Actually, with some very few exceptions,[11] these compounds are generally regarded as considerably better alkylating agents than are all other alkyl halides.[12] In this study it is shown that even the thiocyanate ion and the selenocyanate ion can be easily displaced from the methylene carbon atom. Due to the facility by which this class of compound undergoes displacement reactions, the present study appears to be one of the very few studies on substitution reactions toward aliphatic carbon in which both the forward and the reverse rate constants together with equilibrium constants have been determined. The results therefore provide information on not only the nucleophilicity and the leaving group ability of the employed anions but also on their carbon basicity.[13] Data on basicity toward aliphatic carbon are most rare in the literature.[13-16]

In Table 3 are listed some ratios between the second-order rate constants for the various reactions studied. In Table 4 are listed some average nucleophilicities, average leaving group abilities and the carbon basicity of Br^-, Cl^-, $NCSe^-$ and NCS^-. These latter numbers are calculated from the data

Table 3. The ratio between second-order rate constants for various nucleophiles reacting with 2-substituted 1-phenylethanones, RX, in acetonitrile at 25.0 °C.

	$\frac{k_f(NCSe^-)}{k_f(NCS^-)}$	$\frac{k_f(NCSe^-)}{k_f(Cl^-)}$	$\frac{k_f(NCSe^-)}{k_f(Br^-)}$	$\frac{k_f(Br^-)}{k_f(Cl^-)}$
RBr	8	0.6		
RCl	11		~0.3	
RSeCN	20	2.5	~1.1	~2.3
RSCN	15	1.1	~0.5	~2.1

Table 4. The average nucleophilicity, the average leaving group ability and the carbon basicity of Br^-, Cl^-, $NCSe^-$ and NCS^- for reactions with 2-substituted 1-phenylethanones in acetonitrile at 25.0 °C. (Relative values to NCS^-.)

	Br^-	Cl^-	$NCSe^-$	NCS^-
Nucleophilicity [a]	15	7	10	1
L. group ability [b]	2×10^4	75	10	1
Carbon basicity [c]	1.4×10^{-3}	0.14	1.2	1

[a] Average values calculated from rate constants listed in Table 2 and rate ratios in Table 3. [b] Average values calculated from relative rate constants, k_{rel}, in Table 2, column 4. [c] Values from equilibrium constants, K, in Table 2.

in Tables 2 and 3 and are relative to the values for the thiocyanate ion.

The nucleophilicity of Br^-, Cl^-, $NCSe^-$ and NCS^-. The data in Tables 2 and 4 suggest that the bromide ion, the chloride ion and the selenocyanate ion are approximately of the same nucleophilic strength toward the methylene carbon atom in the various 2-substituted 1-phenylethanones. These ions appear to be about ten times as nucleophilic as is the thiocyanate ion. The same trend in reactivity has previously been observed for substitution reactions toward methyl iodide in acetonitrile.[17] None of the ions therefore seem to prefer the methylene carbon to the methyl carbon in methyl iodide to any significant extent.

The calculated rate ratios, listed in Table 3, indicate clearly that the effect of the leaving group upon the reactivity of the various ions is not pronounced, especially when taking into account that the reactivity of the various substrates spans over more than four powers of ten (column 4 in Table 2). Apparently, only when the leaving groups are very dissimilar *i.e.* the iodide ion and the tosylate ion,[18,19] may nucleophiles show significant preference for one or the other leaving group. In the present study all leaving groups, and thus all nucleophiles, are on the soft side of the scale[20] and the nucleophilicity of the various ions is not anticipated to be strongly dependent upon the leaving group. The data in Table 3, however, suggest that the selenocyanate ion favours slightly the selenocyanate ion as leaving group while the halide ions prefer slightly a halide ion as leaving group. This finding accords with the idea of maximum stabilization of the transition state in alkylation reactions when the entering and the leaving groups are similar.[18]

The leaving group ability of Br^-, Cl^-, $NCSe^-$ and NCS^-. The bromo-substituted compound is clearly the most reactive of the various ω-substituted 1-phenylethanones. The average rate ratio between RBr and RCl, ~300 (column 4 in Table 2 and Table 4), is considerable but is in no way exceptional for alkylation reactions in dipolar aprotic solvents.[21] In protic solvents considerably lower RBr/RCl ratios are generally observed which is predominantly due to the preferential solvation of the chloride ion which increases the leaving group ability of this ion in this class of solvent. In dipolar aprotic solvents, however, where the solvation of the chloride ion is negligible, large rate ratios between alkyl bromides and alkyl chlorides are observed which reflect the large difference in the bond energy of the carbon-bromine and of the carbon-chlorine bond.

The organic selenocyanate, RSeCN, reacts approximately 10 times as rapidly as does the corresponding thiocyanate, RSCN, with all the nucleophiles. Apparently, the weaker carbon-selenium bond is the cause of the higher reactivity of the selenocyanato-substituted compound. Several organic selenocyanates, RSeCN, are well-known to isomerize considerably more rapidly to the iso-substituted derivatives, RNCSe, than do the corresponding thiocyanates, RSCN ($R = Ph_2CH$ *etc.*).[22] The better leaving group ability of the selenocyanate ion from aliphatic carbon appears to be the probable cause of this observation.

The carbon basicity of Br^-, Cl^-, $NCSe^-$ and NCS^-. The bromide ion is clearly the least basic of the anions studied and this ion is about two orders of magnitude less basic than is the chloride ion. This observation agrees with the results by Parker[13] on the carbon basicity of the chloride ion and the bromide ion toward the butyl carbon atom in nitrobenzene at 80 °C and the methyl carbon atom in acetone at 25 °C. The basicity of the thiocyanate ion, however, toward the butyl carbon atom in

nitrobenzene is reported by Parker[13] to be of the same order of magnitude as that of the bromide ion which is not in agreement with the results obtained in the present study; the thiocyanate ion and the selenocyanate ion being even more basic than the chloride ion.

The selenocyanate ion is slightly more basic than is the thiocyanate ion, even though the former ion is a considerably better leaving group. While the leaving group ability is a function of the energy of the bond to be broken and the solvation energy of the displaced ion, the carbon basicity is also a function of the nucleophilicity of the ion. Since the reactivity of nucleophilic species in substitution reactions toward aliphatic carbon is strongly dependent upon the polarizability of the nucleophile,[20] the carbon basicity is therefore also a function of the polarizability of the attacking nucleophile. The carbon basicity should therefore not parallel the hydrogen basicity to any significant extent when the nucleophilic atom is altered. This conclusion was arrived at by Bunnett[14] and Hine[16] several years ago. Since the nucleophilicity and the leaving group ability of nucleophilic species in substitution reactions toward aliphatic carbon is strongly dependent upon the structure of the transition state[1,20] which in turn is a function of the solvent[13] and the organic substrate,[1] it is obvious that no absolute order of carbon basicity of nucleophiles can be arrived at.

REFERENCES

1. Thorstenson, T., Eliason, R. and Songstad, J. *Acta Chem. Scand. A 31* (1977) 276.
2. Austad, T., Songstad, J. and Åse, K. *Acta Chem. Scand. 25* (1971) 331.
3. Dykerhoff, A. *Ber. Dtsch. Chem. Ges. 10* (1877) 199.
4. Hofmann, G. *Justus Liebigs Ann. Chem. 250* (1888) 298.
5. Martinsen, A. and Songstad, J. *Acta Chem. Scand. A 31* (1977) 645.
6. Bulka, E., Ahlers, K.-D. and Tucek, E. *Chem. Ber. 100* (1967) 1367.
7. Jones, R. N. and Spinner, E. *Can. J. Chem. 36* (1958) 1020.
8. Slator, A. and Twiss, D. F. *J. Chem. Soc. 95* (1909) 93.
9. Conant, J. B. and Kirner, W. R. *J. Am. Chem. Soc. 46* (1924) 233.
10. Conant, J. B. and Hussey, R. E. *J. Am. Chem. Soc. 47* (1925) 476, 488.
11. Ross, S. D., Finkelstein, M. and Petersen, R. C. *J. Am. Chem. Soc. 90* (1968) 6411.
12. Bordwell, F. G. and Brannen, W. T., Jr. *J. Am. Chem. Soc. 86* (1964) 4645.
13. Parker, A. J. *Proc. Chem. Soc. London* (1961) 371.
14. Bunnett, J. F., Hauser, C. F. and Nahabedian, K. V. *Proc. Chem. Soc. London* (1961) 305.
15. Matsui, T., Yamane, F. and Tokura, N. *Bull. Chem. Soc. Jpn. 44* (1971) 290.
16. Hine, J. and Weimar, R. D., Jr. *J. Am. Chem. Soc. 87* (1965) 3387.
17. Austad, T., Engemyr, L. B. and Songstad, J. *Acta Chem. Scand. 25* (1971) 3535.
18. Pearson, R. G. and Songstad, J. *J. Org. Chem. 32* (1967) 2899.
19. Engemyr, L. B. and Songstad, J. *Acta Chem. Scand. 26* (1972) 4179.
20. Pearson, R. G. and Songstad, J. *J. Am. Chem. Soc. 89* (1967) 724.
21. Thorstenson, T. and Songstad, J. *Acta Chem. Scand. A 30* (1976) 724.
22. Tarantelli, T. and Leonesi, D. *Ann. Chim. Rome 53* (1963) 1113.

Received September 12, 1977.

Acta Chemica Scandinavica A 32 (1978) 141 – 148

Molecular Structure of Some Sulfur-substituted Schiff Bases of 1,2-Diamines with Two Molecules of Acetylacetone and Their Metal Complexes as Obtained from Absorption and Circular Dichroism Spectra and from X-Ray Diffraction Methods

H. P. JENSEN,[a] B. SAUSTRUP KRISTENSEN,[a] H. MOSBÆK[a] and I. SØTOFTE[b]

[a] Chemistry Department A, Building 207 and [b] Chemistry Department B, Building 301, Technical University of Denmark, DK-2800 Lyngby, Denmark

The Schiff base condensation products between one molecule of 1,2-diamines and two molecules of acetylacetone where the oxygen atoms have been substituted with sulfur and their metal complexes were studied by absorption and circular dichroism spectroscopy and by X-ray diffraction methods.

Only when the spatial separation between the chromophoric groups of the dimers is small exciton splitting in the electronic spectra is observed, and in the case of optically active dimers the associated Cotton effect may then be used to study rotational conformers around the substituted ethylene bridge linking the two monomeric parts together.

The crystal structure of the compound 4,4′-(*R*,*R*-$(-)_D$-1,2-cyclohexanediimine)di(3-penten-2-thione) has been determined in two different crystalline modifications. Both modifications are orthorhombic, space group $P\,2_12_12_1$. Mod 1: $a=12.403(3)$ Å, $b=16.567(2)$ Å, $c=17.833(1)$ Å, $Z=8$. Mod 2: $a=10.255(5)$ Å, $b=13.210(3)$ Å, $c=13.304(2)$ Å, $Z=4$. The structures have been refined to an R value of 0.085 and 0.072, respectively. The two crystallographically independent molecules of Mod 1 and the molecule of Mod 2 are not significantly different. The angle between two thioacetylacetone planes is about 80°. The absolute configuration of the molecule has been determined. The S – S distances in the molecules are 6.0 – 6.4 Å.

Through UV absorption and circular dichroism spectroscopy it has been possible within an exciton formalism to study rotational conformations around the substituted ethylene bridge in various Schiff base condensates of one molecule of 1,2-diamines and two molecules of β-diketones (ONNO).[1-3] Furthermore it has been possible to use the formalism in the case of neutral complexes of Cu^{2+}, Ni^{2+} and VO^{2+} assigning ligand field transitions and absolute configurations,[4] one of which [4,4′-(*R*-propylenediiminato)di(3-penten-2-one)copper(II)] was confirmed by X-ray structural analysis.[5]

This tempted us to investigate optically active sulfur analogous of ONNO, the oxygen atoms of the Schiff bases being substituted with sulfur (=SNNS).[6-8] The fact that equivalent distributions between the tautomers I, II and III of Fig. 1 have been found for the monomeric parts (ON and SN) of the dimers ONNO and SNNS,[6,9,10] the most abundant being represented by tautomer III, suggests large structural similarities. Hence it seems reasonable to assume an essentially unpertubed polarisation of the $\pi\rightarrow\pi^*$ transition dipole moment within the planar chromophore SN as compared to the case of ON or acetylacetone (OO), *i.e.* only

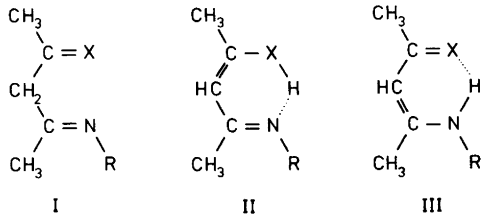

Fig. 1. Tautomeric forms of Schiff base condensate and S-substituted derived from amine and acetylacetone. X = O or S.

slightly off the sulfur-nitrogen direction. This conclusion has been confirmed through an extended Hückel calculation using orbital ionization energies for the diagonal elements and the Wolfsberg-Helmholtz approximation for the off-diagonal elements.[11] In both ON and SN the $\pi\rightarrow\pi^*$ transition dipole moment is found to be polarized some 10° off the nitrogen-chalcogen direction.

If there is no electron transfer or orbital overlap between the two chromophores in a dimer the excited states of the two halves interact only though a coupling of electronic motions resulting in a splitting of the $\pi\rightarrow\pi^*$ transition band inversely proportional with the spatial separation of the two chromophores to the third power (Eqn. 6 of Ref. 1), *i.e.*, when the separation is small (~ 3 Å)[1-4] we observe a splitting in the UV absorption, and in the case of optically active dimers these should furthermore exhibit circular dichroism with rotatory strengths of opposite signs for the two transitions; accordingly it is possible from the sign of the rotatory strength of, *e.g.*, the low energy component to assign an absolute configuration (Δ or Λ)[12] in terms of chirality of the $\pi\rightarrow\pi^*$ transition dipole moments contained in the two chromophore planes.[1,13]

When the spatial separation is big (6–7 Å), however, exciton splitting is expected to be negligible. This was observed with the species tn(acacH)$_2$,[1] tn(fmcH)$_2$[2] or *R*-1,3-bn(fmcH)$_2$,[2] and in the case of optically active dimers, as, *e.g.*, the two latter compounds, it is only possible to observe the inherent Cotton effect from the presumed $n\rightarrow\pi^*$ transitions.

EXPERIMENTAL

Schiff bases of diamines and acetylacetone (ratio 1:2) were prepared in analogy with the procedures given by McCarthy *et al.*[14] and converted to thiones according to Wei *et al.*[7,8] and Gerlach and Holm.[6] Diamines were obtained and resolved as described in the experimental sections of Refs. 2 and 15. UV absorption spectra were measured with a Cary 14 spectrophotometer, and circular dichroism spectra with a Roussel-Jouan dichrograph II and a Jobin-Yvon dichrograph III. ^{13}C NMR spectra were recorded at 22.63 MHz with a Bruker WH 90. The identities of the prepared compounds were established through chemical analyses.

When recrystallized from methanol *R*-chxn-(SacacH)$_2$ exists in two different modifications. Mod 1 appears when the compound is dissolved in methanol at 50 °C and then rapidly cooled to 0 °C. Mod 2 appears when the compound is dissolved in methanol at 20 °C and the solution is allowed to evaporate slowly at room temperature.

Molar absorptions and circular dichroisms in Figs. 5–8 are given in units of 1000 cm^2/mol.

Abbreviations

Amines. ma = methylamine, *R*-pn = (*R*)-(−)$_D$-1,2-propanediamine, *S*-pn = (*S*)-(+)$_D$-1,2-propanediamine, *R*-chxn = *trans*-(*R*,*R*)-(−)$_D$-1,2-cyclohexanediamine, tn = 1,3-propanediamine, *R*-1,3-bn = (*R*)-(−)$_D$-1,3-butanediamine, *S*-stien = (*S*,*S*)-(−)$_D$-1,2-diphenyl-1,2-ethanediamine. Assignments of absolute configurations of optically active diamines are according to Gillard[16] and Balieu *et al.*[17]

Diones. acacH = acetylacetone (2,4-pentanedione), fmcH = formylcamphor (3-formyl-1,7,7-trimethylbicyclo[2.2.1]heptan-2-one) obtained from natural (+)$_D$-camphor.

Condensates. ma(acacH)(4-methylimino-3-penten-2-one) *etc.* symbolizes condensates of an amine with acetylacetone. ma(SacacH)(4-methylimino-3-penten-2-thione) *etc.* symbolizes compounds where the oxygen atoms in the acetylacetone condensates have been substituted with sulfur.

CRYSTAL DATA

4,4′-(*R*,*R*-(−)$_D$-1,2-cyclohexanediimine)di(3-penten-2-thione); $C_{16}H_{26}N_2S_2$; M = 310.5. Orthorhombic. Systematic absences: *h*00 when *h* odd, 0*k*0 when *k* odd, 00*l* when *l* odd; space group $P2_12_12_1$ (No. 19).

Mod 1: $a = 12.403(3)$ Å, $b = 16.567(2)$ Å, $c = 17.833(1)$ Å. $V = 3664$ Å^3. $Z = 8$. $D_c = 1.13$ g cm^{-3}, $D_o = 1.15$ g cm^{-3} (flotation). $F(000) = 1344$.

Mod 2: $a = 10.255(5)$ Å, $b = 13.210(3)$ Å, $c = 13.304(2)$ Å. $V = 1802$ Å^3. $Z = 4$. $D_c = 1.14$ g cm^{-3}, $D_o = 1.15$ g cm^{-3} (flotation). $F(000) = 672$.

$\mu(\mathrm{MoK}\alpha) = 2.8$ cm^{-1}, $\mu(\mathrm{CuK}\alpha) = 25.7$ cm^{-1}.

X-RAY TECHNIQUE

Lattice type and space group were established from photographs taken with Cu*K*α and Mo*K*α radiation. Intensities were measured by a ω scanning technique on an Enraf Nonius CAD-4-F diffractometer. Graphite monochromated Mo*K*α radiation was used. Harmonics were excluded by means of a pulse height discriminator. Reflections with $\sin\theta/\lambda \leqslant 0.53$ Å^{-1} were measured for both

modifications. For Mod 1 the 5054 reflections measured were reduced to 1423 independent observed reflections which had $I > 2\sigma(I)$, where $\sigma(I)$ is calculated from counting statistics. For Mod 2 2566 reflections were reduced to 1131 independent observed reflections. The dimensions of the crystals used were $0.07 \times 0.16 \times 0.27$ mm and $0.15 \times 0.15 \times 0.30$ mm for Mod 1 and Mod 2, respectively. No correction for absorption was applied. The following computer programmes were used: programmes written at Chemistry Department B for processing the diffractometer output, MULTAN[18] and the X-RAY system[19] for the crystal structure analysis, and ORTEP II[20] for the illustrations. All calculations were carried out on an IBM 370/165 computer situated at the Technical University of Denmark.

The atomic scattering factors used were those of Cramer and Mann.[21] The anomalous dispersion corrections to the scattering factor of the sulfur atom were those of Cramer and Liebermann.[22]

STRUCTURE DETERMINATION

For Mod 1 the multiple-tangent-formula method, MULTAN, failed to solve the structure even after changing the starting point. Therefore the coordinates for the four sulfur atoms were deduced from the three-dimensional Patterson function. The positions of the remaining nonhydrogen atoms were derived from successive Fourier syntheses. For Mod 2 the coordinates of all nonhydrogen atoms except two were determined using MULTAN. The position of the last two carbon atoms were found in a Fourier map. The structures were refined by full least-squares minimization of $\Sigma w(|F_o| - c|F_c|)^2$. With anisotropic temperature factors and for Mod 1 use of the weighting scheme[23] $w^{-1} = 16.397 - 0.723|F| + 0.015|F|^2 - 1.640 \sin\theta/\lambda$, the refinement resulted in $R = 0.085$ ($R_w = 0.086$). For Mod 2 the weighting scheme used was $w^{-1} = 4.122 - 0.148|F| + 0.006|F|^2 - 5.348 \sin\theta/\lambda$, and the refinement resulted in $R = 0.072$ ($R_w = 0.078$). Hydrogen atoms have not been included in the structure determinations. The asymmetric carbon atoms in the $(-)_D$-1,2-cyclohexanediamine part of the ligand is known to have the *R*-configurations.[16] Even though the anomalous dispersion correction of the scattering factor of sulfur is small with Cu$K\alpha$ radiation, the absolute configuration of Mod 1 was confirmed by comparison of the observed and calculated intensity differences (Table 1). The reflections used were $4kl$ and $4\bar{k}l$ collected on a semiautomatic equi-inclination diffractometer (Stoe & Cie, Darmstadt, DBR).

Table 1. Observed and calculated structure amplitudes of Bijvoet pairs.

h k l	$F_c(hkl)$	Observed relations	$F_c(h\bar{k}l)$
4 1 9	483	>	455
4 3 3	430	>	418
4 4 1	160	<	190
4 4 2	334	>	316
4 5 2	422	<	449
4 5 3	449	>	430
4 8 1	418	>	396
4 8 5	463	<	475
4 11 6	187	<	208

The final positional parameters and their estimated standard deviations are listed in Table 2 (labelling of the atoms is given in Fig. 2). The final thermal parameters and their estimated standard deviations and a list of observed and calculated structure factors may be obtained from the authors on request.

DESCRIPTION OF THE STRUCTURES

Bond lengths and bond angles together with estimated standard deviations are listed in Tables 3 and 4. By inspection of the tables it is apparent that there are only minor differences between the two independent molecules of Mod 1 and between molecules of Mod 1 and 2. The standard deviations are rather large due to the small number of

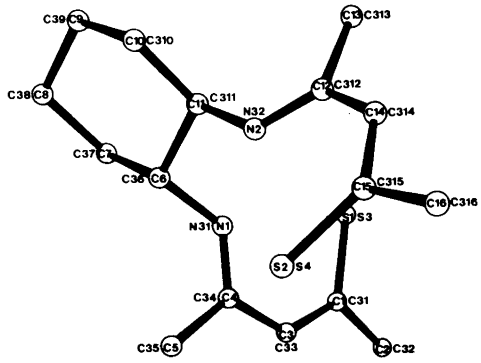

Fig. 2. Mod 2 viewed along the *b*-axis. The labelling inside the atoms corresponds to Mod 2 and one of the molecules in Mod 1. The labelling outside the atoms refers to the atoms of the other molecule of Mod 1.

Table 2. Atomic coordinates. The estimated standard deviations are given in parenthesis.

Atom	Mod 1			Mod 2		
	z	*y*	*z*	*x*	*y*	*z*
S1	0.1773(5)	0.5131(3)	0.4931(3)	0.6943(3)	0.0196(3)	0.6293(3)
S2	0.6798(5)	0.6093(3)	0.4898(4)	0.7468(3)	0.4870(3)	0.5442(2)
N1	0.3561(11)	0.5615(8)	0.5941(8)	0.8930(9)	0.1792(6)	0.6078(6)
N2	0.5442(11)	0.4766(9)	0.5475(9)	0.8068(10)	0.3503(6)	0.7157(6)
C1	0.1698(18)	0.6137(12)	0.4943(11)	0.7145(11)	0.0402(8)	0.5028(9)
C2	0.0744(18)	0.6567(15)	0.4542(11)	0.6352(12)	−0.0283(10)	0.4342(10)
C3	0.2446(16)	0.6632(11)	−0.5368(11)	0.7975(11)	0.1118(7)	0.4608(9)
C4	0.3313(15)	0.6385(11)	0.5817(10)	0.8862(12)	0.1787(8)	0.5090(8)
C5	0.3981(16)	0.7051(12)	0.6200(12)	0.9684(12)	0.2480(9)	0.4475(9)
C6	0.4351(14)	0.5334(10)	0.6481(10)	0.9861(12)	0.2391(8)	0.6685(9)
C7	0.3732(16)	0.5141(12)	0.7223(10)	1.0934(13)	0.1700(9)	0.7091(10)
C8	0.4547(18)	0.4788(14)	0.7803(11)	1.1827(14)	0.2277(10)	0.7806(11)
C9	0.5044(20)	0.4030(12)	0.7493(11)	1.1050(16)	0.2733(10)	0.8668(11)
C10	0.5618(17)	0.4174(12)	0.6756(13)	0.9950(13)	0.3432(9)	0.8274(10)
C11	0.4849(15)	0.4555(11)	0.6171(9)	0.9077(12)	0.2832(8)	0.7571(8)
C12	0.5633(15)	0.4292(11)	0.4903(12)	0.6956(12)	0.3740(8)	0.7601(8)
C13	0.5100(18)	0.3491(11)	0.4825(12)	0.6528(13)	0.3212(9)	0.8579(9)
C14	0.6335(15)	0.4574(11)	0.4323(10)	0.6078(12)	0.4459(8)	0.7210(9)
C15	0.6879(15)	0.5334(13)	0.4277(12)	0.6231(10)	0.5009(8)	0.6309(9)
C16	0.7676(20)	0.5377(15)	0.3580(13)	0.5184(11)	0.5811(9)	0.6055(11)
S3	−0.2355(5)	0.7997(4)	0.8731(3)			
S4	0.2225(5)	0.7649(3)	0.7761(3)			
N31	−0.0920(14)	0.8992(10)	0.7798(10)			
N32	0.1007(11)	0.8886(9)	0.8607(9)			
C31	−0.2547(17)	0.7712(11)	0.7824(14)			
C32	−0.3383(18)	0.6992(13)	0.7692(14)			
C33	−0.2050(16)	0.8038(13)	0.7189(13)			
C34	−0.1239(14)	0.8645(12)	0.7143(14)			
C35	−0.0798(20)	0.8876(17)	0.6397(12)			
C36	−0.0152(14)	0.9654(10)	0.7785(10)			
C37	−0.0723(16)	1.0506(12)	0.7668(12)			
C38	0.0102(18)	1.1194(12)	0.7765(15)			
C39	0.0612(18)	1.1170(16)	0.8495(14)			
C310	0.1263(16)	1.0394(12)	0.8596(13)			
C311	0.0437(15)	0.9653(11)	0.8564(11)			
C312	0.1277(14)	0.8577(12)	0.9283(12)			
C313	0.0877(16)	0.8902(15)	0.9976(12)			
C314	0.1957(15)	0.7869(12)	0.9293(12)			
C315	0.2439(17)	0.7427(12)	0.8699(12)			
C316	0.3148(20)	0.6724(12)	0.8895(15)			

observed reflections. For Mod 1 the ratio number of observations to number of variables is about four and for Mod 2 about six. Therefore the data do not permit a close comparison of bond lengths and bond angles or a discussion of the bond character of the C−C bonds and the C−N bonds, however, it is apparent that the bonds are not localized. The thioacetylacetonimine parts are nearly planar with angles between the two planes in the molecule of 85 and 80° for the two independent molecules in Mod 1. In Mod 2 the angle is 80°. For Mod 1, molecule 1, the angles between a plane through four atoms of the cyclohexane ring (C7, C8, C10, C11) and the two chromophoric parts are 66 and 84°. The corresponding angles for molecule 2 are 57 and 80° and for Mod 2, 77 and 77°. The bond lengths and angles and the planarity of the chromophoric parts are in agreement with the

results obtained for 4,4'-(*R*-propylenediiminato)di-(3-penten-2-one)copper(II).[5]

For Mod 1 the S–S distances in the two molecules are 6.433(9) and 5.966(9) Å, respectively. However, there are shorter S–S distances between the molecules, *viz* S1(x,y,z)–S3($-x,-\frac{1}{2}+y,\frac{3}{2}-z$) of 4.324(8) Å and S2($x,y,z$)–S4($\frac{1}{2}+x,\frac{3}{2}-y,1-z$) of 5.207(9) Å. For Mod 2 the S–S distance in the molecule is 6.300(5) Å and between S1(x,y,z) and

Table 3. Bond lengths in Å. The estimated standard deviations are given in parenthesis.

	Mod 1	Mod 2
S1–C1	1.67(2)	1.717(12)
C1–C2	1.56(3)	1.521(17)
C1–C3	1.45(3)	1.390(16)
C3–C4	1.40(3)	1.421(16)
C4–C5	1.54(3)	1.490(17)
C4–N1	1.33(2)	1.317(14)
N1–C6	1.45(2)	1.480(15)
C6–C7	1.56(3)	1.529(18)
C6–C11	1.53(3)	1.542(16)
C7–C8	1.56(3)	1.524(20)
C8–C9	1.50(3)	1.521(21)
C9–C10	1.51(3)	1.548(20)
C10–C11	1.55(3)	1.517(17)
C11–N2	1.48(2)	1.470(15)
N2–C12	1.31(3)	1.321(15)
C12–C13	1.49(3)	1.540(16)
C12–C14	1.43(3)	1.408(16)
C14–C15	1.43(3)	1.411(16)
C15–C16	1.59(3)	1.546(16)
C15–S2	1.68(2)	1.724(12)
S3–C31	1.70(3)	
C31–C32	1.60(3)	
C31–C33	1.40(3)	
C33–C34	1.43(3)	
C34–C35	1.49(3)	
C34–N31	1.36(3)	
N31–C36	1.45(2)	
C36–C37	1.59(3)	
C36–C311	1.57(3)	
C37–C38	1.54(3)	
C38–C39	1.45(4)	
C39–C310	1.53(3)	
C310–C311	1.60(3)	
C311–N32	1.46(2)	
N32–C312	1.35(3)	
C312–C313	1.44(3)	
C312–C314	1.46(3)	
C314–C315	1.42(3)	
C315–C316	1.50(3)	
C315–S4	1.73(2)	

Table 4. Bond angles (°). The estimated standard deviations are given in parenthesis.

	Mod 1	Mod 2
S1–C1–C3	122.3(16)	125.1(9)
S1–C1–C2	119.6(17)	115.4(8)
C2–C1–C3	117.9(17)	119.4(11)
C1–C3–C4	128.6(18)	129.3(11)
C3–C4–N1	123.5(17)	119.2(10)
C3–C4–C5	117.3(17)	119.8(10)
C5–C4–N1	119.2(16)	121.0(10)
C4–N1–C6	125.1(14)	125.6(9)
N1–C6–C7	107.3(14)	109.7(9)
N1–C6–C11	107.6(14)	106.4(9)
C11–C6–C7	109.3(14)	109.3(10)
C6–C7–C8	108.7(15)	110.8(10)
C7–C8–C9	109.5(16)	110.8(11)
C8–C9–C10	112.4(16)	111.2(11)
C9–C10–C11	111.0(17)	109.1(10)
C10–C11–N2	110.7(15)	109.4(9)
C10–C11–C6	110.4(14)	111.1(10)
C6–C11–N2	107.7(14)	107.9(9)
C11–N2–C12	126.9(15)	125.6(9)
N2–C12–C13	121.8(18)	121.1(10)
N2–C12–C14	118.6(16)	123.1(10)
C13–C12–C14	119.5(17)	115.8(10)
C12–C14–C15	128.0(17)	126.1(11)
C14–C15–C16	112.2(18)	117.4(10)
C14–C15–S2	126.4(16)	126.6(9)
C16–C15–S2	121.3(16)	116.0(9)
S3–C31–C33	127.0(16)	
S3–C31–C32	116.0(17)	
C32–C31–C33	117.0(20)	
C31–C33–C34	129.0(21)	
C33–C34–N31	117.0(20)	
C33–C34–C35	119.4(21)	
C35–C34–N31	123.5(18)	
C34–N31–C36	119.7(16)	
N31–C36–C37	112.4(15)	
N31–C36–C311	106.8(14)	
C311–C36–C37	108.9(14)	
C36–C37–C38	110.2(16)	
C37–C38–C39	111.8(19)	
C38–C39–C310	111.1(20)	
C39–C310–C311	107.6(16)	
C310–C311–N32	110.8(14)	
C310–C311–C36	109.2(15)	
C36–C311–N32	105.9(14)	
C311–N32–C312	119.9(18)	
N32–C312–C313	122.6(18)	
N32–C312–C314	117.5(18)	
C313–C312–C314	119.8(19)	
C312–C314–C315	131.0(19)	
C314–C315–C316	118.3(19)	
C314–C315–S4	123.1(16)	
C316–C315–S4	118.6(16)	

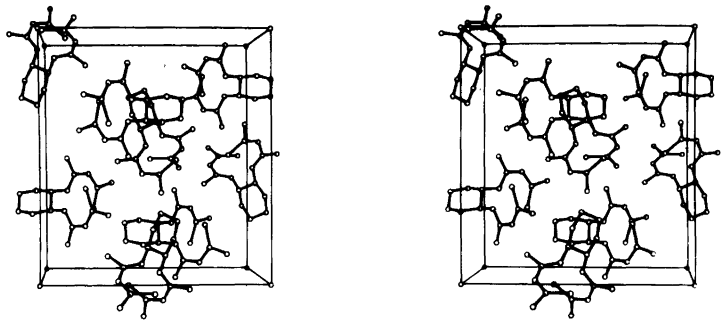

Fig. 3. Stereo view along the *a*-axis of the structure of Mod 1.

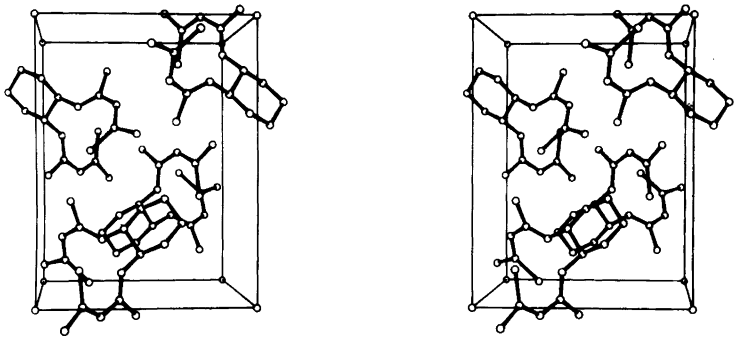

Fig. 4. Stereo view along the *b*-axis of the structure of Mod 2.

S2($-\frac{1}{2}+x$, $\frac{1}{2}-y$, $1-z$) there is a shorter S–S distance of 5.138(5) Å. The packing of a unit cell is shown for Mod 1 in Fig. 3 and for Mod 2 in Fig. 4. All intermolecular distances are larger than the sum of the van der Waals radii[24] of the atoms. The shortest distance between two carbon atoms is in both structures 3.53 Å.

SPECTROSCOPIC RESULTS AND DISCUSSION

The basis for adopting the exciton model to the Schiff bases of acetylacetone was the observation of a splitting in the UV absorption of, *e.g.*, *R*-chxn-(acacH)$_2$ correlated with circular dichroism bands of opposite signs.[1] However, the S-substituted 1,2-cyclohexanediamine derivatives show no splitting in the $\pi\rightarrow\pi^*$ transition region and only a single circular dichroism band (Fig. 5). In order to investigate whether tautomerisation occurs during the dissolution process we have, for *R*-chxn(SacacH)$_2$, measured the absorption and circular dichroism spectra of microcrystals suspended in KBr matrices, and the ^{13}C NMR spectrum in $CDCl_3$ solution. From the facts that the electronic spectra (Abs and CD) are equal in KBr and in $CHCl_3$, and that the ^{13}C NMR spectra show 8 peaks (*R*-chxn(SacacH)$_2$

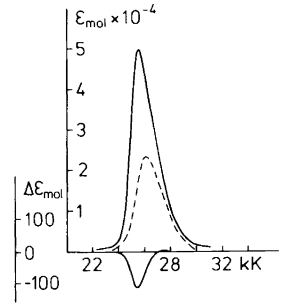

Fig. 5. Molar absorption and circular dichroism in $CHCl_3$ of *R*-chxn(SacacH)$_2$ (———) and ma(SacacH) (– – –).

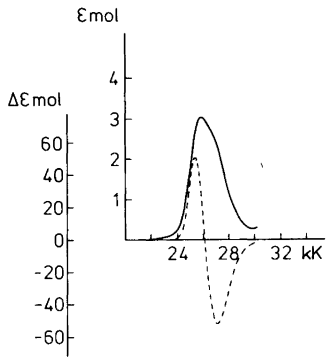

Fig. 6. Molar absorption (———) and circular dichroism (– – –) in CH_3OH of *S*-stien(SacacH)$_2$.

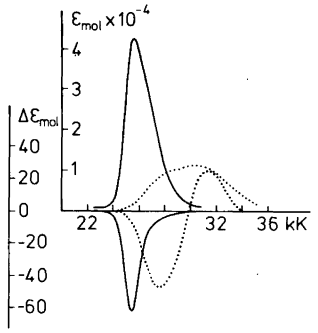

Fig. 7. Molar absorption and circular dichroism in $CHCl_3$ of *R*-pn(SacacH)$_2$ (———) and Zn *S*-pn(Sacac)$_2$ (. . .).

contains 16 C atoms), it is concluded that no tautomerisation occurs.

Since a dimer shows a dipole strength twice that of a monomer (Fig. 5) and no exciton splitting as a consequence of the above demonstrated large spatial separation of the two chromophoric parts, the observed Cotton effect may be identified as due to an $n \rightarrow n^*$ transition. This assignment is in accordance with the observation that ε_{max} is found at another wavelength than $\Delta\varepsilon_{max}$ (388 nm and 392 nm) showing that the two bands may have different causes, the absorption being mainly $\pi \rightarrow \pi^*$.

In the case of either bulky substituents on the ethylene bridge of the Schiff base condensates, or complexation, it should be possible to minimize the spatial separation of the two monomeric parts of the dimer, SNNS, with exciton coupling as a result.

These situations are demonstrated by *S*-stien(SacacH)$_2$ (Fig. 6) which, from the sign of the low energy component in the Cotton effect, may be assigned the same absolute configuration as *S*-chxn(acacH)$_2$,[1] and by Zn *S*-pn(Sacac)$_2$ (Fig. 7) which from a similar argumentation may be assigned the same absolute configuration as Cu *S*-pn(acac)$_2$ (the mirror image of Fig. 2 in Ref. 4). The intensity of the $\pi \rightarrow \pi^*$ transition band in the complex is somewhat reduced compared with the free ligand, but the reduction is comparable with findings in the case of pn(acacH)$_2$ and its Cu^{2+} complex.[4]

For the sake of further comparison we have prepared Cu *R*-pn(Sacac)$_2$ electronic spectra of which are shown in Fig. 8, exhibiting a profound similarity with the spectra of Cu *R*-pn(acac)$_2$ (Fig. 1 of Ref. 4). This similarity means that the model presented in Ref. 4 and further investigated in Refs. 5

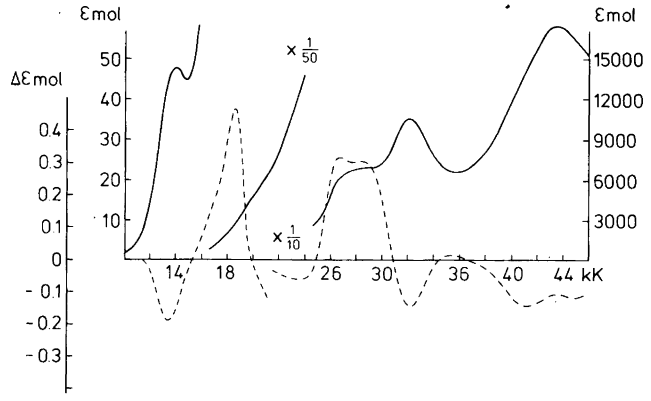

Fig. 8. Molar absorption (———) and circular dichroism (– – –) in CH_3OH of Cu *R*-pn(Sacac)$_2$.

and 25 for assignments of electronic transitions in Cu *R*-pn(acac)$_2$ may also be valid for Cu *R*-pn(Sacac)$_2$. Consequently the structure in solution of the two copper complexes is the same (Fig. 2 of Ref. 4) as seen from the signs of the Cotton effects associated with the high energy exciton components. This structural assignment is supported by the similarities in signs and positions of the ligand field transitions of the two complexes.

The only major difference between the two sets of spectra is found in the 25 – 26 kK region. This is. however, the region where we expect to find transitions originating in σ^n(non-bonding chalcogen orbitals)$\rightarrow\pi^*$,[5,25] and therefore differences are quite eligible and actually support the given interpretation of bands in this region.

Acknowledgement. We thank Mrs. L. Penzien for valuable assistance.

REFERENCES

1. Larsen, E. *Acta Chem. Scand. 23* (1969) 2158.
2. Jensen, H. P. and Larsen, E. *Acta Chem. Scand. A 29* (1975) 157.
3. Jensen, H. P. and Larsen, E. *Gazz. Chim. Ital. 107* (1977) 143.
4. Jensen, H. P. and Larsen, E. *Acta Chem. Scand. 25* (1971) 1439.
5. Larsen, E., Larsen, S., Røen, S. and Watson, K. J. *Acta Chem. Scand. A 30* (1976) 125.
6. Gerlach, D. H. and Holm, R. H. *J. Am. Chem. Soc. 91* (1969) 3457.
7. Blum, P. R., Wei, R. M. C. and Cummings, S. C. *Inorg. Chem. 13* (1974) 450.
8. Wei, R. M. C. and Cummings, S. C. *Inorg. Nucl. Chem. Lett. 9* (1973) 43.
9. Dudek, G. O. and Holm, R. H. *J. Am. Chem. Soc. 83* (1961) 2099.
10. Dudek, G. O. and Holm, R. H. *J. Am. Chem. Soc. 83* (1961) 3914.
11. Ballhausen, C. J. and Gray, H. B. *Molecular Orbital Theory*, Benjamin, New York 1964.
12. *IUPAC Inorg. Chem. 9* (1970) 1.
13. Schellman, J. A. *Acc. Chem. Res. 1* (1968) 144.
14. McCarthy, P. J., Hovey, R. J., Ueno, K. and Martell, A. C. *J. Am. Chem. Soc. 77* (1955) 5820.
15. Gullotti, M., Pasini, P., Fantucci, R., Ugo, R. and Gillard, R. D. *Gazz. Chim. Ital. 102* (1972) 855.
16. Gillard, R. D. *Tetrahedron 21* (1965) 503.
17. Balieu, E., Boll, P. M. and Larsen, E. *Acta Chem. Scand. 23* (1969) 2191.
18. Germain, G., Main, P. and Woolfson, M. *Acta Crystallogr. A 27* (1971) 368.
19. Stewart, J. M. *The X-RAY SYSTEM*, Technical Report TR-192 Computer Science Center, University of Maryland, College Park 1972.
20. Johnson, C. K. *ORTEP II*, Report ORNL-3794, Oak Ridge National Laboratory, Oak Ridge 1970.
21. Cramer, D. and Mann, J. B. *Acta Crystallogr. A 24* (1968) 321.
22. Cramer, D. and Liebermann, D. *J. Chem. Phys. 53* (1970) 1891.
23. Nielsen, K. *Acta Crystallogr. A 33* (1977) 1009.
24. Bondi, A. *J. Phys. Chem. 68* (1964) 441.
25. Jensen, H. P. *Acta Chem. Scand. A 30* (1976) 137.

Received September 16, 1977.

Acta Chemica Scandinavica A 32 (1978) 149 – 151

Acetylcamphor Condensed with Amines. The Structure in Solution as Obtained by NMR, UV Absorption and Circular Dichroism Spectroscopy

HANS PETER JENSEN

Chemistry Department A, Building 207, Technical University of Denmark, DK-2800 Lyngby, Denmark

The structures of Schiff base type condensation products of various 1,2-diamines with acetylcamphor are rationalized within the molecular exciton theory to give information about the relative orientation of the two camphor groups. It is shown that condensation products of acetylcamphor resemble acetylacetone analogues, and consequently indirect information is obtained about the cause of the stereochemical complexity of Schiff base condensates of formylcamphor.

Recently Schiff base type condensation products of various β-diketones and diamines have been investigated and the molecular structure in solution rationalized, *e.g.* within the molecular exciton theory.[1-4] It was, however, shown that erroneous conclusions were drawn relying on the exciton theory alone and omitting an independent check on the chromophore configuration itself. Consequently assignments of molecular structure based on Schiff bases (really enamines) of acetylacetone, which have $\pi \rightarrow \pi^*$ transitions polarized approximately in the N – O direction in a planar *syn* or (*Z*) structured chromophore with intramolecular hydrogen bonding, will be erroneous if the tautomer distribution for some β-diketones is different from that of acetylacetone. This was exactly the case when comparing Schiff bases of formylcamphor and acetylacetone in hydrogen bonding media (*e.g.* methanol), since for the former it was demonstrated through NMR-measurements that the chromophore took on an *anti* or (*E*) structure of the ketoenamine, which in non-hydrogen bonding media, however, could rearrange to the *syn* tautomer.

The basis in the study of rotational conformations around a substituted ethylene-bridge in condensates of planar *syn* structural β-diketones and 1,2-diamines is the strong exciton coupling taking place in the molecules where the chromophores are *gauche*. This leads to a splitting of the UV absorption band, and from the circular dichroism connected to the exciton transitions of optically active dimers it is determined which chiral rotamer is dominating in solution. Details about the method and reservations about its quantitative application have been given earlier.[1-3]

Even with the structural problem of the formylcamphor chromophore solved it is difficult to elucidate the general trends of the overall structure of the Schiff bases in terms of interactions between the asymmetric bulky β-diketone and substituents on the ethylene-bridge linking two chromophores together. To clarify whether the complexity of the formylcamphor Schiff bases compared with the acetylacetone condensation products has its origin in the asymmetric bulkiness of the camphor skeleton or in the lack of a methyl group on the side chain carbonyl group, the Schiff base condensates of acetylcamphor have been investigated.

EXPERIMENTAL

Preparations of optical active amines, acetylcamphor and Schiff base condensation products were all according to the known simple procedures.[1,2,5] The identity of the compounds was established from chemical analyses and NMR-spectra. Circular dichroism spectra were obtained with a Roussel-Jouan Dichrographe II and absorp-

tion spectra with a Cary 14 spectrophotometer. ^{13}C NMR spectra were recorded at 22.63 MHz with a Bruker WH 90 and ^{1}H NMR spectra at 90 MHz with a Bruker HX-90 E.

Abbreviations

Diketones. acacH = acetylacetone (2,4-pentanedione); accH = 3-acetylcamphor, fmcH = 3-formylcamphor, both from $(+)_D$-camphor.

Amines. ma = methylamine; en = 1,2-ethanediamine; *R*-pn = $(R)-(-)_D$-1,2-propanediamine; S-pn = $(S)-(+)_D$-1,2-propanediamine; *R*-chxn = *trans*-(*R*,*R*)-$(-)_D$-1,2-cyclohexanediamine.

Condensates. *R*-pn(accH)$_2$ *etc.* symbolizes the Schiff base condensate formed from one molecule of diamine and two molecules of diketone.

RESULTS AND DISCUSSION

First of all it is appropriate to investigate whether the Schiff base condensation between acetylcamphor and amines is analogous to the condensation between formylcamphor and amines, *i.e.*, occurring at the acetyl group. For this purpose ^{13}C NMR spectra were recorded using $CDCl_3$ as medium. The chemical shift relative to TMS of the carbonyl carbon atom in camphor is 218.4 ppm;[6] acetylcamphor, however, shows four peaks in the carbonyl carbon resonance region, namely 211.9(193), 210.7(132), 203.8(121) and 200.1(222) all ppm relative to TMS and with relative intensities given in parentheses. This reflects keto and enol tautomers in solution and the data may be correlated with investigations on acetylcamphor in CCl_4 using the ^{1}H NMR technique[7] resulting in a percentage distribution of tautomers as follows: 67 % keto form and 33 % enol form with intramolecular hydrogen bonding (*syn* form). From these data combined with peak intensities in the ^{13}C NMR spectrum and with knowledge of chemical shifts for carbonyl carbon atoms in acetone and acetylacetone[6] (acetone: 206.0 ppm; acetylacetone, keto: 201.9 ppm, enol: 191.4 ppm) the following assignments are made to the peaks in the ^{13}C NMR spectrum of acetylcamphor:

211.9 ppm: camphor carbonyl carbon atom in keto form
210.7 ppm: camphor carbonyl carbon atom in enol form
203.8 ppm: acetyl carbonyl carbon atom in enol form
200.1 ppm: acetyl carbonyl carbon atom in keto form

By condensing ethylenediamine with two molecules of acetylcamphor [en(accH)$_2$] and measuring the ^{13}C NMR spectrum, which shows 13 peaks, it is demonstrated that only one tautomer is present in solution ($CDCl_3$). The carbonyl signals of acetylcamphor are now observed at 205.3 and 152.9 ppm (relative to TMS), the latter assignable to an enamine group and the former to a carbonyl group. Returning to acetylacetone and its Schiff bases [*e.g.* en(acacH)$_2$] a shift in the carbonyl position from 201.9 to 194.9 ppm is observed by condensation; furthermore the camphor carbonyl carbon atom is found at 205.8 ppm in condensation products between amines and formylcamphor. Consequently the signal at 205.3 ppm in the ^{13}C NMR spectrum of en(accH)$_2$ is assigned to the camphor carbonyl carbon atom from which it follows that the condensation between acetylcamphor and amines occurs at the acetyl group.

To clarify whether a *syn*/*anti* tautomerisation depending on solvent is operative for acetylcamphor as was found in the case of formylcamphor,[2,3] ^{1}H NMR spectra were measured and no variation with time and/or solvent was found. The chemical shift of the amine protons in, *e.g.*, en(accH)$_2$ is 9.0 ppm relative to TMS, *i.e.* typical of hydrogen bonding; the peak furthermore carries the full intensity of two protons thus reflecting a *syn* structure of the chromophore as the only species present in solution. Consequently with Schiff bases of acetylcamphor it is possible to make structural assignemnts in the strong exciton coupling limit directly from electronic spectra.

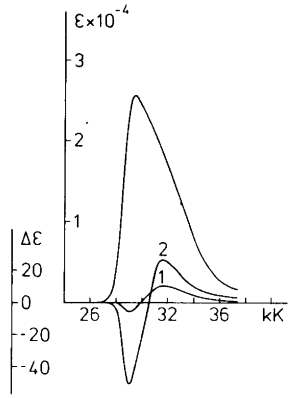

Fig. 1. Molar absorption and circular dichroism of en(accH)$_2$ in $CHCl_3$ (1) at room temperature and (2) at −60 °C.

Table 1. Wavelength of absorption maxima and the associated molar absorptivity to the left and corresponding circular dichroism data to the right.

Compound	Abs	$D \times 10^{19}$	CD			
	λ nm	$cm^3\ cm^{-1}$	λ nm	$\Delta\varepsilon$	λ nm	$\Delta\varepsilon$
ma(accH)	314	0.9	326	4.3		
en(accH)$_2$	340	1.8	344	−5.9	316	10.9
R-pn(accH)$_2$	340	1.9	342	−84.4	311	35.3
S-pn(accH)	340	1.9	342	80.2	301	−33.3
R-chxn(accH)$_2$	340	2.0	344	−71.5	314	28.5

Spectra of representative condensation products are given in Figs. 1 and 2 and in Table 1.

Compared with previous results on acetylacetone [1] the present spectra certainly demonstrate that both in acetylacetone and in acetylcamphor condensation products of 1,2-diamines it is the asymmetry of the diamine which is the stereochemically determining factor since the same rotamers exist for the same stereoisomeric diamine condensed with the two different diketones.

The structural assignments to acetylcamphor condensates are seen to be quite straightforward as the set of formulae derived by Larsen [1] for the strong exciton coupling limit is obeyed, *i.e.* the dipole strength of a dimer is double the dipole strength of a monomer and an optically active dimer exhibits circular dichroism with rotatory strengths of opposite signs for the two transitions.

As acetylcamphor is, however, asymmetric in itself there is also stereochemical induction from that group. This is seen in the CD spectrum of en(accH)$_2$ at low temperature (Fig. 1), since the character changes from a spectrum typical of intrinsic $n \rightarrow \pi^*$ transition to a spectrum typical of exciton splitting originating from compounds with (*R*) asymmetric carbon atoms (*i.e.* Δ). This behaviour is different from what was found with en(fmcH)$_2$ in which the low energy rotamer seems to be of Λ configuration even though *R*- and *S*-pn(fmcH)$_2$ have the same and opposite low energy configuration (Δ).

The difference in behaviour between en(fmcH)$_2$ and en(accH)$_2$ must be attributable to the additional methyl group on the carbonyl chromophore in the latter compound in which the methyl group influences the way en(accH)$_2$ achieves minimum potential energy. The interaction between the camphor groups is greater for condensation products of formylcamphor compared with condensation products of acetylcamphor as the methyl groups in the latter case prevent close contact.

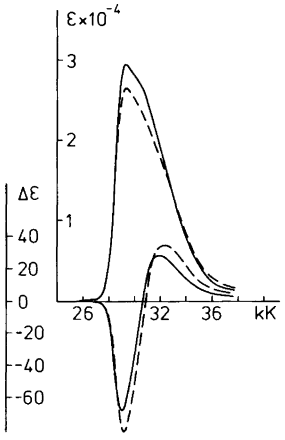

Fig. 2. Molar absorption and circular dichroism of *R*-chxn(accH)$_2$ (———) and *R*-pn(accH)$_2$ (– – –) in $CHCl_3$.

Acknowledgement. The valuable assistance of Mrs. L. Penzien is highly appreciated.

REFERENCES

1. Larsen, E. *Acta Chem. Scand. 23* (1969) 2158.
2. Jensen, H. P. and Larsen, E. *Acta Chem. Scand. A 29* (1975) 157.
3. Jensen, H. P. and Larsen, E. *Gazz. Chim. Ital. 107* (1977) 143.
4. Gullotti, M., Pasini, P., Fantucci, R., Ugo, R. and Gillard, R. D. *Gazz. Chim. Ital. 102* (1972) 855.
5. Brühl, J. W. *Ber. Dtsch. Chem. Ges. 37* (1904) 746.
6. Johnson, L. F. and Jankowski, W. C. *Carbon-13 NMR Spectra*, Wiley, New York 1972.
7. Springer, C. S., Sievers, R. E. and Feibush, B. *Inorg. Chem. 10* (1971) 1242.

Received September 23, 1977.

Acta Chemica Scandinavica A 32 (1978)153–156

Linear and Circular Dichroism in Single Crystals of Dichloro(ethylenediamine)platinum(II) and -palladium(II)

HANS PETER JENSEN*

Chemistry Department A, Building 207, Technical University of Denmark, DK-2800 Lyngby, Denmark

The linear and circular dichroisms in single crystals of dichloro(ethylenediamine)platinum(II) and dichloro(ethylenediamine)palladium(II), which are isomorphous and crystallize in the orthorhombic space group $C222_1$, are measured and the difference in appearance of the circular dichroism spectra of the two compounds is explained through different distortion of the over-all planar coordination sphere, the Pd(II) complex having the major distortion.

A recent X-ray diffraction study[1] has shown that crystals of *cis*-M(en)Cl_2 (M = Pt, Pd; en = 1,2-ethanediamine) are isomorphous and belong to the orthorhombic system, space group $C222_1(D_2^5)$. The metal atoms are surrounded by two Cl and two N atoms in an almost *cis* square-planar arrangement, and the C atoms in the ethylene bridge are twisted out of this plane, one above and the other below; furthermore the molecules stack in a nearly linear array with a uniform spacing of 3.381 Å (Pt) and 3.369 Å (Pd), respectively.

As indicated by Hald and Rasmussen[2] and by Berg[3] the space group symmetry D_2^5 permits the crystal to rotate the polarization direction of linearly polarized light, *i.e.* the molecular units in the single crystals may be dissymmetric due to the ethylenediamine rings exhibiting only one of the two possible conformations λ or δ. Consequently circular dichroism should be detectable in the crystalline phase as it was also indicated by Hald and Rasmussen[2] (see the footnote on p. 1412 in Ref. 3), who tried to measure the circular dichroisms having the two complexes diluted through solid dispersion of single crystals in KBr matrices.

Another way of proceeding for the detection of the inherent circular anisotropy of the M(en)Cl_2 crystals is to measure directly single crystal circular dichroism, which, however, presents the problem of static linear anisotropy coexisting in the crystals.[4,5] As a matter of fact, the problem of linear dichroism has precluded detection of circular dichroism until very recently, where the questions of instrumentation,[6] mathematical formulation,[7,8] measuring conditions and limitations,[8,9] together with actual experiments[10,11] were settled.

The crystals M(en)Cl_2 have an exceptionally ideal orientation of the molecular units for the study of polarization directions of transitions through investigation of linear dichroism since the chains of stacked molecules are directed along the orthorhombic *c* axis and the symmetry axis and permanent dipole moment of every molecule are in the $\pm b$ direction. The crystals grow as thin plates with developed face (100) and show under the microscope pronounced fibrous grooves very often along the longest dimension. These grooves were by X-ray diffraction analysis determined to be parallel to the *c* axis,[3] a fact which makes orientation of the crystals in an experimental coordinate system very easy.

In this investigation we will choose the same molecular Cartesian coordinate system as Martin *et al.*,[4,5] *i.e.* with *z* axis normal to the molecular plane and *y* axis along the molecular symmetry axis from which it follows that the axes *x*, *y* and *z* are conveniently directed parallel to the crystallographic axes *a*, *b* and *c*, respectively. As it was also pointed out by Martin *et al.* with this choice of axes the d_{xy} orbital is used for σ bonding, so that the lowest unfilled orbital on the metal center is the antibonding orbital involving d_{xy}.

* Visitor at Institute of Molecular Biology, University of Oregon, Eugene, Oregon 97403, USA.

Among the ligand field transitions three are electric dipole allowed in the symmetry group C_{2v} (which will be used for assigning transitions in the complexes even though M(en) Cl_2 strictly possesses only the symmetry C_2), and this is the transitions $A_1 \rightarrow B_1$ ($d_{xz} \rightarrow d_{xy}$) with $z(c)$ polarization and $A_1 \rightarrow B_2$ ($d_{z^2} \rightarrow d_{xy}$ and $d_{x^2-y^2} \rightarrow d_{xy}$) with $x(a)$ polarization, but none with $y(b)$ polarization.

Martin *et al.* present a detailed discussion of the polarized absorption spectra of Pt(en)Cl_2; especially they discuss the two *b* polarized bands at 33 100 cm^{-1} and 39 100 cm^{-1}, respectively, in terms of ionized excitons (or alternatively M←L charge-transfer bands) and acknowledge, on the basis of earlier assignments by Chatt *et al.*,[12] three bands in the ligand field range namely, a *c* polarized band at 25 000 cm^{-1} assigned as spin-forbidden $d_{xz} \rightarrow d_{xy}$, a *b* polarized band at 22 000 – 27 000 cm^{-1} assigned as a spin-forbidden ligand field transition with vibronic reinforcement and another *b* polarized band at 28 000 cm^{-1} assigned as spin-allowed $d_{x^2-y^2} \rightarrow d_{xy}$ with vibronic reinforcement. These three bands are those which will be discussed further in the present paper.

EXPERIMENTAL

Crystals were obtained from Berg, who prepared them as described by him.[3] Crystals of suitable thickness (0.06 – 0.01 mm) were mounted on microscope slides and centered in the light beam of a microscope built into a phasemodulation spectrophotometer, the construction of which is described elsewhere.[6,10] The photocurrent is processed and analysed as described by Jensen[9,10] and Jensen *et al.*[8] using the intensity ratios of Ref. 10, which are derived under the condition that the Mueller matrix representing the medium has the form presented by Troxell and Scheraga.[13] This requires that the actual values of the anisotropies are less than 1, a condition which was fulfilled since the measured linear and circular dichroisms never exceeded ~0.1 and ~0.01 absorbance units, respectively.

The ratios between linear and circular dichroisms around absorption maxima are such that the "true" circular dichroism is obtained, provided the proper correction for linear dichroism in the intensity ratio I_{AC}/I_{DC} is performed. This notion may be gathered in considering an optically active copper(II) complex for which the linear and circular dichroisms of single crystals were also obtained through phase modulation spectroscopy together with the circular dichroism of microcrystals dispersed in KBr matrices.[10,14]

The signs and the scaling of the spectra were established as described earlier[10,11] using pseudoisocyanin-*N*,*N*'-diethyl iodide in a streched PVA-film as standard. Concentrations and molar absorptivities were calculated as described in Ref. 11.

The reproducibility of the spectra was checked from 2 – 3 single crystals of each compound, and as far as concerns the circular dichroism spectra none of these crystals were enantiometric of each other.

RESULTS AND DISCUSSION

Linear dichroism and circular dichroism spectra of Pt(en)Cl_2 and Pd(en)Cl_2 in the ligand field range are given in Figs. 1 and 2, respectively. There is a surprising difference between the two sets of spectra, the Pt-compound only showing two bands in the linear dichroism spectrum whereas the Pd-compound has three; furthermore the Cotton effect associated with the *c* polarized absorption band is ~10 times greater for Pd(en)Cl_2 than for Pt(en)Cl_2. However, with the differences acknowledged it should also be noted that the *b* polarized bands in the near UV spectral region for both complexes have very similar appearances both in the linear and circular dichroism spectra.

The lack of a second *b* polarized band in the high wavelength region of the Pt-complex need not be essential, since already Martin *et al.* pointed out that bands of such polarization achieve intensity by vibronic coupling and therefore have fairly low intensity in comparison with the *c* polarized band

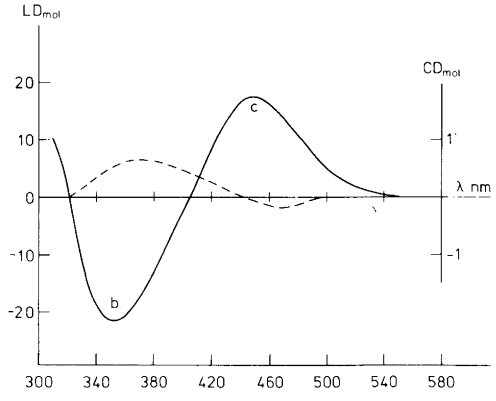

Fig. 1. Linear (———) and circular (– – –) dichroism in a single crystal of Pt(en)Cl_2. The experimental orientation of the crystal is so that $Abs_c - Abs_b$ is obtained.

Table 1. Fractional coordinates and anisotropic temperature factors of $Pt(en)Cl_2$ according to Benson[18]. Space group: $C222_1$, $a=12.437 \pm .002$, $b=8.120 \pm .002$, $c=6.777 \pm .001$.

	x/a	y/b	z/c			β
Pt	0.0	0.00247	0.250			
Cl	0.1371	0.1972	0.250			
N	0.1075	−0.1876	0.2262			3.0192
C	0.0492	−0.3439	0.2166			5.898
	β_{11}	β_{22}	β_{33}	β_{12}	β_{23}	β_{13}
Pt	0.00342	0.00767	0.01499	0	0	0.0031
Cl	0.00714	0.0159	0.03398	−0.00573	−0.00421	0.00692

$d_{xz} \rightarrow d_{xy}$. This means, small differences in orbital energy between Pt and Pd in the complexes taken into consideration, that the two compounds show linear dichroism spectra which are in accordance with each other and with the polarized spectra of Martin *et al.*[4,5]

Besides the mere fact that the predicted circular anisotropy of the title compounds is obtainable, a discussion of the intensity difference of the Cotton effects under the *c* polarized absorption band is relevant. It has above been anticipated that experimental problems exist in attempts to isolate the circular dichroism from a linearly anisotropic system; this mixing of effects in the photocurrent, however, could be less serious than the possibility of a contribution to the rotatory strength from electric quadrupole terms arising from the electric dipole transition and induced by the electric field gradient of the electromagnetic wave.[15-17] That, however, need not be considered here, as such contributions according to Barron[17] would be greater for a Pt- than for a Pd-compound.

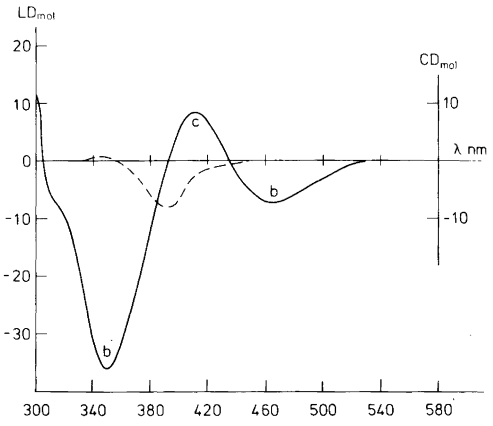

Fig. 2. Linear (———) and circular (– – –) dichroism in a single crystal of $Pd(en)Cl_2$. Experimental orientation as in Fig. 1.

The explanation of the difference in rotatory strength between the two compounds under discussion seems to be that the ethylenediamine group is twisted more with respect to the coordination plane in the Pd-compound than is the case with the Pt-compound, as such a twist would influence the *c* polarized transition greatly since this transition involves an orbital engaged in σ bonding to the diamine group. This conclusion is in disagreement with the results of Iball *et al.*,[1] which give $Pd(en)Cl_2$ less twist of the C−C bond than $Pt(en)Cl_2$. However, the *R*-value for the refinement of the Pt-compound is considerably greater (0.073) than for the Pd-compound (0.057) and this means that the structural determination of $Pt(en)Cl_2$ is rather uncertain. Furthermore there exists another X-ray investigation of $Pt(en)Cl_2$ performed by Benson[18] based on 35 % more reflections and with a comparable *R*-value (0.083) which certainly shows less distortion for $Pt(en)Cl_2$ than found by Iball *et al.* for both of the complexes $M(en)Cl_2$ (Table 1).

On these grounds it seems reasonable to accept the ten-fold difference in Cotton effects as due to less distortion from planarity (twist) of the ethylenediamine group in $Pt(en)Cl_2$ as compared with $Pd(en)Cl_2$.

Acknowledgement. The author is indebted to Dr. R. W. Berg for the crystals used in this work and to Professor J. A. Schellman, University of Oregon, for the opportunity to use his equipment. Furthermore financial support from "Otto Mønsteds Fond" is acknowledged.

REFERENCES

1. Iball, J., MacDougall, M. and Scrimgeour, S. *Acta Crystallogr. B 31* (1975) 1672.
2. Hald, N. C. P. and Rasmussen, K. *Personal communication.*
3. Berg, R. W. *Spectrochim. Acta A 31* (1975) 1409.
4. Martin, D. S., Jacobson, R. A., Hunter, L. D. and Benson, J. E. *Inorg. Chem. 9* (1970) 1276.
5. Martin, D. S., Hunter, L. D., Kroening, R. and Coley, R. F. *J. Am. Chem. Soc. 93* (1971) 5433.
6. Hofrichter, H. J. and Schellman, J. A. *Jerusalem Symposia on Quantum Chemistry and Biochemistry V*, The Israel Academy of Sciences and Humanities, Jerusalem 1973, p. 787.
7. Jensen, H. P. *Spectrosc. Lett. 10* (1977) 471.
8. Jensen, H. P., Schellman, J. A. and Troxell, T. *Appl. Spectrosc. In press.*
9. Jensen, H. P. *Chem. Phys. Lett. 52* (1977) 559.
10. Jensen, H. P. *Acta Chem. Scand. A 30* (1976) 137.
11. Jensen, H. P. and Galsbøl, F. *Inorg. Chem. 16* (1977) 1294.
12. Chatt, J., Gamlen, G. A. and Orgel, L. E. *J. Chem. Soc.* (1958) 486.
13. Troxell, T. and Scheraga, H. A. *Macromolecules 4* (1971) 519.
14. Larsen, E., Larsen, S., Røen, S. and Watson, K. J. *Acta Chem. Scand. A 30* (1976) 125.
15. Gō, N. *J. Chem. Phys. 43* (1965) 1275.
16. Buckingham, A. D. and Dunn, M. B. *J. Chem. Soc. A* (1971) 1988.
17. Barron, L. D. *Mol. Phys. 21* (1971) 241.
18. Benson, J. E. *Personal communication.*

Received September 30, 1977.

Acta Chemica Scandinavica A 32 (1978) 157 – 162

The Crystal Structure of Tetrakis(ethylenethiourea)-tellurium(II) Hexachlorotellurate(IV)

HOLLY K. AULT and STEINAR HUSEBYE

Department of Chemistry, University of Bergen, N-5014 Bergen-Univ., Norway

Crystals of tetrakis(ethylenethiourea)tellurium(II) hexachlorotellurate(IV), $[Te(etu)_4][TeCl_6]$, are orthorhombic, space group, $C222_1$, with cell dimensions $a = 12.0687(4)$ Å, $b = 15.8058(6)$ Å, $c = 15.0231(5)$ Å. There are four formula units in the cell. Reflection intensities were collected on a diffractometer and the structure was solved and refined by conventional X-ray crystallographic methods to an R value of 0.056. The structure is built up of $[Te(etu)_4]^{2+}$ cations and $[TeCl_6]^{2-}$ anions stacked in chains along a. The coordination around the central tellurium atoms are square planar and octahedral for the cations and the anions, respectively. The average Te(II) – S bond length is 2.681 Å, whereas the average Te(VI) – Cl bond length is 2.530 Å.

The solution of the structure of the complex salt, $[TeC_3H_6N_2S)_4]^{2+}[TeCl_6]^{2-}$, was undertaken as a part of a study of the stereochemical activity of the unshared electron pair in highly coordinated complexes of tellurium(IV). Tellurium(IV) has an electron configuration of $4d^{10}5s^2$. Thus, according to the valence shell electron pair repulsion theory (VSEPR),[1,2] a hexacoordinate tellurium(IV) complex should have a lone pair of electrons occupying the seventh position of a pentagonal bipyramid, or situated above one of the rectangular faces of a trigonal prism, or above one of the faces of an octahedron such that great distortion from octahedral symmetry occurs. It has been found, however, that several ions in the lower right-hand corner of the periodic table with electron configurations $(n-1)d^{10}ns^2$ form complexes with stereochemically inert lone pairs.[3-5] This has been found true for several octahedral and dodecahedral complexes of tellurium(IV).[6-9] This effect has been explained as being caused by delocalization of the lone pair on the ligands,[10,11] a three-center four-electron bond system,[12] or steric effects.[2,13] Mössbauer studies indicate the presence of three-center four-electron bonding in octahedral tellurium(IV) complexes.[14] Recently it has been indicated that the lone pair may become stereochemically active in such complexes.[15] The structure of $TeCl_6^{2-}$ has been previously determined with small cations.[16,17] The present investigation was partly undertaken in order to determine whether the influence of a larger cation will affect the stereochemical activity of the lone pair.

EXPERIMENTAL

The preparation of tetrakis(ethylenethiourea)-tellurium(II) hexachlorotellurate(IV) has been previously reported.[18] The crystals are orthorhombic with $a = 12.0687(4)$ Å, $b = 15.8058(7)$ Å, and $c = 15.0231(5)$ Å. There are four formula units per cell. Calculated and observed densities are 2.03 and 2.01 g/cm^3, respectively.

The crystal chosen for data collection was mounted along the prism axis, a. It had a length of 0.25 mm and its cross section was 0.12×0.12 mm^2. Weissenberg photographs showed systematic extinctions of reflections hkl when $h+k = 2n+1$, and of $00l$ when $l = 2n+1$, corresponding to space group $C222_1$. This space group has eight general positions, therefore the tellurium atoms must be located in special positions on two-fold axes. Reflections hkl also appear to be systematically weak when $h = 2n+1$ or $k = 2n+1$.

A Siemens papertape-controlled single crystal diffractometer (AED-1) was used for data collection. The diffractometer was operated as a three-circle instrument using Mo$K\alpha$ radiation. The intensities of 2326 independent reflections with $\theta \leq 30°$ were measured using a scintillation counter, the "five-value" measurement, and $\theta - 2\theta$ scan[19] at a speed

of 2.5°/min with automatic setting of greater speed for strong reflections. To reduce counting losses, attenuation filters were automatically inserted in the beam. The reflections were scanned between $\theta_1 = \theta - 0.32$ and $\theta_2 = \theta + 0.32 + 0.35\text{tg}\theta$ (units are degrees), where θ is the Bragg angle for the α_1 peak. Three reference reflections were measured twice each at intervals of fifty reflections and used to scale the intensities of the recorded reflections. The intensities were corrected for Lorentz and polarization effects, but not for absorption ($\mu = 26.5$ cm^{-1}). Of the reflections measured, 279 had intensities less than twice the standard deviation in net intensities and were regarded as unobserved. Cell dimensions were determined by means of a least-squares procedure based on accurate measurements of the Bragg angle for the α_1 peak of 20 high order reflections ($\theta > 20°$).

STRUCTURE ANALYSIS

The Patterson map gave the position of one tellurium atom on the twofold axis 0,y,1/4, and the other on the twofold axis ½,y,1/4 in the asymmetric unit. The asymmetric unit thus contains two half tellurium atoms, one from the anion and one from the cation, and both were found to have $y \approx 1/8$. This is also consistent with the observed pseudo-extinctions. A Fourier map based on these tellurium positions was then calculated. Tentative positions for the chlorine and sulfur atoms were then found, but they were heavily obscured because of false mirror planes resulting from the special y-coordinates for the tellurium atoms in the special positions above. After refinement of the possible trial structures, the correct structure emerged.

The structure was then further refined by means of full matrix least squares procedures. The computer programs used in this investigation are those of the X-ray system, version of 1972.[20] The weights used in the refinement were set equal to $1/\sigma(F_{\text{rel}})$ squared.

After the hydrogen atoms had been found, the conventional R-factor[12] converged to the final value of 0.056. In the presence of the heavy atoms the hydrogen parameters did not refine well. The hydrogen atoms were therefore held fixed at positions found from a difference map and use of a molecular model. Likewise the U values for these atoms were held constant and set equal to 0.044. Further refinement of the enantiomorphous structure demonstrated that the correct structure had been chosen.[21]

A final difference map revealed peaks of about 7e/Å^3 located near the tellurium atoms, indicating that these atoms should be moved such that their y-coordinates would have values closer to 1/8. Because of their positions at $y \approx 1/8$ the tellurium atoms contribute mostly to the structure factors of the strong reflections which are given low weight. A new weighting scheme which gives unit weight to all reflections was then introduced. Thus, the reflections to which tellurium contributes most, were given greater weight. The new weighting scheme resulted in a shift in the positions of both tellurium atoms less than 0.0001 Å towards $y = 1/8$ and only a small decrease in the height of the spurious peaks in the difference map. As a result of this refinement, the tellurium-ligand bond lengths changed less than one standard deviation. As this new refinement was also accompanied by an

Table 1. Atomic coordinates for atoms in the asymmetric unit in fractions of cell edges. Standard deviations are in parentheses.

	x	y	z
Te1	0	0.11624(6)	0.2500
Te2	0.5000	0.11060(6)	0.2500
Cl1	0.5000	0.2702(3)	0.2500
Cl2	0.5000	−0.0481(2)	0.2500
Cl3	0.3038(3)	0.1110(3)	0.1877(2)
Cl4	0.4134(3)	0.1089(3)	0.4035(2)
S1	0.0368(3)	0.2322(2)	0.1182(2)
S2	0.0411(2)	0.0010(2)	0.1284(2)
C1	−0.0875(10)	0.2840(7)	0.1098(8)
C2	−0.2096(11)	0.3854(9)	0.0619(10)
C3	−0.2705(12)	0.3278(9)	0.1261(11)
C4	−0.0841(9)	−0.0519(7)	0.1122(7)
C5	−0.2636(11)	−0.0937(9)	0.1183(11)
C6	−0.1957(11)	−0.1547(9)	0.0619(11)
N1	−0.1044(9)	0.3454(7)	0.0497(7)
N2	−0.1764(9)	0.2701(7)	0.1559(7)
N3	−0.1768(9)	−0.0371(7)	0.1502(8)
N4	−0.0911(8)	−0.1155(6)	0.0566(7)
H1	−0.024	0.355	0.025
H2	−0.172	0.432	0.072
H3	−0.262	0.389	0.010
H4	−0.260	0.355	0.180
H5	−0.353	0.293	0.123
H6	−0.201	0.195	0.192
H7	−0.202	0.023	0.161
H8	−0.310	−0.058	0.091
H9	−0.276	−0.122	0.151
H10	−0.206	−0.182	−0.001
H11	−0.184	−0,210	0.097
H12	−0.035	−0.152	0.034

Table 2. Components of atomic vibration tensors, $U \times 10^4$, in Å^2, with standard deviations, referred to crystallographic axes. The expression is $\exp\{-2\pi^2(h^2a^{-2}U_{11}+k^2b^{-2}U_{22}+l^2c^{-2}U_{33}+2hka^{-1}b^{-1}U_{12}+2klb^{-1}c^{-1}U_{23}+2hla^{-1}c^{-1}U_{13})\}$

	(U_{11}, U_{12},	U_{22}, U_{23}	U_{33}) U_{13})
Te1	206(4)	319(4)	278(5)
	0	0	−9(4)
Te2	212(4)	427(5)	235(4)
	0	0	53(4)
Cl1	734(34)	383(20)	806(34)
	0	0	281(40)
Cl2	707(32)	378(18)	665(29)
	0	0	191(38)
Cl3	316(15)	880(25)	565(18)
	0(18)	15(21)	−80(15)
Cl4	535(17)	829(23)	325(14)
	−132(19)	−82(17)	118(14)
S1	315(14)	365(14)	443(16)
	−21(11)	87(13)	37(13)
S2	330(13)	359(13)	415(16)
	3(13)	−76(13)	37(14)
C1	430(57)	307(53)	300(59)
	−22(47)	−46(46)	−3(54)
C2	464(76)	436(70)	610(82)
	130(67)	104(75)	55(64)
C3'	686(89)	624(83)	440(89)
	239(74)	148(76)	120(78)
C4	325(50)	333(52)	284(57)
	29(44)	−11(45)	−56(49)
C5	539(70)	632(103)	472(98)
	−93(73)	−184(83)	8(75)
C6	371(66)	456(78)	761(97)
	69(63)	−278(75)	−97(68)
N1	478(58)	462(60)	516(62)
	71(51)	199(52)	98(53)
N2	323(57)	491(61)	480(63)
	63(50)	94(51)	92(52)
N3	264(52)	549(62)	599(75)
	−5(48)	−284(58)	51(55)
N4	458(53)	306(47)	479(54)
	−51(50)	−143(50)	38(48)

The isotropic vibration tensor for the hydrogen atoms is fixed at 44×10^{-3} Å^2, where the expression used is $\exp\{-8\pi^2U(\sin^2\theta/\lambda^2)\}$.

increase in the standard deviations of the atomic parameters, and only a slight reduction of the *R*-value, it was abandoned in favour of the former scheme.

Atomic scattering factors were taken from the *International Tables*.[22] Those for tellurium, sulfur, and chlorine were corrected for anomalous dispersion.[20] Final atomic parameters are given in Tables 1 and 2. Interatomic distances and angles are listed in Tables 3 and 4. The structure factor table can be obtained from the author St. H. upon request.

Table 3. Bond lengths in Å, with standard deviations.

Cation		Anion	
Te1 – S1	2.735(3)	Te2 – Cl1	2.520(4)
Te1 – S2	2.627(3)	Te2 – Cl2	2.508(4)
S1 – C1	1.714(12)	Te2 – Cl3	2.546(3)
S2 – C4	1.744(11)	Te2 – Cl4	2.531(3)
C1 – N1	1.34(2)		
C1 – N2	1.30(2)		
C4 – N3	1.28(2)		
C4 – N4	1.31(1)		
C2 – C3	1.52(2)		
C5 – C6	1.51(2)		
C2 – N1	1.43(2)		
C3 – N2	1.52(2)		
C5 – N3	1.46(2)		
C6 – N4	1.41(2)		

DISCUSSION

The structure of the complex salt is shown in Fig. 1. The configuration around Te(II) (Te1 in the

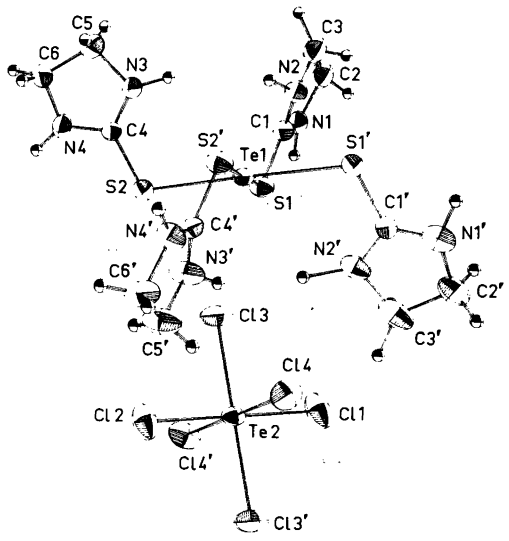

Fig. 1. The complex as seen along the original *c* direction after rotating the cell thirty degrees around *a*. Unprimed letters denote atoms in the symmetry related halves of the two complex ions.

Table 4. Bond angles in degrees, with standard deviations. Atoms related to those in the asymmetric unit by twofold symmetry axes are marked by primes.

Cation		Anion	
S1 – Te1 – S2	86.00(9)	Cl1 – Te2 – Cl2	180.00
S1 – Te1 – S1′	95.86(10)	Cl1 – Te2 – Cl3	89.85(10)
S1 – Te1 – S2′	177.40(9)	Cl1 – Te2 – Cl4	90.60(9)
S2 – Te1 – S2′	92.21(10)	Cl2 – Te2 – Cl3	90.15(10)
Te1 – S1 – C1	103.4(4)	Cl2 – Te2 – Cl4	89.40(9)
Te1 – S2 – C4	105.4(4)	Cl3 – Te2 – Cl4	87.18(11)
S1 – C1 – N1	121.9(9)	Cl3′ – Te2 – Cl4	92.82(11)
S1 – C1 – N2	127.2(9)	Cl3 – Te2 – Cl3′	179.70(13)
N1 – C1 – N2	110.9(10)	Cl4 – Te2 – Cl4′	178.80(14)
C1 – N1 – C2	111.7(11)		
N1 – C2 – C3	104.2(11)		
C2 – C3 – N2	100.7(11)		
C3 – N2 – C1	111.0(11)		
S2 – C4 – N3	127.5(9)		
S2 – C4 – N4	120.8(8)		
N3 – C4 – N4	111.6(10)		
C4 – N3 – C5	111.7(11)		
N3 – C5 – C6	100.7(11)		
C5 – C6 – N4	103.6(11)		
C6 – N4 – C4	111.1(10)		

cation) is approximately square planar with an average Te – S bond length of 2.682(4) Å, which is in agreement with those found previously for square planar complexes of Te(II) with sulfur-containing ligands.[23] This is much larger than 2.41 Å, the sum of the covalent radii of tellurium and sulfur, indicating the presence of a linear three-center four-electron bonding system based on overlap of the *p*-orbitals of tellurium and sulfur. It has indeed been shown from Mössbauer studies that only the *p*-orbitals of the tellurium atom contribute to the bonding in such complexes.[14] Here the system is very nearly linear, as can be seen from the S1 – Te1 – S2′ bond angle of 177.40(9)°. As can be seen from Table 3 there is a significant difference in the lengths of the two Te – S bonds.

The ethylenethiourea rings are nearly planar with deviations in atomic positions of 0.01 – 0.07 Å from the plane. Average S – C bond lengths are 1.73 Å and C – N partial double bonds are 1.31 Å. C – N and C – C single bonds average 1.46 and 1.52 Å, respectively. These values are normal for ethylenethiourea ligands.[23,24] The angles on the nitrogen atoms and C1 and C4 atoms correspond to sp^2 hybridization. The average C – H and N – H bond lengths are 0.95 and 1.09 Å, respectively. The angles on the ethylene carbons correspond to sp^3 hybridization.

The configuration around Te(IV) (Te2 in the anion) is octahedral, in agreement with previous investigations.[6,16] The Te – Cl bond lengths range from 2.508 Å to 2.546 Å with an average value of 2.533 Å. This is close to values around 2.54 Å which has been found previously in octahedral complexes of tellurium(IV).[6,16] Again the bonding probably is of the three-center four-electron type.[14,25,26] The Cl3 – Te2 – Cl4 angle and the interplanar angle Te2Cl1Cl3/Te2Cl1Cl4 are both close to 87°, which differs somewhat from the 90° expected with ideal octahedral coordination. This is probably due to a weak interaction between Cl3 and Te1 (of the cation), and will be discussed later. The seventh valency electron pair on tellurium appears again to be stereochemically inert.

The packing of the complex ions is shown in Fig. 2. There is an interaction between Te1 (of the cation) and Cl3 of two neighbouring anions, one of each side of the cation along the *a* axis with a Te – Cl distance of 3.785(3) Å, such that divalent tellurium tends toward octahedral coordination. This appears to be a very weak interaction, only 0.22 Å shorter than the sum of the van der Waals radii of Te and Cl, and it does not appear to significantly lengthen the Te2 – Cl3 bond. It may, however, distort the octahedral coordination of the tetravalent tellurium atom, by decreasing the Cl3 – Te2 – Cl4 bond angle.

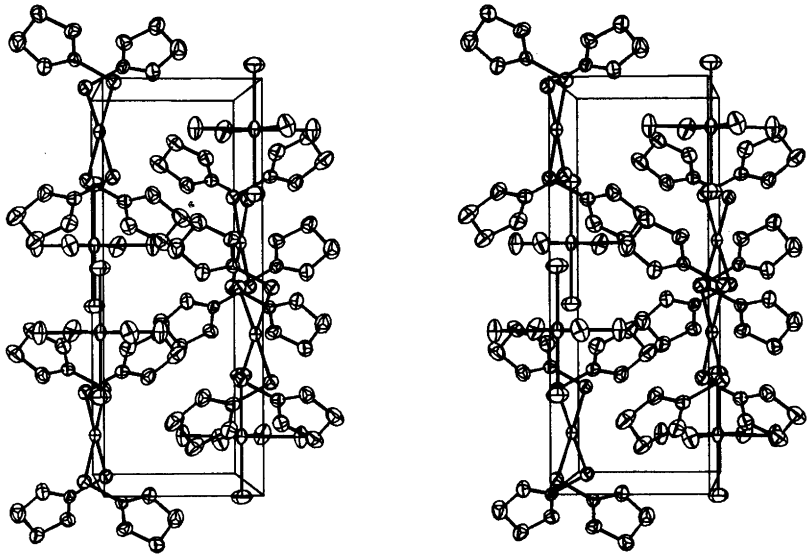

Fig. 2. A stereo view of the complex salt as seen along *c*. One half of a unit cell is outlined with *a*/2 being horizontal and *b* vertical. Hydrogen atoms are omitted.

The Te1 – Cl3 – Te2 angle is 144.12(9)°. Thus the anions and cations are stacked in zigzag chains parallel with the *a*-axis. The chain containing the asymmetric unit is shown in Fig. 3. All tellurium atoms in this chain of alternating octahedral anions and square planar cations containing tetravalent and divalent tellurium central atoms, respectively, have *y* coordinates close to 1/8 and *z* coordinates equal to 1/4. The *x* coordinates are $0, \pm\frac{1}{2}, \pm 1$ *etc.* starting with a cation. This stacking system, as expected, resembles similar ones found for Pt(II)/Pt(IV) complexes with the same coordination.[27]

The stereochemistry of tellurium resembles that of palladium and platinum. In the divalent state, square planar complexes predominate, whereas in the tetravalent state, octahedral complexes are often found. Zero-valent complexes of palladium and platinum have been known for some time, and recently a tellurium(0) complex has been found.[28] *trans*-Effects are also well known for all three elements,[23,29,30] and they are all soft acids with large radii.

For palladium and platinum, complexes of the type $[M(II)L_4][M(II)X_4]$ and $[M(II)L_2X_2][M(IV)L_2X_4]$ with chain structures are well known.[27] Here L is a neutral ligand like NH_3 and X is a uninegative ligand, often a halogen ion. Complexes of the first

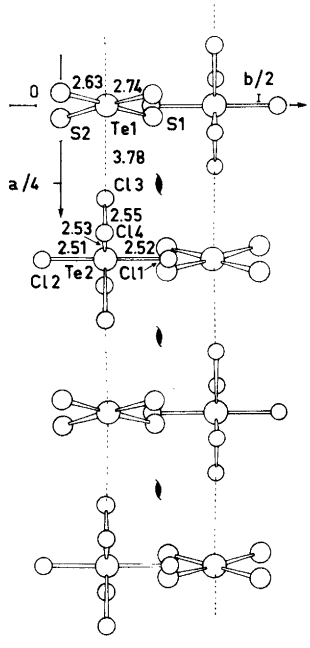

Fig. 3. Two neighbour anion-cation chains seen along *c*, with Te1···Cl3 interactions indicated as dotted lines. Bond lengths (in Å) in the asymmetric unit are indicated, and the lighter atoms are omitted for clarity.

type are salts and are stacked in chains held together by M(II)···M(II) interactions. The ionic planes in alternating anions and cations are parallel. Complexes of the second type are held together by ···M(II)···X–M(IV)–X···M(II)··· interactions. Here the molecular plane of the M(II) complex is normal to the ···X–M(IV) bond.

Neighbour chains (Fig. 3) are related by two-fold screw axes parallel to *c*, so that the tellurium atoms in neighbour chains are ½ above or below the original ones in the *z* direction. Also the tellurium atoms of the anions in the original chain have the same *x*-coordinate as the tellurium atoms in the cations in the neighbour chains and *vice versa*. Thus interactions between chains take place primarily between anions and cations. There are hydrogen bonds[31] Cl4···H1–N1 with Cl4···H1 = 2.33(15) Å, Cl4···N1 = 3.26(1) Å and ∠Cl4···H1–N1 = 148(9)° holding neighbouring chains together.

Acknowledgements. The authors would like to thank Professor Olav Foss for some of the films used. We would also like to thank Knut Maartmann-Moe for assistance with the computations. H.K.A. is indebted to the Rotary Foundation of the Rotary International for financial assistance.

REFERENCES

1. Gillespie, R. J. *Can. J. Chem. 38* (1960) 818.
2. Gillespie, R. J. *J. Chem. Educ. 47* (1970) 18.
3. Morss, L. R. and Robinson, W. R. *Acta Crystallogr. B 28* (1972) 653.
4. Goldberg, I. and Herbstein, F. H. *Acta Crystallogr. B 28* (1972) 400.
5. Wynne, K. J. *J. Chem. Educ. 50* (1973) 328.
6. Husebye, S. and George, J. W. *Inorg. Chem. 8* (1969) 313.
7. Esperås, S., Husebye, S. and Sværen, S. E. *Acta Chem. Scand. 25* (1971) 3539.
8. Esperås, S. and Husebye, S. *Acta Chem. Scand. 27* (1973) 706.
9. Husebye, S. and Sværen, S. E. *Acta Chem. Scand. 27* (1973) 763.
10. Urch, D. S. *J. Chem. Soc.* (1964) 5775.
11. Couch, D. A., Wilkins, C. J., Rossman, G. R. and Gray, H. B. *J. Am. Chem. Soc. 92* (1970) 307.
12. Esperås, S., George, J. W., Husebye, S. and Mikalsen, Ø. *Acta Chem. Scand. A 29* (1975) 141.
13. Gillespie, R. J. *Molecular Geometry*, Van Nostrand Reinhold Co., London 1972, p. 158.
14. Cheyne, B. M., Jones, C. H. W. and Vasudek, P. *Can. J. Chem. 50* (1972) 3677.
15. Esperås, S., George, J. W., Husebye, S. and Mikalsen, Ø. *Acta Chem. Scand. 27* (1973) 1089.
16. Hazell, A. C. *Acta Chem. Scand. 20* (1966) 165.
17. Engel, G. *Z. Kristallogr. 90* (1935) 341.
18. Foss, O. and Fossen, S. *Acta Chem. Scand. 15* (1961) 1620.
19. Troughton, P. G. H. *Siemens Rev.* XXXVII (1970) fourth special issue, p. 9.
20. Stewart, J. M., Kruger, G. J., Ammon, H. L., Dickinson, C. and Hall, S. R., Eds., *The X-Ray System*, Computer Science Center, University of Maryland, College Park 1972.
21. Hamilton, W. C. *Acta Crystallogr. 18* (1965) 502.
22. *International Tables for X-Ray Crystallography*, Kynoch Press, Birmingham 1962, Vol. III, p. 204.
23. Foss, O. In Andersen, P., Bastiansen, O. and Furberg, S., Eds., *Selected Topics in Structure Chemistry*, Universitetsforlaget, Oslo 1967, p. 145.
24. Åse, K., Bøyum, K., Foss, O. and Marøy, K. *Acta Chem. Scand. 25* (1971) 2462.
25. Nakamura, D., Ito, K. and Kubo, M. *J. Am. Chem. Soc. 84* (1962) 163.
26. Nakamura, D., Ito, K. and Kubo, M. *Inorg. Chem. 2* (1963) 61.
27. Cotton, F. A. and Wilkinson, G. *Advanced Inorganic Chemistry*, 3rd. Ed., Interscience, New York 1972, p. 1034.
28. Austad, T., Rød, T., Åse, K., Songstad, J. and Norbury, A. H. *Acta Chem. Scand. 27* (1973) 1939.
29. Yatsimirskii, K. B. *Pure Appl. Chem. 38* (1974) 341.
30. Emeleus, H. J. and Sharpe, A. G. *Modern Aspects of Inorganic Chemistry*, 4th. Ed., Routledge and Kegan Paul, London 1973, p. 547.
31. Pimentel, G. C. and McClellan, A. L. *The Hydrogen Bond*, Freeman, London 1960, p. 285.

Received August 8, 1977.

Acta Chemica Scandinavica A 32 (1978)163 – 168

Crystal Structure of 1-Methylsulfonyl-2-methylsulfoxyethane, A Case of Chiral Disorder

ØIVIND BERG,[a,*] TORGER BRUUN [b,†] and FRODE MO [a]

[a] Institutt for røntgenteknikk and [b] Institutt for organisk kjemi, Universitetet i Trondheim-NTH, N-7034 Trondheim-NTH, Norway

The structure was refined in space group $P\bar{1}$ with $a=5.511(4)$, $b=5.308(2)$, $c=7.478(6)$ Å, $\alpha=93.98(2)$, $\beta=101.72(3)$, $\gamma=116.34(2)°$ and $Z=1$. Two equivalent sets of counter data were collected to a limit in $\sin\theta/\lambda$ of 0.704 $Å^{-1}$, corrected for absorption and averaged. The final R was 0.050 after full-matrix least-squares refinement based on 993 F_o. Both chiral forms of the molecule are present in the crystal, and superimposed sulfoxide and sulfone groups give rise to an apparent centrosymmetric molecule with partial atomic disorder. Bond lengths and angles involving sulfur in this averaged structure are changed relative to the corresponding parameters of the parent di-sulfoxide, in agreement with theory. A short central C – C bond of 1.515 Å is a common feature of the two molecules.

The structure of the title compound was determined as part of our studies on oxygenated 1,2-bis(methylthio)ethanes. These small sulfur-containing molecules are interesting structurally because they allow, *a priori*, a systematic investigation of changes in electronic structure with changes in the oxidation state and hybridization of sulfur. A structure analysis of the first compound in the series, *meso*-ethane-1,2-bis(methyl sulfoxide), hereinafter called DIOX, was reported previously.[1]

EXPERIMENTAL

1-Methylsulfonyl-2-methylsulfoxyethane, hereinafter OXON, was available.[2] The molecule has one chiral centre, both enantiomers exist in solution. Thin, plateformed crystals were grown from methanol. Preliminary Weissenberg photographs showed triclinic symmetry with **c*** orthogonal to the face of the plate. The diffraction spots at low 2θ angles frequently contained short streaks in the ω direction; for some specimens the spots also were slightly blurred in certain regions of reciprocal space. These features were not of the magnitude and systematic nature typical, for instance, of disordered structures of the OD type,[3] nor were there systematically weak reflections to indicate that any of the axes should be doubled. We infer, however, that other lattice defects were present to a varying extent in all examined specimens. A crystal $0.55\times0.26\times0.065$ mm was used for the X-ray measurements.

Collection and processing of intensities. Cell dimensions were obtained from the setting angles of 19 reflections, and centring of these reflections was repeated five times during and after data collection. The cell parameters in Table 1 are averages; standard deviations reflect the spread in each set of measurements. All cell axes increased slightly during data collection. The OXON cell is very similar to that of DIOX (*cf.* Table 1). However, crystals of the former were much more stable under X-radiation. The intensities of 2305 reflections comprising the two sets $\pm h+k\pm l$ and $\pm h-k\pm l$ were measured without attenuators to a 2θ-limit of 60° with Nb-filtered Mo$K\alpha$-radiation on a Picker diffractometer controlled by the Vanderbilt disk-oriented program system.[4] The scan mode was $\omega/2\theta$ at 2° min^{-1} in 2θ, basic scan width was $2\theta(\alpha_1)-1.45°$ to $2\theta(\alpha_2)+1.5°$, and backgrounds were measured for 20 s at each limit of the scan. Intensities below $2\theta=18.5°$ were remeasured with reduced low-angle scan widths to minimize errors caused by the NbK absorption edge. Three standard reflections were monitored at intervals of 60 reflections. The data were scaled with a polynomial fit to the average standard decay and were also corrected for coincidence loss.[5,6] The experimental recovery constant with this particular

* Present address: FFI Avd. for undervannskrigføring, Boks 115, N-3191 Horten, Norway.

† Deceased November, 1977.

Table 1. Crystal data of 1-methylsulfonyl-2-methylsulfoxyethane (OXON) and *meso*-ethane-1,2-bis(methyl sulfoxide)[1] (DIOX).

	OXON	DIOX
Composition	$C_4H_{10}S_2O_3$	$C_4H_{10}(SO)_2$
F.W.	170.25	154.25
Space group	$P\bar{1}$	$P\bar{1}$
a (Å)	5.511(4)	5.305(4)
b	5.308(2)	5.261(3)
c	7.478(6)	7.280(8)
α (°)	93.98(2)	94.79(4)
β	101.72(3)	98.87(7)
γ	116.34(2)	116.22(2)
Z	1	1
D_x (g cm^{-3})	1.50	1.44
λ (Å)	0.71069	1.5418
μ (cm^{-1})	6.17	59.0
M.p. (°C)	136–137	174–175

crystal was 1.9×10^{-8} counts^{-1}. Absorption coefficients were in the range 1.162 to 1.041, and corrections were applied to the intensities with a modified version of the program ABSOR[7] which is based on the analytical method.[8]

Weighted averages of F^2 and $\sigma(F^2)$ were calculated from pairs of equivalents, averages of four measurements were used for the $h0l$ reflections. For an F_i^2: $\sigma(F_i^2)=\sigma(I_i)(\mathrm{Lp})^{-1}(\mathrm{scale})$ and $\sigma^2(I_i)=\sigma^2_{i\,\mathrm{count}}+(SI_{i\,\mathrm{net}})^2$; $i=1, 2$. The agreement index $D=\Sigma|F_1^2-F_2^2|/\Sigma F^2_{\mathrm{ave}}$, was 0.035. The parameter S was adjusted to 0.015 to make the weighted mean of the differences $\Delta_i=|F_i^2-F^2_{\mathrm{ave}}|$ follow a normal distribution. Of the 1100 averaged intensities, 13 at low 2θ were deleted because the NbK edge interfered with the peak itself. Another 94 reflections with $F^2<\sigma(F^2)$ were given zero weight.

Programs used for analyses and corrections of the data are described elsewhere.[9] Other crystallographic programs were from the X-RAY 76 system.[10] Molecular drawings were made with ORTEP.[11]

STRUCTURE DETERMINATION AND REFINEMENT

Since the OXON molecule has no inherent centrosymmetry and $Z=1$, space group $P1$ was assumed. The two S atoms were placed according to the S–S vector peak in the Patterson map. A ΔF map showed the positions of all C atoms with densities of about 6 e Å^{-3} and maxima corresponding to O(A) and O(C) (see Formula 1) of densities about

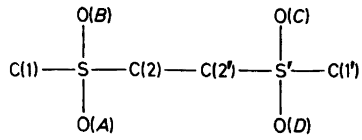

8 e Å^{-3}. In addition, there were two weaker maxima, approximately 4 e Å^{-3}, for a fourth atom bonded in a tetrahedral arrangement about each S. These peaks were less well-defined, a ridge of density extending from each (assigned O(B) and O(D), respectively) towards the nearest S position. Isotropic refinement of all non-H atoms excluding O(B) and O(D) gave a crystallographic R index $(=\Sigma\|F_o|-K|F_c\|/\Sigma|F_o|)$ of 0.24. Refinements without O(B) but with unit weight for O(D), and *vice versa*, gave $R=0.19$, and the densest maximum in subsequent ΔF maps appeared in the position of the absent O(B), respectively O(D) atom. A model with half weight assigned to both O(B) and O(D) refined to $R=0.18$, and anisotropic refinement of this model reduced R to 0.06. We ascribe these results to the presence of both chiral forms of OXON in the crystal. In the averaged X-ray structure, sulfoxide and sulfone groups superimpose, but not exactly, because their common structural features are not identical, and partial disorder arises. The drastic drop in R following anisotropic refinement lends support to this interpretation. Non-centrosymmetric refinement including isotropic H atoms did not converge properly. At an R of 0.043 there were several physically untenable bond lengths, thermal parameters and, for O(B) and O(D), population parameters. Correlation coefficients between parameters related by a pseudo-centre of symmetry were in the range 0.60–0.95, average 0.83.

The strong correlation clearly favours refinement of a structure with a centre of symmetry in the C–C bond. A starting model including all non-H atoms was shifted accordingly. Anisotropic refinement in $P\bar{1}$ also gave $R=0.06$. Symmetry restricts the population parameter of O(2) to 0.5; see Fig. 1 for final atomic numbering. Further full-matrix least-squares refinement of 66 parameters which include isotropic H atoms was based on 993 F_o with weights $w=1/\sigma^2(F_o)$. The final maximum parameter shift was less than 5×10^{-3} of the corresponding e.s.d., $R=0.050$ and $R_w\{=[\Sigma w(|F_o|-K|F_c|)^2/\Sigma w F_o^2]^{\frac{1}{2}}\}=0.041$.

Several more elaborate models were tried in order to describe the disorder more completely. The

Table 2. Final atomic parameters. Thermal parameters, U_{ij}(Å$^2 \times 10^4$) for C, O and S, and U(Å$^2 \times 10^4$) for H, are defined by: $\exp[-2\pi^2(U_{11}a^{*2}h^2+\cdots+2U_{12}a^*b^*hk+\cdots)]$ and $\exp[-8\pi^2U(\sin^2\theta/\lambda^2)]$, respectively. E.s.d.'s appear in parentheses.

Atom	x	y	z	U_{11}	U_{22}	U_{33}	U_{12}	U_{13}	U_{23}
C(1)	0.6442(5)	0.3475(5)	0.3068(4)	459(12)	373(12)	600(15)	77(9)	−74(11)	90(11)
C(2)	0.1471(4)	0.1217(4)	0.0398(3)	428(10)	256(9)	498(12)	170(8)	26(9)	67(9)
O(1)	0.3360(3)	−0.2060(3)	0.1937(2)	617(9)	316(8)	825(11)	256(7)	−69(8)	75(8)
O(2)	0.1583(6)	0.0418(7)	0.3712(4)	562(17)	585(20)	453(16)	187(15)	152(14)	137(15)
S	0.3079(1)	0.0488(1)	0.2481(1)	451(3)	291(3)	521(3)	140(2)	−32(2)	59(2)

Atom	x	y	z	U	Atom	x	y	y	U
H(11)	0.733(5)	0.358(5)	0.199(4)	595(70)	H(21)	0.263(4)	0.152(4)	−0.044(3)	388(55)
H(12)	0.612(6)	0.519(7)	0.327(4)	865(90)	H(22)	0.133(5)	0.267(6)	0.071(3)	545(68)
H(13)	0.742(6)	0.318(6)	0.399(4)	761(86)					

best of them involved two anisotropic S atoms with population parameters fixed at 0.5. The number of variables increased from 66 to 75, corresponding final values of R and R_w were 0.040 and 0.031, respectively. Straightforward application of Hamilton's R-test[12] classifies this as a significant improvement; however, parameters of the two S atoms were strongly correlated and there were obvious inconsistencies in their U_{ij} values. We believe, therefore, that this model is not a better description physically; it is mainly useful in showing that the S positions of the disordered end groups are too close to be resolved in a meaningful way by the least-squares technique. Rae[13] has described a modified least-squares method by which a pseudo-centrosymmetric structure may be refined in a non-centrosymmetric space group. While this scheme might have made refinement in $P1$ possible, the problem of partial atomic disorder still remains.

Only results from the normal refinement in $P\bar{1}$ will be discussed in the following. Final coordinates and thermal parameters from this refinement are in Table 2. A list of structure factors is available from the authors. Scattering factors were those of Doyle and Turner[14] except for H.[15] Anomalous dispersion corrections[16] were applied for S.

RESULTS AND DISCUSSION

The averaged structure of OXON is shown in Fig. 1. Table 3 gives bond lengths and angles together with some corresponding values of DIOX. The fact that H parameters can be refined to give reasonable X-ray values of C−H bond lengths and angles seems to justify a more detailed discussion of the structure. The apparent shortening of the S−O(2) bond can be attributed largely to the elongated density between these atoms in the first ΔF map. Valency angles and the bond involving O(2) will not be considered in comparing parameters of OXON and DIOX.

A short C−C bond in DIOX, also found in a number of related structures, was explained[1] as a secondary effect of rehybridization of the S atom. A set of general rules relating properties of chemical bonds and the degree of hybridization were for-

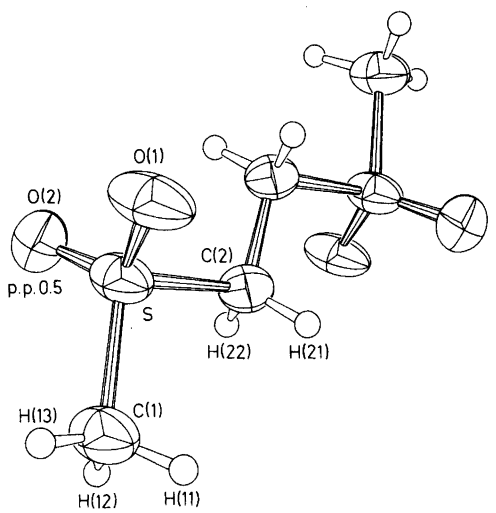

Fig. 1. Averaged centrosymmetric conformation and atomic numbering of OXON. Thermal ellipsoids correspond to a 50 % probability.

Table 3. Bond lengths and angles of OXON, some relevant values of DIOX[1] are also given. E.s.d.'s of the parameters are in parentheses.

Bond lengths (Å)

	OXON	DIOX		OXON
S–C(1)	1.762(2)	1.788(2)[a]	C(1)–H(11)	1.02(3)
S–C(2)	1.786(3)	1.802(2)	C(1)–H(12)	1.01(4)
S–O(1)	1.468(2)	1.501(2)[a]	C(1)–H(13)	0.85(3)
S–O(2)	1.347(4)		C(2)–H(21)	0.95(3)
C(2)–C(2′)	1.515(3)	1.516(2)	C(2)–H(22)	0.83(3)

Bond angles (°)

	OXON	DIOX
C(1)–S–C(2)	100.7(1)	97.0(1)
C(1)–S–O(1)	108.2(1)	106.8(1)
C(1)–S–O(2)	113.5(2)	
C(2)–S–O(1)	106.5(1)	106.3(1)
C(2)–S–O(2)	107.3(2)	
O(1)–S–O(2)	118.9(2)	
S–C(2)–C(2′)	109.2(2)	109.4(1)

	OXON		OXON
S–C(1)–H(11)	110(1)	S–C(2)–H(21)	109(1)
S–C(1)–H(12)	105(2)	S–C(2)–H(22)	106(2)
S–C(1)–H(13)	107(2)	C(2′)–C(2)–H(21)	113(1)
H(11)–C(1)–H(12)	110(3)	C(2′)–C(2)–H(22)	108(2)
H(11)–C(1)–H(13)	108(3)	H(21)–C(2)–H(22)	112(2)
H(12)–C(1)–H(13)	117(3)		

[a] 'Minimum' corrections[22] applied to these bonds are in the range 0.001 to 0.002 Å.

mulated by Walsh[17] and further extended and substantiated by Bent.[18,19] According to the theory, substitution of the lone pair (formally an atom of zero electronegativity) at S in sulfoxide with the strongly electronegative O in sulfone will effect less *p* character in all σ-bonds from S. Decreasing *p* character implies shorter bonds and larger valency angles. Table 3 shows that all bonds involving S are shorter and all valency angles at S, except one, are larger in the averaged structure of OXON, in agreement with the theory. The C(2)–S–O(1) angles are equal. Theory also predicts that the primary rehybridization is relayed in an attenuated manner throughout the bonded system.[19] Thus, if these molecules were purely σ-bonded systems, one would expect shortening of the C–C bond next to S, the magnitude increasing from DIOX to OXON. Both angles S–C(2)–C(2′) and bonds C(2)–C(2′) are equal in the two compounds, however. Interestingly, this bond length is unchanged, 1.515 Å, in the fully oxygenated di-sulfone.[20]

The final ΔF map calculated in the S–C(2)–C(2′) plane (Fig. 2) shows surprisingly well-defined deformation density in the C(2)–C(2′) bond. There are similar features in both S–C bonds. Excess density of about 0.4 e Å^{-3} in the S position is evidence of residual disorder not accounted for by the refinement. In the ΔF map through O(1)–S–O(2) (not shown) both O positions are on zero density level.

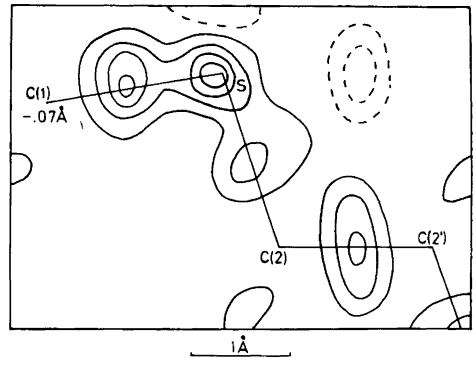

Fig. 2. Residual electron density calculated in the plane S–C(2)–C(2′). Atom C(1) is 0.07 Å below this plane. Contours are at intervals of 0.10 e Å^{-3}; solid lines are positive, broken lines negative. Zero contour is not shown.

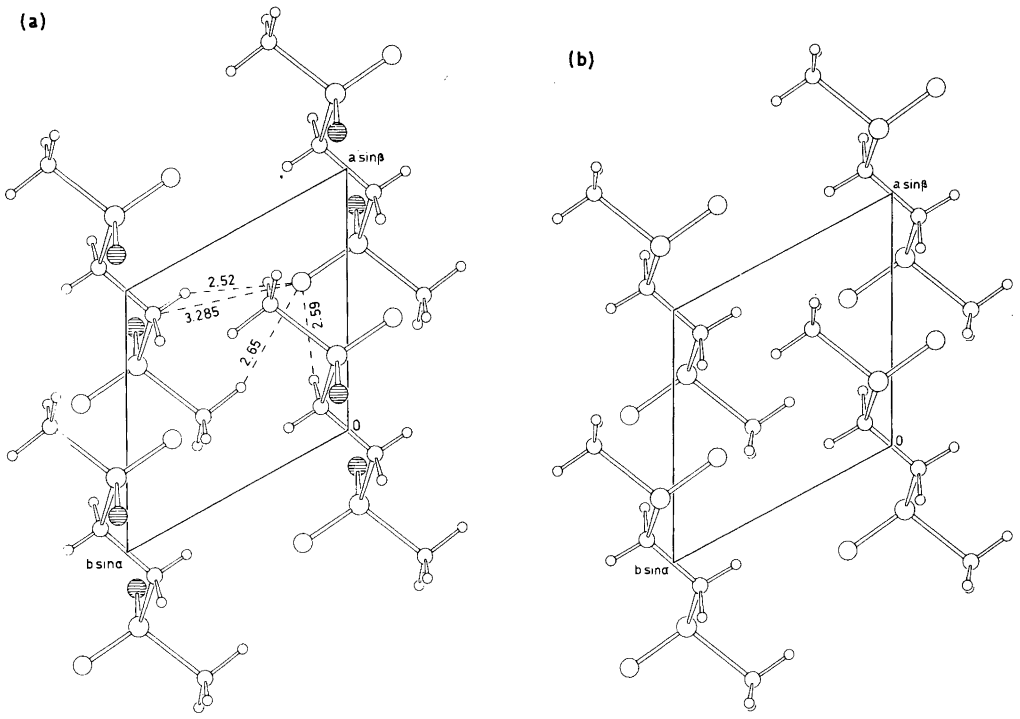

Fig. 3. Molecular packing of OXON (a) and DIOX (b) as seen down c. In the packing diagram of OXON, the oxygen site of 50 % occupancy is hatched and some short intermolecular contacts are given.

Fig. 3(a) shows the molecular packing of OXON. O(1) participates in three intermolecular van der Waals contacts with atoms of the methyl and methylene groups, the shortest distance being O(1)···H(22) at $x,y-1,z$, 2.52 Å. There are two normal contacts between O(2) and C(1) in symmetry-related molecules. In addition, O(2) makes one short contact with its centrosymmetrically related partner in the half-molecule at $-x,-y,1-z$. The distance, 2.783 Å, is significantly less than a normal O···O van der Waals contact, 3.05 Å,[21] and it is further shortened if a normal S–O(2) bond length is assumed. In view of this, a random distribution of both chiral forms throughout the crystal appears to be energetically unfavourable. A more plausible model of the disorder involves a block structure, each block containing ideally only one or the other enantiomer. The short O···O contact then would occur only at the boundaries between blocks in the c* direction. The weak attractive forces along c* are reflected in the mechanical strength and shape of the crystals.

Both the conformation and packing of the molecules are very similar in the OXON and DIOX structures, *cf.* Figs. 3(a) and 3(b). Crystals of DIOX were unstable under X-radiation, the *a* and *c* axes increasing almost linearly with exposure, the angle α contracting and β expanding.[1] The signed shifts suggest (*cf.* Table 1) that the proposed autoxidation of sulfoxide groups may involve a transformation of DIOX into OXON in the solid state.

"Norges Tekniske Høgskoles Fond" is thanked for a grant to F.M.

REFERENCES

1. Svinning, T., Mo, F. and Bruun, T. *Acta Crystallogr. B 32* (1976) 759.
2. Bruun, T. *Unpublished results.*
3. Dornberger-Schiff, K. *Lehrgang über OD-Strukturen*, Akad.-Verlag, Berlin 1966.
4. Lenhert, P. G. *J. Appl. Crystallogr. 8* (1975) 568.

5. Chipman, D. R. *Acta Crystallogr. A 25* (1969) 209.
6. Mo, F. and Jensen, L. H. *Acta Crystallogr. B 31* (1975) 2867.
7. Templeton, L. K. and Templeton, D. H. *Am. Crystallogr. Assoc. Meeting*, Storrs, Connecticut, June 1973, Abstract E 10, p. 143.
8. de Meulenaer, J. and Tompa, H. *Acta Crystallogr. 19* (1965) 1014.
9. Svinning, T. and Mo, F. *XRDATA* Tekn. Rapport 30-RII-77. Inst. for røntgenteknikk, UNIT-NTH, Trondheim 1977.
10. *The X-RAY 76 System.* Stewart, J. M., Machin, P. A., Dickinson, C. W., Ammon, H. L., Heck, H. and Flack, H., Eds., Technical Report TR-446, Computer Science Center, Univ. of Maryland, College Park 1976.
11. Johnson, C. K. (1976) *ORTEP II*, Report ORNL-5138, Oak Ridge National Laboratory, Oak Ridge 1976.
12. Hamilton, W. C. *Acta Crystallogr. 18* (1965) 502.
13. Rae, A. D. *Acta Crystallogr. A 30* (1974) 761.
14. Doyle, P. A. and Turner, P. S. *Acta Crystallogr. A 24* (1968) 390.
15. Stewart, R. F., Davidson, E. R. and Simpson, W. T. *J. Chem. Phys. 42* (1965) 3175.
16. *International Tables for X-Ray Crystallography*, Kynoch Press, Birmingham 1974, Vol. 4, p. 149.
17. Walsh, A. D. *Discuss. Faraday Soc. 2* (1947) 18.
18. Bent, H. A. *J. Inorg. Nucl. Chem. 19* (1961) 43.
19. Bent, H. A. *Chem. Rev. 61* (1961) 275.
20. Mo, F. and Berg, Ø. *To be published.*
21. Kitaigorodskii, A. I. *Molecular Crystals and Molecules*, Academic, New York 1973, p. 17.
22. Busing, W. R. and Levy, H. A. *Acta Crystallogr. 17* (1964) 142.

Received September 5, 1977.

Acta Chemica Scandinavica A 32 (1978) 169 – 171

The Crystal and Molecular Structure of Acetylhydrazonium Chloride at 110 K

TOR OTTERSEN

Department of Pharmacy, University of Oslo, Oslo 3, Norway

The structure of the title compound, $C_2H_7N_2O^+Cl^-$, has been determined using 1506 reflections collected at 110 K. The crystals are orthorhombic, space group $Pca2_1$ with cell dimensions: $a = 14.768(3)$ Å, $b = 4.767(1)$ Å, $c = 7.522(1)$ Å. The structure model was refined to an R of 0.029. In order to reduce the influence of valence electron asphericity low-angle data were excluded from the final refinements. The heavy atom parameters converged for a minimum sin θ/λ cutoff of 0.65 Å^{-1}, leaving 863 reflections, the R is 0.037. The molecule, excluding the hydrogen atoms, is nearly planar with the oxygen and $-NH_3^+$ group *synplanar*.

The structure determination of acetylhydrazonium chloride is part of a series of structure investigations of 3,6-pyridazinediones and related compounds, of which part of the purpose is to study the effect of hydrogen bonding on the N–C=O fragment. The experimental results have been complemented by a series of theoretical studies (for a review see Refs. 1 and 2). The structure investigation of acetylhydrazonium chloride was carried out in order to study the effect on the N–C=O fragment of introducing a hydrazonium group instead of an amine or hydrazine group.

EXPERIMENTAL

Oscillation and Weissenberg photographs revealed orthorhombic symmetry and the systematic absences characteristic of the space groups $Pca2_1$ and $Pcam$. The density indicated four molecules in the unit cell, and the later structure determination showed the space group to be $Pca2_1$.

A platy crystal of approximate dimensions $0.1 \times 0.4 \times 0.2$ mm was used in the experiments. A computer-controlled Syntex $P\bar{1}$ four-circle diffractometer with graphite-monochromatized Mo$K\alpha$ radiation and equipped with a modified Enraf-Nonius liquid nitrogen cooling device was utilized in the determination of unit cell parameters and the recording of intensity data. Cell constants were determined by a least-squares treatment of the angular coordinates of fifteen reflections with 2θ-values between 43 and 55°. The temperature at crystal site was 110 K.

Three-dimensional intensity data were recorded using the $\omega - 2\theta$ scanning mode with scan speed variable from 2.0 to 6.0° min^{-1}, depending on the peak intensity of the reflection. Background counting time was equal to 0.7 × (scan time) and the scan area was from $2\theta(\alpha_1) - 0.9°$ to $2\theta(\alpha_2) + 0.9°$. All reflections with 2θ-values less than 55° were recorded, whereas for the reflections above this limit only those were recorded which had intensities larger than 6 cps determined in a 2 s scan. The intensities of three standard reflections which were remeasured after every sixty reflections were essentially constant throughout the recording run.

The estimated standard deviations were taken as the square-root of the total counts with a 2 % addition of the net intensities for experimental uncertainties. Of the 1546 reflections measured ($2\theta_{max} = 85°$), the 1506 which had intensities larger than twice their standard deviations were used in the refinements. The intensities were corrected for Lorentz and polarization effects. The computer program used, as well as programs subsequently employed, is part of a local assembly of computer programs which is described in Ref. 3.

The atomic scattering factors used were those calculated by Doyle and Turner[4] for chloride, oxygen, nitrogen and carbon and of Stewart *et al.*[5] for hydrogen.

CRYSTAL DATA

Acetylhydrazonium chloride, $C_2H_7N_2O^+Cl^-$, $M=120.55$ amu. Space group $Pca2_1$, cell dimensions at 110 K: $a=14.768(3)$ Å, $b=4.767(1)$ Å, $c=7.522(1)$ Å, $V=529.5(1)$ Å^3. D_{obs} (flotation, 19 °C)$=1.50$ g cm^{-3}, $Z=4$, $D_{calc}=1.512$ g cm^{-3}, F (000)$=232$.

STRUCTURE DETERMINATION AND REFINEMENTS

The phase problem was solved by the MULTAN program assembly[6] (modified assembly). The heavy atom structure model was refined with anisotropic temperature factors to a conventional R of 0.035. The hydrogen atoms were found as the seven largest peaks in a difference Fourier synthesis calculated using this structure model. These were included in the refinement with isotropic thermal parameters. Full-matrix least-squares refinemnt of all positional and thermal parameters converged to an R of 0.029 and an R_w of 0.040. The "goodness of fit" $(\{[\Sigma w(F_o-|F_c|)^2]/(m-s)\}^{\frac{1}{2}})$ (G) is 2.22.

In order to remove the influence of the valence electron asphericity on the heavy atom parameters, the minimum sin θ/λ cutoff value for data used in the refinements was increased systematically. The heavy atom parameters converged to their final values for a cutoff of 0.65 Å^{-1}. The variations in the parameters between this refinement and the refinement with a minimum sin θ/λ cutoff of 0.75 Å^{-1} were all less than twice their e.s.d.'s. The number of reflections in the refinement, final R, R_w and G factors are as follows: cutoff 0.65 Å^{-1}: 863, 0.037, 0.051, 2.02; cutoff 0.75 Å^{-1}: 562, 0.040, 0.053, 1.83. The heavy atom parameters from the refinement with a minimum sin θ/λ cutoff of 0.65 Å^{-1} are listed in Table 1, together with the hydrogen parameters obtained in the refinement using all data. A list of observed and calculated structure factors is available from the author upon request.

DISCUSSION

Bond lengths and bond angles are listed in Fig. 1 where also the numbering of the atoms is indicated. There is one intermolecular hydrogen bond involving the N−C=O fragment: N3−H3···O (in position: $x,1+y,z$), N···O distance 2.821(3) Å, ∠N3−H3···O: 160°. This hydrogen bond is similar to the one found for related molecules.[1] Compared to 1,2-diformylhydrazine the C=O bond is probably significantly shortened while the C−N bond is significantly lengthened; in 1,2-diformylhydrazine these bonds are 1.2380(2) and 1.3316(2) Å, respectively, and in the present structure 1.230(3) and 1.362(3) Å. Taking into consideration the lengthening of the C−N and C=O bonds induced by the introduction of a methyl group at the carbon atom (C=O: 0.008 Å, C−N: 0.012 Å, see Ref. 2 for a discussion of this), the substitution of an ammonia group leads to a significant decrease in the conjugation over the N−C=O fragment. The N−N bond [1.415(3) Å] is of the same length as those found in carbohydrazide[8] [1.4103(3) and 1.4156(3) Å], where the hybridizations of the nitrogen atoms are similar

Table 1. Fractional atomic coordinates and thermal parameters with estimated standard deviations. The anisotropic temperature factor is given by: exp $\{-2\pi^2[U_{11}(a^*h)^2+\cdots+2U_{23}(b^*c^*kl)]\}$. The parameters given for nonhydrogen atoms are those obtained in the refinement using only data with sin $\theta/\lambda \geq 0.65$ Å^{-1}.

Atom	x	y	z	U_{11}	U_{22}	U_{33}	U_{12}	U_{13}	U_{23}
Cl	.89031(4)	.71534(11)	.84253(0)	.0203(3)	.0118(2)	.0135(2)	−.0002(1)	.0005(2)	.0010(2)
O1	.90306(17)	−.14609(41)	.31975(26)	.0225(9)	.0089(5)	.0185(10)	.0018(4)	.0007(5)	.0002(4)
C2	.86931(15)	.08875(40)	.33358(42)	.0154(7)	.0105(5)	.0123(6)	.0001(4)	−.0007(8)	−.0000(7)
N3	.88610(17)	.29066(46)	.20970(26)	.0187(8)	.0089(5)	.0160(6)	.0010(6)	.0009(6)	.0008(5)
N4	.95079(17)	.22887(47)	.07654(28)	.0205(9)	.0112(6)	.0133(6)	.0006(6)	.0004(5)	.0013(5)
C5	.80732(23)	.17847(58)	.48058(42)	.0220(11)	.0176(10)	.0196(9)	.0032(7)	.0044(7)	−.0007(7)

Atom	x	y	z	B	Atom	x	y	z	B
H3	.878(1)	.466(5)	.234(4)	2.1(5)	H41	1.010(2)	.225(4)	.126(4)	2.4(5)
H42	.938(1)	.042(5)	.027(3)	2.0(5)	H43	.950(1)	.370(5)	−.005(3)	1.5(4)
H51	.761(2)	.042(5)	.498(4)	4.7(7)	H52	.835(3)	.176(7)	.570(6)	5.8(9)
H53	.781(2)	.357(5)	.457(5)	3.7(6)					

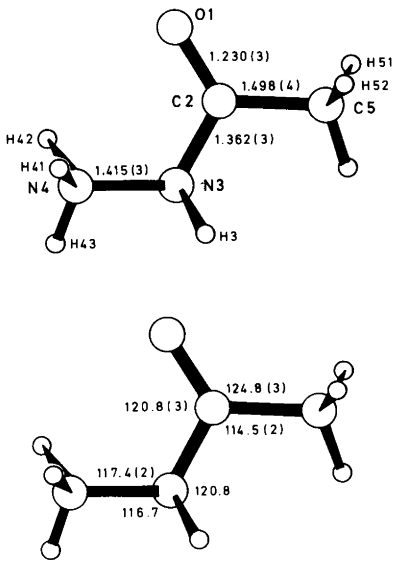

Fig. 1. Bond lengths (Å) and bond angles (°).

to those in the present structure. The N3 lone pair is probably involved in the N–N bonding which decreases its possibility of participating in the conjugation over the N–C=O fragment.[1]

The molecule is less planar than 1,2-diformylhydrazine;[7] deviations from a least-squares plane through O1, C2 and N3 are: C5, −0.015 Å; N4, 0.142 Å and H3, 0.250 Å. The planarity around N3 is similar to that found for the corresponding atoms in carbohydrazide.[8] The dihedral angle O1–C2–N3–N4 is −6.5° (4).

Both the O1–C2–N3 and the C2–N3–N4 angles have decreased significantly compared with those found for 1,2-diformylhydrazine [123.56(1) and 119.38(1)°, respectively] and for carbohydrazide[8] (*synplanar* O–C–N–N arrangement: 122.37(2) and 120.74(2)°, respectively). These decreases and the synplanar O1–C2–N3–N4 arrangement may indicate a weak charge-transfer bonding between the oxygen and $-NH_3^+$ group.

Some details of the hydrogen bonding are shown in Fig. 2. In addition to the N3–H3···O1 hydrogen bond mentioned above there are three hydrogen bonds from the ammonia group to chloride atoms. The hydrogen bond data are as follows: N4–H41···Cl (in position: $2-x,1-y,-0.5+z$), N4···Cl: 3.095(2) Å, ∠N4–H41···Cl: 154°; N4–H2···Cl ($x,-1+y,-1+z$), N4···Cl: 3.145(2) Å, ∠N4–H42···Cl: 160°; N4–H43···Cl ($x,y,-1+z$), N4···Cl: 3.045(2) Å, ∠N4–H43···Cl: 156°. These four bonds give hydrogen-bonded layers in (100) plane. The layers are kept together by van der Waals' contacts.

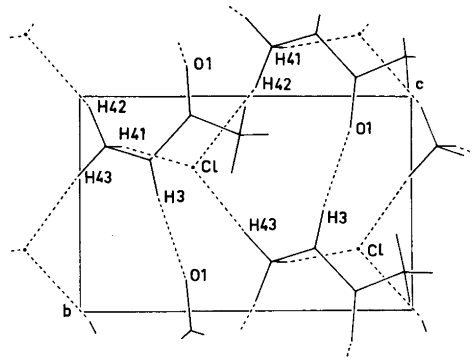

Fig. 2. Projection of the crystal structure as viewed along the *a*-axis. Atoms located between $-0.25 \leq X \leq 0.25$ are shown. Hydrogen bonds are shown by broken lines.

Acknowledgements. The author thanks Ulla Sørensen and Carsten Cristophersen for supplying the crystals, and Per Groth for help in solving the crystal structure.

REFERENCES

1. Ottersen, T. *Adv. Mol. Relaxation Processes 9* (1976) 105.
2. Ottersen, T. *Acta Chem. Scand. A 32* (1978) 127.
3. Groth, P. *Acta Chem. Scand. 27* (1973) 1837.
4. Doyle, P. A. and Turner, P. S. *Acta Crystallogr. A 24* (1968) 390.
5. Stewart, R. F., Davidson, E. R. and Simpson, W. T. *J. Chem. Phys. 42* (1965) 3175.
6. Germain, G., Main, P. and Woolfson, M. M. *Acta Crystallogr. A 27* (1971) 368.
7. Hope, H. and Ottersen, T. *To be published.*
8. Ottersen, T. and Hope, H. *To be published.*

Received September 14, 1977.

Acta Chemica Scandinavica A 32 (1978) 173 – 177

Phase Transitions in MnAs

ANDRZEJ ZIĘBA,[a] KARI SELTE,[b] ARNE KJEKSHUS[b] and ARNE F. ANDRESEN[c]

[a] Institute of Nuclear Physics and Techniques, Academy of Mining and Metallurgy, 30-059 Kraków, Poland, [b] Kjemisk Institutt, Universitetet i Oslo, Blindern, Oslo 3, Norway and [c] Institutt for Atomenergi, N-2007 Kjeller, Norway

The transformation properties of MnAs are studied by magnetization measurements in external magnetic fields up to 250 kOe and by neutron diffraction measurements between 4.2 and 400 K. The results are used to propose a qualitative explanation of the phase transitions in this compound.

The peculiar and apparently unique phase transitions in MnAs[1] are, although certainly recognized among solid state specialists, perhaps not commonly appreciated outside this limited sphere. A probable reason for this lack of general appreciation is that the theoretical understanding of the behaviour of MnAs is rather poor.

The object of this communication is to present a qualitative basis for a theoretical model for the transition properties of MnAs, using fresh experimental results as well as facts summarized in Ref. 1.

EXPERIMENTAL

The samples were prepared as described in Ref. 2, their homogeneity being ascertained from powder X-ray (Guinier) photographs. Experimental details concerning the pulsed field magnetization measurements and the neutron diffraction measurements are given in Refs. 1 and 3.

RESULTS

Near room temperature MnAs [like the Mn-rich $Mn_{1-t}T_tAs$ (T: V, Cr, Fe, or Co) samples discussed in Ref. 1] exhibits, as shown in Fig. 1, a first-order phase transition between ferromagnetic and paramagnetic states with NiAs and MnP type structures, respectively. This combined crystallographic and magnetic transition (conveniently abbreviated[1] as NiAs,$F \rightarrow$ MnP,P for increasing temperature) is only quasi-reversible, as demonstrated by the hysteresis loop in Fig. 1. The Curie temperatures for increasing ($T_{C,i}$) and decreasing ($T_{C,d}$) temperature in Fig. 1 are slightly higher than the values $T_{C,i} = 317$ K and $T_{C,d} = 306$ K obtained in weak sinusoidal fields. This discrepancy is a consequence of the experimental conditions which give rise to the magnetocalorimetric effect outlined in Ref. 1. The maximum magnetocalorimetric effect occurs in the vicinity of T_C and amounts to $\Delta T \approx 10$ K. Apart from supplementary measurements with other techniques, no attempt has been made to correct the present data for this deficiency.

Several parallel evidences suggest that the NiAs,F type state of MnAs should be assigned a substantially higher Curie temperature than expressed above:

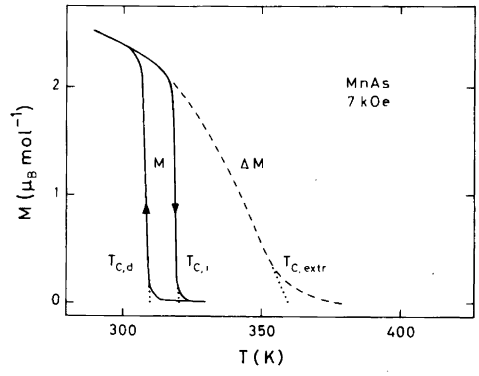

Fig. 1. Magnetization *versus* temperature for MnAs at 7 kOe (solid curves); magnetization increment *versus* temperature at the metamagnetic transition above $T_{C,i}$ (broken curve).

(*i*) The magnetization increment (ΔM) at the metamagnetic transition above $T_{C,i}$ (Fig. 1) joins nicely to the magnetization [M(T)] curve. The ΔM(T) curve gives an extrapolated Curie temperature ($T_{C,extr.}$) of ~360 K.

(*ii*) The relative magnetization ($M/M_{0\,K}$) for the NiAs,F type state of MnAs is known from magnetization[4] and neutron diffraction (*vide infra*) measurements. Assuming that MnAs behaves like a typical ferromagnet (say Fe or Ni) $T_{C,extr.} \approx 360$ K would result, whereas the extrapolation of $M/M_{0\,K}$ according to a Brillouin function gives a slightly higher value.[5]

(*iii*) The Clausius-Clapeyron equation may be used to predict that maximum values of the transition fields H_F and H_P should be found close to the Curie temperature. The maxima in H_F and H_P (Fig. 2) occur at 360 and 365 K, respectively.

(*iv*) In an attempt to account for the thermodynamic properties of MnAs, Grønvold *et al.*[6] concluded that it was necessary to assume incomplete spin randomization above $T_{C,i}$. The observed MnP,$P \rightleftharpoons$NiAs,F type transition can be looked upon as composed of two hypothetical transitions of the types MnP,$P \rightleftharpoons$NiAs,P and NiAs,$P \rightleftharpoons$NiAs,F. The splitting of the total energy into the contributions from these two processes is difficult to assess on an experimental basis. However, extrapolation of the data of Grønvold *et al.*[6] suggests that the internal energy of the MnP,P type state lies between the energies of the NiAs,P and NiAs,F type states below ~360 K. The energy associated with the hypothetical NiAs,$P \rightleftharpoons$NiAs,F type transition can be estimated by means of the molecular field theory.[5] It may be taken as a reasonable proof of selfconsistency that $T_C = T_{C,extr.} = 360$ K and $S = 3/2$ leads to a somewhat higher transition energy than observed.[6]

The temperature *versus* applied magnetic field phase diagram for MnAs in Fig. 2 has the same general appearance as those for $Mn_{1-t}T_tAs$.[1] However, due to the fact that the NiAs,F type state exists at $H = 0$ kOe for MnAs, Fig. 2 is simpler below T_C than the corresponding diagrams in Ref. 1. The stability of the NiAs,F type state is also reflected in the shift of the phase borders H_P and H_F to lower fields in MnAs. (The situation may be illustrated by quoting the critical field $H_{F,max.}$ (in kOe) for a few samples: MnAs, 97; $Mn_{0.99}Cr_{0.01}As$, 127; $Mn_{0.97}Cr_{0.03}As$, 154; $Mn_{0.97}Co_{0.03}As$, 176; $Mn_{0.95}Co_{0.05}As$, >250.) This, together with comparison of Fig. 2 with Figs. 7–10 of Ref. 1, serves to emphasize that a pure, good quality sample is required in any attempt to establish the intrinsic properties of MnAs.

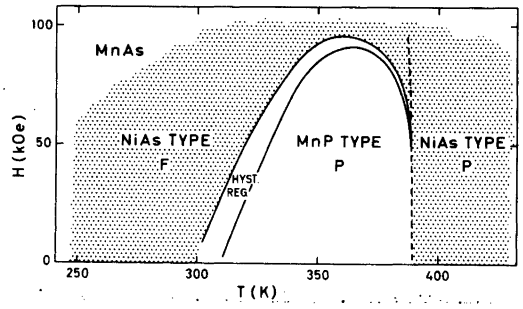

Fig. 2. Phase diagram in T,H space for MnAs.

The neutron diffraction data show that on cooling, MnAs retains the NiAs type crystal structure down to 4.2 K. This is in complete accordance with earlier findings (see Refs. 6 and 7), and there is no evidence for a partial NiAs→MnP type transition at ~160 K as was indicated in Ref. 8.

The value $\mu_{F,tot.} = 3.3 \pm 0.1\ \mu_B$ at 4.2 K obtained by neutron diffraction corresponds well with that (3.1 μ_B) obtained by magnetization measurements, and is also reasonably consistent with the value $2S_{Mn} = 3.6 \pm 0.2$ derived for the NiAs,P type state (using the "spin only" approximation). The temperature dependence of $\mu_{F,tot.}$ over the interval 4.2–297 K follows nicely the Brillouin function for $S = 3/2$ assuming a Curie temperature of 360 K, thus supporting the conclusion drawn from the magnetization data (*vide supra*). The present work concurs with the results of Bacon and Street[7] apart from a somewhat temperature-dependent deviation of the moment from the direction perpendicular to c ($\mu_{F,tot.}$, $\mu_{F,\parallel c}$, $\mu_{F,\perp c}$ are 3.31(10), 1.31(13), 3.03(11) and 2.46(16), 0.81(42), 2.32(20) at 4.2 and 298 K, respectively; as derived by least squares profile refinement of the neutron diffraction data; standard deviations in brackets).

DISCUSSION

The present data shed new light on the peculiar transformation properties of MnAs, which are summarized in the bottom part of Fig. 3. In order to illustrate our points, Fig. 3 also shows a sketch of the temperature variations in the shortest (bonding) Mn–As (averaged in MnP type state) and Mn–Mn distances. In addition, Table 1 gives a comparison between the NiAs,P NiAs,F and MnP,P type states

Table 1. Structural and magnetic parameters for real and hypothetical states of MnAs at 4.2 and 298 K. (NiAs and MnP type structures are referred to space groups $P6_3/mmc$ and *Pnma*, respectively. Extrapolations are based on data from Refs. 1, 2, 10–12, 15, 17–19.)

Structure type	NiAs			MnP		
T (K)	4.2	298	Temp. extrap. to 298	Conc. extrap.; 4.2	Temp. extrap. to 298	Conc. extrap.; 298
a (Å)	3.730	3.722	3.672	5.566	5.704	5.695
b (Å)				3.498	3.655	3.644
c (Å)	5.668	5.702	5.691	6.164	6.365	6.329
x_{Mn}				0.0003	0.005	0.0045
z_{Mn}				0.2141	0.222	0.2160
x_{As}				0.1963	0.224	0.2196
z_{As}				0.5828	0.582	0.5774
$(Mn-As)_{av.}$ (Å)	2.578	2.579	2.553	2.498	2.56	2.560
Mn–Mn (Å)	2.834	2.851	2.846	2.815	2.87	2.883
Mn–Mn (Å)	3.730	3.722	3.672	3.24	3.37	3.27
$2S_{Mn}$, magn. state	3.2 (av.), F [a]	2.5, F [a]	3.6, P	1.9, H [b]	"low spin", P	"low spin", P

[a] Magn. moments 67° (4.2 K) and 71° (298 K) off c; $T_{C,extr.} \approx 360$ K.
[b] $\alpha = 54°$, $\phi = 75°$, $\beta = 90°$ (fixed); $T_N \approx 210$ K (Refs. 1 and 19).

at 298 K and the NiAs,F and MnP,H type states at 4.2 K, including data extrapolated according to temperature or concentration.

The situation in the NiAs,P type state may conveniently be chosen as the starting point for the following brief considerations. At, say, 600 K the atomic arrangement of MnAs is of the "typical" NiAs type with two short Mn–Mn distances of 2.90 Å along the hexagonal axis and six longer Mn–Mn distances of 3.70 Å within the basal plane. As the temperature is lowered towards 400 K, these distances, as well as the Mn–As distances, decrease slightly. At 393 K the structure changes to the MnP type, and a marked shrinkage of the second shortest Mn–Mn distance is observed as the temperature is lowered to ~320 K.

The driving force of the NiAs→MnP type transformation is considered to be the "strive" to establish four close metal–metal contacts.[13] The bonding nature of these metal–metal contacts is still essentially unknown. The transformation from NiAs type to "idealized" MnP type structure [Ref. 13; *inter alia* characterized by four (2+2) short metal–metal distances of virtually equal lengths] proceeds continuously over an appreciable temperature interval which amounts to ~200 K in $MnAs_{0.9}P_{0.1}$[14] and ~500 K in $Mn_{0.9}Fe_{0.1}As$.[15] Fig. 3 indicates that the stability range (~70 K) of the MnP type structure is much too narrow to obtain the "idealized" MnP type atomic arrangement for MnAs.

When the temperature is lowered to ~310 K, the atomic arrangement of MnAs converts back to the NiAs type. The driving force of this transformation is almost certainly the magnetic exchange interactions. Due to the marked dissimilarity between the two pairs of short Mn–Mn distances (2.86 *versus* ~3.3 Å), the exchange interactions corresponding to the closest Mn–Mn contacts will dominate. Hence, the structural rearrangement to the NiAs type is a natural consequence of this imbalance.

The fact that $T_{C,extr.}$ is substantially higher than the observed transformation temperature (~310–~320 K), may be explained by the competition between the two direct magnetic exchange paths. The extrapolated Néel temperature for the hypothetical MnP,H type mode of MnAs is ~210 K.[1] The NiAs,F and hypothetical MnP,H type modes have in common notable similarities in magnetic arrangements, since the spin directions are (approximately) perpendicular to a common direction in the two structure types (c_{NiAs} and a_{MnP}). As seen from Table 1, there is a dissimilarity between the shortest and the second shortest Mn–Mn distances also in the hypothetical MnP,H type mode of MnAs.

In complete accordance with our neutron diffraction results, the temperature dependence of the Mn–As and Mn–Mn distances gives no evidence

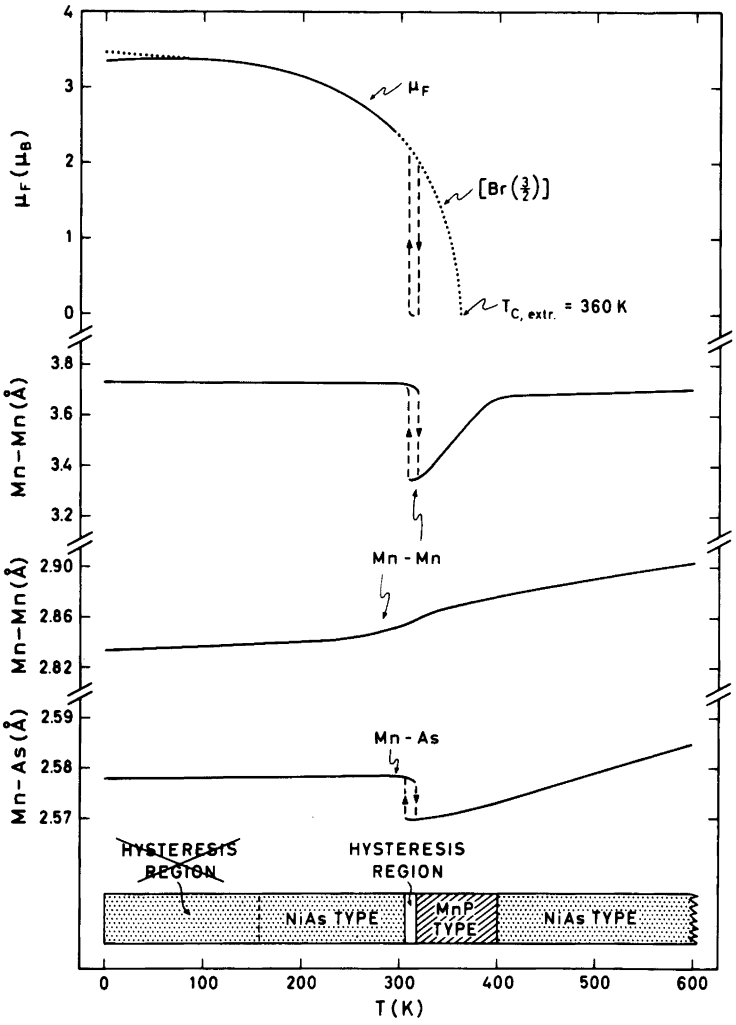

Fig. 3. Structural changes with temperature in MnAs quoted from Ref. 1. Temperature dependence of Mn–As (averaged for MnP type) and Mn–Mn distances according to this study and data from Refs. 9–12. μ_F *versus* T as observed by neutron diffraction.

for the indicated,[8] partial NiAs,$F \rightarrow$MnP,H type transition at ~160 K. Such a transition can, however, be induced by the application of a comparatively small external pressure[16] or by small substitutions of another transition metal for Mn.[1,2,17–19] The fact that the application of an external pressure on MnAs is able to decrease the second shortest Mn–Mn distance, is consistent with expectation, and the pressure induced MnP,H mode[16] thus provides additional support for the above considerations.

Acknowledgements. The authors are grateful to cand.mag. P. G. Peterzéns for help in the neutron diffraction experiments. This work has received financial support from The Norwegian Research Council for Science and the Humanities.

REFERENCES

1. Selte, K., Kjekshus, A., Andresen, A. F. and Zięba, A. *J. Phys. Chem. Solids 38* (1977) 719.
2. Selte, K., Kjekshus, A. and Andresen, A. F. *Acta Chem. Scand. A 28* (1974) 61.

3. Selte, K., Kjekshus, A. and Andresen, A. F. *Acta Chem. Scand. 26* (1972) 3101.
4. Bean, C. P. and Rodbell, D. S. *Phys. Rev. 126* (1962) 104.
5. Smart, J. S. *Effective Field Theories of Magnetism*, Sanders, Philadelphia – London 1966.
6. Grønvold, F., Snildal, S. and Westrum, E. F. *Acta Chem. Scand. 24* (1970) 285.
7. Bacon, G. E. and Street, R. *Nature 175* (1955) 518.
8. Menyuk, N., Kafalas, J. A., Dwight, K. and Goodenough, J. B. *Phys. Rev. 177* (1969) 942.
9. Willis, B. T. M. and Rooksby, H. P. *Proc. Phys. Soc. London Sect. B 67* (1954) 290.
10. Kornelsen, R. O. *Can. J. Phys. 39* (1961) 1728.
11. Wilson, R. H. and Kasper, J. S. *Acta Crystallogr. 17* (1964) 95.
12. Kjekshus, A. and Pearson, W. B. *Prog. Solid State Chem. 1* (1964) 83.
13. Endresen, K., Furuseth, S., Selte, K., Kjekshus, A., Rakke, T. and Andresen, A. F. *Acta Chem. Scand. A 31* (1977) 249.
14. Hall, E. L., Schwartz, L. H., Felcher, G. P. and Ridgley, D. H. *J. Appl. Phys. 41* (1970) 939.
15. Selte, K., Kjekshus, A. and Andresen, A. F. *Acta Chem. Scand. 27* (1973) 3607.
16. Yoshie, H. and Hihara, T. *J. Phys. Soc. Jpn. 40* (1976) 427.
17. Selte, K., Kjekshus, A., Valde, G. and Andresen, A. F. *Acta Chem. Scand. A 30* (1976) 8.
18. Selte, K., Kjekshus, A., Valde, G. and Andresen, A. F. *Acta Chem. Scand. A 30* (1976) 468.
19. Selte, K., Kjekshus, A., Peterzéns, P. G. and Andresen, A. F. *Acta Chem. Scand. In press.*

Received September 19, 1977.

Acta Chemica Scandinavica A 32 (1978) 179 – 185

Structural and Magnetic Properties of $Cr_{1-t}Ni_tAs$, $Mn_{1-t}Ni_tAs$, and $Fe_{1-t}Ni_tAs$

INGER LISE ANDREASSEN DELPHIN,[a] KARI SELTE,[a] ARNE KJEKSHUS[a] and ARNE F. ANDRESEN[b]

[a] Kjemisk Institutt, Universitetet i Oslo, Blindern, Oslo 3, Norway and [b] Institutt for Atomenergi, N-2007 Kjeller, Norway

The pseudo-binary systems CrAs – NiAs, MnAs – NiAs, and FeAs – NiAs have been investigated by X-ray and neutron diffraction and magnetic susceptibility measurements. All systems are characterized by incomplete solid solubility. The structures of the ternary, random solid solution phases are either of the MnP or NiAs type. The double, *c* axis helimagnetic ordering in CrAs extends slightly into the ternary region (to $0.02 < t < 0.05$) of $Cr_{1-t}Ni_tAs$. $Mn_{0.95}Ni_{0.05}As$ takes the double, *a* axis helimagnetic ordering characteristic of other Mn rich $Mn_{1-t}T_tAs$ phases (*T*: V, Cr, Fe, Co).

The authors have earlier studied pseudo-binary *T*As – *T'*As (*T*,*T'*: V, Cr, Mn, Fe, Co) system where *T*As and *T'*As both take the MnP type structure. In the present paper we report the results of similar studies on systems where *T'*As = NiAs has the closely related[1,2] NiAs type structure.

EXPERIMENTAL

The binary compounds CrAs, MnAs, and FeAs were prepared as described in Refs. 3 – 5, and NiAs [from 99.999 % Ni (Johnson, Matthey & Co.; turnings from rods) and As (Koch-Light Laboratories)] by three heat treatments at 900 °C for one week. Ternary $T_{1-t}Ni_tAs$ samples were made similarly from the binary compounds, and finally either quenched (from 600 – 1000 °C) or slowly cooled to room temperature. It proved difficult to obtain thermodynamic equilibrium for $Mn_{1-t}Ni_tAs$, particularly in the region $0.6 \leqq t \leqq 0.8$. The experimental details concerning the X-ray and neutron diffraction and magnetic susceptibility measurements have been reported earlier.[4]

RESULTS AND DISCUSSION

(i) *Homogeneity ranges and atomic arrangements.* Isothermal cross-sections of $Cr_{1-t}Ni_tAs$, $Mn_{1-t}Ni_tAs$, and $Fe_{1-t}Ni_tAs$ as derived for samples quenched from 600 °C, show that the three systems exhibit two-phase miscibility gaps for $0.50 \pm 0.03 < t < 0.68 \pm 0.03$, $0.07 \pm 0.03 < t < 0.30 \pm 0.05$, $0.40 \pm 0.05 < t < 0.60 \pm 0.05$, respectively. The limits of the solubility ranges have been determined from the variation in the unit cell dimensions with *t* (Fig. 1), and further confirmed by application of the disappearing phase principle to the X-ray (Guinier) data. From the variation of the unit cell dimensions (particularly the volume *V*) with *t* it may be suggested that complete miscibility can be obtained for $Cr_{1-t}Ni_tAs$ and $Mn_{1-t}Ni_tAs$ at suitable experimental conditions, whereas such a situation is not expected for $Fe_{1-t}Ni_tAs$. Samples with metal/nonmetal atomic ratios different from 1.00 have not been studied.

Fig. 1a,c shows that the MnP type structure prevails at room temperature in the Cr and Fe rich phases of $Cr_{1-t}Ni_tAs$ and $Fe_{1-t}Ni_tAs$, whereas the NiAs type is stable in the Ni rich phases. At room temperature, $Mn_{1-t}Ni_tAs$ takes the NiAs type structure in the Ni rich phase and in a narrow region near MnAs. Throughout the rest of the Mn rich phase the MnP type structure prevails (Fig. 1b). A second or higher order MnP$\rightleftharpoons$NiAs type transition is detected by high temperature, X-ray diffraction measurements in $Cr_{1-t}Ni_tAs$ and $Fe_{1-t}Ni_tAs$ (Fig. 2). The transformation in $Mn_{0.95}Ni_{0.05}As$ is more difficult to detect, but magnetic susceptibility data (not presented here) suggest that it takes place

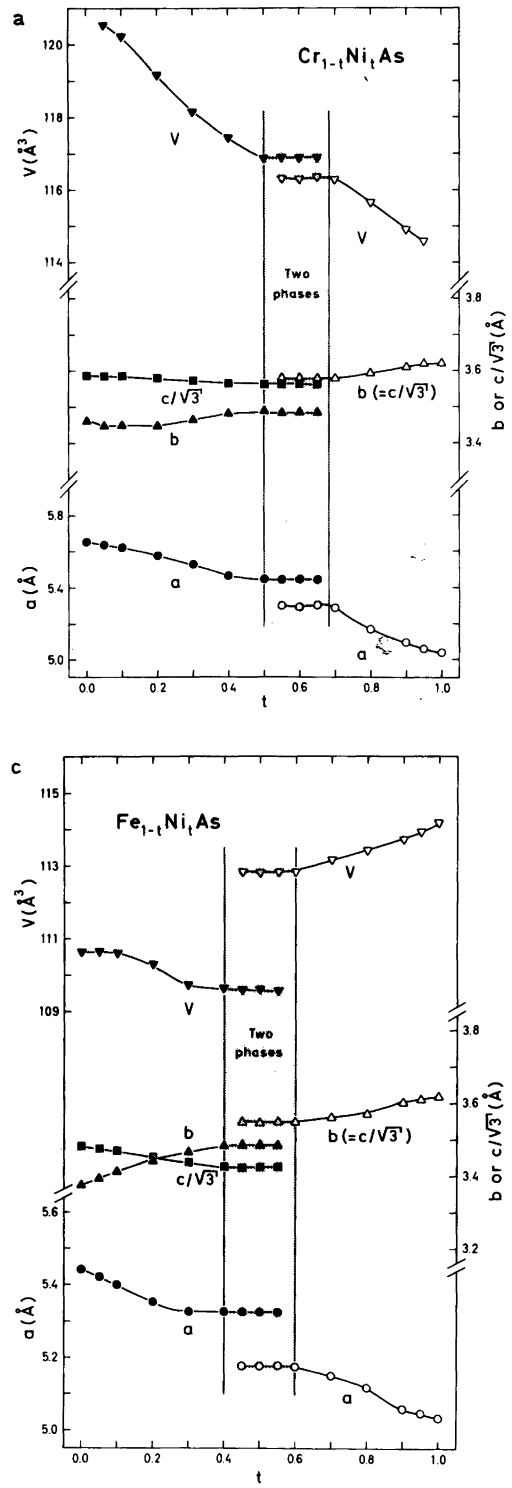

Fig. 1. Room temperature unit cell dimensions of (a) $Cr_{1-t}Ni_tAs$, (b) $Mn_{1-t}Ni_tAs$, and (c) $Fe_{1-t}Ni_tAs$ as functions of t. Open and filled symbols refer to NiAs and MnP type structures, respectively, both described in terms of space group *Pnma*.

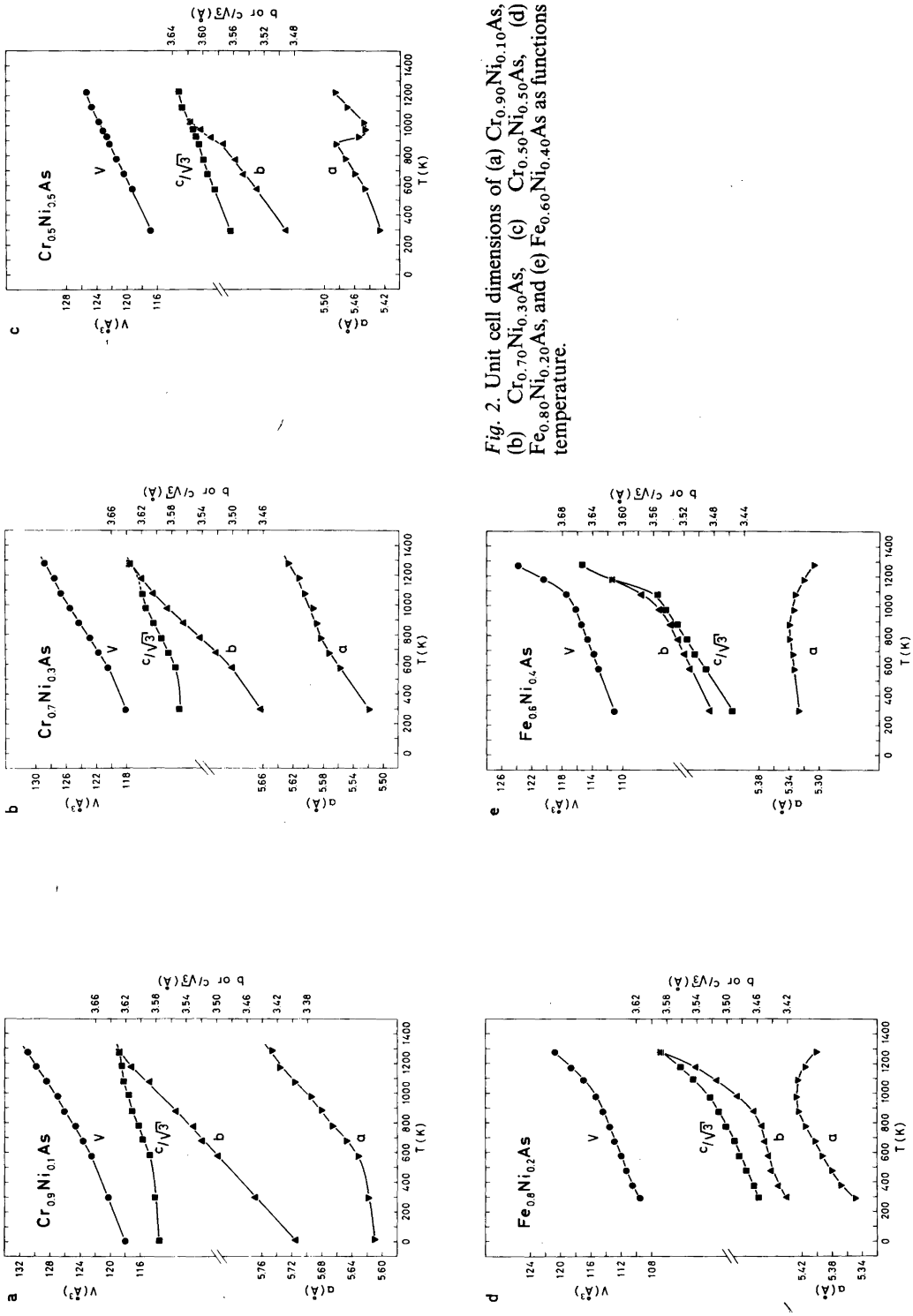

Fig. 2. Unit cell dimensions of (a) $Cr_{0.90}Ni_{0.10}As$, (b) $Cr_{0.70}Ni_{0.30}As$, (c) $Cr_{0.50}Ni_{0.50}As$, (d) $Fe_{0.80}Ni_{0.20}As$, and (e) $Fe_{0.60}Ni_{0.40}As$ as functions temperature.

Table 1. Unit cell dimensions and positional parameters with standard deviations for selected $T_{1-t}Ni_tAs$ samples as derived by least squares profile refinements of neutron diffraction data. (Space group *Pnma*; positions 4(*c*); overall profile reliability factors ranging between 0.021 and 0.038.)

T	*t*	T(K)	*a*(Å)	*b*(Å)	*c*(Å)	x_T	z_T	x_X	z_X
Cr	0.02	10	5.5908(7)	3.5787(4)	6.1277(6)	0.0089(13)	0.2009(10)	0.2046(5)	0.5861(13)
		80	5.5939(7)	3.5794(4)	6.1343(7)	0.0078(14)	0.2035(11)	0.2043(5)	0.5844(15)
		293	5.6371(9)	3.4513(5)	6.1999(10)	0.0078(9)	0.2017(8)	0.2009(4)	0.5766(5)
Cr	0.05	10	5.6175(7)	3.3886(4)	6.1997(6)	0.0086(16)	0.1980(14)	0.1983(13)	0.5741(8)
		80	5.6173(5)	3.3932(2)	6.1990(4)	0.0092(11)	0.1978(10)	0.1996(9)	0.5734(5)
		293	5.6278(7)	3.4488(2)	6.2002(5)	0.0081(11)	0.1993(9)	0.2016(5)	0.5758(6)
Cr	0.10	10	5.6011(10)	3.3954(6)	6.1928(11)	0.0075(9)	0.2003(7)	0.1982(5)	0.5743(6)
		293	5.6055(9)	3.4443(4)	6.1966(9)	0.0084(8)	0.2030(6)	0.2012(4)	0.5755(5)
Mn	0.05	10	5.5413(7)	3.4980(4)	6.1546(10)	0.0041(22)	0.2081(24)	0.1963(9)	0.5831(10)
		80	5.5467(6)	3.5044(3)	6.1638(8)	0.0052(19)	0.2048(22)	0.1975(8)	0.5816(9)
		293	5.6592(5)	3.6375(6)	6.3340(11)	0.0088(25)	0.2242(27)	0.2210(9)	0.5876(16)

just above room temperature. The two kinds of metal atoms are randomly distributed over the metal sub-lattices in the two types of atomic arrangement. The unit cell dimensions and positional parameters at and below room temperature for $Cr_{0.98}Ni_{0.02}As$, $Cr_{0.95}Ni_{0.05}As$, $Cr_{0.90}Ni_{0.10}As$, and $Mn_{0.95}Ni_{0.05}As$ are listed in Table 1.

Among the quasi-binary MnAs–*T*As systems those with *T*=V or Cr exhibit complete miscibility, whereas a two-phase region is found in the systems with *T*=Fe, Co, or Ni. Since MnAs takes the NiAs type structure (except between ~50 and 120 °C), and VAs, CrAs, FeAs, and CoAs take the MnP type, a structural change must occur in $Mn_{1-t}T_tAs$ with *T*=V, Cr, Fe, or Co. The miscibility gaps in MnAs–FeAs and MnAs–CoAs are directly associated with the structural change, and are therefore not unexpected. Similar considerations apply to the incomplete solid solubility in CrAs–NiAs and FeAs–NiAs. As MnAs and NiAs both take the same structure type, the change to the MnP type structure in MnAs–NiAs is, at first sight, surprising. However, the finding is less surprising when it is recalled that application of hydrostatic pressure or chemical substitution of either Mn with V, Cr, Fe, or Co, or As with P induce corresponding structural changes. Without taking up the question of cause and origin, it should be noted that both the application of pressure and chemical substitution lead to a reduction in the unit cell volume.

(ii) *Magnetic susceptibility.* The temperature characteristics of the reciprocal magnetic susceptibility show systematic variations with the composition parameter *t* for $Cr_{1-t}Ni_tAs$ and $Mn_{1-t}Ni_tAs$ (Fig. 3). The $Fe_{1-t}Ni_tAs$ samples were contaminated by traces of ferromagnetic impurities, and the data for this system are not included here.

None of the $\chi^{-1}(T)$ curves for $Cr_{1-t}Ni_tAs$ (data for the two-phase sample with $t=0.60$ and the borderline sample with $t=0.50$ are included among the proper characteristics) follows the Curie-Weiss Law. For $Mn_{1-t}Ni_tAs$ the one-phase samples with t=0, 0.05, 0.30, and 0.40 show linear $\chi^{-1}(T)$ curves to a very good approximation over the measured temperature intervals (Fig. 3). The values for θ (paramagnetic Curie temperature in K), μ_P (paramagnetic moment in μ_B), $2S$ ("spin only" spin quantum number) for these samples are 270, 4.5, 3.6; 270, 4.4, 3.5; 210, 3.2, 2.4; and 160, 2.9, 2.1 (uncertainties 10, 0.3, 0.2) for $t=0$, 0.05, 0.30, and 0.40, respectively. The $\chi^{-1}(T)$ curves for $0.50 \leqq t \leqq 0.95$ become gradually more convex towards the temperature axis. However, even for $t=0.80$ the Curie-Weiss Law represents a useful approximation below ~600 K, leading to $\theta = -75 \pm 10$ K, $\mu_P = 1.7 \pm 0.2\ \mu_B$, and $2S = 1.0 \pm 0.2$.

(iii) *Magnetic structures.* NiAs is the only binary end member of the investigated systems which does not exhibit cooperative magnetism at low temperature.[6] CrAs and FeAs both take helimagnetic arrangements of the double, *c* axis type below ~260–270 and 77 ± 1 K,[3,4] whereas MnAs is ferromagnetic below ~310–320 K.[7] Since the cooperative magnetic states of FeAs[4] and $Fe_{1-t}Co_tAs$[8] were difficult

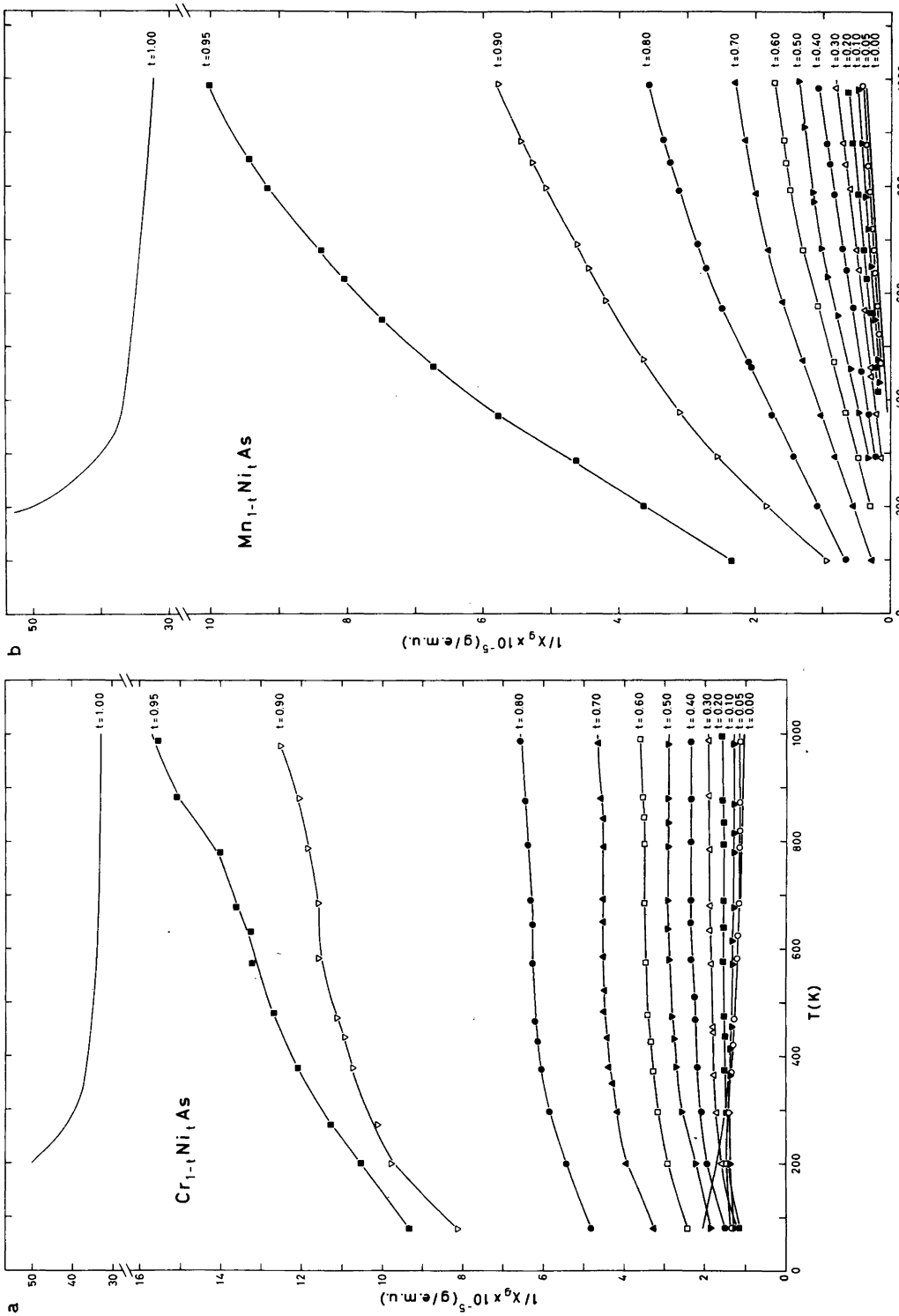

Fig. 3. Reciprocal magnetic susceptibility *versus* temperature for (a) $Cr_{1-t}Ni_tAs$ and (b) $Mn_{1-t}Ni_tAs$. Data for $Cr_{0.40}Ni_{0.60}As$, $Mn_{0.90}Ni_{0.10}As$, and $Mn_{0.80}Ni_{0.20}As$ refer to two-phase samples.

to explore due to their low moments, $Fe_{1-t}Ni_tAs$ samples were not subjected to neutron diffraction examination.

The helimagnetic ordering in CrAs extends only slightly into the ternary composition range (to $0.02 < t < 0.05$) of $Cr_{1-t}Ni_tAs$. Comparatively small changes were observed in the variable parameters (angle between moment and spiral axis, β, fixed at 90°) on going from CrAs [80 K: $\mu = 1.70(5)$ μ_B (magnetic moment per metal atom), $\tau/2\pi\mathbf{c}^* = 0.353(1)$ (spiral propagation vector), $\phi = -133(1)°$ (phase angle between independent spirals)][3] to $Cr_{0.98}Ni_{0.02}As$ (10 K: $\mu = 1.73(5)$ μ_B, $\tau/2\pi\mathbf{c}^* = 0.357(6)$, $\phi = -118(1)°$; 80 K: $\mu = 1.68(5)$ μ_B, $\tau/2\pi\mathbf{c}^* = 0.351(7)$, $\phi = -126(1)°$). However, the 2 % substitution of CrAs by NiAs has led to an appreciable lowering of the Néel temperature (T_N) from ~260–270 to 170–208 K (±2 K). Significant indications of reflections characteristic of the helimagnetic arrangement were not found for $t = 0.05$ and 0.10. The transition to the cooperative magnetic state in $Cr_{0.98}Ni_{0.02}As$ is associated with hysteresis and involves two distinct MnP type phases. Thus, $Cr_{0.98}Ni_{0.02}As$ fits nicely into the pattern of CrAs[3] and CrAs rich samples of $V_{1-t}Cr_tAs$,[9] $Cr_{1-t}Mn_tAs$,[10] $Cr_{1-t}Fe_tAs$,[11] $Cr_{1-t}Co_tAs$,[8] and $CrP_{1-x}As_x$.[12] The spiral parameters ϕ and τ vary little with temperature and composition for all these phases. In fact, the only magnetic parameter which changes rapidly is T_N, thus confirming our earlier suggestion[8] that the breakdown of the cooperative magnetism in $Cr_{1-t}T_tAs$ and $CrP_{1-x}As_x$ is associated with corresponding, rapid variations in the magnetic exchange interactions with t or x.

The hystereses in structural and cooperative magnetic parameters around T_N show that the transition in $Cr_{0.98}Ni_{0.02}As$ is of a combined first and second (or higher) order. [To denote this type of quasi-reversible crystallographic and magnetic transition we suggest the abbreviation MnP(I),$H \rightleftharpoons$ MnP(II),P.] The transition has been most extensively studied for CrAs itself, for which it has been demonstrated that changes in unit cell dimensions, positional parameters, sub-lattice magnetizations, specific heat, and electrical resistivity are associated with the transition, whereas no significant changes hitherto have been detected for magnetic susceptibility, Hall coefficient and thermoelectric power.[3,10,13] Despite the distinct changes in unit cell dimensions and positional parameters at the MnP(II),$P \rightarrow$MnP(I),H transition, it is difficult to detect a clear-cut pattern for the variation of the bonding interatomic distances in the systems studied. The only systematic trend we have found so far is that the shortest metal–metal contact shrinks 1–2 % during the transition. No such shrinkage has been observed for samples lacking this cooperative magnetic behaviour, but with almost the same substitution of VAs, CoAs, and NiAs for CrAs. The origin of the quasi-reversible MnP(I),$H \rightleftharpoons$MnP(II),P transition of CrAs is virtually unknown. Boller and Kallel[13] have suggested that the first order contribution is due to an electronic transition between localized and collective states. Although this interpretation appeared to be satisfactory in view of the structural data provided by these authors, it seems less likely on the basis of the structural data given here and in Refs. 3, 8, and 9.

The cooperative magnetic state of the Mn rich $Mn_{1-t}Ni_tAs$ phase follows the pattern found in other Mn rich $Mn_{1-t}T_tAs$ phases (T: V, Cr, Fe, Co) by associating a ferromagnetic mode with the low temperature, NiAs type structure and a double, a axis helimagnetic mode with the MnP type structure.[5,14–16] Although the NiAs,F state ($0 \leqq t < 0.05$) has not been experimentally studied for $Mn_{1-t}Ni_tAs$, experience[7,17] suggests that its magnetic parameters differ only insignificantly from those of MnAs itself.

At $T_N = 202 \pm 3$ K $Mn_{0.95}Ni_{0.05}As$ undergoes a second (or higher) order MnP,$P \rightleftharpoons$MnP,H type transition, and below this temperature it takes a similar helimagnetic arrangement to that in $Mn_{1-t}V_tAs$ ($0.05 \leqq t \leqq \sim 0.40$),[14] $Mn_{1-t}Cr_tAs$ ($0.10 \leqq t \leqq 0.35$),[16] $Mn_{1-t}Fe_tAs$ ($\sim 0.01 < t < \sim 0.12$),[5,18] and $Mn_{1-t}Co_tAs$ ($0.05 \leqq t \leqq 0.15$).[15] The parameters specifying the magnetic structure are: $\mu = 1.6(1)$ μ_B, $\tau = 0.155(3) \times 2\pi\mathbf{a}^*$, $\phi = 92(2)°$ at 10 K and $\mu = 1.6(1)$ μ_B, $\tau = 0.155(3) \times 2\pi\mathbf{a}^*$, $\phi = 98(2)°$ at 80 K ($\beta = 90°$; fixed). The constraint $\beta = 90°$ was relaxed in the preliminary refinements since the magnetic susceptibility measurements had given indication of a ferromagnetic component in $Mn_{0.95}Ni_{0.05}As$. However, by far the best agreement between the observed and calculated intensity data was obtained for $\beta = 90°$.

The spiral parameters and T_N for $Mn_{0.95}Ni_{0.05}As$ fit in with corresponding data for the other $Mn_{1-t}T_tAs$ phases. The temperature dependence of the relative (integrated) intensity for the strongest satellites $000^{\pm}$ and $001^{\pm}$ (Fig. 4) also show marked similarities with corresponding observations for the other $Mn_{1-t}T_tAs$ phases, and the spiral parameters of $Mn_{0.95}Ni_{0.05}As$ vary with temperature as found

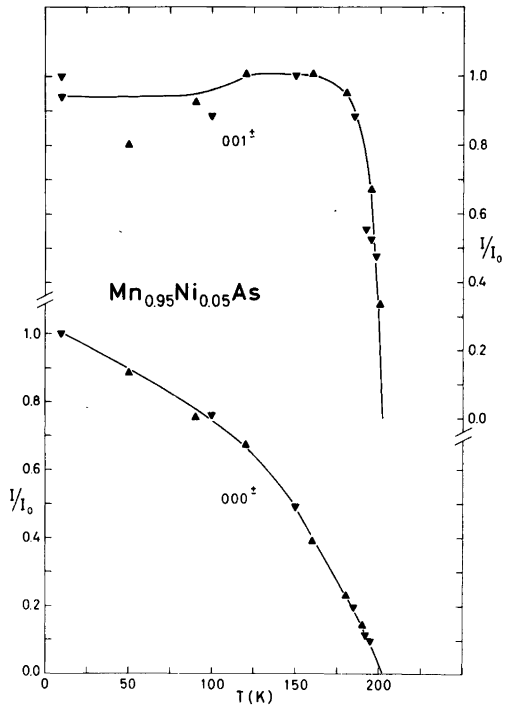

Fig. 4. Relative intensities of satellite reflections $000^{\pm}$ and $001^{\pm}$ as functions of temperature for $Mn_{0.95}Ni_{0.05}As$.

earlier.[5,14-16,18] Probably, the chemical and magnetic phase boundary of $Mn_{1-t}Ni_tAs$ coincide at $t=0.07\pm0.03$. Thus, among the $Mn_{1-t}T_tAs$ phases, the MnP,*H* state of $Mn_{1-t}Ni_tAs$ is characterized by the narrowest compositional stability range. For further discussions on the cooperative magnetic and associated transformational properties of MnAs and $Mn_{1-t}T_tAs$ reference is made to earlier communications.[5,7,14-17]

Acknowledgements. The authors are grateful to cand.mag. P. G. Peterzéns for help in the neutron diffraction experiments. This work has received financial support from The Norwegian Research Council for Science and the Humanities.

REFERENCES

1. Selte, K. and Kjekshus, A. *Acta Chem. Scand. 27* (1973) 3195.
2. Endresen, K., Furuseth, S., Selte, K., Kjekshus, A., Rakke, T. and Andresen, A. F. *Acta Chem.* Scand. *A 31* (1977) 249.
3. Selte, K., Kjekshus, A., Jamison, W. E., Andresen, A. F. and Engebretsen, J. E. *Acta Chem. Scand. 25* (1971) 1703.
4. Selte, K., Kjekshus, A. and Andresen, A. F. *Acta Chem. Scand. 26* (1972) 3101.
5. Selte, K., Kjekshus, A. and Andresen, A. F. *Acta Chem. Scand. A 28* (1974) 61.
6. Kjekshus, A. and Pearson, W. B. *Prog. Solid State Chem. 1* (1964) 83.
7. Zięba, A., Selte, K., Kjekshus, A. and Andresen, A. F. *Acta Chem. Scand. A 32* (1978) 173.
8. Selte, K., Kjekshus, A., Aaby, S. and Andresen, A. F. *Acta Chem. Scand. A 29* (1975) 810.
9. Selte, K., Hjersing, H., Kjekshus, A. and Andresen, A. F. *Acta Chem. Scand. A 29* (1975) 312.
10. Kazama, N. and Watanabe, H. *J. Phys. Soc. Jpn. 30* (1971) 1319.
11. Selte, K., Kjekshus, A. and Andresen, A. F. *To be published.*
12. Selte, K., Hjersing, H., Kjekshus, A., Andresen, A. F. and Fischer, P. *Acta Chem. Scand. A 29* 1975) 695.
13. Boller, H. and Kallel, A. *Solid State Commun. 9* (1971) 1699.
14. Selte, K., Kjekshus, A., Valde, G. and Andresen, A. F. *Acta Chem. Scand. A 30* (1976) 8.
15. Selte, K., Kjekshus, A., Valde, G. and Andresen, A. F. *Acta Chem. Scand. A 30* (1976) 468.
16. Selte, K., Kjekshus, A., Peterzéns, P. G. and Andresen, A. F. *Acta Chem. Scand. In press.*
17. Selte, K., Kjekshus, A., Andresen, A. F. and Zięba, A. *J. Phys. Chem. Solids 38* (1977) 719.
18. Selte, K., Kjekshus, A., Peterzéns, P. G. and Andresen, A. F. *Acta Chem. Scand. A 30* (1976) 671.

Received September 26, 1977.

Acta Chemica Scandinavica A 32 (1978) 187–188

Short Communication

A Simplified Force Field for Glucopyranose

STEEN MELBERG * and
KJELD RASMUSSEN

Chemistry Department A, The Technical University of Denmark, Building 207, DK-2800 Lyngby, Denmark

In a former paper[1] we developed a force field for reproduction of the structures and the equilibrium distribution of α- and β-D-glucopyranoses through energy minimisation. The force field is simple and conventional: harmonic functions for bond and angle deformations, Pitzer terms for torsional motions, and Buckingham potentials for non-bonded interactions.

Some reflexions on the nature of torsional potentials (Ref. 2, p. 87) led us to the abandonment of this particular interaction. The rotation around single bonds in polyatomic molecules is truly hindered by a potential energy barrier, but only a very minor fraction of this barrier is a property of a bond which to a fair approximation is a sigma bond. The barrier arises from the interactions between charge clouds on atoms in vicinal positions to each other. Therefore a torsional term should simply not appear, leaving the hindered rotation around single bonds as the result of a pure non-bonded interaction.

The removal of torsional terms means a further simplification of our force field; yet, as we shall show, it achieves the same agreement with experimental observations. Because of technical difficulties in the complete removal of torsions, and because we wanted to keep the possibility of calculating torsional angles, the only change we made was in K_ϕ, where we use the value 0.02 kJ mol^{-1} or 0.005 kcal mol^{-1}. Otherwise the force field, called FF300, is identical to FF3 of the previous paper.[1] Minimisation in FF300 presents no problems.

In Table 1 we show deviations (calculated minus measured values) of bond lengths and angles. Comparison was made with neutron and X-ray diffraction structures of α- and β-D-glucopyranose[3,4] and of methyl-α- and -β-D-glucopyranoside, which have recently been published.[5,6] For bonds we list the anomeric bond and the maximum, mean and mean square root deviations: there is no difference from one force field to the other. For valence angles, we list the maximum, mean and mean square root deviations, with the same conclusion. For torsions, the maximum and mean square root deviations are listed: the endocyclic and hybrid torsions show a slight improvement from FF3 to FF300.

Although none of the two force fields was selected to reproduce frequencies a comparison of calculated and measured vibrational spectra might be used to test the neglect of torsional potential terms. Our programme allows for a full normal coordinate calculation (Ref. 2, p. 162) of the minimised structure, which was carried out for the two anomers in both force fields.

As expected, any significant difference is seen in the range below 500 cm^{-1}. On the other hand, no experimental data, on basis of which a choice between the two force fields can be made, are available in this frequency range, because no assignments have yet been made.

The equilibrium distributions on anomers α:β are calculated to 0.39:0.61 in FF3 and 0.37:0.63 in FF300, based on the total energy as before.[1] Using a recent addition to our programme[7] for evaluating statistical mechanical sums over the internal degrees of freedom, we find, based on the free enthalpy, the distributions 0.35:0.65 in FF3 and 0.31:0.69 in FF300. The calculations were done at 298 K and should be compared with measurements at 273 K (0.362:0.638),[8] 273 K (0.374:0.626),[8] 303 K (0.36:0.64)[9] and 308 K (0.36:0.64).[10] On this basis, FF3 is better than FF300. However, the validity of the statistical sums depends on the validity of the calculated frequencies, which, as mentioned above, cannot yet be checked.

Conclusion. The neglect of torsional potential terms leads to a very slight improvement in ring geometry and on the whole to no significant changes. In consequence, the simpler force field should be preferred in future work.

* To whom correspondence should be addressed.

1. Kildeby, K., Melberg, S. and Rasmussen, K. *Acta Chem. Scand. A 31* (1977) 1.

Table 1. Deviations of calculated values from observed internal coordinates for -D-glucopyranoses.

	FF3				FF300			
	α-Neutron[3]	Me-α-Neutron[5]	β-X-ray[4]	Me-β-X-ray[6]	α-Neutron[3]	Me-α-Neutron[5]	β-X-ray[4]	Me-β-X-ray[6]
Bond lengths, Å								
anomeric	0.036	0.024	0.039	0.044	0.036	0.024	0.039	0.044
max, others	0.019	0.048	0.019	0.014	0.019	0.048	0.019	0.014
mean, all	0.003	0.006	0.006	0.006	0.003	0.006	0.006	0.006
mean sq.rt., all	0.011	0.014	0.014	0.015	0.011	0.014	0.015	0.015
Valence angles, °								
max	4.5	−3.7	−4.4	−2.8	4.5	−3.7	−4.5	−3.1
mean	0.2	0.1	0.2	0.2	0.2	0.0	0.2	0.2
mean sq.rt.	1.6	1.7	1.8	1.5	1.6	1.7	1.7	1.5
Endocyclic torsions, °								
max	4.2	2.4	4.5	5.8	2.0	2.5	3.6	5.0
mean sq.rt.	2.4	1.4	3.2	3.4	1.3	1.9	2.5	3.1
Hybrid torsions, °								
max	3.6	6.5	4.5	5.6	3.1	7.7	3.3	4.7
mean sq.rt.	2.1	4.0	3.2	4.1	1.7	4.2	2.5	3.7
Exocyclic torsions, °								
max	165	150	120	8	174	160	121	8
mean sq.rt.	114	107			114	112		

2. Niketić, S. R. and Rasmussen, K. *The Consistent Force Field: A Documentation*, Lecture Notes in Chemistry, Vol. 3, Springer, Heidelberg 1977.
3. Brown, G. M. and Levy, H. A. *Science 147* (1965) 1038.
4. Chu, S. S. C. and Jeffrey, G. A. *Acta Crystallogr. B 24* (1968) 830.
5. Jeffrey, G. A., McMullan, R. K. and Takagi, S. *Acta Crystallogr. B 33* (1977) 728.
6. Jeffrey, G. A. and Takagi, S. *Acta Crystallogr. B 33* (1977) 738.
7. Hald, N. C. P. and Rasmussen, K. *To be published.*
8. Isbell, H. S. and Pigman, W. W. *J. Res. Natl. Bur. Stand. 18* (1937) 141.
9. Rudrum, M. and Shaw, D. F. *J. Chem. Soc.* (1965) 52.
10. Lemieux, R. U. and Stevens, J. D. *Can. J. Chem. 44* (1966) 249.

Received October 17, 1977.

Acta Chemica Scandinavica A 32 (1978) 189 – 194

The Crystal and Molecular Structure of μ-Aqua-bis(μ-dichloroacetato-*O*,*O*′)bis(dichloroacetato)bis(*N*,*N*,*N*′,*N*′-tetramethylethylenediamine)dinickel(II), $Ni_2(C_6H_{16}N_2)_2(Cl_2C_2HO_2)_4H_2O$

MARKKU AHLGRÉN, URHO TURPEINEN and REIJO HÄMÄLÄINEN

Department of Inorganic Chemistry, University of Helsinki, SF-00100 Helsinki 10, Finland

The crystal and molecular structure of the title compound has been determined from three-dimensional X-ray data. The green crystals belong to the triclinic system with $a=9.713(7)$ Å, $b=11.795(21)$ Å, $c=16.823(9)$ Å, $\alpha=79.01(11)°$, $\beta=105.19(5)°$, $\gamma=95.34(11)°$, $Z=2$. The structure was solved by the heavy-atom method and refined by block-diagonal least-squares procedures to an R value of 0.044 for 4145 independent reflections. The complex molecule is binuclear, the nickel-nickel distance being 3.657(1) Å. The nickel(II) ions are joined by a bridging water molecule and two bridging carboxylate groups, with average bond lengths of Ni – O(water) 2.132 Å and Ni – O(carboxylate) 2.048 Å. The octahedral environment around each nickel(II) ion is completed by the nitrogen atoms of the diamine molecule and the carboxyl oxygen atom of the dichloroacetate ion, the average bond lengths being 2.164 and 2.092 Å, respectively. The two noncoordinated dichloroacetate oxygen atoms form strong intramolecular hydrogen bonds with the bridging water molecule, the average O···O interaction being 2.586 Å.

This work is part of a systematic investigation of dimeric nickel(II) complexes having the general formula $Ni_2(C_6H_{16}N_2)_2(carboxylate)_4H_2O$. In previous papers five crystal and molecular structures were presented, where the carboxylate ions were acetate, chloroacetate, propionate, 2-chloropropionate or 3-chloropropionate.[1] In this paper the results of a three-dimensional X-ray structure analysis of μ-aqua-bis(μ-dichloroacetato-*O*,*O*′)bis(dichloroacetato)bis(*N*,*N*,*N*′,*N*′-tetramethylethylenediamine)dinickel(II) are reported.

EXPERIMENTAL

Preparation and analyses. $Ni_2(C_6H_{16}N_2)_2(Cl_2C_2HO_2)_4H_2O$ was prepared by adding 0.05 mol of *N*,*N*,*N*′,*N*′-tetramethylethylenediamine (Fluka AG) to an ethanol solution containing 0.05 mol of nickel(II) dichloroacetate prepared from nickel(II) carbonate (J. T. Baker) and dichloroacetic acid (Fluka AG). After several days the green crystals were filtered off, washed with water and dried in air.

Nickel was analyzed gravimetrically as nickel dimethylglyoxime. Anal. Calc. for $Ni_2(C_6H_{16}N_2)_2(Cl_2C_2HO_2)_4H_2O$: Ni, 13.35 %. Found: Ni, 13.34 %. The density, 1.598 g/cm^3, was measured by the flotation method using carbon tetrachloride and methyl iodide. The calculated value with $Z=2$ is 1.601 g/cm^3.

Space group, unit cell and intensity data. Preliminary rotation and Weissenberg photographs taken with Cu$K\alpha$ radiation ($\lambda=1.5418$ Å) showed that the crystals belong to the triclinic system, space group $P1$ or $P\bar{1}$. The latter space group was chosen and subsequent refinement indicated that this choice was the correct one.

Measurements of the unit cell parameters and reflection intensities were carried out on a Syntex $P2_1$ automatic diffractometer using graphite-monochromatized Mo$K\alpha$ radiation ($\lambda=0.71069$ Å). The crystal selected for the intensity measurements was approximately $0.25\times0.50\times0.70$ mm^3. Intensity data were collected ($5°<2\theta<48°$) at room temperature using the ω-scan technique and a scan rate varying from 2.55 to 29.3° min^{-1} depending upon the peak intensity. The intensity of one standard reflection, recorded after every 99 measurements to monitor the crystal stability, remained essentially constant throughout the data collection. Out of 5716 measured intensities 4145 were considered as ob-

served on the basis of $I > 3\sigma(I)$. The data were corrected for Lorentz and polarization effects and for absorption from ϕ-scan data. The following crystal data were obtained:

a =	9.713(7) Å	α =	79.01(11)°
b =	11.795(21) Å	β =	105.19(5)°
c =	16.823(9) Å	γ =	95.34(11)°
V =	1824.0 Å^3	Z =	2
D_m =	1.598 g/cm^3	D_c =	1.601 g/cm^3
μ(MoKα) =	16.6 cm^{-1}	Space group:	$P\bar{1}$

Table 1. Fractional atomic coordinates ($\times 10^4$, except Ni $\times 10^5$) and anisotropic thermal parameters[a] ($\times 10^3$, except Ni $\times 10^4$) for non-hydrogen atoms. Estimated standard deviations are given in parentheses.

Atom	x	y	z	U_{11}	U_{22}	U_{33}	U_{12}	U_{13}	U_{23}
Ni1	10996(7)	18875(6)	25059(4)	350(4)	259(3)	330(4)	52(3)	117(3)	−54(3)
Ni2	29137(7)	47515(6)	23908(4)	327(4)	263(3)	290(4)	52(3)	98(3)	−33(3)
N1	766(5)	271(4)	3284(3)	47(3)	35(3)	42(3)	7(2)	14(2)	−6(2)
C1	−800(7)	41(6)	3080(5)	49(4)	49(4)	77(5)	0(3)	26(4)	4(4)
C2	−1428(8)	387(6)	2160(5)	48(4)	44(4)	84(6)	−5(3)	2(4)	−7(4)
C3	1297(9)	299(6)	4200(4)	100(6)	45(4)	43(4)	13(4)	24(4)	3(3)
C4	1489(8)	−677(5)	3119(4)	69(5)	29(3)	59(4)	13(3)	22(4)	0(3)
C5	−2091(7)	2349(7)	2076(5)	42(4)	61(5)	90(6)	15(3)	18(4)	−12(4)
C6	−1371(8)	1822(7)	936(5)	56(5)	85(6)	51(4)	1(4)	−6(4)	−17(4)
N2	−1117(5)	1627(4)	1872(3)	39(3)	37(3)	52(3)	6(2)	9(2)	−9(2)
N3	4237(5)	6042(4)	3045(3)	41(3)	37(3)	34(3)	6(2)	7(2)	−8(2)
C7	5294(7)	6461(5)	2556(4)	45(4)	42(4)	57(4)	−10(3)	21(3)	−14(3)
C8	4599(7)	6551(5)	1626(4)	60(4)	42(4)	44(4)	−12(3)	29(3)	−2(3)
C9	4974(8)	5555(6)	3918(4)	61(4)	57(4)	36(4)	5(3)	−6(3)	−10(3)
C10	3406(7)	7019(6)	3079(4)	56(4)	42(4)	49(4)	−2(3)	9(3)	−21(3)
C11	5212(8)	4682(6)	1424(5)	57(4)	55(4)	67(5)	7(3)	35(4)	−15(3)
C12	3094(8)	5563(6)	561(4)	81(5)	59(4)	29(3)	7(4)	12(3)	4(3)
N4	4033(5)	5410(4)	1419(3)	46(3)	33(3)	34(3)	4(2)	13(2)	−3(2)
O1	3188(4)	1847(3)	3155(3)	41(2)	35(2)	52(3)	5(2)	4(2)	4(2)
O2	4411(4)	3551(3)	2960(3)	40(2)	31(2)	46(2)	9(2)	9(2)	4(2)
C13	4266(6)	2502(5)	3245(3)	36(3)	38(3)	29(3)	9(2)	10(2)	−4(2)
C14	5659(7)	1968(5)	3813(4)	41(3)	40(3)	43(4)	14(3)	4(3)	−1(3)
Cl1	5765(3)	2171(2)	4847(1)	109(2)	107(2)	37(1)	39(1)	−4(1)	−12(1)
Cl2	5812(2)	524(2)	3776(1)	70(1)	49(1)	93(1)	30(1)	5(1)	−10(1)
O3	562(5)	2755(3)	3329(3)	58(3)	40(2)	47(2)	−3(2)	26(2)	−17(2)
O4	1950(5)	4389(4)	3365(3)	51(3)	46(3)	49(3)	−10(2)	28(2)	−18(2)
C15	1059(6)	3660(5)	3585(4)	43(3)	31(3)	44(3)	−1(3)	18(3)	−15(3)
C16	516(9)	3978(6)	4294(5)	78(5)	57(4)	63(5)	−24(4)	42(4)	−35(4)
Cl3	782(6)	2901(3)	5172(2)	343(6)	97(2)	74(2)	8(3)	112(3)	−6(2)
Cl4	−1333(3)	4263(3)	3914(2)	82(2)	186(3)	195(3)	3(2)	62(2)	−124(3)
O5	1700(4)	1070(3)	1639(3)	53(3)	32(2)	47(2)	5(2)	27(2)	−6(2)
O6	2591(5)	2556(3)	845(3)	87(3)	28(2)	60(3)	6(2)	42(3)	−7(2)
C17	2399(6)	1519(5)	1115(3)	44(3)	32(3)	33(3)	7(3)	9(3)	−5(2)
C18	2997(7)	612(5)	762(4)	51(4)	43(4)	52(4)	10(3)	24(3)	−11(3)
Cl5	4210(3)	−232(2)	1569(1)	103(2)	77(1)	79(1)	58(1)	40(1)	21(1)
Cl6	3777(3)	1205(2)	−62(1)	114(2)	81(1)	75(1)	46(1)	62(1)	12(1)
O7	1399(4)	5962(3)	1808(3)	37(2)	35(2)	56(3)	8(2)	1(2)	−11(2)
O8	−516(5)	4975(4)	1172(3)	47(3)	33(2)	82(3)	7(2)	−13(2)	−19(2)
C19	126(6)	5851(5)	1409(4)	41(3)	31(3)	40(3)	9(2)	7(3)	−8(2)
C20	−780(6)	6922(5)	1220(4)	41(3)	33(3)	50(4)	5(3)	7(3)	−9(3)
Cl7	−1334(2)	7004(2)	2129(1)	69(1)	69(1)	91(1)	5(1)	48(1)	−19(1)
Cl8	188(2)	8218(1)	934(1)	67(1)	34(1)	67(1)	4(1)	20(1)	2(1)
O9	1507(4)	3508(3)	1775(2)	42(2)	30(2)	31(2)	9(2)	10(2)	−7(2)

[a] The anisotropic thermal parameters are of the form $\exp[-2\pi^2(h^2a^{*2}U_{11}+\ldots+2hka^*b^*U_{12}+\ldots)]$.

Structure determination and refinement. The structure was solved by the heavy-atom method. All computations in the structure determination were performed on a Univac 1108 computer using programs of the *X-Ray* 72 system.[2] The approximate positions of the nickel atoms were deduced from a three-dimensional Patterson map, and positions of other non-hydrogen atoms were located by three-dimensional Fourier syntheses.

Block-diagonal least-squares refinement was carried out on F. The function minimixed was $\Sigma w[|F_o|-|F_c|]^2$ with the weighting scheme $w=1/[45.0+|F_o|+0.005|F_o|^2]$. Scattering factors for Ni, Cl, O, N and C were taken from Cromer and Mann[3] and those for H atoms from Stewart, Davidson and Simpson.[4] Corrections for anomalous dispersion[5] were applied to the nickel and chlorine atoms.

Refinement of a model including all non-hydrogen atoms with individual isotropic thermal parameters led to an R value of 0.136 $[R=\Sigma\|F_o|-|F_c\|/\Sigma|F_o|]$. Further refinement with anisotropic thermal parameters reduced the R factor to 0.057. At this point all of the 38 hydrogen atoms were located from a difference Fourier map. Also the water hydrogen atoms were found clearly, the peaks of maximum density being 0.51 and 0.40 $e^-/Å^3$. The peaks of this height are very probably significant, since they are considerably larger than the random "noise" in the final difference Fourier map. Three more least-squares cycles were then computed with the non-hydrogen atoms assigned anisotropic and the hydrogen atoms isotropic thermal parameters. After the last cyle the final R value for 4145 observed reflections was 0.044. The C–H and the two O–H bonds thus obtained were of reasonable length (0.85–1.27 Å), the mean value being 1.00 Å.

The final atomic coordinates and thermal parameters together with their estimated standard deviations are given for the non-hydrogen atoms in Table 1 and for the hydrogen atoms in Table 2. A list of the observed and calculated structure factors is obtainable on request from the authors.

RESULTS AND DISCUSSION

The interatomic distances and angles together with their standard deviations are given in Table 3. The structure of the complex molecule, as shown in Fig. 1, is composed of two nickel(II) ions joined by one bridging water molecule and two bridging dichloroacetate ions. The octahedral environment around each nickel(II) ion is completed by the nitrogen atoms of the diamine molecule and the carboxyl oxygen atom of the monodentate dichloroacetate ion. The strong intramolecular hydrogen bonds O6···H1–O9 [O6···O9 = 2.564(7) Å, O9–H1 = 0.98(8) Å, O6···H1 = 1.63(8) Å, O6···H1–O9 = 159(6)°] and O8···H2–O9 [O8···O9 = 2.608(6) Å, O9–H2 = 0.85(8) Å, O8···H2 = 1.80(8) Å, O8···H2–

Table 2. Fractional atomic coordinates ($\times 10^3$) and isotropic temperature factors ($\times 10^2$) with their standard deviations for hydrogen atoms.

Atom	x	y	z	U	Atom	x	y	z	U
H1(C1)	−127(8)	56(6)	338(4)	7(2)	H2(C8)	525(6)	683(5)	138(3)	3(2)
H2(C1)	−113(9)	−73(7)	327(5)	9(3)	H1(C9)	426(8)	519(7)	427(5)	9(3)
H1(C2)	−251(8)	18(6)	202(4)	7(2)	H2(C9)	571(8)	617(6)	418(5)	8(2)
H2(C2)	−120(10)	−15(8)	187(6)	11(3)	H3(C9)	548(7)	493(6)	393(4)	6(2)
H1(C3)	115(6)	−54(5)	455(4)	5(2)	H1(C10)	411(6)	747(5)	342(4)	4(2)
H2(C3)	237(10)	64(8)	438(6)	13(3)	H2(C10)	255(9)	664(7)	336(5)	9(3)
H3(C3)	93(7)	96(5)	432(4)	5(2)	H3(C10)	295(5)	740(4)	256(3)	2(1)
H1(C4)	137(6)	−136(5)	349(3)	3(1)	H1(C11)	586(8)	466(6)	193(4)	8(2)
H2(C4)	265(6)	−41(5)	326(4)	5(2)	H2(C11)	488(7)	395(6)	130(4)	5(2)
H3(C4)	107(7)	−86(5)	256(4)	5(2)	H3(C11)	584(8)	500(7)	100(5)	8(2)
H1(C5)	−187(7)	227(6)	274(4)	6(2)	H1(C12)	244(8)	611(6)	50(5)	8(2)
H2(C5)	−312(7)	220(6)	176(4)	6(2)	H2(C12)	266(8)	486(6)	41(5)	7(2)
H3(C5)	−190(7)	306(6)	182(4)	5(2)	H3(C12)	347(7)	590(6)	15(4)	6(2)
H1(C6)	−73(7)	129(6)	80(4)	6(2)	H(C14)	646(7)	243(6)	371(4)	6(2)
H2(C6)	−111(10)	290(8)	79(6)	13(3)	H(C16)	101(7)	472(5)	451(4)	5(2)
H3(C6)	−240(8)	158(6)	69(5)	8(2)	H(C18)	220(8)	6(7)	51(5)	8(3)
H1(C7)	599(5)	581(4)	267(3)	2(1)	H(C20)	−165(8)	688(6)	74(5)	8(2)
H2(C7)	573(7)	722(5)	270(4)	5(2)	H1(O9)	197(7)	333(6)	137(4)	6(2)
H1(C8)	366(6)	707(5)	146(4)	5(2)	H2(O9)	71(9)	382(7)	157(5)	8(3)

Table 3. Bond lengths (Å) and angles (°) with standard deviations for non-hydrogen atoms.

The nickel environments					
Ni1 – N1	2.146(5)	N1 – Ni1 – N2	84.4(2)	N2 – Ni1 – O3	91.7(2)
Ni1 – N2	2.160(5)	N1 – Ni1 – O3	89.8(2)	N2 – Ni1 – O5	89.5(2)
Ni1 – O1	2.037(4)	N1 – Ni1 – O5	92.8(2)	N2 – Ni1 – O9	97.9(2)
Ni1 – O3	2.063(5)	O3 – Ni1 – O9	89.3(2)	N2 – Ni1 – O1	170.6(2)
Ni1 – O5	2.118(5)	O5 – Ni1 – O9	88.2(2)	O1 – Ni1 – N1	87.3(2)
Ni1 – O9	2.130(4)	N1 – Ni1 – O9	177.6(1)	O1 – Ni1 – O3	92.4(2)
		O3 – Ni1 – O5	177.3(2)	O1 – Ni1 – O5	86.8(2)
		Ni1 – O9 – Ni2	118.1(2)	O1 – Ni1 – O9	90.6(1)
Ni2 – N3	2.171(5)	N3 – Ni2 – N4	84.4(2)	N4 – Ni2 – O2	91.4(2)
Ni2 – N4	2.179(5)	N3 – Ni2 – O2	90.4(2)	N4 – Ni2 – O7	88.3(2)
Ni2 – O2	2.042(4)	N3 – Ni2 – O7	89.8(2)	N4 – Ni2 – O9	98.3(2)
Ni2 – O4	2.051(5)	O2 – Ni2 – O9	91.8(1)	N4 – Ni2 – O4	170.7(2)
Ni2 – O7	2.066(4)	O7 – Ni2 – O9	88.0(1)	O4 – Ni2 – N3	87.0(2)
Ni2 – O9	2.135(4)	N3 – Ni2 – O9	176.5(2)	O4 – Ni2 – O2	92.2(2)
		O2 – Ni2 – O7	179.6(2)	O4 – Ni2 – O7	88.0(2)
				O4 – Ni2 – O9	90.2(2)
The diamine ligand molecules					
N1 – C1	1.480(9)	Ni1 – N1 – C1	105.2(3)	Ni1 – N2 – C2	103.4(4)
N1 – C3	1.498(9)	Ni1 – N1 – C3	113.5(4)	Ni1 – N2 – C5	113.9(4)
N1 – C4	1.480(10)	Ni1 – N1 – C4	112.0(4)	Ni1 – N2 – C6	113.0(4)
C1 – C2	1.498(11)	C1 – N1 – C3	109.1(6)	C2 – N2 – C5	110.7(6)
N2 – C2	1.479(8)	C1 – N1 – C4	110.6(5)	C2 – N2 – C6	107.9(6)
N2 – C5	1.472(11)	C3 – N1 – C4	106.5(5)	C5 – N2 – C6	107.9(5)
N2 – C6	1.504(9)	N1 – C1 – C2	110.3(6)	N2 – C2 – C1	111.5(6)
N3 – C7	1.472(9)	Ni2 – N3 – C7	104.6(4)	Ni2 – N4 – C8	102.0(4)
N3 – C9	1.485(7)	Ni2 – N3 – C9	112.5(4)	Ni2 – N4 – C11	114.1(1)
N3 – C10	1.484(9)	Ni2 – N3 – C10	112.4(3)	Ni2 – N4 – C12	113.9(4)
C7 – C8	1.521(9)	C7 – N3 – C9	110.0(5)	C8 – N4 – C11	110.9(5)
N4 – C8	1.475(8)	C7 – N3 – C10	109.9(5)	C8 – N4 – C12	109.3(5)
N4 – C11	1.491(10)	C9 – N3 – C10	107.4(5)	C11 – N4 – C12	106.6(6)
N4 – C12	1.480(7)	N3 – C7 – C8	110.4(5)	N4 – C8 – C7	110.9(5)
The dichloroacetate ligand ions					
C13 – O1	1.236(7)	Ni1 – O1 – C13	138.7(4)	C13 – C14 – Cl1	107.3(5)
C13 – O2	1.249(7)	Ni2 – O2 – C13	130.4(4)	C13 – C14 – Cl2	114.6(4)
C13 – C14	1.547(8)	O1 – C13 – O2	130.0(5)	Cl1 – C14 – Cl2	111.3(3)
C14 – Cl1	1.776(7)	O1 – C13 – C14	116.3(5)		
C14 – Cl2	1.737(7)	O2 – C13 – C14	113.8(5)		
C15 – O3	1.236(7)	Ni1 – O3 – C15	131.6(5)	C15 – C16 – Cl3	112.3(5)
C15 – O4	1.238(7)	Ni2 – O4 – C15	136.5(4)	C15 – C16 – Cl4	109.0(5)
C15 – C16	1.542(11)	O3 – C15 – O4	130.5(7)	Cl3 – C16 – Cl4	110.2(5)
C16 – Cl3	1.734(7)	O3 – C15 – C16	117.4(6)		
C16 – Cl4	1.782(8)	O4 – C15 – C16	112.1(6)		
C17 – O5	1.260(8)	Ni1 – O5 – C17	127.2(4)	C17 – C18 – Cl5	110.0(4)
C17 – O6	1.237(7)	O5 – C17 – O6	128.1(6)	C17 – C18 – Cl6	113.7(4)
C17 – C18	1.540(10)	O5 – C17 – C18	112.7(5)	Cl5 – C18 – Cl6	110.7(4)
C18 – Cl5	1.757(6)	O6 – C17 – C18	119.1(6)		
C18 – Cl6	1.752(8)				
C19 – O7	1.252(7)	Ni2 – O7 – C19	131.2(4)	C19 – C20 – Cl7	108.2(4)
C19 – O8	1.233(7)	O7 – C19 – O8	128.1(6)	C19 – C20 – Cl8	112.2(4)
C19 – C20	1.542(9)	O7 – C19 – C20	116.4(5)	Cl7 – C20 – Cl8	109.2(4)
C20 – Cl7	1.772(8)	O8 – C19 – C20	115.5(5)		
C20 – Cl8	1.772(6)				

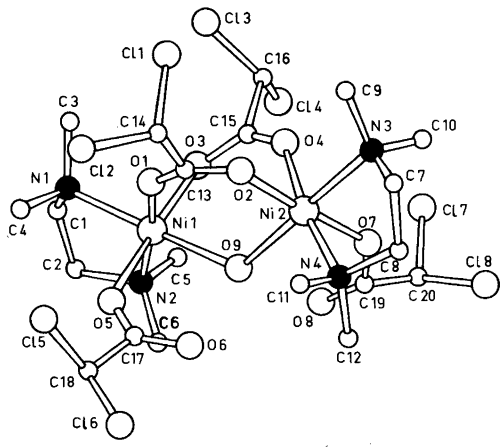

Fig. 1. Molecular structure and atom labeling scheme.

O9 = 158(8)°] formed between the bridging water molecule and the uncoordinated carboxyl oxygen atoms stabilize the complex molecule.

The complex molecules possess approximately a diad axis passing through O9 and are held in the crystal lattice by van der Waals forces. The intermolecular distances below 3.6 Å are between the atoms O6···C20^{I} [3.423(7) Å], O8···C12^{I} [3.428(8) Å], C4···C10^{II} [3.454(10) Å] and C7···Cl7^{III} [3.510(8) Å] where the equivalent position I = $(-x,1-y,-z)$, II = $(x,y-1,z)$ and III = $(1+x,y,z)$. Also these shortest C–C and C–Cl intermolecular interactions are consistent with van der Waals contact distances calculated by Bondi.[6] The structure is similar to the structures of dimeric nickel(II) carboxylate complexes with *N,N,N',N'*-tetramethylethylenediamine examined earlier by us, and selected relevant structural parameters for these complexes are presented in Table 4.

The nickel-oxygen distances of the bridging dichloroacetate ions fall within the range 2.037–2.063 Å. They are somewhat shorter than the corresponding distances of 2.066 and 2.118 Å for the nonbridging dichloroacetate ions and 2.130 and 2.135 Å for the bridging water molecule. The same trend has been found in the compared structures, as can be seen from Table 4.

The nickel–nitrogen distances vary from 2.146 to 2.179 Å, the mean value being 2.164 Å. These values are in the same range as in the compared complexes. Although the mean values seem to increase slightly with increasing basicity of the carboxylate ion, the trend is not clear-cut.

The nickel–nickel distance of 3.657 Å is about 0.1 Å greater than in the other nickel(II) dimers. This difference may be due in part to the decreased basicity of the carboxylate ligand and the steric interactions within the complex molecule. Our failure to prepare the corresponding trichloroacetate crystals in stable form is largely explained by these properties.

In dimeric copper(II) carboxylates there appears to be a slight opening of the O–C–O angle in the case of haloacetates.[7] This trend is also observable in the dimeric nickel(II) complexes. Moreover, in the present compound the O–C–O angles of the bridging dichloroacetate ions are slightly greater than those of the nonbridging ones.

Table 4. Selected relevant structural parameters[a] for $Ni_2(C_6H_{16}N_2)_2(carboxylate)_4H_2O$.

Carboxylate		Acetate	Chloro-acetate	Dichloro-acetate	Propionate	2-Chloro-propionate	3-Chloro-propionate
Ni–Ni	Å	3.563(1)	3.567(3)	3.657(1)	3.497(1)	3.566(3)	3.549(3)
Ni–N	Å	2.192(7)	2.172(12)	2.164(5)	2.191(6)	2.164(11)	2.174(15)
Ni–O(bridg. RCOO)	Å	2.037(6)	2.040(9)	2.048(5)	2.035(4)	2.028(9)	2.038(13)
Ni–O(nonbridg. RCOO)	Å	2.072(6)	2.117(9)	2.092(5)	2.109(4)	2.076(9)	2.062(13)
Ni–O(water)	Å	2.088(4)	2.088(9)	2.133(4)	2.073(4)	2.112(7)	2.109(10)
N–Ni–N	degr.	83.4(2)	84.1(4)	84.4(2)	83.8(2)	84.2(4)	84.4(5)
Ni–O(water)–Ni	degr.	117.2(2)	117.4(4)	118.1(2)	115.0(2)	114.6(5)	115.2(4)
Dihedral angle[b]	degr.	78.3	64.9	66.9	63.0	64.0	64.1
O–C–O	degr.	126.0(7)	127.7(11)	129.2(6)	126.7(6)	128.8(13)	128.1(17)

[a] When more than one chemically equivalent distance or angle is present, the mean value is tabulated. The estimated standard deviations in the parentheses are average e.s.d.'s for an *individual* distance or angle. [b] Dihedral angle refers to the angle between planes I and II presented in Table 5 and corresponding angles in the other structures.

Table 5. Deviations (Å) of atoms from least-squares planes.

Plane I: N1, N2, O1, O9				Plane II: N3, N4, O4, O9			
N1	0.049	Ni1	0.028	N3	−0.015	Ni2	−0.055
N2	−0.044	C1	0.306	N4	0.014	C7	−0.221
O1	−0.048	C2	−0.437	O4	0.015	C8	0.521
O9	0.043			O0	−0.014		
Plane III: O1, O2, C13, C14				**Plane IV: O3, O4, C15, C16**			
O1	0.003	Ni1	−0.071	O3	0.000	Ni1	0.207
O2	0.003	Ni2	0.374	O4	0.000	Ni2	−0.290
C13	−0.007	Cl1	1.699	C15	0.001	Cl3	1.343
C14	0.002	Cl2	−0.853	C16	0.000	Cl4	−1.533
Plane V: O5, O6, C17, C18				**Plane VI: O7, O8, C19, C20**			
O5	−0.006	Ni1	0.472	O7	0.005	Ni2	0.332
O6	−0.006	O9	0.227	O8	0.005	O9	0.155
C17	0.016	Cl5	1.439	C19	−0.014	Cl7	1.674
C18	−0.004	Cl6	−0.190	C20	0.004	Cl8	−1.027

The acetate groups in the dichloroacetate ligands are approximately planar but the chlorine atoms do not lie in these planes (Table 5). The C−O bond distances are equal but the O−C−C angles are nonequivalent, with the greater one located at the side of the oxygen atom nearest the α-chloro-substituents.

The dimensions of the *N,N,N',N'*-tetramethylethylenediamine ligands are as expected.[8] The diamine chelate rings are in normal unsymmetric *gauche* configuration as in the other similar nickel(II) dimers.

REFERENCES

1. a. Turpeinen, U., Ahlgrén, M. and Hämäläinen, R. *Finn. Chem. Lett.* (1977) 246; b. Turpeinen, U. *Finn. Chem. Lett.* (1976) 173; c. Ahlgrén, M., Hämäläinen, R. and Turpeinen, U. *Cryst. Struct. Commun.* 6 (1977) 829; d. Turpeinen, U. *Finn. Chem. Lett.* (1977) 36; e. Turpeinen, U. *Finn. Chem. Lett.* (1977) 123.
2. *The X-RAY System, Version of June 1972*, Technical Report TR-192, Computer Science Center, University of Maryland, College Park 1972.
3. Cromer, D. and Mann, J. B. *Acta Crystallogr. A 24* (1968) 321.
4. Stewart, R. F., Davidson, E. R. and Simpson, W. T. *J. Chem. Phys. 42* (1965) 3175.
5. *International Tables for X-Ray Crystallography*, Kynoch Press, Birmingham 1974, Vol. IV, p. 149.
6. Bondi, A. *J. Phys. Chem. 68* (1964) 441.
7. Doedens, R. J. *Prog. Inorg. Chem. 21* (1976) 227.
8. Turpeinen, U. *Ann. Acad. Sci. Fenn. Ser. A 2 182* (1977) 15.

Received October 12, 1977.

Acta Chemica Scandinavica A 32 (1978) 195 – 201

Preparations and Reactions of a Coordinatively Unsaturated Surface Compound of Nickel(II) on Silica Gel

BERND REBENSTORF

Division of Inorganic Chemistry I, Chemical Center, University of Lund, Box 740, S-220 07 Lund 7, Sweden

The preparation of a coordinatively unsaturated surface compound of nickel(II) on silica gel is described. CO, C_2H_4, NO and NO_2 are adsorbed by this compound at room temperature with an accompanying colour change. Stoichiometric measurements are explained on the basis that three (CO) or two ligands (CO, NO) can be adsorbed by one nickel(II) surface ion, which is thought to be connected to the silica gel by two oxygen ligands. The oligomerization of C_2H_2 to benzene is catalysed by this surface compound at room temperature, but the oligomerization of C_2H_4 to various hexenes was observed only at higher temperatures.

To date four divalent transition metal ions are known to bind to silica gel, presumably through two oxygen ligands. These are chromium(II),[1] manganese(II),[2] iron(II)[3] and cobalt(II).[4] A fifth member of this group, nickel(II), is described in this article.

In connection with investigations on the catalytic properties of metallic nickel on silica gel, surface compounds of nickel(II) have been described.[5] However, the samples had a rather high nickel content of 5 % or more (together with a relatively low pretreatment temperature of 500 °C) and so comparison to low-content samples as used in this work (less then 1 %) may prove difficult.

Low-content nickel(II) silica gels have been investigated by some authors.[6-10] The results[7-10] indicate that a coordinatively unsaturated surface compound of nickel(II) on silica gel may exist, but the attributed tetrahedral coordination[7] and the connection to the silica gel surface by three oxygen ligands[9,10] seems rather unlikely, compared with the properties of the other members of the group of surface compounds mentioned above.

EXPERIMENTAL

The experimental conditions were in general the same as those described in Refs. 3 and 4.

Nickel(II) samples were prepared according to Ref. 4 by impregnating silica gel "Merck 7733"[11] with nickel(II) chloride and were analysed, after destroying the silica gel with hydrofluoric acid, by dimethylglyoxime.[12]

RESULTS

After impregnation and drying at 120 °C in air the colour of the sample is light green (Fig. 1, Curve 1) due to $Ni(H_2O)_6^{2+}$ with O^h symmetry. After vacuum heat treatment at 200 °C the colour changes to yellow (Fig. 1, Curve 2), at 500 °C to brownish pink (Fig. 1, Curve 3) and at 1000 °C (Fig. 1, Curve 4) the sample has the same light green colour as after impregnation. Surprisingly, reflection spectra* of the sample vacuum heat treated at 1000 °C and that of the just impregnated and dried sample have the same two bands near 15 and 25×10^3 cm^{-1}. A third band near 7×10^3 cm^{-1} (Fig. 1, Curve 4) cannot be represented in Fig. 1, Curve 1 because of the intense water and SiOH bands (see note below).

Adsorption of C_2H_4 at room temperature to the sample with pretreatment at 1000 °C gives rise to a colour change to blue (Fig. 2, Curve 2), which, after evacuating the sample, changes to light violet blue (Fig. 2, Curve 3). This behaviour is strong evidence for a coordinatively unsaturated surface compound of nickel(II) on silica gel in this sample.

* Two sharp peaks at 7.3 and 4.5×10^3 cm^{-1} belong to overtones or combination vibrations of the SiOH surface groups.

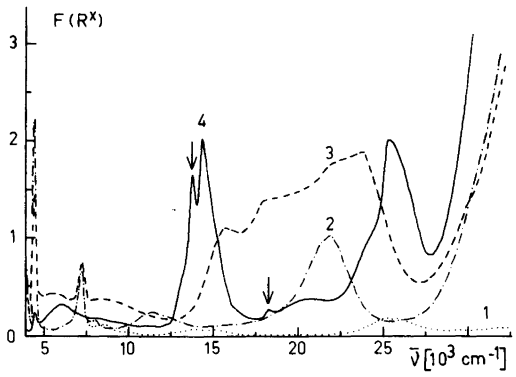

Fig. 1. Reflectance spectra of nickel-containing silica gel with vacuum heat treatment (10^{-2} Torr) at 1, 120 °C (air); 2, 200; 3, 500; 4, 1000 °C [0.6 % nickel(II)].

Adsorption of CO yields a violet compound which changes colour after a few seconds to light gray blue (Fig. 3, Curve 2) and after evacuation to light yellow (Fig. 3, Curve 3). As in the case of adsorbed C_2H_4 the above-mentioned three bands, or in these cases band groups, seem to represent the spectra.

A green compound is the result of the adsorption of NO (Fig. 4, Curve 2). Remarkably there is a difference between the spectra when NO is added directly to the coordinatively unsaturated surface compound (Fig. 4, Curve 2) or when first CO is adsorbed and then displaced by NO (Fig. 4, Curve 3).

The coordinatively unsaturated nickel(II) compound and the water complex of this compound

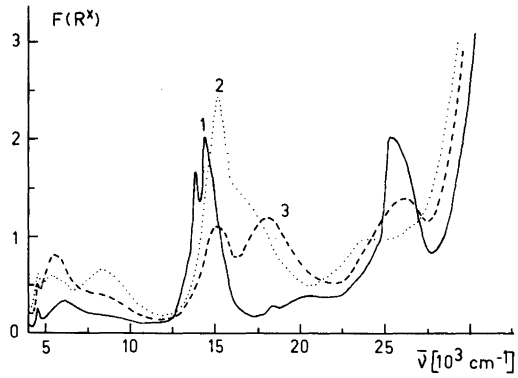

Fig. 2. Reflectance spectra of nickel-containing silica gel with vacuum heat treatment at 1, 1000 °C; 2, with adsorbed C_2H_4 at 760 Torr/20 °C; and 3, with adsorbed C_2H_4 at 1 Torr/20 °C.

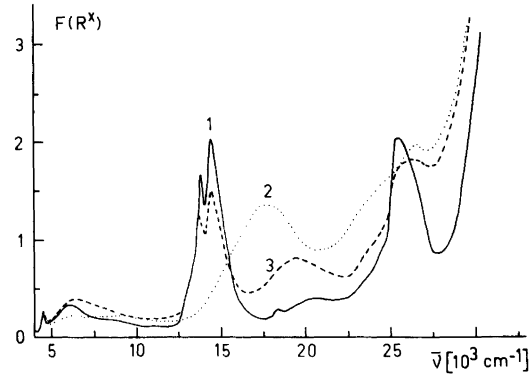

Fig. 3. Reflectance spectra as in Fig. 2 but with adsorbed CO at 2, 760 Torr/20 °C; and 3, 1 Torr/20 °C.

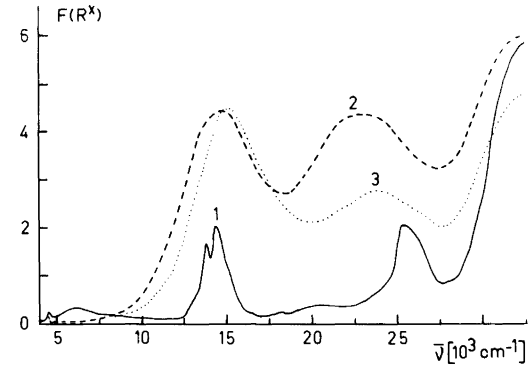

Fig. 4. Reflectance spectra as in Fig. 2 but with adsorbed NO at 2, 1 Torr/20 °C; and 3, 1 Torr/20 °C after displacing CO.

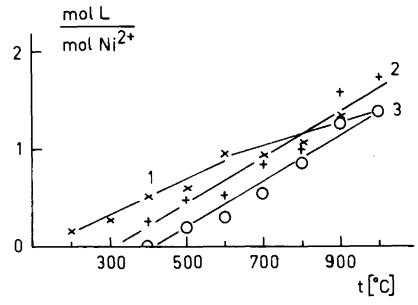

Fig. 5. Effect of the pretreatment temperature on the adsorption of NO and CO at 0 °C on the nickel-containing silica gel [0.6 % nickel(II); 1, NO/1 Torr; 2, CO/760 Torr; 3, CO/1 Torr].

(both are light green) can not be visually distinguished.

As shown before for other members of this group of surface ions[3,4] the adsorption of CO rises with increasing temperature of the vacuum heat treatment (Fig. 5). In contrast to the adsorption of NO, which shows a deviation from linearity and crosses the CO adsorption line, the latter does increase linearly when either 760 or 1 Torr are applied (Fig. 5).

The group behaviour is also apparent when the "concentration effect"[3,4] is investigated (Fig. 6), which causes samples with lower metal content to show higher ligand per metal ion ratios during adsorption of various ligands. The best results are nearly three molecules CO per nickel(II) ion at 0.3 % nickel(II) content. NO is, as is also known for chromium(II),[13] iron(II)[3] and cobalt(II),[4] at low metal ion concentrations adsorbed with a ratio of two molecules per metal ion. The same ratio is observed here with nickel(II) for CO under 1 Torr pressure. No difference in the stoichiometric ratio between NO and the nickel(II) surface ion was observed if NO was adsorbed directly by the surface ion or if CO was first adsorbed and then displaced by NO.

The "concentration effect" is explained on the basis that with rising concentration more nickel(II) ions build small metal oxide or chloride crystals which cannot react as coordinatively unsaturated compounds. With this in mind the stoichiometric ratios at low nickel(II) concentrations are thought to be the "real" values. Referring to the spectra

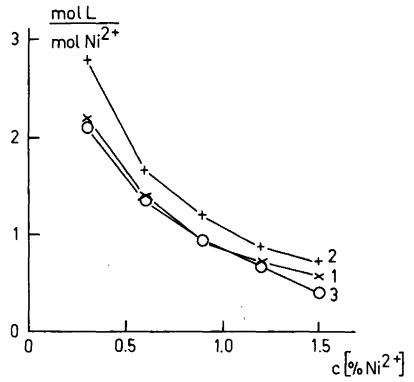

Fig. 6. Adsorption of NO and CO at 0 °C on nickel-containing silica gel with different nickel(II) concentrations (pretreatment: 1000 °C/10^{-2} Torr; 1, NO/1 Torr; 2, CO/760 Torr; 3, CO/1 Torr).

above, this gives a ratio for CO/760 Torr of three to one and for CO/1 Torr of two to one.* The latter ratio is thought to be valid also for the NO spectra. C_2H_4 displaces CO and so is bonded somewhat more strongly. This points to nearly the same or somewhat higher stoichiometric ratios at conditions similar to those of the reflectance spectra.

Adsorption of N_2 or O_2 was not detected. In contrast to the chromium(II)–NO[14] and iron(II)–NO[3] complexes the nickel(II) surface compound does not react with O_2 to yield NO_2-complexes. However, NO_2 is adsorbed to give a light green colour.

After adsorption of C_2H_2 at 760 Torr and 20 °C oligomerization to benzene (detected by mass spectrometry) was observed. A corresponding reaction with C_2H_4 was observed only at temperatures higher than 70 °C at 760 Torr together with a colour change to yellow. As products of this reaction four different hexenes were detected. In Ref. 6 butenes were reported for this reaction, but the preparation of the nickel catalyst was different there. At temperatures higher than 250 °C the colour of the sample changed to black (deposition of carbon or reduction to nickel(O)) and various C_4 and C_3 molecules were detected together with C_2H_6 and the above-mentioned hexenes.

Heating the coordinatively unsaturated nickel(II) compound in a stream of CO gave rise to a colour change to black at temperatures higher then 250 °C and metallic nickel (mirror) was deposited on the glass walls (a glass column was used as the sample container). This points to the reduction of nickel(II) to $Ni(CO)_4$, which decomposed later on the hotter glass walls.

IR spectra of CO adsorbed by the coordinatively unsaturated surface compound of nickel(II) on silica gel show only one very strong signal at 2042 cm^{-1}. On occasion two additional very weak signals at 2132 and 2192 cm^{-1} can be observed (Fig. 7). At these conditions (1 Torr/20 °C) the stoichiometric ratio is thought to be two molecules CO per metal surface ion (see above).

On heating this sample in vacuum at higher temperatures (50 and 100 °C) only the decrease of the signal at 2042 cm^{-1} was observed, but no increase in the intensities of the other two signals. This points to a direct breakdown of the CO com-

* The slight temperature difference between the stoichiometric measurements and the spectra (20 °C) introduces a small error.

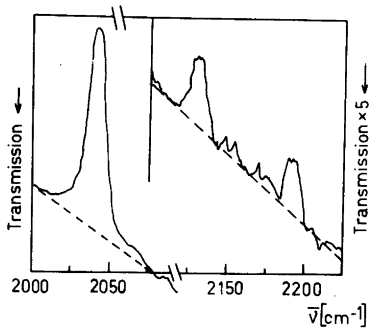

Fig. 7. IR spectrum of adsorbed CO at 20 °C/1 Torr [nickel(II) content: 0.6 %, pretreatment: 1000 °C/ 10^{-2} Torr].

plex without the other two CO complexes being involved as intermediate compounds. Samples with 1.5 % nickel and a pretreatment temperature of 500 °C showed a somewhat stronger band at 2192 cm^{-1}.

IR spectra of NO adsorbed by the nickel(II) surface compound show two signals at 1832 and 1878 cm^{-1} (Fig. 8, Curve 1). Again a difference can be seen between IR spectra when NO is directly adsorbed by the surface compound (Fig. 8, Curve 1) or when CO is adsorbed by the surface compound and then displaced by NO (Fig. 8, Curve 2). Under these conditions (1 Torr/20 °C) the stoichiometric ratio of NO per metal ion is thought to be two to one. Calculation of the angle between the two NO molecules according to Ref. 15 gives a value between 95 and 100°. IR bands at 1842 and 1872 cm^{-1} were reported for the deep green $Ni(NO)_2Cl_2$.[16] By comparison with the analogous compound of $Pd(NO)_2Cl_2$[17,18] a tetrahedral structure can be assigned to $Ni(NO)_2Cl_2$ and also (a distorted one)

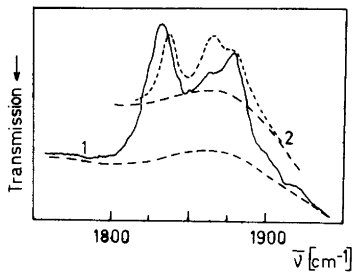

Fig. 8. IR spectra of adsorbed NO: 1, directly adsorbed; 2, after displacing CO [nickel(II) content 0.6 %; pretreatment 1000 °C, 10^{-2} Torr].

to the NO complex of the nickel(II) surface compound on silica gel. This is an important indication of four ligands around the nickel(II) surface ion, which then directly leads to the conclusion that the nickel(II) surface ion is bonded to the silica gel surface by two oxygen ligands.

DISCUSSION

The three bands observed in reflectance spectra of the sample with vacuum heat treatment at 1000 °C and that of the just impregnated and dried sample are in good agreement with the electronic spectra of octahedral nickel(II) complexes,[13] which have three spin-allowed transitions from the $^3A_{2g}$ state to the $^3T_{2g}$, $^3T_{1g}(F)$ and $^3T_{1g}(P)$ excited states, respectively [$(7-13)\times10^3$, $(11-20)\times10^3$, and $(19-27)\times10^3$ cm^{-1}]. Two spin-forbidden transitions, ^1E_g [$(11-14)\times10^3$ cm^{-1}] and $^1T_{2g}$[$(18-21)\times10^3$ cm^{-1}], are often observed. These are evident in the spectrum of the sample with vacuum heat treatment at 1000 °C (Fig. 1/4, near 14 and 18×10^3 cm^{-1}) (arrows). This indicates that the above spectrum arises from nickel(II) ions. However, as will be shown below, the actual symmetry must be C_{2v} and the actual coordination number is thought to be only two in the case of the sample with vacuum heat treatment at 1000 °C.

A model for the coordinatively unsaturated transition metal ions on silica gel with oxidation- and coordination-number two has been proposed before.[19,4] The reactions which may occur during the vacuum heat treatment were discussed in Refs. 3 and 4 and can be applied also to the nickel(II)/silica gel system.

Comparing the IR absorptions of the CO complexes with other coordinatively unsaturated surface compounds reveals a strong difference to the one observed above at 2042 cm^{-1} for nickel(II). So for chromium(II) a band at 2186,[20] for iron(II) at 2165[3] and for cobalt(II)[4] two bands at 2170 and 2184 cm^{-1} were observed and ascribed to CO metal ion ratios of 2:1 or 1:1 [iron(II)]. These bands all have higher wavenumbers than gaseous CO (2143 cm^{-1}). Only the very weak band at 2192 mentioned above would fit compared with the CO complexes of the other three surface compounds. High content nickel/silica gel systems[5] have a strong CO band near 2195 cm^{-1} after vacuum heat treatment at 500 °C and show bands near 2130 and 2050 cm^{-1} after reduction with hydrogen at that temperature. Consequently the IR bands are assigned to surface

compounds of nickel(II), nickel(I) and nickel(O), respectively.

Two arguments suggest that this explanation will not explain the observations stated above for the CO complex of the nickel(II) surface compound: 1, If $Ni(CO)_4$ is produced, it should leave the silica gel surface under vacuum and higher temperature (100 °C). This was not observed. Also $Ni(CO)_4$ was not detected in the gas phase above the samples under vacuum by mass spectrometry; 2, Nickel(0) is a d^{10} electronic system, which means that it has no allowed $d-d$ transitions and so should show no bands below 25×10^3 cm^{-1} [$Ni(CO)_4$ is colourless]. However, the spectra of CO adsorbed at the nickel(II) surface compound show bands in this region.

With four ligands, two oxygen ligands from the silica gel surface and two CO ligands, around the surface metal ion, three different configurations are possible: 1, tetrahedral; 2, *cis* square-planar (Fig. 12a); 3, *trans* square-planar (Fig. 12b). It is a well-established law of ligand field theory that the separation of the energy states in tetrahedral complexes is 4/9 of the separation in octahedral complexes.[21] So if the CO complexes had tetrahedral configurations the bands of the electronic spectra should be shifted to lower wavenumbers. This is not observed for the CO complexes of chromium(II),[22] iron(II)[3] and cobalt(II)[23] surface compounds on silica gel, so that only the two square-planar configurations are left.

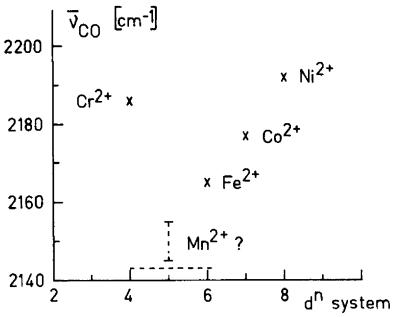

Fig. 9. IR absorptions of CO adsorbed by transition metal ion surface compounds *versus* number of d electrons of the metal ions.

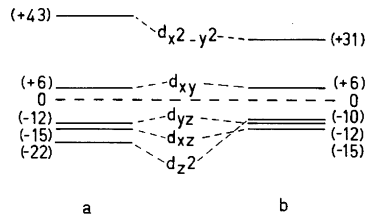

Fig. 10 . Splitting of d orbitals derived from Fig. 9 with the baseline at a, 2143 cm^{-1} and b, 2155 cm^{-1}. The numbers in brackets are the relative distance from zero in cm^{-1}.

In Fig. 9 the position of the IR bands from the CO complexes with the surface compounds (Cr, 2186; Fe, 2165; Co, 2177 (arithmetic mean value of 2170 and 2184), Ni: 2192 cm^{-1}) are shown *versus* the number of d electrons. With the assumption that the wavenumber of the gaseous CO can be used as the base line, this figure resembles the variation of the ligand field stabilisation energy when drawn for different d electron systems surrounded by a square-planar ligand field.[24]

In Fig. 10a the splitting of the d orbitals as derived from Fig. 9 (base line: gaseous CO) is shown. Again a correspondence with the diagram of the d orbitals split by a square-planar ligand field as shown in Refs. 21 and 24 can be seen. The fact that the manganese(II) surface compound binds the CO molecules only very weakly [2] can be explained by the d^5 electronic system of manganese(II) and so fits well in the above figures.

The assumption that the CO frequency can be used as a quantitative measure of the bond strength between the CO molecules and the surface compound is supported by Fig. 11. From preliminary adsorption measurements[23] it can be concluded that the IR absorption of CO adsorbed by the

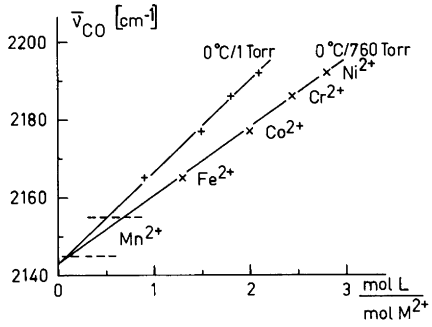

Fig. 11. IR absorptions of CO adsorbed by transition metal ion surface compounds *versus* ratio of adsorbed CO per metal ion (metal content: around 0.3 %). Fe, Co and Ni see Refs. 3, 4 and this paper. Chromium content: 0.3 %, oxydation number: 2.2, preparation see Ref. 34, absorption of CO see Ref. 23).

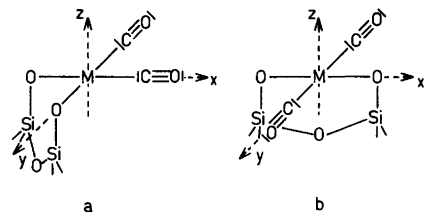

Fig. 12. Model of CO complexes with the transition metal ion surface compounds for a, *cis* and b, *trans* square-planar configuration.

manganese(II) surface compound may lie between 2145 and 2155 cm^{-1}. With the latter value Fig. 10b is redrawn from Fig. 10a, but no substantial difference can be seen between the two figures.

Referring to Fig. 12a a deformation of the (not drawn) d_{xy}, d_{xz} and the d_{yz} orbitals can be assumed on the basis of the electronegativity difference of the oxygen ligands and the metal ions. Together with the low electronegativity difference between the metal ion and the carbon of CO and the relatively high positive charge of two compared with other metal carbonyls this may lead to an electron decrease for the d_{xy}, d_{xz} and the d_{yz} orbitals oriented towards the CO molecules. This can explain why weak or no back donation at all from the metal to the CO is observed with chromium(II), [manganese(II)], iron(II) and cobalt(II) if one assumes a *cis* square-planar configuration.

A third ligand in the z direction can use partly electrons from the deformed d_{xz} or d_{yz} orbitals for back donation and so may have wavenumbers below that of gaseous CO.[20,25]

Referring to Fig. 12b a deformation of the d_{xy} and the d_{xz} orbitals may be assumed, with only weak deformation of the d_{yz} orbital. The two CO ligands can now share the two electrons, each receiving one in the case of a d^8 electronic system [nickel(II)], assuming a splitting as shown in Fig. 10a. This provides for a back donation and can explain the observed CO stretching frequency of 2042 cm^{-1}. That this back donation is only observed for the nickel(II) surface compound may be due to the half filled d_{yz} orbital in the case of the other four metal ions and to the smaller ion radius of the nickel(II).[24]

A *trans* square-planar configuration for the nickel(II) CO complex explains also the fact that only one IR signal is found. Fig. 11 supports the assumption that the actual energies of the *cis* and the *trans* square-planar configuration are not very different. The two IR signals for CO adsorbed by the cobalt(II) surface compound support on the other hand a *cis* square-planar configuration. The single IR absorption for the CO complex with iron(II) may be explained by the stoichiometry of one CO molecule per metal ion.[3]

On samples with high nickel content and low pretreatment temperatures a transformation from a *cis* to a *trans* square-planar configuration may be prevented.

The model of a *cis* or *trans* square-planar configuration may also help to explain the rather complicated IR spectra of CO adsorbed by the surface compound of chromium(II).[20] As stated above the peak of this signal is at 2186 cm^{-1} but two shoulders are also observed at 2181 and 2191 cm^{-1}. After evacuation the main signal decreases but the shoulders remain nearly unchanged.

The IR band with the peak at 2186 cm^{-1} may be assigned to a CO complex with a *trans* square-planar configuration because the peak was recorded under conditions (40 Torr/CO pressure) where two CO molecules are bonded to the chromium(II) surface compound (Fig. 11). The two bands at 2191 and 2181 cm^{-1} may be assigned to a *cis* square-planar configuration and can be compared with those of the cobalt(II) surface compound[4] at 2184 and 2170 cm^{-1}: The two signals have in both cases nearly equal intensities, which means an angle of 90° between the two CO ligands according to Ref. 15 and the splitting in each case, 10 and 14 cm^{-1}, is very similar.

It is known that of the total amount of the chromium(II) surface compound only 5 to 20 %[26-28,30] reacts as the catalytic center of the polymerization of C_2H_4, which is thought to be the catalytic reaction of the Phillips process.[29] Now the intensity of the two IR bands at 2191 and 2181 cm^{-1} is just around 20 % of the total intensity when the peak at 2186 cm^{-1} has its highest intensity.[20] On this basis the chromium(II) surface compound which forms the CO complex with the two IR bands may be the precursor of the catalytic center for the polymerization of C_2H_4, which may start with the oxidative cyclo-addition of two C_2H_4 molecules.

The missing link between the CO complex and the starting mechanism of the polymerization, the C_2H_4 adsorption with the formation of a *cis* square-planar complex with the chromium(II) surface compound, although yet not proved, is easy to imagine as C_2H_4 complexes are known with all five metal ion surface compounds on silica gel.[2-4,30]

The model for the coordinatively unsaturated transition metal ions on silica gel with the oxidation- and coordination-number two implies that four ligands can be adsorbed to raise the coordination number of the metal ion to six. Four different types of ligands can be distinguished by their behaviour during adsorption:

1. Ligands with stoichiometric ratios of one molecule to one metal ion, for instance chelate ligands.[31]

2. Ligands with stoichiometric ratios of 2:1, for example NO.

3. Ligands with the stoichiometric ratio of up to three to one or even four to one such as CO (or C_2H_4). With these ligands a more or less linear increase in the ligand/metal ion ratio is observed with decreasing temperature and increasing pressure.[30]

4. Ligands with the stoichiometric ratio of up to 4:1 such as H_2O or NH_3 [32] but with a discrete step at the 2:1 ratio.

After adsorbing less than four ligands the free coordination sites can be occupied by other ligands to yield mixed ligand complexes. This is especially well-established for NO as the first two ligands and various other ligands adsorbed thereafter, such as CO, H_2O, NH_3 *etc.*[33] (but not NO).

Acknowledgement. This work was made possible by a stipend from the Deutsche Forschungsgemeinschaft. The author thanks Dr. R. Larsson for valuable discussions.

REFERENCES

1. Krauss, H. L. and Stach, H. *Z. Anorg. Allg. Chem. 366* (1969) 34.
2. Möseler, R. *Diss.*, Freie Universität Berlin, Berlin 1976.
3. Rebenstorf, B. *Acta Chem. Scand. A 31* (1977) 547.
4. Rebenstorf, B. *Acta Chem. Scand. A 31* (1977) 208.
5. Peri, J. B. *Discuss. Faraday Soc. 42* (1966) 121.
6. Anderson, J. H. *J. Catal. 26* (1972) 277.
7. Kaverinskii, V. A., Borovkov, V. Yu., Shvets, V. A. and Kazanskii, V. B. *Kinet. Catal. USSR 15* (1974) 819, Engl. 739.
8. Borovkov, V. Yu. and Kazanskii, V. B. *Kinet. Catal. USSR 15* (1974) 1283, Engl. 1136.
9. Kazansky, V. B., Borovkov, V. Yu. and Zhidomirov, G. M. *J. Catal. 39* (1975) 205.
10. Borovkov, V. Yu., Kaverinsky, V. A. and Kazansky, V. B. In Delmon, B. and Jannes, G., Eds., *Catalysis, Heterogeneous and Homogeneous*, Elsevier, Amsterdam 1975, p. 253.
11. Krauss, H. L. and Naumann, D. *Z. Anorg. Allg. Chem. 430* (1977) 23.
12. Snell, F. D. and Snell, C. T. *Colorimetric Methods of Analysis*, D. van Nostrand, Princeton 1959, pp. 55, 263.
13. Lever, A. B. P. *Inorganic Electronic Spectroscopy*, Elsevier, Amsterdam 1968.
14. Krauss, H. L. and Weisser, B. *Z. Anorg. Allg. Chem. 412* (1975) 82.
15. Beck, W., Melnikoff, A. and Stahl, R. *Chem. Ber. 99* (1966) 3721.
16. Iqbal, Z. and Waddington, T. C. *J. Chem. Soc. A* (1969) 1092.
17. Griffith, W. P., Lewis, J. and Wilkinson, G. *J. Chem. Soc.* (1959) 1775.
18. Manchot, W. and Waldmuller, A. *Ber. Dtsch. Chem. Ges. 59* (1926) 2363.
19. Krauss, H. L. *Proc. Int. Congr. Catal. 5th 1972, 1* (1973) 207.
20. Zecchina, A., Garrone, E., Ghiotti, G. and Coluccia, S. *J. Phys. Chem. 79* (1975) 972.
21. Cotton, F. A. and Wilkinson, G. *Advanced Inorganic Chemistry*, Interscience, New York 1972.
22. Krauss, H. L., Rebenstorf, B., Westphal, U. and Schneeweiss, D. In Delmon, B., Jacobs, P. A. and Poncelet, G., Eds., *Preparation of Catalysts*, Elsevier, Amsterdam 1976, p. 489.
23. Rebenstorf, B. *Unpublished results.*
24. Schläfer, H. L. and Gliemann, G. *Einführung in die Ligandenfeldtheorie*, Akademische Verlagsgesellschaft, Frankfurt 1967.
25. Schmidt, H. *Diss.*, Technische Universität München, München 1973.
26. Eden, C., Feilchenfelder, H. and Haas, Y. *J. Catal. 11* (1968) 263.
27. Hogan, J. P. *J. Polym. Sci. 8* (1970) 2637.
28. Krauss, H. L. and Schmidt, H. *Z. Anorg. Allg. Chem. 392* (1972) 258.
29. Clark, A., Hogan, J. P., Banks, R. L. and Lanning, W. C. *Ind. Eng. Chem. 48* (1956) 1152.
30. Rebenstorf, B. *Diss.*, Freie Universität Berlin, Berlin 1975.
31. Hierl, G. and Krauss, H. L. *React. Kinet. Catal. Lett. 3* (1975) 47.
32. Hierl, G. and Krauss, H. L. *Z. Anorg. Allg. Chem. 401* (1973) 263.
33. Zecchina, A., Garrone, E., Ghiotti, G. and Coluccia, S. *J. Phys. Chem. 79* (1975) 984.
34. Rebenstorf, B., Larsson, L. and Larsson, R. *Acta Chem. Scand. A 31* (1977) 877.

Received October 12, 1977.

Acta Chemica Scandinavica A 32 (1978) 203 – 208

Substituted Propanes. XIII. The Vibrational Spectra of 2,2-Dichloropropane-d_6

P. KLÆBOE,[a] A. P. MATHER[a] and B. N. CYVIN[b]

[a] Department of Chemistry, University of Oslo, Oslo 3, Norway and [b] Division of Physical Chemistry, University of Trondheim, N-7034-NTH Trondheim, Norway

The infrared spectra of 2,2-dichloropropane-d_6 as a vapour, liquid and crystalline solid at −180 °C were recorded in the region 4000 – 200 cm^{-1}. Raman spectra of the liquid were obtained and polarization data presented.

The fundamental frequencies have been assigned in terms of C_{2v} symmetry. A normal coordinate analysis reproduced the fundamentals of 2,2-dichloropropane and the d_6-derivative satisfactorily. The assignments for the parent molecule were slightly changed on the basis of this work.

We have been interested in halogenated propanes for some time and have reported the vibrational spectra of certain 2-halopropanes[1-3] and 2,2-dihalopropanes[4] as well as force fields derived for these molecules.[5,6] Since the spectra of isopropylhalides are not complicated by the conformational equilibria present in the propyl halides, they can therefore be interpreted with some confidence. The spectra of 2,2-difluoropropane were published by Crowder and Jackson[7] who also derived a force field for this compound.

The spectra of 2,2-dichloropropane were reinvestigated by Green and Harrison[8] (hereafter referred to as GH) who changed some of the earlier[4] assignments.

Since the fully deuterated molecule 2,2-dichloropropane-d_6 is now commercially available, we decided to study its spectrum. We hoped that these data would be useful for developing a more reliable force field which might settle some of the controversial assignments for the parent molecule.

EXPERIMENTAL

The sample of 2,2-dichloropropane-d_6 was a commercial product from Merck, Sharp & Dohme of Canada Limited, investigated without purification. No impurity peaks were detected by gas chromatographic analysis. The isotopic purity was high since no IR or Raman bands were observed which could be attributed to C – H stretch. Moreover, the most intense IR vapour bands at 1119 and 669 cm^{-1} of the parent compound[4,8] were not detected in the spectra of the fully deuterated species.

The infrared spectra were recorded in the region 4000 – 200 cm^{-1} with a Perkin-Elmer model 225 spectrometer. Vapour cells with windows of KRS-5 and CsI had path lengths of 1 m and 10 cm, respectively. Sealed cells having KBr and CsI windows were used for the liquid, while a conventional cryostat with CsI windows was employed for the crystalline solid at −180 °C.

Raman spectra of the liquid were obtained with a modified[9] Cary 81 spectrometer using the 5145 and 4880 Å lines from an argon ion laser (CRL 52 G) for excitation.

SPECTRAL INTERPRETATION

2,2-Dichloropropane-d_6. The present compound, obviously has C_{2v} symmetry like the parent molecule. Assuming tetrahedral angles and the bond distances: C – C = 1.54, C – D = 1.09 and C – Cl = 1.795 Å we calculated the following principal moments of inertia: $I_A = 170.57$, $I_B = 228.06$ and $I_C = 260.06$ a.m.n. Å.[2] Since the orientation of the I_A, I_B and I_C axes were parallel with those of the parent molecule[4] the various IR active fundamentals should have the same rotational contours for both molecules. The *PR* sparations were esti-

Table 1. Infrared and Raman spectral data for 2,2-dichloropropane-d_6.

Infrared			Raman	Assignments
Vapour	liquid	Solid (−180 °C)	liquid	
2960 vw	2960 vw	2960 vw	2962 vw	
2430 vw		2405	2395 vw	
2258 m, 2252 s	2265	2265	2264 m,P	ν_1 a_1 fund
	2246 s	2252	2247 s,D	ν_{22} b_2 fund
2248 m, 2242 s, 2235 w C	2238 s	2249, 2239	2242, m,D	ν_{15} b_1 fund
			2215 w,D	ν_{10} a_2 fund
2160 m	2151	2155		
2153 m	2142	2140	2142 m,P	A_1 comb
2131 m	2122		2122 vs,P	ν_2 a_1 fund
2118 m	2110		2111 s,P	A_1 comb FR
2109, 2101 m, 2092 C?	2093		2095 w,D	ν_{16} b_1 fund
2077 w	2070	2065	2069 w,P	A_1 comb
2025 w	2015		2022 w,P	A_1 comb
1288 w	1275	1280		
1212 m, 1207 s, 1205 vs, 1203 s, 1202 s, 1200 s, 1194 m C	1200	1205, 1198	1204 w,D	ν_{17} b_1 fund hot bands
1143 s, 1138 s, 1135 s, 1129 s B	1127	1132	1134 m,P	ν_3 a_1 fund
1113 w, 1105 w, 1097 w	1105	1108, 1090	1108 vw	ν_{23} b_2 fund
			1068 vw	ν_{11} a_2 fund
	1056 w	1055		
1062 s, 1052 s, 1048 s A	1048	1058, 1045	1049 m,D	ν_{24} b_2 fund
1042 s C	1037	1035	1037 w	ν_{18} b_1 fund
1023 s, 1016 s, 1013 s, 1006 s B	1005	1011, 1005	1011 vs,P	ν_4 a_1 fund
980 vs, 973 vs, 962 s C?	963	952	963 m,P	ν_5 a_1 fund
932 s, 920 vs, 914 s C	922	919	924 vw	ν_{19} b_1 fund
852 m	839			
830 m,C	826	827		

Table 1. Continued.

822 m 813 w 788 s		806			
782 s 779 s 772 s	B	778	785 780	782 s,P?	ν_6 a_1 fund
				744 w	ν_{12} a_2 fund
750 w 739 m 732 w	C	736	740		ν_{20} b_1 fund
654 s 649 s 646 s 638 s	B?	648	668 652		*A* comb?
618 vs 610 vs 602 vs	A	598	604 582	598 vs,D	ν_{25} b_2 fund
538 s 530 s 527 m 520 s	B	526	530 523 520	525 vs,P	ν_7 a_1 fund
485 vw		482	470	487 vw	
450 w			455	430 vw?	
359 m 350 m 341 m	C	350	353	352 w	ν_{21} b_1 fund
329 w 322 w 319 w 313 w	B	325	324	327 s,P	ν_8 a_1 fund
302 w		291		290 vw	ν_{26} b_2 fund
				252 s,D	ν_{13} a_2 fund
240 m		245	250	244 m,P?	ν_9 a_1 fund
		204 vw	205 m	204 vw	ν_{27} b_2 fund

[a] The weak infrared and Raman bands in the regions 5000 – 2400 cm^{-1} and 2000 – 1300 cm^{-1} are omitted. [b] Abbreviations: s, strong; m, medium; w, weak; v, very; P, polarized; D, depolarized; A, B and C denote vapour contours.

mated[10] to be 14, 16 and 18 cm^{-1} for *A* (b_1), *B* (a_1) and *C* (b_2) contours, respectively.

Many of the observed vapour contours were well resolved, while others were more diffuse and not as valuable for the assignments as in the parent molecule. The Raman polarization data are very useful for determining the polarized a_1 modes, but cannot differentiate between the b_1 and b_2 modes. Moreover, the IR inactive a_2 fundamentals are often very weak in the Raman spectra and their identification therefore uncertain.

The actual IR and Raman spectral curves are not reproduced for the sake of brevity, but the wave numbers for the observed bands are listed in Table 1. In Table 2 the assigned fundamentals are collected together with the results of the normal coordinate calculations.

The nine fundamentals of species a_1 can be assigned with considerable confidence to strongly polarized Raman bands of generally high intensities at 2264, 2122, 1134, 1011, 525 and 327 cm^{-1} while those at 963, 782 and 244 cm^{-1} were only slightly polarized. Generally, these Raman bands corresponded to infrared bands with prominent *B*-contours in the vapour, such as 1136, 1014, 780, 528 and 320 cm^{-1} which had the expected *PR* as well as the *QQ* splitting. Exceptions were the vapour bands around 973 cm^{-1} which had a sharp *Q*-branch

Table 2. Observed and calculated fundamental frequencies (in cm^{-1}) for 2,2-dichloropropane-d_6.

Species	No.	Obs.[a]	Calc.	Potential energy distribution[b]	Approximate motions
a_1	ν_1	2252	2250	$97(s-t)$	CD_3 as.str.
	ν_2	2131	2131	$97(s+t)$	CD_3 sym.str
	ν_3	1136	1169	$52r+33\gamma^+$	C−C str.
	ν_4	1014	1023	$85\gamma^-$	CD_3 as.bend
	ν_5	973	981	$43\gamma^+ + 23(\varepsilon-\delta)+23\alpha$	CD_3 sym.bend
	ν_6	781	764	$47(\varepsilon-\delta)+21r$	CD_3 rock
	ν_7	528	523	$44d+26r$	C−Cl str.
	ν_8	320	315	$112\beta+90\alpha$	mixed
	ν_9	240	247	$31\beta+22\alpha$	
a_2	ν_{10}	2215[c]	2223	$98(s-t)$	CD_3 as.str.
	ν_{11}	1068[c]	1061	$90\gamma^-$	CD_3 as.bend
	ν_{12}	744[c]	766	$91(\varepsilon-\delta)$	CD_3 rock
	ν_{13}	252[c]	248	92β	ClCC bend
	ν_{14}	–	203	83τ	torsion
b_1	ν_{15}	2242	2237	$98(s-t)$	CD_3 as.str.
	ν_{16}	2101	2116	$97(s+t)$	CD_3 sym.str.
	ν_{17}	1205	1233	$65r+19\gamma^+$	C−C str.
	ν_{18}	1042	1038	$90\gamma^-$	CD_3 as.bend
	ν_{19}	920	917	$66\gamma^+$	CD_3 sym.bend
	ν_{20}	739	738	$72(\varepsilon-\delta)$	CD_3 rock
	ν_{21}	350	351	$72\beta+17r$	ClCC bend
b_2	ν_{22}	2246[d]	2238	$98(s-t)$	CD_3 as.str.
	ν_{23}	1105[d]	1101	$41(\varepsilon-\delta)+21\beta+21d$	CD_3 rock
	ν_{24}	1052	1044	$81\gamma^-$	CD_3 as.bend
	ν_{25}	610	586	$54(\varepsilon-\delta)+48d$	C−Cl str.
	ν_{26}	302	304	$49\beta+28d+22\tau$	ClCC bend
	ν_{27}	204	200	66τ	torsion

[a] Infrared vapour values except when noted. [b] Terms below 15 are omitted. [c] Raman liquid values. [d] Infrared liquid values.

suggesting *C*-contour.

Our remaining four a_1 fundamentals had vapour contours which were ill-defined and of no aid to the assignments. Some additional Raman bands appeared polarized (*e.g.* at 2142, 2111, 2069 and 2022 cm^{-1}) which could all be explained as combination bands or overtones of species A_1.

The a_2 fundamentals ($\nu_{10}-\nu_{12}$) were assigned to the weak or very weak Raman bands at 2215, 1068, 744 with unknown polarization ratios. Since the 2215 and 744 cm^{-1} bands were 23 and 8 cm^{-1} removed from IR liquid bands they are not as definite choices for a_2 as would be preferred. A strong, depolarized Raman band at 252 cm^{-1} appears as a good choice for ν_{13}. No likely Raman band was observed for the CD_3 torsional mode ν_{14}.

Vapour bands, having *C*-type contours with sharp central *Q*-branches were observed at 2242, 2101, 920, 739 and 350 cm^{-1} and should therefore be assigned as b_1-modes. The polarization ratios for some of the Raman counterparts were not known because of low intensities. The sharp peaks commencing at 1207 cm^{-1} with 2 cm^{-1} spacing and diminishing intensities apparently form a hot band progression of the *Q*-branches. A very sharp band at 1042 cm^{-1} is apparently the central branch of a *C*-type band but the contours are obscured by the neighbouring *A*-type band. As mentioned previously, the a_1 modes at 973 and 530 cm^{-1} have contours more like *C* than *B*, but the polarized Raman counterparts rule out the possibility for b_1-modes.

Vapour bands with definite *A*-contours were

Table 3. Observed and calculated fundamental frequencies (in cm^{-1}) for 2,2-dichloropropane.

Species	No.	Obs.	Calc.	Potential energy distribution[a]	Approximate motions
a_1	ν_1	3010	3012	$99(s-t)$	CH_3 as.str.
	ν_2	2943	2943	$99(s+t)$	CH_3 sym.str.
	ν_3	1440	1427	$85\gamma^- + 16(\varepsilon-\delta)$	CH_3 as.bend
	ν_4	1391	1360	$86\gamma^+ + 16r$	CH_3 sym.bend
	ν_5	1163	1163	$57(\varepsilon-\delta)+20\alpha$	CH_3 rock
	ν_6	915	937	$48r+17d$	C–C str.
	ν_7	562	575	$44d+26r+19\alpha$	C–Cl str.
	ν_8	359	358	$112\beta+89a+18d$	mixed
	ν_9	258	249	$34\beta+20\alpha$	mixed
a_2	ν_{10}	*2990*[b]	2978	$99(s-t)$	CH_3 as.str.
	ν_{11}	1447	1470	$88\gamma^-$	CH_3 as.bend
	ν_{12}	*1020*[c]	1000	$90(\varepsilon-\delta)$	CH_3 rock
	ν_{13}	*287*	294	$67\tau+20\beta$	torsion
	ν_{14}	–	269	$78\beta+19\tau$	ClCC bend
b_1	ν_{15}	2993	3000	$99(s-t)$	CH_3 as.str.
	ν_{16}	2943	2922	$99(s+t)$	CH_3 sym.str.
	ν_{17}	1453	1457	$83\gamma^-$	CH_3 as.bend
	ν_{18}	1377	1352	$64\gamma^+ + 30r$	CH_3 sym.bend
	ν_{19}	1119[c]	1121	$27\gamma^+ + 27r + 27(\varepsilon-\delta) + 16\beta$	mixed
	ν_{20}	954	954	$58(\varepsilon-\delta)+25r$	CH_3 rock
	ν_{21}	388	387	$77\beta+17r$	ClCC bend
b_2	ν_{22}	*2993*[c]	2998	$99(s-t)$	CH_3 as.str.
	ν_{23}	1463	1480	$83\gamma^-$	CH_3 as.bend
	ν_{24}	*1192*[b]	1198	$51(\varepsilon-\delta)+19\beta$	CH_3 rock
	ν_{25}	669	704	$52r+35(\varepsilon-\delta)+28\beta$	C–Cl str.
	ν_{26}	*359*[c]	339	$41\tau+32d+29\beta$	mixed
	ν_{27}	–	271	$44\tau+28\beta$	torsion + ClCC bend

[a] Terms below 15 are omitted. [b] In variance with Ref. 4 and GH Ref. 8. [c] According to GH, Ref. 8, in variance with Ref. 4.

observed at 1052 and 610 cm^{-1}, most certainly the b_2-fundamentals ν_{24} and ν_{25}. The remaining modes of this symmetry species are more uncertain; thus ν_{22} was assigned to the strong bands at 2246 cm^{-1} (IR liquid) and 2247 cm^{-1} (Raman), overlapping ν_1 and ν_{15} in the vapour phase. A weak IR vapour band at 1105 cm^{-1} with possible *A*-contour appeared as a shoulder on the intense ν_3, but having a very weak Raman couterpart was assigned as ν_{23}. The two low frequency b_2 fundamentals ν_{26} and ν_{27} are tentatively attributed to the weak IR bands at 302 cm^{-1} (vapour) and 204 cm^{-1} (liquid), respectively, both having very weak Raman counterparts.

2,2-Dichloropropane. From the force field developed for these molecules (see below) and from spectral analogies with the fully deuterated compound, we have revised the assignments for the parent molecule. The fundamentals which are revised compared to our earlier assignments are written in italics in Table 3, in many cases they agree with those of GH.[8] No revisions were made for the a_1 modes ($\nu_1-\nu_9$). The CH stretch of species a_2 was reassigned to the depolarized Raman band at 2990 cm^{-1} which overlaps ν_{15} as a consequence of the force constant calculations. The Raman band at 2908 cm^{-1} previously[4] assigned as ν_{15} can be explained as $\nu_{17}+\nu_{23}$. Moreover, we agree with GH's[8] attributions of the Raman bands at 1020 and 287 cm^{-1} as ν_{12} and ν_{13}, respectively, while the torsional mode ν_{14} remains unobserved.

Among the b_1 fundamentals all our previous assignments[4] were supported by the force field calculations. Since the CH_3 rocking mode of species b_2 according to the calculations is expected at higher

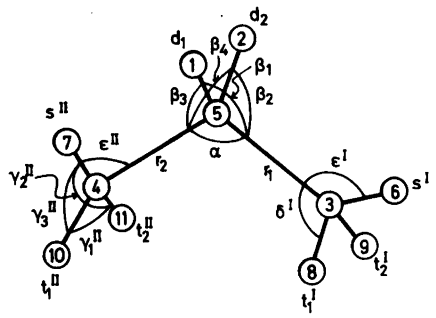

Fig. 1. Definition of the valence coordinates for the propane molecular model. r, d, s and t are stretchings. The γ type bendings are shown only for the methyl group II while the δ's are exemplified by δ_1^I only. The torsions τ_1 and τ_2 (not shown on the figure) involve the atoms 6-3-5-4 and 7-4-5-3, respectively.

wavenumbers than the corresponding b_1 fundamental, we have not followed GH in substituting 1119 cm^{-1} with 1192 cm^{-1} for ν_{19}, although the contour looks more like *A* than *C*. The asymmetric CH_3 stretch ν_{22} of species b_2 has been considered accidentally degenerate with ν_{15} (b_1). For ν_{24} we have assigned the band at 1192 cm^{-1}, previously attributed[4] to ν_{12}, but shown by GH[8] to have an IR counterpart. We have verified that our previous[4] weak band at 332 cm^{-1} was due to an impurity. Thus, there is no other apparent choice for ν_{26} than assuming overlap with ν_8 at 359 cm^{-1} as suggested by GH.[8] No good choice was found for ν_{27}, which as a torsional fundamental should be very weak and might be hidden by ν_9.

NORMAL COORDINATE ANALYSIS

As a help in the assignment discussed above a normal coordinate analysis based on symmetry coordinates was performed. It seems of little interest to go into any details of these calculations here. Finally calculated frequencies for 2,2-dichloropropane-d_6 and 2,2-dichloropropane including the potential energy distributions (PED) are given in Tables 2 and 3, respectively. The potential energy distributions are expressed in terms of the valence coordinates defined in Fig. 1.

Acknowledgement. Financial support from Norges Almenvitenskapelige Forskningsråd and a grant to APN from IAESTE are acknowledged.

REFERENCES

1. Klæboe, P. *Spectrochim. Acta Part A 26* (1970) 87.
2. Klæboe, P., Linde, A. and Cyvin, B. N. *Spectrochim. Acta Part A 30* (1974) 1513.
3. Gustavsen, J. and Klæboe, P. *Spectrochim. Acta Part A 32* (1976) 755.
4. Klæboe, P. *Spectrochim. Acta Part A 26* (1970) 977.
5. Cyvin, B. N. and Cyvin, S. J. *Acta Chem. Scand. 26* (1972) 3943.
6. Andresen, I.-L., Cyvin, S. J., Larsen, B. and Törset, O. *Acta Chem. Scand. 25* (1971) 473.
7. Crowder, G. A. and Jackson, D. *Spectrochim. Acta Part A 27* (1971) 1217.
8. Green, J. H. S. and Harrison, D. J. *Spectrochim. Acta Part A 27* (1971) 1217.
9. Gilbert, B. and Duyckaerts, G. *Spectrochim. Acta Part A 26* (1970) 2197.
10. Seth-Paul, W. A. and Dijkstra, G. *Spectrochim. Acta Part A 23* (1967) 2861.

Received October 5, 1977.

Acta Chemica Scandinavica A 32 (1978) 209 – 217

Pyrite-like Phases in the Rh—Te System

ARNE KJEKSHUS,[a] TROND RAKKE[a] and ARNE F. ANDRESEN[b]

[a] Kjemisk Institutt, Universitetet i Oslo, Blindern, Oslo 3, Norway and [b] Institutt for Atomenergi, N-2007 Kjeller, Norway

The phase and structural relations in the Rh – Te system (from 66 to 74 atomic % Te; between 400 and 1100 °C) have been studied by X-ray and neutron diffraction, density, metallographic, and DTA measurements. $Rh_{1-t}Te_2$ (max. comp. range $0.00 \leqq t \leqq 0.20$) takes a pyrite type structure with disordered distribution of Rh atoms and vacancies. In the pyrite-like, Rh_3Se_8 type structure of Rh_3Te_8, Rh atoms and vacancies are ordered.

Rather fragmentary information is available on the Rh – Te system. Wöhler *et al.*[1] were apparently the first to make a distinct rhodium telluride, $RhTe_2$. Their synthesis was repeated by Biltz[2] who claimed that the composition was Rh_2Te_5 and suggested that the structure is of a pseudo FeS_2-*p* (*p* = pyrite) type. Later work by Geller[3] and Steen[4] could not confirm this suggestion. Geller[3] describes three phases: RhTe (NiAs type), $RhTe_2$, (FeS_2-*p* type), and $RhTe_2$ [$Cd(OH)_2$ type]. Non-stoichiometry of the FeS_2-*p* type phase is suggested by Steen.[4] However, the only phase properly characterized both with respect to composition and structure is Rh_3Te_2.[5]

With this background, a comprehensive examination of the entire Rh – Te system is required, and such a study is presently being carried out at this Institute. Since our original interest in this system concerned the FeS_2-*p* type phase, the research programme was initially designed to clarify the properties of this phase. The present report therefore focuses attention on phases occurring from 66 to 74 atomic % Te.

EXPERIMENTAL

The samples were prepared from 99.999 % Rh powder (Johnson, Matthey & Co.) and 99.999 % Te (Koch-Light Laboratories) by heating in evacuated, sealed silica capsules at fixed temperatures between 400 and 1200 °C (interrupted, when necessary, by crushings). Below 400 °C the reaction rates are extremely low, and no attempts have been made to obtain equilibrium conditions below this temperature. More details concerning temperature regulation and quenching experiments are described in Refs. 6 and 7.

All samples were examined microscopically and by powder X-ray (Guinier) diffraction [Cu$K\alpha_1$ radiation, KCl ($a = 6.2919$ Å) as internal standard] at room temperature (unit cell dimensions derived by applying the method of least squares). Most samples were also examined metallographically (etched with aqueous solutions of HNO_3 or HNO_3/HCl). The density of single phase samples (~ 2 g) was measured pycnometrically with kerosene as displacement liquid. The pycnometer was filled with kerosene under vacuum to remove gases adsorbed by the samples.

DTA and high temperature powder X-ray data were collected and treated as described in Ref. 7.

Room temperature powder neutron diffraction data were obtained using cylindrical sample holders of vanadium or aluminium and neutrons of wavelength 1.877 Å from the reactor JEEP II. The nuclear scattering lengths (in 10^{-12} cm) $b_{Rh} = 0.584$ and $b_{Te} = 0.580$ were taken from Ref. 8. In all cases, the least squares profile refinement programme of Rietveld[9] was applied in the final fitting of the variable parameters.

PHASE ANALYSIS

The Rh – Te system has proved to be rather complicated in the compositional range between 40 and 66 atomic % Te. Below 40 and above 74 atomic % Te the system appears, on the other hand, to be simple. However, our investigations in these compositional ranges are still in progress and the fol-

lowing comments on the phase relationships from 0 to 66 and from 74 to 100 atomic % Te are tentative.

(i). Comments on the Rh–Te system in the range 0 to 66 atomic % Te. The most metal-rich, intermediate phase in the Rh–Te system appears to be Rh_3Te_2.[5] This phase exists at temperatures above ~550 °C and exhibits no appreciable range of homogeneity. Below ~550 °C Rh_3Te_2 disproportionates into Rh (no solid solubility of Te in Rh could be detected) and a phase of approximate composition $RhTe_{0.9}$ (structure unknown). The latter does not appear to exist above ~550 °C where disproportionation into Rh_3Te_2 and an "NiAs-like" phase occurs. The NiAs type phase that Geller[3] reported to be of equi-atomic composition is, in fact, close to $RhTe_{1.1}$ [hexagonal; $a=3.987(1)$, $c=5.661(1)$ Å] with only a very narrow range of homogeneity. Below ~600 °C the NiAs type phase transforms to an "NiAs-like" phase with unknown superstructure.

In the compositional range from $RhTe_{1.1}$* to $RhTe_{1.9}$ there exists some 18 phases depending on composition, temperature, and various details concerning the preparational conditions. Some of these phases are, however, difficult to obtain (particularly in a pure state) since the reaction rates for their formation are low. The structures of these phases are, except for possibly four or five of them, probably intermediate between the NiAs and $Cd(OH)_2$ types with ordered or partially ordered distributions of Rh atoms and vacancies.

The $Cd(OH)_2$ type phase, $Rh_{1+u}Te_2$, covers a range of compositions at high temperatures. Fig. 1 shows the dependence of the room temperature (trigonal) unit cell dimensions (derived from quenched samples) on the compositional parameter u. The widest range of homogeneity, $0.225 \geqq u \geqq 0.055$ ($RhTe_{1.633}$ to $RhTe_{1.896}$), corresponds to the highest quenching temperature (1100 °C) used in these experiments. (Quenching experiments from above 1100 °C showed an unacceptable degree of irreproducibility.) High temperature X-ray diffraction fully confirms these results for the Te-rich side of $Rh_{1+u}Te_2$, but suggests that the homogeneity range is somewhat wider on the Rh-rich side than found by quenching. At 1100 °C this correction may shift the phase boundary to $u=0.30$ ($RhTe_{1.54}$). There is accordingly no indication of a continuous NiAs to $Cd(OH)_2$ type solid solution.

* Gross formulae or atomic % Te are used to denote nominal compositions.

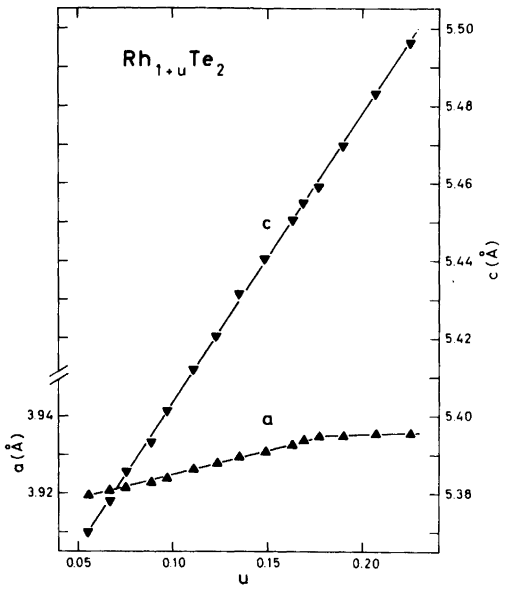

Fig. 1. Unit cell dimensions of (trigonal) $Rh_{1+u}Te_2$ as function of compositional parameter u. Samples quenched from 1100 °C. (Probable errors do not exceed size of symbols.)

The complication in determining the Rh-rich phase boundary below 1100 °C arises from the above-mentioned phases occurring between $RhTe_{1.1}$ and $RhTe_{1.9}$. The same complication renders the determination of the Te-rich phase boundary difficult below 550 °C.

(ii). The range 66 to 74 atomic % Te. Within the range 66 to 74 atomic % Te in the Rh–Te system there exist two intermediate phases (above 400 °C): a cubic (FeS_2-*p* type) phase, $Rh_{1-t}Te_2$, with Rh vacancies (*vide infra*) and a rhombohedrally deformed FeS_2-*p*-like phase, Rh_3Te_8 ($Rh_{0.75}Te_2$). Fig. 2 shows the room temperature unit cell edge and volume (the rhombohedral deformation, $\alpha=90.72°$, for Rh_3Te_8 is not shown) for quenched samples as a function of the compositional parameter t. From the numerous quenching experiments performed during this study, those samples shown to be pure according to X-ray diffraction, were further examined by metallographic methods and density measurements to ensure single phase preparations. The maximum compositional interval covered by the $Rh_{1-t}Te_2$ phase is $0.00 \leqq t \leqq 0.20$ as indicated in the upper part of Fig. 2. There is a distinct gap in composition between $Rh_{1-t}Te_2$ and Rh_3Te_8. The

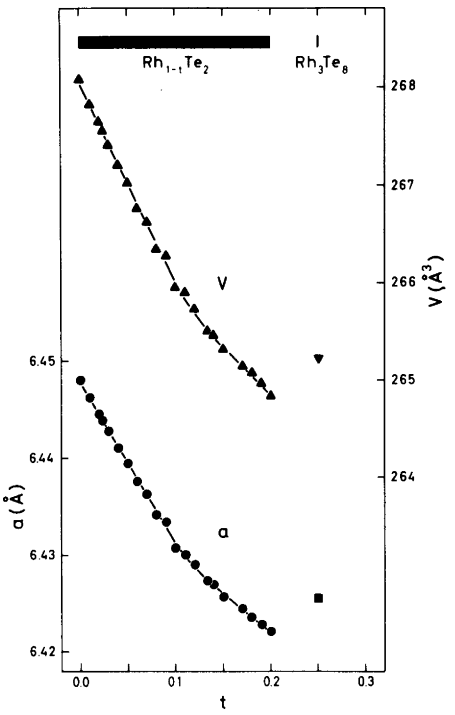

Fig. 2. Unit cell dimension and volume *versus* compositional parameter t for (cubic) $Rh_{1-t}Te_2$ (quenched samples). Data for Rh_3Te_8 are included for comparison. (Probable errors do not exceed size of symbols.)

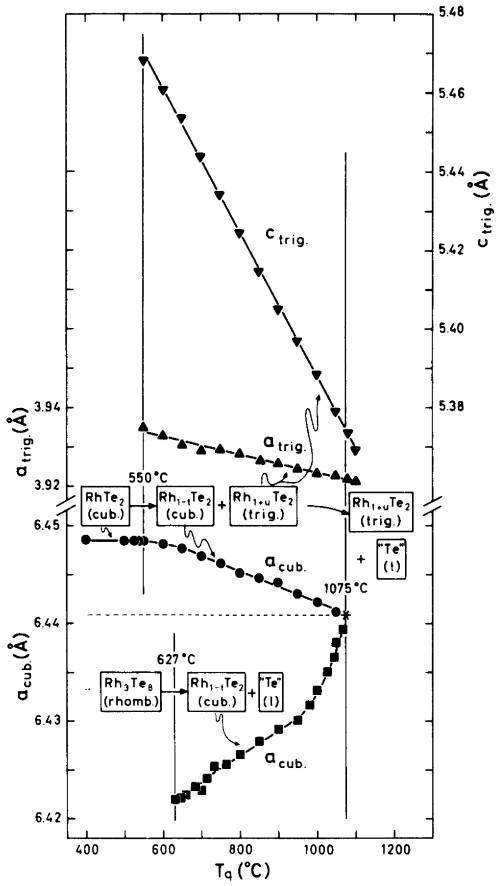

Fig. 3. Room temperature unit cell dimensions for samples of $RhTe_2$ and Rh_3Te_8 quenched from various temperatures T_q. (Probable errors do not exceed size of symbols.) Decomposition reactions are indicated and the notation "Te(l)" is conveniently used for a Te-rich (>95 atomic % Te; see text) liquid.

latter phase exhibits no appreciable range of homogeneity.

The homogeneity range of $Rh_{1-t}Te_2$ is sensitive to temperature, and below 550 °C the stoichiometric 1:2 composition is reached. The homogeneity range does not extend to lower Te contents than $RhTe_2$ at temperatures $\geqq$400 °C. The results of X-ray diffraction and metallographic examinations of quenched samples of $RhTe_2$ are summarized in Fig. 3. By combining the data in Figs. 2 and 3, the Rh-rich phase boundary of $Rh_{1-t}Te_2$ (Fig. 4) is obtained. Peritectic decomposition of $Rh_{1-t}Te_2$ ($t=0.040$) occurs at 1075±6 °C.

The presence of trigonal $Rh_{1+u}Te_2$ in $RhTe_2$ samples quenched from 550 °C is evident from metallographic examinations, whereas X-ray methods failed to detect the trigonal phase. For samples quenched from 600 °C, X-ray diffraction showed three lines. The unit cell dimensions for the trigonal phase at 550 and 600 °C in Fig. 3 therefore refer to measurements on more Rh-rich samples. The Te-rich boundary of the $Rh_{1+u}Te_2$ phase in Fig. 4 is determined by combining the data in Figs. 1 and 3.

In attempts to synthesize samples of nominal composition $RhTe_2$, reaction temperatures above 1075 °C produce the trigonal $Rh_{1+u}Te_2$ phase and liquid (Fig. 4). On cooling to 1075 °C, the peritectic composition, $Rh_{0.960}Te_2$, of the cubic phase and $Rh_{1.058}Te_2$ of the trigonal phase is first formed. At this temperature, equilibrium is established almost instantaneously. At lower (annealing) temperatures, equilibrium (stoichiometric $RhTe_2$ cannot be ob-

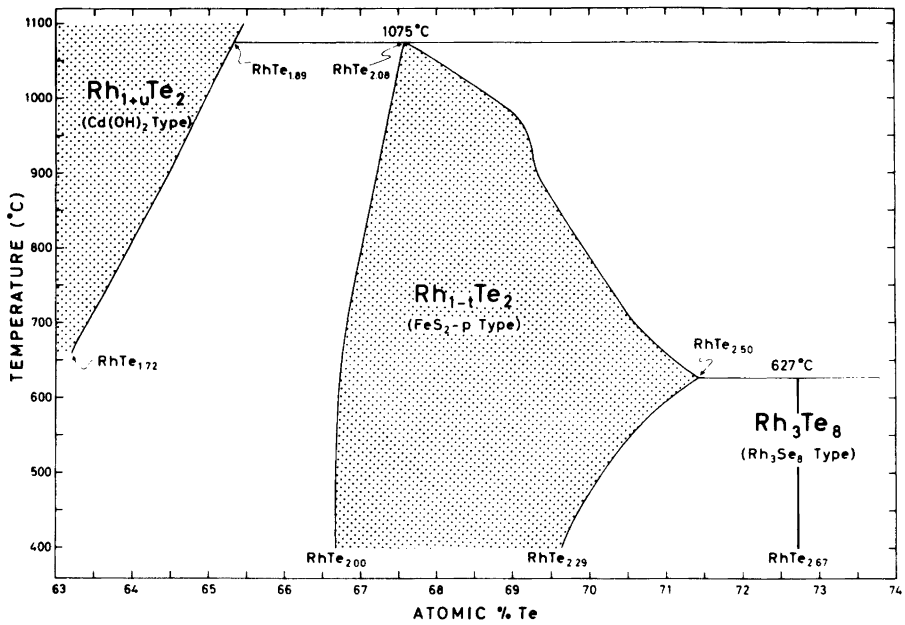

Fig. 4. Section of Rh – Te phase diagram.

tained above 550 °C; see above) is gradually attained more slowly, and even at 900 °C no change from the peritectic composition of the cubic phase could be detected within a few hours. Annealing for about a week at 900 °C is needed to establish true equilibrium conditions, which may explain how Geller[3] could find $a = 6.441(1)$ Å for the composition $RhTe_2$. This value for the cell edge matches, in reality, that for the peritectic composition, $Rh_{0.960}Te_2$.

Rh_3Te_8 decomposes peritectically at 627 ± 3 °C, explaining why Geller[3] and Steen[4] missed this phase by applying too high reaction and annealing temperatures. The quenching experiments on Rh_3Te_8 (Fig. 3) also serve to determine the Te-rich phase boundary of $Rh_{1-t}Te_2$ above 627 °C. At the peritectic temperature, the most Te-rich composition of $Rh_{1-t}Te_2$ ($t = 0.200$) is found.

The Te-rich phase boundary of $Rh_{1-t}Te_2$ below 627 °C is determined from a separate set of quenched samples, making, *inter alia*, use of the relation between unit cell dimension and composition shown in Fig. 2. On gradually turning to lower temperatures, these experiments become more and more time-consuming due to the long annealing periods required to obtain equilibrium. Below 400 °C overall annealing periods of up to two years were insufficient to achieve equilibrium conditions.

(iii). Comments on the Rh – Te system in the range 74 to 100 atomic % Te. At temperatures above 400 °C, no intermediate phase appears to exist between 74 and 100 atomic % Te. Over the compositional range 74 to 90 atomic % Te, DTA peaks at 450, 627, and 1075 °C could be interpreted as eutectic, peritectic, and peritectic temperatures, respectively. At still higher Te contents, the DTA curves were featureless except for the 450 °C peak. Metallographic examination of quenched samples has not yet been fully accounted for, but it seems that the liquidus reaches 1100 °C at 95 atomic % Te. The liquidus is probably lowered to 950 °C at 97 atomic % Te, and the eutectic composition must be located very near to 100 atomic % Te. (No solid solubility of Rh in Te could be detected.)

STRUCTURES

(i). Structure of the $Rh_{1-t}Te_2$ phase. The $Rh_{1-t}Te_2$ phase exhibits cubic symmetry and density (ranging between 8.84 g/cm^3 for $RhTe_2$ and 8.43 g/cm^3 for $Rh_{0.800}Te_2$); measurements show four $Rh_{1-t}Te_2$ formula units per unit cell. The systematic extinctions in the X-ray and neutron powder diffraction patterns (12 to 15 observed reflections) strongly suggest an overall FeS_2-*p* type atomic arrangement.

Table 1. Structural data for selected compositions of the $Rh_{1-t}Te_2$ phase.

	$RhTe_2$	$Rh_{0.980}Te_2$	$Rh_{0.950}Te_2$	$Rh_{0.931}Te_2$	$Rh_{0.900}Te_2$	$Rh_{0.862}Te_2$	$Rh_{0.820}Te_2$
a (Å)	6.4481(7)	6.4442(6)	6.4394(7)	6.4363(8)	6.4307(8)	6.4272(9)	6.4234(9)
x	0.3671(5)	0.3681(4)	0.3697(4)	0.3699(5)	0.3697(5)	0.3700(4)	0.3701(5)

At temperatures $\geqq 400$ °C, no superstructure reflections originating from an ordering of Rh atoms and vacancies (denoted □ in the formulae) could be detected for $t \neq 0$. (The possibility of ordered structures at temperatures below 400 °C is, on the other hand, open for further investigation.) According to space group $Pa3$ appropriate to the FeS_2-p type structure assumed for $Rh_{1-t}\square_tTe_2$, Rh atoms and vacancies are statistically distributed in position 4(*a*), and Te in 8(*c*).

Seven different samples: $RhTe_2$, $Rh_{0.980}Te_2$, $Rh_{0.950}Te_2$, $Rh_{0.931}Te_2$, $Rh_{0.900}Te_2$, $Rh_{0.862}Te_2$, and $Rh_{0.820}Te_2$ were subjected to structural refinements by the powder neutron diffraction/profile refinement technique. The assumption of FeS_2-p type structure for $Rh_{1-t}\square_tTe_2$ was confirmed by the rather low values of 0.019 to 0.034 obtained for the final neutron diffraction reliability factors. The defect concentrations (t) were also verified by varying the occupation numbers in preliminary refinement cycles.

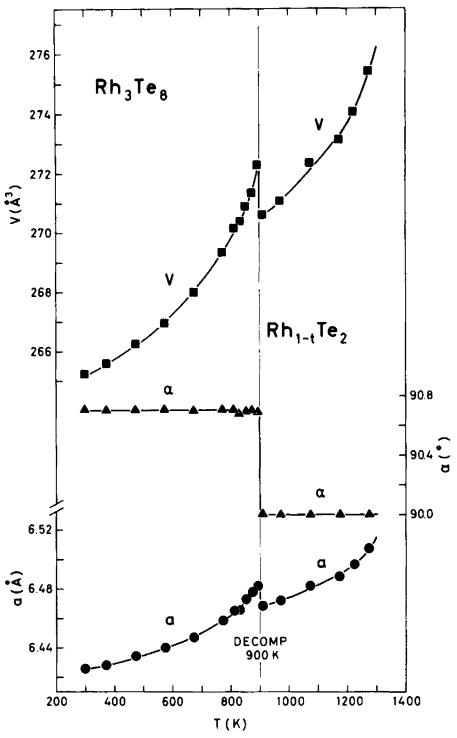

Fig. 5. Unit cell dimensions of (rhombohedral) Rh_3Te_8 *versus* temperature. For $T \geqq 900$ K: $Rh_3Te_8 \rightarrow Rh_{1-t}Te_2$ with variable t. (Probable errors do not exceed size of symbols.)

The room temperature (22 °C) values of the unit cell edge (a) and the positional parameter (x) for Te are listed in Table 1. The data show that the size of the unit cell decreases steadily (see also Fig. 2) with increasing number of vacancies, whereas x increases in the sequence $RhTe_2$, $Rh_{0.980}Te_2$, $Rh_{0.950}Te_2$, and remains approximately constant for higher values of t. The derived interatomic distances and angles are discussed in section *iii*.

(ii). Structure of the Rh_3Te_8 phase. The compound Rh_3Te_8 exhibits rhombohedral symmetry, and density (8.30 g/cm^3) measurements confirm one Rh_3Te_8 formula unit per unit cell. The additional reflections superimposed on the FeS_2-p type diffraction pattern, suggest an ordered, rhombohedrally distorted FeS_2-p type variant, $Rh_{0.75}\square_{0.25}Te_2$, isostructural with Rh_3Se_8.[10] As judged from high temperature X-ray diagrams, not even a partial disordering of the Rh atoms and vacancies occurs above room temperature. Fig. 5 shows the unit cell dimensions of Rh_3Te_8 as function of temperature, the apparent transition to cubic symmetry at 900 K being in reality a peritectic decomposition according to $Rh_{0.75}Te_2 \rightarrow Rh_{0.80}Te_2 + \text{liq}$.

As pointed out in Ref. 10, the only possible rhombohedral space groups permitting an atomic arrangement similar to the FeS_2-p type are $R3$ and $R\bar{3}$. Choosing $R\bar{3}$, places Rh in position 3(*e*) and the two crystallographically non-equivalent Te_I and Te_{II} atoms in 2(*c*) and 6(*f*), respectively.

The room temperature unit cell dimensions (a,α), the positional parameters (x_I, x_{II}, y_{II}, z_{II}) for Te_I and Te_{II}, and interatomic distances and angles are listed in Table 2. The rather low value of 0.038 for the final neutron diffraction reliability factor (based on profile refinement of 28 observed reflections) shows

Table 2. Structural data for the Rh_3Te_8 phase.

a (Å)		6.4255(4)	$Rh-Te_I$(Å)	×2 2.668(8)
α (°)		90.724(7)	$Rh-Te_{II}$(Å)	×2 2.653(6)
x_I		0.3683(12)	$Rh-Te_{II}$(Å)	×2 2.704(6)
x_{II}		0.8823(9)	□ $-Te_{II}$(Å)	×6 2.615(6)
y_{II}		0.1279(9)	Te_I-Te_I(Å)	×1 2.894(22)
z_{II}		0.6326(9)	$Te_{II}-Te_{II}$(Å)	×1 2.820(16)
$Te_I-Rh-Te_{II}$(°)	×2	86.2(2)	$Rh-Te_I-Rh$ (°)	×3 118.0(3)
$Te_I-Rh-Te_{II}$(°)	×2	93.8(2)	$Rh-Te_I-Te_I$(°)	×3 98.3(3)
$Te_I-Rh-Te_{II}$(°)	×2	82.8(2)	$Rh-Te_{II}-Rh$(°)	×1 114.9(2)
$Te_I-Rh-Te_{II}$(°)	×2	97.2(2)	□ $-Te_{II}-Rh$(°)	×1 116.1(2)
$Te_{II}-Rh-Te_{II}$(°)	×3	86.4(2)	□ $-Te_{II}-Rh$ (°)	×1 120.4(2)
$Te_{II}-Rh-Te_{II}$(°)	×2	93.6(2)	$Rh-Te_{II}-Te_{II}$(°)	×1 97.7(2)
$Te_{II}-$□$-Te_{II}$ (°)	×6	82.8(2)	$Rh-Te_{II}-Te_{II}$(°)	×1 100.0(2)
$Te_{II}-$□$-Te_{II}$ (°)	×6	97.2(2)	□ $-Te_{II}-Te_{II}$ (°)	×1 101.7(2)

that the assignment of an Rh_3Se_8 type structure to Rh_3Te_8 must be essentially correct.

(iii). Comparison between the $Rh_{1-t}Te_2$ and Rh_3Te_8 structures. Starting from $RhTe_2$ and its regular FeS_2-*p* type structure, the coordination polyhedron around Rh is that of a slightly distorted $Rh-Te_6$ octahedron (equal Rh – Te distances, Te – Rh – Te angles about 6° different from 90°). The immediate surroundings of Te amount to a distorted $Te-TeRh_3$ tetrahedron (with Te – Rh and Te – Te distances of different length and correspondingly different Rh – Te – Rh and Rh – Te – Te

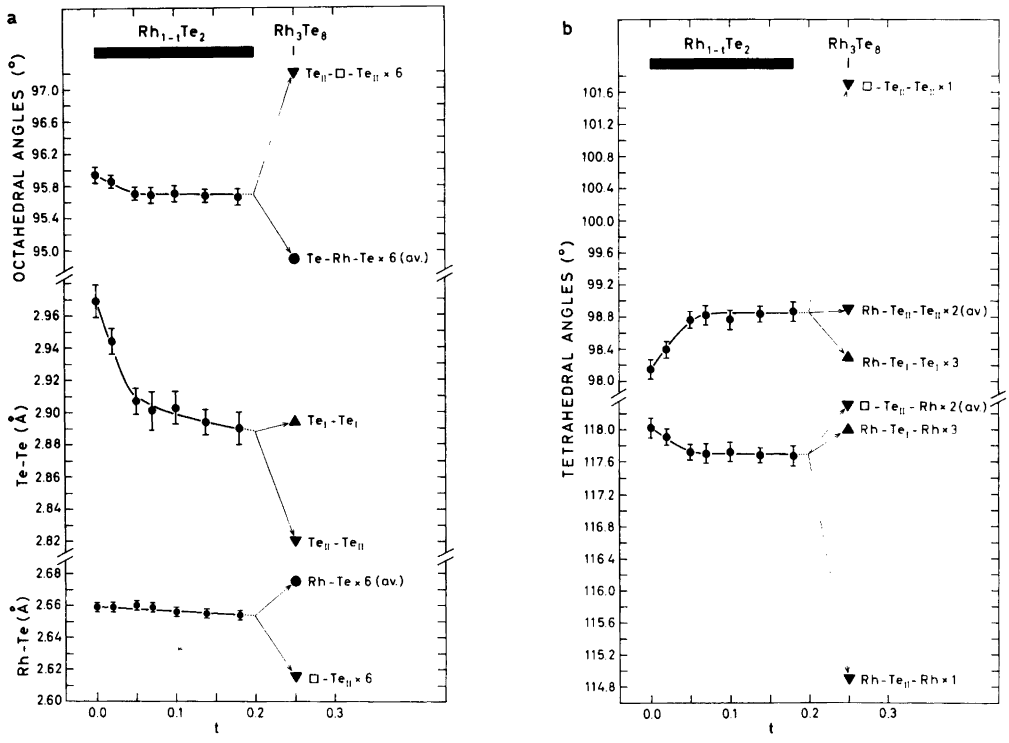

Fig. 6. Variation of bond lengths and bond angles for $Rh_{1-t}Te_2$ with t and in relation to Rh_3Te_8.

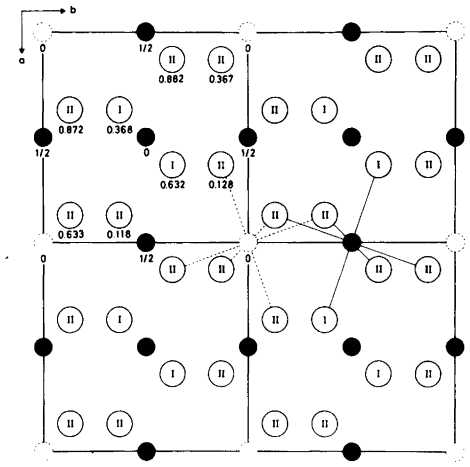

Fig. 7. Four unit cells of the Rh_3Te_8 structure projected along $[00\bar{1}]$, neglecting the rhombohedral distortion. Rh and Te atoms are indicated by filled and open circles, respectively, Rh vacancies by broken circles. (Fractions give z coordinates.)

angles). On turning to the metal deficient $Rh_{1-t}\square_tTe_2$ phase, the Rh–Te (□–Te) and Te–Te bonding interatomic distances, octahedral and tetrahedral bonding interatomic angles vary with t as shown in Fig. 6.

The perhaps most interesting feature emerging from Fig. 6 concerns the Te–Te distance and its functional dependence on t. For $RhTe_2$ this distance amounts to 2.97 Å, which must be considered as a rather long bonding Te–Te distance. For increasing t in $Rh_{1-t}\square_tTe_2$, the Te–Te distance decreases gradually towards the more common value 2.89 Å. Less marked are the overall decrease in the Rh–Te distance and the variations in the independent bond angles.

The kind of ordering of Rh and vacancies in Rh_3Te_8 is illustrated in Fig. 7, where the rhombohedral distortion from an FeS_2-*p* type arrangement is neglected in the plane of projection. An idealized version of the Rh_3Te_8 structure can be described in terms of only one variable parameter (x_0) as follows: $x_I = x_0$, $x_{II} = 1/2 + x_0$, $y_{II} = 1/2 - x_0$, and $z_{II} = 1 - x_0$. Extrapolation of the trend for $Rh_{1-t}Te_2$ (Table 1) gives for a hypothetical, disordered $Rh_{0.75}Te_2$, $x_0 = 0.370$ which may also represent a reasonable value in the idealized Rh_3Te_8 structure. The actual Rh_3Te_8 atomic arrangement is obtained from the idealized structure by further displacement of the atoms, *inter alia*, to make the Rh–Te_6 and □–Te_6 octahedra different (Fig. 6). Another, probably important difference concerns the Te–Te bond lengths: 2.89 Å for Te_I–Te_I *versus* 2.82 Å for Te_{II}–Te_{II}. (This distinction in bond lengths is not reported[10] for the corresponding Se_I–Se_I and Se_{II}–Se_{II} bonds in the isostructural Rh_3Se_8. To proceed further in the understanding of the rhodium tellurides, the latter result should be verified, and a redetermination of the Rh_3Se_8 structure is now being carried out by the present authors.)

The coordination polyhedron around Rh in Rh_3Te_8 is a distorted octahedron (Table 2). The three independent Rh–Te distances and the corresponding Te–Rh–Te angles are averaged in Fig. 6. The immediate surroundings of the vacancy are, on the other hand, similar to the octahedral arrangement in the FeS_2-*p* type structure. Te_I is surrounded by a Te_IRh_3 tetrahedron similar to that in stoichiometric $RhTe_2$, whereas Te_{II} "sees" one Te_{II}, two Rh, and a vacancy in a distorted tetrahedral arrangement (Table 2 and Fig. 6).

CORRESPONDING PHASES IN RELATED SYSTEMS

Unexpectedly Rh_3Te_8 decomposes peritectically rather than undergoing transformation to the disordered state characteristic of the $Rh_{1-t}Te_2$ phase. The reason for this behaviour is not understood and complementary data for related systems would be most helpful. In common with the rhodium tellurides, most of these systems have, however, only been fragmentarily studied. To remedy this situation, systematic studies on other systems have been started at this Institute. Here we shall briefly consider phases occurring between 66 and 74 atomic % X (X = S, Se, Te) on the basis of our preliminary results and literature data.

A separate $Rh_{1-t}S_2$ phase appears not to exist in the Rh–S system (*cf.* Ref. 11), whereas we can unequivocally confirm the occurrence of a rhombohedrally distorted phase. This phase has a composition very close to Rh_3S_8, $a = 5.5910(17)$ Å, but an unexpectedly small rhombohedral distortion, $\alpha = 90.19(3)°$. Further investigations are needed to determine its structure and to establish whether or not rhomohedral Rh_3S_8 transforms into a cubic (disordered) phase at higher temperatures.

The system Rh–Se appears to be more similar to the Rh–Te system in that the cubic phase, $Rh_{1-t}Se_2$, and the rhombohedral, Rh_3Se_8 [a=

5.9632(4) Å, $\alpha = 90.774(8)°$], both exist. However, close to the composition $RhSe_2$ an additional phase,[12] isostructural with $IrSe_2$,[13] occurs, and the location and temperature dependence of the homogeneity range of $Rh_{1-t}Se_2$ is reported[12] to differ substantially from that of $Rh_{1-t}Te_2$. According to our results, the difference is far less than earlier assumed, and mainly concerns the fact that the composition $RhSe_2$ is never reached for the $Rh_{1-t}Se_2$ phase. Apart from this, the shape of the Rh-rich phase boundary of $Rh_{1-t}Se_2$ appears to be similar to that for $Rh_{1-t}Te_2$ (Fig. 4).

The Se-rich phase boundary of $Rh_{1-t}Se_2$ is reported[12] to extend to $t \approx 0.25$ at temperatures between 800 and 900 °C, where the decomposition of Rh_3Se_8 is also assumed.[12] Hence, a phase transition between the rhombohedral and a cubic structure is possible. We have not, however, found any indications that this is the case, and although $Rh_{1-t}Se_2$ extends to larger t values than $Rh_{1-t}Te_2$, there is a distinct gap in composition between $Rh_{1-t}Se_2$ and Rh_3Se_8. Rh_3Se_8 disappears at ~855 °C (according to quenching experiments and high temperature X-ray data, but not detectable by DTA), where a peritectic reaction gives the cubic $Rh_{1-t}Se_2$ phase ($t \sim 0.23$).

Apart from Munson's[14] preparation of FeS_2-*p* type IrS_2 by high pressure–high temperature methods, cubic $Ir_{1-t}S_2$ or $Ir_{1-t}Se_2$ phases have not been synthesized in the Ir–S or Ir–Se systems by more conventional methods. However, phases with approximate compositions IrS_2 and $IrSe_2$ do exist[15] (*cf.* also Ref. 11), but these exhibit the $IrSe_2$ type structure[13] rather than the FeS_2-*p* type. Phases with compositions Ir_3S_8 and Ir_3Se_8 and with FeS_2-*p*-like structures are, on the other hand, registered in these systems.[10,11,15,16] The actual structures and transformation properties of these phases are hitherto unpublished. Our findings indicate that the formula Ir_3S_8 is very nearly correct and that the structure of this phase is of the Rh_3S_8 type. The situation is more complicated in the Ir–Se system, where two distinct FeS_2-*p*-like phases appear to exist with composition around Ir_3Se_8. One of these phases is probably of the Rh_3S_8 type.

Two phases $IrTe_2$ and Ir_3Te_8 have previously been found[17] in the Ir–Te system. $IrTe_2$ exhibits the $Cd(OH)_2$ type structure which is presently confirmed [trigonal; $a = 3.9297(8)$, $c = 5.3958(15)$ Å] to be of the stoichiometric 1:2 composition without any appreciable range of homogeneity [thus contrasting the $Cd(OH)_2$ type phase in the Rh–Te system]. At temperatures below ~650 °C, a new phase (not detected by Hockings and White[17]) is stabilized. This phase, of yet unknown structure, appears to be a proper low temperature modification in that it attains the same stoichiometric 1:2 composition. Transformations between the two modifications of $IrTe_2$ are slow and are not detectable by DTA methods. Ir_3Te_8 is reported[17] to take the FeS_2-*p* type structure, *viz.* $Ir_{0.75}\square_{0.25}Te_2$ with Ir atoms and vacancies statistically distributed. This phase has presently been confirmed, $a = 6.4138(6)$ Å, but we have not yet refined the structure, nor determined the exact composition (between $IrTe_{2.67}$ and $IrTe_{2.72}$). No appreciable range of homogeneity as a function of temperature (between 650 and 920 °C) could be found for this phase, thus contrasting $Rh_{1-t}Te_2$ both in this respect and also with regard to the number of vacancies which may be accommodated in the metal sublattice.

The disordered, FeS_2-*p* type Ir_3Te_8 phase transforms at lower temperatures to either another cubic phase (distinctly different from the disordered FeS_2-*p* type structure), $a = 6.4177(9)$ Å, or to a rhombohedral phase, $a = 6.4183(8)$ Å and $\alpha = 90.47(2)°$, depending on the preparational conditions (particularly the thermal history of the sample). High temperature X-ray studies of both these "low temperature" phases suggest that they transform continuously to the disordered FeS_2-*p* type at 650 °C (undetectable by DTA). The reverse reactions are very slow and reaction periods of the order of a year may be indicated, thus explaining why Hockings and White[17] did not detect these phases. A DTA signal at 920 °C could be interpreted as the peritectic $Ir_{0.75}Te_2 \rightarrow IrTe_2 + \text{liq.}$ decomposition.

The low temperature rhombohedral (probably isostructural with Rh_3Te_8) and cubic (or nearly cubic; allowing for uncertainty due to somewhat diffuse X-ray reflections) phases of Ir_3Te_8 appear to be essentially of the same type with respect to ordering of Rh atoms and vacancies. Thus, it seems possible to obtain an ordered structure with no (or very small) rhombohedral distortion.

On concluding the present survey on these phases, it appears appropriate to emphasize that the FeS_2-*p*-like phases in the Rh–S, Ir–S, Ir–Se, and Ir–Te systems are markedly similar with respect to the existence of only 3:8 compounds, which may transform from ordered to disordered structures. The Rh–Se and Rh–Te systems differ from the

others by taking two compositionally different FeS_2-*p*-like phases of which $Rh_{1-t}Se_2$ and $Rh_{1-t}Te_2$ exhibit broad ranges of homogeneity. Although Rh_3Se_8 and Rh_3Te_8 have well-defined stoichiometric compositions, they differ from their homologues in the degree of rhombohedral deformation and also by undergoing peritectic decompositions rather than order-disorder transformations at higher temperatures.

REFERENCES

1. Wöhler, L., Ewald, K. and Krall, H. G. *Ber. Dtsch. Chem. Ges. 66* (1933) 1638.
2. Biltz, W. *Z. Anorg. Allg. Chem. 233* (1937) 282.
3. Geller, S. *J. Am. Chem. Soc. 77* (1955) 2641.
4. Steen, Ø. *Thesis*, University of Oslo, Oslo 1955.
5. Zachariasen, W. H. *Acta Crystallogr. 20* (1966) 334.
6. Kjekshus, A. and Rakke, T. *Acta Chem. Scand. A 29* (1975) 443.
7. Kjekshus, A. and Rakke, T. *Acta Chem. Scand. A 31* (1977) 517.
8. *The 1977-Compilation of the Neutron Diffraction Commission.*
9. Rietveld, H. M. *J. Appl. Crystallogr. 2* (1969) 65.
10. Hohnke, D. and Parthé, E. *Z. Kristallogr. 127* (1968) 164.
11. Parthé, E., Hohnke, D. and Hulliger, F. *Acta Crystallogr. 23* (1967) 832.
12. Rummery, T. E. and Heyding, R. D. *Can. J. Chem. 45* (1967) 131.
13. Barricelli, L. B. *Acta Crystallogr. 11* (1958) 75.
14. Munson, R. A. *Inorg. Chem. 7* (1968) 389.
15. Sövold, L. *Thesis*, University of Oslo, Oslo 1954.
16. Biltz, W., Laar, J., Ehrlich, P. and Meisel, K. *Z. Anorg. Allg. Chem. 233* (1937) 257.
17. Hockings, E. F. and White, J. G. *J. Phys. Chem. 64* (1960) 1042.

Received September 30, 1977.

Acta Chemica Scandinavica A 32 (1978) 219 – 224

The Electron Density Distribution in Hexahydro-3,6-pyridazinedione

TOR OTTERSEN and JAN ALMLØF

Department of Chemistry, University of Oslo, Oslo 3, Norway

The electron density deformation in hexahydro-3,6-pyridazinedione has been determined by $X-X_{HO}$ Fourier synthesis. These experimental results are compared with densities calculated by *ab initio* Hartree-Fock methods. In the theoretical densities the effect of thermal smearing has been approximately accounted for. The crystallographic results are based on a data set consisting of 1712 non-zero reflections collected at −165 °C. The heavy-atom parameters converged to their final values for a minimum sin θ/λ cutoff of 0.75 $Å^{-1}$, leaving 1026 reflections in the refinement. The final R_w is 0.046.

The present study was carried out as part of a series of deformation electron density investigations of compounds containing the N−N−C=O fragment. A series of structure investigations of such compounds has been carried out in which the experimental results have been complemented by theoretical calculations (for a review see Refs. 1 and 2). It has been found[1] that the readily delocalized π-system in the N−C=O fragment is one of the major factors in the ability of this fragment (the peptide linkage) to form hydrogen bonds, and that the conformation around the N−N bond is dominated by the degree of participation of the nitrogen lone-pairs in the conjugation.[2] Electron deformation density studies of these compounds may give a better understanding of these phenomena, and also of the biologically important peptide linkage.

In order to gain more information on the density distribution it was decided to complement the experimental results with theoretically computed deformation densities. Comparisons between experimental results and thermally smeared theoretical densities may also give information on systematic differences in the two methods,[3] and experimental densities may be utilized to test variations in basis sets used in the theoretical calculations.[3,4] Further, within a series of closely related molecules where the systematic differences between the experimental and theoretical results have been mapped, one may compare theoretical results in order to remove the effects of thermal vibrations inherent in the experimental results.

An earlier low-temperature structure determination of hexahydro-3,6-pyridazinedione[5] (HP) implied that this molecule was well-suited for deformation density studies within the series, which at the moment comprise 1,2-diformylhydrazine,[6] carbohydrazide,[7] and acetamide.[3] HP crystallizes in the centrosymmetric space group *Ibca* with only half a molecule in the asymmetric unit, the molecule having a crystallographically determined C_2 symmetry. The studies of 1,2-diformylhydrazine[6] and carbohydrazide[7] implied that it was possible by refinements using only high-angle data to obtain reasonable positional parameters for the hydrogen atoms [1,2-diformylhydrazine: C−H: 1.07(2) Å, N−H: 1.02(2) Å], and the redetermination of HP could be used to study such refinements further.

EXPERIMENTAL

Crystals of HP[5] were grown by slow evaporation of ethyl alcohol. A rhomb-shaped platy crystal of dimensions 0.44 × 0.36 × 0.10 mm was mounted on a computer-controlled Syntex $P\bar{1}$ four-circle diffractometer equipped with an incident-beam graphite monochromator and a modified Enraf-Nonius low-temperature device (liquid N_2). The temperature at crystal site was −165 °C. The angular coordinates of 13 Mo$K\alpha$ reflections (λ=0.71069 Å) with 2θ-values from 61 to 76° were used in a least-squares

calculation to determine the crystal orientation and cell dimensions. The cell dimensions are: $a=9.126(1)$ Å, $b=17.082(3)$ Å, $c=6.185(1)$ Å, $V=964.2(3)$ Å^3; space group: *Ibca*, $Z=8$.

Three-dimensional intensity data were recorded using the ω-2θ scanning mode with a scan speed of 2.0° (2θ) min^{-1} and a scintillation detector with pulse-height analyse. Each reflection was scanned from $[2\theta(\alpha_1)-0.7°]$ to $[2\theta(\alpha_2)+1.1°]$. Background counting time was equal to 0.35 × scan time at each end of the scan range. In order to study the electron density deformation all reflections within a quadrant with sin θ/λ values less than 0.65 Å^{-1} were recorded, whereas for reflections with sin θ/λ values between 0.65 Å^{-1} and 1.19 Å^{-1} only those were recorded which had integrated counts above 4 cps determined in a 2 s scan over the reflection, and for reflections with sin θ/λ values above 1.19 Å^{-1} only those with integrated counts above 2 cps. The intensities of three check reflections which were remeasured for every seventy reflections showed no systematic variations throughout the data collection.

The estimated standard deviations of the net intensities, I, were calculated as:

$$\sigma(I)=[(B_1+B_2)\times\left(\frac{\text{scan time}}{2\times\text{background time}}\right)^2+I_s+(0.010\times I)^2]^{\frac{1}{2}}$$

where B_1 and B_2 are the two background counts and I_s is the integrated intensity. The factor 0.010 reproduces the observed variance in the check reflections. Of the 2224 symmetry-independent reflections measured ($2\theta_{max}=134°$), the 1712 which had net intensities larger than twice their e.s.d.'s were used in the refinement procedure.

The intensities were corrected for the truncation error. Using the notation of Denne,[8] the formula utilized is:

$$I_{corr}=I/[A_1C_1+A_2C_2+\tfrac{1}{2}(\lambda_a-\lambda_b)\{A_1[I_1(\lambda_a)+I_1(\lambda_b)]+A_2[I_2(\lambda_a)+I_2(\lambda_b)]\}]$$

The line widths and relative intensity data were obtained from Compton and Allison.[9]

Lorentz and polarization corrections were applied to the corrected net intensities. The polarization factor includes the polarization by the monochromator crystal assuming this to be half perfect. The computer program used, as well as programs subsequently employed, is part of a local assembly of computer programs for CYBER-74 and is described in Ref. 10.

REFINEMENT

The quantity $\Sigma w(F_{obs}-K|F_{calc}|)^2$ was minimized in full-matrix least-squares refinements with $w=1/\sigma^2(F_{obs})$. The atomic scattering factors used were those calculated by Doyle and Turner[11] for carbon, nitrogen and oxygen, and the contracted spherical scattering factors calculated by Stewart *et al.*[12] for hydrogen.

The sin θ/λ cutoff value was varied systematically, refinements were performed with minimum cutoff values of 0, 0.40, 0.50, 0.65, 0.75, and 0.85 Å^{-1}. A summary of the results from these refinements is given in Table 1. The standard deviations in hydrogen atomic parameters increased rapidly for cutoffs above 0.40 Å^{-1} (see Table 1). These parameters were, therefore, not refined for cutoffs above 0.65 Å^{-1}.

The C–H and N–N bond lengths obtained in the refinements are listed in Table 1. The variations in these lengths with increasing sin θ/λ minimum cutoff follow the pattern found in the refinements of diformylhydrazine[6] and carbohydrazide.[7] The bond

Table 1. Summary of results from the refinements. $R=\Sigma|kF_{obs}-|F_{calc}||/\Sigma kF_{obs}$, where k is the scale factor, R_t is R-factor taken over all observed reflections, $R_w=[\Sigma w(kF_{obs}-|F_{calc}|)^2/\Sigma wkF_{obs}{}^2]^{\frac{1}{2}}$, $G=[\Sigma w(kF_{obs}-|F_{calc}|)^2/(n-m)]^{\frac{1}{2}}$, where n is the number of observations and m is the number of parameters. The numbering of the atoms may be found in Fig. 1.

$(\sin\theta/\lambda)_{min}$ (Å^{-1})	n	m	R(%)	R_w(%)	R_t(%)	G	k	Bond lengths N–H	C2–H2	C2–H3
0	1712	49	4.76	4.42	4.76	2.22	0.318(1)	0.926(12)	0.969(9)	0.967(11)
0.40	1586	49	4.51	3.99	4.63	1.58	0.328(1)	0.888(17)	0.891(16)	0.949(16)
0.50	1473	49	4.64	4.15	4.67	1.42	0.329(1)	0.817(32)	0.856(30)	0.939(26)
0.65	1229	49	4.83	4.53	4.86	1.28	0.330(1)	1.021(69)	0.984(71)	0.988(75)
0.75	1026	37	5.20	4.60	4.86	1.12	0.330(2)			
0.85	808	37	5.76	5.32	5.06	1.13	0.332(3)			

Table 2. Fractional atomic coordinates and temperature factors with estimated standard deviations. The heavy atom parameters are from the refinement with $(\sin\theta/\lambda)_{min}$ cutoff of 0.75 Å^{-1} and the hydrogen parameters from the refinement with $(\sin\theta/\lambda)_{min}$ cutoff of 0.65 Å^{-1}. The anisotropic temperature factor is given by: $\exp\{-2\pi^2[U_{11}(a^*h)^2\cdots+2U_{23}(b^*c^*kl)]\}$.

Atom	x	y	z	$U_{11}(B)$	U_{22}	U_{33}	U_{12}	U_{13}	U_{23}
O	.04205(5)	.60423(5)	.04555(17)	.0071(1)	.0115(2)	.0173(3)	.0002(1)	−.0010(2)	−.0015(2)
N	−.17349(7)	.54101(3)	−.00006(19)	.0076(1)	.0078(1)	.0161(2)	.0000(1)	.0006(2)	−.0010(2)
C1	−.09423(7)	.60561(5)	.04037(18)	.0074(1)	.0086(2)	.0124(3)	.0006(1)	.0000(2)	−.0004(2)
C2	−.18343(8)	.67877(4)	.07550(18)	.0091(2)	.0086(2)	.0196(3)	.0005(2)	−.0017(2)	−.0028(2)
H1	−.110(6)	.492(4)	−.014(12)	1.91(79)					
H2	−.125(7)	.727(4)	.061(10)	1.76(63)					
H3	−.211(9)	.677(4)	.230(12)	2.22(84)					

lengths decrease with increasing $(\sin\theta/\lambda)_{min}$ with the shortest lengths obtained for the 0.50 Å^{-1} cutoff. At the 0.65 Å^{-1} cutoff the hydrogens shift away from the heavy atoms and the N−H bond increases to the reasonable value of 1.02(7) Å. The two C−H bonds obtained are still too short (0.99 Å). The results obtained in the refinements of diformylhydrazine[6] and carbohydrazide[7] implied that hydrogens bonded to carbon atoms should converge to their "true" (nuclear) positions for the 0.65 Å^{-1} cutoff, whereas hydrogens bonded to nitrogen atoms converge to their nuclear positions for the 0.75 Å^{-1} cutoff. At present we have no decent theoretical explanation of this most remarkable behavior of the X−H bond length as a function of the $\sin\theta/\lambda$ cutoff. However, the e.s.d.'s of the hydrogen positional parameters in the present study are large and one may only observe that the hydrogen positional shifts follow the pattern obtained in the highly accurate studies of diformylhydrazine and carbohydrazide. The overdetermination ratio in the refinement with $(\sin\theta/\lambda)_{min}$ of 0.65 Å^{-1} in the present case is 25.1, and in the studies of diformylhydrazine and carbohydrazide 63.4 and 36.0, respectively.

The heavy atom parameters converged to their final values for the 0.75 Å^{-1} cutoff, in agreement with the results found for diformylhydrazine,[6] carbohydrazide[7] and acetamide.[3] All parameters changed less than twice their e.s.d.'s when the cutoff was increased to 0.85 Å^{-1}. The correlation coefficients between the scale factor and the B_{ii}'s in this refinement were in the order of −0.3 to −0.5, and the correlation between the O and Cl x-parameters is −0.40, and between the y-parameters −0.45. The absolute values of other coefficients are less than 0.3.

Final atomic parameters are listed in Table 2. A list of observed and calculated structure factors is available from the authors upon request. (May also be obtained from: Department of Chemistry, University of Oslo, Oslo 3, Norway.) Standard deviations in molecular parameters were calculated from the correlation matrix ignoring standard deviations in cell dimensions.

The r.m.s. difference between the observed U_{ij}'s (refinement using only data above 0.75 Å^{-1}) and those calculated from the "rigid body" model[13] is 0.0002 Å^2, which implies that the molecule may be regarded as a rigid body. The atomic positions were accordingly corrected for the librational motion. The eigenvalues of **T** are 0.10, 0.09 and 0.09 Å^2, and the librational amplitudes are 4.07, 1.79 and 1.36°. The major librational axis is very nearly parallel with a line through O and O′.

DESCRIPTION OF THE STRUCTURE

Bond lengths and bond angles are listed in Fig. 1 where also the numbering of the atoms is given. The torsional angles Cl−N−N′−Cl′ and Cl−C2−C2′−Cl′ are 25.6(3) and 56.3(2)°, respectively, and N−Cl−C2−C2′ is −37.0(2)°. Deviations from least-squares planes may be found in the legends to Figs. 2 and 3. Apart from H2 and H3 the other atoms in the asymmetric unit are coplanar.

The molecular parameters are essentially the same as those found in the earlier low-temperature, high-angle data structure determination.[5] The maximum deviation occurs in the values of the N−N bond length which earlier was found to be 1.402(1) Å and in the present structure model is 1.398(1) Å. These small deviations do not alter the conclusions made in the earlier publication.[5]

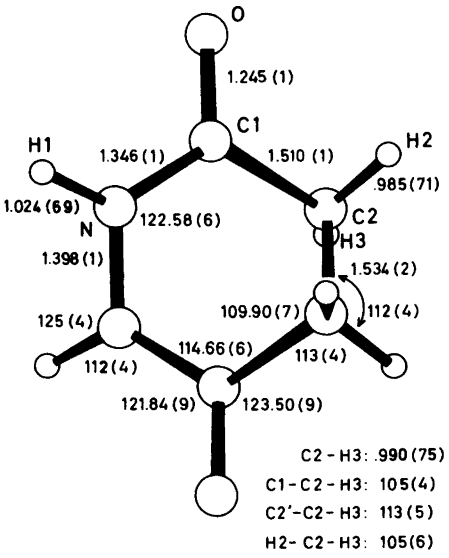

Fig. 1. Bond lengths (Å) (corrected for thermal vibration effects) and bond angles (°) with estimated standard deviations.

CALCULATION OF ELECTRON DENSITY DEFORMATIONS

a. *Experimental densities.* The electron difference densities were obtained using the 904 observed reflections with sin θ/λ-values ≤ 0.85 Å^{-1} in the Fourier summation. The F_{calc}'s are calculated utilizing the heavy atom parameters found in the refinement with a $(\sin\theta/\lambda)_{min}$ cutoff of 0.75 Å^{-1} and the hydrogen parameters obtained in the refinement with a $(\sin\theta/\lambda)_{min}$ cutoff of 0.65 Å^{-1}. The scale factor for the F_{obs}'s [0.322(1)] was obtained by refinement using this structure model and subset of data, in accordance with other studies of similar structures.[3,6,7] Difference density maps through various sections of the molecule are plotted in Figs. 2, 3 and 4. A difference density map calculated using the same structure model and subset of data but with the scale factor obtained in the refinement with $(\sin\theta/\lambda)_{min}$ cutoff of 0.75 Å^{-1} (0.330), showed positive densities in the atomic positions, whereas there were only minor differences in bond and lone-pair densities between this map and the one presented here.

b. *Theoretical densities.* The theoretical deformation densities were obtained from *ab initio* calculations within the Hartree-Fock approximation. The MOLECULE[14] program system was used, employing a basis set of contracted Gaussians. For each of C, N and O, a 7*s*3*p* basis set[15] was contracted to 4*s*2*p*, whereas for H a 4*s* basis[16] was contracted to 2*s*. Thus, the entire basis for the molecular calculation comprised 92 basis functions.

From the wavefunction obtained, the total electron density was computed. The deformation density was then found by subtracting calculated densities for the isolated atoms in their ground states. The atomic densities were calculated using exactly the same contracted basis sets as in the

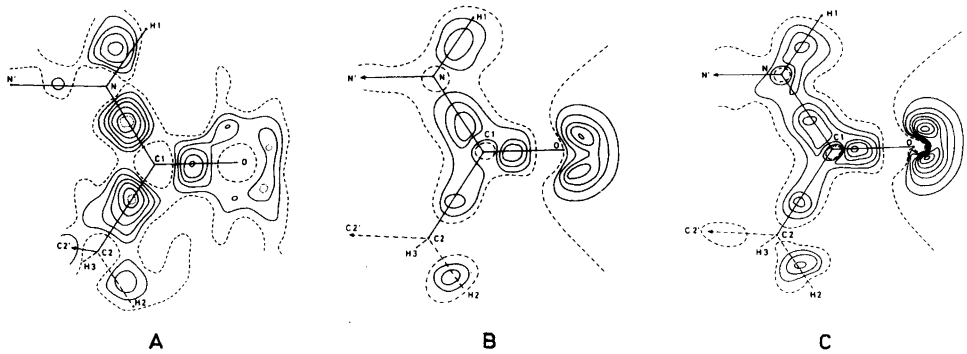

Fig. 2. Deformation electron densities in the least-squares plane through O, N, C1 and C2. Distances of the atoms from this plane are: O: 0.001 Å; N: 0.001 Å; C1: −0.004 Å; C2: 0.001 Å, N′: −0.046 Å, C2′: 0.986 Å, H1: −0.061 Å, H2: 0.266 Å, H3: −0.948 Å. The contours are given at intervals of 0.1 e Å^{-3} for the experimental map, 0.2 e Å^{-3} for the theoretical ones. The zero-line is broken, whereas the dotted lines indicate differences of 0.05 e Å^{-1}. A, Experimental results; B, thermally smeared theoretical results; C, theoretical results.

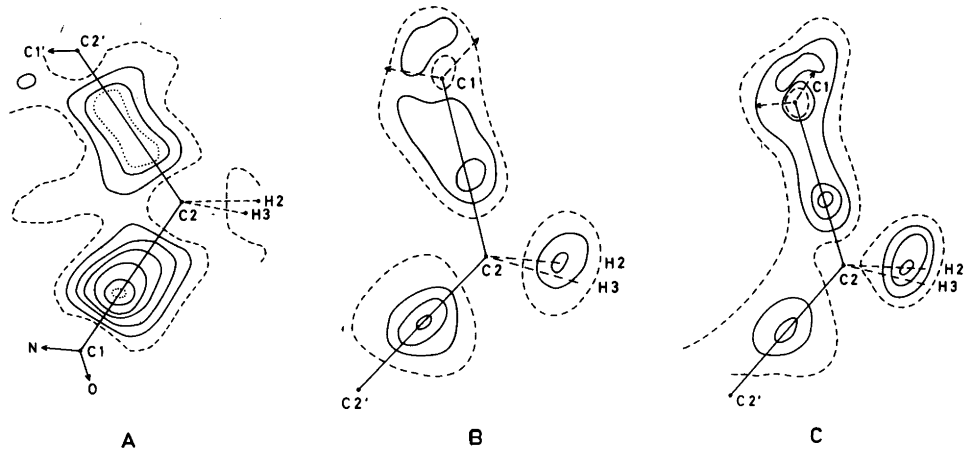

Fig. 3. Deformation electron densities in the plane defined by C1, C2 and C2′. Distances of other atoms from this plane are: N: −0.734 Å; C1′: −1.179 Å; H2: 0.735 Å; H3: −0.819 Å. Contour levels are as in Fig. 2. A, Experimental results; B, thermally smeared theoretical results; C, theoretical results.

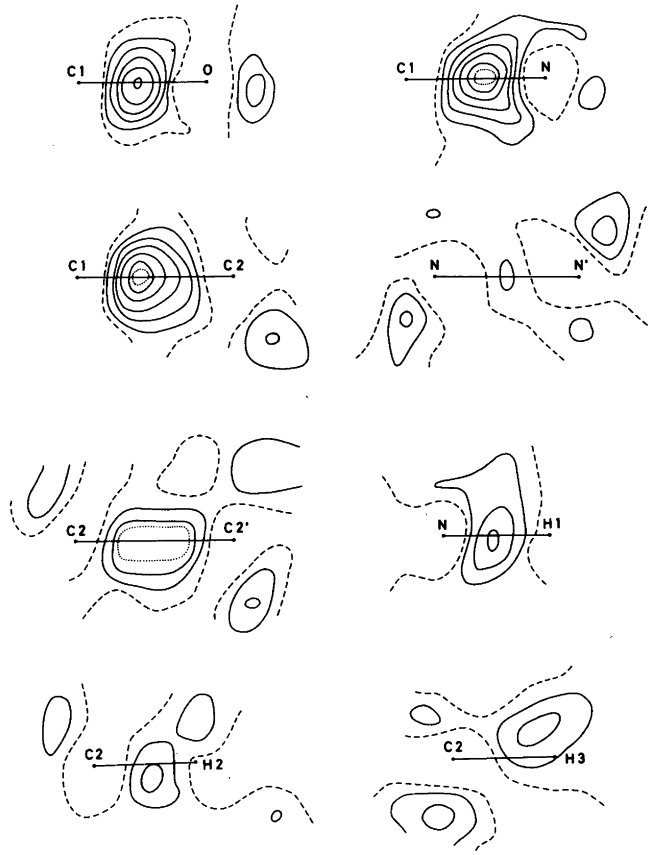

Fig. 4. Experimental deformation electron densities in the bonds normal to the plane through O, N, C1, C2, except for C2−C2′ which is given normal to the plane of C1, C2, C2′. Contour levels are as in Fig. 2.

molecule. This ensures a close cancellation of possible errors due to deficiencies in the basis sets used.

A direct comparison between experimental and theoretical deformation densities is somewhat complicated by the fact that the former have been smeared out as a result of thermal vibration. It is not trivial to apply the same thermal smearing to the theoretical densities, since these are not uniquely decomposable into fragments that can be associated to individual atoms. Therefore, the thermal effects have been only roughly accounted for in the theoretical maps by applying an isotropic, overall smearing factor according to the formula:

$$\rho(r)=(\frac{\alpha}{\pi})^{3/2}\int\rho_0(r')\exp[-\alpha(r'-r)^2]\,dv'$$

Here, ρ_0 and ρ are the computed densities before and after the smearing is applied. A value of 40 was used for the parameter α, corresponding to a conventional B factor of about 1.0.

DISCUSSION

When comparing the experimental deformation density maps with those obtained from the quantum-mechanical calculations, one should first note that the agreement is encouragingly good. It would seem reasonable to interpret the minor discrepancies that still occur as largely due to imperfections in the theoretical maps, resulting from the limited basis set and the approximate theory used in the calculations. Typical such features in the theoretical maps are exaggerated densities in the lone-pair regions on oxygen, and also too low bond densities. The latter are frequently displaced from the centre of the bond as compared to the experimental results. In systematic studies on similar systems[4] such effects have been suggested to originate from the truncations of the basis set used. It can thus be anticipated that a more flexible basis also would have yielded an even better agreement in this work.

The abnormally low density at the centre of the N – N bond obtained in the experimental map may look improbable at first sight. Since the bond is centred on a two-fold axis one could suspect this result to be an artifact, due to the usual accumulation of experimental errors at symmetry elements in the structure. However, this feature is also found in the theoretical maps, where no such accumulation is likely to occur. Furthermore, recent investigations on other, similar systems have also shown very low N – N bond densities.[3,6,7]

Besides the somewhat abnormal N – N bond, the deformation densities – both the experimental and the theoretical ones – show only effects that one would expect on simple, valence-theoretical grounds, *i.e.* accumulation of charge in covalent bonds and in the lone-pair regions. The theoretically obtained integrated density in these regions corresponds to 0.15 – 0.25 electrons in the C – C and C – N covalent bonds, 0.40 – 0.60 in C – H and N – H, and about 0.30 electrons in each of the oxygen lone-pairs. The excess of charge in these parts of the molecule necessitates a flow of charge from other regions in order for the number of electrons to remain constant. The most dominant charge-deficient regions occur close to the nuclei of the heavy atoms. This deficiency of charge can be rationalized in terms of a valence state being the best approximate representation of the atom in the molecule. In the ground state, exactly *two* 2*s* electrons contribute to the density at the nucleus of the atom. In the valence state, on the contrary, a distribution of the valence electrons into sp^n hybrides will always result in *less than* two 2*s* electrons. Although this picture is extremely over-simplified, the number of 2*s* electrons on each atom is always less than two, according to a Mulliken population analysis.

REFERENCES

1. Ottersen, T. *Adv. Mol. Relaxation Processes 9* (1976) 105.
2. Ottersen, T. *Acta Chem. Scand. A 32* (1978) 127.
3. Ottersen, T., Almløf, J. and Hope, H. *To be published.*
4. Almløf, J. *To be published.*
5. Ottersen, T. *Acta Chem. Scand. A 29* (1975) 690.
6. Hope, H. and Ottersen, T. *Acta Crystallogr. In press.*
7. Ottersen, T. and Hope, H. *To be published.*
8. Denne, W. A. *Acta Crystallogr. A 33* (1977) 438.
9. Compton, A. H. and Allison, S. K. *X-Rays in Theory and Experiments.* MacMillan, London 1935, pp. 640 and 745.
10. Groth, P. *Acta Chem. Scand. 27* (1973) 1837.
11. Doyle. P. A. and Turner, P. S. *Acta Crystallogr. A 24* (1968) 390.
12. Stewart, R. F., Davidson, E. R. and Simpson, W. T. *J. Chem. Phys. 42* (1965) 3175.
13. Shoemaker, V. and Trueblood, K. N. *Acta Crystallogr. B 24* (1968) 63.
14. Almløf, J. *USIP Report 74 – 29*, University of Stockholm, Stockholm 1974.
15. Roos, B. and Siegbahn, P. *Theor. Chim. Acta 17* (1970) 199.
16. Huzinaga, S. *J. Chem. Phys. 42* (1965) 1293.

Received October 21, 1971.

Acta Chemica Scandinavica A 32 (1978) 225 – 230

Conformational Analysis. XIV. The Structure of Gaseous 1,3-Dichlorohexafluoropropane, $(CF_2Cl)_2CF_2$, as Determined by Electron Diffraction and Compared with Molecular Mechanics Calculations

LIV FERNHOLT,[a] RAGNHILD SEIP[a] and REIDAR STØLEVIK[b]

[a] Department of Chemistry, University of Oslo, Blindern, Oslo 3, Norway and [b] Department of Chemistry, University of Trondheim, NLHT, Rosenborg, N-7000 Trondheim, Norway

Gaseous 1,3-dichlorohexafluoropropane has been studied at a nozzle temperature of 20 °C. Three conformers *AA*, *AG* and *GG* were detected. Results are presented with error limits (2σ). The following values for bond lengths (r_g) and bond angles ($\angle$) are average parameters for the conformers: r(C–F) = 1.337 (4) Å, r(C–C) = 1.560 (6) Å, r(C–Cl) = 1.755 (6) Å, $\angle$CCC = 114.3° (2.0), $\angle$CCCl = 109.9° (0.8), $\angle$C2C1F = 108.9 (0.8), $\angle$FC2F = 106.6 (2.0). *AA* has an all staggered conformation, while *AG* and *GG* have torsion angles close to the staggered values. The conformational composition is: 53 % (6) of *AA*, 39 % (8) of *AG* and less than *ca.* 10 % of *GG*.

A normal coordinate analysis has been carried out, and calculated values of the vibrational amplitudes were included in the structural analysis.

The diffraction data are consistent with the results obtained from molecular – mechanics calculations.

The results have been compared with those obtained for $(CH_2Cl)_2CH_2$.

This work is part of a systematic conformational study of halogenated propanes. Classically the number of staggered conformers in $(CF_2X)_2CF_2$ is nine. Four conformers are distinguishable by vibrational spectroscopy.

Assuming all-staggered conformations, the distinguishable forms are characterized as follows (X = Cl):

AA:

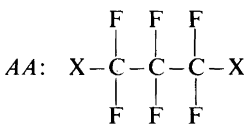

AG:

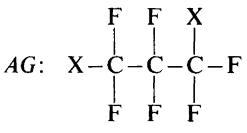

GG:

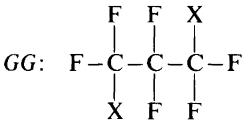

GG(1:3):

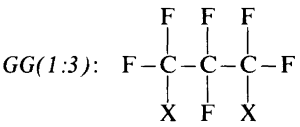

The conformer *GG (1:3)* possesses one parallel (1:3) X···X interaction and therefore the conformational energy of this conformer is significantly higher than the energies of the other conformers. The classical multiplicities are 1, 4, 2, and 2 for *AA*, *AG*, *GG*, and *GG(1:3)*, respectively.

CALCULATIONS

Calculation of conformational energies, structural parameters, torsional barriers and force constants. The energy model is a molecular – mechanics calculation which includes atom-atom potentials and valence force constants, as described in Ref. 1. Energy parameters were taken from the work of Abraham *et al.*[2] The polar terms were not included

in this work. The diagonal force constants in Table 3 were used.

The parameter values in Table 1 correspond to the minima found by minimizing the energy function. Clearly *AG* and *GG* have nearly (1:2) staggered conformations while *AA* is exactly staggered and *GG(1:3)* is far from staggered. According to the energy values of Table 1, *AA* is the energetically most stable conformer. Zero-point vibrational energies for the conformers have not been included here.

Torsional barriers are shown in Table 2. Each energy value has been obtained gy adjusting bond lengths and bond angles. At the minima the values of the torsion angles were also adjusted (see Table 1). The value $\phi_{1-2}=60°$ and values of ϕ_{2-3} equal to $\pm 60°$ correspond to (1:2) *eclipsed* transition forms. All conformers correspond to well – defined minima of the energy function. The lowest barriers correspond to transitions involving the conformer *AG*: 5.4 kcal/mol (*AG*→*AA*), 5.7 kcal/mol (*GG*→*AG*) and 4.1 kcal/mol (*GG(1:3)*→*AG*).

Torsional force constants were calculated at the conformational minima. The values were numerically computed according to the definitions given below:

(mdyn Å (rad)$^{-2}$)	*AA*	*AG*	*GG*
$F_\phi(1-2)=\partial^2E/\partial\phi_{1-2}^2$	0.24	0.28	0.27
$F_\phi(2-3)=\partial^2E/\partial\phi_{2-3}^2$	0.24	0.24	0.27
$F_{\phi\phi'}=\partial^2E/\partial\phi_{1-2}\partial\phi_{2-3}$	−0.09	−0.15	−0.19

The symbol F_ϕ represents the diagonal force constant while $F_{\phi\phi'}$ represents the non-diagonal interaction term.

Values of the diagonal force constants were also calculated according to the formula in Ref. 3. The values estimated in this way were: $F_\phi(1-2)=F_\phi(2-3)=0.27$ for *AA*, $F_\phi(1-2)=0.27$ and $F_\phi(2-3)=0.29$ for *AG*, and $F_\phi(1-2)=F_\phi(2-3)=0.29$ for *GG* in units of mdyn Å (rad)$^{-2}$. The agreement with values based on molecular – mechanics calculations is good.

Calculation of vibrational quantities. Only an approximate force field is needed in order to compute vibrational amplitudes for the internuclear distances. For the compound studied here spectroscopic force constants were not available. However, valence force constants of F_3C-CF_3,[4] Cl_2CF_2,[5] $CH_3-CF_2-CH_3$[6] and $CH_2Cl-CH_2-CH_2Cl$[7] were available. Based on the information from these four compounds, values of the valence force

Table 1. Calculated conformational energy parameters for 1,3-dichlorohexafluoropropane.

Conformer	*AA*	*AG*	*GG*	*GG(1:3)*
ΔE (kcal/mol)[a]	0	1.06	2.01	3.55
ϕ_{1-2}(°)[b]	0(0)	+114.5(120)	+118.6(120)	−109.2(−120)
ϕ_{2-3}(°)[b]	0(0)	+3.5(0)	+118.6(120)	+109.2(+120)
∠CCC(°)[c]	112.5	114.9	117.4	117.4
r(CC)[d] (Å)	1.535	1.538	1.541	1.543

[a] Conformational energy $\Delta E=E-E(AA)$. [b] Torsion angles. Values corresponding to exactly (1:2) staggered conformation are given in parentheses. [c] Reference value 110.0°. [d] Reference value 1.513 Å.

Table 2. Torsional barriers (kcal/mol) between conformers of 1,3-dichlorohexafluoropropane. All values are relative to $E_{AA}=0$.

ϕ_{1-2} / ϕ_{2-3}	0°	60°	120°	180°
180°	8.5	22.8	11.2	∞
120°	1.1(*AG*)	7.7	2.0(*GG*)	11.2
60°	6.5	17.5	7.7	22.8
0°	0(*AA*)	6.5	1.1(*AG*)	8.5
−60°	6.5	17.5	7.6	22.8
−120°	1.1(*AG*)	7.6	*3.5 GG(1:3)*	11.2
−180°	8.5	22.8	11.2	∞

constants were selected. The torsional part of the force field could not be obtained in this way.

In previous works on halogenated propanes (Conformational Analysis I–XIII)[8] an average diagonal force constant for the torsional part of the force field was adjusted to fit theelectron diffraction data. The data for the title compound contain less information for this purpose than the data of previously mentioned compounds. The vibrational amplitude u(Cl...Cl) for the most abundant conformer *AA* (54 %) is essentially independent of the torsional force constant value. The value of u(Cl...Cl) for the conformer *GG* depends strongly on the torsional force constant value. However, *GG* is present in too small an amount (*ca.* 7 %) to give significant information about the force constant values of that conformer. The presence of *AG* (39 %) and the value of u(X···X) could, in principle, provide information about the torsional force constants of that conformer. Based on these considerations and similar arguments for the remaining u-values, it was decided to include only an average torsional force constant ($\bar{F}_\phi$) for the conformers. The value selected for $\bar{F}_\phi$ was 0.27 mdyn Å (rad)$^{-2}$ as calculated from the formula in Ref. 3. For the partial force constants F^*(FF), F^*(CF), F^*(XF), and F^*(CX) the values 0.021, 0.065, 0.048 and 0.110 in units of mdyn Å(rad)$^{-2}$ were used. The value of $\bar{F}_\phi$ was not adjusted, however, the torsional frequency values calculated with $\bar{F}_\phi$ equal to 0.18, 0.27 and 0.36 mdyn Å(rad)$^{-1}$ are given below.

Table 3. Valence force constants for 1,3-dichlorohexafluoropropane (X=Cl). Symbol in parentheses indicates atom or bond which is common for the interaction term.

Stretch (mdyn/Å)		Bend[mdyn Å(rad)$^{-2}$]	
C–F	5.68	FCX	1.40
C–X	3.30	FCF	1.69
C–C	4.57	CCX	1.17
		CCC	0.90
Stretch/bend (mdyn/rad)		CCF	0.79
CC/CCC	0.39(CC)		
CC/CCX	0.29(CC)		
CC/CCF	0.19(CC)	Stretch/stretch (mdyn/Å)	
CC/FCF	−0.19(C)	CF/CF	0.99(C)
CC/FCX	−0.20(C)	CF/CX	0.81(C)
CX/CCX	0.55(CX)	CC/CX	0.35(C)
CX/FCX	0.32(CX)	CC/CF	0.51(C)
CX/FCF	−0.21(C)		
CF/FCF	0.28(CF)		
CF/CCF	0.29(CF)	Torsion [mdyn Å(rad)$^{-2}$]	
CF/CCF	−0.29(C)	F_ϕ=0.27 (all conformers)	
CF/XCF	0.31(CF)	$F_\phi = F_\phi(1-2) = F_\phi(2-3)$	
CF/XCF	−0.15(C)	$F_{\phi\phi'}$0 (interaction term)	
CF/CCC	−0.22(C)		

Table 4. Calculated mean amplitudes of vibration (u). The range of u values and corresponding internuclear distances (r) are given including values for the conformers *AA*, *AG* and *GG*. (X=Cl).

Type of dist.	r (Å)	u (Å)
C–F	1.336	0.046
C–C	1.559	0.051
C–X	1.754	0.052
F···F	2.14–2.19	0.056
C···F	2.36	0.070
F···X	2.54	0.062
C···C	2.62	0.071
C···X	2.71	0.067
X···F(g)	2.88–2.97	0.129–0.134
X···F(a)	3.89	0.068
C···F(g)	2.85–2.96	0.125
C···F(a)	3.75	0.071
F···F(g)	2.61–2.87	0.121–0.122
F···F(a)	3.50	0.069
C···X(g)	3.34	0.135
C···X(a)	4.15	0.070
$F_1\cdots F_3$(gg)	2.55–2.66	0.192–0.193
$F_1\cdots F_3$(gg)	3.25–3.44	0.188
$F_1\cdots F_3$(ag)	4.07–4.22	0.121–0.124
$F_1\cdots F_3$(aa)	4.72	0.088
$X_1\cdots F_3$(gg)	2.91	0.209
$X_1\cdots F_3$(gg)	3.92	0.207
$X_1\cdots F_3$(ag)	4.50–4.56	0.126–0.127
$X_1\cdots F_3$(aa)	5.06	0.091
$X_1\cdots X_3$(gg)	3.95	0.230
$X_1\cdots X_3$(ag)	4.87	0.141
$X_1\cdots X_3$(aa)	5.41	0.094

A normal coordinate analysis[9] was carried out for each of the conformers. Calculated values of the torsional frequencies in cm^{-1} are as follows:

	($\bar{F}_\phi$=0.18)	($\bar{F}$=0.27)	($\bar{F}_\phi$=0.36)
AA:	54–60	66–72	76–82
AG:	50–62	61–74	70–82
GG:	46–66	55–79	63–89

The lowest values of remaining frequencies are 103, 104 and 106 cm^{-1} for *GG*, *AG* and *AA*, respectively, and essentially independent of the torsional force constant value. The highest values are 1257, 1266, and 1271 cm^{-1} for *AA*, *AG* and *GG*, respectively. The final force constant values used in this work are shown in Table 3. Mean amplitudes of vibration (u) were computed[10] and their values are given in Table 4.

EXPERIMENTAL AND DATA REDUCTION

A commercial sample of the compound was used. The purity was *ca.* 99 %. Electron density photographs were made at a nozzle temperature of 20 °C in the Balzer apparatus[11,12] under conditions summarized below.

Nozzle-to-plate distance (mm)	500.12	250.12
Electron wave length (Å)	0.05845	0.05850
Number of plates	4	5
Range of data in s (Å^{-1})	1.25 – 15.50	2.25 – 30.50
Data interval Δs (Å^{-1})	0.125	0.250
Uncertainty in s-scale(%)	0.14	0.14

The electron wave length was determined by calibration against TlCl and benzene.[13] The data were reduced in the usual way[14] to yield an intensity curve for each plate. Average curves for each set of distances were formed. A composite curve was then made by connecting the two average curves after scaling. The final experimental intensity curve is shown in Fig. 1. The intensities have been modified by $s|f'_{Cl}|f'_{C}|^{-1}$. Scattering amplitudes (f') were calculated by the partial-wave method[15] using Hartree-Fock atomic potentials.[16] The radial distribution (RD) curve[14] is shown in Fig. 2.

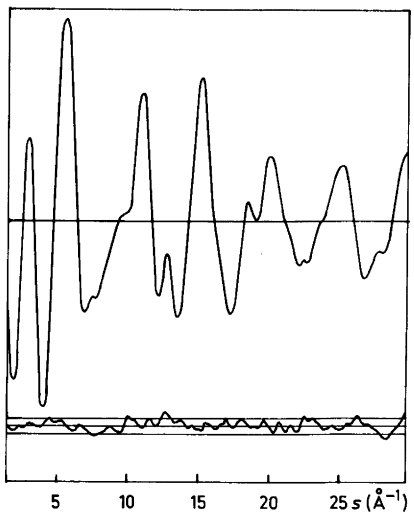

Fig. 1. Experimental intensity curve and difference curve between experimental and theoretical intensities. The straight lines give the experimental uncertainties as ±3 times the average standard deviations.

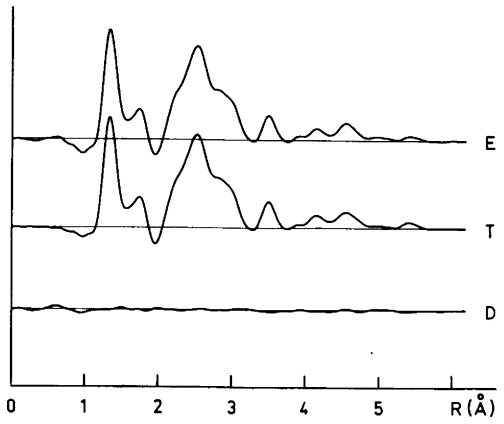

Fig. 2. Experimental (E) and theoretical (T) RD curves computed with an artificial damping constant of 0.002 Å^2. D = E − T.

STRUCTURE ANALYSIS

Radial distribution (RD) curves are shown in Fig. 2 and the final intensity curve in Fig. 1. Both conformers, *AA*, and *AG*, contribute to the RD-curve peaks at 2.5 – 3.2, 3,5, 3.8 – 4.2 and 4.6 Å, while only *AA* contributes to the peak at 5.4 Å and mainly *AG* contributes to the peak at 5.0 Å. The longest internuclear distance is $X_1 \cdots X_3$ (*AA*) at 5.41 Å. Internuclear distances are found in Table 4. The conformers *AA* and *AG* are clearly present in considerable amounts.

According to the energy values in Table 1, *GG(1:3)* is 3.6 kcal/mol less stable than *AA*, corresponding to a percentage of *GG(1:3)* less than 1 %. A small percentage of *GG* has to be expected at the experimental temperature.

In calculating the intensities for the least-squares refinements[14] it was decided not to include a contribution from the *GG(1:3)* conformer. The least-squares program is a modified version of the program described in Ref. 14. Models for the conformers were constructed in terms of the following average conformational parameters:
r(C – F), r(C – C), r(C – X), ∠CCC, ∠CCX, ∠C2C1F, ∠FC2F, ϕ_{1-2}, ϕ_{2-3} and ∠(FC1F)* which is the projection of the FC1F angle on a plane perpendicular to the C2 – C1 axes. Also adjusted were the composition parameters $\alpha(AA)$ and $\alpha(AG)$ with $\alpha(GG) = 100 - \alpha(AA) - \alpha(AG)$. Non-bonded distances were computed as dependent parameters restricted by the constraints of the conformational models.

It is assumed that: the $C-CF_2X$ groups are equivalent and possess C_s symmetry, the $C-CF_2-C$ group possesses C_{2v} symmetry, all C–F bonds have equal length, and thus the conformers have identical structures except for the values of the torsion angles ϕ_{1-2} and ϕ_{2-3} which define the rotation around the C–C bonds.

The expected conformational differences in structural parameters as derived by molecular-mechanics calculations are found in Table 1.

RESULTS

Parameters from the final least-squares refinements and standard deviations (σ) corrected for correlation in the experimental data[17] are given below. In the final refinements, intensities beyond $s=29.75$ Å^{-1} were not included. Using a diagonal weight matrix, all intensities between $s=3.0$ Å^{-1} and $s=28.0$ Å^{-1} were given equal weight. The remaining intensities were given reduced weight.

Calculated mean amplitudes of vibration were included in the analysis as fixed parameters.

The following average values were obtained for the independent bond lengths, r_g(Å), and bond angles, ∠ (in deg), of the conformers (X=Cl):

$r_g(C-F)=1.337$ (2) ∠CCC = 114.3(1.0)
∠CCX = 109.9 (0.4)
$r_g(C-C)=1.560$ (3) ∠C2C1F = 108.9 (0.4)
∠FC2F = 106.6 (1.0)
$r_g(C-X)=1.755$ (3) ∠(FC1F)* = 120.0 (assumed)

The uncertainty in the s-scale (0.14 %) has been included in the standard deviations for bond lengths.

The values of the *dependent* bond angles are: ∠C1C2F = 108.9°(0.4), ∠FC1F = 110.2°(0.5) and ∠XC1F = 109.6°(0.5).

The torsion angles were not refined independently. However, a relationship between a deviation parameter (ϕ_0) and the torsion angles was introduced as suggested by the molecular–mechanics calculations. For the *AG* conformer it was assumed that $\phi_{1-2}=120°-\phi_0$ and $\phi_{2-3}=0.5\,\phi_0$. The parameter ϕ_0 was refined and the value obtained was $\phi_0=7.2°$ with $\sigma=2.4°$. For *AA* and *GG* exactly (1:2) staggered conformations were assumed.

Composition parameters (α) and torsion angles (ϕ) for the conformers are given below:

Conformer	*AA*	*AG*	*GG*
α (in %)	53(3)	39(4)	7(3)
ϕ_{1-2} (in deg.)	0	112.8(2.4)	120
ϕ_{2-3} (in deg.)	0	3.6(1.2)	120

For the conformer *AG* these values agree with those in Table 1. The differences are not statistically significant.

The following correlation coefficients (ρ) had absolute values greater than 0.5: $\rho(2,6)=-0.54$, $\rho(4,8)=-0.57$, $\rho(8,11)=-0.58$, $\rho(8,12)=0.60$, $\rho(4,12)=-0.52$, $\rho(11,12)=-0.76$.

The numbering of parameters is: r(C–C)=2, ∠C2C1F=6, $\phi_0=8$, $\alpha(AA)=11$ and $\alpha(AG)=12$.

DISCUSSION

Assuming equal values of the vibrational partition functions[7] for the conformers, the values of the conformational energies are:
$E(AG)-E(AA)=1.0\pm0.2$ kcal/mol and
$E(GG)-E(AA)\geq1.0$ kcal/mol. The percentage of *GG* being 7 % ($\sigma=3$ %), only a rough lower limit of the difference $E(GG)-E(AA)$ can be estimated. With $\alpha(GG)=7$ % the value of $E(GG)-E(AA)$ is 1.6 kcal/mol.

The conformational energy of *GG(1:3)* was not determined experimentally at the present temperature. However, according to the energy values of Table 1, *AG* is 1.1 kcal/mol less stable than *AA* and *GG* is 2.0 kcal/mol less stable than *AA*, in agreement with the experimental values above. According to the values in Table 1 *GG(1:3)* is 3.6 kcal/mol less stable than *AA*. The fact, that *GG(1:3)* was not included in the conformational analysis, seems justified.

Clearly the values of the vibrational amplitudes (u-values) fit the experimental data well. The average torsional force constant value 0.27 mdyn Å(rad)$^{-1}$ derived from the formula in Ref. 3, and in agreement with the values based on molecular–mechanics calculations, is also consistent with the experimental data. Although the torsional interaction terms $F_{\phi\phi'}$ were not determined in this work, the values of $F_{\phi\phi'}$ derived from molecular–mechanics calculations seem reasonable.

In conclusion, it has been established that the values of the conformational energy parameters, the torsional force constants, and the structural parameters derived from molecular–mechanics calculations agree with the experimentally determined values.

The experimental results for $(CF_2X)_2CF_2$ and $(CH_2X)_2CH_2$[7] are compared below. Standard deviations are shown in parentheses (σ).

X=Cl	$(CF_2X)_2CF_2$	$(CH_2X)_2CH_2$
Nozzle temperature (°C)	20	38
Percentage of conformers (*AA*, *AG*, *GG*)	53,39,7	3,24,73
r_g(C−C) in Å	1.560(3)	1.531(4)
∠CCC in deg.	114.3(1.0)	112.9(0.5)
r_g(C−X) in Å	1.755(3)	1.798(3)
∠CCX in deg.	109.9(0.4)	111.6(0.1)
$\bar{F}_\phi$ (average torsional force constant) in mdyn Å(rad)$^{-2}$	0.27	0.17

The conformational distributions of the two compounds at room temperature are clearly different. The difference in the C−C and C−X bond lengths as well as the difference in the CCX bond angles, are statistically significant. The difference in the CCC bond angles is expected, but hardly statistically significant.

Acknowledgements. We are grateful to Hans Volden for measuring the intensities. Financial support from Norges almenvitenskapelige forskningsråd is acknowledged.

REFERENCES

1. Stølevik, R. *Acta Chem. Scand. A 28* (1974) 327.
2. Abraham, R. J. and Parry, K. J. *J. Chem. Soc. B* (1970) 539.
3. Stølevik, R. *Acta Chem. Scand. A 31* (1977) 359.
4. Carney, R. A., Piotrowski, E. A., Meister, A. G., Braun, J. H. and Cleveland, F. F. *J. Mol. Spectrosc. 7* (1961) 209.
5. Dowling, J. M. *J. Chem. Phys. 22* (1954) 1789.
6. Crowder, G. A. and Jackson, D. *Spectrochim. Acta. Part A 25* (1971) 2505.
7. Grindheim, S. and Stølevik, R. *Acta Chem. Scand. A 30* (1976) 625.
8. Grindheim, S. and Stølevik, R. *Acta Chem. Scand. A 30* (1976) 625.
9. Gwinn, W. D. *J. Chem. Phys. 55* (1971) 477.
10. Stølevik, R., Seip, H. M. and Cyvin, S. J. *Chem. Phys. Lett. 15* (1972) 263.
11. Zeil, W., Haase, J. and Wegmann, L. *Z. Instrumentenkd. 74* (1966) 84.
12. Bastiansen, O., Graber, R. and Wegmann, L. *Balzer High Vacuum Report 25* (1969) 1.
13. Tamagawa, K., Iijima, T. and Kimura, M. *J. Mol. Struct. 30* (1976) 243.
14. Andersen, B., Seip, H. M., Strand, T. G. and Stølevik, R. *Acta Chem. Scand. 23* (1969) 3224.
15. Yates, A. C. *Computer Physics Commun. 2* (1971) 175.
16. Strand, T. G. and Bonham, R. A. *J. Chem. Phys. 40* (1964) 160.
17. Seip, H. M. and Stølevik, R. In Cyvin, S. J., Ed., *Molecular Structures and Vibrations*, Elsevier, Amsterdam 1972.

Received October 21, 1977.

Acta Chemica Scandinavica A 32 (1978) 231 – 233

Synthesis and Properties of Δ,Λ-μ-Hydroxo-μ-sulfato-bis-[bis(ethylenediamine)chromium(III)] Salts

JOHAN SPRINGBORG

Chemistry Department, Royal Veterinary and Agricultural University, Thorvaldsensvej 40, DK-1871 Copenhagen V, Denmark

The binuclear ion Δ,Λ-$[(en)_2Cr(OH)_2Cr(en)_2]^{4+}$ reacts rapidly with sulfuric acid to give the novel sulfato bridged cation Δ,Λ-$[(en)_2Cr(OH)(SO_4)Cr(en)_2]^{3+}$, isolated as its perchlorate, chloride plus tetrachlorozincate and dithionate salts. The sulfato bridged cation is very robust in the $[H^+]$ region $10^{-7} \leq [H^+] \leq 4$ M. In basic solution it deprotonates ($pK \simeq 12$) giving a blue μ-oxo-μ-sulfato complex which undergoes rapid sulfato bridge cleavage giving the cation Δ,Λ$[(OH)(en)_2Cr(OH)Cr(en)_2(OH)]^{3+}$ as the major product. The oxo bridged cation was isolated as the perchlorate, Δ,Λ-$[(en)_2Cr(O)(SO_4)Cr(en)_2](ClO_4)_2.H_2O$.

Recent studies on the *meso* diol,[1,2] Δ,Λ-$[(en)_2Cr(OH)_2Cr(en)_2]^{4+}$, showed that cleavage of the first bridge by addition of water giving monool, Δ,Λ-$[(H_2O)(en)_2Cr(OH)Cr(en)_2(OH)]^{4+}$, occurs several orders of magnitude faster than cleavage of the second bridge. Similar results have recently been obtained for the *racemic* isomers[3] of this diol and of the mixed diol, Δ,Λ-$[(en)_2Cr(OH)_2Co(en)_2]^{4+}$.[4,5] It is now of interest to investigate the reaction of these and of other diols with nucleophiles other than water. The present work describes the novel reaction of *meso* diol with sulfuric acid, and was initiated because of its relevance to the chemistry of chromium tanning.

RESULTS AND DISCUSSION

On dissolution of Δ,Λ-$[(en)_2Cr(OH)_2Cr(en)_2](ClO_4)_4$ in 0.5 M H_2SO_4 (20 °C), the initially purple solution within minutes changes colour giving a wine-red solution from which Δ,Λ-$[(en)_2Cr(OH)(SO_4)Cr(en)_2](ClO_4)_3$ was isolated nearly quantitatively (96 %). From this crude product pure and crystalline salts with the anions perchlorate, chloride plus tetrachlorozincate, and dithionate have been obtained.

The chemical properties of this new dimer provided unambiguous evidence for the proposed structure. The compound reacted neutrally and showed no buffer capacity in the region $1 \leq pH \leq 10$ as indicated by glass-electrode measurements. Furthermore the visible absorption spectrum showed no dependence on $[H^+]$ in the region $10^{-6} \leq [H^+] \leq 4$ M. These results clearly excluded structures having terminal aqua or hydroxo groups, and thereby provided strong evidence for the proposed structure. Other properties mentioned below supported this structure assignment. This assignment has recently been further corroborated by an X-ray structure analysis[6] on the dithionate salt, Δ,Λ-$[(en)_2Cr(OH)(SO_4)Cr(en)_2]_2(S_2O_6)_3.2H_2O$.

The reaction between *meso* diol and sulfuric acid is quantitative and very fast with $k_{obs} = 2.3 \times 10^{-3}$ s^{-1} in 1.0 M sulfuric acid (23 °C). The reaction is therefore unusually rapid as compared to most other reactions involving substitution at a Cr(III) center. This is, however, not surprising as the reaction between *meso* diol and water giving monool similarly has been found to be very rapid.[1] A detailed kinetic study of the reaction between *meso* diol and sulfuric acid is now in progress.

This new dimer is robust in acid and neutral solution but as the pH is increased the sulfato bridge is cleaved rather fast as discussed in the following. When strong base is added to an aqueous solution of Δ,Λ-$[(en)_2Cr(OH)(SO_4)Cr(en)_2](ClO_4)_3$, the colour instantaneously changes from red to blue. The reaction is reversible and is probably due

to deprotonation of the acid hydroxo bridge ($pK \simeq 12$, 20 °C, water) giving the blue μ-oxo-μ-sulfato cation. This cation was isolated as its perchlorate, Δ,Λ-$[(en)_2Cr(O)(SO_4)Cr(en)_2](ClO_4)_2.H_2O$. Similar acid properties of the hydroxo bridge have recently been observed for both *meso* and *racemic* isomers of the ethylenediamine diol.[1,3] The μ-oxo-μ-sulfato ion is not stable in solution and the blue solution turns reddish-purple within minutes (1 M NaOH, 20 °C) due to sulfato bridge cleavage, giving monool, Δ,Λ-$[(OH)(en)_2Cr(OH)Cr(en)_2(OH)]^{3+}$. Thus, by acidifying the product solution, it was then possible to isolate re-formed *meso* diol as perchlorate (42 %). Products formed by hydroxo bridge cleavage have not been observed.

The results presented here may prove to be relevant to the chemistry involved in the chromium tanning process. The basic chromium(III) sulfate solutions, used as tanning agent, contain a large number of polynuclear chromium(III) complexes, and it is now well-established that both sulfate and hydroxide are important bridging groups.[7-9] One of the more well-established species is $[H_2O)_4Cr(OH)(SO_4)Cr(H_2O)_4]^{3+}$, characterized in solution only.[8,9] Studies on its ethylenediamine analogue described in this paper might therefore contribute to a better understanding of the chemistry of this class of complexes.

EXPERIMENTAL

Materials. Δ,Λ-$[(en)_2Cr(OH)_2Cr(en)_2](ClO_4)_4$ was prepared as described in literature.[10] All other materials were of analytical grade.

Analysis. Cr and Zn analyses were determined by atomic absorption spectrophotometry. C, N, H, Cl, and S analyses were made by the microanalytical laboratory at the H.C. Ørsted Institute, Copenhagen.

Instruments. A Cary Model 117 spectrophotometer was used for spectrophotometric measurements in the visible region. For the spectrophotometric data given below the absorbancy ε has been given in l mol^{-1} cm^{-1} and the wavelength λ has been given in nm. Infrared spectra of the compounds in potassium bromide discs were recorded on a Perkin-Elmer 459 grating infrared spectrophotometer.

Preparations. 1. Δ,Λ-μ-Hydroxo-μ-sulfato-bis[bis(ethylenediamine)chromium(III)] perchlorate. Δ,Λ-$[(en)_2Cr(OH)(SO_4)Cr(en)_2](ClO_4)_3$. A solution of Δ,Λ-$[(en)_2Cr(OH)_2Cr(en)_2](ClO_4)_4$ (4.00 g, 5.15 mmol) in 0.5 M sulfuric acid (40 ml, 20 mmol) was kept at room temperature with stirring for 1½ h. The colour of the solution changed from violet to red within minutes after its preparation and after approximately 10 min precipitation of red crystals of Δ,Λ-$[(en)_2Cr(OH)(SO_4)Cr(en)_2](ClO_4)_3$ commenced. After 1½ h a saturated solution of sodium perchlorate (40 ml) was added to the suspension and after a further 20 min the precipitate was filtered off. Washing with 96 % ethanol and drying in the air yielded 3.75 g (96 %). The crude product (2.00 g) was dissolved in 0.5 M hydrochloric acid (70 ml) at room temperature and a saturated solution of sodium perchlorate (30 ml) was then added to the filtered solution. The precipitate was isolated as above. Yield 1.76 g. Anal. $[Cr_2(C_2N_2H_8)_4(OH)(SO_4)](ClO_4)_3$: Cr, C, N, H, Cl, S. Spectral data in 1 M sulfuric acid: $(\varepsilon,\lambda)_{max} = (204,508), (104,382)$; $(\varepsilon,\lambda)_{min} = (46,434)$. The salt is sparingly soluble in pure water, but dissolves readily in, *e.g.*, 1 M solution of sulfuric acid, hydrochloric acid or lithium chloride.

2. Δ,Λ-μ-Hydroxo-μ-sulfato-bis[bis(ethylenediamine)chromium(III)] chloride tetrachlorozincate. Δ,Λ-$[(en)_2Cr(OH)(SO_4)Cr(en)_2]ZnCl_4.Cl.4H_2O$. Crude perchlorate (4.00 g, 5.29 mmol) was dissolved in 0.5 M hydrochloric acid (140 ml) and 4 M Li_2ZnCl_4 (20 ml) was then slowly added to the filtered solution with stirring. After 10 min the precipitate was filtered off, washed with 96 % ethanol and dried in the air. Yield 3.50 g (86 %). The crude salt (2.0 g) was dissolved in water (30 ml) at room temperature, and 4 M Li_2ZnCl_4 (5 ml) was then added slowly to the filtered solution. The precipitate was isolated as above. Yield 1.68 g. Anal. $[Cr_2(C_2N_2H_8)_4(OH)(SO_4)]ZnCl_5.4H_2O$: Cr, Zn, C, N, H, Cl, S. Spectral data in water ($pH \simeq 6$): $(\varepsilon,\lambda)_{max} = (205,508), (105,382)$, $(\varepsilon,\lambda)_{min} = (45,434)$; in 1 M sulfuric acid: $(\varepsilon,\lambda)_{max} = (205,508), (105,382)$; $(\varepsilon,\lambda)_{min} = (45,434)$; in 4 M sulfuric acid: $(\varepsilon,\lambda)_{max} = (208,508), (105,382)$; $(\varepsilon,\lambda)_{min} = (46,434)$. For each medium the spectra changed less than 1 % in absorbancies within 30 min at room temperature.

3. Δ,Λ-μ-Hydroxo-μ-sulfato-bis[bis(ethylenediamine)chromium(III)] dithionate. Δ,Λ-$[(en)_2Cr(OH)(SO_4)Cr(en)_2]_2(S_2O_6)_3.2H_2O$. The dithionate salt was obtained nearly quantitatively by dissolution of the tetrachlorozinkate in a saturated solution of sodium dithionate. The following procedure, which gives a lower yield, was found to give crystals of suitable size for an X-ray crystallographic investigation.[6] To an ice-cold solution of Δ,Λ-$[(en)_2Cr(OH)(SO_4)Cr(en)_2]ZnCl_4.Cl.4H_2O$ (0.85 g, 1.10 mmol) in water (120 ml) was added a saturated (20 °C) solution of sodium dithionate (40 ml) and the solution was kept overnight at 0–5 °C. The crystals were washed with 96 % ethanol and dried in the air. Yield 0.42 g (53 %). Anal. $[Cr_2(C_2N_2H_8)_4(OH)(SO_4)]_2(S_2O_6)_3.2H_2O$: Cr, C, N, H, S. Spectral

data in 1 M H_2SO_4: $(\varepsilon,\lambda)_{max}=(200,508)$, (101,382); $(\varepsilon,\lambda)_{min}=(44,434)$. This salt is nearly insoluble in water.

4. Δ,Λ-μ-Oxo-μ-sulfato-bis[bis(ethylenediamine)-chromium(III)] perchlorate. Δ,Λ-$[(en)_2Cr(O)(SO_4)Cr(en)_2](ClO_4)_2.H_2O$. A suspension of Δ,Λ-$[en)_2Cr(OH)(SO_4)Cr(en)_2](ClO_4)_3$ (2.00 g, 2.65 mmol) in a mixture of 2 M sodium hydroxide (15 ml) and a saturated solution of sodium perchlorate (5 ml) was stirred at room temperature for 10 min. By this the μ-hydroxo-μ-sulfato complex dissolves and simultaneously bluish-green crystals of Δ,Λ-$[(en)_2Cr(O)(SO_4)Cr(en)_2](ClO_4)_2.H_2O$ separate. The product was washed with 96 % ethanol and then with ether and dried in the air. Yield 1.50 g (84 %). Anal. $[Cr_2(C_2N_2H_8)_4(O)(SO_4)](ClO_4)_2.H_2O$: Cr, C, N, H, Cl. The hydroxo bridged complex is re-formed on acidification: To Δ,Λ-$[(en)_2Cr(O)(SO_4)Cr(en)_2](ClO_4)_2.H_2O$ (0.25 g, 0.37 mmol) was added 1 M $HClO_4$ (4 ml) and the suspension was stirred at room temperature for some minutes. The resulting red precipitate was washed with 96 % ethanol and dried in the air. Yield 0.25 g (89 %). The product was identified as Δ,Λ-$[(en)_2Cr(OH)(SO_4)Cr(en)_2](ClO_4)_3$ by its infrared spectrum.

Sulfato bridge cleavage. Conversion of Δ,Λ-$[(en)_2Cr(OH)(SO_4)Cr(en)_2](ClO_4)_3$ to *meso* diol perchlorate was established *via* base hydrolysis as follows: Δ,Λ-$[(en)_2Cr(OH)(SO_4)Cr(en)_2](ClO_4)_3$ (1.75 g, 2.32 mmol) was dissolved in 1.0 M sodium hydroxide (60 ml) by vigorous stirring at 25 °C for 15 min. Initially formed is a blue suspension containing μ-oxo-μ-sulfato dimer partially precipitated as perchlorate. The final reddish-purple solution containing monool, Δ,Λ-$[(OH)(en)_2Cr(OH)Cr(en)_2(OH)]^{3+}$, as a major product was cooled in ice and then acidified to pH ≃ 7 with 6 M perchloric acid. Then solid sodium perchlorate monohydrate (60 g) was added, and the stirred solution was cooled 1 h. During this time, monool was transformed nearly quantitatively into diol which precipitated as perchlorate. The solid was filtered, washed with 96 % ethanol and dried in the air. Yield 0.75 g (42 %). This product was identified as Δ,Λ-$[(en)_2Cr(OH)_2Cr(en)_2](ClO_4)_4$ by comparing its infrared spectrum with that of an authentic[10] sample.

Spectrophotometric measurements. The formation of Δ,Λ-$[(en)_2Cr(OH)(SO_4)Cr(en)_2]^{4+}$ was followed spectrophotometrically in the region 600 – 350 nm at 23 °C. The changes in the spectrum of a 3×10^{-3} M solution of Δ,Λ-$[(en)_2Cr(OH)_2Cr(en)_2](ClO_4)_4$ in 1.0 M sulfuric acid were timed and after 10 min the spectrum remained constant for at least further 20 min. The final spectrum was identical, within experimental error, with the spectrum of Δ,Λ-$[(en)_2Cr(OH)(SO_4)Cr(en)_2](ClO_4)_3$ in 1 M sulfuric acid. First-order plots of log $(OD_t - OD_\infty)$ *vs.* time were linear for at least three half-lifes. From the gradients ($k_{obs}/2.303$) values of the rate-constant, k_{obs}, were calculated and gave $k_{obs}=2.3\times10^{-3}$ s^{-1} independently of the wavelength (λ = 520, 510 and 500 nm).

REFERENCES

1. Springborg, J. and Toftlund, H. *Acta Chem. Scand. A 30* (1976) 171.
2. Kaas, K. *Acta Crystallogr. B 32* (1976) 2021.
3. Toftlund, H. and Springborg, J. *Chem. Commun.* (1976) 1017.
4. Springborg, J. and Schäffer, C. E. *Inorg. Chem. 15* (1976) 1744.
5. Springborg, J. and Schäffer, C. E. *Acta Chem. Scand. A 30* (1976) 787.
6. Kaas, K. *Acta Crystallogr. To be published.*
7. Ellis, M. J., Shuttleworth, S. G. and Sykes, R. L. *J. Am. Leather Chem. Assoc. 58* (1963) 358; Erdmann, H. *Leder 17* (1966) 10; *14* (1963) 249; Slabbert, N. P. *J. Inorg. Nucl. Chem. 39* (1977) 883, and references therein.
8. Finholt, J. E., Caulton, K., Kimball, K. and Uhlenhopp, E. *Inorg. Chem. 7* (1968) 610.
9. Indubala, S. and Ramaswamy, D. *J. Inorg. Nucl. Chem. 35* (1973) 2055.
10. Springborg, J. and Schäffer, C. E. *Inorg. Synth. 18* (1977). *In press.*

Received October 13, 1977.

Acta Chemica Scandinavica A 32 (1978) 235–240

The Crystal Structure of *catena*-μ-(*N*-Salicylidene-L-tyrosinato-*O*,*O*′)copper(II)

REIJO HÄMÄLÄINEN, MARKKU AHLGRÉN, URHO TURPEINEN and MARTTI RANTALA

Department of Inorganic Chemistry, University of Helsinki, SF-00100 Helsinki 10, Finland

The crystal structure of the Schiff base-type complex *catena*-μ-(*N*-salicylidene-L-tyrosinato-*O*,*O*′)-copper(II) {$a = 12.310(8)$ Å, $b = 5.838(5)$ Å, $c = 20.357(11)$ Å, $Z = 4$ and space group $P2_12_12_1$} has been solved by three-dimensional Patterson and Fourier methods and refined by block-diagonal least-squares technique, hydrogen atoms included, to the R value 0.052. The coordination sphere around the copper(II) atom is square pyramidal (4+1). The basal plane consists of the tridentate *N*-salicylidene-L-tyrosine group and an oxygen atom of the adjacent carboxylate group [Cu–O1 = 1.915(8), Cu–O4 = 1.874(9), Cu–N1 = 1.938(8) and Cu–$O2_1$ = 1.986(7) Å]. The other oxygen atom of the carboxylate group occupies the axial position [Cu–$O1_1$ = 2.490(8) Å]. The oxygen atoms of the carboxylate group (in *syn-anti* configuration) coordinate to different copper(II) atoms, joining the adjacent complex units together so that a chain-like structure is formed in the direction of the *b*-axis.

Although a substantial amount of information is available about transition metal complexes of Schiff bases,[1] those derived from salicylaldehyde and amino acids are less well-known.[2-11] Transition metal complexes of salicylaldehyde-amino acid Schiff bases are analogous to those of pyridoxal-amino acid Schiff bases, which are of considerable importance in nonenzymatic catalysed transamination reactions.[12-14] We have used three-dimensional X-ray data to investigate the crystal structures of copper(II) complexes of Schiff bases derived from salicylaldehyde, L-tyrosine and L-phenylalanine. In this study we present the structure of *catena*-μ-(*N*-salicylidene-L-tyrosinato-*O*,*O*′)copper(II).

EXPERIMENTAL

Preparation. Equimolar quantities of salicylaldehyde (2.12 cm^3) and copper(II) acetate monohydrate (4.0 g) were dissolved in a mixture of hydrochloric acid (1 M, 70 cm^3) and ethanol (30 cm^3) according to the method of Laurie.[15] After heating to 50 °C, L-tyrosine (3.62 g), dissolved in a minimum volume of the same acidified ethanol mixture was added, and then 0.2 M sodium hydroxide until a pH of 4.5 was obtained. The crude product was filtered, washed with water and dried in air. The compound was recrystallized from hot water and dark green, prismatic crystals were obtained. Copper was analysed electrolytically, carbon and nitrogen by microanalytical methods. Calc. for $CuC_{16}H_{13}NO_4$ (F.W. 346.81): Cu 18.32; C 55.41; N 4.04. Found: Cu 18.28; C 54.34; N 3.91 %. The crystals were thermally stable to about 240 °C (236 °C given by Laurie), after which they turned brown.

Unit cell and intensity measurements. Weissenberg photographs showed systematic absences of $h00$, $0k0$ and $00l$ reflections with h, k and l odd, indicating the orthorhombic space group $P2_12_12_1$.[16] The approximate cell parameters were refined by the least-squares technique with data obtained from a powder film (Cu$K\alpha$ radiation; $\lambda = 1.5418$ Å), using CaF_2 as internal standard ($a = 5.4630$ Å). Lattice parameters were $a = 12.310(8)$ Å, $b = 5.838(5)$ Å, $c = 20.357(11)$ Å and $V = 1463.0$ Å^3. Density measurements by flotation method showed that there were four formula units per unit cell ($d_{obs} = 1.56$ g cm^{-3} and $d_{calc} = 1.575$ g cm^{-3}).

The intensities of 1372 reflections from six layers ($h0l - h5l$) were collected on a semi-automatic STOE-Güttinger diffractometer with Cu$K\alpha$ radiation. A crystal of dimensions about $0.2 \times 0.4 \times 0.2$ mm was mounted along the b axis. The $10\bar{0}1$ reflections having $I > 2\sigma(I)$ were included in the structure determination. The data were corrected for Lorentz

Table 1. Fractional atomic coordinates ($\times 10^4$; for hydrogen atoms $\times 10^3$) and thermal parameters[a] ($\times 10^3$) with their standard deviations.

Atom	x	y	z	U_{11}	U_{22}	U_{33}	U_{12}	U_{13}	U_{23}
Cu	1315(1)	2494(3)	2509(1)	32(1)	58(1)	21(1)	3(1)	5(1)	13(1)
O1	279(5)	4907(12)	2376(3)	38(4)	48(5)	21(4)	−2(4)	8(3)	6(3)
O2	−596(5)	6868(13)	1637(3)	37(3)	58(5)	20(3)	25(4)	−3(3)	−9(3)
O3	3272(6)	3305(16)	−1564(3)	59(5)	77(6)	42(4)	−27(5)	30(4)	−36(4)
O4	2335(5)	148(16)	2607(3)	31(4)	78(6)	31(4)	10(4)	2(3)	27(4)
N1	1741(6)	3230(15)	1617(3)	39(4)	36(5)	19(3)	−1(4)	−6(3)	6(3)
C1	178(7)	5631(17)	1806(4)	29(4)	29(6)	19(4)	1(5)	12(4)	−7(4)
C2	1077(8)	5000(19)	1310(4)	37(5)	46(7)	11(4)	6(5)	3(4)	−5(4)
C3	532(7)	4142(20)	659(4)	33(5)	51(8)	15(4)	12(5)	−1(4)	−2(5)
C4	1310(8)	3906(20)	84(4)	27(4)	56(7)	20(4)	10(5)	4(4)	9(4)
C5	1289(8)	1964(19)	−298(4)	48(6)	39(7)	21(4)	−14(6)	2(4)	1(4)
C6	1936(9)	1749(20)	−857(5)	46(6)	35(7)	44(6)	−2(6)	14(5)	−13(5)
C7	2624(9)	3448(23)	−1020(5)	41(6)	69(8)	32(5)	−14(6)	10(5)	−13(6)
C8	2681(9)	5355(23)	−644(5)	57(7)	47(7)	35(5)	−21(7)	5(5)	−10(6)
C9	2002(9)	5651(21)	−109(5)	51(6)	36(7)	33(5)	−1(6)	1(5)	−14(5)
C10	3069(8)	−498(22)	2186(5)	27(5)	51(7)	41(5)	2(6)	−7(4)	16(6)
C11	3732(9)	−2417(24)	2310(6)	52(6)	50(7)	65(7)	2(8)	−21(5)	12(7)
C12	4557(9)	−3120(23)	1873(7)	53(7)	48(9)	99(10)	43(7)	−29(7)	−3(8)
C13	4721(11)	−1953(25)	1292(7)	69(8)	64(10)	71(9)	36(8)	−11(7)	−5(7)
C14	4091(11)	−96(28)	1171(6)	57(7)	83(11)	58(8)	13(8)	8(6)	1(9)
C15	3265(8)	635(21)	1576(5)	27(5)	54(7)	35(5)	1(6)	15(4)	1(5)
C16	2605(7)	2536(23)	1338(4)	23(4)	48(6)	37(5)	5(6)	9(4)	−15(6)
H1	858(6)	135(15)	377(4)	18(23)					
H2	983(6)	44(16)	444(4)	26(23)					
H3	1005(9)	822(23)	427(6)	52(41)					
H4	922(8)	595(18)	518(5)	53(31)					
H5	791(6)	512(14)	594(3)	23(19)					
H6	689(6)	719(15)	683(4)	25(21)					
H7	690(8)	197(18)	568(4)	50(28)					
H8	790(6)	165(15)	488(4)	1(23)					
H9	345(13)	707(33)	247(8)	199(69)					
H10	491(6)	577(14)	202(4)	3(22)					
H11	559(8)	733(19)	98(5)	44(30)					
H12	433(8)	114(19)	75(5)	59(33)					

[a] The anisotropic thermal parameters are of the form $\exp[-2\pi^2(h^2a^{*2}U_{11}+\ldots+2hka^*b^*U_{12}+\ldots)]$.

and polarization effects but not for absorption [μ(Cu$K\alpha$) = 23.1 cm^{-1}].

Structure determination. The Patterson and Fourier programs of the *X-Ray* 76 system were used in solving the structure.[17] From a first Fourier summation, phased on the copper atom, it was possible to locate the nitrogen and oxygen atoms. The carbon atoms were obtained by successive Fourier syntheses. The refinement of the structure was carried out by block-diagonal least-squares method with isotropic thermal parameters to $R=0.124$ and with anisotropic parameters to $R=0.072$ ($R=\Sigma\|F_o|-|F_c\|/\Sigma|F_o|$). The hydrogen atoms were located from a difference Fourier map, and after five further cycles, with isotropic parameters for the hydrogen atoms and anisotropic parameters for the others, the R value reached 0.052, the final average shift/error being 0.35. One hydrogen atom (H13) joined to a nitrogen atom could not be located unambiguously and is therefore excluded. The weighting scheme was $w=1/(40.0+|F_o|+0.03|F_o|^2)$ and the function minimized of the form $\Sigma w(|F_o|-|F_c|)^2$. The scattering factors for the non-hydrogen atoms were from Cromer and Mann,[18] and for the hydrogen atoms from Stewart *et al.*[19] Anomalous dispersion corrections were applied for the copper atom, using the values of $\Delta f'$ and $\Delta f''$ from International Tables for X-Ray Crystallography given by Cromer and Liberman.[20] Calculations were carried out on a UNIVAC 1108 computer using the *X-Ray* 76 program system.

Table 2. Interatomic distances (Å) and angles (°). I refers to equivalent position $-x, y-\frac{1}{2}, \frac{1}{2}-z$ and II to position $-x, \frac{1}{2}+y, \frac{1}{2}-z$.

Cu – $O1_I$	2.490(8)	C5 – C6	1.392(16)
Cu – O1	1.915(8)	C6 – C7	1.348(19)
Cu – $O2_I$	1.986(7)	C7 – C8	1.357(20)
Cu – O4	1.874(9)	C8 – C9	1.385(17)
Cu – N1	1.938(8)	C9 – C4	1.386(18)
O1 – C1	1.244(12)	C10 – C11	1.408(20)
O2 – C1	1.247(13)	C11 – C12	1.409(20)
O3 – C7	1.369(14)	C12 – C13	1.371(23)
O4 – C10	1.304(14)	C13 – C14	1.365(24)
N1 – C2	1.446(15)	C14 – C15	1.370(19)
C1 – C2	1.537(15)	C15 – C10	1.419(17)
C2 – C3	1.569(14)	C15 – C16	1.462(18)
C3 – C4	1.515(14)	C16 – N1	1.280(14)
C4 – C5	1.374(17)		
Cu – O1 – Cu_{II}	163.1(4)	C4 – C5 – C6	122.5(11)
O1 – Cu – $O2_I$	87.8(3)	C5 – C6 – C7	119.1(12)
O1 – Cu – O4	177.9(3)	C5 – C4 – C9	116.3(10)
O1 – Cu – N1	83.2(3)	C6 – C7 – C8	120.5(12)
O4 – Cu – N1	94.8(4)	O3 – C7 – C6	121.1(12)
O4 – Cu – $O1_I$	94.2(3)	O3 – C7 – C8	118.4(12)
O4 – Cu – $O2_I$	94.1(3)	C7 – C8 – C9	120.1(13)
N1 – Cu – $O1_I$	115.9(3)	C8 – C9 – C4	121.2(13)
N1 – Cu – $O2_I$	169.0(3)	O4 – C10 – C11	120.9(12)
C2 – N1 – C16	120.4(9)	O4 – C10 – C15	123.7(12)
O1 – C1 – O2	122.1(9)	C11 – C10 – C15	115.4(11)
O1 – C1 – C2	117.2(9)	C10 – C11 – C12	122.5(13)
O2 – C1 – C2	120.7(9)	C11 – C12 – C13	119.9(14)
C1 – C2 – C3	108.9(9)	C12 – C13 – C14	118.0(14)
C1 – C2 – N1	107.2(8)	C13 – C14 – C15	123.9(15)
N1 – C2 – C3	112.6(9)	C10 – C15 – C14	120.1(13)
C2 – C3 – C4	114.0(9)	C10 – C15 – C16	123.7(10)
C3 – C4 – C5	120.2(10)	N1 – C16 – C15	123.9(10)
C3 – C4 – C9	123.3(10)		

RESULTS AND DISCUSSION

The atomic coordinates and thermal parameters with their standard deviations are given in Table 1. The structure and numbering scheme of the compound is shown in Fig. 1. A list of observed and calculated structure factors is obtainable on request from the authors.

The oxygen atoms of the same carboxylate group coordinate in *syn-anti* configuration to different copper ions and thereby join the adjacent complex units together to form a chain structure in the direction of the *b*-axis.

The copper(II) ion has a distorted square-pyramidal coordination geometry (4+1). The tridentate *N*-salicylidene-L-tyrosine group occupies three of the square-planar coordination sites and the carboxyl oxygen atom $O2_I$ of the adjacent complex completes the plane. The carboxyl oxygen atom $O1_I$ occupies the apical site at the distance 2.490 Å. The coordination distances and angles around the copper atom are given in Table 2. The values are comparable with those found earlier in related compounds.[10,11]

The complex unit consists of four, approximately planar groups: atoms of the coordination plane, the carboxylate group, and the rings of the tyrosine and salicylidene residues. The displacements of selected atoms from least-squares planes and the angles between the planes are presented in Table 3. The copper atom is situated almost in the coordination plane (deviation <0.06 Å), which is consistent with

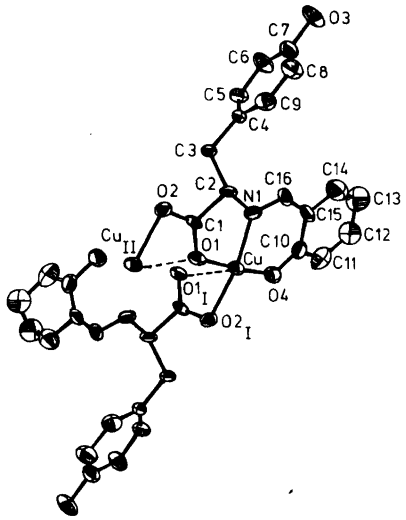

Fig. 1. The structure and numbering scheme of the compound.

the observation that only an oxygen–copper separation of less than ≃2.45 Å results in an interaction sufficient to displace the copper atom from the coordination plane.[21]

The deviation of the nitrogen atom from the carboxylate plane, 0.244 Å, is clearly smaller than the 0.35 Å in *N*-salicylideneglycinatoaquacopper(II) hemihydrate[10] and 0.44, 0.58 and 0.31 Å in α-, β- and γ-glycine, respectively,[22–24] but greater than the deviation 0.12 Å in *N*-salicylideneglycinatoaquacopper(II) tetrahydrate.[11]

The bond distances and angles in the benzene rings fluctuate in the range 1.35–1.42 Å and 115.4–123.9 °, which are fairly large deviations but still comparable with corresponding values in the literature.[25–28] The planarity of both aromatic rings is satisfactory (Table 3) and the exocyclic atoms in the tyrosine residue, C3 and O3, are situated almost in the plane (0.07 Å and 0.03 Å, respectively). The deviations agree, for example, with values of diaquabis(L-tyrosinato)nickel(II) bismethanol.[25]

Ueki *et al.*[11] have examined the bonding around the nitrogen atom in connection with the *N*-salicylideneglycinatoaquacopper(II) tetrahydrate structure and established that the bond lengths are of two different types. In Type I, the bond A between the nitrogen atom and the carbon atom of the amino acid part is shorter than the usual single bond

Table 3. Deviations (Å) from least-squares planes. Atoms indicated with an asterisk were omitted from the calculations.

Plane 1.					
O1	.054	O4	.048	Cu*	.058
$O2_I$	−.050	N1	−.053		
Plane 2.					
O1	.003	C2	.003	N1*	−.244
O2	.003	Cu*	−.409	C16*	−.159
C1	−.008	O4*	−.823	Cu_{II}*	.277
Plane 3.					
C4	.005	C7	−.012	O3*	−.034
C5	.012	C8	.029	C3*	−.069
C6	−.008	C9	−.026		
Plane 4.					
C10	.014	C13	−.009	Cu*	−.069
C11	−.011	C14	.013	O1*	−.200
C12	.008	C15	−.015	O4*	.034
				N1*	−.308

Angle (°) between	
planes 1 and 2	14.6
planes 2 and 3	79.5
planes 2 and 4	19.2
planes 3 and 4	60.7

Table 4. The most significant intermolecular distances (Å).

$O2-O1_I$	2.706(11)	$C1-O1_I$	3.051(14)
$O4-O3_{II}$	2.729(14)	$Cu-O3_{III}$	3.141(10)
$O2-O4_I$	2.828(11)	$O3-O2_{IV}$	3.150(14)
$O1-O3_{III}$	2.995(11)	$Cu-Cu_I$	4.358(2)
$O1-O1_I$	3.041(11)		

I $= -x, \frac{1}{2}+y, \frac{1}{2}-z$ III $= \frac{1}{2}-x, 1-y, \frac{1}{2}+z$

II $= \frac{1}{2}-x, -y, \frac{1}{2}+z$ IV $= \frac{1}{2}+x, \frac{3}{2}-y, -z$

(1.47 – 1.49 Å), and the bond B between the nitrogen atom and the carbon atom of the aldehyde or ketone part has the usual C = N bond dimensions. In Type II, on the other hand, the bond A is normal, wherease the bond B is clearly shorter than normal (1.29 – 1.30 Å). Because in both types one bond, A or B, is shorter than normal, it can be concluded that the nitrogen atom carries more electrons than usual and that one of the bonds is electron-rich. In Type I the mean value expected for bond A is 1.453 Å and for bond B 1.285 Å; in Type II the corresponding values are 1.480 Å and 1.247 Å. The values 1.446 Å for bond A and 1.280 Å for bond B in the present compound agree well with the bond values of Type I.

Table 4 presents some selected intermolecular distances. The H – C and H – O bond lengths vary from 0.60(19) to 1.26(12) Å. It is interesting to note that the hydroxyl oxygen atom O3 in the tyrosine group has not been able to take a sixth place in the coordination sphere of the copper(II) atom but is situated at hydrogen bond distance from the oxygen atoms of the adjacent carboxylate and salicylidene groups ($O1-O3_{III} = 2.995$ Å and $O4-O3_{II} = 2.729$ Å). Thus the hydroxyl oxygen atom lies aside from the axial position and the distance between the copper ion and the hydroxyl oxygen is relatively long ($Cu-O3_{III} = 3.141$ Å).

REFERENCES

1. Holm, R. H., Everett, G. W. and Chakravorty, A. *Prog. Inorg. Chem. 7* (1966) 83.
2. Nakahara, A. *Bull. Chem. Soc. Jpn. 32* (1959) 1195.
3. Kishita, M., Nakahara, A. and Kubo, M. *Aust. J. Chem. 17* (1964) 810.
4. Burrows, R. C. and Bailar, J. C. *J. Am. Chem. Soc. 88* (1966) 4150.
5. Nakao, Y., Sakurai, K. and Nakahara, A. *Bull. Chem. Soc. Jpn. 40* (1967) 1536.
6. O'Connor, M. J., Ernst, R. E., Schoenborn, J. E. and Holm, R. H. *J. Am. Chem. Soc. 90* (1968) 1744.
7. Theriot, L. J., Carlisle, G. O. and Hu, H. J. *J. Inorg. Nucl. Chem. 31* (1969) 2891.
8. Carlisle, G. O., Ganguli, K. K. and Theriot, L. J. *Inorg. Nucl. Chem. Lett. 7* (1971) 527.
9. Carlisle, G. O., Syamal, A., Ganguli, K. K. and Theriot, L. J. *J. Inorg. Nucl. Chem. 34* (1972) 2761.
10. Ueki, T., Ashida, T., Sasada, Y. and Kakudo, M. *Acta Crystallogr. B 22* (1967) 870.
11. Ueki, T., Ashida, T., Sasada, Y. and Kakudo, M. *Acta Crystallogr. B 25* (1969) 328.
12. Snell, E. E., Braunstein, A., Severin, E. S. and Torchinsky, Y. M. *Pyridoxal Catalysis: Enzymes and Model Systems*, Interscience, New York 1968.
13. Snell, E. E., Fasella, P. M., Braunstein, A. and Ross-Fannelli, A. *Chemical and Biological Aspects of Pyridoxal Catalysis*, McMillan, New York 1963.
14. Doctor, V. M. and Oro, J. *Biochem. J. 112* (1969) 691.
15. Laurie, S. H. *Aust. J. Chem. 20* (1967) 2597.
16. *International Tables for X-Ray Crystallography*, Kynoch Press, Birmingham 1969, Vol. 1.
17. *The X-Ray System – Version of 1976.* Technical Report TR-446, Computer Science Center, University of Maryland, College Park 1976.
18. Cromer, D. T. and Mann, J. B. *Acta Crystallogr. A 24* (1968) 321.
19. Stewart, R. F., Davidson, E. R. and Simpson, W. T. *J. Chem. Phys. 42* (1965) 3175.
20. Cromer, D. T. and Liberman, D. *J. Chem. Phys. 53* (1970) 1891.
21. Morosin, B. and Howatson, J. *Acta Crystallogr. B 26* (1970) 2062.
22. Marsh, R. E. *Acta Crystallogr. 11* (1958) 654.
23. Iitaka, Y. *Acta Crystallogr. 13* (1960) 35.
24. Iitaka, Y. *Acta Crystallogr. 14* (1961) 1.

25. Hämäläinen, R., Lajunen, K. and Valkonen, J. *Finn. Chem. Lett.* (1977) 108.
26. Wei, L., Stogsdill, R. M. and Lingafelter, E. C. *Acta Crystallogr. 17* (1964) 1058.
27. Van der Helm, D. and Tatsch, C. E. *Acta Crystallogr. B 28* (1972) 2307.
28. Llewellyn, F. J. and Waters, T. N. *J. Chem. Soc.* (1960) 2639.

Received November 16, 1977.

Acta Chemica Scandinavica A 32 (1978) 241 – 244

Crystal Structure of Tetramethylammonium Hexachloroplatinate(IV)

ROLF W. BERG and INGER SØTOFTE

Chemistry Department A and B, The Technical University of Denmark, DK-2800 Lyngby, Denmark

The room-temperature structure of $\{(CH_3)_4N\}_2[PtCl_6]$ has been reinvestigated using single crystal X-ray diffraction methods. Within reasonable approximation, the structure could be described in the cubic system, space group $Fm3m$, $a = 12.720 \pm 0.004$ Å. Weighted full matrix least squares anisotropic minimization for 113 independent averaged reflections resulted in a final $R_w = 0.026$ and a flat difference Fourier map. All atoms except hydrogen were found. Some indications of a yet unknown noncubic super-structure in the crystal at room temperature are presented and discussed.

An increasing number of crystalline systems exhibiting structural phase transitions have been studied over the past few years. Thus, it has been shown[1-3] that compounds of the type $\{(CH_3)_4N\}_2[MCl_6]$ with M = Sn, U, Zr, Te, exhibit phase transitions at lower temperatures. The origin of these transitions is not clear and the structural behaviour during the transformations is not understood. Recently, the phase transformation was detected at *ca.* 175 K in $\{(CH_3)_4N\}_2PtCl_6$ as well,[4] using variable low temperature far infrared and Raman spectroscopy. Although the room temperature structure of this compound has been studied[5] by single crystal methods in 1926, we found it of interest to undertake an accurate determination. A number of authors[6-10] have concluded from optical examination of crystals or from powder X-ray diffraction experiments that the compound $\{(CH_3)_4N\}_2PtCl_6$ crystallizes with cubic symmetry, whereas Adams and Morris[11] reported the presence of weak forbidden lines of high *hkl* indices in their powder X-ray photographs. Therefore, as a first step towards an understanding of what happens during the low temperature phase transition, the present work was undertaken, so that at least an accurate determination of the room temperature structure was available.

EXPERIMENTAL

Orange red tetramethylammonium hexachloroplatinate(IV) was prepared by mixing equivalent amounts of $(CH_3)_4NCl$ and H_2PtCl_6 dissolved in dilute hydrochloric acid. A crystal of convenient size *ca.* $0.25 \times 0.12 \times 0.12$ mm, showing octahedral faces was obtained by slowly cooling a solution saturated at *ca.* 80 °C. With this crystal mounted on a CAD4F ENRAF-NONIUS automatic four circle diffractometer and using graphite monochromated Mo$K\alpha$ radiation ($\lambda = 0.71069$ Å), two data sets having reflections within a maximum value of $\sin\theta/\lambda = 0.571$ were measured ($0 \leq h,k,l \leq 14$). Three standard reflections, {006}, were repeatedly recorded to check that long term stability remained. 473 and 624 reflections resulted with intensity I larger than $2\sigma(I)$, where $\sigma(I)$ was determined from the counting statistics. The intensities were Lp corrected, but no correction was made for absorption or anomalous dispersion. The data set with 624 reflections is described below. The lattice parameters obtained from the first data set were $a = 12.725(2)$ Å, $b = 12.716(2)$ Å, $c = 12.719(3)$ Å, $\alpha = 89.99(2)°$, $\beta = 90.02(1)°$, $\gamma = 90.01(1)°$. Assuming cubic symmetry, the reflections could be averaged into a set consisting of 113 independent reflections. The internal agreement factor over the set of reflections $R_{int}(F_{obs}^2) = \sum|F_{obs}^2 - \langle F_{obs}^2\rangle|/\sum F_{obs}^2$ was then 0.034. The subsequent crystallographic calculations were done using the X-ray system,[12] and ORTEP.[13] Atomic scattering factors for Pt, Cl, N and C were those of Cromer and Mann.[14] Hydrogen atoms were included near the end of refinement but were finally neglected. A list of the observed and calculated structure factors is obtainable from the authors.

Table 1. Positional and thermal parameters (U_{ij} in units of 10^{-4} Å^2) with estimated standard deviations for independent ones. The temperature factor expression is exp $[-2\pi^2\sum_{ij}h_ih_ja_i^*a_j^*U_{ij}]$.

Atom	X/a	Y/b	Z/c	U_{11}	U_{22}	U_{33}	U_{12}	U_{13}	U_{23}
Pt	0.0	0.0	0.0	447(5)	447	447	0	0	0
Cl	0.1803(3)	0.0	0.0	436(20)	1585(28)	1585	0	0	0
N	0.25	0.25	0.25	493(38)	493	493	0	0	0
C	0.3174(8)	0.3174	0.3174	1927(95)	1927	1927	−667(71)	−667	−667

CRYSTAL DATA

$\{(CH_3)_4N\}_2PtCl_6$. M = 556.1 g/mol. Cubic-(pseudo): $a = 12.720(4)$ Å at 21 °C. $V = 2058.03$ Å^3. $Z = 4$. $D_c = 1.79$. $D_o = 1.81$ g/cm^3 at 16 °C[7] and 1.802(1) g/cm^3.[9] $F(000) = 1064$; $\mu(MoK\alpha) = 79.3$ cm^{-1}. Systematic absences according to space group $Fm3m$ (No. 225, O_h^5): hkl when $h+k$, $k+l$ and $l+h$ are odd. However, weak super lattice reflexes were observed, corresponding to a doubling of the lattice constant in at least two directions.

RESULTS AND DISCUSSION

The cubic lattice parameter obtained above is in reasonable accord with previous results (10.65 Å,[5] 10.66 Å,[11] and 10.72 Å for a crystal with 5 % Ir substitution[10]). Therefore, the space group $O_h^5 = Fm3m$ suggested in the literature[5] was tested against the intensity data, using full matrix least squares minimization and anisotropic temperature factors. Indeed a reasonable structure resulted, see Table 1. The function minimized was $\sum w(|F_o| - |F_c|)^2$. The weights used were estimated by Nielsen's method:[15] $w = xy$, with $x = 1$ for $\sin\theta/\lambda \geq a$; $x = ([\sin\theta/\lambda]/a)^2$ for $\sin\theta/\lambda < a = 0.3294$ and $y = b/F_o$ or F_o/b for $F_o \geq b$ or $F_o < b$, respectively, with $b = 84.10$. For all unobserved reflections $w = 0$. In a normal probability plot, a correlation coefficient $\rho = 0.994$ was obtained,[15] indicating an almost normal distribution of the weighted residuals. The final R-values were: $R = \sum||F_o| - |F_c||/\sum F_o = 0.027$ and $R_w = (\sum w(F_o - F_c)^2/\sum wF_o^2)^{\frac{1}{2}} = 0.026$, and no pronounced peak was seen in the difference Fourier map.

In the final structure these atoms were localized: 4 Pt occupy Wyckoff position a(0,0,0); 24 Cl $e(x,0,0)$; 8 N c(1/4,1/4,1/4) and 32 C $f(x,x,x)$. The chlorine parameter ≈ 0.185 which can be calculated from Huggins' results[5] compares very well with our value of 0.1803 ± 0.0003. The carbon parameter has not been determined previously.

As discussed in detail by Ohe,[2] there are for carbon two possible values of x which would satisfy *both* the C – N bond length *and* the symmetry of the space group: (*i*) all methyl groups point towards platinum ($x \approx 0.18$) and (*ii*) all methyl groups point towards the empty $b(\frac{1}{2},\frac{1}{2},\frac{1}{2})$ position of the cell ($x \approx 0.32$). The value determined here was 0.3174(8) which shows the second case as the one realised. It is of interest to note that this configuration was also found for $\{(CH_3)_4N\}_2SnCl_6$,[16] $\{(CH_3)_4N\}_2CeCl_6$,[17] and $\{(CH_3)_4N\}_2PtF_6$[18] and is probably the most favourable one in all crystals of this kind. Furthermore, the bond lengths and angles obtained were indeed very close to commonly accepted values (Table 2). A stereoscopic view of the structure is shown in Fig. 1.

The anisotropic parameters (Table 1) show quite large values for U_{22}^{Cl} and U_{33}^{Cl}, and for carbon. Although absorption and anomalous dispersion may partly be responsible for this, the obtained values hint to either quite intensive oscillations of the rigid ions or an unresolved superposition of different orientations of octahedra and tetrahedra, or (less probably) to distortions of these highly symmetric ions.

Table 2. Interatomic distances (Å) of the structure, compared with values of the literature.

	This work		Other works
Pt – Cl	2.293(4)		2.323(1)[a]
Pt – C	5.205(8)		
Pt – N	5.508(1)		
Cl – Cl	3.243(4),	5.751(4)	3.285(2)[a]
Cl – C	3.719(5),	4.658(1)	3.75(4)[b], 3.78[d]
Cl – N	4.584(1)		>4.0[b]
C – N	1.484(6),	5.635(10)	1.48(1)[c]
C – C	2.423(10),	4.647(15)	2.44(3)[b]

[a] In K_2PtCl_6.[19] [b] In $(CH_3)_3NHCl$, average value.[20] [c] In $\{(CH_3)_4N\}_2B_6H_6$.[21] [d] In $(CH_3)_4NCl$.[22]

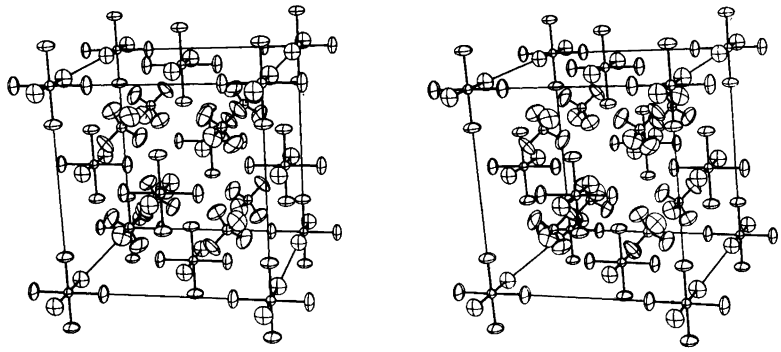

Fig. 1: Stereoscopic view of the structure of tetramethylammonium hexachloroplatinate(IV), in the cubic approximation. Thermal ellipsoids of 40 % charge density are shown. The hydrogen atoms are not shown.

Disordered models were tried with isotropic thermal parameters, but were not significantly better than the anisotropic simple model of Table 1.

EVIDENCE FOR A NONCUBIC SUPER-LATTICE STRUCTURE

As noted, Adams and Morris[11] found noncubic features in their X-ray powder photographs. We found the following noncubic features, each of which taken alone is not convincing; but taken as a whole they indicate that the crystal structure as described above is not strictly adequate:

(*i*) With the *Fm3m* extinction conditions relaxed, we remeasured the complete octant $0 \leq h,k,l \leq 14$ in order to see if the structure could be solved in a less symmetric cell. In this way we got the second data set, with 151 extra integer *hkl* reflections not being *Fm3m* permitted but satisfying the $I > 2\sigma(I)$ criterion. Of these, 58, 29 and 12 reflections were above the 3, 4, or 5 $\sigma(I)$ level, respectively. Very prominent ($I \gtrapprox 5\sigma(I)$) were all permutations within the sets {550}, {552}, {330} and {863}; observed were also all of {772} and {634}. On the other hand, none of these reflections have $|F_o|$ greater than 6 % of the greatest observed values of {004} and {111}. No obvious symmetry governed the intensities of the reflections. *E.g.* (869) was at the 3.6 $\sigma(I)$ level, while (896) *etc.* all were very weak. The length of the axes obtained from the reflections in the second data set were $a = 12.719(2)$ Å, $b = 12.713(2)$ Å, $c = 12.714(2)$ Å, which also tend to indicate a noncubic cell (*cf.* the values of the first data set, which gave the same trend).

(*ii*) Using photographic single crystal X-ray techniques (Cu$K\alpha$ radiation, oscillation and Weissenberg mode) we were able to record additional reflections from this and another crystal in positions corresponding to doubling of two or three of the 12.72 Å axes of the basic unit cell. We did not determine accurate intensities of these "superlattice" reflections, because the crystal seemed to be twinned with respect to the superstructure and because of the problems caused by the short wavelength (Mo$K\alpha$) available at the diffractometer.

(*iii*) A finely powdered sample was tested by neutron scattering. Preliminary results could not be interpreted using the 12.72 Å cubic *Fm3m* cell. Either a lower symmetry or another set of axes was necessary to explain the full structure, including hydrogen atoms.

(*iv*) The optical isotropy was examined in a petrographic microscope and a weak but nonvanishing double refraction was found in all crystallites examined.

(*v*) The angles between the external faces of a several millimeter large single crystal was measured using a two-circle precision reflection goniometer. Deviations were found from the theoretical angles of a cuboctahedron but they were just within the estimated standard deviation of the measurement (0.1°), so that no safe evidence against the cubic description was obtained in this way.

Taken together all these experiments, and especially (*i*) to (*iii*), point to a noncubic symmetry. We have tried to use the reflections from the second diffractometer data set for an estimation of the structure. However, the attempt was not particularly successful. It was possible to get convergence

($R = 0.13$) in a $P4/m$ cell of the same 12.72 Å size but with 42 parameters. In a similar cell with triclinic symmetry and 133 parameters, an R-value of 0.093 could be obtained. Taking into account the increased number of parameters, we do not consider such models as more appropriate.[23] On the other hand, it was gratifying that the refinements of these data produced values for the parameters, very similar to those derived from the first data set.

This situation is not unique. As an example we can compare our results with those obtained on $Cs_2LiCr(CN)_6$, having a quite analogous structure with Li in the center of the cell.[24] Although the structure was shown[24] by other means *not* to be cubic, it was possible to refine its X-ray structure in space group $Fm3m$ down to $R = 0.025$. This was taken as evidence for only a slight distortion from the highly symmetric structure. Other similar examples found in the fluorides of type A_2MF_6 have been discussed in Ref. 25 and papers cited there.

Therefore, also for our compound it must be concluded that the strong scattering power of Pt, combined with other features such as absorption and a probable multiple twinned superstructure make a complete structure determination difficult, especially when the distortion is small. The cell found here by X-ray diffraction is probably the basic fragment of a noncubic cell with larger dimensions, which hopefully can be more accurately determined in the future with the help of neutron diffraction on the perdeuterated compound.

Acknowledgement. The authors are indebted to Dr. Gordon A. Mackenzie (Danish Atomic Energy Commission, Research Establishment, Risø) for his recording and interpretation of the preliminary neutron scattering results on the hydrogen-compound. Dr. J. Engell of this University and Dr. J. Rose-Hansen of the University of Copenhagen did the goniometry and petrographic examination.

REFERENCES

1. Satten, R. A. and Wong, E. Y. *J. Chem. Phys. 43* (1965) 3025.
2. Ohe, W. von der *J. Chem. Phys. 62* (1975) 3933; *63* (1975) 2949.
3. Berg, R. W., Poulsen, F. W. and Bjerrum, N. J. *J. Chem. Phys. 67* (1977) 1829.
4. Berg, R. W. *J. Chem. Phys. In press.*
5. Huggins, M. L. *Phys. Rev. 27* (1926) 638.
6. Topsøe, H. *Overs. K. Dan. Vidensk. Selsk. Forh.*, Copenhagen 1882; *Z. Kristallogr. 8* (1882) 259.
7. Ries, A. *Z. Kristallogr. 49* (1911) 521.
8. Vorländer, D. *Ber. Dtsch. Chem. Ges. 64* (1931) 1736.
9. Staritzky, E. and Singer, J. *Acta Crystallogr. 5* (1952) 536.
10. Jørgensen, C. K. *Acta Chem. Scand. 17* (1963) 1034.
11. Adams, D. M. and Morris, D. M. *J. Chem. Soc. A* (1967) 1666.
12. Stewart, J. M., Kundell, F. A. and Baldwin, J. C. *The X-Ray System, Version 1972*, Univ. of Maryland, College Park 1972.
13. Johnson, C. K. *ORTEP*, Report ORNL-3794, Oak Ridge National Laboratory, Oak Ridge 1965.
14. Cromer, D. T. and Mann, J. B. *Acta Crystallogr. A 24* (1968) 321.
15. Nielsen, K. *Acta Crystallogr. A 33* (1977) 1009.
16. Wyckoff, R. W. G. and Corey, R. B. *Am. J. Sci. 18* (1929) 437.
17. Cromer, D. T. and Cline, R. J. *J. Am. Chem. Soc. 76* (1954) 5282.
18. Mironov, Yu. I., Zemskov, S. V., Tzarkova, G. I., Obmoin, B. I. and Nikonorov, Yu. I. *Izv. Sib. Otd. Acad. Nauk SSSR, Ser. Khim. Nauk 76* (5) (1976) 95.
19. Williams, R. J., Dillin, D. R. and Milligan, W. O. *Acta Crystallogr. B 29* (1973) 1369.
20. Lindgren, J. and Olovsson, I. *Acta Crystallogr. B 24* (1968) 554.
21. Schaeffer, R., Johnson, Q. and Smith, G. S. *Inorg. Chem. 4* (1965) 917.
22. Harmon, K. M., Gennick, I. and Madeira, S. L. *J. Phys. Chem. 78* (1974) 2585.
23. Hamilton, W. C. *Acta Crystallogr. 18* (1965) 502.
24. Ryan, R. and Swanson, B. I. *Phys. Rev. B 13* (1976) 5320.
25. Zemskov, S. V. and Gabuda, S. P. *Russ. J. Struct. Chem. 17* (1976) 772.

Received October 31, 1977.

Acta Chemica Scandinavica A 32 (1978) 245–249

The Molecular Structure and Conformational Composition of Gaseous Methyl Chloroformate as Determined by Electron Diffraction

QUANG SHEN

Department of Chemistry, University of Trondheim, NLHT Rosenborg, N-7000 Trondheim, Norway

The molecular structure of methyl chloroformate has been studied at two different temperatures, 20 and 200 °C. Particular attention was paid to the conformational composition of the gaseous mixture. Both data sets are consistent with the presence of only the *syn* form. There is no evidence for the presence of the *anti* conformer, but models with 0 % (15 %) (20 °C) and 10 % (20 %) (200 °C) *anti* conformer cannot be ruled out by the electron diffraction experiment. For the *syn* form at 20 °C, the principal bond distances (r_a), and angles with error estimates of 2σ are: r(C–H) = 1.092(24) Å, r(C=O) = 1.190(4) Å, r(OC–O) = 1.325(6) Å, r(O–CH_3) = 1.443(7) Å, r(C–Cl) = 1.754(4) Å, ∠O=C–O = 128.1(6)°, ∠O–C–Cl = 108.7(4)°, ∠C–O–C = 114.4(17)° and ∠H–C–O = 110.0° (assumed).

The molecular conformation of methyl chloroformate has been the subject of considerable interest for a number of years.[1-9] Support for the existence of both *syn* and *anti* forms (Fig. 1) are discussed in a review by Jones and Owen.[10] The only structural parameter values reported were by O'Gorman *et al.*[2] in an early electron diffraction study. During the course of our study, Durig and Griffin[11] reported the vibrational and the microwave spectra of gaseous methylchloroformate. In agreement with the earlier electron diffraction study, they concluded that the *syn* form was the prevailing conformer at room temperature, although small amounts of a second conformer could not be excluded. Due to various assumptions introduced, the uncertainties in the structural parameters were quite large. In order to supply accurate geometrical parameter values and to add information about the possible presence of a second conformer, we shall report our electron diffraction studies of methyl chloroformate at 20 and 200 °C.

EXPERIMENTAL

The sample of methyl chloroformate (>97 %, Merck) was checked by gas chromatography before use. The diffraction experiment was carried out at nozzle temperatures of 20 and 200 °C in the Oslo Balzers apparatus.[12] The experimental conditions are summarized in Table 1. The backgrounds were hand-drawn on the averaged curves from each of the two nozzle-to-plate distances. Before the averaging, the curves were plotted for visual check of uniformity.

STRUCTURE ANALYSIS

The structure analysis was carried out in the usual way.[13] The atomic scattering and phase factors used were obtained from Schäfer, Yates and Bon-

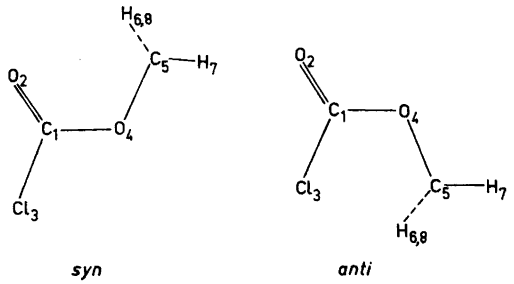

Fig. 1. Diagrams of the *syn* and *anti* forms of methyl chloroformate with atom numbering.

Table 1. Experimental conditions.

Nozzle temp. (°C)	20	200
Wave length (Å)[a]	0.05859	0.05859
Voltage (kV)	42	42
Bath temp. (°C)	0	0
Camera height (mm)	500.12	499.21
Plates used	4	4
s range (Å^{-1})	1.25 – 15.50	1.00 – 15.00
Δs	0.25	0.25
Camera height (mm)	250.12	249.27
Plates used	4	6
s range (Å^{-1})	6.00 – 29.00	7.50 – 26.50
Δs	0.25	0.25

[a] Wave length calibrations were carried out by using benzene and TlCl as standards.

ham's tables.[14] Refinements of the structure were carried out by the method of least squares based on intensity curves by adjusting a single theoretical curve to the two average curves (one each from the long and short camera distances) using a unit weight matrix. The composites of these two experimental curves for 20 and 200 °C are shown in Fig. 2. The *syn* form of the molecule can be described by the following geometrical parameters: r(C – H), r(C = O), $\langle C-O\rangle = (r(C_1-O_4)+r(C_5-O_4))/2$, $\Delta(C-O) = r(C_5-O_4)-r(C_1-O_4)$, r(C – Cl), $\angle O = C-O$, $\angle O-C-Cl$, $\angle C-O-C$, $\angle H-C-O$ and τ (the H – C – O – C torsional angle with zero taken as when one of the C – H bond is eclipsing the C_1-O_4 bond). In all refinements $\angle H-C-O = 110.0$ and $\tau = 60.0°$ were assumed.

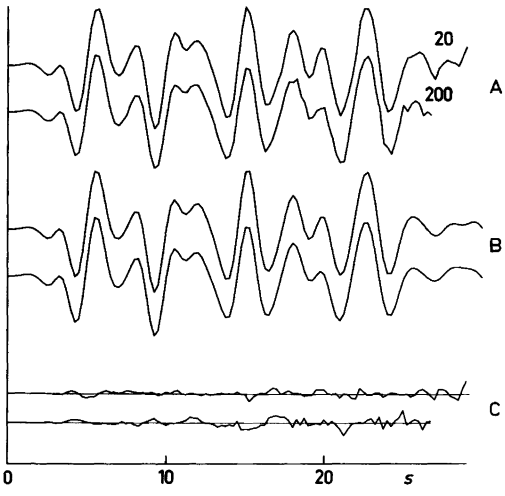

Fig. 2. Experimental (A), theoretical (B) and difference (C) intensity curves for methyl chloroformate at 20 and 200 °C. All curves are on the same scale and are in the form $sI_m(s)$ (see Ref. 13).

NORMAL COORDINATE CALCULATION

The amplitudes of vibration were calculated[15] using a valence force field similar to those reported for ethyl formate and ethyl chloroformate[16] adjusted to fit the frequencies reported for methyl chloroformate.[11] However, the starting values for the OC – O and O – CH_3 force constants used were the ones reported by Susi for methyl formate[17] since Charles *et al.*[16] have reservations about their values. Also these two C – O distances are found to differ by 0.1 Å in both methyl formate[18,19] and methyl chloroformate and are likely to have different force constants. The calculated potential energy distribution shows a rather complicated picture with substantial mixing between the different modes and hardly allows a straightforward assignment. The assignments in general agreed with the description given by Charles *et al.* for ethyl chloroformate.[16] We felt that the force field is adequate for the calculation of amplitudes which are not too sensitive to the force field employed.

From the methoxy torsion force constant obtained from the analysis (fitting the 163 cm^{-1} frequency), values of δ (root mean square amplitude of torsion motion around the C_1-O_4 bond) were estimated to 14° at 20 °C and 18° at 200 °C. These δ values were used in the least square refinements.[13] The calculated amplitudes were used whenever they are not refined in the least squares analyses. In cases where several amplitudes were refined as a group, their calculated differences were maintained. The same force field was used in calculating the amplitudes of vibration for the *anti* form.

CONFORMATION

The experimental radial distribution curves at both temperatures were found to be in good agreement with a model consisting of only the *syn* conformer. The RD-curves corresponding to the final model (100 % *syn*) are shown in Fig. 3. If an *anti* conformer were present, the shape of the curve in

Table 2. Final results for methyl chloroformate at 20 and 200 °C.[a]

	20 °C		200 °C	
	r_a	l[b]	r_a	l
C–H	1.092(24)	0.078	1.092	0.078
⟨C–O⟩	1.384(6)		1.395(8)	
Δ(C–O)	0.117(8)		0.122(10)	
C–Cl	1.754(4)	0.044(5)	1.757(6)	0.047(6)
∠O=C–O	128.1(0.6)		128.8(0.8)	
∠O–C–Cl	108.7(0.4)		108.0(0.7)	
∠C–O–C	114.4(1.7)		112.7(2.4)	
∠H–C–H	110.0		110.0	
τ(H–C–O–C)	60.0		60.0	
C=O	1.190(4)	0.042	1.188(7)	0.037
C–O	1.325(6)	0.050 (6)	1.334(8)	0.046 (9)
O–C	1.443(7)	0.055	1.457(10)	0.051
$O_2\cdots Cl_3$	2.602(7)	0.057	2.604(11)	0.065
$O_4\cdots Cl_3$	2.516(7)	0.059	2.513(10)	0.067
$O_2\cdots O_4$	2.263(8)	0.053	2.276(12)	0.057
$C_1\cdots C_5$	2.327(18)	0.071	2.324(32)	0.082
$O_4\cdots H_6$	2.084(18)	0.107	2.098(8)	0.111
$H_6\cdots H_7$	1.772(38)	0.127	1.777(8)	0.128
$C_5\cdots Cl_3$	3.876(12)	0.074(14)	3.878(19)	0.078(14)
$C_5\cdots O_2$	2.682(28)	0.104	2.675(50)	0.120
$Cl_3\cdots H_6$	4.235(19)	0.161	4.230(32)	0.183
$Cl_3\cdots H_7$	4.595(21)	0.112	4.609(15)	0.119
$O_2\cdots H_6$	2.687(28)	0.347	2.657(64)	0.430
$O_2\cdots H_7$	3.753(32)	0.121	3.750(46)	0.137
$C_1\cdots H_6$	2.617(25)	0.189	2.609(41)	0.222
$C_1\cdots H_7$	3.249(24)	0.103	3.255(22)	0.108
R[c]	0.100		0.122	

[a] Distances (r_a) and amplitudes (l) in Ångströms; angles in degrees. Parenthesized value are 2σ and they include estimates of systematic uncertainties and correlations among the data. [b] Braced values were refined as a group. [c] $R = [\Sigma\Delta_i^2/\Sigma I_i(\text{obs})^2]^{\frac{1}{2}}$ where $\Delta_i = I_i(\text{obs}) - I_i(\text{calc})$.

Table 3. Correlation matrix for methyl chloroformate 20 °C results.[a]

Parameters	σ[b]											
C–H	0.006	100										
C=O	0.001	15	100									
⟨C–O⟩	0.001	15	15	100								
Δ(C–O)	0.002	−38	−8	27	100							
C–Cl	0.001	−18	−32	−30	23	100						
∠O=C–O	0.155	2	−4	−11	15	48	100					
∠O–C–Cl	0.119	9	10	−40	−13	−14	−37	100				
∠C–O–C	0.415	−17	−15	−38	−15	−2	−40	41	100			
l_{12}	0.002	39	11	14	−39	−25	−15	−12	10	100		
l_{13}	0.002	−31	9	19	29	−6	−13	−32	11	13	100	
l_{35}	0.005	−7	14	15	−1	−1	−35	−11	9	12	24	100

[a] Angles in degrees and distances in Ångströms. [b] Standard deviations from least squares.

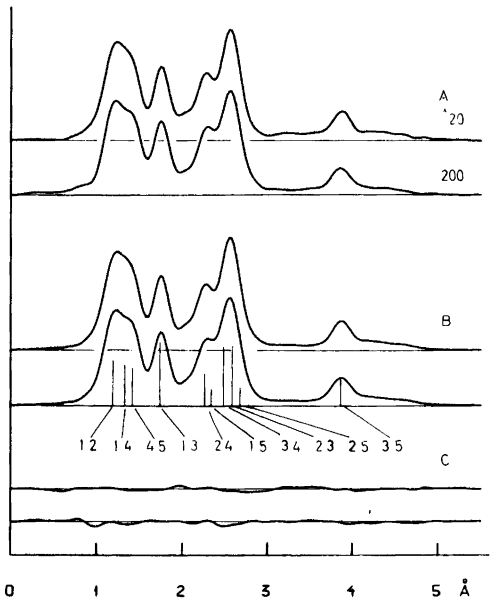

Fig. 3. Experimental (A), theoretical (B) and difference (C) radial distribution curves for methyl chloroformate at 20 and 200 °C. The lengths of the vertical bars are proportional to the weights of the distances.

the region $r > 3.0$ Å would be different due to the increase of the $O_2 \cdots C_5$ distance and the decrease in the $C_5 \cdots Cl_3$ distance.

The possible presence of an *anti* conformer (assumed to have the same structure as the *syn* conformer except for the O=C−O−C torsion angle) was tested by refining the composition parameter simultaneously with other structural parameters and values of 0 % ($2\sigma = 15$ %) and 10 % ($2\sigma = 20$ %) were obtained for the 20 and 200 °C data, respectively. The *R* factors (see Table 2) were virtually the same as those obtained assuming pure *syn* conformer. Radial distribution curves calculated with more *anti* conformer than the 2σ showed poorer agreement. There is no significant change in the gaseous composition between 20 and 200 °C. There is no evidence for the presence of significant amount of the *anti* in either set of data. Thus in the final refinements a model with pure *syn* was assumed for both temperatures. The final results are shown in Table 2 and the corresponding theoretical intensity and radial distribution curves are shown in Figs. 2 and 3. Table 3 is the correlation matrix for the results from the 20 °C experiment.

STRUCTURE

In Table 4 the values of the geometrical parameters obtained for methyl chloroformate from this, the microwave[11] and the earlier electron diffraction[2] investigations are shown together with those for methyl formate.[19] The parameter values from these investigations are consistent within experimental errors except for the OC−O bond where in the microwave work[11] for methyl chloroformate a rather large value of 1.36(2) Å was obtained. Judging from our results and the results obtained for methylformate [1.342(7) Å from ED[19] and 1.334(10) Å from MW[18]] we felt that our value of 1.325(6) Å was a more reasonable one. Comparing the molecular structures of methyl formate and methyl chloroformate it is not surprising that both the C=O and the CO−O bonds are shorter in the latter since

Table 4. Bond lengths (Å) and angles (°) for methyl chloroformate and methyl formate.

	$ClCOOCH_3$	$ClCOOCH_3$	$ClCOOCH_3$	$HCOOCH_3$
C−H	1.092(24)	1.07(2)	–	1.081(20)
C=O	1.190(4)	1.19(2)	1.19(3)	1.206(5)
C−O	1.325(6)	1.36(2)	1.36(4)	1.342(7)
O−CH_3	1.443(7)	1.43(2)	1.47(4)	1.445(4)
C−X	1.754(4)	1.73(2)	1.75(2)	1.101
∠O=C−O	128.1(6)	125(2)	126(4)	126.8(1.6)
∠O−C−X	108.7(4)	109(2)	111(4)	109.3
∠C−O−C	114.4(1.7)	115(2)	112(3)	114.3(2.9)
ϕ(O=C−O−C)	0 [a]	0	0−20	0
Method	E.D.	M.W.	E.D.	E.D.
Ref.	This work	11	2	18

[a] Zero degree corresponding to *syn*.

substitution of a proton by a chlorine atom usually decreases the adjacent bond distances. The $O-CH_3$ bonds, however, remain unchanged. The $O-C(sp^2)$ and $O-C(sp^3)$ bonds in methyl formate[19] [1.342(7) and 1.445(5) Å] are, respectively, shorter and longer than the corresponding ones in methylvinyl ether[20] [1.360(3) and 1.428(3) Å]. These changes may be attributed to the increased conjugation in the $O-C(sp^2)$ bond by lone pair participation and a consequential weakening of the $O-C(sp^3)$ bond caused by replacing the methylene group by a more electronegative oxygen atom. The C–Cl bond of 1.754(4) Å lies in between the $C(sp^2)-Cl$ bonds of 1.746(10) Å for phosgene[21] and 1.798(2) Å for acetyl chloride.[22]

Acknowledgement. The author would like to express his appreciation to Siv. ing. Ragnhild Seip for taking the electron diffraction photographs.

REFERENCES

1. Mizushima, S. and Kubo, M. *Bull. Chem. Soc. Jpn. 13* (1938) 174.
2. O'Gorman, J. M., Shand, W., Jr. and Schomaker, V. *J. Am. Chem. Soc. 72* (1950) 4222.
3. Collingwood, B., Lee, H. and Wilmshurst, J. K. *Aust. J. Chem. 19* (1966) 1637.
4. Bock, E. and Iwacha, D. *Can. J. Chem. 45* (1967) 3177.
5. Nyquist, R. A. *Spectrochim. Acta Part A 28* (1972) 285.
6. Cohen, A. J. and Whitehead, M. A. *J. Chem. Soc. Faraday Trans. 2, 68* (1972) 649.
7. Oki, M. and Nakanishi, H. *Bull. Chem. Soc. Jpn. 45* (1972) 1552.
8. Katon, J. E. and Griffin, M. G. *J. Chem. Phys. 59* (1973) 5868.
9. Lester, P. J. and Owen, N. L. *J. Chem. Soc. Faraday Trans. 2, 69* (1973) 1036.
10. Jones, J. I. L. and Owen, N. L. *J. Mol. Struct. 18* (1973) 1.
11. Durig, J. R. and Griffin, M. G. *J. Mol. Spectrosc. 64* (1977) 252.
12. Bastiansen, O., Garber, R. and Wegmann, L. *Balzer's High Vacuum Report 25* (1969) 1.
13. Hagen, K. and Hedberg, K. *J. Am. Chem. Soc. 95* (1973) 1003.
14. Schäfer, L., Yates, A. C. and Bonham, R. A. *J. Chem. Phys. 55* (1971) 3055.
15. Cyvin, S. J. *Molecular Vibrations and Mean Square Amplitudes*, Universitetsforlaget, Oslo and Elsevier, Amsterdam 1968.
16. Charles, S. W., Jones, G. I. L., Owen, N. L., Cyvin, S. J. and Cyvin, B. N. *J. Mol. Struct. 16* (1973) 225, and private communication with Prof. S. J. Cyvin.
17. Susi, H. and Scherer, J. R. *Spectrochim. Acta Part A 25* (1969) 1243.
18. Curl, R. F., Jr. *J. Chem. Phys. 30* (1959) 1529.
19. Shen, Q. *Acta Chem. Scand. A 31* (1977) 795.
20. Samdal, S. and Seip, H. M. *J. Mol. Struct. 28* (1975) 193.
21. Moule, D. C. and Foo, P. D. *J. Chem. Phys. 55* (1971) 1262.
22. Tsuchiya, S. and Kimura, M. *Bull. Chem. Soc. Jpn. 45* (1972) 736.

Received October 12, 1977.

Acta Chemica Scandinavica A 32 (1978) 251 – 258

On the Heats of Solvation of the Zinc(II), Cadmium(II) and Mercury(II) Ions, and of their Neutral Halide Complexes, in Water and Dimethyl Sulfoxide at 25 °C

STEN AHRLAND, LENNART KULLBERG and ROBERTO PORTANOVA *

Inorganic Chemistry 1, Chemical Center, University of Lund, P.O.Box 740, S-220 07 Lund, Sweden

Heats of solution have been determined for the zinc(II), cadmium(II) and mercury(II) halides in dimethyl sulfoxide (DMSO), and for the cadmium-(II) halides also in water. Combined with data from the literature, the values measured yield the solvation enthalpies of the neutral complexes ML_2. These are much larger for zinc(II) and cadmium(II) than for mercury(II), indicating that the solvent molecules are much more loosely bound in the latter case. Evidently, in the nearly linear complexes HgL_2 no solvent molecules are really close to the metal ion which they certainly are in the complexes ZnL_2 and CdL_2.

From the heats of solvation, the complex formation enthalpies and the lattice enthalpies, the sums of the solvation enthalpies of the ions present in each compound ML_2 can be calculated. If two reasonable extrathermodynamic assumptions are introduced, the solvation enthalpies of the ions Zn^{2+}, Cd^{2+} and Hg^{2+} in both water and DMSO can also be found. In both solvents, Zn^{2+} is more strongly solvated than Cd^{2+} which, however, is somewhat less strongly solvated than Hg^{2+}. The difference between Zn^{2+} and Cd^{2+} is larger in water than in DMSO, while the difference between Cd^{2+} and Hg^{2+} is smaller in water than in DMSO. These trends reflect the different character of the bonds formed by the various acceptors.

For the past few years the thermodynamics of metal complex formation in dimethyl sulfoxide, DMSO, have been studied in this laboratory and the results compared to those found previously for analogous reactions in aqueous solutions. Particularly the complexes formed between the divalent d^{10} ions of the zinc group and the heavy halides Cl^-, Br^- and I^- have been thoroughly investigated. These metal ions vary greatly in their bonding properties, from the distinctly hard Zn^{2+} *via* the mildly soft Cd^{2+} to the very soft Hg^{2+}. Also the bonding character of the ligands spans a wide range, from the mildly soft Cl^- *via* the softer Br^- to the very soft I^-. This means that in these systems complexes of widely different bonding characteristics are formed.

Both in water and DMSO the three metal ions mentioned are certainly all surrounded by six solvent molecules in a regular octahedral arrangement.[1-4] Their halide complexes are formed according to different patterns, however.[3,5-9] The final complex formed is without exception the tetrahedral ML_4^{2-}. For mercury(II) the neutral complexes HgL_2 generally have a linear structure which has no counterpart for cadmium(II) or zinc(II). The linear HgL_2 complexes have long been known both in crystalline and gaseous phases.[10] By recent X-ray diffraction measurements, linear or nearly linear complexes have been proved to exist also in solutions.[8,9] For cadmium(II) and zinc-(II), thermodynamic data also strongly suggest that the switch is directly from octahedral to tetrahedral coordination.[11,12] They indicate, moreover, that the change of coordination generally occurs at an earlier step for Zn^{2+} than for Cd^{2+}. This happens earlier in DMSO than in water. For the zinc chloride and bromide systems, the switch seems mainly to take place already at the first step in DMSO but at the second step in water. On account

* Present address: Istituto Impianto Nucleari, Universita di Palermo, Viale delle Scienze, I-90128 Palermo, Italy.

of the weak complex formation, no definite conclusions can be drawn for the zinc iodide system in water. In DMSO, however, it seems that the change occurs mainly at the second step. For the cadmium halide systems, the change of coordination takes place at the second step in DMSO but at the third step in water.

Complex formation equilibria in solution depend very much upon the solvation of the various species involved. This is why a knowledge of such parameters as the free energy, enthalpy and entropy of solvation is likely to shed light on the thermodynamic parameters of the complex formation reactions.

The free energy and heat of solvation should increase with the number of solvent molecules entering into close contact with the acceptor. Other factors will of course also influence the solvation parameters. The charge and size of acceptor and ligand, their capacities for covalent bonding, and the donor properties of the solvent all intricately contribute to the final outcome.

The heat of solvation of neutral complexes can be determined without any extrathermodynamic assumptions, by combining the heat of sublimation and the heat of solution which can both be experimentally determined. In this investigation, the heats of solvation of the neutral chloride, bromide, and iodide complexes of the zinc group metals in water and DMSO have been determined. Heats of sublimation have been obtained from literature data and heats of solution have been measured calorimetrically.

From the results obtained, heats of solvation of the free ions have also been derived. The heat of solvation of individual ions cannot be found without an extrathermodynamic assumption. Any evaluation from experimental data always gives the sum of the heats of solvation of the positive and negative ions of the electrolyte involved. In the present study, the quantities primarily obtained are therefore the sum of the heats of solvation of M^{2+} ($=Zn^{2+}$, Cd^{2+} or Hg^{2+}) and $2L^-$ ($=Cl^-$, Br^- or I^-). These are found by combining the heats of reaction measured, the lattice enthalpies found by means of a Born-Haber cycle and the enthalpy changes for the complex formation reactions which have been obtained previously. By means of extrathermodynamic assumptions that we consider reasonable, the individual heats of solvation for the halide ions have been calculated both in water and in DMSO. From these, we have been able to calculate the heats of solvation of Zn^{2+}, Cd^{2+} and Hg^{2+} in both solvents.

CALCULATIONS AND NOTATIONS

The heat of solvation of the neutral complex ML_2, $\Delta H^\circ_{sv}(ML_2)$, pertaining to the reaction

$$ML_2(g) \rightarrow ML_2(solv)$$

is obtained from the heat of sublimation, $\Delta H^\circ_{sub}(ML_2)$, pertaining to

$$ML_2(s) \rightarrow ML_2(g)$$

and the heat of solution, $\Delta H^\circ_s(ML_2)$, pertaining to

$$ML_2(s) \rightarrow ML_2(solv)$$

through the relation

$$\Delta H^\circ_{sv}(ML_2) = \Delta H^\circ_s(ML_2) - \Delta H^\circ_{sub}(ML_2) \qquad (1)$$

If the complex ML_2 is not very stable in solution, a more or less extensive dissociation will take place when the salt is dissolved. In many systems reactions involving a disproportionation of the complex also occur. The heats actually measured have to be corrected for effects due to such reactions, in order to provide the quantity $\Delta H^\circ_s(ML_2)$. This requires not only that the compositions of the equilibrium solutions can be calculated from the pertinent stability constants, but also that the enthalpy changes of all the dissociation and disproportionation reactions involved are known. As regards the present systems, extensive dissociation and/or disproportionation takes place for the zinc and cadmium halides, while the mercury ones remain virtually unchanged. The stability constants and enthalpy changes necessary for the calculation of $\Delta H^\circ_s(ML_2)$ for the zinc and cadmium complexes have all been measured,[11-13] though the values determined for the very weak zinc complexes formed in aqueous solution are not sufficiently precise for the present purpose.[13] These measurements all refer to a temperature of 25 °C and to ionic media of 1 M $NaClO_4$ in water and 1 M NH_4ClO_4 in DMSO. Consequently, the same conditions have been chosen for the present study.

For the ion solvation reaction

$$M^{2+}(g) + 2L^-(g) \rightarrow M^{2+}(solv) + 2L^-(solv)$$

the enthalpy change is

$$\Delta H^\circ_{sv}(M,2L) = \Delta H^\circ_{sv}(M) + 2\,\Delta H^\circ_{sv}(L) \quad (2)$$

where $\Delta H^\circ_{sv}(M)$ and $\Delta H^\circ_{sv}(L)$ are the heats of solvation of M^{2+} and L^-, respectively. The quantity $\Delta H^\circ_{sv}(M,2L)$ is related to the enthalpy change $\Delta H^\circ_s(M,2L)$ of the solution reaction

$$ML_2(s) \rightarrow M^{2+}(solv) + 2\,L^-(solv)$$

according to

$$\Delta H^\circ_{sv}(M,2L) = \Delta H^\circ_s(M,2L) + \Delta H^\circ_{lat} \quad (3)$$

where ΔH°_{lat} is the lattice enthalpy of the salt ML_2, *i.e.* the enthalpy change of the reaction

$$M^{2+}(g) + 2\,L^-(g) \rightarrow ML_2(s)$$

The heats of solution pertaining to the ions and to the neutral complex are related according to

$$\Delta H^\circ_s(M,2L) = \Delta H^\circ_s(ML_2) - \Delta H^\circ_{\beta 2} \quad (4)$$

where $\Delta H^\circ_{\beta 2}$ is the enthalpy change of the reaction

$$M^{2+}(solv) + 2\,L^-(solv) \rightarrow ML_2(solv)$$

For the calculation of $\Delta H^\circ_{sv}(M,2L)$, the values of $\Delta H^\circ_{\beta 2}$ have thus to be known not only for the zinc and cadmium, but also for the mercury(II) systems.

EXPERIMENTAL

Materials. The salts used were all of analytical grade. Dry zinc chloride and bromide were prepared by heating the pure "anhydrous" salts in a stream of dry hydrogen chloride and bromide gas, respectively. Traces of these gases were afterwards removed by a stream of dry nitrogen. The zinc iodide was recrystallized from water and then dried by heating in a dry nitrogen atmosphere. The dry salts are extremely hygroscopic and have to be very carefully protected from moisture.

The cadmium halides were dehydrated by heating to 80 °C overnight.

The mercury(II) chloride, bromide, and iodide (red) were recrystallized from hot water, alcohol, and acetone, respectively, and dried over silica gel.

The sodium and ammonium perchlorates and the DMSO were purified and analyzed as described before.[14-15]

The calorimetric apparatus and procedure have been described previously.[16] Varying amounts of the salts (0.05 – 0.5 g) were transferred into ampoules in a dry-box. The ampoules were sealed in the box and then weighed. The salts were dissolved in 80.0 ml of solution which in no case took more than 10 min. At least six separate experiments were performed for each salt and solvent. All the measurements were performed at 25 °C.

Table 1. Solvation enthalpies for neutral complexes, ML_2, in water and DMSO, *i.e.* $\Delta H^\circ_{sv}(ML_2)$ for the reactions $ML_2(g) \rightarrow ML_2(solv)$, calculated from the dissolution and sublimation enthalpies of the solid compounds according to eqn. (1). Values in kJ mol^{-1}; 25 °C.

ML_2	ΔH°_{sub}	Water		DMSO	
		ΔH°_s	ΔH°_{sv}	ΔH°_s	ΔH°_{sv}
$ZnCl_2$	149.0[a]			−70.0	−219
$ZnBr_2$	145.0[a]			−75.9	−221
ZnI_2	140.4[a]			−84.1	−224.5
$CdCl_2$	180[b]	−13.7	−194	−41.2	−221
$CdBr_2$	163[b]	−7.3	−170	−46.2	−209
CdI_2	146[b]	4.9	−141	−45.2	−191
$HgCl_2$	83.1[c]	14.0[d]	−69	−21.2	−104
$HgBr_2$	83.7[b]	20[e]	−64	−17.0	−101
HgI_2	91.2[b]	28.9[f]	−62	−4.3	−95.5

[a] From Ref. 20. [b] From Ref. 21. [c] From Ref. 22. [d] From Ref. 19; in 1 M $HClO_4$. [e] From Ref. 18; at variable ionic strength. [f] From Ref. 17; in 0.5 M $(Na,H)ClO_4$.

MEASUREMENTS AND RESULTS

Heats of solvation of neutral complexes. In the present investigation, heats of solution have been measured for all the halides in DMSO, and for the cadmium halides also in water. The values of $\Delta H_s^\circ(ML_2)$ found are collected in Table 1. These values are fairly precise with random errors estimated to 0.5–0.8 kJ mol^{-1} in DMSO and even less, <0.2 kJ mol^{-1}, in water. The degree of dissociation and disproportionation of a salt depends on its concentration. We found the same value of $\Delta H_s^\circ(ML_2)$ independent of the amount of salt dissolved so the corrections introduced to account for these reactions are evidently correct.

The mercury(II) bromide is very sparingly soluble in water and the iodide even less. A determination of $\Delta H_s^\circ(ML_2)$ by means of the present calorimetric method is therefore not feasible for these systems. For HgI_2, a value has nevertheless been determined calorimetrically, from measurements including the precipitation reaction.[17] For $HgBr_2$, on the other hand, one has to be content with a value calculated from the temperature coefficient of the solubility.[18] The value given for $HgCl_2$ has been determined calorimetrically, by much the same method as used in the present work.[19] The errors of the chloride and iodide values given in Table 1 are estimated to ±1 kJ mol^{-1}, while the precision of the bromide value is probably only ±4 kJ mol^{-1}.

The heats of sublimation listed in Table 1 are claimed to be correct within 2 or 3 kJ mol^{-1}. In all but the $HgBr_2$ case, these errors thus contribute most to the errors of ΔH_{sv}°.

Heats of solvation of individual ions. The total heats of solution, $\Delta H_s^\circ(M,2L)$, of the halide salts, calculated from eqn. (4) by using the values of $\Delta H_s^\circ(ML_2)$ in Table 1, are given in Table 2, where the values of $\Delta H_{\beta 2}^\circ$ are also stated. The values of $\Delta H_s^\circ(M,2L)$ for the zinc halide systems in water have been obtained directly from calorimetric determinations of the heats evolved when the salts are dissolved.[25]

The lattice enthalpies, ΔH_{lat}°, at 25 °C, wanted for the calculation of $\Delta H_{sv}^\circ(M,2L)$ have been obtained by the Born-Haber cycle given in Fig. 1. The data used in these calculations are listed in Table 3. The heat of solvation values, $\Delta H_{sv}^\circ(M,2L)$, obtained from eqn. (3) are given in Table 4.

From the difference $\Delta H_{sv}^\circ(M,2L) - \Delta H_{sv}^\circ(M,2L')$, the difference in the heat of solvation between the two halide ions can be obtained. Values of $\Delta H_{sv}^\circ(Cl-L)$ have been calculated between the chloride ion and the bromide and iodide ions. For each of the two solvents, the three metal ions ought to give the same differences which they do, within the experimental errors, as is demonstrated by the values listed in Table 4. In Fig. 2, the differences are plotted *vs.* the ionic radii of the halide ions. In both solvents, $-\Delta H_{sv}^\circ(L^-)$ decreases in the sequence $Cl^- > Br^- > I^-$, *i.e.* with increasing radius of the halide ion. The decrease is much slower in DMSO than in water, however. From studies involving only alkali halides, Halliwell and Nyburg[31] found

Table 2. Heats of solution, $\Delta H_s^\circ(M,2L)$, in water and DMSO. The values calculated from $\Delta H_s^\circ(ML_2)$, see Table 1, and $\Delta H_{\beta 2}^\circ$ according to eqn. (4). All values in kJ mol^{-1}.

ML_2	Water		DMSO	
	$\Delta H_{\beta 2}^\circ$	$\Delta H_s^\circ(M,2L)$	$\Delta H_{\beta 2}^\circ$	$\Delta H_s^\circ(M,2L)$
$ZnCl_2$		−67.2[d]	23.1[e]	−93.1
$ZnBr_2$		−59.4[d]	36.9[e]	−112.8
ZnI_2		−51.0[d]	48.4[e]	−132.5
$CdCl_2$	2.6[a]	−16.3	8.7[f]	−49.9
$CdBr_2$	−6.5[b]	−0.8	13.1[f]	−59.3
CdI_2	−12.3[a]	17.2	29.4[f]	−74.6
$HgCl_2$	−53.6[c]	68	−49.3[g]	28.1
$HgBr_2$	−87.0[c]	107	−57.5[g]	40.5
HgI_2	−143.1[c]	172	−73.1[g]	68.8

[a] From Ref. 23. [b] From Ref. 24; in 3 M $NaClO_4$. [c] From Ref. 17; in 0.5 M ($NaClO_4$, $HClO_4$). [d] From Ref. 25; in 2 M HNO_3 ($ZnCl_2$ and $ZnBr_2$) and in 2 M $HClO_4$ ($ZnBr_2$). [e] From Ref. 12. [f] From Ref. 11. [g] From Ref. 26.

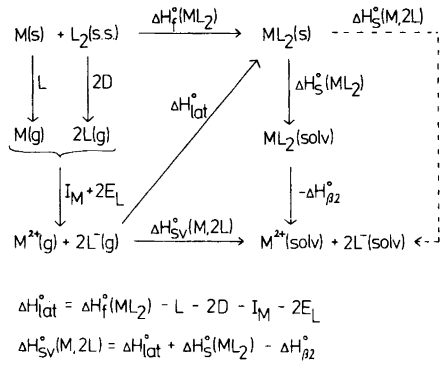

Fig. 1. The Born-Haber cycle used for the calculation of ΔH°_{lat} and $\Delta H^\circ_{sv}(M,2L)$.

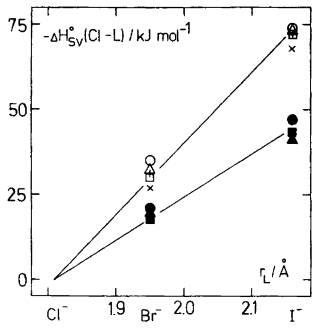

Fig. 2. Differences $\Delta H^\circ_{sv}(Cl-L)$ between halide ions in water and DMSO plotted *vs.* the ionic radii. Circles, squares and triangles refer to values obtained from ZnL_2, CdL_2 and HgL_2, respectively; open signs refer to water, filled signs to DMSO. The signs × and + refer to the values found for water by Halliwell and Nyburg[31] and by Morris,[32] respectively.

differences $-\Delta H^\circ_{sv}(Cl-Br)=27$ kJ mol^{-1} and $-\Delta H^\circ_{sv}(Cl-I)=68$ kJ mol^{-1} while Morris[32] found 31 and 72 kJ mol^{-1}, respectively. Especially the latter values agree nicely with ours; *cf.* Fig. 2 and Table 4.

There is, as has been pointed out above, no purely thermodynamic way to separate $\Delta H^\circ_{sv}(M,2L)$ into its constituent parts $\Delta H^\circ_{sv}(M^{2+})$ and $2\Delta H^\circ_{sv}(L)$, *cf.* eqn. (2). Large efforts have been made to effect a reasonable partition by means of various extrathermodynamic assumptions. Aqueous solutions have naturally attracted the largest interest. The focal point of this discussion has been how to calculate the "best" value of the solvation enthalpy of the proton, $\Delta H^\circ_{aq}(H^+)$. The most satisfactory approach seems to be the semi-empirical one used by Halliwell and Nyburg.[31] By this method Morris[32] found $-\Delta H^\circ_{aq}(H^+)=1103\pm12$ kJ mol^{-1}. With this value as reference Morris determined, *i.a.*, the heats of hydration of the halide ions, Table 4, note *a*. These values have been used in the calculation of heats

Table 3. Calculation of lattice enthalpies, ΔH°_{lat}, for the reactions $M^{2+}(g)+2L^-(g)\rightarrow ML_2(s)$, from the Born-Haber cycle, Fig. 1. All values in kJ mol^{-1}.

ML_2	ΔH°_f [a]	D [b]	E [c]	L [d]	I [e]	$-\Delta H^\circ_{lat}$
$ZnCl_2$	−416.7	121.8	−348.5	130.5	2638.0	2731.8
$ZnBr_2$	−328.0	111.7	−324.7	130.5	2638.0	2670.5
ZnI_2	−208.4	106.7	−295.4	130.5	2638.0	2599.5
$CdCl_2$	−389.1	121.8	−348.5	111.9	2497.8	2545.4
$CdBr_2$	−317.1	111.7	−324.7	111.9	2497.8	2500.8
CdI_2	−202.5	106.7	−295.4	111.9	2497.8	2434.8
$HgCl_2$	−223.4	121.8	−348.5	61.3	2815.0	2646.3
$HgBr_2$	−170.3	111.7	−324.7	61.3	2815.0	2620.6
HgI_2	−105.9	106.7	−295.4	61.3	2815.0	2604.8

[a] Standard heats of formation of the crystalline halides, *i.e.* ΔH°_f for the reactions $M(s)+\frac{1}{2}L_2(s,s)\rightarrow ML_2(s)$. The values (at 298 K) from Ref. 27. [b] Heats of atomization of the halogens, *i.e.* D for the reactions $\frac{1}{2}L_2(s,s)\rightarrow L(g)$. The values (at 298 K) from Ref. 28. [c] Electron affinities of the halogen atoms, *i.e.* E for the reactions $e^-+L(g)\rightarrow L^-(g)$. The values (at 0 K) from Ref. 29. [d] Heats of sublimation of the metals, *i.e.* L for the reactions $M(s)\rightarrow M(g)$. The values (at 298 K) from Ref. 27. [e] Ionization potentials of the metal atoms, *i.e.* I for the reactions $M(g)\rightarrow M^{2+}(g)+2e^-$. The values (at 0 K) from Ref. 30.

Table 4. Solvation enthalpies of pairs of ions and determination of single-ion heats of solvation. All values in kJ mol^{-1}.

$M^{2+}+2L^-$	Water			DMSO		
	$-\Delta H^\circ_{sv}(M,2L)$	$-\Delta H^\circ_{sv}(Cl-L)$	$-\Delta H^\circ_{sv}(M^{2+})^a$	$-\Delta H^\circ_{sv}(M,2L)$	$-\Delta H^\circ_{sv}(Cl-L)$	$-\Delta H^\circ_{sv}(M^{2+})^b$
$Zn^{2+}+2Cl^-$	2799	0	2067	2825	0	2131
$Zn^{2+}+2Br^-$	2730	35	2060	2783	21	2121
$Zn^{2+}+2I^-$	2651	74	2063	2732	47	2118
			Av. 2063			Av. 2123
$Cd^{2+}+2Cl^-$	2562	0	1830	2595	0	1901
$Cd^{2+}+2Br^-$	2502	30	1832	2560	18	1898
$Cd^{2+}+2I^-$	2418	72	1830	2509	43	1895
			Av. 1831			Av. 1898
$Hg^{2+}+2Cl^-$	2578	0	1846	2618	0	1923
$Hg^{2+}+2Br^-$	2514	32	1844	2580	19	1917
$Hg^{2+}+2I^-$	2433	73	1845	2536	41	1922
			Av. 1845			Av. 1921

[a] Calculated from heat of hydration values of the halide ions given in Ref. 32: $-\Delta H^\circ_{aq}=366$, 335 and 294 kJ mol^{-1} for Cl^-, Br^- and I^-, respectively. [b] From heats of hydration given in Ref. 32 and heats of transfer given in Ref. 37; the heats of solvation of the halide ions in DMSO have been calculated to be $-\Delta H^\circ_{s}=347$, 331 and 307 kJ mol^{-1} for Cl^-, Br^- and I^-, respectively.

of hydration of Zn^{2+}, Cd^{2+}, and Hg^{2+}, Table 4. For each metal ion the three halides should give the same value of $\Delta H^\circ_{aq}(M^{2+})$. Indeed the values found agree within a few kJ mol^{-1}, Table 4. The values of $\Delta H^\circ_{aq}(M^{2+})$ also agree well with those given by Noyes[33] in a compilation of ion hydration data. Recalculating Noyes' values to the same reference point as ours, *i.e.* $-\Delta H^\circ_{aq}(H^+)=1103$ kJ mol^{-1}, gives $-\Delta H^\circ_{aq}=2071$, 1833, and 1848 kJ mol^{-1} for Zn^{2+}, Cd^{2+}, and Hg^{2+}, respectively. Values of $\Delta H^\circ_{aq}(M^{2+})$ for these ions have also been reported by Ladd and Lee.[34] Their values for Zn^{2+} and Cd^{2+}, *viz.* 2067 and 1837 kJ mol^{-1} are close to ours, while the value quoted for Hg^{2+} is considerably more exothermic. Ladd and Lee calculated their $\Delta H^\circ_{aq}(Hg^{2+})$ value from measurements on $HgCl_2$, $HgBr_2$, and $Hg(CN)_2$. By means of eqn. (3) above, they found from these measurements $-\Delta H^\circ_{aq}(Hg^{2+})=1908$, 1942, and 2042 kJ mol^{-1}, respectively. In their evaluation Ladd and Lee apparently assumed that these mercury(II) salts are all completely dissociated in aqueous solution. In fact, they dissociate very little even at low concentrations. Ladd and Lee's values can be corrected by subtracting the enthalpy changes, $\Delta H^\circ_{\beta 2}$, from the calculated hydration enthalpies; *cf.* eqn. (4). Christensen *et al.*[17,35] have determined the enthalpy changes for the complex formation in the mercury(II) halide and cyanide systems. Using their $\Delta H^\circ_{\beta 2}$-values we find the corrected values $-\Delta H^\circ_{aq}(Hg^{2+})=1854$, 1853, and 1840 kJ mol^{-1} from the $HgCl_2$, $HgBr_2$ and $Hg(CN)_2$ data, respectively. These values agree satisfactorily among themselves and the mean, 1849 kJ mol^{-1}, is indeed very close both to our value and to the modified Noyes value quoted above.

The solvation enthalpies of ions differ relatively little between different solvents. The differences are defined as enthalpies of transfer, ΔH°_{tr}. Values of ΔH°_{tr} for salts are readily determined as differences between the values of ΔH°_s in the solvents concerned. Just as for ΔH°_{sv}, however, the values of the individual ions cannot be calculated except by the introduction of an extrathermodynamic assumption. Again, several such assumptions have been proposed. Of these, the assumption that $\Delta H_{tr}(Ph_4As^+)=\Delta H_{tr}(Ph_4B^-)$ has become most widely used, as being both very reasonable and also easy to apply.[36] Based on that assumption Krishnan and Friedman[37] determined values of ΔH°_{tr} of single ions for the transfer between the three solvents propylene carbonate, DMSO, and water. For the halide ions Cl^-, Br^-, and I^-, ΔH°_{tr} (W → DMSO) were found to be 18.8, 3.5, and -12.8 kJ mol^{-1}, respectively, with errors not exceeding 1 or, at most, 2 kJ (*cf.*

also Ref. 38, p. 19. These values together with the $\Delta H^\circ_{aq}(L^-)$-values given by Morris[32] yield the absolute heats of solvation of the halide ions in DMSO, see note *b* of Table 4. From these, the values of the heats of solvation of Zn^{2+}, Cd^{2+}, and Hg^{2+} in DMSO, can be calculated, Table 4. The results show that also in DMSO, the values of $\Delta H^\circ_{sv}(M^{2+})$ obtained from the chloride, bromide, and iodide data agree very well for each metal ion.

DISCUSSION

For the metal ions studied the heat of solvation is more exothermic in DMSO than in water, indicating a preference for DMSO. For Zn^{2+}, Cd^{2+}, and Hg^{2+}, ΔH°_{tr} (W → DMSO) is found to be −60, −67, and −76 kJ mol^{-1}, respectively, Table 4. Thus, the softer the metal ion, the stronger its preference for DMSO. In both water and DMSO the heat of solvation decreases considerably from Zn^{2+} to Cd^{2+} but increases a little from Cd^{2+} to Hg^{2+}. The total heat is composed of contributions from electrostatic as well as covalent interactions between the metal ion and the solvent molecules. The electrostatic interaction decreases with increasing radius of the ion, *i.e.* in the order $Zn^{2+} > Cd^{2+} > Hg^{2+}$ (for recent values of the octahedral ionic radii, see Refs. 4 and 39). The covalent interaction, on the other hand, increases as the metal ion becomes softer, *i.e.* in the order $Zn^{2+} < Cd^{2+} < Hg^{2+}$. Evidently the sum of the two contributions might pass through a minimum, as is in fact observed for Cd^{2+}.

The heats of solvation of the neutral complexes, ML_2, should follow the same trend as those of the metal ions, if no special effects intervene. For all halides studied, $-\Delta H^\circ_{sv}(ML_2)$ is considerably higher in DMSO than in water, Table 1. This is, as previously noted, also the case for the free metal ions. For the complexes, however, the heat differences between the two solvents are relatively much larger than for the free ions. This is evident from the ratio ΔH°_{tr} (W → DMSO)/ΔH°_{aq} which for the free metal ions is ≈0.04, much lower than for any of the complexes. For the complexes HgL_2, the ratio even reaches values as high as ≈0.5. The solvents thus interact much more specifically with the complexes ML_2 than with the free metal ions. In fact, the absolute values of $-\Delta H^\circ_{tr}$ (W → DMSO) for the complexes, 30 to 50 kJ mol^{-1} are not much smaller than for the free ions, 60 to 76 kJ mol^{-1}; Table 1.

For both water and DMSO the values of $-\Delta H^\circ_{sv}(ML_2)$ are much higher for the zinc and cadmium halides than for the mercury halides. The reason is certainly that solvent molecules enter into a much closer contact with the metal ion in the case of ZnL_2 and CdL_2 than in the case of HgL_2. The second zinc and cadmium complexes are in solution either octahedral or tetrahedral,[11,12,38] with solvent molecules coordinated about as closely as the other ligands. In the nearly linear mercury complexes, on the other hand, the solvent to metal bonds are certainly all long[8,9] and the interaction consequently much weaker.

Another very striking fact is that while for HgL_2 and CdL_2 the values of $-\Delta H^\circ_{sv}(ML_2)$ in both water and DMSO distinctly decrease in the order $Cl^- > Br^- > I^-$, the values for Zn^{2+} increase slowly in the same order. This is probably due to a combination of the following two effects.

Firstly, in the complexes ZnL_2, where the forces between L^- and the hard acceptor Zn^{2+} are of a mainly electrostatic character, the effective charge on the metal ion will be higher the lower the charge density on the ligand, and the higher the effective charge, the stronger the solvation. As the charge density decreases in the sequence $Cl^- > Br^- > I^-$, the effective charge will increase and the solvation consequently become stronger in the same sequence. On the other hand, in complexes like CdL_2 and HgL_2 where the metal ions are soft, the interactions between the ligands and the central ions are of a rather covalent character. The effective charge on the metal ion will in such cases be lower the more covalent the bonding, *i.e.* the softer the ligand. As the softness increases in the sequence $Cl^- < Br^- < I^-$, the effective charge for these soft metal ions decreases, and the solvation consequently becomes weaker in the same sequence.

Secondly, in the zinc chloride and bromide systems, the switch from octahedral to tetrahedral coordination in DMSO occurs mainly at the first step and is certainly complete at the second, while the process occurs later in the zinc iodide and in all the cadmium halide systems. Consequently, the heats of solvation of $ZnCl_2$ and $ZnBr_2$, forming exclusively tetrahedral complexes, should be expected to be relatively low compared to the other complexes which are more extensively solvated. For $ZnCl_2$, the value of $-\Delta H^\circ_{sv}$ is in fact even somewhat lower than that of $CdCl_2$, though the opposite could be expected considering the values of ΔH°_{sv} of the respective metal ions.

The two effects discussed are most likely interwoven. The high effective charge left on zinc iodide complexes permits the coordination of more solvent molecules at a later stage of the complex formation than in the case of the chloride and bromide systems, where the effective charge is lower.

Acknowledgement. We gratefully acknowledge the support given to this investigation by Statens naturvetenskapliga forskningsråd (The Swedish Natural Science Research Council).

REFERENCES

1. Bol, W., Gerrits, G. J. A. and van Panthaleon van Eck, C. L. *J. Appl. Crystallogr. 3* (1970) 486.
2. Johansson, G. *Acta Chem. Scand. 25* (1971) 2787.
3. Ohtaki, H., Maeda, M. and Ito, S. *Bull. Chem. Soc. Jpn. 47* (1974) 2217.
4. Sandström, M., Persson, I. and Ahrland, S. *To be published.*
5. Sandström, M. *Acta Chem. Scand. A 31* (1977) 141.
6. Sandström, M. and Johansson, G. *Acta Chem. Scand. A 31* (1977) 132.
7. Johansson, G., Pocev, S. and Triolo, R. *Personal communication.*
8. Gaizer, F. and Johansson, G. *Acta Chem. Scand. 22* (1968) 3013.
9. Sandström, M. *To be published.*
10. Wells, A. F. *Structural Inorganic Chemistry*, 4th Ed., Clarendon Press, Oxford 1975.
11. Ahrland, S. and Björk, N. O. *Acta Chem. Scand. A 30* (1976) 257.
12. Ahrland, S., Björk, N. O. and Portanova, R. *Acta Chem. Scand. A 30* (1976) 270.
13. Gerding, P. *Acta Chem. Scand. 23* (1969) 1695.
14. Ahrland, S. and Kullberg, L. *Acta Chem. Scand. 25* (1971) 3457.
15. Ahrland, S. and Björk, N. O. *Acta Chem. Scand. A 28* (1974) 823.
16. Kullberg, L. *Acta Chem. Scand. A 28* (1974) 979.
17. Christensen, J. J., Izatt, R. M., Hansen, L. D. and Hale, J. D. *Inorg. Chem. 3* (1964) 130.
18. Tyrrel, H. J. V. and Richards, J. *J. Chem. Soc.* (1953) 3812; see *Gmelin Hg B2*, p. 766.
19. Gallagher, P. K. and King, E. L. *J. Am. Chem. Soc. 82* (1960) 3510.
20. Rice, D. W. and Gregory, N. W. *J. Phys. Chem. 72* (1968) 3361.
21. Brewer, L., Somayajulu, G. R. and Brackett, E. *Chem. Rev. 63* (1963) 111.
22. Cubicciotti, D., Eding, H. and Johnson, J. W. *J. Phys. Chem. 70* (1966) 2989.
23. Gerding, P. and Jönsson, I. *Acta Chem. Scand. 22* (1968) 2247.
24. Gerding, P. *Acta Chem. Scand. 20* (1966) 79.
25. Bernhard, M. A., Busnot, F. and Le Querler, J. F. *Bull. Soc. Chim. Fr.* (1972) 4523.
26. Ahrland, S., Persson, I. and Portanova, R. *To be published.*
27. Lewis, G. N. and Randall, M. *Thermodynamics* (revised by Pitzer, K. S. and Brewer, L.) Appendix 7, McGraw-Hill, New York 1961.
28. Sharpe, A. G. In Gutmann, V., Ed., *Halogen Chemistry*, Academic, London and New York 1967, Vol. 1.
29. Berry, R. S. and Reimann, C. W. *J. Chem. Phys. 38* (1963) 1540.
30. *Handbook of Chemistry and Physics*, 55th Ed., CRC, Cleveland, Ohio 1974.
31. Halliwell, H. F. and Nyburg, S. C. *Trans. Faraday Soc. 59* (1963) 1126.
32. Morris, D. F. C. *Struct. Bonding (Berlin) 4* (1968) 63.
33. Noyes, R. M. *J. Am. Chem. Soc. 84* (1962) 513.
34. Ladd, M. F. C. and Lee, W. H. *J. Inorg. Nucl. Chem. 13* (1960) 218.
35. Christensen, J. J., Izatt, R. M. and Eatough, D. *Inorg. Chem. 4* (1965) 1278.
36. Cox, B. G. and Parker, A. J. *J. Am. Chem. Soc. 95* (1973) 402.
37. Krishnan, C. V. and Friedman, H. L. *J. Phys. Chem. 73* (1969) 3934.
38. Ahrland, S. In Lagowski, J. J., Ed., *The Chemistry of Non-Aqueous Solvents*, Academic, New York and London 1978, Vol. V, p. 1.
39. Shannon, R. D. and Prewitt, C. T. *Acta Crystallogr. B 25* (1969) 925.

Received November 22, 1977.

Acta Chemica Scandinavica A 32 (1978) 259–265

Tentative Assignments of Fundamental Vibrations of Thio- and Selenoamides. IV. Addition Compounds of Tetramethylthiourea with Iodine, Methyl Iodide and Metal Halides

G. BORCH,[a] P. KLÆBOE,[b] P. H. NIELSEN[c] and L. M. PEDERSEN[c]

[a] Chemistry Department A, The Technical University of Denmark, DK-2800 Lyngby, Denmark, [b] Department of Chemistry, University of Oslo, Oslo 3, Norway and [c] Chemical Laboratory II, The H. C. Ørsted Institute, DK-2100 Copenhagen, Denmark

The perturbations of the vibrational modes of tetramethylthiourea (TMTU) in addition compounds (complexes) with iodine, methyl iodide, and methyl halides ($ZnCl_2$, $CdCl_2$, CdI_2, $HgCl_2$, and HgI_2) have been studied. The changes of force constants obtained from normal coordinate analyses agreed well with the charge redistributions calculated in the CNDO-MO approximation using model compounds. A limited CNDO/S-CI procedure was used to assign the main UV transitions for TMTU and its addition compounds with iodine, methyl iodide, and strong acids. The CNDO occupied orbital eigenvalues and assignments for the photoelectron spectrum of TMTU in the 7–13 eV range are in agreement with experimental results. The study demonstrates that the semiempirical CNDO/S method may serve to explain infrared, ultraviolet, and photoelectron spectra of TMTU and some of its addition compounds. Some limitations for the interpretation of the infrared spectra are discussed.

We have previously shown [1] that certain IR absorption bands of thioureas (termed A–G bands) behave in a characteristic way when the thioureas are deuterated, *S*-alkylated, transformed into metal complexes, or when sulfur is replaced with selenium. Recently, the vibrational spectra of tetramethylthiourea (TMTU) including a normal coordinate treatment of TMTU and five isotopic species [2] and of tetramethylselenourea and two deuterated species [3] were published. In the present paper we report the changes in the IR spectra of TMTU when forming addition compounds with iodine ($TMTU \cdot I_2$), methyl iodide ($TMTU \cdot CH_3I$ or *S*-methylisothiouronium iodide), and metal halides (2:1 complexes with HgI_2, $CdCl_2$, CdI_2 and $ZnCl_2$, and 1:1 complex with $HgCl_2$). In a forthcoming paper the vibrational spectra of the addition compound between tetramethylselenourea and iodine will be discussed in connection with a normal coordinate analysis (NCA).

Recently, the charge transfer complex formed between tetramethylurea and iodine was studied in nonpolar solvents by IR spectroscopy.[4] From an NCA it was concluded that mainly the CO and CN stretching and the $(CH_3)_2N$ deformation vibrations are perturbed by complex formation. Qualitatively, this was explained by electronic redistribution caused by charge transfer from tetramethylurea to iodine.[4,5]

TMTU forms a very strong 1:1 complex with iodine [6,7] and the IR spectrum of a solution has been reported.[8–10] Since the IR results are partly conflicting we have reinvestigated the spectrum of $TMTU \cdot I_2$ in solution and as a film on a KBr-disc. The Raman bands below 300 cm^{-1} may be correlated with the strength of the donor-acceptor interaction [11] and this region was therefore recorded for $TMTU \cdot I_2$ in chloroform solution.

The IR spectrum of $TMTU \cdot CH_3I$ has only been incompletely reported [1] and was recorded in the 200–4000 cm^{-1} range. Though the IR and Raman spectra of metal halide complexes of TMTU have been discussed in several papers,[12–18] complete listings of the observed frequencies in the region 200–2000 cm^{-1} have not appeared. Therefore, we

determined the IR spectra of five selected metal halide complexes. Since the frequency shifts of the TMTU bands on complex formation with the metal halides were quite similar, we used the mean values of these shifts as characteristic for a typical complex.

Generalised valence force fields (GVFF) of these complexes are correlated with CNDO/S electronic densities for feasible model compounds. The usefulness of the CNDO/S method is further demonstrated by correlation with ultraviolet and photoelectron data.

EXPERIMENTAL

The IR spectra were recorded on Perkin-Elmer models 180, 225, 283 and/or 337 spectrometers. Spectra of TMTU solutions without and with addition of iodine were recorded on the same paper and are believed to be correct within $1-2\ cm^{-1}$ for well-resolved bands. All shifts were determined in *ca.* 1 M solutions in CS_2 and $CHCl_3$. In CS_2, even with a double excess of iodine, only a 50 % conversion of TMTU to the iodine complex took place. This complies with thermodynamic evidence[6] that polar solvents like $CHCl_3$ stabilize strong charge-transfer complexes such as $TMTU \cdot I_2$ more than do nonpolar solvents (CS_2). The measurements in $CHCl_3$ solution were carried out in solutions with

Table 1. Observed and calculated shifts (cm^{-1}) of the infrared bands of tetramethylthiourea on addition of methyl iodide, iodine, and metal halides.

Species[b] and No.		Tetramethylthiourea Position[b]	Description (PED, %)[c]	Shifts[a] on addition of CH_3I[d] Obs	Calc	I_2[e] Obs	Calc	Metal halide[f] Obs	Calc
a	ν_7	1499	$\nu_{as}N_2CS(30)$, $\delta NCN(15)$, $\rho Me_2N(25)$, $\nu_{as}Me_2N(16)$	+94	+98	+47	+48	+51	+52
	ν_{12}	1360	$\nu CH_3^{cis}N(11)$, $\delta CH_3^{cis}(98)$	+29	+32	+19	+20	+17	+12
	ν_{14}	1275	$\nu_s NCN(25)$, $\delta CH_3^{tr}NC(20)$, $\nu CH_3^{cis}N(35)$	−12	−10	−9	−9	+7	+12
	ν_{15}	1137	$\nu_{as}N_2CS(27)$, $\nu_{as}Me_2N(36)$, $\rho CH_3(30)$	+6	+2	0	−4	0	0
	ν_{16}	1113	$\rho CH_3(83)$, $\delta CH_3(12)$	−7	−7	−7	−3	−12	−4
	ν_{17}	1061	$\rho CH_3(89)$	−10	−5	0	0	0	−3
	ν_{19}	960	$\nu_s N_2CS(10)$, $\nu_s Me_2N(56)$, $\rho CH_3(30)$	+6	+1	−10	−9	−12	−10
	ν_{20}	631	$\nu_s N_2CS(43)$, $\nu_s Me_2N(16)$, $\delta Me_2N(29)$	−20	−15	−12	−14	0	+1
	ν_{21}	492	$\nu CS(51)$, $\delta CH_3^{tr}NC(22)$	−41	−39	−24	−22	−14	−18
	ν_{22}	396	$\delta CH_3^{cis}NC(29)$, $\delta Me_2N(33)$, $\nu_s NCN(15)$	−4	−4	0	−1	−13	−10
	ν_{23}	303	$\tau CN(43)$, $\delta NCN(24)$, $\delta CH_3^{tr}NC(16)$	+19	+9	0[g]	0	+3	+2
b	ν_{38}	1369	$\nu_{as}NCN(10)$, $\delta NCS(6)$, $\rho Me_2N(27)$, $\nu_{as}Me_2N(29)$	+30	+25	+16	+14	+21	+20
	ν_{39}	1360	$\nu CH_3^{cis}N(12)$, $\delta CH_3^{cis}(98)$	+21	+24	+19	+18	+17	+11
	ν_{40}	1334	$\delta_s CH_3(93)$, $\nu CH_3^{tr}N(16)$	−5	−5	0	−2	0	+6
	ν_{41}	1214	$\nu_{as}NCN(18)$, $\nu CH_3^{tr}N(26)$, $\rho CH_3(45)$	−10	−7	−4	−6	0	−5
	ν_{42}	1137	$\rho CH_3(64)$, $\tau CN(8)$, $\nu_{as}NCN(4)$	+6	−2	0	−1	0	0
	ν_{43}	1094	$\nu_{as}NCN(25)$, $\rho CH_3(47)$	+10	+14	0	+4	+3	+8
	ν_{44}	1061	$\rho CH_3(87)$	−10	−5	0	−1	0	−3
	ν_{46}	930	$\nu CH_3^{cis}N(48)$, $\nu CH_3^{tr}N(21)$	+3	+9	0	+3	0	+2
	ν_{47}	886	$\tau CN(47)$, $\nu CH_3^{tr}N(17)$	−13	−10	−12	−12	0	+2
	ν_{49}	442	$\nu_{as}NCN(7)$, $\delta CH_3^{tr}NC(46)$	−26	−23	−8	−6	0	0

[a] 24 fundamentals of TMTU (Ref. 2) display shifts of 2 cm^{-1} or less in the IR spectra ($200-4000\ cm^{-1}$) and are not included. The corresponding calculated shifts do not exceed 3 cm^{-1}. The region below 200 cm^{-1} has not been investigated. [b] As used in the calculations of Ref. 2. [c] Based upon the L-matrix and PED of parent TMTU. The abbreviations are ν=stretch, δ=deformation, ρ=rock, τ=torsion. The subscripts as=antisymmetric and s=symmetric refer to the local symmetry of the groups in question. The designations cis and tr refer to the methyl groups *cis* and *trans* relative to sulfur. [d] Spectra run in KBr-discs (in the region $200-400\ cm^{-1}$ in CsI-discs). [e] Values from solution spectra ($CHCl_3$). [f] Mean values of the spectra of $TMTU_2ZnCl_2$, $TMTU_2CdI_2$, $TMTU_2CdCl_2$, $TMTU_2HgI_2$, and $TMTUHgCl_2$ run in CsI and KBr-discs. [g] Raman value ($CHCl_3$ solution).

TMTU to iodine mol. ratios varying from 1:½ to 1:3. The best spectra were obtained with a 50 % excess of iodine. Spectra of this solution were recorded with different cell-thicknesses and the mean values for the iodine shifts are given in Table 1. The shifts determined when the spectrum of TMTU · I_2 was run as a film on a KBr-disc were somewhat larger (listed in the same order as in Table 1): +59, +22, −14, +3, −10, 0, −17, −19, −22, 0, 0 cm^{-1} in species *a* and +27, +22, 0, −6, +3, 0, 0, 0, −12, −15 cm^{-1} in species *b*. The IR spectra of TMTU · CH_3I and of the metal halide complexes were recorded in the range 200−4000 cm^{-1} in KBr and CsI discs with different concentrations. The mean values for the shifts are listed in Table 1.

The Raman spectra of TMTU · I_2 in $CHCl_3$ solution were recorded with a Cary 81 spectrometer equipped with a He−Ne laser (6328 Å) in the axial illumination mode. The following lines were observed in the region below 200 cm^{-1} ($CHCl_3$): 114 m (I_3^-), 138 s (probably [11] I−I stretch), 182 w, 193 w,sh. The ultraviolet spectra were recorded on a Cary 11 spectrophotometer at room temperature in a concentration range of TMTU and the acceptor generally between 10^{-2} and 10^{-4} M. The results are given in Table 3. Noise-decoupled ^{13}C NMR spectra were determined with a Bruker WH 90 system (22.63 MHz) operating in the Fourier transform mode. The spectra of TMTU and TMTU · I_2 were examined as 1 M solutions in $CDCl_3$ and shieldings were measured relative to internal TMS. He(I) photoelectron spectra were obtained on a Perkin-Elmer PS 18 spectrometer calibrated by measuring the $^2P_{3/2}$ peaks of Ar and Xe present with the samples.

CALCULATIONS

Since the molecular structure of TMTU I_2 has not been determined, the geometry of TMTU was

Table 2. A general valence force field (GVFF) of tetramethylthiourea (TMTU)[a] and the changes calculated for the addition products with methyl iodide, iodine, and metal halides (MeX_2).

Symbol[a]	Description[b]	GVFF of TMTU[c]	Changes relative to TMTU		
			TMTU · CH_3I	TMTU · I_2	TMTU · MeX_2
Stretching					
K_D	νCS	4.029	−0.76	−0.48	−0.51
K_R	νCN	4.799	+0.17	−0.08	+0.08
F_R	νCN/νCN	1.613	−0.16	−0.05	−0.07
K_{P_1}	$\nu CH_3^{cis}-N$	5.414	+0.20	+0.14	+0.16
K_{P_2}	$\nu CH_3^{trans}-N$	5.393	+0.23	−0.08	−0.10
The N−CS−N grouping					
H_{δ_1}	δNCN	1.123	+0.91	+0.21	+0.13
H_{δ_2}	δNCS	0.800	+0.04	+0.06	0
$F_{R\delta_2}$	νCN/δNCS	0.981	+0.54	+0.38	+0.61
$F_{R\delta_3}$	νCN/δNCS	0.408	+0.48	+0.33	+0.55
The $(CH_3)_2NC$ grouping					
H_{γ_1}	$\delta CH_3^{cis}NC$	1.657	−0.37	−0.01	−0.42
H_{γ_2}	$\delta CH_3^{trans}NC$	1.916	−0.42	−0.12	+0.29
H_{γ_3}	δCH_3NCH_3	1.065	+0.25	+0.05	+0.19
Others					
H_β	δHCN	0.711	+0.01	+0.01	0
F_β	δHCN/δHCN	−0.059	+0.019	+0.010	+0.007
$F_{P_2\beta}$	$\nu CH_3^{trans}-N/\delta$HCN	0.373	+0.16	+0.06	+0.03
H_{τ_3}	τCN	1.013	+0.01	−0.05	+0.01

[a] The GVFF of Ref. 2 was transferred directly except for the force constants listed in the table and for K_r, H_α, H_Δ, H_{τ_1} and H_{τ_2} where calculations produced no change. [b] For abbreviations *cf.* footnote *c*, Table 1. [c] In units of mdyn/Å (stretch constants), mdyn/rad (stretch-bend interaction constants), and mdynÅ/(rad)^2 (bending and torsion constants).

used in all calculations. A recent determination of the crystal structure of the related *N*-methylthiocaprolactam–iodine 1:1 complex[19] showed that bond lengths and bond angles are not significantly altered on iodine complex formation. The iodine molecule coordinates to sulfur with a C–S–I angle of 105–110° with the iodine molecule nearly co-planar with the N–CS–C group.[19,20] From the 1:1 thiourea–iodine adduct, however, a 2:1 compound is eventually formed and the crystal structure shown to be ionic.[20] The C_2-symmetry of TMTU apparently breaks down on complex formation with iodine, and strictly we should distinguish between the $(CH_3)_2N$-groups *cis* and *trans* to to iodine. In the metal halide complexes the CS distance increases,[21,22] but the remaining distances and interbond angles are not significantly altered. When thiourea is converted to *S*-methylthiouronium salts the geometry is hardly changed[23,24] and we have used the geometry of TMTU both in the case of TMTU · CH_3I and in the TMTU · metal halide adducts.

The NCA of TMTU was started with a least-squares fit identical to that described previously[2] except that all the observed frequencies of the isotopically labelled compounds were removed and only the fundamentals of the parent molecule were included. This was done since the IR shifts of isotopically labelled addition compounds have not been determined. Since the NCA led to physically unrealistic values for the force constants the following constraints were introduced to reduce the number of independent constants to a tractable number: (1) The diagonal force constants should be included in order to secure that all internal coordinates were taken into account, and (2) only those interaction constants which were necessary to reproduce the shifts observed in the addition compounds were allowed to vary. All other force constants were given the previous values.[2]

Among the 54 vibrational modes for TMTU,[2] 21 are shifted 2 cm^{-1} or more upon complex formation as observed in the IR spectra of TMTU · I_2, TMTU · CH_3I and TMTU · metal halide. These vibrational fundamentals are included in Table 1, while the remaining 33 modes which were perturbed less than 2 cm^{-1} are not included. Simultaneous NCA were now performed on the spectra of TMTU and the three complexes. With the inclusion of the five interaction constants F_R, $F_{R\delta_2}$, $F_{R\delta_3}$, F_β and $F_{P_2\beta}$ listed in Table 2 (the number of off-diagonal elements were kept as low as possible) converging solutions were obtained with good agreement between experimental and calculated shifts (Table 1). However, the force constants given in Table 2 should be taken with due reservation. In addition to the errors caused by the approximated geometry, exploratory calculations indicate that the choice of other interaction constants leads to alternative solutions which have only the gross features (discussed below) in common with the force field of Table 2.

Semi-empirical all valence-electron molecular orbital calculations were carried out using both the CNDO/2 and the CNDO/S[25] parametrisations, but since the electronic densities were almost identical, only the CNDO/S densities are reproduced (Fig. 1). A modified CNDO/S-CI program[26] was provided by Professor G. Pfister-Guillouzo and extended to molecules containing 40 atoms/100 orbitals. Excited states were calculated from the ground state occupied and virtual orbitals by a CI procedure limited to the 20 lowest-energy, single-excited configurations. Calculations were made on TMTU and the TMTU · CH_3^+ ion. TMTU *S*-oxide served as a model substance for the TMTU · I_2 complex using an S–O distance of 1.50 Å and a C–S–O angle of 106°. For the TMTU · metal halide complexes we used a hypothetical 1:1 TMTU · $MgCl_2$ complex with Mg–S and Mg–Cl distances of 2.60 and 2.53 Å, respectively, and C–S–Mg and Cl–Mg–Cl angles of 110°. The calculated energies and transitions are compared with our experimental results in Tables 3 and 4.

RESULTS AND DISCUSSION

In Table 1 are summarised the observed and calculated shifts with a description of the fundamentals in terms of the contributing skeletal modes. Gosavi *et al.*[10] claim the significant change in the spectrum of TMTU on complex formation with iodine to be a shift to lower frequency and increased intensity of a band near 990 cm^{-1}. However, this band does not occur in our spectra of TMTU[2] and is presumably due to a solvent (CCl_4) band.

In one instance (the overlapping fundamentals ν_{15} and ν_{42} near 1137 cm^{-1}) the shifts in Table 1 cannot be regarded as conclusive. On iodine addition to TMTU the band becomes much weaker and at the same time a band near 1150 cm^{-1} (in TMTU assigned[2] a combination mode) gains intensity and finally becomes much stronger than the band near

Table 3. Ultraviolet absorption of tetramethylthiourea (TMTU) and its compounds with methyl iodide, iodine and sulfuric acid assigned from CNDO/S-CI calculations.

Compound	Solvent	Transitions[a]							
		$n_S \rightarrow \pi^*_{N_2CS}$		$\pi_S \rightarrow \pi^*_{N_2CS}$		$\pi_N \rightarrow \pi^*_{N_2CS}$		Others	
		obs[b]	calc[c]	obs[b]	calc[c]	obs[b]	calc[c]	obs[b]	calc[c]
TMTU	isooctane	330 (211)	464 (0.003)	261 (15810)	294 (0.165)	240sh (9000)	239 (0.115)	219 (5200)	$n_S \rightarrow \sigma^*_S/\pi^*_S$ 211(0.0009) 204(0.0015)
TMTU·CH_3I	ethanol	–	–	220 (15600)	251 (0.12)	252 (13300)	260 (0.09)	211sh (10000)	$\pi_S \rightarrow \sigma^*_S/\pi^*_S$ 214(0.0015) 201(0.0061)
TMTU·I_2[e]	perfluormethyl-cyclohexane	–	–	–	332 (0.094)	252	243 (0.055)	235 210 br	$\pi_S \rightarrow \sigma^*_S/\pi^*_S$ 280(0.005) 237(0.048)
TMTU·H^+[d]	conc. H_2SO_4	–	–	230 (8710)	247 (0.115)	246 (9120)	269 (0.147)	–	–

[a] Approximate description based upon the CI-coefficients. [b] λ_{max} (nm), and, in parenthesis, ε_{max} (l mol^{-1} cm^{-1}). [c] Transition wave length (nm) and, in parenthesis, the oscillator strength. [d] From Ref. 31. [e] Charge transfer bands omitted. The calculated values are for tetramethylthiourea *S*-oxide. The observed bands are not well separated from TMTU and only approximate values are given in the table.

Table 4. Vertical ionization energies and CNDO/S orbital assignments of tetramethylthiourea compared with the shifts in the PES[a] of tetramethylselenourea.

Tetramethylthiourea			Tetramethylselenourea	
Exp. (eV)	Calc. (eV)	Electron density (%)	Exp. (eV)	Shift (eV)
7.80	8.76	n_S (92)	7.35	−0.45
8.15	9.24	π_S (77)	7.70	−0.45
8.60	10.98	π_N (61)	8.60	0
11.25	13.43	σ_{CS} (C=22, S=48)	11.05	−0.20
12.10	13.58	π_{N_2CS} (N=30, C=24, S=7)	11.95	−0.15

[a] Photoelectron spectra.

1137 cm^{-1}. This can have two possible explanations. (1) One or both bands at 1137 cm^{-1} are actually displaced by *ca.* 15 cm^{-1} towards higher frequencies. This is contradicted by the results of the NCA which predict a small shift in the opposite direction. (2) The band in TMTU near 1150 cm^{-1} has been incorrectly assigned[2] and is instead the fundamental ν_{42} *b*. This attribution is supported by the results obtained for tetramethylselenourea.[3] In the IR spectrum of this compound (which is very similar to the spectrum of TMTU) the band near 1150 cm^{-1} of species *b* is stronger than in TMTU and therefore supports the latter assignment.

From the results in Table 1 we can relate the IR shifts to perturbation of the skeletal modes in TMTU as was made for tetramethylurea.[4] However, a more precise description can be given by discussing the GVFF changes of Table 2 in relation to the CNDO/S electronic densities of Fig. 1.

The ground state electronic distribution of TMTU (top of Fig. 1) indicates a net charge of the $(CH_3)_2N$ groups (+0.08) and the thiocarbonyl carbon (+0.40) while the sulfur atom has acquired a net negative charge of −0.57. The predicted charge-densities are probably too high (*cf.* the charge-density of −0.18 found for sulfur in TMTU by X-ray emission

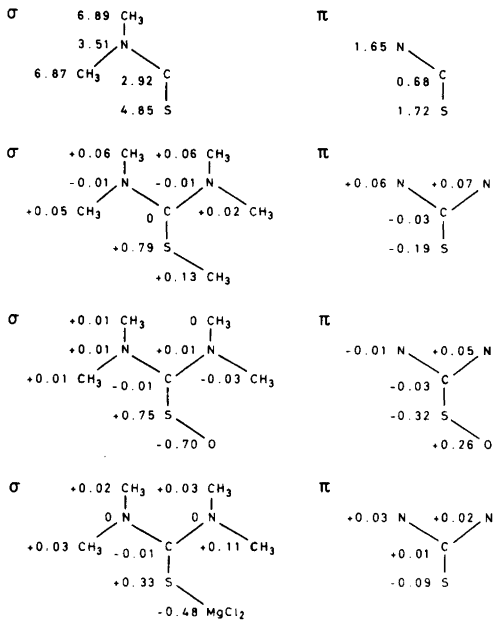

Fig. 1. The CNDO/S σ- and π-electron density for TMTU and the changes on conversion to methiodide, *S*-oxide and metal halide complex. (Lower and higher densities relative to TMTU are indicated by the signs + and −, resp. The π-densities are taken at right angles to the N−CS−N plane).

spectroscopy[27]) while the signs and relative magnitudes are probably correct. The opposite σ and π orbital donor/acceptor properties of the N−CS−N group are general features of CNDO calculations.[28] Conversion of TMTU to the charge-transfer complex TMTU · I_2 (exemplified by the *S*-oxide in Fig. 1) leads to an increased positive charge of sulfur (+0.43) while the rest of the molecule is almost unaffected apart from the atoms closest to oxygen. In accordance with this the largest change in the GVFF (Table 2) is a decrease of K_D upon charge-transfer of 0.48 mdyn/Å. The negligible decrease in K_R, F_R, and H_τ suggest that the electron density of the CN bonds might decrease slightly. By varying the GVFF of TMTU · I_2 it appears that only the sum of the force constants H_{γ_1}, H_{γ_2}, and H_{γ_3} is significant. In accordance with CNDO/S predictions this sum is almost unchanged from TMTU to TMTU · I_2. The increase in the force constants K_{P_1}, H_{δ_1}, and H_{δ_2} might be connected with the increased resistance to stretching and bending caused by steric hindrance of coordinated iodine.

The force field of a metal halide complex of TMTU follows closely the pattern of TMTU · I_2 (considering only the sum of $H_{\gamma_1} - H_{\gamma_3}$) except that the force constants K_R and H_τ have increased relative to TMTU. This trend agrees with the CNDO/S π-electron changes indicating an increased charge transfer from N to S, *i.e.* an increased weight of $^+N{=}C{-}S^-$ in classical terms. The same, but more pronounced trend occurs in the case of TMTU · CH_3I. In agreement with a calculated enhanced $^+N{=}C{-}S^-$ polarisation, K_R shows a substantial increase relative to TMTU (+0.17) and the resistance towards NCN bending (H_{δ_1}) also rises sharply (+0.91). The sum of the force constants H_{γ_1}, H_{γ_2}, and H_{γ_3} is also less than in TMTU in accordance with the decreased electron density at nitrogen.

^{13}C NMR data have been obtained for TMTU and TMTU · I_2. The chemical shift observed for the CS group at 180.3 ppm in the iodine complex is shifted 13.8 ppm upfield relative to TMTU (194.1 ppm). This is consistent with the CNDO/S prediction (Fig. 1) of an increased thiocarbonyl carbon shielding (−0.04) in the charge-transfer complex. However, since the mean excitation energy also exerts a strong influence on the chemical shift[29] this result does not necessarily support the results of the CNDO/S calculations.

The UV spectrum of TMTU has been the subject of empirical[30,31] and theoretical (Hückel)[32,33] investigations as has the charge-transfer spectra of the iodine complex.[6-9] Since the thioureide group is non-planar the spectra are in many ways anomalous[31] and may therefore function as a sensitive test for the predictability of the CNDO/S−CI calculations. The observed and calculated transitions are given in Table 3. The UV-spectrum of the iodine complex was recorded in perfluoromethylcyclohexane in order to avoid the contact charge-transfer spectrum of iodine.[34] It is seen from the table that the calculated values for the $\pi_S \rightarrow \pi^*_{N_2CS}$ (and especially the $n_S \rightarrow \pi^*_{N_2CS}$) transitions are too high. However, the CNDO/S−CI values reproduce the signs but not the magnitudes of the shifts of the $\pi_S \rightarrow \pi^*_{N_2CS}$ and $\pi_N \rightarrow \pi^*_{N_2CS}$ transitions from TMTU to the addition compounds. Tentatively, a few other bands in the short wave length region have been assigned to $n_S/\pi_S \rightarrow \sigma^*_S/\pi^*_S$ transitions in accordance with the calculated results.

The first four bands at *ca.* 7.80, 8.15, 8.60, and 11.25 eV in the photoelectron spectrum of TMTU were assigned by Guimon *et al.*[35] to ionisations in

the order n, π, π, σ by comparison with the calculated (CNDO/S) and experimental spectra of related thioureas. In a comparative study of amides, thioamides, ureas, and thioureas, Mines and Thompson[36] considered instead the order of the first three bands to be π, n, π. The results of our CNDO/S calculations (Table 4) support the former assignment. It is seen that the third band (8.60 eV) is calculated to rise from ionisation of an electron from an orbital localized on the nitrogen atoms while the four other bands originate in orbitals partly located on sulfur. Comparison with the photoelectron spectrum of tetramethylselenourea (Table 4) shows that the ionisation potential of the third band is unchanged while those of the other four bands are lowered. Since seleno compounds have spectra[37] similar to those of sulfur compounds except for bands due to ionisation from orbitals with S(Se) character, the orbital assignments of the CNDO/S method are supported by these results.

Acknowledgements. We wish to thank Dr. L. Henriksen for his assistance in recording and interpreting the photoelectron spectra and Dr. H. Eggert for assistance with the ^{13}C NMR spectra and stimulating discussions. This research was supported by grants from the Danish Natural Science Research Council and the Norwegian Research Council for Science and the Humanities.

REFERENCES

1. Jensen, K. A. and Nielsen, P. H. *Acta Chem. Scand. 20* (1966) 597.
2. Anthoni, U., Nielsen, P. H., Borch, G., Gustavsen, J. and Klæboe, P. *Spectrochim. Acta A 33* (1977) 403.
3. Anthoni, U., Nielsen, P. H., Borch, G. and Klæboe, P. *Spectrochim. Acta. In press.*
4. Muller, J.-P., Maes, G. and Zeegers-Huyskens, T. *J. Chem. Phys. 71* (1974) 893.
5. Dorval, C. and Zeegers-Huyskens, T. *Ann. Chim. Paris 10* (1975) 5.
6. Lang, R. P. *J. Phys. Chem. 72* (1968) 2129.
7. Grand, A. F. and Tamres, M. *Inorg. Chem. 8* (1969) 2495.
8. Niedzielski, R. J., Drago, R. S. and Middaugh, R. L. *J. Am. Chem. Soc. 86* (1964) 1694.
9. Bhaskar, K. R., Gosavi, R. K. and Rao, C. N. R. *Trans. Faraday Soc. 62* (1966) 29.
10. Gosavi, R. K., Agarwala, U. and Rao, C. N. R. *J. Am. Chem. Soc. 89* (1967) 235.
11. Klæboe, P. *J. Am. Chem. Soc. 89* (1967) 3667.
12. Schafer, M. and Curran, C. *Inorg. Chem. 5* (1966) 265.
13. Gosavi, R. K. and Rao, C. N. R. *J. Inorg. Nucl. Chem. 29* (1967) 1937.
14. Marcotrigiano, G. and Battistuzzi, R. *J. Nucl. Chem. 36* (1974) 3719.
15. Devore, E. C. and Holt, S. L. *J. Inorg. Nucl. Chem. 34* (1972) 2303.
16. Wynne, K. J., Pearson, P. S., Newton, M. G. and Golen, J. *Inorg. Chem. 11* (1972) 1192.
17. Wynne, K. J. and Pearson, P. S. *Chem. Commun.* (1971) 293.
18. Wynne, K. J. and Pearson, P. S. *Inorg. Chem. 10* (1971) 2735.
19. Ahlsen, E. L. and Strømme, K. O. *Acta Chem. Scand. A 28* (1974) 175.
20. Hung-Yin Lin, G. and Hope, H. *Acta Crystallogr. B 28* (1972) 643.
21. Husebye, S. and George, J. W. *Inorg. Chem. 8* (1969) 313.
22. Spofford, W. A., Griffith, E. A. H. and Amma, E. L. *Chem. Commun.* (1970) 533.
23. Stam, C. H. *Acta Crystallogr. 15* (1962) 317.
24. Kennard, O. and Walker, J. *J. Chem. Soc.* (1963) 5513.
25. Bene, J. D. and Jaffé, H. H. *J. Chem. Phys. 48* (1968) 1807.
26. Arbelot, M., Guimon, C., Gonbeau, D. and Pfister-Guillouzo, G. *J. Mol. Struct. 20* (1974) 487, and earlier papers.
27. Takahashi, Y., Yabe, K. and Sato, T. *Bull. Chem. Soc. Jpn. 42* (1969) 2707.
28. Clementi, E. *Chem. Rev. 68* (1968) 341.
29. Martin, G. J., Martin, M. L. and Odiot, S. *Org. Magn. Reson. 7* (1975) 2.
30. Gosavi, R. K. and Rao, C. N. R. *Can. J. Chem. 45* (1967) 1897.
31. Fabian, J., Viola, H. and Mayer, R. *Tetrahedron 23* (1967) 4323.
32. Figuera, J. M. and Menéndez, V. *An. Quim. 67* (1971) 1169.
33. Chatterjee, K. K. *Indian J. Chem. 11* (1973) 678.
34. Julien, L. M. and Person, W. B. *J. Phys. Chem. 72* (1968) 3059.
35. Guimon, C., Pfister-Guillouzo, G., Arbelot, M. and Chanon, M. *Tetrahedron 30* (1974) 3831; Guimon, C., Gonbeau, D., Pfister-Guillouzo, G., Åsbrink, L. and Sandström, J. *J. Electron Spectrosc. Relat. Phenom. 4* (1974) 49.
36. Mines, G. W. and Thompson, H. W. *Spectrochim. Acta 31 A* (1975) 137.
37. Betteridge, G., Henriksen, L., Sandström, J., Wennerbeck, I. and Williams, M. A. *Acta Chem. Scand. A 31* (1977) 14.

Received October 26, 1977.

Acta Chemica Scandinavica A 32 (1978) 267–270

The Crystal Structure of Serotonin Hydrogen Oxalate

A. AMIT,[a] L. MESTER,[a] B. KLEWE[b] and S. FURBERG[b]

[a] Institut de Chimie de Substances Naturelles, Gif-sur-Yvette, France and [b] Kjemisk institutt, Universitetet i Oslo, Oslo 3, Norway

An X-ray analysis of serotonin oxalate has been carried out. The space group is $P2_1/n$ with cell dimensions $a=18.385(5)$ Å, $b=5.620(2)$ Å, $c=12.034(4)$ Å, $\beta=96.57(2)°$. The structure was refined to $R=0.069$ for 1767 observed reflections. The serotonin cations have a nearly planar *trans* conformation and are linked by hydrogen bonds to the hydrogen oxalate anions, which form infinite chains.

The biological importance of serotonin (5-hydroxytryptamine) and related substances has prompted a number of investigations of their structure. Crystal structure analyses have been carried out on serotonin creatinine sulfate,[1] serotonin picrate,[2] and a number of structural relatives.[3-6] Different side-chain conformations have been found, which have been discussed with the view of establishing structure-activity relationships.[7,8] One of us has prepared sugar derivatives of serotonin, using the oxalate salt as starting material.[9] These compounds show unexpected biological behaviours.[10-12] It was thought to be of interest to determine the conformation of serotonin in its hydrogen oxalate salt.

EXPERIMENTAL

From a sample of serotonin oxalate supplied by Sigma Co., St. Louis, a single crystal of dimensions $0.37\times0.31\times0.06$ mm^3 was selected, coated by a thin layer of epoxy glue, and used for the X-ray diffraction work. Data were collected at room temperature on an automatic Syntex $P\bar{1}$ diffractometer using monochromatic Mo$K\alpha$ radiation and $\theta-2\theta$ scan technique; $2\theta_{max}=55°$, scan speed $1.5-3°$ min^{-1} (in 2θ), background to scanning time ratio 0.7. An experimental fluctuation of 2 % as calculated from the measurements of three monitoring reflections registered at regular intervals was included in the standard deviations based upon counting statistics. 1767 of the 3025 reflections had intensities greater than 2σ and were subsequently used in the refinement. The cell dimensions were determined from the measurements of all setting angles for 30 reflections.

On crystallization from methanol a different modification of serotonin oxalate was obtained. The crystals were unstable in air, turning opaque in the course of a few hours, but were stable in closed capillaries containing methanol. Weissenberg and precession diagrams showed these crystals to be orthorhombic, space group $P2_12_12_1$, with approximate cell dimensions $a=13.21$ Å, $b=19.5$ Å, $c=5.60$ Å. The density as measured by flotation corresponds to an additional cell content of four methanol molecules, and we believe these unstable crystals to be a methanol solvate of serotonin oxalate. They were not further investigated.

CRYSTAL DATA

Serotonin oxalate (5-hydroxy-3-indolethylammonium hydrogen oxalate). $C_{12}H_{14}N_2O_5$, *F.W.* $=266.25$. Space group $P2_1/n$, $a=18.385(5)$ Å, $b=5.620(2)$ Å, $c=12.034(4)$ Å, $\beta=96.57(2)°$, $V=1235.1$ Å^3, $Z=4$, $D_m=1.4$ g cm^{-3}, $D_x=1.43$ g cm^{-3}, λ(Mo$K\alpha$)$=0.71069$ Å, μ(Mo$K\alpha$)$=1.05$ cm^{-1}.

STRUCTURE DETERMINATION AND REFINEMENT

The structure was determined by the MULTAN program. The hydrogen atoms were localized from a difference electron density map. Full matrix least-squares refinement of $M=\Sigma[(F_o-F_c)/\sigma(F_o)]^2$ yielded a final R-value of 0.069 ($R_w=0.067$, "goodness of fit" $=2.67$), using anisotropic temperature factors

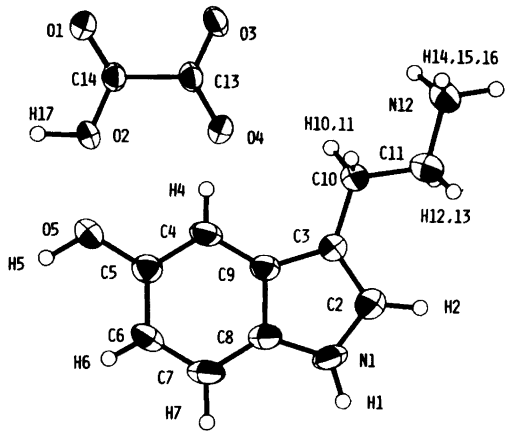

Fig. 1. Thermal ellipsoids viewed perpendicular to the cation and anion planes.

for heavy atoms and isotropic ones for the hydrogen atoms. The thermal ellipsoids are shown in Fig. 1. Atomic form factors were taken from Refs. 13 and 14. The final parameters are given in Table 1. A list of observed and calculated structure factors is available from one of the authors (S.F.) upon request. Bond distances and angles and hydrogen bond parameters are listed in Table 2. The numbering of atoms can be seen from Fig. 1. The figures have been prepared by the ORTEP 2 program. Other programs used are described in Ref. 15.

RESULTS AND DISCUSSION

As seen in Fig. 1, the ethylamine side-chain is in the extended *trans* planar conformation. The torsional angles C9–C3–C10–C11 and C3–C10–C11–N12 are 171.7 and 175.8°, respectively, and the entire serotonin cation is approximately planar except for the side chain hydrogen atoms. The conformation is similar to that found in, *e.g.*, serotonin-creatinine sulfate,[1] whereas non-planar conformations are observed in 5-methoxytryptamine.[4,6] Distances from a plane fitted to the indole ring are given in Table 3. The indole ring appears to be very slightly bent about C9–C8, the six-membered ring being planar to within 0.008 Å and the five-membered ring to within 0.002 Å, the angle between them being 1.0°. Bond lengths and angles agree within three times the estimated standard deviations with those given by Falkenberg and Carlström,[3] and found also in subsequent investigations,[4–6] except for C4–C9 and C10–C11, which both are about 0.03 Å shorter than expected. We do not, however, believe these deviations to be real.

The dimensions of the anion correspond closely to those reported in the literature.[16] The bond

Table 1. Positional and thermal parameters. The anisotropic temperature factor is $\exp[-2\pi^2(h^2a^{*2}U_{11}+\cdots+2klb^*c^*U_{23})]$.

ATOM	x	y	z	U11	U22	U33	U12	U13	U23
O1	.7866(2)	.7864(5)	.4487(2)	.0818(24)	.0319(17)	.0426(17)	-.0057(17)	.0278(17)	.0015(15)
O2	.8395(2)	.5524(5)	.2984(2)	.0589(21)	.0192(15)	.0428(17)	.0012(15)	.0167(15)	.0014(14)
O3	.8281(2)	1.1420(5)	.3788(2)	.0675(22)	.0210(15)	.0365(16)	-.0006(16)	.0075(15)	-.0008(14)
O4	.8888(2)	.9807(5)	.2257(2)	.0648(21)	.0312(16)	.0387(16)	-.0005(16)	.0215(15)	.0016(14)
O5	.5531(2)	-.1828(6)	.3688(2)	.0611(22)	.0475(21)	.0379(17)	.0108(18)	.0128(16)	-.0051(16)
N1	.3806(2)	.4243(7)	.1266(3)	.0473(24)	.0661(29)	.0249(19)	.0078(23)	-.0059(18)	.0022(22)
N12	.3203(3)	.8662(9)	.5545(3)	.0574(30)	.0497(27)	.0489(23)	.0116(26)	.0139(22)	-.0039(22)
C2	.3413(3)	.5620(9)	.2129(4)	.0481(27)	.0492(30)	.0411(25)	.0067(26)	.0062(21)	.0088(24)
C3	.3774(2)	.4823(7)	.3114(3)	.0369(24)	.0364(25)	.0318(21)	.0048(21)	.0025(19)	-.0005(20)
C4	.4698(3)	.1376(8)	.3479(4)	.0518(29)	.0426(27)	.0249(22)	-.0065(24)	.0099(21)	-.0045(21)
C5	.5044(2)	-.0411(8)	.2953(3)	.0447(26)	.0368(26)	.0334(22)	-.0004(24)	.0092(20)	.0018(21)
C6	.4994(3)	-.0736(9)	.1794(4)	.0545(32)	.0544(33)	.0346(25)	.0092(29)	.0118(23)	-.0144(28)
C7	.4424(3)	.0728(9)	.1149(3)	.0436(27)	.0663(35)	.0265(22)	-.0033(27)	.0034(21)	-.0101(25)
C8	.4068(2)	.2624(8)	.1679(3)	.0343(24)	.0529(29)	.0268(21)	-.0034(25)	.0023(19)	-.0027(22)
C9	.4210(2)	.2638(8)	.2846(3)	.0369(25)	.0420(27)	.0269(20)	.0010(22)	.0078(19)	-.0004(20)
C10	.3764(3)	.5618(10)	.4278(4)	.0656(36)	.0399(30)	.0317(24)	.0105(29)	.0043(24)	-.0002(24)
C11	.3213(3)	.7638(11)	.4385(4)	.0667(37)	.0536(35)	.0358(27)	.0097(33)	.0088(25)	-.0035(27)
C13	.8398(2)	.9748(7)	.3154(3)	.0437(27)	.0232(23)	.0385(22)	-.0018(21)	.0007(20)	.0031(19)
C14	.8124(2)	.7256(7)	.3582(3)	.0410(25)	.0246(23)	.0293(21)	-.0019(21)	.0028(19)	.0040(19)

ATOM	x	y	z	B	ATOM	x	y	z	B
H1	.341(3)	.436(9)	.052(4)	5.6(12)	H2	.384(2)	.691(7)	.202(3)	3.1(9)
H4	.478(3)	.168(8)	.423(4)	6.1(12)	H5	.585(3)	-.385(9)	.322(4)	7.1(14)
H6	.514(2)	-.189(7)	.148(3)	2.7(9)	H7	.429(2)	.044(8)	.031(3)	4.1(10)
H10	.428(3)	.678(10)	.458(4)	7.8(17)	H11	.377(2)	.467(7)	.485(3)	2.8(9)
H12	.321(3)	.887(10)	.398(4)	6.5(16)	H13	.278(4)	.676(12)	.427(5)	11.8(24)
H14	.371(3)	.957(11)	.574(5)	8.8(19)	H15	.324(3)	.788(11)	.684(5)	9.1(18)
H16	.284(3)	.988(11)	.564(4)	6.1(16)	H17	.818(4)	.388(15)	.328(6)	15.1(26)

Table 2. Bonding parameters.

BOND DISTANCES (A)

N1 -C2	1.367(6)	C4 -C5	1.384(6)	C8 -C9	1.407(5)	C11-N12	1.502(6)	O3 -C13	1.247(5)
C2 -C3	1.365(6)	C5 -C6	1.401(6)	C8 -N1	1.371(6)	C5 -O5	1.372(5)	O4 -C13	1.232(5)
C3 -C9	1.433(6)	C6 -C7	1.376(6)	C3 -C10	1.501(6)	O1 -C14	1.213(4)	C13-C14	1.553(5)
C9 -C4	1.377(6)	C7 -C8	1.386(6)	C10-C11	1.483(7)	O2 -C14	1.290(5)		

BOND ANGLES (°)

N1-C2-C3	109.7(4)	C4-C5-C6	120.5(4)	C9 -C3 -C10	123.4(4)	O1-C14-O2	125.8(4)
C2-C3-C9	106.7(4)	C5-C6-C7	121.2(5)	C3 -C10-C11	113.9(4)	O3-C13-C14	114.2(3)
C3-C9-C8	106.8(4)	C6-C7-C8	118.0(4)	C10-C11-N12	110.8(4)	O4-C13-C14	118.7(4)
C9-C8-N1	107.5(4)	C7-C8-C9	121.2(4)	C4 -C5 -O5	117.9(4)	O3-C13-O4	127.2(4)
C8-N1-C2	109.3(4)	C8-C9-C4	120.1(4)	C6 -C5 -O5	121.6(4)		
C3-C9-C4	133.1(4)	C7-C8-N1	131.3(4)	O1 -C14-C13	120.6(4)		
C9-C4-C5	119.0(4)	C2-C3-C10	129.8(4)	O2 -C14-C13	113.6(3)		

HYDROGEN BONDS

	BOND LENGTH (A)				ANGLE (°)		EQUIV. POS.		
O2 -H17	1.08	O2...O3	2.520	H17..O3	1.47	O2 -H17..O3	164	x,	-1+y, z
O5 -H5	1.01	O5...O4	2.735	H5...O4	1.73	O5 -H5...O4	172	3/2-x,	-3/2+y, 1/2-z
N1 -H1	.93	N1...O3	3.014	H1...O3	2.12	N1 -H1...O3	161	-1/2+x,	3/2-y, -1/2+z
N12-H14	.92	N12..O5	2.896	H14..O5	1.99	N12-H14..O5	167	1-x,	1-y, 1-z
N12-H15	1.08	N12..O4	2.874	H15..O4	1.89	N12-H15..O4	150	-1/2+x,	3/2-y, 1/2+z
N12-H16	1.06	N12..O1	3.144	H16..O1	2.13	N12-H16..O1	160	1-x,	2-y, 1-z
N12-H16	1.06	N12..O3	2.951	H16..O3	2.22	N12-H16..O3	124	1-x,	2-y, 1-z

Table 3. Distances (Å) from the least-squares plane of the nine indole ring atoms.

N1	0.010	O5	0.046
C2	0.009	C10	0.050
C3	−0.010	C11	−0.153
C4	0.004	N12	0.021
C5	0.013	H1	−0.026
C6	−0.002	H2	−0.043
C7	−0.010	H4	0.007
C8	−0.004	H5	0.138
C9	−0.012	H6	0.011
		H7	−0.078

lengths are significantly different in the two halves of the anion, and the twist angle between the COO planes is 6.7°. Values between 0 and 14° have been reported for this angle in hydrogen oxalates.[16]

The crystal packing is shown in Fig. 2. The hydrogen oxalate anions are linked together by strong unsymmetrical hydrogen bonds (length 2.520 Å) to roughly planar infinite chains, as is commonly found for these ions.[16] They run nearly parallel to *b*. The repeat distance in such chains is about 5.6 Å and it may be inferred that they occur also in the unstable solvate mentioned above, being parallel to *c* in this case. The serotonin cations occur as

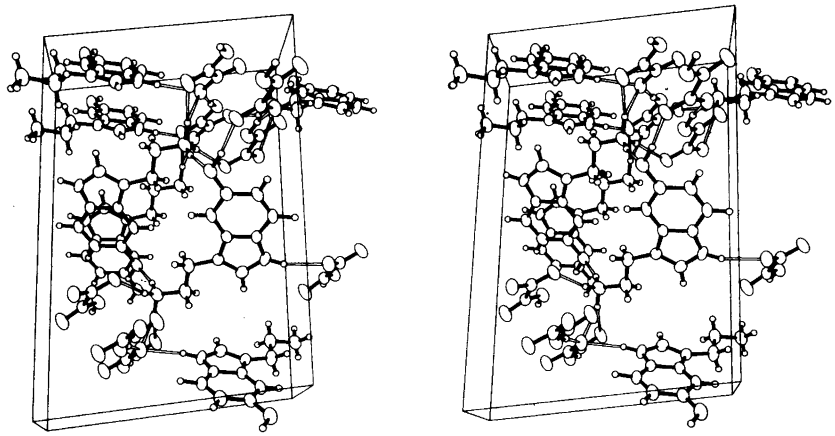

Fig. 2. Stereoscopic view of the structure in the *b* direction.

centrosymmetrical dimers formed by hydrogen bonds N12–H14···O5 between NH_3^+ and hydroxyl groups. The cations are linked to the anion chains by four hydrogen bonds (involving H1, H5, H15 and H16). One of these (H16) is possibly bifurcated, as indicated by the data on the hydrogen bonds given in Table 2.

The biological implications of the structure will be discussed in a forthcoming paper.[1,2]

REFERENCES

1. Karle, I. L., Dragonette, K. S. and Brenner, S. A. *Acta Crystallogr. 19* (1965) 713.
2. Bugg, C. E. and Thewalt, U. *Science 170* (1970) 852.
3. Falkenberg, G. and Carlström, D. *Acta Crystallogr. B 27* (1971) 411.
4. Quarles, W. G., Templeton, D. H. and Zalkin, A. *Acta Crystallogr. B 20* (1974) 95, 99.
5. Petscher, T. J. and Weber, H. P. *J. Chem. Soc. Perkin Trans. 2* (1974) 946.
6. Sakaki, T., Sogo, A., Wakahara, A., Kanai, T., Fujiwara, T. and Tomita, K. *Acta Crystallogr. B 32* (1976) 3235.
7. Chothia, C. and Pauling, P. *Proc. Natl. Acad. Sci. U.S.A. 63* (1969) 1063.
8. Courriere, P., Coubeils, J. L. and Pullman, B. *C.R. Acad. Sci. Paris 272* (1971) 1697.
9. Mester, L. and Mester, M. *J. Carbohydr. Nucleos. Nucleot. 2* (1975) 141.
10. Mester, L. and Mester, M. *French Patent* No. 75-22577 (1975).
11. Mester, L. and Mester, M. In Khadem, H. S., Ed., *Synthetic Methods for Carbohydrates, ACS Symposium Series No. 39* (1976) 240.
12. Mester, L. *et al. In preparation.*
13. Doyle, P. A. and Turner, P. S. *Acta Crystallogr. A 24* (1968) 390.
14. Stewart, R. F., Davidson, E. R. and Simpson, W. T. *J. Chem. Phys. 42* (1965) 3175.
15. Groth, P. *Acta Chem. Scand. 27* (1973) 1837.
16. Thomas, J. O. and Renne, N. *Acta Crystallogr. B 31* (1975) 2161.

Received October 7, 1977.

Acta Chemica Scandinavica A 32 (1978) 271 – 273

Molecular Structure of Gaseous Pyrimidine

LIV FERNHOLT and CHRISTIAN RØMMING

Department of Chemistry, University of Oslo, Oslo 3, Norway

From an electron-diffraction investigation of pyrimidine the following structural data were obtained, assuming *2mm* (C_{2v}) symmetry: r_a(N–C)= 1.340(2) Å; r_a(C–C)=1.393(2) Å; ∠NCN= 127.6(3)°; ∠CNC=115.5(2)°; ∠CCC=116.8°.

The crystal structure of pyrimidine was investigated by Wheatley in 1960 by X-ray methods.[1] The uncertainty in the measured bond lengths was, owing to the rather severe thermal effects in the crystals, estimated to be as high as ±0.015 Å. In view of the importance of this model molecule and also because of a demand for more accurate data in the course of an investigation of 2,2′-bipyrimidyl,[2] a structure determination of the free pyrimidine molecule was undertaken by means of gas phase electron diffraction methods.

EXPERIMENTAL

The sample of pyrimidine used in the experiments was supplied by SIGMA. The electron-diffraction data were collected on the Oslo apparatus.[3] The diagrams were recorded on two sets of photographic plates with nozzle-to-plate distances of 480.82 mm (6 plates) and 200.82 mm (5 plates), respectively. The nozzle temperature was 21 °C and the wavelength 0.064690 Å. The intensity was measured on a photometer for each 0.25 mm of the plates; each plate was oscillated about the centre of the diffraction diagram and the intensity integrated over the arc.

The data were treated in the way described in Ref. 4; the molecular intensities were modified by $s/(|f'_N||f'_C|)$. The scattering amplitudes were calculated from the atomic potentials.[5]

The least-squares refinement procedure used to refine the parameters estimated from the experimental radial distribution curve was based on a composite intensity curve ranging from $s=1.625$ Å^{-1} to $s=43.75$ Å^{-1} with full weight from $s=3.0$ Å^{-1} to $s=37.0$ Å^{-1}. The s-intervals were 0.125 Å^{-1} for $s \leq 8.0$ Å^{-1} and 0.25 Å^{-1} for higher s-values.

STRUCTURE ANALYSIS AND RESULTS

In Fig. 1 a drawing of the molecule with the numbering of the atoms is shown. The refinement was performed with the following constraints: The molecule was assumed to be planar with *2mm* (C_{2v}) symmetry. The bond distances C–C, C–N and C–H and the angles N–C–N, C–N–C and N3–C4–H8 were chosen as independent parameters. All C–N bonds were treated as equal, as were the C–H bonds. Mean amplitudes of vibration were calculated as described in Ref. 6; the force field was designed as for 2,2′-bipyrimidyl.[2] Vibrational parameters were not varied in the refinement which converged to an R_2-value ($(\Sigma w\Delta^2/\Sigma wI^2)^{\frac{1}{2}}$) of 0.051.

The experimental and theoretical intensity curves were Fourier transformed into the corresponding radial distribution (RD) functions using an artificial damping constant of $k=0.002$ Å^2. As shown in Fig. 1 there is a good agreement between the two RD curves; this is also indicated by the difference curve.

The peak at about 1.35 Å corresponds to the bond lengths in the molecule. The complex at 2.35 Å consists of distances between atoms separated by one atom and the one at 2.7 Å represents distances between the heavier atoms separated by two atoms. The long N···H and C···H distances are involved in the two outer peaks.

DISCUSSION

The structural data arrived at in the present investigation are presented in Table 1. The param-

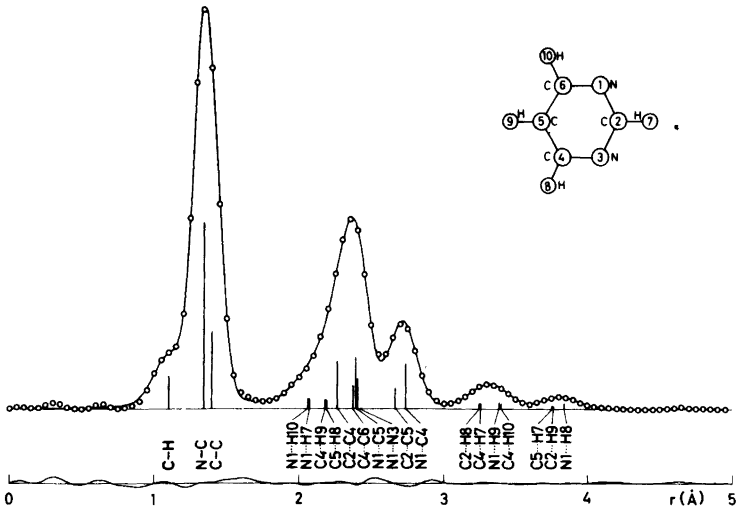

Fig. 1. Experimental (open circles) and theoretical (solid line) RD-functions for pyrimidine, and (below) the corresponding difference curve.

eters varied in the least-squares refinement are those for which estimated standard deviations are given. Shrinkage corrections were not applied.

The two pairs of chemically equivalent N–C bonds, N1–C2, N3–C2 and N1–C6, N3–C4, are of too similar length to be resolved by the current method. They were accordingly treated as equal, and the mean value was found to be 1.340(2) Å. There is evidence, however, indicating that the difference from this mean for each of the bond

Table 1. Parameter values for pyrimidine. Distances (r_a) and the corresponding calculated r.m.s. amplitudes of vibration (u) in Å, angles in degrees. The estimated standard deviations given in parentheses apply to the last digit given, they are corrected for uncertainties in the electron wave length and correlation between intensity data.

	r_a	u		r_a	u
C–C	1.393(2)	0.046	$N_1 \cdots H_{10}$	2.065	0.100
N–C	1.340(2)	0.045	$N_1 \cdots H_9$	3.389	0.094
C–H	1.099(7)	0.077	$N_1 \cdots H_8$	3.837	0.093
$N_1 \cdots N_3$	2.405	0.053	$C_2 \cdots H_8$	3.249	0.096
$N_1 \cdots C_4$	2.739	0.059	$C_2 \cdots H_9$	3.761	0.093
$N_1 \cdots C_5$	2.394	0.054	$C_4 \cdots H_7$	3.255	0.095
$C_2 \cdots C_4$	2.267	0.055	$C_4 \cdots H_9$	2.180	0.098
$C_2 \cdots C_5$	2.662	0.060	$C_4 \cdots H_{10}$	3.396	0.093
$C_4 \cdots C_6$	2.373	0.055	$C_5 \cdots H_7$	3.761	0.093
$N_1 \cdots H_7$	2.075	0.099	$C_5 \cdots H_8$	2.189	0.097
Angle					
∠NCN	127.6(3)				
∠CNC	115.5(2)				
$\angle N_3C_4H_8$	115.3(2.8)				
$\angle C_5C_4N_3$	122.3				
$\angle C_4C_5C_6$	116.8				
$\angle C_4C_5H_9$	121.6				

lengths does not exceed the estimated standard deviation. In an X-ray crystallographic study of 5-methylpyrimidine, a molecule which may be expected to have a geometry nearly identical to pyrimidine near the nitrogen atoms, the N1–C2 and N1–C6 bond lengths differ by only 0.003 Å.[7] Secondly, the principal moments of inertia calculated from the pyrimidine geometry found are 80.65, 83.03, and 163.69 amu Å^2, respectively; the experimental values according to a microwave spectroscopic study of pyrimidine are 80.514, 83.296 and 163.844 amu Å^2.[8] Even though the two sets of moments of inertia are based upon the operational parameters in electron diffraction and microwave spectroscopy, r_a and r_o, respectively, which do not represent the same physical quantity, the agreement is remarkably good.

The C–C bond was found to be 1.393(2) Å; there is thus no significant shortening relative to the benzene C–C bond corresponding to that observed in pyridazine.[9] The internal ring angles given in Table 1 are in good agreement with those found in the crystal structure determination of pyrimidine.[1]

The asymmetry in the external angles at C4 and C6, the N–C–H angle being 115° and the H–C–C angle 122°, is probably significant. No steric repulsion would be expected between the H8 and H9 atoms, their separation being 2.56 Å and thus well above the normal van der Waals' distance. The effect may, however, the explained by the VSEPR model as the nitrogen atom is more electronegative than carbon. A corresponding difference in H–C–N and H–C–C angles is also observed in pyridine (116.03 and 120.17°)[10] and in pyridazine (111.7 and 124.6°).[9]

Acknowledgement. The authors are grateful to Cand.real. A. Almenningen for recording the electron diffraction data.

REFERENCES

1. Wheatley, P. J. *Acta Crystallogr. 13* (1960) 80.
2. Fernholt, L. and Rømming, C. *Acta Chem. Scand. To be published.*
3. Bastiansen, O., Hassel, O. and Risberg, E. *Acta Chem. Scand. 9* (1955) 232.
4. Andersen, B., Seip, H. M., Strand, T. G. and Stølevik, R. *Acta Chem. Scand. 23* (1969) 3224.
5. a. Yates, A. C. *Comput. Phys. Commun. 2* (1971) 175; b. Stewart, R. F., Davidson, E. R. and Simpson, W. T. *J. Chem. Phys. 42* (1965) 3175; c. Strand, T. G. and Bonham, R. A. *J. Chem. Phys. 40* (1964) 1686.
6. Stølevik, R., Seip, H. M. and Cyvin, S. J. *Chem. Phys. Lett. 15* (1962) 263.
7. Furberg, S. and Smedsrud, B. *Private communication.*
8. Blackman, G. L., Brown, R. D. and Burden, F. R. *J. Mol. Spectrosc. 35* (1970) 444.
9. Almenningen, A., Bjørnsen, G., Ottersen, T., Seip, R. and Strand, T. G. *Acta Chem. Scand. A 31* (1977) 63.
10. Sørensen, G. O., Mahler, L. and Rastrup-Andersen, N. *J. Mol. Struct. 20* (1974) 119.

Received November 16, 1977.

Acta Chemica Scandinavica A 32 (1978) 275–281

Short Communications

Brønstedian Energetics and the Gibbs-Duhem Equation

TORBEN KNUDSEN

Instituttet for Silikatindustri, Danmarks Tekniske Højskole, Bygning 204, DK-2800 Lyngby, Denmark

In his third paper in Acta Chemica Scandinavica about energetics,[1] Torben Smith Sørensen discusses the Gibbs-Duhem equation and its bearing on non-equilibrium thermodynamics. The first part of Sørensens paper is concerned with the possible extension of the Gibbs-Duhem equation to include external forces. Sørensen concludes that the straightforward addition of a term representing the effect of the external field yields an equation not verified by experiment. In the opinion of the present author the apparent impossibility of a straightforward extension of the Gibbs-Duhem equation to include the effect of external fields is due to an incorrect treatment of the role played by the pressure. When allowing for external forces in the Gibbs-Duhem equation, the external force nature of the pressure should be recognized.

Continuing to systems with temperature gradients Sørensen correctly states that, the equation: $d\mu_1 + \bar{S}_1 dT = 0$, is unable to predict a Soret effect for a two-component system. This is not remarkable, since it was never intended to do so. The relevant equation for two-component systems reads:

$$d\mu_1 + \bar{S}_1 dT - \frac{\partial \mu_1}{\partial X} dX = 0 \qquad (1)$$

X being the mol fraction.

One-component systems in a gravitational field. The reason why the so-called generalized Gibbs-Duhem equation for continous media in a gravitational or other external field has brought about confusion, as stated in Sørensens article, is in my opinion to be found in the failing to recognize the pressure as another external field. External forces acting on the small volume element under consideration are not merely gravitational, but include surface forces from the outside pressure. The reason why this obvious contribution to the external forces is overlooked is probably due to the pressure already being included in the purely thermodynamic equation:

$$d\mu - V dP = 0 \qquad (2)$$

But the pressure appearing in (2) has a specific thermodynamic significance. It is the pressure inside the volume element, acting when this element changes its volume through a spatial basic process, giving rise to the work term $-V dP$, when the volume V is transported between P and $P+dP$. The external pressure or the outside pressure is "active" when the volume element changes its position in the pressure field, without change of volume. It contributes the term $V dP$. As the volume element is infinitesimal the two pressures are of course measured at the same point in space, and are phenomenologically identical. The generalized Gibbs-Duhem with the inclusion of all external forces now reads:

$$d\mu - V dP + V dP + M d\phi = 0 \qquad (3)$$

where M is the mass of the volume element and ϕ the gravitational potential. The nominal content of eqn. (3) is of course:

$$d\mu + M d\phi = 0 \qquad (4)$$

which can be taken as the statement of the constancy of the gravi-chemical potential. Eqn. (4) could have been derived by adding the purely mechanical equilibrium condition:

$$V dP + M d\phi = 0 \qquad (5)$$

to the purely thermodynamic one (2).

Another way of arguing would be to consider the build up of the small volume element and keeping all potentials constant during this process. This is perfectly possible, although stated to the contrary in Sørensens article. Infinitesimal contributions of quantities to the system should merely extend this in horizontal directions, thus keeping the gravitational potential constant. Besides the three obvious terms: $N\mu$, $M\phi$ and $-PV$, being the chemical, gravitational and spatial energy terms, the term PV enters into the calculation of the total

energy of the sub-system. This last term stems from the fact that, the sub-system built up in this experiment is "floating" in the rest of the system, and the transport of the sub-system, keeping the volume constant, to levels of zero pressure would contribute the work term PV. Thus the total energy is $N\mu + M\phi$, corresponding to the Gibbs-Duhem equation (4).

Equilibrium of matter in temperature gradients. As stated in the beginning of this note eqn. (1) is the equation to be employed for two-component systems with temperature gradients. Transforming this equation it reads:

$$d\mu_1 + (\bar{S}_1 - \frac{\partial \mu_1}{\partial X}\frac{dX}{dT})dT = 0 \qquad (6)$$

The quantity dX/dT is a measure of the Soret effect. Its value depends on the specific components constituting the system. For metalline conductors, considered as two-component systems, composed of positive ions and negative electrons, it must be concluded that $dX/dT = 0$, since the simpler equation $d\tilde{\mu}_1 + \bar{S}_1 dT = 0$, $\tilde{\mu}_1$ is now the electro-chemical potential, can accurately predict the relation between thermo-emf and the Peltier heat.

As dX/dT for any system is a purely dynamical quantity, depending on the specific interactions between phonons and chemical constituents, it takes but little imagination to concieve its directional nature, as for instance in single crystals. Thus there seems only little difficulty in explaining the thermo-emf observed for cells composed of identical single crystals oriented in different directions. $\bar{S}_1$ and $\partial\mu_1/\partial X$ remains of course functions of temperature only, whereas the dynamical quantity dX/dT depends on direction, giving rise to different values of $d\mu_1$ when going in different directions in the single crystal.

Defining now the entropy of transport $\bar{S}_1^*$ by:

$$\bar{S}_1^* = \bar{S}_1 - \frac{\partial \mu_1}{\partial X}\frac{dX}{dT} \qquad (7)$$

eqn. (6) will read:

$$d\mu_1 + \bar{S}_1^* dT = 0 \qquad (8)$$

which is equivalent to Sørensens eqn. (28).

The author of this note fails to see the entirely "new principle of non-equilibrium thermodynamics", inherent in eqn. (8). It is derivable through the thermodynamic eqn. (1), which is a well-established equation from equilibrium thermodynamics. Its application on non-equilibrium systems is granted by the "local equilibrium" or the Brønsted "work principle for infinitesimally diverging systems".

1. Sørensen, T. S. *Acta Chem. Scand. A 31* (1977) 437.

Received January 27, 1978.

Generalised Gibbs-Duhem Equations and Quasi-thermostatic Methods

TORBEN SMITH SØRENSEN

Fysisk-Kemisk Institut, Technical University of Denmark, DK-2800 Lyngby, Denmark

Matter in gravitational and electric fields. In my third paper in the series "Towards a Rational Thermodynamics"[1] I pointed out that a straightforward generalisation of the Gibbs-Duhem equation to include the effect of external fields – such as proposed by La Mer, Foss and Reiss[2] – leads to contradictions with well-established facts, *e.g.* that pressure gradients exist at equilibrium in gravitational fields. In a short communication[3] by Torben Knudsen my propositions are criticised. He argues that the "generalised" Gibbs-Duhem equation should rather be (in the case of only a single component present)

$$d\mu - V dP + V dP + M d\phi = 0 \qquad (1)$$

where the first $-V dP$ term is the "normal" Gibbs-Duhem term due to local equilibrium or – in Brønsted's terminology – the work principle, applied to infinitesimally diverging systems. The second $+V dP$ term should then be a work term due to the change in position of the volume elemnt (V) as a whole in the pressure gradient regarded as an "external field".

To me Knudsen's arguments seem to be of an *ad hoc* nature. It is very confusing to operate with two sorts of pressures: an internal and an external. It is very confusing – and inconsistent with usual lines of thought in physics and irreversible thermodynamics – to speak about pressure as an external field. In the momentum balance equation the action of external fields shows up as a source term [see, *e.g.*, Ref. 4, eqn. (1.31)], since momentum is introduced into the volume element from distant momentum-reservoirs through the action of the external fields. On the contrary, pressure may be considered as a flux of momentum from neighbouring volume elements. Although pressure gradients are sometimes consequences of the action of external fields, they do not generically belong to the class of external fields. Finally, trying to follow the arguments of Knudsen, it is difficult to understand why the "internal" pressure should contribute the term $-V dP$ to the Gibbs-Duhem equation, while the "external" pressure contributes with $+V dP$. A clear cut Brønstedian process of building up the system is lacking in Knudsen's communication.

It was exactly such a procedure for building up the system which I devised in my paper (see Ref. 1, Fig. 1) to explain why a homogeneous integration of the total internal energy (Gibbs' internal energy + potential energy) is not possible – and similarily not a "generalisation" of the Gibbs-Duhem equation. However, there is one important comment in Knudsen's paper regarding this point: It *is* indeed possible to build up a system in a one-dimensional gravitational field by adding quantities in fixed proportions without changing any of the potentials. One just has to add quantities in a direction perpendicular to the field. Thus, with *this* interpretation of the differentials (dK) a homogeneous integration of the complete internal energy to $E = \Sigma PK$ is possible and a generalised Gibbs-Duhem equation of the form

$$S dT - V dP + \Sigma n_i d\tilde{\mu}_i = 0 \qquad (2)$$

can be derived. It might have been this interpretation of the generalised G.D. equation which La Mer, Foss and Reiss had in mind, but then it is confusing that they speak about eqn. (2) in connection with discussion of the equilibrium conditions ($d\tilde{\mu}_i = 0$) in the direction of the field.

A similar example where a generalisation of Gibbs-Duhem's equation is possible – and highly useful – is given by the case of an electric double layer at a liquid-liquid interface. We consider the system as composed of bulk phase I with surface layer α and bulk phase II with surface layer β. The two dividing surfaces and the interfacial surface are selected so that phases I and II are electroneutral and the positive surface charge of α corresponds to the negative surface charge of β. By building up the system in the directions of the interface we derive the following generalised Gibbs-Duhem equation (T and P taken as constants for brevity)

$$\sum_{\mathrm{I}} n_i^{\mathrm{I}} d\tilde{\mu}_i^{\mathrm{I}} + \sum_{\mathrm{II}} n_i^{\mathrm{II}} d\tilde{\mu}_i^{\mathrm{II}} + A \sum_{\alpha} \Gamma_i^{\alpha} d\tilde{\mu}_i^{\alpha} + \sum_{\beta} \Gamma_i^{\beta} d\tilde{\mu}_i^{\beta} + A d\sigma = 0 \qquad (3)$$

where A is the interfacial area of the final system, Γ_i are surface excess concentrations and σ is the interfacial tension. Since we have electroneutrality in the bulk solutions we have separately for each bulk solution

$$\Sigma n_i d\tilde{\mu}_i = \Sigma n_i d\mu_i + (\Sigma z_i F n_i) d\psi = \Sigma n_i d\mu_i = 0 \qquad (4)$$

Due to equilibrium between bulk solution and surface, the bulk electrochemical potentials equal the surface electrochemical potentials, and we obtain

$$d\sigma = -\sum_{\alpha} \Gamma_i^{\alpha} d\tilde{\mu}_i^{\alpha} - \sum_{\beta} \Gamma_i^{\beta} d\tilde{\mu}_i^{\beta} \qquad (5)$$

From eqn. (5) it is a simple matter to derive the classical Lippmann equation[5] of relevance for the study of effects of electrocapillarity at an interface between mercury and an electrolyte solution. The derivation given here is the one usually given (see, *e.g.*, Ref. 6), but unfortunately not very many thermodynamicians pose themselves fundamental questions concerning when and why generalisations of the Gibbs-Duhem equation can be made. The rule which has been found in Ref. 1 and here is straightforward: Whenever a way of building up the system in question can be found, such as by adding the quantities in fixed proportions to the different localities in the system, all the potentials remain constant, we are able to integrate the internal energy to $E=\Sigma PK$ and thereby to obtain a generalised Gibbs-Duhem equation $\Sigma K\mathrm{d}P=0$.

Matter in temperature gradients and the use of quasi-thermostatic arguments. Knudsen's critique of my treatment of the equilibrium of matter in temperature gradients is based upon a misinterpretation of what I have written in Ref. 1. I have never doubted that his eqns. (1) or (6) apply. On the contrary, I used the same equation (Ref. 1, p. 442, 1st column, line 15 from above). But this equation is just a "passive" expression of local equilibrium and therefore useless as an equation of dynamic balance. Just as we have for equilibrium in an electric field at isothermal and isobaric conditions

$$\mathrm{d}\tilde{\mu}_i = \mathrm{d}\mu_i + z_i F\,\mathrm{d}\psi = 0 \qquad (6)$$

together with the obvious equation $\mathrm{d}\mu_i - \sum_{j=1}^{n-1}(\partial\mu_i/\partial X_j)\mathrm{d}X_j = 0$, it would be tempting to use

$$\mathrm{d}\tilde{\mu}_i + \bar{S}_i\mathrm{d}T = 0 \qquad (7)$$

as a general balance equation for matter in temperature gradients. In Ref. 1 I have shown, how it is possible to derive the relation between thermo-emf and Peltier-entropy using eqn. (7). Another variant of this "quasi-thermostatic" method was used already by Thomson in 1854.[7] The two effects are according to this argumentation related, since the partial molar entropy of the electron appears in both expressions. This method of using equilibrium thermodynamics on non-equilibrium problems is far from unproblematic, however, as understood already by Thomson himself. It is therefore somewhat unfortunate, that Brønsted[8] used the same kind of arguments at a time where irreversible thermodynamics had reached recognition of the connection between thermo-emf and Peltier-effect as being due to the Onsager reciprocal relations.

Since many chemists still have a "quasi-thermostatic" picture of the world, however, I wanted to point out clearly the inconsistencies connected with the use of eqn. (7). In the case of a single, neutral solute in a temperature gradient, the use of (7) precludes any Soret-effect. Also, the experiments of of Denbigh and Raumann on thermo-osmosis with rubber membranes[9] show clearly that the "entropies of transport" have nothing to do with partial molar entropies. I would not expect either that the entropy of transport of the electron should have anything to do with the partial molar entropy of the electron, but at present I am not aware of any independent method of measuring partial molar entropies of electrons in metallic conductors.

1. Sørensen, T. S. *Acta Chem. Scand. A 31* (1977) 437.
2. La Mer, V. K., Foss, O. and Reiss, H. *Acta Chem. Scand. 3* (1949) 1238.
3. Knudsen, T. *Acta Chem. Scand. A 32* (1978) 275.
4. Glansdorff, P. and Prigogine, I. *Thermodynamic Theory of Structure, Stability and Fluctuations*, Wiley-Interscience, London, New York, Sydney, Toronto 1971, p. 7.
5. Lippmann, G. *Ann. Chim. Phys. 5* (1875) 494.
6. Sanfeld, A. *Introduction to the Thermodynamics of Charged and Polarized Layers*, Wiley-Interscience, London, New York, Sydney, Toronto 1968, pp. 165–167.
7. Thomson, W. *Proc. R. Soc. Edinburgh 3* (1854) 225.
8. Brønsted, J. N. *Principer og Problemer i Energetiken*, Københavns Universitets Festskrift, Bianco Luno, København 1946, Kapitel VII, sektion 1.
9. Denbigh, K. G. and Raumann, G. *Proc. R. Soc. London Ser. A 210* (1951) 377, 518.

Received February 17, 1978.

Crystal Conformation of 1,4,7,10-Tetraoxacyclododecane at −150 °C

P. GROTH

Department of Chemistry, University of Oslo, Oslo 3, Norway

As part of a study of conformational problems of tetraoxacycloalkanes 1,4,7,10-tetraoxacyclododecane has been synthesized.[1] In five known complexes with this cyclomer three different ring conformations occur. In $Na(C_8H_{16}O_4)_2Cl.5H_2O$,[2] $Na(C_8H_{16}O_4)_2OH.8H_2O$[3] and $Ca(C_8H_{16}O_4)Cl_2.8H_2O$,[4] the ring symmetry is C_4. In $Cu(C_8H_{16}O_4)Cl_2$[5] it is C_s and in $Mg(H_2O)_6Cl_2.C_8H_{10}O_4$[6] a C_i geometry is obtained. For $C_8H_{16}O_4$ itself no definite conclusions about the ring conformation could be drawn on the basis of NMR-data, and the crystal structure is now reported.

The crystals belong to the triclinic system with space group $P\bar{1}$, cell dimensions (for Dirichlet's reduced cell) $a=4.704(3)$ Å, $b=7.282(4)$ Å, $c=7.520(5)$ Å, $\alpha=64.10(5)°$, $\beta=85.12(5)°$, $\gamma=76.52(4)°$, and $Z=1$ ($D_x=1.30$ g cm^{-3}). The melting point was ~0 °C and the density was not measured.

With $2\theta_{max}=50°$, Mo$K\alpha$-radiation, and an observed – unobserved cutoff at 2.5 $\sigma(I)$, 715 independent reflections were recorded as observed on an automatic four-circle diffractometer at −150 °C (the crystals were grown at −10 °C and rapidly transferred into the cold stream). No corrections for absorption or secondary extinction were applied (crystal size 0.3 × 0.4 × 0.4 mm).

The structure was solved by direct methods[7] (assuming space group $P1$) and refined by full-matrix least squares technique.[8] After three cycles of isotropic refinement, the correlation matrix strongly indicated a centrosymmetric structure, and coordinates were transformed to $P\bar{1}$. Hydrogen atom positions were calculated. Anisotropic temperature factors were introduced for O and C atoms and weights in least squares were calculated from the standard deviations in intensities, $\sigma(I)$, taken as

$$\sigma(I)=[C_T+(0.02C_N)^2]^{\frac{1}{2}}$$

where C_T is the total number of counts and C_N the net count. The form factors used were those of Hanson *et al.*[9] except for hydrogen.[10] The final R-value was 3.0 % (weighted value 3.8 %) for 715 observed reflections.

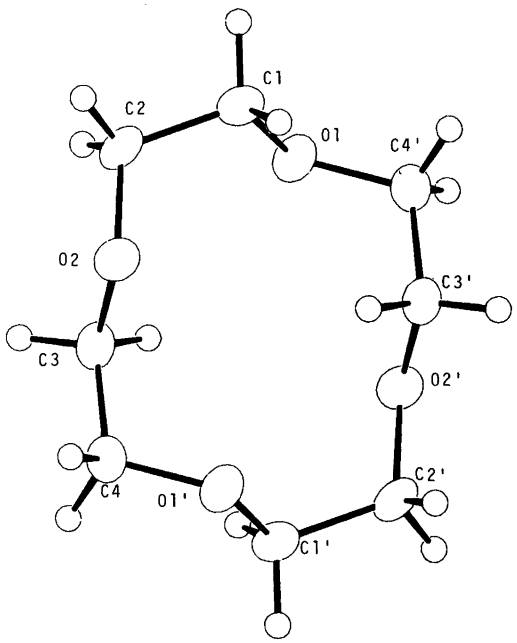

Fig. 1. Schematic drawing of the molecule.

Table 1. Final fractional coordinates and thermal parameters with estimated standard deviations. The expression for anisotropic vibration is $\exp[-2\pi^2(h^2a^{*2}U11+\cdots+2klb^*c^*U23)]$. Atom H_{mn} is bonded to C_m.

ATOM	X	Y	Z	U11	U22	U33	U12	U13	U23
O1	.07414(19)	-.20886(13)	.31532(12)	.0309(5)	.0297(5)	.0286(5)	-.0138(4)	.0053(4)	-.0156(4)
O2	.16389(18)	.22456(13)	.02679(12)	.0265(5)	.0311(5)	.0237(5)	-.0101(4)	.0037(3)	-.0127(4)
C1	.31366(29)	-.10866(21)	.31288(20)	.0263(7)	.0323(7)	.0233(7)	-.0103(5)	-.0001(5)	-.0125(6)
C2	.21132(30)	.12415(21)	.23625(18)	.0306(7)	.0330(7)	.0240(7)	-.0141(6)	.0044(5)	-.0176(6)
C3	-.13607(27)	.28563(21)	-.03263(19)	.0247(7)	.0250(7)	.0308(7)	-.0065(5)	.0038(5)	-.0155(6)
C4	-.15293(32)	.36594(20)	-.25370(20)	.0344(7)	.0219(6)	.0303(7)	-.0086(5)	.0000(5)	-.0107(5)

ATOM	X	Y	Z	B	ATOM	X	Y	Z	B
H11	.4684(31)	-.1340(20)	.2274(20)	1.7(3)	H12	.3919(29)	-.1665(21)	.4497(21)	1.8(3)
H21	.3713(31)	.1770(21)	.2625(20)	2.1(3)	H22	.0363(31)	.1585(21)	.3040(20)	1.9(3)
H31	-.2388(30)	.3962(22)	.0858(19)	1.8(3)	H32	-.2313(30)	.1668(22)	.0354(19)	1.8(3)
H41	-.0103(31)	.4551(22)	-.3162(21)	1.9(3)	H42	-.3580(32)	.4506(23)	-.3013(20)	2.2(3)

Table 2. Bond distances, bond angles, and dihedral angles with estimated standard deviations. Left columns: present compound. Right columns: $Mg(H_2O)_6Cl_2C_8H_{16}O_4$.

Distance	(Å)	(Å)	Distance	(Å)	(Å)
O1–C1	1.430(1)	1.428(2)	O1–C4′	1.431(2)	1.428(2)
O2–C2	1.429(1)	1.435(2)	O2–C3	1.423(2)	1.430(2)
C1–C2	1.502(2)	1.495(3)	C3–C4	1.505(2)	1.494(3)
Angle	(°)	(°)	**Angle**	(°)	(°)
O1–C1–C2	110.3(1)	110.5(1)	C1–O1–C4′	113.1(1)	113.0(1)
O2–C2–C1	111.9(1)	111.7(2)	C2–O2–C3	114.1(1)	116.4(2)
O2–C3–C4	108.5(1)	108.0(2)	C3–C4–O1′	112.3(1)	112.1(2)
	Dihedral angle		(°)	(°)	
	C4′–O1–C1–C2		140.2(1)	116.8(2)	
	C3–O2–C2–C1		102.7(1)	98.0(2)	
	C4–C3–O2–C2		−173.6(1)	−147.3(2)	
	O2–C2–C1–O1		−75.4(1)	−83.1(2)	
	O2–C3–C4–O1		74.5(1)	71.0(2)	
	C3–C4–O1′–C1′		85.2(1)	91.1(2)	

Final fractional coordinates together with the thermal parameters are listed in Table 1. The principal thermal vibration ellipsoids for oxygen and carbon atoms were calculated from the thermal parameters of this table, and the maximum r.m.s. amplitudes range from 0.184 to 0.200 Å.

Bond distances, bond angles and dihedral angles may be found as the left columns of Table 2. The standard deviations, given in parentheses, are estimated from the correlation matrix of the final least squares refinement cycle. The right columns show corresponding values for the $C_8H_{16}O_4$ ring in the $Mg(H_2O)_6.Cl_2$ complex[6] (after turning the molecules to their best fit). Fig. 1 is a schematic drawing of the molecule giving a view of its C_i geometry and indicating the numbering of atoms.

As may be seen from Table 2, corresponding bond distances of the two rings are equal within error limits. Also the angles agree closely except for C2–O2–C3, which is somewhat larger for the complexed ring. However, for dihedral angles the deviations are considerable. In particular the angles at C1–O1 and C3–O2 are about 25° larger in the cyclomer itself than in the hydrogen-bonded ring of the complex.

C–H bond distances range from 0.99 to 1.01 Å and no short inter-molecular distances are observed.

Acknowledgement. The author thanks Dr. G. Borgen for preparing the crystals.

1. Borgen, G. and Dale, J. *To be published.*
2. van Remoortere, F. P. and Boer, F. P. *Inorg. Chem. 13* (1974) 2071.
3. Boer, F. P., Neuman, M. A., van Remoortere, F. P. and Steiner, E. C. *Inorg. Chem. 13* (1974) 2826.
4. North, P. P., Steiner, E. C., van Remoortere, F. P. and Boer, F. P. *Acta Crystallogr. B 32* (1976) 370.
5. van Remoortere, F. P., Boer, F. P. and Steiner, E. C. *Acta Crystallogr. B 31* (1975) 1420.
6. Neuman, M. A., Steiner, E. C., van Remoortere, F. P. and Boer, F. P. *Inorg. Chem. 14* (1975) 734.
7. Germain, G., Main, P. and Woolfson, M. M. *Acta Crystallogr. A 27* (1971) 368.
8. Groth, P. *Acta Chem. Scand. 27* (1973) 1837.
9. Hanson, H. P., Herman, F., Lea, J. D. and Skillman, S. *Acta Crystallogr. 17* (1964) 1040.
10. Stewart, R. F., Davidson, E. R. and Simpson, W. T. *J. Chem. Phys. 42* (1965) 3175.

Received February 2, 1978.

Acta Chemica Scandinavica A 32 (1978) 283–288

On the Accuracy of Stability Constants of Carboxylate Complexes from Potentiometric Measurements of Central Ion Concentrations

ÅKE OLIN and PÄR SVANSTRÖM

Institute of Chemistry, University of Uppsala, P.O.B. 531, S-751 21 Uppsala, Sweden

The influence of the liquid junction potential, E_j, and varying activity coefficients, y, on the values of stability constants obtained from emf measurements of central ion concentrations is discussed. It is found both experimentally and theoretically that β_1 is quite insensitive to errors in E_j and to non-constant y whereas β_2 may be substantially changed thereby. The choice of expression for E_j in carboxylate systems is discussed. It is also suggested that β values should be calculated using different assumptions about the value of E_j in order to obtain better estimates of the uncertainties in the numerical values of equilibrium constants.

In an aqueous solution of two electrolytes A and B the mean activity factors will vary when the composition of the solution is changed from one of pure A to one of pure B at constant ionic strength. The variations often follow Harned's rule.[1] Since composition changes must necessarily be made in complexation studies the principle of specific interactions of ions[2] is used in the design of the electrolyte background employed to reduce activity coefficient and liquid junction potential changes. Thus the concentration of the anion of the medium is kept constant when the complex formation between mainly cationic species is studied and *vice versa*. The success of this approach to damp activity changes was demonstrated by Biedermann and Sillén.[3] They also provided evidence showing that the medium effects upon an ion from changes in the composition of the ions of opposite charge could be expressed by the relation $\lg y_B = k[A]$. y_B is the activity coefficient of ion B, k is a constant and [A] the concentration of an ion exchanged in the medium.

For exchanges made at constant equivalent concentration there is now ample evidence[4,5] indicating that the above relation is also followed when the charges on A and B are of the same sign. The k values are small and neglect of activity coefficient variations will be a main concern only in studies of weak complex formation where large concentrations of the ligand must be used. For the same reason the values of the stability constants of the higher complexes will in general be effected. These remarks are also pertinent to the influence of a neglect of liquid junction potentials when the emf method is used.

STUDIES ON CARBOXYLATE BUFFERS

In two recent studies[6,7] the complex formation between Pb^{2+} and aliphatic dicarboxylic acids, H_2A, has been investigated by central ion measurements. Since the complexation is of moderate strength with the dicarboxylate ion and the protonated complexes are weak, it was felt necessary to estimate and correct for the effects mentioned in the introduction. This has been attempted by measurement of the cell

$$\text{Glass} \mid H_nA,\ H_{n-1}A \mid \text{Ref.} \qquad \text{(I)}$$

$$E = E^\circ - g \ln a_H - E_j \qquad (1)$$

The experimental details of this measurement and those to be described later can be found in Refs. 6 and 8. The ionic medium employed was 1 M $Na(ClO_4)$ and the activity scales chosen so that $y \rightarrow 1$ when the composition of the equilibrium solution $\rightarrow 1$ M $NaClO_4$. E_j is the liquid junction potential and $g = RTF^{-1}$. $[H_nA]^*$ *etc.* represent the formal concentrations of the components of the buffer. The ratio $[H_nA]^*/[H_{n-1}A]^*$ was kept con-

stant in each run and E was measured as a function of the total concentration of the buffer. An approximate hydrogen ion concentration, h, can be found from eqn. (1) putting $y_{H^+} = 1$ and then inserted together with $[OH^-]$ into the expression

$$\phi = ([H_nA]^* - h + [OH])([H_{n-1}A]^* + h - [OH])^{-1} \quad (2)$$

The approximate nature of the concentrations of H^+ and OH^- is not serious since they are small compared to the concentrations of the buffer components. For a N-basic acid we have

$$[H_nA]^* + [H_{n-1}A]^* = \sum_0^N [H_mA] = [A]_{tot} \quad (3)$$

$$n[H_nA]^* + (n-1)[H_{n-1}A]^* = \sum_0^N m[H_mA] + h - [OH] \quad (4)$$

so that eqn. (2) can be written

$$\phi = (\sum_0^N (1 + m - n)[H_mA])(\sum_0^N (n - m)[H_mA])^{-1} \quad (5)$$

The use of eqn. (5) will be illustrated with acetic acid as an example. Then $N = n = 1$ and $\phi = [HA]/[A]$. The protonation constant, β_1 of the acid is defined by

$$\beta_1 = [HA][A]^{-1} y_{HA} y_A^{-1} a_H^{-1} \quad (6)$$

Eqns. (1), (5), and (6) yield

$$E - E^\circ + g \ln \phi = g \ln \beta_1 + g \ln (y_A y_{HA}^{-1}) - E_j \quad (7)$$

In Fig. 1 the left hand side of eqn. (7) has been plotted as a function of $[A]_{tot}$ for various buffer ratios. Straight lines are obtained which have a common intercept within 0.1 mV. From the intercept the protonation constant at infinite dilution in the medium can be calculated. $\beta_1 = 3.91 \times 10^4$ M^{-1} obtained for acetic acid agrees very well with the value found by Ahrland.[9] An iterative procedure must be used for diprotic acids.

It has been observed that the slopes of the lines representing eqn. (7) can be expressed as linear functions of $[H_nA]$ and $[H_{n-1}A]$, *i.e.*

$$g \ln (y_{H_{n-1}A} y_{H_nA}^{-1}) - E_j = k_n [H_nA] + k_{n-1} [H_{n-1}A] \quad (8)$$

The linearity is in agreement with the Guggenheim and Setchenow relations for activity coefficients[10] and the linearized form of Henderson's equation.[11]

The values of the coefficients, k_m, in eqn. (8) obtained for acetic acid and the series of dicarboxylic acids from oxalic to adipic acid were in reasonable agreement with the values estimated from Henderson's equation for the charged species. The coefficients for the acids were in the range $1-2$ mVM^{-1}. It was therefore concluded that the observed effects mainly arose from variations in the liquid junction potential and that the activity coefficients could be considered as invariant. A correction term $E_j = \sum_0^N k_m[H_mA]$ would then be

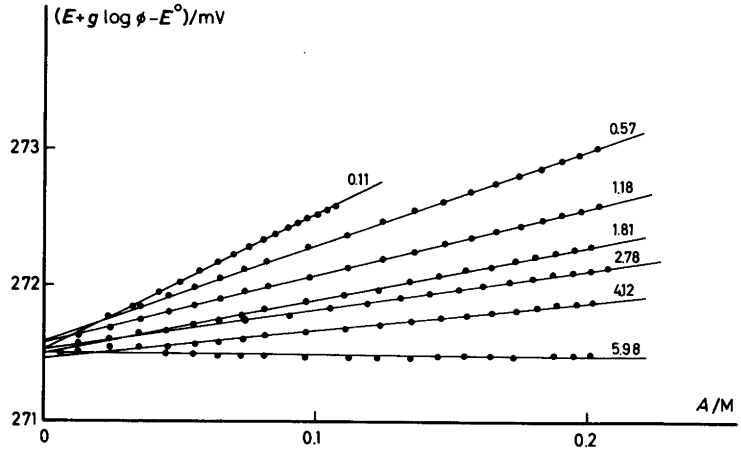

Fig. 1. The experimental values of $E + g \log \phi - E^\circ$ [see eqn. (7)] in the acetate system plotted against A at different values of the quotient $[HA]^*/[A]^*$. In this figure $g = 59.16$ mV.

applicable to the emf of other electrodes as well. A similar correction has been applied by Sandell,[12] who demonstrated that in this way the stability constants calculated from central ion measurements were brought into better agreement with those from ligand measurements.

When data obtained for benzoic and some other aromatic acids were treated in the way described above, it was found that some of the coefficients were considerably greater than expected for a pure liquid junction potential. It must therefore be concluded that changes in the activity coefficients and/or dimerisation of the acids occur.

The dimerisation of carboxylic acids has been much debated and it is hardly likely that the arguments can be settled from thermodynamic measurements alone.[13] This can be seen if the ϕ-function is used. One would then have

$$\phi = ([HA] + [HA_2] + 2[H_2A_2])([A] + [HA_2])^{-1} \quad (9)$$

Assuming constant activity coefficients and introducing the equilibrium constants K_1 and K_2 of the reactions $HA + A \rightleftharpoons HA_2$ and $2HA \rightleftharpoons H_2A_2$ eqn. (10) is obtained from eqn. (9)

$$\phi = h\beta_1(1 + K_1[A] + 2K_2[HA])(1 + K_1[HA])^{-1} = h\psi \quad (10)$$

A combination of eqns. (1) and (10) leads to

$$E - E^\circ + g \ln \phi = g \ln \psi - E_j \quad (11)$$

In cases where K_1 and K_2 are small, $\ln \psi$ is approximately

$$\ln \psi \approx \ln \beta_1 + K_1[A]^* + (2K_2 - K_1)[HA]^* \quad (12)$$

A plot of the left hand side of eqn. (11), where ϕ is calculated from eqn. (2), as a function of $[A]_{tot}$ should at a constant buffer ratio then give a straight line as is observed in Fig. 1. One is thus faced with a situation where activity coefficient and liquid junction potential changes, and dimerisation lead to the same type of deviation from a horizontal line for a plot of $E - E^\circ + g \ln \phi$ as a function of the total concentration of the buffer. When K_1 and K_2 have comparatively large values, as appears to be the case for aromatic acids, eqn. (12) is no longer valid. Calculations on models show, however, that deviations from a linear relationship become significant only if a very broad range in [HA]/[A] and $[A]_{tot}$ is investigated.

For the most thoroughly investigated system, acetic acid-acetate ion, Danielsson and Stenius,[14] and Persson[15] concluded that the observed effects are mainly due to changes in activity coefficients and liquid junction potentials. Farrer and Rossotti[16] made an attempt to compensate for these variations and obtained values for K_1 and K_2. Indirect evidence for and against dimerisation has been obtained in complexation studies.[15,17] It appears plausible that the course of the plots of eqn. (7) cannot be solely attributed to E_j for the following reasons: (*i*) the emfs of cells without a liquid junction[15] cannot be explained by the simple $H + A \rightleftharpoons HA$ equilibrium (*ii*) the coefficients in eqn. (8) are different from those, $k_{HA(H)}$ and $k_{A(OH)}$ from measurements of cell (I) with an excess of H^+ or OH^-. See Table 1 for experimental results. It may be noted that $k_{A(OH)}$ is close to the values estimated from the Henderson equation.

Activity coefficient changes also seem to be present. $k_{HA(H)}$ is definitely observed to be $\neq 0$ and the most reasonable cause is variations of the activity coefficients. This is further corroborated by measurements on the cell

$$\text{Glass} \mid \text{HB, B, A} \mid \text{Ref.} \quad \text{(II)}$$

where HB−B is a buffer present at a constant concentration. It is chosen so that there is virtually

Table 1. Experimental values of the coefficients from eqn. (8) in mVM^{-1}. $k_{HA(H)}$ and $k_{A(OH)}$ refer to results from cell (I) with an excess of H^+ or OH^-.

Acid	k_{HA}	$k_{HA(H)}$	k_A	$k_{A(OH)}$	Medium ($NaClO_4$) (M)
Acetic	1.4	2.6	−13.5	−7.2	1
Acetic	–	3.4[a]	–	−2.9; −6.3[a]	3
p-Hydroxybenzoic	−47	6.8	−25.3	−9.5[b]	1
Benzoic	–	–	–	−3.2	3

[a] Ref. 15. [b] Benzoate ion.

no proton transfer from HB to A. The concentration of A was varied from 0 to 0.2 M. With B = borate or tris(hydroxymethyl)aminomethane, and A = acetate or benzoate it was found that E as a function of [A] could be represented by straight lines. Their slopes were different from $k_{A(OH)}$, which indicates that $y_B y_{HB}^{-1}$ changes with [A] unless some quite unfamiliar species are postulated to form.

MODELLING

Modelling of the influence of varying liquid junction potentials and activity coefficients on calculated stability constants. When the complexation of a metal ion, M^{z+}, is studied by central ion measurements, the correct value of E_j to be used is somewhat difficult to ascertain. This difficulty is enhanced when the ligand contains carboxylate groups due to the alleged dimerisation. Variations of the activity coefficients will further add to the uncertainty of the model proposed. An instructive case can be found in Ref. 18. In the actual case, calculations of the stability constants under various assumptions will provide an estimate of the uncertainties in these constants and hence in the proposed model. It is, however, instructive to obtain semi-quantitative information from a study of a simple case.

Let it be assumed to simplify matters that M^{z+} forms only the complexes ML and ML_2 with the ligand L. The species present are thus M, L, ML and ML_2. The metal ion activity, a_M, is determined from potentiometric measurements

$$E = E^\circ + g \ln a_M + E_j; a_M = m y_M; g = RT(zF)^{-1} \quad (13)$$

It is further assumed that the total concentration of the metal, M, is small compared to the total concentration of the ligand. The concentration of non-complexed L, l, can therefore be considered as known. The relation between E and the composition of the solution is found from the equations

$$M = m + [ML] + [ML_2] \quad (14)$$

and

$$\beta_1 = [ML] m^{-1} l^{-1} y_1^{-1}; \; \beta_2 = [ML_2] m^{-1} l^{-2} y_2^{-1} \quad (15)$$

where y_1 and y_2 are combinations of the individual activity coefficients. Eqns. (13)–(15) yield

$$E = E^\circ + g \ln M + g \ln y_M - g \ln (1 + \beta_1 l y_1 + \beta_2 l^2 y_2) + E_j \quad (16)$$

Since it has been found experimentally that E_j and $\ln y$ are linear functions of l and if in addition M is kept constant eqn. (16) can be written

$$E = E^{\circ\prime} - g \ln (1 + \beta_1 l y_1 + \beta_2 l^2 y_2) + kl \quad (17)$$

In this equation y_1 and y_2 are largely unknown and the value of k subject to some ambiguity. When solving eqn. (17) for the β values, y_1 and y_2 are given a value = 1 when the ionic medium method is used. The uncertainty in β caused thereby can be estimated as follows.

In the relation $g \ln y = kl$ the constant k is generally less than 20 mVM^{-1}. This corresponds to moderate changes in y when $l < 0.2$ M and the relation can therefore be written

$$y = 1 + p_1 l + p_2 l^2; \; p_1 = k g^{-1} \text{ and } p_2 = 0.5\, p_1^2 \quad (18)$$

Inserting this into eqn. (17) yields

$$E = E^\circ - g \ln (1 + \beta_1 l + (\beta_2 + \beta_1 p_{11}) l^2 + (\beta_1 p_{12} + \beta_2 p_{21}) l^3 + \beta_2 p_{22} l^4) + kl \quad (19)$$

With k known eqn. (19) will yield stability constants, β', which are related to the values at infinite dilution by

$$\beta'_1 = \beta_1 \text{ and } \beta'_2 = \beta_2 + \beta_1 p_{11} \quad (20)$$

β_1 is thus expected to be little effected by changes in the activity factors whereas the error in β_2 (and higher β) can be considerable. The values of β'_3 and β'_4 are so small that they can hardly be mistaken for real constants. However, varying activity coefficients could lead to a systematic trend in E_{calc} amounting to a few tenths of a millivolt. One should therefore be cautions to interprete small trends as indicating the formation of higher complexes.

The influence of a change in k on the values of β is found upon differentiation of eqn. (17) putting $y_1 = y_2 = 1$.

$$(1 + \beta_1 l + \beta_2 l^2) \Delta k = g (\Delta\beta_1 + l \Delta\beta_2) \quad (21)$$

From this equation it can be seen that if the complex formation is strong enough to allow ML_2 and higher complexes to be present in considerable amounts, it is not possible to fully compensate a change in k

Table 2. Stability constants of cadmium and lead benzoate complexes calculated using various expressions for the liquid junction potential (see text for further details). Three times the estimated standard deviation from the least-squares calculation is given within parenthesis.

E_j	β_1/M^{-1}	$\beta_2 \times 10^{-2}/M^{-2}$	$\sigma(E_{Pb})$/mV	β_1/M^{-1}	$\beta_2 \times 10^{-2}/M^{-2}$	$\sigma(E_{Cd})$/mV
(1) No Correction	73.4(1.0)	8.75(0.17)	0.09	10.9(0.5)	55.1(0.7)	0.02
(2) $6.8[HA]-9.5[A^-]$	74.1(0.6)	7.59(0.10)	0.05	10.2(0.4)	43.5(0.5)	0.01
(3) (2) + HA_2^-	73.8(0.6)	7.78(0.11)	0.06	10.2(0.1)	44.9(0.7)	0.01
(4) $-25.4[A^-]$	74.8(0.1)	5.76(0.02)	0.01	9.10(0.03)	26.4(0.4)	0.01

by changes in the values of β. In this case the extension of the program LETAGROP by Ulmgren and Wahlberg to treat k as an adjustable parameter would be useful to find the best set of β_1, β_2, and k. Their paper[5] should be further consulted for suggestions on the treatment of data in systems where uncertainties in the activity factors and liquid junction potentials are present.

When the complex formation is weak so that ML_2 does not become predominant, Δk can be largely compensated for by the following changes in β

$$\Delta\beta_1 = \Delta k g^{-1};\ \Delta\beta_2 = \beta_1 \Delta k g^{-1} = \beta_1 \Delta\beta_1 \qquad (22)$$

as can be seen from eqn. (21). In this case simultaneous refinement of k, β_1, and β_2 would tend to fail. It is also to be noted that β_2 is much more sensitive to Δk than β_1.

The conclusions reached here were corroborated by calculations made on "theoretical" data with the program LETAGROP.[19] $\Delta\beta_2$ was in general greater than estimated by eqn. (22) which is not surprising in view of the term $\beta_2 l^2$ in eqn. (21). A real case is shown in Table 2, where the result of a study of the complex formation between Pb^{2+}, Cd^{2+} and the benzoate ion is presented.[8] The expressions for the E_j correction in eqn. (13) were obtained as follows; $E_j(2)$ uses the coefficients $k_{HA(H)}$ and $k_{A(OH)}$ obtained from cell (I) with excess of H^+ or OH^-; $E_j(3)$ includes the species HA_2^- with a stability constant determined from measurements of cell (I) using the corrections suggested by Farrer and Rossotti,[16] *i.e.* $E_j(2)$; $E_j(4)$ uses the coefficients k_{HA} and k_A obtained when the same data as used for finding $E_j(3)$ were treated according to eqns. (7) and (8). In accordance with the predictions β_1 is quite insensitive to the choice of E_j and β_2 subject to large variations. It can also be observed that when the complexation is weak as for Cd^{2+}, the covariation between E_j and β in all cases leads to small $\sigma(E_{Cd})$. This is no longer the case when the complexation becomes stronger, as for Pb^{2+}.

Another example is given in Table 3, which

Table 3. Stability constants of lead acetate complexes for various expressions of the liquid junction potential $E_j = k_1[HA] + k_2[A]$. In (8) and (9) k_1 and k_2 were included in the least-squares refinement. k_1 and k_2 have been taken from Table 1. Three times the estimated standard deviation from the refinements is given within parenthesis.

E_j/mV	$\beta_1 \times 10^{-2}/M^{-1}$	$\beta_2 \times 10^{-3}/M^{-2}$	$\beta_3 \times 10^{-3}/M^{-3}$	$\sigma(E_{pb})$mV
(1) No correction	0.95(0.04)	1.37(0.06)		0.36
(2) $2.6[HA]-7.2[A]$	0.99(0.02)	1.23(0.03)		0.17
(3) $2.6[HA]-7.2[A]$	1.03(0.02)	1.06(0.05)	1.1(0.3)	0.10
(4) $1.4[HA]-13.5[A]$	1.00(0.01)	1.11(0.01)		0.09
(5) $1.4[HA]-13.5[A]$	1.02(0.01)	1.05(0.04)	0.38(0.02)	0.08
(6) (2) + $HA_2 + H_2A_2$	1.01(0.01)	1.28(0.02)		0.10
(7) (6) + $PbHA_2$	0.996(0.01)	1.27(0.01)	[a]	0.08
(8) $5.4[HA]-13.6[A]$	1.020(0.004)	1.11(0.02)		0.03
(9) $-3.0[HA]-11.9[A]$ + $HA_2 + H_2A_2$	1.002(0.006)	1.17(0.04)		0.05

[a] $\beta(PbHA_2) = 1.1 \times 10^6\ M^{-3}$.

presents results for the lead–acetate system from titrations covering a broad range of buffer quotients, $[HA]/a = 0.1$, 1, and 2. With the types of coefficients in Table 1, cases (1)–(5), $\sigma(E_{Pb})$ is greater than 0.08 mV. Allowance for the dimerisation of acetic acid does not improve $\sigma(E_{Pb})$, cases (6)–(7). However, simultaneous refinement of the β values and the coefficients in E_j results in a substantial improvement in $\sigma(E_{Pb})$, cases (8)–(9).

Individual sets of coefficients in E_j for the glass and the amalgam electrodes seem to give the best result, a situation that is not unexpected if changes in activity coefficients occur. From measurements in only one buffer (or a narrow range of buffer quotients) this will hardly show up due to the partial interdependence between β and the coefficients in E_j.

CONCLUSIONS

Liquid junction potentials and activity coefficient changes can have considerable effect on the numerical values of stability constants obtained from emf measurements of central ion concentrations as can be seen in Tables 2 and 3. Realistic estimates of the uncertainties in these constants can therefore be obtained only by a study of these influences. It will not be possible, in general, to derive simple expressions for finding them. Instead, one has to make calculations for a number of reasonable models with the least-squares program at hand and use the changes in the values of β as a measure of the uncertainties.

In complicated systems, for instance, when the ligand is the conjugate base of a di- or triprotic acid, the number of parameters in E_j will be great. Simultaneous refinement of these parameters and a large number of equilibrium constants can be anticipated to cause problems. Use of the E_j correction obtained from glass electrode measurements in buffers appears to yield good estimates of the β values in many systems. A better fit seems to be obtained by this correction than by the Farrer and Rossotti correction.[16] This result is probably partly fortuitous, since with a large E_j correction there is a smaller part of $E-E^{\circ\prime}$ in eqn. (17) to be accounted for by complex formation. In all probability results with the Farrer and Rossotti correction are more accurate than those obtained by the more common "$E_j = 0$" correction. Large values of k obtained from buffers probably indicate association reactions in the ligand system and E_j values from such measurements would then tend to overestimate E_j.

REFERENCES

1. Robinson, R. A. and Stokes, R. H. *Electrolyte Solutions*, 2nd Ed., Butterworths, London 1959, p. 438.
2. Ref. 1, p. 436.
3. Biedermann, G. and Sillén, L. G. *Ark. Kemi 5* (1953) 425.
4. Ohtaki, H. and Biedermann, G. *Bull. Chem. Soc. Jpn. 44* (1971) 1515.
5. Ulmgren, P. and Wahlberg, O. *Chem. Scr. 8* (1975) 126.
6. Olin, Å. and Svanström, P. *Acta Chem. Scand. A 29* (1975) 849.
7. Hammam, A., Olin, Å. and Svanström, P. *Acta Chem. Scand. A 31* (1977) 384.
8. Olin, Å. and Svanström, P. *Acta Chem. Scand. To be published.*
9. Ahrland, S. *Acta Chem. Scand. 5* (1951) 199.
10. King, E. J. *Acid-Base Equilibria*, Pergamon, Oxford 1965, p. 20.
11. Baes, C. F., Jr. and Mesmer, R. E. *The Hydrolysis of Cations*, Wiley, New York 1976, p. 431.
12. Sandell, A. *Acta Chem. Scand. 25* (1971) 1795.
13. Lee, Y.-H. and Lundgren, G. *Trans. R. Inst. Technol., Stockholm* (1972) No. 267.
14. Danielsson, I. and Stenius, P. *Trans. R. Inst. Technol., Stockholm* (1972) No. 254.
15. Persson, H. *Acta Chem. Scand. 25* (1971) 1775.
16. Farrer, H. N. and Rossotti, F. J. C. *Acta Chem. Scand. 17* (1963) 1824.
17. Rossotti, F. J. C. and Whewell, R. J. *J. Chem. Soc. Dalton Trans.* (1977) 1223.
18. Leden, I. *Acta Chem. Scand. 6* (1952) 971.
19. Brauner, P., Sillén, L. G. and Whiteker, R. *Ark. Kemi 31* (1969) 365.

Received December 14, 1977.

Acta Chemica Scandinavica A 32 (1978) 289–296

Association Equilibria and Micelle Formation of Fatty Acid Sodium Salts. V. Investigation of Branched Chain Salts by Vapour Pressure Osmometry

RAUNO FRIMAN [a] and PER STENIUS [b]

[a] Department of Physical Chemistry, Åbo Akademi, Porthansgatan 3–5, SF-20500 Åbo 50, Finland and [b] The Swedish Institute for Surface Chemistry, Box 5607, S-114 86 Stockholm, Sweden

The association of sodium pentanoate, sodium 3-methylbutyrate and sodium 2,2-dimethylpropionate in aqueous solution was studied by vapour pressure osmometry. The mean aggregation numbers calculated from these data are in good agreement with those calculated from previously reported determinations of the stability constants of the complexes. At low ionic strengths, the mean activity coefficients of the salts follow Harned's rule. The excess Gibbs' energies were calculated and clearly indicate that the association decreases with increasing branching of the hydrocarbon chain. Otherwise the thermodynamic properties are not easily interpreted.

The aggregation processes in solutions of short-chain carboxylates have been studied extensively in order to elucidate the steps in the aggregation leading to micelle formation.[1-6] It has been clearly established that the association to micelles is preceded by the formation of small amounts of aggregates with 3–5 monomers at concentrations below and around the c.m.c.[5] The potentiometric method used to determine the stability constants of the complexes, however, requires the use of constant ionic strength and high concentrations of the associating species. The ionic medium method as a device to eliminate the influence of variations in the activity coefficients in this case is open to some criticism.[7] Hence, it becomes very important to confirm the potentiometric results by other methods. In this paper we report vapour pressure osmometric studies of systems that were previously investigated by potentiometry.[1,3] It is possible to clearly distinguish between the effects of association and the effects of changes in the mean activity coefficients.

EXPERIMENTAL

1. *Chemicals.* The sodium salts of pentanoic acid, 3-methylbutyric acid and 2,2-dimethylpropionic acid were prepared by neutralization of the acids (Fluka Ag, *puriss.*) with NaOH (Merck Titrisol) at the boiling point. The salts were dried and their purity checked as described previously.[3] The NaCl and KCl (Merck *zur Analyse*) were dried for a week at 200 °C. The doubly distilled and de-ionized water has a spec. conductivity of 0.5 μS cm^{-1}.

2. *Solutions.* The solutions were prepared by mixing sodium carboxylate and NaCl of equal concentrations in different volumetric proportions. The molalities of the solutions were calculated from known NaCl solution densities[14] and pycnometrically determined densities of the carboxylate solutions. The contraction on mixing is of the order 0.1 ‰, which causes smaller changes in the concentrations than could be detected with the osmometer. Hence, the contraction was neglected throughout in the calculations.

3. *Water activities.* The activity of water was measured using a Mechrolab Vapor Pressure Osmometer Model 301. NaCl solutions of suitable concentrations were used as reference solutions. The procedure used is described in Ref. 2.

4. *Conductivities.* The conductivities were measured with a Metrohm E 365 B conductoscope, which was calibrated with 0.01 mol dm^{-3} KCl.

List of symbols

A_1 = integral in eqn. 5.
B = carboxylate ion.
a_i = activity of species i.
G^E = excess Gibbs' energy.
m_i = molality of species i.
m = total molality.
$\bar{q}_2$ = mean aggregation number of carboxylate ions.
R = universal gas constant.
T = temperature.
$u_i = m_{ir}/m \quad i=1, 2.$
$x_i = m_i/m \quad i=1, 2.$
$z_i = m_{ir}\,\phi_{ir} \quad i=1, 2.$
β_{pq} = stability constant of complex H_pB_q.
γ_i = mean activity coefficient of species i.
ϕ_i = osmotic coefficient of species i.
ν_i = number of ions formed by each NaCl (i = 1) or Na carboxylate (i = 2) molecule.
ν = mean amount of ions per unit amount of mixed electrolyte.

Subscripts. 1 denotes NaCl, 2 Na carboxylate, w water and r reference solution.

Calculations

Calculation of mean activity coefficients and aggregation numbers. For the system under consideration, the Gibbs-Duhem equation takes the form

$$-m_w\,\mathrm{d}(\ln a_w) = m_1\,\mathrm{d}(\ln a_1) + m_2\,\mathrm{d}(\ln a_2) \tag{1}$$

(for notation see the list of symbols.) We assume that the molality of free Na^+ ions is $m_{Na} = m_1 + m_2 = m$, *i.e.*, that no sodium ions are bound to the carboxylate aggregates. This is probably a good approximation except in solutions containing aggregates of micellar size. Then

$$\begin{aligned} \nu m &= m_{Na} + m_{Cl} + m_{aggr} \\ &= m(2 - x_2) + m_{aggr} \end{aligned} \tag{2}$$

where ν is the number of moles of ions formed by one mol of mixed electrolyte and m_{aggr} is the molality of the aggregates formed by the carboxylate ions, including monomers. Since two ions are formed by each NaCl molecule and ν_2 ions by each NaB molecule,

$$a_1 = \gamma_1^2 m^2 x_1\,;\, a_2 = [x_2(\nu_2 - 1)]^{\nu_2 - 1}(\gamma_2 m)^{\nu_2} \tag{3}$$

Substituting in (1), we obtain for constant m

$$\begin{aligned} -m_w\,\mathrm{d}(\ln a_w) = {} & 2\,x_1 m\,\mathrm{d}(\ln \gamma_1) + \\ & + x_2 m\,\mathrm{d}[\ln (\nu_2 - 1)^{\nu_2 - 1}\gamma_2^{\nu_2}] + \\ & + m(\nu_2 - 2)\mathrm{d}x_2 \end{aligned} \tag{4}$$

In a previous paper[2] we have shown, that the following equation for γ_1 may be derived on the basis of (4) and the corresponding equation for a pure NaCl solution with the same vapour pressure (reference solution, quantities pertaining to it are denoted by subscript r)

$$\begin{aligned} \ln \gamma_1 &= \ln(\gamma_{1r} u_1) - \int_0^{z_1} \frac{1}{m_{1r}} \left[x_2 \left(\frac{\partial u_1}{\partial x_2} \right)_{m_{1r}} - u_1 + 1 \right]_{x_2} \mathrm{d}z_1 \\ &= \ln(\gamma_{1r} u_1) - A_1 \end{aligned} \tag{5}$$

The equation was derived on the basis of a method suggested by McKay and Perring.[8] The equation is valid provided two ions are formed by every NaCl molecule dissolved. If this is the case for the sodium carboxylate, an exactly analogous equation is valid for its mean activity coefficient (γ_2). However, we have good reason to believe that the carboxylate ions associate. It is experimentally found that for a given m, A_1 in eqn. (5) is close to zero[2] for systems in which there is no association (*e.g.* sodium acetate/NaCl or sodium propionate/NaCl). We may then assume that values of A_1 that deviate substantially from 0 indicate association. It can be shown that ν is given by[2]

$$\nu = 2e^{A_1} \tag{6}$$

if only the carboxylate ions associate.

The mean aggregation number of the carboxylate ions, including the monomers may be calculated from

$$\bar{q}_2 = \frac{m_2}{m_{aggr}} = \frac{x_2}{\nu + x_2 - 2} \tag{7}$$

When ν is known, the mean activity coefficient of NaB *with the association taken into account* may be calculated from

$$\begin{aligned} \ln \gamma_2 = {} & \ln m + \frac{1}{\nu_2} \left\{ \ln \frac{(\nu_{2r} - 1)^{\nu_{2r} - 1}(m_{2r}\gamma_{2r})^{\nu_{2r}}}{(\nu_2 - 1)^{\nu_2 - 1}} \right. \\ & \left. - \int_0^{z_2} \frac{1}{m_{2r}} \left[\left(\frac{\partial u_2}{\partial x_1} \right)_{m_{1r}} x_1 - u_2 + 1 \right]_{x_1} \mathrm{d}z_2 \right\} \end{aligned} \tag{8}$$

ν_{2r}, the number of ions formed by NaB in a solution without NaCl, is calculated by extrapolation of the ν to $x_1 = 0$. γ_1, γ_2, ν and $\bar{q}_2$ were calculated from vapour pressure data for seven different total molalities and seven equidistant x_2 values using a numerical procedure programmed in Algol for a Univac 1108 computer.

Calculation of excess Gibbs' energies. In accordance with Harned and Robinson,[9] the excess Gibbs'

energy of the mixed solution is defined as the Gibbs' energy possessed by the solution over and above that possessed by the single electrolyte solutions, *i.e.*, as the Gibbs' energy for the process

x_1 kg H_2O x_1 I mol NaCl	+	x_2 kg H_2O x_2 I mol NaB	→	1 kg H_2O I mol (NaCl + NaB)

In terms of the activities of the components, this excess Gibbs' energy is given by

$$G^E/RT = m_w \ln a_w + x_2 m \ln a_2 + x_1 m \ln a_1 - x_2 m_w \ln a_{w(2)} - x_2 m \ln a_2^\circ - x_1 m_w \ln a_{w(1)} - x_1 m \ln a_1^\circ \quad (9)$$

where a_w is the water activity in the solution of two electrolytes and $a_{w(1)}$ and $a_{w(2)}$ the water activities in the solutions of NaCl and NaB, respectively, at the molality m. a_1 and a_1° are the activities of NaCl in the mixed and pure NaCl solutions, respectively, and a_2, a_2° are the corresponding quantities for NaB.

To calculate G^E, we integrate eqn. (4) (i) from a solution at molality m containing only NaCl (mean activity coefficient γ_1°) to one in which the molality of NaCl is $x_1 m$, (ii) from a solution at molality m containing only NaB (mean activity coefficient γ_2°) to $x_2 m \equiv (1-x_1)m$. The resulting integrals are multiplied by x_1 and x_2, respectively, and added; we then obtain the sum $x_1 \ln a_w + x_2 \ln a_w \equiv \ln a_w$ which is inserted into (9). By rearrangement of terms, eqn. (9) then becomes

$$\frac{G^E}{RT} = -2x_1 m \int_{\ln \gamma_1^\circ}^{\ln \gamma_1} x_1 \, d(\ln \gamma_1) - x_1 m \int_{\ln[(\nu_2^\circ - 1)^{\nu_2^\circ - 1} \gamma_2^{\circ \nu_2^\circ}]}^{\ln[(\nu_2 - 1)^{\nu_2 - 1} \gamma_2^{\nu_2}]} x_2 \, d[\ln(\nu_2 - 1)^{\nu_2 - 1} \gamma_2^{\nu_2}] - 2x_2 m \int_{\ln \gamma_1^*}^{\ln \gamma_1} x_1 \, d(\ln \gamma_1) - x_2 m \int_{\ln[(\nu_2^* - 1)^{\nu_2^* - 1} \gamma_2^{*\nu_2^*}]}^{\ln[(\nu_2 - 1)^{\nu_2 - 1} \gamma_2^{\nu_2}]} x_2 \, d[\ln(\nu_2 - 1)^{\nu_2 - 1} \gamma_2^{\nu_2}] - x_1 m \int_0^{x_2} (\nu_2 - 2) dx_2 - x_2 m \int_1^{x_2} (\nu_2 - 2) dx_2 + x_1 m \ln \gamma_1^2 / \gamma_1^{\circ 2} + x_2 m \ln \frac{(\nu_2 - 1)^{\nu_2 - 1} \gamma_2^{\nu_2} m^{\nu_2}}{(\nu_2^\circ - 1)^{\nu_2^\circ - 1} \gamma_2^{\circ \nu_2^\circ} m^{\nu_2^\circ}} \quad (10)$$

where γ_1^* is the value for γ_1 at molality m when extrapolated to $x_1 = 0$, γ_2^* the similarly extrapolated value for γ_2 at $x_2 = 0$ and ν_2^* the value for ν_2 extrapolated to $x_2 = 0$. By partial integration, this equation becomes

$$\frac{G^E}{RT} = m \int_0^{x_2} \ln \frac{(\nu_2 - 1)^{\nu_2 - 1} \gamma_2^{\nu_2}}{\gamma_1^2} dx_2 - x_2 m \int_0^1 \ln \frac{(\nu_2 - 1)^{\nu_2 - 1} \gamma_2^{\nu_2}}{\gamma_1^2} dx_2 - m \int_0^{x_2} (\nu_2 - 2) dx_2 + x_2 m \int_0^1 (\nu_2 - 2) dx_2 + x_2 m \ln \frac{m^{\nu_2}}{m^{\nu_2^\circ}} \quad (11)$$

This equation was used to calculate G^E from the known values of γ_1, γ_2, ν_2 as functions of x_2 at constant m.

Calculation of $\bar{q}_2$ from concentrations of complexes. The stability constants of the complexes formed by the three salts investigated here have been determined potentiometrically at ionic strength 3 mol dm^{-3} and are given in Table 1.[4] Knowing these, we

Table 1. Complex formation by different isomers of sodium pentanoate. The stability constants are defined by eqn. (12). $\beta_{p,q}$ = stability constant of complex H_pB_q (from Refs. 4 and 11).

Sodium pentanoate	
$CH_3(CH_2)_3COO^-Na^+$	
$-\log \beta_{1,1}$	9.20 ± 0.2
$-\log \beta_{2,5}$	17.40 ± 0.06
$-\log \beta_{3,5}$	25.26 ± 0.05
$-\log \beta_{1,11}$	12.06 ± 0.20
Sodium 3-methylbutyrate	
$(CH_3)_2CH-CH_2-COO^-Na^+$	
$-\log \beta_{1,1}$	9.23 ± 0.02
$-\log \beta_{1,4}$	9.17 ± 0.05
$-\log \beta_{0,15}$	6.35
Sodium 2,2-dimethylpropionate	
$(CH_3)_3C-COO^-Na^+$	
$-\log \beta_{1,1}$	8.859 ± 0.002
$-\log \beta_{1,4}$	9.85 ± 0.07
$-\log \beta_{2,4}$	17.48 ± 0.07

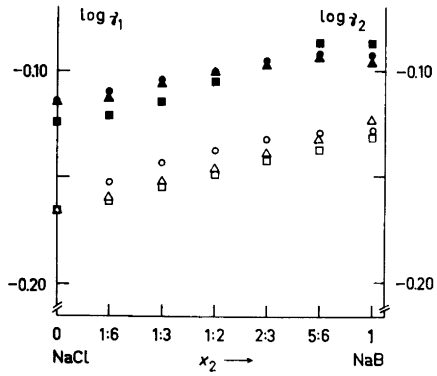

Fig. 1. The mean activity coefficient of the sodium chloride and sodium carboxylate in mixtures of sodium chloride and sodium pentanoate (△/▲), sodium 3-methylbutyrate (□/■) and sodium 2,2-dimethylpropionate (○/●) at constant total molality 0.5 mol kg^{-1} and 25 °C.

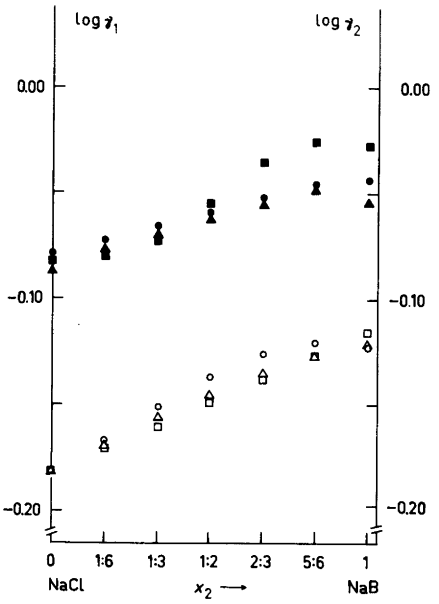

Fig. 2. As Fig. 1, total molality 1.0 mol kg^{-1}.

may calculate $\bar{q}_2$ at any total concentration of carboxylate. Since the electrode system used in the potentiometric titrations was calibrated against an excess of base, the stability constants obtained are the base constants, defined for the complex H_pB_q by

$$\beta_{pq} = (OH)^p (B)^{-q} (H_pB_q) \qquad (12)$$

(Parentheses denote concentrations (mol dm^{-3});

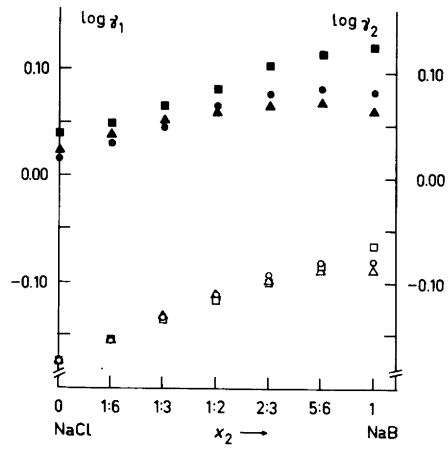

Fig. 3. As Fig. 1, total molality 2.0 mol kg^{-1}.

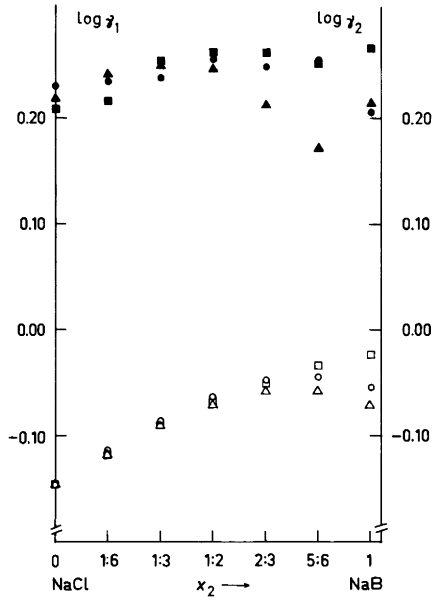

Fig. 4. As Fig. 1, total molality 3.0 mol kg^{-1}.

charge signs are omitted.) For any (OH) we may calculate (B) by numerically solving the mass balance equation

$$c_B = (B) + \sum_{p,q} q(H_pB_q) = (B) + \sum_{p,q} q(OH)^{-p} (B)^{-q} \beta_{pq} \qquad (13)$$

for (B). We then use (B) to calculate (H_pB_q) from (12) and $\bar{q}_2$ from

$$\bar{q}_2 = \frac{\sum_{p,q} q(H_pB_q)}{\sum_{p,q} (H_pB_q)} \qquad (14)$$

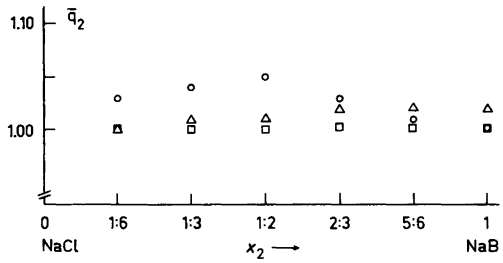

Fig. 5. The mean aggregation number of sodium pentanoate (△), sodium 3-methylbutyrate (□) and sodium 2,2-dimethylprionate (○) in mixtures with NaCl at constant total molality, 0.5 mol kg^{-1}.

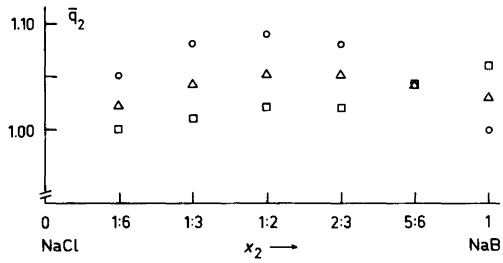

Fig. 6. As Fig. 5, total molality 1.0 mol kg^{-1}.

RESULTS

In Figs. 1–4 we give the logarithms of the mean activity coefficients for NaCl and NaB at four different total molalities, for each of the salts investigated, and with the fraction of NaB as the abscissa.

Values for $\bar{q}_2$ calculated from eqn. (7) using eqn. (6) to calculate the ν are given for the same total molalities in Figs. 5–8. Finally, we give the excess Gibbs' energies for the molalities 1 mol kg^{-1} and 3 mol kg^{-1} in Figs. 9 and 10.

A comparison between $\bar{q}_2$ values calculated from eqn. (7) and from eqn. (14) at pOH = 7.5 is given in

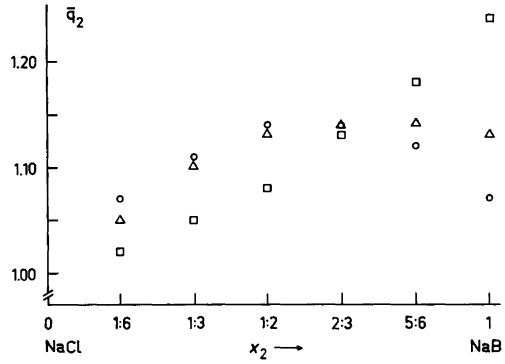

Fig. 7. As Fig. 5, total molality 2.0 mol kg^{-1}.

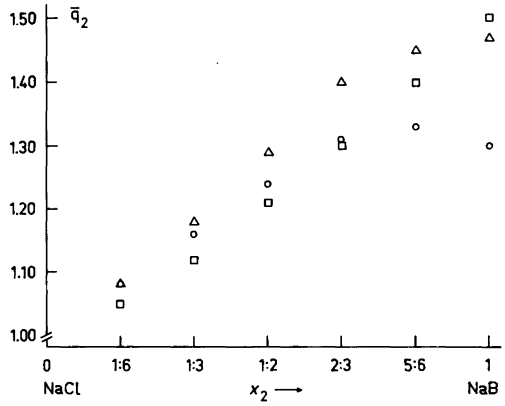

Fig. 8. As Fig. 5, total molality 3.0 mol kg^{-1}.

Table 2. A comparison of $\bar{q}_2$ values calculated from eqn. (7) with those calculated from eqn. (14). The former are given for constant total molality 3.5 mol kg^{-1}, the latter for ionic strength 3 mol dm^{-3} and pOH = 7.5.

m_2	Sodium pentanoate		3-Methylbutyrate		2,2-Dimethylpropionate	
mol kg^{-1}	$\bar{q}_2$ (pot)	$\bar{q}_2$ (VPO)	$\bar{q}_2$ (pot)	$\bar{q}_2$ (VPO)	$\bar{q}_2$ (pot)	$\bar{q}_2$ (VPO)
0.5	1.00	1.09	1.01	1.05	1.00	1.07
1.0	1.02	1.15	1.05	1.14	1.02	1.18
1.5	1.08	1.35	1.13	1.24	1.05	1.29
2.0	1.17	1.50	1.22	1.36	1.10	1.41
2.5	1.29	1.65	1.31	1.50	1.16	1.50
3.0	1.42	1.74	1.41	1.63	1.22	1.52
3.5	1.55	1.78	1.52	1.73	1.28	1.51

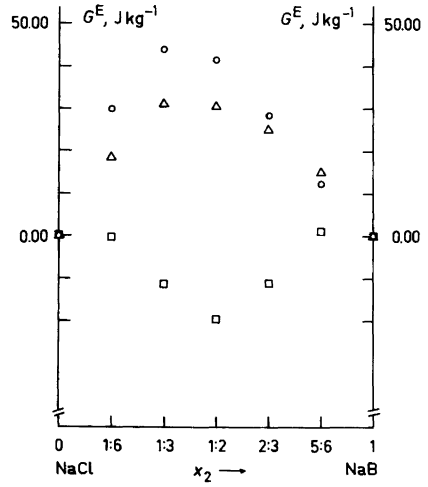

Fig. 9. The excess Gibbs' energy of mixing sodium pentanoate (△), sodium 3-methylbutyrate (□) and sodium 2,2-dimethylpropionate (○) with NaCl at constant total molality 1.0 mol kg^{-1}.

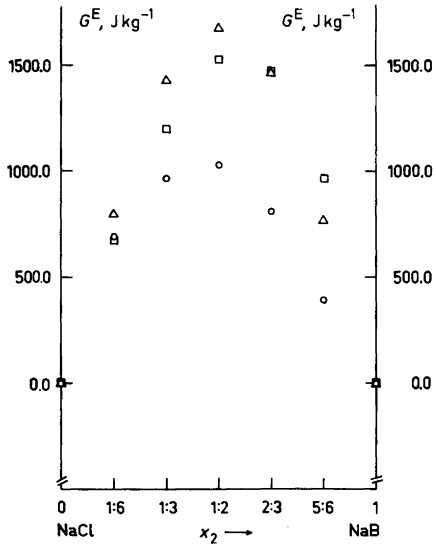

Fig. 10. As Fig. 9, total molality 3.0 mol kg^{-1}.

Table 2. Since we know the stability constants at ionic strength 3 mol dm^{-3} only, we have used the v values at the highest total molality investigated by vapour pressure measurements to calculate the $\bar{q}_2$ for the comparison.

DISCUSSION

A comparison of the aggregation numbers calculated from the potentiometric and osmometric measurements, respectively, (see Table 2) shows that these agree very satisfactorily, in particular considering the lengthy calculations needed to obtain the osmometric aggregation numbers from the primary experimental data. The osmometric aggregation numbers are consistently somewhat higher than the potentiometric, but both vary with concentration in the same way. Moreover, both investigations show an increasing tendency to associate in the order 2,2-dimethylpropionate < 3-methylbutyrate < pentanoate. It is also obvious from both investigations that the association is so weak that there are no dramatic changes in the mean aggregation numbers. Hence, we conclude that the two independent methods both indicate association of the salts to polynuclear aggregates. The osmometric results, of course, do not allow us to draw any conclusions concerning the size distribution of the aggregates. The potentiometric measurements show a formation of aggregates with 4–5 anions as well as small micelles in 3-methylbutyrate and pentanoate solutions.[4,11]

As is clearly seen from Figs. 1–4, the changes in the mean activity coefficients at lower ionic strengths follow the wellknown Harned's rule:

$$\log \gamma_i = \log \gamma_i^{tr} + \alpha m_i \qquad (15)$$

where γ_i^{tr} denotes the trace mean activity coefficient, *i.e.*, the value of the mean activity coefficient of the salt i at infinite dilution at this ionic strength. Figs. 1–4 also show that the slope α of the log γ_1 *vs.* x_2

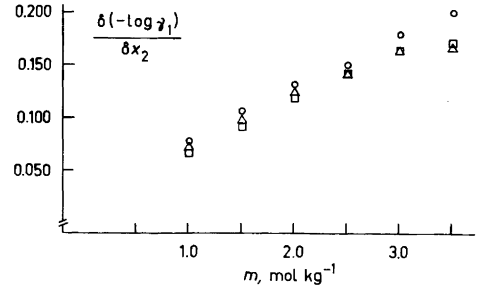

Fig. 11. The limiting slopes of the log γ_1 *vs.* x_2 plots extrapolated to $x_2 = 0$ for the sodium pentanoate (△), sodium 3-methylbutyrate (□) and sodium 2,2-dimethylpropionate (○) as a function of the total molality in mixtures with NaCl.

Table 3. The trace mean activity coefficients for sodium chloride and sodium carboxylates at ionic strength 2.0 mol kg^{-1} the molar conductivity at infinite dilution and the Stokes' radii for sodium pentanoate, sodium 3-methylbutyrate and sodium 2,2-dimethylpropionate at 25 °C.

	λ^{∞} ($cm^2\ \Omega^{-1}\ mol^{-1}$)	r_{Stokes} (nm)	γ_1^{tr}	γ_2^{tr}
Sodium pentanoate	78.7	0.116	0.815	1.060
Sodium 3-methylbutyrate	87.3	0.105	0.859	1.070
Sodium 2,2-dimethylpropionate	83.5	0.110	0.830	1.004

plot increases with increasing ionic strength. This is more clearly seen in Fig. 11 where we have plotted the slopes as functions of the total molality. There is no obvious explanation to this systematic variation. At very high total molalities the 3-methylbutyrate and the pentanoate show deviations from the linear dependence. This may be due to the formation of micelles, *i.e.*, the assumption that no sodium ions are bound in aggregates is probably no longer valid and, consequently, the procedure of calculating the mean activity coefficients with the association taken into account is no longer valid.

A comparison of the γ_1 values when the chloride ion is replaced with the carboxylate ion in the three systems shows that they are roughly equal for pentanoate and 3-methylbutyrate at low ionic strengths, while they are higher for the latter salt at higher ionic strength. The mean activity coefficients are lowest for the 2,2-dimethylpropionate throughout. This probably reflects differences in the way straight and branched hydrocarbon chains affect the water structure.

The excess Gibbs' energies of mixing chloride with carboxylate is shown in Fig. 9 for ionic strength 1 mol kg^{-1}. These curves clearly reflect the differences in the interaction with the surrounding water between linear and branched hydrocarbon chains with the same number of carbon atoms. The excess energy is positive throughout for the almost spherical 2,2-dimethylpropionate, and for pentanoate passes from negative to positive for the 3-methylbutyrate. At ionic strength 3 mol kg^{-1} the 2,2-dimethylpropionate and pentanoate excess energies behave similarly as at 1.0 mol kg^{-1}, but are roughly ten times higher. The excess energy of the 3-methylbutyrate behaves quite differently: this is now strongly positive. This certainly partially is an effect of the dissociation of micelles and pre-micellar aggregates when the solutions are mixed; this may also be the cause of the inflection points in the curve for ionic strength 1 mol kg^{-1}. The excess energies thus clearly show the increasing tendency to associate with decreasing branching of the hydrocarbon chains. All the same, they also serve to stress the complicated nature of the hydrophobic interactions in water. Excess energies are often interpreted in terms of changes in solvent-solute interactions rather than association. We have shown, however, that by assuming that all effects are due to association of the carboxylate ions we arrive at aggregation numbers that are in good agreement with independent potentiometric results.

Backlund[12] has correlated the trace ionic activity coefficients for straight-chain carboxylates with the hydrocarbon chain length, calculated according to Tanford.[13] From the linear relationship between these two quantities, he concluded that the energy of interaction between the ions and the surrounding solvent is proportional to the size of the hydrocarbon moiety of the ions. In order to investigate whether this correlation could be extended to branched hydrocarbon chains we have calculated the Stokes' radii of the three carboxylate ions discussed here from measurements of their molar conductivities at infinite dilution.[10] The results are given in Table 3, together with γ_1^{tr} and γ_2^{tr}. γ_1^{tr} is inversely proportional to the radius, but there is no correlation between the carboxylate mean activity coefficient, γ_2^{tr}, and the radius of the ion.

Acknowledgements. Mr. Sune Backlund and Mr. Folke Eriksson are thanked for discussions on parts of this work. Part of this work was financed by the Finnish Research Council for Natural Sciences.

REFERENCES

1. Stenius, P. and Zilliacus, C.-H. *Acta Chem. Scand. 25* (1971) 2232 (Part I).
2. Stenius, P. *Acta Chem. Scand. 27* (1973) 3435 (Part II).

3. Stenius, P. *Acta Chem. Scand. 27* (1973) 3452 (Part III).
4. Stenius, P. *Acta Chem. Scand. 27* (1973) 3897 (Part IV).
5. Friman, R., Pettersson, K. and Stenius, P. *J. Colloid Interface Sci. 53* (1975) 90.
6. Danielsson, I. and Stenius, P. *J. Colloid Interface Sci. 37* (1971) 264.
7. Danielsson, I. and Stenius, P. *Trans. R. Inst. Technol., Stockholm, Pure Appl. Chem. 34* (1972) 81.
8. McKay, H. A. C. and Perring, J. K. *Trans Faraday Soc. 49* (1953) 163.
9. Harned, H. S. and Robinson, R. A. *Multicomponent Electrolyte Solutions*, Pergamon, Oxford 1968, p. 32 f.
10. Robinson, R. A. and Stokes, R. H. *Electrolyte Solutions*, Butterworths, London 1959, pp. 44, 124.
11. Stenius, P. and Filén, L.-A. *Progr. Colloid Polymer Sci. 56* (1975) 21.
12. Backlund, S. *Personal communication; to be published.*
13. Tanford, C. *J. Phys. Chem. 76* (1972) 3020.
14. Landolt-Börnstein, *Physikalisch-Chemische Tabellen, II Erg. Bd.*, Springer, Berlin 1935.

Received November 2, 1977.

Acta Chemica Scandinavica A 32 (1978) 297 – 302

Reaction Rate Studies of the Acid Hydrolysis of Some Chromium(III) Complexes. IX. Angular Overlap Model Calculations on Transition State Structures for Chromium(III) Substitution Reactions

O. MØNSTED

Chemistry Department I, Inorganic Chemistry, The H. C. Ørsted Institute, University of Copenhagen, DK-2100 Copenhagen, Denmark

Linear correlations between enthalpies of activation for ligand hydrolysis reactions and single-ligand Δ-parameters, derived from visible absorption spectra, are found experimentally for the pentaamine- and the pentaaquachromium(III) series of complexes. These empirical correlations have been rationalized using the angular overlap model of the ligand field, and in this way information on possible transition state structures for the substitution reactions has been obtained. It is concluded firstly that the metal-to-leaving-ligand bond is probably weakened but not completely broken in the transition state, and secondly that the most symmetrical transition state which accommodates the experimental data is one having square pyramidal coordination of the nonreacting ligands and symmetrical coordination of the entering and leaving ligand with respect to the fourfold axis defined by the five nonreacting ligands. Consequently the results reported here support the associative interchange mechanism proposed previously for these reactions.

The significance of the ligand field for the kinetic and thermodynamic behaviour of transition metal complexes is well established, and there are numerous examples of successful qualitative rationalizations of the variation in chemical behaviour of various metal ions with similar coordination spheres.[1]

Most discussions of the influence of the ligand field on the kinetic behaviour of transition metal complexes have been limited to exchange reactions which have been handled assuming ground state and transition state structures of high symmetry. Descriptions of structures of lower symmetry usually require many parameters unless simplifying assumptions are introduced. The angular overlap model[2] is one such attempt at simplification, and in combination with the assumption of ligand-parameter transferability between different complexes with identical central metal atoms the number of parameters necessary for a description of low symmetry structures may be greatly reduced. The recent availability of angular overlap model parameters for a variety of ligands coordinated to chromium(III)[3] provides the possibility of carrying out a detailed treatment of the kinetic consequences of the ligand field from an experimental point of view. It should thus be possible to rationalize the empirical correlations which exist between spectroscopic and kinetic parameters, and thereby gain additional insight into the geometry of the transition states for substitution reactions.

METHOD OF CALCULATION

General equations facilitating the construction of ligand field matrices for all d^n configurations in all symmetries have recently been given.[4] In this work the ligand field part of the energy matrices

for the quartet states* was generated using the relationship given in the footnote on p. 282 in Ref. 4, and the interelectronic part as described in Ref. 3. Tensorial parameters were calculated from angular overlap model parameters by use of the set of relations given by eqns. 61 and 62 in Ref. 4, with angular overlap matrix element products taken from Tables 3, 4, and 5 in Ref. 2.

RESULTS

A considerable number of empirical correlations between kinetic and spectroscopic parameters for chromium(III) complexes can be found in the literature. However, many of these are not well suited to a more detailed theoretical analysis since either positions of spectral bands are used as spectroscopic parameters, or rate constants are used as kinetic parameters, and neither band component sums nor the entropy part of the free energy can be handled by ligand field models at their present stage of evolution.

Consequently the chosen basis for the present investigation is the linear correlation between the enthalpies of activation for hydrolysis of ligands bound to a chromium(III) centre, as in the following generalized reaction scheme:

$$[CrJ_5X]^{(3-i)+} + H_2O \rightarrow [CrJ_5(OH_2)]^{3+} + X^{i-} \quad (1)$$

* Attempts have been made previously to account for the enthalpies of activation for chromium(III) substitution reactions in terms of ligand field effects only.[5] This was only possible if a doublet excited electronic state was assumed for the transition state. However, comparisons with kinetic data for tripositive metal ions in which ligand field effects should be absent do not provide support for this approach. For the transition state geometries discussed in this paper electronic ground states are invariably quartet states.

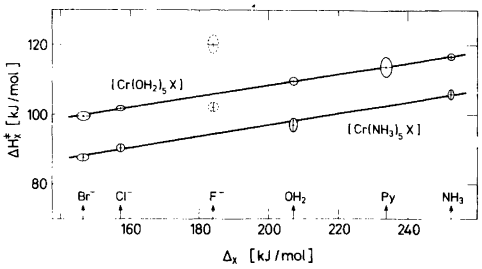

Fig. 1. Linear correlations between $\Delta H_X^{\ddagger}$ and Δ_X for pentaaqua(⊖-points) and pentaamminechromium-(III) complexes (⊕-points). Experimental values are indicated by contour ellipses of the probability density function drawn at the 68 % probability level.

($J = NH_3$ or OH_2; $X^{i-} = Br^-$, Cl^-, (F^-), OH_2, C_5H_5N or NH_3; see Table 1), and the energy difference between the σ- and π-interactions between the substituted ligands and the central metal atoms

$$\Delta = \Delta'_\sigma - \Delta'_\pi$$

which for $J = OH_2$ has been noted previously.[3] The correlations are shown in Fig. 1 and are described quantitatively in Table 2.

The existence of such correlations is strong evidence in favour of similar reaction mechanisms for these reactions, except in the case of hydrolysis of coordinated fluoride ion. This difference between the reactions of the coordinated fluoride ion and those of the other ligands has also been observed in other contexts and has been ascribed to protonation of the basic fluoride ligand in the transition state,[6] a mechanism which is also known to operate for the hydrolysis of other basic ligands.

For the remaining ligands in each of the two series of complexes the differences in enthalpies of

Table 1. Enthalpies of activation for the ligand substitution processes of eqn. 1.

X^{i-}	$[Cr(OH_2)_5X]^{(3-i)+}$ kJ/mol	Ref.[a]	$[Cr(NH_3)_5X]^{(3-i)+}$ kJ/mol	Ref.[a]
Br^-	99.6±1.3	6	88.8±1.3	12,13
Cl^-	101.7±0.8	7	90.4±1.3	12,14
F^-	120.1±2.5	7	102.1±1.3	15
OH_2	109.6±1.3	8	97.1±2.0	16
Py[b]	113.8±2.9	9	—	
NH_3	116.7±0.8	10,11	105.9±1.3	10,17

[a] Where two references are given the enthalpy quoted is obtained as the weighted average of the two results. [b] In this table and throughout the paper Py is used as an abbreviation for pyridine.

Table 2. Estimated parameters (mean values ± standard deviations upon the mean values) for the linear correlation between $\Delta H_X^{\neq}$ and Δ_X. (*cf.* Fig. 1).

Complexes	$\alpha^{a,b}$	$\beta^{a,b}$ kJ/mol
$[Cr(NH_3)_5X]^{(3-i)+}$	0.160 ± 0.007	65.1 ± 1.4
$[Cr(OH_2)_5X]^{(3-i)+}$	0.159 ± 0.005	76.6 ± 0.9

[a] The functional relation between $\Delta H^{\neq}$ and Δ is given by $\Delta H^{\neq} = \alpha\Delta + \beta$, and α and β are estimated by minimization of $\Sigma(\Delta H^{\neq} - \alpha\Delta - \beta)^2/[\sigma^2(\Delta H^{\neq}) + \alpha^2\sigma^2(\Delta)]$, where $\sigma^2(\Delta H^{\neq})$ and $\sigma^2(\Delta)$ are the variances upon $\Delta H^{\neq}$ and Δ, respectively. [b] The two cases involving hydrolysis of coordinated fluoride have not been included in the calculations since these two reactions proceed *via* a different mechanism.[6]

activation are accurately described by differences in the ligand field parameter Δ of the leaving ligand. It therefore seems reasonable to assume that the major part of these enthalpy differences is the result of ligand field effects, and that other energetic consequences of the variation of the leaving ligand are of less importance.

This limits the following considerations to the α parameters of Table 2, which will be rationalized using the angular overlap model on a single reactant pair, a simplification of the treatment of an ensemble of reactants,[18] which, however, since only the *variation* in a series of similar reactions is considered, should have little effect on the following conclusions.

The ligand field stabilization energy of the octahedral ground state of the $[CrJ_5X]^{(3-i)+}$ complex is $-(\Delta_J + \frac{1}{5}\Delta_X)$. If the leaving ligand, X, is completely dissociated in the transition state, the ligand field stabilization of this state will be independent of X irrespective of the transition state geometry. For the D mechanism it can thus be seen that the contribution to the enthalpy of activation from the ligand field of the X ligand is given by $\frac{1}{5}\Delta_X$. This differs from the experimentally observed variation (*cf.* Fig. 1 and Table 2), the implication being that the bond between the leaving ligand and the chromium(III) center is not completely broken in the transition state.

Evaluation of the role of the leaving ligand in transition states in which the bond between the metal centre and the leaving ligand is not completely broken is clearly a more difficult problem. The contribution from the ligand field to the enthalpy of activation for the ligand exchange process:

$$CrJ_5J' + J'' \rightarrow CrJ_5J'' + J' \qquad (2)$$

$$(J = J' = J'')$$

has previously been computed for all d^n electronic configurations, assuming a transition state of pentagonal bipyramidal geometry.[1] For the d^3 electronic configuration, however, the electronic ground state of such a transition state structure will be doubly degenerate, and such a geometry therefore cannot be expected to be stable for chromium(III) complexes.

All the evidence therefore points towards transition states with lower symmetry. The majority of substitution reactions of chromium(III) complexes which have been studied so far proceed with retention of configuration. Therefore, only *cis* attack of the entering ligand will be considered here, and two transition state structures based on such a restriction are shown in Fig. 2.

The two structures in Fig. 2 are easily handled by the angular overlap model: For the I_ϕ structure, the ligand field contribution, $\Delta L^{\neq}$, to the enthalpy of activation is computed to be:

$$I_\phi\colon\ \Delta L^{\neq} = \frac{1}{20}(1 - 5\cos 4\phi)\,\Delta_J \qquad (3a)$$

Results for the II_ϕ structure are less easily reported since both the separation of Δ into contributions from σ- and π-bonding, as well as the inter-electronic repulsions are of importance. Results for selected sets of parameter values are shown graphically in Fig. 3 and may be compared with the values calculated from eqn. 3a for the I_ϕ structure. For ϕ values less than about 45° $\Delta L^{\neq}$ for the II_ϕ structure

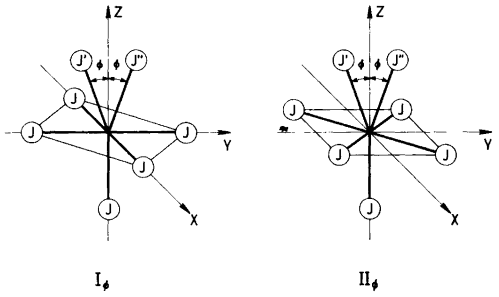

I_ϕ II_ϕ

Fig. 2. Transition state structures discussed in the text. Both the leaving ligand, J', and the entering ligand, J'', lie in the *YZ* plane.

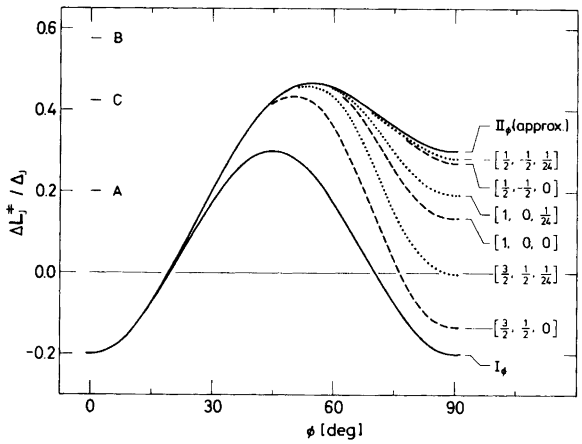

Fig. 3. Ligand field contribution to enthalpies of activation for exchange reactions of metal ions with a d^3 electronic configuration and octahedrally coordinated in the ground state with linearly ligating ligands. Parameters for the calculations without approximations for the II_ϕ transition state are given in the form: $[\Delta'_{\sigma J}/\Delta_J, \Delta'_{\pi J}/\Delta_J, b/\Delta_J]$. A, B and C are values for a tetragonal pyramid, a trigonal bipyramid and a pentagonal bipyramid, respectively.

is seen to be a function of ϕ and Δ only, and it may easily be verified that the approximation:

$$II_\phi^*: \Delta L^{\neq} \sim \frac{1}{80}(19 - 20\cos 2\phi - 15\cos 4\phi)\Delta_J \quad (3b)$$

is valid for this range of values of ϕ.

The results given by eqns. 3a and 3b apply only to exchange processes of the type given by eqn. 2. However, most of the experimental material displayed in Fig. 1 is for reactions of the type:

$$CrJ_5X + Y \rightarrow CrJ_5Y + X$$

For such reactions proceeding *via* transition states similar to those shown in Fig. 2, with X = J′ and Y = J″, the following approximate expressions similar to those for the exchange process may be derived:

$$I_\phi: \Delta L^{\neq} \sim \frac{1}{40}[8\Delta_X - (3 + 5\cos 4\phi)(\Delta_X + \Delta_Y)] \quad (4a)$$

$$II_\phi: \Delta L^{\neq} \sim \frac{1}{160}[32\Delta_X + (3 - 20\cos 2\phi - 15\cos 4\phi)(\Delta_X + \Delta_Y)] \quad (4b)$$

It is immediately seen that the contribution to $\Delta L^{\neq}$ from the ligand which is substituted, X, is a function of Δ_X only, and it can readily be verified that values of ϕ of 26.5 and 25.4°, for the I_ϕ and II_ϕ structures, respectively, reproduce the experimental variation of $\Delta H_X^{\neq}$ with Δ_X. The approximations inherent in both of the equations 4a and 4b have been tested by diagonalization of complete energy matrices for the quartet states of the d^3 electronic configuration. The results, which are depicted in Fig. 4, are seen to support the validity of the use of eqns. 4a and 4b.

The preceding results have all been obtained using the assumption of single ligand parameter transferability between different chromium(III) complexes. This assumption has been investigated previously in connection with parametrizations of the ligand field spectra of a variety of chromium(III) complexes, and for this purpose was found to be a useful approximation which permitted the estima-

* Results for a transition state structure similar to II_ϕ with $\phi = 45°$ and $\phi = 54.74°$ have been given previously.[19] These results do not include the effects of interelectronic repulsion, and are limited to the value 2.0 for the crystal field parameter ratio, I^2/I^4. In terms of angular overlap model parameters this ratio is:[2]

$$I^2/I^4 = (20\Delta'_\sigma + 15\Delta'_\pi)/36\Delta$$

which gives experimental values from 0.56 for ammonia coordinated to chromium(III) to 0.98 for fluoride coordinated to chromium(III).[3] From Fig. 3 these values and the neglect of interelectronic repulsion are seen not to affect the 45° results but to limit the applicability of the results for the larger ϕ angle.

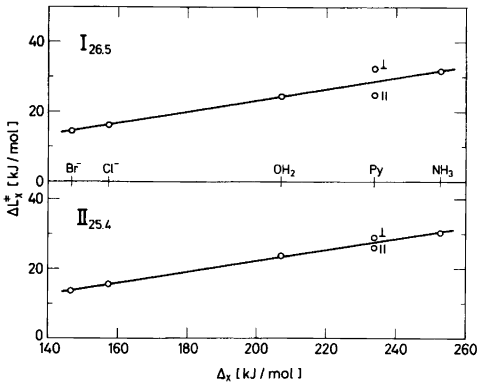

Fig. 4. Calculated values (○-points) for the ligand field contribution to enthalpies of activation for the ligand substitution processes given by eqn. 1, proceeding *via* the two transition states: I_ϕ with $\phi = 26.5°$ and II_ϕ with $\phi = 25.4°$. Single ligand Δ'_σ and Δ'_π parameters were taken from Table IV in Ref. 3. Differences between the two series of complexes, *i.e.* that with $J = NH_3$ and that with $J = OH_2$, are too small to be seen on the figure. The span of possible values for the pyridine complex, caused by the nonlinear ligation of the pyridine ligand,[3] is between the two values indicated. For both transition state structures the upper value corresponds to the situation where the plane of the pyridine ring is perpendicular to the plane defined by the entering ligand, the metal atom, and the donor atom of the leaving ligand. The lower values are for the situation were these two planes are coplanar. A value for the angle between the two planes of about 45° will place the computed value for the pyridine complex on the indicated straight line, which has been drawn with the experimentally determined slope 0.160 (*cf.* Table 2).

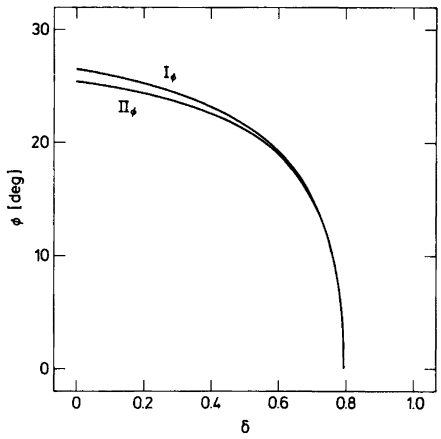

Fig. 5. Values of ϕ which rationalize the data of Fig. 1 and Table 2, drawn as a function of the degree of dissociation, δ, of the leaving ligand (*cf.* eqn. 5) in the I_ϕ and II_ϕ transition state structures.

tion of empirical Δ'_σ and Δ'_π parameters for a series of ligands.[3] In the angular overlap model Δ'_σ and Δ'_π are empirical measures of σ- and π-interactions between a ligand and the central metal atom, and for a given ligand they are a function of the metal-to-ligand bond distance. Metal-to-ligand bond distances in octahedral ground states are rarely very dependent on the other ligands in the coordination sphere, and this may be one reason for the usefulness of the transferability assumption.

In the transition states for the substitution reactions studied here the metal-to-ligand bonds, although not completely broken, are almost certainly stretched compared to those in the ground state. The empirical ligand parameters cannot therefore be expected to have the same values for the transition states as for the ground states. In this case $\Delta L^{\neq}$ may be expressed by a set of equations similar to 4a and 4b, but will contain the ligand Δ parameters for the transition states. These are not known but will be smaller than those for the ground states, and the degree of dissociation of the leaving ligand in the transition state, δ, may be defined as

$$\delta \equiv 1 - \frac{\Delta_{X(TS)}}{\Delta_{X(GS)}} \qquad (5)$$

Defined in this way δ will have values between 0 ($\Delta_{X(TS)} = \Delta_{X(GS)}$) for the A mechanism to 1 ($\Delta_{X(TS)} = 0$) for the D mechanism. Fig. 5 illustrates the relationship between values of δ and ϕ for the two different transition state structures which rationalize the experiments. Again the inaccessibility of a D mechanism is seen.

DISCUSSION

The analysis outlined in the preceding sections shows that it is possible to rationalize the variation in enthalpies of activation as a function of spectroscopic parameters of the leaving ligand on the basis of angular overlap model calculations on a single reactant pair. Complete dissociation of the leaving ligand does not occur in the transition state, and the

highest symmetry of the transition state is that attending symmetrical coordination of the entering and leaving ligand with respect to a fourfold axis defined by the five nonreacting ligands (*cf.* Fig. 2). A rather small angle between the bonds from chromium to the reacting ligands, $2\phi \lesssim 50°$, is predicated by the quantitative calculations (*cf.* Fig. 5). It is thus plausible that the metal to ligand bonds, in order to compensate for an increase in ligand-ligand interactions, are stretched when the transition states are formed. That part of the net energetic consequences of such ligand motion which is a function of the leaving ligand is, however, apparently small when compared with the effects of the ligand field of this ligand, since Fig. 1 for the various ligands in question would otherwise be hard to understand. The total energy required to stretch the metal-to-ligand bonds to form the transition state is difficult to assess. It can be crudely estimated, however, that a number of the relevant energy contributions comprise a positive fraction of the $\Delta H°$ values for the processes. Since $\Delta H^{\neq}$ and $\Delta H°$ are positively correlated this will have the effect of reducing acceptable δ values to numbers smaller than the 0.8 indicated by Fig. 5.

The material presented here is therefore additional evidence in favour of the associative interchange, I_a, mechanism for reactions of complexes within the pentaammine- and pentaaquachromium(III) series. It is thus in agreement with conclusions reached from other types of evidence, in that the observation of negative volumes of activation for water exchange reactions and the existence of linear free energy relationships having slopes significantly smaller than 1.00 have been interpreted analogously.[20]

The analysis carried out in this paper has been restricted to a transition metal ion with a d^3 electronic configuration but could easily be extended to other systems. At present, however, experimental values for angular overlap model parameters and substitution kinetic parameters for series of ligands bound to metal centers other than chromium(III) do not appear to be available. The practical application of such extended analyses is therefore limited at present, and it is not possible to say to what extent the behaviour of other metal ions will reflect the rather simple picture obtained here for chromium(III).

Acknowledgement. The author wishes to thank C. E. Schäffer for stimulating discussions on the ligand field part of this paper and Martin Hancock for revising the manuscript.

REFERENCES

1. Basolo, F. and Pearson, R. G. *Mechanisms of Inorganic Reactions*, 2nd Ed., New York 1967.
2. Schäffer, C. E. *Struct. Bonding (Berlin) 14* (1973) 69.
3. Glerup, J., Mønsted, O. and Schäffer, C. E. *Inorg. Chem. 15* (1976) 1399.
4. Harnung, S. E. and Schäffer, C. E. *Struct. Bonding (Berlin) 12* (1972) 257.
5. Spees, S. T., Perumareddi, J. R. and Adamson, A. W. *J. Am. Chem. Soc. 90* (1968) 6626.
6. Guthrie, F. A. and King, E. L. *Inorg. Chem. 3* (1964) 916.
7. Swaddle, T. W. and King, E. L. *Inorg. Chem. 4* (1965) 532.
8. Stranks, D. R. and Swaddle, T. W. *J. Am. Chem. Soc. 93* (1971) 2783.
9. Bakac, A. and Orhanovic, M. *Inorg. Chem. 10* (1971) 2443.
10. Mønsted, L. and Mønsted, O. *Acta Chem. Scand. A 28* (1974) 569.
11. Bakac, A., Butkovic, V. and Orhanovic, M. *Croat. Chem. Acta 48* (1976) 35.
12. Data from: Levine, M. A., Jones, T. P., Harris, W. E. and Wallace, W. J. *J. Am. Chem. Soc. 83* (1961) 2453, recalculated in Ref. 15.
13. Ramasami, T. and Sykes, A. G. *Inorg. Chem. 15* (1976) 2885.
14. Duffy, N. V. and Early, J. E. *J. Am. Chem. Soc. 89* (1967) 272.
15. Jones, T. P. and Phillips, J. K. *J. Chem. Soc. A* (1968) 674.
16. Swaddle, T. W. and Stranks, D. R. *J. Am. Chem. Soc. 94* (1972) 8357.
17. Guastalla, G. and Swaddle, T. W. *Inorg. Chem. 13* (1974) 61.
18. Glasstone, S., Laidler, K. J. and Eyring, H. *The Theory of Rate Processes*, 1st Ed., p. 153ff. New York 1941.
19. Hush, N. S. *Aust. J. Chem. 15* (1962) 378.
20. Swaddle, T. W. *Coord. Chem. Rev. 14* (1974) 217, and references therein.

Received November 7, 1977.

Acta Chemica Scandinavica A 32 (1978) 303 – 308

The Crystal Structure of Tris(1-phenyl-1,2-propanedione-2-oximato)cobalt(III) –Benzene(1/1), $[Co(C_9H_8NO_2)_3].C_6H_6$

HEIKKI SAARINEN, JORMA KORVENRANTA and ELINA NÄSÄKKÄLÄ

Department of Inorganic Chemistry, University of Helsinki, SF-00100 Helsinki 10, Finland

The title compound crystallizes in the triclinic space group $P\bar{1}$ with $Z=2$ and with unit cell dimensions $a=10.316(10)$, $b=12.318(10)$, $c=12.695(19)$ Å, $\alpha=76.34(10)$, $\beta=74.42(11)$, and $\gamma=89.36(7)°$. The structure was solved by direct methods with the MULTAN program and refined by full-matrix least-squares technique to an R value 0.041 for 2646 observed reflections. The cobalt(III) in the complex is octahedrally coordinated by three oxime nitrogen and three carbonyl oxygen atoms such that the three nitrogen atoms are mutually *cis*. There are no closer interactions between the complex and the solvent benzene molecules. The average C – N, N – O, C – O, C1 – C2 bond lengths and the CNO angle are 1.348(7), 1.252(6), 1.279(6), 1.421(8) Å, and 121.4(5)°, respectively. The results are compared with those obtained earlier for similar ligands in free and metal-coordinated states.

In earlier X-ray studies we found the metal chelates formed by 1,2-nitrosonaphthols $\rightleftharpoons$ 1,2-naphthoquinone oximes to have a quinone oximato structure.[1-3] For comparative purposes the investigation has now been extended to include a typical carbonyl-oxime ligand of aliphatic character. Unlike 1,2-nitrosonaphthols, aliphatic carbonyl-oximes are poor metal chelating agents and the complexes, if formed at all, are often amorphous and unstable.[4] The crystalline cobalt(III) chelate of 1-phenyl-1,2-propanedione-2-oxime is easily prepared, however, and the results of an X-ray structure analysis of it are given here. The structure of the uncoordinated ligand acid has been described earlier by the authors.[5]

EXPERIMENTAL

Crystal preparation. The complex compound was prepared by adding $Na_3[Co(NO_2)_6]$ (1 mol), dissolved in a small quantity of water, to a hot methanolic solution of 1-phenyl-1,2-propanedione-2-oxime (3 mol). The precipitated product was dissolved in a benzene – chloroform mixture (1:1), from which brown-red prisms were separated after the solution had slowly evaporated almost to dryness. Anal. C, H, N. The amount of solvent was determined thermogravimetrically as 12 % (calc. 12.5 %).

Crystal and intensity data. Preliminary photographic work showed the crystals to be triclinic. The space group $P\bar{1}$ was assumed and later confirmed by successful refinement of the structure. A crystal with approximate dimensions $0.3 \times 0.3 \times 0.3$ mm was mounted on a Syntex $P2_1$ diffractometer and precise cell parameters were determined by a least-squares refinement of 15 automatically centered reflections. The crystal data for $[Co(C_9H_8NO_2)_3].C_6H_6$ are:
$a=10.316(10)$, $b=12.318(10)$, $c=12.695(19)$ Å,
$\alpha=76.34(10)$, $\beta=74.42(11)$, $\gamma=89.36(7)°$,
Space group $P\bar{1}$, $Z=2$, $D_x=1.37$ g cm^{-3}, $D_m=1.3$ g cm^{-3} (by flotation),
$\lambda(MoK\alpha)=0.7107$ Å, $\mu=6.5$ cm^{-1} ($MoK\alpha$)

X-Ray intensities were measured by the ω scan technique ($3° < 2\theta < 50°$) with graphite monochromated $MoK\alpha$ radiation. The scan rate varied from 2 to 29° min^{-1}, depending on the intensity of the reflection. The three reflections checked periodically during the data collection showed no crystal decomposition. Of the 3946 recorded reflections, 2646 with $I > 3\sigma(I)$ were used for the structure analysis. The intensities were corrected for Lorentz and polarization effects.

Structure determination and refinement. The structure was solved by direct methods with the MULTAN program.[6] The cobalt and the atoms in its coordination sphere could be localized in the

Table 1. Fractional atomic coordinates ($\times 10^4$) and anisotropic thermal parameters[a] ($\times 10^3$) for non-hydrogen atoms. The three different values for the parameters refer to atoms in ligands A, B and C, respectively. The values in Table 2 and Figure 2 refer to the same order of ligands.

Atom	x	y	z	U_{11}	U_{22}	U_{33}	U_{12}	U_{13}	U_{23}
C1	2227(5)	4434(4)	1053(4)	39(3)	44(3)	42(3)	6(2)	−15(2)	−4(2)
	4610(5)	3630(4)	3432(4)	31(3)	43(3)	34(3)	−2(2)	−0(2)	−3(2)
	201(5)	2390(4)	4634(4)	35(3)	34(3)	47(3)	2(2)	−14(2)	0(2)
C2	3233(6)	3737(4)	624(4)	48(4)	40(3)	40(3)	2(2)	−1(3)	−5(2)
	4520(5)	2436(4)	3870(4)	27(3)	50(3)	46(3)	−1(2)	−4(2)	−2(2)
	69(5)	1721(4)	3907(5)	35(3)	35(3)	51(3)	−1(2)	−7(3)	−8(2)
C3	3898(7)	3750(5)	588(5)	72(5)	70(4)	43(4)	8(3)	0(3)	−7(3)
	5363(7)	1730(5)	4528(5)	57(4)	58(4)	71(4)	9(3)	−23(3)	−3(3)
	−1085(6)	945(5)	4009(5)	38(4)	58(4)	69(4)	−9(3)	−10(3)	−16(3)
C4	1846(6)	5485(4)	374(4)	53(4)	43(3)	37(3)	−1(3)	−10(3)	−6(2)
	5658(5)	4401(5)	3495(4)	40(3)	57(3)	34(3)	−11(3)	−8(2)	−4(3)
	−776(5)	2363(4)	5738(4)	38(3)	43(3)	46(3)	6(2)	−11(2)	−8(2)
C5	517(6)	5809(5)	656(5)	61(4)	50(3)	60(4)	2(3)	−19(3)	−8(3)
	5328(6)	5488(5)	3538(5)	51(4)	61(4)	47(3)	−8(3)	−8(3)	−10(3)
	−1012(6)	3342(5)	6111(5)	60(4)	61(4)	56(4)	−6(3)	−14(3)	−15(3)
C6	172(7)	6816(5)	73(6)	59(5)	63(4)	98(5)	15(3)	−35(4)	−18(4)
	6284(8)	6269(6)	3539(6)	90(6)	69(4)	69(5)	−19(4)	−20(4)	−23(4)
	−1908(8)	3330(6)	7145(6)	87(5)	81(5)	78(5)	21(4)	−14(4)	−45(4)
C7	1145(8)	7531(5)	−769(6)	117(7)	51(4)	66(4)	19(4)	−35(4)	−2(3)
	7577(8)	5957(6)	3511(6)	79(6)	92(5)	83(5)	−36(4)	−31(4)	−12(4)
	−2530(8)	2341(7)	7823(6)	88(6)	94(6)	72(5)	2(4)	13(4)	−27(4)
C8	2465(8)	7230(5)	−1027(6)	101(6)	51(4)	59(4)	6(4)	−15(4)	6(3)
	7925(6)	4882(6)	3476(6)	40(4)	105(6)	79(5)	−23(4)	−20(4)	−3(4)
	−2308(7)	1360(6)	7478(6)	71(5)	80(5)	68(5)	−7(4)	17(4)	−5(4)
C9	2826(7)	6210(5)	−480(5)	65(4)	53(4)	54(4)	−0(3)	−12(3)	1(3)
	6985(6)	4103(5)	3451(5)	46(4)	74(4)	57(4)	−8(3)	−15(3)	−2(3)
	−1441(6)	1364(5)	6432(5)	66(4)	53(4)	48(4)	6(3)	10(3)	−6(3)
N	3474(4)	2918(3)	1449(4)	35(3)	42(3)	50(3)	−2(2)	−3(2)	−8(2)
	3470(4)	1962(3)	3673(4)	40(3)	38(2)	51(3)	−4(2)	−9(2)	1(2)
	1128(4)	1896(3)	2974(4)	46(3)	36(2)	47(3)	−1(2)	−11(2)	−7(2)
O1	1592(3)	4166(3)	2102(3)	43(2)	42(2)	40(2)	−1(2)	−7(2)	−4(2)
	3725(4)	4068(3)	2958(3)	39(2)	41(2)	49(2)	−4(2)	−13(2)	−1(2)
	1236(3)	3074(3)	4339(3)	42(3)	45(2)	42(2)	−8(2)	−8(2)	−8(2)
O2	4304(4)	2199(3)	1250(3)	61(3)	58(3)	62(3)	20(2)	5(2)	−9(2)
	3209(4)	921(3)	4013(4)	73(3)	37(2)	78(3)	−9(2)	−22(2)	7(2)
	1181(4)	1388(3)	2219(3)	60(3)	59(2)	53(2)	−6(2)	−9(2)	−25(2)
Co	2443(1)	2976(1)	2910(1)	39(1)	36(1)	40(1)	−5(1)	−6(1)	−2(1)

Table 1. Continued.

The benzene molecule									
C11	7127(10)	−528(8)	2607(8)	135(8)	104(7)	113(8)	−5(6)	4(6)	−33(6)
C12	6081(9)	−297(7)	2173(9)	90(7)	96(6)	153(9)	−6(5)	−16(6)	−41(6)
C13	6253(13)	−378(9)	1031(11)	184(12)	129(9)	184(12)	−26(8)	−109(10)	33(8)
C14	7576(14)	−715(9)	446(9)	247(14)	131(9)	87(7)	−42(9)	−15(8)	−15(6)
C15	8530(11)	−889(8)	1017(10)	150(9)	98(7)	181(11)	−11(7)	23(8)	−69(9)
C16	8341(10)	−825(8)	2066(10)	120(8)	93(7)	166(10)	−15(6)	−36(7)	−3(7)

[a] The anisotropic thermal parameters are of the form exp $[-2\pi(h^2a^{*2}U_{11} + \cdots + 2klb^*c^*U_{23})]$.

initial E map, and subsequent Fourier syntheses gave the positions of the other non-hydrogen atoms. The refinement was carried out by block-diagonal least-squares calculations (X-RAY system, 1976)[7] with the non-hydrogen atoms refined anisotropically. All hydrogen atoms except those of the benzene molecule were located on a difference Fourier map. The refinement was then continued with a mixed thermal mode, with the hydrogen atoms isotropic. The function to be minimized was

Table 2. Fractional atomic coordinates ($\times 10^3$), isotropic thermal parameters ($\times 10^3$) and bond distances (Å) for hydrogen atoms.

Atom	x	y	z	U_{iso}	Bond length
H1(C3)	479(7)	406(6)	−84(6)	112(24)	0.94(7)
	578(7)	212(5)	490(5)	95(22)	0.93(8)
	−188(5)	113(4)	449(4)	54(16)	0.95(5)
H2(C3)	394(6)	295(5)	−68(5)	93(22)	1.02(7)
	601(6)	138(5)	408(5)	93(21)	0.93(6)
	−87(6)	14(5)	430(5)	73(18)	1.02(6)
H3(C3)	334(6)	417(5)	−108(5)	74(19)	1.01(6)
	474(8)	107(6)	516(6)	126(27)	1.07(6)
	−130(7)	101(6)	328(6)	120(28)	0.99(8)
H(C5)	−9(5)	529(4)	123(5)	64(17)	0.93(5)
	443(4)	571(4)	357(4)	34(13)	0.96(5)
	−56(6)	400(5)	563(5)	76(18)	0.93(5)
H(C6)	−86(6)	700(5)	36(5)	75(19)	1.07(6)
	597(7)	705(6)	356(6)	106(24)	1.01(7)
	−215(6)	402(5)	733(5)	90(21)	0.94(7)
H(C7)	93(7)	825(5)	−112(6)	101(23)	0.95(6)
	825(6)	652(5)	347(5)	91(21)	0.97(7)
	−315(8)	234(6)	859(6)	124(27)	1.01(7)
H(C8)	314(7)	782(6)	−156(6)	109(24)	1.01(6)
	888(8)	468(6)	329(6)	121(27)	0.99(8)
	−276(7)	69(6)	792(6)	111(24)	0.93(6)
H(C9)	378(6)	596(5)	−64(5)	72(18)	1.01(9)
	724(6)	333(4)	336(5)	70(18)	1.01(9)
	−125(5)	61(4)	618(4)	61(16)	1.05(6)

$w(|F_o| - |F_c|)^2$, where $w = 1/(50.0 + |F_o| + 0.006|F_o|^2)$. The final R value ($R = \Sigma||F_o| - |F_c||/\Sigma|F_o|$) was 0.041 for 2646 observed reflections; the average shift/e.s.d. value of variable parameters was 0.09.

The atomic scattering factors for the non-hydrogen atoms were those of Cromer and Mann[8] and for the hydrogen atom those of Stewart, Davidson and Simpson.[9] The anomalous dispersion corrections ($\Delta f'$, $\Delta f''$) were included for Co.[10]

Atomic parameters for the non-hydrogen and hydrogen atoms are listed in Tables 1 and 2, respectively. The calculated C–H bond distances in the complex moiety are also included in Table 2. The solvent benzene molecules are relatively loosely bound in the structure, and the benzene carbon atoms show considerably higher thermal vibrations than the other non-hydrogen atoms, as is common. The observed C–C bond lengths in the benzene molecule are in the range 1.31 – 1.47 Å, with a mean standard deviation of 0.02 Å.

A list of the observed and calculated structure factors is obtainable from the authors on request.

DESCRIPTION AND DISCUSSION OF THE STRUCTURE

Fig. 1 illustrates the molecular structure. The same numbering scheme has been adopted for each of the three ligand molecules, which are distinguished from each other by the letters A, B and C. The bond lengths and angles for the non-hydrogen atoms of the complex constituents are shown in Fig. 2.

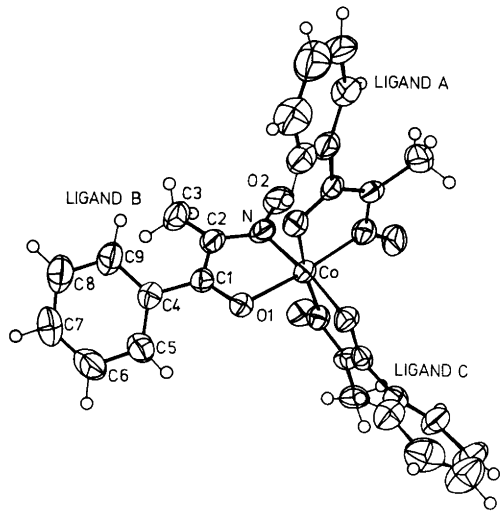

Fig. 1. ORTEP drawing of the complex molecule showing the atom numbering scheme used. The non-hydrogen atoms are represented by their thermal ellipsoids with 50 % probability.

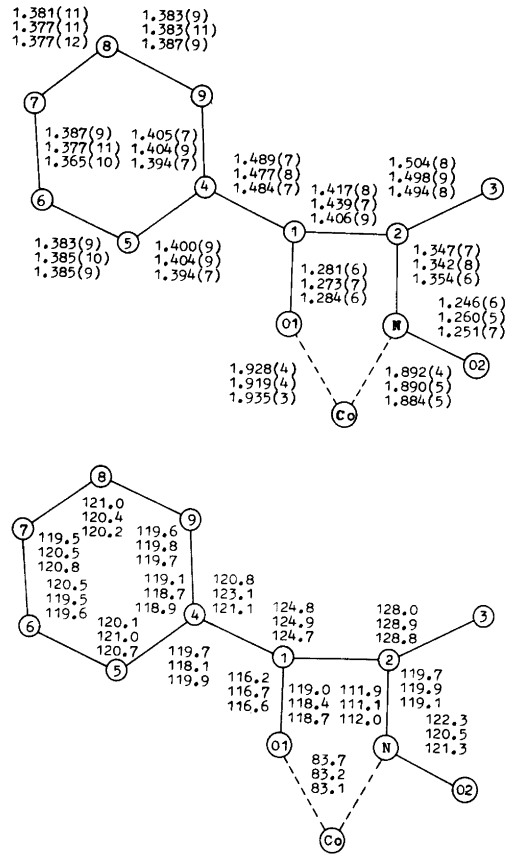

Fig. 2. Bond lengths (Å) and angles (°). The estimated standard deviations for the bond angles are 0.2 – 0.7°.

The coordination about cobalt is *cis*-octahedral with five-membered chelate rings. Such geometry could be anticipated: thus far the presence of five-membered chelate rings, *i.e.* coordination through oxime nitrogen and quinone oxygen, has been established in all complexes of the series,[1-3,11-14] and *cis*-octahedral geometry about the metal has been found in those few cases where tris chelates have been studied.[12-14]

The three Co–N bond lengths are in the range 1.884 – 1.892 Å, with a mean of 1.889 Å, and the equivalent values for Co–O are 1.919 – 1.935 Å with a mean of 1.927 Å. These distances are very similar to those found in *fac*-tris(isonitrosoacetylacetonato)cobalt(III) (mean distances 1.891 and 1.925 Å),[14] which is the only other cobalt complex of known structure containing a carbonyl-oxime

Table 3. Selected structural details.

Torsion angles (°)	Ligand A	Ligand B	Ligand C
NC2C1O1	−6.6	1.1	1.5
C3C2C1O1	166.5	−175.3	−174.1
C4C1C2N	172.8	−179.2	−178.2
Deviations (Å) from the plane CoNO1			
C1	0.190	−0.016	−0.022
C2	0.125	−0.004	−0.005
O2	−0.101	0.036	0.035

function. The coordination octahedron about cobalt found here is not seriously distorted from regular octahedral with the N−Co−N angles of *ca.* 94°, N−Co−O angles in the range 83−94°, and O−Co−O angles of 89−93°.

Although the bond lengths and angles in the chelate rings appear to be essentially equivalent, some differences in the chelation conformation do exist. The chelate rings involving ligands B and C are relatively planar, whereas slight but significant deviations from planarity can be found for ligand A. The different puckering of the chelate ring of ligand A as compared with the other two rings, and which most probably arises from packing considerations, is revealed in the values of the torsion angle NC2C1O1 together with the deviations of atoms C1 and C2 from the plane CoNO1. These values for each of the chelate rings, together with some other structural details, are listed in Table 3.

In our studies on nitrosonaphtholato⇌naphthoquinone oximato complexes[1-3] we have observed that chelation with a metal ion (Cu^{2+}, Ni^{2+} or Zn^{2+}) brings about the following changes in the ligand geometry: (*i*) the C=O and C=N distances are lengthened from their respective free ligand values of 1.22±0.02 and 1.30±0.01 Å to 1.28±0.02 and 1.36±0.02 Å, (*ii*) the N−O and C1−C2 distances are shortened from their free ligand values of 1.37±0.02 and 1.49±0.03 Å to 1.26±0.01 and 1.43±0.01 Å, and (*iii*) the CNO angle of 112±2° is opened up to 121±2°. The mean values of the present C1−O1, C2−N, C1−C2, and N−O2 bond lengths and the C2NO2 bond angle are 1.279, 1.348, 1.421, 1.252 Å, and 121.4°, respectively. The corresponding free ligand values have been previously reported as 1.231(4), 1.278(4), 1.501(5), 1.405(4) Å, and 113.0(2)° (in the free ligand the oxime nitrogen and carbonyl oxygen are roughly in *trans*-position, the torsion angle NC2C1O1 being 155°).[5] These values are in excellent agreement with the results given above for the free and metal-coordinated naphthoquinone oximes. The C−O and C−N bond lengths, and the CNO angle obtained in this study are also very similar to those reported for the iron(II) and cobalt(III) complexes of isonitrosoacetylacetone, which seem to be the only other metal chelates of aliphatic carbonyl-oximes studied by X-rays. However, the N−O bond [1.22(2) Å] in these two complexes is possibly somewhat shorter than the one found here.[14] As a whole it can still be maintained that aliphatic carbonyl-oximes and nitrosophenol⇌quinone oxime compounds yield metal chelates of essentially similar basic structure with no marked effects arising from the aromatic ring system.

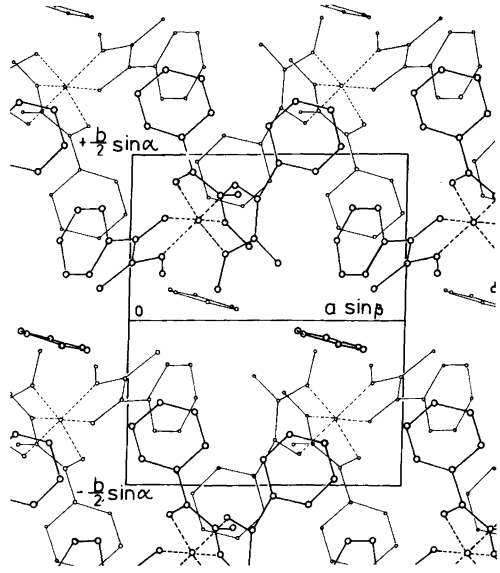

Fig. 3. A packing diagram of $[Co(C_9H_8NO_2)_3]\cdot C_6H_6$ as viewed down the *c* axis.

The low density of the present compound (1.3 g cm^{-3}) suggests a loose packing of the complex and the solvent in the unit cell. In fact, there are only four intermolecular distances below 3.45 Å, and none of these is associated with the solvent benzene molecule, which simply fills gaps in the structure and is held by van der Waals forces. It may be noted, too, that three of the intermolecular contacts mentioned (3.23−3.35 Å), comprising two oxime oxygen−carbon contacts and a carbon−carbon contact, occur between A ligands, while the

fourth is an oxime oxygen – carbon contact of 3.29 Å between ligands B and C. Fig. 3 shows a view of the molecular packing.

Acknowledgement. The financial support of the Science Research Council of Finland is gratefully acknowledged.

REFERENCES

1. Saarinen, H., Korvenranta, J. and Näsäkkälä, E. *Acta Chem. Scand. A 31* (1977) 213.
2. Saarinen, H., Korvenranta, J. and Näsäkkälä, E. *Finn. Chem. Lett.* (1977) 155.
3. Korvenranta, J., Saarinen, H. and Näsäkkälä, E. *Acta Chem. Scand. A 31* (1977) 689.
4. Chakravorty, A. *Coord. Chem. Rev. 13* (1974) 1.
5. Saarinen, H., Korvenranta, J. and Näsäkkälä, E. *Cryst. Struct. Commun. 6* (1977) 557.
6. Main, P., Woolfson, M. M., Decleroqk, I. and Germain, G. *MULTAN, a Computer Programme for the Automatic Solution of Crystal Structures*, Dec. 1974.
7. *X-Ray 76, Program System for X-Ray Crystallography*, Technical Report TR-446, Computer Science Center, University of Maryland, College Park.
8. Cromer, D. T. and Mann, J. B. *Acta Crystallogr. A 24* (1968) 321.
9. Stewart, R. F., Davidson, E. and Simpson, W. *J. Chem. Phys. 42* (1968) 3175.
10. *International Tables for X-Ray Crystallography*, Kynoch Press, Birmingham 1974, Vol. IV, p. 149.
11. McPartlin, M. *Inorg. Nucl. Chem. Lett. 9* (1973) 1207.
12. Candeloro, S., Grdenic, D., Taylor, N., Thomson, B., Viswamitra, M. and Hodgin, D. C. *Nature (London) 224* (1969) 589.
13. Carrek, P. W., Charalambous, J., Kensett, M. J. McPartlin, M. and Sims, R. *Inorg. Nucl. Chem. Lett. 10* (1974) 749.
14. Figgins, B. N., Raston, C. L., Sharma, R. P. and White, A. H. *Seventh Australian Conference on Coordination and Metal-Organic Chemistry (COMO) Abstracts*, Melbourne, Feb. 1977.

Received November 28, 1977.

Acta Chemica Scandinavica A 32 (1978) 309–311

Crystal Structure Refinements of ZrCoP, NbCoP, NbNiP and TaFeP

NARONGSAK CHAICHIT, PRAMODE CHALUGUNE, SURAPOL RUKVICHAI, PILAI CHOOSANG, VALAPHA KAEWCHANSILP, CHA-ON PONTCHOUR, PATHANA PHAVANANTHA and SUPANICH PRAMATUS

Faculty of Science, Chulalongkorn University, Bangkok 5, Thailand

ZrCoP, NbCoP, NbNiP and TaFeP crystallize with the Co_2P (*anti*-$PbCl_2$)-type structure. The crystal structures have been refined from X-ray single crystal data obtained by visual intensity estimation from Weissenberg films. The special character of the Co–Co interaction in compounds of the type investigated is revealed by the distribution of interatomic distances in the structures.

A large number of ternary transition metal phosphides and arsenides crystallize with the Co_2P-type structure.[1-7] The chemical and physical properties of these compounds and related phases have been studied extensively (see, for example, Refs. 8–11), and many interesting relationships between properties and atomic arrangement have been observed. ZrFeP has so far been the only ternary phosphide or arsenide for which accurate crystallographic data are available.[1] Detailed structural information on further representatives of this class of compound is thus desirable. In the present paper we report the results from structure refinements of four of the ternary phosphides.

EXPERIMENTAL

Single crystals were obtained from alloys originally prepared by Rundqvist and Nawapong.[1] The crystals selected were almost cylindrical, with the *b* axes directed along the cylinder axes. The crystals were mounted on a Nonius Weissenberg camera with *b* axis as rotation axis. Intensity data were recorded with zirconium-filtered Mo*K* radiation by the multiple-film technique. In the case of NbNiP, light exposed and developed X-ray films were used as absorbers between successive films in the multiple pack. For ZrCoP, NbCoP and TaFeP, the films were interleaved with thin iron foils. The (*h*0*l*) and (*h*1*l*) zones were recorded for NbNiP, ZrCoP and NbCoP. For TaFeP, only (*h*0*l*) reflexions were recorded. The intensities of the reflexions were measured by visual comparison with intensity scales obtained by timed exposures of one reflexion from each crystal. Absorption corrections were applied to the intensity data by approximating the crystal shape to a cylindrical form.

The crystals were assumed to be isostructural with ZrFeP (space group *Pnma*), and positional parameters and isotropic temperature factors were refined directly by the least-squares method. Atomic scattering factors and corrections for dispersion were taken from the International Tables.[12] Weights were assigned according to Cruickshank's formula,[13] $w=1/(c_1+|F_0|+c_2|F_0|^2)$, where the constants c_1 and c_2 were given appropriate values as judged from weight analyses calculated between successive cycles in the least-squares refinement procedure. The calculations were performed on a CDC 3100 computer using standard crystallographic programs adapted by R. Liminga, University of Uppsala. Unit cell dimensions were taken from the work of Rundqvist and Nawapong, and their standard deviations were assumed to be as reported for ZrFeP.[1]

RESULTS AND DISCUSSION

The refinements for all four crystals converged satisfactorily, and the final difference syntheses calculated revealed no significant maxima or minima. The final conventional *R*-values of ZrCoP, NbCoP, NbNiP and TaFeP were 0.06, 0.09, 0.09

and 0.10 for the 153, 114, 224 and 130 observed reflexions, respectively. The structure data obtained are presented in Table 1, where the notations M(1) and M(2) for the two metal positions are the same as those used by Rundqvist and Nawapong: M(1) being occupied by the 3*d* transition metal component, and M(2) by the 4*d* or 5*d* metal component. Due to the approximate character of the absorption corrections, the values for the temperature factors in Table 1 should be regarded with caution, while the positional parameter values can be treated with much greater confidence.

Interatomic distances are given in Table 2. A detailed analysis of these distances provides some information on a curious feature originally pointed out by Rundqvist and Tansuriwongs.[2] They observed that, for ternary Co_2P-type phases with the general formula M(1)M(2)X (where M(1) is a 3*d* transition metal, M(2) is a 4*d* or 5*d* metal, and X is phosphorus, arsenic, silicon or germanium), compounds with cobalt as the M(1) component invariably have the smallest unit-cell volume for any fixed combination of M(2) and X components. This is somewhat surprising since the normal metal

Table 1. Structure data for ZrCoP, NbCoP, NbNiP and TaFeP. Space group *Pnma* (No 62); all atoms in 4*c* positions, M(1)=Fe, Co, Ni; M(2)=Zr, Nb, Ta. *a*, *b*, *c* in Å; *B* in Å^2.

		ZrCoP	NbCoP	NbNiP	TaFeP
a		6.332(1)	6.112(1)	6.108(1)	6.099(1)
b		3.698(1)	3.587(1)	3.578(1)	3.574(1)
c		7.160(1)	6.978(1)	7.091(1)	6.976(1)
M(1)	*x*	0.1401(4)	0.1442(10)	0.1471(5)	0.1444(17)
	z	0.5620(4)	0.5609(8)	0.5662(4)	0.5618(13)
	B	0.30(4)	0.15(10)	0.47(4)	0.53(10)
M(2)	*x*	0.0205(3)	0.0249(6)	0.0221(3)	0.0236(4)
	z	0.1833(2)	0.1730(5)	0.1683(3)	0.1751(3)
	B	0.17(3)	−0.12(8)	0.15(2)	0.08(2)
P	*x*	0.2716(8)	0.2764(15)	0.2804(10)	0.269(4)
	z	0.8845(7)	0.8804(16)	0.8765(8)	0.876(3)
	B	0.27(7)	0.07(15)	0.31(7)	0.77(27)

Table 2. Interatomic distances in ZrCoP, NbCoP, NbNiP and TaFeP, (Å). Distances up to 3.5 Å included. M(1)=Fe, Co, Ni; M(2)=Zr, Nb, Ta.

	ZrCoP	NbCoP	NbNiP	TaFeP
M(1)−2P	2.312(4)	2.244(7)	2.282(4)	2.272(16)
−P	2.365(6)	2.285(11)	2.276(7)	2.317(25)
−P	2.455(6)	2.372(12)	2.346(6)	2.333(25)
−2M(1)	2.712(4)	2.655(9)	2.704(5)	2.653(15)
−2M(2)	2.789(2)	2.781(5)	2.794(3)	2.759(7)
−M(2)	2.815(3)	2.804(7)	2.830(4)	2.796(9)
−2M(2)	2.965(3)	2.814(5)	2.795(3)	2.814(8)
−M(2)	2.981(3)	2.842(7)	2.923(4)	2.843(10)
M(2)−2P	2.660(4)	2.598(7)	2.591(5)	2.549(16)
−P	2.666(5)	2.556(11)	2.602(6)	2.568(23)
−2P	2.688(4)	2.605(8)	2.614(5)	2.600(17)
−P	3.473(5)	3.467(11)		3.498(24)
−2M(2)	3.221(2)	3.023(6)	2.995(3)	3.041(3)
−2M(2)	3.307(1)	3.240(2)	3.266(2)	3.224(1)

Table 3. Average near–neighbour distances. M(1)=Fe, Co, Ni; M(2)=Zr, Nb, Ta.

Compound	M(1)–2M(1)	M(1)–6M(2)	M(1)–4P	M(2)–4M(2)	M(2)–5P
ZrFeP	2.776	2.883	2.359	3.265	2.690
ZrCoP	2.712	2.884	2.361	3.264	2.672
NbCoP	2.655	2.806	2.286	3.132	2.592
NbNiP	2.704	2.822	2.297	3.131	2.602
TaFeP	2.653	2.798	2.299	3.133	2.573

radius for nickel is smaller than that of cobalt.

The anomalous unit-cell volume for cobalt-containing crystals is accompanied by a specific distribution of interatomic distances. In order to illustrate this feature more clearly, average near-neighbour distances have been calculated and are given in Table 3, including also distances for ZrFeP.[1] The data in Table 3 reveal that the major difference between NbCoP and NbNiP lies in the Co–Co and Ni–Ni distances. The latter distances exceed the former by more than three times the difference between any other pair of corresponding average distance. An analogous situation occurs for ZrCoP and ZrFeP as regards the Co–Co and Fe–Fe distances; the differences between other distances are here almost insignificant. The singular character of Co–Co metal interactions in ternary phosphides and arsenides of the Co_2P-type, and also the closely related Fe_2P- and Cu_2Sb-types, has been stressed by Fruchart and coworkers (see, for example, Ref. 5). The present results are indeed in good accordance with Fruchart's ideas.

Acknowledgements. We wish to express our gratitude to Prof. Stig Rundqvist, Uppsala, for his valuable advice and encouragement. We also wish to thank Prof. Rune Liminga, Uppsala, for his help in adapting the crystallographic programs to our computer. Thanks are also due to Dr. J. O. Thomas, Uppsala, for his careful revision of the English text. We are indebted to the International Seminars, University of Uppsala, and the Swedish International Development Authority (SIDA) for their extensive financial support during this work to P. Choosang, V. Kaewchansilp, C-O. Pontchour and S. Pramatus.

We wish to thank Prof. Vichai Hayodom, Dean of the Faculty of Science, Chulalongkorn University, for his interest. The work has also been supported by the Thai University Development Commission.

REFERENCES

1. Rundqvist, S. and Nawapong, P. C. *Acta Chem. Scand. 20* (1966) 2250.
2. Rundqvist, S. and Tansuriwongs, P. *Acta Chem. Scand. 21* (1967) 813.
3. Fruchart, R., Roger, A. and Sénateur, J. P. *J. Appl. Phys. 40* (1969) 1250.
4. Nylund, A., Roger, A., Sénateur, J. P. and Fruchart, R. *J. Solid State Chem. 4* (1972) 115.
5. Roy-Montreuil, Mme, Deyris, B., Michel, A., Rouault, A., l'Héritier, P., Nylund, A., Sénateur, J. P. and Fruchart, R. *Mater. Res. Bull. 7* (1972) 813.
6. Deyris, B., Roy-Montreuil, J., Rouault, A., Krumbügel-Nylund, A., Sénateur, J.-P., Fruchart, R. and Michel, A. *C.R. Acad. Sci. Ser. C 278* (1974) 237.
7. Guérin, R. and Sergent, M. *Mater. Res. Bull. 12* (1977) 381.
8. Roger, A. *Thesis*, University of Paris, Faculty of Sciences, Orsay 1970.
9. Wäppling, R., Häggström, L., Rundqvist, S. and Karlsson, E. *J. Solid State Chem. 3* (1971) 276.
10. Sénateur, J. P., Rouault, A., l'Héritier, P., Krumbügel-Nylund, A., Fruchart, R., Fruchart, D., Convert, P. and Roudaut, E. *Mater. Res. Bull. 8* (1975) 229.
11. Krumbügel-Nylund, A. *Thesis*, University of Paris, Faculty of Sciences, Orsay 1974.
12. *International Tables for X-Ray Crystallography*, Kynoch Press, Birmingham 1974, Vol. 4.
13. Cruickshank, D. W. J., Philling, D. E., Bujosa, A., Lovell, F. M. and Truter, M. R. In *Computer Methods and the Phase Problem*, Pergamon, Oxford 1961, p. 32.

Received October 26, 1977.

Acta Chemica Scandinavica A 32 (1978) 313–318

The Crystal Structure of the Chloroform Solvate of Thallium(I) Diethyldithiocarbamate, $[TlS_2CN(C_2H_5)_2]_2.CHCl_3$

SAM-HYO HONG [a] and PER JENNISCHE [b]

[a] Department of Inorganic Chemistry, Arrhenius Laboratory, University of Stockholm, S-106 91 Stockholm, Sweden and [b] Institute of Chemistry, University of Uppsala, Box 531, S-751 21 Uppsala, Sweden

The crystal structure of $[TlS_2CN(C_2H_5)_2]_2.CHCl_3$ has been determined at 0 °C from X-ray data collected on an automatic two-circle diffractometer. The crystals are monoclinic, space group $P2_1/c$; cell dimensions $a=13.102(2)$ Å, $b=11.734(4)$ Å, $c=16.042(3)$ Å, $\beta=112.95(2)°$, $Z=4$. The thallium atoms coordinate four sulfur atoms at distances 2.9 to 3.5 Å in dimeric, centrosymmetric molecules $[TlS_2CN(C_2H_5)_2]_2$, which are packed with the molecular centres in layers at $x=0$ and $x=0.5$. Each thallium atom also coordinates one sulfur atom in another layer, at 3.7 or 3.8 Å, and two chlorine atoms, at 3.9 to 4.5 Å, belonging to chloroform molecules situated between the layers.

The crystal structures of six dialkyldithiocarbamates of thallium(I) have been determined.[1-6] They all contain dimeric molecules with the two thallium atoms coordinated to four sulfur atoms in a plane between them. Interaction between the molecules augments the coordination number of thallium to five, six or seven. The arrangement of the intermolecular Tl–S bonds depends on the size of the alkyl groups; the highest thallium coordination number is found in the compound with the smallest alkyl group, methyl. The internal geometries of the dimers are distorted to various degrees. Large distortions are related to strong intermolecular interactions.

The chloroform solvate of thallium(I) diethyldithiocarbamate was obtained during attempts to prepare highly concentrated solutions.[7]

EXPERIMENTAL

Semitransparent crystals of $[TlS_2CN(C_2H_5)_2]_2.CHCl_3$ were obtained from a solution of $TlS_2CN(C_2H_5)_2$ in $CHCl_3$, saturated at 35 °C, by cooling to room temperature. Since the preparation was unstable in air, crystallization was performed in a thin-walled glass capillary, which was afterwards sealed with a mixture of glass powder and cyanoacrylate.

The chloroform content was determined from the loss of weight of a sample kept in air for a week at 50 °C. The density was measured by flotation in a mixture of $CHCl_3$ and $CHBr_3$.

Preliminary unit cell parameters at 25 °C were determined from small interval zero level oscillation photographs. The film radii were calibrated from α-quartz reflections. Unit cell parameters at 0 °C were determined by least squares refinement based on 73 medium or high θ-values from crystals rotated about a or b on a two-circle diffractometer. The β value remained constant at the lowered temperature, but the unit cell edges decreased by 0.99 %.

Crystal data at 0 °C. Formula unit: $[TlS_2CN(C_2H_5)_2]_2.CHCl_3$. Space group: $P2_1/c$. Unit cell parameters: $a=13.102(2)$ Å, $b=11.734(4)$ Å, $c=16.042(3)$ Å, $\beta=112.95(2)°$. $Z=4$. $D_m=2.40(1)$ g cm^{-3}. $D_x=2.412$ g cm^{-3}. $\mu(CuK\alpha)=335$ cm^{-1}. Systematic absences: $h0l$ for $l=2n+1$; $0k0$ for $k=2n+1$.

The intensities were recorded on a STOE 2-circle diffractometer using graphite monochromatized $CuK\alpha$ radiation. The intensity collection procedure was similar to that used in Ref. 8. The maximum value of $\sin\theta/\lambda$ was 0.51. Since heat development from the diffractometer's stepping motors has been observed to affect crystal volume and alignment, the temperature of the crystal was held constant at 0 °C in this experiment by a stream of dry air cooled with dry ice.[9]

Table 1. Atomic coordinates and thermal parameters. The anisotropic temperature factor is expressed as $\exp(-\beta_{11}h^2 \ldots -2\beta_{12}hk \ldots)$. The values of β_{ij} in the table have been multiplied by 10^4.

Atom	x	y	z	B/Å^2
Tl1	0.1485(3)	0.0015(3)	0.0708(2)	
Tl2	0.6541(3)	0.0215(3)	0.0728(2)	
Cl1	0.655(2)	0.499(1)	0.076(1)	
Cl2	0.733(2)	0.322(2)	0.209(1)	
Cl3	0.792(1)	0.321(1)	0.053(1)	
S11	0.008(2)	0.208(1)	0.001(1)	
S12	0.046(1)	0.053(1)	−0.128(1)	
S21	0.452(1)	0.011(1)	0.121(1)	
S22	0.426(1)	0.205(1)	0.000(1)	
N1	0.033(3)	0.283(3)	−0.148(3)	4(1)
N2	0.431(3)	0.229(3)	0.164(3)	4(1)
C	0.681(4)	0.351(4)	0.092(3)	5(1)
C10	0.036(4)	0.194(5)	−0.097(4)	5(1)
C11	0.025(5)	0.402(5)	−0.115(4)	6(1)
C12	−0.084(5)	0.443(5)	−0.150(4)	7(1)
C13	0.034(4)	0.267(4)	−0.239(3)	4(1)
C14	0.149(5)	0.274(5)	−0.234(4)	7(1)
C20	0.430(4)	0.161(4)	0.098(3)	4(1)
C21	0.417(4)	0.353(4)	0.146(3)	5(1)
C22	0.301(5)	0.395(6)	0.118(4)	8(2)
C23	0.439(4)	0.187(5)	0.256(4)	6(1)
C24	0.556(5)	0.189(5)	0.327(4)	6(1)

Atom	β_{11}	β_{22}	β_{33}	β_{12}	β_{13}	β_{23}
Tl1	98(12)	116(3)	60(2)	3(2)	25(1)	17(2)
Tl2	106(12)	79(2)	67(2)	−10(2)	21(2)	−30(2)
Cl1	194(24)	98(16)	105(13)	−11(16)	39(13)	9(13)
Cl2	183(24)	209(25)	67(11)	29(18)	47(12)	16(14)
Cl3	152(21)	128(17)	67(10)	9(14)	37(10)	0(11)
S11	270(28)	78(15)	52(9)	20(15)	77(12)	7(10)
S12	182(23)	54(13)	62(10)	−6(12)	62(11)	4(9)
S21	166(22)	67(15)	74(11)	14(12)	60(12)	12(10)
S22	147(21)	70(13)	35(8)	−19(11)	24(9)	−4(8)

Ten well-formed cylindrical crystals in sealed capillaries were used. Average cross section and length were 0.14 and 0.27 mm. Interlayer scale factors were calculated from the common reflections registered about a ($0 \leq h \leq 10$) and b ($0 \leq k \leq 1$). The intensities were corrected for Lorentz, polarization and absorption effects.

The Patterson map would fit two alternative thallium atom positions. In the successful alternative, one thallium position (0.157, 0.0, 0.071) was determined from the map. Because of the low intensities of reflections with odd h the other one was placed $a/2$ from the first one. These coordinates and isotropic temperature factors were refined by Fourier and least squares calculations. The positions of the sulfur, chlorine, nitrogen and carbon atoms were located from difference syntheses alternating with least squares refinements. Hydrogen atoms were not located. The interlayer scale factors were included and anisotropic temperature factors used for thallium, chlorine and sulfur. The final reliability index $R = \Sigma \| F_o | - | F_c \| / \Sigma | F_o |$ was 0.074 which was based on 1319 observed reflections with $I_o > 1.5\sigma(I_o)$. 17 of these violating $0.5 < |F_o/F_c| < 2.0$ were excluded in the refinement. The expression minimized was $\Sigma(|F_o| - |F_c|)^2$. In the final cycle of the full matrix program refinement the shifts were less than 0.2 of the estimated standard deviations. A difference synthesis calculated with the final atomic parameters shown in Table 1 showed no spurious peaks higher than 0.08 eÅ^{-3}. Atomic scattering factors were taken from Ref. 10 (Tl, Cl, S) and Ref. 11 (N, C). Anomalous dispersion corrections [11] were applied to Tl, Cl and S. The computer programs are described in Ref. 12.

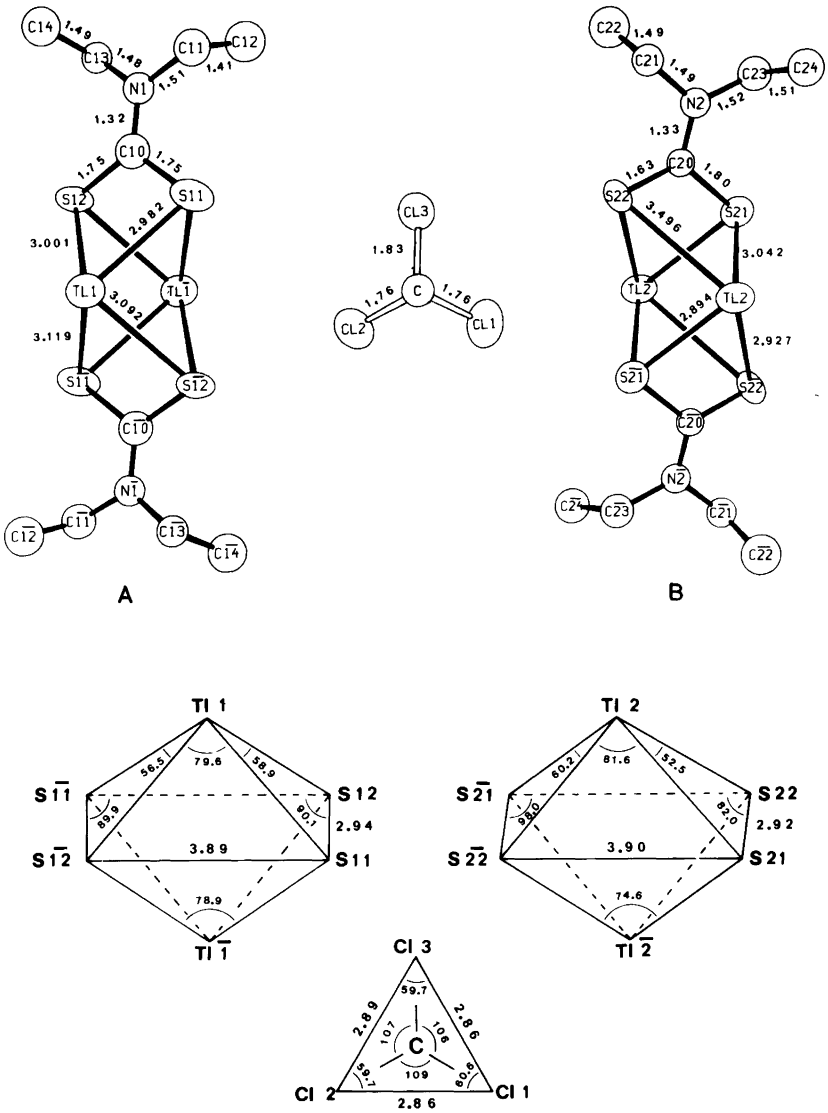

Fig. 1. Geometrical structures of the two dimeric, centrosymmetrical molecules A and B, and the chloroform molecule. The estimated standard deviations (Å) of the distances are for Tl–S 0.017, S–S 0.02, S–C 0.05, Cl–C 0.05, N–C 0.07 and C–C 0.08.

RESULTS AND DISCUSSION

The crystal contains dimeric molecules, $[TlS_2CN(C_2H_5)_2]_2$, packed so as to form a stack of layers parallel to the (*b*,*c*)-plane, with the molecular centres of symmetry at $x=0$ and $x=0.5$ and with interleaving chloroform molecules. Tl–S bonds connect the dimeric molecules from different layers to form infinite chains parallel to **a**.

The two independent dimeric molecules, A and B, Fig. 1, have the same structure as the molecules of the unsolvated compound.[5] The same type of molecule is also found in the other thallium dialkyldithiocarbamates (alkyl = methyl,[3] propyl,[1]

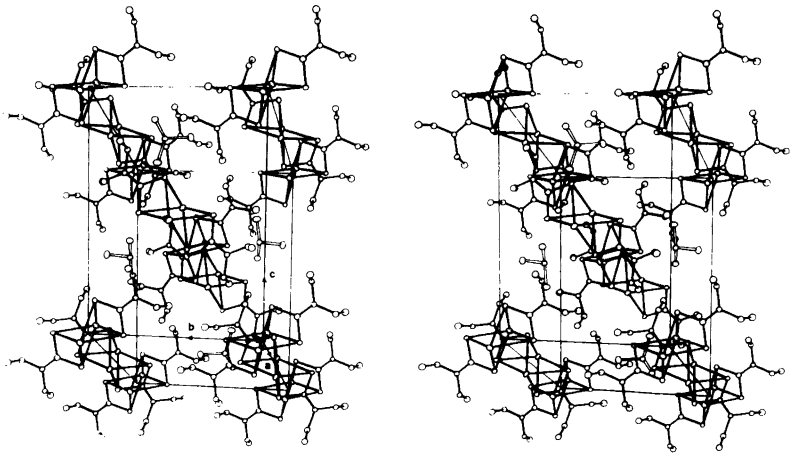

Fig. 2. Stereoscopic illustration of the stacking of the layers viewed along the normal to the (*b*,*c*)-plane. Two layers of molecules A are seen at $x=0$ and $x=1$, and one layer of molecules B at $x=0.5$. The chloroform molecules are situated between the layers.

isopropyl,[2] butyl[6] and isobutyl[4]) and in the potassium,[13] rubidium[13] and cesium[14] dibutyldithiocarbamates. Some interatomic distances are given in Fig. 1. The intramolecular Tl–Tl distances are 3.661(6) Å (A) and 3.829(7) Å (B). The S_2CNC_2 parts of the ligands are planar within experimental error. The S_4 planes of the molecules are somewhat inclined to the layers, 13.2° for A and 22.5° for the less regular B.

Molecule A is more regular than B as indicated by: (1) the smaller range of Tl–S distances, (2) the smaller angle between the Tl_2 vector and the normal to the S_4 plane (2.9° *vs.* 10.6°) and (3) the smaller angle between the S_2CNC_2 plane and the S_4 plane (9.7° *vs.* 19.6°).

The chloroform molecule has the expected structure, with average distances Cl–Cl (2.87(3) Å) and C–Cl [1.79(5) Å] agreeing with those in solid chloroform at 185 K [2.86(1) and 1.75(2) Å[15]].

The dimeric molecule may be formally obtained from that of the isopropyl compound, $[TlS_2CN(C_3H_7)_2]_2$, by replacing one methyl group in each isopropyl chain by a hydrogen atom. The molecules of the isopropyl compound form the same type of layer as the title compound, with similar dimensions. The molecules are quite regular, and the S_4 plane is inclined by only 4.3° to the layer plane. Unsolvated thallium(I) diethyldithiocarbamate, on the other hand, contains no such layers. Evidently the chloroform molecules stabilize the layers by filling the vacancies corresponding to the methyl groups replaced. Two vacancies in layer A cooperate to form one large cavity housing the Cl_3 tripod. If the glide planes were normal to the long axis, as in the isopropyl compound, the vacancies would be dispersed, producing narrow crevices which are unsuitable for accommodating the solvent molecules.

The stacking of the layers. The stacking is shown in Fig. 2. The stacking distance is longer than in the isopropyl compound, 6.03 compared to 5.55 Å, but short interatomic distances between the layers show that the layers are in contact [*e.g.* *D*(C12,C22)= 3.61(9) Å; *D*(C13,C23)= 3.89(8) Å]. The chloroform molecules are situated between the layers, the CH apices pointing towards layer B and the Cl_3 tripod towards layer A. In comparison to the isopropyl compound each solvent molecule, crystal volume[15] 104 Å^3, replaces four methylene groups, combined theoretical volume[16] 106 Å. Despite the similarities of the two values the crystal volume of one dimeric molecule + one chloroform molecule in the solvate, 568 Å^3, is actually 26 Å^3 larger than the crystal volume of one dimeric molecule in the isopropyl compound. Evidently the methylene vacancies are not perfectly located to fit the unsymmetrical solvent molecules. The Cl_3 tripod fits well into the vacancies of layer A but the CH apex is incapable of filling the vacancies in layer B.

The chains of dimeric molecules. The stacking produces chains containing alternating molecules A and B oriented crosswise, Fig. 3. The correspond-

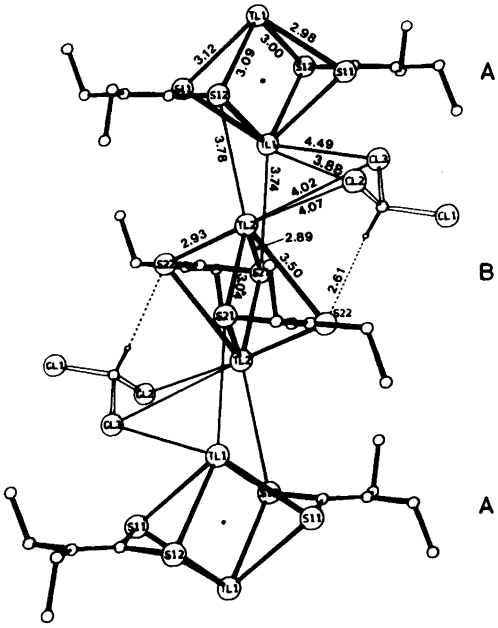

Fig. 3. Perspective illustration of the chain formed by alternating molecules A and B having their centres of symmetry along the *a*-axis which is oriented downwards. The chloroform hydrogen atom has been positioned at 2.31 Å from the three chlorine atoms.

ing chains in the isopropyl compound contain parallel molecules due to a different stacking with only one layer type and a stacking period of one layer. In the propyl compound there is one layer type but a two-layer stacking period, which again gives a crosswise orientation.

The molecules in the chain are linked by Tl–S bonds which are considerably longer than those within the dimeric molecules, D(T11,S21) = 3.74(2) Å: D(T12,S12) = 3.78(2) Å. The five sulfur atoms form a distorted rectangular pyramid about the thallium atom, the apical Tl–S bond being inclined by 25° (A) and 39° (B) to the normal of the equatorial S_4 plane.

The thallium coordination geometry is similar to that of the isopropyl compound in which the apical distance is 3.86 Å. In the unsolvated ethyl compound the coordination geometry is trigonal prismatic; apart from the four sulfur atoms in the dimeric molecule the thallium atom coordinates two extra sulfur atoms in an adjacent dimer at distances 3.7–3.9 Å.

Two chlorine atoms also appear in the vicinity of each thallium atom, D(T11,C12) = 3.88(2) Å, D(T11,C13) = 4.49(2) Å, D(T12,C12) = 4.07(2) Å, D(T12,C13) = 4.02(2) Å. Although longer than in TlCl[17] (3.27 Å) and in $TlCl_2$[18] (3.27 and 3.29 Å), the shortest of the Tl–Cl distances, 3.88 Å, is comparable to the intermolecular Tl–S distances, 3.78 and 3.74 Å. Since the van der Waals radii[19] of Cl and S are similar, 1.74 to 1.80 Å depending on the bonding conditions, Tl–Cl bonds stronger than van der Waals contacts cannot be rejected.

The chloroform carbon atom is close to one of the sulfur atoms in molecule B, D(C,S22) = 3.53(5) Å. Fig. 3 shows that the Tl–Cl and the C–H···S interactions cooperate to connect the chloroform molecule to dimer B. A hydrogen atom positioned at 2.31 Å from the three chlorine atoms, as in solid chloroform,[15] is close to the sulfur atom, D(H,S22) = 2.61 Å. This distance is less than the sum of the van der Waals radii,[19] 3.0 Å. Distances of the same kind and length were interpreted as corresponding to C–H···S hydrogen bonds in tris(morpholyldithiocarbamato)ruthenium(III). $2\frac{1}{2}$ chloroform.[16] The long Tl2–S22 bond, 3.50 Å, should then be attributed to a combination of the two interactions.

Acknowledgements. We wish to thank Professor Ivar Olovsson for experimental facilities, Dr Åke Olin for communicating his discovery of the compound and Dr Rolf Hesse for stimulating discussions. The work has been supported by grants from the Swedish Natural Science Research Council.

REFERENCES

1. Nilson, L. and Hesse, R. *Acta Chem. Scand. 23* (1969) 1951.
2. Jennische, P., Olin, Å. and Hesse, R. *Acta Chem. Scand. 26* (1972) 2799.
3. Jennische, P. and Hesse, R. *Acta Chem. Scand. 27* (1973) 3531.
4. Anacker-Eickhoff, H., Jennische, P. and Hesse, R. *Acta Chem. Scand. A 29* (1975) 51.
5. Pritzkow, H. and Jennische, P. *Acta Chem. Scand. A 29* (1975) 60.
6. Elfwing, E., Anacker-Eickhoff, H., Jennische, P. and Hesse, R. *Acta Chem. Scand. A 30* (1976) 335.
7. Olin, Å. *Personal communication.*
8. Hong, S.-H. and Olin, Å. *Acta Chem. Scand. 27* (1973) 2309.
9. Olovsson, I. *Ark. Kemi 16* (1960) 437.
10. Hanson, H. P., Herman, F., Lea, J. D. and Skillman, S. *Acta Crystallogr. 17* (1964) 1040.

11. *International Tables for X-Ray Crystallography*, Kynoch Press, Birmingham 1962, Vol. 111.
12. Lundgren, J.-O. *UUIC B13-4-02*, 1975.
13. Wahlberg, A. *Acta Chem. Scand. A 30* (1976) 614.
14. Aava, U. and Hesse, R. *Ark. Kemi 30* (1968) 149.
15. Fourme, R. and Renaud, M. *C.R. Acad. Sci. Ser. A 263b* (1966) 69; *Structure Reports B 31* (1974) 33.
16. Fischer, W. *Personal communication;* Fischer, W. and Koch, E. *Acta Crystallogr. A 31* (1975) S170.
17. Wells, A. F. *Structural Inorganic Chemistry*, 3rd Ed., Oxford University Press, London 1962.
18. Thiele, G. and Rink, W. *Z. Anorg. Allg. Chem. 414* (1975) 231.
19. Bondi, A. *J. Phys. Chem. 68* (1964) 441.

Received September 5, 1977.

Acta Chemica Scandinavica A 32 (1978) 319–327

Studies on Polynuclear Complexes. II. On the Formation of Polynuclear Cobalt(III) Complexes in Aged Solutions of Aquahydroxo[tris(2-aminoethyl)amine]cobalt(III) Perchlorate

EVA PORZSOLT,* TORSTEN BERG and JANNIK BJERRUM

Chemistry Department I, Inorganic Chemistry, H. C. Ørsted Institute, University of Copenhagen, Universitetsparken 5, DK-2100 Copenhagen Ø

Ageing reactions in solutions of aquahydroxo[tris-(2-aminoethyl)amine]cobalt(III) perchlorate have been studied. In our initial experiments we employed a temperature of 80 °C. However, the cobalt–nitrogen bonds were not sufficiently robust at this temperature and a series of unidentified decomposition products were formed during the ageing procedures. Experiments were therefore made at room temperature, the most important observation then being the slow formation of an orange-red polymer in 0.01 M solutions of the cobalt(III) monomers. A stationary state entailing transformation of up to 60 % of the cobalt into the polymer is established after about one year, and analysis of the aged solutions showed that no polymers other than the orange-red complex are formed in the diaqua-aquahydroxo buffer range. The isolated polymer is labile and is rapidly converted back into the monomers in acid solution. It has no acid-base properties in the pH range 4–9 and its absorption maxima (λ(nm), ε (l mol^{-1}cm^{-1}): 500,134; 355,113) are situated ~5 nm lower than those of the diaqua(tren) complex. The polymer was not isolated in the solid state, but it could be estimated from the experiments that ~1.6 protons per cobalt monomer are set free when the polymer is formed from the diaqua tren complex and a plausible constitution consistent with this observation is discussed. Some Co–N bound-rupture occurs in the more basic solutions, tris{[di-μ-hydroxo(tren)]cobalt(III)}-cobalt(III) perchlorate being isolated as one of the products formed.

During a study[1,2] of the acid-base equilibria in the diaquabis(ethylenediamine)cobalt(III) system it was found that solutions of monomers in the buffer region showed spectral changes attended by a fall in pH in the course of a few weeks or months. It was first believed that this was due to the process:

$$2\mathrm{Co\,en_2(H_2O)_2}^{3+} \rightleftharpoons \mathrm{en_2CO\overset{OH}{\underset{HO}{}}Co\,en_2}^{4+} + 2\,\mathrm{H}^+ \quad (1)$$

However, the absorption spectrum of solutions prepared from tetrakis(ethylenediamine)di-μ-hydroxodicobalt(III) nitrate changed in the course of a few days until they became identical with that of solutions of the monomeric system at the pH in question. This clearly rules out the possibility of explaining the ageing process by eqn. (1).

The formation of chain or ring polymers of the type:

$$-\mathrm{Co\,en_2}-\mathrm{OH}-\mathrm{Co\,en_2}-\mathrm{OH}-\mathrm{Co\,en_2}-\mathrm{OH}-\mathrm{Co\,en_2}-\mathrm{OH}-$$

was another possibility. However, just as in "diol" formation, this type of polymerization cannot explain the fact that solutions of the aquahydroxo-bis(ethylenediamine) salt with one OH per cobalt monomer produce hydrogen ions during the polymerization process.

The two chelated ethylenediamine molecules were at first thought not to be engaged in the ageing reactions. However, it was noted that the

* On leave from Institute of Physical Chemistry, Kossuth Lajos University, 4010 Debrecen 10, Hungary.

solutions changed more rapidly in glass than in paraffined vessels and that addition of charcoal had a striking effect. Charcoal evidently catalyzes dissociation of ethylenediamine with the results that the solutions instead of becoming more acidic became more basic. The experiments mentioned were all performed at room temperature, but some subsequent experiments performed by Sven Harnung of this department have shown that the use of higher temperatures also results in some decomposition of the complexes leading to an increase in pH.

In the hope of avoiding such decomposition we have studied the ageing reactions occurring in the analogous cobalt(III) system with the tetradentate ligand tris(2-aminoethyl)amine (in the following abbreviated tren). This ligand has the advantage for our purposes that it occupies four facial positions for steric reasons, so that only two *cis* positions are left for the ageing reactions, assuming that the Co – N bonds are sufficiently robust.

In order to obtain results in a reasonably short time, our first experiments with the cobalt(III) tren complexes were made at 80 °C. However, contrary to expectations some cobalt-nitrogen bond rupture took place at this temperature and separation of the reaction mixture on Sephadex columns showed that a complex mixture of unidentified products was formed. In the following section the experiments at 80 °C are dealt with. We then describe the more successful experiments at room temperature, in which cobalt-nitrogen bond rupture was unimportant in relation to the ageing reactions.

Ageing experiments with the cobalt(III)tren complexes in 1 M $NaClO_4$ at 80 °C. The solutions of the aqua-hydroxo complex were made up in 1 M $NaClO_4$ from the anhydrous perchlorate salt, $[Co\ tren(OH)H_2O](ClO_4)_2$. Solutions of this salt with or without addition of $HClO_4$ and (or) NaOH are characterized in the following by their cobalt concentration C_{Co} and by $\bar{v}$, the average number of protons released initially per cobalt atom:

$$\bar{v} = \frac{C_{Co} - C_{HNO_3} + C_{NaOH} + [H^+] - [OH^-]}{C_{Co}} \qquad (2)$$

if $|C_{HNO_3} - C_{NaOH}| \lesssim C_{Co}$.

The way in which the ageing reactions influence pH in ~0.01 M complex solutions with different $\bar{v}$ is shown in Fig. 1. The reactions are surface catalyzed and therefore not completely reproducible. However, Fig. 1 shows clearly that the initial

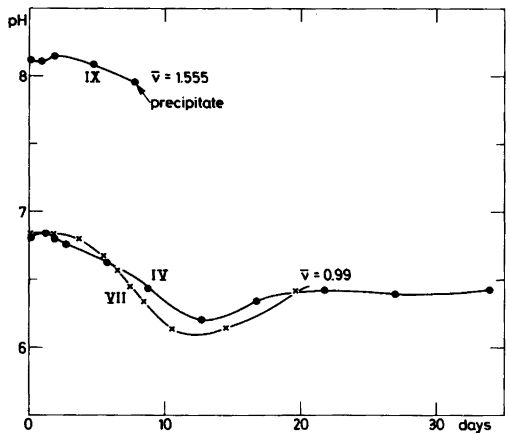

Fig. 1. The change in pH with time at 80 °C for solutions with various $\bar{v}$. $C_{NaClO_4} = 1.00$ M in the solutions and the cobalt concentrations C_{Co} were as follows: IV, 0.00997; VII, 0.01028; IX, 0.00965 M. The measurements were made at 25 °C on samples taken at intervals.

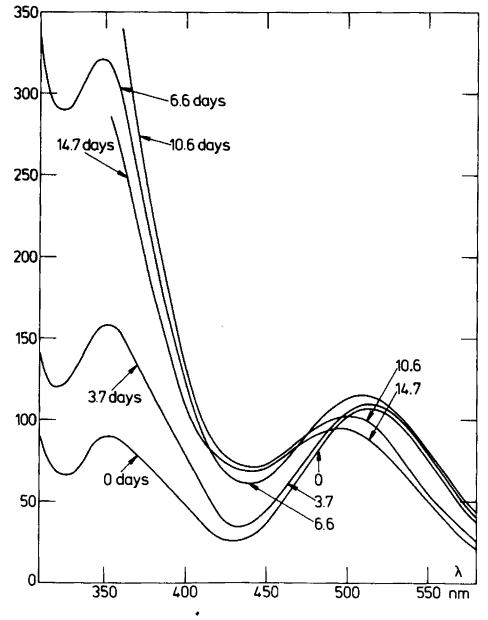

Fig. 2. Changes in the absorption spectrum of solution VII ($C_{Co} = 0.0128$ and $\bar{v} = 0.99$) during the ageing process at 80 °C. Samples were taken at intervals and measurements made at 25 °C. The figures on the curves indicate the number of days from the start of the experiment.

reactions for solutions with $\bar{\nu} = 0.99$ and 1.555 produce a decrease in pH which is followed after some days by reactions which increase pH, and which for $\bar{\nu} = 1.555$ lead to precipitation.

The effect of the ageing reactions on the absorption spectrum of solution VII with $\bar{\nu} = 0.99$ is shown in Fig. 2. The band in the visible region shows, like the changes in pH, two opposite effects: first a small intensity increase followed, after about one week, by a decrease, the absorption maximum in both cases shifting towards lower wavelength. On the other hand, the very large increase in the ultraviolet absorption intensity suggests extensive decomposition of the complexes.

In the case of solution VII the formation of a very complex mixture of compounds during the ageing reactions was shown directly by separation on Sephadex columns. Some analytical results from this experiment, in which the percentage of cobalt in each fraction was determined by atomic absorption spectrometry (see Experimental), are shown in Table 1. It can be seen that at least six coloured fractions are formed in the solution after keeping it at 80 °C for about 12 days.

Table 1. Separation of the components of solution VII ($\bar{\nu} = 0.99$) at various stages of the ageing process. 0.2 – 0.6 M $NaClO_4$ solutions (pH ~3) were used as eluent.

Days	Colour of fractions	Co %
3.7	red	93
	orange-red	weak
	violet	~1
6.6	orange-red	13
	red	86
	reddish brown	2
	greyish	Residue
7.5	orange-red	31
	red	67
	brown	4
	greyish	Residue
12.5	violet	38
	orange-red	20
	reddish brown	2
	violet	20
	yellow	8
	brown	11
	greyish	Residue

Their presence is indicative of the existence of a number of new polymeric cobalt(III) complexes, although identification of these will require further work. However, the red fraction dominating during the first week of the reaction can be ascribed to the equilibrium mixture of the monomeric cobalt(III) tren complexes. It should be noted that an orange-red fraction appears to be the initial reaction product. This compound will be dealt with in more detail in the following section.

Results of the ageing experiments at room temperature. Portions of solutions Nos. I – X which were to be used in the experiments at 80 °C were set aside and used to follow the slow ageing reactions at room temperature. Changes in pH and extinction coefficients for solutions Nos. I – VII (having $\bar{\nu} \sim 0.5$ and ~1.0) after about 500 days are described in Table 2. All of these solutions have become considerably more acidic during the 16 months in which they have been maintained at room temperature. It is also noteworthy that the five solutions having $\bar{\nu} \sim 1$ and C_{Co} varying from 0.005 to 0.02 M have exhibited very similar pH- and extinction coefficient changes. It is known from the separation experiments on Sephadex columns that apart from the mononuclear complexes only one polymer is formed in the solutions having $\bar{\nu} \lesssim 1$. This polymer is probably identical with the orange-red complex formed initially in the experiments at 80 °C, and it should be mentioned that after 500 days solution I was found to contain ~21 % of the cobalt in the form of this polymer, ~75 % in the mononuclear aquahydroxo system, and only about 3 % as unidentified residue. By making certain assumptions it should therefore be possible to calculate the spectrum of the polymer from the data given in Table 2.

Calculation of the absorption spectrum of the orange-red polymer. In order to calculate the spectrum of the orange-red polymer it is necessary to know the number of protons per cobalt which are released during its formation. For this purpose we know that solutions VIII and IX in Table 5, both having $\bar{\nu} \sim 1.5$, become more acidic during the ageing process, whereas solution X having $\bar{\nu} = 1.9$ becomes more basic. We have therefore tentatively assumed that 1.6 protons per cobalt are released during the formation of the polymer from the diaqua tren complex.

If we denote the formal cobalt concentration in the polymer by x and the average number of protons released from the diaqua complex in the

Table 2. Extinction coefficients for the diaqua-, dihydroxo- and aquahydroxotren cobalt(III) ions, and the changes in pH and extinction coefficients during ageing of solutions I–VII with $\bar{v} \leqq 1.00$. $C_{NaClO_4} = 1.00$ M, 25 °C.

Solution	C_{Co}	$\bar{v}$	pH	days	560	530	510	490	450	430	410 nm
Diaqua	0.00809	0	~2	0	47.0	90.0	107.1	101.6	41.8	19.8	17.9
Dihydroxo	0.00798	2	~11	0	77.0	116.0	117.0	92.8	28.7	21.6	44.9
Aquahydroxo	–	1	–	0	69.0	103.4	110.0	95.0	38,2	27.7	40.1
I	0.01006	0.494	5.68	0	55.5	95.0	110.0	100.8	41.7	25.2	28.6
	0.01006	0.494	5.68	21	55.8	95.0	109.4	99.4	40.7	24.4	28.8
	0.01006	0.494	4.86	499	48.2	95.5	115.1	108.2	43.7	22.4	23.8
II	0.00994	0.591	5.83	0	58.5	97.5	110.0	100.1	36.0	30.6	30.6
	0.00994	0.591	4.93	499	49.3	98.8	118.5	111.9	44.3	22.2	24.6
III	0.00515	0.979	6.79	0	68.0	104.3	112.5	97.3	38.9	29.5	39.0
	0.00515	0.979	5.12	500	48.5	104.9	130.0	123.1	48.5	25.2	29.1
IV	0.00997	0.989	6.82	0	68.4	103.4	111.4	95.4	37.4	26.9	39.1
	0.00997	0.989	5.12	500	49.1	103.1	125.2	116.2	44.1	24.1	30.1
V	0.01992	0.997	6.85	0	67.3	103.4	112.4	95.2	36.9	26.9	38.7
	0.01992	0.997	5.12	500	52.1	(106)	–	–	48.2	26.2	32.6
VI	0.01007	0.969	6.75	0	68.0	104.0	113.0	98.3	39.1	28.3	37.2
	0.01007	0.969	5.19	499	51.7	106.2	131.0	122.0	46.9	26.0	31.5
VII	0.01028	0.991	6.83	0	62.2	98.8	106.1	–	36.4	25.6	37.0
	0.01028	0.991	6.70	20	68.5	104.8	113.0	97.8	40.4	30.3	43.5
	0.01028	0.991	519	470	49.8	104.4	129.2	122.5	48.5	27.2	32.6

equilibrium system of the monomers by $\bar{n}$, we obtain the following equation which is valid subject to the assumptions made:

$$\bar{v}C_{Co} = \bar{n}(C_o - x) + 1.6x$$

or

$$x = \frac{C_{Co}(\bar{v} - \bar{n})}{(1.6 - \bar{n})} \qquad (3)$$

From this expression x can be calculated. C_{Co} and $\bar{v}$ are known for the initial solutions, and $\bar{n} = \alpha_1 + 2\alpha_2$ as well as the fractions of diaqua (α_0), aquahydroxo (α_1) and dihydroxo (α_2) ions can be calculated from the pH in the aged solutions and the dissociation constants of the diaqua ion: $pK_1 = 5.69$, $pK_2 = 8.04$ (see Experimental).

If we furthermore introduce the molar extinction coefficients of the diaqua (ε_0), aquahydroxo (ε_1) and dihydroxo (ε_2) ions at a given wavelength, the extinction coefficient (ε_x) of the polymer at this wavelength can be calculated from eqn. (4).

$$x\varepsilon_x = C_{Co}\varepsilon_{av} - (C_{Co} - x)(\alpha_0\varepsilon_0 + \alpha_1\varepsilon_1 + \alpha_2\varepsilon_2) \qquad (4)$$

where ε_{av} is the experimental extinction coefficient for the aged solutions. The values of ε_0 and ε_2 given in Table 2 were measured directly for acidic and basic solutions, and the value of ε_1 was calculated from the average spectrum of the solutions having $\bar{v} \sim 0.99$ and the following distribution of the complexes: $\alpha_0 = 0.064$, $\alpha_1 = 0.882$, $\alpha_2 = 0.054$.

Results of the calculations for solutions I–VII are shown in Table 3. The fraction $\alpha_x = x/C_{Co}$ of the polymer varies from 0.25 for $\bar{v} \sim 0.5$ to as much as ~0.6 for $\bar{v} = 1$. The value $\alpha_x = 0.25$ for solution I is seen to be in good agreement with the value of 0.21 obtained in the previously-mentioned direct determination employing Sephadex columns. It should also be noted that there is fair agreement between the values of the extinction coefficients for the polymer calculated for the various solutions.

Table 3. Calculated extinction coefficients for the orange-red polymer in aged solutions of the cobalt(III) tren system.

No.	C_{Co}	$\bar{v}$	$\bar{n}$	x	560	530	510	490	450	430	410 nm
I	0.01006	0.494	0.129	0.00250	43	106	138	132	51	27	34
II	0.00994	0.591	0.147	0.00303	47	113	145	136	51	24.7	33
III	0.00515	0.979	0.214	0.00292	46	114	147	141	54.5	28.1	34
IV	0.00997	0.989	0.213	0.00565	46	109	136	127	46	25.6	35
V	0.01992	0.997	0.212	0.01130	52	122	142	140	53.5	29.2	41
VI	0.01007	0.969	0.242	0.00563	69	117	149	140	51.5	28.4	45
VII	0.01028	0.991	0.239	0.00575	46	113	146	140	55	31.5	40

Table 4. Calculated extinction coefficients for the hypothetical polymer in aged solutions of the cobalt(III) bis(ethylenediamine) system (based on data given by Rasmussen and Bjerrum [2]). Extinction coefficients of the *cis-trans* equilibrium mixture of the monomers are also given.

C_{Co}	$\bar{v}$	pH	$\bar{n}$	x	540	520	500	440	420	410	380 nm
0.01013	0.50	5.047	0.147	0.00246	93	126	124	24	21	31	134
0.00989	0.49	5.837	0.166	0.00223	106.5	143	140	24.6	22	34	104
0.00855	1.00	5.577	0.371	0.00438	93	125	124	26.7	24.4	26.2	101
0.00974	1.00	5.747	0.468	0.00457	92	124	123	24.7	22.5	32	96.6
				Average	96	129	128	25	22.4	30.8	109
				Diaqua	41.6	62.6	79.4	29.6	14.9	14.2	44.0
				Dihydroxo	63.6	71.0	65.6	20.6	24.2	37.0	73.6
				Aquahydroxo	61.5	71.2	71.1	32.9	37.4	46.2	73.6

An analogous calculation of the extinction coefficients of a corresponding hypothetical polymer in aged solutions of the cobalt(III) bis(ethylenediamine) system was made using the data given by Rasmussen and Bjerrum.[2] The results of such a calculation for solutions showing a sufficient change in pH during ageing for more than 400 days (solutions 2, 3, 5 and 6) are shown in Table 4. The values for the extinction coefficients of the equilibrated *cis/trans* diaqua, dihydroxo and aquahydroxo monomers used in the calculation are also also given. Eqns. (3) and (4) were used, and the calculations of α_0, α_1, α_2 and $\bar{n}$ were made using the following dissociation constants for the *cis/trans* equilibrated diaqua ions: $pK_1 = 5.81$, $pK_2 = 8.10$ (1 M KNO_3, 25 °C).[1]

The absorption spectrum and extinction coefficients estimated for the orange-red polymeric tren and ethylenediamine species are compared in Fig. 3 with the spectra of the corresponding diaqua and dihydroxo monomers.

Direct measurements of the spectrum of the orange-red tren cobalt(III) polymer. Data for the solutions used for these measurements are given in Table 5. The aged solutions are probably all very close to being at equilibrium. For example, it was observed that the spectrum of VIII did not change significantly after about 400 days. During the first year of ageing solutions VIII and IX, both having $\bar{v} \sim 1.5$, deposited a few milligrams of irregular, almost black crystals. These crystals were identified by analysis and by their solution spectrum (λ_{max} 622, 495 and 310 nm) as tris{[di-μ-hydroxo(tren)]cobalt(III)}-cobalt(III) perchlorate, analogous to the so-called "Werner's brown salts",[3] (see Experimental).

The aged solutions referred to in Table 5 were analyzed on Sephadex columns and the results are summarized in Table 6. The first fractions contained the orange-red polymer and the second fractions the equilibrium mixture of the monomers. It will also be noted that the orange-red polymer is so labile that a change in the pH of the eluent from ~5 to ~2 (in the case of solution IX) reduces the percentage of isolated polymer from 66 to 10 % and increases the percentage of the aquahydroxo mixture from 6 to 72 %. The violet labile third frac-

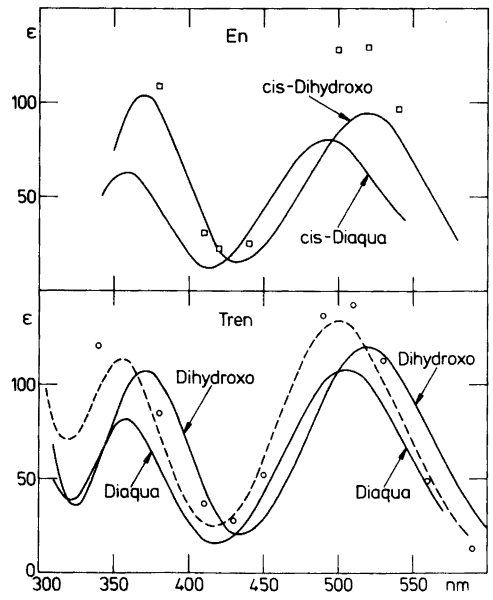

Fig. 3. The lower part of the figure shows the directly-measured spectrum of the orange-red polymer (– – –) and of the diaqua- and dihydroxo(tren)-cobalt(III) complexes. The O-points show the extinction coefficients (from Table 3) for the polymer calculated on the basis of data for the aged solutions.

The upper part of the figure shows the spectra of the *cis*-diaqua- and *cis*-dihydroxobis(ethylenediamine)cobalt(III) complexes, and the □-points show the calculated values (from Table 4) for the hypothetical polymer formed in aged bis(ethylenediamine)cobalt(III) solutions.

Table 5. Data for solutions of the aquahydroxo-(tren)cobalt(III) salt in 1 M $NaClO_4$ ($\bar{\nu} > 1$) aged at room temperature.

No.	C_{Co}	$\bar{\nu}$	pH	Time of ageing (days)
VIII	0.00942	1.437	7.43	0
	0.00866	–	6.42	866
IX	0.00965	1.555	8.14	0
	0.00936	–	6.70	816
X	0.00788	1.90	9.02	0
	0.00788	–	9.53	383

Table 6. Sephadex column separations of the components of the aged solutions referred to in Table 5. 0.15 – 0.7 M $NaClO_4$ solutions were used as eluents for VIII and IX, and 0.2 – 0.5 M NH_4Cl,NH_3 buffer solutions for X. Figures give the percentage of total cobalt present.

pH in eluent	VIII ~5	IX ~5	IX ~2	X ~9
1. Fraction, % Co	52	66	10	62
2. Fraction, % Co	44	6	72	11
3. Fraction, % Co	–	16	4	4
Left on column, % Co	5	12	14	23

tion obtained from solution IX could not be identified. The brownish-yellow third fraction obtained from solution X was found to contain tris{[di-μ-hydroxo(tren)]cobalt(III)}cobalt(III) complex. The amount of higher polymers and decomposition products left on the columns, which was negligible in the case of the more acidic solutions for $\bar{\nu} \lesssim 1$, is seen to increase with increasing basicity of the solutions.

The absorbance and the cobalt concentration of isolated fractions of the orange-red polymer were measured in several cases, and the extinction coefficients obtained are summarized in Table 7. It is especially noteworthy how well the extinction coefficients estimated indirectly from measurements on solutions I – VII (Table 3) agree with the directly measured extinction coefficients obtained for the isolated polymer fractions from solutions VIII – X. The best spectrum, especially in the ultraviolet part of the spectrum, was observed for a polymer fraction from solution X in which the cobalt concentration had been increased about 10 fold by repeated elution.[4] The lack of acid-base properties, and the essential constancy of the absorption spectrum (within $\leq 1\,\%$) of the orange-red polymer in the pH-range 4 to 9 was also established using this fraction. Unfortunately the cobalt concentration in this fraction was poorly determined and the extinction coefficients have therefore been fitted to the other data by assuming $\varepsilon_{510} = 130\ \mathrm{l\ mol^{-1}\ cm^{-1}}$.

The orange-red polymer is very labile at low pH as can be seen from the data shown in Table 6 and decomposes in acidic solution to give the diaqua-(tren) complex.

The solutions employed in the experiments discussed until now all had $C_{Co} \sim 0.01$ M. More pronounced polymer formation would be expected

Table 7. Comparison of calculated and directly measured molar extinction coefficients for the orange-red cobalt(III) tren polymer. C_{Co} in the isolated fractions varied from 0.3 to 0.7 mM in VIII and IX, to ~5 mM in X.

No.	Method	560	530	510	490	450	430	410 nm
VIII	Direct	52	100	125	122	62.5	46	54
IX	Direct	44	103	134	128	52	30	38
X	Direct	54	104	(130)	130	61	32	27
I–VII	Calc.	49	113	143	137	52	28	37

in solutions with a higher cobalt concentration and to examine this a solution having $C_{Co}=0.067$ M and $\bar{v}=1.5$ was studied. The results of the analysis of this solution after ageing for 380 days are shown in Table 8. It can be seen that as many as 7 fractions are obtained in this case. The first fraction contains the orange-red polymer and the second fraction the equilibrium mixture of the monomers. Of the other fractions only the 7th, showing maxima at 620, 426 and 308 nm, could be identified as containing the tris{[di-μ-hydroxo(tren)]cobalt(III)}cobalt(III) complex. Considerably more work will be necessary to identify (and if possible obtain solid salts of) the complexes present in the remaining fractions. In this connection it can be mentioned that an attempt to isolate the iodide salt of the labile orange-red polymer led to the precipitation after some hours of a small quantity of crystalline material which was analyzed for aquahydroxo(tren)cobalt(III) iodide.

DISCUSSION

The main result of the work described here is the observation of the slow formation of an orange-red polymeric complex in dilute (~0.01 M) solutions of the aquahydroxo(tren)cobalt(III) system. A stationary state involving up to 60 % of the cobalt in the form of the polymer is attained after about one year at room temperature. Furthermore, analysis of aged solutions of the monomeric system having a neutralization degree $\bar{v}\leq 1$ has shown that no polymers other than the orange-red species are formed at room temperature. Solutions with $\bar{v}\simeq 1.5$ become more acidic, and solutions with $\bar{v}=1.9$ more basic during the ageing process (see Table 5). Some formation of other complexes occurs in aged solutions with $\bar{v}\geq 1.5$, but there is nothing to indicate that tren functions as a tridentate ligand by the formation of the orange-red polymer. The cobalt(III) ions must therefore have only two coordination sites remaining for bridged complex formation and this restriction reduces the number

Table 8. Analysis of a more concentrated cobalt(III) tren solution ($C_{Co}=0.067$ M, $\bar{v}=1.5$) aged at room temperature for about 380 days. NaCl solution was used as eluent.

No. of fraction	Co %	Colour of fraction	pH	Band maxima (λ in nm)	$\varepsilon(\sim 500)/\varepsilon(\sim 360)$
1	~35	orange-red	4–9	500, 354	~1.25
2	~5	as monomers	4	500, 358	~1.32
			9	508, 358	~1.25
3	~30	red	4	508, 361	~1.3
			9	513, 362	~0.85
4	~25	violet	4–9	523, 360	~1.25
5	~1.3	red	4–9	510, ~365	
6	~1.2	blue	4–9	528, 368	~1.0
7	~0.5	brownish	4–9	620, 496, 308	
Residue	~2	red			

Table 9. Absorption maxima for some cobalt(III) tren complexes.

Complex	$\lambda_{max,1}$	ε	$\lambda_{max,2}$	ε	$\lambda_{max,3}$	ε	Reference
Orange polymer	500	134	355	113			This paper
Co tren$(H_2O)_2^{3+}$	505	107.5	360	81			This paper
	504	109	360	81			Scheidegger [5]
Co tren$(OH)H_2O^{2+}$	512	110	355	82			This paper
	513	100	355	65			Bösch [6]
Co tren$(OH)_2^{+}$	520	120	370	107			This paper
	520	119	370	117			Scheidegger [5]
{tren Co$(OH)_2$Co tren$\}_3^{4+}$	526	129	368	170	300	3890	Bösch [6]
Co{$(OH)_2$Co tren$\}_3^{6+}$	622	117	495	372	310	6020	This paper
	623	135	500	468	311	7410	Bösch [6]

of possibilities for the constitution of the complex. The proposal expressed by eqn. (5) corresponding

$$\text{Co tren}(OH)H_2O^{2+} + 2\text{Co tren}(OH)_2^{+} \rightarrow O(\text{Co tren OH})_3^{4+} + 2H_2O \quad (5)$$

to $\bar{\nu} = 1.67$ is consistent with the data. In Fig. 3 (lower part) the absorption spectrum of the polymer is compared with those of the diaqua and dihydroxo-(tren)cobalt(III) complexes. The data for the absorption maxima are given in Table 9 and it will be noted that the absorption maxima for the polymer are situated ~5 nm lower than those for the diaqua tren complex. This is consistent with the orange colour of the polymer and supports our assumption that the four Co – N bonds remain intact during the formation of the polymer. However, the relatively low absorption intensity in the ultraviolet may not support our assumption (*cf.* Table 9). Furthermore, although the ease with which the polymer is eluted from Sephadex columns is consistent with a relatively low charge per cobalt atom, we have still to explain the fact that the three OH-groups in the proposed polymer do not show acid-base properties in the pH-range 4 – 9. As regards the latter problem, it is possible that the compound has a structure in which the three OH-groups are strongly hydrogen bonded to each other. To bring them within bonding distances the angle Co – O – Co has to be 120 – 125°, compared to 115° in H_3O^{+}. In the basic chromium-(III) acetate, $O\left(Cr\left\{\begin{matrix}O\\O\end{matrix}\right>CCH_3\right\}_2H_2O\Big)_3^{+}$, the three chromium atoms and the central oxygen lie in the same plane,[7] but this is not a prerequisite in the case of diamagnetic cobalt(III) structures with no possibility of stabilization *via* π-bonding. A model of $O(\text{Co tren OH})_3^{4+}$ with a distance from cobalt to the central oxygen atom of 2.0 Å shows, however, that the structure is so compact that only with difficulty is it possible to place the coordinated NH_2-groups sufficiently far apart, *e.g.* 2.7 Å, from each other. On the other hand, the assumptions made are consistent with the fact that the polymer slowly undergoes changes when isolated from the solution in which it is formed and rapidly hydrolyzes to give the monomers in acidic solution.

The spectra of the diaqua- and dihydroxobis-(ethylenediamine)cobalt(III) complexes and the λ,ε-values calculated for the hypothetical polymer in this system from the data of Rasmussen and Bjerrum[2] (see Table 4) are shown in the upper part of Fig. 3. The data provide some support for the proposal that this polymer has a constitution similar to that of the orange-red polymer in the tren system, but this remains to be confirmed by direct isolation of the polymer.

EXPERIMENTAL

Preparation of complexes. Aquahydroxo(tren)-cobalt(III) perchlorate was prepared from the corresponding carbonato complex:

[Co tren(CO_3)]ClO_4.aq has been prepared previously by Scheidegger.[5] Our procedure was as follows: A solution of $CoCl_2.6H_2O$ (23.8 g, 0.1 mol) in a mixture of 30 % H_2O_2 (50 ml) and water (250 ml) was slowly added to solid $KHCO_3$ (100 g). The green mixture was heated and vigorously stirred. After 10 min solid tren.3HCl (25.4 g, 0.1 mol) was added in small portions. The solution became reddish-brown and after heating for 10 min all the solid had dissolved. The solution was then evaporated to about one half of its original volume and after cooling to room temperature three volumes of methanol were added. About 90 % of the KCl

was precipitated in this way and after filtration the methanol was removed from the solution by evaporation and the remaining chloride by adding 0.2 M $AgClO_4$ dropwise until precipitation ceased. The mixture was filtered and after adding 3.5 M $LiClO_4$ (100 ml) the solution was cooled in ice and the carbonato perchlorate precipitated by adding ethanol (500 ml). The dark red crystals of $[Co\ tren(CO_3)]ClO_4.2H_2O$ were washed with ethanol and dried in air. The crude product was purified as follows: 50 g of the salt was stirred mechanically with 150 ml of 99 % ethanol for 1 h in order to remove the remaining $LiClO_4$. After filtration the procedure was repeated twice.

$[Co\ tren(OH)H_2O](ClO_4)_2$. $[Co\ tren(CO_3)]ClO_4.2H_2O$ (40 g, 0.1 mol) was dissolved in the minimum volume of water at 80 °C and 5 M $HClO_4$ was then added dropwise until CO_2 evolution ceased. The solution was maintained at 80 °C for a further 30 min and allowed to cool. After addition of saturated $NaClO_4$ (20 ml) the ice-cold solution was slowly neutralized by addition of 2 M NaOH. At pH 5–6 $[Co\ tren(OH)H_2O](ClO_4)_2$ began to precipitate as red-violet crystals. Continuing with the neutralization 95–98 % of the salt could be precipitated. The crystals were washed with ethanol and recrystallized from water. *Anal.* Calc. for $Co\ tren(OH)H_2O(ClO_4)_2$: Co 13.42; C 16.14; H 4.82; N 12.76; Cl 16.15. Found: Co 13.39; C 16.26; H 4.79; N 12.81; Cl 15.94.

$Co\{(OH)_2Co\ tren\}_3(ClO_4)_6$, which separated from some of the aged solutions of the cobalt(III) tren monomers, has recently been characterized by Bösch[6] (see Table 9). The following preparative route has been devised by us: $Co(ClO_4)_2.6H_2O$ (18.0 g, 0.05 mol) was dissolved in water (25 ml) and tren (5.6 g, 0.0375 mol) was added and the dark red mixture was filtered to remove a slight precipitate of cobalt oxide. The solution was stirred vigorously and aerated for 2 h and was then placed in a refrigerator at 5 °C. After 5 days the precipitate of crude $Co\{(OH)_2Co\ tren\}_3(ClO_4)_6.aq$ (9.8 g) was isolated by filtration. The salt was recrystallized from water at 60 °C.

The dark brown irregular crystals were subjected to an X-ray analysis by Mrs. Eva Bang. They crystallize in the monolinic system with the unit cell dimensions $a=23.67$ Å, $b=13.47$ Å, $c=32.96$ Å and $\beta=98.22°$. Weissenberg photographs show an ordered-disordered structure and oscillation diagrams around the *b*-axis clearly show equatorial symmetry.

Solutions. The solutions of cobalt(III) tren complexes in 1 M $NaClO_4$ were prepared by weighing the complex salt and pipetting or titrating from stock solutions of $NaClO_4$ (5 M), $HClO_4$ and NaOH.

pH-Measurements. Hydrogen ion concentrations were measured relative to $10^{-3}-10^{-2}$ M solutions of $HClO_4$ in 1 M $NaClO_4$, using a Radiometer PHM 52 digital pH-meter. A selected Radiometer glass electrode (type 620 2 B) with the theoretical pH-dependence was used, and a 1 M NaCl/calomel electrode was employed as reference.

The acid dissociation constants of the diaqua(tren)-cobalt(III) complex were determined according to the method of Bjerrum and Rasmussen[1] from measurements of the hydrogen ion concentration in a number of solutions having $\bar{v}\sim0.5$ and $\bar{v}\sim1.5$. The following values were obtained: $pK_1=5.69$, $pK_2=8.04$ (1 M $NaClO_4$, 25 °C).

Spectrophotometric measurements. The absorption spectra were measured on a Cary 14 spectrophotometer with a thermostatted (25 °C) cell compartment. In a few cases a Cary 118 spectrophotometer was also used. Cells of pathlength 0.1 to 5 cm were used, the reference cells being filled with 1 M $NaClO_4$ solution.

Analysis. The Co(III) species in the aged solutions were separated by cation-exchange chromatography on columns of Sephadex SP C-25. When necessary the eluates were concentrated employing the technique used by Andersen *et al.*[4] The cobalt content in the various fractions was determined by atomic absorption spectrometry using a Perkin-Elmer, model 403, instrument.

Acknowledgements. This investigation was supported by a maintenance grant from "Statens Naturvidenskabelige Forskningsråd" to Dr. Eva Porzsolt which is gratefully acknowledged. Mrs. Eva Bang took part in some of the work. Our thanks are also due to Claus Schäffer for helpful discussions and to Dr. Martin Hancock for revising the English manuscript.

1. Bjerrum, J. and Rasmussen, S. E. *Acta Chem. Scand. 6* (1952) 1265.
2. Rasmussen, S. E. and Bjerrum, J. *Acta Chem. Scand. 9* (1955) 735.
3. Werner, A. *Ber. Dtsch. Chem. Ges. 47* (1914) 1977.
4. Andersen, P., Berg, T. and Jacobsen, J. *Acta Chem. Scand. A 29* (1975) 381.
5. Scheidegger, H. A. *Diss.*, No. 3878, Eidgenöss. Techn. Hochschule, Zürich 1966.
6. Bösch, J. *Diss.*, No. 4579, Eidgenöss. Techn. Hochschule, Zürich 1971.
7. Chang, S. C. and Jeffrey, G. A. *Acta Crystallogr. B 26* (1970) 673.

Received November 4, 1977.

Acta Chemica Scandinavica A 32 (1978) 329 – 332

Powder Diffraction Studies of the Ionic Conductor $K_{0.72}(In_{0.72}Sn_{0.28})O_2$

CLAUDE DELMAS[a] and PER-ERIK WERNER[b]

[a] Laboratoire de Chimie du Solide du C.N.R.S., Université de Bordeaux I, 351, cours de la Libération, F-33405 Talence-Cedex, France and [b] Department of Structural Chemistry, Arrhenius Laboratory, University of Stockholm, S-106 91 Stockholm, Sweden

The crystal structure of the sheet oxide $K_{0.72}(In_{0.72}Sn_{0.28})O_2$ has been investigated by profile analysis of a Guinier-Hägg powder diffraction record. The hexagonal unit cell has $a = 3.2314(4)$ Å, $c = 12.820(5)$ Å, $Z = 2$ and space group $P\bar{6}m2$. The structure consists of sheets of octahedra $(MO_2)_n$ (M = In,Sn) between which are inserted the potassium ions. It was found that the structure can be described as having the In and Sn atoms statistically distributed over two non-identical positions, which are 0.72 Å apart. The distribution of the potassium ions in two types of trigonal prisms has been studied. The conventional R value calculated from 32 structure factors is 0.128. Because of the limited amount of data and the statistical character of the structure, however, only the metal positions in the structure can be accurately described.

In connection with studies of ionic condustivity of new sheet phases in the KLO_2-MO_2 (L = In, Sc; M = Zr, Hf, Sn, Pb) systems,[1] structural studies of $K_{0.72}(In_{0.72}Sn_{0.28})O_2$ have been performed in order to correlate the ionic conductivity properties and the structural parameters. It has been concluded that these phases are isomorphous with the bronze $K_{0.67}CoO_2$. The potassium ions are located in trigonal prismatic sites between the $[(L,M)O_2]_n$ sheets and show a high mobility (*cf.* Fig. 1). The conductivity is better than that of β-alumina in its usual utilization range, *i.e.* above 200 °C.

Because of the equal number of electrons around In^{3+} and Sn^{4+} it was expected that the distribution of the potassium ions could be studied in a KMO_2 model of formula $K_{0.72}(In_{0.72}Sn_{0.28})O_2$. Furthermore, at room temperature the conductivity of the compound is relatively low, $5.6 \times 10^{-7} \Omega^{-1}$ cm^{-1}.

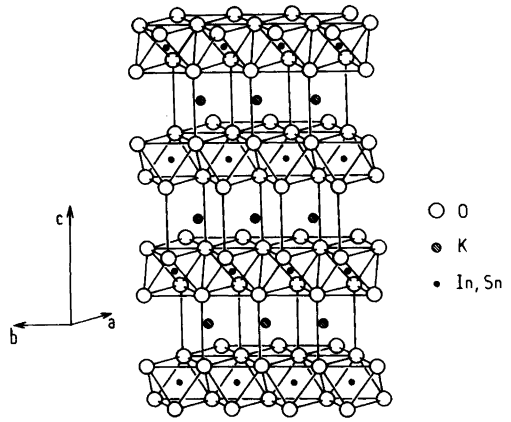

Fig. 1. The arrangement of $(In,Sn)O_6$ octahedra and KO_6 trigonal prisms in $K_{0.72}(In_{0.72}Sn_{0.28})O_2$. The potassium ions are shown in one of the two possible types of trigonal prisms.

Therefore, the potassium ions were expected to be fixed at definite positions at this temperature and in a zero electric field. Due to lack of single crystals, however, the study had to be based on powder data. Since the primary interest in this study was to obtain information about the metal atoms in the structure, X-ray rather than neutron diffraction data were collected.

EXPERIMENTAL

The sample $K_{0.72}(In_{0.72}Sn_{0.28})O_2$ used in this study was prepared and characterized in the way described in Ref. 1.

A powder diffraction photograph was taken in a focussing camera of the Guinier-Hägg type, with strictly monochromatized Cu$K\alpha_1$ radiation ($\lambda = 1.54056$ Å). Silicon ($a = 5.430880(34)$ Å at 25 °C)[2] was added as an internal theta-standard. Since the sample was strongly hygroscopic it had to be protected from moisture by being sealed between two pieces of adhesive tape with low X-ray absorption coefficient. The exposure time was 1 h, and single-coated film was used so that a back-layer profile would be avoided and the background diminished, thus improving the signal-to-noise ratio. Peak positions and step-scan intensities were evaluated by an automatic film-scanner system.[3] The 2θ-step used was 0.03169° and the upper limit in 2θ was 85.7°.

From the similarities between the observed pattern and a diffraction pattern obtained from $K_{0.67}CoO_2$[4] approximate unit cell dimensions were derived. The least-squares[5] refined hexagonal cell dimensions, $a = 3.2314(4)$ Å and $c = 12.820(5)$ Å, were derived from peak positions obtained by a parabolic correction curve calculated from the positions of the internal standard lines. The observed and calculated powder pattern is given in Table 1. The correctness of the unit cell is confirmed by a de Wolff figure of merit,[6] $M = 102$, for the 14 strongest observed lines with indices obtained from the most closely approximating calculated theta values, thus disregarding the overlaps.

Table 1. X-Ray powder diffraction data for $K_{0.72}(In_{0.72}Sn_{0.28})O_2$. Cu$K\alpha_1$ radiation ($\lambda = 1.54056$). Internal standard; Si ($a = 5.43088$ Å at 25 °C).

d_o (Å)	d_c (Å)	$h\,k\,l$	I_o
6.411	6.410	0 0 2	1588
3.204	3.205	0 0 4	406
2.7986	2.7985	1 0 0	1091
2.5643	2.5647	1 0 2	1868
2.3398	2.3411	1 0 3	235
2.1072	2.1080	1 0 4	1168
1.6992	1.6982	1 0 6	315
1.6159	1.6157	1 1 0	749
1.5669	1.5667	1 1 2	588
1.4428	1.4427	1 1 4	402
1.3994	1.3992	2 0 0	253
	1.3671	2 0 2	
1.3669	1.3669	1 1 5	381
1.2822	1.2823	2 0 4	353
	1.2820	0 0 10	
1.1703	1.1706	2 0 6	170

STRUCTURAL STUDIES

a. Indium and tin. The structure was studied by means of the Rietveld profile analysis procedure.[7] The original Rietveld program which was written for neutron diffraction data has been rewritten for Guinier data[8] and now further extended for simultaneous structure refinement of two phases present in a powder sample.[9]

Fractional atomic coordinates derived from the study of $K_{0.67}CoO_2$[4] were used as starting parameters for a number of different refinements in space group $P6_3/mmc$. It was not found possible, however, to reach any R_F $(= \Sigma|\sqrt{I_{obs}} - \sqrt{I_{calc}}|\Sigma\sqrt{I_{obs}})$ value below 0.23 using this space group. Furthermore, efforts to refine an (In,Sn)-position in the non-centric space group $P\bar{6}m2$ failed. The most notable differences between observed and calculated structure factors were found for the reflections (110), (112), (114) and (202). The calculated intensities for these reflections were always considerably less than the observed values. No changes in potassium or oxygen parameters could in any significant way reduce the R_F value. The different ionic radii for In^{3+}, 0.790 Å,[10] and Sn^{4+}, 0.690 Å,[10] made it conceivable, however, that these atoms were situated in two non-identical positions inside the oxygen octahedra, both with site position 2(*h*) in space group $P\bar{6}m2$. A least-squares profile refinement of the In and Sn positions converged at $R_F = 0.17$ with the In and Sn coordinates (1/3, 2/3, 0.244) and (1/3, 2/3, 0.301), respectively (*cf.* Table 2). Since the atomic scattering factors for In^{3+} and Sn^{4+} are almost identical it is impossible to prove from the diffraction data that In and Sn are not mixed within each of the two positions. If the two kinds of ions are assumed to be differently situated, as

Table 2. Atomic coordinates and occupancies.

Atom	Point set	x	y	z	Occupancy
In	2(h)	1/3	2/3	0.239(1)	0.72
Sn	2(h)	1/3	2/3	0.295(2)	0.28
K1	1(c)	1/3	2/3	0	0.117(8)
K2	1(d)	1/3	2/3	1/2	0.117(8)
K3	1(a)	0	0	0	0.243(8)
K4	1(f)	2/3	1/3	1/2	0.243(8)
O1	2(i)	2/3	1/3	0.108[a]	1.0
O2	2(g)	0	0	0.316[a]	1.0

[a] These parameters should not be considered as oxygen coordinates (*cf.* text).

described above, the observed occupancies correspond to the stoichiometry. A mixing also seems unlikely because of the differences in radius and charge of the ions. The obtained z-coordinate values for In^{3+} and Sn^{4+} certainly tend to decrease the electrostatic repulsion between the ions.

As was seen from the observed intensity curve no super-structure lines are present in the pattern. Thus it may also be concluded that the In and Sn atoms despite their particular positions are statistically distributed within the structure without any detectable long-range order. Furthermore, from charge considerations it may be expected that they are also statistically distributed within the $[(L,M)O_2]_n$ sheets.

b. Oxygen. Because of the limited amount of data available, it was not possible to refine the oxygen positions. The difficulties were aggrevated by the expected short-range order of the structure. The relatively large difference, 0.72 Å, along the c-axis between the two statistically occurring In^{3+} and Sn^{4+} positions should give rise to more than one oxygen position within each one of the point sets 2(*i*) and 2(*g*). Furthermore, although the potassium ions are all in special positions, having no variable positional parameter, the statistical distribution of them, as concluded from the ionic conductivity,[1] makes it extremely difficult to interpret any formally refined oxygen coordinate as a real positional parameter. Therefore, the formal "oxygen coordinates" obtained from least-squares refinements of the structure and given in Table 2, should not be regarded as simple arithmetic means of two discrete oxygen positions. It should be kept in mind that the statistical nature of all structural parameters, not only the In^{3+} and Sn^{4+}, will affect the structure factors.

c. Potassium. There are two different types of trigonal prismatic sites available for the potassium ions between the $[(In,Sn)O_2]_n$-sheets. The sites are schematically illustrated in Fig. 2. If K^+ is located in positions 1(c) or 1(d), referred to as type A below, trigonal KO_6 prisms share faces with InO_6 and/or SnO_6 octahedra. If K^+ is located in 1(a) or 1(f), called type B positions, the trigonal prisms share edges with InO_6 and/or SnO_6 octahedra. Since there is no variable positional parameter in any one of the four possible potassium sites it was thought that the statistical distribution of the ions between the two types of sites could be derived from the diffraction data.

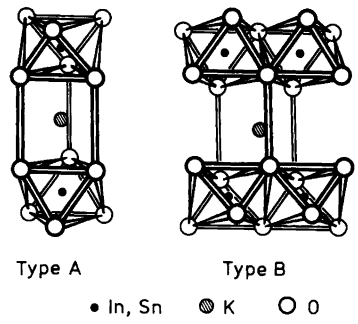

Fig. 2. Type A and B arrangements of trigonal KO_6 prisms and $(In,Sn)O_2$ octahedra in $K_{0.72}(In_{0.72}Sn_{0.28})O_2$.

With the composition of the compound fixed and the occupancies of the positions 1(c), 1(d) (type A) and 1(a), 1(f) (type B) assumed pairwise equal (*i.e.* the structure containing the same number of potassium ions of each type in each layer) a least-squares profile refinement was made. The formal "oxygen atoms" were held in average positions obtained from earlier refinements, and the refinement was considered complete when all shifts were less than 10 % of the standard deviation of the corresponding parameter. The parameters refined were the z coordinates for In and Sn, one parameter describing the distribution of the potassium ions (*i.e.* occupancy parameters with a constraint function), one isotropic over-all temperature factor, one scale factor, one asymmetry and two half-width parameters. The final R_F-value obtained was 0.128. The corresponding conventional R-value calculated from the structure was found to be identical with the R_F-value. The observed and calculated structure factors are given in Table 3. The structure factors were derived from the observed and calculated profile intensities.

The over-all temperature factor obtained was -1.6 Å^2. No physical significance, however, can be given to the negative "temperature factor" because of the strong correlations between absorption, scale factor and temperature factor.[9]

From the occupancy factor obtained it may be concluded that approximately 1/3 of the potassium ions occupy type A and 2/3 type B positions. This is also in agreement with the conclusion that the type B positions corresponding to longer In,Sn···K distances, should be more electrostatically favourable (*cf.* Fig. 2). It may also be mentioned that

Table 3. Observed and calculated structure factors obtained from least-squares profile analysis refinement of X-ray Guinier-Hägg powder diffraction data for $K_{0.72}(In_{0.72}Sn_{0.28})O_2$.

$(h\,k\,l)$	$\lvert F_{obs}\rvert$	$\lvert F_{calc}\rvert$	$(h\,k\,l)$	$\lvert F_{obs}\rvert$	$\lvert F_{calc}\rvert$
0 0 2	63	69	1 1 4	69	71
0 0 4	71	80	2 0 0	75	68
1 0 0	80	73	2 0 1	3	4
1 0 1	9	4	1 0 8	35	36
1 0 2	81	80	2 0 2	67	72
1 0 3	32	25	1 1 5	15	16
0 0 6	66	30	2 0 3	15	19
1 0 4	77	72	1 1 6	36	29
1 0 5	7	15	2 0 4	67	66
1 0 6	62	52	0 0 10	6	6
1 1 0	117	115	1 0 9	15	18
1 1 1	1	1	2 0 5	5	13
0 0 8	46	47	1 1 7	14	9
1 1 2	77	59	2 0 6	54	49
1 0 7	19	14	1 0 10	35	26
1 1 3	12	10	1 1 8	44	45

various least-squares profile refinements using other "oxygen parameters" show no significant deviations from the remaining structural parameters given in Table 2.

In order to illustrate the sensitivity of the method used for determination of the potassium distribution a number of least-squares profile refinements with various fixed potassium occupancy parameters were carried out. The R_F values obtained with K^+ situated entirely at A or B were 0.167 and 0.263, respectively. The minimum value $R_F = 0.128$ was found for 67.5 % K^+ at B and 32.5 % at A.

DISCUSSION

The conductivity of the material is caused by a two-dimensional transport of potassium ions between the $[(In,Sn)O_2]_n$ sheets. This means that the potassium ions of the structure model illustrated in Fig. 1 must shift between the type A and B positions during the transport. As discussed above, however, the type A positions are less electrostatically favourable than the type B positions. This effect is probably enhanced if any of the neighbouring MeO_6 octahedra contain Sn^{4+} because of this ion's large deviation from the ideal position $z = 0.25$. As a consequence it seems likely that the mobility of K^+ in such type A positions is strongly reduced. This may also explain why the activation energy is as high as 0.69 eV,[1] *i.e.* why the conductivity is small at lower temperatures.

We could not find any correlation between the probability of presence of the In^{3+} and Sn^{4+} ions in the adjacent sites and the distribution of potassium between the type A and B positions. It is tempting to correlate the shift of the z-coordinates of In^{3+} and Sn^{4+} from the ideal value with the neighbourhood of the K^+ ions, but the existence of only one cobalt position in the CoO_2 sheets of the analogous metallic $K_{0.67}CoO_2$ phase seems to indicate that the driving force of the shift is not repulsion by K^+ ions, but rather the differences in charge and size of the In^{3+} and Sn^{4+} ions.

Acknowledgements. This investigation has been performed in connection with a research program on chemical storage of energy sponsored jointly by the Swedish Natural Science Research Council and the Centre National de la Recherche Scientifique. One of us (C.D.) is grateful for the support which has made possible his stay at the Arrhenius Laboratory. The interest shown and encouragement given by Professors P. Hagenmuller and A. Magnéli are highly appreciated The skilful technical assistance of Mr. L. Göthe and Mr. S. Salomé is gratefully acknowledged.

REFERENCES

1. Delmas, C., Fouassier, C., Réau, J.-M. and Hagenmuller, P. *Mater. Res. Bull. 11* (1976) 1081.
2. Hubbard, C. R., Swanson, H. E. and Mauer, F. A. *J. Appl. Crystallogr. 8* (1975) 45.
3. Malmros, G. and Werner, P.-E. *Acta Chem. Scand. 27* (1973) 493.
4. Delmas, C., Fouassier, C. and Hagenmuller, P. *J. Solid State Chem. 13* (1975) 165.
5. Werner, P.-E. *Ark. Kemi 31* (1969) 513.
6. De Wolff, P. M. *J. Appl. Crystallogr. 1* (1968) 108.
7. Rietveld, H. M. *J. Appl. Crystallogr. 2* (1969) 65.
8. Malmros, G. and Thomas, J. O. *J. Appl. Crystallogr. 10* (1977) 7.
9. Werner, P.-E., Salomé, S., Malmros, G. and Thomas, J. O. *J. Appl. Crystallogr. To be published.*
10. Shannon, R. D. and Prewitt, C. T. *Acta Crystallogr. B 25* (1969) 925.

Received December 5, 1977.

Acta Chemica Scandinavica A 32 (1978) 333–343

Studies on the Hydrolysis of Methylmercury(II) and its Complex Formation with Some Aliphatic Carboxylic and Aminocarboxylic Acids

MOHAMMAD JAWAID,[a] FOLKE INGMAN[a] and DJIET HAY LIEM[b]

[a] Department of Analytical Chemistry and [b] Department of Inorganic Chemistry, The Royal Institute of Technology (KTH), S-100 44 Stockholm, Sweden

The hydrolysis of methylmercury(II), the protonation of formic acid and acetic acid, glycine, alanine and valine (=HL) and their complex formation with methylmercury(II) ions have been studied by a potentiometric method at 25 °C and 1.0 M $(Na,H)NO_3$ ionic medium. The data were computer analyzed using the ETITR-LETAGROP program and indicate the formation of the species MeHgOH, $(MeHg)_2OH^+$ and 1:1, 1:2 and 2:1 complexes between $MeHg^+$ and the acid HL.

The following values of log K were obtained for the equilibrium reactions: $MeHg^+ + H_2O \rightleftharpoons MeHgOH + H^+$, −4.686; $2MeHg^+ + H_2O \rightleftharpoons (MeHg)_2OH^+ + H^+$, −1.725; $MeHgOH(s) \rightleftharpoons MeHg^+ + OH^-$, −13.66 (in water); $MeHg^+ + L^- \rightleftharpoons MeHgL$, 2.681 (formic acid), 3.204 (acetic acid), 7.518 (glycine), 7.516 (α-alanine), 7.268 (DL-valine); $MeHg^+ + 2L^- \rightleftharpoons MeHgL_2^-$, 9.468 (glycine), 9.450 (α-alanine), 9.157 (DL-valine); $2MeHg^+ + L^- \rightleftharpoons (MeHg)_2L^+$, 5.279 (acetic acid).

Organomercurial compounds have been shown to cause hazardous environmental pollution. The harmful ecological effects of these substances and their metabolism in nature have previously been reported.[1-3] Although the use of these substances as fungicides in seed dressing has been discontinued in many countries including Sweden, because of their toxic nature, yet there is experimental evidence that inorganic and metallic mercury from the industrial waste is partially transformed into methylmercury and dimethylmercury by certain bacteriological processes.[4,5] The organic form of mercury is easily absorbed and accumulated by the living organisms and thus it may endanger the health of man and animals.

Studies on the complex formation between these compounds and the ligands that are commonly found in nature are of importance for a better understanding of their ecological behaviour. The equilibria of complex formation between methylmercury(II) and certain organic and inorganic ligands have been studied by different methods, such as ion-exchange,[6] solvent extraction,[7-10] polarography,[7] NMR,[11,12] conductance measurements[13] and potentiometry.[14-16] In our previous publications, we have reported the results of solvent extraction studies on the complex formation between methylmercury and some ligands that are commonly present in natural waters, such as chloride,[8] bromide[9] and phosphate.[10] However, only a few studies on the complex formation of methylmercury with organic ligands have been reported in the literature.[7,11]

In the present paper we report the results of the hydrolysis of methylmercury(II) and its complex formation with some model aliphatic carboxylic acids, *i.e.* formic and acetic acid and the aminocarboxylic acids glycine, alanine and valine in 1.0 M $NaNO_3$ ionic medium. These acids were chosen as model ligands, since they contain functional groups which are of analytical and biochemical interest. In preliminary experiments we also studied, in the same medium, the protonation of the acids by potentiometric titration, and the equilibrium constants evaluated by LETAGROP[17] were used in subsequent calculations where the complex formation of methylmercury(II) ions with these acids was considered.

PREVIOUS WORK

Formation of methylmercury(II) and other alkylmercury(II) hydrolysis species. Maynard and Howard[18] – as well as Johns *et al.*[19] – from conductance data of MeHgOH aqueous and ethanol solutions assumed the formation of the MeHgOH complex. Schwarzenbach and Schellenberg[15] explained their potentiometric data in 0.1 M KNO_3 medium with the formation of the species MeHgOH and $(MeHg)_2OH^+$. They were the first to report the formation of dimeric hydrolyzed species by EMF measurements of systems with varying $C_{MeHg} = 5.85 \times 10^{-4}$ to 2.19×10^{-2} M. Zanella *et al.*[16] reported the formation of only RHgOH species in 0.1 M KNO_3 for R = Me, Et, Pr and Bu. Waugh *et al.*[20] assumed the formation of RHgOH (R = Me, Et, and Ph) to explain their potentiometric titration data. Libich and Rabenstein[11] from NMR data of MeHg(II) solutions of different pH, found indications of the formation of MeHgOH and $(MeHg)_2OH^+$ species. Using NMR and Raman spectroscopy, Rabenstein *et al.*[12] reported evidence for the formation of MeHgOH and $(MeHg)_2OH^+$ species in (Na.H)ClO_4 medium. Ingman and Liem[10] explained their distribution data of MeHg(II) in the two-phase system *o*-xylene/1.0 M (Na,H)(Cl,NO_3,-PO_4) by the formation of MeHgCl in both phases and MeHgOH and $MeHgHPO_4^-$ in the aqueous phase.

Woodward *et al.*[21] studied the Raman spectra of methylmercury(II) hydroxide solution in nitrate medium and explained their data by assuming the formation of the species MeHgOH and $(MeHg)_2OH^+$ which they assigned to the bands at 577 and 511 cm^{-1}.

Formation of methylmercury(II) complexes with alkylcarboxylic acids and aminocarboxylic acids. Simpson[7] from polarographic data assumed the formation of the complex MeHgAc between methylmercury(II) and acetate ions, the species $MeHgHY^{2-}$, $MeHgY^{3-}$ and $(MeHg)_2Y^{2-}$ with EDTA (= H_4Y) and the complex MeHgSR with cysteine and glutathione (RSH) and $MeHgNH_2$(his) with histidine. Libich and Rabenstein[11] used NMR technique to study the pH dependence of the chemical shift of the methyl group of CH_3Hg(II) and that of the protons of several derivatives of alkylcarboxylic acids in aqueous solution of approximately 0.4 M ionic strength. These authors explained their experimental data assuming the formation of 1:1 complexes between methylmercury(II) and all the carboxylic acids they studied.

EXPERIMENTAL

$NaNO_3$ (*p.a.* Merck) was dried at 110 °C and used without further purification. NaOH, HNO_3 (*p.a.* Merck) stock solutions were prepared and standardized as described previously.[9] Formic acid, acetic acid (*p.a.* Merck) and glycine, alanine and DL-valine (Merck, Biopur grade) were used without further purification and assayed potentiometrically by the method described by Pehrsson and coworkers.[22] Boiled double distilled water was used to prepare all solutions.

EMF titration. The cell used for the EMF titration may be represented as follows:

Reference half cell	v ml 1.0 M Na,(OH,NO_3) / V_0 ml 1.0 M (Na,H,MeHg)(L,NO_3)	Glass electrode

where L is the ligand anion of the organic acid HL, v the volume of titrant added and V_0 the initial volume in the titration vessel. Additions of titrant were made with a pneumatically operated burette (AGA, Sweden) which can deliver any volume between 0.5 to 5.0 ml with a high degree of reproducibility.

The $[H^+]$ is measured potentiometrically using a combined glass electrode (Ingold 2293) with a built-in reference half cell of saturated KCl solution/Ag,AgCl in conjunction with a digital voltmeter (Systemteknik Type S1016H). In the Nernst relationship (1) the E'_0 and j for correction of the pH dependent parts of the liquid junction potential and the activity coefficients were determined, as a rule, before and after each titration as described elsewhere.[22] The E'_0 value found before and after each titration was constant within 0.1 mV and $j = -19$ mV/M.

$$E = E'_0 + 59.156 \log [H^+] + j[H^+] \quad (1)$$

During the experiment, the solution was protected from atmospheric CO_2 by bubbling N_2 gas that passed through "Ascarite" and 1.0 M $NaNO_3$. All experiments were carried out in a thermostated room at 25.0±0.5 °C and the titration vessel immersed in a thermostatic bath of 25±0.05 °C.

Chemical model. We assume the formation of the species $(H^+)_p(MeHg^+)_q(HL)_r$ with the equilibrium constant

$$K_{pqr} = [(H^+)_p(MeHg^+)_q(HL)_r]\text{-}[H^+]^{-p}[MeHg^+]^{-q}[HL]^{-r} \quad (2)$$

A species may thus be characterized by the set of numbers (p,q,r), *e.g.* $(MeHg)_2OH^+$ will be denoted by (−1,2,0) and MeHgL by (−1,1,1). The formation of $(MeHg)_2OH^+$ is given by (8) and that of MeHgL

by the reaction: $MeHg^+ + HL \rightleftharpoons MeHgL + H^+$; $K_{-111} = [MeHgL][H^+][MeHg^+]^{-1}[HL]^{-1}$. For the reagent components MeHg(II) and HL the following material balance equations are valid:

$$C_{MeHg} = [MeHg^+] + \Sigma q K_{pqr}[H^+]^p[MeHg^+]^q[HL]^r \quad (3)$$

$$C_L = [HL] + \Sigma r K_{pqr}[H^+]^p[MeHg^+]^q[HL]^r \quad (4)$$

$$C_H = [H^+] + \Sigma p K_{pqr}[H^+]^p[MeHg^+]^q[HL]^r \quad (5)$$

Given the values of $[H^+]$, C_{MeHg}, C_L and the set of constants K_{pqr} for the formation of the species (p,q,r), we can calculate for each point the values for $[MeHg^+]$ and $[HL]$ from (3) and (4) and $C_{H(calc)}$ from (5). In the ETITR-LETAGROP program this is calculated using the procedure BDTV.[23] In the EMF titration the following applies for the proton excess:

$$C_{H(exp)} = (C_H^* V_0 - C_{OH}^* \cdot v)/(V_0 + v) \quad (6)$$

where C_H^* = the initial molarity of acid in the titration vessel,
C_{OH}^* = the molarity of NaOH in the titrant,
V_0 = the initial volume of solution in the titration vessel,
v = the volume of titrant added.

Computer analysis of the data. The data have been computer analyzed by the ETITR-LETAGROP program. In this program for the assumed set of complexes $(H^+)_p(MeHg^+)_q(HL)_r$, the program adjusts the set of constants $K_1, K_2 \ldots K_n$ for their formation so as to minimize the error-square sum $U = \sum_1^{Np} (y_{calc} - y_{exp})^2$. Np represents the number of experimental points, y a parameter which is a function of the equilibrium constants $K_1, K_2 \ldots$ and the known experimental parameters, such as C_{MeHg}, C_L, $\log [H^+]$. In ETITR-LETAGROP with Typ = 1, we minimize the square-sum of the error $\Delta H = H_{calc} - H_{tot}$, where H_{calc} is calculated from (5) and H_{tot} from (6). The "best" model accepted, is the one which gives the least error-square sum, U_{min}, and within the limit of the experimental errors gives the simplest description of the data. Once the "best" model has been found, one can make use of the HALTAFALL program,[23] to calculate titration or distribution curves for the given reaction conditions.

RESULTS

The primary data are available on request from the authors (F.I. or D.H.L.).

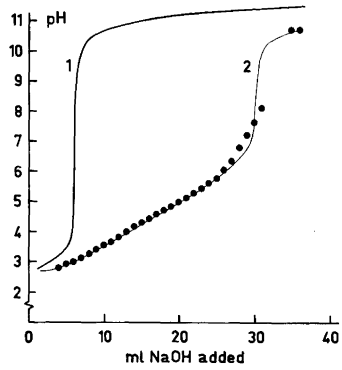

Fig. 1. Titration of 100.04 ml solution S against v ml 1.0 M $Na(OH,NO_3)$, $[OH] = 0.033294$ M. The initial composition of S is 8.002×10^{-3} M $MeHgNO_3$, 1.994×10^{-3} HNO_3, 0.990 M $NaNO_3$. The drawn curves have been calculated assuming in one case no formation of $MeHg(II) - OH^-$ species (Curve 1) and in another case the formation of MeHgOH and $(MeHg)_2OH^+$ species with the equilibrium constants given in Table 1 (Model II, Curve 2).

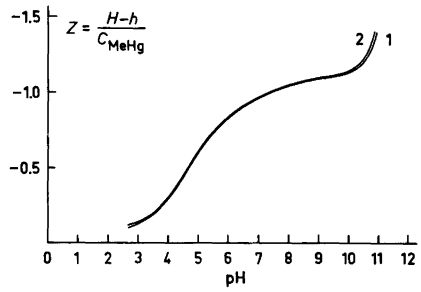

Fig. 2. Titration of 1.0 M $(H,Na,MeHg)NO_3$ against 1.0 M $Na(OH,NO_3)$ given as Z, the average number of OH bound per MeHg(II), *versus* pH. The initial concentration of $MeHgNO_3$ in the titrated solution is 8.002×10^{-3} M (Curve 1) and 4.804×10^{-3} M (Curve 2).

Formation of methylmercury(II) hydrolyzed species. EMF titration data for the hydrolysis were taken at different concentrations of methylmercury. In Fig. 1, two titration curves are shown. The curve marked 1 is a normal acid-base potentiometric titration, and the one marked 2 represents the same titration conditions, but with methylmercury(II) ions present in the solution. Comparing the two titration curves, one can clearly observe the higher buffer capacity at low pH-values of the solution containing methylmercury(II) ions, indicating the

Table 1. Equilibrium constant log K_{pq} for the formation of $(H^+)_p(MeHg^+)_q$ species in 1.0 M (Na.H)(NO_3) ionic medium at 25 ± 0.05 °C for various assumptions of chemical models which minimize the error-square sum $U = \sum_1^{89}(H_{calc} - H_{exp})^2$. The limits given correspond approximately to log $[K \pm 3\sigma(K)]$.

Model No.	Equilibrium reactions	log $(K \pm 3\sigma)$	U_{min}	σ(H)
I	$MeHg^+ + H_2O \rightleftharpoons MeHgOH + H^+$	-4.648 ± 0.130	29.373	0.577
II	$MeHg^+ + H_2O \rightleftharpoons MeHgOH + H^+$ $2MeHg^+ + H_2O \rightleftharpoons (MeHg)_2OH^+ + H^+$	-4.686 ± 0.045 -1.725 ± 0.090	2.257	0.161
III	$MeHg^+ + H_2O \rightleftharpoons MeHgOH + H^+$ $2MeHg^+ + H_2O \rightleftharpoons (MeHg)_2OH^+ + H^+$ $3MeHg^+ + 2H_2O \rightleftharpoons (MeHg)_3(OH)_2{}^+ + 2H^+$	-4.688 ± 0.057 -1.728 ± 0.102 -5.638 max. -4.410	2.226	0.162

formation of hydrolyzed methylmercury(II) species. In Fig. 2 the number of OH^- bound per MeHg(II), $Z = (H_{tot} - h)/C_{MeHg}$, h denoting the concentration of free hydrogen ions, is plotted as a function of *pH*. As can be seen, the Z curve levels off with increasing *pH* to a limiting value, indicating the predominant formation of the MeHgOH species. Furthermore, the Z-curves for different C_{MeHg} values (8.002×10^{-3} M and 4.801×10^{-3} M) do not fully coincide over the pH range studied, which indicates the additional formation of polynuclear methylmercury(II) hydrolyzed species. In Table 1, we summarize the results of the computer calculations for the formation of $(H^+)_p(MeHg^+)_q$ species, using $Np = 89$ points. Model No. 1, in which the formation of methylmercury(II) hydrolyzed species, MeHgOH only, is assumed, gives a large error-square sum ($U_{min} = 29.373$, $\sigma(H) = 0.577$) compared with the other models. Model No. 2, assuming the formation of MeHgOH and $(MeHg)_2OH^+$, seems to give the best description of the data with $U_{min} = 2.257$ and $\sigma(H) = 0.161$. Model No. 3, with the additional formation of $(MeHg)_3(OH)_2^+$ species, does not give a significant improvement to U or σ(H). Moreover, the standard deviation, $\sigma(K)$, found for the formation constant of $(MeHg)_3(OH)_2^+$ species is higher than the value of the constant K itself, $[\sigma(K) = 5.30K]$, thus indicating that no such species is formed under the present experimental conditions.

We may thus conclude that our data can be explained by assuming the formation of species MgHgOH and $(MeHg)_2OH^+$ with the following equilibrium constants:

$$MeHg^+ + H_2O \rightleftharpoons MeHgOH + H^+$$
$$\log (K \pm 3\sigma) = -4.686 \pm 0.045 \qquad (7)$$

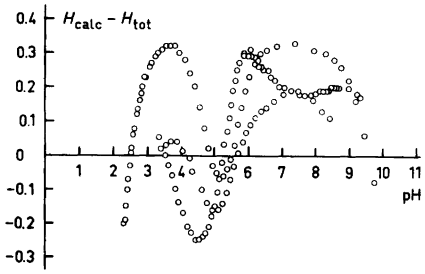

Fig. 3. The distribution of the error $(H_{calc} - H_{tot})$ in the titration of 1.0 M (H,Na,MeHg)NO_3 against 1.0 M Na(OH,NO_3) solution as a function of pH. The error $(H_{calc} - H_{tot})$ has been calculated assuming the formation of the species MeHgOH and $(MeHg)_2OH^+$ with the equilibrium constants given in Table 1 (Model II).

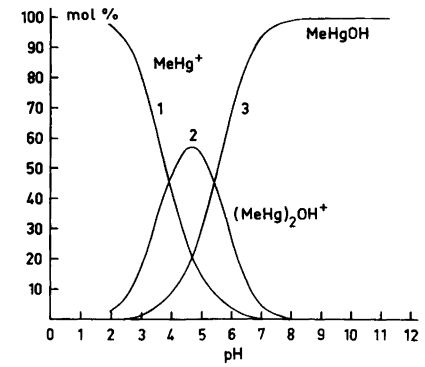

Fig. 4. The mol % of the different MeHg(II) species in 1.0 M (H,Na,MeHg)(NO_3OH) solution as a function of pH for $C_{MeHg} = 8.00 \times 10^{-3}$ M. The curves have been calculated assuming the formation of MeHgOH and $(MeHg)_2OH^+$ species with the equilibrium constants given in Table 1, Model II).

Table 2. Solubility of MeHgOH(s) in water at 25 °C.

$-\log [H^+]$	C_{MeHg^+} (mol/l)	$[MeHg^+]$ (calc. from eqn. 11)	$\log K_{so}$
8.80	0.0598	2.832×10^{-9}	−13.75
12.46	0.1142	8.562×10^{-13}	−13.61
12.69	0.1087	4.921×10^{-13}	−13.62
			$\log K_{so} \pm \sigma = -13.66 \pm 0.08$

$$2MeHg^+ + H_2O \rightleftharpoons (MeHg)_2OH^+ + H^+$$
$$\log (K \pm 3\sigma) = -1.725 \pm 0.090 \quad (8)$$

Assuming the ionization constant of water $K_w = [H^+][OH^-] = 10^{-13.95}$ M^2 at $I = 1.0$ (Ref. 26), the formation of these MeHg(II) species may also be described by the following equilibrium reactions:

$$MeHg^+ + OH^- \rightleftharpoons MeHgOH$$
$$\log (K \pm 3\sigma) = 9.264 \pm 0.045 \quad (9)$$

$$MeHgOH + MeHg^+ \rightleftharpoons (MeHg)_2OH^+$$
$$\log (K \pm 3\sigma) = 2.961 \pm 0.049 \quad (10)$$

In Fig. 3 the error $H_{calc} - H_{tot}$ is plotted *versus* pH for the best model assumed (*cf.* Table 1, model 2). In Fig. 4 using the HALTAFALL program[24] the distribution of the methylmercury(II) species is given as a function of pH for $C_{MeHg} = 8.002 \times 10^{-3}$ M, assuming the formation of MeHgOH and $(MeHg)_2OH^+$ with the equilibrium constants given in (7) and (8).

Solubility equilibrium of methylmercury hydroxide. The solubility of MeHgOH(s) has been studied as a function of pH and the data given in Table 2. Assuming the formation of the species MeHgOH and $(MeHg)_2OH^+$ with the constant of formation given in (7) and (8), we have the following equation for the solubility of MeHg(II):

$$C_{MeHg} = [MeHg^+] + [MeHgOH] + 2[(MeHg)_2OH] = [MeHg^+] + 10^{-4.686}[MeHg^+][H^+]^{-1} + 2 \times 10^{-1.725}[MeHg^+]^2[H^+]^{-1} \quad (11)$$

Given the values of C_{MeHg} and $[H^+]$ one can calculate $[MeHg^+]$ from (11) and hence the solubility product for MeHgOH(s). For $K_w = 10^{-14.0}$ M^2, the following value for K_{so} has been obtained:

$$MeHgOH(s) \rightleftharpoons MeHg^+ + OH^-$$
$$\log K_{so} = -13.66 \pm 0.08$$

Dissociation equilibria of the acids HL. The dissociation equilibria of the acids HL have been studied by potentiometric acid-base titration. The data have been computer analyzed using the ETITR-LETAGROP program and the results of the calculations summarized in Table 3. In Fig. 5

Table 3. Equilibrium constants $\log K_{pq}$ for the protonation of the acids, $(H^+)_p(L^-)_q$ in 1.0 M (Na,H)(NO_3,L) ionic medium at 25 ± 0.05 °C which minimize the error-square sum $U = \sum_1^{Np} (H_{calc} - H_{exp})^2$. The limits given correspond approximately to $\log [K \pm 3\sigma(K)]$.

Acid	Equilibrium reactions	$\log(K \pm 3\sigma)$	U_{min}	σ(H)	Np (number of points)
Formic acid	$H^+ + L^- \rightleftharpoons HL$	3.472 ± 0.006	0.0033	0.011	28
Acetic acid	$H^+ + L^- \rightleftharpoons HL$	4.509 ± 0.001	0.0013	0.007	29
Glycine	$H^+ + L^- \rightleftharpoons HL$	9.642 ± 0.002	0.0766	0.031	79
	$2H^+ + L^- \rightleftharpoons H_2L^+$	12.073 ± 0.009			
α-Alanine	$H^+ + L^- \rightleftharpoons HL$	9.746 ± 0.005	0.4470	0.076	80
	$2H^+ + L^- \rightleftharpoons H_2L^+$	12.161 ± 0.022			
β-Alanine	$H^+ + L^- \rightleftharpoons HL$	10.155 ± 0.003	0.1041	0.040	66
	$2H^+ + L^- \rightleftharpoons H_2L^+$	13.838 ± 0.010			
DL-Valine	$H^+ + L^- \rightleftharpoons HL$	9.565 ± 0.007	0.7011	0.095	80
	$2H^+ + L^- \rightleftharpoons H_2L^+$	11.881 ± 0.029			

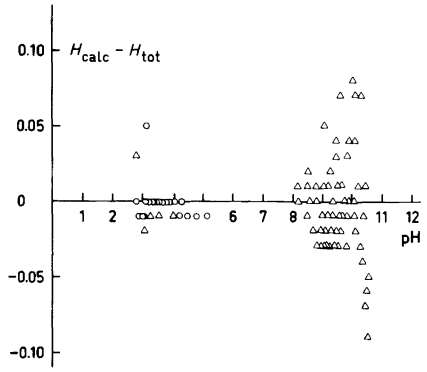

Fig. 5. The distribution of the error $(H_{calc} - H_{tot})$ *versus* pH for the titration of 1.0 M (H,Na)(L,NO_3) against 1.0 M Na(OH,NO_3) solution, where L = formate (□) and L = acetate (△). The error $(H_{calc} - H_{tot})$ has been calculated assuming the formation of HL with the equilibrium constants given in Table 3.

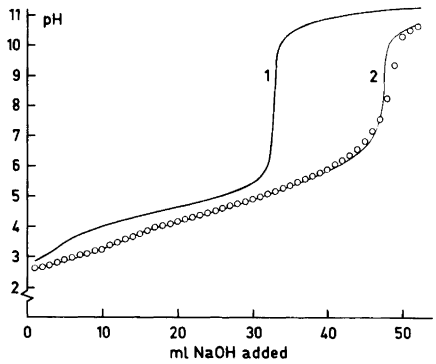

Fig. 6. Titration of 80.03 ml of solution S against v ml 1.0 M Na(OH,NO_3), [OH] = 0.0333 M, given as pH *versus* v. The initial composition of S is 6.007×10^{-3} M $MeHgNO_3$, 1.50×10^{-3} M HNO_3, 1.214×10^{-2} M HAc and 0.9804 M $NaNO_3$. Curve 1 has been calculated assuming the formation of only MeHgOH and $(MeHg)_2OH^+$ species, whereas in case of Curve 2 we assume the additional formation of the species MeHgAc and $(MeHg)_2Ac^+$ with the equilibrium constants given in Table 4 (Model IV for HAc).

the error $H_{calc} - H_{tot}$ is shown as a function of pH, assuming the set of constants which minimize the error-square sum $U = \sum_1^{Np} (H_{calc} - H_{tot})^2$. The dissociation equilibria of the different acids in 1 M (Na,H)NO_3 medium may thus be described by the reactions given in Table 5.

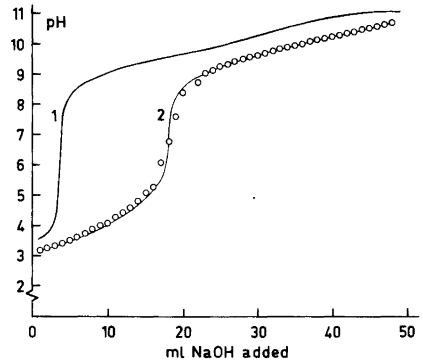

Fig. 7. Titration of 80.03 ml of solution S against v ml 1.0 M Na(OH,NO_3), [OH] = 0.0333 M. Solution S has the initial composition: 6.007×10^{-3} M $MeHgNO_3$, 1.500×10^{-3} M HNO_3, 1.247×10^{-2} M glycine, 0.9800 M $NaNO_3$. Curve 1 has been calculated assuming the formation of MeHgOH and $(MeHg)_2OH^+$ species only, while in Curve 2, we also assume the additional formation of the species MeHgGly and $MeHg(Gly)_2^-$ with the equilibrium constants given in Table 4 (Model III for glycine).

Formation of methylmercury(II) complexes with the acids HL. In Figs. 6 and 7, a part of the titration data for acetic acid and glycine, respectively, have been plotted as calculated titration curves where the curve 1, as before, depicts a normal acid-base titration. The curves marked 2 in both figures, represent the case where the titration is made in the presence of methylmercury(II) ions. These curves have been calculated taking into account the protolysis of the acids given in Table 3, and the equilibrium constants of complex formation between methylmercury and these acids given in Table 5. The experimental points from the actual titration fall essentially on curve 2, thus supporting the assumptions made in the computer analysis of the data. The results of these analyses are summarized in Table 4. In these analyses, the formation of MeHgOH and $(MeHg)_2OH^+$ species and the protolysis of the acids were taken into account and their equilibrium constants found previously were kept constant during the computer calculations. The results of these calculations indicate that formic acid forms 1:1, and acetic acid 1:1 and 2:1, whereas all the aminocarboxylic acids that is, glycine, α-alanine and DL-valine, predominantly form 1:1 and 1:2 complexes with methylmercuric ion.

Table 4. The equilibrium constant log K_{pqr} for the formation of $(H)_p(MeHg)_q(HL)_r$ species in 1.0 M (Na,H)(NO_3,L) ionic medium at 25 ± 0.05 °C for various assumptions of chemical models which minimize the error-square sums $U=\sum_1^{Np}(H_{calc}-H_{exp})^2$. The limits given correspond approximately to $\log[K\pm3\sigma(K)]$. The equilibrium constants for the hydrolysis of MeHg(II) were not varied except in model I in each case. The values of the hydrolysis constants are those given in Table 1 (Model II).

Model	Equilibrium reactions	$\log(K\pm3\sigma)$	U_{min}	σ(H)
Formic acid; $Np=60$				
I	$MeHg^+ + H_2O \rightleftharpoons MeHgOH + H^+$	−4.793 max. −4.548	20.741	0.627
	$2MeHg^+ + H_2O \rightleftharpoons (MeHg)_2OH^+ + H^+$	−0.850 max. −0.143		
II[a]	$MeHg^+ + L^- \rightleftharpoons MeHgL$	2.681±0.066	0.863	0.121
III	$MeHg^+ + L^- \rightleftharpoons MeHgL$	2.718±0.039	0.795	0.117
	$MeHg^+ + 2L^- \rightleftharpoons MeHgL_2^-$	3.973 max. 4.350		
IV	$MeHg^+ + L^- \rightleftharpoons MeHgL$	2.718±0.040	0.863	0.122
	$2MeHg^+ + L^- \rightleftharpoons (MeHg)_2L^+$	$K=0$		
Acetic acid; $Np=90$				
I	$MeHg^+ + H_2O \rightleftharpoons MeHgOH + H^+$	−4.685±0.146	15.967	0.428
	$2MeHg^+ + H_2O \rightleftharpoons (MeHg)_2OH^+ + H^+$	−0.745±0.131		
II	$MeHg^+ + L^- \rightleftharpoons MeHgL$	3.231±0.045	2.072	0.152
III	$MeHg^+ + L^- \rightleftharpoons MeHgL$	3.229±0.046	2.072	0.152
	$MeHg^+ + 2L^- \rightleftharpoons MeHgL^-$	$K=0$		
IV[a]	$MeHg^+ + L^- \rightleftharpoons MeHgL$	3.204±0.044	1.453	0.128
	$2MeHg^+ + L^- \rightleftharpoons (MeHg)_2L^+$	5.279±0.256		
Glycine; $Np=91$				
I	$MeHg^+ + H_2O \rightleftharpoons MeHgOH + H^+$	−4.102 max. −3.883	50.543	0.754
	$2MeHg^+ + H_2O \rightleftharpoons (MeHg)_2OH^+ + H^+$	−1.277 max. −0.870		
II	$MeHg^+ + L^- \rightleftharpoons MeHgL$	7.514±0.061	3.713	0.203
III[a]	$MeHg^+ + L^- \rightleftharpoons MeHgL$	7.518±0.050	2.316	0.161
	$MeHg^+ + 2L^- \rightleftharpoons MeHgL_2^-$	9.468±0.225		
IV	$MeHg^+ + L^- \rightleftharpoons MeHgL$	7.509±0.057	3.046	0.185
	$2MeHg^+ + L^- \rightleftharpoons (MeHg)_2L^+$	9.958 max. 10.231		
α-Alanine; $Np=75$				
I	$MeHg^+ + H_2O \rightleftharpoons MeHgOH + H^+$	−4.194 max 3.979	46.686	0.708
	$2MeHg^+ + H_2O \rightleftharpoons (MeHg)_2OH^+ + H^+$	−1.377 max. −0.973		
II	$MeHg^+ + L^- \rightleftharpoons MeHgL$	7.514±0.064	3.036	0.202
III[a]	$MeHg^+ + L^- \rightleftharpoons MeHgL$	7.516±0.052	2.471	0.163
	$MeHg^+ + 2L^- \rightleftharpoons MeHgL_2^-$	9.450±0.227		
IV	$MeHg^+ + L^- \rightleftharpoons MeHgL$	7.524±0.058	3.302	0.188
	$2MeHg^+ + L^- \rightleftharpoons (MeHg)_2L^+$	9.952 max. 10.248		
β-Alanine; $Np=95$				
I	$MeHg^+ + H_2O \rightleftharpoons MeHgOH + H^+$	−5.027±0.105	6.459	0.264
	$2MeHg^+ + H_2O \rightleftharpoons (MeHg)_2OH^+ + H^+$	−2.049±0.263		
II	$MeHg^+ + L^- \rightleftharpoons MeHgL$	$K=0$	12.779	0.367
III	$MeHg^+ + L^- \rightleftharpoons MeHgL$	$K=0$		
	$MeHg^+ + 2L^- \rightleftharpoons MeHgL_2^-$	$K=0$	12.970	0.367
IV	$MeHg^+ + L^- \rightleftharpoons MeHgL$	$K=0$		
	$2MeHg^+ + L^- \rightleftharpoons (MeHg)_2L^+$	$K=0$	12.958	0.367
DL-Valine; $Np=95$				
I	$MeHg^+ + H_2O \rightleftharpoons MeHgOH + H^+$	−4.284 max. −4.078	44.050	0.688
	$2MeHg^+ + H_2O \rightleftharpoons (MeHg)_2OH^+ + H^+$	−1.561 max. −1.156		
II	$MeHg^+ + L^- \rightleftharpoons MeHgL$	7.514±0.064	3.885	0.203
III[a]	$MeHg^+ + L^- \rightleftharpoons MeHgL$	7.268±0.056	2.821	0.174
	$MeHg^+ + 2L^- \rightleftharpoons MeHgL_2^-$	9.157±0.259		
IV	$MeHg^+ + L^- \rightleftharpoons MeHgL$	7.280±0.063	3.834	0.203
	$2MeHg^+ + L^- \rightleftharpoons (MeHg)_2L^+$	9.191 max. 9.967		

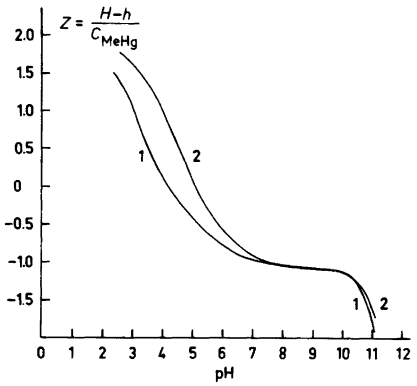

Fig. 8. Titration of 1.0 M (H,Na,MeHg)(L,NO_3) against 1.0 M Na(OH,NO_3) given as Z, the average number of OH bound per MeHg(II), *versus* pH. Curve 1 applies for L = formate, initial total concentrations $C_{MeHg} = 6.007 \times 10^{-3}$ M, $C_{HL} = 1.190 \times 10^{-2}$ M and $C_{HNO_3} = 1.52 \times 10^{-3}$ M. Curve 2 applies for L = acetate with initial total concentrations $C_{MeHg} = 6.007 \times 10^{-3}$ M, $C_{HL} = 1.214 \times 10^{-2}$ M and $C_{HNO_3} = 1.500 \times 10^{-3}$ M.

This conclusion is based on the choice of different models tried taking into account the most probable equilibrium reactions that may take place in the solution under the present experimental conditions (see Table 4). In Fig. 8, the typical formation curves

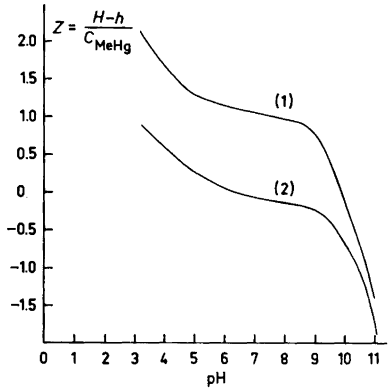

Fig. 9. Titration of 1.0 M (H,Na,MeHg)(Gly,NO_3) against 1.0 M Na(OH,NO_3) given as Z, average number of OH per MeHg(II), *versus* pH. Curve 1 applies for a solution with initial total concentrations $C_{MeHg} = 6.007 \times 10^{-3}$ M, $C_{HNO_3} = 1.490 \times 10^{-3}$ M and $C_{HGly} = 1.248 \times 10^{-2}$ M, whereas for Curve 2 $C_{MeHg} = 3.202 \times 10^{-3}$ M, $C_{HNO_3} = 3.795 \times 10^{-3}$ M and $C_{HGly} = 2.997 \times 10^{-3}$ M.

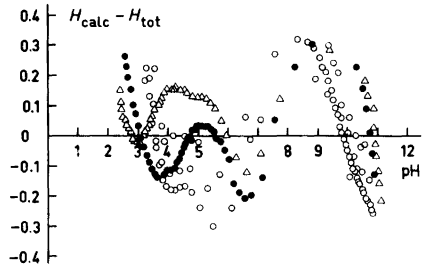

Fig. 10. The distribution of the error ($H_{calc} - H_{tot}$) in the titration of 1.0 M (H,Na,MeHg)(L,NO_3) *versus* 1.0 M Na(OH,NO_3) as a function of pH, where L = formate (△), acetate (●) and glycinate (○). The error ($H_{calc} - H_{tot}$) has been calculated assuming the formation of the MeHg(II) − HL species with the equilibrium constants given in Table 4 (Model II for formic acid; Model IV for acetic acid; Model III for glycine).

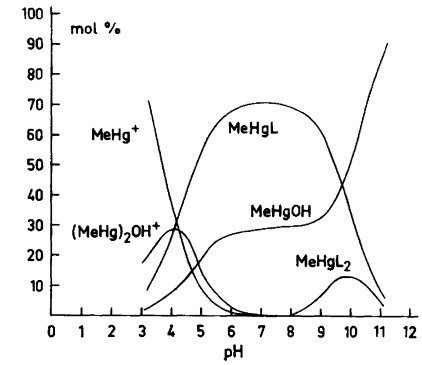

Fig. 11. The distribution of the species $(H)_p(MeHg)_q(HGly)_r$ as a function of pH. The curves have been calculated using the HALTAFALL program [24] assuming the formation of the MeHg(II) species with the equilibrium constants given in Table 4, Model III for glycine. The initial total constants given in Table 4, Model III for glycine. The initial total concentrations of $C_{MeHg} = 6.007 \times 10^{-3}$ M and $C_{HGly} = 1.247 \times 10^{-2}$ M were assumed.

for methylmercury-formate and methylmercury-acetate complexes are plotted showing $Z = (H_{tot} - h)/C_{MeHg}$ as a function of pH. Similar curves are shown in Fig. 9 for the complex formation of methylmercury with one of the amino acids, that is glycine; at two different concentrations of the acid with respect to methylmercury. The distribution of error, $H_{calc} - H_{tot}$ as a function of pH, for the accepted model assuming the formation of the

Table 5. Equilibrium constants for the formation of $(H)_p(MeHg)_q(HL)_r$ complexes in various systems.

$\log K_{MeHgOH}$	$\log K_{(MeHg)_2OH^+}$		Ref.
Hydrolysis			
-4.59^a	-2.53^a		14, 15
-4.78^a			16
-4.70^b	-2.33^b		11
-4.40 ± 0.07^c			10
-4.686 ± 0.045^d	-1.725 ± 0.090^d		This work
$\log K_{MeHgL}$	$\log K_{MeHgL_2^-}$	$\log K_{(MeHg)_2L^+}$	
Formic acid			
2.681 ± 0.066^d			This work
2.67^b			11
Acetic acid			
3.192 ± 0.034^d		5.223 ± 0.257	This work
3.18^b			11
3.55 ± 0.03^e			13
$\sim3.6^e$			7
Glycine			
7.518 ± 0.050^d	9.468 ± 0.225^d		This work
α-Alanine			
7.516 ± 0.05^{2d}	9.450 ± 0.227^d		This work
β-Alanine			
$K=0$	$K=0$	$K=0$	This work
DL-Valine			
7.268 ± 0.056^d	9.157 ± 0.259^d		This work

[a] 0.1 M $(K,H)NO_3$. [b] Aqueous. [c] 1.0 M $(Na,H)(NO_3,Cl,PO_4)$. [d] 1.0 M $(Na,H)NO_3$. [e] Undefined.

species $(H)_p(MeHg)_q(HL)_r$ with the equilibrium constants given in Table 5, is shown in Fig. 10. The error is rather small and is almost uniformly distributed over the whole pH range. In Fig. 11, the equilibrium distribution of methylmercury(II) complexes with glycine at $C_{MeHg} = 6.007\times10^{-3}$ M and $C_{HL} = 1.247\times10^{-2}$ M, is given as a function of pH. In Table 5, the available results on the hydrolysis of methylmercury(II) and its complex formation with some carboxylic and aminocarboxylic acid are summarized.

DISCUSSION

Our results show that the predominant methylmercury(II) hydrolyzed species formed are MeHgOH and $(MeHg)_2OH^+$. This supports the results reported by other authors that are summarized in Table 5.

The structure of $(MeHg)_2OH^+$ may be expected to be similar to that of Hg(II) hydrolyzed species, as given by Johansson.[25] From the liquid X-ray diffraction studies, Johansson has reported that the structure of polynuclear complexes of hydrolyzed Hg(II) is expected to contain predominantly the linear building elements O–Hg–O, where the oxygen atoms from both OH^- and H_2O may contribute to the bonding. The only possible structure for a dinuclear $Hg_2OH(H_2O)_2^{3+}$ complex was concluded to consist of two linear O–Hg–O groups, having an oxygen in common. The author found from scattering data distances of 3.64 Å for Hg–Hg and 2.10 Å for Hg–O. This will give an angle of ~120° for HgOHg. The stability constants of the 1:1 complexes of methylmercury(II) with formate and acetate ions are in good agreement with those reported by Libich and Rabenstein[11] from NMR studies. Simpson[7] has also studied the com-

plex formation of methylmercury(II) with acetate-ions polarographically. However, the present results show that the value of the stability constant, log $K = 3.6$ that he has reported is definitely too high. The formation of a 1:2 acetate complex with methylmercury(II) is rather surprising from structural considerations, especially under the present experimental conditions where even a two-fold excess of acetate with respect to methylmercury(II) has been used. The calculations indicate that it is present in very small amounts compared with the 1:1 complex. Further studies, such as NMR or infrared spectroscopy, are therefore required to verify the existence of such a species.

The complexing ability of α-aminocarboxylic acids with methylmercury(II) is considerably higher than that of simple carboxylic acids. This is not unexpected, because with a chelating agent like $NH_2CH_2COO^-$, both metal – nitrogen and metal – oxygen bonds are involved in the complexation.

Our experiments with β-alanine indicate that it does not seem to form any complex with methylmercury(II) although its complexes with most of the metals including Hg(II) are known.[26] In the computer calculations, the stability constant of its complex formation with methylmercury(II) is invariably reduced to zero (*cf.* Table 4) meaning that no detectable complexation takes place under the present experimental conditions. This may be explained considering the steric effects partly due to the β-position of the amino group and partly due to the presence of a methyl group on Hg(II).

Several investigators,[11,27,28] have reported that approximate linear relationships exist between the

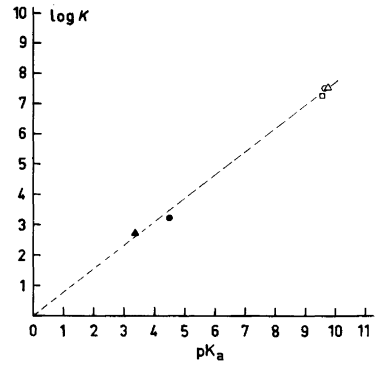

Fig. 12. The formation constant K for MeHgL as a function of the acid constant K_a of HL, for formic acid (▲), acetic acid (□), glycine (□), α-alanine (△) and DL-valine (○).

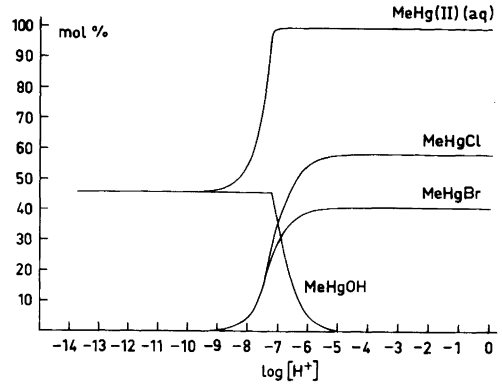

Fig. 13. The distribution of MeHg(II) species as a function of $\log[H^+]$ for initial total concentrations $C_{MeHg} = 1.00 \times 10^{-4}$ M, $C_{Cl} = 1.00 \times 10^{-3}$ M, $C_{Br} = 1.00 \times 10^{-4}$ M and $C_{NO_3} = 1.00$ M. The curves have been calculated using the HALTAFALL program,[24] assuming the formation of MeHgCl(aq), MeHgCl(s), MeHgOH(aq), MeHgOH(s), $(MeHg)_2OH^+$(aq), MeHgBr(aq), MeHgBr(s) and $MeHgBr_2^-$(aq) with equilibrium constants given in the present work and in others.[9]

stability constants of first 1:1 metal-ligand complex and the corresponding proton-ligand complex, formed by a given metal with a series of closely-related ligands. Such a relationship is important and can provide a basis for predicting the stability constants of other complexes in the series, if the stability constant of a closely related complex has been measured. The theoretical background and the conditions under which such a relationship holds, as well as its analytical significance, have been discussed by Irving and Rossotti.[29] A similar relationship has been found to exist between the pK_a values of the acids that we have studied and the stability constants of their corresponding complexes with methylmercury(II) ions (Fig. 12). In Fig. 13 we use the HALTAFALL program to simulate the equilibria of a lake that has been contaminated with methylmercury(II). The calculations are based on the formation of $(H^+)_p(MeHg^+)_q(Br^-)_r(Cl^-)_s$ species with equilibrium constants determined in the present and previous works. Moreover, the formation of solid phases of MeHgCl(s), MeHgBr(s) and MeHgOH(s) has also been considered in these calculations. This indicates that the equilibrium analysis may contribute to a better understanding of our ecological problems.

Acknowledgements. This work has been financially supported by the Swedish Natural Science Research Council. The authors are grateful to Professor Ingmar Grenthe for his keen interest in this work and to Dr. Georg Johansson for valuable discussions on structural aspects.

REFERENCES

1. *FAO Fish. Rep.* No. 99, Rome 1971.
2. Irkayama, K. *Adv. Water Pollut. Res. 3* (1967) 153.
3. Westöö, G. and Rydäl, M. *Vår Föda* 7–8 (1971); *Report on Mercury in Foods*, by the Joint FAO/WHO Expert Committee on Food Additives, 1970.
4. Wood, J. M., Kennedy, F. M. and Rosen, C. G. *Nature 220* (1968) 173.
5. Jensen, S. and Jernelöv, A. *Nature 223* (1969) 753.
6. Rizzardi, G., Pietropaolo, R. and Barbini, R. *Gazz. Chim. Ital. 96* (1965) 1371.
7. Simpson, R. B. *J. Am. Chem. Soc. 83* (1961) 4711.
8. Budevsky, O., Ingman, F. and Liem, D. H. *Acta Chem. Scand. 27* (1973) 1277.
9. Jawaid, M., Ingman, F., Liem, D. H. and Wallin, T. *Proc. Conference on the Effects of Toxic Metal on Man and Environment*, Luleå 1976, Sweden; *Acta Chem. Scand. A 32* (1978) 7.
10. Ingman, F. and Liem, D. H. *Acta Chem. Scand. A 28* (1974) 947.
11. Libich, S. and Rabenstein, D. L. *Anal. Chem. 45* (1973) 118.
12. Rabenstein, D. L., Evans, C. A., Tourangeau, M. C. and Fairhurst, M. J. *Anal. Chem. 47* (1975) 338.
13. Maguire, R. J., Anand, S., Chew, H. and Adams, W. A. *J. Inorg. Nucl. Chem. 38* (1976) 1659.
14. Schellenberg, M., *Diss.*, ETH, Zürich 1963.
15. Schellenberg, M. and Schwarzenbach, G. *Helv. Chim. Acta 48* (1965) 28.
16. Zanella, P., Plazzogna, G. and Tagliavini, G. *Inorg. Chim. Acta 2* (3) (1968) 340.
17. Brauner, P., Sillén, L. G. and Whiteker, R. *Ark. Kemi 31* (1968) 365.
18. Maynard, J. L. and Howard, H. C. *J. Chem. Soc. 123* (1923) 960.
19. Johns, I. B., Peterson, W. D. and Hixen, R. M. *J. Phys. Chem. 34* (1930) 2218.
20. Waugh, T. D., Harled, F. W. and Laswick, J. A. *J. Phys. Chem. 59* (1955) 395.
21. Goggin, P. L. and Woodward, L. A. *Trans. Faraday Soc. 56* (1960) 1591.
22. Pehrsson, L., Ingman, F. and Johansson, A. *Talanta 23* (1976) 769.
23. Arnek, R., Sillén, L. G. and Wahlberg, O. *Ark. Kemi 31* (1969) 353.
24. Ingri, N., Kakolowicz, W. and Sillén, L. G. *Talanta 14* (1967) 1261.
25. Johansson, G. *Acta Chem. Scand. 25* (1971) 2799.
26. Sillén, L. G. and Martell, E. A., Eds., *Stability Constants*, The Chemical Society, Special Publications Nos. 17 and 25, London 1964 and 1972.
27. Martell, E. A. and Kalvin, M. *Chemistry of Metal Chelate Compounds*, Prentice-Hall, New York 1952.
28. Theirs, G. F., Van Poucke, L. C. and Herman, M. A. *J. Inorg. Nucl. Chem. 30* (1968) 1543.
29. Irving, H. and Rossotti, H. *Acta Chem. Scand. 10* (1956) 72.

Received October 11, 1977.

Acta Chemica Scandinavica A 32 (1978) 345–352

Equilibrium Studies of the Pyruvate Protonation and Metal Pyruvate Complexes in Aqueous Solutions

OVE FORSBERG, BERTIL GELLAND, PER ULMGREN and OLOF WAHLBERG

Departments of Inorganic and Structural Chemistry, Arrhenius Laboratory, University of Stockholm, S-106 91 Stockholm, Sweden

The protonation of pyruvic acid (HPyr) has been studied in 3 M (Na)ClO_4 and in 0.3 M (Na)ClO_4 aqueous solutions at 25 °C. The total concentration of pyruvic acid varied between 0.01000 M and 1.000 M. The equilibrium data obtained from emf measurements could be described by a single dissociation step.

The cadmium(II) and iron(II) complexes of pyruvic acid have been studied in 3 M (Na)ClO_4 medium, while the calcium pyruvate equilibria have been studied both in 0.3 M and in 3 M (Na)ClO_4 media. Formation constants of the main species are given in this article. Altogether 428 equilibrium solutions are studied.

Pyruvate ion frequently occurs as a reactant or a reaction product of chemical reactions[1,2] in living organisms. Pyruvic acid, or 2-oxo-propanoic acid is a monobasic acid with $pK_a = 2.49$ in pure water at 25 °C.[3] Complexes of the type $MPyr^+$ and $MPyr_2$ have been reported (*cf.* Table 1). The crystal structure of the sodium salt has been determined by X-ray diffraction methods.[9] Pyruvic acid dimerizes in aqueous solution. In pure water this reaction is rather slow provided that pH ≤ 5. The presence of CN^-, OH^- or metal ions speeds up the dimerization of HPyr.[7c] The dimer is a dibasic weak acid with $pK_{a1} = 1.73$ and $pK_{a2} = 3.72$ in 1 M NaCl medium.[7c]

The present study has been undertaken to determine the main complexes of Cd^{2+}, Ca^{2+} and Fe^{2+} with pyruvic acid. In man calcium and iron are two of the most abundant metals, while cadmium occurs only in very low concentrations. The complex formation with calcium has been investigated by Davies[4] and by Schubert and Lindebaum.[5] They found one complex, $CaPyr^+$, with $\beta \sim 10\ M^{-1}$. The complex formation of the pyruvate ion with Fe^{2+} and Cd^{2+} does not seem to have been studied earlier. Part of this report concerns the protonation of pyruvic acid, which had to be determined in the ionic media used. The influence of the diffusion potentials and the activity coefficients on the measured data also had to be investigated. In order to determine the influence of Na^+ on the complex formation, measurements have been made both in 0.3 M $NaClO_4$ medium and in 3 M $NaClO_4$ medium.

The equilibria studied are generally written as

$$pH^+ + qM^{2+} + rPyr^- \rightleftharpoons M_qPyr_rH_p^{2q+p-r} \quad (1a)$$

The equilibrium constant for the formation of a complex can be written as

$$\beta_{pqr} = h^{-p}b^{-q}c^{-r}c_{pqr} \quad (1b)$$

where h, b, c and c_{pqr} are the concentrations of the species H^+, M^{2+}, Pyr^- and $M_qPyr_rH_p^{2q+p-r}$, respectively.

EXPERIMENTAL

Chemicals and analyses

Sodium perchlorate, *perchloric acid*, *sodium chloride* and *sodium hydroxide* were prepared and analyzed as described in Ref. 11. The preparations of cadmium perchlorate solutions, calcium perchlorate solutions and iron(II) perchlorate solutions have been described elsewhere.[11b,c,d]

Table 1. Metal-pyruvate complexes in aqueous solution. A literature survey. HPyr = pyruvic acid. Temperature is 25 °C.

Investigation	Notes	Species	log β_{pqr}
Method = Solubility			
Davies[4]	→0	$CaPyr^+$	1.08
Method = Ionic exchange			
Schubert and Lindenbaum[5a]	0.16 M NaCl	$CaPyr^+$	0.8
Schubert and Lindenbaum[5a]	0.16 M NaCl	$SrPyr^+$	0.5
Schubert, Russell and Meyers[5b]	0.16 M NaCl	$RaPyr^+$	0.89
Chibnall and Cannan[6]	0.16 M NaCl	$RaPyr^+$	1.9
Method = Potentiometry			
Leussing and Shultz[7a]	0.65 M KCl	$MnPyr^+$	1.26
Gelles and Hay[8]	→0	$CuPyr^+$	2.3
Gelles and Hay[8]	→0	$CuPyr_2$	4.9
Leussing and Shultz[7a]	0.65 M KCl	$NiPyr^+$	1.15
Leussing and Hanna[7b]	0.5 M KCl	$NiPyr^+$	1.12
Tallman and Leussing[7c]	1.0 M NaCl	$NiPyr^+$	0.883
Leussing and Hanna[7b]	0.5 M KCl	$NiPyr_2$	0.46
Tallman and Leussing[7c]	1.0 M NaCl	$NiPyr_2$	0.948
Leussing and Shultz[7a]	0.65 M KCl	$ZnPyr^+$	1.28
Leussing and Hanna[7b]	0.5 M KCl	$ZnPyr^+$	1.26
Tallman and Leussing[7c]	1.0 M NaCl	$ZnPyr^+$	1.16
Leussing and Hanna[7b]	0.5 M KCl	$ZnPyr_2$	1.98
Tallman and Leussing[7c]	1.0 M NaCl	$ZnPyr_2$	2.00

Sodium pyruvate $NaC_3H_3O_3$. The analytical grade reagent from BDH was used. The molecular weight was determined by titration of solutions containing accurately weighed samples of sodium pyruvate acidified with perchloric acid. As a titrant, a standard sodium hydroxide solution was used. The experimental value, 110.1 ± 0.1 g/mol equals the theoretical value within the stated error. From proton resonance spectra it was found that 5 % of the pyruvate had formed pyruvate dimer.

Pyruvic acid solutions were prepared by adding perchloric acid to sodium pyruvate solutions.

Apparatus

The measurements of emf were performed with an *automatic titration system*, which includes a master digital voltmeter (Solartron Instruments) and a digital computer (Philips P855). A complete description will be given elsewhere.[10] The NMR measurements were made with a Varian model XL 100 Spectrometer. The saltbridge, electrodes and thermostat are described in Ref. 11. The glass electrodes (Beckman No. 39303) were checked against hydrogen electrodes.

THE TITRATION PROCEDURE

All solutions studied contained sodium perchlorate as an ionic medium to hold the activity coefficients approximately constant and to eliminate the influence of the diffusion potentials on the data. The concentration of ClO_4^- was kept constant either at 3 M or 0.3 M, while Na^+ was varied within the following ranges: $2.830 \leq [Na^+] \leq 3.160$ M or $0.270 \leq [Na^+] \leq 0.320$ M, respectively. From one or two burets, V_T ml of a solution with known analytical concentration of H^+ ($\equiv H_T$) were introduced into V_0 ml of a solution with an analyzed concentration of H^+ ($\equiv H_0$) to yield ($V_0 + V_T$) ml of a solution with

$$H = (V_0 H_0 + V_T H_T)/(V_0 + V_T) \quad (2)$$

The total concentrations of pyruvic acid ($\equiv C$) and metal ion ($\equiv B$) were held constant in each titration except in four experiments (see below). In some titrations, where an acidified solution of pyruvic acid was made gradually more alkaline, a sodium hydroxide solution and a pyruvic acid solution were introduced from two separate burets. The two

solutions were immediately mixed by stirring to disperse locally concentrated solutions of hydroxide ions.

THE EXPRESSION FOR EMF

The solutions studied were analyzed for $[H^+]$ by the following cells

$$-\text{Ag, AgCl(s)}\,\big|\,[Cl^-]=0.010\ \text{M}\,\big|\,\begin{matrix}\text{Equilibrium}\\ \text{solution}\\ \text{studied}\end{matrix}\,\Big|\,\begin{matrix}\text{Glass}\\ \text{elec-}\\ \text{trode}\end{matrix}\,+ \quad (3a)$$

$$-\text{Ag, AgCl(s)}\,\Big|\,\begin{matrix}\text{Equilibrium}\\ \text{solution contain-}\\ \text{ing 0.01 M NaCl}\end{matrix}\,\Big|\,\begin{matrix}\text{Glass}\\ \text{electrode}\end{matrix}\,+ \quad (3b)$$

Sodium perchlorate was added to all solutions so that $[ClO_4^-]=3$ M or 0.3 M. Proton concentrations were calculated from

$$E = E_0' + (RT\ln 10/F)\lg h + E_j', \text{ where}$$
$$RT\ln 10/F = 59.155\ \text{mV at 25 °C} \quad (3c)$$

The constant E_0' was determined for each titration from measurements in solutions with $0.8<\text{pH}<1.4$ where $C\approx[\text{HPyr}]$. The contribution of protons to h from dissociated HPyr was, however, taken into account. The variations of the activity coefficients and the diffusion potentials in the cell (3a) were for practical reasons expressed as two terms[11e] E_0' and E_j' where

$$E_0' = E_{00} + j_C C \text{ and} \quad (3d)$$

$$E_j' = \Sigma j_{pr} c_{pr} \text{ (summation over all } p,r) \quad (3e)$$

E_0' is a constant for each titration with constant C, and E_j' is expected to vary at most a few mV. As a first approximation we set $E_j'=j_{10}h$. From studies of $E=f(C)_h$ in solutions dominated by HPyr or Pyr^-, respectively, two terms $j_{11}[\text{HPyr}]$ and $j_{01}[Pyr^-]$ in eqn. (3e) could be estimated. The term $j_{10}h$ is known from earlier experiments.[11] Our second approximation of E_j' is then

$$E_j' = -16.8[H^+] + j_{01}[Pyr^-] + j_{11}[\text{HPyr}] \quad (3f)$$

The computer program LETAGROP[12a,b] was used to refine the parameters j_{pr} in eqn. (3e) and if necessary to introduce new terms in the expression for E_j'.

Attainment of equilibrium

The attainment of equilibrium between monomeric pyruvic acid and protons is rapid, while the formation of dimer is slow. For each measured data point a stable emf value was obtained within a few minutes after mixing of a solution. This value remained stable within ± 0.2 mV for at least 8 h in acid solution and for a few hours in neutral solution. The emf values were read 10 min after the mixing of solutions for each experimental data point.

Each titration was completed within 6 h, when studying the systems $Ca^{2+}-H^+-Pyr^-$ and $Cd^{2+}-H^+-Pyr^-$, but within 3 h for the systems H^+-Pyr^- and $Fe^{2+}-H^+-Pyr^-$, thus before appreciable formation of pyruvate dimers. The concentration of pyruvate dimer was found to be approximately 5 % for all data points. No data points were measured at low Z-values for the iron(II) pyruvate system, since stable emf values could not be obtained within a few minutes. The Ca^{2+}-pyruvate data in Fig. 3b are restricted to $1.0>Z_{H/C}>0.2$ representing the points used in the graphic treatment described below. The data at low Z-values were discarded in the graphic treatment since we wanted to keep the influence of pyruvate dimers low. However, all the data, even those at low Z-values, were used in the final refinement of the equilibrium model whereby the dissociation of the pyruvate dimer was taken into account. Back titrations show that the data can be explained by equilibrium models for reversible processes, within the limits of the experimental uncertainty (*cf.* Figs. 2, 3). The iron solutions used in the experiments were carefully reduced before each titration (*cf.* Ref. 11d).

SURVEY OF EXPERIMENTAL DATA*

The primary data consist of measured volumes, emf values and analyzed total concentrations. In four titrations (Fig. 1) the total concentration of pyruvic acid was varied at constant pH. For most measurements, however, both B and C were held constant for each titration. The emf of the cell (3a) or (3b) was measured and from eqn. (3c) h was calculated. These data were transformed to the formation functions $Z_{H/C}$ and $Z_{C/B}$ by eqns. (4a, b).

* The primary data are available on request to the Department of Inorg. and Structural Chemistry, Arrhenius Laboratory, University of Stockholm, S-106 91 Stockholm, Sweden.

$$Z_{H/C} = (H-h)/C \quad (4a)$$

$$Z_{C/B} = (C-c)/B \quad (4b)$$

The data transformed to $Z_{H/C}(\log h)_{B,C}$ or $Z_{C/B}(\log c)_{B,C}$ are shown in Figs. 2, 3 and 4. E_0' (which is a function of C, *cf.* eqn. 3d) was estimated for each titration from five or six acid points by the computer program TRAVE[11f] which accounts for the dissociation of HPyr. E_j' has been estimated by separate experiments. In the refinement of the final equilibrium model we search for a better estimation of E_j'. The least-squares sum $(Z_{calc}-Z_{exp})^2$ has been minimized (*cf.* eqn. 3e). Z_{calc} was obtained from the eqns. (1b), (4a), (4c), (4d) and (4e). Z_{exp} was obtained from eqns. (2), (3c) and (4a).

$$H = h + \Sigma p c_{pqr} \quad (4c)$$

$$B = b + \Sigma q c_{pqr} \quad (4d)$$

$$C = c + \Sigma r c_{pqr} \quad (4e)$$

TREATMENT OF DATA

All solutions contained 5 % pyruvate dimer as measured by NMR. Calculations by the program HALTAFALL[12c] show that the influence of 5 % dimer on the data is at most 2 % of H. Since the effect of dimers is so small in the present case, the dimers were taken into account only in the final least-squares calculations. The data treatment is divided into two main sections: (1) Estimation of the relationship between activity coefficients and the liquid junctions as a function of the pyruvate concentration and the determination of pK_a for pyruvic acid. (2) Determination of the main metal complexes of pyruvic acid with Ca^{2+}, Cd^{2+} and Fe^{2+}.

1a. Estimations of $E_0'+E_j'$. The data have been plotted in Fig. 1 as $E=f(C)_{pH}$. Straight lines were obtained. Forward and backward titrations agree indicating that no irreversible reactions take place in the solutions studied. The eqns. (5a) and (5b) were calculated to describe these data in 3 M $(Na)ClO_4$:

$$E_0'+E_j' = E_{00}+(5.6\pm0.5)C \text{ at pH}=0 \text{ where } C=[\text{HPyr}] \quad (5a)$$

$$E_0'+E_j' = E_{00}-(8.5\pm0.5)C \text{ at pH}=4.4 \text{ and } 5.0 \text{ where } C=[\text{Pyr}^-] \quad (5b)$$

The measurements at pH = 0 were performed in 1.00 M $HClO_4$ solutions. The measurements at

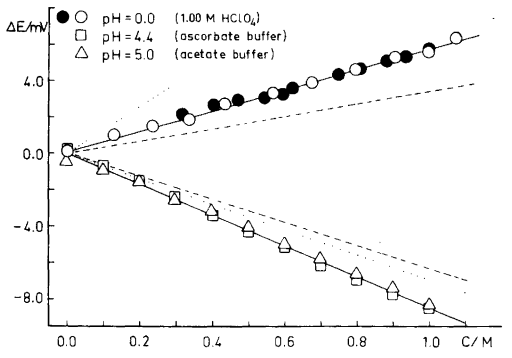

Fig. 1. E as a function of C at constant log h. The symbols represent experimental data points for pyruvic acid. The solid lines correspond to eqns. (5a) and (5b). The dotted lines refer to ascorbic acid [11e] and the broken lines refer to acetic acid (14).

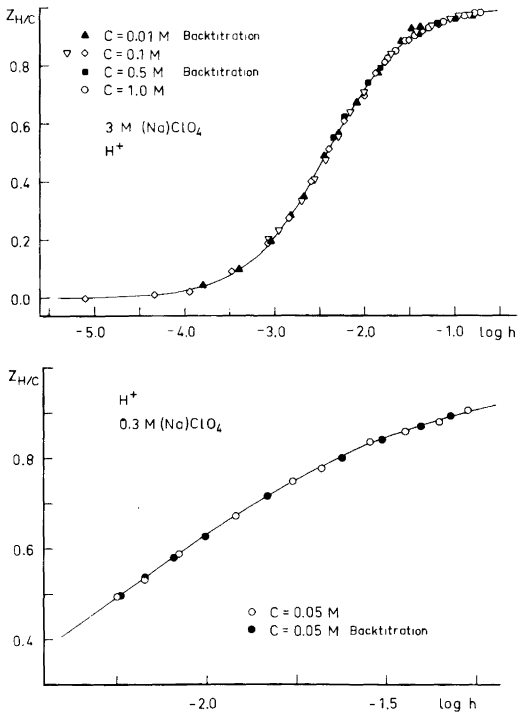

Fig. 2. Z(= the average number H^+ bound per C) as a function of log h. The solid curve corresponds to a normalized function and $pK_a = 2.40$ in 3 M $(Na)ClO_4$ and $pK_a = 2.20$ in 0.3 M $(Na)ClO_4$.

pH = 4.4 and 5.0 were performed in ascorbate and acetate buffers, respectively. Thus, using one value of E_0' for each titration with constant C, the variations of activity coefficients and liquid junction potentials for each titration are approximated by

$$E_j' = -14.1\,c - 16.8\,h \qquad (5c)$$

while now $E_0' = E_{00} + 5.6\,C$ (*cf.* eqns. (3d), (3e), (5a) and (5b))

1b. The protonation of the pyruvate ion. The formation function $Z_{H/C}$ (log h)$_C$ is represented in Fig. 2. All the experimental data could be explained by assuming the presence of HPyr and Pyr^- in the solutions. From eqns. (1b) and (4a), (4c) and (4e) one obtains

$$Z_{H/C} = (\beta_{101}h)/(1+\beta_{101}h) \qquad (5d)$$

The normalized function $u/(1+u) = f(\log u)$ was fitted to the experimental $Z(\log h)_C$. The "best" fit gave

$$pK_a = \log \beta_{101} = \log u - \log h = 2.4 \pm 0.1 \text{ for 3 M (Na)ClO}_4 \qquad (5e)$$

and $pK_a = 2.2 \pm 0.1$ for 0.3 M (Na)ClO_4.

1c. Least-squares treatment of the data. Least-squares refinements of pK_a by program LETAGROP[12a,b] (*cf.* Table 2a) yielded the values given below (*cf.* eqn. (7)).

No significant change was observed when models with different hypotheses for E_j' were refined. This fact was interpreted to mean that the errors caused

Table 2a. Least-squares treatment of data for equilibrium between pyruvic acid and protons. $U_Z = (Z_{calc} - Z_{exp})^2$. K_{D1} and K_{D2} are the acidity constants of the pyruvic acid dimer H_2Pyr_2. The systematic errors δE_0 and δH have been adjusted. n.v. = not varied.

[(Na)ClO_4]	Np	$U \times 10^4$	$(\sigma Z) \times 10^3$	$\log(\beta_{101} \pm 3\sigma)$	$-\log(K_{D1} \pm 3\sigma)$	$-\log(K_{D2} \pm 3\sigma)$
3 M	89	8.64	8.64	2.415 ± 0.009	–	–
		8.62	8.63	2.403 ± 0.009	2.2 ± 0.4[a]	3.6 ± 0.4[a]
0.3 M	20	1.61	2.94	2.244 ± 0.005	–	–
		1.39	2.70	2.202 ± 0.004	1.73 n.v.[b]	3.72 n.v.[b]
		1.39	2.69	2.196 ± 0.004	1.9 ± 0.7[a]	3.7 ± 1.1[a]

[a] The dimers were included only to show the very small effect that 5 % pyruvate dimer has on the measured emf. [b] Values determined by Leussing and Tallman [7c] in 1 M NaCl at 25 °C.

Table 2b. Least-squares treatment of data for equilibria between Cd(II), Ca(II) or Fe(II) ions, pyruvic acid and protons. $U_Z = (Z_{calc} - Z_{exp})^2$. K_{D1} and K_{D2} are the acidity constants of the pyruvic acid dimer H_2Pyr_2. The systematic errors δE_0 and δH have been adjusted. n.v. = not varied.

M^{2+}	[(Na)ClO_4]	Number of points	$U \times 10^4$	$(\sigma Z) \times 10^3$	$\log(\beta_{101} \pm 3\sigma)$	$\log(\beta_{011} \pm 3\sigma)$	$-\log K_{D1}$	$-\log K_{D2}$
Cd^{2+}	3 M	159	118	8.4	2.415 n.v.	0.961 ± 0.015	–	–
Ca^{2+}	3 M	102	55.2	7.4	2.415 n.v.	0.571 ± 0.012	–	–
			49.1	7.0	2.403 n.v.	0.554 ± 0.011	1.73 n.v.[b]	3.72 n.v.[b]
			44.0	6.6	2.403 n.v.	0.581 ± 0.010	2.2 n.v.[a]	3.6 n.v.[a]
Ca^{2+}	0.3 M	20	0.42	1.5	2.244 n.v.	0.619 ± 0.014	–	–
			0.37	1.4	2.202 n.v.	0.596 ± 0.013	1.9 n.v.[a]	3.7 n.v.[a]
Fe^{2+}	3 M	38	12.9	5.9	2.403 n.v.	0.69 ± 0.04	2.2 n.v.[a]	3.6 n.v.[a]
			12.6	5.8	2.415 n.v.	0.67 ± 0.04	–	–

[a] The dimers were included only to show the very small effect that 5 % pyruvate dimer has on the measured emf. *Cf.* Table 2. [b] Values determined by Leussing and Tallman [7c] in 1 M NaCl at 25 °C.

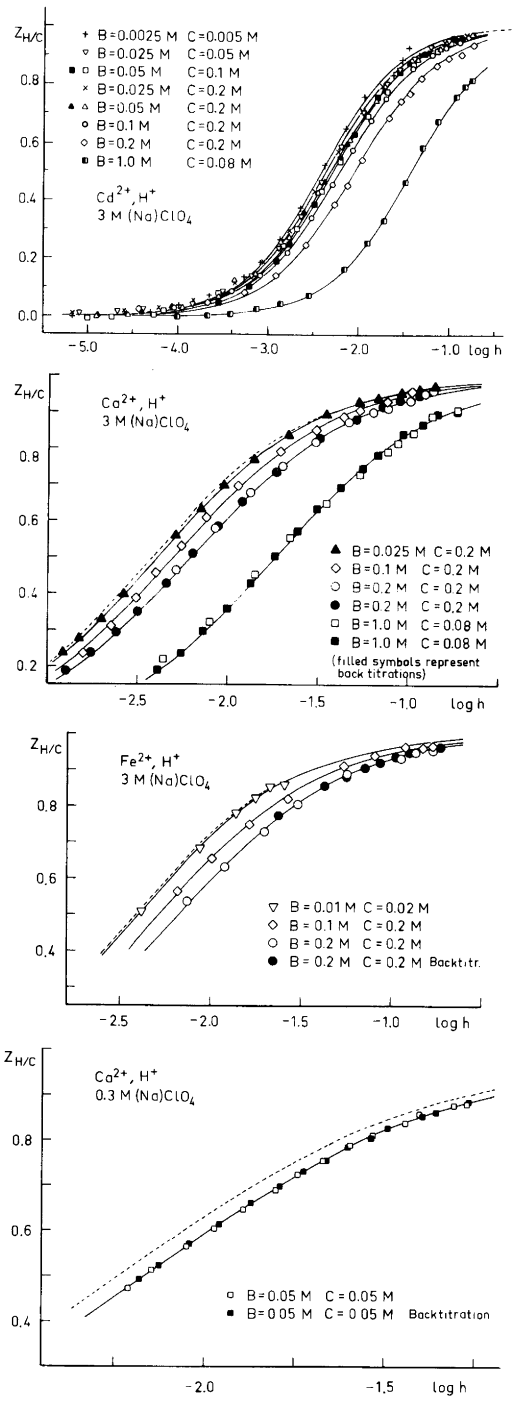

Fig. 3. $Z=Z_{H/C}$, =the average number of H^+ bound per C, as a function of log *h*. The solid curves have been calculated by the program HALTAFALL[12c] using the final equilibrium constants. The broken curves correspond to pyruvate solutions with metal ions absent.

by activity coefficients and diffusion potentials have been accounted for by E_0'. The fit of the model with the data was improved very little when the dimers were taken into account. Rough estimates of pK_a for the dimer are $pK_{a1}=2.2\pm0.5$ and $pK_{a2}=3.6\pm0.5$ (*cf.* Table 2a). Certainly, the dimers have very little influence on the present data.

2. Determination of the equilibrium constants for the formation of metal pyruvate complexes. In this equilibrium analysis we have first deduced a model by studying the graphs of $Z_{H/C}$ (log $h)_{B,C}$ and $Z_{C/B}$ (log $c)_{B,C}$ in Figs. 3 and 4. The least-squares program LETAGROP[12a,b] was then used for refinement of the model. The hydrolysis of the metal ion could be neglected in the pH-regions studied.[3] All equilibrium solutions studied contained 5 % pyruvate dimer, which caused the small deviation at $Z_{H/C}\approx0.01$ evident in Fig. 3a. In the final least-squares refinement we have taken into account also the pyruvate dimers.

2a. Graphic analysis of the data. In Figs 3a–d the average number of H^+ bound per Pyr^- has been plotted as a function of log $[H^+]$ for several total concentrations of the metal ion. The influence of the metal ion on the curves $Z_{H/C}$(log $h)_{B,C}$ is larger for pyruvate than for ascorbate for pH ≤5 (*cf.* Ref. 11). For the pyruvate metal complexes $Z_{H/C}\geq0$ for all data (Fig. 3), in contrast to the ascorbate–metal complexes, which form chelated species at pH ≥5 giving $Z_{H/C}<0$ (Ref. 11b).

As a first approximation we have assumed that the complexes are of the type $M_q(Pyr)_r^{2q-r}$ (thus with $p=0$). Using this assumption we can easily calculate the average number of Pyr^- bound per M^{2+} as a function of $c=[Pyr^-]$ (*cf.* Ref. 11a). The function $Z_{C/B}$(log $c)_{B,C}$ is shown in Figs. 4a–c. The theoretical expression for $Z_{C/B}$ is

$$Z_{C/B} = \Sigma r\beta_{qr}b^qc^r/(b+\Sigma q\beta_{qr}b^qc^r) \qquad (6a)$$

All the experimental points in Figs. 4a–c can be fitted by the normalized function $[u/(1+u)]=f(\log u)$, assuming one complex with $q=r=1$. The translation of the normalized curve to the "best" fit with the experimental curves $Z_{C/B}$(log $c)_{B,C}$ gives log $\beta_{11}=\log u-\log c=1.0\pm0.1$ for Cd^{2+}. The corresponding value for Fe^{2+} was 0.7 ± 0.1 and for Ca^{2+} 0.6 ± 0.1 (both in 3 M $NaClO_4$ and in 0.3 M $NaClO_4$).

2b. Least-squares treatment by the LETAGROP method.[12a,b] Models with additional species were tried, but no significant improvement of the fit with

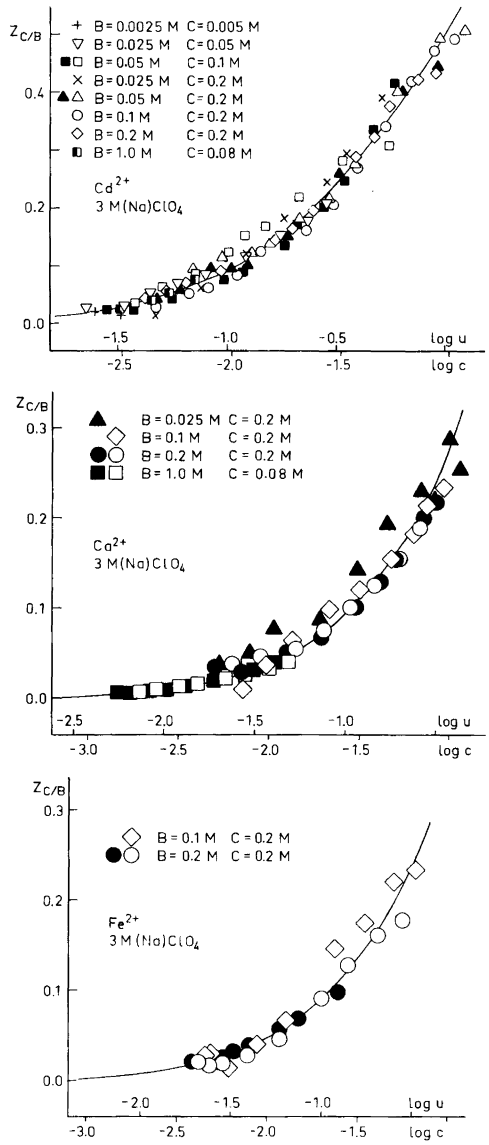

Fig. 4. $Z_{C/B}$ = the average number of C bound per B as a function of $c = [Pyr^-]$. $B \equiv Cd^{2+}$, Ca^{2+} or Fe^{2+} and $C \equiv Pyr^-$. The solid curves correspond to the final values of the constants (Table 2b).

the data was obtained. Errors were assumed in the chemical analysis of H^+ in the stock solutions. The corresponding parameters suggest negligible errors; $|\delta Z| = 0.005 - 0.01$. The final equilibrium constants are given below.

FINAL RESULTS AND DISCUSSION

We propose the following reactions and constants valid at 25 °C

$H^+ + Pyr^- \rightleftharpoons HPyr$	$\log \beta_{101} = 2.40 \pm 0.01$ in 3 M $NaClO_4$	
	$\log \beta_{101} = 2.20 \pm 0.01$ in 0.3 M $NaClO_4$	
$Ca^{2+} + Pyr^- \rightleftharpoons CaPyr^+$	$\log \beta_{011} = 0.59 \pm 0.02$ in 3 M $NaClO_4$	(7)
	$\log \beta_{011} = 0.56 \pm 0.02$ in 0.3 M $NaClO_4$	
$Fe^{2+} + Pyr^- \rightleftharpoons FePyr^+$	$\log \beta_{011} = 0.69 + 0.04$ in 3 M $NaClO_4$	
$Cd^{2+} + Pyr^- \rightleftharpoons CdPyr^+$	$\log \beta_{011} = 0.98 \pm 0.02$ in 3 M $NaClO_4$	

The errors given are three times the standard deviations. The values of pK_a for pyruvic acid agree with those reported earlier, *viz.* $pK_a = 2.49 (\mu \rightarrow 0)$,[13] 2.35-(0.5 M KCl),[7b] 2.39(0.65 M KCl),[7a] 2.10(1.0 M NaCl),[7c] all at 25 °C. The presence of 5 % dimer was taken into account. The roughly estimated values $pK_{a1} = 2.2$ and $pK_{a2} = 3.6$ for the dimers agree with those determined by Leussing and Tallman[7c] in 1 M NaCl, *viz.* $pK_{a1} = 1.73$ and $pK_{a2} = 3.72$. The expression used by us for description of the variation of activity coefficients and liquid junction potentials in 3 M (Na)ClO_4 is $E_j' = 5.6[HPyr] - 8.5[Pyr^-] - 16.8\ h$ [now with $E_0' = E_{00}$; *cf.* eqn. (3d)]. This expression may be compared with Persson's[14] expression for acetic acid in 3 M $Na(ClO_4)$, *viz.* $E_j' = 3.40[HAc] - 6.32[Ac^-]$ and our[11e] expression for ascorbic acid in 3 M $Na(ClO_4)$, *viz.* $E_j' = 13\ [H_2Asc] - 7[HAsc^-] - 16.8\ h$. The first term in E_j' is rather different for the three acids while the second term only differs slightly. If the medium is changed from 0.3 M $NaClO_4$ to 3 M $NaClO_4$ the value of pK_a changes 0.2 units, but the formation constant for $CaPyr^+$ remains the same within the limits of error. Our value of $\log \beta_{011}$ for $CaPyr^+$ is lower than Davies[4] value of 1.08 (extrapolated to zero ionic strength) and the value obtained by Schubert and Lindenbaum,[5] *viz.* 0.8 in 0.16 M NaCl. The only metal complexes formed in appreciable amounts in these systems over a time scale of a few hours seem to be $MePyr^+$. It should be noted that we also measured a few data points in more alkaline solutions than shown in Fig. 3a, which indicates a very low buffer capacity for pH ≥ 5.

Table 3. Formation constants, log β_{011} for $M^{2+} + X^- \rightleftharpoons MX^+$.

X^-	M^{2+}		
	Ca^{2+}	Fe^{2+}	Cd^{2+}
Pyr^-	0.59	0.69	0.98
$HAsc^-$	0.00	0.20	0.45

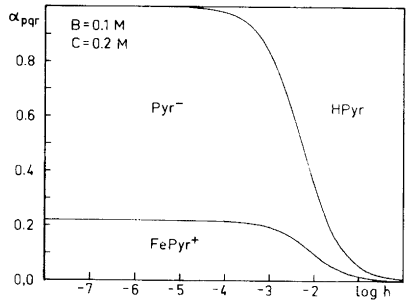

Fig. 5. The distribution of pyruvic acid among different species as a function of log *h*, calculated by means of HALTAFALL.[12c] The distribution curves for Fe^{2+} are very similar to those of Cd^{2+} and Ca^{2+}.

The metal–pyruvate complexes $MPyr^+$ are stronger than the corresponding metal–ascorbate complexes $MHAsc^+$ as can be seen in Table 3 of formation constants for metal–pyruvate and metal–ascorbate complexes.

The complexes $CdPyr^+$ and $CdHAsc^+$ are both weaker than the cadmium acetate complex $CdAc^+$. The value $\log \beta_{011} = 1.30$ for $CdAc^+$ was determined by Leden[15] and later by Gerding[16] ($\log \beta_{011} = 1.33$) in the same medium at the same temperature. The distribution of pyruvate on different species in an iron(II) pyruvate solution is demonstrated in Fig. 5.

Acknowledgements. We thank Professor Peder Kierkegaard and Professor Arne Magnéli for placing excellent facilities at our disposal. We are obliged to Miss Evelin Ehlers and Mr Ove Pettersson for their help with some of the experiments and calculations in connection with this work. Mr Anders Eriksson kindly helped us with the NMR-measurements. The English of this article was revised by Dr Don Koenig.

This investigation is financially supported by the Swedish Natural Research Council.

REFERENCES

1. Garfinkel, D., Anderson, J. and Achs, M. J. *Comput. Biomed. Res. 4* (1971) 1–125.
2. Lehninger, A. *Biochemistry*, Worth Publishers, New York 1970.
3. Sillén, L. G. and Martell, A. E. *Stability Constants, Chem. Soc. Spec.Publ. No. 17*, London 1964, and *Suppl. No. 1*, London 1969.
4. Davies, C. W. *J. Chem. Soc.* (1938) 277.
5. a. Schubert, J. and Lindenbaum, A. *J. Am. Chem. Soc. 74* (1952) 3529; b. Schubert, J., Russell, E. R. and Meyers, L. S. *J. Biol. Chem. 185* (1950) 387.
6. Chibnall, B. K. and Cannan, R. A. *Biochem. J. 27* (1933) 945.
7. a. Leussing, D. L. and Schultz, D. C. *J. Am. Chem. Soc. 86* (1964) 4846; b. Leussing, D. L. and Hanna, E. M. *J. Am. Chem. Soc. 88* (1966) 693; c. Tallman, D. E. and Leussing, D. L. *J. Am. Chem. Soc. 91* (1969) 6253.
8. Gelles, E. and Hay, R. W. *J. Chem. Soc.* (1958) 3673.
9. Tavale, S. S., Pant, L. M. and Biswas, A. B. *Acta Crystallogr. 14* (1961) 1281.
10. Forsberg, O., Johansson, K. E. and Kierkegaard, P. *To be published.*
11. a. Ulmgren, P. and Wahlberg, O. *Acta Chem. Scand. 25* (1971) 1000; b. Wahlberg, O. *Acta Chem. Scand. 25* (1971) 1045; c. Forsberg, O., Johansson, K., Ulmgren, P. and Wahlberg, O. *Chem. Scr. 3* (1973) 153; d. Ulmgren, P. and Wahlberg, O. *Acta Chem. Scand. A 28* (1974) 631; e. Ulmgren, P. and Wahlberg, O. *Chem. Scr. 8* (1975) 126; f. Ulmgren, P. and Wahlberg, O. *Chem. Commun. Univ. Stockholm* (1970) No. 4.
12. a. Arnek, R., Sillén, L. G. and Wahlberg, O. *Ark. Kemi 31* (1968) 353; b. Brauner, P., Sillén, L. G. and Whiteker, R. *Ark. Kemi 31* (1968) 365; c. Ingri, N., Kakolowicz, W., Sillén, L. G. and Warnqvist, B. *Talanta 14* (1967) 1261.
13. Pedersen, K. J. *Acta Chem. Scand. 6* (1952) 243.
14. Persson, H. *Acta Chem. Scand. 25* (1971) 1775.
15. Leden, I. *Sven. Kem. Tidskr. 58* (1946) 129.
16. Gerding, P. *Acta Chem. Scand. 22* (1968) 1283.

Received November 17, 1977.

Acta Chemica Scandinavica A 32 (1978) 353 – 359

An ESCA Investigation of Ambident Ions and Tautomerism. *N*-Cyanobenzamides and Benzohydroxamic Acids

BERNT LINDBERG,[a] ANDERS BERNDTSSON,[a] ROY NILSSON,[a] RALF NYHOLM[a] and OTTO EXNER[b]

[a] Institute of Physics, University of Uppsala, P.O.Box 530, S-751 21 Uppsala, Sweden and [b] Institute of Organic Chemistry and Biochemistry, Czechoslovak Academy of Science, Flamingovo náměstí 2, Praha 6, CSSR

Solid state N1*s* and O1*s* electron binding energies have been measured by means of ESCA for some *N*-cyanobenzamides, their alkali salts, benzohydroxamic acids, their alkali salts and one hydrochloride, as well as for reference compounds. The electron binding energy shifts are discussed in terms of the electronic structure and tautomerism of the ambident ions. Similarities of shifts imply a similar charge distribution pattern in the anions of *N*-cyanobenzamide and 4-nitrobenzohydroxamic acid, indicating that the latter behaves as an N-acid. The data for the unsubstituted benzohydroxamic acid are compatible with O-acidity. The data for benzohydroxamic acid hydrochloride are consistent with O-protonation.

The structure of prototropic (tautomeric) molecules has been studied for over a century. While the structure of undissociated molecules, *i.e.* the position of the hydrogen atom, may now be established by a variety of methods,[1] there still remains the question of the electronic structure of the corresponding ambident anion, *i.e.* the distribution of the negative charge. The available methods are then more restricted, also owing to the unfavourable physical properties of the salts. Some of them can be investigated in the solid state only. For instance *N*-cyanoamides can easily be proven[2] to exist virtually in the structure Ia (Scheme 1). It is, however, more difficult to describe the electronic structure of their anions either in terms of the charges on individual atoms or in terms of the mesomeric formulae IIa–c. In particular the prevalence of Ia does not infer IIa to be the structure of the anion.

If a prototropic molecule bears more than one potentially acidic hydrogen, an additional problem arises. The anion has still at least one hydrogen and its position is to be determined in addition to the electronic structure of the molecule. For instance, the structure of hydroxamic acids was shown[3] to be IIIa (Scheme 2), and the anion may have three different structures, IVa⟷IVb, IVc or IVd. If we accept spectroscopic and other arguments in favour of the first structure,[3–5] the question of its charge distribution still remains. Similarly for the cation of hydroxamic acids[4] two structures are possible, Va⟷Vb or Vc, corresponding to O-protonation or N-protonation, respectively.

The present investigation is an attempt to apply ESCA to these problems. The experimental O1*s* and N1*s* electron binding energies of the structures

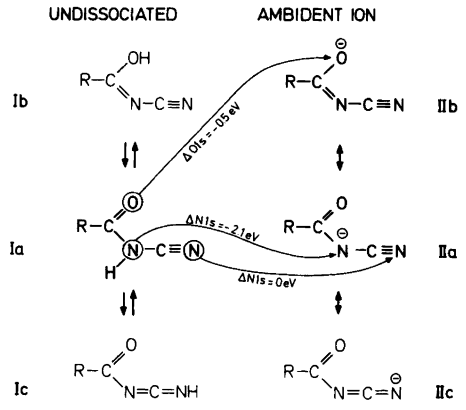

Scheme 1. N-Cyanoamides.

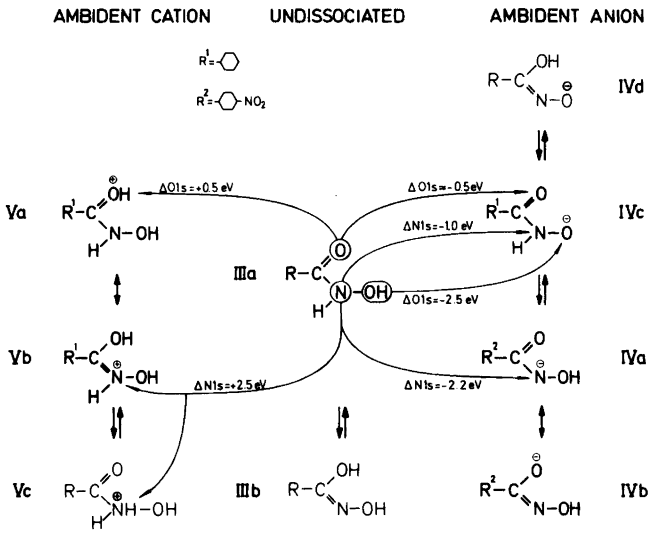

Scheme 2. Hydroxamic acids.

I–V and of reference compounds are compared and discussed in terms of chemical structure and charge pattern of the molecules. Owing to the involatility of the salts they were investigated in the solid state, and the lattice effects thus represent an inherent difficulty of the approach. However, one must take into account that many other methods are not at all applicable to non-volatile and slightly soluble compounds.

Since crystal lattice data are often lacking for organic salts their shifts can only be discussed on the level of "intuitive charges" used by chemists.[6a,7] It has been argued that the "intuitive charge" distributions are really reflexions of the potential at a given site of a molecule rather than of the actual charge distribution. This has received support by the finding that within a series of similar compounds, the core electron binding energies often correspond very well to those changes in charge distribution which would be predicted from the substituent effects on reactivity.[8]

EXPERIMENTAL

The samples were excited by Al$K\alpha$ radiation and the spectra recorded with a magnetic double-focussing spectrometer[9] equipped with a multichannel detector system.[10] The base pressure during the recordings was 1 mPa both in the sample and the analyzer compartments.

All the samples were studied in the solid state pressed on a silver backing. The C1*s* peak from the hydrocarbons ($E_b = 285.0$ eV), which coincides with the C1*s* peak from the phenyl groups, was used as a reference line to determine the binding energies.[11] This composite peak was so intense that it almost obscured other structures from chemically different carbon atoms. Thus no C1*s* binding energies were determined. Since the samples are insulators the irradiation may cause charging. The charging depends on sample thickness, geometrical arrangements in the sample compartment and the X-ray intensity (in our case the X-ray power was maintained at 40 mA/10 kV). In order to minimize the sample charging we made the samples thin. By recording spectra both from a grounded metal piece and the hydrocarbon layer on the sample surface we could compensate for the unavoidable charging. This is always possible since the hydrocarbon layer attains the same potential as the sample surface.[11] Inhomogeneous surface charging tends to broaden the electron lines, but thin and uniform samples will reduce this effect. We recorded spectra from several samples prepared from the same substance. The error in the absolute binding energies was estimated to ± 0.3 eV. However, the binding energy shifts are determined more accurately, since systematical errors do not enter.

Compounds *8*–*19* (Table 1) were characterized in previous works[2,3,5] and compounds *1a*, *b*, *2*, *4*, *5* and *7* were commercial laboratory reagents. Samples of compound *19*, which is very hygroscopic, were prepared in dry nitrogen atmosphere. In vacuum

the sample releases HCl. The resulting spectrum is thus a superposition of the spectra of compounds *9* and *19*, but chemical shifts of the N1*s* and O1*s* levels between the hydrochloride and the parent compound are large enough for the different chemical states to be easily identified in the electron spectrum.

In most cases the peaks in the spectra were sufficiently well-separated to allow a straightforward energy determination. For composite peaks we assumed that all components had the same line width. The number of components and their relative intensities are known from the chemical formulae. With these assumptions it is possible to make an analytical deconvolution using Voigt functions for the line profiles. For the deconvolution the narrowest observed line width for single peaks was used as a standard line width. This procedure was used for compounds *8*–*11*, *15*, *18* and *19*.

An attempt to run a spectrum of cyanamide in the vapour state failed due to polymerization when the sample was heated in order to evaporate it under vacuum.

RESULTS

The measured N1*s* and O1*s* electron binding energies are given in Table 1. The relevant shifts of the amidic nitrogen, cyano nitrogen, carbonyl oxygen and hydroxyl oxygen are graphically represented in Figs. 1–3.

Cyanobenzamides. Cyanamide (*4*) and cyanobenzamides (Nos. *9*–*11*) contain two types of nitrogen in the same molecule. (*N*-benzylcyanamide (*8*) exists as a trimer in the solid state.) For cyanamide the nitrogen peak is not broad enough to warrant a decomposition into two peaks of different binding energies, therefore the two nitrogen atoms are found to have about equal N1*s* binding energies in the solid state. The same is the case for the cyanobenzamide salts (*12*–*14*) but the N1*s* binding energy is shifted to a lower value compared to cyanamide (0.5 eV). In the undissociated cyanobenzamides there is a considerable internal nitrogen shift (2.1 eV). The lowest binding energy is assigned to the cyano nitrogen.

Table 1. Experimental N1*s* and O1*s* electron binding energies (eV).

	Compound [e]	N1*s*			O1*s*		
		N–H	C≡N	NO_2	C=O	O–H	Other
1a	Cl–C_6H_4–COOH [a]				532.3	533.6	
1b	C_6H_5–CO_2Na						531.6
2	C_6H_5–$CONH_2$	399.7			532.4		
3	H_3C–CN		399.8 [b]				
4	H_2N–CN	399.4	399.4				
5	NaO–CN		398.7				532.0
6	C_6H_5–CN		399.4 [c]				
7	O_2N–C_6H_4–CN		399.2	405.8			532.2
8	[C_6H_5–CH_2NHCN]$_3$	400.7	398.4				
9	C_6H_5–CONHCN	401.2	398.9		532.1		
10	H_3C–C_6H_4–CONHCN	400.6	398.7		532.5		
11	Br–C_6H_4–CONHCN	401.2	399.1		532.1		
	Mean value (*9*–*11*)	401.0	398.9		532.2		
12	C_6H_5–CONCN/Na	399.0	399.0		531.8		
13	H_3C–C_6H_4–CONCN/Na	398.9	398.9		531.5		
14	Br–C_6H_4–CONCN/Na	398.9	398.9		531.8		
	Mean value (*12*–*14*)	398.9	398.9		531.7		
15	C_6H_5–CONHOH	401.4			531.8	533.8	
16	O_2N–C_6H_4–CONHOH	401.0		405.8	——	532.6 [d]	——
17	C_6H_5–CONOH/K	400.4			531.3	531.3	
18	O_2N–C_6H_4–CONOH/Na	398.8		406.1	——	532.2 [d]	——
19	C_6H_5–$CONH_2$OH/Cl	403.9			532.3	534.7	

[a] The unsubstituted benzoic acid was too volatile in the vacuum of the spectrometer. [b] From Ref. 20 adjusted to solid state. [c] From Ref. 17. [d] Undeconvoluted O1*s* peaks. [e] Compounds *1a*, *7*, *10*, *11*, *13*, *14*, *16* and *18* are 4-substituted.

Table 2. Internal N1*s* electron binding energy shifts $\Delta(N^2-N^1)$, eV.

Compound	Calculated CNDO/2[a]		Found
	TPM	GPM	
$PhCON^2HCN^{1\,b}$	4.5	3.9	2.2
$H_2N^2CN^{1\,c}$	2.9	2.7	<0.5

[a] Geometrical data (bond angles and bond lengths) are estimated within the limits of standard values. [b] For the −CONH− group geometrical data from acetobenzohydroxamic acid were used [21]. [c] Data from Ref. 22.

In order to support this assignment of the N1*s* binding energies we performed CNDO/2 calculations on the two neutral compounds (*4* and *9*) using geometrical data based on the *Z*-conformation around the C−N bond as determined from solution dipole moments.[2] The lattice effects cannot be accounted for in a calculation unless the crystal structure is known. Especially for ionic salts these can be of great importance. Thus, we restricted ourselves to neutral compounds. We used both the ground state potential model (GPM)[6b] and the transition state potential model (TPM),[12-14] the latter accounting for relaxation energies. The results are given in Table 2 and both models give the same assignment. Our assignment is also supported by comparing the N1*s* binding energies with those of other compounds investigated, taking account of appropriate substituent effects.

The amide nitrogen in the neutral compound has a lower binding energy than that of the corresponding salt ("salt shift" of −2.1 eV), as would be expected for the creation of a formal negative charge on this atom (limiting structure IIa). The O1*s* binding energies situated in the carbonyl region also have lower values in the salts (−0.5 eV). The cyano nitrogen is unaffected by salt formation.

The experimental internal N1*s* shifts listed in Table 2 are about 2 eV smaller than the calculated ones. Levelling effects of this kind have previously been attributed to hydrogen bonding.[6c,15] Thus for acetic acid the binding energy difference of O1*s* between the =O and −OH groups is 1.8 eV in the vapour state but is not resolved in the solid state due to intermolecular $=O\cdots HO-$ hydrogen bonding.[6c] Similar levelling effects on anticipated internal shifts can be visualized for cyanobenzamides by intermolecular hydrogen bonding, involving either the cyano nitrogen or the carbonyl oxygen.

Benzohydroxamic acids. For 4-nitrobenzohydroxamic acid (*16*) the N1*s* salt shift is −2.2 eV, just equal to that in cyanobenzamides. The similarity of these salt shifts would be in agreement with structure IVa, b for the 4-nitrobenzohydroxamate (*18*). In the unsubstituted benzohydroxamic acid the N1*s* salt shift is much smaller, −1.0 eV suggesting structure IVc for the salt.

The highest O1*s* binding energies in the unsubstituted benzohydroxamic acid and its protonated form are assigned to the N−OH group, and the lower to the C=O group. This is done in analogy to the carboxylic acids where the −OH group has a binding energy about 1−2 eV higher than that of the >C=O group[6d,16] (in compound *1a*, 1.3 eV). In 4-nitrobenzohydroxamic acid and its salt the O1*s* spectra include components from the nitro group oxygens and could not be deconvoluted with any confidence. In the alkali salt of unsubstituted benzohydroxamic acid (*17*) the high binding energy

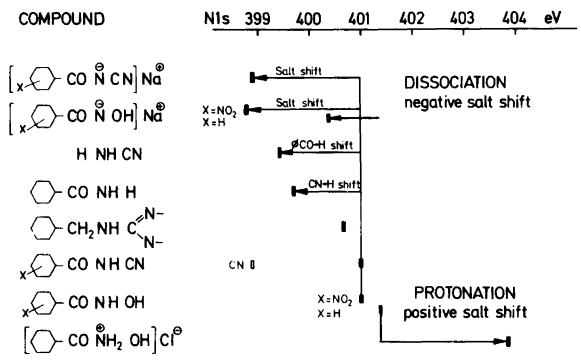

Fig. 1. Chart of N1*s* electron binding energies for amide nitrogen in a series of aromatic amidic compounds.

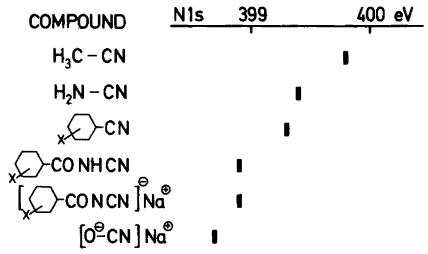

Fig. 2. Chart of N1*s* electron binding energies for cyano nitrogen in a series of cyano compounds.

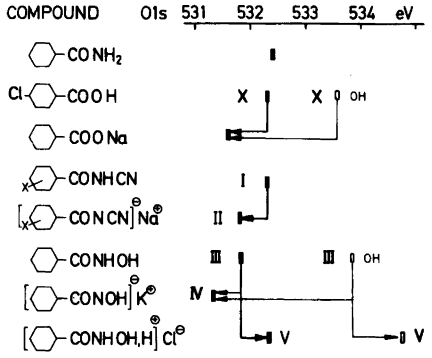

Fig. 3. Chart of O1*s* electron binding energies for carbonyl oxygen in a series of aromatic carbonyl compounds.

O1*s* component disappears. The narrowness of the O1*s* peak indicates that the two oxygen atoms have closely equal binding energies.

In the protonated benzohydroxamic acid (*19*) both the N1*s* and O1*s* salt shifts are in the opposite direction to those of the corresponding alkali salt and of a similar magnitude.

DISCUSSION

Amide nitrogen. With our assignment the substituent effects on the N1*s* binding energies of the cyanoamides indicated in Fig. 1 are consistent with previously known group shifts [17] for the substituents. The amide N1*s* electron binding energy for benzohydroxamic acids is about the same as for cyanobenzamides. The substituent effects of $-CN$ and $-OH$ are thus similar in these compounds.

Cyano nitrogen. For the cyano nitrogen (Fig. 2) there are significant substituent effects although effects from more distant atoms (second-order substituent effects) are usually small in ESCA.[18] However, in the present compounds the cyano nitrogen is a terminal atom in a conjugated structure. In such cases mesomeric electron displacements may cause significant second-order effects, and shifts up to 1 eV have previously been observed.[18,19] Also in this case the substituent effects cover a shift span of -1 eV from the acetonitrile (*3*) as a reference. This indicates strong $+M$ effects.

Carbonyl oxygen. For the cyanobenzamides we observe a small but significant O1*s* salt shift towards lower binding energy (-0.5 eV, Fig. 3). The shift is in the same direction as in going from carboxylic acid or benzamide to carboxylate, which indicates a delocalization of charge to the carbonyl oxygen in the salts (IIa↔IIb). For the unsubstituted benzohydroxamic acid there is a similar O1*s* salt shift (-0.5 eV) suggesting a similar charge delocalization pattern.

Hydroxyl oxygen. If we assume $N-H$ acidity for the benzohydroxamic acids we would expect to find the O1*s* $-OH$ component shifted according to the weight of the limiting structures IVa, b. Limiting structure IVa would require a slight shift towards lower binding energies due to a negatively charged adjacent nitrogen. For the unsubstituted benzohydroxamic acid, however, this component suffers a large shift (-2.5 eV), which is of the same magnitude as the salt shift for benzoic acid (-2.0 eV, Fig. 3). This is more consistent with $O-H$ acidity (IVc) which would be further supported by the smaller N1*s* salt shift (-1.0 eV) for the unsubstituted benzohydroxamic acid as compared with that of the 4-nitrosubstituted acid (-2.2 eV). This shift as well as the still smaller carbonyl shift (-0.5 eV) could well be explained as a potential effect caused by the neighbouring negative oxygen in IVc. These results indicate different tautomeric forms for 4-nitrobenzohydroxamate and benzohydroxamate in the solid state. Other spectroscopic and p*K* investigations indicate that in solution stronger hydroxamic acids are with certainty pure N-acids while in the weaker ones some O-dissociation may take place.[3,5] A more definite interpretation of the O1*s* as well as the N1*s* shifts in the salts would require knowledge of the crystal structure and a better understanding of the lattice effects on the ESCA shifts.

Benzohydroxamic acid. The protonated benzohydroxamic acid has previously been assumed to have structure Va↔Vb.[4] The N1*s* shift between the

acid and its protonated form (+2.5 eV) would in this case be consistent with a considerable weight of limiting structure Vb, *i.e.* O-protonation. A large N1*s* shift would, however, also be consistent with structure Vc, *i.e.* N-protonation. This is, however, less likely because of the loss of conjugation in this structure.[4]

The O1*s* component in the carbonyl region can be discussed in more detail on the basis of the carboxylic acid–carboxylate model VI (Scheme 3). Because of the symmetry of the anion VIa, b the carbonyl O1*s* salt shift (−0.7 eV) may serve as a standard salt shift for anions, where the limiting structures of type VIIIa↔VIIIb have equal weight. The smallness of this shift indicates a considerable counter ion effect. The creation of half a negative charge unit on oxygen would in a free ion be expected to cause a shift of about −3 eV.[6c] By analogy the O1*s* shift for a protonated carboxyl group (VII) would reasonably be expected to have the same magnitude but in the opposite direction. This may similarly serve as a standard salt shift for a protonation, where the limiting structures of the cations IXa↔IXb have equal weight.

The aromatic amidic compounds under investigation are of similar size and shape as the benzoic acid models Nos. *1a, b*. It thus seems reasonable to assume similar lattice effects. By analogy similar carbonyl O1*s* shifts would thus be expected for compounds of type VI/VIII and VII/IX, respectively. The difference of −0.5 eV between Ia and IIa, b (Scheme 1) may thus serve as a standard shift for VIII. We would thus expect a shift of about +0.5 eV for IX. Consequently the carbonyl shift of +0.5 eV for protonated benzohydroxamic acid would be consistent with structure Va↔Vb.

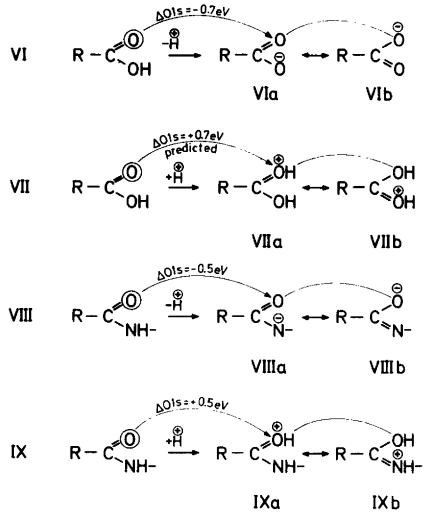

Scheme 3. Carbonyl groups.

SUMMARY

1. Cyanobenzamides and 4-nitrobenzohydroxamic acid have similar N1*s* and O1*s* salt shifts indicating similar structures with similar charge delocalization patterns for the corresponding anions.

2. *Cyanobenzamides.* The O1*s* salt shift indicates a delocalization of the negative charge in the anion to the carbonyl oxygen (IIa, b), similar to that occurring in carboxylate anions. The N1*s* shift of cyano nitrogen indicates negligible contribution of IIc.

3. *Benzohydroxamic acid.* The N1*s* salt shift for 4-nitrobenzohydroxamic acid is consistent with N–H acidity and delocalization of the charge to the carbonyl oxygen in the anion (IVa, b).

A smaller N1*s* salt shift for the unsubstituted benzohydroxamic acid could account for O–H acidity, which is also favoured by the O1*s* shift of the −OH group. For protonated benzohydroxamic acid the shifts are reversed when compared to the corresponding alkali salt shifts. The carbonyl O1*s* shift in conjunction with the N1*s* shift suggests O-protonation with a considerable delocalization of the positive charge to nitrogen (Va, b).

Acknowledgements. We thank Rein Maripuu for technical assistance. This work has been supported by the Swedish Natural Science Research Council.

REFERENCES

1. Elguero, J., Marzin, C., Katritzky, A. R. and Linda, P. *The Tautomerism of Heterocycles*, Academic, London 1976.
2. Janák, P. and Exner, O. *Collect. Czech. Chem. Commun. 40* (1975) 2052.
3. Bauer, L. and Exner, O. *Angew. Chem. 86* (1974) 419.
4. Exner, O. and Kakáč, B. *Collect. Czech. Chem. Commun. 28* (1963) 1656.
5. Exner, O. and Simon, W. *Collect. Czech. Chem. Commun. 30* (1965) 4078.
6. a. Siegbahn, K., Nordling, C., Johansson, G., Hedman, J., Hedén, P. F., Hamrin, K., Gelius, U., Bergmark, T., Werme, L. O. and Baer, Y. *ESCA Applied to Free Molecules*, North-

Holland, Amsterdam 1971, and references therein; b. *Ibid.* Chapter 5.4; c. *Ibid.* p. 126; d. *Ibid.* p. 120.
7. Clark, D. T., Chambers, R. D., Kilcast, D. and Musgrave, K. R. *J. Chem. Soc. Faraday Trans. 2 68* (1972) 309.
8. Lindberg, B., Svensson, S., Malmquist, P. Å., Basilier, E., Gelius, U. and Siegbahn, K. *Chem. Phys. Lett. 40* (1976) 175.
9. Nordberg, R., Hedman, J., Hedén, P. F., Nordling, C. and Siegbahn, K. *Ark. Fys. 37* (1968) 489.
10. Gelius, U., Basilier, E., Svensson, S. and Siegbahn, K. *J. Electron Spectrosc. Relat. Phenom. 2* (1973) 405.
11. Johansson, G., Hedman, J., Berndtsson, A., Klasson, M. and Nilsson, R. *J. Electron Spectrosc. Relat Phenom. 2* (1973) 295.
12. Siegbahn, H., Medeiros, R. and Goscinski, O. *J. Electron Spectrosc. Relat. Phenom. 8* (1976) 149.
13. Howat, G. and Goscinski, O. *Chem. Phys. Lett. 30* (1975) 87.
14. Davis, D. W. and Shirley, D. A. *J. Electron Spectrosc. Relat. Phenom. 3* (1974) 137.
15. Clark, D. T. In Dekeyser, W., Fiermans, L., Vanderkelen, G. and Vennik, J., Eds., *Electron Emission Spectroscopy*, Reidel Publishing Co, Dordrecht-Holland 1973, p. 441.
16. Schwartz, M. E., Switalski, J. D. and Stronski, R. In Shirley, D. A., Ed., *Electron Spectroscopy*, North-Holland, Amsterdam 1972, p. 605.
17. Lindberg, B. J. and Hedman, J. *Chem. Scr. 7* (1975) 155.
18. Lindberg, B. J. *XXIIIrd IUPAC Congress, Boston 1971*, Butterworths, London 1971, Vol. 7, p. 33.
19. Lindberg, B. J. and Hamrin, K. *Acta Chem. Scand. 24* (1970) 3661.
20. Stucky, G. D., Matthews, D. A., Hedman, J., Klasson, M. and Nordling, C. *J. Am. Chem. Soc. 94* (1972) 8009.
21. Bracher, B. M. and Small, R. W. H. *Acta Crystallogr. B 26* (1970) 1705.
22. Tyler, J. K., Thomas, L. F. and Sheridan, J. *Proc. Chem. Soc. London* (1959) 155.

Received November 14, 1977.

Acta Chemica Scandinavica A 32 (1978) 361–366

The Crystal and Molecular Structure of the Violet Form of Tris(β-alaninato)cobalt(III) Tetrahydrate

H. SOLING

Chemistry Department B, Structural Chemistry Group, Technical University of Denmark, DK-2800 Lyngby, Denmark

The crystals of the title compound are monoclinic, space group $P2_1/n$, with four formula units in a unit cell with $a=5.666(2)$ Å, $b=12.868(1)$ Å, $c=22.215(3)$ Å, $\beta=90.66(3)°$ at 22 °C. The solution and refinement of the structure was based on 1577 unique non-zero reflections measured with a four-circle diffractometer. The full matrix least squares refinement terminated with $R=0.046$, $R_w=0.048$. The configuration of the tris(β-alaninato)cobalt complex is *meridional*. The average Co-ligator distance is 1.929 Å. No characteristic Co–O or Co–N distance is found. The bond lengths and angles of the β-alanine residue are normal. The conformations of the chelate rings are twist-boat; the sense of the twist of one ring is opposite to that of the other two. One molecule of water of crystallization connects four complex molecules by hydrogen bonds. The remaining three water molecules, which complete the tetrahydrate formula, are randomly distributed in channels around $x,0,0$ and $x,\frac{1}{2},\frac{1}{2}$.

The development of elaborate methods for calculating the minimum energy conformation of complexes of trivalent metals with bidentate ligands has created an interest in accurate structural data. Conformational analyses of tris(diamino) compounds of Co(III) have been undertaken by Niketić and Woldbye.[1] The results of the crystal structure analysis of tris(β-alaninato)cobalt(III) tetrahydrate, reported in this paper, provide data for the more complicated case of a bidentate ligand with different ligators.

EXPERIMENTAL

Needle-like, bluish-violet crystals of tris(β-alaninato)cobalt(III) tetrahydrate, henceforth called $Co(\beta\text{-ala})_3$ were prepared by S.R. Niketić, University of Beograd.[2] A single crystal, approximately $0.17\times0.12\times0.05$ mm^3, was picked directly from the mother liquor.

The unit cell dimensions, the space group extinctions as well as a unique set of reflection intensities were measured with a CAD4 four-circle diffractometer. Monochromatized (graphite) Mo$K\alpha$ radiation ($\lambda=0.71069$ Å) was used. The crystal data and some technicalities of the collection and treatment of data are as follows:

$Co(C_3H_6NO_2)_3.4H_2O$, FW = 395.2
$a=5.666(2)$ Å, $b=12.868(1)$ Å, $c=22.215(3)$ Å,
$\beta=90.66(3)°$, $V=1619.6$ Å^3 at 22 °C.
D_m (flot.) = 1.62 g cm^{-3}, $D_x(Z=4)=1.621$ g cm^{-3}.
μ(Mo$K\alpha$) = 11.6 cm^{-1}.

Systematically absent reflections: $h0l$ for $h+l$ odd, $0k0$ for k odd. Space group $P2_1/n$. Coordinates of general positions $\pm(x,y,z)$ and $\pm(\frac{1}{2}-x,\frac{1}{2}+y,\frac{1}{2}-z)$.

All unique reflections in the interval $4°<\theta<28°$ were $\omega/2\theta$ scanned. The width of the scan was $(1.2+0.35\tan\theta)°$. The width of the variable horizontal detector aperture was $(2.5+\tan\theta)$ mm. The intensity of a control reflection of medium intensity, remeasured at intervals of ~4000 s of exposure time, did not show significant variations.

The solution and refinement of the structure was based on 1577 unique reflections having $|F|<\sqrt{2}\sigma(F)$. The number of variables involved in the refinement was 280.

Computional details. The observed net intensities, I, were reduced to relative structure factors and assigned a standard deviation calculated from the counting statistics. The usual Lorentz and polariza-

tion corrections were applied, but no corrections were made for absorption, extinction or anomalous dispersion. All crystallographic calculations were made with the X-RAY program system,[3] which also generates atomic form factors from given constants.[4,5] Form factors for neutral atoms were used. The full matrix, least squares calculation minimizes $\Sigma w(\Delta F_o)^2$, $\Delta F = \| F_o | - | F_c \|$. During the final stages of refinement a weight function $1/w = 0.193 + 1.66(\sigma F)^1 + 0.0590|F| - 0.000220|F|^2 - 1.152 \sin\theta/\lambda$ was used. The coefficients of the function were determined by a least squares calculation[6] minimizing

$$S = 1 + \frac{\Sigma w(\Delta F)^2 \log (w(\Delta F)^2}{\log N}$$, where N is the number of reflections.

The residual $R = \Sigma|\Delta F|/\Sigma F_0$; the weighted residual

$$R_w = \left(\frac{\Sigma w(\Delta F)^2}{\Sigma w F_o{}^2}\right)^{\frac{1}{2}}.$$

SOLUTION AND REFINEMENT OF THE STRUCTURE

The sites of all non-hydrogen atoms of the complex molecule and 1 molecule of water of crystallization were determined by the heavy atom method. The refinement, which initially proceeded steadily, came to a halt at $R = 0.1$. A difference electron density map showed positive regions indicating the presence of disordered water molecules. A thermogravimetric analysis supported this interpretation; 3 water molecules out of 4 were loosely bond. When 6 oxygen half-atoms were placed in the intermolecular channels extending in the a-direction, the refinement process continued. All hydrogen atoms, except those of the disordered water molecules, showed up on another difference map. After two more cycles of least squares calculations the refinement was completed. The final residual indexes were $R = 0.046$ and $R_w = 0.048$. A final difference Fourier map did not show any

Table 1. Fractional atomic coordinates and anisotropic thermal parameters for the non-hydrogen atoms of the complex. Standard deviations in parentheses. The form of the temperature factor expression is $\exp[-2\pi^2 \Sigma_{ij} h_i h_j a_i^* a_j^* U_{ij}]$. All U-values have been multiplied by 10^3.

	x	y	z	U_{11}	U_{22}	U_{33}	U_{12}	U_{13}	U_{23}
Co	0.2222(1)	0.06243(6)	0.034917(3)	22.3(3)	35.6(4)	27.5(4)	2.2(4)	−2.3(2)	0.4(4)
Ligand 1									
N	0.0128(8)	0.0126(4)	0.2857(2)	25(2)	40(3)	38(3)	2(2)	−4(2)	2(2)
O1	0.4755(6)	0.0942(3)	0.2964(2)	27(2)	51(3)	36(2)	−6(2)	−2(2)	5(2)
O2	0.6435(7)	0.1409(4)	0.2124(2)	38(2)	65(3)	50(3)	−10(2)	8(2)	10(2)
C1	0.115(1)	−0.0075(5)	0.2258(3)	37(3)	64(4)	35(3)	−6(3)	−4(3)	−8(3)
C2	0.246(1)	0.0857(6)	0.2042(3)	38(3)	87(3)	33(3)	−8(3)	−2(3)	7(3)
C3	0.4678(9)	0.1089(5)	0.2397(3)	29(3)	40(3)	47(4)	3(3)	2(3)	6(3)
Ligand 2									
N	0.3687(7)	−0.0712(4)	0.3599(2)	31(2)	45(3)	32(2)	6(2)	−1(2)	−1(2)
O1	−0.0299(6)	0.0332(3)	0.4031(2)	33(3)	47(2)	33(2)	10(2)	4(2)	−9(2)
O2	−0.2645(7)	−0.0573(4)	0.4610(2)	29(2)	79(3)	42(2)	4(2)	6(2)	9(2)
C1	0.226(1)	−0.1591(5)	0.3807(3)	43(4)	42(4)	47(4)	3(3)	3(3)	3(3)
C2	0.1067(11)	−0.1332(5)	0.4387(3)	45(4)	51(4)	43(4)	9(3)	11(3)	9(3)
C3	−0.0732(9)	−0.0484(5)	0.4344(2)	30(3)	53(4)	26(3)	−2(3)	−4(2)	−7(3)
Ligand 3									
N	0.4226(8)	0.1184(4)	0.4144(2)	37(3)	52(3)	34(3)	7(2)	−9(2)	−7(2)
O1	0.0771(7)	0.1947(3)	0.3325(2)	44(2)	35(2)	40(2)	5(2)	−7(2)	−1(2)
O2	−0.0546(3)	0.3522(3)	0.3487(2)	62(3)	41(3)	59(3)	12(2)	1(2)	3(2)
C1	0.448(1)	0.2307(6)	0.4169(3)	53(4)	57(5)	52(4)	−6(3)	−19(3)	−2(3)
C2	0.217(2)	0.2835(6)	0.4201(4)	102(6)	48(4)	56(5)	11(4)	−19(4)	−15(4)
C3	0.069(1)	0.2766(5)	0.3633(3)	39(3)	38(4)	41(4)	−1(3)	8(3)	9(3)

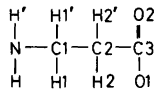

Scheme 1. Labelling scheme for the atoms of the β-alanine residue.

distinct features. The atomic coordinates and the temperature factors are listed in Tables 1 and 2. A list of observed and calculated structure factors may be obtained from this institute.

RESULTS AND DISCUSSION

The present crystal structure analysis confirms the result of previous, mainly spectroscopic, investigations.[2] The configuration of the complex is *meridional.*

The coordination polyhedron, shown schematically in Fig. 1, is a slightly deformed octahedron. The distances from the Co atom to the ligators O and N vary from 1.907(4) to 1.967(5) Å. No characteristic Co–N or Co–O distance is found. On the other hand, the Co–O distance is always the smaller in each particular chelate ring. The same holds for all the complexes quoted in Table 3 except for the A

Table 2. Fractional atomic coordinates and isotropic thermal parameters of hydrogen and oxygen (water) atoms. [a] Standard deviations in parentheses.

	x	*y*	*z*	*B*(Å^2)
Ligand 1				
H	−0.061(9)	−0.037(4)	0.293(2)	3.9
H′	−0.089(9)	0.059(4)	0.281(2)	3.9
H1	0.214(9)	−0.069(4)	0.230(2)	3.9
H1′	−0.020(9)	−0.030(4)	0.197(2)	3.9
H2	0.275(9)	0.075(4)	0.163(2)	3.9
H2′	0.135(9)	0.150(4)	0.210(2)	3.9
Ligand 2				
H	0.432(9)	−0.089(4)	0.327(2)	3.9
H′	0.467(4)	−0.071(4)	0.386(3)	3.9
H1	0.110(9)	−0.176(4)	0.354(2)	3.9
H1′	0.328(9)	−0.219(4)	0.389(2)	3.9
H2	0.039(9)	−0.186(4)	0.451(3)	3.9
H2′	0.226(9)	−0.112(4)	0.467(2)	3.9
Ligand 3				
H	0.361(9)	0.102(4)	0.447(3)	3.9
H′	0.550(9)	0.093(4)	0.413(2)	3.9
H1	0.555(9)	0.253(4)	0.452(2)	3.9
H1′	0.522(9)	0.250(4)	0.381(2)	3.9
H2	0.138(9)	0.250(4)	0.453(2)	3.9
H2′	0.237(9)	0.349(4)	0.431(2)	3.9
Water				
O	0.8221(8)	0.3380(4)	0.2290(2)	4.1(1)
H	0.858(9)	0.354(4)	0.254(2)	3.9
H′	0.763(9)	0.289(4)	0.221(3)	3.9
W1	0.149(3)	0.097(2)	0.039(1)	13.3(7)
W2	0.266(3)	0.103(1)	0.0345(8)	10.0(6)
W3	0.681(4)	0.050(2)	0.0950(9)	13.4(7)
W4	0.775(3)	0.166(1)	0.0922(8)	12.2(7)
W5	0.593(4)	−0.004(2)	0.0585(9)	13.2(7)
W6	0.841(4)	−0.027(2)	0.074(1)	15.0

[a] W = oxygen half-atom.

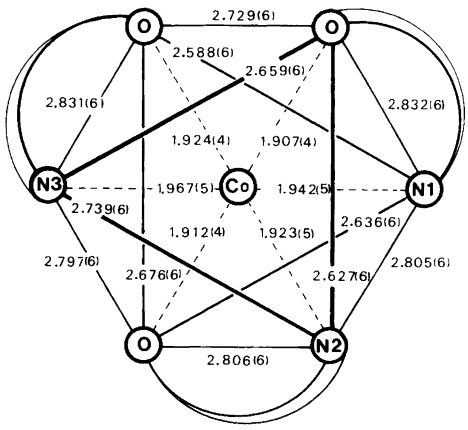

Fig. 1. Interatomic distances (Å), with standard deviations, in the coordination octahedron.

molecule in $Cu(\beta\text{-ala})_2.4H_2O$. The reversal in the A molecule is due to the repulsive force of the carbonyl O atom of the adjacent B molecules occupying the *trans* positions of the A molecule.

Bond lengths and angles involving only non-hydrogen atoms of the three β-alanine residues are shown in Fig. 2. The average N–H and C–H bond lengths are 0.82(3) and 0.95(6) Å, respectively.

In Table 3 average values of the bonds are compared with results from the recent literature. The C3–O1 bond, as well as the N–C1 bond, in the cited complexes is the same as in the pure amino acid. The C3–O2 bond, as well as the bonds C1–C2 and C2–C3, is significantly shorter in the complexes, (except C2–C3 in $KCo(\beta\text{-ala})_2(NO_2)_2$). In addition to the complexes mentioned above only two other β-alaninato compounds have been reported,[11] *viz.* $Ni(\beta\text{-ala})_2.2H_2O$ and $Cu(\beta\text{-ala})_2$.-

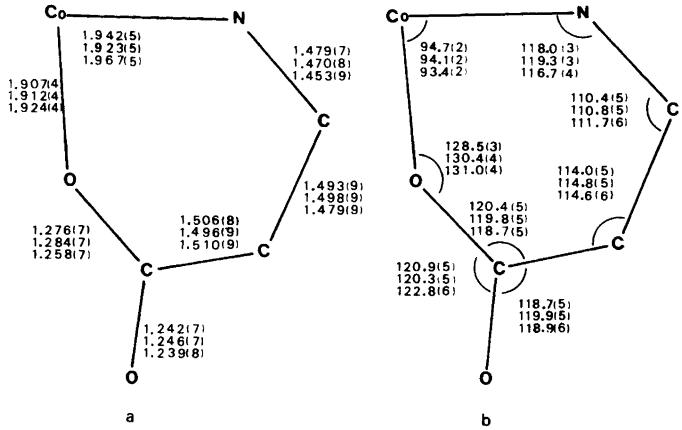

Fig. 2. a. Bond lengths (Å), and *b.* bond angles (°) in the chelate rings. Standard deviations in parentheses.

Table 3. Bond lengths in (Å) in β-alanine and some β-alaninato complexes. $\tilde{\beta}$ = β-alaninato. tn = 1,3-diaminopropane. Standard deviations in parentheses.

Bond	β-Alanine Ref. 7	$KCO\tilde{\beta}_2(NO_2)_2$ Ref. 8	$Co\tilde{\beta}tn(NO_2)_2$ Ref. 9	$Cu\tilde{\beta}_2.4H_2O$ Ref. 10 A	B	$Co\tilde{\beta}_3.4H_2O$ This paper		
Co–O1		1.913(8)	1.912(5)	2.015(3)	1.960(4)	1.907(4)	1.812(4)	1.924(5)
Co–N		1.956(9)	1.962(6)	1.967(4)	1.987(3)	1.942(5)	1.923(4)	1.967(5)
N–C1	1.478(10)	1.463(14)	1.469(9)	1.473(6)	1.483(7)	1.467(14)		
C3–O1	1.287(9)	1.279(13)	1.272(8)	1.276(6)	1.274(7)	1.273(13)		
C3–O2	1.292(9)	1.227(13)	1.238(8)	1.250(7)	1.247(5)	1.242(4)	Average[a]	
C1–C2	1.551(10)	1.521(15)	1.492(10)	1.511(8)	1.503(8)	1.490(10)		
C2–C3	1.553(10)	1.543(15)	1.513(10)	1.507(8)	1.507(8)	1.504(7)		

[a] Sample standard deviation = $[\sum_i (d_i - \bar{d})^2/(n-1)]^{\frac{1}{2}}$.

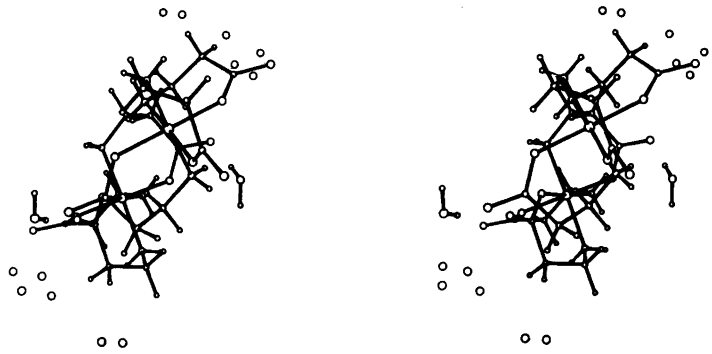

Fig. 3. Stereo pair showing two Co(β-ala)$_3$.4H_2O units related by a center. The disordered water molecules, W in Table 2, are shown as isolated open circles.

6H_2O. In general the structures of these compounds are in agreement with the results of this investigation. A detailed comparison, however, is prohibited by the low accuracy of the reported data.

The chelate rings of Co(β-ala)$_3$.4H_2O have the twist-boat conformation. The twisting is easily seen on the ORTEP[12] stereo drawing, Fig. 3. The sense of the twist of one ligand (No. 3 in Table 1) is opposite to that of the other two. Quantitatively, the twist may be expressed in terms of the torsion angles listed in Table 4. Inspection of all available data on torsion angles reveals rather large varia-

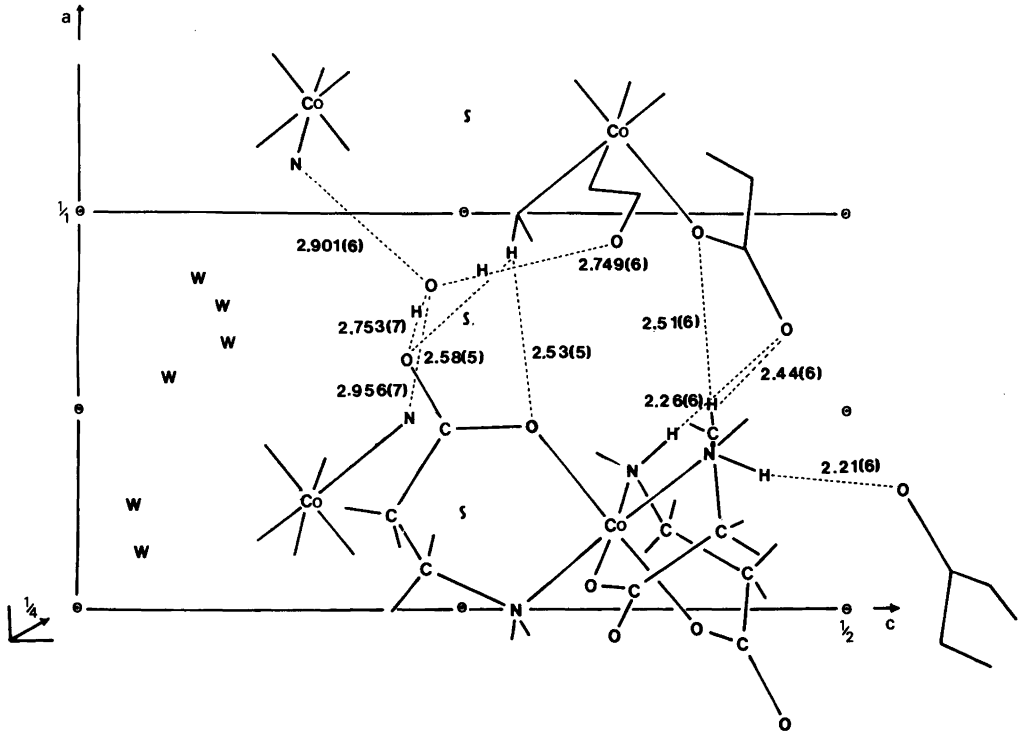

Fig. 4. Schematic projection of the structure on the *ac*-plane, showing the hydrogen bonds and the short *inter*-complex contacts (Å). Standard deviations in parentheses. The disordered water molecules, W in Table 2, have been calculated as oxygen half-atoms.

Table 4. Torsion angles with standard deviations. Signs as recommended by the IUPAC-IUB commission.[13]

Atoms	Angles (°) Ligand 1	Ligand 2	Ligand 3
N–Co–O1–C3	19.8(5)	0.7(5)	−16.7(5)
Co–O1–C3–C2	−9.6(8)	9.2(7)	8.4(8)
O1–C3–C2–C1	−36.8(8)	−42.2(8)	36.6(9)
C3–C2–C1–N	68.5(7)	65.4(7)	−69.2(8)
C2–C1–N–Co	−53.0(6)	−55.4(6)	55.7(6)
C1–N–Co–O1	12.8(4)	22.8(4)	−16.2(4)

tions. There is no fixed standard conformation of the β-alaninato chelate ring. A constant feature, though, is the coplanarity of the atoms C2, C3, O1, O2.

The packing of the complexes and the water molecules in the unit cell is illustrated in Fig. 4. The short *inter*-complex contacts are all of the type H···O. One molecule of water connects four complexes by hydrogen bonds. The remaining three water molecules, which complete the tetrahydrate formula, are randomly distributed in the channels around $x,0,0$ and $x,\frac{1}{2},\frac{1}{2}$.

Acknowledgements. I thank S. R. Niketić for supplying the crystals, and B. Saustrup Kristensen for performing the thermogravimetric analysis.

REFERENCES

1. Niketić, S. R. and Woldbye, F. *Acta Chem. Scand. 27* (1973) 621, 3811; *A 28* (1974) 248.
2. Ćelap, M. B., Niketić, S. R., Jantić, T. J. and Nikolić, V. N. *Inorg. Chem. 11* (1967) 2063.
3. *X-RAY Program System for X-Ray Crystallography 1972*, Computer Science Center, University of Maryland, College Park 1972.
4. Cromer, D. T. and Man, J. B. *Acta Crystallogr. A 24* (1968) 321.
5. Stewart, R. F., Davidson, E. and Simpson, W. *J. Chem. Phys. 42* (1968) 3175.
6. Nielsen, K. *Acta Crystallogr. A 33* (1977) 1009.
7. José, P. and Pant, L. M. *Acta Crystallogr. 18* (1965) 806.
8. Prelesnik, B., Ćelap, M. B. and Herak, R. *Inorg. Chim. Acta 9* (1973) 569.
9. Herak, R. M., Ćelap, M. B. and Krstanović, I. *Private communication.*
10. Mitsui, Y., Iitaka, Y. and Sakagucki, H. *Acta Crystallogr. B 32* (1976) 1734.
11. Freeman, H. C. *Adv. Protein Chem. 22* (1967) 257.
12. Johnson, C. K., *ORTEP*, Report ORNL 3794, Oak Ridge National Laboratory, Oak Ridge 1965.
13. IUPAC-IUB Commission on Biochemical Nomenclature *J. Mol. Biol. 52* (1970) 1.

Received November 3, 1977.

Acta Chemica Scandinavica A 32 (1978) 367–376

Short Communications

Dichroism and Depolarization of Vibration Spectra of Polyphenylene Oxides

J. J. LINDBERG, G. LUNDSTRÖM, S.-L. KORPPI-TOMMOLA, B. LÖFGREN, and A. SAARINEN

Department of Wood and Polymer Chemistry, University of Helsinki, SF-00100 Helsinki 10, Finland

In connection with studies on the structure and properties of 2,6-disubstituted polyphenylene oxides it was found necessary to determine the orientation and anisotropy of unstressed and stressed polymers in the solid state.[1] Recent reviews on investigations of the vibration spectra of solid polymers indicate that these phenomena can conveniently be examined by measuring frequency shifts,[2] Raman spectroscopic dichroism effects[3,4] or infrared spectroscopic dichroism.[5] As a continuation of our previous spectroscopic work on polymers in the solid state[6] we have examined the vibration spectra of stressed and unstressed poly-2,6-dimethyl-(1,4-phenylene oxide) (PPO) and poly-2,6-dimethoxy-(1,4-phenylene oxide) (PPOO) films.

Experimental. PPO was of commercial origin. PPOO was synthesized by polymerization of 2,6-dimethoxy phenol in the presence of silver oxide in triethylamine–chloroform.[7] The viscosity average molecular weights $\overline{M}_v$ obtained were 62 000 for PPO and 150 000 for PPOO.

From chloroform solutions (PPO – $CHCl_3$ = 1:7 and PPOO – $CHCl_3$ = 1:10 by weights) 60 μm thick films were drawn by a spiral roller on polytetrafluoroethylene plates. The moist films were detached and stretched by 40–60 %, after which they were clamped in metal frames and carefully dried. The effect of mechanical stress on the vibrational spectra of these polymers was examined by dichroic ratios of infra-red absorption peaks and by laser Raman spectroscopy.

The infrared spectra were recorded with a grating spectrometer, model Perkin-Elmer 621. The dichroism was measured with an AgBr wire-grid polarizer. In the cell compartment the direction of strain made an angle of 45° with the vertical. The plane of the polarizer was either in the direction of strain or perpendicular to it. With such a measuring method it was possible to work with a constant attenuation of the light beam and to compare directly the absorbances $A_{\parallel}$ and $A_{\perp}$. All measurements were made at room temperature. The Raman spectroscopic studies were performed with a Jarrell-Ash 25–300 spectrometer. The 488.0 nm exciting line of an Ar–Kr laser (2 W) was used, with plasma filtering to protect the samples against heat. The samples were illuminated for several hours to reduce the fluorescence background, which interferes with the recording of the spectra.

The orientation process was also investigated with a polarizing microscope. In the unstretched films no polarizing effect could be observed, whereas in stretched ones a strong orientation was evident.

Results. The general feature and assignments of the infrared and Raman spectra together with the infrared dichroism and Raman spectroscopic depolarization ratios are given in Table 1.

The positions of the bands given are in good agreement with earlier infrared data.[8,9] From the point of view of the present investigation, the bands associated with the chain motion, at about 1200 and 920–960 cm^{-1}, and with the substituents ($-CH_3$ and $-OCH_3$), at 1420–1490 and 1300–1380 cm^{-1}, are of special interest.

The bands at 1221, 1203, 925 and 845 cm^{-1} are shifted about 1–2 cm^{-1} toward lower frequencies when the PPOO films are stretched. Similar spectral trends have been observed by, among others, Evans and Hallam[2] in Raman spectra of polypropene, polycarbonate, polystyrene and nylon-6,6 on tensile-testing dumbbells and by Korsakov and coworkers[10] in the infrared.

From Table 1 it is evident that, in contrast to the very small infrared spectral shifts on stretching the films, large changes in dichroism ratios are observed. Thus in PPO and PPOO no dichroism is noted in the unstretched state, whereas on stretching both σ-dichroism ($A_{\parallel}/A_{\perp} < 1$) and π-dichroism ($A_{\parallel}/A_{\perp} > 1$) up to 50 % are observed for several of the infrared bands. Especially involved are the bands at 1605, 1492, 1446, 1417, 1126 and 991 cm^{-1} in PPOO. Similar trends are observed for the corresponding bands in PPO.

Table 1. Infrared and Raman spectroscopic data of poly-2,6-dimethyl-(phenylene oxide) (PPO) and poly-2,6-dimethoxy-(phenylene oxide) (PPOO).

Assignment	PPO				PPOO			
	IR (cm^{-1})	$A_{\parallel}/A_{\perp}$	Raman (cm^{-1})	$A_{\parallel}/A_{\perp}$	IR (cm^{-1})	$A_{\parallel}/A_{\perp}$	Raman (cm^{-1})	$A_{\parallel}/A_{\perp}$
					3620 w			
					3460 w			
ν CH	3020 w				3000 m	1.0		
ν_{as}					2965 m		2950 w	0.86
ν_{as} CH_3	2953 m				2935 m	0.94		
ν_s	2922 m	1.0	2925 w	1.0				
$2\delta_{as}$ CH_3	2850 w							
ν_s CH_3					2838 m	1.0	2842 w	1.10
$2\delta_s CH_3$	2785 w							
	1697 w							
ν C–C	1605 s	1.1	1605 w		1605 s	1.06	1605 s	1.0
δ_{as} CH_3	1470 s				1492 s	1.30		
δ_{as}+ CH_3	1438 m				1464 s	0.79		
δ_{as}+ CH_3	1425 m				1446 s	1.40		
($-OCH_3$)					1417 s	0.90		
δ_s CH_3	1380 m	1.3	1380 w	1.10				
δ_s CH_3	1362 m				1355 w			
CH_3					1330 w	1.43	1334 m	0.89
CH_3	1307 m		1308 w	0.82				
					1221 w	0.82	1215 w	0.90
$\nu_a(O\phi)$[a]	1190 s				1203 s	1.50		
	1142 w							
ν_s OCH_3					1126 s	0.90		
δ CH	1115 w	1.1						
OCH_3					1105 m			
δ_{as}– CH_3	1021 s	(2.0)			1035 m	1.08	1048 m	0.99
					991 s	1.33		
$\nu_s(O\phi)$	960 m	1.2	962 w	0.70				
					925 s	1.0	930 w	0.34
γ CH	859 m	0.9			845 m	1.33	850 m	0.97
1,2,3,5-tetra(ϕ)	832 m	1.5	835 w	1.67	813 m	0.82		
*para*subst.(ϕ)	758 m				775 m			
arom. C=C	668 w				665 w			
1,2,3,5-tetra(ϕ)	595 w		575	0.95	620 w		604 w	1.10
	475 w				521 w			
							373	1.0
							77	0.86

[a] ϕ = Phenyl.

It is generally a difficult task to get sufficiently strong depolarization effects in the Raman spectra of polymers, owing to internal interactions in the materials. The best results are presently obtained with thin films and polymer melts.[11] Oriented films, fibers and fiber bundles have also been tested.[12,13]

In the present case only one real depolarized band was observed: namely, in connection with the ν_s ($\phi-O-\phi$) vibration at 962 and 930 cm^{-1} for PPO and PPOO, respectively. This effect indicates, however, the strong influence of the orientation of the material on the chain motion.

Discussion. The above effects have been interpreted in several ways. According to Evans and Hallam[2] and Cunningham and co-workers[14] dichroism in IR spectra and changes in Raman spectra, *e.g.*, in poly(ethylene terephthalate) may

be caused, on drawing, by changes in molecular conformations. Zhurkov, Korsukov and co-workers[10] and Gubanov,[15] on the other hand, favour an interpretation based on the stressing of the interatomic bands in the molecule.

It is difficult to decide between the two interpretations on the basis of the present data alone. Earlier thermodynamic work on PPO and PPOO by our group[16] indicated that the increased volume of side chain groups in PPOO causes the glass transition to move to a lower temperature. This effect is attributable to both the flexibility of the side chain substituents and the decreased intermolecular effects. In the light of the above-mentioned results, the present dichroism and depolarization effects could be attributed partly to changes in intermolecular effects due to changes in free volume on orientation and partly to changes in valence angle motions of the main chain due to locking of the bulky side groups.

Acknowledgement. The work was supported in part by the Foundation of the Investigation of the Natural Resources of Finland and in part by the Finnish Society of Science.

1. Lindberg, J. J., Jauhiainen, T.-P. and Savolainen, A. *Pap. Puu. 54* (1972) 91.
2. Evans, R. A. and Hallam, H. E. *Polymer 17* (1976) 838.
3. Hendra, P. J. *Adv. Polymer Sci. 6* (1969) 151.
4. Turrell, G. *Infrared and Raman Spectra of Crystals*, Academic, London – New York 1972.
5. Dechant, J. *Ultrarotspektroskopische Untersuchungen an Polymeren*, Akademie-Verlag, Berlin 1972.
6. Lindberg, J. J., Stenman, F. and Laipio, I. *J. Polymer Sci.*, Symposium No. 42 (1973) 925.
7. Jauhiainen, T.-P. and Lindberg, J. J. *TTA, Tutkimus ja Tekniikka 2* (1975) 32.
8. Lindberg, J. J., Savolainen, A. and Starck, P. *Suom. Kemistil. B 42* (1969) 120; Savolainen, A. *Thermodynamic and Relaxation Studies on 2,6-Disubstituted Polyphenylene Oxides*, Thesis, Helsinki 1974.
9. Hay, A. S. *J. Polymer Sci. 58* (1962) 581.
10. Zhurkov, S. N., Vettergren, V. I., Korsukov, V. E. and Novak, I. I., *Proc. 2nd Int. Conf. Fracture*, Brighton (1969) 545; Korsukov, V. E. and Vettergren, V. I. *Strength Mater. (USSR) 2* (1971) 51.
11. Vasko, P. D. and Koening, J. L. *Macromolecules 3* (1970) 597.
12. Snyder, R. G. *J. Mol. Spectrosc. 36* (1970) 222.
13. Carter, V. B. *J. Mol. Spectrosc. 34* (1970) 356.
14. Cunningham, A., Ward, I. M., Willis, H. A. and Zichy, V. *Polymer 15* (1974) 749.
15. Gubanov, A. I. *Mekh. Polim. 3* (1967) 771.
16. Savolainen, A. *Makromol. Chem. 172* (1973) 213.

Received March 1, 1978.

A Potentiometric Study on the Complex Equilibria between Uranyl Ions and 3-Hydroxy-5,7-disulfo-2-naphthoic Acid

LAURI H. J. LAJUNEN * and MIKKO KARVO

Department of Chemistry, University of Oulu, SF-90100 Oulu 10, Finland

In the preceding papers the complex equilibria between Cu^{2+}, Be^{2+} or Al^{3+} ions and 3-hydroxy-5,7-disulfo-2-naphthoic acid have been investigated.[1-6] In addition to the binary systems, the formation of ternary complex species of copper and beryllium ions with 3-hydroxy-5,7-disulfo-2-naphthoic acid as one of the ligands has also been studied.[1-5] In the binary systems the data clearly indicated the formation of ML and ML_2 complexes (M = Cu^{2+}, Be^{2+} or Al^{3+} ion, and L = unprotonated 3-hydroxy-5,7-disulfo-2-naphthoic acid anion), and in the case of the ternary systems the formation of mixed ligand complex compounds with composition MXY (M = Cu^{2+} or Be^{2+} ion, X = 3-hydroxy-5,7-disulfo-2-naphthoic acid, and Y = 3,5-disulfosalicylic, 1-hydroxy-4,7-disulfo-2-naphthoic, catechol-3,5-disulfonic or chromotropic acid).

The present investigation was carried out to determine the species formed in the binary systems of uranyl ions and 3-hydroxy-5,7-disulfo-2-naphthoic acid. This study was carried out in the same conditions [$t = 25$ °C and $I = 0.5$ ($NaClO_4$)] as were the earlier investigations of 3-hydroxy-5,7-disulfo-2-naphthoic acid.

Experimental. Reagents. The preparation and purification of the disodium salt of 3-hydroxy-5,7-disulfo-2-naphthoic acid has been described earlier.[1,4]

Stock solutions of uranyl ions were prepared from the corresponding nitrate (E. Merck AG, 99.9 %). The concentrations of these solutions were determined by potentiometric neutralization titrations, after passage through a cation exchanger.

Apparatus. The potentiometric titrations were carried out automatically with a Radiometer digital titration system DTS 633, consisting of an autoburette ABU 13, a pH meter PHM 64, a digital titrator TTT 61, and an equal increment accessory constructed in this laboratory.

The other details of the apparatus are described in the earlier papers.[1-4]

Methods. Two different types of titration were carried out for resolving the stability constants:

(a) During the titrations of the first kind the total concentrations of uranium C_M, and 3-hydroxy-5,7-disulfo-2-naphthoic acid, C_L, were kept constant. The ratio C_L:C_M was varied systematically between 1 and 7 in the separate titrations. The free hydrogen ion concentration, $[H^+]$, was decreased by adding sodium hydroxide. The reversibility of the equilibria system was tested by also reversing some of the titrations by adding standardized perchloric acid into the solution to be titrated.

(b) In the titrations of the second kind the total concentration of protons, C_H, and 3-hydroxy-5,7-disulfo-2-naphthoic acid was kept constant. The ratio C_L:C_M was varied during the measurements by adding a standardized solution of uranyl ions. The readings of the titration steps were taken in the range where the ratio C_L:C_M was between 10 and 0.5.

Precipitates appeared in neutral and alkaline solutions, and hence the available $-\log[H^+]$ range was restricted to an upper limit of 6 – 7.

Because of the poor solubility of 3-hydroxy-5,7-disulfo-2-naphthoic acid, the total concentrations of uranium and 3-hydroxy-5,7-disulfo-2-naphthoic acid were varied within the limits of 0.001 and 0.010 M.

A constant ionic medium of 0.5 M $NaClO_4$ was used in order to avoid the changes in the activity coefficient. The buffer solutions, the solutions to be titrated and the titrant solutions were all 0.5 M with regard to $NaClO_4$.

The calibration of the glass electrode and the determination of the liquid junction potential, E_j, were performed as described earlier.[4]

Calculations. The values 10.92 and 2.14 were used for the logarithms of the first and second protonation constants of the ligand anion, respectively.[1]

The experimental values of the $\bar{n}$ function were calculated by means of the following equation:[7]

$$\bar{n}(\text{exp}) = \{C_L - [C_H - ([H^+] - K_w[H^+]^{-1})]/\bar{n}_H\}/C_M \quad (1)$$

where K_w is the stoichiometric ionic product of water, $\bar{n}_H$ the average number of protons bound to ligand anion ($\bar{n}_H = \sum_{i=1}^{2} i\beta_i[H^+]^i / \sum_{i=0}^{2} \beta_i[H^+]_i$, β_i is the overall protonation constant of the acid H_iL).

The values of the constants were calculated as overall stability constants β_{qpr} with the programmes SCOGS[8] and MINIQUAD[9] on a Univac 1100/20 computer.

The overall stability constant of a general complex $M_qH_pL_r$ is defined by

$$\beta_{qpr} = [M_qH_pL_r]/[M]^q[H]^p[L]^r \quad (2)$$

where the square brackets indicate the concentrations of the free metal, hydrogen and ligand ions.

Table 1. The stability constants of uranyl, beryllium, copper and aluminum complexes of 3-hydroxy-5,7-disulfo-2-naphthoic acid at $I=0.5$ ($NaClO_4$) and 25 °C. $\{k_n=K(ML_{n-1}+L=ML_n)$ and $R=[\sum_i\phi_i^{obs}-\phi_i^{calc})^2/\sum_i(\phi_i^{obs})^2]^{1/2}\}$. The values in parentheses are the standard deviations.

M	$\log\beta_{101}$	$\log\beta_{102}$	$\log k_2$	$\log(\beta_1/k_2)$	R	χ^2	Refs.
UO_2^{2+} [a]	9.809(3)	17.398(5)	7.59	2.2	0.0005	6.5	This work
Be^{2+}	10.18	18.17	7.99	2.2			1, 4
Cu^{2+}	8.18	14.11	5.93	2.3			1, 4
Al^{3+}	10.81	19.26	8.45	2.4			6

[a] No. of titrations: 11; No. of data points: 385.

The programme MINIQUAD calculates, along with the stability constants, their standard deviations, an agreement index R and a χ^2 statistics.[9,10]

Results and discussion. The data were visualized by presenting experimental values of $\bar{n}$ *versus* $-\log$ [L] (Fig. 1). It can be seen from this plot that the function $\bar{n}(-\log$ [L]) seems to be independent of C_L, C_M and C_H, thus indicating the formation of stepwise metal complexes $UO_2L_r^{-(4r-2)}$. The highest experimental value of $\bar{n}$ is about 1.6, which means that at least two successive complex compounds are formed in the conditions studied. Because of precipitations, the measurements were only possible in the acidic pH region, and that is why the experimental $\bar{n}$ values are all under 1.6.

Computations with the programmes SCOGS and MINIQUAD showed that the data were well explicable with two complex compounds: UO_2L^{2-} and $UO_2L_2^{6-}$. The best stability constants with the corresponding standard deviations, and the values of R and χ^2, are given in Table 1. For the sake of comparison, the table also shows the stability constants of the corresponding complexes of copper(II), beryllium(II) and aluminum(III) ions. According to the values of the standard deviations, R and χ^2, the model of two parameters, β_{101} and β_{102}, must be considered a good approximation. At a 95 % confidence level the value of χ^2 should be less than 12.6 (χ^2 is the measure of the conformity to normal distribution of the residuals $\phi_i^{obs}-\phi_i^{calc}$).[11] The value of R should be as small as possible.

The complex equilibria between UO_2^{2+}, Be^{2+}, Cu^{2+} and Al^{3+} ions with 3-hydroxy-5,7-disulfo-2-naphthoic acid at $I=0.5$ ($NaClO_4$) and 25 °C in the acidic pH region are similar: two successive complex compounds, ML and ML_2, are formed and the data give no evidence of protonated, hydrolyzed or polynuclear complex species. The stability of the complexes of 3-hydroxy-5,7-disulfo-2-naphthoic acid decreases in the order Al, Be, UO_2, Cu. Also, the ratio $\log(\beta_1/k_2)$ is equal for all the metal systems, indicating that addition of the second

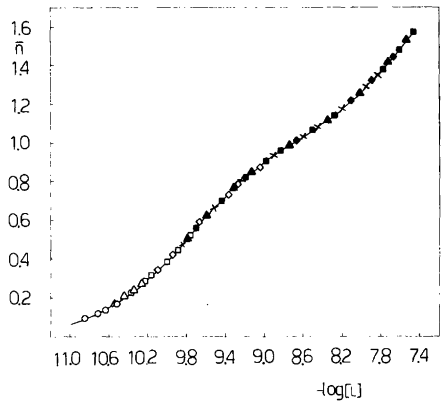

Fig. 1. Experimental values of $\bar{n}$ *versus* $-\log$ [L] calculated from a few different titrations. □, $C_H=5.90\times10^{-3}$ M, $C_L=3.95\times10^{-3}$ M; △, $C_H=4.90\times10^{-3}$ M, $C_L=3.95\times10^{-3}$ M; ○, $C_H=3.90\times10^{-3}$ M, $C_L=3.95\times10^{-3}$ M; ◇, $C_H=2.90\times10^{-3}$ M, $C_L=3.95\times10^{-3}$ M. Titrant in the first four titrations = 0.1 M $UO_2(NO_3)_2$ solution; ×, $C_M=2.00\times10^{-3}$ M, $C_L=5.93\times10^{-3}$ M; ▲, $C_M=1.00\times10^{-3}$ M, $C_L=4.94\times10^{-3}$ M; ■, $C_M=1.00\times10^{-3}$ M, $C_L=7.90\times10^{-3}$ M; ◆, $C_M=3.00\times10^{-3}$ M, $C_L=7.90\times10^{-3}$ M, titrant in the last four titrations = 0.1 M NaOH solution.

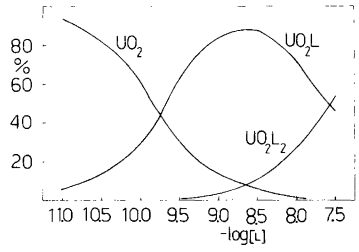

Fig. 2. Distribution of the different metal species as a function of $-\log$ [L].

ligand molecule to the monocomplexes is equally hindered in every case.

The distribution of the different uranyl species in the $-\log [L]$ region studied is presented in Fig. 2.

1. Saarinen, H., Raikas, T. and Lajunen, L. *Finn. Chem. Lett.* (1974) 104.
2. Lajunen, L. H. J. *Finn. Chem. Lett.* (1975) 1.
3. Lajunen, L. H. J. *Finn. Chem. Lett.* (1975) 71.
4. Lajunen, L. H. J. *Ann. Acad. Sci. Fenn. Ser. A II* (1976) No. 179.
5. Lajunen, L. H. J. and Tikanmäki, M. *Finn. Chem. Lett.* (1978) 96.
6. Lajunen, L. H. J. *Finn. Chem. Lett. In press.*
7. Rosotti, H. S. *Talanta 21* (1974) 813.
8. Sayce, I. G. *Talanta 15* (1968) 1397; *18* (1971) 653; Sayce, I. G. and Sharma, V. S. *Ibid. 19* (1972) 831.
9. Sabatini, A., Vacca, A. and Gans, P. *Talanta 21* (1974) 53.
10. Lajunen, L. H. J. and Karvo, M. *Anal. Chim. Acta 97* (1978) 423.
11. Sabatini, A. and Vacca, A. *Coord. Chem. Rev. 16* (1975) 161.

Received March 29, 1978.

X-Ray Investigation of *p*-Nitroanisole

H. J. TALBERG

Department of Chemistry, University of Oslo
Oslo 3, Norway

The following is an account of an X-ray structural study of *p*-nitroanisole based on diffraction data collected at −165 °C. The measurements were done using a SYNTEX $P\bar{1}$ diffractometer and a prismatic crystal of dimensions $0.3 \times 0.3 \times 0.1$ mm. Apart from the following details, data relevant to data collection and data treatment may be found in publications devoted to X-ray investigations of *C*-nitroso compounds performed in this laboratory.[1] Within a quadrant of reciprocal space and with $2\theta_{max} = 65°$ (Mo$K\alpha$ radiation) 1427 reflections were measured; 759 had intensities larger than $2.5\sigma(I)$ and were used in the further work. The scan limits were $2\theta(\alpha_1) - 1.1°$ and $2\theta(\alpha_2) + 1.3°$. Atomic scattering factors and computer programs used are referred to in the publications mentioned.[1] The crystal data for *p*-nitroanisole at −165 °C are: $C_7H_7O_3N$, monoclinic, space group $P2_1/c$, $a = 9.045(3)$ Å, $b = 10.573(6)$ Å, $c = 7.533(2)$ Å, $\beta = 100.56(2)°$, $V = 708.2$ Å^3, $M = 153.14$, $D_{calc} = 1.436$ g cm^{-3}, $Z = 4$, $F(000) = 320$.

The structure was determined by use of the MULTAN program package. Isotropic least-squares full matrix refinement yielded a conventional R factor of 17.4 %. The improvement achieved by introducing anisotropy was unusually large, R dropping to 8.8 %. At this stage all hydrogen atoms could be located in a subsequently calculated ΔF map. The refinement converged to $R = 0.048$, a weighted R_w of 0.042 and a goodness of fit S of 1.8. Final parameters are given in Table 1. The estimated standard deviations are from 0.003 to 0.006 Å in bond lengths and 0.4 − 0.5° in angles involving only non-hydrogen atoms. The C − H bond lengths are in the range 0.87 − 1.10 Å with e.s.d.'s of 0.03 − 0.04 Å. Other structural results are given in Fig. 1. In this the view is down the normal to planes containing edge-to-edge and head-to-tail packed molecules. Some interlayer contacts are: O41···O41′: 3.049 Å, N4···O1: 3.244 Å and C2···C5: 3.429 Å. Both the benzene ring with O1 and N4 and the CNO_2 group are planar. The corresponding interplanar angle is 7.3° while the torsion about the C − OMe bond is 5.9(6)°. The title compound resembles *p*-nitrophenol closely as to the bond lengths, especially in the nitro group, considering the α-form of the phenol.[2] For all the corresponding bond lengths $\Delta R_{rms} = 0.011$ Å. The only significant difference is in the C5 − C6 distance. This is gratifying in view of the identical IR-KBr-ω_{NO}

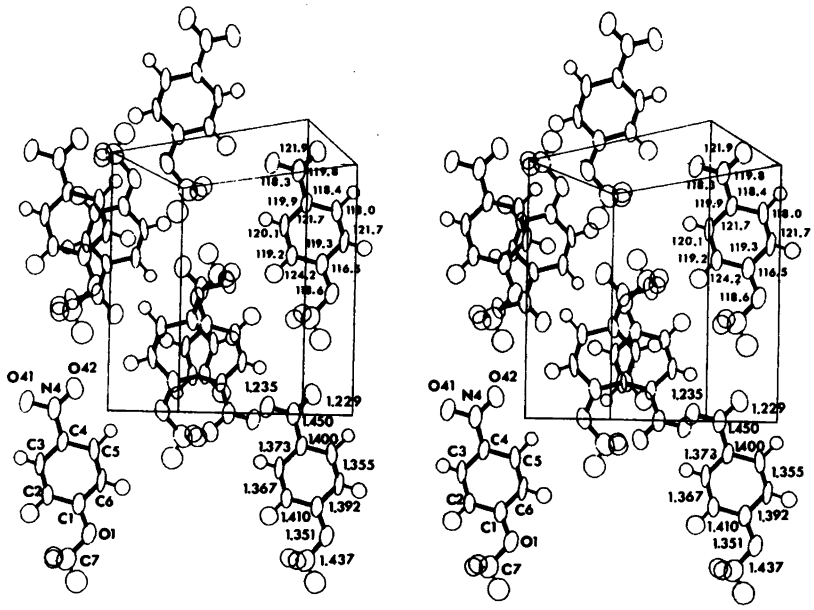

Fig. 1. A stereoscopic illustration of the structure including numbering of atoms and bond lengths (Å) and angles (°). The ellipsoids are those of 50 % probability.

Table 1. Fractional atomic coordinates and thermal parameters. The anisotropic temperature factors are expressed as: $\exp[-2\pi^2(h^2a^{*2}U_{11} + \cdots + 2klb^*c^*U_{23})]$. Estimated standard deviations in parentheses.

ATOM	X	Y	Z	U11	U22	U33	U12	U13	U23
O1	.14468(29)	.08871(41)	.39346(38)	.0344(14)	.0843(29)	.0433(17)	-.0113(28)	.0185(13)	-.0069(22)
O41	.41471(27)	.52755(28)	.65244(36)	.0484(16)	.0987(31)	.0363(16)	-.0098(17)	.0084(13)	-.0134(18)
O42	.22189(34)	.58449(33)	.45777(44)	.0615(20)	.0877(38)	.0542(22)	.0101(21)	.0036(17)	.0001(28)
N4	.30178(37)	.58173(47)	.53943(44)	.0319(19)	.0994(43)	.0263(18)	-.0033(26)	.0066(15)	-.0064(27)
C1	.19808(41)	.12049(53)	.43568(52)	.0265(25)	.0856(49)	.0235(25)	-.0074(25)	.0119(20)	.0004(27)
C2	.32718(41)	.15249(53)	.54864(51)	.0235(21)	.0774(42)	.0264(23)	-.0053(27)	.0047(19)	.0066(28)
C3	.36253(41)	.27723(56)	.57099(53)	.0172(20)	.0984(47)	.0217(21)	-.0078(26)	.0002(16)	.0023(28)
C4	.26486(39)	.36964(53)	.50466(49)	.0236(22)	.0762(41)	.0286(23)	-.0077(23)	.0058(18)	-.0075(23)
C5	.12683(48)	.34015(53)	.39335(54)	.0289(21)	.0958(48)	.0203(19)	.0061(27)	.0023(17)	-.0054(28)
C6	.09319(38)	.21651(52)	.36840(52)	.0182(21)	.1023(49)	.0189(21)	-.0096(27)	-.0085(16)	-.0062(29)
C7	.23382(64)	-.10188(69)	.48689(77)	.0622(34)	.0936(68)	.0497(35)	-.0145(37)	.0262(29)	-.0004(36)

ATOM	X	Y	Z	B	ATOM	X	Y	Z	B
H5	.0648(34)	.4174(29)	.3381(43)	2.6(8)	H6	.0027(38)	.1918(38)	.2816(46)	3.7(9)
H3	.4477(33)	.3084(33)	.6468(44)	3.8(9)	H2	.4851(42)	.0788(37)	.6876(50)	5.3(11)
H71	.1986(43)	-.1986(45)	.4426(59)	7.2(15)	H72	.3339(48)	-.1821(34)	.4442(49)	5.3(10)
H73	.2458(36)	-.0916(33)	.6143(54)	4.6(9)					

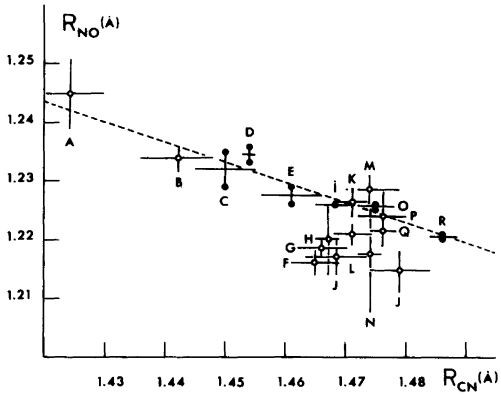

Fig. 2. A plot of the N–O bond length (R_{NO}) against the C–N bond length (R_{CN}) in the compounds potassium *o*-nitrophenolate hemihydrate (A),[3] *p*-nitrophenol α form (B),[2] *p*-nitroanisole (C), 4-nitropyridine *N*-oxide (D),[2] 4(nitrobenzendiazo-4′-methoxythiophenolate (E),[4] *p*-nitrodiphenyl (F),[2] *p*-nitroacetophenone (G),[2] α-chloro-4-nitrobenzaldoxime (H),[2] 3,5-dimethyl-4-nitropyridine *N*-oxide tetragonal form (i),[5] *p*-dimethylaminobenzylidene-*p*-nitroaniline (J),[2] *p*-nitrobenzaldoxime (K),[2] *p*-methylbenzylidene-*p*-nitroaniline (L),[2] 4-nitro-*N*-methylbenzaldoxime (M),[2] *m*-nitrophenol (N),[2] 2-(*p*-nitrobenzoyloxy)-3-phenyl-2-pentene-4-one (O),[6] *p*-nitrobenzylidene-*p*-dimethylaminoaniline (P),[2] *p*-nitrobenzoic acid (Q),[7] and 2,4-dinitrophenol (R).[8] Vertical bars show ΔR_{NO} while horizontal bars indicate the e.s.d. in R_{CN}. The least-squares line shown is for the ●-points (low temperature or librational correction).

wavenumbers for the two compounds. The title compound is compared with some recently studied nitrobenzenes and pyridines in an R_{NO}/R_{CN} plot in Fig. 2 (X-ray, complete data sets). It appears that the point for this investigation (C) lies close to a correlation line established by points being weakly influenced by thermal vibration effects (B, C, D and O are for low temperature studies). Mutual conjugation seems to cause a 0.025 Å shortening of the C–N bond in *p*-nitroanisole. A rigid body analysis of the entire molecule shows moderate agreement between observed and calculated tensor elements: $\Delta U_{rms} = 0.0044$ Å^2. The r.m.s. eigenvalues of **L** are 4.2, 3.1 and 2.2° and those of **T** 0.30, 0.13 and 0.13 Å. It appears from Fig. 1. that the unusually strong translational oscillation is in the direction of the *b* axis. This anisortopy in the translational oscillation is paralleled by anisotropy in the dependency of the unit cell dimensions upon temperature: *a* and *c* decrease the usual 2–3 % while *b* is constant when lowering the temperature from 20 to −165 °C.

1. Talberg, H. J. *Acta Chem. Scand. A 30* (1976) 829.
2. Kennard, O. and Watson, D. G. *Molecular Structures and Dimensions*, Oosthoek, Scheltema and Holkema, Utrecht, Vols. 1–8.
3. Andersen, E. K. K. *Thesis*, Odense 1971.
4. Reiding, J., de Kok, A. J., de Graaff, R. A. and Romers, C. *Acta Crystallogr. B 32* (1976) 2676.
5. Shiro, M., Yamakawa, M. and Kubota, T. *Acta Crystallogr. B 33* (1977) 1549.
6. Stezowski, J. *Acta Crystallogr. B 32* (1976) 2557.
7. Colapietro, M. and Domenicano, A. *Acta Crystallogr. B 33* (1977) 2240.
8. Iwasaki, F. and Kawano, Y. *Acta Crystallogr. B 33* (1977) 2455.

Received February 20, 1978.

X-Ray Investigation of Methyl *m*-Azoxy-*trans*-cinnamate

H. J. TALBERG

Department of Chemistry, University of Oslo, Oslo 3, Norway

In an attempt to derive methyl *m*-nitrosocinnamate from the corresponding nitro compound by use of a standard method[1] golden coloured crystals melting at 175 °C were obtained. The present X-ray structure analysis at −165 °C has shown this compound to be methyl *m*-azoxy-*trans*-cinnamate. The crystals formed upon slow evaporation of an acetone solution of a sample purified by sublimation. Film investigation at room temperature showed monoclinic symmetry and unit cell dimensions deviating less than 3 % from those at low temperature. The diffractometer measurements were done using a prismatic crystal of dimensions $0.57 \times 0.12 \times 0.04$ mm. High crystal perfection prevented overlap between the reflections: $(\Delta 2\theta)_{min} = 1.07°$ along c^* (Mo$K\alpha$ radiation). The scan width was $[2\theta(\alpha_1) - 0.6] - [2\theta(\alpha_2) + 0.6]°$. Within a quadrant of reciprocal space and with $2\theta_{max} = 70°$, 1847 reflections were measured; 1231 had intensities larger than $2.5\sigma(I)$ and were used in the further work. Other details in connection with the data collection, the data treatment, the atomic scattering factors and the computer programs used may be found in publications devoted to studies of *C*-nitroso compounds performed in this laboratory.[2] The crystal data for methyl *m*-azoxy-*trans*-cinnamate at −165 °C are: $C_{20}H_{18}O_5N_2$, monolinic, space group $P2_1/c$, $a = 3.8251(8)$ Å, $b = 5.825(1)$ Å, $c = 38.364(7)$ Å, $\beta = 90.73(2)°$, $V = 854.7$ Å^3, $M = 366.38$, $Z = 2$, $D_{calc} = 1.424$ g cm^{-3}, $F(000) = 384$.

An approximate and centrosymmetrical structural model was obtained by use of the MULTAN program package. Fully ordered it is that of methyl *m*-nitroso-*trans*-cinnamate in an azo dioxide dimeric state, *i.e.* an *N*-oxide derivative of the title compound. Including hydrogen atoms (from ΔF-maps) and with anisotropic temperature factors for the heavy atoms this model was refined to a conventional *R*-factor of 0.11 (full matrix least-squares refinement). Then all structural results but the B_{11} value for the nitroso oxygen atom (O6) appeared reasonable. Introduction of half occupancy at the O6 site and subsequent refinement yielded a lowering of *R* to 0.059. This, in connection with the finding by MS of $M = 366$, showed that the compound under investigation was actually the title compound. The best model then consists of two half azoxy molecules superimposed so that all atoms apart from the O6 atom coincide. The final weighted R_w and goodness of fit *S* were 0.047 and 1.67, respectively. The parameter values at convergence are listed in Table 1. For bond lengths involving only heavy atoms the estimated standard deviations range from 0.003 to 0.005 Å. Bond

Table 1. Fractional atomic coordinates and thermal parameters. The anisotropic temperature factors are expressed as: $\exp[-(B_{11}h^2 + \cdots + B_{23}kl)]$. Estimated standard deviations in parentheses.

ATOM	x	y	z	B11	B22	B33	B12	B13	B23
O11	0.6416(5)	0.9529(4)	0.18419(4)	0.068(2)	0.0252(8)	0.00025(1)	-0.009(2)	0.0009(2)	-0.0003(2)
O12	0.8513(5)	0.6350(4)	0.21055(4)	0.084(2)	0.0335(9)	0.00023(1)	-0.007(2)	-0.0016(3)	0.0018(2)
O6	0.7238(10)	0.7163(6)	0.02021(8)	0.060(3)	0.0170(13)	0.00031(3)	0.034(3)	0.0005(4)	-0.0005(3)
N6	0.9469(6)	0.5290(4)	0.01482(5)	0.051(2)	0.0253(9)	0.00045(2)	-0.026(2)	0.0035(3)	-0.0038(2)
C1	0.7844(7)	0.7434(5)	0.18450(7)	0.041(2)	0.0252(12)	0.00029(2)	-0.025(3)	-0.0002(3)	-0.0001(2)
C2	0.8528(7)	0.6661(5)	0.14850(6)	0.041(2)	0.0198(10)	0.00027(2)	-0.007(2)	-0.0003(3)	0.0009(2)
C3	1.0022(7)	0.4665(5)	0.14168(7)	0.037(2)	0.0219(11)	0.00033(2)	-0.013(3)	-0.0012(3)	0.0027(2)
C4	1.0782(6)	0.3715(5)	0.10724(7)	0.021(2)	0.0120(9)	0.00051(2)	-0.005(2)	-0.0001(3)	0.0007(2)
C5	0.9883(7)	0.4846(5)	0.07647(7)	0.029(2)	0.0099(9)	0.00041(2)	-0.001(2)	0.0010(3)	-0.0005(2)
C6	1.0630(7)	0.3899(5)	0.04423(7)	0.036(2)	0.0196(10)	0.00041(2)	-0.018(2)	0.0015(3)	-0.0014(2)
C7	1.2213(8)	0.1764(6)	0.04239(11)	0.037(3)	0.0260(14)	0.00105(4)	-0.017(3)	0.0044(5)	-0.0072(4)
C8	1.3090(8)	0.0621(6)	0.07284(13)	0.031(2)	0.0128(11)	0.00167(5)	0.005(3)	0.0004(5)	-0.0034(4)
C9	1.2407(8)	0.1590(5)	0.10467(10)	0.032(2)	0.0134(10)	0.00101(3)	-0.007(2)	-0.0012(4)	0.0019(3)
C10	0.5550(10)	1.0466(7)	0.21854(8)	0.069(3)	0.0340(15)	0.00028(2)	-0.013(4)	0.0007(4)	-0.0017(3)

ATOM	x	y	z	B	ATOM	x	y	z	B
H2	0.776(6)	0.759(4)	0.1302(6)	2.0(6)	H3	1.063(7)	0.379(5)	0.1611(6)	2.9(6)
H5	0.872(6)	0.623(4)	0.0768(6)	2.0(6)	H7	1.267(9)	0.112(6)	0.0223(8)	5.3(9)
H8	1.429(9)	-0.082(6)	0.0712(8)	6.0(9)	H9	1.303(8)	0.082(5)	0.1255(7)	3.9(7)
H101	0.382(8)	0.948(5)	0.2280(7)	3.8(8)	H102	0.769(8)	1.052(5)	0.2333(7)	3.6(7)
H103	0.464(9)	1.203(6)	0.2125(7)	5.3(9)					

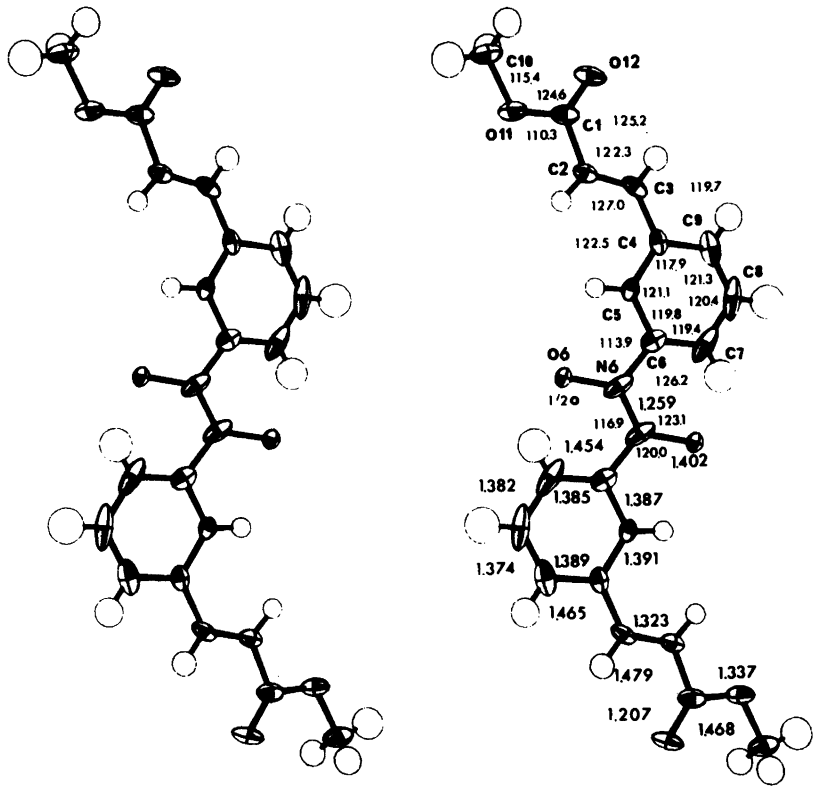

Fig. 1. Bond lengths (Å), bond angles (°), numbering of atoms and 50 % probability ellipsoids. The projection of the *c* axis intersects the C8 – H and the O11 – C10 bond midway while the *a* axis is normal to the paper plane.

lengths, angles and other structural results are given in Fig. 1.

The packing pattern is similar to those for smectogenic compounds in that the molecules are arranged in layers having carbomethoxy boundaries. However, the title compound seems not to have a smectic mesophase (countrary to its *para* analogue). This may probably be due to the fact that the molecules are close-packed rather than stacked within these layers.[3]

Apparently the disorder determines to a large extent the shape of the probability ellipsoids of all atoms but the O6 atom. In the azoxy group the structural results indicate the NO nitrogen atom to reside in the ring-far half of the N6 ellipsoid. The average CNONC fragment is planar and inclined 12.3° to the planar benzene ring. This conformation is somewhat different from that of the smectogenic and nearly planar ethyl *p*-azoxybenzoate.[3]

1. Alway, F. J. and Bonner, W. D. *Am. Chem. J. 32* (1902) 385.
2. Talberg, H. J. *Acta Chem. Scand. A 30* (1976) 829.
3. Krigbaum, W. R. and Barber, P. G. *Acta Crystallogr. B 27* (1971) 1884.

Received February 22, 1978.

Acta Chemica Scandinavica A 32 (1978) 377 – 380

Linear Free Energy Relationships and Activation Volumes for Water Exchange Reactions as Measures of the Degree of Association in the Transition State for Octahedral Substitution Reactions

LENE MØNSTED

Department I, Inorganic Chemistry, H. C. Ørsted Institute, University of Copenhagen, Universitetsparken 5, DK-2100 Copenhagen Ø

The controversy which is encountered in the literature concerning the associative character of substitution reactions in the pentaamminechromium(III) series of complexes has been resolved by a redetermination of the association constant for $[Cr(NH_3)_5(OH_2)]^{3+} + Br^-$ at 50 °C. Both linear free energy relationships and activation volumes then predict an increase in the associative character of substitution reactions along the series: $Co(NH_3)_5X < Ir(NH_3)_5X < Rh(NH_3)_5X < Cr(NH_3)_5X < Cr(OH_2)_5X$, where X is one of a number of single charged anions or water.

An important aspect of substitution reactions of metal complexes is the extent to which the entering and leaving ligands are associated with the metal center in the transition state. Several approaches to this problem have been made, two of the more successful being based upon determinations of volumes of activation for solvent exchange reactions, and investigations of the existence of linear free energy relations for series of similar complexes, respectively.

These two approaches have led to the same conclusions for both the pentaamminecobalt(III) and the pentaaquachromium(III) series of complexes. In the former series of complexes the volume of activation for water exchange in the pentaammineaquacobalt(III) ion is positive, *viz.* $+1.2$ cm^3 mol^{-1}.[1] This indicates that *dissociation* of the reacting ligand is important in the formation of the transition state,[1] a conclusion which is further supported by the existence of a linear correlation (with slope, α, equal to 1.00) between ΔG^* and ΔG° for the process

$$[Co(NH_3)_5X]^{(3-n)+} + H_2O \rightleftharpoons [Co(NH_3)_5OH_2]^{3+} + X^{n-}$$

for a large number of X-ligands.[2]

Water exchange in the hexaaquachromium(III) ion is characterized by a negative volume of activation, *viz.* -9.3 cm^3 mol^{-1}.[3] This indicates the importance of *association* of the reacting ligands in the transition state,[1,3] and this conclusion is supported by the fact that α is 0.56[4] for a variety of reactions of the type:

$$[Cr(OH_2)_5X]^{3-n} + H_2O \rightleftharpoons [Cr(OH_2)_6]^{3+} + X^{n-}.$$

In the pentaamminechromium(III) series a different situation is encountered. The volume of activation for water exchange in the pentaammineaquachromium(III) ion is found to be -5.8 cm^3 mol^{-1},[5] a result which has been taken as evidence of significant association of the reacting ligands in the transition state.[5] However, contrary to this an α value of 0.91 has been found and this has been taken as evidence of the operation of a dissociative mechanism for the series of reactions:[6]

$$[Cr(NH_3)_5X]^{(3-n)+} + OH_2 \rightleftharpoons [Cr(NH_3)_5OH_2]^{3+} + X^{n-}.$$

The latter discrepancy would clearly appear to invalidate conclusions derived from the use of such data, and a closer examination of the agreement concerning the classification of reaction mechanisms reached on the basis of these two criteria was therefore of interest.

EXPERIMENTAL

Materials. Ion exchanged water, distilled from alkaline permanganate in an all-quartz apparatus, was employed throughout. $HClO_4$ (Merck 70 % *p.a.*) was used without further purification. NaBr (Merck, "reinst") was recrystallized once from water. $[Cr(NH_3)_5Br]Br_2$ and $[Cr(NH_3)_5(OH_2)]Br_3$ were prepared by literature methods.[20]

Equilibrium measurements. Pentaammine chromium(III) complexes lose ammonia at a rate which renders equilibrium measurements in acid bromide solutions impractical. Instead, synthetic mixtures with varying $[Cr(NH_3)_5Br]^{2+}/[Cr(NH_3)_5OH_2]^{3+}$ ratios were prepared and solutions with negligible initial variation in absorbance at 270 nm as function of time were assumed to contain the pentaammine complex ions in their equilibrium concentrations. This assumption was supported by decreasing absorbances for ratios larger than the equilibrium value and increasing absorbances for smaller ratios. In aqueous 0.5 M NaBr + 0.3 M $HClO_4$ solution with a total chromium(III) concentration of 3.5 mM the concentration equilibrium constant:

$$K = \frac{([Cr(NH_3)_5Br]^{2+})}{([Cr(NH_3)_5(OH_2)]^{3+})(Br^-)}$$

was thus found to have the value $(0.019 \pm 0.002)\ M^{-1}$ at 50 °C.

RESULTS AND DISCUSSION

In addition to the data for the various series of complexes already mentioned, data may be found in the literature which permit $\Delta G^*/\Delta G^\circ$ plots to be constructed for the aquation reactions of a limited number of pentaamminerhodium(III)[7-9] and pentaammineiridium(III)[10,11] complexes. These plots are shown in Fig. 1 and are found to have α-values of 0.72 and 0.85, respectively. As a measure of association in the transition state these values are consistent with volumes of activation for water exchange of -4.1 cm^3 mol^{-1}[12] and -3.2 cm^3 mol^{-1}[13] for the pentaammineaquarhodium(III) and -iridium(III) ions, respectively. Additional evidence for the importance of association in the transition state in the reactions of pentaamminerhodium(III) and -iridium(III) complexes comes from studies of the chloride and bromide anation of the pentaammineaqua ions, reactions which are found to be significantly faster than water exchange.[7,14]

The value of α of 0.91 for aquation of the pentaamminechromium(III) series of complexes is derived from data obtained at 50 °C. A limited number of

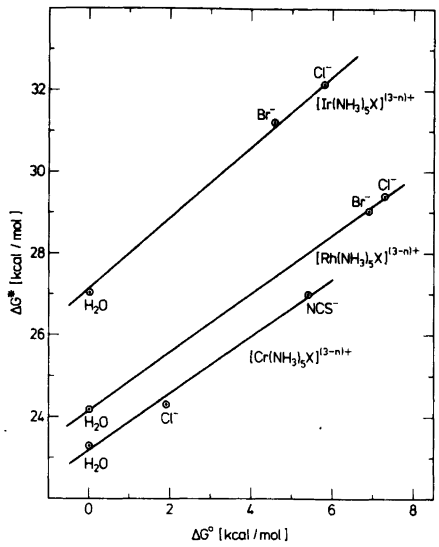

Fig. 1. Relationship between the free energy of activation, ΔG^*, and the free energy of reaction, ΔG°, for the acid-independent aquation of $M(NH_3)_5X^{(3-n)+}$ [M = Cr(III) (25 °C) Rh(III) (65 °C), and Ir(III) (95 °C)]. ΔG° values are calculated from

$$K = \frac{[M(NH_3)_5OH_2{}^{3+}][X^{n-}]}{[M(NH_3)_5X^{(3-n)+}][H_2O]}$$

with $[H_2O]$ taken as 55.5 M.

rate and equilibrium measurements which have been carried out at, or may be extrapolated to 25 °C[12,15-18] may be found in the literature. These data are also shown in Fig. 1 and they yield an α value of 0.70. This is significantly lower than the value derived from data at 50 °C, and indicates a degree of association in the transition state which is in agreement with that predicted on the basis of the activation volume.

The temperature dependence of α may be evaluated from:[19]

$$\alpha_T = \gamma_H \times \frac{\beta^\circ(T-\beta^*)}{\beta^*(T-\beta^\circ)}$$

where γ_H is the slope of a plot of ΔH^* *vs.* ΔH°, and β^* and β° are the slopes of plots of ΔH^* *vs.* ΔS^* and ΔH° *vs.* ΔS°, respectively. For reactions of series of complexes for which all these quantities are known this equation predicts only a slight temperature dependence of α. Thus for the pentaaquachromium-

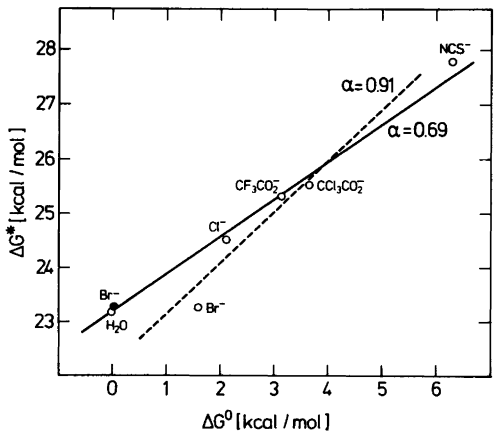

Fig. 2. Relationship between the free energy of activation, ΔG^*, and the free energy of reaction, $\Delta G°$, for the acid-independent aquation of $Cr(NH_3)_5X^{(3-n)+}$ complexes at 50 °C. The open circles are values calculated from data given in Refs. 5 and 6, and the filled circle is the value for bromide obtained in the present work. The dotted line is that obtained in Ref. 5, whereas the full line is obtained after correction of the association constant for the bromido complex.

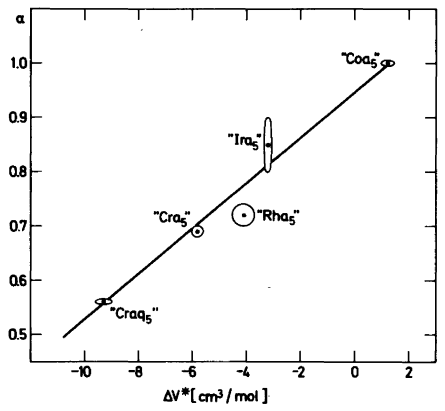

Fig. 3. Correlation between ΔV^* and α for the indicated series of complexes (see the text, $a = NH_3$ and $aq = OH_2$). Experimental values are indicated by contour ellipses of the probability density function drawn at the 68 % probability level.

(III) series of complexes, where α (25 °C) = 0.56, a value for α (90 °C) of 0.57 may be computed.* This result casts doubt on the reality of the apparently large temperature dependence of α for the pentaamminechromium(III) series of complexes, and the agreement between the activation volume and the $\Delta G^*/\Delta G°$ data at 25 °C focus attention primarily upon the $\Delta G^*/\Delta G°$ data for 50 °C. The latter data are shown in Fig. 2 and have been supplemented with data for the water exchange reaction.[5]

Attempts in this laboratory to reproduce the reported[6] association constant ($K = 0.21$ M^{-1}) for the process

$$[Cr(NH_3)_5OH_2]^{3+} + Br^- \overset{K}{\rightleftharpoons} [Cr(NH_3)_5Br]^{2+} + H_2O$$

were unsuccessful. An aqueous 0.5 M NaBr + 0.3 M $HClO_4$ solution with the chromium species calculated from this constant to be at equilibrium showed a decreasing absorbance at 270 nm as function of time. From spectrophotometric measurements we find a value which is approximately 10 times smaller ($K \sim (0.019 \pm .002)$ M^{-1}). This new value brings the $\Delta G^*/\Delta G°$ data for the pentaammineaquachromium(III) ion into agreement with the remaining data for the pentaamminechromium(III) series of complexes, the resulting value of α being 0.69 (Fig. 2). This value is in good agreement with that estimated from the data at 25 °C, Fig. 1.

Fig. 3 shows that a correlation exists between ΔV^* and α obtained from the corrected and the new data. Predictions based on the two types of criteria are thus in agreement and furthermore the *degree of association* of the reacting ligands in the transition state may be expected to increase along the series:

$$Co(NH_3)_5X < Ir(NH_3)_5X < Rh(NH_3)_5X < Cr(NH_3)_5X < Cr(OH_2)_5X$$

The degree of association in the transition state is therefore not only dependent on the central metal ion, but also on the non-reacting ligands.

Acknowledgement. The author wishes to thank Dr. Martin Hancock for revising the English manuscript.

* From data given in Ref. 4 values of $\gamma_H = 0.45$, $\beta^* = -280$ K and $\beta° = -190$ K are obtained. Neither ΔH^* *vs.* ΔS^* nor $\Delta H°$ *vs.* $\Delta S°$ gives a single straight line, two *parallel* lines being obtained in both cases. The data for the Cl^-, Br^- and I^- complexes lie one line and the data for the H_2O, NCS^- and NH_3 complexes on the other.

Note added in proof. Additional evidence for the assignment of an associative mechanism to the series of pentaamminechromium(III) complexes has recently been given: Palmer, D. A. and Kelm, H. *Inorg. Chem. 16* (1977) 3139.

REFERENCES

1. Hunt, H. R. and Taube, H. *J. Am. Chem. Soc. 80* (1958) 2642.
2. Haim, A. *Inorg. Chem. 9* (1970) 426.
3. Stranks, D. R. and Swaddle, T. W. *J. Am. Chem. Soc. 93* (1971) 2783.
4. Swaddle, T. W. *Coord. Chem. Rev. 14* (1974) 217.
5. Swaddle, T. W. and Stranks, D. R. *J. Am. Chem. Soc. 94* (1972) 8357.
6. Ramasami, T. and Sykes, A. G. *Chem. Commun. 14* (1976) 378.
7. Monacelli, F. *Inorg. Chim. Acta 2* (1968) 263.
8. Lalor, G. C. and Bushnell, G. W. *J. Chem. Soc. A* (1968) 2520.
9. Lamb, A. B. *J. Am. Chem. Soc. 61* (1939) 699.
10. Lamb, A. B. and Fairhall, L. T. *J. Am. Chem. Soc. 45* (1923) 378.
11. Borghi, E. and Monacelli, F. *Inorg. Chim. Acta 5* (1971) 211.
12. Swaddle, T. W. and Stranks, D. R. *J. Am. Chem. Soc. 94* (1972) 8357.
13. Tong, S. B. and Swaddle, T. W. *Inorg. Chem. 13* (1974) 1538.
14. Borghi, E., Monacelli, F. and Prosperi, T. *Inorg. Nucl. Chem. Lett. 6* (1970) 667.
15. Levine, M. A., Jones, T. P., Harris, W. E. and Wallace, W. J. *J. Am. Chem. Soc. 83* (1961) 2453.
16. Guastalla, G. and Swaddle, T. W. *Can. J. Chem. 51* (1973) 821.
17. Swaddle, T. W. and Guastalla, G. *Inorg. Chem. 7* (1968) 1915.
18. Adamson, A. W. and Wilkins, R. G. *J. Am. Chem. Soc. 76* (1954) 3379.
19. Edwards, J. O. *Inorganic Reaction Mechanisms*, Benjamin, New York 1964, p. 156.
20. Mori, M. *Inorg. Synth. 5* (1957) 130.

Received December 16, 1977.

Acta Chemica Scandinavica A 32 (1978) 381 – 390

On the Hydrolysis of the Manganese(III) Ion

GEORG BIEDERMANN and ROBERTO PALOMBARI

Department of Inorganic Chemistry, The Royal Institute of Technology, 100 44 Stockholm, Sweden

The protolysis equilibria of the Mn^{3+} ion have been studied at 25 °C and in the ionic medium 3 M ($H^+ - Li^+$), ClO_4^- by measuring with iridium electrodes the redox potential of the $Mn^{3+} - Mn^{2+}$ couple as a function of the ratio $[Mn(III)][Mn^{2+}]^{-1}$ at acidity levels ranging from 0.26 to 3 M. The emf data may be explained by the equilibria

$Mn^{3+} + H_2O \rightleftharpoons MnOH^{2+} + H^+$;
$\log {}^*K_1 = 0.4 \pm 0.1$

and

$Mn^{3+} + 2H_2O \rightleftharpoons Mn(OH)_2{}^+ + 2H^+$;
$\log {}^*\beta_2 = 0.1 \pm 0.1$

The standard potential of the $Mn^{3+} - Mn^{2+}$ half-cell in 3 M lithium perchlorate medium has been determined to 1559 ± 3 mV.

For the study of equilibria in solutions possessing a slight redox buffer capacity an experimental approach is presented that may find a wide application.

The present communication represents the first part of a series dealing with the redox and the complex formation equilibria of the manganese(III) ion. A prerequisite for the correct interpretation of these reactions is that all the steps of the hydrolysis mechanism are ascertained, hence the choice of our first subject.

Since the Mn^{3+} ion represents a strong and rapid oxidizing agent, and it plays a central role in the complicated redox reactions involving permanganate and mangan dioxide, the hydrolysis and complex formation equilibria of the manganese(III) species have received considerable attention in the last decades.

In connection with a comprehensive kinetic study, Diebler and Sutin[1] have estimated, on the basis of the influence of the acidity level on the visible spectrum of manganese(III) perchlorate solutions, $\log {}^*K_1$ for the first step of hydrolysis to amount to such a high value as 0.3. Essentially the same conclusion was deduced by Fackler and Chawla[2] who have studied the spectra of the numerous manganese(III) complexes. Rosseinsky,[3] who first explored the conditions required to prepare stable manganese(III) perchlorate solutions, confirmed in a kinetic study, carried out in collaboration with Nicol, that the Mn^{3+} ion is an acid of exceptional strength and has given kinetic evidence for a $\log {}^*K_1$ value near to zero at 20 °C. A careful spectrophotometric investigation on this subject was published in 1967 by Wells and Davies[4] who concluded that the hydrolysis may be described by the formation of $MnOH^{2+}$ and have found $\log {}^*K_1 = \log [MnOH^{2+}][H^+][Mn^{3+}]^{-1}$ to equal 0.0 in 4 M perchlorate medium.

As in order to deduce this equilibrium constant the molar absorptivities of the reacting manganese species must be evaluated, it is understandable that the simplest hypothesis was chosen to describe the hydrolysis process.

In this work an attempt has been made to utilize the greater power of potentiometry for obtaining a detailed picture of the hydrolysis reaction. Our starting point was the pioneering investigation of Ciavatta and Grimaldi.[5] These authors have demonstrated that under the proper experimental conditions the $Mn^{3+} - Mn^{2+}$ couple yields reversible potentials, and they have given convincing evidence that the manganese(III) species prevailing in perchloric acid solutions are mononuclear.

METHOD OF INVESTIGATION

In the present work the hydrolysis equilibria have been studied by determining the formal standard

potential of the Mn(III) – Mn^{2+} couple as a function of the hydrogen ion concentration.

In each experiment we started with a solution of the general composition Mn^{2+} B_0, H^+ H, Li^+ (3.00 M – 2 B_0 – H), ClO_4^- 3.00 M, which for the sake of compactness in the following discussion will be denoted by TS_0, while the solution arising from TS_0 by oxidation of the Mn^{2+} to Mn(III) will be symbolized by TS. Usually a B_0 value of around 15 mM has been chosen and in the different series of experiments the hydrogen ion concentration level, H, was made to increase from 0.26 to 3 M.

In an attempt to minimize the activity factor variation of the reacting species in TS, the perchlorate ion concentration was maintained at the 3 M level by introducing lithium perchlorate. This solvent salt was chosen since, according to the measurements of Rush and Johnson,[6] the activity factor of perchloric acid varies only slightly when at the ionic strength 3 M lithium ions are replaced by hydrogen ions. As the reference state 3 M $LiClO_4$ will be taken, thus the activity factors of the reacting species are defined to tend to unity as the composition of TS approaches this pure solvent salt solution.

In order to generate manganese(III) ions, the test solution was placed in the anode compartment of the electrolysis circuit

$$\left[\text{Au}\,|\,\text{TS}\,|\,\text{HClO}_4\ H,\ \text{LiClO}_4\ (3.00\ \text{M} - H)\,|\,|\,\text{HClO}_4\ 3.00\ \text{M},\ \text{AgClO}_4\ 0.100\ \text{M}\,|\,\text{Ag}\right]_{\text{constant current supply}}$$

and ensuing each step of oxidation, involving usually the removal of a few tenths of a micromol of electrons from TS, the emf of the cell (R), where TS

$$\text{RE}\,\Big|\,\text{TS}\,\Big|\begin{matrix}\text{Au}\\ \text{and}\\ \text{Ir}\end{matrix}\Big|\,+ \qquad \text{(R)}$$

is the symbol for a solution of the composition Mn(III) B_3, Mn^{2+} ($B_0 - B_3$), H^+H, Li^+ (3.00 M – $2B_0 - H$), ClO_4 3.00 M and

$$\text{RE} = |\text{HClO}_4\ H,\ \text{LiClO}_4\ (3.00\ \text{M} - H)|\text{HClO}_4\ 3.00\ \text{M},\ \text{AgClO}_4\ 0.010\ \text{M}\,|\,\text{Ag}$$

was determined.

The emf of this cell may at 25 °C be expressed by eqn. (1), where e_0 represents the standard potential,

$$E_R = e_0 + 59.16 \log \frac{[Mn^{3+}]}{[Mn^{2+}]} + e_j - e_{RE} \qquad (1)$$

e_j is the liquid junction potential arising between TS and the bridge solution, while the potential of the reference half-cell, RE, is denoted by e_{RE}. In some cases to save time a 3 M $LiClO_4$ solution was employed in the salt bridges, but of course some gain in accuracy was attained by choosing the same acidity level as in TS.

Because of the instability of the manganese(III) species, in the course of a series of oxidation experiments the maximum manganese(III) concentration we have been able to generate never exceeded 0.25 mM. As a consequence, either low yield at the anodic oxidation or inadvertent or intentional reconversion of Mn(III) to Mn^{2+} may influence appreciably the hydrogen ion concentration in TS_0 which was chosen to range between 0.3 and 3 M. We shall therefore introduce in the following calculations the approximation that the equilibrium concentration of hydrogen ions equals the starting value H.

The interpretation of the $E_R([Mn(III)])_H$ data is further simplified by the fact that the hydrolysis of the manganese(II) ion is suppressed entirely[6a] in the acidity interval studied by us, and therefore the $[Mn^{2+}]$ value may always be set equal to $B_0 - [Mn(III)]$.

For reasons that will be discussed in the second part of this section, we have generally not been able to attain a theoretical yield for the anodic oxidation of Mn^{2+} to Mn(III). In order to find the [Mn(III)] present in the test solution when E_R is being determined, we have been forced to withdraw a sample from TS and analyze it for [Mn(III)]. By the coulometric method of I_3^- analysis which is described in the Experimental Section, a few tenths of a micromol of Mn(III) could be determined with an uncertainty of 1 – 2 %. Thus the complication arising from the low current yield which at the lowest hydrogen ion concentration, 0.26 M, was as low as 36 %, did not significantly influence the accuracy of the $E_R([Mn(III)])_H$ data.

After having terminated the electrolysis experiment, a slightly platinized platinum foil was inserted into TS and N_2 was replaced by H_2. In the presence of this catalyst the reaction

$$2Mn^{3+} + H_2 \rightarrow 2Mn^{2+} + 2H^+$$

has been found, by measuring E_R, to go to completion within a couple of hours.

When the E_R value indicated a practically complete reduction, the platinum foil was connected to the potentiometric equipment and we started with the determination of the emf of the cell (H), where

$$H_2|TS_0|RE+ \qquad (H)$$

we may use the symbol TS_0 as the hydrogen ion concentration change ensuing an oxidation reduction cycle is certainly less than the analytical uncertainty.

It took usually another 2–3 h to saturate TS_0 with hydrogen of the prevailing partial pressure and to obtain an emf value remaining constant to within 10 μV overnight.

The emf of cell (H) may at 25 °C be described by eqn. (2), where $p_{H_2} = p_{atm} - p_{H_2O}$. The relevant water

$$E_H = e_{RE} - 59.16 \log (H/\sqrt{p_{H_2}}) - e_j \qquad (2)$$

vapor pressure values could be estimated by interpolating Rush's and Johnson's osmotic coefficient data.[6]

By adding eqn. (2) to (1) and by substracting from the resulting equation the experimentally determined expression 59.16 log $\{[Mn(III)]p_{H_2}^{\frac{1}{2}}/[Mn^{2+}]H\}$ we may calculate for each point the value of the function (3) which does not contain the

$$e_0 + 59.16 \log \frac{[Mn^{3+}]}{[Mn(III)]} \equiv \varepsilon^0 \qquad (3)$$

terms e_j and e_{RE} complicating the evaluation of the $[Mn^{3+}]$ from the emf data.

This ε^0 function will serve as the basis for ascertainment of the hydrolysis mechanism. Before turning to this question which forms the subject of the Results Section, some *general comments on the experimental conditions* might be of value partly for enabling the reader to assess the accuracy of the final conclusions, and partly because the experience gathered in the course of this work seems to be utilizable for the study of other unstable oxidizing agents such as Ag^{2+} and Co^{3+}.

To prepare manganese(III) solutions of a concentration sufficient to obtain reversible redox potentials, one must primarily retard the establishment of the equilibrium

$$2Mn^{3+} + 2H_2O \rightleftharpoons MnO_2 + 4H^+ + Mn^{2+} \qquad (4)$$

which according to our preliminary data has a log K value in the vicinity of 8.4, and one must work with solutions containing a minimum amount of reducing contaminants.

These requirements exclude the introduction of reagent solutions (which inevitably contain contaminants and floating solid material catalyzing the attainment of equilibrium (4)) and necessitate *anodic oxidation*. We have not been able to prepare by ozonization MnO_2 or MnO_4^--free mangan(III) solutions.

In accordance with the experience of Ciavatta and Grimaldi[5] we have found a gold-plated platinum net as the most suitable anode material. Whatever precautions are taken to minimize by stirring the accumulation of Mn(III) in the vicinity of the anode and thereby the acceleration of equilibration (4), the decisive factor in building up a local excess of Mn(III) remains the current density. For obvious practical reasons this cannot be lowered under a certain level and a compromise is inevitable. We have applied current densities varying between 2 to 100 $\mu A/cm^2$ which enabled us to attain even at the lowest acidity level an [Mn(III)] value of 60 μM without the formation of visible amounts of MnO_2 on the anode surface.

With conventionally purified reagents one cannot attain a practical current yield, especially at low acidity, a great part of the generated Mn^{3+} is lost by route (4) and another is reconverted by the impurities to Mn^{2+}. We have attempted to solve this problem by a *preoxidation* procedure. Each series of E_R measurement was preceded by the generation of 50 to 100 μmol of manganese(III). A high portion of this amount always decayed (as it could be recognized by E_R measurement) oxidizing the contaminants in the ionic medium and the perchloric acid. This test solution was allowed to stand overnight, the anode was then replaced by a platinized platinum electrode and all the remaining manganese(III) was reduced by H_2. The anode was now reinserted, the H_2 replaced by N_2 and finally the principal series of measurements could be started. The efficiency of this *preoxidation* treatment was tested by several experiments.

First, we have found that a second purification step does not significantly improve the current yield for Mn^{3+} generation. More importantly, the theoretical current efficiency to within 1 % was attained both in a 3 M $HClO_4$ solution prepared from doubly recrystallized $HClO_4(H_2O)_2(s)$ and in a 3 M solution of this acid purified by preoxidation.

A further important point was to find an electrode material yielding reversible and stable *redox potentials* at manganese(III) concentrations as low as 10–20 μM. Iridium metal has proved to be superior to gold while, as it has been pointed out in Ref. 5, platinum has shown an erratic behavior and seemed to catalyze the formation of MnO_2. We must emphasize that at [Mn(III)] values exceeding 50 μM gold and iridium gave E_R data agreeing to within 1 mV and this result we consider as a test that our E_R measurements provide the correct redox potential of TS. Whenever the two metals differed, the iridium potential was higher and it was accepted as the true E_R value.

Another minor difficulty was encountered by the slow decline of E_R due to the *oxidation of water*

$$2Mn^{3+} + H_2O \rightarrow 2Mn^{2+} + 2H^+ + \tfrac{1}{2}O_2 \qquad (5)$$

In each series of experiments the last point, usually corresponding to the highest manganese(III) concentration, was measured for several hours to get an idea of the magnitude of this source of error. Independently of the acidity and the manganese concentration level, E_R was found to decrease with a rate of 0.02 to 0.01 mV per hour, thus for a complete series of measurements, requiring about 40 to 50 h, an error of about 1 mV arises by decomposition through route (5). This instability is of importance for us only at the 3 M $HClO_4$ level at which the [Mn(III)] was calculated to save time on the basis of coulometry. The E_R data were in these cases corrected for reaction (5); the magnitude of the correction has barely exceeded the experimental uncertainty.

Further details of our experimental approach are summarized in the following section.

EXPERIMENTAL

Manganese(II) perchlorate solutions have been prepared by oxidizing at room temperature manganese metal, being introduced in excess, by thallium(I) ions:

$$2\,Tl^+ + Mn(s) \rightarrow 2\,Tl(s) + Mn^{2+} \qquad (6)$$

At a log H value of around −3 this reaction proceeds rapidly while the rate of dissolution of manganese metal is negligible, consequently the hydrogen ion concentration of the thallium perchlorate reagent solution remains unchanged and no appreciable amounts of chloride ions are formed.

To prepare 0.5 l of 0.1 M manganese perchlorate solution by this method requires about 24 h. The completion of the oxidation was checked by withdrawing samples and testing them for the presence of Tl^+ by adding I^-. We were always working with so great volumes that no appreciable loss occurred by this sampling.

The manganese concentration of the resulting stock solution has been checked each time and it has always proved to agree with the value calculated on the basis of the amount of thallium perchlorate introduced to within 0.2 %. The manganese analyses were made gravimetrically by precipitating $MnNH_4PO_4H_2O$ as recommended by Winkler.[7]

Since the hydrolysis of the Mn^{2+} ion is negligible for log $H > -6$, the stoichiometric proton excess of the stock could easily be determined by titration with coulometrically generated hydroxide ions. The equivalence point was evaluated potentiometrically by using a glass electrode.

We encountered in this synthesis only one *difficulty*. All the high purity (designation 4 N) manganese samples commercially available have been found to contain a trace of MnS, originating presumably from the concentrated manganese sulfate solution which served as the catholyte when the metal was prepared. Contacting this impure metal with the $TlClO_4$ solution gave rise to the evolution of some H_2S which was driven out by the vigorous stream of N_2 that was allowed to pass through the perchlorate solution throughout the synthesis.

Our choice of *$TlClO_4$ as a reagent* was dictated by the narrow hydrogen ion concentration range available for the oxidation of manganese metal. At acidities exceeding 1 mM some chloride formation from ClO_4^- is inevitably occurring even at 0 °C, while at higher pH values $Mn(OH)_2$ may precipitate because of low buffer capacity.

Moreover, thallium perchlorate can conveniently be prepared in a state of high purity by oxidizing cathodically deposited thallium metal with oxygen [eqn. (7)] in a perchloric acid solution. Crystals may

$$O_2 + 4Tl(s) + 2H_2O \rightarrow 4Tl^+ + 4OH^- \qquad (7)$$

finally be obtained by adding an excess of $HClO_4$ and cooling.

This somewhat lengthy method must be used instead of dissolving commercial Tl_2CO_3 in perchloric acid. All the Tl_2CO_3 samples we could acquire were contaminated with chloride which could not be removed by recrystallization because the influence of temperature on the solubility of TlCl and Tl_2CO_3 is very similar. This complication might be of interest for the analytical chemists who often employ thallium carbonate as an ultimate standard. The only safe way to prepare this

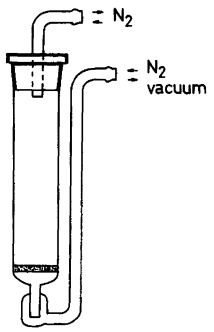

Fig. 1. Apparatus for the preparation of perchloric acid dihydrate.

substance in a state of high purity seems to be to introduce a stream of CO_2 in a solution of TlOH made by reaction (7) using a platinum vessel.

In the initial phase of this work *perchloric acid* solutions were made from crystalline perchloric acid dihydrate. This phase was separated from commercial perchloric acid of azeotropic composition at about −32 °C. Provided the viscous liquid was seeded with $HClO_4(H_2O)_2$, crystal formation was rapid and a yield of 10 – 20 % could be obtained. By two steps of crystallization the iron(III) and chloride contamination could be brought down to 0.1 μmol/mol $HClO_4$. The simple vessel shown in Fig. 1 was useful to agitate the solution, to protect it against atmospheric humidity and to remove the supernatant.

As we have discussed in the Method of Investigation section, the main part of the measurements was carried out with solutions of commercial perchloric acid purified by the preoxidation treatment. We consider the satisfactory agreement between the redox potential data with these two methods as an important argument for the reliability of our results.

The perchloric acid stock solutions were standardized either coulometrically or by titration against a sodium-free $KHCO_3$ preparation which serves as a primary standard in this laboratory; the analyses by the two approaches were found to agree to within 0.1 %.

Silver- and lithium perchlorate solutions were prepared and analyzed as usual in this laboratory.

In each series of redox potential measurements the test solution was protected by *a nitrogen stream;* floating matter was first removed by passing the gas through a tower filled with molecular sieve. The gas was then presaturated with water vapor and finally led through a sintered glass disc of porosity G4.

Gold electrodes were prepared by dipping a platinum gauze into a 0.1 M $AuCl_4^-$ solution containing hydrochloric acid. The gauze covered with a film of the gold solution was then inserted into an oven kept at 300 °C. At this temperature rapid decomposition to gold metal and chlorine occurs, and, provided the platinum support is clean, a coherent layer of gold is formed.

Any time we suspected the electrode was contaminated, the surface could be renewed by this treatment. In our experiments of one to two days duration, renewal often was necessary and usually entailed a redox potential increase of several mV's.

Gold deposited cathodically from a tetracyanoaurate solution has been found quite unsuitable as a redox electrode. Gold-plated platinum foils have always shown very low redox potential values and they could not be used either for the generation of Mn^{3+} ions. The failure is probably due to our inability to remove from the electrode surface the last traces of cyanide ions, they are known to form strong complexes with manganese(III).

When two gold electrodes were immersed in the same test solution, they agreed to within one or two mV's provided the [Mn(III)] exceeded 50 – 60 μM. This has also been found to be the case when one of the gold electrodes served as the anode. At lower manganese(III) concentrations, however, the gold electrodes have proved to be unreliable. In contrast to what we found at higher concentrations, several hours were needed to obtain a stationary redox potential value and electrodes prepared as identically as possible differed considerably. When one of the gold electrodes was employed as the anode, the difference often was as high as 5 mV.

These observations led us to believe that a thin layer of a gold oxide is formed on the electrode surface by oxidation with Mn^{3+}. Until the layer covers the surface, the manganese(III) concentration in the vicinity of the electrode will, because of the reaction, be lower than in the bulk. A further argument for this hypothesis is the observation that pretreatment with a manganese(III) solution entailed in many cases a considerable improvement. On the other hand in this case the electrode transfer, the necessary washing and the final drying often caused contamination, resulting in an unpredictable behavior. Moreover, we lose in this way the possibility to renew the active surface which represents a desideratum when working with solutions of a low redox buffer capacity.

No difficulties were encountered, however, by using *iridium* redox electrodes. At manganese(III) concentration levels as low as 10 – 20 μM they attained within a few minutes a constant redox potential value exceeding the gold electrode potential by several mV's. Moreover, when several iridium electrodes were inserted into the same test solution they never differed more than 1 mV. A

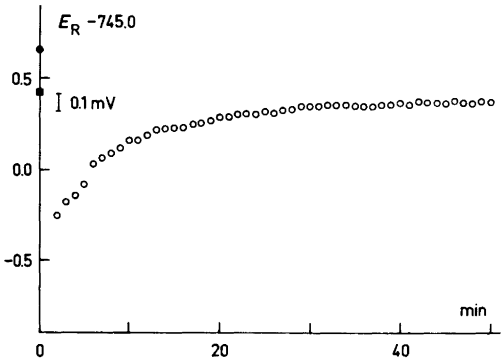

Fig. 2. Illustration of the behavior of the iridium electrodes. In a solution of $H=1$ M, [Mn(III)] = 51 μM and $[Mn^{2+}]=7.5$ mM two iridium electrodes were inserted. One of them was removed at zero time, was ignited and then reintroduced. ○, the reattainment of the reversible redox potential; ●, emf value prior to removal; ■, emf value of the second Ir-electrode.

typical experiment illustrating their excellent performance is shown in Fig. 2. Indeed, without the iridium electrodes we would not have been able to bring this investigation to a completion.

Unfortunately, we could not find a method for preparing a fresh iridium surface for each experiment. In an attempt to remove the impurities accumulated during the previous run, prior to a new series of measurements the iridium foils were brought, with a hydrogen-oxygen flame, to a temperature of around 2000 °C. Repetition of this ignition did not further improve the electrode behavior. In many cases, especially at the higher acidity levels, the ignition step could be omitted without influencing the results.

In view of this discussion it is easily understandable that whenever a difference of significance arose between the iridium and the gold electrodes, we always preferred the redox potential value shown by the former.

At the very low redox buffer capacity levels we had to work at, it was imperative to minimize the risk of contamination with reducing agents such as stopcock grease and the organic matter always present in the laboratory air. The vessel, illustrated in Fig. 3, which forms a part of a complete coulometric cell arrangement that has been described elsewhere, has proved therefore to be indispensable. Only the stopcocks containing the channels leading to the reference half-cell and the cathode compartments were coated lightly with silicon grease pretreated with 3 M $HClO_4$ and then washed with water and dried.

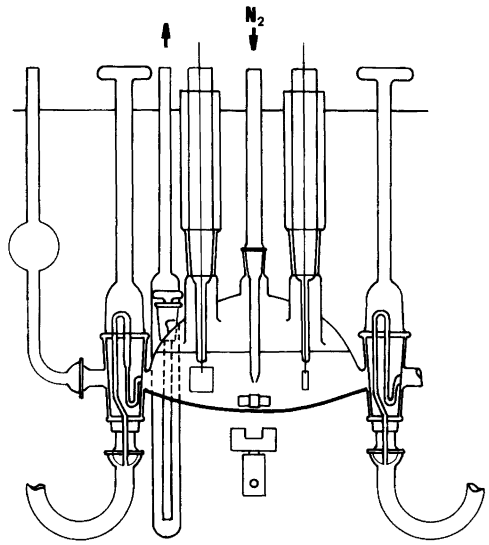

Fig. 3. All-glass vessel used for the redox potential measurements and for the generation of manganese(III) ions.

For the determination of the actual *manganese(III) concentration* 5.00 or 10.00 ml samples were withdrawn from the test solution and they were immediately introduced into a deoxygenated 0.1 M NaI solution. The reaction

$$2Mn^{3+} + 3I^- \rightarrow 2Mn^{2+} + I_3^- \qquad (8)$$

has been found to proceed to completion instantaneously even at the lowest manganese(III) concentration level studied in this work, 10 μM.

The amount of triiodide ions formed was determined potentiometrically, using Pt-foil electrodes, with coulometrically generated I_3^- ions. In each step about 0.15 μmoles of I_3^- were generated. Ensuing the anodic oxidation the redox potential, $E_{I_3^-}$, of the resulting solution was determined with at least two Pt-electrodes, one of them serving as the anode. Under the present conditions $E_{I_3^-}$, the emf of the redox half-cell against the silver reference half-cell, may simply be expressed by eqn. (9).

$$E_{I_3^-} = \eta^\circ - 29.58 \log \frac{\mu^\circ + \mu}{2} \qquad (9)$$

In this equation η° represents a constant including (1) the standard potential of the $I_3^- - I^-$ couple, (2) the potential of the Ag^+/Ag reference half-cell and (3) the constant term 29.58 log $[I^-]^3$ $V_{solution}$. The number of moles of electrons withdrawn at the anode are denoted by μ and μ° is the symbol for

the moles of manganese(III) ions which are sought for.

The most probable value for μ° was calculated in two steps. First a plot of $10^{-E_{I_3^-}/29.58}$ *versus* μ was made and the intercept on the μ-axis was determined. In the vicinity of this graphically estimated μ° value, several others were assumed and with each of them η° was calculated for every point, $E_{I_3^-}(\mu)$, of the titration. The μ° choice giving rise to an η° value constant to within 0.1 mV being accepted as the correct one.

By this method a few tenths of a μmol of triiodide ions could be determined with an uncertainty not exceeding 1 %. With 1 μmol, an accuracy of 0.1 % has been found to be easily attainable.

In this type of analysis two main difficulties are encountered. Oxygen must of course be rigorously excluded and the iodine contamination of the sodium iodide preparation must be reliably determined.

The first requirement could be fulfilled by employing for the titration an air-tight cell arrangement similar to that used for the manganese redox potential measurement, *cf.* Fig. 3. The sodium iodide solution was prepared *in situ* and oxygen was expelled with a stream of purified nitrogen which was switched off when the manganese sample had been introduced. The absence of oxygen was often controlled by letting the last solution of the titration stand overnight; during this time the redox potential change never exceeded a few tenths of an mV.

The iodine contamination of our sodium iodide sample ("specially purified" by the Merck Co., Darmstadt) was measured in blank experiments which were conducted as the manganese(III) titrations. Our sample was found to contain 1 ± 0.1 μmol of iodine per mol sodium iodide. When significant, this amount was substracted from the direct analysis result.

Some additional experiments were made to find whether any decomposition of manganese(III) might occur during the sampling. Varying the residence time of the manganese sample in the pipette from 30 s to 5 min was without effect, likewise rinsing the pipette with a few milliliters of the test solution prior to the sampling did not appreciably influence the result of the analysis. Nevertheless, rinsing was usually applied as a precaution to avoid accidental contamination.

Each series of measurements was carried out with the programmable *data acquisition system* of our laboratory. To bring our long series of measurements to a successful completion without automatization would certainly have met with great difficulties.

The E_R values with the several iridium and gold electrodes as well as the E_H data were determined with a precision of 0.01 mV by using an IDVM with 10^{10} Ω input impedance. The current supply for the electrolysis has been synchronized with a digital counter; the actual current level strength was continuously monitored by measuring with the IDVM the potential drop caused by the electrolysis along a resistance of NBS type. The current fluctuations seldom exceeded one part in 10^4. By choosing electrolysis periods long enough to make the synchronization uncertainty of around 0.01 sec, arising from the relay switchings, negligible, the number of ampere seconds passed through during an electrolysis step could always be determined with an uncertainty not exceeding 0.01 %.

RESULTS AND DISCUSSION

We have studied the five acidity levels, shown in Table 1, which cover, in about equal logarithmic steps, the interval 0.26 to 3 M. At lower hydrogen ion concentrations we have not been able to generate an amount of manganese(III) sufficient for reliable E_R measurements. The higher limit was chosen to maintain the same total molarity level at which the other triply charged ions have been previously studied in this laboratory and elsewhere.

At every H level at least two series of measurements comprising generally ten E_R determinations have been made. At each of the acidities the function $\varepsilon^\circ = e^\circ + 59.16 \log [Mn^{3+}][Mn(III)]^{-1}$ has proved to remain constant as the manganese(III) concentration was stepwise increased between the limits indicated in Table 1. This result shows that in these dilute manganese(III) solutions mononuclear hydrolysis products are formed only. Thus we can write

$$\varepsilon^\circ = e^\circ + 59.16 \log \frac{[Mn^{3+}]}{[Mn(III)]} = e^\circ - 59.16 \log (1 + \sum {}^*\beta_p H^{-p}) \quad (10)$$

Table 1. Summary of conditional standard potentials.

H M	ε° mV	Mn(III) concentration range investigated, μM
0.258	1473 ± 1	30 – 61
0.5676	1503 ± 1	32 – 63
1.000	1519 ± 1	27 – 104
1.500	1528 ± 1	34 – 104
2.968	1541 ± 0.5	40 – 287

where $*\beta_p = [Mn(OH)_p]H^p[Mn^{3+}]^{-1}$ symbolizes the equilibrium constant for the reaction step

$$Mn^{3+} + pH_2O \rightleftharpoons Mn(OH)_p^{(3-p)+} + pH^+$$

As a consequence we may call ε° the conditional standard potential of the Mn(III)–Mn^{2+} couple valid at a certain H level.

A typical series of measurements is illustrated in Table 2; each [Mn(III)] value represents the result of a iodometric analysis and each E_R datum is the mean of two redox potential determinations differing at most 0.2 mV.

In order to check the influence of accidental contamination, several series were made at each acidity levels. For instance, the three experiments at $H = 0.258$ M afforded the ε° values 1472.8, 1473.3 and 1474.1 mV whence the average included in Table 1 is calculated by taking into account the spread within the individual series as well. In the last series the reversibility was tested by building up first an [Mn(III)] of 61 μM which was then reduced stepwise to 37 μM.

The starting value of the manganese concentration was usually chosen to lie between 10 and 20 mM. In a few special experiments, measurements were made with $B_0 = 3.8$ as well as with 16.2 mM; *e.g.* at $H = 1.5$ M both series yielded the ε° value 1528 ± 1 mV. No appreciable difference in ε° was ever found when B_0 was varied between the indicated limits.

To find the composition of the hydrolysis products and the corresponding formation constants, the $\varepsilon' = \varepsilon^\circ$ (log H) data have been compared with model functions representing different hypotheses. With the assumption that a single reaction product, $Mn(OH)_p^{(3-p)+}$, is formed, no fit could be achieved. Comparison with the model based on the formation of $MnOH^{2+}$ and $Mn(OH)_2^+$

$$Y = -59.16 \log(1 + v + lv^2) \equiv Y(\log v)_l \qquad (11)$$

where $v = *K_1 H^{-1}$ and $l = *\beta_2 *K_1^{-2}$ yielded, however, a satisfactory agreement, as it is shown in Fig. 4. Model functions with l values ranging from 0.05 to 1 were calculated and superimposed on the ε° data. The closest fit was found with $l = 0.2$, and we read off from the magnitude of the lateral translation needed to bring the model function $Y(\log v)_{0.2}$ in coincidence with the experiments the most probable value for $\log *K_1 = \log v - (-\log H)$ to equal 0.4, and from the vertical translation e°, the standard potential of $Mn^{3+} - Mn^{2+}$, to equal 1559 mV.

As it is illustrated in Fig. 4 the uncertainty of our ε° determinations give rise to the following limits of uncertainty

$$e^\circ = 1559 \pm 3 \text{ mV} \qquad (12)$$

$$\log *K_1 = 0.4 \pm 0.1 \qquad (13)$$

$$\log *\beta_2 = 0.1 \pm 0.1 \qquad (14)$$

Eqns. (12) and (14) may be regarded as the final results of this work.

Our $\log *K_1$ value is thus seen to be in reasonable agreement with the estimates of the previous

Table 2. An example for a series of measurements. Hydrogen ion concentration level 0.999_8 M. Initial manganese(II) concentration 7.345 mM. After the series had been terminated, manganese(III) was reduced with H_2 and E_{H_2} was determined to 645.1 mV.

E_R (iridium) mV	[Mn(III)] μM	$E_R - 59.16 \log \frac{[Mn(III)]}{[Mn^{2+}]}$
728.6	27.2	872.4
743.0	48.0	872.1
748.2	58.8	872.0
753.6	69.2	873.2
756.2	74.8	873.8

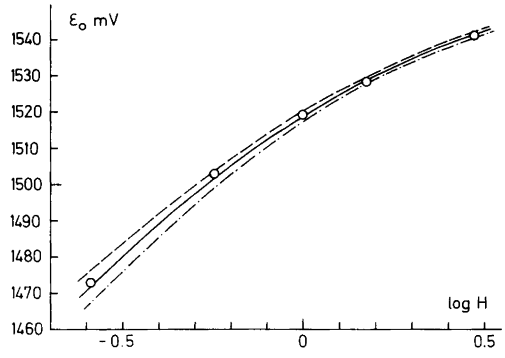

Fig. 4. The conditional standard potential, ε°, as a function of log H. The full-drawn curve represents the equation $\varepsilon^\circ = 1559 \text{ mV} - 59.16 \log(1 + 2.5H^{-1} + 1.25H^{-2})$. The broken curve corresponds to the choice $e^\circ = 1562$ mV, $\log *K_1 = 0.5$ and $l = 0.1$, while the dotted curve illustrates the choice: $e^\circ = 1556$ mV, $\log *K_1 = 0.3$, $l = 0.375$.

investigators[1-3] who studied such acidic solutions that the second step became much suppressed and who wanted to give only the order of magnitude of the protolysis constant for this strong acid.

In the light of the present results we have reinterpreted Wells' and Davies' spectrophotometric data[4] by assuming the magnitudes of log $*K_1$ and of log $*\beta_2$ in their 4 M perchlorate medium to equal our values. As the medium effect estimates of the next paragraph indicate, no serious error is likely to arise from this assumption.

The spectrophotometric data at 300 nm were recalculated to the form $\log A(1+*K_1H^{-1}+*\beta_2H^{-2})$ *versus* log H and they were compared with the model function $\log(1+u+lu^2)=Y(\log u)_l$. In these formulas A represents the absorbance of the manganese(III) species, u is the normalized variable $\varepsilon(MnOH^{2+})\varepsilon(Mn^{3+})^{-1}*K_1H^{-1}$ and l is the parameter $*\beta_2*K_1{}^{-2}\varepsilon(Mn^{3+})\varepsilon(Mn(OH)_2{}^{+})\varepsilon(MnOH^{2+})^{-2}$.

The best fit has been found with $l=0.03$; we derived then on the basis of the coordinate translations the molar absorptivities $\varepsilon(Mn^{3+})=30$, $\varepsilon(MnOH^{2+})=243$, and $\varepsilon(Mn(OH)_2{}^{+})=308$ cm^2 mol^{-1}. The fit is illustrated in Fig. 5.

To enable us to estimate other manganese(III) equilibria, we attempted to assess the magnitude of the standard potential and that of log $*K_1$ in the *conventional reference state:* dilute aqueous solution. Assuming the validity of the specific interaction theory and postulating the interaction coefficients of the manganese(III) and iron(III) species to be equal, we obtained that $e^\circ_{standard}=1604$ mV and log $*K_{1,standard}$ $-\log *K_1$ (3 M) is less than the uncertainty of our log $*K_1$ (3 M) determination.

For the $e^\circ_{standard}$ calculations we used the interaction coefficients derived in a previous communication.[8] The medium effect on log $*K_1$ was estimated by considering the log $*K_1(Fe^{3+})$ data in 3, 1 and 0.5 M $NaClO_4$ solutions.[9] The formation of $Fe(OH)_2{}^{+}$ seems to have been studied only in 3 M $NaClO_4$, so we are not able to derive a value for log $*\beta_{2,standard}$.

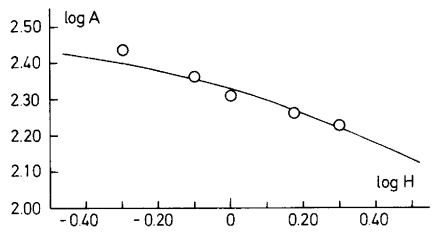

Fig. 5. Recalculation of Davies' and Wells' spectrophotometric data,[4] logarithm of the manganese(III) absorbance as a function of log H. The curve has been calculated with the log $*K_1$ and log $*\beta_2$ values of (13) and (14) and with the molar absorptivities of the text.

Since the radii of the triply charged cations of the 3*d* series have been estimated to vary but little, for each of them a value near to 0.65 Å has been deduced,[10] we have to seek *an explanation for the exceptional acid strength of the* Mn^{3+} *ion* on the basis of the properties of the *d* orbitals.

A correlation between the aquo acidity (as measured by log $*K_1$) and the crystal field stabilization energy of the octahedrally coordinated $Me^{3+}(H_2O)_6$ ions is easy to recognize. The following $p*K_1$ values have been reported, valid, with the exception of Ti^{3+}, in a 3 M $NaClO_4$ medium: Ti^{3+} 2.55 (3 M KBr medium),[11] V^{3+} 2.7,[12] Cr^{3+} 4.6,[13] Fe^{3+} 3.05[14] and $Co^{3+}\geq 2.0$.[15] Titanium(III) cannot be studied at room temperature with conventional methods in this medium because it reduces $ClO_4{}^{-}$ rapidly to Cl^{-}. The investigation of the more sluggish reducing agent V^{3+} involves also some complications and the $p*K_1$ value cited has to be regarded as a first estimate only.

Thus Cr^{3+} with the greatest C.F.S.E. represents the weakest acid, while for V^{3+}, with only 8 Dq, $*K_1$ is seen to be raised at least one hundred times. One would be inclined to ascribe the high $p*K_1$ for Fe^{3+} to the special stability of a half-filled shell.

From these data we would interpolate a $p*K_1$ value of around 2.5 to 3 for Mn^{3+} which has been shown in the present work to behave as a strong acid. This discrepancy can be made intelligible by assuming for $MnOH^{2+}$ a ligand configuration giving rise to four low energy orbitals capable of accomodating all the *d* electrons of Mn(III). A five-coordinated $MnOH^{2+}(H_2O)_4$ ion with the ligands in the square pyramid arrangement and with the OH^{-} ion near to the high-level orbital, satisfies this requirement and it provides a greater C.F.S.E. than the octahedral coordination.

Postulating the same structure for the other $MeOH^{2+}$ ions of the series a parallelism arises between log $*K_1$ and the difference in C.F.S.E. for the square pyramid and the octahedral coordination. For this difference the following estimates have been made by Basolo and Pearson[16] (who intended to explain kinetic data but have realized the potential value of their calculations for the interpretation of equilibria) Mn^{3+} 3.14, V^{3+} 1.14, Co^{3+} and Ti^{3+} 0.57, Fe^{3+} zero, Cr^{3+} -2.00. Hence

we may have little doubt that the hydrolysis of these ions is greatly influenced by ligand field effects.

On the basis of these speculations we may expect the Mn^{3+} ion to form complexes of extraordinary strength not only with OH^- but also with other singly charged anions. Equilibria of this type are now being studied in this laboratory and the results will form the subject of a forthcoming publication.

Acknowledgements. We would like to express our appreciation to Mr. Sture Lind who constructed and maintained many parts of our complicated equipment.

The present work represents a part of a research project financially supported by Statens Naturvetenskapliga Forskningsråd (Swedish Natural Science Research Council).

REFERENCES

1. Diebler, H. and Sutin, N. *J. Phys. Chem. 68* (1964) 174.
2. Fackler, J. P., Jr. and Chawla, I. D. *Inorg. Chem. 3* (1964) 1130.
3. Rosseinsky, D. R. and Nicol, M. J. *J. Chem. Soc. A* (1968) 1022.
4. Wells, C. F. and Davies, G. *J. Chem. Soc. A* (1967) 1858.
5. Ciavatta, L. and Grimaldi, M. *J. Inorg. Nucl. Chem. 31* (1969) 3071.
6. a. Rush, R. M. and Johnson, J. S. *J. Phys. Chem. 72* (1968) 767. b. Fontana, S. and Brito, F. *Inorg. Chim. Acta 2* (1968) 179.
7. Winkler, L. W. *Ausgewählte Untersuchungsverfahren für das chemische Laboratorium*, Enke Verlag, Stuttgart 1931.
8. Biedermann, G. *Dahlem Workshop on the Nature of Seawater*, Dahlem Konferenzen, Berlin 1975.
9. Sillén, L. G. and Martell, A. E. *Stability Constants*, Special Publications Nos. 17 and 25, The Chemical Society, London 1964 and 1971.
10. The radius values preferred by Basolo and Pearson[16] do not differ significantly from the estimates of Geller quoted by Wells, A.F. in *Structural Inorganic Chemistry*, 3rd Ed., Oxford 1962, p. 69. The most recent (1952) and the oldest (1925) radius estimates shown in the comparative Table of Landolt-Börnstein, I Bd., 4. Teil, 1955, p. 522, are also in reasonable agreement with each other and with the previously mentioned deductions which were made later.
11. Paris, M. R. and Gregoire, C. *Anal. Chim. Acta 42* (1968) 439.
12. Brito, F., quoted in Ref. 9.
13. This value is the result of a recent study in this laboratory. The mononuclear hydrolysis was studied by measuring with a glass electrode the hydrogen ion concentration of coulometrically alkalified dilute (<1 mM) chromium(III) solutions in 3 M $NaClO_4$ medium.
14. Hedström, B. O. A. *Ark. Kemi 6* (1953) 1.
15. Warnqvist, B. *Inorg. Chem. 9* (1970) 682.
16. Basolo, F. and Pearson, R. G. *Mechanisms of Inorganic Reactions*, Wiley, New York 1958.

Received December 5, 1977.

Acta Chemica Scandinavica A 32 (1978) 391 – 400

Conformational Analysis of Coordination Compounds. IV. Tris(1,2-ethanediamine)- and Tris(2,3-butanediamine)cobalt(III) Complexes *

SVETOZAR R. NIKETIĆ ** and KJELD RASMUSSEN ***

Chemistry Department A, The Technical University of Denmark, Building 207, DK-2800 Lyngby, Denmark

A fast convergent energy minimisation programme is used to calculate equilibrium conformations of three series of tris(diamine) coordination complexes with the amines 1,2-ethanediamine and *rac*- and *meso*-2,3-butanediamine. All possible isomers and conformers are treated, their minimum energies are given, and examples of equilibrium conformations are shown in stereo. Ob-lel and axial-equatorial energy differences are derived and compared, and the influence of various non-bonded interactions in determining conformations is analysed. Shapes of chelate rings and of coordination polyhedra MN_6 are discussed in terms of deviations from regular octahedral microsymmetry.

Equilibrium conformations of $M(en)_3$ are compared with summaries of recent crystal structure determinations of $[Co(en)_3]^{3+}$ and $[Cr(en)_3]^{3+}$ salts, which are referenced.

As part of our continuing efforts in developing a consistent force field (CFF)[2] for coordination compounds we have studied the conformations of tris-alkanediamine complexes of cobalt(III) and chromium(III) containing 5-membered metal chelate rings of 1,2-ethanediamine (en) and 2,3-butanediamine (2,3-bn).

In the previous paper[3] we have presented an analysis of the conformations of tris(1,3-propanediamine) and tris(2,4-pentanediamine) Co(III) and Cr(III) systems. The results reported in this paper confirm our assertion that convergent energy minimisation is an expedient method to find equilibrium conformations, and that our present force field, though not ideal, is able to provide some insight into the interactions which determine the shapes of chelate amine coordination compounds.

CHOICE OF THE SYSTEMS

There is no need to emphasise the importance of $M(en)_3$ as a prototype of a family of propeller-like tris(alkanediamine) complexes. On this molecule a number of theoretical models have been developed in parallel with an accumulation of experimental data of a very good quality, comprising X-ray analyses,[4] ORD/CD studies,[5] eleetronic spectra of single crystals at low temperature,[6,7] NMR studies,[8] vibrational spectra[9] and stability constants.[10] $M(en)_3$ therefore represents an indispensable model system for an optimisation of a force field for tris-alkanediamine coordination complexes.

The $M(2,3\text{-bn})_3$ system was chosen because it provides additional sources of isomerism, which will be described in detail below. The possibility for a later comparison of our results with the experimental thermodynamic data on 2,3-bn complexes obtained recently in this laboratory[11] was another incitement for our choice.

ISOMERISM AND NOMENCLATURE

In the present study we have included all theoretically possible isomers and conformers of

* Presented at the XX Annual Meeting of the Serbian Chemical Society, Beograd, Yugoslavia, January 1977. For synopsis see Ref. 1. For Part III see Ref. 3.

** Present address: Department of Chemistry, Faculty of Science, University of Beograd, Studentski trg 16, POB 550, YU-11001 Beograd, Yugoslavia.

*** To whom correspondence should be addressed.

$M(en)_3$ and $M(2,3\text{-bn})_3$ systems. The principal features of their static stereochemistry are those characteristic of three-bladed chiral propeller molecules.[12] Their configurational chirality gives rise to a pair of enantiomers (designated as Λ and Δ according to the IUPAC nomenclature[13]) for each structure.

The $M(en)_3$ system. The source of conformational isomerism in the $M(en)_3$ system is the nonplanarity of the 5-membered metal chelate rings. Considering the two stable chiral (skew) conformations of chelate rings (designated as λ and δ according to the IUPAC nomenclature[13]) four conformationally unique conformers of $M(en)_3$ can be constructed for each absolute configuration:

$$\lambda\lambda\lambda,\ \lambda\lambda\delta,\ \lambda\delta\delta,\ \text{and}\ \delta\delta\delta \qquad (1)$$

As in our previous writings[14] we shall use the chirality invariant nomenclature in which the two possible conformations of an individual ethylenediamine chelate ring in $M(en)_3$ are named *lel* and *ob*, respectively, connoting that the central C–C bond of the ring is (approximately) para*lel* and *ob*lique with respect to the C_3 or pseudo-C_3 symmetry axis. Thus, the four conformers (11) are symbolised as:

$$lel_3,\ lel_2ob,\ ob_2lel\ \text{and}\ ob_3 \qquad (2)$$

and this type of isomerism as lel-ob isomerism. The symbol lel_3, for example, denotes either $\Delta(\lambda\lambda\lambda)$ or $\Lambda(\delta\delta\delta)$, which are energetically identical.

The $M(2,3\text{-bn})_3$ system. Due to the presence of the two chiral centres 2,3-bn exists in optically active (2*R*,3*R*- or 2*S*,3*S*-) and in *meso* (*RS*) form. For convenience, we shall discuss separately $M(2,3\text{-bn})_3$ complexes with optically active (or racemic) forms of 2,3-bn, and with *meso*-2,3-bn.

*Racemic (*rac*) or optically active (*RR- *or* SS-*) 2,3-bn.* By coordination of the *rac*-2,3-bn twenty theoretically possible and conformationally unique forms of $M(2,3\text{-bn})_3$ can be formed (Table 1). They can be systematically enumerated on the basis of the following two principles. Firstly, optically active 2,3-bn forms a chelate ring in which the two methyl groups are either both equatorial (*e.g.*, for λ ring conformation of 2*R*,3*R*-bn) or both axial (*e.g.*, for δ ring conformation of 2*R*,3*R*-bn). Therefore, in the $M(bn)_3$ system with coordinated optically active 2,3-bn, four different species with respect to the methyl group orientation, namely eq_6, eq_4ax_2, eq_2ax_4, and ax_6, are possible. We will refer to this as an eq-ax isomerism. Secondly, the $M(2,3\text{-bn})_3$ system has the same four possibilities for the ring conformations (lel_3, lel_2ob, ob_2lel, and ob_3) as the parent $M(en)_3$ system. By the interplay of lel-ob and eq-ax isomerism, 16 isomers and conformers of $M(2,3\text{-bn})_3$ with racemic amine are generated. However, for conformers whose parent skeletons lack a C_3-axis (lel_2ob and ob_2lel) the degeneracy between otherwise identical rings is lifted, and we get two instead of one representative for eq_4ax_2 and for eq_2ax_4 structures [pairs 6/7, 8/9, 12/13, and 14/15 in Table 1], so that we arrive at a total of 20 isomers and conformers of $M(rac\text{-}2,3\text{-bn})_3$.

Eight of them (two groups of four in each) represent structures containing only one enantiomer of 2,3-bn: either 2*R*,3*R*-bn in structures 4, 9, 13, 17; or 2*S*,3*S*-bn in structures 1, 6, 14, 20; all cases pertaining to Λ configuration. The remaining 12 are "mixed" forms containing both enantiomers of 2,3-bn coordinated to the same metal ion. The former 8 structures are relevant from the point of view of a practicing chemist because they represent all species that are theoretically obtainable from a synthesis with an optically active form of the amine. For example, the coordination of 2*S*,3*S*-bn may produce isomers 1, 6, 14, 20 of Λ configuration, and the enantiomeric forms of 4, 9, 13, and 17 having Δ configuration (Table 1).

In Table 1 the 20 isomers and conformers of $M(2,3\text{-bn})_3$ are given the full IUPAC designation[13] and a shorthand notation which is used in this paper. The chirality invariant shorthand notation emphasizes the conformationally relevant features lel/ob for rings, and eq/ax for methyl groups, and is unambiguous on the condition that the sequence of designators, as written, is consistently adhered to. For example, the (ob lel_2)(eq_4ax_2) designation implies the following sequence of rings: ob ring (eq CH_3 groups), lel ring (eq CH_3 groups), lel ring (ax CH_3 groups), and therefore corresponds to the Λ-[M(2*S*,3*S*-bn)(2*R*,3*R*-bn)(2*S*,3*S*-bn)$\delta\lambda\lambda$] configuration, or to its enantiomer Δ-[M(2*R*,3*R*-bn)-(2*S*,3*S*-bn)(2*R*,3*R*-bn)$\lambda\delta\delta$].

Meso-*2,3-bn.* Coordination of *meso*-2,3-bn gives rise to twelve theoretically possible conformationally unique isomers and conformers of $M(2,3\text{-bn})_3$ (Table 2). In contrast to the optically active form, *meso*-2,3-bn forms chelate rings with one of the methyl groups equatorial and the other axial, both for λ and for δ ring conformation. Therefore, there is no eq-ax isomerism and all tris

Table 1. Twenty isomers and conformers of M(rac-2,3-bn)$_3$. Numbering and nomenclature.

No.	Shorthand notation	Full IUPAC notation for Λ-series
1	(eq$_6$)(lel$_3$)	Λ-[M2*S*,3*S*-bn)$_3\delta\delta\delta$]
2	(eq$_6$)(lel$_2$ob)	Λ-[M(2*S*,3*S*-bn)$_2$(2*R*,3*R*-bn)$\delta\delta\lambda$]
3	(eq$_6$)(lel ob$_2$)	Λ-[M(2*S*,3*S*-bn)(2*R*,3*R*-bn)$_2\delta\lambda\lambda$]
4	(eq$_6$)(ob$_3$)	Λ-[M(2*R*,3*R*-bn)$_2\lambda\lambda\lambda$]
5	(eq$_4$ax$_2$)(lel$_3$)	Λ-[M(2*S*,3*S*-bn)$_2$(2*R*,3*R*-bn)$\delta\delta\delta$]
6	(eq$_4$ax$_2$)(lel$_2$ob)	Λ-[M(2*S*,3*S*-bn)$_3\delta\delta\lambda$]
7	(eq$_4$ax$_2$)(lel ob lel)	Λ-[M(2*S*,3*S*-bn)(2*R*,3*R*-bn)$_2\delta\lambda\delta$]
8	(eq$_4$ax$_2$)(lel ob$_2$)	Λ-[M(2*S*,3*S*-bn)(2*R*,3*R*-bn)(2*S*,3*S*-bn)$\delta\lambda\lambda$]
9	(eq$_4$ax$_2$)(ob$_2$lel)	Λ-[M(2*R*,3*R*-bn)$_3\lambda\lambda\delta$]
10	(eq$_4$ax$_2$)(ob$_3$)	Λ-[M(2*R*,3*R*-bn)$_2$(2*S*,3*S*-bn)$\lambda\lambda\lambda$]
11	(eq$_2$ax$_4$)(lel$_3$)	Λ-[M(2*S*,3*S*-bn)(2*R*,3*R*-bn)$_2\delta\delta\delta$]
12	(eq$_2$ax$_4$)(lel$_2$ob)	Λ-[M2*S*,3*S*-bn)(2*R*,3*R*-bn)(2*S*,3*S*-bn)$\delta\delta\lambda$]
13	(eq$_2$ax$_4$)(ob lel$_2$)	Λ-[M(2*R*,3*R*-bn)$_3\lambda\delta\delta$]
14	(eq$_2$ax$_4$)(lel ob$_2$)	Λ-[M(2*S*,3*S*-bn)$_3\delta\lambda\lambda$]
15	(eq$_2$ax$_4$)(oblel ob)	Λ-[M2*R*,3*R*-bn)$_2$(2*S*,3*S*-bn)$\lambda\delta\lambda$]
16	(eq$_2$ax$_4$)(ob$_3$)	Λ-[M(2*R*,3*R*-bn)(2*S*,3*S*-bn)$_2\lambda\lambda\lambda$]
17	(ax$_6$)(lel$_3$)	Λ-[M(2*R*,3*R*-bn)$_3\delta\delta\delta$]
18	(ax$_6$)(lel$_2$ob)	Λ-[M(2*R*,3*R*-bn)$_2$(2*S*,3*S*-bn)$\delta\delta\lambda$]
19	(ax$_6$)(lel ob$_2$)	Λ-[M(2*R*,3*R*-bn)(2*S*,3*S*-bn)$_2\delta\lambda\lambda$]
20	(ax$_6$)(ob$_3$)	Λ-[M(2*S*,3*S*-bn)$_3\lambda\lambda\lambda$]

Table 2. Twelve isomers and conformers of M(*meso*-2,3-bn)$_3$. Numbering and nomenclature. All are eq$_3$ax$_3$.

No.	Shorthand notation	Full IUPAC notation for Λ-series
1	fac-(lel$_3$)	*fac*-Λ-[M(2*R*,3*S*-bn)$_3\delta\delta\delta$]
2	fac-(lel$_2$ob)	*fac*-Λ-[M(2*R*,3*S*-bn)$_3\delta\delta\lambda$]
3	fac-(lel ob$_2$)	*fac*-Λ-[M(2*R*,3*S*-bn)$_3\delta\lambda\lambda$]
4	fac-(ob$_3$)	*fac*-Λ-[M(2*R*,3*S*-bn)$_3\lambda\lambda\lambda$]
5	mer-(lel$_3$)	*mer*-Λ-[M(2*R*,3*S*-bn)$_2$(2*S*,3*R*-bn)$\delta\delta\delta$]
6	mer-(lel$_2$ob)	*mer*-Λ-[M(2*R*,3*S*-bn)$_2$(2*S*,3*R*-bn)$\delta\delta\lambda$]
7	mer-(leloblel)	*mer*-Λ-[M(2*R*,3*S*-bn)$_2$(2*S*,3*R*-bn)$\delta\lambda\delta$]
8	mer-(oblel$_2$)	*mer*-Λ-[M(2*R*,3*S*-bn)$_2$(2*S*,3*R*-bn)$\lambda\delta\delta$]
9	mer-(lelob$_2$)	*mer*-Λ-[M(2*R*,3*S*-bn)$_2$(2*S*,3*R*-bn)$\delta\lambda\lambda$]
10	mer-(oblelob)	*mer*-Λ-[M(2*R*,3*S*-bn)$_2$(2*S*,3*R*-bn)$\lambda\delta\lambda$]
11	mer-(ob$_2$lel)	*mer*-Λ-[M(2*R*,3*S*-bn)$_2$(2*S*,3*R*-bn)$\lambda\lambda\delta$]
12	mer-(ob$_3$)	*mer*-Λ-[M(2*R*,3*S*-bn)$_2$(2*S*,3*R*-bn)$\lambda\lambda\lambda$]

complexes of *meso*-2,3-bn are eq$_3$ax$_3$. Another consequence of the difference in chiralities at the C-2 and C-3 atoms is the existence of facial and meridional isomers. Fac-mer isomerism, well-known in the case of tris-bidentate complexes of, *e.g.*, amino acids and β-diketonates, has been recognized in M(*meso*-2,3-bn)$_3$ for a long time,[15] but has only recently been demonstrated.[16]

Since there is no variation in the number of equatorial and axial methyl groups there are only four conformers of the facial isomer of M(*meso*-2,3-bn)$_3$: lel$_3$, lel$_2$ob, ob$_2$lel, and ob$_3$. These have C-atoms of the same chirality adjacent to the ligators spanning an octahedral face. The number of meridional isomers is eight. They have C-atoms of the same chirality adjacent to the ligators spanning an octahedral meridian. They include two sets (lel$_2$ob and ob$_2$lel) of three heteroconformational forms each, arising from the intrinsic non-equivalence of all three rings in meridional structures.

Table 2 illustrates the use of chirality invariant shorthand symbolism for 12 M(*meso*-2,3-bn)$_3$ isomers and conformers along with the full IUPAC specification.

CREATION OF INITIAL STRUCTURES

Initial cartesian atomic coordinates of the four M(en)$_3$ conformers were generated from the standard values of bond lengths and valence angles by our CFF programmes[2] by specifying the appropriate torsional angles.

Thirty-two isomers and conformers of M(2,3-bn)$_3$ were built by adding methyl groups on the conformations of the M(en)$_3$-like skeleton, in turn, in a systematic way, with help of a small (~40 statements) FORTRAN programme written for this purpose, which also labels the conformers as required and stores the sets of coordinates as a member of a partitioned data set compatible with the system of CFF programmes.

Table 3. Force field for coordination compounds. All units are such that energies are given in kJ mol^{-1}; distances are in Å; angles are in rad.

Bond stretching: $E_b = \frac{1}{2}K_b(b-b_0)^2$		
Bond	K_b	b_0
M–N	1052.9	2.00
N–C	3610.0	1.47
C–C	3008.3	1.54
C–H	3008.3	1.093
N–H	3369.3	1.011
Angle bending: $E_t = \frac{1}{2}K_\theta(\theta-\theta_0)^2$		
Angle	K_θ	θ_0
N–M–N	409.13	1.571
M–N–H	120.33	1.911
M–N–C	240.66	1.911
N–C–C	601.66	1.911
N–C–H	311.08	1.911
H–N–H	318.88	1.911
C–N–H	391.08	1.911
H–C–H	312.86	1.911
H–C–C	601.66	1.911
Torsional: $E_p = \frac{1}{2}K_\phi(1+\cos n\phi)$		
	K_ϕ	n
C–C and C–N	12.55	3
M–N	0.0	12
Non-bonded: $E_{nb} = A\exp(-Br) - C/r^6$		
Interaction	$A\times10^{-4}$	B	C
H···H	2.76	4.08	205.9
H···C	13.14	4.20	506.7
H···N	11.76	4.32	415.1
C···N	88.74	4.44	1020.9
C···C	97.16	4.32	1246.0
N···N	77.99	4.55	836.8
M···H	13.14	4.20	506.7
M···C	99.16	4.32	1246.0

CALCULATIONS

Method. A full documentation of the method and programmes for CFF calculations is presented elsewhere.[2]

Force field. Our force field was that used in previous work,[3,14] with slight changes. In the torsional function we used the concept of group torsion rather than bond torsion,[17] whereby only one torsion is counted for each bond rather than nine for an sp^3-sp^3 bond. The change was made because it entailed much fewer internal coordinates, thus easing a vibrational analysis to follow later. The modification caused insignificant differences in computed structures (less than 0.003 Å and 0.02 rad) and in energies (less than 2.0 kJ mol^{-1}).

The potential energy functions and their parameters are shown in Table 3. Bond stretching and angle bending parameters for the hydrocarbon part of our force field were taken over from Wiberg's force field.[17-19] It was supplemented with parameters defining harmonic deformations of bonds and angles involving metal and coordinated nitrogen atoms, which were assumed on the basis of the normal coordinate analyses of Nakagawa and Shimanouchi[20] on ammine complexes of cobalt(III).

Several sets of non-bonding parameters were tried. Our final choice was a set of parameters for the Buckingham-type function developed by Liquori.[21]

Torsional parameters (the same value for both C–C and C–N bonds) were adjusted so that the

force field could reproduce the rotational barrier of about 12.55 kJ mol^{-1} in ethane using the aforementioned non-bonded functions.

The application of this force field for the octahedral trisbidentate metal chelate complexes implied some special considerations: (1) Since the geminal (1,3-) interactions were accounted for in the angle bending terms, they were automatically left out of calculations of non-bonded interactions, wherefore the N···N parameters of Table 3 were actually not in use. (2) Valence angles defined by ligating atoms in *trans* position ($\sim 180°$), as well as those between ligators from different chelate rings were not treated. In this way only three chelate angles were considered at the octahedral metal atom. (3) Exclusion of the so called core field potential (non-bonded interactions involving the central metal atom in our force field M···C and M···H contributions) has practically no significance on the results of force field calculations.[22] This was demonstrated[3] by test computations in which core field terms included with the appropriate parameters for M were set equal to those of C.

Minimisation. A typical minimisation of one molecule using the steepest-descent and modified Newton algorithms required about 150 s on an IBM 370/165. All minimisations were carried through to a gradient norm of less than 10^{-6} kJ mol^{-1} $Å^{-1}$.

RESULTS AND DISCUSSION

Relative energies. All energy contributions and total and relative energy values are listed in Tables 4–6. Energies are in kJ mol^{-1}. The columns headed $\nabla \times 10^9$ give the final gradient norms in kJ mol^{-1} $Å^{-1}$.

All complexes are shown on a common energy scale in Fig. 1. They fall distinctly into six groups according to the presence of axial and equatorial methyl groups. The tables show that from one group to another the various types of energy contributions change in a parallel way. Such regularity was not found for complexes with six-membered rings.[3]

ax-eq Differences. Table 6 shows that the total energy increases in a regular way when two methyl groups are changed from equatorial to axial configuration of the same conformation. An ax-eq energy difference of (15.0 ± 1.0) kJ mol^{-1} reproduces quite well all data for the intermediate groups, including those of Table 5 where all members have the eq_3ax_3 configuration. In earlier work[14b] using

Table 4. Energy contributions for $M(en)_3$ conformers.

Conformer	$\nabla \times 10^9$	E_b	E_t	E_p	E_{nb}	E_T	ΔE
ob_3	192	1.34	8.08	19.44	−16.96	11.91	4.75
$lelob_2$	105	1.39	8.24	19.11	−16.81	11.93	4.77
lel_2ob	92	1.26	8.38	18.21	−18.01	9.84	2.68
lel_3	197	1.11	8.84	16.89	−19.68	7.16	0.00

Table 5. Energy contributions for twelve isomers and conformers of M(*meso*-bn)$_3$.

	Conformer	$\nabla \times 10^9$	E_b	E_t	E_p	E_{nb}	E_T	ΔE
12	mer-(ob_3)	21	4.60	22.79	37.72	−17.32	47.78	8.55
11	mer-(ob_2lel)	430	4.82	23.90	36.28	−15.84	49.16	9.93
10	mer-(oblelob)	100	4.86	24.24	37.08	−15.36	50.83	11.60
9	mer-($lelob_2$)	167	4.47	21.36	35.98	−17.73	44.08	4.85
8	mer-($oblel_2$)	251	4.77	21.97	35.19	−15.79	46.13	6.90
7	mer-(leloblel)	8	4.58	21.96	34.72	−17.30	43.96	4.73
6	mer-(lel_2ob)	96	4.49	21.74	36.32	−17.45	45.10	5.87
5	mer-(lel_3)	42	4.32	19.99	34.06	−19.14	39.23	0.00
4	fac-(ob_3)	13	4.91	24.94	37.08	−16.02	50.91	11.68
3	fac-($lelob_2$)	201	4.84	23.78	36.16	−15.84	48.94	9.71
2	fac-(lel_2ob)	122	4.52	21.76	35.79	−17.55	44.52	5.29
1	fac-(lel_3)	71	3.99	20.37	36.37	−21.26	39.47	0.24

Table 6. Energy contributions for twenty isomers and conformers of M(*rac*-bn)$_3$.

	Conformer	$\nabla \times 10^9$	E_b	E_t	E_p	E_{nb}	E_T	ΔE
20	$(ax_6)(ob_3)$	71	5.81	40.25	59.74	−11.16	94.64	96.72
19	$(ax_6)(lelob_2)$	723	6.03	42.13	55.70	−10.25	93.62	95.70
18	$(ax_6)(lel_2ob)$	1393	5.79	39.41	55.58	− 9.76	91.02	93.10
17	$(ax_6)(lel_3)$	163	5.27	32.78	57.77	− 9.18	86.65	88.73
16	$(eq_2ax_4)(ob_3)$	79	4.55	29.78	48.29	−16.44	66.18	68.26
15	(eq_2ax_4)(oblelob)	1033	4.82	32.01	43.97	−15.48	65.32	67.40
14	$(eq_2ax_4)(lelob_2)$	130	4.69	29.11	45.22	−16.74	62.28	64.36
13	$(eq_2ax_4)(oblel_2)$	42	4.69	30.69	42.72	−15.33	62.77	64.85
12	$(eq_2ax_4)(lel_2ob)$	184	4.46	27.68	42.93	−16.71	58.36	60.44
11	$(eq_2ax_4)(lel_3)$	159	4.14	24.20	43.30	−17.35	54.30	56.38
10	$(eq_4ax_2)(ob_3)$	172	3.42	20.79	34.52	−23.13	35.59	37.67
9	$(eq_4ax_2)(ob_2lel)$	104	3.64	22.28	32.98	−20.04	36.86	38.94
8	$(eq_4ax_2)(lelob_2)$	79	3.54	20.91	31.35	−23.15	32.66	34.74
7	(eq_4ax_2)(leloblel)	134	3.38	19.73	31.54	−23.02	31.63	33.71
6	$(eq_4ax_2)(lel_2ob)$	50	3.29	19.59	27.60	−25.07	25.42	27.50
5	$(eq_4ax_2)(lel_3)$	126	3.10	17.76	39.14	−25.58	24.42	26.50
4	$(eq_6)(ob_3)$	426	2.33	12.77	18.40	−30.68	2.82	4.90
3	$(eq_6)(lelob_2)$	67	2.36	12.93	18.12	−30.41	3.00	5.08
2	$(eq_6)(lel_2ob)$	142	2.24	13.01	17.29	−31.68	0.86	2.94
1	$(eq_6)(lel_3)$	33	2.07	13.53	16.03	−33.72	−2.08	0.00

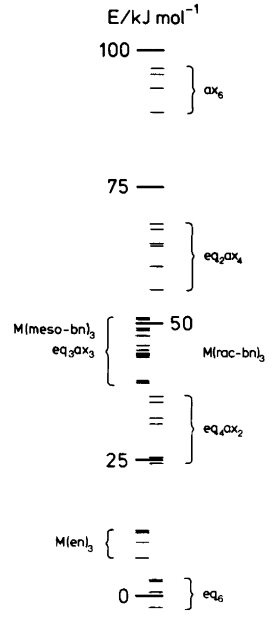

Fig. 1. Relative energies of four conformers of M(en)$_3$ and thirty-two isomers and conformers of M(2,3-bn)$_3$ on a common energy scale.

essentially the same force field but a rather primitive minimisation programme an ax-eq difference of 8.2 kJ mol^{-1} was found. DeHayes and Busch,[23] using a programme essentially the same as ours, and a force field of the same form, though with rather different parameters, also found 8.2 kJ mol^{-1}. The standard value of the ax-eq free enthalpy difference for only one group on a cyclohexane ring is 7.1 kJ mol^{-1}.[24]

When the M(en)$_3$ series is fitted into this picture, we find that the presence of a methyl group in an equatorial position changes the energy by −1.53 kJ mol^{-1}, and in an axial position by 13.52 kJ mol^{-1}. This applies, of course, only to the present force field.

ob-lel Differences. When we examine the energy differences between conformers having the same methyl group disposition but different ring conformations, we find a clear-cut regularity, but no pronounced additivity. Fig. 2 shows that an ob_3 conformation has only slightly higher energy than the corresponding $lelob_2$ conformation whereas the $lelob_2$-lel_2ob and lel_2ob-lel_3 differences are larger, as a rule. We can derive the following average ob-lel energy differences: M(en)$_3$ 1.6±0.9; fac-M(*meso*-bn)$_3$ 3.8±1.1, mer-M(*meso*-bn)$_3$ 2.9±1.8, all M(*meso*-bn)$_3$ 3.3±1.6; M(*rac*-bn)$_3$ eq_6 1.7±1.0, M(*rac*-bn)$_3$ eq_4ax_2 4.9±1.9, M(*rac*-bn)$_3$ eq_2ax_4

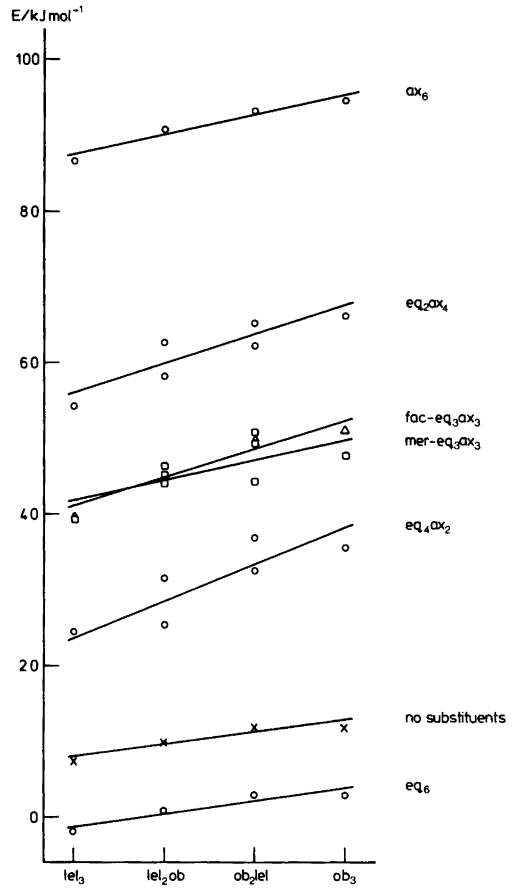

Fig. 2. Relationship between ring conformation (lel/ob), methyl group orientation (eq/ax) and energy of four $M(en)_3$ and thirty-two isomers and conformers of $M(2,3\text{-bn})_3$.

3.9 ± 1.2, $M(rac\text{-bn})_3$ ax_3 2.7 ± 1.1, all $M(rac\text{-bn})_3$ 3.3 ± 1.6; all values in kJ mol^{-1}. These data are illustrated in Fig. 2. The large spread is obvious, as are the deviations from the traditionally accepted value of 0.6 kcal mol^{-1} or 2.5 kJ mol^{-1}. The average value for all our cases is 3.2 kJ mol^{-1}. In the earlier work,[14b] a value of 3.3 kJ mol^{-1} was found.

Non-bonded interactions. A histogram analysis in intervals of 0.2 Å was made for all non-bonded interactions in an attempt to detect clear trends in the relative influence of the various contributions. For each type of interaction we considered only the shorter distances involved, as the interaction energy changes appreciably only at distances shorter than and around the minimum on the potential energy curve.

We found no such clear trends for the $M(en)_3$ and $M(meso\text{-bn})_3$ complexes, but for the $M(rac\text{-bn})_3$ complexes the following observations were made.

H---H. The short-range (2.0 – 2.2 Å), most strongly repulsive, interactions increase in number on going from one group of configurations to the next (eq_6 to eq_4ax_2 *etc*), whereas the number is constant or nearly so within a group. Longer ranges (2.2 – 2.4 and 2.4 – 2.6 Å), weakly repulsive, are almost constant in number.

C---H. Interactions in the shortest range (2.4 – 2.6 Å), strongly repulsive, reveal the same pattern as for H---H, while the range 2.6 – 2.8 Å, weakly repulsive, becomes slightly less populated from one group to the next.

N---H. Interactions in the shortest range (2.4 – 2.6 Å), weakly repulsive, increase in number from one group to the next, and also, within each group, on going from lel to ob conformation. The range (2.6 – 2.8 Å), weakly attractive, shows the reverse trend.

C---C. The shortest interactions found (3.3 – 3.2 Å) include the minimum on the potential energy curve and are thus strongly attractive. Their numbers are constant within a group: 3, 2, 1, and 0, representing the vicinal interactions of methyl carbons within a ring. The next interactions are found much farther out.

C---N. The shortest interactions found (3.0 – 3.6 Å) are all strongly or weakly attractive, and they all increase in frequency from one group to the next. The range (3.2 – 3.4 Å) represents interactions between a methylene carbon in one ring and an amino nitrogen in another and are almost constant through the series. The range (3.0 – 3.2 Å) is interactions between an axial methyl carbon in one ring and an amino nitrogen in another.

The following conclusions may thus be drawn: (1) The vicinal methyl carbon – methyl carbon interactions favour the ax-ax dispositions. (2) This is countered by hydrogen – hydrogen and carbon – hydrogen repulsions between both methyl groups and between a methyl group in one ring and an amino group in another. (3) Nitrogen-hydrogen interactions play a less determining role. (4) Carbon-nitrogen interactions favour the axial disposition of methyl groups. (5) The preference for lel conformation is caused largely by nitrogen-hydrogen interactions.

Shapes of chelate rings. The puckering of a five-

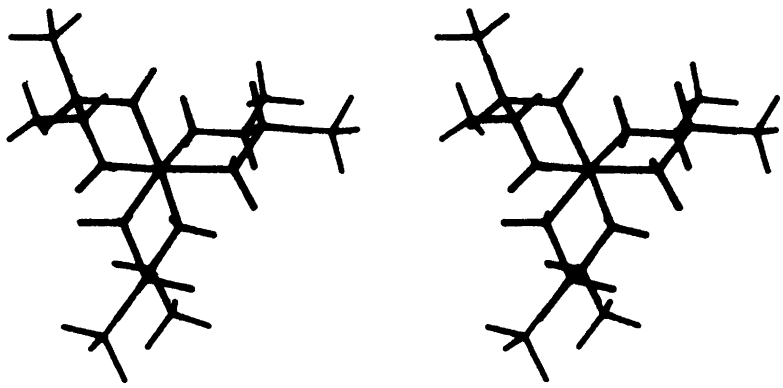

Fig. 3. Stereoscopic pair showing the equilibrium structure of lel$_3$-M(2*S*,3*S*-bn)$_3$ superimposed on the lel$_3$-M(en)$_3$ structure. The rings have practically the same shape. Conformers depicted are those which are expected to predominate in an equilibrium in solution.

membered chelate ring can be conveniently expressed through the torsional angle ϕ = N−C−C−N around the central C−C bond and through the dihedral angle τ defined by lines joining the C−C and N---N atoms.

All 108 chelate rings in the 36 isomers and conformers studied here fall into three distinct groups according to these two ring puckering descriptors. (1) When a ring carries no methyl groups or two equatorial ones (see Fig. 3) it is highly puckered, and both descriptors have a very small range: $\phi=(55.3\pm1.5)°$ and $\tau=(28.5\pm1.0)°$. These values are similar to those found by Duesler and Raymond[25] and Iwata *et al.*[26] in crystal structure determinations, but differ from the older works of Nakatsu *et al.*[27-29] who found less puckered rings. (2) A ring carrying two axial methyl groups is flattened, with a large range for the descriptors: $\phi=(38.5\pm4.5)°$ and $\tau=(20.0\pm2.5)°$. (3) A ring carrying an equatorial and an axial methyl group (all rings of the M(*meso*-bn)$_3$ series) is almost as puckered as the former, and with the same range: $\phi=(49.0\pm2.0)°$ and $\tau=(25.0\pm1.0)°$. These details of ring shape are thus largely determined by the disposition of methyl groups, whether the rings have lel or ob conformation. The ring flattening described above was also found by DeHayes and Busch.[23] The effect of methyl substitution is exemplified in Figs. 3 and 4.

There is a strictly linear relationship between the two ring puckering descriptors for all 108 rings: $\tau=0.51\phi$. This is hardly surprising, as all distances and angles are almost equal, and as all rings have strict or approximate twofold symmetry.

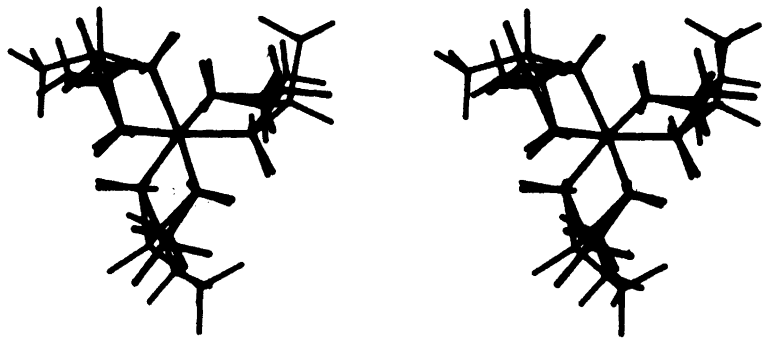

Fig. 4. Stereoscopic pair showing the equilibrium structure of *fac*-lel$_3$-M(*meso*-2,3-bn)$_3$ superimposed on the lel$_3$-M(en)$_3$ structure. The axial methyl groups flatten the rings and remove their twofold symmetry.

Table 7. Average bond lengths and angles in M(en) rings.

	MN	NC	CC	NMN	MNC	NCC
Present work	2.018	1.475	1.541	86.6	106.7	107.7
Early crystal structures, M = Co[27-29]	2.00	1.47	1.54	87.4	107	110
Saito's average ring, M = Co[4]	1.991	1.494	1.567	85.5	108.7	105.4
Recent crystal structures, M = Co[25,26,33-43]	1.973	1.486	1.509	85.3	109.1	107.4
Recent crystal structures, M = Cr[38,39,44-47]	2.067	1.493	1.514	82.9	109.6	107.9

Shapes of coordination octahedra. We use three descriptors for the discussion of departure from octahedral microsymmetry: (1) The twist angle ω,[4] which is zero for a trigonal prismatic and 60° for a regular octahedral arrangement. (2) The tilt angle θ, formerly[4,30] called the polar angle, subtended by a threefold or pseudo-threefold axis and a metal–nitrogen bond; for a regular octahedron $\theta = 54.8°$. It is related to the compression ratio[31] by $s/h = 0.865$ tg θ. (3) The pitch angle ψ[30] defined by a threefold or pseudo-threefold axis and an N---N line. For a regular octahedron $\psi = 35.3°$.

The following observations may be mentioned: (1) ω is about 55° for unsubstituted and hexaequatorially substituted complexes. A similar magnitude and direction of trigonal twisting was observed in a series of crystal structures of lel_3 tris(diamine)cobalt(III) complexes reported by Saito and co-workers.[32] Axial substitution lowers ω and widens its range; the lowest value found is 48° for ax_6ob_3. (2) All complexes are slightly compressed, $\theta = (55.5 \pm 2.0)°$. (3) The pitch angle for all complexes is slightly less than the regular value, $\psi = (33 \pm 4)°$. (4) For all three descriptors, unsubstituted and hexaequatorially substituted complexes show a much smaller range than the rest of the complexes.

Comparison with crystal structures. Crystal structures have been determined for many salts of $[Co(en)_3]^{3+}$[25-29,33-43] and some salts of $[Cr(en)_3]^{3+}$;[38,39,44-47] all four combinations of ring conformers have been found, with no significant differences in bond lengths and angles between lel and ob conformations.

Our calculations give almost identical bond lengths and valence angles for lel and ob conformations of M(en) rings. Average values are shown in Table 7 together with averages evaluated for crystal structure determinations. Our force field was originally developed to reproduce the early crystal structure data. This goal is almost achieved, but comparison with the more recent data is also quite favourable. It is seen that our M–N bond lengths are intermediate between the experimental values for Co–N and Cr–N bonds; our C–N values are a little too short and C–C much too long; the chelate angles and the N–C–C angles are almost correct; and the M–N–C angles are too small. This comparison gives us directions on how to improve our force field at a later stage.

No crystal structure determination of tris-complexes of 2,3-bn with Co(III) or Cr(III) is known to us, but our predicted chelate ring geometries and shapes of coordination octahedra agree well with those found in crystal structures of tris-complexes with other symmetrically substituted 1,2-ethanediamines: 1,2-diphenylethylenediamine,[48] *trans*-cyclopentanediamine,[49] and *trans*-cyclohexanediamine.[50,51]

Acknowledgements. We thank the Institute of Mathematics, Beograd, for the use of their IBM 360/44 in the initial stages of this work. All major computations were done by the Technical University Computer Centre NEUCC and were payed for by a grant from the Danish Natural Science Research Council, which is gratefully acknowledged. Stereo drawings were produced from the coordinates of the equilibrium conformers with a programme MONSTER written by Mr. Per Jacobi of the Royal Danish Academy of Fine Arts, Laboratory of Datalogy.

REFERENCES

1. Niketić, S. R. *Glas. Hem. Drust. Beograd 42* (1977). *In press.*
2. Niketić, S. R. and Rasmussen, K. *The Consistent Force Field: A Documentation*, Lecture Notes in Chemistry, Vol. 3, Springer, Berlin–Heidelberg–New York 1977.
3. Niketić, S. R., Rasmussen, K., Woldbye, F. and Lifson, S. *Acta Chem. Scand. A 30* (1976) 485.
4. Saito, Y. *Coord. Chem. Rev. 13* (1974) 305.
5. Mason, S. F. In Ciardelli, F. and Salvadori, P., Eds., *Fundamental Aspects and Recent Advances in Optical Rotatory Dispersion and Circular*

Dichroism, Heyden, London 1973, p. 196; Mason, S. F. and Seal, R. H. *Mol. Phys. 31* (1976) 755.
6. Dingle, R. and Ballhausen, C. J. *K. Dan. Vidensk. Selsk. Mat.-Fys. Medd. 35* (1967) No. 12.
7. McCarthy, P. J. and Vala, M. T. *Mol. Phys. 25* (1973) 17.
8. Sudmeier, J. L. and Blackmer, G. L. *Inorg. Chem. 10* (1971) 2010; Sudmeier, J. L., Blackmer, G. L., Bradley, C. H. and Anet, F. A. L. *J. Am. Chem. Soc. 94* (1972) 757.
9. Rasmussen, K. *Spectrochim. Acta A 30* (1974) 1763, and references therein.
10. Bjerrum, J. *Metal Ammine Formation in Aqueous Solution*, Haase & Søn, Copenhagen 1941, reprint 1957.
11. Bang, O. *Thesis*, The Technical University of Denmark, 1976.
12. Mislow, K., Gust, D., Finocchiaro, P. and Boettcher, R. J. *Top. Curr. Chem. 47* (1974) 1.
13. *Inorg. Chem. 9* (1970) 1.
14. a. Niketić, S. R. and Woldbye, F. *Acta Chem. Scand. 27* (1973) 621; b. *Ibid.* 3811; c. *Ibid. A 28* (1974) 248.
15. Woldbye, F. *Studier over Optisk Aktivitet*, Polyteknisk Forlag, København 1969.
16. Kojima, M., Funaki, H., Yoshikawa, Y. and Yamasaki, K. *Bull. Chem. Soc. Jpn. 48* (1975) 2801.
17. Gleicher, G. J. and Schleyer, P. von R. *J. Am. Chem. Soc. 89* (1967) 582.
18. Wiberg, K. B. *J. Am. Chem. Soc. 87* (1965) 1070.
19. Harris, H. A. *Ph.D. Thesis*, Yale University, 1966.
20. Nakagawa, I. and Shimanouchi, T. *Spectrochim. Acta 22* (1966) 759, 1707.
21. Liquori, A. M. In Engström, A. and Strandberg, E., Eds., *Eleventh Nobel Symposium on Symmetry and Function of Biological Systems at the Macromolecular Level*, Almquist and Wiksell, Stockholm 1969, p. 101.
22. Dwyer, M. and Searle, G. H. *Chem. Commun.* (1972) 726.
23. DeHayes, L. J. and Busch, D. H. *Inorg. Chem. 12* (1973) 1505.
24. Hirsch, J. A. *Top. Stereochem. 1* (1967) 204.
25. Duesler, E. N. and Raymond, K. N. *Inorg. Chem. 10* (1971) 1486.
26. Iwata, M., Nakatzu, K. and Saito, Y. *Acta Crystallogr. B 25* (1969) 2562.
27. Nakatsu, K., Saito, Y. and Kuroya, H. *Bull. Chem. Soc. Jpn. 29* (1956) 428.
28. Nakatsu, K., Shiro, M., Saito, Y. and Kuroya, H. *Bull. Chem. Soc. Jpn. 30* (1957) 158.
29. Nakatsu, K. *Bull. Chem. Soc. Jpn. 35* (1962) 832.
30. Pignolet, L. H. *Top. Curr. Chem. 56* (1975) 91.
31. Stiefel, E. I. and Brown, G. F. *Inorg. Chem. 11* 1972) 434.
32. Saito, Y. *Proc. XIV Int. Conf. Coord. Chem.*, Toronto 1972, p. 91.
33. Enemark, J. H., Quinby, M. S., Reed, L. L., Steuck, M. J. and Walthers, K. K. *Inorg. Chem. 9* (1970) 2397.
34. Hodgson, D. J., Hale, P. K. and Hatfield, W. E. *Inorg. Chem. 10* (1971) 1061.
35. Veal, J. T. and Hodgson, D. J. *Inorg. Chem. 11* (1972) 597.
36. Witiak, D., Clardy, J. C. and Martin, Jr., D. S. *Acta Crystallogr. B 28* (1972) 2694.
37. Bok, L. D. C., Leipoldt, J. G. and Basson, S. S. *Z. Anorg. Allg. Chem. 389* (1972) 307.
38. Whuler, A., Brouty, C., Spinat, P. and Herpin, P. *Acta Crystallogr. B 31* (1975) 2069.
39. Whuler, A., Brouty, C., Spinat, P. and Herpin, P. *Acta Crystallogr. B 32* (1976) 194.
40. Haupt, M. J., Huber, F. and Preut, H. *Z. Anorg. Allg. Chem. 422* (1976) 255.
41. Tada, T., Kushi, Y., Yoneda, H. *Chem. Lett.* (1977) 379.
42. Brouty, C., Spinat, P., Whuler, A. and Herpin, P. *Acta Crystallogr. B 32* (1976) 2153.
43. Kushi, Y., Kuramoto, M. and Yoneda, H. *Chem. Lett.* (1976) 135.
44. Raymond, K. N., Corfield, P. W. R. and Ibers, J. A. *Inorg. Chem. 7* (1968) 1362.
45. Raymond, K. N. and Ibers, J. A. *Inorg. Chem. 7* (1968)2333.
46. Kushi, Y., Kuramoto, M. and Yoneda, H. *Chem. Lett.* (1976) 339.
47. Robinson, P. R., Schlemper, E. O. and Murmann, R. K. *Inorg. Chem. 14* (1975) 2035.
48. Kuroda, R. and Mason, S. F. *J. Chem. Soc. Dalton Trans.* (1977) 1016.
49. Ito, M., Marumo, F. and Saito, Y. *Acta Crystallogr. B 27* (1971) 2187.
50. Marumo, F., Utsumi, Y. and Saito, Y. *Acta Crystallogr. B 26* (1970) 1492.
51. Kobayashi, A., Marumo, F. and Saito, Y. *Acta Crystallogr. B 28* (1972) 2709.

Received December 20, 1977.

Acta Chemica Scandinavica A 32 (1978) 401 – 405

The Crystal and Molecular Structure of Ethyl *m*-Nitroso-*trans*-cinnamate

HANS JØRGEN TALBERG

Department of Chemistry, University of Oslo, Oslo 3, Norway

The crystal and molecular structure of ethyl *m*-nitroso-*trans*-cinnamate, $C_{11}H_{11}O_3N$, has been determined from X-ray diffraction data collected at −165 °C and refined by least squares methods. The space group is $P2_1/n$ with cell dimensions $a = 12.065(4)$ Å, $b = 15.626(3)$ Å, $c = 5.387(2)$ Å and $\beta = 92.44(2)°$ at −165 °C. The final R factor was 5.4 % and the estimated standard deviations in bond lengths involving only non-hydrogen atoms ranged from 0.003 to 0.005 Å. The C−NO bond length (1.451 Å) is longer and the N−O bond length (1.229 Å) probably shorter in this molecule than in any previously studied nitrosobenzene. Other bond lengths and angles are very similar to those of cinnamic acid and some of its derivatives. The molecule is essentially planar.

The present structure investigation of ethyl *m*-nitroso-*trans*-cinnamate (I) is part of a series of investigations of *C*-nitroso compounds. The earlier parts of this series have been devoted to nitrosobenzenes shown to have molecular structures consistent with substantial mutual conjugation between an oxide,[1,2] a dialkylamino[3,4] and a hydroxyl[5] group and the nitroso group. Absence of mutual conjugation in the title compound makes it a reference substance to the molecules previously investigated.

An X-ray investigation has shown that the natural reference compound, nitrosobenzene, exists in an azo dioxide dimeric state in its stable crystals.[6] This seems to be the case also for *all* other potential reference molecules studied. The azo dioxide dimeric state is indicated by IR spectroscopy or solely by absence of colour in these cases (Ref. 7 and references therein). Interestingly, dealkylation of (I) gives an acid forming very stable colourless crystals whereas only green coloured crystals have so far been found for the title compound.

EXPERIMENTAL

The title compound was derived from the corresponding nitro compound by use of a standard method.[8] Using a somewhat modified method described by Mijs *et al.*[9] only the corresponding azoxy compound could be isolated (golden coloured, m.p. 90 °C, IR-KBr-ω_{NNO} bands at 1455 and 1300 cm^{-1}). Monomeric ethyl *m*-nitroso-*trans*-cinnamate crystallizes in two forms. The one investigated (α) collected in the condenser and separated from the distillate upon steam distillation. The β form separated from the filtrated reaction mixture over a period of a week in the refrigerator. The light green and crisp needle-shaped β crystals melt at 55 °C. They have monoclinic symmetry, a needle axis of 4.02 Å, a unique axis of 15.36 Å and a somewhat smaller unit cell volume (1015 $Å^3$) than the α crystals. The IR-KBr-ω_{NO} band is at 1480 cm^{-1}. Sublimation by use of a cold finger gave reformation of the β form. Also subsequent evaporation of a diethyl ether solution resulted in β crystals. Continued recrystallization from diethyl ether, however, gave increasing amounts of the α form. Crystals suited for diffractometer measurements could not be found. The emerald-coloured elongated tabular α crystals melt at 65 °C. In contrast to the β crystals they are plastic. The α crystal used for the diffractometer measurements was grown from a melt. This was accomplished by carefully melting α crystals until near completion followed by controlled recrystallization on a "THERMOPAN" melting point apparatus. The crystal was perfectly shaped and of dimensions $0.44 \times 0.16 \times 0.08$ mm. Apart from the following details the experimental conditions in connection with the diffractometer measurements were as those described in Ref. 3. The temperature at the crystal site was −165 °C. The scan limits were $2\theta(\alpha_1) - 1.1°$ and $2\theta(\alpha_2) + 1.1°$ and a quadrant of reciprocal space was examined. Reflections up to 65° in 2θ were measured; below 40° all, above 40° those having integrated counts larger than a

preset value during a 2s scan over the peak. Out of 2151 unique reflections measured 1303 had intensities larger than $2.5\sigma(I)$ where $\sigma(I)$ is the standard deviation of the intensity based on counting statistics adding 2 % uncertainty due to experimental fluctuations. The atomic scattering factors for the heavy atoms were those of Doyle and Turner[10] and for hydrogen those of Stewart *et al.*[11] All programs except for the ORTEP program (Ref. 11 in Ref. 3) and the MULTAN program (Ref. 12 in Ref. 3) applied during the investigation are described in Ref. 12.

CRYSTAL DATA

Ethyl *m*-nitroso-*trans*-cinnamate or *trans*-3-(3-nitrosophenyl)propenoic acid ethyl ester, $C_{11}H_{11}O_3N$, monoclinic α form, space group $P2_1/n$ (No. 14). Dimensions of the unit cell at −165 °C: $a=12.065(4)$ Å, $b=15.626(3)$ Å, $c=5.387(2)$ Å and $\beta=92.44(2)°$; $V=1014.7$ Å^3. At 18 °C (film): $a=12.99$ Å, $b=15.83$ Å, $c=5.46$ Å, $\beta=103°$; $V=1115$ Å^3. $M=205.22$, $F(000)=432$, $D_{calc}(18\ °C)=1.22$ g cm^{-3}, $D_{calc}(-165\ °C)=1.343$ g cm^{-3}, $Z=4$.

STRUCTURE DETERMINATION

The structure was determined by direct methods (MULTAN) and refined by full matrix least squares techniques.[12] Initial positional parameters for hydrogen atoms were obtained from a ΔF synthesis. The refinement including all atoms and all observed reflections converged with $R=0.054$, a weighted

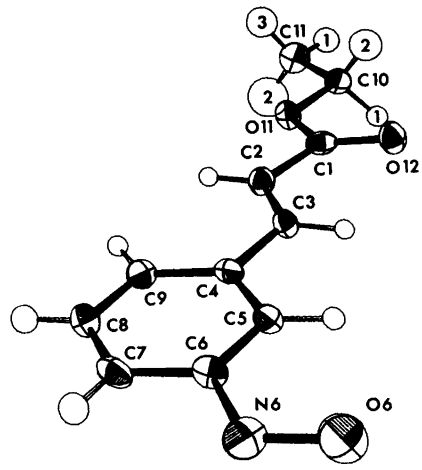

Fig. 1. 50 % probability ellipsoids and numbering of atoms.

R_w factor of 0.043 and a goodness of fit S of 1.6. A list of structure amplitudes is available from the author. Final parameters from the refinement with all the observed reflections are given in Table 1. Magnitudes and directions of the principal axes of the vibrational ellipsoids are indicated in Fig. 1. A rigid body analysis of the entire molecule shows a fairly good agreement between observed and calculated vibration tensor elements ($\Delta U_{rms}=0.0030$ Å^2). The agreement is slightly better for the nitrosophenyl moiety ($\Delta U_{rms}=0.0025$ Å^2). For the entire molecule the r.m.s. eigenvalues of **T** are 0.15, 0.14

Table 1. Fractional atomic coordinates and thermal parameters. The anisotropic temperature factors are expressed as: $\exp[-2\pi^2(h^2a^{*2}U_{11}+\cdots+2klb^*c^*U_{23})]$. Estimated standard deviations in parentheses.

ATOM	X	Y	Z	U11	U22	U33	U12	U13	U23
O11	.46517(19)	.25593(12)	.81444(44)	.0381(13)	.0166(11)	.0241(13)	-.0030(9)	-.0055(10)	-.0007(9)
O12	.49378(19)	.37636(13)	1.02978(44)	.0398(14)	.0191(11)	.0258(14)	-.0029(11)	-.0049(11)	-.0024(11)
O6	.31816(21)	.78578(14)	.52102(46)	.0458(16)	.0267(13)	.0377(16)	-.0030(12)	.0019(13)	-.0024(13)
N6	.26899(25)	.75634(16)	.33558(57)	.0388(18)	.0272(17)	.0326(18)	-.0025(13)	.0091(15)	-.0074(13)
C1	.45188(26)	.34196(19)	.80861(66)	.0268(20)	.0158(15)	.0261(21)	-.0010(14)	.0059(17)	.0010(16)
C2	.38912(26)	.38448(20)	.64478(62)	.0239(20)	.0196(18)	.0220(19)	-.0016(14)	-.0006(16)	-.0025(15)
C3	.38329(25)	.46965(20)	.64038(66)	.0225(20)	.0238(18)	.0158(18)	-.0014(14)	.0003(16)	-.0034(15)
C4	.32361(24)	.52348(18)	.45488(58)	.0176(17)	.0196(15)	.0186(18)	.0002(13)	.0029(14)	.0039(14)
C5	.32428(26)	.61167(19)	.48665(62)	.0195(19)	.0224(17)	.0182(19)	-.0012(14)	.0001(15)	.0019(14)
C6	.26702(27)	.66383(19)	.31702(59)	.0218(20)	.0185(16)	.0224(22)	.0042(13)	.0019(16)	.0012(14)
C7	.21167(27)	.62967(21)	.11189(67)	.0239(19)	.0285(19)	.0210(19)	.0068(16)	.0012(15)	.0102(16)
C8	.21123(29)	.54186(21)	.07612(66)	.0266(21)	.0271(18)	.0217(19)	-.0001(15)	.0003(16)	-.0005(16)
C9	.26714(26)	.48950(20)	.24503(65)	.0243(19)	.0221(17)	.0229(17)	-.0013(14)	.0041(15)	-.0031(16)
C10	.51557(29)	.28899(20)	1.00873(67)	.0266(20)	.0183(16)	.0260(19)	.0062(16)	-.0022(16)	.0045(17)
C11	.56927(33)	.11556(21)	.94228(80)	.0332(21)	.0186(18)	.0398(25)	.0064(17)	-.0027(19)	.0038(17)

ATOM	X	Y	Z	B	ATOM	X	Y	Z	B
H2	.394(2)	.349(2)	.621(5)	1.0(6)	H3	.422(2)	.508(2)	.763(5)	.7(6)
H5	.362(2)	.634(2)	.626(5)	.8(6)	H7	.174(2)	.666(2)	.906(5)	.1(6)
H8	.168(2)	.516(2)	-.069(6)	2.9(8)	H9	.264(2)	.428(2)	.211(5)	.9(6)
H101	.594(2)	.231(2)	1.022(5)	1.2(6)	H102	.486(2)	.225(2)	1.169(6)	2.0(8)
H111	.554(2)	.884(2)	1.069(6)	2.0(7)	H112	.542(3)	.103(2)	.764(7)	5.4(10)
H113	.433(3)	.894(2)	.950(6)	2.9(8)					

Table 2. Bond lengths (Å) and angles (°).

Bond lengths			
O6–N6	1.229(3)	C4–C5	1.391(4)
O11–C1	1.360(3)	C5–C6	1.388(4)
O12–C1	1.201(4)	C6–C7	1.385(4)
O11–C10	1.449(4)	C7–C8	1.385(4)
N6–C6	1.451(4)	C8–C9	1.378(5)
C1–C2	1.470(5)	C9–C4	1.396(4)
C2–C3	1.333(4)	C10–C11	1.505(5)
C3–C4	1.474(4)		
Bond angles			
O11–C1–O12	122.7(3)	C2–C3–C4	127.3(3)
O11–C1–C2	111.1(3)	C3–C4–C5	118.3(3)
O12–C1–C2	126.2(3)	C3–C4–C9	122.7(3)
O6–N6–C6	113.5(3)	C4–C5–C6	119.5(3)
N6–C6–C5	124.6(3)	C5–C6–C7	121.1(3)
N6–C6–C7	114.2(3)	C6–C7–C8	119.4(4)
C10–O11–C1	114.7(3)	C7–C8–C9	120.0(4)
C11–C10–O11	107.5(3)	C8–C9–C4	121.0(3)
C1–C2–C3	119.3(3)	C9–C4–C5	119.0(3)
Inter-molecular contacts			
O11···N6(a)	3.282	N6···C10(c)	3.379
O6···C10(b)	3.225	O12···C3(b)	3.306
O6···C1(a)	3.372	O12···C5(b)	3.333
Torsion angles			
O6–N6–C6–C5	0.7(5)	O12–C1–C2–C3	−4.6(5)
C11–C10–O11–C1	−178.6(3)	C2–C3–C4–C9	2.7(5)
C10–O11–C1–O12	0.3(4)		

Symmetry code
(a): $-x+3/2, y+\frac{1}{2}, -z+\frac{1}{2}$, (b): $-x+2, -y+1, -z+1$, (c): $-x+1, -y+1, -z+1$

and 0.13 Å, and of **L** 3.7, 1.4 and 0.8°, corresponding to librational bond lengthenings in the range 0.001–0.003 Å. The estimated standard deviations (e.s.d.'s) were derived from the final correlation matrix of the least squares refinement. The C–H bond lengths are in the range 0.90–1.07 Å with e.s.d.'s of 0.03 Å. Other bond lengths and angles involving non-hydrogen atoms are given in Table 2.

DISCUSSION

The crystal structure is similar to that of the related methyl *p*-hydroxy-*m*-nitro-*trans*-cinnamate, (II).[13] Characteristic for both is the infinite layers of edge-to-edge packed molecules close to (10*l*) planes and the existence of several nearly linear *intra*-layer CH···O(N) contacts which stabilize the sheet-like arrangement of molecules.[13] The nitroso oxygen atom, however, is only participating in non-linear and loose H-contacts (above 2.66 Å). The COOEt group has one *intra*-layer neighbouring NO group and is sandwiched by two nitroso groups. These structural features are illustrated in Fig. 2 which also reveals nearly "close" packing normal to the (10–3) plane. A C3···C3′ contact of 3.387 Å (3.295 Å from the benzene ring plane) and a C3···C8 contact of 3.391 Å are the only C···C *inter*-layer contacts shorter than 3.65 Å. The lack of extensive *inter*-molecular $\pi-\pi$ overlapping apparently makes the present structure rather loose (packing coefficient of 0.76) and may explain the drastic change in a and β when the temperature is increased to 18 °C. These changes seem to involve a considerable (0.4 Å) increase in the *inter*-molecular spacing, indicating a starting-up of coordinated flipping of the stacked terminal groups. The latter is

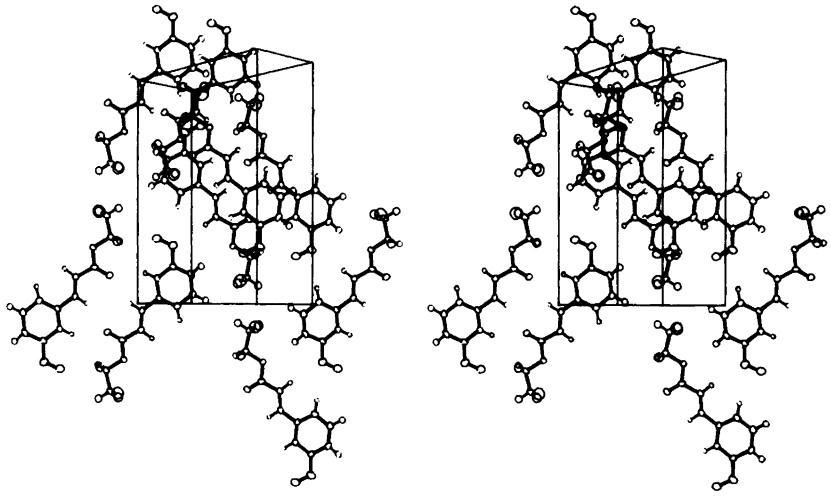

Fig. 2. A stereoscopic illustration of the structure.

consistent with the plastic character of the crystal at 18 °C.

The molecular structure. The ethyl ester of *m*-nitroso-*trans*-cinnamic acid (I) conforms with most other alkyl cinnamates and cinnamic acids in having three nearly coplanar parts each being planar within the accuracy of the experiment.[14] In the present case the three parts are the phenyl ring with N6 and C3, the four-atom olefinic group and the CCOOC fragment. More details are given in Table 3. The molecule as a whole is also essentially planar as the twist about the $O-CH_2$ and the C–NO bond is less than 1.5°. In agreement with all other *trans* alkyl cinnamates the conformation about the C–OEt and the C–COOEt bond is, respectively, *anti* (the R groups are *anti*) and *syn*.[13-15] The *anti* $C_{Ar}-C$ conformation, however, makes (I) a unique *meta* substituted cinnamate.[13-15]

Table 3. Deviation (Å) of atoms from least squares planes. Atoms defining the planes are marked with an asterisk.

Atom/Plane	A	B	C
O11	0.052		0.000*
O12	0.159	−0.092	0.000*
O6	0.030		
N6	0.013		
C1	0.100	−0.007*	0.000*
C2	0.068	0.006*	0.000*
C3	0.013	0.009*	0.094
C4	0.003*	−0.008*	
C5	−0.003*	−0.056	
C6	0.003*		
C7	−0.002*		
C8	0.002*		
C9	−0.003*		
C10	0.071		0.008
C11	0.047		−0.027

Inter-planar angles: AB, 2.7°; BC, 4.6°; AC, 1.9°

Owing to different libration effects it is difficult to compare directly the bond lengths with those of (II), *p*-methoxycinnamic acid (III)[14] and of cinnamic acid (IV).[14] Otherwise, however, such a comparison seems appropriate as judged from the experimental technique used, the *R* factors, the e.s.d.'s and the resolution achieved. If one excludes the C–O bonds in the acids there are only six significant differences between bond lengths in (I) and corresponding ones in the other molecules (in the range 0.013–0.025 Å). Three involve distances in the side chain as compared to (II) and may possibly be ascribed to libration effects. The others conform with expected conjugation involving the *para* substituents. The average ring bond length is the same within 0.001 Å for all four molecules. Using reasonably enlarged e.s.d.'s (by a factor $\sqrt{2}$) a χ^2 test gives a probability of 0.5 for the ring bond lengths being randomly distributed about the mean value [1.387(6) Å] in (I). Although of limited value, this gives reason for not discussing in detail the spread in the ring bond lengths. The latter is actually smaller than in cinnamic acid (probably due to

libration effects). In consistency with the finding of an essentially unperturbed benzene ring the C–NO bond length ($R_{CN} = 1.451(4)$ Å) is close to that usually accepted for a "pure" C(sp^2)–N(sp^2) single bond (1.458 Å).[16] Comparison with 5-nitrososalicylic acid (V) shows that R_{CN} is 0.025 Å longer and that the N–O bond length [$R_{NO} = 1.229(3)$ Å] is 0.005 Å shorter in (I) than in (V). Although the latter difference is rather uncertain (e.s.d. of 0.004 Å) it seems reasonable on the basis of a previously found relationship between R_{NO} and R_{CN}.[2] Using this relationship a regression of 0.010 Å (to 1.223 Å) is obtained for R_{NO} upon changing R_{CN} from 1.426 Å [as in (V)] to 1.451 Å. The nitrogen bond angle [113.5(3)°] is smaller than in any of the other nitrosobenzenes. This strengthens an earlier assumption concerning the connection between ∠CNO and the conjugation over the C–N–O group.[2,5] In short it may be stated that the geometry of the nitroso group in (I) is consistent with a smaller charge displacement to the group than in any other nitrosobenzene investigated.

REFERENCES

1. Talberg, H. J. *Acta Chem. Scand. A 29* (1975) 919.
2. Talberg, H. J. *Acta Chem. Scand. A 31* (1977) 37.
3. Talberg, H. J. *Acta Chem. Scand. A 30* (1976) 829.
4. Talberg, H. J. *Acta Chem. Scand. A 31* (1977) 743.
5. Talberg, H. J. *Acta Chem. Scand. A 31* (1977) 485.
6. Dieterich, D. A., Paul, I. C. and Curtin, D. Y. *J. Am. Chem. Soc. 96* (1974) 6372.
7. Azoulay, M., Stymme, B. and Wettermark, G. *Tetrahedron 32* (1976) 2961.
8. Alway, F. J. and Bonner, W. D. *Am. Chem. J. 32* (1902) 385.
9. Mijs, W. J., Hoekstra, S. E., Ulmann, R. M. and Havinga, E. *Recl. Trav. Chim. Pays-Bas 77* (1958) 746.
10. Doyle, P. A. and Turner, P. S. *Acta Crystallogr. A 24* (1968) 390.
11. Stewart, R. F., Davidson, E. R. and Simpson, W. T. *J. Chem. Phys. 42* (1965) 3175.
12. Groth, P. *Acta Chem. Scand. 27* (1973) 1837.
13. Hanson, A. W. *Acta Crystallogr. B 31* (1975) 1963.
14. Bryan, R. F. and Freyberg, D. P. *J. Chem. Soc. Perkin Trans. 2* (1975) 1835.
15. Leiserowitz, L. and Schmidt, G. M. J. *Acta Crystallogr. 18* (1965) 1058.
16. Fischer-Hjalmars, I. and Sundbom, M. *Acta Chem. Scand. 22* (1968) 2237.

Received January 3, 1978.

Acta Chemica Scandinavica A 32 (1978) 407 – 414

A Large-angle X-Ray Scattering Study of 9-Molybdomonophosphate Complexes in Aqueous Solution

GEORG JOHANSSON,[a] LAGE PETTERSSON[b] and NILS INGRI[b]

[a] Department of Inorganic Chemistry, Royal Institute of Technology, S-100 44 Stockholm 70, Sweden and [b] Department of Inorganic Chemistry, University of Umeå, S-901 87 Umeå, Sweden

Radial distribution curves have been calculated from X-ray scattering measurements on two solutions which according to equilibrium data contain complexes of the compositions $(H^+)_{15}(MoO_4^{2-})_9(HPO_4^{2-})$ and $(H^+)_{16}(MoO_4^{2-})_9(HPO_4^{2-})$. Comparison with calculated peak shapes for intramolecular interactions within the complex $Mo_9PO_{31}(OH_2)_3^{3-}$, which is known from a crystal structure determination, shows the complexes in solution to have the same basic structure. Small differences in the interatomic distances are, however, found, which can be ascribed to slightly changed positions of the Mo atoms.

The aqueous three component equilibria $pH^+ + qMoO_4^{2-} + rHPO_4^{2-} \rightleftharpoons (H^+)_p(MoO_4^{2-})_q(HPO_4^{2-})_r$ have been extensively studied mainly by means of emf methods at 25 °C and in 3.0 M $Na(ClO_4)$ medium.[1-4] The existence of two series of complexes has been established. For $B/C \leq 2.5$ (with B the total molybdenum concentration and C the total phosphorus concentration in the solution) the predominant ternary complexes formed are $(H^+)_p(MoO_4^{2-})_5(HPO_4^{2-})_2$ with $p=8$, 9 and 10. For $B/C \geq 9$ and $-\log [H^+] < 5$ the predominant complexes are $(H^+)_p(MoO_4^{2-})_9(HPO_4^{2-})$ with $p=14$, 15, 16 and 17. For simplicity these complexes will in the following often be referred to by their (p,q,r) values.

By slow evaporation of equilibrium solutions, crystalline phases with compositions corresponding to those of all the three proposed pentamolybdodiphosphates and one of the four 9-molybdomonophosphates have been obtained. Structure determinations have shown the crystals to contain discrete polyanions $Mo_5P_2O_{23}^{6-}$,[5,6] $HMo_5P_2O_{23}^{5-}$,[7] $H_2Mo_5P_2O_{23}^{4-}$,[8] (corresponding to the (8,5,2) (9,5,2) and (10,5,2) complexes, respectively) and $Mo_9PO_{31}(OH_2)_3^{3-}$,[9,10] (corresponding to the (17,9,1) complex). Since the number of water molecules in a complex cannot be deduced from the emf data, $(H^+)_8(MoO_4^{2-})_5(HPO_4^{2-})_2$ is equivalent to $Mo_5P_2O_{23}^{6-}$, $(H^+)_{17}(MoO_4^{2-})_9(HPO_4^{2-})$ to $Mo_9PO_{31}(OH_2)_3^{3-}$ etc.

X-Ray diffraction measurements on solutions of the pentamolybdodiphosphates were reported in a previous paper,[11] in which a comparison was made between the structure of the pentamolybdodiphosphates in solution and the structure of the discrete $Mo_5P_2O_{23}$ groups found in crystals. In the present paper a similar investigation of the 9-molybdomonophosphate complexes is reported.

EXPERIMENTAL

Solutions investigated. In order to get significant effects in the diffraction curves high concentrations of the complexes in the solutions are necessary. For $B/C=9$, the ratio at which an optimal amount of 9-molybdomonophosphate complexes is formed, solutions with concentrations larger than about 1.6 M in molybdate cannot be prepared. By means of the stability constants given by Pettersson,[3] the fraction of molybdenum bound in the different complexes has been calculated for a molybdophosphate solution as a function of $-\log [H^+]$ for $B=1.60$ M and $C=0.178$ M ($B/C=9$). The distribution of complexes is shown in Fig. 1. Provided that the stability constants are valid at this high concentration, it should, therefore, be possible to prepare solutions, which are practically pure in either the (15,9,1) or the (16,9,1) complex, *i.e.* in $(H^+)_p(MoO_4^{2-})_9(HPO_4^{2-})$ with $p=15$ or 16.

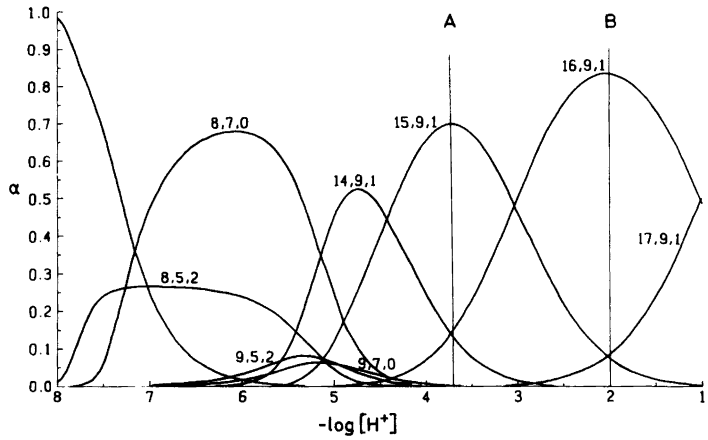

Fig. 1. The fraction of molybdenum, α, bound in different complexes in a 1.6 M molybdate solution with an Mo(VI)/P(V) ratio of 9.0, as a function of log[H^+]. The stability constants given by Pettersson [3] have been used for the calculation.

Solutions with compositions given by A and B in Fig. 1 and in Table 1 were chosen for the diffraction measurements. For the analysis of the X-ray data three reference solutions, C, D, and E, were used, the compositions of which are given in Table 1. These solutions should contain all molybdenum bound as $Mo_5P_2O_{23}^{6-}$, $Mo_7O_{24}^{6-}$ and MoO_4^{2-}, respectively.[11]

X-Ray measurements. The scattering measurements and the data treatment were carried out as described in previous papers.[11-14] Ag$K\alpha$-radiation was used. The measured intensities were normalized to a stoichiometric unit of volume containing one molybdenum atom. For one of the solutions the normalized intensity values, $I(s)$, the independent coherent scattering $\sum_i f_i^2$, with the summation carried out over all atoms in a stoichiometric unit, and the incoherent scattering reaching the counter are shown in Fig. 2 as a function of $s=4\pi\lambda^{-1}\sin\theta$, ($\lambda=0.5608$ Å). The scattering factors, f_i, were taken from the same sources as in the previous work.[11]

The corresponding reduced intensity values

Table 1. Composition of solutions.

	A (15,9,1)	B (16,9,1)	C (8,5,2)	D (8,7,0)	E (0,1,0)
Concentrations in mol/l					
Mo	1.600	1.600	1.770	2.040	2.035
P	0.178	0.178	0.710	–	–
Na	3.378	3.378	4.250	4.080	4.070
Cl	2.489	2.678	2.120	2.330	–
O	61.6	61.7	62.5	61.9	59.0
H	91.9	90.8	91.7	91.1	101.6
Number of atoms in the unit of volume, V					
Mo	1	1	1	1	1
P	0.111	0.111	0.401	–	–
Na	2.111	2.111	2.401	2.000	2.000
Cl	1.556	1.674	1.198	1.142	–
O	38.5	38.6	35.3	30.3	29.0
H	57.4	56.7	51.8	44.7	49.9
V/Å^3	1038	1038	938.2	814.0	816.0
ρ_0/el^{2}Å^{-3}	202.8	204.4	196.2	168.9	146.4

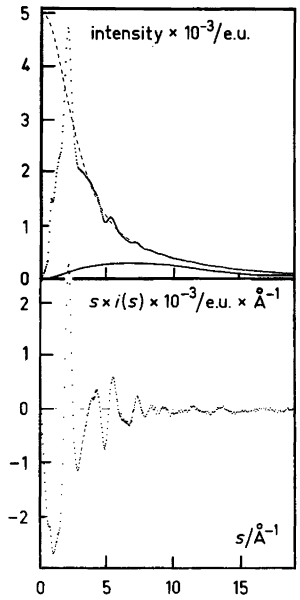

Fig. 2. The normalized intensity values (dots), the independent coherent scattering (dashed line) and the incoherent scattering, estimated to reach the counter (solid line), as a function of $s=4\pi\lambda^{-1}\sin\theta$, for the solution B (upper part) and the reduced intensity values, given as $si(s)$, for the same solution (lower part).

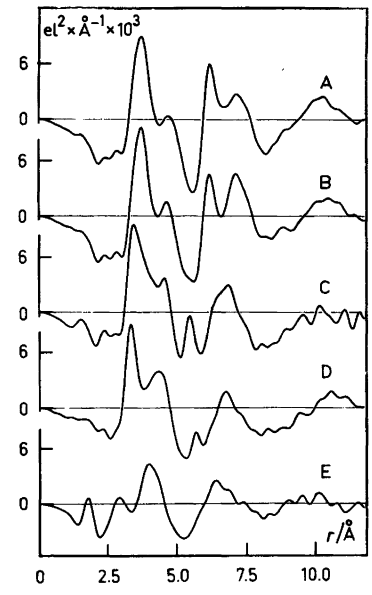

Fig. 3. The $D(r)-4\pi r^2\rho_0$ functions for the solutions A and B and for the reference solutions C, D, and E, the compositions of which are given in Table 1.

$i(s)=I(s)-\sum_i f_i^2$, multiplied by s, are shown in the same figure. The radial distribution functions, $D(r)$, were calculated as

$$4\pi r^2\rho_0+\frac{2r}{\pi}\int_0^{s_{max}} s\,i(s)\,M(s)\sin(rs)\,ds.$$

The modification function, $M(s)$, was chosen to be $\{f_{Mo}^2(0)/f_{Mo}^2(s)\}\exp(-0.01s^2)$. The functions $D(r)-4\pi r^2\rho_0$ are shown in Fig. 3.

ANALYSIS OF THE DATA

The representation of the scattering data, that seems best suited for the analysis, is the distribution function $D(r)-4\pi r^2\rho_0$ given in Fig. 3. The pronounced peaks obtained for the solutions A and B are indicative of the occurrence of polynuclear complexes. This is particularly apparent when comparing with the corresponding function for the alkaline molybdate solution (E in Fig. 3) in which only mononuclear tetrahedral MoO_4^{2-} ions should be present.

Approximate shape functions for the polymolybdates in the solutions A and B were derived by the following procedure, which makes use of the scattering data from the reference solutions C, D and E, for which the structures of the complexes are known.[11]

Theoretical $i(s)$ values can be calculated by summing over all pair interactions. Assuming the solutions to contain discrete complexes: $(H^+)_p(MoO_4^{2-})_q(HPO_4^{2-})_r, ClO_4^-, Na^+$, and H_2O, the summation can be separated into intra- and intermolecular interactions:

$$i(s)=\sum_j n_j\{i_{intra}(s)+i_{inter}(s)\}$$

where n_j is the number of molecules "j" in the stoichiometric unit of volume, V. A simple approximation for the intermolecular interactions is to assume each complex to occupy a spherical hole of radius R_j in a uniform scattering density. The following expressions will then hold for each complex:[14]

Table 2. Parameter values used in the calculations of the shape functions.

Complex	Intramolecular distances, Å	Temperature coefficients Mo–Mo	Mo–O	O–O	Intermolecular interactions R	B
MoO_4^{2-}	Mo–O 1.79	–	0.003	0.0002	3.0	0.02
ClO_4^-	Cl–O 1.43	–	0.002	0.002	2.8	0.02
H_2O	–				1.8	0.02
$Mo_5P_2O_{23}$	see Ref. 5	0.004	0.002	0	5.0	0.02
Mo_7O_{24}	see Ref. 18	0.002	0.004	0.006	5.5	0.02
Mo_9PO_{34}	see Ref. 9	0.006	0.006	0.006	6.5	0.02
$Mo_{18}P_2O_{62}$	see Ref. 15	0.006	0.006	0.006	8.5	0.02

$$i_{intra}(s) = \sum_{u \neq v} \Sigma f_u f_v \sin sr_{uv}/(sr_{uv}) \exp(-b_{uv}s^2)$$

$$i_{inter}(s) \approx i_{sphere}(s) =$$

$$-(4\pi R_j^3)/(3V)3[\sin sR_j - sR_j \cos sR_j]/(sR_j)^3 \times$$

$$\exp(-B_j s^2) \sum_{u=1}^{m} f_u \sin(sr_u)/(sr_u) \sum_{n=1}^{n_{stoich}} n_i f_i$$

where the last two summations are over the number of atoms in the complex (m) and the number of atoms (n_{stoich}) in the stoichiometric unit of volume, respectively. Distances within a molecule are represented by r_{uv} and b_{uv} and B_j are temperature factors.

The total expression for $i(s)$ can now be written as

$$i(s) = \sum_j n_j \{i_{intra}(s) + i_{sphere}(s)\} + i_{corr}$$

where i_{corr} represents contributions from remaining structure in the solution not taken into account by the idealized model.

A Fourier transformation of each separate term in the expression for $i(s)$ gives the corresponding contribution to the distribution function:

$$D(r) - 4\pi r^2 \rho_0 = \sum_j n_j \{P_j(\text{intra}) + P_j(\text{sphere})\} + P_{corr}$$

From the experimental distribution curves and the known structures of the complexes the P_{corr} terms can easily be derived for the reference solutions C, D and E. If the values obtained are used as approximations for the corresponding terms for the solutions A and B the peak shapes for the molybdate complexes in these solutions can be derived.

The parameter values used in the calculations are given in Table 2. The resulting shape functions as derived from the C, D, and E reference solutions, respectively, are shown in Fig. 4. The differences between them are minor, in particular between the shape functions derived with the use of the two reference solutions C and D, which both contain polynuclear complexes. This may be taken as a confirmation that differences between the P_{corr} terms do not seriously affect the derived shape functions.

Information from crystal structure determinations. From (16,9,1) solutions (B in Table 1) two types of

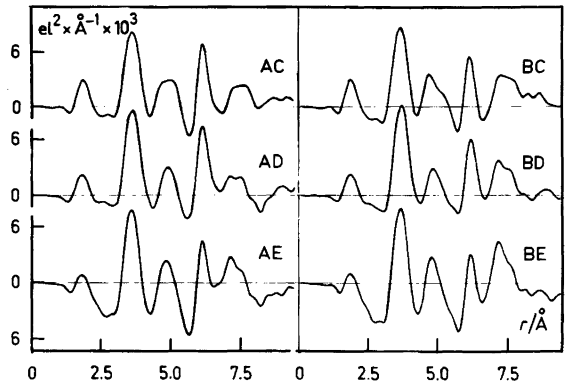

Fig. 4. The shape functions for the polymolybdate complexes in the solutions A and B derived with the use of the reference solutions C, D, and E, respectively.

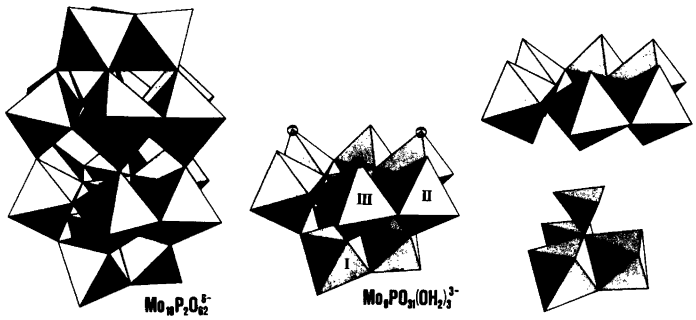

Fig. 5. The structures of the $Mo_9PO_{31}(OH_2)_3^{3-}$ and the $Mo_{18}P_2O_{62}^{6-}$ complexes as found in the crystal structure determinations of $Na_3H_6Mo_9PO_{34}(H_2O)_{12-13}$ and $Na_6Mo_{18}P_2O_{62}(H_2O)_{24}$ by Strandberg.[9,15] The water molecules bonded to the MoIII atoms in $Mo_9PO_{31}(OH_2)_3^{3-}$ are marked by circles. In the right-hand side of the figure the Mo_9PO_{34} group is separated into two parts: The ring of six MoO_6 octahedra and the compact group of three edge-sharing octahedra with the attached PO_4 tetrahedron.

crystals with the compositions $Na_3H_6Mo_9PO_{34}(H_2O)_{12-13}$ and $Na_6Mo_{18}P_2O_{62}(H_2O)_{24}$ can be obtained. Crystal structure determinations carried out by Strandberg show both of them to contain discrete polyanions with the formulae $Mo_9PO_{31}(OH_2)_3^{3-}$,[9] and $Mo_{18}P_2O_{62}{}^{6-}$,[15] respectively. Their structures are illustrated in Fig. 5.

Apart from the number of protons, the Mo_9PO_{34} group has a composition which is equivalent to that derived from emf measurements ($Mo_9PO_{34}^{9-} + 6H^+ + 6H_2O = (H^+)_{17}(MoO_4^{2-})_9(HPO_4^{2-})$). Its structure is related to the well-known Keggin model for $PW_{12}O_{40}{}^{3-}$,[16] from which it can be derived by removing three of the twelve MoO_6 octahedra. The $Mo_{18}P_2O_{62}$ group is closely related to the structure of the $P_2W_{18}O_{62}$ group determined by Dawson,[17] although the molybdenum atoms within the two six-fold rings are zigzagged. The group may be considered as being built up by a condensation of two $Mo_9PO_{31}(OH_2)_3^{3-}$ groups.

The parameters from the crystal structure determination were used to calculate the expected contribution from an Mo_9PO_{34} complex to the radial distribution curve. The resulting "molecular peak shape" normalized to the same molybdenum concentration and the same stoichiometric unit of volume as the experimental data, is compared in Fig. 6 with the shape function derived for the solutions A and B. The same has been done for the $Mo_{18}P_2O_{62}$ complex and for a fraction of the Mo_9PO_{34} group Mo_6PO_{28}, *i.e.* the ring of six MoO_6 octahedra with the attached PO_4 tetrahedron. These units are illustrated in Fig. 5.

Since the same characteristic unit of six edge and corner sharing MoO_6 octahedra occurs in all the three complexes used for the comparison, many of the characteristic features in their shape functions are similar. The same features appear also in the shape functions derived from the scattering data. It is obvious, however, that the number of interactions – as judged by the peak sizes – in the experimental curves are in best agreement with those calculated for the Mo_9PO_{34} unit.

Structural differences between the Mo_9PO_{34} group in solution and in crystals. Although the shape

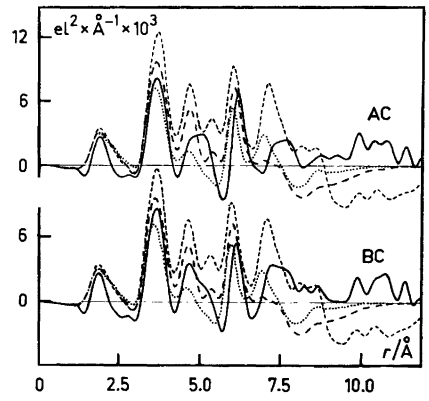

Fig. 6. Comparison between the derived shape functions for the polymolybdate complexes in the solutions A and B (solid lines) and the sum of the peak shapes calculated from the crystal structure parameters for the complexes $Mo_{18}P_2O_{62}$ (short dashes), Mo_9PO_{34} (long dashes), and Mo_6PO_{28} (dots). The parameter values used are summarized in Table 2.

function derived from the experimental distribution curves is consistent with the calculated shape function for the Mo_9PO_{34} group, deviations occur primarily in the region around 5 to 6 Å. The two peaks at 4.7 and 5.4 Å in the calculated function correspond to a single broad peak in the experimental curve. This is independent of the reference solution used for the derivation of the shape function (Fig. 4) and, therefore, probably reflects a difference in structure between the complex in the crystalline state and in solution.

In Fig. 7 the separate contributions from the different types of intramolecular interactions to the shape function of the Mo_9PO_{34} complex are given. The O – O interactions, although the largest in number, result in a rather smooth curve, which does not significantly contribute to the characteristic features of the total curve. The Mo – O interactions, which are also large in number, give more pronounced contributions to the curve, but the main features are caused by the well-defined Mo – Mo (and Mo – P) interactions. Minor changes in the structure leading to changed Mo – Mo distances should, therefore, show up clearly in the distribution curves, while corresponding changes in the Mo – O distances would probably to a large extent average out causing only minor changes. The search for a structural interpretation of the differences between the observed and the calculated distribution curves was, therefore, limited to the Mo positions, assuming the Mo – O, P – O, and O – O interactions to be unchanged.

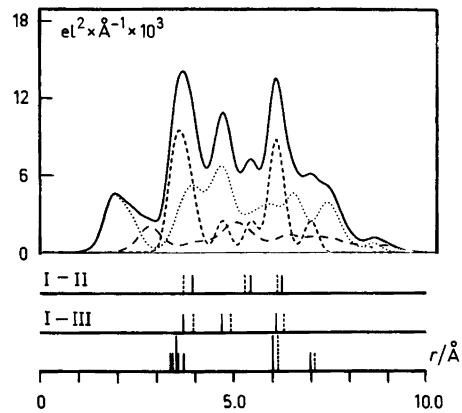

Fig. 7. The shape function for the Mo_9PO_{34} complex (solid line) as calculated from the crystal structure parameters (Table 2). Separately shown are the contributions to the shape function from O – O interactions (long dashes), Mo(P) – O interactions (dots), and Mo(P) – Mo(P) interactions (short dashes). The distances between the Mo atoms (MoI – MoII and MoI – MoIII on the two upper lines and remaining distances on the lower line) are marked by vertical lines having heights proportional to the frequency of the distances. Full lines are calculated from the crystal structure parameters. Dashed lines are calculated for the modified structure giving the best agreement with the distribution curves.

The Mo – Mo distances calculated with the use of the crystal structure parameters[9] are marked in Fig. 7. Three crystallographically independent Mo atoms occur within the Mo_9PO_{34} group: MoI in the compact group of three octahedra sharing edges, MoII and MoIII in the ring of six octahedra sharing corners and edges (Fig. 5). The MoIII atoms are closer to MoI than are the MoII atoms. In relation to the best plane through the Mo atoms in the ring of six MoO_6 octahedra, which is parallel to a plane through the three MoI atoms, MoIII is situated 0.3 Å below while Mo II is 0.3 Å above this plane. The three water molecules, incorporated into the complex in the crystals, are bonded to the MoIII atoms, which leads to a long distance, 2.21 Å, from MoIII to its apex oxygen, compared to only 1.70 Å for the corresponding MoII – O distance.

The two separated peaks at 4.7 and 5.4 Å observed in the shape function calculated from the crystal structure parameters result from the different MoIII – MoI and MoII – MoI distances. Con-

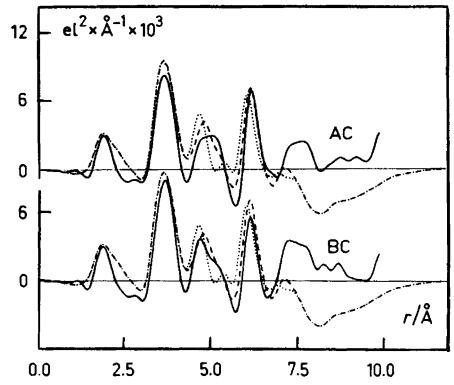

Fig. 8. Comparison of the derived shape functions (solid lines) for the polymolybdate complexes in solutions A and B with calculated functions for a Mo_9PO_{34} complex. The dotted lines are obtained with the crystal structure parameters, and the dashed lines with the modified parameter values.

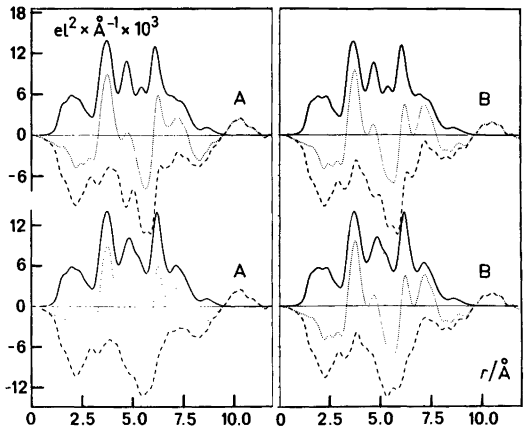

Fig. 9. Comparison between the $(D(r)-4\pi r^2\rho_0)$ functions (dotted lines) for the solutions A and B and the shape function for an Mo_9PO_{34} complex (solid lines) calculated from the crystal structure parameters (upper part) and from the modified parameter values (lower part). Dashed lines are corresponding differences.

ceivably, therefore, since these peaks are not separated in the shape function derived for the complexes in solution, the corresponding distances in solution are more equal, possibly as a result of a change in the number of protons attached to the oxygen atoms of MoIII and MoII. A markedly improved agreement between observed and calculated shape functions is obtained by making the MoI – MoIII and MoI – MoII distances more equal and by slightly enlarging the six-ring. From systematic variations of the Mo positions a "best" set of parameter values was obtained, which corresponded to almost equal MoIII – MoI and MoII – MoI distances, with all the MoII and MoIII atoms positioned in a plane parallel to the plane through the MoI atoms. The resulting shape function is shown in Fig. 8. The relation between the Mo – Mo distances obtained with this set of parameter values and the Mo – Mo distances in the crystal structure is shown in Fig. 7.

The parameter values giving the best agreement between observed and calculated shape functions (Fig. 8) also lead to the smoothest background curves when the corresponding peak shapes are subtracted from the $D(r)-4\pi r^2\rho_0$ functions (Fig. 9).

For solution B the results indicate that the same conclusions are valid as those derived for A. There are, however, indications that in B part of the molybdenum may occur as larger complexes, probably as $Mo_{18}P_2O_{62}$, since the peak at 7.2 Å is relatively more pronounced than for solution A. The additional intramolecular interactions of $Mo_{18}P_2P_{62}$ compared to those of Mo_9PO_{34} are, however, rather evenly distributed over the shape function and, therefore, do not lead to any characteristic differences between the two complexes, (Fig. 6), apart from the long distances for $r>6$ Å. This makes the distribution curves less useful for a differentiation between them.

DISCUSSION OF THE RESULTS

The scattering data confirm that the (15,9,1) complex, *i.e.* $(H^+)_{15}(MoO_4^{2-})_9(HPO_4^{2-})$, used by Pettersson for the interpretation of emf data on molybdophosphate solutions (Fig. 1), has the same basic structure as the discrete polyanions $Mo_9PO_{31}(OH_2)_3^{3-}$, found in crystals of $Na_3H_6Mo_9PO_{34}(H_2O)_{12-13}$.[9] In a slightly more acid solution, which according to emf data should contain the (16,9,1) complex (Fig. 1), part of the molybdate seems to be bonded in larger complexes, probably dimers of $Mo_9PO_{31}(OH_2)_3^{3-}$ which have the formula $Mo_{18}P_2O_{62}^{6-}$ and are found as discrete polyanions in crystals of $Na_6Mo_{18}P_2O_{62}(H_2O)_{24}$.[15]

These conclusions are supported by Raman measurements.[4] Raman spectra of solution A and of $Na_3H_6Mo_9PO_{34}(H_2O)_{12-13}$ are similar. In the Raman spectrum of solution B, however, a new strong peak appears, which is also present in Raman spectra from crystals of $Na_6Mo_{18}P_2O_{62}(H_2O)_{24}$.

The slight difference between the structure of the Mo_9PO_{34} complexes in solution and in crystals as indicated by the radial distribution curves can be ascribed to slightly changed positions of the Mo atoms in the ring of six octahedra, which forms part of the Mo_9PO_{34} structure (Fig. 5). The structural change may be caused by a change in the positions of the protons attached to the group.

Acknowledgements. The work has been supported by the Swedish Natural Science Research Council. We thank ing. Ernst Hansen for skilful technical assistance.

REFERENCES

1. Pettersson, L. *Acta Chem. Scand. 25* (1971) 1959.
2. Pettersson, L., Andersson, I., Lyhamn, L. and Ingri, N. *Trans. R. Inst. Technol. Stockholm* (1972) No. 256.
3. Pettersson, L. *Chem. Scr. 7* (1975) 145.
4. Pettersson, L. *Equilibrium and Structure Studies of Aqueous Three Component Polyanion Complexes Formed in the Systems* $H^+ - MoO_4^{2-} - HPO_4^{2-}$, $H^+ - MoO_4^{2-} - HAsO_4^{2-}$ *and* $H^+ - MoO_4^{2-}$ – D-*mannitol*, Diss., Umeå Universitet, Umeå 1974.
5. Strandberg, R. *Acta Chem. Scand. 27* (1973) 1004.
6. Hedman, B. *Acta Cryst. B 33* (1977) 3083.
7. Hedman, B. and Strandberg, R. *Personal communication.*
8. Hedman, B. *Acta Chem. Scand. 27* (1973) 3335.
9. Strandberg, R. *Acta Chem. Scand. A 28* (1974) 217.
10. Hedman, B. *Acta Chem. Scand. A 32* (1978). *In press.*
11. Johansson, G., Pettersson, L. and Ingri, N. *Acta Chem. Scand. A 28* (1974) 1119.
12. Johansson, G. *Acta Chem. Scand. 25* (1971) 2787; *20* (1966) 553.
13. Pocev, S. and Johansson, G. *Acta Chem. Scand. 27* (1973) 2146.
14. Johansson, G. and Sandström, M. *Chem. Scr. 4* (1973) 195.
15. Strandberg, R. *Acta Chem. Scand. A 29* (1975) 350.
16. Keggin, J. F. *Proc. R. Soc. London 144* (1934) 75.
17. Dawson, B. *Acta Crystallogr. 6* (1953) 113.
18. Sjöbom, K. and Hedman, B. *Acta Chem. Scand. 27* (1973) 3673.

Received December 31, 1977.

Acta Chemica Scandinavica A 32 (1978) 415–421

Extraction du Gallium de l'Indium et de Quelques Autres Métaux en Milieu Thiocyanate par le Dibutylphénacylphosphonate (HDBPP)

J. P. BRUNETTE,[a] M. J. F. LEROY,[a] B. CECCAROLI[b] et J. ALSTAD[b]

[a] Laboratoire de Chimie Minérale, Ecole Nationale Supèrieure de Chimie de Strasbourg, Université Louis Pasteur, 1, rue Blaise Pascal, 67008 Strasbourg Cedex, France et [b] Section of Nuclear Chemistry, Department of Chemistry, University of Oslo, Oslo 3, Norway

The extraction of gallium(III), indium(III), iron(III), vanadium(IV) and some other metals from aqueous thiocyanate media by dibutylphenacylphosphonate (HDBPP) in toluene has been studied. $Ga(NCS)_3(HDBPP)_3$, $In(NCS)_3(HDBPP)_3$ $Fe(NCS)_3(HDBPP)_3$ and $VO(NCS)_2(HDBPP)_3$, together with the thiocyanic acid, are extracted. HDBPP is bonded to the extracted metals only through one atom, probably the oxygen of the P=O group.

Les extractions du gallium(III), de l'indium(III), du fer(III), du vanadium(IV) et de quelques autres métaux en milieu thiocyanate par le dibutylphénacylphosphonate (HDBPP) dans le toluène ont été étudiées. Les espèces $Ga(NCS)_3(HDBPP)_3$, $In(NCS)_3(HDBPP)_3$, $Fe(NCS)_3(HDBPP)_3$ et $VO(NCS)_2(HDBPP)_3$, ainsi que l'acide thiocyanique, sont extraits. Le HDBPP n'est lié aux métaux extraits que par l'intermédaire d'un seul atome vraisemblablement l'oxygène du groupement P=O.

De nombreuses publications sur l'extraction des métaux en milieu thiocyanate ont paru ces dernières années: Sekine, Hasegawa et coll.,[1-7] Specker et coll.,[8,9] Golub et coll.[10] et Khopkar et coll.,[11] en particulier, ont étudié l'extraction des terres rares, de In, Ga, Zn, Hg, Be... par des extractants neutres tels que le phosphate de tributyle, l'oxyde de trioctylphosphine et la méthylisobutylcétone. D'autres auteurs ont utilisé des extractants échangeurs d'anions: Mikheev et coll. ont étudié l'extraction du gallium par la tri-n-octylamine[12] et nous nous sommes intéressés à la séparation de l'aluminium, du gallium et de l'indium par la trilaurylamine.[13] Certaines études ont finalement conduit à des applications.[14,15]

Le travail présenté ici concerne essentiellement l'extraction du gallium, de l'indium et de quelques autres métaux en milieu thiocyanate par le dibutylphénacylphosphonate $(BuO)_2P(O)CH_2C(O)C_6H_5$, noté HDBPP, en solution dans le toluène. Cela fait partie d'une étude plus générale des propriétés extractives des β-cétophosphonates. De tels composés sont *à priori* intéressants du fait de la dissymétrie du pouvoir donneur des deux groupements fonctionnels C=O et P=O qui peut conduire à une grande sélectivité, et de la présence d'un groupe méthylène à hydrogène mobile qui en fait potentiellement des chélatants acides asymétriques. Peu d'études concernant l'utilisation des β-cétophosphonates comme extractants ont été publiées à ce jour. Nous citerons les travaux de Meider-Gorican et coll.[16-17] concernant l'extraction des couples de métaux Zr–Hf et Nb–Ta ainsi que nos propres travaux qui ont porté essentiellement sur l'extraction de l'uranium.[18]

PARTIE EXPERIMENTALE

Phases organiques. Ce sont des solutions de HDBPP dans du toluène "Fluka *purum*" à des concentrations telles que $0{,}01\ M \leq [HDBPP] \leq 0{,}4\ M$. Le HDBPP a été préparé suivant la méthode décrite précèdemment[18] qui fait intervenir la réaction de la bromoacétophénone sur le phosphite de tributyle.

Phases aqueuses. Elles sont obtenues par attaque de 1 g de métal par 15 ml d'acide nitrique concentré ou par dissolution aqueuse de son équivalent en nitrate. La solution est ensuite diluée; la concentration en KSCN et le pH de la solution sont ajustés par addition de solutions de KSCN ou de HNO_3 concentrées. Dans le cas du vanadium nous avons dissous du sulfate de vanadyle dans de l'eau acidifiée par H_2SO_4; l'utilisation de métavanadate d'ammonium est également possible du fait de la réduction qui se fait en présence d'ions thiocyanates. (concentrations métalliques utilisées lors des extractions: Al = 200 mg/l Ga = 200 mg/l; In = 500 mg/l; Zn = 250 mg/l; Cd = 200 mg/l; Fe = 100 mg/l et V = 250 mg/l).

Extractions. Elles ont été réalisées par agitations manuelles de volumes égaux des deux phases pendant cinq minutes à une température de 19 ± 1 °C. Les pH des solutions aqueuses à l'équilibre ont été mesurés à l'aide d'un pH mètre digital Philips PW 9408 équipé d'une électrode de verre Ingold 40I.88 NS KI9. Un spectrophotomètre d'absorption atomique IL 453 a été utilisé pour la mesure des concentrations métalliques dans les deux phases. Dans le cas du vanadium, c'est la colorimétrie de l'ion peroxyvanadyle $[VO(O_2)]^+$ a 460 nm qui a été choisie comme méthode de dosage.

Dosage de HSCN. Afin de doser l'acide thiocyanique extrait en phase organique ce dernier est réextrait par plusieurs lavages successifs de 5 ml de solution organique par une solution aqueuse de soude molaire. La solution de lavage est recueillie quantitativement, acidifiée par HNO_3 puis dosée par $AgNO_3$ 0,01 M. Le point d'équivalence est déterminé par potentiométrie.

RESULTATS – DISCUSSION

Généralités

En milieu thiocyanate, la plupart des métaux sont susceptibles de se complexer suivant les équilibres:

$$M^{m+} + n SCN^- \overset{\beta_n}{\rightleftharpoons} M(NCS)_n^{m-n}$$

$$\beta_n = \frac{[M(NCS)_n^{m-n}]}{[M^{m+}][SCN^-]^n} \qquad (1)$$

L'agitation d'une telle solution aqueuse avec un extractant neutre S dissous dans un solvant organique peut faire passer le métal M d'une phase à l'autre suivant l'équilibre:

$$M^{m+} + m SCN^- + x\bar{S} \overset{K}{\rightleftharpoons} \overline{M(NCS)_m S_x}$$

$$K = \frac{[\overline{M(NCS)_m S_x}]}{[M^{m+}][SCN^-]^m [\bar{S}]^x} \qquad (2)$$

(les espèces de la phase organique sont surlignées)

Si l'on suppose que x ne puisse prendre qu'une seule valeur, le coefficient de distribution D_M du métal M s'écrit alors:

$$D_M = \frac{\bar{C}_M}{C_M} = \frac{[\overline{M(NCS)_m S_x}]}{\Sigma[M(NCS)_n^{m-n}]}$$

ce qui entraîne, en tenant compte des équations (1) et (2)

$$D_M = \frac{K[SCN^-]^m[\bar{S}]^x}{\sum_n \beta_n [SCN^-]^n}$$

soit, pour $[SCN^-]$ constant

$$\log D_M = \text{cte} + x \log [\bar{S}] \qquad (3)$$

Si le HDBPP se comporte vis-à-vis des métaux en milieu thiocyanate comme un simple extractant neutre, les courbes $\log D_M = f(\log[HDBPP])$, établies à diverses concentrations en ions SCN^- constantes, seront donc des droites de pentes égales au nombre de molécules de HDBPP fixées sur chaque atome de métal extrait. Avant d'étudier de telles courbes, nous avons évalué l'importance de l'extraction d'acide thiocyanique par le HDBPP dans les conditions d'extraction des métaux.

Extraction de l'acide thiocyanique par le HDBPP

Les extractions ont été réalisées à partir de solutions aqueuses molaires en KSCN en faisant varier le pH et la concentration en HDBPP de la phase organique. Soit D_{SCN} le rapport des concentrations en SCN^- des phases organique et aqueuse à l'équilibre; il apparait (Fig. 1) que les courbes $\log D_{SCN} = f(pH)$ sont des droites de pentes voisines de -1, ce qui montre que l'extraction des ions SCN^- se fait sous la forme d'acide thiocyanique HSCN associé au HDBPP. Les courbes $\log D_{SCN} = f(\log[HDBPP])$ à divers pH constants (Fig. 2) sont des droites de pentes voisines de 0,7, ce qui reste compatible avec l'équilibre d'extraction suivant:

$$H^+ + SCN^- + \overline{HDBPP} \rightleftharpoons \overline{HSCN.HDBPP} \qquad (4)$$

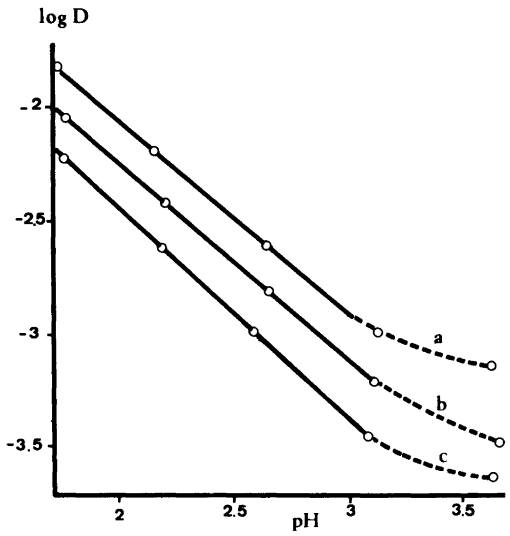

Fig. 1. Extraction de SCN^- par le HDBPP: log $D_{SCN}=f$ (pH). ([KSCN]=1 M. a: [$\overline{HDBPP}$]=0,2 M; pente= −0,85. b: [$\overline{HDBPP}$]=0,1 M; pente = −0,85. c: [HDBPP]=0,05 M; pente= −0,95).

La similitude des courbes d'extraction de l'acide thiocyanique par le HDBPP et par le TBP (Fig. 3) confirme l'équilibre d'extraction (4) proposé ci-

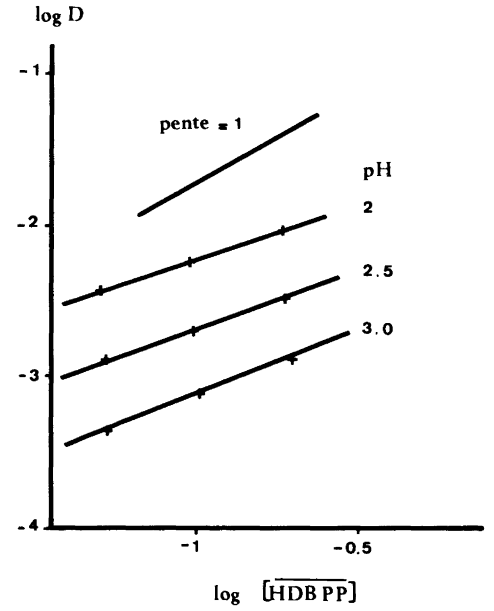

Fig. 2. Extraction de SCN^- par le HDBPP: log $D=f$(log[$\overline{HDBPP}$]) ([KSCN]=1 M).

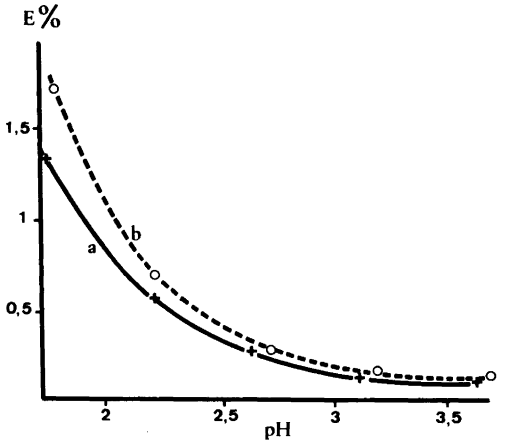

Fig. 3. Pourcentage de SCN^- extrait (E %) par le HDBPP et par le TBP. ([KSCN]=1 M; a: [$\overline{HDBPP}$]=0,2 M; b: [TBP]=0,2 M) les volumes des deux phases étant égaux.

dessus: Khopkar et coll.[11] ont en effet montré que l'acide thiocyanique est extrait par le TBP sous la forme $\overline{HSCN.TBP}$. Ceci montre par ailleurs que c'est le groupement phosphoryle qui joue une rôle prépondérant lors de l'extraction, le groupement carbonyle n'ayant vraisemblablement qu'un effet secondaire. HDBPP et TBP ont également des pouvoirs extractants très voisins vis-à-vis des autres acides minéraux lesquels sont extraits sous la forme $\overline{HX.S}$ où HX=HCl, $HClO_4$ ou HNO_3 et S=TBP ou HDBPP.[18]

Extraction du gallium et de l'indium

Influence du pH. Au dessus de pH 2, les extractions du gallium et de l'indium en milieu SCN^- par le HDBPP dans le toluène sont indépendantes du pH de la solution aqueuse, les autres paramètres restant inchangés (Fig. 4); ceci montre que l'extraction se fait par simple addition. Si le pH devient inférieur à 2, l'extraction diminue ce qui s'explique par une extraction non négligeable d'acide thiocyanique (voir Fig. 3).

Influence de la concentration en SCN^-. Si l'indium et le gallium sont extraits par le HDBPP sous la forme $M(NCS)_3$ $(HDBPP)_x$, pour une concentration donnée en HDBPP, l'extraction est alors proportionnelle à la fraction de complexe neutre $M(NCS)_3$ présent en phase aqueuse. L'importance de l'extraction dépend alors directement des valeurs des constantes de formation des com-

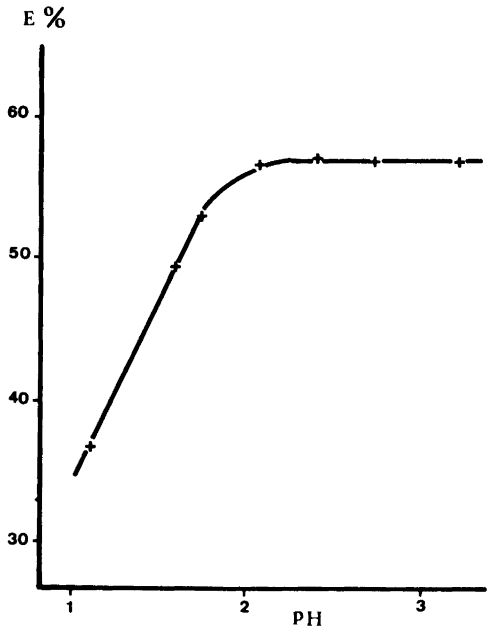

Fig. 4. Influence du pH sur le pourcentage d'indium extrait (E %). ([KSCN] = 1 M; [HDBPP] = 0,05 M). les volumes des deux phases étant égaux.

plexes successifs $M(NCS)_n^{3-n}$ et de la concentration en ions SCN^- de la phase aqueuse.

Dans le cas de l'indium, l'extraction par le HDBPP passe par un maximum pour $[SCN^-]$ ~0,5 M ce qui est en bon accord avec les valeurs des constantes β_n (équation 1) déterminées par Hasegawa et Sekine.[7] Pour $[SCN^-] > 0{,}5$ M, la formation d'espèces anioniques $In(NCS)_{3+n}^{n-}$ non extractibles, aux dépens de l'espèce extractible $In(NCS)_3$, est responsable de la diminution de l'extraction.

En ce qui concerne le gallium, l'extraction croît régulièrement en fontion de la concentration croissante en ions SCN^- dans de domaine étudié ($0 \leq [SCN^-] \leq 2$ M), ceci est conforme au fait que les espèces cationiques ou neutres $Ga(NCS)_n^{3-n}$ ($n \leq 3$) prédominent en phase aqueuse dans les conditions expérimentales.[12]

Ainsi, le comportement différent du gallium et de l'indium vis-à-vis des ions SCN^- en milieu aqueux est le facteur déterminant qui permet la séparation des deux métaux. Des faits similaires ont d'ailleurs pu être observés lors de l'étude de l'extraction du gallium et de l'indium en milieu thiocyanate par la trilaurylamine.[13]

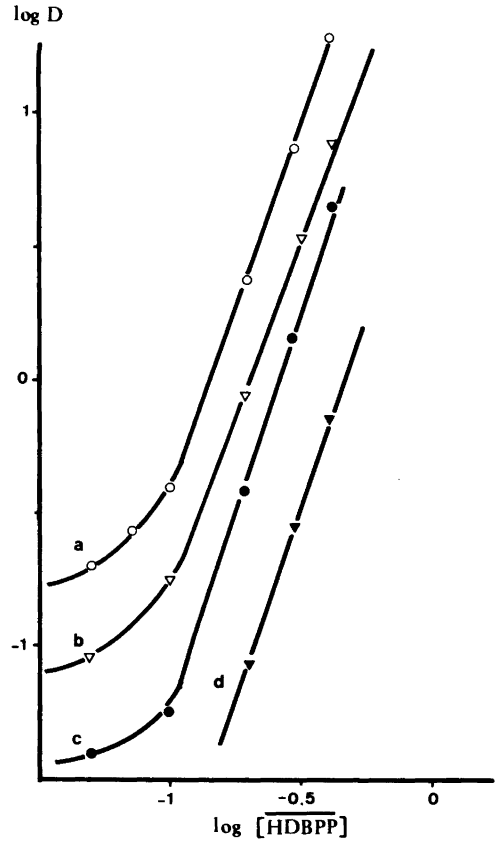

Fig. 5. Extraction du gallium. a: [KSCN] = 2 M; pente = 2,7. b: [KSCN] = 1 M; pente = 2,75. c: [KSCN] = 0,5 M; pente = 3,0. d: [KSCN] = 0,2 M; pente = 3,0.

Influence de la concentration en HDBPP. Dans le but de déterminer la composition des espèces extraites, nous avons étudié l'influence de la concentration en HDBPP sur les extractions du gallium et de l'indium. Les courbes $\log D = f(\log [\overline{HDBPP}])$, obtenues sont reportées sur les Fig. 5 et 6. Il s'agit de droites dont les pentes sont très voisines de 3. Conformément à l'équation (3) et au raisonnement qui s'y rapporte, les espèces extraites peuvent s'écrire $Ga(NCS)_3(HDBPP)_3$ et $In(NCS)_3(HDBPP)_3$.

Les coordinences du gallium et de l'indium étant au maximum de 6, le dibutylphénacylphosphonate ne peut-être coordiné sur ces métaux que par un seul atome d'oxygène donneur. Le caractère généralement plus donneur des groupements phos-

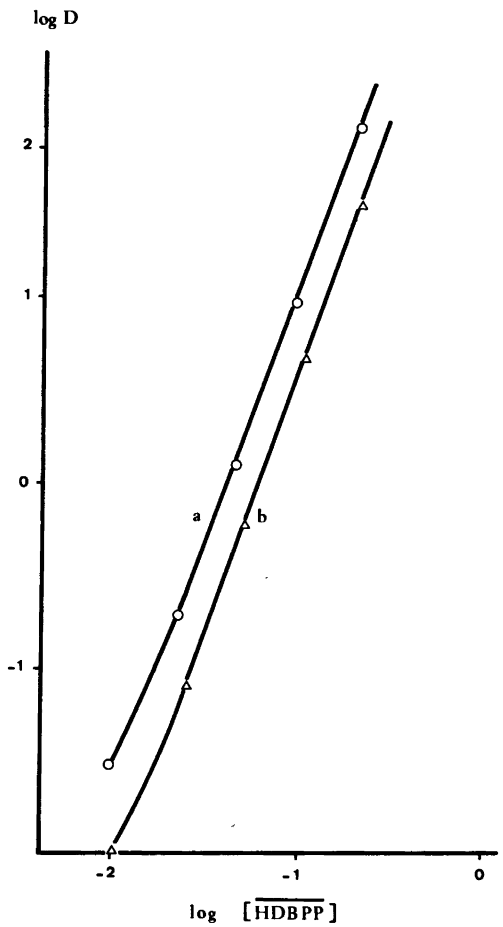

Fig. 6. Extraction de l'indium. a: [KSCN]=0,5 M; pente=3,05. b: [KSCN]=0,1 M, pente=3,10).

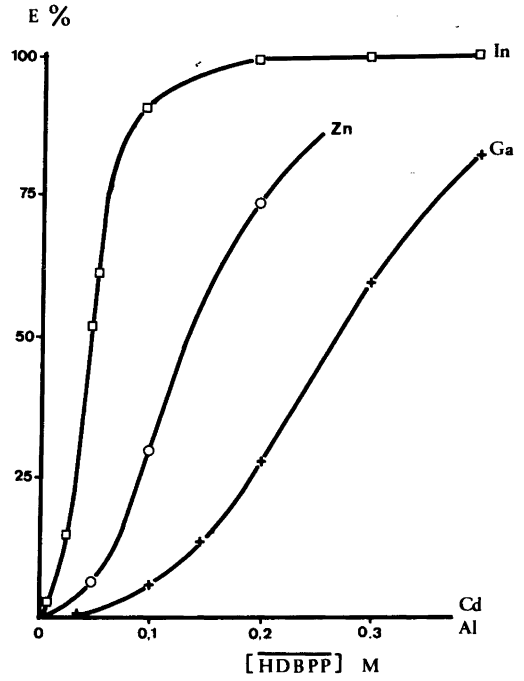

Fig. 7. Pourcentage d'extraction (E %) de Al, Ga, In, Zn et Cd. [KSCN]=0,5 M; valeur optimale permettant la séparation Ga-In, les volumes des deux phases étant égaux.

phoryles par rapport aux groupements carbonyles ainsi que les comportements très voisins du HDBPP et du TBP dans les mêmes conditions, laissent penser que le HDBPP joue ici un rôle d'extractant solvatant dont la fonction active est le groupement P=O. Une étude infrarouge a d'ailleurs montré qu'il en était ainsi dans le complexe $UO_2(NO_3)_2(HDBPP)_2$. Le HDBPP ne se coordine en fait par ses deux atomes d'oxygène que dans des conditions bien définies; c'est le cas, par exemple, lors de l'extraction acide de l'uranium qui ne peut être réalisée qu'à des pH élevés.[18]

Extraction d'autres métaux

Extractions comparées des éléments Al, Ga, In, Zn et Cd. La Fig. 7 représente les courbes d'extraction de ces métaux à partir de solutions aqueuses 0,5 M en KSCN. Pour des concentrations en HDBPP comprises entre 0 et 0,4 M, cadmium et aluminium ne sont pas extraits ce qui peut permettre une séparation quantitative de l'indium de ces métaux en un seul équilibrage des phases organique et aqueuse: l'indium est en effect complètement extrait pour $[\overline{HDBPP}] \geq 0{,}3$ M. Zinc et gallium peuvent être séparés du cadmium et de l'aluminium, mais plusieurs étages d'extraction sont nécessaires. Dans une moindre mesure les séparations In−Ga et In−Zn sont également possibles puisque pour $[\overline{HDBPP}]=0{,}05$ M, 57 % de l'indium est extrait contre 6 % du zinc et 4 % du gallium, et pour $[\overline{HDBPP}]=0{,}1$ M, 91 % de l'indium est extrait contre 5 % du gallium.

Extraction du fer et du vanadium. Les Fig. 8 et 9 représentent les courbes d'extraction log $D=f$(log

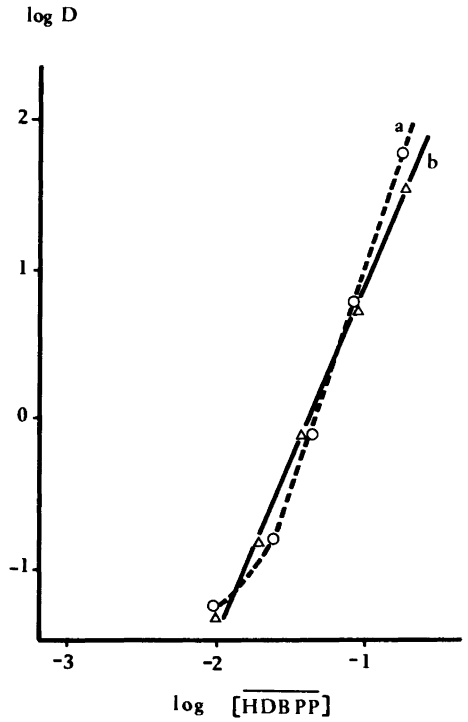

Fig. 8. Extraction du fer(III). a: [KSCN] = 0,5 M; pente = 2,9. b: [KSCN] = 0,3 M; pente = 2,7.

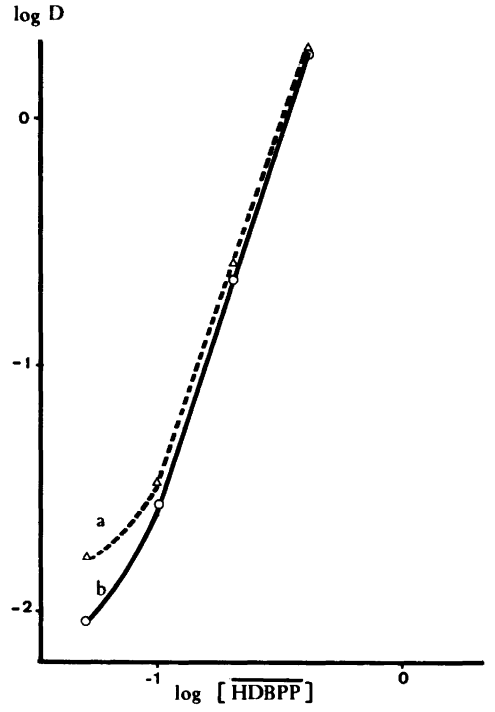

Fig. 9. Extraction du vanadium(IV). (a: [KSCN] = 0,5 M; pente = 2,98. b: [KSCN] = 2 M; pente = 3,03).

[$\overline{\text{HDBPP}}$]) du fer(III) et du vanadium(IV) à diverses concentrations en KSCN. Dans tous les cas, il s'agit de droites dont les pentes sont voisines de 3, ce qui montre que les espèces extraites sont $Fe(NCS)_3(HDBPP)_3$ et $VO(NCS)_2(HDBPP)_3$. Là encore, compte tenu de la coordinence maximum de 6 de Fe(III) et de V(IV), le dibutylphenacylphosphonate n'est lié aux deux autres métaux que par l'intermédiaire de son groupement phosphoryle. Le HDBPP semble agir de la même façon vis-à-vis des terres rares; cependant, à des pH plus élevés ($pH \geq 5$), l'extraction prend un caractère acide marqué malgré la présence en solution aqueuse des ions SCN^-; l'extraction fait alors vraisemblablement intervenir la forme anionique chélatante $DBPP^-$ du HDBPP.[18]

Remerciements. Les auteurs tiennent à remercier la Centre National de la Recherche Scientifique, (Paris) pour son soutien financier: ce travail s'inscrit dans le cadre de l'Action Thématique Programmée «Epargne d'Energie et opérations chimiques industrielles».

BIBLIOGRAPHIE

1. Sekine, T. *Bull. Chem. Soc. Jpn. 38* (1965) 1972.
2. Sekine, T. et Ishu, T. *Bull. Chem. Soc. Jpn. 43* (1970) 2422.
3. Hasegawa, Y. *Bull. Chem. Soc. Jpn. 43* (1970) 2665.
4. Sekine, T., Komatsy, Y. et Sakairi, M. *Bull. Chem. Soc. Jpn. 44* (1971) 1480.
5. Moriya, M. et Sekine, T. *Bull. Chem. Soc. Jpn. 44* (1971) 3347.
6. Hasegawa, Y., Takenchi, H. et Sekine, T. *Bull. Chem. Soc. Jpn. 45* (1972) 1388.
7. Hasegawa, Y. et Sekine, T. *J. Inorg. Nucl. Chem. 36* (1974) 421.
8. Specker, H. et Bankmann, E. *Z. Anal. Chem. 149* (1956) 97.
9. Henning, K. et Specker, H. *Z. Anal. Chem. 241* (1968) 81.
10. Golub, A. M., FamWang Ch'a et Samoilenko, V. M. *Russ. J. Inorg. Chem. 16* (1971) 282.
11. Khopkar, P. K. et Narayanakkutty, P. *J. Inorg. Nucl. Chem. 34* (1972) 2617.
12. Mikheev, N. B., Elfimova, G. J., Mikheeva, L. M. et Rumer, I. A. *Vestnik. Mosk. Univ. Khim. 25* (1970) 742.

13. Brunette, J. P., Araujo-Barreira, M. L., Taheri, M. et Leroy, M. J. F. *J. Inorg. Nucl. Chem. Accepté pour publication.*
14. Gandon, L. et Goulaouic, M. *French Pat.* 2. 129.916 (1972).
15. Gaudernack, B., Hannestad, G. et Hundere, I. *U.S. Pat.* 3. 751.553 (1973).
16. Sevdic, D. et Meider-Gorican, H. *J. Less. Common Metals 37* (1974) 103.
17. Bronzan, P. et Meider-Gorican, H. *J. Less. Common Metals 29* (1972) 407.
18. Martin, J. L. et Leroy, M. J. F. (soumise a *J. Chem. Res.*).

Reçu le 28 Novembre 1977.

Acta Chemica Scandinavica A 32 (1978) 423–428

On the Study of Triple Ion Formation

PER BERONIUS and TURE LINDBÄCK

Department of Physical Chemistry, University of Umeå, S-901 87 Umeå, Sweden

The formation of triple ions of lithium bromide in 1-octanol at 25 °C has been studied by electrical conductance measurements over the concentration range 0.42×10^{-4} to 42×10^{-4} M assuming equal probabilities of forming Li_2Br^+ and $LiBr_2^-$. The conductivity data at concentrations below 3.5×10^{-4} M, where triple ion formation was found to be negligible, which is in accord with theory, were employed to calculate the ion pair association constant (K_A) and the limiting conductivity of simple ions (Λ_∞). The triple ion association constant (K_T) and the limiting conductivity of ion triples (Λ_∞^T) were computed from a conductance equation involving these quantities as adjustable parameters. A mobility correction factor was incorporated in this equation to correct for ion atmosphere effects. Two different forms of this correction factor were investigated.

There exists a vast literature on ion pair formation in organic electrolyte systems as studied by means of electrical conductance measurements, *cf.* Refs. 1–5. A survey of the literature reveals, however, that comparatively few investigations of this kind concerning the formation of higher aggregates, such as triple ions, quadrupoles *etc.*, have been performed. There is an urgent need for further research in this field.

Previous investigations of triple ion formation are based on rather arbitrary assumptions concerning the limiting conductivity of these species. Ion atmosphere effects have not infrequently been neglected in the calculations. The objective of the present research is to investigate the formation of triple ions by means of electrical conductance measurements taking ion atmosphere effects into account. In this article, where conductance data for lithium bromide in 1-octanol at 25 °C are reported, a method for the derivation of both the triple ion association constant and the limiting conductivity of ion triples is outlined.

EXPERIMENTAL

Materials. The solvent (1-octanol, Fisher, *puriss*) was dried by shaking with Drierite (anhydrous calcium sulfate) for 24 h and fractionally distilled. The corrected[6] density at 25 °C, determined by means of a Lipkin type pycnometer[6] of 11 cm^3 capacity, was 0.82172 g cm^{-3} (lit.[7] 0.82209 g cm^{-3}). The electrolytic conductivity was 1×10^{-11} Ω^{-1} cm^{-1}. The literature[8] values, $\varepsilon = 9.85$ for the relative permittivity, and $\eta = 0.073$ P for the viscosity, were used.

Lithium bromide (Merck, *suprapur*) was dried for 2 h at 200 °C.

Solutions were prepared by weight. The density, 0.82377 g cm^{-3}, of the most concentrated stock solution used (0.02623 M) was determined as above. A linear[9] relationship between the density of the solution and the concentration of lithium bromide was assumed in the calculations.

Measurements. Conductivity measurements were performed at 25.00±0.02 °C using a Leeds and Northrup 4666 conductivity bridge. The conductivity cell, which was fitted with bright platinum electrodes, was of the Daggett-Bair-Kraus type.[10] The cell constant, determined by several calibrations using aqueous potassium chloride,[11] was 0.062026 cm^{-1}.

A portion of the pure solvent was transfered to the cell and its resistance established. Several 10 ml portions from a stock lithium bromide solution were then added by means of a syringe. The exact amount of each portion added was determined by differential weighing of the syringe. After each addition the cell resistance was established by measurements at different frequencies between 2 and 3.3 kHz and extrapolation to infinite frequency performed.

Because the resistances were in most instances outside the range of the conductivity bridge a 20 kΩ precision resistor was connected in parallel with the cell. For checking purposes a few measurements were performed using a 30 kΩ precision resistor.

Table 1. Conductance data for LiBr in 1-octanol at 25.0 °C.

$c \times 10^4$ M	Λ cm^2 Ω^{-1} mol^{-1}	$c \times 10^4$ M	Λ cm^2 Ω^{-1} mol^{-1}
0.42394	1.9040	7.2871	0.64228
0.44963	1.8649	7.6699	0.63148
0.85233	1.4983	8.0810	0.61588
0.90227	1.4667	8.4187	0.60814
1.2910	1.2853	8.8939	0.59244
1.3633	1.2565	9.1844	0.58715
1.7017	1.1557	9.6630	0.57270
1.7901	1.1318	11.818	0.53004
2.1024	1.0632	14.054	0.49496
2.2171	1.0383	16.284	0.46741
2.4953	0.99347	18.456	0.44535
2.6387	0.96949	20.620	0.42675
2.8915	0.93699	22.787	0.41098
3.0533	0.91425	24.635	0.39893
3.6810	0.85067	26.755	0.38686
3.9438	0.82424	28.785	0.37693
4.5339	0.78156	30.626	0.36817
4.8031	0.76075	32.548	0.36020
5.3342	0.73173	34.366	0.35315
5.6220	0.71363	36.251	0.34664
6.1154	0.69227	38.093	0.34061
6.4569	0.67449	39.914	0.33497
6.8852	0.65983	41.831	0.32954

Almost identical resistances of the cell were obtained for the two different shunt resistors used.

RESULTS AND DISCUSSION

The molar conductivity (Λ), corrected for the conductivity of the solvent, is given in Table 1 for several different concentrations, c, of lithium bromide.

Concentration range for ion pair formation. To determine the upper concentration limit for which triple ion formation is negligible the following procedure was used. The conductance equation,

$$\Lambda = \Lambda_\infty - Sc_i^{1/2} + Ec_i{}^{10}\log c_i + J_1 c_i - J_2 c_i^{3/2} - K_A c_i \alpha \gamma^2 \Lambda \quad (1)$$

where

$$\Lambda_\infty = \lambda_\infty(Li^+) + \lambda_\infty(Br^-) \quad (2)$$

and c_i is the concentration of free ions, was fitted to the seven lowest concentration points (c,Λ) to obtain the values of Λ_∞ and K_A which minimize $\sigma(\Lambda)$, the standard deviation between experimental and calculated Λ-values. This procedure was repeated upon increasing successively the upper limit of the concentration interval studied, *i.e.* eqn. (1) was fitted to the eight, nine, *etc.* lowest concentration points.

Two different forms of eqn. (1) were used, *viz.* the Pitts' equation[12] in the form of Fernández-Prini and Prue[13] ("PFPP" equation) and the Fuoss-Hsia equation[14,15] in the form of Fernández-Prini[16] ("FHFP" equation).

The coefficients S and E in eqn. (1), which are of the same form in the PFPP and FHFP equations, respectively, are functions of Λ_∞, ε, η, and the temperature. The J-coefficients, which are of different forms for the two conductance equations concerned are, in addition, functions of R, the maximum center-to-center distance between the ions in the ion pair. The distance parameter, R, was set equal to the Bjerrum radius, *cf.* Refs. 17–19, which for octanol at 25 °C amounts to 28.45 Å for the charge type of electrolyte concerned.

The degree of dissociation, α, was calculated from the law of mass action for the equalibrium between free ions and ion pairs,

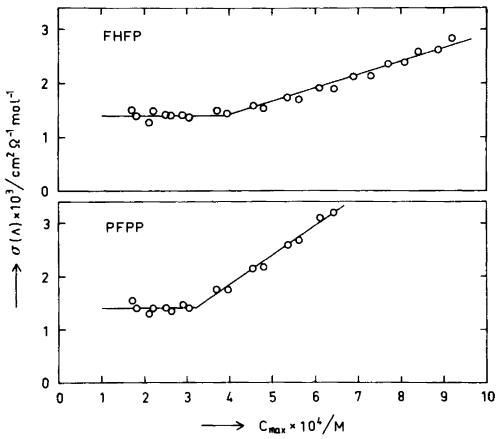

Fig. 1. Dependence of $\sigma(\Lambda)$ on maximum electrolyte concentration for application of the PFPP and FHFP versions of eqn. (1) to conductivity data of LiBr in 1-octanol at 25 °C.

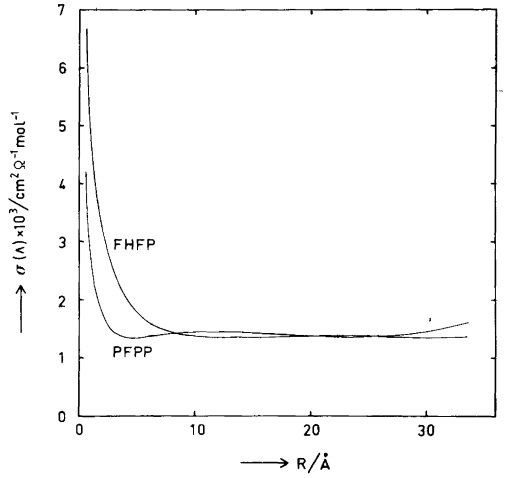

Fig. 2. Dependence of $\sigma(\Lambda)$ on distance parameter, R, for application of the PFPP and FHFP versions of eqn. (1) to conductivity data of LiBr ($c \leq 3.0533 \times 10^{-4}$ M) in 1-octanol at 25 °C.

$$K_A = (1-\alpha)/(c\gamma^2\alpha^2) \quad (3)$$

where γ is the mean molar activity coefficient of free ions, which was calculated from the Debye-Hückel equation,

$$^{10}\log\gamma = -11.465c_i^{1/2}/(1+26.401c_i^{1/2}) \quad (4)$$

corresponding to the values of ε and R quoted above.

The computer program used to calculate Λ_∞, K_A, and $\sigma(\Lambda)$ for a given value of R has been described.[20]

Graphical representations of the dependence of $\sigma(\Lambda)$ on the maximum concentration of lithium bromide are shown in Fig. 1 for the two different forms of eqn. (1) discussed. For concentrations above approximately 3.5×10^{-4} M the fit of eqn. (1) to the experimental points gradually deteriorates as reflected by the increasing values of $\sigma(\Lambda)$. This is so for both the PFPP and FHFP versions of eqn. (1). The effect observed may be ascribed the formation of triple ions, *cf.* Ref. 21 and references therein.

For 1:1-electrolyte solutions at 25 °C Fuoss has derived the following relationship,[5]

$$c_{max} = 3.2 \times 10^{-7}\,\varepsilon^3 \quad (5)$$

between the maximum concentration, for which triple ion formation is negligible, and the permittivity of the solvent. For the solvent studied eqn. (5) yields, $c_{max} = 3.1 \times 10^{-4}$ M, which is in excellent agreement with the experimental value of 3.5×10^{-4} M arrived at above.

It is concluded that the 14 lowest concentration points in Table 1 may be used to compute the constants of eqn. (1). With $R = 28.45$ Å the following values were obtained. PFPP equation: $\Lambda_\infty = 3.9214$ cm^2 Ω^{-1} mol^{-1}; $S = 41.07$; $E = 890.4$; $J_1 = 5610$; $J_2 = 123\,600$; $K_A = 56\,180$ (M^{-1}); FHFP equation: $\Lambda_\infty = 3.9479$; $S = 41.21$; $E = 897.5$; $J_1 = 5152$; $J_2 = 61\,100$; $K_A = 57\,100$.

It may be noted that $\sigma(\Lambda)$ is quite insensitive to the value of R within the 5–30 Å range, see Fig. 2.

Triple ion formation. In the interpretation of the conductivity data in the higher concentration range ($c \geq 3.681 \times 10^{-4}$ M; *cf.* Table 1) equal probabilities of forming the two different kinds of triple ions, Li_2Br^+ and $LiBr_2^-$, will be assumed.

The following equilibria will be considered.

$$Li^+ + Br^- \rightleftharpoons LiBr \quad (I)$$

$$LiBr + Li^+ \rightleftharpoons Li_2Br^+ \quad (IIa)$$

$$LiBr + Br^- \rightleftharpoons LiBr_2^- \quad (IIb)$$

The equilibrium constants of (IIa) and (IIb), being equal according to the assumption above, are denoted K_T. Putting,

$$[Li^+] = [Br^-] = c\alpha \quad (6)$$

$$[Li_2Br^+] = [LiBr_2^-] = c\alpha_T \quad (7)$$

we obtain eqn. (8) for the concentration of ion pairs.

$$[LiBr] = c(1-\alpha-3\alpha_T) \quad (8)$$

Hence,

$$K_A = (1-\alpha-3\alpha_T)/(c\gamma^2\alpha^2) \quad (9)$$

$$K_T = \alpha_T/[c\alpha(1-\alpha-3\alpha_T)] \quad (10)$$

The molar conductivity is given by the expression,

$$\Lambda = m(\alpha\Lambda_\infty + \alpha_T\Lambda_\infty^T) \quad (11)$$

where

$$\Lambda_\infty^T = \lambda_\infty(Li_2Br^+) + \lambda_\infty(LiBr_2^-) \quad (12)$$

and m is a mobility correction factor, which corrects Λ for ion atmosphere effects. This correction factor was calculated from the expression,

$$m = (\Lambda_\infty - Sc_i^{1/2} + Ec_i^{10}\log c_i + J_1c_i - J_2c_i^{3/2})/\Lambda_\infty \quad (13)$$

where the coefficients are the same as in eqn. (1) and,

$$c_i = c(\alpha+\alpha_T) \quad (14)$$

Eqn. (11) was fitted to the experimental conductivity data of the higher concentration range using a computer program operating as follows.

For each experimental point (c,Λ) a first approximation for α was calculated from eqn. (9) putting $\gamma = 1$ and $\alpha_T = 0$ using the K_A-value computed above from the conductivity data of the lower concentration range.

Using a preselected value of K_T a preliminary value of α_T was then obtained from eqn. (10).

A preliminary value for γ was calculated from the activity coefficient expression, eqn. (4), using c_i according to eqn. (14).

The new values of α_T and γ were inserted into eqn. (9) to obtain a better estimate of α, and so on.

These calculations were repeated until the difference between successive α-values, as well as between successive α_T-values, was less than 1×10^{-6}.

After attainment of the desired convergence in α and α_T the mobility correction term was calculated from eqn. (13) using the values of Λ_∞, S, E, J_1, and J_2 computed above.

Using a preselected value of Λ_∞^T eqn. (11) yielded a calculated Λ-value and, hence, the difference,

$$\Delta\Lambda = \Lambda(\text{exp}) - \Lambda(\text{calc}) \quad (15)$$

The expression,

$$\sigma(\Lambda) = \left(\frac{\Sigma(\Delta\Lambda)^2}{N-2}\right)^{1/2} \quad (16)$$

where N is the number of experimental points, was used to obtain the standard deviation between experimental and computed Λ-values.

To find the values of K_T and Λ_∞^T which minimize $\sigma(\Lambda)$ the dependence of $\sigma(\Lambda)$ on K_T was established for a series of values of the quotient, $\Lambda_\infty^T/\Lambda_\infty$. Since it seems improbable that the limiting conductivity of the triple ions would exceed that of the simple ions the calculations were restricted to values of $\Lambda_\infty^T/\Lambda_\infty \leq 1$.

Some results of these calculations are shown graphically in Fig. 3, which reveals that well-defined minima are obtained.

In Fig. 4 the conditional minimum $\sigma(\Lambda)$ has been plotted *vs.* the ratio, $\Lambda_\infty^T/\Lambda_\infty$. The corresponding

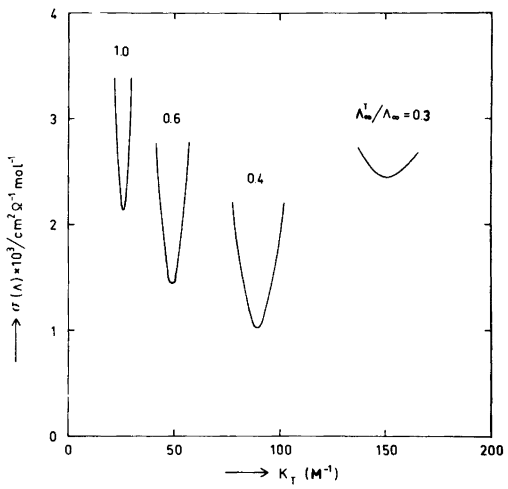

Fig. 3. Dependence of $\sigma(\Lambda)$ on K_T and the ratio, $\Lambda_\infty^T/\Lambda_\infty$, for application of the F version of eqn. (11) to conductivity data of LiBr ($c \geq 3.681 \times 10^{-4}$ M) in 1-octanol at 25 °C.

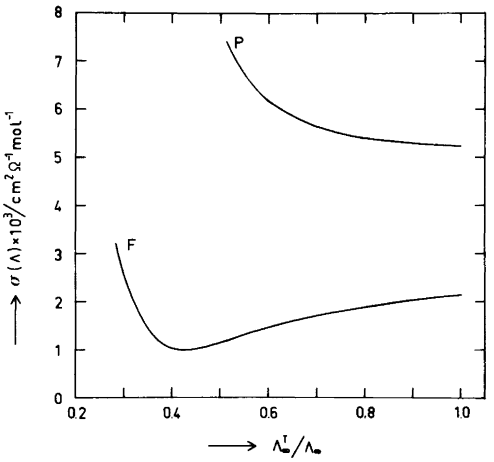

Fig. 4. Dependence of conditional minimum $\sigma(\Lambda)$ on the ratio, $\Lambda_{\infty}^{T}/\Lambda_{\infty}$, for application of the P and F versions of eqn. (11) to conductivity data for LiBr ($c \geq 3.681 \times 10^{-4}$ M) in 1-octanol at 25 °C.

graph of the dependence of K_T on this ratio is shown in Fig. 5. The curves labelled "P" and "F" in Figs. 4 and 5 were obtained using the two different versions of eqn. (11) based on the conductance parameter values quoted above for the PFPP and FHFP equations, respectively. According to the curves in Fig. 4 the F version of eqn. (11) results in the better fit to the experimental points.

By contrast with the P curve in Fig. 4 the F curve exhibits a minimum, which appears at a limiting conductivity of the triple ions corresponding to $\Lambda_{\infty}^{T} \simeq 0.4\Lambda_{\infty}$. This observation suggests that the limiting conductivity of the triple ions is about half that of the single ions. Compare previous studies in which the limiting conductivity of the triple ions has been assumed equal to 1/3 of that of the simple ions in some investigations, *e.g.* in Ref. 21, and equal to 2/3 in others, see for instance Ref. 22.

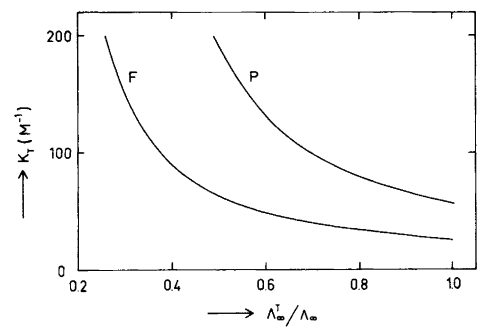

Fig. 5. Dependence of K_T on the ratio, $\Lambda_{\infty}^{T}/\Lambda_{\infty}$, for LiBr in 1-octanol at 25 °C.

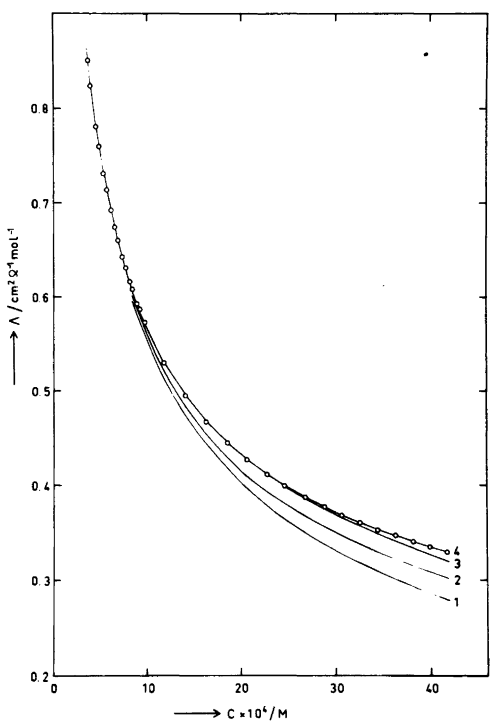

Fig. 6. Experimental and calculated values of Λ *vs.* concentration of LiBr in 1-octanol at 25 °C. Curves 1 and 2: PFPP and FHFP versions, respectively, of eqn. (1). Curves 3 and 4: P and F versions, respectively, of eqn. (11).

The experimental points (c,Λ) of the higher concentration range are shown graphically, together with calculated curves, in Fig. 6. Curve 1 is an extrapolation of the PFPP version of eqn. (1) from the lower to the higher concentration range, while curve 2 is the corresponding extrapolation of the FHFP version of eqn. (1). Curve 3 represents the P version of eqn. (11) for $\Lambda_{\infty}^{T}/\Lambda_{\infty} = 1$ and $K_T = 57$ referring to the minimum value of $\sigma(\Lambda)$ of curve P in Fig. 4. Curve 4 is the corresponding representation of the F version of eqn. (11) referring to the minimum of curve F in Fig. 4 for $\Lambda_{\infty}^{T}/\Lambda_{\infty} = 0.43$ and $K_T = 80$. As may be seen from Fig. 6 an excellent fit of eqn. (11) to the experimental points of the higher concentration range is obtained in this latter case.

As mentioned above previous investigations are based on rather arbitrary assumptions concerning the limiting conductivity of the triple ions. According to the present study the minimum value of $\sigma(\Lambda)$ corresponds to a limiting conductivity of the triple ions, which is about half that of the single ions. It is a matter for further research to verify whether the location of this minimum, *cf.* Fig. 4, indeed reflects the true value of the limiting conductivity of the triple ions.

The present formalism used to analyze conductance data assuming ion pair and triple ion formation necessarily involves a great number of adjustable parameters. Furthermore, the numerical value of the triple ion association constant may be rather strongly dependent on basic assumptions made, *e.g.* concerning ion atmosphere effects, *cf.* Fig. 5. Consequently, it seems worthwhile to stress that the calculated value of K_T should be used with caution.

Acknowledgements. The authors thank Mrs. Margareta Ögren for technical assistance and the Swedish Natural Science Research Council for financial support.

REFERENCES

1. Gordon, J. E. *The Organic Chemistry of Electrolyte Solutions*, Wiley, New York 1975.
2. Covington, A. K. and Dickinson, T., Eds., *Physical Chemistry of Organic Solvent Systems*, Plenum, London 1973.
3. Janz, G. J. and Tomkins, R. P. T. *Nonaqueous Electrolytes Handbook*, Academic, New York 1972, Vol. 1.
4. Conway, B. E. and Barradas, R. G., Eds., *Chemical Physics of Ionic Solutions*, Wiley, New York 1966.
5. Fuoss, R. M. and Accascina, F. *Electrolytic Conductance*, Interscience, New York 1959.
6. Bauer, N. and Lewin, S. Z. In Weissberger, A., Ed., *Physical Methods of Organic Chemistry*, 3rd Ed., Interscience, New York 1959, Vol. I, Part I, Chapter IV.
7. Weissberger, A., Ed., *Technique of Chemistry, Organic Solvents*, 3rd Ed., Wiley-Interscience, New York 1970, Vol. II, p. 181.
8. Shkodin, A. M., Sadovnichaya, L. P. and Podolyanko, V. A. *Ukr. Khim. Zh. 35* (1969) 144.
9. Nilsson, A.-M. and Beronius, P. *Z. Phys. Chem. (Frankfurt am Main) 79* (1972) 83.
10. Daggett, Jr., H. M., Bair, E. J. and Kraus, C. A. *J. Am. Chem. Soc. 73* (1951) 799.
11. Lind, Jr., J. E., Zwolenik, J. J. and Fuoss, R. M. *J. Am. Chem. Soc. 81* (1959) 1557.
12. Pitts, E. *Proc. R. Soc. London A 217* (1953) 43.
13. Fernández-Prini, R. and Prue, J. E. *Z. Phys. Chem. (Leipzig) 228* (1965) 373.
14. Fuoss, R. M. and Hsia, K.-L. *Proc. Natl. Acad. Sci. U.S.A. 57* (1967) 1550.
15. Fuoss, R. M. and Hsia, K.-L. *Proc. Natl. Acad. Sci. U.S.A. 58* (1968) 1818.
16. Fernández-Prini, R. *Trans. Faraday Soc. 65* (1969) 3311.
17. Justice, J.-C. *Electrochim. Acta 16* (1971) 701.
18. Beronius, P. *Acta Chem. Scand. A 29* (1975) 289.
19. Beronius, P. *Acta Chem. Scand. A 30* (1976) 115.
20. Beronius, P. *Acta Chem. Scand. A 28* (1974) 77.
21. Robinson, R. A. and Stokes, R. H. *Electrolyte Solutions*, Butterworths, London 1965, Chapter 14.
22. Ralph, E. K. and Gilkerson, W. R. *J. Am. Chem. Soc. 86* (1964) 4783.

Received December 27, 1977.

Acta Chemica Scandinavica A 32 (1978) 429–434

Studies on Cobalt(II) Halide Complex Formation. II. Cobalt(II) Chloride Complexes in 10 M Perchloric Acid Solution

L. H. SKIBSTED[a] and JANNIK BJERRUM[b]

[a] Chemistry Department, Royal Veterinary and Agricultural University, DK-1871 Copenhagen V, Denmark and [b] Chemistry Department I, Inorganic Chemistry, H. C. Ørsted Institute, University of Copenhagen, DK-2100 Copenhagen Ø, Denmark

The stability constants K_1 and β_4 for the chlorocobalt(II) complexes in 10 M $H(Cl,ClO_4)$ aqueous solutions are calculated from spectrophotometric measurements to have the values $10^{1.34}$ l/mol and $10^{2.57}$ l^4/mol^4, respectively. The dichloro and trichloro complexes are shown to have a negligibly small range of existence. The greatly increased stability of the tetrachlorocobaltate(II) ion relative to that in dilute aqueous solutions can be accounted for entirely by the change in the chloride ion activity coefficient, and the general validity of so-called "effective formation constants" is discussed.

The change in colour of cobalt(II) chloride solutions from red to blue with increasing chloride concentration has been the subject of numerous studies, and it is now generally recognized that the colour change is caused by the reaction:

$$Co(H_2O)_6^{2+} + 4Cl^- \rightleftharpoons CoCl_4^{2-} + 6H_2O$$

Chloride ion activities sufficiently large for almost complete conversion of the hexaaqua ion into the tetrachlorocobaltate(II) ion are reached in saturated aqueous solutions of lithium chloride and hydrochloric acid, and in a recent paper[1] the present authors have estimated values of the stepwise formation constants for the tetrachloro complex from spectrophotometric measurements. The latter study utilized the fact that the tetrachloro ion is the only complex absorbing in the wavelength range 610–690 nm for chloride concentrations higher than 5 M. Activity corrections were included semiquantitatively by means of a one-parameter function for the chloride ion activity, and using the concept of effective stepwise formation constants[2] it was shown that a common set of activity constants is valid for the complex equilibria in solutions of cobalt(II) in lithium chloride, calcium chloride and hydrochloric acid at high chloride ion concentrations ($C_{Cl^-} \gtrsim 5$ M).

Since the so-called effective stepwise formation constants are approximately equal to the true activity formation constants, they ought to be valid for any aqueous solution when combined with the appropriate activity function.

The chloro complex formation and the accompanying change in configuration of the complexes in cobalt(II) chloride solutions are strongly promoted by lowering the water activity.[2,3] In order to clarify this influence on the chloro complex formation and to prove the general validity of the effective stepwise formation constants, the stability constants in 10 M $H(Cl,ClO_4)$ medium were determined, in concentration terms, spectrophotometrically. In 10 M $HClO_4$ the water activity is less than 4 % of that in pure water.[4]

EXPERIMENTAL

Cobalt(II) hydroxide-carbonate from MERCK was dissolved in perchloric acid and cobalt(II) perchlorate was precipitated by addition of 70 % perchloric acid. The cobalt(II) perchlorate was dissolved in sufficient water and 70 % perchloric acid to give a perchloric acid concentration of 10.0 M. Cobalt(II)- and acid concentrations in the stock solutions were determined by standard complexometric and alkalimetric titrations, respectively. Perchloric acid and hydrochloric acid were of

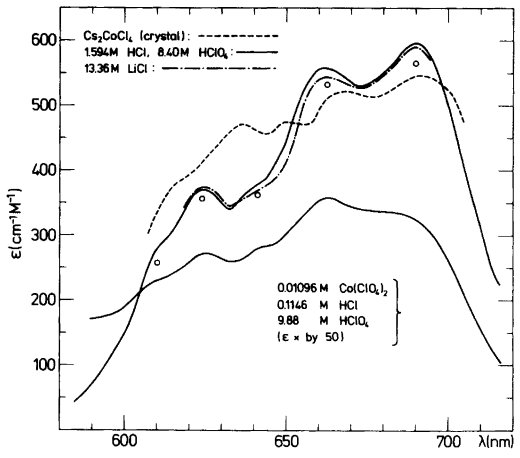

Fig. 1. Absorption spectra of $\sim 10^{-3}$ M Co(II) in 13.36 M LiCl[1] and in 1.594 M HCl plus 8.40 M $HClO_4$ compared with the solid state spectrum[5,6] of Cs_2CoCl_4 crystal (in arbitrary absorbance units). The O points indicate the molar absorptivities of the tetrachlorocobaltate(II) ion obtained from regression analysis at selected wavelengths; see text. The spectrum of 0.01096 M $Co(ClO_4)_2$ in 0.1146 M HCl + 9.88 M $HClO_4$ with the molar absorptivities multiplied by 50 is also shown.

analytical grade. The water used was doubly-distilled.

Densities were determined by weighing known volumes at 25 °C.

Spectrophotometric measurements were made on a Zeiss DMR 21 recording spectrophotometer using 1 and 5 cm cells thermostatted at 25.0 °C. Since the hydrogen-chloride vapour pressure over a 10.0 M acid solution is considerable, spectra were recorded immediately after mixing the solutions.

DETERMINATION OF STABILITY CONSTANTS

Formation of the tetrachlorocobaltate(II) ion is nearly complete in ≈ 13 M lithium chloride. As shown in Fig. 1, almost the same absorption spectrum is observed for a solution with hydrochloric and perchloric acid concentrations of 1.6 and 8.4 M, respectively. Fig. 1 also outlines the solid-state spectrum of Cs_2CoCl_4 which is known to contain tetrahedral tetrachlorocobaltate(II) ions. This spectrum (in arbitrary absorbance units[5,6]) displays the same characteristic absorption bands between 600 and 700 nm, although they are shifted ~ 5 nm towards longer wavelengths. It can thus be concluded that formation of the tetrachlorocobaltate(II) ion in 10.0 M $H(Cl,ClO_4)$ solutions is nearly complete at hydrochloric acid concentrations of around 1.6 M.

In order to determine the concentration stability constants in this medium, absorption spectra of a series of solutions of $Co(ClO_4)_2$ in 10.0 M $H(Cl,ClO_4)$ were recorded. One such spectrum is shown in Fig. 1. The hydrochloric acid concentration ranged from *ca.* 0.07 to *ca.* 0.9 M. To ensure a fair constancy of the ionic medium, higher concentrations were not included in the series. After correction for the absorption of the medium, the apparent molar absorptivities (ε_λ) at the wavelengths $\lambda = 610$, 624, 641, 662, and 690 nm were calculated for each solution.

The concentration stability constants in a constant salt medium are defined according to eqn. (1).

$$K_n = \frac{[CoCl_n^{2-n}]}{[CoCl_{n-1}^{3-n}][Cl^-]}, \text{ where } \beta_n = K_1 K_2 \ldots K_n \quad (1)$$

The following relationships are valid for each solution:

$$[Cl^-] = C_{HCl} - \sum_{n=1}^{4} n\beta_n [Co^{2+}][Cl^-]^n \quad (2)$$

$$[Co^{2+}] = C_{Co(ClO_4)_2} - \sum_{n=1}^{4} \beta_n [Co^{2+}][Cl^-]^n \quad (3)$$

$$\alpha_n = \frac{[CoCl_n^{2-n}]}{C_{Co(ClO_4)_2}} = \beta_n [Cl^-]^n \Big/ \sum_{n=0}^{4} \beta_n [Cl^-]^n \quad (4)$$

$$\varepsilon_\lambda = \sum_{n=0}^{4} \alpha_n \varepsilon_{\lambda,n} \quad (5)$$

The experiments determine ε_λ as a function of the total concentrations C_{HCl} and $C_{Co(ClO_4)_2}$. For a given set of stability constants, $[Cl^-]$ and $[Co^{2+}]$ were calculated from C_{HCl} and $C_{Co(ClO_4)_2}$ [eqns. (2) and (3)] by Newton-Raphson iteration. Within the framework of non-linear regression analysis, the following expression was minimized as a function of the stability constants and the molar absorptivities for the complexes:

$$\sum_{\lambda} \sum_{i} \frac{[\varepsilon_{\lambda,i}(\text{calc}) - \varepsilon_{\lambda,i}(\text{obs})]^2}{\sigma_{\lambda,i}^2}$$

where the index i refers to solution-numbers. The uncertainties σ_λ were assumed to be proportional to the observed $\varepsilon_{\lambda,i}$ values.

Attempts to calculate the four stability constants and the molar absorptivities for the five species present showed that further information or certain assumptions had to be introduced. The ambiguities which arise in such simultaneous calculation of absorptivities and stability constants have recently been discussed by the present authors.[7] A preliminary calculation was therefore made based on the assumption that only the tetrachlorocobaltate(II) ion absorbs in the wavelength range of interest, justifying the use of the simple relationship: $\alpha_4 = \varepsilon_\lambda/\varepsilon_{\lambda,4}$. The spectrum of Co(II) in 0.1146 M HCl, 9.88 M $HClO_4$ (multiplied by 50; see Fig. 1) shows that this assumption is not of general validity under the present conditions. Not only the intensity but also the shape (especially the ratio $\varepsilon_{690}/\varepsilon_{662}$) of the absorption band changes with increasing chloride ion concentration. However, these preliminary calculations showed clearly that the species $CoCl_2$ and $CoCl_3^-$ have a negligibly small range of existence. This seems to be even more pronounced in 10.0 M $H(Cl,ClO_4)$ than in lithium chloride solutions.[1] Calculations based on eqns. (1)–(5) confirmed the validity of this assumption, and in the final calculations the dichloro and trichloro complexes were not taken into account. Table 1 gives the observed absorptivities together with the values calculated from the final numerical treatment at the three wavelengths 641, 662 and 690 nm. The resulting estimates of the stability constants are: $\log K_1 = 1.34 \pm 0.11$ and $\log \beta_4 = 2.57 \pm 0.09$. The molar absorptivity of the tetrachloro complex (ε_4) for the 5 wavelengths (given in Fig. 1 and Table 3) was obtained by regression analysis of the data for each wavelength. The molar absorptivities of Co^{2+} and $CoCl^+$ appear, within the estimated uncertainties, to be equal to zero at these wavelengths.

DISCUSSION

Spectra of chlorocobalt(II) complexes. These near-infrared ligand field spectra are not significantly influenced by the medium. For example, it can be seen from Table 3 and Fig. 1 that changing the salt medium from 13.4 M LiCl to 1.6 M HCl in

Table 1. Observed and calculated molar absorptivities (in $cm^{-1}\ M^{-1}$) of Co(II) in 10.0 M $H(Cl,ClO_4)$ at 641, 662, and 690 nm.[a]

$C_{Co(ClO_4)_2}$	C_{HCl}	$[Cl^-]$	ε_{641} obs.	calc.	ε_{662} obs.	calc.	ε_{690} obs.	calc.
0.01147	0.0738	0.0669	1.52	1.50	1.78	1.77	1.45	1.46
0.01126	0.0905	0.0830	2.61	2.69	3.13	3.20	2.74	2.70
0.01096	0.1146	0.1064	5.57	5.56	7.14	7.04	6.48	6.39
0.01068	0.1374	0.1286	9.87	9.81	13.01	12.99	12.27	12.34
0.01059	0.1447	0.1357	11.56	11.53	15.51	15.43	14.64	14.81
0.01041	0.1590	0.1497	15.56	15.45	21.1	21.0	20.4	20.5
0.01016	0.1796	0.1697	23.1	22.4	31.6	31.0	30.8	30.7
0.00999	0.1928	0.1825	28.1	27.7	38.7	38.6	37.6	38.5
0.00968	0.218	0.207	40.1	39.6	55.7	55.8	54.9	56.2
0.00911	0.264	0.251	66.3	66.7	94.1	95.1	94.0	96.7
0.001526	0.361	0.358	144.0	147.3	208	212	210	217
0.001239	0.379	0.376	164.6	161.3	237	232	243	238
0.001526	0.397	0.393	176.0	173.9	250	251	254	257
0.001239	0.498	0.494	243	237	350	343	363	352
0.001239	0.548	0.544	261	261	376	377	394	388
0.001239	0.598	0.594	281	280	406	405	425	417
0.001239	0.647	0.643	291	295	424	427	444	439
0.001239	0.697	0.693	299	307	437	445	458	458
0.001239	0.796	0.791	317	325	463	471	491	485
0.001526	0.893	0.887	333	337	490	487	514	502

[a] ε(obs.) are apparent molar absorptivities based on the total Co(II) concentrations. ε(calc.) are calculated from the estimated stability constants and molar absorptivities for the complex ions; see text.

10.0 M $H(Cl,ClO_4)$ alters the molar absorptivities of $CoCl_4^{2-}$ by less than 3 %.

The molar absorptivities of $CoCl_4^{2-}$ calculated by regression analysis are as much as 6 % smaller than those measured directly in 10.0 M $H(Cl,ClO_4)$. This is only an apparent difference. It reflects accumulated errors from the rather lengthy extrapolation with $\alpha_4 \approx 0.90$ at the highest chloride ion concentration included in the final numerical treatment. A series of measurements on solutions with chloride ion concentrations varying up to 1.6 M was tentatively incorporated in the calculations. This treatment gave values for ε_λ which were a few percent higher but it was clear that the ionic medium had been changed too much to justify the use of the concentration constants defined according to eqn. (1).

The ratio $\varepsilon_{690}/\varepsilon_{625} \approx 1.55$ is constant in 7.0 M $Na(Cl,ClO_4)$ over a 1000-fold change in absorption, indicating that one species, the tetrachloro complex, is mainly responsible for the absorption in this wavelength range.[8] Almost the same value for this ratio is calculated from the limiting spectra measured with the other salt media quoted in Table 3, except for the spectrum in 9.0 M $H(Cl,ClO_4)$ reported by Belousov *et al.*[3]

Chloride ion activity. The overall effective formation constant determined previously[1] is assumed to approximate to the true activity constant:

$$\beta_4^* = \frac{[CoCl_4^{2-}]}{[Co^{2+}]\, a_{Cl^-}^4} \approx \frac{a_{CoCl_4^{2-}}}{a_{Co^{2+}}\, a_{Cl^-}^4}$$

By combining β_4^* ($= 10^{-6.62}$) with the concentration constant β_4 ($= 10^{2.57}$) valid in 10.0 M $H(Cl,ClO_4)$ it is possible to estimate the effective activity coefficient based on molar concentrations for the chloride ion in this actual medium:

$$\gamma_{Cl^-}^C = \sqrt[4]{\beta_4/\beta_4^*} \approx 200,$$

and it is satisfying that a similar estimate using the values for K_1 and K_1^* (see Table 2) leads to a value of the same order of magnitude.

A linear relationship between $\log \gamma_\pm^m$ and molality of an electrolyte in binary electrolyte mixtures at constant total molality is known as Harned's rule.[9] For γ_{HCl}^m (the mean activity coefficient based on molal concentrations) in an $H(Cl,ClO_4)$ medium this rule can be formulated as eqn. (6).

$$\log \gamma_{HCl}^m = \log \gamma_{HCl}^{m,o} - \varkappa_{HCl}\, m_{HClO_4} \qquad (6)$$

Table 2. Comparison of stability constants for the cobalt(II) chloride system.

Medium	$\log K_1$	$\log K_2$	$\log K_3$	$\log K_4$	$\log \beta_4$
10.0 M $H(Cl,ClO_4)$[a]	1.34±0.11				2.57±0.09
10.0 M $H(Cl,ClO_4)$[b]	0.82±0.09	0.44	0.35	−0.17	1.43±0.22
$LiCl-H_2O$[c]	−1.05±0.38	−2.69±0.90	−1.54±0.89	−1.34±0.13	−6.62±0.24

[a] This paper. Constants based on concentrations. [b] Belousov *et al.*[3] Constants based on concentrations. [c] Bjerrum *et al.*[1] Constants are effective constants, denoted in the text by an asterisk.

Table 3. Molar absorptivities of $CoCl_4^{2-}$ in $cm^{-1}\ M^{-1}$ at 25 °C.

Medium	ε_{610}	ε_{624}	ε_{641}	ε_{662}	ε_{690}	$\varepsilon_{690}/\varepsilon_{624}$
$LiCl-H_2O$[a]	279	380	372	550	600	1.58
$HCl-H_2O$[a]	279	380	380	560	610	1.61
1.59 M HCl, 8.40 M $HClO_4$	277	370	378	557	597	1.61
10.0 M $H(Cl,ClO_4)$[b]	258±5	356±5	362±4	532±5	564±6	1.58
7.0 M $Na(Cl,ClO_4)$[c]						1.55[c]
9.0 M $H(Cl,ClO_4)$[d]		180[d]			615	3.42[d]

[a] Extrapolated from data for solutions saturated with LiCl and HCl, respectively; see Ref. 1. [b] Calculated by non-linear regression; see text. [c] From Ref. 8, ratio $\varepsilon_{690}/\varepsilon_{625}$. [d] From Ref. 3, ratio $\varepsilon_{690}/\varepsilon_{623}$.

where $\gamma^{m,o}_{HCl}$ is the activity coefficient for HCl in pure hydrochloric acid at the molality in question. $\varkappa_{HCl}$ denotes the Harned coefficient. 10.0 M $HClO_4$ has a density of 1.575 and a molality m of 17.5. The activity coefficient of HCl in 17.5 m $HClO_4$ is not known, but $\gamma^{C}_{Cl^-} \approx 200$ (corresponding to $\gamma^{m}_{HCl} \approx 200/1.75 = 114$) seems to be a reasonable assumption. From data in the literature[10] it can be estimated that $\gamma^{m,o}_{HCl} \approx 60$ in 17.5 m HCl. When these values for γ^{m}_{HCl} and $\gamma^{m,o}_{HCl}$ together with $m_{HClO_4} = 17.5$ are inserted in (6), $\varkappa_{HCl}$ is calculated to be -0.016. For comparison it can be mentioned that Harned's rule is known to be approximately valid in 1.0 m H(Cl,ClO_4), where $\varkappa_{HCl} \approx -0.020$.[11]

The remarkable increase in the stability of the tetrachlorocobaltate(II) ion which is observed can therefore be accounted for entirely by the dramatic change in the activity of the chloride ion. Fig. 2 shows the molar absorptivity of Co(II) at 624 nm as a function of increasing chloride ion activity. The curve is calculated from the effective constants and the molar absorptivity of the tetrachlorocobaltate-(II) ion. The measurements in lithium chloride and

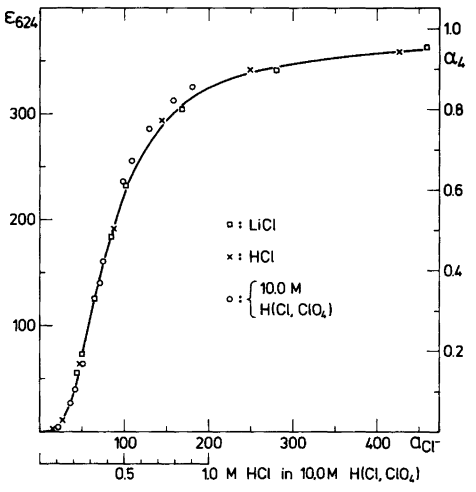

Fig. 2. The molar absorptivity of Co(II) at 624 nm as a function of chloride ion activity. The curve is calculated from the effective formation constants (see Table 2) and the molar absorptivity of $CoCl_4^{2-}$. The values for LiCl and HCl are from Ref. 1 and the chloride ion activity is calculated to be $a_{Cl^-} = [Cl^-] \times 10^{B[Cl^-]-0.5}$, with $B = 0.170$ and $B = 0.185$ in the case of LiCl and HCl, respectively. The measurement in 10.0 M H(Cl,ClO_4) is from the present investigation, and the chloride activity is calculated to be $a_{Cl^-} = 200[Cl^-]$.

in hydrochloric acid solutions are seen to follow this curve. With the estimated value of $\gamma^{C}_{Cl^-} \approx 200$ in 10.0 M H(Cl,ClO_4), the experimental absorptivities in this medium lie close to this same curve. This indicates the general validity of the effective formation constants.

Intermediate complexes. Smithson and Williams[8] showed the existence of $CoCl^+$ and $CoCl_4^{2-}$ species in 7.0 M Na(Cl,ClO_4) spectrophotometrically but found no intermediate complexes. The same conclusion can be drawn from the present calculations based on the measurement of the absorbance of Co(II) in 10.0 M H(Cl,ClO_4). In the previous investigation[1] of chlorocobalt(II) complex formation in lithium chloride solutions it was shown that the dichloro and trichloro complexes have a very small range of existence, and the calculated values for K_2^* and K_3^* were only crude estimates. The principal conclusion to be drawn concerning these two species, however, is that they can normally be neglected in calculations relating to aqueous solutions.

The above results contrast with the rather large range of existence for the dichloro and trichloro complexes which is predicted by the constants determined by Belousov *et al.*[3] in 10.0 M H(Cl,ClO_4) and the latter values are undoubtedly incorrect for aqueous solutions. However, a complex distribution of the type predicted by Belousov *et al.*[3] is observed in non-aqueous solvents such as acetic acid.[12] In acetone[13] and dimethyl sulfoxide[14] the dominant species have been shown to be $CoCl_3^-$ and $CoCl_4^{2-}$. These solvents have lower solvating power toward Co(II), and in addition to the different complex distribution a much stronger complex formation is found. In aqueous solution the entirely different distribution, with $CoCl^+$ and $CoCl_4^{2-}$ as the dominant complexes, does not seem to be significantly influenced by the bulk of electrolyte present.

Acknowledgement. The authors are most grateful to Ole Mønsted for helpful advice concerning the computer calculations and to Martin Hancock for revising the English manuscript.

REFERENCES

1. Bjerrum, J., Halonin, A. S. and Skibsted, L. H. *Acta Chem. Scand. A 29* (1975) 326.
2. Marcus, Y. *Rec. Chem. Prog. 27* (1966) 105.
3. Belousov, E. A., Bocharow, V. V. and Mironov, V. E. *Russ. J. Inorg. Chem. 17* (1972) 1717.

4. Jones, K. M. and Bjerrum, J. *Acta Chem. Scand. 19* (1965) 974.
5. Smith, H. W. and Stratton, W. J. *Inorg. Chem. 16* (1977) 1640.
6. Ferguson, J. *J. Chem. Phys. 39* (1963) 116.
7. Bjerrum, J. and Skibsted, L. H. *Acta Chem. Scand. A 31* (1977) 673.
8. Smithson, J. M. and Williams, R. J. P. *J. Chem. Soc.* (1958) 457.
9. Robinson, R. A. and Stokes, R. H. *Electrolyte Solutions*, 2nd. Ed., Butterworths, London 1959, p. 438.
10. Robinson, R. A. and Stokes, R. H. *Trans. Faraday Soc. 45* (1949) 612.
11. Murdock, P. G. and Barton, R. C. *J. Am. Chem. Soc. 54* (1932) 4480.
12. Sawada, K. and Tanaka, M. *J. Inorg. Nucl. Chem. 36* (1974) 1971.
13. Carunchio, V., Ceipidor, U. B. and Messina, A. *Inorg. Chim. Acta 6* (1972) 613.
14. Magnell, K. R. and Reynolds, W. L. *Inorg. Chim. Acta 6* (1972) 571.

Received December 23, 1977.

Acta Chemica Scandinavica A 32 (1978) 435–438

The Complex Formation of H^+, Cd^{2+} and Pb^{2+} with the Benzoate, Phthalate and Isophthalate Ions

ÅKE OLIN and PÄR SVANSTRÖM

Institute of Chemistry, University of Uppsala, P.O.B. 531, S-751 21 Uppsala, Sweden

By potentiometric measurements with an amalgam electrode the stability constants for the formation of H^+, Cd^{2+} and Pb^{2+} complexes with benzoate, phthalate and isophthalate ions have been determined in 1 M $Na(ClO_4)$ at 25 °C. Stability constants for the formation of BA, BA_2, BHA and B(HA)A are reported.

The complex formation of Cd^{2+} and Pb^{2+} (=B) with the phthalate and isophthalate ligands (=A) has been studied by Jain, Kumar and Gaur[1,2] using the polarographic technique. The formation of BA, BA_2 and BA_3 was reported. The numerical values of the stability constants are, however, somewhat unexpected. Thus the stabilities of the Pb^{2+} and Cd^{2+} complexes were found to be quite close, whereas in general Cd(II)–carboxylate complexes are substantially weaker than the lead(II) complexes.[3] Also the stabilities of the PbA complexes were reported to be smaller than the corresponding benzoate complex. It was therefore considered appropriate to re-investigate these systems and at the same time extend the pH range so that the formation of protonated complexes would be detected. Due to its low solubility it was not possible to include terephthalic acid in the measurements.

EXPERIMENTAL

Potentiometric measurements. The experiments have been carried out as potentiometric titrations at 25.0 °C in a 1 M $Na(ClO_4)$ medium using an automatic titrator. In general the ligand was added as a buffer with a constant quotient between the total concentration of H^+, H and the total concentration of carboxylic acid, A. The free hydrogen ion concentration, h, was measured with the cell

(−) Glass | Equilibrium solution | Ref (+) (I)

$$E_g = E_g^\circ - 59.16\,(\text{mV})\log(h/\text{M}) - E_j \quad (1)$$

and the concentration of the uncomplexed metal ion, b, with the cell

(−) B(Hg) | Equilibrium solution | Ref (+) (II)

$$E_B = E_B^\circ - 29.58\,(\text{mV})\log(b/\text{M}) - E_j \quad (2)$$

The liquid junction potential, E_j, can be expressed by

$$E_j = kh + l[H_2A] + m[HA^-] + na;\ (a = [A^{2-}]) \quad (3)$$

where k, l, m and n are constants. E_j was determined from titrations with buffers as described previously.[4] The quantity so determined will contain contributions from the "true" liquid junction potential, activity coefficient changes and dimerisation reactions in the buffer.[5]

Chemicals and analysis. Benzoic acid (Fluka *p.a.*) was recrystallized from water and the formula weight as determined by alkalimetric titration was 121.1 (calc. 121.1). *Sodium benzoate* (Merck *zur Analyse*) was used as received. *4-Hydroxybenzoic acid* (Fluka *puriss.*), formula weight 138.3 (calc. 138.1) was used without further purification. *Phthalic acid* (Fluka *p.a.*). The formula weight was found to be 166.3 (calc. 166.1). *Isophthalic acid* (Fluka *purum*) was purified by repeated recrystallizations from water after treatment with charcoal. The formula weight of the final product was 166.5 (calc. 166.1).

Cadmium perchlorate was prepared by dissolving CdO in a small excess of $HClO_4$. The oxide was prepared from the nitrate (Merck *zur Analyse*) as described by Biedermann and Ciavatta.[6] The cadmium content of the stock solution was determined gravimetrically as $CdNH_4PO_4H_2O$[7] and

as $CdSO_4$ after evaporation with H_2SO_4. The results agreed within 0.1 %. The analytical hydrogen ion concentration was determined by potentiometric titrations with $HClO_4$ and the equivalence point was found from Gran plots.

The cadmium amalgam electrode was prepared by dissolving cadmium metal in mercury (Kebo redist.). The cadmium metal, electrolytically prepared,[8] was a gift from Professor F. Nydahl. The cadmium concentration in the amalgam was 0.1 % (weight) and the electrode was stable within ± 0.02 mV for at least 12 h at a total metal ion concentration of 5×10^{-4} M or more. The preparation and analysis of the other chemicals used have been described earlier.[4]

RESULTS AND CALCULATIONS

In the complexation of the metal (B) HA^- and A^{2-} can be regarded as the ligands. The stability constants will then be defined by

$$B + sHA + tA \rightleftharpoons B(HA)_sA_t$$
$$\beta_{s,t} = [B(HA)_sA_t]\, b^{-1}[HA]^{-s}a^{-t} \quad (4)$$

since it will be shown that only mononuclear complexes are formed. It is sometimes more convenient to write the above reaction with H^+, B, and A^{2-} as components

$$pH + qB + rA \rightleftharpoons H_pB_qA_r \; (q=1)$$
$$\beta_{pqr} = [H_pB_qA_r]h^{-p}b^{-q}a^{-r} \quad (5)$$

With $q=0$ eqn. (5) includes the proton complexes of A^{2-}.

The preliminary analysis of the titration data was made graphically by studying $(B/b-1)/a$ as a function of a at different values of the buffer quotient $\emptyset = [HA]/a$. The details of this treatment are presented in Ref. 9. For the final calculation of the stability constants the least-squares program Letagrop Vrid, version Etitr[10] was used.

The small solubilities of the lead(II) carboxylates did not allow studies of metal in concentrations higher than about 1×10^{-3} M. A lower limit is set by the amalgam electrode which does not work satisfactorily for total metal ion concentrations below 2×10^{-4} M. The lead(II) benzoate and phthalate systems were measured at $0.2 < B/\text{mM} < 0.5$. Even then the solutions appear to be supersaturated. The exchange of the perchlorate ions of the medium by the ligands is generally less than 10 %. When the solubility of H_2A was sufficient the measurements were, however, extended to $[A^{2-}] = 0.1$ M.

The proton carboxylate systems

The proton–benzoate system. This system was investigated in the range $0.01 < \bar{n} < 0.91$ at a total benzoate concentration of 0.010 M. $\bar{n}$ is the average number of protons bound per A. The liquid junction potential for the exchange of ClO_4^- by A^-, E_{j,A^-}, was determined in a buffer with $[HA]/a = 0.05$ and found to be $E_{j,A^-} = -25.4a$ mV M^{-1}. This is a rather large value in comparison with $E_j \approx -8a$ estimated from the Henderson equation. By the method of Farrer and Rossotti[11] the expression for E_j was found to be $E_{j,FR} = 6.8[HA] - 9.5a$. The coefficient for HA was found from measurements on 4-hydroxybenzoic acid, which has a higher solubility than benzoic acid.

Using $E_{j,FR}$ as correction in eqn. (1), the large value of the coefficient in E_{j,A^-} can be accounted for by assuming an association between HA and A^-. The least-squares treatment of the data yielded $\beta_{101} = (1.068 \pm 0.001) \times 10^4$ M^{-1}. The quoted error here and in the following is equal to three standard deviations. The value of $\beta_{102} = 8.5 \times 10^3$ M^{-2} should be regarded as an estimate since the constant is calculated from measurements on only one buffer.

The proton–phthalate system. The stability constants were determined from measurements at $A = 0.010$ and 0.020 M in the range $0.05 < \bar{n} < 1.75$. The liquid junction potentials in buffers with $H/A = 0.13$, 0.33, 0.50, 0.67, 0.99 and 1.5 could be expressed by $E_j = 1.3[H_2A] - 25.5[HA^-] - 26.3a$. The coefficient for $[HA^-]$ is large and indicates association reactions. In order to find the stability constants for these reactions $E_{j,FR} = 6.8[H_2A] - 9.5[HA^-] - 25a$ was used. The coefficients for $[H_2A]$ and $[HA^-]$ were taken from the benzoate system and the factor for a was determined with the phthalate ion. The following constants were obtained; $\beta_{101} = (4.729 \pm 0.011) \times 10^4$ M^{-1}; $\beta_{201} = (2.303 \pm 0.007) \times 10^7$ M^{-2}; $\beta_{202} = (5.74 \pm 0.19) \times 10^8$ M^{-3}; $\beta_{302} = (1.31 \pm 0.08) \times 10^{12}$ M^{-4}; $\beta_{402} = (5.1 \pm 0.7) \times 10^{14}$ M^{-5}. The β_{101} and β_{201} values are close to those reported by Lumme *et al.*[12]

The proton–isophthalate system. Due to the low solubility of isophthalic acid the $\bar{n}$ range has been limited to values less than 0.6 at $A = 6 \times 10^{-3}$ M. A solution of the acid was neutralized to $\bar{n} = 0.05$ and then titrated with dilute $HClO_4$ until a per-

Table 1. Stability constants of Pb(II) and Cd(II) benzoate, phthalate and isophthalate complexes in 1 M $NaClO_4$ at 25 °C. The figures within parentheses are three times the estimated standard deviations.

System	$\beta_{011} \times 10^{-2}$ M^{-1}	$\beta_{012} \times 10^{-3}$ M^{-2}	$\beta_{111} \times 10^{-5}$ M^{-2}	$\beta_{112} \times 10^{-7}$ M^{-3}	$\beta_{1,0}$ M^{-1}	$\beta_{1,1} \times 10^{-3}$ M^{-2}
Pb(II) – benzoate	0.738(0.006)	0.778(0.011)				
Cd(II) – benzoate	0.102(0.001)	0.0449(0.0002)				
Pb(II) – phthalate (1)	5.95(0.03)	10.7(0.3)	8.32(0.09)	10.4(0.5)	17.6	2.2
Pb(II) – phthalate (2)	6.01(0.02)	10.2(0.2)	6.90(0.05)	6.0(0.3)	14.6	1.3
Cd(II) – phthalate (1)	0.722(0.003)	0.792(0.006)	2.31(0.02)	0.92(0.04)	4.9	0.2
Cd(II) – phthalate (2)	0.733(0.004)	0.755(0.008)	1.42(0.03)	0.30(0.05)	3.0	0.06
Pb(II) – isophthalate	1.464(0.007)	2.27(0.02)	8.8(0.4)	1.7(0.5)	60.3	1.2
Cd(II) – isophthalate	0.213(0.001)	0.149(0.001)	0.96(0.05)	–	6.6	–

manent precipitate was formed. The constants obtained were; $\beta_{101} = (1.46 \pm 0.02) \times 10^4$ M^{-1}; $\beta_{201} = (3.7 \pm 0.2) \times 10^7$ M^{-2}. No attempt was made to identify dimeric species in this system.

The metal carboxylate systems

The Cd^{2+} – and Pb^{2+} – benzoate systems. The results from titrations to $A = 0.1$ M with a buffer having $[HA]/a = 0.05$ can be explained by the formation of BA and BA_2. The discussion in Ref. 5, where the results are presented in more detail, suggests that the E_j correction proposed by Farrer and Rossotti leads to the best estimate of the stability constants. The β values so calculated are given in Table 1. The experimental data from the cadmium-benzoate system presented by Vartak and Shetiya[13] are in good agreement with our results. The numerical values of the equilibrium constants differ from our values since they have been calculated with $E_j = 0$.

The Pb^{2+} – phthalate system. The measurements were carried out with $0.25 < B/\text{mM} < 0.5$ in the buffers (H/A, A_{max}/M); 0.11, 0.017; 0.21, 0.023; 0.55, 0.022; 0.86, 0.022; 0.96, 0.067; 1.63, 0.041. The highest value of A reached during a titration is denoted by A_{max}. The concentration ranges are limited by the solubilities of phthalic acid and lead phthalate. The experimental data can be explained by the formation of PbA, PbA_2, Pb(HA), and Pb(HA)A. In Table 1, two sets of stability constants are given (1) on the assumption that dimeric species are formed and thus $E_{j,FR}$ is valid and (2) that the E_j coefficients found from buffers are measures of activity changes and "true" liquid junction potentials. In both cases $\sigma(E_{Pb})$ is 0.02 – 0.04 mV.

The Cd^{2+} – phthalate system. The experiments were carried out with $B = 1.0 \times 10^{-3}$ M and the buffers (H/A, A_{max}/M); 0.14, 0.11; 0.51, 0.074; 0.99, 0.12; 1.35, 0.075. A model including the complexes CdA, CdA_2, Cd(HA), and Cd(HA)A gave the smallest value of $\sigma(E_{Cd}) = 0.03 - 0.04$ mV for both assumptions on E_j presented above. The constants are given in Table 1.

The Pb^{2+} – isophthalate system. Titrations were performed with $B = 1.0 \times 10^{-3}$ M and the buffers (H/A, A_{max}/M); 0.05, 0.106; 0.25, 0.024; 0.35, 0.015. Again the data could be explained by the formation of PbA, PbA_2, Pb(HA) and Pb(HA)A. The inclusion of Pb(HA)A lowers the value of $\sigma(E_{Pb})$ from 0.05 mV to 0.02 mV. The constants are given in Table 1.

The Cd^{2+} – isophthalate system. Measurements carried out at $B = 1.0 \times 10^{-3}$ M in the buffers (H/A, A_{max}/M); 0.05, 0.10; 0.31, 0.020 are well explained by the formation of the complexes CdA, CdA_2, and Cd(HA). $\sigma(E_{Cd})$ was 0.02 mV and the constants are given in Table 1.

DISCUSSION

The formation of the complexes BA and BA_2 is well established. No evidence for BA_3, reported by Kumar *et al.*,[2] was found at the ligand concentrations (< 0.1 M) studied here. The constants determined by them in 2 M $NaClO_4$ and 30 °C are in disagreement with our values, particularly for Pb^{2+}. $\beta_{011} = 65$ and 52.5 M^{-1} for the phthalate and isophthalate complex, respectively, are remarkably small. They are even smaller than the constant for the benzoate complex, $\beta_{011} = 70$ M^{-1}, determined by the same authors.[1] This value is in agreement with our results.

The formation of protonated complexes in these systems has not been reported earlier but is in accordance with findings for other dicarboxylic

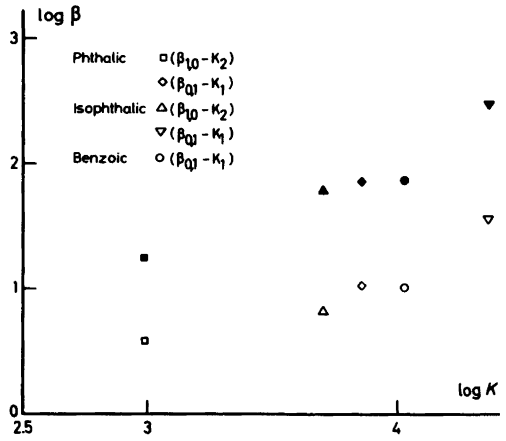

Fig. 1. Statistically corrected stability constants for the metal complexes (mean values from Table 1) plotted *versus* the corresponding constants for the proton complexes. Filled symbols are used for Pb(II). The data on which the points are based are indicated in the figure.

acids.[9] The variation of $\beta_{1,1}$ with the nature of the complex forming system indicates that the evidence for B(HA)A is real and not caused by an erroneous E_j, since the same expression for E_j has been used in the two systems. The numerical values of $\beta_{1,1}$ and $\beta_{1,0}$ are, however, very sensitive to the choice of E_j as can be seen from Table 1.

Fig. 1 shows the correlation between lg $\beta_{1,0}$ and lg $(2K_2)$, and lg $(\beta_{0,1}/2)$ and lg $(K_1/2)$, *i.e.* statistically corrected constants have been used. For structurally related complexes such correlations are often found to be linear. Then it may be inferred that the phthalate complexes have an extra stability which indicates that this ligand acts bidentately forming a seven-membered ring. A ring of the same size can be formed by succinic acid, but a plot similar to that in Fig. 1 indicates that this ligand is essentially non-chelating. The difference in behaviour could be caused by the greater rigidity of the aromatic ligand.

REFERENCES

1. Jain, D. S., Kumar, A. and Gaur, J. N. *J. Polarogr. Soc. 13* (1967) 120.
2. Kumar, A. and Gaur, J. N. *Electroanal. Chem. 49* (1974) 317.
3. Yasuda, M., Yamasaki, K. and Ohtaki, H. *Bull. Chem. Soc. Jpn. 33* (1960) 1067.
4. Olin, Å. and Svanström, P. *Acta Chem. Scand. A 29* (1975) 849.
5. Olin, Å. and Svanström, P. *Acta Chem. Scand. A 32* (1978) 283.
6. Biedermann, G. and Ciavatta, L. *Acta Chem. Scand. 16* (1962) 2221.
7. Vogel, A. I. *A Textbook of Quantitative Inorganic Analysis*, Longmans, London 1951.
8. Nydahl, F. *Talanta 21* (1974) 1259.
9. Olin, Å. and Svanström, P. *Acta Chem. Scand. A 31* (1977) 384.
10. Brauner, P., Sillén, L. G. and Whiteker, R. *Ark. Kemi 31* (1969) 365.
11. Farrer, H. N. and Rossotti, F. J. C. *Acta Chem. Scand. 17* (1963) 1824.
12. Lumme, P. and Esko, K. *Acta Chem. Scand. A 29* (1975) 117.
13. Vartak, D. G. and Shetiya, R. S. *Indian J. Chem. 3* (1965) 533.

Received January 6, 1978.

Acta Chemica Scandinavica A 32 (1978) 439–446

Multicomponent Polyanions. 18. A Neutron Diffraction Study of $Na_3Mo_9PO_{31}(OH_2)_3.12—13H_2O$, a Compound Containing 9-Molybdomonophosphate Anions with Molybdenum-coordinated Water Molecules*

BRITT HEDMAN

Department of Inorganic Chemistry, University of Umeå, S-901 87 Umeå, Sweden

A single crystal neutron diffraction study of $Na_3Mo_9PO_{31}(OH_2)_3.12-13H_2O$ has been made. Full-matrix least-squares refinements based on 1175 independent reflexions resulted in an *R*-value of 0.091. The structure contains the $Mo_9PO_{31}(OH_2)_3^{3-}$ anion, which is an end member in a proton-series of 9:1-molybdophosphates.

The results of the investigation show that the hydrogen atoms are attached in pairs to Mo-coordinated oxygens of the heteropolyanion. Thus three Mo atoms formally coordinate one water molecule each. This arrangement excludes the possibility of the presence of H_3O^+ in the structure. The other members of the proton-series are obtained by step-wise emission of one hydrogen per water molecule.

The anions are held together in a three-dimensional framework by hydrogen bonds involving anion and water hydrogen atoms and by O–Na–O links. Large diameter channels along 0,0,*z* penetrate the framework. These channels are filled with water molecules, most of which are non-structural, giving the crystal a zeolitic character. The hydrogen bonding within the framework is described, and the partly occupied positions found for the water in the channels are given. The total amount of water located accounts for approximately 5 of the 12 to 13 H_2O indicated by the formula.

Aqueous equilibrium studies of the $H^+ - MoO_4^{2-} - HPO_4^{2-}$ system have shown that $(H^+)_p(MoO_4^{2-})_q(HPO_4^{2-})_r$ complexes are formed. In solutions with $[MoO_4^{2-}]/[HPO_4^{2-}] \sim 9$ a series of complexes with composition (*p*,9,1), where $p = 14$, 15, 16 and 17, dominates.[1,2] In crystallization experiments performed parallel with the equilibrium studies only one crystalline (*p*,9,1) phase was obtained, $Na_3H_6Mo_9PO_{34}(H_2O)_{12-13}$. This phase, corresponding to the (17,9,1) complex, was investigated by X-ray methods.[3] The structure was shown to consist of 9-molybdomonophosphate anions connected by Na^+ ions. No water molecules could be located with certainty.

In the X-ray investigation, three of the Mo–O distances (crystallographically equivalent) were found to be extremely long, 2.21(1)* Å, for a terminal O atom, *i.e.* an atom coordinated to only one Mo atom (expected value 1.69 – 1.73 Å[4,5]). The oxygens were therefore assumed to be protonized with the six hydrogens in the formula situated either as two H^+ on each of the three oxygens, or as one H^+ on each of the three oxygens and the remaining H^+ as H_3O^+ ions within the structure. The existence of six H_3O^+ was considered unlikely.

For proton-series of hetero- and isopolyanions of this kind, the presence of oxonium ions has often been assumed, *e.g.* in $H_3Mo_{12}PO_{40}(H_2O)_{29-31}$ (broad-line ^1H NMR spectra,[6] single crystal X-ray diffraction[7]). Recently $H_5O_2^+$ ions were located in a neutron diffraction study of $H_3W_{12}PO_{40}(H_2O)_6$.[8]

* A preliminary report of this work was presented at the ECM-4, Oxford, 1977 (PII.81).

* Throughout this paper, numbers in parentheses represent the estimated standard deviation and refer to the last decimal place.

However, hydrogens have also been found attached to the anions, for example those attached to O atoms shared between Mo and Cr in $Na_3CrMo_6O_{24}H_6 \cdot 8H_2O$[9] or to O atoms coordinated to P in $Na_4H_2Mo_5P_2O_{23}(H_2O)_{10}$.[4]

The present neutron diffraction study was undertaken primarily to determine the positions of the six hydrogens in "$H_6Mo_9PO_{34}^{3-}$" in an attempt to understand how deprotonation occurs when p changes from 17 to 14 in the proton-series. An additional aim of the study was to investigate to what extent the crystal water is ordered or present in a non-structural way in channels. An independent X-ray structure determination of this crystalline phase has been reported,[10,11] but no further information on the hydrogens or crystal water was obtained.

CRYSTAL DATA[3]

$Na_3Mo_9PO_{31}(OH_2)_3 \cdot xH_2O$, $x = 12-13$: F.W. = 1729.6 ($x=12$), space group $P6_3$ (No. 173), $a = 14.248(1)$ Å, $c = 10.83(1)$ Å, $V = 1904.0$ Å^3, $Z = 2$, $D_m = 3.038(3)$ g cm^{-3}, $D_x = 3.02$ ($x=12$); 3.05 ($x=13$) g cm^{-3}, μ(neutrons) = 0.85 cm^{-1} (determined experimentally).

EXPERIMENTAL

Yellowish single crystals with a hexagonal prismatic form were grown from an aqueous solution by slow evaporation at room temperature. The composition of the solution was as reported previously[3] except that an addition of 10 % ethanol was made in order to avoid the initial formation of a large number of small crystals. The crystal used in the data collection had six boundary faces of the form $\{10\bar{1}0\}$. It was bounded at one end by a small cap and at the other by a rough face which were approximated to $(000\bar{1})$ and (0001), respectively. The crystal volume was 10.3 mm^3. The crystal was sealed in a thin-walled quartz glass tube to prevent it from losing water.

The neutron diffraction data were collected at the Swedish Atomic Energy R2 reactor in Studsvik, using a computer-controlled Hilger & Watts four-circle diffractometer at ~20 °C. The experimental arrangement has been described previously.[12] The flux at the specimen was 1.26×10^6 n cm^{-2} s^{-1} and the wavelength 1.210 Å. Reflexions with all three indices ≥ 0 (1/12 of reciprocal space) and out to $(\sin\theta)/\lambda = 0.693$ Å^{-1} were measured using an $\omega - 2\theta$ step-scan technique. The fluctuations observed in the intensities of the three standard reflexions monitored at regular intervals throughout the data collection were random and negligible. The values of I and $\sigma_o(I)$ (calculation based on counting statistics) were corrected for Lorentz and absorption effects. The linear absorption coefficient, μ, was determined experimentally to be 0.85 cm^{-1}, which corresponds to a value of 26 barns for the incoherent scattering cross-section for hydrogen. The transmission factor varied from 0.83 to 0.88. Of the 2253 reflexions measured in all, 1862 were unique. Of these, only 1175 reflexions had $F_o^2 \geq 2\sigma_c(F_o^2)$ and 956 reflexions had $F_o^2 \geq 3\sigma_c(F_o^2)$. This may be attributed to the high level of background caused by the large incoherent scattering contribution from the hydrogen atoms.

STRUCTURE REFINEMENT

A three-dimensional difference Fourier synthesis based on the anion Mo, P and O parameters obtained in the X-ray study revealed the positions of the anion H atoms, the Na^+ ion and the water O atoms O(Aq1) and O(Aq2), (Figs. 3, 4). In a difference Fourier synthesis with these atoms included, two rather weak minima around each of O(Aq1) and O(Aq2) were interpreted as hydrogens. They were included in the refinement, one at a time, and each caused a significant improvement seen as a reduction in the R-value.[13,14] Unusually high temperature factors and comparatively low amplitudes of the difference Fourier maxima/minima for all atoms in these two water molecules indicated partial vacancies, and the occupancy factors were therefore refined. During the refinements, the hydrogens approached the O position even when the H occupancy factor was varied separately from the O factor. Since the geometries of the water molecules and the bonding situation around them as given from the Fourier synthesis were considered quite reasonable, the H atoms were constrained to give the O–H distances and H–O–H angles found in the synthesis. The H temperature factors were in each molecule constrained to the same values as those for the O atom.

Two additional, partly occupied water O positions were located in the Fourier maps, but their H atoms could not be found. These O atoms were included with isotropic temperature factors. In all, the water found accounts for ~5 of the 12–13 crystal water molecules indicated by water analysis and density measurements.[3] The effect of the remaining non-structural water on the intensities

and, hence, on the positional and thermal parameters is difficult to estimate. The largest discrepancies between F_o and F_c were found for weak reflexions and for reflexions at high (sin θ)/λ. Therefore, no comparison will be made between the positional and thermal parameters obtained in the X-ray structure investigation and those obtained in the neutron refinements.

The structure was refined using full-matrix least-squares methods minimizing the function $\Sigma w_i(|F_o|-|F_c|)^2$. Due to the low core memory capacity of the computer, the final refinements were divided into two extensively overlapping blocks. A weighting scheme was applied in which the weights were modified according to $w^{-1}=\sigma^2(F_o)+(0.04F_o)^2$. The presence of extinction was tested both by inclusion of one isotropic extinction parameter and by inclusion of six anisotropic (type I or II) extinction parameters in the refinements *ad modum* Coppens and Hamilton,[15] but no indication of extinction effects was discovered. Final refinements based on the 1175 reflexions with $F_o^2 \geq 2\sigma_c(F_o^2)$ converged with R-values $R=\Sigma||F_o|-|F_c||/\Sigma|F_o|=0.091$ and $R_w=[\Sigma w_i(|F_o|-|F_c|)^2/\Sigma w_i|F_o|^2]^{1/2}=0.100$. The R-value based on reflexions with $F_o^2 \geq 3\sigma_c(F_o^2)$ is 0.079. In the final cycle the parameter shifts were less than 0.1σ.

The coherent scattering amplitudes used were $\bar{b}_{Mo}=0.660$, $\bar{b}_P=0.510$, $\bar{b}_O=0.575$, $\bar{b}_{Na}=0.351$ and $\bar{b}_H=-0.372$ (10^{-12} cm).[16] Data reduction was performed with the programs STUKC and DATAPH on the IBM 1800 and IBM 370/155 computers at the University of Uppsala.[17] All other computations were made with previously described programs[18] on the CD 3300 and CD CYBER 172 computers at the University of Umeå. Final atomic positional and thermal parameters are presented in Table 1. A list of observed and calculated structure factors may be obtained from the author on request.

DESCRIPTION AND DISCUSSION OF THE STRUCTURE

The $Mo_9PO_{31}(OH_2)_3^{3-}$ anion. The anion is shown in Figs. 1 and 2, and a detailed description of the arrangement of the Mo, P and O atoms may be found in Ref. 3. With the exception of a few minor individual discrepancies, the dimensions of the

Table 1. Fractional atomic coordinates ($\times 10^4$), occupancy factors (for statistically disordered atoms), anisotropic thermal parameters ($\times 10^4$) and, for two water oxygens, isotropic temperature factors (Å^2). The expression for the anisotropic temperature factor is $\exp[-(\beta_{11}h^2+...+2\beta_{12}hk+...)]$. For the anion O atoms, numbers within parentheses in the symbol denote the Mo atom(s) to which it is bonded.

	x	y	z	occupancy	β_{11}/B	β_{22}	β_{33}	β_{12}	β_{13}	β_{23}
Mo1	7571(4)	4917(4)	1[a]		22(3)	23(3)	22(3)	13(2)	-1(3)	0(3)
Mo2	7200(5)	5996(4)	3215(6)		31(3)	23(3)	44(4)	16(3)	2(4)	-5(4)
Mo3	4646(4)	4020(4)	2638(6)		25(3)	32(3)	24(4)	18(3)	5(3)	-4(3)
P	2/3	1/3	2750(11)		22(4)	22(4)	14(8)	11(2)	0	0
O(1)	8270(5)	5906(6)	-1062(7)		26(4)	33(4)	35(5)	12(3)	0(4)	8(4)
O(11')	7896(5)	3768(5)	- 688(6)		33(4)	24(4)	23(4)	14(3)	5(4)	1(3)
OP(11'1'')	2/3	1/3	1310(11)		21(3)	21(3)	25(9)	11(2)	0	0
O(12)	7315(6)	5590(5)	1215(8)		37(4)	26(4)	35(5)	18(3)	6(4)	0(4)
O(13)	8880(5)	5144(5)	1076(7)		26(4)	31(4)	27(5)	14(3)	-3(4)	-3(4)
O1(2)	7741(7)	7322(6)	2830(9)		53(5)	28(4)	65(8)	23(4)	-4(5)	-14(5)
O2(2)	7058(7)	5973(7)	4783(8)		57(6)	55(6)	38(6)	27(5)	-3(5)	-25(5)
O1(23)	8516(5)	5895(6)	3213(7)		25(4)	35(4)	41(5)	19(3)	1(4)	-5(4)
O2(23)	5714(5)	5499(5)	2719(7)		31(4)	29(4)	38(5)	19(3)	0(4)	-2(4)
OP(23)	6300(5)	4117(5)	3195(7)		28(4)	25(3)	29(4)	15(3)	-3(4)	-4(4)
O1(3)	3527(6)	4123(7)	2467(8)		29(4)	55(5)	46(6)	30(4)	4(4)	-7(5)
O2(3)	4611(7)	4260(7)	4671(8)		48(5)	51(6)	35(6)	34(5)	0(4)	-6(5)
H1[O2(3)]	4752(17)	4961(15)	4995(19)		104(17)	72(12)	91(17)	56(13)	-30(15)	-43(13)
H2[O2(3)]	4731(30)	3873(25)	5281(20)		238(40)	153(27)	59(16)	143(30)	-4(21)	2(18)
Na	3390(29)	1716(22)	6753(26)		167(32)	86(18)	124(26)	69(21)	12(24)	8(18)
O(Aq1)	5097(24)	3303(17)	6432(17)	0.67(6)	257(37)	133(20)	93(20)	125(22)	75(18)	58(14)
H1(Aq1)[b]	5357(24)	3691(17)	7191(17)	0.67(6)						
H2(Aq1)[b]	5367(24)	2801(17)	6391(17)	0.67(6)						
O(Aq2)	2491(16)	2221(20)	5220(18)	0.44(4)	76(15)	121(22)	74(18)	73(16)	12(14)	25(15)
H1(Aq2)[b]	2980(16)	2757(20)	4675(18)	0.44(4)						
H2(Aq2)[b]	2230(16)	2497(20)	5855(18)	0.44(4)						
O(Aq3)	1793(37)	-250(36)	5830(46)	0.27(4)	4.4(8)					
O(Aq4)	1797(34)	303(35)	7326(43)	0.37(4)	6.1(8)					

a, Arbitrarily fixed.

b, Atomic, occupancy and thermal parameters constrained to those of the corresponding oxygen atom; see text.

anion calculated from the neutron data parameters (Table 2) do not differ significantly from those obtained in the X-ray study.[3] The hydrogens are attached in pairs to a single O atom, [O2(3)], in every second octahedron in the ring of six octahedra in the anion, *cf.* Figs. 1 and 2. This coordination of water molecules to Mo atoms induces a non-planar arrangement of the Mo2 and Mo3 atoms in the ring, with 'water-free' Mo2 displaced ~0.62 Å outside the Mo3 atoms. The Mo−OH_2 distance is 2.232(11) Å, which may be compared to the Mo−OH_2 distances found in $MoO_3.2H_2O$[19] [2.274(2), 2.276(2), 2.290(2) and 2.294(2) Å] and α-$MoO_3.H_2O$[20] [2.346(7) Å]. In the coordinated water molecules the O−H distances are 0.98(2) and 0.93(3) Å with an H−O−H angle of 110(2)°, *i.e.* the expected values for ordinary water molecules.[21]

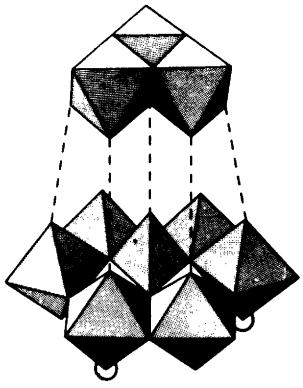

Fig. 1. The $Mo_9PO_{31}(OH_2)_3^{3-}$ anion depicted using idealized polyhedra. The rings denote the positions for two of the three water molecules.

As mentioned above, the equilibrium studies established the series of (17,9,1), (16,9,1), (15,9,1) and (14,9,1) complexes.[1] However, crystals could be obtained for only the (17,9,1) complex. For the others large-angle X-ray scattering measurements were made. Solutions containing predominantly the (16,9,1) or (15,9,1) complexes were investigated for both the $H^+ - MoO_4^{2-} - HPO_4^{2-}$ system[22] and the analogous $H^+ - MoO_4^{2-} - HAsO_4^{2-}$ system,[23,24] while the (14,9,1) complex was investigated only for the latter system. The investigations clearly showed that the basic anion structure (Mo, P/As and O atoms) for the complexes is the same as that in the $Mo_9PO_{31}(OH_2)_3^{3-}$ anion with minor changes in the dimensions. Since the six hydrogens have been shown in the present study to be attached to the anion, it may be concluded that three of them are emitted one by one to obtain (16,9,1), (15,9,1) and (14,9,1), which have five, four and three hydrogens, respectively. Further removal of hydrogens appears to destabilize the anion which decomposes forming pentamolybdodiphosphates and heptamolybdates.[1]

The dimerization in solution[1] according to $2Mo_9PO_{31}(OH_2)_3^{3-} \rightleftharpoons Mo_{18}P_2O_{62}^{6-} + 6H_2O$ causes a removal of the Mo-coordinated water molecules. The structure of the dimer has been determined in X-ray investigations of $Na_6Mo_{18}P_2O_{62}(H_2O)_{24}$[25] and $Na_4H_2Mo_{18}P_2O_{62}.nH_2O, n \sim 20$.[11] In the latter investigation the presence of two H_3O^+ ions was suggested. There is, however, great similarity in the two structures, most of the cell and atomic parameters being the same within statistical errors except for one Na and two water O atoms, which are missing in the latter determination. It is therefore suggested that this phase is the same as the one in Ref. 25.

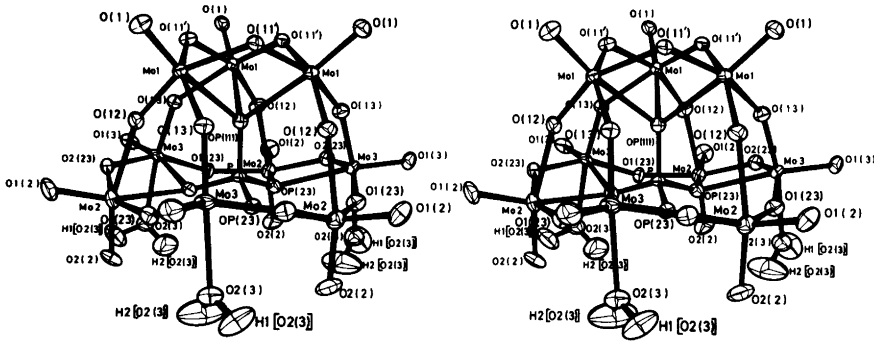

Fig. 2. A stereoscopic view of the $Mo_9PO_{31}(OH_2)_3^{3-}$ anion. The thermal ellipsoids are scaled to include 50 % probability.[29]

Table 2. Distances (Å) and angles (°) within the $Mo_9PO_{31}(OH_2)_3^{3-}$ anion. The superscipts refer to the following symmetry operations: (I) $1-y,x-y,z$; (II) $1+y-x,1-x,z$.

	Neutron	X-ray		Neutron	X-ray
Mo1 – Mo1^{II}	3.396(9)	3.411(1)	Mo1^{II} – Mo1 – Mo2	116.46(10)	116.50(4)
Mo1 – Mo2	3.946(8)	3.933(3)	Mo1^{I} – Mo1 – Mo3^{II}	118.00(12)	118.00(4)
Mo1 – Mo3^{II}	3.680(7)	3.690(3)	Mo3 – Mo2 – Mo3^{II}	116.84(22)	117.23(4)
Mo2 – Mo3	3.362(8)	3.364(1)	Mo2 – Mo3 – Mo2^{I}	117.01(22)	117.04(4)
Mo2 – Mo3^{II}	3.696(8)	3.703(1)			
P – Mo1	3.565(11)	3.564(11)			
P – Mo2	3.513(6)	3.516(2)			
P – Mo3	3.475(5)	3.486(1)			
Mo1 – O(1)	1.703(8)	1.713(9)	Mo3 – O1(3)	1.684(9)	1.697(9)
– O(11′)	2.052(8)	2.080(7)	– O2(3)	2.232(11)	2.213(10)
– O(11′)^{I}	1.821(8)	1.826(8)	– O(13)^{I}	1.799(10)	1.813(9)
– O(12)	1.770(8)	1.778(8)	– O1(23)^{I}	1.849(9)	1.825(8)
– O(13)	2.082(8)	2.075(8)	– O2(23)	1.886(8)	1.886(7)
– OP(11′1″)	2.419(8)	2.419(9)	– OP(23)	2.369(9)	2.375(7)
Mo2 – O1(2)	1.697(9)	1.708(9)	P – OP(11′1″)	1.560(17)	1.567(20)
– O2(2)	1.709(11)	1.695(12)	– OP(23)	1.528(7)	1.532(8)
– O(12)	2.268(11)	2.258(9)			
– O1(23)	1.952(9)	1.971(7)	O2(3) – H1[O2(3)]	0.98(2)	
– O2(23)	1.942(9)	1.942(8)	– H2[O2(3)]	0.93(3)	
– OP(23)	2.319(8)	2.312(7)			

Hydrogen bonding in the crystal structure. The anions are connected to a framework, illustrated in Fig. 3, through electrostatic O – Na – O links and hydrogen bonds O2(3) – H1[O2(3)]...O(13)^{II}. The framework contains cavities located between anions which are one unit cell apart in the z-direction. The cavities are filled with Aq1 molecules hydrogen bonded to O2(3). There are no O atoms available as possible acceptors within hydrogen bond distances from O(Aq1). The hydrogens are, however,

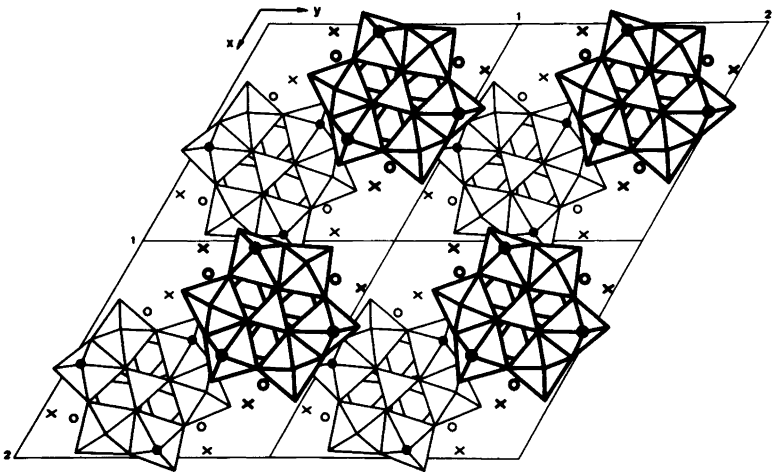

Fig. 3. The framework of anions around the 0,0,z channels. The anions are drawn as linked polyhedra. Filled circles = Mo-coordinated waters; open circles = Na^+ ions; crosses = Aq2 waters; thin lines = atoms at z; heavy lines = atoms at $z+1/2$.

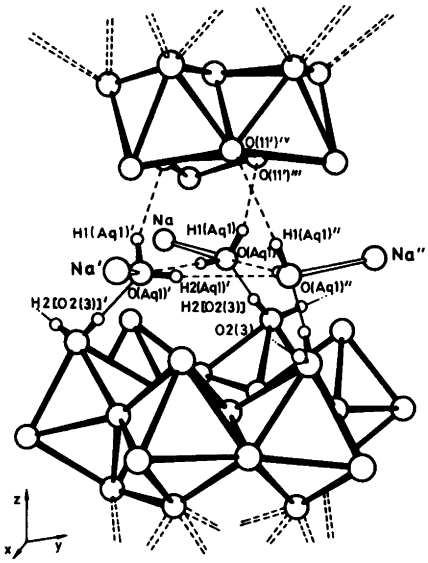

Fig. 4. The arrangement of Aq1 waters in the cavities between anions one unit cell apart along *z*. The anions are drawn as linked polyhedra. Thin full lines = hydrogen bonds; single dashed lines = direction to nearest neighbour O atom for H(Aq1). The superscripts refer to the following symmetry operations: (I) $1-y,x-y,z$; (II) $1+y-x,1-x,z$; (III) $1-y,x-y,1+z$; (IV) $x,y,1+z$.

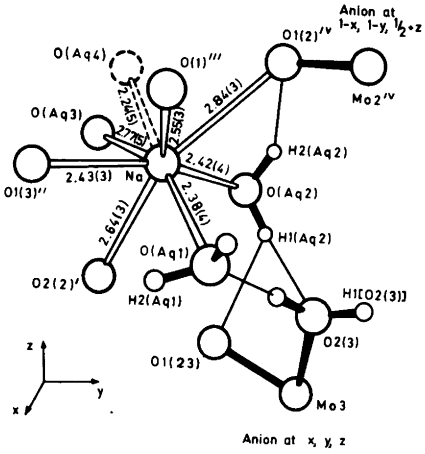

Fig. 5. The sodium-oxygen arrangement with bond distances (Å), and hydrogen bonds involving Aq2. (Aq3 and Aq4 are not present simultaneously; see text.) The superscripts refer to the following symmetry operations: (I) $1-y,x-y,z$; (II) $y,y-x,1/2+z$; (III) $1-y,x-y,1+z$; (IV) $1-x,1-y,1/2+z$.

directed towards O(11'), 3.44(2) Å, and towards the O atom of a symmetry-related Aq1 molecule, 3.84(5) Å away, *cf.* Fig. 4. The presence of an Na^+ ion in the opposite direction completes a tetrahedral coordination around O(Aq1). The occupancy factor for Aq1 is 0.67(6), *i.e.* ~two molecules are present around the three-fold axis. This is probably caused by the lack of hydrogen bond acceptors and

Table 3. Distances (Å) and angles (°) within the hydrogen bond system. Values for the atoms closest to O(Aq1) have also been included despite the fact that they exceed the hydrogen bond range. The geometry of Aq1 and Aq2 has been constrained; see text. The superscripts refer to the following symmetry operations: (I) $1-y,x-y,z$; (II) $y,1+y-x,1/2+z$; (III) $1-y,x-y,1+z$; (IV) $1-x,1-y,1/2+z$.

	H1–O	O–H2	H1–H2	∠H1–O–H2
H1[O2(3)]–O2(3)–H2[O2(3)]	0.98(2)	0.93(3)	1.57(4)	110(2)
H1(Aq1)–O(Aq1)–H2(Aq1)	0.96(3)	0.97(3)	1.54(3)	107(3)
H1(Aq2)–O(Aq2)–H2(Aq2)	0.94(3)	0.96(3)	1.59(3)	114(3)

	H···O	O···O	∠O–H···O
O2(3)–H1[O2(3)]···O(13)^{II}	2.02(2)	2.98(1)	165(2)
O2(3)–H2[O2(3)]···O(Aq1)	1.71(4)	2.63(2)	173(3)
O(Aq1)–H1(Aq1)···O(11')^{III}	2.54(2)	3.44(2)	157(2)
O(Aq1)–H2(Aq1)···O(Aq1)^{I}	2.89(4)	3.84(5)	165(3)
O(Aq2)–H1(Aq2)···O1(23)^{I}	2.33(2)	3.00(2)	128(2)
O(Aq2)–H1(Aq2)···O2(3)	2.24(2)	3.02(2)	140(2)
O(Aq2)–H2(Aq2)···O1(2)^{IV}	2.15(2)	2.96(2)	141(2)

might explain the observed variation in the cell parameter *c*.[3]

Additional hydrogen bonds in the framework are formed *via* the Aq2 molecules. They are situated in the outermost part of channels through the framework around 0,0,*z* (Fig. 3) and are also coordinated to Na^+. The atomic positions are only partly occupied and the waters probably enter the channels in a statistical way as non-structural water. Also rotational behaviour of the Aq2 molecule might be induced by non-structural channel water giving a variety of possible hydrogen bond acceptors. The hydrogen positions found indicate for H1(Aq2) a bifurcated hydrogen bond to O2(3) and $O1(23)^{I}$, and for H2(Aq2) a bond to $O1(2)^{IV}$. The Aq2 molecules in this way connect adjacent anions in the *z*-direction in the manner shown schematically to the right in Fig. 5. Hydrogen bond distances and angles are given in Table 3.

The sodium-oxygen arrangement. The Na^+ ion coordinates seven O atoms, of which four are anion and three are water O atoms. The anion oxygens are donated by four different anions which implies that there are several different O–Na–O links in the framework. The water positions are all partly occupied. In addition the O(Aq3)–O(Aq4) distance is too short (1.80 Å) for the molecules to be present simultaneously. The resulting coordination around Na^+, assuming full occupation on Aq1, Aq2 and one of Aq3 or Aq4, is irregular with the Na–O distances varying between 2.24 and 2.84 Å, *cf.* Fig. 5.

The channel. The channel is limited by atoms such as O(1), O1(3), O(12) and O1(23) forming an approximate cylinder along 0,0,*z* with a diameter of ~10.6 Å. The channel passages are narrower, however, at the two *z*-levels in each cell where the O1(2) oxygens protrude into the channel, *cf.* Fig. 3. Here the O–O distance is ~6.3 Å, with the diameter of a circle through the O positions of ~7.3 Å. If the average radius of an O atom is considered to be approximately 1.4 Å,[26] the open passage in the channel would have a cross-section of ~48 $Å^2$ and, at the narrow section, $\gtrsim$16 $Å^2$, the inequality sign being used as there is additional space outside the circle.

A rough estimation of the channel volume would then give ~22–24 $Å^3$/water molecule for the ~20 channel waters in each unit cell. This may be compared to a value of ~25 $Å^3$ for the water and Na^+ in the zeolite phillipsite[27] and to ~32–33 $Å^3$ for ice structures, for example. In phillipsite the channel cross-sections are ~9 and 12 $Å^2$, and it might be assumed that the wider channel in the present structure allows a more dense packing of water.

As mentioned above, most of the water in the channel is non-structural. Indications for three partly occupied water positions were found, but for two, O(Aq3) and O(Aq4), only the presence of one at a time is possible due to the short internal distance. In thermobalance analyses the loss of water upon heating was seen to first occur in three steps, while the temperature was increased to ~115 °C in which a total of ~10.2 H_2O were emitted (probably channel water). An additional ~2.4 H_2O was gradually emitted with a further increase of temperature to ~250 °C. At 400 °C the samples retained their hexagonal prismatic form and yellowish colour but displayed large cracks along *z*. At ~700 °C they decomposed rather quickly.

This type of channel containing non-structural water has also been reported for other structures containing large, compact heteropolyanions, *e.g.* in $H_3Mo_{12}PO_{40}(H_2O)_{29-31}$[7] and $(NH_4)_7Na_2[H_2GaW_{11}O_{40}].15H_2O$.[28]

Acknowledgements. I thank Professor Nils Ingri for his valuable advice, for his great interest in my work, and for the facilities which he placed at my disposal. I am grateful to Drs. Lage Pettersson and Rolf Strandberg for stimulating discussions. I am also grateful to Dr. Lage Pettersson for information on as yet unpublished results. I am indebted to Drs. John O. Thomas and Roland Tellgren, University of Uppsala for help in the data collection and reduction and for valuable discussions. Linguistic corrections have been made by Dr. Kenneth Wing. This work has been financially supported by the Swedish Natural Science Research Council.

REFERENCES

1. Pettersson, L. *Chem. Scr.* 7 (1975) 145.
2. Pettersson, L. *Equilibrium and Structure Studies of Aqueous Three Component Polyanion Complexes Formed in the Systems* $H^+-MoO_4^{2-}-HPO_4^{2-}$, $H^+-MoO_4^{2-}-HAsO_4^{2-}$ and $H^+-MoO_4^{2-}$–(D-)*mannitol*, Diss., University of Umeå, Umeå 1974.
3. Strandberg, R. *Acta Chem. Scand. A 28* (1974) 217.
4. Hedman, B. *Acta Chem. Scand. 27* (1973) 3335.
5. Hedman, B. *Acta Crystallogr. B 33* (1977) 3083.
6. Wada, T. *C. R. Acad. Sci. Ser. C 259* (1964) 553.

7. Strandberg, R. *Acta Chem. Scand. A 29* (1975) 359.
8. Brown, G. M., Noe-Spirlet, M.-R., Busing, W. R. and Levy, H. A. *Acta Crystallogr. B 33* (1977) 1038.
9. Perloff, A. *Inorg. Chem. 9* (1970) 2228.
10. d'Amour, H. and Allman, R. *Naturwissenschaften 61* (1974) 31.
11. d'Amour, H. *Acta Crystallogr. B 32* (1976) 729.
12. Tellgren, R., Ramanujam, P. S. and Liminga, R. *Ferroelectrics 6* (1974) 191.
13. Hamilton, W. C. *Acta Crystallogr. 18* (1965) 502.
14. Pawley, G. S. *Acta Crystallogr. A 26* (1970) 691.
15. Coppens, P. and Hamilton, W. C. *Acta Crystallogr. A 26* (1970) 71.
16. *International Tables for X-Ray Crystallography*, Kynoch Press, Birmingham 1974, Vol. IV, pp. 270–271.
17. Lundgren, J.-O. *Crystallographic Computer Programs*, UUIC-B13-4-03, Institute of Chemistry, University of Uppsala, Uppsala 1976.
18. Antti, B.-M. *Acta Chem. Scand. A 30* (1976) 24.
19. Åsbrink, S. and Brandt, B. G. *Chem. Scr. 1* (1971) 169.
20. Böschen, I. and Krebs, B. *Acta Crystallogr. B 30* (1974) 1795.
21. Ferraris, G. and Franchini-Angela, M. *Acta Crystallogr. B 28* (1972) 3572.
22. Johansson, G., Pettersson, L. and Ingri, N. *Acta Chem. Scand. A 32* (1978) 407.
23. Pettersson, L. *Acta Chem. Scand. A 29* (1975) 677.
24. Johansson, G., Pettersson, L. and Ingri, N. *Acta Chem. Scand. Submitted for publication.*
25. Strandberg, R. *Acta Chem. Scand. A 29* (1975) 350.
26. Pauling, L. *The Nature of the Chemical Bond*, Cornell University Press, New York 1960.
27. Steinfink, H. *Acta Crystallogr. 15* (1962) 644.
28. Evans, H. T., Jr. In Dunitz, J. D. and Ibers, J. A., Eds., *Perspectives in Structural Chemistry*, Wiley, New York 1971, Vol. IV, Chapter 1.
29. Johnson, C. K. *ORTEP-II*, Report ORNL-5138, Oak Ridge National Laboratory, Oak Ridge 1976.

Received January 25, 1978.

Acta Chemica Scandinavica A 32 (1978) 447–453

Ion Activities and Zinc Electrode Reactions in Aqueous Sulfate Solutions

TOR HURLEN and TURID R. BREIVIK

Department of Chemistry, University of Oslo, Blindern, Norway

Thermodynamic and kinetic studies have revealed conventional mean-ion and convenient single-ion activity coefficients for zinc(II), magnesium and sulfate ions and standard rate data for the Zn(I)/Zn(II) electron-transfer step (the Zn/Zn(I) step appears inaccessibly fast) at solid zinc in 0.005 *m* $ZnSO_4$ + (*x* − 0.005) *m* $MgSO_4$ and partly in *x m* $ZnSO_4$ (for *x* = 0.2 − 3.0) at 25 °C. With increasing *x*, the anion activity coefficient steadily falls, the cation activity coefficients go through a minimum at *x* = 0.5 to 1, and the standard rate falls. The results show that the main electroactive Zn(I)/Zn(II) couple is one of purely hydrated ions, and they suggest that it may be $Zn(H_2O)_6^+/Zn(H_2O)_6^{2+}$ of fully hexahydrated ions. Double layer effects are considered and discussed.

After some initial work,[1] a convenient scale for single-ion activities has recently been introduced,[2,3] and some convenient single-ion activity data have been accumulated.[1–8] This mostly applies to chloride solutions.[1–5] The present work backs up and extends the little there is for sulfate solutions.[6,7] Such activity determinations are important for the evaluation of ionic interactions and reactions in solutions and at electrodes and other interfaces.

From its polarization behaviour[2,9–12] in comparison with that[3,13–16] of the Zn(Hg)/Zn(II) electrode, the Zn/Zn(II) electrode appears to react in two consecutive steps with the Zn(I)/Zn(II) electron-transfer step as the rate-determining one. Little is known as to the electroactive Zn(I) and Zn(II) species,[2,9,15] which in sulfate solution most likely are purely hydrated ions. This is pursued in the present work by studies on kinetic water-activity and double-layer effects. It is hoped that this may assist in elucidating also the double-layer properties of the solid zinc electrode.[17–19]

EXPERIMENTAL

The experimental work comprises equilibrium potential measurements on saturated and well-equilibrated Zn(Hg)/Zn(II) and Hg/Hg_2SO_4 electrodes *vs.* SCE and kinetic polarization measurements on etched (in hot 4 M H_2SO_4) high-purity (99.999 %) zinc wire electrodes (exposed surface area near 0.3 cm^2) in the two solution series:

$$0.005\ m\ ZnSO_4 + (x - 0.005)\ m\ MgSO_4 \quad \text{(A)}$$
$$x\ m\ ZnSO_4 \quad \text{(B)}$$

with *x* = 0.2 − 3.0 and addition of H_2SO_4 to pH about 3, all at 25 °C. The solutions were prepared from *p.a.* quality salts and acid and twice distilled water, deoxygenated with purified and premoistened nitrogen, and kept under nitrogen atmosphere during the measurements.

The kinetic studies mostly are by galvanostatic single-pulse measurements in unstirred solutions and quasi-stationary overvoltage measurements in vigorously stirred (by nitrogen bubbling) solutions. All measurements have been performed with equipment and procedures essentially as previously described.[1,2] This includes capacity (purity) checking and ohmic drop correction by the slope and the gap of galvanostatic transients on the 10 μs scale.[2] For "good" zinc wire electrodes, the capacity appeared to be about 55 μF cm^{-2}. "Bad" electrodes with lower capacity usually could be improved by strong anodic loads for a few seconds in the test solution. The ohmic drop mostly was well below 1 V/A cm^{-2}.

ACTIVITY DATA

The conventional mean molal activity coefficient ($\gamma_\pm$) and the convenient single-ion ones (γ'_{2+} and γ'_{2-}) for zinc(II) and sulfate ions in the test solutions should[2,3] be given by eqns. (1)–(3).

$$\gamma_{\pm} = m^{\circ} m_{2+}^{-\frac{1}{3}} m_{2-}^{-\frac{1}{3}} \exp\left[f(E'_{2+} - E'_{2-}) - f(E^{\circ}_{2+} - E^{\circ}_{2-})\right] \quad (1)$$

$$\gamma'_{2+} = m^{\circ} m_{2+}^{-1} \exp\left[2f(E'_{2+} - (\phi_t - \phi_r) - E^{\circ}_{2+} + 0.241)\right] \quad (2)$$

$$\gamma'_{2-} = m^{\circ} m_{2-}^{-1} \exp\left[-2f(E'_{2-} - (\phi_t - \phi_r) - E^{\circ}_{2-} + 0.241)\right] \quad (3)$$

where m° is the standard molality (1 mol kg^{-1}), m_{2+} and m_{2-} respectively, are the zinc(II) and the sulfate molality, f means F/RT, E'_{2+} and E'_{2-} respectively, are the apparent (including liquid junction) reversible Zn/Zn(II) and Hg/Hg_2SO_4 potentials in V(SCE), E°_{2+} and E°_{2-} are the standard potentials of these electrodes in V(SHE), $\phi_t - \phi_r$ is the liquid-junction potential difference between test and reference (saturated KCl) solution in V, and 0.241 V(SHE) is the recommended value[20] for $E^{\circ}(Hg/Hg_2Cl_2) - f^{-1}\ln(a_{\pm}(\text{sat. KCl})/a^{\circ})$, all at 25 °C. These activity coefficients are bare-ion ones.

Table 1 presents E' values measured, $\phi_t - \phi_r$ values estimated,[7] and γ values hence obtained from (1)–(3) for the solution series (A), when use is made of the E°/V(SHE) values −0.763 and 0.612 for Zn/Zn(II) and Hg/Hg_2SO_4,[22,23] respectively. The table moreover reproduces mean ionic and water activity data[21] for pure magnesium sulfate solutions. These data are presently accepted for the solution series (A), and they partly have been used in determining γ'_{2+}(Mg) from its equality to $(\gamma_{\pm}(MgSO_4))^2/\gamma'_{2-}(SO_4)$. Table 2 presents data correspondingly obtained for the solution series (B), when the $\phi_t - \phi_r$ values of Table 1 are accepted also for this series. The mean-ion coefficient values of Table 2 check well with previously tabulated ones.[21]

In Fig. 1, a comparison is made of the three ionic activity coefficients of zinc sulfate with those of

Table 1. Data for 0.005 *m* $ZnSO_4 + (x - 0.005)$ *m* $MgSO_4 + H_2SO_4$ (to pH about 3) at 25 °C (see text).

x	0.2	0.5	1.0	1.5	2.0	2.5	3.0
Potential data							
E'_{2+}(Zn)/V(SCE)	−1.099	−1.100	−1.100	−1.097	−1.093	−1.088	−1.082
$E'_{2-}(SO_4)$/V(SCE)	0.419	0.420	0.420	0.422	0.423	0.424	0.424
$(\phi_t - \phi_r)$/V	−0.001	0.000	0.001	0.001	0.002	0.002	0.003
Activity data							
$\gamma_{\pm}(ZnSO_4)$	0.12	0.070	0.050	0.042	0.041	0.043	0.050
$\gamma_{\pm}(MgSO_4)$[a]	0.11	0.068	0.049	0.043	0.042	0.044	0.049
$\gamma'_{2-}(SO_4)$	0.11	0.044	0.024	0.014	0.010	0.008	0.007
γ'_{2+}(Zn)	0.13	0.11	0.10	0.13	0.17	0.25	0.36
γ'_{2+}(Mg)	0.11	0.10	0.10	0.13	0.17	0.24	0.35
a_w[a]	0.996	0.991	0.981	0.969	0.953	0.932	0.905

[a] For x *m* $MgSO_4$.[21]

Table 2. Data for x *m* $ZnSO_4 + H_2SO_4$ (to pH about 3) at 25 °C (see text).

x	0.2	0.5	1	2	3
Potential data					
E'_{2+}(Zn)/V(SCE)	−1.052	−1.042	−1.028	−1.010	−0.992
$E'_{2-}(SO_4)$/V(SCE)	0.423	0.422	0.428	0.433	0.437
Activity data					
$\gamma_{\pm}(ZnSO_4)$	0.10	0.062	0.043	0.035	0.041
$\gamma'_{2-}(SO_4)$	0.080	0.038	0.013	0.0047	0.0025
γ'_{2+}(Zn)	0.12	0.10	0.14	0.27	0.67
a_w[a]	0.996	0.991	0.983	0.985	0.911

[a] For x m $ZnSO_4$.[21]

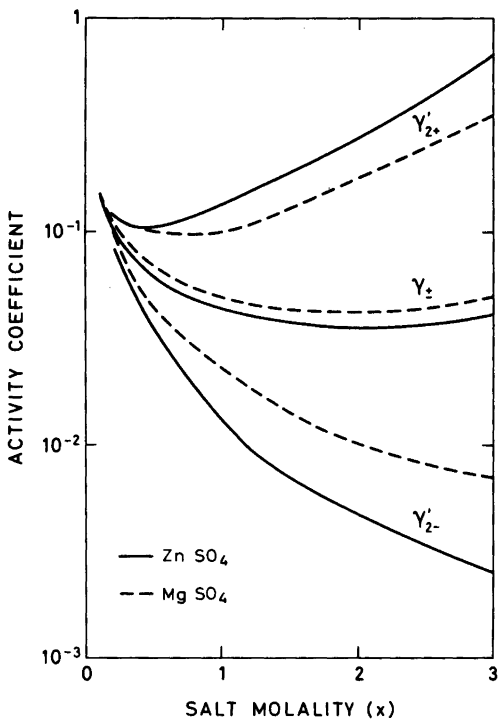

Fig. 1. Molal bare-ion activity coefficients in essentially pure solutions of zinc sulfate (solid curves) or magnesium sulfate (dashed curves) at 25 °C.

magnesium sulfate in essentially pure solutions of these salts. Since the activity coefficient for traces of zinc sulfate in magnesium sulfate solution nearly is the same as for the main salt (Table 1), this comparison essentially also is for the limiting activity coefficients of zinc sulfate in mixed solutions with magnesium sulfate (at zero and infinite zinc/magnesium ratio).

The convenient single-ion activity coefficients are related to absolute ones[2,3] by $\gamma'_z = \gamma_z r^{-z/2}$ where r is the ratio γ_+/γ_- for potassium chloride in saturated pure solution at the temperature concerned, and z is the charge number (with sign) of the ion concerned. The ratio r is not yet exactly known, but it appears to be near unity at 25 °C.[4] For any complex species, the activity should be proportional to the mass-action activity product of its constituent bare ions and molecules. This is made use of in the kinetic studies below.

KINETIC DATA

The kinetic data of the present work apply to pre-etched zinc wire electrodes in the solution series (A). A slightly unstable and stirring dependent open-circuit potential, somewhat positive to the reversible Zn/Zn(II) potential (Table 1), was generally obtained. This invalidated any attempt of directly determining the charge-transfer resistance near equilibrium of the electrode, and only Tafel data

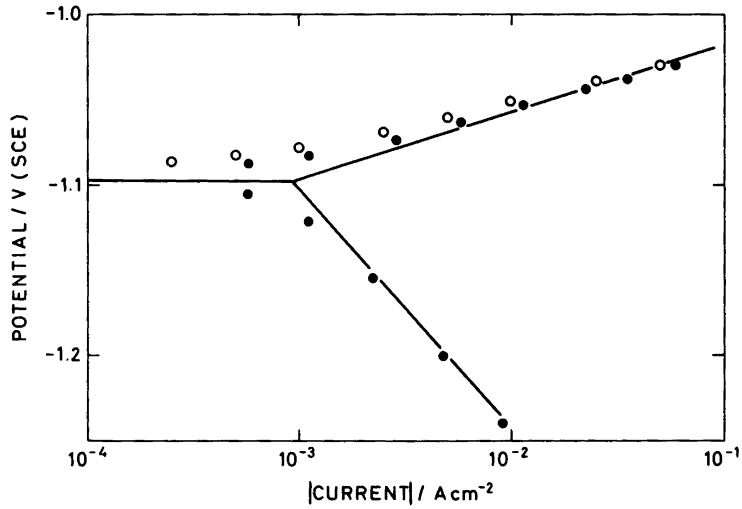

Fig. 2. Charge-transfer data for solid zinc in 0.005 *m* $ZnSO_4$ + 1.495 *m* $MgSO_4$ + H_2SO_4 (to pH about 3 at 25 °C from (○) slow measurements in vigorously stirred solution and (●) fast galvanostatic transients in unstirred solution.

Table 3. Exchange data for Zn(I)/Zn(II) at solid zinc in 0.005 *m* $ZnSO_4$ + (*x* − 0.005) *m* $MgSO_4$ + H_2SO_4 (to pH about 3) at 25 °C (see text).

x	0.5	1.0	1.5	2.0	2.5	3.0
i_{o2}/mA cm^{-2}	0.70	0.50	0.50	0.45	0.45	0.40
I_{o2}/A cm^{-2}	0.20	0.15	0.12	0.09	0.07	0.05

will presently be considered. Examples of such data are given in Fig. 2.

Tafel slopes. In all solutions (A), charge-transfer controlled anodic and cathodic Tafel lines were obtained with *E*/ln *i* slopes of typically $2RT/3F$ and $-2RT/F$, respectively. This agrees with a two-step charge-transfer mechanism in which the Zn(I)/Zn(II) electron-transfer step is rate determining (see Introduction) and essentially symmetric ($\alpha_2 = \frac{1}{2}$). A more exact determination of the slopes was impeded both by the Tafel-linear regions covered being too small and by the reproducibility of the cathodic data being too poor.

Exchange rates. The anodic data of the present work are well reproducible and warrant further treatment. With the reaction mechanism proposed, the anodic Tafel lines should intersect with the reversible potential applying (Table 1) at twice the exchange current of the rate-determining Zn(I)/Zn(II) electron-transfer step.[24] Values accordingly obtained for this exchange current (i_{o2}) are given in Table 3. The exchange current (i_{o1}) of the Zn/Zn(I) ion-transfer step appears to be inaccessibly high for the present measurements.

From ordinary electrode kinetics,[24] i_{o2} should depend on the bare-ion activity of Zn(II) by (when $\alpha_2 = \frac{1}{2}$):

$$i_{o2} = I_{o2}\,(a'_{2+}/a^{o})^{3/4} = I_{o2}\,(\gamma'_{2+} m_{2+}/m^{o})^{3/4} \qquad (4)$$

where I_{o2} is a bare-zinc-ion standardized exchange rate which still depends on ligand activities and double-layer effects. Also values accordingly obtained for I_{o2} from i_{o2} and activity data (Table 1) are given in Table 3.

Double-layer and ligand effects. With increasing concentration of the supporting salt ($MgSO_4$), I_{o2} clearly falls (Table 3). This fall is steeper than can be expected solely from activity effects by water or sulfate ions as ligands in the electroactive species, and double-layer effects must be invoked. Since the sulfate-ion activity ($\gamma'_{2-} m_{2-}$) is nearly constant over the solution series concerned (Table 1), this may be illustrated by a log-log plot of I_{o2} against the water activity applying. Such a plot is given in Fig. 3,

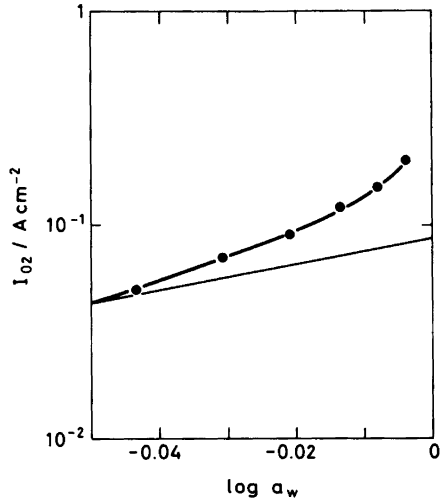

Fig. 3. Log-log plot of I_{o2} *vs.* a_w for solid zinc in 0.005 *m* $ZnSO_4$ + (*x* − 0.005) *m* $MgSO_4$ + H_2SO_4 (to pH about 3) at 25 °C. The straight line slopes as for sole sixth-order water dependence.

where also comparison is made to a line sloping as for sole sixth-order water dependence.

The double-layer properties of solid zinc is not well-known, but its potential of zero charge may be near −0.9 V(SCE).[17,18] The present rate data then apply to negatively charged zinc electrodes with little or no ions specifically adsorbed. The double-layer effect accordingly should be mainly by the Frumkin factor:[24]

$$\exp\,[f(\tfrac{1}{2} - z)\phi_2] \qquad (5)$$

where ϕ_2 is regarded the pre-electrode potential, *z* is the net charge number (with sign) of the electroactive Zn(II) species, and use has been made of $\alpha_2 n = \frac{1}{2}$ for the reaction step considered.

Under the electrode conditions noted, φ_2 is negative, $|\phi_2|$ decreases with increasing salt concentration, and so consequently does also the Frumkin factor (5) for $z = 2$ (but not for $z = 0, -2$, *etc.*). The results in Fig. 3 agree qualitatively with

the expectations from the Frumkin factor for $z=2$ (but not for $z=0,-2$, *etc.*). The main electroactive Zn(I)/Zn(II) couple hence appears to be one of purely hydrated ions ($z=2$) and not one of sulfato-complexes ($z=0,-2$, *etc.*).

Further double-layer studies. The results of Fig. 3 are at present difficult to separate genuinely into water-activity and double-layer effects. However, if it be assumed that the electroactive zinc ions are fully hexa-hydrated, and that no unconsidered effect contributes to the changes in I_{o2}, one should have:

$$\Delta\ln(I_{o2}/a_w^6) = -3f\Delta\phi_2/2 \qquad (6)$$

for connected differences in the parameters noted. This equation enables changes in ϕ_2 to be obtained from those of I_{o2} and a_w.

Fig. 4 presents the results accordingly obtained for the variation of ϕ_2 with x (from an arbitrary zero at $x=1$) in the solution series (A). A $\Delta\phi/\log x$ presentation is chosen for easy comparison to expectations from the Gouy-Chapman diffuse-layer theory. Such expectations are given by a dashed line in Fig. 4. This line is partly extrapolated (beyond $x=1$) from data in Russel's tables[25] for Gouy-Chapman values of $|z|\phi_2$ at mercury in solutions of an unadsorbed and unassociated $z:z$ electrolyte like NaF, and it applies to electrodes with sufficiently negative charge to make $d\phi_2/d\ln c$ essentially invariant to changes in this charge. The dashed line thus gives the steepest variation allowed by the Gouy-Chapman theory. The variation should be smaller if the electrode charge be less negative than considered.

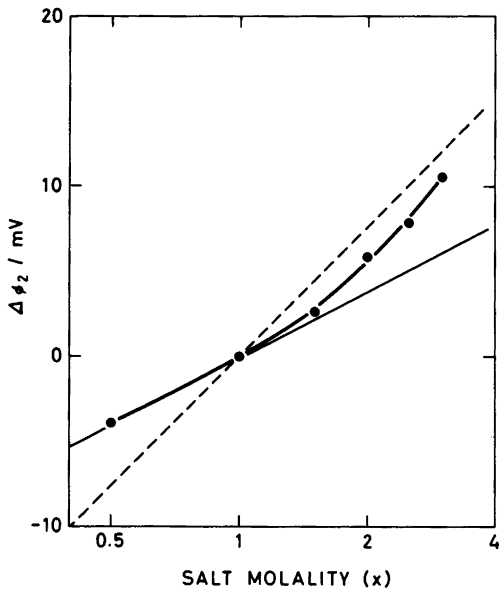

Fig. 4. Values from (6) for $\Delta\phi_2=\phi_2(x)-\phi_2(x=1)$ *vs.* log x for solid zinc around -1.05 V(SCE) in 0.005 *m* $ZnSO_4+(x-0.005)$ *m* $MgSO_4+H_2SO_4$ (to pH about 3) at 25 °C.

At low salt concentration (x), the results follow a $\Delta\phi_2/\log x$ line with about half the Gouy-Chapman slope. The increasing deviation from this line at higher salt concentration accompanies an increasing instability of the test electrode (especially in cathodic studies) and an increasing deviation of its open-circuit potential from the reversible Zn/Zn(II) potential (see above). These deviations may be due to some side effect (*e.g.* precipitation of some compound at the electrode surface) which, with increasing salt concentration, increasingly comes in and makes the observed rates increasingly too low.

The kinetic data underlying the results of Fig. 4 mostly apply to potentials around -1.05 V(SCE). This is only 150 mV negative to the above-noted value for the zero-charge potential of solid zinc. Since also Gouy-Chapman values for $|\phi_2|$ may be too high,[4,26,27] the ϕ_2-variation obtained from (6) is not unacceptable. This means that the main electroactive Zn(I)/Zn(II) couple could be one of fully hexahydrated zinc ions as presumed. Due to the Franck-Condon principle, one must expect the two electroactive species of an electron-transfer couple to have one and the same coordination.[28]

DISCUSSION

The present results are already somewhat discussed in connection with their presentation, and only some closing remarks shall be made on the activities, the kinetics and the double-layer properties revealed.

Activities. Besides being needed and used in the present kinetic evaluations, the convenient single-ion activity data of the present work carry information on the energetics of ion and cosphere interactions in the test solutions, and more so than do the conventional mean-ion data. This includes information on complex formation. The single-ion data partly depend on the validity of the values used for the liquid-junction potential difference $\phi_t-\phi_r$, however.

Some interaction information may be read rather easily from the data collection of Fig. 1. The interpretation and quantitative evaluation of these data, however, require more than can presently be given. The activity data, therefore, are left with previous ones of the same kind[1-8] for future treatment.

Kinetics. The kinetic results of the present work agree with the two-step mechanism of the Zn/Zn(II) electrode (see Introduction). They further show that the main electroactive Zn(I)/Zn(II) couple in the sulfate solutions used is one of purely hydrated ions, and they suggest that these ions may be fully hexacoordinated solution species. The latter in case agrees with previous kinetic results on zinc in chloride solutions,[2] and it compares well with corresponding results on manganese,[4] nickel,[1] and copper.[8] The kinetic results say nothing about the thermodynamically most stable Zn(I) and Zn(II) species, nor about the electroactive species of the Zn/Zn(I) couple.

Double-layer properties. The present separation of double-layer effects from other effects is not a fool-proof one, but a likely one. It does not yield the pre-electrode potential (ϕ_2) itself, but the sign and changes of this potential. Provided sulfatocomplexes participate negligibly and the electrode charge be sufficiently negative, these changes may seem to be lower than expected from the Gouy-Chapman diffuse-layer theory. This in case adds to similar results on liquid amalgam electrodes[4,26] in suggesting that Gouy-Chapman values of $|\phi_2|$ may be too high. This agrees qualitatively with more recent double-layer theory.[27]

It appears that the bare-zinc-ion and water standardized Zn(I)/Zn(II) exchange rate at solid zinc is a little lower (by a factor of about 1.2) in 1 *m* magnesium sulfate solution (present work) than in 1 M alkali chloride solutions,[3] and that the Zn(II) reduction in 0.5 *m* (or M) magnesium sulfate solution of 0.005 *m* (or M) Zn(II) is slower (by about half a decade) at solid zinc (present work) than at mercury.[14] These comparisons apply to data obtained at potentials around −1.05 V(SCE) and 25 °C. They support that ϕ_2 be negative at solid zinc (but less so than at mercury) under the conditions applying, and that z be positive (not zero or negative) for the main electroactive Zn(I)/Zn(II) couple. These conclusions partly imply that the electrode material (Zn or Hg) *per se* means little for the rate of electron transfer between a metallic electrode and species in solution.[29]

REFERENCES

1. Hurlen, T. *Electrochim. Acta 20* (1975) 499.
2. Hurlen, T. and Fischer, K. P. *J. Electroanal. Chem. 61* (1975) 165.
3. Hurlen, T. and Eriksrud, E. *J. Electroanal. Chem. 63* (1975) 157.
4. Hurlen, T. *J. Electroanal. Chem. 73* (1976) 285.
5. Hurlen, T. *J. Electroanal. Chem. 77* (1977) 181.
6. Hurlen, T., Staurset, A. and Eriksrud, E. *J. Electroanal. Chem. 83* (1977) 263.
7. Barba, W. D. and Hurlen, T. *J. Electroanal. Chem. In press.*
8. Kurnikov, B. D. and Hurlen, T. *J. Electroanal. Chem. In press.*
9. Heusler, K. E. and Knödler, R. *Electrochim. Acta 18* (1973) 855; Gaiser, L. and Heusler, K. E. *Electrochim. Acta 15* (1970) 161.
10. Bockris, J. O'M., Nagy, Z. and Damjanovic, A. *J. Electrochem. Soc. 119* (1972) 285.
11. Armstrong, R. D. and Bell, M. F. *J. Electroanal. Chem. 55* (1974) 201.
12. Clarke, J. T. and Hampson, N. A. *J. Electroanal. Chem. 26* (1970) 307.
13. Salie, G. *Z. Phys. Chem. 244* (1970) 1.
14. Van der Pol, F., Sluyters-Rehbach, M. and Sluyters, J. H. *J. Electroanal. Chem. 58* (1975) 177.
15. Despic, A. R., Jovanovic, D. and Rakic, T. *Electrochim. Acta 21* (1976) 63.
16. Eriksrud, E. *J. Electroanal. Chem. 76* (1976) 27.
17. Perkins, R. S. and Andersen, T. N. In Bockris, J. O'M. and Conway, B. E., Eds., *Modern Aspects of Electrochemistry, No. 5*, Butterworths, London 1969, Chapter 3.
18. Trasatti, S. *J. Electroanal. Chem. 33* (1971) 351.
19. Frumkin, A., Damaskin, B., Grigoryev, N. and Bagotskaya, I. *Electrochim. Acta 19* (1974) 69.
20. Ives, D. J. G. and Janz, G. J. *Reference Electrodes*, Academic, New York and London 1961, p. 160.
21. Robinson, R. A. and Stokes, R. H. *Electrolyte Solutions*, 2nd Ed. (revised), Butterworths, London 1970.
22. Pourbaix, M. *Atlas of Electrochemical Equilibria in Aqueous Solutions*, Pergamon, Oxford 1966, p. 408.
23. Noer, S. and Grønlund, F. *Ber. Bunsenges. 79* (1975) 517.
24. Delahay, P. *Double Layer and Electrode Kinetics*, Interscience, New York 1965.
25. Russel, C. D. *J. Electroanal. Chem. 6* (1963) 486.
26. Hurlen, T., Barba, W. D. and Glasner, I. *J. Electroanal. Chem. In press.*
27. Krylov, V. S. and Levich, V. G. *Russ. J. Phys. Chem. 37* (1963) 50; Krylov, V. S. *Electrochim. Acta 9* (1964) 1247.

28. Phillips, C. S. G. and Williams, R. J. P. *Inorganic Chemistry, II. Metals*, Oxford Univ. Press, Oxford 1966, p. 447.
29. Parsons, R. *Surface Sci. 2* (1964) 418; Capon, A. and Parsons, R. *J. Electroanal. Chem. 46* (1973) 215.

Received January 27, 1978.

Acta Chemica Scandinavica A 32 (1978) 455–459

Pulse Radiolysis of *para*-Substituted Phenyl Selenides and Tellurides in Methanolic Solution. I

J. BERGMAN,[a] N. EKLUND,[a] T. E. ERIKSEN[b] and J. LIND[b]

Departments of [a] Organic and [b] Nuclear Chemistry, The Royal Institute of Technology, S-100 44 Stockholm 70, Sweden

The pulse radiolysis of Ar_2Se, Ar_2Se_2, Ar_2Te and Ar_2Te_2 (Ar = *p*-methoxyphenyl) in neutral and acid methanolic solution permitted the observation of transients assigned to the radicals ArSe·, ArSeSe· and ArTe·.

Hydrogen atoms react with both mono- and diselenide producing the same radical ArSe· and solvated electrons react with monoselenide producing ArSe· through an acid catalyzed reaction.

For the diselenide two reaction modes are proposed, one producing ArSe· and the other ArSeSe·. In mono- and ditelluride solution only the ArTe· radical was observed.

Reliable studies on organoselenium and organotellurium radicals have only recently been made.[1-3] Thus Chu *et al.*[2] found evidence for the formation of the radicals $C_6H_5CH_2Se$· and $C_6H_5CH_2SeSe$· during the photolysis of benzyl diselenide and Marsh *et al.*[1] proposed an organotellurium radical fragment in the photodecomposition of bis(benzoylmethyl)tellurium dichloride.

In this paper we report the results from pulse radiolysis of Ar_2Se and Ar_2Se_2 (Ar = *p*-methoxyphenyl) and the corresponding tellurides in methanolic solution. Evidence for the formation of radicals of the type ArSe·, ArTe· and ArSeSe· was obtained.

EXPERIMENTAL

The selenium and tellurium compounds were synthesized as described below. Melting points were determined on a micro hot stage and are uncorrected. Mass spectra were obtained with an LKB 9000 A instrument using the direct inlet technique. The electron energy was 70 eV. $SeOCl_2$ (Merck), $TeCl_4$ (Merck) and KSeCN (BDH) were used as received.

Ar_2Se and Ar_2Te were synthesized from Ar_2SeCl_2 and Ar_2TeCl_2 respectively, according to Bergman.[4] The preparation of Ar_2SeCl_2 was carried out according to Alqvist[5] with some modifications. A solution of $SeOCl_2$ (16.6 g, 0.1 mol) and anisole (21.6 g, 0.2 mol) in dry ether (100 ml) was stirred for 20 h, at 25 °C. After concentration the solid formed was collected, washed with cold ether, dried and recrystallized from ethanol. Yield: 91 %, m.p. 159–160 °C (lit.[5] 163 °C). Ar_2TeCl_2 was synthesized according to Bergman.[4] ArSeCN was prepared as described by Behagel.[6] MS, *m/e* (rel. intensity) 215 (6), 213 (31), 211 (16), 210 (6), 209 (6), 187 (9), 172 (5), 170 (7), 144 (5), 134 (10), 133 (100), 103 (10). Only peaks above *m/e* 100 and stronger than 4 % of the base peak are listed.

Ar_2Se_2 was prepared using the method of Rheinboldt and Giesbrecht[7] with some modifications. ArSeCN (1 g) was stirred for 5 h in 2 M NaOH (25 ml), at 25 °C. The solid formed was collected, dried and recrystallized from ethanol. It is important that the ArSeCN is pure. If not, the crude diselenide is very difficult to purify. Yield 80 %, m.p. 49.5–50.0 °C (lit.[8] 50.7–51.6 °C). MS, *m/e* (rel. intensity) 376 (14), 375 (7), 374 (42), 373 (9), 372 (38), 371 (15), 370 (23), 369 (7), 368 (9), 214 (10), 199 (5), 189 (19), 188 (10), 187 (100), 186 (7), 185 (50), 184 (19), 183 (20), 172 (18), 170 (9), 144 (12), 142 (6). Only peaks above *m/e* 100 and stronger than 4 % of the base peak are listed.

Ar_2Te_2 was synthesized from $ArTeCl_3$[9] by reduction with hydrazine.[4]

The methanol used as solvent (Fluka, *p.a.*) was distilled in a packed column after addition of 2,4-dinitrophenylhydrazine and H_2SO_4. The solutions were freed from oxygen by purging with Ar (Aga SR-quality) for half an hour. The N_2O (Aga) was

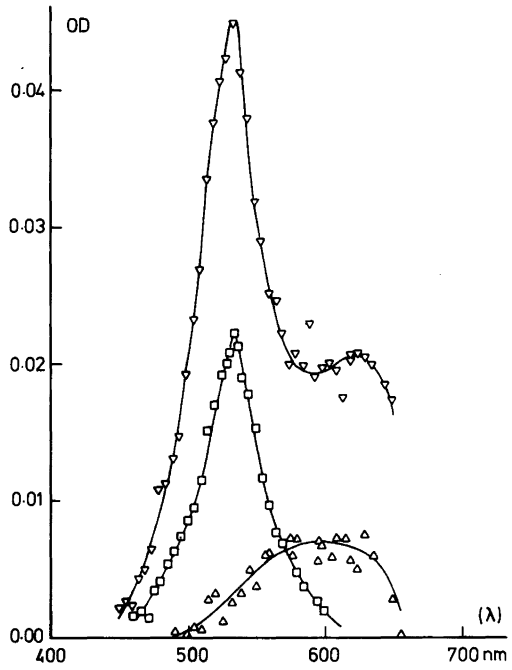

Fig. 1. Transient absorptions in pulse irradiated methanolic solutions of Ar_2Se and Ar_2Se_2. □, $\sim 10^{-2}$ mol dm^{-3} Ar_2Se in acid (0.5×10^{-3} mol dm^{-3} H_2SO_4) and neutral solution. Dose: 3.3 krad. $\sim 10^{-3}$ mol dm^{-3} Ar_2Se_2, neutral solution; ▽, immediately after electron pulse; △, 40 μs after electron pulse; Dose: 2.40 krad.

used as received. The solutions were acidified with H_2SO_4 (Merck, *p.a.*).

The accelerator and pulse radiolysis set up are described elsewhere.[10,11] The irradiation cell used was of 2 cm optical path length. Conductivity measurements could be started 0.5 μs after electron pulse.

RESULTS AND DISCUSSION

About 10^{-9} s after the radiation induced decomposition of methanol the main products are $CH_3O\cdot$, $\cdot CH_2OH$, e_s^- and H·. The *G*-values are $G(CH_3O\cdot + \cdot CH_2OH) = 2.5$, $G(e_s^- + H\cdot) = 3.7$ and $G(e_s^-) \simeq 1.3$.[12] $CH_3O\cdot$ is converted into $\cdot CH_2OH$ within 10^{-7} s. On addition of H^+ or N_2O the solvated electrons (e_s^-) are converted into H· or $\cdot CH_2OH$ radicals, respectively.

The transient absorption spectra obtained from pulse irradiated solutions of Ar_2Se and Ar_2Se_2 are shown in Fig. 1. In acid (5×10^{-3} mol dm^{-3} H_2SO_4) and neutral Ar_2Se solutions an absorption with maximum at 535 nm was obtained. In acid Ar_2Se_2 solutions a more intense but otherwise identical absorption was obtained, whereas in neutral solution a shoulder on the low energy side of the spectrum with absorption maximum at ~600 nm appeared immediately after the electron pulse. This absorption was found to decay much slower than the 535 nm absorption. The transient decayed without the formation of any optically observable products in the wavelength range 420–650 nm. On N_2O-saturating neutral and slightly acid (5×10^{-7} mol dm^{-3} H_2SO_4) 0.87×10^{-2} mol dm^{-3} methanolic solutions of Ar_2Se the absorption intensity at 535 nm decreased by a factor of 2.5 and 2.33, respectively, (Table 1) clearly indicating that the 535 nm absorption must be assigned to a radical/radical ion with both the solvated electron and H· as precursors. The plot of 1/OD at 535 nm *versus* $1/C(Ar_2Se)$ in pulse irradiated acid solution (10^{-2} mol dm^{-3} H^+) (Fig. 2) gives a straight line. From the intercept of this plot we obtain $G\varepsilon = 9000$ whereas in acid solution of Ar_2Se_2 $G\varepsilon$ was found to be concentration independent in the concentration range ($10^{-4} - 10^{-3}$) mol dm^{-3} and equal to 14 700. No change in electrical conductivity was detected in slightly acid or neutral solutions of Ar_2Se.

Table 1. Effect of proton concentration and N_2O on intensity of the transient absorption at 535 nm on pulse radiolysis of 0.87×10^{-2} mol dm^{-3} methanolic solution of Ar_2Se. Dose 3.6 krad.

C_{H^+} mol dm^{-3}	Purging gas	OD_{235}	(OD_{Ar}/OD_{N_2O})
1.2×10^{-2}	Ar	0.012(1)	
Neutral	Ar	0.010(1)	2.5
Neutral	N_2O	0.004(1)	
10^{-6}	Ar	0.014(1)	2.33
10^{-6}	N_2O	0.006(1)	

In alkaline methanol an irreversible decomposition of the selenium compound seems to take place.

To accomodate the experimental results we assign the 535 nm absorption to the only possible common uncharged selenium centered radical ArSe· and propose the reactions.

$$e_s^- + Ar_2Se \xrightarrow[H^+, CH_3OH]{k_1} ArSe\cdot + ArH \qquad (1)$$

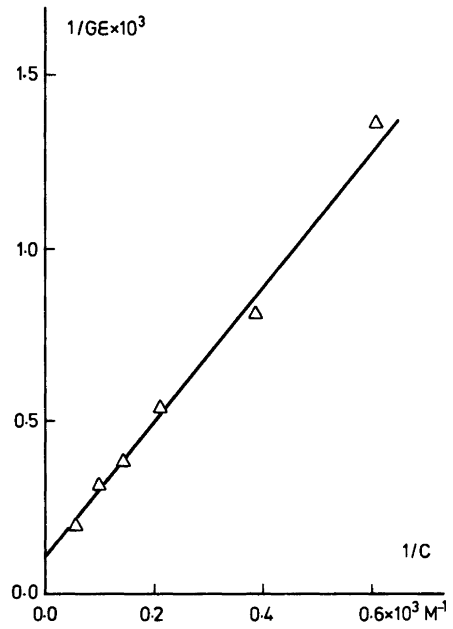

Fig. 2. $1/G\varepsilon$(535 nm) in pulse irradiated methanolic solutions of Ar_2Se *vs.* $1/C(Ar_2Se)$.

$$H\cdot + Ar_2Se \xrightarrow{k_2} ArSe\cdot + ArH \qquad (2)$$

According to this mechanism $ODAr/OD_{N_2O}$ at 535 nm equals the ratio $[G(e_s^-)+G(H)]/G(H)$ when all e_s^- and H· react with Ar_2Se. From Fig. 2 it is estimated that in 0.87×10^{-2} mol dm^{-3} Ar_2Se solution ~38 % of all H· radicals react with Ar_2Se. Taking this into account and using the G-values given above $ODAr/OD_{N_2O}$ is calculated to be 2.43 which is in very good agreement with the values 2.5 and 2.33 obtained from the experimental data in Table 1.

The kinetic plot in Fig. 2 is explained by the competition between reactions (2) and (3)

$$H\cdot + CH_3OH \xrightarrow{k_3} H_2 + \cdot CH_2OH \qquad (3)$$

and from the slope we obtain $k_2/k_3 = 1.36\times10^3$. Assuming $k_3 = 1.6\times10^6$ M^{-1} s^{-1} [13] the rate constant k_2 is calculated to be $(2.2\pm0.2)\times10^9$ M^{-1} s^{-1}.

The transient absorptions in acid (5×10^3 mol dm^{-3} H_2SO_4) 1.5×10^{-5} mol dm^{-3} Ar_2Se solution 2 and 15 μs after pulse irradiation are shown in in Fig. 3. The absorption with maximum at 305 nm is assigned to a cyclohexadienyl type radical and

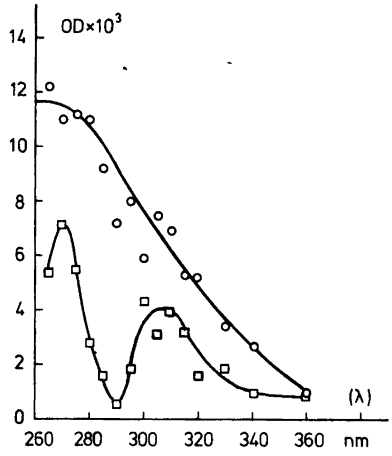

Fig. 3. Transient absorption in pulse irradiated 1.5×10^{-5} mol dm^{-3} acid (5×10^{-3} mol dm^{-3} H_2SO_4) solution of Ar_2Se. ○, 2 μs after electron pulse; □, 15 μs.

the rate constant for the reaction of $\cdot CH_2OH$ with Ar_2Se is estimated from the growing in of the 305 nm and the decay of the $\cdot CH_2OH$ absorption to be $\sim10^9$ M^{-1} s^{-1}.

The two absorption bands obtained in neutral $ArSe_2$ solutions are suggestive of two reaction modes according to reactions (4) and (5) and we assign the 600 nm absorption to the radical ArSeSe·.

$$e_s^- + Ar_2Se_2 \xrightarrow{CH_3OH,H^+} ArSe\cdot + ArSeH \qquad (4)$$

$$\searrow\ ArSeSe\cdot + ArH \qquad (5)$$

Using Baxendales and Mellows [12] methanol data $G(H\cdot + e_s^-)$ ~3.7 G(scavengable radicals) ~6.5 and the ratio of the experimental G-values ~1.63 in acid solution at least 83 % of all accessible radicals other than hydrogen atoms were found to react with Ar_2Se_2 to give ArSe·, *i.e.* the hydroxymethyl radical reacts according to eqn. (6).

$$\cdot CH_2OH + Ar_2Se_2 \rightarrow ArSe\cdot + \text{prod.} \qquad (6)$$

The decay of the 535 nm absorption in Ar_2Se solutions follows pseudo first-order kinetics and from the plot in Fig. 4 of the observed first-order rate constant *versus* Ar_2Se concentration the rate constant of reaction 7 was found to be $k_7 = 8\times10^5$ M^{-1} s^{-1}.

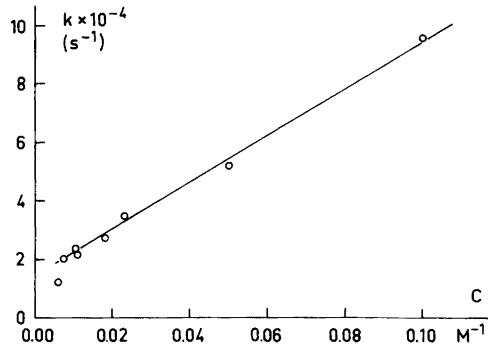

Fig. 4. The observed rate constant for the reaction $ArSe\cdot + Ar_2Se \rightarrow$ prod. *vs.* Ar_2Se concentration ($k_7 = 8 \times 10^5$ M^{-1} s^{-1}).

$$ArSe\cdot + ArSe \xrightarrow{k_7} \text{prod.} \qquad (7)$$

The fact that the straight line in Fig. 4 does not pass through origo indicates competition between reaction (7) and second-order reactions at low Ar_2Se concentration.

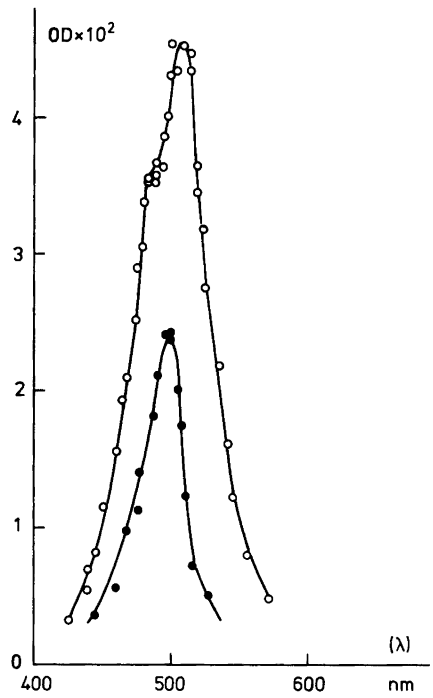

Fig. 5. Transient spectra in pulse irradiated Ar_2Te_2 and Ar_2Te solution in ○, methanol; ●, cyclohexane.

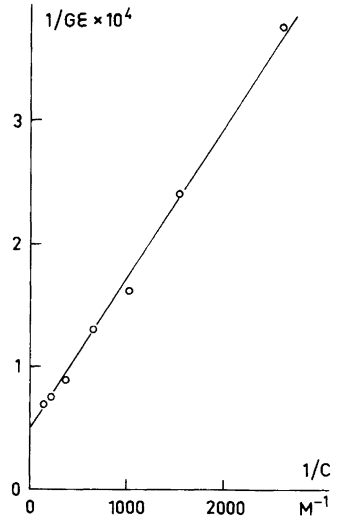

Fig. 6. $G\varepsilon$ at 508 nm in pulse irradiated methanolic Ar_2Te solutions *vs.* Ar_2Te concentration.

In acid and neutral methanolic solutions of the corresponding tellurides and ditellurides a transient absorption with maximum at 508 nm and a small shoulder on the high energy side of the spectrum ($\lambda \sim 490$ nm) was obtained (Fig. 5). In cyclohexane, however, a transient absorption with no shoulder and the maximum shifted to 498 nm was obtained. The absorptions are assigned to the tellurium centered radical ArTe·.

A plot of $1/G\varepsilon$ at 508 nm *versus* $1/C(Ar_2Te)$ in pulse irradiated solutions gives a straight line in accordance with the competition between reactions (8) and (3).

$$H\cdot + Ar_2Te \rightarrow ArTe\cdot + ArH \qquad (8)$$

From the intercept and slope of the plot in Fig. 6 the rate constant is calculated to be $k_8 = 1.5 \times 10^{10}$ M^{-1} s^{-1}.

The $G\varepsilon$ -values were found to be the same in methanolic solutions of both telluride and ditelluride. This clearly indicatesthat the hydroxymethyl radicals react very slowly or not at all with Ar_2Te_2.

Acknowledgement. The financial support by the Swedish Atomic Research Council is gratefully acknowledged.

REFERENCES

1. a. Günther, W. H. H., Chu, J. Y. C. and March, D. G. *Chem. Scr. A 8* (1975) 115; b. Marsh, D. G., Chu, J. Y. C., Lewicki, J. W. and Weaver, J. L. *J. Am. Chem. Soc. 98* (1976) 8432.
2. Chu, J. Y. C., Marsh, D. G. and Günther, W. H. H. *J. Am. Chem. Soc. 97* (1975) 4905.
3. Schmidt, U., Müller, A. and Markau, K. *Chem. Ber. 97* (1964) 405.
4. Bergman, J. *Tetrahedron 28* (1972) 3323.
5. Alqvist, F. N. and Nelson, R. E. *J. Am. Chem. Soc. 53* (1931) 4033.
6. Behagel, O. and Rollman, M. *J. Prakt. Chem. 123* (1929) 336.
7. Rheinboldt, H. and Giesbrecht, E. *Chem. Ber. 88* (1955) 666.
8. Rheinboldt, H. In Houben-Weyl, *Methoden der organischen Chemie*, Vol. IX, Schwefel-Selen und Tellurverbindungen, 4th Ed., Thieme, Stuttgart 1955, p. 1095.
9. Reichel, L. and Kirschbaum, E. *Justus Liebigs Ann. Chem. 523* (1936) 211.
10. Rosander, S. *Diss. 1974*, TRITA-EPP-74-16, p. 28.
11. Eriksen, T. E., Lind, J. and Reitberger, T. *Chem. Scr. 10* (1976) 5.
12. Baxendale, J. H. and Mellows, F. W. *J. Am. Chem. Soc. 83* (1961) 4720.
13. Neta, P. and Dorfman, L M. *J. Phys. Chem. 73* (1969) 413.

Received December 27, 1977.

Acta Chemica Scandinavica A 32 (1978) 461 – 465

Catalysis by Coordinatively Unsaturated Surface Compounds of Chromium(II), Iron(II), Cobalt(II) and Nickel(II) on Silica Gel. II. Decomposition of N_2O, Reduction of N_2O by CO and Oxidation of CO by O_2

BERND REBENSTORF, LENNART LARSSON and RAGNAR LARSSON

Division of Inorganic Chemistry 1, Chemical Center, University of Lund, Box 740, S-220 07 Lund 7, Sweden

The coordinatively unsaturated surface compounds of chromium(II), iron(II), cobalt(II) and nickel(II) on silica gel catalyse the reduction of N_2O by CO, the oxidation of CO by O_2 and, with the exception of chromium(II), the decomposition of N_2O. No simple increase or decrease of the catalytic activity was observed in the series from chromium to nickel. On the basis of the chemisorption of N_2O, CO and O_2 by the surface compounds reaction mechanisms are discussed including the reduction of NO by CO.

In the first paper of this series[1] we reported the catalytic activity of the four coordinatively unsaturated surface compounds of chromium(II),[2] iron(II),[3] cobalt(II)[4] and nickel(II)[5] on silica gel for the decomposition of NO and the reduction of NO by CO.

On the basis that firstly CO,[2-5] and N_2O[6] in the case of chromium(II), are known to be chemisorbed by the coordinatively unsaturated surface compounds and secondly that O_2 reacts with some of these compounds (chromium(II),[2] iron(II)[3]), catalytic reactions may be expected. In fact for cobalt(II), the catalytic oxidation of CO by O_2 has been observed previously.[4]

EXPERIMENTAL

The preparation of the catalyst samples has been described previously for chromium(II),[1] iron(II),[3] cobalt(II)[4] and nickel(II).[5] The metal content of the samples was 0.7 % for iron(II) and 0.6 % for the others.

The catalytic reactions were performed with the samples placed in a column with an inner diameter of 8 mm, a heated length of 200 mm and an effective sample mass of about 6 g. The gases were dried before entering the column by a molecular sieve and phosphorus pentoxide. The gas flow was adjusted to 10 ml/min for N_2O (N_2O decomposition), 5 ml/min for both N_2O and CO (N_2O reduction by CO), 2 ml/min for O_2 and CO with 16 ml/min for N_2 (CO oxidation by O_2) and 12, 5 and 3 ml/min for CO, N_2O and NO, respectively (N_2O/NO reduction by CO).

N_2O, NO, N_2, CO and O_2 were determined using a Perkin-Elmer F 17 gas chromatograph equipped with a separation column filled with molecular sieve 13 X, mesh 45/60.

RESULTS

N_2O decomposition. During the decomposition of N_2O only one reaction occurs:

$$N_2O \rightarrow N_2 + \tfrac{1}{2}O_2$$

In contrast to the NO decomposition[1] the catalytic activity is higher for cobalt(II) than for iron(II) and is also higher for all three surface ions than for the decomposition of NO (Fig. 1). As in the case of the NO decomposition, the oxygen produced destroys the surface compound of chromium(II) by oxidising it to chromium(VI) and therefore no catalytic activity was observed in this case.

N_2O reduction by CO. Only one reaction occurs also during the reduction of N_2O by CO:

$$N_2O + CO \rightarrow N_2 + CO_2$$

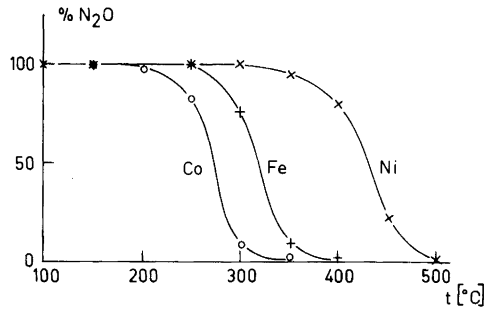

Fig. 1. Decrease of N_2O over iron(II), cobalt(II) and nickel(II) on silica gel as a function of temperature for the decomposition of N_2O.

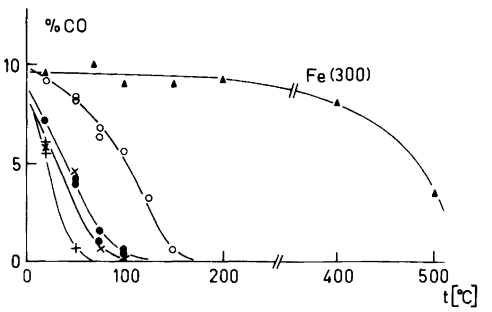

Fig. 3. CO decrease during oxidation of CO by O_2 over chromium(II), iron(II), cobalt(II) and nickel(II) on silica gel (pretreatment at 1000 °C/10^{-2} Torr) and iron(II) (pretreatment at 300 °C) *versus* temperature.

The nickel(II) surface compound has a relatively high catalytic activity in this reaction, while the three other surface ions show the same order when compared to the reduction of NO by CO (Fig. 2). Again the catalytic activity is higher for the reduction of N_2O than for NO.

Oxidation of CO by O_2. Also here only one reaction has to be considered:

$$O_2 + 2CO \rightarrow 2CO_2$$

During this reaction the highest activity is shown by iron(II), followed by nearly equal activity for chromium(II) and nickel(II) (Fig. 3). Cobalt(II) has the lowest activity.

In Fig. 3 the catalytic activity of a sample of iron(II) pretreated in a vacuum at 300 °C (low compared with the pretreatment temperature of 1000 or 800 °C (Cr) for the other samples used in this work) is shown to be very low. In fact, the catalytic activity increases only when the temperature is raised to a value at which the coordinatively unsaturated iron(II) surface compound is produced.[3] This is an indication that the coordinatively unsaturated surface ions really are the catalytic centers in this reaction. This does not hold for chromium(II) because of its oxidation to chromium(VI). On the basis of the above observation and with the results of both the NO decomposition and the NO reduction by CO[1] in mind, the conclusion that the coordinatively unsaturated surface compounds are the catalytic centers is thought to be valid also for the other two catalytic reactions above.

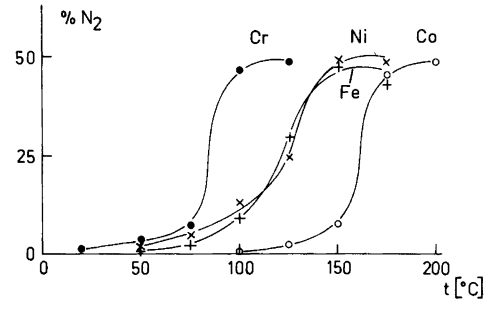

Fig. 2. N_2 production by N_2O reduction with CO over chromium(II), iron(II), cobalt(II) and nickel(II) on silica gel as a function of temperature.

Combined reduction of NO and N_2O by CO. For the NO reduction by CO the problem of whether N_2O is only a reaction product formed in a distinct temperature region[1,7] or an intermediate reaction product[8,9] is still not resolved in a satisfactory way. For this reason the combined reduction of NO and N_2O by CO was examined. Three reactions may occur:

1. $2\,NO + 2CO \rightarrow N_2 + 2\,CO_2$
2. $2\,NO + CO \rightarrow N_2O + CO_2$
3. $N_2O + CO \rightarrow N_2 + CO_2$

This catalytic reaction was only examined with iron(II). As Fig. 4 shows the N_2O only reacted after all NO had been transformed to N_2O (or N_2), although the reaction of N_2O alone with CO takes place at a lower temperature than that of NO with CO. This indicates that as long as NO is not transformed entirely it is bound to the catalytic active sites and blocks them.

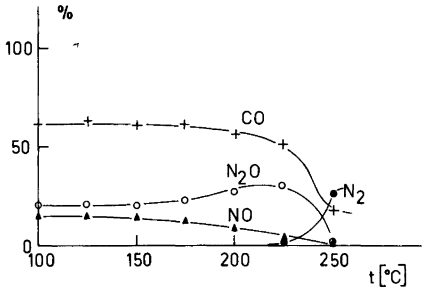

Fig. 4. Combined reduction of NO and N_2O by CO over iron(II) on silica gel *versus* temperature.

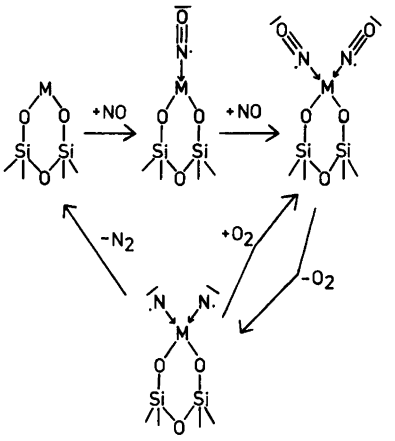

Scheme 1.

DISCUSSION

During the reduction of NO by CO, the first product after raising the temperature is N_2O (later replaced by N_2) while during decomposition of NO only N_2 is produced. In contrast to this difference the catalytic activity decreases nearly in the same order from chromium(II) to nickel(II) (reduction of NO by CO) or from iron(II) to nickel(II) (decomposition of NO). This may point to a reaction model in which the rate-determining step involves the same intermediate species or partly so.[1]

The catalytic activity of the three surface metal ions during the decomposition of N_2O can be correlated with the adsorption enthalpy of the N_2O chemisorption (at least qualitatively), which has the values 34, 12, 20 and 9 (arbitrary scale, 760 Torr/20 °C) for chromium(II), iron(II), cobalt(II) and nickel(II), respectively.[10] In contrast to the decomposition of NO, which reaches in the best case [iron(II)] only 75 % conversion[1] and is possibly controlled by product O_2, the decomposition of N_2O reaches 100 % (Fig. 1). While it may be concluded that during the decomposition of NO the reaction product O_2 can be readsorbed and react with the two adsorbed nitrogen atoms to yield the starting compound again, *i.e.* the surface compound with the two adsorbed NO molecules (Scheme 1), this cannot occur for the decomposition of N_2O.

The order of the catalytic activity between nickel(II) and cobalt(II) for the decomposition of N_2O is the reverse of that for the reduction of N_2O by CO. This may be an indication that N_2O and CO compete for adsorption at the catalytic sites. In fact the adsorption enthalpies of CO lie in the same range as those of N_2O with values of 26, 14, 20 and 28.5 (arbitrary scale, 760 Torr/20 °C) for chromium(II), iron(II), cobalt(II) and nickel(II), respectively. However, a simple quantitative correlation does not exist.

Similarly, the catalytic activity of the surface ions during the oxidation of CO by O_2 may be explained by the assumption that for cobalt(II) and nickel(II) CO is predominantly adsorbed while for chromium(II) and iron(II) O_2 is bonded more strongly. For the latter two surface ions, chromium(II) forms by oxidation to chromium(VI) the most strongly bonded oxygen and may be relatively difficult to reduce thereafter,[2] at least when compared with the product of the oxidation or chemisorption of iron(II) and oxygen.

Fig. 4 shows that in a mixture of NO, N_2O, CO, N_2 and CO_2 the most strongly bound molecule is NO. The same was observed by measuring the adsorption enthalpies and it should be noted that this was also shown for transition metal oxide catalysts.[11] However, this does not provide a solution to the problem of whether N_2O is a necessary intermediate or only a reaction product in a certain temperature region. The following discussion may provide some arguments for the case of a reaction product in a certain temperature region only.

In Ref. 1 it was observed that only for chromium(II) does N_2O reach the peak value of nearly 33 % during the reduction of NO by CO. For iron(II) nearly 18 % (for both the preparation temperatures of 1000 and 500 °C), for cobalt(II) 25 % and for nickel(II) 21 % were found. Similar observations have been reported by other authors.[12] The best explanation for this behaviour seems to

be the assumption that while N_2O is produced, the additional reaction step to N_2 has already begun in the case of iron(II), cobalt(II) and nickel(II). Such a reaction is thought to be proof of the reaction mechanism in Ref. 1, as it seems rather unlikely that N_2O can displace NO at the catalytic active centers while NO is still in the gas mixture. However, as will be shown below, N_2O may be reduced by CO at higher temperatures under these conditions.

In Ref. 12 (Fig. 1) NO surplus (CO/NO: 1.2/1.9) was used and an unusual reaction was observed. At appropriate conditions NO was reduced almost entirely to N_2O at certain temperatures. However at higher temperatures, when the product of the reduction is N_2, NO reappeared and reached nearly half of its initial value. If N_2O is an absolute intermediate of the NO reduction then this observation would mean that N_2O disproportionates at higher temperatures than NO and N_2. Such a reaction was not observed during the decomposition of N_2O mentioned above and is most unlikely as the N=N bond should be conserved. However, in the reaction mechanism where N_2O is only produced at a certain temperature region, an apparent disproportionation is occurring as the formation of N_2 is taking place after the reduction of the second NO molecule (Ref. 1).

Fig. 3 in Ref. 12 has the initial conditions N_2O:CO:NO of 0.7, 1.4 and 2.2 and with increasing temperature additional N_2O is produced, as would be expected, to give ratios of the above gases of 1.2, 0.7 and 1.0 (220 °C). At 300 °C all N_2O reacts to N_2, while the amount of NO in the gas phase rises again (0, 0, 1.5). The reduction of N_2O in the presence of NO can be explained by the assumption that after the complex with two NO molecules at the transition metal ion surface compound is formed, CO and N_2O compete for the fifth coordination site. More specifically, it may be suggested that after a CO molecule has been chemisorbed, reacted to CO_2 and a chemisorbed nitrogen atom and left the surface ion, an N_2O molecule may be chemisorbed, react to N_2 by oxidising the adsorbed nitrogen atom to NO and desorb as an N_2 molecule (Scheme 2).

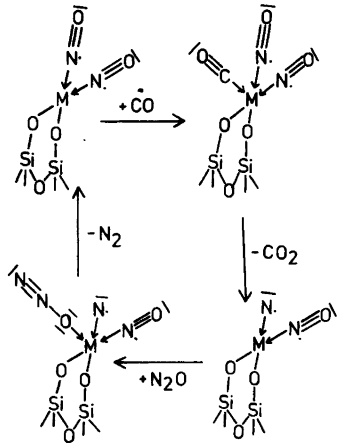

Scheme 2.

This reaction mechanism does not discredit the result of the above discussion that N_2O is only a product in a certain temperature region, because in that case nearly all NO had reacted and so the basis for the above reduction does not exist.

All five catalytic reactions discussed above are known to occur also on transition metal oxides. This seems to be a basis for applying reaction mechanisms and models of the catalytic center gained for the reactions with the coordinatively unsaturated surface compounds on silica gel, as shown above, also to transition metal oxide surfaces. It may be further suggested that the coordinatively unsaturated surface compounds on silica gel may be used as "model surface sites" of transition metal oxides.

Acknowledgement. This work has been financially supported by the Swedish Board of Technical Development and by the Deutsche Forschungsgemeinschaft. The latter agency has given a grant to one of us (B. R.), which made it possible for him to work in Sweden.

REFERENCES

1. Rebenstorf, B., Larsson, L. and Larsson, R. *Acta Chem. Scand. A 31* (1977) 877.
2. Krauss, H. L. and Stach, H. *Z. Anorg. Allg. Chem. 366* (1969) 34.
3. Rebenstorf, B. *Acta Chem. Scand. A 31* (1977) 547.
4. Rebenstorf, B. *Acta Chem. Scand. A 31* (1977) 208.
5. Rebenstorf, B. *Acta Chem. Scand. A 32* (1978) 195.
6. Krauss, H. L. and Weisser, B. *Z. Anorg. Allg. Chem. 412* (1975) 82.
7. Shih, S. S., Shihabi, D. S. and Squires, R. G. *Proc. 6th Int. Congr. Catal.* (1976) *2* (1977) 978.
8. Shelef, M. and Kummer, J. T. *AIChE Symp. Ser. 67* (115) (1971) 74.
9. Shelef, M. *Catal. Rev.-Sci. Eng. 11* (1975) 1.

10. Rebenstorf, B. *Unpublished results.*
11. Winter, E. R. S. *J. Catal. 22* (1971) 158; Amirnazmi, A., Benson, J. E. and Boudart, M. *J. Catal. 30* (1973) 50.
12. Shelef, M. and Otto, K. *J. Catal. 10* (1968) 408.

Received January 13, 1978.

Acta Chemica Scandinavica A 32 (1978) 467–470

Short Communications

Ion Pair Formation of Rubidium Iodide in 1-Butanol at 25 °C

PER BERONIUS

Department of Physical Chemistry,
University of Umeå, S-901 87 Umeå, Sweden

As part of a study of the structure of univalent electrolytes in n-alcohols the association constant for ion pair formation of rubidium iodide in 1-butanol at 25 °C was determined by electrical conductance measurements. A survey of the literature reveals that precise conductance data referring to this solvent are available for only a few salts, see, *e.g.*, Ref. 1.

Experimental. The solvent (Merck, *pro analysi*) was dried using a molecular sieve (Fischer, type 4A) and fractionally distilled; electrolytic conductivity, $\kappa = 2.5 \times 10^{-9}$ S cm^{-1}; $d = 0.80601$ g cm^{-3} (lit.[2] 0.8060 g cm^{-3}). The values, $\eta = 0.0246$ P and $\varepsilon = 17.51$, for the viscosity[1] and relative permittivity,[2] respectively, were used in the calculations. Rubidium iodide (Merck, *suprapur*) was dried for 4 h at 110 °C.

The two conductivity cells used, each of 300 cm^3 capacity, were of the Daggett-Bair-Kraus type.[3] They were fitted with bright platinum electrodes. The cell constants were 0.055727 and 0.056040 cm^{-1}. Conductivity measurements were performed at 25.00±0.03 °C and different frequencies between 2 and 5 kHz using a Leeds and Northrup conductivity bridge and extrapolated to infinite frequency.

Table 1. Dependence of molar conductivity on concentration of rubidium iodide in 1-butanol at 25 °C.

Run A $c \times 10^4$ M	Λ S cm^2 mol^{-1}	Run B $c \times 10^4$ M	Λ S cm^2 mol^{-1}
1.9994	14.298	1.9213	14.405
3.9532	12.619	3.9274	12.629
6.0083	11.484	5.9695	11.506
8.0462	10.649	7.9974	10.668
10.053	10.041	10.055	10.041
12.033	9.5517	11.989	9.5684

Calculations and results. Molar conductivities, Λ, for different rubidium iodide concentrations, c, are given in Table 1. To avoid disturbances due to formation of higher aggregates than ion pairs the measurements were confined to concentrations below 1.7 mM. This concentration limit was derived from the condition,[4]

$$c \leq 3.2 \times 10^{-7}\, \varepsilon^3 \qquad (1)$$

New expressions for the relaxation and electrophoretic terms, $\Delta X/X$ and $\Delta\Lambda_e$, in the conductance equation for pairwise associated symmetrical electrolytes,

$$\Lambda = \alpha[\Lambda_\infty(1 - \Delta X/X) - \Delta\Lambda_e] \qquad (2)$$

where α is the degree of dissociation and Λ_∞ is the limiting molar conductivity, have recently been derived by Fuoss.[5,6]

The association constant, K_A, Λ_∞, and $\sigma(\Lambda)$, *i.e.* the standard deviation between experimental and computed Λ values, were calculated from eqn. (2) and the law of mass action for the equilibrium between free and paired ions,

$$K_A = (1 - \alpha)/c\gamma^2\alpha^2 \qquad (3)$$

using a computer programme[7] similar to that outlined in Ref. 8. In eqn. (3) γ is the mean molar activity coefficient of free ions. The maximum center-to-center distance, R, between the ions in the ion pair was set equal to the Bjerrum radius.[9] The results of these calculations are given in Table 2 where "F75" refers to eqn. (2), *i.e.* the Fuoss equation[5,6] from 1975. For comparison the values of K_A and Λ_∞ according to the modified Fuoss-Hsia ("FHFP") and Pitts' ("PFPP") conductance equations[10,11] are included. Errors quoted are standard deviations.

Eqns. (2) and (3) may be combined to yield,

$$(\Lambda - HY)/(1 + RX) = \Lambda_\infty - K_A c\alpha\gamma^2\Lambda/(1 + RX) \qquad (4)$$

where $RX = -\Delta X/X$, and $HY = -\Delta\Lambda_e$. A graph according to eqn. (4) is shown in Fig. 1.

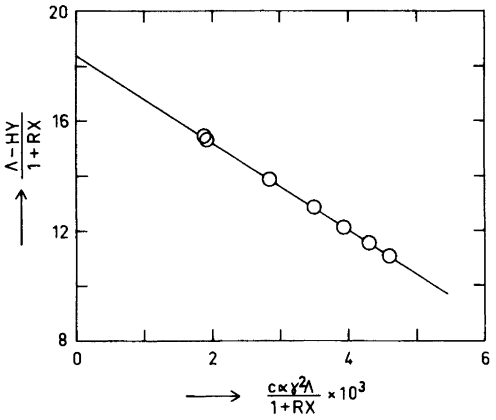

Fig. 1. Graph corresponding to eqn. (4) for rubidium iodide in 1-butanol at 25 °C.

Table 2. Data for rubidium iodide in 1-butanol at 25 °C.

Conductance equation	K_A M^{-1}	Λ_∞ S cm^2 mol^{-1}	$\sigma(\Lambda)$ S cm^2 mol^{-1}
F75	1593± 6	18.40±0.02	0.01
FHFP	1743± 7	18.48±0.02	0.01
PFPP	1663±13	18.32±0.04	0.02

An estimate of the distance of closest approach, a, of the ions in the ion pair may be obtained from the Bjerrum theory.[9] Using the value of K_A derived from the F75 equation (Table 2) one arrives at $a=3.0$ Å, which is close to the crystal radii sum for Rb^+ and I^-.

Acknowledgements. The author thanks Mrs. Margareta Ögren for technical assistance and the Swedish Natural Science Research Council for financial support.

1. Janz, G. J. and Tomkins, R. P. T. *Nonaqueous Electrolytes Handbook*, Academic, New York 1972, Vol. I.
2. Riddik, J. A. and Bunger, W. B. *Techniques of Chemistry, Organic Solvents*, 3rd Ed., Wiley-Interscience, New York 1970, Vol. II.
3. Daggett, H. M., Bair, E. J. and Kraus, C. A. *J. Am. Chem. Soc. 73* (1951) 799.
4. Fuoss, R. M. and Accascina, F. *Electrolytic Conductance*, Interscience, New York 1959, Chapter 18.
5. Fuoss, R. M. *J. Phys. Chem. 79* (1975) 525.
6. Fuoss, R. M. *J. Phys. Chem. 79* (1975) 1983.
7. Beronius, P. *Unpublished.*
8. Beronius, P. *Acta Chem. Scand. A 28* (1974) 77.
9. Bjerrum, N. *K. Dan. Vidensk. Selsk., Mat.-Fys. Medd. 7* (1926) No. 9.
10. Fernández-Prini, R. *Trans. Faraday Soc. 65* (1969) 3311.
11. Fernández-Prini, R. and Prue, J. E. *Z. Phys. Chem. (Leipzig) 228* (1965) 373.

Received April 21, 1978.

Properties of Sodium Iodide in 1-Octanol at 25 °C. A Conductimetric Study

PER BERONIUS

Department of Physical Chemistry,
University of Umeå, S-901 87 Umeå, Sweden

Comprehensive information regarding various interactions in electrolyte solutions may be provided by the very precise conductimetric method. In connection with investigations of solvent effects on the character of ion pairs, which may consist of ions in contact or of pair of ions separated by solvent molecules,[1] conductance measurements of highly diluted solutions of sodium iodide in 1-octanol at 25 °C were undertaken. The objective of this communication is to report the results and a few conclusions. This system has been studied previously by Shkodin *et al.*[2] but their data are of insufficient precision for our purposes.

Experimental. The electrolyte (sodium iodide, Merck, *suprapur*) was predried for 2 h at 110 °C and again dried under these conditions immediately before use. Precautions were taken to avoid absorption of moisture from the air. The solvent (1-octanol, Riedel De Haen AG), containing less than 0.018 vol.% of water according to Karl Fisher titration, was flushed for 3 h with dry nitrogen to remove dissolved oxygen; electrolytic conductivity, $\kappa = 2.9 \times 10^{-9}$ (Run A) and 3.8×10^{-9} S cm^{-1} (Run B).

The equipment used and the method of performing the conductivity measurements have been described.[3]

Table 1. Experimental data for NaI in 1-octanol at 25 °C.

Run A $c \times 10^4$ M	Λ S cm^2 mol^{-1}	Run B $c \times 10^4$ M	Λ S cm^2 mol^{-1}
0.62619	2.1529	0.54937	2.2333
0.83114	1.9624	1.0937	1.7793
1.0342	1.8192	1.6331	1.5412
1.2355	1.7096	2.1676	1.3868
1.4350	1.6203	2.6973	1.2769
1.6327	1.5450		
1.8287	1.4810		
2.0229	1.4255		
2.2154	1.3774		
2.4062	1.3347		
2.5954	1.2967		
2.7830	1.2625		
2.9689	1.2312		

Results and conclusions. Conductance data for two different runs are given in Table 1, where the molar conductivity, Λ, is quoted for several different sodium iodide concentrations in the interval, $5 \times 10^{-5} < c < 3 \times 10^{-4}$ M. The measurements must necessarily be confined to this narrow concentration interval because of disturbing triple ion formation at higher concentrations[4] and deteriorating precision at lower concentrations.

The ion pair association constant, K_A, and the limiting molar conductivity, Λ_∞, were calculated from the recent conductance equation of Fuoss,[5] which for pairwise associated symmetrical electrolytes may be written,

$$\Lambda = \Lambda_\infty(1 - \Delta X/X) - \Delta\Lambda_e - K_A c\alpha\gamma^2\Lambda \qquad (1)$$

where $\Delta X/X$ is the relaxation term, $\Delta\Lambda_e$ is the electrophoretic term, α is the unassociated fraction of the electrolyte, and γ is the mean activity coefficient of free ions, which was calculated from the Debye-Hückel equation in the form used in Ref. 6. The distance parameter in eqn. (1) and in the Debye-Hückel equation was set equal to the Bjerrum radius, which for univalent electrolytes in 1-octanol at 25 °C (relative permittivity,[2] $\varepsilon = 9.85$) amounts to 28.45 Å. The value, $\eta = 0.073$ P, for the viscosity[2] of the solvent was used. The computer programme used for these calculations is similar to that outlined in Ref. 6.

The values of K_A and Λ_∞ computed are given together with their standard deviations in Table 2, where $\sigma(\Lambda)$ is the standard deviation[6] between measured and calculated Λ values.

A graph according to eqn. (1), rewritten in linear form, is shown in Fig. 1. It is evident from this graph that the evaluation of Λ_∞ implies a quite long extrapolation. In spite of this Λ_∞ was obtained with a relative standard deviation of only a few tenth's percent, *cf.* Table 2.

Table 2. Conductance parameters for NaI in 1-octanol at 25 °C.

Run	$K_A \times 10^{-2}$ M^{-1}	Λ_∞ S cm^2 mol^{-1}	$\sigma(\Lambda)$ S cm^2 mol^{-1}
A	364 ± 1	4.389 ± 0.008	0.0007
B	353 ± 2	4.327 ± 0.016	0.0013
A + B	357 ± 2	4.353 ± 0.018	0.0025

Table 3. Data corresponding to eqn. (1) for 1-octanol as solvent at 25 °C.

Salt	$K_A \times 10^{-2}$ M^{-1}	Λ_∞ S cm^2 mol^{-1}
NaI	357	4.35
LiBr	518	3.85

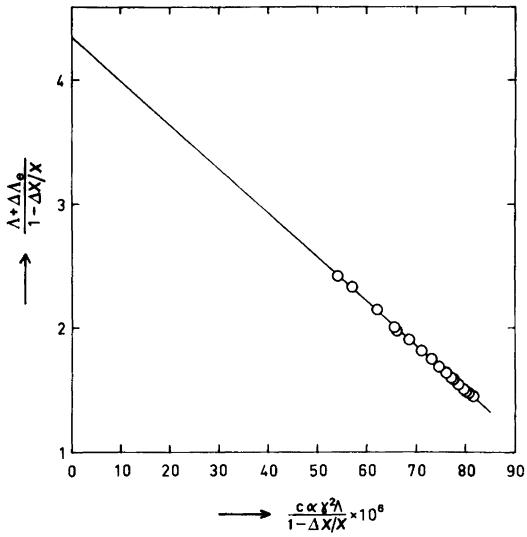

Fig. 1. Graph corresponding to eqn. (1) for NaI in 1-octanol at 25 °C.

Data according to eqn. (1) for lithium bromide [3] and sodium iodide in 1-octanol are compared in Table 3. It is found that $K_A(\text{LiBr}) > K_A(\text{NaI})$. This finding indicates that lithium bromide forms more tight ion pairs than does sodium iodide. The fact that $\Lambda_\infty(\text{LiBr}) < \Lambda_\infty(\text{NaI})$ reflects stronger ion-solvent interactions for Li^+ and Br^- as compared with Na^+ and I^-, respectively. In view of the different surface charge densities of the naked ions this is what might be expected.

Limiting molar conductivities of the iodide ion, $\lambda_\infty(I^-)$, in methanol, ethanol, 1-propanol, and 1-butanol at 25 °C have been previously established [7,8] (Table 4). The limiting transport number [9] of the iodide ion, $t_\infty^-(\text{NaI})$, in these alcohols varies but slightly, *viz.* from 0.567 to 0.580. The value of $\lambda_\infty(I^-)$ referring to 1-octanol in Table 4 was calculated assuming $t_\infty^-(\text{NaI}) = 0.57$ in this solvent.

The conductivity and viscosity data in Table 4 were used to calculate the Stokes' radius of the iodide ion from the expression,[10]

Table 4. Data referring to n-alcohols at 25 °C.

Solvent	$\lambda_\infty(I^-)$ S cm^2 mol^{-1}	Ref.	η P	Ref.
MeOH	63.12	7	0.005445	11
EtOH	27.36	7	0.01078	11
PrOH	13.87	7	0.01952	12
BuOH	9.66	8	0.0246	13
OctOH	2.48	This work	0.073	2

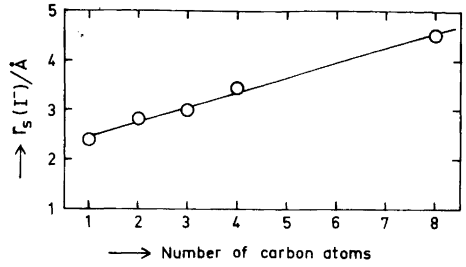

Fig. 2. Stokes' radius of the iodide ion in n-alcohols at 25 °C as a function of the number of carbon atoms in the solvent molecule.

$$r_s(I^-) = |z|F^2/(6\pi N\eta\lambda_\infty) \quad (2)$$

where z is the valency of the ion, F is the Faraday constant, and N is the Avogadro constant. The results, shown in graphical form in Fig. 2, indicate that $r_s(I^-)$ increases linearly with the number of carbon atoms in the solvent molecule.

Acknowledgements. The author thanks Mrs. Margareta Ögren for technical assistance and the Swedish Natural Science Research Council for financial support.

1. Winstein, S., Clippinger, E., Fainberg, A. H. and Robinson, G. C. *J. Am. Chem. Soc. 76* (1954) 2597.
2. Shkodin, A. M., Sadovnichaya, L. P. and Podolyanko, V. A. *Ukr. Khem. Zh. 35* (1969) 144.
3. Beronius, P. and Lindbäck, T. *Acta Chem. Scand. A 32* (1978) 423.
4. Fuoss, R. M. and Accascina, F. *Electrolytic Conductance*, Interscience, New York 1959, Chapter 18.
5. Fuoss, R. M. *J. Phys. Chem. 79* (1975) 525 and 1983.
6. Beronius, P. *Acta Chem. Scand. A 28* (1974) 77.
7. Beronius, P. *Unpublished.*
8. Vehlow, J. and Marx, G. *Naturwissenschaften 58* (1971) 320.
9. Ström, E. S. and Beronius, P. *Radiochem. Radioanal. Lett. 18* (1974) 143.
10. Robinson, R. A. and Stokes, R. H. *Electrolyte Solutions*, Butterworths, London 1965, p. 43.
11. Riddik, J. A. and Bunger, W. B. *Techniques of Chemistry, Organic Solvents*, 3rd Ed., Wiley-Interscience, New York 1970, Vol. II.
12. Evans, D. F. and Gardam, P. *J. Phys. Chem. 72* (1968) 3281.
13. Janz, G. J. and Tomkins, R. P. T. *Nonaqueous Electrolytes Handbook*, Academic, New York 1972, Vol. I.

Received June 5, 1978.

Acta Chemica Scandinavica A 32 (1978) 471 – 478

Metal Complexes with Mixed Ligands. 18. A Potentiometric and Spectrophotometric Study of the Systems Ni^{2+}—Cl^-, Ni^{2+}—Imidazole and Ni^{2+}—Cl^-—Imidazole in 3.0 M $(Na)ClO_4$,Cl Media

WILLIS FORSLING

Department of Inorganic Chemistry, University of Umeå, S-901 87 Umeå, Sweden

Equilibria between nickel(II), imidazole ($C_3H_4N_2$), OH^- and Cl^- were studied at 25 °C by means of potentiometric (glass electrode) and spectrophotometric titrations in media consisting of 3.0 M $(Na)ClO_4$, 3.0 M (Na)Cl and mixtures of these two with $0 \leq |Cl^-| \leq 3.0$ M. Besides pure binary species NiL_n^{2+}, $n=1$, 2, 3, 4, and $NiCl^+$, data can be explained with the ternary complexes $NiLCl^+$, NiL_2Cl^+, NiL_2Cl_2 and NiL_4Cl_2, ($L=C_3H_4N_2$). Formation constants for the ternary chloride species and molar absorption coefficients for the different binary species were evaluated within the wavelength range 350 – 750 nm. Data were analyzed with the least squares computer program LETAGROPVRID.

In parts 10[1] and 16[2] of this series equilibria in the system $Ni^{2+} - OH^- - C_3H_4N_2$ were studied in the media 3.0 M $(Na)ClO_4$, 3.0 M (Na)Cl and 1.0 M (Na)Cl. The results showed that besides the formation of stepwise metal complexes NiL_n^{2+}, $n=1,2,3,4$, also ternary species $Ni(OH)L^+$ [3.0 M $(Na)ClO_4$, 3.0 M (Na)Cl and 1.0 M (Na)Cl] and $Ni(OH)L_3^+$ [1.0 M (Na)Cl] were formed. However, differences in the complexation in the 3.0 M $(Na)ClO_4$ and 3.0 M (Na)Cl media indicate the formation of ternary $Ni^{2+} - C_3H_4N_2 - Cl^-$ species.

The present investigation was made to evaluate the possible formation of ternary $Ni^{2+} - C_3H_4N_2 - Cl^-$ complexes and the measurements were performed in media consisting of mixtures of 3.0 M $(Na)ClO_4$ and 3.0 M (Na)Cl with $0 \leq |Cl^-| \leq 3.0$ M. To determine the difference in absorbance in the chloride media due to the formation of ternary species, spectrophotometric titrations were employed in which both log $[H^+]$ and absorbance values were measured. This method was also used in an attempt to obtain a value of the constant for the formation of $NiCl^+$.

EXPERIMENTAL

Chemicals and analysis. All solutions used were prepared and analyzed as described earlier.[1]

Apparatus. The cell arrangement and experimental details of the emf measurements are fully described earlier.[1]

The spectrophotometer used was a Heath model 721 single beam instrument with an automatic sample-reference changer and was equipped with an automated potentiometric titrator. A detailed description of the automated potentiometric and spectrophotometric titration system will be given in a forthcoming paper by Ginstrup, Lyhamn and Ingri.[3] The sample cells were of flow-through type with path lengths of 1.001 cm (HELLMA, type 05) or 2.000 cm (HELLMA, type 05).

Method. The present study was carried out as a series of titrations in which both emf and absorbance values were measured, as in the system $H^+ - Ni^{2+} - C_3H_5N_2^+$ in 3.0 M $(Na)ClO_4$ and 3.0 M (Na)Cl media. However, in the investigations of the systems $H^+ - Ni^{2+} - C_3H_5N_2^+ - Cl^-$ and $Ni^{2+} - Cl^-$ in the mixed media 3.0 M $(Na)ClO_4$,Cl just emf-values resp. absorbance values were measured.

The potentiometric titrations were similar to those described in earlier papers.[1,4] The equilibrium solutions contained $|ClO_4^-| + X = 3.0$ M, where X

is the chloride concentration. The general compositions of the solutions were: B mM Ni^{2+}, C mM $C_3H_5N_2^+$, H mM H^+, X mM Cl^- ($|ClO_4^-| + X - C - H - 2B$) mM Na^+ and $3000 - X$ mM ClO_4^-. In the titrations the total concentrations of nickel (II), B, and imidazole, C, were varied, while the ratio C/B was always held constant. The total concentration of hydrogen ions, H, was calculated over the zero level, Ni^{2+}, $C_3H_5N_2^+$ and H_2O and the free hydrogen ion concentration, h, was varied by addition of OH^- and measured with a glass electrode. h was determined according to the relation

$$E = E_o + 59.157 \log h + E_j \quad (1)$$

where E_o is a constant determined in acid solutions where complex formation could be neglected. The liquid junction potential $E_j = -16.7\,h$ mV was used in 3.0 M (Na)ClO_4, 3.0 M (Na)Cl as well as in mixtures of these two media. It has earlier been shown by Sjöberg[4] that within the chloride concentration range $0 \le X \le 3.0$ M with $|ClO_4^-| + X = 3.0$ M the concentration scale for H^+ remains constant. No change in E_o could be found on replacing ClO_4^- by Cl^- or *vice versa*.

We will assume the presence of four-component equilibria of the general form

$$pH^+ + qNi^{2+} + rC_3H_5N_2^+ + sCl^- \rightleftharpoons (H^+)_p(Ni^{2+})_q(C_3H_5N_2^+)_r(Cl^-)_s;\ \beta_{pqrs} \quad (2)$$

It is convenient to write complexes where $-p = r$ as $Ni_q(C_3H_4N_2)_nCl_s^{(2q-s)+}$ and the stability constant as β_{nqs}. This terminology is used throughout this paper.

In addition to the four-component equilibria in (2) we have

(i) the complex formation between Ni^{2+} and Cl^-

$$Ni^{2+} + sCl^- \rightleftharpoons NiCl_s^{(2-s)+}; \quad (3)$$

(ii) the imidazole equilibria, which within the concentration range

$0 \le X \le 3.0$ M with $|ClO_4^-| + X = 3.0$ are

$$C_3H_5N_2^+ \rightleftharpoons C_3H_4N_2 + H^+;\ K_a \quad (4)$$

$$C_3H_5N_2^+ + Cl^- \rightleftharpoons C_3H_4N_2Cl^- + H^+;\ \beta_{101} \quad (5)$$

$$C_3H_5N_2^+ + 2Cl^- \rightleftharpoons C_3H_4N_2Cl_2^{2-} + H^+;\ \beta_{102} \quad (6)$$

with $\log K_a = -7.940$. $\log \beta_{101} = -8.641$ and $\log \beta_{102} = -9.279$.[4,5]

(iii) the nickel(II) imidazole equilibria

$$pH^+ + qNi^{2+} + rC_3H_5N_2^+ \rightleftharpoons H_pNi_q(C_3H_5N_2)_r^{(q+p+r)+}; \quad (7)$$

with equilibrium constants given in Table 1. In the present study the C/B-ratios were kept at high values, where the hydrolytic equilibria of the nickel(II) ion as well as formation of ternary nickel(II) – OH^- – L complexes could be neglected. The species $NiOHL^+$ is formed only at low C/B-ratios ($C/B \le 4$) and low B concentrations ($B < 5$ mM).

Equilibria (3)–(7) were determined in separate investigations and are assumed to be known in calculations concerning the four component equilibria.

The measurements using the combined emf and spectrophotometric method were performed in the following way: For each titration point the emf of the glass electrode was measured until equilibrium was obtained and then the transmittance, T, was recorded at a number of different wavelengths ($N\lambda$). As reference a 3.0 M $NaClO_4$ or 3.0 M NaCl solu-

Table 1. Results of the final LETAGROP calculations giving the formation constants for the "best fitting" complexes. The formation constants are related according to the reaction $nL + qNi^{2+} + sCl^- \rightleftharpoons L_nNi_qCl_s^{(2q-s)+}$, where L stands for $C_3H_4N_2$. When no $3\sigma(\log \beta_{nqs})$ is given, the formation constant has not been varied.

No. of titr./ no. of points	$\sigma(C-c)$ × 1000	$NiCl^+$ $\log(\beta_{011} \pm 3\sigma)$	NiL^{2+} $\log(\beta_{110} \pm 3\sigma)$	$NiLCl^+$ $\log(\beta_{111} \pm 3\sigma)$	NiL_2Cl^+ $\log(\beta_{211} \pm 3\sigma)$	NiL_3Cl^+ $\log(\beta_{311} \pm 3\sigma)$	NiL_2Cl_2 $\log(\beta_{212} \pm 3\sigma)$	NiL_4Cl_2 $\log(\beta_{412} \pm 3\sigma)$
19/271	0.28	−0.47	3.37[a]	3.16 ±0.03	5.48 ±0.12	8.29 ±0.07	5.70 ±0.03	10.17 ±0.06
6/39	0.14	−0.53 ±0.10	3.37 ±0.01	3.14 ±0.09				

[a] Ref. 1.

tion was used. The absorbance, OD, at a particular wavelength λ is given by the relation

$$OD_\lambda = l\Sigma\varepsilon_i c_i$$

where ε_i is the molar absorption coefficient for the absorbing species i at the wavelength λ and c_i the concentration of the same species. Thus the spectrophotometric measurements give data (OD, log h, H, B, C, $X)_{N\lambda}$.

Data treatment. It is possible to reduce the four component system $H^+ - Ni^{2+} - C_3H_5N_2^+ - Cl^-$ to the three component system $C_3H_4N_2 - Ni^{2+} - Cl^-$ under the assumption that $-p = r$ in eqn. (2), which means that only complexes of the type $Ni_qL_nCl_s^{(2q-s)+}$ are formed. With this assumption $|C_3H_4N_2|$ can be calculated according to the relation

$$|C_3H_4N_2| = K_a h^{-1}|C_3H_5N_2^+| = K_a h^{-1}(C-(h-H)); \quad (8)$$

where K_a is the acidity constant of $C_3H_5N_2^+$ in 3.0 M (Na)ClO_4. Thus as input to the computer, data in the form (A, log $|C_3H_4N_2|$, B, $X)_N$, $A = C - c$ are given instead of (H, log h, B, C, $X)_N$. This was done to save computer time, which is considerably greater with four components.

The mathematical analysis of the emf-data were performed with the least squares computer program LETAGROPVRID[6] (version ETITR).[7] On treating the data, the error squares sum $U = \Sigma(A_{calc} - A_{exp})^2$ was minimized, where A denotes $C - c$, *i.e.* the total imidazole concentration not obtained as $C_3H_5N_2^+$.

In calculations on the combined emf- and spectrophotometric data, the LETAGROP version TITRER-SPEFO[8] was used and $U = \Sigma(OD_{calc} - OD_{exp})^2$ was minimized.

The different standard deviations given, $3\sigma(\log \beta)$ and $\sigma(\varepsilon)$ were defined and calculated according to Sillén.[9] The computation was performed on a CDC3300 and a CYBER 172 computer.

DATA, CALCULATIONS AND RESULTS

Results from earlier measurements concerning the complex formation between nickel(II) and imidazole are given in Ref. 1.

The spectrophotometric measurements were performed to obtain accurate values of the molar absorption coefficients ε_{-nin} for the different nickel(II) species and both log h and absorbance were thereby measured.

Many workers have reported formation of a $NiCl^+$ complex and even $NiCl_2$ in aqueous solutions.[10] Only the former seems to be of importance at chloride concentration levels up to 3.0 M, but the reported log β_{11}-values for the formation of $NiCl^+$ are widely spread. An attempt to determine a value of β_{11} valid in the 3.0 M ionic medium was made by performing spectrophotometric titrations at a constant acidity level, where hydrolysis reactions are negligible.

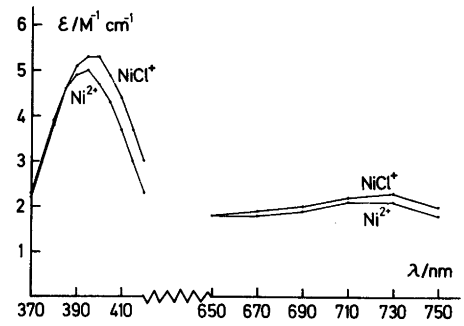

Fig. 1. Molar absorption coefficients, ε cm^{-1} M^{-1}, as a function of the wavelength, λ nm, plotted for the species $Ni(H_2O)_6^{2+}$ and $NiCl(H_2O)_5^+$.

The results obtained in the different investigations are given below.

(i) Nickel(II) chloride in mixtures of 3.0 M (Na)ClO_4 and 3.0 M (Na)Cl. Four different titrations were performed yielding 33 titration points and 528 absorbance values at 16 different wavelengths in the range 370–750 nm. The concentration ranges studied were $0.096 \leq B \leq 0.302$ M and $1.25 \leq X \leq 3.0$ M and the titrations were performed at a constant acidity level of $|H^+| = 0.030$ M. The calculations showed that within the concentration ranges investigated, the formation of the complex $NiCl^+$ could be established with log $K(Ni^{2+} + Cl^- \rightleftharpoons NiCl^+) = -0.47 \pm 0.10$. The standard deviations σ(OD) at the different wavelengths were all very small (0.001–0.002) thus indicating a good fit to experimental data (*cf.* Fig. 1).

(ii) Nickel(II) imidazole in 3.0 M (Na)ClO_4 medium. Four different titrations including 197 titration points were performed. 24 different wavelengths ranging from 350 to 750 nm were investigated and thus 4728 measured absorbance values were collected. The following concentration ranges were investigated: $0.018 \leq B \leq 0.062$ M, 0.115 M $\leq C \leq 0.240$ M, $1.2 \leq -\log h \leq 7.7$ with $C/B = 2, 4, 5$ and 11. Only mononuclear $Ni(C_3H_4N_2)_n^{2+}$ species are formed at these concentration ranges and the

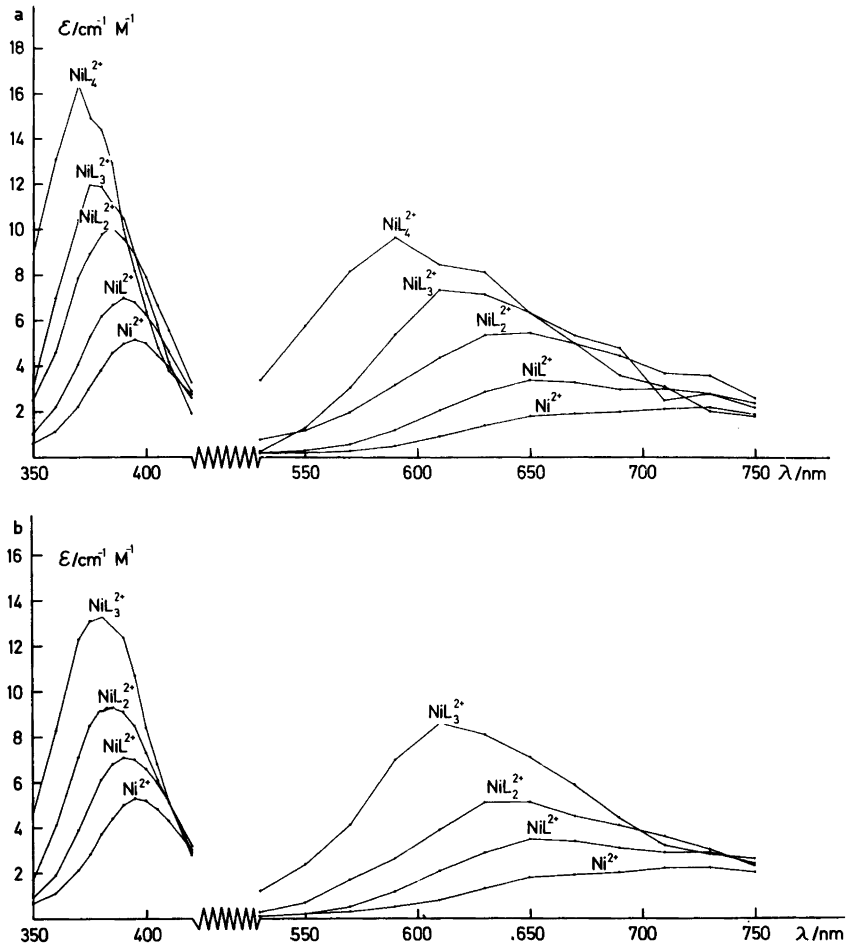

Fig. 2. Molar absorption coefficients, ε cm^{-1} M^{-1}, as a function of the wavelength, λ nm, plotted for the mononuclear species $Ni(C_3H_4N_2)_n^{2+}$, $n=0$, 1, 2, 3 and 4. (a) 3.0 M (Na)ClO_4 and (b) 3.0 M (Na)Cl medium. L stands for $C_3H_4N_2$. The errors $\sigma(\varepsilon)$ for the different species are ≤ 0.01 (Ni^{2+}), $0.02-0.07$ (NiL^{2+}), $0.02-0.10$ (NiL_2^{2+}), $0.05-0.3$ (NiL_3^{2+}) and ≤ 0.5 (NiL_4^{2+}), with the errors $\sigma(OD)=0.001-0.005$. A complete list of the molar absorption coefficients obtained at different wavelengths is available upon request.

molar absorption coefficients ε_{-n1n} for each of the different nickel(II) species were calculated at the wavelengths studied. The formation constants for the complexes were taken from Ref. 1 and a satisfactory fit to experimental data was obtained. Owing to the small absorption of the complexes no attempt to determine the formation constants β_{-n1n} from spectrophotometric data was made. The molar absorption coefficients ε_{-111} and ε_{-212} were determined in the range $0 \leq \bar{n} \leq 1.8$ and ε_{-313} and ε_{-414} in the range $1.8 \leq \bar{n} \leq 2.8$, where the first two were kept constant. Molar absorption coefficients (with standard deviations) of the different NiL_n^{2+}-species are given in Fig. 2.

(iii) Nickel(II) imidazoles in 3.0 M (Na)Cl medium. Four different titrations yielding 122 titration points were performed and the same wavelengths as in (ii) were covered, thus giving 2928 absorbance values. The following concentration ranges were investigated: $0.029 \leq B \leq 0.058$ M,

$0.086 \leq C \leq 0.353$ M, $0.85 \leq -\log h \leq 7.6$ with $C/B =$ 1.2, 5, 6 and 12. As in 3.0 M (Na)ClO_4 only mononuclear NiL_n^{2+} species are formed and no attempt to determine the β_{-n1n} values was made. The calculation of the molar absorption coefficients was performed as in (ii), but since precipitation appeared at $n_- \sim 2.5$ the value of ε_{-414} was not determined. As chloride ions are coordinated in the different species, the formation constants and molar absorption coefficients in 3.0 M (Na)Cl must be considered as conditional. However, only very small shifts to higher wavelengths are obtained for the different species and thus it seems to be impossible to evaluate the ternary $Ni^{2+} - C_3H_4N_2 - Cl^-$ complexes from spectrophotometric data. Molar absorption coefficients with standard deviations are given in Fig. 2.

(iv) Nickel(II) imidazoles in mixtures of 3.0 M (Na)ClO_4 and 3.0 M (Na)Cl. To evaluate the formation of the ternary $Ni^{2+} - C_3H_4N_2 - Cl^-$ complexes measurements were performed in the four-component system $H^+ - Ni^{2+} - C_3H_5N_2^+ - Cl^-$. The total nickel, B, the total imidazole, C, and the total chloride, X, were varied within the limits $0.0043 \leq B \leq 0.090$ M, $0.020 \leq C \leq 0.201$ M, $0 \leq X \leq$ 3.0 M and the ratios C/B between $1.4 \leq C/B \leq 40$. The titrations were performed at different constant Z-values ($Z = 0.4$, 0.6, 0.9, 1.1, 1.4, 1.7, 2, 2.3, 2.5, 2.6 and 3.2) $Z = (h - H)/B$ and X was varied by the addition of 3.0 M NaCl medium to a solution with $|ClO_4^-| = 3.0$ M or *vice versa*. The formation constants of the binary species NiL_n^{2+}, $n = 1$, 2, 3, 4, obtained in the 3.0 M (Na)ClO_4 medium and $NiCl^+$ obtained from (i) were supposed to be exactly known and they were not varied until some final calculations. Owing to the small difference in absorbance between the ternary nickel(II) complexes no attempt to evaluate formation constants and molar absorption coefficients of these species from spectrophotometric data were made.

Bjerrum plots $\bar{n}(\log |C_3H_4N_2|)$ are calculated using the acidity constant valid in 3.0 M (Na)ClO_4. This $\bar{n}$ is given by

$$\bar{n} = (h - H - [L] - [LCl^-] - [LCl_2^{2-}])/B =$$

$$\left(h - H - (C + H - h)h^{-1}\{K_a - X(\beta_{101} + X\beta_{102})\}\right)/B$$

and thus correction for the complexes $C_3H_4N_2Cl^-$ and $C_3H_4N_2Cl_2^{2-}$ in the mixed chloride media is

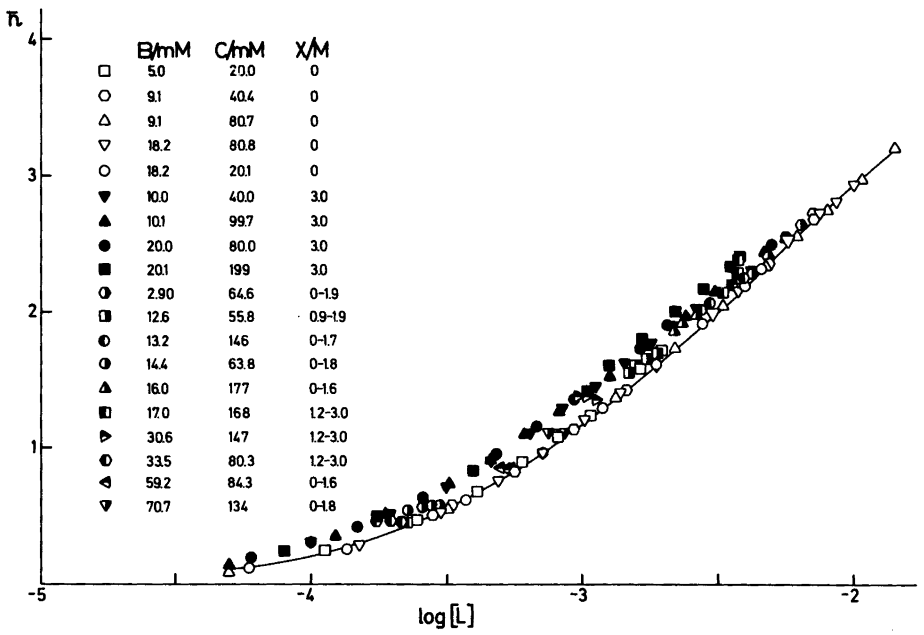

Fig. 3. Experimental data plotted as curves $\bar{n}(\log[C_3H_4N_2])$. Open symbols refer to titrations in 3.0 M (Na)ClO_4 and filled symbols to 3.0 M (Na)Cl. Half-filled symbols are obtained in mixtures of the two media. A complete list of experimental data is available upon request.

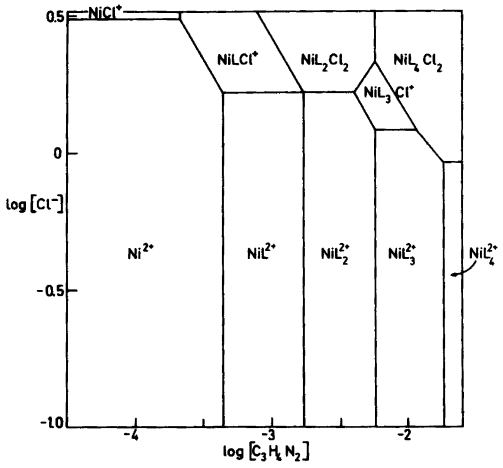

Fig. 4. Predominance area diagram for the different nickel(II) imidazole complexes. (The dominating species at every fixed $\lg[Cl^-] - \lg[L]$ level is given.) The computer program SOLGASWATER[17] was used in the calculations.

made. The plot is given in Fig. 3. The total data material comprised 19 titrations with 271 titration points. The best explanation of experimental data was obtained with the species $NiLCl^+$, NiL_2Cl^+, NiL_3Cl^+, NiL_2Cl_2 and NiL_4Cl_2. The complexes $NiLCl_2$, NiL_3Cl_2 and NiL_4Cl^+ were rejected by the computer in a covariation with the other species. The final calculation ended at $\sigma(A)=0.28$ and the result is shown in Table 1.

In a data set consisting of six titrations with 39 titration points where $Z<0.5$ the formation constant of $NiCl^+$ was varied together with the species NiL^{2+} and $NiLCl^+$. This calculation gave a value of the formation constant of $NiCl^+$ in an indirect way and this value was in a good agreement with the separately determined one. The results are given in Table 1. In order to visualize the amounts of the ternary species, we have made a predominance area diagram, which is shown in Fig. 4. It is seen from the diagram that the ternary nickel(II)-chloro-imidazole species are generally obtained in great amounts, at high chloride concentration levels ($[Cl^-]>1.5$ M).

DISCUSSION

The present investigation has confirmed the existence of ternary nickel(II) – imidazole – Cl^- complexes. Besides the series NiL_nCl^+, $n=1, 2, 3$, the complexes NiL_2Cl_2 and NiL_4Cl_2 are obtained in rather large amounts.

The NiL_nCl^+ series can be considered as stepwise reactions in which imidazole molecules are successively coordinated to an $NiCl^+$ core or alternatively as chloride ions coordinated to NiL_n^{2+} cores with $n=1, 2, 3$. Stepwise constants of these reactions are given in Table 2. The similarities between this and the corresponding copper(II) –[4] and zinc(II) – imidazole – Cl^- [5] systems are remarkable. Thus the species $MeLCl^+$, MeL_2Cl^+, MeL_3Cl^+ and MeL_2Cl_2 are obtained in all systems and the even coordination numbers 2, 4, 6 are usually favoured compared with the odd numbers 1, 3, 5.

The crystal and molecular structures of the crystalline phases in the nickel(II) imidazole system investigated by X-ray diffraction techniques are all octahedral of the form NiL_6^{2+}. However, several other compounds containing nickel(II) – Cl^- – imidazole or substituted imidazole have been prepared and characterized by analytical data, spectral and conductivity measurements,[11-13] differential thermal analysis (DTA), thermogravimetry (TG) and *X*-ray powder diffraction technique.[14]

Table 2. Some stepwise reactions with constants calculated by means of formation constants given in Ref. 1 and Table 5. The different reactions define the stepwise uptake of the ligands $C_3H_4N_2$ (L) and Cl^- are to be read horizontally. (NiL_2Cl^+ 2.82 NiL_3Cl^+ stands for $NiL_2Cl^+ + L \rightleftharpoons NiL_3Cl^+$ with $\log K = 2.82$.)

	log *K*		log *K*		log *K*		log *K*	
Ni^{2+}	3.37	NiL^{2+}	2.77	NiL_2^{2+}	2.25	NiL_3^{2+}	1.73	NiL_4^{2+}
$NiCl^+$	3.65	$NiLCl^+$	1.82	NiL_2Cl^+	2.82	NiL_3Cl^+		
Ni^{2+}	−0.5	$NiCl^+$						
NiL^{2+}	−0.21	$NiLCl^+$						
NiL_2^{2+}	−0.66	NiL_2Cl^+	0.22	NiL_2Cl_2				
NiL_3^{2+}	−0.10	NiL_3Cl^+						

Thus the compounds NiL_4Cl_2 (L=imidazole, 1-vinyl-imidazole, 2-methyl-imidazole), $NiL_4(H_2O)_2Cl_2$ (L=imidazole), $NiL_2(H_2O)_2Cl_2$ (L=imidazole), $|NiL_2Cl_2(H_2O)_2|.2H_2O$ (L=1-vinyl-2-methyl-imidazole) and $NiLCl_2$ (L=imidazole, 1-vinyl-imidazole) have been prepared and characterized. The arrangement around nickel seems to be octahedral in all these cases with the chlorine atoms generally coordinated to the nickel atom. Thus the complexes $NiL_2Cl_2(H_2O)_2$ and NiL_4Cl_2 are obtained both in the solid state and in solution while the compound $NiLCl_2$, which has a polymeric structure with chlorine atoms acting as bridges between the nickel atoms, is probably obtained as $NiLCl^+$ in solution.

Furthermore, the crystal and molecular structure of tetrakispyrazolenickel chloride, $Ni(C_3H_4N_2)_4Cl_2$ has been determined by X-ray diffraction techniques.[15] It was found that the $Ni(C_3H_4N_2)_4Cl_2$ molecule is centrosymmetric, with the nickel atom at the center of an octahedron formed by two chlorine atoms, and a nitrogen atom from each of the four pyrazole molecules. The corresponding imidazole complex should have a similar configuration.

The crystal structure of $NiCl_2.6H_2O$ has been determined by neutron diffraction[16] and it was found that the nickel atom is octahedrally coordinated to four oxygen and two chlorine atoms. The two chlorines are located on the two normals to the oxygen plane which is formed by the water molecules with the nickel at the center. By exchanging the water molecules around nickel with two respectively four imidazole molecules the complexes $NiL_2Cl_2(H_2O)_2$ respectively NiL_4Cl_2 are obtained.

In accordance with the spectrochemical series the strength of the ligand field increases within the series $Cl^- < H_2O < C_3H_4N_2$. However, the differences are very small and the possibility to evaluate the ternary $Ni^{2+}-C_3H_4N_2-Cl^-$ species from spectrophotometric data seems to be very limited. In the binary system $Ni^{2+}-Cl^-$ the different ε-values $\varepsilon_{Ni^{2+}}$ and ε_{NiCl^+}, could be sufficiently separated to permit calculation of the formation constant of $NiCl^+$. The log K-value obtained, -0.47 ± 0.10 is a rather good mean value of several earlier investigations.[10] The corresponding constant determined from potentiometric data in an indirect way is of the same order (log $K=-0.53\pm0.10$) and the agreement is quite satisfactory.

Concerning the binary NiL_n^{2+} species it is seen from the figures that the strength of the ligand field increases with the number of the coordinated $C_3H_4N_2$-molecules, (λ_{max} decreases) and ε_{max} also increases with n. These findings are in conformity with the corresponding Cu(II)-system,[4] and are summarized in Table 3.

Table 3. The wavelengths, λ_{max}, with corresponding molar absorption maxima, ε_{max}, for the nickel(II) species.

Complex	λ_{max}/nm	ε_{max}/cm^{-1} M^{-1}
Ni^{2+}	395 730	5.0–5.2 2.1–2.2
$NiCl^+$	395–400 730	5.3 2.3
NiL^{2+}	390 650	7.0 3.4
NiL_2^{2+}	385 630–650	10.1 5.4–5.5
NiL_3^{2+}	375–380 610	11.9–12.0 7.4
NiL_4^{2+}	370 590	16.4 9.7

Acknowledgements. I thank Professor Nils Ingri for much valuable advice, for his great interest and for all the facilities placed at my disposal. Thanks are also due to Lab. ing Agneta Nordin for valuable help with some of the measurements. I also wish to thank Dr Staffan Sjöberg for many helpful discussions and valuable comments on the manuscript. The English of the present paper has been corrected by Dr Michael Sharp. The work forms part of a program financially supported by the Swedish Natural Science Research Council.

REFERENCES

1. Forsling, W. and Sjöberg, S. *Acta Chem. Scand. A 29* (1975) 569.
2. Forsling, W. *To be published.*
3. Ginstrup, O., Lyhamn, L. and Ingri, N. *To be published.*
4. Sjöberg, S. *Acta Chem. Scand. A 31* (1977) 718.
5. Forsling, W. *Acta Chem. Scand. A 31* (1977) 783.
6. Ingri, N. and Sillén, L. G. *Ark. Kemi 23* (1964) 97.
7. Arnek, R., Sillén, L. G. and Wahlberg, O. *Ark. Kemi 31* (1969) 353; Brauner, P., Sillén, L. G. and Whiteker, R. *Ark. Kemi 31* (1969) 365.

8. Lyhamn, L. *Chem. Scr. 10* (1976) 49.
9. Sillén, L. G. *Acta Chem. Scand. 16* (1962) 159; Sillén, L. G. and Warnqvist, B. *Ark. Kemi 31* (1969) 341.
10. Sillén, L. G. and Martell, A. E. (compilers) *Stability Constants, Chem. Soc. London Spec. Publ.* No. *17* (1964) and No. *25* (1971).
11. Dash, K. C. and Pujari, P. *J. Inorg. Nucl. Chem. 37* (1975) 2061.
12. Goodgame, D. M. L., Goodgame, M., Hayward, P. J. and Rayner-Canham, G. W. *Inorg. Chem. 11* (1968) 2447.
13. Taylor, C. E. and Underhill, A. E. *J. Chem. Soc. A* (1969) 368.
14. Van Dam, J. C., Hakvort, G., Jansen, J. C. and Reedijk, J. *J. Inorg. Nucl. Chem. 37* (1975) 713.
15. Reimann, C. W., Mighell, A. D. and Mauer, F. A. *Acta Crystallogr. 23* (1967) 135.
16. Kleinberg, R. *J. Chem. Phys. 50* (1969) 4690.
17. Eriksson, G. *To be published.*

Received February 3, 1978.

Acta Chemica Scandinavica A 32 (1978) 479–484

Phase Analyses of Potassium, Rubidium and Cesium Tungsten Bronzes

ALTAF HUSSAIN

Department of Inorganic Chemistry, Arrhenius Laboratory, University of Stockholm, S-106 91 Stockholm, Sweden

The formation of the various phases of alkali tungsten bronzes, M_xWO_3, where M = K, Rb and Cs, has been investigated mainly within the temperature range 700–950 °C. Intergrowth tungsten bronzes, ITB, and hexagonal tungsten bronzes, HTB, form with all these metals: ITB for $0.06 \leq x \leq 0.10$ and HTB for $0.19 \leq x \leq 0.33$. Potassium also forms a tetragonal tungsten bronze phase, TTB, within the range $0.42 \leq x \leq 0.57$; for $x > 0.48$ it could not be prepared in the normal way from K_2WO_4, WO_3, and WO_2, however, but only by hydrogen reduction of a potassium tungstate mixture. HTB forms at all temperatures investigated, ITB only above 800 °C, while the TTB phase is stable up to 900 °C and decomposes above this temperature. The relationships between composition and unit cell parameters have also been studied for the TTB and HTB phases.

The alkali metal tungsten bronzes are the best studied and longest known compounds among the oxide bronzes. They are non-stoichiometric compounds of the general formula, M_xWO_3, where M represents an alkali metal. As early as 1823, Wöhler [1] prepared sodium tungsten bronzes and somewhat later Laurent,[2] von Knorre [3] and Schäfer [4] reported the same type of compounds with potassium, lithium and rubidium, respectively. These compounds were believed to be stoichiometric until 1935 when Hägg [5] in a systematic study using X-ray diffraction techniques found that all sodium tungsten bronzes of cubic symmetry belong to a continuous series of solid solutions. Later Magnéli and Blomberg [6] prepared the corresponding cesium compound in a study of the alkali metal tungsten bronzes.

Alkali metal tungsten bronzes adopt four different types of structures. These are (i) perovskite tungsten bronzes, *PTB*, formed by Li and Na,[5,6] (ii) tetragonal tungsten bronzes, *TTB*, with Na and K,[5,7] (iii) hexagonal tungsten bronzes, *HTB*[8] and (iv) intergrowth tungsten bronzes, *ITB*,[9] the latter bronze types with K, Rb and Cs. The Li and Na atoms in PTB partially fill the *A* positions of the perovskite structure, ABO_3. The symmetry is lower than cubic for low x-values. The structures of TTB and HTB are built up by corner sharing of WO_6 octahedra, which give rise to tri-, tetra-, penta- and hexagonal tunnels formed by linkage of 3, 4, 5 and 6 octahedra, respectively. The trigonal tunnels are too small to accommodate alkali atoms with the possible exception of lithium.[10] The alkali atoms in TTB are located in tetra- and pentagonal tunnels [7,11,12] and in HTB in the hexagonal tunnels.[8] The structure of ITB can be considered as an intergrowth of WO_3 and HTB elements, which gives rise to a family of closely related phases.[9] Each member in this family is characterized by specific thickness of slabs of the two structure elements. The alkali content is determined by two factors: the relative proportion of the HTB-type elements in the structure and the occupancy of the alkali sites in the HTB tunnels.

The perovskite type bronzes have been studied rather extensively whereas there has been no systematic study of the TTB, HTB and ITB phases formed in the K, Rb and Cs systems. This led us to undertake a thorough investigation of the phase relationship of these systems. The results are reported here.

EXPERIMENTAL

Preparation and materials. The bronzes were synthesized by the following methods:

(a) Samples of various compositions with $0.01 \leq x \leq 0.80$ were prepared from the appropriate amounts of M_2WO_4, WO_3 and WO_2 according to the following formula:

$$\frac{x}{2}M_2WO_4 + (1-x)WO_3 + \frac{x}{2}WO_2 \rightarrow M_xWO_3$$

The finely ground, intimate mixtures were introduced into silica tubes which were evacuated and sealed. The sealed tubes were heated in a furnace at various temperatures between 700 and 950 °C for periods of time ranging from 15 h to several weeks. In some cases, the samples were packed tightly in a small gold or platinum tube sealed at one end and pressed tightly or sealed at the other end. This metal tube was then placed in a silica tube, thoroughly evacuated, and sealed.

(b) Tetragonal tungsten bronzes were also prepared by reduction of polytungstate mixtures with the gross composition $K_2O.nWO_3$, where $n>1$, in a slow stream of hydrogen at 600 °C for about 40 min.[7] The potassium polytungstate mixtures used were prepared by heating appropriate amounts of potassium tungstate and tungsten trioxide at 800 °C for one week. This method was employed to prepare tetragonal bronzes with higher alkali metal content. TTB obtained in this way was also reheated at 800, 850 and 950 °C in evacuated sealed silica tubes for a few days to a week.

K_2WO_4 was commercially available (BDH, reagent grade) whereas Rb_2WO_4 and Cs_2WO_4 were prepared from corresponding carbonate (BDH, reagent grade) and WO_3 (Koch-Light Laboratories Ltd., 99.9 %, or obtained by dehydrating tungstic acids, Merck, puriss). Tungsten dioxide was prepared from WO_3 by reduction with an H_2/H_2O mixture.

Identification of the various phases. The characteristic colours of the various phases (ITB black, HTB dark blue and TTB red violet) facilitated their preliminary identification under a microscope. Definitive evidence was obtained from their X-ray powder patterns. These were recorded both before and after purification of the products with a Guinier-Hägg focusing camera using monochromatic Cu$K\alpha_1$ radiation ($\lambda = 1.54051$ Å). KCl ($a = 6.2919$ Å) was used as an internal standard whenever unit cell parameters were to be calculated.

Purification. The bronzes could be purified from the unreacted material and other non-bronze phases (including possible contamination from the reaction tubes at higher temperatures). Use was made of the unusual chemical inertness of tungsten bronzes and the purification consisted of successive treatment with boiling aqueous solution of HF (40 %), conc. HCl and 10 % NaOH with thorough washing with water after each step.[6] In some cases a final treatment with *aqua regia* was employed. The remaining bronze was finally washed with alcohol and then dried at 60 °C.

Chemical analysis. The method for the analysis of the alkali metal content in tungsten bronzes has recently been reported elsewhere.[13] Bronzes were oxidized in air at 550–600 °C and then dissolved in 1 M sodium hydroxide solution. The alkali metal content of the solution was then determined by atomic absorption spectrometry. The compositions given in this article were obtained in this way.

Since most of the syntheses were made in silica tubes under reducing conditions there is a risk of contamination by silicon. To check this two K-HTB samples prepared at 900 and 950 °C with relatively high alkali content (where the risk for contamination should be greatest) were analysed by plasma emission spectroscopy after oxidation and dissolution as above. A blank containing the same starting materials, not heat treated, was also run. All three samples gave a Si content of approximately 25 ppm. There was no significant difference between the blank and the heat treated samples in this respect, indicating that no silicon had been introduced during the annealing.

RESULTS AND DISCUSSIONS

The results of the present phase analysis are summarized in Fig. 1. The formation regions are almost the same for all the three systems (K, Rb

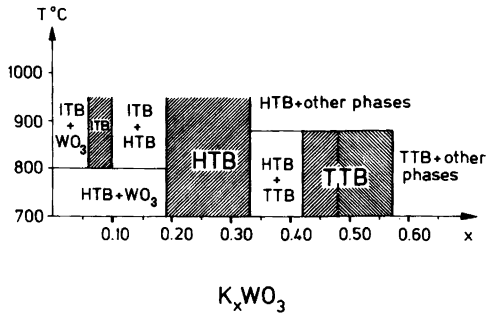

Fig. 1. Formation temperature *versus* potassium content for potassium tungsten bronzes (ITB: intergrowth, HTB: hexagonal and TTB: tetragonal tungsten bronzes). Rubidium and cesium have practically the same formation diagram except that they do not form a TTB phase. TTB with $x>0.48$ (to the right of the dotted line) could be prepared only by hydrogen reduction of polytungstate mixtures.

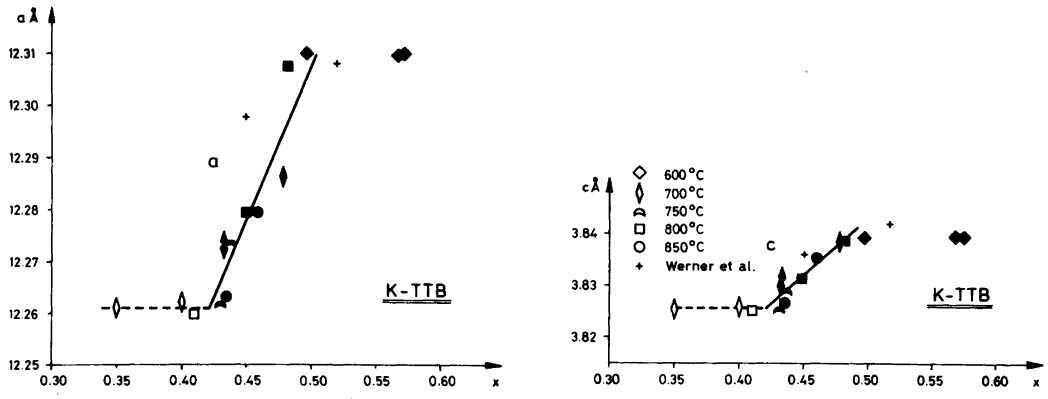

Fig. 2. Cell parameters *versus* potassium content for K-TTB phase. Filled symbols represent single phase samples. Unfilled symbols represent samples containing several phases and the compositions indicated in these cases are not the composition of the TTB phase but the gross compositions.

and Cs) except that a TTB phase is formed with potassium but not with rubidium and cesium.

Tetragonal tungsten bronzes, TTB. Of the alkali metals investigated here only potassium forms a TTB phase. The theoretical upper compositional limit is $x=0.60$, a value reached when all tetragonal and pentagonal tunnels are completely filled with potassium. However, in the present investigation the observed x values never exceeded 0.57, in agreement with Magnéli's results.[7] The lower limit of the range is close to 0.42. The limit can be obtained from the variation in the lattice parameters (Fig. 2). Samples with gross composition in the range $0.33 \leq x \leq 0.42$ were always mixtures of TTB and HTB. The potassium content at the limit could not be checked by chemical analysis as TTB cannot be separated from HTB by chemical means. From a refinement of the potassium occupancy parameter in the crystal structure of K-TTB Kihlborg and Klug[11] found a composition $x=0.371\pm0.008$ in the crystal investigated. X-Ray fluorescence analysis of another crystal from the same batch gave $x=0.34\pm0.02$. These values are outside the range found in this investigation, but it is to be noted that the preparation conditions were rather different (see below). Kihlborg and Klug used rather short heating times and the limit found in the present investigation is therefore more likely to represent equilibrium conditions.

Phases with $x>0.48$ could only be prepared by hydrogen reduction of polytungstate (method b) and not by the normal solid state synthesis (method a). Samples with nominal composition $x\geq0.50$ prepared according to method (a) were always phase mixtures as indicated by the presence of a few weak extra reflections in the diffraction patterns in addition to the TTB lines. The unknown phase could be removed by the usual purification process and the analysis of the remaining TTB consistently gave $x\leq0.48$. In method (b) the temperature (600 °C) was lower and the reaction time ($\approx$40 min) shorter compared with the conditions normally used in method (a). In order to check whether the TTB with $x>0.48$ is stable at higher temperature, samples prepared by method (b) having $x>0.48$ were heated at 800 and 850 °C for 2 days. The X-ray patterns obtained were identical to those of the original samples before heat treatment. The potassium content was also analysed and found to have the same value both before and after heat treatment indicating stability at temperatures up to 850 °C. Réau *et al.*[14] prepared TTB phases with compositions up to $x=0.59$ at 750 °C by the normal solid state synthesis. However, they did not report any analysis and apparently considered the bronzes to have the same composition as the starting mixtures.

At 900 °C and above, TTB phases are not stable (see Fig. 1). After treatment at these temperatures, samples having gross compositions $x>0.35$ were mixtures of mainly HTB, hexatungstate and tritungstate. In addition there were some weak lines, which came from some unidentified, probably reduced, phase. These samples had obviously not reached a state of equilibrium. The same mixtures were obtained when pure TTB was heated at 900 °C or above for few days and thus seem to be

the result of thermal decomposition of TTB. In order to obtain large single crystals Magnéli [7] and later Kihlborg and Klug [11] prepared TTB by heating for 15–20 min at temperatures between 900 and 1100 °C. The TTB obtained in those experiments was always contaminated by HTB. In the light of the present findings it is likely that the TTB obtained in those experiments was in a metastable or transient state at the higher temperatures.

In Fig. 2 the unit cell parameters of the TTB phase are plotted *versus* x and compared with previously reported values. Both cell parameters are seen to increase up to $x \approx 0.50$ and are then practically constant. This does not mean that $x \approx 0.50$ is the upper limit of composition, however, since the analysis of carefully purified samples gave values up to $x = 0.57$. It is interesting to note that this region of nearly constant lattice parameters is approximately the same as that in which the solid state synthesis does not work. The preparation conditions may thus influence the unit cell parameters. The variation of the cell parameters with respect to potassium content within the linear range ($x = 0.42 - 0.48$) has been refined by the least squares method with the resulting equation $a = (12.006 + 0.605x)$ Å and $c = (3.733 + 0.222x)$ Å [indicated by solid lines in Fig. 2].

Hexagonal tungsten bronzes, HTB. In the potassium, rubidium and cesium systems the HTB phase forms as a single phase in the range $0.19 \leq x \leq 0.33$ for all temperatures investigated (700–950 °C) (see Fig. 1). The upper compositional limit, $x = 1/3$, is reached when all the available alkali sites in the hexagonal tunnels are occupied. Samples with gross composition $x < 0.19$ were not homogeneous HTB phase but mixtures of HTB and other phases (Fig. 1). Chemical analysis of pure HTB phase obtained as single phase, directly or by purification, showed the lower limit to be approximately 0.19. Only about 57 % of the available alkali sites are occupied in this case.

In the potassium system, HTB with even lower x values was obtained when samples having a gross composition $x > 0.35$ were heated at 900 °C or above. Low potassium HTB ($x \geq 0.13$) could thus be obtained as one of the products resulting from thermal decomposition of TTB but not by the synthesis method normally employed. Banks and Goldstein [10] report on potassium HTB with x as low as 0.13. They prepared their samples in the normal way from W, WO_3 and K_2WO_4 but used a lower temperature (500 °C) and a longer reaction time (500 h) than generally used here. Attempts were therefore made here to prepare HTB with $x < 0.19$ under these conditions. The product obtained was mainly unreacted WO_3 with a small amount of HTB phase. After purification, there remained too little HTB to allow a reliable analysis. However, one sample was analysed and found to have $x = 0.17$, but this sample still contained a small amount of WO_3 as judged from its X-ray pattern and the x value of the HTB phase should accordingly be somewhat higher. The range of x observed in the present investigation agrees fairly well, however, with that reported by Réau *et al.*[14] for K ($0.22 \leq x \leq 0.31$) and Wanlass and Sienko [15] for Rb ($0.20 \leq x \leq 0.33$). No corresponding study of the Cs system has been made previously.

The unit cell parameters of some of the M_xWO_3 are presented graphically *versus* composition in Fig. 3. Some previously reported values are included for comparison. The parameters obtained for rubidium and cesium are seen to vary rather smoothly with x but the values for potassium scatter considerably, in particular the c parameter. The a value remains practically constant with x while the length of the c-axis in general seems to increase with x. Values for samples with nearly the same x-value prepared at different temperatures are seen to differ but no systematic variation is obvious. Although the values obtained by Werner *et al.*[16] for one composition are in good agreement with the present data the results reported by Banks and Goldstein [10] are rather different. These authors found an almost smooth increase in both a and c with x (see Fig. 3) and the c values are considerably higher than observed here. Moreover, the samples prepared at the same temperature as that used by Banks and Goldstein (500 °C) give c values which deviate most from their values. Similar variations in the lattice parameters for K-HTB have been observed in a study of the oxidation-reduction transformation between K-HTB and corresponding tungstate.[17] This could then lead to the suspicion that the differences are due to slight variations in the oxygen content of the samples. In order to check this, some samples were prepared deliberately understoichiometric in oxygen. These would then be expected to have extreme lattice parameters. This was not the case, however, as seen in Fig. 3. Oxidizing treatment with *aqua regia* and subsequent heating in air at 200 °C was also performed with some samples but did not change the lattice parameters significantly. The reason for this scattering and

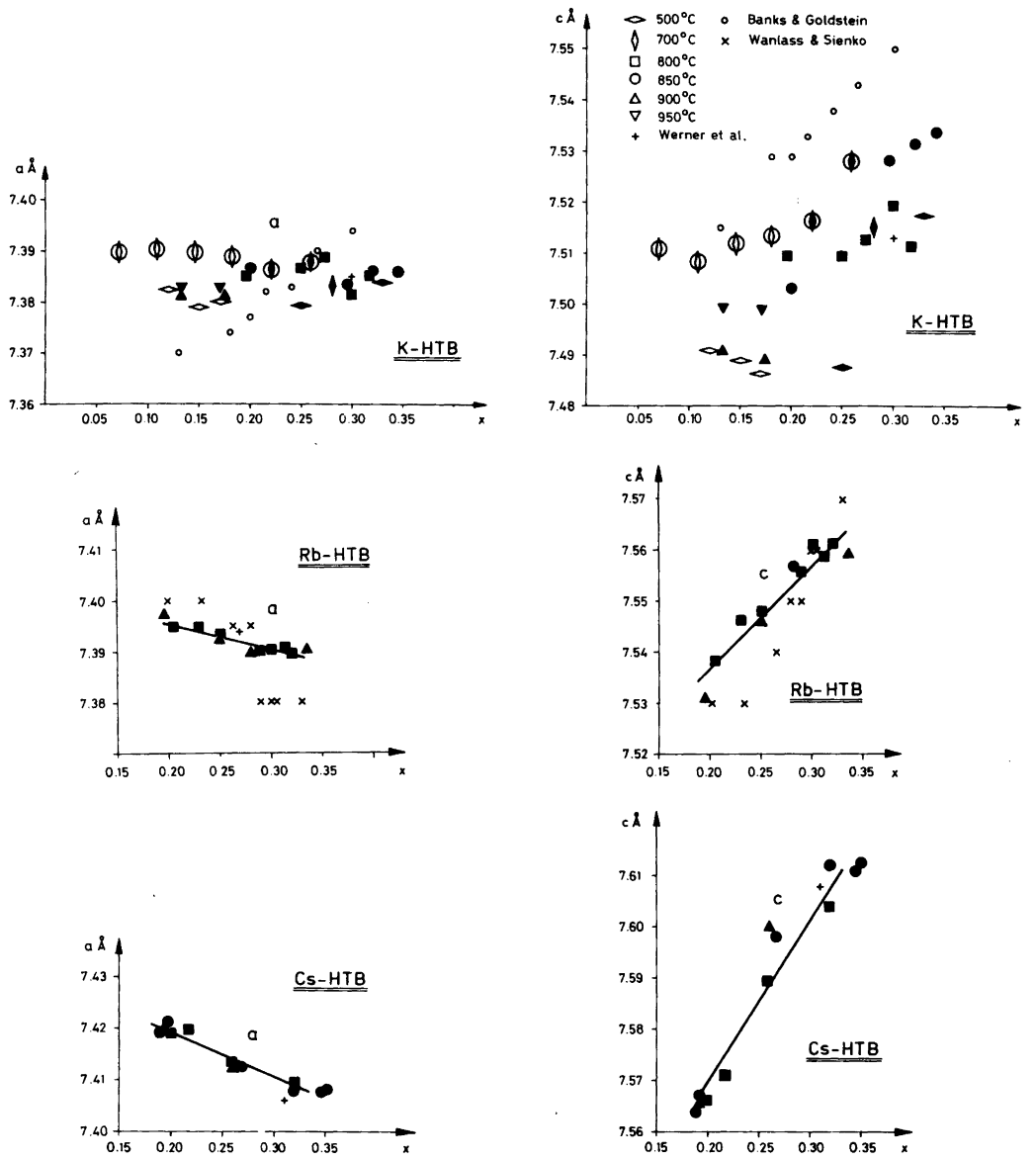

Fig. 3. Lattice parameters *versus* alkali metal content of potassium, rubidium and cesium HTB. Encircled symbols represent the samples being understoichiometric in oxygen in the gross initial compositions. Filled and large unfilled symbols have the same meaning as in Fig. 2.

disagreement is thus still obscure but may be due to some structural feature not yet detected, for example partial ordering of potassium ions, which is sensitive to the preparation conditions and which influences the lattice parameters.

In contrast to the above behaviour the cell parameters observed for Rb- and Cs-HTB scatter very little and vary smoothly with x. With increasing x the length of the a axis decreases slightly and that of the c axis increases. The rate of change is almost twice as large for Cs than for Rb. The same trend has been observed by Wanlass and Sienko,[16] but

the absolute values of the cell parameters are slightly different (Fig. 3). As seen in Fig. 3, it is possible that the cell parameters for both Rb- and Cs-HTB are constant for x values above 0.30 but the scattering is too large to allow a definite conclusion about this. The following equations were obtained for the least squares lines fitted to the points in the linear ranges, namely for Rb $a=(7.406-0.050x)$ Å, $c=(7.497+0.202x)$ Å and for Cs $a=(7.436-0.085x)$ Å, $c=(7.507+0.314x)$ Å.

Intergrowth tungsten bronzes, ITB. Optical microscope examination and the X-ray powder patterns revealed that samples of gross composition $0.06 \leq x \leq 0.10$ contained only ITB phases. The purified ITB crystals from various batches were analysed and the alkali metal content was found to be in the range $0.06 \leq x \leq 0.10$. The reproducibility in the analyses was not as good as for the other phases, however, which may be due to the fact that the ITB bronzes formed were always mixtures of different members and never obtained as true single phases. In the potassium system a mixture of ITB and HTB was obtained in the range $0.11 \leq x \leq 0.18$ (see Fig. 1). Rubidium and cesium gave a mixture of HTB and WO_3 in the same range. This anomalous behaviour seems to indicate that the samples had not reached an equilibrium state. In order to check whether equilibrium had been reached in these cases, some samples within this range of these two systems were reground and reheated at 850 °C for one week. The X-ray patterns of the samples were almost the same as before but a few ITB crystals were seen under the optical microscope in several cases. After 2 months, a considerable amount of ITB had formed even if the starting materials were HTB and WO_3 and were kept at separate places in the reaction tube. This indicates that chemical vapour transport must take place. It is thus evident that also for Rb and Cs the stable phases in this region are ITB and HTB but the HTB phase once formed reacts rather slowly with WO_3.

The temperature is rather critical for the formation of ITB phases. The lower limit is close to 800 °C as samples prepared at this temperature sometimes contained ITB, sometimes only HTB and WO_3. The ITB phases were obtained up to 950 °C, the upper limit of temperature used in this investigation. The variations of the cell parameters with composition of the ITB phases could not be studied because true single phases were not obtained.

Acknowledgements. The author is deeply indebted to Professor Arne Magnéli and Dr. Lars Kihlborg for their continuous interest in this investigation and for valuable comments on the manuscript. The spectrographic silicon analysis was kindly made by Mr. E. Söderman at the laboratories of the Swedish Geological Survey. This work forms a part of a research project financially supported by the Swedish Natural Science Research Council.

REFERENCES

1. Wöhler, F. *Ann. Chim. Phys.* [2] *43* (1823) 29.
2. Laurent, A. *Ann. Chim. Phys.* [2] *67* (1838) 215.
3. von Knorre, G. *J. Prakt. Chem.* [2] *27* (1883) 49.
4. Schäfer, E. *Z. Anorg. Allg. Chem. 38* (1903) 142.
5. Hägg, G. *Nature 135* (1935) 847; *Z. Phys. Chem. B 29* (1935) 192.
6. Magnéli, A. and Blomberg, B. *Acta Chem. Scand. 5* (1951) 372.
7. Magnéli, A. *Ark. Kemi 1* (1949) 213.
8. Magnéli, A. *Acta Chem. Scand. 7* (1953) 315.
9. Hussain, A. and Kihlborg, L. *Acta Crystallogr. A 32* (1976) 551.
10. Banks, E. and Goldstein, A. *Inorg. Chem. 7* (1968) 966.
11. Kihlborg, L. and Klug, A. *Chem. Scr. 3* (1973) 207.
12. Takusagawa, F. and Jacobson, R. A. *J. Solid State Chem. 18* (1976) 163.
13. Hussain, A. and Kihlborg, L. *Anal. Chim. Acta 90* (1977) 283.
14. Réau, J. M., Fouassier, C., Le Flem, G., Barraud, J. Y., Doumerc, J. P. and Hagenmuller, P. *Rev. Chim. Miner. 7* (1970) 975.
15. Wanlass, D. R. and Sienko, M. J. *J. Solid State Chem. 12* (1975) 362.
16. Werner, P., Kiekegaard, P. and Magnéli, A. *Acta Chem. Scand. 15* (1961) 427.
17. Hussain, A., Kihlborg, L. and Klug, A. *J. Solid State Chem. 25* (1978) 189.

Received February 10, 1978.

Acta Chemica Scandinavica A 32 (1978) 485–491

The Stability of *u-fac*-Bis[di(2-aminoethyl)sulfide]cobalt(III) and the Charcoal-catalyzed Racemization of the $(-)_D$ Enantiomer in Acidic Solution

A. HAMMERSHØI and ERIK LARSEN

Chemistry Department I, The H. C. Ørsted Institute, Universitetsparken 5, DK-2100 Copenhagen Ø, Denmark.

The charcoal catalyzed racemization of optically active *unsymmetrical facial bis*[di(2-aminoethyl)-sulfide]cobalt(III) ion has been investigated. The complex is inert to racemization in the absence of the catalyst but in the presence of charcoal racemization occurs even in 0.01 M acid medium without any detectable decomposition. The formation constant for the complex has been determined from potentiometric measurements together with the available formation constant data for the corresponding cobalt(II) complex. The stability constant is compared to that for bis(diethylenetriamine)-cobalt(III), also measured in this work, and it is concluded that the sulfur atom of the thioether function is only a weak ligator for cobalt(III). It is proposed that the catalyzed racemization entails the transient loss of a sulfur from the coordination sphere, resulting in a symmetrical transition state.

Recently, Mureinik and Spiro[1-3] carried out an extensive investigation of the racemization of optically active tris(ethylenediamine)cobalt(III), $[Co(en)_3]^{3+}$, in acidic medium. These authors found that charcoal alone did not catalyze racemization under these conditions, whereas charcoal and iodide ions in combination were found to catalyze racemization with only a slight decomposition of the complex. Their results were discussed in terms of the softness of the counter anion, and since iodide was the only efficient halide ion in this respect it was suggested that only a very soft anion in combination with charcoal could catalyze the racemization. This proposal lead us to study the charcoal catalyzed racemization of the recently prepared *u-fac* isomer of $(-)_D$-bis[di(2-aminoethyl)sulfide]-cobalt(III), $(-)_D$-$[Co(daes)_2]^{3+}$. In this complex a presumably soft ligator in the form of a thioether is already present in the inner-coordination sphere and on the basis of the above-proposed one might therefore expect that $[Co(daes)_2]^{3+}$ would undergo charcoal-catalyzed racemization under acid conditions.

$(-)_D$-$[Co(daes)_2]^{3+}$ has been found[4] to racemize much more rapidly in aqueous solution in the presence of charcoal than $[Co(en)_3]^{3+}$. However, at neutral pH the mechanism of the charcoal-catalyzed racemization may be independent of a soft counter ion or another soft donor. It is possible that charcoal partly reduces some cobalt(III) so that an electron-transfer equilibrium between Co(III) and Co(II) complexes of the type described previously by Dwyer and Sargeson may be established.[5] In the case of buffered acid solutions such a mechanism should produce $Co(H_2O)_6^{2+}$ in amounts according to the equilibrium constants for the total system, and therefore a study of the stability of $[Co(daes)_2]^{3+}$ ion was undertaken. The Co(II)-daes equilibrium system has been studied by Douglas *et al.*[6] and their data have been used to calculate the stability constant β_2 for the reaction

$$Co^{3+} + 2\ daes \rightleftharpoons [Co(daes)_2]^{3+}.$$

A knowledge of the Co(II)/Co(III)/daes equilibrium should enable us to assess the likelihood of a reductive mechanism for the catalysis by charcoal of $[Co(daes)_2]^{3+}$ racemization.

To date, very few stability constants have been measured for Co(III) complexes. To put the meas-

ured β_2 in perspective we therefore also measured the stability of a corresponding cobalt(III) complex with the amine analog of daes, *viz.* diethylenetriamine (dien).

Comparison of the two β_2 values suggests that the thioether function is very loosely bound to cobalt(III). This result will be discussed below in relation to the racemization of $[Co(daes)_2]^{3+}$.

EXPERIMENTAL

Materials. $(-)_D$-*u-fac*-$[Co(daes)_2]Cl_3.2H_2O$ and $(+)_D$-*u-fac*-$[Rh(daes)_2]Cl_3.2H_2O$ were prepared as described previously.[4,7] $[Co(daes)_2](NO_3)_3.H_2O$ used in the equilibrium study was prepared by ion exchange. Anal. $C_8H_{26}N_7O_{10}S_2Co$: C, H, N, S. $[Co(dien)_2](NO_3)_3.H_2O$ (a mixture of geometric isomers) was prepared from $Co(NO_3)_2.6H_2O$ and the ligand (Fluka, techn.) by air oxidation with charcoal as catalyst. Anal. $C_8H_{28}N_9O_{10}Co$: C, H, N.

The charcoal used throughout this work was Norit W supplied by Norit Sales Co. Ltd., Amsterdam, Holland.

Physical measurements. Absorption spectra were recorded on a Cary 118 spectrophotometer and circular dichroism spectra were measured on Roussell-Jouan mark I and III dichrographs. Radiometer PHM 52 and PHM 64 pH-meters in conjunction with Radiometer electrodes were used for pH measurements.

Kinetic of racemization. Reactions were performed in a 200 ml water-jacketed glass vessel maintained at 60.0 ± 0.2 °C by circulating water from a thermostat. The vessel was fitted with a polyethylene lid having holes for a thermometer and for glass and calomel electrodes. There was also an opening allowing the introduction of reagents as well as permitting sample collection. Light was excluded by wrapping the vessel in Al-foil. The apparatus was not completely air-tight, slight evaporation from the reaction mixture being observed over long runs.

Before each experiment a weighed amount of charcoal and a magnetic stirred bar were placed in the dry vessel and 100.0 ml of a pre-prepared solution of sodium nitrate and nitric acid was introduced. The mixture was stirred for at least 15 h. When the potential was constant (± 0.005 pH) over a period of 1 h equilibration of the charcoal and solution was considered to be complete. A weighed amount of the solid complex salt was then introduced at $t = 0$. At suitable intervals 3 ml aliquots of the stirred mixture were withdrawn using a simple glass tube, and each aliquot was filtered through fine porosity filter paper. The removal of the charcoal and cooling to room temperature were achieved within 1 min, so that the catalytic reaction was quickly quenched.

The absorbance at 485 nm (the maximum of the first band) and the circular dichroism at 512 nm and 457 nm were measured for each sample filtrate. The absorbance measurements revealed a small continuous loss of complex in solution during each run due to adsorption. This adsorption corresponded to at most 13 % of the initial amount of complex when the optical activity had reached half its initial value. Repeated attempts to detect cobalt (II) as $H_2Co(NCS)_4$ by extraction into amyl alcohol were all unsuccessful.

The degree of racemization of $(-)_D$-$[Co(daes)_2]^{3+}$ was determined as the ratio of the difference between the negative CD peak at 512 nm and the positive peak at 457 nm to the absorbance at the absorption maximum of 485 nm. This ratio is concentration independent since for 1 cm cell length $\Delta(\Delta A)/A = [\Delta A(512) - \Delta A(457)]/A(485) = [\Delta\varepsilon(512) - \Delta\varepsilon(457)]/\varepsilon(485)$. The experimental rate constants for the rate law

$$\ln\left[\frac{\Delta[\Delta A(0)]}{A(0)} \Big/ \frac{\Delta[\Delta A(t)]}{A(t)}\right] = 2kt$$

were found by a least squares fit.

Equilibrium measurements. Stock solutions of 0.2000 M HNO_3 ("Fixanal", Riedel-de-Haen), 0.5 M daes, 1.0 M dien, 0.4 M $Co(NO_3)_2$, 0.4 M $[Co(daes)_2](NO_3)_3.H_2O$ and 0.2 M $[Co(dien)_2](NO_3)_3$ were prepared and analysed. The concentration of the ligand solutions were determined by titration with the nitric acid. The cobalt-containing solutions were analysed by atomic absorption with a Perkin Elmer 403 instrument.

For each experiment weighed amounts of KNO_3 and charcoal were introduced into a measuring flask together with measured amounts of acid and ligand. Nitrogen was passed through the mixture for 15 min before the measured amounts of Co(II) and Co(III) solutions and water were added to make up the final solutions. The mixture was shaken to ensure complete mixing and then introduced into the measuring vessel similar to the one used for the kinetic runs. The solution was thermostated to 30.0 ± 0.2 °C and was protected from atmospheric oxygen by bubbling oxygen-free nitrogen through it with an excess pressure corresponding to 5 mm H_2O.

The potential difference between a saturated calomel electrode and a platinum spiral immersed in the solution was followed until a constant value was obtained (0–60 min). The potential was noted when it had been constant for at least 10 min.

Racemization of $(+)_D$-u-fac-$[Rh(daes)_2]^{3+}$. Using a method similar to that employed for the kinetic runs mentioned above the charcoal catalyzed racemization of the rhodium complex was followed in a chloride medium. The absorbance maximum

at 312 nm and the circular dichroism peaks at 336 and 308 nm were used to follow the racemization. No change in the absorption spectrum other than that due to a 10 % decrease in concentration was observed during the operations.

The complex $(+)_D$-$[Rh(en)_3]Cl_3.2H_2O$ (supplied by Dr. F. Galsbøl) was found not to racemize under exactly the same conditions.

Molecular sieves as a racemization catalyst. To a solution of 1 g of $(-)_D$-$[Co(daes)_2]Cl_3.2H_2O$ in 25 ml of water was added 2 g of 10 Å Molecular Sieves (Merck, powder). The mixture was shaken and kept at 60 °C for 24 h. After filtration the filtrate was found to contain the fully optically active complex. The molecular sieves were strongly coloured by adsorbed complex and were treated with 10 ml of 2 M $Al_2(SO_4)_3$. After degradation of the aluminosilicate 20 ml of water was added and after 1 h most of the silicate could be filtered off. The filtrate contained the completely racemized complex. No cobalt(II) species were detected.

RESULTS AND DISCUSSION

Kinetic results. The experimental conditions and data for the rate of racemization of $(-)_D$-$[Co(daes)_2]^{3+}$ in acidic (sodium) nitrate solutions with activated charcoal as catalyst are summarized in Table 1. The experimental conditions were chosen such that the complex adsorbed on the charcoal at most amounts to *ca.* 10 % of the cobalt(III) complex. Complete adsorption equilibrium between the catalyst and the reaction medium was ensured by allowing the mixture to attain a constant pH before introducing the complex. For low $[Co(daes)_2^{3+}]/[H^+]$ ratios the pH remained constant during an experiment, whereas for the highest ratios the pH decreased by up to 0.2 pH units.

As predicted by Mureinik and Spiro the racemization rate, $V = k \times C_{Co}$, obeys the McKay equation (see Table 1). The deviations from the average values may represent the uncertainties which are otherwise hard to estimate. Within uncertainty, however, the results suggest that the rate, V, is proportional to $[H^+]^{-1}$. The rate is also influenced by the concentration of inert salt, an effect which is believed to reflect competition for the active sites on the charcoal. The cobalt complex cation may compete strongly with the sodium ions due to its high charge whereas the hydrogen ion may compete efficiently because of more specific bonding.

From the observed simple rate law it is not possible to deduce any mechanism for the reaction. In fact it is at present not clear that charcoal equilibrates the complex or only causes it to racemize. Judging from the results of the equilibrium study (*vide infra*) the latter would appear to be the case.

Stability constants. Very few determinations of stability constants for cobalt(III) systems have been made since J. Bjerrum's early work in this field.[8] In a sense it is surprising that it is possible to measure equilibrium constants for robust systems. However, when an electron-transfer equilibrium with the corresponding labile cobalt(II) complex of known stability can be established then simple

Table 1. Rate constants, k, for the charcoal catalysed racemization of $(-)_D$-*u-fac*-$[Co(daes)_2]Cl_3$ in acid solution at 60 °C.

$C_{[Co(daes)_2]Cl_3}$[a] mM	C_{HNO_3}[a] mM	$C_{NO_3^-}$[a] M	Charcoal g/l	$10^6 \times k$ s^{-1}	$10^9 \times V$[b] $M\ s^{-1}$	$10^9 \times V C_{HNO_3}$ $M^2\ s^{-1}$
1.25	10	1	2	36	46	0.46
1.66	10	1	2	29	48	0.48
2.50	10	1	2	15	38	0.38
5.00	10	1	2	8	41	0.41
2.50	10	0.1	2	28	70	
2.50	7.5	1	2	23	58	0.43
5.00	7.5	1	2	12	69	0.52
5.00	7.5	1	1	2.6	1.3	
2.50	5.0	1	2	45	111	0.56
5.00	5.0	1	2	23	117	0.58

[a] C denotes a total starting concentration. [b] $V = kC_{[Co(daes)_2]Cl_3}$, the first four results demonstrate the typical variance in the experimental results.

Table 2. Redox potentials of solutions of varying ratios $[Co(daes)_2^{3+}]/[Co(daes)_2^{2+}]$ and of varying hydrogen ion concentration at 30.0 °C.

$C_{Co(daes)_2(NO_3)_3}$ (M)	$C_{Co(NO_3)_2}$ (M)	C_{daes} (M)	C_{HNO_3} (M)	[daes] (M)	$-\log[H^+]$	I (M)	$0.0601 \log \frac{[Co(daes)_2^{3+}]}{[Co(daes)_2^{2+}]}$ (V)	E (V)	E_H (V)	E° (V)
0.0167	0.0155	0.137	0.0800[a]	0.026	9.15	1.23	0.0020	−0.1589	0.0828	0.0808
0.0167	0.0155	0.171	0.0800[a]	0.060	9.51	1.23	0.0019	−0.1590	0.0827	0.0808
0.0244	0.00724	0.156	0.0800[a]	0.062	9.53	1.25	0.0318	−0.1297	0.1120	0.0802
0.00828	0.0229	0.193	0.0800[a]	0.068	9.57	1.20	−0.0266	−0.1868	0.0549	0.0815
0.00414	0.0267	0.193	0.0800[a]	0.060	9.51	1.19	−0.0487	−0.2097	0.0320	0.0807
0.00814	0.0217	0.185	0.0800[a]	0.062	9.53	1.19	−0.0256	−0.1901	0.0516	0.0772
0.00814	0.0217	0.176	0.0200[a]	0.112	10.39	1.13	−0.0256	−0.1897	0.0520	0.0776
0.00814	0.0217	0.176	0.0200[b]	0.112	10.39	1.19	−0.0256	−0.1917	0.0500	0.0756
0.00814	0.0217	0.185	0.120[c]	0.022	8.90	1.19	−0.0255	−0.1910	0.0507	0.0762
0.00814	0.0219	0.195	0.120[c]	0.031	9.06	1.19	−0.0257	−0.1896	0.0521	0.0778
mean[d]										0.0788 ± 0.0022

[a] $C_{KNO_3} = 1.00$ M. [b] $C_{KNO_3} = 1.06$ M. [c] $C_{KNO_3} = 0.96$ M. [d] All the reported measurements were obtained with 20 mg charcoal/50 ml solution to ensure fast equilibrium.

Table 3. Redox potentials of solutions of varying ratios $[Co(dien)_2^{3+}]/[Co(dien)_2^{2+}]$ and of varying hydrogen ion concentrations at 30.0 °C.

$C_{Co(dien)_2(NO_3)_3}$ (M)	$C_{Co(NO_3)_2}$ (M)	C_{dien} (M)	C_{HNO_3} (M)	[dien] (M)	$-\log[H^+]$	I (M)	$0.0601 \log \frac{[Co(dien)_2^{3+}]}{[Co(dien)_2^{2+}]}$ (V)	E (V)	E_H (V)	E° (V)
0.0236	0.0228	0.124	0.0600	0.019	9.44	1.27	0.0009	−0.4620	−0.2203	−0.2212
0.0238	0.0236	0.207	0.0600	0.100	10.16	1.27	0.0001	−0.4625	−0.2208	−0.2209
0.0238	0.0236	0.249	0.0600	0.142	10.31	1.27	0.0001	−0.4621	−0.2208	−0.2209
0.0117	0.0347	0.209	0.0600	0.079	10.06	1.23	−0.0284	−0.4885	−0.2468	−0.2184
0.00778	0.0385	0.209	0.0600	0.072	10.02	1.22	−0.0417	−0.5010	−0.2593	−0.2176
0.00786	0.0395	0.188	0.0600	0.049	9.95	1.26	−0.0421	−0.5013	−0.2596	−0.2175
0.0236	0.00785	0.125	0.0600	0.050	9.90	1.26	0.0287	−0.4300	−0.1883	−0.2170
0.0393	0.00785	0.125	0.0600	0.050	9.90	1.32	0.0421	−0.4200	−0.1783	−0.2204
0.0236	0.0231	0.207	0.0600	0.101	10.17	1.27	0.0006	−0.4630	−0.2213	−0.2219[a]
0.00685	0.0200	0.128	0.0521	0.036	9.78	1.15	−0.0283	−0.4881	−0.2464	−0.2181
0.0204	0.0199	0.135	0.0517	0.043	9.86	1.23	0.0007	−0.4619	−0.2202	−0.2209
0.00693	0.0203	0.114	0.0530	0.020	9.52	1.15	−0.0279	−0.4883	−0.2466	−0.2187
mean[b]										−0.2195 ± 0.0017

[a] All the reported measurements except this one were obtained with 20 mg charcoal/50 ml solution. [b] $C_{KNO_3} = 1.00$ M for all solutions.

potentiometric measurements are sufficient to obtain the necessary information about the cobalt(III) system. In the case of di(2-aminoethyl)sulfide and diethylenetriamine equilibrium data for the cobalt(II) systems are available.[6,9,10] In order to use these published data we have used the same experimental conditions, *viz.* 30 °C and 1 M KNO_3 medium, as in the previous investigations.

Typical sets of experimental data are given in Tables 2 and 3. The reported data were obtained using 20 mg of charcoal per 50 ml of solution, but other experiments indicate that charcoal is not essential for obtaining equilibrium under the rather basic conditions used in the equilibrium work. The measured potentials of the Pt-electrode relative to SCE were then calculated relative to the standard hydrogen electrode.

The standard potential for the electron-transfer reaction between CoL_2^{2+} and CoL_2^{3+} was calculated from

$$E^\circ = E_H - 0.0601 \log([CoL_2^{3+}]/[Co_2^{2+}]),$$

in which $[CoL_2^{3+}]$ is obtainable directly from the analytical composition of the solution and $[CoL_2^{2+}]$ is calculated from the composition and the stability constants of the cobalt(II) system. The conditions were chosen to be such that $[CoL_2^{2+}]$ constituted at least 99 % of the total concentration of cobalt(II). Inspection of Tables 2 and 3 shows that the above Nernst equation is obeyed. The spread in the data may arise from the presence of uncertain amounts of oxygen adsorbed to the charcoal and from the minor variation in the ionic strength, I, in the series of runs.

The standard potentials obtained were used in combination with Bjerrum's[8] value of $E^\circ = 1.837$ for $Co^{3+} + e \rightleftharpoons Co^{2+}$ in 1 M HNO_3 at 30 °C to calculate the cumulative stability constant, β_2^{III}, for the cobalt(III)–L system:

$$\log \beta_2^{III} = \log \beta_2^{II} + (E^\circ_{Co^{3+}/Co^{2+}} - E^\circ_{CoL_2^{3+}/CoL_2^{2+}})/0.0601,$$

where β_2^{II} is the cumulative stability constant for CoL_2^{2+}.

We then obtain for $[Co(daes)_2]^{3+}$ $\log \beta_2 = 38.3$ and for $[Co(dien)_2]^{3+}$ $\log \beta_2 = 48.8$. Using an estimated value for $\log \beta_2$ per nitrogen donor of 8.1 one arrives at $\log K \sim 3$ for the complexity constant of the thioether function to cobalt(III). This indicates a very low affinity of >S for Co(III). In this connection it is interesting to note that thioether sulfur of a methionine residue in both oxidized and reduced forms of cytochrome *c* coordinates to the iron ions.[11,12] The reduced enzyme contains iron(II) which is isoelectronic with cobalt(III) but with the metal having a lower charge one might expect Fe(II) to have even less affinity to thioether sulfur than has Co(III). The Fe(II) surrounded by a porphyrine ligand may have affinities unusual for this metal ion. However, it seems substantiated[13,14] that thioether sulfur is only a very weak ligator in iron(II) porphyrins in accordance with the above prediction.

Racemization on charcoal occurs without any detectable formation of cobalt(II). From the complexity constant, β_2, and the acidity constants pK_{a1} (8.8) and pK_{a2} (9.6) the equilibrium constant for the process

$$[Co(daes)_2]^{3+} + 4\,H^+ \rightleftharpoons Co^{3+} + 2\,daesH_2^{2+}$$

can be estimated to be ~ 0.1. The most acidic solutions employed in the kinetic runs should accordingly contain $\sim 10^{-4}$ M Co^{3+}. The aqua cobalt(III) ion is reduced by water and the solution is thereby further acidified. Thus, under the experimental conditions of the racemization studies, the system is thermodynamically unstable relative to its conversion to $Co(H_2O)_6^{2+}$. Although we observed decreases in pH, our failure to detect cobalt(II) shows that the catalyst for the racemization cannot be catalyzing the above equilibration process. The decrease in pH which was observed in runs at highest $[Co(daes)_2^{3+}]/[H^+]$ ratios is attributed to the ion-exchange effect by the charcoal rather than to a reduction process.

Dwyer and Sargeson explained charcoal catalyzed racemization of tris(ethylenediamine)cobalt(III) in terms of an electron-transfer equilibrium between the cobalt(III) complex and the corresponding labile cobalt(II) complex.[5] Their experimental conditions were such that both complexes were stable, *i.e.* rather basic conditions. This approach has since been employed quite often in the establishment of equilibrium between isomers of cobalt(III) complexes. Harnung *et al.*[15] showed that equilibrium between the isomers of tris(propylenediamine)-cobalt(III) could be achieved with charcoal. These authors noticed that the rearrangement leading to equilibrium between the Δ and Λ forms takes place at a much faster rate than does the rearrangement between geometric isomers. Keene and Searle[16]

determined the equilibrium distribution of the three geometric isomers of $[Co(dien)_2]^{3+}$. There is thus a general concensus that charcoal is a catalyst for the electron-transfer reaction between cobalt(III) and cobalt(II) complexes of otherwise identical constitution. Under preparative conditions charcoal may also act as a catalyst in the $[Co(daes)_2]^{3+}/[Co(daes)_2]^{2+}$ system. However, this catalysis is apparently not operative under acidic conditions such as those used in the racemization experiments in the present work.

Charcoal in acidic medium was used by Bjerrum and Rasmussen as a catalyst for the *trans-cis* isomerization of $[Co(en)_2(H_2O)_2]^{3+}$ in 0.05 M HNO_3.[17] In this case the mechanism of the catalysis cannot involve the same kind of electron-transfer reaction as that discussed above because the corresponding cobalt(II) complexes are highly unstable in 0.05 M HNO_3. This is therefore one of a number of examples of partial catalysis by charcoal for which no mechanistic postulates have so far appeared. The reaction also proceeds without catalysis, unlike the racemization of $[Co(daes)_2]^{3+}$.

In view of the low affinity of cobalt(III) for the thioether sulfur atom of the daes ligand it is tempting to propose that the racemization of $[Co(daes)_2]^{3+}$ entails Co–S bond rupture. The labilizing effect of the charcoal might arise from a hydrophobic interaction which simply distorts a ligand sufficiently to remove a sulfur atom from the coordination sphere.

This model for the catalytic action of charcoal on the racemization of $[Co(daes)_2]^{3+}$ is not easily verifiable. However, if it is essentially correct then one would predict that the racemization of the corresponding rhodium(III) complex would likewise be catalyzed by charcoal. We have found this to be true. The process was followed during a period of one week and it was indicated that the racemization of $[Rh(daes)_2]^{3+}$ is approximately 500 times slower than it is for the cobalt complex. For economic reasons the process has not been studied extensively.

The above mechanistic model would also lead one to predict that the racemization of tris(ethylenediamine)rhodium(III) should not be catalyzed by charcoal, and in agreement with this we were unable to detect any such racemization in agreement with an earlier result.[18]

Another obvious prediction to make on the basis of the model is that any material having accessible pores of the right size should produce some catalytic effect. Such an effect has indeed been observed with 10 Å molecular sieves. These sieves are rather basic and all sorts of trace impurities could play a role in the catalysis. However, we failed to observe any racemization of $[Co(en)_3]^{3+}$ under the same experimental conditions. This does not entirely exclude the possibility of the type of base hydrolysis often encountered in reactions of cobalt(III) complexes taking place on the surface of the catalysts. Further work is in progress to decide this possibility. However, the predictions based on the mechanistic model involving Co–S bond rupture are fulfilled by the experiments and this gives it some credibility although the suggested mechanism has not before been considered for reactions of coordination compounds. However, a mechanism of the type proposed is generally accepted to be involved in the hydrolysis of substrates by proteolytic enzymes, and since it is so widespread it may also be worth-while to consider the relevance of this mechanism in coordination chemistry.

Acknowledgements. We are grateful for a university scholarship (to A.H.), a grant from the Danish Science Research Council (No. 511–6670) enabling the purchase of a dichrograph, to Dr. F. Galsbøl for a gift of optically active $[Rh(en)_3]Cl_3.2H_2O$, and to Dr. M. Hancock for help in preparation of the manuscript.

REFERENCES

1. Mureinik, R. J. and Spiro, M. *J. Chem. Soc. Dalton Trans.* (1974) 2480.
2. Mureinik, R. J. and Spiro, M. *J. Chem. Soc. Dalton Trans.* (1974) 2486.
3. Mureinik, R. J. and Spiro, M. *J. Chem. Soc. Dalton Trans.* (1974) 2493.
4. Searle, G. H. and Larsen, E. *Acta Chem. Scand. A 30* (1976) 193.
5. Dwyer, F. P. and Sargeson, A. M. *Nature 187* (1960) 1022.
6. Douglas, B. E., Fernelius, W. C. and Gonick, E. *J. Am. Chem. Soc. 76* (1954) 4671.
7. Galsbøl, F., Hammershøi, A. and Larsen, E. *Acta Chem. Scand. A 32* (1978). *In press.*
8. Bjerrum, J. *Metal Ammine Formation in Aqueous Solution*, Haase, Copenhagen 1941.
9. Jonassen, H. B., Hurst, G. G., Leblanc, R. B. and Meibohm, A. H. *J. Phys. Chem. 56* (1952) 16.
10. Jonassen, H. B., LeBlanc, R. B., Meibohm, A. W. and Rogan, R. M. *J. Am. Chem. Soc. 72* (1950) 2430.

11. Swanson, R., Trus, B. L., Mandel, N., Mandel, G., Kallai, O. and Dickersen, R. E. *J. Biol. Chem. 252* (1977) 759.
12. Takano, T., Trus, B. L., Mandel, N., Mandel, G., Kallai, O., Swanson, R. and Dickerson, R. E. *J. Biol. Chem. 252* (1977) 776.
13. Harburg, H. A., Cronin, J. R., Fanger, M. W., Hettinger, T. P., Murphy, A. J., Myer, Y. P. and Vinogradov, S. N. *Proc. Natl. Acad. Sci. U.S.A. 54* (1965) 1658.
14. Castro, C. E. *Bioinorg. Chem. 4* (1974) 45.
15. Harnung, S. E., Kallesøe, S., Sargeson, A. M. and Schäffer, C. E. *Acta Chem. Scand. A 28* (1974) 385.
16. Keene, F. R. and Searle, G. H. *Inorg. Chem. 11* (1972) 148.
17. Bjerrum, J. and Rasmussen, S. E. *Acta Chem. Scand. 6* (1952) 1265.
18. Sen, D. and Fernelius, W. C. *J. Inorg. Nucl. Chem. 10* (1959) 269.

Received January 31, 1978.

Acta Chemica Scandinavica A 32 (1978) 493–499

The Crystal Structure of {2-[(3-Aminopropyl)amino]ethanolato}-copper(II) Bromide Tetramer Trihydrate, $[Cu_4(C_5H_{13}N_2O)_4]Br_4.3H_2O$

KARI NIEMINEN and AARNE PAJUNEN

Department of Inorganic Chemistry, University of Helsinki, SF-00100 Helsinki 10, Finland

The title compound crystallizes in the monoclinic space group $P2_1/n$ with unit cell dimensions $a=18.648(8)$, $b=22.013(8)$, $c=9.327(5)$ Å, $\beta=90.08(4)°$ and $Z=4$. The crystal structure has been determined by direct and Fourier methods from 3914 independent reflections collected with an automated four-circle diffractometer and refined by block-diagonal least-squares methods to an R value of 0.049. The complex has a tetranuclear structure with Cu···Cu distances 3.186–3.555 Å and a cubane-type Cu_4O_4 core. Four of the twelve Cu–O distances are long (2.521–2.633 Å) and eight short (1.951–1.976 Å). Two of the longer distances are perpendicular to the other two. The amine is coordinated tridentately forming 6- and 5-membered rings. The cation $[Cu_4(C_5H_{13}N_2O)_4]^{4+}$ has S_4 pseudosymmetry. Each copper(II) ion has a distorted octahedral (4+2)-coordination with four atoms in equatorial positions at average distances Cu(i)–N(i1) 1.991 Å, Cu(i)–N(i2) 2.025 Å, Cu(i)–O(i) 1.955 Å, Cu(i)–O(j) 1.969 Å, and an oxygen atom and a bromide ion at average distances 2.583 and 3.240 Å in apical positions. One of the four bromide ions forms a bridge between the tetranuclear units in the direction of the c-axis.

In recent years several structures with a cubane-type Cu_4O_4 core have been reported.[1-9] In all these structures an approximately tetrahedral array of copper(II) ions has been bridged by an also roughly tetrahedral array of the alkoxy-group oxygen atoms of different ligands. In each cube there are eight short and four long Cu–O distances. According to Mergehenn and Haase,[8] two types of cores can be distinquished: one having all four stretching directions parallel, and the other having two stretched edges perpendicular to the other two. The coordination around copper(II) ions varies, being either distorted square pyramidal, distorted octahedral or distorted bipyramidal.

The compounds have also been studied magnetically and found to have nearly normal magnetic moments at room temperature.[1,2,6,10-16] Nishida and Kida [15] have distinguished four different types of magnetic behaviour for polynuclear alkoxy-bridged copper(II) complexes on the basis of χ_M-T curves. Two types of these apply to tetranuclear Cu_4O_4 cubane-type cores, one (*type-B*) obeying the Curie-Weiss law with positive Weiss constant, and the other (*type-C(a)*) obeying the Curie-Weiss' law with negative Weiss constant.

The present determination of the crystal structure of the one-to-one complex formed by 2-[(3-aminopropyl)amino]ethanol and copper(II) bromide continues a series of investigations in this laboratory on structures having the above-described cubane-type Cu_4O_4 core, and was performed to obtain more information on the coordination around the copper(II) ions and the effects of different anions on the geometry of the core.

EXPERIMENTAL

The preparation of the blue plate-like crystals has been reported earlier.[16] The approximate dimensions of the crystal used for data collection were $0.4\times0.3\times0.1$ mm^3. Both the crystal data and the intensity data were measured on an automated Syntex $P2_1$ four-circle diffractometer using graphite-monochromated Mo$K\alpha$ radiation ($\lambda=0.7107$ Å).

The space group is monoclinic $P2_1/n$ (No. 14), and not orthorhombic as reported earlier.[16]

The cell dimensions were obtained by least-squares refinement of setting angles for 14 well-centered reflections and the intensity data were collected by the $\theta/2\theta$-scanning method (scan range 1.0°, scan speed 2.00–14.50° min^{-1} and $5.0° \leq 2\theta \leq 45.0°$). Of the 6128 reflections recorded, 3914 had $I > 2.0\ \sigma(I)$ and were regarded as observed. Data were corrected for Lorentz and polarization effects and also for absorption from ϕ-scan data. The standard reflections measured periodically during the data collection varied irregularly by about ±6 %.

Table 1. Fractional atomic coordinates ($\times 10^4$) and thermal parameters[a] ($\times 10^3$). Estimated standard deviations are given in parentheses.

Atom	X/a	Y/b	Z/c	U_{11}	U_{22}	U_{33}	U_{12}	U_{13}	U_{23}
Br(1)	−2450(1)	2825(1)	−1554(1)	31(1)	43(1)	40(1)	1(1)	−1(1)	4(1)
Br(2)	113(1)	2640(1)	3448(1)	43(1)	42(1)	26(1)	1(1)	0(1)	2(1)
Br(3)	2544(1)	1939(1)	−1391(1)	35(1)	40(1)	45(1)	5(1)	−1(1)	−1(1)
Br(4)	2267(1)	−161(1)	−2735(2)	72(1)	46(1)	50(1)	2(1)	−6(1)	−1(1)
Cu(1)	−899(1)	2206(1)	−2267(1)	27(1)	21(1)	24(1)	−6(1)	−3(1)	3(1)
Cu(2)	−169(1)	3009(1)	195(1)	18(1)	19(1)	32(1)	−1(1)	2(1)	−2(1)
Cu(3)	539(1)	2888(1)	−3215(1)	18(1)	17(1)	31(1)	1(1)	3(1)	4(1)
Cu(4)	825(1)	1880(1)	−830(1)	29(1)	19(1)	26(1)	1(1)	−3(1)	2(1)
O(1)	−514(4)	2189(3)	−315(7)	25(4)	20(4)	24(4)	−2(3)	−2(3)	5(3)
O(2)	763(4)	2763(3)	−566(7)	17(4)	18(4)	28(4)	−4(3)	1(3)	2(3)
O(3)	−438(4)	3000(3)	−2518(8)	19(4)	20(4)	32(4)	−1(3)	−5(3)	−0(3)
O(4)	452(4)	2014(3)	−2767(7)	35(4)	17(4)	20(4)	7(3)	−6(3)	2(3)
N(11)	−1239(5)	2166(5)	−4318(9)	41(6)	40(6)	19(4)	−11(5)	−0(4)	−2(4)
N(12)	−1489(4)	1495(4)	−1599(9)	22(5)	7(4)	30(5)	−4(4)	−9(4)	0(4)
N(21)	−1111(5)	3312(5)	850(11)	23(5)	40(6)	40(6)	11(5)	−7(4)	−7(5)
N(22)	370(5)	3736(4)	964(9)	21(5)	28(5)	29(5)	−10(4)	8(4)	−6(4)
N(31)	1554(5)	2817(4)	−3806(11)	34(6)	18(5)	49(6)	9(4)	3(5)	−5(5)
N(32)	404(5)	3727(4)	−4067(9)	32(5)	19(5)	28(5)	4(4)	5(4)	−1(4)
N(41)	1101(6)	1717(5)	1196(11)	38(6)	34(6)	38(6)	8(5)	−6(5)	5(5)
N(42)	996(5)	1011(4)	−1513(10)	30(5)	12(4)	37(5)	−10(4)	3(4)	6(4)
C(11)	−1440(7)	1569(6)	−4927(12)	41(8)	49(8)	27(6)	−9(6)	−10(6)	−6(6)
C(12)	−1956(7)	1215(6)	−4015(13)	45(8)	42(8)	35(6)	−8(6)	−24(6)	−6(6)
C(13)	−1666(7)	968(6)	−2591(13)	44(8)	39(7)	35(6)	−1(6)	2(6)	−13(6)
C(14)	−1181(6)	1282(5)	−206(12)	24(6)	33(7)	31(6)	−1(5)	−8(5)	0(5)
C(15)	−953(6)	1830(6)	608(12)	23(6)	37(7)	36(6)	−5(5)	6(5)	3(5)
C(21)	−1259(6)	3957(6)	931(14)	26(7)	35(7)	50(8)	16(6)	1(6)	−6(6)
C(22)	−692(8)	4308(6)	1781(17)	43(8)	35(8)	73(10)	13(7)	7(7)	−14(7)
C(23)	43(7)	4354(6)	1055(14)	32(7)	33(7)	47(7)	15(6)	1(6)	−16(6)
C(24)	1075(6)	3759(5)	234(12)	35(7)	20(6)	36(6)	−9(5)	6(5)	−13(5)
C(25)	1332(6)	3116(5)	94(12)	13(5)	33(6)	38(6)	−6(5)	−8(5)	−8(5)
C(31)	1984(6)	3391(6)	−3849(14)	17(6)	30(7)	55(8)	−7(5)	9(6)	−2(6)
C(32)	1652(7)	3854(6)	−4874(14)	37(7)	33(7)	51(8)	−10(6)	16(6)	21(6)
C(33)	1002(6)	4163(6)	−4271(15)	27(7)	27(7)	67(9)	−11(6)	6(6)	7(6)
C(34)	−252(6)	3993(5)	−3434(15)	29(7)	24(6)	59(8)	13(6)	2(6)	−1(6)
C(35)	−791(6)	3509(5)	−3208(12)	26(6)	18(6)	38(6)	10(5)	6(5)	2(5)
C(41)	921(7)	1114(6)	1817(12)	40(7)	28(7)	33(6)	3(6)	−6(6)	8(5)
C(42)	1178(7)	600(6)	959(15)	40(7)	42(8)	57(9)	14(7)	5(7)	31(7)
C(43)	817(8)	500(6)	−478(14)	59(9)	29(7)	48(8)	10(7)	−3(7)	17(6)
C(44)	623(7)	946(5)	−2888(14)	37(7)	13(5)	48(7)	1(5)	−6(6)	−5(5)
C(45)	693(6)	1531(5)	−3688(11)	33(7)	33(7)	19(5)	14(5)	−8(5)	−11(5)
O(5)	2160(7)	581(6)	−5838(13)	94(9)	81(9)	69(7)	−13(7)	−19(7)	17(7)
O(6)	3170(5)	572(5)	−220(11)	56(6)	55(6)	56(6)	−7(5)	−16(5)	0(5)
O(7)	3326(7)	11(6)	2536(13)	85(9)	67(8)	80(8)	−12(7)	0(7)	−20(6)

[a] The anisotropic thermal parameters are of the form $\exp[-2\pi^2(h^2a^{*2}U_{11} + \cdots + 2hka^*b^*U_{12} + \cdots)]$.

Table 2. Fractional atomic coordinates ($\times 10^3$) for hydrogen atoms.

Atom	X/a	Y/b	Z/c	Atom	X/a	Y/b	Z/c
H(101)	−122(7)	232(7)	−504(15)	H(304)	243(7)	324(7)	−428(15)
H(102)	−163(8)	228(6)	−371(15)	H(305)	162(7)	366(6)	−587(14)
H(103)	−100(7)	139(6)	−497(14)	H(306)	212(7)	410(6)	−507(15)
H(104)	−172(7)	168(7)	−572(15)	H(307)	77(7)	437(6)	−521(14)
H(105)	−240(7)	152(7)	−377(14)	H(308)	112(8)	436(6)	−345(15)
H(106)	−211(7)	85(6)	−469(15)	H(309)	20(7)	361(6)	−484(15)
H(107)	−209(7)	69(6)	−222(15)	H(310)	−44(8)	431(6)	−388(15)
H(108)	−137(7)	85(6)	−307(15)	H(311)	−3(8)	417(6)	−256(15)
H(109)	−193(7)	176(7)	−169(14)	H(312)	−119(7)	366(6)	−257(15)
H(110)	−148(7)	104(6)	30(15)	H(313)	−93(7)	330(7)	−422(15)
H(111)	−87(7)	101(6)	−40(14)	H(401)	82(8)	206(6)	166(15)
H(112)	−72(7)	173(7)	178(15)	H(402)	142(7)	166(6)	144(14)
H(113)	−145(8)	205(6)	101(15)	H(403)	39(7)	99(7)	186(15)
H(201)	−69(7)	352(6)	135(15)	H(404)	126(7)	103(6)	295(15)
H(202)	−135(7)	315(6)	44(15)	H(405)	170(7)	69(6)	79(14)
H(203)	−140(8)	413(7)	−8(15)	H(406)	99(7)	34(6)	156(15)
H(204)	−176(7)	399(7)	116(15)	H(407)	104(8)	21(6)	−101(15)
H(205)	−69(8)	402(7)	284(15)	H(408)	24(7)	51(6)	−40(14)
H(206)	−115(7)	451(6)	193(15)	H(409)	136(7)	118(6)	−129(14)
H(207)	1(7)	454(6)	−5(15)	H(410)	21(7)	80(7)	−278(15)
H(208)	38(7)	453(7)	167(14)	H(411)	79(7)	49(7)	−336(14)
H(209)	52(7)	363(7)	188(14)	H(412)	33(7)	147(6)	−452(14)
H(210)	148(7)	403(6)	96(15)	H(413)	130(7)	150(6)	−401(14)
H(211)	105(7)	386(6)	−68(15)	H(51)	234(7)	107(7)	−598(15)
H(212)	146(8)	306(6)	111(15)	H(52)	222(7)	49(6)	−486(15)
H(213)	169(7)	315(6)	−31(15)	H(61)	285(7)	46(6)	−73(14)
H(301)	179(7)	256(6)	−319(14)	H(62)	300(7)	86(7)	51(15)
H(302)	139(8)	300(6)	−324(15)	H(71)	330(7)	21(6)	181(15)
H(303)	200(7)	357(6)	−289(15)	H(72)	293(7)	32(6)	298(15)

CRYSTAL DATA

$[Cu_4(C_5H_{13}N_2O)_4]Br_4.3H_2O$, FW = 1096.52
Crystal system: Monoclinic (*b* unique)
Space group: $P2_1/n$ (No. 14)
$a = 18.648(8)$, $b = 22.013(8)$, $c = 9.327(5)$ Å,
$\beta = 90.08(4)°$, $V = 3828(3)$ Å^3, $Z = 4$,
$F(000) = 2168$, $\mu(\text{MoK}\alpha) = 67.5$ cm^{-1},
$D_m = 1.91$ g cm^{-3}, $D_x = 1.90$ g cm^{-3}

STRUCTURE DETERMINATION AND REFINEMENT

The structure was solved by direct methods and Fourier syntheses. The four bromide and four copper(II) ions were located from the eight largest maxima of an F_o statistical map. The other non-hydrogen atoms were located from successive Fourier syntheses and the hydrogen atoms from a difference Fourier map.

In the calculations of F_c, atomic scattering factors computed from numerical Hartree-Fock wave functions were used for all nonhydrogen atoms [17] and for hydrogen atoms those reported by Stewart *et al.*[18] The anomalous dispersion coefficients for copper and bromine atoms were also included in the calculations.[19]

Atomic coordinates were refined by block-diagonal least-squares techniques to an R values of 0.049 ($R = \Sigma||F_o| - |F_c||/\Sigma|F_o|$) with the weighting scheme $w = 1/(40.0 + |F_o| + 0.0035|F_o|^2)$ in minimizing the function $\Sigma w(|F_o| - |F_c|)^2$. Anisotropic thermal parameters were used for all non-hydrogen atoms and a fixed isotropic thermal parameter ($U = 0.06$ Å^2) for all hydrogen atoms. The computations were performed on a UNIVAC 1108 computer with the X-Ray 76 program system.[20] The figures were drawn by the ORTEP program.

DESCRIPTION OF THE STRUCTURE AND DISCUSSION

The atomic coordinates and thermal parameters with their standard deviations for non-hydrogen atoms are given in Table 1 and the coordinates of hydrogen atoms in Table 2. A list of observed and calculated structure factors can be obtained from the authors. The distances between the copper(II) ions are shown in Table 3, and the intramolecular distances and angles in the complex $\{[Cu_4(C_5H_{13}N_2O)_4]Br_3\}^+$ are shown in Table 4. A stereoscopic drawing of the complex is seen in Fig. 1 (hydrogen atoms are omitted for clarity).

Table 3. Interatomic distances (Å) between the copper(II) ions.

Cu(1)···Cu(2)	3.200(2)
Cu(1)···Cu(3)	3.199(2)
Cu(1)···Cu(4)	3.555(2)
Cu(2)···Cu(3)	3.455(2)
Cu(2)···Cu(4)	3.244(2)
Cu(3)···Cu(4)	3.186(2)

The structure consists of tetranuclear cations $[Cu_4(C_5H_{13}N_2O)_4]^{4+}$ having the same cubane-type Cu_4O_4 core as found in the structures of {2-[(3-aminopropyl)amino]ethanolato}copper(II) chloride tetramer tetrahydrate, $(CuLCl)_4.4H_2O$,[5] and {2-[(3-aminopropyl)amino]ethanolato}copper(II) nitrate tetramer dihydrate, $(CuLNO_3)_4.2H_2O$.[9] However, the difference between the longest and shortest Cu···Cu distances, 0.369 Å, is greater in the present compound than in $(CuLCl)_4.4H_2O$, 0.235 Å, and $(CuLNO_3)_4.2H_2O$, 0.219 Å. The eight short Cu–O distances in the Cu_4O_4 core are identical to those

Table 4. Intramolecular distances (Å) and angles (°) in $[Cu_4(C_5H_{13}N_2O)_4]Br_3^+$.

	i=1	i=2	i=3	i=4
Cu(i)–Br(1)	3.266(2)$^{l=1}$	3.185(2)$^{l=2}$	[a]3.256(2)$^{l=2}$	3.251(2)$^{l=3}$
Cu(i)–O(i)	1.956(7)	1.954(7)	1.951(7)	1.957(7)
Cu(i)–O(j)	1.962(7)$^{j=3}$	1.975(7)$^{j=1}$	1.976(7)$^{j=4}$	1.962(7)$^{j=2}$
Cu(i)–O(k)	2.597(7)$^{k=4}$	2.579(7)$^{k=3}$	2.521(7)$^{k=2}$	2.633(7)$^{k=1}$
Cu(i)–N(i1)	2.017(9)	1.977(10)	1.979(10)	1.991(10)
Cu(i)–N(i2)	2.013(8)	2.020(9)	2.025(9)	2.043(9)
N(i1)–C(i1)	1.48(2)	1.45(2)	1.50(2)	1.49(2)
C(i1)–C(i2)	1.50(2)	1.53(2)	1.53(2)	1.47(2)
C(i2)–C(i3)	1.53(2)	1.53(2)	1.50(2)	1.52(2)
C(i3)–N(i2)	1.52(2)	1.49(2)	1.48(2)	1.52(2)
N(i2)–C(i4)	1.49(1)	1.48(1)	1.48(2)	1.46(2)
C(i4)–C(i5)	1.49(2)	1.50(2)	1.48(2)	1.49(2)
C(i5)–O(i)	1.43(1)	1.45(1)	1.45(1)	1.44(1)

	Range		Range
O(i)–Cu(i)–Br(1)	96.5(2)–101.2(2)	Cu(i)–O(i)–Cu(j)	108.2(3) –111.9(3)
O(j)–Cu(i)–Br(1)	91.1(2)– 92.8(2)	Cu(i)–O(i)–Cu(k)	98.5(3) –101.7(3)
O(k)–Cu(i)–Br(1)	162.7(2)–164.7(2)	Cu(j)–O(i)–Cu(k)	87.7(3) – 89.9(3)
O(i)–Cu(i)–O(j)	86.9(3)– 88.6(3)	Cu(i)–N(i1)–C(i1)	117.0(7) –121.0(8)
O(i)–Cu(i)–O(k)	78.1(3)– 80.8(3)	N(i1)–C(i1)–C(i2)	111.3(10)–113.9(10)
O(j)–Cu(i)–O(k)	70.5(3)– 72.5(3)	C(i1)–C(i2)–C(i3)	113.2(11)–116.8(11)
O(i)–Cu(i)–N(i1)	174.0(4)–175.6(4)	C(i2)–C(i3)–N(i2)	109.4(10)–111.2(10)
O(j)–Cu(i)–N(i1)	93.5(3)– 95.3(4)	C(i3)–N(i2)–Cu(i)	117.4(7) –123.3(7)
O(k)–Cu(i)–N(i1)	96.1(3)– 97.7(3)	Cu(i)–N(i2)–C(i4)	106.9(6) –107.8(7)
O(i)–Cu(i)–N(i2)	84.1(3)– 84.7(3)	C(i3)–N(i2)–C(i4)	111.0(9) –114.6(9)
O(j)–Cu(i)–N(i2)	163.9(3)–167.5(3)	N(i2)–C(i4)–C(i5)	107.0(9) –109.6(9)
O(k)–Cu(i)–N(i2)	116.6(3)–120.3(3)	C(i4)–C(i5)–O(i)	107.7(9) –108.2(9)
N(i1)–Cu(i)–Br(1)	84.6(3)– 87.3(3)	C(i5)–O(i)–Cu(i)	109.2(6) –111.9(6)
N(i2)–Cu(i)–Br(1)	75.4(3)– 80.4(3)	C(i5)–O(i)–Cu(j)	122.7(6) –124.5(6)
N(i1)–Cu(i)–N(i2)	93.7(4)– 95.1(4)	C(i5)–O(i)–Cu(k)	118.5(6) –122.1(6)

[a] Equivalent position $x,y,z-1$ of Br(2).

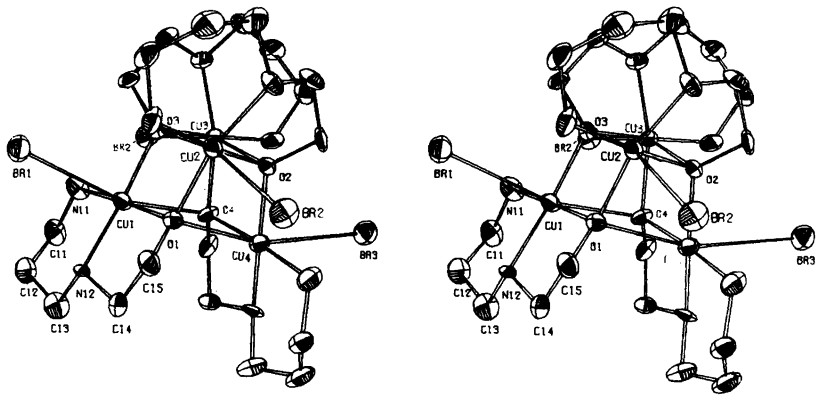

Fig. 1. Stereo view of the complex $[Cu_4(C_5H_{13}N_2O)_4]Br_3^+$.

of $(CuLCl)_4.4H_2O$ and $(CuLNO_3)_4.2H_2O$. The four long Cu–O distances are also identical within standard deviation to those of $(CuLNO_3)_4.2H_2O$, but are considerably longer than those of $(CuLCl)_4.4H_2O$, 2.448 Å. In the Cu_4O_4 core, as also in the Cu_4O_4 cores of $(CuLCl)_4.4H_2O$ and $(CuLNO_3)_4.2H_2O$, two stretched distances are perpendicular to the other two. The deviations of atoms from the limiting planes of the cube and the angles between the planes are shown in Table 5. The cation $[Cu_4(C_5H_{13}N_2O)_4]^{4+}$ has S_4 pseudo-symmetry in the direction of the *b*-axis.

The average Cu···Br distance 3.240 Å is smaller than the Cu···Cl distance 3.335 Å in $(CuLCl)_4.4H_2O$. Since the sum of the ionic radii of Cu^{2+} and Br^- ions is 3.23 Å,[21] it can be assumed that there is a semicoordination bond between copper(II) and bromide ions. On the opposite side of each copper(II) ion lies an oxygen atom O(k) at average distance 2.583 Å, corresponding to a semicoordination bond.[21] The two nitrogen atoms and the oxygen atoms O(i) of amine (i) and O(j) of amine (j) lie almost in a plane (Table 6) nearly perpendicular to the line Br···O(k). The angle between the normal of the plane and the line is about 16°. In the plane the average bond distances are Cu(i)–N(i1) 1.991 Å, Cu(i)–N(i2) 2.025 Å, Cu(i)–O(i) 1.955 Å, and Cu(i)–O(j) 1.969 Å. Thus the coordination around the copper(II) ion is distorted octahedral (4+2). The dihedral angles between planes [Cu(i),N(i1), N(i2)] and [Cu(i),O(i),O(j)] are 12.3, 11.4, 14.7 and 10.6° for i=1, 2, 3 and 4, respectively, indicating some tetrahedral distortion. The octahedral copper(II) coordination is also found in

Table 5. Deviations (Å) of atoms from least-squares planes for Cu_4O_4, and the angles (°) between the planes.

Plane 1:	Cu(1)	Cu(2)	O(1)	O(3)	Plane 4:	Cu(1)	Cu(4)	O(1)	O(4)
	−0.11	−0.09	0.11	0.08		−0.06	−0.06	0.07	0.07
Plane 2:	Cu(2)	Cu(3)	O(2)	O(3)	Plane 5:	Cu(1)	Cu(3)	O(3)	O(4)
	0.08	0.08	−0.08	−0.08		−0.07	−0.09	0.10	0.07
Plane 3:	Cu(3)	Cu(4)	O(2)	O(4)	Plane 6:	Cu(2)	Cu(4)	O(1)	O(2)
	0.10	0.12	−0.09	−0.13		0.11	0.08	−0.08	−0.12

Angles (°) between the planes

Plane	2	3	4	5	6
1	80.6	20.4	80.5	87.6	88.7
2		79.0	0.3	80.5	80.8
3			79.1	89.4	87.7
4				80.7	80.6
5					18.7

Table 6. Least-squares planes through N(i1), N(i2), O(i), O(j) and the distances (Å) of some atoms from these planes.

N(11)	N(12)	O(1)	O(3)	Cu(1)	O(4)	Br(1)
0.13	−0.14	0.15	−0.14	0.06	2.42	−3.16
N(21)	N(22)	O(2)	O(1)	Cu(2)	O(3)	Br(2)
0.11	−0.13	0.13	−0.13	0.05	2.40	−3.09
N(31)	N(32)	O(3)	O(4)	Cu(3)	O(2)	Br(2)[a]
0.14	−0.16	0.17	−0.16	0.08	2.36	−3.13
N(41)	N(42)	O(4)	O(2)	Cu(4)	O(1)	Br(3)
−0.12	0.13	−0.14	0.13	−0.03	−2.41	3.18

[a] Equivalent position $x,y,z-1$.

Table 7. Bond lengths (Å) and angles (°) in water molecules. Interatomic distances and angles between the bromide ions, the hydrogen atoms of water molecules and the oxygen atoms of water molecules.

O(5)−H(51)	1.14(14)	H(51)−O(5)−H(52)	106(11)
O(5)−H(52)	0.94(14)	H(61)−O(6)−H(62)	111(13)
O(6)−H(61)	0.80(14)	H(71)−O(7)−H(72)	86(12)
O(6)−H(62)	0.99(14)	[a]Br(1)···H(51)−O(5)	170(10)
O(7)−H(71)	0.81(14)	Cu(1)···[a]Br(1)···H(51)	126(3)
O(7)−H(72)	1.09(14)	Br(4)···H(52)−O(5)	156(12)
[a]Br(1)···H(51)	2.52(14)	H(52)···Br(4)···H(61)	107(4)
Br(4)···H(52)	2.45(14)	Br(4)···H(61)−O(6)	156(13)
Br(4)···H(61)	2.56(14)	Br(3)···H(62)−O(6)	112(13)
Br(3)···H(62)	3.08(14)	O(6)···H(71)−O(7)	169(14)
O(6)···H(71)	2.07(14)	[b]O(5)···H(72)−O(7)	158(11)
[b]O(5)···H(72)	1.90(14)	H(71)···O(6)−H(61)	121(11)
		H(71)···O(6)−H(62)	70(9)
		H(72)···[b]O(5)−[b]H(51)	90(8)
		H(72)···[b]O(5)−[b]H(52)	114(9)

[a] Equivalent position $\frac{1}{2}+x,\frac{1}{2}-y,-\frac{1}{2}+z$. [b] Equivalent position $x,y,z+1$.

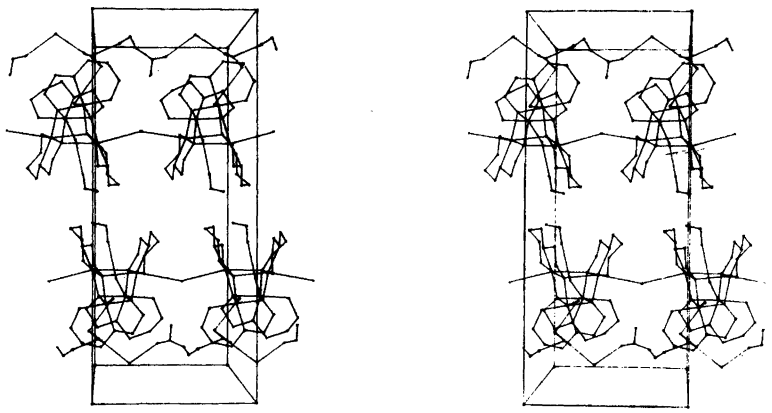

Fig. 2. Stereo view of the packing along the *a*-axis. (The front part of the unit cell is omitted for clarity.)

$(CuLNO_3)_4.2H_2O$, but the other compounds having the cubane-type Cu_4O_4 core have either distorted square-pyramidal or distorted bipyramidal copper(II) coordination sphere.

As reported earlier, the amine coordinates tridentately forming six- and five-membered rings.[5,9] The bond distances correspond to single bond values and are in agreement with those reported for $(CuLCl)_4.4H_2O$ and $(CuLNO_3)_4.2H_2O$. All the bond angles are also normal for the amine. The angles around the oxygen atoms vary between 88 and 125° having the average value 109°, which can be assumed to correspond to sp^3-hybridization. The distortion of the angles can be thought of as the effect of the Cu_4O_4 core. The six-membered ring is in chair conformation.

There are three types of bromide ions in the structure: (*a*) Br(1) is semicoordinated to Cu(1) and Br(3) to Cu(4), and water molecules are joined to these ions by hydrogen bonds. (*b*) Br(2) is joined to two copper(II) ions by semicoordination bonds, forming a bridge between Cu(2) and Cu(3) (at $x,y,z+1$) in the direction of the *c*-axis; (*c*) Br(4) is joined to the structure by water molecules. The bond lengths and angles for the water molecules forming hydrogen bonds with bromide ions and with each other are shown in Table 7. One of the three water molecules, $H_2O(5)$, is joined to bromide ion Br(1) (at $\frac{1}{2}+x,\frac{1}{2}-y,-\frac{1}{2}+z$) and to the free bromide ion Br(4). A second water molecule, $H_2O(6)$, is located between Br(4) and Br(3) ions, and the third water molecule, $H_2O(7)$, joins together water molecules $H_2O(6)$ and $H_2O(5)$ (at $x,y,z+1$). A stereo view of the packing is shown in Fig. 2.

The magnetic data of this compound have been published earlier.[16] A detailed interpretation of the relation between the molecular geometries and magnetic properties will be given later.

REFERENCES

1. Bertland, J. and Kelley, J. *Inorg. Chim. Acta 4* (1970) 203.
2. Haase, W. *Chem. Ber. 106* (1973) 3132.
3. Dixon Estes, E. and Hodgson, D. *Inorg. Chem. 14* (1975) 334.
4. von Mergehenn, R., Haase, W. and Allmann, R. *Acta Crystallogr. B 31* (1975) 1847.
5. Pajunen, A. and Nieminen, K. *Finn. Chem. Lett.* (1975) 67.
6. Matsumoto, N., Ueda, I., Nishida, Y. and Kida, S. *Bull. Chem. Soc. Jpn. 49* (1976) 1308.
7. von Mergehenn, R., Merz, L., Haase, W. and Allmann, R. *Acta Crystallogr. B 32* (1976) 505.
8. von Mergehenn, R. and Haase, W. *Acta Crystallogr. B 33* (1977) 1877.
9. Nieminen, K. *Acta Chem. Scand. A 31* (1977) 693.
10. Uhlig, E. and Steiger, K. *Z. Anorg. Allg. Chem. 346* (1966) 21.
11. Uhlig, E. and Steiger, K. *Z. Anorg. Allg. Chem. 360* (1968) 39.
12. Näsänen, R., Luukkonen, E., Kalmi, H. and Nieminen, K. *Suom. Kemistil. B 44* (1971) 327.
13. Merz, L., Haase, W. and Keller, G. *Ber. Bunsenges. Phys. Chem. 80* (1976) 305.
14. Merz, L. and Haase, W. *Z. Naturforsch. Teil A 31* (1976) 177.
15. Nishida, Y. and Kida, S. *J. Inorg. Nucl. Chem. 38* (1976) 451.
16. Nieminen, K. and Pajunen, S. *Suom. Kemistil. B 45* (1972) 391.
17. Cromer, D. and Mann, J. *Acta Crystallogr. A 24* (1968) 321.
18. Stewart, R., Davidson, E. and Simpson, W. *J. Phys. Chem. 42* (1965) 3175.
19. *International Tables for X-Ray Crystallography*, Kynoch Press, Birmingham 1962, Vol. 3, Table 3.3.2C.
20. Stewart, J. M., Ed., *The X-Ray System, Version of 1976*, Technical Report TR-446, Computer Science Center, University of Maryland, College Park 1976.
21. Pauling, L. *The Nature of the Chemical Bond*, 3rd. Ed., Cornell University Press, Ithaca 1960, pp. 160, 252, 260.

Received February 6, 1978.

Acta Chemica Scandinavica A 32 (1978) 501 – 507

The Crystal Structure of (—)$_D$-*u-fac*-Bis[di(2-aminoethyl)-sulfide]cobalt(III) Chloride Dihydrate and the Absolute Configuration of the Cation

A. HAMMERSHØI, ERIK LARSEN and SINE LARSEN

Chemistry Departments I and IV, The H. C. Ørsted Institute, Universitetsparken 5, DK-2100 Copenhagen, Denmark

The crystal structure of (−)$_D$-*u-fac* bis[di(2-aminoethyl)sulfide]cobalt(III) chloride dihydrate has been determined by X-ray diffraction methods. The crystals are orthorhombic, space group $P2_12_12_1$, $Z=4$, with the unit cell dimensions $a=14.665(3)$ Å, $b=15.821(3)$ Å, and $c=7.979(2)$ Å. Cu$K\alpha$ and Mo$K\alpha$ diffraction data were collected on an automatic four circle diffractometer. The structure was determined from Patterson and Fourier methods. The final refinement of 3284 reflections (Mo radiation) led to $R=0.040$ and $R_w=0.046$.

The structure determination confirms an earlier assignment of the structure as unsymmetrical facial. The Cu-data were used to establish the absolute configuration Δ in agreement with an earlier assignment based on the empirical correlation between circular dichroism spectra and absolute configuration. All four five-membered chelate rings have λ conformations. A full description of the cation is therefore (−)$_D$-Δ($\lambda\lambda\lambda\lambda$)-*u-fac*.

The complex bis[di(2-aminoethyl)sulfide]cobalt(III), $[Co(daes)_2]^{3+}$, could in principle exist in three geometric isomers (*symmetrical facial*, *unsymmetrical facial* and *meridional*) each of which would have the possibility of forming several conformers. Recently, an analysis was made of the reaction products from a number of preparative routes leading to $[Co(daes)_2]^{3+}$ including some routes commonly believed to involve equilibrium.[1] This analysis revealed that only one geometric isomer was formed in measurable yield. The result is astonishing in view of the fact that all three geometrical isomers of the corresponding complex bis(diethylenetriamine)-cobalt(III), $[Co(dien)_2]^{3+}$, are formed in approximately equal amounts.[2] Because the bond angle for C−S−C is generally found to be *ca.* 100° the *mer* isomer of $[Co(daes)_2]^{3+}$ would be highly strained and this may well be the reason for the absence of *mer* form. However, from model considerations there seems to be no apparent reason why one of the *fac* forms and not the other should be stable. It was concluded[1] that the found form of $[Co(daes)_2]^{3+}$ was the unsymmetrical *facial* because the complex could be resolved in optically active forms with a pronounced circular dichroism. The *u-fac* form must have a chiral disposition of the chelate rings – a configurational dissymmetry – whereas the *s-fac* isomer can have only a conformational dissymmetry presumably with much less circular dichroism and a low barrier towards racemization. The present structure determination has confirmed that the configuration is *u-fac*.

Since Saito first determined the absolute configuration of a cobalt(III) complex[3] a large body of empirical material has been collected which shows that there is a rather general correlation between the circular dichroism exhibited by a complex with five-membered chelate rings and its absolute configuration[4] expressed for example in terms of Δ and Λ. For cobalt(III) complexes of six nitrogen ligators empirical correlations have been specially successful and extensions to complexes with other ligating atoms than nitrogen have been attempted apparently with good reliability. Thus it seems that cobalt(III) complexes of the absolute configuration Δ have a dominating negative circular dichroism connected to the absorption related to the spin allowed transition having lowest energy in an

octahedral complex. This behaviour was observed for $(-)_D$-$[Co(daes)_2]Cl_3$ and on this basis the absolute configuration was predicted to be Δ.[1] This is substantiated in the present work and with this confirmation of the prediction based on the empirical rule more reliability may be connected to future empirical conclusions also for chelates containing a thioether as a ligator.

During the initial experiments a number of racemic complex salts as well as optically active salts were investigated to search for crystals most suitable for the single crystal X-ray investigation. It was hereby found that the racemic chloride and the optically active chloride were isomorphous. This is a relatively rare situation and accordingly the $(-)_D$-$[Co(daes)_2]Cl_3.2H_2O$ was selected for further work.

EXPERIMENTAL

$(-)_D$-$[Co(daes)_2]Cl_3.2H_2O$ was prepared as published earlier.[1] Crystals suitable for diffraction work were obtained by recrystallization from a 50 % water/ethanol mixture. The water content is not well defined and depending on humidity and temperature water contents were found by thermogravimetry to vary between 2 and 2.5. Found: C 21.5; H 6.5; N 12.6; S 14.6; Cl 23.7. Calc. for $C_8H_{29}N_4O_{2.5}S_2Cl_3Co$: C 21.3; H 6.5; N 12.4; S 14.2; Cl 23.6. Specific rotations for the sample at 25 °C (0.2 % aqueous solution, 2 cm cell length): $[\alpha]_{589}$ −322°; $[\alpha]^{578}$ −446°; $[\alpha]^{546}$ −895°; $[\alpha]_{436}$ +597°.

The compound crystallizes as orange red prisms. X-Ray diffraction photographs showed that the crystals are orthorhombic, the space group being uniquely determined to be $P2_12_12_1$. Crystals from the racemic sample were found to have the same space group and identical unit cell parameters. Powder photographs taken of both the optically active and the racemic samples confirmed this observation. The powder diffraction patterns were obtained using a Hägg-Guinier camera XDC 700 with Cu$K\alpha$ radiation monochromated by a quartz crystal employing silicon as an internal standard.

The density of the crystals was measured by flotation in a mixture of α-bromonaphthalene and 1,2-dibromopropane.

Data collection. A single crystal with dimensions $0.09 \times 0.13 \times 0.32$ mm^3 limited by 20 faces was chosen for the data collection and for the determination of unit cell parameters on a Picker FACS-1 diffractometer. Two sets of data were collected at 22 °C using graphite monochromated Cu$K\alpha$ and Mo$K\alpha$ radiation, respectively.

Both data sets were obtained by operating the diffractometer in a $\theta-2\theta$ scan mode at a rate in 2θ of 2° min^{-1} for the Cu-data and 1° min^{-1} for the Mo-data. The scan was symmetrical and increased with 2θ following the expression $\Delta 2\theta_{SC} = 2A + 2D + \tan\theta$, where with Cu$K\alpha$ radiation $A = 1.6°$, $D = 0.143°$ and for Mo$K\alpha$ radiation $A = 1.5°$ and $D = 0.346°$. Background counts were made at each end of the scan range for 10 s for the Cu-data and for 20 s for the Mo-data. The intensities of standard reflections were measured after every 40 reflections. In both cases these measurements showed that no deterioration or misalignment of the crystal occurred during the data collections. The intensity data were measured for reflections in two octants which were not symmetry related (hkl, $h\bar{k}l$). The Cu-data were obtained for $6° < 2\theta < 127.5°$ and the Mo-data for $6° < 2\theta \leq 54°$. The criterion $I/\sigma(I) > 2.0$ was used to classify a reflection as observed. The data obtained with Cu$K\alpha$ radiation consist of 2867 independent reflections of which 2706 were observed. The data obtained with Mo radiation consist of 4022 independent reflections of which 3284 were observed. The two data sets were corrected for Lorentz and polarization effects and absorption.

For the crystallographic calculations the unit cell parameters used were those resulting from the least-squares refinement of the setting angles of 12 reflections measured with Cu$K\alpha$ radiation.

The following computer programs were used during the computations: The Vanderbilt system [5] for diffractometer operations, a data reduction program of local origin, ORTEP II for the illustrations,[6] the X-ray system [7] for the crystal structure analysis, and Simplex [8] for weight analysis.

The atomic scattering factors employed were those reported by Cromer and Mann [9] taking the values for the uncharged non-hydrogen atoms. For hydrogen the scattering factor calculated by Stewart *et al.*[10] was used. The anomalous dispersion corrections added to the scattering factors for cobalt, sulfur, and chlorine were from Cromer and Liberman.[11]

CRYSTAL DATA

$(-)_D$-Bis[di(2-aminoethyl)sulfide]cobalt(III) chloride dihydrate; $C_8H_{29}N_4O_{2.5}S_2Cl_3Co$; M = 450.8. Orthorhombic, $a = 14.665(3)$ Å, $b = 15.821(3)$ Å, $c = 7.979(2)$ Å; $V = 1851.2$ Å^3; $d_{obs} = 1.609$ g/cm^3; $Z = 4$; $d_{calc} = 1.617$ g/cm^3. μ(Cu$K\alpha$) = 138.2 cm^{-1}, μ(Mo$K\alpha$) = 15.78 cm^{-1}. $F(000) = 920$. Space group $P2_12_12_1$ (No. 19). Developed forms, {110}, {011}, {111} and {120}.

STRUCTURE DETERMINATION AND REFINEMENT

The intensity measurements with Cu$K\alpha$ radiation were performed first and this data set was used to solve the structure. The position of the cobalt atom could be deduced from the three-dimensional Patterson function. The other non-hydrogen atoms were located by Fourier syntheses.

The structure was refined by the method of least-squares minimizing $R=\Sigma w(|F_o|-K|F_c|)^2$. After a full matrix refinement with unit weights of the scale factor, the atomic parameters, anisotropic thermal parameters for Co, S and Cl, and isotropic temperature factors for the other atoms the R-value was 0.078. A difference Fourier calculated after this refinement contained a large peak at a distance of approximately 2.5 Å from one of the oxygen atoms which exhibited a very large temperature factor. From this it was concluded that one of the water molecules in the structure is distributed between at least two sites. The population parameters for the two oxygen atoms placed at these sites were included in the following least-squares refinements. Two cycles of refinement were performed with fixed temperature factors allowing the populations to vary. This was followed by two cycles in which the populations were fixed while the temperature factors were varied.

The sum of population parameters for the two partly occupied sites tended to be bigger than 1.0 and the anisotropic temperature factors for the oxygen atoms took physically unrealistic values. An analysis of the difference Fourier calculated without including the disordered water molecule showed that the water was located in a banana-shaped area that could contain more than one water molecule. A better description of this disorder was obtained by using four different sites each having independent population and isotropic thermal parameters. For the other non-hydrogen atoms anisotropic temperature factors were used.

The 24 hydrogen atoms on the ligands were located in a difference Fourier based on the Mo$K\alpha$ data. The positional parameters of the hydrogen atoms were also included in the least-squares refinement. The thermal parameters for the hydrogen atoms were not refined but were given the refined isotropic temperature factor of the atom to which they are attached.

The weights used were $w=1/(A+B\sigma(F)^2+CF+DF^2)$. The numerical values for A, B, C and D were obtained as described and programmed by Nielsen.[8] During the final cycles of least-squares refinements the coefficients in the weighting function were A, B, C, D (Cu$K\alpha$) = 5.78, 0.75, 0.31, 0.0059 and A, B, C, D (Mo$K\alpha$): 0.0, 1.02, 0.033, 0.0005. This refinement was continued until the maximum change in the population and thermal parameters for the disordered oxygen atom was less than 0.5σ between two successive refinements. The maximum change of the other parameters was 0.05σ. The unit weighted and weighted residuals R and R_w are 0.040 and 0.046 respectively for Mo$K\alpha$ data. For the Cu$K\alpha$ data $R=0.051$ and $R_w=0.059$.

In order to establish the absolute configuration of the complex the mirror image of the structure was refined as well using both data sets. For the Cu-data $R=0.120$ and $R_w=0.154$ and the corresponding values for the Mo-data are $R=0.049$ and $R_w=0.058$. Using Hamilton's R-value test[12] the latter solution can be rejected on a significance level much lower than 0.005 even on the Mo-data alone. By inspecting the list of observed and calculated structure factors of the Cu-data for the two catoptric forms the same conclusion is reached.

The two parameter sets resulting from the refinements using the Cu- and Mo-data sets were compared by performing two full normal probability plots for the positional and thermal parameters, respectively. These plots had the correct slope but did not pass through 0.0 thus indicating the presence of systematic errors. We suspect that insufficient correction for absorption in the Cu-data may have caused the error since the great number of faces made measurements of the crystal inaccurate. The parameters given in Tables 1–3 are thus those obtained from the Mo-data since these are considered the most reliable. Lists of structure factors may be obtained from the authors.

DESCRIPTION AND DISCUSSION OF THE STRUCTURE

The hexacoordinated cobalt(III) complex has the unsymmetrical *facial* configuration with the sulfur atoms *cis* as shown in Fig. 1. The cation has effectively C_2 symmetry when corresponding bond distances, bond angles, and dihedral angles (see Tables 4 and 5) are compared. The bond angles at the cobalt atom are close to the octahedral values. The bite angles are slightly less than 90° and the other bond angles are opened correspondingly.

Table 1. Final fractional coordinates. The estimated standard deviations are given in parentheses. The labelling corresponds to Fig. 1.

Atom	*x*	*y*	*z*
Co	0.01455(4)	0.11854(3)	0.05597(7)
S1	−0.03216(7)	−0.00633(6)	−0.04623(16)
S2	0.14111(8)	0.05713(7)	0.15821(15)
N1	−0.0942(3)	0.1685(2)	−0.0506(7)
N2	−0.0560(3)	0.0930(2)	0.2597(5)
N3	0.0555(3)	0.2246(2)	0.1601(6)
N4	0.0856(3)	0.1444(3)	−0.1498(6)
C1	−0.1248(3)	0.1223(4)	−0.2017(7)
C2	−0.1325(4)	0.0288(3)	−0.1637(7)
C3	−0.0827(4)	−0.0468(3)	0.1469(7)
C4	−0.1239(3)	0.0241(3)	0.2428(7)
C5	0.1165(4)	0.2101(3)	0.3042(8)
C6	0.1916(4)	0.1500(4)	0.2590(8)
C7	0.2024(3)	0.0529(4)	−0.0379(7)
C8	0.1853(4)	0.1308(4)	−0.1377(8)
Cl1	0.05997(9)	0.01449(9)	0.5576(2)
Cl2	0.18657(8)	0.35138(8)	−0.0433(2)
Cl3	−0.1099(1)	0.2974(1)	0.4061(3)
O1	0.2357(4)	0.3378(3)	0.5665(6)
H1(N1)	−0.085(4)	0.216(4)	−0.075(7)
H2(N1)	−0.141(4)	0.170(3)	0.019(7)
H1(C1)	−0.078(4)	0.135(3)	−0.279(7)
H2(C1)	−0.187(4)	0.152(3)	−0.244(6)
H1(C2)	−0.140(4)	−0.009(3)	−0.255(7)
H2(C2)	−0.194(3)	0.019(3)	−0.100(6)
H1(C3)	−0.028(3)	−0.075(3)	0.197(6)
H2(C3)	−0.127(3)	−0.088(3)	0.108(6)
H1(C4)	−0.144(3)	0.005(3)	0.368(6)
H2(C4)	−0.176(4)	0.046(3)	0.195(6)
H1(N2)	−0.012(3)	0.077(3)	0.338(6)
H2(N2)	−0.077(4)	0.134(3)	0.290(7)
H1(N3)	0.008(4)	0.248(3)	0.180(7)
H2(N3)	0.085(3)	0.258(3)	0.084(6)
H1(C5)	0.076(4)	0.187(3)	0.404(6)
H2(C5)	0.141(4)	0.247(4)	0.332(7)
H1(C6)	0.216(4)	0.129(4)	0.341(8)
H2(C6)	0.238(4)	0.169(3)	0.177(7)
H1(C7)	0.180(3)	0.001(3)	−0.085(6)
H2(C7)	0.260(4)	0.052(3)	−0.010(6)
H1(C8)	0.208(4)	0.124(3)	−0.261(7)
H2(C8)	0.217(4)	0.179(3)	−0.085(7)
H1(N4)	0.069(4)	0.115(3)	−0.244(7)
H2(N4)	0.067(4)	0.194(4)	−0.181(7)

Table 2. Refined parameters for the disordered water molecules. Estimated standard deviations in parentheses.

Atom	Population	*x*	*y*	*z*	$U \times 10^2$ Å^2
O2	0.58(1)	−0.0392(6)	0.3179(6)	−0.203(1)	7.4(2)
O3	0.50(1)	0.0009(8)	0.2950(7)	−0.272(1)	7.6(3)
O4	0.42(3)	−0.102(1)	0.339(1)	0.078(2)	8.2(5)
O5	0.12(2)	−0.109(2)	0.337(3)	0.021(5)	3.7(9)

Table 3. Final thermal parameters, u_{ij}, in units of $Å^2 \times 10^{-2}$. The expression for the temperature factors is $\exp\{-2\pi^2(u_{11}h^2a^{*2}+\cdots+2u_{12}hka^*b^*+\cdots)\}$. The estimated standard deviations are given in parentheses.

Atom	u_{11}	u_{22}	u_{33}	u_{12}	u_{13}	u_{23}
Co	2.00(2)	1.95(2)	2.45(2)	−0.06(2)	0.06(2)	0.10(2)
S1	3.05(5)	2.23(4)	3.27(5)	−0.13(4)	−0.01(5)	−0.43(5)
S2	2.66(6)	2.93(6)	3.49(6)	0.47(5)	−0.38(5)	−0.19(5)
N1	2.9(2)	1.9(2)	4.5(2)	0.1(1)	0.0(2)	0.3(2)
N2	3.3(2)	2.3(2)	2.7(2)	0.0(2)	0.1(2)	0.1(2)
N3	2.9(2)	2.5(2)	4.2(2)	0.0(2)	0.0(2)	−0.4(2)
N4	3.2(2)	4.2(2)	3.4(2)	−0.3(2)	0.8(2)	0.7(2)
C1	3.0(2)	4.3(3)	3.6(3)	0.0(2)	−0.9(2)	0.6(2)
C2	3.5(3)	3.4(3)	3.4(2)	−0.3(2)	−0.9(2)	−0.4(2)
C3	3.6(3)	2.7(2)	4.5(3)	−0.7(2)	−0.2(2)	0.5(2)
C4	2.7(3)	3.4(3)	3.8(3)	−0.8(2)	0.2(2)	0.8(2)
C5	4.7(3)	3.0(3)	4.8(3)	−0.8(2)	−1.0(3)	−1.1(2)
C6	3.6(3)	4.6(3)	4.5(3)	−0.2(2)	−1.4(3)	−1.0(3)
C7	2.3(2)	5.2(3)	4.1(3)	0.8(2)	0.5(2)	−1.3(3)
C8	3.0(3)	4.8(3)	4.6(3)	−0.1(2)	1.5(2)	−0.6(3)
Cl1	4.89(7)	6.77(8)	3.08(6)	0.81(6)	−0.08(7)	−0.36(7)
Cl2	4.12(6)	3.55(5)	5.50(8)	−0.68(5)	0.51(7)	0.47(7)
Cl3	5.00(9)	7.06(11)	10.65(16)	−0.88(8)	0.56(10)	−0.91(11)
O1	10.0(4)	7.5(3)	5.8(3)	3.1(3)	−2.3(3)	−1.4(3)

The Co−S bond lengths of 2.241 and 2.243 Å are identical to those observed [13] in the complex *u-cis*-$[Co(ete)(NO_2)Cl]^+$ (where ete = 3,7-dithianonane-1,9-diamine). The corresponding bond lengths in 6,9-diaza-2,13-dithiatetradecane-5,10-dicarboxylato cobalt(III) monocation is 2.267 Å.[14] In this complex the thioethers are terminal ligators of the hexadentate ligand and therefore not forced closer to the cobalt atom by surrounding chelate rings. All four Co−N distances are substantially equal (mean: 1.973 Å) and in accordance with results obtained for other cobalt(III) chelates with terminal amino groups. The C−S and C−N distances are all found to assume normal values. The C−C distances (mean: 1.493 Å) are somewhat shorter than usually observed. Similar short bonds have been found in a number of free and complexed cyclic ethers and thioethers.

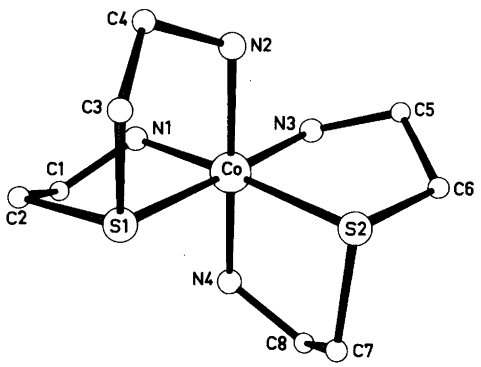

Fig. 1. An ORTEP drawing of the $(-)_D$-$\Delta(\lambda\lambda\lambda\lambda)$-*u-fac*$[Co(daes)_2]^{3+}$ ion illustrating the atomic labelling.

It has been established that the $(-)_D$ catoptric form of the complex has the absolute configuration Δ. This result thus confirms the tentative assignment of the absolute configuration given on the basis of the circular dichroism spectrum of the isomer.[1] The four individual five-membered chelate rings take λ

Table 4. Bond lengths (Å) in $[Co(daes)_2]Cl_3$. Standard deviations in parentheses.

Co−S1	2.244(1)	Co−S2	2.248(1)
Co−N1	1.973(4)	Co−N3	1.965(4)
Co−N2	1.968(4)	Co−N4	1.988(5)
N1−C1	1.480(7)	N3−C5	1.475(8)
C1−C2	1.514(8)	C5−C6	1.500(8)
C2−S1	1.830(6)	C6−S2	1.831(6)
S1−C3	1.826(6)	S2−C7	1.806(6)
C3−C4	1.487(7)	C7−C8	1.489(8)
C4−N2	1.482(7)	C8−N4	1.481(7)

Table 5. Selected bond angles (°).

S1 – Co – S2	90.19(5)	N1 – Co – N3	95.0(2)
S1 – Co – N1	87.1(2)	S2 – Co – N3	87.9(1)
S1 – Co – N2	87.6(1)	S2 – Co – N4	87.5(1)
S1 – Co – N4	92.4(1)	S2 – Co – N2	92.6(1)
N1 – Co – N2	90.8(2)	N3 – Co – N4	90.7(2)
N1 – Co – N4	89.2(2)	N3 – Co – N2	89.2(2)
Co – N1 – C1	113.5(3)	Co – N3 – C5	112.5(3)
N1 – C1 – C2	110.0(4)	N3 – C5 – C6	110.9(5)
C1 – C2 – S1	109.8(4)	C5 – C6 – S2	108.5(4)
C2 – S1 – Co	99.5(2)	C6 – S2 – Co	98.4(2)
C2 – S1 – C3	102.2(2)	C6 – S2 – C7	102.1(3)
S1 – C3 – C4	109.5(3)	S2 – C7 – C8	110.4(4)
C3 – C4 – N2	109.2(4)	C7 – C8 – N4	108.8(4)
C4 – N2 – Co	115.4(3)	C8 – N4 – Co	115.7(4)
Dihedral angles			
N1 – C1 – C2 – S1	– 44.8(5)	N3 – C5 – C6 – S2	– 49.4(6)
N2 – C4 – C3 – S1	– 50.7(5)	N4 – C8 – C7 – S2	– 51.5(5)

conformations. So the isomer studied here can be characterized as $(-)_D$-$\Delta(\lambda\lambda\lambda\lambda)$-*u-fac*-$[Co(daes)_2]^{3+}$. The structure of the closely analogous complex $(-)_D$-*u-fac*-$[Co(dien)_2]^{3+}$ (as a salt of $[Co(CN)_6]^{3-}$) contains the two conformers $\Delta(\lambda\lambda\lambda\lambda)$ and $\Delta(\lambda\delta\lambda\delta)$.[15] This may reflect a smaller degree of conformational rigidity and a smaller energy difference between conformers of the dien complex relative to the daes complex.

The packing in the crystal is determined by hydrogen bonding. In the stereo pair shown in Fig. 2 the hydrogen bonds are illustrated. Two of

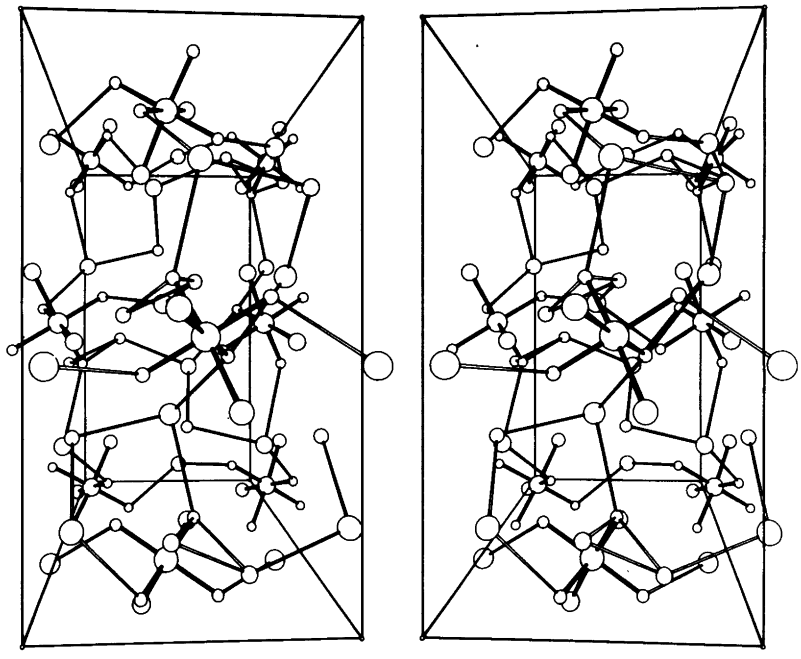

Fig. 2. Stereo pair of the packing viewed along the *c* axis.

the chloride ions Cl1 and Cl2 are hydrogen bonded to the complex ion. Thus Cl1 bridges N2 and N4 of different cations so that chains along the direction of the *c* axis are formed. The distances are Cl1 – N2 3.175 Å and Cl1 – N4 3.133 Å. The two Cl1 – H – N angles are both 162°. Correspondingly Cl2 connects the two nitrogen atoms N1 and N3 (lying in the CoS_2-plane) from different cations making chains along the *a* axis. These interactions are slightly weaker (Cl2 – N1 3.218 Å, Cl2 – N3 3.316 Å). The third chloride is hydrogen bonded to N3, Cl3 – N3 3.326 Å.

The ordered water molecule in the structure has interactions to Cl2 and Cl3 (Cl2 – O1 3.202 Å, Cl3 – O1 3.122 Å). The sites for the disordered water molecules are in an area where it is possible to form hydrogen bonds to Cl1, Cl3, and N1. The distance between the two sites O3 and O4 is 3.25 Å making it possible to fit more than one water molecule into this area.

The efficient hydrogen bonding network described above may account for the spontaneous resolution that occurs when the racemic compound crystallizes. One could imagine that a hypothetical crystal structure which contained both enantiomers in the unit cell would have higher free energy than the crystal structure described here. From solutions of racemic mixtures of the salt at various different temperatures were grown large single crystals (0.01 – 1 cm^3). These crystals were found to have circular dichroism corresponding to the completely resolved samples or at some instances to consist of twinned crystals.

REFERENCES

1. Searle, G. H. and Larsen, E. *Acta Chem. Scand. A 30* (1976) 143.
2. Keene, F. R. and Searle, G. H. *Inorg. Chem. 11* (1972) 148.
3. Saito, Y., Nakatsu, K., Shiro, M. and Kuroya, H. *Acta Crystallogr. 8* (1955) 729.
4. Hawkins, C. J. *Absolute Configuration of Metal Complexes*, Wiley-Interscience, N.Y. 1971.
5. Lehnert, P. G. *J. Appl. Crystallogr. 8* (1975) 568.
6. Johnson, C. K. *ORTEP, A Fortran Ellipsoid Plot Program for Crystal Structure Illustrations*, Report ORNL-3794, Second Rev., Oak Ridge National Laboratory, Oak Ridge 1970.
7. Stewart, J. M. *et al. The X-Ray System 1972*, Technical Report Tr-192, Computer Science Center, University of Maryland, College Park 1972.
8. Nielsen, K. *Acta Crystallogr. A 31* (1977) 1009.
9. Cromer, D. T. and Mann, J. B. *Acta Crystallogr. A 24* (1968) 321.
10. Stewart, R. F., Davidson, E. R. and Simpson, W. T. *J. Chem. Phys. 42* (1965) 3175.
11. Cromer, D. T. and Liberman, D. *J. Chem. Phys. 53* (1970) 1891.
12. Hamilton, W. C. *Acta Crystallogr. 18* (1965) 502.
13. Murray-Rust, J. and Murray-Rust, P. *Acta Crystallogr. B 29* (1973) 2606.
14. Geue, R. and Snow, M. *Acta Crystallogr. B 33* (1977) 70.
15. Konno, M., Marumo, F. and Saito, Y. *Acta Crystallogr. B 29* (1973) 739.

Received February 24, 1978.

Acta Chemica Scandinavica A 32 (1978) 509–514

Crystal Structure of α-Tetraethylammonium Trichloromercurate(II)

MAGNUS SANDSTRÖM and DJIET HAY LIEM

Department of Inorganic Chemistry, Royal Institute of Technology, S-100 44 Stockholm 70, Sweden

The structure of the compound $[N(C_2H_5)_4]HgCl_3$ was determined from three-dimensional single-crystal X-ray diffraction data collected at room temperature on an automatic Syntex $P2_1$ four-circle diffractometer. The unit cell is triclinic, space group $P\bar{1}$, with $a=7.644(1)$, $b=9.749(2)$, $c=10.325(2)$ Å, $\alpha=62.78(1)$, $\beta=86.91(1)$, $\gamma=86.07(1)°$, and $Z=2$. The structure, refined to a final conventional R value of 0.039, comprises planar trigonal $HgCl_3^-$ anions and NEt_4^+ cations of almost regular S_4 symmetry. The average Hg–Cl bond length is 2.43 Å. Two long Hg–Cl contacts at 3.054(3) and 3.017(3) Å complete a trigonal bipyramidal configuration around Hg and bridge adjacent $HgCl_3^-$ ions, giving rise to infinite chains parallel to the x axis. A comparison is made with other structures where mercury(II) is surrounded by halide ions in a trigonal bipyramidal configuration. A probable structure change is proposed for the transition from the α to the β form of $[NEt_4]HgCl_3$.

Crystal structure determinations of trihalidomercurate(II) salts show a variety of different mercury(II) coordinations.[1] Planar trigonal coordination occurs for several compounds containing HgX_3^- ions (X=I, Br and Cl), where two long Hg–X interactions complete a trigonal bipyramidal configuration.[2-7]

Tetrahedral coordination in chains of HgX_4 tetrahedra sharing two apexes is found in several compounds.[8-13] Distorted tetrahedral coordination also occurs in the discrete dimeric $Hg_2X_6^{2-}$ complexes with X=I[14] or Br[15,16] where two tetrahedra share an edge.

For several trichloromercurate(II) salts distorted octahedral coordination with two short digonal Hg–Cl bonds, is found. These octahedra can share apexes to form sheets[17,18] or a distorted perovskite structure as in $CsHgCl_3$,[19,20] or edges to give a double-rutile chain structure.[21-22]

By X-ray diffraction methods the HgI_3^- and $HgBr_3^-$ ions are found to be pyramidal in aqueous and dimethyl sulfoxide (DMSO) solutions. Coordinated solvent molecules probably complete a tetrahedral coordination (for $HgBr_3^-$ in DMSO possibly distorted trigonal bipyramidal).[23-25]

In concentrated aqueous solutions with the mol ratio Cl/Hg≈3 polymeric Hg–Cl complexes occur, probably with the distorted octahedral coordination mentioned above.[26] In DMSO solutions, however, monomeric $HgCl_3^-$ ions are found with an average Hg–Cl bond length of 2.434(4) Å.[25] The X-ray diffraction and Raman data are consistent with a planar trigonal structure with two DMSO oxygen atoms completing a trigonal bipyramidal coordination.[25] Since spectroscopic data indicated the compound α-$[NEt_4]HgCl_3$ to contain discrete $HgCl_3^-$ ions,[13] its structure was determined in the present work to provide a comparison with the solution data.

EXPERIMENTAL

Colourless crystals of α-$[NEt_4]HgCl_3$ were prepared as described previously.[13] The compound was identified by its strong ν_1(Hg–Cl) Raman line at 269 cm^{-1}.[13] Its density, $D_m=2.10(2)$, was determined by the apparent loss of weight in benzene.

The X-ray data were obtained using graphite-monochromatized Mo$K\alpha$ radiation ($\lambda=0.71069$ Å) at room temperature on a prismatic crystal with a largest dimension of about 0.15 mm. The unit cell parameters were determined by the standard procedure on the computer-controlled Syntex $P2_1$ four-circle diffractometer,[27] and refined by least-squares methods for 25 centred reflections, all with $2\theta>30°$. A triclinic unit cell was found with $a=7.644(1)$, $b=9.749(2)$, $c=10.325(2)$ Å. $\alpha=62.78(1)$, $\beta=86.91(1)$, $\gamma=86.07(1)°$, $V=682.5(2)$ Å^3, and $D_x=2.128$ for $Z=2$.

The ω scan technique with variable scan speeds from 0.5° min^{-1} upwards was used. Four check reflections were measured regularly every 100th reflection. All their intensities increased continuously, but markedly more for the strong low-angle reflections, indicating extinction changes. The largest increase, 27 %, was obtained for the 011 check reflection. Of the 2396 possible independent hkl, $h\bar{k}l$, $hk\bar{l}$ and $h\bar{k}\bar{l}$ reflections measured for $2\theta < 50°$, 2183 reflections had intensities larger than $1.96\sigma(I)$ and were considered observed.

A semi-empirical absorption correction method was applied on the data, as described previously.[27] The largest variation obtained in the relative intensity correction factors was from 1 to 0.63. The linear absorption coefficient μ(Mo$K\alpha$) is 121 cm^{-1}.

Further data reduction to scaled $|F_o|$ values was performed as previously, using computer programs and scattering factors from the same sources.[27] Anomalous dispersion corrections were included for the Hg and Cl atoms.

STRUCTURE DETERMINATION AND REFINEMENT

From a three-dimensional Patterson peak listing, centrosymmetrical positions of the two Hg and six Cl atoms of the unit cell could be deduced, consistent with the space group $P\bar{1}$ (No. 2). Full-matrix least-squares refinements of these initial parameters using isotropic temperature factors yielded a conventional R value of 0.15 and weighted R_w of 0.22, defined as before.[27] A difference Fourier synthesis revealed the positions of all non-H atoms and refinements with the Hg and Cl atoms anisotropic gave $R = 0.040$ and $R_w = 0.066$. Refinements with all atoms anisotropic further decreased R to 0.039 and R_w to 0.062, which is a significant improvement according to the Hamilton test.[28] A total of 118 parameters was refined. The parameter shifts in the last refinement cycle were all less than 1 % of the corresponding standard deviation. The highest of the peaks in a final difference Fourier map was 0.92 e $Å^{-3}$. Only a few of these peaks corresponded to any of the 20 possible H atom positions. Therefore, no H atoms were included in the final model.

The final parameter values are given in Tables 1 and 2.

The function minimized in the least-squares refinement was $\Sigma w\|F_o| - |F_c\|^2$. The weighting function w was chosen as $w = 1/\{\sigma^2(F_o) + (0.04F_o)^2\}$. This gave a satisfactory weighting scheme according to statistical analyses of the error distribution, except for some of the weakest reflections indicating systematic errors in this part of the measured data. All 119 reflections with $|F_o| < 10$ have therefore been omitted in the refinements reported here, which caused a decrease in the final R value from 0.041 to 0.039.

DISCUSSION

General. The structure comprises planar trigonal $HgCl_3^-$ anions, stacked in columns parallel to the x axis and surrounded by discrete $[N(C_2H_5)_4]^+$ cations (Figs. 1 and 2). Some interatomic distances and angles are given in Table 3.

The $HgCl_3^-$ ion. The average Hg–Cl bond length in the planar $HgCl_3^-$ unit is 2.43_2 Å. The deviations

Table 1. Final fractional atomic positional parameters with estimated standard deviations in parentheses.

Atom	x	y	z
Hg	0.25071(5)	0.04711(5)	0.42529(4)
Cl1	0.2609(4)	0.2006(4)	0.1601(3)
Cl2	0.0598(4)	0.1372(4)	0.5694(4)
Cl3	0.4324(4)	−0.1900(3)	0.5328(4)
N	0.2334(10)	0.6633(9)	0.1679(9)
C1	0.2945(15)	0.8083(12)	0.1739(13)
C2	0.4893(17)	0.8184(14)	0.1708(13)
C3	0.3013(16)	0.6503(17)	0.0320(14)
C4	0.2404(19)	0.7827(18)	0.8899(13)
C5	0.3097(15)	0.5247(12)	0.2946(13)
C6	0.2571(14)	0.5095(14)	0.4445(11)
C7	0.0341(14)	0.6727(16)	0.1757(13)
C8	0.0526(17)	0.4655(15)	0.8097(15)

Table 2. Final anisotropic thermal parameters (Å^2) with estimated standard deviations in parentheses. The expression used for the temperature factor is $\exp[-1/4(B_{11}h^2a^*+\cdots+2B_{12}hka^*b^*+\cdots)]$.

Atom	B_{11}	B_{22}	B_{33}	B_{12}	B_{13}	B_{23}
Hg	3.93(2)	3.32(2)	2.88(2)	0.50(1)	0.21(1)	−1.30(2)
Cl1	4.23(11)	4.52(13)	2.81(11)	−0.30(10)	0.07(9)	−1.51(10)
Cl2	3.78(11)	4.42(13)	5.65(15)	−0.82(10)	1.45(10)	−3.42(12)
Cl3	3.94(11)	3.32(11)	5.24(14)	0.85(9)	−1.28(10)	−2.49(11)
N	3.0(3)	2.6(3)	2.6(3)	−0.4(3)	0.4(3)	−1.5(3)
C1	4.9(5)	2.3(4)	4.2(5)	−0.6(4)	0.1(4)	−2.1(4)
C2	5.2(6)	4.1(5)	3.2(5)	−1.3(5)	0.9(4)	−1.2(4)
C3	4.1(5)	6.4(7)	3.6(5)	−0.7(5)	1.3(4)	−3.2(5)
C4	6.4(7)	7.2(8)	1.8(4)	−0.3(6)	−0.4(4)	−2.2(5)
C5	3.9(5)	3.0(4)	3.6(5)	0.6(4)	−0.8(4)	−1.3(4)
C6	4.1(5)	4.3(5)	2.2(4)	−0.9(4)	0.0(4)	−0.8(4)
C7	2.6(4)	6.0(6)	4.0(5)	0.4(4)	−0.5(4)	−2.8(5)
C8	4.5(6)	4.3(6)	4.4(6)	−0.9(5)	0.4(5)	−0.9(5)

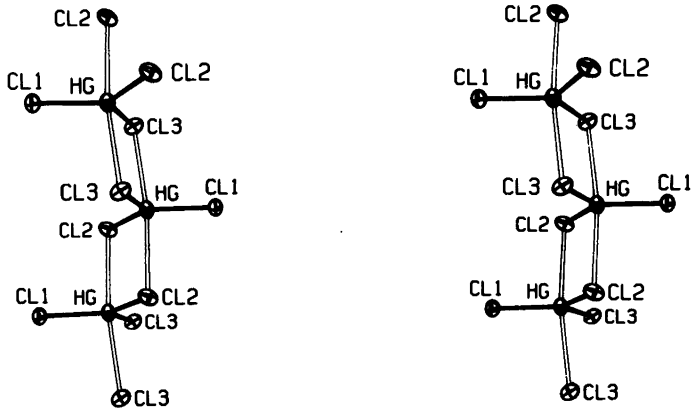

Fig. 1. A stereoscopic view of the chain of $HgCl_3^-$ anions. The long bridging interactions are shown by the unfilled bonds. The thermal ellipsoids include 30 % probability.

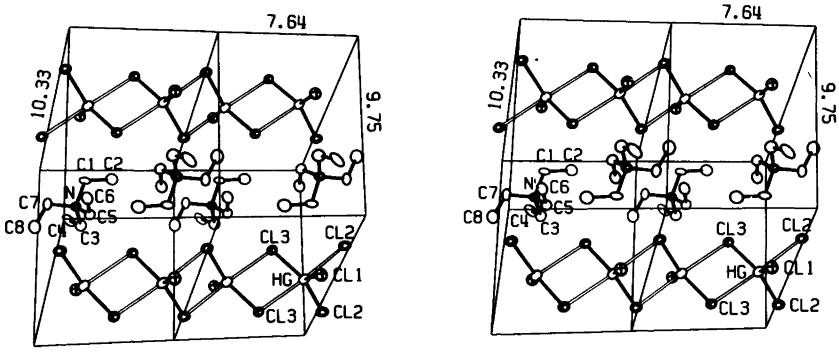

Fig. 2. A stereoscopic illustration of the molecular packing viewed almost perpendicular to the *b* edge. The cell edges of two unit cells are outlined with their lengths in Å. The thermal ellipsoids enclose 30 % probability. The long Hg−Cl bridging interactions are shown by the unfilled bonds.

Table 3. Some interatomic distances (Å) and bond angles (°). Estimated standard deviations are given in parentheses. The superscripts imply the following symmetry operations relative to *x*, *y*, *z* in Table 1: [a] $\bar{x}$, $\bar{y}$, 1-*z* and [b] 1-*x*, $\bar{y}$, 1-*z*.

Hg–Cl1	2.444(3)	Cl1–Hg–Cl2	118.9(1)
Hg–Cl2	2.426(3)	Cl1–Hg–Cl3	118.3(1)
Hg–Cl3	2.426(3)	Cl2–Hg–Cl3	122.9(1)
Hg–Cl2[a]	3.054(3)	Cl2[a]–Hg–Cl3[b]	171.1(1)
Hg–Cl3[b]	3.017(3)	Cl1–Hg–Cl2[a]	94.9(1)
Hg–Hg[a]	4.050(1)	Cl1–Hg–Cl3[b]	93.6(1)
Hg–Hg[b]	4.070(1)	Cl2–Hg–Cl2[a]	85.4(1)
N–C1	1.546(16)	Cl2–Hg–Cl3[b]	92.9(1)
N–C3	1.524(16)	Cl3–Hg–Cl2[a]	89.8(1)
N–C5	1.494(15)	Cl3–Hg–Cl3[b]	83.8(1)
N–C7	1.518(13)	C1–N–C3	113.0(9)
C1–C2	1.495(18)	C1–N–C5	107.7(8)
C3–C4	1.514(19)	C1–N–C7	106.5(8)
C5–C6	1.518(16)	C3–N–C5	106.0(9)
C7–C8	1.483(22)	C3–N–C7	111.3(9)
		C5–N–C7	112.3(9)
		N–C1–C2	114.6(10)
		N–C3–C4	114.4(11)
		N–C5–C6	116.0(10)
		N–C7–C8	115.6(11)

from a weighted least-squares plane are for Hg −0.0001(4) Å, for Cl1, Cl2 and Cl3 0.002(3) Å. Two long Hg–Cl interactions at 3.054(3) and 3.017(3) Å to the adjacent $HgCl_3^-$ ions complete a slightly distorted trigonal bipyramidal configuration (the sum of the van der Waals radii of Hg[29] and Cl is 3.3_0 Å), where the bipyramids share two of their long edges on opposite sides (Figs. 1 and 3). These bridging chlorine atoms form asymmetric double bridges between the Hg atoms giving rise to infinite $(HgCl_3^-)_n$ chains (Fig. 2).

Comparison with other trigonal bipyramidal Hg–X configurations. The same type of chain as in the present structure has been found in the compounds $Hg_3I_6(en)_2$ where en = ethylenediamine, $C_2H_8N_2$,[4] in $[S(CH_3)_3]HgI_3$,[2] and recently in $[S(CH_3)_3]HgCl_3$,[6] where the average bond length in the trigonal $HgCl_3^-$ unit is 2.42_7 Å and the long Hg–Cl interactions 3.040(5) and 3.049(5) Å. The $(HgBr_3^-)_n$ chain in $[N(CH_3)_4]HgBr_3$ can also be described in this way even though the Hg atoms are all displaced approximately 0.3 Å above the plane through the bromine atoms in the $HgBr_3^-$ units,[11] thus giving a pseudotetrahedral coordination intermediate to the chains of HgX_4-tetrahedra sharing two apexes (*cf.* Fig. 3) found in, *e.g.*, $KHgBr_3.H_2O$,[10] $KHgI_3.H_2O$[9] and $[N(CH_3)_4]HgI_3$.[8]

Neither in the vibrational spectra of the compounds $[S(CH_3)_3]HgCl_3$,[6] α-$[NEt_4]HgCl_3$ and $[S(CH_3)_3]HgI_3$,[13] with the bipyramidal arrangement described above (*cf.* Fig. 3), nor in that of $[N(CH_3)_4]HgBr_3$,[13] were bridging Hg–X modes found, implying that the long Hg–X interactions are quite weak. However, infrared bands which can be assigned to bridging frequencies occur in the spectrum of $[N(CH_3)_4]HgI_3$,[13] consistent with the structure reported for this compound.[8] Similar bridging frequencies are also found[13] in the spectrum of the high-temperature form, β-$[NEt_4]HgCl_3$, of the compound studied in the present work. Consequently, it seems probable that the same type of apex-sharing chains of HgX_4-tetrahedra[8] occur in these compounds, and thus that the α to β transition of $[NEt_4]HgCl_3$ consists only of a displacement of the Hg atoms approximately 0.4 Å perpendicular to the plane through the chlorine atoms in the $HgCl_3^-$ unit (Fig. 3).

The bipyramidal chain type discussed above leaves only one non-bridging halogen atom in each HgX_3^- unit. Another arrangement, giving two non-bridging halogen atoms, is found in the $(HgCl_3^-)_n$ chain in $[S_4N_3]HgCl_3$ (*cf.* Ref. 7, Fig. 2). One of the chlorine atoms of each planar $HgCl_3^-$ unit has two long interactions, 3.022(8) and 3.204(9)

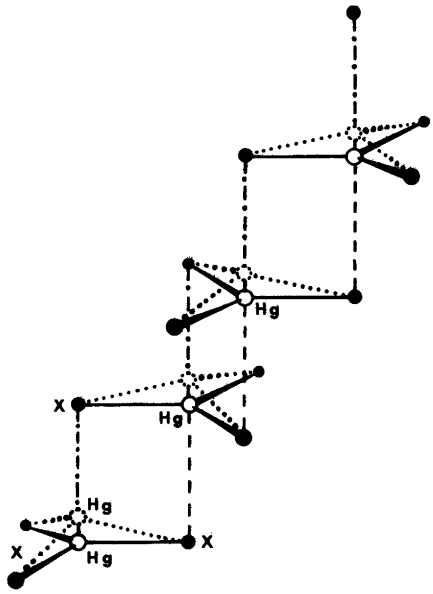

Fig. 3. A perspective view showing the probable structure change of the $(HgCl_3^-)_n$ chain due to a displacement of the mercury atoms (open circles) at the α to β transition of $[N(C_2H_5)_4]HgCl_3$. The solid and dashed lines show the the bipyramidal arrangement in the α form. The lines with dots visualize the chain of $HgCl_4$ tetrahedra sharing two apexes which probably occur in β-$[N(C_2H_5)_4]HgCl_3$. The same types of coordination occur in several other HgX_3 compounds (see text).

Å, to the Hg atoms of the adjacent $HgCl_3^-$ ions thus forming a double-chain of bipyramids on top of each other, fused by sharing the two long edges on the same side of each bipyramid. The average Hg–Cl bond length in the $HgCl_3^-$ unit is 2.42_3 Å.[7]

There seems to be no correlation between the short Hg–X bond lengths for bridging and non-bridging halogen atoms in either of the two chain types, which is an additional indication of the weakness of these bridging interactions.

Columns of HgX_3^- ions joined by interjacent equidistant halide ions, thus forming single chains of apex-sharing bipyramids on top of each other with all the three halogen atoms of HgX_3^- non-bridging, are found in the compounds Hg_2NHBr_2 [5] and $K_2HgI_4.3H_2O$ [3] (*cf.* Ref. 1, Fig. 1).

Discrete regular trigonal bipyramidal $HgCl_5^{3-}$ complex ions also occur, but have shorter axial, 2.518(4) Å, than equatorial, 2.640(4) Å, bond lengths.[30] The ratio is 0.954(3) which can be compared with the corresponding ratios ranging between 1.25 and 1.33 for the bipyramidal configurations in the $(HgX_3^-)_n$ chains.

The $[N(C_2H_5)_4]^+$ ion. The tetraethylammonium ion is well-ordered and has an almost regular S_4 symmetry (*cf.* Fig. 2 and Table 3). The deviations from the two almost perpendicular (87.8°) planes through the N atom and the C atoms of the opposite ethyl groups are less than 0.011 Å (which is less than 1σ) for all atoms except C8 (deviation 0.187(14) Å). The ethyl groups are in contact with the Cl atoms of the $HgCl_3^-$ ions. The closest approach is C5–Cl3, 3.45(1) Å, which is slightly shorter than the sum of the van der Waals radii, 3.6 Å.[31]

The average bond lengths found, C–N 1.52(2) Å and C–C 1.50(2) Å, are in good agreement with average values reported in a recent precise determination, C–N 1.528(3) Å and C–C 1.504(13) Å.[32]

Acknowledgements. The authors wish to thank the Swedish Natural Science Research Council and the foundation "Knut & Alice Wallenbergs Stiftelse" for economic support. Professor Ingmar Grenthe, Dr. Georg Johansson and Mr. Ivaylo Toromanov are gratefully thanked for their interest in this work.

REFERENCES

1. Sandström, M. *Thesis*, Royal Institute of Technology, Stockholm 1978. (Available on request).
2. Fenn, R. H. *Acta Crystallogr. 20* (1966) 20.
3. Gerken, V. A. and Pakhomov, V. I. *Zh. Strukt. Khim. 10* (1969) 753.
4. Grdenić, D., Sikirica, M. and Vicković, I. *Acta Crystallogr. B 33* (1977) 1630.
5. Brodersen, K. *Acta Crystallogr. 8* (1955) 723.
6. Biscarini, P., Fusina, L., Nivellini, G. and Pelizzi, G. *J. Chem. Soc. Dalton Trans.* (1977) 664.
7. Weidenhammer, K. and Ziegler, M. L. *Z. Anorg. Allg. Chem. 434* (1977) 152.
8. Fedorov, P. M. and Pakhomov, V. I. *Koord. Khim. 1* (1975) 1140.
9. Nyqvist, L. and Johansson, G. *Acta Chem. Scand. 25* (1971) 1615.
10. Padmanabhan, V. M. and Yadava, V. S. *Acta Crystallogr. B 25* (1969) 647.
11. White, J. G. *Acta Crystallogr. 16* (1963) 397.
12. Herlinger, A. H. *Spectrosc. Lett. 8* (1975) 787.
13. Barr, R. M. and Goldstein, M. *J. Chem. Soc. Dalton Trans.* (1976) 1593, and references therein.

14. Beurskens, P. T., Bosman, W. P. J. H. and Cras, J. A. *J. Cryst. Mol. Struct. 2* (1972) 183.
15. Harris, G. S., Inglis, F., McKechnie, J., Cheung, K. K. and Ferguson, G. *Chem. Commun. 9* (1967) 442.
16. Gal, A. W., Beurskens, G., Cras, J. A., Beurskens, P. T. and Willemse, J. *Recl. Trav. Chim. Pays-Bas 95* (1976) 157.
17. Harmsen, E. J. *Z. Kristallogr. 100* (1938) 208.
18. Barr, R. M. and Goldstein, M. *J. Chem. Soc. Dalton Trans.* (1974) 1180.
19. Zvonkova, Z. V., Samodurova, V. V. and Vorontsova, L. G. *Dokl. Akad. Nauk. SSSR 102* (1955) 1115.
20. Scaife, D. E. *Aust. J. Chem. 24* (1971) 1753.
21. Sagisawa, K., Kitahama, K., Kiriyama, H. and Kiriyama, R. *Acta Crystallogr. B 30* (1974) 1603, and references therein.
22. Authier-Martin, M. and Beauchamp, A. L. *Can. J. Chem. 53* (1975) 2345.
23. Gaizer, F. and Johansson, G. *Acta Chem. Scand. 22* (1968) 3013.
24. Sandström, M. and Johansson, G. *Acta Chem. Scand. A 31* (1977) 132.
25. Sandström, M. *Acta Chem. Scand. A 32* (1978). *In press.*
26. Sandström, M. *Acta Chem. Scand. A 31* (1977) 141.
27. Sandström, M. and Persson, I. *Acta Chem. Scand. A 32* (1978) 95, and references therein.
28. *International Tables for X-Ray Crystallography*, Kynoch Press, Birmingham 1968 and 1974, Vols. 3 and 4.
29. Grdenić, D. *Q. Rev. Chem. Soc. 19* (1965) 303.
30. Clegg, W., Greenhalgh, D. A. and Straughan, B. F. *J. Chem. Soc. Dalton Trans.* (1975) 2591.
31. Harmon, K. M., Gennick, I. and Madeira, S. L. *J. Phys. Chem. 78* (1974) 2585, and references therein.
32. Elder, R. C. and Pesa, F. *Acta Crystallogr. B 34* (1978) 268.

Received February 13, 1978.

Acta Chemica Scandinavica A 32 (1978) 515 – 517

The Crystal Structure of a β-V_3S-Type Modification of Ta_3P

PATHANA PHAVANANTHA,[a] CHA-ON PONTCHOUR,[a] SUPANICH PRAMATUS,[a] YVONNE ANDERSSON[b] and STIG RUNDQVIST[b]

[a] Faculty of Science, Chulalongkorn University, Bangkok 5, Thailand and [b] Institute of Chemistry, University of Uppsala, Box 531, S-751 21 Uppsala, Sweden

Ta_3P occurs in two modifications: low-temperature α-Ta_3P with the Ti_3P-type structure, and high-temperature β-Ta_3P with the β-V_3S-type structure. The crystal structure of β-Ta_3P has been refined from X-ray single-crystal diffraction data: space group $P4_2/nbc$ (No. 133), $a=10.1542(4)$ Å, $c=5.0137(3)$ Å, Ta(1) in 8*j*: $x=0.1576(1)$, Ta(2) in 8*j*: $x=0.5490(1)$, Ta(3) in 8*i*: $x=0.6048(1)$, P in 8*h*: $x=0.544(1)$, (origin at $\bar{1}$).

The occurrence of a tantalum phosphide with the approximate composition Ta_3P was observed in a cursory examination of the Ta–P system at elevated temperatures.[1] The powder diffraction pattern was indexed on a primitive tetragonal unit cell of dimensions $a=10.154$ Å, $c=5.012$ Å. In analogy to a number of Me_3P-type phosphides previously discovered in systems related to Ta–P it was assumed that Ta_3P crystallizes with the Ti_3P-type structure.[2]

During studies of various alloys containing transition metals and phosphorus, the X-Ray Crystallography Group at Chulalongkorn University isolated a tantalum phosphide single crystal fragment. Photographic X-ray data obtained by the Weissenberg method for this crystal indicated a primitive tetragonal symmetry, with unit cell dimensions closely the same as those reported previously for Ta_3P.[1] The Laue symmetry was 4/*mmm*, however, while a Ti_3P-type structure should possess the lower Laue symmetry 4/*m*. Subsequent structure analysis made by the Chulalongkorn group showed that the crystal was in fact isostructural with β-V_3S.[3]

In a re-examination of the Ta-P system at Uppsala,[4] preliminary studies of crystals obtained in tantalum-rich alloys showed that Ta_3P actually occurs in two modifications: one with the β-V_3S-type and the other with the Ti_3P-type structure. For both types of crystal, X-ray diffraction data were collected by single-crystal diffractometry. The present paper gives an account of the structure analyses made at the Chulalongkorn and Uppsala Universities for the β-V_3S-type tantalum phosphide.

EXPERIMENTAL DETAILS AND RESULTS

Preparation and powder diffraction work. Tantalum monophosphide was synthesized by heating tantalum metal (S.A. Lindberg & Co.) and red phosphorus, both of purities higher than 99 %, at 1040 °C in evacuated and sealed silica tubes. Ta_3P alloys were prepared by heating appropriate mixtures of tantalum monophosphide and tantalum in an arc furnace or an induction furnace under a protective atmosphere of argon. β-V_3S-type Ta_3P crystals were obtained directly from the as-cast arc-melted alloys, while Ti_3P-type crystals were found in alloys, which had been annealed at 1700 °C in the induction furnace. This indicates that the β-V_3S and the Ti_3P-type phases are high- and low-temperature modifications of Ta_3P, respectively. In the following, the low-temperature form is denoted by α-Ta_3P, and the high-temperature form by β-Ta_3P.

Powder diffraction patterns were recorded in Hägg-Guinier-type focussing cameras (Philips XDC-700) with Cu$K\alpha_1$ or Cr$K\alpha_1$ radiation and silicon ($a=5.431065$ Å)[5] as internal calibration standard. The powder patterns of the two forms of Ta_3P were very similar, with almost insignificant differences in diffraction angles and only minor differences in intensity between corresponding lines.

The unit cell dimensions were refined by the least-squares method using the local program CELNE.[6]

Structure refinement based on photographic data. Intensity data were recorded with zirconium-filtered MoK radiation in a Nonius Weissenberg camera. The multiple-film technique was used with thin iron foils interleaved with the films. The needle-shaped crystal was mounted with the tetragonal axis as rotation axis and $hk0$ and $hk1$ reflexions were recorded. The intensities of the reflexions were measured by visual comparison with an intensity scale obtained by timed exposures of one reflexion. Absorption corrections were applied to the intensity data, the crystal shape being approximated to a cylindrical form. The structure was refined by the least-squares method, initial values for the positional parameters being taken from the β-V_3S structure.[3] Atomic scattering factors and anomalous dispersion corrections were taken from International Tables.[7] Weights were applied according to Cruickshank's formula.[8] The calculations were carried out on IBM 1800 and IBM 370/155 computers using programs described in Ref. 9. The refinement converged with a final conventional R-value of 0.135 for the 102 independent observed reflexions. The results are given in Table 1.

Structure refinement based on diffractometer data. Intensities were recorded with a PDP8/A-controlled Nonius CAD-4F diffractometer using graphite-monochromatized Mo$K\alpha$ radiation. An $\omega-3/4\theta$ scanning mode was used, and instrumental stability was checked by remeasuring three standard reflexions regularly. A total number of 1590 reflexions, of these 862 independent, was recorded up to 90° in 2θ. In the region $0<2\theta\leq 15°$, the corresponding indices were $-7\leq h\leq 7$, $-7\leq k\leq 7$, $-3\leq l\leq 3$, and for $15<2\theta\leq 90°$, $0\leq h\leq 20$, $0\leq k\leq 20$, $0\leq l\leq 9$. Corrections for absorption were applied using the Gaussian grid method. Due to unavoidable errors in the description of the crystal form in combination with the extremely strong absorption ($\mu=1254\ \mathrm{cm}^{-1}$, transmissions varying between 0.07 and 0.22), some systematic absorption errors affected the final intensity material. Equivalent reflexions were averaged and refinement of the structure was performed by the least-squares method in a similar manner as for the photographic intensity data. The function minimized was $w(|F_o^2|-|F_c^2|)^2$. Weights were assigned to the reflexions according to the formula $w^{-1}=\sigma^2(F_o^2)+(pF_o^2)^2$, where $\sigma^2(F_o^2)$ is based on counting statistics and the empirical factor p was set to 0.03. A scale factor, positional parameters and individual isotropic temperature factors were refined. The three strongest reflexions were affected by extinction and were eventually assigned zero weight in the refinement.

For the 859 reflexions refined the following agreement factors were finally obtained: $R(F^2)=0.134$, $R(F)=0.108$, $R_w(F^2)=0.224$, where $R(F^n)=\Sigma\|F_o^n|-|F_c^n\|/\Sigma|F_o^n|$, and $R_w(F^n)=[\Sigma w(|F_o^n|-|F_c^n|)^2/\Sigma w|F_o^n|^2]^{\frac{1}{2}}$.

The final structure data obtained are presented in Table 1. Interatomic distances, based on the positional parameters and standard deviations derived from the diffractometer data, are given in Table 2.

Table 1. Structure data for β-Ta_3P, based on space group $P4_2/nbc$, origin at $\bar{1}$.

Atom	x	y	z	B
Diffractometer data				
Ta(1) in 8j	0.1576(1)	(=x)	1/4	0.14(2)
Ta(2) in 8j	0.5490(1)	(=x)	1/4	0.21(2)
Ta(3) in 8i	0.6048(1)	1/4	1/2	0.20(2)
P in 8h	0.544(1)	1/4	0	0.4(1)
Film data				
Ta(1) in 8j	0.1563(7)	(=x)	1/4	0.38(12)
Ta(2) in 8j	0.5497(6)	(=x)	1/4	0.13(9)
Ta(3) in 8i	0.6038(8)	1/4	1/2	0.14(9)
P in 8h	0.544(6)	1/4	0	0.6(8)

Table 2. Interatomic distances in β-Ta_3P. Distances shorter than 3.5 Å are listed.

Distance	Å	Distance	Å
Ta(1)−2P	2.579(8)	Ta(3)−2P	2.557(8)
− Ta(1)	2.653(2)	−2P	2.581(2)
−2Ta(2)	2.952(1)	− Ta(2)	2.859(1)
− Ta(2)	2.968(2)	− Ta(2)	2.859(1)
−2Ta(3)	3.091(1)	− Ta(3)	2.948(3)
−4Ta(1)	3.131(1)	−2Ta(1)	3.091(1)
−2Ta(2)	3.176(1)	−4Ta(3)	3.260(1)
		−2Ta(2)	3.333(1)
Ta(2)−2P	2.575(4)	P−2Ta(3)	2.557(8)
−2Ta(3)	2.859(1)	−2Ta(2)	2.575(4)
−2Ta(2)	2.875(1)	−2Ta(1)	2.579(8)
−2Ta(1)	2.952(1)	−2Ta(3)	2.581(2)
− Ta(1)	2.968(2)	−2Ta(2)	3.285(1)
−2Ta(1)	3.176(1)		
−2P	3.285(1)		
−2Ta(3)	3.333(1)		

CONCLUDING REMARKS

The principal features of the β-V_3S-type structure were presented and discussed by Pedersen and Grønvold,[3] and our results for β-Ta_3P are in general agreement with those obtained for β-V_3S. The close relationship between the four tetragonal structure types Fe_3P, Ti_3P, α-V_3S and β-V_3S has been stressed in many previous discussions.[10,11] With the discovery of β-Ta_3P, all four of these types are now represented among the transition metal phosphide structures. A more detailed crystal chemical analysis of this structure family is deferred to a forthcoming paper.

Acknowledgements. This work has partly been supported by grants from the Swedish Natural Science Research Council. The authors from Chulalongkorn University wish to thank the International Seminars, University of Uppsala and the Swedish International Development Authority (SIDA) for their generous financial support. A part of this work has been supported by the Thai University Development Commission Program.

REFERENCES

1. Rundqvist, S. *Nature 211* (1966) 847.
2. Lundström, T. and Snell, P.-O. *Acta Chem. Scand. 21* (1967) 1343.
3. Pedersen, B. and Grønvold, F. *Acta Crystallogr. 12* (1959) 1022.
4. Björkegren, J. and Andersson, Y. *New Phases in the Ta-P System*, Institute of Chemistry, University of Uppsala, Uppsala 1976, UUIC-B18-53.
5. Deslattes, R. D. and Henins, A. *Phys. Rev. Lett. 31* (1973) 972.
6. Ersson, N.-O. Institute of Chemistry, University of Uppsala. *Unpublished.*
7. *International Tables for X-Ray Crystallography*, Kynoch Press, Birmingham 1974, Vol. IV.
8. Cruickshank, D. W. J., Philling, D. E., Bujosa, A., Lovell, F. M. and Truter, M. R. In *Computer Methods and the Phase Problem*, Pergamon, Oxford 1961, p. 32.
9. Lundgren, J.-O., Ed., *Crystallographic Computer Programs*, Institute of Chemistry, University of Uppsala, Uppsala 1975, UUIC-B13-04-2.
10. Rundqvist, S. *Ark. Kemi 20* (1962) 67.
11. Lundström, T. *Ark. Kemi 31* (1969) 227.

Received January 25, 1978.

Acta Chemica Scandinavica A 32 (1978) 519–525

Crystal and Molecular Structure of Hexakis(dimethyl sulfoxide)cadmium(II) Perchlorate, $[Cd((CH_3)_2SO)_6](ClO_4)_2$

MAGNUS SANDSTRÖM

Department of Inorganic Chemistry, Royal Institute of Technology, S-100 44 Stockholm 70, Sweden

The title compound crystallizes in the orthorhombic space group $Fd2d$ with $a=12.54(1)$, $b=20.23(1)$, $c=25.53(1)$ Å, and $Z=8$. The X-ray data were collected at room temperature by a computer-controlled Syntex $P2_1$ four-circle diffractometer using Mo$K\alpha$ radiation. The structure determination was performed on a data-set with 1244 independent reflections and refined by least-squares methods to a conventional R value of 0.039.

The structure is built up of discrete $[Cd(DMSO)_6]^{2+}$ and perchlorate ions. Six DMSO oxygen atoms are coordinated to each Cd atom, forming an almost regular octahedron. The average Cd–O bond length is 2.27 Å. Two symmetry-related DMSO ligands and one of the two crystallographically different perchlorate groups are disordered between two alternative positions. Both perchlorate groups perform large librational movements.

As part of an investigation into the structures of solvated Cd(II) and Hg(II) ions in solutions and in crystals,[1–4] the crystal structure of the compound $[Cd(DMSO)_6](ClO_4)_2$ was determined.

EXPERIMENTAL

Preparation. The compound $Cd(ClO_4)_2.6DMSO$, prepared as described previously,[5] was recrystallized from DMSO. On slow evaporation, colourless prismatic crystals were formed from a saturated 0.70 M solution at room temperature. They were filtered off and washed with cold acetone. Methods and results of analyses are given elsewhere.[1,5]

X-Ray data collection and reduction. The lattice parameters were determined and refined using 15 centred reflections, by the standard method on the computer-controlled Syntex $P2_1$ diffractometer.[2] The unit cell was found to be orthorhombic with $a=12.54(1)$, $b=20.23(1)$, $c=25.53(1)$ Å, $D_m=1.58(1)$, and $D_x=1.60$ for $Z=8$. Graphite-monochromatized Mo$K\alpha$ radiation ($\lambda=0.71069$ Å) was used.

Two separate data sets were collected using two different crystals enclosed in capillaries. Both data collections were performed in three parts, 0–20, 20–40 and 40–50° in 2θ for one octant (hkl). Different scan speeds were used, the lowest speed being 1° min^{-1}. After every 50th reflection four check reflections were measured. For the first set their intensity variations were within $\pm 3\sigma(I)$, for the second set within ± 3 % in the first two parts ($2\theta<40°$) but a decrease of 10 % occurred in the last part.

The first data set was collected on a prismatic crystal of maximum dimensions about 0.15 mm. The ω scan method was used. The second data set was measured using the $\theta-2\theta$ scan technique on a crystal of maximum dimensions 0.3 mm.

All reflections within the first part ($2\theta<20°$) were recorded for both data sets. Conditions limiting possible reflections were found to be: hkl: $h+k=2n$, $k+l=2n$, $hk0$: $h+k=4n$ ($h,k=2n$), $0kl$: $k+l=4n$ ($k,l=2n$). This is characteristic of the non-centrosymmetric space group $Fd2d$, non-standard setting of No. 43. The general position is 16-fold with coordinates of equivalent positions (x,y,z), $(\bar{x},y,\bar{z})$, $(1/4-x, 1/4+y, 1/4+z)$ and $(1/4+x, 1/4+y, 1/4-z)$ with translations $(0,\frac{1}{2},\frac{1}{2})$, $(\frac{1}{2},0,\frac{1}{2})$, $(\frac{1}{2},\frac{1}{2},0)$. There were in both data sets about 10 reflections with intensities larger than $3\sigma(I)$ violating the condition $h+k=2n$. Since they were not the same in the two sets and most of them were not centred in the scan range, they were considered spurious. For $2\theta<50°$, 1467 independent reflections are possible. Of these, 1244 in the first and 1218 in the second data set had intensities larger than $1.96\,\sigma(I)$ and were considered observed.

The data were reduced and converted to scaled $|F_o|$ values as described previously using the same computer programs.[2]

STRUCTURE DETERMINATION AND REFINEMENTS

The first data set. The structure was solved using this data set which was considered to be the better. From a three-dimensional Patterson synthesis, the 8 Cd and the 16 Cl atoms of the unit cell were found to occupy the special positions 8(*a*) on two-fold rotation axes. The origin was fixed by giving the Cd atoms the *y* coordinate 0. Possible starting parameters for the Cl and two of the three expected 16-fold S positions could then be obtained. Full-matrix least-squares refinements with these atoms isotropic gave $R=0.20$ ($R_w=0.27$), where the conventional *R*-value is $R=\Sigma\|F_o|-|F_c\|/\Sigma|F_o|$ and the weighted $R_w=(\Sigma w\|F_o|-|F_c\|^2/\Sigma w|F_o|^2)^{\frac{1}{2}}$.

A difference Fourier map revealed two peaks with heights 4.5 and 3.0 e $Å^{-3}$ corresponding to two different possible locations S3 and S4, of the third S atom. They were both included and refined. Subsequent Fourier difference peak listings revealed possible positions of all non-H atoms. A refinement with Cd anisotropic varying the occupancy factors of S3 and S4 gave $R=0.082$ ($R_w=0.12$). All atoms anisotropic lowered the *R* value to 0.042 ($R_w=$ 0.053).

From geometric considerations of the symmetry of the disordered DMSO ligands, it became evident that the very elongated thermal ellipsoid obtained for their DMSO oxygen atoms was very probably caused by two alternative positions, O3 and O4, about 0.8 Å apart.

A Fourier map showed alternative oxygen positions for one of the two different perchlorate groups. Refinements with only O3 and O4 isotropic, including the occupancy factors of all alternative positions, gave $R=0.039$ ($R_w=0.047$). The parameter values obtained are given in Tables 1 and 2.

The largest remaining peak found in a final difference Fourier map was 0.43 $eÅ^{-3}$. Definite H-atom positions could not be ascertained.

The semi-empirical absorption correction[6] discussed previously[2] was tested on this data set, but did not improve the results (μ(Mo$K\alpha$)= 12.6 cm^{-1}).

The second data set. For comparisons, especially of the parameters of the disordered groups, refinements were also performed with this data set. The final refinements with only O3 and O4 isotropic gave $R=0.13$ ($R_w=0.17$). No significant differences between any parameter values of this set and those

Table 1. Final fractional atomic positional parameters with estimated standard deviations for refined parameters in parentheses. The *G* values are the refined occupancy factors.

Atom	*x*	*y*	*z*	*G*	B/Å^2
Cd	0	0	0		
Cl1	0	0.3380(5)	0		
Cl2	0	0.6839(3)	0		
S1	0.2389(2)	−0.0437(1)	0.0441(1)		
S2	0.1840(3)	0.1091(2)	−0.0385(1)		
S3	0.0769(4)	−0.1263(3)	−0.0847(2)	0.67(1)	
S4	0.1547(7)	−0.0945(4)	−0.0827(3)	0.32(1)	
O1	0.1416(5)	−0.0015(5)	0.0557(3)		
O2	0.0798(8)	0.0751(6)	−0.0522(4)		
O3	0.1046(17)	−0.0641(14)	−0.0517(9)	0.57(6)	7.5(8)
O4	0.0691(17)	−0.0916(11)	−0.0377(8)	0.48(5)	5.6(7)
O5	0.457(3)	−0.111(1)	−0.028(1)	0.77(6)	
O6	0.099(4)	0.327(3)	−0.023(3)	0.57(10)	
O5A	0.436(5)	−0.224(3)	−0.019(3)	0.32(6)	
O6A	−0.020(7)	0.328(3)	0.049(1)	0.35(9)	
O7	0.071(2)	0.654(1)	−0.033(7)		
O8	0.0573(15)	0.7217(10)	0.0340(6)		
C1	0.3421(9)	−0.0082(8)	0.0829(6)		
C2	0.2156(13)	−0.1198(8)	0.0786(6)		
C3	0.1811(14)	0.1846(8)	−0.0754(8)		
C4	0.2831(16)	0.0700(10)	−0.0760(6)		
C5	0.1498(20)	0.1586(8)	0.1036(6)		
C6	0.0638(14)	0.0716(7)	0.1712(6)		

Table 2. Final anisotropic thermal parameters (Å^2) with estimated standard deviations of refined parameters in parentheses. The temperature factor expression used is $\exp[-1/4(B_{11}h^2a^{*2}+\cdots+2B_{12}hka^*b^*+\cdots)]$.

Atom	B_{11}	B_{22}	B_{33}	B_{12}	B_{13}	B_{23}
Cd	3.28(3)	3.55(3)	2.73(3)	0	0.23(4)	0
Cl1	5.5(2)	10.4(4)	6.7(3)	0	1.3(2)	0
Cl2	7.5(3)	7.7(3)	4.8(2)	0	−1.0(2)	0
S1	4.6(1)	5.9(1)	4.0(1)	1.37(11)	−0.62(9)	−0.20(9)
S2	6.2(1)	8.6(2)	4.9(1)	−3.10(15)	0.62(12)	0.02(13)
S3	5.0(3)	6.9(3)	5.7(2)	−0.75(20)	0.50(17)	−2.64(19)
S4	4.5(5)	4.5(4)	4.3(4)	0.05(31)	−0.90(29)	−1.56(27)
O1	5.0(3)	7.0(4)	4.7(3)	2.2(4)	−1.6(3)	−1.4(4)
O2	8.3(6)	11.7(7)	6.5(5)	−6.0(5)	−1.5(4)	5.0(5)
O5	18(3)	14(2)	21(3)	4.8(18)	0.4(20)	4.2(19)
O6	9(2)	21(5)	16(4)	−2.8(21)	5.4(26)	−6.8(32)
O5A	10(4)	10(3)	23(7)	−5.2(25)	−2.5(39)	−1.4(34)
O6A	11(5)	20(5)	5(2)	−2.2(34)	2.6(18)	1.4(19)
O7	27(3)	21(2)	12(1)	8.7(2)	7.6(16)	−5.0(15)
O8	12(1)	15(1)	11(1)	−2.0(10)	−2.5(10)	−3.3(9)
C1	5.1(5)	7.7(8)	7.8(7)	0.3(6)	−2.3(5)	−0.1(7)
C2	9.2(9)	6.6(8)	8.1(8)	0.7(7)	0.6(7)	2.8(7)
C3	8.5(9)	6.2(8)	14(1)	−2.1(7)	3.3(10)	0.8(9)
C4	11(1)	10(1)	6.1(7)	−2.2(9)	1.6(7)	−0.1(7)
C5	18(2)	7.3(9)	6.3(8)	−3.8(10)	0.7(10)	−0.1(7)
C6	10(1)	6.2(7)	6.6(7)	−2.6(7)	−0.6(7)	−0.6(6)

of the first set were found. The temperature factors, however, increased about 20 % on the average.

Refinement conditions and scattering factors. The least-squares refinements minimized the sum $\Sigma w\|F_o|-|F_c\|^2$ for all reflections with $|F_o|>3.92\sigma(F_o)$. The weighting function was $w=\{\sigma^2(F_o)+0.03(F_o)^2\}^{-1}$, which, according to analyses of the error distribution, gave a satisfactory weighting scheme. A total of 193 parameters was varied in the final refinements with a largest parameter shift in the last cycle of refinement less than 0.2σ for the first and 1.0σ for the second data set.

The scattering factors were calculated from analytical expressions for the neutral atoms.[7] Anomalous dispersion corrections were included for Cd, Cl and S.[7]

DESCRIPTION AND DISCUSSIONS OF THE STRUCTURE

General. The crystal structure comprises discrete $Cd(DMSO)_6^{2+}$ cations and ClO_4^- anions. Both the Cd and the Cl atoms are found in layers with $z=n/4$ ($n=0, 1, 2,\ldots$) parallel to the xy-plane. Each $Cd(DMSO)_6^{2+}$ complex ion is almost circularly surrounded by six perchlorate groups within such a layer but is in contact with other Cd-complexes diagonally. The closest intermolecular approaches between the Cd-complexes are Cd – C5 of 4.36(2) Å and Cd – C6 of 4.75(2) Å, which are shorter than some of the intramolecular Cd – C distances given in Table 3.

A stereoscopic view of the $Cd(DMSO)_6^{2+}$ complex ion is shown in Fig. 1 and a unit cell view in Fig. 2.

The $Cd(DMSO)_6^{2+}$ complex ion. Each Cd atom is coordinated to six DMSO oxygen atoms forming a fairly regular octahedron around Cd (Table 3). The arrangement of the DMSO ligands is more irregular than the rather symmetric distribution found for the $Hg(DMSO)_6^{2+}$ ion, in which also the S atoms surround the Hg atom almost octahedrally.[2] In the Cd complex, several of the ligands are closer together giving it a more flattened shape.

A peculiar feature is the alternative orientations found for two symmetry-related DMSO ligands (Fig. 1), with the apex atoms, S3 and S4, of the pyramidal DMSO groups in opposite directions. The C atom positions, C5 and C6, of the two orientations almost coincide and cannot be resolved, but the O atom positions, O3 and O4, are 0.81(4) Å apart. Since there were no provisions in the programs for coupling the occupancy factors within the al-

Table 3. Some intramolecular atomic distances (Å) and angles (degrees). Estimated standard deviations are given in parentheses. The superscript *i* refers to the equivalent position $-x,y,-z$ relative to x,y,z in Table 1.

Cd–O1	2.278(7)	O1–Cd–O1^i	178.5(3)
Cd–O2	2.257(11)	O1–Cd–O2	91.9(3)
Cd–O3	2.270(24)	O1–Cd–O2^i	89.2(3)
Cd–O4	2.262(22)	O1–Cd–O3	84.5(7)
Cd–S1	3.323(3)	O1–Cd–O3^i	94.6(7)
Cd–S2	3.343(4)	O1–Cd–O4	87.5(6)
Cd–S3	3.485(5)	O1–Cd–O4^i	91.3(6)
Cd–S4	3.448(8)	O2–Cd–O2^i	95.3(4)
Cd–C1	4.791(12)	O2–Cd–O3	77.6(7)
Cd–C2	4.152(16)	O2–Cd–O3^i	170.3(7)
Cd–C3	4.779(17)	O2–Cd–O4	97.5(6)
Cd–C4	4.290(19)	O2–Cd–O4^i	166.9(6)
Cd–C5	4.565(18)	O3–Cd–O3^i	110.3(9)
Cd–C6	4.678(15)	O3–Cd–O4	20.3(8)
S1–O1	1.519(8)	O3–Cd–O4^i	90.1(8)
S2–O2	1.520(11)	O4–Cd–O4^i	69.9(8)
S3–O3	1.554(26)	Cd–O1–S1	120.9(4)
S4–O4	1.574(22)	Cd–O2–S2	123.4(6)
S1–C1	1.782(13)	Cd–O3–S3	130.5(14)
S1–C2	1.800(16)	Cd–O4–S4	127.1(12)
S2–C3	1.796(18)	O1–S1–C1	104.5(6)
S2–C4	1.759(19)	O1–S1–C2	104.8(6)
S3–C5	1.754(16)	C1–S1–C2	101.0(7)
S3–C6	1.737(17)	O2–S2–C3	104.2(7)
S4–C5	1.769(18)	O2–S2–C4	106.2(8)
S4–C6	1.747(17)	C3–S2–C4	96.4(9)
Cl1–O5	1.37(3)	O3–S3–C5	97.2(11)
Cl1–O6	1.39(5)	O3–S3–C6	105.6(11)
Cl1–O5A	1.58(6)	C5–S3–C6	101.0(9)
Cl1–O6A	1.30(4)	O4–S4–C5	114.1(11)
Cl2–O7	1.36(3)	O4–S4–C6	98.6(10)
Cl2–O8	1.36(2)	C5–S4–C6	100.0(9)

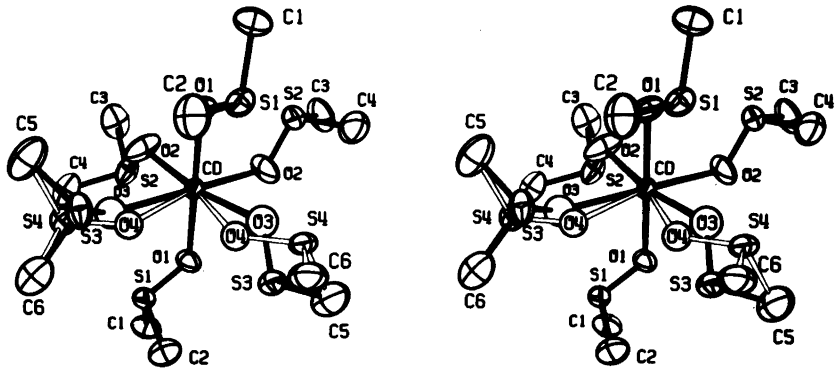

Fig. 1. A stereoscopic view of the $Cd(DMSO)_6^{2+}$ cation. The alternative positions of the two symmetry-related ligands are marked by unfilled bonds. The thermal ellipsoids enclose regions of 30 % probability.

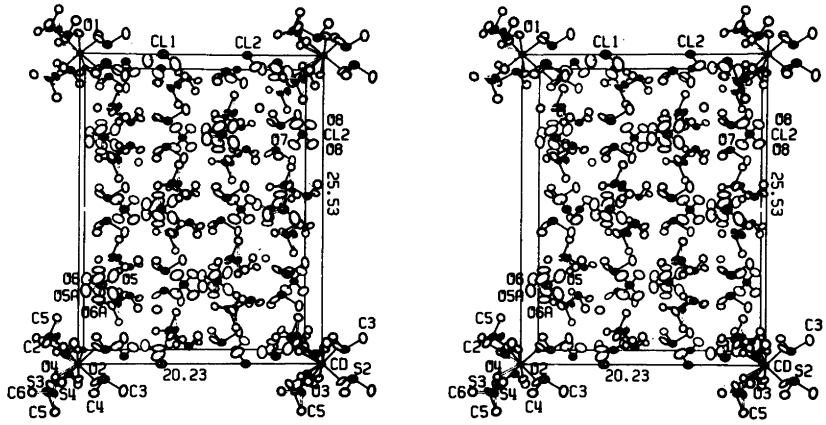

Fig. 2. A stereoscopic view along the *a* edge of the unit cell. The lengths in Å of the *b* and *c* edges are plotted. The alternative positions of the DMSO and $Cl1-O_4$ groups are indicated by unfilled bonds. All atoms are represented by 20 % probability ellipsoids. For the C and O atoms the boundary ellipsoids only are shown.

ternative orientations, they were independently refined. For S3 and O3 their values were found to be 0.67(1) and 0.57(6) for the first and 0.62(4) and 0.41(13) for the second data set, respectively. Corresponding values for S4 and O4 are 0.32(1) and 0.48(5) for the first and 0.29(4) and 0.50(12) for the second data set. The values obtained are not significantly different within each DMSO orientation or between the data sets and show that the DMSO ligands are indeed statistically distributed between the two alternative orientations, approximately in the ratio 2:1. The thermal parameters for the disordered ligands (Tables 1 and 2) are of the same order of magnitude as for the non-disordered ones, which supports the correctness of the occupancy factors obtained (Table 1).

There is sufficient room in the structure to allow for the different orientations. The closest non-bonded interatomic distances to S3 are: C2 3.68(2), O7 3.69(2), O1 3.80(1), and O8 3.74(2) Å. To S4 they are: S1 3.56(1), O2 3.64(1) and C4 3.70(2) Å. However, the rather short distance S1–S4 (van der Waals radius of S 1.75 to 1.85 Å)[8] may explain why the S3 position is preferred.

The disorder observed could also possibly be explained by ordered layers, the stacking of which is disordered in the *z*-direction (*cf.* Fig. 2). The structure would then be of the order-disorder (OD) type, which would give streaks within additional layer lines in the intensity data. However, neither by Weissenberg films and oscillation photos on the diffractometer, nor by the statistical distribution of errors in F_c caused by removal of one of the disordered DMSO positions, could any indications of an OD-structure be found.

The average values of the well-defined S–O and S–C bond distances within the non-disordered DMSO ligands are 1.52 and 1.77 Å, respectively, in good agreement with previously reported results.[2,9,10] The corresponding values for the disordered groups are not significantly different (Table 3).

None of the Cd–O bond lengths differs significantly from their average value, 2.27 Å, but the thermal ellipsoids of the O2 and S2 atoms of the DMSO ligands are elongated (Fig. 1). This is probably due to a slight disorder, corresponding to the alternative O3 or O4 positions opposite O2, and causes a slight apparent shortening of the calculated Cd–O2 bond length. Only the well-defined Cd–O1 bond distance, 2.276(7) Å, seems to be unaffected by the disorder. This value is also close to the mean Cd–O bond length, 2.28 Å, found for the $Cd(H_2O)_6^{2+}$ ion in the structure of $[Cd(H_2O)_6](NH_4)_2(SO_4)_2$,[11] and is not significantly different from the value 2.291(4) Å found for the $Cd(DMSO)_6^{2+}$ ion in solution.[1]

The ClO_4^- ions. There are two crystallographically different perchlorate groups in the structure, $Cl1-O_4$ and $Cl2-O_4$. An examination of a Fourier map showed large librational movements of both groups and also two alternative positions of the $Cl1-O_4$

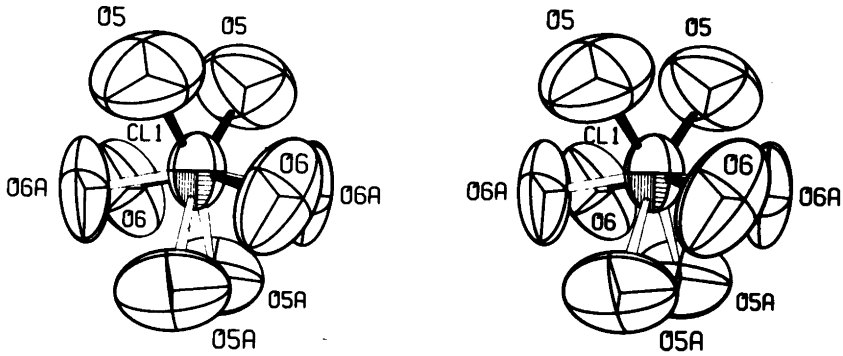

Fig. 3. A stereoscopic view of the disordered Cl1 – O_4 perchlorate ion. The unfilled Cl – O bonds correspond to the alternative oxygen positions, O5A and O6A. The two-fold rotational axis through the Cl atom is vertical in the picture. The thermal ellipsoids are shown at the 30 % probability level.

group. These positions are approximately related to each other by a 180° rotation perpendicular to the twofold rotational axis through the Cl1 atom and a displacement along this axis of about 0.4 Å (Fig. 3). The resulting new oxygen positions are denoted O5A and O6A. The two slightly displaced Cl1 positions could not be resolved by least squares refinements, but are shown by the elongation of the thermal ellipsoid of the Cl1 atom (Fig. 3) and by the asymmetry of the Cl1 – O bond lengths (Table 3).

The apparent shortening of the average Cl – O bond length, 1.38 Å, from the expected value of 1.42_6 Å,[12] is certainly an effect of the large librational movements, as discussed for the disordered perchlorate ion found in the structure of $[Hg(DMSO)_6](ClO_4)_2$.[2] The thermal ellipsoids of the perchlorate oxygens are also here very large (Fig. 3 and Table 2). The bond angles within the two positions of the disordered Cl1 – O_4 group show large deviations from tetrahedral values, probably mainly due to the displacement of the Cl1 atom position. They range from 71 to 163°. For Cl2 – O_4 the bond angles range from 102 to 127°.

The sum of the refined occupancy factors of the symmetry-related oxygen positions in Cl1 – O_4 for the first data set is 2.06(16), close to the expected value of 2.0. The sum for the second data set is 1.5(3).

Judging from the refined occupancy factors (Table 1) there seems to be a correlation between the alternative positions of the DMSO and the Cl1 – O_4 groups. This perchlorate ion is situated between the disordered DMSO ligands of two different Cd-complexes, as can be seen in Fig. 2. The simultaneously occupied positions would then be S3,O3 and O5,O6 or S4,O4 and O5A,O6A, with the shortest distance S4 – O5A 4.52(8) Å. It is noticeable that for the other configuration the closest distance would be much shorter, *viz.* S4 – O5 4.05(4) Å, although still much longer than the sum of the van der Waals radii.[8]

Acknowledgements. The author wishes to thank Prof. Sten Ahrland and Mr. Ingmar Persson for providing the salt and for their interest in the work. Dr. Georg Johansson's valuable help in solving the structure and Prof. Ingmar Grenthe's helpful comments on the manuscript are gratefully acknowledged. This work has been supported financially by the Swedish Natural Science Research Council and by the foundation "Knut and Alice Wallenbergs Stiftelse".

REFERENCES

1. Sandström, M., Persson, I. and Ahrland, S. *Acta Chem. Scand. A 32* (1978). *In press.*
2. Sandström, M. and Persson, I. *Acta Chem. Scand. A 32* (1978) 95.
3. Sandström, M. *Acta Chem. Scand. A 32* (1978) 533.
4. Johansson, G. and Sandström, M. *Acta Chem. Scand. A 32* (1978) 109.
5. Ahrland, S. and Björk, N.-O. *Acta Chem. Scand. A 28* (1974) 823.
6. Kopfmann, G. and Huber, R. *Acta Crystallogr. A 24* (1968) 348; North, A. C. T., Phillips, D. C. and Scott Mathews, F. *Ibid* 351.
7. *International Tables of X-Ray Crystallography*, Kynoch Press, Birmingham 1974, Vol 4.
8. Pauling, L. *The Nature of the Chemical Bond*, 3rd Ed., Cornell Univ. Press, New York 1960, p. 260.

9. Biscarina, P., Fusina, L., Nivellini, G. D., Mangia, A. and Pelizzi, G. *J. Chem. Soc. Dalton Trans.* (1974) 1846.
10. Björk, N.-O. and Cassel, A. *Acta Chem. Scand. A 30* (1976) 235.
11. Montgomery, H. and Lingafelter, E. C. *Acta Crystallogr. 20* (1966) 728.
12. Berglund, B., Thomas, J. O. and Tellgren, R. *Acta Crystallogr. B 31* (1975) 1842.

Received February 13, 1978.

Acta Chemica Scandinavica A 32 (1978) 527–532

Crystal and Molecular Structure of $Hg(ClO_4)_2.4(CH_3)_2SO$, a Dimeric Addition Compound

MAGNUS SANDSTRÖM

Department of Inorganic Chemistry, Royal Institute of Technology, S-100 44 Stockholm 70, Sweden

The crystal structure of the compound $Hg(ClO_4)_2.4DMSO$ has been determined from three-dimensional X-ray diffraction data collected at room temperature on an automatic Syntex $P2_1$ four-circle diffractometer. The unit cell is monoclinic, space group $P2_1/n$, with $a=12.490(6)$, $b=22.88(1)$, $c=17.27(1)$ Å, $\beta=105.67(4)°$ and $Z=8$. The structure, refined to a conventional R-value of 0.087 for 1812 independent reflections, is built up of dimeric $Hg_2(DMSO)_8^{4+}$ entities and perchlorate ions. Two dimethyl sulfoxide (DMSO) oxygen atoms form a double bridge between the mercury atoms, with the distances 2.54(4) and 2.51(3) Å to Hg1, and 2.45(4) and 2.37(3) Å to Hg2. The Hg1 atom coordinates four more DMSO oxygen atoms at 2.17(7), 2.25(5), 2.29(4), and 2.40(6) Å, completing a distorted octahedron. The Hg2 atom is bonded to only two more DMSO oxygen atoms at 2.13(4) and 2.16(4) Å in a highly distorted tetrahedral configuration. Two long perchlorate oxygen contacts to Hg2 at 2.78(5) and 3.04(9) Å complete a very distorted octahedral arrangement.

All four crystallographically independent perchlorate groups in the structure perform large librational movements.

A series of X-ray diffraction and spectroscopic investigations of the structures of the hexasolvated Hg(II) and Cd(II) ions, coordinating water and DMSO molecules, have been performed.[1-4] Discrete octahedral complexes, with six oxygen atoms bonded to the metal atoms both in solution and in solid perchlorates, were found. In order to investigate how this regular octahedral coordination, for mercury rarely found, had changed in the novel tetrasolvate, $Hg(ClO_4)_2.4DMSO$,[1] its structure was determined.

EXPERIMENTAL

Preparations. The crystals were prepared and analyzed as described previously.[2] The recrystallization from methanol solutions was performed at about 5 °C. At room temperature another phase was formed, large colourless crystals with almost quadratic faces. They were found to be monoclinic with $a=11.18(1)$, $b=10.83(1)$, $c=22.90(1)$ Å, and $\beta=91.18(7)°$. No analyses of this compound were performed.

From large colourless twinned crystals of the $Hg(ClO_4)_2.4DMSO$ phase, obtained at about 5 °C, single crystals of irregular shape were cut out and sealed into capillaries.

X-Ray data collection and reduction. The lattice parameters were determined and refined for 25 centred reflections by the standard method on the automatic Syntex four-circle diffractometer of type $P2_1$.[2] A monoclinic unit cell with $a=12.490(6)$, $b=22.88(1)$, $c=17.27(1)$ Å, $\beta=105.67(4)°$, $D_m=1.96(2)$ and $D_x=1.99$ g cm^{-3} for $Z=8$ was found. Two separate data sets on different crystals, both with maximum dimensions less than 0.2 mm, were collected at room temperature. Graphite-monochromatized Mo$K\alpha$ radiation ($\lambda=0.71069$ Å) was used.

For the first set, all 3232 possible independent reflections below 35° in 2θ were measured by the ω scan technique using variable scan speeds, from 1°/min upwards.

For the second set, only 2251 of the independent reflections for $2\theta<35°$ (but all below 30°) were collected. The $\theta-2\theta$ scan mode was used with 2°/min as the lowest scan speed.

The $h0l$ reflections for $h+l=2n+1$ and $0k0$ for $k=2n+1$ were systematically absent. This is characteristic of the space group $P2_1/n$, non-standard setting of No. 14. The general setting is four-fold: $\pm(x,y,z;\ 1/2-x,1/2+y,1/2-z)$. Of the 3027 possible non-extinct reflections for $2\theta<35°$ 1812 in the first

data set and 1229 in the second had intensities larger than 1.96 $\sigma(I)$, and were considered observed. Nine strong reflections, apparently suffering from effects of extinction or double diffraction, were removed from the first set of data.

Check reflections were measured regularly every 100th reflection, four for the first data set and three others for the second set. All their intensities decreased almost linearly at nearly the same relative rate as a function of the exposure time. The total decrease was 32 % for the first and 25 % for the second set.

A linear correction therefore seemed to be justified and was applied on intensities and sigma-values of the first data set.

The absorption coefficient $\mu(\mathrm{Mo}K\alpha)$ is 72.2 cm^{-1}. A semi-empirical absorption correction method[5] was applied on both data sets in the way described previously.[2] The largest measured intensity ratio was 1:0.51 for the first and 1:0.59 for the second data set.

The data reduction was performed as described previously. The same computer programs were used.[2]

STRUCTURE DETERMINATION AND REFINEMENTS

First data set. A three-dimensional Patterson function was calculated. The eight Hg atoms of the unit cell were assumed to occupy two of the general four-fold positions. Due to overlapping vectors, several different choices of parameter sets of these positions were possible. One of them gave markedly lower R values than the others. Isotropic least-squares refinements gave the conventional R value 0.29 and the weighted $R_w = 0.34$, defined as in the preceding paper.[4] Subsequent difference Fourier syntheses followed by full-matrix least-squares refinements revealed possible positions of all 54 non-H atoms of the asymmetric unit. Refinements with anisotropic temperature factors for the Hg, S and Cl atoms gave $R = 0.087$ ($R_w = 0.099$). The corresponding parameter values are given in Tables 1 and 2. A subsequent difference Fourier synthesis showed a seemingly random background variation not exceeding 1.2 e $\mathrm{Å}^{-3}$.

When these final refinements were repeated for data without the linear intensity correction, $R = 0.10$ ($R_w = 0.13$) was obtained. The corresponding difference Fourier map had peaks up to 1.8 e $\mathrm{Å}^{-3}$ around the Hg atoms.

Second data set. Refinements with the final model gave $R = 0.089$ ($R_w = 0.091$). No significant differences between any of the parameter values of the two data sets were obtained, but the estimated standard deviations were on the average 50 % larger in the second set. The background variation in the final difference Fourier map did not exceed 1.1 e $\mathrm{Å}^{-3}$.

Refinement conditions. The least-squares refinements were based on the minimization of $\Sigma w \| F_o | - | F_c \|^2$ for all reflections with $|F_o| > 3.92\sigma(F_o)$ using the same weighting function, w, and scattering factors as previously.[2] A total of 287 parameters was varied in the final refinements. The largest shift of the parameter values in the last refinement cycle was 0.1σ for the first data set and 1.0σ for the second.

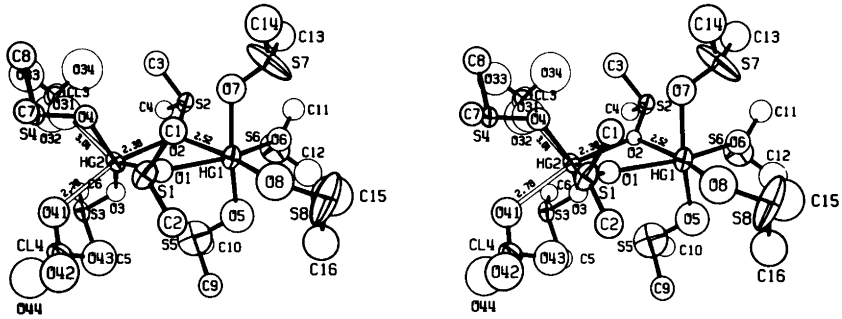

Fig. 1. A stereoscopic view of the dimeric $Hg_2(DMSO)_8^{4+}$ complex ion (filled bonds). The long interactions from Hg2 to the perchlorate oxygen atoms O31 and O41 are shown by unfilled bonds. The distances are given in Å. The thermal ellipsoids are drawn at the 30 % probability level.

Table 1. Final fractional atomic positional parameters and isotropic temperature factor coefficients in $Å^2$. Estimated standard deviations are given in parentheses.

Atom	*x*	*y*	*z*	*B*
Hg1	0.2494(2)	0.1377(1)	0.2572(1)	
Hg2	−0.0608(2)	0.1330(1)	0.2646(1)	
S1	0.1238(14)	0.2256(6)	0.3882(9)	
S2	0.0363(13)	0.1199(6)	0.0894(8)	
S3	−0.1994(13)	0.0193(6)	0.2847(9)	
S4	−0.2124(14)	0.2465(7)	0.2728(9)	
S5	0.1772(26)	0.0301(10)	0.3543(17)	
S6	0.3003(24)	0.0342(10)	0.1245(16)	
S7	0.3050(31)	0.2419(13)	0.1431(16)	
S8	0.5275(20)	0.1671(13)	0.3774(21)	
Cl1	0.5330(15)	0.3659(9)	0.3561(10)	
Cl2	−0.0256(24)	0.3949(11)	0.1459(11)	
Cl3	0.6317(19)	0.1294(10)	0.0738(14)	
Cl4	−0.0807(17)	0.1259(8)	0.4719(9)	
O1	0.1173(30)	0.1791(17)	0.3320(20)	6.7(9)
O2	0.0538(24)	0.1150(11)	0.1777(16)	3.5(7)
O3	−0.1054(31)	0.0414(15)	0.2526(19)	6.6(10)
O4	−0.1098(32)	0.2224(15)	0.2499(19)	6.7(9)
O5	0.2816(55)	0.0541(29)	0.3179(36)	16.7(21)
O6	0.3318(34)	0.0922(21)	0.1630(22)	8.9(11)
O7	0.2252(41)	0.2169(21)	0.1768(26)	11.0(14)
O8	0.4041(55)	0.1801(26)	0.3542(32)	15.5(19)
O11	0.426(6)	0.360(3)	0.355(4)	17(2)
O12	0.597(6)	0.327(3)	0.403(4)	18(2)
O13	0.547(4)	0.365(2)	0.282(3)	13(2)
O14	0.562(7)	0.418(4)	0.401(5)	23(3)
O21	0.044(11)	0.417(7)	0.126(8)	34(6)
O22	−0.084(11)	0.441(7)	0.132(8)	38(8)
O23	−0.026(7)	0.385(3)	0.222(5)	22(3)
O24	−0.085(8)	0.357(4)	0.098(6)	25(4)
O31	0.715(7)	0.139(3)	0.141(5)	20(3)
O32	0.583(9)	0.073(5)	0.063(6)	29(4)
O33	0.567(7)	0.172(4)	0.068(4)	20(3)
O34	0.677(10)	0.135(5)	0.004(7)	33(5)
O41	−0.129(4)	0.152(2)	0.403(3)	11.9(15)
O42	−0.020(5)	0.160(3)	0.535(4)	16(2)
O43	−0.006(6)	0.090(3)	0.453(3)	16(2)
O44	−0.155(7)	0.095(4)	0.502(4)	21(3)
C1	0.188(5)	0.280(3)	0.351(3)	7.2(16)
C2	0.230(5)	0.211(3)	0.469(3)	7.7(16)
C3	−0.042(6)	0.187(3)	0.061(4)	10.0(20)
C4	−0.068(5)	0.066(2)	0.046(3)	7.2(16)
C5	−0.130(5)	−0.040(3)	0.357(3)	8.3(17)
C6	−0.280(5)	−0.016(2)	0.200(3)	6.7(15)
C7	−0.149(4)	0.308(2)	0.340(3)	5.8(14)
C8	−0.280(6)	0.295(3)	0.187(4)	9.4(19)
C9	0.267(5)	0.019(2)	0.452(3)	7.5(16)
C10	0.171(5)	−0.034(3)	0.317(3)	7.2(16)
C11	0.315(5)	0.042(3)	0.018(4)	9.3(18)
C12	0.407(8)	−0.002(4)	0.154(5)	13.8(28)
C13	0.297(7)	0.229(3)	0.054(5)	11.7(23)
C14	0.296(8)	0.312(4)	0.146(5)	14.9(29)
C15	0.526(10)	0.114(6)	0.321(8)	22.7(49)
C16	0.530(7)	0.095(5)	0.408(5)	14.5(27)

Table 2. Final anisotropic thermal parameter values (Å^2) with estimated standard deviations in parentheses. The temperature factor expression used is: $\exp[-1/4(B_{11}h^2a^{*2}+\cdots+2B_{12}hka^*b^*+\cdots)]$

Atom	B_{11}	B_{22}	B_{33}	B_{12}	B_{13}	B_{23}
Hg1	4.7(1)	6.7(2)	6.5(2)	0.47(16)	1.40(11)	−1.19(14)
Hg2	6.9(2)	2.7(1)	6.8(2)	−0.76(12)	4.02(12)	−0.65(10)
S1	6.4(11)	4.7(9)	6.8(9)	0.7(8)	1.0(9)	−2.6(7)
S2	5.1(9)	7.0(11)	5.1(8)	0.9(8)	1.1(7)	−0.9(7)
S3	6.0(10)	2.6(7)	9.2(10)	−1.1(7)	4.6(9)	−0.4(7)
S4	7.5(12)	6.9(10)	7.0(10)	3.2(9)	4.6(9)	1.8(7)
S5	19.0(26)	8.3(15)	17.3(22)	−0.7(16)	4.4(20)	−4.0(14)
S6	17.3(23)	7.0(13)	17.0(20)	−1.1(15)	7.5(18)	−3.0(13)
S7	31.7(37)	14.9(23)	15.1(20)	−8.5(23)	18.0(24)	−1.7(16)
S8	6.3(15)	15.1(22)	28.7(33)	4.5(14)	−1.0(17)	−7.3(23)
Cl1	6.8(12)	8.4(11)	6.4(9)	1.5(11)	1.9(8)	−0.2(9)
Cl2	12.6(18)	11.2(16)	6.7(11)	−4.0(15)	2.2(12)	0.9(10)
Cl3	8.7(14)	7.2(12)	12.7(15)	2.1(12)	3.3(13)	1.0(11)
Cl4	9.9(12)	6.9(10)	5.3(9)	0.7(11)	3.1(9)	0.0(8)

DESCRIPTION AND DISCUSSION OF THE STRUCTURE

The crystal structure is composed of $Hg_2(DMSO)_8^{4+}$ entities, di-μ-dimethyl sulfoxide-*O*-{[bis-(dimethyl sulfoxide)mercury(II)] [tetra(dimethyl sulfoxide)mercury(II)]} ions, and perchlorate ions. A stereoscopic view of the molecular geometry of the dimeric complex is given in Fig. 1. A unit cell view is shown in Fig. 2. Some interatomic distances and angles are given in Table 3.

The dimeric complex. The two unique Hg atoms within the asymmetric unit are joined by a double DMSO oxygen bridge to discrete dimeric entities. Four more DMSO oxygen atoms complete a distorted octahedral coordination around the Hg1 atom with a largest deviation of 19° from regular octahedral angles. The Hg2 atom is bonded to only two more DMSO oxygen atoms in a highly distorted tetrahedral coordination with the angles at Hg2 between 76 and 149°. There are, however, two long

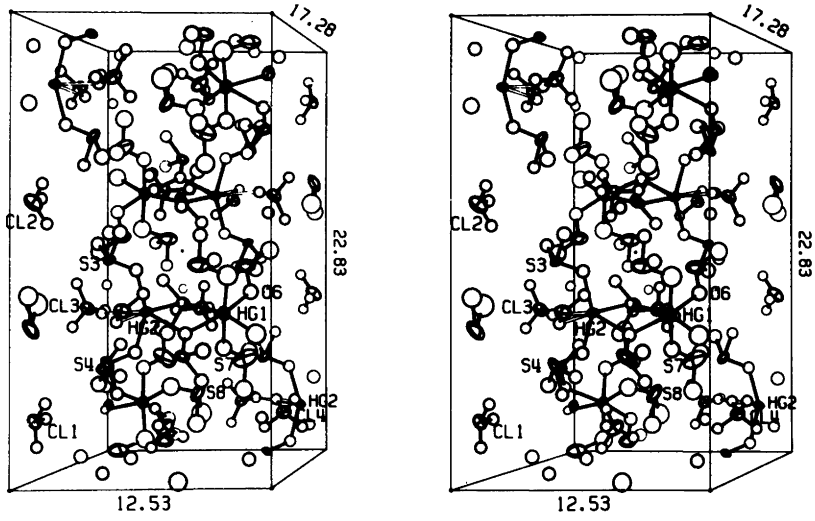

Fig. 2. A stereoscopic unit cell view. The lengths in Å of the unit cell edges are plotted. The thermal ellipsoids enclose 20 % probability. The perchlorate oxygen atoms have for clarity been given the *B* value 5 Å^2.

Table 3. Selected interatomic distances (Å) and angles (degrees). Estimated standard deviations are given in parentheses.

Hg1 – O1	2.54(4)	O1 – Hg1 – O2	72(1)
Hg1 – O2	2.51(3)	O1 – Hg1 – O5	98(2)
Hg1 – O5	2.17(7)	O1 – Hg1 – O6	166(1)
Hg1 – O6	2.39(4)	O1 – Hg1 – O7	91(2)
Hg1 – O7	2.25(5)	O1 – Hg1 – O8	90(2)
Hg1 – O8	2.40(6)		
Hg2 – O1	2.45(4)	O1 – Hg2 – O2	76(1)
Hg2 – O2	2.37(3)	O1 – Hg2 – O3	130(1)
Hg2 – O3	2.16(4)	O1 – Hg2 – O4	81(1)
Hg2 – O4	2.13(4)	O1 – Hg2 – O31	149(2)
Hg2 – O31	3.04(9)	O1 – Hg2 – O41	89(1)
Hg2 – O41	2.78(5)	O31 – Hg2 – O41	99(2)
Hg1 – O1 – Hg2	103(1)	Hg2 – O4 – S4	123(2)
Hg1 – O1 – S1	134(2)	Hg1 – O5 – S5	114(4)
Hg2 – O1 – S1	121(2)	Hg1 – O6 – S6	126(3)
Hg1 – O2 – Hg2	106(1)	Hg1 – O7 – S7	126(3)
Hg1 – O2 – S2	113(2)	Hg1 – O8 – S8	133(4)
Hg2 – O2 – S2	134(2)	Hg2 – O31 – Cl3	161(5)
Hg2 – O3 – S3	120(2)	Hg2 – O41 – Cl4	123(3)

interactions between Hg2 and the perchlorate oxygen atoms O41 and O31. The distances Hg2 – O41 and Hg2 – O31 are found to be 2.78(5) and 3.04(9) Å, respectively, from the first set of data, and 2.62(7) and 2.92(9) Å from the second. At least the O41 atom seems to be within the effective coordination sphere of Hg2. The sum of the van der Waals radii for Hg and O is 1.5 + 1.4 = 2.9 Å.[6] These contacts complete a very distorted octahedral oxygen coordination around Hg2. The largest angular deviation from a regular symmetry is 40°.

Dimeric complexes with almost symmetrical double bridges, formed by oxygen donor atoms, have also been found in the crystal structures of the adducts $3HgCl_2.SDMSO$ and $[(HgCl_2.(C_6H_5)_3AsO)_2]$.[7,8] The bridging Hg – O bonds for a specific Hg atom are found to be longer in all three compounds than the non-bridging where the oxygen atom forms only one donor-acceptor bond, as was first observed by Bränden.[8]

The Hg – Hg distance is significantly shorter in the present study, 3.913(4) Å, than in $3HgCl_2.2DMSO$, 4.01_6 Å.[7] This is due to the lower coordination number for Hg2 than for Hg1, which causes a shortening of the Hg2 – O bond lengths.

In the DMSO molecules the average distances found, S – O 1.51(9) Å and S – C 1.72(13) Å, do not differ significantly from the expected values, 1.52 and 1.77 Å, respectively. The sulfur atoms S7 and S8 are found to be extremely anisotropic (Fig. 1) from refinements for both data sets. Approximate anisotropic thermal parameters obtained for the DMSO oxygen atoms show similar elongated thermal ellipsoids of the O5, O7 and O8 atoms, the two latter parallel to the ellipsoids of the corresponding sulfur atoms. This may be an effect of a slight disorder of these DMSO ligands or of the decomposition of the crystal during the data collection.

The perchlorate ions. There are four crystallographically different ClO_4^- ions in the structure.

Examination of Fourier maps showed that all perchlorate groups performed large librational movements. Distinct alternative positions were not found, however. All perchlorate oxygen atoms have large temperature factors (Table 1), of which the smallest is found for O41 which is within the coordination sphere of the Hg2 atom, as discussed above. Meaningful refinements of anisotropic temperature factors could not be performed, since the standard deviations became too large compared with the parameter values.

The apparent shortening of the average Cl – O bond length, 1.33(8) Å, from the expected value 1.42_6 Å,[9] is probably an effect of this freedom of movement in the absence of hydrogen bonds, as discussed previously.[2] The bond angles obtained did not differ significantly from tetrahedral values.

Acknowledgements. The author is indebted to Dr. G. Johansson for valuable help in solving the Patterson function. Thanks are due to Prof. S. Ahrland and Mr. I. Persson for suggesting the problem and providing the salt and to Prof. I. Grenthe for helpful comments on the manuscript. Financial support was given by The Swedish Natural Science Research Council and the foundation "Knut and Alice Wallenbergs Stiftelse".

REFERENCES

1. Sandström, M., Ahrland, S. and Persson, I. *Acta Chem. Scand. A 32* (1978). *In press.*
2. Sandström, M. and Persson, I. *Acta Chem. Scand. A 32* (1978) 95.
3. Johansson, G. and Sandström, M. *Acta Chem. Scand. A 32* (1978) 109.
4. Sandström, M. *Acta Chem. Scand. A 32* (1978) 525.
5. Kopfmann, G. and Huber, R. *Acta Crystallogr. A 24* (1968) 348; North, A. C. T., Phillips, D. C. and Scott Mathews, F. *Ibid.* 351.
6. Grdenić, D. *Q. Rev. Chem. Soc. 19* (1965) 303.
7. Biscarina, P., Fusina, L., Nivellini, G. D., Mangia, A. and Pelizzi, G. *J. Chem. Soc. Dalton Trans.* (1974) 1846.
8. Bränden, C.-I. *Ark. Kemi 22* (1964) 485 and 501.
9. Berglund, B., Thomas, J. O. and Tellgren, R. *Acta Crystallogr. B 31* (1975) 1842.

Received February 13, 1978.

Acta Chemica Scandinavica A 32 (1978) 533 – 538

The Crystal Structures of 7-Nitroso-8-hydroxyquinoline-5-sulfonic Acid [⇌7-(Hydroxyimine)-8-oxo-quinoline-5-sulfonic Acid] and Its Disodium Salt Monohydrate

JORMA KORVENRANTA, MATTI NÄSÄKKÄLÄ, HEIKKI SAARINEN and ELINA NÄSÄKKÄLÄ

Department of Inorganic Chemistry, University of Helsinki, SF-00100 Helsinki 10, Finland

Crystals of H_2L [L = 7-nitroso-8-oxidoquinoline-5-sulfonate, $(C_9H_4O_5N_2S)^{2-}$] are monoclinic, a = 8.342(4), b = 8.568(3), c = 13.428(5) Å, β = 90.15(4)°, Z = 4, space group $P2_1/n$. Crystals of $Na_2L.H_2O$ are triclinic, a = 8.046(4), b = 8.528(4), c = 9.669(5) Å, α = 86.23(4), β = 67.63(4), γ = 71.74(4)°, Z = 2, space group $P\bar{1}$. The structures were solved by direct methods with the MULTAN program and refined by least-squares methods to the R values 0.061 (H_2L) and 0.041 ($Na_2L.H_2O$) for 1382 and 1916 observed reflections, respectively.

The C7 – N [1.299(7) Å], N – O [1.368(6) Å] bond lengths, the C – N – O bond angle [112.2(4)°] and the C8 – O bond distance [1.229(6) Å] together indicate that H_2L exists in a tautomeric oxime form in which the oxime group and the carbonyl oxygen are in the *anti* configuration. The acid has a zwitterion structure, the sulfonic acid proton being attached to the quinoline nitrogen atom.

The organic anion in $Na_2L.H_2O$ has an oximato-like structure with bond lengths C7 – N, 1.351(3); N – O 1.281(4) and C8 – O, 1.253(4) Å and bond angle C7 – N – O, 116.3(3)°. One of the sodium ions is in a strongly distorted octahedral environment, while the other is surrounded by only five atoms. Two hydrogen bonds are present in both structures.

Our preceding communications have shown that sulfonic acid derivatives of 1-nitroso-2-naphthol and 2-nitroso-1-naphthol exist in their tautomeric quinone oxime forms in the solid state and that the quinonoid character of the ligands is retained in their metal complexes.[1,2] Our study on free and metal-coordinated nitrosophenol⇌quinone oxime compounds has now been extended with solid 7-nitroso-8-hydroxyquinoline-5-sulfonic acid, which is very similar in structure to the 2-nitroso-1-naphthol sulfonates studied earlier. The present compound is particularly interesting as a metal-chelating ligand because it has two coordination sites: one like that of 2-nitroso-1-naphthol and one like 8-hydroxyquinoline, the hydroxyl group being functional at both sites. This acid and its disodium salt have been specially selected for X-ray investigation to facilitate our prospective research on the metal chelates of the ligand.

EXPERIMENTAL

The preparation and crystallization of 7-nitroso-8-hydroxyquinoline-5-sulfonic acid (= H_2L) and its disodium salt monohydrate (= $Na_2L.H_2O$) have been described earlier.[3]

Crystal data for H_2L are:

a = 8.342(4), b = 8.568(3), c = 13.428(5) Å,
β = 90.15(4)°, Z = 4, Space group $P2_1/n$,
D_x = 1.759 g cm^{-3}, D_m = 1.78 g cm^{-3} (by flotation)
V = 959.8 Å^3, μ = 31.1 cm^{-1} (Cu$K\alpha$)

Cell dimensions for H_2L were determined from Weissenberg photographs and refined using the data obtained from a powder photograph taken with a Hägg-Guinier camera with Cu$K\alpha$ radiation and calcium fluoride as an internal standard. The space group, from systematic absences, is $P2_1/n$.

The crystal selected for the data collection had dimensions *ca.* 0.2 × 0.2 × 0.2 mm. Intensity data from levels $0kl - 7kl$ were collected with a Stoe-Güttinger diffractometer using Ni-filtered Cu radiation (Cu$K\alpha$, λ = 1.5418 Å). Of the 1694 recorded reflections, 1382 with $I > 3\sigma(I)$ were used for the structure analysis. The data were corrected for Lorentz and polarization effects.

Crystal data for $Na_2L.H_2O$ are:

$a=8.046(4)$, $b=8.528(4)$, $c=9.669(5)$ Å,
$\alpha=86.23(4)$, $\beta=67.63(4)$, $\gamma=71.74(4)°$,
$Z=2$, Space group $P\bar{1}$, $D_x=1.805$ g cm^{-3},
$D_m=1.82$ g cm^{-3} (by flotation), $V=581.6$ Å^3,
$\mu=3.9$ cm^{-1} (Mo$K\alpha$)

Preliminary Weissenberg photographs showed the crystals of $Na_2L.H_2O$ to be triclinic. Unit cell dimensions and intensity data were measured on a Syntex $P2_1$ diffractometer with graphite-monochromatized Mo radiation (Mo$K\alpha$, $\lambda=0.7107$ Å). The cell parameters given above are the results of a least-squares refinement of automatically centered reflections.

The intensity data of a single crystal ($0.2\times0.3\times0.3$ mm) were collected by the $\theta-2\theta$ scan mode ($5°<2\theta<60°$). The intensity of a test reflection remeasured after every 40 reflections showed no significant change during the data collection. The absorption correction was made from ϕ-scan data and corrections for Lorentz and polarization effects were then applied.[4] Of the 3105 recorded reflections, 1916 with $F_o>9\sigma(F_o)$ were used in the calculations.

Determination and refinement of the structures. The structures were both solved by direct methods with the MULTAN program.[5] The non-hydrogen atoms were localized in E maps. The positional and isotropic temperature parameters for the non-hydrogen atoms were refined by block-diagonal least-squares technique (X-RAY system).[6] All hydrogen atoms were located on the respective difference Fourier maps. Finally, the parameters for the non-hydrogen atoms in the structures were refined anisotropically; those for the hydrogen atoms of $Na_2L.H_2O$ were refined isotropically, and a fixed temperature factor $U=0.04$ Å^2 was used for the hydrogen atoms in H_2L. The atomic scattering factors for the non-hydrogen atoms were taken from Ref. 7 and those for the hydrogen atoms from Ref. 8. The weighting scheme used in the calculations was $w=1/(A+|F_o|+B|F_o|^2)$ with $A=40.0$ and 20.0, and $B=0.015$ and 0.020 for H_2L and $Na_2L.H_2O$, respectively. The final R value was 0.061 for H_2L and 0.041 for $Na_2L.H_2O$.

The atomic coordinates with standard deviations for the non-hydrogen atoms in H_2L and in $Na_2L.H_2O$ are given in Tables 1 and 2, respectively; the atomic parameters and bond lengths for the hydrogen atoms in Tables 3 and 4. Lists of the observed and calculated structure factors and the anisotropic thermal parameters for the non-

Table 1. Fractional atomic coordinates ($\times10^4$) for the non-hydrogen atoms in H_2L.

Atom	X/a	Y/b	Z/c	Atom	X/a	Y/b	Z/c
C2	3504(7)	2635(7)	466(4)	N1	2009(6)	2930(5)	147(3)
C3	4794(7)	2873(7)	−162(4)	N2	−1799(6)	4857(5)	−2171(3)
C4	4522(7)	3399(7)	−1120(4)	O1	−1050(5)	3570(5)	−362(3)
C5	2515(7)	4225(6)	−2461(4)	O2	−1986(5)	5500(5)	−3097(3)
C6	986(7)	4568(6)	−2708(4)	S	4004(2)	4481(1)	−3396(1)
C7	−331(6)	4427(6)	−2003(4)	O3	4910(5)	5850(4)	−3048(3)
C8	−21(6)	3780(6)	−1002(4)	O4	4985(5)	3069(4)	−3371(3)
C9	1700(6)	3460(6)	−775(4)	O5	3151(5)	4740(5)	−4311(3)
C10	2949(6)	3699(6)	−1448(4)				

Table 2. Fractional atomic coordinates ($\times10^4$) for the non-hydrogen atoms in $Na_2L.H_2O$.

Atom	X/a	Y/a	Z/c	Atom	X/a	Y/b	Z/c
C2	601(5)	6794(4)	347(4)	N2	7239(4)	689(3)	−1897(4)
C3	220(5)	6760(4)	1885(4)	O1	4464(4)	2988(3)	−2584(2)
C4	1318(5)	5462(4)	2408(3)	O2	8494(4)	−347(3)	−1498(3)
C5	4125(4)	2834(4)	1790(3)	S	3892(1)	2587(1)	3689(1)
C6	5565(5)	1705(4)	743(3)	O3	5452(4)	1120(3)	3670(3)
C7	5785(4)	1752(4)	−805(3)	O4	2075(4)	2332(3)	4512(3)
C8	4450(4)	2986(4)	−1284(3)	O5	4027(4)	4082(3)	4232(3)
C9	3013(4)	4315(4)	−136(3)	O6	8915(3)	2100(3)	4016(3)
C10	2805(4)	4202(4)	1382(3)	Na1	7051(2)	4574(2)	3403(1)
N1	1943(4)	5600(3)	−646(3)	Na2	6667(2)	860(2)	5615(1)

Table 3. Fractional atomic coordinates and bond distances (Å) for the hydrogen atoms in H_2L.

Atom	*X/a*	*Y/b*	*Z/c*	Bond length
H(C2)	0.361(7)	0.222(7)	0.117(4)	1.02(6)
H(C3)	0.606(7)	0.265(7)	0.014(4)	1.14(6)
H(C4)	0.546(7)	0.355(7)	−0.165(4)	1.06(6)
H(C6)	0.082(7)	0.500(7)	−0.345(4)	1.07(6)
H(N1)	0.093(7)	0.260(7)	0.063(4)	1.15(6)
H(O2)	−0.342(7)	0.576(7)	−0.315(4)	1.22(6)

hydrogen atoms are obtainable from the authors on request.

DESCRIPTION AND DISCUSSION OF THE STRUCTURES

The molecular dimensions of H_2L can be seen in Fig. 1. They show that the acid has a quinone oxime structure rather than a nitroso-hydroxyquinoline structure. This is revealed in the C7−N2 [1.299(7) Å], N2−O2 [1.368(6) Å] bond lengths and in the C7−N2−O2 bond angle [112.2(4)°] which are all typical values for an oxime group,[1,9] and in the C8−O1 distance [1.229(6) Å] which is almost equal to the C=O double bond length found in naphthoquinone compounds (average 1.22 Å)[10] and thus markedly shorter than the C−O(H) single bond [1.330(5) Å] reported for 2-methyl-8-hydroxyquinoline-5-sulfonic acid.[11] The quinonoid nature of the hexagonal C5−C10 carbon ring is further indicated by the considerable shortening of the C5−C6 bond as compared with the other C−C bonds in the ring. Such localization cannot

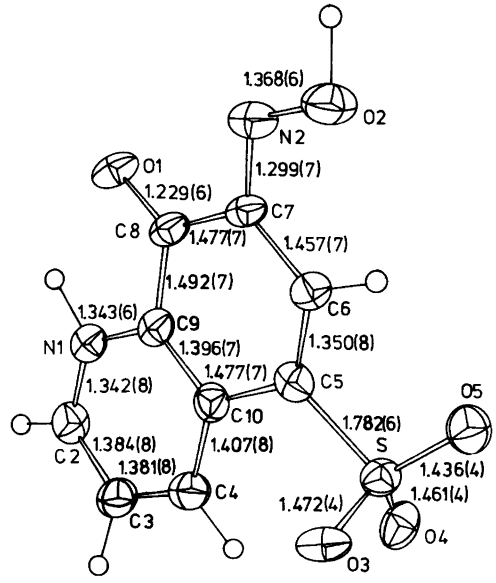

Fig. 1. ORTEP drawing of H_2L showing bond lengths (Å). The non-hydrogen atoms are represented by their thermal ellipsoids with 50 % probability.

be found in 2-methyl-8-hydroxyquinoline-5-sulfonic acid where both of the rings in the quinoline nucleus are clearly aromatic. As a whole the structure of the H_2L molecule closely resembles the known structures of 1,2-naphthoquinone-2-oxime-sulfonic acids; in all these compounds the oxime group is in the *anti* configuration with respect to the quinone oxygen atom.

The acid H_2L is a zwitter-ion compound, the proton being transferred from the sulfonic acid group to the quinoline nitrogen. Since the acidity

Table 4. Fractional atomic coordinates, isotropic thermal parameters and bond distances (Å) for the hydrogen atoms in $Na_2L.H_2O$.

Atom	*X/a*	*Y/b*	*Z/c*	*U*	Bond length
H(C2)	−0.010(6)	0.770(6)	−0.003(5)	0.046(13)	0.95(5)
H(C3)	−0.086(6)	0.759(5)	0.261(5)	0.034(11)	0.98(3)
H(C4)	0.108(6)	0.548(6)	0.344(5)	0.047(13)	0.94(5)
H(C6)	0.652(6)	0.087(5)	0.096(5)	0.032(11)	0.95(4)
H1(O6)	0.962(6)	0.151(6)	0.319(5)	0.050(14)	0.86(4)
H2(O6)	0.977(7)	0.227(7)	0.424(6)	0.070(17)	0.85(7)

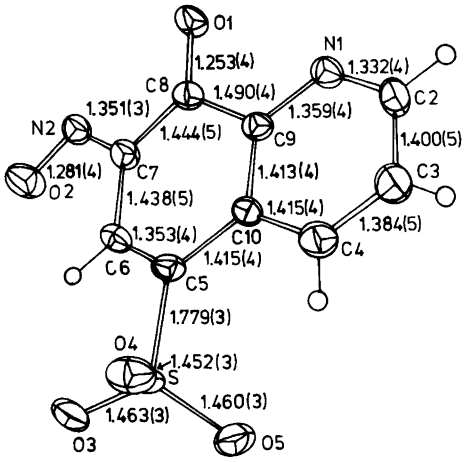

Fig. 2. ORTEP drawing of the organic anion in $Na_2L.H_2O$ showing bond lengths (Å).

of the sulfonic acid is distinctly greater than that of the $-NH^+$ group, this transfer could well be anticipated, and it has been observed in several related compounds, *e.g.* in 2-methyl-8-hydroxyquinoline-5-sulfonic acid.[11]

The bond lengths of the organic anion in $Na_2L.H_2O$ are presented in Fig. 2, and the bond angles in both of the present compounds are collected in Table 5. It can be seen that removal of the protons brings about some changes in the bond lengths of the quinoline ring, the shortening of the C5–C10 distance being most prominent. However, the differences between the degree of the localization of the ring structures in these two compounds are not very marked, and the most significant changes are rather associated with the oxime group: the C7–N2 bond is lengthened to 1.351(3) Å, the N2–O2 is shortened to 1.281(4) Å, and the C7–N2–O2 angle is opened to the value 116.3(3)°. Another observation, although not very significant, is that the C8–O1 bond is lengthened to 1.253(4) Å. It is interesting to note that all these changes are very similar to those found as a result of coordination of transition metal ions (Cu^{2+}, Ni^{2+} or Zn^{2+}) to naphthoquinone oximato ligands, in which cases the chelation occurs through oxime nitrogen and quinone oxygen atoms.[1,2]

The coordinations about the two sodium cations in the structure of $Na_2L.H_2O$ are distinctly different. One of the sodium ions (Na2) is in a strongly distorted octahedral environment, being surrounded by one nitrogen atom and five oxygen atoms. The nitrogen atom is the oxime nitrogen, one of the oxygen atoms is the quinone oxygen of the same molecule, three other oxygens are derived from two separate sulfonate groups, and the sixth is the water oxygen. The water oxygen also takes part in the coordination environment of Na1, which consists additionally of two sulfonate oxygens, the quinoline nitrogen and the quinone oxygen, the last two from the same molecule. Thus there are only five bond contacts, the distance from Na1 to the next nearest atom (which is another Na1 in the structure) being 3.464(2) Å. The spatial arrangement of the atoms is such that the coordination geometry of Na1 may be best described as trigonal bipyramidal, with the quinone oxygen $(1-x,1-y,-z)$ and the water

Table 5. Bond angles (°) related to Figs. 1 and 2.

	H_2L	$Na_2L.H_2O$		H_2L	$Na_2L.H_2O$
C2–N1–C9	122.2(5)	118.1(3)	C6–C7–N2	125.2(5)	123.3(3)
N1–C2–C3	120.1(5)	123.0(3)	C8–C7–N2	115.3(5)	115.9(3)
C2–C3–C4	119.3(5)	119.1(3)	C7–C8–O1	124.8(5)	123.6(2)
C3–C4–C10	120.1(5)	119.6(3)	C9–C8–O1	120.3(4)	120.2(3)
C4–C10–C5	124.8(5)	124.4(3)	C7–N2–O2	112.2(4)	116.3(3)
C4–C10–C9	117.9(4)	116.7(3)	C10–C5–S	121.1(4)	121.1(2)
C5–C10–C9	117.3(5)	118.9(2)	C6–C5–S	117.4(4)	117.6(3)
C10–C5–C6	121.5(5)	121.4(3)	C5–S–O3	103.4(2)	105.9(1)
C5–C6–C7	122.4(5)	121.2(3)	C5–S–O4	105.9(2)	107.5(2)
C6–C7–C8	119.5(5)	120.8(2)	C5–S–O5	106.1(3)	107.4(2)
C7–C8–C9	114.9(4)	116.3(3)	O3–S–O4	111.5(2)	111.1(2)
C8–C9–N1	115.6(4)	115.9(3)	O3–S–O5	113.7(2)	112.1(2)
C8–C9–C10	124.1(4)	120.7(3)	O4–S–O5	115.1(2)	112.4(2)
N1–C9–C10	120.3(5)	123.4(2)			

Table 6. Interatomic angles (°) related to Fig. 3; the coordination spheres of sodium ions.

The coordination sphere of sodium ion Na1			
O5 – Na1 – O6	101.1(1)	O6 – Na1 – $O1^{II}$	173.5(1)
O5 – Na1 – $O5^{I}$	86.8(1)	O6 – Na1 – $N1^{II}$	106.2(1)
O5 – Na1 – $O1^{II}$	84.6(1)	$O5^{I}$ – Na1 – $O1^{II}$	89.1(1)
O5 – Na1 – $N1^{II}$	102.1(1)	$O5^{I}$ – Na1 – $N1^{II}$	155.4(1)
O6 – Na1 – $O5^{I}$	94.3(1)	$O1^{II}$ – Na1 – $N1^{II}$	69.2(1)
The coordination sphere of sodium ion Na2			
O3 – Na2 – O6	86.9(1)	O6 – Na2 – $O4^{IV}$	113.8(1)
O3 – Na2 – $O1^{III}$	104.4(1)	$O1^{III}$ – Na2 – $N2^{III}$	66.8(1)
O3 – Na2 – $N2^{III}$	167.8(1)	$O1^{III}$ – Na2 – $O3^{IV}$	95.3(1)
O3 – Na2 – $O3^{IV}$	75.7(1)	$O1^{III}$ – Na2 – $O4^{IV}$	136.9(1)
O3 – Na2 – $O4^{IV}$	97.5(1)	$N2^{III}$ – Na2 – $O3^{IV}$	96.3(1)
O6 – Na2 – $O1^{III}$	104.1(1)	$N2^{III}$ – Na2 – $O4^{IV}$	84.8(1)
O6 – Na2 – $N2^{III}$	103.1(1)	$O3^{IV}$ – Na2 – $O4^{IV}$	54.8(1)
O6 – Na2 – $O3^{IV}$	156.7(1)		

[I] Symmetry relations for atoms in Fig. 3 and in Table 6: [I] $1-x,1-y,1-z$ [II] $1-x,1-y,-z$ [III] $x,y,1+z$ [IV] $1-x,-y,1-z$

Table 7. Hydrogen bonding details.

X – H···Y	Position of acceptor atom	X···Y (Å)	X – H (Å)	H···Y (Å)	X – H···Y (°)
H_2L:					
N1 – H···O4	$-\frac{1}{2}+x,\frac{1}{2}-y,\frac{1}{2}+z$	2.749(5)	1.15(6)	1.66(6)	157(5)
O2 – H···O3	$-1+x,y,z$	2.608(6)	1.22(6)	1.40(6)	169(5)
$Na_2L.H_2O$:					
O6 – H1···O2	$2-x,-y,-z$	2.677(3)	0.86(4)	1.83(4)	169(6)
O6 – H2···O4	$1+x,y,z$	2.827(5)	0.85(7)	1.98(7)	170(5)

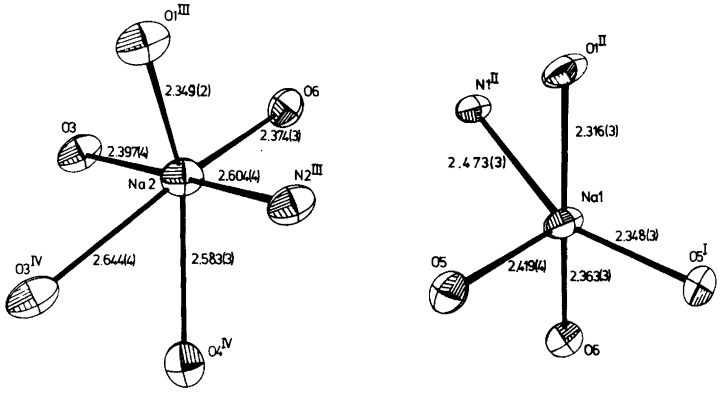

Fig. 3. ORTEP drawing of the coordination environments of the sodium ions showing bond lengths (Å).

oxygen in the apical positions. The bond contacts around the sodium ions Na1 and Na2 shown in Fig. 3 are normal, ranging from 2.316 to 2.644 Å. The respective angles are presented in Table 6.

There are two hydrogen bonds in $Na_2L.H_2O$ both of which are associated with the water molecule. One of these bonds is a relatively weak interaction with a sulfonate oxygen atom: O···O 2.827(5) Å, O–H···O angle 170(5)°; the other is formed with the oxime oxygen atom: O···O separation 2.677(3) Å and O–H···O angle 169(6)°.

In the structure of H_2L there are layers made up of infinite parallel chains running along the *a*-axis. Successive molecules within each chain are connected by a hydrogen bond of 2.608(6) Å, with O–H···O angle of 169(5)° from the oxime oxygen to a sulfonate oxygen atom. Between the chains of separate layers there is also hydrogen-bond interaction of 2.749(6) Å involving the N–H···O angle of 157(5)°, formed *via* the quinoline nitrogen and a neighbouring sulfonate oxygen. Details of the hydrogen bonding in the structures are given in Table 7.

Acknowledgement. The financial support of the Science Research Council of Finland is gratefully acknowledged.

REFERENCES

1. Saarinen, H., Korvenranta, J. and Näsäkkälä, E. *Acta Chem. Scand. A 31* (1977) 213.
2. Korvenranta, J., Saarinen, H. and Näsäkkälä, E. *Acta Chem. Scand. A 31* (1977) 689.
3. Saarinen, H., Orama, M. and Korvenranta, J. *Finn. Chem. Lett.* (1978) 74.
4. *Syntex XTL Operations Manual*, 2nd Ed., Syntex Analytical Instruments, Cupertino, California 1976.
5. Main, P., Woolfson, M. M., Declercq, J-P. and Germain, G. MULTAN, *A Computer Programme for the Automatic Solution of Crystal Structures*, Dec. 1974.
6. *X-RAY 76*, Technical Report TR-446, Computer Science Center, University of Maryland, College Park 1976.
7. Cromer, D. T. and Mann, J. B. *Acta Crystallogr. A 24* (1968) 321.
8. Stewart, R. F., Davidson, E. and Simpson, W. *J. Chem. Phys. 42* (1968) 3175.
9. Chakravorty, A. *Coord. Chem. Rev. 13* (1974) 1.
10. Gaultier, P. J. and Hauw, C. *Acta Crystallogr. 18* (1965) 179.
11. Merritt, L. L. and Duffin, B. *Acta Crystallogr. B 26* (1970) 734.

Received January 27, 1978.

Acta Chemica Scandinavica A 32 (1978) 539–544

Structural Studies of the Solid Electrolyte High-$LiTa_3O_8$

ANDERS G. NORD[a] and JOHN O. THOMAS[b]

[a] Departments of Inorganic and Structural Chemistry, Arrhenius Laboratory, University of Stockholm, S-106 91 Stockholm, Sweden and [b] Institute of Chemistry, University of Uppsala, Box 531, S-751 21 Uppsala, Sweden

The high temperature modification of $LiTa_3O_8$ has been studied by X-ray single-crystal and neutron powder diffraction techniques. The orthorhombic unit cell ($Z=4$) has the dimensions $a=16.705(2)$, $b=3.836(1)$, $c=8.928(1)$ Å. A structural model has been proposed based on the space group *Pmma* (No. 51) and refined by least squares to $R(F)=0.045$ on the basis of 1206 independent X-ray reflections. A mechanism of the isotropic electrical conductivity of the compound is discussed in relation to the proposed structure and the slight disorder which may be attributed to it.

The last ten years have witnessed a steadily growing interest in the study of solid electrolytes for their potential use as battery and energy storage materials. General reviews of the field have been given by many authors (*cf.* Refs. 1, 2). As part of a project on energy-related research, investigations of solid electrolyte compounds have been started at the Arrhenius Laboratory. The present paper reports on the high temperature form of the trimorphic compound $LiTa_3O_8$, referred to hereafter as high-$LiTa_3O_8$. This compound is structurally related to $LiNb_6O_{15}F$.[3,4] High-$LiTa_3O_8$ has been shown to be a solid electrolyte with moderately good conduction properties: at 500 K the conductivity of a pellet is about 10^{-2} ohm^{-1}m^{-1} with an activation energy of 0.78 eV.[5] Measurements on large single crystals prepared at the Arrhenius Laboratory have shown the electrical conductivity to be isotropic rather than anisotropic.[6] The purpose of the present work has been to elucidate the essential structural features of high-$LiTa_3O_8$ and relate these to the conduction properties of the material.

EXPERIMENTAL

Preparation. High-$LiTa_3O_8$ was prepared by mixing absolutely dry Li_2CO_3 (Merck, *pro analysi*) and Ta_2O_5 (Fluka, 99.9 %) in the molar ratio 1:3. The mixture was slowly heated in a platinum crucible, placed in an iridium-wound electric furnace, until it melted at about 1900 K. Large, slightly pink crystals up to a few cubic millimeters in volume can be obtained by very slow crystallization from the melt. The high temperature modification of $LiTa_3O_8$ thus obtained is metastable at room temperature.

Preliminary X-ray studies. X-Ray powder photographs of the sample were taken with a Guinier-Hägg type focusing camera using strictly monochromatized Cu$K\alpha_1$ radiation ($\lambda=1.54050$ Å) and with potassium chloride as an internal standard ($a=6.29294$ Å).[7] The unit cell parameters were refined by least squares. Of 76 powder reflections, 72 could be indexed; four very weak lines originated from a slight impurity of $LiTaO_3$. The dimensions of the orthorhombic unit cell at 298 K are: $a=16.705(2)$, $b=3.836(1)$, $c=8.928(1)$ Å, and $V=572.1$ Å^3. The density was determined experimentally by the apparent loss of weight in benzene. It was found to be 7.81 ± 0.05 g cm^{-3} which compares favourably with the theoretical value of 7.86 g cm^{-3} ($Z=4$).

Comparison of the unit cell dimensions and visual inspection of the Guinier photographs for high-$LiTa_3O_8$ and $LiNb_6O_{15}F$ (*Pmma* symmetry[3]) clearly indicated that their crystal structures must be closely related. Refinement of the Guinier powder profile of high-$LiTa_3O_8$ utilizing the Rietveld technique[8,9] and with $LiNb_6O_{15}F$ structural parameters as a start gave an $R(F)$ value of 0.082. This also indicates a close resemblance between the two structures.

Weissenberg photographs were recorded about the *a* and *b* axes. Orthorhombic symmetry was confirmed, and no evidence of superstructure could be

detected. The only systematic extinctions were $hk0$ reflections for $h=2n+1$, suggesting as possible space groups *Pmma*, *Pm2a*, and $P2_1ma$.

Single-crystal data (X-ray diffractometer data). A small prismatic single crystal with the approximate dimensions $0.03\times0.14\times0.05$ mm^3 was used for recording the single-crystal data. These were collected with a Siemens automatic four-circle diffractometer (graphite monochromator, Mo$K\alpha$ radiation, $\theta-2\theta$ scan with $\theta_{max}\approx35°$). Of about 1300 measured reflections, 1206 had $\sigma(I)/I<0.5$ and were regarded as significantly observed. These were corrected for Lorentz, polarization, and absorption effects ($\mu=603$ cm^{-1}; transmission factors in the range 0.066 – 0.161).

STRUCTURE INVESTIGATIONS (X-RAY SINGLE-CRYSTAL DATA)

The layers $h0l$, $h1l$, $h2l$, *etc.*, were very similar, indicating that practically all atoms are situated in one plane perpendicular to the short b axis. A Patterson synthesis confirmed that all tantalum atoms could be placed in or near the $y=0$ plane. The centric space group *Pmma* (*cf.* $LiNb_6O_{15}F$ [3]) was chosen to begin the refinements. Only the tantalum atoms were included in the first stages. Hughes' weighting function [10] was always used. The atomic scattering factors used were those for Ta^{5+} and O^{2-} including the real and imaginary anomalous dispersion terms.[11,12] The conventional R factor, defined as $R(F)=\Sigma\|F_o|-|F_c\|/\Sigma|F_o|$, dropped to 0.104 when the tantalum atoms, all at $y=0$, were refined with isotropic temperature factors. The temperature factor was noted to be about three times larger for Ta(4) [*cf.* below] than for the other tantalums. After three cycles of refinement with anisotropic temperature factors, the R value fell to 0.081. Ta(4) now acquired a large amplitude in the direction of the b axis. Moreover, the standard deviations obtained were anomalously large.

At this stage, the possibility of a lower, non-centric symmetry was considered. Statistical tests based on the normalized structure factors were undecisive as to the question of the existence of a centre of symmetry. Neither could a Giebe-Scheibe piezoelectric tester produce definite results in this respect. Therefore refinements were also made in the two feasible non-centric space groups *Pm2a* and $P2_1ma$ with Ta(4) shifted slightly from its former position. No significant improvement could be observed, however ($R=0.090$ with isotropic and 0.076 with anisotropic tantalums, respectively, for space group *Pm2a*). Returning to *Pmma*, the Ta(4) atoms were then "split" to lie disordered on either side of the mirror plane at $y=0$. This refinement, with all atoms vibrating isotropically (still no oxygens included), with an R value of 0.078 and very reasonable standard deviations, was a significant improvement on earlier refinements.

The subsequent difference Fourier synthesis revealed almost all oxygen atoms situated in (or near) the $y=0$ plane, and close to the corresponding positions in $LiNb_6O_{15}F$.[3] The oxygen atoms in the $y=1/2$ plane were, however, much more difficult to identify. A large number of refinements were made, also with "split" (disordered) oxygen atoms, but with no greater improvements. Although some of the oxygen atoms may well be disordered, the authors prefer at this stage to report a structural model (*cf.* Fig. 1) in which only Ta(4) is disordered and all other atoms lie at $y=0$ or $y=1/2$. Also, only isotropic temperature factors are used henceforward. This model gave an R value of 0.054, which was further improved to 0.045 on the inclusion of an isotropic extinction parameter ($g=0.073\pm0.006$)[13] in the refinement. The atomic and thermal parameters are given in Table 1. A general survey of the computer programs has been published earlier.[14] The structure factor list can be obtained on request from the Arrhenius Laboratory (The Secretariat, Inorganic Chemistry).

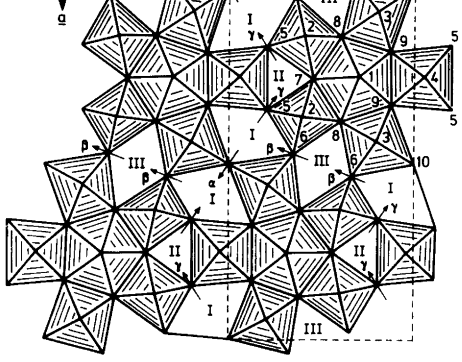

Fig. 1. Projection of the crystal structure of high-$LiTa_3O_8$ along the b axis. Numbers 1 – 4 refer to tantalum (at $y\approx0$) and oxygen (at $y=1/2$) atoms. Numbers 5 – 10 refer to oxygen atoms at $y=0$. Tunnels I – III are parallel to the b axis. Migration paths α, β, and γ are also indicated.

Table 1. Fractional atomic coordinates and isotropic temperature factors for high-$LiTa_3O_8$ described in *Pmma* ($Z=4$). X-Ray as well as neutron-determined values are given, the latter in *italics*. In the neutron powder diffraction refinement, the tantalum positions were fixed at their X-ray determined values, and overall temperature factors were used (see the text).

Atom	Position	x	y	z	B (Å^2)
Li(I)[a]	4(*j*)	–	–	–	–
		0.087(4)	1/2	*0.049(7)*	
Li(II)[a]	4(*j*)	–	–	–	–
		0.171(4)	1/2	*0.238(8)*	
Li(III)[a]	4(*j*)	–	–	–	–
		−0.019(4)	1/2	*0.391(8)*	
Ta(1)	2(*e*)	1/4	0	0.6871(1)	0.57(2)
Ta(2)	4(*i*)	0.1328(1)	0	0.3921(1)	0.55(1)
Ta(3)	4(*i*)	0.0601(1)	0	0.8109(1)	0.53(2)
Ta(4)[b]	4(*k*)	1/4	0.0387(3)	0.0532(1)	0.52(2)
O(1)	2(*f*)	1/4	1/2	0.688(2)	0.8 (2)
		1/4	1/2	*0.685(4)*	
O(2)	4(*j*)	0.130(1)	1/2	0.400(3)	3.4 (4)
		0.115(1)	1/2	*0.411(2)*	
O(3)	4(*j*)	0.061(2)	1/2	0.825(3)	4.0 (5)
		0.056(2)	1/2	*0.809(3)*	
O(4)	2(*f*)	1/4	1/2	0.057(5)	3.6 (6)
		1/4	1/2	*0.073(4)*	
O(5)	4(*i*)	0.162(2)	0	0.185(3)	3.3 (4)
		0.164(1)	0	*0.196(2)*	
O(6)	4(*i*)	0.019(2)	0	0.344(3)	2.6 (4)
		0.013(1)	0	*0.345(3)*	
O(7)	2(*e*)	1/4	0	0.450(2)	1.3 (3)
		1/4	0	*0.464(3)*	
O(8)	4(*i*)	0.133(1)	0	0.620(1)	0.8 (2)
		0.133(1)	0	*0.627(2)*	
O(9)	4(*i*)	0.176(1)	0	0.877(2)	1.3 (2)
		0.175(1)	0	*0.889(2)*	
O(10)	2(*a*)	0	0	0	0.8 (2)
		0	*0*	*0*	

[a] The occupancies for the lithiums are less than unity (compare text). [b] Ta(4) has an occupancy of 0.5.

NEUTRON DIFFRACTION STUDIES

The large difference in X-ray scattering power for tantalum and lithium meant that all efforts to locate the lithium ions in the difference Fourier maps would be fruitless. The situation for neutron scattering is, however, more favourable. The scattering amplitudes b (in *cm*) are -0.194×10^{-12} for lithium, 0.70×10^{-12} for tantalum, and 0.575×10^{-12} for oxygen.[15] Neutron powder diffraction data have been collected at the Studsvik R2 reactor from 2 cm^3 of powdered high-$LiTa_3O_8$ ($\lambda=1.56$ Å with a flux of 10^6 neutrons cm^{-2} s^{-1}; $3\leq\theta\leq42°$ with $\Delta(\theta)=0.04°$). The Rietveld full-profile refinement procedure[8] was then used, fixing the tantalums from the X-ray study and refining the oxygens only. This gave a final $R(I)$ factor of 0.160 with overall temperature factors B(Ta) = 1.0(2) and B(O) = 1.2(1) Å^2. This is poorer agreement than expected and can presumably be attributed to disorder in the structure, as discussed above. The largest negative peaks [b(Li) is negative] in the difference Fourier map appeared in the $y=1/2$ plane (see Fig. 2). These peaks suggest that the lithium ions occupy the structural tunnels, labelled I – III in Fig. 1, although this is a very simplified model.

In the final refined model, the tantalum positions were again fixed at their X-ray determined values, while the lithium and oxygen positions were refined (*cf.* Table 1). For simplicity, the four lithium ions

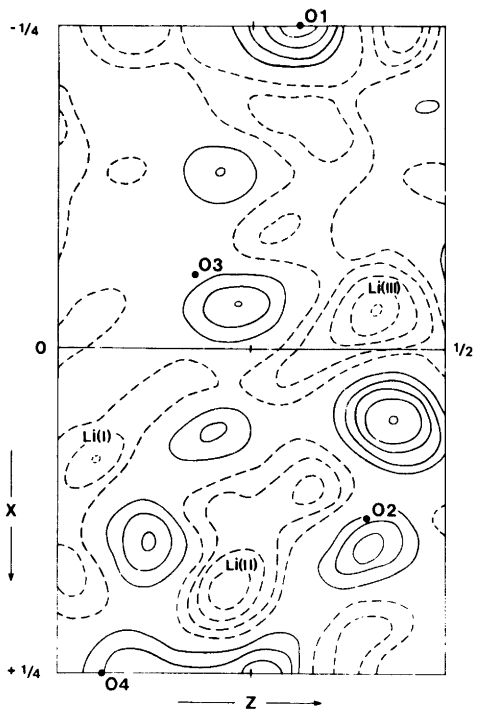

Fig. 2. Neutron difference Fourier map at the section $y=1/2$ (see text).

per unit cell were assumed to be uniformly distributed among three 4(*j*) positions so that there is one "half" lithium at $y=1/2$ in each tunnel, *i.e.* the occupancy factors for Li(I)–Li(III) are 0.5, 0.25 and 0.25, respectively. The overall isotropic temperature factors refined to $B(\mathrm{Li})=-8.7(6)$, $B(\mathrm{Ta})=1.0(2)$, and $B(\mathrm{O})=1.0(1)$ Å^2. Scale factor, zero-point, cell parameters and half-width parameters[8] were also refined. The final agreement factors were: $R_I=0.127$, $R_p=0.180$, and $R_{pw}=0.193$.

It can be noted from Table 1 that the e.s.d.'s for the neutrondetermined oxygen positions are comparable with those from the X-ray study. It may be significant that poor agreement is found for O(4) and O(7). Their *y*-values successfully refined in a later trial refinement, but they acquired anomalously large individual temperature factors. The *R* values, though, improved significantly (0.093, 0.161, and 0.172). This reinforces earlier suspicions that at least certain of the atoms are disordered or do not conform to the centrosymmetric space group *Pmma*. The negative temperature factor for lithium may again be some artefact of an oversimplified model.

STRUCTURAL CONSIDERATIONS AND IONIC CONDUCTIVITY

The structure of high-$LiTa_3O_8$ comprises a polygonal network built up of pentagonal Ta(1)O_7 bipyramids each surrounded through edge-sharing by five TaO_6 octahedra to form a kind of "five-pointed" star (*cf.* Fig. 1). It may also be regarded as a layer structure with its layers in the $y=0$ plane, and held together through the O(1)–O(4) atoms between the layers. Ta(4) is situated 0.15 Å out of the $y=0$ plane on a 50 % disordered site. From packing considerations it would seem likely that the Ta(4)O_6 octahedra arrange themselves in rows parallel to the *b* axis such that each individual row is ordered [*i.e.* Ta(4) is displaced from the $y=0$ plane in the *same* way *within* a row], and that the disordering occurs *between* rows. The physical meaning of the Ta(4) displacement is not clear as regards the lithium ion transport in the structure. The pentagonal bipyramids and octahedra are fairly regular. Some interatomic distances have been listed in Table 2.

Table 2. Some interatomic distances (Å) within the lithium-oxygen and tantalum-oxygen polyhedra of high-$LiTa_3O_8$. The X-ray coordinates have been used except for the lithium atoms (*cf.* Table 1).

Central atom X	Coord. number	Average distance ⟨X–O⟩	Shortest X–O dist.	Longest X–O dist.
Li(I)	9	2.59(4)	X–O(3): 2.05(7)	X–O(9): 2.87(5)
Li(II)	4	1.92(4)	X–O(2): 1.62(7)	X–O(4): 2.08(7)
Li(III)	7	2.39(4)	X–O(3): 2.05(7)	X–O(8): 2.70(5)
Ta(1)	7	2.04(2)	X–O(1): 1.92(1)	X–O(7): 2.12(2)
Ta(2)	6	1.96(2)	X–O(5): 1.91(2)	X–O(8): 2.04(1)
Ta(3)	6	1.97(2)	X–O(6): 1.91(3)	X–O(8): 2.09(1)
Ta(4)	6	1.94(2)	X–O(4): 1.77(1)	X–O(4'): 2.07(1)

It is clear from the two crystallographic studies that some of the atoms are disordered, or ordered within a lower symmetry space group. Their positions, as given in Table 1, should thus be regarded as "average" positions with respect to the space group *Pmma*. This is true, in particular, of the lithium ions and the oxygen atoms at the extremities of the stars referred to above.

Measurements on high-$LiTa_3O_8$ have shown that the electrical conductivity is isotropic rather than anisotropic.[6] This is in good accordance with the structure (Fig. 1). The lithium ions, which are responsible for the electrical conductivity, reside in sites corresponding to the widest parts of the tunnels I – III. The distribution of charge carriers is supposed to be uniform so that there is 0.5 Li^+ ion in each tunnel (for $0 \leq y \leq 1$). Actually an occupancy smaller than unity is a necessary requirement if the basic conduction mechanism is a lithium "jump" from one position to a neighbouring empty position. Different possible "migration paths" have been indicated in Fig. 1. The obvious ones are along the tunnels I – III for ion transport parallel to the *b* axis. The alternative paths (α, β, and γ) are approximately at $y = 1/2$ and lead ions from one tunnel to another. Each of these six paths contains a "bottleneck". These occur along the tunnels at $y \approx 0$, and between the tunnels at $y \approx 1/2$.

To ascertain the more probable paths of migration, the largest solid sphere which can pass through a bottleneck has been computed for the six different paths. The atomic parameters used are those listed in Table 1 (X-ray data); $r(O^{2-})$ is 1.40 Å. The results show that lithium transport is most unlikely along the tunnels II and III since the lithium radius (~0.6 Å) is about double the "radius" of the II and III bottlenecks at $y = 0$. All four remaining bottlenecks allow the passage of a solid sphere of radius 0.5 – 0.6 Å. This gives structural support to the observed three-dimensional electrical conductivity. In such considerations, however, it must be remembered, firstly, that atoms behave as elastic rather than as solid spheres. Moreover, the thermal motion of the atoms is considerably larger at temperatures where the conductivity is higher. Finally, and most important: the suspected disorder among certain of the oxygen atoms tends to widen the bottlenecks, since these are defined to a large extent by the probably somewhat disordered oxygens at the extremities of the five-pointed stars.

The rest-positions for the lithium ions together with the suggested migration paths constitute a highly simplified picture of the ionic conduction mechanism in high-$LiTa_3O_8$, but one which is in agreement with experiments. [Other structural studies made by Werner and Marinder[16] based on X-ray powder profile refinements support the present structural proposal.] It is evident, however, that much work remains in elucidating the structure completely. One is here reminded of the structural complexity of the much-studied solid electrolyte beta-alumina [*cf. Refs.* 2, 17 – 20]. Efforts to grow single crystals of high-$LiTa_3O_8$ large enough for a neutron diffraction study are currently being made at the Arrhenius Laboratory.

Acknowledgements. The authors would like to thank Professors Arne Magnéli, Peder Kierkegaard, and Ivar Olovsson for their encouragement, advice, and support during this work. They are also grateful to Professor Paul Hagenmuller, Dr. Jean-Maurice Réau and their co-workers at the Laboratoire de Chimie du Solids in Bordeaux for valuable cooperation. This work has been performed as part of a research program on chemical storage of energy supported financially by the Swedish Natural Science Research Council.

REFERENCES

1. Whittingham, M. S. and Huggins, R. A. In Anderson, J. S., Ed., *7th Int. Symp. React. Solids*, Chapman & Hall, Bristol 1972.
2. *Superionic Conductors*, Mahan, G. D. and Roth, W. L., Eds., Plenum, New York 1976.
3. Lundberg, M. *Acta Chem. Scand. 19* (1965) 2274.
4. Roth, R. S., Parker, H. S., Brower, W. S. and Waring, J. L. In van Gool, W., Ed., *Fast Ion Transport in Solids*, North-Holland, Amsterdam 1973.
5. Réau, J. M., Magniez, G., Chaminade, J. P., Pouchard, M. and Hagenmuller, P. *Acta Chem. Scand. A 31* (1977) 88.
6. Magniez, G. *Contribution à l'étude de noveaux électrolytes solides du lithium*, Diss., University of Bordeaux, Bordeaux 1976.
7. Hambling, P. G. *Acta Crystallogr. 6* (1953) 98.
8. Rietveld, H. M. *J. Appl. Crystallogr. 2* (1969) 65.
9. Malmros, G. and Thomas, J. O. *J. Appl. Crystallogr. 10* (1977) 819.
10. Hughes, E. W. *J. Am. Chem. Soc. 63* (1941) 1737.
11. *International Tables for X-Ray Crystallography*, Kynoch Press, Birmingham 1974, Vol. IV, Table 2.2A.

12. *Ibid.* 1968, Vol. III, Table 3.3.2C.
13. Coppens, P. and Hamilton, W. C. *Acta Crystallogr. A 26* (1970) 71.
14. Nord, A. G. *Chem. Commun. Univ. Stockholm* (1973) No. 15.
15. *International Tables for X-Ray Crystallography*, Kynoch Press, Birmingham 1974, Vol. IV, Table 2.6.
16. Werner, P. E. and Marinder, B. O. *To be published.*
17. Bragg, W. L., Gottfried, C. and West, J. *Z. Kristallogr. 77* (1931) 255.
18. Beevers, C. A. and Ross, M. A. S. *Z. Kristallogr. A 97* (1937) 59.
19. Felsche, J. *Z. Kristallogr. 127* (1968) 94.
20. Peters, C. R., Bettman, M., Moore, J. W. and Glick, M. D. *Acta Crystallogr. B 27* (1971) 1826.

Received February 8, 1978.

Acta Chemica Scandinavica A 32 (1978) 545–548

Preparation and Chromatographic Separation of Diastereoisomeric Ions of Tris[(*R*)-1-phenyl-1,2-ethanediamine]cobalt(III)

N. BERNTH and ERIK LARSEN

Chemistry Department I, The H. C. Ørsted Institute, Universitetsparken 5, DK-2100 Copenhagen Ø, Denmark

Racemic 1-phenyl-1,2-ethanediamine has been prepared and resolved in its catoptric forms. The $(-)_D$-*R* isomer was used in preparation of the tris-[(*R*)-1-phenyl-1,2-ethanediamine]cobalt(III) cation of which four diastereoisomers are expected to form. By means of chromatography on Sephadex SP-C25 the diastereoisomers have been separated and three of them have been isolated and characterized by their visible–UV absorption and circular dichroism spectra and ^{1}H NMR spectroscopy. It is shown that the *meridional* lel_3 and *facial* lel_3 forms have different circular dichroism spectra.

Since Werner's work on optically active cobalt(III) complexes the tris-diamine cobalt(III) complexes have been the subject of very detailed investigations in order to unravel the connection between the chiroptical properties and the varied configurational and conformational structures. In this respect the tris(1,2-propanediamine)cobalt(III) complexes, $[Co(pn)_3]^{3+}$, have played an important role in clarifying our understanding of the stereochemistry and also in developing experimental techniques to separate and characterize the altogether 24 different cations. One of these isomers was characterized by X-ray diffraction to be the *fac*-Δ-$[Co(R\text{-}pn)_3]^{3+}$.[1] At this time it had already been realized[2] that the synthetic route could yield a mixture of the *fac* and *mer* isomers of Δ-$[Co(R\text{-}pn)_3]^{3+}$. The crystal structure determination was made from the bulk crystalline material of a preparation and from considerations about the statistical ratio of the *fac* and *mer* geometric isomers this sample was expected to contain about three times more of the *mer* isomer that of the *fac* isomer. It was noted that a single crystal taken from a batch was not necessarily representative of the whole batch.[3] MacDermott[4,5] succeeded in separating the geometric isomers of Δ-$[Co(R\text{-}pn)_3]^{3+}$ after having realized that the bromide of the *fac* form but not that of the *mer* isomer is crystalline. After precipitating the *fac* bromide the *mer* form could be isolated as the crystalline dithionate.

The chromatographic separation on Sephadex of the *fac* and *mer* Δ-$[Co(R\text{-}pn)_3]^{3+}$ isomers was achieved much later and an extensive study of the isomer distribution of $[Co(pn)_3]^{3+}$ was reported by Harnung *et al.*[6] In these investigations and in similar studies (*e.g.* Ref. 7) it was found that the absorption and circular dichroism spectra of *fac* and *mer* pairs of isomers were nearly if not totally indistinguishable. If this result is general it means that a theoretical model for optical activity of these complexes need only be concerned with the spatial distribution of the nearest and next nearest neighbouring atoms to the central metal ions. The present work was started to test this point with complexes of a ligand considered more unsymmetric than 1,2-propanediamin, *i.e.* 1-phenyl-1,2-ethanediamine (phenen). The ligand is not commercially available but obtainable from acetophenone by a synthetic route which is convenient only for rather small amounts. Therefore the investigation was restricted to the four tris complexes formed by $(-)_D$-1-phenyl-1,2-ethanediamine: (*fac* or *mer*)-(Δ or Λ)-$[Co((-)_D\text{-}phenen)_3]^{3+}$. This system has been studied[8] to some extent previous to the development of conformational analysis of chelate rings and therefore not with the same intentions as ours.

EXPERIMENTAL

Physical measurements. Absorption spectra were recorded on a Cary 118 spectrophotometer and circular dichroism on a Roussel-Jouan Dichrographe IIIS. ^{1}H NMR spectra were obtained on a Bruker HX-270 spectrometer. A Perkin-Elmer AA 305 was used for atomic absorption analyses.

Preparations

Isonitrosoacetophenone was prepared by Claisen condensation from acetophenone and butylnitrite added to sodium ethanolate in ethanol.

Phenylglyoxime[9] was obtained from isonitrosoacetophenone (100 g) in 150 ml of water to which was added 500 ml of ethanol, 100 g hydroxylammonium chloride, 170 ml 6 M acetic acid and 25 g of sodium acetate. The mixture was refluxed for 2 h and then left to cool to room temperature. Crystallization of the desired product was initiated by scratching. Yield 48 g (~45 %).

Phenylethylenediamonium chloride. 44 g of phenylglyoxime dissolved in 1 l of absolute ethanol was reduced with *ca.* 130 g sodium. After cooling, first 100 ml 4 M hydrochloric acid then excess 12 M hydrochloric acid were added. After filtration the red solution was evaporated to 400 ml and again filtered. The pH of the filtrate was adjusted to 3–4 with 2 M sodium hydroxide and to this solution was added 90 g of wet picric acid dissolved in 1 l of boiling water. After cooling to room temperature the picrate was filtered, washed with water and then suspended in 300 ml of water. Picric acid was liberated and to a large extent removed by filtration after the addition of 300 ml of 12 M hydrochloric acid. The yellow filtrate was evaporated to near dryness. The addition of 300 ml of ethanol dissolved the remaining picric acid and precipitated most of the amine as the hydrochloride. The product was washed with ether or acetone. Characteristic yield 25–30 g (45–55 %).

Resolution of racemic phenen.2HCl.[10] 33.3 g (0.154 mol) phenen.2HCl was dissolved in 200 ml of water. The solution was placed on a column of IRA-402 anion exchanger in the OH^- form (length 35 cm, diameter 7.5 cm) and eluted with water. The basic part of the eluate was collected and to this was added 23.0 g (0.154 mol) of $(+)_D$-tartaric acid. The volume of the solution was then reduced until precipitation commenced. Thereafter the resolving procedure of Reilen *et al.*[10] was followed.

$[Co((-)_D$-phenen$)_3]Cl_3$. The complex was prepared by the method analogous to that of Michelsen.[11] 3 g (10.5 mmol) $(-)_D$-phenylethylenediammonium $(+)_D$-tartrate was added to a solution of 0.81 g (19.2 mmol) $LiOH.H_2O$ in 8 ml of hot water. The solution was cooled in an ice bath and 20 ml of ethanol and later 30 ml pyridine were added. After removal of the lithium tartrate by filtration the filtrate was poured into a suspension of 1.5 g (2.54 mmol) *trans*-dichloridotetrapyridinecobalt(III) chloride hexahydrate in 30 ml of pyridine. The mixture was stirred for 20 min at room temperature and then evaporated to dryness. The yellow product was kept evacuated over sulfuric acid for 24 h to remove most pyridine.

Chromatographic separation of diastereoisomers. 7 g of the crude product was dissolved in 500 ml 0.1 M sodium perchlorate at 60–70 °C and approximately 45 ml swollen Sephadex SP-C25 was added under stirring. The slurry of the ion exchange material was placed on top of a column of the same material (35 cm long, 7.5 cm diameter). The column was eluted with 0.2 M sodium perchlorate. A number of red bands moved relatively fast down the column leaving an orange band on the top. This band separated slowly into four bands, in the following denoted A, B, C, D in order of their increasing elution time on the Sephadex. The first two were eluted from the column whereas the latter two bands were separated by removing the Sephadex from the top and placing each coloured fraction on a smaller column. The complex was then liberated from the Sephadex ion exchanger with 1 M hydrochloric acid. The complexes from the various fractions were each concentrated on a weak cation exchange resin (Bio-Rex 70) and eluted with 0.1 M hydrochloric acid. From the eluates the slightly soluble perchlorates were precipitated by addition of a 5 M sodium perchlorate solution. In this way pure samples of the diastereoisomers from band A, C, and D were isolated. Band B was the least intensely coloured band and it was not completely separated from band A. Therefore, the amount of complex in the fraction considered to contain only the compound B was small and not enough was isolated to allow both analysis and characterization of the complex.

Similar chromatographic separations on a smaller scale were used to compare the relative amounts of cobalt(III) complex in each band by absorption spectroscopy. Analysis C, H, N, Cl, Co.

Equilibrium studies

A few experiments were performed in order to establish equilibrium between the diastereoisomers of $[Co((-)_D$-phenen$)_3]^{3+}$. A typical example is: 0.805 g (1.0 mmol) of the diastereoisomer from band C (demonstrated to be Δ-*mer*-$[Co(R$-phenen$)_3](ClO_4)_3.2H_2O$ (*vide infra*), 0.160 g (1.2 mmol) $(-)_D$-phenen and 70 mg charcoal (Norit W) were added to 125 ml of water. The pH was

adjusted to 7.0 by addition of 1 M perchloric acid. Under a slow nitrogen flow the mixture was stirred at 60 °C for 48 h. The charcoal was removed by filtration and the solution was analysed by the above-mentioned chromatographic technique. The amount of complex in each band was measured by absorption and atomic absorption spectroscopy.

RESULTS AND DISCUSSION

Tris{(−)$_D$-1-phenyl-1,2-ethanediamine}cobalt(III) chloride, [Co((−)$_D$-phenen)$_3$]Cl$_3$, has been prepared from *trans*-dichloridotetrapyridincobalt(III) chloride and (−)$_D$-phenen as the (+)$_D$-tartrate in pyridine. The resulting crude material was separated into four diastereoisomers (A, B, C, and D in order of increasing elution time) by ion exchange chromatography on Sephadex SP-C25. The preparative route need not give an isomer distribution close to that determined by the relative stabilities of the isomers. However, it was found that pure samples of isomer C (or A or D) in the presence of the free ligand and activated charcoal could equilibrate at 60 °C during 48 h to the same relative mixture of diastereoisomers. Different independent preparations and equilibrated samples gave the relative amounts A:B:C:D = 0.26:0.05:2.9:1.0. The very small amounts of fraction B present prevented us from isolating enough of this isomer for its characterization. The three isomers A, C, and D have identical or nearly identical absorption spectra in the visible and ultraviolet region. The first spin allowed band has maximum at 468 nm ($\varepsilon = 126$). The second band is only observed as a shoulder due to the rising absorption from the phenyl group (Fig. 1).

The circular dichroism spectra of the diastereoisomers A, C, and D are shown in Fig. 1. The CD spectrum of A consists of a single component under the first absorption band with its maximum approximately coinciding with that of the absorption. This kind of behaviour has often been noticed (see, *e.g.*, Ref. 6) for tris(α,β-diamine)cobalt(III) complexes but only for ob$_3$ complexes. The CD spectra of C and D are also typical, however, for lel$_3$ complexes. The observed signs for the Cotton effects under the first absorption band dictate the absolute configuration of the cations and from the knowledge[12] that the absolute configuration of (−)$_D$-phenen is *R*, it follows that A is Λ-(λλλ)-ob$_3$- and C and D are Δ-(λλλ)-lel$_3$-[Co(*R*-phenen)$_3$]$^{3+}$. The assignment is completed by using the approximate 3:1 ratio found between the isomers A:B and C:D, respectively. This is the ratio expected between *mer*:*fac* geometric isomers. The perchlorate of isomer C was found to be a relatively insoluble material albeit a glass as judged from the absence of lines in the X-ray powder photographs. Isomer D is more insoluble and crystalline. In view of MacDermott's experiences with the corresponding isomer of tris(1,2-propanediamine)cobalt(III) bromide this information was taken as further evidence for the assignment Δ-lel$_3$-*mer*[Co(*R*-phenen)$_3$]$^{3+}$ for band C.

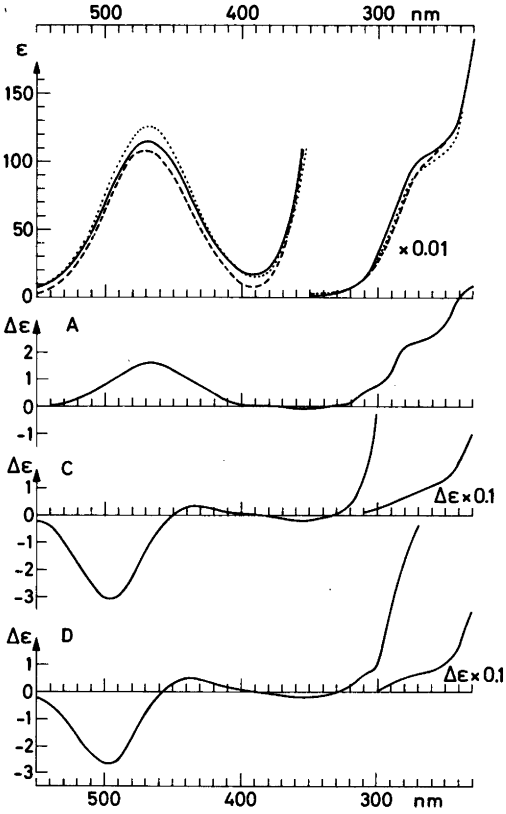

Fig. 1. Absorption spectra of *mer*-Λ-ob$_3$-, ...; *mer*-Δ-lel$_3$, ——; and *fac*-Δ-lel$_3$-[Co((−)$_D$-phenen)$_3$]-(ClO$_4$)$_3$, – – –. A, C, and D are the circular dichroism spectra of the same isomers.

The assignment was finally tested with ^{1}H NMR spectroscopy. Spectra of the *N*-deuterated diastereoisomers as perchlorates in dimethyl sulfoxide-d_6 were recorded at 270 MHz. The spectrum originating from band D was clearly more simple than those of the bands A and C demonstrating the presence of a molecular three-fold axis of symmetry in D but

not in A and C. The coupling constants for the protons of isomer D were determined. The *geminal* and the *trans* coupling constants are both 13 Hz and the remaining *vicinal* coupling constant is 4 Hz. These values show that the phenyl group indeed is an equatorial substituent of the chelate ring as expected and not an axial substituent as has been detected [13] in a Schiff base complex of nickel(II).

Having assigned the structure of each of the found diastereoisomers we can now discuss the question of similarity between two geometric isomers, namely the *fac*- and *mer*-Δ-$[Co(R\text{-phenen})_3]^{3+}$. The circular dichroism spectra shown in Fig. 1 clearly demonstrate a qualitative similarity between the CD of the two isomers. The first CD maximum falls at 497 nm for the *fac* isomer and at 496 nm for the *mer* isomer. However, the intensitives, $\Delta\varepsilon$, are widely different: -2.68 and -3.11, respectively, for the two. The second CD component under the first absorption band (at 435 nm *mer*, and at 433 nm *fac*) is more intense ($\Delta\varepsilon = 0.49$) for the *fac* isomer than for the *mer* isomer ($\Delta\varepsilon = 0.33$) whereas the CD band under the second spin allowed octahedral transition falls at 355 nm for both isomers and the intensities are the same within approx. 10 %. We feel that these findings are important for testing theoretical models for introducing rotatory strengths in $d-d$ transitions. A simple "ligating atom displacement" model seems for example to be unable to explain the observed difference in rotatory strengths while other models may prove more successful.

Acknowledgements. E.L. acknowledges the award of grant No. 511-6670 from the Danish Science Research Council making the purchase of a Dichrographe-IIIS possible.

REFERENCES

1. Iwasaki, H. and Saito, Y. *Bull. Chem. Soc. Jpn. 39* (1966) 92.
2. Dwyer, F. P., Garvan, F. L. and Shulman, A. *J. Am. Chem. Soc. 81* (1959) 290.
3. Legg, J. I. *Chem. Commun.* (1967) 675.
4. MacDermott, T. E. *Chem. Commun.* (1968) 223.
5. MacDermott, T. E. *Inorg. Chim. Acta 2* (1968) 81.
6. Harnung, S. E., Kallesøe, S., Sargeson, A. M. and Schäffer, C. E. *Acta Chem. Scand. A 28* (1974) 385.
7. Kojima, M., Yoshikawa, Y. and Yamasaki, K. *Bull. Chem. Soc. Jpn. 46* (1973) 1687.
8. Lifschitz, I. and Dijkema, K. M. *Proc. K. Ned. Akad. Wet. 43* (1940) 874.
9. Ponzio, G. and Avogadro, L. *Gazz. Chim. Ital. 53* (1922).
10. Reihlen, H., Weinbrenner, E. and von Hessling, O. *Justus Liebigs Ann. Chem. 494* (1932) 143.
11. Michelsen, K. *Acta Chem. Scand. A 28* (1974) 478.
12. Raeymaekers, A. H. M., Roevens, L. F. C. and Janssen, P. A. J. *Tetrahedron Lett.* (1967) 1467.
13. Larsen, E. and Schaumburg, K. *Acta Chem. Scand 25* (1971) 962.

Received February 24, 1978.

Acta Chemica Scandinavica A 32 (1978) 549 – 553

The Crystal Structure of *N*-Salicylidene-L-phenylalaninato-aquacopper(II) Dimer

REIJO HÄMÄLÄINEN, URHO TURPEINEN, MARKKU AHLGRÉN and MARTTI RANTALA

Department of Inorganic Chemistry, University of Helsinki, SF-00100 Helsinki 10, Finland

The Schiff base-type complex *N*-salicylidene-L-phenylalaninatoaquacopper(II) dimer crystallizes in the monoclinic system with $Z = 12$. The space group is $C2$ and the lattice parameters are $a = 22.053(6)$ Å, $b = 12.715(3)$ Å, $c = 16.476(3)$ Å and $\beta = 89.98(2)°$. The compound was studied by single-crystal X-ray diffraction using the counter method and the structure was solved by direct methods combined with Fourier syntheses. Refinement by block-diagonal least-squares technique reduced the R value to 0.090 for 2091 reflections. The compound consists of dimeric units with copper – copper distances of 3.30(1) Å. The asymmetric unit is made up of one and a half dimeric units. The copper atoms are five-coordinated (4 + 1), a tridentate *N*-salicylidene-L-phenylalanine group and a water molecule forming the coordination plane. The Cu – O distances in these planes vary between 1.89 and 1.99 Å and the Cu – N distances between 1.91 and 1.92 Å. The fifth coordination atom, an oxygen atom from an adjacent salicylidene group, lies at the apex of the square pyramid at 2.41 – 2.45 Å from the copper ion. This contact also serves to join the monomeric complexes into dimeric units. The sixth site is taken up by the phenylalanine ring of the adjacent complex, the closest carbon atom lying at a distance of 3.31 – 3.40 Å from the copper atom. The hydrogen bond distances between the dimeric units vary between 2.66 and 3.10 Å.

The syntheses of several copper complexes formed with salicylaldehyde and amino acids have been reported in the literature.[1-2] As part of a series of investigations on metal chelate structures where at least one component is an amino acid,[3-5] we have synthesized and investigated the structure of the Schiff base copper(II) complex formed with salicylaldehyde and L-phenylalanine.

EXPERIMENTAL

Preparation and analyses. The title compound was synthesized according to Laurie[1] by dissolving equimolar quantities of salicylaldehyde (2.12 cm^3) and copper(II) acetate monohydrate (4.0 g) in a mixture of 1 M hydrochloric acid (30 cm^3) and ethanol (30 cm^3). The solution was heated to 50 °C and a stoichiometric amount of L-phenylalanine (Merck AG) dissolved in a minimum volume of the same mixture was added. The pH of the solution was adjusted to 5 by dropwise addition of 0.2 M sodium hydroxide. Microscopic examination of the fine green powder which separated as product, revealed two different crystalline forms. Thus, in addition to the Schiff base complex, one or other of the possible bis complexes seemed to be formed. However, further concentration of the mother liquid gave green prismatic crystals of one kind only. These were of expected composition and suitable for X-ray data collection. To check the composition, copper was analyzed by electrodeposition. The decomposition temperature and density were measured, and the IR-spectrum and thermogravimetric curve were recorded. All results were in agreement with values given in the literature.[1]

Measurements. Preliminary rotation and equi-inclination Weissenberg photographs taken with Ni-filtered Cu$K\alpha$ radiation showed that the crystals belong to the monoclinic system. The cell parameters were calculated by least-squares treatment of the 2θ values of fourteen high order reflections measured on a SYNTEX-$P2_1$ diffractometer using graphite monochromated Mo$K\alpha$ radiation ($\lambda = 0.71069$ Å). Crystal data:

$a = 22.053(6)$ Å	$V = 4620.1$ Å^3
$b = 12.715(3)$	$F.W. = 348.85$
$c = 16.476(3)$	$D_{obs} = 1.52$ g cm^3
$\beta = 89.98(2)°$	$D_{calc} = 1.52$ g cm^3
$Z = 12$	Space group $C2$

The intensities of 4447 reflections were collected by the ω-scan technique with $2\theta_{min} = 5.0°$ and $2\theta_{max} = 50.0°$ and variable scan rate ($2.0 - 15.0°$ min^{-1}). The crystal used in data collection had the approximate dimensions $0.15 \times 0.20 \times 0.40$ mm and it was mounted with the c axis nearly parallel to the spindle axis of the goniometer head. Systematic absences for hkl when $h+k$ odd, $h0l$ when h odd and $0k0$ when k odd indicated $C2$, Cm or $C2/m$[6] as the possible space groups; and since the compound has

Table 1. Fractional atomic coordinates ($\times 10^4$) and thermal parameters[a] ($\times 10^3$) with standard deviations in parentheses.

	x	y	z	U_{11}	U_{22}	U_{33}	U_{12}	U_{13}	U_{23}
CuA	4653(2)	1605(3)	888(2)	37(2)	22(2)	34(2)	−4(2)	−5(1)	1(2)
CuB	5659(2)	4633(3)	2448(2)	31(2)	26(2)	34(2)	−13(2)	−1(1)	−3(2)
CuC	6006(2)	3588(3)	4222(2)	23(2)	30(2)	35(2)	−2(2)	3(1)	−1(2)
O1A	4384(8)	1373(13)	−221(11)	31(10)	7(9)	48(12)	9(8)	−1(9)	1(8)
O2A	4905(8)	1871(17)	2013(11)	24(10)	50(15)	36(11)	−3(10)	−9(8)	−2(10)
O3A	4848(11)	1112(20)	3250(16)	64(17)	52(16)	84(19)	−10(14)	−14(14)	−3(14)
O4A	4676(8)	3154(13)	772(10)	42(11)	3(7)	24(9)	−6(8)	4(8)	−12(7)
O1B	5650(9)	5187(17)	3542(12)	49(13)	44(14)	31(11)	23(11)	−15(9)	13(9)
O2B	5687(8)	4152(16)	1300(11)	28(11)	38(11)	34(11)	2(9)	−15(9)	−15(9)
O3B	6010(11)	4545(18)	97(14)	69(16)	35(12)	62(15)	−9(13)	4(12)	−8(12)
O4B	4902(8)	3846(14)	2548(11)	15(9)	32(11)	42(11)	−30(8)	2(8)	−14(9)
O1C	6274(8)	3325(14)	3148(11)	23(9)	24(11)	49(11)	7(8)	8(8)	17(9)
O2C	5772(8)	3852(14)	5336(10)	40(11)	30(12)	25(9)	34(9)	−3(8)	13(8)
O3C	6150(9)	4107(19)	6578(12)	27(11)	72(15)	42(12)	−38(11)	3(9)	−3(11)
O4C	5236(9)	2830(18)	4100(13)	33(12)	47(14)	56(13)	−6(10)	7(10)	18(12)
NA	4400(10)	263(16)	1287(13)	40(13)	12(12)	36(13)	38(11)	21(11)	25(10)
NB	6184(11)	5700(20)	2039(12)	56(16)	34(13)	11(11)	−16(13)	11(10)	2(11)
NC	6802(10)	3886(17)	4627(13)	28(12)	22(13)	36(13)	−3(10)	1(10)	8(10)

	x	y	z	U		x	y	z	U
C1A	3999(14)	−352(28)	955(19)	43(8)	C1B	6314(13)	6606(26)	2393(17)	34(7)
C2A	3798(13)	−197(24)	117(18)	38(7)	C2B	6138(12)	6838(22)	3253(16)	28(7)
C3A	3352(18)	−900(32)	−185(22)	63(11)	C3B	6296(14)	7867(26)	3525(18)	41(8)
C4A	3196(17)	−869(31)	−1012(22)	54(10)	C4B	6177(14)	8125(25)	4324(18)	36(7)
C5A	3371(15)	−127(29)	−1498(21)	52(9)	C5B	5863(15)	7447(28)	4806(20)	48(8)
C6A	3770(13)	638(24)	−1197(17)	32(7)	C6B	5708(14)	6440(26)	4582(19)	40(8)
C7A	3994(12)	603(21)	−403(16)	23(6)	C7B	5815(15)	6133(26)	3766(20)	44(8)
C8A	4798(11)	1089(20)	2492(15)	21(6)	C8B	6003(12)	4645(24)	835(16)	30(6)
C9A	4579(13)	60(22)	2159(17)	30(7)	C9B	6399(17)	5576(32)	1222(22)	60(10)
C10A	5080(14)	−732(24)	2225(18)	39(7)	C10B	7070(13)	5192(23)	1076(17)	33(7)
C11A	4875(13)	−1896(24)	2045(18)	35(7)	C11B	7524(15)	6003(26)	1309(20)	45(8)
C12A	4869(16)	−2284(30)	1221(21)	54(9)	C12B	7735(16)	6289(28)	2109(21)	57(10)
C13A	4650(25)	−3388(54)	1076(32)	119(18)	C13B	8093(22)	7091(41)	2278(28)	92(14)
C14A	4448(23)	−3937(42)	1748(30)	93(16)	C14B	8382(19)	7655(34)	1587(24)	71(12)
C15A	4500(15)	−3607(27)	2490(19)	49(9)	C15B	8135(18)	7436(34)	799(23)	62(10)
C16A	4685(19)	−2525(36)	2680(24)	73(11)	C16B	7753(14)	6671(29)	709(18)	42(8)
C1C	7343(14)	3596(30)	4303(19)	48(8)	C9C	3160(11)	4207(20)	4535(15)	22(6)
C2C	7353(14)	3220(25)	3413(19)	40(8)	C10C	7023(12)	5412(22)	5515(16)	28(6)
C3C	7935(12)	2933(22)	3149(16)	29(6)	C11C	7655(13)	5700(24)	5382(17)	36(7)
C4C	8003(14)	2565(25)	2290(18)	38(8)	C12C	7846(17)	5848(31)	4616(22)	64(10)
C5C	7480(15)	2522(28)	1836(19)	46(8)	C13C	8439(22)	6086(39)	4429(28)	85(14)
C6C	6903(12)	2724(21)	2125(16)	24(6)	C14C	8865(18)	6097(31)	5074(24)	70(11)
C7C	6800(11)	3085(20)	2897(15)	20(6)	C15C	8660(19)	5867(35)	5795(25)	71(12)
C8C	3782(14)	4044(25)	4173(18)	40(7)	C16C	8070(16)	5686(31)	6031(21)	58(10)

[a] The anisotropic thermal parameters are of the form $\exp[-2\pi^2(h^2a^{*2}U_{11} + \cdots + 2hka^*b^*U_{12} + \cdots)]$.

only one enantiomer the structure determination was based on *C*2. During the data collection, the intensity of one standard reflection was measured every 60 reflections. The intensities were corrected for Lorentz and polarization effects but not for absorption $\{\mu(\text{Mo}K\alpha)=15.1\ \text{cm}^{-1}\}$.

Structure determination. The structure was solved with the MULTAN -74 system[7] and Fourier methods of the X-Ray-76 program system.[8] Atomic coordinates were refined by the block-diagonal least-squares method with isotropic thermal parameters to an *R* value of 0.116 (2091 reflections with $|F_o|>6.25\sigma|F_o|$ were included) and with anisotropic parameters for copper, oxygen and nitrogen atoms to the final value 0.090 ($R=\Sigma\|F_o|-|F_c\|/\Sigma|F_o|$). The weighting scheme used was $w=1/(65.0+|F_o|+0.01|F_o|^2)$ and the average shift/error ratio in the last cycle was 0.24. The positional and thermal parameters are listed in Table 1. The atomic scattering factors were those given by Cromer and Mann.[9] Anomalous dispersion corrections were applied for the copper atom, using the values from International Tables for X-Ray Crystallography given by Cromer and Liberman.[10] Calculations were carried out on a UNIVAC 1108 computer.

A list of the observed and calculated structure factors is obtainable on request from the authors.

STRUCTURE OF THE COMPOUND

The geometry and numbering scheme of one asymmetric unit is shown in Fig. 1. The structure is composed of dimeric units with CuB–CuC and $CuA-CuA_I$ ($I=-x+1,y,-z$) distances of 3.30 Å; the asymmetric unit consists of one and a half dimeric units.

Table 2. Interatomic distances (Å) and angles (°).

The complex unit	A	B	C
The copper(II) environment			
Cu–O1	1.94(2)	1.94(2)	1.89(2)
Cu–O2	1.96(2)	1.99(2)	1.94(2)
Cu–O4	1.98(2)	1.96(2)	1.96(2)
Cu–N	1.91(2)	1.91(2)	1.92(2)
Cu–O1[a]	2.41(2)	2.44(2)[b]	2.45(2)[c]
The salicylaldehyde residue			
O1–C7	1.34(3)	1.31(4)	1.27(3)
N–C1	1.30(4)	1.32(4)	1.36(4)
C1–C2	1.46(4)	1.50(4)	1.54(4)
C2–C3	1.42(5)	1.43(4)	1.40(4)
C2–C7	1.40(4)	1.42(4)	1.50(4)
C3–C4	1.41(5)	1.38(4)	1.49(4)
C4–C5	1.30(5)	1.36(4)	1.38(4)
C5–C6	1.40(5)	1.38(5)	1.38(4)
C6–C7	1.40(4)	1.42(5)	1.37(4)
The phenylalanine residue			
O2–C8	1.29(3)	1.21(3)	1.30(3)
O3–C8	1.25(3)	1.22(3)	1.25(4)
N–C9	1.51(4)	1.44(4)	1.44(3)
C8–C9	1.50(4)	1.60(5)	1.51(4)
C9–C10	1.50(4)	1.58(5)	1.59(4)
C10–C11	1.58(4)	1.49(4)	1.46(4)
C11–C12	1.45(5)	1.44(5)	1.34(5)
C11–C16	1.38(5)	1.40(4)	1.41(5)
C12–C13	1.50(7)	1.30(5)	1.38(6)
C13–C14	1.38(7)	1.44(6)	1.42(6)
C14–C15	1.30(6)	1.48(6)	1.30(6)
C15–C16	1.47(6)	1.32(6)	1.38(6)
The copper(II) environment			
O1–Cu–N	107.8(8)	94.4(9)	94.3(8)
O1–Cu–O2	178.2(8)	176.4(9)	177.3(8)
O1–Cu–O4	93.2(7)	95.6(8)	95.0(8)
O2–Cu–O4	85.0(8)	87.0(8)	87.2(8)
O2–Cu–N	84.9(9)	82.2(9)	83.0(9)
O4–Cu–N	158.2(8)	155.9(9)	157.7(9)
The salicylaldehyde residue			
O1–C7–C2	126(2)	123(3)	122(2)
N–C1–C2	121(3)	122(3)	118(3)
C1–C2–C7	126(3)	125(3)	124(3)
C1–C2–C3	117(3)	115(3)	113(3)
C1–N–C9	118(2)	116(3)	114(2)
C2–C3–C4	120(3)	118(3)	118(3)
C2–C7–C6	119(3)	118(3)	116(2)
C3–C4–C5	123(4)	120(3)	116(3)
C4–C5–C6	118(3)	124(3)	125(3)
C5–C6–C7	122(3)	118(3)	122(3)
The phenylalanine residue			
O2–C8–O3	125(3)	126(3)	123(3)
O2–C8–C9	120(2)	116(3)	118(2)
O3–C8–C9	114(2)	118(3)	119(3)
N–C9–C8	106(2)	106(3)	107(2)
N–C9–C10	112(2)	119(3)	110(2)
C8–C9–C10	109(2)	103(3)	110(2)
C9–C10–C11	114(2)	112(3)	119(2)
C10–C11–C12	120(3)	129(3)	118(3)
C10–C11–C16	119(3)	119(3)	120(3)
C11–C12–C13	118(3)	125(4)	123(4)
C11–C16–C15	118(3)	128(3)	114(3)
C12–C13–C14	117(5)	118(4)	118(4)
C13–C14–C15	124(5)	116(4)	117(4)
C14–C15–C16	122(4)	120(4)	129(4)

[a] Refers to equivalent position $-x+1,y,-z$. [b] The distance CuB–O1C. [c] The distance CuC–O1B.

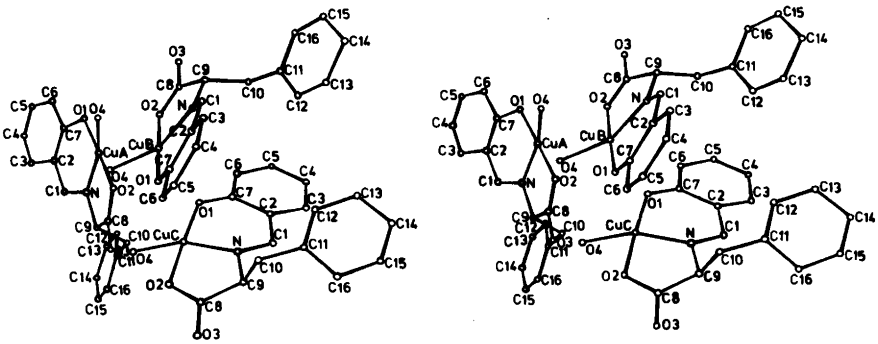

Fig. 1. Stereoscopic view of the asymmetric unit.

Table 3. Deviations (Å) of selected atoms from least-squares planes. Atoms indicated with an asterisk were omitted from the calculations.

		A	B	C
Plane 1	O1	.14	.15	.15
	O2	.16	.18	.17
	O4	−.15	−.16	−.15
	N	−.15	−.17	−.16
	Cu*	.18	.20	.18
	O3*	−.26	−.22	−.30
	C8*	−.05	−.00	−.10
	C9*	−.08	−.09	−.17
Plane 2	O2	−.00	−.01	.00
	O3	−.00	−.01	.00
	C8	.01	.03	−.00
	C9	−.00	−.01	.00
	N*	−.33	−.32	−.27
	Cu*	−.27	−.24	−.27
Plane 3	C2	.03	.02	.03
	C3	−.06	−.02	−.02
	C4	.04	.02	−.01
	C5	.01	−.03	.03
	C6	−.03	.03	−.02
	C7	.01	−.02	−.01
	C1*	.10	.05	.03
	N*	.17	.04	.07
	Cu*	−.22	−.28	−.29
Plane 4	C11	−.01	.03	.02
	C12	.01	.02	−.03
	C13	.02	−.07	.01
	C14	−.05	.07	.02
	C15	.04	−.03	−.03
	C16	−.02	−.03	.01
Angles between planes (°)				
1 and 2		10.9	10.8	12.5
1 and 3		23.8	23.4	24.2
1 and 4		38.6	21.9	24.2

Table 4. Intermolecular distances below 3.10 Å. I = x,y,z II = $-x+1,y,-z$ and III = $-x+1,y,-z+1$.

O2A − $O4B_I$	2.66(3)	O4A − $O2B_{II}$	2.73(3)
O4A − $O2B_I$	2.71(3)	O1A − $O1A_{II}$	2.81(3)
O3A − $O4C_I$	2.73(3)	O4A − $O4A_{II}$	2.92(2)
O1B − $O1C_I$	2.81(3)	O4B − $O3C_{III}$	2.75(2)
O4B − $O4C_I$	2.96(2)	O2C − $O4C_{III}$	2.74(3)
O4A − $O4B_I$	3.10(2)		

The monomeric complexes in the dimeric units are joined together through the coordinated salicylidene oxygen atoms which each in turn occupies the apical position of the square pyramid of the adjacent monomer (Cu − O distance 2.41 − 2.45 Å). The shortest copper − copper distance between the dimeric units is 5.13 Å. There are hydrogen bonds between the coordinated carboxyl oxygen atom O2A and the water oxygen O4B (2.66 Å) and between the uncoordinated carboxyl oxygen atom O3A and the coordinated water oxygen O4C (2.73 Å). Further contacts are found between O4A and O2B (2.71 Å), between O4A and O4B (3.10 Å), and between O4B and O4C (2.96 Å). Contact distances (< 3.10 Å) between asymmetric units, are listed in Table 4.

Each monomeric complex may be described in terms of four approximately planar groups, as was found also in *catena*-μ-(*N*-salicylidene-L-tyrosinato-O,O′)copper(II):[5] the coordination plane, the salicylidene and phenylalanine rings, and the carboxylate group. The angles between the above-mentioned planes in the same complex molecule vary in the range 10.9 − 38.6, 10.8 − 23.4 and 12.5 − 24.2° for complexes A, B and C, respectively. Deviations of selected atoms from least-squares planes and angles between the planes are given in Table 3.

The coordination geometry about the copper atoms is square pyramidal (4+1). The tridentate *N*-salicylidene-L-phenylalanine group occupies three of the square planar coordination sites, with the oxygen atom of the water molecule completing the plane. The fifth coordinated atom, the salicylidene oxygen of the monomeric partner, lies at the apex of the pyramid. The sixth site is taken up by the phenylalanine ring of the adjacent molecule, with the closest carbon atom lying 3.31 – 3.40 Å from the copper ion. The bond lengths and angles around the copper atoms (Table 2) are in fairly good agreement with the values found in *N*-salicylideneglycinatoaquacopper(II) tetrahydrate,[11] *N*-salicylideneglycinatoaquacopper(II) hemihydrate[12] and *catena*-μ-(*N*-salicylidene-L-tyrosinato-*O*,*O*')-copper(II).[5]

All the copper ions are displaced from the square plane towards the apical salicylidene oxygen atom (0.18 – 0.29 Å), which is a common feature of the square pyramid configuration of the copper(II) ion in the crystalline state. The shift of the nitrogen atom from the carboxyl plane, 0.27 – 0.33 Å, agrees with the values found in *N*-salicylideneglycinatoaquacopper(II) hemihydrate[12] and *catena*-μ-(*N*-salicylidene-L-tyrosinato-*O*,*O*')-copper(II).[5]

There are no significant differences in molecular dimensions as found in the three monomers, and the bond lengths and angles are, if standard deviations are taken into account, compatible with values given in the literature for analogous compounds.[5,11]

REFERENCES

1. Laurie, S. H. *Aust. J. Chem. 20* (1967) 2597.
2. Nakao, Y., Sakurai, K.-I. and Nakahara, A. *Bull. Chem. Soc. Jpn. 40* (1967) 1536.
3. Hämäläinen, R., Lajunen, K. and Valkonen, J. *Finn. Chem. Lett. 4 – 5* (1977) 108.
4. Hämäläinen, R. *Finn. Chem. Lett. 4 – 5* (1977) 113.
5. Hämäläinen, R., Ahlgrén, M., Turpeinen, U. and Rantala, M. *Acta Chem. Scand. A 32* (1978) 235.
6. *International Tables for X-Ray Crystallography*, Kynoch Press, Birmingham 1969, Vol. 1.
7. Main, P., Woolfson, M. M., Lessinger, L., Germain, G. and Declercq, J.-P. *MULTAN 74, A System of Computer Programs for the Automatic Solution of Crystal Structures from X-Ray Diffraction Data.*
8. *The X-Ray System, Version of 1976*, Technical Report TR-446, Computer Science Center, University of Maryland, College Park 1976.
9. Cromer, D. T. and Mann, J. B. *Acta Crystallogr. A 24* (1968) 321.
10. Cromer, D. T. and Liberman, D. *J. Chem. Phys. 53* (1970) 1891.
11. Ueki, T., Ashida, T., Sasada, Y. and Kakudo, M. *Acta Crystallogr. B 25* (1969) 328.
12. Ueki, T., Ashida, T., Sasada, Y. and Kakudo, M. *Acta Crystallogr. 22* (1967) 870.

Received January 30, 1978.

Acta Chemica Scandinavica A 32 (1978) 555–557

The Crystal Structure of Silver Ethylenediamine Perchlorate

EVA BANG

Department I, Inorganic Chemistry, H. C. Ørsted Institute, University of Copenhagen, Universitetsparken 5, DK-2100 Copenhagen Ø, Denmark

The crystal structure of $Ag(NH_2CH_2CH_2NH_2)ClO_4$ has been determined from three-dimensional X-ray data, using Mo$K\alpha$ radiation. The crystals are monoclinic, space group $P2_1/c$, $a=8.834(4)$, $b=9.885(2)$, $c=9.893(4)$ Å, $\beta=125.09(2)°$, $Z=4$. The coordination of the silver atom is almost linear (175.8°) with bond distances Ag–N 2.17(1) Å. The complex forms infinite chains with a bridging ethylenediamine between the silver atoms.

Equilibrium studies of aqueous silver(I) and ethylenediamine solutions have led to detection of dimeric species $Ag_2(NH_2CH_2CH_2NH_2)_2^{2+}$ and a ring structure has been suggested.[1] Dimeric silver complexes with ring structures and Ag–Ag distances as short as in the silver metal are found in several crystal structures.[2,3] The structural investigation reported here was suggested by G. Schwarzenbach and led to further investigations of the aqueous system.

EXPERIMENTAL

The crystals of $Ag(NH_2CH_2CH_2NH_2)ClO_4$ were kindly provided by G. Schwarzenbach, Zürich, and were flat needles of rather poor quality. They were assigned to space group $P2_1/c$ through Weissenberg and precession photographs. Intensity data were collected on a Picker FACS-1 diffractometer with graphite-monochromated Mo$K\alpha$ ($\gamma=0.7107$ Å) radiation. The measurements were carried out in the θ-2θ mode. The scan rate was 2° min^{-1}, the scan range 3.6° and increasing with 2θ. The background counts were made for 20 s at each end of the scan range.

From the 5238 reflections measured 1985 independent reflections had $I/\sigma(I)>1.0$. $\sigma(I)$ is the standard deviation of the intensity calculated from counting statistics. 1669 reflections for which $0<\sin\theta/\lambda<0.66$ were used in the final refinement. The crystal size was $0.14\times0.04\times0.33$ mm^3. The large face was (010) with the needle axis as c. During the exposure the crystal changed from almost colourless to completely black, but this did not seem to affect the intensity measurements. The cell dimensions were refined from powder diagrams obtained from a Hägg-Guinier camera using Cu$K\alpha$ radiation ($\lambda=1.5405$ Å) and Si as internal standard.

The X-ray system[4] was used in the crystal structure analyses and the Ortep II[5] for the illustrations.

CRYSTAL DATA

$AgC_2N_2H_8ClO_4$; Monoclinic, $P2_1/c$; $a=8.834(4)$, $b=9.885(2)$, $c=9.893(4)$, $\beta=125.09(2)$, $V=706.85$ Å^3, $D_m=2.40$, $D_x=2.51$ g cm^{-3}, $Z=4$, μ(Mo$K\alpha$)=31 cm^{-1}.

SOLUTION OF THE STRUCTURE

The silver atom was located through the Patterson function. The solution went then straightforward through Fourier methods. No determination of the position of hydrogen atoms has been attempted. The structure was refined isotropically

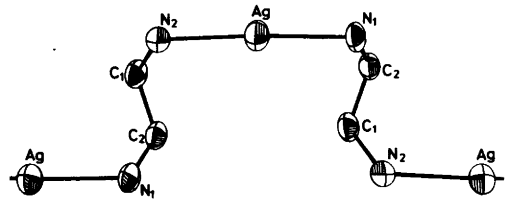

Fig. 1. The Ag complex. Thermal ellipsoids are at 50 % probability.

Table 1. Fractional atomic coordinates ($\times 10^4$), anisotropic thermal parameters ($Å^2 \times 10^2$). The anisotropic temperature factor is of the form $T=\exp[-2\pi^2(U_{11}h^2a^{*2}+\cdots+2U_{12}hka^*b^*+\cdots)]$.

	x	y	z	$U_{11}(U)$	U_{22}	U_{33}	U_{12}	U_{13}	U_{23}
Ag	1929(1)	914(1)	685(1)	5.29(5)	4.64(4)	4.28(4)	−0.50(3)	3.51(4)	−0.40(3)
N1	2073(11)	3990(8)	3569(10)	5.4 (5)	3.8 (4)	3.7 (4)	0.2 (4)	3.2 (4)	0.2 (3)
N2	1923(11)	945(8)	2874(10)	4.8 (4)	4.4 (4)	4.3 (4)	−0.9 (4)	3.7 (4)	−0.6 (4)
C1	3521(13)	1689(10)	4293(11)	4.2 (5)	4.2 (5)	3.7 (5)	0.6 (4)	2.9 (4)	0.6 (4)
C2	3645(14)	3132(10)	3881(12)	4.4 (4)	4.8 (5)	4.5 (5)	−0.3 (4)	3.5 (5)	0.1 (4)
Cl	7821(3)	1905(2)	3975(2)	3.61(10)	3.53(10)	3.17(10)	−0.04(8)	2.50(9)	−0.06(8)
O1	6419(11)	909(9)	3014(10)	5.8 (2)					
O2	9466(12)	1542(9)	4072(10)	6.1 (2)					
O3	8286(11)	3053(8)	628(10)	5.3 (2)					
O4	7146(13)	3191(10)	3240(11)	6.6 (2)					

Table 2. Bond lengths (Å) and selected distances.

Ag−N1	2.171(11)	Cl−O1	1.433(8)
Ag−N2	2.170(11)	Cl−O2	1.445(12)
N1−C2	1.500(16)	Cl−O3	1.440(10)
N2−C1	1.492(11)	Cl−O4	1.414(9)
C1−C2	1.504(15)		
N1−O1	3.198(12)		
N1−O2	3.310(12)		
N1−O3	3.054(9)		
N2−O2	3.069(18)		
N2−O3	3.274(13)		
N2−O3	3.374(11)		
N2−O4	3.217(15)		
Ag−Ag	3.377(1)		

Table 3. Selected angles (°).

N1−Ag−N2	175.8(3)	O1−Cl−O2	109.0(6)
Ag−N1−C2	112.7(6)	O1−Cl−O3	110.3(6)
Ag−N2−C1	113.7(8)	O1−Cl−O4	109.2(5)
N1−C2−C1	112.9(11)	O2−Cl−O3	108.2(5)
N2−C1−C2	112.9(9)	O2−Cl−O4	111.6(7)
		O3−Cl−O4	108.6(6)

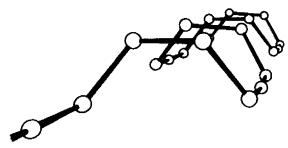

Fig. 2. The chain Ag(en).

until $R=0.11$ and then anisotropically for all atoms apart from oxygen. The final R value was 0.07. Unit weights were used. The atomic parameters are given in Table 1, bond-lengths and angles in Tables 2 and 3. A list of observed and calculated structure factors can be obtained from the author on request.

DESCRIPTION OF THE STRUCTURE

The complex forms infinite chains, Figs. 1 and 2. All Ag−N bonds are very nearly parallel to the c-axis and the almost linear group N−Ag−N is

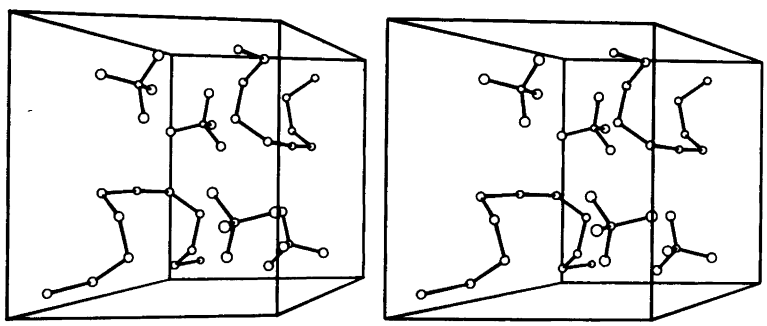

Fig. 3. Stereoscopic view perpendicular to the *ab* plane.

connected to the two neighbouring groups through the glide plane, Fig. 3. The carbon atoms are all on the same side of the chain, Fig. 2. The complex possesses a pseudo symmetry plane through the silver atom perpendicular to the *c*-axis. The chlorine atom in the shortest distance from the silver atom lies almost in this plane. The conformation of the ethylenediamine is reasonable, the torsion angle N–C–C–N being 67(1)°. The Ag–N distances are slightly larger than found in diimidazole silver nitrate,[2,6] 2.12–2.13, and in glycinato silver,[2] 2.11–2.14 Å.

The perchlorate ion is not disordered. For each nitrogen atom there is one short distance to the oxygen atoms, which could indicate hydrogen bonds, 3.05–3.09 Å. The infinite chains and the perchlorate ions form double layers parallel to the *bc* plane. The interactions between these layers are very weak. This is consistent with the easy splitting of the crystal along the *c*-axis.

Solution experiments are in progress in this laboratory to investigate if further polymerization takes place in aqueous solution.

REFERENCES

1. Schwarzenbach, G., Ackermann, H., Maissen, B. and Anderegg, G. *Helv. Chim. Acta 35* (1952) 2337.
2. Acland, C. B. and Freeman, H. C. *Chem. Commun.* (1971) 1016.
3. Baenziger, N. C. and Struss, A. W. *Inorg. Chem. 15* (1976) 1807.
4. Stewart, J. M., Kundell, F. A. and Baldwin, J. C. *The X-Ray System 1972*, Technical Report 92, Computer Science Center, University of Maryland, College Park.
5. Johnson, C. K. *Ortep: A Fortran Ellipsoid Plot Program for Crystal Structure Illustrations*, Report ORNL-3794, Sec. Rev., Oak Ridge National Laboratory, Oak Ridge 1970.
6. Antti, C.-J. and Lundberg, B. *Acta Chem. Scand. 25* (1971) 1758.

Received February 6, 1978.

Acta Chemica Scandinavica A 32 (1978) 559 – 563

Kinetic Isotope Effect and Tunnelling in the Proton-transfer Reaction between 4-Nitrophenylnitromethane and Tetramethylguanidine in Toluene: A Reinvestigation

OTTO ROGNE

Norwegian Defence Research Establishment, Division for Toxicology, N-2007 Kjeller, Norway

The reaction of the deuterated analogue of 4-nitrophenylnitromethane with tetramethylguanidine in toluene shows complex kinetics compared to the corresponding proton-transfer reaction. The complex kinetics can be accounted for by an H – D exchange mechanism. Comparison of experimental data and data calculated from the assumed reaction mechanism suggests a kinetic isotope effect of about 11 at 30 °C which is confirmed in experiments using deuterated tetramethylguanidine. The results are not in agreement with previously reported values and suggest that the isotope effect and degree of tunnelling is much less than previously supposed.

The proton-transfer reaction (1) between 4-nitrophenylnitromethane (4-NPNM) and the strong base tetramethylguanidine [TMG; $HN=C(NMe_2)_2$] has been found exceptionally suitable for studies of the tunnel effect.[1-3]

$$NO_2C_6H_4CH_2NO_2 + B \underset{k_b}{\overset{k_f}{\rightleftharpoons}} NO_2C_6H_4\bar{C}HNO_2\overset{+}{H}B \quad (1)$$

In solvents of low polarity such as toluene and chlorobenzene, large isotopic rate ratios ($k^H/k^D \approx 50$ at 25 °C) are observed. These isotope effects and their temperature vairations are only explainable in terms of tunnelling.

The isotope effect in the reaction of 4-NPNM with TMG in toluene is among the highest so far recorded for a simple proton-transfer in solution, and is generally accepted as some of the most convincing evidence for tunnelling in such reactions.[4,5] It would therefore be of interest to have it confirmed in similar reactions. This has so far proved unsuccessful. Thus, for the reaction of 4-NPNM in toluene with the following bases: tributylamine, triethylamine, quinuclidine,[6] *N,N*-diethyl-n-alkylamidines,[7] 1,5-diazabicyclo[5.4.0]undec-5-ene (DBU),[8] 1,5-diazabicyclo[4.3.0]non-5-ene (DBN)[9] and pentamethylquanidine,[10] the isotope effects are *ca.* 10 – 15.

The large effects observed with TMG as compared to trialkylamines have been attributed to an unusually narrow potential energy barrier due to the sp^2 hybridisation of the basic nitrogen atom.[3] Since no similar effects are observed with any of the last four bases mentioned above, this explanation must be questioned, and the rather special position of TMG among the bases so far studied must be regarded as largely unexplained.

In previous studies[11,12] we have observed that deuteron-transfer reactions of [$^2H_2$]-4-NPNM exhibit complex kinetics as a result of isotopic exchange. Such exchange may give rise to apparent deuteron-transfer rate constants which are too small and hence to erroneously large isotope effects. These complications are particularly pronounced in reactions with bases containing an exchangeable proton on the basic nitrogen atom such as the amidines. In view of the special position of TMG noted above, and of the fact that TMG also has an exchangeable proton on the basic nitrogen atom, the possibility arises that the deuteron-transfer reaction of TMG is affected by exchange and that the original data are in error. We have therefore reinvestigated the reaction of 4-NPNM with TMG in toluene[2] at 30 °C with particular emphasis on the kinetic behaviour of the deuteron-transfer reaction.

EXPERIMENTAL

Materials. 4-Nitrophenylnitromethane was prepared by the method of Cooke and MacBeth;[13] m.p. 90–91 °C (lit. 91 °C), and the deuterated analogue was prepared from this by exchange with sodium methoxide-methan(²H)ol in deuterium oxide.[14] The ^{1}H NMR spectrum of the deuterated acid was identical to that for the proton acid except for the absence of the methylene proton signal.

Tetramethylguanidine (Koch-Light) was dried with potassium hydroxide and fractionally distilled at reduced pressure, b.p. 23 °C/0.4 mmHg. Deuteration was accomplished by shaking a few milliliter in light petroleum with an excess of D_2O. Sufficient NaOD in D_2O was then added to extract the base into the organic phase, and the aqueous phase discarded. This operation was repeated four times. The solution was then cooled in ice and the solvent evaporated under vacuum. These operations yielded deuterated material containing about 98 % D on the imine nitrogen as judged from the ^{1}H NMR spectrum.

Toluene was refluxed over sodium with a Dean-Stark trap and fractionally distilled under dry nitrogen.

Apparatus and procedure. Rate constants were generally determined by following the increase with time of the absorbance at 435 nm, using a Canterbury SF-3A stopped-flow spectrophotometer (Nortech Laboratories Ltd.). The signal from the stopped-flow apparatus was digitalized and read out on a typewriter by an Intertechnique Didac 800 digital data-processing system. All kinetic measurements were made under first-order conditions with the base in excess. First-order rate constants were calculated by fitting 15–20 readings of approximately equally spaced absorbance to the first-order rate equation by the LSKINI programme of DeTar.[15]

Theoretical runs from the H–D exchange mechanism shown in Scheme 1 were calculated as previously described[12] from the variation with time of the concentrations of the four ion pairs I–IV in Scheme 1 by the REMECH programme of DeTar[16] after assigning rate constants to each step and a set of initial concentrations for the acid and the base. Assignment of rate constants to the various steps in Scheme 1 was done as follows. Since the proton-transfer reaction is free from complications, the forward (k_f^H) and backward (k_b^H) rate constants for this reaction are known. These give values for $k_9 = k_f^H$ and $k_5 = k_{10} = k_b^H$. By assuming a value for the isotope effect equal for the forward and backward reaction (*i.e.* equilibrium isotope effect = 1), values for the forward (k_f^D) and backward (k_b^D) deuterium transfer reaction can be calculated. This gives value for $k_1 = k_f^D$. In the half-deuterated species a statistical factor of 2 in assumed so that $k_2 = k_7 = \frac{1}{2}k_b^D$, $k_3 = k_8 = \frac{1}{2}k_b^H$, $k_4 = \frac{1}{2}k_f^H$ and $k_6 = \frac{1}{2}k_f^D$. A secondary isotope effect of 15 % was initially included in the appropriate rate constants; this had, however, only a small effect on the calculated results (3–4 %) and was therefore subsequently omitted.

To prevent H–D exchange with the glass in the reaction with deuterated TMG all glass apparatus was treated with dimethyldichlorosilane followed by a methanol rinse and drying.

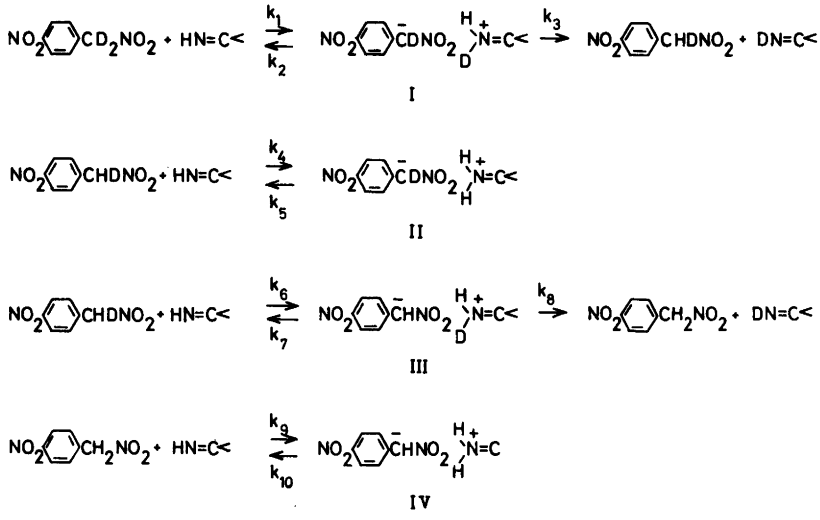

Scheme 1.

RESULTS

The proton-transfer reaction showed good first-order kinetics in runs with the base in excess, and gave rate constants in agreement with published values.[2] This reaction was therefore not studied further.

The deuteron-transfer reaction shows small systematic deviations from first-order kinetics in a manner similar to that observed previously in the reaction of 4-NPNM with alkylamidines.[11,12] The departure from accurate first-order kinetics is not easily detected from the oscilloscopic trace of the reaction, but becames apparent when the data are fitted to the first-order expression by the least-squares program LSKIN1 of De Tar.[15] This program generates a plot of the residuals, ($A_{obs} - A_{calc}$) *vs.* percent of reaction, which is particularly convenient for visual examination of systematic deviations from first-order behaviour.[17] An example is shown in Fig. 1 for the reaction of 4-[$^2H_2$]-NPNM with TMG in toluene at 30 °C with concentrations of acid and base equal to 2×10^{-5} M and 7.83×10^{-3} M, respectively (filled circles). The dashed lines represent about two standard deviations for a normal first-order proton-transfer reaction. If the data conformed to the first-order expression, there should be no trend.

The kinetic behaviour of the deuteron-transfer reaction can be reproduced by the H – D exchange mechanism shown in Scheme 1. Theoretical runs can be calculated from Scheme 1 by the REMECH program of DeTar if the forward, k_f^H, and backward, k_b^H, rate constants for proton-transfer are known, and if a value for the isotope effect is assumed.[12] The open circles in Fig. 1 illustrate data from a calculated run based on published values[2] for $k_f^H = 2544$ mol^{-1} dm^3 s^{-1} and $k_b^H = 19.2$ s^{-1} in toluene at 30 °C, an assumed isotope effect of 11, and the same concentrations of acid and base as in the experimental run. The isotope effect of 11 was found by trial and error to give the best quantitative reproduction of the experimental data. A significantly worse fit was obtained with a variation of ±2 in the assumed isotope effect. In our stopped-flow apparatus about 3 – 15 % of the initial reaction is lost due to the dead-time of the apparatus and the sampling mode of the data-acquisition system. In the experimental run in Fig. 1, 15 % was lost and the theoretical run was therefore adjusted accordingly. Thus the two runs illustrated in Fig. 1 represent the last 85 % of the complete reaction. The assumed isotope effect of 11 corresponds to a value for $k_f^D = 231$ dm^3 mol^{-1} s^{-1}, in contrast to the reported value[2] of 67.3 dm^3 mol^{-1} s^{-1} at 30 °C.

The S-shaped plot of the residuals in Fig. 1 is characteristic for the deuteron-transfer reaction and is independent of the concentration of the reactants. The quantitative deviation from first-order kinetics as measured by the standard deviation of the fit of the data does, however, decrease with increasing base concentration. Thus the standard deviation is reduced by a factor of 2 – 3 for concentrations of base above 0.04 M compared to those below 0.02 M.

Since the data show systematic deviations from first-order kinetics, the apparent first-order rate constant will depend systematically on the extent of reaction covered. It is nevertheless convenient to use the first-order expression,[17] and provided all data refer to the same extent of reaction within a few

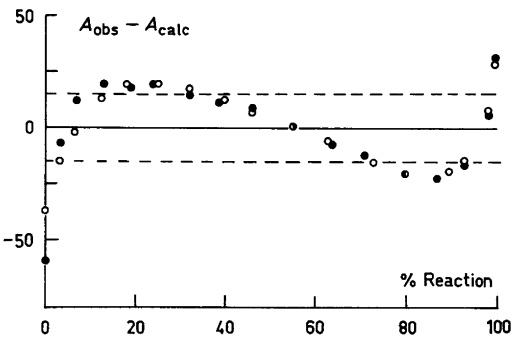

Fig. 1. Plot of residuals against percent reaction for an experimental (filled circles) and a calculated run (open circles). Total change in A is *ca.* 0 – 900.

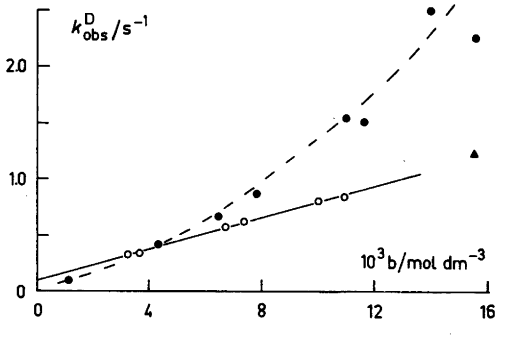

Fig. 2. Plot of k_{obs}^D against base concentration. Filled circles are experimental points and dashed line is calculated from the Scheme with $k^H/k^D = 11$. Open circles are values at 30 °C from Ref. 18.

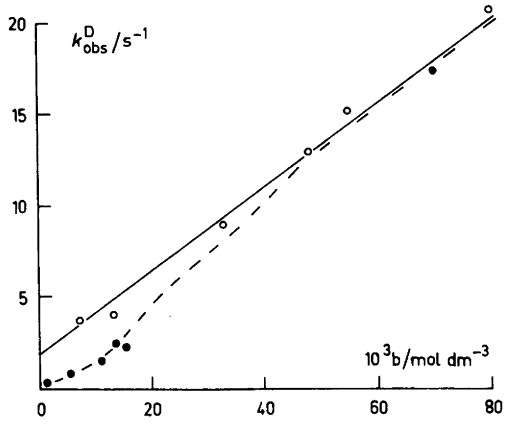

Fig. 3. Plot of k^D_{obs} against base concentration. Filled circles are experimental points using ordinary TMG, open circles are experimental points using deuterated TMG. Full line and dashed line are calculated from eqn. (2) and Scheme 1, respectively.

percent, valid comparisons between observed and calculated rate constants can be made.

Figs. 2 and 3 show experimentally determined apparent first-order rate constants at various base concentrations (filled circles) and calculated values from Scheme 1 based on an assumed isotope effect of 11 (dashed line). The filled triangle in Fig. 2 illustrates the value of the apparent first-order rate constant obtained for the highest base concentration if only the last 30 % of the reaction is used. For comparison, the data[2,18] of Caldin and Mateo at 30 °C are shown in Fig. 2 as open circles. The open circles in Fig. 3 are the experimentally observed first-order rate constants obtained when deuterated TMG ($DN=C(NMe_2)_2$) is used in place of ordinary TMG. A least-squares treatment of these data gives $k^D_f = 244 \pm 8$ mol^{-1} dm^3 s^{-1} and $k^D_b = 1.3 \pm 0.4$ s^{-1}. The straight line in Fig. 3 is calculated from eqn. (2).

$$k^D_{obs} = k^D_b + k^D_f B \qquad (2)$$

which follows from eqn. (1) when the base is in large excess, and with values of $k^D_f = 231$ mol^{-1} dm^{-3} s^{-1} and $k^D_b = 1.74$ s^{-1} as used in Scheme 1 to calculate the dashed line.

Although better first-order kinetics were obtained with deuterated TMG than with ordinary TMG, we find it impossible to get completely satisfactory kinetics in the deuteron-transfer reaction as compared to the proton-transfer reaction. We attribute this to difficulties in maintaining TMG fully deuterated in solution and to the presence of adventitions protons in the solvent.

DISCUSSION

The reaction of 4-NPNM and its deuterated analogue with TMG in toluene has been shown by kinetic data, ^{1}H NMR and absorption spectroscopy to be a reversible proton- or deuteron-transfer giving rise to an ion-pair.[2] The kinetics and spectrophotometric determination of the equilibrium constant for the proton-transfer reaction is consistent with the mechanism in eqn. (1). Similar results have been obtained for the reaction of 4-NPNM with butylamidine[7] and DBU[8] in toluene, and with triethylamine in acetonitrile.[14] No evidence indicates that the deuteron reaction gives other or additional products than the proton reaction.

The kinetic behaviour of the deuteron-transfer reaction between 4-[$^2H_2$]-NPNM and TMG is not consistent with the simple mechanism of eqn. (1). In runs with the base in excess the deuteron-transfer is not first-order in acid (Fig. 1). If the deviations from first-order kinetics are ignored, the reaction is apparently also not first-order in base (Fig. 2), and inconsistent with eqn. (2). The same behaviour was observed in the reaction with alkylamidines and attributed to H−D exchange as shown in Scheme 1.[11,12] The same mechanism can account for the observed kinetics in the present reaction if an isotope effect of 11 at 30 °C is assumed, as shown by the good agreement between calculated and observed data in Figs. 1, 2 and 3. The fact that improved first-order kinetics as well as a linear relation between k_{obs} and base concentration are obtained with deuterated TMG is consistent with the proposed mechanism. In this case no exchange can occur and Scheme 1 reduces to eqn. (1) where the observed first-order rate constant is related to the forward and backward rate constants and base concentration through eqn. (2). Fig. 3 shows that the observed first-order rate constants obtained with deuterated TMG agree with the line calculated from eqn. (2) with the same values of k^D_f and k^D_b as were used in Scheme 1 to reproduce the experimental data obtained with ordinary TMG. It is evident from Fig. 3 that the discrepancy between the observed value for k^D_{obs} and the value expected if the mechanism was that of eqn. (1) decreases as

the base concentration increases. Thus at base concentrations above 0.05 M almost the same value for k_{obs}^{D} is calculated either from Scheme 1, or from eqn. (2), as obtained experimentally using either TMG or deuterated TMG. This is consistent with the assumed H−D exchange mechanism since as the base concentration increases the relative importance of the back reaction will decrease and the observed rate will be dominated by the k_1 or k_f step in Scheme 1 and eqn. (1), respectively. Unfortunately the most convenient base concentrations for the present type of studies are usually below 0.01 − 0.02 M, and thus fall in the range where the back reaction, and hence exchange, become important.

In the previous study of the present reaction[2] it was found that the plots of k_{obs}^{D} *vs.* base concentration had intercepts close to zero, and that k_b^D could therefore not be obtained reliably. An example, with data at 30 °C from the original thesis,[18] is shown in Fig. 2 where $k_f^D = 67.3 \pm 2.3$ dm^3 mol^{-1} s^{-1} and $k_b^D = 0.11 \pm 0.02$ s^{-1}. We believe that the small intercepts and k_b^D values are misleading and a consequence of H−D exchange by the mechanism in Scheme 1. The small k_b^D value at 30 °C is inconsistent with the value estimated from $k_b^D = k_f^D/K^D$. At 30 °C $K^D = 120 \pm 50$ dm^3 mol^{-1} and hence $k_b^D = 0.56 \pm 0.23$ s^{-1}. Alternatively, since the isotope effect on the equilibrium constant is small,[2] $K^H = 125 \pm 4$ dm^3 mol^{-1} may be used in place of K^D, in which case $k_b^D = 0.54 \pm 0.02$ s^{-1}. Such a value for k_b^D is not in agreement with the intercept of the straight line in Fig. 2. Thus the original data are either internally inconsistent, or there is a large inverse equilibrium isotope effect ($K^H/K^D = 0.19$). The latter is unreasonable and contrary to the statement that the equilibrium isotope effect is small. A similar estimate of k_b^D as above with $k_f^D = 231$ dm^3 mol^{-1} s^{-1}, *i.e.* corresponding to an isotope effect of 11, gives $k_b^D = 1.8$ s^{-1}, in reasonable agreement with the intercept of 1.3 in the k_{obs}^{D} *vs.* base plot for the reaction with deuterated TMG (Fig. 3).

The present results show that the deuteron-transfer rate constants for the reaction of TMG with 4-NPNM in toluene are considerably larger, and hence the isotope effects smaller, than previously suggested.[2] Thus the degree of tunnelling will also be less than supposed. At 30 °C the results indicate an isotope effect of about 11, a value about the same as that observed in other reactions of 4-NPNM in toluene.[6-10]

It is to be expected that the complications due to H−D exchange will diminish with increasing polarity of the solvent. As the solvent polarity increases the ion-pair will be increasingly better stabilized and the importance of the back reaction, and exchange, will be reduced. Thus it seems likely that the isotope effects of about 30 − 50 reported[2] for the present reaction in cyclohexene, mesitylene, dibutyl ether and chlorobenzene in addition to toluene, are also affected by scrambling. On the other hand, the results in the more polar solvent acetonitrile, dichloromethane and tetrahydrofuran, where k^H/k^D is *ca.* 11 − 13, are probably much more reliable.

Acknowledgements. The author is indebted to Professor E. F. Caldin for copies of data from Ref. 18, to J. H. Blanch for valuable discussions and help with the computer programs, and to Mrs. I Heggen for experimental assistance.

REFERENCES

1. Caldin, E. F. and Mateo, S. *Chem. Commun.* (1973) 854.
2. Caldin, E. F. and Mateo, S. *J. Chem. Soc. Faraday Trans. 1, 71* (1975) 1876.
3. Caldin, E. F. and Wilson, C. J. *Discuss. Faraday Soc. 10* (1975) 121.
4. Bell, R. P. *Chem. Soc. Rev. 3* (1974) 513.
5. Lewis, E. S. In Caldin, E. F. and Gold, V., Eds., *Proton-Transfer Reactions*, Chapman & Hall, London 1975, p. 317.
6. Caldin, E. F. and Mateo, S. *J. Chem. Soc. Faraday Trans. 1, 72* (1976) 112.
7. Caldin, E. F., Rogne, O. and Wilson, C. J. *J. Chem. Soc. Faraday Trans. 1, 74* (1978) 1796.
8. Caldin, E. F. and Rogne, O. *J. Chem. Soc. Faraday Trans. 1, 74* (1978) 2065.
9. Caldin, E. F., Kaehler, H. C. and Rogne, O. *Unpublished results.*
10. Heggen, I., Lindstrøm, J. and Rogne, O. *J. Chem. Soc. Faraday Trans. 1, 74* (1978) 1263.
11. Rogne, O. *Chem. Commun.* (1977) 695.
12. Blanch, J. H. and Rogne, O. *J. Chem. Soc. Faraday Trans. 1, 74* (1978) 1254.
13. Cooke, R. G. and McBeth, A. K. *J. Chem. Soc.* (1938) 1024.
14. Caldin, E. F., Jarcsewski, A. and Leffek, K. T. *Trans. Faraday Soc. 67* (1971) 110.
15. DeTar, D. F. In DeTar, D. F., Ed., *Computer Programs for Chemistry*, Benjamin, New York 1968, Vol. I, p. 126.
16. Ref. 15, Vol. II, p. 16.
17. DeTar, D. F. and Day, V. M. *J. Phys. Chem. 70* (1966) 495.
18. Mateo, S. *Ph. D. Thesis* (1974), University of Kent.

Received March 8, 1978.

Acta Chemica Scandinavica A 32 (1978) 565–570

The Synthesis and Vibrational Spectra of Some Dihalides of Divalent Tellurium

P. KLÆBOE,[a] C. J. NIELSEN,[a] R. SUCHI[a] and O. VIKANE[b]

[a] Department of Chemistry, University of Oslo, Oslo 3, Norway and [b] Department of Chemistry, University of Tromsø, N-9001 Tromsø, Norway

Salts containing $[ArTeXY]^-$ X = I, Br; Y = I, Br, Cl were synthesized and preliminary X-ray crystallographic data are reported. The infrared and Raman spectra of six salts containing the $[ArTeXY]^-$ ion were recorded below 400 cm^{-1}, and compared with spectra of the cations. From these data the three fundamentals connected with the approximately linear X–Te–Y linkage (two stretches and a bending mode) were tentatively assigned. Simple force fields were derived for the anions which reproduced the wave numbers of the observed fundamentals satisfactorily.

Aryltellurenylhalides and pseudohalides, ArTeX (X = uninegative ion), are known to be relatively unstable. The first members of this class to be prepared were *p*-methoxyphenyltellurenyl methanethiosulfonate and *p*-methoxyphenyltellurenyl benzenethiosulfonate.[1] For several years the only known tellurenyl halide was 2-naphthyltellurenyl iodide.[2] Recently several aryltellurenyl bromides and iodides, comprising C_6H_5TeBr, C_6H_5TeI, 4-$(CH_3O)C_6H_4TeI$, 4-$(C_6H_5)C_6H_4TeBr$, 4-(C_6H_5)-C_6H_4TeI, and 3,4-$(CH_3)_2C_6H_3TeI$, were reported.[3]

We have recently published the synthesis[4] and infrared and Raman spectra[5] of tetramethylammonium phenyldithio- and phenyldiselenocyanatotellurate(II), and in a recent paper Petragnani *et al.* report the synthesis and Raman spectra of several tetraorganylphosphonium dihaloaryltellurates(II). However, attempts to prepare methyltriphenylphosphonium diiodophenyl- and bromoiodophenyltellurate(II) were reported to be unsuccessful.[6]

In the present paper we investigate the syntheses, crystal data and the infrared and Raman spectra of six salts containing the dihaloaryltellurate(II) ion. The anions in the present compounds are: diiodophenyltellurate(II), $C_6H_5TeI_2^-$, bromoiodophenyltellurate(II), $C_6H_5TeBrI^-$, dibromophenyltellurate(II), $C_6H_5TeBr_2^-$, bromochlorophenyltellurate(II), $C_6H_5TeBrCl^-$, together with 4-$(C_2H_5O)C_6H_4TeI_2^-$, and 4-$(C_2H_5O)C_6H_4TeBrI^-$.

From the known stability of phenyltellurenylbromide and iodide, at least in aprotic solvents,[3] the most plausible reaction path to the isolated products is:

$$C_6H_5TeTeC_6H_5 + X_2 = 2C_6H_5TeX \quad (1)$$

$$C_6H_5TeX + (C_6H_5)_4AsY = [(C_6H_5)_4As][C_6H_5TeXY] \quad (2)$$

Here X_2 is bromine or iodine, and Y is chloride, bromide, or iodide. Due to the large cation used, the compounds crystallized readily from acetonitrile. Attempts to prepare the compounds in protic solvents like methanol were not successfull.

EXPERIMENTAL

Diphenylditelluride was prepared as described by Haller and Irgolic.[7] Space groups and unit cell dimensions were determined from single-crystal oscillation and Weissenberg photographs, using Cu$K\alpha$ radiation. The unit cell dimensions are believed to be accurate to within 0.5 %. Densities were determined by flotation. Melting points are uncorrected.

Tetraphenylarsonium diiodophenyltellurate(II), $[(C_6H_5)_4As][C_6H_5TeI_2]$ (Number I, Table 1). To a solution of 1.25 mmol (0.5 g) of diphenylditelluride in 30 ml warm acetonitrile was added, under

Table 1. Numbering and formula of the tellurium(II) compounds studied as well as certain reference substances.

Number	
I	$[(C_6H_5)_4As](C_6H_5TeII)$
II	$[(C_6H_5)_4As](C_6H_5TeIBr)$
III	$[(C_6H_5)_4As](C_6H_5TeBrBr)$
IV	$[(C_6H_5)_4As](C_6H_5TeBrCl)$
V	$[(C_6H_5)_3PCH_3](C_2H_5OC_6H_4TeII)$
VI	$[(C_6H_5)_3PCH_3](C_2H_5OC_6H_4TeIBr)$
VII	$[(C_6H_5)_4As]Cl$
VIII	$[(C_6H_5)_4As]Br$
IX	$[(C_6H_5)_4As]I$
X	$[(C_6H_5)_3PCH_3]Br$
XI	$[(C_6H_5)_3PCH_3]I$

vigorous stirring, 1.25 mmol (0.32 g) of iodine dissolved in 15 ml acetonitrile. To the clear, dark red solution was added 2.5 mmol (1.28 g) of tetraphenylarsonium iodide dissolved in 30 ml acetonitrile. After filtering, the volume of the solution was reduced to 20 ml in vacuum. The clear dark red solution was placed in a refrigerator overnight. Yield 1.86 g (88 %). M.p. 174–176 °C. Anal. $C_{30}H_{25}AsI_2Te$: C, H, As, I, Te. The crystals form red monoclinic prisms, extended along the $a-c$ diagonal, with $a=9.94$ Å, $b=23.12$ Å, $c=13.59$ Å, $\beta=108.4°$. There are four formula units per unit cell, density, calc. 1.89, found 1.88 g/cm^3. The space group, from systematic absences is $P2_1/n$ (No. 14).

Tetraphenylarsonium bromoiodophenyltellurate-(II), $[(C_6H_5)_4As][C_6H_5TeBrI]$ (Number II, Table 1), was prepared in the same way as compound I, starting with 1.25 mmol (0.5 g) of diphenylditelluride, 1.25 mmol (0.2 g) of bromine, and 2.5 mmol (1.28 g) of tetraphenylarsonium iodide. The compound crystallized from 20 ml of acetonitrile. Yield 86 %. M.p. 168–170 °C. Anal. $C_{30}H_{25}AsBrITe$: C, H, As, Br, I, Te.

The crystals are isomorphous with those of the diiodo analogue, and show the same colour and morphology. The unit cell dimensions are: $a=9.89$ Å, $b=23.09$ Å, $c=13.48$ Å, $\beta=108.5°$, and density calc. 1.81, found 1.82 g/cm^3.

Tetraphenylarsonium dibromophenyltellurate(II), $[(C_6H_5)_4As][C_6H_5TeBr_2]$, (Number III, Table 1), was prepared in the same way as the diiodo analogue, I, starting with 1.34 mmol (0.55 g) of diphenylditelluride, 1.25 mmol (0.2 g) of bromine, and 2.72 mmol (1.26 g) of tetraphenylarsonium bromide. The compound crystallized from 15 ml of acetonitrile. Yield 1.6 g (85 %) based on the amount of bromine added. M.p. 158–160 °C. Anal. $C_{30}H_{25}AsBr_2Te$: C, H, As, Br, Te.

The crystals are orange red triclinic plates with $a=13.14$ Å, $b=13.79$ Å, $c=19.22$ Å, $\alpha=110.2°$, $\beta=110.1°$, $\gamma=61.5°$. The density, calc, for four formula units per unit cell is 1.77, found 1.77 g/cm^3.

Tetraphenylarsonium bromochlorophenyltellurate-(II), $[(C_6H_5)_4As][C_6H_5TeBrCl]$, (Number IV, Table 1), was prepared in the same way as the dibromo analogue, III, starting with 1.34 mmol (0.55 g) of diphenylditelluride, 1.25 mmol (0.2 g) of bromine, and 2.27 mmol (1.13 g) of tetraphenylarsonium chloride. The compound crystallized from 10 ml of acetonitrile. Yield 1.4 g (80 %) based on the amount of bromine added. M.p. 138–140 °C. Anal. $C_{30}H_{25}AsBrClTe$: C, H, As, Br, Cl, Te. The crystals are isomorphous with those of the dibromo analogue, and show the same colour and morphology. The unit cell dimensions are: $a=13.08$ Å,

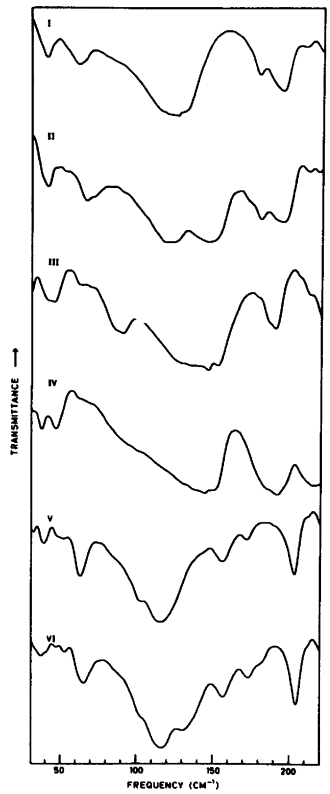

Fig. 1. Far infrared transmission spectra in the region 30–220 cm^{-1} of compounds I–VI as polyethylene pellets, concentrations *ca.* 30 mg of I–IV and *ca.* 18 mg of V and VI, resolution 4 cm^{-1}, beamsplitter 12 μm mylar, 30 scans.

Table 2. The far infrared (IR) and Raman (R) spectral data for tetraphenylarsonium salts of dihalophenyltellurium(II)

I[a] I, I[b] IR	R	II[a] I, Br[b] IR	R	III[a] Br, Br[b] IR	R	IV[a] Br, Cl[b] IR	R	Interpretation
359 s[c]		356 s		361 s		362 s		*[d]
350 s		351 s		352 s		352 s		*
				346 s		345 s		
260 w	259 w	260 w	262 w		266 w		266 m	*
							259 m	
244 vw				240 w	240 m		239 s	*
	236 w		237 w					
227 vw	229 w	228 w	229 vw	228 m	228 m	232 w	230 m	*
193 m		189 w		190 m		217 m	218 w	
179 w		180 w				212 w	213 m	
127 m }		144 s	146 w	138 s		188 s		ν_a(X–Te–Y).
120 s }								
	110 vs	121 s	120 m	151 w	150 vs	148 m	150 vs	ν_s(X–Te–Y).
						138 m		
	86 vw							
			112 s		111 w,br			
	92 vw							
	76 w,br		75 w,br					
61 m		70 w		89 m	92 vw	98 w	105 m,br	δ(X–Te–Y).
					75 m		78 w,br	
							58 w	
56 vw		66 m		45 vw		46 w		
40 w		40 w		37 vw		38 w		*

[a] Roman numerals refer to compounds listed in Table 1. [b] Substituents (X–Te–Y) in approximately linear arrangement. [c] Abbreviations: s, strong; m, medium; w, weak; v, very; br, broad. [d] Asterisks indicate bands attributed to the cation.

$b=13.71$ Å, $c=19.18$ Å, $\alpha=110.3°$, $\beta=110.0°$, $\gamma=61.5°$. Density, calc. 1.69, found 1.68 g/cm^3.

Triphenylmethylphosphonium diiodo-*para*-ethoxyphenyltellurate(II) (Number V, Table 1) and triphenylmethylphosphonium bromoiodo-*para*-ethoxyphenyltellurate(II) (Number IV, Table 1), were prepared as reported previously.[6]

Spectral. The far IR spectra of the samples I–VI as well as of the cations VII–XI were recorded with an evacuable fast scan Fourier transform interferometer (Model 114 c) from Bruker. The interferometer was connected to a Nicolet 1180 computer and an interactive disc system. Beamsplitters of mylar of thicknesses 3.5, 6, 12 and 23 μm were employed and most of the spectra were recorded with resolution 4.0 cm^{-1}, using *ca.* 30 scans. Pellets were pressed, containing *ca.* 15 mg and 30 mg of the salts mixed with 200 mg polyethylene (Rigidex).

A Cary model 81 Raman spectrometer equipped with a Spectra Physics model 125 A helium-neon laser and a Coherent Radiation Laboratory model 52 G argon ion laser were employed for the Raman recordings. Because of the yellow-brownish colour of the salts, spectra excited with the 6328 Å helium-neon laser were superior to those excited with the argon ion laser. The samples were illuminated in the 180° mode with *ca.* 50 mw of laser energy on the sample.

RESULTS AND DISCUSSION

The observed infrared curves in the region 30 to 220 cm^{-1} obtained with a 12 μm beam splitter of the compounds I–VI are shown in Fig. 1. The wave numbers of the IR and Raman bands of the tetra-phenyl arsonium salts (I–IV) and the triphenylmethylphosphonium salts (V and VI) are listed in Tables 2 and 3, respectively. For comparison, the bands of the reference compounds containing the appropriate cations are listed in Table 4.

Table 3. The far infrared (IR) and Raman (R) spectral data for triphenyl methyl phosphonium salts of paramethoxyphenyltellurium(II).

V II IR	R	VI I Br IR	R	Interpretation
362 m[a]		362 w		*[b]
316 m		318 m		*
	229 w		228 w	*
203 s		204 s		*
172 vw		173 vw		*
156 w		156 w		*
114 vs	119 m	128 m	126 w	ν_a(X−Te−Y)
103 m	100 m	114 vs	120 m	ν_s(X−Te−Y)
	93 vw		103 m	
	76 m		76 m	
63 m		65 m		δ(X−Te−Y)
41 vw		49 w		

[a] Abbreviations, see Table 1. [b] Attributed to the cation.

While divalent tellurium generally forms four-coordinated complexes, it is well known that when a phenyl group is one of the ligands, the position *trans* to the phenyl group is vacant, making the compounds three-coordinated. Extensive X-ray crystallographic studies of three-coordinated tellurium (II) compounds revealed that the molecules have a T-shaped geometry. Crystallographic work including compounds I and II demonstrate a nearly linear arrangement of the X−Te−Y group.[8] The results are in complete agreement with earlier work on phenyltellurium(II) complexes with halides and thiourea or selenourea as ligands. In all these compounds the deviation form linearity of the X−Te−Y groups is less than 8° and the Te−C bond nearly bisects the angle of the three-centre system.[9-14]

The vibrational modes of the X−Te−Y group can as a first approximation be separated from those of the rest of the molecule. This can be done with some confidence regarding the two X−Te−Y stretching vibrations which should be fairly independent of the bisecting phenyl group and appear as very intense bands. Much more uncertain are attempts to assign an "X−Te−Y bending mode". It is quite likely that the "linear, isolated molecule approximation" breaks down, giving rise to two bending vibrations. One of these is in the X−Te(C)−Y plane and is mixed with C−Te stretch. We have only concerned ourselves with the other bending mode which is perpendicular to this plane and of quite low frequency.

In the "linear, isolated molecule approximation" the compounds I, III and V should have $D_{\infty h}$ symmetry, giving rise to one Raman active (Σ_g^+)

Table 4. The far infrared (IR) and Raman (R) spectral data for tetraphenylarsonium halides (VII−IX) and triphenylmethylphosphonium halides (X, XI).

VII I IR	R	VIII Br IR	R	IX Cl IR	R	X I IR	R	XI Br IR	R
366 s[a]		365 s		364 s					
350 s			350 s		351 s				
				341 s					
	283 m		283 m		283 m			285 vw	
	272 m				265 m	261 w	260 vs	267 vw	267 m
249 w	248 s				246 s	256 m	255 vs	257 s	
	235 s	237 s	239 s	238 m	238 w	242 s	241 s	241 s	
223 s	222 vw			231 w	229 m			188 m	188 w
181 s		187 s	186 w	189 s	192 vw	168 s	167 m	166 m	167 w
	119 w		111 m		111 m		111 w		117 w
	105 m	105 w					89 w		96 w
				95 s	93 m			76 s	70 s
			83 w	85 vs	83 w	63 s	65 m		
76 s	77 s	76 m	75 m						
					56 m	46 s		53 s	

[a] Abbreviations, see Table 1.

and two IR active (Σ_u^+ and π_u) fundamentals. The less symmetric compounds II, IV and VI, however, should have $C_{\infty v}$ symmetry, with all the three fundamentals (Σ^+, Σ^+ and π) active in Raman and IR. Because of the pseudosymmetry of the three latter molecules we would expect the symmetric stretching mode to be intense in Raman, while the asymmetric mode should be intense in IR.

The asymmetric ν_a(X–Te–Y) and symmetric ν_s(X–Te–Y) stretching modes can be assigned with reasonably good confidence from the experimental data. For I, II and IV the ν_a was supposedly at higher wave numbers than ν_s, while the opposite was true for compound III. Comparison between Tables 1 and 3, reveals that most of the IR and Raman bands not assigned to the X–Te–Y group can be attributed to cation vibrations. Our assignment of the bending mode δ(X–Te–Y) (because of the presence of the Te–C bond to the phenyl group) should be considered very tentative.

In Table 2 the corresponding assignments are listed for compounds V and VI. They differ somewhat from those reported by Petragnani *et al.*[6] which were based upon Raman spectra only. Our results for compounds I–IV reveal without doubt that the far IR data are essential for assigning ν_a(X–Te–Y) in the symmetric (I and III) as well as in the asymmetric (II and IV) compounds. As apparent from Table 3 a very strong IR band at 114 cm^{-1} is observed for V as well as for VI and is attributed as ν_s and ν_a, respectively. We might state very approximately that the "C–I and C–Br stretching modes" are observed at 120 cm^{-1} (114 cm^{-1} in IR) and 128 cm^{-1} (126 cm^{-1} in Raman), respectively in compound IV. The two stretching modes ν_s and ν_a for V and VI were at somewhat lower wave numbers than for the corresponding I and II, indicating weaker bonds in the former molecules.

Force constant calculations. As was done in our earlier spectroscopic study of three-coordinated tellurium(II) compounds,[5] force fields were derived for the present molecules. These calculations are very simple for the "linear isolated molecule approximation". In the quadratic force field, two stretching constants k_1 and k_2 and an interaction term k_{12} are sufficient to calculate the two stretching frequencies ν_a and ν_s. One bending constant k_α is sufficient to calculate the bending frequency δ(X–Te–Y).

Using the bond distances Te–I = 2.95, Te–Br = 2.87 and Te–Cl = 2.70 Å, preliminary values of $k_{Te-I}=k_{Te-Br}=k_{Te-I}=0.8$ mdyn/Å and $k_{12}=0.3$ mdyn/Å were employed. With the aid of an iteration procedure the three k_{Te-X} force constants were allowed to vary while the specific interaction term k_{12} was assumed to be common for all the molecules. The results are listed in Table 5, and as is apparent the agreement between the 8 observed stretching frequencies of compounds I–IV and the calculated values are satisfactory, employing the following four independent parameters: $k_{Te-I}=0.66$, $k_{Te-Br}=0.73$, $k_{Te-Cl}=0.64$ and k_{12} (Te–X/Te–Y) = 0.29 mdyn/Å. Since the assigned fundamentals for compounds V and VI were systematically lower than for I–IV (of different chemical surroundings) they were not included in the calculations. The following values for the bending force constant k_α were calculated: $k_{I-Te-I}=0.40$, $k_{I-Te-Br}=0.47$, $k_{Br-Te-Br}=0.68$, $k_{Br-Te-Cl}=0.60$ mdyn Å/rad^2.

Table 5. Observed and calculated vibrational fundamentals of the X–Te–Y group.

Compound	Linkage	ν_a		ν_s		δ
		obs	calc	obs	calc	obs[a]
I	I–Te–I	120	121	110	113	61
II	I–Te–Br	144	145	120	118	70
III	Br–Te–Br	138	144	150	147	89
IV	Br–Te–Cl	188	191	150	143	98
V[b]	I–Te–I	114	–	100	–	63
VI[b]	I–Te–Br	128	–	120	–	65

[a] The bending force constants k_α were adjusted to make the observed and calculated frequencies equal. [b] Not included in the least squares fit because of different chemical surroundings.

It was attempted to calculate the splittings of the X–Te–Y bending modes by introducing the third ligand, the phenyl group, as a point mass. Using the same k_α for the "in plane" and "out of plane" bending and $k_{C-Te}=2.2$ mdyn/Å a splitting of the bending modes of only a few wavenumbers were calculated.

Acknowledgement. The Fourier transform spectrometer was partly finance by a grant from NAVF. R.S. acknowledges a fellowship sponsored by IAESTE.

REFERENCES

1. Foss, O. *Acta Chem. Scand.* 6 (1952) 306.
2. Vicentini, G., Giesbrecht, E. and Pitombo, L. *Chem. Ber.* 92 (1959) 40.

3. Schulz, P. and Klar, G. *Z. Naturforsch. Teil B 30* (1975) 40.
4. Hauge, S. and Vikane, O. *Acta Chem. Scand. 27* (1973) 3596.
5. Klæboe, P. and Vikane, O. *Acta Chem. Scand. A 31* (1977) 120.
6. Petragnani, N., Torres, L., Wynne, K. J. and Williams, D. J. *J. Organometal. Chem. 76* (1974) 241.
7. Haller, W. S. and Irgolic, K. J. *J. Organometal. Chem. 38* (1972) 97.
8. Vikane, O. *To be published.*
9. Hauge, S. and Vikane, O. *Acta Chem. Scand. A 29* (1975) 755.
10. Vikane, O. *Acta Chem. Scand. A 29* (1975) 738.
11. Vikane, O. *Acta Chem. Scand. A 29* (1975) 763.
12. Vikane, O. *Acta Chem. Scand. A 29* (1975) 787.
13. Foss, O. and Marøy, K. *Acta Chem. Scand. 20* (1966) 123.
14. Foss, O. and Husebye, S. *Acta Chem. Scand. 20* (1966) 132.

Received March 16, 1978.

Acta Chemica Scandinavica A 32 (1978) 571 – 594

The Adjusted Screened Potential/Excluded Volume (ASPEV) Theory of Strong Electrolytes in Solution

TORBEN SMITH SØRENSEN

Fysisk-Kemisk Institut, Technical University of Denmark, DK-2800 Lyngby, Denmark

By analogy with the virial expansion of the equation of state of real gases a Debye-Hückel/Excluded Volume (DHEV) theory is proposed for electrolyte solutions. The second virial coefficients are interpreted as excluded volume between anion and cation using the principle of specific interaction of ions of Brønsted. The calculated ionic radii for many 1 – 1, 2 – 1 and 1 – 2 electrolytes follow a clear-cut pattern, but the radii are too large.

This is explained to be due to the screening effect of counterions which lowers the interaction energy between ions and lowers the contribution to the term in the expression for the activity coefficients proportional to the square root of ionic strength. A statistical-mechanical theory of screened potential is evaluated. The theory yields a semi-quantitative explanation of the effect of screening.

A semi-empirical Adjusted Screened Potential/ Excluded Volume (ASPEV) theory is proposed giving an excellent fit for the mean ionic molar activity coefficients $f_\pm$ for all combinations of H, Li, Na, K, Rb, Cs and Cl, Br, I in water at 25 °C up to concentrations around 3 – 5 mol/dm^3. In the formula there is only one adjustable parameter – the excluded volume – from which one calculates cationic radii well in accordance with radii derived from ionic conductivties at infinite dilution.

The Debye and Hückel theory of strong electrolytes proposed in 1923[1] has had such far-reaching influence on the later development of electrochemistry that it has to a certain degree overshadowed the many subsequent efforts to rationalise the theory or to extend its applicability to higher electrolyte concentrations. The ionic strength has to stay below 0.001 mol/dm^3 for the Debye-Hückel limiting law of electrolytes to be valid. This corresponds to such high dilution that one should properly speak about "slightly polluted solvents" where the activity coefficients are so close to unity that the interest in their calculation is quite low. An exception – of course – is the use of the D.H. theory for making extrapolations to "infinite dilution".

There has been two general lines of investigation. Some researchers have tried to enlarge the concentration range by making empirical and semi-empirical assumptions. Already the original papers of Debye and Hückel used the concept of distance of closest approach of the two ions (*a*). Instead of the dependence of activity coefficients on the square root of the ionic strength $\sqrt{I}$ the dependence should rather be on $\sqrt{I}/(1+b\sqrt{I})$ where b is proportional to a and can be fitted individually for each salt. The quantity b has a value around unity and many authors put $b=1$ mol$^{-1/2}$ dm$^{3/2}$ (Güntelberg approximation). This approximation is useful up to 0.01 mol/dm^3 but it may give deviations to the wrong side of the limiting law in exceptional cases (*e.g.* ammonium halides[2] and tetraalkyl ammonium iodides[3]). To account for the minimum and subsequent increase in ln $\gamma_\pm$ *vs.* $\sqrt{I}$ ($\gamma_\pm$ being the mean ionic molal activity coefficient) – found for most strong electrolytes – an empirical "salting-out" term Bm (m=molality) is also added. Even a third term Cm^2 has been found necessary in some cases and quite recently Pitzer and Mayorga[4] have claimed the B-coefficient to be a quite complicated function of ionic strength. Those authors have furthermore added still another term proportional to $\ln(1+b\sqrt{I})$. The hydration theory of Bjerrum[5,6] and later of Robinson and Stokes[7] seems much simpler and the latter has been widely cited, but it is inconsistent in several respects (see Appendix II). Somewhat more convincing are the later arguments of Glueckauf,[8] Jacobsen and Skou[9] and Stokes and Robinson.[10]

Other researchers have concentrated more on the fundamental weaknesses of the original D.H. theory. The technique of Debye and Hückel was to combine the statistical Boltzmann-distribution with the macroscopic Poisson eqn. from electrostatics and to solve the linearised Poisson-Boltzmann eqn. For the linearisation to be valid one must have that $z_iF\psi_j/RT$ is much less than unity (ψ_j is the electric potential around the j'th ion at the position of the i'th ion with charge z_i). La Mer *et al.*[11,12] obtained series expansions in $z_iF\psi_j/RT$, and Guggenheim[13-15] has made computer calculations on the non-linear Poisson-Boltzmann eqn. He concluded that the expansions of La Mer *et al.* do not give significant improvements in comparison to the D. H. solution for aqueous solutions of uni-univalent electrolytes and that the expansion terms are not sufficient for higher valence types.

On a more fundamental level Onsager[16] has shown that the non-linear Poisson-Boltzmann eqn. is inconsistent with the principles of statistical mechanics, since the conditional probability of finding an ion i at $r=r$ given an ion j at $r=0$ is not equal to the conditional probability of finding ion j at r given ion i at 0 for unsymmetrical electrolytes according to the non-linear P.B. eqn. This is due to the mixing of microscopic and macroscopic concepts in the hybrid P.B. eqn. Luckily, however, the inconsistency disappears when the P.B. eqn. is linearised. Onsager also showed that the so-called Debye charging process yields different results from the so-called Güntelberg charging process (see Appendix I) when non-linearities are taken into account – even for symmetrical electrolytes. Nevertheless, solution of the nonlinear P.B. eqn. has become popular among some electrochemists and among researchers studying macro-ions.[17]

Mayer[18] applied the principles of statistical mechanics to the problem of finding the thermodynamic properties of an ensemble of charged hard spheres among solvent molecules. He succeeded in deriving a virial expansion by the cluster integral method and found the D.H. limiting law at high dilution avoiding the questionable P.B. eqn. and the problematic charging procedures. The same was done with somewhat different methods by Kirkwood and Poirier.[19] Although the finding of the possibility of stratification of the average space charge around each ion by those latter authors seemed promising – being reminiscent of the space oscillations of the pair correlation functions in simple liquids – the approximations done were too rough for direct comparison between theory and experiments. In 1968 Résibois (Ref. 20, p. 47) could state – after an excellent survey of the results of applying the Bogolubov-Born-Green-Kirkwood-Yvon (BBGKY) hierarchy of equations on the electrolyte problem – that "unfortunately, the considerable effort which has been put into this problem has not resulted in much interest. No rigourous theory is presently available beyond the limiting-law region".

Some light has broken through the dimness in recent years with the appearance of the hypernetted chain theory (HNC) and the mean spherical approximation method (MSA). Friedman and coworkers[21,22] have performed the first successful calculations for a wide range of concentrations and salts with the HNC-eqns. However, the HNC method invokes the solution of a transcendental integral eqn. and is therefore not apt for rapid and practical calculations. The MSA-model, proposed by Lebowitz and coworkers,[23,24] seems to be considerably more manageable,[25] and Triolo *et al.*[26] have fitted osmotic coefficients of 23 uni-univalent salts using this model. We shall see, however, that the fit is somewhat unsatisfactory for the activity coefficient data (see Appendix III) and the cationic radii found are also sometimes less than the Pauling radii and not consistent among different electrolytes with common cations.

In the present paper I shall try to manoeuvre safely between Scylla and Charybdis: on one hand I shall avoid mere curve fitting without fundamental ideas, on the other hand the sophisticated mathemathics without practical results. A simple one parameter model is proposed – with the excluded volume between the positive and negative ion as the single adjustable parameter – which can explain the activity data from 0.001 up to 3–5 mol/dm^3 for hydrogen- and alkali halides in aqueous solution. Hopefully, the model can also be extended to electrolytes of other valence types and to electrolyte mixtures. Even if the end result appears simple and the sum of radii seems to follow a consistent pattern with hydration numbers of the cations in reasonable accordance with numbers calculable from other sources, the chain of argumentation has many links and subtilities. Therefore, I shall start with the description of a simple Debye-Hückel/Excluded Volume theory (DHEV). This model also yields a consistent pattern of ionic radii, but the radii are generally too large and the concentration range not very big. Next, a modification of the D.H. theory – the "screened potential" theory will be presented,

and it will be explained why plots of $\ln f_{\pm}$ vs. $\sqrt{I}$ for many electrolytes above 0.001 mol/dm^3 yield almost straight lines with slopes around 0.7–0.9 times the value predicted by the D.H. limiting law. Finally, the DHEV-theory and the screened potential theory will be merged into a semi-empirical "Adjusted Screened Potential/Excluded Volume" (ASPEV) theory yielding reasonable ionic radii when tested on uni-univalent RX-electrolytes with R=H, Li, Na, K, Rb, Cs and X=Cl, Br, I.

DEBYE-HÜCKEL/EXCLUDED VOLUME (DHEV) THEORY

In this section I shall assume the following formula for the molar activity coefficient in a mixture of n different ionic species in electroneutral solvent (0)

$$\ln f_i = -A_{\mathrm{D.H.}} z_i^2 \sqrt{I} + \sum_{j=1}^{n} B_{ij} c_j \quad (i=1,n) \tag{1}$$

where z_i is the number of unit charges carried by species No. i, $A_{\mathrm{D.H.}}$ is the Debye-Hückel slope, I is the ionic strength $=(1/2)\Sigma c_i z_i^2$ and c_j the concentration of the j'th ionic species. The coefficients B_{ij} are just phenomenological interaction coefficients between the ions. We notice that the usual Debye-Hückel expression can be Taylor-expanded in the following way

$$-A_{\mathrm{D.H.}} z_i^2 \frac{\sqrt{I}}{1+b\sqrt{I}} \cong -A_{\mathrm{D.H.}} z_i^2 \{\sqrt{I} - bI\} \tag{2}$$

so that the effect of the denominator in the D.H. theory can be approximated by eqn. (1) for ionic strengths small enough. Due to the Maxwell conditions we have

$$\frac{\partial \ln f_i}{\partial c_j} = \frac{\partial \ln f_j}{\partial c_i} \quad (i \neq j) \tag{3}$$

and since

$$\frac{\partial \ln f_i}{\partial c_j} = -\frac{z_i^2 z_j^2}{4} \frac{A_{\mathrm{D.H.}}}{\sqrt{I}} + B_{ij} \tag{4}$$

we have the requirements

$$B_{ij} = B_{ji} \tag{5}$$

for purely thermodynamic reasons.

We now want to calculate the osmotic pressure Π of an electrolyte solution. For the change in chemical potential of the solvent caused by addition of electrolyte we have (at constant T)

$$\mathrm{d}\mu_0 = V_0 \mathrm{d}p + RT \mathrm{d} \ln a_0 \tag{6}$$

where V_0 is the partial molar volume of the solvent and a_0 its activity. If the pressure p is equal to Π we have $\mathrm{d}\mu_0 = 0$, *i.e.*

$$\frac{\mathrm{d}\Pi}{RT} = -\frac{\mathrm{d} \ln a_0}{V_0} \tag{7}$$

When we combine the Gibbs-Duhem eqn. (const. T, V total volume, n_i number of mol)

$$-V\mathrm{d}p + n_0 \mathrm{d}\mu_0 + \sum_{i \neq 0} n_i \mathrm{d}\mu_i = 0 \tag{8}$$

with the requirement

$$V = n_0 V_0 + \sum n_i V_i \tag{9}$$

and with eqn. (6) and the analogous eqns for $i \neq 0$ we obtain

$$\mathrm{d} \ln a_0 = -\frac{1}{c_0} \sum_{i \neq 0} c_i \mathrm{d} \ln a_i \tag{10}$$

Inserting (10) into (7) and introducing the molar activity coefficients f_i we have

$$\frac{\mathrm{d}\Pi}{RT} = \frac{1}{c_0 V_0} \left\{ \sum_{i \neq 0} \mathrm{d}c_i + \sum_{i \neq 0} c_i \mathrm{d} \ln f_i \right\} \tag{11}$$

To integrate for the osmotic pressure one should know $c_0 V_0$ as a function of the various salt concentrations. In moderately dilute solutions, however, we have to a good approximation

$$c_0 V_0 \cong 1 \tag{12}$$

We then have for the osmotic pressure

$$\frac{\Pi}{RT} \cong \sum_{i \neq 0} c_i + \sum_{i \neq 0} \int_0^{c_i} c_i' \mathrm{d} \ln f_i' \tag{13}$$

Since Π is of course independent of the path of integration, we shall choose the simplest possible. We put

$$c_i' = l c_i \tag{14}$$

where the parameter l runs from 0 to 1. For the integrals in (13) we then obtain [using eqn. (1)]

$$\int_{l=0}^{1} c_i' \, \mathrm{d} \ln f_i' = -A_{\mathrm{D.H.}} \times \tfrac{1}{2} c_i z_i^2 \times \tfrac{2}{3} \sqrt{I} + \tfrac{1}{2} \sum_{j \neq 0} B_{ij} c_i c_j \qquad (15)$$

and for the osmotic pressure

$$\frac{\Pi}{RT} = \sum_{i \neq 0} c_i - \tfrac{2}{3} A_{\mathrm{D.H.}} I^{3/2} + \tfrac{1}{2} \sum_{i \neq 0} \sum_{j \neq 0} B_{ij} c_i c_j \qquad (16)$$

We shall now make an analogy to the case of a mixture of moderately dilute gases. According to Ref. 27, eqns. (7−61) and (7−1) we have for a mixture of gases ($c_{\mathrm{tot}} = \Sigma c_i$, N_0 = Avogadro number)

$$\frac{P}{RT} = c_{\mathrm{tot}} + c_{\mathrm{tot}}^2 N_0 \sum_i \sum_i x_i x_j B_2(ij) \qquad (17)$$

with x_i being the mol fraction of the i'th species and the second virial coefficients are given by [Ref. 27, eqn. (7.27)]

$$B_2(ij) = -2\pi \int_0^{\infty} \{ \mathrm{e}^{-U_{ij}(r_{ij})/kT} - 1 \} r_{ij}^2 \mathrm{d}r_{ij} \qquad (18)$$

where U_{ij} is the pair potential between the i'th and the j'th species which is function of the distance r_{ij}. It can be rigorously shown [28] that it is allowable to use exactly the same formalism for the osmotic pressure in a moderately dilute solution as for the pressure of a mixture of moderately dilute gases. The pair potential has just to be interpreted as the pair potential of average forces. The average force between two solute molecules separated by a distance of r_{ij} is given by the direct force between the two solute molecules *plus* the average of a fluctuating force due to the fact that two solute molecules fixed at a distance r_{ij} perturb the spherical symmetry of solvent molecules around each solute species. Thus, for a solution of electroneutral species we obtain

$$\frac{\Pi}{RT} = \sum_{i \neq 0} c_i + N_0 \sum_{i \neq 0} \sum_{j \neq 0} c_i c_j B_2(ij) \qquad (19)$$

The virial coefficients are given by (18) with U_{ij} interpreted as the potentials of the average force. In this paper we shall consider only the simplest interaction, *i.e.* hard core interaction

$$U_{ij} = \begin{cases} 0 & r_{ij} \geq R_i + R_j \\ \infty & r_{ij} < R_i + R_j \end{cases} \qquad (20)$$

From eqn. (18) we then get the second virial coefficients in terms of excluded volumes

$$B_2(ij) = \frac{2\pi}{3} (R_i + R_j)^3 \qquad (21)$$

If we compare (19) with (16) we see that they are identical except for the Debye-Hückel term. The simplest assumption is therefore that it is possible to superpose the D.H. osmotic pressure on the hard core osmotic pressure. We than have

$$B_{ij} = 2N_0 B_2(ij) \qquad (22)$$

so that the interaction coefficients B_{ij} in (1) may be calculated from assumptions of certain ionic radii.

Two years before the advent of the D.H. theory, Lewis and Randall [29] had introduced the concept of ionic strength and stated the principle that "in dilute mixed electrolyte solutions (up to $I' = 0.05$ mol/kg solvent) the activity coefficient of a given strong electrolyte is the same in all solutions of the same ionic strength". This principle was shortly after repudiated by Brønsted [30] who instead advocated his principle of specific interaction of ions: "In a dilute salt solution of constant total concentration ions will be uniformly influenced by ions of their own sign". From the context it appears that Brønsted meant that only ions of opposite signs would have a specific interaction on the activity coefficients of each other. If we interpret "uniformly influenced" to be an influence through the ionic strength and a "specific interaction" to a B_{ij}-interaction, Brønsted's principle combined with the present theory may be stated as follows

$$B_{ij} = \begin{cases} \dfrac{4\pi N_0}{3} (R_i + R_j)^3 & \text{if } z_i z_j < 0 \\ 0 & \text{if } z_i z_j > 0 \end{cases} \qquad (23)$$

The principle of superposition of the D.H. term and the second virial terms supposed in the DHEV-theory is of course far from obvious. One cross-coupling between the $c^{3/2}$ term and the c^2 terms in the expression for the osmotic pressure might very well be, that excluded volumes of ions of like signs should not be accounted for, since the ions are kept apart by the electrostatic forces already accounted

for in the D.H. term. We shall see that this seems to be the case, experimentally.

We shall now concentrate on solutions of single, binary electrolytes dissociating into ν_+ cations and ν_- anions. The cation is given the number 1 and the anion the number 2. We have now for the mean ionic activity coefficient

$$\ln f_\pm = -A_{\mathrm{D.H.}}|z_+z_-|\sqrt{I} + \frac{c_s}{\nu_+ + \nu_-} \{B_{11}\nu_+^2 + 2B_{12}\nu_+\nu_- + B_{22}\nu_-^2\} \quad (24)$$

where c_s is the salt concentration and $B_{11} = B_{22} = 0$ if Brønsted's principle of specific interaction of ions is valid. Newman[31] (Chap. 4, Section 30) gives the following formula for the *molal* activity coefficient (I' = molal ionic strength)

$$\ln \gamma_\pm = -|z_+z_-|\frac{A'_{\mathrm{D.H.}}\sqrt{I'}}{1+b\sqrt{I'}} + \frac{4\nu_+\nu_-}{\nu_+ + \nu_-}\beta m \quad (25)$$

together with tables of b and β for various electrolytes in water at 25 °C. Power expanding the denominator according to eqn. (2) we obtain

$$\ln \gamma_\pm \cong -A'_{\mathrm{D.H.}}|z_+z_-|\sqrt{I'} + \left\{\frac{4\nu_+\nu_-}{\nu_+ + \nu_-}\beta + \mu|z_+z_-|A'_{\mathrm{D.H.}}b\right\}m \quad (26)$$

with

$$\mu = \tfrac{1}{2}\{z_+^2\nu_+ + z_-^2\nu_-\} \quad (27)$$

Table 1. Calculation of DHEV-radii for various 1 – 1 electrolytes.

Electrolyte	β[a] kg/mol ~ dm³/mol	B_{12} dm³/mol	R_1+R_2 Å	R_2 Å	R_1 Å	R_1 (Pauling) Å	Hydration shell volume (Å³)	Hydration number
HCl	0.27	1.72	8.8	1.8				
HBr	0.33	1.84	9.0	2.0	7.0(1)	0	1440	48
HI	0.36	1.90	9.1	2.2				
LiCl	−0.21	1.62	8.6	1.8				
LiBr	0.22	1.70	8.8	2.0	6.8(1)	0.61	1320	44
LiI	0.26	1.88	9.1	2.2				
NaCl	0.15	1.48	8.4	1.8				
NaBr	0.17	1.52	8.4	2.0	6.5(1)	0.96	1150	39
NaI	0.21	1.60	8.6	2.2				
KCl	0.10	1.38	8.2	1.8				
KBr	0.11	1.40	8.2	2.0	6.3(1)	1.33	1040	35
KI	0.15	1.48	8.4	2.2				
RbCl	0.06	1.30	8.0	1.8				
RbBr	0.05	1.28	8.0	2.0	6.0(2)	1.48	890	30
RbI	0.04	1.26	7.9	2.2				
CsCl	0.00	1.18	7.8	1.8				
CsBr	0.00	1.18	7.8	2.0	5.8(2)	1.66	800	27
CsI	−0.01	1.16	7.7	2.2				
HNO_3	0.20	1.58	8.6		7.0			
$LiNO_3$	0.21	1.60	8.6		6.8			
$NaNO_3$	0.04	1.26	7.9	1.4(4)	6.5			
KNO_3	−0.11	0.96	7.3		6.3			
$RbNO_3$	−0.14	0.90	7.1		6.0			
$CsNO_3$	−0.15	0.88	7.0		5.8			

[a] All data for water at 25 °C from Ref. 31, Table 30-1. For all electrolytes $b = 1$ (kg/mol)$^{\frac{1}{2}} \sim 1$ (dm³/mol)$^{\frac{1}{2}}$. Numbers in parenthesis indicate uncertainty on the preceding cipher.

Table 2. Calculation of DHEV-radii for various 2−1 and 1−2 electrolytes.

Electrolyte	b [a] (kg/mol)‡ ~(dm³/mol)‡	2β [a] kg/mol ~dm³/mol	B_{12} dm³/mol	R_1+R_2 Å	R_2 Å	R_1 Å	R_1 (Pauling) Å
$MgCl_2$	1.59	0.36	8.79	15.2	1.8	13.3(1)	0.65
$MgBr_2$	1.62	0.50	9.09	15.3	2.0		
$CaCl_2$	1.54	0.29	8.45	15.0	1.8		
$CaBr_2$	1.62	0.37	8.96	15.3	2.0	13.3(1)	0.99
$SrCl_2$	1.56	0.22	8.49	15.0	1.8	13.2	1.13
$SrBr_2$	1.62	0.30	8.89	15.2	2.0		
$BaCl_2$	1.56	0.11	8.38	14.9	1.8	13.0(1)	1.35
$BaBr_2$	1.56	0.24	8.51	15.0	2.0		
$Mg(NO_3)_2$	1.53	0.36	8.47	15.0		13.3	
$Ca(NO_3)_2$	1.39	0.09	7.46	14.4	1.3(4)	13.3	
$Sr(NO_3)_2$	1.39	−0.07	7.30	14.2		13.2	
Li_2SO_4	1.41	−0.11	7.36	14.3		6.8	
Na_2SO_4	1.27	−0.28	6.45	13.7		6.5	
K_2SO_4	1.07	−0.15	5.52	13.0	7.5(7)	6.3	
Rb_2SO_4	1.33	−0.25	6.80	13.9		6.0	
Cs_2SO_4	1.33	−0.20	6.85	14.0		5.8	

[a] All data for water at 25 °C from Ref. 31, Table 30-2.

For sufficiently dilute solutions we can neglect the difference between the molality and salt concentration except that we have to use $A_{D.H.} = 1.1779$ $dm^{3/2}mol^{-1/2}$ instead of $A'_{D.H.} = 1.1762\,kg^{1/2}mol^{-1/2}$ (Ref. 31, Table 28 − 1). We have then by comparison with (23) and (24)

$$B_{12} \cong 2\beta + \frac{b}{2}\mu\frac{\nu_+ + \nu_-}{\nu_+\nu_-}A_{D.H.}|z_+z_-| \qquad (28)$$

From the figures in Newman's tables (Ref. 31, Table 30−1 and Table 30−2) we calculate by means of (28) the excluded volume B_{12} for various uni-univalent electrolytes (Table 1) and for various 2−1 and 1−2 electrolytes (Table 2). Furthermore, we get the sum of radii from (23). Comparing the sum of radii for alkali halides with the same cation, we observe that the differences correspond very well to the differences in the crystallographic radii between the halogenide ions. Therefore, the anions are assumed unhydrated and the radii of the cations can be estimated. The hydration numbers of the cations are calculated from the volume in the spherical shell between the calculated radius and the Pauling radius, assuming that each water molecule occupies 30.0 Å³ as in pure water at 25 °C. This is just a rough approximation, since many electrolytes are known to have negative partial molar volumes in water; see Bernal and Fowler (Ref. 32, Table V). However, the approximation is good enough to demonstrate that the hydration numbers calculated by the DMEV-theory are much too large to have any realistic significance.

Apart from that, the pattern shown in Table 1 and Table 2 is fairly consistent. The radii of the series H^+, Li^+, Na^+, K^+, Rb^+ and Cs^+ as well as the series Mg^{2+}, Ca^{2+}, Sr^{2+} and Ba^{2+} decrease monotonically, since the smallest ions are the most hydrated. The earth alkali ions are more hydrated that the alkali ions due to the double charge. The "radius" of the NO_3^- ion in alkali nitrates is 1.4 ± 0.4 Å and the "radius" of the SO_4^{2-} ion in alkali sulfates is 7.5 ± 0.7 Å. Those values are remarkably constant when one considers that attractive forces and orientation dependent forces must play important roles for those ions − making a simple excluded volume theory quite inappropriate. The constancy of those anionic radii should also be seen in the light of the

wildly fluctuating values of the b- and the β-values taken apart.

The reason for the exaggeration of the values of the sum of radii is that the Debye-Hückel slope $A_{D.H.}$ grossly exaggerates the effect of ionic strength for ionic strengths above 0.001 mol/dm^3 due to the screening of ions by their counterions. In the next section it will be explained why slopes less than $A_{D.H.}$ (0.7 to 0.9 $A_{D.H.}$) give a much better fit for electrolytes of all valence types between ionic strengths 0.001 and 0.05 mol/dm^3, and why even smaller slopes may be expected for larger ionic strengths. It is then clear that the excluded volume in (24) will be exaggerated.

THEORY OF SCREENED POTENTIAL

The point of departure in the classical theory of Debye and Hückel is the following pair distribution of ion j in the field of ion i

$$n_{ji}(r) = \rho_i \rho_j \exp[-z_j F \psi_i(r)/RT] \tag{29}$$

where ρ_i is the mean number density of the i'th ion, ψ_i the electric potential due to the i'th ion in the distance r from this ion and F is the Faraday number. We shall require that

$$F\psi_i/RT \ll 1 \tag{30}$$

The local charge density $\rho_q^{(i)}$ around the i'th ion can then be approximated by (using the condition of electroneutrality for the mean densities)

$$\rho_q^{(i)} \cong -\frac{2F^2}{RT} I \psi_i \tag{31}$$

Combination of (31) with the Poisson eqn. of electrostatics yields the linearised Poisson-Boltzmann eqn. for the distribution of the electric potential

$$\nabla^2 \psi_i = \varkappa^2 \psi_i \tag{32}$$

with the definition

$$\varkappa = F\sqrt{\frac{2I}{RT\varepsilon}} \tag{33}$$

where ε is the absolute permittivity of the solvent medium. The solution to (32) for a point charge z_i is

$$\psi_i^{D.H.} = \frac{z_i F e^{-\varkappa r}}{4\pi\varepsilon N_0 r} \tag{34}$$

and the charge density around ion i is to a first approximation

$$\rho_q^{(i)}(D.H.) = -\frac{\varkappa^2 z_i F e^{-\varkappa r}}{4\pi N_0 r} \tag{35}$$

Already at ionic strengths around 0.001 mol/dm^3, however, we have a pronounced screening of the interactions between ions due to the atmosphere of the counterions. From (35) we get a first approximation to the charge in the ionic cloud inside a sphere with radius R

$$q_{cloud}^{(D.H.)}(R) = \int_0^R 4\pi r^2 \rho_q^{(i)} dr = -\frac{z_i F}{N_0}\{1 - g(\varkappa R)\} \tag{36}$$

with the definition

$$g(\varkappa R) = (1 + \varkappa R)e^{-\varkappa R} \tag{37}$$

To get the total "effective charge" inside the sphere with radius R we have to add the ionic charge $z_i F/N_0$ to q_{cloud}. We obtain

$$z_i^{eff}(R) = g(\varkappa R) z_i \tag{38}$$

The basic eqn. (29) was obtained by using simple Boltzmann statistics and noting that the interaction energy of ion j in the field of ion i is $z_j F \psi_i / N_0$. A much better approximation of the interaction energy is, however

$$z_j^{eff}(r) F \psi_i(r)/N_0$$

since $z_j^{eff}(r)$ is the part of the charge z_j effectively "seen" from the central ion i. Just imagine, that the ionic cloud was effectively finished at a distance smaller than r. Then, there cannot be any electrostatic interaction between ion i and ion j, and the local densities of those species are uncorrelated with a pair distribution function $n_{ji}(r) = \rho_i \rho_j$. Replacing z_j with $g(\varkappa r) z_j$ in (29) and using the Debye-Hückel condition (30) we obtain as a second approximation for the local charge density (the "screened potential" approximation)

$$\rho_q^{(i)}(SP) = -\frac{2F^2}{RT} I\, g(\varkappa r) \psi_i(r) \tag{39}$$

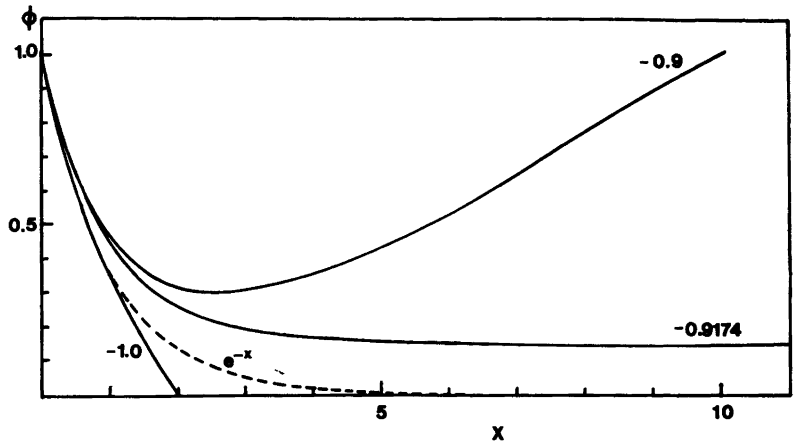

Fig. 1. Finding the screened potential function by trial and error. See text.

Inserting this into the Poisson eqn. we get the "screened potential" version of the linearised P.B. eqn.

$$\nabla^2\psi_i^{SP} = \varkappa^2 g(\varkappa r)\psi_i^{SP} \tag{40}$$

Introducing the dimensionless variable

$$x = \varkappa r \tag{41}$$

the Laplacian in spherical coordinates and the new function

$$\Phi = \psi_i^{SP} x \tag{42}$$

we get the differential eqn.

$$\frac{d^2\Phi}{dx^2} = g(x)\Phi \tag{43}$$

This differential eqn. has been solved by computer using a third order Runge-Kutta algorithm with a steplength in x equal to $h=0.1$ and an error of $O(h^4)$; see Ref. 33, No. 25.5.22.

Some results are shown in Fig. 1. One can choose Φ and $d\Phi/dx$ at $x=0$ to be arbitrary values. We choose $\Phi(x=0)$ to be 1, since another value will just amount to a scale factor. For the chosen value of $\Phi(x=0)$ there will only be one value of $[d\Phi/dx]_{x=0}$ with a solution with the property that $\Phi \to 0$ when $x \to \infty$ (see Fig. 1). If the initial slope is -0.9173 the $\Phi(x)$ curve finally rises and goes to ∞ when $x \to 0$. On the other hand, the curve with initial slope -0.9174 cuts the x-axis around $x=4170$, while the curve with initial slope -0.9175 cuts at $x=202$. The initial slope must therefore be between -0.9173 and -0.9174, but the curve with slope -0.9174 will be very close to the true curve for x less than 1000. Because of the importance of this potential curve for the present and future studies we have tabulated it in Table 3. We notice especially the long "tail" of the potential curve in comparison to the solution $\exp(-x)$ to the simple linearised P.B.

Table 3. The screened potential function $\phi(x)$.

x	ϕ	x	ϕ
0	1.0000	2.2	0.2406
0.1	0.9131	2.4	0.2245
0.2	0.8353	2.6	0.2113
0.3	0.7657	2.8	0.2003
0.4	0.7035	3.0	0.1912
0.5	0.6479	3.5	0.1744
0.6	0.5982	4.0	0.1638
0.7	0.5538	5.0	0.1525
0.8	0.5140	6.0	0.1478
0.9	0.4784	7.0	0.1459
1.0	0.4465	8.0	0.1450
1.1	0.4179	9.0	0.1447
1.2	0.3922	10.0	0.1445
1.3	0.3691	20.0	0.1441
1.4	0.3483	50.0	0.1430
1.5	0.3296	80.0	0.1419
1.6	0.3127	100.0	0.1413
1.7	0.2975	150.0	0.1396
1.8	0.2837		
1.9	0.2713		
2.0	0.2600		

eqn. The ionic cloud is less concentrated in the screened case since the interactions between ions are weaker.

In the classical Debye-Hückel theory the transition from potential function to activity coefficients is made by various charging processes (Debye charging, Güntelberg charging), but since those procedures can be criticized from several points of view (see Appendix I), we shall apply instead a more satisfactory method given, *e.g.*, in the monograph of Résibois (Ref. 20, pp. 34–40). From simple mathematical properties of the configuration integral and the pair distribution function we obtain for the electrostatic contribution to the Helmholtz free energy per unit volume

$$\frac{A_{el}}{\Omega} = \frac{1}{2}\int_0^1 \frac{d\lambda}{\lambda} \int d\mathbf{r} \sum_{i,j} \lambda \cdot U_{ij}^{el}(r) n_{ij}(r,\lambda) \tag{44}$$

where λ is a parameter measuring the strength of electrostatic interaction with the Coulombic interaction energy λU_{ij}^{el} given by

$$\lambda U_{ij}^{el} = \frac{\lambda z_i z_j F^2}{4\pi N_0^2 \varepsilon_0 r_{ij}} \tag{45}$$

with ε_0 being the permittivity of vacuum. The pair distribution function n_{ij} in (44) is determined by the U_{ij}^{el}-interactions as by the short range quantum mechanical forces between ions and between ions and solvent. The Debye-Hückel approximation is now to suppose that the only contribution of short range forces are the ion-dipole forces between ions and solvent molecules, and to assume that those interactions can be adequately accounted for by substituting the permittivity of the solvent ε instead of ε_0 in (45). Furthermore, the Debye-Hückel pair distribution function is used, *i.e.*

$$n_{ij} \cong \rho_i \rho_j \left[1 - \frac{z_i F \psi_j}{RT}\right] = \rho_i \rho_j \left[1 - \frac{z_i z_j F^2 e^{-\kappa r}}{4\pi RT\varepsilon N_0 r}\right] \tag{46}$$

When the interaction strength is only the fraction λ of the full interaction, we can proceed formally by replacing z_i by $\sqrt{\lambda} z_i$. We then have $\kappa' = \sqrt{\lambda}\kappa$ and

$$n_{ij}(r,\lambda) \cong \rho_i \rho_j \left[1 - \frac{\lambda z_i z_j F^2 e^{-\sqrt{\lambda}\kappa r}}{4\pi RT\varepsilon N_0 r}\right] \tag{47}$$

Using the electroneutrality condition for the mean densities ρ_i and transforming the variable $d\mathbf{r} = 4\pi r^2 dr$ we obtain from (44), modified (45) and (47)

$$\frac{A_{el}}{\Omega} = -\frac{1}{2}\int_0^1 \lambda d\lambda \sum_{i,j} \left\{ \frac{z_i^2 z_j^2 F^4 c_i c_j}{N_0 4\pi RT\varepsilon^2} \int_0^\infty e^{-\sqrt{\lambda}\kappa r} dr \right\} \tag{48}$$

Carrying out the integrations we obtain

$$\frac{A_{el}}{\Omega} = -\frac{RT}{12\pi N_0}\kappa^3 \tag{49}$$

which is exactly the result of Debye and Hückel for point charges.

We are now going to introduce the corrections for screening. According to (39) and (40) the charge distribution around the i'th ion in the SP-approximation is given by

$$\rho_q^{(i)}(\mathrm{SP}) = -\varepsilon\kappa^2 g(\kappa r)\psi_i^{SP} = -\varepsilon\kappa^2 \frac{g(\kappa r)}{\kappa r} C_i \Phi \tag{50}$$

where Φ is given in Table 3 and C_i is a scaling factor for the potential distribution. It can be found by requiring that the total charge in the ionic cloud counterbalances the charge on the central ion

$$\int_0^\infty \rho_q^{(i)} 4\pi r^2 dr = -\frac{4\pi\varepsilon}{\kappa} C_i \int_0^\infty g(x)\Phi(x) x dx = -\frac{z_i F}{N_0}$$

so that

$$C_i = \frac{z_i F}{N_0} \frac{\kappa}{4\pi\varepsilon \int_0^\infty x g(x)\Phi(x) dx} \tag{51}$$

The potential around the i'th ion is then given by

$$\Psi_i^{SP} = \frac{z_i F}{N_0 4\pi\varepsilon J_1} \times \frac{\Phi(\kappa r)}{r} \tag{52}$$

with

$$J_1 = \int_0^\infty x g(x)\Phi(x) dx \tag{53}$$

The pair distribution function is given by

$$n_{ij}(r) \cong \rho_i \rho_j \left[1 - \frac{z_i F\, g(\kappa r)\psi_i^{SP}}{RT}\right] \tag{54}$$

or – when the Coulumbic interaction strength is less than unity –

$$n_{ij}(r\lambda) \cong \rho_i \rho_j \left[1 - \frac{\lambda z_i z_j g(\sqrt{\lambda}\kappa r) F^2}{4\pi\varepsilon N_0 RT J_1} \times \frac{\Phi(\sqrt{\lambda}\kappa r)}{r}\right] \tag{55}$$

The screened potential interaction energy is

$$U_{ij}^{el} = \frac{z_i z_j g^2(\varkappa r) F^2}{4\pi N_0^2 \varepsilon r_{ij}} \tag{56}$$

Introducing (55) and (56) in (44) and using the electroneutrality condition for the mean densities ρ_i and ρ_j we obtain

$$\frac{A_{el}}{\Omega} = -\frac{1}{2} \times \frac{F^4}{4\pi\varepsilon^2 N_0 RTJ_1} \int_0^1 \lambda d\lambda \int_0^\infty \sum_{i,j} c_i c_j z_i^2 z_j^2 \, g^3(\sqrt{\lambda}\varkappa r)\Phi(\sqrt{\lambda}\varkappa r)dr \tag{57}$$

In the last integral we change variable to $p = \sqrt{\lambda}\kappa r$. Furthermore, we use that

$$\sum_{i,j} c_i c_j z_i^2 z_j^2 = (\sum_i c_i z_i^2)(\sum_j c_j z_j^2) = 4I^2 \tag{58}$$

Then (57) can be written

$$\frac{A_{el}}{\Omega} = -\frac{I^2 F^4 J_2}{2\pi\varepsilon^2 N_0 RTJ_1 \varkappa} \int_0^1 \sqrt{\lambda} d\lambda \tag{59}$$

with

$$J_2 = \int_0^\infty g^3(p)\Phi(p)dp \tag{60}$$

Carrying out the λ-integration and using the definition of κ in (33) we obtain

$$\frac{A_{el}}{\Omega} = -\frac{RT}{12\pi N_0}\left(\frac{J_2}{J_1}\right)\varkappa^3 \tag{61}$$

The activity coefficient of the i'th ion is given by

$$RT \ln f_i = \left[\frac{\partial}{\partial c_i}\left(\frac{A_{el}}{\Omega}\right)_{\Omega,T} = -\left(\frac{J_2}{J_1}\right)\frac{\sqrt{2}F^3 z_i^2 \sqrt{I}}{8\pi N_0 \varepsilon^{3/2}\sqrt{RT}}\right. \tag{62}$$

or

$$\ln f_i = -\left(\frac{J_2}{J_1}\right) A_{D.H.} z_i^2 \sqrt{I} \tag{63}$$

with the Debye-Hückel constant

$$A_{D.H.} = \frac{\sqrt{2}F^3}{8\pi N_0 (RT\varepsilon)^{3/2}} \tag{64}$$

The only difference from the D.H. limiting law is the factor J_2/J_1 which has to be evaluated numerically. The two integrals have been calculated by computer by means of Simpson integration with steplength $h = 0.1$. We obtain

$$J_1 = 0.8555 \pm 0.0005 \quad J_2 = 0.6055 \pm 0.0005$$

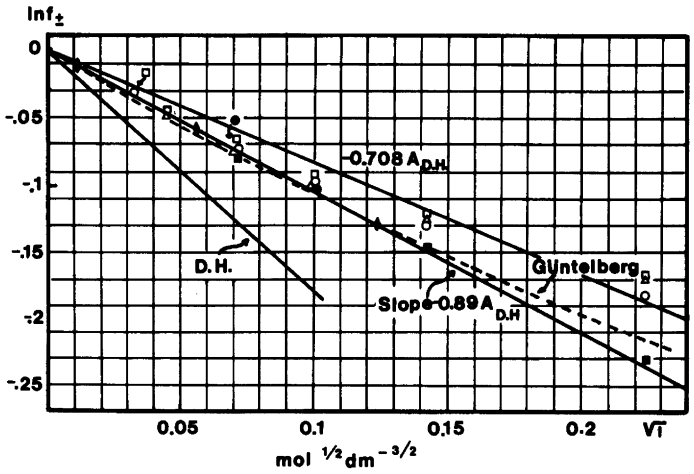

Fig. 2. Logarithm of molar mean ionic activity coefficient *vs.* square root of molar ionic strength at moderate concentrations for various electrolytes. Water at 25 °C.
○, HCl; □, LiBr; △, KI; ●, RbCl; ■, CsCl+CsBr; ◆, $Co(NH_3)_6^{3+}Co(CN)_6^{3-}$. (Data from Ref. 34 at 18 °C have been multiplied by $(A_{D.H.}^{25}/A_{D.H.}^{18} \times 3^2)$ to make them compatible.)

We have then for the mean ionic molar activity coefficient in the screened potential approximation

$$\ln f_{\pm} = -0.708|z_+z_-|A_{\mathrm{D.H.}}\sqrt{I} \tag{65}$$

In Fig. 2 we have plotted some experimental results for various electrolytes against the square root of the ionic strength. From the figure it is clear that the D.H. limiting law is grossly in error even at such low concentrations as 0.001 mol/dm^3 where measurements start for most electrolytes. The experimental results for the lowest concentrations (up to ionic strenths around 0.01 mol/dm^3) seem to follow quite closely a straight line with slope -0.89 $A_{\mathrm{D.H.}}$, but around $I=0.02$ mol/dm^3 the slope -0.708 $A_{\mathrm{D.H.}}$ is more appropriate. The concentration region shown in Fig. 2 is then a transition region between the Debye-Hückel situation and the screened potential situation. We could repeat the whole procedure once more and obtain a third approximation and so on. It is clear from the formalism used that for each new iteration we would find an expression of the same form as (65), but the factor would differ. Sketchy calculations seem to indicate that the factor will diminish even further, but a detailed investigation of this point as well as an investigation of the influence of the ionic size on the effect of screening will be left for future study. Here we shall just anticipate that the empirical facts show (see next paragraph) that the numerical value of the effective slope in (65) diminishes with increasing ionic strength, until it reaches a stationary value which seems to be greater the greater the excluded volume is between anion and cation.

ADJUSTED SCREENED POTENTIAL/ EXCLUDED VOLUME (ASPEV) THEORY

We have seen that the DHEV-theory gave a quite consistent picture of excluded volumes for many electrolytes, but the sum of radii was too big. In the preceding paragraph we showed that the Debye-Hückel limiting law is exaggerating the effect of Coulombic forces, since it doesn't take into account the shielding of ions by their counterions in the expression for the interaction energy between two ions. As a straightforward generalisation of (24) I shall try to apply the following equation

$$\ln f_{\pm} = -A^*x + B^*x^2 \tag{66}$$

where B^* in conformation with (23) and (24) is given by

$$B^* = \frac{2\mu\nu_+\nu_-}{\nu_+ + \nu_-} B_{12} \tag{67}$$

and x is the square root of the ionic strength. In accordance with the points of view in the preceding paragraph, A^* is around $0.7|z_+z_-|A_{\mathrm{D.H.}}$, but it might be varying in an individual way for each electrolyte with varying ionic strength. In the present section we shall fit (66) to the mean ionic activity coefficients of various hydrogen- and alkali halides.

If (66) were a true parabola (*i.e.* A^* and B^* are independent of x) one should have

$$x_{\min} = \frac{A^*}{2B^*} \tag{68a}$$

$$(\ln f_{\pm})_{\min} = -\frac{(A^*)^2}{4B^*} \tag{68b}$$

$$x_{-\frac{1}{2}} = \frac{A^*}{2B^*}\left(1 - \frac{1}{\sqrt{2}}\right) \tag{68c}$$

$$x_{+\frac{1}{2}} = \frac{A^*}{2B^*}\left(1 + \frac{1}{\sqrt{2}}\right) \tag{68d}$$

$$x_0 = \frac{A^*}{B^*} \tag{68e}$$

For the definitions of $x_{-1/2}$, $x_{+1/2}$ and x_0 see Fig. 3. The data for mean ionic activity coefficients (molal) as a function of molality have been collected from various sources.[35-37] Molal activity coef-

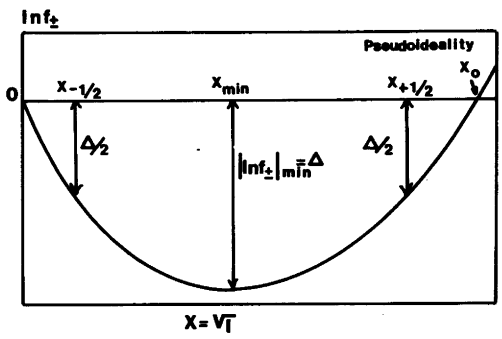

Fig. 3. Various characteristics for $\ln f_{\pm}$ *vs.* $\sqrt{I}$ curves.

Table 4. Characteristics of the $\ln f_{\pm}$ *vs* $\sqrt{I}$ curves for various uni-univalent electrolytes.

Electrolyte	$-(\ln f_{\pm})_{min}$	$x_{-\frac{1}{2}}$	$x_{-0.9}$	x_{min}	$x_{+0.9}$	$x_{+\frac{1}{2}}$	x_0	Ref. No.
HCl	0.270	0.150		0.60		1.115	1.322	37
HBr	0.240	0.130		0.50		0.965	1.162	37
HI	0.202	0.105		0.42		0.820	0.982	37
LiCl	0.305	0.150		0.65		1.235	1.452	37
LiBr	0.276	0.150		0.60		1.080	1.298	35
LiI	0.214	0.125		0.42		0.930	1.100	37
NaCl	0.400	0.240		1.0		1.855	2.175	37,35
NaBr	0.352	0.240		0.85		1.550	1.845	37
NaI	0.300	0.175		0.65		1.300	–	35
KCl	0.493	0.305		1.3		(2.43)[a]	–	37
KBr	0.452	0.270		1.2		2.20	–	37($I \leqq 0.05$), 36($I \geq 0.1$)
KI	0.415	0.245		1.0		1.835	–	35
RbCl	0.533	0.328	0.870	1.3	1.845	–	–	37,35
RbBr	0.540	0.330	0.895	1.4	1.900	–	–	35
RbI	0.528	0.320	0.850	1.3	1.750	–	–	35
CsCl CsBr	0.627	0.380	0.960	1.45	1.950	–	–	37,35
CsI	~0.65	~0.4	?	?	?	–	–	35

[a] Extrapolated value.

ficients have been transformed to molar activity coefficients and molality to molarity by means of the formula and tabulation for c/m given in Ref. 35, Table (12-1-1A), p. 725. A smooth curve was drawn for $\ln f_{\pm}$ as a function of the square root of ionic strength and x_{min}, $(\ln f_{\pm})_{min}$, $x_{-1/2}$, $x_{+1/2}$ and x_0 were found for the investigated electrolytes. The tabulation together with the data sources is given in Table 4. Since $\ln f_{\pm}$ *vs.* x is not precisely a parabola one has to make some choice about the concentration range of fitting. When $(\ln f_{\pm})_{min}$, $x_{-1/2}$, $x_{+1/2}$ and x_0 are fixed to their experimental values and A^* is chosen to some value, B^* may be calculated from (68b–e). The B^*-values calculated for the various A^*-values by the four formulae are plotted for H I in water at 25 °C in Fig. 4. One observes that in optimum 1, the depth of the minimum, the x-value of half-minimum to the right of the minimum and the pseudoideal point is reproduced by the parabola, but not the x-value of half-minimum to the left of the minimum. In optimum 2, the depth of the minimum and the $x_{-1/2}$ value fit, but not $x_{+1/2}$ and x_0. Similar plots

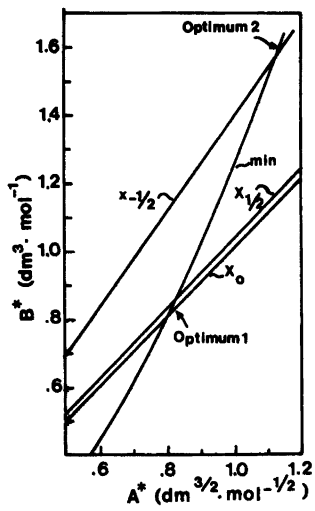

Fig. 4. Finding optimal values for A^* and B^*. Here HI in water at 25 °C.

Table 5. Optimal values of A^* and B^*.

Electrolyte	A^*_{opt} $(dm^3/mol)^{\frac{1}{2}}$	B^*_{opt} dm^3/mol	B^* (adjusted to regress.) dm^3/mol	B^* (final adj.) dm^3/mol
HCl	0.83	0.63	0.64	0.64
HBr	0.84	0.74	0.74	0.74
HI	0.82	0.84	0.94	0.94
LiCl	0.865	0.60	0.54	0.54
LiBr	0.87	0.68	0.62	0.62
LiI	0.78	0.71	0.78	0.78
NaCl	0.75	0.35	0.355	0.355
NaBr	0.765	0.415	0.415	0.415
NaI	0.795	0.52	0.52	0.52
KCl	0.705	0.25	0.25	0.27
KBr	0.715	0.28	0.29	0.29
KI	0.78	0.365	0.35	0.35
RbCl	(0.76)	(0.27)	0.26	0.25
RbBr	(0.75)	(0.26)	0.25	0.25
RbI	(0.80)	(0.30)	0.27	0.26
CsCl + CsBr	(0.845)	(0.285)	0.23	0.16
CsI	–	–	–	0.16

were made for most of the electrolytes given in Table 4. In most cases the $x_{+1/2}$ and the x_0 curves even coincided completely.

The values of A^* and B^* in optimum 1 are given in Table 5. Values for rubidium and caesium halides have been estimated from $x_{-0.9}$, $x_{+0.9}$ and $(\ln f_\pm)_{min}$, since $x_{+1/2}$ and x_0 could not be safely extrapolated from experimental data. When two data sources disagree about the numerical values of $f_\pm$ we have proceeded with the values which seemed to follow the excluded volume pattern most closely. Especially some of the data given by Latimer[37] in more concentrated solutions seem to need careful scrutiny before use, see Fig. 11 for an example (KBr).

In Fig. 5 we have plotted the optimum values (optimum 1) of A^* found *vs.* the optimum values of of B^*. There seems to be a linear correlation between the two parameters. The lower the excluded volume, the lower the optimum A^*. A qualitative explanation may be that for smaller ions, the screening effects described in the preceding paragraph – leading to an A^* lower than $A_{D.H.}$ – are allowed to evolve to a greater extent at increasing ionic strength than for the larger ions where the excluded volume forces come into action at lower ionic strengths. The linear regression involving all

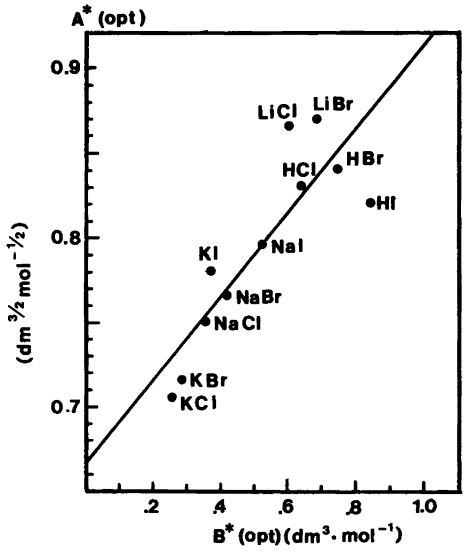

Fig. 5. Linear regression for optimal A^* on optimal B^*.

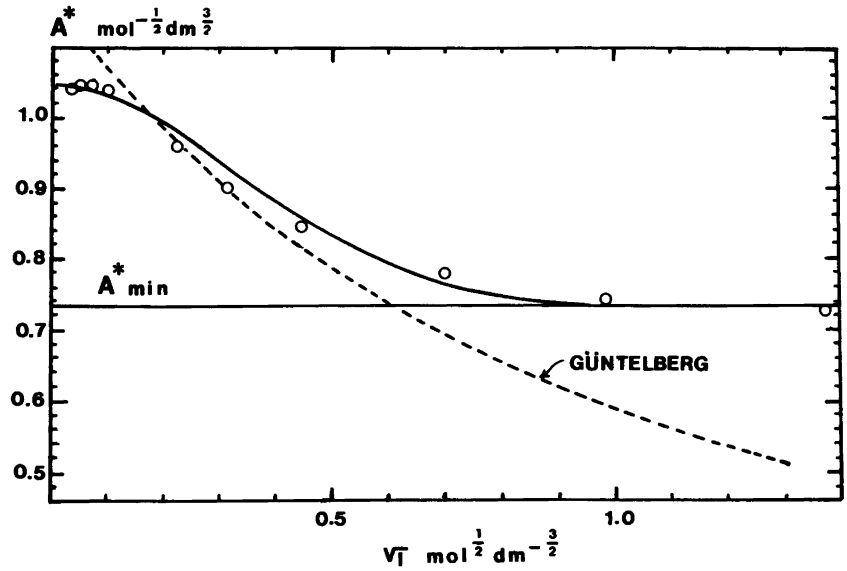

Fig. 6. The variation of A^* with ionic strength. ○ Calculated from experimental data for KCl in water at 25 °C with $B^*_{opt} = 0.27$ dm^3/mol. Full line: $0.734 + (0.89 A_{D.H.} - 0.734)\exp(-18 \times 0.27I)$.

the points in Fig. 5 (where LiI and Rb and Cs halides have been omitted) is found to be

$$A^*_{opt} = 0.247\, B^*_{opt} + 0.667 \tag{69}$$

No systematic variation between the parameters in optimum 2 (Fig. 4) is found. What I have done now is simply to force the deviating points to lie somewhere on the regression line without disturbing the good fit of the parabola too much. In this way I have obtained a one parameter expression for $\ln f_\pm$ for concentrations from the minimum in $\ln f_\pm$ and above. The chosen B^* values are listed in the fourth column of Table 5. What remains is then the concentration region from around 0.001 mol/dm^3 to the concentrations of minimum $\ln f_\pm$. If we calculate A^* as a function of ionic strength by means of

$$A^* = \frac{-\ln f_\pm + B^*_{opt} I}{\sqrt{I}} \tag{70}$$

we observe that the variation in A^* is quite well described by the expression (see Fig. 6)

$$A^* = A^*_{min} + (0.89\, A_{D.H.} - A^*_{min})e^{-\alpha I} \tag{71}$$

Expressions of the type $\exp(-\alpha'\sqrt{I})$ have also been tried, but they yield a bad fit. The classical D.H. expression taking into account ionic size in the electrostatic contribution to $\ln f_\pm$ would lead to the following variation of A^*:

$$A^* = \frac{A_{D.H.}}{1 + b\sqrt{I}} \tag{72}$$

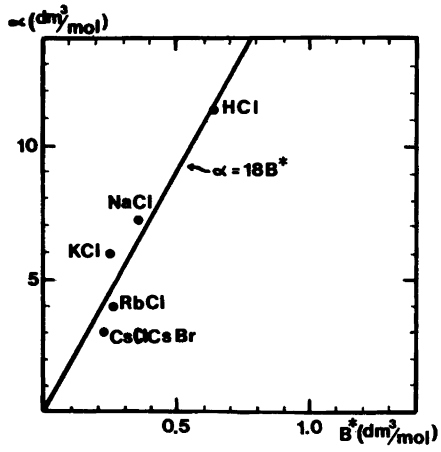

Fig. 7. Regression of α *vs.* B^*_{opt}.

When $b=1$ mol$^{-\frac{1}{2}}$ dm$^{3/2}$ one speaks about the Güntelberg approximation. This is indicated in Fig. 6 by a dashed line. The Güntelberg approximation as well as the more general D.H. relation fail to describe the asymptotic behaviour of A^* towards a minimum value A^*_{min} ($=A^*_{opt}$). Notice, that the experimentally determined slope of $0.89A_{D.H.}$ for small values of $\sqrt{I}$ (see Fig. 2) has been built into (71). This eqn. should therefore not be used for exact calculations below $I=0.001$ mol/dm^3.

Some of the α-values are plotted against B^* in Fig. 7. The regression yields a linear correlation given by

$$\alpha = 18.0B^* \qquad (73)$$

The final result is that $\ln f_\pm$ can be calculated from knowledge of the excluded volume only, by means of the formula

$$\ln f_\pm = -\{A^*_{min} + (0.89\,A_{D.H.} - A^*_{min})e^{-18B^*I}\}\sqrt{I} + B^*I \qquad (74)$$

[with $A^*_{min}=A^*_{opt}$ given by (69)] valid for all the uni-univalent electrolytes investigated in this paragraph.

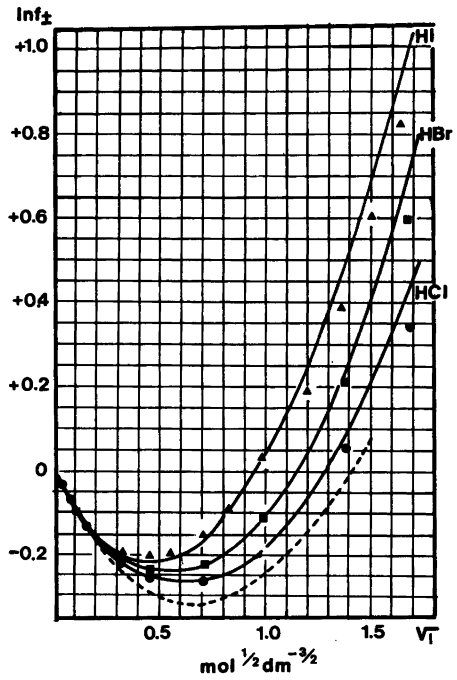

Fig. 8. ●, HCl (Ref. 37); ■, HBr (Ref. 37); ▲, HI (Ref. 37).

Dashed line: Calculation according to MSA-theory for HCl, see Appendix III. Text common to Figs. 8 – 12: Logarithm of molar mean ionic activity coefficients *vs.* square root of molar ionic strength in water at 25 °C. Full lines calculated from eqns. (69) and (74).

The expression (74) yields very fine correspondence with experimental values, see Figs. 8 – 12. The values of B^* for Rb and Cs halides were the most uncertainly determined due to lack of data for $x_{+\frac{1}{2}}$ and x_0. For these electrolytes, (74) has simply been taken for granted, and B^* has been fitted to give the best correspondence up to the greatest possible ionic strengths. Small changes in B^* have also been made for some of the other electrolytes. In that way, the values in the last column of Table 5 have appeared.

Thus, we have here a very simple one parameter formula which can easily compete with the more complicated two parameter formula of Robinson and Stokes[7] and with multi-parameter formulae such as given by Pitzer *et al.*[4] Eqn. (74) is also much simpler than the eqn. derived from the MSA-theory (see Appendix III). Furthermore, it will be shown in the next paragraph that the B^*-values found constitute a nice illustration of the principle of specific interaction of ions of Brønsted and yield values of the radii of the hydrated cations in reasonable accordance with radii estimated from ionic conductivity data.

RADII OF HYDRATED CATIONS FROM ASPEV-THEORY AND FROM CONDUCTANCE DATA

I have calculated the sum of radii ($R_+ + R_-$) from the final values of B^* (Table 5, column 5) using eqns. (67) and (23), *i.e.* the principle of specific interaction of ions of Brønsted is used. The results are given in Table 6. If the anions are assumed to be unhydrated, their radii are given by the Pauling radii and the values of the cationic radii given in Table 6, column 4 are found.

To have an independent check of those radii we have also considered data for ionic conductivities at infinite dilution (λ^0_i). The advantage of those data are that they can be ascribed completely to one single ion in pure solvent. The most obvious idea is to try to apply the Stokes-Einstein formalism, *i.e.* to assume the macroscopic, hydrodynamic law of

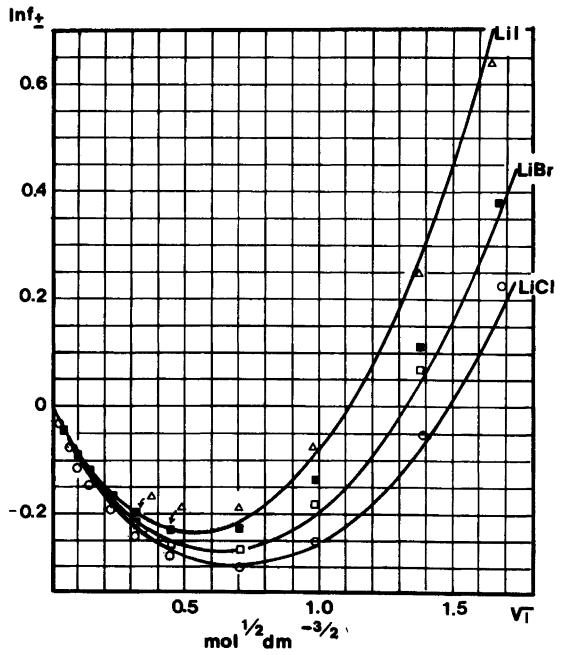

Fig. 9. ○, LiCl (Ref. 37); □, LiBr (Ref. 35); ■, LiBr, probably erroneous data (Ref. 37); △, LiI (Ref. 37).

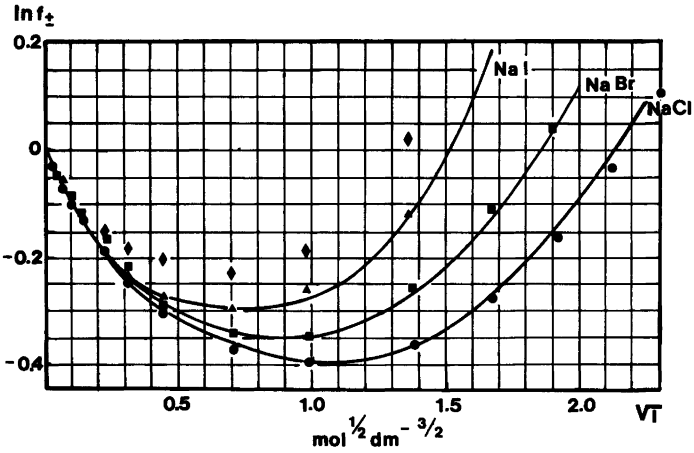

Fig. 10. ●, NaCl (Ref. 37); ■, NaBr (Ref. 37); ▲, NaI (Ref. 35); ◆, NaI, probably erroneous data (Ref. 37).

Stokes valid for the microscopic "friction coefficient". As is well-known, this procedure yields reasonable results for macromolecules. Calculating the cationic radii from

$$R_i = \frac{|z_i| F^2}{6\pi\eta\lambda_i^0} \tag{75}$$

(η = macroscopic viscosity for water at 25 °C) we obtain the values of the cationic radii given in Table 6, column 5. For K^+, Rb^+ and Cs^+ the

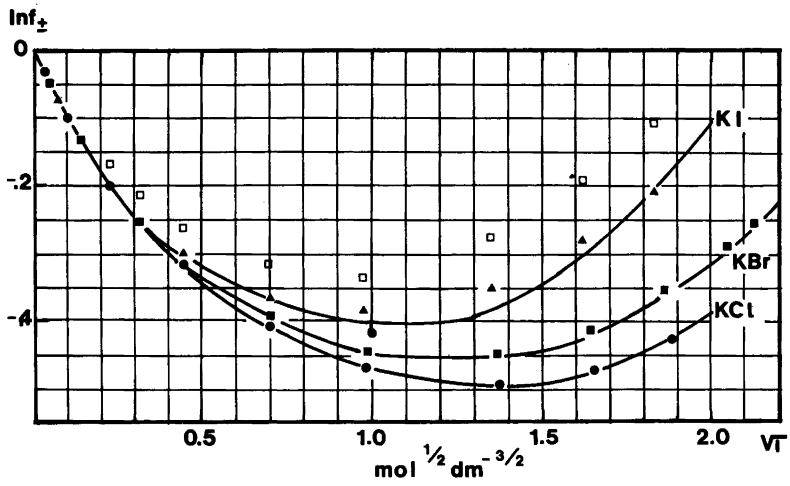

Fig. 11. ●, KCl (Ref. 37); ■, KBr (Ref. 37 $I \leqq 0.05$, Ref. 36 $I \geq 0.1$); ▲, KI (Ref. 35); □, KI, probably erroneous data (Ref. 37).

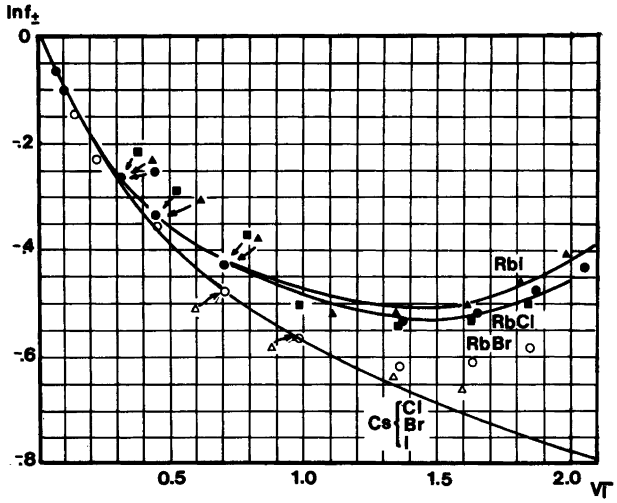

Fig. 12. ●, RbCl (Ref. 37, Ref. 35); ■, RbBr (Ref. 35); ▲, RbI (Ref. 35); ○, CsCl+CsBr (Ref. 37, Ref. 35); △, CsI (Ref. 35).

Stokes radii are less than the Pauling radii which cannot be true.

It is far from obvious, however, that Stokes' law can be used for an ion of approximately the same size as the solvent. One would expect – at least – that a "microscopic" viscosity should be applied instead of the macroscopic viscosity. Furthermore, as Frank[38] has pointed out, it seems to be beglected by most researchers that for small ions in highly dielectric solvents there is a substantial dielectric relaxation drag on a moving ion. In contrast to the so-called "relaxation effect" discussed in Onsager's theory of concentration dependence of equivalent conductivities of strong electrolytes, the ion-dipole relaxation effect operates also at infinite dilution. The effect was first discussed by Born,[39] rediscovered by Fuoss[40] and quantified in terms of modern dielectric theory by Boyd[41]

Table 6. Cationic radii from ASPEV-calculations and from other sources.

Electro-lyte	$R_+ + R_-$ (ASPEV) Å	R_- (Pauling) Å	R_+ (ASPEV) Å	R_+ (Stokes) Å	R_+ (modif.BFBZ) Å	$R_+ + R_-[\Lambda(c)]$ Å	R_+(MSA) Å
HCl	6.3	1.80				–	2.07
HBr	6.6	1.95	4.7(3)	–	–	–	2.13
HI	7.2	2.16				–	2.10
LiCl	6.0	1.80				–	1.94
LiBr	6.3	1.95	4.3(2)	2.35	5.35	–	1.95
LiI	6.7	2.16				–	1.94
NaCl	5.2	1.80				3.5 [a]	1.30
NaBr	5.5	1.95	3.5(2)	1.81	4.05	–	1.34
NaI	5.9	2.16	2.16			–	1.29
KCl	4.7	1.80				2.80,[b] 2.85,[c] 3.20[d]	0.91
KBr	4.9	1.95	2.9(1)	1.23	2.50	–	0.83
KI	5.2	2.16				–	0.75
RbCl	4.6	1.80				–	0.80
RbBr	4.6	1.95	2.6(2)	1.17	2.10	–	0.59
RbI	4.7	2.16				–	0.35
CsCl	4.0	1.80				–	0.58
CsBr	4.0	1.95	2.0(2)	1.17	2.15	–	0.37
CsI	4.0	2.16				2.41,[b] 2.56,[c] 3.49[d]	0.10

[a] Ref. 45. [b] Ref. 46, Table I, $D = 78.54$, first entry. [c] Ref. 46, Table I, $D = 78.54$, second entry. [d] Ref. 46, Table VI, $D = 78.54$.

and Zwanzig.[42] Here we shall call it the BFBZ-theory. According to this theory one has

$$\lambda_i^0 = \frac{|z_i| A R_i^3}{C + R_i^4} \tag{76}$$

For water at 25 °C and with R_i in Å and λ_i^0 in Ω^{-1} cm^2/mol we have $A = 91.7$ and C is around 10 Å^4. We see that for large values of R_i, Stokes' law is approached. It is interesting to observe that the BFBZ-theory predicts a maximum for the ionic conductivity. Such a maximum is actually found for the series F^-, Cl^-, Br^- and I^- when λ_i^0 is plotted against the crystallographic radii (see Fig. 13), but the maximum value of λ_i^0 predicted by the BFBZ-theory is too low. However, in view of the small sizes of the species involved, it is to be expected that the "macroscopic" constants A and C in (76) have to be adjusted. Using the height and the position of the maximum we find for the adjusted constants $A = 209$ and $C = 5.33$ Å. In this way the "modified BFBZ" curve in Fig. 13 was found. This curve, together with the values of the limiting ionic conductivities were used for calculation of the cationic radii given in Table 6, column 6. There will be two values of R_+ giving the same λ_i^0, but the larger of the values was always used.

In Table 6, column 7 some values of $R_+ + R_-$ are given which are derived from the deviation from the simple Onsager formula for equivalent conductivities (Λ) at higher concentrations.[44–46] These calculations are very involved and not really clarified, so that those values for the distance of closest approach cannot be regarded with much confidence.

The last column in Table 6 contains the values of R_+ found by Triolo *et al.*[26] by fitting the MSA-model to data for the concentration dependence of the osmotic coefficient, using Pauling radii for the anions. For the K, Rb and Cs halides the cationic radii are quite inconsistent and also less than the Pauling radii (see Table 7, column 3). The radii are generally much lower than the radii obtained from

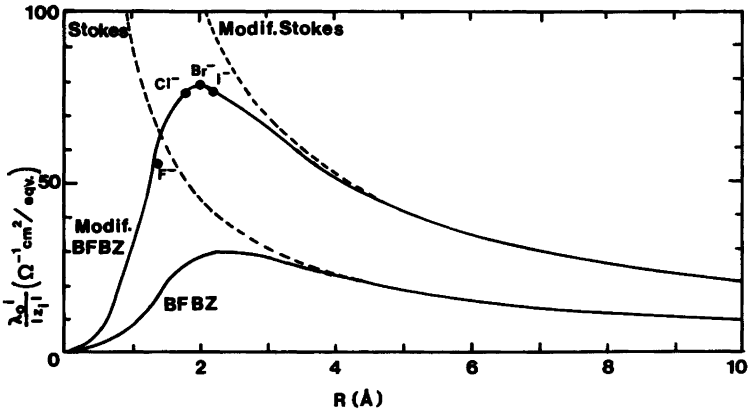

Fig. 13. Estimating ionic radii from Stokes' law and from the Born-Fuoss-Boyd-Zwanzig theory of dielectric relaxation drag; see text.

ASPEV or from modified BFBZ. In Appendix III I have calculated $\ln f_{\pm}$ for HCl from the MSA-theory using the radii of Triolo *et al.* The fit to experimental data is not very good (dashed curve in Fig. 8). Thus, it might be that the other radii given by Triolo *et al.* are not optimally fitted either.

Fig. 14 shows a comparison between the cationic radii calculated by the two independent semi-empirical methods (ASPEV and modified BFBZ). The radii are quite consistent and it is observed, that the ions with the smallest crystallographic radii are the largest, *i.e.* the most hydrated. The hydration numbers are estimated in Table 7. The values of the apparent ionic volumes used to correct the volume in the spherical shell between the Pauling radius and the ASPEV radius are the volumes reported by Bernal and Fowler (Ref. 32, Table V). We have

$$V_{\text{ion}}^{\text{app}} = \frac{4}{3}\pi R_{\text{p}}^3 + n\Delta V \qquad (77)$$

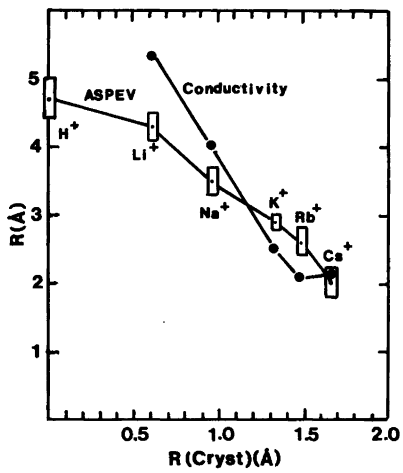

Fig. 14. Radii of hydrated cations calculated from ASPEV-theory compared to radii estimated from conductivity data. Abscissa: crystallographic radii of unhydrated cations.

Table 7. ASPEV-calculations of hydration numbers of cations.

Ion	R(ASPEV) Å	R(Pauling) Å	$(4\pi/3)(R^3 - R_{\text{P}}^3)$ Å^3	$V_{\text{ion}}^{\text{app}}$ Å^3 [a]	Hydration number, n	n(Ref. 43)	n(Ref. 7)
H^+	4.7	0	435	−8	15	–	9±1
Li^+	4.3	0.61	332	−8	11	5±1	8±1
Na^+	3.5	0.96	176	−8.5	6	5±1	4±1
K^+	2.9	1.33	92	+8	3	4±2	2±0.5
Rb^+	2.6	1.48	60	+15.5	2	3±1	1±0.3
Cs^+	2.0	1.66	14	+27	0.2	–	–

[a] Apparent (=partial) ionic volumes taken from Ref. 32.

where ΔV is the volume change per molecule water bound and n is the number of bound water molecules. Since a "normal" water molecule at 25 °C occupies 30.0 Å^3 we have

$$\frac{4}{3}\pi(R^3 - R_p^3) = n(30 + \Delta V) \tag{78}$$

From (77) and (78) and the data in Table 7 we can calculate the hydration numbers n shown in Table 7, column 6. They agree with the values of primary hydration numbers given by Bockris and Reddy[43] (column 7) except for Li^+. The ASPEV hydration numbers also agree roughly with the hydration numbers according to the theory of Stokes and Robinson (Ref. 7, Table I) which values are given in Table 7, column 8. This theory is criticized for a number of reasons in Appendix II, however.

The substantial success of the ASPEV-theory in giving radii of cations of uni-univalent electrolytes in agreement with radii and hydration numbers derived from other sources seems promising for future treatment of electrolytes of other valence types, for which the DHEV-theory also gave a consistent picture (though the radii were all too large). It is also my intention to scrutinise the existing data for electrolyte mixtures in the light of the ASPEV theory and to consider temperatures different from 25 °C.

Acknowledgement. The author is grateful to Niels Østerberg, Jørgen Birger Jensen, Jørgen Koefoed, Torben Jacobsen and Sven Atlung for stimulating discussions.

APPENDIX I. CRITIQUE OF COMMONLY APPLIED CHARGING PROCEDURES

The solution to the linearised P.B.-eqn. (32) is given by

$$\psi_i = C_i \frac{e^{-\varkappa r}}{r} \tag{A-I-1}$$

The constant C_i can be determined by using (31) and requiring the net charge between $r = a$ and $r = \infty$ to be equal to the charge on the central ion with opposite sign. We obtain

$$\psi_i = \frac{z_i F}{4\pi\varepsilon N_0} \times \frac{e^{-\varkappa(r-a)}}{r} \tag{A-I-2}$$

Two charging procedures commonplace in litterature (see, *e.g.*, Ref. 31, pp. 80–83 and Ref. 47, pp. 21–23) are the Debye charging process and the Güntelberg charging process. In the Debye method we calculate the electrostatic contribution to Helmholtz' free energy as the net work the surroundings have to do by first stripping the ions for their charges in infinite dilution (with a Coulomb-potential around each ion) and then charging all the ions simultaneously at the given concentration. We obtain (with charging and discharging in the distance $r = a$ from the central ions)

$$\Delta A_{el} = \sum_i n_i \frac{z_i^2 F^2}{4\pi N_0 \varepsilon a} \left\{ \int_0^1 \left[\frac{\xi}{1 + a\varkappa\xi} - \xi \right] d\xi \right.$$

$$= -\sum_i n_i \frac{z_i^2 F^2 \varkappa}{4\pi N_0 \varepsilon} \int_0^1 \frac{\xi^2}{1 + a\varkappa\xi} d\xi$$

$$= -\frac{F^2 \varkappa}{4\pi N_0 \varepsilon} \tau(\varkappa a) \sum_i n_i z_i^2 \tag{A-I-3}$$

where n_i is the number of mol of the i'th ion and ξ is the charging parameter. We have introduced the function

$$\tau(x) \equiv \frac{1}{x^3}\left[\ln(1+x) - x + \frac{1}{2}x^2\right] = \frac{1}{3} - \frac{1}{4}x + \frac{1}{5}x^2 - \ldots. \tag{A-I-4}$$

The electrostatic contribution to the chemical potential of the i'th ion is now

$$\mu_i^{el} = \left[\frac{\partial\left(\frac{\Delta A_{el}}{\Omega}\right)}{\partial c_i}\right]_{\Omega, T, c_j} = -\frac{F^2 z_i^2 \varkappa}{4\pi N_0 \varepsilon}\left[\tau(\varkappa a) + \right.$$

$$\left. \frac{1}{2}\frac{d}{d(\varkappa a)}(\varkappa a \tau(\varkappa a))\right] = -\frac{F^2 z_i^2}{8\pi N_0 \varepsilon} \times \frac{\varkappa}{1 + \varkappa a} \tag{A-I-5}$$

The Güntelberg charging process is more direct. Here we charge one single ion in a mixture of ions already charged. The electrostatic contribution to the chemical potential is then

$$\mu_i^{el} = \frac{z_i^2 F^2}{4\pi N_0 \varepsilon a} \int_0^1 \left[\frac{\xi}{1 + a\varkappa} - \xi\right] d\xi$$

$$= -\frac{z_i^2 F^2}{8\pi N_0 \varepsilon} \times \frac{\varkappa}{1 + \varkappa a} \tag{A-I-6}$$

identical to the expression (A-I-5). There is a serious drawback in connection with both charging processes, however. For small enough ionic strengths $a\kappa \ll 1$. Then the integrands in both (A-I-3) and (A-I-6) vanish and the electrostatic contribution to the chemical potential becomes nil. But the potential distribution given by (34) is still very different from a Coulomb-distribution (where κr should be approximately zero for all practical r). Then it is absurd that there should be no electrosatic contribution to the chemical potential.

The difficulties arise from the inaccurate use of a as sometimes the distance of closest approach and sometimes the ionic radii. Tanford[48] has given a more thorough derivation. He considers the potential around the central ion (1) in the following three regions:

I. The "interior" of ion 1.

II. The "excluded volume" between ion 1 and the counterion (2), *i.e.* the region from $r=R_1$ and $r=a=R_1+R_2$.

III. The region of the ionic cloud ($r>a$). In regions I and II there can be no charge (the charge of the central ion is visualized to be smeared out uniformly at the interface between I and II) and the Laplace eqn. therefore applies for the electric potential. In region III the linearised P.B. eqn. applies. Solving those eqns. together with the continuity conditions for ψ and $d\psi/dr$ at the interfaces I/II and II/III one obtains

$$\psi_1^{(I)} = \frac{z_1 F}{4\pi N_0 \varepsilon R_1}\left[1 - \frac{\kappa R_1}{1+\kappa a}\right] \qquad \text{(A-I-7a)}$$

$$\psi_1^{(II)} = \frac{z_1 F}{4\pi N_0 \varepsilon R_1}\left[1 - \frac{\kappa r}{1+\kappa a}\right] \qquad \text{(A-I-7b)}$$

$$\psi_1^{(III)} = \frac{z_1 F}{4\pi N_0 \varepsilon} \times \frac{e^{\kappa a}}{1+\kappa a} \times \frac{e^{-\kappa r}}{r} \qquad \text{(A-I-7c)}$$

For the electrical work in a Güntelberg charging process we have now

$$\mu_1^{el} = \frac{z_1^2 F^2}{4\pi N_0 \varepsilon R_1}\left[\int_0^1 \left[1 - \frac{\kappa R_1}{1+\kappa a}\right]\xi d\xi - \int_0^1 \xi d\xi\right] \qquad \text{(A-I-8)}$$

and we again find (A-I-5) or (A-I-6) but in a much more satisfactory way, since we can put $\kappa a \ll 1$ before the integration without having $\mu_1^{el}=0$.

Also the Tanford charging procedure can be criticised on a more fundamental level, however. For small κa we obtain for the potential at $r=a$ from (A-I-7b and c)

$$\psi_1(r=a) \cong \frac{z_1 F}{4\pi N_0 \varepsilon a} \qquad \text{(A-I-9)}$$

Very near to the central ion, the Debye-Hückel condition therefore takes the form

$$\frac{F^2}{4\pi R T N_0 \varepsilon a} \ll 1 \qquad \text{(A-I-10)}$$

However, calculating the quantity on the l.h.s. of the inequality (A-I-10) with $F=96\,500$ C, $a=5\times10^{-10}$ m, $\varepsilon=6.9\times10^{-10}$ Farad/m, $N_0=6.02\times10^{23}$, $T=298$ K and $R=8.31$ J/molK we find the number 1.44! Thus, the assumption behind the linearisation of the P.B. eqn. is far from valid at the position where the solution is applied in the charging process. As rescue for the charging procedures Güntelberg[49] calculated that 97 % of the potential at $r=a$ originated from ions at distances $r>2a$ and 88 % from ions at distances $r>5a$ at an ionic strength of 10^{-3} mol/dm^3. Since the D.H. assumption is valid at those distances, it does not mean so much that it fails near to the central ion. The whole procedure becomes quite artificial and unpedagogical, however, and the Résibois charging method used in the main text should be applied instead.

APPENDIX II. CRITIQUE OF THE THEORY OF STOKES AND ROBINSON

The hydration theory of Stokes and Robinson[7] has been much cited in electrochemical textbooks. Here we shall follow the derivation given in Ref. 47, pp. 30–32 which shows the fundamental assumptions more clearly than the original text. For the Gibbs' free energy of a mixture of n_0 mol solvent and one mol electrolyte we have

$$G = n_0\mu_0 + \nu_+\mu_+ + \nu_-\mu_- = (n_0 - h)\mu_0' + \nu_+\mu_+' + \nu_-\mu_-' \qquad \text{(A-II-1)}$$

h is the number of solvent molecules bound to 1 molecule of the electrolyte, and the primed chemical potentials correspond to the chemical potential of

free solvent and of solvated electrolyte. It is assumed that

$$\mu_0' = \mu_0 \qquad \text{(A-II-2)}$$

When the chemical potentials are split up into standard and variable terms one obtains from (A-II-1) and (A-II-2)

$$\frac{\nu_+(\mu_+^0 - \mu_+^{0'})}{RT} + \frac{\nu_-(\mu_-^0 - \mu_-^{0'})}{RT} + \frac{h\mu_0^0}{RT}$$

$$= -h \ln a_0 - \nu \ln \frac{n_0 + \nu - h}{n_0 + \nu} - \nu_+ \ln \gamma_+^{\times} - \nu_- \ln \gamma_-^{\times}$$
$$+ \nu_+ \ln (\gamma_+')^{\times} + \nu_- \ln (\gamma_-')^{\times} \qquad \text{(A-II-3)}$$

where $\nu = \nu_+ + \nu_-$ and $\gamma^{\times}$ are activity coefficients based on mol fractions. At infinite dilution $n_0 \to \infty$ and all the terms on the r.h.s. of (A-II-3) become zero. The l.h.s. of (A-II-3) must then be zero in all cases. Introducing this in (A-II-3), changing to molal activity coefficients instead of rational activity coefficients using

$$n_0 = 1\,000/M_0 m \qquad \text{(A-II-4)}$$

$$\gamma_{\pm}{}^{\times} = \gamma_{\pm}^{m}[1 + 0.001\, \nu\, M_0 m] \qquad \text{(A-II-5)}$$

(M_0 = molecular weight of solvent) and introducing mean ionic activity coefficients, we obtain from (A-II-3)

$$\ln \gamma_{\pm}^{m} = \ln (\gamma_{\pm}')^{\times} - \frac{h}{\nu} \ln a_0 - \ln [1 + 0.001\, M_0(\nu - h)m] \qquad \text{(A-II-6)}$$

With the following identification

$$\ln (\gamma_{\pm}')^{x} = -\frac{A_{\text{D.H.}} |z_+ z_-| \sqrt{I}}{1 + b\sqrt{I}} \qquad \text{(A-II-7)}$$

formula (A-II-6) is the formula used by Stokes and Robinson. The solvent activity coefficient is calculated by means of data for the osmotic coefficient Φ_m

$$\ln a_0 = -0.001\, M_0 m \nu \Phi_m = -\frac{c_s \nu}{c_o} \Phi_m \qquad \text{(A-II-8)}$$

Whereas the postulate (A-II-2) seems reasonable enough, the identification (A-II-7) has no basis in D.H. theory, whatever. According to D.H. theory it is $\ln f_{\pm}$ which is equal to the r.h.s. of (A-II-7) and certainly not the logarithm of the rational activity coefficient! Furthermore, data for the osmotic coefficient as a function of concentration has to be used to calculate the r.h.s. of (A-II-6), but from such data activity coefficients can be calculated directly by means of the exact thermodynamic formula

$$-\ln \gamma_{\pm}^{m} = (1 - \Phi_m) + \int_0^m (1 - \Phi_m) \mathrm{d} \ln m \qquad \text{(A-II-9)}$$

[see Ref. 47, p. 8, eqn. (50)]. Therefore, the whole fitting procedure of Stokes and Robinson seems to be a redundance. Better derivations of similar hydration theories have been performed later by Glueckauf,[8] Jacobsen and Skou[9] and Stokes and Robinson,[10] but the formula (A-II-6) with (A-II-7) and (A-II-8) is the one most cited and used. At any rate, such expressions are two parameter formulae with the distance of closest approach as one parameter (a) and the hydration number (h) as the other. But those parameters are not independent, and are united in the excluded volume parameter in the ASPEV-theory.

APPENDIX III. SAMPLE CALCULATION OF ACTIVITY COEFFICIENTS IN THE MEAN SPHERICAL APPROXIMATION MODEL

Triolo *et al.* [Ref. 26, eqn. (24)] give the following formula for the osmotic coefficient in the mean spherical approximation (MSA) model

$$\Phi_m = \frac{\Pi}{\Pi_{\text{ideal}}} = -\frac{\Gamma^3}{3\pi\nu} + 1 + \beta_2 c_s N_0 + \beta_3 c_s^2 N_0^2 \qquad \text{(A-III-1)}$$

The generalised inverse Debye length Γ is found as solution to the algebraic eqn. [Ref. 26, eqn. (9)]

$$2\Gamma = \frac{\varkappa}{\sqrt{2}} \times f(\Gamma) = \frac{\varkappa}{\sqrt{2}} \sqrt{\sum_i \frac{\nu_i z_i^2}{(1 + \Gamma\sigma_i)^2}} \qquad \text{(A-III-2)}$$

where κ is given by eqn. (33) in the main text and σ_i is the hard core diameter of ion number i. The β-terms in (A-III-1) are of the Percus-Yevick type with

$$\beta_2 = \frac{\pi}{2}(\zeta_3/3 + \zeta_1\zeta_2/\zeta_0) \qquad \text{(A-III-3)}$$

Table 8. Example of mean spherical approximation calculation of activity coefficients.[a]

Conc. mol/dm^3	$\Gamma_0 = \kappa/2$ Å^{-1}	Γ_1 Å^{-1}	Γ_2 Å^{-1}	Γ_3 Å^{-1}	Γ_4 Å^{-1}	$g(\Gamma_4)$	$2\beta_2 N_0 c_s$	$(3/2)\beta_3 N_0^2 c_s^2$	$\ln f_\pm$
0.001	0.0052	0.00510			0.00510	−0.0358	0.0003	–	−0.0355
0.005	0.0117	0.0112			0.0112	−0.0770	0.0015	–	−0.0755
0.01	0.0164	0.0154	0.0155		0.0155	−0.1046	0.0030	–	−0.1016
0.05	0.0368	0.0322	0.0327		0.0327	−0.208	0.015	–	−0.193
0.1	0.052	0.0433	0.0445		0.0444	−0.271	0.030	0.0002	−0.241
0.5	0.117	0.0806	0.0892	0.087	0.0870	−0.470	0.148	0.005	−0.322
1.0	0.164	0.101	0.118	0.113	0.114	−0.559	0.295	0.020	−0.244
2.0	0.231	0.122	0.151	0.146	0.148	−0.664	0.590	0.081	+0.007

[a] All calculations: Hard core diameters $\sigma_+ = 4.14$ Å, $\sigma_- = 3.60$ Å.

$$\beta_3 = \frac{\pi^2}{36}[\zeta_3^2 + 6\zeta_2(\zeta_1\zeta_3 + \frac{1}{2}\zeta_2^2)/\zeta_0] \qquad \text{(A-III-4)}$$

and

$$\zeta_n = \sum_i \nu_i \sigma_i^n \quad (n = 0, 1, 2, 3) \qquad \text{(A-III-5)}$$

Since the ideal osmotic pressure is $\Pi_{id} = RT\nu c_s$ we have from (A-III-1) that

$$\frac{\Pi}{RT} = h(\Gamma) + \nu c_s + \nu\beta_2 N_0 c_s^2 + \nu\beta_3 N_0^2 c_s^3 \qquad \text{(A-III-6)}$$

From eqn. (13) in the main text we have

$$\frac{\Pi}{RT} = \nu c_s + \nu \int_0^{c_s} c_s' \, \mathrm{d} \ln f_\pm' \qquad \text{(A-III-7)}$$

Introducing

$$\ln f_\pm' = g(\Gamma') + Bc_s' + Cc_s'^2 \qquad \text{(A-III-8)}$$

in (A-III-7) we obtain

$$\frac{\Pi}{RT} = \nu \int_0^{c_s} c_s' \frac{\mathrm{d}g}{\mathrm{d}\Gamma'} \frac{\mathrm{d}\Gamma'}{\mathrm{d}c_s'} \mathrm{d}c_s' + \nu c_s + \frac{\nu}{2} B c_s^2 + \frac{2\nu}{3} C c_s^3 \qquad \text{(A-III-9)}$$

Comparison with (A-III-6) makes obvious that the integral amounts to the h-function, and

$$\ln f_\pm = g(\Gamma) + 2\beta_2 N_0 c_s + \frac{3}{2}\beta_3 N_0^2 c_s^2 \qquad \text{(A-III-10)}$$

Blum and Høye [Ref. 25, eqn. (3.11)] have given the following formula for $g(\Gamma)$ according to the MSA-model

$$g(\Gamma) = -\frac{\kappa^2 \Gamma}{16\pi N_0 c_s} \sum \frac{\nu_i z_i^2}{1 + \Gamma\sigma_i} \qquad \text{(A-III-11)}$$

This is a very interesting formula, since it is to my knowledge the only example of a modern statistical mechanical theory yielding a formalism somewhat similar to the original D.H. expression (A-I-6). Take a uni-univalent electrolyte, for example, and put $\sigma_+ = \sigma_- = a$. From (A-III-2) it is obvious, that Γ for small concentrations is equal to $\kappa/2$. Inserting this and the definition of κ in (A-III-11) we again find the D.H. expression (A-I-6).

Triolo *et al.* have fitted the MSA-model to osmotic coefficient data for 23 uni-univalent electrolytes. For HCl they have found $\sigma_+ = 4.14$ Å and $\sigma_- = 3.60$ Å. From those diameters Γ can be calculated from (A-III-2) inserting $\Gamma_0 = \kappa/2$ on the r.h.s., thereby calculating Γ_1 and so on. Three or four iterations are necessary for a precision of 1 %. Then $\ln f_\pm$ can be calculated by (A-III-10 & 11). The results are given in Table 8 and represented as the dashed line in Fig. 8. The fit to experimental data does not seem very good, so perhaps the values of the hard core diameters found by Triolo *et al.* should be reconsidered.

REFERENCES

1. Debye, P. and Hückel, E. *Phys. Z. 24* (1923) 185.
2. Scatchard, G. and Prentiss, S. S. *J. Am. Chem. Soc. 54* (1932) 2696.

3. Lange, J. *Z. Phys. Chem. 168 A* (1934) 147.
4. Pitzer, K. S. and Mayorga, G. *J. Phys. Chem. 77* (1973) 2300.
5. Bjerrum, N. *Medd. K. Vetenskapsakad. Nobelinst. 5* (1919) 16.
6. Bjerrum, N. *Z. Anorg. Allg. Chem. 109* (1920) 275.
7. Stokes, R. H. and Robinson, R. A. *J. Am. Chem. Soc. 70* (1948) 1870.
8. Glueckauf, E. *Trans. Faraday Soc. 51* (1955) 1235.
9. Jacobsen, T. and Skou, E. *Electrochim. Acta 22* (1977) 161.
10. Stokes, R. H. and Robinson, R. A. *J. Solution Chem. 2* (1973) 173.
11. Gronwald, T. H., La Mer, V. K. and Sandved, K. *Phys. Z. 29* (1928) 358.
12. La Mer, V. K., Gronwald, T. H. and Greiff, L. J. *J. Phys. Chem. 35* (1931) 2245.
13. Guggenheim, E. A. *Trans. Faraday Soc. 55* (1959) 1714.
14. Guggenheim, E. A. *Trans. Faraday Soc. 56* (1960) 1152.
15. Guggenheim, E. A. *Trans. Faraday Soc. 58* (1962) 86.
16. Onsager, L. *Chem. Rev. 13* (1933) 73.
17. Morawetz, H. *Macromolecules in Solution*, Interscience, New York 1965, p. 336.
18. Mayer, J. E. *J. Chem. Phys. 18* (1950) 1426.
19. Kirkwood, J. G. and Poirier, J. C. *J. Phys. Chem. 58* (1954) 591.
20. Résibois, P. M. V. *Electrolyte Theory*, Harper and Row, New York, Evanston, London 1968.
21. Rasaiah, J. C. and Friedman, H. L. *J. Chem. Phys. 48* (1968) 2742.
22. Ramanathan, P. S., Krishnan, C. V. and Friedman, H. L. *J. Solution Chem. 1* (1972) 237.
23. Lebowitz, J. L. and Percus, J. K. *Phys. Rev. 144* (1966) 251.
24. Waisman, E. and Lebowitz, J. L. *J. Chem. Phys. 56* (1972) 3086, 3093.
25. Blum, L. and Høye, J. S. *J. Phys. Chem. 81* (1977) 1311.
26. Triolo, R. and Grigera, J. R., Blum, L. *J. Phys. Chem. 80* (1976) 1858.
27. Reed, T. M. and Gubbins, K. E. *Applied Statistical Mechanics*, McGraw-Hill Chemical Engineering Series 1973.
28. Mayer, J. E. *J. Chem. Phys. 10* (1942) 629.
29. Lewis, G. N. and Randall, M. *J. Am. Chem. Soc. 43* (1921) 1112.
30. Brønsted, J. N. *K. Dan. Vidensk. Selsk. Mat.-Fys. Medd. IV* (1921) 4.
31. Newman, J. S. *Electrochemical Systems*, Prentice-Hall, Englewood Cliffs, N.J. 1973.
32. Bernal, J. D. and Fowler, R. H. *J. Chem. Phys. 1* (1933) 515.
33. Abramowitz, M. and Stegun, I. A. *Handbook of Mathematical Functions*, Dover, New York 1965.
34. Brønsted, J. N. and Brumbaugh, N. J. *J. Am. Chem. Soc. 48* (1926) 2015.
35. Harned, H. S. and Owen, B. B. *The Physical Chemistry of Electrolyte Solutions*, 3rd Ed., Van Nostrand – Reinold, New York 1958, Appendix A, pp. 731 – 735.
36. Robinson, R. A. and Stokes, R. H. *Electrolyte Solutions*, 2nd Ed., Butterworths, London 1959, Appendix 8.10.
37. Latimer, W. M. *Oxidation Potentials*, 2nd Ed., Prentice-Hall, Englewood Cliffs, N.J. 1952, Appendix II.
38. Frank, H. S. *Solvent Models and the Interpretation of Ionization and Solvation Phenomena*, pp. 53 – 66 in Conway, B. E. and Barradas, R. G., Eds., Chemical Physics of Ionic Solutions, Wiley, New York – London – Sydney 1966.
39. Born, M. *Z. Phys. 1* (1920) 221.
40. Fuoss, R. M. *Proc. Natl. Acad. Sci. U.S.A. 45* (1959) 807.
41. Boyd, R. H. *J. Chem. Phys. 35* (1961) 1281.
42. Zwanzig, R. *J. Chem. Phys. 38* (1963) 1603.
43. Bokris, J.O'M. and Reddy, A. K. N. *Modern Electrochemistry*, Plenum, New York 1970, Table 2.18, Vol. 1, p. 119.
44. Murphy, T. J. and Cohen, E. G. D. *Biosystems 8* (1977) 255.
45. Cohen, E. G. D. and Murphy, T. J. *J. Chem. Phys. 53* (1970) 2173.
46. Fuoss, R. M., Onsager, L. and Shinner, J. F. *J. Phys. Chem. 69* (1965) 2581.
47. Koryta, J., Dvořák, J. and Boháčková, V. *Electrochemistry*, Methuen, London 1970.
48. Tanford, C. *Physical Chemistry of Macromolecules*, Wiley, New York – London – Sydney 1961, pp. 461 – 466.
49. Güntelberg, E. *Studier over Elektrolyt-aktiviteter i Vandige Opløsninger*, Diss., G.E.C. Gads Forlag, København 1938, p. 24.

Received January 13, 1978.

Acta Chemica Scandinavica A 32 (1978) 595–602

Enthalpies of Mixing in Binary Liquid Alkali Hydroxide Mixtures

B. K. ANDERSEN * and O. J. KLEPPA

The James Franck Institute and The Department of Chemistry, The University of Chicago, Chicago, Illinois 60637, U.S.A.

The enthalpies of mixing in the binary liquid alkali hydroxide mixtures have been determined by direct high temperature calorimetry. The measurements were performed over wide ranges of composition at 773 K.

The results are discussed and interpreted in terms of the conformal solution theory for fused salts of Reiss, Katz, and Kleppa as modified by Blander and by Davis and Rice. The enthalpies of mixing at the 50:50 compositions are well represented by the semiempirical expression

$$4\Delta H^{M}_{0.5} = U_0^{++} + (17.8/\text{Å}^2)\Delta\alpha\delta_{12} - (1250/\text{Å}^{-2})\delta_{12}^2, \text{ kJ mol}^{-1}$$

In this expression, $\delta_{12}=(d_1-d_2)/d_1d_2$, where d_1 and d_2 are characteristic interionic distances in the two salts; U_0^{++} represents a numerical estimate of the positive contribution to the enthalpy of mixing, which arises from the London–van der Waals interaction between next nearest neighbour cations; $\Delta\alpha$ is the difference in polarizability between the two cations.

A large number of binary molten salt systems have been studied by means of direct high temperature heat of mixing calorimetry. Thus, among the monovalent symmetrical salts with a common anion, AX-BX, extensive studies have now been carried out on the alkali halides and on the alkali nitrates. So far, no comparable thorough study has been made of the binary alkali hydroxides, which are of interest both from a practical and theoretical point of view. For example, it is well known that the ionic radius of OH^- is roughly comparable to that of F^-. However, the former ion has much greater polarizability, and also has a permanent dipole moment. Hence a comparison of the liquid hydroxides with the liquid fluorides is of special interest.

To our knowledge the only direct calorimetric measurements carried out on molten alkali hydroxides are those of Aghai-Khafri *et al.*[1] However, these authors studied only the NaOH–KOH system and only in very dilute solutions. Prior to this, Lumsden[2] had calculated excess chemical potentials in this system from the phase diagram of Reshetnikov and Vilutis,[3] using the thermochemical data given by Douglas and Dever,[4] and by Kelley.[5]

EXPERIMENTAL

Apparatus. All the calorimetric experiments were carried out in a single unit Calvet-type microcalorimeter suitable for work at temperatures up to about 1400 K. Apart from its single (rather than twin) construction and the higher operating temperature, the calorimeter is similar to that previously described by Kleppa.[6]

Due to the corrosive nature of molten alkali hydroxides, these cannot, unlike most other salts which have been studied previously, be handled in fused silica containers and by the usual "break-off" technique. Separate tests showed that the attack on Palau (20 % Pd and 80 % Au) by alkali hydroxide melts kept in an inert atmosphere was negligible. Therefore, this alloy was chosen as the only material in contact with the hydroxide melts during the mixing experiments. These were carried out in an atmosphere of pure dry argon.

* Present address: Fysisk-Kemisk Institut, The Technical University of Denmark, DK-2800 Lyngby, Denmark.

Table 1. Supplier and purity of chemicals.

Chemicals	Supplier Purity	Content of Alk_2CO_3 in mol %	Impurities by spectroscopic analysis in weight %
LiOH	Baker Chemical Co. Analytical Reagent	0.32	NaOH + KOH 0.07 Others ≤ 0.003
NaOH	Baker Chemical Co. Analytical Reagent	0.36	KOH 0.002 Others ≤ 0.003
KOH	Baker Chemical Co. Analytical Reagent	0.15	NaOH + RbOH 0.11 Others ≤ 0.015
RbOH	Kawecki Berylco Industries, Inc. High purity	0.30	KOH 0.42, CsOH 0.22 Others ≤ 0.10
CsOH	Kawecki Berylco Industries, Inc. High purity	0.24	NaOH + KOH + RbOH 0.09 Others ≤ 0.06

The experimental arrangements inside the calorimeter proper are the same as those previously used by Andersen and Kleppa.[7] Both the plunger and the dipper-crucible could be manipulated from outside the calorimeter proper.

Chemicals. The chemicals used in the present work and their purities are shown in Table 1.

The alkali hydroxides, which as received contained up to 12 weight % of water, were dried by heating them slowly in an atmosphere of dry argon up to 700–800 K over a period of 24 h. Silver was found to be a reasonably satisfactory container material. Because of the instability of LiOH (probably due to the reaction $2LiOH \rightarrow Li_2O + H_2O$) and the volatility of RbOH and CsOH care was taken to avoid prolonged heating at elevated temperatures.

The carbonate contents determined by means of a CO_2-evolution technique were 0.15–0.36 mol percent, and they were hence of the same order of magnitude in all the hydroxides. Therefore enthalpy contributions due to reciprocal reactions of the type

$$Alk^{I}_2CO_3(1) + 2Alk^{II}OH(1) \rightarrow Alk^{II}_2CO_3(1) + 2Alk^{I}OH(1)$$

could be neglected.

The alkali hydroxides are extremely hygroscopic. In order to avoid the pick-up of H_2O and CO_2 the filling and weighing processes were carried out in a dry box in an atmosphere of dry argon.

Procedure. Immediately before insertion into the calorimeter, the fused silica liner with its content was preheated for a period of 15 min about 50 K above the operating temperature of the calorimeter. In typical runs the total time elapsed prior to mixing was about 2 h. All systems were studied at the temperature 773 ± 1 K.

Due to the instability and volatility of the hydroxides at more elevated temperatures we did not study the temperature dependence of the enthalpies of mixing.

The mixing of the two salts was achieved by vertical manipulation of the plunger and dipper. After the initial mixing process three additional stirring operations were carried out at one minute intervals to assure complete mixing. Each stirring operation gave rise to a small reproducible heat effect, which had to be corrected for in some of the experiments.

In each run a total of 80 to 250 mmol of salt was used. The calibration of the calorimeter was achieved by dropping weighed pieces of 2 mm gold wire from room temperature into the calorimeter. The evaluation of the resulting endothermic heat effects was based on Kelley's equation for the heat content of gold.[5] At 773 K the weight losses because of vaporization and decomposition of the hydroxides were small, less than 0.2 %, and could be neglected. Also, the correction which is made for the heat pick-up of the gold pieces during the fall into the calorimeter was very small; from data given by Melnichak[8] this correction was estimated to be 0.1 % or less.

The temperature-sensing device of the calorimeter consists of a 54 + 54 junction Pt-Pt/13 %Rh thermopile, the output of which is amplified by means of a Leeds & Northrup D.C. amplifier and recorded on a Type H-Azar recorder. The emf *versus* time curves were integrated by means of an

Ott precision planimeter. In this way the area between the curve and the "base line", which is proportional to the total heat effect, could be determined with a precision of about ±0.3 %. The error due to uncertainty in drawing the base line was in most experiments estimated to be about ±1 %. However, in some experiments, especially those on the KOH–RbOH, KOH–CsOH, and RbOH–CsOH systems, which have very small enthalpies of mixing, this relative error was much larger.

RESULTS

All the ten binary alkali hydroxide systems were investigated. The concentration dependence of the enthalpy of mixing was studied for all the lithium and sodium containing systems. For the three remaining systems (KOH–RbOH, KOH–CsOH, and RbOH–CsOH) the heat effects were small and

Table 2. Molar enthalpies of mixing of binary liquid alkali hydroxide mixtures. x_1 is the mol fraction of the salt with the smaller cation.

Mol fraction x_1	Total, mol	ΔH^M/ kJ mol^{-1}	$(\Delta H^M/x_1x_2)$/ kJ mol^{-1}
LiOH–NaOH			
0.1499	0.19565	−0.843	−6.617
0.1505	0.17573	−0.885	−6.921
0.2503	0.22867	−1.243	−6.625
0.2513	0.24393	−1.353	−7.193
0.3607	0.17295	−1.627	−7.055
0.4010	0.20050	−1.678	−6.987
0.5512	0.22328	−1.718	−6.944
0.8010	0.25397	−1.087	−6.820
0.8464	0.17349	−0.937	−7.207
0.9002	0.27949	−0.636	−7.077
LiOH–KOH			
0.05045	0.10112	−0.558	−11.651
0.1000	0.13188	−1.135	−12.609
0.1508	0.13267	−1.704	−13.304
0.1996	0.16809	−2.274	−14.232
0.2999	0.15755	−3.266	−15.556
0.3001	0.15234	−3.074	−14.637
0.4000	0.14742	−3.574	−14.890
0.5002	0.16926	−4.324	−17.295
0.5503	0.18262	−4.283	−17.308
0.5999	0.17121	−4.075	−16.979
0.7000	0.21776	−3.758	−17.896
0.8003	0.22927	−2.950	−18.457
0.8483	0.16875	−2.438	−18.942
0.9000	0.21886	−1.756	−19.514
0.9202	0.24742	−1.437	−19.562
LiOH–RbOH			
0.05004	0.10112	−0.492	−10.345
0.1000	0.12370	−1.048	−11.644
0.1997	0.07887	−1.758	−10.997
0.2514	0.13841	−2.366	−12.572
0.3001	0.15930	−2.879	−13.705
0.4000	0.15984	−3.382	−14.093
0.5501	0.18421	−4.093	−16.538
0.6500	0.18502	−4.088	−17.970
0.7521	0.19726	−3.404	−18.252
0.9201	0.24090	−1.488	−20.247
LiOH–CsOH			
0.05194	0.10894	−0.412	−8.369
0.2000	0.08560	−1.781	−11.130
0.3000	0.11309	−2.416	−11.507
0.4001	0.16377	−3.450	−14.376
0.4505	0.13329	−3.661	−14.788
0.5806	0.16209	−3.561	−14.624
0.9000	0.23144	−1.850	−20.559
0.9500	0.26970	−1.038	−21.851
NaOH–KOH			
0.1998	0.12685	−0.4193	−2.622
0.1999	0.12631	−0.3901	−2.439
0.2003	0.14481	−0.3611	−2.255
0.2517	0.12357	−0.4937	−2.621
0.4997	0.18120	−0.6072	−2.429
0.6009	0.16501	−0.5113	−2.132
0.8800	0.17567	−0.2263	−2.143
0.8801	0.15160	−0.2298	−2.176
0.9004	0.21219	−0.1825	−2.035
0.9001	0.18303	−0.2048	−2.278
NaOH–RbOH			
0.2000	0.13486	−0.6211	−3.882
0.4010	0.12907	−0.8663	−3.606
0.8801	0.17088	−0.3623	−3.433
0.9001	0.17512	−0.3178	−3.533
NaOH–CsOH			
0.2506	0.11301	−0.5934	−3.160
0.4002	0.13298	−0.7974	−3.322
0.7998	0.15368	−0.4651	−2.905
0.8959	0.16969	−0.2890	−3.099
0.9002	0.15683	−0.2964	−3.299
KOH–RbOH			
0.2998	0.13034	0.0468	0.223
0.7502	0.14087	0.0323	0.172
KOH–CsOH			
0.2001	0.10837	0.1633	1.020
0.9000	0.13470	0.1249	1.389
RbOH–CsOH			
0.3499	0.11198	0.0541	0.238
0.8500	0.11285	0.0322	0.252

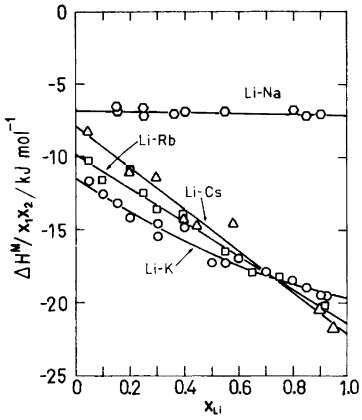

Fig. 1. Plots of $\Delta H^M/x_1x_2$ *versus* x_{Li} for LiOH–AlkOH mixtures.

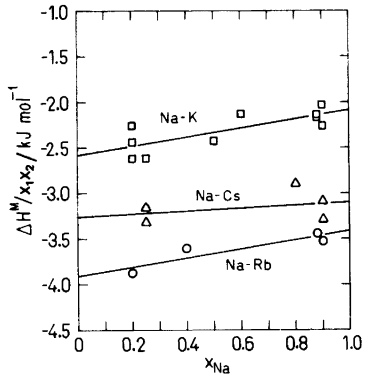

Fig. 2. Plots of $\Delta H^M/x_1x_2$ *versus* x_{Na} for NaOH–KOH, NaOH–RbOH, and NaOH–CsOH mixtures.

values for two mixtures only in each system were determined.

The experimental results are tabulated in Table 2. In Figs. 1 and 2 the enthalpy interaction parameter, $\Delta H^M/x_1x_2$, is plotted *versus* the mol fraction of the salt with the smaller cation.

By means of the least squares method the experimental data for the seven systems shown in Figs. 1 and 2 were fitted to linear expressions of the form

$$\Delta H^M/x_1x_2 = a + bx_1 \quad (1)$$

For LiOH–KOH a curve of second degree

$$\Delta H^M/x_1x_2 = a + bx_1 + cx_1x_2 \quad (2)$$

was found to give a much better fit. In Table 3 we give the values of the coefficients a, b and c as well as the enthalpies of mixing at the 50:50 composition.

DISCUSSION

The enthalpies of mixing are interpreted in light of the conformal solution theories for fused salts developed by Reiss, Katz, and Kleppa (RKK),[9] by Blander,[10] and by Davis and Rice (DR).[11]

We have chosen to represent the enthalpy of mixing for a given binary system by $4\Delta H^M_{0.5}$, *i.e.*, by the calculated value of the interaction parameter, $\Delta H^M/x_1x_2$, at the equimolar composition. To these values we have applied a correction by estimating the values of U_0^{++}, the change on mixing in the London-van der Waals dispersion energy between next nearest neighbour cations. The method of

Table 3. Integral enthalpies of mixing for binary alkali hydroxides at 773 K ($\Delta H^M = x_1x_2(a+bx_1+cx_1x_2)$ kJ mol^{-1}; x_1 is mol fraction of salt with the smaller cation).

System	a	b	c	$4\Delta H^M_{0.5}$	S.D.
LiOH–NaOH	−6.80	−0.30		−6.95	0.20
LiOH–KOH	−11.43	−8.28	−4.34	−16.66	0.47
	(−12.13)	(−8.31)		(−16.29)	0.55
LiOH–RbOH	−9.79	−11.61		−15.60	0.58
LiOH–CsOH	−7.81	−14.28		−14.95	0.82
NaOH–KOH	−2.58	+0.49		−2.34	0.14
NaOH–RbOH	−3.91	+0.49		−3.66	0.11
NaOH–CsOH	−3.26	+0.16		−3.18	0.19
KOH–RbOH				+0.20	
KOH–CsOH				+1.21	
RbOH–CsOH				+0.25	

estimating U_0^{++} is the same as previously used by Hersh and Kleppa.[12] However, in the present work we have in the London expression adopted the uncorrected values of the ionization potential of the alkali ions, I, rather than the value $0.75I$. This choice was dictated by more recent work on the dispersion energy, which generally suggests that the earlier estimate was significantly too low (see, *e.g.*, Pitzer[25]). We have made use of the ionic radii of the alkali metals given by Melnichak and Kleppa.[13] The same method and values were used also by Østvold and Kleppa[14] and by Andersen and Kleppa.[7] The relevant interatomic distances were calculated from the ionic radii of the ions. For the hydroxide anion we adopted the thermochemical radius, $r(OH^-)=1.40$ Å, as given by Kapustinskii.[15] The importance of the choice of ionic radii will be discussed later. The polarizabilities are those reported by Tessman *et al.*[16] Table 4 shows the ionic radii, polarizabilities, and ionization potentials used in the calculations. In Fig. 3 the corrected interaction parameter, $4\Delta H^{M}_{0.5}-U_0^{++}$, is plotted *versus* the square of the distance parameter, δ_{12} ($\delta_{12}=(d_1-d_2)/d_1d_2$ where d_1 and d_2 are characteristic interionic distances in the two salts; $d=r_+ + r_-$). It will be noted that the points representing the LiOH–NaOH, LiOH–KOH and NaOH–KOH systems fall close to a straight line through the origin, while most of the points which represent the rubidium or cesium containing systems fall below this line.

The ionic conformal solution theory of Reiss, Katz, and Kleppa as modified by the perturbation theory of Davis and Rice, predicts that the enthalpies of mixing for families of related fused salt solutions should be of the form

$$\Delta H^{M}/x_1x_2 = U_0 + U_1\delta_{12} + U_2\delta_{12}^2 \qquad (3)$$

Table 4. Ionic radii, polarizabilities, and ionization potentials for the alkali metal ions.

Ion	r^a Å	r^b Å	α^c Å^3	I^d kJ mol^{-1}
Li^+	0.57	0.60	0.03	7296
Na^+	0.96	0.95	0.41	4563
K^+	1.34	1.33	1.33	3069
Rb^+	1.49	1.48	1.98	2653
Cs^+	1.68	1.69	3.34	2422

[a] Melnichak and Kleppa.[13] [b] Pauling.[17] [c] Tessman *et al.*[16] [d] "Handbook of Chemistry and Physics".[24]

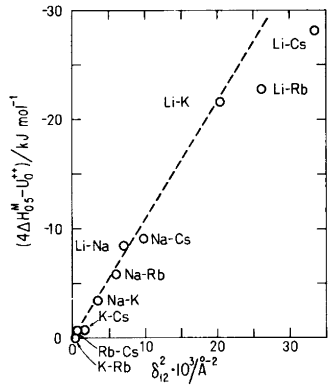

Fig. 3. Dependence of the corrected enthalpy interaction parameter, $4\Delta H^{M}_{0.5}-U_0^{++}$, on the size parameter δ^2_{12} in alkali hydroxide mixtures.

According to the DR theory the leading term in U_1, for a given common anion family, should be proportional to $\Delta\alpha=\alpha_1-\alpha_2$, *i.e.*, the difference between the polarizbilities of the two cations. Taking this into account and substituting U_0^{++} for U_0 we may write eqn. (3) as follows:

$$\Delta H^{M}/x_1x_2 = U_0^{++} + A(\alpha_1-\alpha_2)\delta_{12} + B\delta_{12}^2 \qquad (4a)$$

or for $x_1=x_2=0.5$

$$(4\Delta H^{M}_{0.5}-U_0^{++})/(\alpha_1-\alpha_2)\delta_{12} = A + B\delta_{12}/(\alpha_1-\alpha_2) \qquad (4b)$$

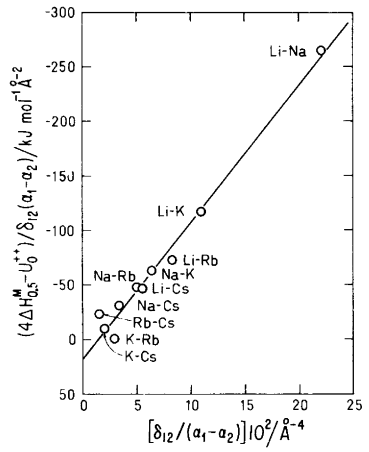

Fig. 4. Dependence of the quantity $(4\Delta H^{M}_{0.5}-U_0^{++})/\delta_{12}(\alpha_1-\alpha_2)$ on the parameter $\delta_{12}/(\alpha_1-\alpha_2)$ in mixtures of molten alkali hydroxides. Melnichak's radii for the alkali metal ions are used.

In these expressions A and B are unknown coefficients to be determined from experiments.

A plot of the left hand side of eqn. (4b) *versus* $\delta_{12}/(\alpha_1-\alpha_2)$ is given in Fig. 4, and indicates that the alkali hydroxide family is in fact very well represented by this equation. A least squares treatment of all the data yields the following values

$A = +17.8$ kJ Å^{-2} mol^{-1}
$B = -1250$ kJ Å^2 mol^{-1}

According to Davis and Rice the quantity B should mainly reflect the sum of the coulombic energy of mixing predicted by the RKK theory plus a term which arises from nearest neighbour dispersion interactions.

The numerical values of A and B depend greatly on the actual choice of the interionic distances. For example, if we use the original Pauling radii[17] for the alkali metal ions instead of the Melnichak radii we obtain the following constants

$A' = +36.3$ kJ Å^{-2} mol^{-1}
$B' = -1650$ kJ Å^2 mol^{-1}

A plot of the left hand side of eqn. (4b) *versus* $\delta_{12}/(\alpha_1-\alpha_2)$, where U_0^{++} and δ_{12} are calculated by use of the Pauling radii, is shown in Fig. 5. Except for the Li^+-ion, where the Pauling radius is 0.60 Å and the Melnichak radius 0.57 Å, the two set of ionic radii differ only by 0.01 Å or less. Actually very little is known about the interionic distances in the molten alkali hydroxides, and it does not seem possible to choose between the two sets of cationic radii. Furthermore, the choice of the thermochemical radius for the OH^--ion also is open to question. Fortunately, small changes in $r(OH^-)$ cause relatively small changes in δ_{12},δ_{12}^2, and U_0^{++}. Therefore, the fundamental conclusions in this discussion are not influenced by this choice.

Dantzer and Kleppa[18] have expressed doubt whether the small non-zero values of the constant A in the nitrate, chloride, and bromide families are physically significant. However, for the fluorides,[13] sulfates,[14] carbonates,[7] and hydroxides it is evident that significant positive values of A are obtained. In these families it seems that the cation–anion dispersion interactions may give rise to relatively large positive contributions to the enthalpy interaction parameters. These contributions vary linearly with the size parameter δ_{12} and with $(\alpha_1-\alpha_2)$. This effect might account for the deviations from linearity in the plot of corrected interaction parameter versus δ_{12}^2 given in Fig. 3.

The data in Table 3 show that the lithium containing hydroxide mixtures exhibit quite large values of the asymmetry parameter b, which numerically increases sharply in the sequence Li–Na < Li–K < Li–Rb < Li–Cs. According to Blander's calculation[10] of the higher order terms of the RKK theory it may be expected that this parameter should depend on ionic size through the third power of δ_{12}. Such a behaviour is in fact found for the lithium containing hydroxide mixtures as

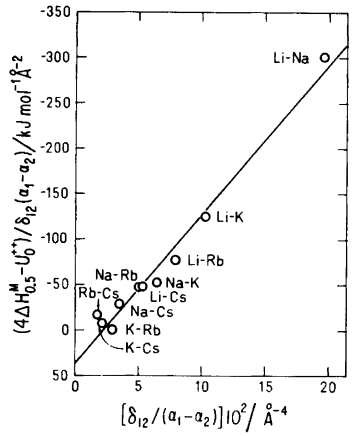

Fig. 5. Dependence of the quantity $(4\Delta H^M_{0.5}-U_0^{++})/\delta_{12}(\alpha_1-\alpha_2)$ on the parameter $\delta_{12}/(\alpha_1-\alpha_2)$ in mixtures of molten alkali hydroxides. Pauling's radii for the alkali metal ions are used.

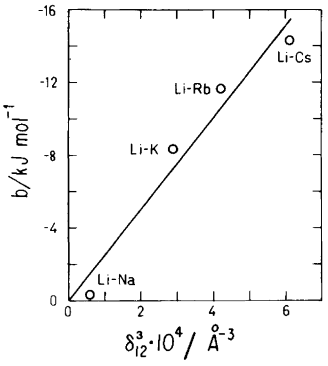

Fig. 6. Dependence of the asymmetry parameter b on the size parameter δ_{12}^3 for the mixtures of lithium hydroxide with the other alkali hydroxides. For the Li–K system the constant b from the linear plot has been used.

illustrated in Fig. 6. A similar dependence of b on δ_{12}^3 is found also for the lithium mixtures of other anion families.

Comparison with earlier data. Aghai-Khafri *et al.*[1] obtained the following values for the limiting partial molar excess enthalpies of potassium hydroxide in liquid sodium hydroxide and of sodium hydroxide in liquid potassium hydroxide, respectively.

$H^{E,\infty}(KOH) = -2430 \pm 210$ J mol^{-1} *
$(-2090 \pm 140$ J mol$^{-1})$
$H^{E,\infty}(NaOH) = -3050 \pm 170$ J mol^{-1} *
$(-2580 \pm 140$ J mol$^{-1})$

The data given in the parentheses are those obtained from the results of the present investigation. The agreement between the two sets of data is good when the very considerable experimental difficulties are taken into account.

From the NaOH branches of the liquidus and solidus curves of the phase diagram of Reshetnikov and Vilutis,[3] Lumsden[2] calculated a Gibbs excess energy interaction parameter of about -1260 J mol^{-1}. This is about one-half of the corresponding values of the enthalpy interaction parameter obtained in the present work, and points toward small negative excess entropies. This is consistent with what is found in many simple fused salt mixtures.

The thermochemical radius of the hydroxide ion ($r_{OH^-} = 1.40$ Å) is very close to the ionic radius of the fluoride ion ($r_{F^-} = 1.36$ Å). To a first approximation one therefore should expect the enthalpies of mixing of the alkali hydroxide mixtures to be comparable to those of the corresponding fluorides. The similarities of the alkali hydroxides and fluorides are also reflected in the small enthalpy changes of the following reciprocal reactions:

LiF(1) + KOH(1) = LiOH(1) + KF(1)
$\Delta H^0(800\ K) = -12.1$ kJ mol^{-1} *
NaF(1) + KOH(1) = NaOH(1) + KF(1)
$\Delta H^0(800\ K) = -3.1$ kJ mol^{-1} *

Table 5 shows results from the present investigation compared with data on the fluorides obtained by Holm and Kleppa[22] and by Holm.[23] The consistency between the two sets of data is fairly good. Even so, there are some interesting systematic differences. Thus we note that the enthalpies of mixing of the lithium hydroxide containing systems consistently are less negative than those of the corresponding fluorides.

It is possible that these differences may be explained by the high ionic potential of the small Li^+-ion, which would tend to limit the rotational freedom of the OH^--ions in the melts, and perhaps even give rise to some formation of Li^+OH^- ion pairs. If the OH^--ion is free to rotate (or rather "tumble"), the higher polarizability of the OH^--ion ($\alpha_{OH^-} = 1.2$ Å^3)[16] compared to the F^--ion ($\alpha_{F^-} = 0.64$ Å^3),[16] presumably would give rise to somewhat more negative mixing enthalpies in the hydroxides than in the fluorides. This is consistent with the new enthalpy data for the mixtures involving sodium and the larger alkali cations. Hence it is possible that the enthalpy of mixing data may reflect a structural difference between the liquid hydroxides and the liquid fluorides, which should be most pronounced for the lithium salts. This possible structural difference may also be involved in making the melting points lower in the hydroxides than in the fluorides. In this context, it is of interest to note that the highest melting alkali hydroxide is LiOH (m.p. 744 K), while the highest melting fluoride is NaF (m.p. 1269 K).

* According to least squares calculations carried out by the present authors $H^{E,\infty}(KOH) = -2410 \pm 350$ J mol^{-1} and $H^{E,\infty}(NaOH) = -2790 \pm 240$ J mol^{-1}.

Table 5. Enthalpies of mixing in equimolar mixtures of liquid alkali hydroxides and fluorides ($4\Delta H^M_{0.5}$/kJ mol^{-1}).

Alkali metals	Hydroxides[a]	Fluorides[b]
Li–Na	−6.95	−8.08
Li–K	−16.66	−19.45
Li–Rb	−15.60	−20.29
Li–Cs	−14.95	−16.15
Na–K	−2.34	−0.38
Na–Rb	−3.66	+0.38
Na–Cs	−3.18	(+3.55)[c]
K–Rb	+0.20	+0.36
K–Cs	+1.21	(+2.05)[c]
Rb–Cs	+0.25	–

[a] This investigation. [b] Holm and Kleppa[22] and Holm.[23] [c] Calculated from phase diagram data.

* The thermochemical data used are those tabulated in JANAF.[24] The fluorides are in a hypothetical state below their normal melting points.

Acknowledgements. We are indebted to Dr. J. Ito who carried out the spectrochemical analyses of the chemicals.

This investigation has been supported by a grant from the National Science Foundation (NSF-CHE 75-13936) and has also benefitted from the general support of Materials Science at University of Chicago provided by NSF-MRL.

One of the authors (BKA) wishes to acknowledge financial support from the Danish Natural Science Research Council (Denmark).

REFERENCES

1. Aghai-Khafri, H., Bros, J. P. and Gaune-Escard, M. *J. Chem. Thermodyn. 3* (1976) 331.
2. Lumsden, J. *Thermodynamics of Molten Salt Mixtures*, Academic, New York 1966, p. 146.
3. Reshetnikov, N. A. and Vilutis, N. I. *Russ. J. Inorg. Chem. 4* (1959) 49.
4. Douglas, T. B. and Dever, J. L. *J. Res. Natl. Bur. Stand. 53* (1954) 81.
5. Kelley, K. K. *U.S.Bur.Mines, Bull.* (1960) No. 584.
6. Kleppa, O. J. *J. Phys. Chem. 64* (1960) 1937.
7. Andersen, B. K. and Kleppa, O. J. *Acta Chem. Scand. A 30* (1976) 751.
8. Melnichak, M. E. *Ph.D. Thesis*, The University of Chicago, Chicago 1972.
9. Reiss, H., Katz, J. L. and Kleppa, O. J. *J. Chem. Phys. 36* (1962) 144.
10. Blander, M. *J. Chem. Phys. 34* (1961) 192.
11. Davis, H. T. and Rice, S. A. *J. Chem. Phys. 41* (1964) 14.
12. Hersh, L. S. and Kleppa, O. J. *J. Chem. Phys. 42* (1965) 1309.
13. Melnichak, M. E. and Kleppa, O. J. *Rev. Chim. Miner. 9* (1972) 63.
14. Østvold, T. and Kleppa, O. J. *Acta Chem. Scand. 25* (1971) 919.
15. Kapustinskii, A. F. *Quart. Rev. 10* (1956) 283.
16. Tessman, J. R., Kahn, A. H. and Shockley, W. *Phys. Rev. 92* (1953) 890.
17. Pauling, L. *The Nature of the Chemical Bond*, 3rd Ed., Cornell University Press, New York 1960.
18. Dantzer, P. and Kleppa, O. J. *J. Chim. Phys. 71* (1974) 216.
19. Michaud, M. *C.R.Acad.Sci. Ser. C 264* (1967) 1939.
20. Ostrovityanova, S. E. and Itkina, L. S. *Russ. J. Inorg. Chem. 14* (1969) 299.
21. JANAF Thermochemical Tables. 2nd Ed., Stull, D. R. and Prophet, H. *Natl. Stand. Ref. Data Ser., Natl. Bur. Stand. 37* (1971).
22. Holm, J. L. and Kleppa, O. J. *J. Chem. Phys. 49* (1968) 2425.
23. Holm, J. L. *Dr. Techn. Thesis*, The University of Trondheim, NTH, Trondheim 1971.
24. *Handbook of Chemistry and Physics*, 57th Ed., Chemical Rubber Co., Cleveland 1976.
25. Pitzer, K. S. *Inter- and Intramolecular Forces and Molecular Polarizability.* In Prigogine, I., Ed., *Advances in Chemical Physics*, Interscience, New York 1959, Vol. 2.

Received February 20, 1978.

Acta Chemica Scandinavica A 32 (1978) 603–606

The Crystal Structure of Iron(III) Hydrogen Biselenite, $FeH(SeO_3)_2$

JUSSI VALKONEN and MARKUS KOSKENLINNA*

Department of Chemistry, Helsinki University of Technology, Otaniemi, SF-02150 Espoo 15, Finland

The crystal structure of the title compound has been determined by X-ray methods from 1193 observed reflections collected by counter method. The crystals are monoclinic, space group $P2_1/c$ (No. 14), with unit cell dimensions $a=6.409(2)$ Å, $b=9.921(3)$ Å, $c=8.108(3)$ Å and $\beta=92.76(3)°$. The structure was solved by direct methods and refined to the conventional R-factor 0.047. The structure consists of edge-sharing pairs of FeO_6-octahedra connected by one of the two non-equivalent Se atoms into layers. The layers are held together by the other Se atom. The range of Se–O bonds is 1.669(7)–1.742(7) Å and the range of Fe–O bonds 1.955(7)–2.137(7) Å.

In our studies on the selenite compounds of divalent manganese the coordination octahedra around the metal atoms were found to be irregularly distorted in $MnSeO_3.D_2O$ and $MnSeO_3.2H_2O$.[1,2] In the first case the distortion was mainly due to the rigidity of the selenite ion, in the latter case to the stretching of the Mn–O bonds by hydrogen bonds. Thus, in these two compounds the spherically distributed d-electron density of the metal ion allows a marked distortion of the MnO_6-octahedron. The question then arose whether the same phenomenon would be encountered in the selenite compounds of the isoelectronic trivalent iron.

EXPERIMENTAL

Preparation of the compound. Dropwise addition of 1 mol/dm^3 solution of $KHSeO_3$ to a 1 mol/dm^3 solution of iron(III) nitrate yielded amorphous, green iron(III) selenite hydrate as a precipitate. After addition of 10–15 cm^3 of 3 mol/dm^3 selenous acid to 0.2 g of the iron(III) selenite hydrate the mixture was sealed in an ampoule and kept for 6–7 weeks at 150 °C.

The ampoule was then broken; among the green bar-like crystals of the title compound a few large enough for X-ray diffraction studies were found and selected for the measurements. The method of preparation is analogous to that described by Pinaev and Volkova for $Fe_2O_3.4SeO_2.H_2O$.[3] All reagents were of analytical grade.

Structure analysis. A computer–controlled Syntex $P2_1$ (Fortran version) four-circle diffractometer with graphite monochromatized Mo$K\alpha$-radiation was utilized in the determination of unit cell parameters and the collection of intensity data. Crystal size was $0.25\times0.2\times0.1$ mm and the temperature 298 K. Cell dimensions were calculated from diffractometer measurements of setting angles for 24 reflections (Table 1). Intensity data were collected in the interval $5°<2\theta<60°$ using the $\theta/2\theta$ technique and a scan speed of 2°/min. Of the 1587

Table 1. Crystal data for $FeH(SeO_3)_2$.

Formula	$FeH(SeO_3)_2$
Formula weight	310.77
Lattice constants	$a=6.409(2)$ Å
	$b=9.921(3)$ Å
	$c=8.108(3)$ Å
	$\beta=92.76(3)°$
Cell volume	$V=514.9(3)$ Å^3
Molecules per unit cell	$Z=4$
Space group	$P2_1/c$ (No. 14)
Density (calc.)	$D_x=4.01$ g cm^{-3}
Density (pycnometer)	$D_m=4.0$ g cm^{-3}
Linear absorption coefficient	μ(Mo$K\alpha$)$=168.8$ cm^{-1}

*Present address: Ministry of Trade and Industry, Aleksanterinkatu 10, SF-00170 Helsinki 17, Finland.

unique reflections measured, 1193 had intensities larger than three times their standard deviations. The space group $P2_1/c$ (No. 14) was determined on the basis of systematic absences in the original intensity data. Empirical absorption corrections were made from the ϕ-scan with 8 different 2θ values after which Lorentz and polarization corrections were applied.

The solving, refinement and drawing of the figures were carried out with the X-Ray 76 program package and a UNIVAC 1108 computer.[4] Scattering factors for neutral atoms were taken from Cromer and Mann.[5] The atomic positions of Fe and Se were determined by direct methods from the *E*-map calculated with 315 *E*-values larger than 1.2. The positional parameters of the Fe and the two Se atoms were then refined to an *R* of 17.9 %, and the subsequent difference Fourier map gave the positions of all the oxygen atoms. After refinement with isotropic temperature factors the value of *R* was reduced to 5.8 %, and after full-matrix refinement with anisotropic temperature factors the final *R*-value was 4.7 %. The $|F_o|$ and $|F_c|$ listing is available from the authors upon request.

RESULTS AND DISCUSSION

The positional and thermal parameters of the Fe, Se and O atoms are given in Table 2 and some selected bond lengths and angles in Table 3. There are two non-equivalent Se atoms in the compound, and all the O atoms are bonded to one or the other of the Se atoms. Thus, no water of crystallization is present (*cf.* Ref. 3) and the formula of the compound is written as $Fe(HSeO_3)(SeO_3)$ or more shortly as $FeH(SeO_3)_2$.

A characteristic feature of the structure is that the FeO_6-octahedra appear as edge-sharing pairs,

Table 2. Atomic coordinates and anisotropic temperature coefficients with their estimated standard deviations. The temperature coefficients are of the form $\exp[-2\pi^2(h^2a^{*2}U_{11}+k^2b^{*2}U_{22}+l^2c^{*2}U_{33}+2hka^*b^*U_{12}+2hla^*c^*U_{13}+2klb^*c^*U_{23})]$, and have been multiplied by 10^4.

Atom	*x*	*y*	*z*	U_{11}	U_{22}	U_{33}	U_{12}	U_{13}	U_{23}
Se1	0.0691(1)	0.9074(1)	0.2016(1)	44(4)	99(4)	125(4)	−7(4)	−15(4)	−6(4)
Se2	0.5940(1)	0.7132(1)	0.0213(1)	55(4)	30(4)	11(4)	6(4)	−13(4)	0(4)
Fe	0.4448(2)	0.5066(1)	0.2989(2)	25(5)	26(5)	3(5)	0(4)	−7(4)	−2(4)
O1	0.2488(10)	0.0279(7)	0.2313(9)	69(30)	31(30)	136(33)	−3(24)	−10(25)	−42(26)
O2	0.0257(14)	0.8640(12)	0.4043(12)	177(42)	604(73)	220(45)	−135(45)	−71(35)	279(49)
O3	0.8560(11)	0.0021(9)	0.1598(10)	38(21)	212(39)	174(36)	30(28)	0(26)	55(31)
O4	0.3938(11)	0.6250(7)	0.1076(9)	99(31)	71(31)	89(31)	−11(25)	−4(25)	50(25)
O5	0.4774(11)	0.8714(7)	0.0024(8)	142(32)	30(28)	12(26)	16(24)	−35(23)	−4(23)
O6	0.5632(12)	0.6640(7)	0.8219(8)	257(40)	42(30)	18(28)	9(27)	−18(26)	−26(23)

Table 3. Bond lengths (Å) and selected angles (°) with standard deviations in parentheses.

Fe−O1	2.002(7)	O1−Fe−O3	174.5(3)
Fe−O3	1.973(7)	O4−Fe−O5	175.3(3)
Fe−O4	1.961(7)	O5[a]−Fe−O6	156.1(3)
Fe−O5	2.137(7)	O1−Fe−O5	87.9(3)
Fe−O5[a]	2.049(7)	O3−Fe−O6	93.6(3)
Fe−O6	1.955(7)	O4−Fe−O5[a]	106.8(3)
Se1−O1	1.669(7)	O1−Se1−O2	100.5(4)
Se1−O2	1.734(10)	O1−Se1−O3	100.2(4)
Se1−O3	1.679(8)	O2−Se1−O3	99.5(4)
Se2−O4	1.728(7)	O4−Se2−O5	99.7(3)
Se2−O5	1.742(7)	O4−Se2−O6	100.7(4)
Se2−O6	1.691(7)	O5−Se2−O6	98.4(3)

[a] $-x, -y, -z$.

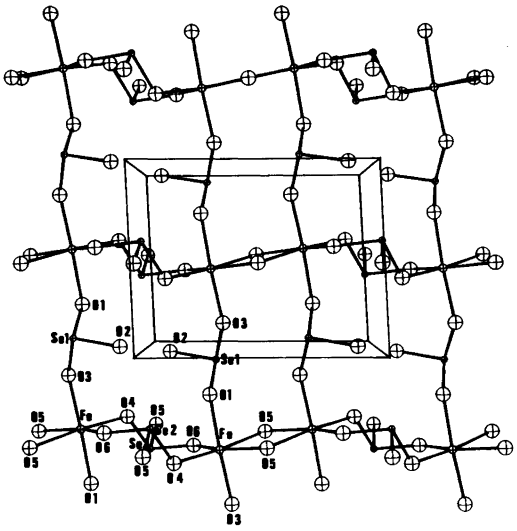

Fig. 1. Perspective view of the layer structure along *b*-axis. The *c*-axis is horizontal.

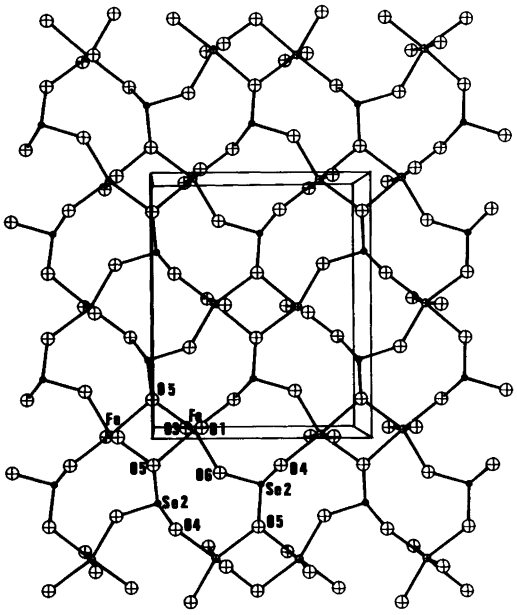

Fig. 2. Perspective view of the layer structure along *a*-axis. The *c*-axis is horizontal.

and these pairs of coordination polyhedra are then knitted by the Se2 atoms into layers parallel to the *ab*-plane (Figs. 1 and 2). One Se2 atom links together three pairs of FeO_6-octahedra. This

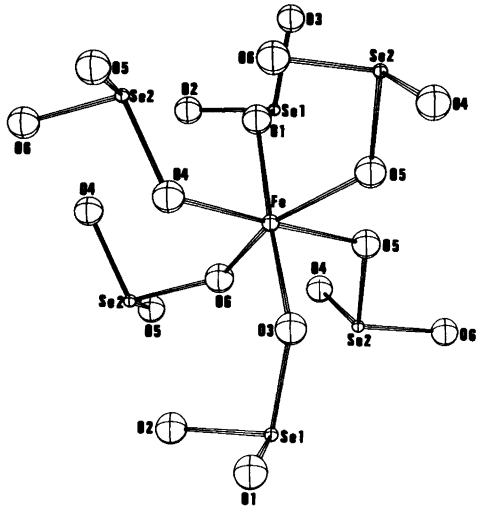

Fig. 3. Bonding scheme of the selenite groups to iron.

structural arrangement is possible because O5, which forms the two vertices of the shared edge, is within bonding distance of three atoms. The angles in the pyramidal arrangement of the bonds of O5 are 104.3(3), 114.6(3) and 129.0(4)° for Fe-O5-Fe', Fe-O5-Se and Se-O5-Fe', respectively. In $MnSeO_3.D_2O$, which also has an oxygen simultaneously coordinated to two metal atoms and to one selenium atom, the angles, in corresponding order, are 119.8, 125.0 and 97.9°.[1]

The layers are connected by Se1 atoms into a three-dimensional network. Both the non-equivalent selenite groups act as bridging ligands. The selenite group formed by Se2 joins four Fe atoms and that by Se1 two Fe atoms. Thus, one Fe atom is joined to ten others *via* six different selenite groups (Fig. 3).

The Se1 – O2 bond is stretched as compared with the other two bonds in the $Se1O_3$-group. Since O2 is not coordinated to Fe, it is plausible to assume that this oxygen has the hydrogen atom attached to it and is thus capable of acting as hydrogen bond donor. Such stretching is frequently observed in compounds containing hydrogenselenite groupings, and the relative difference between the shortest and longest bond in the group in the present case is compatible with the difference detected in $PrH_3(SeO_3)_2(Se_2O_5)$ and $MnH(SeO_3)(Se_2O_5)$ for a hydrogenselenite group likewise involved in hydrogen bonding.[6,7] The O – O distances around O2

(less than 3.0 Å) are O2 – O1 2.617 Å, O2 – O3 2.604 Å and O2 – O4 2.814 Å of which the first two are in the same selenite group. Thus it might be possible that the hydrogen atoms exists between O2 and O4, which would explain the stretching of the Se2 – O4 bond.

The $Se2O_3$-pyramid is more distorted than the $Se1O_3$-pyramid, and also more distorted than the selenite group in $MnSeO_3.D_2O$. In both compounds the bond between the Se and the three-coordinated oxygen is the longest: 1.742(7) Å in the present case and 1.720(8) Å in the latter.

The two bond distances Fe – O5 [2.137(7) and 2.049(7) Å] are significantly longer than the other Fe – O distances in the compound, and especially the former distance approaches the bond lengths detected in compounds of divalent iron. It is notable that the metal-oxygen bond was found to be stretched also in $MnSeO_3.D_2O$, when the coordination number of the oxygen atom was three.[1] This structurally plausible stretching of the Fe – O bonds distorts the regularity of the FeO_6-octahedron and the angle O5 – Fe – O5′ deviates from 90° to a smaller value by 14.3(3)°. The mean of the four short bonds is 1.973 Å, which agrees well with the mean bond length found in regular FeO_6-octahedra, for example 1.986 Å reported for $[Fe(H_2O)_6](NO_3)_3.3H_2O$.[8]

Acknowledgement. We are indebted to Professor Lauri Niinistö for his interest in this work.

REFERENCES

1. Koskenlinna, M. and Valkonen, J. *Acta Chem. Scand. A 31* (1977) 752.
2. Koskenlinna, M., Niinistö, L. and Valkonen, J. *Cryst. Struct. Commun. 5* (1976) 663.
3. Pinaev, G. F. and Volkova, V. P. *Russ. J. Inorg. Chem. 21* (1976) 734.
4. Steward, J. M., Ed., *The X-Ray System, Version of 1976*, Technical Report TR-446, Computer Science Center, University of Maryland, College Park 1976.
5. Cromer, D. and Mann, J. *Acta Crystallogr. A 24* (1968) 321.
6. Koskenlinna, M. and Valkonen, J. *Acta Chem. Scand. A 31* (1977) 457.
7. Koskenlinna, M. and Valkonen, J. *Acta Chem. Scand. A 31* (1977) 638.
8. Hair, N. J. and Beattie, J. K. *Inorg. Chem. 16* (1977) 245.

Received February 15, 1978.

Acta Chemica Scandinavica A 32 (1978) 607–625

On the Coordination around Mercury(II), Cadmium(II) and Zinc(II) in Dimethyl Sulfoxide and Aqueous Solutions. An X-Ray Diffraction, Raman and Infrared Investigation

MAGNUS SANDSTRÖM,[a] INGMAR PERSSON[b] and STEN AHRLAND[b]

[a] Department of Inorganic Chemistry, Royal Institute of Technology, S-100 44 Stockholm 70, Sweden and [b] Inorganic Chemistry 1, Chemical Center, University of Lund, P.O.B. 740, S-220 07 Lund, Sweden

The structures of the solvated metal ions in dimethyl sulfoxide (DMSO) solutions of mercury(II) and cadmium perchlorates have been determined by X-ray diffraction measurements. In both cases, regularly octahedral hexasolvates are formed, with DMSO coordinated *via* the oxygen atom. The bond lengths are: Hg–O 2.393(5), Cd–O 2.292(4) Å. The value of Hg–O is significantly longer than in the solid hexasolvate, while that of Cd–O is virtually the same in both phases. The bond angles Hg–O–S, 120.2(1.0)° and Cd–O–S, 125.7(1.0)°, are not significantly different from the average angles found in the solid solvates. A recalculation of earlier X-ray diffraction data pertaining to mercury(II) perchlorate in aqueous solution confirms that the hydrate formed is indeed regularly octahedral. The bond length Hg–O is 2.41(1) Å, *i.e.* close to the value found in DMSO solution. These bond lengths correspond to octahedral ionic radii of Cd^{2+} and Hg^{2+} of 0.94 and 1.05 Å, respectively.

The Raman spectra of perchlorate solutions of mercury(II), cadmium and zinc in DMSO confirm that the metal ions are all coordinated *via* oxygen. The spectra also reflect the change in character of the M–O bond from mercury(II) to zinc. Both the decreasing covalency and the increasing electrostatic interaction are clearly indicated.

In the aprotic solvent dimethyl sulfoxide (DMSO), the neutral mercury halides $HgCl_2$, $HgBr_2$ and HgI_2 are all easily soluble.[1,2a] In the solvated HgX_2 molecules, the angles X–Hg–X (X=Cl, Br, I) deviate significantly[2] from the value 180° found in the gaseous and solid halides (except for red HgI_2).[3,4] On the addition of excess halide further ligands are taken up, resulting in the formation of HgX_3^- and finally, HgX_4^{2-}. The HgI_3^- and $HgBr_3^-$ ions are pyramidal, slightly flattened relative to a regularly tetrahedral arrangement.[1] In all the systems the fourth complex is a regular tetrahedron.[1,2]

In aqueous solution, the complexes HgX_2 should be less bent than in DMSO, on account of the weaker interaction with the solvent,[4,5] but the solubilities in this protic solvent are too low for a structure determination by X-ray diffraction. The complexes $HgBr_3^-$ and HgI_3^- are again slightly flattened pyramids, derived from tetrahedra.[6] As in DMSO, the mononuclear complexes HgX_4^{2-} finally formed are all regular tetrahedra.[6,7]

In the numerous solid compounds where linear HgX_2 units exist, four longer contacts usually complete a distorted octahedral coordination around Hg.[2b,3,8–15] Planar HgX_3^-, with two long contacts forming a trigonal bipyramid,[16–21] pyramidal HgX_3^-, with a bridging X atom completing a distorted tetrahedral coordination,[22–24] and tetrahedral HgX_4^{2-},[25–29] also exist in solid state. Even discrete bipyramids $HgCl_5^{3-}$ have been found.[30]

Both in water and in DMSO, the formation of the third complex thus involves a drastic change of the digonal coordination characteristic of the second complex. In the case of bromide and iodide, the new arrangements very probably are approximately tetrahedral, while the picture is less clear for the chloride complexes.

Another drastic change of coordination very probably occurs in both solvents, as the digonal

second complex is formed when halide is added to a solution of the solvated mercury(II) ion. The solvated perchlorates $[Hg(H_2O)_6](ClO_4)_2$ and $[Hg(DMSO)_6](ClO_4)_2$ have been crystallized, the structures of which contain octahedrally coordinated solvate ions as discrete entities.[31,32] It is therefore very plausible that such species exist also in solution. In aqueous perchlorate solution, the existence of the hexahydrate has in fact been proved by X-ray diffraction measurements.[33]

In aqueous solution, the switch from digonal to tetrahedral coordination at the formation of the third complex is also clearly indicated by abrupt changes of the magnitude of the enthalpy changes ΔH_j° of the consecutive formation reactions. These become much less exothermic for the two later steps.[34]

Changes of ΔS_j° also occur, but they are not clear-cut enough to yield further evidence.[34] As to the postulated change from an initial octahedral coordination to an intermediate digonal one, relatively little can be learned from the thermodynamic data. Neither ΔH_j°, nor ΔS_j° differ very drastically between the first and second step. This must mean that water molecules are expelled from the close vicinity of the mercury atoms at both stages. The first ligand displaces one water molecule and loosens the bonds of the others except the one in *trans* position to the ligand which might be held even more tightly than before.[33] This is supported by the high acidities of the HgX^+ and $HgOH^+$ species compared with the acidity of the Hg^{2+} ion.[35] The second ligand replaces this water molecule and relegates the remaining ones to even more distant positions. Under such conditions, the thermodynamic functions of the first two steps need not be very different. The hydration of the HgX_2 complexes is indeed quite weak as is shown by their low heats of solvation.[36]

In DMSO, the thermodynamics of the formation of mercury(II) halide complexes follows a pattern which is quite different from that found in water. The values of ΔH_j° do not vary much between the different halides or, perhaps even more remarkable, between the consecutive steps.[37,38] This levelling of the ΔH_j° values is brought about by a combination of several causes.[38] Firstly, the heat of solvation of the mercury(II) ion is considerably larger in DMSO than in water,[36] which tends to decrease the values of $-\Delta H_j^\circ$, and preferentially for the first steps. Secondly, the differences between the heats of solvation of the halide ions are much smaller in DMSO than in water.[36,39] Evidently, it so happens that the sum of these changes rather nicely counterbalances the change of ΔH_j° due to the switch from digonal to tetrahedral coordination. The switch will therefore not be marked by any drastic change of ΔH_j°. The values of ΔS_j° found in DMSO are, on the other hand, very informative.[38] For all the halide systems, extremely large positive values of ΔS_1° clearly show that a very extensive desolvation takes place when the first complex is formed. Smaller, though still quite large values of ΔS_2° indicate a less extensive, though still quite substantial desolvation in the second step. The values of ΔS_3° are quite small which means that already the HgX_2 complexes are relatively weakly solvated. This has also been confirmed by a determination of their heats of solvation which are indeed low compared to those of the presumably tetrahedral solvated CdX_2 and ZnX_2 molecules.[36]

In analogy with the mercury(II) ion, the cadmium ion finally forms four-coordinated halide complexes CdX_4^{2-} in DMSO as the ligand ion concentration is increased.[40] The same is most probably true also in water, although in this solvent the chloride complexes are fairly unstable.[41-43] The complex CdI_4^{2-} has been found by X-ray diffraction measurements to be a regular tetrahedron in both solvents.[44,45] There is every reason to believe that $CdBr_4^{2-}$ and $CdCl_4^{2-}$ have the same structure.

Also in analogy with Hg(II), both DMSO and aqueous solutions of Cd(II) and Zn(II) perchlorates very probably contain hexacoordinated metal ions solvates. This is strongly indicated already by the existence of the crystalline solvates $[M(DMSO)_6](ClO_4)_2$,[46] and $[M(H_2O)_6](ClO_4)_2$,[47] where M = Zn or Cd. Several crystal structure determinations[48-52] confirm the existence of discrete octahedrally coordinated solvate cations. By means of X-ray diffraction measurements,[44,53] the hexahydrates have been found to exist also in aqueous solution, while no such direct proof of the existence of the hexasolvates in DMSO has so far been produced.

Contrary to mercury(II), cadmium(II) does not form any linear complexes. Therefore, only a change from the initial octahedral coordination to the final tetrahedral one is to be expected as halide is added to a solution of a cadmium(II) hexasolvate. The thermodynamic functions of the consecutive formation reactions also indicate that the change mainly occurs at a certain step of the complex formation. This step is characterized by values of ΔH_j° and ΔS_j° which are abnormally positive relative to the values

of the neighbouring steps. The switch takes place at different steps in the two solvents, *viz.* at the formation of the third complex in water but at the formation of the second one in DMSO.[40]

In the solids $[Hg(DMSO)_6](ClO_4)_2$, $Hg(ClO_4)_2$.4DMSO, and $[Cd(DMSO)_6](ClO_4)_2$, the solvent molecules are coordinated *via* oxygen.[32,46,48,54] For the very soft acceptor mercury(II), a coordination *via* the soft sulfur atom would perhaps rather have been expected. The most important reason why this does not occur is presumably that the donor properties of the sulfur atom are very considerably reduced by its bonding to the electronegative oxygen. Also sterically, the oxygen coordination is certainly much more favourable. Rather as expected, the infrared spectra also indicate[46,55] that the hard acceptor zinc(II) is oxygen coordinated in the solids $[Zn(DMSO)_6](ClO_4)_2$ and $Zn(ClO_4)_2$.5DMSO. It might be presumed that, for all three acceptors, oxygen coordination prevails also in solution but this has so far not been proved.

A direct structure determination of the solvates formed by these acceptors in DMSO would evidently decide whether the solvation number and mode of coordination inferred are indeed correct. While the mercury(II) and cadmium perchlorates are sufficiently soluble to allow a determination of the solvate structure by means of X-ray diffraction, this is unfortunately not the case for the zinc perchlorate. The concentrations of the solutions in equilibrium with the solid hexasolvates are 0.93, 0.70 and 0.29 M, respectively, at room temperature. On the other hand, recent improvements in the evaluation technique has allowed a considerable refinement of the parameters determined earlier for the hydrated mercury(II) ion in solution.[33]

In order to obtain further information about the nature and strength of the various acceptor to solvent bonds Raman spectra of the saturated solutions of the zinc, cadmium and mercury(II) perchlorates have been recorded. With the modern laser technique, all these solutions yield spectra of high resolution. The bands principally due to the M–O stretching modes are discerned in both solvents and, in DMSO, also bands due to the M–O bending vibrations. The solution spectra are compared to those obtained for solid hydrates and DMSO solvates. In order to facilitate the assignments, the infrared spectra of the solid solvates have also been recorded.

Table 1. Compositions of the DMSO solutions at 25 °C in mol l^{-1}. The linear absorption coefficient, μ, is calculated for Mo$K\alpha$-radiation.

Hg(II)	Cd(II)	ClO_4^-	DMSO	μ/cm^{-1}
–	0.685	1.370	13.33	7.2
0.932	–	1.864	13.00	26.8
0.434	–	0.868	13.55	15.0

EXPERIMENTAL

Preparation and analysis of solvates and solutions. The DMSO solutions investigated were prepared by dissolving DMSO solvates of the metal perchlorates in DMSO. The solvent had been purified as described earlier.[46] The water content, determined by Karl Fischer titration,[56] was <0.08 %. The composition of the solutions, checked by EDTA titration,[57] is given in Table 1. Their densities were determined pycnometrically.

The solvates $[Zn(DMSO)_6](ClO_4)_2$ and $[Cd(DMSO)_6](ClO_4)_2$ were prepared as described previously.[46] The mercury(II) hexasolvate prepared previously[46] was, on the other hand, not pure and stable enough to meet the demands of the present investigations, or of the potentiometric and calorimetric measurements also in progress.[36,38] Its mercury(II) content was generally somewhat too low and varied significantly between different preparations. Moreover, the compound, as well as the DMSO solutions prepared from it, decomposed appreciably in a few weeks even at ordinary temperature. In a few months, the solutions might even turn dark yellow, with a very sizable reduction of the mercury(II) concentration. Instant decomposition of the solid solvate also took place at a much lower temperature (Table 2) than for the pure $[Hg(DMSO)_6](ClO_4)_2$ that has now been prepared by another route.[32] While the impure solvate decomposed violently immediately upon melting, the pure one survives its melting by $\simeq 80$ °C. Remarkably enough, the melting point of the pure compound is only slightly higher than that of the impure one. By a modified method of preparation, described below, a pure tetrasolvate was first obtained. From a saturated DMSO solution of the tetrasolvate, the pure hexasolvate crystallized.[32]

The solid solvates were analysed for metal and sulfur as described before.[46,57] Especially for the mercury compounds, the results are very close to the theoretical values, Table 2. As mentioned, this was not the case for the mercury hexasolvate prepared previously, whose values have also been entered.

Melting and decomposition points were determined using a Bücki apparatus. Measured densities,

Table 2. The crystalline DMSO solvates.

Compound	M.p./°C	Dec.p./°C	Metal/% Calc.	Metal/% Found	Sulfur/% Calc.	Sulfur/% Found	D_m/g cm^{-3}	D_x/g cm^{-3}
$[Zn(DMSO)_6](ClO_4)_2$	168–174	195–205	8.92	8.98	27.43	27.04	1.52(2)	1.54
$[Cd(DMSO)_6](ClO_4)_2$	188–190	200–210	14.41	14.14	24.66	24.49	1.58(1)	1.60
$[Hg(DMSO)_6](ClO_4)_2$	126–129	204–207	23.10	23.12	22.15	22.20	1.96(2)	1.99
$[Hg(DMSO)_6](ClO_4)_2$[46]	125–128	125–128	23.10	22.57	22.15	22.05	–	–
$Hg(ClO_4)_2.4DMSO$	167–168	170–174	28.17	28.19	18.02	18.00	1.76(3)	1.82

D_m, were obtained from the apparent loss of weight in benzene. They are compared to calculated densities, D_x, from unit cell dimensions found in the structure determinations.[32,48,54] The unit cell for $[Zn(DMSO)_6](ClO_4)_2$ was found to be trigonal with $a=b=20.818(1)$ and $c=12.659(2)$ Å, by X-ray diffraction methods.

Preparation of $Hg(ClO_4)_2.4DMSO$. Mercury(II) perchlorate trihydrate[46] (0.01 mol) was dissolved in a minimum amount of methanol (100 ml). A few drops of concentrated perchloric acid had previously been added to the methanol in order to minimize the hydrolysis of mercury(II). Still it was sometimes necessary to decant the solution in order to remove a slight solid residue. About 0.06 mol DMSO was then added and the solution cooled to about −78 °C. Very small white crystals precipitated which were filtered in dry air at the low temperature and then dried in vacuum over silica gel at room temperature, in order to remove the methanol. This resulted in a recrystallization of the phase obtained originally into the tetrasolvate. Larger crystals, suitable for investigation by single X-ray diffraction technique,[54] were obtained by recrystallization at lower temperature, ~5 °C. The compound seems to be stable for years when stored over silica gel at room temperature.

Warning. Metal perchlorates and nitrates solvated by DMSO are generally powerful explosives and under certain conditions a violent reaction is easily triggered.[46,58,59] During one of the earlier attempts to prepare a mercury(II) solvate, the compound obtained at room temperature from a methanol solution exploded with extreme violence, after having been kept for about two weeks in a desiccator over sulfuric acid. The explosion seemingly occurred without outer provocation. On the other hand, the solvates described above explode only when subjected to very unmild mechanical treatment and stand fairly high temperatures before a rapid decomposition occurs, Table 2. Generally, the sensitivity seems to decrease with increasing purity. This does not exclude that even pure DMSO solvates might be very explosive as is no doubt the case[46] with $Ag(ClO_4)_2.2DMSO$.

Great caution must also be exercised when handling DMSO solutions of poisonous substances, such as mercury and cadmium salts, since these are easily carried through the skin by the DMSO which penetrates lipid tissues at an astonishing rate.[59] DMSO dissolves many natural and synthetic polymers.[59] The unusual solvent properties must of course be taken into account in the design of the apparatus, and also in order to ensure good personal protection.

X-RAY DATA

Data collection

The X-ray scattering of Mo$K\alpha$-radiation ($\lambda=0.71069$ Å) was measured from the free surface of the DMSO solutions, as described in previous papers.[33,60] The solutions were enclosed in an airtight shield, with a cylindrical beryllium window for the X-rays. The scattered intensity was repeatedly measured at discrete points between the θ values 1.5 and 70°, where 2θ is the scattering angle. Intervals of 0.1° for $1.5°<\theta<15°$ and 0.25° for $15<\theta<70°$ were used. At least 100 000 counts were accumulated for each point which corresponds to a statistical error of about 0.3 %. All measurements were performed at 25±1 °C.

Data reduction and corrections

All calculations were carried out by means of the KURVLR and PUTSLR programs.[61] The measured intensities were corrected for background, polarization, and double scattering, and normalized to a stoichiometric unit of volume, V, corresponding to the average volume per metal atom in the solutions. The normalization was done by comparing the high angle region of the corrected intensities to the calculated sum of the independent coherent scattering and the fraction of the incoherent scattering reaching the counter. The correction for double scattering did not exceed 3 % for any of the

three DMSO solutions. A few points clearly outside estimated statistical error limits were removed.

Only the low-absorbing cadmium solution (Table 1) had to be corrected for absorption effects.[62] The largest correction of the intensity curve (at $\theta=45°$) was 3.3 %.

RHF scattering factors, f, for the neutral atoms[63,64] were used, except for H, where the spherical form factors proposed by Stewart *et al.* were employed.[65] For the recalculation of the aqueous mercury(II) perchlorate solution *A*1 of Ref. 33, spherical form factors for the H_2O molecule were used.[66] Anomalous dispersion corrections, $\Delta f'$ and $\Delta f''$, were applied for all atoms.[64] The incoherent scattering factors, I_{incoh}, were taken from the same sources as before.[6] Correction for the Breit-Dirac factor[67,68] in the appropriate form for a radiation counter, $(\lambda/\lambda')^2$, were applied.[69]

The reduced intensity curves, $i(s)$, were calculated for each experimental point from:

$$i_{obs}(s) = I_{obs}(s) - \sum_m \{(f_m(s) + \Delta f_m')^2 + (\Delta f_m'')^2 + \\ + del(s)\ (\lambda/\lambda')^2 I_{m,incoh}(s)\}$$

Here $I_{obs}(s)$ are the corrected and normalized intensities and $s=4\pi\lambda^{-1}\sin\theta$. The summations are performed over all the atoms m in a stoichiometric unit of volume, V. The function $del(s)$, describing the fraction of the incoherent radiation which passes the monochromator, was determined as follows. The apparent shape of the spectrum of the Mo-tube was measured after reflection by the (200) lattice planes in the LiF-monochromator used. For radiation scattered incoherently, the wavelength (in Å) is increased: $\lambda'=\lambda+0.02426\,(1-\cos 2\theta)$.[64] The relative intensity at the wavelength λ' from the measured spectrum compared to the peak intensity at $\lambda(K\alpha)$ then gives $del(s)$ for the scattering angle 2θ.

An independent check of this function at high angles ($2\theta>135°$) was obtained by measurements with a Zr-filter.[70]

The electronic radial distribution functions, $D(r)$, were calculated as $D(r)=4\pi r^2\rho_0+(2r/\pi)\int_0^{s_{max}} si(s)\times Mod(s)\sin(rs)ds$ where the modification function, $Mod(s)$, was $\{f_M^2(0)/f_M^2(s)\}\exp(-0.01s^2)$, (M = Cd or Hg) and $\rho_0=\{(\sum_m(f_m+\Delta f_m'))^2+(\sum_m\Delta f_m'')^2\}/V$.

Finally, a correction was made for errors giving low-frequency additions to the $i(s)$ curves. Small spurious peaks below 1 Å in the $D(r)$ functions, which could not be related to interatomic distances, were removed by a Fourier transformation procedure.[70]

The calculations of intramolecular intensity contributions and peak shapes were carried out as described previously.[6,61]

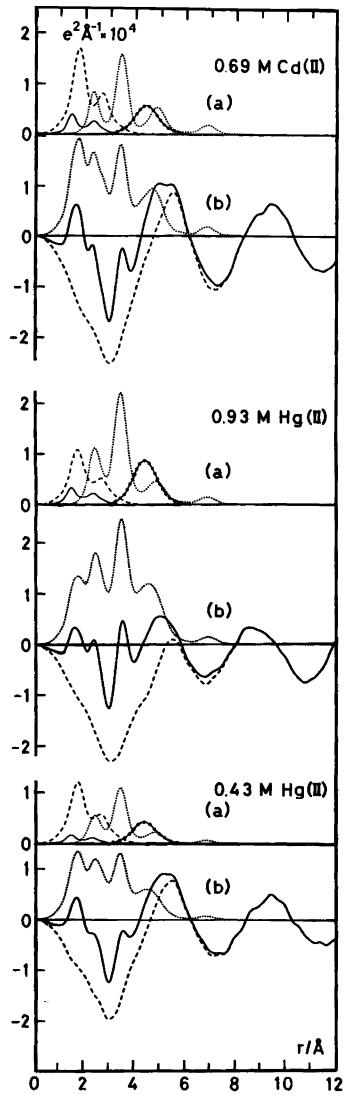

Fig. 1. (a) Peak shapes calculated for the refined models of the DMSO solutions, using the parameter values in Table 3, columns *B*. Dotted lines refer to M−O, M−S, S−S and O−O interactions, solid lines with large dots to M−C interactions within the complex $[M(DMSO)_6]^{2+}$. Dashed lines refer to S−O, S−C, O−C and C−C interactions within DMSO, and solid lines to Cl−O and O−O interactions within ClO_4^-. (b) $D(r)-4\pi r^2\rho_0$ functions (solid lines) compared with sums of calculated peak shapes (dotted lines). The differences are shown by the dashed lines.

Results

Intensity curves and radial distribution functions (RDF). The experimental distribution functions, $D(r)-4\pi r^2\rho_0$, are shown in Fig. 1. The peaks found at about 2.3 and 3.4 Å in the RDF's fit in with the M–O and M–S distances expected for an octahedral complex and are close to corresponding values found in the crystal structures of the hexasolvates.[32,48]

Intramolecular DMSO-distances should occur at about 1.52 (S–O), 1.78 (S–C) and 2.7 Å (O–C and C–C).[10,32,48,71,72] The S–O and S–C interactions explain the observed peak at 1.6–1.7 Å (Fig. 1). Expected Cl–O and O–O distances within the tetrahedral ClO_4^- ion are 1.43 and 2.33 Å, respectively.[73] Two broad peaks at about 5–6 and 9–10 Å also occur in the RDF's. They are, as well as the sharp intensity peak at $s\sim1.5$ Å^{-1} (Fig. 2), features also found in an X-ray diffraction study of liquid DMSO,[2a] and are very probably mainly caused by intermolecular interactions between DMSO molecules.

For the 0.93 M mercury(II) perchlorate solution, a separation of the intensity contributions from the various interactions can be performed with fair accuracy. This has been done in Fig. 3, where the functions *si(s)* have been plotted separately for the various types of intramolecular interaction taking place in the solution, *viz.* those due to the complex formation, and those originating from the DMSO molecules and the perchlorate ions. The interactions due to the complex formation have been further divided so that the contributions from Hg–O, Hg–S, O–O and S–S have been combined, while the contribution from Hg–C has been separated.

For all three solutions investigated, the sum of

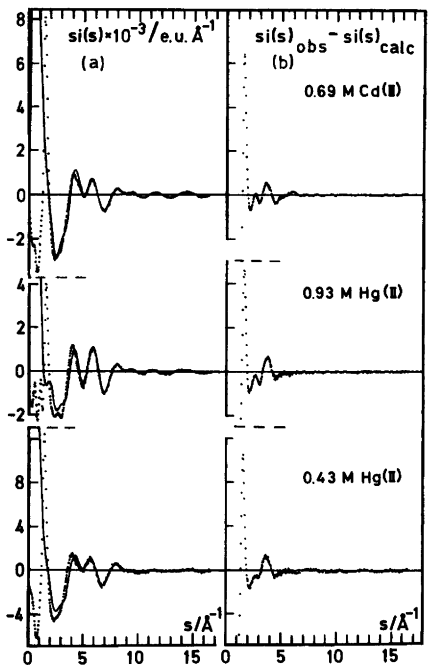

Fig. 2. (a) Reduced intensities multiplied by *s* for the DMSO solutions investigated. Experimental values are denoted by dots, values calculated for the refined model (with the parameter values in Table 3, columns *B*) by solid lines. (b) Differences between experimental and calculated values.

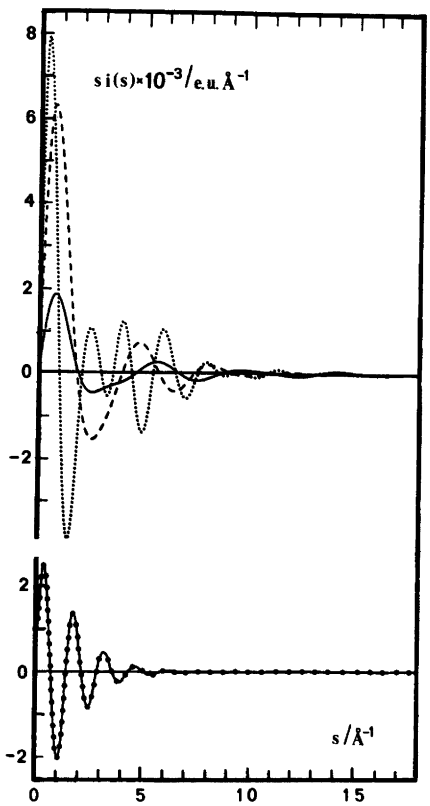

Fig. 3. Separation of the reduced intensities between various interactions for 0.93 M mercury(II) perchlorate in DMSO. The various lines refer to the same interactions as in Fig. 1a. For clarity, the highly damped curve of the Hg–C interactions is shown separately in the lower part of the figure.

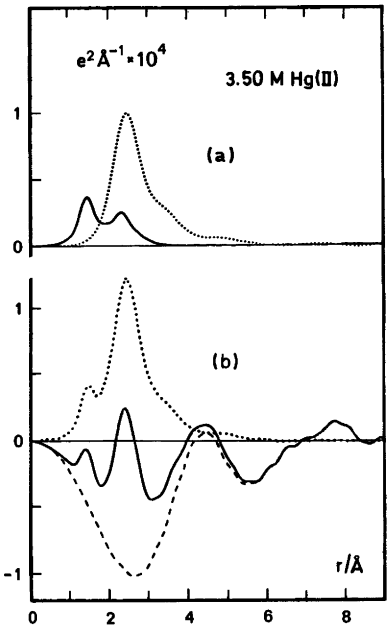

Fig. 4. (a) Peak shapes calculated for intramolecular interactions within the $[Hg(H_2O)_6]^{2+}$ complex (dotted line) and the ClO_4^- ion (solid line), using the parameter values in Table 4, column *B*. (b) $D(r)-4\pi r^2\rho_0$ function for the acidic aqueous 3.50 M $Hg(ClO_4)_2$ solution (solid line), the sum of the calculated peak shapes (dotted line), and the difference between them (dashed line).

all the calculated intramolecular reduced intensity contributions, $i_{calc}(s)$, are compared with the experimental $i_{obs}(s)$ curves of Fig. 2*a*, after multiplication by s. As can be seen from the differences $si_{obs}-si_{calc}$ in Fig. 2*b*, these intramolecular intensities are the dominant contributors to the high angle regions of the observed intensity curves, where the effect of the highly damped intermolecular contributions become negligible.[6]

A recalculation of the aqueous mercury(II) perchlorate solution *A*1 in Ref. 33 (3.50 M $Hg(ClO_4)_2$ + 0.64 M $HClO_4$) was performed, since it was felt that, with the better scattering factors now available and the efficient data treatment now possible,[61] a more precise value of the Hg–O bond length could be obtained, to be compared with the present data. The $D(r)-4\pi r^2\rho_0$ curve obtained is shown in Fig. 4. Distinct peaks are found at 1.4 and 2.4 Å. The shorter distance can be identified with Cl–O in the perchlorate ion[73] and the longer one with Hg–O in the hydrated Hg^{2+} ion.[31] A contribution to the peak at 2.4 Å also comes from the O–O interactions in ClO_4^-. These assignments are founded on the distances determined in crystal structures. The broad peak at about 4.5 Å is mainly caused by intermolecular interactions in the solutions as is discussed later.

Least-squares refinements. The parameter values of the models used for calculations of intramolecular intensity contributions can be refined using the high angle regions of the intensity curves. A series of refinements were performed where a minimum was sought[6,61] for the weighted error-square-sum $\sum_{s_{min}}^{s_{max}} w(s)\{i_{obs}(s)-i_{calc}(s)\}^2$. The weighting function, $w(s)$, was proportional to $I_{obs}^{-2}\cos\theta$, which gives each part of the refined $i(s)$ curve a weight corresponding approximately to its statistical precision and also compensates for the unequal spacing between the points caused by the constant $\Delta\theta$ interval used during the intensity measurements.

To check for correlations between the parameters of the refined models, different combinations of parameters were refined. Those held constant were systematically given different values within their probable limits of variation.[74] The influence of systematic errors in different parts of the intensity curves were estimated by using different s ranges in the refinements. Especially the lower s limit was varied.[6]

For the DMSO solutions, the model selected in the final refinements consisted of the following parts.

1. Oxygen coordinated $M(DMSO)_6^{2+}$ complexes, where the distances d of the M–O and M–S interactions, the coefficients b of their temperature factors $\exp(-bs^2)$ and, in some cases, the number of distances, n, were refined. The contributions from the O–O and S–S interactions, assuming octahedral arrangements around the metal atoms as in the crystal structure of $[Hg(DMSO)_6](ClO_4)_2$,[32] were also introduced.

2. Pyramidal DMSO molecules, where in some cases the S–O and S–C distances and a b value, common to S–O and S–C, were refined. The O–C and C–C distances were taken from the crystal structure of pure DMSO at 5 °C.[71] The b values of these interactions were assumed to be twice as large as the refined one for the S–O and S–C interactions. The C–H distance 1.08 Å and $b_{C-H}=0.0030$ Å^2 were used.[75] All DMSO molecules,

Table 3. Results of the least-squares refinements of the DMSO solutions. The refined parameters, d = distance (Å), b = temperature factor coefficient (Å^2) and n = number of distances per metal atom, are obtained for the range $6 < s < 16$ Å^{-1} of the reduced intensity curves. Estimated standard deviations are given within parentheses for refined parameters. In columns *A* all parameters in the table have been independently refined, in columns *B* a few are held constant.

Complex	Interaction	Parameter	0.69 M $Cd(ClO_4)_2$		0.93 M $Hg(ClO_4)_2$		0.44 M $Hg(ClO_4)_2$
			A	*B*	*A*	*B*	*B*
$M(DMSO)_n^{2+}$	M–O	*d*	2.290(3)	2.294(2)	2.394(3)	2.392(3)	2.39(1)
		b	0.0041(5)	0.0044(3)	0.010(1)	0.0098(3)	0.013(1)
	M–S	*d*	3.417(3)	3.422(3)	3.426(3)	3.427(3)	3.437(5)
		b	0.016(1)	0.0154(4)	0.018(1)	0.0190(3)	0.016(1)
	M–O and M–S	*n*	6.5(4)	6	5.6(2)	6	6
ClO_4^-	Cl–O	*d*	1.425(3)	1.426	1.447(5)	1.426	1.426
DMSO	S–O	*d*	1.559(3)	1.53	1.51(1)	1.53	1.53
	S–C	*d*	1.814(3)	1.80	1.78(1)	1.80	1.80
		b	0.0032(2)	0.0031(2)	0.0036(3)	0.0036(2)	0.0034(4)

Table 4. Results of least-squares refinements of an aqueous 3.5 M $Hg(ClO_4)_2$ solution in 0.64 M $HClO_4$. The refined parameters with the estimated standard deviation within parentheses are obtained for the range $4 < s < 16$ Å^{-1} of the reduced intensity curve. In column *A* only Hg–H_2O and Cl–O interactions are taken into account, while in column *B* also H_2O–H_2O interactions along the edges of a regular octahedron are included. Spherical formfactors are used for the water molecules.[66]

Complex	Interaction	Parameter	*A*	*B*
$Hg(H_2O)_n^{2+}$	Hg–H_2O	*d*	2.40(1)	2.41(1)
		b	0.022(3)	0.026(1)
		n	5.4(4)	6.0(4)
	H_2O–H_2O	*d*		$2.41 \times \sqrt{2}$
		b		0.022(7)
		n		12
ClO_4^-	Cl–O	*d*	1.423(4)	1.420(4)

bonded or non-bonded, were accounted for in this way.

3. Regular tetrahedral ClO_4^- ions, for which only one parameter, determining all distances, was independently refined. The *b* values were taken from mean-square amplitudes of vibration calculated from spectroscopic data.[76] The values $b_{Cl-O} = 0.00074$ and $b_{O-O} = 0.0016$ Å^2 were used.

For the aqueous solution the model used in the final refinements was the hydrated Hg(II) ion, where the three parameters *d*, *b* and *n*, describing the Hg–H_2O interactions, were refined. H_2O–H_2O interactions, assuming octahedral coordination around mercury, were introduced. A regular ClO_4^- tetrahedron was included as described above.

The parameter values of the DMSO solutions, from refinements in the range $6 < s < 16$ Å^{-1}, are summarized in Table 3, and the ones of the aqueous solution, in the range $4 < s < 16$ Å^{-1}, in Table 4. Significant deviations occurred in the values when the lower *s* limit was $\lesssim 5$ for DMSO and $\lesssim 3$ for water. This is also indicated by the differences between experimental and calculated *si*(*s*) curves for the DMSO solutions in Fig. 2*b*.

The standard deviations given in Tables 3 and 4 are those calculated in the least-squares process. From the variation of the results with different ranges of *s*, it seems that the inherent systematic errors may be of the same order of magnitude and the estimated standard deviations given in the text have been accordingly increased to give a more realistic error estimate.[74]

Discussion

The solvated Cd^{2+} and Hg^{2+} ions in DMSO. If assumed to be the same, the number of M–O and M–S distances obtained in the least-squares refinements (columns *A* in Table 3) is six, within the estimated limits of error. Also when the number is allowed to vary independently for the two interactions, the same result emerges, though the error becomes larger. This of course further confirms that the lower peaks at 2.3 Å are due to M–O and the higher ones at 3.4 Å to M–S interactions, *i.e.* that both Cd^{2+} and Hg^{2+} are in fact coordinated *via* oxygen.

When the constant contributions from O–O and S–S interactions within the same complex, assuming octahedral configurations, were included in the refinements, the error-square-sum decreased 3–4 %. A coefficient *b* corresponds to a root-mean-square variation, $l=\sqrt{2b}$, in the average distance. This *l* value includes both mean-square amplitudes from thermal vibrations[75] and more permanent variations of the distance for a specific type of interaction. The b_{S-S} was therefore given a rather large value, 0.04 $Å^2$ ($l=0.28$ Å), corresponding to the expected large variation in the individual S–S distances.[32,48]

An inclusion in the refinements of the M–C interactions, which vary considerably around an average of 4.4 Å[32,48] in the crystal structures did not reduce the error-square-sum for the refined high angle regions of the intensity curves ($s>6\ Å^{-1}$). This indicates that large variations in the M–C distances occur also in the solutions, corresponding to the estimated large *b* value $\simeq 0.07\ Å^2$.

Especially for M–O, the number of distances, *n*, is strongly correlated to the *b* value. Therefore, calculations have also been performed with a constant coordination number of six. This results in more precise *b* values, but the other parameters do not change significantly, Table 3.

The b_{Cd-O} value corresponds to $l=0.085(4)$ Å. This is not much larger than the expected vibrational amplitude. The spread of the Cd–O distances is thus small, confirming that the coordination is regularly octahedral.

The b_{Hg-O} is significantly larger, corresponding to $l=0.15(1)$ Å. This probably does not reflect any permanent deviation from regular octahedral symmetry, however, since the Hg–O peak (Fig. 1) seems too symmetrical to contain Hg–O interactions from a markedly distorted octahedral configuration. If any of the bonds were markedly shorter and stronger, they also ought to have small *b* values and therefore be prominent in the outermost parts of the intensity curves. No sign of such an influence has been detected, however.

Comparisons between the RDF's and the calculated peak shapes for the refined model (see above) using the parameter values in Table 3, columns *B*, are made in Fig. 1. The M–C interactions are also included, with the average distance 4.4 Å and the estimated $b_{M-C}=0.07\ Å^2$ ($l=0.37$ Å). Smooth difference curves are obtained showing that the refined model accounts for all distinct intramolecular interactions.

The hydrated Hg^{2+} ion. Within the estimated limits of error six oxygen atoms are found to be coordinated to Hg (Table 4). The parameters obtained, when only the Hg–H_2O and the intramolecular interactions in ClO_4^- are taken into account, are listed in column *A*, Table 4. There is, however, a small shoulder at 3.4 Å in the RDF (Fig. 4) corresponding to O–O distances along the edges of a regular octahedral complex. Such expected O–O interactions were therefore included in the refinements, adjusting only the b_{O-O} independently (column *B*, Table 4). The error-square-sum then decreased by 5 %.

The *b* value of the Hg–O distances is rather large, corresponding to a root-mean-square variation $l=0.23(1)$ Å. For the same reasons as discussed for $Hg(DMSO)_6^{2+}$, however, the average symmetry seems to be regularly octahedral (*cf.* Fig. 5, Ref. 33). This is also supported by the relatively small average $l=0.21(3)$ Å obtained for the non-bonded O–O distances along the octahedral edges.

Peak shapes, calculated from the parameter values in column *B*, Table 4, have been subtracted from the RDF of the aqueous solution. A smooth difference curve was obtained (Fig. 4), which supports the assumption of a regular octahedral coordination around mercury.

Comparison of the structures of the DMSO solvates of Hg^{2+} and Cd^{2+} in solution and in crystals. In the octahedrally oxygen coordinated solid compounds $[M(DMSO)_6](ClO_4)_2$, the orientation of the DMSO ligands differ for Cd^{2+} and Hg^{2+}.[48] For the Cd complex even alternative orientations are found. In solution, the DMSO ligands certainly have a considerable freedom of movement. As the methyl groups have a rather large free volume available,[32,48] rotations around the M–O and S–O bonds should be possible. This would give

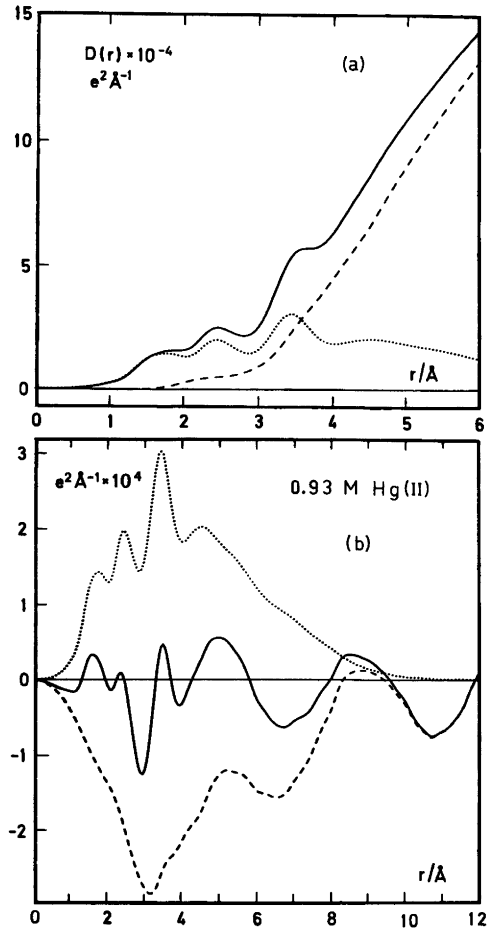

Fig. 5. (a) $D(r)$ curve (solid line) for the 0.93 M $Hg(ClO_4)_2$ solution in DMSO, compared with the sum of the calculated peak shapes (dotted line) for all intramolecular interactions within $[Hg(DMSO)_6]^{2+}$, free DMSO and ClO_4^-. For $[Hg(DMSO)_6]^{2+}$ the positional parameters from the crystal structure determination in Ref. 32 were used, except for the Hg–O distances which were lengthened to 2.393 Å. The dashed line gives the difference between the functions. (b) $D(r)-4\pi r^2\rho_0$ function (solid line), the sum of the calculated peaks (dotted line), and the difference between them (dashed line).

constant M–O and M–S, but varying M–C distances, as is in fact found. There are therefore no reasons to believe that the different shapes found in the crystals would persist in solution.

Discrete dinuclear complexes with a double DMSO oxygen bridge are found in the structure of $Hg(ClO_4)_2.4DMSO$.[54] The Hg–Hg distance is 3.913(4) Å. Also in the structure of $3HgCl_2.2DMSO$ such a double bridge exists. In this case, the Hg–Hg distance is 4.01_6 Å.[10] Therefore, the RDF's were checked for signs of bridge-formation. No trace of such Hg–Hg distances could be found, however.

The complex $Hg(DMSO)_6^{2+}$ in the crystals of $[Hg(DMSO)_6](ClO_4)_2$ has been used to calculate peak shapes for a comparison with the RDF of the 0.93 M $Hg(ClO_4)_2$ solution (Fig. 5). The positional parameters obtained in the structure determination were used,[32] except for the Hg–O distance which was lengthened to 2.39 Å. The freedom of rotation of the DMSO ligands was accounted for by giving the appropriate interactions rather large b values. The intramolecular interactions of ClO_4^- and non-bonded DMSO were also included in the same way as described before. The main difference between this model and the previously refined one is that all intramolecular interactions within $Hg(DMSO)_6^{2+}$ are now taken into account. Subtraction of peak shapes, calculated with this model, from the RDF's give smooth background curves with fairly low electron pair densities up to 4–5 Å (dashed curves in Fig. 5). This indicates that intermolecular interactions from the heavy metal atoms to the ClO_4^- ion and to free DMSO molecules are not frequently occurring within a radius of about 5 Å from the metal atoms. This is consistent with an approximately octahedral arrangement of the S atoms, just as in the solid compound. The remaining broad peaks at about 5.5 and 9 Å in the back-ground curve, agree with peaks found for intermolecular interactions in liquid DMSO.[2] In the solution, non-coordinated DMSO molecules, as well as ClO_4^- ions, are evidently kept away from the mercury rather efficiently by the movements of the DMSO ligands attached to the mercury atoms.

Comparison of the structure of the hydrated Hg^{2+} in solution and in crystal. The very concentrated solution used, 3.5 M $Hg(ClO_4)_2$ in 0.64 M $HClO_4$, contains less than five non-bonded H_2O molecules per $Hg(H_2O)_6^{2+}$ complex. A comparison with intermolecular interactions involving Hg atoms in the structure of the solid hydrate, $[Hg(H_2O)_6](ClO_4)_2$ is therefore of immediate interest. In this compound a slight deviation from a regular octahedral O_h symmetry for the $Hg(H_2O)_6^{2+}$ complexes is observed.[31] This is probably an effect of H-bonds between the complexes leading to Hg–Hg distances

of 5.34 Å. There are no indications of such Hg–Hg interactions in the RDF (Fig. 4), and H-bonds between the complexes are evidently not formed in the solution.

In the solid hydrate each Hg is surrounded by six equidistant ClO_4^-. There are therefore six Hg–Cl distances at 4.75 Å, 12 Hg–O distances at 4.39 Å, and another six at 4.64 Å. They correspond very well to the large and broad peak from about 4 to 5 Å which remains in the "back-ground" curve discussed above (dashed curve in Fig. 4). This strongly indicates that in this concentrated solution the complex $Hg(H_2O)_6^{2+}$ is surrounded by ClO_4^- ions at much the same distance as in the solid (*cf.* the results of the refinements in Table 3, Ref. 33).

Bond lengths, bond angles and ionic radii. The Cd–O bond length 2.292(4) Å, found in DMSO solution of $Cd(DMSO)_6^{2+}$, does not differ significantly from the well-defined Cd–O1 bond length, 2.278(7) [2.291]* Å, in the crystalline solvate $[Cd(DMSO)_6](ClO_4)_2$.[48] Also in aqueous solution, much the same bond lengths have been found, *viz.* 2.289 ± 0.013 and 2.31 ± 0.02 Å,[53,44] and these are not significantly different from the average Cd–O bond length in the crystalline hydrate $[Cd(H_2O)_6](NH_4)_2(SO_4)_2$, *viz.* 2.28 Å.[49]

On the other hand, the average Hg–O bond length is significantly longer in the solutions studied than in the crystalline solvates. In aqueous and DMSO solutions (Tables 3 and 4) the values found are 2.41(1) and 2.393(5) Å, respectively, while 2.341(6) [2.349]* Å is found in $[Hg(H_2O)_6](ClO_4)_2$ and 2.338 [2.350]* in $[Hg(DMSO)_6](ClO_4)_2$.[31,32]

In solution, the average values of the angle M–O–S are 120.2(1.0) and 125.7(1.0)° for the Hg and Cd solvates, respectively. This is not significantly different from the corresponding values 123 and 125° in the crystalline solvates.[32,48]

Nor do the intramolecular S–O and S–C distances obtained in the refinements (Table 3) in the DMSO molecules in solution differ significantly from the values found in crystals of DMSO[71] or oxygen coordinated solvates,[32,48] see also surveys in Refs. 10 and 72.

The Cl–O bond length in ClO_4^- found in the least squares refinements agrees very well with that found in crystal structures, especially where only weak hydrogen bonding occurs.[73]

From the average bond lengths obtained, the ionic radii of Cd^{2+} and Hg^{2+} in octahedral coordination can be derived. If the radii of oxygen are taken as 1.35 Å in the two-coordination of the DMSO solvates and as 1.36 Å in the three-coordination of the hydrates,[77] virtually the same radii, $r(Cd^{2+}) = 0.94$ Å and $r(Hg^{2+}) = 1.05$ Å, are found for both DMSO and aqueous solutions. From the crystalline DMSO solvates, $r(Cd^{2+}) = 0.92$ Å and $r(Hg^{2+}) = 0.99$ Å are calculated, from the hydrates 0.92 Å and 0.98 Å. The radii found for the solids are thus somewhat shorter than found for the solutions, and in the case of Hg^{2+} the difference is certainly significant. The radii derived from crystal structures by Shannon and Prewitt[77] are somewhat longer than the present ones, however, *viz.* $r(Cd^{2+}) = 0.95$ Å and $r(Hg^{2+}) = 1.02$ Å, *i.e.* rather close to the values presently found in solution.

While the octahedral bond length relative to oxygen is $\simeq 0.1$ Å longer for Hg(II) than for Cd(II), the bond lengths do not differ significantly in the tetrahedral tetraiodo complexes. The Cd–I bonds are 2.79 Å both in DMSO[45] and in aqueous solution[44] and the Hg–I bonds are 2.80 and 2.785(3) Å, respectively.[1,6] In the tetrachloro complexes, on the other hand, the bond length of Hg(II) seems again to be slightly longer than of Cd(II). Admittedly, only one reliable determination has so far been performed in solution, *viz.* for $HgCl_4^{2-}$ in water,[7] where the distance Hg–Cl is 2.47(1) Å. This result agrees well with those found for solids,[26,25] *viz.* 2.46_4 and 2.50 Å. Thus, in the case of this complex, the distance seems to be the same in solution and in crystalline compounds. For $CdCl_4^{2-}$, the average distance Cd–Cl in two recently investigated solid compounds[78] is 2.45_4 Å, *i.e.* most probably shorter than the mean of the values found for Hg–Cl.

The bond distance Hg–L thus becomes shorter relative to Cd–L as the ligand atom L becomes softer, and the bonding hence more covalent, in the sequence O < Cl < I. As might be expected, the softer acceptor Hg^{2+} is able to utilize the covalent bonding capacities of the softer ligands more efficiently than Cd^{2+}, with the result that the bonds Hg–L are strengthened, and consequently also markedly shortened relative to the bonds Cd–L. For the very soft iodide ion, the effect becomes so considerable that the bond lengths, and hence the radii of Hg^{2+} and Cd^{2+}, become virtually equal. For even softer ligands, $r(Hg^{2+})$ might well be even shorter than $r(Cd^{2+})$. Such an inversion has in fact been observed between the neighbour acceptors

* Corrected for thermal motion assuming oxygen to ride on the metal atom.

gold(I) and silver(I). In the bidentate complexes MCl(PP),[79] the bonds Au–P are 0.1 and 0.15 Å shorter than the corresponding bonds Ag–P while Au–Cl is 0.3 Å longer than Ag–Cl.

RAMAN AND INFRARED SPECTRA

Data collection

The Raman spectra were recorded in the range 1550 to 150 cm^{-1}, with a Cary 82 argon ion laser spectrophotometer using the 4880 Å line. Glass tubes of 1 mm diameter were used both for the solids and the solutions. The infrared spectra were recorded in the range 4000 to 230 cm^{-1}, with a Perkin-Elmer 221 or a Beckman IR-9 spectrometer. In the low-frequency range, 400 to 150 cm^{-1}, the measurements were carried out on an RIIC FS-720 Fourier spectrometer at liquid nitrogen temperature. All other measurements were carried out at room temperature. Depending upon substance and frequency, various techniques had to be used (polyethene or KRS-5 windows; KBr pellets).

Results and discussion

DMSO solvates of Zn^{2+}, Cd^{2+} and Hg^{2+} in solids and solutions. The Raman and infrared spectra recorded display a large number of bands. These can be divided into three distinct groups, *viz.* bands

Table 5. Raman bands (cm^{-1}) of pure DMSO(l), of solid solvates $[M(DMSO)_6](ClO_4)_2$, M = Zn, Cd, Hg and $Hg(ClO_4)_2.4DMSO$ (= Hg 4), and of the saturated DMSO solutions of the hexasolvates. Intensities: vs = very strong, s = strong, m = medium, w = weak, vw = very weak.

	Hexasolvates				Solutions[a]			
DMSO(l)	Zn	Cd	Hg	Hg 4	Zn	Cd	Hg	Vibration
	~416 w	~412 w	422 m	~420 m	415 vw	~411 vw	425 w	M–O str, sym
	176 w	197 m	221 m		175 vw	195 w	202 m	M–O bend
1420 m	1425 vs	1425 s	1405 s			1422 s	1420 s	C–H def, asym
1310 w	1325 vw	1305 vw	1320 w			1312 w	1313 w	C–H def, sym
1045 vs	1042 m				1047 s	1047 s	1048 s	S–O str
	1021 s	1028 s	1028 s	1029 w			1025 m[b]	S–O str
997 vw	1003 m	1007 m	1001 m	998 w	1000 vw	1005 vw	996 vw	C–H rock
995 m	954 m	962 m	960 vw		955 m	955 w	950 ww	C–H rock
928 vw	912 m	912 m	909 m		912 w	912 w	911 w	C–H rock
	717 s	717 s	717 s	718 s		~712 m[b]	713 m[b]	C–S str, asym
699 s					698 m	700 m	700 m	C–S str, asym
	683 vs	681 vs	683 vs	683 vs				C–S str, sym
670 vs					668 vs	672 vs	674 vs	C–S str, sym
			399 m	402 m			397 w[b]	C–S–O def, sym
382 m					383 m	384 m	384 m	C–S–O def, sym
	345 s	343 s	342 s	341 s				C–S–O def, asym
332 s					334 s	338 s	336 s	C–S–O def, asym
	317 s	315 s	316 s	314 m				C–S–C def
308 m					308 m	311 m	310 m	C–S–C def
	1102 m	1100 m	1100 m	1093 m				Cl–O
	935 vs	932 vs	932 vs	932 s	932 s	933 s	933 s	Cl–O
	626 m	626 m	625 w	621 w	[c]	625 w	626 w	Cl–O
	460 m	460 m	459 w	463 w	457 w	458 w	460 w	Cl–O

[a] Concentrations: Zn, 0.29 M; Cd, 0.71 M; Hg, 0.93 M. [b] Shoulders. [c] Covered by the very strong C–S stretch at 668 cm^{-1}.

Table 6. Infrared bands (cm^{-1}) of pure DMSO(l), and of solid solvates $[M(DMSO)]_6(ClO_4)_2$, M = Zn, Cd, Hg, and $Hg(ClO_4)_2.4DMSO$ (= Hg 4).

	Hexasolvates				
DMSO(l)	Zn	Cd	Hg	Hg 4	Vibration
	431 m	418 m	445 s		M–O str, asym
	192, 178 w	191, 195 w			M–O bend
2985 s	2978 vw	2970 vw	2980 vw	2985 vw	C–H str
2902 s	2900 vw	2899 vw	2900 vw	2900 vw	C–H str
1432 s		1418 m	1425 vw	1429 w	C–H def, asym
1401 s	1412 vw	1395 m	1397 vw	1397 w	C–H def, asym
1305 m	1303 vw	1304 w		1305 w	C–H def, sym
1048 vs	1015 m	1019 m	1025 m	1015 s	S–O stretch
949 m	948 m	947 m	948 m	945 s	C–H rock
690 m	694 w	695 w	692 w	697 w	C–S stretch, asym
660 w	660 vw	665 vw	666 vw	665 vw	C–S stretch, sym
378 m	368 w	370 w	370 w	371 m	C–S–O def, sym
327 m	321 w	320 w	322 w	340 m	C–S–O def, asym
	1100 w	1088 m	1100 w	1088 s	Cl–O
	621 vs	621 vs	621 vw	621 vw	Cl–O

due to the coordinate bond, to the bonds within DMSO, and to the bonds within ClO_4^-.

The well-known frequencies[80] of the Cl–O bands are, as expected, not shifted in the present solids or solutions, Tables 5 and 6.

On the other hand, the frequencies found in pure DMSO[81] are shifted considerably when the solvent molecules are coordinated to a metal atom. As might be expected, the shifts are larger, the closer the bond associated with the vibration is to the site of coordination. As will be further discussed below, the direction of the shifts depends upon whether the metal ion is coordinated *via* oxygen or *via* sulfur. Especially the S–O stretching frequency, strongly active in both Raman and infrared, exhibits very characteristic shifts. Those found in the infrared spectra have repeatedly been used to discern between different modes of coordination in solid solvates.[82–85,46]

In addition to the ClO_4^- and DMSO bands, the solvates display two new bands of low energy, with wavenumbers just above 400 cm^{-1} and just below 200 cm^{-1}, Tables 5 and 6. The bands observed are of weak to medium intensity. The higher frequency band has been found earlier[55] in the infrared spectra of DMSO hexasolvates of several divalent metal ions, including Zn^{2+}. It has been assigned to the M–O stretching mode.[55] It seems natural to assign the band of lower frequency now discovered to M–O bending modes. Evidence supporting this assignment will be presented below.

A coordination of a metal ion to the O-atom in DMSO should bring about a lowering of the S–O bond order and hence a decrease of the S–O stretching frequency relative to free DMSO. Conversely, a coordination to the S-atom should bring about an increase of the S–O bond order, and hence of the S–O stretching frequency.[83,84] These inferences have later been amply confirmed by complete structure determinations of several of those solids which were used in the previous studies of infrared spectra.[32,48,72,86]

The present Raman spectra of the solid hexasolvates show, as expected, shifts in the S–O stretching frequency very similar to those found in the infrared spectra, Table 5. The latter have moreover been checked, Table 6, with results that agree very well with those previously found.[46] The wavenumbers found in the pure solvent, 1045 cm^{-1} in Raman and 1048 cm^{-1} in infrared, are in all the solvates lowered by 20 to 30 cm^{-1} as expected for O-coordination. The same applies to the actually dimeric[54] $Hg(ClO_4)_2.4DMSO$.

In solutions of these solvates, free DMSO predominates over coordinated DMSO, even if the solutions are saturated. It might be hoped, however, that the bands due to free and coordinated DMSO are resolved in the laser Raman spectra. Unfortu-

nately, the shifts are not large enough for such a resolution. Especially for Zn^{2+}, but also for Cd^{2+}, the solubility is so low that the bands due to coordinated DMSO only appear as rather insignificant shoulders on the low frequency side of the intense band due to free DMSO. For Hg^{2+}, however, where the solubility is higher, a well-developed shoulder is observed, consistent with a downward shift of the S–O stretching band in coordinated DMSO to $\simeq 1025$ cm^{-1}, *i.e.* to the value found for the solid hexasolvate, Table 5. This is of course in line with the result of the structure determination reported above for $Hg(DMSO)_6^{2+}$ in solution.

The decrease of the S–O bond order brought about by a coordination of a metal ion via the O atom should induce a compensatory increase in the C–S bond order. Consequently the wavenumbers of the C–S stretching modes, both the symmetric and the antisymmetric ones, should increase. Such shifts, ranging from 10 to 30 cm^{-1}, have in fact been observed in infrared for the antisymmetric mode.[84,85] For the solvates studied here, corresponding shifts have been found for both modes, though smaller, only $\simeq 5$ cm^{-1}, Table 6. Especially the bands due to the symmetric vibrations are of low intensity, however, so the determinations are not very precise. For the pure solvent, these bands are found at 660 and 690 cm^{-1} for the symmetric and antisymmetric mode, respectively. The values agree very well with those originally found by Cotton *et al.*[82] and differ only slightly from later determinations which generally record wavenumbers $\simeq 10$ cm^{-1} higher.[84,85] Also in the present Raman measurements, somewhat higher wavenumbers are found for these vibrations, *viz.* 670 and 699 cm^{-1}, in accord with earlier determinations,[81] Table 5. For the solid solvates, upward shifts are again found, somewhat larger than in infrared, *viz.* 10 to 13 cm^{-1} for the symmetric and 16 to 17 cm^{-1} for the antisymmetric mode, Table 5. Most probably, the differences found between the infrared and Raman shifts are mainly due to the relatively low precision of the infrared measurements. There is no doubt, however, that the wavenumbers of the C–S stretching modes increase on the coordination of a metal ion to the O-atom, just as expected.

In saturated solutions of the mercury and cadmium solvates, these shifts appear as shoulders on the high frequency side of the bands due to free DMSO. The shoulders are especially marked for the bands due to the antisymmetric stretching, where the shifts are larger. For the less soluble zinc solvate, on the other hand, the concentration of coordinated DMSO is too low to bring about any perceptible shoulders of the DMSO bands.

In contrast to earlier work,[55] we have found that also other vibrations involving the C–S bond, *viz.* the symmetric C–S–C deformation, and the symmetric and antisymmetric C–S–O deformations, increase their wavenumbers perceptibly in the solid solvates, Table 5. This is borne out beyond doubt by the Raman spectrum of the mercury(II) hexasolvate where all three modes are represented by bands of medium to strong intensity. For zinc and cadmium, the symmetric C–S–O bands presumably overlap with the M–O stretching bands which would imply upward shifts of $\simeq 30$ cm^{-1}. Considering that shifts of more than 40 cm^{-1} have been found for lanthanide DMSO solvates,[87] this seems quite plausible. Moreover, at least the cadmium band has a deformed shape indicating a composite absorption.

Generally, the complex formation does not bring about large shifts of the vibrations involving the C–H bonds, Tables 5 and 6. Evidently, these are too far from the site of coordination to be much affected by the new bond. The C–H rocking band at 928 cm^{-1} has moved markedly downwards, however. Virtually the same shift is observed when liquid DMSO is vaporized, or diluted by carbon tetrachloride.[81b] Most likely, therefore, this shift is due to the disappearance of the molecular packing preferred by the pure solvent.

Not surprisingly, the most direct information about the M–O coordinate bonds is provided by their own vibrations. The antisymmetrical stretching modes are displayed by the infrared spectra of the solid hexasolvates, Table 6. For zinc, the band is in exactly the same position as found in an earlier study.[55] In the Raman spectra, bands assigned to the symmetrical M–O stretching modes are found for all the hexasolvates, Table 5. For zinc and cadmium, the intensities are fairly low while the mercury band is well-developed. The frequencies are markedly lower than for the anti-symmetric stretching bands recorded in infrared. As the Raman data are more complete, and certainly are more precise, they will serve as the main basis for the following discussion.

Also the Raman spectra of the saturated solutions yield both the M–O bending and the M–O stretching bands, Table 5. In the case of zinc and cadmium, however, the concentrations are so low

that the bands are barely perceptible. For mercury they are stronger and, for some unknown reason, the wavenumber of the bending mode is lower than for the solid solvate.

The wavenumber of the stretching modes decreases from zinc to cadmium and then increases again the mercury, Tables 5 and 6. The latter value is even higher than that of zinc. This certainly holds even if, as postulated above, the zinc and cadmium bands in the Raman spectra are somewhat affected by the overlap with the C–S–O deformation frequency. For regularly octahedral complexes like the present ones, the stretching force constants are approximately proportional to the square of the wavenumbers for a symmetric stretching (*cf.* below) which means that they vary in a similar manner, with a marked minimum at cadmium, Table 8. The force constants of course do not measure the total strength of the M–O bonds but rather their resistance to a small disturbance.[88] Nevertheless, the minimum indicates that the Cd–O bond is most probably weaker than both Zn–O and Hg–O. The conclusion is moreover convincingly vindicated by the similar trend found for the heats of solvation, as will be further discussed below. The reason for the remarkable minimum of bond strength at Cd^{2+} must be the rapid change of bond character along the series Zn^{2+}, Cd^{2+}, Hg^{2+}. The small and hard acceptor Zn^{2+} forms a strong bond of a markedly electrostatic character. The very soft and much larger acceptor Hg^{2+} forms a strong bond of a rather covalent character. The intermediate Cd^{2+} is evidently handicapped by being on one hand much larger than Zn^{2+}, on the other much less soft than Hg^{2+}. The outcome is a bond of a lower overall strength than developed by either Zn^{2+} or Hg^{2+}.

This topic will be further discussed later on when the comparison can be extended to stretching force constants for bonds in other complexes of the three metal ions considered, and also to quantities connected with the total strength of these bonds.

The wavenumber of the vibration assigned to the M–O bending mode increases monotonously from zinc to mercury, Table 5. The resistance to this deformation thus increases as the bond becomes more covalent, and hence the directional forces stronger. This is evidently just what to expect for a bending mode and strongly confirms the assignment done for this vibration.

Hydrates of Zn^{2+}, Cd^{2+} and Hg^{2+} in solids and solutions. In the spectral studies of the hydrates, the interest has been focussed on the M–O bonds. In Raman, the symmetric stretching frequencies are found for all the solid solvates, and also for all the saturated solutions, Table 7. The wavenumbers are throughout lower than in DMSO. As in DMSO, a minimum is found at cadmium. In water, the wavenumber for mercury is lower than for zinc, however. The implications of these differences will be discussed below.

The wavenumbers found agree fairly well with those reported previously[89,90] for near-saturated aqueous nitrate and perchlorate solutions (385–390 cm^{-1} for zinc, *ca.* 356 cm^{-1} for cadmium and 380 cm^{-1} for mercury).

For the solid hydrates, faint bands presumably due to the M–O bending mode are observed at $\simeq 175$ cm^{-1}. These bands are too poorly developed, however, to allow a reliable determination of the shifts between the various hydrates.

Force constants and bond strengths. For the present octahedral solvates, a valence force field approach allows a simple calculation of the primary

Table 7. Raman bands (cm^{-1}) of the solid hydrates $[M(H_2O)_6](ClO_4)_2$, M = Zn, Cd, Hg, and of their saturated aqueous solutions.[a]

Solvates			Solutions[b]			
Zn	Cd	Hg	Zn	Cd	Hg	Vibration
385 w	352 m	360 s	~380 m	352 m	370 m	M–O stretch
933 vs	933 vs	933 vs	933 s	933 s	933 s	Cl–O
631 s	630 s	627 s	630 m	627 m	629 m	Cl–O
463 s	465 s	466 s	464 m	461 m	462 m	Cl–O

[a] No measurements at wavenumber >1000 cm^{-1}. [b] Concentrations: Zn, 3.26 M; Cd, 3.23 M; Hg, 3.50 M (+0.64 M $HClO_4$).

stretching force constants F_r. If it is assumed that the frequency is determined solely by the interaction between the metal ion and the oxygen ligand atom and if the secondary interaction constants are neglected, the following relation holds for the symmetric mode[91]

$$F_r = 4\pi^2 c^2 \bar{\nu}^2 N^{-1} A_L$$

where c = the velocity of light, $\bar{\nu}$ = the wavenumber, N = the Avogadro number and A_L = the atomic weight of the ligand atom.

Especially for the DMSO solvates, this approach is a considerable simplification of the actual conditions, as the vibrations of the ligand atom are influenced by the bond joining it to the rest of the DMSO molecule. The values of F_r calculated in this manner, listed in Table 8, will evidently represent the lower limits of the force constants in the present approximation. The other extreme, *viz.* insertion of the total mass of DMSO, would certainly yield values of F_r much further from the truth. However, the influence of the mixing with the bending modes is probably larger for the DMSO solvates than for the hydrates and would counteract the effect of a too small effective ligand mass in the calculations.

This is also borne out by a comparison with the corresponding values of F_r found for the hydrates (Table 8), where insertion of the mass of the whole ligand H_2O certainly is the best approximation. The values of F_r found are not very different from the lower limits calculated for the DMSO solvates. As there is no reason to believe, that the M–O bond strength differs radically between the hydrates and the DMSO solvates, the true values of F_r for the DMSO solvates should be fairly close to those calculated by insertion of the mass of the oxygen atom. Even when this minimum mass is applied, the values for the DMSO solvates are higher, and the M–O bonds, therefore, presumably stronger than for the hydrates. Comparisons between complexes of different acceptors with the same ligand are of course not influenced by this uncertainty.

It is also of interest to compare stretching force constants of these solvates with those found for other complexes of the acceptors studied. As to the gaseous linear[3,92,93] halides MX_2, the symmetric stretching frequencies are so far known only in the case of mercury. The antisymmetric stretching frequencies are, on the other hand, known for all the halides. Again assuming that the secondary interaction constant is negligible, the primary stretching force constant F_r can be calculated from[94]

$$F_r = 4\pi^2 c^2 \bar{\nu}^2 N^{-1} \frac{A_L}{1 + 2A_L A_M^{-1}}$$

where A_M = the atomic weight of the metal. The values of F_r thus found are listed in Table 8. For the mercury systems, they differ somewhat from the set published previously[92] which was calculated as the mean between the values of F_r found from the symmetric and antisymmetric stretching frequencies. It seems better, however, to compare data calculated on the same basis. It is nevertheless reassuring that the values calculated from the symmetric and antisymmetric stretching frequencies do not differ very much.

Table 8. Stretching force constants of the M–O bonds in solid hexasolvates and of the M–X bonds in gaseous dihalides (10^5 dyn cm^{-1}).

	M–O			M–X		
	H_2O[a]	H_2O[b]	DMSO[a]	Cl^-	Br^-	I^-
Zn^{2+}	1.40	1.57	1.63	2.67	2.33	1.77
Cd^{2+}	1.17	1.32	1.60	2.34[c]	1.93	1.61
Hg^{2+}	1.22	1.38	1.68	2.63	2.25	1.85

[a] Force constants calculated with A_L = atomic weight of oxygen atom. [b] with A_L = molecular weight of water. [c] Corrected value, calculated from ν_3 of Ref. 92.

For all the dihalides, the value of F_r displays that minimum at cadmium which has already been noticed for the solvates, coordinated via oxygen. The lower bond strength of Cd^{2+} relative to both Zn^{2+} and Hg^{2+} thus persists even if the character of the coordinating ligand varies greatly. Moreover, Hg^{2+} is favoured relative to Zn^{2+} by a typically soft ligand as I^- (and also by DMSO!) while the reverse is true for a typically hard ligand as H_2O. The ligands Cl^- and Br^- are intermediate, as might be expected.

The heats of solvation measure the total strength of the M–O bonds while, as already pointed out, the stretching force constants measure their resistance to a limited deformation. As the potential curves of different M–O bonds generally do not conform, the two quantities cannot be expected to vary according to quite the same pattern between different systems. The minimum at Cd^{2+} nevertheless persists also in the heats of solvation, both for

Table 9. Solvation enthalpies,[36] ΔH°_{sv}, and coordination bond energies,[95] CBE, of Zn^{2+}, Cd^{2+} and Hg^{2+} (kJ mol^{-1}).

	$-\Delta H^{\circ}_{sv}$		CBE		
	H_2O	DMSO	Cl^-	Br^-	I^-
Zn^{2+}	2063	2123	2590	2530	2460
Cd^{2+}	1831	1898	2360	2340	2290
Hg^{2+}	1845	1921	2570	2540	2520

DMSO and water,[36] Table 9. As expected, it is more marked for the softer ligand DMSO. The total bond strength is considerably higher for Zn^{2+} than for Hg^{2+} in both cases.

For the gaseous halides, the coordinate bond energies,[95] *i.e.* the enthalpy changes for the reactions $MX_2(g) \rightarrow M^{2+}(g) + 2X^-$, provide a measure of the total strength of the M–X bonds. For all three ligands, the minimum at Cd^{2+} is again evident, Table 9. For the complexes of the very soft ligand I^-, the total bond strength is even higher for Hg^{2+} than for Zn^{2+}, while for the less soft Br^- they are practically equal. For the least soft halide Cl^-, the bond strength is again higher for Zn^{2+} than for Hg^{2+}. This ligand thus reverts to a pattern similar to that found for DMSO and water. As might be expected, however, the difference between Zn^{2+} and Hg^{2+} is much smaller for Cl^- than for the considerably harder oxygen donors.

Conclusion

The Raman spectra confirm that the acceptors Zn^{2+}, Cd^{2+} and Hg^{2+} form DMSO solvates coordinated *via* oxygen not only in solids but also in solutions. They clearly indicate an increase of the covalency of the M–O interaction in the order $Zn^{2+} < Cd^{2+} < Hg^{2+}$, and also a simultaneous decrease of its electrostatic character. These variations thus counteract each other which results in a minimum of M–O bond strength at Cd^{2+}, as is also found from other evidence. The M–O bonds are more covalent in the DMSO solvates than in the hydrates, but the bond strength minimum at Cd^{2+} nevertheless persists also for the harder water ligand.

Acknowledgements. We have been fortunate to have the advice of Dr. Georg Johansson, Stockholm, on the X-ray measurements, and of Dr. Ragnar Larsson, Lund, on the Raman and infrared spectra. We are most grateful for their valuable and generous help.

Our thanks are also due to Professor Kåre Larsson who made the Raman spectrophotometer available. The infrared spectra have been recorded by Dr. Jan Lindgren, Uppsala and Mrs. Karin Trankell, Lund.

We gratefully acknowledge the support given to these investigations by "Naturvetenskapliga forskningsrådet" (The Swedish Natural Science Research Council).

REFERENCES

1. Gaizer, F. and Johansson, G. *Acta Chem. Scand. 22* (1968) 3013.
2. a. Sandström, M. *Acta Chem. Scand. A 32* (1978) 627; b. Sandström, M. *Thesis*, Royal Institute of Technology, Stockholm 1978.
3. Wells, A. F. *Structural Inorganic Chemistry*, Clarendon Press, Oxford 1975.
4. Waters, D. N. and Kantarci, Z. *J. Raman Spectrosc. 6* (1977) 251.
5. Smith, J. H. and Brill, T. B. *Inorg. Chim. Acta 18* (1976) 225.
6. Sandström, M. and Johansson, G. *Acta Chem. Scand. A 31* (1977) 132.
7. Sandström, M. *Acta Chem. Scand. A 31* (1977) 141.
8. Grdenić, D. *Q. Rev. Chem. Soc. 19* (1965) 303; *Angew. Chem. Int. Ed. Engl. 12* (1973) 435.
9. Brusset, H. and Madaule-Aubry, F. *Bull. Soc. Chim. Fr. 10* (1966) 3122 and references therein.
10. Biscarini, P., Fusina, L., Nivellini, G. D., Mangia, A. and Pelizzi, G. *J. Chem. Soc. Dalton Trans.* (1973) 159; (1974) 1846.
11. Brotherton, P. D. and White, A. H. *J. Chem. Soc. Dalton Trans.* (1973) 2698.
12. Sagisawa, K., Kitahama, K., Kiriyama, H. and Kiriyama, R. *Acta Crystallogr. B 30* (1974) 1603 and references therein.
13. Aurivillius, K. and Stålhandske, C. *Acta Chem. Scand. A 30* (1976) 735 and references therein.
14. Leligny, H., Frey, M. and Monier, J. C. *Acta Crystallogr. B 28* (1972) 2104 and references therein.
15. Brodersen, K., Thiele, G. and Görz, G. *Z. Anorg. Allg. Chem. 401* (1973) 217.
16. Biscarini, P., Fusina, L., Nivellini, G. and Pelizzi, G. *J. Chem. Soc. Dalton Trans.* (1977) 664.
17. Sandström, M. and Liem, D. H. *Acta Chem. Scand. A 32* (1978) 509.
18. Grdenić, D., Sikirica, M. and Vicković, I. *Acta Crystallogr. B 33* (1977) 1630.
19. Gerken, V. A. and Pakhomov, V. I. *Zh. Strukt. Khim. 10* (1969) 753.

20. Brodersen, K. *Acta Crystallogr. 8* (1955) 723.
21. Weidenhammer, K. and Ziegler, M. L. *Z. Anorg. Allg. Chem. 434* (1977) 152.
22. White, J. G. *Acta Crystallogr. 16* (1963) 397.
23. Barr, R. M. and Goldstein, M. *J. Chem. Soc. Dalton Trans.* (1976) 1593.
24. Herlinger, A. W. *Spectrosc. Lett. 8* (1975) 787.
25. Ferguson, G., Jeffreys, J. A. D. and Sim, G. A. *J. Chem. Soc. B* (1966) 454.
26. Clegg, W., Brown, M. L. and Wilson, L. J. A. *Acta Crystallogr. B 32* (1976) 2905.
27. Kamenar, B. and Nagl, A. *Acta Crystallogr. B 32* (1976) 1414.
28. Fenn, R. H. *Acta Crystallogr. 20* (1966) 24.
29. Pakhomov, B. I., Fedorov, P. M., Alymov, I. M., Ivanova-Korfini, I. N. and Semin, G. K. *Izv. Akad. Nauk. SSSR Ser. Fiz. 39* (1975) 2519 and references therein.
30. Clegg, W., Greenhalgh, D. A. and Straughan, B. P. *J. Chem. Soc. Dalton Trans.* (1975) 2591.
31. Johansson, G. and Sandström, M. *Acta Chem. Scand. A 32* (1978) 109.
32. Sandström, M. and Persson, I. *Acta Chem. Scand. A 32* (1978) 95.
33. Johansson, G. *Acta Chem. Scand. 25* (1971) 2787, 2799.
34. a. Gallagher, P. K. and King, E. L. *J. Am. Chem. Soc. 82* (1960) 3510; b. Arnek, R. *Ark. Kemi 24* (1965) 531.
35. a. Ahlberg, I. and Leden, I. *Transactions of the Royal Institute of Technology*, Stockholm *249* (1972) 17; b. Sjöberg, S. *Acta Chem. Scand. A 31* (1977) 705.
36. Ahrland, S., Kullberg, L. and Portanova, R. *Acta Chem. Scand. A 32* (1978) 251.
37. Arnek, R. and Poceva, D. *Acta Chem. Scand. A 30* (1976) 59.
38. Ahrland, S., Persson, I. and Portanova, R. *To be published.*
39. Criss, C. M. and Salomon, M., In Covington, A. K. and Dickinson, T. Eds., *Physical Chemistry of Organic Solvent Systems*, Plenum, London and New York 1973, Chapter 2, Part 4, Appendix 2.11.15.
40. Ahrland, S. and Björk, N.-O. *Acta Chem. Scand. A 30* (1976) 249, 257.
41. Leden, I. *Z. Phys. Chem. Abt. A 188* (1941) 160.
42. Vanderzee, C. E. and Dawson, H. J., Jr. *J. Am. Chem. Soc. 75* (1953) 5659.
43. Mironov, V. E., Kulba, F. Y. and Nazarov, V. A. *Russ. J. Inorg. Chem. 8* (1963) 470.
44. Ohtaki, H., Maeda, M. and Ito, S. *Bull. Chem. Soc. Jpn. 47* (1974) 2217.
45. Pocev, S., Triolo, R. and Johansson, G. *Acta Chem. Scand. A 32* (1978). *In press.*
46. Ahrland, S. and Björk, N.-O. *Acta Chem. Scand. A 28* (1974) 823.
47. West, C. D. *Z. Kristallogr. A 91* (1935) 980.
48. Sandström, M. *Acta Chem. Scand. A 32* (1978) 519.
49. Montgomery, H. and Lingafelter, E. C. *Acta Crystallogr. 17* (1964) 1295; *20* (1966) 728.
50. Ferrari, A., Braibanti, A., Manotti Lanfredi, A. M. and Tiripicchio, A. *Acta Crystallogr. 22* (1967) 240.
51. Ray, S., Zalkin, A. and Templeton, D. H. *Acta Crystallogr. B 29* (1973) 2741.
52. Black, W. H., Griffith, E. A. H. and Robertson, B. E. *Acta Crystallogr. B 31* (1975) 615.
53. Bol, W., Gerrits, G. J. A. and van Panthaleon van Eck, C. L. *J. Appl. Crystallogr. 3* (1970) 486.
54. Sandström, M. *Acta Chem. Scand. A 32* (1978) 527.
55. Berney, C. W. and Weber, J. H. *Inorg. Chem. 7* (1968) 283.
56. Karlsson, R. and Karrman, K. J. *Talanta 18* (1971) 459.
57. Schwarzenbach, G. *Complexometric Titrations*, Methuen, London 1957.
58. Reynolds, W. L. *Prog. Inorg. Chem. 12* (1970) 1.
59. Martin, D. and Hauthal, H. G. *Dimethyl Sulphoxide*, van Nostrand Reinhold, Wokingham, Berkshire 1975, pp. 448–449.
60. Johansson, G. *Acta Chem. Scand. 20* (1966) 553.
61. Johansson, G. and Sandström, M. *Chem. Scr. 4* (1973) 195.
62. Milberg, M. E. *J. Appl. Phys. 29* (1958) 64.
63. Doyle, P. A. and Turner, P. S. *Acta Crystallogr. A 24* (1968) 390.
64. *International Tables of X-Ray Crystallography*, Vols. 3 and 4, Kynoch Press, Birmingham 1968 and 1974, respectively.
65. Stewart, R. F., Davidson, E. R. and Simpson, W. T. *J. Chem. Phys. 42* (1965) 3175.
66. Narten, A. H. and Levy, H. A. *J. Chem. Phys. 55* (1971) 2263.
67. Breit, G. *Phys. Rev. 27* (1926) 362.
68. Dirac, P. A. M. *Proc. R. Soc. London A 111* (1926) 405.
69. Dwiggins, C. W. and Park, D. A. *Acta Crystallogr. A 27* (1971) 264.
70. Levy, H. A., Danford, M. D. and Narten, A. H. *Data Collection and Evaluation with an X-Ray Diffractometer Designed for the Study of Liquid Structure*, Report ORNL-3960, Oak Ridge National Laboratory, Oak Ridge 1966.
71. Thomas, R., Shoemaker, C. L. and Eriks, K. *Acta Crystallogr. 21* (1966) 12.
72. Björk, N. O. and Cassel, A. *Acta Chem. Scand. A 30* (1976) 235.
73. Berglund, B., Thomas, J. O. and Tellgren, R. *Acta Crystallogr. B 31* (1975) 1842.
74. Seip, H. M. in *Molecular Structure by Diffraction Methods*, Vol. 1, p. 53, *Specialist Periodical Reports*, The Chemical Society, London 1973.

75. Cyvin, S. J. *Molecular Vibrations and Mean Square Amplitudes*, Elsevier, Amsterdam 1968.
76. Müller, A. and Nagarajan, G. *Z. Naturforsch. Teil B 21* (1966) 508.
77. Shannon, R. D. and Prewitt, C. T. *Acta Crystallogr. B 25* (1969) 925.
78. a. Richardson, M. F., Franklin, K. and Thompson, D. M. *J. Am. Chem. Soc. 97* (1975) 3204; b. Oleksyn, B. J., Stadnicka, K. M. and Hodorowicz, S. A. *Acta Crystallogr. B 34* (1978) 811.
79. Barrow, M., Bürgi, H. B., Johnson, D. K. and Venanz, L. M. *J. Am. Chem. Soc. 98* (1976) 2356.
80. Cohn, H. *J. Chem. Soc.* (1952) 4282.
81. a. Horrocks, W. D. and Cotton, F. A. *Spectrochim. Acta 17* (1961) 134; b. Forel, M.-T. and Tranquille, M. *Ibid. 26 A* (1970) 1023.
82. Cotton, F. A., Francis, R. and Horrocks, W. D., Jr. *J. Phys. Chem. 64* (1960) 1534.
83. Drago, R. S. and Meek, D. *J. Phys. Chem. 65* (1961) 1446.
84. Selbin, J., Bull, W. E. and Holmes, L. H., Jr. *J. Inorg. Nucl. Chem. 16* (1961) 219.
85. Currier, W. F. and Weber, J. H. *Inorg. Chem. 6* (1967) 1539 and references therein.
86. Bennett, M. J., Cotton, F. A., Weaver, D. L., Williams, R. J. and Watson, W. H. *Acta Crystallogr. 23* (1967) 788.
87. Kawano, Y. and Osorio, V. K. L. *J. Inorg. Nucl. Chem. 39* (1977) 702.
88. Jones, L. H. *Coord. Chem. Rev. 1* (1966) 351.
89. a. Hester, R. E. and Plane, R. A. *Inorg. Chem. 3* (1964) 768, 769; b. Macklin, J. W. and Plane, R. A. *Ibid. 9* (1970) 821.
90. Bulmer, J. T., Irish, D. E. and Ödberg, L. *Can. J. Chem. 53* (1975) 3806.
91. Jones, L. *Inorganic Vibrational Spectroscopy*, Marcel Dekker, New York 1971, Vol. 1, pp. 48, 95.
92. Klemperer, W. *J. Chem. Phys. 25* (1956) 1066 and *J. Electrochem. Soc. 110* (1963) 1023 and references therein.
93. Vilkov, L. V., Rambidi, N. G. and Spiridonov, V. P. *J. Struct. Chem. 8* (1967) 715 and references therein.
94. Herzberg, G. *Infrared and Raman Spectra of Polyatomic Molecules*, van Nostrand, New York 1945, p. 172.
95. Pearson, R. G. and Mawby, R. J. In Gutmann, V., Ed., *Halogen Chemistry*, Academic, London and New York 1967, Vol. 3.

Received March 29, 1978.

Acta Chemica Scandinavica A 32 (1978) 627–641

An X-Ray Diffraction and Raman Study of Chloride, Bromide and Iodide Complexes of Mercury(II) in Dimethyl Sulfoxide Solution and of Mercury(II) Chloride in Methanol Solution

MAGNUS SANDSTRÖM

Department of Inorganic Chemistry, Royal Institute of Technology, S-100 44 Stockholm 70, Sweden

The structures of solvated mercury(II) halide complexes in concentrated dimethyl sulfoxide (DMSO) solutions have been studied by X-ray diffraction and Raman methods. Tetrahedral HgX_4^{2-} (X=I, Br and Cl) complexes are found to dominate for mol ratios X/Hg ≥ 4, with no direct coordination of solvent molecules to mercury. The Hg–Br bond length in $HgBr_4^{2-}$ is found to be 2.636(4) Å, and in the slightly pyramidal $HgBr_3^-$ 2.548(4) Å. The $HgCl_3^-$ complex seems to have a planar trigonal structure with a bond length of 2.434(4) Å. Coordination of DMSO molecules through the oxygen atom to mercury is suggested by Raman spectra for all HgX_3^- and HgX_2 complexes and confirmed by X-ray diffraction.

The bond length found for HgI_2 is 2.625(2), $HgBr_2$ 2.455(3), and $HgCl_2$ 2.350(4) Å. The angle X–Hg–X is 159(2)° for HgI_2 and 165(3)° for $HgBr_2$. The bent structure is consistent with the occurence of a ν_3 band in the Raman spectra of these molecules. A methanol solution of $HgCl_2$ was studied and the significantly shorter bond length found, 2.308(3) Å, reflects the much weaker solvation. Still, a slight deviation from linearity is indicated by the appearance of a weak ν_3 band in the Raman spectra.

The Raman spectra of concentrated $HgXClO_4$ solutions in DMSO did not indicate the HgX^+ species to be dominant. A disproportionation, especially of $HgCl^+$, to solvated Hg^{2+} ions and HgX_2 molecules occurs. For the $HgIClO_4$ solution about half the mercury seems to be present in dimeric complexes formed by a single I-bridge.

A 2 M $HgBrNO_3$ solution in DMSO was also studied. The data are consistent with a dominant $[O(HgBr)_2]$ complex with an Hg–O–Hg angle of about 113°.

The coordination changes of the mercury(II) atom in solution upon the stepwise addition of halide ligands have been the subject of several structural studies.[1] A point of special interest is the strong preference for linear coordination, for which $d-s$ hybridization has been proposed.[2] The halide ions, with the exception of the F^- ion which forms very weak complexes, form an interesting series for a study of changes in covalency of the metal–ligand bond (which is expected to increase in the sequence $Cl^- < Br^- < I^-$). The coordination of solvent molecules will also play an important role in determining the structure of the halide complexes in solution.

X-Ray diffraction methods have been applied to concentrated aqueous solutions.[3–7] Due to the low solubilities of the HgX_2 complexes and the formation of polynuclear complexes in the Hg(II)–Cl^- system,[6] only the structures of the pyramidal $HgBr_3^-$ and HgI_3^- ions and the tetrahedral HgX_4^{2-} complexes have been unambiguously determined. The hydrated Hg^{2+} ion was found to coordinate six water molecules forming an almost regular octahedral arrangement.[7,8]

For a more complete structural study of the mononuclear HgX_n^{2-n} ($n=0, 1, \ldots, 4$) complexes by X-ray diffraction and spectroscopic methods, the solvent dimethyl sulfoxide was chosen. In solution, the solvated Hg^{2+} ion was found to have a regular octahedral coordination of six DMSO molecules through their oxygen atoms.[7] Recently reliable potentiometric and calorimetric investigations of the mercury(II) halide systems in DMSO have been performed.[9,10] The thermodynamic data obtained are discussed in Ref. 7 and indicate that successive desolvation of the octahedral $[Hg(DMSO)_6]^{2+}$

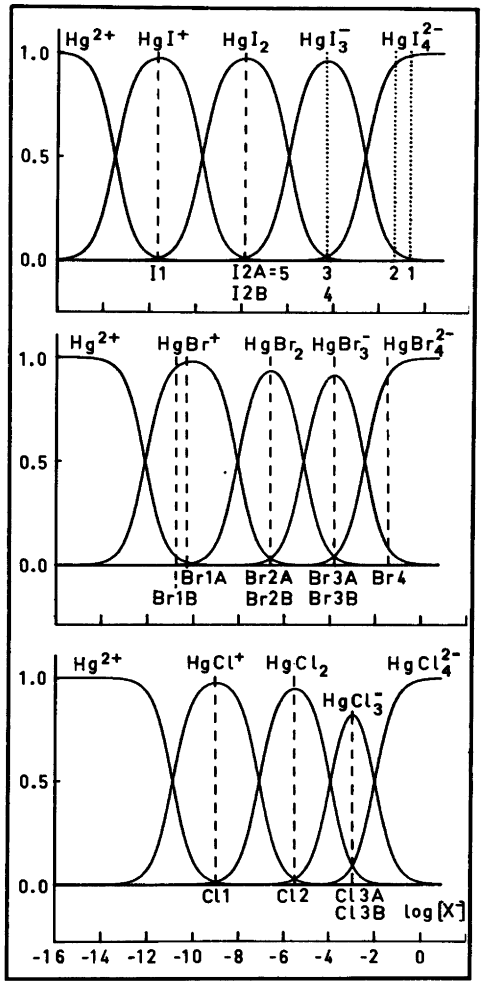

Fig. 1. Relative distributions of the mercury(II) halide complexes in dilute DMSO solutions as a function of the free halide ion concentration. Equilibrium constants from Ref. 9, determined by potentiometric methods with an ionic medium of 1 M NH_4ClO_4, have been used. The calculated compositions of the solutions investigated by X-ray diffraction, assuming the same equilibrium constants to be valid, are indicated by the vertical dashed lines. The dotted lines and the numbers correspond to the iodide solutions studied previously (Ref. 12).

complex takes place when the first and second halide ligands are coordinated. The HgX_2 complexes were found to be only relatively weakly solvated.[10] All HgX_n^{2-n} complexes have well-separated ranges of domination,[9] Fig. 1. If this situation persists even in concentrated solutions without ionic medium, these systems are particularly well-suited for X-ray diffraction and Raman studies, since the solubilities are high. Other favourable points are the strong solvation ability of DMSO for cations[11] and the rather large scattering power of the S atoms, which faciliate the study of solvent coordination.

The HgI_2, HgI_3^- and HgI_4^{2-} complexes have been studied previously by X-ray diffraction in DMSO and DMF solutions.[12] An approximately linear coordination was reported for HgI_2, pyramidal for HgI_3^-, and tetrahedral for HgI_4^{2-}. No definite conclusions were reached with regard to the coordination of solvent. During the present investigation, data for the previously studied 2.5 M HgI_2 solution in DMSO were recalculated, since improvements in the data evaluation technique[13] allow more precise results to be derived.

A recent spectroscopic study[14] of $HgCl_2$ and $HgBr_2$ complexes in various solvents indicated increasing deviations from linearity as the donor strength of the solvent increases. To study the solvent effect on the structure, a solution of $HgCl_2$ in methanol, where the solvation is much weaker than in DMSO,[11] was also investigated here.

EXPERIMENTAL

The solutions investigated were prepared by dissolving weighed amounts of mercury(II) halide, $Hg(NO_3)_2 \cdot \frac{1}{2}H_2O$, sodium or lithium halide (all analytical reagents), and $Hg(ClO_4)_2 \cdot 4DMSO$,[7] in DMSO or methanol (*p.a.*). Their compositions are given in Table 1.

The halide salts and the mercury(II) nitrate had been gently heated and stored in vacuum desiccators for several months prior to use. After this treatment the mercury content of the mercury(II) nitrate was checked by analysis[8a] (found 61.1 %, calculated for $Hg(NO_3)_2$ 61.8 %, for $Hg(NO_3)_2 \cdot \frac{1}{2}H_2O$ 60.1 %). The DMSO was repeatedly distilled in vacuum over calcium hydride. Its water content was determined by Karl-Fischer titrations and was normally below 0.02 %. Such titrations could not be performed in Hg(II) solutions due to reduction of mercury, but a gas-chromatographic check of the water content was made for several of the solutions. The highest values were as expected found for the nitrate solution, Br1B. About 0.3 weight % H_2O was found before and 0.5 % after the X-ray measurements, during which the solutions were enclosed in an air-tight shield with a cylindrical Be-window for the X-rays.

Table 1. Concentrations in mol dm^{-3} of the solutions investigated by X-ray diffraction. The solvent is DMSO except for Sol. Cl2B where methanol was used. The linear absorption coefficient $\mu(cm^{-1})$, is calculated for Mo$K\alpha$ radiation.

Solution	Hg(II)	X^-	ClO_4^-	NO_3^-	Na^+	Li^+	Solvent	μ
I2A	2.50	5.00	–	–	–	–	11.3	84.4
I2B	4.39	8.78	–	–	–	–	9.0	144.6
I1	1.27	1.27	1.27	–	–	–	12.7	39.9
Br4	0.606	2.40	–	–	1.19	–	13.1	32.8
Br3A	0.55	1.65	–	–	0.55	–	13.2	27.1
Br3B	1.00	3.01	–	–	1.00	–	12.7	45.4
Br2A	1.00	2.00	–	–	–	–	13.1	39.4
Br2B	3.18	6.36	–	–	–	–	11.2	115.0
Br1A	1.54	1.47	1.61	–	–	–	12.3	49.2
Br1B	2.01	2.00	–	2.02	–	–	12.3	62.4
Cl3A	1.00	3.00	–	–	1.00	–	13.0	28.8
Cl3B	1.49	4.46	–	–	–	1.49	12.6	40.4
Cl2A	1.00	2.00	–	–	–	–	13.3	28.4
Cl2B	1.50	3.00	–	–	–	–	22.9	36.3
Cl1	1.30	1.30	1.30	–	–	–	13.0	35.5

The diffracted intensity of Mo$K\alpha$ radiation ($\lambda = 0.71069$ Å) was measured at 25 ± 1 °C from the free surface of the solutions as described previously.[5] Laser-Raman spectra were recorded with a Cary 82 Spectrophotometer in the same way as before.[6] The accuracy of the frequencies reported is estimated to be within $\pm 2\ cm^{-1}$, unless otherwise indicated.

X-Ray diffraction measurements were also made on pure DMSO, but due to inadequate geometrical limitations during the data collection for this low-absorbing liquid ($\mu = 4.8\ cm^{-1}$), the results are not of very high quality and are only used for comparison (Figs. 2c and 3c). With the geometrical arrangement used, absorption corrections are not required for solutions with linear absorption coefficients $\mu > \sim 15\ cm^{-1}$.[15]

DATA TREATMENT

All calculations were carried out by means of the KURVLR and PUTSLR programs.[13] The same data reduction and correction procedures as described previously[13,5,7] were followed. The experimental intensities were normalized to a stoichiometric unit of volume containing one mercury atom (for pure DMSO one molecule). The correction for double scattering did not exceed 3 % for any of the solutions. Scattering factors were obtained from the same sources as before.[5,6] The reduced intensity curves $i_{obs}(s)$, multiplied by s, are shown in Figs. 2, 5 and 7 with the first ten points estimated by extrapolation. By a Fourier transformation, corresponding electronic radial distribution functions, $D(r)$ and $D(r) - 4\pi r^2 \rho_0$ curves, were obtained (Figs. 3, 4, 6 and 8) using the same modification function as previously.[5]

RESULTS

The Raman spectra were used to identify the dominating species in the solutions and to obtain additional information on the solvent coordination. Frequencies of interest are reported in Table 3. The assignments were made by comparison with previously reported values in DMSO or other solvents.

The RDF's for all DMSO solutions (Figs. 3, 4 and 8) show a peak at 1.5 – 1.7 Å corresponding to distances within the DMSO molecules.[7] In the perchlorate solutions, Cl – O distances also contribute.[7] The sharp peak found in the range 2.3 to 2.8 Å corresponds to expected Hg – X distances within the mercury(II) halide complexes and also includes Hg – O distances from coordinated solvent molecules. At about 3.5 – 3.8 Å, another peak or shoulder is found (except for Sol. Br4) corresponding to expected Hg – S distances (*cf.* Fig. 4) from coordinated DMSO molecules.[7,16,17] Distinct peaks corresponding to probable I – I or Br – Br distances within the complexes can be discerned at 5.1 Å in Sols. I2A and I2B, at 4.8 Å in Sol. Br2B, and at

4.3 Å in Sols. Br4 and Br3B. The broad peaks at about 5.5 and 9 Å, found in the RDF's of all DMSO solutions except the most concentrated ones, also occur in the RDF of pure DMSO (Fig. 3c) and are probably mainly caused by intermolecular interactions between DMSO molecules.

The appearance of the RDF of Sol. Br1B (Fig. 8) differs markedly from the others and will be discussed later.

For the RDF of the 1.5 M methanol solution of $HgCl_2$ (Fig. 6), the intramolecular methanol distances correspond to the peak at 1.4 Å.[18] The distinct peak at 2.3 Å originates from Hg–Cl interactions[19] and the broad peak at about 4 Å mainly from the structure of liquid methanol.[20]

Least-squares refinements of distinct intramolecular interactions were performed minimizing the sum $\sum_{s(\min)}^{s(\max)} w(s)\,[i_{obs}(s)-i_{calc}(s)]^2$ following the same procedure as before.[5,7]

The expected contributions to the calculated reduced intensities, $i_{calc}(s)$, from the intramolecular DMSO, ClO_4^- and CH_3OH interactions were held constant during the refinements. The parameter values used for the calculations were taken from crystal structures,[21,22] an electron diffraction study,[18] vibrational amplitudes,[23,24] and from results of another X-ray diffraction study.[7]

A summary of the results is given in Table 2, where the standard deviations given are those calculated in the least-squares process. From variations in the parameter values when different ranges of the high angle parts ($s > \sim 4$ Å^{-1}) of the intensity curves were used in the refinements, the inherent systematic errors can be estimated to be of the same order of magnitude as the standard deviations given. To give a more realistic error estimate, the standard deviations in the text have been increased accordingly.[25]

The parameter values of Table 2 have been used to calculate reduced intensities, which together with the constant contributions mentioned above, are compared with the experimental values in Figs. 2, 5 and 7. As can be seen, the agreement is satisfactory in the high-angle ranges used for the refinements. The intermolecular intensity contributions, which decrease rapidly with increasing s values, do not seem to give significant contributions in this range ($s > \sim 4$ Å^{-1}).

The consistency of the refined models is also checked by comparing peak shapes, obtained by Fourier transformation of the calculated $i_{calc}(s)$ values, with the RDF's (Figs. 3, 4, 6 and 8). Subtraction of these peaks from the experimental curves should then give fairly smooth background curves showing that all distinct intramolecular interactions are accounted for, as is in fact observed (dashed lines in Figs. 3, 4, 6 and 8).

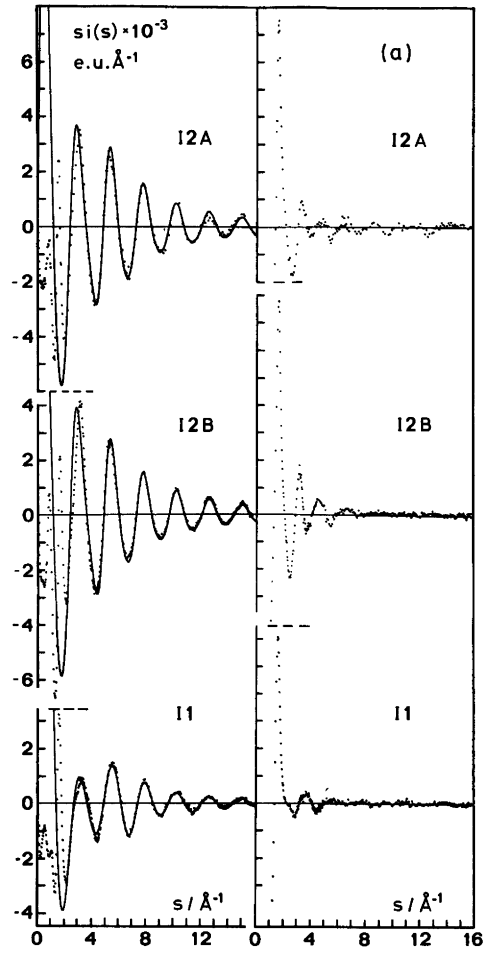

Fig. 2. (a–c) Reduced intensities, $i(s)$, multiplied by s, are shown in the left-hand half of the figure for the DMSO solutions investigated. Experimental values are denoted by dots (the first ten are obtained by extrapolation), values calculated for the refined model by solid lines. The right-hand half of the figure shows the differences, $s\,i_{obs}(s)-s\,i_{calc}(s)$, between experimental and calculated values.

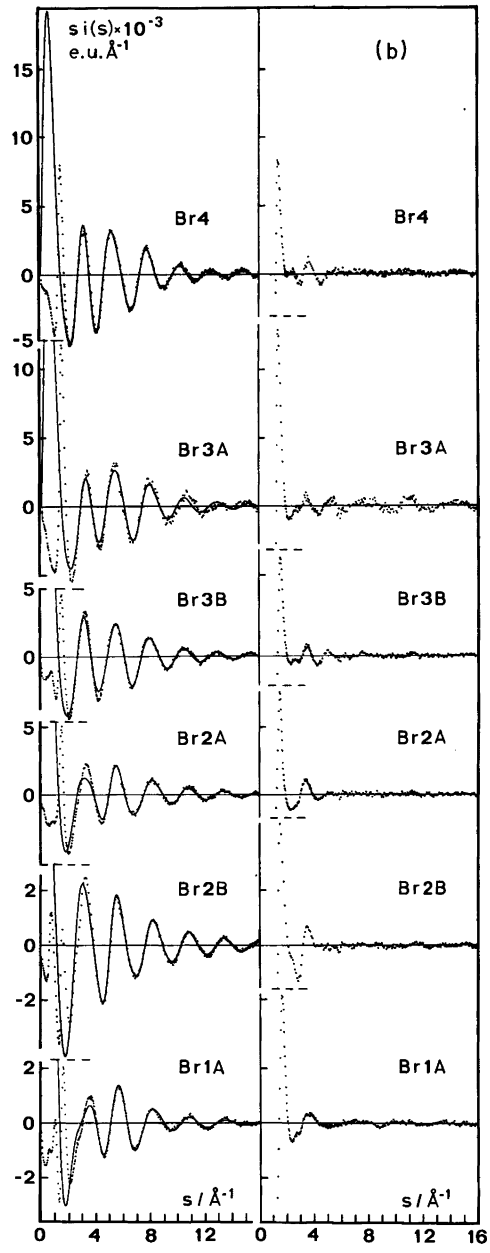

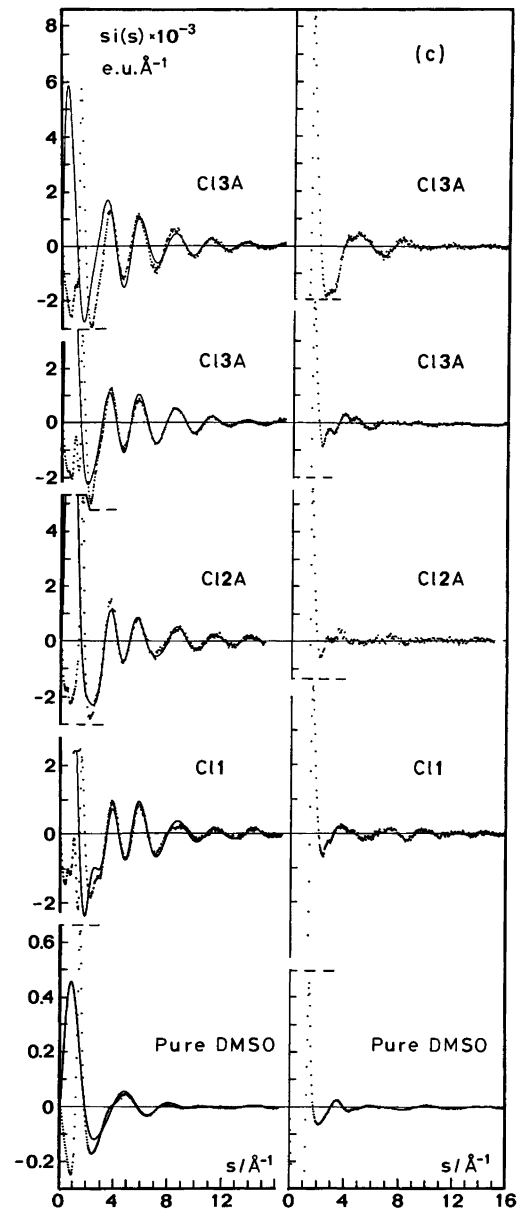

Fig. 2. Contd.

DISCUSSION

The HgX_4^{2-} complexes. The dominating complexes in Sols. I4, Br4 and Cl4 are HgX_4^{2-}, if the complex distributions in these concentrated solutions (*cf.* Table 3) are approximately the same as those in Fig. 1. That the HgX_4^{2-} complexes dominate is supported by the Raman spectra obtained (Table 3), where the observed frequencies are close to previously reported values for $\nu_1(HgX_4^{2-})$.[14,26-30] The spectroscopic results indicate a regular tetrahedral coordination,[27,28] which has been cor-

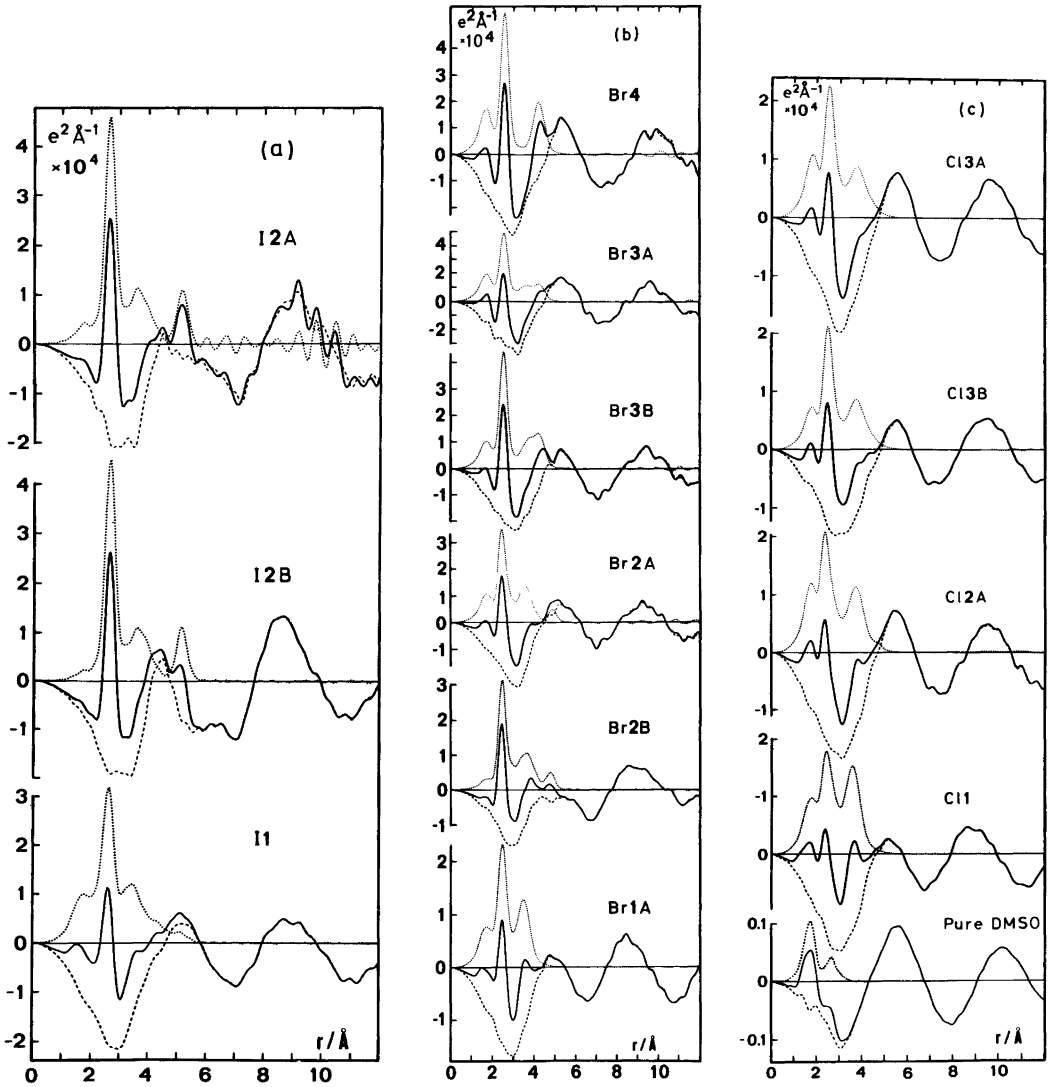

Fig. 3. (a–c) $D(r)-4\pi r^2\rho_0$ functions (solid lines) compared with sums of calculated peak shapes of the refined models (dotted lines). The parameter values given in Table 2 and in the text have been used. The differences are shown by the dashed lines.

roborated by X-ray diffraction studies of solutions.[4-6,12]

In the present investigation only $HgBr_4^{2-}$ has been studied by X-ray diffraction. The Hg–Br bond length, $d_{Hg-Br}=2.636(4)$ Å, was obtained for Sol. Br4 after correction for the calculated amount of $HgBr_3^-$ (~9 %) present (*cf.* Fig. 1), using the distances from Table 2. The ratio d_{Hg-Br}/d_{Br-Br} is 0.611(2), close to the value 0.6124 expected for a regular tetrahedral complex. The numbers of Hg–Br and Br–Br distances obtained (Table 2) are also consistent with a tetrahedral structure.

The frequency variation observed for $\nu_1(HgX_4^{2-})$ in different solvents has been interpreted as indicating a second sphere solvation mechanism,[14] where electron donation to the solvent results in a weaken-

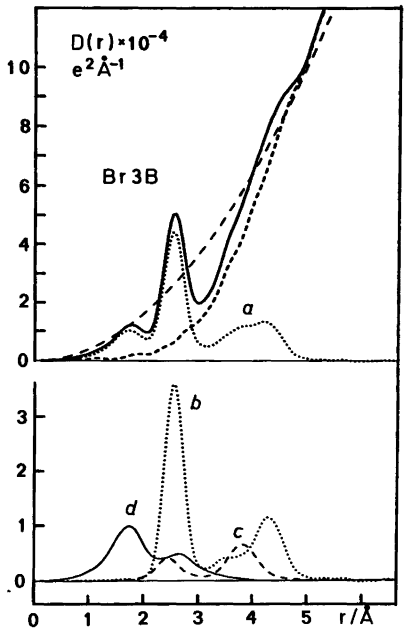

Fig. 4. The radial distribution function, $D(r)$ (solid line), and the $4\pi r^2\rho_0$ curve (long dashes) for Sol. Br3B (1 M $NaHgBr_3$ in DMSO). The sum of the calculated peak shapes for intramolecular contributions is given by the dotted curve *a*, which gives a rather smooth difference curve (short dashes) when subtracted from the $D(r)$ curve. Individual contributions to the peak shapes are shown separately in the lower part of the figure (note the larger ordinate scale). The dotted curve *b* corresponds to the sum of the Hg–Br, Br–Br and Br–O contributions according to the parameters in Table 2. The dashed curve *c* shows the Hg–O and Hg–S contributions expected for two DMSO molecules coordinated to an $HgBr_3^-$ complex (Table 2), and the solid line *d* the intramolecular contributions from all DMSO molecules in the solution.

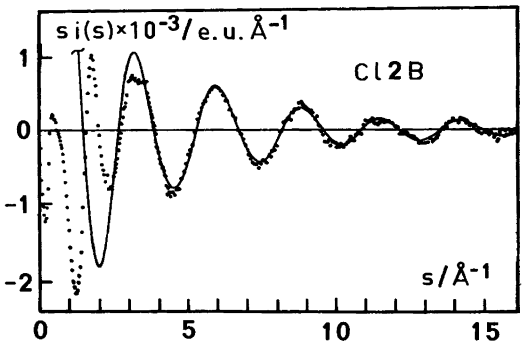

Fig. 5. Reduced intensities multiplied by s for the 1.5 M solution of $HgCl_2$ in methanol (Sol. Cl2B). Experimental values are denoted by dots, calculated values by the solid line.

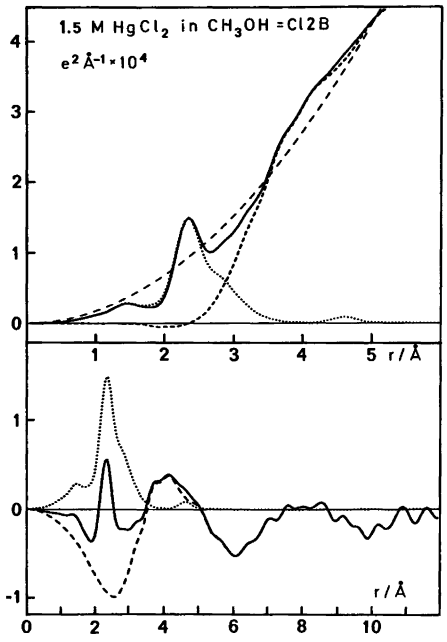

Fig. 6. RDF's for Sol. Cl2B (1.5 M $HgCl_2$ in methanol). The upper part of the figure shows the $D(r)$ curve (solid line) and the $4\pi r^2\rho_0$ function (long dashes). The $D(r)-4\pi r^2\rho_0$ curve is shown by the solid line in the lower part. The sum of the calculated peak shapes of the refined model (dotted lines) gives smooth background curves (dashes) after subtraction from the RDF's.

ing of the Hg–X bond and a decrease of the $\nu_1(HgX_4^{2-})$ frequency. Slightly lower ν_1 values indicating stronger solvation, are obtained for HgX_4^{2-} in DMSO[14] (Table 3) than in H_2O,[28–30] supporting the debated[31] suggestion that large polarizable anions should be more solvated in DMSO.[32] This is also consistent with the observed tendency towards lengthening of the bonds: $d_{Hg-Br}=2.610(5)$ in H_2O[5] and 2.636(4) Å in DMSO, $d_{Hg-I}=2.785(3)$ in H_2O[5] and 2.80 Å in DMSO.[12]

The HgX_3^- ions. In the complex distributions for dilute solutions represented in Fig. 1, the HgX_3^-

Table 2. Results of the least-squares refinements on the reduced X-ray intensity curves. The parameters descriptive of an atomic pair interaction are: d=distance (Å), b=temperature factor coefficient (Å^2) and n=number of distances per Hg atom. The standard deviation given within parentheses for refined parameters is obtained from the least-squares process and does not include systematic errors. The intramolecular intensity contributions from the solvent molecules (DMSO for all solutions except the methanol solution Cl2B) and from the ClO_4^- ions, if present, were calculated and held constant during the refinements.

Interaction		I2A	I2B	I1	Cl3A	Cl3B	Cl2A	Cl2B	Cl1
Hg–I	d	2.620(2)	2.627(1)	2.626(5)	2.432(3)	2.436(2)	2.350(3)	2.308(2)	2.32(1)
or	b	0.0037(4)	0.0022(1)	0.0026(8)	0.0029(3)	0.0038(3)	0.0013(3)	0.0015(3)	0.000(1)
Hg–Cl	n	2.2(1)	2.03(2)	1.2(1)	3	3	2	2	1
Hg–S	d			3.51(2)	3.68(3)	3.63(3)	3.68(2)		3.51(1)
	b			0.047(5)	0.022(3)	0.054(4)	0.043(3)		0.034(3)
	n			4.4(4)	2	2	4		4.9(3)
Hg–O	d			2.33(1)	2.60	2.60	2.53(3)	2.66(2)	2.42(1)
	b			0.008(1)	0.010	0.010	0.021(4)	0.015(3)	0.012(2)
	n			$=n$(Hg–S)	2	2	4	2.2(6)	$=n$(Hg–S)
I–I	d	5.11(1)	5.123(6)		4.23	4.23	4.68	4.60	
or	b	0.006(2)	0.006(1)		0.03	0.03	0.004	0.004	
Cl–Cl	n	1.1(2)	1.03(8)		3	3	1	1	

Interaction		Br4	Br3A	Br3B	Br2A	Br2B	Br1A	Interaction		Br1B
Hg–Br	d	2.628(2)	2.542(3)	2.552(2)	2.452(2)	2.457(2)	2.435(2)	Hg–Hg	d	3.514(5)
	b	0.0058(4)	0.0024(3)	0.0031(2)	0.0015(2)	0.0018(1)	0.0061(3)		b	0.0094(10)
	n	4.1(2)	3	3	2	2	1.1(1)		n	1.04(4)
Hg–S	d		3.81(4)	3.73(2)	3.57(3)	3.63(3)	3.49(1)	Hg–Br	d	2.452(3)
	b		0.011(3)	0.015(2)	0.029(7)	0.052(10)	0.029(6)		b	0.0072(5)
	n		2	2	4.3(11)	3.9(11)	4.2(6)		n	0.97(3)
Hg–O	d		2.60	2.49(9)	2.64(7)	2.66(3)	2.43(4)	Hg···Br	d	5.66(2)
	b		0.010	0.003(1)	0.031(8)	0.023(7)	0.006(2)		b	0.028(8)
	n		2	2	$=n$(Hg–S)	$=n$(Hg–S)	$=n$(Hg–S)		n	0.85(13)
Br–Br	d	4.31(1)	4.31	4.31(2)	4.82	4.828(14)		Hg–O	d	2.1
	b	0.026(8)	0.016	0.018(2)	0.004	0.004			b	0.005
	n	6(2)	3	3	1	1			n	1

complexes have the narrowest ranges of domination.[9] However, Raman spectra of the Sols. I3, Br3A, Br3B, Cl3A and Cl3B (Table 3), compared with spectra of essentially monomeric HgX_3^- anions in the solid state[33–36] and in DMSO solution,[14,27,33] are consistent with completely dominating HgX_3^- complexes. This is confirmed by Raman spectra showing the stepwise formation of complex anions as the ratio X^-/Hg^{2+} is increased (*cf.* Fig. 1 in Ref. 14). For all these HgX_3^- solutions oxygen coordination of DMSO molecules to the Hg atom is indicated by a shoulder at about 1020 cm^{-1} on the strong S–O stretching band found at 1048–1050 cm^{-1} (Table 3).[7]

The HgI_3^- complex has been studied previously by X-ray diffraction in DMSO, DMF and aqueous solutions,[12,5] where a pyramidal structure has been found. The Hg–I bond lengths obtained were in DMSO 2.733(2),[12] in DMF 2.752(5),[12] and in water 2.76(1) Å.[5] From spectroscopic results a planar structure has been suggested in TBP solution[26] while planar trigonal anions with two long Hg—I contacts completing a bipyramidal configuration are found in crystal structures.[37–39]

However, the present Raman results in combination with the previous X-ray diffraction study,[12] are consistent with an approximately tetrahedral coordination around Hg in DMSO with a DMSO

Table 3. Raman frequencies of interest observed for some mercury(II) halide solutions. The solvent is DMSO except for Sol. Cl2B where methanol was used. The abbreviations are: vs = very strong, s = strong, m = medium, w = weak, sh = shoulder and br = broad.

Sol.	C_{Hg}/M	Mol ratio X to Hg	Dominating Hg species	Hg-frequencies/cm^{-1} ν_1 (Hg–X)	Others (assignment)	S–O bands/cm^{-1} Free	Coordinated
I4	1.00	4.00	HgI_4^{2-}	118 vs		1050 m	
I3	1.00	3.00	HgI_3^-	130 vs		1050 m	~1010 w,sh
I2C	4.00	2.00	HgI_2	144 vs	195 m(ν_3 HgI_2)	1050 w	1008 m,br
I2D	1.00	2.00	HgI_2	145 vs	195 w(ν_3 HgI_2)	1048 s	~1010 w,sh
I1	1.27	1.00	HgI_2, Hg–I–Hg	144 vs	173 m(ν_1 Hg–I–Hg)	1047 s	~1025 w,sh
Br4	0.61	3.96	$HgBr_4^{2-}$	164 vs		1048 s	
Br3B	1.00	3.01	$HgBr_3^-$	178 vs		1045 s,br	~1005 w,sh
Br2A	1.00	2.00	$HgBr_3$	194 vs	~238 w,sh(ν_3 $HgBr_2$)	1045 m	~1010 w,sh
Br2B	3.18	2.00	$HgBr_2$	195 vs	240 w (ν_3 $HgBr_2$)	1050 m,br	1010 m–s,br
Br1A	1.54	0.96	$HgBr_2$,$HgBr^+$, $Hg(DMSO)_6^{2+}$	193 vs	~225 w,br (ν_1 $HgBr^+$) ~425 w (ν_1 Hg–O)	1047 m	~1025 m,br
Br1B	2.01	1.00	$O(HgBr)_2$, $HgBr^+$, $HgBr_2$	237 s 225 w	110 s (ν_1 Hg–O–Hg), 195 w(ν_1 $HgBr_2$)	1042 s	
Cl4	0.40	4.00	$HgCl_4^{2-}$	260 s		1043 s	
Cl3A	1.00	3.00	$HgCl_3^-$	278 s		1050 s	~1020 w,sh
Cl3B	1.49	3.00	$HgCl_3^-$	280 vs		1050 s	~1020 w,sh
Cl2A	1.00	2.00	$HgCl_2$(in DMSO)	303 s		1040 s	~1020 w,sh
Cl2B	1.50	2.00	$HgCl_2$(in CH_3OH)	322 vs	365 w (ν_3 $HgCl_2$)		
Cl1	1.30	1.00	$HgCl_2$,$HgCl^+$, $Hg(DMSO)_6^{2+}$	305 s	~428 w (ν_1 Hg–O) ~200 w (Hg–O bend)[7]	1050 s	~1025 w,sh

oxygen atom bonded in the fourth vertex.

For the $HgBr_3^-$ ion in DMSO solution (Sols. Br3A and Br3B), an average Hg–Br bond length of 2.548(4) Å was obtained (Table 2). The Br–Br distance found for Sol. Br3B 4.31(2) Å, is intermediate between the calculated value for a planar trigonal structure, 4.42 Å, and that for a pyramid derived from a tetrahedral structure, 4.17 Å. There is a shoulder at about 3.7 Å in the RDF's (Figs. 3b and 4) which corresponds to expected Hg–S distances for weakly oxygen coordinated DMSO molecules. The number of DMSO ligands could not be unambiguously determined by least-squares refinements. However, a model assuming two DMSO ligands completing an approximately bipyramidal arrangement gave about 30 % lower values of the error-square-sum than a tetrahedral model with one DMSO ligand. Moreover, the bipyramidal model fits the peaks in the RDF somewhat better than does the tetrahedral one.

The *b* values obtained (Table 2) correspond to root-mean-square variations, $l = \sqrt{2b}$, of 0.080(3) Å for the Hg–Br and 0.18(1) Å for the Br–Br distances. They are in fairly good agreement with the corresponding mean amplitudes of vibration, 0.058 and 0.20 Å, respectively, calculated for $HgBr_3^-$ in TBP solution,[40] where the spectroscopic data obtained indicated a non-planar structure.[26]

The $HgBr_3^-$ ion is pyramidal in aqueous solution. By X-ray diffraction the distances $d_{Hg-Br} = 2.58(1)$ and $d_{Br-Br} = 4.24(3)$ Å were obtained.[5]

In the crystal structure of $[N(CH_3)_4]HgBr_3$, long (2.9 Å) bridging Hg–Br interactions cause a slight but significant deviation from planarity of the $HgBr_3^-$ ions, which have an average bond length of 2.52 Å.[41] Only one structure containing planar $HgBr_3^-$ units ($d_{Hg-Br} = 2.6 \pm 0.1$ Å), with two long Hg–Br interactions at 3.0_8 Å completing a trigonal bipyramidal configuration, has been proposed from powder diffraction data.[42]

For the $HgCl_3^-$ complex, the Hg–Cl bond length is found to be 2.434(4) Å (Table 2). Although there are clearly distinguishable Hg–S peaks at about 3.7 Å and, at least for Sol. Cl3B, a small peak possibly corresponding to a Cl–Cl distance of about 4.25 Å (Fig. 3c), neither the number of Hg–Cl

distances nor the parameters of the Cl–Cl interaction could be satisfactorily determined by least-squares refinements. Two possible models were then compared. A pyramidal $HgCl_3^-$ ion with a DMSO oxygen coordinated in the fourth vertex would, for a regular tetrahedral structure, give Cl–Cl distances of 4.00 Å. A planar $HgCl_3^-$ ion with Hg coordinating two DMSO oxygen atoms in a trigonal bipyramidal configuration, would give Cl–Cl distances of 4.24 Å. The calculated peak shapes for the bipyramidal model using the parameter values in Table 2 gave a slightly better fit to the experimental RDF's (Fig. 3c).

Recently, planar trigonal $HgCl_3^-$ ions have been found in the structures of $[S(CH_3)_3]HgCl_3$,[33] and $[S_4N_3]HgCl_3$,[43] and in α-$[N(C_2H_5)_4]HgCl_3$.[35] The average bond lengths found are 2.42_3, 2.42_7 and 2.43_2 $[2.43_9]$* Å, respectively, not significantly different from the value found in DMSO solution, 2.434(4) Å. Two long axial Hg–Cl contacts at 3.0 to 3.2 Å complete a bipyramidal configuration around Hg in all three structures.

In the structure of the adduct between mercury(II) chloride and histidin hydrochloride,[44] two long axial interactions, Hg–O 2.5_4 and Hg–Cl 3.2_5 Å, with a slightly pyramidal $HgCl_3^-$ ion, give a distorted bipyramidal arrangement similar to that proposed for the solvated $HgBr_3^-$ ion in DMSO.

Assuming the same average angle Hg–O–S of 120° as found in the $[Hg(DMSO)_6]^{2+}$ complexes in solution,[7] the observed Hg–S distances of 3.6 to 3.7 Å (Table 2) lead to Hg–O distances of about 2.6 Å, which is a reasonable value[44,45] for the weak interactions expected.

The Raman and X-ray data of the HgX_3^- solutions do not indicate the formation of polynuclear complexes. Edge-sharing bitetrahedra, $Hg_2X_6^{2-}$, as found in crystal structures for X=Br[46,47] and I,[48] would give distinct and clearly marked Hg–Hg peaks at about 3.8 and 4.0 Å, respectively, which do not occur in the RDF's. Neither Hg–Hg distances corresponding to the double chloride bridges found in aqueous solution[6] nor the double DMSO oxygen bridges occurring in crystal structures[17,49] are consistent with the RDF's in Fig. 3. Moreover, no Raman frequencies due to bridge-formation[34] were detected.

The HgX_2 molecules. The solubility of HgI_2 in DMSO is very high and an almost saturated 4.4 M solution (Sol. I2B) was studied by X-ray diffraction. The mol ratio DMSO/HgI_2 is only 2.06 and, therefore, rather short intermolecular distances must occur between the HgI_2 molecules. In the RDF (Fig. 3a) there is a large and broad peak at 4.4 Å, very probably corresponding to intermolecular HgI_2 interactions, besides the Hg–I and I–I peaks at 2.63 and 5.1 Å.

The Raman spectrum of a 4.0 M HgI_2 solution shows a decrease of the S–O stretching frequency indicating that virtually all DMSO oxygen atoms are coordinated to Hg (Table 3). Only a shoulder remains of the S–O band at 1050 cm^{-1} corresponding to non-coordinated DMSO molecules.[7]

In order to study the effect of a concentration change, data for a previously investigated 2.5 M HgI_2 solution[12] were recalculated (I2A in Table 1). Despite the poorer quality of the data from this early study, noticeable in the spurious peaks at large distances in Fig. 3a, the Hg–S peak at 3.6 Å from coordinated DMSO molecules is now distinguishable in the RDF. The relative size of the peak at 4.4 Å is much smaller than for Sol. I2B, confirming its intermolecular character.

Double DMSO oxygen bridges, as found in crystal structures giving well-defined Hg–Hg distances of 3.913(4) and 4.01_6 Å,[17,49] would give distinct peaks in the RDF's. The broadness and relatively long (4.4 Å) distance found, indicate that single DMSO oxygen bridges, formed by sharing weakly coordinated DMSO oxygen atoms between the Hg atoms, are predominating.

The refined Hg–I and I–I distances are not significantly different for Sols. I2A and I2B (Table 2). The average values obtained are 2.625(2) Å for Hg–I and 5.12(1) Å for I–I. The number of distances obtained in the refinements are consistent with expected values for an HgI_2 molecule. The *b* values correspond to root-mean-square variations of 0.063(2) Å for the Hg–I and 0.10(1) Å for the I–I distances, which are only slightly larger than corresponding mean amplitudes calculated from vibration frequencies in the gas phase, 0.050 and 0.069 Å, respectively.[23] For linear HgI_2 molecules, these vibrational amplitudes should lead to an apparent shortening of the observed I–I distance, compared with its expected value of twice the Hg–I distance, of 0.044 Å.[23] The shrinkage effect obtained here is 0.13(2) Å (Table 2). This unexpectedly large value cannot be explained merely by the slightly larger variations obtained in the distances. Taking the calculated shrinkage into account the angle I–Hg–I would be 159(2)°.

* Corrected for thermal motion assuming Cl to ride on Hg.

Such a slightly bent structure is supported by the appearance of the ν_3 antisymmetric stretching mode[26] at 193 cm^{-1} (Table 3) in the Raman spectra of both 1.0 and 4.0 M HgI_2 solutions.

For a simple valence force field, providing the valence interaction force constant, F_{rr}, is small compared with the bond stretching constant, F_r,[50] the interbond angle can be estimated from the frequency data.[51,14] The calculated angle is insensitive to the ν_2 value, for which the values reported for a TBP solution were used.[26] The I–Hg–I angle was estimated in this way from the values in Table 3 ($\nu_2 = 52$ cm^{-1}) to 138°, which is about 21° too low. This probably reflects inadequacies in the assumptions made above but, for the homologous HgX_2 species, comparisons can still be of interest.

Two $HgBr_2$ solutions were investigated, Sol. Br2A (1.0 M) and Sol. Br2B (3.2 M, supersaturated). For the highly concentrated Sol. Br2B (mol ratio DMSO/Hg = 3.52) a large and broad peak was found in the RDF at about 4.4 Å, just as for the HgI_2 solutions (*cf.* Figs. 3a and 3b), thus supporting the suggestion that DMSO oxygen atoms are shared between the Hg atoms of the HgX_2 molecules. The S–O stretching frequency is shifted to 1010 cm^{-1} and its intensity is considerably larger than for the band at about 1050 cm^{-1} (Table 3) from non-coordinated DMSO, showing that the majority of the DMSO oxygen atoms are coordinated to Hg. For the 1.0 M $HgBr_2$ solution, the lower proportion of coordinated DMSO molecules gives only a shoulder at ~1010 cm^{-1} on the broad band at about 1045 cm^{-1} (Table 3), and in the RDF (Fig. 3b) the Hg–S distances appear as a shoulder at 3.7 Å.

The average Hg–Br distance is 2.455(3) Å and the corresponding root-mean-square variation is $l = 0.060(2)$ Å, which is only slightly larger than the mean amplitude 0.045 Å obtained from vibrational frequencies in the gas phase.[23] The Br–Br distance from the refinements, 4.828(14) Å, is 0.082(14) Å shorter than twice the Hg–Br distance. The shrinkage effect for a linear molecule is 0.039 Å, calculated from the gas phase vibration frequencies.[23] Taking this effect into account, the Br–Hg–Br angle is found to be 165(3)°. Also here the ν_3 frequency is observed in the Raman spectra for both 1.0 and 3.2 M solutions (Table 3), supporting a slightly bent structure.[14] An angle estimation from the spectroscopic data as for the HgI_2 molecule, gives 139°, which is about 26° too low. The ν_2 value 66 cm^{-1} was used.[26]

For the $HgCl_2$ complex in DMSO, the Hg–Cl bond length, 2.350(4) Å, could be obtained, but not the Cl–Cl distance due to its relatively small contribution to the scattering curves. The root-mean-square variation l(Hg–Cl) of 0.058(5) Å is comparable to the calculated mean vibrational amplitude[23] 0.044 Å and the experimental value[52] 0.052(5) Å in the gas phase. The Hg–S peak at 3.7 Å is clearly distinguishable (Fig. 3c) and is consistent with about four Hg–S interactions. The coordination of DMSO oxygen atoms to Hg gives rise to a shoulder at about 1020 cm^{-1} on the 1050 cm^{-1} S–O band in the Raman spectrum (Table 3). The expected $\nu_3(HgCl_2)$ frequency could not be detected due to solvent interference, but from the correlations between ν_1 and ν_3 frequencies from $HgCl_2$ molecules in various solvents and solvent properties which express electron donating power,[14] a Cl–Hg–Cl angle of about 140° can be estimated from spectroscopic data. The actual angle would then presumably be about 165°, assuming the same degree of underestimation with this method as before. This is supported by the angles found in crystal structures of sulfoxide adducts to $HgCl_2$, 166.0(3) and 164.0(2)°, where two[49] and three[53] sulfoxide oxygen atoms, respectively, are coordinated to mercury.

The weakening of the solvation going from $Hg(DMSO)_6^{2+}$ ions to solvated HgX_2 molecules which is proposed from thermochemical studies,[9,10] is reflected by a corresponding increase in the Hg–S distance from 3.427(5)[7] to about 3.7 Å and in the Hg–O bond length from 2.393(5)[7] to about 2.6 Å in the HgX_2 solutions. The number of coordinated DMSO molecules could not be precisely determined by least-squares refinements but the RDF's are satisfactorily explained by assuming four DMSO ligands.

For the 1.5 M solution of $HgCl_2$ in methanol an Hg–Cl bond length of 2.308(3) Å is obtained, significantly shorter than in DMSO. This shortening is certainly due to the much weaker solvation in methanol.[11,54] This is also evident in the crystal structure of the adduct $HgCl_2.2CH_3OH$, where the bond length in the linear $HgCl_2$ unit is 2.31 ± 0.03 Å and a distorted octahedral coordination around Hg is completed by two long Hg–O distances of 2.82 ± 0.05 Å and two Hg–Cl distances of 3.07 ± 0.03 Å.[19]

A still shorter bond length, 2.252(5) Å, has been found for gaseous mercury(II) chloride.[52]

In the crystal structure of pure methanol, every

oxygen atom is H-bonded to two others at 2.66 ± 0.03 Å,[55] which also is in accordance with an X-ray diffraction study of liquid methanol.[20] The parameter values obtained in the refinement of the interaction labelled Hg–O (Sol. Cl2B in Table 2) would correspond well to such H-bonded O–O interactions, provided these H-bonds can exist to an appreciable extent in this concentrated solution. The number of Hg–O interactions obtained, $n(\mathrm{Hg-O}) = 2.2(6)$, equals about 2.9(8) O–O interactions per oxygen atom. It is not possible, however, to determine the proportions of Hg–O and O–O contributions to this interaction from the present data, although the solvent interference with the $HgCl_2$ molecule is evidently strong enough to cause a slight deviation from linearity, as is indicated by the appearance of a weak ν_3 band in the Raman spectrum (Table 2).[54] A Cl–Hg–Cl angle estimation from the spectroscopic data as previously,[51,14] with $\nu_2 = 97$ cm^{-1},[26] gives about 146°. This value is, as found for the HgI_2 and $HgBr_2$ molecules, probably about 25° too low.

The $HgXClO_4$ solutions. Although the calculated complex distributions in Fig. 1 indicate that mononuclear HgX^+ complexes are dominant in the I1, Br1A and Cl1 solutions, the Raman spectra show strong bands corresponding to the $\nu_1(HgX_2)$ frequencies (Table 3). By comparing their relative intensities with those of the HgX_2 solutions, at least 1/3 of the total Hg(II) amount is estimated to be present in HgX_2 groups in all three solutions. Oxygen coordination of DMSO molecules to Hg(II) is indicated by shoulders at 1020–1030 cm^{-1} on the S–O stretching frequency (Table 3). Distinct Hg–S peaks, increasingly pronounced for the solutions I1, Br1A and Cl1 are found in the RDF's at 3.5 Å, (Figs. 3a–c). The shorter average Hg–O and Hg–S distances obtained compared with those of the HgX_2 solutions (Table 2) are, together with the Raman results, consistent with a partial disproportionation of the HgX^+ species to $[Hg(DMSO)_6]^{2+}$ ions[7] and solvated HgX_2 molecules, which is especially extensive in the Cl1 solution.

In dilute solutions, a very large entropy gain is found for the formation of HgX^+ from Hg^{2+} and X^-, indicating an extensive desolvation (ΔS_1^0 is 3–4 times larger than ΔS_2^0 for the successive formation of HgX_2,[9] *cf.* the discussion in Ref. 7). In the concentrated solutions studied here, where the mol ratios DMSO/Hg do not exceed 10 (*cf.* Table 1), a higher degree of order is probably imposed on the small amount of remaining bulk solvent, which reduces the entropy stabilization of HgX^+ and favours the disproportionation.

For Sol. Br1A there is a small peak at 4.8 Å in the RDF corresponding to expected Br–Br distances in an $HgBr_2$ molecule. The weak band found at about 225 cm^{-1} in the Raman spectrum is probably the ν_1 (Hg–Br) frequency from the solvated $HgBr^+$ complex. Comparable values in other less coordinating solvents occur between 230 and 240 cm^{-1}.[30,56,57]

In the RDF of Sol. I1 there is a small peak at 4.3 Å and probably one also at 5.12 Å, the expected I–I distance in I–Hg–I units, overlapping the large and broad peak from intermolecular DMSO interactions. In the Raman spectrum there is a band of medium intensity at 173 cm^{-1}, besides the strong $\nu_1(HgI_2)$ frequency. This band corresponds to the ν_1 frequency 168 cm^{-1} ascribed to the the $[Hg-I-Hg]^{3+}$ ion in aqueous solution (the HgI^+ frequency is reported to be 191 cm^{-1}).[56] An Hg–Hg distance of 4.3 Å, corresponding to the peak found in the RDF, would give an Hg–I–Hg angle of about 110° which is a plausible value. The number of Hg–I interactions obtained in the least-squares refinements (Table 2) and the fit to the RDF of the calculated peak shapes including the Hg–Hg interaction (Fig. 3a), are consistent with about 50 % of the mercury atoms in complexes with single iodide bridges. A rather large $b_{\mathrm{Hg-Hg}}$ value, 0.05 Å^2, had to be assumed, implying substantial variations in the Hg–I–Hg angle. Such variations are also found in the corresponding angles, 89.4(2)° and 97.2(2)°, of the infinite $(HgI^+)_n$ chain found in a crystal structure.[58]

The $HgBrNO_3$ solution. An exchange of the anion from ClO_4^- to NO_3^- gives quite different results (*cf.* Sols. Br1A and Br1B in Figs. 3b and 8). The RDF of Sol. Br1B shows large and distinct peaks at 2.45, 3.55 and 5.6 Å. The refined parameter values (Table 2) are consistent with a dominating dimeric complex, formed by a single oxide bridge between two HgBr groups, as shown in Fig. 9. Calculated peak shapes and theoretical intensities for all interactions within the $[O(HgBr)_2]$ complex in Fig. 9, assuming the Hg atoms to be weakly solvated by four DMSO molecules as in the HgX_2 solutions, satisfactorily account for the experimental peaks in the RDF (Fig. 8) and for the high-angle part of the reduced intensity curves (Fig. 7).

The Raman spectrum (Table 3) is also compatible with a dominant $[O(HgBr)_2]$ complex. The sharp

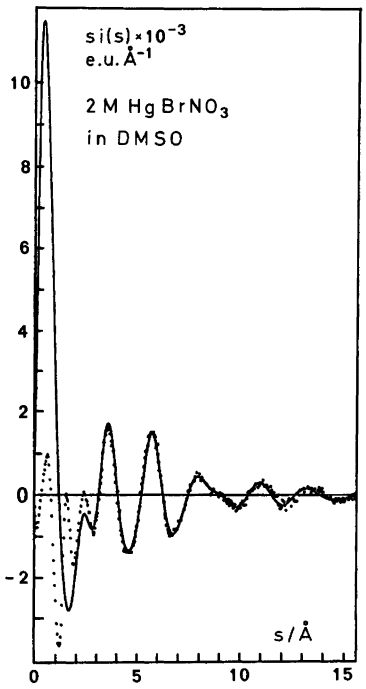

Fig. 7. Reduced intensities multiplied by s for Sol. Br1B corresponding to the distribution curves in Fig. 8. The experimental values are denoted by dots and the calculated values (see text) by the solid line.

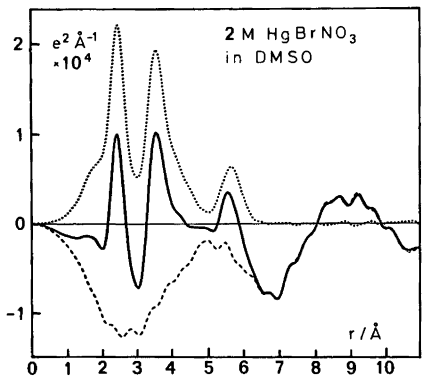

Fig. 8. $D(r)-4\pi r^2\rho_0$ curve (solid line) for Sol. Br1B. The sum of the calculated peak shapes for the intramolecular interactions of the complex in Fig. 9 assuming each Hg atom to be weakly solvated by four DMSO molecules, and for the DMSO molecules of the solvent, is shown by the dotted line and the difference by the dashed line.

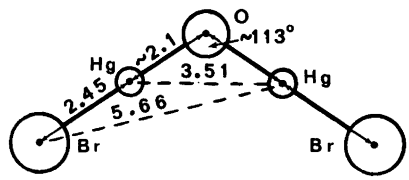

Fig. 9. The probable structure of the dominating complex $[O(HgBr)_2]$ in Sol. Br1B. The distances are given in Å.

polarized (depolarization ratio $\rho=0.0$) band at 110 cm^{-1} probably corresponds with the symmetric Hg–O–Hg stretching[59] and the strong polarized ($\rho=0.12$) band at 237 cm^{-1} with the ν_1(O–Hg–Br) frequency (ν_1 values from 233 to 246 cm^{-1} with ρ values 0.07 to 0.17 have been reported for the mixed X–Hg–Br complexes in various solvents).[57] There are additional weak bands at 195 cm^{-1} and possibly at 225 cm^{-1}, corresponding to $\nu_1(HgBr_2)$ and $\nu_1(HgBr^+)$ respectively, indicating that small amounts of these complexes are present.

A discrete dinuclear complex with an oxide bridge, but with CN^- instead of Br^- ligands, has been found in a crystal structure.[60] Moreover, discrete complexes with single oxygen bridges, mostly with an oxide ion coordinating three mercury(II) atoms, and with terminating halide ligands, have been found in crystal structures of several mercury(II) oxide halides.[59–61] The Hg–Hg distances are around 3.5–3.6 Å and the bridging Hg–O bond lengths about 2.1 Å in good agreement with the present results.

Only oxide and hydroxide[62] ions have been found in this type of bridge.[15] In solution Br1B oxide ions are probably formed by an oxidation of DMSO to dimethyl sulfone[11] by the nitrate ions:

$$(CH_3)_2SO+2NO_3^-+2Hg^{2+}+2Br^- \rightarrow (CH_3)_2SO_2+2NO_2+O(HgBr)_2$$

Since no nitrate frequencies[63] could be detected in the Raman spectrum, the reaction seems to be virtually complete. This would explain the dominance of the $[O(HgBr)_2]$ complex and the anomalous behaviour of this solution compared with the perchlorate solution Br1A.

Decomposition reactions with gas evolution have previously been observed between DMSO and alkali nitrates,[64] supporting the reaction proposed

above. Moreover, in an attempt to prepare a water-free mercury(II) nitrate solution in DMSO, the colour of the solution darkened gradually from yellow to dark brown during a few days, indicating a slow reaction.[65] The $HgBrNO_3$ solution (Br1B), however, was almost colourless.

CONCLUSIONS

The aim of this work was to study the coordination changes around mercury(II) when the number of halide ligands increases. The regular octahedral coordination in the $[Hg(DMSO)_6]^{2+}$ ion[7] changes to a slightly bent digonal configuration in the HgX_2 complexes. The angle X–Hg–X is found to be 159(2)° for the HgI_2 and 165(3)° for the $HgBr_2$ complex, and probably has a similar value for $HgCl_2$ in DMSO. The deviation from linearity is certainly due to the coordination of DMSO molecules to Hg *via* oxygen. However, the solvation of HgX_2 is much weaker than that of Hg^{2+}, causing a lengthening of both the Hg–O and Hg–S distances by about 0.2 Å. Even for $HgCl_2$ in methanol, where the solvation is much weaker than in DMSO and the Hg–Cl bond length is significantly shorter, a slight deviation from linearity due to solvent interference is indicated by the appearance of a weak ν_3 ($HgCl_2$) band in the Raman spectrum.

No structural information concerning the HgX^+ complexes could be obtained since they do not seem to be dominant in the investigated concentrated $HgXClO_4$ solutions in DMSO, due to a partial disproportionation to Hg^{2+} and HgX_2. Moreover, in the $HgIClO_4$ solution, complexes with single iodide bridges between mercury atoms occur.

In the pyramidal HgI_3^- complex[12] a DMSO oxygen atom probably completes a slightly flattened tetrahedral coordination around mercury. The $HgBr_3^-$ ion still has a more flattened pyramidal configuration, while for the $HgCl_3^-$ ion the structure probably is planar trigonal. For both $HgCl_3^-$ and $HgBr_3^-$, two DMSO oxygen atoms presumably complete an approximately trigonal bipyramidal coordination around mercury. The HgX_4^{2-} complexes are, however, all regular tetrahedra.

Only for the most concentrated HgI_2 and $HgBr_2$ solutions, is sharing of weakly coordinated DMSO oxygen atoms between the Hg atoms indicated. The single oxygen bridge found in the dominant complex, probably $[O(HgBr)_2]$, in the 2 M $HgBrNO_3$ solution investigated, is of another kind and is very probably formed by oxide ions produced by an oxidation of DMSO by nitrate ions.

Acknowledgements. The author wishes to thank Dr. Georg Johansson for his continuous interest and guidance during this investigation and for providing data for the recalculation of the HgI_2 solution. Professor Sten Ahrland and Mr. Ingmar Persson are gratefully thanked for providing results from their potentiometric and thermochemical investigations prior to publication, for preparing the $Hg(ClO_4)_2.4DMSO$ salt, and for many stimulating discussions. Thanks are due to Professor Kåre Larsson for kindly making the laser Raman apparatus available, and to Dr. Anthony Bristow for linguistic revision. The financial support by the Swedish Natural Science Research Council is hereby gratefully acknowledged.

REFERENCES

1. Deacon, G. B. *Rev. Pure Appl. Chem. 13* (1963) 189.
2. Orgel, L. E. *J. Chem. Soc.* (1958) 4186.
3. van Panthaleon van Eck, C. L. *Thesis*, Leiden 1958, see *Gmelins Handbuch der Anorganischen Chemie*, Hg-B2, Verlag Chemie Weinheim/Bergstr. 1967.
4. Furey, D. A. *Thesis*, Kent State University 1967 (Univ. Microfilms, Ann Arbor, Mich., Access No. 68-6207).
5. Sandström, M. and Johansson, G. *Acta Chem. Scand. A 31* (1977) 132.
6. Sandström, M. *Acta Chem. Scand. A 31* (1977) 141.
7. Sandström, M., Persson, I. and Ahrland, S. *Acta Chem. Scand. A 32* (1978) 607.
8. a. Johansson, G. *Acta Chem. Scand. 25* (1971) 2787; b. *Ibid.*, 2799.
9. Ahrland, S., Persson, I. and Portanova, R. *To be published.*
10. Ahrland, S., Kullberg, L. and Portanova, R. *Acta Chem. Scand. A 32* (1978) 251.
11. Martin, D. and Hauthal, H. G. *Dimethyl Sulphoxide*, van Nostrand Reinhold, Wokingham, Berkshire 1975, Chapter 4.
12. Gaizer, F. and Johansson, G. *Acta Chem. Scand. 22* (1968) 3013.
13. Johansson, G. and Sandström, M. *Chem. Scr. 4* (1973) 195.
14. Waters, D. N. and Kantarci, Z. *J. Raman Spectrosc. 6* (1977) 251.
15. Sandström, M. *Thesis*, Royal Institute of Technology, Stockholm 1978.

16. Sandström, M. and Persson, I. *Acta Chem. Scand. A 32* (1978) 95.
17. Sandström, M. *Acta Chem. Scand. A 32* (1978) 527.
18. Kimura, K. and Kubo, M. *J. Chem. Phys. 30* (1959) 151.
19. Brusset, H. and Madaule-Aubry, F. *Bull. Soc. Chim. Fr. 10* (1966) 3122.
20. Wertz, D. L. *Thesis*, Univ. of Arkansas 1967, (Access No. 67-8719 Univ. Microfilms, Ann Arbor, Michigan).
21. Thomas, R., Shoemaker, C. L. and Eriks, K. *Acta Crystallogr. 21* (1966) 12.
22. Berglund, B., Thomas, J. O. and Tellgren, R. *Acta Crystallogr. B 31* (1975) 1842.
23. Cyvin, S. J. *Molecular Vibrations and Mean Square Amplitudes*, Elsevier, Amsterdam 1968.
24. Müller, A. and Nagarajan, G. *Z. Naturforsch. Teil B*, (1966) 508.
25. Seip, H. M. In *Molecular Structure by Diffraction Methods, Chem. Soc. Spec. Per. Reports*, London 1973, Vol. 1, Chapter 1.
26. Waters, D. N., Short, E. L., Tharwat, M. and Morris, D. F. C. *J. Mol. Struct. 17* (1973) 389.
27. Hooper, M. A. and James, D. W. *Aust. J. Chem. 24* (1971) 1345 and 1331.
28. Adams, D. M. *Metal-Ligand and Related Vibrations*, Edward Arnold, London 1967.
29. Davies, J. E. D. and Long, D. A. *J. Chem. Soc. A* (1968) 2564.
30. Macklin, J. W. and Plane, R. A. *Inorg. Chem. 9* (1970) 821.
31. Rodewald, R. F., Mahendran, K., Bear, J. L. and Fuchs, R. *J. Am. Chem. Soc. 90* (1968) 6698.
32. Le Demezet, M. *Bull. Soc. Chim. Fr. 12* (1970) 4550.
33. Biscarina, P., Fusina, L., Nivellini, G. and Pelizzi, G. *J. Chem. Soc. Dalton Trans.* (1977) 664.
34. a. Barr, R. M. and Goldstein, M. *J. Chem. Soc. Dalton Trans.* (1976) 1593; b. *Ibid.* (1974) 1180.
35. Sandström, M. and Liem, D. H. *Acta Chem. Scand. A 32* (1978) 509.
36. Herlinger, A. W. *Spectrosc. Lett. 8* (1975) 787.
37. Fenn, R. H. *Acta Crystallogr. 20* (1966) 20.
38. Grdenić, D., Sikirica, M. and Vicković, I. *Acta Crystallogr. B 33* (1977) 1630.
39. Gerken, V. A. and Pakhomov, V. I. *Zh. Strukt. Khim. 10* (1969) 753.
40. Sanyal, N. K., Goel, R. K. and Pandry, A. N. *Indian J. Phys. 49* (1975) 546.
41. White, J. G. *Acta Crystallogr. 16* (1963) 397.
42. Brodersen, K. *Acta Crystallogr. 8* (1955) 723.
43. Weidenhammer, K. and Ziegler, M. L. *Z. Anorg. Allg. Chem. 434* (1977) 152.
44. Adams, M. J., Hodgkin, D. C. and Raeburn, U. A. *J. Chem. Soc. A* (1970) 2632.
45. McPhail, A. T. and Sim, G. A. *Chem. Commun.* (1966) 21.
46. Beurskens, P. T., Bosman, W. P. J. H. and Cras, J. A. *J. Cryst. Mol. Struct. 2* (1972) 183.
47. Harris, G. S., Inglis, F., McKechnie, J., Cheung, K. K. and Ferguson, G. *Chem. Commun. 9* (1967) 442.
48. Gal, A. W., Beurskens, G., Cras, J. A., Beurskens, P. T. and Willemse, J. *Recl. Trav. Chim. Pays-Bas, 95* (1976) 157.
49. Biscarini, P., Fusina, L., Nivellini, G. D., Mangia, A. and Pelizzi, G. *J. Chem. Soc. Dalton Trans.* (1974) 1846.
50. Jones, H. L. *Inorganic Vibrational Spectroscopy*, Marcel Dekker, New York 1971, Vol. 1, p. 70.
51. Herzberg, G. *Infrared and Raman Spectra of Polyatomic Molecules*, Van Nostrand, New York 1945, p. 170.
52. Kashiwabara, K., Konaka, S. and Kimura, M. *Bull. Chem. Soc. Jpn. 46* (1973) 410.
53. McEwen, R. S., Sim, G. A. and Johnson, C. R. *Chem. Commun.* (1967) 885.
54. Smith, J. H. and Brill, T. B. *Inorg. Chim. Acta 18* (1976) 225.
55. Tauer, K. J. and Libscomb, W. N. *Acta Crystallogr. 5* (1952) 606.
56. Clarke, J. H. R. and Woodward, L. A. *Trans. Faraday Soc. 61* (1965) 207.
57. Ammlung, R. L. and Brill, T. B. *Inorg. Chim. Acta 11* (1974) 201.
58. Köhler, K., Breitinger, D. and Thiele, G. *Angew. Chem. Int. Ed. Engl. 13* (1974) 821.
59. Köhler, K., Thiele, G. and Breitinger, D. *Z. Anorg. Allg. Chem. 418* (1975) 79; Köhler, K. *Dissertation*, Erlangen 1973.
60. Aurivillius, K. *Ark. Kemi 24* (1965) 151 and references therein.
61. Aurivillius, K. and Stålhandske, C. *Acta Crystallogr. B 30* (1974) 1907.
62. Matkovic, B., Ribar, B., Prelesnik, B. and Gerak, R. *Inorg. Chem. 13* (1974) 3006 and references therein.
63. Cooney, R. P. J. and Hall, J. R. *Aust. J. Chem. 22* (1969) 337; *25* (1972) 1159.
64. Kenttämaa, J. *Suom. Kemistil. B 33* (1960) 179.
65. Persson, I. *Personal communication.*

Received March 29, 1978.

Acta Chemica Scandinavica A 32 (1978) 643–646

The Bis[di(2-aminoethyl)sulfide]rhodium(III) Ion. Preparation of the *u-fac* Isomer, its Resolution, and the Determination of the Absolute Configuration of the $(+)_D$-Enantiomer

F. GALSBØL, A. HAMMERSHØI and ERIK LARSEN

Chemistry Department I, The H.C. Ørsted Institute, Universitetsparken 5, DK-2100 Copenhagen, Denmark

Bis[di(2-aminoethyl)sulfide]rhodium(III) chloride has been prepared and characterized as the *unsymmetrical facial* geometric isomer. Resolution into the catoptric forms has been accomplished by the use of arsenyl $(+)_D$-tartrate. The absolute configuration of the $(+)_D$-isomer of the complex ion has been determined to be Δ by a new modification of the method of active racemates. The circular dichroism of this isomer is very similar to that of the corresponding Δ-$(-)_D$-cobalt(III) complex.

Recently, a study of several synthetic pathways leading to bis[di(2-diaminoethyl)sulfide]cobalt(III), $[Co(daes)_2]^{3+}$, was published.[1] It was shown that one geometrical isomer is formed exclusively and the latter was assigned the *u-fac* geometry on the basis of the circular dichroism of the resolved complex. This assignemnt has been verified by determination of the crystal structure of Δ-$(-)_D$-$[Co(daes)_2]Cl_3.2H_2O$.[2] At present it is not known why only the *u-fac* and not the *s-fac* and *mer* geometrical isomers are formed. The stability of $[Co(daes)_2]^{3+}$ is much lower than that of $[Co(dien)_2]^{3+}$ (dien = diethylenetriamine),[3] all three possible geometrical isomers of the latter being formed in approximately equal amounts when a preparative route involving equilibration is employed.[4]

There is a general tendency for the metals of the second transition series to exhibit a greater affinity towards sulfur than do the elements in the first transition series. Therefore, it seems possible that both *facial* isomers of $[Rh(daes)_2]^{3+}$ could be prepared. However, in the work described here only the *u-fac* isomer was found and characterized.

EXPERIMENTAL

Instrumentation. Absorption spectra were recorded on a Cary 118 spectrophotometer, and circular dichroism spectra on a Roussel Jouan Dichrographe III. Optical rotations were measured at 25 °C on a Perkin-Elmer 141 polarimeter. X-Ray powder diffraction photographs were obtained with a Hägg-Guinier focusing camera XDC 700 using Cu$K\alpha$ radiation (quartz monochromator).

Preparations

$[Rh(daes)_2]Cl_3.2H_2O$. To doubly distilled di(2-aminoethyl)sulfide (6.60 g, 55.0 mmol) in 35 ml of water was added a solution of $RhCl_3.3H_2O$ (6.57 g, 25 mmol; Johnson Matthey Chemicals Ltd.) in 30 ml of water over a period of 6 h. The reaction mixture was kept at 55–60 °C and vigorously stirred during the addition and for 1 h after it was completed. Carbon dioxide was excluded by the attachment of an absorption tube containing CaO. After dilution with 50 ml of water a yellowish solid byproduct was removed by filtration and the orange filtrate was evaporated to dryness on a rotary vacuum evaporator. The residue was subsequently heated at 130 °C for 20 min. The resulting sticky product was dissolved in 10 ml of boiling water and to this solution was added 10 ml of ethanol. Crystallization was initiated by stirring and scraping and aided by slow addition of a further 10 ml of ethanol and subsequent cooling to 0 °C. The creamcoloured crystalline product was filtered off, washed twice with a mixture of 1.5 ml of water and 8 ml of ethanol and then twice with ethanol. Yield 6.0 g. Prolonged standing of the mother liquor resulted in the formation of a second crop of 1.5 g. Total yield 7.5 g (62 %). Anal. $C_8H_{28}Cl_3N_4O_2S_2Rh$: C, H, N.

Resolution of $[Rh(daes)_2]Cl_3.2H_2O$. Sodium arsenyl $(+)_D$-tartrate[5] (1.96 g, 7.5 mmol) was dissolved in a hot solution of $[Rh(daes)_2]Cl_3.2H_2O$ (2.43 g, 5.0 mmol) in 15 ml of water. A slight amount of precipitate was removed by filtration while hot. Slow cooling of the solution to 0 °C resulted in the formation of a crystalline precipitate. The latter was filtered off, washed with 8 ml of ice-cold water, 8 ml of 50 % ethanol and 8 ml of absolute ethanol. Yield 1.6 g (60 %) of $(+)_D$-$[Rh(daes)_2][AsO(+)_D$-tart$]_3.H_2O$ having $[\alpha]_{578} = 40.7$, $[\alpha]_{546} = 46.3$, and $[\alpha]_{436} = 71.5$. The product was recrystallized from boiling water until the specific rotations remained unchanged (4 times) giving the values (0.6 % solution, 1 dm cell length) $[\alpha]_{578} = 58.5$, $[\alpha]_{546} = 66.2$, and $[\alpha]_{436} = 103$. Anal. $C_{20}H_{38}N_4O_{22}S_2As_3Rh$: C, H, N, S.

The diastereoisomer was converted into the chloride salt by cation exchange on Bio-Rex 70. 0.54 g (0.5 mmol) of $(+)_D$-$[Rh(daes)_2][AsO(+)_D$-tart$]_3.H_2O$ was dissolved in 75 ml of 0.03 M LiOH and the cation was adsorbed on a column (1.5 cm long, 1.2 cm diameter) of the ion exchanger in the Li-form. After careful washing of the resin the complex was eluted with 10 ml of 1 M HCl. The last 8 ml of the eluate was collected and evaporated to dryness, and the residue was recrystallized from 2 ml of water by addition of 8 ml of ethanol and cooling in ice. The precipitate was removed by filtration and washed with 85 % and 96 % ethanol. Yield 0.17 g of $(+)_D$-$[Rh(daes)_2]Cl_3.2H_2O$. Specific rotations at 25 °C: $[\alpha]_{589} = 101$, $[\alpha]_{578} = 107$, $[\alpha]_{546} = 120$, $[\alpha]_{436} = 190$, and $[\alpha]_{364} = -187$.

"*Active racemates*". A: a solution of Δ-$(-)_D$-*u-fac*$[Co(daes)_2]Cl_3.2H_2O$ (22 mg, 0.05 mmol) and $(+)_D$-*u-fac*$[Rh(daes)_2]Cl_3.2H_2O$ (24 mg, 0.05 mmol) in 0.5 ml of water was allowed to evaporate slowly. Examination under a microscope showed that the resulting crystals were uniformly red coloured.

B: a solution of Λ-$(+)_D$-*u-fac*$[Co(daes)_2]Cl_3.2H_2O$ (22 mg) and $(+)_D$-*u-fac*$[Rh(daes)_2]Cl_3.2H_2O$ (24 mg) in 0.5 ml of water was similarly allowed to evaporate. Examination of the resulting crystals under a microscope revealed them to be a mixture of discrete white and red crystals.

RESULTS AND DISCUSSION

A compound having the correct analytical composition for bis[di(2-aminoethyl)sulfide]rhodium-(III) has been prepared by a route similar to that used in the preparation of tris(diamine)rhodium-(III)[6,7] and has been resolved into enantiomers. The absorption and circular dichroism spectra of the $(+)_D$ catoptric form are shown in Fig. 1 together with the spectra of the corresponding cobalt(III)

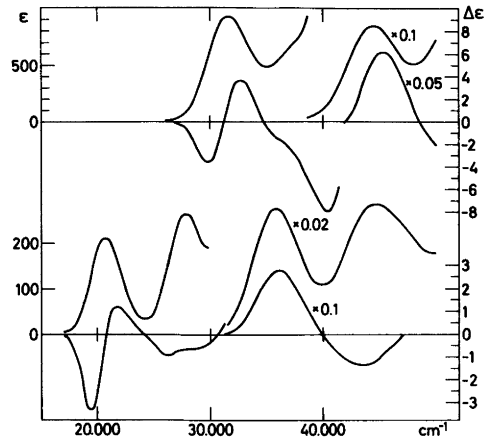

Fig. 1. The absorption and circular dichroism spectra of $(+)_D$-$[Rh(daes)_2]^{3+}$ (top) and $(-)_D$-$[Co(daes)_2]^{3+}$ (bottom).

complex which is known to be the Δ-*u-fac* isomer. A comparison of the two sets of spectra leaves little doubt that the $(+)_D$-$[Rh(daes)_2]^{3+}$ ion also possesses the Δ-*u-fac* configuration. The racemic $[Rh(daes)_2]Cl_3.2H_2O$ and *u-fac*-$[Co(daes)_2]Cl_3.2H_2O$ give very similar X-ray powder diagrams (*vide infra*), thereby substantiating our conclusion that *u-fac*-$[Rh(daes)_2]Cl_3.2H_2O$ has indeed been isolated. The relatively low yield of this product (62 %), however, could indicate that a more soluble isomer has remained in solution. This possibility was examined by carrying out chromatography on Sephadex SP-C25, a procedure similar to that employed in previous work with the cobalt complex.[1] However, this procedure resulted in considerable reduction to rhodium metal and no absolutely conclusive results were obtained.

The absolute configuration of $(+)_D$-$[Rh(daes)_2]^{3+}$ is predicted to be Δ on the basis of the similarity of the circular dichroism of this isomer to that of Δ-$(-)_D[Co(daes)_2]^{3+}$ (see Fig. 1). Both cations are obtained as the less soluble diastereoisomeric arsenyl $(+)_D$-tartrates, information which provides further evidence for the assignment of the absolute configuration of the rhodium complex. However, in this particular case there is unequivocal proof of the Δ absolute configuration of $(+)_D$-$[Rh(daes)_2]^{3+}$ since the absolute configuration of Δ-$(-)_D$-$[Co(daes)_2]^{3+}$ has been established[3] by X-ray diffraction:

Table 1. Indexed Guinier X-ray powder diffraction lines for Δ-$(-)_D$-*u-fac*-$[Co(daes)_2]Cl_3.2H_2O$, I; Δ-$(+)_D$-*u-fac*-$[Rh(daes)_2]Cl_3.2H_2O$, II; and crystals containing a mixture of the two cations, III.

	I			II			III		
h k l	I_{obs}	d_{obs} Å	d_{calc} Å	I_{obs}	d_{obs} Å	d_{calc} Å	I_{obs}	d_{obs} Å	d_{calc} Å
0 2 0	mw	7.931	7.933	m	7.962	7.961	m	7.952	7.946
2 0 0	vs	7.338	7.339	s	7.434	7.437	vs	7.387	7.387
0 1 1	vs	7.156	7.146	vs	7.169	7.174	vs	7.155	7.156
1 2 0	vs	6.972	6.979	vs	7.011	7.019	vs	6.994	6.998
2 1 0							w	6.693	6.699
1 1 1	vs	6.430	6.425	vs	6.462	6.462	vs	6.435	6.440
0 2 1	mw	5.634	5.634	w	5.647	5.656	m	5.645	5.643
2 2 0	mw	5.393	5.387	mw	5.440	5.435	m	5.408	5.410
2 1 1	mw	5.119	5.120	m	5.166	5.163	m	5.142	5.140
2 2 1	m	4.467	4.469	m	4.503	4.502	ms	4.487	4.484
0 3 1	m	4.411	4.412	ms	4.429	4.429	ms	4.419	4.419
2 3 0	mw	4.291	4.291	mw	4.319	4.320	m	4.306	4.305
1 3 1				m	4.246	4.245	m	4.236	4.234
3 2 0				mw	4.205	4.209	mw	4.187	4.186
3 1 1	w	4.040	4.037	w	4.079	4.079	mw	4.058	4.057
0 0 2	w	4.006	4.002	w	4.020	4.018	mw	4.008	4.007
0 1 2				mw	3.895	3.896	w	3.885	3.886
1 0 2							w	3.869	3.867
1 4 0	m	3.829	3.829	mw	3.844	3.845	w	3.838	3.837
2 3 1	mw	3.782	3.782	mw	3.806	3.805	w	3.792	3.792
3 3 0	w	3.595	3.592						
4 1 0	w	3.575	3.575	mw	3.622	3.621			
2 0 2				mw	3.535	3.535			
1 4 1	vvw	3.456	3.454	mw	3.469	3.469	mw	3.461	3.461
2 1 2	vvw	3.433	3.430	mw	3.449	3.451	mw	3.440	3.439
4 0 1	mw	3.336	3.336	vvw	3.375	3.375	w	3.354	3.354
4 1 1				w	3.301	3.301			
2 2 2	m	3.213	3.213	vw	3.230	3.231	w	3.220	3.220
2 4 1				vw	3.214	3.216	w	3.205	3.207
1 3 2	m	3.119	3.118				w	3.122	3.124
Refined unit cell dimensions assuming orthorhombic unit cell (Å)									
	$a = 14.656(4)$			$a = 14.873(4)$			$a = 14.774(4)$		
	$b = 15.834(6)$			$b = 15.932(6)$			$b = 15.893(5)$		
	$c = 7.986(3)$			$c = 8.036(3)$			$c = 8.014(2)$		

Racemic and optically active *u-fac*$[Co(daes)_2]Cl_3.2H_2O$ crystallize in the same chiral space group $P2_12_12_1$. The compound thus exhibits the phenomenon of spontaneous resolution, and large single crystals having the required optical rotations of the fully resolved complex have been obtained from solutions of the racemate. The crude product of $[Rh(daes)_2]Cl_3.2H_2O$ behaves similarly.

When Δ-$(-)_D$-$[Co(daes)_2]Cl_3.2H_2O$ and $(+)_D$-$[Rh(daes)_2]Cl_3.2H_2O$ are co-recrystallized crystals are obtained which contain both $[Co(daes)_2]^{3+}$ and $[Rh(daes)_2]^{3+}$. However, when Λ-$(+)_D$-$[Co(daes)_2]Cl_3.2H_2O$ and $(+)_D$-$[Rh(daes)_2]Cl_3.2H_2O$ are co-recrystallized only red crystals of the cobalt complex and white crystals of the rhodium complex are formed. These experiments prove conclusively that $(+)_D$-*u-fac*$[Rh(daes)_2]^{3+}$ has the Δ absolute configuration.

When small amounts of the rhodium complex are used the effect is hard to appreciate with the naked eye since twinned crystals may occur. However, under a microscope the difference between the two co-recrystallizations is easily recognized. X-Ray powder photographs provide conclusive proof even

when small amounts are used: Table 1 lists the observed d-spacings for the pure cobalt and rhodium complexes as well as those for the mixed salt $\{\Delta\text{-}(-)_D\text{-}[Co(daes)_2],\Delta\text{-}(+)_D\text{-}[Rh(daes)_2]\}Cl_3.2H_2O$ prepared from solution A (see Experimental). Crystals obtained from solution B, containing $\Lambda\text{-}(+)_D\text{-}[Co(daes)_2]^{3+}$ and $\Delta\text{-}(+)_D\text{-}[Rh(daes)_2]^{3+}$, gave X-ray powder photographs which exhibit all the lines observed for both of the pure complexes and no extra lines. The powder photographs of crystals obtained from solution A were indexed and refined assuming an orthorhombic unit cell. The unit cell parameters for the solid mixture lie between those for the pure cobalt and rhodium complexes.

The method for correlating absolute configurations presented above is limited to cases in which the racemate crystallizes in a chiral space group. However, when this condition is fulfilled the method has an appealing simplicity because the experiment can often be performed without the use of sophisticated apparatus.

Acknowledgements. E.L. acknowledges the award of grant No. 511-6670 from the Danish Science Research Council making the purchase of the Dichrographe-III S possible.

REFERENCES

1. Searle, G. H. and Larsen, E. *Acta Chem. Scand. A 30* (1976) 143.
2. Hammershøi, A., Larsen, E. and Larsen, S. *Acta Chem. Scand. A 32* (1978) 501.
3. Hammershøi, A. and Larsen, E. *Acta Chem. Scand. A 32* (1978) 485.
4. Keene, F. R. and Searle, G. H. *Inorg. Chem. 13* (1974) 2173.
5. Schlessinger, G. *Inorg. Synth. 12* (1970) 267.
6. Galsbøl, F., Steenbøl, P. and Sørensen, B. S. *Acta Chem. Scand. 26* (1972) 3605.
7. Galsbøl, F. *Inorg. Synth. 12* (1970) 269.

Received February 24, 1978.

Acta Chemica Scandinavica A 32 (1978) 647–651

Uranyl(VI) Compounds. I. The Crystal Structure of Ammonium Uranyl Sulfate Dihydrate, $(NH_4)_2UO_2(SO_4)_2.2H_2O$

LAURI NIINISTÖ, JUKKA TOIVONEN and JUSSI VALKONEN

Department of Chemistry, Helsinki University of Technology, Otaniemi, SF-02150 Espoo 15, Finland

The crystal structure of $(NH_4)_2UO_2(SO_4)_2.2H_2O$ has been determined by single crystal X-ray diffraction techniques. The compound crystallizes in the space group $P2_1/c$ with unit cell dimensions $a=7.783(5)$, $b=7.403(2)$, $c=20.918(9)$ Å, $\beta=102.25(4)°$, and $Z=4$. Least-squares refinement with anisotropic temperature factors for the uranium and sulfur atoms resulted in an R-value of 0.053 for 2251 significant reflections. The coordination polyhedron around uranium is a pentagonal bipyramid. Sulfate groups join the polyhedra into a layered structure where the ammonium ions and half of the water molecules are located between the layers. The mean bond lengths are: U–O(uranyl)=1.82, U–O(sulfate)=2.36, and U–O(water)=2.52 Å. The IR spectrum of the compound has also been recorded and interpreted.

Uranyl compounds, including the sulfates, have received considerable attention during recent years. Thus, the structures of normal sulfates, $UO_2SO_4.2\frac{1}{2}H_2O$ and $UO_2SO_4.3\frac{1}{2}H_2O$,[1,2] as well as of the complex ones, $Cs_2(UO_2)_2(SO_4)_3$ and $K_4UO_2(SO_4)_3$,[3,4] have been determined by X-ray diffraction methods. The results indicate that although the coordination polyhedron around uranium in the sulfate structures is invariably a pentagonal bipyramid, the polyhedra may be linked together in three dimensions quite differently.

The present work was initiated as part of a systematic study on the structures and spectroscopic and thermal properties of the complex uranium sulfates. The ammonium compound $(NH_4)_2UO_2(SO_4)_2.2H_2O$ was chosen for single crystal structure analysis because its stoichiometry corresponds to the complex anion $[UO_2(SO_4)_2]^{2-}$; although determined as one of the main species in solution,[5] this anion has not previously been structurally characterized in the solid state. Another interesting feature of this compound is the role of water molecules in the structure as compared with the anhydrous $Cs_2(UO_2)_2(SO_4)_3$ and $K_4UO_2(SO_4)_3$.

EXPERIMENTAL

The compound was crystallized at room temperature from an aqueous solution containing ammonium and uranyl sulfates in equimolar amounts.[6] The yellow crystals, strongly fluorescent in UV-light, corresponded well to the description given by Traill.[7] The crystal data are summarized in Table 1. The unit cell is given here in the standard setting ($P2_1/c$); another choice would be $P2_1/n$.[7]

The single crystal intensity data in the interval $5°<2\theta<60°$ were collected with a Syntex $P2_1$ (Fortran version) automatic diffractometer, using the $\theta/2\theta$ technique and graphite monochromatized Mo$K\alpha$-radiation. The scan speed was 1°/min. The crystal had approximate dimensions $0.3\times0.1\times0.1$ mm. A total of 2251 independent reflections satisfying the criterion $I>3\sigma(I)$ were used in the subsequent calculations. The intensities were corrected for Lorentz and polarization effects and for absorption from the ϕ-scan data.

A three-dimensional Patterson function revealed the position of the uranium atom and its coordinates

Table 1. Crystal data of $(NH_4)_2UO_2(SO_4)_2.2H_2O$.

Space group $P2_1/c$ (No. 14)
$a=7.783(5)$, $b=7.403(2)$, $c=20.918(9)$ Å,
$\beta=102.25(4)°$, $V=1177.8$ Å^3,[a] $Z=4$, $D_m=3.0$ g cm^{-3}, $D_x=3.01$ g cm^{-3}, μ(Mo$K\alpha$)=135 cm^{-1}

[a] Diffractometer data at 25 °C based on 25 reflections. Mo$K\alpha$-radiation ($\lambda=0.7107$ Å).

Table 2. Atomic coordinates and temperature factors for $(NH_4)_2UO_2(SO_4)_2.2H_2O$. Estimated standard deviations have been given in parentheses. The anisotropic parameters U_{ij} (Å^2) are of the form $\exp[-2\pi^2(h^2a^{*2}U_{11}+\ldots+2klb^*c^*U_{23})]$. All thermal parameters have been multiplied by 10^2.

Atom	x	y	z	U_{11} or U	U_{22}	U_{33}	U_{12}	U_{13}	U_{23}
U	0.2306(1)	0.3892(1)	0.3772(1)	1.07(2)	1.36(2)	1.12(3)	−0.08(2)	0.06(2)	−0.01(2)
S(1)	0.5489(5)	0.7161(5)	0.4545(2)	1.50(15)	1.39(16)	1.37(21)	−0.13(13)	0.14(13)	0.02(13)
S(2)	0.1432(5)	0.7270(6)	0.2477(2)	2.32(18)	1.76(17)	1.46(22)	0.18(15)	−0.06(15)	0.20(15)
O(1)	0.4144(16)	0.3612(17)	0.3371(6)	2.4(3)					
O(2)	0.0423(15)	0.4176(16)	0.4151(6)	2.2(2)					
O(3)	0.4009(16)	0.2562(18)	0.4741(6)	2.5(3)					
O(4)	0.3690(16)	0.6325(17)	0.4400(6)	2.3(3)					
O(5)	0.5350(16)	0.8914(19)	0.4222(6)	2.6(3)					
O(6)	0.6770(17)	0.5984(19)	0.4316(7)	2.8(3)					
O(7)	0.1381(17)	0.6475(18)	0.3127(7)	2.9(3)					
O(8)	0.0437(17)	0.2750(18)	0.2831(7)	2.7(3)					
O(9)	0.2097(21)	0.5977(24)	0.2068(8)	4.2(4)					
O(10)	0.2453(19)	0.8926(22)	0.2598(7)	3.7(3)					
O(11)	0.2205(17)	0.0495(16)	0.3774(7)	2.3(2)					
O(12)	0.7598(23)	0.1996(23)	0.4336(9)	4.5(4)					
N(1)	0.6517(27)	0.7293(29)	0.2964(10)	4.4(5)					
N(2)	0.9788(26)	0.8422(26)	0.4455(10)	4.1(4)					

Table 3. Selected interatomic distances (Å) and angles (°).

Environment of uranium			
U−O(1)	1.818(14)	O(1)−U−O(2)	178.3(5)
−O(2)	1.819(13)	O(1)−U−O(3)	89.7(5)
Mean	1.819	O(1)−U−O(4)	91.9(5)
		O(1)−U−O(7)	90.2(5)
U−O(8)	2.344(13)	O(1)−U−O(8)	88.9(5)
−O(4)	2.351(12)	O(1)−U−O(11)[a]	85.1(5)
−O(7)	2.364(14)	O(2)−U−O(3)	91.8(5)
−O(3)	2.385(12)	O(2)−U−O(4)	89.1(5)
−O(11)[a]	2.516(12)	O(2)−U−O(7)	88.8(5)
Mean	2.392	O(2)−U−O(8)	89.6(5)
		O(2)−U−O(11)[a]	95.0(5)
O(3)−U−O(4)	74.7(4)		
O(4)−U−O(7)	75.4(4)	Possible hydrogen bonds	
O(7)−U−O(8)	75.7(5)	O(11)[a]−O(5)	2.695(18)
O(8)−U−O(11)[a]	68.1(4)	−O(10)	2.765(21)
O(11)[a]−U−O(3)	66.3(4)	O(5)−O(11)[a]−O(10)	84.1(6)
Sulfate groups			
S(1)−O(5)	1.457(14)	S(2)−O(9)	1.450(19)
−O(3)	1.477(14)	−O(10)	1.453(17)
−O(6)	1.478(15)	−O(7)	1.489(15)
−O(4)	1.501(13)	−O(8)	1.503(13)
Mean:	1.478	Mean:	1.474
O(4)−S(1)−O(3)	107.3(8)	O(7)−S(2)−O(8)	105.9(8)
O(5)−S(1)−O(6)	111.4(8)	O(9)−S(2)−O(10)	114.1(10)
Mean:	109.4[b]	Mean:	109.2[b]

[a] Oxygen atom belonging to a water molecule. [b] Mean value of all O−S−O angles.

were refined. The subsequent electron density map showed the positions of all the remaining non-hydrogen atoms.

A block-diagonal least-squares refinement with anisotropic temperature factors for uranium and sulfur led to the final value of 0.053 for the conventional R index; the weighted R index was 0.072 $[w=1/\sigma^2(F_o^2)]$. In the refinement scattering fractors for neutral atoms were used, and, for uranium, a correction for the anomalous scattering was applied.[8] It was not possible to locate any of the hydrogen atoms from a difference Fourier map calculated after the final refinement.

All calculations were performed with the UNIVAC 1108 computer using the X-RAY 76 program system.[9] A listing of structure factors is available from the authors upon request.

The infrared spectrum in the range 4000–250 cm^{-1} was recorded on a Perkin-Elmer 521 spectrophotometer with the KBr pellet technique. The compound showed no reaction with KBr.

DESCRIPTION AND DISCUSSION OF STRUCTURE

The atomic coordinates and temperature factors are given in Table 2. Selected interatomic bond lengths and angles involving uranium and sulfur atoms are given in Table 3.

The coordination polyhedron around uranium is, as expected, a pentagonal bipyramid. Our X-ray data are in full agreement with the linearity and symmetry of the uranyl group (Table 3) and also with the nearly planar arrangement of uranium and the five equatorial oxygens (Table 4).

Table 4. Deviations of atoms (Å) from the least-squares plane.

Atom	Deviation (Å)
U	−0.027
O(3)	−0.031
O(4)	0.006
O(7)	0.040
O(8)	−0.053
O(11)	0.065

The UO_7-polyhedra are joined into a layer structure by sulfate groups (Fig. 1). The basic building unit of the structure consists of two symmetry-related UO_7-polyhedra joined together by $S(1)O_4$ tetrahedra. These double polyhedra are connected by $S(2)O_4$ bridging groups into an infinite layer $[UO_2(H_2O)(SO_4)_2]_n^{2n-}$.

The sulfate tetrahedra are not significantly distorted in this process although S–O distances involving oxygens bonded to uranium are generally slightly longer than the free S–O bonds. In the coordination polyhedron of uranium, however, the U–O(sulfate) distances are significantly shorter than the U–O(water) distance. The water molecule O(11) is probably involved in strengthening the layer structure through hydrogen bonding to neighbouring sulfate oxygens O(5) and O(10); this

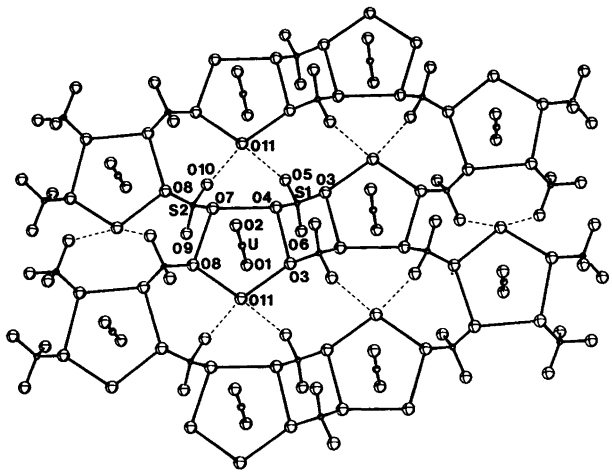

Fig. 1. The $[UO_2(H_2O)(SO_4)_2]_n^{2n-}$ layer viewed roughly perpendicular to the equatorial plane of the UO_7-polyhedra. Possible hydrogen bonds are shown as broken lines.

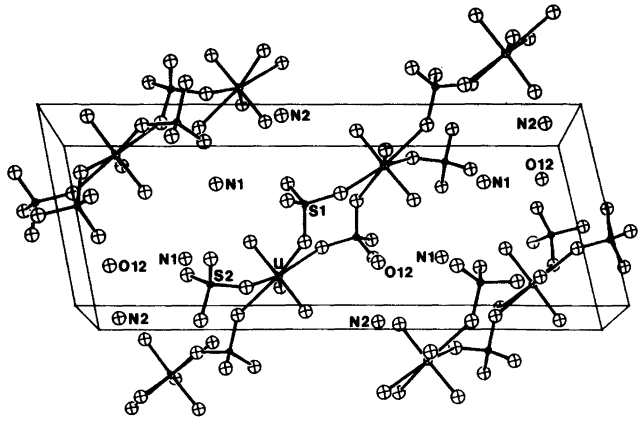

Fig. 2. A perspective view showing the unit cell contents of $(NH_4)_2UO_2(SO_4)_2.2H_2O$. The *a*-axis is vertical and the *c*-axis is horizontal.

may cause the difference in bond lengths (*cf.* Table 3 and Fig. 1).

Half of the water molecules and the ammonium ions do not form part of the layers but are located between them and joined to the structure probably by hydrogen bonding (Fig. 2). Table 5 gives the nearest neighbours of these atoms. Possible hydrogen bonds for the water molecule O(12) are also suggested in this table.

Table 5. The environment of ammonium ions and the noncoordinated water molecule (up to 3.2 Å).

N(1)–O(1)^{ii} [a]	2.900(25)
–O(9)^{ii}	2.939(28)
–O(10)^{ii}	2.939(28)
–O(6)	2.956(26)
–O(8)^{ii}	3.190(28)
–O(5)	3.194(27)
N(2)–O(12)^{i}	2.907(24)
–O(6)	2.928(24)
–O(11)	3.009(26)
–O(12)	3.128(27)
O(12)–O(2)	2.820(22)
–O(5)	2.854(22)
–O(6)	3.021(22)
–O(9)^{ii}	3.089(26)
–O(3)	3.115(24)
O(6)–O(12)–O(9) (°)	106.6(7)

[a] The superscripts denote the symmetry operations: ^{i} $-x,-y,-z$ and ^{ii} $-x,1/2+y,1/2-z$.

There are several possible hydrogen bond acceptors for the ammonium ions at distances less than 3.2 Å. However, the angles calculated at both N(1) and N(2) are not acceptable for a regular

Table 6. Infrared absorption frequencies in the region 4000–400 cm^{-1}.

Observed frequency	Assignment
3600 m, 3500 m	$\nu(H_2O)$
3175 vs	$\nu_3(NH_4)$
3000 sh	$\nu_1(NH_4)$
2850 m	$2\nu_4(NH_4)$
1990 w	$2\nu_1(SO_4)$
1620 m, 1595 m	$\delta(H_2O)$
1425 s	$\nu_4(NH_4)$
1205 s, 1165 sh, 1120 vs, 1060 s, 1020 sh	$\nu_3(SO_4)$
990 vs	$\nu_1(SO_4)$
924 s	$\nu_3(UO_2)$
836 m	$\nu_1(UO_2)$
640 m, 610 m, 590 sh, 580 s	$\nu_4(SO_4)$
470 w, 455 w, 435 w, 425 sh	$\nu_2(SO_4)$

hydrogen bonding scheme. Thus, it seems probable that the ammonium ions are in static or dynamic disorder.[10]

THE INFRARED SPECTRUM

The IR spectrum of $(NH_4)_2UO_2(SO_4)_2.2H_2O$ was recorded and interpreted in this work (Table 6). Narasimham and Girija earlier studied the same compound by absorption spectroscopy but their main emphasis was on the uranyl group.[11]

On the basis of the IR spectrum it is possible to deduce some of the main features of the structure: (i) the splitting of sulfate ν_3 and ν_4 vibrations into three peaks indicates C_{2v} symmetry for the sulfate group (bidentate ligand, bridging or chelate), and (ii) the splitting of the bending vibration of H_2O around 1600 cm^{-1} indicates two types of water molecules in the structure.

Further structural conclusions based on the IR spectrum alone are not warranted until the absorption spectra of a larger number of uranyl sulfates have been compared with the X-ray diffraction results.

Acknowledgement. Financial aid from the Neste Oy Foundation to one of the authors (J.T.) is gratefully acknowledged.

REFERENCES

1. Putten, N. and Loopstra, B. O. *Cryst. Struct. Commun. 3* (1974) 377.
2. Brandenburg, N. P. and Loopstra, B. O. *Cryst. Struct. Commun. 2* (1973) 243.
3. Ross, M. and Evans, H. T. *J. Inorg. Nucl. Chem. 15* (1960) 338.
4. Mikhailov, Yu. N., Kokh, L. A., Kuznetsov, V. G., Grevtseva, T. G., Sokol, S. K. and Ellert, G. V. *Koord. Khim. 3* (1977) 508.
5. Ahrland, S. *Acta Chem. Scand. 5* (1951) 1151.
6. Colani, A. *Bull. Soc. Chim. Fr. 43* (1928) 754.
7. Traill, R. J. *Am. Mineral. 37* (1952) 394.
8. *International Tables for X-Ray Crystallography*, Kynoch Press, Birmingham 1974, Vol. 4, pp. 71, 150.
9. Stewart, J. M., Ed., *The X-Ray System, Version of 1976*, Technical Report TR-446, Computer Science Center, University of Maryland, College Park.
10. Khan, A. A. and Bauer, W. H. *Acta Crystallogr. B 28* (1972) 693.
11. Narasimham, K. V. and Girija, M. *Indian J. Pure Appl. Phys. 6* (1968) 231.

Received April 5, 1978.

Acta Chemica Scandinavica A 32 (1978) 653–657

Magnetic Structures and Properties of $Mn_{1-t}Cr_tAs$ ($0 < t \leq 0.40$)

KARI SELTE,[a] ARNE KJEKSHUS,[a] PER G. PETERZÉNS[a] and ARNE F. ANDRESEN[b]

[a] Kjemisk Institutt, Universitetet i Oslo, Blindern, Oslo 3, Norway and [b] Institutt for Atomenergi, Kjeller, Norway

$Mn_{1-t}Cr_tAs$ (MnP type structure) takes a double, helimagnetic structure with propagation vector along *a* for $\sim 0.10 \leq t \leq 0.35$ and along *c* for $0.40 \leq t \leq 1$. The spirals are conical for $0.25 \leq t \leq 0.35$. The results are discussed in relation to data for other $Mn_{1-t}T_tAs$ phases (T= V, Fe, Co, Ni). At low temperatures $Mn_{1-t}Cr_tAs$ shows a small miscibility gap ($0.01 < t < 0.10$ at 10 K).

Among the binary and ternary 3*d* transition metal mono arsenides with the MnP type structure, Mn rich $Mn_{1-t}T_tAs$ phases have recently received considerable attention due to their interesting variety of helimagnetism. For T= V, Fe, Co, and Ni the cooperative magnetic state is of the double, *a*-axis spiral type,[1-5] whereas for T=Cr a simpler antiferromagnetic arrangement has been proposed.[6] However, the brief experimental data presented in Ref. 6 are apparently also consistent with the double, *a*-axis spiral structure, and, for this reason, a reexamination of $Mn_{1-t}Cr_tAs$ has been undertaken.

EXPERIMENTAL

Samples were made from initial batches of MnAs and CrAs (preparational details, including purity of elements are given in Refs. 1 and 7) by a first heat treatment at 850 °C for one week. All samples were crushed and subjected to 2–3 further annealings for one week at 850 °C, before finally being cooled slowly to room temperature. The experimental details concerning X-ray and neutron diffraction are described in Ref. 8.

RESULTS AND DISCUSSION

(i) *Chemical crystal structure.* The room temperature unit cell dimensions of $Mn_{1-t}Cr_tAs$ are shown in Fig. 1 as functions of the composition parameter *t*. The revised phase diagram for the pseudo-binary MnAs–CrAs system on the basis of these and other findings is presented in Fig. 2.

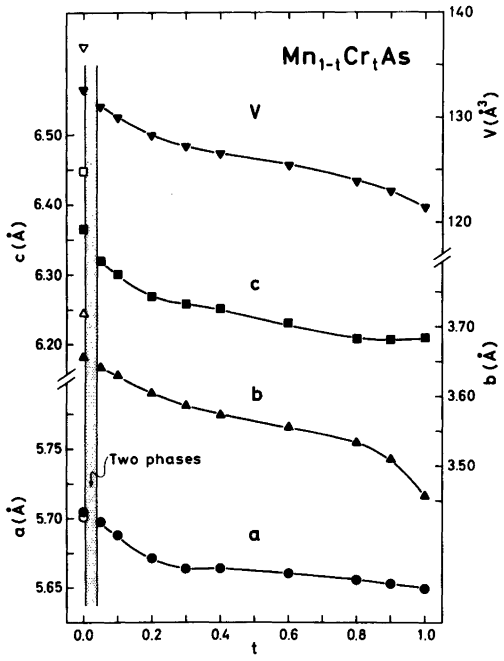

Fig. 1. Room temperature (extrapolated for MnAs) unit cell dimensions of ternary solid solution series MnAs–CrAs *versus* composition. Error limits do not exceed size of symbol. Open symbols for MnAs represent data for its NiAs type structure at room temperature.

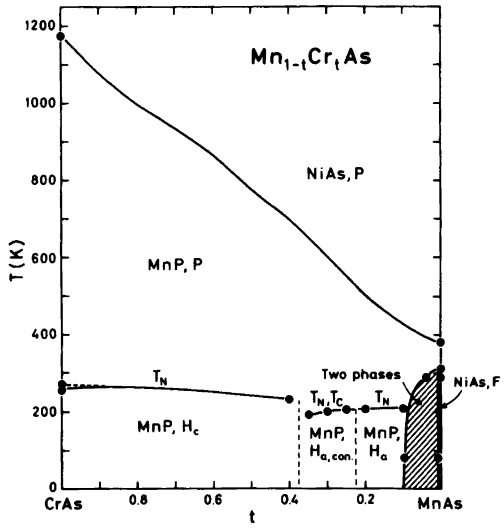

Fig. 2. Phase diagram for the pseudo-binary MnAs–CrAs system. Magnetic state is indicated by: P, para; F, ferro; H, helical.

This diagram differs *inter alia* from Kazama and Watanabe's version by the small, low temperature pocket of two phases near MnAs. The gap in the solid solubility of MnAs and CrAs is so narrow that this feature was overlooked until the structural and magnetic properties of the most Mn rich samples were compared. The present study has not been concerned with samples with (Mn+Cr)/As ratios different from 1.00.

At room temperature the MnP type atomic arrangement is stable in the interval $0.04 \leq t \leq 1$, whereas the NiAs type prevails in the immediate vicinity of MnAs. The diffraction data show that the substituted atoms are distributed randomly in the metal sub-lattice, unit cell dimensions and positional parameters for the samples studied by neutron diffraction being given in Table 1.

In common with other pseudo-binary systems of the type MnAs–*T*As,[1-5] Mn rich $Mn_{1-t}Cr_tAs$ samples take an NiAs type atomic arrangement as both low (I) and high (II) temperature form, separated by a temperature interval where the

Table 1. Unit cell dimensions and positional parameters with standard deviations for some $Mn_{1-t}Cr_tAs$ samples as derived by least squares profile refinements of neutron diffraction data. (Space group *Pnma*; positions 4(*c*); overall profile reliability factors ranging between 0.029 and 0.056.)

t	T(K)	*a* (Å)	*b* (Å)	*c* (Å)	x_T	z_T	x_X	z_X
0.05	293	5.6974(4)	3.6431(16)	6.3190(30)	0.0064(21)	0.2169(19)	0.2194(8)	0.5808(30)
0.10	6	5.5655(5)	3.4908(4)	6.1596(8)	0.0046(17)	0.2035(17)	0.1974(7)	0.5822(8)
	80	5.5681(11)	3.4966(9)	6.1671(16)	0.0056(35)	0.1996(34)	0.2009(13)	0.5786(17)
	293	5.6877(6)	3.6286(14)	6.3007(25)	0.0090(30)	0.2190(27)	0.2149(9)	0.5783(25)
0.20	8	5.5767(6)	3.4917(4)	6.1728(8)	0.0052(22)	0.2092(29)	0.1981(7)	0.5809(10)
	293	5.6701(4)	3.5985(4)	6.2795(8)	0.0050(24)	0.2119(23)	0.2119(6)	0.5825(8)
0.25	10	5.5807(15)	3.4825(10)	6.1750(18)	0.006(3)	0.213(3)	0.2001(7)	0.5795(9)
	100	5.5941(17)	3.4940(11)	6.1917(21)	0.008(3)	0.227(4)	0.1984(7)	0.5796(9)
	293	5.6668(11)	3.5870(9)	6.2657(16)	0.011(3)	0.223(4)	0.2102(7)	0.5733(10)
0.30	10	5.5954(5)	3.4844(3)	6.1903(6)	0.002(3)	0.208(3)	0.1995(5)	0.5793(7)
	80	5.5914(7)	3.4856(4)	6.1879(8)	0.012(3)	0.207(4)	0.1987(7)	0.5802(9)
	170	5.6057(6)	3.5093(3)	6.2061(7)	0.009(3)	0.205(3)	0.2029(6)	0.5784(8)
	293	5.6626(4)	3.5807(3)	6.2609(6)	0.004(3)	0.216(3)	0.2094(4)	0.5790(8)
0.35	10	5.6042(6)	3.4812(3)	6.1951(7)	0.003(5)	0.219(5)	0.2002(6)	0.5803(7)
	293	5.6642(5)	3.5783(3)	6.2562(7)	0.008(4)	0.205(4)	0.2095(5)	0.5832(8)
0.40	10	5.6359(10)	3.5925(11)	6.2082(18)	−0.006(8)	0.211(7)	0.2053(6)	0.5798(18)
	220	5.6473(10)	3.5754(5)	6.2335(5)	0.003(7)	0.217(7)	0.2065(5)	0.5812(12)
	235	5.6480(5)	3.5642(4)	6.2313(7)	0.011(6)	0.222(6)	0.2068(5)	0.5783(8)
	293	5.6599(5)	3.5694(4)	6.2464(8)	0.012(7)	0.213(6)	0.2091(5)	0.5781(8)

MnP type prevails. The second or higher order MnP⇌NiAs(II) type transition in $Mn_{1-t}Cr_tAs$ has been described by Kazama and Watanabe,[6] and we have earlier discussed the MnP⇌NiAs(I) type transition in Ref. 9.

(ii) *Magnetic structures.* As deduced from the two-phase sample of nominal composition $Mn_{0.95}Cr_{0.05}As$ (Fig. 2), the ferromagnetic mode of MnAs[10,11] extends to $t \approx 0.01$ of $Mn_{1-t}Cr_tAs$.

The double, *a*-axis type helimagnetic ordering, characteristic of $Mn_{1-t}V_tAs$ ($0.05 \leq t < \sim 0.40$),[2] $Mn_{1-t}Fe_tAs$ ($\sim 0.01 < t < \sim 0.12$),[1,4] $Mn_{1-t}Co_tAs$ ($0.05 \leq t \leq 0.15$),[3] and $Mn_{1-t}Ni_tAs$ ($0.05 \leq t < 0.07$)[5] is also found for $Mn_{1-t}Cr_tAs$ ($\sim 0.10 \leq t \leq 0.35$). For $Mn_{0.60}Cr_{0.40}As$ a double, *c*-axis type helimagnetic ordering like that of CrAs[6,7] is observed. According to Kazama and Watanabe[6] this mode covers the whole range $0.40 \leq t \leq 1$. Parameters describing these helimagnetic arrangements, are magnetic moment per metal atom (μ_T), spiral propagation vector (τ_a or τ_c), phase angle between independent spirals (ϕ_a or ϕ_c), and angle between moment and spiral axis (β), numerical values being given in Table 2 together with the Néel temperature (T_N). The two types of spiral arrangement are illustrated in Fig. 5 of Ref. 1, where also the phase relationship between the two pairs of spirals is described.

The temperature dependence of the integrated intensity of the satellites $000^{\pm}$ and $001^{\pm}$ of $Mn_{1-t}Cr_tAs$ ($0.10 \leq t \leq 0.35$) and of the satellites $000^{\pm}$, 101^{+}, 002^{-}, and 011^{-} of $Mn_{0.60}Cr_{0.40}As$ are shown in Fig. 3. From the positions and intensities of the satellite reflections, the temperature variation of μ_T, ϕ_a, and α_a (spiral turn angle) were obtained as shown in Fig. 4. Not included are curves for μ_T and ϕ_a for samples with $0.25 \leq t \leq 0.35$, due to a larger uncertainty, caused by reduced intensities of the satellites and a ferromagnetic contribution originating from a conical deformation of the spirals

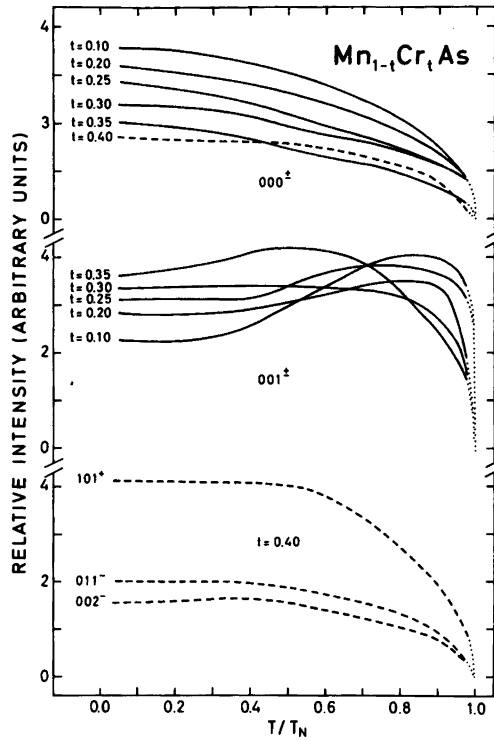

Fig. 3. Relative, integrated satellite intensities *versus* reduced temperature for $Mn_{1-t}Cr_tAs$.

(*cf.* Table 2). The appreciable variation in phase angle with temperature is characteristic for the double, *a*-axis helical mode in $Mn_{1-t}T_tAs$ (T=V, Fe, Co, Ni).[1-5] For the double, *c*-axis helical mode of $Mn_{0.60}Cr_{0.40}As$ the phase angle (Table 2) is approximately temperature independent, a feature which seems to be common for phases with this type of helimagnetic arrangement (*cf.* Refs. 5,7,8, 12–14). The turn angle increases moderately (10–15° from 0 K to T_N) independent of the

Table 2. Helimagnetic parameters for $Mn_{1-t}Cr_tAs$. Spiral propagation vector along *a* for $0.10 \leq t \leq 0.35$, along *c* for $t = 0.40$.

t	0.10		0.20	0.25	0.30	0.35	0.40
T (K)	6	80	6	10	10	10	10
$\tau_a/2\pi a^*$ or $\tau_c/2\pi c^*$	0.133(2)	0.136(2)	0.120(2)	0.097(2)	0.088(2)	0.071(3)	0.252(2)
$\mu_{T,\text{tot.}}$ (μ_B)	1.60(10)	1.60(10)	1.55(10)	1.7(1)	1.7(2)	1.6(2)	1.9(1)
ϕ_a or ϕ_c (°)	71(5)	73(5)	68(5)	60(10)	50(20)	56(20)	−122(5)
β (°)	90	90	90	62(5)	55(15)	56(15)	90
T_N (K)	210±1		208±1	205±2	202±2	195±5	232±2

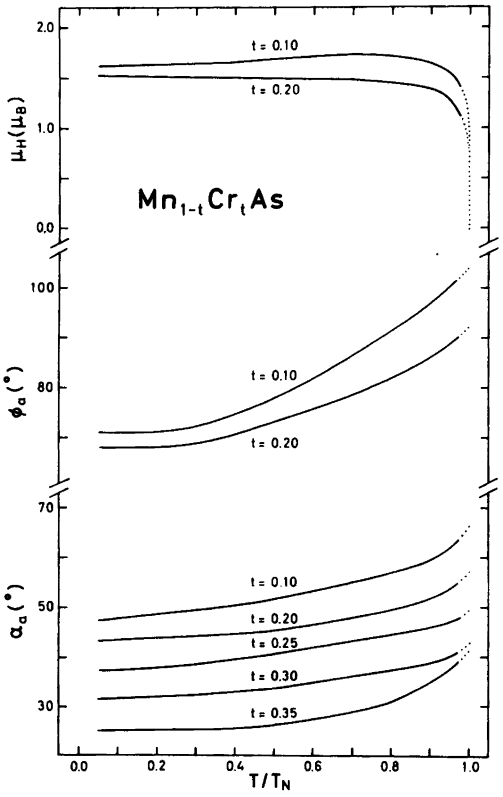

Fig. 4. Phase and turn angles and magnetic moments for *a*-axis spirals in $Mn_{1-t}Cr_tAs$ as functions of reduced temperature.

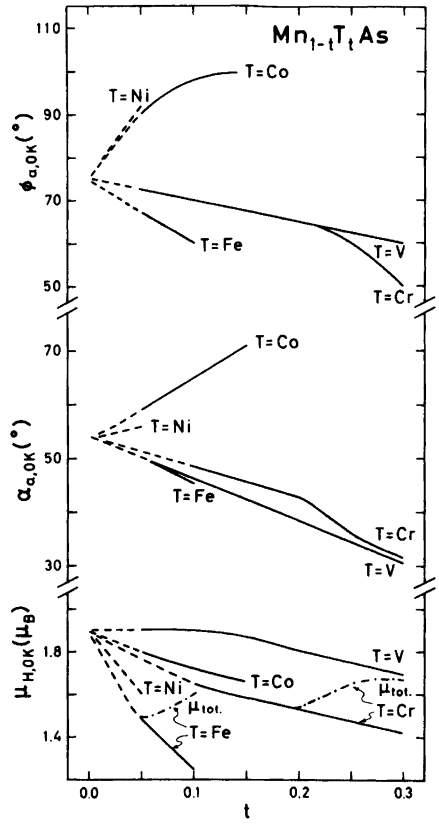

Fig. 5. Magnetic moment, turn and phase angle as functions of t in $Mn_{1-t}T_tAs$. Data refer to 0 K (extrapolated). Both helical (μ_H) and total ($\mu_{tot.}$) magnetic moments are shown for conical regions.

propagation direction of the spirals.

The variation of T_N with t (Table 2, Fig. 2) matches very closely the curves derived by Kazama and Watanabe[6] apart from the region $\sim 0.2 < t < \sim 0.5$. The designation T_N,T_C in Fig. 2 reflects the fact that the conical deformation of the double, *a*-axis helical mode (with β approximately constant) is maintained throughout the cooperative magnetic state. The consistent trend in T_N *versus* t for the different $Mn_{1-t}T_tAs$ phases is illustrated in Fig. 1 of Ref. 9. As opposed to T_N, which shows minor variation with T, the spiral parameters μ_T, α_a, and ϕ_a change markedly (Fig. 5). However, the individual characteristics extrapolate nicely to specific values for the spiral parameters of a hypothetical, helimagnetic state of MnAs ($\mu_{H,\,0\,K} = 1.9\,\mu_B$, $\alpha_{a,\,0\,K} = 54°$, $\phi_{a,\,0\,K} = 75°$, $T_N = 210$ K [9]). The implication of this on the properties of MnAs is discussed in Ref. 11.

As seen from Fig. 5, the conical deformation occurs when Mn is substituted by the nearest neighbours, Cr or Fe, in the Periodic System. The ferromagnetic component of the magnetic moment appears to be a supplement to the intrinsic helimagnetic moment. This extra contribution seems to have minor effect on the spiral parameters. However, more information is needed to explain the occurrence of the cones.

The total magnetic moment throughout the entire $Mn_{1-t}Cr_tAs$ phase shows altogether surprisingly little variation with t (between 1.6 and 1.9 μ_B). The same applies to T_N which varies between 195 and $\sim$265 K. According to considerations based on molecular field theory, this may suggest that the summed magnetic exchange interactions are approximately independent of t. On empiric basis it is commonly assumed that there is a relation between the magnetic exchange parameters and correspond-

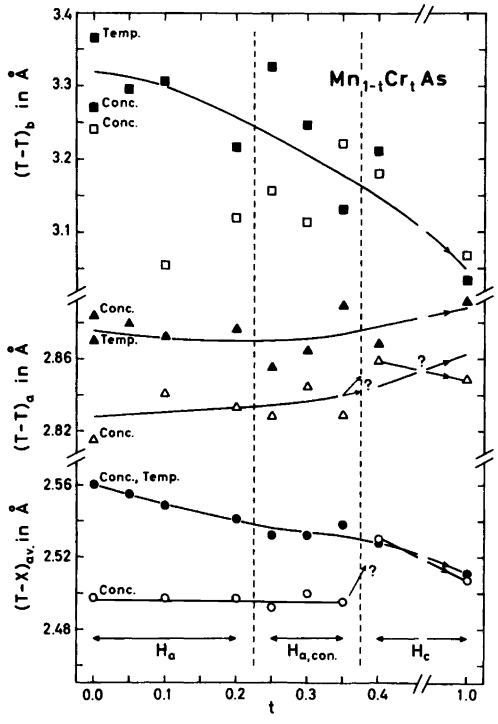

Fig. 6. Interatomic distances (average $T-X$, $T-T$ zig-zags along *a* and *b*) as functions of t in $Mn_{1-t}Cr_tAs$. Open and filled symbols refer to ~10 and 293 K, respectively. Concentration and temperature extrapolated data for MnP type MnAs are taken from Ref. 11.

ing interatomic distances. The variations with t of the shortest interatomic distances in $Mn_{1-t}Cr_tAs$ at 10 and 293 K are shown in Fig. 6. No clear-cut correlation between interatomic distances and magnetic structure is, however, evident from this illustration. In particular, the $T-T$ distance within the zig-zag chains along the *b*-axis shows large, unsystematic scattering in the experimental points.

Acknowledgement. This work has received financial support from The Norwegian Research Council for Science and the Humanities.

REFERENCES

1. Selte, K., Kjekshus, A. and Andresen, A. F. *Acta Chem. Scand. A 28* (1974) 61.
2. Selte, K., Kjekshus, A., Valde, G. and Andresen, A. F. *Acta Chem. Scand. A 30* (1976) 8.
3. Selte, K., Kjekshus, A., Valde, G. and Andresen, A. F. *Acta Chem. Scand. A 30* (1976) 468.
4. Selte, K., Kjekshus, A., Peterzéns, P. G. and Andresen, A. F. *Acta Chem. Scand. A 30* (1976) 671.
5. Delphin, I. L. A., Selte, K., Kjekshus, A. and Andresen, A. F. *Acta Chem. Scand. A 32* (1978) 179.
6. Kazama, N. and Watanabe, H. *J. Phys. Soc. Jpn. 30* (1971) 1319.
7. Selte, K., Kjekshus, A., Jamison, W. E., Andresen, A. F. and Engebretsen, J. E. *Acta Chem. Scand. 25* (1971) 1703.
8. Selte, K., Kjekshus, A. and Andresen, A. F. *Acta Chem. Scand. 26* (1972) 3101.
9. Selte, K., Kjekshus, A., Andresen, A. F. and Zięba, A. *J. Phys. Chem. Solids 38* (1977) 719.
10. Bacon, G. E. and Street, R. *Nature 175* (1955) 518.
11. Zięba, A., Selte, K., Kjekshus, A. and Andresen, A. F. *Acta Chem. Scand. A 32* (1978) 173.
12. Selte, K., Hjersing, H., Kjekshus, A. and Andresen, A. F. *Acta Chem. Scand. A 29* (1975) 312.
13. Selte, K., Hjersing, H., Kjekshus, A., Andresen, A. F. and Fischer, P. *Acta Chem. Scand. A 29* (1975) 695.
14. Selte, K., Kjekshus, A., Aaby, S. and Andresen, A. F. *Acta Chem. Scand. A 29* (1975) 810.

Received February 15, 1978.

Acta Chemica Scandinavica A 32 (1978) 659–662

Optical Properties of Bis(histidinato)cobalt(III) Complexes

SVEN BAGGER and HANS PETER JENSEN

Chemistry Department A, Building 207, The Technical University of Denmark, DK-2800 Lyngby, Denmark

Dedicated to Jannik Bjerrum on the occasion of his 70th birthday

The isomer all-*cis*-[Co(L-his)(D-his)]$^+$ has been resolved. Improved procedures for the preparation and separation of *trans*-imidazole- and *trans*-amine-[Co(L-his)$_2$]$^+$ are given. The electronic spectra of all the geometrical isomers of bis(histidinato)cobalt(III) are discussed in terms of the angular overlap model.

An octahedral bis(histidinato)cobalt(III) complex gives rise to five geometrical isomers, four of which are chiral. The nine different theoretical structures are shown in Fig. 1.

The absorption spectra of the isomers *trans*-i, *trans*-a, *trans*-c and all-*cis* are reported in the literature.[1,2] The circular dichroism (CD) spectra

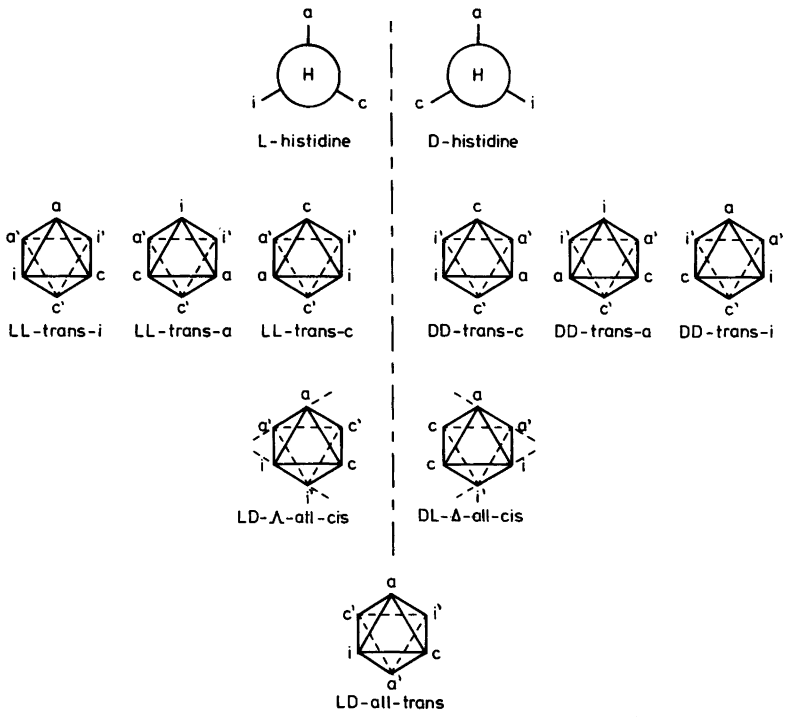

Fig. 1. Newman projections of histidine, and the structures of the bis(histidinato)cobalt(III) isomers.

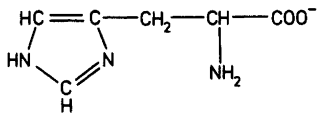

Fig. 2. Histidinate; L-histidine has the (*S*)-configuration in the Cahn-Ingold-Prelog notation.

of *trans*-i, *trans*-a and *trans*-c are also known.[2] The achiral all-*trans* isomer, however, has not yet been isolated and characterized.

In this work CD spectrum of the all-*cis* isomer is reported.

Schmidtke[3] has successfully used the angular overlap model (AOM), proposed by Schäffer and Jørgensen,[4] to explain the absorption spectra of the three isomers known at that time, namely *trans*-i, *trans*-a and *trans*-c. We have reexamined the application of the model to bis(histidinato)cobalt(III) complexes taking into account all the spectral data now available.

NOMENCLATURE

In formulas histidinate (Fig. 2) is abbreviated his^-.

The letters a, i and c are used as symbols for amino, imidazole and carboxylate, respectively.

The IUPAC rules for the designation of absolute configurations of octahedral complexes[5] may be adapted to all-*cis*-$[Co(his)_2]^+$ using the pairs of non-orthogonal skew lines indicated in Fig. 1.

EXPERIMENTAL RESULTS

The racemic isomer all-*cis*-[Co(L-his)(D-his)]Br has been resolved chromatographically using a Sephadex column. The antipodes separate into two distinct zones, indicating complete resolution.

The absorption and CD spectra are shown in Fig. 3.

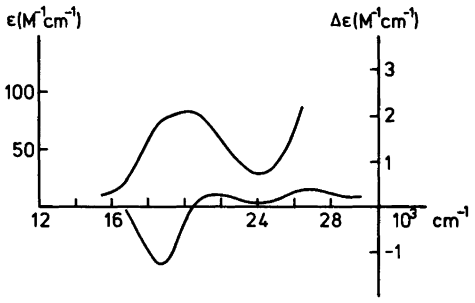

Fig. 3. Spectra of the $(-)_{589}$ antipode of the all-*cis*-$[Co(L\text{-}his)(D\text{-}his)]^+$ isomer in H_2O.

An improved procedure for obtaining pure samples of *trans*-i-$[Co(L\text{-}his)_2]ClO_4.1\frac{1}{2}H_2O$ and *trans*-a-$[Co(L\text{-}his)_2]ClO_4.2H_2O$ has been worked out. Previously the two isomers were separated by chromatography,[6] whereas the new method makes use of the different crystallization rates of the perchlorates.

Resolution of rac-*all*-cis-[*Co*(D-*his*)(L-*his*)]*Br*. The complex is prepared as the bromide[2] and is subsequently resolved chromatographically on SP-Sephadex C-25 with 0.1 M aqueous sodium antimonyl-*d*-tartrate as eluent. Our column was 30 cm long and had a diameter of 3 cm; 20 mg complex was eluted with a flow-rate of 0.5 ml/min. After 21 h two separate 1.5 cm broad zones had developed with centers 23 and 27 cm from the top of the column. The $(+)_{589}$ antipode is eluted first.

Preparation of trans-*imidazole*-$[Co(L\text{-}his)_2]ClO_4.1\frac{1}{2}H_2O$ *(red isomer) and* trans-*amine*-$[Co(L\text{-}his)_2]ClO_4.2H_2O$ *(orange isomer).* 3.57 g $CoCl_2.6H_2O$ (15 mmol) and 4.65 g L-histidine (30 mmol) are dissolved in 50 ml H_2O, and 0.5 g activated charcoal is added. The solution is heated to 75 °C and aerated for 90 min. Then 1 ml 30 % H_2O_2 is added, and the solution is kept at 75 °C for 30 min. The reaction mixture is cooled to *ca.* 0 °C, and the wall of the flask is scratched with a glass rod to insure that possible small amounts of unwanted products are precipitated. Subsequently the cooled solution is filtered. The volume is adjusted to 50 ml with water, and a solution of 20 g $NaClO_4.H_2O$ in 50 ml H_2O is added. After cooling in an ice bath for 30 min a precipitate of the red isomer is filtered off. Recrystallization from hot (70 °C) water. The mother liquid from the precipitation of the red isomer is left in a refrigerator for a couple of days and crystals of the orange isomer slowly form. Recrystallization from hot (70 °C) water.

Apparatus. A Cary 11 spectrophotometer and a Roussel-Jouan Dichrograph II were used for the measurements of optical spectra.

THEORETICAL RESULTS

The semi-empirical *angular overlap model*[4] is a useful tool for calculating energy levels in transition metal complexes. Application of the concept *holohedrized symmetry*,[4] which for low-symmetry molecules is higher than the actual symmetry, is a simplifying approximation which makes the model easy to deal with. The literature[3,4] should be consulted

for a description of the model and its underlying principles.

The holohedrized symmetry of all the bis(histidinato)cobalt(III) isomers is D_{2h}. On lowering the symmetry from O_h to D_{2h} the $^1T_{1g} \leftarrow {}^1A_{1g}$ parent transition in cobalt(III) is decomposed into $B_{1g} \leftarrow A_{1g}$, $B_{2g} \leftarrow A_{1g}$, and $B_{3g} \leftarrow A_{1g}$.

In his treatment of the *trans*-c, *trans*-a, and *trans*-i isomers Schmidtke[3] gave the energies of the three component transitions, abbreviated $\Delta E(B_1)$, $\Delta E(B_2)$, and $\Delta E(B_3)$, in terms of the special AOM parameters. We prefer to express these energies as functions of the usual cubic ligand field parameters for carboxylate (Δ_c), amine (Δ_a), and imidazole (Δ_i). This is possible for low-spin d^6-systems, as already pointed out by Schäffer and Jørgensen.[4] Otherwise we have used the procedure described by Schmidtke,[3] and we arrive at the following energy expressions:

trans-c:

$$\Delta E(B_1) = \frac{1}{2}(\Delta_a + \Delta_i)$$
$$\Delta E(B_2) = \Delta E(B_3) = \frac{1}{4}(\Delta_a + \Delta_i + 2\Delta_c) \quad (1)$$

trans-a:

$$\Delta E(B_1) = \Delta E(B_3) = \frac{1}{4}(2\Delta_a + \Delta_i + \Delta_c)$$
$$\Delta E(B_2) = \frac{1}{2}(\Delta_i + \Delta_c) \quad (2)$$

trans-i:

$$\Delta E(B_1) = \Delta E(B_2) = \frac{1}{4}(\Delta_a + 2\Delta_i + \Delta_c)$$
$$\Delta E(B_3) = \frac{1}{2}(\Delta_a + \Delta_c) \quad (3)$$

all-*cis*:

$$\Delta E(B_1) = \frac{1}{4}(2\Delta_a + \Delta_i + \Delta_c)$$
$$\Delta E(B_2) = \frac{1}{4}(\Delta_a + 2\Delta_i + \Delta_c) \quad (4)$$
$$\Delta E(B_3) = \frac{1}{4}(\Delta_a + \Delta_i + 2\Delta_c)$$

all-*trans*:

$$\Delta E(B_1) = \frac{1}{2}(\Delta_a + \Delta_i)$$
$$\Delta E(B_2) = \frac{1}{2}(\Delta_i + \Delta_c) \quad (5)$$
$$\Delta E(B_3) = \frac{1}{2}(\Delta_a + \Delta_c)$$

These equations immediately tell that all-*cis* and all-*trans* have three bands under the $T_{1g} \leftarrow A_{1g}$ parent transition, whereas each of the isomers *trans*-c, *trans*-a, and *trans*-i because of degeneracy only have two.

Using the assumption of Schmidtke[3]

$$\Delta_a > \Delta_i > \Delta_c$$

which is in accordance with the spectrochemical series,[7,8] it is easily deduced that the relative magnitudes of the transition energies are:

trans-c: $\Delta E(B_1) > \Delta E(B_2) = \Delta E(B_3)$ (6)

trans-a: $\Delta E(B_1) = \Delta E(B_3) > \Delta E(B_2)$ (7)

trans-i: $\Delta E(B_1) = \Delta E(B_2) > \Delta E(B_3)$ (8)

all-*cis*: $\Delta E(B_1) > \Delta E(B_2) > \Delta E(B_3)$ (9)

all-*trans*: $\Delta E(B_1) > \Delta E(B_3) > \Delta E(B_2)$ (10)

These five relations may be used for the assignment of the transitions in the experimental spectra.

DISCUSSION

It appears from eqns. (1)–(5) that if the energies of any three transitions in the five isomers are empirically known, the AOM will predict the energies of all the others.

Three of the transitions may be assigned and quite accurately read from the known experimental absorption spectra, namely the low-energy band of the *trans*-c isomer, and the high-energy bands of the *trans*-a and *trans*-i isomers, respectively. These three bands are marked by arrows in Fig. 4.

Simple calculations yield the values for the three cubic ligand field parameters as well as the transition energies listed in Table 1.

Table 1. Wavenumbers (in units of $10^3 \cdot cm^{-1}$) of the $T_{1g} \leftarrow A_{1g}$ components in $[Co(his)_2]^+$ isomers.

Isomer	$\Delta E(B_1)$	$\Delta E(B_2)$	$\Delta E(B_3)$
trans-c	21.9	18.7 [a]	18.7 [a]
trans-a	20.6 [a]	18.1	20.6 [a]
trans-i	20.0 [a]	20.0 [a]	19.3
all-*cis*	20.6	20.0	18.7
all-*trans*	21.9	18.1	19.3

[a] Experimentally determined values.

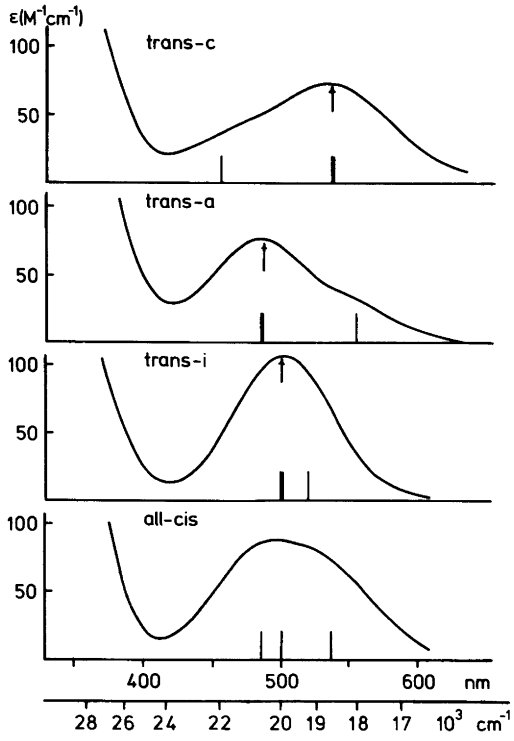

Fig. 4. Experimental absorption spectra of the four known geometrical isomers of the bis(histidinato)-cobalt(III) complex. Vertical lines indicate the position of transitions from Table 1.

The energy values from Table 1 are depicted as vertical lines in Fig. 4. The agreement between the experimental spectra and the AOM results is seen to be very satisfactory.

Table 1 includes a prediction of the unknown spectrum of the all-*trans* isomer, which so far has escaped isolation.[2]

The cubic ligand field parameters obtained, $\Delta_a = 23.1 \times 10^3$ cm^{-1}, $\Delta_i = 20.7 \times 10^3$ cm^{-1} and $\Delta_c = 15.5 \times 10^3$ cm^{-1}, are in good agreement with expected values from the literature.[7]

The fact that all-*cis*-[Co(D-his)(L-his)]$^+$ has been resolved into optical antipodes is a confirmation of its structure[2,9] since the other possibility, all-*trans*-[Co(D-his)(L-his)]$^+$, has a symmetry centrum and would therefore be nonresolvable.

The CD spectra of the four chiral isomers of [Co(his)$_2$]$^+$ turn out to be of little use for the purpose of determining transition energies. Their shapes are typical for so-called "residual wing absorptions", which arise when positive and negative contributions partially cancel each other.[10]

Since chirality vanishes on holohedrization the simple AOM used above is not appropriate for a detailed discussion of circular dichroism.

Acknowledgement. We wish to acknowledge the skilful technical assistance of Mrs. Lise Penzien.

REFERENCES

1. Zompa, L. J. *Chem. Commun.* (1969) 783.
2. Bagger, S., Gibson, K. and Sørensen, C. S. *Acta Chem. Scand. 26* (1972) 2503.
3. Schmidtke, H. H. *Chem. Phys. Lett. 4* (1969) 451.
4. a. Schäffer, C. E. and Jørgensen, C. K. *K. Dan. Vidensk. Selsk., Mat.-Fys. Medd. 34* (1965), No. 13; b. *Mol. Phys. 9* (1965) 401.
5. IUPAC *Inorg. Chem. 9* (1970) 1.
6. Bagger, S. and Gibson, K. *Acta Chem. Scand. 27* (1973) 3227.
7. Jørgensen, C. K. *Modern Aspects of Ligand Field Theory*, North-Holland, Amsterdam 1971, pp. 346–348.
8. Epstein, L. M., Straub, D. K. and Maricondi, C. *Inorg. Chem. 6* (1967) 1720.
9. Thorup, N. *Acta Chem. Scand. A 31* (1977) 203.
10. Jensen, H. P. and Galsbøl, F. *Inorg. Chem. 16* (1977) 1294.

Received April 21, 1978.

Acta Chemica Scandinavica A 32 (1978) 663–671

Two Quadruply-bonded Dimolybdenum Tetra(dithiocarboxylato) Compounds

F. A. COTTON, P.E. FANWICK, R. H. NISWANDER and J. C. SEKUTOWSKI

Department of Chemistry, Texas A&M University, College Station, Texas 77843, U.S.A.

Dedicated to Jannik Bjerrum on the occasion of his 70th birthday

Structural data for compounds of the type $Mo_2(S_2CR)_4L_2$ are reported for the first time. The compounds studied are those with $R=CH_3$ and C_6H_5; in both cases L=tetrahydrofuran. The dithioacetate is a new compound and a superior method of preparation is given for the benzoate. They are found to be fairly stable toward air when in crystalline form, and, unlike the xanthato compound, they do not give stable addition products with Br_2 or I_2. The acetate forms triclinic crystals in space group $P\bar{1}$ with $Z=2$ and unit cell dimensions $a=10.937(2)$ Å, $b=14.358(3)$ Å, $c=9.132(1)$ Å, $\alpha=93.43(1)°$, $\beta=111.33(1)°$, $\gamma=88.98(1)°$. Each molecule lies on an inversion center. The benzoate forms monoclinic crystals in space group $P2_1/c$ with $Z=2$ and $a=9.192(3)$ Å, $b=19.701(6)$ Å, $c=11.658(3)$ Å, $\beta=110.95(1)°$, and the molecules are equivalent and reside on inversion centers. In both compounds there are tetrahydrofuran molecules loosely coordinated in the axial positions. The dimensions of the central $Mo_2S_8O_2$ units are very similar in all three crystallographically independent molecules and have the following values: Mo–Mo=2.138(4) Å; Mo–S=2.465(8) Å; Mo–O=2.70(3) Å; ∠Mo–Mo–S=99.4(2)°.

Carboxylato-bridged species, $M_2(O_2CR)_4$, have played a prominent role in the developing chemistry of compounds with quadruple bonds between metal atoms,[1] especially Cr_2 and Mo_2 species, and many have been studied structurally.[2,3] It is therefore surprising that only one dithiocarboxylate, $Mo_2(S_2CR)_4$, has ever been reported, namely, the dithiobenzoate,[4,5] and only two monothiocarboxylates,[5] and no structure has previously been reported. In order to see what effect the replacement of RCO_2 by RCS_2 might have on the metal-to-metal bonding, we have begun an investigation of several $Mo_2(S_2CR)_4$ compounds. The first step has been to develop convenient, general and minimally odoriferous preparative methods. The second has been to obtain accurate structural information on representative compounds. For this second purpose we have chosen a compound with the simplest aliphatic R group, *viz.*, $Mo_2(S_2CCH_3)_4$, and a compound with the simplest aromatic R group, $Mo_2(S_2CC_6H_5)_4$. The results of x-ray crystallographic studies of both these compounds, each in the form of its tetrahydrofuran adduct, are reported here. We have also conducted some exploratory studies of the chemical reactivity of the $Mo_2(S_2CR)_4$ compounds to see whether they might resemble chemically the xanthato compound, $Mo_2(S_2COEt)_4$.[6,7]

EXPERIMENTAL

Materials and analyses. $Mo_2(O_2CCH_3)_4$ was prepared by reaction of $Mo(CO)_6$ with acetic acid in refluxing diglyme. C_6H_5MgBr and CH_3MgBr were purchased from Aldrich Chemical Company, Inc. Carbon disulfide was obtained from Fischer Scientific Company and dried over molecular sieves prior to use. All other compounds and solvents were of reagent grade or better from commercial sources. Tetrahydrofuran, THF, was always distilled shortly before use. Carbon and hydrogen analyses were performed at the Center for Trace Characterization, Texas A&M University.

Preparation of $Mo_2(S_2CC_6H_5)_4.2THF$. Under nitrogen, 5 ml of a 3 M solution of C_6H_5MgBr were added to 50 ml of THF. To this stirred solution, 2 ml of CS_2 were added very slowly at room temperature. The mixture was then allowed to react for one hour. $Mo_2(O_2CCH_3)_4$, 1.67 g, was added and the mixture stirred for an additional hour.

Deoxygenated methanol, 100 ml, was added slowly producing a burgundy-red crystalline precipitate. The product was stirred for 15 min, filtered, and washed with 50 ml of deoxygenated methanol. After it had been dryed under vacuum at room temperature, the compound appeared to be quite air stable. Elemental analysis indicated the compound was solvated with THF. *Anal.* Calc. for $Mo_2(S_2CC_6H_5)_4 \cdot 2C_4H_8O$: C 45.57; H 3.80. Found: C 45.6; H 3.76.

THF appears to be easily replaced by other donor molecules such as glyme, diglyme, and pyridine. When the compound is placed in these solvents, slight color and physical changes are apparent. Products, however, were not isolated or characterized.

Attempted preparation of $Mo_2(S_2CC_6H_5)_4I_2$. In 100 ml of deoxygenated chloroform $Mo_2(S_2CC_6H_5)_4.2THF$, 0.80 g (1.25 mmol), and 0.32 g (1.25 mmol) of I_2 were mixed. The mixture was stirred for 6 h at room temperature without conspicuous change. The product was filtered, washed with 50 ml of deoxygenated hexane and dried under vacuum at room temperature for 3 h. Elemental analysis indicated that the product had the composition $Mo_2(S_2CC_6H_5)_4I_2$. *Anal.* Calc. C 31.76; H 1.89. Found: C 31.2; H 1.86. This compound was then dissolved (under nitrogen) in THF, the solution filtered and a layer of deoxygenated hexane placed gently over the filtrate. After three days, small crystals had formed at the interface of the two liquids. These crystals were collected by filtration and dried by passing nitrogen through the filter. One of these crystals was chosen for X-ray analysis. However, this was found to be the unreacted dithiobenzoate and no iodide (or iodine) was found. This identification was later substantiated by elemental analysis of the crystals.

Preparation of $Mo_2(S_2CCH_3)_4.2THF$. In a procedure similar to that used for benzoate, 10 ml of a 2.8 M solution of CH_3MgBr was added to 50 ml of THF. To this stirred solution 4 ml of CS_2 was added very slowly and the reaction was cooled by means of an ice bath. The mixture was stirred for 2 h while the flask was allowed to warm to room temperature. $Mo_2(O_2CCH_3)_4$, 3.11 g, was added, whereupon an orange-red product precipitated. After addition of 100 ml of deoxygenated methanol, stirring was continued for 30 min. The compound was then collected by filtration, washed with 50 ml of deoxygenated methanol, and dried under vacuum at room temperature for 3 h. The dry product appeared to be quite air stable. Elemental analysis indicated the product obtained as above was not solvated. *Anal.* Calc. for $Mo_2(S_2CCH_3)_4$: C 17.27; H 2.16. Found: C 17.7; H 2.18.

Crystals suitable for X-ray analysis were grown by gently placing a layer of hexane over a saturated THF solution of the compound. The crystals which formed were solvated with THF. *Anal.* Calc. for $Mo_2(S_2CCH_3)_4.2C_4H_8O$: C 24.43; H 4.00. Found: C 24.8; H 3.68.

X-Ray crystallography of $Mo_2(S_2CC_6H_5)_4.2THF$. A crystal measuring approximately $0.3 \times 0.2 \times 0.2$ mm was mounted on a glass fiber and coated with epoxy resin. The crystal was examined on a Syntex $P\bar{1}$ four-circle automated diffractometer.[8] Both rotation photographs and ω-scans were used to determine the quality of the crystal. Preliminary examination indicated that the crystal was monoclinic. Cell constants, determined by a least-squares fit of 15 reflections having $18° < 2\theta(MoK\alpha) < 30°$, were: $a = 9.192(3)$ Å, $b = 19.701(6)$ Å, $c = 11.658(3)$ Å, $\beta = 110.95(1)°$, and $V = 1972(1)$ Å^3. The observed volume is consistent with $Z = 2$.

Data were collected at 22 ± 2 °C using the Syntex $P\bar{1}$ autodiffractometer, with graphite-monochromated $MoK\alpha$ radiation and the $\theta - 2\theta$ scan technique. Variable scan rates from 4° to 24°/min were used, depending on the intensity. The scan range was from $K\alpha_1 - 0.9°$ to $K\alpha_2 + 1.0°$. The systematic absences, k odd for $0k0$ and l odd for $h0l$, indicated the space group to be $P2_1/c$ (No. 14). A total of 2866 reflections having $0° < 2\theta(MoK\alpha) < 45°$ were collected. Of these, 1499 unique reflections with $I > 3\sigma(I)$ were used to solve and refine the structure. Three standard reflections were checked after every 97 measurements and were found to remain effectively constant. Lorentz and polarization corrections were applied but absorption was neglected.

The presence of only two formula units in the unit cell requires each one to reside on an inversion center. The position of one crystallographically unique Mo atom was determined from a three-dimensional Patterson function. The positions of the other atoms were obtained from subsequent difference Fourier maps. The function minimized in least squares refinement was $\Sigma w(|F_o| - |F_c|)^2$ and the parameter ρ in the expression[8] for the weights was assigned a value of 0.07. The discrepancy indices used are defined as follows:

$$R_1 = \Sigma \| F_o | - | F_c \| / \Sigma | F_o |$$

$$R_2 = [\Sigma w(|F_o| - |F_c|)^2 / \Sigma w |F_o|^2]^{1/2}$$

The structure was refined to convergence with all temperature parameters anisotropic. The final discrepancy indices were $R_1 = 0.046$ and $R_2 = 0.057$. The estimated standard deviation of an observation of unit weight was 1.18. A final difference Fourier revealed no features of structural significance.

X-Ray crystallography of $Mo_2(S_2CCH_3)_4.2THF$. An approximately equidimensional crystal with a mean thickness of about 0.25 mm was wedged in a

soft glass capillary, immersed in mineral oil and mounted on a Syntex $P\bar{1}$ autodiffractometer. Procedures for preliminary examination and data collection were essentially the same as those just described for the benzoate. In this case there was an overall decline of about 10 % in the standards and a linear correction was made for this before the 2558 unique data having $I > 3\sigma(I)$ were used to solve and refine the structure.

The preliminary examination showed that the crystal belonged to the triclinic system with the following unit cell dimensions: $a = 10.937(2)$ Å, $b = 14.358(3)$ Å, $c = 9.132(1)$ Å, $\alpha = 93.43(1)°$, $\beta = 111.33(1)°$, $\gamma = 88.98(1)°$, and $V = 1333(1)$ Å^3. This volume is consistent with $Z = 2$, and a formula unit of $Mo_2(S_2CCH_3)_4.2C_4H_8O$.

The structure was solved by conventional heavy atom methods and successfully refined in the space group $P\bar{1}$ using anisotropic thermal parameters for the Mo and S atoms and isotropic ones for the C and O atoms. Each molecule in the unit cell resides on one of the inversion centers at the origin and 1/2, 1/2, 1/2 so that the asymmetric unit consists of half of each molecule. The final values of the residuals, defined above, were $R_1 = 0.050$ and

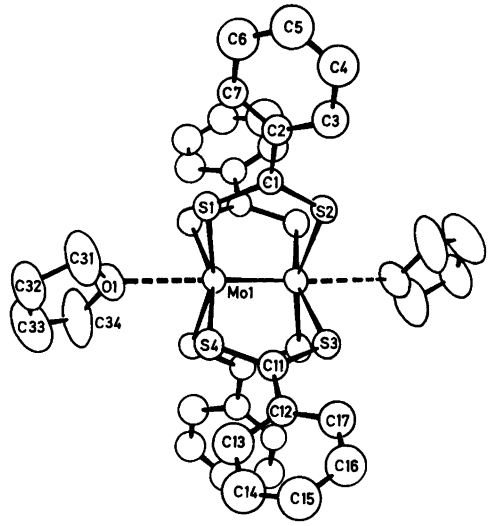

Fig. 1. An ORTEP drawing of the $Mo_2(S_2CC_6H_5)_4.2THF$ molecule in which each atom is represented by its ellipsoid of thermal vibration scaled to enclose 50 % of its electron density.

Table 1. Positional and thermal parameters and their estimated standard deviations for $Mo_2(S_2CC_6H_5)_4.2THF$.[a]

Atom	x	y	z	β_{11}	β_{22}	β_{33}	β_{12}	β_{13}	β_{23}
Mo(1)	0.1080(1)	0.01751(5)	0.06531(7)	0.0140(1)	0.00304(2)	0.00576(5)	−0.0018(1)	0.0060(1)	0.00005(8)
S(1)	0.2036(3)	0.0838(1)	−0.0724(2)	0.0165(4)	0.00395(9)	0.0074(2)	−0.0045(3)	0.0075(4)	0.0012(2)
S(2)	−0.0912(3)	0.0332(1)	−0.2526(2)	0.0162(4)	0.00361(9)	0.0068(2)	−0.0030(3)	0.0064(4)	0.0009(2)
S(3)	−0.0250(3)	−0.1254(1)	−0.1266(2)	0.0176(4)	0.00336(9)	0.0082(2)	−0.0012(3)	0.0070(4)	−0.0010(2)
S(4)	0.2741(3)	−0.0776(1)	0.0520(2)	0.0157(4)	0.00365(9)	0.0088(2)	−0.0006(3)	0.0078(4)	−0.0007(2)
O(1)	0.3958(8)	0.0558(5)	0.2216(6)	0.016(1)	0.0068(3)	0.0108(7)	−0.003(1)	0.006(1)	0.0029(8)
C(1)	0.072(1)	0.0787(5)	−0.2161(8)	0.015(1)	0.0031(3)	0.0076(7)	0.000(1)	0.009(1)	0.0009(8)
C(2)	0.100(1)	0.1184(5)	−0.3149(8)	0.018(1)	0.0034(3)	0.0086(8)	−0.000(1)	0.011(2)	0.0017(9)
C(3)	0.033(1)	0.0954(7)	−0.4374(8)	0.018(2)	0.0079(5)	0.0071(7)	−0.003(2)	0.006(2)	0.0051(11)
C(4)	0.060(1)	0.1324(8)	−0.5274(9)	0.023(2)	0.0114(6)	0.0085(9)	−0.012(2)	0.005(2)	0.0068(13)
C(5)	0.151(1)	0.1913(8)	−0.4988(11)	0.019(2)	0.0096(6)	0.0162(12)	−0.001(2)	0.010(3)	0.0135(13)
C(6)	0.223(1)	0.2133(7)	−0.3781(10)	0.030(2)	0.0060(5)	0.0145(10)	0.001(2)	0.022(2)	0.0066(12)
C(7)	0.199(1)	0.1754(6)	−0.2868(9)	0.023(2)	0.0038(4)	0.0138(9)	−0.002(1)	0.023(2)	0.0019(10)
C(11)	0.165(1)	−0.1348(5)	−0.0479(7)	0.018(1)	0.0035(3)	0.0076(7)	−0.001(1)	0.015(1)	0.0016(8)
C(12)	0.246(1)	−0.1986(5)	−0.0709(9)	0.024(2)	0.0029(3)	0.0127(9)	−0.000(1)	0.021(2)	0.0006(9)
C(13)	0.390(1)	−0.2177(6)	0.0169(11)	0.023(2)	0.0050(4)	0.0171(14)	0.008(1)	0.012(3)	0.0001(13)
C(14)	0.458(1)	−0.2756(7)	−0.0058(14)	0.024(2)	0.0055(5)	0.0342(21)	0.005(2)	0.023(3)	−0.0058(17)
C(15)	0.392(1)	−0.3123(6)	−0.1162(13)	0.031(2)	0.0039(4)	0.0318(15)	0.001(2)	0.042(2)	−0.0044(14)
C(16)	0.253(1)	−0.2924(6)	−0.2008(11)	0.031(2)	0.0038(4)	0.0243(13)	−0.002(2)	0.034(2)	−0.0053(12)
C(17)	0.178(1)	−0.2354(6)	−0.1819(9)	0.033(2)	0.0039(4)	0.0130(10)	−0.003(2)	0.022(2)	−0.0023(11)
C(31)	0.517(2)	0.0781(11)	0.1843(14)	0.021(2)	0.0161(11)	0.0180(15)	−0.014(2)	0.013(3)	0.0064(21)
C(32)	0.664(1)	0.0668(9)	0.2877(12)	0.017(2)	0.0119(9)	0.0147(14)	−0.005(2)	0.006(3)	0.0046(19)
C(33)	0.620(2)	0.0342(12)	0.3757(15)	0.025(3)	0.0181(12)	0.0199(16)	−0.008(3)	0.009(3)	0.0184(22)
C(34)	0.453(2)	0.0369(13)	0.3428(13)	0.020(2)	0.0186(12)	0.0133(14)	−0.016(3)	0.007(3)	−0.0005(24)

[a] The form of the anisotropic thermal parameter is: $\exp[-(\beta_{11}h^2 + \beta_{22}k^2 + \beta_{33}l^2 + \beta_{12}hk + \beta_{13}hl + \beta_{23}kl)]$.

$R_2 = 0.074$, and the esd for an observation of unit weight was 1.61.

Structure factor tables. A complete list of the observed and final calculated structure factors for each compound may be obtained, on request, from FAC.

RESULTS

Structural. Tables 1 and 2 list the atomic positional and thermal vibration parameters for the benzoate and acetate, respectively. The $Mo_2(S_2CC_6H_5)_4.2THF$ molecule is shown in Fig. 1, where the atom numbering scheme used in all tables pertaining to this molecule is defined. The molecule resides on a crystallographic inversion center; all unlabelled atoms may be identified, when necessary, by primed labels corresponding to those given for atoms related by the inversion operation. Fig. 2 shows one of the two independent molecules of $Mo_2(S_2CCH_3)_4.2THF$, and its numbering scheme. In the other molecule a related set of numbers, Mo(2), Mo(2)', S(5), S(6), *etc.* is used. The relationship will be quite clear from the tables of bond lengths and angles in the dithioacetate, where corresponding dimensions of the two molecules are listed side by side.

The two molecules of $Mo_2(S_2CC_6H_5)_4.2THF$ in the unit cell are equivalent and there is a crystallographically rigorous center of symmetry at the midpoint of the Mo–Mo bond. The bond lengths and angles are listed in Tables 3 and 4 and it may

Table 2. Positional and thermal parameters and their estimated standard deviations for $Mo_2(S_2CCH_3)_4.2THF$.[a]

Atom	x	y	z	β_{11}[b]	β_{22}	β_{33}	β_{12}	β_{13}	β_{23}
Mo(1)	0.39747(8)	0.48341(6)	0.45406(9)	0.00681(7)	0.00427(4)	0.0103(1)	0.0000(1)	0.0071(1)	0.0012(1)
Mo(2)	0.09856(8)	−0.02419(6)	0.04901(9)	0.00765(8)	0.00448(5)	0.0110(1)	−0.0010(1)	0.0080(1)	−0.0000(1)
S(1)	0.4070(3)	0.3261(2)	0.3340(3)	0.0114(3)	0.0048(1)	0.0153(4)	−0.0017(4)	0.0113(5)	−0.0026(4)
S(2)	0.3109(3)	0.6291(2)	0.5366(3)	0.0095(3)	0.0055(2)	0.0192(4)	0.0025(3)	0.0139(5)	0.0014(4)
S(3)	0.3378(3)	0.5438(2)	0.1906(3)	0.0104(3)	0.0071(2)	0.0117(3)	−0.0008(4)	0.0064(5)	0.0043(4)
S(4)	0.6200(3)	0.5894(2)	0.3157(3)	0.0103(3)	0.0061(2)	0.0134(3)	−0.0017(3)	0.0118(4)	0.0029(4)
S(5)	0.1521(3)	0.0351(2)	0.3239(3)	0.0115(3)	0.0072(2)	0.0117(4)	−0.0023(4)	0.0054(5)	−0.0015(4)
S(6)	−0.1205(3)	0.1000(2)	0.1898(3)	0.0125(3)	0.0061(2)	0.0151(4)	0.0011(4)	0.0152(5)	−0.0016(4)
S(7)	0.2157(3)	0.1127(2)	0.0124(3)	0.0090(3)	0.0055(2)	0.0196(4)	−0.0027(3)	0.0113(5)	0.0015(4)
S(8)	−0.0557(3)	0.1804(2)	−0.1228(3)	0.0104(3)	0.0050(1)	0.0169(4)	−0.0004(4)	0.0099(5)	0.0028(4)
O(1)	0.1440(8)	0.4363(6)	0.3320(9)	6.4(2)					
O(2)	0.3444(9)	−0.0945(7)	0.1731(10)	7.2(2)					
C(10)	0.0893(14)	0.3459(11)	0.330(2)	8.0(4)					
C(11)	−0.0575(15)	0.3615(11)	0.244(2)	8.2(4)					
C(12)	−0.0859(14)	0.4641(11)	0.238(2)	7.6(4)					
C(13)	0.0428(15)	0.5066(12)	0.261(2)	8.7(4)					
C(14)	0.4518(15)	−0.0654(11)	0.128(2)	8.5(4)					
C(15)	0.5711(15)	−0.0836(11)	0.261(2)	8.5(4)					
C(16)	0.5335(17)	−0.1370(13)	0.369(2)	9.8(5)					
C(17)	0.3893(14)	−0.1545(11)	0.300(2)	7.6(4)					
C(20)	0.5629(9)	0.2996(7)	0.365(1)	3.7(2)					
C(21)	0.5964(12)	0.2046(9)	0.302(1)	5.9(3)					
C(30)	0.4725(10)	0.5874(7)	0.175(1)	4.1(2)					
C(31)	0.4596(12)	0.6293(9)	0.018(1)	5.9(3)					
C(40)	0.0226(10)	0.0910(7)	0.344(1)	4.1(2)					
C(41)	0.0317(13)	0.1336(9)	0.502(1)	6.2(3)					
C(50)	0.1068(10)	0.1952(7)	−0.075(1)	4.0(2)					
C(51)	0.1580(12)	0.2868(9)	−0.104(1)	5.8(3)					

[a] The form of the anisotropic thermal parameter is: $\exp[-(\beta_{11}h^2+\beta_{22}k^2+\beta_{33}l^2+\beta_{12}hk+\beta_{13}hl+\beta_{23}kl)]$.
[b] For atoms refined isotropically this column gives B_{iso} in Å^2.

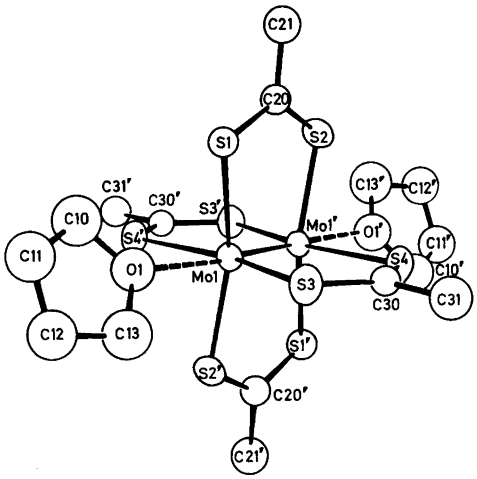

Fig. 2. An ORTEP drawing of Molecule I of $Mo_2(S_2CCH_3)_4.2THF$. Atoms are represented by ellipsoids or spheres of thermal vibration scaled to enclose 50 % of the electron density.

be seen that the central portion of the molecule, that is, the $Mo_2(S_2CC)_4O_2$ part, has essentially D_{4h} symmetry. The THF molecules violate this and so also do the phenyl rings. As shown in Table 5 these rings are twisted out of coplanarity with their respective CS_2 planes by 21.1° and 25.0°. This may be only a result of intermolecular packing.

Table 3. Bond distances (Å) for $Mo_2(S_2CC_6H_5)_4.2THF$.[a,b]

Mo(1)–Mo(1)'	2.139(2)	S(3)–C(11)	1.67(1)
Mo(1)–S(1)	2.462(2)	S(4)–C(11)	1.67(1)
Mo(1)–S(2)'	2.455(2)	C(11)–C(12)	1.53(1)
Mo(1)–S(3)'	2.449(3)	C(12)–C(13)	1.40(2)
Mo(1)–S(4)	2.456(3)	C(13)–C(14)	1.37(2)
Mo(1)–O(1)	2.727(7)	C(14)–C(15)	1.41(2)
S(1)–C(1)	1.683(9)	C(15)–C(16)	1.37(2)
S(2)–C(1)	1.666(9)	C(16)–C(17)	1.38(2)
C(1)–C(2)	1.49(1)	C(17)–C(12)	1.42(1)
C(2)–C(3)	1.41(1)	O(1)–C(31)	1.40(1)
C(3)–C(4)	1.37(2)	O(1)–C(34)	1.37(2)
C(4)–C(5)	1.40(2)	C(31)–C(32)	1.47(2)
C(5)–C(6)	1.39(2)	C(32)–C(33)	1.39(2)
C(6)–C(7)	1.38(1)	C(33)–C(34)	1.44(2)
C(7)–C(2)	1.41(1)		

[a] The esd in the least significant digit is given in parentheses. [b] Atoms with primed symbols are related by the inversion center to those with the same unprimed symbol.

Table 4. Bond angles (deg.) for $Mo_2(S_2CC_6H_5)_4.2THF$.[a,b]

Mo(1)'–Mo(1)–S(1)	99.43(7)
–S(2)'	99.45(7)
–S(3)'	100.41(8)
–S(4)	98.55(8)
–O(1)	175.2(2)
S(1)–Mo(1)–S(2)'	161.08(9)
–S(3)'	87.18(9)
–S(4)	89.36(9)
S(2)'–Mo(1)–S(3)'	88.18(9)
–S(4)	89.09(9)
S(3)'–Mo(1)–S(4)	161.04(9)
O(1)–Mo(1)–S(1)	78.6(2)
–S(2)'	82.7(2)
–S(3)'	83.9(2)
–S(4)	77.1(2)
Mo(1)–S(1)–C(1)	108.6(3)
Mo(1)'–S(2)–C(1)	109.2(3)
S(1)–C(1)–S(2)	123.2(5)
–C(2)	118.5(7)
S(2)–C(1)–C(2)	118.3(7)
C(1)–C(2)–C(3)	118.7(9)
–C(7)	120.9(9)
C(3)–C(2)–C(7)	120.2(9)
C(2)–C(3)–C(4)	118(1)
C(3)–C(4)–C(5)	121(1)
C(4)–C(5)–C(6)	122(2)
C(5)–C(6)–C(7)	117(1)
C(6)–C(7)–C(2)	121(1)
Mo(1)'–S(3)–C(11)	108.1(4)
Mo(1)–S(4)–C(11)	109.2(4)
S(3)–C(11)–S(4)	123.7(6)
–C(12)	118.2(8)
S(4)–C(11)–C(12)	118.0(8)
C(11)–C(12)–C(13)	118(1)
–C(17)	120(1)
C(13)–C(12)–C(17)	122(1)
C(12)–C(13)–C(14)	117(1)
C(13)–C(14)–C(15)	122(1)
C(14)–C(15)–C(16)	120(1)
C(15)–C(16)–C(17)	121(1)
C(16)–C(17)–C(12)	118(1)
Mo(1)–O(1)–C(31)	124.5(8)
–C(34)	122.6(8)
C(31)–O(1)–C(34)	110(1)
O(1)–C(31)–C(32)	107(1)
C(31)–C(32)–C(33)	105(1)
C(32)–C(33)–C(34)	110(1)
C(33)–C(34)–O(1)	106(1)

[a] The esd in the least significant digit is given in parentheses. [b] Atoms with primed symbols are related by the inversion center to those with the same unprimed symbol.

Table 5. Planes and dihedral angles for $Mo_2(S_2CC_6H_5)_4.2THF$.[a]

Plane	Atom	Distance from Plane
1	C(2)	0.023(11)
	C(3)	−0.013(13)
	C(4)	−0.014(14)
	C(5)	0.022(14)
	C(6)	0.002(13)
	C(7)	−0.022(11)
2	C(12)	−0.008(11)
	C(13)	0.016(12)
	C(14)	−0.018(14)
	C(15)	0.009(14)
	C(16)	0.003(13)
	C(17)	0.005(12)
3	S(1)	0.000(3)
	S(2)	0.000(3)
	C(1)	0.000(10)
4	S(3)	0.000(3)
	S(4)	0.000(3)
	C(11)	0.000(10)

Dihedral Angles

	Plane	Angle
1	3	−25.0
2	4	21.1

[a] The esd in the least significant digit is given in parentheses.

Table 6. Bond distances (Å) for $Mo_2(S_2CCH_3)_4.2THF$.[a,b]

Molecule I		Molecule II	
Mo(1)−Mo(1)′	2.141(1)	Mo(2)−Mo(2)′	2.133(1)
Mo(1)−S(1)	2.469(2)	Mo(2)−S(5)	2.462(2)
Mo(1)−S(2)	2.470(2)	Mo(2)−S(6)	2.467(2)
Mo(1)−S(3)	2.461(2)	Mo(2)−S(7)	2.469(2)
Mo(1)−S(4)	2.472(2)	Mo(2)−S(8)	2.481(2)
Mo(1)−O(1)	2.667(7)	Mo(2)−O(2)	2.712(6)
S(1)−C(20)	1.665(8)	S(5)−C(40)	1.677(9)
S(2)−C(20)	1.673(8)	S(6)−C(40)	1.690(9)
C(20)−C(21)	1.54(1)	C(40)−C(41)	1.51(1)
S(3)−C(30)	1.667(9)	S(7)−C(50)	1.681(9)
S(4)−C(30)	1.657(9)	S(8)−C(50)	1.682(9)
C(30)−C(31)	1.54(1)	C(50)−C(51)	1.51(1)
O(1)−C(10)	1.43(1)	O(2)−C(14)	1.45(1)
O(1)−C(13)	1.48(1)	O(2)−C(17)	1.42(1)
C(10)−C(11)	1.53(2)	C(14)−C(15)	1.46(2)
C(11)−C(12)	1.50(2)	C(15)−C(16)	1.46(2)
C(12)−C(13)	1.48(2)	C(16)−C(17)	1.49(2)

[a] The esd in the least significant digit is given in parentheses. [b] Atoms with primed symbols are related by the inversion center to those with the same unprimed symbol.

The unit cell of $Mo_2(S_2CCH_3)_4.2THF$ contains two molecules. Each one has a crystallographically rigorous center of inversion at the midpoint of the Mo−Mo bond. Neglecting the orientations of the THF rings and the hydrogen atoms of the methyl groups (which were not included in the refinement) the $Mo_2(S_2CC_4)O_2$ core of the molecule has symmetry approximating very closely to D_{4h}. Thus, the various distances and angles that ought to be equal on the basis of that symmetry are equal within a few times their esd's. These internal dimensions are recorded in Tables 6 and 7.

Chemical. The preparation of $Mo_2(S_2CR)_4$ compounds has been shown to be relatively simple and odor-free if the RCS_2^- ion is generated by reaction of the Grignard reagent, RMgBr, with CS_2 and reacted *in situ* with $Mo_2(O_2CCH_3)_4$. The solid $Mo_2(S_2CR)_4$ compounds are stable toward ordinary laboratory air for periods of at least several days. It has also been shown that, in contrast to the behavior of $Mo_2(S_2COEt)_4$, the dithiocarboxylato compounds do not react with Br_2 or I_2 to give stable, well-defined addition products. The benzoate gave a product of composition $Mo_2(S_2CC_6H_5)_4I_2$ but upon attempted recrystallization, the iodine was lost.

DISCUSSION

Preparative chemistry. As noted at the outset $Mo_2(S_2CC_6H_5)_4$, $Mo_2(OSCC_6H_5)_4$ and $Mo_2(OSCCH_3)_4$ were the only known thioacid[4,5] derivatives of quadruply-bonded M_2 units until now. Lack of interest in such compounds may have stemmed in part from the offensive odor generated by acids such as HS_2CR. Although it is the sodium salt that is normally used to prepare the complex, previous methods[9,10] have called for the intermediate formation of the free acid. In the earlier preparation[4] of $Mo_2(S_2CC_6H_5)_4$, the reaction of CS_2 with the Grignard reagent C_6H_5MgBr was followed first by acidification and then by neutralization and reaction with $Mo_2(O_2CCH_3)_4$.

We sought a procedure which does not at any point involve the free acid. An attempt to react the Grignard salt, $C_6H_5CS_2MgBr$, directly with $Mo_2(O_2CCH_3)_4$ was successful and suggested that, in general, the acidification step, which was primarily employed to purify the thio acid, could be omitted. The general effectiveness of this simple procedure was then confirmed by preparing for the first time the dithioacetate.

For unknown reasons, attempts to use C_6H_5Li and CH_3Li instead of the respective Grignard reagents were unsuccessful.

It was shown[7] recently that $Mo_2(S_2COR)_4$ molecules react with I_2 and Br_2 to yield products in which the Mo–Mo bond order is reduced from 4 to 1 because the oxidative addition of X_2 is accompanied (followed?) by an unprecedented rearrangement of the xanthate groups relative to the metal atoms. We have examined the reactions of Br_2 and I_2 with the $Mo_2(S_2CR)_4$ species to see if they would undergo simple oxidative addition to afford triply-bonded products. The stoichiometric reactions of I_2 and Br_2 with $Mo_2(S_2CCH_3)_4$ in $CHCl_3$ or THF did not result in simple oxidative addition

Table 7. Bond angles (deg) for $Mo_2(S_2CCH_3)_4.2THF$.[a,b]

Molecule I		Molecule II	
Mo(1)′–Mo(1)–S(1)	99.18(7)	Mo(2)′–Mo(2)–S(5)	99.22(7)
–S(2)	99.50(7)	–S(6)	99.59(7)
–S(3)	99.31(7)	–S(7)	99.65(7)
–S(4)	99.46(7)	–S(8)	99.16(7)
–O(1)	177.6(2)	Mo(2)′–Mo(2)–O(2)	177.1(2)
S(1)–Mo(1)–S(2)	161.31(9)	S(5)–Mo(2)–S(6)	161.18(9)
–S(3)	88.10(8)	–S(7)	87.65(9)
–S(4)	89.04(8)	–S(4)	89.41(9)
–O(1)	78.5(2)	–O(2)	81.52(2)
S(2)–Mo(1)–S(3)	88.20(9)	S(6)–Mo(2)–S(7)	88.51(8)
–S(4)	88.59(8)	–S(8)	88.31(8)
–O(1)	82.8(2)	–O(2)	79.73(2)
S(3)–Mo(1)–S(4)	161.22(9)	S(7)–Mo(2)–S(8)	161.19(9)
S(3)–Mo(1)–O(1)	80.0(2)	–O(2)	83.16(2)
S(4)–Mo(1)–O(1)	81.2(2)	S(8)–Mo(2)–O(2)	78.03(2)
Mo(1)–S(1)–C(20)	109.0(3)	Mo(2)–S(5)–C(40)	110.1(3)
Mo(1)–S(2)–C(20)	108.6(3)	Mo(2)–S(6)–C(40)	109.4(3)
Mo(1)–S(3)–C(30)	108.4(3)	Mo(2)–S(7)–C(50)	109.7(3)
Mo(1)–S(4)–C(30)	108.0(3)	Mo(2)–S(8)–C(50)	109.5(3)
S(1)–C(20)–S(2)	123.6(5)	S(5)–C(40)–S(6)	121.6(5)
S(1)–C(20)–C(21)	119.6(7)	S(5)–C(40)–C(41)	119.9(7)
S(2)–C(20)–C(21)	116.8(6)	S(6)–C(40)–C(41)	118.5(7)
S(3)–C(30)–S(4)	124.7(5)	S(7)–C(50)–S(8)	120.0(5)
S(3)–C(30)–C(31)	118.0(7)	S(7)–C(50)–C(51)	118.5(7)
S(4)–C(30)–C(31)	117.3(7)	S(8)–C(50)–C(51)	119.4(7)
Mo(1)–O(1)–C(10)	126.6(7)	Mo(2)–O(2)–C(14)	122.7(8)
–C(13)	120.7(7)	–C(17)	125.7(7)
C(10)–O(1)–C(13)	112.7(9)	C(14)–O(2)–C(17)	111.2(9)
O(1)–C(10)–C(11)	103(1)	O(2)–C(14)–C(15)	105(1)
C(10)–C(11)–C(12)	110(1)	C(14)–C(15)–C(16)	107(1)
C(11)–C(12)–C(13)	103(1)	C(15)–C(16)–C(17)	109(1)
C(12)–C(13)–O(1)	107(1)	C(16)–C(17)–O(2)	104(1)

[a] The esd in the least significant digit is given in parentheses. [b] Atoms with primed symbols are related by the inversion center to those with the same unprimed symbol.

Table 8. Mean values of distances (Å) and angles (deg) common to all $Mo_2(S_2CR)_4.2THF$ molecules.

Distance or angle	$R=C_6H_5$	$R=CH_3$ I	$R=CH_3$ II	Grand average
Mo–Mo	2.139(2)	2.141(1)	2.133(1)	2.138(4)
Mo–S	2.456(5)	2.468(5)	2.470(8)	2.465(8)
Mo–O(THF)	2.727(7)	2.667(7)	2.712(6)	2.70(3)
Mo–Mo'–S	99.46(80)	99.36(15)	99.40(20)	99.4(2)

products. Elemental analyses indicated incomplete reactions, though the products were completely different in appearance from the starting material. They were non-crystalline, insoluble substances which defied attempts at recrystallization. The exact nature of these products is still uncertain, with the possibility that they are polymeric with bridging halide ions being conceivable.

The reaction of Br_2 with $Mo_2(S_2CC_6H_5)_4$ also resulted in an insoluble substance, but the reaction of I_2 gave a slightly soluble product resembling the starting compound. Elemental analysis of this product suggested complete oxidative addition. However, attempts to recrystallize the material resulted in its decomposition back to the starting compound. Since it seems unlikely that reductive elimination could take place under such mild conditions, it is unlikely that the "reacted" compound was an oxidative addition product. It may possibly be an inclusion compound or even a weak π-complex between I_2 and the benzene rings.

The failure of the $Mo_2(S_2CR)_4$ species to react with Br_2 and I_2 in the way that the $Mo_2(S_2COR)_4$ molecules do, or in any other simple, definite way suggests that simple oxidative addition is not in itself an important reaction even for the xanthates and that the unusual bonding of two of the xanthato groups in the products is crucial to the occurrence of the reaction.

Structural. The structures are qualitatively as expected, and there are no significant differences between the structures of the two compounds studied here (see Table 8), nor between these structures and that of the xanthato compound.[6]

There are slight but real differences between the bond lengths for the two crystallographically independent molecules of the dithioacetate, and these are in accord with the well-known[2,3,11] inverse relationship between the strength of M–M and $M-L_{ax}$ bonds. The molecule which has the slightly shorter Mo–Mo bond, 2.133(1) Å has the slightly longer Mo–O axial bond, 2.716(6) Å, while the longer Mo–Mo distance in the other molecule, 2.141(1) Å, is accompanied by the shorter Mo–O bond, 2.667(7) Å.

In all three compounds with bridging dithio units that have now been studied, the Mo–S distances are practically identical. Those in the structures reported here (see Table 8) average 2.465(8) Å while those in the xanthate have a mean of 2.477(2) Å.

It is clear that the Mo–Mo distances in the compounds bridged by dithiocarboxylates and xanthate are about 0.045 Å longer than those in the carboxylato bridged species,[1,3] such as $Mo_2(O_2CCH_3)_4$, 2.093(1) Å, $Mo_2(O_2CCF_3)_4$, 2.090(4) Å, and $Mo_2(O_2CC_6H_5)_4$, 2.096(1) Å. In all of the latter (and other) cases, there are only loose intermolecular axial interactions, with Mo···O distances around 2.85 Å. Even when fairly strong axial donors are brought in as in $Mo_2(O_2CCF_3)_4.2py$,[12] where Mo–N=2.55 Å and Mo–Mo=2.129(2) Å and $Mo_2(O_2CC_6H_5)_4.2diglyme$,[13] where Mo–O=2.72 Å and Mo–Mo=2.100 Å, the Mo–Mo distances increase rather little, *viz.*, 0.039 Å for the very short Mo–N bond but <0.01 Å for the benzoate where the axial Mo–O distance is similar to those in the dithiocarboxylates reported here. We therefore conclude that while a part of the increase in Mo–Mo distances may be attributed to the presence of axial THF molecules in each of the dithio cases, this cannot account fully for the difference. The steric and electronic properties of the XCS_2^--type ligand must themselves favor a slightly greater Mo–Mo distance.

Acknowledgement. We are grateful to the National Science Foundation for financial support.

REFERENCES

1. Cotton, F. A. *Chem. Soc. Rev.* 4 (1975) 27.
2. Cotton, F. A., Extine, M. W. and Rice, G. W. *Inorg. Chem.* 17 (1978) 176.

3. Cotton, F. A., Extine, M. and Gage, L. D. *Inorg. Chem. 17* (1978) 172.
4. Steele, D. F. and Stephenson, T. A. *Inorg. Nucl. Chem. Lett. 9* (1973) 777.
5. Holste, G. *Z. Anorg. Allg. Chem. 425* (1976) 57.
6. Ricard, L., Kargiannides, P. and Weiss, R. *Inorg. Chem. 12* (1973) 2179.
7. Cotton, F. A., Extine, M. W. and Niswander, R. H. *Inorg. Chem. 17* (1978) 692.
8. Crystallographic procedures are conventional ones and details that may be peculiar to This Laboratory have been fully described many times before. See, for example, Refs. 2 and 3.
9. Bost, R. W. and Mattox, J. W. *J. Am. Chem. Soc. 52* (1930) 332.
10. Bost, R. W. and Shealy, O. L. *J. Am. Chem. Soc. 73* (1951) 25.
11. Cotton, F. A. and Hall, W. T. *Inorg. Chem. 16* (1977) 1867.
12. Cotton, F. A. and Norman, J. G., Jr. *J. Am. Chem. Soc. 94* (1972) 5697.
13. Collins, D. M., Cotton, F. A. and Murillo, C. A. *Inorg. Chem. 15* (1976) 2950.

Received February 20, 1978.

Acta Chemica Scandinavica A 32 (1978) 673 – 674

Short Communication

Synthesis of *trans*-Dichloro- and *trans*-Difluorotetrakis(pyridine)-cobalt(III) Salts

JØRGEN GLERUP,[a] CLAUS ERIK SCHÄFFER[a] and JOHAN SPRINGBORG[b]

[a]Chemistry Department I (Inorganic Chemistry), University of Copenhagen, H. C. Ørsted Institute, Universitetsparken 5, DK-2100 Copenhagen Ø, Denmark and [b]Chemistry Department, Royal Veterinary and Agricultural University, Thorvaldsensvej 40, DK-1871 Copenhagen V, Denmark

Dedicated to Jannik Bjerrum on the occasion of his 70th birthday

Only a few tetrakis(pyridine)cobalt(III) complexes have been reported in the literature. Thus the *trans*-dichloro- and *trans*-diaquatetrakis(pyridine)cobalt-(III) cations [1,2] are the only *trans* complexes which have been described until now.

The main purpose of this communication is to describe the preparation of the new classical complex, *trans*-difluorotetrakis(pyridine)cobalt(III) perchlorate whose chromium(III) analogue has proved most interesting spectroscopically [3] and useful for preparative purposes.[4,5]

Two methods are described for the preparation of *trans*-difluorotetrakis(pyridine)cobalt(III) perchlorate. One method starts from *trans*-dichlorotetrakis(pyridine)cobalt(III) chloride hexahydrate, for which an improved synthesis is also reported. This complex is treated with mercury(II) ions (added as mercury(II) acetate) in liquid hydrogen fluoride at −70 °C. The second method employs the new complex aquadifluorotris(pyridine)cobalt(III) perchlorate which is heated in pyridine at 70 °C. Aquadifluorotris(pyridine)cobalt(III) perchlorate itself is prepared from carbonatochlorotris-(pyridine)cobalt(III) by treatment of the latter with liquid hydrogen fluoride. The configuration of the aquadifluorotris(pyridine)cobalt(III) cation is probably meridional, but we do not know whether the coordinated fluoride ions are *cis* or *trans*. However, the behaviour of the complex indicated that we are dealing with a single compound. Preliminary experiments [6] suggest that the reaction between some other tris(pyridine)cobalt(III) complexes and pyridine also gives *trans*-tetrakis(pyridine)cobalt(III) complexes.

The cation *trans*-$[CoF_2(py)_4]^+$ behaves as a base in strongly acidic media. When the complex is formed in the anhydrous hydrogen fluoride the colour is green, becoming red when the solution is diluted with methanol. Similarly, the red perchlorate salt dissolves in 70 % perchloric acid giving a green colour, and on dilution of this solution with ice-water the colour changes to red and the original compound reprecipitates. These colour changes are undoubtedly associated with a protonation reaction involving one or both of the coordinated fluorides.

Materials. Carbonatochlorotris(pyridine)cobalt-(III) perchlorate was prepared according to the literature.[2] All other chemicals were of analytical grade.

Spectra. Absorption spectra in the 300 – 650 nm region, recorded using a Cary 14 spectrophotometer, were used as a check of purity and as characterization of the compounds. Data for maxima and minima are given below with the molar absorptivity ε in liter mol^{-1} cm^{-1} and the wavelength λ in nm.

Preparations. 1. *trans*-$[CoCl_2(py)_4]Cl.6H_2O$. (*CAUTION.* Personal communication from R. D. Gillard; when this synthesis is performed by the classival method, in which gaseous chlorine is employed, an explosion of severe character has sometimes resulted. The present method has been used in this laboratory at least a dozen times without ever giving rise to difficulties of this sort). Pyridine (500 ml, 6.2 mol) and methanol (750 ml) were heated under mechanical stirring in a 2 l three-necked flask. To the solution was added anhydrous cobalt-(II) chloride (100 g, 0.77 mol) in small portions and the resulting blue solution was heated under reflux for 15 min. The blue solution was poured into a 4 l beaker equipped with a mechanical stirrer and cooled with dry ice and acetone. When the temperature had fallen to 10 °C the red complex $CoCl_2(py)_4$ began to precipitate. When the temperature had reached −40 °C, liquid chlorine (30 ml, 1.33 mol) was added to the solution and the cooling bath was removed. (The liquid chlorine was condensed from a cylinder into a beaker cooled with dry ice and acetone). Over a period of *ca.* 30 min the temperature rose to 0 °C, and the colour changed from red to a mixture of red and green. In order to prevent the temperature from increasing beyond 25 °C it was necessary at this stage to cool again with the dry ice and acetone bath (alternatively

the solution could also be cooled by pouring liquid N_2 directly into it).

After the oxidation was complete the mixture was a green porridge. It was then heated to 40 °C and 4 M hydrochloric acid (2.5 l) was added gradually. When approximately 700 ml of hydrochloric acid had been added the precipitate had redissolved and on adding more hydrochloric acid the green complex began to precipitate again. After keeping the solution at −18 °C overnight it was filtered and the precipitate washed with ice-cold water and air dried. Yield 340 g (75 %). The crude *trans*-$[CoCl_2(py)_4]Cl.6H_2O$ (160 g) was recrystallized by dissolving it in 1:1 aqueous ethanol (640 ml) preheated to 50 °C. The filtered solution was kept at −18 °C overnight and the crystals were filtered off, washed with ice-cold water and air dried. Yield 126 g. Anal. $[CoCl_2(py)_4]Cl.6H_2O$: Co, C, N, H, Cl. Spectral data in 0.01 M HCl: $(\varepsilon,\lambda)_{max}$: (43.1,631), (29.8,505). $(\varepsilon,\lambda)_{min}$: (16.5,559), (24.1,470).

2. *trans*-$[CoF_2(py)_4]ClO_4.\frac{1}{2}H_2O$. *trans*-$[CoCl_2(py)_4]Cl.6H_2O$ (50 g, 0.1 mol) was dissolved in anhydrous hydrogen fluoride (150 ml) cooled to −70 °C with dry ice. To the green solution was added portion-wise mercury(II) acetate (48 g, 0.15 mol). After standing for 30 min, methanol (150 ml) precooled with dry ice was added when the colour changed from green to red. The solution was filtered (Whatman No. 450) and evaporated overnight in an effective hood by means of a fan (*CAUTION*. HF is poisonous!). During this evaporation water is taken up from the air and a reddish-purple solution containing some precipitated mercury(II) chloride remains. The complex was precipitated from this mixture by addition of 70 % perchloric acid (15 ml) followed by a saturated aqueous solution of sodium perchlorate (20 ml). It was then filtered off on a plastic Büchner funnel and washed with water.

For recrystallization the product was dissolved in 0.01 M perchloric acid (1500 ml) preheated to 60 °C. 70 % perchloric acid (40 ml) was added to the cooled, filtered solution. The reddish-purple crystals were filtered off and washed with ice-cold water. After two such recrystallizations the yield was 38 g (73 %). Anal. $[CoF_2(py)_4]ClO_4.\frac{1}{2}H_2O$: Co, C, N, H, Cl. Spectral data in 0.01 M $HClO_4$: $(\varepsilon,\lambda)_{max}$: (27.5,567), (37.8,479), (62.2,371.5), $(\varepsilon,\lambda)_{min}$: (24.0,532), (14.0,423), (20.3,332.5).

3. $[CoF_2(H_2O)(py)_3]ClO_4$. Liquid hydrogen fluoride (100 ml) was cooled in an 800 ml polyethylene beaker by addition of an excess of dry ice in small lumps and finely powdered $[Co(CO_3)Cl(py)_3]$ (40 g, 0.102 mol) was added to the cold mixture. The carbonato complex dissolved slowly with evolution of carbon dioxide gas and formation of a reddish-purple solution. The latter was allowed to stand for 3−4 h with thorough ventilation to attain room temperature. During this time the hydrogen fluoride had almost completely evaporated and a purple product had been formed. The last traces of hydrofluoric acid were removed by extraction with 5 % (v/v) methanol in ether (4 × 200 ml). The sample was then collected on a filter, washed with ether and sucked as dry as possible. This almost dry product was dissolved in 0.012 M perchloric acid (250 ml) and a small amount of brownish impurities and red cobalt(II) fluoride was removed by filtration. Icecold 70 % perchloric acid (50 ml) was then added to the filtrate with stirring and cooling in ice, when purple crystals of $[CoF_2(H_2O)(py)_3]ClO_4$ began to separate immediately. After cooling for one hour the precipitate was filtered off, washed with ice-cold water (3 × 40 ml) and then with 96 % ethanol (40 ml). Drying in air yielded 35.4 g (77 %) of the almost pure perchlorate. This was purified by reprecipitation from perchloric acid: 5 g was dissolved in 0.012 M perchloric acid (700 ml) at room temperature. 70 % perchloric acid (70 ml) was added to the filtered solution with stirring and cooling in ice. After cooling for one hour the precipitate was filtered off and washed as described above. The yield was 3.65 g (73 %). The sample reprecipitated three times gave a constant absorption spectrum, indicating that only one isomer was present. Anal. $[CoF_2(H_2O)(py)_3]ClO_4$: Co, C, N, H, F, Cl. Spectral data in 0.1 M HCl: $(\varepsilon,\lambda)_{max}$: (40.5,520), (48.0,381). $(\varepsilon,\lambda)_{min}$: (10.2,443), (23.7,344.5).

4. *trans*-$[CoF_2(py)_4]ClO_4.\frac{1}{2}H_2O$. Crude $[CoF_2(H_2O)(py)_3]ClO_4$ (4.00 g, 8.86 mmol) was added to pyridine (15 ml) in a conical flask equipped with a condenser and a calcium chloride tube. The sample dissolved to give a reddish-purple solution and on heating at 70 °C for 15 min the solution turned red owing to the formation of the cation *trans*-$[CoF_2(py)_4]^+$. Cooling in ice caused precipitation of large red crystals of the perchlorate salt. To the cold solution was then added ether (40 ml) to obtain a quantitative precipitation. The product was filtered off, washed thoroughly with ether and dried in air. Yield 4.5 g. The crude product was reprecipitated once as described in Preparation 2. Drying in air yielded 2.82 g (61 %). Anal. $[CoF_2(py)_4]ClO_4.\frac{1}{2}H_2O$: Co, C, N, H, F, Cl. Spectral data as those given in Preparation 2.

1. Werner, A. and Feenstra, R. *Ber. Dtsch. Chem. Ges. 39* (1906) 1543.
2. Springborg, J. and Schäffer, C. E. *Acta Chem. Scand. 27* (1973) 3312.
3. Glerup, J., Mønsted, O. and Schäffer, C. E. *Inorg. Chem. 15* (1976) 1399.
4. Glerup, J., Josephsen, J., Michelsen, K., Pedersen, E. and Schäffer, C. E. *Acta Chem. Scand. 24* (1970) 247.
5. Glerup, J. and Schäffer, C. E. *Inorg. Chem. 15* (1976) 1408.
6. Springborg, J. *Unpublished results.*

Received August 1, 1978.

Acta Chemica Scandinavica A 32 (1978) 675–680

A Discussion of the Expansivity and the Compressibility of Liquid Water

AASE HVIDT

Chemistry Laboratory III, H. C. Ørsted Institute, Universitetsparken 5, DK-2100 Copenhagen Ø, Denmark

The expansivity, the compressibility and the internal pressure of water and other liquids at atmospheric pressure are compared. The anomalous behaviour of water is discussed on the basis of the assumption that structural equilibria exist in liquid water for which $\Delta H^{\ominus}\Delta V^{\ominus}<0$. The discussion supports the conclusion that the structural transitions predominant in water at the lower temperatures are highly cooperative long-range interactions. It is tentatively suggested that the bulky low-energy state of water resembles "normal" liquids, but that the dense, high-energy state is atypical of liquids at atmospheric pressure.

In a recent paper[1] it is pointed out that a great many of the theories of liquid water presented with the years are essentially elaborations of the simple model of water proposed by Röntgen[2] nearly one hundred years ago. Röntgen suggested that liquid water is an "aggregate" of two molecular species. One is an "icelike" form which upon heating is converted to the other (less bulky) form. In Ref. 1 the model is described as two structural components of water in rapid equilibrium

$$B \rightleftharpoons D \qquad (1)$$

B is a bulky ("icelike") form of a lower energy than the dense ("normal") form, D.

Experimental data on the variation of the enthalpy and the volume of water with temperature and pressure are discussed in Ref. 1 on the basis of the Röntgen model, and the discussion leads to the statement that "it is difficult to avoid the conclusion that the model is inadequate".[1]

The present paper follows the lines of the approach suggested in Ref. 1, with only slight modifications. It is the aim of this sequel of the discussion to illustrate that available thermodynamic data on water are in accordance with the basic idea of Röntgen's model, that equilibria exist in liquid water, for which the changes in standard volume and enthalpy are of the opposite sign. The terms "icelike" and "normal" must, however, be used with care in attempts to characterize the two forms of water more closely.

EXPERIMENTAL DATA

Available experimental data on liquid water at atmospheric pressure are shown in Figs. 1–3. The (isobaric) thermal expansivity (the coefficient of thermal expansion), α, the (isothermal compressibility, κ, and the internal pressure, P_i, are plotted

$$\alpha = V^{-1}(\partial V/\partial T)_P \qquad (2)$$

$$\kappa = -V^{-1}(\partial V/\partial P)_T \qquad (3)$$

$$P_i = (\partial U/\partial V)_T = T(\partial S/\partial V)_T - P \qquad (4)$$

as functions of the temperature, see eqns. (2)–(4). Data on a few organic liquids are included in the figures for comparison with water.

Atypical features of water at atmospheric pressure, illustrated in Figs. 1–3, are

1. The thermal expansivity is below the normal range, and *negative* at temperatures below 4 °C.

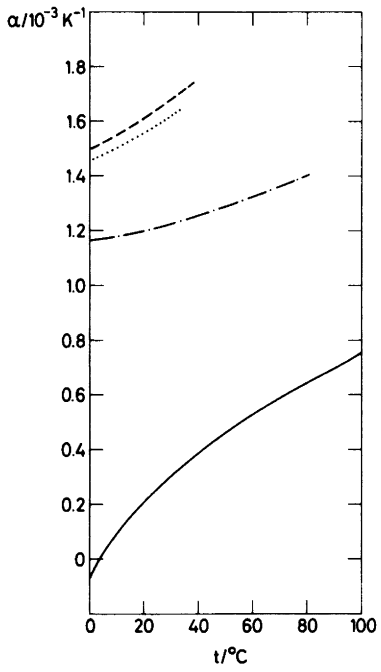

Fig. 1. Available data on the thermal expansivity at atmospheric pressure of water[3] ——, benzene[4] –·–, *n*-pentane[4] ..., and diethyl ether[4] – – –.

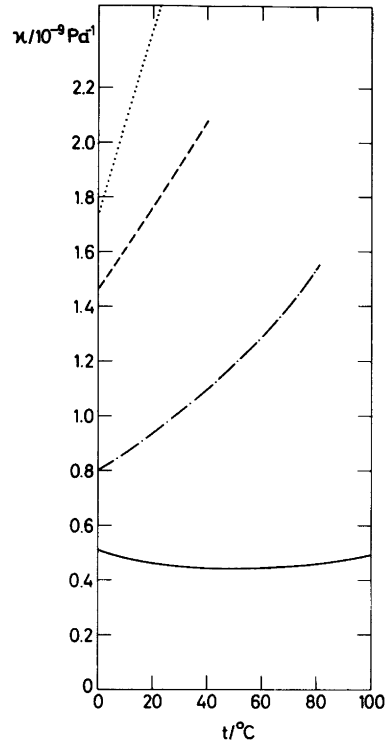

Fig. 2. Available data on the compressibility at atmospheric pressure of water[3] – – –, benzene[5] –·–, *n*-pentane[6] ..., and diethyl ether[6] – – –.

2. The compressibility is unusually low, and *decreases* with increasing temperature ($\partial\kappa/\partial T<0$) at temperatures below 40 °C.

3. The internal pressure *increases* with increasing temperature from *negative* values below 4 °C to values *above* the normal range at temperatures above 60 °C.

The internal pressure of liquids at atmospheric pressure is normally about 300×10^6 Pa (*i.e.* $P_i \gg P \cong 0.1\times10^6$ Pa), slightly decreasing with increasing temperature. The negative values of P_i observed for water reflect the phenomenon that what keeps water molecules together in liquid water below 4 °C is not an energetic cohesion between the molecules ($\partial U/\partial V<0$), but a positive entropic contribution to the free energy upon expansion ($-T(\partial S/\partial V)>0$.

In the following, this anomalous behaviour of liquid water is tentatively discussed on the basis of the assumption that structural equilibria like (1) exist in liquid water, for which $\Delta H^{\ominus}>0$.

THE MODEL

The equilibrium (1) is thought to be due to the ability of water molecules to associate through hydrogen bonding, and as such it is tentatively expressed as

$$\underset{\text{B}}{(H_2O)_n} \rightleftharpoons \underset{\text{D}}{nH_2O}, \qquad \Delta H^{\ominus}>0,\ \Delta V^{\ominus}<0. \tag{5}$$

The dissociation of a polymer of water to monomers does proceed through a series of reactions

$$(H_2O)_{i+1} \rightleftharpoons H_2O_i + H_2O \qquad i=1,2,3,\ldots \tag{6}$$

but due to the kind of cooperation intrinsic to water association (in the sense that hydrogen bonding promotes hydrogen bonding) it is assumed that the distribution of *i*-mers in liquid water has a sufficiently sharp maximum (for $i=n$), that the formulation (5) is a reasonably good approximation of the reactions (6).

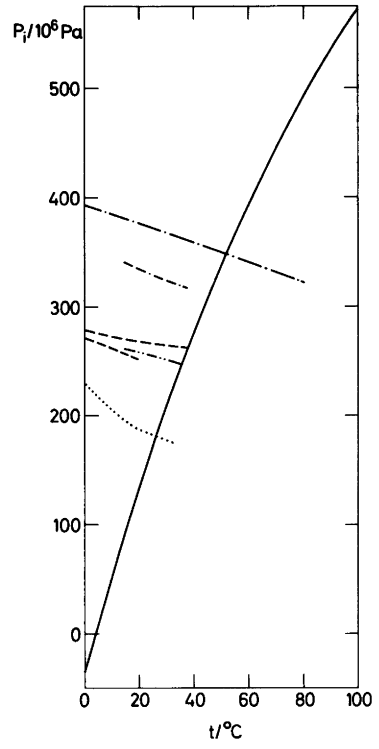

Fig. 3. The internal pressure $P_i = T\alpha/\kappa - P$ calculated on the basis of available data on water[3] ——, benzene[4,6,7] –·–, *n*-pentane[4,6] ..., diethyl ether[4,6,8] – – –, heptane[7] –··–, and acetone[7] – – ·– –.

In accordance with the procedure applied in Ref. 1 the molar volume and the molar enthalpy of water are expressed as

$$V = xV_D + (1-x)V_B = V_B + x\Delta V \tag{7}$$

and

$$H = xH_D + (1-x)H_B = H_B + x\Delta H \tag{8}$$

x is the fraction of water molecules present as monomers. $\Delta V = V_D - V_B$ (<0), and $\Delta H = H_D - H_B$ (>0) are the differences between the molar volume and the molar enthalpy, respectively, of water in the monomeric (dense) and in the associated (bulky) state. The relation between ΔV, ΔH and $\Delta V^\ominus$, $\Delta H^\ominus$ of eqn. (5) is $\Delta V^\ominus = n\Delta V$ and $\Delta H^\ominus = n\Delta H$.

The temperature and the pressure dependence of the volume obtained from (7) and (8) are

$$\frac{\partial V}{\partial T} = \underbrace{x\frac{\partial V_D}{\partial T} + (1-x)\frac{\partial V_B}{\partial T}}_{\text{static}} + \underbrace{\Delta V\frac{\partial x}{\partial T}}_{\text{relaxational}} \tag{9}$$

and

$$\frac{\partial V}{\partial P} = \underbrace{x\frac{\partial V_D}{\partial P} + (1-x)\frac{\partial V_B}{\partial P}}_{\text{static}} + \underbrace{\Delta V\frac{\partial x}{\partial P}}_{\text{relaxational}} \tag{10}$$

The sum of the first two terms on the r.h.s. of these expressions (and of similar expressions following) is denoted the *static* contribution to the derivative, and the last term is denoted the *relaxational* contribution.

The equilibrium constant of (5) is

$$\frac{[H_2O]^n}{[(H_2O)_n]} = K_c/(\text{mol dm}^{-3})^{n-1}$$

or

$$\frac{x^n}{(1-x)/n} = K_c V^{n-1} = K_x \tag{11}$$

In the following, the volume dependence of K_x is ignored and the subscript x of this constant is omitted, $K_x = K$.

It follows from (11) that

$$\frac{\partial \ln K}{\partial x} = \frac{n(1-x)+x}{x(1-x)} \tag{12}$$

so that the terms $\frac{\partial x}{\partial T}$ and $\frac{\partial x}{\partial P}$ in (9) and (10) may be expressed as

$$\frac{\partial x}{\partial T} = \frac{\partial x}{\partial \ln K}\frac{\partial \ln K}{\partial T} = \frac{x(1-x)}{n(1-x)+x}\cdot\frac{n\Delta H}{RT^2} = F(n,x)\frac{\Delta H}{RT^2} \tag{13}$$

and

$$\frac{\partial x}{\partial P} = \frac{\partial x}{\partial \ln K}\frac{\partial \ln K}{\partial P} = -\frac{x(1-x)}{n(1-x)+x}\frac{n\Delta V}{RT} = -F(n,x)\frac{\Delta V}{RT} \tag{14}$$

where $F(n,x) = nx(1-x)/[n(1-x)+x]$.

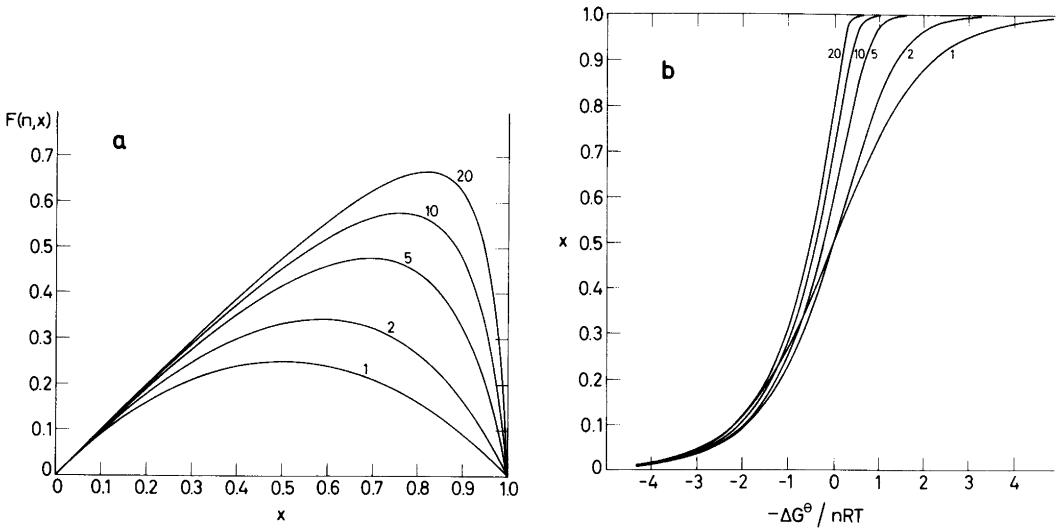

Fig. 4. a. $F(n,x)=nx(1-x)/[n(1-x)+x]$ calculated as a function of x for $n=1$, 2, 5, 10 and 20. $F(n,x)$ enters the expressions (15) and (16) in the text. *b.* x as a function of $n^{-1}\ln K=-\Delta G^{\ominus}/nRT$, calculated according to eqn. (11) in the text for $n=1$, 2, 5, 10 and 20. x is the fraction of water molecules present in the dense, monomeric state. $\Delta G^{\ominus}$ and n refer to eqn. (5). The values of n are indicated in the figure.

Expressions of the thermal expansivity, α, and the compressibility, κ, derived from eqns. (11)–(14), are

$$\alpha = \frac{1}{V}\frac{\partial V}{\partial T} = \frac{x}{V}\frac{\partial V_D}{\partial T} + \frac{(1-x)}{V}\frac{\partial V_B}{\partial T} + F(n,x)\frac{\Delta V}{V}\frac{\Delta H}{RT^2} = \phi_D\alpha_D + \phi_B\alpha_B + F(n,x)\frac{\Delta V}{V}\frac{\Delta H}{RT^2} \quad (15)$$

and

$$\kappa = -\frac{1}{V}\frac{\partial V}{\partial P} = \phi_D\kappa_D + \phi_B\kappa_B + F(n,x)\frac{\Delta V}{V}\frac{\Delta V}{RT} \quad (16)$$

where $\phi_D=xV_D/V$ and $\phi_B=(1-x)V_B/V$ are the volume fractions of water in the monomeric and the associated state, respectively.

The function $F(n,x)=n\partial x/\partial \ln K$ as a function of x, and x as a function of $n^{-1}\ln K=-\Delta G^{\ominus}/nRT$, are shown in Fig. 4 for various values of n. Straightforward calculations from (11) show that $F(n,x)$, or $\partial x/\partial(n^{-1}\ln K)$, exhibits a maximum ($F(n,x)=n/(1+n^{\frac{1}{2}})^2$) for $x/(1-x)=n^{\frac{1}{2}}$, *i.e.* for $x=n^{\frac{1}{2}}/(1+n^{\frac{1}{2}})$.

COMPARISON BETWEEN THE EXPERIMENTAL DATA AND THE MODEL

As already discussed by Röntgen[2] the negative expansivity of water below 4 °C is a strong indication that equilibria, for which $\Delta H^{\ominus}\Delta V^{\ominus}<0$, play an important role in the volumetric behaviour of liquid water. Eqn. (5) is undoubtedly an oversimplification of the equilibria present in water, but this simple model may suffice as a starting point in a chemical-thermodynamic approach to the peculiar properties of water. The main purpose of the treatment suggested in this paper is to outline the possible influence of equilibria like (5) on the temperature dependence of the thermal expansivity and the compressibility of liquid water.

In eqn. (15) the thermal expansivity, α, is expressed as a sum of a static and a relaxational contribution. Experimental data on water (Fig. 1) indicate that at temperatures below 4 °C the (negative) relaxational contribution to α is numerically larger than the (positive) static one. The temperature dependence of α, however, suggests that the relaxational contribution vanishes rapidly with increasing temperature, such as is the case if, at 0 °C, $F(n,x)$ in eqn. (15) is about maximal (Fig. 4) or $\Delta G^{\ominus}/nRT$ of the equilibrium (5) is small and

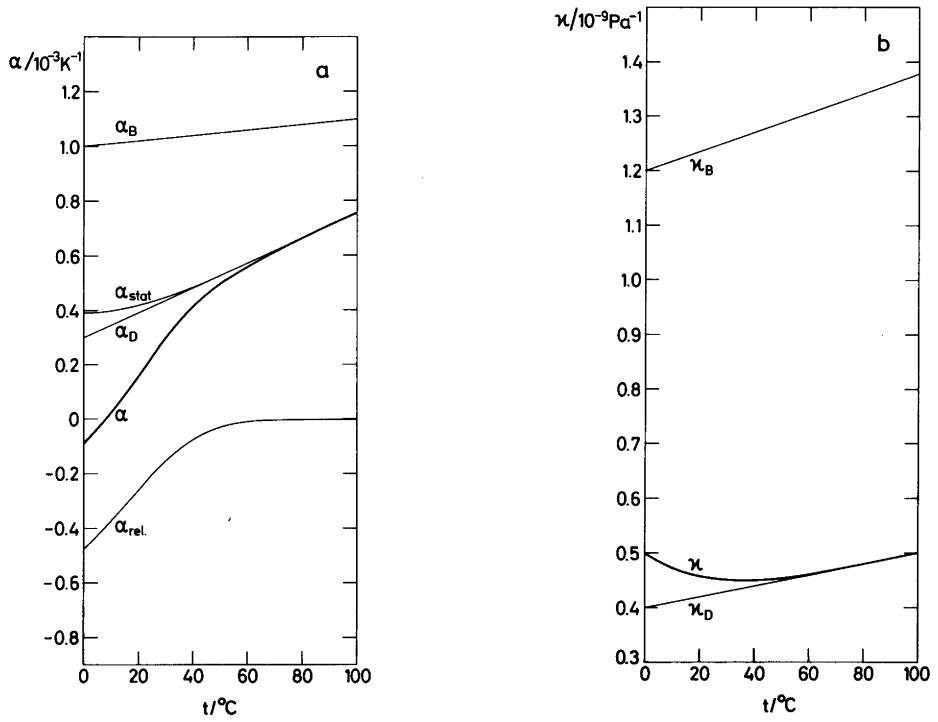

Fig. 5. The temperature dependence of the thermal expansivity (a) and the compressibility (b) of the water model calculated according to eqn. (15) and (16) for the following values of the thermodynamic quantities mentioned in the text: $\Delta H^{\ominus}=75$ kJ mol^{-1}, $\Delta S^{\ominus}=300$ J K^{-1} mol^{-1}, $n=15$, $\alpha_B=(1+10^{-3}t)10^{-3}$K^{-1}, $\alpha_D=0.3(1+1.5\times10^{-2}t)10^{-3}$ K^{-1}, $\kappa_B=1.2(1+1.5\times10^{-3}t)$ 10^{-9} Pa^{-1}, $\kappa_D=0.4(1+2.5\times10^{-3}t)$ 10^{-9} Pa^{-1}. α_{stat} is the static contribution to the expansivity, $\alpha_{stat}=\phi_D\alpha_D+\phi_B\alpha_B$, and α_{rel} is the relaxational contribution, $\alpha_{rel}=F(n,x)\,\frac{\Delta H}{V}\,\frac{\Delta H}{RT^2}$ (see eqn. (15)). As it is explained in the text the relaxational contribution to the compressibility is vanishingly small.

negative, and if $\Delta H^{\ominus}=50-100$ kJ mol^{-1}, *e.g.* $\Delta H=5-10$ kJ mol^{-1} and $n=10$ (Fig. 5).

Fig. 5 illustrates the functions α and κ, calculated according to the eqns. (15) and (16) for the following values of the thermodynamic parameters of eqn. (5): $\Delta H^{\ominus}=75$ kJ mol^{-1} ($n=15$, $\Delta H=5$ kJ mol^{-1}), $\Delta S^{\ominus}=300$ J K^{-1} mol^{-1}, and $\Delta V^{\ominus}=-30$ cm^3 mol^{-1} ($\Delta V/V=-0.1$). For these values of the thermodynamic parameters x varies from 0.89 at 0 °C to practically one at 100 °C. The relaxational contribution to κ is vanishingly small ($F(n,x)(\Delta V)^2/VRT<5\times10^{-12}$ Pa^{-1} in eqn. (16)).

In the calculations illustrated in Fig. 5 it is assumed that the expansivity and the compressibility of water in the bulky state are within the normal range for liquids at atmospheric pressure, $\alpha_B=10^{-3}\times(1+10^3t)K^{-1}$ and $\kappa_B=1.2\times10^{-9}(1+1.5\times10^{-3}t)$ Pa^{-1}, but the expansivity and the compressibility of water in the dense state are assumed to be smaller, and more strongly dependent on the temperature, $\alpha_D=0.3\times10^{-3}(1+1.5\times10^{-2}t)K^{-1}$ and $\kappa_D=0.4\times10^{-9}(1+2.5\times10^{-3}t)$ Pa^{-1}. Had it not been for the tradition, which dates back to Röntgen,[2] to call the bulky state of water "icelike" and the dense state "normal", these assumptions might not have seemed surprising. Bulky liquids are generally more compressible than dense ones, and flexible chains of associated water molecules do in many respects resemble the molecules present in normal liquids. The atypical liquid state of water is the dense, monomeric state; with respect to volume properties this state appears "solid-like", but with respect to

enthalpy or entropy it seems rather "gas-like".

A comparison between the calculated curves in Fig. 5 and the experimental curve in Figs. 1 and 2 shows a fairly good agreement between the calculated and the experimental data. No attempt has been made to estimate the values of the parameters of the model by a numerical fitting to the experimental data. The choice of values underlying the curves in Fig. 5 is based on a judgement in great outline of the data in Figs. 1–3, combined with the observation[1,9] that at pressures above 5×10^8 Pa (5000 atm) the thermal expansivity of water at 25 °C is about "normal". For $\Delta V^\ominus = -30$ cm^3 mol^{-1}, we have $\partial \ln K/\partial P = -\Delta V^\ominus/RT \cong 10^{-8}$ Pa^{-1}, so an increase in pressure of 5×10^8 Pa, or more, will significantly perturb the equilibrium (5) in favour of the dense state. This dense state of liquid water apparently resembles other liquids elevated pressures.[1,9]

The presence in liquid water of equilibria for which $\Delta S^\ominus = 300$ J K^{-1} mol^{-1} and $\Delta V^\ominus = -30$ cm^3 mol^{-1}, *i.e.* $\Delta S^\ominus \Delta V^\ominus = -10$ J K^{-1}cm^{-3} $= -10^7$Pa K^{-1} may counterbalance the positive value of $\partial S/\partial V \cong 10^6$Pa K^{-1} which is common of liquids at 0 °C (see Fig. 3 and eqn. (4)), and thus explain the negative internal pressure of water at this temperature. The value of $\Delta H^\ominus = 75$ kJ mol^{-1} makes $\Delta G^\ominus$ slightly negative at 0 °C, and accounts for the temperature dependence of α and P_i.

The equilibria are assumed to be associations-dissociations of the water molecules through hydrogen bonding. Estimates of the strength of a hydrogen bond between water molecules are uncertain,[10] but the above-mentioned values of $\Delta H^\ominus$, $\Delta S^\ominus$ and $\Delta V^\ominus$ seem to show, that the structural transitions predominant in liquid water at the lower temperatures involve many hydrogen bonds ($n = 15$ in eqn. (5)). In the primitive model of water here discussed it is implicitly assumed that n is independent of the temperature, and the presence of dimers, trimers *etc.* of water is ignored. There is all experimental evidence that lower associates of the molecules exist in liquid water,[10] and they ought to be taken into account in more refined water models.[11,12]

CONCLUSIONS

Experimental data on the expansivity and the compressibility of water indicate that the molecules in liquid water fluctuate between bulky low-energy states and dense high-energy states. The large changes in enthalpy, entropy and volume of the fluctuations predominant at the lower temperatures suggest that the fluctuations are due to highly co-operative, long-range structural transitions of the water molecules. Judged from the experimental data considered, the bulky state of water resembles other liquids at atmospheric pressure, but the dense state is atypical.

REFERENCES

1. Kauzmann, W. In Alfsen, A. and Berteaud, A. J., Eds., *L'Eau et les Systèmes Biologiques*, Editions du Centre National de la Recherche Scientifique, 15, quai Anatole-France, 75700 Paris, (1976), p. 63.
2. Röntgen, W. C. *Annalen der Physik und Chemie, Neue Folge 45, 281* (1892) 91.
3. Kell, G. S. *J. Chem. Eng. Data 20* (1975) 97.
4. Landolt-Börnstein *Physikalisch-Chemische Tabellen II, 5. Auflage* (1923) 1232.
5. *Handbook of Chemistry and Physics 55* (1974–1975) F-16.
6. Landolt-Börnstein *Physikalisch-Chemische Tabellen I, 5. Auflage* (1923) 97–100.
7. Westwater, W., Frantz, H. W. and Hildebrand, J. H. *Phys. Rev. 31* (1928) 135.
8. Hildebrand, J. H. *Phys. Rev. 34* (1929) 984.
9. Frank, H. S. *Science 169* (1970) 635.
10. Eisenberg, D. and Kauzmann, W. *The Structure and Properties of Water*, Oxford Univ. Press, Oxford 1969.
11. Némethy, G. and Scheraga, H. A. *J. Chem. Phys. 36* (1962) 3382.
12. Owicki, J. C. and Scheraga, H. A. *J. Am. Chem. Soc. 99* (1977) 7403.

Received April 25, 1978.

Acta Chemica Scandinavica A 32 (1978) 681 – 688

A Large-angle X-Ray Scattering Investigation of Some Polynuclear Molybdoarsenate Complexes in Aqueous Solution

GEORG JOHANSSON,[a] LAGE PETTERSSON[b] and NILS INGRI[b]

[a] Department of Inorganic Chemistry, Royal Institute of Technology, S-100 44 Stockholm 70, Sweden and [b] Department of Inorganic Chemistry, University of Umeå, S-901 87 Umeå, Sweden

The structures of heteropoly complexes formed in aqueous $H^+ - MoO_4^{2-} - HAsO_4^{2-}$ solutions have been investigated by large-angle X-ray scattering (LAXS) measurements. The complexes $(H^+)_p(MoO_4^{2-})_9(HAsO_4^{2-})$, with $p = 14-16$, present at Mo/As ratios ~9 according to results of potentiometric measurements, have been shown to have the same basic structure as the discrete units $Mo_9AsO_{31}(OH_2)_3^{3-}$ found in the crystalline compound $Na_3Mo_9AsO_{31}(OH_2)_3.12-13H_2O$. The complex $(H^+)_{12}(MoO_4^{2-})_6(HAsO_4^{2-})_2$, which according to potentiometric measurements should be dominant in acid solutions at Mo/As ratios ~3, is shown by the scattering data to lack long Mo – Mo distances and, therefore, may contain fewer than six Mo atoms.

In the aqueous system $H^+ - MoO_4^{2-} - HAsO_4^{2-}$, heteropoly complexes are formed according to the reaction

$$pH^+ + qMoO_4^{2-} + rHAsO_4^{2-} \rightleftharpoons (H^+)_p(MoO_4^{2-})_q(HAsO_4^{2-})_r$$

Potentiometric and spectrophotometric measurements by Pettersson[1,2] have been interpreted by assuming the formation of two series of complexes. For Mo/As ratios ~9 the predominant complexes found are $(H^+)_p(MoO_4^{2-})_9(HAsO_4^{2-})$ with $p = 14$, 15, 16 and 17. For Mo/As ratios ~3 the species $(H^+)_p(MoO_4^{2-})_6(HAsO_4^{2-})_2$ with $p = 10$, 11 and 12, and, to a minor extent, $(H^+)_8(MoO_4^{2-})_5(HAsO_4^{2-})_2$, are dominant. For the analogous system $H^+ - MoO_4^{2-} - HPO_4^{2-}$ potentiometric and spectrophotometric measurements were explained by a similar set of complexes, excluding those containing six molybdenum atoms.[2,3] In the following, the complexes formed will often the denoted by their p, q and r values only, thus (14,9,1) will indicate the complex $(H^+)_{14}(MoO_4^{2-})_9(HAsO_4^{2-})$ or, written differently, $Mo_9AsO_{31}(OH)_3^{6-}$, which is equivalent because the number of water molecules in the formula cannot be determined from equilibrium analyses in aqueous solution.

Crystals containing discrete (17,9,1) complexes as well as discrete (8,5,2), (9,5,2) and (10,5,2) complexes have been obtained from the molybdophosphate system and the crystal structures have been determined. The structures of the complexes in solution have been shown by X-ray scattering measurements to be basically the same as those in the crystals.[4,5] Therefore, the correct formula for a (17,9,1) complex is $Mo_9PO_{31}(OH_2)_3^{3-}$, $[Mo_9PO_{31}(OH_2)_3^{3-} + 6\ H_2O = (H^+)_{17}(MoO_4^{2-})_9(HPO_4^{2-})]$, and for an (8,5,2) complex $Mo_5P_2O_{23}^{6-}$, $[Mo_5P_2O_{23}^{6-} + 5H_2O = (H^+)_8(MoO_4^{2-})_5(HPO_4^{2-})_2]$. Also from the molybdoarsenate system crystals can be obtained which according to a crystal structure determination contain discrete (17,9,1) complexes having the same structure as the corresponding molybdophosphate.[6] It has not, however, been possible to prepare crystals containing (p,6,2) or (p,5,2) complexes from the molybdoarsenate solutions.

In order to obtain information on the structures of the molybdoarsenate complexes in solution, the X-ray scattering has been measured from solutions which, according to results from the potentiometric measurements, should contain optimal amounts of the different complexes.

Table 1. Compositions of solutions.

	A (14,9,1)	B (15,9,1)	C (15,9,1)	D (16,9,1)	E (12,6,2)	F (12,6,2)	G (8,5,2)	H (8,7,0)
Concentrations in mol/l								
Mo	1.608	1.608	1.600	1.600	1.608	1.400	1.770	2.040
As	0.178	0.178	0.178	0.178	0.536	0.467	–	–
Na	1.072	0.893	3.556	3.556	1.072	3.733	4.250	4.080
Cl	–	–	2.667	2.844	–	2.800	2.120	2.330
O	58.4	58.3	61.8	61.9	58.8	62.1	69.5	61.9
H	105.2	105.1	90.9	89.8	104.1	90.0	91.7	91.1
P	–	–	–	–	–	–	0.710	–
Number of atoms in the unit of volume, V								
Mo	1	1	1	1	1	1	1	1
As	0.111	0.111	0.111	0.111	0.333	0.333	–	–
Na	0.667	0.556	2.223	2.223	0.667	2.666	2.401	2.000
Cl	–	–	1.667	1.778	–	2.000	1.198	1.142
O	36.3	36.8	38.6	38.7	36.5	47.3	35.3	30.3
H	65.4	65.4	56.8	56.1	64.8	64.3	51.8	44.7
P	–	–	–	–	–	–	0.401	–
$V/Å^3$	1032.7	1032.7	1037.8	1037.8	1032.7	1186.1	938.2	814.0
$\rho_0/el^2\,Å^{-3}$	161.3	159.7	207.1	208.4	168.4	241.4	196.2	168.9

EXPERIMENTAL

The compositions of the six solutions, A – F, used for the X-ray scattering measurements are given in Table 1. The total concentration of molybdenum was kept as high as possible and the composition of each solution was chosen so as to yield an optimal amount of one of the complexes. The best compositions were selected by means of the stability constants given by Pettersson [1] (Fig. 1). These constants were derived from potentiometric measurements performed in solutions containing 3 M $Na(ClO_4)$ as the ionic medium but with the highest molybdate concentration less than about one tenth of that used here. For the analysis of the scattering data two reference solutions, G and H, were used (Table 1). As shown in a previous work [4] all molybdenum in these solutions should occur as $Mo_5P_2O_{23}^{6-}$ (G) or as $Mo_7O_{24}^{6-}$ (H) complexes, the structures of which are known.

Preparation of solutions: The solutions were prepared either by adding a standarized NaOH solution to weighed amounts of MoO_3 (Merck *p.a.*) and $Na_2HAsO_4.7H_2O$ (Merck *p.a.*) (solutions A, B and E), or by adding a standardized $HClO_4$ solution to weighed amounts of $Na_2MoO_4.2H_2O$ (Mallinckrodt *p.a.*) and $Na_2HAsO_4.7H_2O$ (Merck *p.a.*) (solutions C, D and F). The first procedure was used for the (14,9,1) solution (A) in order to prevent a precipitation of isopolymolybdates, and for one

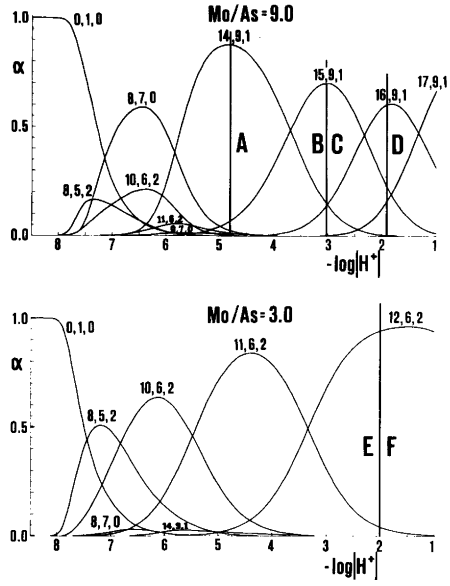

Fig. 1. The fraction, α, of molybdenum bound in different complexes as a function of $-\log[H^+]$. The total concentration of molybdenum is 1.60 M. The stability constants given by Pettersson [1] have been used for the calculation. The compositions of the solutions, A – F, used for the scattering measurements are indicated by vertical lines.

of the (12,6,2) solutions (E) in order to reach the same total molybdenum concentration (1.60 M) as for the other solutions. With the second procedure the molybdenum concentration of the (12,6,2) solution could not be increased beyond about 1.40 M (F). Two (15,9,1) solutions having equal concentrations of molybdate were prepared, one (B) by means of the first procedure and therefore holding a low concentration of Na^+ with no ClO_4^- and the other (C) by the second procedure resulting in a high concentration of $NaClO_4$. They were both subjected to diffraction measurements in order to study the influence of the presence of sodium perchlorate in the solutions.

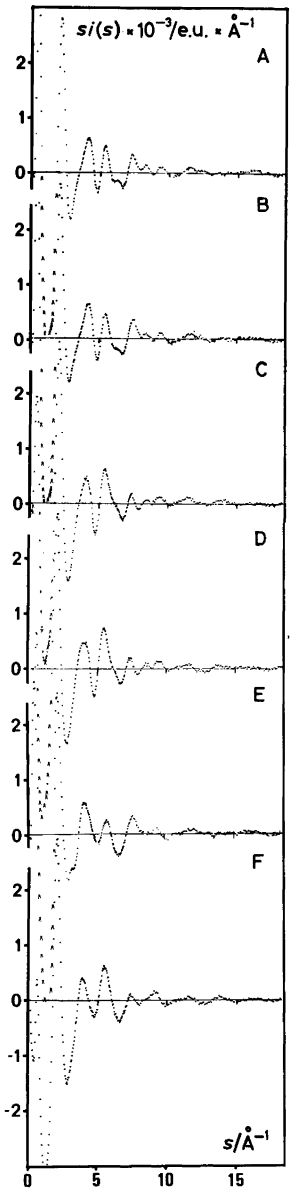

Fig. 2. Reduced intensity values, $si(s)$, as a function of s for the six solutions investigated.

X-Ray measurements. The scattering measurements and the treatment of the X-ray data were carried out as described in previous papers.[4,7-9] Ag$K\alpha$ radiation ($\lambda = 0.5608$ Å) was used and the scattering data were normalized to a stoichiometric unit of volume containing one molybdenum atom. The scattering factors, f_i, were taken from the same sources as in the previous work.[4]

The reduced intensity functions, $i(s) = I(s) - \sum_i f_i^2$, multiplied by $s = 4\pi \sin\theta/\lambda$ are shown in Fig. 2 for the six solutions investigated. The radial distribution functions were calculated according to the expression $D(r) = 4\pi r^2\rho_0 + (2r/\pi)\int_0^{s_{max}} si(s)M(s)\sin(rs)ds$ with $M(s) = \{f_{Mo}^2(0)/f_{Mo}^2(s)\}\exp(-0.01\,s^2)$.[9]

The functions $D(r) - 4\pi r^2\rho_0$ for the six molybdoarsenate solutions, A–F, and the two reference solutions, G and H, are compared in Fig. 3.

ANALYSIS OF DATA

A comparison between the distribution functions (Fig. 3) for the solutions A to D, *i.e.* those solutions that according to the potentiometric measurements (Fig. 1) should contain the complexes (14,9,1), (15,9,1), or (16,9,1), shows no significant differences apart from those that can be ascribed to the presence of perchlorate in two of the solutions (C and D) but not in the other two (A and B). This is consistent with the deductions from the potentiometric measurements that the dominant complexes in these solutions differ only in the number of protons.[1]

The two solutions E and F, which according to the same investigation [1] should contain the complex (12,6,2) also are similar apart from differences ascribable to the presence of perchlorate in solution F but not in solution E.

Because of these similarities the following analysis will be limited to only two of the solutions: C, containing the (15,9,1) complex, and F containing the (12,6,2) complex. Both of these solutions contain perchlorate which makes their compositions correspond more closely to those of the two reference solutions G and H (Table 1).

A comparison between the distribution functions for the (15,9,1) solution (C) and a corresponding

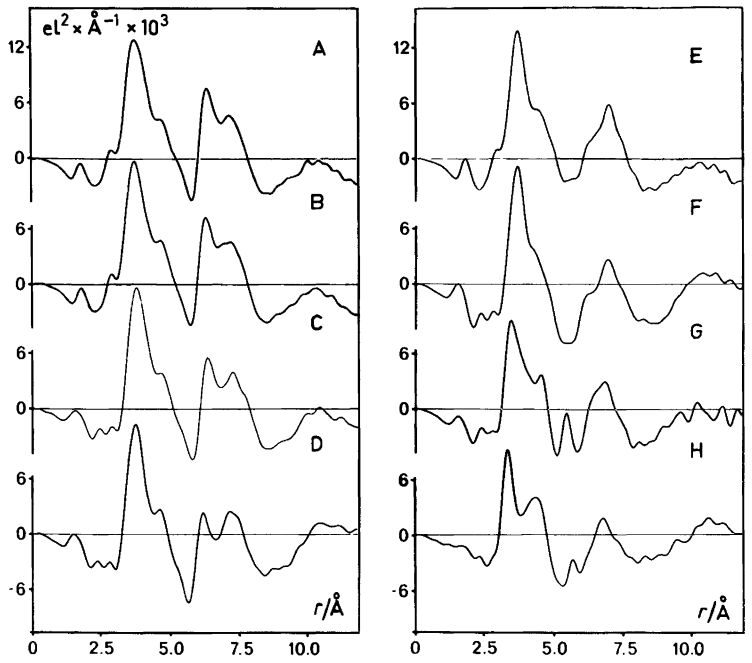

Fig. 3. The functions $D(r)-4\pi r^2\rho_0$ for the six investigated solutions of the molybdoarsenate system (A – F) and for the two reference solutions (G and H).

solution for the phosphate system, previously shown[5] to contain the molybdenum bonded in Mo_9PO_{34} groups, is shown in Fig. 4 together with the shape functions calculated from the crystal structure parameters for the complexes $Mo_9AsO_{31}(OH_2)_3^{3-}$ [6] and $Mo_9PO_{31}(OH_2)_3^{3-}$.[10] It is obvious that the distribution function for the arsenate solution shows the features expected for a dominant complex of this type.

From Fig. 3 a similar comparison can be made between the (12,6,2) solution (F) and a corresponding solution in the phosphate system (G), previously shown to contain all molybdenum bonded in $Mo_5P_2O_{23}^{6-}$ complexes. The two curves do not agree and cannot, therefore, correspond to similar complexes. This is consistent with the conclusions from the potentiometric measurements.

In order to separate, as far as possible, the intramolecular interactions of the unknown molybdoarsenate complexes from those of other interactions in the solution a procedure was used which has been described in a previous paper.[5] It makes use of the scattering data from a closely related reference solution containing complexes for which

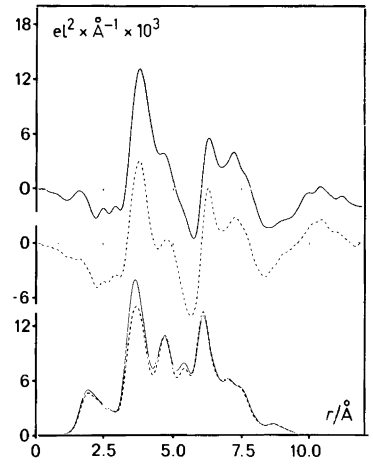

Fig. 4. A comparison between the $D(r)-4\pi r^2\rho_0$ functions for a (15,9,1) solution in the molybdoarsenate system (solid line) and in the phosphate system (dashed line). In the lower part of the figure are given the shape functions, calculated from the crystal structure parameters, for an Mo_9AsO_{34} group (solid line) and an Mo_9PO_{34} group (dashed line).

the structures are known. A theoretical distribution curve can be calculated for this solution, if a suitable approximation to the intermolecular interactions can be found, for example by assuming the complexes to occupy spherical holes in an evenly distributed electron density. Deviations from the distribution function calculated from the experimental intensities result from intermolecular interactions not taken into account by the idealized model. By assuming the same deviations to be applicable to the solution under investigation an approximate shape function for the unknown complex can be derived. The approximations, inherent in this method of derivation, can to some extent be estimated by using more than one reference solution.

Two different reference solutions were used: one, G, previously shown to contain all molybdenum as $Mo_5P_2O_{23}^{6-}$ complexes and the other, H, containing all molybdenum as $Mo_7O_{24}^{6-}$ complexes. The shape functions derived from the scattering data for the solutions C and F with the use of each of the two reference solutions, G and H, are shown in Figs. 5 (CG and CH) and 6 (FG and FH). The parameters used in the derivations are given in Table 2.

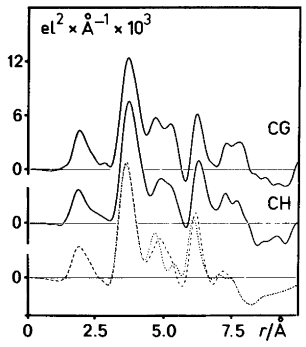

Fig. 5. The shape function (solid lines) for the molybdoarsenate complexes in the (15,9,1) solution (C) derived with the use of the reference solution G (upper drawing) and H (lower drawing). For comparison the shape function for an Mo_9AsO_{34} group calculated from the crystal structure parameters and assuming a radius of 6.4 Å, is also plotted (dotted line). The dashed line gives the corresponding shape function after modifying the Mo positions as described in a previous paper.[5]

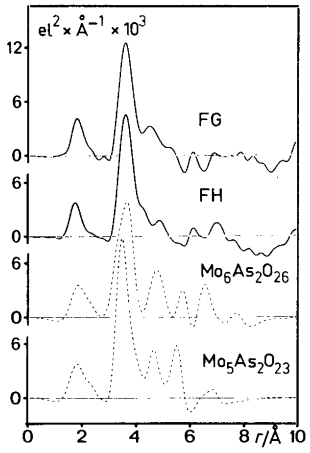

Fig. 6. The shape function (solid lines) for the molybdoarsenate complexes in the (12,6,2) solution (F) derived with the use of the reference solutions G (FG) and H (FH). For comparison the calculated shape functions for two assumed groups $Mo_6As_2O_{26}$ and $Mo_5As_2O_{23}$ (dashed lines), illustrated in Fig. 7, have been plotted.

Table 2. Parameters used in the calculations of shape functions. A formula given within brackets indicates that the corresponding complex has not been found in discrete form in a crystal structure.

Complex	Intramolecular distances	Temperature coefficients [Å²]			Intermolecular interactions	
		Mo–Mo	Mo–O	O–O	R[Å]	B[Å²]
Mo_9AsO_{34}	Ref. 6	0.006	0.006	0.006	6.4	0.02
$Mo_5P_2O_{23}$	Ref. 15	0.004	0.002	0.000	5.0	0.02
$[Mo_5As_2O_{23}]$						
$[Mo_6As_2O_{26}]$	Ref. 1, 11	0.010	0.010	0.010	5.5	0.02
$[Mo_3AsO_{16}]$	Ref. 6	0.006	0.006	0.006	4.5	0.02
Mo_7O_{24}	Ref. 16	0.002	0.004	0.006	5.5	0.02
ClO_4	Cl–O 1.43 Å		0.002	0.002	2.8	0.02
H_2O					1.8	0.02
Na						

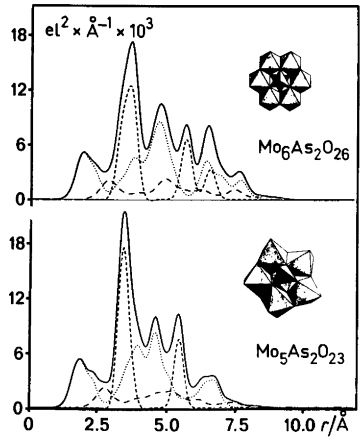

Fig. 7. Calculated shape functions for an $Mo_6As_2O_{26}$ group with the structure suggested by Pettersson (upper drawing) and an $Mo_5As_2O_{23}$ group assumed to have the same structure as $Mo_5P_2O_{23}^{6-}$. The separate contributions from Mo(As) – Mo(As) (short dashes), Mo(As) – O (dots), and O – O (long dashes) interactions are also given.

In agreement with the conclusions already made, the (15,9,1) solution gives a shape function closely similar to that calculated from the crystal structure parameters[6] for the Mo_9AsO_{34} unit. Similar deviations, although apparently somewhat less pronounced, seem to occur as were found for the corresponding phosphate and which were then related to a slight difference between the Mo positions when the complexes occurred in crystals and in solutions.[5]

The (12,6,2) solution leads to a shape function which is characteristically different from that of the (15,9,1) complex. It indicates the absence of long intramolecular distances, which seems to suggest that the (12,6,2) complex is a small complex. A structure for the (*p*,6,2) complexes, based on the structure of $TeMo_6O_{24}^{6-}$ determined by Evans,[11] has been suggested by Pettersson,[1] and is shown in Fig. 7. A (10,6,2) complex with this structure would have the formula $Mo_6As_2O_{26}^{6-}$ and a (12,6,2) complex would correspond to its disprotonated from. Filowitz and Klemperer[12] have interpreted ^{17}O NMR spectra of the anions $(OAs)_2Mo_6O_{24}^{6-}$ and $(C_6H_5As)_2Mo_6O_{24}^{4-}$ in solution to be consistent with such a structure. The same structure has been found for the anions $Mo_8O_{26}^{4-}$ in crystals of $[N(C_4H_9)_4]_4Mo_8O_{26}$[13] and $(CH_3As)_2Mo_6O_{24}^{4-}$ in crystals of $[N(CH_3)_4]_2Na_2[(CH_3As)_2Mo_6O_{24}]\cdot 6H_2O$.[14] The calculated shape function for an $Mo_6As_2O_{26}$ group having this structure is given in Fig. 7 and is compared in Fig. 6 with the shape function derived from the (12,6,2) solution. In the same figures similar comparisons are made for an assumed $Mo_5As_2O_{23}$ group having the same structure as $Mo_5P_2O_{23}^{6-}$, which, in its diprotonated form, would be the dominant complex in the molybdophosphate system at the concentrations used for the (12,6,2) molybdoarsenate solution. It seems unlikely that the structure of the complexes in the (12,6,2) solution can be closely related to any of these complexes, because of the absence in the derived shape function of the long intramolecular interactions, clearly recognizable in the functions calculated for the $Mo_6As_2O_{26}$ and the $Mo_5As_2O_{23}$ structures. No clear indications of long intramolecular interactions are present in the distribution curve, with the possible exception of the small peak at about 6.1 Å that can be observed in both the FG and the FH curves in Fig. 6. Its position corresponds approximately to that of the second largest peak in the shape function for the Mo_9AsO_{34} group (Figs. 4 and 5) and it may, therefore, indicate the presence of a minor amount of this complex in the solution.

Thus, if we accept the conclusions from the potentiometric and the spectrophotometric measurements, that the (12,6,2) solution contains a single dominant molybdoarsenate complex, the scattering data strongly suggest that this complex cannot contain as many as 6 Mo atoms. Because of experimental difficulties the potentiometric measurements could not be carried out over as wide a concentration range as would have been desirable.[1] Therefore, although the ratio between the number of Mo and As atoms in the complex is probably well established, the number of Mo atoms in the complex is less certain. A recalculation of the potentiometric data, using a slightly extended set of data, shows that the inclusion of a (6,3,1) complex in addition to the original (12,6,2) complex improves the agreement between observed and calculated data. The (12,6,2) complex, however, remains the dominant complex.

A (6,3,1) complex would be more consistent with the scattering data since the MoO_6 octahedra can be directly connected without the occurrence of long Mo – Mo distances. Two conceivable structures for a complex of this type are shown in Fig. 9. They have both been cut out from the Mo_9AsO_{34} structure and can be written as $Mo_3AsO_{16}^{9-}$ – or as $H_7Mo_3AsO_{16}^{2-}$ in order to correspond to a

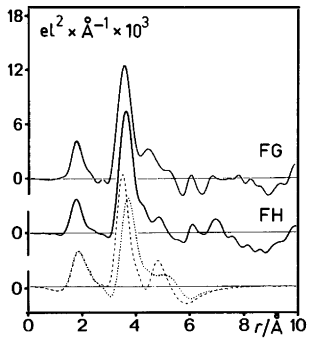

Fig. 8. The shape functions FG and FH (solid lines) compared with calculated shape functions for an Mo_3AsO_{16} group containing edge-sharing MoO_6 octahedra (dashed line) or corner sharing MoO_6 octahedra (dotted line). The assumed structures are illustrated in Fig. 9. Values of 4.5 Å were used for the radii.

(6,3,1) complex. In one of them the three MoO_6 octahedra are joined by common edges and in the other by common corners. The corresponding shape functions calculated with the use of the crystal structure parameters for the Mo_9AsO_{34} group, are compared in Fig. 8 with the shape function derived from the (12,6,2) solution.

CONCLUSIONS

The results of the X-ray scattering measurements on molybdoarsenate solutions are in the main consistent with results previously obtained from potentiometric and spectrophotometric measurements.[1,2] For solutions with Mo/As ratios ~9 the occurrence of complexes with the composition $(H^+)_p(MoO_4^{2-})_9(HAsO_4^{2-})$ has been suggested on the basis of emf data.[1,2] This is consistent with the results of the scattering measurements which show the structure of the complexes in such solutions to be independent of the hydrogen ion concentration and to be basically the same as that of the $Mo_9AsO_{31}(OH_2)_3^{3-}$ complexes found in crystals of $Na_3Mo_9AsO_{31}(OH_2)_3.12-13H_2O$.[6] Similar results have been previously obtained for the molybdophosphate system.[2,3,5] Thus the existence of a series of protonated heteropolymolybdates with the general formula $H_yMo_9O_{31}(OH)_3^{(6-y)-}$, where X stands for pentavalent phosphorus or arsenic, with $y=0-3$, seems to be firmly established.

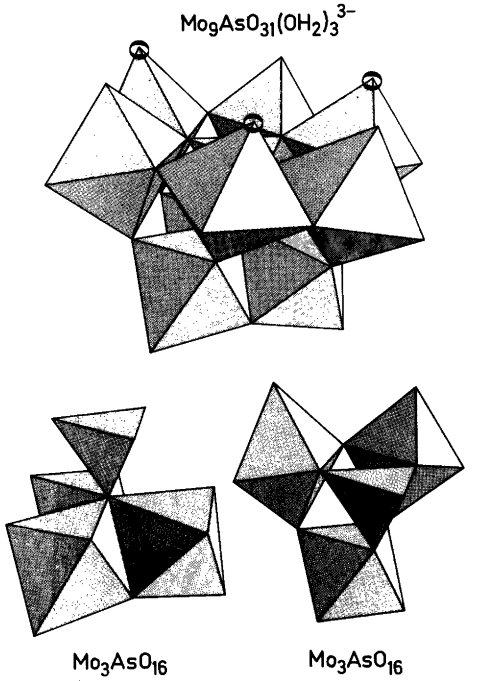

Fig. 9. The structure of an Mo_9AsO_{34} group as found in crystals of $Na_3Mo_6AsO_{31}(OH_2)_3.12-13$ H_2O.[6] The Mo-coordinated water molecules are marked by circles. Two groups which have both been cut out from this structure and which both have the composition Mo_3AsO_{16} are illustrated in the lower half of the figure.

For solutions with Mo/As ratios ~3 the best interpretation of the emf data has indicated the predominant complexes to have the composition $(H^+)_p(MoO_4^{2-})_6(HAsO_4^{2-})_2$ with $p=10-12$. This type of complexes was not found in the phosphate system, where complexes $(H^+)_p(MoO_4^{2-})_5(HPO_4^{2-})_2$, with $p=8-10$ present only to a minor extent in the arsenate system, were found to be dominant and to have the same structure as that of the discrete units $Mo_5P_2O_{23}^{6-}$ occurring in crystals. The scattering data confirm that the structure of the complexes in (12,6,2) molybdoarsenate solutions differs from that found for the complexes in corresponding molybdophosphate solutions. The structure of the (12,6,2) molybdoarsenate complexes cannot be uniquely derived from the limited information contained in the solution scattering data, but these data indicate that the complexes are small and may contain fewer Mo atoms than the six previously suggested. The

(12,6,2) complex can be obtained in high concentration in solution in contrast to the first two members of the series (Fig. 1), which might indicate a difference in structure. Since the (10,6,2) and the (11,6,2) complexes cannot be obtained in sufficiently high concentrations a comparison by means of LAXS measurements cannot be made. To clarify this point, further potentiometric measurements, covering a larger concentration range, and structure determinations of crystals prepared from these solutions will be needed. Work in this direction is in progress.

Acknowledgements. The work has been supported by the Swedish Natural Science Research Council. We thank Ing. Ernst Hansen for skilful technical assistance.

REFERENCES

1. Pettersson, L. *Acta Chem. Scand. A 29* (1975) 677.
2. Pettersson, L. *Equilibrium and Structure Studies of Aqueous Three Component Polyanion Complexes Formed in the Systems* $H^+ - MoO_4^{2-} - HPO_4^{2-}$, $H^+ - MoO_4^{2-} - HAsO_4^{2-}$ *and* $H^+ - MoO_4^{2-}$ *–(D-)mannitol*, Diss., Umeå Universitet, Umeå 1974.
3. Pettersson, L. *Chem. Scr. 7* (1975) 145.
4. Johansson, G., Pettersson, L. and Ingri, N. *Acta Chem. Scand. A 28* (1974) 1119.
5. Johansson, G., Pettersson, L. and Ingri, N. *Acta Chem. Scand. A 32* (1978) 407.
6. Johansson, G. *Acta Chem. Scand. To be published.*
7. Johansson, G. *Acta Chem. Scand. 25* (1971) 2787; *20* (1966) 553.
8. Pocev, S. and Johansson, G. *Acta Chem. Scand. 27* (1973) 2146.
9. Johansson, G. and Sandström, M. *Chem. Scr. 4* (1973) 195.
10. Strandberg, R. *Acta Chem. Scand. A 28* (1974) 217.
11. Evans, H. T., Jr. *Acta Crystallogr. B 30* (1974) 2095.
12. Filowitz, M. and Klemperer, W. G. *Chem. Commun.* (1976) 233.
13. Fuchs, J. and Hartl, H. *Angew. Chem. 88* (1976) 385.
14. Kwak, W., Rajković, L. M., Stalick, J. K., Pope, M. T. and Quicksall, C. O. *Inorg. Chem. 15* (1976) 2778.
15. Strandberg, R. *Acta Chem. Scand. 27* (1973) 1004.
16. Sjöbom, K. and Hedman, B. *Acta Chem. Scand. 27* (1973) 3673.

Received April 17, 1978.

Acta Chemica Scandinavica A 32 (1978) 689–699

Structural Studies on the Phosphorus—Nitrogen Bond. I. The Crystal Structure of Tris(morpholino)phosphine and Tris(piperidino)phosphine

CHRISTIAN RØMMING[a] and JON SONGSTAD[b]

[a] Department of Chemistry, University of Oslo, Oslo 3, Norway and [b] Department of Chemistry, University of Bergen, 5014 Bergen-Univ., Norway

The structures of the title compounds $[O(CH_2CH_2)_2N]_3P$, I, and $[CH_2(CH_2CH_2)_2N]_3P$, II, have been determined by X-ray diffraction techniques. I is triclinic, space group $P\bar{1}$, with $a=8.734(3)$ Å, $b=9.299(2)$ Å, $c=11.357(3)$ Å; $\alpha=73.91(2)°$, $\beta=83.29(2)°$ and $\gamma=117.88(2)°$, $Z=2$. II is monoclinic, space group $P2_1/c$, with (at -150 °C) $a=8.931(4)$ Å, $b=23.507(6)$ Å, $c=15.428(4)$ Å and $\beta=90.44(3)°$, $Z=8$. Full-matrix least-squares refinement led to a final R-value of 0.062 for 2056 reflections for I, and 0.072 for 5218 reflections for II.

The two compounds exhibit several similar structural features: (*i*) Two small NPN bond angles of 98° and one large of 110°; (*ii*) two short P–N bonds between 1.69 and 1.70 Å while the third is longer, 1.726 Å; (*iii*) one of the nitrogen atoms, the one linked through the long bond to the phosphorus atom, is essentially sp^3 hybridized and its lone pair is *anti* to the phosphorus lone pair; (*iv*) the remaining two nitrogen atoms are mainly sp^2 hybridized and their lone pairs are roughly normal to the phosphorus lone pair and also to each other. The main difference between the two molecules is that in I two of the morpholino groups are twisted in opposite directions whereas in II two piperidino groups are twisted in the same direction.

A correlation between the sums of the bond angles around the nitrogen atoms and the corresponding P–N bond lengths has been observed.

In recent years there has been a controversy with regard to the structure of tris(dialkylamino)phosphines, $(R_2N)_3P$.[1–4] The main subject for the dispute has been the direction of the nitrogen lone pairs relative to that of the phosphorus lone pair and whether these compounds possess local C_{3v} or C_s symmetry (for a detailed review, *cf.* Ref. 5). Some of the possible models suggested so far are shown in Fig. 1. Several other models are just as conceivable, *e.g.* those having the nitrogen lone pairs skew to the phosphorus lone pair in a propeller-like arrangement.[4] It should be emphasized, however, that the structural models considered for this class of tervalent phosphorus compounds are based upon the assumption that the nitrogen atoms are sp^2 hybridized. An X-ray study of difluorodimethylaminophosphine, Me_2NPF_2,[6] has revealed that the nitrogen atom and its neighbours are coplanar. Similar conclusions have been arrived at from electron diffraction studies of tris(dimethylamino)phosphine, $(Me_2N)_3P$,[7] and from microwave studies of related compounds.[8,9]

Recently, from studies of tris(dialkylamino)phosphines by photoelectron spectroscopy, the

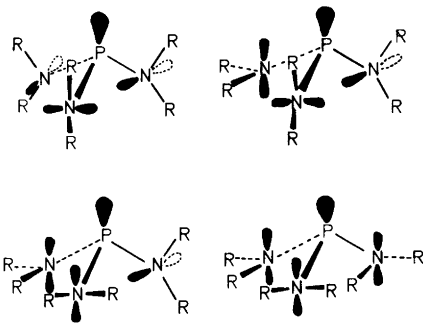

Fig. 1. Models suggested for the lone pair directions in tris(dialkylamino)phosphines.

accuracy and thus the structural conclusions from the electron-diffraction experiments have been seriously critisized.[1,4,5] Furthermore, the occurrence of nitrogen atoms with coplanar bonds may not be as general as has been believed; Me_2NPF_2, for example, does not have a planar nitrogen configuration in the gas phase.[10] It is also difficult to understand how tris(dialkylamino)phosphines can act as powerful nitrogen nucleophiles toward a number of substrates[11,12] when the nitrogen atoms have a planar structure.

Finally, the problem with regard to the bond order of the phosphorus-nitrogen bond arises.[13] Two opposing views have been forwarded as to the direction of the charge transfer in this type of bond; the $p_N \rightarrow d_P$ transfer mechanism has been preferred by some authors,[14-17] whereas others find evidence for the reverse transfer without the use of *d*-orbitals, that is, electron transfer from the phosphorus atom to the more electronegative nitrogen atom.[18-23]

In an attempt to solve some of the many problems with regard to both structure and bonding in aminophosphines and related compounds we have started a structural investigation of this class of compounds. In the present paper the X-ray crystal structure determinations of tris(morpholino)phosphine, I, and tris(piperidino)phosphine, II, are reported. Since the steric demands of the substituents in the two compounds would be expected to be comparable to those of other dialkylamino groups, the structures of I and II may be typical for

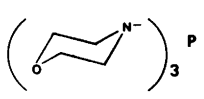

I

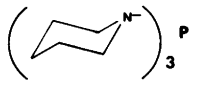

II

the structure of $(R_2N)_3P$ (R = Me, Et, Pr *etc.*). The latter compounds are not readily attacked by X-ray methods since they are liquids, even at low temperatures, whereas I and II both are crystalline at room temperatures and stable provided atmospheric moisture is excluded.

EXPERIMENTAL

Materials. Tris(morpholino)phosphine, I, was prepared from phosphorus trichloride and morpholine as previously described.[24] The product was repeatedly crystallized from toluene to remove traces of morpholine hydrochloride. Suitable crystals were grown from acetonitrile; the specimen used for the X-ray experiments was cut to approximate dimensions $0.3 \times 0.3 \times 0.1$ mm. Tris(piperidino)-phosphine, II, was made in a similar way but in diethyl ether as solvent. After filtration and removal of the solvent the oily product was dissolved in a large volume of diethyl ether and kept for several days at -20 °C to allow traces of piperidine hydrochloride to precipitate. A crystalline product separated from a fairly concentrated etheral solution at dry ice temperature. Crystals suitable for the X-ray study were obtained by sublimation; the specimen used had approximate dimensions $0.2 \times 0.2 \times 0.2$ mm.

X-Ray data. Data for the measurements of cell dimensions and intensity data were obtained on a SYNTEX $P\bar{1}$ diffractometer at 18 ± 1 °C (I) and -150 °C (II), respectively, using graphite crystal monochromated Mo$K\alpha$ radiation ($\lambda = 0.71069$ Å). Cell parameters were determined by a least-squares fit to the diffractometer settings for 15 general reflections with $20° < 2\theta < 30°$. Intensities were collected with the $\theta - 2\theta$ scan technique, scan speed 4 ° min^{-1} for compound I and 3–6 ° min^{-1} depending on the peak intensity for compound II, scan width $\pm 1.2°$ (I) and $\pm 0.6°$ (II), up to a sin θ/λ value of 0.60 Å^{-1} for I and 0.70 Å^{-1} for II. Background counts were taken for 0.35 times the scan time at each of the scan limits. Three standard reflections were measured at regular intervals during the data collection; variations less than 2.5 % were observed for I, whereas a decrease of 15 % in the intensity of the standard reflections was observed for II; the intensities were adjusted according to this drift. Out of the 2639 unique reflections recorded from I, 2056 with $I > 2.5\sigma(I)$ were retained for the structure analysis; the corresponding numbers for II were 6203 and 5218. The standard deviations for the intensities were calculated by $\sigma(I) = [C_T + (0.03C_N)^2]^{\frac{1}{2}}$, where C_T is the total number of counts and C_N is the scan count minus background count. The intensities were corrected for Lorentz and polarization effects but not for absorption.

Description of the computer programs applied for the structure analyses is given in Ref. 25. In the full-matrix least-squares program the quantity minimized was $\Sigma w \Delta F^2$ where w is the inverse of the variance of the observed structure factors; for reflections with sin $\theta/\lambda < 0.45$ Å^{-1} w was multiplied with a function of sin θ/λ to give less weight to low-order reflections. Atomic form factors were those of Doyle and Turner[26] for P, O, N and C and of Stewart, Davidson and Simpson[27] for H.

CRYSTAL DATA

I. Tris(morpholino)phosphine, $C_{12}H_{24}O_3N_3P$, m.p. 157 °C. Triclinic, $a=8.734(3)$ Å; $b=9.299(2)$ Å; $c=11.357(3)$ Å; $\alpha=73.91(2)°$; $\beta=83.29(2)°$; $\gamma=117.88(2)°$; $V=749.6$ Å^3; ($t=18\pm1$ °C); $M=289.31$; $Z=2$; F (000)=312; μ(Mo$K\alpha$)=2.2 cm^{-1}; D_m (flotation)=1.27 g cm^{-3}; $D_x=1.282$ g cm^{-3}. Space group $P\bar{1}$ (No. 2).

II. Tris(piperidino)phosphine, $C_{15}H_{30}N_3P$, m.p. 37 °C. Monoclinic, $a=8.931(4)$ Å; $b=23.507(6)$ Å; $c=15.428(4)$ Å; $\beta=90.44(3)°$; $V=3238.8$ Å^3; ($t=-150$ °C); $M=283.40$; $Z=8$; F (000)=1248; μ(Mo$K\alpha$)=1.0 cm^{-1}; $D_x=1.162$ g cm^{-3}. Absent reflections: ($h0l$) for l odd, ($0k0$) for k odd. Space group $P2_1/c$ (No. 14).

STRUCTURE DETERMINATIONS

The structure of tris(morpholino)phosphine was determined from Patterson functions; that of tris-(piperidino)phosphine (with *two* molecules per asymmetric unit) was solved by the use of the program assembly MULTAN.[28] All positions of the heavy atoms were found after some cycles of successive Fourier syntheses. The refinement proceeded by least-squares methods, initially with isotropic temperature factors, subsequently with anisotropic temperature factors for the heavy atoms. Hydrogen positions were calculated from stereochemical considerations and refined; they were assigned isotropic temperature factors which were refined with the constraint that all hydrogen atoms with about the same distance from the central phosphorus atom were to have the same B-value. The refinements converged to conventional R-factors of 0.063 (I) and 0.072 (II); the R_w-values were 0.069 (I) and 0.092 (II) and the standard deviation of an observation of unit weight, $[\Sigma w\Delta F^2/(m-n)]^{\frac{1}{2}}$, was 2.1 (I) and 2.5 (II), respectively. The overdetermination ratios were 8.4 (I) and 9.9 (II).

The two molecules in the asymmetric unit of II are nearly related by a *pseudo* screw axis along the a-axis close to $y=\frac{1}{4}$, $z=\frac{1}{8}$. No correlation larger than 0.5 was found between positional parameters, however. The geometry of the two molecules is nearly identical, there are no significant differences in bond lengths and angles nor in P–N torsional angles.

Final atomic parameters are listed in Table 1. Tables of observed and calculated structure factors with standard deviations are available from the authors.

ORTEP drawings of molecule I and one of the molecules II are shown in Fig. 2, where the numbering of the atoms is also indicated.

RESULTS

In Table 2 bond lengths, bond angles, torsional angles and other structural data are given. Estimated standard deviations are calculated from the variance-coveriance matrix. In Fig. 3 are shown the Newman projections of the P–N bonds. As the nitrogen bonds are nearly coplanar for some of the nitrogen atoms, the definition of the torsional angle about the P–N bond given by Holywell[10] cannot be applied. According to the IUPAC recommendations[29] the lone pair directions on the phosphorus and nitrogen atoms decide the description of the conformation. In the present case where neither of the atoms exhibit three-fold symmetry, these direc-

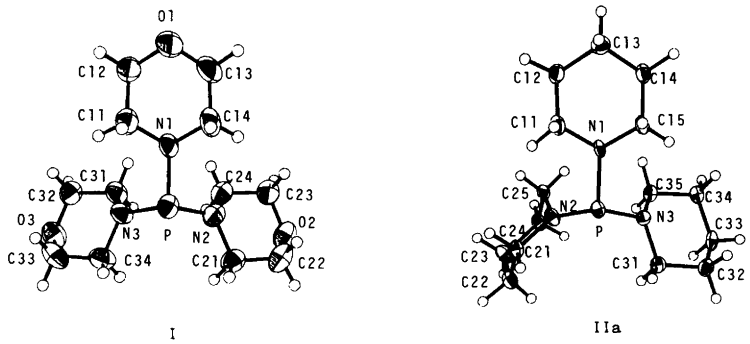

Fig. 2. ORTEP drawings of tris(morpholino)phosphine (I) and tris(piperidino)phosphine (IIa). The atoms of the piperidino substituents of the second molecule of II (IIb) have first index by 3 larger.

Table 1. Fractional atomic coordinates and thermal parameters with estimated standard deviations for tris(morpholino)phosphine (I) and tris(piperidino)phosphine. The anisotropic temperature factor is given by $\exp -2\pi^2(U_{11}a^{*2}h^2 + \ldots + 2U_{12}a^*b^*hk + \ldots)$.

I

ATOM	X	Y	Z	U11	U22	U33	U12	U13	U23
P	.3703(1)	.1252(1)	.1535(1)	.0355(5)	.0393(5)	.0536(6)	.0137(4)	-.0044(4)	-.0131(4)
O1	.7819(3)	.0301(4)	.3116(4)	.0459(15)	.0853(20)	.1449(28)	.0392(15)	-.0410(17)	-.0521(20)
O2	.2861(4)	.4778(3)	.3225(3)	.0696(17)	.0560(15)	.0748(16)	.0376(13)	-.0056(14)	-.0194(13)
O3	-.1570(3)	-.3953(3)	.2848(3)	.0443(14)	.0608(16)	.1040(24)	.0099(12)	-.0278(15)	-.0326(16)
N1	.4946(3)	.0718(3)	.2445(3)	.0260(13)	.0391(14)	.0778(20)	.0110(11)	-.0152(13)	-.0263(13)
N2	.3409(4)	.2525(3)	.2236(3)	.0480(16)	.0466(15)	.0612(18)	.0253(13)	-.0112(13)	-.0137(13)
N3	.1807(3)	-.0776(3)	.2077(3)	.0333(13)	.0467(15)	.0539(16)	.0127(12)	-.0156(12)	-.0151(12)
C11	.5257(5)	-.0617(5)	.2232(4)	.0439(20)	.0557(21)	.0911(30)	.0250(18)	-.0199(19)	-.0370(21)
C12	.6142(5)	-.1150(6)	.3176(5)	.0526(22)	.0661(24)	.1250(40)	.0364(20)	-.0396(25)	-.0496(26)
C13	.7529(5)	.1605(6)	.3295(5)	.0409(21)	.0783(28)	.1170(38)	.0275(21)	-.0345(23)	-.0538(27)
C14	.6695(4)	.2218(5)	.2342(4)	.0338(18)	.0468(20)	.0993(32)	.0103(16)	-.0140(19)	-.0339(21)
C21	.2813(5)	.3658(5)	.1540(4)	.0537(22)	.0565(21)	.0679(25)	.0318(18)	-.0145(18)	-.0154(18)
C22	.3461(7)	.5244(5)	.1888(4)	.0757(28)	.0525(22)	.0746(28)	.0368(22)	-.0043(22)	-.0132(19)
C23	.3510(5)	.3725(5)	.3878(4)	.0491(21)	.0581(21)	.0711(25)	.0272(18)	-.0096(18)	-.0249(19)
C24	.2824(5)	.2030(5)	.3610(3)	.0537(22)	.0485(19)	.0592(22)	.0271(17)	-.0085(17)	-.0144(16)
C31	.0029(5)	-.1869(4)	.3431(3)	.0309(18)	.0493(19)	.0581(21)	.0135(15)	-.0124(16)	-.0171(16)
C32	-.0341(5)	-.3762(5)	.3591(4)	.0436(19)	.0456(19)	.0774(27)	.0165(16)	-.0115(18)	-.0157(18)
C33	-.0607(7)	-.2929(6)	.1538(5)	.0673(27)	.0848(31)	.1005(36)	.0293(25)	-.0499(28)	-.0501(28)
C34	.0551(5)	-.1014(5)	.1308(4)	.0541(22)	.0705(25)	.0648(25)	.0308(20)	-.0276(19)	-.0224(20)

ATOM	X	Y	Z	B	ATOM	X	Y	Z	B
H111	.595(6)	-.019(5)	.134(4)	4.8(2)	H112	.414(6)	-.167(6)	.229(4)	4.8
H121	.638(6)	-.201(6)	.299(4)	5.6(3)	H122	.512(6)	-.176(6)	.410(4)	5.6
H131	.873(6)	.259(6)	.325(4)	5.6	H132	.671(7)	.116(6)	.417(5)	5.6
H141	.747(6)	.270(5)	.145(4)	4.8	H142	.649(5)	.310(5)	.254(4)	4.8
H211	.150(6)	.285(5)	.180(4)	4.8	H212	.329(6)	.401(5)	.081(4)	4.8
H221	.305(6)	.599(6)	.156(4)	5.6	H222	.479(7)	.590(6)	.157(4)	5.6
H232	.313(6)	.354(6)	.477(5)	5.6	H232	.489(7)	.441(6)	.360(4)	5.6
H241	.143(6)	.132(5)	.393(4)	4.8	H242	.324(6)	.142(6)	.400(4)	4.8
H311	.010(6)	-.149(5)	.378(4)	4.8	H312	.167(6)	-.174(5)	.395(4)	4.8
H321	.102(6)	-.449(6)	.446(5)	5.6	H322	.045(6)	-.421(6)	.334(4)	5.6
H331	.145(7)	-.307(6)	.104(4)	5.6	H332	.023(5)	-.333(6)	.120(4)	5.6
H341	.024(6)	-.056(5)	.157(4)	4.8	H342	.113(6)	-.042(6)	.049(5)	4.8

II

ATOM	X	Y	Z	U11	U22	U33	U12	U13	U23
P1	.9179(1)	.1092(0)	.0402(1)	.0256(6)	.0194(5)	.0131(5)	-.0016(5)	.0027(4)	-.0011(4)
P2	.4225(1)	.3932(0)	.2157(1)	.0247(6)	.0200(5)	.0132(5)	.0012(5)	.0012(4)	-.0003(4)
N1	1.1112(4)	.1067(1)	.0387(2)	.0274(19)	.0179(16)	.0141(15)	-.0019(16)	.0064(13)	.0040(13)
N2	.0915(4)	.0915(1)	.1456(2)	.0296(20)	.0263(19)	.0147(15)	-.0072(16)	.0034(14)	-.0003(13)
N3	.8980(4)	.1798(1)	.0271(2)	.0212(19)	.0205(18)	.0180(16)	-.0024(15)	-.0023(14)	-.0012(13)
N4	.6155(4)	.3941(1)	.2166(2)	.0248(18)	.0192(16)	.0139(15)	-.0018(16)	.0005(13)	.0009(13)
N5	.3933(4)	.4092(1)	.1102(2)	.0293(20)	.0256(19)	.0121(15)	.0102(16)	.0031(14)	.0006(14)
N6	.4014(3)	.3216(1)	.2296(2)	.0208(18)	.0207(18)	.0167(16)	.0015(15)	.0051(13)	-.0003(13)
C11	1.1744(5)	.0806(2)	.0615(3)	.0353(25)	.0183(22)	.0297(21)	.0031(20)	.0115(18)	.0034(17)
C12	1.1397(5)	.0551(2)	.0792(3)	.0340(26)	.0251(22)	.0291(22)	.0059(20)	.0053(19)	.0061(17)
C13	1.4222(5)	.0304(2)	.0017(3)	.0281(24)	.0292(24)	.0314(22)	.0020(20)	.0024(19)	-.0021(18)
C14	1.3502(5)	.1365(2)	-.0259(2)	.0325(25)	.0243(23)	.0232(21)	.0015(20)	.0062(18)	.0046(17)
C15	1.1831(5)	.1286(2)	-.0404(2)	.0282(24)	.0292(23)	.0128(19)	-.0006(20)	.0043(17)	.0038(16)
C21	.7827(5)	.0485(2)	.1706(2)	.0296(25)	.0170(20)	.0195(20)	-.0029(19)	.0017(18)	.0003(16)
C22	.6753(5)	.0717(2)	.2385(3)	.0293(26)	.0237(25)	.0278(23)	-.0016(21)	.0074(20)	.0016(19)
C23	.7592(5)	.0975(2)	.3156(3)	.0341(28)	.0365(30)	.0224(21)	-.0060(23)	.0130(20)	-.0035(19)
C24	.8759(5)	.1404(2)	.2854(2)	.0291(25)	.0264(23)	.0182(19)	-.0042(20)	.0040(17)	-.0008(16)
C25	.9783(4)	.1131(2)	.2188(2)	.0232(22)	.0266(22)	.0138(17)	-.0024(19)	.0011(15)	.0051(16)
C31	.7443(4)	.1987(2)	.0113(2)	.0250(23)	.0258(22)	.0189(19)	.0002(18)	.0014(17)	-.0006(16)
C32	.7394(5)	.2549(2)	-.0376(2)	.0297(26)	.0299(25)	.0202(21)	.0031(19)	-.0017(18)	.0025(17)
C33	.8295(5)	.3004(2)	.0101(2)	.0422(26)	.0207(22)	.0150(19)	.0037(20)	.0018(17)	.0032(16)
C34	.9880(5)	.2792(2)	.0267(2)	.0312(25)	.0206(21)	.0220(19)	-.0022(19)	.0027(18)	.0014(16)
C35	.9855(5)	.2222(2)	.0755(2)	.0287(24)	.0202(21)	.0168(20)	-.0021(18)	-.0032(17)	-.0027(16)
C41	.6790(5)	.4501(2)	.1947(2)	.0301	.0231	.0244	-.0036	-.0007	.0002
C42	.8450(5)	.4443(2)	.1755(3)	.0341	.0209	.0282	-.0072	.0037	.0008
C43	.9291(5)	.4188(2)	.2533(3)	.0295	.0305	.0279	-.0042	.0011	-.0008
C44	.8552(5)	.3629(2)	.2809(2)	.0287	.0258	.0231	-.0026	-.0022	.0006
C45	.6984(5)	.3718(2)	.2967(2)	.0283	.0285	.0183	-.0050	-.0005	.0017
C51	.2860(5)	.4531(2)	.0854(2)	.0319	.0177	.0224	.0047	.0009	.0036
C52	.1766(5)	.4315(2)	.0167(3)	.0319	.0312	.0293	.0099	-.0022	.0043
C53	.2604(5)	.4065(2)	-.0612(3)	.0378	.0438	.0214	.0096	-.0071	-.0030
C54	.3753(5)	.3627(2)	-.0323(2)	.0319	.0282	.0146	.0046	.0014	-.0012
C55	.4792(4)	.3882(2)	.0364(2)	.0251	.0271	.0133	.0047	.0056	-.0010
C61	.2478(4)	.3034(2)	.2455(2)	.0227	.0274	.0171	.0010	-.0028	-.0023
C62	.2424(5)	.2471(2)	.2936(3)	.0306	.0306	.0211	-.0083	.0052	.0003
C63	.3304(5)	.2014(2)	.2453(2)	.0352	.0231	.0165	-.0036	-.0006	.0027
C64	.4887(5)	.2219(2)	.2289(2)	.0341	.0197	.0197	.0006	.0032	.0038
C65	.4857(5)	.2789(2)	.1804(2)	.0274	.0212	.0208	.0009	.0062	-.0018

Table 1. Continued.

ATOM	X	Y	Z	B	ATOM	X	Y	Z	B
H111	1.156	.021	.014	1.6	H112	1.111	.036	.109	1.6
H121	1.372	.012	.093	2.2	H122	1.356	.082	.130	2.2
H131	1.415	.051	-.044	1.7	H132	1.531	.084	.011	1.7
H141	1.408	.154	-.078	2.2	H142	1.366	.168	.020	2.2
H151	1.175	.098	-.088	1.6	H152	1.139	.167	-.056	1.6
H211	.832	.013	.185	1.6	H212	.725	.034	.127	1.6
H221	.602	.040	.261	2.2	H222	.614	.098	.219	2.2
H231	.814	.067	.350	1.7	H232	.685	.116	.355	1.7
H241	.942	.155	.332	2.2	H242	.830	.175	.263	2.2
H251	1.032	.086	.244	1.6	H252	1.054	.138	.202	1.6
H311	.686	.204	.066	1.6	H312	.702	.168	-.021	1.6
H321	.636	.269	-.047	2.2	H322	.783	.252	-.095	2.2
H331	.773	.308	.072	1.7	H332	.837	.332	-.023	1.7
H341	1.047	.312	.060	2.2	H342	1.052	.274	-.029	2.2
H351	.935	.230	.131	1.6	H352	1.092	.209	.082	1.6
H411	.664	.478	.242	1.6	H412	.621	.464	.147	1.6
H421	.887	.482	.162	2.2	H422	.854	.418	.127	2.2
H431	.920	.446	.304	1.7	H432	1.039	.416	.243	1.7
H441	.914	.350	.334	2.2	H442	.865	.333	.231	2.2
H451	.682	.403	.347	1.6	H452	.645	.335	.307	1.6
H511	.363	.487	.056	1.6	H512	.224	.472	.135	1.6
H521	.111	.464	-.006	2.2	H522	.122	.402	.045	2.2
H531	.315	.440	-.096	1.7	H532	.180	.390	-.103	1.7
H541	.438	.350	-.082	2.2	H542	.324	.328	-.006	2.2
H551	.531	.424	.008	1.6	H552	.548	.360	.063	1.6
H611	.192	.301	.192	1.6	H612	.191	.331	.279	1.6
H621	.134	.235	.308	2.2	H622	.291	.250	.351	2.2
H631	.266	.197	.194	1.7	H632	.321	.165	.291	1.7
H641	.537	.190	.193	2.2	H642	.546	.228	.283	2.2
H651	.433	.273	.119	1.6	H652	.588	.291	.167	1.6

tions are not precisely defined. We have chosen to define the torsional angle as the angle between the lines bisecting the larger of the angles between the projection along the P – N bond of the other P – N bonds and the N – C bonds. The lines thus defining the torsional angles are indicated with broken lines in Fig. 3. It may be noted, however, that the directions thus defined for the phosphorus lone pair direction do not necessarily coincide exactly for the three P – N torsional angles of one molecule.

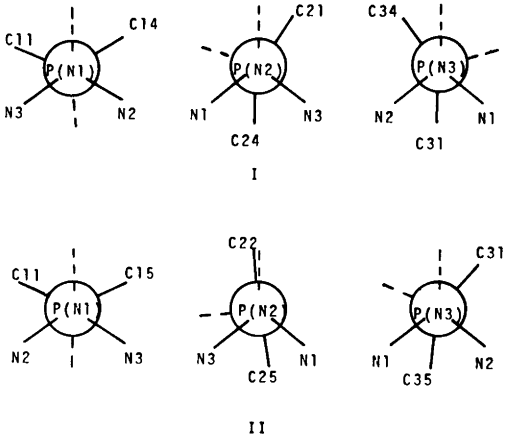

Fig. 3. Newman projections along the P – N bonds in tris(morpholino)phosphine (I) and tris(piperidino-phosphine (II).

Several features in the two structures are similar: Both molecules have two short P – N bonds (1.69 – 1.70 Å); the third P – N bond being significantly longer (1.726 Å). The nitrogen atoms involved in the long P – N bond are essentially sp^3 hybridized and the lone pair of this nitrogen atom in both compounds is *anti* to the phosphorus lone pair. The remaining nitrogen atoms are mainly sp^2 hybridized and their lone pairs are partly orthogonal to that of the phosphorus atom. Two of the N – P – N angles are about 98° while the third N – P – N angle in both I and II (between bonds to sp^2 hybridized nitrogen atoms) is about 110°. The sum of the N – P – N bond angles in I and II are 306.6 and 305.0°, respectively.

The significant differences in the two structures are as follows: In II, one of the nitrogen atoms is sp^2 hybridized, whereas in I all three nitrogen atoms have some sp^3 character. Furthermore, in I, the two morpholino groups linked through short bonds to the phosphorus atom are twisted in opposite directions (torsional angles of opposite signs), while in II the corresponding piperidino groups are twisted in the same direction.

The morpholino and piperidino parts of the molecule are both in the expected chair conformation. The hybridization of the nitrogen atoms influences slightly the bond angles and bond lengths in these group (*cf.* Table 3). All N – P bond directions correspond approximately to that of an

Table 2. Structural data for tris(morpholino)phosphine (I) and the two crystallographically non-equivalent molecules (a and b) of tris(piperidino)phosphine (II).

Bond lengths (Å)

I			IIa			IIb		
P	N1	1.726(3)	P1	N1	1.727(3)	P2	N4	1.724(3)
P	N2	1.691(3)	P1	N2	1.692(3)	P2	N5	1.689(3)
P	N3	1.696(3)	P1	N3	1.705(3)	P2	N6	1.708(3)
N1	C11	1.467(4)	N1	C11	1.476(5)	N4	C41	1.472(5)
C11	C12	1.493(6)	C11	C12	1.504(7)	C41	C42	1.521(6)
C12	O1	1.431(5)	C12	C13	1.530(6)	C42	C43	1.533(6)
O1	C13	1.410(5)	C13	C14	1.527(5)	C43	C44	1.532(6)
C13	C14	1.503(6)	C14	C15	1.519(6)	C44	C45	1.526(6)
C14	N1	1.472(4)	C15	N1	1.476(4)	C45	N4	1.488(5)
N2	C21	1.468(5)	N2	C21	1.456(5)	N5	C51	1.457(5)
C21	C22	1.498(6)	C21	C22	1.526(5)	C51	C52	1.523(6)
C22	O2	1.416(5)	C22	C23	1.526(6)	C52	C53	1.538(6)
O2	C23	1.429(5)	C23	C24	1.526(6)	C53	C54	1.519(6)
C23	C24	1.495(5)	C24	C25	1.523(5)	C54	C55	1.526(6)
C24	N2	1.458(5)	C25	N2	1.457(5)	C55	N5	1.464(4)
N3	C31	1.464(5)	N3	C31	1.461(5)	N6	C61	1.459(5)
C31	C32	1.508(5)	C31	C32	1.522(6)	C61	C62	1.519(6)
C32	O3	1.419(5)	C32	C33	1.524(6)	C62	C63	1.528(6)
O3	C33	1.414(6)	C33	C34	1.520(6)	C63	C64	1.517(6)
C33	C34	1.503(6)	C34	C35	1.537(5)	C64	C65	1.534(5)
C34	N3	1.455(5)	C35	N3	1.467(5)	C65	N6	1.469(5)

Bond angles (°)

I				IIa				IIb			
N1	P	N2	98.0(1)	N1	P1	N2	98.9(2)	N4	P2	N5	98.8(2)
N2	P	N3	110.7(1)	N2	P1	N3	109.2(2)	N5	P2	N6	108.9(2)
N3	P	N1	97.9(1)	N3	P1	N1	97.0(2)	N6	P2	N4	97.0(2)
P	N1	C11	114.4(2)	P1	N1	C11	113.3(3)	P2	N4	C41	113.4(3)
P	N1	C14	115.0(2)	P1	N1	C15	116.4(3)	P2	N4	C45	115.7(2)
P	N2	C21	116.7(2)	P1	N2	C21	121.0(3)	P2	N5	C51	120.5(2)
P	N2	C24	125.9(2)	P1	N2	C25	126.0(3)	P2	N5	C55	126.6(3)
P	N3	C31	124.3(2)	P1	N3	C31	114.6(3)	P2	N6	C61	114.5(3)
P	N3	C34	115.6(2)	P1	N3	C35	123.7(3)	P2	N6	C65	123.5(2)
N1	C11	C12	110.2(3)	N1	C11	C12	110.7(3)	N4	C41	C42	110.1(3)
C11	C12	O1	112.7(4)	C11	C12	C13	111.3(3)	C41	C42	C43	110.8(3)
C12	O1	C13	109.4(3)	C12	C13	C14	110.5(3)	C42	C43	C44	110.1(3)
O1	C13	C14	112.8(4)	C13	C14	C15	110.3(3)	C43	C-4	C45	110.6(3)
C13	C14	N1	109.6(3)	C14	C15	N1	110.7(3)	C44	C45	N4	109.7(3)
C14	N1	C11	108.2(3)	C15	N1	C11	109.9(3)	C45	N4	C41	109.8(3)
N2	C21	C22	109.8(3)	N2	C21	C22	111.0(3)	N5	C51	C52	111.3(3)
C21	C22	O2	111.9(3)	C21	C22	C23	111.7(3)	C51	C52	C53	111.0(3)
C22	O2	C23	109.7(3)	C22	C23	C24	110.9(3)	C52	C53	C54	111.2(3)
O2	C23	C24	110.9(3)	C23	C24	C25	110.0(3)	C53	C54	C55	110.1(3)
C23	C24	N2	109.7(3)	C24	C25	N2	110.6(3)	C54	C55	N5	110.7(3)
C24	N2	C21	110.6(3)	C25	N2	C21	112.9(3)	C55	N5	C51	112.5(3)
N3	C31	C32	109.8(3)	N3	C31	C32	111.7(3)	N6	C61	C62	111.8(3)
C13	C32	O3	111.0(3)	C31	C32	C33	110.9(3)	C61	C62	C63	110.9(3)
C32	O3	C33	110.0(3)	C32	C33	C34	109.8(3)	C62	C63	C64	109.9(3)
O3	C33	C34	111.5(4)	C33	C34	C35	110.5(3)	C63	C64	C65	110.3(3)
C33	C34	N3	109.8(3)	C34	C35	N3	110.6(3)	C64	C65	N6	110.6(3)
C34	N3	C31	110.6(3)	C35	N3	C31	112.1(3)	C65	N6	C61	111.9(3)

Torsional angles (°)

I					II (average for a and b)				
N2	P	N1	C11	171.9(2)	N2	P1	N1	C11	61.5(3)
N2	P	N1	C14	-61.9(3)	N2	P1	N1	C15	-170.0(3)
N3	P	N1	C11	59.5(3)	N3	P1	N1	C11	172.1(2)
N3	P	N1	C14	-174.3(3)	N3	P1	N1	C15	-59.4(3)
N1	P	N2	C21	164.3(2)	N1	P1	N2	C21	132.6(3)
N1	P	N2	C24	-47.6(3)	N1	P1	N2	C25	40.6(3)
N3	P	N2	C21	-94.2(3)	N3	P1	N2	C21	126.7(3)
N3	P	N2	C24	54.0(3)	N3	P1	N2	C25	-60.0(3)
N1	P	N3	C31	52.2(3)	N1	P1	N3	C31	171.1(2)
N1	P	N3	C34	-164.8(3)	N1	P1	N3	C35	-46.1(3)
N2	P	N3	C31	-49.5(3)	N2	P1	N3	C31	-87.1(3)
N2	P	N3	C34	93.6(3)	N2	P1	N3	C35	55.8(3)

Table 2. Continued.

Various derived and averaged data

	I			II (average for a and b)		
Nx	N1	N2	N3	N1	N2	N3
$\overline{N-C}$ (Å)	1.470	1.463	1.460	1.478	1.459	1.464
$\overline{C-C}$ (Å)	1.498	1.497	1.505	1.524	1.526	1.526
$\overline{C-O}$ (Å)	1.421	1.423	1.417			
Deviation of Nx from plane PCC (Å)	0.43	0.23	0.27	0.42	0.05	0.29
Sum of N bond angles (°)	337.6	353.2	350.5	339.3	359.8	350.1
Torsional angle Lone pair(P)-P-N-Lone pair(N) (°)	170.6	-70.9	73.2	-178.9	-96.3	-66.6
$\overline{C-H}$ (Å)		0.99(6)			1.00(5)	
Sum of P bond angles (°)		306.6			305.0	

Short intramolecular distances (Å)

I			II (average for a and b)		
P	H111(a)	2.87	P1	H111(a)	2.98
P	H112(e)	2.82	P1	H112(e)	2.65
P	H141(a)	2.89	P1	H151(a)	3.07
P	H142(e)	2.83	P1	H152(e)	2.82
P	H212(e)	2.69	P1	H212(e)	2.83
P	H312(e)	2.90	P1	H252(e)	2.80
P	H341(a)	3.03	P1	H312(e)	2.64
P	H342(e)	2.69	P1	H352(e)	2.92
N1	H242(e)	2.59	N1	H252(e)	2.62
N1	H312(e)	2.63	N1	H352(e)	2.54
N2	H142(e)	2.57	N2	H112(e)	2.45
N3	H112(e)	2.54	N3	H152(e)	2.52
H241(a)	H311(a)	2.38			

equatorial bond of the morpholine and piperidine rings.

In both I and II the packing of the molecules in the crystals is of normal van der Waals' type, the contacts being mainly between hydrogen atoms.

DISCUSSION

Conformational considerations. Recent NMR studies of acyclic amino phosphines of the general type X_2PNR_2 (X = F and Cl) and related substances have revealed that the synclinal *(gauche)* conformation is the best representation of the ground state geometry, regardless whether the nitrogen atom is sp^2 or sp^3 hybridized.[30] The preference for this conformation is generally thought to be due to the lone pair repulsion which is at its minimum in the synclinal conformation. This orthogonality of lone-pair electrons appears to be quite general and is apparent in compounds with S – S,[31] N – N,[32] N – S,[33] and O – O[34] bonds. For a detailed discussion of the "*gauche*" effect, *cf.* Ref. 35.

However, when the phosphorus atom is bonded to *three* atoms, each with a lone pair as in tris-(dialkylamino) phosphines, the situation is more complex. Cowley *et al.*[1] have argued convincingly in favour of a conformation where only two nitrogen lone pairs are orthogonal to the phosphorus lone pair. The results from the present study, however, suggest that the steric demands of the substituents linked to the nitrogen atoms must be taken into account when the conformation of tris(dialkylamino)phosphines is to be considered. Evidently, a complex interplay of effects due to lone pair repulsions, phosphorus-nitrogen bond lengths, hybridization of nitrogen atoms, bond angles around the phosphorus atom and the spatial requirements of the substituents determine the geometry.

For the discussion of the lone pair directions the same difficulty arises as when defining the torsional angles. We take as the direction of the lone pair on a trivalent atom that of the normal to the plane through three points in unit distance from the atom along the bonds. In Table 3 are listed angles between such directions in the present molecules.

In both I and II, two of the nitrogen lone pairs are partly orthogonal to the phosphorus lone pair in agreement with the suggestion by Cowley.[1] The third lone pair is nearly antiparallel to that of the phosphorus atom, all nitrogen lone pairs are thus

Table 3. Angles (°) between lone pair directions of the P and N atoms of I and the two molecules (a and b) of II (for definition, see text).

Atoms	Molecule I	Molecule IIa	Molecule IIb
P N1	170.6	169.4	169.6
P N2	70.9	79.8	79.4
P N3	73.2	68.3	68.8
N1 N2	114.9	71.0	71.0
N2 N3	83.4	74.2	73.7
N1 N3	109.1	119.1	118.8

also partly orthogonal to each other. According to the figures given in Table 3 none of the structures proposed in Fig. 1 are representative of the structure of I and II in their crystalline state. Because of the close similarity of the structures of I and II, and because the spatial demands of the usual dialkylamino groups are quite comparable to those of the piperidino and the morpholino groups, one may conclude that tris(dialkylamino)-phosphines $(R_2N)_3$(R = Me, Et *etc.*), generally have geometries of the same type as have I and II. The close similarity in the structures of tris(morpholino)-phosphine selenide, tris(piperidino)phosphine selenide and tris(dimethylamino)phosphine selenide[36] substantiates this conclusion.

The important factor which is primarily responsible for the geometry of tris(dialkylamino)-phosphines appears thus to be the accommodation of two, but only two, nitrogen atoms in positions whereby their lone pair directions are close to be orthogonal to the phosphorus lone pair.[1] The third substituent will then be accommodated where vacant space is available. It is noteworthy that the structures of I and II bear no resemblance to that of triaryl phosphines, Ar_3P, where the aryl groups are twisted to propeller-shaped molecules.[37] Apparently the repulsive forces between lone pairs will not allow geometries of this type for tris(dialkylamino)phosphines.

Bond angles around the phosphorus atom. The sum of the bond angles, $\Sigma\angle$ NPN, in I and II are 306.6 and 305.0°, respectively, which is approximately the same as in Ar_3P.[37] Except for PH_3 and the sterically very hindered phosphine, tris-*tert*-butyl phosphine,[38] the sum of bond angles around the phosphorus atom in tervalent phosphorus compounds is generally in the range 295 – 310° and is not very dependent on the substituents. It is an interesting observation in the present compounds that one of the NPN bond angles, the angle between bonds to the essentially sp^2 hybridized nitrogen atoms, is considerably larger (110°) than the two remaining NPN bond angles (98°). This increase in the one bond angle is probably due to the steric demands of the two substituents whose nitrogen atoms have their lone pair orthogonal to the phosphorus lone pair.

Bond angles around the nitrogen atoms. In both I and II there are actually three different nitrogen atoms, the sum of their bond angles being 337.6, 353.2 and 350.2° in I and 339.3, 359.8 and 350.1° in II. The nitrogen atom with its lone pair *anti* to the phosphorus lone pair is essentially sp^3 hybridized in both I and II as seen from the sum of the bond angles, 337.6 and 339.3°, respectively. It may well be that when no significant "through-space" σ or π interaction with the phosphorus lone pair takes place due to the unsuitable spatial orientation of the nitrogen lone pair, the sp^3 state is the favourable hybridization of the nitrogen atom.[23] Furthermore, increased *p*-character of the nitrogen atom is accompanied by a significant lengthening of the phosphorus-nitrogen bond, which may be of some advantage when the substituent is to be accommondated on the fairly crowded central phosphorus atom.

The phosphorus – nitrogen bond lengths. In recent years a number of X-ray, electron diffraction and microwave studies of compounds with phosphorus-nitrogen bonds have appeared and the P – N bond is known to range from 1.84 to 1.47 Å (*cf.* Refs. 13 and 39 for a survey of P – N bond lengths). It is generally accepted that P^V – N bond lengths shorter than 1.77 Å and P^{III} – N bond lengths shorter than 1.80 Å reflect bond orders higher than unity.[40-42] Bond orders higher than unity seem invariably to be connected with some deviation from sp^3 hybridization of the nitrogen atom.

In both I and II the two shorter bonds (1.69 – 1.70 Å), and the longer bond (1.726 Å), are considerably shorter than the length for a single P – N bond according to Pauling (1.80 Å),[40] and also shorter than the Schomaker-Stevenson value (1.76 Å).[42] In Fig. 4 is plotted the sum of the nitrogen bond angles *versus* the corresponding P – N bond lengths in I and II. There seems to be a linear dependence, and the least-squares straight line is indicated. From extrapolation to an angle sum of 325 – 330° a $P^{III}-N_{sp^3}$ bond length of 1.74 – 1.75 Å may be obtained as the measure for an authentic P^{III} – N single bond. This is slightly shorter than the

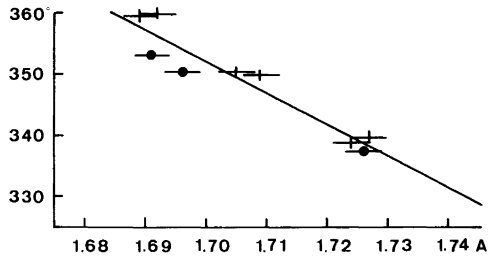

Fig. 4. The P – N bond length *vs.* the nitrogen bond angle sum in tris(morpholino)phosphine (circles) and tris(piperidino)phosphine (crosses).

current estimate of a P – N single bond, 1.77 Å, the bond length in the monoamidophosphate anion,[41] which, however, exists in the betaine form.

IR studies of tris(dimethylamino)phosphine and tris(pyrrolidino)phosphine have shown two peaks in the P – N stretching region which have been assigned to symmetric and asymmetric stretching.[14,43] In view of the present results indicating that in this class of compounds there are at least two different P – N bonds, the IR assignments ought to be reconsidered.

The torsional angles. Apart from the torsional angle of the P – N bonds for the essentially sp^3 hybridized nitrogen atoms which are about 180°, the remaining angles are in the range 69 – 96°, most of them around 70° (Table 2). None of the lone pairs of the nitrogen atoms are ideally orthogonal to the phosphorus lone pair. It appears that the value of 70° for the torsional angle is the optimum compromise between steric repulsion of the atomic cores and the electronic energy. This value has previously been found in tris(dimethylamino)difluorophosphorane.[44] However, the P – N2 torsional angle of II of 96° is associated with the shortest (strongest) P – N bond and with the most coplanar nitrogen bonds of all in the present analysis; furthermore, this N2 lone pair is also the one closest to being orthogonal to the phosphorus lone pair (80°).

The structure of the substituents. The morpholino and piperidino substituents are all in the expected chair conformation and linked to the phosphorus atom in an approximately equatorial direction. As indicated in Table 2, the bond angles and, to some extent the bond lengths, are significantly dependent upon the hybridization of the nitrogen atoms. A detailed discussion of bond lengths and angles in the morpholino and the piperidino group will appear in a later paper in this series.

Intramolecular contacts. Several short intramolecular nonbonded contacts have been observed and are listed in Table 2.

In compound I the four hydrogen atoms of C11 and C14 are about equidistant from P [2.82 – 2.89 Å]; the equatorial hydrogen atoms of C11 and C14 are also in van der Waals' contact with N3 and N2, respectively [2.54 and 2.57 Å]. The equatorial hydrogen atoms of C24 and C31 are both at van der Waals' distance from N1 [2.59 and 2.63 Å, respectively], and the axial hydrogen atoms of the same carbon atoms are in contact with each other [2.38 Å]. Probably these interactions are responsible for the asymmetry in the external angles at N2 and N3 [$\angle$ P – N2 – C21 = 116.7°, $\angle$ P – N2 – C24 = 125.9°; $\angle$ P – N3 – C34 = 115.6°, $\angle$ P – N3 – C31 = 124.3°]; they are counterbalanced only by the interactions between the equatorial hydrogen atoms at C21 and P[2.69 Å] and C34 and P[2.69 Å]. The steric demands of the substituents are also the probable cause for the N2 – P – N3 angle being as large as 110.7°.

The situation is somewhat different in compound II since the P – N2 twist is in the opposite direction as compared to the P – N3 twist in I (*cf.* Fig. 2). Since the molecules *a* and *b* of II are nearly identical, mean values are used in the discussion. As in I the four hydrogen atoms of C11 and C15 of II are in contact with the phosphorus atom [2.65 – 3.07 Å] and the equatorial ones in contact with N2 and N3 [2.45 and 2.52 Å, respectively]. The atoms of the ring associated with N3 have mainly contacts analogous to those described for compound I [equatorial hydrogen of C35 to N1: 2.54 Å, that of C31 to P: 2.64 Å] and the same asymmetry in the external angles of N3 is observed [$\angle$ P – N3 – C31 = 114.6°, $\angle$ P – N3 – C35 = 123.6°]. There are no contacts between hydrogens of C35 and C25, however. The equatorial hydrogen atom of C25 is separated from N1 by 2.62 Å and from P by 2.80 Å; the equatorial hydrogen atom of C21 is at a distance 2.83 Å from P. The asymmetry in the external angles of N2 is less pronounced than for N3 [$\angle$ P1 – N2 – C21 = 120.8°, $\angle$ P1 – N2 – C25 = 126.3°]; the angle N2 – P – N3 [109.1°] is slightly smaller than in I.

Comments on the reactivity of I and II. From a recent kinetic study of reactions with methyl iodide it has been found that II is considerably more nucleophilic than I.[45] However, the similarity in the

structure of I and II including bond lengths and bond angles does not signal such a difference in reactivity. The presence of one essentially sp^3 hybridized nitrogen atom in I and II agrees with the fact that tris(dialkylamino)phosphines may act as nitrogen nucleophiles toward several substrates.[11,12]

CONCLUSIONS

None of the structural models considered for the structure of tris(dialkylamino)phosphines, Fig. 1, are in accordance with the structure of tris(piperidino)phosphine and tris(morpholino)phosphine. In this class of compounds two substituents appear to be accommodated with essentially sp^2 hybridized nitrogen atoms in positions whereby their lone pairs are partly orthogonal to the phosphorus lone pair. The position of the third substituent appears to be mainly governed by the steric demands. In both I and II the nitrogen atom of this third substituent is essentially sp^3 hybridized and has its lone pair *anti* relative to the phosphorus lone pair. The results indicate that in tris(dialkylamino)phosphines there are nitrogen atoms with at least two different hydridizations and thus at least two types of P–N bonds in each molecule. In view of this, it appears as if the results from recent IR, Raman and photoelectron spectral studies of tris(dialkylamino)-phosphines and related compounds ought to be reconsidered.

REFERENCES

1. Cowley, A. H., Dewar, M. J. S., Goodman, D. W. and Schweiger, J. R. *J. Am. Chem. Soc. 95* (1973) 6506.
2. Lappert, M. F., Pedley, J. B., Wilkins, B. T., Stelzer, O. and Unger, E. *J. Chem. Soc. Dalton Trans.* (1975) 1207.
3. Cowley, A. H., Goodman, D. W., Knebler, N. A., Sanchez, M. and Verkade, J. G. *Inorg. Chem. 16* (1977) 854.
4. Hargis, J. H. and Worley, S. D. *Inorg. Chem. 16* (1977) 1886.
5. Cowley, A. H. *Phosphorus and Sulphur 2* (1976) 283.
6. Morris, E. D. and Nordman, C. E. *Inorg. Chem. 8* (1969) 1673.
7. Vilkov, L. V., Khaikin, L. S. and Evdokimov, V. V. *Zh. Strukt. Khim. 13* (1972) 7.
8. Brittain, A. H., Smith, J. E., Lee, P. L., Cohn, K. and Schwendeman, R. H. *J. Am. Chem. Soc. 93* (1971) 6772.
9. Forti, P., Damiani, D. and Favero, P. G. *J. Am. Chem. Soc. 95* (1973) 756.
10. Holywell, G. C., Rankin, D. W. H., Beagley, B. and Freeman, J. M. *J. Chem. Soc. A* (1971) 785.
11. Simonnin, M. P., Charrier, C. and Burgada, R. *Org. Magn. Reson. 4* (1972) 113.
12. Hudson, R. F. and Brown, C. *Acc. Chem. Res. 5* (1972) 204.
13. Clardy, J. C., Kolpa, R. L. and Verkade, J. G. *Phosphorus 4* (1974) 133.
14. Mathis, R., Lafaille, L. and Burgada, R. *Spectrochim. Acta A 30* (1974) 357.
15. Gilje, J. W. and Seff, K. *Inorg. Chem. 11* (1972) 1643.
16. Bach, M. C., Brian, C., Crasnier, F., Labarre, J.-F., Leibovici, C. and Dargelos, A. *J. Mol. Struct. 17* (1973) 23.
17. Emsley, J. and Hall, D. *The Chemistry of Phosphorus*, Harper and Row, London 1976, p. 394.
18. Hoffmann, R., Howell, J. M. and Muetterties, E. L. *J. Am. Chem. Soc. 94* (1972) 3047.
19. Strich, A. and Veillard, A. *J. Am. Chem. Soc. 95* (1973) 5574.
20. Hoffmann, R. *Acc. Chem. Res. 4* (1971) 1.
21. Czismadia, I. G., Cowley, A. H., Taylor, M. W., Tel, L. M. and Wolfe, S. *Chem. Commun.* (1972) 1147.
22. Czismadia, I. G., Cowley, A. H., Taylor, M. W. and Wolfe, S. *Chem. Commun.* (1974) 432.
23. Lambert, J. B. *Top. Stereochem. 6* (1971) 19.
24. Stangeland, L. J., Austad, T. and Songstad, J. *Acta Chem. Scand. 27* (1973) 3919.
25. Groth, P. *Acta Chem. Scand. 27* (1973) 1837.
26. Doyle, P. A. and Turner, P. S. *Acta Crystallogr. A 24* (1968) 390.
27. Stewart, R. F., Davidson, E. R. and Simpson, W. T. *J. Chem. Phys. 42* (1965) 3175.
28. Germain, G., Main, P. and Woolfson, M. M. *Acta Crystallogr. A 27* (1971) 368.
29. IUPAC Commission on Nomenclature of Organic Chemistry, *Pure Appl. Chem. 45* (1976) 11.
30. Cowley, A. H., Dewar, M. J. S., Jackson, W. R. and Jennings, W. B. *J. Am. Chem. Soc. 92* (1970) 1085, 5206.
31. Foss, O. In Kharasch, N., Ed., *Organic Sulfur Compounds*, Pergamon, New York 1961, Vol. 1, Chapter 8.
32. Dewar, M. J. S. and Jennings, W. B. *J. Am. Chem. Soc. 91* (1969) 3656.
33. Raban, M., Kenney, K. W. J., Jr. and Jones, F. B. *J. Am. Chem. Soc. 91* (1969) 6677.
34. Fink, W. H. and Allen, L. C. *J. Chem. Phys. 46* (1967) 2261.
35. Wolfe, S. *Acc. Chem. Res. 5* (1972) 102.
36. Rømming, C. and Songstad, J. *Acta Chem. Scand. To be published.*

37. Corbridge, D. E. C. *The Structural Chemistry of Phosphorus*, Elsevier, Amsterdam 1974, p. 330.
38. Labarre, M.-C. and Hausard, M. *J. Mol. Struct. 26* (1975) 17.
39. Vilkov, L. V. and Khaikin, L. S. *Top. Curr. Chem. 53* (1975) 25.
40. Pauling, L. *Nature of the Chemical Bond*, Cornell University Press, New York 1960.
41. Cruickshank, D. W. J. *Acta Crystallogr. 17* (1964) 671.
42. Schomaker, V. and Stevenson, D. P. *J. Am. Chem. Soc. 63* (1941) 37.
43. Raüchle, F., Pohl, W., Blaich, B. and Goubeau, J. *Ber Bunsenges. Phys. Chem. 75* (1971) 66.
44. Oberhammer, H. and Schmutzler, R. *J. Chem. Soc. Dalton Trans.* (1976) 1454.
45. Thorstenson, T. and Songstad, J. *Acta Chem. Scand. A 30* (1976) 781.

Received April 24, 1978.

Acta Chemica Scandinavica A 32 (1978) 701 – 703

^{13}C NMR Chemical Shifts in Donor—Acceptor Systems. A Model for the Alternating Substituent Effect

LARS HENRIKSEN and HANNE EGGERT

Department of General and Organic Chemistry, University of Copenhagen, The H. C. Ørsted Institute, Universitetsparken 5, DK-2100 Copenhagen Ø, Denmark

^{13}C chemical shifts in three donor-acceptor substituted ethylenes respond characteristically to changes of the donor substituents. An increased electron donating capacity causes downfield shifts for atoms removed from the donor atoms by an odd number of bonds and upfield shifts for atoms removed by an even number of bonds. The shifts are qualitatively predicted by a simple perturbation MO model which also applies to other molecules with donor atoms adjacent to a π-system.

A great deal of attention has been focused on the effects of substitution on ^{13}C chemical shifts. Recently, several papers have reported on systems, saturated as well as unsaturated, where this effect is alternating along a carbon chain.[1-5] These examples of alternating substituent effects may be rationalized on the basis of charge alternation predicted by CNDO[6] as well as *ab initio* calculations.[7] In the present communication we present the result of a ^{13}C NMR study of a series of donor–acceptor systems (*1–3*, *a–c*), which show pronounced alternating chemical shift changes along the carbon chain C-1–C-3(C-3′) upon change of the C-1 sulfur substituent (see Table 1). In donor–acceptor systems electron density is transferred from a donor group (the sulfur substituent) to an acceptor group (the remaining molecule). These compounds can therefore not immediately be subjected to treatments that neglect charge transfer effects as in Ref. 8. As an alternative treatment we suggest that induced charge variations in series of related systems of the donor–acceptor type may be predicted approximately by applying second-order perturbation theory to the charge transfer process.

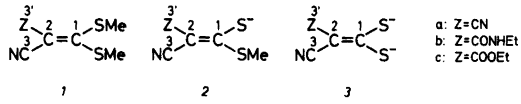

1 *2* *3*

EXPERIMENTAL

Compounds 1 (*a–c*) and *3* (*a–c*) were obtained by literature methods.[9] Compounds *2* (*a–c*) were prepared as sodium salts by treatment of *3* (*a–c*) with equimolar amounts of methyl iodide in aqueous methanol. They were isolated as a mixture with sodium iodide by evaporation of the reaction mixture, dissolution in acetone, filtration and precipitation with methylene chloride. No organic contaminants were detected on the basis of the ^{1}H NMR spectra of these products. Noise decoupled ^{13}C NMR spectra were determined with a Bruker WH 90 NMR instrument. All samples were examined at *ca.* 35 °C in DMSO-d_6 solution (~0.5 M) and shieldings measured relative to TMS. Unambiguous signal assignments were made by comparison with spectra of compounds *1c–3c* specifically ^{13}C labeled at C-1, prepared from ethyl cyanoacetate and $^{13}CS_2$.[9]

RESULTS AND DISCUSSION

The ^{13}C NMR results (see Table 1) in each of the three series (*a–c*) clearly demonstrate the following: C-1 becomes progressively more deshielded in going from neutral to dianionic species. A downfield shift of ~45 ppm at C-1 upon increasing electron-donating power of the substituent is remarkable. This places the actual chemical shift of C-1 in the dianion at the very low-field end of the chemical shift scale (~220 ppm) in spite of the gross negative

Table 1. ^{13}C chemical shifts in ppm relative to TMS.

	1a	*2a*	*3a*	*1b*	*2b*	*3b*	*1c*	*2c*	*3c*
C-1	185.7	202.5	224.6	166.8	190.1	214.3	181.2	203.7	225.6
C-2	74.4	64.0	67.5	106.3	95.1	96.6	98.2	89.0	90.2
C-3	113.1	119.6[a]	123.5	116.1	121.0	127.4	115.9	122.2	125.8
C-3′	113.1	118.3[a]	123.5	160.5	165.6	167.9	161.5	164.7	166.7

[a] Shift assignments may be interchanged.

charge of this species. Shifts towards lower field are also observed for the carbon atoms 3 and 3′. C-2, separated by two bonds from the donor centers, becomes more shielded in going from neutral to charged species, but is slightly less shielded in the dianion than in the monoanion. If these features of ^{13}C shifts are interpreted in terms of charge density variations,* the charge redistribution induced by *increasing* the electron donating power of the sulfur substituent (going from *1* to *3*) results in *decreased* charge density on the carbon atoms one and three bonds removed from the substituent.

Considering the theoretical predictions[6,7] that a small amount of charge transfer implicates an additional charge separation, the perturbation model can be used on the charge transfer process in donor–acceptor systems. In the perturbation approach charge transfer is equivalent to interactions between occupied and unoccupied substructure orbitals and orbital interactions are inversely proportional to the energy difference between the interacting orbitals. While there is usually a large energy gap between occupied and unoccupied substructure orbitals in organic compounds, donor acceptor systems are characterized by a relatively small energy difference between the donor HOMO and acceptor LUMO. The perturbation treatment suggests that the interaction of these two orbitals which is most heavily felt in the compound HOMO[11] is the major source of transfer and, thereby, of charge separation. As a consequence the induced charge variations in these systems may be predicted approximately by evaluating the changes in the compound HOMO which results from changing the (donor) substituent (going from *1* to *3*) keeping the remaining substructure constant. The compound HOMO can be represented as the donor (the sulfur substituent) HOMO combined out-of-phase with the acceptor (the remaining molecule) HOMO and incorporating a smaller in-phase contribution from acceptor LUMO. This is shown for the systems *1a*–*3a* in Fig. 1; phase and relative amplitudes at each atom are represented by the vectors. The successive replacement of two CH_3S^- with S^- donors through the series *1*–*3* increases the donor-HOMO energy by concentrating electron density on sulfur. The predicted result of this change is an increased incorporation of acceptor LUMO leading to increased charge transfer. At the same time the compound HOMO is depleted at C-1 and C-3 where acceptors HOMO and LUMO are out-of-phase (vectors in opposite direction) and concentrated on C-2 and N where these orbitals are in phase. These changes are in accord with the observed ^{13}C NMR results assum-

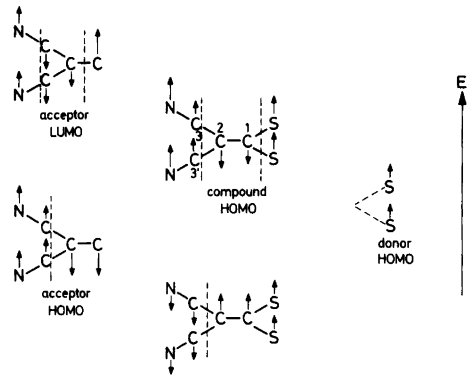

Fig. 1. Combination of donor and acceptor substructure orbitals to give compound HOMO. Phase and relative amplitude at each atom are represented by the vectors.

* An alternative interpretation would involve a predominating contribution from *changes* in the mean electronic excitation energy.[10] This alternative seems unlikely as the absorption spectra are largely unchanged through each of the series *1*–*3*, *e.g.* $\lambda_{max} = 334$, 341, and 342 nm for *1c*, *2c*, and *3c*, respectively and CNDO calculations[12] show only a small shift in the lowest $n \rightarrow \pi^*$ transition while they predict the development of positive charge at C-1.

ing that chemical shift changes are influenced primarily by charge density variations. The model does not predict the slight but consistent upfield shift at C-2 in the monoanion relative to the dianion but neither does the CNDO calculation of total charge.[12] However, it should be noted that both models operate on the isolated molecule and do not include medium effects.

The range of applicability of this approach has been tested against data from the literature. The model presented here predicts the variation in ^{13}C NMR substituent shifts for donor substituted ethylenes,[5] butadienes,[1] and arenes.[13] The observed attenuation in the two latter systems does not emerge from this simple picture. However, already the introduction into the interaction scheme of the subjacent unoccupied orbital of the skeleton substructure will bring forth such an effect.

REFERENCES

1. Kayimoto, O. and Fueno, T. *Tetrahedron Lett.* (1972) 3329.
2. Grahn, W. and Reichardt, C. *Tetrahedron 32* (1976) 125.
3. Morishima, I., Yoshikawa, K., Okada, K., Yonezawa, T. and Goto, K. *J. Am. Chem. Soc. 95* (1973) 165.
4. Terui, Y., Tori, K. and Tsuji, N. *Tetrahedron Lett.* (1976) 621.
5. Miyajima, G., Takahashi, K. and Nishimoto, K. *Org. Magn. Reson. 6* (1974) 413.
6. Pople, J. A. and Gordon, M. *J. Am. Chem. Soc. 89* (1967) 4253.
7. Newton, M. D. and Lipscomb, W. N. *J. Am. Chem. Soc. 89* (1967) 4261.
8. Sardella, D. J. *J. Am. Chem. Soc. 95* (1973) 3809; *98* (1976) 2100.
9. a. Jensen, K. A. and Henriksen, L. *Acta Chem. Scand. 22* (1968) 1107; b. Gompper, R. and Töpfl, W. *Chem. Ber. 95* (1962) 2861; c. Söderbäck, E. *Acta Chem. Scand. 24* (1970) 228.
10. Ditchfield, R. and Ellis, P. D. In Levy, G. C., Ed., *Topics in Carbon-13 NMR Spectroscopy*, Wiley-Interscience, New York 1974, Vol. 1.
11. Betteridge, D., Henriksen, L., Sandström, J., Wennerbeck, I. and Williams, M. A. *Acta Chem. Scand. A 31* (1977) 14.
12. Sandström, J. and Henriksen, L. *Unpublished results.*
13. Stothers, J. B. *Carbon-13 NMR Spectroscopy*, Academic, New York 1972, p. 196.

Received April 13, 1978.

Acta Chemica Scandinavica A 32 (1978) 705–714

Tentative Assignments of Fundamental Vibrations of Thio- and Selenoamides. V. Tetramethylthiouram Disulfide

U. ANTHONI,[a] G. BORCH,[b] P. KLÆBOE[c] and P. H. NIELSEN[a]

[a] Chemical Laboratory II, The H. C. Ørsted Institute, DK-2100 Copenhagen, Denmark, [b] Chemistry Department A, The Technical University of Denmark, DK-2800 Lyngby, Denmark and [c] Department of Chemistry, University of Oslo, Oslo 3, Norway

The infrared and Raman spectra of tetramethylthiouram disulfide (TMTD) and four ^{13}C, ^{15}N and deuterium labelled analogues have been studied in the solid state and in solution in the region below 4000 cm^{-1}. A normal coordinate analysis has been accomplished for these compounds as a 24-body problem utilizing a general valence force field. By fitting 26 force constants to reproduce *ca.* 300 observed frequencies, the normal modes of vibration are described in terms of the potential energy distribution between the symmetry coordinates. A tentative assignment of the fundamentals of TMTD and the perdeuterated compound is given based upon intensities, Raman depolarisation ratios, the $^{13}C/^{15}N$ shifts and the calculated values. The results indicate the need for revision of previous assignments for TMTD.

In the present paper, the IR and Raman spectra of tetramethylthiouram disulfide, $[(CH_3)_2NCSS]_2$ (TMTD), and the four isotopically substituted derivatives $[(CD_3)_2N-CSS]_2$ (TMTD-d_{12}), $[(CH_3)_2N-{}^{13}CSS]_2$ (TMTD-^{13}C), $[(CH_3)_2{}^{15}N-CSS]_2$ (TMTD-^{15}N), and $[(CD_3)_2N-{}^{13}CSS]_2$ (TMTD-d_{12}-^{13}C) were measured in solution and in the solid state in the region below 4000 cm^{-1}. Semiquantitative Raman depolarisation data were also obtained, but with a few exceptions vibrations of species *a* and *b* overlap completely. The assignments were supported by the results of a full normal coordinate analysis (NCA) (*i.e.* including treatment of the methyl groups) based upon the general valence force field (GVFF) derived for related compounds,[1,2] assuming C_2 symmetry.

The IR and Raman spectra of TMTD have previously been measured by Coleman *et al.*[3] in the region below 2000 cm^{-1}. A partial assignment of the fundamental vibrations was proposed from a simplified NCA treating the methyl groups as point masses. The isotopic shifts observed in our spectra were incompatible with the assignment proposed by Coleman *et al.* and it has been necessary to reinvestigate the spectrum of TMTD in some detail. A reproduction of the IR spectrum of TMTD in the range 4000–250 cm^{-1} has been reported[4] for use as reference spectrum in pesticide research. Contreras and Cortés[5] reported some major IR shifts of TMTD on complex formation with cobalt(II).

STRUCTURE

In a preliminary report[6] the crystal and molecular structure of TMTD has been given but has since been refined by least-squares methods to $R=0.095$ for 426 non-zero observed reflections (personal communication from the author). TMTD consists of two planar C_2NCS_2 units with a dihedral C–S–S–C angle of 88.3°. The most important bond distances are: CH_3-N: 1.483(21) and 1.506(18) Å, C–N: 1.319(15) Å, C=S: 1.634(13) Å, C–S: 1.829(15) Å, and S–S: 2.005(7) Å. The positions of the hydrogen atoms were estimated by assuming tetrahedral configuration of the methyl group and standard C–H distances. The final Cartesian coordinates correspond to an overall C_2 symmetry and may be obtained on request.

^1H NMR studies of TMTD in solution indicate a restricted rotation around the C(S)–N bond with an energy barrier of *ca.* 15 kcal/mol.[6–10] Splittings due to the restricted rotation around the C–S and

S–S bonds have not been observed in these spectra. Likewise the ^{13}C NMR spectrum of TMTD ($CDCl_3$) showed only splittings due to the C–N barrier at temperatures down to −15 °C, the lowest temperature obtainable without the precipitation of TMTD. Probably the barriers around the C–S and S–S bonds do not exceed 10 kcal/mol.[11] On the NMR time scale, TMTD can therefore be considered composed by two planar dimethyldithiocarbamate units joined by the S–S bond, *i.e.*, the C_2-symmetry is retained. Since new bands do not appear in the vibrational spectra of TMTD on dissolution we assume TMTD to occur in solution only as one isomer most probably of C_2-symmetry.

EXPERIMENTAL

The preparation of the compounds as well as the techniques and equipment used for recording the IR and Raman spectra have been given in a previous paper.[1] Infrared spectra were also run in CCl_4 and CS_2 solution but the spectra were identical within a few cm^{-1} with those recorded in $CHCl_3$ and no indication of the presence of more than one isomer was found.

Noise-decoupled ^{13}C NMR spectra were determined with a Bruker WH 90 system (22.63 MHz) operating in the Fourier transform mode. The samples were examined as saturated solutions in $CDCl_3$ and shieldings measured relative to internal TMS. The following values were obtained at room temperature: 42.0 and 47.5 ppm (CH_3) and 193.5 ppm (*C*S). The spectrum was also obtained of the ^{13}C substituted TMTD, but we were unable to discern and long-range coupling due to the $^{13}C-S-S-^{13}C$ grouping.

NORMAL COORDINATE ANALYSIS

The NCA was performed as a 24-body problem assuming C_2-symmetry of TMTD. Treatment of TMTD under point group C_2 reduced the normal modes of vibration to the irreducible representation $T_{vib}=34A+32B$, and the standard GF[12] programs[13] were employed. The potential field employed was of the general valence force field type similar to that described in previous papers.[1] Of the 66 normal modes of vibration possible, 32 are out-of-phase combinations (species *B*) of the two dimethyldithiocarbamate units joined by the S–S bond. The remaining 34 of species *A* are composed of the 32 corresponding in-phase combinations together with the S–S stretching and C–S–S–C

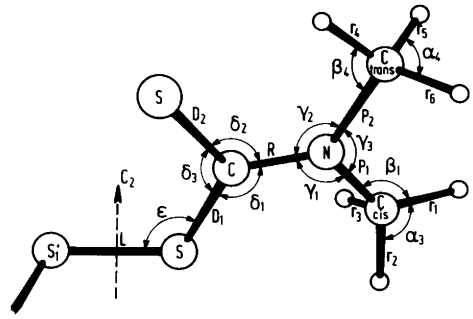

Fig. 1. Internal coordinates for TMTD (one half shown). The following coordinates are not shown on the figure: $CH_3^{cis}-N$ torsion τ_1, $CH_3^{trans}-N$ torsion τ_2, $CH_3^{cis}-N-C-S$ torsion τ_3, $CH_3^{trans}-N-C-S$ torsion τ_4, $N-C-S-S$ torsion τ_5, $S=C-S-S$ torsion τ_6, and S–S torsion τ_7. The twofold axis of symmetry indicated is perpendicular to the plane of the paper.

torsional modes. The internal coordinates used in setting up the *F* matrix are simply the changes in bond lengths and interbond angles. The symmetry coordinates are defined by the in-phase and out-of-phase combinations (Fig. 1).

The initial values for the force constants were first chosen in accordance with the NCA reported by Coleman *et al.*[3] but only a very poor agreement was achieved especially for the isotopic shifts. The values were then adjusted to comply with the force fields previously obtained for tetramethylthiourea[1] and dimethyldithiocarbamates.[2] This allowed assignment of more than 250 experimental frequencies by slight refinements of the diagonal elements of the *F* matrix using the Jacobian matrix of frequencies *vs.* force constants as a guide. However, attempts to refine this force field by the usual least-squares procedure failed and led only to non-converging solutions. Inspection of the correlation matrix (*cf.* Knoeck and Witt[14]) showed that several of the matrix elements related to the coordinates γ_1/γ_2 and P_1/P_2 were approaching 1. Accordingly, the isotopic substitution is insufficient for determining separate force fields for the *cis* and *trans* methyl groups, and the constraints $F_{R\gamma 1}=F_{R\gamma 2}$, $F_{P_1\gamma 1}=F_{P_2\gamma 2}$ and $F_{P_1\gamma 3}=F_{P_2\gamma 3}$ were introduced. Furthermore, the number of torsional force constants was reduced by setting $H_{\tau 3}=H_{\tau 4}$ and $H_{\tau 5}=H_{\tau 6}$. A new least-square adjustment of the force field to the observed frequencies revealed that several of the important interaction force constants (*e.g.* $F_{D_1D_2}$)

Table 1. Final valence force constants for tetramethylthiouram disulfide.

Force type	Constants symbol	Group[a]	Coordinate(s) involved	Atoms common to interacting coordinates	Value[b]
Stretch	K_r	CH_3	C-H		4.69
	K_P	CH_3-N	C-N		5.00
	K_R	N-C(S)	N-C		6.81
	K_{D_2}	C=S	C=S		3.02
	K_{D_1}	C-S	C-S		2.13
	K_L	S-S	S-S		2.58
Stretch-Stretch	F_r	CH_3	C-H,C-H	C	0.038
	F_{RD_1}	N-C-S	N-C,C-S	C	1.52
	F_{RP}	CH_3-N-C	C-N,N-C	N	0.27
	F_P	CH_3-N-CH_3	C-N,N-C	N	0.30
Bend	H_α	CH_3	<HCH		0.524
	H_β	CH_3-N	<HCN		0.773
	$H_{\gamma_1}=H_{\gamma_2}$	CH_3-N-C	<CNC		1.59
	H_{γ_3}	CH_3-N-CH_3	<CNC		2.26
	$H_{\delta_1}=H_{\delta_2}$	N-C=S/N-C-S	<NCS		0.68
	H_{δ_3}	S=C-S	<SCS		1.29
	H_ϵ	C-S-S	<CSS		0.83
Stretch-bend	$F_{R\gamma_1}=F_{R\gamma_2}$	CH_3-N-C	<CNC,N-C	N-C	0.68
	$F_{P_1\gamma_1}=F_{P_2\gamma_2}$	CH_3-N-C	<CNC,CH_3-N	CH_3-N	0.90
	$F_{P_1\gamma_3}=F_{P_2\gamma_3}$	CH_3-N-CH_3	<CNC,CH_3-N	CH_3-N	1.33
	$F_{P\beta}$	CH_3-N	<HCN,CH_3-N	CH_3-N	0.34
Bend-bend	F_β	CH_3-N	<HCN,<HCN	C-N	-0.047
Torsion	$H_{\tau_1}=H_{\tau_2}$	CH_3-N	CH_3-N		0.0314
	$H_{\tau_3}=H_{\tau_4}$	N-CS_2	N-CS_2		0.305
	$H_{\tau_5}=H_{\tau_6}$	C-S	C-S		0.177
	H_{τ_7}	S-S	S-S		0.198

[a] The force constants referring to the CH_3^{cis} and CH_3^{trans} groups have been assumed identical.

[b] In units of mdyn/A (stretch constants), mdyn/rad (stretch-bend interaction constants) and mdyn·A/(rad)^2 (bending and torsion constants).

were very poorly determined, and that a drastic reduction in the number of force constants was necessary. Using only the 26 force constants of Table 1 we finally obtained satisfactory convergence and good agreement between observed and calculated frequencies and $^{15}N/^{13}C$ shifts (Table 2 and 3). However, the number of independent constants of the force field has been reduced to the point where detailed considerations based upon their relative values are not clearly justified. We shall only point out that the gross features are in accordance with expectations (e.g. $K_{D_2} > K_{D_1}$, $K_R > K_P$) and that the final values are physically reasonable.

RESULTS AND DISCUSSION

The IR spectrum of TMTD in the range 250–4000 cm^{-1} is reproduced in a collection of reference spectra[4] and the region below 2000 cm^{-1}, together with the Raman spectrum, in Coleman's paper.[3] The IR spectra correspond in detail to the spectra obtained by us except for a splitting in the strong band near 1500 cm^{-1} into two branches at 1497 and 1506 cm^{-1} attributed[3] to the in-phase and out-of-phase CN stretching modes of species *a* and *b*. This splitting does not appear in any of our spectra in the solid phase nor in solution, and the calculations indicate (Table 2) that the fundamentals in question ($\nu_7 a$ and $\nu_{41} b$) are accidentally degener-

ate. The agreement of our Raman spectra with that given by Coleman *et al.* is good.

The ^{13}C and ^{15}N shifts included in Tables 2 and 3 are not in all cases definite though the quality of the spectra is excellent. For example, the IR spectrum of TMTD displays two very strong bands at 970 and 977 cm^{-1} together with a weaker band at 952 cm^{-1}. In the ^{13}C-labelled compounds we observe the corresponding three bands at 974 (medium strength), 954 (strong), and 939 cm^{-1} (very strong). Based upon the results of the NCA this is explained (Table 2) as a shift of the funda-

Table 2. Observed and calculated vibrational frequencies (cm^{-1}) of tetramethylthiouram disulfide and frequency shifts obtained by comparison with $[CH_3)_2N-{}^{13}CSS]_2$ and $[(CH_3)_2{}^{15}N-CSS]_2$.

Infrared[a]				Raman[a]				Calculated[b]			Assignment and Description[c]
solid, disc			solution	solid			solution				(PED, %)[d]
parent	^{13}C-sh	^{15}N-sh	$CHCl_3$	parent	^{13}C-sh	^{15}N-sh	$CHCl_3$	parent	^{13}C-sh	^{15}N-sh	
3010w,br	0	0		3017w	0	0					
				2980w	0	0	2988m(0.41)				
				2960w,sh	0	0					
2932m	0	0	2938m	2933s	0	0	2936s(0.14)	2954 2949 2947 2947	0 0 0 0	0 0 0 0	$\nu_1{}^a$, $\nu_{35}{}^b$, $\nu_{as}CH(99)$ $\nu_2{}^a$, $\nu_{36}{}^b$, $\nu_{as}CH(99)$ $\nu_3{}^a$, $\nu_{37}{}^b$, $\nu_{as}CH(99)$ $\nu_4{}^a$, $\nu_{38}{}^b$, $\nu_{as}CH(99)$
				2924m,sh	0	0					$2\cdot\nu_8{}^A$
2895vw				2893m,sh	0	0					$\nu_8+\nu_{11}{}^A$
2851w	0	2	2860w	2859m	0	0	2868m(0.19)	2866 2866	0 0	0 0	$\nu_5{}^a$, $\nu_{39}{}^b$, $\nu_s CH(100)$ $\nu_6{}^a$, $\nu_{40}{}^b$, $\nu_s CH(100)$
				2854w,sh			2857w,sh				$\nu_8+\nu_{12}{}^A$
				2848w	2						$\nu_{10}+\nu_{12}{}^A$
				2808w	-1	0	2809w(0.08)				$2\cdot\nu_{12}{}^A$
2790vw			2800vw	2787w		2	2793vw,sh				$\nu_{12}+\nu_{13}{}^A$
				1508vw	0	0	1508vw,sh				$\nu_{18}+\nu_{24}{}^A$
1500s	18	21	1504s	1490vw			1498m,br(0.56)	1493	10	12	$\nu_7{}^a$, $\nu_{41}{}^b$, $\nu CN(29)$, $\delta CH_3(36)$, $\rho CH_3(24)$
1454w,sh	0			1465m,br	6	2	ca. 1453m,br	1466 1462 1459	0 0 0	0 0 0	$\nu_8{}^a$, $\nu_{42}{}^b$, $\delta CH_3(83)$ $\nu_9{}^a$, $\nu_{43}{}^b$, $\delta CH_3(85)$ $\nu_{10}{}^a$, $\nu_{44}{}^b$, $\delta CH_3(87)$
				1433w	0	-1		1442	7	7	$\nu_{11}{}^a$, $\nu_{45}{}^b$, $\delta CH_3(71)$, $\nu CN(18)$
1400m	1	1	1409w	1400s	1	0	1408m(0.85)	1407	1	1	$\nu_{12}{}^a$, $\nu_{46}{}^b$, $\delta CH_3(100)$
1375s	8	9	1380s	1375s	8	9	1382s(0.67)	1385	7	5	$\nu_{13}{}^a$, $\nu_{47}{}^b$, $\delta CH_3(84)$, $\nu CN(17)$
1335vw			1335vw	1336vw	-1		1335vw				$2\cdot\nu_{21}{}^A$
1294vw	16	1	1297vw								$\nu_{53}+\nu_{59}{}^A$
1235s	4	19	1245s	1239w	4	20	ca. 1245w	1248	6	18	$\nu_{14}{}^a$, $\nu_{48}{}^b$, νCH_3-N(51), $\delta CH_3NC(33)$, $\rho CH_3(25)$
1150s	15/4	1	1152s	1150s	13/0	0	1156(0.58)	1158 1155	12	2	$\nu_{15}{}^a$, $\nu_{49}{}^b$, $\rho CH_3(61)$, $\nu CN(12)$ $\nu_{16}{}^a$, $\nu_{50}{}^b$, $\rho CH_3(80)$, $\delta CH_3(17)$
				1134w		3	1131vw,sh				$2\cdot\nu_{22}{}^A$
1110vw	2	3	1115w,sh	1105w	0	0					$\nu_{55}+\nu_{57}{}^A$
1090vw	0	0	1095vw	1091w	0	4	1090vw	1091	0	0	$\nu_{17}{}^a$, $\nu_{51}{}^b$, $\rho CH_3(86)$, $\delta CH_3(13)$
1039s	1	5	1049m	1041w	0	4	1050w	1048	1	6	$\nu_{18}{}^a$, $\nu_{52}{}^b$, $\rho CH_3(57)$, νCH_3-N(39)
977vs	3	4	985s,sh	977vs	3	2					$\nu_{55}+\nu_{59}{}^A$
970vs	31	3	976vs	977vs	30	2	986s(0.23)	982	22	3	$\nu_{19}{}^a$, $\nu_{53}{}^b$, $\nu_{as}CSS(37)$, $\nu CN(20)$, νCH_3-N(31)
952s	-2	4	960s,sh	958m,sh	0	7	964w,sh				$\nu_{26}+\nu_{55}{}^B$
				898vw	0	0					$2\cdot\nu_{24}{}^A$
849s	-2/13	2	855m	852s	0/13	2	857s(0.32)	857 856	7 7	3 3	$\nu_{20}{}^a$, νCH_3-N(81) $\nu_{54}{}^b$, νCH_3-N(82)
839w,sh	2	2									$\nu_{24}+\nu_{25}{}^A$
				824vw	3						$\nu_{22}+\nu_{27}{}^A$
790vw	1	1		795vw	2	2					$2\cdot\nu_{58}{}^A$
				773vw	0	0					$2\cdot\nu_{25}{}^A$
674vw				676vw	2	0		676	3	4	$\nu_{21}{}^a$, $\delta(CH_3)_2N(50)$, $\rho CH_3(13)$
667vw				667vw				670	3	5	$\nu_{55}{}^b$, $\delta(CH_3)_2N(57)$, $\rho CH_3(14)$

Table 2. Continued.

Infrared[a]				Raman[a]				Calculated[b]			Assignment and Description[c] (PED,%)[d]
solid, disc			solution $CHCl_3$	solid			solution $CHCl_3$				
parent	^{13}C-sh	^{15}N-sh		parent	^{13}C-sh	^{15}N-sh		parent	^{13}C-sh	^{15}N-sh	
563m/w	3	3	563m/w	561vs	2	3	565vs(0.14)	558	0	0	$\nu_{22}a$, νS-S(75)
542w,sh	16/10	3	540w	536vw,sh		3	542vw,sh	538	13	4	$\nu_{23}a$, τCN(65), τC-S(22)
520vw,sh	12	0						526	12	5	$\nu_{56}b$, τCN(69), τC-s(22)
				502vw	1	0	502vw				$2\cdot\nu_{27}A$
				490vw	0	0	493vw				$\nu_{57}+\nu_{66}A$
			475vw	480vw	0	0					$\nu_{59}+\nu_{61}A$
441m	0	1	444m	443s	0	1	447s(0.28)	442 439	0	2	$\nu_{57}b$, νC=S(36), δCH_3NC(40) $\nu_{24}a$, νC=S(38), δCH_3NC(39)
396m	0	1	396m	395s	0	1	395s(0.20)	395 390	0	0	$\nu_{58}b$, $\nu_{as}CSS$(72), $\delta(CH_3)_2N$(20) $\nu_{25}a$, $\nu_{s}CSS$(73), $\delta(CH_3)_2N$(17)
358w	0	0		361w	0	0					$2\cdot\nu_{61}A$
312vw,sh	0	0		317m	1	1	314m(0.5)	312	0	1	$\nu_{59}b$, δC-S-S(24), δS=C-S(33)
284w,sh	0	2		283w				290	1	4	$\nu_{26}a$, τCN(54), τC-S(16)
275m	1	5		267m	0	0		266	2	3	$\nu_{60}b$, τCN(66), τC-S(15)
268w,sh				255vw				252	1	1	$\nu_{27}a$, δS=C-S(39, δNCS(16), νCN(12)
218vw,br											$\nu_{33}+\nu_{61}B$
				203w	0	0					$2\cdot\nu_{32}A$
178m				179m	0	1	175m(0.6)	175	0	0	$\nu_{61}b$, δNCS(64), δCH_3NC(17)
151vw				158vw							$\nu_{32}+\nu_{66}B$
144vw				142vw				145	0	0	$\nu_{28}a$, τCH_3(95)
135vw				133vw	0	0		136 133 133 131	1 0 0 0	0 0 0 0	$\nu_{29}a$, δS-S-C(30), τCN(19), τC-S(20) $\nu_{30}a$, δNCS(64), δCH_3NC(15) $\nu_{62}b$, τCH_3(66) $\nu_{63}b$, τCH_3(39), δC-S-S(19), τCN(11), τC-S(14
				125vw	1	0		125 124	0 0	0 0	$\nu_{31}a$, τCH_3(87) $\nu_{64}b$, τCH_3(80)
117w				116w	0	1					lattice mode
110w				110m	0	0					lattice mode
				97vw				96	0	0	$\nu_{32}a$, τC-S(55), τCN(34)
91w,sh								93	0	0	$\nu_{65}b$, τC-S(65), τCN(29)
84m				75s	2						lattice mode
68w				64m,sh	0	0					lattice mode
50w								51	0	0	$\nu_{66}b$, τC-S(61), δC-S-S(25)
				44s	0			47	0	0	$\nu_{33}a$, τC-S(60), δC-S-S(21)
38vw				37m,sh	0			39	0	0	$\nu_{34}a$, τS-S(65)
32w											lattice mode

[a] The following abbreviations have been used: s, strong; m, medium; w, weak; br, broad; sh, shoulder. The Raman depolarisation ratio is given in parenthesis. Weak bands between 1550 and 2750 cm^{-1} have been omitted.

[b] Iteration based upon all isotopic species.

[c] Abbreviations: ν = stretching, δ, Δ = deformation, ρ = rocking, ω = wagging, t = twisting, τ = torsion, and, as subscripts, s = symmetric, as = antisymmetric.

[d] The potential energi distribution (PED) is defined as $\underline{x}_{ik} = 100\underline{F}_{ii}\underline{L}^2_{ik}/\underline{\lambda}_k$. The stated PED's are only approximative and small contributions have been neglected.

mental $\nu_{19}a$ at 970 cm^{-1} by 31 cm^{-1} to 939 cm^{-1}, while the two other bands are considered combination modes which are hardly displaced on ^{13}C substitution. Though this interpretation is supported by the Raman spectra the results remain ambiguous.

Raman depolarisation measurements have been performed for both TMTD and TMTD-d_{12} in $CHCl_3$ solution. The fundamentals belonging to species *a* should give rise to polarised Raman lines whereas those of species *b* should appear depolarised. However, the in-phase and out-of-phase combinations in most cases superimpose to give one band which appears polarised. Therefore, only the assignments of $\nu_{23}a$, $\nu_{59}b$, and $\nu_{61}b$ in the

spectrum of TMTD and $\nu_{21}a$, $\nu_{22}a$, $\nu_{59}b$, and $\nu_{61}b$ in TMTD-d_{12} are supported from these measurements.

The CH_3 and CD_3 stretching modes. The four asymmetric CH stretching modes of species *a* are expected to fall within a narrow frequency range (7 cm^{-1} according to the NCA) coincident with the corresponding modes of species *b*. Furthermore, the NCA predicts the symmetric modes to coincide to one band at a lower frequency. The two strongest bands found both in the IR and the Raman spectrum of TMTD have been assigned to these overlapping fundamentals (Table 2). Some of the remaining bands are easily explained as overtones or binary

Table 3. Observed and calculated vibrational frequencies (cm^{-1}) of perdeuterotetramethylthiouram disulfide and frequency shifts obtained by comparison with $[(CD_3)_2N-{}^{13}CSS]_2$.

Infrared[a]			Raman[a]			Calculated[b]		Assignment and Description[c] (PED,%)[d]
solid, disc		solution	solid		solution			
parent	^{13}C-sh	$CHCl_3$	parent	^{13}C-sh	$CHCl_3$	parent	^{13}C-sh	
2262w,br		2265w,sh	2265w,br		2270w,sh			$\nu_8+\nu_{11}^A$
		2240m,sh	2232m,sh		2240m,sh	2220	0	ν_1^a, $\nu_{35}b$, $\nu_{as}CD(95)$
2221w	0	2233m	2223s	2	2232s(0.50)	2204 2200 2199	0 0 0	ν_2^a, $\nu_{36}b$, $\nu_{as}CD(97)$ ν_3^a, $\nu_{37}b$, $\nu_{as}CD(98)$ ν_4^a, $\nu_{38}b$, $\nu_{as}CD(98)$
2176w	3	2190w	2177w	4	2188w			$\nu_9+\nu_{11}^A$
2135w	3	2143m	2135s	4	2143s(0.23)			$\nu_{10}+\nu_{14}^A$
2108w	0	2114w,sh	2113w,sh		2115w,sh			$2\cdot\nu_{11}^A$
		2107m	2102m	2	2105m(0.33)			$2\cdot\nu_{12}^A$
2087vw	0	2094w,sh	2090w,sh		2093w,sh			$2\cdot\nu_{13}^A$
2060m	0	2070s	2062m	1	2070s(0.28)	2066 2065	0 0	ν_5^a, $\nu_{39}b$, $\nu_s CD(98)$ ν_6^a, $\nu_{40}b$, $\nu_s^a CD(98)$
1538vw	8		1540vw					$2\cdot\nu_{20}^A$
1505vw,sh			1509vw		~1500vw,br			$\nu_{16}+\nu_{21}^A$
1443vs,sh	2				1447m,sh			$\nu_{12}+\nu_{24}^A$
1437s	22	1437vs	1433s	21	1438s(0.79)	1434	26	ν_7^a, $\nu_{41}b$, $\nu CN(70)$
1419w,sh			1417vw,sh		1418vw,sh			$\nu_{51}+\nu_{56}^A$
1296vw	2		1302vw					$\nu_{20}+\nu_{22}^A$
1258vw,sh			1259vw					$\nu_{15}+\nu_{27}^A$
1210s	4		1214w	4		1211	8	ν_8^a, $\nu_{42}b$, νCD_3-N(64), $\delta CD_3NC(42)$
1166vw	2		1156vw					$2\cdot\nu_{21}^A$
1147vw	7		1144vw	5				$\nu_{20}+\nu_{25}^A$
			1124vw,sh					$2\cdot\nu_{55}^A$
1111m	3	1120m	1112w		1119w(0.9)	1111	1	ν_9^a, $\nu_{43}b$, $\delta CD_3(84)$, νCD_3-N(24)
1100w,sh	0	1104w,sh	1104w,sh	3		1106	4	ν_{10}^a, $\nu_{44}b$, $\delta CD_3(80)$, νCD_3-N(32)
			1078w	1				$\nu_{18}+\nu_{27}^A$
			1074w,sh	1				$\nu_{54}+\nu_{59}^A$
1057s	2		1058w	2	~1064w,br	1053	0	ν_{11}^a, $\nu_{45}b$, $\delta CD_3(87)$
1042vw,sh			1045vw			1050 1045 1043	0 0 0	ν_{12}^a, $\nu_{46}b$, $\delta CD_3(83)$ ν_{13}^a, $\nu_{47}b$, $\delta CD_3(88)$ ν_{14}^a, $\nu_{48}b$, $\delta CD_3(92)$
1017s	16/4	1012m	1013m	15	1021m(0.35)	1006	11	ν_{15}^a, $\nu_{49}b$, $\rho CD_3(37)$, $\delta(CD_3)_2N(17)$, $\nu C{=}S(12)$
946w,sh	0		942w		944w			$\nu_{21}+\nu_{25}^A$
925vw,sh			928w,sh	0	928w,sh	928	0	ν_{16}^a, $\nu_{50}b$, $\rho CD_3(75)$
910s	0/8	914s	914s	8	921s(0.60)	917	18	ν_{17}^a, $\nu_{51}b$, $\nu_{as}CSS(29)$, $\nu CN(18)$, νCD_3-N(17)
889m	12	899s	892m	10	899m,sh(0.81)			$\nu_{22}+\nu_{25}^A$
837vw	0		834w	0	833w,sh	832	0	ν_{18}^a, $\nu_{52}b$, $\rho CD_3(91)$
816m	2		817w	1	824w(0.7)	824	1	ν_{19}^a, $\nu_{53}b$, $\delta CD_3(80)$
770m	6		773m	5		770 769	3 3	ν_{20}^a, νCD_3-N(55), $\rho CD_3(11)$ $\nu_{54}b$, νCD_3-N(57), $\rho CD_3(10)$
750vw	2		753vw					$2\cdot\nu_{25}^A$
618vw			615vw					$\nu_{25}+\nu_{27}^A$
			585vw					$2\cdot\nu_{59}^A$
572w	1	576w	573m	1	578m(0.45)	589	0	ν_{21}^a, νS-S(43), $\rho CD_3(12)$, $\delta(CD_3)_2N(12)$

Table 3. Continued.

Infrared[a]			Raman[a]					
solid, disc		solution	solid		solution	Calculated[b]		Assignment and Description[c] (PED, %)[d]
parent	^{13}C-sh	$CHCl_3$	parent	^{13}C-sh	$CHCl_3$	parent	^{13}C-sh	
566w,sh			566w,sh		567w,sh	559	1	$\nu_{55}b$, $\delta(CD_3)_2N(33)$, $\rho CD_3(27)$
539w,sh		538w,sh	544w,sh					$2\cdot\nu_{26}A$
528vs	2	532s	529s	1	528vs (0.31)	528	1	$\nu_{22}a$, $\nu S\text{-}S(37)$, $\delta(CD_3)_2N(28)$
518vw	6/10		522w,sh			520	13	$\nu_{23}a$, $\tau CN(58)$, $\tau C\text{-}S(22)$
509vw	19	504vw,sh	505vw,sh		504vw,sh	506	13	$\nu_{56}b$, $\tau CN(64)$, $\tau C\text{-}S(24)$
487vw,br	0	480vw,sh	484vw,sh					$2\cdot\nu_{27}A$
396m	2		400m	2	400m	410 406	0 0	$\nu_{57}b$, $\nu C\text{=}S(39)$, $\delta CD_3NC(35)$ $\nu_{24}a$, $\nu C\text{=}S(39)$, $\delta CD_3NC(34)$
			387w		390m			$\nu_{26}+\nu_{62}B$
375m	1		375s	0		379 377	0 0	$\nu_{58}b$, $\nu_s CSS(68)$, $\delta(CD_3)_2N(25)$ $\nu_{25}a$, $\nu_a CSS(68)$, $\delta(CD_3)_2N(21)$
342vw	0		343m	0	340w			$2\cdot\nu_{61}B$
298m	2		300s	0	293s(0.6)	301	0	$\nu_{59}b$, $\delta C\text{-}S\text{-}S(21)$, $\delta S\text{=}C\text{-}S(34)$
271m	0		269w	0		271	1	$\nu_{26}a$, $\tau CN(48)$, $\tau C\text{-}S(17)$
			255vw			249	1	$\nu_{60}b$, $\tau CN(65)$, $\tau C\text{-}S(17)$
246m			242m	0		242	0	$\nu_{27}a$, $\delta S\text{=}C\text{-}S(39)$, $\delta NCS(15)$, $\nu CN(12)$
207vw								$\nu_{30}+\nu_{63}B$
193vw			192vw	0				$\nu_{63}+\nu_{64}A$
178w			177m	0	171m(0.5)	168	0	$\nu_{61}b$, $\delta NCS(59)$, $\delta CD_3NC(18)$
158w			160w		160w(0.7)			$\nu_{34}+\nu_{62}B$
138vw			132vw	0		132	1	$\nu_{28}a$, $\delta S\text{-}S\text{-}C(39)$, $\tau CN(17)$, $\tau C\text{-}S(21)$
122vw			125vw	0		127 123	1 0	$\nu_{62}b$, $\delta S\text{-}S\text{-}C(31)$, $\tau CN(11)$, $\tau C\text{-}S(23)$ $\nu_{29}a$, $\delta NCS(64)$, $\delta CD_3NC(18)$
117m			115w	0	115w	112	0	$\nu_{30}a$, $\tau CD_3(93)$
			105m	0	102w	98	0	$\nu_{63}b$, $\tau CD_3(66)$, $\tau C\text{-}S(22)$, $\tau CN(12)$
89w,sh			93w	0		90 89	0 0	$\nu_{31}a$, $\tau CD_3(74)$, $\tau C\text{-}S(14)$ $\nu_{64}b$, $\tau CD_3(90)$
83w						87 82	0 0	$\nu_{32}a$, $\tau CD_3(25)$, $\tau CN(30)$, $\tau C\text{-}S(41)$ $\nu_{65}b$, $\tau CD_3(33)$, $\tau CN(21)$, $\tau C\text{-}S(44)$
76vw			76vw					lattice mode
67w			67s	0				lattice mode
61m			63m,sh	0				lattice mode
56m								lattice mode
43w			43s	0		47 44	0 0	$\nu_{66}b$, $\tau C\text{-}S(61)$, $\delta C\text{-}S\text{-}S(24)$ $\nu_{33}a$, $\tau C\text{-}S(58)$, $\delta C\text{-}S\text{-}S(17)$
			37m,sh	0		38	0	$\nu_{34}a$, $\tau S\text{-}S(62)$

[a]See footnote to Table 2 for abbreviations. Weak absorption in the range 1550 - 2000 cm^{-1} has been omitted.

[b,c,d,e]See footnotes to Table 2.

combination modes. However, the ^{13}C and ^{15}N shifts of three weak bands in the upper part of this region (2960 – 3017 cm^{-1}) are negligible and must stem from combination modes of fundamentals which also remain unchanged. Since no such fundamentals are available they probably arise through ternary combination modes.

In the spectra of TMTD-d_{12} (Table 3) the pattern is quite similar, except that one of the asymmetric CD stretching bands ($\nu_1 a$, $\nu_{35} b$) is predicted to be shifted *ca.* 20 cm^{-1} towards higher frequency relative to the other asymmetric CD stretching vibrations. These fundamentals have been assigned to the strong rather broad absorption near 2230 cm^{-1} with a prominent shoulder at *ca.* 2240 cm^{-1}. The NCA predicts the four symmetric CD stretching modes to be coincident at *ca.* 2065 cm^{-1} corresponding to the strongest band in the IR spectrum in this region. However, in the Raman spectrum of TMTD-d_{12} in the solid phase the strongest band in this region occurs at 2135 cm^{-1}. In $CHCl_3$ solution this band moves to 2143 cm^{-1} and becomes comparable in intensity to the band at 2070 cm^{-1}. Since the NCA strongly contradicts this to be a

fundamental it is instead assumed to be an unusually strong combination mode. Only a combination of the CD_3 deformation modes (*e.g.* $\nu_{10}+\nu_{14}A$) can be expected to achieve the necessary intensity enhancement by Fermi resonance with the fundamentals of this region, and the band has been assigned accordingly. The assignment of the remaining bands of TMTD-d_{12} is straightforward.

The thioureide band ν_7/ν_{41}. In the IR spectrum of TMTD, the prominent band near 1500 cm^{-1} (known as the thioureide band[15]) is assigned to the overlapping fundamentals $\nu_7 a$ and $\nu_{41} b$. Coleman's results showed[3] this band to consist essentially of CN stretching (81 %) weakly coupled to C=S and CH_3-N stretching. The results of the present NCA (including full treatment of the CH_3 groups instead of considering them to be point masses) rather indicate this band to consist of CN stretching (29 %) strongly coupled to CH_3 deformation and rocking (total 60 %). On deuteration the coupling is removed and the corresponding band in TMTD-d_{12} near 1435 cm^{-1} consists mainly of CN stretching (70 %). Though our NCA probably overestimates the contribution of CH_3 modes to this band in TMTD (the ^{13}C and ^{15}N shifts are calculated too small) there is hardly any doubt that both CN stretching and CH_3 deformation and rocking modes contribute to this band. On complex formation with cobalt(II) chloride the frequency of this vibration is raised by 30 cm^{-1} reflecting the concomitant increase in double bond character of the CN bond.[5]

The CH_3 *and* CD_3 *deformation and rocking vibrations.* The four $\delta_{as}CH_3$ and two $\delta_s CH_3$ modes of species *a* are predicted by the NCA to be coincident with the corresponding six bands of species *b* and to appear in the range 1380–1470 cm^{-1} in the spectrum of TMTD. Since only four bands are observed in this region, the broad and unresolved absorption occurring in both the Raman and IR spectrum of TMTD near 1450–1460 cm^{-1} has been assigned to the overlapping fundamentals $\nu_8-\nu_{10}a/\nu_{42}-\nu_{44}b$. In the case of $\nu_{13}a/\nu_{47}b$ the observation of ^{13}C (8 cm^{-1}) and ^{15}N (9 cm^{-1}) shifts supports the occurrence of a weak coupling to CN stretching as indicated by the calculations. In the spectrum of TMTD-d_{12} (Table 3) the corresponding CD_3 deformation modes occur in the range 1040–1120 cm^{-1} and are easily assigned in accordance with the results of the NCA.

The ρCH_3 modes are expected from the calculations to give rise to four bands in the 1000–1200 cm^{-1} region each consisting of overlapping fundamentals of species *a* and *b*. On ^{13}C substitution, part of the strong band near 1150 cm^{-1} (Table 2) is displaced by 13–15 cm^{-1} towards lower frequencies while part of the absorption remains unchanged. The NCA indicates that the fundamentals $\nu_{15}a/\nu_{49}b$ are distinguished by a major ^{13}C shift of 12 cm^{-1} arising from coupling with the CN stretching mode while the ρCH_3 mode $\nu_{16}a/\nu_{50}b$ occurs at almost identical frequencies but is not diplaced by ^{13}C substitution. The 1150 cm^{-1} band is therefore assigned to all four fundamentals. The remaining fundamentals are assigned following the condition that $\nu_{17}a/\nu_{51}b$ is neither displaced by ^{13}C nor by ^{15}N substitution, while $\nu_{18}a/\nu_{52}b$ should shift by *ca.* 6 cm^{-1} on ^{15}N substitution as a result of coupling to the CH_3-N stretching mode. A few remaining weak bands in this region are assigned to overtones and combination modes.

Three of the ρCD_3 modes in TMTD-d_{12} should give rise to bands which are not displaced by ^{13}C substitution and, again, with complete overlap between fundamentals of species *a* and *b*. These have been identified with the weak absorption occurring near 928, 833 and 824 cm^{-1}. The overlapping fundamentals $\nu_{15}a/\nu_{49}b$, however, are calculated to exhibit a ^{13}C-shift of 11 cm^{-1} because of coupling with the C=S stretching and $(CD_3)_2N$ deformation modes. These are assigned the medium to strong bands observed in both the IR and Raman spectra near 1015 cm^{-1} displaying a ^{13}C shift of 15–16 cm^{-1}.

The skeletal modes of TMTD in the range 800–1300 cm^{-1}. In the IR spectrum of TMTD a strong band occurs at 1245 cm^{-1} ($CHCl_3$) which is shifted 4 cm^{-1} on ^{13}C substitution and 19 cm^{-1} on ^{15}N substitution towards lower frequencies. The Raman counterpart is much weaker but occurs at identical frequencies and with almost identical isotopic shifts. In good agreement with the NCA this band is assigned as overlapping $\nu_{14}a/\nu_{48}b$ fundamentals due to CH_3-N stretching (51 %) weakly coupled to CH_3NC deformation and CH_3 rock. In TMTD-d_{12} the coupling with CH_3 rock is removed and the corresponding band $\nu_8 a/\nu_{42}b$ is found at *ca.* 30 cm^{-1} lower frequencies. Coleman *et al.*[3] assigned this band to CH_3 rocking, but this seems excluded by the isotopic shifts reported here.

One of the strongest bands in both the IR and Raman spectrum of TMTD is observed near 980 cm^{-1}. The ^{15}N shift is only *ca.* 2 cm^{-1} but on ^{13}C substitution it displays a large shift of 30 cm^{-1}.

These characteristics allow an unambiguous assignment to the overlapping fundamentals $\nu_{19}a/\nu_{53}b$ arising from an out-of-phase stretching mode of the $(CH_3)_2N-CSS$ group of TMTD involving $\nu_{as}CSS$-(37 %), νCN(20 %) and νCH_3-N(31 %). In TMTD-d_{12} the counterpart is calculated to appear at 917 cm^{-1} displaying a ^{13}C shift of 18 cm^{-1}. However, two strong bands occur near this position in both the IR and Raman spectra of TMTD-d_{12}, one near 915 cm^{-1} (^{13}C-shift 8 cm^{-1}) and one near 890 cm^{-1} (^{13}C shift 10–12 cm^{-1}). Since the *sum* of the observed ^{13}C shifts corresponds quite closely to the predicted value, an explanation could be the occurrence of an overtone or combination mode with the following features: (i) The ^{13}C shift should be negligible since the observed ^{13}C shifts of this region can be explained entirely as arising from the fundamental. (ii) At least one of the components should involve skeletal modes of the $(CH_3)_2N-CSS$ group in order that Fermi resonance with the $\nu_{17}a/\nu_{51}b$ fundamental may achieve the necessary intensity. In our opinion the assigned combination mode, $\nu_{22}+\nu_{25}A$, most closely corresponds to these demands.

The overlapping fundamentals $\nu_{20}a/\nu_{51}b$ are calculated to appear at *ca.* 855 cm^{-1} with small ^{15}N and ^{13}C shifts. Considering the PED in comparison with the elements of the *L*-matrix, it consists of more than 80 % of symmetric $(CH_3)_2N$ stretching. Except for some ambiguity in the interpretation of the experimental ^{13}C shifts these features agree with the experimental spectra. In TMTD-d_{12} weak coupling occurs to the CD_3 rocking mode,

The region below 700 cm^{-1} of TMTU and TMTU-d_{12}. The band observed at 565 cm^{-1} in the Raman spectrum of TMTD in $CHCl_3$ solution is the strongest band in the spectrum; furthermore, it is the band having the lowest depolarisation ratio (0.14). It must accordingly be of species *a* and originate in vibrations producing a strong Raman scattering. The counterpart in the IR spectrum is only of weak to medium strength indicating the change of dipole moment during the vibration to be small. The observed ^{13}C and ^{15}N shifts are negligible (2–3 cm^{-1}). These features indicate strongly (*cf.* Bellamy [16]) that this band should be assigned to $\nu_{22}a$, due to the S–S stretching mode (75 % according to our NCA). The corresponding force constant $K_L=2.58$ mdyn/Å, is intermediate between the values for aliphatic sulfides (3.10 mdyn/Å [17]) and the value proposed by Coleman *et al.* for TMTD [3] (2.30 mdyn/Å). The latter value is obtained on the assumption, that the band with maximum S–S stretching character (91 % according to their NCA) is instead the strong, polarised Raman band at 447 cm^{-1} also observed with weak to medium strength in the IR at 444 cm^{-1}. Their NCA indicate the band at 565 cm^{-1} to originate in a vibration involving stretching and bending of the $CH_3-N-C-S$ part of the molecule, which, in our opinion, is not likely to be an adequate description of the strongest band in the Raman spectrum. Unfortunately, the results obtained for TMTD-d_{12} do not unambigously support our interpretation, since the S–S stretching character is equiparted between the two strong Raman bands at 578 and 528 cm^{-1} ($CHCl_3$), the latter of which also appear very strong in the IR contrary to expectations. If Coleman's assignment was correct, the band originating primarily in S–S stretching in the spectrum of TMTD-d_{12} should be the Raman line of medium strength at 400 cm^{-1} also having an IR counterpart of similar intensity. At present a decisive interpretation cannot be given for these bands.

Torsional vibrations of the $C_2N-C-S-S-NC_2$ chain give rise to the fundamentals ν_{23}, ν_{26}, ν_{32}, ν_{33}, and $\nu_{34}a$ and ν_{56}, ν_{60}, ν_{65}, and $\nu_{66}b$. These are only tentatively identified except in the case of $\nu_{23}a$ and $\nu_{56}b$, which are distinguished by displaying ^{13}C shifts calculated to *ca.* 13 cm^{-1}. In TMTU they appear as two weak bands at *ca.* 540 and 520 cm^{-1} and in TMTU-d_{12} they are displaced by *ca.* 20 cm^{-1} towards lower frequencies. In both cases the ^{13}C shifts have been difficult to establish with certainty, especially in the Raman spectrum where this region is completely dominated by the strong $\nu_{22}a$. Though the shifts are somewhat irregular, varying from 6 to 19 cm^{-1} according to the IR spectra, we believe these fundamentals to be correctly identified. They were not observed by Coleman *et al.*[3], likewise vibrations concerned with out-of-plane deformations and torsions were not included in their NCA. According to our NCA, some coupling occur to the τCH_3 bands of TMTD in the 120–50 cm^{-1} range and to the τCD_3 bands of TMTU-d_{12} between 80 and 120 cm^{-1}.

The symmetric stretching vibration of the CSS group is expected [2] to contribute significantly to strong Raman bands occurring in the 400–500 cm^{-1} region. In the Raman spectrum of TMTU we observe two strong, polarised bands at 447 and 395 cm^{-1} ($CHCl_3$) which might both comply with these demands. The NCA indicates the band at highest frequencies to originate in C=S stretching (36–

38 %) coupled to CH_3NC deformation (39 – 40 %), of which the former component explains the observed Raman intensity. The Raman line near 395 cm^{-1} is predominantly due to the ν_sCSS mode (72 – 73 %) but with a weak coupling to $(CH_3)_2N$ deformation (17 – 20 %). This assignment is in agreement with the shifts observed on deuteration. It differs considerably from the assignments of this region by Coleman *et al.*, however, their agreement between observed and calculated values in this range is not good.

The two skeletal deformation modes, $\nu_{59}b$ due to the S=C–S–S chain and $\nu_{27}a$ originating in the N–CS_2 group, are assigned to bands near 315 and 255 cm^{-1}, respectively, in the spectra of TMTD. In the spectra of TMTD-d_{12} both bands are shifted towards lower frequencies and are found near 300 and 245 cm^{-1}, respectively. These assignments are based exclusively upon the agreement with the results of the NCA. The in-phase and out-of-phase combinations of NCS deformation (with small contributions from CH_3NC deformation $\nu_{30}a$ and $\nu_{61}b$, are assigned to bands near 135 and 175 cm^{-1} in TMTD. The latter band has been observed in $CHCl_3$ solution as a Raman line with depolarisation ratio 0.6, not far from full depolarisation (0.75). The counterparts in the spectrum of TMTD-d_{12} are quite similar. The two bands originating from NCS deformation were calculated by Coleman *et al.*[3] to fall near 79 and 92 cm^{-1}, which is at much lower frequencies than our assignment for TMTD. However, their force constants for S=C–S and S=C–N bending were found to be 1.98 and 0.13 mdyn Å/(rad)^2, respectively, which seems to be a much more unrealistic result than the values found by us (Table 1). Furthermore, their calculated values for the region below 600 cm^{-1} seem to be severely hampered by the omission of torsional vibrations which, as discussed above, give rise to several bands in this region.

Acknowledgements. We thank Mrs. J. E. Gustavsen who recorded many of the IR and Raman spectra and Dr. Kjartan Marøy, Bergen for making some unpublished results concerning the structure of TMTD available to us. This research was supported by grants from the Danish Natural Science Research Council and the Norwegian Research Council for Science and the Humanities.

REFERENCES

1. Anthoni, U., Borch, G., Gustavsen, J., Klæboe, P. and Nielsen, P. H. *Spectrochim. Acta A 33* (1977) 403.
2. Dahl, B. M., Jensen, K. A., Nielsen, P. H. and Borch, G. *Acta Chem. Scand. 25* (1971) 2029, 2039; *26* (1972) 2241.
3. Coleman, M. M., Koenig, J. L. and Shelton, J. R. *J. Phys. Sci., Polym. Phys. Ed. 12* (1974) 1001.
4. Gore, R. C., Hannah, R. W., Pattacini, S. C. and Porro, T. J. *J. Assoc. Off. Anal. Chem. 54* (1971) 1040.
5. Contreras, H. and Cortés, H. *Inorg. Nucl. Chem. Lett. 6* (1970) 225.
6. Brinkhoff, H. C., Grotens, A. M. and Steggerda, J. J. *Recl. Trav. Chim. Pays-Bas 89* (1970) 11; Marøy, K. *Personal communications.*
7. Brinkhoff, H. C. and Grotens, A. M. *Recl. Trav. Chim. Pays-Bas 111* (1971) 252.
8. Wilson, N. K. *J. Phys. Chem. 75* (1971) 1067.
9. Schlottmann, B. U. *Tetrahedron Lett.* (1971) 4051.
10. Edgar, B. L., Duffy, D. J., Palazzotto, M. C. and Pignolet, L. H. *J. Am. Chem. Soc. 95* (1973) 1125.
11. Fraser, R. R., Boussard, G., Saunders, J. K., Lambert, J. B. and Mixan, C. E. *J. Am. Chem. Soc. 93* (1971) 3822.
12. Wilson, E. B., Jr. *J. Chem. Phys. 7* (1939) 1047; *9* (1941) 76.
13. Snyder, R. G. and Schachtschneider, J. H. *Spectrochim. Acta 21* (1965) 169.
14. Knoeck, J. and Witt, J. *Spectrochim. Acta A 32* (1976) 149.
15. Jensen, K. A. and Nielsen, P. H. *Acta Chem. Scand. 20* (1966) 597.
16. Bellamy, L. J. *The Infra-red Spectra of Complex Molecules*, 3rd Ed., Chapman & Hall, London 1975.
17. Scott, D. W. and El-Sabban, M. Z. *J. Mol. Spectrosc. 30* (1969) 317; *31* (1969) 362.

Received May 8, 1978.

Acta Chemica Scandinavica A 32 (1978) 715–719

The Crystal Structure of a Tetranuclear Bismuth(III) Complex, $(C_5H_5NH)_6Bi_4Cl_{18}$

BENGT AURIVILLIUS and CLAES STÅLHANDSKE

Division of Inorganic Chemistry 2, Chemical Center, The Lund Institute of Technology, P.O.Box 740, S-220 07 Lund 7, Sweden

The crystal structure of $(C_5H_5NH)_6Bi_4Cl_{18}$ has been determined and refined from 2605 independent counter reflections (Mo$K\alpha$) to a final R-value of 0.039. The crystals are monoclinic, space group $C2/m$ with $a=17.224(3)$, $b=14.874(2)$, $c=13.043(2)$ Å, $\beta=123.94(2)°$ and $Z=2$. The structure is built up of pyridinium ions and isolated $Bi_4Cl_{18}^{6-}$ groups, the latter representing a new type of halide complex. The $Bi_4Cl_{18}^{6-}$ complex consists of two pairs of edge-sharing octahedra joined by their top ligands. Of the six Bi–Cl bonds, the three short terminals vary between 2.57 and 2.61 Å and the long bridgings are 2.83–2.94 Å.

It has long been known that the presence of a large cation in a crystal structure will promote the formation of large anion complexes. These views have been summarized by Basolo[1] in 1968 and more recently by Martinsen and Songstad.[2] Whereas comprehensive studies have been made in the solid state on complexes between Bi^{3+} and Br^- and I^- [3-5] only a few complex bismuth(III) chlorides have been investigated. We started with the pyridinium ion as cation and chose the previously known compound $(C_5H_5NH)_3Bi_2Cl_9$.[6]

EXPERIMENTAL

Crystal data. $(C_5H_5NH)_6Bi_4Cl_{18}$; F.W. 1954.73. Monoclinic, space group $C2/m$; $a=17.224(3)$ Å, $b=14.874(2)$ Å, $c=13.043(2)$ Å, $\beta=123.94(2)°$, $V=2272.2$ Å^3. $D_m=2.33$ g cm^{-3}, $Z=2$, $D_x=2.34$ g cm^{-3}, $\mu=129$ cm^{-1} (Mo$K\alpha$).

Single crystals of the title compound were prepared in the following way: 7.8 g bismuth oxide chloride was dissolved in 30 ml hot dilute (15 %) hydrochloric acid. 4.8 ml pyridine was added dropwise to the hot solution under constant stirring. The solution was then cooled very slowly and after about 30 min colourless quadratic crystals were formed. Analyses gave Bi 42.27 (42.76), Cl 32.19 (32.65), C 19.13 (18.43), N 4.17 (4.30) and H 1.90 (1.84). Calculated values are given within parentheses.

Preliminary precession photographs indicated the Laue symmetry $2/m$. The only systematic absences were $h+k+l=2n+1$, which are characteristic of the space groups Im, $I2$ and $I2/m$. Before indexing the powder photographs the body-centered cell [$\beta=103.47(2)°$] was transformed to a C-centered cell [$\beta=123.94(2)°$].

The dimensions of the single crystal used were $0.11\times0.17\times0.22$ mm^3. Intensity data were collected on a computer-controlled Enraf-Nonius CAD-4 diffractometer with Mo$K\alpha$ radiation and a graphite monochromator ($\lambda=0.70930$ Å). The $\omega-2\theta$ scan technique was used with a peak scan interval $\Delta\omega=(0.80+0.50\tan\theta)°$ and a maximum time of 4 min for each reflection. In one quadrant of reciprocal space 4195 independent reflections with $3°<\theta<30°$ were measured. Out of these, 2605 with $I>3\sigma(I)$ were used in the structure analysis. Corrections were applied for Lorentz-polarization and absorption effects. The transmission factors, evaluated by numerical integration, varied from 0.15 to 0.27.

STRUCTURE DETERMINATION AND REFINEMENT

The positions of the bismuth atoms were deduced from the three-dimensional Patterson function, assuming space group $C2/m$. As the positions of all other non-hydrogen atoms could be found from three-dimensional fourier maps no other space

Table 1. Positional and thermal parameters obtained in the least-squares refinement. Estimated standard deviations are given within parentheses. The anisotropic temperature factors U_{ij} (Å^2) for the bismuth and chlorine atoms are based on the expression: $\exp[-2\pi^2(U_{11}a^{*2}h^2+\cdots+2U_{23}b^*c^*kl)]$.

Atom	x	y	z	U_{11}	U_{22}	U_{33}	U_{12}	U_{13}	U_{23}
Bi	.37709(2)	.18982(2)	.31101(3)	.0300(2)	.0259(2)	.0378(2)	.0002(1)	.0173(1)	−.0012(1)
Cl(1)	.3677(4)	0	.3099(5)	.1352(50)	.0291(18)	.0959(36)	0	.0700(36)	0
Cl(2)	.3538(2)	.1778(2)	.0992(2)	.0527(13)	.0625(16)	.0425(11)	.0129(12)	.0265(10)	.0011(11)
Cl(3)	.3821(2)	.3632(2)	.3026(2)	.0442(12)	.0276(9)	.0581(14)	.0002(9)	.0299(11)	−.0005(10)
Cl(4)	.5754(2)	.1965(2)	.4346(2)	.0409(11)	.0516(14)	.0518(12)	.0102(11)	.0268(10)	.0017(11)
Cl(5)	.1990(2)	.1987(2)	.2235(3)	.0347(10)	.0547(15)	.0671(15)	−.0068(11)	.0271(11)	−.0012(13)

Atom	x	y	z	B	Atom	x	y	z	B
C(1)	.1683(13)	0	.9910(18)	5.6(4)	C(7)	.7822(10)	.0798(10)	.5212(13)	6.1(3)
C(2)	.1224(9)	.0815(9)	.9580(12)	5.5(3)	C(8)	.7378(14)	0	.5085(19)	6.0(4)
C(3)	.0261(11)	.0783(11)	.8858(14)	6.7(3)	C(9)	.6828(13)	0	.1640(17)	5.4(4)
C(4)	−.0217(15)	0	.8537(20)	6.3(4)	C(10)	.6472(8)	.0798(8)	.1690(10)	4.5(2)
C(5)	.9166(11)	0	.5620(15)	4.3(3)	C(11)	.5708(9)	.0809(9)	.1793(12)	5.3(3)
C(6)	.8729(7)	.0804(7)	.5474(9)	4.0(2)	C(12)	.5331(13)	0	.1828(18)	5.6(4)

groups were tried. The resulting atomic positions were refined by means of least-squares calculations, using anisotropic temperature factors for the bismuth and chlorine atoms and isotropic ones for the other non-hydrogen atoms. The hydrogen atoms were not included in the calculations. The nitrogen and carbon atoms in the pyridine groups could not be unequivocally distinguished and therefore all non-hydrogen atoms in the rings were treated as carbon atoms.

In the final refinement a parameter was included to correct for secondary extinction.[7] The final R-factors were $R=0.039$ and $R_w=0.049$, with the isotropic extinction parameter $g=0.33(3)$. The value of S, defined by $[\Sigma w_i(|F_o|-|F_c|)^2/(m-n)]^{1/2}$, where m and n are the numbers of observations and parameters varied, was 1.36. The function minimized was $\Sigma w_i(|F_o|-|F_c|)^2$, with $w_i^{-1}=\sigma^2(|F_o|)+(0.025\times|F_o|)^2$. The scattering factors used were those of Doyle and Turner.[8]

The final coordinates and thermal parameters are listed in Table 1. Lists of observed and calculated structure factors are available on request from Division of Inorganic Chemistry 2.

RESULTS AND DISCUSSION

Selected distances and angles within the present structure are given in Table 2 which also includes the deviations of the atoms for their respective best planes in the pyridinium ions. For notations of the atoms and rings, *cf.* Tables 1, 2.

The pyridine rings. The carbon and nitrogen atoms of the pyridine rings could as mentioned not be distinguished with certainty. Hydrogen atom positions were geometrically deduced in order to calculate possible N−H···Cl hydrogen bonds. The numbering of the H atoms is the same as for the corresponding 'carbon' atoms. Assuming C(N)−H bonds of 0.95 Å, the two shortest Cl−H contacts, Cl(4)−H(6) and Cl(5)−H(10), were calculated to 2.52 and 2.56 Å. The distances Cl(4)−C(6) and Cl(5)−C(10) are 3.41 and 3.38 Å and the corresponding C(N)−H−Cl angles 157 and 145°. Thus if there exist N−H···Cl hydrogen bonds they are weak and it does not seem unreasonable to assume that the atoms C(6) and C(10) in the pyridinium ions II and III, respectively, stand for (0.5 C+0.5 N) each and that the pyridinium ion I is completely disordered with respect to the nitrogen atom. Similar disordering has been found in other pyridinium compounds containing anionic halide complexes where the N−H···X hydrogen bonds are weak or absent; for a survey, *cf.* Ref. 9.

The chloro bismuthate(III) complex. A stereoview of the content of one unit cell of the title compound is given in Fig. 1. It is seen that the crystal structure contains discrete $Bi_4Cl_{18}^{6-}$ groups centred about the crystallographic points $0,\frac{1}{2},\frac{1}{2}$; $\frac{1}{2},0,\frac{1}{2}$, which coincide with the point position 2(*d*) in the space group used,

Table 2. Selected bond distances (Å) and angles (°) in the crystal structure of $(C_5H_5NH)_6Bi_4Cl_{18}$. Distances (Å) from the best planes through the rings I – III are also given.

Within the pyridinium ions

Ring I			
C(1) – C(2)	1.38(2)	C(2) – C(1) – C(2)	123(2)
C(2) – C(3)	1.38(2)	C(1) – C(2) – C(3)	116(1)
C(4) – C(3)	1.35(2)	C(2) – C(3) – C(4)	122(2)
		C(3) – C(4) – C(3)	119(2)
Ring II			
C(5) – C(6)	1.37(1)	C(6) – C(5) – C(6)	122(1)
C(6) – C(7)	1.40(2)	C(5) – C(6) – C(7)	119(1)
C(8) – C(7)	1.37(2)	C(6) – C(7) – C(8)	120(1)
		C(7) – C(8) – C(7)	120(2)
Ring III			
C(9) – C(10)	1.35(1)	C(10) – C(9) – C(10)	122(2)
C(10) – C(11)	1.39(2)	C(9) – C(10) – C(11)	119(1)
C(12) – C(11)	1.38(2)	C(10) – C(11) – C(12)	119(1)
		C(11) – C(12) – C(11)	121(2)

Distances from the best planes through the rings

I		II		III	
C(1)	−0.001	C(5)	0.013	C(9)	−0.004
C(2)	0.006(x2)	C(6)	−0.008(x2)	C(10)	0.001(x2)
C(3)	−0.016(x2)	C(7)	−0.001(x2)	C(11)	0.005(x2)
C(4)	0.021	C(8)	0.005	C(12)	−0.008

Within the $Bi_4Cl_{18}^{6-}$ complex

Bi – Cl(2)	2.567(3)	Cl(1) – Bi – Cl(3)	177.7(1)
Cl(3)	2.585(2)	Cl(2) – Bi – Cl(4)	91.7(1)
Cl(5)	2.611(2)	Cl(4) – Bi – Cl(4)	82.5(1)
Cl(1)	2.828(1)	Cl(4) – Bi – Cl(5)	90.6(1)
Cl(4)	2.850(2)	Cl(5) – Bi – Cl(2)	95.4(1)
Cl(4)	2.941(3)		

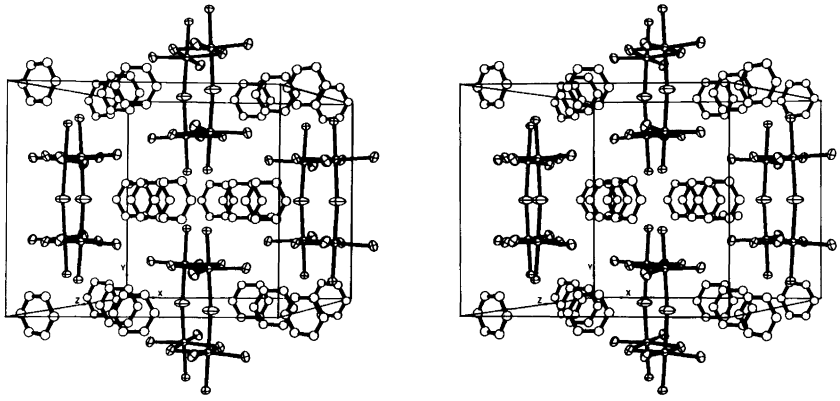

Fig. 1. A stereoview of the unit cell of $(C_5H_5NH)_6Bi_4Cl_{18}$, showing the $Bi_4Cl_{18}^{6-}$ complexes and the pyridine rings.

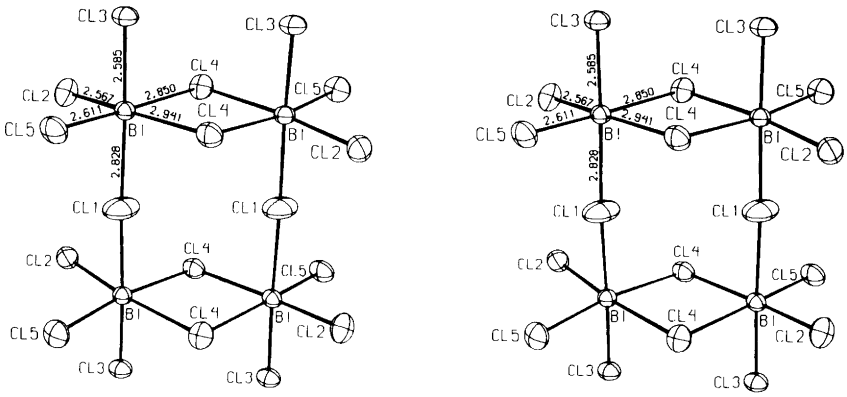

Fig. 2. A stereoview showing the discrete $Bi_4Cl_{18}^{6-}$ complex. The bond distances Bi–Cl are given.

$C2/m$. The complex thus as a whole has the symmetry $2/m$. The independent Bi–Bi distances within the complex are 4.35, 5.65 and 7.13 Å and the next nearest distance (to another complex) is 6.97 Å. The longest Bi–Cl bond distance within the complex is 2.941 Å and the shortest Bi–Cl distance between two complexes is slightly less than 5 Å. Thus the complexes are isolated. The complex $Bi_4Cl_{18}^{6-}$ consists of two pairs of edge-sharing octahedra joined by their top ligands (Fig. 2). The terminal chlorine atoms Cl(5) and the bridging Cl(4) may be joined by weak hydrogen bonds to pyridinium ions II and III respectively.

The short terminal Bi–Cl bonds to the atoms Cl(2), Cl(3) and Cl(5) are 2.567(3)–2.611(2) Å and the long bridging to Cl(4)(× 2) and Cl(1) are 2.828(1) –2.941(3) Å (Fig. 2). The short bonds observed in the present structure are longer than the corresponding ones in $BiCl_3$[10] [2.468(4)–2.518(7) Å]. The bismuth atoms of the present compound are thus (3+3)-coordinated but have a larger tendency towards 6-coordination than is found for solid $BiCl_3$. In $Cs_2NaBiCl_6$[11] the bismuth atom with the site symmetry $m3m$ is strictly octahedrally coordinated with the Bi–Cl distance 2.66(2) Å, which falls between the long and the short Bi–Cl bonds in the present structure.

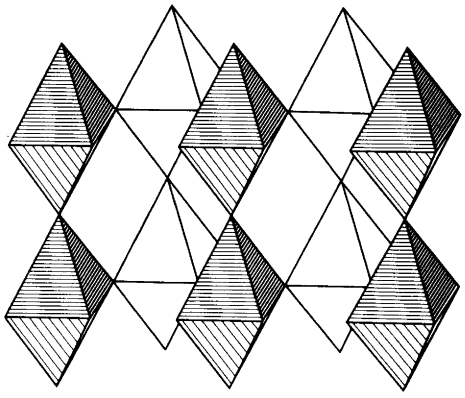

Fig. 3. A perspective view of part of the endless double chain, formed from linked $BiCl_6$ octahedra in $Cs_3Bi_2Cl_9$.[12]

A compound closely related to the present one is $Cs_3Bi_2Cl_9$,[12] in which the octahedra of the ion $Bi_2Cl_9^{3-}$ are joined to an endless double chain extending along the crystallographic a-axis. An idealized picture of part of this chain is given in Fig. 3. The authors of Ref. 12 have, however, chosen to give another description of the coordination of bismuth in this compound. They depict $BiCl_3$ molecules and this formulation is based on the fairly short three nearest Bi–Cl bonds of 2.48(5)–2.56(5) Å.

Acknowledgement. The authors wish to thank Dr. Karin Aurivillius for valuable discussions. This investigation has been financially supported by grants from the Swedish Natural Science Research Council.

REFERENCES

1. Basolo, F. *Coord. Chem. Rev. 3* (1968) 213.
2. Martinsen, A. and Songstad, J. *Acta Chem. Scand. A 31* (1977) 645.
3. Lazarini, F. *Acta Crystallogr. B 33* (1977) 1954.

4. Lazarini, F. *Acta Crystallogr. B 33* (1977) 2686.
5. Lazarini, F. *Acta Crystallogr. B 33* (1977) 2961.
6. Vanino, L. and Hauser, O. *Ber Dtsch. Chem. Ges. 34* (1901) 416.
7. Zachariasen, N. H. *Acta Crystallogr. 23* (1967) 558.
8. Doyle, P. A. and Turner, P. S. *Acta Crystallogr. A 24* (1968) 390.
9. Brassay, C., Robert, R., Bachet, B. and Chevalier, R. *Acta Crystallogr. B 32* (1976) 1371.
10. Nyburg, S. C., Ozin, G. A. and Szymański, J. T. *Acta Crystallogr. B 27* (1971) 2298.
11. Morss, L. R. and Robinson, W. R. *Acta Crystallogr. B 28* (1972) 653.
12. Kihara, K. and Sudo, T. *Acta Crystallogr. B 30* (1974) 1088.

Received April 28, 1978.

Acta Chemica Scandinavica A 32 (1978) 721 – 729

EMF of Concentration Cells with Liquid-liquid Junction Established by Free Diffusion. Part I. Experimental Results for HCl/$BaCl_2$ Junctions at Various Concentrations

NIELS OLAF ØSTERBERG, JØRGEN BIRGER JENSEN and TORBEN SMITH SØRENSEN

Fysisk-Kemisk Institut, DTH 206, DK-2800 Lyngby, Denmark

Emf's have been measured at 25 °C on the following cell:

$$Pt|Ag|AgCl,BaCl_2(C_1)\|HCl(C_2),AgCl|Ag|Pt$$

where C_1 is ranging between 5.0×10^{-4} and 1.0 mol dm^{-3} and C_2 is ranging between 1.0×10^{-3} and 1.0×10^{-1} mol dm^{-3}.

The liquid junction between the two half cells is established as free diffusion.

The results are compared with the simple model of Henderson. A detailed description for the preparation of reliable Ag/AgCl electrodes is given.

In a great number of potentiometric measurements the reference electrode is connected to the test solution by means of a salt bridge. In pH-measurements as well as in measurements with ion selective electrodes a calomel electrode together with a saturated KCl-solution is most often used as reference electrode. In such measurements it is postulated that the liquid junction potential created when the salt bridge is immersed in the test solutions containing different ions with different charges and concentrations is zero or at least constant from one test solution to another.

Surprisingly, only a limited number of important contributions to the understanding of this problem has been reported. The first contributions were given by Helmholtz[1] and Nernst,[2] who gave a description of electrolyte diffusion and pointed out that most often an electric diffusion potential is created when two electrolyte solutions are brought into contact. Two other important features of the liquid junction potentials were stated by Cumming and Gilchrist[3] in their study of KCl/HCl and HCl/HCl liquid junction potentials: (1) The emf-values are affected by variations in the nature of the liquid boundary and (2) the potentials of KCl/HCl solutions varied with the time the two solutions had been in contact with each other. Guggenheim,[4] Guggenheim and Unmack,[5] and MacInnes[6] pointed out the importance of controlled experimental conditions and reported values for two different 1:1 salts measured under different boundary and initial conditions.[7] A more detailed description of the most commonly used liquid junctions was given by Smyrl and Newman.[8] Among the recent contributions to the understanding of 1:1 liquid junction potentials we must mention the paper of Lindeberg and Østvold[9] treating a mixed boundary between HCl and KCl, the paper of Spiro[10] dealing with a Henderson model for completely dissociated uni-univalent electrolyte solutions, and the book of Newman[11] containing numerous – mostly theoretically calculated – values of liquid junction potentials and literature references. Only very few experimental results of emf's with liquid junction potentials caused by other electrolytes than 1:1 salts are reported in the literature. Those reported by Henderson[12] are of questionable value, since the experimental conditions were not properly stated. Jones and Doyle[13] have computed the transference number of $BaCl_2$ at various concentrations from emf measurements on concentration cells with liquid junctions. However, in such cases with only a single electrolyte present it is well known that the liquid junction potentials are independent of the initial conditions.

Obviously, there is a lack of reliable data on emf

measurements on cells with liquid junctions between two electrolytes where at least one is not a 1:1 electrolyte. In the present paper we intend to amend the present lack in knowledge. Emf measurements have been carried out on the following cell:

$$\mathrm{Pt|Ag|AgCl,BaCl_2}(C_1)\|\mathrm{HCl}(C_2),\mathrm{AgCl|Ag|Pt} \quad (1)$$

where C_1 is ranging between 5.0×10^{-4} and 1.0 mol dm^{-3} and C_2 is ranging between 1.0×10^{-3} and 1.0×10^{-1} mol dm^{-3}. The electrolytic contact was established with "free diffusion" boundary conditions. The technique is described in detail in the experimental section. The reason why the $BaCl_2$/HCl system was selected can be summarized in the following points:

(1) To support previous investigations carried out in this institute.[14]

(2) This system is used as example in the calculations made by Pleijel.[15] His model gives a theoretical treatment of liquid junction potentials between two electrolytes of different valence types during steady interdiffusion in a fixed layer.

(3) Activity coefficients of $BaCl_2$/HCl mixtures are reported in the literature.[16]

(4) Due to the common ion in the $BaCl_2$/HCl system, the same type of measuring electrode – i.e. Ag/AgCl – can be used in the two electrolytes. This enables us to correct for inevitable asymmetric potentials between the two Ag/AgCl-electrodes.

(5) To the best of our knowledge, apart from in this institute,[14] no experimental values for the $BaCl_2$/HCl system with specified boundary conditions have been reported.

(6) Due to the great difference in mobility of the H^+-ion and the Ba^{2+}-ion, it is to be expected that $BaCl_2$/HCl junction potential contributes reasonably to the total cell-emf and therefore the possibilities of estimating the liquid junction potential with reasonable accuracy are enhanced.

In this paper we shall limit ourselves to give a brief theoretical introduction, a more detailed experimental description, and to report the experimental values together with preliminary calculations. As liquid junction potentials in principle are immeasurable with ordinary electrochemical devices, the results will be presented as total emf-values.

In a subsequent paper the $BaCl_2$/HCl system will be treated theoretically. New models for liquid junction potentials will be developed and compared with those of Planck, Pleijel, Henderson and others.

THEORY

Assuming one dimensional diffusion the liquid junction potential between two electrolyte solutions of arbitrary compositions can be written:

$$\Delta\phi = -\frac{RT}{F}\int_{x=-\delta_1}^{x=+\delta_2}\sum_i \frac{t_i}{z_i}\frac{\partial \ln a_i}{\partial x}\,dx \quad (2)$$

where δ_1 and δ_2 indicate the boundary of the diffusion zone (see Fig. 1), t_i is the transport number, a_i is the activity and z_i is the valency of the ith ion.

The conditions pertaining to emf-measurements in cells with liquid junctions are: (1) the electric current density is zero and (2) the liquid junction potentials are created due to concentration gradients in the cell. Since transport numbers are defined according to the conditions (1) electric current is passing through the cell and (2) there are

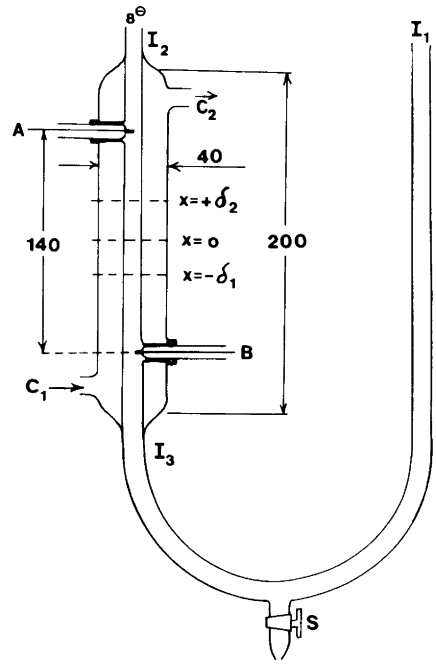

Fig. 1. Diffusion column with attached plastic tubes. Dimensions in mm. The free diffusion junction established at $x=0$. Distance from $x=-\delta_1$ to $x=+\delta_2$ indicates length of diffusion zone at the time $t=\tau$. Emf measured between the two Ag/AgCl electrodes A and B. C_1: thermostated water inlet, C_2: thermostated water outlet. I_1 and I_3: inlet of lower electrolyte. I_2: inlet of upper electrolyte. S: cock for connection to water pump.

no concentration gradients in the cell, the interpretation of eqn. (2) is far from simple. This equation cannot be derived by simple arguments about "passing a Faraday through the cell". Although such arguments are the ones most frequently found in textbooks they are of the "quasithermostatic" type analogous to the arguments of Thomson[28] in connection with thermo emf.

In connection with liquid junction potentials, Helmholz[1] was the first to apply quasi-thermostatic arguments. However, Onsager[26] realized that the correct proof of such methods rested on extra-thermostatic principles, *viz.* the reciprocal relations. Therefore, the identity of transference numbers measured by means of the Hittorf method and the transference numbers obtained by emf-measurements in liquid junctions can be taken as an experimental proof of the validity of Onsager's reciprocal relations. See for example Miller (Ref. 17, p. 395, eqn. (11.59)). See also Wagner[27] for a careful comparison between the "quasi-thermostatic" method and the method of "irreversible thermodynamics".

In the single-electrolyte case – for example when the two electrolytes both are $BaCl_2$ at various concentrations – eqn. (2) yields:

$$\Delta\phi = \frac{RT}{F} \ln \frac{a_{Cl^-}(1)}{a_{Cl^-}(2)}$$

$$- \frac{RT}{F} \int_{\ln a_{BaCl_2(1)}}^{\ln a_{BaCl_2(2)}} \frac{t_{Ba^{2+}}}{2} \, d \ln a_{BaCl_2} \qquad (3)$$

The liquid junction potential cannot be measured directly due to the first term in eqn. (3). This term can be eliminated by measuring the total emf of the following cell:

$$Pt|Ag|AgCl,BaCl_2\,(a_1)\|BaCl_2\,(a_2),AgCl|Ag|Pt \qquad (4)$$

including the liquid junction potential under examination. The expression for EMF of cell (4) has the form:

$$EMF = \frac{RT}{2F} \int_{\ln a_{BaCl_2(2)}}^{\ln a_{BaCl_2(1)}} t_{Ba^{2+}} \, d \ln a_{BaCl_2} \qquad (5)$$

Because $t_{Ba^{2+}}$ is a function of a_{BaCl_2} only, the integral in eqns. (3) and (5) can be calculated numerically from table-data of $t_{Ba^{2+}}$ and $\ln a_{BaCl_2}$ as functions of concentration. This means that emf's of concentration cells including liquid junctions with only one electrolyte present are invariant with time and therefore independent of the manner in which the liquid junctions arliquid junctions are formed.

If we have simultaneously two different electrolytes in the junction – for example when cell (1) is examined instead of cell (4) – the emf expression takes the form:

$$EMF(1)_{t=\tau} = - \frac{RT}{2F} \int_{x=-\delta_1}^{x=+\delta_2} t_{Ba^{2+}} \left(\frac{\partial \ln a_{BaCl_2}}{\partial x} \right)_{t=\tau} dx$$

$$- \frac{RT}{F} \int_{x=-\delta_1}^{x=+\delta_2} t_{H^+} \left(\frac{\partial \ln a_{HCl}}{\partial x} \right)_{t=\tau} dx \qquad (6)$$

Although eqns. (5) and (6) are very much alike some difficulties – not existing in eqn. (5) – arise when eqn. (6) is applied. Due to the fact that both the two transport numbers and the two activities are functions of *two* concentrations – *i.e.* C_{BaCl_2} and C_{HCl} – it is necessary to know how the concentration profiles vary with time along the diffusion zone, *i.e.* the path of integration in $C_{BaCl_2} - C_{HCl}$ space must be known. This is normally not known and can only be simulated by using a specific model of electrodiffusion.[18]

After some time the concentration profiles have in practice reached their final pattern. In the free diffusion case the diffusion profiles only become functions of time *through* the Boltzmann parameter $x/\sqrt{t}$, where t is the time elapsed from a hypothetical "infinitely sharp" step in the concentrations around $x=0$. When those "Boltzmann-profiles" have been reached the liquid junction potential (or cell emf) can be shown again to be independent of time (but *not* of the profiles).[18]

Even when the concentration profiles have reached their final pattern it is only possible to calculate those profiles by numerical calculations. The period of building up the concentration profiles will experimentally be observed as a drift in the measured emf (eqn. (6)). The dependence of the profile-pattern on the *boundary conditions* is observed as a variation in the (stable) measured emf.[7]

EXPERIMENTAL

Chemicals. The hydrochloric acid solutions were made from Titrisol ampullas containing 1.0 mol HCl by dilution. The barium chloride solutions were made from analytical grade $BaCl_2.2H_2O$ (Riedel-de Haen), predried for one week at 50 °C. The silver plating solution was made of analytical grade

$KAg(CN)_2$ (Merck) used without further purification. For all solutions distilled and deionized water was used.

Apparatus. The diffusion column was made of Pyrex glass. The column consists of a tube with circular cross section – inside diameter 8 mm – covered with a water jacket in which the temperature was kept at 25 ± 0.1 °C. For further details see Fig. 1.

Measuring devices. For the preliminary measurements the cell emf was measured with a Hewlett-Packard 3420 A DC differential voltmeter to which a Radiometer recorder, REC 61, was connected. With this experimental set-up it should be possible to measure potentials with an accuracy down to ± 1 μV. We experienced that the measured potentials were affected by the choice of sensitivity ranges on the instruments. With two different HP 3420 A DC/ REC 61 instruments we found it impossible to measure the asymmetric potential (the potential developed when two Ag/AgCl electrodes are placed in the same chloride solution) with an accuracy greater than $\pm 0.2 - 0.3$ mV, and we also observed that the voltmeter and the recorder affected well prepared Ag/AgCl electrodes so that the asymmetric potentials during the measurements became time dependent and instable, even if in all measurements the electrodes were connected to the voltmeter with shielded cables connected to earth. Based on the above observations we decided to give up the possibility of continuous recording of emf, and measure the potential only by means of a single digital mV-meter. We found that with a high impedance Data Technology $3\frac{1}{2}$ digits millivoltmeter (input impedance = 10^9 Ω for 500 mV full scale) the asymmetric potentials could be reproduced within ± 0.05 mV.

Preparation of silver-silver chloride electrodes. In order to be able to obtain emf-values with an accuracy and reproducibility of 0.1 mV it is absolutely necessary to have reliable electrodes with short response time. Numerous different methods for electrolytic preparations of Ag/AgCl electrodes can be found in the literature.[19-23] We have tried some of these methods, but did not succeed in preparing electrodes with the required qualifications. Many of the reported methods are so troublesome, that in practice it is almost impossible to control all the parameters during the preparation. Besides this we found the electrodes were slow to come to equilibrium and to give different asymmetric potentials when placed in different chloride solutions. Furthermore we found that the electrodes were greatly affected by the daylight as visualized in Fig. 2. We have therefore developed our own method for electrolytic preparations of Ag/AgCl

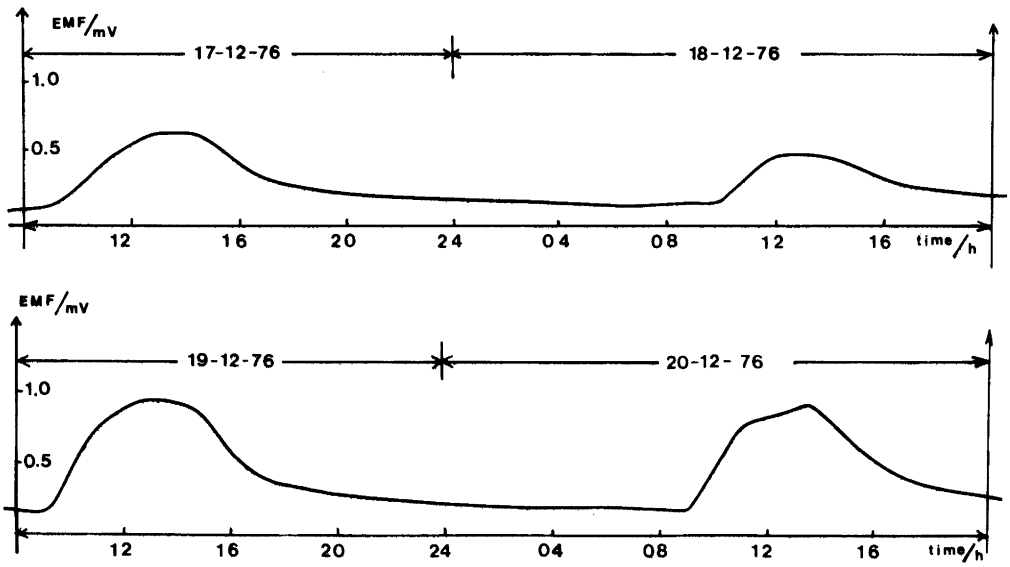

Fig. 2. Illustration of light dependence on Ag/AgCl electrode potentials. Continuous registration of emf between A and B (Fig. 1) in four subsequent days and nights with diffusion column filled with 0.1 mol dm^{-3} HCl. Hours and dates are read on figure. The Ag/AgCl electrodes were prepared according to Güntelberg.[20] Although the electrodes were not exposed to direct sunshine the influence from daylight on the measured EMF is clearly illustrated.

electrodes. Also, we decided to carry out all measurements in darkness in order to insure no influence from daylight on the silver-silver chloride electrodes. The electrodes were prepared as follows: A Radiometer platinum electrode, P 1312, was placed in concentrated nitric acid. In this solution the electrode was cleansed with electrolytic H_2 and O_2 evolution on the electrode, 10 min as cathode and 10 min as anode. This procedure was followed twice. The Pt electrode was rinsed for about 1 min in running distilled water and surrounded by an Ag-spiral in a distance of 2–3 mm. Immediately afterwards the Pt electrode and the Ag-spiral were placed in a well-stirred aqueous $KAg(CN)_2$-solution, 10 g dm^{-3}, through which purified nitrogen had been bubbled for at least 1 h in advance. The Pt-electrode was cathodically electrolyzed at a current density of 5 mA cm^{-2} for 60 min. The Ag-spiral served as anode. The Pt-electrode was rinsed for another minute in running distilled water. A part of the silver layer on the Pt electrode was electrolytically converted into AgCl in an aqueous 0.1 mol dm^{-3} HCl-solution with a current density of 5 mA cm^{-2} for 2 min. The silver-silver chloride electrode was now ready for use.

The Ag/AgCl electrodes prepared as described above have asymmetric potentials rarely exceeding 0.05 mV, (A potential between +0.05 mV and −0.05 mV is indicated on the Data Technology voltmeter by the reading .0000 V with a fluctuating + and − sign). The useful life is somewhat uncertain. We made the observation, that generally an electrode pair may be used for five to fifteen experiments in a period of one to two months, and, generally, equilibrate with the cell solutions within half an hour. Failure of an electrode pair is indicated by increasing values in asymmetric potential and longer equilibration periods.

Measuring technique. A plastic tube was connected to the bottom of the diffusion column at I_3 (Fig. 1). Before each experiment the whole system was thoroughly rinsed several times with distilled and deionized water. Then the system was rinsed twice with absolute ethyl alcohol and allowed to dry under suction at least one hour. The screw-cock, S, was closed, the two Ag/AgCl electrodes were mounted in the diffusion column, and the lower part of the diffusion column was filled with the more dense electrolyte through inlet I_3 *via* I_1. The walls of the plastic tubes were pressed together with two screw-taps in order to close the connection between I_3 and I_1 and the surface of the more dense electrolyte was then at the position $x=0$ (Fig. 1). Very carefully the second electrolyte was then placed on top of the first one by means of a semi-automatic burette adjusted to give a flow of 4.5 ml h^{-1}. Except for the cases where the densities of the two electrolytes were approximately equal, the liquid junction could in this way be formed with a sharp boundary as could be observed by means of the difference in the refraction index of the two electrolytes. Electrode A was covered with electrolyte approximately half an hour after the formation of the liquid junction. From this time emf of the cell was measured during a period of at least 24 h. Before and after each emf measurement on the concentration cell the asymmetric potential was measured in one of the two electrolytes used in the experiments.

Further, before each experiment the electrodes A and B were allowed to equilibrate at least one hour in the electrolytes applied to the measurements.

RESULTS AND DISCUSSION

Fig. 3 shows the time dependence of emf from four experiments carried out on cell (1). The time $t=0$ is selected when the first drop of the upper electrolyte was placed on the lower one. The first measuring points on the upper, middle and lower figures refer to the time when electrode A was covered with electrolyte. The individual curves in Fig. 3 can be roughly divided into three sections. In section one a variation in the measured emf is observed during the first 3–4 hours of the experiment. Section two is characterized by constant emf values, and in section three a continuous fall in the measured emf is observed. We assume that the emf variations in section one are mainly due to variations in the potential of electrode A. At the time when electrode A is covered with the upper electrolyte, electrode B has been covered with the lower electrolyte and the diffusion zone has been developed so long that both the potential of electrode B and the concentration profiles in the diffusion zone have most probably been well established. Experiences from measurements of asymmetric potentials show that at least the electrode potential of electrode B should be stable, when electrode A is covered with electrolyte. However, although the emf variations are different from experiment to experiment and although duplicate esperiments on the same $HCl-BaCl_2$ solutions give different curves, it is seen from the upper Fig. 3 that the constant emf value can be reproduced and determined with a few tenths of millivolts. This constant emf value is selected as the true emf of cell (1). The emf fall shown on the right-hand side of Fig. 3 shows that the diffusion zone now has reached at least one of the measuring electrodes.

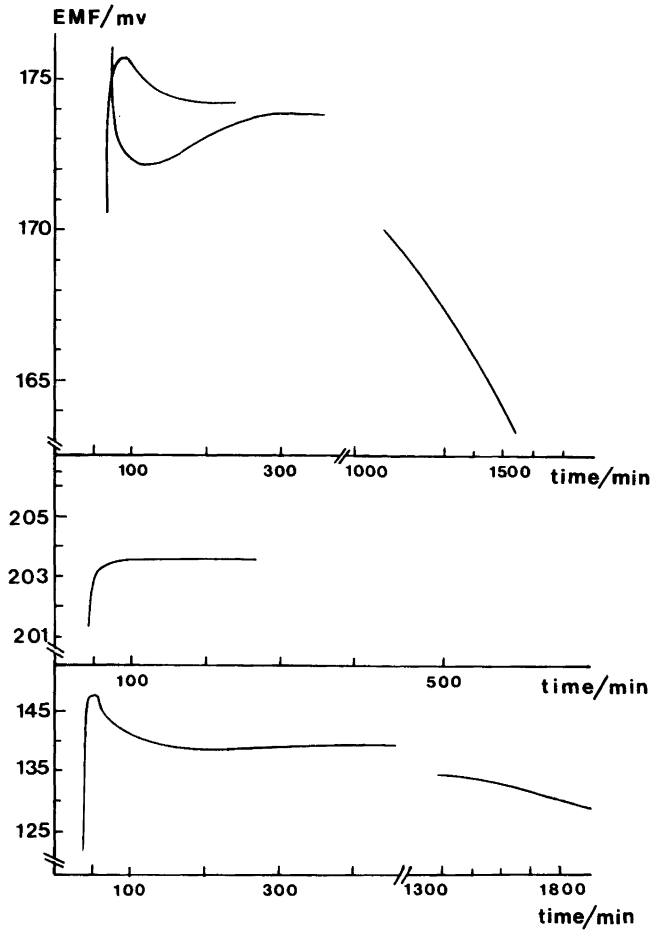

Fig. 3. Measured emf on cell (1) *versus* time. Emf measurements were performed on the diffusion column at 25 °C. Upper curves: $C_1 = 0.001$ mol dm^{-3}, $C_2 = 0.1$ mol dm^{-3} (duplicate experiments). Middle curve: $C_1 = 0.0005$ mol dm^{-3}, $C_2 = 0.1$ mol dm^{-3}. Lower curve: $C_1 = 0.001$ mol dm^{-3}, $C_2 = 0.05$ mol dm^{-3}.

Emf values from different $HCl-BaCl_2$ pairs, determined as described above, are collected in Table 1. The integers (in parenthesis) indicate the number of emf determinations.

Due to complex formation between Cl^--ions and crystalline AgCl[24] it was impossible to exceed $C_{HCl} = C_{BaCl_2} \cong 0.1$ mol dm^{-3} with electrodes prepared as described above. Some experiments have been carried out with $C_{BaCl_2} = 1.0$ mol dm^{-3}. In these experiments it was necessary to cover the Ag/AgCl electrodes with ten times the amount of AgCl as described earlier. Similar experiments with $C_{HCl} = 1.0$ mol dm^{-3} have not been performed until now.

The ./. signs in Table 1 indicate $HCl/BaCl_2$ ratios when the densities of the two electrolytes are so much alike that we found it impossible to establish a free diffusion zone. Further in Table 1 is shown [in parenthesis] the corresponding emf-values from Sørensen.[14] As these measurements all were carried out at 17 °C, it is not directly possible to compare our results with those made by Sørensen, but generally it is shown that his values are smaller than ours. To our knowledge, besides Sørensen, only Henderson[12] has reported experimentally emf-values from cells with $HCl/BaCl_2$ liquid junctions. Since Henderson indicates almost no experimental details and since he further in two papers gives two

Table 1. Experimental emf-values of cell (1) together with the estimated accuracies. (Temp. 25.0±0.1 °C). The integers in parenthesis indicate the number of experiments. The corresponding values from Ref. 14 are given in brackets [ ] (Temp. 17.0±0.1 °C).

C_{HCl}	C_{BaCl_2} 0.0005	0.001	0.005	0.010	0.050	0.100	1.000
0.001		−5.3±0.5 (2)		43.7±0.4 (5)		86.8±1.0 (2)	126.4±1.0 (3)
0.005	·/·	−54.8±0.1 (1)					
0.010	−111.2±0.1 (2)	·/·	−30.2±0.1 (2)	−15.8±0.6 (2)		40.7±0.2 (2) [37.7±1.0]	82.9±1.0 (2) [79.2±1.5]
0.050		−138.9±0.1 (1)	·/·	−61.7 (1)			
0.100	−203.3±0.2 (2)	−174.0±0.1 (3)	−113.6±0.1 (2)	./. [−92.4±0.7]	−32.7±0.1 (2)	−16.3±1.0 (2) [−22.2±1.8]	40.6±0.2 (2)

different values for the same experiment, we are unable to compare our results with his.

Probably the most simple model for calculating the liquid junction potential of, for example, cell (1) is the one given by Henderson.[12] This model, combined with the ideal Nernst equation for electrode potentials, gives the following equation for the total emf of cell (1):

$$\mathrm{EMF}=\frac{RT}{F}\left[\frac{2C_1(U_{Ba^{2+}}-U_{Cl^-})-C_2(U_{H^+}-U_{Cl^-})}{2C_1(2U_{Ba^{2+}}+U_{Cl^-})-C_2(U_{H^+}+U_{Cl^-})}\ln\left(\frac{2C_1}{C_2}\times\frac{U_{Cl^-}+2U_{Ba^{2+}}}{U_{H^+}+U_{Cl^-}}\right)+\ln\frac{2C_1}{C_2}\right] \quad (7)$$

where C_1 is the concentration of $BaCl_2$. C_2 is the concentration of HCl. U_i is the mobility of the i'th specie, i=H^+, Ba^{2+}, Cl^-. For $C_1 \ll C_2$ eqn. (7) gives:

$$\mathrm{EMF}_{C_1\ll C_2}=\frac{RT}{F}\left[\left(\frac{U_{H^+}-U_{Cl^-}}{U_{H^+}+U_{Cl^-}}+1\right)\ln\frac{2C_1}{C_2}+\frac{U_{H^+}-U_{Cl^-}}{U_{H^+}+U_{Cl^-}}\ln\left(\frac{U_{Cl^-}+2U_{Ba^{2+}}}{U_{H^-}-U_{Cl^-}}\right)\right] \quad (8)$$

and for $C_2 \ll C_1$

$$\mathrm{EMF}_{C_2\ll C_1}=\frac{RT}{F}\left[\left(\frac{U_{Ba^{2+}}-U_{Cl^-}}{2U_{Ba^{2+}}+U_{Cl^-}}+1\right)\ln\frac{2C_1}{C_2}+\frac{U_{Ba^{2+}}-U_{Cl^-}}{2U_{Ba^{2+}}+U_{Cl^-}}\ln\left(\frac{U_{Cl^-}+2U_{Ba^{2+}}}{U_{H^+}-U_{Cl^-}}\right)\right] \quad (9)$$

In Fig. 4 eqn. (7) is plotted together with our experimental results. As in the Henderson model it is assumed that the ionic mobilities were independent of concentration and the values at zero concentration were used to make the plot. These values were calculated from the corresponding ionic equivalent conductivities taken from Robinson and Stokes.[25] It is seen that there is only a rough agreement between the experimental data and data calculated from the model, *i.e.* by means of the model an experimental result can be calculated only with an accuracy of about 10 mV. Another comparison between calculated and experimental results is made in Fig. 4. Eqn. (7) predicts linear dependence of emf *vs.* $\log\frac{C_1}{C_2}$ when $C_2 \gg C_1$ [eqn. (8)] and when $C_1 \gg C_2$ (eqn. (9)). As seen in the figure also the experimental results fit a straight line under these conditions.

Another more general conclusion can be drawn. If a liquid junction is established between two electrolytes, both consisting of one salt and the conditions from eqn. (8) or (9) are fulfilled, then the liquid junction potential between the two electrolytes is determined only by the ionic mobilities – or ionic transport numbers – of the more concentrated electrolyte. This situation is approximately obtained in practical emf measurements in dilute solutions with a saturated calomel electrode as reference electrode. Here the liquid junction potentials are impressed by the saturated KCl-salt bridge.

More detailed discussions concerning comparison of experimental results with results calculated from theoretical models will be given in part II.

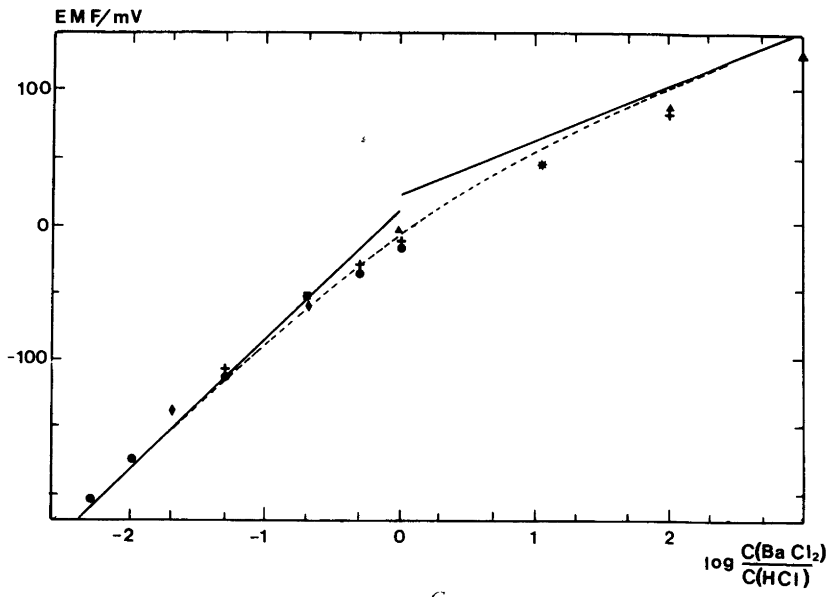

Fig. 4. Measured emf on cell (1) as function of log $\frac{C_{BaCl_2}}{C_{HCl}}$. Emf measurements were performed on the diffusion column at 25 °C. C_{HCl}/mol dm^{-3}: 0.1 (●), 0.01 (+), 0.001 (▲), 0.05 (■), 0.005 (◆). In cases where the experimental values coincide, the symbol ✱ is used. The dotted curve is a plot of eqn. (7). The straight lines indicate the two asymptotes to the dotted curve. The mathematical expressions of these asymptotes are given by eqns. (8) and (9).

Acknowledgements. Thanks are due to Mr. P. S. Rasmussen, Fysisk-Kemisk Institut, for keen interest in preparing the Ag/AgCl electrodes, and to Mr. L. E. Mikkelsen, Kemisk Laboratorium A, for manufacturing the diffusion column. One of the authors, (Torben Smith Sørensen) wishes to thank Drs. T. Førland, T. Østvold, and S. K. Ratkje, The University of Trondheim, for inspiring discussions during his visit to Trondheim.

REFERENCES

1. Helmholtz, H. *Ann. Phys. 3* (1878) 201.
2. Nernst, W. *Z. Phys. Chem. 2* (1888) 613.
3. Cumming, C. and Gilchrist, E. *Trans. Faraday Soc. 9* (1913) 174.
4. Guggenheim, E. A. *J. Am. Chem. Soc. 52* (1930) 1315.
5. Guggenheim, E. A. and Unmack, A. *K. Dan. Vidensk. Selsk. Mat-Fys. Medd. X*, 14 (1931).
6. MacInnes, D. A. *The Principles of Electrochemistry*, Dover Publications, New York 1961 (1939), pp. 220–245.
7. Ref. 6, p. 230.
8. Smyrl, W. H. and Newman, J. *J. Phys. Chem. 72* (1968) 4660.
9. Lindeberg, G. B. and Østvold, T. *Acta Chem. Scand. A 28* (1974) 563.
10. Spiro, M. *Electrochim. Acta 11* (1966) 569.
11. Newman, J. S. *Electrochemical Systems*, Prentice-Hall, Englewood Cliffs, N. J. 1973, pp. 124–138.
12. Henderson, P. *Z. Phys. Chem. 59* (1907) 118; *63* (1908) 325.
13. Jones, G. and Dole, M. *J. Am. Chem. Soc. 51* (1929) 1073.
14. Sørensen, T. S. *Studier over Fysisk-Kemiske Systemers Statik, Dynamik, Kinetik*, Ph.D. Thesis, Technical University of Denmark, Lyngby 1973, Vol. II, Chapter 3 (in Danish).
15. Pleijel, H. *Z. Phys. Chem. 72* (1910) 1.
16. Harned, H. S. and Gary, R. *J. Am. Chem. Soc. 76* (1954) 5924.
17. Miller, D. G. In Hanley, H. J. M., Ed., *Transport Phenomena in Fluids*, Dekker, New York 1969, p. 395.
18. Sørensen, T. S. and Jensen, K. F. *J. Chem. Soc. Faraday Trans. 2, 71* (1975) 1805.
19. Noyes, A. A. and Ellis, J. H. *J. Am. Chem. Soc. 39* (1917) 2532.
20. Güntelberg, E. *Z. Phys. Chem. 123* (1926) 199.
21. Brown, A. S. *J. Am. Chem. Soc. 56* (1934) 646.

22. Ives, D. J. G. and Janz, G. J. *Reference Electrodes*, Academic, London 1961.
23. Harzdorf, C. *Z. Anal. Chem. 270* (1974) 23.
24. Kolthoff, M. I. and Sandell, E. B. *Textbook of Quantitative Inorganic Analysis*, The MacMillan Company, New York 1952.
25. Robinson, R. A. and Stokes, R. H. *Electrolyte Solutions*, Butterworths, London 1965 (1959).
26. Onsager, L. *Phys. Rev. 37* (1931) 405; *38* (1931) 2265.
27. Wagner, C. *Adv. Electrochem. Eng. 4* (1966) 1.
28. Thomson, W. *Proc. R. Soc. Edinburgh 3* (1854) 225.

Received May 12, 1978.

Acta Chemica Scandinavica A 32 (1978) 731 – 735

On the Structural and Magnetic Properties of $Cr_{1-t}Fe_tP$, $Mn_{1-t}Co_tP$ and $Fe_{1-t}Co_tP$

KARI SELTE, LEIF BIRKELAND and ARNE KJEKSHUS

Kjemisk Institutt, Universitetet i Oslo, Blindern, Oslo 3, Norway

The pseudo-binary CrP – FeP, MnP – CoP, and FeP – CoP systems have been investigated by X-ray diffraction and magnetic susceptibility measurements. The three systems show complete solid solubility with MnP type structure and random distribution of the metal atoms. The paramagnetic susceptibilities follow the Curie-Weiss Law only for samples rich in MnP.

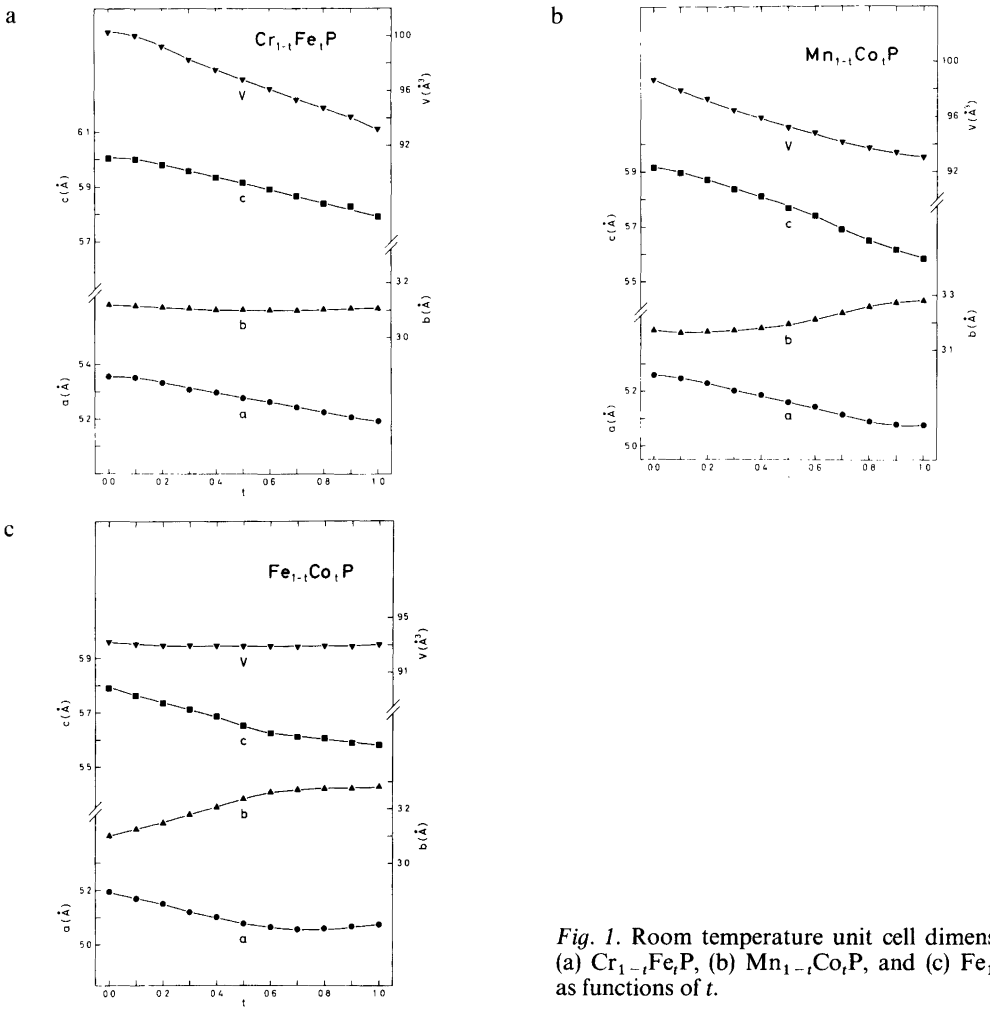

Fig. 1. Room temperature unit cell dimensions of (a) $Cr_{1-t}Fe_tP$, (b) $Mn_{1-t}Co_tP$, and (c) $Fe_{1-t}Co_tP$ as functions of t.

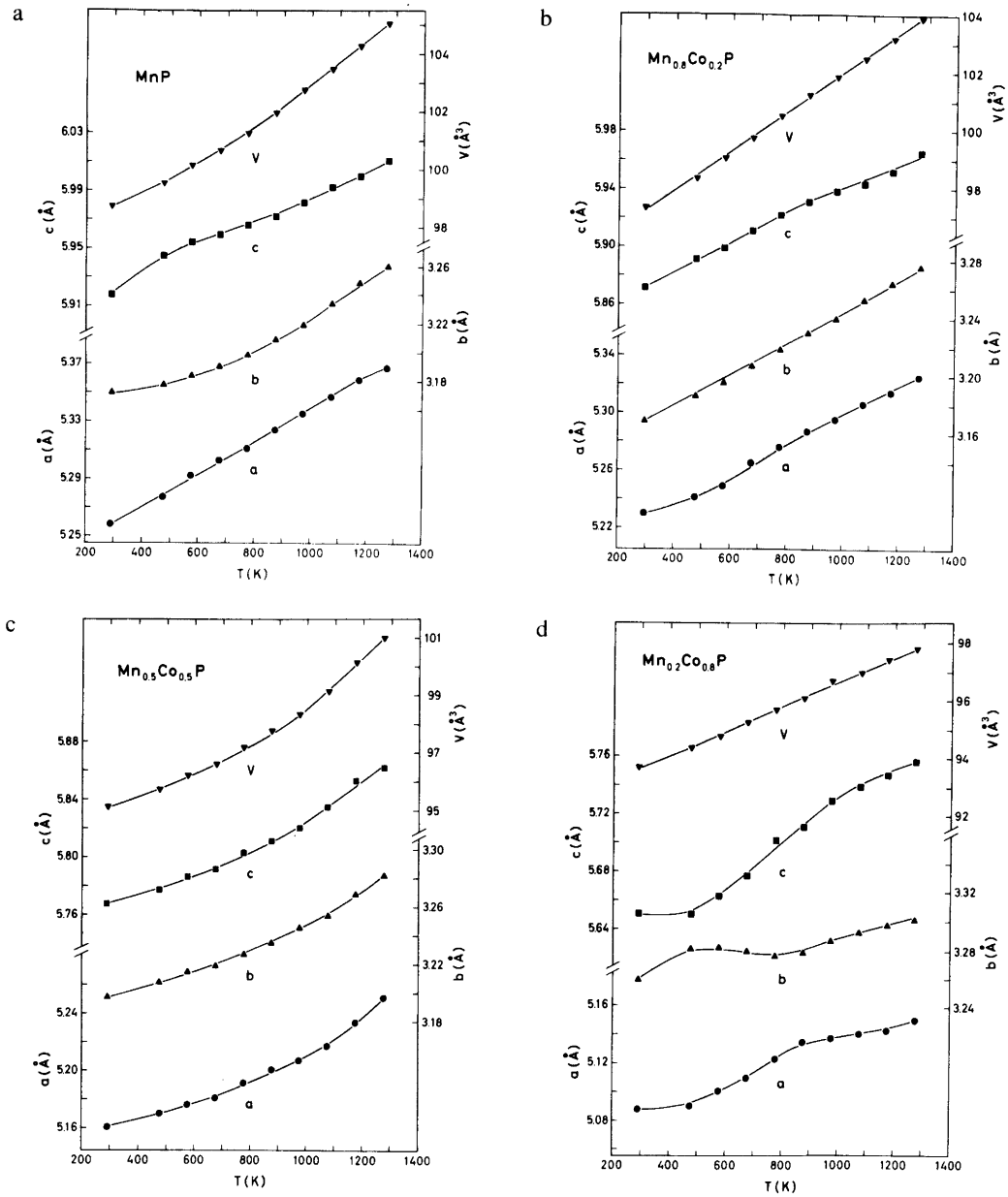

Fig. 2. Unit cell dimensions of (a) MnP, (b) $Mn_{0.8}Co_{0.2}P$, (c) $Mn_{0.5}Co_{0.5}P$, (d) $Mn_{0.2}Co_{0.8}P$, (e) FeP,

The mono-phosphides and -arsenides of the transition metals Cr, Mn, Fe, and Co take the MnP type structure. The structural and magnetic properties of the mono-arsenides (both binary and pseudo-binary) have been extensively studied at this Institute and are now well characterized. The corresponding properties of the mono-phosphides have been given less attention. The behaviour of the binary compounds is mainly disclosed,[1-13] whereas only a few characteristics have been reported for the pseudo-

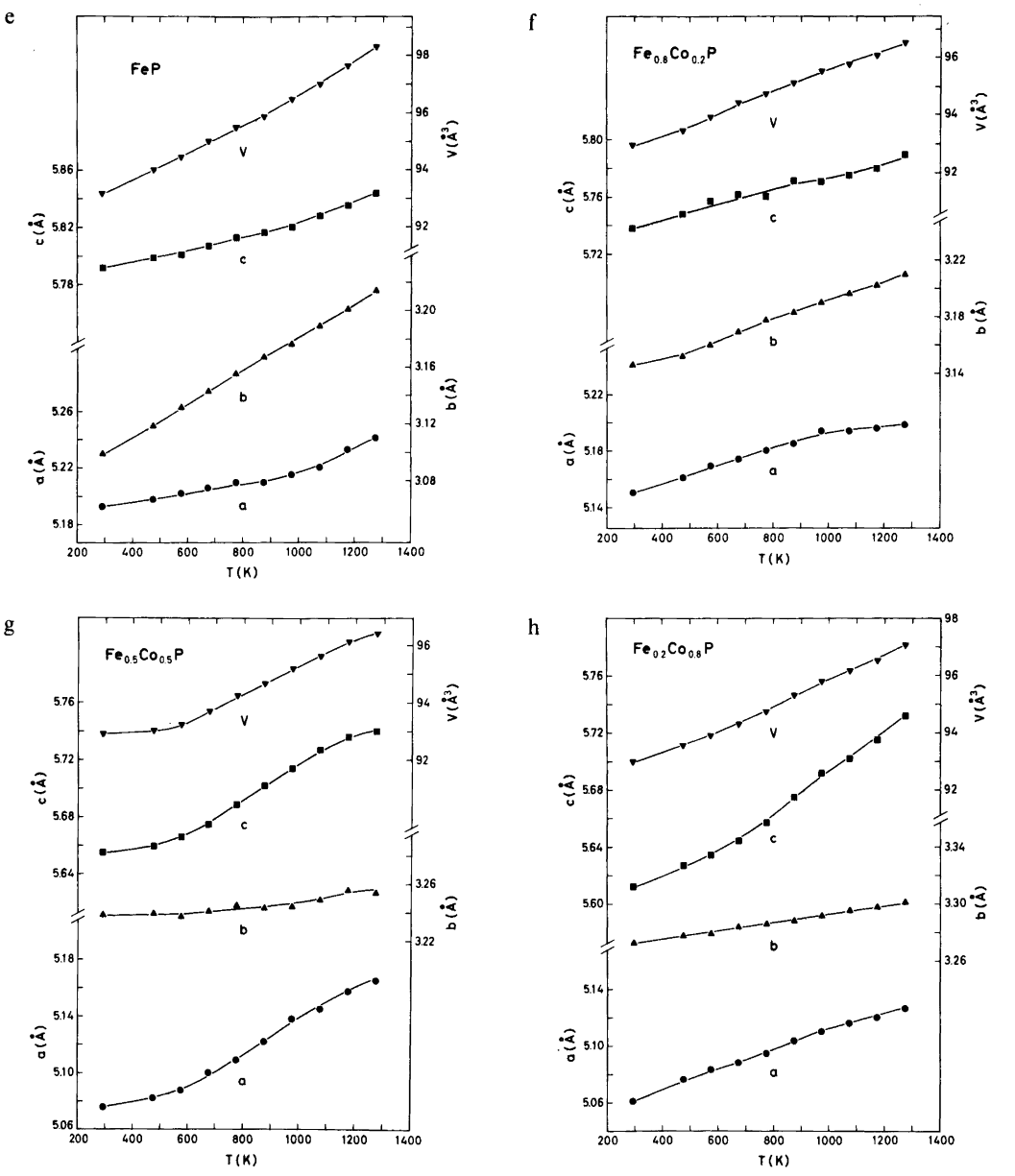

(f) $Fe_{0.8}Co_{0.2}P$, (g) $Fe_{0.5}Co_{0.5}P$, and (h) $Fe_{0.2}Co_{0.8}P$ as functions of temperature.

binary mono-phosphides.[14-18] As a continuation of our programme on MnP type phases, attention has now been focussed on these ternary phosphides.

EXPERIMENTAL

Samples were made from 99.99 % Mn and Fe, 99.99+ % Co (Johnson, Matthey & Co.; crushed Mn flakes, turnings from rods of Fe and Co), 99.999 % crushed Cr flakes and red P (Koch-Light

Laboratories). Binary samples of FeP and CrP were prepared as described in Refs. 10 and 11. CoP was obtained after two heat treatments, one at 1000 °C for 2 d, followed by 1 d at 1200 °C and 2 d at 1000 °C. MnP was prepared by a first heat treatment at 650 °C for 1 week, the second at 1100 °C for 1 h followed by slow cooling to 600 °C. Ternary samples were made from the binary compounds by one heat treatment at 1000 °C for 2 d followed by another of 1 d at 1000 °C, 1 week at 850 °C, slow cooling to 600 °C and then quenching. The experimental details concerning X-ray diffraction and magnetic susceptibility measurements have been reported earlier.[19]

RESULTS

(i) *Homogeneity ranges and atomic arrangement.* Isothermal cross-sections of $Cr_{1-t}Fe_tP$, $Mn_{1-t}Co_tP$, and $Fe_{1-t}Co_tP$, as derived for samples quenched from 600 °C, show (Fig. 1) that these systems exhibit complete solid solubility. Only ternary samples with metal/non-metal atomic ratios equal to 1.00 have

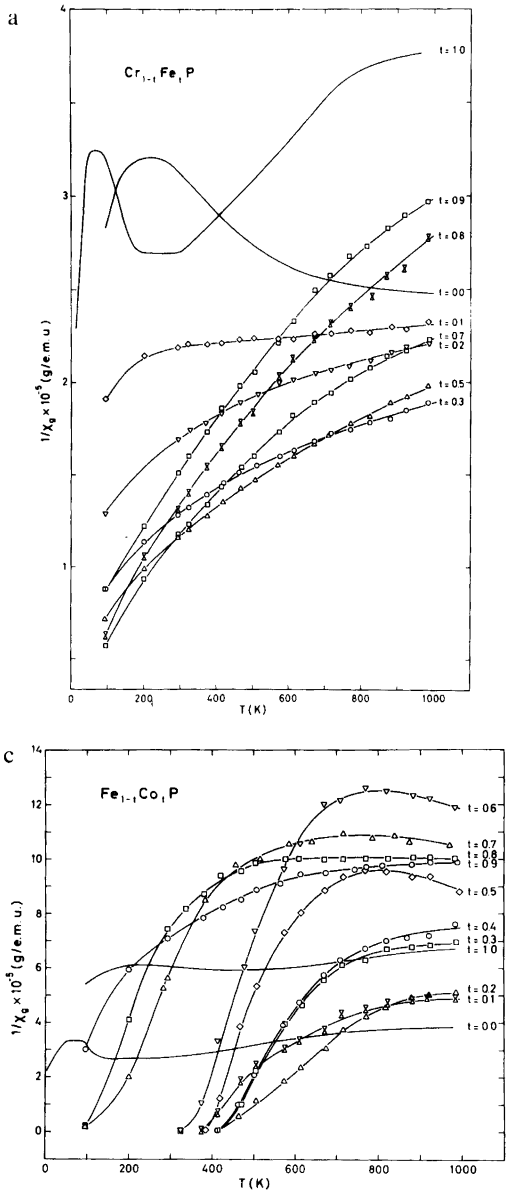

Fig. 3. Reciprocal magnetic susceptibility *versus* temperature for (a) $Cr_{1-t}Fe_tP$, (b) $Mn_{1-t}Co_tP$, and (c) $Fe_{1-t}Co_tP$.

Table 1. Curie constant (θ), paramagnetic moment ($\mu_P = \sqrt{8C_M}$), and number of unpaired electrons ($n = 2S_T$) for $Mn_{1-t}Co_tP$ samples which fulfil Curie-Weiss Law.

t	θ (K)	μ_P (μ_B)	$2S_T$
0.00	310±10	2.6±0.1	1.8±0.1
0.05	300±10	2.4±0.1	1.6±0.1
0.10	255±10	2.2±0.1	1.5±0.1
0.20	190±10	2.1±0.1	1.3±0.1
0.30	130±15	1.9±0.1	1.2±0.1
0.40	80±20	1.7±0.1	1.0±0.1

been examined. The diffraction data show that $Cr_{1-t}Fe_tP$, $Mn_{1-t}Co_tP$, and $Fe_{1-t}Co_tP$ ($0 \leq t \leq 1$) take the orthorhombic MnP type structure with random distribution of the two kinds of metal atoms. This applies also to samples of approximate composition $Mn_{0.2}Co_{0.8}P$ and $Fe_{0.4}Co_{0.6}P$ for which the axial ratio c/b is $\sqrt{3}$ and hexagonal symmetry (*e.g.*, NiAs type structure) could have been a possibility. This confirms the findings of Rundqvist.[14]

A second or higher order transition to the NiAs type structure has been detected above room temperature for many binary and ternary MnP type arsenide phases.[20,21] However, the high temperature, X-ray diffraction measurements on $Mn_{1-t}Co_tP$ and $Fe_{1-t}Co_tP$ samples with $t = 0$, 0.2, 0.5, and 0.8 (results for CrP and CoP being presented earlier[20]) show no such transition, as demonstrated by the results given in Fig. 2.

(ii) *Magnetic susceptibility.* The temperature characteristics of the reciprocal magnetic susceptibility show systematic variation with the composition parameter t for $Cr_{1-t}Fe_tP$, $Mn_{1-t}Co_tP$, and $Fe_{1-t}Co_tP$ (Fig. 3). No signs of ferri- or ferromagnetic impurities were found. The $\chi^{-1}(T)$ curves for $Cr_{1-t}Fe_tP$ and $Fe_{1-t}Co_tP$ are generally nonlinear and convex towards the temperature axis. The same applies to $Mn_{1-t}Co_tP$ for $t > 0.4$. $\chi^{-1}(T)$ is, on the other hand, linear to a very good approximation for $0 \leq t \leq 0.4$. The Curie-Weiss Law is accordingly fulfilled, and values for the Curie constant, paramagnetic moment, and number of unpaired electrons according to the "spin only" approximation are listed in Table 1. With decreasing content of Mn there is a gradual reduction in these magnetic parameters. The present findings for $Mn_{1-t}Co_tP$ concur with those of Huber and Ridgley[1] for the paramagnetic state of MnP, and are also reasonably consistent with data (*cf.*, *e.g.*, Refs. 1 and 4) on its ferromagnetic state. It may be worth noting that MnP itself and its Mn rich ternary derivatives are the only phases with MnP type structure hitherto that fulfil the Curie-Weiss Law over an appreciable temperature interval.

Acknowledgement. This work has received financial support from The Norwegian Research Council for Science and the Humanities.

REFERENCES

1. Huber, E. E. and Ridgley, D. H. *Phys. Rev. 135* (1964) A1033.
2. Rundqvist, S. and Nawapong, P. C. *Acta Chem. Scand. 19* (1965) 1006.
3. Komatsubara, T., Kinoshita, K. and Hirahara, E. *J. Phys. Soc. Jpn. 20* (1965) 2036.
4. Felcher, G. P. *J. Appl. Phys. 37* (1966) 1056.
5. Forsyth, J. B., Pickart, S. J. and Brown, P. J. *Proc. Phys. Soc. 88* (1966) 333.
6. Bellavance, D., Vlasse, M., Morris, B. and Wold, A. *J. Solid State Chem. 1* (1969) 82.
7. Ishikawa, Y., Komatsubara, T. and Hirahara, E. *Phys. Rev. Lett. 23* (1969) 532.
8. Wäppling, R., Häggström, L., Rundqvist, S. and Karlsson, E. *J. Solid State Chem. 3* (1971) 276.
9. Felcher, G. P., Smith, F. A., Bellavance, D. and Wold, A. *Phys. Rev. B 3* (1971) 3046.
10. Selte, K. and Kjekshus, A. *Acta Chem. Scand. 26* (1972) 1276.
11. Selte, K., Kjekshus, A. and Andresen, A. F. *Acta Chem. Scand. 26* (1972) 4188.
12. Selte, K., Hjersing, H., Kjekshus, A., Andresen, A. F. and Fischer, P. *Acta Chem. Scand. A 29* (1975) 695.
13. Westerstrandh, B., Lundgren, L., Gäfvert, U. and Karlsson, B. *Phys. Scr. 15* (1977) 276.
14. Rundqvist, S. *Acta Chem. Scand. 16* (1962) 287.
15. Roger, A. and Fruchart, R. *C.R. Acad. Sci. Ser. C 264* (1967) 508.
16. Bonnerot, J., Fruchart, R. and Roger, A. *Phys. Lett. A 26* (1968) 536.
17. Sénateur, J.-P., Roger, A., Fruchart, R. and Chappert, J. *C.R. Acad. Sci. Ser. C 269* (1969) 1385.
18. Maeda, Y. and Takashima, Y. *J. Inorg. Nucl. Chem. 35* (1973) 1219.
19. Selte, K., Kjekshus, A. and Andresen, A. F. *Acta Chem. Scand. 26* (1972) 3101.
20. Selte, K. and Kjekshus, A. *Acta Chem. Scand. 27* (1973) 3195.
21. Selte, K., Kjekshus, A., Andresen, A. F. and Zięba, A. *J. Phys. Chem. Solids 38* (1977) 719.

Received April 18, 1978.

Acta Chemica Scandinavica A 32 (1978) 737–746

Lattice Vibrations of the Water Molecules in $Ba(ClO_3)_2.H_2O$ and $K_2C_2O_4.H_2O$

ANDERS ERIKSSON and JAN LINDGREN

Institute of Chemistry, University of Uppsala, Box 531, S-751 21 Uppsala, Sweden

Infrared spectra of $Ba(ClO_3)_2.H_2O$ and $K_2C_2O_4.H_2O$ between 40 and 4000 cm^{-1} have been studied at 100 K. The isotopic species H_2O, D_2O, HDO and $H_2{}^{18}O$ have been used to identify the lattice vibrations of the water molecules. Infrared bands at 467, 457 and 396 cm^{-1} for $Ba(ClO_3)_2.H_2O$ have been assigned to rocking, twisting and wagging; bands at 743 and 651 cm^{-1} for $K_2C_2O_4.H_2O$ to wagging and rocking. The twisting mode for $K_2C_2O_4.H_2O$ has not been observed but is predicted to have almost the same wavenumber as the wagging mode (743 cm^{-1}). A translational mode for the water molecule out of the molecular plane has been established at 78 cm^{-1} for $Ba(ClO_3)_2.H_2O$ and at 98 cm^{-1} for $K_2C_2O_4.H_2O$.

Lattice vibrations of water molecules in crystal hydrates are found in the region 300–900 cm^{-1} (rotational vibrations) and 50–500 cm^{-1} (translational vibrations). This has been verified, for example, in studies of infrared wavenumber shifts on deuterium substitution. Rotational vibrations have been assigned to bands having a wavenumber ratio $\nu_{H_2O}/\nu_{D_2O} \sim 1.36$ and translational vibrations to bands with a ratio ~ 1.04.

A subdivision of the rotational modes can be made assuming rotations about the principal inertial axes of the water molecule, to give the familiar twisting, wagging and rocking vibrations. The translational vibrations can be assumed, to a first approximation, to occur along the principal inertial axes.

It is quite difficult to make unambiguous assignments in these terms using experimental data from infrared and Raman spectra or neutron inelastic scattering, however. Several complications arise, such as the occurrence of bands from several water molecules in the crystal unit cell or low band intensities. The use of single crystals, studied with polarized radiation, should permit correct assignments when the water molecules are found at sites with symmetries C_{2v}, C_s or C_2. Such investigations are rare, however.

The water molecules in $Ba(ClO_3)_2.H_2O$ and $K_2C_2O_4.H_2O$ are found at sites with the symmetry C_2. The space group is $C2/c$ (C_{2h}^6) in both cases.[1,2] The corresponding unit cell groups are thus isomorphous with the point group C_{2h}. In the case of $Ba(ClO_3)_2.H_2O$, single crystal infrared and Raman data exist,[3] whereas only a Raman study has been performed on single crystals of $K_2C_2O_4.H_2O$.[4] Both hydrates have been studied as single crystals using neutron inelastic scattering.[5] In the latter study it was possible to assign the rocking modes definitely. The two remaining rotational modes in each case could not be distinguished. Even with the combined use of Refs. 3 and 5 some ambiguities remain for $Ba(ClO_3)_2.H_2O$ mainly as regards the twisting mode.

In the present investigation we have studied infrared spectra of powders of the two hydrates using the isotopic species H_2O, D_2O, HDO and $H_2{}^{18}O$. From these data and the results of Refs. 3 and 5, we will show that the three rotational vibrations and the translational vibration perpendicular to the water molecular plane can be assigned.

EXPERIMENTAL

Commercial analytical grade $Ba(ClO_3)_2.H_2O$ and $K_2C_2O_4.H_2O$ were used as starting materials for the preparation of the various isotope sub-

stituted hydrates. The salts were dried for about 30 h at 140 and 90 °C, respectively, in order to obtain the anhydrous salts. The results were checked by weighing. An appropriate amount of liquid water with the required isotopic composition was then added with a micro syringe. The system of anhydrous salt and water was allowed to reach its equilibrium state in a closed vessel at room temperature. It was found that about two days were enough if the exposed area of the salt was not too small.

The degrees of isotopic enrichment of original D_2O and $H_2{}^{18}O$ liquids were 99.9 and 97 %, respectively.

For the infrared measurements a Beckman IR-9 grating spectrometer was used in the region 400–4000 cm^{-1}. For sample preparation the mull technique was applied with nujol and fluorolube as complementary suspension agents. The hydrates of potassium oxalate were also studied with hexachlorobutadiene mulls in the 600–800 cm^{-1} region. The samples were carried as thin films between plates of KBr or KRS-5.

The far infrared region was scanned using a computer-controlled RIIC FS-720 Fourier spectrometer. An average of several scans (~10) was computed for sample and background (nujol plus polyethene plates) before the ratio was calculated. This reduced the noise to a low level and spectra of good quality were obtained in the region 30–300 cm^{-1}. Between 300 cm^{-1} and 430 cm^{-1} the noise level was somewhat high especially near 400 cm^{-1}. Therefore KRS-5 plates were used to improve the quality of the spectra in this region. The low temperature studies (100 K) were carried out with a Beckman-RIIC VLT2 variable temperature unit.

The spectrometers were calibrated using standard gas bands.[6] The resolution was about 3 cm^{-1} in the region 30–400 cm^{-1} (FS-720 spectrometer) and 2 to 3 cm^{-1} in the region 400–3600 cm^{-1}. For narrow bands the given wavenumbers should be accurate to ±2 cm^{-1} if registered with the IR-9 spectrometer and ±1 cm^{-1} with the FS-720 spectrometer. In order to obtain reliable values for isotopic ratios in the low wavenumber region the relevant spectra were plotted together using a Calcomp plotter. It was then found that positions of narrow bands relative to each other could be measured with an accuracy of about ±0.3 cm^{-1}. At 100 cm^{-1} this corresponds to a maximum error in the isotopic ratios of ±0.006.

Table 1. Infrared absorption wavenumbers of $Ba(ClO_3)_2.H_2O$, $Ba(ClO_3)_2.D_2O$ and $Ba(ClO_3)_2.H_2{}^{18}O$ in the region 470–40 cm^{-1}.

$Ba(ClO_3)_2.H_2O$		$Ba(ClO_3)_2.D_2O$		$Ba(ClO_3)_2.H_2{}^{18}O$		Assignments
100 K	298 K	100 K	298 K	100 K	298 K	
467 m	451			468 m	451	rocking H_2O
457 w				455 w		twisting H_2O
		437 [a]				out of plane H, HDO
		406 [a]				rocking HDO
396 s	390			395 s	390	wagging H_2O
		362 m	351			rocking D_2O
		340 w				twisting D_2O
		317 [b]				out of plane D, HDO
		292 s	290			wagging D_2O
246 m	235	237 m	225	236 m	224	in plane transl.H_2O,D_2O
		241 [c]				in plane transl. HDO
217 m	208	209 m	200	211 m	203	in plane transl.H_2O,D_2O
184 m	176	183 m	174	183 m	173	External vibrations
172 m	165	172 m	165	172 m	165	
153 m	149	152 m	148	152 m	146	
143 m	139	142 m	139	143 m	140	
136 m	134	136 m	134	137 m	134	
130 s	126	130 s	126	130 s	125	
109 s	107	109 s	106	109 s	106	
97.1 m	95	96.1 m	95	96.1 m	94	
77.6 m	75	76.0 m	74	75.0 m	72	out of plane transl., H_2O,D_2O

s = strong, m = medium, w = weak. [a] Measured using a ratio H/D = 5/95. [b] Measured using a ratio H/D = 95/5. [c] Measured using a ratio H/D = 50/50.

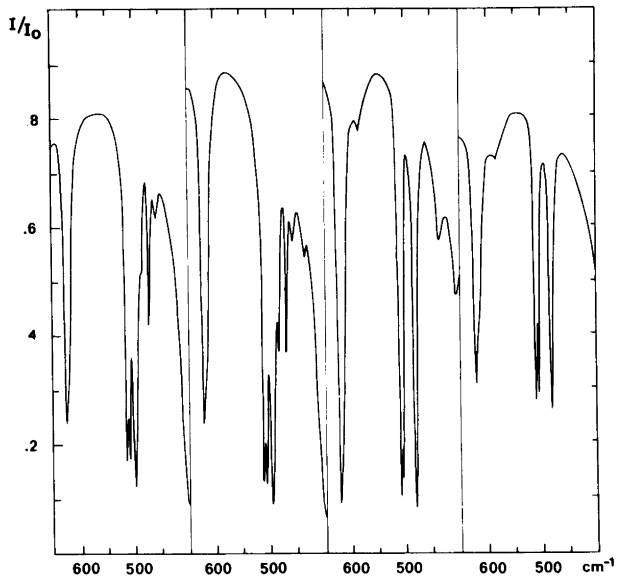

Fig. 1. Infrared spectra (nujol mulls) of $Ba(ClO_3)_2.H_2O$ containing different amounts of deuterium at 100 K in the region of rotational vibrations of the H_2O molecules. From left to right 100, 95, 5 and 1 % H.

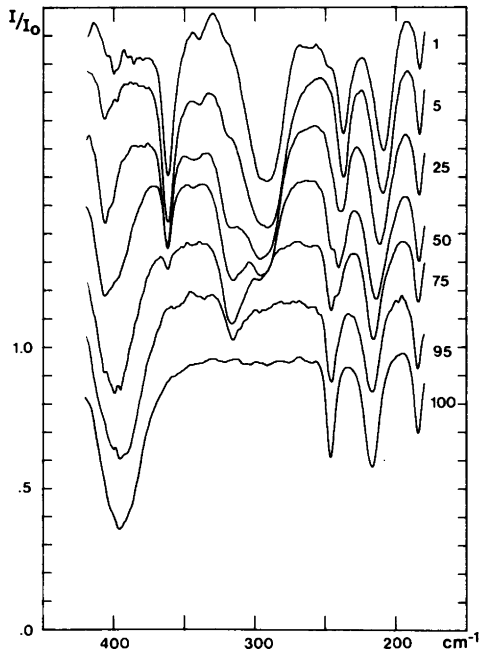

Fig. 2. Far infrared spectra (nujol mulls) of $Ba(ClO_3)_2.H_2O$ containing different amounts of deuterium at 100 K in the region of rotational vibrations of the D_2O molecules. The percentages of H are given in the figure.

RESULTS AND DISCUSSION

Our results for $Ba(ClO_3)_2.H_2O$ in the region above 470 cm^{-1} are in agreement with those of Ref. 3 where survey spectra can be found. The discussion is therefore limited to the low wavenumber region where the rotational and translational vibrations of the water molecule are found. The spectra considered are shown in Figs. 1–3. Wavenumbers and assignments are given in Table 1.

Survey spectra of $K_2C_2O_4.H_2O$ and $K_2C_2O_4.D_2O$ at 100 K between 400 and 3600 cm^{-1} are shown in Fig. 4 and those between 40 and 400 cm^{-1} including that of $K_2C_2O_4.H_2{}^{18}O$ in Fig. 5. Spectra showing the bands from rotational vibrations of the water molecule with different H/D ratios are shown in Fig. 6. Wavenumbers and assignments of the observed bands are found in Table 2. A vibrational analysis in terms of internal and external vibrations together with symmetry correlation diagrams for $K_2C_2O_4.H_2O$ is given in Ref. 4.

In the following the rotational and translational vibrations of the water molecules are discussed separately. Finally, some further aspects of the spectrum of $K_2C_2O_4.H_2O$ are given.

Table 2. Infrared absorption wavenumbers for $K_2C_2O_4.H_2O$, $K_2C_2O_4.D_2O$ and $K_2C_2O_4.H_2{}^{18}O$.

$K_2C_2O_4.H_2O$		$K_2C_2O_4.D_2O$		$K_2C_2O_4.H_2{}^{18}O$		Assignment of fundamental vibrations
100 K	298 K	100 K	298 K	100 K	298 K	
(3436)sh[d]				(3414)sh		
(3351)sh	(3350)sh,b			(3341)sh	(3350)sh,b	
		3249 w,b				OH-stretching HDO
3244 vs,vb	3270 s,vb			3233 vs,vb	3260 s,vb	ν_3 and ν_1,H_2O
(3156)sh				(3130)sh		
		(3092)vw	(3084)vw			
		(3045)vw	(3042)vw			
(2920)w	(2917)w	(2917)w	(2911)w		(2914)vw	
(2751)vw	(2747)vw	(2753)vw	(2745)vw	(2749)vw	(2743)vw	
(2723)vw		(2724)vw		(2725)vw	(2728)vw	
		(2590)sh	(2590)sh			
		2433 s,b	2475 s,vb			ν_3 D_2O
		2387 m,sh				ν_1 D_2O
(1878)w,b	(1868)vw	(1875)vw,b		(1879)w,b	(1868)vw	
1709 w	1690 sh			1705 w	1688 sh	ν_2 H_2O
		(1670)w				
1612 sh	1608 sh	1612 sh		1616 sh	1612 sh	oxalate antisymm. stretching
1598 vs,b	1596 vs,b	1597 vs,b	1595 vs,b	1596 vs,b	1595 vs,b	
(1569)sh	(1568)sh	(1567)sh	(1564)sh	(1568)sh	(1567)sh	
		1489 m[a]	1476 m[a]			bending HDO
(1446)w,b						
(1409)m	(1408)m	(1407)m	(1405)m	(1408)m	(1406)m	
1322 s	1318 s	1322 s	1318 s	1322 s	1318 s	oxalate symm. stretching
1315 s	1310 s,b	1313 s	1310 s,b	1313 s	1309 s,b	
(1299)sh		(1299)sh		(1299)sh		
		1236 m	1225 m			ν_2 D_2O
		(1070)w,vb	(1060)w,vb			
785 s	775 s	775 s	775 s	785 s	775 s	oxalate angle deformation
		771 s	769 s			
		746[b]				out of plane H, HDO
743 s	723 m,b			740 s	723 m,b	wagging H_2O
651 s	620 m,b			648 s	617 m,b	rocking H_2O
		553 s	551 sh			wagging D_2O
		553[c]				out of plane D, HDO
		540[c]				rocking HDO
529 s	526 s	538 w	530 s	529 s	527 s	oxalate angle deformation
525 s		526 s		524 s		
		475 s	454 m,b			rocking D_2O
357 m	353 w	357 sh	349 w	356 m	353 w	oxalate angle deformation
		353 m				
223 s,b	214 s,b	217 s,b	208 s,b	217 s,b	207 s,b	in plane transl., H_2O, D_2O
191 sh		184 sh		184 sh		in plane transl., H_2O, D_2O
174 vs,b	166 vs,b	173 vs,b	165 vs,b	174 vs,b	166 vs,b	external vibrations
138 sh		137 sh		137 sh		
136 m	130 m	135 m	129 m	135 m	129 m	
124 m	117 sh	124 m	116 sh	124 m	117 sh	
97.9 m	95 m	96.7 m	94 m	93.9 m	92 m	out of plane transl., H_2O, D_2O
60 w	56 w	60 w	56 w	60 w	56 w	external vibration

s = strong, m = medium, w = weak, v = very, b = broad, sh = shoulder. [a] Measured using a ratio H/D = 50/50. [b] Measured using a ratio H/D = 5/95. [c] Measured using a ratio H/D = 95/5. [d] Wavenumbers within parantheses are used for combination bands.

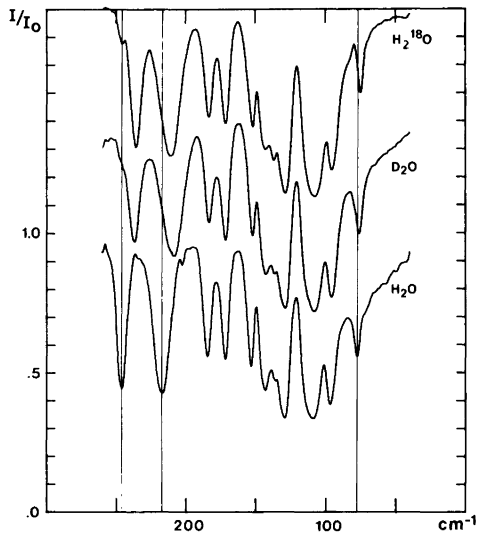

Fig. 3. Far infrared spectra (nujol mulls) of $Ba(ClO_3)_2.H_2O$, $Ba(ClO_3)_2.D_2O$ and $Ba(ClO_3)_2.H_2{}^{18}O$ at 100 K in the region of translational vibrations of the water molecules. Vertical lines are drawn to facilitate the observation of bandshifts.

Rotational vibrations of the water molecules

Inelastic neutron scattering spectra of the hydrates using single crystals have been obtained at 120 K.[5] The spectra were restricted to the region where the rotational vibrations of the water molecules are expected. Using different orientations of the wave vector transfer the authors were able to distinguish the rocking mode (where the hydrogens move in the plane of the molecule) from the twisting and wagging modes (where the hydrogens move perpendicular to the plane).

For $Ba(ClO_3)_2.H_2O$ the rocking mode was found at 477 cm^{-1}. Two additional bands were found at 457 and 398 cm^{-1}. These should correspond to the remaining two rotational modes, but they could not be differentiated in this experiment. In an infrared spectrum the twisting band is expected to have a low intensity[7] since the direction of the dipole moment of the water molecule is unchanged and only changes in the magnitude of the induced dipole moment will give rise to absorption. In the infrared spectrum of $Ba(ClO_3)_2.H_2O$ a band at 395 cm^{-1} (Ref. 3) was assigned as wagging. Due to

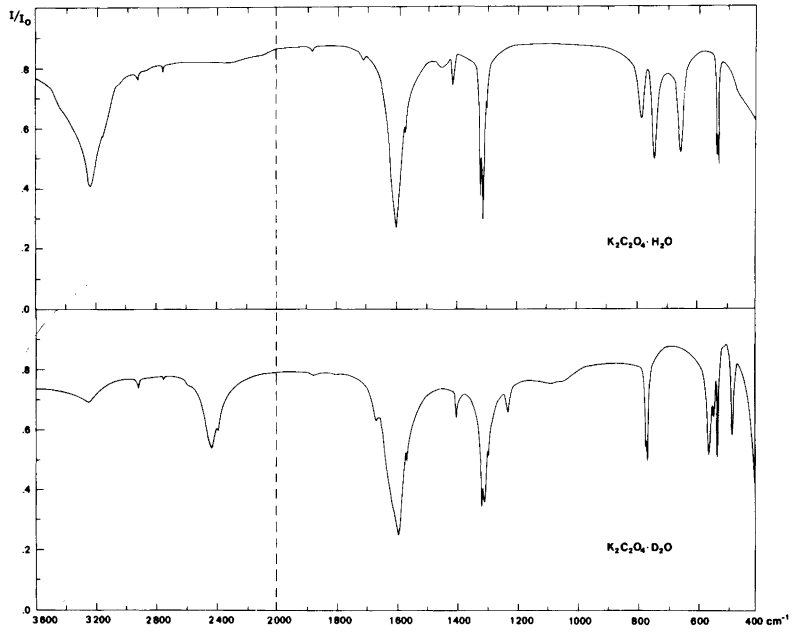

Fig. 4. Infrared spectra of $K_2C_2O_4.H_2O$ and $K_2C_2O_4.D_2O$ at 100 K. Combined spectra from mulls in nujol, fluorolube and hexachlorobutadiene.

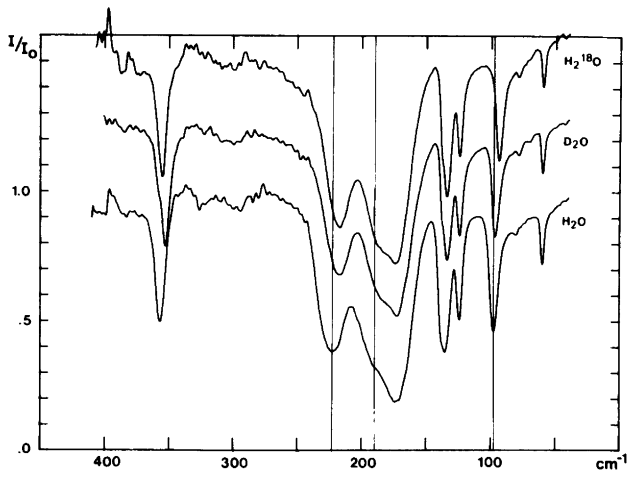

Fig. 5. Far infrared spectra (nujol mulls) of $K_2C_2O_4.H_2O$, $K_2C_2O_4.D_2O$ and $K_2C_2O_4.H_2{}^{18}O$ at 100 K. Vertical lines are drawn to facilitate the observation of bandshifts.

the polarization behaviour of the bands in the infrared spectra a component at 395 cm^{-1} was assigned as twisting. These assignments are thus partly in contradiction with the results of the neutron scattering study.

For $K_2C_2O_4.H_2O$ the rocking mode was found at 644 cm^{-1} in the neutron spectrum,[5] but only one additional band at 738 cm^{-1} was found where two were expected for wagging and twisting. Since intensities of comparable magnitude are expected for twisting and wagging bands in the neutron spectra (the intensities are proportional to the mean square amplitudes of hydrogen motions) an explanation for the single band observed could be that it actually is an unresolved doublet. In the infrared spectra of $K_2C_2O_4.H_2O$[8] a band at 737

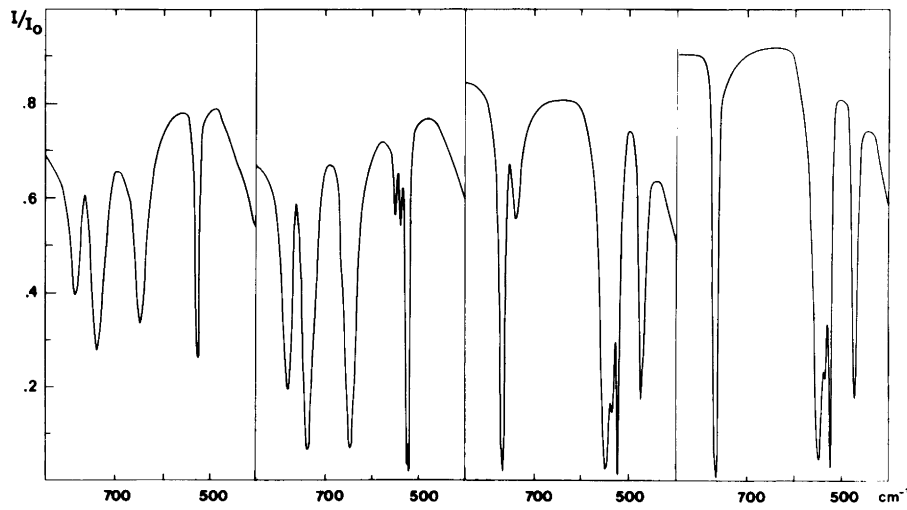

Fig. 6. Infrared spectra (combined from mulls in nujol and hexachlorobutadiene) of $K_2C_2O_4.H_2O$ containing different amounts of deuterium at 100 K in the region of rotational vibrations of the water molecules. From left to right 100, 95, 5 and 1 % H.

cm^{-1} was assigned to wagging but the twisting band was not observed.

In order to resolve the remaining ambiguities we have studied the infrared spectra of $K_2C_2O_4.H_2O$ and $Ba(ClO_3)_2.H_2O$ containing various amounts of HDO. It has been pointed out[9-12] that the use of partially deuterated compounds would be helpful in the assignments of rotational vibrations of water molecules.

We have recently[13] performed a model calculation of the vibrations of a water molecule placed in a simulated crystal environment. The vibrational frequencies and normal modes for H_2O, HDO, D_2O and $H_2{}^{18}O$ were calculated. Some important results found concerning the rotational vibrations will be summarized here. The isotopic ratio ν_{H_2O}/ν_{HDO} was found in the range 1.15 – 1.22 for the rocking mode. The other two modes of HDO could be described as essentially an out-of-plane H motion (H-mode) and an out-of-plane D motion (D-mode). Furthermore, the wavenumber of the H-mode is close to the average wavenumber of wag (H_2O) and twist (H_2O) and the D-mode close to the average of wag (D_2O) and twist (D_2O).

To obtain a straightforward interpretation of spectra from samples containing HDO, two conditions must be fulfilled. No large correlation field effects may exist and the dispersion of the rotational frequencies as functions of the wavevector must be small. In the present hydrates the correlation field effects are small since the Raman[3,4] and infrared frequencies nearly coincide. The dispersion is small since the bands in the neutron scattering study which represent averages over the wavevectors are relatively narrow.

A schematic representation of the rotational bands discussed in the following is given in Fig. 7.

$Ba(ClO_3)_2.H_2O$. Wag (D_2O) for $Ba(ClO_3)_2.D_2O$ is found at 292 and rock (D_2O) at 362 cm^{-1} in the infrared spectra in agreement with Ref. 3. From Fig. 2 it can be seen that, when the percentage of deuterium is decreased, the intensities of the wag (D_2O) and rock (D_2O) bands are decreased and they finally disappear for 5 % D. At the same time a new band at 317 cm^{-1} appears with increasing intensity relative to wag and rock (D_2O). This band is still visible in the 5 % D spectrum and is hence assigned as the D-mode of HDO. In Fig. 1 two bands are found at 437 and 406 cm^{-1}, in the 5 % H 95 % D spectrum, which are the remaining rotational bands of HDO. The band at 406 cm^{-1} and rock (H_2O) at 467 cm^{-1} give a ratio ν_{H_2O}/ν_{HDO}

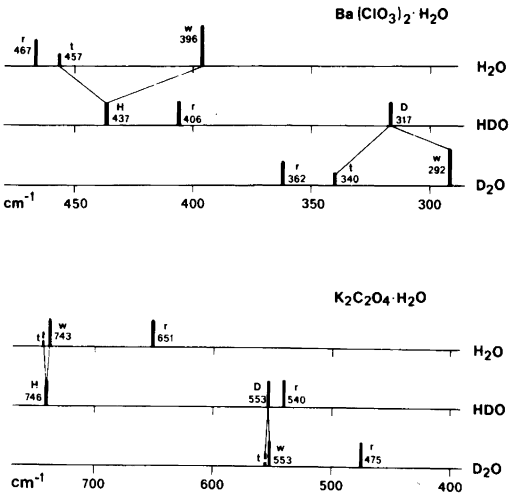

Fig. 7. A summary of the rotational vibration band positions of H_2O, HDO and D_2O for $K_2C_2O_4.H_2O$ and $Ba(ClO_3)_2.H_2O$.

= 1.15 and the 406 cm^{-1} band is accordingly assigned as rock (HDO). The band at 437 cm^{-1} therefore corresponds to the H-mode of HDO. The H-mode is in fact also visible in Fig. 1 in the 95 % H 5 % D spectrum whereas rock (HDO) is overlapped by wag (H_2O).

The H- and D-modes of HDO are thus located 41 and 25 cm^{-1} from wag (H_2O) and wag (D_2O), respectively. Since the wavenumber of the H-mode should be close to the average of wag (H_2O) and twist (H_2O) and correspondingly for the D-mode, it is then clear that twist (H_2O) and twist (D_2O) cannot coincide with wag (H_2O) and wag (D_2O) as suggested in Ref. 3. In fact we have observed two new bands in the spectra of $Ba(ClO_3)_2.H_2O$ and $Ba(ClO_3)_2.D_2O$ at 457 and 340 cm^{-1} (see Figs. 1 and 2), which we assign as twist (H_2O) and twist (D_2O). These very weak bands were discovered only because we used thick samples in order to see the bands from the isotopically dilute HDO molecules. The assignment of the band at 457 cm^{-1} to twist (H_2O) is of course strongly corroborated by the peak at 457 cm^{-1} found in the neutron inelastic scattering spectrum.

$K_2C_2O_4.H_2O$. In the infrared spectrum of $K_2C_2O_4.H_2O$ we observed two rotational bands of H_2O at 743 and 651 cm^{-1} (see Fig. 4). The band at 651 cm^{-1} corresponds to the peak at 644 ± 12 cm^{-1} in the neutron inelastic scattering spectrum

and therefore arises from rock (H_2O). The band at 743 cm^{-1} then arises from wag (H_2O) since the band from twist (H_2O) is expected to have a low intensity (see also Ref. 8). In the spectra of samples containing 5 % H and 95 % H in Fig. 6, three bands at 746, 553 and 540 cm^{-1} from isotopically dilute HDO molecules have been observed. The band at 746 cm^{-1} practically coincides with wag (H_2O) and is assigned as the H-mode of HDO. It follows that the D-mode of HDO is expected to have a wavenumber close to that of wag (D_2O) at 553 cm^{-1}. Therefore we assign the HDO band, also at 553 cm^{-1}, to the D-mode. For the reasons discussed above we then assume that the bands from twist (H_2O) and twist (D_2O) are situated very close to the ones of wag (H_2O) and wag (D_2O), respectively. Finally, the HDO band at 540 cm^{-1} should be rock (HDO) giving a ratio $\nu_{H_2O}/\nu_{HDO} = 1.21$.

This assignment of the twisting and wagging modes is confirmed by the single peak at 738 ± 12 cm^{-1} found in the neutron inelastic scattering spectrum. The single peak evidently corresponds to an unresolved doublet.

In the neutron scattering experiment[5] two orientations of each hydrate were investigated. This was done to differentiate between in- and out-of-plane motions of the hydrogen atoms. In addition to the main peaks observed and discussed above, some smaller peaks or shoulders were seen. These were explained as arising from two phonon processes involving lower lying modes. Since wagging and rocking each form the representation $B_g + B_u$ under the unit cell group the symmetry permits a coupling between these modes. Such a coupling leads to an out-of-plane component of the motion of the H-atoms for the mainly rocking vibration and an in-plane component for the mainly wagging vibration. We believe that this is the main reason for the additional peaks in the neutron spectra.

Translational vibrations of the water molecules

Below 300 cm^{-1} the IR spectra show essentially three bands that are sensitive to isotopic substitutions in the water molecule. For $K_2C_2O_4.H_2O$ these bands are found at 223, 191 and 97.9 cm^{-1} at 100K (Fig. 5). Corresponding wavenumbers for $Ba(ClO_3)_2.H_2O$ are 246, 217 and 77.6 cm^{-1} (Fig. 3). The latter band was not observed by Bertie *et al.*[3] The intensity of this band increased together with other bands with increasing thickness of the sample. In particular, the band vanished completely if the sample scans were carried out with only nujol between the polyethylene plates. Thus it is ruled out that the band originates from polyethylene.

$K_2C_2O_4.H_2O$. The band at 97.9 cm^{-1} for $K_2C_2O_4.H_2O$ shows a larger shift for substitution with $H_2{}^{18}O$ than with D_2O ($\nu_{H_2O}/\nu_{D_2O} = 1.012$ and $\nu_{H_2O}/\nu_{H_2{}^{18}O} = 1.043$) (Fig. 5). The increase in the total mass is the same for the two substitutions. Therefore the vibration cannot be a pure translation. To account for the different shifts, a rotational component in the motion must be introduced so that the change of the moment of inertia is larger for the $H_2{}^{18}O$-substitution. The above-mentioned calculation[13] resulted in a low wavenumber vibration in which only the oxygen is vibrating out of the molecular plane. Such a mode has a rotational axis through the hydrogens but can equally well be thought of as translational in character because the centre of mass of the water molecule is not fixed in the vibration. The wavenumber ratio obtained in the calculation was 1.054 for $H_2{}^{18}O$ substitution and 1.000 for D_2O-substitution. If the rotational axis is displaced somewhat towards or away from the oxygen the non-zero shift for D_2O substitution is explained. Actually the model calculations reproduced this situation when the initial restriction implying a stationary environment was relaxed. The existence of a vibration with a low wavenumber and a rotational component as described above is in agreement with the result from the neutron diffraction study of $K_2C_2O_4.H_2O$ at room temperature.[2] Namely, the total out-of-plane amplitude for oxygen was found to exceed that for the hydrogens. Finally, it has been shown[14] that an out-of-plane mode, rotational in character and with a low wavenumber, explains the temperature dependence of the deuteron quadrupole splittings that are measured using a single crystal of $K_2C_2O_4.D_2O$. In view of all this information we assign the vibration at 97.9 cm^{-1} to be an out-of-plane vibration with a rotational component so that the amplitude for oxygen is larger than for the hydrogens.

The band at 223 cm^{-1} is broad and that at 191 cm^{-1} is a shoulder (Fig. 5). The location of these bands is therefore not very precise and accordingly one cannot make definite conclusions from the isotopic ratios.

$Ba(ClO_3)_2.H_2O$. The far IR spectrum of $Ba(ClO_3)_2.H_2O$ has a band at 77.6 cm^{-1} (Fig. 3).

The evidence for an assignment similar to the one for the band at 97.9 cm^{-1} in $K_2C_2O_4.H_2O$ is very much the same for model calculations,[13] neutron diffraction[1] and IR. The isotopic substitutions give the ratios $\nu_{H_2O}/\nu_{D_2O} = 1.021$ and $\nu_{H_2O}/\nu_{H_2{}^{18}O} = 1.035$. Furthermore, the magnitudes of the out-of-plane atomic motions found in the neutron diffraction work are nearly identical for oxygen and hydrogen. This indicates that the rotational component is somewhat smaller as compared to the situation in $K_2C_2O_4.H_2O$. It should also be noted that another band at 97.1 cm^{-1} in $Ba(ClO_3)_2.H_2O$ is shifted to 96.1 cm^{-1} both for D_2O and $H_2{}^{18}O$ substitution. Obviously, some water motion is included in the corresponding vibration.

The remaining bands in $Ba(ClO_3)_2.H_2O$ (246 and 217 cm^{-1}, Fig. 3) have been discussed by Bertie *et al.*[3] One of the bands should be of symmetry type A_u, the other of type B_u. In terms of translational motion of the water molecule the A-type vibration is along the bisector of the OH bonds. According to Ref. 3 Raman data indicated that the band at 246 cm^{-1} is of A-type while the band at 217 cm^{-1} could not be classified from the experiment. Our investigation gives additional wavenumber ratios for $H_2{}^{18}O$ substitution (Table 1), from which one can conclude that the vibration at 217 cm^{-1} has some rotational contribution.

Further aspects of the spectrum of $K_2C_2O_4.H_2O$

For $K_2C_2O_4.H_2O$ Tomar *et al.*[8] observed a broad absorption band with two peaks at 3400 and 3250 cm^{-1} (liquid nitrogen temperature). Those peaks were assigned to the antisymmetric and symmetric stretching vibrations of the water molecule. In our low temperature spectrum (100 K) (Fig. 4) a strong peak appears at 3244 cm^{-1} with shoulders at 3436, 3351 and 3156 cm^{-1}. The spectrum of $K_2C_2O_4.D_2O$ shows a main peak at 2433 cm^{-1} and shoulders at 2590 and 2387 cm^{-1}. Application of the isotopic dilution technique resulted in wavenumbers for the uncoupled OH and OD stretchings at 3249 and 2418 cm^{-1}.[15] These vibrations are expected to be found between respective antisymmetric (ν_3) and symmetric (ν_1) stretching vibrations on the wavenumber scale. Moreover, Schiffer *et al.*[16] have plotted $\nu_3 - \nu_1$ as a function of the uncoupled OH and OD vibrational wavenumbers. Extrapolation of the plots to include the wavenumber regions of $K_2C_2O_4.H_2O$ and $K_2C_2O_4.D_2O$ gives approximate values for $\nu_3 - \nu_1$ of 10 cm^{-1} for H_2O and 60 cm^{-1} for D_2O. In view of this we assign antisymmetric and symmetric stretching motions to the D_2O peaks at 2433 and 2387 cm^{-1}, respectively. Also, we strongly believe that the peak at 3244 cm^{-1} in the $K_2C_2O_4.H_2O$ spectrum is two unresolved bands corresponding to the antisymmetric and symmetric H_2O stretching motions.

A very similar case is found for $LiHC_2O_4.H_2O$.[17] Although the water molecule is on a C_1 site in this compound the OH bonds are nearly equivalent. In the IR spectrum, the D_2O stretching bands are found at 2465 and 2420 cm^{-1}, while in the H_2O stretching region one strong band centred at 3291 cm^{-1} is found. The uncoupled OH (two bands) and OD stretching bands appear at 3297, 3292 and 2451 cm^{-1}.

The water bending vibration in $K_2C_2O_4.H_2O$ has been placed at 1615 cm^{-1} by Tomar *et al.*[8] We observe a band at 1236 cm^{-1} in $K_2C_2O_4.D_2O$ which certainly is due to the D_2O bending vibration. Using intermediate degrees of deuteration a band observed by us at 1489 cm^{-1} must arise from the HDO bending vibration. Moreover, we observe a new weak band at 1709 cm^{-1}. The wavenumber ratio H_2O/D_2O is 1.35 for the free water molecule and for solid hydrates typically around 1.36.[18] The ratio 1709/1236 is 1.38 while the ratio 1615/1236 is 1.31. The band at 1709 cm^{-1} disappears on deuteration while nothing seems to happen around 1600 cm^{-1}. In particular, a weak shoulder at 1612 cm^{-1} in our spectrum is not influenced by deuteration. Instead, a new band appears at 1670 cm^{-1}. We assign the band at 1709 cm^{-1} in $K_2C_2O_4.H_2O$ to the water bending vibration but leave the band at 1670 cm^{-1} in $K_2C_2O_4.D_2O$ unassigned.

We assign bands at 785, 529, 525 and 357 cm^{-1} in $K_2C_2O_4.H_2O$ at 100K to angle deformation vibrations in the oxalate ion. The bands at 529 and 525 cm^{-1} are obviously the A_u and B_u components of the same internal oxalate vibration. On deuteration the band at 785 cm^{-1} splits into two bands at 775 and 771 cm^{-1} while the band at 357 cm^{-1} splits into two bands at 357 (shoulder) and 353 cm^{-1}. The behaviour on deuteration is probably due to a small interference from the water rotational vibrations of which one is of A_u type (twisting) and the others are of B_u type. The small factor group splittings (≤ 4 cm^{-1}) are in agreement with those obtained in the Raman investigation for the A_g

and B_g modes.[4] The band at 357 cm^{-1} in $K_2C_2O_4.D_2O$ has previously been assigned by Fukushima[19] to a rotational vibration of D_2O with the corresponding H_2O band at 524 cm^{-1}. As we have assigned all the rotational and translational vibrations of the water molecule to bands at other wavenumbers, we believe that Fukushima's assignment is not correct.

Acknowledgements. The authors would like to thank Professor I. Olovsson for the facilities made available to us. The technical assistance of Mrs Margit Hillberg, Mrs Gunilla Lindh and Mr Rune Nordlund is greatly appreciated. This work is supported by grants from the Swedish Natural Science Research Council which are gratefully acknowledged.

REFERENCES

1. Sikka, S. K., Momin, S. N., Rajagopal, H. and Chidambaram, R. *J. Chem. Phys. 48* (1968) 1883.
2. Sequeira, A., Srikanta, S. and Chidambaram, R. *Acta Crystallogr. B 26* (1970) 77.
3. Bertie, J. E., Heyns, A. M. and Oehler, O. *Can. J. Chem. 51* (1973) 2275.
4. Eriksson, A. and Nielsen, O. F. *J. Mol. Struct. 48* (1978) 343.
5. Thaper, C. L., Dasannacharya, B. A., Sequeira, A. and Iyengar, P. K. *Solid State Commun. 8* (1970) 497.
6. Tables of Wavenumbers for the Calibration of Infrared Spectrometers, I.U.P.A.C., *Pure Appl. Chem. 1* (1961) 537; *Ibid. 33* (1973) 605.
7. Miyazawa, T. *Bull. Chem. Soc. Jpn 34* (1961) 202.
8. Tomar, V. S., Bist, H. D. and Khandelwal, D. P. *Appl. Spectrosc. 24* (1970) 598.
9. Lutz, H. D., Klüppel, H.-J., Pobitschka, W. and Baasner, B. *Z. Naturforsch. Teil B 29* (1974) 723.
10. Ichida, K., Kuroda, Y., Nakamura, D. and Kubo, M. *Spectrochim. Acta A 28* (1972) 2433.
11. Thomas, G. H., Falk, M. and Knop, O. *Can. J. Chem. 52* (1974) 1029.
12. Falk, M. and Knop, O. *Can. J. Chem. 55* (1977) 1736.
13. Eriksson, A. and Lindgren, J. *J. Mol. Struct. 48* (1978) 417.
14. Berglund, B., Eriksson, A., Lindgren, J. and Tegenfeldt, J. *J. Mol. Struct. In press.*
15. Berglund, B., Lindgren, J. and Tegenfeldt, J. *J. Mol. Struct. 43* (1978) 169.
16. Schiffer, J., Intenzo, M., Hayward, P. and Calabrese, C. *J. Chem. Phys. 64* (1976) 3014.
17. de Villepin, J. and Novak, A. *J. Mol. Struct. 30* (1976) 255.
18. Falk, M. and Knop, O. In Franks, F., Ed., *Water, a Comprehensive Treatise*, Plenum, New York 1973, Vol. 2, p. 55.
19. Fukushima, K. *Bull. Chem. Soc. Jpn 44* (1971) 372.

Received May 19, 1978.

Acta Chemica Scandinavica A 32 (1978) 747–751

Adsorption of Protium and Deuterium Oxides on Cation Exchange Resins

AARRE KELLOMÄKI

Department of Biomedical Sciences, University of Tampere, P.O.Box 607, SF-33101 Tampere 10, Finland

The adsorption of protium and deuterium oxides at 298.15 K on the lithium, sodium, potassium, and barium forms of Dowex 50W-X8 cation exchanger was studied. In the whole humidity range the resinates adsorb larger mol amounts of H_2O than of D_2O. In the low humidity range the observations fit well the two parameter B.E.T. isotherm. The Gibbs energy changes of transfer of the resinates from H_2O to D_2O were $\Delta G_t = 2400$ J/mol. About 2200 J/mol of this is believed to be caused by the anions. Thus, in their interactions with the isotopically different waters the resinates resemble ordinary salts. The relative magnitudes of the ΔG_t values reveal different surface effects between the resin matrix bound sulfonate groups and the two kinds of water.

The cation exchangers based on strong sulfonic acid resins are polyelectrolytes with their negative charge bound to the resin matrix. A special feature of these resinates is their great ability to adsorb water even from the vapor phase.[1] The purpose of this study was to examine, if there are any differences in this feature when the ordinary water, protium oxide, is replaced with the isotopically different kind of water, deuterium oxide.

EXPERIMENTAL

The cation exchange resin used was a commercial sulfonated polystyrene resin Dowex 50W-X8, 50 to 100 mesh, manufactured by Dow Chemicals Co. The resin in the H^+ form was first washed with methanol in a Soxhlet apparatus and then with distilled water. The exchange capacity determined by a standard titrimetric method[2] was 5.060 mmol/g dry acid form resin, which gives a molecular weight of 197.6. (One mol of resin is defined as the amount which contains a number of sulfonic acid groups equal to Avogadro's number.) Portions of the resin were converted to salt forms in a column using a tenfold amount of Merck's analytical grade lithium, sodium, potassium, and barium chlorides. According to the manufacturer, Norsk Hydro-elektrisk Kvaelstofaktieselskab, the deuterium fraction of the heavy water employed in the experiments was 0.997.

The isopiestic measurements were conducted in a stainless steel humidistat shown in Fig. 1. It was modified from the type described by Boyd and Soldano[3] to facilitate rapid weighings below a balance without opening the vessel. The basic part of the humidistat was a 5 l pot with a 3 cm wide rim with eight fastening bolts (A) and a channel for an O-ring seal (B). The cover was furnished with holes for the fastening bolts, a plastic window (C), and eight pipes (D) which could be closed with rubber plugs. The air in the humidistat was stirred with a paddle stirrer (E) and slave magnets (F) fixed to it. The stirrer was rotated with a master magnet (G) driven at one revolution per second by a small synchronous electric motor. A proper saturated salt solution was placed in a nickel dish (H) which was stirred at times with a glass rod. The samples were in eight open porcelain crucibles (I) equipped with metal wire bails. The whole humidistat was sub-

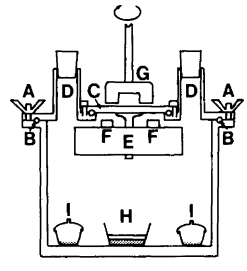

Fig. 1. The isopiestic apparatus.

merged up to the rim in a constant temperature water bath (25.00 ± 0.05 °C) below the balance.

For each ionic form two samples were used, and their dry weights (0.6 to 1.0 g) were determined after drying for 24 h at 120 °C. The dry samples and the first saturated salt solution were placed in the humidistat, which in the case of the deuterium oxide run was predried with phosphorus pentoxide, the vessel was closed tightly and placed in the water bath. To determine the water uptake of a sample the plug of the respective pipe (D) was removed, a hook-ended wire was threaded through to grip the bail on the crucible, and the sample was weighed in the humidistat below the balance. Because this procedure did not change the humidity of the isopiestic apparatus, it greatly speeded up reaching an equilibrium. When constant weights were registered, the salt solution was replaced with the next one. To avoid the effect of possible hysteresis the experiments were performed in such a succession that every second equilibrium was approached from below, every second from above. The relative humidities of the saturated salt solutions in D_2O were taken from the paper by Becker *et al.*[4] The corresponding values for the H_2O solutions were from the measurements by Stokes and Robinson.[5]

RESULTS

Since the samples were rather big, and the porcelain crucibles did not conduct heat well, the samples reached constant weights fairly slowly, typically in a week. The equilibrium was reached more slowly from above than from below, and more slowly with D_2O than with H_2O, which is, no doubt, caused by the slower diffusion of D_2O through the resin matrix. Further, the equilibrium was established slower with increasing molecular weight of the counter ion. Especially with the barium resinate such a slowness caused a distinct hysteresis effect at some humidities.

The results of the experiments are given in Table 1, each the mean of two samples consistent within a few hundredths of mol/mol resinate. For a more convenient comparison the lithium resinate data are presented also in Fig. 2. The results are most accurate in the low humidity range; in higher humidities the experimental points may differ from the average adsorption curves by as much as 0.1 to

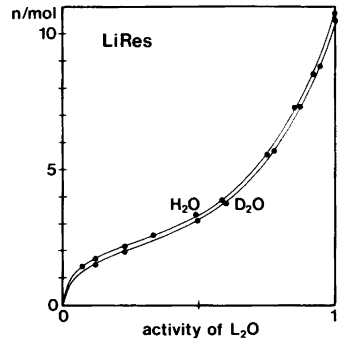

Fig. 2. The amounts of H_2O and D_2O adsorbed on one mol of the lithium resinate at various relative humidities at 298.15 K.

Table 1. The amounts of protium and deuterium oxides adsorbed by resinates at 298.15 K expressed in mol of water species per mol of resin. For $BaRes_2$ the molecular weight of 265.3 was used.

Resinate	Saturated salt solution and its relative vapor pressure										
		NaOH	LiCl	KAc	$MgCl_2$	KNO_2	NaBr	NaCl	KCl	KNO_3	L_2O
	H_2O	0.070	0.113	0.222	0.330	0.482	0.582	0.751	0.842	0.920	1.000
	D_2O		0.116	0.226		0.495	0.598	0.771	0.865	0.943	1.000
LiRes	H_2O	1.41	1.67	2.13	2.55	3.31	3.81	5.50	7.29	8.44	10.71
	D_2O		1.50	1.93		3.12	3.74	5.65	7.34	8.75	10.42
NaRes	H_2O	1.37	1.62	2.00	2.35	3.03	3.36	4.65	6.18	7.16	9.54
	D_2O		1.43	1.84		2.82	3.24	4.71	6.22	7.44	9.20
KRes	H_2O	1.16	1.37	1.67	1.95	2.49	2.73	3.63	4.60	5.61	7.99
	D_2O		1.20	1.53		2.28	2.57	3.61	4.82	5.80	7.49
$BaRes_2$	H_2O	1.38	1.59	1.92	2.13	2.74	2.89	3.45	4.24	5.69	6.12
	D_2O		1.39	1.79		2.43	2.61	3.35	4.29	4.62	5.49

0.2 mol/mol resinate. In this study as in the earlier ones[3,6,7] the adsorption from the vapor phase gave lower values for 100 % relative humidity than those obtained with a centrifugal method from water solution.[8] During the D_2O run the dry weights of the resinates increased by 1 to 3 mg/g resinate, which, however, is negligible compared with other experimental errors. The effect is due to the deuteration of the resin matrix found in an earlier study.[9] The present adsorption curves are similar to the sigmoidal curves obtained by other investigators. In the case of lithium, sodium, and potassium the H_2O adsorption can be directly compared with the results of Boyd and Soldano,[3] and the agreement is good. For the D_2O adsorption no comparative values were found in the literature.

DISCUSSION

Each of the resinates studied adsorbs larger mol amounts of protium oxide than of deuterium oxide in the whole humidity range. The difference is produced already at the steeply rising low humidity part of the adsorption curves, where the water is thought to be used mainly to form hydration shells on sulfonate groups.[3,7] Then the water dipoles preferably orient themselves with hydrogen ends towards the negatively charged sulfonate groups, and we may expect differences in the behavior of various kinds of water. When the relative humidity is raised the cations, too, begin to be hydrated but the orientation of the water dipoles is the opposite and there are no special differences between the different kinds of water. Thus, the difference of the adsorption curves remains essentially constant in the plateau range, and the situation continues in the higher humidities, where adsorption takes place on the nonionic resin matrix.

As Gregor and his coworkers stated [6] the Raoult's law diagrams like Fig. 3 reveal special features of the binary system resin-water. At low water mol fractions the components behave as if they were completely miscible. Where the water activity becomes one the components become completely immiscible. Thus, there is a solubility gap in the range corresponding to dilute solutions of ordinary electrolytes. According to Fig. 3, the system exhibits a large negative deviation from Raoult's law indicating strong interactions between the resinates and the two waters. As the deviation is larger for H_2O, the resinate binds H_2O more tightly than D_2O.

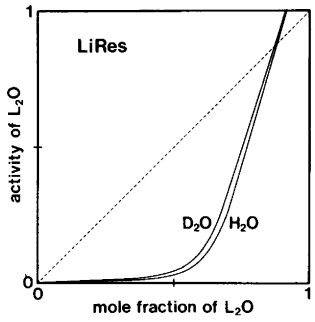

Fig. 3. The Raoult law diagrams of the system L_2O-LiRes.

The Raoult's law relations for a number of salt solutions in protium and deuterium oxides can be calculated from the osmotic coefficients reported by Kerwin [10] and Rasaiah.[11] Because the ordinary salts have limited solubilities, only the upper right corner in the Raoult's law diagram is reached.

In the case of alkali halides and zink sulfate the D_2O and H_2O curves lie very close to one another and generally the former curve is to the right of the latter one. Cesium chloride and zink sulfate, however, resemble the resinates in that the D_2O curves lie to the left of the H_2O curves. This does not, however, prove any deeper relationship between the mentioned salts and resinates. The same comparison can also be made by calculating the osmotic coefficients for the resinate solutions. Then it must be noted that the sulfonate groups bound to the resin matrix have no osmotic effect.[6] According to such calculations the osmotic coefficients for the resinates are larger in H_2O than in D_2O as in the case of cesium chloride and zink sulfate.

The measurements provide data for calculating free energy changes of adsorption.[6,12,13] According to the Gibbs-Duhem equation, the Gibbs energy change for a process, where a dry resinate adsorbs water isothermally up to the relative humidity of 100 %, is

$$\Delta G = -RT \int_0^1 \frac{n}{a} \mathrm{d}a \qquad (1)$$

In this equation n is the number of water moles adsorbed at the water activity a, R is the gas constant and T the absolute temperature. The integral can be evaluated best with graphic integration by plotting n/a against a.

Table 2. The B.E.T. parameters and Gibbs energy changes for adsorption of different kinds of water on resinates.

		B.E.T. parameters		Gibbs energy changes	
		C	n_m	ΔG J/mol	ΔG_t J/mol
LiRes	H_2O	35.78	1.808	−26100	
	D_2O	30.75	1.657	−23660	2440
NaRes	H_2O	50.14	1.647	−24870	
	D_2O	39.49	1.529	−22170	2700
KRes	H_2O	60.25	1.357	−21040	
	D_2O	51.43	1.235	−18640	2400
$BaRes_2$	H_2O	165.83	1.466	−29130	
	D_2O	175.38	1.339	−27110	2020

For calculations the observations were first plotted in a large scale and the best fitting adsorption curves (Fig. 2) were drawn considering the possible hysteresis. The two parameter B.E.T. isotherm[14] was found to represent the observations very well in the low humidity range. The equation of this isotherm is

$$\frac{a}{1-a}\frac{1}{n} = \frac{1}{Cn_m} + \frac{(C-1)a}{Cn_m} \qquad (2)$$

where a and n are the same quantities as above, C and n_m are parameters. The observations were fitted to eqn. (2) by least squares, and the parameters are given in Table 2. The missing points for $a(D_2O) = 0.330$ were estimated from the large scale adsorption curves. In the B.E.T. isotherm theory the parameter n_m is the amount of the adsorbate needed to form a monomolecular layer. From the n_m values we can estimate that the adsorption areas of the resinates are 320 to 570 m^2/g, which is very reasonable. The point must not, however, be taken too literally, since we get smaller areas with D_2O than with H_2O.

The integrals (1) were calculated with Simpson's formula. In the range $a = 0 - 0.35$ the B.E.T. isotherm values were used. The integral can be evaluated also at the lower limit, because $\lim_{a\to 0} n/a = Cn_m$. In the range above $a = 0.35$ the n values were taken from the large scale adsorption curves. The calculated Gibbs energy changes are given in Table 2 and their cumulation with increasing relative humidity calculated with the trapeze rule in Fig. 4. The errors of the Gibbs energy changes are estimated to be a few hundred J/mol at most, except for the barium resinate, which is less accurate.

The difference $\Delta G_t = \Delta G(D_2O) - \Delta G(H_2O)$ is the Gibbs energy change for the transfer process

$$MRes(H_2O) \rightarrow MRes(D_2O) \qquad (3)$$

where the adsorbed protium oxide is replaced with deuterium oxide. Within the experimental errors the ΔG_t values for the resinates are the same, 2400 J/mol. They are somewhat larger than, but of the same sign as, those obtained for ordinary salts.[15,16] The Gibbs energy changes of transfer of metal ions are believed to be only a few hundred J/mol.[16]

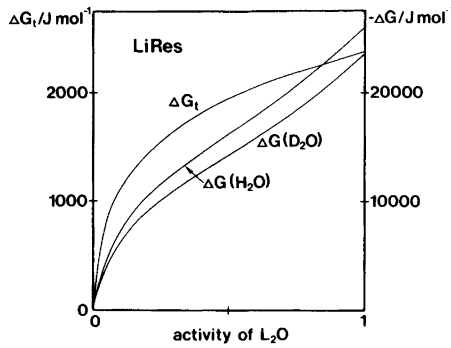

Fig. 4. The cumulative Gibbs energy changes of adsorption for the lithium resinate.

Thus, the transfer of the resin matrix bound sulfonate groups from H_2O to D_2O causes a Gibbs energy change of about 2200 J/mol. It is larger than obtained for other anions[16] giving evidence of special surface effects in this case. The fact that a larger part of the ΔG_t value of a resinate is due to the anion is seen also from Fig. 4: ΔG_t increases very steeply just in the low humidity range, where the hydrate shells of the sulfonate groups are being filled.

The present adsorption experiments show that the resinates of strong sulfonic acid cation exchangers are rather normal electrolytes in their interactions with the isotopically different kinds of water. As usual, the isotopic effects are mainly due to the anions. The magnitude of the transfer Gibbs energies suggests, however, that there are special surface effects between the resin matrix bound sulfonate groups and the two kinds of water.

Acknowledgement. The English language of the manuscript was checked by Ms. Kyllikki Kauppinen-Walin, translator.

REFERENCES

1. Pietrzyk, D. J. *Ion Exchanger-Solvent Interactions: Properties and Methodology.* In Campbell, B., Ed., *CRC Critical Reviews in Analytical Chemistry*, CRC Press, Inc. Cleveland 1976, Vol. 6, p. 131.
2. Kunin, R. *Ion Exchange Resins*, Robert E. Krieger Publishing Company, Huntington, N.Y. 1972, p. 341.
3. Boyd, G. E. and Soldano, B. A. *Z. Elektrochem. 57* (1953) 162.
4. Becker, M., Schälike, W. and Zirwer, D. *Z. Naturforsch. Teil A 24* (1969) 684.
5. Stokes, R. H. and Robinson, R. A. *Ind. Eng. Chem. 41* (1949) 2013.
6. Gregor, H. P., Sundheim, B. R., Held, K. M. and Waxman, M. H. *J. Colloid Sci. 7* (1952) 511.
7. Lal, B. B. and Douglas, W. J. M. *Ind. Eng. Chem., Fundam. 13* (1974) 223.
8. Howery, D. G., Shore, L. and Kohn, B. H. *J. Phys. Chem. 76* (1972) 578.
9. Kellomäki, A. and Jutila, M. *Finn. Chem. Lett.* (1977) 158.
10. Kerwin, R. E. *Ph.D. Thesis*, University of Pittsburg, Pittsburg 1964.
11. Rasaiah, J. C. *Ph.D. Thesis*, University of Pittsburg, Pittsburg 1965.
12. Bull, H. B. *J. Am. Chem. Soc. 66* (1944) 1499.
13. Dole, M. and McLaren, A. D. *J. Am. Chem. Soc. 69* (1947) 651.
14. Adamson, A. W. *Physical Chemistry of Surfaces*, Wiley, New York 1976, Chapter XIV.
15. Arnett, E. M. and McKelvey, D. R. In Coetzee, J. F. and Richie, D. C., Eds., *Solute-Solvent Interactions*, Dekker, New York 1969, Chapter 6.
16. Kellomäki, A. *Ann. Acad. Sci. Fenn. Ser. A 2 166* (1972).

Received May 19, 1978.

Acta Chemica Scandinavica A 32 (1978) 753–756

Conformational Analysis of Coordination Compounds. V. Tris(2-methyl-1,2-propanediamine)- and (2,3-Butanediamine)bis-(1,2-ethanediamine)cobalt(III) Complexes

NIELS CHRISTIAN POUL HALD and KJELD RASMUSSEN*

Chemistry Department A, The Technical University of Denmark, Building 207, DK-2800 Lyngby, Denmark

For all members of the $[Co(ibn)_3]$ series and those members of the $[Co(rac\text{-}bn)en_2]$ series containing equatorial methyl groups, equilibrium conformations are found by convergent energy minimization in a force field developed for tris(diamine) complexes of cobalt(III). Ob-lel and axial-equatorial energy differences are compared with earlier results, and shapes of chelate rings and coordination polyhedra are discussed in terms of deviations from regular octahedral microsymmetry. The energetics of the tris-(ibn) series closely follows that of the tris(*m*-bn) series studied previously; the ring distortions are shown in stereo. The energetics of the $(rac\text{-}bn)en_2$ series fits those of the tris(en) and tris-(rac-bn) series; the geometries are less regular.

Recently, some insight in the energetics and structures of tris(diamine) chelate complexes of cobalt was gained from convergent conformational energy minimization using the Consistent Force Field System,[1] particular concerning the shapes of the chelate rings.[2,3] Both works reported studies on symmetrically substituted diamines, and we thought it might be interesting to include in this series a study of a system with a non-symmetrical diamine, 2-methyl-1,2-propanediamine (="isobutylenediamine"=ibn). In a tris(ibn) complex each ring will have one methyl group in each of the configurations traditionally termed axial and equatorial, as in tris(*meso*-2,3-butanediamine) complexes. In contrast to these tris-(*m*-bn) complexes, the methyl groups in tris(ibn) complexes are situated two at one carbon atom in each ring, and it might be expected that the regularity of *m*-bn chelate rings is distorted.

In addition to tris-(ibn) complexes, we included in this work a study of the conformers of a mixed complex, $[Co(rac\text{-}2,3\text{-}bn)(en)_2]$ (en=ethylenediamine=1,2-ethanediamine) in order to see to which extent the ob-lel conformational differences of the Coen ring[3] are modified by the presence of the methyl group, and to see whether there is any difference in the geometry of a Co(rac-2,3-bn) ring between this series and the $Co(rac\text{-}2,3\text{-}bn)_3$ series. We have found no references to earlier studies of these series, neither from a computational nor from a structural point of view.

ISOMERISM AND NOMENCLATURE

Analogously to the tris-(*meso*-2,3-bn) complexes,[3] the tris(ibn) series has 12 conformationally distinct members within the overall Λ (or Δ) configuration, 4 having facial (*fac*) and 8 having meridional (*mer*) configuration. Their numbering in the series and their notation will be completely analogous to the tris(*meso*-2,3-bn) series (Ref. 3, Table 2) and shall not be repeated here.

In the $Co(rac\text{-}2,3\text{-}bn)(en)_2$ series we only deal with equatorial disposition of the methyl groups. Considering only the Λ absolute configuration, the two ligands 2*S*,3*S*-bn and 2*R*,3*R*-bn will then have the conformations lel and ob. The two en rings of each molecule can each take the conformations lel and ob. Altogether we get 6 isomers and conformers, which are listed in Table 1.

* To whom correspondence should be addressed.

Table 1. Six conformers of M(*rac*-2,3-bn)(en)$_2$. Both methyl groups are equatorial, and the overall configuration is Λ.

No.	Shorthand notation	Full notation for Λ-series
1	lellel$_2$	[M(2*S*,3*S*-bn)(en)$_2\delta\delta\delta$]
2	lellelob	[M(2*S*,3*S*-bn)(en)$_2\delta\delta\lambda$]
3	lelob$_2$	[M(2*S*,3*S*-bn)(en)$_2\delta\lambda\lambda$]
4	oblel$_2$	[M(2*R*,3*R*-bn)(en)$_2\lambda\delta\delta$]
5	oblelob	[M(2*R*,3*R*-bn)(en)$_2\lambda\delta\lambda$]
6	obob$_2$	[M(2*R*,3*R*-bn)(en)$_2\lambda\lambda\lambda$]

CALCULATIONS

Method. A full documentation of the methods and programmes for Consistent Force Field calculations is available.[1]

Force Field. Exactly the same force field as in the previous work[3] was used.

Initial structures. Starting conformations of the tris-(ibn) series were constructed with a modification of a small programme used for the tris(*m*-bn) series;[2] for the (rac-2,3-bn)(en)$_2$ series they were taken from the minimized conformations of the tris(rac-2,3-bn) series[2] by substituting hydrogen atoms for four methyl groups of Nos. 1, 6, 14, 13, 9, and 4 of the previous work (Ref. 3, Table 1).

Minimization. The steepest-descent and modified Newton algorithms were used. The resources required per molecule were on average as in the previous study.[3]

RESULTS AND DISCUSSION

Relative energies. All energy contributions and total and relative energy values are listed in Tables 2 and 3. Energies are in kJ mol^{-1}. The columns headed $\nabla \times 10^9$ give the final gradient norms in kJ mol^{-1} Å^{-1}, which is a good measure of the success of the minimization.

When the absolute energies are plotted on a common energy scale, pictures exactly like Figs. 1 and 2 of the previous study[3] result. The tris-(ibn) system lies 10.5 kJ mol^{-1} below the tris-(*m*-bn) system, with the same spread of 12 kJ mol^{-1}, and with the same relative positions, to within 0.5 kJ mol^{-1}, for corresponding conformations. The (*rac*-

Table 2. Energy contributions for twelve iso- and conformers of M(ibn)$_3$. E in kJ mol^{-1}, ∇ in kJ mol^{-1} Å^{-1}.

	Conformer	$\nabla \times 10^9$	E_b	E_t	E_p	E_{nb}	E_T	ΔE
12	mer(ob$_3$)	3	4.48	16.30	36.75	−20.84	36.70	8.12
11	mer(ob$_2$lel)	21	4.74	16.89	36.01	−18.86	38.78	10.20
10	mer(oblelob)	67	4.78	17.21	36.67	−18.13	40.54	11.96
9	mer(lelob$_2$)	25	4.33	14.64	35.54	−21.81	32.69	4.11
8	mer(oblel$_2$)	29	4.66	14.82	34.80	−19.20	35.08	6.50
7	mer(leloblel)	29	4.62	15.13	34.10	−19.59	34.25	5.67
6	mer(lel$_2$ob)	13	4.43	14.69	36.34	−20.91	34.54	5.96
5	mer(lel$_3$)	398	4.32	13.14	33.36	−22.24	28.58	0.00
4	fac(ob$_3$)	13	4.86	18.39	35.94	−18.62	40.58	12.00
3	fac(lelob$_2$)	42	4.76	16.84	35.60	−18.67	38.54	9.96
2	fac(lel$_2$ob)	88	4.46	14.87	35.48	−20.88	33.94	5.46
1	fac(lel$_3$)	38	4.04	13.61	36.07	−24.65	29.07	0.49

Table 3. Energy contributions for six conformers of M(*rac*-bn)en$_2$. E in kJ mol^{-1}, ∇ in kJ mol^{-1} Å^{-1}.

	Conformer	$\nabla \times 10^9$	E_b	E_t	E_p	E_{nb}	E_T	ΔE
6	obob$_2$	38	1.68	9.65	19.09	−21.45	8.97	4.79
5	oblelob	25	1.71	9.83	18.79	−21.29	9.04	4.86
4	oblel$_2$	209	1.58	10.03	17.85	−22.52	6.94	2.76
3	lelob$_2$	42	1.73	9.75	18.81	−21.18	9.10	4.92
2	lellelob	25	1.61	9.86	17.98	−22.45	6.99	2.81
1	lellel$_2$	96	1.43	10.42	16.60	−24.28	4.18	0.00

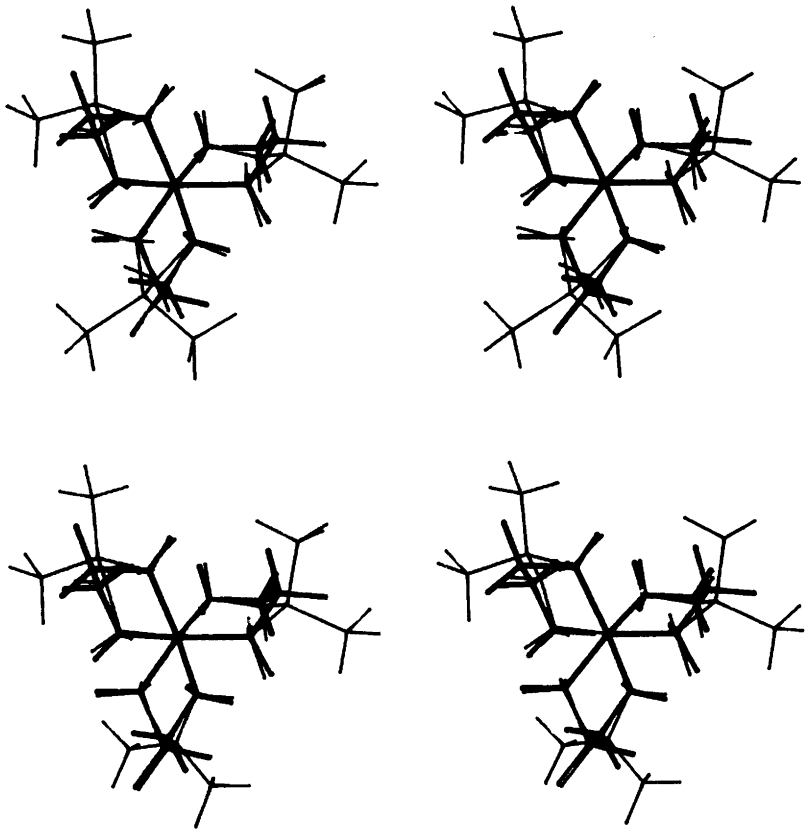

Fig. 1. Stereo drawings of (upper) Λ-*fac*-[Co(ibn)$_3$δδδ] and (lower) Λ-*mer*-[Co(ibn)$_3$δδδ], the lel$_3$ conformations.

bn)(en)$_2$ system conforms strikingly to a linear combination of the tris(en) and the tris(*rac*-bn) eq$_6$ systems.

ob-lel Differences. For the energy differences between chelate rings having ob and lel conformations, we find much the same results as for the series studied previously:[3] *fac*-M(ibn)$_3$ 3.9 ± 0.9, *mer*-M(ibn)$_3$ 2.7 ± 2.2, all M(ibn)$_3$ 3.3 ± 1.8; M(*rac*-bn)-(en)$_2$ 1.6 ± 0.9 kJ mol^{-1}.

ax-eq Differences. Previously,[3] an equatorially placed methyl group was found to change the energy by -1.53 kJ mol^{-1}, whereas an axial methyl group would add 13.52 kJ mol^{-1} to the energy. The (*rac*-bn)(en)$_2$ series conforms singularly well to this picture, giving an average of -1.46 kJ mol^{-1} per equatorial methyl group. The tris(ibn) series, as pointed out above, is displaced 10.5 kJ mol^{-1} down the energy scale from the corresponding tris(*m*-bn) series, which also has the eq$_3$ax$_3$ configuration. This is hardly surprising, as the chelate ring would be expected to deform when an "axial" and an "equatorial" methyl group are placed on the same carbon atom. Fig. 1 shows this deformation, tending to give both methyl groups on a ring axial as well as equatorial character.

Non-bonded interactions. A histogram analysis of all non-bonded interactions revealed no clear trends as to the importance of any particular type of interaction for either set of molecules. This is analogous to what was found for the tris(en) and tris(*m*-bn) series.[3]

Shapes of chelate rings. The introduction of two methyl groups on one carbon atom induces slight changes in the calculated values of bond lengths, valence angles and torsional angles connected with that atom. Table 4 shows that, with two methyl

Table 4. Structures of the twelve isomers and conformers of $M(ibn)_3$, with methyl groups on C1, compared with $M(en)_3$. The average values and ranges found in the calculations are shown.

Bonds/Å	$M(ibn)_3$	$M\,en_3$
M – N1	2.026 ± 0.003	2.018 ± 0.002
M – N2	2.018 ± 0.006	
C1 – N1	1.483 ± 0.003	1.475 ± 0.001
C2 – N2	1.474 ± 0.002	
C1 – C2	1.548 ± 0.001	1.540 ± 0.001
Angles/°		
N – M – N	84.9 ± 0.6	86.7 ± 0.3
M – N1 – C1	111.2 ± 0.8	106.5 ± 0.6
M – N2 – C2	107.0 ± 1.2	
N1 – C1 – C2	108.4 ± 0.5	107.8 ± 0.1
N2 – C2 – C1	108.8 ± 0.8	
Torsions/°		
N2 – M – N1 – C1	3.7 ± 3.7	15.6 ± 1.3
C2 – N2 – M – N1	23.8 ± 4.5	
M – N1 – C1 – C2	24.8 ± 3.7	40.2 ± 1.2
C1 – C2 – N2 – M	44.3 ± 3.0	
N1 – C1 – C2 – N2	44.6 ± 3.3	55.5 ± 1.2

groups on C1, the bonds M – N1, N1 – C1 and C1 – C2 increase slightly, while the M – N1 – C1 angle opens and the N1 – M – N2 closes; torsions around M – N1, N1 – C1 and C1 – C2 are most affected. C1 is found almost in the (M,N1,N2) plane. The valence and torsional angle changes, in particular, are seen in stereo in Fig. 1. There are no significant differences between rings in *fac* and *mer* isomers of the tris(ibn) series.

Table 5 shows, together with Table 4, that bonds, angles and torsions are very alike for the two systems $M(en)_3$ and $M(rac\text{-bn})en_2$. From the previous study we see that also the $M(rac\text{-bn})_3$ system is very close hereto.

The ring puckering descriptors, the N – C – C – N torsional angle ϕ and the dihedral angle τ defined by lines joining the C – C and N---N atoms, are, for the tris(ibn) series, almost like those found[3] in the tris(*rac*-bn) eq_6 and tris(en) series: $\phi = 44.6 \pm 3.3$ and $\tau = 23.5 \pm 1.3$, with the ratio $\tau:\phi = 0.53$. For the $(rac\text{-bn})(en)_2$ series the correspondence is even closer: $\phi = 55.2 \pm 1.2$ and $\tau = 28.1 \pm 1.3$, and their ratio is 0.51 as found in the earlier work.[3]

Shapes of coordination octahedra. As before,[3] we use three angles to describe deviations of the MN_6 octahedron from a regular one: the twist ω (regular: 60°), the tilt θ (regular: 54.8°) and the pitch ψ (regular: 35.3°). All ω values range from 50 to 58°, showing that the octahedron is twisted towards a trigonal prism ($\omega = 0°$) as befits tris-chelates with five-membered rings. All θ values are approximately regular, 51 – 58°; all ibn rings are slightly compressed along the threefold or pseudo-threefold axis; the $(rac\text{-bn})(en)_2$ series shows a larger variation, with cases of elongation, though with no apparent regularity. The degree of helicity, as measured by ψ, ranges from 31 to 35° for the tris(ibn) series and from 25 to 44° for the $(rac\text{-bn})(en)_2$ series.

Table 5. Structures of the six conformers of $M(rac\text{-bn})en_2$. The average values and ranges found in the calculations are shown.

Bonds/Å	*rac*-bn	en
M – N	2.015 ± 0.001	2.019 ± 0.002
C – N	1.476 ± 0.001	1.474 ± 0.001
C – C	1.547 ± 0.001	1.540 ± 0.001
Angles/°		
N – M – N	86.5 ± 0.3	86.4 ± 0.6
M – N – C	107.0 ± 0.6	106.5 ± 0.5
N – C – C	107.5 ± 0.2	107.8 ± 0.2
Torsions/°		
N – M – N – C	15.0 ± 1.6	15.0 ± 2.0
M – N – C – C	40.6 ± 0.6	50.7 ± 1.6
N – C – C – N	55.2 ± 1.2	55.5 ± 1.2

Acknowledgement. Computations were done on an IBM 370/165 at the Technical University Computer Centre NEUCC and were paid for with a grant from the Danish Natural Science Research Council, which is gratefully acknowledged. Stereo drawings were produced from the coordinates of the equilibrium conformers with a programme MONSTER written by Mr. Per Jacobi of The Royal Danish Academy of Fine Arts, Laboratory of Datalogy.

REFERENCES

1. Niketić, S. R. and Rasmussen, K. *The Consistent Force Field: A Documentation*, Lecture Notes in Chemistry, Vol. 3, Springer, Berlin-Heidelberg-New York 1977.
2. Niketić, S. R., Rasmussen, K., Woldbye, F. and Lifson, S. *Acta Chem. Scand. A 30* (1976) 485.
3. Niketić, S. R. and Rasmussen, K. *Acta Chem. Scand. A 32* (1978) 391.

Received April 5, 1978.

Acta Chemica Scandinavica A 32 (1978) 757–761

The Preparation, Separation, and Characterization of the lel_3- and ob_3-Isomers of Tris(*trans*-1,2-cyclohexanediamine)iridium(III) Complexes

F. GALSBØL

Chemistry Department I, Inorganic Chemistry, H. C. Ørsted Institute, University of Copenhagen, Universitetsparken 5, DK-2100 Copenhagen Ø, Denmark

Dedicated to Jannik Bjerrum on the occasion of his 70th birthday

The isomers $\Delta(+)[Ir\{(-)chxn\}_3\lambda\lambda\lambda]^{3+}$ (lel_3), $\Lambda(+)[Ir\{(-)chxn\}_3\lambda\lambda\lambda]^{3+}$ (ob_3), $\Lambda(-)[Ir\{(+)chxn\}_3\delta\delta\delta]^{3+}$ (lel_3), and $\Delta(-)[Ir\{(+)chxn\}_3\delta\delta\delta]^{3+}$ (ob_3) (chxn = *trans*-1,2-cyclohexanediamine) have been isolated as chlorides and nitrates, and characterized by their electronic and circular dichroism spectra and their optical rotation. The nitrates are isomorphous with the corresponding Cr, Co, and Rh compounds. The lel_3-isomers form sparingly soluble hexachloroiridate(III) salts which are isomorphous with the analogous Co and Rh hexachloroiridates.

The formula $[Ir\{(\pm)chxn\}_3]^{3+}$ (chxn = *trans*-1,2-cyclohexanediamine) represents eight isomers (four possible combinations for the chelate ring conformations within each of the absolute configurations Δ and Λ). The present work is confined to the two pairs of isomers which arise when three (−)chxn or three (+)chxn ligands are bound to the central atom. *trans*-(−)-1(*R*),2(*R*)-Cyclohexanediamine, (−)chxn, has the λ and (+)chxn the δ conformation (IUPAC 1968).[1] Each enantiomer of chxn forms two diastereoisomeric tris-complexes, *e.g.* $\Delta(+)[Ir\{(-)chxn\}_3\lambda\lambda\lambda]^{3+}$ and $\Lambda(+)[Ir\{(-)chxn\}_3\lambda\lambda\lambda]^{3+}$, denoted[2] lel_3 and ob_3, respectively, using an obvious extension of the original notation of Corey and Bailar[3] whereby the mixed tris-complexes containing both (−)chxn and (+)chxn would be described as lel_2ob and ob_2lel.

The attempt of Jaeger and Bijkerk[4] to prepare tris(*trans*-1,2-cyclohexanediamine)iridium(III) by a method analogous to that for the corresponding rhodium compound, *i.e.* from sodium hexachloroiridate(III) and (−)chxn in a water-ethanol mixture, was only partly successful. The reaction mixture precipitated a nearly colourless, poorly crystalline compound which on the basis of elemental analysis was assumed to be $(+)[Ir\{(-)chxn\}_3][IrCl_6]$.aq. In the present work the lel_3-isomer $\Delta(+)[Ir\{(-)chxn\}_3\lambda\lambda\lambda][IrCl_6]$.aq and the analogous Co- and Rh-hexachloroiridates have been precipitated from solutions of the constituent ions* and it seems very probable that the iridium-compound is identical to the precipitate obtained by Jaeger and Bijkerk. The latter authors' failure to induce this compound to react further is probably due to the low solubility of the compound and the kinetic inertness of iridium(III).

In the procedure described here an aqueous solution of (−)chxn or (+)chxn (*ca.* 25 % excess) is allowed to react with soluble iridium(III) chloride. Carbon dioxide appears to catalyze the reaction. To complete the reaction the mixture is kept at 170 °C for approx. 300 h and then evaporated to dryness. The residue is a mixture of the lel_3- and ob_3-isomers from which the lel_3-isomer can be extracted with *ca.* 80 % ethanol in which the ob_3-isomer is only slightly soluble. It is difficult to remove coloured impurities from these two diastereoisomeric chlorides but the nitrates of both

* The ob_3-isomers are not precipitated by $[IrCl_6]^{3-}$ under the same experimental conditions.

isomers have a rather high solubility temperature coefficient and a rather low solubility at room temperature, and are easily prepared as colourless crystals. Purification as the nitrate salts was therefore chosen.

EXPERIMENTAL

Materials. Iridium(III) chloride hydrate (52.39 % Ir, *i.e.* 3.8 mol H_2O/mol Ir) was obtained from Johnson, Matthey and Co. *trans*-Cyclohexanediamine was purified and resolved as described earlier.[5]

Physical measurements. Absorption spectra were recorded on a Cary 118C spectrophotometer and circular dichroism on a Roussel-Jouan Dichrographe II. Optical rotation was measured using a Perkin-Elmer polarimeter 141 and thermogravimetric measurements were performed with the thermobalance described by Pedersen.[6] X-Ray powder photographs were taken using a focussing Guinier type camera and Cu$K\alpha$ radiation.

Preparation and separation of the lel_3- and ob_3-isomers. A 6.28 g sample of (−)chxn (55.0 mmol, *ca.* 25 % excess) was dissolved in 6.5 ml of water in a test tube, and carbon dioxide was bubbled through the solution until a slight amount of white precipitate had formed (*ca.* 1 min). 5.35 g of $IrCl_3$.aq (14.5 mmol) were then added. (It is sometimes necessary to moderate the reaction by cooling the tube under the water tap). After 5 min the mixture was carefully heated to boiling and then boiled until an orange-brown solution containing a small amount of fine precipitate had formed. The test tube was sealed, placed in an autoclave containing a little water, and the autoclave was kept in an oven at 170 °C for approx. 300 h and then allowed to cool to room temperature. At this point the reaction mixture consisted of large colourless crystals in a light yellow solution. After opening the tube the content was dissolved in water and the solution was filtered (Whatman No. 50). The filtrate was evaporated to dryness on a rotating vacuum evaporator (RVE) using a final water-bath temperature of 90 °C. The resulting beige solid was extracted using a mixture of 193 ml of ethanol and 34 ml of water by heating the mixture under reflux for 5 min and then leaving it to stand overnight. The mixture was filtered and the residue was washed with a mixture of 50 ml of ethanol and 5 ml of water. (The filtrate and washings were reserved for the isolation of the lel_3-isomer).

The almost white residue (ob_3-chloride) was dissolved in the minimum necessary volume of boiling water (*ca.* 40 ml) and 18 ml of 14 M HNO_3 were added. The mixture was heated under reflux for 1 h and then allowed to stand overnight. The white precipitate was filtered off, washed with water and dissolved in the minimum necessary volume of boiling water (*ca.* 125 ml). After filtering the solution, the filtrate was heated to boiling, 50 ml of 14 M HNO_3 were added, and the mixture was allowed to stand overnight. The white precipitate was then filtered off, washed with water and dried in air. Yield 2.8 g (25 %) of $\Lambda(+)[Ir\{(-)C_6H_{14}N_2\}_3\text{-}\lambda\lambda\lambda](NO_3)_3.3H_2O$. (Found: C 27.79; N 16.34; H 6.20. Calc: C 27.90; N 16.27; H 6.24).

The ob_3-nitrate was dissolved in 90 ml of 12 M HCl by heating to boiling and the solution was heated under reflux for 5 min. It was then allowed to stand for 30 min before being evaporated to dryness on an RVE. The white residue was dissolved in the minimum necessary volume of boiling water (*ca.* 35 ml), 12 ml of 12 M HCl were added and the solution was then left to stand overnight. The resulting crystals of ob_3-chloride were isolated by filtration, washed, first with two 1 ml portions of 4 M HCl, then with 1 ml of water, and dried in air. Yield 2.2 g of $\Lambda(+)[Ir\{(-)C_6H_{14}N_2\}_3\lambda\lambda\lambda]Cl_3$.aq.* (Found: C:N:Cl, 18.00:6.033:3.000).

The ethanolic solution of lel_3-chloride (remaining from the separation of the diastereoisomers) was evaporated to dryness on an RVE. The light brown residue was dissolved in the minimum necessary volume of boiling water (*ca.* 32 ml) and 15 ml of 14 M HNO_3 were added. The mixture was heated under reflux for 1 h and then allowed to stand overnight. The resulting light brown precipitate was filtered off, washed with water and extracted with 450 ml of water under reflux. The mixture was then filtered to remove a brown voluminous impurity. The filtrate was heated to boiling after which 180 ml of 14 M HNO_3 were added and the mixture left to stand overnight. The white precipitate was isolated by filtration, washed with water and dried in air. Yield 6.5 g (57 %) of $\Delta(+)[Ir\{(-)C_6H_{14}N_2\}_3\text{-}\lambda\lambda\lambda](NO_3)_3.3H_2O$. (Found: C 27.82; N 16.34; H 5.97. Calc: C 27.90; N 16.27; H 6.24).

The lel_3-nitrate was dissolved in 150 ml of 12 M HCl by heating under reflux for 5 min. The solution was then allowed to stand for 30 min before being evaporated to dryness on an RVE. The white residue was dissolved in the minimum necessary volume of boiling water (*ca.* 30 ml), 1.3 ml of 12 M HCl were added and the solution was left to stand overnight. The crystals of lel_3-chloride were filtered off, washed, first with two 1.5 ml portions of 0.5 M HCl, then with 1.5 ml of water, and dried in air. Yield 4.8 g of $\Delta(+)[Ir\{(-)C_6H_{14}N_2\}_3\lambda\lambda\lambda]$-

* The content of water of crystallization is somewhat variable. Between 0.5 and 1.2 mol H_2O/mol Ir were found by thermogravimetry.

Cl_3.aq.* (Found: C:N:Cl, 18.00:6.008:3.013).

The catoptromeric lel_3- and ob_3-complexes were prepared in an identical manner and with identical yields using (+)chxn.

Preparation of hexachloroiridate(III) salts. A solution of $[IrCl_6]^{3-}$ was prepared as follows: 0.373 g of $IrCl_3$.aq (1.02 mmol) was dissolved in 10 ml of boiling water. After the addition of 20 ml of 12 M HCl and a few crystals of ascorbic acid, the solution was heated to boiling and then allowed to cool. 6 ml portions of this solution were then added to solutions containing *ca.* 0.2 mmol of $[M(chxn)_3]Cl_3$.aq (M = Co, Rh, and Ir) in 2 ml of water, *i.e.* the mixtures from which the hexachloroiridates were precipitated were *ca.* 6 M in HCl and *ca.* 0.025 M in $[M(chxn)_3]^{3+}$ and $[IrCl_6]^{3-}$.

1. $\Delta(+)_{589}[Co\{(-)C_6H_{14}N_2\}_3\lambda\lambda\lambda][IrCl_6]$.aq. 0.117 g of $\Delta(+)_{589}[Co\{(-)chxn\}_3\lambda\lambda\lambda]Cl_3.4H_2O$ (0.202 mmol) was dissolved in 2 ml of water. On adding the 6 ml of hexachloroiridate(III) solution (0.203 mmol) a voluminous precipitate immediately formed. After 2 h the mixture was heated to boiling and allowed to cool. After a further 2 h a few crystals of ascorbic acid were added and the mixture was heated to boiling and then allowed to stand overnight. This heat treatment facilitated the settling of the precipitate. The product was filtered off, washed, first with two 1 ml portions of 6 M HCl, then with two 1 ml portions of water, and dried in air. Yield 0.16 g. (Found: C 25.52; N 9.90; H 5.63; Cl 23.83, *i.e.* C:N:H:Cl, 18.00:5.99:47.3:5.69).

2. $\Delta(+)[Rh\{(-)C_6H_{14}N_2\}_3\lambda\lambda\lambda][IrCl_6]$.aq was prepared in an analogous manner from 0.127 g of $\Delta(+)[Rh\{(-)chxn\}_3\lambda\lambda\lambda]Cl_3.4H_2O$ (0.203 mmol). Yield 0.13 g (Found: C 24.12; N 9.50; H 5.19; Cl 24.22, *i.e.* C:N:H:Cl, 18.00:6.08:46.2:6.12).

3. $\Delta(+)[Ir\{(-)C_6H_{14}N_2\}_3\lambda\lambda\lambda][IrCl_6]$.aq was prepared in an analogous way using 0.142 g of $\Delta(+)[Ir\{(-)chxn\}_3\lambda\lambda\lambda]Cl_3.3\frac{1}{2}H_2O$ (0.202 mmol). Yield 0.18 g (Found: C 22.14; N 8.65; H 4.68; Cl 21.76; Ir 39.32, *i.e.* C:N:H:Cl:Ir, 18.00:6.03:45.3:5.99:2.00. Thermogravimetry: 2.5 H_2O).

4. An attempt to prepare a hexachloroiridate(III) salt of an ob_3-isomer using the same procedure as described above but starting with a solution of 0.109 g of $\Lambda(+)[Rh\{(-)chxn\}_3\lambda\lambda\lambda]Cl_3.\frac{1}{2}H_2O$ (0.194 mmol) in 3 ml of water resulted in the formation of a white precipitate – denser than the previous ones – which shrank considerably on washing with water. The residue (0.05 g) was identified by its X-ray powder photograph as the ob_3-chloride.

* The content of water of crystallization is somewhat variable. Between 3.3 and 4.5 mol H_2O/mol Ir were found by thermogravimetry.

RESULTS

The absolute configurations of the iridium complexes have been assigned by correlation of the lel_3-isomers to $\Lambda(-)_{589}[Co\{(+)chxn\}_3\delta\delta\delta]Cl_3.5H_2O$, using the method of active racemates.[7]

The specific and molar rotations of the chlorides and nitrates are given in Table 1 and the electronic and circular dichroism spectra of the chlorides are shown in Fig. 1 (allowance has to be made for the variable content of water of crystallization of the weighed samples). Fig. 2 shows the spectra of the nitrates. It is noteworthy that the CD curve for the ob_3-isomer is all positive in the $d-d$ transition region and that $\Delta\varepsilon_{max}$ for the main band of the ob_3-isomer is numerically *ca.* four and a half times $\Delta\varepsilon_{max}$ for the main band of the lel_3-isomer (for the

Table 1. Specific rotations, [α], and molar rotations, [M], of the $\Delta(+)[Ir\{(-)chxn\}_3\lambda\lambda\lambda]^{3+}$ (lel_3) and $\Lambda(+)[Ir\{(-)chxn\}_3\lambda\lambda\lambda]^{3+}$ (ob_3) chlorides and nitrates in aqueous solution at 25 °C. Conc. *ca.* 1.6 mmol/l. [M] = [α]M/100 ([α] in deg. ml g^{-1} dm^{-1}; M = molecular weight).

		313 nm	364 nm	436 nm	546 nm	578 nm	589 nm
$\Delta(+)[Ir\{(-)chxn\}_3\lambda\lambda\lambda]Cl_3.3\frac{1}{2}H_2O$	[α]	915	640	412	243	214	205
	[M]	6440	4510	2900	1710	1510	1440
$\Lambda(+)[Ir\{(-)chxn\}_3\lambda\lambda\lambda]Cl_3.\frac{1}{2}H_2O$	[α]	392	278	102	45	38	35
	[M]	2550	1810	665	290	250	230
$\Delta(+)[Ir\{(-)chxn\}_3\lambda\lambda\lambda](NO_3)_3.3H_2O$	[α]	818	586	377	222	196	186
	[M]	6340	4540	2920	1720	1520	1440
$\Lambda(+)[Ir\{(-)chxn\}_3\lambda\lambda\lambda](NO_3)_3.3H_2O$	[α]	322	230	83.2	36	31	30
	[M]	2500	1780	645	280	240	230

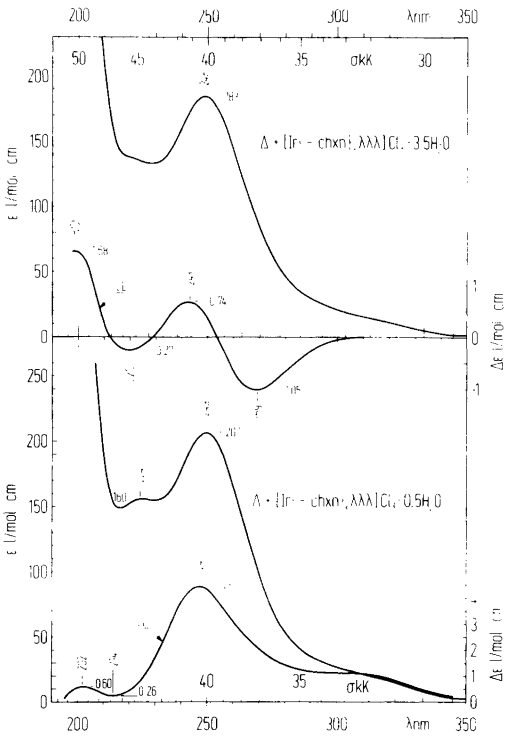

Fig. 1. Absorption and circular dichroism spectra of $\Delta(+)[Ir\{(-)chxn\}_3\lambda\lambda\lambda]Cl_3.aq$ (lel_3) and $\Lambda(+)[Ir\{(-)chxn\}_3\lambda\lambda\lambda]Cl_3.aq$ (ob_3).

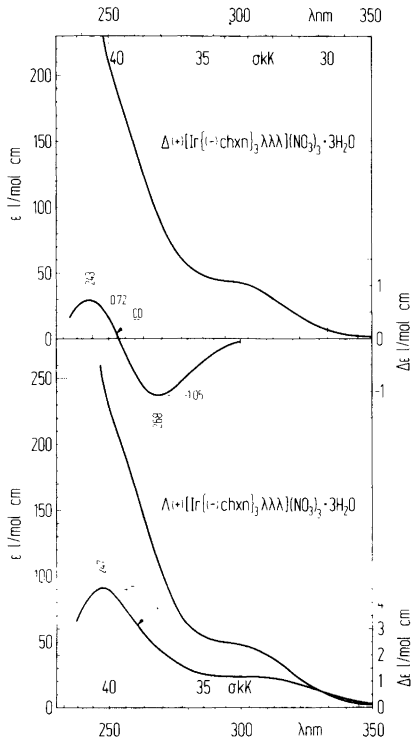

Fig. 2. Absorption and circular dichroism spectra of $\Delta(+)[Ir\{(-)chxn\}_3\lambda\lambda\lambda](NO_3)_3.3H_2O$ (lel_3) and $\Lambda(+)[Ir\{(-)chxn\}_3\lambda\lambda\lambda](NO_3)_3.3H_2O$ (ob_3).

analogous Cr, Co, and Rh compounds this ratio is *ca.* 1.6, 1.8, and 2.2, respectively). Apart from this the spectra show features similar to those of the corresponding Cr,[8] Co,[9] and Rh [5] complexes except for a triplet in $\Lambda(+)[Ir\{(-)chxn\}_3\lambda\lambda\lambda]^{3+}$ giving rise to some CD-intensity on the low energy side of the first spin allowed absorption band. The triplet can just be seen in the absorption spectra of both the lel_3- and ob_3-chlorides of iridium (Fig. 1). In the absorption spectra of the nitrates (Fig. 2) a combination of the absorption of this triplet and that of the nitrate ion which has an absorption band at *ca.* 300 nm ($\varepsilon_{max} = 7.2$ l mol^{-1} cm^{-1}) results in a plateau around *ca.* 295 nm.

X-Ray powder photographs show that the three compounds of the lel_3-series $\Delta[M\{(-)chxn\}_3\lambda\lambda\lambda](NO_3)_3.aq$ (M = Cr, Co, Rh, and Ir) are isomorphous, as are the members of the ob_3-series [10] $\Lambda[M\{(-)chxn\}_3\lambda\lambda\lambda](NO_3)_3.aq$. Saito *et al.* have determined the structure of one member of each series, *viz.* $\Lambda(+)[Rh\{(-)chxn\}_3\lambda\lambda\lambda](NO_3)_3.3H_2O$ [11] and $\Delta(+)[Rh\{(-)chxn\}_3\lambda\lambda\lambda](NO_3)_3.3H_2O$.[12] The analogous Cr- and Rh-compounds of both the lel_3- and ob_3-series have been syncrystallized and the chromium ESR spectra recorded.[13] The powder photographs also indicate great structural similarities between these two series, in accordance with the fact that both series belong to the hexagonal space group $P6_3$ ($Z = 2$). Both types of complex ions have rigorous threefold symmetry and are oriented with the C_3-axis parallel to the *c*-axis of the crystal.[11,12]

X-Ray powder photographs also show that the three complexes in the lel_3-series $\Delta[M\{(-)chxn\}_3\lambda\lambda\lambda][IrCl_6].aq$ (M = Co, Rh, and Ir) are isomorphous. A similar series of hexachlororhodate(III) salts can be prepared in an analogous fashion but the latter have been found to be non-isomorphous.

REFERENCES

1. IUPAC, *Information Bulletin 33* (1968) 68; *Inorg. Chem. 9* (1970) 1.
   IUPAC, *Nomenclature of Inorganic Chemistry*, 2nd Ed., Definitive rules 1970, Butterworths, London 1971, p. 75.
2. Andersen, P., Galsbøl, F. and Harnung, S. E. *Acta Chem. Scand. 23* (1969) 3027.
3. Corey, E. J. and Bailar, J. C., Jr. *J. Am. Chem. Soc. 81* (1959) 2620.
4. Jaeger, F. M. and Bijkerk, L. *Z. Anorg. Allg. Chem. 233* (1937) 97.
5. Galsbøl, F., Steenbøl, P. and Sørensen, B. S. *Acta Chem. Scand. 26* (1972) 3605.
6. Pedersen, E. *J. Sci. Instrum.* [2] *1* (1968) 1013.
7. Andersen, P., Galsbøl, F., Harnung, S. E. and Laier, T. *Acta Chem. Scand. 27* (1973) 3973.
8. Harnung, S. E. and Laier, T. *Acta Chem. Scand. A 32* (1978) 41.
9. Harnung, S. E., Sørensen, B. S., Creaser (Olsen), I., Maegaard, H., Pfenninger, U. and Schäffer, C. E. *Inorg. Chem. 15* (1976) 2123.
10. Andersen, P. and Galsbøl, F. *To be published.*
11. Kuroda, R., Sasaki, Y. and Saito, Y. *Acta Crystallogr. B 30* (1974) 2053.
12. Miyamae, H., Sato, S. and Saito, Y. *Acta Crystallogr. B 33* (1977) 3391.
13. Pedersen, E. *To be published.*

Received May 26, 1978.

Acta Chemica Scandinavica A 32 (1978) 763 – 769

The Reactions between Bis(styrene)bis(triphenylphosphine)-ruthenium(0) and Cyclohexene; its Relevance to the Alkene Isomerisation Reaction and to the Catalytic Disproportionation of Cyclohexene

BRUNO N. CHAUDRET,[a] DAVID J. COLE-HAMILTON[b] and GEOFFREY WILKINSON[b]

[a] Laboratoire de Chimie de Coordination, C.N.R.S., 31030 Toulouse, France and [b] Chemistry Department, Imperial College of Science and Technology, London SW7 2AY, United Kingdom

Dedicated to Jannik Bjerrum on the occasion of his 70th birthday

The reaction between bis(styrene)bis(triphenylphosphine)ruthenium(0) and cyclohexene produces the 1-5-η-cyclohexadienylhydridobis(triphenylphosphine)ruthenium(II) complex, $RuH(1\text{-}5\text{-}\eta\text{-}C_6H_7)(PPh_3)_2.C_6H_{10}$, whose structure has been determined by X-ray diffraction, and also two isomers of $RuH(1\text{-}3\text{-}\eta\text{-}C_6H_7)(PPh_3)_2.C_6H_{10}$.

$RuH(1\text{-}5\text{-}\eta\text{-}C_6H_7)(PPh_3)_2$ can be prepared by the reaction of $RuH_2(PPh_3)_4$ and cyclohexa-1,3-diene. In solution these complexes exist as a mixture of the 1-5-η and 1-3-η complexes and cyclohexene and detailed ^1H and ^{31}P nuclear magnetic resonance studies have been made. The complex $RuH(1\text{-}3\text{-}\eta\text{-}C_6H_7)(PPh_3)_2(C_6H_{10})$ undergoes a reversible insertion of alkene into the Ru – H bond. The relevance of this observation to the mechanism of alkene isomerisation is discussed. The catalytic disproportionation of cyclohexene to benzene and cyclohexane in solution has also been studied.

The reversible insertion of alkenes into metal hydrogen bonds is a key step in the isomerisation of alkenes using transition metal complex hydridic catalysts in homogeneous solution. The only system in which this reaction has been demonstrated[1] to occur on the NMR time scale, is the reversible insertion of ethylene into the M – H bond of $MoH(C_2H_4)_2(diphos)_2^+$, formed by protonation of $Mo(C_2H_4)_2(diphos)_2$. Stable hydrido alkene complexes in which insertion is slow on the NMR time scale are also known.[2] No systems in which alkene coordination to a complex metal hydride is followed by such a reversible insertion have been studied although this prior coordination is usually assumed. Hence no spectroscopic information is available for determining the relative rates of alkene coordination and insertion and for ascertaining which of these steps is rate determining in the isomerisation of alkenes using hydride metal catalysts in solution.

We have studied[2,3] the reactions of various alkenes with hydrido ruthenium(II) and ruthenium(0) triphenylphosphine species and have shown that these reactions involve alkene coordination and insertion reactions although in some cases dehydrogenation of the alkene occurs, *e.g.*, of but-1-ene to give a buta-1,3-diene complex.

We now describe the reaction between the styrene complex, $Ru(C_8H_8)_2(PPh_3)_2$, and cyclohexene. This reaction gives several products and ^1H and ^{31}P NMR studies on these provide some insight into the mechanism of the isomerisation of alkenes using hydridic ruthenium(II) complex catalysts.

RESULTS AND DISCUSSION

The reaction of the ruthenium(0) complex $Ru(C_8H_8)_2(PPh_3)_2$ with cyclohexene gives a series

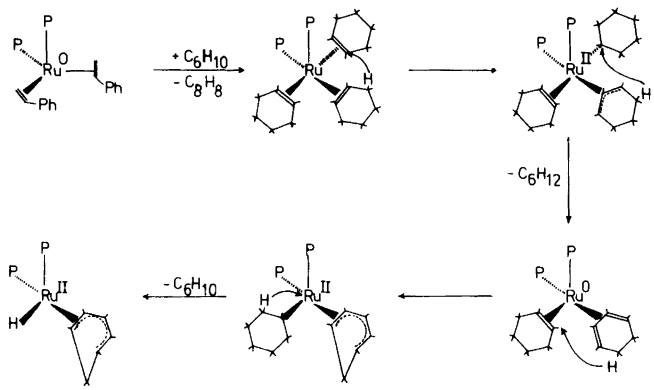

Scheme 1. Proposed mechanism for the formation of cyclohexadienylhydrido complexes from the interaction of cyclohexene and $Ru(C_8H_8)_2(PPh_3)_2$; $P = PPh_3$. Arrows indicate hydride shifts. Conformations of rings are not shown.

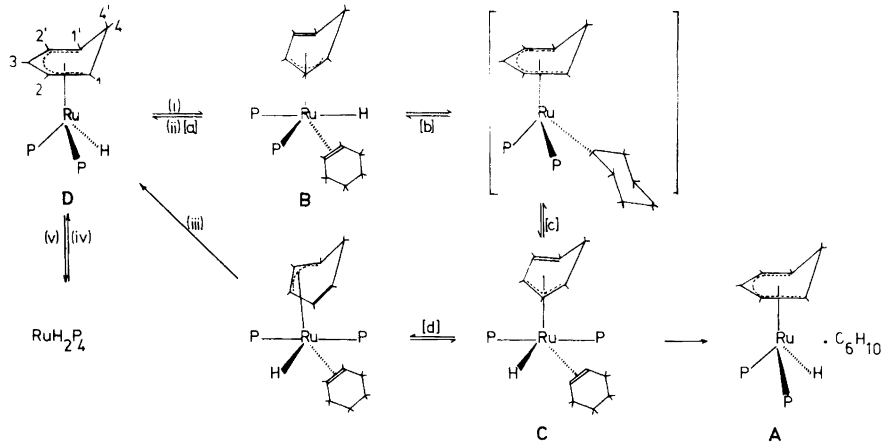

Scheme 2. The reaction of cyclohexene with $RuH(C_6H_7)(PPh_3)_2$. (i) cyclohexene, (ii) argon sweep of toluene solution, (iii) recrystallise or stand in Nujol mull, (iv) cyclohexa-1,3-diene, (v) add PPh_3 and warm.

of products all of which have to be formulated as hydridobis(triphenylphosphine)ruthenium(II) species. These hydrido species are formed by reactions involving hydride transfer from cyclohexene to ruthenium as shown in Schemes 1 and 2.

The most stable compound, which can be isolated as yellow crystals, has the stoichiometry $RuH(C_6H_7)(PPh_3)_2.C_6H_{10}$ (**A**). It has to be formulated as a 1-5-η-cyclohexadienyl species that contains uncoordinated cyclohexene in the crystal lattice. The structure of this compound, determined[4] by X-ray crystallography, confirms that the cyclohexene molecule is not coordinated and that the complex has the structure shown in Fig. 1.

An absorption at 2015 cm^{-1} in the infrared spectrum of **A** is assigned to $\nu Ru-H$, whilst peaks at 2790 and 2760 cm^{-1} arise from $\nu C-H_{(exo)}$ of the methylene group of the coordinated 1-5-η-cyclohexadienyl moiety[5] and from uncoordinated cyclohexene (*cf.* 2703 cm^{-1} for free cyclohexene[6]).

On carrying out the reaction between $Ru(C_8H_8)_2(PPh_3)_2$ and cyclohexene under slightly different conditions (see Experimental), two other compounds, **B** and **C**, also of formula $RuH(C_6H_7)(PPh_3)_2(C_6H_{10})$ may be isolated. Recrystallisation of **B** or **C*** gives **A**.

* **C** is also converted quantitatively to **A** if a Nujol mull is allowed to stand for some hours.

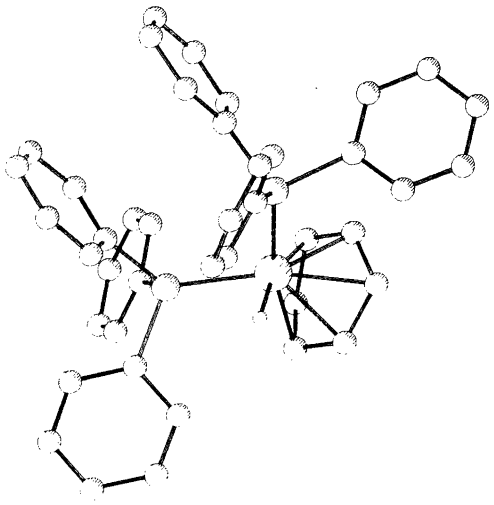

Fig. 1. The structure of 1-5-η-cyclohexadienyl-hydridobis(triphenylphosphine)ruthenium(II).cyclohexene (1/1) as determined by X-ray diffraction. The cyclohexene is not coordinated to the metal and is omitted.

Evaporating a solution of **A**, **B** or **C** in toluene to dryness with an inert gas (to remove cyclohexene) produces another complex, $RuH(C_6H_7)(PPh_3)_2$ (**D**). The latter is more easily prepared by interaction of $RuH_2(PPh_3)_4$ with cyclohexa-1,3-diene and is a 1-5-η-cyclohexadienyl compound identical with **A** except that no cyclohexene is present.

The compounds **B**, **C** and **D** all show absorptions in the IR spectrum attributable to $\nu Ru-H$ and to $\nu C-H_{(exo)}$ of the methylene group of a coordinated cyclohexadienyl ligand, together with other peaks attributable to triphenylphosphine (see Experimental).

From the methods of preparation of the various compounds it appears that the transformations shown in Schemes 1 and 2 occur.

Other 1-5-η-cyclohexadienyl complexes of ruthenium are well-known and may be formed by nucleophilic attack of hydride on coordinated π-benzene complexes such as $[(C_6H_6)_2Ru]^{2+}$ [7] and $[C_6H_6RuL_3]^+$.[8]

^1H and ^{31}P NMR spectroscopy. The ^1H NMR spectrum of the compound **D**, RuH(1-5-η-C_6H_7)-$(PPh_3)_2$, in toluene at 25 °C consists of a series of poorly resolved resonances at δ 4.9(1), 4.8(2), 2.6(3), 1.6(1) (relative intensities in parentheses) which can be assigned to protons 3; 2 and 2′; 1, 1′ and 4; and 4′ (Scheme 2), the *exo* proton of the methylene group resonating to high field of the *endo* proton.

The hydride resonance is a sharp triplet at δ −12.4 (J_{PH} = 27 Hz). This is entirely consistent with the structure shown in Fig. 1.

The complex is isoelectronic and essentially isostructural with (1-5-η-C_5H_5)$RuH(PPh_3)_2$ [9] and (1-5-η-PhO)$RuH(PPh_3)_2$.[10]

The noise decoupled ^{31}P NMR spectrum consists of a single resonance at δ 61.5 ppm,* which splits into a doublet (J_{PH} = 27 Hz) when coupling to the hydride is introduced, and a doublet of doublets (J_{PH} = 27 and 8 Hz) when the phenyl region is selectively decoupled. This last observation suggests that the phosphorus atoms are coupled to one proton of the cyclohexadienyl moiety and we tentatively suggest that this is the *endo* proton. On cooling, the single ^{31}P resonance broadens and splits (coalescence temperature ≈ 253 K) so that at −70 °C an **AB** quartet (δ_A = 63.9, δ_B = 59.7, J_{AB} = 17 Hz) is observed. The two phosphorus atoms are thus non-equivalent and we suggest that this is caused by the adoption by the cyclohexadienyl ring of a conformation which destroys the two-fold axis of the rest of the molecule, as is found in the solid state when cyclohexene is present in the lattice[4] (Fig. 1). Once again, the resonances split further into doublets (J_{PH} = 27 Hz) when coupling to the hydride is introduced.

The ^1H NMR spectra of **A**, **B** and **C** at room temperature in benzene or toluene** are all identical and consist of resonances from RuH(1-5-η-C_6H_7)-$(PPh_3)_2$(**D**) and from free cyclohexene together with a broad resonance at δ −5.6 and a sharper resonance at 2.65 ppm. This same spectrum is obtained if cyclohexene is added to RuH(1-5-η-C_6H_7)$(PPh_3)_2$ (**D**) but the resonances mentioned above grow only slowly; similarly, freshly prepared solutions of $RuH(C_6H_7)(PPh_3)_3.C_6H_{10}$ (**A**) do not show the resonances at δ 2.65 and −5.6 ppm but these grow slowly with time.

This suggests that these two resonances are from either **B** or **C** and since **C** is apparently thermodynamically more stable than **B** they probably arise from **C**.

On cooling cyclohexene solutions of **A**, **B** or **C**,

* All ^{31}P chemical shifts are to high frequency of external 85 % H_3PO_4.

** In CD_2Cl_2 an identical spectrum is obtained but, on standing, the resonances disappear and are replaced by resonances attributable to CD_2HCl, $RuHCl(PPh_3)_3$,[11] $(\pi$-$C_6H_6)RuH(PPh_3)_2^+Cl^-$,[10] benzene and cyclohexene.

the resonance at δ −5.6 broadens until at *ca.* −20 °C it is no longer visible. Further cooling causes little observable change until at −60 °C a broad peak is observed at δ −17.6. This sharpens considerably when the solution is irradiated in the position of the phosphorus resonance for this compound, but viscosity broadening and crystallisation problems have meant that we have been unable to achieve the low temperature limiting spectrum. Similar effects are observed in C_7D_8 but the resonance at δ −17.6 is much weaker presumably because in the absence of excess cyclohexene the equilibrium (a) in Scheme 2 lies further to the left.

On account of the presence of excess cyclohexene it is difficult to detect what other resonances the resonance at δ −5.6 gives rise to on cooling. However, new broad resonances are observed at δ 4.3, 2.8 and 2.2 ppm. These could arise from olefinic, *endo* and *exo* protons of the cyclohexene groups respectively. The sharp resonance at δ 2.65 disappears. It is clear that the resonance at δ −5.6 ppm which is present at room temperature and which sharpens to a triplet ($J_{PH} \approx 6$ Hz) on warming to 60 °C arises from dynamic exchange between a hydrido ligand (δ −17.6 at −70 °C) and some aliphatic protons.

The actual number of aliphatic protons taking part in the exchange reaction is difficult to assess, but since J_{PH} for hydrido protons in this kind of complex is typically[3,10] *ca.* 30 Hz, and since the average J_{PH} in the fast exchange situation is 6 Hz, it seems likely that the total number of protons taking part in the exchange is five (one hydridic and four aliphatic).

From this evidence it seems probable that **B** and **C** contain a coordinated cyclohexene moiety and that the cyclohexadienyl group is only 1-3-η-, *i.e.*, it is bound by only three carbon atoms in a η_3-allylic system, and has in addition an uncoordinated double bond. The free double bond in these complexes should show νC=C near 1655 cm^{-1}[12,13] but it is apparently too weak to be observed in our complexes; this kind of vibration is often weak.[13]

Even at −80 °C we do not observe resonances from the 1-3-η-cyclohexadienyl ring but this is probably caused by ring gliding as in Equilibrium (d), Scheme 2, which we assume to be a low energy process. This would make the ring appear as a 1-5-η- ring on the NMR time scale and cause the resonances to lie underneath those from $RuH(1\text{-}5\text{-}\eta\text{-}C_6H_7)(PPh_3)_2$ (**D**). A similar effect has been reported for the 1-3-η-C_5H_5 ring of $(C_5H_5)_2W(CO)_2$.[14,15]

The temperature dependence of the ^{1}H NMR spectrum of **C**, the thermodynamically more stable product and hence, presumably, the one present in solution, is then best explained in terms of a reversible insertion of the cyclohexene group into the M−H bond (Equilibrium (c) in Scheme 2). If the insertion and elimination reactions both occur with the same stereochemistry, then the hydride will exchange with four protons on the cyclohexene ring.

Thus, if the inversion and elimination reactions are stereospecifically *cis*, the metal will effectively move around on one side of the ring and exchange with the four methylene protons on one side of the ring. If no invertion of the ring occurs the metal would alternate between axial and equatorial positions. However, since the metal is a bulky substituent it presumably would prefer to be in an equatorial position and the ring would probably invert at each 1,2-shift, thus rendering equivalent the two olefinic protons and the four methylene protons which are not exchanging with the hydride ligand. This then accounts for the sharp singlet at δ 2.6 observed in the room temperature ^{1}H NMR spectrum. (The mean position expected for this resonance based on the individual chemical shifts is δ 3.1).

If, on the other hand, the insertion and elimination reactions are stereospecifically *trans*, the metal would move around the equatorial positions of the ring and the remaining six protons would be rendered equivalent despite the fact that no ring inversion would occur. (The mean position expected for the non-exchanging proton in this case would be *ca.* δ 2.9). It would appear that in either case the position of the resonance due to the protons exchanging with the hydride should be *ca.* δ −2 rather than −5.6 and we are unable to explain this anomaly unless the chemical shift of one or more of the protons is itself temperature dependent.

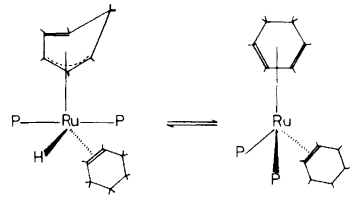

Scheme 3. Alternative pathway for exchange of metal hydride with aliphatic protons in $RuH(C_6H_7)(PPh_3)_2(C_6H_{10})$ (**C**).

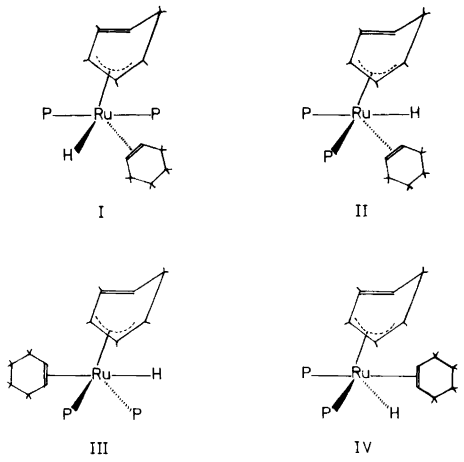

Fig. 2. Possible structures of (1-3-η-cyclohexadienyl)-hydridoruthenium(II) species.

On the basis of the ^{1}H NMR evidence we cannot unequivocally rule out the possibility that the hydride is exchanging with some protons on the cyclohexadienyl moiety (Scheme 3), but we feel that this would not explain the resonances present in the low temperature spectrum satisfactorily. It would also not account for the ready formation of benzene and cyclohexane when a solution of **C** or **D** is warmed to 60 °C for a few minutes (see below). The non-reversible insertion of cyclohexene into an Fe–H bond to give a cyclohexyl complex has been reported.[16]

It remains to assign the stereochemistries of **B** and **C**, for which the four possibilities are shown in Fig. 2, I–IV. Since in **C** the reversible insertion of alkene into the M–H bond is occurring, it is probable that the alkene and hydride are mutually *cis*. This, together with the fact that a single sharp ^{31}P NMR resonance (δ 59.7) is observed at all temperatures, suggests that **C** has structure I. Since **B** is so readily converted to **C** it is probable that here again the alkene and the hydride are mutually *cis* and that **B** has structure II or IV.

The compound **C** may then readily be formed from **B** by insertion of alkene into the M–H bond followed by elimination in a different sense to give **C** ((b) in Scheme 1). The formation of these complexes from $Ru(C_8H_8)_2(PPh_3)_2$ and cyclohexene is outlined in Schemes 1 and 2. It is interesting to note that complexes analogous to **B** and **C** which contain hydrido, alkene and 1-3-η-allyl ligands are obtained[3] from the reaction of $Ru(C_8H_8)_2(PPh_3)_2$ with hex-1-ene.

Implications for the alkene insertion reaction. It is clear from the NMR data presented above that the equilibrium (a) in Scheme 2 is *slow* on the NMR time scale, even at 60 °C, while the rate of the insertion reaction (Equilibrium (c)) is *comparable with* the NMR time scale. This then represents the first spectroscopically observable system in which it can be unequivocally stated that the rate determining step in the isomerisation of alkenes using catalysts of this kind is alkene coordination rather than hydrogen transfer from the metal to the alkene. The same conclusion has also been reached for other hydridic Ru^{II} systems on the basis of kinetic studies.[17]

In principle it is possible to calculate the relative rates of the coordination and insertion steps from NMR data but, in view of the complexity of the system we can be satisfied with the qualitative result.

Although we are unable to say from our data whether the stereochemistry of addition of the Ru–H bond across the double bond of cyclohexene is *cis* or *trans*, the fact that only four of the methylene protons take part in the exchange with the metal hydride indicates that the stereochemistry of this addition must be the same as that of elimination from the cyclohexyl ruthenium species to re-form the hydrido alkene complex.

Catalytic disproportionation of cyclohexene to benzene and cyclohexane. When solutions of $RuH(C_6H_7)(PPh_3)_2(C_6H_{10})$ (**A**, **B** or **C**) are heated to 60 °C in deuteriotoluene they become red and all the peaks in the ^{1}H NMR spectrum below δ 6 disappear to be replaced by sharp resonances attributable to benzene and cyclohexane (GLC evidence shows that benzene and cyclohexane are formed in an approximately 1:1 ratio).

The most rational explanation of this observation is that transfer of hydrogen from the methylene group of the cyclohexadienyl moiety to the transient cyclohexyl group (formed by the insertion of cyclohexene into the Ru–H bond of **C**) occurs. This provides direct evidence for the type of mechanism that we have postulated for the removal of hydrogen from the *ortho* position of triphenylphosphine, propene, but-1-ene, pent-1-ene, and cyclooctadiene in related ruthenium systems.[2,3] We think it unlikely that the hydrogen transfer occurs *via* the metal, but transfer to the metal evidently can occur since heating $RuH(C_6H_7)(PPh_3)_2$ in the

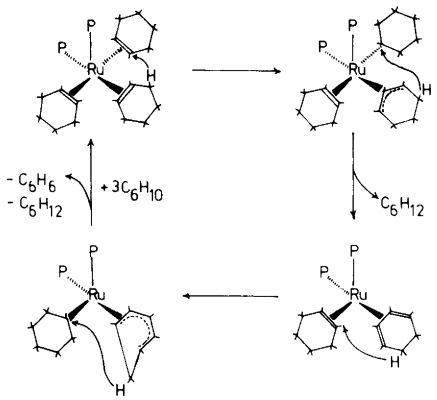

Scheme 4. Catalytic cycle for the conversion of cyclohexene to benzene and cyclohexane.

presence of PPh_3 causes quantitative conversion to $RuH_2(PPh_3)_4$.

The disproportionation of benzene to cyclohexene is evidently catalytic since if 0.2 g $Ru(C_8H_8)_2(PPh_3)_2$ is refluxed in cyclohexene (5 ml) for 16 h, GLC data show that 9.8 % of cyclohexane and 4.5 % of benzene are formed. After a further 20 h, 23.7 % cyclohexane and 10 % benzene are present, which represents about 25 catalytic cycles. Note that although in the decomposition of **C** equimolar amounts of benzene and cyclohexane are formed, in the catalytic reaction *two* mol of cyclohexane must be formed per mol of benzene.

The catalytic reaction is slowly poisoned as a black solid, assumed to be ruthenium metal, slowly precipitates. However, at room temperature the reaction will proceed without decomposition to black solid, albeit much more slowly. NMR evidence suggests that $RuH(C_6H_7)(PPh_3)_2$ and $RuH(C_6H_7)$-$(PPh_3)_2(C_6H_{10})$ (**C**) are present at all times in the solution. The proposed mechanism of this reaction is outlined in Scheme 4.

The catalytic disproportionation of cyclohexene to benzene and cyclohexane does not appear to have been previously observed in homogeneous systems but it is known to occur heterogeneously[18] and the related catalytic disproportionation of ethylene to ethane and butadiene has been reported,[19] using a titanium catalyst. Polyhydride complexes of iridium catalyse[20] the disproportionation of terminal alkenes with chain length greater than C_4 to alkane and diene.

EXPERIMENTAL

Microanalyses by Butterworth Microanalytical Consultancy Limited, Pascher, Bonn and Imperial College Microanalytical Laboratories. Nuclear magnetic resonance spectra were obtained using Perkin-Elmer R12 (60 MHz) and Varian XL-100-12 (^{31}P) spectrometers, the latter operating in the Fourier transform mode with noise proton decoupling. Narrow band decoupling studies were carried out on a Jeol FX60 60 MHz spectrometer. Infrared spectra were measured on a Perkin-Elmer 457. GLC analyses were carried out on Perkin-Elmer F33 chromatograph with Infotronics integrator attachment using a 4 m column packed with 20 % $AgNO_3$ – ethyleneglycol on a Chromosorb P support. Melting points were determined in closed capillaries under argon on an Electrothermal melting point apparatus and are uncorrected.

All solvents were thoroughly dried and degassed before use and cyclohexene was purified by shaking with acidified iron(II) ammonium sulfate, washed with water and dried by passing down an alumina column. Cyclohexa-1.3-diene was used from a new bottle without further purification but was stored under nitrogen. The petroleum used has boiling range 40–60 °C.

All operations were carried out under dry oxygen free argon using standard suba-seal and catheter tubing techniques.

1. *Hydrido(1-5-η-cyclohexadienyl)bis(triphenylphosphine)ruthenium(II). cyclohexene (1/1)* (**A**). $Ru(C_8H_8)_2(PPh_3)_2$[3] (0.15 g) was stirred with petroleum (5 ml) containing cyclohexene (1.5 ml) at room temperature for 90 min. The resulting yellow solution was filtered and after standing for 3 h the walls of the flask were scratched to induce crystallisation. The pale yellow crystals so formed were collected, washed with petroleum (1 ml) and dried *in vacuo*. On standing, more of the complex crystallised from the mother liquors. Total yield *ca.* 70 %. This compound was also obtained on recrystallisation of **A**, **B** or **C** from cyclohexene or on crystallisation of **B** or **C** from toluene–petroleum. M.p. 109(d) °C; Anal. $RuP_2C_{48}H_{48}$: C, H, P. ^1H and ^{31}P NMR, see text.

IR (Nujol mull, CsI plates) 3130vw, 3040ms, 3000vw, 2790m, 2760m, 2010m, 1580m, 1570w, 1430s, 1305w, 1295w, 1180m, 1175w, 1150w, 1080ms, 1040w, 1025w, 995w, 960w, 930w, 900w, 870vw, 850w, 830w, 790w, 745s, 735s, 720w, 690s, 650m, 615w, 590m, 530s, 515s, 505s, 490s, 455m, 425m, 420m.

2. *Hydrido(1-3-η-Cyclohexadienyl)cyclohexene-bis(triphenylphosphine)ruthenium(II)* (**B**). $Ru(C_8H_8)_2(PPh_3)_2$ (0.5 g) was stirred in petroleum (10 ml) containing cyclohexene (3 ml) at room temperature for 16 h. The resulting yellow solid was

collected, washed with petroleum (5 ml) and dried *in vacuo*. Yield *ca* 80 %. M.p. 115(d) °C; Anal. $RuP_2C_{48}H_{48}$: C, H, P. ^1H and ^{31}P NMR, see text.

IR 3130vw, 3035m, 3002m, 2760s, 1960mbr, 1580w, 1568w, 1480s, 1472s, 1432s, 1427s, 1309w, 1298m, 1260w, 1180m, 1178wsh, 1152w, 1145vw, 1132vw, 1118vw, 1085s, 1068w, 1042w, 1027w, 999w, 992vwsh, 962vw, 955vw, 931w, 914w, 901m, 875w, 860vw, 849w, 835m, 821w, 790m, 749s, 742ssh, 739s, 736ssh, 720m, 705ssh, 698vssh, 692vs, 682ssh, 648m, 618w, 600m, 581w, 538vs, 522vs, 511vs, 499s, 480s, 470wsh, 460m, 432s, 425msh.

3. *Hydrido(1-3-η-cyclohexadienyl)cyclohexene-bis(triphenylphosphine)ruthenium(II)* (**C**). $Ru(C_8H_8)_2(PPh_3)_2$ was stirred in cyclohexene (2.5 ml) for 2 h whereupon the yellow solution so formed began to precipitate the complex as pale yellow microscrystals. After stirring for a further 1 h, the precipitate was collected, washed with petroleum (2 ml) and dried *in vacuo*. Yield *ca* 60 %, m.p. 85–90(d) °C. Anal. Found: C 72.6; H 6.1; P 7.8. Calc. for $RuP_2C_{48}H_{48}$: C 73.2; H 6.1; P 7.9. ^1H and ^{31}P NMR, see text.

IR 3072msh, 3050m, 3010m, 2770m, 2040mbr, 1582w, 1570w, 1475s, 1432ssh, 1430s, 1308w, 1299w, 1262w, 1182m, 1158w, 1145w, 1138w, 1082m, 1069w, 1045w, 1026w, 999w, 990vw, 969w, 931w, 919w, 902w, 876w, 855vw, 849vw, 836w, 820vw, 789w, 752s, 739s, 721m, 702vssh, 698vs, 690vs, 682ssh, 650m, 643wsh, 620w, 537vs, 521vs, 510vs, 492vs, 458m, 431m, 425msh, 418msh.

4. *Hydrido(1-5-η-cyclohexadienyl)bis(triphenyl-phosphine)ruthenium(II)*. (**D**) (a) $RuH_2(PPh_3)_4$ (0.18 g) was warmed to 100 °C in toluene (5 ml) containing cyclohexa-1,3-diene (0.5 ml) for 3 min. After cooling at room temperature the resulting pale yellow solution was treated with petroleum (35 ml) and cooled to −20 °C. The yellow crystals that separated over 2 days were collected and dried *in vacuo*. The mother liquors were evaporated to dryness and dissolved with warming in a mixture of toluene (0.5 ml), cyclohexa-1,3-diene (0.5 ml) and petroleum (25 ml). On cooling to −20 °C a further crop of the compound was obtained as yellow microcrystals. Total yield *ca*. 60 %. When cyclohexene was omitted from this last procedure, the compound dissolved but a copious yellow precipitate of $RuH_2(PPh_3)_4$ was rapidly obtained.

(b) $RuH(1\text{-}3\text{-}\eta\text{-}C_6H_7)(PPh_3)_2(C_6H_{10})$ (**B**) (0.1 g) was dissolved in toluene (5 ml) and the solution evaporated to dryness in a slow stream of nitrogen. On the basis of its infrared spectrum the pale yellow solid was identified as **D** but was not further purified. Yield, *ca*. 95 %, m.p. 90–95 (d) °C. Anal. $RuP_2C_{42}H_{38}$: C, H, P. ^1H and ^{31}P NMR spectra, see text.

IR 3060msh, 3020m, 3006w, 2780m, 1945mbr, 1580w, 1568w, 1432s, 1429s, 1310w, 1299m, 1203 m, 1174m, 1153w, 1127m, 1088s, 1082ssh, 1068m, 1040w, 1024m, 998w, 965vw, 955vw, 931vw, 919vw, 899w, 881vw, 866vw, 845vw, 832vw, 821w, 775w, 751s, 741s, 737ssh, 721m, 708msh, 699vssh, 695vs, 682msh, 650w, 618w, 599w, 571vw, 537ssh, 535vs, 522vs, 510vs, 495vs, 485msh, 469w, 460w, 438w, 432w, 420m.

Acknowledgements. We are greatly indebted to Dr. W. McFarlane, City of London Polytechnic, for narrow band decoupling NMR spectra and to Dr. M. B. Hursthouse, Queen Mary College, for permission to quote X-ray results. We thank Johnson Matthey Limited for the loan of ruthenium and Albright and Wilson Limited for gifts of triphenylphosphine.

REFERENCES

1. Byrne, J. W., Blaser, H. V. and Osborn, J. A. *J. Am. Chem. Soc. 97* (1975) 3871.
2. Cole-Hamilton, D. J. and Wilkinson, G. *Nouv. J. Chim. 1* (1977) 141, and references therein.
3. Chaudret, B. N., Cole-Hamilton, D. J. and Wilkinson, G. *J. Chem. Soc. Dalton Trans.* (1978). *In press.*
4. Hursthouse, M. B., Queen Mary College, London. *Personal communication.*
5. Churchill, M. R. and Scholer, F. R. *Inorg. Chem. 8* (1969) 1950.
6. *Infrared Spectra of Selected Chemical Compounds*, Heyden, London 1961.
7. Jones, D., Pratt, L. and Wilkinson, G. *J. Chem. Soc.* (1962) 4458.
8. Robertson, D. R. and Stephenson, T. A. *J. Organomet. Chem. 142* (1977) C31.
9. Blackmore, T., Bruce, M. I. and Stone, F. G. A. *J. Chem. Soc. A* (1971) 2376.
10. Cole-Hamilton, D. J., Young, R. J. and Wilkinson, G. *J. Chem. Soc. Dalton Trans.* (1976) 1995.
11. Hallman, P. S., McGarvey, B. R. and Wilkinson, G. *J. Chem. Soc. A* (1968) 3143.
12. Greco, A., Green, M. and Stone, F. G. A. *J. Chem. Soc. A* (1971) 285.
13. Robinson, S. D. and Shaw, B. L. *J. Chem. Soc.* (1964) 5002.
14. Tang Wong, K. L. and Brintzinger, H. H. *J. Am. Chem. Soc. 97* (1975) 5143.
15. Huttner, G., Brintzinger, H. H., Bell, L. G., Friedrich, P., Bejenke, V. and Neugebauer, D. *J. Organomet. Chem. 145* (1978) 285.
16. Bianco, V. D., Daranzo, S. and Gallo, N. *J. Organomet. Chem. 124* (1977) C43.
17. Pennella, F. *Coord. Chem. Rev. 16* (1975) 51.
18. German, J. E. *Catalytic Conversion of Hydrocarbons*, Associated Press, 1969, p. 115, and references therein.
19. Pez, G. P. *Chem. Commun.* (1977) 560.
20. Clerici, M. G., Di Gioacchino, S., Maspero, F., Perrotti, E. and Zanobi, A. *J. Organomet. Chem. 84* (1975) 379.

Received May 9, 1978.

Acta Chemica Scandinavica A 32 (1978) 771 – 780

Equilibrium Constants for the Axial Coordination of *meso*-Tetraphenylporphinatomanganese(II) and -chromium(III) Complexes

FRED BASOLO, ROBERT D. JONES and DAVID A. SUMMERVILLE

Department of Chemistry, Northwestern University, Evanston, Illinois 60201, U.S.A.

Dedicated to Jannik Bjerrum on the occasion of his 70th birthday

The reaction of molecular oxygen at −78 °C in toluene with five-coordinate *meso*-tetraphenylporphinatomanganese(II) complexes, Mn(II)(TPP)(L), where L represents a neutral N-, P-, or S-donor ligand, is described. Spectrophotometric titrations of toluene solutions of these complexes at −78 °C with molecular oxygen confirm the stoichiometry of the porphinatomanganese dioxygen complexes as Mn(TPP)(O_2). Equilibrium constants for the reaction are reported. Equilibrium constants for axial ligation reactions of Cr(III) and Mn(II) tetraphenylporphinato complexes are reported and the results discussed.

Variations in the biological role of the naturally occurring heme proteins are intimately associated with changes in the axial ligation of the heme moiety. Relevant to our understanding of the mechanism of the action of the heme proteins is an understanding of the manner in which axial ligation affects the electronic structure and reactivity of a metalloporphyrin system. Such studies are particularly important since the reactivities of the metal center in some metalloporphyrin complexes have been shown to differ significantly from the reactivities that would be predicted by comparison with Werner-type complexes containing the same metal center. For example, whereas classical Cr(III) and Co(III) Werner-type complexes are known to be substitution inert,[1] substitution of axial ligands has been shown to occur quite rapidly in Cr(III)[2] and Co(III)[3] metalloporphyrin complexes.

Recently we have been engaged[4,5] in studying the reactions of some metalloporphyrin systems with both neutral nitrogen-, phosphorus-, and sulfur-donor ligands. We have further been investigating the chemical and spectroscopic properties of the dioxygen carrying porphinato complexes of iron(II)[6] and manganese(II).[5] In this paper we report on the equilibrium constants for the bonding of dioxygen to *meso*-tetraphenylporphinatomanganese(II) complexes, as well as on the relative affinities of neutral donor ligands to *meso*-tetraphenylporphinatomanganese(II) and chromium(III) complexes.

NOMENCLATURE

The abbreviations used in this paper are: TPP, the *meso*-tetraphenylporphinato dianion; L represents a neutral ligand such as pyridine; py, pyridine; 1-MeIm, 1-methylimidazole; *sec*-$BuNH_2$, *sec*-butylamine; 3,4-lut, 3,4-lutidine(3,4-dimethylpyridine); 4-CN-py, 4-cyanopyridine; Co(benacen), *N*,*N*′-ethylenebis(benzoylacetiminato)cobalt(II); $(n\text{-}Bu)_3P$, tri-n-butylphosphine.

EXPERIMENTAL

Reagents. Toluene was reagent grade and was distilled under N_2 from sodium-benzophenone ketyl immediately prior to use. Acetone was Baker Spectrophotometric grade. Pyridine and 1-methylimidazole were dried over BaO and KOH respectively, and were distilled prior to use. The 4-cyanopyridine was recrystallized from benzene/heptane several times. The N_2 was Matheson pre-purified grade and was passed through a Ridox column to remove O_2 and water. Gaseous dioxygen

was Airco Ultra Pure (containing less than 2 ppm H_2O) and was further dried by passing the gas over molecular sieves at −130 °C. All other reagents were reagent grade and were used as received without further purification.

Syntheses. *meso*-Tetraphenylporphine ($TPPH_2$) was prepared by the method of Adler and coworkers[7] and was purified (to remove any *meso*-tetraphenylchlorin impurity) by refluxing[8] with 2,3-dichloro-5,6-dicyanobenzoquinone in CH_2Cl_2. Chloro-*meso*-tetraphenylporphinatochromium(III), Cr(III)(TPP)(Cl), was prepared and purified using literature methods.[4] Chloro-*meso*-tetraphenylporphinatomanganese(III), Mn(III)(TPP)(Cl), was synthesized and reduced to the porphinatomanganese(II) complex pyridine-*meso*-tetraphenylporphinatomanganese(II), Mn(II)(TPP)(py), using published procedures.[5] All the above complexes were characterized by comparison with published spectra. Suitable analyses were obtained for Cr(III)(TPP)(Cl) and Mn(II)(TPP)(py). The base-free complex *meso*-tetraphenylporphinatomanganese(II), Mn(II)(TPP), was prepared from the corresponding monopyridine adduct, Mn(II)(TPP)(py), by heating the solid material in a vacuum line at 250 °C. The loss of pyridine from the solid was monitored with a thermocouple vacuum gauge. Heating was continued until the vacuum gauge indicated that no further pyridine was being evolved. In all instances, heating for 2 h resulted in complete removal of pyridine. *Anal.* Calc. for $Mn(C_{44}H_{28}N_4)$: C 79.15; H 4.23; N 8.39. Found: C 79.67; H 4.34; N 8.51.

The series of complexes Mn(II)(TPP)(L), where L represents a nitrogen, phosphorus, or sulfur-donor ligand, were prepared by two different methods, depending on the ligand, L. Where L equals 1-MeIm, 4-CN-py, or *sec*-$BuNH_2$, the complexes were prepared by the reduction of Mn(III)(TPP)(Cl) with $NaBH_4$ in the presence of excess ligand, L, using a similar procedure with that in Ref. 5 for the preparation of Mn(II)(TPP)(py). The complex Mn(II)(TPP)(L), where L is 3,4-lutidine, $(n\text{-}Bu)_3P$, thioanisole, and $(C_2H_5O)_3P$ were prepared by dissolving the base-free complex Mn(II)(TPP) in a toluene solution containing the ligand, L, and precipitation of the solid Mn(II)(TPP)(L) by the addition of either CH_3OH (for L equal to 3,4-lutidine or $(n\text{-}Bu)_3P$), hexane (for L equal to thioanisole) or isooctane (for L equal to $(C_2H_5O)_3P$). The solids were washed several times with the solvent used for precipitation and were dried *in vacuo* overnight. In all cases, optical spectra of the complex Mn(II)(TPP)(L) dissolved in a toluene solution containing approximately 10 % v/v of the ligand, L, were identical with the spectra obtained from a toluene solution of the complex at −78 °C, when correction is made for solvent contraction. Cooling to −78 °C is necessary since dissolving Mn(II) (TPP)(L) at room temperature under N_2 results in the formation of an equilibrium mixture of Mn(II) (TPP) and Mn(II)(TPP)(L) in solution.

Equilibrium constant determinations. Equilibrium constants for the dioxygen replacement reaction

$$\text{Mn(II)(TPP)(L)} + O_2 \overset{K^{Mn}}{\rightleftharpoons} \text{Mn(TPP)}(O_2) + \text{L} \qquad (1)$$

were measured in toluene at −78 °C by a spectrophotometric titration technique using a 4 cm path length low-temperature visible cell.[9] Aliquots of O_2 were added from a gas manifold to the system *via* a gas tight valve and the solution was stirred until equilibrium was obtained (~5 min). The pressure of dioxygen above the solution was determined with an MKS Baratron, Type 221 Series pressure gauge having a range of 0−1000 Torr. Pressures were obtained in a digital format from a Data Precision digital voltmeter (Model No. 1450). Values for K^{Mn} were then determined by monitoring the optical spectra of the solution at different pressures of O_2.

Data from the spectrophotometric titration were fitted to eqn. (2), where

$$\log \frac{y^2}{1-y} = n \log P_{O_2} + \log K^{Mn}([\text{Mn(TPP)(L)}]_{total}) \qquad (2)$$

$[Mn(TPP)(L)]_{total}$ represents the initial concentration of the manganous prophyrin complex. In this expression y is the fraction of manganese(II) sites binding dioxygen, *i.e.*, $y = [Mn(TPP)(O_2)]/[Mn(TPP)(L)]_{total}$ which can be related to the experimentally observed absorbances by the relation

$$y = \frac{A_{deoxy} - A_{obs}}{A_{deoxy} - A_{oxy}} \qquad (3)$$

where

A_{obs} = absorbance differences at two different wavelengths at a specific oxygen pressure, P_{O_2};
A_{deoxy} = absorbance difference at two wavelengths of the parent complex, Mn(II)(TPP)(L); and
A_{oxy} = absorbance difference at two wavelengths of the totally oxygenated complex, $Mn(TPP)O_2$.

To eliminate any problems arising from baseline drift in obtaining the optical spectra, the absorbances at two different wavelengths were monitored to determine the percentage of oxy and deoxy species present. Data were collected at the maximum of either the α or β band of the deoxy species, Mn(II)(TPP)(L), (570 to 620 nm) with the second wavelength being chosen in a region where

the manganese porphyrin complexes do not absorb strongly, ~650 nm.

Eqn. (2) is readily derived from the equilibrium expression

$$K^{Mn} = \frac{[Mn(TPP)(O_2)_n][py]}{[Mn(TPP)(py)]P_{O_2}^n} \quad (4)$$

where n represents the number of dioxygen molecules being bound to the manganese center. For a plot of $y^2/(1-y)$ *vs.* log P_{O_2} the parameter n represents the slope of the straight line. For a simple replacement reaction $n=1.00$. The data obtained from the spectrophotometric titration were fitted to eqn. (2) using a non-weighted linear least-squares method. Values for $K^{Mn}[Mn(TPP)(L)]_{total}$ were obtained from the y-intercept of the regression line for a plot of log $y^2/(1-y)$ *vs.* log P_{O_2}.

In several cases the equilibrium constants, K^{Mn}, for the reaction of eqn. 1 were so low that oxygenation of the manganous porphyrin complex was not complete at a P_{O_2} of 1000 Torr. In these cases calculated values for the absorbances of the solutions at 100 % oxygenation were used to determine a value of y. The calculated values for the absorbance of the fully oxygenated solution, A_∞, were determined by systematically varying A_∞ to obtain a best straight-line fit to eqn. 2.

The concentrations of Mn(II)(TPP)(L) used in measuring K^{Mn} were in the range $1-4\times10^{-5}$ M. Data points were generally taken between 25 and 95 % oxygenation. Over this range the concentration of base-free Mn(II)(TPP) was calculated to be present in insignificant amounts.

Equilibrium constants for the reaction

$$Mn(II)(TPP) + 4\text{-CN-py} \overset{K^{Mn}_{4-CN-py}}{\rightleftharpoons} Mn(II)(TPP)(4\text{-CN-py}) \quad (5)$$

in toluene were measured by a spectrophotometric titration method. Aliquots of a toluene solution containing 4-CN-py were added to a toluene solution of Mn(II)(TPP) in a 1 cm optical cell at 0.0, 23.0 and 40.0 ± 0.1 °. In general the spectra were recorded in the 630 to 530 nm region during the titration.

The data were fitted to the Hill equation[10]

$$\log y/(1-y) = n \log [4\text{-CN-py}] + \log K^{Mn}_{4-CN-py} \quad (6)$$

where in this case y equals the fraction of Mn(II)(TPP) binding 4-CN-py; *i.e.*, $y=[Mn(TPP)(4\text{-CN-py})]/[Mn(TPP)]_{total}$ and n represents the number of molecules of 4-CN-py binding to the manganese(II) center.

In this expression, y can be experimentally determined from the expression

$$y = \frac{A_{obs} - A_0}{A_\infty - A_0} \quad (7)$$

where

A_{obs} = the observed absorbance at a specific concentration of 4-CN-py;
A_0 = initial absorbance of Mn(II)(TPP)
A_∞ = final absorbance, *i.e.* Mn(II)(TPP) present totally as Mn(II)(TPP)(4-CN-py).

Values for log $K^{Mn}_{4-CN-py}$ were determined from the y-intercept of the regression line for a plot of log $y/(1-y)$ *vs.* log[4-CN-py]. Values for the equilibrium constant were found to be independent of the wavelength used.

Equilibrium constants for the replacement reaction, eqn. 8, were measured in

$$Cr(III)(TPP)(Cl)(acetone) + L \overset{K^{Cr}}{\rightleftharpoons} Cr(III)(TPP)(Cl)(L) + acetone \quad (8)$$

solutions of 60 % acetone in toluene (v/v) at 23.0 ± 0.1 °C, using a spectrophotometric titration method and analysis of data analogous with that used for determining $K^{Mn}_{4-CN-py}$. In all cases good isosbestic points were maintained throughout most of the titration. Deviations from isosbestic behavior during the latter stages of the titration could be quantitatively related to dilution effects. Since the equilibrium constants were measured in the presence of 60 % acetone, the equilibrium constants determined from experiment, K^{Cr}_{obs}, were corrected for acetone concentration by the expression $K^{Cr} = K^{Cr}_{obs}$[acetone].

RESULTS

Spectrophotometric titrations for the oxygenation of Mn(II)(TPP)(L), eqn. (1), where L represents a neutral donor ligand, were performed in toluene at −78 °C. The results from a typical titration are shown in Fig. 1. Good isosbestic points were maintained throughout the titration. Plots of log $y^2/(1-y)$ *vs.* log P_{O_2} (see experimental section for details) gave straight lines (Fig. 2) with slopes of 1.00 ± 0.10, with the exception that for the oxygenation of Mn(II)(TPP)(1-MeIm) slopes of 1.14 and 1.18 were observed. Values for the slopes and the calculated equilibrium constants are given in Table 1. Equilibrium constants were checked at a second wavelength and proved independent of the wavelength chosen.

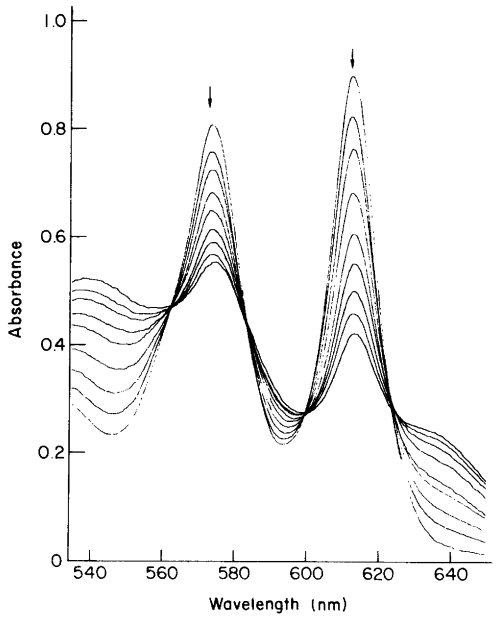

Fig. 1. Optical spectral changes on the addition of molecular oxygen to a 1.1×10^{-4} M toluene solution of Mn(II)(TPP)(*sec*-BuNH$_2$) at −78 °C. The final spectrum was run at a pressure of O_2 of 1004 torr. At this pressure the manganous porphin is 79 % oxygenated.

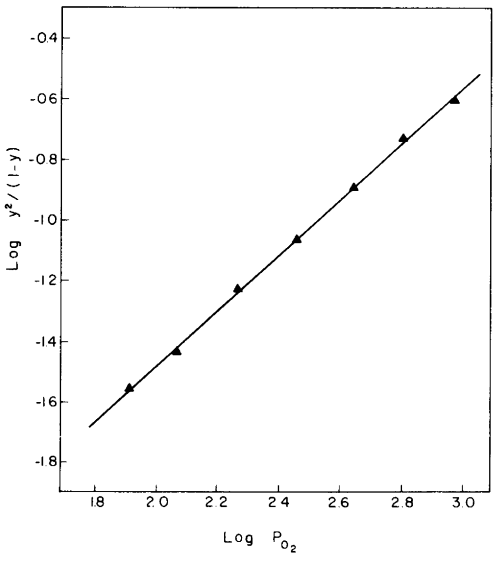

Fig. 2. Plot of $\log y^2/(1-y)$ *vs.* $\log P_{O_2}$ for the oxygenation of Mn(II)(TPP)((n-Bu)$_3$P) in toluene solution at −78 °C. The slope is 0.91 and $\log K = -8.44$. An *R*-factor of 0.9998 was calculated.

Table 1. Equilibrium constants for the reaction $\mathrm{Mn(II)(TPP)(L)} + \mathrm{O_2} \overset{K^{Mn}}{\rightleftharpoons} \mathrm{Mn(II)(TPP)(O_2)} + \mathrm{L}$ at −78 °C in toluene.

L	n[a]	$-\log K^{Mn}$
4-CN-py[a]	1.08	5.57
$pK_a = 1.86$[b]	0.93	5.58
py	1.09	5.91
$pK_a = 5.27$[c]	1.06	5.95
	1.06	5.97
	1.01	6.02
3,4-lut	1.04	7.09
$pK_a = 6.46$[c]	1.10	7.19
1-MeIm	1.14	7.94
$pK_a = 7.25$[c]	1.18	8.00
sec-BuNH$_2$[c]	0.93	7.33
$pK_a = 8.43$	1.00	7.39
(n-Bu)$_3$P[d]	1.00	8.52
$pK_a = 8.43$	0.91	8.44
(C$_2$H$_5$O)$_3$P	0.91	5.43
$pK_a = 3.50$[e]	0.91	5.59
Thioanisole	1.03	7.43
	0.99	7.46

[a] Calculated from a least-squares analysis of $\log y^2/(1-y)$ *vs.* $\log P_{O_2}$. See text for details. K^{Mn} has units of mol/L Torr. From a least-squares analysis of the data all values for $\log K^{Mn}$ fell within ±0.1. [b] Schofield, K. *Hetero-Aromatic Nitrogen Compounds*, Plenum, New York 1967, p. 146. [c] Albert, A. *Phys. Methods Heterocyclic Chem. 1* (1963). [d] Streuli, C. A. *Anal. Chem. 32* (1960) 985. [e] Estimated value, see Ref. 23.

Heating solid Mn(II)(TPP)(py) *in vacuo* at 250 °C for several hours results in the formation of the corresponding four-coordinate, base-free Mn(II)-(TPP) complex. The identity of this complex has been confirmed both by elemental analysis and by the spectrophotometric titration of these complexes with toluene solutions containing an N-donor ligand (*vide infra*).

Spectrophotometric titrations of toluene solutions of Mn(II)(TPP) with toluene solutions containing 4-CN-py were performed at several temperatures. Plots of $\log y/(1-y)$, where y equals $[\mathrm{Mn(II)(TPP)(4\text{-}CN\text{-}py)}]/[\mathrm{Mn(II)(TPP)}]_{total}$, *vs.* log[4-CN-py] gave straight lines with slopes of 1.0±0.2. Good

Table 2. Equilibrium constants for the addition of 4-cyanopyridine to Mn(II)(TPP) in toluene

$$\text{Mn(II)(TPP)} + \text{4-CN-py} \overset{K^{Mn}_{4-CN-py}}{\rightleftharpoons} \text{Mn(II)(TPP)(4-CN-py)}$$

Ligand	t (°C)[a]	Slope(n)[b]	log $K^{c}_{4-CN-py}$
4-Cyanopyridine	40.0	0.94	3.16
	40.0	1.05	3.04
	23.0	1.14	3.60
	23.0	1.17	3.59
	23.0	1.08	3.55
	0.0	1.12	4.19
	0.0	1.20	4.21
	−78 (extrapolated)		7.63

[a] ±0.1°. [b] Slope from fitting the data to the Hill equation (eqn. 6). [c] Errors estimated at ±0.1. Thermodynamic constants for the addition of 4-CN-py are $\Delta H = -10.7 \pm 0.4$ kcal/mol, and $\Delta S = -19.8 \pm 1.5$ eu.

isosbestic points were maintained throughout the titration. Values for the slopes and equilibrium constants for the addition of 4-CN-py to Mn(II)(TPP) are given in Table 2. Values for the equilibrium constant were found to be independent of the wavelength used.

Spectrophotometric titrations at 23 °C of 60 % acetone/toluene (v/v) of Cr(III)(TPP)(Cl) with toluene solutions of a nitrogenous ligand, L, were performed. The results from a typical titration are shown in Fig. 3. Plots of log $y/(1-y)$ where $y = [\text{Cr(III)(TPP)(Cl)(L)}]/[\text{Cr(III)(TPP)(Cl)}]_{\text{total}}$ *vs.* log [L] gave straight lines with slopes of 1.00±0.1. Values for the slopes obtained from the titrations as well as the observed equilibrium constants are given in Table 3.

Table 3. Equilibrium constants[a] for the reaction

$$\text{Cr(III)(TPP)(Cl)(acetone)} + \text{L} \overset{K^{Cr}}{\rightleftharpoons} \text{Cr(III)(TPP)(Cl)(L)} + \text{acetone}.$$

L[b]	Slope[c]	log K^{Cr}
4-CN-py	1.03	3.20±0.03
	1.00	3.12±0.07
py	1.03	4.28± .06
	1.01	4.28± .04
3,4-Lut	1.02	5.01±0.12
	0.97	5.01±0.13
sec-$BuNH_2$	1.03	5.47±0.08
	0.99	5.43±0.17
1-MeIm	1.00	6.71±0.13
	0.94	6.44±0.16

[a] Measured in 60 % acetone/toluene (v/v) at 23.0±0.1 °C. Log K^{Cr} represents the equilibrium constant corrected for acetone concentration. Errors reported represent deviations of data from a least-squares analysis. [b] Ligands were in toluene solution: 4-CN-py, ~0.6 M; py, 0.1 to 0.6 M; 3,4-Lut, 0.27 M; *sec*-$BuNH_2$, $\sim 2 \times 10^{-2}$ M; 1-MeIm, $\sim 2 \times 10^{-2}$ M. [c] Calculated from a least-squares analysis of log $y/(1-y)$ *vs.* log (L); see text for details.

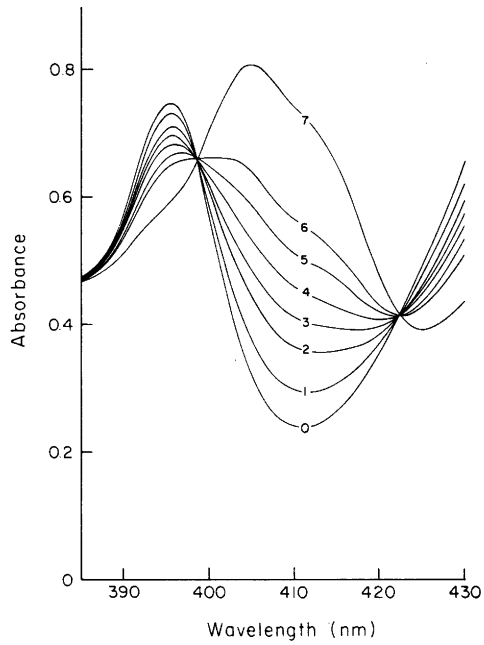

Fig. 3. Visible spectral changes on the addition of pyridine (in 60 % acetone/toluene, v/v) to a 1.50×10^{-5} M solution of Cr(TPP)(Cl) in 60 % acetone/toluene. The addition was performed using a two syringe technique. The spectrum labelled 0 is the spectrum of the initial acetone adduct. Spectra labelled 1 to 6 were obtained from solutions having pyridine concentrations ($\times 10^4$) of 0.56, 1.42, 2.27, 3.42, 5.14 and 8.00, respectively. Spectrum 7 was obtained at a final pyridine concentration of 5.84×10^{-2} M and corresponds to the spectrum of Cr(TPP)(Cl)(py).

DISCUSSION

Until recently, the only synthetic metal complexes of biological interest that had been observed to reversibly bind molecular oxygen were those containing Fe(II) or Co(II) centers.[11] Recently, *meso*-tetraphenylporphinatomanganese(II) complexes of the form Mn(II)(TPP)(L) have been shown to act as reversible oxygen carriers in toluene solution at −78 °C.[12,13] That the formation of tetraphenylporphinatomanganese-dioxygen complex involves the replacement of the coordinated neutral ligand, L, to form Mn(TPP)(O_2) has been inferred[12] both from EPR evidence and from the observation that the dioxygen complex is not observed in the presence of an excess of the ligand L.

The study on the equilibrium reactions of Mn(II)-(TPP)(L) complexes with O_2 at −78 °C in toluene presented here confirms that the reaction of O_2 with the manganous porphyrins occurs *via* replacement of the axial ligand L, eqn. (1). The study also presents us with information as to the affinities of tetraphenylporphinatomanganese(II) complexes for dioxygen and neutral ligands.

Dissolving five-coordinate tetraphenylporphinatomanganese(II) complexes in toluene and cooling to −78 °C results in the manganous porphyrin being present predominantly as the five-coordinate, Mn(II)(TPP)(L), species with almost none of the base-free adduct being present. This result is consistent with an analysis of the cold temperature spectra of Mn(II)(TPP)(L), both in the absence and presence of extra ligand, L. Further, a calculation of the amount of base-free Mn(II)(TPP) present when a 10^{-5} M toluene solution of Mn(II)(TPP)(4-CN-py) is cooled to −78 °C, using the extrapolated value for $K^{Mn}_{4-CN-py}$ (Table 2), reveals that only about 0.2 % of the metalloporphin is present as the base-free complex.

In the presence of molecular oxygen at low temperature in toluene solution, an equilibrium between the five-coordinate mono-ligated species, Mn(II)(TPP)(L), and the dioxygen complex, Mn-(TPP)(O_2) is established, eqn. (1). The good isosbestic behavior and straight-line plots of log $(y^2/(1-y))$ *vs.* log P_{O_2} obtained from the spectrophotometric titrations of the five-coordinate manganous porphins with molecular oxygen confirm that the manganous porphyrins add only one mol of O_2 for every mol of metalloporphyrin, and that the dioxygen complexes have no ligand occupying the vacant axial position.

The possibility that the oxygenation of the ligated manganous porphin complexes, Mn(II)(TPP)(L), proceeds as the simple dioxygen addition reaction can be eliminated for two other reasons: (1) The data obtained from the titrations with molecular oxygen were analyzed using the Hill plot method. The resulting plots of log $y/(1-y)$ *vs.* log P_{O_2} (where y equals the fraction of maganese sites oxygenated) showed both deviations from straight-line behavior, and slopes significantly different from $n = 1.00$, (for example, the results of the titration of Mn(TPP)-($(n\text{-Bu})_3$P) with O_2, shown in Fig. 2, when analyzed according to the Hill equation, eqn. (6), gave a slope of 0.52), and (2) the values obtained for the log of the equilibrium constants for the oxygenation of Mn(TPP)(py) were found to be directly proportional to the log of the concentration of manganese porphin used when the data were analyzed by the Hill method. Such results are inconsistent with the oxygenation of the manganous porphins being a straightforward addition reaction but are consistent with the replacement by oxygen of the axial ligand.

An examination of the dioxygen replacement reaction, eqn. (1), reveals that the equation can be rewritten in terms of the two equilibrium processes

$$\text{Mn(II)(TPP)(L)} \overset{K^{Mn}_{L}}{\rightleftharpoons} \text{Mn(II)(TPP)} + \text{L} \qquad (9)$$

$$\text{Mn(II)(TPP)} + \text{O}_2 \overset{K^{Mn}_{O_2}}{\rightleftharpoons} \text{Mn(TPP)(O}_2\text{)} \qquad (10)$$

From the equilibrium constants for the binding of 4-CN-py to Mn(II)(TPP), Table 2, and the value for the equilibrium constant for oxygenation of Mn(II)(TPP)(4-CN-py) at −78 °C, Table 1, we can estimate a value for the oxygenation of four coordinate Mn(II)(TPP) at −78 °C. From the data in Table 2 we obtain a value for log $K^{Mn}_{4-CN-py}$, extrapolated to −78 °C, of 7.63. Using the value determined for this equilibrium constant for the oxygenation of Mn(TPP)(4-CN-py) at −78 °C, log $K^{Mn} = -5.57$, we calculate the value for the equilibrium constant for the oxygenation of Mn(II)-(TPP) at −78 °C as $K^{Mn}_{O_2} \sim 10^{2.1}$ Torr^{-1}.

A comparison of the equilibrium constants for oxygenation for a series of porphinato metal(II) complexes at −78 °C with the $M^{III/II}$ half-wave reduction potentials (Table 4) shows that, with the exception of Mn(II)(TPP), there is a direct relationship between the affinity of the complex for dioxygen and the ease of oxidation of the metal(II) center. Thus, the $K^{Mn}_{O_2}$ observed for Mn(II)(TPP) at −78 °C

Table 4. Equilibrium constants for the oxygenation of metalloporphyrin complexes at −78 °C.[a]

Complex	Conditions	log K_{O_2}	$E_{\frac{1}{2}}(M^{III/II})$[b]
Co(II)(TPP)(py)	toluene solution	−1.7[c]	+0.13[c]
Co(II)(T(*p*-OMe)PP)(1-MeIm)	toluene solution	−0.8[d]	+0.11[c]
Fe(II)(TpivPP)(1-MeIm)	solid	6.4[e]	−0.11[f]
Mn(II)(TPP)	toluene solution	~2.1[g]	−0.27[h]
Cr(II)(TPP)(py)	solid	large	−0.86[i]

[a] The equilibrium constants reported in this table are for the addition of O_2 to a vacant axial coordination site on the metal(II) center. Values for log K_{O_2} at −78 °C are calculated from thermodynamic data given in the references cited. Units of K_{O_2} are $Torr^{-1}$. [b] In DMSO. Values reported in volt *vs.* SCE. [c] For Co(TPP) and Co(II)(T(*p*-OMe)PP); Walker, F. A., Beroiz, D. and Kadish, K. M. *J. Am. Chem. Soc. 98* (1976) 3484. [d] Walker, F. A. *J. Am. Chem. Soc. 95* (1973) 1154. [e] TpivPP represents the dianion of the "picket-fence" porphyrin. Collman, J. P., Braumau, J. I. and Suslick, K. S. *J. Am. Chem. Soc. 97* (1975) 7185. [f] Kadish, K. M., Morrison, M. M., Constant, L. A., Dickens, L. and Davis, D. G. *J. Am. Chem. Soc. 98* (1976) 8387. [g] This work. [h] Cape, T., Szymanski, T. and Basolo, F. *Unpublished results;* see also Kadish, K. M. and Morrison, M. M. *Bioelectrochem. Bioenergetics 3* (1976) 480. [i] The dioxygen adduct forms irreversibly. Cheung, S. K., Grimes, C. J., Wong, J. and Reed, C. A. *J. Am. Chem. Soc. 98* (1976) 5028.

is several orders of magnitude less than would be predicted on the basis of the half-wave reduction potential.

This apparent anomaly in the bonding of dioxygen to Mn(TPP) compared with the porphinato metal(II) complexes of cobalt, iron and chromium may indicate that the nature of the bond between manganese and dioxygen differs significantly from that observed with these other metals. Although the bonding in the metalloporphin-dioxygen complexes containing Fe, Co, and Cr have been shown to bind dioxygen in an end-on (Pauling) conformation, the geometry of the manganese-dioxygen bond in Mn(TPP)(O_2) has not yet been unambiguously determined. Since we expect the relationship between K_{O_2} and $E_{\frac{1}{2}}$ to be consistent for similarly bonded structures, the anomalous value observed for the oxygen affinity of Mn(II)(TPP) is consistent with a symmetrical, Griffith type conformation of the manganese-dioxygen bond as had been previously suggested on the basis of EPR results.[12] There is, however, another interpretation for the anomalous value for $K_{O_2}^{Mn}$. Basolo and co-workers[9] have reported that whereas five-coordinate complexes of the cobalt(II) Schiff base Co(II)(benacen)(L), where L represents an N-donor ligand, readily bind dioxygen in toluene solution at 0 °C (*e.g.* log $K_{O_2}^{Co}$ = −2.0 at 0 °C for L equal to 1-MeIm) only a small amount of the four-coordinate Co(II)(benacen) complex is oxygenated under one atmosphere of O_2 in toluene at −83 °C. Thus if the dioxygen moiety in Mn(TPP)(O_2) adopts the Pauling conformation, the seemingly low value for log $K_{O_2}^{Mn}$ is consistent with the absence of a sixth axial ligand.

Having determined that Mn(II)(TPP)(L) reacts reversibly with molecular oxygen to form Mn(TPP)-(O_2) it is interesting to compare the chemical properties observed for the tetraphenylporphinatomanganese dioxygen complex with those predicted on the basis of the ground-state electronic configuration as determined from EPR studies. Frozen solution EPR spectra of Mn(TPP)(O_2) have been interpreted[12] in terms of a d^3 electronic configuration about the manganese center. Such an electronic configuration has been interpreted[12] in terms of an Mn(IV)-O_2^{2-} formalism for the metalloporphyrin complex. As such, the chemistry of the manganese dioxygen complex should be expected to be similar to that observed for tetraphenylporphinatochromium(III) complexes that contain a d^3 metal center.

Upon adding a toluene solution containing an N-donor ligand to a solution containing Cr(III)-(TPP)(Cl)(acetone), replacement of the acetone by the N-donor ligand, eqn. (8), is observed to occur.[4] The equilibrium constants for this replacement, K^{Cr}, at 23 °C are given in Table 3. Although we have been unable to obtain equilibrium constants for the addition of a neutral N-donor ligand to five-coordinate Cr(III)(TPP)(Cl) due to the insolubility of Cr(TPP)(Cl) in the absence of a coordinating ligand,[4] we can use the values of K^{Cr}, Table 3, as lower limits for the affinities of five-coordinate Cr(TPP)(Cl) for N-donor ligands. In contrast to the large affinity of five-coordinate Cr(TPP)(Cl) for a sixth N-donor ligand, we observed no tendency for Mn(TPP)(O_2) to bind a sixth ligand at −78 °C.[5]

Such a large difference in behavior for the two d^3-metalloporphin systems is consistent with the dioxygen bonding in a side-bonded Griffith conformation, with repulsive steric interactions between the coordinated oxygen atoms and N-atoms of the porphin ring accounting for the tendency of the d^3 manganese center not to bind a neutral axial ligand.

In addition to studying the equilibrium of manganese(II) tetraphenylporhin complexes with dioxygen, this study gives us information about the bonding of neutral ligands to Cr(III) and Mn(II) tetraphenylporphinato complexes. It is unfortunate that the insolubility of Cr(TPP)(Cl) in toluene has made it impossible for us to obtain any absolute values for the affinity of the five-coordinate Cr(TPP)(Cl) for a sixth ligand. However, replacement of the acetone coordinated to the Cr(III) center in Cr(TPP)(Cl)(acetone) by 1-methylimidazole occurs with an equilibrium constant of 4.0×10^6 (23 °C in 60 % v/v acetone – toluene). Using this value as a lower limit for the affinity of five-coordinate Cr(TPP)(Cl) for 1-MeIm we can contrast this value with the equilibrium constant obtained for the addition of a 1-MeIm to Fe(III)(TPP)(Cl) (in benzene at 25 °C)[14] where $K = 1.3 \pm 0.2$, or of a pyridine to Mn(III)(TPP)(Cl) where $K = 2.5$.[15] Indeed, the binding of the sixth ligand by Cr(TPP)(Cl) compares favorably with the addition of the first imidazole to base-free Fe(II)(TPP) (in benzene at 25 °C)[16] where $K = 8.8 \times 10^3$ M^{-1}.

The imidazole ligand in its binding to metalloporphin complexes has been shown to exhibit unusual behavior compared with other nonhindered nitrogenous bases. The lower lability of the coordinated dioxygen in Fe(TPP)(1-MeIm)(O_2) compared with that observed where pyridine or piperidine occupy the axial position has been attributed to the larger π-donor effect of the imidazole ligand relative to that of pyridine or piperidine.[6] Other anomalous effects of the imidazole ligand have been observed for O_2 and CO bonding to metalloporphyrin and metallophthalocyanin complexes.[9,17-19]

In this bis-imidazole complexes of some Fe(III) porphyrins (the bis-imidazole hemichromes), the imidazole ligand has been implicated as a π-donor from Mössbauer data[20] and as a π-acceptor from NMR studies compared with Hückel calculations.[21] It is therefore of interest to examine our equilibrium data for the binding of nitrogenous bases to Cr(TPP)(Cl).

A plot of log K^{Cr} values for the equilibrium reactions of Cr(TPP)Cl with L, eqn. (8), *versus* the basicity (pK_a for LH^+) of the N-donor ligand L is shown in Fig. 4. The linearity of the plot for the π-acceptor substituted pyridine ligands and the non π-bonding *sec*-butylamine suggests that metal-to-ligand π-bonding is relatively unimportant for these complexes. The anomalously strong binding of 1-MeIm is consistent with ligand-to-metal π-bonding from the imidazole to the chromium(III) being important in these complexes.

The relative affinities of base-free Mn(II)(TPP)

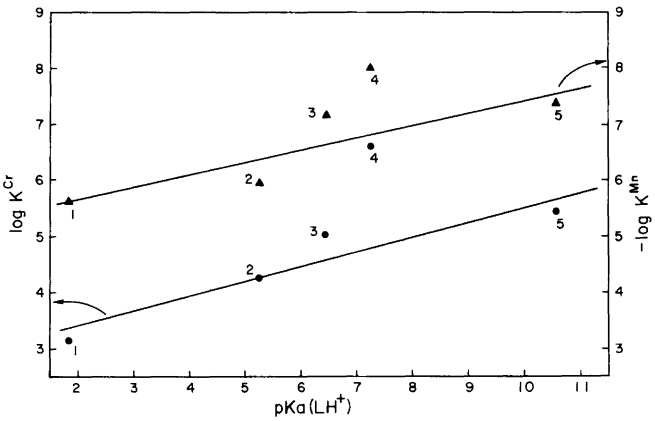

Fig. 4. Correlation between pK_a for the conjugate acids (LH^+) and the log of the equilibrium constants for reactions 1 and 8. The left hand ordinate and represent log K^{Cr} for the reaction Cr(III)(TPP)(Cl)(acetone) + L ⇌ Cr(III)(TPP)(Cl)(L) + acetone; the right hand ordinate and ▲ represent the $-\log K^{Mn}$ for the reaction Mn(II)(TPP)(L) + O_2 ⇌ Mn(TPP)(O_2) + L. Ligands (L) are 1 = 4-cyanopyridine; 2 = pyridine; 3 = 3,4-butadiene; 4 = 1-methylimidazole; 5 = *sec*-butylamine. The straight lines represent regression lines obtained for points 1, 2, 3 and 5.

for a neutral N-, P-, and S-donor ligand in toluene at −78 °C can be determined directly from the data in Table 1. A plot of $-\log K^{Mn}$ *vs.* the σ-donor strength of the N-donor ligands (represented as pK_a for LH^+) is shown in Fig. 4 along with the data for $\log K^{Cr}$ *vs.* L. Construction of a least-squares line for the values of $-\log K^{Mn}$ *vs.* pK_a for the substituted pyridine bases and *sec*-$BuNH_2$, Fig. 4, shows that although there appears to be a general correlation between the parameters, deviations from straight-line behavior are greater than those observed for the binding of these same ligands to Cr(III)(TPP)(Cl). The large deviation of the value of $-\log K^{Mn}$ observed for the 1-MeIm case is similar to that observed previously for the ligation of Cr(III) porphyrins.

An examination of the data for the bonding of the phosphorus-donor ligands, $(C_2H_5O)_3P$ and $(n\text{-}Bu)_3P$, to Mn(II)(TPP) shows an interesting correlation with the data obtained for the nitrogen-donor bases. In comparison with the equilibrium constant data (Table 3) obtained for the substituted pyridine ligands and *sec*-butylamine, $(C_2H_5O)_3P$ and $(n\text{-}Bu)_3P$ show affinities for the manganous porphin that are, respectively, weaker and stronger than would be predicted on the basis of the proton basicity of the P-donor ligands. The fact that a linear relationship is observed between the proton acidities of a series of ligands containing the same donor atom, *i.e.* N or P, and the equilibrium constants observed for the bonding to the manganese(II) center implies either that ligand-metal π-bonding plays a relatively constant role in the bonding of the ligand to the metal center or that there exists an intimate balance between σ- and π-bonding effects. Both σ- and π-bonding have been implicated in the bonding of both pyridine and P-donor ligands to metal centers.[22] The variation in bonding of the neutral ligand to the manganese(II) porphin observed for the N- and P-donor series may therefore reflect differences in π-bonding between the manganese(II) center and the nitrogen- and phosphorus-donor ligands. This effect is similar to that previously reported[23] for the binding of an axial ligand to the four-coordinate diethyl ester of mesoporphyrinatocobalt(II) where it was observed that the influence of σ-donor ability of the ligand (as measured by the pK_a) on the binding of P-donor ligands to the cobaltous porphyrin was much greater than the effect of pK_a obtained for a series of N-donor ligands.

Acknowledgements. This research was supported by grants from the National Institutes of Health and the National Science Foundation. One of us (F.B.) has fond memories of his year (1954–1955) in the laboratory of Professor Jannik Bjerrum, and is delighted to have this opportunity to participate in the celebration of his 70th birthday.

REFERENCES

1. Basolo, F. and Pearson, R. G. *Mechanisms of Inorganic Reactions*, 2nd Ed., Wiley, New York 1967, Chapter 3.
2. Fleischer, E. B. and Krishnamurthy, M. *J. Am. Chem. Soc. 93*, (1971) 3784; *J. Coord. Chem. 2* (1972) 89.
3. Pasternack, R. F. and Cobb, M. A. *Biochem. Biophys. Res. Commun. 51* (1973) 507; Fleischer, E. B., Jacobs, S. and Mestichelli, L. *J. Am. Chem. Soc. 90* (1968) 2527.
4. Summerville, D. A., Jones, R. D., Hoffman, B. M. and Basolo, F. *J. Am. Chem. Soc. 99* (1977) 8195.
5. Jones, R. D., Summerville, D. A. and Basolo, F. *J. Am. Chem. Soc. 100* (1978) 4416.
6. Weschler, C. J., Anderson, D. L. and Basolo, F. *J. Am. Chem. Soc. 97* (1975) 6707.
7. Adler, A. D., Longo, F. R., Finarelli, R. D., Goldmacher, J., Assour, J. and Korsakoff, L. *J. Org. Chem. 32* (1967) 476.
8. Barnett, G. H., Mudson, M. F. and Smith, K. M. *Tetrahedron Lett. 30* (1973) 2887.
9. Carter, M. J., Rillema, D. P. and Basolo, F. *J. Am. Chem. Soc. 96* (1974) 392.
10. Hill, A. V. *J. Physiol. (London) 40* (1910) iv–vii.
11. a. Basolo, F., Hoffman, B. M. and Ibers, J. A. *Acc. Chem. Res. 8* (1974) 384; b. McLendon, G. M. and Martell, A. E. *Coord. Chem. Rev. 19* (1976) 1.
12. Weschler, C. J., Hoffman, B. M. and Basolo, F. *J. Am. Chem. Soc. 97* (1975) 5278; Hoffman, B. M., Weschler, C. J. and Basolo, F. *Ibid. 98* (1976) 5473.
13. Gonzalez, B., Kouba, J., Yee, S., Reed, C. A., Kirner, J. F. and Scheidt, W. R. *J. Am. Chem. Soc. 97* (1975) 3247.
14. Walker, F. A., Lo, M.-W. and Ree, M. T. *J. Am. Chem. Soc. 98* (1976) 5552.
15. Boucher, L. J. *Coord. Chem. Rev. 7* (1972) 289.
16. Brault, D. and Rougee, M. *Biochem. Biophys. Res. Comm. 57* (1974) 654.
17. Walker, F. A. *J. Am. Chem. Soc. 95* (1977) 1154.
18. Stynes, D. V., Stynes, H. C., James, B. R. and Ibers, J. A. *J. Am. Chem. Soc. 95* (1973) 1796.
19. Stynes, D. V. and James, B. R. *J. Am. Chem. Soc. 96* (1974) 2733.

20. Epstein, L. M., Straub, D. K. and Maricondi, C. *Inorg. Chem. 6* (1967) 1720.
21. Satterlee, J. D. and La Mar, G. N. *J. Am. Chem. Soc. 98* (1976) 2804.
22. Huheey, J. E. *Inorganic Chemistry; Principles of Structure and Reactivity*, Harper and Row, New York 1972, pp. 347–358; Horrocks, W. D., Jr. and Taylor, R. C. *Inorg. Chem. 2* (1963) 723.
23. Takayanagi, T., Yamamoto, H. and Kwan, T. *Bull. Chem. Soc. Jpn. 48* (1975) 2618.

Received May 18, 1978.

Acta Chemica Scandinavica A 32 (1978) 781 – 783

Short Communication

The Anodic Dissolution of Iron. IX. Strong, Selective Inhibition Caused by Acetylene

G. BECH-NIELSEN

Chemistry Department A, Building 207,
The Technical University of Denmark,
DK-2800 Lyngby, Denmark

Dedicated to Jannik Bjerrum on the occasion of his 70th birthday

It has been shown that the anodic dissolution of iron takes place *via* two different reactions.[1-5] A transition region separates the I_1 reaction at lower potentials and the I_2 reaction at higher potentials. These experimental observations have been interpreted by two kinetic models,[2,4] both of which assume a stepwise formation of adsorbed intermediates containing Fe(I) or Fe(II) species and OH^--groups. According to the author's model the oxidation of Fe(I) during the I_1 reaction can only take place at a defect site in the surface. The precise characteristics of the transition between the I_1 and the I_2 reactions are explained by adsorption of an Fe(II) intermediate of the I_2 reaction starting at defect sites and thereby blocking the I_1 reaction. As a consequence of this idea it has recently been predicted[5] that a particular type of inhibition should be expected, if the only function of a given inhibitor molecule is to adsorb strongly at defect sites, yet less strongly than the Fe(II) intermediate of the I_2 reaction. We should then expect complete inhibition of the I_1 reaction and rather little influence on the I_2 reaction.

Acetylene was selected for use in the experiments. Earlier reports ascribe the inhibition due to this molecule to strong adsorption at the metal surface,[7] but also secondary products formed by hydrogenation and polymerization are assumed to contribute to the observed effects.[6] In order to avoid formation of secondary products we used the following procedure: A polarization diagram was recorded with an iron electrode in a given electrolyte solution, through which pure nitrogen was being bubbled. Nitrogen was quickly replaced by acetylene, and the polarization diagram for the acetylene saturated solution was recorded. Acetylene was then replaced by nitrogen, and the final polarization diagram was recorded. The changes between the first and the last diagrams were found to be very small. We also found no difference between diagrams obtained with the iron electrode at anodic or cathodic potentials during the introduction of acetylene. These observations indicate a reversible adsorption of acetylene, and the observed short-term effects can be attributed to the simple molecule.

Experimental procedures have been described previously.[1] The acetylene was 99 % pure, the major contaminant being acetone. Two samples were used for rotating disk electrodes, pure iron (Johnson Matthey Chemicals Ltd., metallic impurities <15 ppm) and a 0.12 % carbon steel (annealed at 1350 °C). The disk surface was finished by diamond-polishing or by electro-polishing. Irrespective of the purity of the metal and the method of polishing the results for a given solution were similar.

The diagrams for acetate-perchlorate mixtures and for a 0.5 M $(NH_4)_2SO_4$ solution are well represented by Fig. 1. The agreement with the expectations is good, but in order to verify that the I_1 reaction is completely inhibited at potentials, where the I_2 reaction is unaffected, an additional analysis was performed. In the absence of inhibition the current density (cd) in the transition region is given by:[1,3-5]

$$i = I_1(1-\theta_1) + I_2\theta_1 \qquad (1)$$

where i is the measured cd at a given potential, I_1 and I_2 are extrapolated values according to the two Tafel lines, and θ_1 is a fraction developing according to a Langmuir adsorption isotherm. Plots of $\log[\theta_1/(1-\theta_1)]$ *vs.* potential are linear at not too low values of θ_1 and have slopes close to 0.03 V. Hence inspection of the plots shown in Fig. 2 allows the conclusion that the observed anodic current in the presence of acetylene is a pure I_2-contribution, since plot b (constructed exclusively on the basis of the second term on the rhs of (1)) has very closely the same form as plot a.

Fig. 1 indicates a definite decrease in the cathodic current level in the presence of acetylene. However,

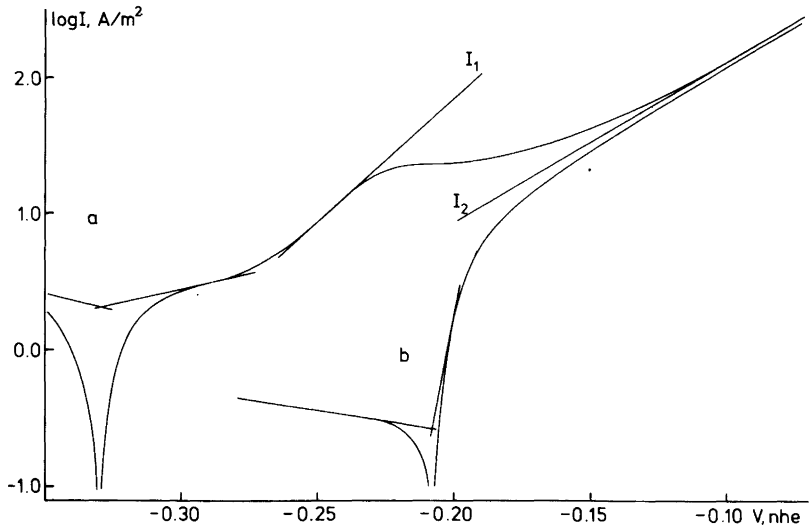

Fig. 1. Polarization diagram for a 0.12 % C-steel electrode in 0.99 M $NaClO_4$, 0.01 M Na-acetate, *ca.* 1 M acetic acid, pH = 2.44. 27 °C. 3000 rpm. Rate of potential sweeps: 5×10^{-4} V/s. The recordings were made going from anodic to cathodic potentials. a: Without acetylene, b: With acetylene saturated solution (1 atm). Extrapolated anodic and cathodic Tafel lines intersect at the corrosion potentials and indicate the magnitudes of the corrosion cd's in the two situations. A decrease in corrosion cd by 87 % is noted in passing from a to b.

Note: The highly increased slope at the low end of the I_1 region is a genuine feature presently being investigated.

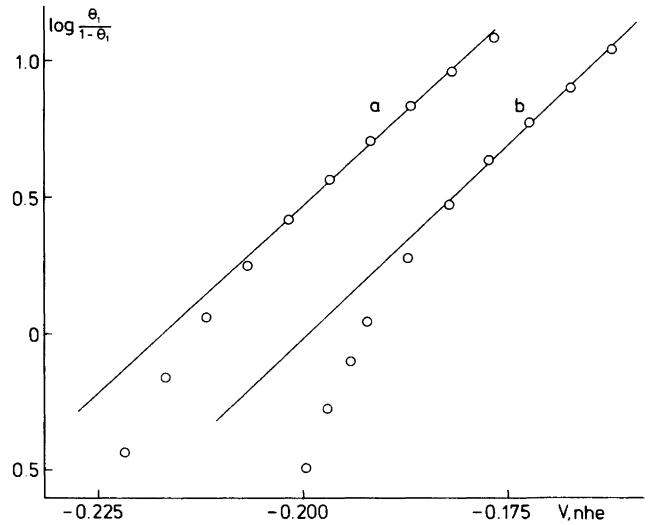

Fig. 2. Diagram of $\log [\theta_1(1-\theta_1)]$ *vs.* potential calculated for the curves shown in Fig. 1, where a and b refer to the experiments without and with acetylene, respectively. The two straight lines are close to parallel, and they have a slope near 0.036 V.

recording of the cathodic current at a fixed potential during the introduction of acetylene showed a considerable increase in current prior to the decrease. This observation obviously explains earlier reports of a short-term increase in corrosion rate prior to the establishment of efficient inhibition.[6]

Acknowledgements. Valuable assistance in the experiments by T. Lyk Christiansen, H. Serup Pedersen and Mrs. T. Brögger Andersen is gratefully acknowledged. The author is indebted to Drs. J. C. Reeve and M. Mogensen for discussions.

1. Nord, H. and Bech-Nielsen, G. *Electrochim. Acta 16* (1971) 849.
2. Bessone, J., Karakaya, L., Lorbeer, P. and Lorenz, W. J. *Electrochim. Acta 22* (1977) 1147.
3. Nilsson, P. and Håkansson, B. *Proc. 8th Scand. Corros. Congr.* Helsinki 1978, Vol. I, p. 41.
4. Bech-Nielsen, G. *Electrochim. Acta 21* (1976) 627.
5. Bech-Nielsen, G. *Jernelektrodens kinetik og ledsagende fænomener i området anodisk opløsning til tidlige stadier af passivering*, Diss., The Technical University of Denmark, Published by teknisk forlag, Copenhagen 1978; references therein.
6. Putilova, I. N. and Chislova, E. N. *Zashch. Met. 2* (1966) 290.
7. Zavorokhin, N. D. *Acetylene and Its Derivatives as Inhibitors of Acid Corrosion*, [in Russian], Diss., Alma-Ata 1956; Ref. 6.

Received May 31, 1978.

Acta Chemica Scandinavica A 32 (1978) 785–788

Preparation of Single Phases and Single Crystals in the Vanadium-Gallium-Antimony System. Crystal Structure of V_6GaSb

SVEND ERIK RASMUSSEN and RITA GRØNBÆK HAZELL

Department of Inorganic Chemistry, Aarhus University, DK-8000 Aarhus C, Denmark

Dedicated to Jannik Bjerrum on the occasion of his 70th birthday

Vanadium-antimony and vanadium-gallium-antimony compounds were prepared by floating zone melting. Single phases of A15 structure were produced for both the V–Sb and the V–Ga–Sb systems. Samples were examined by X-ray diffraction and X-ray fluorescence analysis. A single crystal of nominal composition V_6GaSb was mounted on a four-circle diffractometer for a detailed investigation of order parameters. The A15 structure, space group *Pm3n*, was confirmed. Ga and Sb are distributed at random at the positions 0,0,0 and $\frac{1}{2},\frac{1}{2},\frac{1}{2}$. The vanadium atoms are in an ordered arrangement in the $0,\frac{1}{2},\frac{1}{4}$ positions. A conventional *R*-value of 0.8 % was obtained. Deviations from stoichiometry are discussed. Attempts to introduce In atoms in the A15 structure by reacting V with InSb were unsuccessful.

Vanadium forms a number of intermetallic compounds of general formula $V_{3+y}X$. Several are of A15 structure. The stoichiometry range, defined by the possible values of y, is in general difficult to assess, partly because equilibria are established very slowly at low temperature. The best investigated compound of this class is probably V_3Ga, an important superconductor. Little is known about V_3Sb and we therefore chose to investigate this compound and part of the V_3Ga-V_3Sb system. V_3Ga is stable at both sides of the stoichiometric composition. We found that the stoichiometric range for $V_{3+y}Sb$ also extends to both positive and negative values of y, and we examined the possibility of producing a pure phase of stoichiometry V_6GaSb. General phase diagram considerations indicate that it should be possible to establish a V_3X phase of 25 atomic percentage X in the V_3Ga-V_3Sb pseudo binary system and also one in which $X=\frac{1}{2}Ga+\frac{1}{2}Sb$.

EXPERIMENTAL

The compounds were in general synthesized from pure elements by induction heating in a helium atmosphere. We made GaSb using a graphite crucible and the other compounds using crucible-free methods. Powder mixtures of nominally 99.5 % V and 99.9 % Sb were pressed into nearly cylindrical rods by isostatic pressing. A rod of composition 3V+1Sb was sintered in a helium atmosphere of 0.35 MPa at about 800 °C. Afterwards a molten zone of width 10–15 mm and of temperature 1425 °C was passed through the sample at a speed of about 10 mm/h. The helium pressure was 1.5 MPa in this run. The sample lost 3.7 % of weight as some Sb evaporated. Another specimen, of composition 3V+1.5 Sb was treated in a similar way. Also here some Sb evaporated. Powder mixtures of V and GaSb were pressed, sintered and zone melted as already described and attempts were made to react V and InSb, both in the induction oven and in a high temperature powder diffractometer.

The zone melted rods were cut perpendicular to the cylinder axis into sections using a spark cutting machine. We took samples from the sections by filing with a diamond file and examined the powders by X-ray diffraction using a Guinier camera and in some cases also a powder diffractometer. The cylindrical sections were next ground and polished and examined by metallographic techniques and finally analyzed by X-ray fluorescence analysis.

Measurements and computations were performed essentially in the same way as described by Vicente and Rasmussen.[1] Pure Sb was used as reference sample for antimony for the V_3Sb case and GaSb was used as reference for the V_6GaSb samples. Excitation voltages were chosen near the *K*-absorption edge for each element to avoid secondary enhancement effects. The α-coefficients (Ref. 1) were calculated assuming that the absorption edge was the effective wavelength for each element determined. As a control of the relevance of the absorption coefficients employed the composition of GaSb was determined using pure Ga and pure Sb, respectively, as reference samples. (Found: Ga 36.34; Sb 63.48. Calc.: Ga 36.41; Sb 63.59). Vanadium was not analyzed by fluorescence analysis. One sample was analyzed for vanadium by redox titration of V^{4+} with Fe^{2+}.

Semiconductor grade germanium was used for calibrating Guinier films, assuming a lattice constant $a = 5.6576$ Å. The wavelength of the Cu$K\alpha_1$ radiation used with the camera was taken to be 1.54051 Å.

We selected single crystals of V_6GaSb from crushed fragments and investigated them by X-ray diffraction. Graphite monochromatized radiation was employed with Weissenberg and precession cameras to establish space group and crystal quality. The apparently best suited crystal of those examined was mounted on a Picker fourcircle diffractometer. We collected 598 reflections using Mo$K\alpha$ radiation selected by a graphite monochromator. A scintillation detector was employed in conjunction with a pulse height analyzer.

The crystal was a rod of $0.017 \times 0.017 \times 0.197$ mm, μ(Mo$K\alpha$) is 227.5 cm^{-1}. An absorption correction was applied and gave transmission factors in the range 0.65 – 0.71. The data were averaged according to the symmetry *m*3*m* with an internal agreement of 0.04 giving 48 independent reflections of which only 30 were significant ($I > 3\sigma I$). The X-ray photographs and the diffractometric measurements confirmed the cubic symmetry and the systematic extinctions were

Table 1. Analytical and other results for V – Sb preparations. Samples labelled 271076 were prepared from mixtures of stoichiometry 3 V + 1 Sb before melting. Samples labelled 170976 were prepared from mixtures of stoichiometry 3 V + 1.5 Sb. Estimated standard deviations of a: 0.002 Å. Estimated standard deviation of chemical analysis: 0.1 %.

Sample No.	*w* % V	*w* % Sb	Density g cm^{-3}	Lattice const. Å	Formula	Ref.
271076 –						
2		39.73		4.938	$V_{3.63}Sb$	This paper
3			6.889	4.941	$V_{3.75}Sb$	– –
a	57.4	39.66		4.937	$V_{3.64}Sb$	– –
b	57.4	37.09		4.937	V_4Sb	– –
170976 –						
2				4.945		– –
3				4.940		– –
4		46.08	7.35	4.942	$V_{2.8}Sb$	– –
				4.932		2
				4.9335		3
				4.941		4

Table 2. Analytical and other results for V – Ga – Sb phases. Original stoichiometry before melting was 6V + Ga + Sb. Estimated standard deviation of a: 0.002 Å. Estimated standard deviation of chemical analysis: 0.1 %.

Sample No.	*w* % Ga	*w* % Sb	Density g cm^{-3}	Lattice const. Å	Formula
291076 –					
2	15.54	22.12		4.893	
3	16.31	22.43		4.892	$V_6Ga_{1.12}Sb_{.88}$
4	17.47	23.8	6.904	4.892	$V_6Ga_{1.22}Sb_{.95}$

Table 3. Lattice constants for V_3Ga, V_3Sb and V_6GaSb.

Compound	a	σa	Ref.
V_3Ga	4.818	.001	5
V_6GaSb	4.892	.002	This paper
V_3Sb	4.940	.002	– –

consistent with the space group *Pm3n* (No. 223) to which the A15 structure is assigned.

The majority of the V – Sb samples were badly suited for X-ray fluorescence analysis as most of the slices cut from the zone melted rods were porous but a few were completely homogenous. Table 1 shows analytical results and observed lattice constants for V – Sb compounds. It is evident that the diffraction technique applied is not sensitive enough to indicate analytical composition. The table also shows that the existence range for the A15 structure is at least in the range of 21.6 to 26.3 atomic percent Sb. Table 2 shows similar results for the V – GaSb products. It is again obvious that chemical composition cannot be established from observed lattice constants but that a chemical analysis is necessary.

Our attempts to react vanadium with In by sintering or by melting vanadium with InSb were unsuccessful. Sintered products yielded at room temperature powder diagrams which showed the presence of metallic In and a phase of A15 structure with a lattice constant equal to that of V_3Sb. Samples which had been subjected to zone melting were nearly depleted of their In content as shown by X-ray fluorescence analysis. According to their powder diagrams they were pure phases of V_3Sb structure. For comparison lattice constants of V_3Ga, V_3Sb and V_6GaSb are shown in Table 3.

RESULTS AND DISCUSSION

As a check we calculated a three dimensional Patterson function which was in full agreement with the proposed A15 structure. Thus, the main problem was to determine the degree of order of the atomic arrangement. For this discussion the following considerations are helpful:

In a compound of formula A_3B and space group *Pm3n* the atoms occupy the positions:

A: 0,1/2,1/4; *etc.* (6-fold)
B: 0,0,0; 1/2,1/2,1/2 (2-fold)

The structure factors may for convenience be arranged in the following categories:

I: $h+k+l=2n+1$, with contributions from A-atoms only, and
II: $h+k+l=2n$, with contributions from A- and B-atoms.

In category I the following types of reflections are extinguished:

$h=2n+1, k=2n+1, l=2n+1$
$h=4n, k=4n, l=2n+1$
$h=4n+2, k=4n+2, l=2n+1.$

The reflections with $h=4n+2$, $k=4n$, $l=2n+1$ are generally strong with $F(hkl)=4f_A$.

Category II reflections yield the following structure factors:

$F=2(f_B-f_A)$ for $h=k=2n+1$, $l=4n$
$F=2(f_B+f_A)$ for $h=k=2n+1$, $l=4n+2$
$F=2f_B\pm 6f_A$ for the rest of category II.

Reflections which should be systematically absent were especially carefully examined, both by photographic methods and by counter measurements; none were observable. A model assuming an ordered arrangement of Ga and Sb atoms on the B-sites could therefore be excluded. Since we could observe and measure reflections with $h=k=2n+1$, $l=4n$ we could also exclude a model assuming a completely disordered arrangement of all V, Ga and Sb atoms. Intermediate degrees of order were examined by least-squares refinement of various models. The scattering factors used were those published in Volume IV of International Tables for X-Ray Crystallography. Although we could discard the assumption of an ordered arrangement of Ga and Sb atoms, we did try a refinement of such a model allowing a site occupation parameter to vary. The refinement yielded a parameter value corresponding to equal occupancy of the 0,0,0 and $\frac{1}{2},\frac{1}{2},\frac{1}{2}$ positions.

The possibility of Ga and Sb atoms occupying part of the A-sites instead of vanadium was tested refining the site occupation parameter of the vanadium position. The highest value of this parameter was 1.01 for a model assuming equal amounts of Ga and Sb on the B-sites with full occupancy. Models assuming deficit of Sb gave occupation parameters slightly less than 1. We are not certain about the composition of the particular crystal fragment employed in this analysis but it is most likely to be of a composition near $V_6Ga_{1.12}Sb_{0.88}$; *cf.* Table 2. Thus we consider the A-sites to be fully ordered and

Table 4. Results of two refinements: (a) where the occupation factor for V was kept at 1.0 and (b) where the ratio Ga:Sb was kept at the value 0.56:0.44 found by fluorescence analysis, both with full occupation of the B-sites.

	a	b
Occ (V)	1.0	0.978(5)
U_{11} (V)	0.0086(4)	0.0086(4)
U_{33} (V)	0.0067(4)	0.0067(4)
Occ (Ga)	0.510(10)	0.56
Occ (Sb)	0.490	0.44
U (Ga,Sb)	0.0066(3)	0.0065(3)
Scale factor	0.1802(16)	0.1843(13)
Extinction param.	0.00127(16)	0.00131(16)
Minimum transmiss.	0.82	0.82
$R(F)$	0.0084	0.0084
$R(F^2)$	0.0162	0.0162

occupied by V-atoms within experimental uncertainty. According to site symmetry the vanadium atom may have two different thermal parameters, U_{11} and U_{33}. The GaSb atoms must vibrate isotropically. The introduction of the parameter allowing for anisotropic motion of the vanadium atom lowered the *R*-value from 1.0 % to 0.8 % for two models which differ slightly in stoichiometry but otherwise are similar. Table 4 shows the results from the refinements which yielded the lowest *R*-values. Although the *R*-value is fairly satisfactory the data do not allow an accurate determination of stoichiometry. It appears, however, that it is likely that Sb is present in less than the stoichiometric amount. The uncertainty about stoichiometry is of little consequence for the thermal parameters. The two models a and b of Table 4 yield practically the same u-values. The lighter V atom has the larger movement, but not as much as could be expected from the difference in mass. This is due to the close contacts in the V chain, which also lead to the movement along the chain being less than perpendicular to it, as was also found in V_3Si.[6]

Acknowledgements. We are indebted to Britta Lundtoft for excellent technical assistance. The Danish Science Foundation is thanked for providing the high temperature powder diffractometer. We are also indebted to Carlsbergfondet for providing a spark erosion machine.

REFERENCES

1. Vicente, V. A. and Rasmussen, S. E. *X-Ray Spectrom. 7* (1978) 5.
2. Wood, E. A., Compton, V. B., Matthias, B. T. and Corenzwit, E. *Acta Crystallogr. 11* (1958) 604.
3. Nevitt, M. V. *Trans. AIME 212* (1958) 350.
4. Matthias, B. T., Geballe, T. H. and Compton, V. B. *Rev. Mod. Phys. 35* (1963) 1.
5. Das, B. N. and Ayers, J. D. *J. Cryst. Growth 43* (1978) 397.
6. Staudenmann, J. L., Coppens, P. and Muller, J. *Solid State Commun. 19* (1976) 29.

Received May 29, 1978.

Acta Chemica Scandinavica A 32 (1978) 789–797

Reactions of Nitriles Bound to Cobalt(III) Ammines

DOUGLAS G. BUTLER,* INGE I. CREASER, STANLEY F. DYKE** and ALAN M. SARGESON

Research School of Chemistry, Australian National University, Canberra, A.C.T., 2600, Australia

Dedicated to Jannik Bjerrum on the occasion of his 70th birthday

Rapid intramolecular oxidation of the carbanions $[Co(NH_3)_5N\bar{C}HR]^{2+}$ ($R=C_6H_5$, $CH=CH_2$) generated by rapid H^+ loss from $[Co(NH_3)_5NCH_2R]^{3+}$ yields the nitrile radicals which immediately dimerize. Reduction of coordinated nitriles with BH_4^- and Michael additions of carbanions and PO_4^{3-} to coordinated acrylonitrile occur more thn 10^4-fold faster than the same reactions for the uncoordinated nitriles. Attack of CN^- at the nitrile C atom of $(NH_3)_5CoN\equiv CCH_3^{3+}$ followed by intramolecular condensations yields a tridentate bis(amidine) amino methyl malonate chelate.

When nitriles are coordinated to a metal ion a considerable increase in their reactivity has been observed for several types of reactions.[1-13] The rate of attack of HO^- at the nitrile carbon atom is enhanced by a factor of 10^6-10^8 when the nitrile is attached to the $M(NH_3)_5^{3+}$ moiety (M=Co, Rh, Ru) resulting in the corresponding N-bound amide complex. Furthermore the $Co(NH_3)_5^{3+}$ fragment enhances the activity of the α methylene group by *ca.* 10^6. Using nitriles with sufficiently labile methylene groups such as $NCCH_2CN$, $NCCH_2CO_2C_2H_5$ and $NCCH_2CO_2H$ it was possible to generate the $Co(NH_3)_5N\bar{C}CHR^{2+}$ carbanions in aqueous solution by adding base.[10] The carbanions subsequently decayed by losing an electron to the cobalt(III) centre. They were also found to undergo nucleophilic reactions with added substrates such as methyl iodide, formaldehyde, tolyl chloride and pyruvic acid. The product of the reaction of $[Co(NH_3)_5NCCH_2CO_2C_2H_5]^{3+}$ with excess CH_3I in the presence of base in $(CH_3)_2SO$ was characterized as the disubstituted $[Co(NH_3)_5NCC(CH_3)_2CO_2C_2H_5]^{3+}$ complex. The reduction of the metal ion to cobalt(II) takes place by electron transfer from the carbanion to the metal resulting in a nitrile radical which triggered the polymerisation of acrylonitrile added to the reaction mixture. The results were sufficiently interesting to prompt further exploration into the reactivity of coordinated nitriles, the production and reactions of nitrile radicals, other possible reactions induced by activation from the metal ion and the distance over which such an activation might extend. This paper reports the rapid production and reactions of the coordinated organic radicals PhĊHCN and $NC\dot{C}HCH=CH_2$, the reduction of coordinated nitriles by BH_4^- in aqueous solution, the cyanoethylation reactions of $[Co(NH_3)_5NCCH=CH_2]^{3+}$ with acetyl acetone, nitromethane, malononitrile and phosphate ion and nucleophilic addition of cyanide ion to the coordinated nitrile carbon atom.

EXPERIMENTAL

All chemicals were analytical grade. ^1H NMR spectra were recorded on a JEOL 100 MHz Minimar spectrometer. Cary 14 and 118C spectrophotometers were used for the kinetics and IR spectra were recorded using a Perkin-Elmer PE 225 spectrometer using KBr discs. The mass spectra were recorded on an AEI MS 902 spectrometer.

The nitrile complexes $[Co(NH_3)_5N\equiv CR](ClO_4)_3$ were generally prepared either by dissolving $[Co(NH_3)_5TMP](ClO_4)_3$, (TMP=trimethylphos-

* On leave from the Chemistry Department, York University, Toronto, Canada.

** On leave from the Chemistry Department, University of Bath, Claverton Down, Bath, BA2 7AY, England.

phate), in the appropriate nitrile[14] and leaving the mixture at 40 °C for ~24 h or by treating $[Co(NH_3)_5N_3](ClO_4)_2$ with $NO(CF_3SO_3)$ using the appropriate nitrile as the solvent and leaving the resulting mixture at 40 °C for ~24 h or until it turned yellow. Where the complexes were not soluble in the nitriles a small amount of TMP was added to effect dissolution. The nitrile complexes were isolated from the reaction mixtures upon precipitation with ether. They were recrystallized by dissolving in water (40–50 °C, pH ~4) followed by the addition of $NaClO_4$ or $HClO_4$. Care was taken to keep the reaction mixtures containing the $NCCH_2C_6H_5$ and $NCCH_2CH=CH_2$ complexes acidic by the addition of a few drops of concentrated H_2SO_4 and the complexes were recrystallized from 0.1 M $HClO_4$. For $[Co(NH_3)_5NCCH_2NHCOCH_3](ClO_4)_3$ where the free nitrile is a solid the complex was prepared by mixing $[Co(NH_3)_5TMP](ClO_4)_3$(1 g) with the nitrile (2 g) and heating on a steam bath until the melt turned orange. The mixture was cooled and extracted several times with $CHCl_3$ to remove excess nitrile. The product was dissolved in water and sorbed on a cation exchange column (SP-Sephadex C-25) and eluted with 0.3 M $NaClO_4$ at pH ~4. The eluent containing the main yellow band was collected and taken down to a small volume on a vacuum evaporator. The yellow crystalline product was filtered off, washed with ethanol and ether and recrystallized as above. Anal. $[Co(NH_3)_5NCCH_2NHCOCH_3](ClO_4)_3.H_2O$ ($CoN_7H_{23}C_4Cl_3O_{14}$): C, H, N. IR: 2330 (w) cm^{-1}. Anal. $[Co(NH_3)_5NCCH_2C_6H_5](ClO_4)_3$($CoN_6C_8H_{22}Cl_3O_{12}$): C, H, N. Anal. $[Co(NH_3)_5NCCH_2CH=CH_2](ClO_4)_3$ ($CoN_6C_4H_{20}Cl_3O_{12}$): C, H, N. Anal. $[Co(NH_3)_5$(5-norbornene-2-carbonitrile)$](ClO_4)_3$($CoN_6C_8H_{24}Cl_3O_{12}$): C, H, N. Anal. $[Co(NH_3)_5NCCH=CH_2](ClO_4)_3$-($CoN_6C_3H_{18}Cl_3O_{12}$): C, H, N, Co. Anal. $[Co(NH_3)_5NC(CH_2)_4CN](ClO_4)_3$($CoN_7C_6H_{23}$-$Cl_3O_{12}$): C, H, N, Co. IR: 2260 (w), 2325 (w) cm^{-1}. Anal. $[Co(NH_3)_5NCCH_3](ClO_4)_3$($CoN_6C_2H_{18}$-$Cl_3O_{12}$): C, H, N.

Nitrile dimerization reactions of $[Co(NH_3)_5NCCH_2C_6H_5](ClO_4)_3$ *and* $[Co(NH_3)_5NCCH_2CH=CH_2](ClO_4)_3$. The complex was dissolved in a pH 6 phosphate or citrate buffer and allowed to react over 15 min. In the case of $[Co(NH_3)_5NCCH_2C_6H_5]^{3+}$ a white precipitate was deposited which was collected, washed with water and dried. Yield >90 %, m.p. 140–160 °C. Anal. $(C_8H_6N)_n$: C, H, N. MS [*m/e* (% rel.int)]: 232 (15, M), 116 (100) 89 (20). ^1H NMR [$(CD_3)_2CO$]: δ 1.95 (2 H, s, CH), 2.88 (2 H, s, CH), 3.60 (~0.1 H, s, CH), 3.80 (~0.1 H, s), 5.46 (10 H, s, 2ArH) 5.56 (10 H, s, 2ArH) relative to $\delta_{(CD_3)_2CO}$. After recrystallization from boiling acetic acid ^1H NMR ($(CD_3)_2CO$): δ 2.88 (2 H, s, 2CH) and 5.46 (10 H, s, 2ArH). For $C_6H_5CH_2CN$ ^1H NMR: δ 1.88 (2 H, s, CH_2), 5.30 (5 H, s, ArH) relative to $\delta_{(CD_3)_2CO}$. M.p. of recrystallized product 224–226 °C.

The reaction mixture from the $[Co(NH_3)_5$-$NCCH_2CH=CH_2]^{3+}$ complex was extracted with dichloromethane and the solution dried over calcium sulfate. The solvent was removed on the vacuum evaporator leaving an oil. Anal. $(C_4H_4N)_n$. ^1H NMR (CCl_4): δ 2.6 (2 H, m), 3.6 (1H, m), 5.8 (4 H, m), 6.8 (1 H, m). For $CH_2=CHCH_2CN$ ^1H NMR (CCl_4): δ 3.05 (2 H, d, CH_2), 5.4 (3 H, m, $CH_2=CH$). MS [*m/e* (% rel.int)]: 132 (9, M), 131 (14), 105 (10), 92 (4), 79 (11), 66 (100), 52 (10), 39 (33). Samples of the complexes in pH 6 phosphate buffers were added to (1) a solution of 2,2-diphenyl-1-picrylhydrazyl in acetonitrile, (2) a solution of ~0.05 M Br_2 in a pH 6 phosphate buffer, (3) I_2 in a 1:1 CH_3CN–pH 6 phosphate buffer.

Reduction of $[Co(NH_3)_5NCR](ClO_4)_3$ *with* $NaBH_4$. In a typical experiment $[Co(NH_3)_5NCR](ClO_4)_3$ (2×10^{-3} mol) was dissolved in a "Tris"/HCl buffer ["Tris" = tris(hydroxymethyl)aminomethane] at pH ~9 (30 ml) and mixed with a solution of $NaBH_4$ (Merck, 0.3 g) in the buffer (10 ml). After 6–8 min the reaction mixture was rapidly sorbed on an SP-Sephadex C-25 cation exchange column which had been washed with the buffer. When all the complex was sorbed the column was again washed carefully with the buffer to remove excess borohydride and the complex eluted with 0.5 M $NaClO_4$ at pH ~9. Some +2 amide complex was collected first followed by the main yellow product which analyzed for the corresponding amino-pentammine complex. Yields ~50 %. For $[Co(NH_3)_5NC(CH_2)_2CH(COCH_3)_2](ClO_4)_3$. also the carbonyl groups were reduced so that the isolated product analyzed for $[Co(NH_3)_5NH_2(CH_2)_3CH(CHOHCH_3)_2](ClO_4)_3$. Anal. $CoN_6C_8H_{34}Cl_3O_{14}$: C, N, H, Co. The other reduced nitrile complexes were: $[Co(NH_3)_5NCCH_3](ClO_4)_3$ with the product $[Co(NH_3)_5NH_2CH_2CH_3](ClO_4)_3$. Anal. CoN_6C_2-$H_{22}Cl_3O_{12}$: C, N, H. ^1H NMR (D_2O): δ 1.16 (3 H, t, CH_3), 2.36 (2 H, broad s, CH_2) 3.40 (15 H, broad s, NH_3). $[Co(NH_3)_5NCCH_2CO_2C_2H_5](ClO_4)_3$ with the product $[Co(NH_3)_5NH_2(CH_2)_2CO_2C_2H_5](ClO_4)_3$. Anal. $CoN_9H_{26}C_5O_{11}$: C, N, H. ^1H NMR (D_2O): δ 1.2 (3 H, t, CH_3), 2.80 [4 H, broad s, $(CH_2)_2$], 3.60 (15 H, broad s, NH_3), 4.20 (2 H, q, CH_2). $[Co(NH_3)_5NC(CH_2)_4CN](ClO_4)_3$ with the product $[Co(NH_3)_5NH_2(CH_2)_4CN](ClO_4)_3$. Anal. C, H, N. IR: 2260 (w) cm^{-1}.

Reaction of $[Co(NH_3)_5NCCH=CH_2](ClO_4)_3$ *with acetylacetone.* $[Co(NH_3)_5NCCH=CH_2](ClO_4)_3$ (5 g) was dissolved in water (300 ml) and rapidly mixed with a solution of acetylacetone (10 g) and sodium hydroxide (2 g) in water (100 ml). After 5 s excess concentrated perchloric acid was added to acidify the solution and quench the reaction. The

solution was reduced in volume on the vacuum evaporator. The yellow compound which crystallized out was collected and recrystallized from warm water (pH ~4) and addition of concentrated perchloric acid or solid sodium perchlorate. Yield 45 % of a product which analyzed for $[Co(NH_3)_5NC(CH_2)_2CH(COCH_3)_2](ClO_4)_3$. Anal $CoN_6H_{26}C_8Cl_3O_{14}$: C, N, H, Co. IR: 2320 (w), 1740 (s) cm^{-1}. When the reaction mixture was left for 15 min before being acidified the product analyzed for $[Co(NH_3)_5NH_2CO(CH_2)_2CH(COCH_3)_2](ClO_4)_3.H_2O$. Yield 30 %. Anal. $CoN_6C_8H_{30}Cl_3O_{16}$: C, N, H. IR: no absorption in the C≡N stretching region.

Reaction of $[Co(NH_3)_5NCCH=CH_2]Cl_3$ *with nitromethane.* $[Co(NH_3)_5NCCH=CH_2]Cl_3$ (2.2 g) was dissolved in water (25 ml) and added to a solution of nitromethane (7.2 g) in a "Tris"/HCl buffer at pH ~9 (100 ml). After 20 s the reaction was quenched by adding concentrated perchloric acid. The solution was diluted and sorbed on an SP-Sephadex C-25 cation exchange column and eluted with 0.3 M $NaClO_4$. The eluent containing the major component was taken down in volume on a vacuum evaporator and a yellow product crystallized out which analyzed for $[Co(NH_3)_5NC(CH_2)_3NO_2](ClO_4)_3$. Yield 45 %. Anal. $CoN_7C_4H_{21}Cl_3O_{14}$: C, N, H, Co. IR: 2330 (w) cm^{-1}. ^1H NMR (D_2O): δ 2.50 (2 H, p, CH_2), 3.20 (2 H, t, CH_2CN), 3.90 (15 H, broad, NH_3), 4.70 (2 H, t, CH_2NO_2). When the reaction mixture was left for 15 min before being quenched the product analyzed for $[Co(NH_3)_5NH_2CO(CH_2)_3NO_2](ClO_4)_3$. Anal. $CoN_7H_{23}C_4Cl_3O_{15}$: C, N, H.

Reaction of $[Co(NH_3)_5NCCH=CH_2]Cl_3$ *with malonitrile.* The complex (0.5 g) was dissolved in a "Tris"/HCl buffer at pH 9 saturated with malonitrile. After 10 s the reaction was quenched by the addition of concentrated perchloric acid and the reaction mixture sorbed on an SP-Sephadex C-25 cation exchange column. This was then eluted with 0.5 M $NaClO_4$ and a yellow product was isolated which analyzed for $[\{Co(NH_3)_5NC(CH_2)_2\}_2C(CN)_2](ClO_4)_6.H_2O$. Anal. $Co_2N_{14}C_9H_{40}Cl_6O_{25}$: C, N, H, Co. ^1H NMR (D_2O): δ 2.8 (2 H, t, CH_2C), 3.6 (2 H, t, CH_2CN).

Reaction of $[Co(NH_3)_5NCCH=CH_2]Cl_3$ *with* PO_4^{3-}. $[Co(NH_3)_5NCCH=CH_2]Cl_3$ (1 g) dissolved in water (10 ml) was rapidly mixed with a solution of $K_3PO_4.H_2O$ (0.2 mol) and $K_2HPO_4.3H_2O$ (0.2 mol) in water (65 ml). After 30 s the reaction was quenched with concentrated perchloric acid (55 ml), filtered and diluted to 4 l. The reaction mixture was sorbed on an SP-Sephadex C-25 cation exchange column. The column was then washed with water and eluted with a pH 8 "Tris"/HCl buffer (0.05 M). A small orange band (1) separated out following the front of the eluent. This eluate was acidified with concentrated perchloric acid and reduced to a small volume on a vacuum evaporator and a yellow compound crystallized out (6 %). The column was then eluted with 0.3 M $NaClO_4$ at pH 8. Three bands (2), (3) and (4) separated and all three compounds crystallized as the perchlorates upon acidification and evaporation to a small volume using a vacuum evaporator. Yield of band (2) 39 %. Band (1) analyzed for $[Co(NH_3)_5NH_2CO(CH_2)_2OPO_3H_2](ClO_4)_3.H_2O$. Anal. $CoN_6C_3H_{25}PCl_3O_{18}$: C, N, H, Co. ^1H NMR (D_2O): δ 2.8 (2 H, t, CH_2CO), 4.1 (2 H, q, CH_2OP), 3.4 (15 H, broad, NH_3). Band (2) analyzed for $[Co(NH_3)_5NC(CH_2)_2OPO_3]ClO_4.1\frac{1}{2}HClO_4$. Anal. $CoN_6C_3H_{20.5}Cl_{2.5}PO_{14}$: C, N, H, Co, Cl, P. ^1H NMR (D_2O): δ 3.40 (2 H, t, CH_2CN), 4.30 (2 H, q, CH_2OP), 4.15 (3 H, broad, *cis* NH_3), 3.75 (12 H, broad, *trans* NH_3). ^1H NMR (D_2O) of bands (3) and (4) showed olefin signals and they were assumed to be unreacted acrylonitrile complex and acrylamide complex.

Reaction of $[Co(NH_3)_5NCCH_3](ClO_4)_3$ *with NaCN.* $[Co(NH_3)_5NCCH_3](ClO_4)_3$ (9 g) was dissolved in a mixture of NaCN (34 g), Na_2EDTA (7.5 g) and concentrated $HClO_4$ (30.5 ml) in water (700 ml), pH ~10.5. After 20 min the solution was poured into 2.3 l H_2O containing 50 ml HAc and quickly sorbed on an SP-Sephadex C-25 cation exchange column. The column was eluted with 0.3 M $NaClO_4$ until one orange band remained. This was taken off with 0.5 M $NaClO_4$ and the complex crystallized by evaporation using a vacuum evaporator. Yield 40 %. Anal. $CoN_8C_{14}H_{21}Cl_3O_{12.5}$: C, N, H, Co, Cl. ^1H NMR [$(CD_3)_2SO$]: δ 1.5 (3H, s, CH_3), 3.0 (6 H, s, *cis* NH_3), 3.2 (3 H, s, *trans* NH_3) 5.6 (2 H, s, $CoNH_2$), 6.4 (2 H, s, NH=), 7.8 (2 H, broad s, $NH_2-C=$), 8.2 (2 H, broad s, $NH_2-C=$).

α-Alanine was produced by decomposing the product with H_2S. The complex was dissolved in H_2O and treated with a stream of H_2S. After filtration the solution was reduced to dryness and then dissolved in slightly acidic water (pH ~3) and sorbed on a cation exchange column (Dowex 50 W−X2, 200−400 mesh, NH_4^+ form). The column was washed with water (pH ~3) and then eluted with 1 M NH_3. The eluate was reduced to dryness to give a white product. ^1H NMR (D_2O): δ 1.5 (s).

The product was refluxed with 1 M HCl for 1 ½ h and the resulting material isolated. ^1H NMR (D_2O): δ 1.6 (3 H, d, CH_3), 4.1 (1 H, q, CH). An authentic sample of α-alanine.HCl gave an identical ^1H NMR spectrum. α-Alanine was isolated by adjusting an aqueous solution to pH 6 with aniline and adding ethanol. M.p. = 280−290 °C. M.p. for α-alanine is 295 °C. Anal. Found: C 39.02; H 8.49; N 14.83. Calc. for $C_3H_7NO_2$: C 40.44; H 7.91; N 15.72.

RESULTS AND DISCUSSION

Syntheses. A simple and direct method to prepare cobalt(III) pentaammine nitrile complexes is to treat $[Co(NH_3)_5N_3](ClO_4)_3$ with an excess of $NOCF_3SO_3$ in a solution or suspension of the complex in the nitrile containing some trimethyl phosphate to assist dissolution. The initially formed complex may be wholly or partly $[Co(NH_3)_5TMP]^{3+}$ (TMP = trimethyl phosphate) which on standing exchanges TMP for the nitrile. In the instances when this method was used the NO^+ did not attack double bonds nor aromatic rings. The nitrile complex was then isolated from the reaction mixture by the addition of ether and recrystallization of the precipitated product from water. Care had to be taken with solutions of the $C_6H_5CH_2CN$ and $CH_2=CHCH_2CN$ complexes to keep them acidic at all times to minimize decomposition.

The coordinated nitrile groups were easily characterized by their IR spectra. They all showed C≡N stretching absorptions at ~2330 cm^{-1} while the absorptions of the uncoordinated nitriles appeared at ~2260 cm^{-1}. The adipo nitrile complex spectrum displayed both as expected for a compound with one coordinated and one uncoordinated nitrile group. The same result was previously observed for $[Co(NH_3)_5NCCH_2CN]^{3+}$.[10]

Nitrile radical formation. When the complexes $[Co(NH_3)_5NCCH_2C_6H_5](ClO_4)_3$ or $[Co(NH_3)_5NCCH_2CH=CH_2](ClO_4)_3$ were dissolved in neutral or basic aqueous solution, immediate decomposition of the complexes was observed with the production of cobalt(II), NH_3 and organic products. For $[Co(NH_3)_5NCCH_2C_6H_5]^{3+}$ a white precipitate was deposited which analysed for $(C_8H_6N)_n$. Its mass spectrum indicated it to be a molecule with a molecular weight of 232 ($C_{16}H_{12}N_2$) which readily splits into two halves. The ^1H NMR spectrum exhibited four principal resonances and two minor ones. After recrystallization from boiling acetic acid only two of the resonances remained. They integrated as 1:5. Both spectra were different from that of the starting material $C_6H_5CH_2CN$. When solutions of the free radical 2,2-diphenyl-1-hydrazyl, bromine, or iodine were added to the decomposing mixture their colours faded. During the same period of time no disappearance of colour was observed under identical conditions when the complexes were not present.

The data are consistent with an almost quantitative formation of the dimer 2,3-diphenylsuccinonitrile, $C_6H_5CH(CN)CH(CN)C_6H_5$, (M.W. 232.26) in an approximately equal mixture of the *meso* and racemic forms with minor amounts of two other isomers. On recrystallization from hot acetic acid the racemic form of $C_6H_5CH(CN)CH(CN)C_6H_5$ is transformed into the *meso* form.[15] This means that the two resonances in the ^1H NMR spectrum of the recrystallized product are due to 2 CH protons (δ 2.88) and 10 aromatic protons (δ 5.46) arising from meso $C_6H_5CH(CN)CH(CN)C_6H_5$ and that the resonances at δ 1.95 and 5.56 in the original spectrum arise from the racemic isomer. The melting point of 224–226 °C was lower than that recorded for the pure *meso* form, 238–240 °C,[15] presumably because of traces of the racemic form (M.p. 160 °C).[16] 2,3-Diphenylsuccinonitrile has been synthesized by several methods[15] including condensation and photochemical methods giving good yields (70–90 %) but requiring relatively long reaction times and producing predominently the *meso* form. The method presented here yields the product in seconds by dissolving coordinated benzyl nitrile in water and produces 50 % of the recemic form which can be obtained pure by fractional crystallization.[16]

The $[Co(NH_3)_5NCCH_2CH=CH_2]^{3+}$ complex reacted under similar conditions giving cobalt(II), NH_3 and an oil which analysed for $(C_4H_4N)_n$. The ^1H NMR spectrum revealed four multiplets which integrated roughly as 2:1:4:1. No resonances corresponding to the CH_2 protons in the original nitrile $CH_2=CHCH_2CN$ were observed. The mass spectrum indicated a molecular weight of 132 ($C_8H_8N_2$) and again showed compounds which readily split into two halves. Gas chromatography of the product indicated it to be a rather complex mixture. The results are consistent with an isomeric mixture of dimeric nitriles with the formula $(CH_2=CHCH(CN))_2$.

The rapid formation of dimeric nitriles in these decomposition reactions can be explained by the fast deprotonation of the methylene group of the coordinated nitrile, followed by a rapid oxidation of the coordinated carbanion by cobalt(III) to the radical which then dissociates from the labile cobalt(II) $(NH_3)_5^{2+}$ ion and dimerizes (Scheme 1)

$$Co(NH_3)_5NCCH_2R^{3+} \xrightarrow{HO^-}$$
$$Co(NH_3)_5NCC^-HR^{2+} \longrightarrow$$
$$Co^{II}(NH_3)_5NC\dot{C}HR^{2+} \longrightarrow$$
$$\text{“}Co^{II}(NH_3)_5{}^{2+}\text{”} + NC\dot{C}HR \longrightarrow (NCCHR)_2$$

Scheme 1.

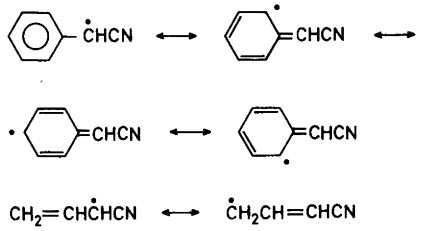

Scheme 2.

or reacts with other radicals or radical trapping agents. However, reactions between radical and coordinated radical cannot be excluded. The presence of radicals is supported by the observation of the reactions with 2,2-diphenyl-1-hydrazyl and bromine or iodine which are known radical trapping agents.

In both the instances above we are dealing with nitrile radicals which are resonance-stabilized (Scheme 2). This could give rise to several isomers when the radicals react with each other. However, for the benzyl nitrile complex, by far the major product is $C_6H_5CH(CN)CH(CN)C_6H_5$ (DL + *meso*) with only small amounts of two other isomers. The resonance forms of the allyl nitrile radical suggest the possible dimerization isomers: $[CH_2=CHCH(CN)]_2$ (DL + *meso*), $(NCCH=CHCH_2)_2$ and $CH_2=CHCH(CN)CH_2CH=CHCN$. Interpretation of the ^{1}H NMR resonances as being due to A: δ 2.6, $-CH_2-$; B: δ 3.6, CHCN; C: δ 5.8, $CH_2=$ and $-CH=$; and D: δ 6.8, $=CHCN$ along with the integration A:B:C:D = 2:1:4:1 indicates either the formation of the unsymmetrical isomer or a 1:1 mixture of the two symmetrical isomers, and possibly some of the unsymmetrical one. The last suggestion seems the most likely as in a fast dimerization of two very reactive radicals the exclusive formation of the unsymmetrical dimer would not be expected.

The $[Co(NH_3)_5NCCH_2NHCOCH_3]^{3+}$ complex partly decomposed in neutral or basic solution. If resonance is a requirement for the formation of the nitrile radicals it may in this case arise from the presence of the enol form: $NCCH_2NHCOCH_3 \longleftrightarrow NCCH_2NC(OH)CH_3$ giving the radicals $NC\dot{C}HN=(OH)CH_3 \longleftrightarrow NCCH=N\dot{C}(OH)CH_3$. However, competition for hydrolysis to the coordinated amide was here the stronger factor. When the benzylcyanide and allylcyanide complexes were treated with strongly basic solution some hydrolysis was also observed. By allowing the decomposition to take place at a low pH this side reaction was depressed. Other nitrile complexes such as $[Co(NH_3)_5NCCH_2CO_2C_2H_5]^{3+}$, $[Co(NH_3)_5NCCH_2CO_2H]^{3+}$ and $[Co(NH_3)_5NCCH_2CN]^{3+}$ have earlier been shown to initiate acrylonitrile polymerisation by radical formation.[10] The radicals formed from these complexes are also resonance stabilized.

The $[Co(NH_3)_5NCCH_2NHCOCH_3](ClO_4)_3$ complex was prepared in the hope that it might prove useful in the synthesis of α-substituted amino acids. By treating the complex in DMSO with alkyl halides in the presence of an equivalent amount of base it was hoped to be able to alkylate the methylene group as was the case for $[Co(NH_3)_5NCCH_2CO_2Et]^{3+}$.[10] Base hydrolysis of the coordinated nitrile and removal of the ligand from the complex would then lead to $NH_2COCR^1R^2NHCOCH_3$ ($R^1=R^2$ or H) which on hydrolysis would give $HO_2CCR^1R^2NH_2$. However, because of the radical formation following the addition of base the complex decomposed before reacting with the alkyl halide.

The prospects for stabilizing radicals and bond migration in a homo-conjugated system were examined by preparing the complex $[Co(NH_3)_5$(2-*endo*-cyano-5-norbornene)$](ClO_4)_3$. Homoallylic participation potentially allows products derived from the involvement of the two radicals shown in Scheme 3, however no decomposition was observed when this complex was dissolved in neutral or basic solution thereby discarding homo-conjugation as a likely stabilizing factor for the formation of nitrile radicals at least in this system.

The radical-producing nitrile complexes were all stable in dilute aqueous acid solutions, but decomposed rapidly in unbuffered neutral solutions and in basic media. By choosing an appropriate pH of the aqueous solution it is possible to control the rate of deprotonation and thereby the production of the radicals. Decomposition of $[Co(NH_3)_5NCCH_2C_6H_5]^{3+}$ and $[Co(NH_3)_5NCCH_2CH=CH_2]^{3+}$ was still observed at pH 4 but was much slower at pH 3. The complexes as the perchlorate

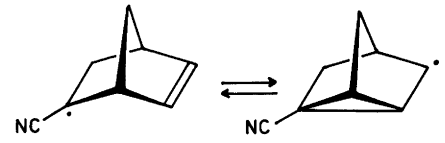

Scheme 3.

salts, are slightly soluble in some organic solvents such as $HCONMe_2$, Me_2SO, Me_2CO and MeCN but decompose rapidly unless acid is added. The same dinitrile dimers were obtained with $[Co(NH_3)_5NCCH_2C_6H_5]^{3+}$ in acetonitrile as in aqueous solution.

These reactions show a particularly facile way of producing a carbanion and then a radical adjacent to a strong electron-withdrawing group under mild conditions. The process is easily controlled by the pH of the aqueous solution and the subsequent one-electron transfer is fast. In some instances useful organic synthesis via carbanion and radical generation could be conducted by this mixture of intra- and intermolecular processes.

Reduction of coordinated nitriles by $NaBH_4$. Normally nitriles require potent reducing agents such as $LiAlH_4$ in a non-aqueous medium to generate the amine. However, if a strong electron-withdrawing group such as a metal ion is applied to the nitrile moiety the carbon centre becomes more susceptible to attack by H^- or BH_4^- and the prospect for a more facile reduction arises. The problem of a reduction of the metal ion also exists and the selectivity between the two processes is a key component in such a strategy.

$[Co(NH_3)_5NCCH_3]^{3+}$ was treated with excess $NaBH_4$ in a pH ~9 buffer for 7–8 min. After separation of the complexes on a cation exchange column the main product was found to be $[Co(NH_3)_5NH_2CH_2CH_3]^{3+}$ together with some $[Co(NH_3)_5NHCOCH_3]^{2+}$ and cobalt(II). When other coordinated nitriles such as $[Co(NH_3)_5NCCH_2CO_2C_2H_5]^{3+}$, $[Co(NH_3)_5NC(CH_2)_4CN]^{3+}$ and $[Co(NH_3)_5NC(CH_2)_2CH(COCH_3)_2]^{3+}$ were treated similarly the corresponding amine complexes were also recovered from the reaction mixtures. Attempts to follow the rates of reduction were frustrated by the side reactions, mainly of the reducing ion BH_4^-. The formation of traces of cobalt(II) species prevented the reaction from being followed by ^1H NMR and the evolution of H_2 from the reaction between BH_4^- and water made it difficult to follow the rates by spectrophotometric methods. However, an estimated half life of ~1 min for the reduction of $[Co(NH_3)_5NCCH_3]^{3+}$ was obtained by sampling the reaction mixture over intervals and separating the components by ion exchange chromatography. The rate of reaction showed some dependence on the BH_4^- concentration but the quantification was difficult to assess accurately. The yield of amine complex seemed markedly dependent on the purity of $NaBH_4$. When uncoordinated acetonitrile was treated with $NaBH_4$ under identical circumstances no sign of reduction was apparent over 10 days. By this time a substantial amount of the BH_4^- ion had decomposed but the ^1H NMR spectra still indicated the presence of H–B signals and thus reducing capacity. It appears therefore that reduction of the coordinated nitrile is enhanced by $>10^4$ over the rate of the uncoordinated one. For the adipic nitrile and the cyanoacetic ethylester complexes only the nitrile groups attached to cobalt(III) were reduced while the other functional groups were unaffected so that some specificity was built into the reaction. Further, no reduction was observed when the N-bound acetamide complex $[Co(NH_3)_5NHCOCH_3]^{2+}$ was treated with $NaBH_4$ for 20 min at room temperature.

The process demonstrates a rapid reduction of a nitrile under very mild conditions in an aqueous medium. In the present cases the complexes are kinetically inert but the implication is that the reduction of a nitrile which is predominantly α-bound to a metal ion should be accelerated for labile complexes as well, provided the complexes are stable around pH 9–10. Metal oxidation states such as Co(II), Cu(II), Ni(II), Pt(II) and Os(II) have been used to accelerate reduction of nitrile by BH_4^- in hydroxylic as well as non-hydroxylic solvents.[17] However, in contrast to the chemistry above these reagents were also capable of reducing amides and nitro compounds to primary amines and the reduction could arise via a metal hydride complex rather than directly from the BH_4^- reagent. The effective metals are those which readily form metal hydrides. In the present case the Co–N–C entity remains intact during the reduction, indicating that the reducing agent is BH_4^- and not a cobalt hydride.

The yields of reduced nitrile complexes were usually ~50 %. The question arises whether the remaining organic residues appeared as free amines or unreacted free nitriles in the reaction mixture. This problem needs further exploration.

The same reactions conducted in more acidic media lead to a preferential reduction of the metal centre presumably *via* the B_2H_6 reagent. The low specificity of BH_4^- ion for the metal centre compared with coordinated unsaturated organic functions is an especially interesting specificity giving rise to real synthetic potential. We presume that whereas B_2H_6 adds rapidly to the filled *d* electron orbitals of the metal ion, the BH_4^- anion has more

difficulty doing so and prefers a nucleophilic role at the unsaturated organic moiety rather than the electron – rich metal centre.

Cyanoethylation reactions. A variety of compounds possessing labile hydrogen atoms add to acrylonitrile in the presence of an alkaline catalyst with the formation of molecules containing the $-CH_2CH_2CN$ moiety in a so-called cyano-ethylation reaction: $RH + CH_2=CHCN \rightarrow RCH_2CH_2CN$. The cyanide group introduces a polarization in the acrylonitrile molecule $\overset{+\delta}{C}H_2=CH\overset{-\delta}{C}\equiv N$ facilitating the attack of the deprotonated reagent R^- at $=\overset{+\delta}{C}H_2$. In aqueous solution these reactions are slow and usually occur with multiple additions in the presence of labile methyl or methylene groups, *e.g.* $RCH_3 + CH_2=CHCN \rightarrow RCH_2CH_2CH_2CN \rightarrow RCH(CH_2CH_2CN) \rightarrow RC(CH_2CH_2CN)_3$. It was of interest therefore to investigate whether the activating influence of a metal ion would extend to the distant carbon atom for these carbanion addition reactions and whether there is any selectivity in these additions.

When a large excess of half-neutralized acetylacetone (pH ~9) was added to an aqueous solution of $[Co(NH_3)_5NCCH=CH_2]^{3+}$ addition of $\bar{C}H(COCH_3)_2$ occurred within 5 s producing $[Co(NH_3)_5NC(CH_2)_2CH(COCH_3)_2]^{3+}$ (~45 %). The product was characterized by its ^1H NMR spectrum, IR spectrum and by elemental analysis. Some reduction to cobalt(II) occurred during the reaction and when left in the basic reaction mixture hydrolysis of the nitrile complex to the coordinated amide complex $[Co(NH_3)_5NHCO(CH_2)_2CH(COCH_3)_2]^{2+}$ took place. For uncoordinated acrylonitrile under the same conditions the additions are very slow ($t_{\frac{1}{2}} > 7$ h for acetylacetone) which indicates an acceleration factor $> 10^4$ for the coordinated nitrile.

Nitro-methane also added to the acrylonitrile complex in a fast reaction producing $[Co(NH_3)_5NC(CH_2)_3NO_2]^{3+}$ in ~50 % yield. Again the nitrile complex hydrolyzed to the corresponding amido complex when left in the basic reaction mixture. ^1H NMR, IR spectra and elemental analysis confirmed the formulae.

Most interestingly PO_4^{3-} added to the double band in coordinated acrylonitrile when $[Co(NH_3)_5NCCH=CH_2]Cl_3$ was treated with a concentrated solution of K_3PO_4 and K_2HPO_4 (pH = 11.3), producing the coordinated monophosphate ester which crystallized as $[Co(NH_3)_5NC(CH_2)_2OPO_3].ClO_4.1\frac{1}{2}HClO_4$ (39 %). Some $[Co(NH_3)_5NH_2CO(CH_2)_2OPO_2H_2](ClO_4)_3$ product arising from base hydrolysis of the nitrile complex was formed as well (6 %). Kinetic studies of the reaction of $[Co(NH_3)_5NCCH=CH_2]^{3+}$ in a solution containing 0.5 M K_3PO_4 and 0.5 M K_2HPO_4 (pH = 11.27, 25 °C) revealed two pseudo first-order rate constants $k^1_{obs} = 49.5 \times 10^{-3}$ s^{-1} and $k^2_{obs} = (9.7 \pm 0.4) \times 10^{-3}$ s^{-1}. When the isolated $[Co(NH_3)_5NC(CH_2)_2OPO_3]ClO_4$ complex was treated similarly only one rate was observed with $k^P_{obs} = (9.6 \pm 0.2) \times 10^{-3}$ s^{-1}. The rate constant k^1_{obs} corresponds to that for the base hydrolysis of $[Co(NH_3)_5NCCH=CH_2]^{3+}$ ($k^1_2 = 27$ M^{-1} s^{-1}); k_2 for this reaction at 25 °C, $\mu = 1.0$, was 35 M^{-1} s^{-1}.[10] The fact that $k^2_{obs} = k^P_{obs}$ implies that the second rate observed in the reaction of $[Co(NH_3)_5NCCH=CH_2]^{3+}$ with phosphate is due to base hydrolysis of $[Co(NH_3)_5NC(CH_2)_2OPO_3]^+$ to the corresponding amide complex with a second-order rate constant of $k^2_2 = k^P_2 = 5.2 \pm 0.2$ M^{-1} s^{-1}. The product $[Co(NH_3)_5NH_2CO(CH_2)_2OPO_3H_2](ClO_4)_3$ was then isolated from the reaction mixture and characterized by ^1H NMR spectroscopy and elemental analysis.

These results demonstrate that PO_4^{3-} adds to the coordinated acrylonitrile double bond at a rate comparable to the base hydrolysis rate of the coordinated nitrile. That PO_4^{3-} was the reactive nucleophile was demonstrated by the fact that no addition took place during the same period with HPO_4^{2-}. Addition of $P_2O_7^{4-}$ and $O_2P(OCH_3)_2^-$ also proved unsuccessful. The reaction described here is interesting in that it demonstrates the very fast addition of PO_4^{3-} to a double bond in aqueous solution producing the monophosphate ester as the only product while most phosphate ester syntheses give rise to a mixture of mono- and diphosphate esters. Attempts to follow the reaction between free acrylonitrile and phosphate were frustrated for lack of a solvent common to both reagents.

The isolated addition products were mostly the monocyanoethylated compounds. Smaller amounts of yellow compounds were detected at the top of the cation exchange columns after elution of the main products. These were hard to elute and may have consisted of higher substituted complexes which would be highly charged, for example $\{(Co(NH_3)_5NC(CH_2)_2\}C(COCH_3)_2^{6+}$ and $\{Co(NH_3)_5NC(CH_2)_2\}_2CHNO_2^{9+}$. However, the amounts were very small and no attempts were made to isolate them. Only in the case of

malononitrile did the isolated compound analyze as the dinuclear complex.

Besides offering extremely fast reactions the coordinated acrylonitrile thus has the additional benefit of producing primarily monocyanoethylated products which are easily separated from smaller amounts of other addition products.

The ligands in all these cobalt(III) complexes can be readily removed from the metal by reduction with acidic BH_4^-, V^{2+}, Cr^{2+} or by treatment with CN^- or S^-.

The reaction of cyanide with $[Co(NH_3)_5NCCH_3]Cl_3$. The product from the reaction of $[Co(NH_3)_5NCCH_3]^{3+}$ and cyanide at pH ~10 was found from an X-ray crystallographic analysis[13] to be the tridentate bis(amidine)aminomethylmalonate complex.

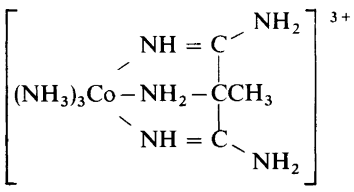

The compound was further characterized by its elemental analysis and ^1H NMR spectrum.

The reaction is assumed to proceed initially by the attack of CN^- at the nitrile carbon producing a coordinated imine, Scheme 4. There appears to be two possibilities for the next step. It may involve deprotonation of a neighbouring NH group followed by nucleophilic attack of coordinated amide at the nitrile C atom to produce a chelated amidine. The rate constants for proton exchange with coordinated NH_3 are large ($\sim 10^6$ $M^{-1}s^{-1}$, 25 °C) in basic media even though the pK_a of the coordinated ammonia is ~14–16. These properties allow for rapid proton transfer in the routes for the suggested condensation which has been observed in other cases.[18] This reaction is then followed by the addition of another CN^- and a second intramolecular amide addition results in the tridentate bis(amidine)aminomethylmalonate complex. The other possibility is the attack of another CN^- on the coordinated imine followed by intramolecular addition of *cis* amide ions. It is known from other cases that coordinated imines are more susceptible to attack by CN^- than the original nitrile[19] which explains why only the tridentate complex was observed.

Release of the diamidine ligand from the complex in aqueous solution followed by rapid hydrolysis should result in the production of amino methylmalonamide which readily hydrolyzes and decarboxylates to α-alanine. This was also observed. On treating an aqueous solution of the complex with H_2S a white compound was isolated whose ^1H NMR spectrum was consistent with $CH_3C(NH_2)(CO_2NH_4)_2$. When this compound was refluxed in acid solution the isolated product exhibited a ^1H

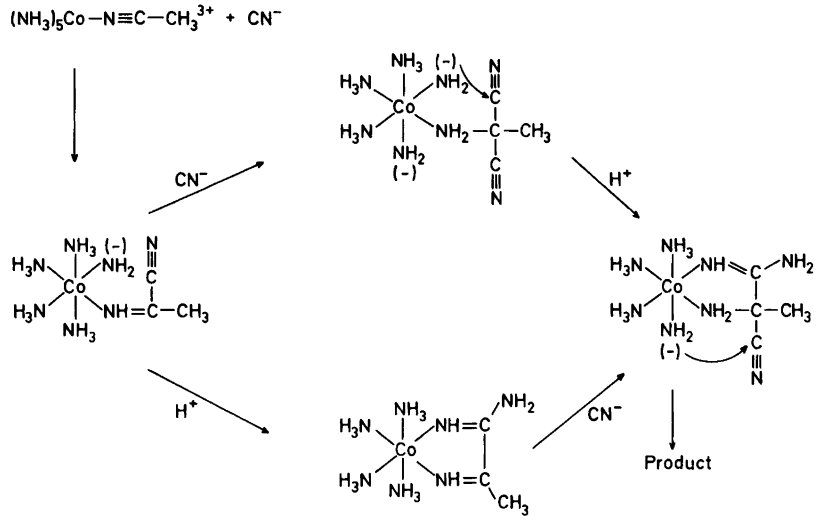

Scheme 4.

NMR spectrum identical to that of α-alanine.HCl and finally α-alanine itself was isolated and analyzed.

The reaction between CN^- and a coordinated nitrile thus introduces the possibility of a general amino acid synthesis from nitriles and a means of labelling the carboxyl group.

Acknowledgements. The authors A.M.S. and I.I.C. would like to acknowledge the stimulus, hospitality and teaching provided by Jannik Bjerrum over many years, and also the A.N.U. Microanalytical Services.

REFERENCES

1. Buckingham, D. A., Keene, F. R. and Sargeson, A. M. *J. Am. Chem. Soc. 95* (1973) 5649.
2. Breslow, R., Fairweather, R. and Keana, J. *J. Am. Chem. Soc. 89* (1967) 2135.
3. Sakai, K., Ito, T. and Watanabe, K. *Bull. Chem. Soc. Jpn. 40* (1967) 1660.
4. Komiya, S., Suzuki, S. and Watanabe, K. *Bull. Chem. Soc. Jpn. 44* (1971) 1440.
5. Barnard, P. F. D. *J. Chem. Soc. A* (1969) 2140.
6. Pinnell, D., Wright, G. B. and Jordan, R. B. *J. Am. Chem. Soc. 94* (1972) 6104.
7. Zanella, A. W. and Ford, P. C. *Inorg. Chem. 14* (1975) 42.
8. Balahura, R. J., Cock, P. and Purcell, W. L. *J. Am. Chem. Soc. 96* (1974) 2739.
9. Rouschias, G. and Wilkinson, G. *J. Chem. Soc. A* (1968) 489.
10. Buckingham, D. A., Keene, F. R., Harrowfield, J. MacB. and Sargeson, A. M. *Unpublished results.*
11. Creaser, I. I. and Sargeson, A. M. *Chem. Commun.* (1975) 324.
12. Creaser, I. I. and Sargeson, A. M. *Chem. Commun.* (1975) 974.
13. Creaser, I. I., Dyke, S. F., Sargeson, A. M. and Tucker, P. A. *Chem. Commun.* (1978) 289.
14. Jordan, R. B., Sargeson, A. M. and Taube, H. *Inorg. Chem. 5* (1966) 1091.
15. Davies, R. B. and Ward, J. A., Jr. *Org. Synth. Coll. Vol. IV* (1963) 392.
16. Coe, D. G., Gale, M. M., Linstead, R. P. and Timmons, L. J. *J. Chem. Soc.* (1957) 123.
17. Satoh, T., Suzuki, S., Suzuki, Y., Miyaji, Y. and Imai, Z. *Tetrahedron Lett. 52* (1969) 4555.
18. Buckingham, D. A., Foxman, B. M., Sargeson, A. M. and Zanella, A. *J. Am. Chem. Soc. 94* (1972) 1007.
19. Harrowfield, J. MacB., Sargeson, A. M. and Springborg, J. *Unpublished results.*

Received May 29, 1978.

Acta Chemica Scandinavica A 32 (1978) 799–803

Ion Activities and Zinc Electrode Reactions in Calcium Chloride Solutions

TURID R. BREIVIK and TOR HURLEN

Department of Chemistry, University of Oslo, Blindern, Norway

The title subjects are studied in various pure and mixed aqueous solutions of zinc and calcium chlorides at 25 °C, but most extensively in slightly acidified 0.005 m $ZnCl_2 + x$ m $CaCl_2$ for $x = 0.2 - 6.0$.* In this solution series, the bare-ion activity coefficients rises strongly for Ca^{2+} and slightly for Cl^- after a minimum at x near 0.5, whereas it strongly falls for Zn^{2+} due to complex formation with chloride ions. In the same solution seires, the Zn/Zn(II) electrode appears to be kinetically controlled by the couple $Zn(H_2O)_4Cl_2^-/Zn(H_2O)_4Cl_2$ at x-values above 0.5 and by corresponding Zn(I)/Zn(II) couples of lower or no chloride content at lower x-values.

As briefly described in two previous contributions from our laboratory,[1,2] the reactions of the Zn/Zn(II) electrode in aqueous solution seem to occur in two consecutive steps of which the Zn(I)/Zn(II) electron-transfer step is the rate-determining one. Our studies moreover suggest that the electroactive Zn(I)/Zn(II) couple be mainly $Zn(H_2O)_6^+/Zn(H_2O)_6^{2+}$ in sulfate[2] and dilute chloride[1] solutions and $Zn(H_2O)_4Cl_2^-/Zn(H_2O)_4Cl_2$ in more concentrated chloride solution,[1] but the water and chloride activity ranges covered by these studies are rather small. The present work pursues this over considerably expanded activity ranges by extending the kinetic studies to a wide concentration range of zinc and calcium chlorides in aqueous solution at 25 °C.

A convenient scale for single-ion activities is introduced in Ref. 1, and its subsequent use is briefly summarized in Ref. 2. The present work extends also such ion-activity studies to a wide concentration range (0.2 – 6.0 m) of calcium chloride in aqueous solution at 25 °C. This follows previous studies of such solutions with nickel (instead of zinc) chloride as a minority salt.[3]

EXPERIMENTAL

The experimental work comprises equilibrium potential measurements on saturated Zn(Hg)/Zn(II) and Ag/AgCl electrodes *vs.* SCE and kinetic polarization measurements on etched (in hot 4 M HCl) high-purity (99.999 %) zinc wire electrodes (exposed surface area near 0.3 cm^2) in the three solution series:

0.005 m $ZnCl_2 + x$ m $CaCl_2$ (A)

x m $ZnCl_2$ (B)

x m $ZnCl_2 + (4 - x)$ m $CaCl_2$ (C)

with $x = 0.2 - 6.0$ in (A) and (B) and $x = 0.005 - 4.0$ in (C) and addition of hydrochloric acid to pH about 2.5, all at 25 °C.

The solutions were prepared from *p.a.* quality salts and acid and twice distilled water, deoxygenated by purified and premoistened nitrogen, and kept under nitrogen atmosphere during the measurements. The measurements have been performed with techniques, equipment and procedures essentially as previously described.[1–3] This includes capacity (purity) checking and ohmic drop correction by the slope and the gap of fast galvanostatic transients.[2] The capacity of "good" zinc wire electrodes essentially was the same (near 55 $\mu F\ cm^{-2}$) in the present chloride solutions as in previously studied sulfate solutions.[2]

* 1 m = 1 mol kg^{-1}.

ACTIVITY DATA

The conventional mean molal activity coefficient ($\gamma_\pm$) and the convenient single-ion ones (γ'_{2+} and γ'_-) for zinc(II) and chloride ions in the test solutions are given by (see Ref. 1):

$$\gamma_\pm = m^\circ m_{2+}^{-1/3} m_-^{-2/3} \exp\{(2/3)f[E'_{2+} - E^\circ_{2+} - (E'_- - E^\circ_-)]\} \quad (1)$$

$$\gamma'_{2+} = m^\circ m_{2+}^{-1} \exp[2f(E'_{2+} - (\phi_t - \phi_r) - E^\circ_{2+} + 0.241)] \quad (2)$$

$$\gamma'_- = m^\circ m_-^{-1} \exp[-f(E'_- - (\phi_t - \phi_r) - E^\circ_- + 0.241)] \quad (3)$$

where m° is the standard molality (1 mol/kg), m_{2+} and m_-, respectively, are the zinc(II) and the chloride molality, f means F/RT, E'_{2+} and E'_-, respectively, are the apparent (including liquid junction) reversible Zn/Zn(II) and Ag/AgCl potentials in V(SCE), E°_{2+} and E°_- are the standard potentials of these electrodes in V(SHE), $\phi_t - \phi_r$ is the liquid-junction potential difference between test and reference (saturated KCl) solution in V, and 0.241 V(SHE) is the recommended value[4] for $E^\circ(\mathrm{Hg/Hg_2Cl_2}) - f^{-1} \ln(a_\pm(\mathrm{sat.KCl})/a^\circ)$, all at 25 °C. These activity coefficients are bare-ion ones.

Table 1 presents the E' values measured and the $\gamma_\pm$ values hence obtained from (1) for zinc chloride in the solution series (A)–(C), when E°/V(SHE) values of 0.222 and −0.763 are used for Ag/AgCl and Zn/Zn(II),[4-6] respectively. The values presently obtained for $\gamma_\pm$ of zinc chloride in essentially pure solutions of this salt, the solution series (B), check well with previously tabulated data.[5] The authors are not aware of data for checking the present results in the mixed solutions of zinc and calcium chlorides, the solution series (A) and (C).

Table 2 presents $\phi_t - \phi_r$ values estimated (from the Henderson equation[7] and mobility data[5]) and γ'_z values hence obtained from (1), (2) and $\gamma'_{2+}(\mathrm{Ca}) = [\gamma_\pm(\mathrm{CaCl_2})]^3/[\gamma'_-(\mathrm{Cl})]^2$ for zinc, chloride and calcium ions in the solution series (A). Values of $\gamma_\pm$ for calcium chloride in pure x m solutions of this salt[5] have then been accepted for it in the corresponding solutions (A). Also values for the water activity (a_w) of such pure calcium chloride solutions[5] are reproduced in Table 2 and are presently accepted for the test solutions (A).

Fig. 1 compares the various activity coefficients in the solution series (A) with each other. It is there clearly shown how the mean-ion and cation activity coefficients of the minority salt ($ZnCl_2$) increasingly separate from those of the main salt ($CaCl_2$) with increasing salt concentration. This separation, which has no counterpart in corresponding $ZnSO_4$–$MgSO_4$ solutions,[2] naturally comes from a rather strong complexing of zinc(II) with chloride ions in the solutions.[5,8,9] Although the present activity data show the formation of such complexes, they hardly reveal their composition and stability.

Table 1. Zn/Zn(II) and Ag/AgCl reversible potentials and mean molal bare-ion activity coefficient of $ZnCl_2$ in various solutions at 25 °C. Potentials in V(SCE) including liquid junction.

x	0.2	0.5	1	2	3	4	6
In 0.005 m $ZnCl_2$ + x m $CaCl_2$							
E'_{2+}	−1.090	−1.090	−1.091	−1.106	−1.118	−1.130	−1.127
E'_-	+0.014	−0.005	−0.021	−0.038	−0.049	−0.060	−0.074
$\gamma_\pm$	0.48	0.43	0.40	0.27	0.20	0.16	0.19
In x m $ZnCl_2$							
E'_{2+}	−1.040	−1.025	−1.010	−0.990	−0.972	−0.952	−0.911
E'_-	+0.019	+0.005	−0.002	−0.002	+0.001	+0.007	+0.021
$\gamma_\pm$	0.46	0.39	0.34	0.29	0.29	0.31	0.42
x	0.005	0.03	0.1	0.3	1	2	4
In x m $ZnCl_2$ + (4−x)m $CaCl_2$							
E'_{2+}	−1.130	−1.105	−1.088	−1.069	−1.034	−0.988	−0.952
E'_-	−0.060	−0.059	−0.057	−0.055	−0.041	−0.015	+0.007
$\gamma_\pm$	0.16	0.17	0.16	0.18	0.20	0.27	0.31

Table 2. Liquid-junction ($\Delta\phi = \phi_t - \phi_r$), single-ion and water data for 0.005 m $ZnCl_2 + x$ m $CaCl_2$ at 25 °C (see text).

x	0.2	0.5	1	2	3	4	6
$\Delta\phi$/V	0.001	0.003	0.005	0.008	0.010	0.011	0.013
γ'_-(Cl)	0.70	0.65	0.65	0.71	0.79	0.95	1.18
γ'_{2+}(Zn)	0.23	0.20	0.15	0.038	0.013	0.0046	0.0050
γ'_{2+}(Ca)	0.22	0.21	0.30	0.99	5.2	28	985
a_w	0.991	0.976	0.945	0.862	0.749	0.624	0.392

KINETIC DATA

The kinetic data of the present work apply to preetched zinc wire electrodes in solutions of series (A). In these calcium chloride solutions, the solid zinc electrode is found to behave somewhat as in magnesium sulfate solutions[2] by showing a slightly unstable and stirring-dependent open-circuit potential (a little positive to the reversible Zn/Zn(II) potential) and exhibiting charge-transfer controlled anodic and cathodic Tafel lines with $E/\ln i$ slopes of typically $2RT/3F$ and $-2RT/F$, respectively. The latter conforms with results also in potassium chloride solutions,[1] and it agrees with the introductionally mentioned two-step mechanism of the Zn/Zn(II) electrode. Examples of Tafel data are given in Fig. 2.

With the reaction mechanism proposed, the Tafel lines should intersect at the reversible potential and twice the exchange current of the rate-determining Zn(I)/Zn(II) electron-transfer step.[7,10] Table 3 gives values accordingly obtained for this exchange current (i_{02}) mostly by extrapolating the more reproducible *anodic* Tafel lines to the reversible potential proper (Table 1). From ordinary electrode kinetics,[7,10] i_{02} should depend on the bare-ion activity of zinc(II) by (when $\alpha_2 = \frac{1}{2}$):

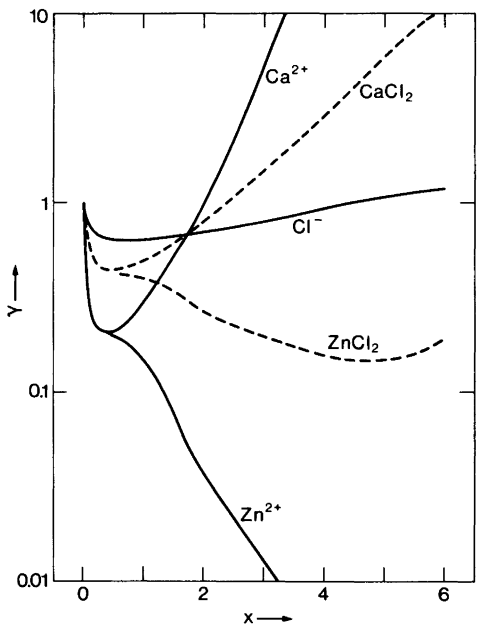

Fig. 1. Conventional mean-ion (dashed curves) and convenient single-ion (solid curves) activity coefficients in 0.005 m $ZnCl_2 + x$ m $CaCl_2$ at 25 °C.

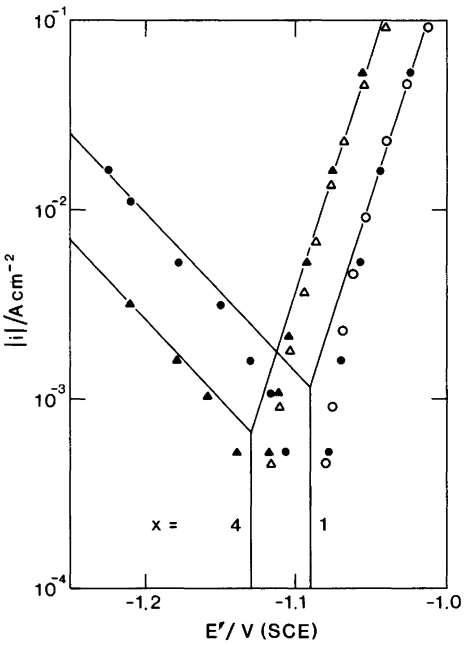

Fig. 2. Tafel data for solid zinc in acidified (pH near 2.5) 0.005 m $ZnCl_2 + x$ m $CaCl_2$ for $x = 1$ and 4 at 25 °C from (closed symbols) fast galvanostatic steps in unstirred solution and (open symbols) slow galvanostatic measurements in vigorously stirred solution.

Table 3. Exchange data for Zn(I)/Zn(II) at solid zinc in 0.005 m $ZnCl_2 + x$ m $CaCl_2$ at 25 °C (see text).

x	0.2	0.5	1	2	3	4	6
i_{02}/mA cm^{-2}	1.0	0.6	0.6	0.7	0.5	0.35	0.25
I_{02}/A cm^{-2}	0.15	0.1	0.15	0.45	0.7	1.05	0.7

$$i_{02} = I_{02}(\gamma'_{2+} m_{2+}/m^\circ)^{3/4} \quad (4)$$

where the bare-zinc-ion standardized exchange rate (I_{02}) still depends on ligand activities and double-layer effects. Table 3 gives also values accordingly obtained for I_{02} from i_{02} and activity data (Table 2).

I_{02} actually is a sum of terms, one term for each different Zn(I)/Zn(II) couple participating, and each term given by:

$$I_{02,ij} = I^\circ_{02,ij}(\gamma'_- m_-/m^\circ)^i a_w^j \quad (5)$$

where i and j are the chloride and water ligand numbers of the couple concerned, and the further standardized exchange rate ($I^\circ_{02,ij}$) still depends on double-layer effects. Hence, I_{02} should exhibit a simple chloride and water activity dependence only when determined predominantly by one of its terms, and then only if double-layer effects be small or nearly constant (or appropriately corrected for).

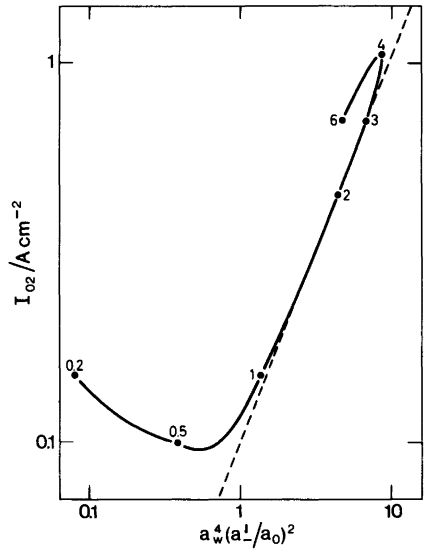

Fig. 3. Bare-zinc-ion standardized Zn(I)/Zn(II) exchange rate I_{02} *vs.* $a_w^4(\gamma'_- m_-/m^\circ)^2$ for solid zinc in 0.005 m $ZnCl_2 + x$ m $CaCl_2$ at 25 °C. Values of x at the points.

In Fig. 3, the values obtained for I_{02} (Table 3) are log-log plotted *vs.* $a_w^4(\gamma'_- m_-/m^\circ)^2$ for the solutions applied (Table 2). There a line of unit slope (dashed line) is nearly obeyed at x-values above 0.5 and is clearly disobeyed at lower x-values. This agrees with $Zn(H_2O)_4Cl_2^-/Zn(H_2O)_4Cl_2$ being the main electroactive Zn(I)/Zn(II) couple at x-values above 0.5 and with corresponding couples of lower or no chloride content taking control at lower x-values.[1] Double-layer effects and the possible participation by higher chloride complexes are briefly considered in the Discussion below.

DISCUSSION

Although connected, the activity data and the kinetic data of the present work may appropriately be discussed separately.

Activities. Besides giving conventional mean-ion data for zinc chloride in various pure and mixed solutions with calcium chloride (Table 1), the present work yields convenient single-ion data for calcium chloride solutions with zinc chloride as a minority salt (Table 2 and Fig. 1). Even though the single-ion data to some extent depend on the validity of the values estimated and used for the liquid-junction potential difference ($\phi_t - \phi_r$), and they hence are less certain than the mean-ion data, they certainly are more informative. Some information is extracted and used in the present kinetic studies, but more is held. It is hoped to treat this in a future more comprehensive analysis of convenient single-ion activity data.

Kinetics. The present results support the introductionally mentioned two-step charge-transfer mechanism of the Zn/Zn(II) electrode (by the Tafel slopes observed) and its rate control by the $Zn(H_2)_4Cl_2^-/Zn(H_2O)_4Cl_2$ couple over a large chloride concentration range (Fig. 3). The results of Fig. 3 further suggest that double-layer effects be rather small (or change rather little) under the experimental conditions, since larger deviations from a line of unit slope should otherwise have occurred.[2] The slight deviations observed at high

x-values may perhaps be due to a retarding diffuse-layer effect (by the Frumkin factor $\exp(\frac{1}{2}f\phi_2)$ with negative ϕ_2)[2] which decreases with increasing salt concentration (by $|\phi_2|$ then decreasing). These deviations, therefore, need not mean that Zn(I)/-Zn(II) couples of higher chloride content come into account.

REFERENCES

1. Hurlen, T. and Fischer, K. P. *J. Electroanal. Chem. 61* (1975) 165.
2. Hurlen, T. and Breivik, T. R. *Acta Chem. Scand. 32* (1978) 447.
3. Hurlen, T. *Electrochim. Acta 20* (1975) 499.
4. Ives, D. J. G. and Janz, G. J. *Reference Electrodes*, Academic, New York and London 1961.
5. Robinson, R. A. and Stokes, R. H. *Electrolyte Solutions*, 2nd Ed. (revised), Butterworths, London 1970.
6. Pourbaix, M. *Atlas of Electrochemical Equilibria in Aqueous Solutions*, Pergamon, Oxford 1966, p. 408.
7. Vetter, K. J. *Electrochemical Kinetics*, Academic, New York and London 1967.
8. Smith, R. M. and Martell, A. E. *Critical Stability Constants, Vol. 4, Inorganic Complexes*, Plenum, New York 1976, p. 108.
9. Skou, E., Jacobsen, T., van der Hoeven, W. and Atlung, S. *Electrochim. Acta 22* (1977) 169.
10. Delahay, P. *Double Layer and Electrode Kinetics*, Interscience, New York 1965, p. 180.

Received May 9, 1978.

Acta Chemica Scandinavica A 32 (1978) 805–809

The Crystal Structure, Thermal Behaviour and IR Spectrum of Copper Tetraammine Dithionate

MARKKU LESKELÄ and JUSSI VALKONEN

Department of Chemistry, Helsinki University of Technology, Otaniemi, SF-02150 Espoo 15, Finland

$Cu(NH_3)_4S_2O_6$ crystals were obtained from ammoniacal copper acetate solution which had been saturated with sulfur dioxide. The compound was characterized by chemical and thermal analyses and IR spectra and the crystal structure was determined from three-dimensional X-ray diffraction data. The dithionate crystallizes in the monoclinic space group $P2_1/c$ (No. 14). The cell parameters are $a=7.148(2)$ $b=10.604(3)$, $c=11.675(3)$ Å, $\beta=145.12(1)°$, $Z=2$. The structure was refined to a final R-value of 5.2 %.

The structure consists of chains formed by Cu-octahedra and dithionate groups. The Cu-atom is six-coordinated by four nitrogen atoms and two oxygen atoms at average distances of 2.05 and 2.62 Å, respectively.

The existence of copper dithionate and copper tetraammine dithionate has been known a long time. In 1926 De Baat prepared copper dithionate from $BaS_2O_6.2H_2O$ and $CuSO_4.5H_2O$.[1] The dithionate ion for $BaS_2O_6.2H_2O$ was prepared from sulfite solution, which had been oxidized with MnO_2. This remains one of the standard methods of producing dithionates. A few years later Garreau[2] prepared $Cu(NH_3)_4S_2O_6$ from a solution containing $(NH_4)_2SO_3$, NH_4OH and $NH_3Cu(OH)_2$, showing that in alkaline solution sulfite ion can be oxidized to dithionate ion by air alone.

Although the crystal structures of several simple dithionates[3–6] and those of some complex ones[7] have been solved, the structures of copper dithionates have remained unknown. Only the IR and molecular spectrum of these compounds have been measured by Duval and Lecomte.[8,9]

EXPERIMENTAL

Crystal preparation and analyses. Crystals suitable for X-ray analysis were obtained by dissolving 2 g of copper acetate in 50 ml of distilled water and adding 30 ml of ammonia (25 %). This deep blue solution was saturated with sulfur dioxide by bubbling it through the solution for 1 h. On evaporation of the solution at room temperature dark violet $Cu(NH_3)_4S_2O_6$ needles were formed. All reactions were carried out in air so that the oxidation could take place.

Elemental analyses were carried out by Novo Microanalytical Laboratory, Novo Industri A/S, DK-2880 Bagsvaerd, Denmark, supervised by Rolf E. Amsler. Found: 21.59 % Cu, 22.29 % S and 19.21 % N. Calc. for $Cu(NH_3)_4S_2O_6$: 21.77 % Cu, 22.01 % S and 19.20 % N.

The thermal decomposition was investigated in a Mettler thermoanalyzer TA-1 by simultaneous recording of the TG, DTG and DTA curves. The investigations were made both in air and in nitrogen. The flow rate of the gases was 100 cm^3/min and the heating rates were 6 °C min^{-1} and 1 °C min^{-1}. The sample holder was a platinum crucible (diam. 7 mm, depth 19 mm). In DTA measurements alumina was used as reference material.

IR spectrum were measured on a Perkin-Elmer 521 instrument using the KBr pellet technique.

Structure determination. The X-ray intensities were recorded with a Syntex $P2_1$ (Fortran version) automatic four-circle diffractometer employing graphite monochromatized Mo$K\alpha$-radiation. The unit cell parameters were calculated by least-squares refinement of 24 reflections. The intensities of 1845 independent reflections up to 2θ of 70° were measured and the 1429 reflections with $I>4\sigma(I)$ were considered significant. The $\theta/2\theta$ scan technique was used and the scan speed was 0.8–3.5°/min. The intensity, I, of each reflection was calculated by subtracting the total background count, BG,

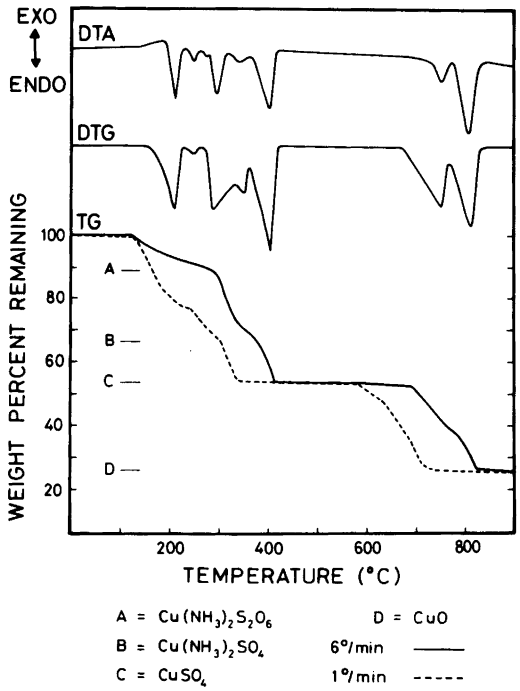

Fig. 1. Thermal decomposition of $Cu(NH_3)_4S_2O_6$ in air. Sample weight 53 mg.

Table 1. Infrared absorption frequencies and their assignments in the region 4000 – 400 cm^{-1}.

Observed frequency	Assignments
3310 s	$\nu_4(NH_3)$
3220 s	$\nu_1(NH_3)$
2330 vw	$\nu_7+\nu_1(S_2O_6)$
2200 vw	$\nu_{10}+\nu_5(S_2O_6)$
2085 vw	$\nu_1+\nu_5(S_2O_6)$
1620 m	$\nu_5(NH_3)$
1600 m	$\nu_1+\nu_8(S_2O_6)$
1390 m	$\nu_1+290(S_2O_6)$ [a]
1245 vs	$\nu_7(S_2O_6)$, ν_2 (NH_3)
1210 s	$\nu_{10}(S_2O_6)$
1090 m	$\nu_1(S_2O_6)$
995 s	$\nu_5(S_2O_6)$
780 m	$\nu_{11}+204(S_2O_6)$ [a]
700 s	$\nu_6(NH_3)$
565 vs	$\nu_{11}(S_2O_6)$
510 s	$\nu_8(S_2O_6)$
420 vw	$\nu_3(NH_3)$

[a] The low frequencies of the $S_2O_6^{2-}$ groups are according to Palmer.[15]

from the total scan count, SC. The standard deviation, $\sigma(I)$ was obtained from $\sigma(I)=(SC+BG)^{1/2}$. The values obtained were then multiplied with the scan rate to compensate for the different scan speeds. The net intensities were corrected for Lorentz and polarization effects. Empirical absorption correction were made on the basis of the ϕ-scan data with 9 different 2θ values. The largest measured relative reduction in intensity was from 1.000 to 0.557. The systematic absences in the original intensity data indicated the space group $P2_1/c$ (No. 14). The dimensions of the crystal were approximately 1.0 × 0.5 × 0.2 mm.

The positions of Cu and S atoms were obtained by direct methods, using the 244 E-values larger than 1.4. Solving, refinement and plotting were carried out with the X-RAY SYSTEM 1976.[10] The scattering factors were those of Cromer and Mann for neutral atoms.[11] After refinement of the positions of Cu and S atoms the value of R was 0.288. The positional parameters of all the oxygens were obtained from the difference Fourier map. The structure was then refined with isotropic temperature factors to an R-value of 0.077 and, after block-diagonal refinement with anisotropic temperature factors, to an R-value of 0.052. No weighting scheme was used, all intensities had a unit weight. The $|F_o|$ and $|F_c|$ listing is available from the authors upon request.

Table 2. Atomic coordinates and anisotropic temperature coefficients with their estimated standard deviations. The temperature coefficients are of the form $\exp[-2\pi^2(h^2a^{*2}U_{11}+\ldots+2klb^*c^*U_{23})]$, and have been multiplied by 10^4.

Atom	x	y	z	U_{11}	U_{22}	U_{33}	U_{12}	U_{13}	U_{23}
Cu	0	0	0	271(5)	232(4)	289(5)	8(4)	240(4)	5(4)
S1	.8638(4)	.0322(1)	.3591(2)	240(6)	280(6)	270(6)	24(5)	209(6)	36(5)
O1	.4161(11)	.5986(5)	.2331(7)	255(21)	381(25)	345(24)	−93(18)	220(21)	−60(19)
O2	.7798(13)	.9161(5)	.2547(7)	442(30)	492(31)	344(26)	35(24)	314(25)	−67(22)
O3	.0899(13)	.1151(5)	.4107(8)	374(27)	571(34)	448(30)	−23(24)	338(27)	136(25)
N1	.8427(15)	.3912(6)	.2877(9)	388(31)	367(29)	338(28)	−25(23)	313(27)	−55(22)
N2	.0830(15)	.6493(5)	.4339(9)	496(36)	284(26)	469(35)	−12(24)	424(32)	26(23)

RESULTS AND DISCUSSION

Thermal analysis. With the heating rate of 6°/min there is first an endothermic reaction in the temperature range 160–230 °C (Fig. 1). The observed weight loss corresponds to two ammonia molecules. In the following stage dithionate decomposes to sulfate and sulfur dioxide is released. Then the two other ammonia molecules are released. At 410 °C there remains only anhydrous copper sulfate, which decomposes as expected in two stages to copper oxide in the temperature range of 690–820 °C. The decomposition was found to proceed similarly in nitrogen atmosphere.

When the heating rate is 1°/min the four ammonia molecules and sulfur dioxide are released in succession so that clear plateaus between the different decomposition stages are not found. As expected, the reactions take place in a temperature range which is 50–80 °C lower than with the higher heating rate.

The results of the thermal analyses correspond well with those obtained by Liptay for zinc tetraammine dithionate.[12]

Infrared analysis. The IR spectrum of copper tetraammine dithionate showed the normal frequencies of the symmetries C_{3v} for NH_3 and D_{3d} for $S_2O_6^{2-}$ (Table 1).[13-15] Outside the investigated range were the following: S–S stretching at 290 cm^{-1}, SO_3 rocking at 205 cm^{-1} and SO_3-SO_3 torsion at 155 cm^{-1}.[15]

Structure analysis. The positional and thermal parameters for nonhydrogen atoms are given in Table 2 and crystal data in Table 3. The Cu atom is

Table 3. Crystal data for $Cu(NH_3)_4S_2O_6$.

Formula	$Cu(NH_3)_4S_2O_6$
Formula weight	291.79
Lattice constants	$a=7.148(2)$
(Å)	$b=10.604(3)$
	$c=11.675(3)$
(°)	$\beta=145.12(1)$
Cell volume (Å^3)	$V=506.1(2)$
Molecules per unit cell	$Z=2$
Space group	$P2_1/c$ (No. 14)
Density (g cm^{-3})	$D_x=1.915$
Linear absorption coefficient (cm^{-1})	$\mu(MoK\alpha)=26.7$

Table 4. Distances (Å) and angles (°) around the Cu atom.

Cu–O1	2.624(5)	(*2)	N1–Cu–N2	91.2(4)
Cu–N1	2.041(10)	(*2)	O1–Cu–N1	91.6(3)
Cu–N2	2.050(10)	(*2)	O1–Cu–N2	94.9(3)

Table 5. Distances (Å) and angles (°) in the dithionate group.

S–O1	1.457(8)	O1–S–O2	114.4(4)
S–O2	1.470(7)	O1–S–O3	113.4(4)
S–O3	1.467(9)	O2–S–O3	113.9(6)
S–S	2.138(4)	S–S–O1	104.9(4)
		S–S–O2	104.2(3)
		S–S–O3	104.7(3)

Table 6. Interatomic S–O and S–S distances in some dithionates.

Compound	S–S distances (Å)	S–O distances (Å)	Ref.
$Li_2S_2O_6.2H_2O$	2.14	1.447–1.457	4
$Na_2S_2O_6.2H_2O$	2.15	1.450–1.463	4
$Na_2S_2O_6.2H_2O$	2.141	1.450–1.457	25
$K_2S_2O_6$	2.14–2.15	1.42–1.43	16
$MgS_2O_6.6H_2O$	2.123	1.447–1.449	17
$BaS_2O_6.2H_2O$	2.15	1.46	5
$NiS_2O_6.6H_2O$	2.123	1.446–1.454	17
$ZnS_2O_6.6H_2O$	2.127	1.448–1.453	17
$NaK_2ClS_2O_6$	2.08	1.44–1.50	7
$NaK_5Cl_2(S_2O_6)_2$	2.08	1.47–1.49	7
$[(NH_3)_3Co(OH)_3Co(NH_3)_3]_2(S_2O_6)_3$	2.119–2.138	1.441–1.455	19
$(NH_4)_3ClS_2O_6$	2.13–2.16	1.41–1.53	18
$[(Cr(en)_2(OH))_2][S_2O_6]_2$	2.127	1.435–1.460	20
$Cu(NH_3)_4S_2O_6$	2.138	1.457–1.470	This work

Table 7. Interatomic distances between Cu – O and Cu – N atoms in some copper tetraammine compounds.

Compound	Cu – O (Å)	Cu – N (Å)	Ref.
$Cu(NH_3)_4SO_4.H_2O$	2.339(9)	2.031(6) – 2.032(6)	21
$Cu(NH_3)_4SeO_4$	2.607(7), 2.451(8)	1.992(1) – 2.017(9)	21
$Cu(NH_3)_4(NO_3)_2$	2.517(5) – 2.706(7)	2.008(5) – 2.029(5)	22
$Cu(NH_3)_4S_2O_6$	2.624(5)	2.041(10) – 2.050(10)	Present work

Table 8. Distances (Å) around nitrogen atoms (less than 3.3 Å).

N1 – N2	2.863(14)
– N2	2.922(8)
– O3	3.097(8)
– O1	3.279(6)
– O2	3.128(14)
– O3	3.078(8)
N2 – O2	2.952(10)
– O1	3.189(14)
– O2	3.105(8)
– O3	3.113(14)

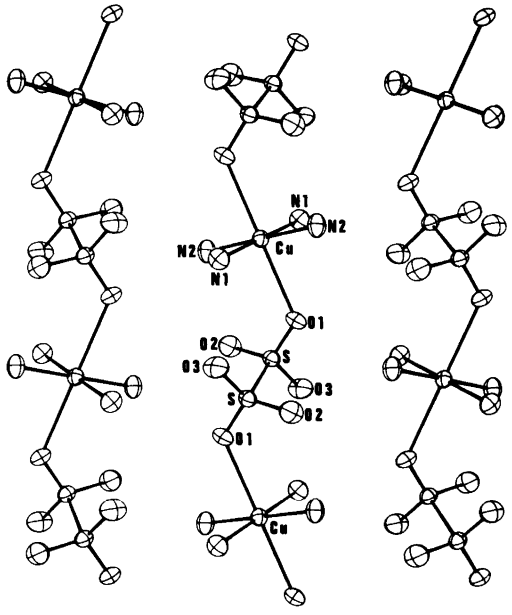

Fig. 2. Perspective drawing showing the chain structure of $Cu(NH_3)_4S_2O_6$. The *x*-axis is vertical and the *y*-axis horizontal.

six-coordinated, of type 4+2; the four nitrogen atoms of the ammine group lie about 2.0 Å from Cu, forming a square planar arrangement around it, while the two oxygen atoms of the dithionate group are situated at a distance of about 2.6 Å (Table 4). The O1 atoms are above and below this plane. The Cu atoms are situated at the centres of symmetry. All distances are quite normal compared with other Cu compounds of the same type (Table 7).

The dithionate group consists of two SO_3 polyhedra connected together centrosymmetrically by an S – S bond of 2.138 Å. The S – O distance is slightly shorter than in sulfites (about 1.5 Å),[23] probably due to the second sulfur atom (Table 5). The distance between the sulfur atoms is longer than usual (about 2.06)[24] but this is observed in all dithionates (Table 6).

The structure consists of chains formed by dithionate and copper atoms (Fig. 2). These Cu – O1 – S – S – O1 – Cu chains are perpendicular to the *yz*-plane and are joined together by hydrogen bonds to ammine groups. Hydrogen atoms could not be located but the possible hydrogen bond distances listed in Table 8 are in good agreement with the distances given for $Cu(NH_3)_4SO_4.H_2O$ and $Cu(NH_3)_4SeO_4$[21] and $Cu(NH_3)_4(NO_3)_2$.[22]

REFERENCES

1. De Baat, W. C. *Recl. Trav. Chim. Pays-Bas 45* (1926) 237.
2. Garreau, Y. *Bull. Soc. Chim. Fr. 1* (1934) 1563.
3. Van Meerssche, M., Dereppe, J. M. and Lobo, P. W. *Acta Crystallogr. 16* (1963) 95.
4. Berthold, I. and Weiss, A. *Z. Naturforsch. Teil A 22* (1967) 1440.
5. Rausell-Colom, J. A. and Garcia-Blanco, S. *Acta Crystallogr. 21* (1966) 672.
6. Chan, J. and Stanley, E. *Z. Kristallogr. 132* (1970) 404.
7. Stanley, E. *Acta Crystallogr. 6* (1953) 187.
8. Duval, C. and Lecomte, J. *C.R. Acad. Sci. Ser. C. 217* (1943) 42.

9. Duval, C. and Lecomte, J. *Bull. Soc. Chim. Fr. 11* (1944) 376.
10. Steward, J. M., Ed., *The X-Ray System, Version of 1976*, Technical Report TR-446, Computer Science Center, University of Maryland, College Park.
11. Cromer, D. and Mann, S. *Acta Crystallogr. A 24* (1968) 321.
12. Liptay, G. *Kem.-Kemi 4* (1977) 387.
13. Vogt, L. H., Katz, J. L. and Wiberley, S. E. *Inorg. Chem. 4* (1965) 1157.
14. Nakagawa, I. and Shimanouchi, T. *Spectrochim. Acta 22* (1966) 759.
15. Palmer, W. G. *J. Chem. Soc.* (1961) 1552.
16. Stanley, E. *Acta Crystallogr. 9* (1956) 897.
17. Black, W. H., Griffith, E. A. H. and Robertson, B. E. *Acta Crystallogr. B 31* (1975) 615.
18. Guttormson, R. J. and Stanley, E. *Acta Crystallogr. B 25* (1969) 971.
19. Thewalt, U. *Z. Anorg. Allg. Chem. 412* (1975) 29.
20. Cline, S. J., Scaringe, R. P., Hatfield, W. E. and Hodgson, D. J. *J. Chem. Soc. Dalton Trans. 17* (1977) 1662.
21. Morosin, B. *Acta Crystallogr. B 25* (1969) 19.
22. Morosin, B. *Acta Crystallogr. B 32* (1976) 1237.
23. Kierkegaard, P. and Nyberg, B. *Acta Chem. Scand. 19* (1965) 2189.
24. Meyer, B. *Chem. Rev. 76* (1976) 367.
25. Kiers, C. T., Piepenbroek, A. and Vos, A. *Acta Crystallogr. B 34* (1978) 888.

Received May 26, 1978.

Acta Chemica Scandinavica A 32 (1978) 811–813

Crystal Structure Refinement of α-Ta_3P

YVONNE ANDERSSON, SUPANICH PRAMATUS* and STIG RUNDQVIST

Institute of Chemistry, University of Uppsala, Box 531, S-751 21 Uppsala, Sweden

The crystal structure of α-Ta_3P has been refined from X-ray single crystal diffractometer data. α-Ta_3P crystallizes with the Ti_3P type structure: space group $P4_2/n$ (No. 86), $a=10.1550(3)$ Å, $c=5.0128(2)$ Å; all atoms in 8*g*, Ta(1) $x=0.15898(7)$, $y=0.65557(7)$, $z=0.7435(2)$; Ta(2) $x=0.10483(7)$, $y=0.25374(7)$, $z=0.5044(2)$; Ta(3) $x=0.05257(7)$, $y=0.54548(7)$, $z=0.2474(2)$; P $x=0.0420(5)$, $y=0.2583(5)$, $z=0.0064(16)$; (origin at $\bar{1}$). The transformation from low-temperature α-Ta_3P to high-temperature β-Ta_3P occurs at a temperature between 2000 and 2100 °C.

In a previous paper[1] on the crystal structure of β-Ta_3P it was mentioned that Ta_3P occurs in two modifications: β-Ta_3P crystallizing with the β-V_3S type structure, and α-Ta_3P with the Ti_3P type structure. In the present paper we give some further information on the α/β transformation and present the results of a single crystal structure refinement of α-Ta_3P.

EXPERIMENTAL DETAILS AND RESULTS

Synthetic and phase-analytical work. As mentioned earlier,[2] TaP and TaP_2 are the only phases formed by reaction between tantalum and phosphorus under the conditions of the ordinary silica tube synthetic technique. At higher temperatures, however, tantalum and TaP react to form a number of intermediate phases.[2,3] β-Ta_3P, crystallizing with the β-V_3S type structure, is obtained by arc melting appropriate mixtures of tantalum and TaP on a water-cooled copper hearth.[1] If this material is annealed at temperatures not too far below the melting-point, α-Ta_3P, crystallizing with the Ti_3P type structure, is rapidly formed.

Since a detailed investigation of the Ta-P equilibrium diagram presents formidable experimental difficulties, we restricted the present studies to a cursory X-ray diffraction examination of some alloys, which has been subjected to different heat-treatments.

X-Ray powder patterns were recorded in Hägg-Guinier-type focussing cameras (Philips XDC-700) using Cu$K\alpha_1$ or Cr$K\alpha_1$ radiation, and zone-refined silicon ($a=5.431065$ Å)[4] as internal calibration standard. Powder diffraction data for the two forms of Ta_3P are given in Table 1. The unit cell dimensions for both forms are almost equal, for α-Ta_3P:

Table 1. Powder diffraction data for α-Ta_3P and β-Ta_3P. Philips XDC-700 camera, Cu$K\alpha_1$ radiation, intensities measured on SAAB automatic film scanner.

		α-Ta_3P		β-Ta_3P				α-Ta_3P		β-Ta_3P	
hkl	d_o (Å)	I_o	I_c	I_o	I_c	hkl	d_o (Å)	I_o	I_c	I_o	I_c
110	7.173	4	3	3	2	331		0	0	-	-
200		0	0	0	3	421	2.069	8	8	4	4
101		0	0	0	1	222	2.056	38	34	31	26
111		0	0	-	-	302		0	0	0	0
220	3.589	6	7	7	5	510	1.992	14	16	12	10
201	3.567	16	16	8	7	312	1.976	14	15	13	21
211		0	0	1	6	431		0	1	0	1
310	3.211	2	2	1	0	501		0	0	0	0
221		0	0	-	-	322		0	0	0	0
301		0	0	0	0	511	1.851	6	8	2	4
311	2.704	33	37	20	16	440		0	1	0	0
400		0	1	0	2	402	1.784	4	6	4	1
002	2.506	4	6	4	4	521		0	2	0	1
321	2.456	100	100	89	100	412		0	0	0	0
102		0	0	0	0	530		0	0	0	1
330	2.394	45	43	35	34	332	1.731	2	3	1	2
112	2.367	67	61	94[a]	48	600		0	1	0	0
420	2.271	35	35	39	30	441		0	0	0	0
401	2.265	24	22		9	422		0	0	0	0
202	2.248	19	17	18	8	103		0	0	0	0
411	2.211	82	87	64	62	531	1.645	2	3	0	1
212		0	0	0	2						

a) overlapped by Ta.

* On leave from the Faculty of Science, Chulalongkorn University, Bangkok 5, Thailand.

$a = 10.1550(3)$ Å; $c = 5.0128(2)$ Å and for β-Ta_3P: $a = 10.1542(4)$ Å; $c = 5.0137(3)$ Å, and remain unchanged within experimental error in alloys of different compositions. As seen from Table 1 there are only minor differences in intensity between corresponding lines, the most prominent difference being exhibited by the pair (220)/(201). The great similarities between the powder patterns made it very difficult to determine the relative proportions of the two Ta_3P forms in samples containing both phases simultaneously. Examination of ground and polished specimens by optical microscopy provided no additional advantage from the phase-analytical point of view.

The heat-treatments of the alloys were made in an induction furnace under a protective atmosphere of argon. Since molten Ta-P alloys were found to attack conventional crucible materials severely, heating was performed using a water-cooled current concentrator specially designed for levitation melting. The temperatures of the samples were measured by optical pyrometry.

The melting-point of Ta_3P was determined to be close to 2100 °C. After rapid quenching the solidified melt was found to consist of β-Ta_3P, as judged from the X-ray diffraction films. When β-Ta_3P was heated at 1100 °C for three days in an evacuated and sealed silica tube, the films gave indications of an inchoate transformation, while heating at 1900 °C for 20 min in the induction furnace produced complete conversion into α-Ta_3P. In an attempt to locate the transformation temperature more accurately, a sample was levitated for several minutes in such a way that the lower part was molten and the upper part solid. The alloy was then quenched rapidly. The part, which had been molten, was found to consist of β-Ta_3P, while the part, which had remained solid, was found to consist of α-Ta_3P. The temperature of the solid α-Ta_3P part was about 2000 °C during the heating.

The results of our experiments indicate that the transformation between high-temperature β-Ta_3P and low-temperature α-Ta_3P occurs at some temperature less than 100 °C below the melting-point of β-Ta_3P. Whether β-Ta_3P melts congruently or not remains to be determined by a complete thermal analysis of the Ta-P system.

X-Ray single crystal work. The intensities were recorded on a Stoe four-circle diffractometer with a graphite monochromator using Mo$K\alpha$ radiation. The measurements were made using the $\omega - 2\theta$ step scan technique, to a maximum in 2θ of 70°. Totally 1418 reflexions were recorded, of these 1136 were nonequivalent. The intensities were corrected for absorption using the Gaussian grid method, and a calculated linear absorption coefficient of 1254 cm^{-1}. The transmissions varied between 0.04 and 0.11. Equivalent reflexions were averaged and the crystal structure was refined by the least-squares method in the same manner as described in Ref. 1.

For the 1133 reflexions refined the following agreement factors were obtained: $R(F^2) = 0.093$, $R(F) = 0.077$ and $R_w(F^2) = 0.124$. The final structure data obtained are presented in Table 2. Calculated interatomic distances are given in Table 3. A table of observed and calculated structure factors can be obtained from the authors on request.

DISCUSSION OF THE RESULTS

The Ti_3P type structure, and its relationships to the Fe_3P, α-V_3S and β-V_3S types, have been described and discussed at length earlier.[5-9] Here, we restrict the discussion to a few observations on Ti_3P-type α-Ta_3P and β-V_3S-type β-Ta_3P.

These two structures are indeed very similar, and movements of the atoms of the order of tenths of an Ångström are sufficient to transform one structure into the other. One might even suspect that the β crystals actually are polysynthetic twins of the α form, but the powder diffraction data (Table 1) and the reasonable values obtained for the temperature factors of the atoms in the β structure[1] definitely exclude this possibility. Regarding the

Table 2. Structure data for α-Ta_3P, including isotropic temperature factors, space group $P4_2/n$ (No. 86), origin at $\bar{1}$. $a = 10.1550(3)$ Å; $c = 5.0128(2)$ Å.

Atom	Position	x	y	z	B
Ta(1)	8*g*	0.15898(7)	0.65557(7)	0.7435(2)	0.38(1)
Ta(2)	8*g*	0.10483(7)	0.25374(7)	0.5044(2)	0.40(1)
Ta(3)	8*g*	0.05257(7)	0.54548(7)	0.2474(2)	0.41(1)
P	8*g*	0.0420(5)	0.2583(5)	0.0064(16)	0.64(6)

Table 3. Interatomic distances in α-Ta_3P. Distances shorter than 3.5 Å are listed.

Ta(1) – P	2.550(6)	Ta(3) – P	2.552(6)
– P	2.572(6)	– P	2.584(6)
– Ta(1)	2.664(1)	– Ta(2)	2.845(1)
– Ta(3)	2.933(1)	– Ta(3)	2.854(2)
– Ta(3)	2.964(1)	– Ta(2)	2.874(1)
– Ta(3)	2.967(1)	– Ta(3)	2.900(2)
– Ta(2)	3.085(1)	– Ta(1)	2.933(1)
– Ta(2)	3.093(1)	– Ta(1)	2.964(1)
– 4Ta(1)	3.136(1)	– Ta(1)	2.967(1)
– Ta(3)	3.178(1)	– P	3.159(5)
– Ta(3)	3.180(1)	– Ta(1)	3.178(1)
		– Ta(1)	3.180(1)
Ta(2) – P	2.561(5)	– Ta(2)	3.274(1)
– P	2.577(8)	– Ta(2)	3.395(1)
– P	2.595(5)	– P	3.414(5)
– P	2.597(8)		
– Ta(3)	2.845(1)	P – Ta(1)	2.550(6)
– Ta(3)	2.874(1)	– Ta(3)	2.552(6)
– Ta(2)	2.950(1)	– Ta(2)	2.561(5)
– Ta(1)	3.085(1)	– Ta(1)	2.572(6)
– Ta(1)	3.093(1)	– Ta(2)	2.577(8)
– 2Ta(2)	3.227(2)	– Ta(3)	2.584(6)
– Ta(3)	3.274(1)	– Ta(2)	2.595(5)
– 2Ta(2)	3.295(2)	– Ta(2)	2.597(8)
– Ta(3)	3.395(1)	– Ta(3)	3.159(5)
		– Ta(3)	3.414(5)

nature of the α/β transition, the structural similarities indicate a diffusion-less mechanism. The available data provide no definite information on this point.

The major structural difference between a β-V_3S type compound and a typical representative of the Ti_3P type structure lies in the nonmetal atom coordination. The phosphorus atoms in β-Ta_3P have eight near metal atom neighbours. Two additional metal atoms are situated at considerably larger distances. In Ti_3P, the phosphorus atoms have nine near metal neighbours at almost the same distances. A tendency to eight-coordination for the non-metal atoms in Ti_3P-type compounds has been observed for Nb_3P [10] and V_3P,[11] and this tendency is most pronounced for α-Ta_3P. The members in the series V_3P, Nb_3P, α-Ta_3P thus exhibit a gradual structural change towards the ultimate β-V_3S-type atomic arrangement. This and other structural features will be discussed in a more extensive survey of coordination and bonding in Fe_3P, Ti_3P, α-V_3S and β-V_3S type compounds to be published later.

Acknowledgements. Financial support from the Swedish Natural Science Research Council is gratefully acknowledged. S.P. thanks the International Seminars at the University of Uppsala and the Swedish International Development Authority (SIDA) for a travel grant.

REFERENCES

1. Phavanantha, P., Pontchour, C.-O., Pramatus, S., Andersson, Y. and Rundqvist, S. *Acta Chem. Scand. A 32* (1978) 515.
2. Rundqvist, S. *Nature (London) 211* (1966) 847.
3. Björkegren, J. and Andersson, Y. *New Phases in the Ta–P System*, Institute of Chemistry, University of Uppsala, Uppsala 1976, UUIC-B18-53.
4. Deslattes, R. D. and Henins, A. *Phys. Rev. Lett. 31* (1973) 972.
5. Rundqvist, S. *Acta Chem. Scand. 16* (1962) 1.
6. Rossteutscher, W. and Schubert, K. *Z. Metallkd. 56* (1965) 813.
7. Lundström, T. and Snell, P. O. *Acta Chem. Scand. 21* (1967) 1343.
8. Rundqvist, S. *Ark. Kemi 20* (1962) 67.
9. Lundström, T. *Ark. Kemi 31* (1969) 250.
10. Nawapong, P. C. *Acta Chem. Scand. 20* (1966) 2737.
11. Jawad, H., Lundström, T. and Rundqvist, S. *Phys. Scr. 3* (1971) 43.

Received May 29, 1978.

Acta Chemica Scandinavica A 32 (1978) 815–832

Conformational Analysis of Coordination Compounds. X. ^{1}H NMR Study of Paramagnetic Five-membered Diamine Chelate Rings

CLIFFORD J. HAWKINS and RUSSELL M. PEACHEY

Department of Chemistry, University of Queensland, Brisbane, Australia 4067

Dedicated to Jannik Bjerrum on the occasion of his 70th birthday

Conformational populations of a number of mono and tris five-membered diamine chelates of nickel(II) have been determined from their proton magnetic resonance spectra by a chemical shift method. Intrinsic chemical shift differences between protons in axial and equatorial orientations were determined directly from the spectra of the nickel(II) complexes of 3,3-dimethyl-1,2-ethanediamine for the primary amine ligands and of *N*,*N*,*N*′,*N*′-tetramethyl-1,2-propanediamine for the tertiary amine ligands. These ligands are stereospecific. The data for the secondary nitrogen ligands were determined by an indirect method based on *N*-methyl-1,2-ethanediamine. The influence of counter-ion and solvent on the conformational populations of $[Ni(en)_3]^{2+}$ has also been studied. In addition activation parameters have been determined for the configurational inversion of $[Ni(en)_3]^{2+}$ in dimethyl sulfoxide (DMSO) and 1.6 M aqueous NaCl and for the nitrogen inversion in mono complexes of secondary amine donors.

A technique based on proton-proton coupling constants has been utilized for the conformational analysis of diamagnetic diamine and aminoalcohol chelate rings.[1,2] For paramagnetic complexes the proton resonances are usually too broad to observe any fine structure due to coupling. A chemical shift technique based on the chemical shift difference between axial and equatorial protons or other nuclei, which has been used extensively for organic systems,[3] has been applied to tris(diamine) complexes of the diamagnetic metal ions, cobalt(III), rhodium(III), ruthenium(II), and platinum(IV).[4] However, for diamagnetic systems, if the determination of the intrinsic chemical shift difference between the axial and equatorial protons in a frozen conformation requires the use of a model compound, such as an analogous compound with a substituent that stereospecifically imposes a particular conformation on the system, long-range anisotropic shielding within the model system can significantly affect the chemical shift difference and make it a crude approximation for the 'intrinsic' value. For paramagnetic systems, in which contact interactions yield large chemical shift differences between axial and equatorial protons, the long-range anisotropic diamagnetic shielding factors are too small to affect the application of model systems. Because of this, complexes of nickel(II) have proven to be ideal for the application of the chemical shift technique to the conformational analysis of chelate rings.[5–10]

Milner and Pratt first reported the ^{1}H NMR spectra of the 1:1 nickel(II) 1,2-ethanediamine complex in aqueous solution in 1962.[11] A single CH resonance was observed. Zamaraev and coworkers varied the metal:ligand ratio and observed a single resonance for the 1:1 and 1:2 complexes and a two line spectrum for the 1:3 complex.[12] The observation of a single resonance for both the 1:1 and 1:2 complexes was attributed to fast conformational interconversion that averaged the CH resonances, whereas the interconversion was considered to be resisted in the 1:3 complex due to the close packing of the rings resulting in separate peaks for axial and equatorial protons.[12] Ho and Reilley later reinvestigated the 1:3 system and analysed the ^{1}H NMR spectrum in terms of incomplete averaging of the axial and equatorial protons due to

a difference in energy of the δ and λ conformations for a particular distribution of chelate rings.[6] The conformational interconversion was considered to be fast on the NMR time scale, but the inversion of the tris(bidentate) complexes was slow on this time scale. Ho and Reilley applied the chemical shift method of conformational analysis to determine the energy difference between the δ and λ conformations.[6] More recently, Cramer and Harris have reinvestigated $[Ni(en)_3]^{2+}$ and also studied a limited solvent and anion dependence of the conformational interconversion equilibrium.[9,10]

Reilley and his coworkers have extended their studies to tris(*meso*-2,3-butanediamine)nickel(II).[7] As the methine proton resonances could not be observed, the calculations of the conformer populations were based on observed methyl frequencies. The analogous system with the racemic isomer of the diamine provided no stereochemical information as only one resonance was observed and this was assigned to overlapped methyl and methine peaks.[7] An earlier report[13] that the 1:3 nickel(II) complexes of *meso*- and *racemic*-2,3-butanediamine have identical optical and ^1H NMR spectra is incorrect.[7]

Ho and Reilley have also applied the chemical shift technique to a number of 1:1 nickel(II) diamine complexes, in particular the complexes formed by *meso*- and *racemic*-*N*,*N*′-dimethyl-1,2-ethanediamine.[5] For this application, as for the above applications of this technique, it was necessary to know the chemical shift difference between an axial and an equatorial proton for the 'frozen' conformation. Five-membered diamine chelate rings invert rapidly on the NMR time scale even at low temperatures,[14,15] and therefore, this intrinsic chemical shift difference cannot be determined directly. A number of indirect methods have been used previously, but as discussed later in this paper, they have weaknesses associated with them. New approaches to this problem are employed in the current study which reinvestigates 1:1 and 1:3 nickel(II) diamine complexes in a number of solvents, and examines the influence of concentration and counter-ions on the conformer populations.

EXPERIMENTAL

Reagents. Anhydrous nickel chloride was prepared by adding freshly distilled thionyl chloride to nickel chloride hexahydrate, stirring for 1 h and removing the excess thionyl chloride under vacuum. The compound was stored over potassium hydroxide *in vacuo*. 1,2-Ethanediamine (en, Ajax) was dried and purified by distillation from sodium metal. 1,2-Propanediamine (pn, Ajax), *N*-methyl- (men), *N*,*N*-dimethyl- (*N*,*N*-dmen), *N*,*N*′-dimethyl- (*N*,*N*′-dmen), and *N*,*N*,*N*′,*N*′-tetramethyl-1,2-ethanediamine (tmen) (Koch-Light), 3,3-dimethyl-1,2-butanediamine (dmbn),[1] and *N*,*N*,*N*′,*N*′-tetramethyl-1,2-propanediamine (tmpn)[16] were distilled from barium oxide. The solvents used in the study, DMSO-d_6, methanol-d_4, acetone-d_6, acetonitrile-d_3, formamide, dimethylformamide and tetrahydrofuran, were purified and dried as has been described previously.[17] The salts employed, sodium chloride, sodium nitrate, sodium nitrite, sodium fluoride, sodium phosphate, sodium perchlorate, and potassium fluoride, were all AnalaR grade.

The 1:1 complexes were prepared in solution by dissolving anhydrous nickel chloride in slight excess over that required for a 1:1 ratio in the solvent required, adding the calculated weight of diamine, and making the solution up to a pre-determined volume.

$[Ni(en)_3]^{2+}$ was made in solution with a nickel:ligand ratio of 1:3.5. For the anion dependence investigations the calculated weight of salt was added before the solution was made up to volume. For the solvent dependence studies, solubility problems required the preparation of tris complexes with different counter-ions. The chloride, nitrate, and acetate salts were prepared by the published method[18] using the different nickel(II) salts. The tetraphenylborate salt was prepared by adding an excess of a filtered aqueous solution of sodium tetraphenylborate to an aqueous solution of $[Ni(en)_3]Cl_2$. The solid, which precipitated, was filtered off, washed well with water, and dried under vacuum. $[Ni(R\text{-pn})_3](MeCO_2)_2$ and $[Ni(dmbn)_3](MeCO_2)_2$ were prepared by an analogous method to the corresponding 1,2-ethanediamine complex.

Spectroscopic studies. All ^1H NMR spectra were recorded on a JEOL-PS-100 with a JEOL JES-VT-3 variable temperature controller. The temperatures were measured with a Chromel-Alumel thermocouple under full operating conditions before and after the recording of the spectra.

In the basic operating mode of Wide Sweep with a sweep width of 10.8 G, serious problems were encountered from the overlap of peaks emanating from the centre-band and the first lower side-band (8 kHz). This problem was overcome by employing Wide Offset, which allows a variable side-band of between 30 Hz and 30 kHz to be selected. In the Wide Sweep mode, both the superstabilizer and the lock cannot be used to minimize field drift. For each spectrum, therefore, four scans (two upfield and two downfield) were recorded to compensate for any small amount of drift. Also the conditions of

measurement, that is, high RF and AF levels, required the sample to be non-spinning and the pre-amplifier gain to be on low to maximize probe balance. The spectra were calibrated using the separation between the first and second lower sidebands which was equal to the preselected frequency of the variable oscillator. Sodium 3-trimethylsilylpropane-1-sulfonate was used as internal reference for the aqueous and DMSO solutions. The contact shifts were calculated from the peak for uncoordinated 1,2-ethanediamine.

RESULTS

Spectral analyses

Octahedral complexes of nickel(II) (S = 1) possess an orbital singlet ground state ($^3A_{2g}$ in O_h symmetry) and hence their isotropic shifts are essentially contact in origin[19] and are described for protons by equation (1),*

$$\delta_i^{iso} = A_i \left(\frac{\gamma_e}{\gamma_H}\right) \frac{g\beta S(S+1)}{6SkT} \qquad (1)$$

where the symbols have their usual meaning. The isotropic shift is proportional to T^{-1} (Curie behaviour) and a plot of δ_i^{iso} against T^{-1} should be a straight line with a slope proportional to A_i, the hyperfine coupling constant. Deviations from this linear relationship are indicative of the presence of equilibria between different structures or different spin states. If all equilibria are absent, a plot of $\delta_i^{iso} \times T$ against T should be independent of T. For a chelate ring undergoing rapid ring inversion, the observed isotropic shift for a particular nucleus will be a time-averaged shift over all species present in the conformational equilibrium and the plots of $\delta \times T$ against T generally will not be independent of T except where one conformation markedly predominates, or the equilibrium is between two conformations of equal energy.

* Resonances which are less shielded than the diamagnetic reference are assigned here a positive isotropic shift according to the normal convention for chemical shifts.

Mono complexes

1,2-Ethanediamine. For the 1:1 complex in water a single peak was observed at δ 93.8 at 300 K. A plot of δ against T^{-1} was a straight line over the range 300 – 365 K and the plot of $\delta \times T$ against T (Fig. 1) was independent of temperature consistent with the rapid chelate ring inversion between the enantiomeric δ and λ conformations. In fact, if wet methanol was used below ambient, the δ against T plot was linear over the range 183 – 365 K. In methanol and DMSO, a single peak was again observed. The plots of δ against T^{-1} were linear over the temperature ranges 189.7 – 301.5 K (methanol) and 301.75 – 455.5 K (DMSO) but the $\delta \times T$ against T plots showed positive deviations from Curie behaviour as the temperature increased (Fig. 1).

3,3-Dimethyl-1,2-butanediamine. At 301.75 K three peaks were observed in water at δ 3.2 (9 H), 11.7 (2 H) and 170.8 (1 H). For $[Ni(R\text{-dmbn})S_4]^{2+}$, where S is the solvent and the (*R*) configuration is assumed to simplify the discussion although the racemate was used, the λ conformation with the *tert*-butyl group equatorial should be stereospecifically favoured because of the severe non-bonded interactions between the axial *tert*-butyl group and an apical ligand in the alternative δ conformation. This stereospecificity was confirmed by the strict observance of Curie behaviour in the δ against T^{-1} and $\delta \times T$ against T plots (Fig. 2) for the

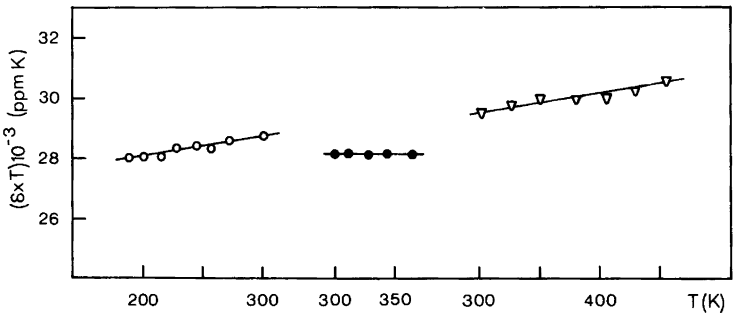

Fig. 1. $\delta \times T$ against T for $[Ni(en)S_4]^{2+}$: ○, S = MeOH; ●, S = H_2O; ▽, S = Me_2SO.

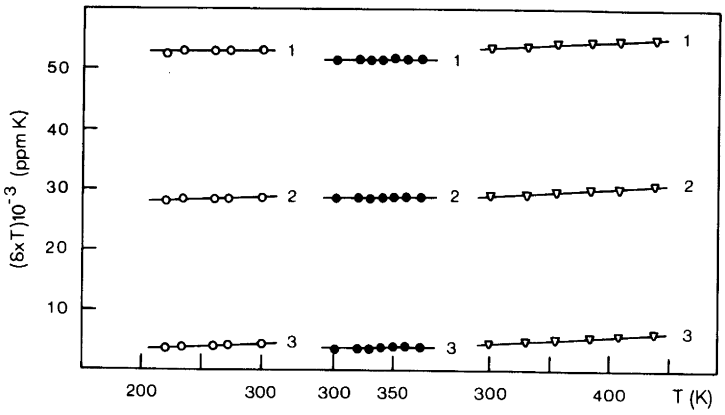

Fig. 2. Plot of $\delta \times T$ against T for $[Ni(dmbn)S_4]^{2+}$: ○, S=MeOH; ●, S=H_2O; ▽, S=Me_2SO for 1. H_{eq}, 2. mean of H_{eq} and H_{ax}, 3. H_{ax}.

individual protons. The 1-proton peak has therefore been assigned to the equatorial methylene proton H2 and the 2-proton peak to the two axial protons H1 and H3 (Fig. 3). This assignment is consistent with the Karplus-like relationship between the isotropic shift and the dihedral angle between the NiNC and NCH planes (Fig. 4).[12] The dihedral

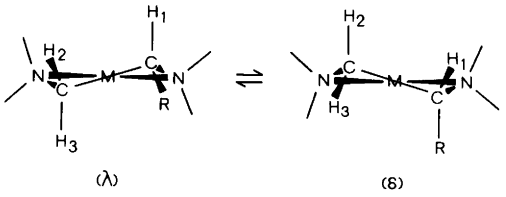

Fig. 3. Conformational interconversion for a C-substituted five-membered diamine chelate ring.

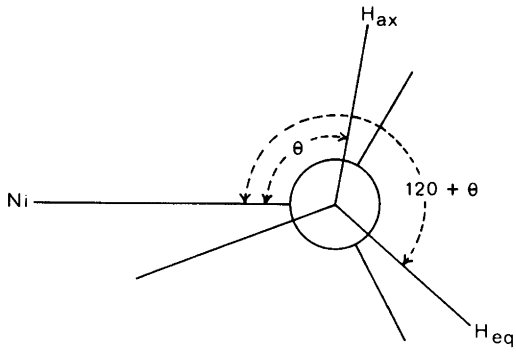

Fig. 4. Dihedral angles for Ni–N–C–H.

angle for the equatorial proton approaches 180° whereas it is in the vicinity of 60° for the axial protons, and hence the equatorial proton should experience a larger isotropic shift.

Considering the mean of the $\delta \times T$ against T lines for the axial and equatorial peaks, a straight line independent of temperature was obtained for the aqueous solution but, for the methanol and DMSO solutions, the line showed a positive deviation with increasing temperature (Fig. 2) as was found for the 1,2-ethanediamine complex.

1,2-Propanediamine. At 329.2 K three peaks were observed in water, at δ 18.0, 21.0, and 148.3 with intensity ratios 3:2:1. For $[Ni(R\text{-pn})S_4]^{2+}$, the λ conformation with the methyl equatorial is preferred but not to the exclusion of the δ conformation with the methyl axial.[20,21] Hence the time-averaged signals for each nucleus will reflect the frozen λ conformation more than the δ. The one-proton peak at δ 148.3 corresponds to the methylene proton that is equatorial in the λ conformation (H2 in Fig. 3). The two-proton peak at δ 21.0 corresponds to the two protons that are axial in the λ conformation (H1 and H3). The remaining signal at δ 18.0 has been assigned to the methyl group.

In the plot of $\delta \times T$ against T (Fig. 5) the lines corresponding to the equatorial and axial protons showed deviations from normal Curie behaviour. For the 'equatorial' proton a negative deviation was noted: as the temperature increased, the chemical shift was less than that for normal Curie behaviour. This arose because, as the temperature increased, the less favoured conformer became more

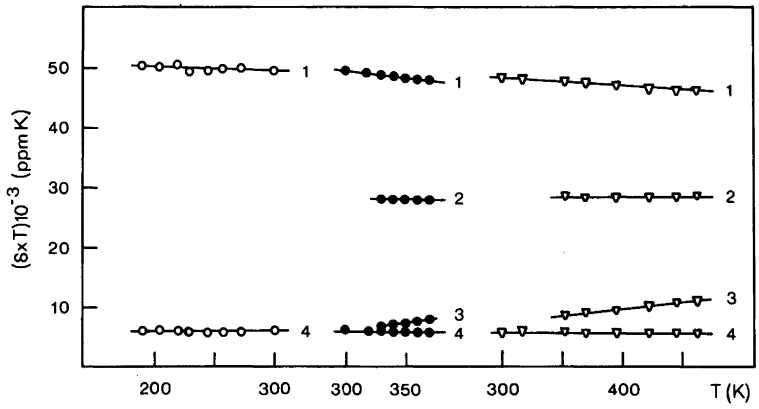

Fig. 5. Plot of $\delta \times T$ against T for $[Ni(pn)S_4]^{2+}$: ○, S=MeOH; ●, S=H_2O; ▽, S=Me_2SO for 1. H_{eq}, 2. mean of H_{eq} and H_{ax}, 3. H_{ax}, 4. CH_3.

populated and the 'equatorial' proton became more weighted towards the axial isotropic shift. The axial proton correspondingly showed a positive deviation.

The pattern of peaks found in methanol and DMSO was similar to that found in water, and hence the same assignments apply. In methanol, the methyl resonance was superimposed on the axial proton resonance at all temperatures, and hence the same chemical shift has been assumed for the protons under the peak. The mean of the $\delta \times T$ against T lines for the axial and equatorial protons again was found to be independent of temperature for the aqueous solution, but showed a positive deviation from Curie behaviour for the methanol and DMSO solutions (Fig. 5).

N-*Methyl-1,2-ethanediamine.* The spectrum of the complex in water had four peaks, which at 300 K were positioned at δ 59.2, 125.4, 133.9 and 140.6. The peak at δ 133.9 was the largest and has been assigned to the methyl protons. The remaining three had intensity ratios 2:1:1 for the above order.

When the coordinated nitrogen has the (*S*) configuration, the λ conformation has the methyl group equatorial, which is preferred to the alternative δ conformation with the methyl axial. As for the 1,2-propanediamine complex, the protons that are predominantly equatorial will resonate at lowest field because of their angular relationship with respect to the paramagnetic nickel. The resonances at δ 140.6 and 125.4 have therefore been assigned to the two protons that are equatorial in the λ conformation. They have different chemical shifts because they experience different contact interactions as one is on a carbon adjacent to a secondary nitrogen and the other is on a carbon adjacent to a primary nitrogen. Ho and Reilley assigned the more downfield peak to the methylene proton adjacent to the primary nitrogen arguing that *N*-alkyl substitution would weaken the Ni–N bond and reduce the coupling with the adjacent methylene protons.[5] From an extended Hückel molecular orbital calculation, Cramer came to the opposite conclusion that the protons adjacent to the substituted nitrogen would resonate at lowest field.[22] This latter conclusion is supported by the observation that the average chemical shift of the methylene protons of the *N,N'*-dimethyl-1,2-ethanediamine complex is greater than that for the 1,2-ethanediamine complex implying that a greater degree of delocalization of unpaired electrons takes place through the secondary nitrogen donor. Therefore the latter assignment will be used in this paper. The remaining peak at δ 59.2 (2 H) has been assigned to the two protons that are axial in the λ conformation. It is interesting to note that the two axial protons showed no observable chemical shift difference arising from the different degrees of substitution at the two nitrogens.

For the aqueous solution, the plot of $\delta \times T$ against T was what was expected for a ring undergoing rapid exchange between conformers of differing populations: the 'equatorial' and 'axial' proton lines showed negative and positive deviations, respectively, while the lines for the methyl protons and the mean of the 'equatorial' and 'axial' protons showed

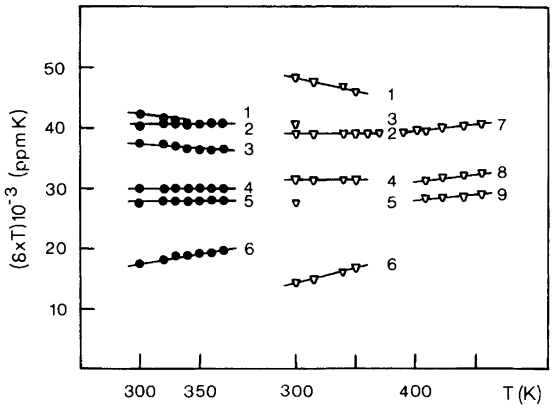

Fig. 6. Plot of $\delta \times T$ against T for $[Ni(men)S_4]^{2+}$: ●, S = H_2O; ▽, S = Me_2SO for 1. $^{s}NCH_{eq}$; 2. NCH_3; 3. $^{p}NCH_{eq}$; 4. mean of $^{s}NCH_{eq}$ and $^{s}NCH_{ax}$; 5. mean of $^{p}NCH_{eq}$ and $^{p}NCH_{ax}$; 6. H_{ax}; 7. NCH_3; 8. NCH_2; 9. $^{p}NCH_2$.

no dependence on T (Fig. 6).

In methanol solution, the pattern of peaks was as for water, and therefore the same assignments were made for the various peaks. However, no variable temperature data were obtained because as the temperature was decreased, the peaks broadened to such an extent that the chemical shifts measured were extremely inaccurate.

In DMSO, the pattern was different to that found for water. At 301.5 K the methyl group was at δ 129.3, approximately the same position as in water, but both equatorial protons were further downfield than in water with the proton adjacent to the primary nitrogen resonating downfield of the methyl group. The plot of $\delta \times T$ against T for the region 300 – 340 K showed the characteristic deviations for the equatorial and axial protons, but the mean of the axial and equatorial lines did not show any temperature dependence. Above 340 K the axial and equatorial $\delta \times T$ against T lines converged at a greater rate than expected from the conformational equilibrium until at 380 K the protons had been completely averaged. Above this temperature, averaged peaks were observed in the spectrum for the two sets of protons. These peaks and the methyl peak all showed positive deviations from Curie behaviour. The averaging of the peaks is due to the inversion of the coordinated secondary nitrogen and an approximate value for the rate of inversion was calculated to be 6.4×10^3 s^{-1} from the expression,

$$k = \frac{\pi \Delta \nu_{ax,eq}}{\sqrt{2}} \qquad (2)$$

where $\Delta \nu_{ax,eq}$, the separation of the axial and equatorial resonances without inversion, was estimated to be 2870 Hz at 380 K by extrapolating the $\delta \times T$ against T curves from where no inversion effects were observed.

N,N-*Dimethyl-1,2-ethanediamine.* As the ligand does not have an asymmetric centre, the δ and λ conformations will be of equal energy. In water, the spectrum consisted of two peaks at δ 99.9 and 65.2 with an intensity ratio of 8:2. Obviously the peaks due to methyl protons and one set of methylene protons overlap under the δ 99.9 peak. As the methylene protons in the 1,2-ethanediamine complex resonated at δ 94.0, the methylene protons adjacent to the primary nitrogen have been assigned to the resonance at δ 99.9 and the methylene protons adjacent to the tertiary nitrogen to the resonance at δ 65.2. The $\delta \times T$ against T plots showed a slight dependence on temperature (Fig. 7).

For the three solvents, water, methanol, and DMSO, there were changes in the relative positions of the resonances for the three types of nuclei. The resonance for the methylene protons adjacent to the primary nitrogen, which was under the methyl peak in water, moved downfield for methanol and DMSO, whereas the resonances for the methyl and the other methylene protons moved upfield. For methanol and DMSO, the $\delta \times T$ against T plots

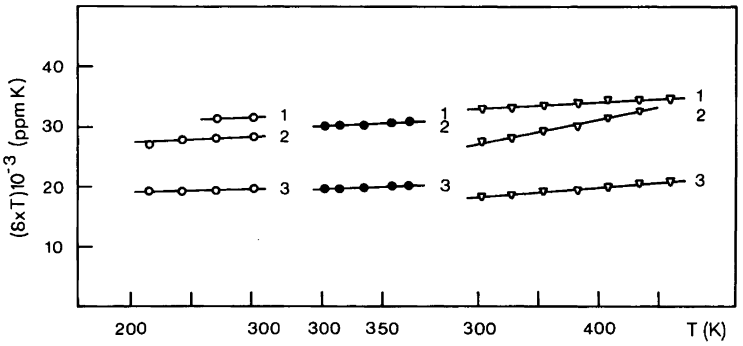

Fig. 7. Plot of $\delta \times T$ against T for $[Ni(N,N\text{-dmen})S_4]^{2+}$: ○, S=MeOH; ●, S=$H_2O$; ▽, S=$Me_2SO$ for 1. $^{P}NCH_2$, 2. NCH_3, 3. $^{t}NCH_2$.

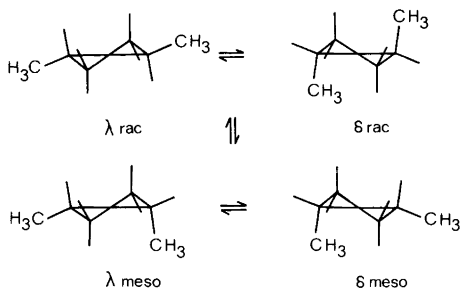

Fig. 8. Chelate rings for *N,N'*-dimethyl-1,2-ethanediamine.

were all straight lines, but as observed for the other complexes showed a dependence on T.

N,N'-*Dimethyl-1,2*-ethanediamine. In $[Ni(N,N'\text{-dmen})S_4]^{2+}$ the two nitrogens are asymmetric and give rise to a racemic and a *meso* form as shown in Fig. 8. In the racemic form, the two methyl groups are either both axial or both equatorial, whereas in the *meso* form both conformations have one equatorial and one axial methyl group.

In water, five peaks were observed at 301.5 K at δ 40.0, 86.7, 129.1, 133.8 and 156.3 with the broad peak with δ 86.7 consisting of two poorly resolved peaks. The same assignments were deduced here as

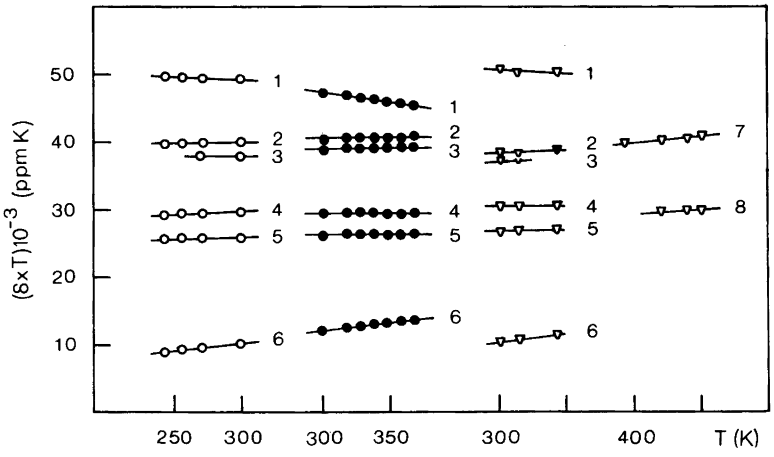

Fig. 9. Plot of $\delta \times T$ against T for $[Ni(N,N'\text{-dmen})S_4]^{2+}$: ○, S=MeOH; ●, S=$H_2O$; ▽, S=$Me_2SO$ for 1. H_{eq}, *rac*; 2. NCH_3, *rac*; 3. NCH_3, *meso*; 4. mean of H_{eq} and H_{ax}, *rac*; 5. $H_{ax,eq}$, *meso*; 6. H_{eq}, *rac*; 7. NCH_3; 8. CH_2.

has been published by Ho and Reilley.[5] The peaks at 129.1 and δ 133.8 arise from the methyl protons of the *meso* and racemic forms. The peaks at δ 40.0 and 156.3 were assigned to the 'axial' and 'equatorial' methylene protons, respectively, in the racemic form. The $\delta \times T$ against T plots for these two resonances showed positive and negative deviations from Curie behaviour, whereas their mean was independent of temperature (Fig. 9). For the *meso* isomer, both conformations are of equal energy and the broad peak corresponding to the four methylene protons had a $\delta \times T$ against T line independent of T. At 301.5 K the ratio of the total areas of the methylene peaks for the racemic and *meso* isomers was 1.3.

The data for methanol were similar to that in water. The $\delta \times T$ against T plots are given in Fig. 9. The racemic:*meso* ratio was calculated to be 2.2 at 300 K. The data for DMSO were also similar until 360 K. Above 360 K all the methyl protons and all the methylene protons were averaged, again due to inversion of the coordinated nitrogen. The two averaged lines had $\delta \times T$ against T plots with a positive deviation from Curie behaviour. At 301.5 K the racemic:*meso* ratio was calculated to be 1.7. The rate of inversion of the asymmetric nitrogens was calculated at the coalescence temperature of 370 K to be 9.0×10^3 s^{-1} based on an estimated $\Delta\nu_{ax,eq}$ value of 4054 Hz.

N,N,N',N'-*Tetramethyl-1,2-ethanediamine.* As the coordinated ligand has no asymmetric centres, the δ and λ conformations are of equal energy, and one peak would be expected for the four methyl groups and one for the four methylene protons. In all three solvents these two resonances were observed with the methyl protons to lower field of the methylene protons. The resonances in water are to lower field of the corresponding resonances in methanol and these in turn are to lower field of the resonances in DMSO.

In water, as the temperature was increased above ambient, a precipitate formed, and therefore, only the probe temperature spectrum was recorded. This did not happen in methanol and DMSO. The $\delta \times T$ against T plots for the methanol solution showed positive deviations from Curie behaviour (Fig. 10). For the DMSO solution, the methylene protons showed a positive deviation but the methyl protons showed a curved line.

N,N,N',N'-*Tetramethyl-1,2-propanediamine.* The complex with this ligand was not sufficiently soluble in water to give a spectrum from which accurate chemical shifts could be obtained. The methanol and DMSO solutions were measured at 300 K. In methanol, the equatorial methylene proton resonated at δ 126.5, the NCH_3 groups at δ 106.7 and 91.2, and the CCH_3 at δ 7.4. The peak for the two axial protons was under the CCH_3 peak. In DMSO the observed chemical shifts were δ 127.7, 100.8, 88.0, and 5.5.

Tris complexes

As has been found previously,[6,9,10,12] the ^1H NMR spectrum of $[Ni(en)_3]^{2+}$ had two CH resonances. These result from the fact that for one distribution of the chelate rings, say Δ, the δ and λ conformations are not equally populated, and therefore the CH resonances are not averaged to one line. Implicit in this is that the $\Delta \rightarrow \Lambda$ inversion is slow on the NMR time scale. In line with the previous work, the downfield peak has been assigned to the protons that are largely equatorial and the upfield resonance to the 'axial' protons.

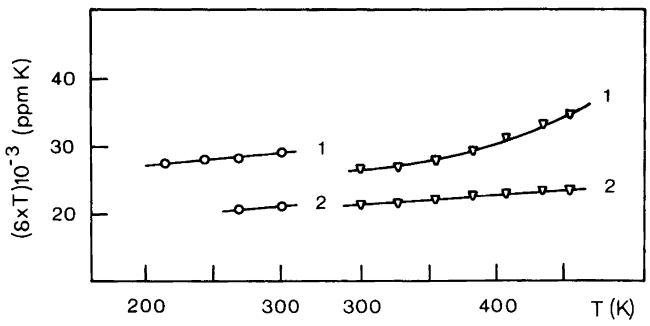

Fig. 10. Plot of $\delta \times T$ against T for $[Ni(tmen)S_4]^{2+}$: ○, S = MeOH; ▽, S = Me_2SO for 1. NCH_3, 2. $^1NCH_2$.

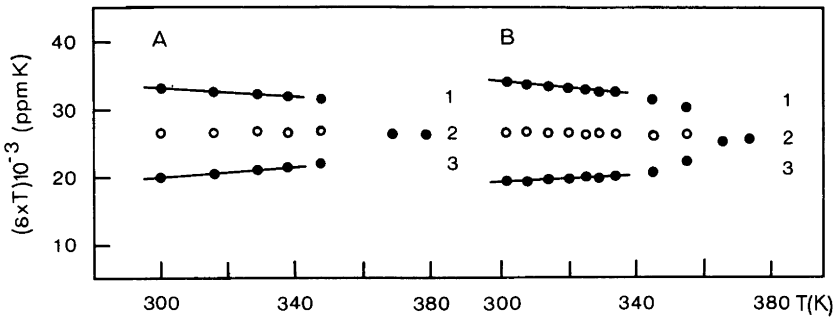

Fig. 11. Plot of $\delta \times T$ against T for aqueous solutions of A. $[Ni(en)_3]Cl_2$; B. $[Ni(en)_3]Cl_2 + 1.6$ M NaCl for 1. H_{eq}, 2. mean of H_{eq} and H_{ax}, 3. H_{ax}.

The plots of $\delta \times T$ against T for these two peaks for $[Ni(en)_3]Cl_2$ in water exhibited deviations from Curie behaviour with the 'equatorial' peak showing a negative deviation and the 'axial' a positive deviation (Fig. 11). The expected horizontal straight-line was observed for the mean of the two lines. As for the mono complexes, the deviations indicate a shift in the equilibrium between the λ and δ conformations. At temperatures above 340 K, the lines deviated at an increased rate and finally coalesced at approximately 373 K. This is due to the rapid configurational inversion of the complex.[6]

The variable temperature ^1H NMR spectra of $[Ni(en)_3]Cl_2$ (0.4 *M*) in the presence of added sodium chloride (1.6 M) showed similar gross features to the above spectra but the chemical shift differences between the exchanging axial and equatorial protons, $\Delta\delta^{obs}$, were significantly larger (Fig. 11). The variable temperature spectra of $[Ni(en)_3](MeCO_2)_2$ in methanol were attempted but, as the temperature was lowered, the peaks broadened to such an extent that all accuracy in chemical shift position was lost.

The effects of counter-ion and solvent were examined at 301.5 K and the results are presented in Table 1. The effects of added salts were also

Table 1. Isotropic shifts and n_λ values for 0.4 M Δ-$[Ni(en)_3]X_2$ at 301.5 K.[a]

Solvent	δ_{ax}	δ_{eq}	$\Delta\delta^{obs}$	n_λ
X = Cl				
H_2O	67.8	107.2	39.4	0.62
$HCONH_2$	57.5	118.8	61.3	0.69
$X = NO_3$				
H_2O	71.4	103.4	32.0	0.60
$HCONH_2$	61.9	112.8	50.9	0.66
Me_2SO	47.4	129.5	82.1	0.76
$X = MeCO_2$				
H_2O	71.0	105.8	34.8	0.61
$HCONH_2$	56.4	117.9	61.5	0.69
MeOH	49.2	129.4	80.2	0.75
$X = BPh_4$[b]				
MeCN			70.2	0.60
Me_2CO			50.1	0.66
THF[c]			50.8	0.66
$HCONMe_2$			31.5	0.72
Me_2SO			87.8	0.78

[a] Solutions prepared from isolated complex salt. [b] en resonances obscured by BPh_4 resonances and therefore only $\Delta\delta$ obs could be determined accurately. [c] Tetrahydrofuran.

Table 2. Isotropic shifts and n_λ values for 0.4 M Δ-$[Ni(en)_3]X_2$ in presence of NaCl at 301.5 K.

[NaCl] (M)	δ_{ax}	δ_{eq}	$\Delta\delta^{obs}$	n_λ
X = Cl				
0.0	69.1	105.5	36.4	0.61
0.2	67.9	106.8	38.9	0.62
0.4	66.9	107.5	40.6	0.63
0.8	66.8	109.6	43.8	0.64
1.2	65.8	110.9	45.1	0.64
1.6	63.9	112.1	48.2	0.65
$X = NO_3$				
0.0	71.3	103.2	31.9	0.60
0.4	69.7	105.6	36.0	0.61
1.6	67.5	108.6	41.1	0.63
2.0	64.9	110.9	46.0	0.64

investigated. Sodium chloride was found to have a significant effect on $\Delta\delta^{obs}$. The results are given in Table 2. However, other salts did not have a marked effect. The maximum concentration of salt added to $[Ni(en)_3]X_2$ (0.4 M) and the observed change in $\Delta\delta^{obs}$ were as follows: for $X^- = Cl^-$, NaF, 0.8 M, 0.2; KF, 3.0 M, 2.7; $NaNO_3$, 1.2 M, 0.3; $NaNO_2$, 2.0 M, 1.4; Na_3PO_4, 0.4 M, 0.4; $NaClO_4$, 0.4 M, 0.0; for $X^- = NO_3^-$, KF, 1.6 M, 2.3; $NaNO_3$, 1.2 M, 1.2; K_3PO_4, 0.8 M, 1.3. These results of a concentration dependence study are given in Table 3. The study showed that the chemical shift difference for both the chloride and nitrate salts increased markedly with concentration. A similar concentration dependence study (0.4 to 1.6 M) with the mono complexes of 1,2-ethanediamine and 1,2-propanediamine showed no detectable change in the peak position. The same result was obtained when sodium chloride (0.2 to 1.2 M) was added to the mono complexes (0.4 M). For all of the above investigations with $[Ni(en)_3]^{2+}$, the mean chemical shift for the axial and equatorial protons did not show a significant variation even for those systems where the individual chemical shifts showed marked changes.

The variable temperature spectra of $[Ni(pn)_3](MeCO_2)_2$ and $[Ni(dmbn)_3](MeCO_2)$ were also studied. Compared to the mono complexes with half-band widths of about 4 ppm, the tris complexes gave rather broad resonances, with half-band widths of the order of 40 ppm. As a result, the 'axial' protons could not be distinguished from other resonances. For $[Ni(pn)_3]^{2+}$, the axial protons were assigned the same chemical shift as the methyl protons at 301.5 K. The equatorial proton resonance for $[Ni(pn)_3]^{2+}$ was found to give a negative deviation from Curie Law confirming changes in conformer populations with temperature, whereas for $[Ni(dmbn)_3]^{2+}$ the equatorial resonance δ 169.2 at 301.5 K strictly followed Curie behaviour consistent with the stereospecificity of this ligand. For $[Ni(pn)_3]^{2+}$, assuming that $\delta \times T$ for the mean of the 'equatorial' and 'axial' resonances is independent of temperature, it is possible to estimate the $\delta \times T$ against T plot for the 'axial' proton. Spectra were also recorded for $[Ni(pn)_3]^{2+}$ in a number of solvents. The results are presented in Table 4. The 'axial' proton's resonance was obscured by the methyl resonance and hence it was assigned the same chemical shift as the methyl.

Table 3. Isotropic shifts and n_λ values of Δ-$[Ni(en)_3]X_2$ as a function of concentration at 301.5 K.

Conc[a] (M)	δ_{ax}	δ_{eq}	$\Delta\delta^{obs}$	n_λ
X = Cl				
0.4	67.8	107.2	39.4	0.62
0.8	65.8	110.0	44.2	0.64
1.2	62.6	113.2	50.6	0.66
$X = NO_3$				
0.4	71.4	103.4	32.0	0.60
1.2	69.4	106.4	37.0	0.62
1.6	67.1	109.0	41.9	0.63

[a] Solutions prepared from isolated complex salt.

Table 4. Isotropic shifts and n_λ values for $[Ni(R\text{-pn})_3]X_2$ at 301.5 K.[a]

Solvent	$\delta_{CH_3}, \delta_{ax}$	δ_{eq}	$\Delta\delta^{obs}$	n_λ
X = Cl[b]				
H_2O	19.1	157.4	138.3	0.94
$HCONH_2$	16.0	153.2	137.2	0.93
$X = NO_3$[c]				
$HCONH_2$	15.9	153.7	137.7	0.93
Me_2SO	19.7	157.7	138.0	0.93
$X = MeCO_2$[c]				
H_2O	17.9	157.1	139.2	0.94
MeOH	18.2	158.2	140.0	0.94
$HCONH_2$	17.6	158.6	141.0	0.94

[a] Solutions prepared from isolated complex salt. [b] At 0.4 M. [c] At 0.8 M.

The approximate rates of the $\Delta \rightleftarrows \Lambda$ inversion were calculated for the aqueous solution containing 1.6 M NaCl and for the DMSO solution by using the equation,[23]

$$k_i = (\pi/\sqrt{2})(\Delta\nu_{ax,eq}^2 - \Delta\nu_T^2)^{\frac{1}{2}} \quad (3)$$

where $\Delta\nu_{ax,eq}$ is the frequency separation in the absence of inversion and $\Delta\nu_T$ is the observed frequency separation at temperature T, both expressed in Hz. The experimental data and the calculated rates are given in Table 5. From these rates, the enthalpies and entropies of activation were calculated from a plot of $-R \ln (k_i h/kT)$ against T^{-1} according to the Eyring equation,

$$-R \ln (k_i h/kT) = \Delta H^{\neq} T^{-1} - \Delta S^{\neq} \quad (4)$$

Table 5. Rates of inversion for $Ni(en)_3)Cl_2$. T is in K, $\Delta\nu_{ax,eq}$ and $\Delta\nu_T$ are in Hz, and k_i is in s^{-1}.

T	$\Delta\nu_{ax,eq}$	$\Delta\nu_T$	k_i
(a) 1.6 M NaCl			
345	33.90	32.2	2355
350	32.30	28.3	3459
355	30.99	22.3	4780
360	29.72	14.7	5738
362.5	28.96	9.7	6062
365	28.20	0	6265
(b) DMSO			
365	59.2	57.8	2843
370	57.3	53.5	4558
375	55.2	49.1	5603
380	53.2	41.8	7311
385	51.4	27.5	9647
390	49.7	13.9	10600
395	49.1	0	10907

The values obtained were for 1.6 M NaCl, $\Delta H^{\neq}$ 48.1 ± 6.2 kJ mol^{-1}, $\Delta S^{\neq}$ -41.2 ± 17.3 JK^{-1} mol^{-1}, $\Delta G^{\neq}$ (300 K) 60.5 ± 11.4 kJ mol^{-1}; for DMSO, $\Delta H^{\neq}$ 50.3 ± 6.0 kJ mol^{-1}, $\Delta S^{\neq}$ -41.3 ± 15.9 JK^{-1} mol^{-1}, $\Delta G^{\neq}$ (300 K) 62.7 ± 10.8 kJ mol^{-1}.

Insufficient data from both Reilley's investigations[6] and this study of $[Ni(en)_3]^{2+}$ in water, prevented a calculation of enthalpies and entropies of activation in this solvent. However, the free energy of activation at coalescence was calculated from the Eyring equation from the rate estimated from eqn. (2). Both sets of data gave $\Delta G^{\neq}$ 65.7 kJ mol^{-1} at 374 K.

Conformation analysis – chemical shift method

Because the conformations interconvert rapidly, the observed chemical shifts, for example δH2 and δH3 for protons H2 and H3 in Fig. 3, are weighted averages of their values in the frozen λ and δ conformations.

$$\delta H2 = n_\lambda \delta H2(\lambda) + n_\delta \delta H2(\delta) \quad (5)$$

$$\delta H3 = n_\lambda \delta H3(\lambda) + n_\delta \delta H3(\delta) \quad (6)$$

where n_λ and n_δ are the mol fractions of the λ and δ conformations, respectively, and are related by

$$n_\lambda + n_\delta = 1 \quad (7)$$

abbreviating eqn. (1) to

$$\delta_i^{iso} = K_i T^{-1} \quad (8)$$

eqns. (5) and (6) can be expressed as

$$T\delta H2 = n_\lambda K_{H2}(\lambda) + n_\delta K_{H2}(\delta) \quad (9)$$

$$T\delta H3 = n_\lambda K_{H3}(\lambda) + n_\delta K_{H3}(\delta) \quad (10)$$

By addition and subtraction of eqns. (9) and (10), the following equations are obtained:

$$T(\delta H2 + \delta H3) = n_\lambda K_{H2}(\lambda) + n_\lambda K_{H3}(\lambda) + n_\delta K_{H2}(\delta) + n_\delta K_{H3}(\delta) \quad (11)$$

$$T(\delta H2 - \delta H3) = n_\lambda K_{H2}(\lambda) - n_\lambda K_{H3}(\lambda) + n_\delta K_{H2}(\delta) - n_\delta K_{H3}(\delta) \quad (12)$$

Reilley made the assumptions that $K_{H2}(\lambda) = K_{H3}(\delta)$ and $K_{H3}(\lambda) = K_{H2}(\delta)$, which imply that the hyperfine coupling constants for H2(λ) and H3(δ) and for H3(λ) and H2(δ) are identical. These assumptions are used here, but their validity will be discussed later. Taking eqns. (11) and (12), and utilizing relation (7) and the above assumptions, the final equations can be expressed as

$$T(\delta H2 + \delta H3) = K_{H2}(\lambda) + K_{H3}(\lambda) \quad (13)$$

$$T(\delta H2 - \delta H3) = (2n_\lambda - 1)\{K_{H2}(\lambda) - K_{H3}(\lambda)\} \quad (14)$$

According to eqn. (13), the product of the temperature and the mean of the chemical shifts for H2 and H3 should be independent of temperature.

From eqn. (8)

$$K_{H2}(\lambda) - K_{H3}(\lambda) = T\{\delta H2(\lambda) - \delta H3(\lambda)\} \quad (15)$$

and eqn. (14) can be rearranged to give

$$n_\lambda = 0.5[1 + (\delta H2 - \delta H3)/\{\delta H2(\lambda) - \delta H3(\lambda)\}] \quad (16)$$

or more simply

$$n_\lambda = 0.5[1 + \Delta\delta^{obs}/\Delta\delta^{int}] \quad (17)$$

where $\Delta\delta^{int}$ is the intrinsic chemical shift difference between axial and equatorial protons in the frozen conformation.

The values of n_λ and hence values of the equilibrium constant, $K_{\lambda\delta}$, and the free energy difference for the $\lambda \rightleftarrows \delta$ equilibrium can be calculated from the experimental data if a value for $\Delta\delta^{int}$ is known. Ho and Reilley determined $\Delta\delta^{int}$ to be 182 at 305.1 K for $[Ni(N,N'\text{-dmen})(OH_2)_4]^{2+}$ by an indirect method based on the assignment of a contact shift of 6 ppm for the "frozen" axial proton.[5] This value was chosen because it was the value found for the ethylenic axial proton in $[Ni(edta)]^{2-}$. The value of $\Delta\delta^{int}$ 182 yielded a good straight-line plot for $\log K_{\lambda\delta}$ against T^{-1}. However, it was found that the correlation coefficient for the fit of Ho and Reilley's data to a straight line approached unity as $\Delta\delta^{int}$ was allowed to increase to unrealistic values. Further, $[Ni(edta)]^{2-}$ is a very poor model compound because the nitrogens are tertiary and the diamine chelate ring in that complex is under considerable strain, which is relieved by the chelate ring being flattened compared to the bidentate situation.[24] For $[Ni(en)_3]^{2+}$, Ho and Reilley determined a value of $\Delta\delta^{int}$ 152 at 305.1 K by using a similar least squares fit method.[6]

In this paper, complexes of 3,3-dimethyl-1,2-butanediamine were used as models to determine $\Delta\delta^{int}$ for primary amines. The *tert*-butyl group stereospecifically restricts the conformation to λ for the (*R*) configuration.[25] In this conformation with the *tert*-butyl group equatorial the geometry of the ring is virtually identical to the related 1,2-ethanediamine chelate ring, and substituted diamine chelates where the substituents are equatorial.[25] The axial and equatorial proton resonances were found to obey Curie Law strictly, consistent with the stereospecificity of this ligand (Fig. 2). The values of $\Delta\delta^{int}$ determined from $[Ni(dmbn)S_4]^{2+}$ were for water 159.6, methanol 162.2, and DMSO 163.6 at 300 K. In the spectrum of $[Ni(dmbn)_3]^{2+}$ the resonance for the axial protons was not observed, but the equatorial proton had δ 169.2 at 301.5 K compared to δ 170.9 for $[Ni(dmbn)(OH_2)_4]^{2+}$. It was assumed therefore that $\Delta\delta^{int}$ is the same for the mono and tris complexes. The value of $\Delta\delta^{int}$ 159.6 at 300 K which corresponds to 158.8 at the ambient temperature of 301.5 K was also used for the tris complexes in methanol and DMSO because, in contrast to the mono complexes, the solvents are not in the primary coordination sphere.

The value of $\Delta\delta^{int}$ for a secondary nitrogen donor was calculated using $\Delta\delta^{int}$ for a primary nitrogen and the $\Delta\delta^{obs}$ values for the primary and secondary nitrogens from the *N*-methyl-1,2-ethanediamine complex. This yielded 196.2, 207.4, and 212.1 for water, methanol and DMSO solutions, respectively, at 300 K.

The complex $[Ni(tmpn)S_4]^{2+}$ was used as the model for the determination of $\Delta\delta^{int}$ for tertiary nitrogens. It has been found to exist exclusively in the conformation with the methyl equatorial because in the alternative conformation there is a severe 1,3-diaxial interaction between methyl groups.[1] Because of insolubility problems, the value for aqueous solution could not be determined, but in methanol and DMSO the values were 119.1 and 122.4, respectively, at 300 K. Based on the trend in $\Delta\delta^{int}$ values with solvent for the primary and secondary nitrogens, the value in water for the tertiary would be of the order of 113. Separate signals were observed for the axial and equatorial NCH_3 groups in $[Ni(tmpn)S_4]^{2+}$. The separation (MeOH, 15.5; Me_2SO, 12.8 at 300 K) gives $\Delta\delta^{int}$ for $N(CH_3)_2$. The value in water would be approximately 18.

With these above values of $\Delta\delta^{int}$, n_λ was computed from eqn. (17), and from this, $K_{\lambda\delta}$ and ΔG were calculated at each temperature, and ΔH and ΔS were determined from a plot of $-R \ln K$ against T^{-1} using a weighted least-squares method of analysis. The results are summarized for the mono complexes in Table 6. For the tris complexes, the free energy differences for the equilibria

$$\Delta(\lambda\lambda\lambda) \rightleftarrows \Delta(\lambda\lambda\delta) \quad (\Delta G_1^\circ)$$
$$\Delta(\lambda\lambda\lambda) \rightleftarrows \Delta(\lambda\delta\delta) \quad (\Delta G_2^\circ)$$
$$\Delta(\lambda\lambda\lambda) \rightleftarrows \Delta(\delta\delta\delta) \quad (\Delta G_3^\circ)$$

can be approximated by assuming that the free energy for each $\lambda \rightleftarrows \delta$ interconversion has the same energy:

$$\Delta G_1^\circ = \Delta G^\circ - RT\ln 3 \tag{18}$$

$$\Delta G_2^\circ = 2\Delta G^\circ - RT\ln 3 \tag{19}$$

$$\Delta G_3^\circ = 3\Delta G^\circ \tag{20}$$

where ΔG° is calculated directly from n_λ and $RT\ln 3$ is a statistical entropy term. The results from this study are presented in Table 7, which also includes published data for these systems.

Table 6. Conformational analysis data for $[NiLS_4]^{2+}$. ΔH and ΔG (300 K) are in kJ mol^{-1} and ΔS is in J K^{-1} mol^{-1}, n_λ at 300 K.

S	n_λ	ΔH	ΔS	ΔG
L = pn				
H_2O	0.95	8.1±0.3	+2.0±0.7	7.5±0.5
MeOH	0.95	[a]	[a]	7.2±0.7
Me_2SO	0.93	5.5±0.2	−2.8±0.4	6.3±0.3
L = men				
H_2O	0.71	2.1±0.1	−0.3±0.3	2.2±0.2
MeOH	0.72	2.2±0.2	0.0±0.5	2.2±0.2
Me_2SO	0.76	2.7±0.1	−0.8±0.3	2.9±0.2
L = een [b]				
H_2O	0.68	1.7±0.2	−0.5±0.6	1.9±0.4
L = *N,N'*-dmen				
H_2O	0.80	2.2±0.1	−3.9±0.2	3.4±0.2
MeOH	0.82	1.2±0.1	−8.4±0.2	3.7±0.2
Me_2SO	0.82	2.2±0.1	−5.2±0.4	3.8±0.2
L = trmen [c]				
H_2O	0.74 [d]			2.6±0.6 [e]

[a] Variable temperature data too inaccurate for meaningful ΔH and ΔS values. [b] *N*-Ethyl-1,2-ethanediamine with chemical shift data taken from Ref. 5. [c] *N,N,N'*-Trimethyl-1,2-ethanediamine with chemical shift data taken from Ref. 5 at 305.1 K. [d] ±0.04 (NMe, 0.73; $^tNCH_2$, 0.78; $^sNCH_2$, 0.70). [e] NMe, 2.5; $^tNCH_2$, 3.2; $^sNCH_2$, 2.2.

DISCUSSION

The assumptions that $K_{H2}(\lambda) = K_{H3}(\delta)$ and $K_{H3}(\lambda) = K_{H2}(\delta)$ imply the dihedral angle between Ni−N and say C−H_{ax} in a λ conformation is identical to the same dihedral angle in a δ conformation. For an achiral ligand this will of course be valid, but for chiral ligands such as pn, men, *N,N'*-dmen, and trmen this need not necessarily be correct. In fact, conformational-energy minimization calculations have shown, for example for *R*-pn chelate rings, that, whereas in the λ conformation with the methyl equatorial, the two ring carbons are equidistant from the NMN plane, in the δ conformation the unfavourable interactions between the axial methyl and the apical ligand are minimized by the ring adopting a conformation in which the two ring carbons are unsymmetrically located with respect to the NMN plane.[21] In addition, conformations with axial substituents tend to be flattened to minimize non-bonded interactions. Both of these factors would remove this above dihedral angle equality. For M−N 200 pm, for which the energy minimization calculations were conducted, the inequality is marked, but for longer M−N bond lengths as apply here (Ni−N, ~210 pm) it becomes less significant. The error in the results due to this cannot be estimated, but it will be of little importance for the *N,N'*-dimethyl-1,2-ethanediamine and 1,2-ethanediamine complexes which maintain symmetric conformations for both δ and λ chelate rings.

Table 7. Conformational analysis data for Δ-$[NiL_3]Cl_2$. Solvent is water unless stipulated, ΔH and ΔG (301.5 K) are in kJ mol^{-1}, ΔS is in J K^{-1} mol^{-1}, and n_λ is at 301.5 K.

Conc (M)	n_λ	ΔH	ΔS	ΔG	ΔG_1	ΔG_2	ΔG_3
L = en							
0.4 [a]	0.63	1.5	0.8	1.3	−1.4	−0.1	+3.9
0.4 [b,c]	0.62	1.3	0.3	1.2	−1.5	−0.3	+3.6
0.8 [d]	0.97	31.9	76.4	9.0	+6.3	+15.3	+27.0
0.8 [e,c]	0.65	2.0	1.8	1.5	−1.2	+0.3	+4.5
0.8 [f,c]	0.64	[g]	[g]	1.4	−1.3	+0.1	+4.2
0.4 [f,c,h]	0.65	2.0	1.6	1.5	−1.2	+0.3	+4.5
[d,i]	0.98	24.4	49.6	9.5	+6.8	+16.3	+28.5
[e,c,i]	0.79	4.2	3.0	3.3	+0.6	+3.9	+9.9
L = pn							
0.8 [f,c]	0.94	5.0	−5.9	6.8	+4.1	+10.9	+20.4

[a] Results from Ref. 6. [b] Data from Ref. 6. [c] Results calculated with $\Delta\delta^{int}$ 158.8. [d] Results from Ref. 9. [e] Data from Ref. 9 for 305 to 340 K. [f] Current data. [g] Insufficient data points for accurate values. [h] Solution contained 1.6 M NaCl. [i] Me_2SO solution at unknown concentration.

The results for $[Ni(R\text{-pn})S_4]^{2+}$ have two surprising features. Firstly, the n_λ and associated $\Delta G_{\lambda\delta}$ values are higher than the values obtained by the coupling constant method for $[Co(R\text{-pn})(NH_3)_4]^{3+}$ (n_λ 0.72, ΔG 2.37 kJ mol^{-1}) and $[Co(R\text{-pn})CN_4]^-$ (n_λ 0.83, ΔG 3.97 kJ mol^{-1}).[1] Energy-minimization calculations had suggested that the non-bonded interactions between an apical water molecule and an axial methyl group attached to a five-membered diamine chelate are less than for an apical ammonia or a cyanide.[25] Further, as the metal–ligand bond lengths for nickel(II) are greater than for cobalt(III), the axial methyl is further away from an apical ligand in the nickel(II) complex, and therefore, unfavourable interactions should be reduced.[1] No explanation for the above result can be offered at this stage. The second surprising feature, which was also observed for the other diamines, was that for the methanol and DMSO systems the $\delta \times T$ values for the average of the axial and equatorial CH chemical shifts increased with temperature. This indicates the presence of a second equilibrium with the species favoured at higher temperatures having a larger contact shift. Several processes such as ion-pairing, hydrogen-bonding, dissociation, and paramagnetic-diamagnetic equilibria can be discounted. Ion-pairing is not affecting the spectra because the spectrum of $[Ni(en)(OH_2)_4]^{2+}$ is independent of added chloride ion. As hydrogen-bonding decreases with increasing temperature, the observed larger contact shifts at higher temperature would suggest that, if a solvated–unsolvated equilibrium is important, the unsolvated species has the larger contact shift. However, DMSO has been found to solvate at the NH_2 of coordinated diamines more strongly than water,[17] and yet the contact shifts in DMSO are greater than in water. Therefore, the results cannot be explained by a solvated-unsolvated equilibrium. Similarly, dissociation and paramagnetic-diamagnetic equilibria would give the opposite result to what was observed.

When methyl substitution is on the N, the energy difference between the axial and equatorial conformations is markedly less than for the C-substituted chelates as predicted by the energy-minimization calculations.[21,25] The men, een, and trmen systems had similar n_λ and $\Delta G_{\lambda\delta}$ values. The *N,N'*-dmen system gave larger values for these two parameters because the equilibrium is between two equatorial methyls and two axial methyls. Based on n_λ for the racemic isomer and the racemic:*meso* isomer ratio, it is possible to calculate the relative populations of the conformations with two equatorial methyls, one equatorial and one axial methyl, and two axial methyls. The ratios at 300 K were found to be 1:0.96:0.25 in water, 1:0.56:0.22 in methanol, and 1:0.72:0.22 in DMSO. These yield free energy differences between the di-equatorial configuration and the equatorial-axial configuration of 0.1 kJ mol^{-1} in water, 1.5 kJ mol^{-1} in methanol, and 0.8 kJ mol^{-1} in DMSO. The *meso* equatorial-axial configuration is stabilized relative to the di-equatorial configuration by a probability entropy term ($RT \ln 2$) of 1.7 kJ mol^{-1} at 300 K, and when this is taken into account, the energy difference between an axial and an equatorial *N*-methyl group for *N,N'*-dmen does not differ markedly from the corresponding energy for the men, een and trmen systems.

Statistically significant differences were found in the thermodynamic parameters for the mono complexes in different solvents. However, because of the complexity of the systems possessing different unidentate ligands and with the possibility of different degrees of solvation at the NH protons, it has not been possible to interpret these differences in the energies.

The observed rate constants for the inversion of the coordinated secondary nitrogen in the DMSO solutions of the mono complexes of *N*-methyl-1,2-ethanediamine and *N,N'*-dimethyl-1,2-ethanediamine are of a similar order of magnitude when the difference in the temperatures and the statistical factor for the two-centre inversion in the latter ligand are taken into account. The observed rates of inversion in DMSO must be higher than in water because the separations of the axial and equatorial resonances are smaller in water and yet no evidence for inversion was obtained up to 373 K. From the study of $[Co(NH_3)_4(men)]^{3+}$,[26] $[Pt(en)(men)]^{2+}$,[27] $[PtCl_2(en)(men)]^{2+}$ [29] and $[Co(NO_2)_2(men)_2]^+$ [28] Buckingham and coworkers have proposed that the nitrogen inversion proceeds *via* a deprotonated intermediate. The above greater rate of inversion in DMSO than in water (pH ~8) could therefore be associated with the higher basicity of DMSO.[29]

Values of n_λ and the free energies, ΔG_1, ΔG_2 and ΔG_3, have been determined by the coupling constant method for the tris(1,2-ethanediamine) complexes of cobalt(III), rhodium(III), and ruthenium(II).[1] The results for cobalt(III) were in excellent agreement with values obtained by an indirect method[30] based on the concentrations of the

various isomers of $[Co(R\text{-pn})_i(S\text{-pn})_{3-i}]^{3+}$, which had been prepared under equilibrium conditions and separated chromatographically. For the above three complexes in water at about 300 K, n_λ values of between 0.64 and 0.70 were found. Similar values were found for $[Ni(en)_3]^{2+}$ in the present study from the current data and the data of Ho and Reilley[6] and Cramer[9] (Table 7). Ho and Reilley's calculative procedure had yielded a similar result,[6] but Cramer[9] had determined an n_λ value of 0.98.

For $[Ni(en)_3]^{2+}$ in DMSO, Cramer determined a similar value for n_λ to that in water even though $\Delta\delta^{obs}$ in the two solvents differed markedly.[9] He rationalized this result on the basis of a proposed difference in ring pucker in the two solvents due to the strong hydrogen-bonding interactions between the complex and DMSO. The proposed greater ring pucker in this solvent would make the $Ni-N-C-H_{eq}$ dihedral angle closer to 180°, which is the optimum angle for electron delocalization, thus making $\Delta\delta^{obs}$ and $\Delta\delta^{int}$ larger in DMSO. However $[Ni(pn)_3]^{2+}$ does not show a similar large variation in $\Delta\delta^{obs}$ with solvent (Table 4), and hence the observed differences between the water and DMSO solution spectra of $[Ni(en)_3]^{2+}$ are not derived from differences in ring pucker, but result from differences in $\Delta G_{\lambda\delta}$. Cramer's method of calculation is therefore called into question.

At 301.5 K and 0.4 M concentration in water Δ-$[Ni(en)_3]^{2+}$ yields for $\lambda \rightleftarrows \delta$ ΔH 1.3 kJ mol^{-1}, ΔS +0.3 JK^{-1} mol^{-1}, and ΔG 1.2 kJ mol^{-1}. The low ΔS value suggests there is not a marked difference in the solvation of the λ and δ conformations by water as the vibrational entropy term is expected to be small.[14] At 0.8 M concentration, both the ΔH and ΔS values are increased. Similar values for ΔH and ΔS were obtained at 0.4 M concentration in the presence of 1.6 M NaCl. Both results suggest that there is stronger ion association for the λ conformation.* Further evidence for this can be gained from Tables 2 and 3. The value of n_λ increased from 0.60 with no chloride in solution to 0.65 with 2.4 M chloride, and it increased by 0.04 from 0.4 M complex to 1.2 M complex.

Although chloride ion affected the conformer populations, a number of other anions including phosphate had no significant effect. The circular dichroism spectrum of Δ-$[Co(en)_3]^{3+}$ in aqueous solution has been found to change markedly on the addition of phosphate.[31,32] The changes have been explained previously in terms of the phosphate hydrogen-bonding to the cation along the complex's C_3 axis: in the $\Delta(\lambda\lambda\lambda)$ configuration three NH_{eq} protons are oriented approximately parallel to the C_3 axis and ideally situated for hydrogen-bonding to the phosphate, whereas in the $\Delta(\lambda\lambda\delta)$, $\Delta(\lambda\delta\delta)$ and $\Delta(\delta\delta\delta)$ configurations the protons are said to be less ideally oriented for a three-pronged hydrogen-bonding interaction. It is claimed that this results in the conformational equilibrium being shifted towards the λ conformation with an associated change in the circular dichroism. However, as pointed out by Sarneski and Urbach, such an interaction renders each nitrogen asymmetric with the same absolute configuration and this will have a major effect on the observed circular dichroism.[33] Further, the differences in the H---H separations for $\Delta(\lambda\lambda\lambda)$ and $\Delta(\lambda\lambda\delta)$ are relatively slight and the differences in the hydrogen-bonding between phosphate and these two configurations would not be marked. Nevertheless, NMR data confirm for $[Co(en)_3]^{3+}$ and $[Rh(en)_3]^{3+}$ that phosphate does increase n_λ, although the errors in n_λ are sufficiently large to make the actual magnitude of the increase uncertain: at 290 K $[Rh(en)_3]^{3+}$ $[PO_4^{3-}]$O, n_λ 0.64±0.06; $[PO_4^{3-}]$ 0.1 M, n_λ 0.68±0.06; $[Co(en)_3]^{3+}$ $[PO_4^{3-}]$O, n_λ 0.70±0.07; $[PO_4^{3-}]$ 0.1 M, n_λ 0.73±0.05; $[PO_4^{3-}]$ 0.3 M, n_λ 0.83±0.08. Chloride on the other hand, has a much smaller effect on the CD of Δ-$[Co(en)_3]^{3+}$,[32] consistent with the fact that the association constant for chloride with $[Co(en)_3]^{3+}$ is an order of magnitude less than for phosphate.[34] In addition, the effect chloride has on the relative rotational strengths of the $^1A_1 \rightarrow {}^1E$ and $^1A_1 \rightarrow {}^1A_2$ components of the $^1A_{1g} \rightarrow {}^1T_{1g}$ cubic absorption band differs from that of phosphate suggesting that the type of interaction is different for the two anions in solution.

Based on the above results for $[Co(en)_3]^{3+}$ and $[Rh(en)_3]^{3+}$ and the significant effect of chloride with $[Ni(en)_3]^{2+}$ it had been anticipated that the addition of phosphate to $[Ni(en)_3]^{2+}$ would induce large changes in the contact shifts of the ring protons. The observed changes were in fact zero for a 1:1 ratio of $[Ni(en)_3]Cl_2$ and phosphate, and 1.29 ppm for a 1:2 ratio of $[Ni(en)_3](NO_3)_2$ and phosphate. This latter result reflects a change in n_λ of less than 0.01. For the dipositive cation, ion association would

* Cramer and Harris claimed that their larger observed chemical shift differences compared to the previous results of Ho and Reilley[6] were caused by a small amount of excess diamine.[9] It has been shown here that the contact shifts for $[Ni(en)_3]^{2+}$ are independent of 1,2-ethanediamine up to a 100 % excess.

be less than for the tripositive $[Co(en)_3]^{3+}$, and therefore a smaller change in n_λ would be expected for $[Ni(en)_3]^{2+}$. However, the question that remains to be answered is why chloride was found here to have a much larger effect with $[Ni(en)_3]^{2+}$ than phosphate and other anions such as fluoride, nitrate and perchlorate. One possible answer to this question relates to the interaction of the anions with the solvent, water. An investigation of the infrared and Raman OH stretching and librational bands of simple salt solutions has yielded the following order for anion-water interactions:[35]

$$PO_4^{3-} > SO_4^{2-} > F^- > NO_3^- > CH_3CO_2^- > Cl^- > ClO_4^-$$

At the high concentrations of the complex salts of the present study, the number of water molecules per ion would be significantly less than for the CD, the diamagnetic NMR and the ion-association constant studies, and the number could be of the order of 16 or less. The degree of hydration of Cl^- would be very low compared to PO_4^{3-} and under these circumstances the chloride may be able to form a contact ion-pair with the complex which differs in stability for the δ and λ configurations. For ClO_4^-, the hydration is less than for Cl^- but it is known to form very unstable ion-pairs.[36] $[Ni(en)_3](NO_3)_2$ showed a concentration dependence but this was less than for the chloride (Table 3), consistent with the above order.

$[Ni(en)_3]^{2+}$ in DMSO showed a marked increase in n_λ over the aqueous solution (Tables 1 and 6). For the $\lambda \rightleftarrows \delta$ equilibrium, both ΔH and ΔS were more positive, consistent with DMSO binding more strongly to the NH_2 groups in the λ configuration. The equatorial NH protons are readily accessible in both the δ and λ conformations, but for the Δ configuration the axial NH protons for a δ conformation are less accessible for solvation due to their interactions with other atoms in the molecule. The greater donor power of DMSO therefore stabilizes the λ more than water. In Table 1, n_λ values are given for a number of solvents and counter ions. The trend in n_λ values for the non-aqueous solvents follows the order of the donor number for the solvents: MeCN 14.1,[29] Me_2CO 17.0,[29] thf 20.0,[29] $HCONH_2$ 24.7,[37] $HCON(Me)_2$ 26.6,[29] Me_2SO 29.8.[29] Water with a donor number of 18.0 gives a smaller n_λ value than would be expected.

The inversion of $[Ni(en)_3]^{2+}$ in water, in 1.6 M NaCl and DMSO was studied at elevated temperatures. Ho and Reilley determined a free energy of activation of 65.7 kJ mol^{-1} at 374 K for the water solution.[6] The other two solvents yielded similar values: 1.6 M NaCl $\Delta G^{\neq}_{374}$ 63.5 kJ mol^{-1}, Me_2SO $\Delta G^{\neq}_{374}$ 65.7 kJ mol^{-1}. Insufficient data points were available for the water solution to calculate $\Delta H^{\neq}$ and $\Delta S^{\neq}$ but these were obtained for the 1.6 M NaCl and the DMSO solutions. These values are in excellent agreement indicating that the same mechanism is occurring in both solvents, and that the solvent does not play a dominant role in the formation of the activated complex. This is consistent with the non-bond-rupture twist mechanism proposed by Ho and Reilley.[6] The large negative entropy of activation has also previously been associated with a twist mechanism.[38]

Zamaraev has proposed that a Karplus-type equation could be applied to the proton contact shifts of diamine chelate rings to estimate the degree of ring pucker:[12]

$$A_i = B_0 + B_2 \cos^2\theta_i \qquad (21)$$

where A_i is the hyperfine coupling constant, B_0 and B_2 are constants, and θ the dihedral angle between the Ni−N−C and N−C−H planes (Fig. 4). Experimental evidence for radicals with rigid geometries has led to the conclusion that B_0 is much less than B_2.[39] This allows the approximation,

$$A_i \simeq B_2 \cos^2\theta_i \qquad (22)$$

and the formulation of the equation,

$$\delta_{ax}/\delta_{eq} = \cos^2\theta_{ax}/\cos^2\theta_{eq} \qquad (23)$$

Eqn. (23) yields four values for the angle θ: θ, $\pi-\theta$, $\pi+\theta$, and $2\pi-\theta$. In calculations the intrinsic contact shifts must be employed; not shifts that are weighted because of the conformational equilibrium present. The intrinsic contact shifts for the axial and equatorail protons for 3,3-dimethyl-1,2-butanediamine are 11.8 and 170.7 ppm at 300 K, and 7.4 and 126.5 ppm at 300 K for *N,N,N',N'*-tetramethyl-1,2-propanediamine. These shifts give θ values of approximately 76° for both rings. This angle was chosen in preference to the remaining three because of the correspondence to the angle of 78° found in the solid state for $[Ni(en)_3](MeCO_2)_2.2H_2O$.[40] The fact the two rings gave similar values for θ shows that the interactions of axial *N*-methyl groups are not sufficiently strong to cause significant flattening

of the chelate ring. The intrinsic contact shifts for the axial and equatorial protons in $[Ni(dmbn)_3]^{2+}$ also gave a value of 76° for θ. The correspondence between this value for the tris(diamine) complex in solution and the value determined by X-ray analysis for the above crystalline complex suggests that the interactions of the solvent do not significantly affect the degree of pucker of the chelate rings.

Cramer studied the degree of pucker of the diamine chelates using an equation similar to (21) in which A_i was replaced by δ_i.[9] He assumed a value of zero for B_0 and estimated a value of B_2 using a contact shift of 300 ppm and a θ value of 180° as found for the α-imino proton of *cis,cis*-1,3,5-tris(pyridine-2-carbonimino)cyclohexanenickel(II).[41] Knowing B_2, the dihedral angles were calculated from the individual contact shifts. Three points arise from Cramer's use of this method. Firstly, the hyperfine coupling constant and not the contact shift is related to the dihedral angle.[12] Secondly, the delocalization of electron density to the α-imino proton in the above compound is influenced by the presence of π-bonding in the ligand framework, which will increase the contact shift relative to the σ-bonded situation.[42] Finally, of the angles 63, 117, 243, and 297° which were solutions for Cramer's equation, he chose 117°, a value dictated by his previous theory that chelate rings are much flatter in solution than in the solid state. A dihedral angle of 117° implies that the ring is approaching planarity which is most unlikely considering the high energy of that conformation.

Acknowledgements. The authors gratefully acknowledge financial support from the Australian Research Grants Committee.

REFERENCES

1. Hawkins, C. J. and Peachey, R. M. *Aust. J. Chem. 29* (1976) 33.
2. Hawkins, C. J. and Palmer, J. A. *Aust. J. Chem. 31* (1978) 1689; Hawkins, C. J. and McEniery, M. L. *Aust. J. Chem. 31* (1978) 1699.
3. Booth, H. *Prog. Nucl. Magn. Reson. Spectrosc. 5* (1969) 149.
4. Beattie, J. K. and Novak, L. H. *J. Am. Chem. Soc. 93* (1971) 620; Beattie, J. K. *Acc. Chem. Res. 4* (1971) 253.
5. Ho, F. F.-L. and Reilley, C.N. *Anal. Chem. 41* (1969) 1835.
6. Ho, F.F.-L. and Reilley, C. N. *Anal. Chem. 42* (1970) 600.
7. Evilia, R. F., Young, D. C. and Reilley, C. N. *Inorg. Chem. 10* (1971) 433.
8. Ho, F. F.-L., Erickson, L. E., Watkins, S. R. and Reilley, C. N. *Inorg. Chem. 9* (1970) 1139; Evilia, R. F. and Reilley, C. N. *J. Coord. Chem. 3* (1973) 7; Sarneski, J. E. and Reilley, C. N. *Inorg. Chem. 13* (1974) 977.
9. Cramer, R. E. and Harris, R. L. *Inorg. Chem. 12* (1973) 2575.
10. Cramer, R. E. and Harris, R. L. *Inorg. Chem. 13* (1974) 2208; Cramer, R. E. and Huneke, J. T. *Inorg. Chem. 17* (1978) 64.
11. Milner, R. S. and Pratt, L. *Discuss. Faraday Soc. 34* (1962) 88.
12. Zamaraev, K. I., Molin, Y. N. and Skubnevskaya, G. I. *J. Struct. Chem. (USSR) 7* (1966) 740.
13. Fitzgerald, R. J. and Drago, R. S. *Inorg. Chem. 8* (1969) 2254.
14. Gollogly, J. R., Hawkins, C. J. and Beattie, J. K. *Inorg. Chem. 10* (1971) 317.
15. Hawkins, C. J., Peachey, R. M. and Szoredi, C. L. *Aust. J. Chem. 31* (1978) 973.
16. Moshier, R. W. and Spialter, L. *J. Org. Chem. 21* (1956) 1050.
17. Hawkins, C. J., Lawrance, G. A. and Peachey, R. M. *Aust. J. Chem. 30* (1977) 2115.
18. State, H. M. *Inorg. Synth. 6* (1960) 200.
19. Jesson, J. P. *J. Chem. Phys. 47* (1967) 582.
20. Corey, E. J. and Bailar, J. C. *J. Am. Chem. Soc. 81* (1959) 2620.
21. Gollogly, J. R. and Hawkins, C. J. *Inorg. Chem. 8* (1969) 1168.
22. Cramer, R. E. *Inorg. Chem. 11* (1972) 1019.
23. Gutowsky, H. S. and Holm, C. H. *J. Chem. Phys. 25* (1956) 1228.
24. Erickson, L. E., Young, D. C., Ho, F.F.-L., Watkins, S. R., Terrill, J. B. and Reilley, C. N. *Inorg. Chem. 10* (1971) 441; Everhart, D. S. and Evilia, R. F. *Inorg. Chem. 14* (1975) 2755.
25. Gollogly, J. R. *Conformational Analysis of Chelate Rings*, Diss., University of Queensland, Brisbane 1970.
26. Buckingham, D. A., Marzilli, L. C. and Sargeson, A. M. *J. Am. Chem. Soc. 89* (1967) 825.
27. Buckingham, D. A., Marzilli, L. G. and Sargeson, A. M. *J. Am. Chem. Soc. 91* (1969) 5227.
28. Buckingham, D. A., Marzilli, L. G. and Sargeson, A. M. *J. Am. Chem. Soc. 89* (1967) 3428.
29. Mayer, U. *Coord. Chem. Revs. 21* (1976) 159.
30. Harnung, S. E., Kallesøe, S., Sargeson, A. M. and Schäffer, C. E. *Acta Chem. Scand. A 28* (1974) 385.
31. Mason, S. F. and Norman, B. J. *Chem. Commun.* (1965) 73; Larsson, R., Mason, S. F. and Norman, B. J. *J. Chem. Soc. A* (1966) 301;

Mason, S. F. and Norman, B. J. *J. Chem. Soc. A* (1966) 307.
32. Smith, H. L. and Douglas, B. E. *Inorg. Chem. 5* (1966) 784.
33. Sarneski, J. E. and Urbach, F. L. *J. Am. Chem. Soc. 93* (1971) 884.
34. Craighead, K. L., Jones, P. and Bryant, R. G. *J. Phys. Chem. 79* (1975) 1868.
35. James, D. W. and Armishaw, R. F. *Aust. J. Chem. 28* (1975) 1179; James, D. W. and Frost, R. L. *Discuss. Faraday Soc. 64* (1977) 48.
36. Erlich, R. H. and Popov, A. I. *J. Am. Chem. Soc. 93* (1971) 5620.
37. Greenberg, M. S., Bodner, R. L. and Popov, A. I. *J. Phys. Chem. 77* (1973) 2449.
38. Ray, P. *Chem. Rev. 61* (1961) 313; Jurado, B. and Springer, C. S. *Chem. Commun.* (1971) 85.
39. Stone, E. W. and Maki, A. H. *J. Chem. Phys. 37* (1962) 1326.
40. Cramer, R. E., Van Doorne, W. and Huneke, J. T. *Inorg. Chem. 15* (1976) 529.
41. Wandiga, S. O., Sarneski, J. E. and Urbach, F. L. *Inorg. Chem. 11* (1972) 1349.
42. Horrocks, W. DeW. and Johnston, D. L. *Inorg. Chem. 10* (1971) 1835.

Received June 2, 1978.

Acta Chemica Scandinavica A 32 (1978) 833–836

The Crystal Structure of *trans*-Difluoro(1,4,8,11-tetraazaundecane)-chromium(III) Perchlorate

EVA BANG and ERIK PEDERSEN

Chemistry Department I (Inorganic Chemistry), H. C. Ørsted Institute, Universitetsparken 5, DK-2100 Copenhagen Ø, Denmark

Dedicated to Jannik Bjerrum on the occasion of his 70th birthday

The complex ion in *trans*-[Cr(1,4,8,11-tetraazaundecane)F_2]ClO_4 was determined from X-ray diffraction to be of the *meso*-type having an *R,S*-configuration of the two inner asymmetric nitrogen ligators. The crystals are monoclinic, space group *Cc* or *C2/c*, $a=21.86(3)$, $b=5.618(4)$, $c=28.39(3)$ Å, $\beta=126.84(3)°$, $Z=8$. After isotropic refinement the final *R* value was 0.13. The oxygen atoms of the perchlorate ions are disordered. The *R,S*-configuration is consistent with the chemical properties.

In their thorough and pioneering studies of cobalt(III) complexes of 1,4,7,10-tetraazadecane (2,2,2-tet), Sargeson and coworkers[1-2] showed that this linear tetradentate ligand has a pronounced tendency to form *cis*-octahedral complexes. The homologous ligands 1,4,8,11-tetraazaundecane (2,3,2-tet) and 1,5,8,12-tetraazadodecane (3,2,3-tet) show an increased preference to form *trans*-complexes. A large number of cobalt(III)[3-8] and a few chromium(III)[7-11] and rhodium(III)[7,8,12] complexes have been studied. The potential of the two inner nitrogen atoms to introduce dissymmetry close to the metal ion has been an important aspect in these investigations. During our studies of such chromium(III) complexes in the late sixties we encountered the present *trans*-complex which resisted optical resolution.

EXPERIMENTAL

The orange-red crystals were prepared as reported earlier.[10] They occur prismatic with parallel extinction and the *b* axes in the length of the crystal, or rhombohedral with diagonal extinction on the large face (100). Weissenberg and precession photographs showed the possible space groups to be *Cc* or *C2/c*. Intensity data were collected on a Picker FACS-1 diffractometer with graphite monochromated Cu$K\alpha$ radiation. ($\lambda=1.5405$ Å). The copper radiation was preferred to the molybdenum on account of the long axes of the unit cell. The data collection was performed in the $\theta-2\theta$ mode. The scan rate was 1°/min, the scan range was 1.5° and increasing with 2θ. The background counts were made for 20 s at each end of the scan range.

Only reflections from two octants were collected. 1756 independent reflections were recorded, but only 696 had $I/\sigma(I)>3.0$. The crystal size was $0.12\times0.05\times0.03$ mm^3. No correction for absorption was applied. The anisotropic temperature factors found later in the refinement showed the influence of absorption to be of minor importance for the gross features of the structure. The cell dimensions were refined from powder diagrams obtained from a Hägg-Guinier camera and Cu$K\alpha$ radiation. The X-ray system[13] was used in the crystal structure analysis, and the Ortep II[14] for the illustrations.

CRYSTAL DATA

[Cr($C_7H_{20}N_4$)F_2]ClO_4. Space group *C2/c* (No. 15) or *Cc* (No. 9). $a=21.86(3)$, $b=5.618(4)$, $c=28.39(3)$ Å, $\beta=126.8(3)°$, $Z=8$, $D_m=1.66$ g cm^{-1}, $D_x=1.67$ g cm^{-1}, μ(Cu$K\alpha$)=97 cm^{-1} (See Fig. 1).

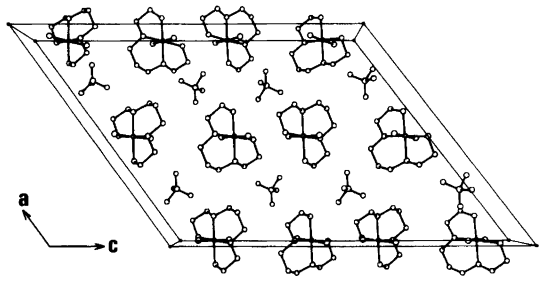

Fig. 1. View of the unit cell along the *b*-axis.

SOLUTION AND DESCRIPTION OF THE STRUCTURE

Direct methods assuming an acentric structure gave the information which led to the solution of the structure. The many peaks in the Patterson function which could be related to the layer *u*,0,*w* indicated that the space group could possibly be *C*2/*c*, or at least a great number of the atoms were centrosymmetrically arranged. The refinement has been carried out both in *Cc* and *C*2/*c* with and without reflections where $I/\sigma(I) \leq 3.0$ and the value of the calculated structure factor was larger than the $\sigma(I)$ limit. The resulting structures were almost identical. Anisotropic refinement was carried out for both space groups, but may not be justified as the number of observed intensities is small, and is also small against the number of parameters. Unit weights were used. The results for isotropic refinement in the centrosymmetric case (696 obs. reflections and 545 LT reflections, *R* 0.13) are given in Tables 1 and 2.

The great number of weak reflections among strong reflections, even for small values of sin θ, can be explained in terms of the positions of some of the atoms. The positions of the cations are such that the chromium, two nitrogen, and two fluorine atoms are close to 0 or 1/4. Furthermore, the vector differences between the chromium and the chlorine atoms are close to 1/4, 1/4, 0.

The two fluorine atoms in the *trans*-positions in the complex, Fig. 2, have the distances 1.85 and 1.90 Å from the chromium atom. This is in agreement with the results for the $[CrF_6]^{3-}$ ion as found in $BaLi[CrF_6]$.[15] The other distances in the complex are Cr–N 2.06–2.08, C–N 1.48–1.56, and C–C 1.51–1.56 Å. The best plane through the Cr, Fl, F2, and C4 atoms is very close to being a mirror plane, corresponding to *R* and *S* configurations of the two asymmetric nitrogen atoms N2 and N3. The three carbon atoms in the trimethylene group and the two nearest carbon atoms in the ethylene groups C2 to C6 are all on the same side of the least squares best plane through the chromium and the four nitrogen atoms. The carbon atom C4 in the middle of the trimethylene group has a shorter

Table 1. Fractional atomic coordinates ($\times 10^4$), isotropic thermal parameters ($Å^2 \times 10^2$).

	x	*y*	*z*	*U*
Cr	0001(2)	0270(7)	3989(1)	3.4(1)
N1	1176(11)	0078(40)	4482(8)	4.5(5)
N2	4973(10)	2771(34)	1532(8)	2.9(4)
N3	1179(10)	0369(35)	1534(7)	3.1(5)
N4	0087(9)	2620(33)	0501(7)	2.4(4)
F1	0020(7)	2815(24)	3582(5)	4.3(3)
F2	4944(7)	2667(23)	4390(5)	3.4(3)
C1	3620(14)	2760(50)	0694(11)	4.0(5)
C2	4188(13)	2679(46)	1369(10)	3.8(6)
C3	4453(13)	3140(45)	2800(10)	4.2(7)
C4	3628(13)	3097(45)	2612(9)	4.6(6)
C5	1584(14)	0404(50)	2212(11)	4.9(7)
C6	1410(15)	2600(52)	1384(11)	3.5(6)
C7	0901(14)	2616(49)	0701(11)	3.3(5)
Cl	2475(4)	2781(15)	3906(3)	5.2(2)
O1	2441(16)	0178(59)	0947(12)	13(4)
O2	1743(18)	2475(61)	3566(13)	12(3)
O3	2928(18)	1405(61)	4361(14)	12(2)
O4	2791(15)	2519(54)	3620(11)	11(2)

Table 2. Bond lengths (Å) and selected angles (°).

CrF1	1.85(2)	N1CrN2	83.9(9)
CrF2	1.90(2)	N1CrN4	99.2(8)
CrN1	2.06(6)	N2CrN3	93.4(8)
CrN2	2.07(2)	N3CrN4	83.5(8)
CrN3	2.07(6)	N1CrN3	177.3(10)
CrN4	2.05(2)	N2CrN4	175.9(10)
		F1CrF2	178.0(7)
N1C1	1.56(4)		
N2C2	1.49(4)	N1C1C2	105(2)
N2C3	1.54(5)	C1C2N2	108(2)
N3C5	1.57(4)	N2C3C4	110(3)
N3C6	1.51(4)	C3C4C5	113(2)
N4C7	1.51(4)	C4C5N3	109(2)
		N3C6C7	104(2)
C1C2	1.54(6)	C6C7N4	106(2)
C3C4	1.54(5)	C2N2C3	109(2)
C4C5	1.56(4)	C5N3C6	107(2)
C6C7	1.56(4)		

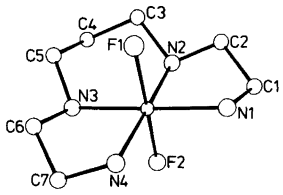

Fig. 2. The chromium complex cation.

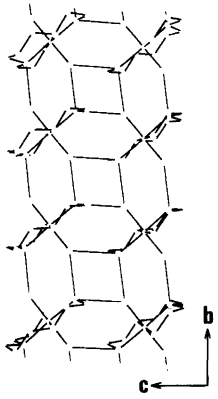

Fig. 3. Contacts formed between complexes in the *bc*-plane along the *b*-axis.

distance, 0.51 Å, than the two others in this group, C3 0.89 Å and C5 0.97 Å. Only C1 and C7 are at the opposite side of the plane, which indicates that the two fluorine atoms are placed in essentially different environments.

The chair configuration of the six-membered ring has also been found in several cobalt(III) complexes.[16-19] In the case of tris(1,3-propanediamine)chromium(III) pentacyanonickelate(II)[20] there are two six-membered rings with the chair configuration whereas the third forms a skew boat.

The complex ions form infinite double-bands in the *bc* plane in the direction of the *b*-axis as shown in Fig. 3. The fluorine-nitrogen intercomplex distances in these bands are 2.80–2.98 Å. Within the complexes these distances are 2.73–2.88 Å. The perchlorate ions are placed between these bands as seen from the view of the unit cell in Fig. 1. Difference syntheses and the large temperature factors indicate disorder of the oxygen atoms in the perchlorate ion. The position of the chlorine excludes the possibility of strong hydrogen bonds from oxygen to nitrogen atoms.

CONCLUSIONS

trans-[Cr(2,3,2-tet)F_2]ClO_4 was prepared by a general procedure[10] for preparation of chromium(III) complexes with two fluorine atoms and four nitrogen atoms as ligators. This procedure yields *trans*-complexes unless it is prevented by steric factors as observed for 2,2,2-tet and tris(2-aminoethyl)amine where *cis*-complexes are formed. Visible absorption spectra of the present compound indicated a *trans*-configuration as now finally shown by X-ray analysis. An earlier procedure[3] yielded almost entirely the *cis*-complex with a small amount of *trans*-complex as an impurity.[4]

This indicates the great flexibility of the 2,3,2-tet ligand. In the *trans*-configuration there are two possible isomers having *R,R/S,S* (racemate) or *R,S* configurations on the two inner nitrogen atoms. These isomers would have a skew boat and a chair configuration in the six-membered ring, respectively. The *R,R/S,S* configuration is possible in cobalt(III) complexes[5] as indicated by their optical resolutions. The *R,S*- or *meso*-configuration is observed in the crystal structure[22,23] of a nickel(II) complex of 2,3,2-tet obtained by cyclizing the amine with 1,3-dibromopropane.

The *R,S*-configuration found in the present complex remains intact even in basic aqueous solution. Our attempts to obtain optical resolution by precipitation as α-bromocamphor-π-sulfonates in weakly acid solution failed both before and after treatment with base.

Another chemical evidence for the *R,S*-configuration obtained at an early stage was the observation that during the reaction of the complex in a 5:1 v/v mixture of 12 M hydrochloric acid and 70 % w/w perchloric acid the *trans*-[Cr(2,3,2-tet)ClF]$^+$ ion was easily obtained. Further substitution of the second fluoride ligand was very slow. This is probably related to the position of the fluorine atom which is partly protected in the chair. For the related *trans*-difluoro complexes with ammonia[24] and ethylenediamine it is difficult to isolate the intermediate product.

REFERENCES

1. Sargeson, A. M. and Searle, G. H. *Inorg. Chem.* *4* (1965) 45.
2. Buckingham, D. A., Marzilli, P. A. and Sargeson, A. M. *Inorg. Chem.* *6* (1967) 1032.

3. Bosnich, B., Gillard, R. D., McKenzie, E. D. and Webb, G. A. *J. Chem. Soc. A* (1966) 1331.
4. Dale Alexander, M. and Hamilton, Jr., H. G. *Inorg. Chem. 8* (1969) 2131.
5. Brubaker, G. R. and Schaefer, D. P. *Inorg. Nucl. Chem. Lett. 6* (1970) 237.
6. Brubaker, G. R. and Schaefer, D. P. *Inorg. Chem. 10* (1971) 811.
7. Bosnich, B. and Harrowfield, J. MacB. *Inorg. Chem. 14* (1975) 828.
8. Bosnich, B., Harrowfield, J. MacB. and Boucher, H. *Inorg. Chem. 14* (1975) 815.
9. Kutal, C. and Adamson, A. W. *Inorg. Chem. 12* (1973) 1990.
10. Glerup, J., Josephsen, J., Michelsen, K., Pedersen, E. and Schäffer, C. E. *Acta Chem. Scand. 24* (1970) 247.
11. Pedersen, E. *Acta Chem. Scand. 24* (1970) 3362.
12. Halliday, R. W. and Court, R. H. *Can. J. Chem. 52* (1974) 3469.
13. Stewart, J. M., Kundell, F. A. and Baldwin, J. C., Eds., *The X-Ray System 1972*, Technical Report 92, Computer Science Center, University of Maryland, College Park.
14. Johnson, C. K. *Ortep: A Fortran Ellipsoid Plot Program for Crystal Structure Illustrations*, Report ORNL-3794, Sec. Rev., Oak Ridge National Laboratory, Oak Ridge 1970.
15. Babel, D. *Z. Anorg. Allg. Chem. 23* (1974) 406.
16. Payne, N. C. *Inorg. Chem. 11* (1972) 1376.
17. Payne, N. C. *Inorg. Chem. 12* (1973) 1151.
18. Corfield, P. W. R., Dobrowiak, J. C. and Gore, E. S. *Inorg. Chem. 12* (1973) 1734.
19. Herak, R. M., Čelap, M. B. and Krstanović, I. *Acta Crystallogr. B 33* (1977) 3368.
20. Jurnak, F. A. and Raymond, K. N. *Inorg. Chem. 13* (1974) 2387.
21. Wismer, R. K. and Jacobsen, R. A. *Inorg. Chim. Acta 7* (1973) 477.
22. Bosnich, R., Poon, C. K. and Tobe, M. L. *Inorg. Chem. 4* (1965) 1102.
23. Bosnich, B., Tobe, M. L. and Webb, G. A. *Inorg. Chem. 4* (1965) 1109.
24. Glerup, J. and Schäffer, C. E. *Inorg. Chem. 15* (1976) 1408.

Received June 5, 1978.

Acta Chemica Scandinavica A 32 (1978) 837–845

Chloro Complexes in Molten Salts. VII. Potentiometric, Spectrophotometric, and Raman Spectroscopic Study of the System KCl—$AlCl_3$—$NbCl_5$ at 300 °C

JENS H. von BARNER, NIELS J. BJERRUM * and G. PEDRO SMITH **

Chemistry Department A, The Technical University of Denmark, DK-2800 Lyngby, Denmark

Dedicated to Jannik Bjerrum on the occasion of his 70th birthday

Potentiometric, spectrophotometric and Raman spectroscopic measurements on the molten system $KCl-AlCl_3-NbCl_5$ at 300 °C indicate the presence of an equilibrium between Nb(V) species as follows: $NbCl_6^- \rightleftarrows NbCl_5 + Cl^-$. For an Nb(V) concentration of 0.1 F this equilibrium holds over the pCl^- range 0.42–5.44 with pK of 4.49±0.05 (in molar units) while at 0.3 F it holds over 0.42–4.72 with a pK of 4.19±0.03. Further support for this interpretation is provided by measurements of the vapor-phase concentration of $NbCl_5$ in equilibrium with the melt. The vapor-liquid distribution coefficient of $NbCl_5$ is independent of other compositional variables and has a value of 0.133± 0.011 at 300 °C.

As part of a general study of the acid-base properties of molten salts,[1-5] an investigation was made of the chloroniobium(V) species in the $KCl-AlCl_3-NbCl_5$ system.

It is well-known that $NbCl_5$ is a Lewis acid and, therefore, has a strong affinity for chloride ions. Examination[6,7] of the $MCl-NbCl_5$ systems (M = Li,Na,K,Rb,Cs) shows that the $NbCl_6^-$ ion is present (except in the $LiCl-NbCl_5$ system) and in cases where structural data are available this complex is found to have an octahedral configuration.[8,9] Bues, Demiray and Øye[9] found that the equilibrium $Nb_2Cl_{10} \rightleftarrows 2NbCl_5$ probably occurs in liquid niobium(V) chloride and that at temperatures above 320 °C almost all niobium(V) chloride is present as $NbCl_5$.

An interesting problem for salt systems containing chlorocomplexes of Nb(V) is whether or not a dinuclear ion such as $Nb_2Cl_{11}^-$ may form under special conditions. Such dinuclear ions are well-known for other Lewis acid chlorides. For example, $Al_2Cl_7^-$ and $Fe_2Cl_7^-$ occur in $MCl-AlCl_3$[1,10-12] and $KCl-FeCl_3$[4] melts. Such a dinuclear ion for Nb(V) should be favored at high Nb(V) concentrations but, unfortunately, the $NbCl_5$ vapor pressure over $MCl-NbCl_5$ melts at high Nb(V) concentrations is very substantial.[6] For this reason we found it necessary to work with melts that are relatively dilute in Nb(V) and, under these conditions, did not find dinuclear complexes.

EXPERIMENTAL

Aluminium trichloride was made from pure metal (99.999 %) and HCl gas (made by reaction between concentrated hydrochloric acid and concentrated sulfuric acid), and further purified by sublimation. Potassium chloride (analytical reagent from Riedel-de Haën) was purified by first passing HCl gas (electronic grade from Matheson) over the solid and then through the melt, then flushing with pure N_2, and finally filtering the melt. Niobium(V) chloride (analytical reagent from Schuchardt) was further purified by 5 distillations under a chlorine pressure of 1/3 atm. An analysis of the material

* To whom correspondence should be addressed.
** Permanent address: Oak Ridge National Laboratory, Post Office Box X, Oak Ridge, Tennessee 37830, U.S.A.

gave a chlorine content of 65.25 ± 0.51 % (theoretical value 65.61 %). The materials that made up a melt were weighed in a nitrogen-filled glove-box with a measured water content of about 5 ppm and continuous gas purification by forced recirculation through external molecular sieves. The oxygen content of the box was not monitored but the box was filled and flushed with nitrogen containing less than 40 ppm of O_2 plus H_2O. In order to minimize the formation of oxychloride, $NbCl_5$ was kept in sealed ampoules until used. The experimental techniques and equipment used in this investigation were almost the same as those used in previous work.[1-5] The densities of the melts used were calculated from the assumption that mixtures of $NbCl_5$ and $KCl-AlCl_3$ behave ideally. This assumption can give rise to only a small error because the amounts of $NbCl_5$ were small compared to the amounts of $KCl-AlCl_3$. The densities of $NbCl_5$ and $KCl-AlCl_3$ were obtained from the work of Nisel'son *et al.*[13] and Morrey and Carter,[14] respectively.

The electrochemical cells were made of Pyrex with glassy carbon rods (Carbone-Lorraine) fused into the bottom and had a shape similar to that of the cells used earlier.[1,2,4,5] The cells were filled with chlorine (Fluka > 99.9 %) at 0.5 atm and then sealed vacuum-tight. Because of the fairly high vapor pressure above the melt the tube connecting the two cell compartment was sealed after chlorine had been added. This could cause an error due to different chlorine pressures in the two cell compartments. Experiments performed at compositions with high chloride activity (and low vapor pressure) showed that there was only a small difference between the results obtained with open and sealed connecting tubes. The same is also probably true at low chloride activity (and high vapor pressure) because the solubility of chlorine in chloride melts is rather low and seems to increase with increasing chloride activity.[15]

The optical cells were of fused quartz. Short pathlengths (less than 0.1 mm) were obtained by placing precision-ground fused-silica inserts into 5 mm cells. The spectra were measured with a Cary 14R spectrophotometer equipped with a Datex digital system for punching out spectral data on paper tape.

The optical cells used for the Raman spectra were the same as those used for the UV-Vis spectra but without inserts. The Raman spectra were recorded using a Coderg PH1 laser spectrometer with 632.8 nm (60–80 mW) excitation and a cooled photomultiplier. A 90° scattering was used and the polarization of the laser beam was kept fixed. The depolarization measurements were made by the conventional method of two different analyzer orientations in the scattered beam ($\rho = 0.75$ for depolarized lines). The uncertainty in the measured Raman shifts due to the instrument was ± 2 cm^{-1}.

When $NbCl_5$ was added to molten $KCl-AlCl_3$, small amounts of Nb(V) oxychlorides were formed, largely from oxide impurities in the solvent. These contributed to the absorption spectrum and it was necessary to take the following steps to minimize this contribution. First, the highest practical concentration of Nb(V) was used. The limitation on this concentration was set by the high molar absorptivities (up to 26×10^3 M^{-1} cm^{-1}) of the chlorocomplexes of Nb(V) formed in the melt in combination with the shortest pathlengths that were practical to use. In order to obtain reproducible results, it was necessary to place the insert in the cell in exactly the same way each time, and to handle the cell in the same manner in each experiment. Finally, measurements were made with two different concentrations of Nb(V), one with the highest concentration at which spectra could be measured and one with 1/3 to 1/2 of this concentration. Since $AlCl_3$ from the same batch was used in both experiments subtraction of these two spectra gave a spectrum with almost no contribution from oxychloride complexes.

The vapour pressure of $NbCl_5$ over acidic melts was so high that a correction was necessary. It was measured spectrophotometrically with a special cell made from a normal cell with a fixed pathlength of 0.5 mm. Fused to the end of this cell was a compartment of about 1.5 cm^3 which contained the melt under examination.

GENERAL CONSIDERATIONS

The nomenclature used in this work is the same as that used in previous publications.[1-4] The initial molar amount of one of the added substances (in the present work KCl, $AlCl_3$, and $NbCl_5$) dissolved in 1 l of melt is defined as its formality, C′. The values used for the self-dissociation reactions of the solvent at 300 °C were 7.78 ± 0.02 and 6.86 ± 0.11 for the reaction $2AlCl_4^- \rightleftarrows Al_2Cl_7^- + Cl^-$ and $Al_2Cl_7^- \rightleftarrows Al_2Cl_6 + Cl^-$, respectively.[16] From other measurements[10,12,16] we realize that the equilibria in the chloroaluminate melts are described better by including a third reaction. However, in the present case two parameters describe the chloride activity of the solvent almost as well as three parameters. The pCl^- value for the $KCl-AlCl_3$ system saturated with KCl at 300 °C was taken to be 0.255 ± 0.03.[16] From what has been said above and as we shall see later, it is clear that at low pCl^- we are dealing with $NbCl_6^-$ in solution. The average experimental coordination number, $\bar{n}$, for Nb(V) is defined as

$(C'_{KCl}+3C'_{AlCl_3}+5C'_{NbCl_5}-[Cl^-]-4[AlCl_4^-]-7-[Al_2Cl_7^-]-6[Al_2Cl_6])/C'_{NbCl_5}$. Since $\bar{n}$ decreases as we increase pCl^-, chloride ions are simultaneously taken away from Nb(V).This can be described by a set of general equations or models where the ratio Cl:Nb for each succesive complex becomes smaller and smaller.

It has previously been shown[2] that close to the 1:1 composition in the $KCl-AlCl_3$ system (from 47 to about 52 mol % KCl), the potential of a concentration cell is within experimental incertainty given by

$$pCl_I^- = -(F/RT\ln 10))\Delta E + pCl_{II}^- \quad (1)$$

where pCl_I^- and pCl_{II}^- are the negative logarithms of the chloride concentration in cell compartments I and II, respectively, and II usually refers to the reference compartment saturated with KCl. From the measured pCl^- of the melt and from the formality of Nb(V), $\bar{n}$ can be calculated. For each of the models mentioned above (to explain the variation of $\bar{n}$ *versus* the pCl^--values) and from arbitrarily chosen equilibrium constants the concentrations of each of the proposed complexes can be calculated. These concentrations can be used to calculate a new $\bar{n}$-value. By varying systematically the values for the equilibrium constants a minimum value for the deviation (least squares) between measured and the calculated $\bar{n}$-values can be found. By looking at different models, the minimum variance for each model can be obtained in this way. The ratio between the minimum variances obtained in this way and the experimental variances (for example obtained in a concentration range where there is only one species present) can then be compared. Based on an F-test the distinction can be made between models with a probability of greater or less than 90 %. Models with higher than 90 % probability are then marked with asterisks in the tables. To obtain $F_\alpha(\phi_N,\phi_D)$ (where $(1-\alpha)\times 100$ % is the probability and ϕ_N and ϕ_D are the numbers of degrees of freedom in the nominator and denonator, respectively) in connection with the potentiometric method, it was assumed that ϕ_N was equal to the number of melt compositions minus the number of equilibrium constants in the equilibria and ϕ_D equal to the number of measurements necessary to determine the average of $\bar{n}$ in the basic region (where the experimental variance is obtained) minus one.

The spectrophotometric measurements are used in this connection to obtain the number of different Nb(V) complexes present in the melt. The Bourger-Beer law and the law of additive absorbances were assumed to be valid.

The variation in the activity coefficients was neglected in all the calculations. This can be justified by the fact that the solvent was $KAlCl_4$ and that the concentrations of solute species were small compared to the concentrations of K^+ and $AlCl_4^-$.

RESULTS AND DISCUSSION

Measurements and calculations for cell potentials in the KCl—$AlCl_3-NbCl_5$ system. In Table 1 are shown the values of $-\Delta E$ at given mol fractions of KCl and $AlCl_3$ for 0.1 and 0.3 F $NbCl_5$ with the composition corrected for the presence of $NbCl_5$ in the gaseous phase. The measurements for 0.3 F $NbCl_5$ could not be performed accurately at pCl^- values much higher than *ca.* 4.7 (corresponding to a $-\Delta E$ of *ca.* 500 mV). Plots of the average experimental coordination number ($\bar{n}$) as a function of the pCl^- values calculated from Table 1 are shown in Fig. 1. From this figure it is clearly indicated by an $\bar{n}$-value close to 6.0 that $NbCl_6^-$ is the only stable species at pCl^- values below 2.1. In this connection it is interesting to examine more accurately the value of $\bar{n}$ at low pCl^- values. In Table 2 the average $\bar{n}$-values for a number of measurements are given. From this table it is clear that the values of $\bar{n}$ for both 0.1 and 0.3 F Nb(V) solutions are very close to 6.00. The variances given in this table are based on the deviation from the average given in $\bar{n}$-units.

From Fig. 1 it can also be seen that the lowest measured value of $\bar{n}$ is around 5.0. More important is to notice that there seems to be a levelling off of the curve around 5.0. Due to the high vapor pressure of the melt at high pCl^- values and even at fairly low Nb(V) concentrations (which makes the potentiometric measurements impossible with the present cells) this effect is only observed for the approx. 0.1 F Nb(V) solutions. In the present case it is furthermore very unlikely that we are dealing with complexes with more than two niobium atoms linked together. This is primarily based upon the fact that we have a fairly dilute solution and that Nb_2Cl_{10} is the highest known polymer for liquid niobium(V) chloride. Together these restrictions give the five models shown in Table 3. Here the data given in Table 1 for pCl^- values higher than

Table 1. Values of cell potential and composition[a] of $NbCl_5$ in molten $KCl-AlCl_3$ at 300 °C.

0.1 F $NbCl_5$			0.3 F $NbCl_5$		
$-\Delta E$ mV	Mol fraction KCl	$AlCl_3$	$-\Delta E$ mV	Mol fraction KCl	$AlCl_3$
586.2	0.4898_2	0.5047_0	508.0	0.4917_6	0.4912_0
553.5	0.4936_3	0.5008_4	462.2	0.4945_3	0.4874_9
531.5	0.4953_4	0.4990_2	410.2	0.4965_7	0.4842_6
519.8	0.4958_9	0.4984_3	365.5	0.4981_5	0.4820_3
507.8	0.4969_2	0.4971_3	346.0	0.4987_5	0.4817_1
483.8	0.4977_7	0.4961_8	244.0	0.5002_5	0.4794_8
476.4	0.4975_7	0.4966_2	109.9	0.5023_2	0.4775_6
414.3	0.4989_1	0.4948_0	55.5_8	0.5061_3	0.4739_1
395.9	0.4991_8	0.4940_5	44.4_2	0.5076_2	0.4725_1
298.2	0.5000_3	0.4933_4	34.2_0	0.5091_9	0.4709_7
203.5	0.5005_0	0.4928_0	18.4_1	0.5124_6	0.4678_4
127.7	0.5016_4	0.4917_0			
87.8_0	0.5032_3	0.4901_8			
55.8_5	0.5059_0	0.4874_7			
54.3_1	0.5061_1	0.4872_9			
32.3_3	0.5094_7	0.4839_5			
29.9_8	0.5096_4	0.4837_5			
18.8_8	0.5124_7	0.4809_3			

[a] Corrected for the presence of $NbCl_5$ in the gaseous phase.

Table 2. Average values of $\bar{n}$ for Nb(V) in the basic region.

Concentration of $NbCl_5$,M	Number of measurements	pCl^- region	$\bar{n}$	Variance $\times 10^4$
0.1	8	0.42 – 2.04	6.006 ± 0.055	29.7
0.3	5	0.42 – 1.22	6.006 ± 0.020	4.1

Table 3. Comparison between different models for 0.1 F and 0.3 F $NbCl_5$ in $KCl-AlCl_3$ at 300 °C. Based on potentiometric measurements.[a]

Equilibria	Model No.	0.1 F $NbCl_5$[b] pK	Variance $\times 10^4$	0.3 F $NbCl_5$[c] pK	Variance $\times 10^4$
$NbCl_6^- \rightleftarrows NbCl_5 + Cl^-$	(1)	4.49 ± 0.05	48.8*	4.19 ± 0.03	5.6*
$2NbCl_6^- \rightleftarrows Nb_2Cl_{10} + 2Cl^-$	(2)	7.95 ± 0.13	99.6	7.70 ± 0.13	54.3
$NbCl_6^- \rightleftarrows NbCl_5 + Cl^-$	(3)	4.49 ± 0.05		4.19 ± 0.03	
$2NbCl_5 \rightleftarrows Nb_2Cl_{10}$		[d]	48.8	[d]	5.6*
$2NbCl_6^- \rightleftarrows Nb_2Cl_{11}^- + Cl^-$	(4)	3.24 ± 0.28		3.57 ± 0.10	
$Nb_2Cl_{11}^- \rightleftarrows Nb_2Cl_{10} + Cl^-$		4.51 ± 0.20	51.9*	4.11 ± 0.10	5.9*
$2NbCl_6^- \rightleftarrows Nb_2Cl_{11}^- + Cl^-$	(5)	4.05 ± 0.80		4.56 ± 0.60	
$Nb_2Cl_{11}^- \rightleftarrows 2NbCl_5 + Cl$		4.91 ± 0.77	52.1*	3.82 ± 0.60	6.0*

[a] Number of measurements, 10 and 6 for 0.1 and 0.3 F $NbCl_5$, respectively. [b] Asterisks based on $F_{0.10}(9.7) = 2.72$ or $F_{0.10}(8.7) = 2.75$ with experimental variance taken from Table 2. [c] Asterisks based on $F_{0.10}(5.4) = 4.05$ or $F_{0.10}(4.4) = 4.11$ with experimental variance taken from Table 2. [d] No minima found here.

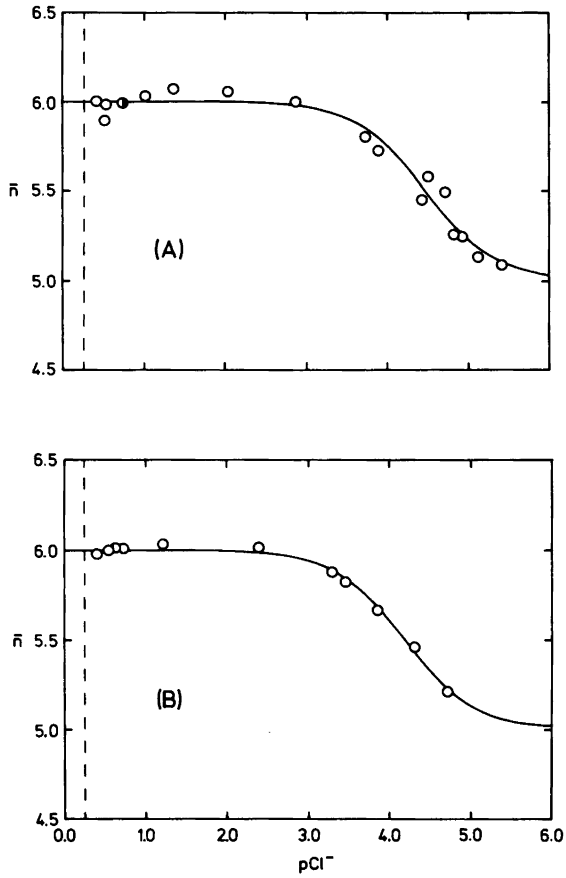

Fig. 1. Average experimental coordination number ($\bar{n}$) for Nb(V) at 300 °C as a function of pCl^-: A, 0.1 F Nb(V), B, 0.3 F Nb(V), compared with calculated lines for the reaction $NbCl_6^- \rightleftarrows NbCl_5 + Cl^-$ (full lines). The vertical dashed lines show the limiting pCl^-, due to saturation with KCl. The half-filled circle represents a coincidence between two open circles. The measurements have been corrected for $NbCl_5$ present in the gaseous phases above the melts.

2.1 ($-\Delta E$ higher than 210 mV) are used in the calculations. As discussed under General Considerations, models marked with asterisks indicate those for which the probability is higher than 90 % as compared with the experimental variances. A problem one should be aware of here is that the experimental variance could be a function of pCl^-.

One way of solving this problem would be to assume that the lowest variance is in fact the correct experimental variance for the examined range. However, this assumption will still give the same picture as shown in Table 3 (*i.e.* none of the asterisks are moved). This leaves us with four possible models, namely: models (1), (3), (4), and (5). It is not possible to distinguish among these models on the basis of potentiometric measurements alone.

It will be seen from Table 3 that model (1) involves only two chromophoric species, whereas models (3), (4) and (5) involve three chromophoric species. In order to distinguish between these possibilities spectrophotometric measurements are needed.

Spectrophotometric measurements on $NbCl_5$ in $KCl-AlCl_3$. The problem with oxychloride formation was partly solved as described in the Experimental Section by subtracting spectra for high and low concentrations of $NbCl_5$. A set of spectra

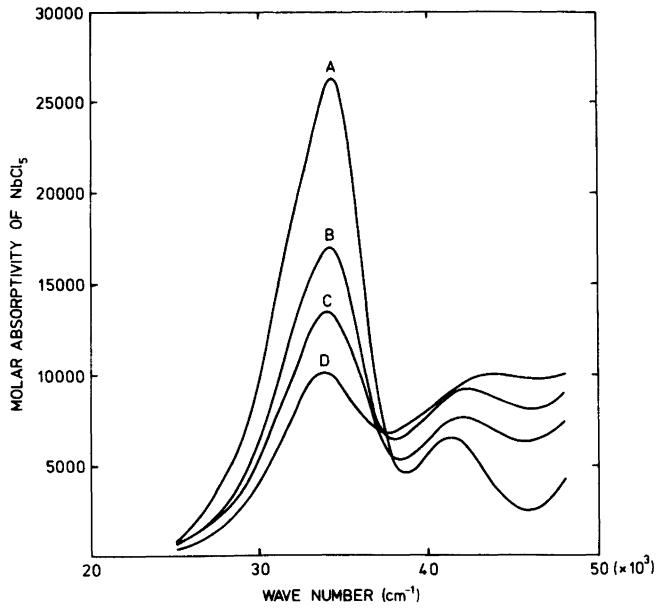

Fig. 2. Spectra of $NbCl_5$ in $KCl-AlCl_3$ at 300 °C. Mol fractions of KCl, $AlCl_3$, and formal concentration of $NbCl_5$, respectively, for the two sets of melts which form the basis for each calculated spectrum; the low concentrations are given in parentheses: A, 0.5105_5 (0.5106_7), 0.4866_6 (0.4881_9), 0.0424 (0.0174); B, 4994_9 (0.4996_9), 0.4978_6 (0.4993_7), 0.0400 (0.0142); C, 0.4988_7 (0.4991_5), 0.4993_0 (0.4998_1) 0.0277 (0.0158); D, 0.4911_6 (0.4917_9), 0.5061_2 (0.5069_2), 0.0408 (0.0194). Based on a pK-value for the reaction $NbCl_6^- \rightleftarrows NbCl_5 + Cl^-$ of 4.49 and the self-dissociation constants for the solvent (given in the text) the average experimental coordination number ($\bar{n}$) for the niobium complex and the pCl^- for the melt could be calculated to be (values for the low concentrations are given in parentheses): A, 6.00_0 (6.00_0), 4.93 (4.88). B, 5.80_8 (5.82_4), 3.85 (3.80); C, 5.59_2 (5.62_7), 4.31 (4.25); D, 5.11_6 (5.11_7), 5.35 (5.35), respectively. All measurements have been corrected for $NbCl_5$ present in the gaseous phase above the melt.

obtained in this way is shown in Fig. 2. An examination of these spectra shows that even if we are not dealing with a perfect two-species system (due to the influence of some oxychloride) the best way to describe the spectra is probably by a two-species model. If only two species are present there is only one model left of the models given in Table 3, namely model (1) ($NbCl_6^- \rightleftarrows NbCl_5 + Cl^-$). Under these circumstances, what we observe as we increase the pCl^- value for the melt is a change from $NbCl_6^-$ ions to $NbCl_5$ molecules. Based on the equilibrium constant given in Table 3 for 0.1 F Nb(V) and the self-dissociation constant for the solvent given under General Considerations, pCl^- and the average experimental coordination number can be calculated for the composition corresponding to each spectrum. These values are given in the caption to Fig. 2. It can be seen that spectrum A represents the spectrum of pure $NbCl_6^-$, whereas spectrum D represents a mixture of 88.4 % $NbCl_5$ and 11.6 % $NbCl_6^-$. In Fig. 3 are shown the spectrum of pure $NbCl_5$ in the melt (calculated from the spectra in Fig. 2) and the spectrum of pure $NbCl_6^-$. It will be seen from these figures that $NbCl_6^-$ has two band maxima located at 34.4×10^3 and 41.3×10^3 cm^{-1}. $NbCl_5$ also has two band maxima located at 33.7×10^3 and 43.8×10^3 cm^{-1}, with molar extinction coefficient that are smaller than those of the $NbCl_6^-$ bands.

Spectrophotometric measurements on $NbCl_5$ in the gas phase. Fig. 4 shows the spectrum of $NbCl_5$ in the gas phase at 300 °C compared with the calculated spectrum of $NbCl_5$ in the melt. It can be seen that in the gas phase two bands are found at 34.8×10^3 and 43.4×10^3 cm^{-1}, respectively. These band positions are close to those of $NbCl_5$ in the $KCl-AlCl_3$ melt, but molar extinction coefficients for $NbCl_5$ in the melt are much smaller than those of $NbCl_5$ in the gas.

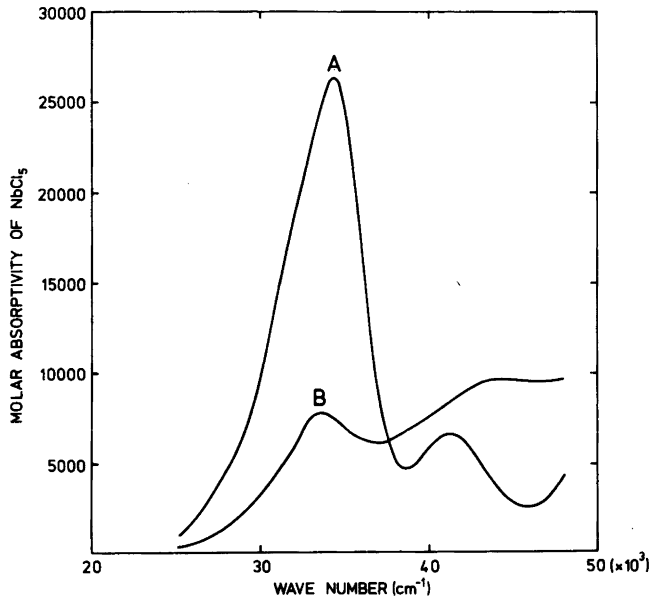

Fig. 3. Comparison between the calculated spectra of $NbCl_6^-$, A, and $NbCl_5$, B, in $KCl-AlCl_3$ at 300 °C.

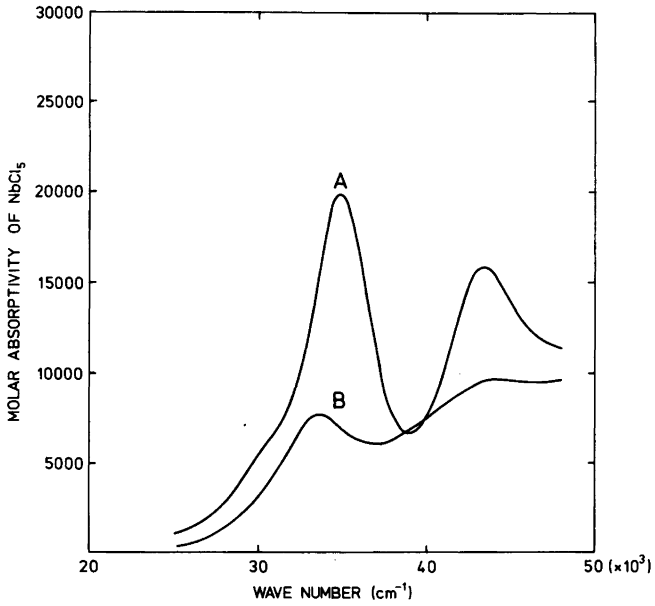

Fig. 4. Comparison between spectra of $NbCl_5$ at 300 °C: A, in the gas phase (concentration of Nb(V), 1.707×10^{-3} M); B, in $KCl-AlCl_3$ (calculated).

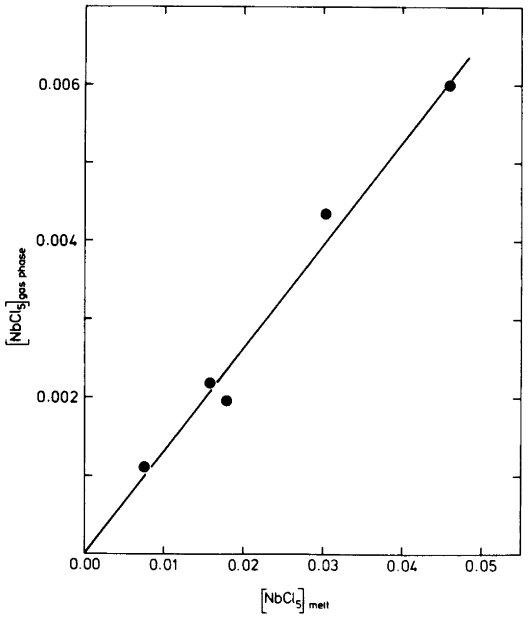

Fig. 5. Measured concentrations of $NbCl_5$ in the gas phase above $KCl-AlCl_3-NbCl_5$ melts at 300 °C *versus* the calculated concentrations of $NbCl_5$ in the melt (based on a p*K*-value of 4.49 for the reaction $NbCl_6^- \rightleftarrows NbCl_5 + Cl^-$ and the self-dissociation constants for the solvent given in the text). The calculated concentrations of $NbCl_5$ in the melt, the calculated pCl^- values, and calculated $\bar{n}$-values were: 7.75×10^{-3} M, 4.24, 5.63_3; 1.57×10^{-2} M, 4.27, 5.61_5; 1.79×10^{-2} M, 5.36, 5.11_5; 3.03×10^{-2} M, 5.31, 5.12_7; 4.59×10^{-2} M, 5.39, 5.10_8, respectively.

Since we know that at high pCl^- values there is a fairly high vapor pressure of Al_2Cl_6 above the melt, it is important to determine whether there is any interference between Al_2Cl_6 and $NbCl_5$ in the gas phase. Addition of Al_2Cl_6 to the gas cell had no influence on the gas spectrum of $NbCl_5$. This we consider to be an indication that no gaseous complexes are formed between $NbCl_5$ and Al_2Cl_6 at the given temperature in contrast to what is usually found between chlorides of transition metals and aluminum chloride.[17,18] A further consequence of this observation is that it is unlikely that $NbCl_5$ is solvated by $AlCl_4^-$ in the melt.

If we now examine the gaseous phase above different $KCl-AlCl_3-NbCl_5$ melts, the measurements show as expected that there is no $NbCl_5$ present if the melt is basic and a fairly high concentration if the melt is acidic. If we take a series of different melts with different pCl^- values and measure the concentration of $NbCl_5$ above the melt and plot this concentration against the concentration of $NbCl_5$ present in the melt calculated from the equilibrium constant given in Table 3 model (1) a plot as shown in Fig. 5 is obtained. There is a very good linear correlation here between the concentration in the gas phase and the concentration in the melt phase independent of the pCl^- of the melt. This is, of course, a further reason to believe that we have obtained the right model for the system. From the slope of this curve the vapor/liquid distribution coefficient is calculated to be 0.133 ± 0.011 at 300 °C. This distribution coefficient can be used to make accurate corrections for the $NbCl_5$ present in the gas phase above a given melt.

Raman spectra of $NbCl_5$ in $KCl-AlCl_3$ melt at 300 °C. In Fig. 6 are shown a series of spectra of 0.2 to 0.3 F $NbCl_5$ dissolved in different $KCl-AlCl_3$ melts (with different pCl^- values). Most of the bands shown are due to the $AlCl_4^-$ complex but a comparison with the spectrum of pure $KAlCl_4$[10,19] reveals that the band around 376 cm^{-1} must be

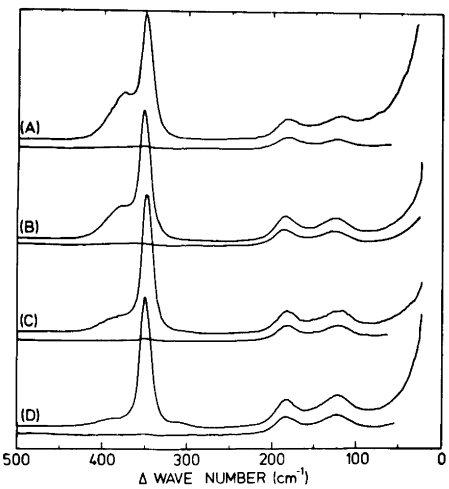

Fig. 6. Series of Raman spectra (parallel and perpendicular polarizations) of $NbCl_5$ dissolved in molten $KCl-AlCl_3$ at 300 °C. The mol fractions of KCl, $AlCl_3$, and the formal concentration of $NbCl_5$ as well as the calculated pCl^- and $\bar{n}$ (based on a p*K*-value of 4.19 for the reaction $NbCl_6^- \rightleftarrows NbCl_5 + Cl^-$) were: A, 0.5135_1, 0.4668_9, 0.2963, 3.89, 6.00_0; B, 0.4964_5, 0.4864_2, 0.2558, 3.97, 5.62_3; C, 0.4884_1, 0.4972_4, 0.2134, 5.18, 5.09_3; D, 0.4824_2, 0.5035_8, 0.2072, 5.54, 5.04_2, respectively.

due to Nb(V). In order to obtain the correct position for this band, the background due to the $AlCl_4^-$ band has been subtracted in the vicinity of 376 cm^{-1}. The band at 376 cm^{-1} must be the ν_1 vibration of the octahedral $NbCl_6^-$ ion (the band position in liquid $CsNbCl_6$ at 600 °C is found[9] at 373 cm^{-1} in complete agreement with our proposed model). In this connection it is interesting to look for the other bands found in $CsNbCl_6$ at 600 °C, *i.e.* at 281 cm^{-1} (E_g) and at 181, 173 cm^{-1} (T_{2g}). The band at 281 cm^{-1} is weak and this is probably the reason why it is not seen. The bands at 181 and 173 cm^{-1} are stronger but they are concealed by the 182 cm^{-1} band due to $AlCl_4^-$.

As the melt is made increasingly acidic a change occurs so that the band at 376 cm^{-1} disappears and a new, weaker band appears. This band, which is also strongly polarized, is located around 397 cm^{-1}. In this connection it is very important to subtract the background due to $AlCl_4^-$ before the band maximum is determined. A comparison with the spectrum of liquid $NbCl_5$ at 300 °C (where the main part of the liquid consists of $NbCl_5$ molecules[9]) shows that the strongest band is located at 397 cm^{-1} and this band is also polarized. According to the work of Bues, Demiray and Øye[9] Nb_2Cl_{10} is characterized by a band at 415 cm^{-1}. Unfortunately, the present spectra are not good enough to reject the possibility of the presence of a smaller band at 415 cm^{-1} in addition to the band at 397 cm^{-1}. However, the observed behavior agrees well with the other types of measurements we performed. As in the case of the $NbCl_6^-$ complex the other bands due to $NbCl_5$ are obscured by bands due to $AlCl_4^-$, *i.e.* the bands at 182 and 122 cm^{-1}.

Acknowledgements. The authors wish to thank O. Faurskov Nielsen for measuring the Raman spectra and to acknowledge the financial support given to J.H.v.B. by "Statens naturvidenskabelige Forskningsråd" and to G.P.S. by the Division of Basic Energy Sciences of the U.S. Department of Energy.

REFERENCES

1. Barner, J. H. von and Bjerrum, N. J. *Inorg. Chem. 12* (1973) 1891.
2. Barner, J. H. von, Bjerrum, N. J. and Kiens, K. *Inorg. Chem. 13* (1974) 1708.
3. Poulsen, F. W., Bjerrum, N. J. and Nielsen, O. F. *Inorg. Chem. 13* (1974) 2693.
4. Andreasen, H. A. and Bjerrum, N. J. *Inorg. Chem. 14* (1975) 1807.
5. Andreasen, H. A. and Bjerrum, N. J. *Inorg. Chem. 18* (1979). *In press.*
6. Huber, K., Jost, E., Neuenschwander, E., Studer, M. and Roth, B. *Helv. Chim. Acta 41* (1958) 2411.
7. Gavrilov, O. R. and Nisel'son, L. A. *Zh. Neorg. Khim. 11* (1966) 209; *Russ. J. Inorg. Chem. 11* (1966) 114.
8. Beattie, I. R., Gilson, T. R. and Ozin, G. A. *J. Chem. Soc. A* (1968) 2765.
9. Bues, W., Demiray, F. and Øye, H. A. *Z. Phys. Chem. N.F. 84* (1973) 18.
10. Rytter, E., Øye, H. A., Cyvin, S. J., Cyvin, B. N. and Klæboe, P. *J. Inorg. Nucl. Chem. 35* (1973) 1185.
11. Boxall, L. G., Jones, H. L. and Osteryoung, R. A. *J. Electrochem. Soc. 120* (1972) 223.
12. Torsi, G., Mamantov, G. and Begun, G. M. *Inorg. Nucl. Chem. Lett. 6* (1970) 553.
13. Nisel'son, L. A., Pustil'nik, A. I. and Sokolova, I. D. *Zh. Neorg. Khim. 9* (1964) 1049; *Russ. J. Inorg. Chem. 9* (1964) 574.
14. Morrey, J. R. and Carter, D. G. *J. Chem. Eng. Data 13* (1968) 94.
15. Flengas, S. N. and Block-Bolten, A. *Adv. Molten Salt Chem. 2* (1973) 43.
16. Brekke, P. B., Barner, J. H. von and Bjerrum, N. J. *Submitted.*
17. Papatheodorou, G. N. *Z. Anorg. Allg. Chem. 411* (1975) 153.
18. Sørlie, M. and Øye, H. A. *J. Inorg. Nucl. Chem. 40* (1978) 493.
19. *Unpublished results.*

Received June 2, 1978.

Acta Chemica Scandinavica A 32 (1978) 847–855

A Double-bridged Binuclear Chromium(III) Complex with 1-(2-Pyridyl)ethylamine. Stereochemical and Magnetic Properties of Di-μ-hydroxobis[bis{1-(2-pyridyl)ethylamine}-chromium(III)] Ions

KIRSTEN MICHELSEN and ERIK PEDERSEN

Chemistry Department I (Inorganic Chemistry), University of Copenhagen, H. C. Ørsted Institute, Universitetsparken 5, DK-2100 Copenhagen Ø, Denmark

Dedicated to Jannik Bjerrum on the occasion of his 70th birthday

The synthesis, resolution and stereochemical and magnetic properties of binuclear complexes of the double-bridged type $[(C_7H_{10}N_2)_2Cr(OH)_2Cr(C_7H_{10}N_2)_2]^{4+}$, where the bidentate ligand $C_7H_{10}N_2$ is 1-(2-pyridyl)ethylamine, are reported for the first time. The ligand apparently chelates stereospecifically in this type of complexes. In the case when the title complex is prepared from racemic ligand, one obtains only one racemic pair of complexes, resolvable into catoptric forms, that are identical with the complexes prepared from $(+)_D$- and $(-)_D$-{1-(2-pyridyl)ethylamine}, respectively.

Based on the circular dichroism in the visible range the $(-)_D$-$[\{(R)(+)_D$-$C_7H_{10}N_2\}_2Cr(OH)_2Cr\{(R)(+)_D$-$C_7H_{10}N_2\}_2]^{4+}$ ion is assigned the absolute configuration ΔΔ. The preliminary results from an X-ray analysis support this assignment.

The magnetic susceptibility of powdered samples of $\Lambda\Lambda(+)_D$-$[\{(S)(-)_D$-$C_7H_{10}N_2\}_2Cr(OH)_2Cr\{(S)(-)_D$-$C_7H_{10}N_2\}_2](S_2O_6)_2.2H_2O$ has been examined in the temperature range 4.5–287 K. The dimer exhibits an antiferromagnetic exchange interaction. The data were fitted to a model assuming independent triplet, quintet and septet energies. The results were almost consistent with the Van Vleck equation and with a triplet energy of 32.95(9) cm^{-1}. The susceptibilities of other active and racemic bromide, dithionate and perchlorate salts were measured in the range 45–300 K. Singlet–triplet splittings were in all cases in the range 31–37 cm^{-1}.

Dimeric chromium(III) complexes with two hydroxo groups as bridging ligands, the so-called diols, have recently received much attention because of their spectroscopic,[1-6] structural and magnetic properties.[7-21]

In a recent paper from this laboratory the synthesis, resolution and properties of the binuclear ion $[(C_6H_8N_2)_2Cr(OH)_2Cr(C_6H_8N_2)_2]^{4+}$, where the bidentate ligand $C_6H_8N_2$ = (2-pyridyl)methylamine (Fig. 1a), were reported.[5] The present work deals with the corresponding compounds of the closely related amine $C_7H_{10}N_2$ = 1-(2-pyridyl)ethylamine (Fig. 1b). We described the preparation and resolution of this ligand in an earlier work,[22] and the absolute chirality of the $(-)_D$-form was found by X-ray analysis to be *S*.[23]

For the di-μ-hydroxo complexes of copper(II), several groups of workers have noted apparently simple correlations between the structural and

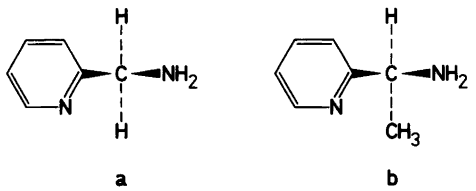

Fig. 1. a. (2-Pyridyl)methylamine, $C_6H_8N_2$. b. 1-(2-Pyridyl)ethylamine, $C_7H_{10}N_2$.

magnetic properties.[21,24] The magnetic interactions seem to be determined essentially by the geometry of the bridging system. A more complex behaviour has been observed for the chromium(III) complexes. It must be born in mind, however, that only a few complexes are known, in which the geometry of the entire bridging systems, including the hydrogen atoms, has been well determined from X-ray diffraction.

We have, therefore, continued such studies on chromium(III) dimers. We here report the magnetic properties of $\Lambda\Lambda(+)_D$-$[\{(S)(-)_D$-$C_7H_{10}N_2\}_2Cr(OH)_2Cr\{(S)(-)_D$-$C_7H_{10}N_2\}_2](S_2O_6)_2.2H_2O$ and the corresponding active and racemic salts in relation to the preliminary results of a determination of the crystal and molecular structure of the optically active salt.[19]

EXPERIMENTAL

Reagents. Racemic 1-(2-pyridyl)ethylamine was prepared and resolved as described before. SP-Sephadex C 25 was purchased from Pharmacia, Uppsala, Sweden. All other chemicals were of reagent grade and were used without further purifications.

Analyses. The chromium analyses were performed on a Perkin Elmer 403 Atomic Absorption Spectrophotometer. The microanalytical laboratory of this institute carried out the carbon, nitrogen, hydrogen and halogen analyses by standard methods.

Physical measurements. Absorption spectra were recorded on a Cary Model 14 spectrophotometer. The spectra are characterized by their maxima and minima (ε,λ), where the molar extinction coefficient ε is in units of 1 mol^{-1} cm^{-1} and λ is in nm. Circular dichroism was measured on a Roussel-Jouan Dichrographe I in the region 650–350 nm, on a Roussel-Jouan Dichrographe III in the region 350–200 nm. The maxima are given below as $(\Delta\varepsilon,\lambda)=[(\varepsilon_l-\varepsilon_r),\lambda]$. Optical rotation was measured on a Perkin Elmer Model 141 polarimeter. In all cases the solvent was 0.1 M hydrochloric acid. The magnetic susceptibility of powdered samples was measured by the Faraday method in the temperature range 4.2 – 300 K at a field strength of 12 000 G. The magnetic field was calibrated with $Hg[Co(NCS)_4]$.[25] A more detailed description of the equipment is published elsewhere.[18,26]

Preparations

1. Racemic ligand complexes. 1 a. Di-μ-hydroxobis[bis{1-(2-pyridyl)ethylamine}chromium(III)] bromide, $[(C_7H_{10}N_2)_2Cr(OH)_2Cr(C_7H_{10}N_2)_2]Br_4.3H_2O$. 1.00 g $[CrBr_2(H_2O)_4]Br.2H_2O$ (2.50 mmol) was dissolved in 2–3 ml 2-methoxyethanol, and a spatula of zinc powder and 0.6 ml racemic 1-(2-pyridyl)ethylamine (~5 mmol) were stirred in. Red crystals immediately precipitated. They were filtered after 15 min and washed with 2-methoxyethanol and ethanol. This crude product was always contaminated with metallic zinc and a zinc compound (perhaps a tetrabromozincate). Pure zinc-free diol could be obtained by conversion to a perchlorate (1 b) or an iodide (1 c) or, as in this case, by ion exchange. A filtered solution of the crude product was absorbed on a short column (length 5 cm, diameter 2.5 cm) of an SP-Sephadex C-25 cation exchanger. Elution with 0.1 M sodium bromide (250 ml) and 0.1 M hydrobromic acid (100 ml) removed the unwanted ions. Finally the diol was eluted with 1 M hydrobromic acid and precipitated with ethanol and ether. Yield: 0.370 g (30 %). In other experiments, yields ranging from 26 to 35 % were obtained. Recrystallization from boiling water (2 ml) with the addition of lithium bromide (0.5 g), ethanol (40 ml) and ether (20 ml) yielded 0.339 g. Anal. $[Cr(C_7H_{10}N_2)_2OH]_2Br_4.3H_2O$: Cr, C, N, H, Br. In other experiments the complex crystallized with 4 or 5 mol of crystal water. $(\varepsilon,\lambda)_{max}$: (200, 535.5), (119, 378). $(\varepsilon,\lambda)_{min}$: (26, 435), (65, 350).

1 b. Di-μ-hydroxobis[bis{1-(2-pyridyl)ethylamine}chromium(III)] perchlorate, $[(C_7H_{10}N_2)_2Cr(OH)_2Cr(C_7H_{10}N_2)_2](ClO_4)_4.3H_2O$. The crude product, prepared from 1.00 g $[CrBr_2(H_2O)_4]Br.2H_2O$ (see 1 a), was dissolved in boiling water (6 ml), and a solution of sodium perchlorate (2 g) in water (1 ml) was added to the filtrate. Cooling on ice. Filtering and washing with ethanol. Yield: 0.599 g (22 %). The compound was recrystallized from boiling water (6 ml). The loss was 25 %. Anal. $[Cr(C_7H_{10}N_2)_2OH]_2(ClO_4)_4.3H_2O$: Cr, C, N, H, Cl. In other experiments the compound crystallized with 2 mol of crystal water. $(\varepsilon,\lambda)_{max}$: (202, 535.5), (119, 378). $(\varepsilon,\lambda)_{min}$: (26, 435), (67, 350).

1 c. Di-μ-hydroxobis[bis{1-(2-pyridyl)ethylamine}chromium(III)] iodide, $[(C_7H_{10}N_2)_2Cr(OH)_2Cr(C_7H_{10}N_2)_2]I_4.3H_2O$. The crude product prepared from 1.00 g $[CrBr_2(H_2O)_4]Br.2H_2O$ (see 1 a) was dissolved in boiling water (6 ml), and a solution of sodium iodide (1 g) in water (1 ml) was added to the filtrate. Cooling on ice. Filtering and washing with ethanol. Yield: 0.501 g (34 %). The compound was recrystallized from boiling water with 70 % recovery. Anal. $[Cr(C_7H_{10}N_2)_2OH]_2I_4.3H_2O$: Cr, C, N, H, I. $(\varepsilon,\lambda)_{max}$: (201, 535.5), 122, 378). $(\varepsilon,\lambda)_{min}$: (28, 434), (71, 350).

2. Resolution of racemic ligand complexes. 2 a. $(-)_D$-Di-μ-hydroxobis[bis{1-(2-pyridyl)ethylamine}chromium(III)] diantimonyl $(+)_D$-tartrate dibromide, $(-)_D$-$[(C_7H_{10}N_2)_2Cr(OH)_2Cr(C_7H_{10}$-

$N_2)_2]\{(+)_D$-$SbOC_4H_4O_6\}_2Br_2.7H_2O$. Compound 1 a (2.20 g, 2.2 mmol) was dissolved in hot water (6–7 ml, 70 °C). Sodium antimonyl $(+)_D$-tartrate (2.6 g, 8.4 mmol) was dissolved in hot water (5 ml, 70 °C). These solutions were mixed, gently heated for a moment and then left at room temperature for 1 h. Filtering and washing with ethanol–water (1:1) and ethanol. Yield: 1.36 g (42 %). Anal. $[Cr(C_7H_{10}N_2)_2OH]_2(SbOC_4H_4O_6)_2Br_2.7H_2O$: Cr, C, N, H, Br. $(\varepsilon,\lambda)_{max}$: (202, 535.5), (122, 378). $(\varepsilon,\lambda)_{min}$: (29, 435), (68, 350). $(\Delta\varepsilon,\lambda)_{max}$: (−5.44, 504.5), (+1.70, 374).

2 b. $(-)_D$-Di-μ-hydroxobis[bis{1-(2-pyridyl)ethylamine}chromium(III)] bromide, $(-)_D$-$[(C_7H_{10}N_2)_2Cr(OH)_2Cr(C_7H_{10}N_2)_2]Br_4.3H_2O$. Compound 2 a (1.10 g, 0.74 mmol) was dissolved in 3–4 ml 1 M sodium hydroxide. Ethanol (80 ml) was added to precipitate sodium antimonyl $(+)_D$-tartrate. The filtrate was acidified with conc. hydrobromic acid, and by the addition of lithium bromide (5 g), ethanol and ether, violet crystals of the active bromide separated. Yield: 0.699 g (94 %). The compound was recrystallized as described for 1 a. Anal. $[Cr(C_7H_{10}N_2)_2OH]_2Br_4.3H_2O$: Cr, C, N, H, Br. $(\varepsilon,\lambda)_{max}$: (199, 535.5), (120, 378). $(\varepsilon,\lambda)_{min}$: (27, 435), (65, 350). $(\Delta\varepsilon,\lambda)_{max}$: (−5.40, 504.5), (+1.67, 374).

2 c. $(-)_D$-Di-μ-hydroxobis[bis{1-(2-pyridyl)ethylamine}chromium(III)] perchlorate, $(-)_D$-$[(C_7H_{10}N_2)_2Cr(OH)_2Cr(C_7H_{10}N_2)_2](ClO_4)_4.2H_2O$. Compound 2 a (0.250 g, 0.17 mmol) was dissolved in boiling water (5 ml). A solution of sodium perchlorate (1 g, 1 ml) was added, and fluffy crystals separated. Filtering and washing with 1 M sodium perchlorate and with ethanol. Yield: 0.135 g (75 %). Anal. $[Cr(C_7H_{10}N_2)_2OH]_2(ClO_4)_4.2H_2O$: Cr, C, N, H, Cl. $(\varepsilon,\lambda)_{max}$: (199, 535.5), (121, 378). $(\varepsilon,\lambda)_{min}$: (27, 435), (68, 350). $(\Delta\varepsilon,\lambda)_{max}$: (−5.43, 504.5), (+1.66, 374).

3. Active ligand complexes. 3 a. $(+)_D$-Di-μ-hydroxobis[bis{$(-)_D$-1-(2-pyridyl)ethylamine}chromium(III)] bromide, $(+)_D$-$[\{(-)_D$-$C_7H_{10}N_2\}_2Cr(OH)_2Cr\{(-)_D$-$C_7H_{10}N_2\}_2]Br_4.3H_2O$. The compound was prepared as 1a except that the racemic ligand was replaced by $(-)_D$-1-(2-pyridyl)ethylamine. The yield was normally 30 %. Anal. $[Cr(C_7H_{10}N_2)_2OH]_2Br_4.3H_2O$: Cr, C, N, H, Br. $(\varepsilon,\lambda)_{max}$: (199, 535.5), (120, 378). $(\varepsilon,\lambda)_{min}$: (28, 434), (67, 350). $(\Delta\varepsilon,\lambda)_{max}$: (5.41, 504), (−1.71, 375).

3 b. $(+)_D$-Di-μ-hydroxobis[bis{$(-)_D$-1-(2-pyridyl)ethylamine}chromium(III)] dithionate, $(+)_D$-$[\{(-)_D$-$C_7H_{10}N_2\}_2Cr(OH)_2Cr\{(-)_D$-$C_7H_{10}N_2\}_2](S_2O_6)_2.5H_2O$. Compound 3a (0.122 g, 0.122 mmol) was dissolved in boiling water (2 ml). Sodium dithionate (0.1 g) was added and dissolved by gentle heating. A few minutes later red, needle-shaped crystals separated. Washing with ice-cold water. Yield: 0.111 g (91 %). Anal. $[Cr(C_7H_{10}N_2)_2OH]_2(S_2O_6)_2.5H_2O$: Cr, C, N, H. In other experiments the complex crystallized with 2, 3 or 4 mol of crystal water. $(\varepsilon,\lambda)_{max}$: (203, 535.5), (120, 378). $(\varepsilon,\lambda)_{min}$: (27, 434), (66, 350).

3 c. $(-)_D$-Di-μ-hydroxobis[bis{$(+)_D$-1-(2-pyridyl)ethylamine}chromium(III)] perchlorate, $(-)_D$-$[\{(+)_D$-$C_7H_{10}N_2\}_2Cr(OH)_2Cr\{(+)_D$-$C_7H_{10}N_2\}_2](ClO_4)_4.2H_2O$. The compound was prepared as 1b except that the racemic ligand was replaced by $(+)_D$-1-(2-pyridyl)ethylamine. The yields varied from 30 to 35 %. Anal. $[Cr(C_7H_{10}N_2)_2OH]_2(ClO_4)_4.2H_2O$: Cr, C, N, H, Cl. $(\varepsilon,\lambda)_{max}$: (200, 535.5), (122, 378). $(\varepsilon,\lambda)_{min}$: (28, 434), (70, 350). $(\Delta\varepsilon,\lambda)_{max}$: (−5.41, 504.5), (+1.73, 374).

3 d. $(+)_D$-Di-μ-hydroxobis[bis{$(-)_D$-1-(2-pyridyl)ethylamine}chromium(III)] perchlorate, $(+)_D$-$[\{(-)_D$-$C_7H_{10}N_2\}_2Cr(OH)_2\{(-)_D$-$C_7H_{10}N_2\}_2](ClO)_4.2H_2O$. The compound was prepared as 1b except that the racemic ligand was replaced by $(-)_D$-1-(2-pyridyl)ethylamine. Yields as above. Anal. $[Cr(C_7H_{10}N_2)_2OH]_2(ClO_4)_4.2H_2O$: Cr, C, N, H, Cl. $(\varepsilon,\lambda)_{max}$: (201, 535.5), (121, 378). $(\varepsilon,\lambda)_{min}$: (27, 434), (67, 350). $(\Delta\varepsilon,\lambda)_{max}$: (+5.40, 504.5), (−1.66, 374).

RESULTS AND DISCUSSION

Synthesis and resolution. We have earlier found[5,6] that di-μ-hydroxo complexes of chromium(III) with the related ligands (2-pyridyl)methylamine and 1,6-bis-(2′-pyridyl)-2,5-diazahexane could be obtained by the reaction of chromium(III) bromide hexahydrate, with the amine in question in the presence of zinc dust. The same method could be used here, but the yields never exceeded 40 %. The byproducts, as revealed by column chromatography, consisted partly of several lavender-coloured polymeric compounds containing ions of a higher charge than four, and partly of a small amount of a monomeric compound. Only one diol-band appeared on the column, just as it was impossible to isolate more than one diol-isomer from the reaction mixture, no matter whether racemic or optically active amine had been used in the preparation. We cannot, however, preclude the existence of other isomers, because they could have evaded our detection if they were formed in sufficiently small amounts.

Like the corresponding diols with (2-pyridyl)-methylamine,[5] 1,6-bis-(2′-pyridyl)-2,5-diazahexane,[6] 1,10-phenanthroline and 2,2′-bipyridine,[3] the diol prepared from racemic 1-(2-pyridyl)ethylamine could be resolved with sodium antimonyl $(+)_D$-tartrate as a resolving agent. The less soluble diastereoisomer was converted into a perchlorate that turned out to be identical with the diol-per-

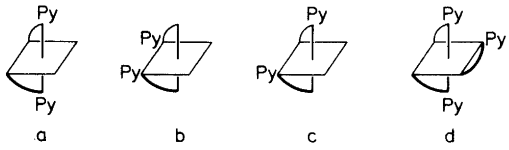

Fig. 2. a, b, c. Geometrical isomers of *cis*-complexes of (2-pyridyl)methylamine with chromium(III). Py symbolizes the pyridine nitrogen. The ligand configurations around the central atoms on the figures are all Λ. a. *α-cis* (Λα). b. *α'-cis* (Λα'). c. *β-cis* (Λβ). d. A meridional isomer of a *tris*-complex of 1-(2-pyridyl)ethylamine with cobalt(III) or chromium-(III), *mer*-Λ.

chlorate prepared direct from $(R)(+)_D$-{1-(2-pyridyl)ethylamine}.

Stereochemistry of the di-μ-hydroxobis[bis{1-(2-pyridyl)ethylamine}chromium(III) ion. The binuclear ion $[(C_7H_{10}N_2)_2Cr(OH)_2Cr(C_7H_{10}N_2)_2]^{4+}$ could in principle exist in several isomeric forms. The isomerism becomes easier to grasp when at first we ignore the methyl group in the amine and consider the isomerism of diols formed with the closely related ligand, (2-pyridyl)methylamine (Fig. 1). This ligand is unsymmetrical, and consequently three geometrical isomers of *cis*-complexes of chromium(III) may occur (Fig. 2 a–c). These *cis*-skeletons are the building stones from which twenty-four diols can be constructed as shown below. From two *α-cis*-skeletons, for instance, we can build up three different isomers (Fig. 3 a–c). Correspondingly we obtain three isomers from two *α'-cis*-skeletons. Two *β-cis*-skeletons result in six isomers. The combination of an *α-cis* and an *α'-cis*-skeleton gives four isomers as do the combinations of *α-cis* and *β-cis*-skeletons and of *α'-cis* and *β-cis* skeletons, respectively.

Molecular models indicate, however, that all compounds containing an *α'-cis* or a *β-cis* skeleton as well as all *meso*-isomers are hindered sterically.

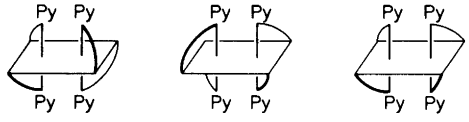

Fig. 3. $[(C_6H_8N_2)_2Cr(OH)_2Cr(C_6H_8N_2)_2]^{4+}$. a–c are the three isomers that can be constructed from two *α-cis*-skeletons. a. ΛαΛα. b. ΔαΔα. c. ΛαΔα.

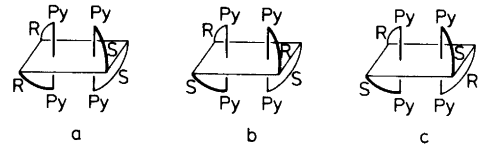

Fig. 4. ΛΛ-$[(C_7H_{10}N_2)_2Cr(OH)_2Cr(C_7H_{10}N_2)_2]^{4+}$. a, b and c show the three different ΛΛ isomers containing two R-amines and two S-amines. a. ΛRR ΛSS. b. ΛRS ΛRS. c. ΛRS ΛSR.

That leaves us with the possibility of finding two isomers only, namely the catoptromers ΛαΛα and ΔαΔα shown in Fig. 3 a and b.

Returning now to 1-(2-pyridyl)ethylamine we find that geometrical isomerism caused by the methyl-groups makes the simplified picture complicated again. Instead of one ΛΛ isomer and one ΔΔ isomer we get the theoretical possibility of seven ΛΛ isomers and seven ΔΔ isomers, namely:

ΛΛ: *RRRR RRRS RRSS RSRS RSSR RSSS SSSS*
ΔΔ: *SSSS SSSR SSRR SRSR SRRS SRRR RRRR*

Fig. 4 shows how the combination of two *R*-amines and two *S*-amines necessarily results in three different complexes with the configuration ΛΛ.

In the case when $[(C_7H_{10}N_2)_2Cr(OH)_2Cr(C_7H_{10}N_2)_2]^{4+}$ was prepared from $(S)(-)_D$-{1-(2-pyridyl)ethylamine} only one optically active complex, namely ΛΛ-$(+)_D$-$[\{(-)_D$-$C_7H_{10}N_2\}_2Cr(OH)_2Cr\{(-)_D$-$C_7H_{10}N_2\}_2]^{4+}$ (abbrev. $\Lambda\Lambda S_4$) was obtained. The expected $\Delta\Delta S_4$ isomer was never detected. When racemic amine was used as a starting material, we were able to find one racemate only, instead of seven as expected. This racemate was resolved, and, as mentioned above, the identity of one of the isolated species proved that we had been dealing with a racemate of $\Delta\Delta R_4$ and $\Lambda\Lambda S_4$.

Results from an earlier work on *tris*-complexes of $(S)(-)_D$-{1-(2-pyridyl)ethylamine} and cobalt-(III)[22] support this evidence of stereospecific coordination. The existence of two meridional isomers, namely *mer*-Λ$(+)_D$-$[Co\{(S)(-)_D$-$C_7H_{10}N_2\}_3]^{3+}$ (abbrev. ΛS_3) and *mer*-Δ$(-)_D$-$[Co\{(S)(-)_D$-$C_7H_{10}N_2\}_3]^{3+}$ (abbrev. ΔS_3) was expected at that time, but we found only one, namely the ΛS_3 isomer.

Recognizing that both a meridional *tris*-complex (Fig. 2 d) and a di-μ-hydroxo complex (Fig. 3 a and b) contain an *α-cis*-skeleton (Fig. 2 a), it is an

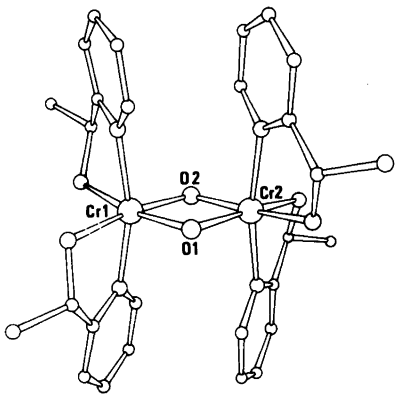

Fig. 5. View of cation in ΛΛ(+)$_D$-[{(*S*)(−)$_D$-$C_7H_{10}N_2$}$_2$Cr(OH)$_2$Cr{(*S*)(−)$_D$-$C_7H_{10}N_2$}$_2$]-$(S_2O_6)_2.2H_2O$. Hydrogen atoms are omitted for clarity. Refer to the text for details of distances and angles.

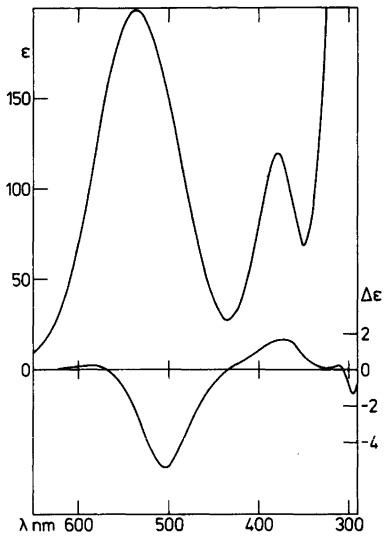

Fig. 6. The absorption spectrum (top) and the circular dichroism (bottom) of (−)$_D$-[{(*R*)(+)$_D$-$C_7H_{10}N_2$}$_2$Cr(OH)$_2$Cr{(*R*)(+)$_D$-$C_7H_{10}N_2$}$_2$]$^{4+}$. Region 620 – 300 nm.

obvious thought that the possible stereospecificity is linked to the α-*cis*-skeleton, and that investigations on α-*cis*-complexes of chromium(III) and cobalt(III) with 1-(2-pyridyl)ethylamine might throw light on the problem.

Configuration and optical activity. The preliminary results from an X-ray analysis of (+)$_D$-[{(*S*)(−)$_D$-$C_7H_{10}N_2$}$_2$Cr(OH)$_2$Cr{(*S*)(−)$_D$-$C_7H_{10}N_2$}$_2$]-$(S_2O_6)_2.2H_2O$[19] (Fig. 5) prove that this compound has the configuration ΛΛ. The catoptromer, (−)$_D$-[{(*R*)(+)$_D$-$C_7H_{10}N_2$}$_2$Cr(OH)$_2$Cr{(*R*)(+)$_D$-$C_7H_{10}N_2$}$_2$]$^{4+}$, whose absorption and circular dichroism spectra (vis. region) are shown in Fig. 6, consequently has the configuration ΔΔ. This is in agreement with the empirical rule that relates a dominant negative CD-band in the region of the cubic $^4A_{2g} \rightarrow {}^4T_{2g}$ $d-d$ absorption of the chromium(III) ion to a ΔΔ configuration.[27] A comparison with spectral data for related compounds is presented in Table 1.

From the X-ray analysis it also appears that (*S*)(−)$_D$-{1-(2-pyridyl)ethylamine} chelates with the conformation δ, thus preferring the conformation in which the methyl group is equatorial. The same amine conformation was earlier found in *fac*-Λ-[Co{(*S*)(−)$_D$-$C_7H_{10}N_2$}$_3$]$^{3+}$.[23]

Table 1. CD-spectral parameters for some di-μ-hydroxo complexes of chromium(III) with (2-pyridyl)-methylamine ($C_6H_8N_2$), 1-(2-pyridyl)ethylamine ($C_7H_{10}N_2$), 1,6-bis(2′-pyridyl)-2,5-diazahexane ($C_{14}H_{18}N_4$), 1,10-phenanthroline ($C_{12}H_8N_2$) and 2,2′-bipyridine ($C_{10}H_8N_2$).

Compound	$\lambda_{ex}(1)$ nm	$\Delta\varepsilon_{ex}(1)$	$\lambda_{ex}(2)$ nm	$\Delta\varepsilon_{ex}(2)$	$\lambda_{ex}(3)$ nm	$\Delta\varepsilon_{ex}(3)$	Ref.
(−)$_D$-[Cr($C_6H_8N_2$)$_2$OH]$_2^{4+}$	588	+0.37	508	−5.55	376	+1.62	5
(−)$_D$-[Cr{(R)(+)$_D$-$C_7H_{10}N_2$}$_2$OH]$_2^{4+}$	~585	~+0.22	504.5	−5.41	374	+1.73	
(+)$_D$-[Cr{(S)(−)$_D$-$C_7H_{10}N_2$}$_2$OH]$_2^{4+}$	~583	~−0.23	504.5	+5.40	374	−1.66	
(−)$_D$-[Cr($C_7H_{10}N_2$)$_2$OH]$_2^{4+}$ (2c)	~583	~+0.23	504.5	−5.43	374	+1.66	
(−)$_D$-[Cr($C_{14}H_{18}N_4$)OH]$_2^{4+}$			520	−5.30	382	+1.10	6
(+)$_D$-[Cr($C_{14}H_{18}N_4$)OH]$_2^{4+}$			520	+5.42	383	−1.13	6
(−)$_D$-[Cr($C_{12}H_8N_2$)$_2$OH]$_2^{4+}$			~520	~−6.2	~400	~+2.6	3
(−)$_D$-[Cr($C_{10}H_8N_2$)$_2$OH]$_2^{4+}$	615	+0.18	518	−6.62	402	+0.79	28

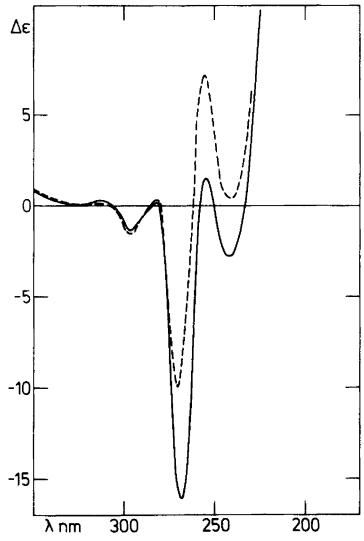

Fig. 7. The circular dichroism spectra of $(-)_D$-$[\{(R)(+)_D$-$C_7H_{10}N_2\}_2Cr(OH)_2Cr\{(R)(+)_D$-$C_7H_{10}N_2\}_2]^{4+}$ (——) and of $(-)_D$-$[(C_6H_8N_2)_2$-$Cr(OH)_2Cr(C_6H_8N_2)_2]^{4+}$ (– – –). Region 350–220 nm.

The CD-spectra of $(-)_D$-$[\{(R)(+)_D$-$C_7H_{10}N_2\}_2$-$Cr(OH)_2Cr\{(R)(+)_D$-$C_7H_{10}N_2\}_2]^{4+}$ and $(-)_D$-$[(C_6H_8N_2)_2Cr(OH)_2Cr(C_6H_8N_2)_2]^{4+}$ in the region 350–220 nm are shown in Fig. 7. The CD-spectrum of the di-μ-hydroxo complex with (2-pyridyl)methylamine is included for comparison. It is not possible to interpret the spectra at the present time, but we find it worthwhile to draw attention to the small, sharp peaks in the region 320–280 nm. Apparently they are closely linked to the binuclear structure of the di-μ-hydroxo complexes, as they were never detected in the corresponding mononuclear *cis*-complexes.

Magnetic and structural properties. The average magnetic susceptibility and effective moment of a powdered sample of $(+)_D$-$[\{(S)(-)_D$-$C_7H_{10}N_2\}_2$-$Cr(OH)_2Cr\{(S)(-)_D$-$C_7H_{10}N_2\}_2](S_2O_6)_2.2H_2O$ as functions of temperature are shown in Fig. 8. Similar results were obtained for the related bromide, dithionate and perchlorate salts with the important difference, however, that the magnetic properties of these salts were measured only in the interval 45–300 K. The susceptibility data were fitted to the expression

$$\chi'_A = -\frac{N}{H}\frac{\sum_i \left(\frac{\partial E_i}{\partial H}\right) e^{-(E_i/kT)}}{\sum_i e^{-(E_i/kT)}} \quad (1)$$

where E_i refers to the energies of the sixteen components of the ground states, by minimization[29] of

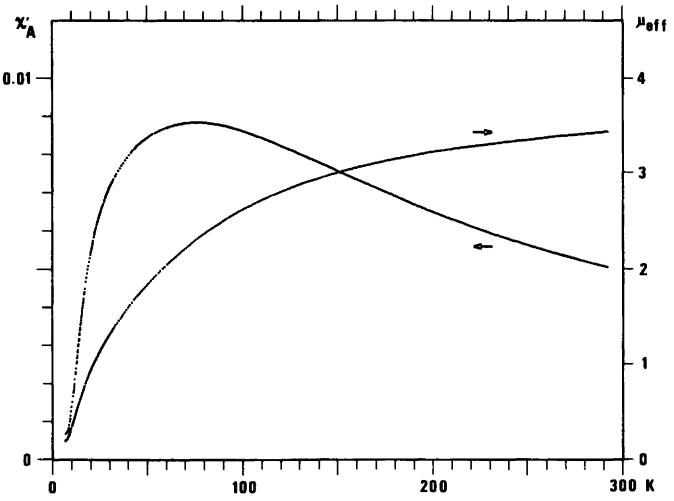

Fig. 8. Magnetic susceptibility (left scale in c.g.s. units) and effective magnetic moment (right scale in Bohr magnetons) of $\Lambda\Lambda(+)_D$-$[\{(S)(-)_D$-$C_7H_{10}N_2\}_2Cr(OH)_2Cr\{(S)(-)_D$-$C_7H_{10}N_2\}_2](S_2O_6)_2.2H_2O$. The dots represent 330 measurements. The theoretical values corresponding to the parameters in Table 2 fall within the areas of the dots.

$$\sum_i (\chi_i^{obs} - \chi_A')^2 / \{\sigma^2(\chi) + \left(\frac{\partial \chi}{\partial T}\right)^2 \sigma^2(T)\} \quad (2)$$

We assumed the Hamiltonian

$$\mathcal{H} = E(S') + g\beta H M_{S'} \quad (3)$$

where $\mathbf{S}' = \mathbf{S}_1 + \mathbf{S}_2$. Since $S_1 = S_2 = 3/2$, S' takes the values 0,1,2 and 3. Eqn. (3) implies independent energies of the singlet, triplet, quintet and septet levels, absence of zero-field splittings within these and furthermore an isotropic Zeeman effect. This is a generalized version of the Van Vleck Hamiltonian which in some cases has been expanded with a biquadratic exchange term according to

$$\mathcal{H} = J\mathbf{S}_1\mathbf{S}_2 + j(\mathbf{S}_1\mathbf{S}_2)^2 \quad (4)$$

The relations between $E(S')$, J and j restricted by eqn. (4) are given by

$$\begin{aligned} E(1) - E(0) &= J - 13/2\, j \\ E(2) - E(0) &= 3J - 27/2\, j \\ E(3) - E(0) &= 6J - 9j \end{aligned} \quad (5)$$

where the J-terms follow the Landé rule.

The results of fitting the susceptibility of the $(+)_D$-dithionate to eqns. (1) and (3) are shown in Table 2. We assumed a normal distribution of errors of each measurement corresponding to standard deviations of the susceptibilities of 0.05 % and of the temperature of 0.05 K plus 0.05 % of the deviation of the actual temperature from that of boiling nitrogen which was used as a reference. The estimated standard deviations of our susceptibility measurements are thus a factor of ten smaller than the accuracy of the standard[25] used for calibration of $H\partial H/\partial x$. This calibration constant, the molecular weight assumed, and the g-factors obtained from our fitting procedure are strongly correlated, g^2 being proportional to the molecular weight and roughly inversely proportional to $H\partial H/\partial x$. The calculated standard deviations of the g-factors as obtained from the fitting procedure and as shown in Table 2 do therefore not reflect the absolute accuracy, estimated to be 0.3 %. The $E(S')$ values, however, are determined from the shape of the susceptibility *vs.* temperature and not correlated with the molecular weight and $H\partial H/\partial x$.

The ratio between the variance and the degrees of freedom indicates good agreement with the model expressed in eqn. (3) according to the estimates of a χ^2-test. This ratio was 1.5 when the data were fitted to eqn. (4). For the other salts for which the low-temperature data are missing the data were fitted to eqn. (4) with and without j fixed to zero. It was found in all cases that zero was within the range of the estimated j-values plus/minus two standard deviations.

The parameters obtained from the $(+)_D$-dithionate are close to the predictions of the simple Van Vleck Hamiltonian although small deviations do occur. In terms of the super-exchange model by Anderson[30] as later clarified by Glerup[20] for interacting d^3-configurations the antiferromagnetism of compounds of the present type can be accounted for[15] in terms of configuration interaction between the $t_2^3 \times t_2^3$ ground states and excited transfer states of the types $t_2^2 \times t_2^4$. In the limiting case of small energy separations in the charge transfer states relative to the excitation energy, the

Table 2. Results of the digital fitting procedure for susceptibilities. $E(1)$, $E(2)$, and $E(3)$ refer to the triplet, quintet, and septet energies, respectively. Other parameters in the procedure were a temperature independent susceptibility term besides the standard diamagnetic corrections (results $30-120\times10^{-6}$ c.g.s. units) and monomeric impurities (results 0–0.3 mol %).

Compound	$E(1)$ cm^{-1}	$E(2)$ cm^{-1}	$E(3)$ cm^{-1}	Degrees of freedom (f)	Variance per f	g
rac-$[Cr(C_7H_{10}N_2)_2OH]_2Br_4.3H_2O$	35.64(4)	3E(1)	6E(1)	327	0.4	1.979(2)
$(-)_D$-$[Cr\{(R)(+)_D$-$C_7H_{10}N_2\}_2OH]_2Br_4.3H_2O$	31.6(1)	3E(1)	6E(1)	309	0.2	1.961(4)
rac-$[Cr(C_7H_{10}N_2)_2OH]_2(ClO_4)_4.3H_2O$	30.53(4)	3E(1)	6E(1)	330	0.9	2.000(2)
$(+)_D$-$[Cr\{(S)(-)_D$-$C_7H_{10}N_2\}_2OH]_2$-$(ClO_4)_4.2\frac{1}{2}H_2O$	33.79(6)	3E(1)	6E(1)	343	0.2	1.989(2)
rac-$[Cr(C_7H_{10}N_2)_2OH]_2(S_2O_6)_2.5H_2O$	36.85(3)	3E(1)	6E(1)	396	0.4	1.976(1)
$(+)_D$-$[Cr\{(S)(-)_D$-$C_7H_{10}N_2\}_2OH]_2$-$(S_2O_6)_2.2H_2O$	32.95(9)	101.2(4)	200(1)	324	1.3	1.993(8)

Table 3. Geometry of the chromium-oxygen ring system and the singlet-triplet splitting for di-μ-hydroxo complexes of chromium(III) with 1,10-phenanthroline ($C_{12}H_8N_2$), 1,2-ethanediamine ($C_2H_8N_2$) and (*S*)(−)$_D$-{1-(2-pyridyl)ethylamine}($C_7H_{10}N_2$). Average values are given for Cr−O and Cr−O−Cr.

	$[Cr(C_{12}H_8N_2)_2OH]_2^{4+}$		$[Cr(C_2H_8N_2)_2OH]_2^{4+}$		$(+)_D$-$[Cr\{(S)(-)_D$-$C_7H_{10}N_2\}_2OH]_2^{4+}$
	Chloride	Iodide	Dithionate	Dichloride Diperchlorate	Dithionate
Cr−Cr (Å)	3.008	2.986	3.032	3.059	3.019
Cr−O (Å)	1.927	1.920	1.979	1.949	1.938
Cr−O−Cr (°)	102.7	102.1	100.0	103.4	102.3
Triplet energy (cm^{-1})	55	53.6	3.68	28[a]	32.95
Ref.	9	11	14	31	19

[a] For the corresponding bromide and perchlorate salts the triplet energies are 24 cm^{-1} and 27 cm^{-1}, respectively.

consequence of such an interaction for the ground states is antiferromagnetism according to the Van Vleck equation. We feel at the present stage that it is too early to correlate the small deviations from the Van Vleck equation with energy separations in the charge transfer states.

The singlet-triplet splittings found for the present compounds are within the range of values observed in other chromium(III) diols. For comparison, average values of known distances and angles as well as of singlet-triplet splittings are given in Table 3, and the view of the ΛΛ-$(+)_D$-$[\{(S)(-)_D$-$C_7H_{10}N_2\}_2Cr(OH)_2Cr\{(S)(-)_D$-$C_7H_{10}N_2\}_2]^{4+}$ cation as found in the dithionate salt[19] is shown in Fig. 5. The positions of the hydrogen atoms on the bridging oxygen atoms have not been determined for the phenanthroline complexes.[9,11] For the other complexes mentioned in Table 3 the hydrogen atoms are at the expected distances from the oxygen atoms, and they are within 5° from the almost planar arrangement of bridging oxygen and chromium atoms, except for the magnetically anomalous ethylenediamine complex dithionate where they are approximately 60° out of the plane. These hydrogen positions appear to be determined by formation of hydrogen bonds to the anions or water molecules. On this basis we expect hydrogen positions close to the bridging plane in the phenanthroline complexes.

According to simple considerations concerning "super-exchange pathways" in systems with two coupled d^3-configurations[15,20] the largest antiferromagnetic couplings in di-μ-hydroxobridged systems are expected when the hydrogen atoms on the bridges are in the bridging plane. This leaves a p_z-orbital perpendicular to this plane available for maximum overlap with the d_{zx}- and d_{yz}-orbitals on the metal atoms.[15]

The magnetic interaction in the ethylenediamine complex dithionate is remarkably small, and this compound has the longest Cr−O distances, and hydrogen positions in the bridging system far away from the bridging plane. Only variations with 3° of the Cr−O−Cr angles are observed.

A simple pattern seems to emerge from these considerations. All data presently available are consistent with the interpretations that out-of-plane positions of the hydrogens lead to reduced π-overlaps between the metals and the bridging oxygen atoms, and consequently small magnetic interactions, and increased metal-to-oxygen distances, the driving force being unpredictable hydrogen bonding effects in the lattice.

Acknowledgements. We are very grateful to Mrs. Solveig Kallesøe who performed the susceptibility measurements and most parts of the computer processing, to Dr. Sine Larsen for information of the crystallographic data and for permission to reproduce Fig. 5, and to The Danish Natural Science Research Council for financial support through grant No. 511-3993.

REFERENCES

1. Inskeep, R. G. and Benson, M. *J. Inorg. Nucl. Chem. 20* (1961) 290.
2. Ferraro, J. R., Driver, R., Walker, W. R. and Wosniak, W. *Inorg. Chem. 6* (1967) 1586.
3. Mason, S. F. and Wood, J. W. *Chem. Commun.* (1968) 1512.
4. Josephsen, J. and Schäffer, C. E. *Acta Chem. Scand. 24* (1970) 2929.
5. Michelsen, K. *Acta Chem. Scand. A 30* (1976) 521.
6. Michelsen, K. *Acta Chem. Scand. A 31* (1977) 429.
7. Earnshaw, A. and Lewis, J. *J. Chem. Soc.* (1961) 396.

8. Morishita, T., Hori, K., Kyono, E. and Tsuchiga, R. *Bull. Chem. Soc. Jpn. 38* (1965) 1276.
9. Veal, J. T., Hatfield, W. E. and Hodgson, D. J. *Acta Crystallogr. B 29* (1973) 12.
10. Veal, J. T., Hatfield, W. E., Jeter, D. Y., Hempel, J. C. and Hodgson, D. J. *Inorg. Chem. 12* (1973) 342.
11. Scaringe, R. P., Singh, P., Eckberg, R. P., Hatfield, W. E. and Hodgson, D. J. *Inorg. Chem. 14* (1975) 1127.
12. Estes, E. D., Scaringe, R. P., Hatfield, W. E. and Hodgson, D. J. *Inorg. Chem. 15* (1976) 1179.
13. Scaringe, R. P., Hatfield, W. E. and Hodgson, D. J. *Inorg. Chim. Acta 22* (1977) 175.
14. Cline, S. J., Scaringe, R. P., Hatfield, W. E. and Hodgson, D. J. *J. Chem. Soc. Dalton Trans.* (1977) 1662.
15. Josephsen, J. and Pedersen, E. *Inorg. Chem. 16* (1977) 2534.
16. Hodgson, D. J. In Interrante, L. V., Ed., *Extended Interactions between Metal Ions*, American Chemical Society, Washington D.C. 1974.
17. Cline, S. J., Kallesøe, S., Hodgson, D. J. and Pedersen, E. *Inorg. Chem. 17* (1978). *In press.*
18. Pedersen, E. *Acta Chem. Scand. 26* (1972) 333.
19. Larsen, S. and Søresen, B. *Acta Chem. Scand. To be published.*
20. Glerup, J. *Acta Chem. Scand. 26* (1972) 3775.
21. Hodgson, D. J. *Progr. Inorg. Chem. 19* (1975) 173, and references therein.
22. Michelsen, K. *Acta Chem. Scand. A 28* (1974) 428.
23. Bang, E. *Acta Chem. Scand. A 31* (1977) 495.
24. Hatfield, W. E. In Interrante, L. V., Ed., *Extended Interactions between Metal Ions*, American Chemical Society, Washington D.C. 1974, and references therein.
25. Figgis, B. N. and Nyholm, R. S. *J. Chem. Soc.* (1958) 4190.
26. Cotton, F. A. and Pedersen, E. *Inorg. Chem. 14* (1975) 388.
27. Mason, S. F. *Q. Rev. Chem. Soc. 17* (1963) 20.
28. Hancock, M. P., Josephsen, J. and Schäffer, C. E. *Acta Chem. Scand. A 30* (1976) 79.
29. Mønsted, O. *Private communication.*
30. Anderson, P. W. *Phys. Rev. 79* (1950) 350.
31. Kaas, K. *Acta Crystallogr. B 32* (1976) 2021.
32. Unpublished results from this laboratory.

Received June 5, 1978.

Acta Chemica Scandinavica A 32 (1978) 857–865

Metal Complexes with Mixed Ligands. 17. An Emf Investigation of the Complex Formation between the Hydroxo Nickel(II) Tetramer and Tris(hydroxymethyl)aminomethane Ligands

WILLIS FORSLING

Department of Inorganic Chemistry, University of Umeå, S-901 87 Umeå, Sweden

Dedicated to Jannik Bjerrum on the occasion of his 70th birthday

Three component equilibria between nickel(II), tris(hydroxymethyl)aminomethane ($H_2NC(CH_2OH)_3$, HL, THAM), and OH^- were studied by means of emf titrations at 25 °C in an ionic medium of 3.0 M (Na)ClO_4. The total nickel, B, and the total THAM, C, were varied within the limits $0.003 \leq B < 0.227$ M and $0.005 \leq C < 0.227$ M and the ratios C/B between $1 \leq C/B < 11$. Data can be explained with the metal complexes $NiHL^{2+}$ and $Ni(HL)_2^{2+}$ together with a series of tetranuclear ternary hydrolytic species $Ni_4(OH)_4(HL)_4^{4+}$, $Ni_4(OH)_4(HL)_3L^{3+}$, $Ni_4(OH)_4(HL)_2L_2^{2+}$ and the trinuclear ternary complex $Ni_3H_{-3}(HL)_3^{3+}$. The equilibrium constants with standard deviations (3σ) are given. Data were analyzed with the least squares computer program LETAGROPVRID.

In earlier papers of this series the three component equilibria in the systems copper(II)–imidazole ($C_3H_4N_2$)–OH^-,[1] nickel(II)–imidazole–OH^- [2,3] and zinc(II)–imidazole–OH^- [4] were investigated.[2] In addition to the metal complexes $Me(C_3H_4N_2)_n^{2+}$, $n=1, 2, 3, 4$, ternary complexes were also formed. Furthermore, there seems to be a strong connection between the binary metal hydrolysis and the ternary hydrolytic species obtained in the various systems. Thus in the copper system investigated by Sjöberg, data clearly indicated the formation of $Cu_2(OH)_2L_2^{2+}$, $Cu_2(OH)_2L_4^{2+}$ and $CuOHL^+$ (L = $C_3H_4N_2$), while the dominating hydrolytic species are $Cu_2(OH)_2^{2+}$ and $CuOH^+$. In the zinc system the main ternary species appeared to be $ZnOHL^+$ and $Zn_2(OH)L_2^{3+}$ in 3.0 M (Na)Cl resp. $Zn(OH)L_3^+$ and $Zn_2(OH)L_3^{3+}$ in 3.0 M (Na)ClO_4, while the binary hydrolytic complexes in the corresponding media are Zn_2OH^{3+} and $ZnOH^+$.

However, in the nickel system only mononuclear ternary species were obtained, *viz.* $NiOHL^+$ (3.0 M (Na)Cl, 3.0 M (Na)ClO_4, 1.0 M (Na)Cl) and $Ni(OH)L_3^+$ (1.0 M (Na)Cl), while the dominating hydrolysis complexes seem to be $Ni_4(OH)_4^{4+}$, Ni_2OH^{3+} together with $NiOH^+$.[5,6] The reason why no polynuclear ternary species are formed may possibly be that the available pH and solubility ranges in the case of imidazole are too restricted to permit such complexes. Thus it seems worthwhile to exchange imidazole for another amine ligand, which fulfills the demands for solubility and acidity strength to form polynuclear ternary hydrolytic species. According to earlier investigations [7–9] two suitable ligands should be triethanolamine (N$(C_2H_4OH)_3$) and tris(hydroxymethyl)aminomethane ($H_2NC(CH_2OH)_3$, THAM).

In an investigation of the system nickel(II)–triethanolamine–OH^- by Cadiot-Smith [7] comprising both potentiometric and spectrophotometric methods, several polynuclear ternary complexes are proposed. The metal complexes NiT^{2+} and NiT_2^{2+} as well as the polynuclear species $T_2Ni_2(OH)_2^{2+}$, $T_4Ni_4(OH)_6^{2+}$ and $T_3Ni_2(OH)_4$ and the mononuclear ternary complexes $TNi(OH)_4^{2+}$ and $TNi(OH)_2$ were reported (T = $N(C_2H_4OH)_3$).

The nickel(II)–tris(hydroxymethyl)aminomethane–OH^- system was studied by Hall *et al.*[8] applying spectrophotometric methods and poten-

tiometric titrations carried out in an ionic medium of 0.5 M $NaClO_4$. They proposed the species $NiHL^{2+}$, $Ni(HL)_2^{2+}$ and NiL^+ to be formed ($HL = H_2NC(CH_2OH)_3$). They also established that a polynuclear ternary species is formed with a ratio of nickel(II) ion to reacted hydroxyl ion of 1:1.5.

The same system is investigated by Bai and Martell[9] at 25 °C and at an ionic strength of 0.10 M. They explained data by assuming the species $NiHL^{2+}$, $Ni(HL)_2^{2+}$, $Ni_2L_3^+$ and $Ni_3(H_{-1}L)_2L^+$ to be formed. Both spectrophotometric and potentiometric methods were used and as the Ni(II)–THAM reaction is very slow, the titrations were performed batchwise using series of bottles.

However, in both investigations the variation ranges in the total concentrations of nickel(II), B, were rather small, which makes the determination of the polynuclear complexes quite difficult.

Any of these ligands is probably a suitable choice for our purposes. However, as THAM is commonly used as an acidimetric standard and is easily purified and dried and has low hygroscopicity while triethanolamine lacks all these qualities, the former was chosen. Furthermore as THAM is used extensively as a buffer in the study of chemical kinetics as well as in biological studies even though the THAM-metal ion interaction has not been completely studied, equilibrium data in the Ni^{2+}–$H_2NC(CH_2OH)_3$–OH^- system should be of great interest.

EXPERIMENTAL

Tris(hydroxymethyl)aminomethane, $H_2NC(CH_2OH)_3$, HL (SIGMA, reagent grade) was used without further purification after drying. Stock solutions of H_2L^+ were prepared by dissolving HL in $HClO_4$. Titration solutions were generally prepared by weighing in HL to nickel(II) solutions. Stock solutions of sodium and nickel perchlorate as well as the dilute perchloric acids and sodium hydroxide solutions were prepared and standardized as earlier.[2]

The cell arrangement and experimental details of the emf measurements are fully described earlier.[2]

METHOD

The titration procedures used were similar to those described in earlier papers.[1,2] During the titrations the total concentrations of nickel, B, THAM, C, were generally kept constant, but dilution experiments were also carried out. In general each titration was performed at a constant C/B-ratio. The free hydrogen ion concentration, h, was varied by adding hydroxide ions or hydrogen ions and measured with a glass electrode. To check the reliability two electrodes were often immersed in the same equilibrium solution. The change in the differences between the emf values was not allowed to exceed 0.2 mV. Owing to formation of precipitates and the reduced reliability of the glass electrodes at high $-\log h$-levels, the available $-\log h$-range was restricted to an upper limit of 7–9. The reproducibility and reversibility of equilibria were tested by performing both forward (increasing $-\log h$) and backward (decreasing $-\log h$) titrations. To check the reversibility, dilution experiments were also carried out at some C/B-ratios. Special efforts were made to cover as wide a concentration range as possible. A constant ionic medium of 3.0 M $(Na)ClO_4$ was used in order to avoid activity coefficient variations. The reactions especially at low quotients C/B are extremely slow and stable potentials of the glass electrodes were not attained until 6–8 h after every change in the composition of the equilibrium solution at the log h-range of ternary complex formation. When equilibrium was obtained the emf-values remained constant to 0.1 mV for several hours. An ordinary titration lasted 2–3 days, which naturally should influence the accuracy of the measurements. However, as the ternary hydroxyl species are obtained in great amounts, minor changes in, for example, E_0 of the glass electrodes owing to the lengthy titration measurements seem to be rather insignificant.

The total concentrations of B and C were varied within the limits $0.003 \leq B < 0.227$ M and $0.005 \leq C < 0.227$ M and the ratios C/B between $1 \leq C/B < 11$.

Calibrations and assumptions in connection with the use of the glass electrodes were the same as described earlier.[2] We will assume the presence of three component equilibria of the general type

$$pH^+ + qNi^{2+} + rH_3NC(CH_2OH)_3^+ \rightleftarrows (H^+)_p(Ni^{2+})_q(H_3NC(CH_2OH)_3^+)_r \quad (1)$$

Applying the law of mass action to these equilibria the conditions for the total concentrations then give

$$B = b + \sum_p \sum_q \sum_r q\beta_{pqr} h^p b^q c^r \quad (2)$$

$$C = c + \sum_p \sum_q \sum_r r\beta_{pqr} h^p b^q c^r \quad (3)$$

$$H = h - k_a h^{-1} c + \sum_p \sum_q \sum_r p\beta_{pqr} h^p b^q c^r \quad (4)$$

where $b = [Ni^{2+}]$ and $c = [H_3NC(CH_2OH)_3^+]$.

The calculational problem is then to find the model (sets of pqr and β_{pqr}) that best can explain the experimental data.

The search for the best model was made by using the least squares computer program LETAGROPVRID[10] (version ETITR).[11] As "best" model or models we will consider those giving the lowest error squares sum

$$U = \Sigma(Z_{calc} - Z_{exp})^2 \text{ where } Z = (h - H)/C.$$

The LETAGROP calculations also give standard deviations $\sigma(Z_c)$, $\sigma(\beta_{pqr})$ and/or $\sigma(\log \beta_{pqr})$, calculated and defined according to Sillén.[12] The computation was performed on a CYBER 172 computer.

Concerning the binary proton THAM equilibrium

$$H_3NC(CH_2OH)_3^+ \rightleftarrows H_2NC(CH_2OH)_3 + H^+ \quad (5)$$

we will make use of the results obtained from separate experiments and for the binary hydrolysis

$$pH^+ + qNi^{2+} \rightleftarrows Ni_qH_p^{(p+2q)+} \quad (6)$$

the results obtained by Burkov-Sillén.[5]

For reaction (5) $\log (K_a \pm 3\sigma)$ was found to be -8.646 ± 0.002. For reaction (6) investigations both of Ohtaki-Biedermann[6] (3.0 M (Na)Cl) and Burkov-Sillén[5] (3.0 M $(Na)ClO_4$) clearly show that the main species in a hydrolyzed Ni^{2+} solution is a hydroxonickel(II) tetramer, $Ni_4(OH)_4^{4+}$ and $\log \beta_{-44} = -27.37$ was reported in 3.0 M $(Na)ClO_4$.

These binary equilibria were assumed to be exactly known and all effects above this level will be treated as being caused by the metal complexes $Ni(HL)_n^{2+}$ and ternary species.

DATA, CALCULATIONS AND RESULTS

The data used to evaluate the binary proton THAM equilibrium comprise 6 titrations with 146 experimental points within the concentration ranges $0.020 \leq C \leq 0.200$ M. The analysis ended at $\sigma(Z) = 0.003$ and the $\log(K_a \pm 3\sigma)$ obtained was -8.646 ± 0.002.

The mathematical analysis of the three component data was started by making a Bjerrum plot $\bar{n}(\log[HL])$. The plot is shown in Fig. 1. It is seen that even at the highest quotient C/B ($C/B \geq 10$) the function $\bar{n}(\log[HL])$ seems to be dependent on B and C thus indicating formation of ternary species $Ni_qH_{-p}(HL)_r^{(2q-p)+}$. However, at sufficiently low log[HL]-values, all data, even at the lowest C/B-ratios, fall on a single curve, thus indicating formation of stepwise mononuclear complexes $Ni(HL)_n^{2+}$. By selecting data from all C/B-ratios fulfilling the condition that $\bar{n}(\log[HL])$ is independent of B and C, it should be possible to obtain accurate values of the $Ni(HL)_n^{2+}$-species. A LETAGROP analysis of these data including 8 titrations and 54 titration points ended at $\sigma(Z_c) = 0.0025$ and the actual $\log \beta_n$-values obtained according to the reaction

Table 1. Results of the final LETAGROP calculations giving the formation constants for the "best fitting" complexes. The formation constants are related according to the relation $pH^+ + qNi^{2+} + rH_2L^+ \rightleftarrows (H^+)_p(Ni^{2+})_q(H_2L^+)_r$. The errors are $3\sigma(\log \beta_{pqr})$.

Number of titr./ number of points	p,q,r	$\log(\beta_{pqr} \pm 3\sigma)$	p,q,r	$\log(\beta_{pqr} \pm 3\sigma)$	p,q,r	$\log(\beta_{pqr} \pm 3\sigma)$	p,q,r	$\log(\beta_{pqr} \pm 3\sigma)$	$\sigma(z)$
6/146	−1,0,1	−8.646 ±0.002							0.003
8/54	−1,1,1	−5.47 ±0.01	−2,1,2	−11.56 ±0.02					0.003
23/328 [a]	−5,3,2	−30.06 ±0.04	−8,4,4	−46.65 ±0.03	−9,4,4	−54.85 ±0.05	−10,4,4	−63.60 ±0.06	0.007

[a] β_{-111} and β_{-212} were not varied.

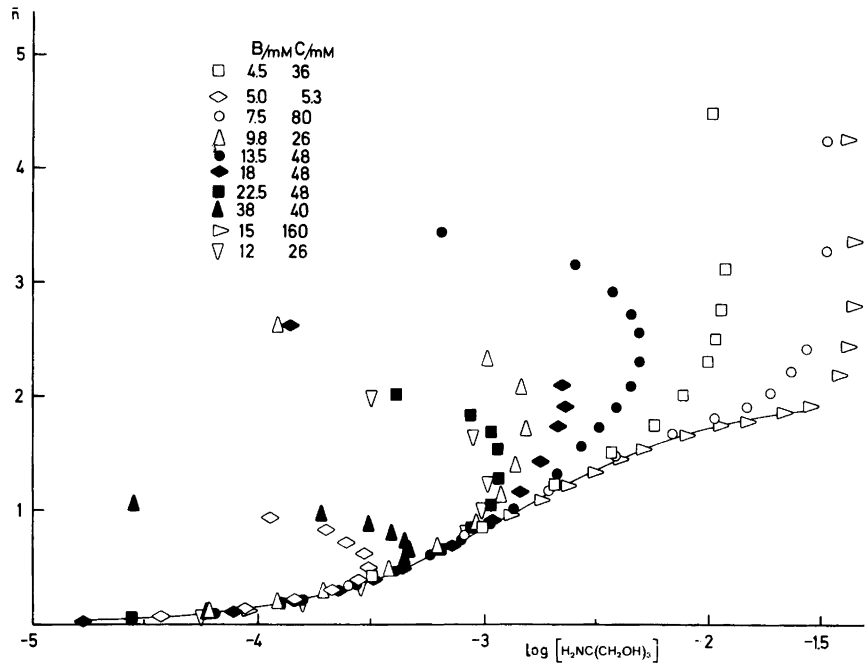

Fig. 1. Experimental data plotted as curves $\bar{n}(\log[HL])$. In order to make the figure clear only a few titrations have been plotted. The full curve has been calculated with the formation constants for the metal species $NiHL^{2+}$ and $Ni(HL)_2^{2+}$ given in Table 1. A complete list of experimental data is available from the author.

$$Ni^{2+} + nH_2L^+ \rightleftarrows Ni(HL)_n^{2+} + nH^+ \quad (7)$$

were $\log(\beta_1 \pm 3\sigma) = -5.47 \pm 0.01$ and $\log(\beta_2 \pm 3\sigma) = -11.56 \pm 0.02$.

These equilibrium constants ($\log K_a$, $\log \beta_1$ and $\log \beta_2$) were then assumed to be exactly known with the values given above and they were not varied until some final calculations. The data used to evaluate the ternary complex model comprises 23 titrations with 328 titration points.

Experimental data fulfilling the condition $Z_c > 1$ *i.e.* $C + H - h < 0$, cannot be visualized by the $\bar{n}(\log[HL])$-function. These data are therefore represented as $Z_c(\log h)$-curves (see Fig. 2) and the accomplishment of the condition $Z_c > 1$ is in itself a demonstration of ternary complex formation.

The search for the ternary species was started with *pqr*-analysis (systematic testing of different *pqr*-complexes) on a representative part of data, comprising 8 titrations with 124 titration points (Table 2). It was soon found that at every *q*-section (corresponding to the number of nickel atoms in the

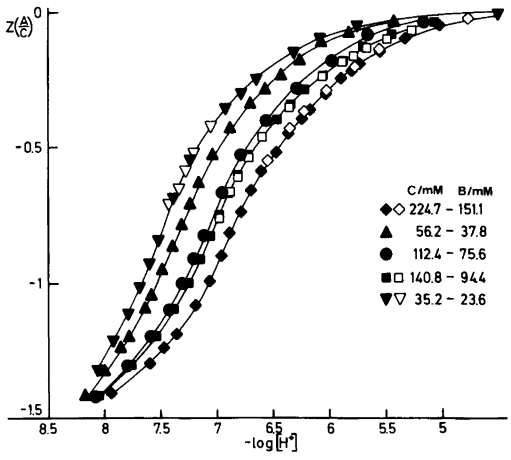

Fig. 2. Experimental data plotted as curves $Z_C((\log h)_{B,C})$ for the quotient $C/B = 1.5$. The full curves have been calculated using the formation constants for the binary and ternary species given in Table 1. Open symbols refer to back titrations.

Table 2. Results of some introductary LETAGROP calculations comprising a representative part of experimental data, no variations of the binary constants given in Table 1 have been made. The constants β_{pqr} are defined in Table 1 and the errors are $3\sigma(\log\beta_{pqr})$; Data I.

Number of titr./ number of points	p,q,r	$\log(\beta_{pqr} \pm 3\sigma)$	p,q,r	$\log(\beta_{pqr} \pm 3\sigma)$	$\sigma(z)$	$U \times 10^{-3}$
8/124	−9,4,4	−53.99±0.09			0.0265	86.1
8/124	−11,5,5	−64.90±0.11			0.0266	86.8
8/124	−8,4,4	−46.25±0.07	−10,4,4	−63.33±0.14	0.0182	40.1
8/124	−9,3,4	−56.78±0.14	−9,5,4	−52.37±0.11	0.0310	112
8/124	−10,5,5	−57.26±0.13	−12,5,5	−73.98±0.25	0.0252	77.3
8/124	−11,4,5	−67.36±0.15	−11,6,5	−63.40±0.24	0.0254	78.7

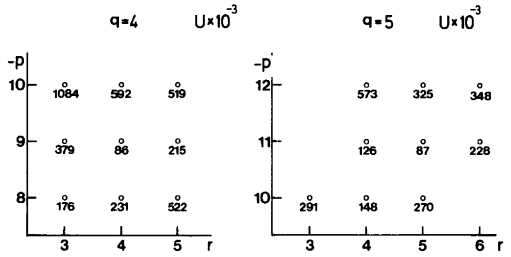

Fig. 3. LETAGROP-search for ternary species. The diagrams give error squares sums $U(pr)_q \times 10^{-3}$, $q=4$, 5, assuming only one complex.

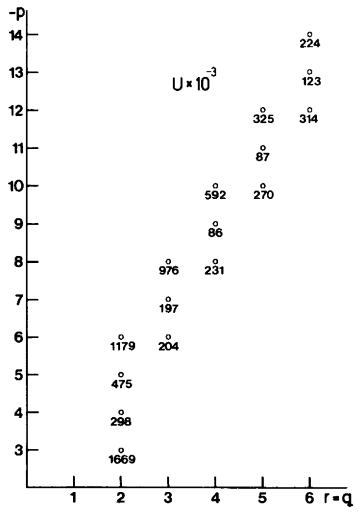

Fig. 4. LETAGROP-search for ternary species. A summary of the error squares sums $U(pr)_q \times 10^{-3}$ concerning the q-sections $2 \leq q \leq 6$, and assuming $r=q$. Only one complex is supposed to be formed.

complexes) the lowest error squares sum was obtained when $r=q$, *i.e.* the numbers of nickel(II) and THAM in the complexes are the same.

A good illustration of this statement is given by the results of the calculations for $q=4$ and $q=5$ in Fig. 3. Thus the calculations can be summarized in one figure, where the error squares sums for the species, fulfilling the condition $r=q$, are given for the different q-sections, $z \leq q \leq 6$; Fig. 4.

It is seen that the lowest error squares sums are obtained for the complexes $Ni_4H_{-5}(HL)_4^{3+}$ and $Ni_5H_{-6}(HL)_5^{4+}$. However, remaining effects indicate the formation of two or more ternary species and the tetranuclear model appeared to give a better fit to experimental data assuming either two or three complexes to be formed. Results of some calculations including probable combinations of tetranuclear and pentanuclear complexes are given in Table 2, calculation denoted Data I. As seen from this table, the best model assuming two complexes seems to include the species $Ni_4H_{-4}(HL)_4^{4+}$ and $Ni_4H_{-6}(HL)_4^{2+}$.

Thus the following conclusions may be drawn from the introductory *pqr*-analysis:

(i) polynuclear and most probably tetranuclear ternary complexes are formed.

(ii) the condition $q=r$ seems to be fulfilled, *e.g.*, complexes of the type $(NiHL)_{q=r}H_{-p}^{(2q-p)+}$ seem to be dominating at least on the average,

(iii) the average number of OH^- bound per nickel in the complexes is ~2.25 calculated over the level H_2O, $H_3NC(CH_2OH)_3^+$ and Ni^{2+}.

The condition $p=r$ indicates that titration experiments at low quotients C/B should be especially favourable for determining the ternary $Ni_qH_{-p}(HL)_r$ species. Owing to the low solubility of the complexes at the ratio $C/B=1$, leading to precipitation of nickel(II) hydroxide, comparative titration ex-

Table 3. Results of LETAGROP calculations for some different assumptions concerning the ternary complexes formed. The constants β_{pqr} are defined in Table 1 and the errors are $3\sigma(\log \beta_{pqr})$. If no 3σ is given the corresponding constant has not been varied. $1 \leq C/B < 11$.

Number of titr./ number of points	p,q,r	log(β_{pqr} $\pm 3\sigma$)	p,q,r	log(β_{pqr} $\pm 3\sigma$)	p,q,r	log(β_{pqr} $\pm 3\sigma$)	p,q,r	log(β_{pqr} $\pm 3\sigma$)	$\sigma(z)$
7/101 [a]	−8,4,4	−46.55 ±0.03	−9,4,4	−54.86 ±0.09	−10,4,4	−63.60 ±0.05			0.0051
23/328	−8,4,4	−46.44 ±0.03	−9,4,4	−54.86 ±0.12	−10,4,4	−63.55 ±0.12			0.0160
23/328	−8,4,4	−46.63 ±0.04	−9,4,4	−54.86	−10,4,4	−63.60	−4,2,2	−24.55 ±0.05	0.0110
23/328 [b]	−6,3,3	−35.34 ±0.02	−9,4,4	−55.12 ±0.15	−10,4,4	−63.46 ±0.07			0.0107
23/328 [c]	−8,4,4	−46.65 ±0.03	−9,4,4	−54.85 ±0.05	−10,4,4	−63.60 ±0.06	−5,3,2	−30.06 ±0.04	0.0073
23/328 [d,e]	−1,1,1	−5.46 ±0.008	−2,1,2	−11.57 ±0.02	−5,3,2	−30.04 ±0.03			0.0071
23/328 [e]	−8,4,4	−46.55 ±0.03	−9,4,4	−54.90 ±0.06	−5,3,2	−30.12 ±0.04	−6,3,2	−38.66 ±0.21	0.0070
23/328 [e]	−8,4,4	−46.65	−9,4,4	−54.85	−5,3,2	−30.11 ±0.05	−2,1,1	−14.58 ±0.25	0.0071
23/328 [e]	−8,4,4	−46.65	−9,4,4	−54.85	−5,3,2	−30.10 ±0.04	−4,2,1	−28.21 ±0.30	0.0070
23/328 [e]	−8,4,4	−46.65	−9,4,4	−54.85	−5,3,2	−30.07 ±0.03	−3,1,1	−23.24 ±0.25	0.0071

[a] $2 < C/B < 11$. [b] $\beta_{-623} < 0$ and $\beta_{-535} < 0$. [c] $\beta_{-432} < 0$ and $\beta_{-633} < 0$. [d] β_{-844} and β_{-944} were not varied. [e] $\beta_{-10,4,4}$ was not varied.

periments were performed at $C/B = 1.5$.

In the evaluation of the ternary complex model experimental data were divided in two or in some calculations three parts consisting of the quotients $C/B = 1$, 1.5 resp. 2 − 11. The different parts of data, each consisting of 7 − 10 titrations with 100 − 150 experimental points, were treated separately but conclusions from one part were applied to the others.

Experimental data comprising titrations with quotients $C/B > 2$ were very well explained assuming the series $Ni_4H_{-4}(HL)_4^{4+}$, $Ni_4H_{-5}(HL)_4^{3+}$ and $Ni_4H_{-6}(HL)_4^{2+}$ to be formed. A data material consisting of 7 titrations with 101 titration points yielded the following formation constants log ($\beta_{pqr} \pm 3\sigma$) related to eqn. 1:

$$\log \beta_{-8,4,4} = -46.55 \pm 0.03$$
$$\log \beta_{-9,4,4} = -54.86 \pm 0.09$$
$$\log \beta_{-10,4,4} = -63.60 \pm 0.05$$

with the standard deviation in ΔZ_c ($\Delta Z_c = Z_{calc} - Z_{exp}$), $\sigma(Z) = 0.005$ indicating a good fit.

However, at lower quotients C/B ($C/B \leq 1.5$) this complex model exhibits a much poorer fit to experimental data leaving considerable deviations in $\Delta Z_c = Z_{calc} - Z_{exp}$. This behaviour demonstrates that either additional ternary complexes exist or at worst that a more or less new complex model has to be determined. A greet number of combinations is possible, but we decided to test complexes fulfilling the condition $r = q$ in the first instance, *e.g.* $(NiHL)_2H_{-n}^{(4-n)+}$, $(NiHL)_3H_{-m}^{(6-m)+}$ and so on. Addition of the species $Ni_2H_{-2}(HL)_2^{2+}$ to the complex model made the error squares sum considerably lower, but a still better fit was obtained by exchanging the species $Ni_4H_{-4}(HL)_4^{4+}$ for $Ni_3H_{-3}(HL)_3^{3+}$.

Thus this set of complexes $Ni_3H_{-3}(HL)_3^{3+}$, $Ni_4H_{-5}(HL)_4^{3+}$ and $Ni_4H_{-6}(HL)_4^{2+}$ provides a good explanation of data at low quotients C/B ($C/B \leq 1.5$), but upon introducing this complex model to the whole data material negative deviations in ΔZ_c appeared in the highest quotients C/B ($C/B > 2$) indicating a poorer fit to experimental data at these concentration ranges.

A reasonable explanation seems to be that the species $Ni_3H_{-3}(HL)_3^{3+}$ actually is a kind of an average complex of two or more other species. A number of combinations were therefore tested and the best explanation of experimental data comprising all quotients C/B, $1 \leq C/B < 11$, was obtained assuming the species $Ni_3H_{-3}(HL)_2^{3+}$, $Ni_4H_{-4}(HL)_4^{4+}$, $Ni_4H_{-5}(HL)_4^{3+}$ and $Ni_4H_{-6}(HL)_4^{2+}$ to be formed. The formation constants with standard deviations (3σ) are given in Table 3 and the analysis ended at $\sigma(Z) = 0.007$. The complex model suggested by Bai-Martell comprising the species $Ni_2L_3^+$ and $Ni_3(H_{-2}L)_2(H_{-1}L)$ were also tested, but the formation constants were obtained either with negative values ($\beta_{-6,2,3} < 0$) or with large standard deviations ($\log(\beta_{-8,3,3} \pm 3\sigma) = -52.5 \pm 0.3$) indicating a poor fit to experimental data.

In connection with the evaluation of the ternary complex model the computer program SOLGASWATER [13] equipped with plotting procedures has been very useful. The theoretical $Z_c(\log h)$-plots calculated by the program were performed in a scale adjusted to the same "plots" of experimental data. In that way a concise picture of the fit to experimental data of several complex models was immediately obtained.

The SOLGASWATER-program was also used to calculate distribution diagrams and predominance area diagrams in order to visualize the amounts of the different species (see Fig. 5, 6).

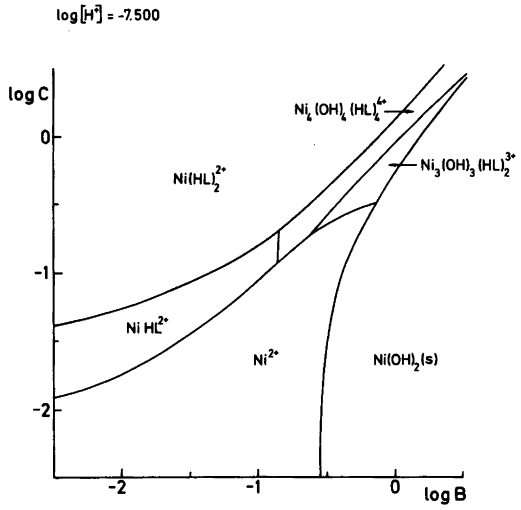

Fig. 5. Predominance area diagrams for the different nickel(II) THAM species. The dominating species at every fixed log B − log C level is given. The solubility product of $Ni(OH)_2(s)$, used in the calculations, is a kind of an average value taken from *Stability Constants.*[16] The computer program SOLGASWATER [13] equipped with plotting procedures was used.

DISCUSSION

The present investigation has given further evidence for the compositional connection between the binary metal hydrolysis and the ternary hydrolytic species. The tetranuclear ternary species $Ni_4H_{-4}(HL)_4^{4+}$, $Ni_4H_{-5}(HL)_4^{3+}$ and Ni_4H_{-6}-

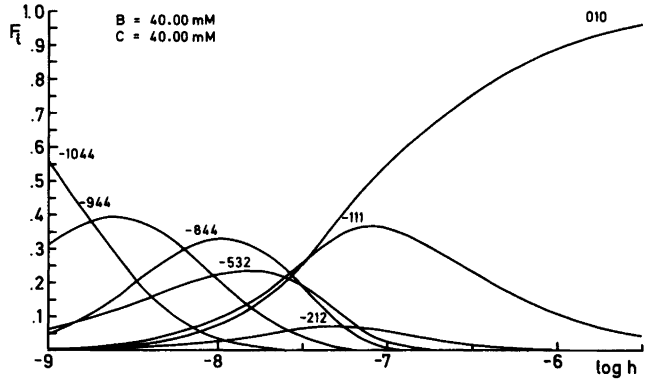

Fig. 6. Distribution diagram $F_i(\log[H^+])_{B,C}$ of the binary and ternary nickel(II) species in the system $H^+ - Ni^{2+} - (CH_2OH)_3CNH_3^+$ in 3.0 M (Na)ClO_4. F_i is defined as the ratio between nickel(II) in the species and total nickel(II). The computer program SOLGASWATER [13] was used in the calculations.

$(HL)_4^{2+}$ are obtained in great amounts. The composition of these species is reflected in the composition of the dominating binary hydroxo nickel species $Ni_4(OH)_4^{4+}$, and then the tetranuclear ternary series should preferably be written $Ni_4(OH)_4(HL)_4^{4+}$, $Ni_4(OH)_4(HL)_3L^{3+}$ and $Ni_4(OH)_4(HL)_2L_2^{2+}$. The complexes $Ni_4(OH)_4(HL)_3L^{3+}$ and $Ni_4(OH)_4(HL)_2L_2^{2+}$ are probably formed by the removal of protons from the hydroxyl groups in the THAM ligand. It is then possible to establish the following equilibria

$$Ni_4(OH)_4^{4+} + 4HL \rightleftarrows Ni_4(OH)_4(HL)_4^{4+}: \quad \log K = 15.30 \tag{8}$$

$$Ni_4(OH)_4(HL)_4^{4+} \rightleftarrows Ni_4(OH)_4(HL)_3L^{3+} + H^+; \quad \log K = -8.25 \tag{9}$$

$$Ni_4(OH)_4(HL)_4^{4+} \rightleftarrows Ni_4(OH)_4(HL)_2L_2^{2+} + 2H^+; \quad \log K = -16.95 \tag{10}$$

It is not possible to establish the structure of the ternary species from emf data. Thus an OH^- group together with an $H_2NC(CH_2OH)_3$ molecule may equally well be regarded as for example $H_2NC(CH_2OH)_2CH_2O^-$ and the complexes proposed could also be $Ni_4L_4^{4+}$, $Ni_4(H_{-1}L)L_3^{3+}$ and $Ni_4(H_{-1}L)_2L_2^{2+}$. Such displacements of the alcoholic protons are suggested in the present system by Hall *et al.*[8] and Bai-Martell.[9] However, the strong connection between the binary hydrolysis and the ternary hydrolytic species in this and other metal systems[1-4] makes the presence of hydroxide groups more probable.

The Ni^{2+} and OH^- ions in the tetramer, $Ni_4(OH)_4^{4+}$, are supposed to form a distorted cube where the nickel and oxygen atoms are arranged tetrahedrally.[14] This structure permits each nickel to interact with three oxygen atoms and *vice versa*.

Quite recently a crystal structure of the compound $Ni_4(OH)_4[C_6H_9(NH_2)_3]_4(NO_3)_4(H_2O)_7$[15] was presented containing $Ni_4(OH)_4^{4+}$ clusters similar to those described above. The three NH_2 groups in the ligand (1,3,5-triamino(*aaa*)cyclohexane denoted "tach") form an equilateral triangle and they are all coordinated to the same nickel ion. Thus three coordination positions at the octahedral nickel ion are left to be occupied by, for example, OH^- ions.

The tetranuclear species obtained in the present system should have a similar structure with the NH_2 group and two hydroxyl groups from the THAM ligand and three OH^- ions coordinated to each nickel ion.

The nickel tetramer built up in this way seems to be very rigid and excess ligand is left quite uncomplexed at high $-\log h$-ranges. As the total amounts of the tetranuclear ternary species are great, large angle X-ray scattering (LAXS) measurements should give valuable information of the structure of these complexes and investigations in this direction are in progress.

It is also possible to compare the acidity strength (tendency to hydrolyze) between the hydrated nickel(II) ion ($Ni(H_2O)_6^{2+}$) and the mononuclear species $Ni(HL)^{2+}$. According to the equilibria

$$4Ni^{2+} + 4H_2O \rightleftarrows Ni_4(OH)_4^{4+} + 4H^+; \quad \log {}^*\beta_{-44} = -27.37 \tag{11}$$

$$4Ni(HL)^{2+} + 4H_2O \rightleftarrows Ni_4(OH)_4(HL)_4^{4+} + 4H^+; \quad \log {}^*\beta_{-44} = -24.77 \tag{12}$$

it seems that the introduction of a THAM ligand increases the acidity strength of the nickel(II) ion. This behaviour was also found in the nickel(II)–imidazole system.[2,3]

In addition to the tetranuclear series a trinuclear ternary species $Ni_3H_{-3}(HL)_2^{3+}$ was laso established. The composition of this complex exhibits no direct relation to the binary hydrolysis species $Ni_4(OH)_4^{4+}$, Ni_2OH^{3+} and $NiOH^+$, but a possible relation between the trinuclear and tetranuclear ternary species is obtained by the equilibria

$$2Ni_3(OH)_3(HL)_2^{3+} + 2H^+ \rightleftarrows Ni_4(OH)_4(HL)_4^{4+} + 2Ni^{2+} + 2H_2O; \log \beta = 13.47 \tag{13}$$

The formation, as well as the decomposition, of the trinuclear ternary species are probably rather slow reactions since the longest waiting periods to obtain stable potentials were obtained at low *C/B*-quotients, where the amounts of this complex are high.

The available $-\log h$-range can be extended to higher values by exchanging the glass electrodes for a hydrogen electrode and/or by performing spectrophotometric titrations. Some preliminary spectrophotometric measurements have been carried out and further experiments are planned. As the reactions of formation and decomposition of the ternary species are slow, kinetic experiments using the stopped-flow technique may be practicable and such studies are planned. In cooperation with

Dr Gun Ivarsson crystal growth experiments have been carried out in order to relate the structures of the species in solution to those formed in the solid state.

Acknowledgements. I thank Professor Nils Ingri for much valuable advice, for his great interest and for all the facilities placed at my disposal. I also wish to thank Fil. Dr. Staffan Sjöberg for many helpful and constructive discussions and valuable comments to the manuscript. Thanks are also due to Lab. ing. Agneta Nordin for help with the titration measurements. The English of the present paper has been corrected by Dr. Michael Sharp. The work forms part of a program financially supported by the Swedish Natural Science Research Council.

REFERENCES

1. Sjöberg, S. *Acta Chem. Scand. 25* (1971) 2149.
2. Forsling, W. and Sjöberg, S. *Acta Chem. Scand. A 29* (1975) 569.
3. Forsling, W. *To be published.*
4. Forsling, W. *Acta Chem. Scand. A 31* (1977) 759.
5. Burkov, K. A., Lilic, L. S. and Sillén, L. G. *Acta Chem. Scand. 19* (1965) 14.
6. Ohtaki, H. and Biedermann, G. *Bull. Chem. Soc. Jpn. 44* (1971) 1822.
7. Cadiot-Smith, M. *J. Chim. Phys. Phys. Chim. Biol. 60* (1963) 957, 976, 991.
8. Hall, J. L., Swischer, J. A., Brannon, D. G. and Liden, T. M. *Inorg. Chem. 1* (1962) 409.
9. Bai, K. S. and Martell, A. E. *J. Inorg. Nucl. Chem. 31* (1969) 1697.
10. Ingri, N. and Sillén, L. G. *Ark. Kemi 23* (1964) 97.
11. Arnek, R., Sillén, L. G. and Wahlberg, O. *Ark. Kemi 31* (1969) 353; Brauner, P., Sillén, L. G. and Whiteker, R. *Ark. Kemi 31* (1969) 365.
12. Sillén, L. G. *Acta Chem. Scand. 16* (1962) 159. Sillén, L. G. and Warnqvist, B. *Ark. Kemi 31* (1969) 341.
13. Eriksson, G. *To be published.*
14. Kolski, G. B., Kildahl, N. K. and Margerum, D. W. *Inorg. Chem. 8* (1969) 1211.
15. Aurivillius, B. *Acta Chem. Scand. A 31* (1977) 501.
16. Sillén, L. G. and Martell, A. E. (compilers), *Stability Constants Chem. Soc. London Spec. Publ.* No. *17* (1964) and No. *25* (1971).

Received June 5, 1978.

Acta Chemica Scandinavica A 32 (1978) 867–877

Kinetics, Mechanism and Equilibria for Halide Substitution Processes of Chloro Bromo Complexes of Gold(III)

L. I. ELDING and A.-B. GRÖNING

Division of Physical Chemistry 1, Chemical Center, University of Lund, P.O.Box 740, S-220 07 Lund 7, Sweden

Dedicated to Jannik Bjerrum on the occasion of his 70th birthday

The over-all process

$$AuCl_4^- + 4Br^- \rightarrow AuBr_4^- + 4Cl^-$$

has been studied at 25.0 °C in a 1.00 M sodium perchlorate medium using stopped-flow spectrophotometry. The stoichiometric mechanism for the reaction has been derived and the twelve rate constants have been determined. The stepwise substitutions take place *via* direct halide displacements, the solvent path being negligible. The kinetics give no evidence for slow formation of long-lived intermediate five-coordinated associates between the square-planar complex and the entering halide, which has been suggested in recent literature.

The kinetic behaviour of analogous platinum(II) and gold(III) complexes is compared. *cis*- and *trans*-effects are of the same order of magnitude, but the nature of the entering group is much more important for the reactions of the gold complexes. The ratio in reactivity Au(III)/Pt(II) is *ca.* 2×10^6 for bromide, 10^5 for chloride and only 10^3 for water as the entering group.

The equilibrium constants,

$$K_n = \frac{[AuCl_{4-n}Br_n^-][Br^-]}{[AuCl_{3-n}Br_{n+1}^-][Cl^-]}$$

determined from kinetics, are 240 ± 40, 98 ± 20, 49 ± 10, and 17 ± 5 for $n = 0$, 1, 2 and 3, respectively. These constants give $\lg(\beta_{4Br}/\beta_{4Cl}) = 7.3 \pm 0.3$ for the over-all stability constants β_{4X} for the halide complexes AuX_4^- (X=Cl,Br). Charge-transfer spectra for the complexes $AuCl_{4-n}Br_n^-$ ($n = 0$, 1, 2, 3, 4) have been obtained and spectral assignments are proposed.

The kinetics for the reaction between $AuCl_4^-$ and bromide have been studied earlier in methanol [1] and in aqueous solution [2,3] giving discordant results. For instance, Louw and Robb [2] observed only one single reaction step for the over-all process (1),

$$AuCl_4^- + 4Br^- \rightleftarrows AuBr_4^- + 4Cl^- \quad (1)$$

which was interpreted to be a rate-determining replacement of the first chloride by bromide. The other two studies [1,3] report two-stage reactions, however. Cattalini *et al.*[1] interpreted these two steps as two consecutive ligand substitutions, whereas Hall and Satchell,[3] in their recent paper, concluded that the first step is the formation of a five-coordinate intermediate complex between $AuCl_4^-$ and bromide, and the second one a formation of $AuCl_3Br^-$ from this intermediate, subsequent substitutions of chloride being assumed to be much slower. The proposed solvent paths [1,2] (the k_1-term in the usual square-planar substitution rate law[4]) are also questionable, since the interpretation of intercepts in the kinetic plots depends on the kinetic model used.

A detailed study of the $AuCl_4^-$-bromide reaction was thus desirable, and this would also enable a comparison of the kinetic behaviour of the gold(III) chloro bromo complexes and the analogous platinum(II) complexes, which have recently been studied.[5]

The present investigation shows that the stepwise substitution reactions (2)

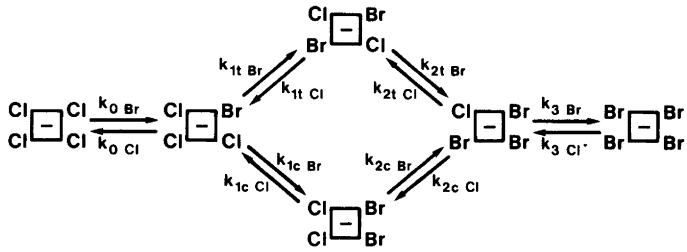

Fig. 1. Stoichiometric model for reaction (1).

$$AuCl_{4-n}Br_n^- + Br^- \underset{k_{nCl}}{\overset{k_{nBr}}{\rightleftharpoons}} AuCl_{3-n}Br_{n+1}^- + Cl^- \quad (2)$$

take place *via* the stoichiometric mechanism in Fig. 1. We have previously used that model for the $PtCl_4^{2-}$-bromide reaction.[5] The halide substitution rate constants defined in the figure are related to the equilibrium constants K_n, $n=0$, 1, 2, 3 by eqn. (3):

$$K_n = k_{nBr}/k_{nCl} = \frac{[AuCl_{3-n}Br_{n+1}^-]}{[AuCl_{4-n}Br_n^-]} \times \frac{[Cl^-]}{[Br^-]} \quad (3)$$

$AuCl_2Br_2^-$ appears as *cis*- and *trans*-isomers, denoted by the subscripts c and t in the following text.

The following reactions have been studied using stopped-flow spectrophotometry:

$$AuCl_4^- + Br^- \underset{k_{0Cl}}{\overset{k_{0Br}}{\rightleftharpoons}} AuCl_3Br^- + Cl^- \quad (4)$$

$$AuClBr_3^- + Br^- \underset{k_{3Cl}}{\overset{k_{3Br}}{\rightleftharpoons}} AuBr_4^- + Cl^- \quad (5)$$

$$AuCl_3Br^- + Br^- \xrightarrow{k_{1tBr}} trans\text{-}AuCl_2Br_2^- + Cl^- \quad (6)$$

$$trans\text{-}AuCl_2Br_2^- + Br^- \xrightarrow{k_{2tBr}} AuClBr_3^- + Cl^- \quad (7)$$

$$cis\text{-}AuCl_2Br_2^- + Br^- \xrightarrow{k_{2cBr}} AuClBr_3^- + Cl^- \quad (8)$$

Equilibrium constants K_n and spectra for the complexes $AuCl_{4-n}Br_n^-$, $n=0$, 1, 2, 3, 4, have also been determined.

EXPERIMENTAL

Chemicals. Hydrogen tetrachloroaurate(III) trihydrate, $HAuCl_4.3H_2O$ (Mallinckrodt or Degussa) was used directly. Anal. Calc.: Au 50.0; Cl 35.5.

Table 1. Reaction (4) followed in the forward and reverse directions. Wavelength 327 nm. $C_{Au}=1.0\times10^{-5}$ M. $[H^+]=2$ mM or 20 mM. Ionic strength 1.00 M.

$10^3[Cl^-]$/M	$10^3[Br^-]$/M	k_{exp}/s^{-1}
$AuCl_4^- + Br^- \rightleftarrows AuCl_3Br^- + Cl^-$		
300	0.3	0.108±0.05
300	0.5	0.120±0.06
300	0.6	0.128±0.007
300	0.8	0.140±0.007
300	1.0	0.153±0.008
500	0.5	0.183±0.009
500	1.0	0.212±0.010
500	1.2	0.233±0.010
500	1.5	0.249±0.012
500	1.7	0.264±0.013
800	0.5	0.249±0.012
800	1.0	0.287±0.014
800	2.0	0.333±0.017
800	3.0	0.396±0.018
$AuCl_3Br^- + Cl^- \rightleftarrows AuCl_4^- + Br^-$		
250	0.15	0.078±0.005
350	0.15	0.102±0.005
450	0.15	0.135±0.007
550	0.15	0.161±0.008
250	0.10	0.077±0.005
350	0.10	0.099±0.005
450	0.10	0.130±0.006
550	0.10	0.155±0.008
250	0.05	0.072±0.005
350	0.05	0.101±0.005
450	0.05	0.132±0.006
550	0.05	0.160±0.008

Table 2. Reaction (5) followed in the forward and reverse directions. Wavelength 400 nm. $[H^+]=20$ mM. C_{Au} was 2.0×10^{-4} or 1.0×10^{-4} M.

$10^3[Br^-]$/M	$10^3[Cl^-]$/M	k_{exp}/s^{-1}
$AuClBr_3^- + Br^- \rightleftarrows AuBr_4^- + Cl^-$		
250	79	47±3
250	74	50±3
250	69	41±2
250	64	41±2
250	59	42±2
350	450	59±3
350	250	70±4
350	79	59±3
350	74	58±3
350	69	59±3
350	64	64±3
350	59	61±3
450	450	84±3
450	250	83±3
450	79	82±3
450	74	79±3
450	69	78±4
450	64	70±3
450	59	83±3
550	450	101±5
550	250	99±4
550	79	99±4
550	74	93±4
550	69	96±5
550	64	100±5
550	59	103±5
$AuBr_4^- + Cl^- \rightleftarrows AuClBr_3^- + Br^-$		
350	200	64.0±0.7
350	300	65.3±0.8
350	400	66.3±0.7
350	500	67.7±0.7
250	200	48.4±0.5
250	300	49.7±0.5
250	400	50.5±0.5
250	500	51.8±0.8
75	100	14.5±0.4
75	200	16.5±0.5
75	300	17.0±0.5
75	400	18.0±0.7
75	500	19.0±0.6

Found: Au(grav.) 49.9±0.3, Cl (Mohr titr.) 35.5±0.2. 1.00 M stock solutions were prepared from perchloric acid (Baker's *p.a.*), sodium perchlorate (Baker's *p.a.*), sodium chloride (Merck's *p.a.*), sodium bromide (Merck's *p.a.*) and water, doubly distilled from quartz vessels.

Kinetics. The reactions were followed at 25.00 ±0.02 °C using a modified Durrum-Gibson stopped-flow instrument. The metal solution (M) contained the gold complex and sometimes also chloride and/or bromide to adjust the mean ligand number at the start of the experiment. The ligand solution (L) contained chloride and/or bromide. Tables 1 to 3 give the concentrations after mixing, all solutions having the ionic strength 1.00 M, with sodium perchlorate as the supporting electrolyte. The hydrogen ion concentration was varied within the interval $2\text{ mM} \leq [H^+] \leq 0.5$ M by substitution of part of the sodium perchlorate of the M-solution by perchloric acid. This variation had no influence on the reaction rates. The equilibrium constant for reaction (9)

$$AuCl_4^- + H_2O \rightleftharpoons AuCl_3OH^- + Cl^- + H^+ \qquad (9)$$

has been determined to 2.4×10^{-6} M[2,6,7] or 7×10^{-7} M[2,8] and for the corresponding bromo complex to 3×10^{-8} M[2,2] or 3×10^{-9} M[2,8] so the hydrogen and halide ion concentrations used were sufficiently large to suppress the formation of hydroxo complexes in all experiments.

Large excess of chloride and bromide compared to gold gave pseudo first-order kinetics. Rate constants were calculated from first-order rate expressions using a least-squares programme and a computer.

The equilibrium reaction (4) was followed from both directions, see Table 1. In one series of experiments, solution M contained 2×10^{-5} M $AuCl_4^-$ and 0.60 M, 0.80 M or 1.00 M NaCl and solution L NaBr (0.6 to 6 mM) and – for $[Cl^-]=0.800$ M – NaCl (0.800 M) also. The reaction product in these runs was mainly $AuCl_3Br^-$; *cf.* Fig. 8. In another series, the gold solution M contained an equilibrium mixture of $AuCl_4^-$ and $AuCl_3Br^-$ (C_{Au} was 2×10^{-5} M, C_{Cl} 0.100 M and C_{Br} 0.300, 0.200 or 0.100 mM; *cf.* Fig. 8), and solution L contained sodium chloride (0.40, 0.60, 0.80 or 1.00 M).

Reaction (5) – see Table 2 – was started either by adding excess bromide ($C_{Br}=0.400$, 0.600, 0.800 or 1.000 M) to an equilibrated gold solution containing mainly $AuClBr_3^-$ and $AuBr_4^-$ (C_{Au} was 2×10^{-4} or 4×10^{-4} M, and C_{Cl} was 0.900, 0.500, 0.158, 0.148, 0.138, 0.128, or 0.118 M; *cf.* Fig. 8), or by adding sodium chloride ($C_{Cl}=0.200$, 0.400, 0.600, 0.800 or 1.000 M) to a solution of $AuBr_4^-$ ($C_{Au}=2\times10^{-4}$ M, C_{Br} was 0.150, 0.500 or 0.700 M) to give a mixture of $AuBr_4^-$ and $AuClBr_3^-$ at equilibrium. Large concentrations of chloride are required, which limits the possibilities to vary the ratio $[Cl^-]/[Br^-]$.

Reaction (6) – see Table 3 – was followed by mixing an M-solution having $C_{Au}=2\times10^{-5}$ M,

Table 3. Reactions (6), (7) and (8). Wavelengths 365 nm (6), 332 or 365 nm (7) 365 nm (8).

$10^3[Br^-]$/M	$10^3[Cl^-]$/M	$10^5 C_{Au}$/M	$[H^+]$/M	k_{exp}/s^{-1}
$AuCl_3Br^- + Br^- \rightarrow$ *trans*-$AuCl_2Br_2^- + Cl^-$				
100	100	1.0	0.100	23±2
150	100	1.0	0.100	34±3
200	100	1.0	0.100	52±4
300	100	1.0	0.100	69±8
400	100	1.0	0.100	93±9
500	100	1.0	0.100	120±11
trans-$AuCl_2Br_2^- + Br^- \rightarrow AuClBr_3^- + Cl^-$				
200	–	2.5	0.500	5.6±0.8
300	–	2.5	0.500	9.3±0.4
400	–	2.5	0.500	11.8±0.5
500	–	2.5	0.500	15.5±0.9
201	50	5.0	0.020	6.1±0.3
301	50	5.0	0.020	8.8±0.3
401	50	5.0	0.020	11.7±0.4
501	50	5.0	0.020	15.6±0.5
cis-$AuCl_2Br_2^- + Br^- \rightarrow AuClBr_3^- + Cl^-$				
200	50	5.0	0.020	90±20
300	50	5.0	0.020	134±20
400	50	5.0	0.020	177±20
500	50	5.0	0.020	230±30

$C_{Cl}=0.200$ M, C_{Br} 0.30 mM, 0.50 mM or 0.80 mM, and $C_{H^+}=0.200$ M with L-solutions of sodium bromide (0.200, 0.300, 0.400, 0.600, 0.800 or 1.000 M). At the start of the kinetics, gold is present mainly as $AuCl_3Br^-$ and $AuCl_4^-$; see Fig. 8. Reaction (6) can be observed as a fast initial process followed by the much slower reaction between $AuCl_4^-$ and bromide; *cf.* the rate constants in Fig. 7.

Reaction (7) – see Table 3 – was started by mixing an L-solution of sodium bromide (0.400, 0.300, 0.800 or 1.00 M) with an M-solution containing 5×10^{-5} M $AuCl_3H_2O^-$ in 1.00 M $HClO_4$. The latter was prepared immediately before use in the kinetic studies by slow addition at 25 °C of 10 ml of 25.0 mM $AgNO_3$ (Merck's *p.a.*) to 10 ml 25.0 mM $HAuCl_4$ dissolved in 1.00 M perchloric acid, and subsequent separation of the silver chloride precipitate. After mixing, the following reactions take place:

$$AuCl_3H_2O \xrightarrow[\text{fast}]{+Br^-} AuCl_3Br^- \xrightarrow[\text{fast}]{+Br^-} \textit{trans}\text{-}AuCl_2Br_2^- \xrightarrow[\text{slow}]{+Br^-} AuClBr_3^-$$

The two fast reactions are complete within less than one half-life of the slow process. The subsequent reaction $AuClBr_3^- \rightarrow AuBr_4^-$ is fast (*cf.* Fig. 7). Table 3 also contains the results of some experiments on reaction (7) performed by mixing L-solutions of sodium bromide (0.400, 0.600, 0.800 or 1.000 M) with an M-solution, having $C_{Au}=1\times10^{-4}$ M, $C_{Cl}=0.100$ M, $C_{Br}=1.60$ mM and $C_{H^+}=0.040$ M. This solution contains mainly the complexes $AuCl_3Br^-$, $AuCl_2Br_2^-$ and $AuClBr_3^-$; *cf.* Fig. 8. After mixing, the following reactions take place

$$AuCl_3Br^- \xrightarrow[\text{fast}]{+Br^-} \textit{trans}\text{-}AuCl_2Br_2^- \xrightarrow[\text{slow}]{+Br^-}$$
$$AuClBr_3^- \xrightarrow[\text{fast}]{+Br^-} AuBr_4^-$$

$$\textit{cis}\text{-}AuCl_2Br_2^- \xrightarrow[\text{fast}]{+Br^-} AuClBr_3^- \xrightarrow[\text{fast}]{+Br^-} AuBr_4^-$$

The fast reactions are complete within less than one half-life of the slow process (7).

Reaction (8) was started by mixing an M-solution, having $C_{Au}=1\times10^{-4}$ M, $C_{Cl}=0.100$ M, $C_{Br}=2$ mM

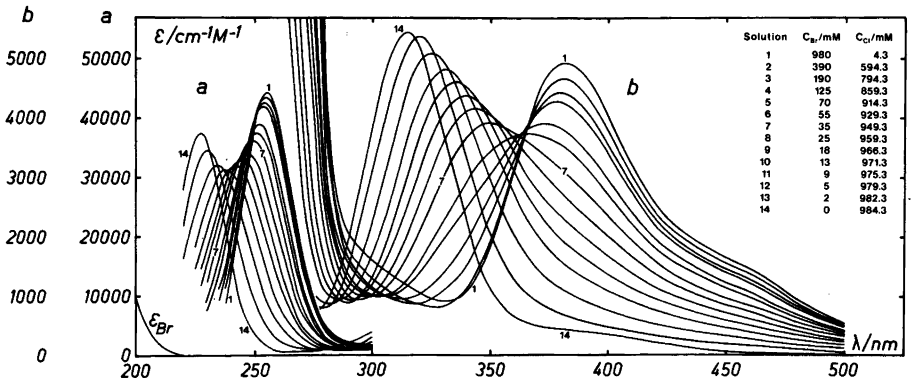

Fig. 2. Molar absorptivities, $\varepsilon = e/C_{Au}$, where e denotes absorptivity for equilibrated solutions with different ratios C_{Br}/C_{Cl}. C_{Au} was 0.171 mM. Curve 14 represents 100 % $AuCl_4^-$, curve 1 100 % $AuBr_4^-$.

and $C_{H^+} = 0.040$ M with L-solutions of sodium bromide ($C_{Br} = 0.400$, 0.600, 0.800 or 1.00 M). The equilibrated M-solution contains mainly the complexes $AuCl_2Br_2^-$, $AuClBr_3^-$ and $AuBr_4^-$, so the following reactions take place after mixing:

$$trans\text{-}AuCl_2Br_2^- \xrightarrow[\text{slow}]{+Br^-} AuClBr_3^- \xrightarrow{+Br^-} AuBr_4^-$$

$$cis\text{-}AuCl_2Br_2^- \xrightarrow[\text{fast}]{+Br^-} AuClBr_3^- \xrightarrow{+Br^-} AuBr_4^-$$

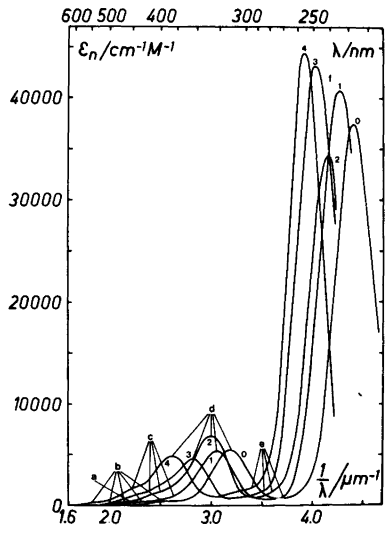

Fig. 3. Molar absorptivities, ε_n, for the complexes $AuCl_{4-n}Br_n^-$, $n = 0$, 1, 2, 3, 4, calculated from the curves in Fig. 2. and the equilibrium constants in Table 5. Assignments, see Table 7.

The reaction of the *cis*-isomer is about fifteen times faster than that of the *trans*-isomer, so these two reactions are kinetically separated. The subsequent reaction $AuClBr_3^- \rightarrow AuBr_4^-$ is only about 4 times slower than the *cis*-$AuCl_2Br_2^- \rightarrow AuClBr_3^-$ reaction, but reaction (8) can be followed at 365 nm, where $AuClBr_3^-$ and $AuBr_4^-$ have equal molar absorptivities (*cf.* Fig. 3).

Spectra. Fig. 2 shows spectra of a series of equilibrated solutions recorded using a Cary 15 Recording Instrument. The resolved spectra of the complexes shown in Fig. 3 were calculated using these curves and the equilibrium constants in Table 5.

RESULTS AND DISCUSSION

Rate expressions. The halide substitutions (4) to (8) can be described by the scheme (10) (*cf.* Refs. 4, 9) with $n = 0$, 1, 2, 3 and with *cis*- and *trans*-isomers for $n = 1$, 2:

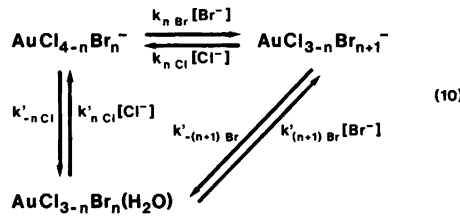

(10)

For excess halide and with steady-state conditions for the intermediate aqua complex the pseudo first-order rate constant is described by eqn. (11). (Integration of rate law for reversible processes, *cf.* Ref. 10).

$$k_{exp} = k_{nCl}[Cl^-] + k_{nBr}[Br^-] + k'_{-nCl} \times \left(1 + \frac{k_{nCl}[Cl^-]}{k_{nBr}[Br^-]}\right) \Big/ \left(1 + \frac{k'_{-nCl}}{k'_{-(n+1)Br}} \times \frac{k_{nCl}[Cl^-]}{k_{nBr}[Br^-]}\right) \quad (11)$$

Reaction (4) ($n=0$) was studied using such chloride and bromide concentrations that the predominant complexes at equilibrium were $AuCl_4^-$ or $AuCl_4^-$ and $AuCl_3Br^-$, *cf.* Table 1. The rate constant k'_{-0Cl} for the acid hydrolysis of $AuCl_4^-$ is about 0.02 s^{-1}.[11,12] The rate constant k'_{-1Br} for acid hydrolysis of the bromide in $AuCl_3Br^-$ is then approximately 0.02/4 s^{-1}, since the leaving ligand effect is negligible (compare rate constants for the corresponding platinum complexes in Ref. 5, Table VIII). The third term in eqn. (11) therefore never amounts to more than about 0.006 s^{-1}, which is much less than the observed rate constants. Thus, the reaction *via* the aqua complex can be neglected for the experimental conditions used, and eqn. (11) is simplified to (12):

$$k_{exp} = k_{nCl}[Cl^-] + k_{nBr}[Br^-] \quad (12)$$

Similarly, for reaction (5), ($n=3$) the chloride and bromide concentrations were chosen to give $AuClBr_3^-$ and $AuBr_4^-$ or $AuBr_4^-$ predominantly at equilibrium. The acid hydrolysis rate constant for $AuBr_4^-$, k'_{-4Br}, is 0.2 s^{-1},[2] so the rate constant for hydrolysis of the chloride in $AuClBr_3^-$, k'_{-3Cl}, is approximately 0.2/4 s^{-1}. In this case, the third term in eqn. (11) is always smaller than about 0.20 s^{-1}, which is also negligible compared to the experimental rate constants. Thus, eqn. (12) is applicable for reaction (5) as well.

For reactions (6) to (8) ($n=1, 2$) all acid hydrolysis rate constants involved are much smaller than the observed rate constants which means that the reactions *via* aqua complexes can also be neglected in these cases. Furthermore, the reverse reactions are suppressed for the halide concentrations used, so eqn. (12) reduces to (13).

$$k_{exp} = k_{nBr}[Br^-] \quad (13)$$

Rate constants. Fig. 4a shows plots of the observed rate constants *vs.* the concentration of entering bromide at constant concentration of chloride for reaction (4) starting from $AuCl_4^-$. According to eqn. (12) the slopes give the rate constant for substitution of chloride by bromide, k_{0Br}, and the intercepts the term $k_{0Cl}[Cl^-]$. Fig. 4b shows the linear plot of the intercepts *vs.* the chloride concentration, the slope of which gives k_{0Cl}. Finally, Fig. 4c, shows a plot of the observed rate constants *vs.* the entering chloride concentration at various concentrations of bromide when reaction (4) is followed in the other direction, starting from a mixture of $AuCl_3Br^-$ and $AuCl_4^-$.

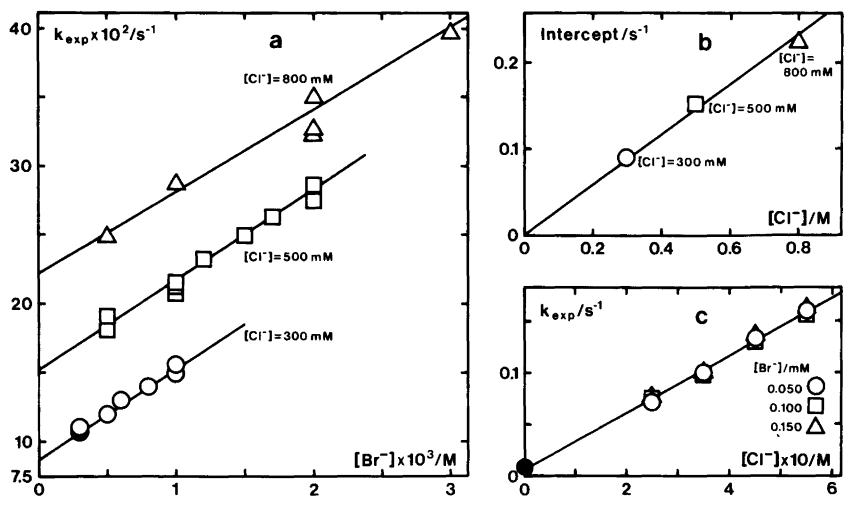

Fig. 4. Reaction (4) followed in the forward direction (a) and in the reverse direction (c). In (b), the intercepts from Fig. 4a have been plotted *vs.* $[Cl^-]$. The symbol ● in Fig. 4c denotes $k_{0Br} \times [Br^-]$, for $[Br^-] = 0.1$ mM, using the k_{0Br} value from Table 4.

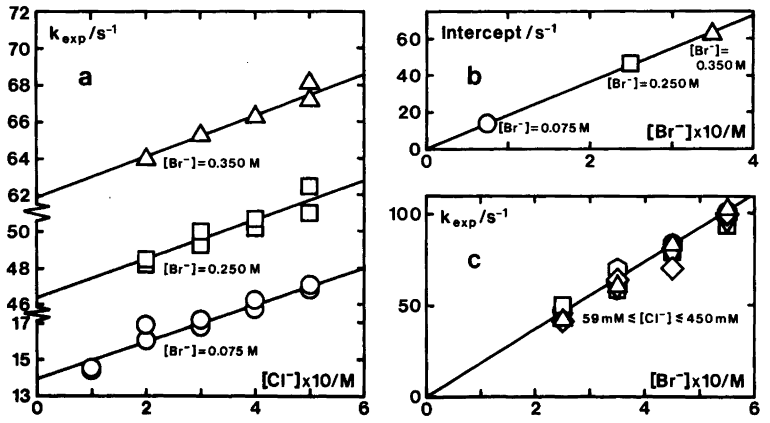

Fig. 5. Reaction (5) followed in the forward direction (c), and in the reverse direction (a). In (b), the intercepts from Fig. 5a have been plotted *vs.* $[Br^-]$.

The slope gives also a value for the rate constant k_{0Cl}.

Fig. 5 shows analogous plots for reaction (5). Fig. 5a gives k_{3Cl} from the slopes and $k_{3Br}[Br^-]$ from the intercepts according to eqn. (12), and Fig 5b gives k_{3Br}. The slope of the plot in Fig. 5c gives k_{3Br} according to eqn. (12), and the intercept $k_{3Cl}[Cl^-]$ is too small to be observable in this case.

Fig. 6 shows plots of the observed rate constants *vs.* the concentration of entering bromide for reactions (6) to (8), the slopes of which give k_{1tBr}, k_{2tBr} and k_{2cBr}, respectively, according to eqn. (13).

The rate constants are given in Table 4. Comparisons of the statistically corrected values of k/m using the relation $k/m=(const)TC_1C_2$ as described in Ref. 5, p. 15 give values of the relative *cis*- and *trans*-effects for these reactions. The reaction pairs

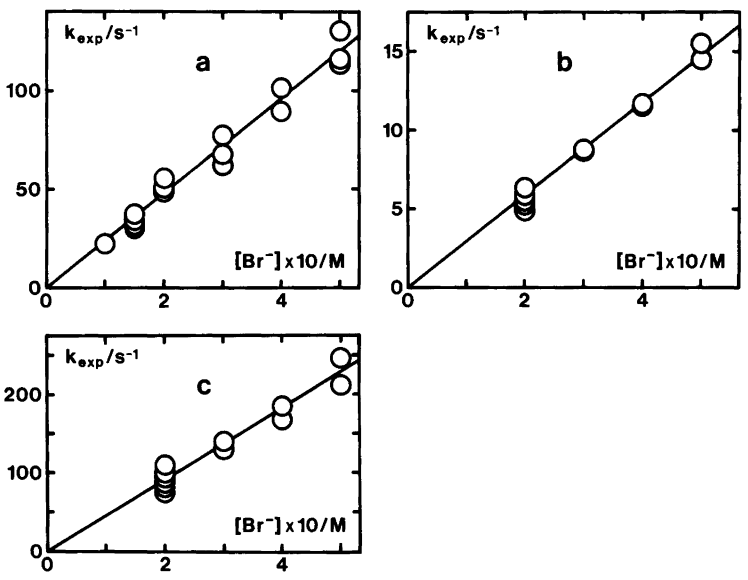

Fig. 6. Reactions (6)–a, (7)–b and (8)–c.

Table 4. Rate constants at 25 °C, 1.00 M perchlorate medium for reactions of gold(III) and platinum(II)[5] complexes.

Reaction	Rate constant	M = Au			M = Pt		$10^{-6}k_{Au}/k_{Pt}$
		k_{Au}/s^{-1} M^{-1}	$(k_{Au}/m)/s^{-1}$ M^{-1} [a]	Method	$10^5k_{Pt}/s^{-1}$ M^{-1} Ref. 5		
A $MCl_4^- + Br^- \rightarrow MCl_3Br^- + Cl^-$	k_{0Br}	63.3±2.3	16	Fig. 4a	4.8		1.3
B $MCl_3Br^- + Br^- \rightarrow t\text{-}MCl_2Br_2^- + Cl^-$	k_{1tBr}	240±20	240	Fig. 6a	8.9		2.7
C $MCl_3Br^- + Br^- \rightarrow c\text{-}MCl_2Br_2^- + Cl^-$	k_{1cBr}	29	14.5	Calc.[b]	2.6		1.1
D $t\text{-}MCl_2Br_2^- + Br^- \rightarrow MClBr_3^- + Cl^-$	k_{2tBr}	29.5±1.5	14.8	Fig. 6b	0.94		3.1
E $c\text{-}MCl_2Br_2^- + Br^- \rightarrow MClBr_3^- + Cl^-$	k_{2cBr}	456±40	228	Fig. 6c	10.0		4.6
F $MClBr_3^- + Br^- \rightarrow MBr_4^- + Cl^-$	k_{3Br}	185±13	185	Fig. 5b, c	2.8		5.8
G $MCl_3Br^- + Cl^- \rightarrow MCl_4^- + Br^-$	k_{0Cl}	0.26±0.03	0.26	Fig. 4b, c	0.45		0.056
H $t\text{-}MCl_2Br_2^- + Cl^- \rightarrow MCl_3Br^- + Br^-$	k_{1tCl}	7.0	3.5	Calc.[c]	4.2		0.13
I $c\text{-}MCl_2Br_2^- + Cl^- \rightarrow MCl_3Br^- + Br^-$	k_{1cCl}	0.45	0.23	Calc.[c]	0.60		0.075
K $MClBr_3^- + Cl^- \rightarrow t\text{-}MCl_2Br_2^- + Br^-$	k_{2tCl}	0.19	0.19	Calc.[c]	0.15		0.113
L $MClBr_3^- + Cl^- \rightarrow c\text{-}MCl_2Br_2^- + Br^-$	k_{2cCl}	6.2	6.2	Calc.[c]	3.1		0.174
M $MBr_4^- + Cl^- \rightarrow MClBr_3^- + Br^-$	k_{3Cl}	10.7±2.5	2.7	Fig. 5a	3.0		0.38

[a] m is a statistical factor, equal to the number of equivalent leaving ligands in the complex. [b] Calculated from reactions A and F and the relative *cis*- and *trans*-effects Br^-/Cl^-. [c] Calculated from reactions G and M and the relative *cis*- and *trans*-effects Br^-/Cl^-, see text.

A;D, B;E and B;F indicate a relative *cis*-effect Cl^-/Br^- of 1,1±0.1. Similarly, reactions B;A, D;F and, if corrections for the *cis*-effects are applied, reactions G;M, E;A, F;A and B;D give a relative *trans*-effect Br^-/Cl^- of 14±3. Both the relative *cis*- and *trans*-effects are of the same order of magnitude as those found for the corresponding platinum(II) complexes.[5]

The acid hydrolysis rate constant for $AuCl_4^-$ is 2.2×10^{-2} s^{-1},[11,12] and for $AuBr_4^-$ 0.25 s^{-1} [12] at 25 °C. If these two rate constants are corrected for the difference in *cis*- and *trans*-effect between chloride and bromide, it appears that there is no difference between chloride and bromide as leaving groups in these complexes. This is also valid for the Pt(II)[5] and Pd(II)[13] complexes. A comparison of k/m for reactions A and G, and F and M, therefore shows that bromide is about 65±5 times better as entering ligand than chloride in the gold complexes, compared to a factor of only about 3 for the corresponding platinum(II) complexes.[5]

The relative *cis*- and *trans*-effects obtained as described above were used to calculate rate constants for reactions C, H, I, K and L in Table 4, which are not accessible experimentally.

Reaction mechanism and reactivities. Fig. 7 reviews the system. Obviously, the over-all process (1) occurs mainly *via* the intermediate complexes $AuCl_3Br^-$, *trans*-$AuCl_2Br_2^-$ and $AuClBr_3^-$. The reaction *via* the *cis*-isomer contributes only with about 10 % to the over-all reaction (k_{1cBr}/k_{1tBr} ≈0.1). In this respect there is a close similarity to

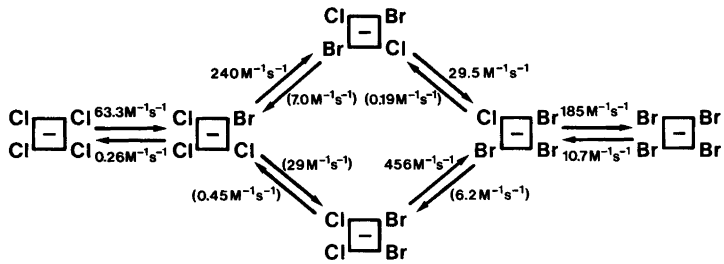

Fig. 7. Rate constants. Values within parenthesis calculated using relative *cis*- and *trans*-effects.

the analogous Pt(II)-system, *cf.* Ref. 5, Fig. 6. In the case of gold, however, each substitution step takes place *via* a direct halide exchange, the solvent path (the k_1-term[4]) being completely negligible. The halide substitutions in the platinum complexes, on the other hand, occur *via* the usual two-term rate law,[4] the solvent path often being the predominant contributor to the over-all rate for the halide concentration ranges accessible.[5]

Table 4 gives a comparison of the reactivities of analogous gold(III) and platinum(II) complexes. For bromide as entering ligand the former react about 2×10^6 times faster than the latter, and for chloride as entering ligand about 10^5 times faster. The difference in relative reactivity by a factor of about 20 ($2\times10^6/10^5$) shows that the nature of the entering ligand is more important for reactions of the gold complexes than for those of the platinum complexes. (This is equivalent to the conclusion in the previous paragraph that bromide is 65 times better as entering ligand than chloride for gold, but only about 3 times better for platinum complexes).

Whereas there is no difference between chloride and bromide as leaving ligands in the gold complexes, a comparison of the rate constant 2.3×10^3 s^{-1} M^{-1} (Bekker and Robb[14]) for the reaction between $AuCl_3H_2O$ and chloride, and the rate constant 1.5 s^{-1} M^{-1} (Rich and Taube[15]) for the isotopic exchange of chloride in $AuCl_4^-$, corrected for the differences in ionic charge (*cf.* Ref. 5), shows that water is about 300 times – $2.3\times10^3/(5\times1.5)$ – better as leaving ligand than chloride. Thus, the influence of the leaving group (Cl, Br, H_2O) appears to be similar for gold(III) and platinum(II) complexes (*cf.* Ref. 5).

The absence of an observable solvent path in the present experiments on the gold complexes is also in accord with the increased importance of the nature of the entering group in the case of gold. The rate constants for the acid hydrolyses (M = Au, Pt; $j=1, 2$)

$$MCl_4^{j-}+H_2O \xrightarrow{k_1} MCl_3OH_2^{1-j}+Cl^-$$

$$MBr_4^{j-}+H_2O \xrightarrow{k_2} MBr_3OH_2^{1-j}+Br^-$$

are $k_{1Au}=0.022$ s^{-1},[11] $k_{1Pt}=4\times10^{-5}$ s^{-1},[5] $k_{2Au}=0.245$ s^{-1},[2] and $k_{2Pt}=19\times10^{-5}$ s^{-1},[5] which give $k_{1Au}/k_{1Pt}=6\times10^2$ and $k_{2Au}/k_{2Pt}=12\times10^2$. For water as entering ligand the ratio in reactivity between gold and platinum is obviously only about 10^3. Summarizing:

Entering ligand	k_{Au}/k_{Pt}
H_2O	$\sim10^3$
Cl^-	$\sim10^5$
Br^-	$\sim2\times10^6$

The relative contribution of the solvent path to the over-all reaction is thus 100 to 1000 times smaller for the gold complexes than for those of platinum when halide is the entering ligand.

These observations support the picture of an associative intimate mechanism and are compatible with Baddley's and Basolo's[16] conclusion that bond formation in the transition state is more important for gold(III) than for platinum(II) complexes.

The four rate constants $k_{0Br}=63.3$ M^{-1} s^{-1}, $k_{1tBr}=240$ M^{-1} s^{-1}, $k_{2tBr}=29.5$ M^{-1} s^{-1} and $k_{3Br}=185$ M^{-1} s^{-1} are so close to each other that the four consecutive reactions in the gold system are not kinetically separated in aqueous solution (*cf.* Fig. 7). If this is valid for methanol solution also, the experiments in Ref. 1, evaluated using a model with two separated rate-determining steps, might give too large values for the rate constants of the first, rapid step. The intercepts of the k_{obs} *vs.* [Y] plots might then be due to a deviation from first-order kinetics, caused by the two consecutive reactions $AuCl_4^- \rightarrow AuCl_3Br^- \rightarrow$ *trans*-$AuCl_2Br_2^-$, and not by a reaction with the solvent. The rather large scatter in the values of the intercepts for different entering ligands Y, $(2.7\pm2.1)\times10^{-3}$ s^{-1}, support this interpretation.

The results in Fig. 7 show clearly that the "single-stage" reaction observed in Ref. 2 is composed of a series of consecutive processes. To treat these consecutive reactions as a first-order process will of course give rate constants, which have no physical significance. A variation of wavelength shows immediately the complexity of the reaction. For the experimental conditions used in Ref. 2, there is a monotonous increase of absorbance at 382 nm, which might be misinterpreted as one reaction, whereas at 300 nm, there is first a rapid decrease, followed by a slower increase, *cf.* Fig. 2.

The equilibrium constants in Table 5 and the graphical representation in Fig. 8 show, that for the chloride and bromide concentrations used in the experiments by Hall and Satchell,[3] $AuClBr_3^-$ and $AuBr_4^-$ will be the products at equilibrium. Spectra of equilibrated solutions are not identical with the $AuCl_3Br^-$ spectrum (see Fig. 3) as assumed by these authors. One single wavelength (nominal 312 nm) was used for all their experiments. Our spectra

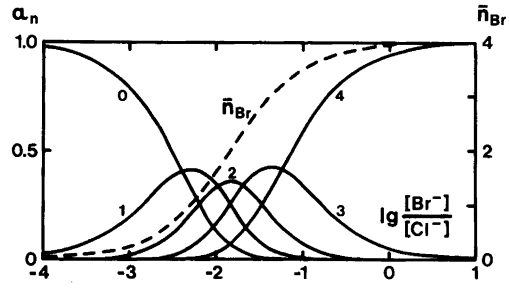

Fig. 8. The distribution of gold between the species $AuCl_{4-n}Br_n^-$, $n=0$, 1, 2, 3, 4 for 25 °C and 1.00 M perchlorate medium calculated from the equilibrium constants in Table 5.

Table 5. Stepwise equilibrium constants, K_n, defined by eqn. (3).

K_n	From kinetics 1 M $NaClO_4$	From Ref. 17 3 M $HClO_4$
K_0	243 ± 40	288
K_1	98 ± 20	135
K_{1c}	64 ± 13	90[a]
K_{1t}	34 ± 7	45[a]
K_2	49 ± 10	64.6
K_{2c}	73 ± 15	97[a]
K_{2t}	153 ± 30	194[a]
K_3	17 ± 5	23.4

[a] Calculated, assuming a statistical distribution [*cis*]/[*trans*] = 2:1.

in Fig. 3 show that at 320 nm, for instance, the absorbance will first increase due to formation of $AuCl_3Br^-$ and $AuCl_2Br_2^-$, and then decrease, when $AuClBr_3^-$ and $AuBr_4^-$ are formed. This is exactly what was observed in Ref. 3. A systematic wavelength error of 8 nm is not at all unusual for a Durrum-Gibson instrument. Experiments performed at other wavelengths, for instance at 382 nm – *cf.* Fig. 2 – immediately show that the mechanistic interpretation made in Ref. 3 cannot be correct.

The "chloride catalysis" reported by Hall and Satchell[3] is also compatible with the model in Fig. 7, the reactions studied being reversible, and the back reactions being chloride dependent; *cf.* eqn. (12). Finally, it seems very unlikely that the rate of formation of a five-coordinate adduct between $AuCl_4^-$ and bromide of the type proposed in Ref. 3 should lie within the stopped-flow region.

Equilibria. The equilibrium constants K_n, $n=0$, 1, 2, 3, given in Table 5 were calculated from the rate constants in Table 4 using eqn. (3). They agree satisfactorily with those previously calculated by Almgren[17] from spectrophotometric equilibrium measurements for a 3 M perchlorate medium. The values of $K_{1c}/K_{1t}=1.9\pm0.7$ and $K_{2t}/K_{2c}=2.1\pm0.8$ indicate that the two isomers of $AuCl_2Br_2^-$ are present at equilibrium in about the statistically expected ratio [*cis*]/[*trans*] = 2:1, which is also a reasonable result. Fig. 8 shows the distribution of gold between the different complexes calculated from these constants. Table 6 shows that the distribution is very nearly statistical.

The equilibrium constants K_n defined by eqn. (3) are related to the over-all stability constants β_{4X} for the chloro and bromo complexes, defined by eqn. (14), by the relation (15).

$$\beta_{4X} = \frac{[AuX_4^-]}{[Au^{3+}][X^-]^4} \tag{14}$$

$$K_0K_1K_2K_3 = \beta_{4Br}/\beta_{4Cl} \tag{15}$$

The constants in Table 5 give $\beta_{4Br}/\beta_{4Cl}=2.0\times10^7$ which is compatible with J. Bjerrum's and Skibsted's[18] calculation $\log \beta_{4Cl}=26$ and $\log \beta_{4Br}=34$ (*cf.* also Refs. 19, 20, 21). Thus, the difference in stability between the bromo and chloro complexes of gold(III) is much larger than the difference for the corresponding platinum(II) complexes, having

Table 6. Statistical and experimental values for the equilibrium constants of the mixed complexes formed from $AuCl_4^-$ and $AuBr_4^-$.

Reaction	lg *K* (found)	lg *K* (statistical)
$3/4\ AuCl_4^- + 1/4\ AuBr_4^- \rightleftharpoons AuCl_3Br^-$	0.56	0.60
$1/2\ AuCl_4^- + 1/2\ AuBr_4^- \rightleftharpoons AuCl_2Br_2^-$	0.73	0.78
$1/4\ AuCl_4^- + 3/4\ AuBr_4^- \rightleftharpoons AuClBr_3^-$	0.59	0.60

Table 7. Wavenumbers, $\lambda^{-1}/\mu m^{-1}$; molar absorptivities, $\varepsilon_n/cm^{-1}M^{-1}$, for $AuCl_{4-n}Br_n^-$, ($n=0$, 1, 2, 3, 4) and proposed assignments for D_{4h} symmetry.

Peak	$AuCl_4^-$	$AuCl_3Br^-$	$AuCl_2Br_2^-$	$AuClBr_3^-$	$AuBr_4^-$	Assignment(D_{4h})	Excited state (D_{4h})
a	~2.25(70)	–	–	–	–	*d*–*d*	
b	2.52(350)	2.31(400)	2.15(400)	~2.0(300)	1.83(200)	$3b_{1g}\leftarrow a_{2g}$	$^1B_{2g}$ (allowed *via* E_u-vibration)
c	–	2.63(800)	2.49(1200)	2.40(1350)	2.21(1350)	$3b_{1g}\leftarrow 3e_u$	^3E_u
d	3.19(5500)	3.05(5500)	3.00(6800)	2.83(4850)	2.62(4950)	$3b_{1g}\leftarrow 3e_u$	^1E_u
e	–	~3.7(800)	3.60(1000)	3.52(1400)	~3.4(1800)	?[a]	–
f	4.39(37500)	4.26(42000)	4.13(34500)	4.03(43500)	3.92(44000)	$3b_{1g}\leftarrow 2e_u$	^1E_u

[a] See footnote g in Table V of Ref. 22, alternatively $3b_{1g}\leftarrow 2e_u$ (^3E_u), *cf.* Table III of Ref. 22.

$\beta_{4Br}/\beta_{4Cl}=133\pm15$.[5] In other words, gold(III) is an extremely soft metal.

Spectra. The charge-transfer spectra of $AuCl_4^-$ and $AuBr_4^-$ shown in Fig. 3 are very similar to those of the corresponding Pd(II) complexes,[22] the bands of the gold complexes being displaced somewhat more towards the visible region. Table 7 gives tentative assignments, which are analogous to those proposed for $PdCl_4^{2-}$ and $PdBr_4^{2-}$.[22] The assignments for bands *d* and *f* agree with those made previously by Chakravorty *et al.*[23] The *d*–*d* bands of the gold complexes are difficult to observe because of their proximity to the high-intensity bands. The band denoted by *b* in Table 7 has a rather large intensity in all the complexes and blue-shifts approximately the same as bands *c* to *f*, so it has been classified as a charge-transfer band (*cf.* Ref. 22).

Acknowledgements. Our thanks are due to Fil. mag. Ingegerd Lind for experimental assistance and to the Swedish Natural Science Research Council and the "*Kgl. Fysiografiska Sällskapet*", Lund, for financial support.

REFERENCES

1. Cattalini, L., Orio, A. and Tobe, M. L. *J. Am. Chem. Soc. 89* (1967) 3130.
2. Louw, W. J. and Robb, W. *Inorg. Chim. Acta 9* (1974) 33.
3. Hall, A. J. and Satchell, D. P. N. *J. Chem. Soc. Dalton Trans.* (1977) 1404.
4. Langford, C. H. and Gray, H. B. *Ligand Substitution Processes*, Benjamin, New York 1965, p. 23.
5. Elding, L. I. and Gröning, A.-B. *Chem. Scr. 11* (1977) 8.
6. Bjerrum, N. *Bull. Soc. Chim. Belg. 57* (1948) 432.
7. Carlsson, L. and Lundgren, G. *Acta Chem. Scand. 21* (1967) 819.
8. Chateau, H., Gadet, M.-C. and Pouradier, J. *J. Chim. Phys. 63* (1966) 269.
9. Elding, L. I. and Gröning, A.-B. *Inorg. Chim. Acta 31* (1978) 243.
10. Frost, A. A. and Pearson, R. G. *Kinetics and Mechanism*, 2nd Ed., Wiley, New York 1961, p. 186.
11. Robb, W. *Inorg. Chem. 6* (1967) 382.
12. Fry, F. H., Hamilton, G. A. and Turkevich, J. *Inorg. Chem. 5* (1966) 1943.
13. Elding, L. I. *Inorg. Chim. Acta 7* (1973) 581.
14. Bekker, P. van Z. and Robb, W. *Inorg. Nucl. Chem. Lett. 8* (1972) 849.
15. Rich, R. L. and Taube, H. *J. Phys. Chem. 58* (1954) 57.
16. Baddley, W. H. and Basolo, F. *Inorg. Chem. 3* (1964) 1087.
17. Almgren, L. *Acta Chem. Scand. 25* (1971) 3713.
18. Skibsted, L. H. and Bjerrum, J. *Acta Chem. Scand. A 31* (1977) 155.
19. Bjerrum, N. and Kirschner, Å. *K. Dan. Vidensk. Selsk. Skrifter, Mat.-Nat. Avd. 8* (1918) 5.
20. Grube, G. and Morita, T. *Z. Elektrochem. 38* (1932) 117.
21. Latimer, W. M. *Oxidation Potentials*, 2nd Ed., Prentice-Hall, New York 1952, p. 193.
22. Elding, L. I. and Olsson, L. F. *J. Phys. Chem. 82* (1978) 69.
23. Grangopadhayay, A. K. and Chakravorty, A. *J. Chem. Phys. 35* (1961) 2206.

Received June 5, 1978.

Acta Chemica Scandinavica A 32 (1978) 879–886

Conformational Analysis of Coordination Compounds. VI. Force Field Calculation of Thermodynamic Properties of Tris(diamine)cobalt(III) Coordination Complexes

NIELS CHRISTIAN POUL HALD and KJELD RASMUSSEN *

Chemistry Department A, The Technical University of Denmark, Building 207, DK-2800 Lyngby, Denmark

Dedicated to Jannik Bjerrum on the occasion of his 70th birthday

An empirical force field developed to reproduce geometries of equilibrium conformers of tris-(diamine)cobalt(III) complexes is used to derive thermodynamic functions and equilibrium distributions through statistical methods. The programme is tested on a series of alkanes prior to application to the coordination compounds.

Differences in thermodynamic properties between different conformers are well reproduced. Good agreement is also obtained for differences between configurational isomers. Calculations of properties of complexes of different ligands fail to reproduce the observed trends.

The Consistent Force Field concept (CFF)[1] was developed to account simultaneously for equilibrium geometry, vibrational spectra, thermodynamic data and other properties of a family of related compounds. A version of the CFF system was constructed at this Department;[2] so far it has been applied to tris(diamine) complexes of Co(III) and Cr(III),[3-5] to mono- and disaccharides[6-9] and to haloalkanes.[10] For coordination complexes, until now only equilibrium geometries and differences in static potential energy were considered;[3-5] the normal coordinate analysis was tested on a chloropropane;[10] and the thermodynamic programmes to be described briefly in this paper were applied to sugars.[7-9]

From the start of this project in 1969 it was our intention to calculate thermodynamic functions of both robust and labile complexes. We cannot yet, with our programme, compare molecules with different numbers and types of atoms, and we therefore confine our interest to such tris(diamine) Co(III) complexes as have been studied before with our CFF system, and for which thermodynamic data for conformers and isomers are available.

Such data have been obtained in recent years, mainly with Bjerrum's classical equilibrium methods,[11-13] and by calorimetric measurements.[14]

We shall first describe our new general programme for calculation of thermodynamic data, and assess its reliability by calculations on simple alkanes. We shall then apply it to robust Co(III) complexes and see to which extent the force field developed entirely to reproduce geometry[3,4] can predict measured differences in thermodynamic properties.

THE PROGRAMME

Method. We use the standard statistical-mechanical methods, assuming that the molecule under treatment is in thermodynamic equilibrium with its surroundings and obeys Boltzmann statistics, and that its total energy is separable and that therefore its partition function can be factorized. We are interested in differences between conformers and isomers; accordingly we do not consider electronic

* To whom correspondence should be addressed.

and nuclear spin degrees of freedom, but only vibrational plus external degrees of freedom. For molecules in solution, generally the case in thermodynamic measurements on coordination compounds, we quench translational and rotational motion.

The formulae we use can be found in any standard textbook on statistical thermodynamics.[15-16] Further simplifying assumptions underlie our choice of formulae: for the rotational partition function we use the high-temperature approximation and treat the molecule as a quasi-rigid body, for the vibrational we assume harmonic vibrations. These simplifications are used almost universally although they are not always stated explicitly. Their validity is investigated in an extensive series of test calculations on alkanes reported in the Appendix. Subsequent work on sugars[7-9] would also serve to justify the approximations.

It will be seen that we give no special treatment of internal rotation, "free" and "restricted". Such motion is simply an internal vibration, usually of low frequency, and is treated as such. The concept of internal rotation was introduced at a time when it was almost impossible to either measure or calculate the lowest frequencies of vibrations. This is now done as a matter of routine, and we shall see that it gives perfectly good results to treat internal rotation as any other vibration.

Implementation. The new programmes are organized as one more overlay branch of the CFF system[2] and are fully compatible with the rest of the system. In this way no extra core store is required, and the user will sense no other change than the possibility of ordering thermodynamic output by specifying the value of just two control digits per molecule. The input manual available to users gives directions on how to choose this control parameter to get data at 298.15 and 313.15 K or at 100, 200, 300 and 400 K, and to include or exclude summation over external degrees of freedom. If summation over rotations is wanted, the symmetry number of the molecule (the order of its pure rotational group) must also be specified. Output consists of energy, enthalpy, free energy, free enthalpy, entropy and heat capacity. The static potential energy is added to the zero-point vibrational energy. As the product of the principal moments of inertia are needed for summation over rotations, we also diagonalize the inertia tensor and print moments of inertia and rotational constants; this gives us the possibility of comparing with the most important results of microwave and rotational-vibrational spectroscopy.

COORDINATION COMPOUNDS

Choice of substances. We choose those five-membered chelate ring systems whose structures have previously been described with the CFF system: $(en)_3$, $(rac\text{-}bn)_3$, $(m\text{-}bn)_3$, $(ibn)_3$ and $(rac\text{-}bn)(en)_2$ complexes of cobalt(III),[4,5] where the abbreviations are: en = 1,2-ethanediamine, bn = 2,3-butanediamine, ibn = 2-methyl-1,2-propanediamine, *rac* = *racem* (= *d* or *l*, or = *R,R* or *S,S*), *m* = *meso* (= *R,S*).

As mentioned before, we do not include translational and rotational motion when evaluating statistical sums for these large molecules in solution. This approach contrasts with the practice of De-Hayes and Busch.[17] The question of how reliable calculations on isolated molecules are when compared to measurements on solutions and on condensed phases in general is partly answered by reference to the comparable work on glucose,[6,7] maltose[8] and cellobiose,[9] where calculated properties nicely reproduce results from measurements on solutions. Earlier papers of the present series[3,4] show that crystal structures are reproduced, and there is an indication[18] that most internal vibrations do not change from crystalline to dissolved state.

We shall see how well the force field developed for a different purpose[3,4] can reproduce thermodynamic differences between conformers and between isomers.

$[Co(en)_3]^{3+}$, *lel-ob equilibrium.* The problem of the equilibrium distribution of the four conformers is the classical one of conformational analysis of chelate compounds since Corey and Bailar.[19] Their simple calculation of non-bonded H---H interaction energy gave $E(ob_3) - E(lel_3) \simeq 4.7$ kJ mol^{-1}. Very little extra insight has been provided by a host of later researchers, including ourselves.[4]

We shall here consider only free enthalpy, and not energy differences. Gollogly *et al.*,[20] using a rather special way of summing over vibrations, estimated free enthalpy differences for the four conformers. De Hayes[21] calculated proper statistical sums, but included translational and rotational terms as if the molecule were in the gaseous state. These results are shown, with our values, in Table 1. All ΔG values refer to $G(lel_3)$ as zero and are cor-

Table 1. Free enthalpy differences and equilibrium distributions of conformers of $[Co(en)_3]^{3+}$. Unit for ΔG is kJ mol^{-1}.

		lel_3	lel_2ob	$lelob_2$	ob_3	lel:ob	Ref.
Calc.	ΔG	0.00	0.15	0.75	1.50		33
	distr.	0.47	0.36	0.13	0.04	0.75:0.25	
Calc.	ΔG	0.00	−0.61	−0.05	1.42		34
	distr.	0.20	0.56	0.22	0.02	0.65:0.35	
Meas.	distr. 290 K					0.75:0.25	35
Calc.	ΔG 298 K	0.00	0.52	2.80	5.80		This work
	distr.	0.45	0.36	0.15	0.04	0.74:0.26	
Meas.	distr. 298 K	0.40	0.40	0.16	0.03	0.73:0.27	36
Calc.	ΔG 313 K	0.00	0.41	2.70	5.85		This work
	distr.	0.43	0.37	0.15	0.05	0.73:0.27	
Meas.	distr. 333 K					0.74:0.26	35
Meas.	distr. 366 K					0.79:0.21	35
Meas.	distr. 373 K	0.35	0.41	0.20	0.04	0.69:0.31	36
Calc.	ΔG 400 K	0.00	−0.20	2.13	6.13		This work
	distr.	0.36	0.39	0.19	0.06	0.69:0.31	

rected with the statistical weights which are 1, 3, 3 and 1 for the four conformers lel_3, lel_2ob, $lelob_2$ and ob_3.

Comparison can be made with equilibrium distributions derived from NMR measurements and chromatographic separations. Sudmeyer *et al.*[22] measured the 251 MHz ^1H NMR spectrum of $[Co(en)_3]^{3+}$ in D_2O using decoupling of ^{59}Co. Under some simplifying assumptions they derived from spin-coupling parameters, through the Karplus equation, the ratio of the gross population lel:ob at three temperatures. Harnung *et al.*[23] measured, by a chromatographic method, distributions in the system $[Co(pn)_3]^{3+}$, pn = 1,2-propanediamine, and derived from these data the distribution for $[Co(en)_3]^{3+}$ at 298 and 373 K. All of these experimental data are shown in Table 1. Our calculations reproduce very closely, also concerning temperature dependence, the distributions derived from chromatographic separation.[23] The distributions derived from NMR measurements,[22] being reproduced at ordinary temperature, show a temperature dependence which is unexpected and not accounted for, and which is at variance with that found by chromatography and in our calculations.

$[Co(rac\text{-}bn)_3]^{3+}$, stereospecificity. A synthesis of the tris-complex, carried out with the resolved amine, will result in complexes having all six methyl groups equatorially disposed. The two configurations Δ and Λ will form with the same statistical probability, but the ob-lel energy difference will change the equilibrium. This energy difference,

Table 2. Free enthalpies for isomers of $[Co(bn)_3]^{3+}$ complexes. Units are kJ mol^{-1}.

System	T/K	ΔG° [12,13]	G_{calc}	$\Delta\Delta G^{\circ}$	ΔG_{calc}	Error
d,l-bn	298	−292.3	1304.0			
l-bn	298	−295.9	1307.4			
	313	−297.1	1302.6			
m-bn	298	−259.2	1349.6			
	313	−260.2	1345.0			
ibn	298	−236.2	1336.2			
	313	−239.0	1331.2			
l-bn	298			−36.0	−44.2	6.2
−*m*-bn	313			−36.9	−42.4	5.5
l-bn	298			−59.7	−28.8	−30.9
−ibn	313			−58.1	−28.6	−29.5
m-bn	298			−23.7	13.4	−37.1
−ibn	313			−21.2	−13.8	−35.0
l-bn −*d,l*-bn	298			−3.6	3.4	−7.0

small though it is, will have some effect, as we can have only homoconformational geometry. With 2*S*,3*S*-bn, for example, we shall have, keeping all methyl groups equatorial, either $\Lambda\delta\delta\delta$ (lel_3) or $\Delta\delta\delta\delta$ (ob_3). At 298 K, we calculate a free enthalpy difference of 5.81 kJ mol^{-1} in favour of the former, which gives an equilibrium ratio for the Λ on Δ configurations of 0.91:0.09. This predicted difference is large enough for detection with a chromatographic method. We have found no report of such an experiment.

$[Co(m\text{-}bn)_3]^{3+}$, fac:mer *ratio.* We calculate the free enthalpies at 298 K for all 4 *fac* and 8 *mer* conformers[4] of this system. After correcting with the statistical weights, which are 1 for the fac lel_3 and fac ob_3 conformers and 3 for the rest, we calculate the entire equilibrium distribution spectrum. Summing over all fac and all mer conformers gives a fac:mer ratio of 0.24:0.76.

Kojima *et al.*[24] separated the equilibrium mixture prepared at room temperature on a Sephadex column and identified the products spectroscopically. Graphical integration of their Fig. 2 gives a fac:mer ratio of 0.42:0.58.

For the closely related system of $[Co(cis\text{-}chxn)_3]^{3+}$, chxn = cyclohexanediamine, Toftlund and Laier[25] separated the fac and mer isomers after equilibration at 363 K; they found a ratio of 0.41:0.59. Our force field thus overestimates the population of the mer isomers by 17 %.

$[Co(ibn)_3]^{3+}$, fac:mer *ratio.* In exactly the same way, we calculated a fac:mer ratio of 0.23:0.77. Graphic integration of Fig. 3 in the paper[26] of Kojima *et al.* gives a ratio of 0.26:0.74. The coincidence could hardly be better.

$[Co(bn)_3]^{3+}$, *stability constants.* A number of stability constants for these complexes are available. Bang measured β_3 at 298 and 313 K for Co(III) with *rac*-bn,[12] *m*-bn[12] and ibn,[13] and derived ΔG°, ΔH° and ΔS°.

With our methods we can calculate free enthalpies. Their absolute values are not of interest, but the differences for series of isomers can be compared with differences in the ΔG° values derived from stability constants. Table 2 shows such comparisons.

For *rac*-bn we average over the four conformers having six equatorial methyl groups,[4] and correct the free enthalpies with a term $-RT\ln 2$ to account for both Δ and Λ configurations, which will form in equal proportion under equilibrium conditions.

For *l*-bn we use averaged data for the eq_6lel_3 and eq_6ob_3 conformers of lowest energy, as the comparison is to be made with measurements on a preparation from optically pure amine.

The calculated data for the *m*-bn and ibn systems have been statistically averaged over all 12 iso- and conformers. Under equilibrium conditions both Δ and Λ configurations will be formed, and we therefore corrected the free enthalpies with the term $-RT\ln 2$.

Table 3. Differences in complexation enthalpy at 298 K. Units are kJ mol^{-1}.

System	H_{strain} [14]	$H°_{calc}$	ΔH_{strain}	$\Delta H°_{calc}$
Δ-$[Co(l\text{-bn})_3]^{3+}$	−5.0	1398.9		
rac-$[Co(m\text{-bn})_3]^{3+}$	20.9	1442.6		
rac-$[Co(ibn)_3]^{3+}$	41.1	1428.4		
l-bn − *m*-bn			−25.9	−43.7
l-bn − ibn			−46.1	−29.5
m-bn − ibn			−20.2	14.2

The comparisons show that we have here struck the limit of realibility, not of the method and programme, but of the present force field. The calculated sequence of stability is *d,l*-bn > *l*-bn > ibn > *m*-bn against the experimentally established *l*-bn > *d,l*-bn > *m*-bn > ibn.

$[Co(l\text{-}bn)(en)_2]^{3+}$, *stability constants.* Bang[13] also reported a ΔG for Λ- and Δ-$[Co(l\text{-bn})en_2]^{3+}$, in which the methyl group preference for equatorial positions causes the l-bn ring to adopt ob and lel conformations, respectively. He found a ΔG difference of 2.06 kJ mol^{-1}; our calculated value is 2.11 kJ mol^{-1}.

Enthalpies of complexation. Enthalpy differences were measured calorimetrically at 298 K by Bagger *et al.*;[14] a more accurate method than deriving the $\Delta H°$ from equilibrium data. Essentially they measured the heat evolved during sulfide decomposition of the complex. Results are shown in Table 3, together with calculated values. H_{strain} is[14] ΔH for the process $[Co(en)_3]^{3+}$ (aq) + 3 bn (aq) → $[Co(bn)_3]^{3+}$ (aq) + 3 en (aq).

Bang[13] also produced calorimetric data for Λ- and Δ-$[Co(l\text{-bn})(en)_2]^{3+}$ where the l-bn ring has ob and lel conformations, respectively. He derived H_{strain} $(\Lambda ob' - \Delta lel') = -0.6$ kJ mol^{-1}, a rather unexpected result. Our calculated value is 2.6 kJ mol^{-1}.

The comparisons show that, as for the free enthalpies, we have reached the limit of reliability of the force field.

Conclusion. We have demonstrated that it is practicable to calculate thermodynamic properties of series of coordination complexes. The agreement with measured data is encouraging for differences between conformers. For differences between isomers, caution should be exercised. When the differences are limited to configurations at the metal atom, the calculations show neat agreement; but when we try to reproduce differences between complexes with different amines we fail.

The remedy is a refinement of the force field on structures and frequencies of vibration. This is a major task now being undertaken.

Acknowledgements. All computations were done on an IBM 370/165 at the Technical University Computer Centre NEUCC. Computational costs were covered by a grant from the Danish Natural Science Research Council, which is gratefully acknowledged. We thank Mr. Klavs Kildeby for checking and correcting our thermodynamic programmes in the initial phase of the work.

APPENDIX: TEST OF ALKANES

Choice of substances. Thermodynamic functions of alkanes are known to a very high degree of precision, and it is evident that we should be able to reproduce them to a fair degree of approximation. The small alkanes are very flexible, and in context with our applications to complexes of 2,3-butanediamines, which contain methyl groups with different degrees of restricted rotation, they are particularly interesting.

We choose two groups of molecules: methane, ethane, propane, isobutane, neopentane and cyclohexane; and butane and pentane. In the first group each molecule exists as only one conformer, in the second as two or more. n-Butane can take two conformations, *anti* (A) and *gauche* (G and −G), the second with a twofold statistical weight. Pentane takes four conformations: AA, AG = GA = −GA = A−G, GG = −G−G and −GG = G−G, with statistical weights 1,4, 2 and 2.

Force field. We use, without changes, the force field which was employed in our earlier work on coordination complexes.[4]

Initial geometries. All thirteen individual conformers were built by the CFF programme from standard values of bond lengths, valence angles and

Table 4. Comparison of calculated and measured alkane structures.

Property	No. of exp. data	Max. dev.	Mean dev.	Ref.
C–H	9	0.036 Å	0.022 Å	27–34
C–C	7	−0.016 Å	−0.013 Å	28–34
C–C–H	6	1.5°	0.7°	28, 30–33
C–C–C	4	2.0°	1.6°	29–30, 32–34
H–C–H	3	−2.0°	−1.0°	29, 31, 34
C–C–C–C	2	−3.5°	−1.3°	32, 34

torsional angles. For all but one, the initial energies and energy gradients indicated that energy minimization would be easy. For n-pentane −GG we found a few very large elements in the gradient vector. This was due to hydrogens of different methyl groups being placed closer to each other than the distance corresponding to the maximum of the Buckingham exp-6 function used for non-bonded interactions. This difficulty was overcome by twisting the methyl groups so that no H---H distance would be shorter than that corresponding to the function maximum, which is 0.85 Å.

Energy minimization. Up to 20 steepest descent and 10 modified Newton iterations were sufficient to get to minimum for all cases but two. For pentane −GG up to 40 Newton iterations had to be used. For neopentane the resultant conformer had a rather high energy gradient. The molecule was therefore "shaken" by adding cartesian coordinate increments generated with a random number routine, whereupon minimization proceeded satisfactorily. All final energy gradient norms were below 10^{-6} kJ mol^{-1} Å^{-1}.

Comparison of geometry. In view of the shortcomings of the present force field in reproducing structures of Co complexes,[3,4] it was to be expected that the calculated alkane conformations would deviate from the measured, particularly with respect to C–H and C–C bond lengths. Table 4 bears this out, in a comparison with published r_g structures found by electron diffraction (the r_a or r_α structure for angles). Another and very fast test of a structure is a comparison of calculated and measured moments of inertia or rotational constants. These are measured with microwave spectroscopy (the r_s structure), or infrared or Raman spectroscopy (the r_0 or r_e structure). A comparison of these properties is shown in Table 5.

The comparisons show that the calculated C–H bond lengths are consistently too short; this tends to give too small moments of inertia and too large rotational constants. C–C bond lengths are calculated too long; this gives moments of inertia and rotational constants with the opposite trend. These trends are well illustrated by the rotational constants in Table 5. Comparison, where possible, is made with spectroscopically determined A_0, B_0 and C_0.

Vibrational spectra. A reasonable reproduction of vibrational frequencies must be secured if statistical summation over internal vibrations is to have any meaning. Here we shall not go into details of vibrational analysis, but simply state that all frequencies are calculated 0–100 cm^{-1} too high, the extremes being exceptions. This is a welcome though slightly unexpected result from a force field

Table 5. Calculated and measured rotational constants of alkanes.

Molecule	Property	Calc.	Meas.	Diff.	Unit	Rel. diff. %	Ref.
Methane	B_0	5.2497	5.2406(11)	−0.0091	cm^{-1}	−0.174	35
Ethane	A_0	2.631	2.671(5)	0.040	cm^{-1}	1.50	36
	B_0	0.66370	0.66313(2)	−0.00057	cm^{-1}	−0.086	37
Propane	A_s	28475.77	29207.36(5)	732.41	MHz	2.51	38
(microwave)	B_s	8488.81	8446.07(5)	−42.74	MHz	−0.51	
	C_s	6768.23	7458.98(5)	−690.75	MHz	−8.12	
Isobutane	B_0	7713.78	7789.45(1)	−75.67	MHz	−0.97	39
Cyclohexane	B_0	0.142528	0.143429(2)	0.000901	cm^{-1}	0.63	40

Table 6. Calculated and correlated[41] thermodynamic functions of alkanes. All units are J mol^{-1} K^{-1}.

Substance	Temp. K	$(H_T^\circ - H_0^\circ)/T$ Calc.	Correl.	S_T° Calc.	Correl.	$C_{p,T}^\circ$ Calc.	Correl.
Methane	200	33.28	33.22	172.5	172.6	33.47	33.51
	400	34.72	34.73	197.3	197.4	40.56	40.63
Ethane	200	35.70	36.28	209.5	201.5	40.56	42.26
	400	43.26	44.81	243.9	246.5	63.33	66.23
Propane	200	40.64	42.72	242.6	245.1	52.73	52.89
	400	55.29	58.07	289.6	294.3	89.48	93.97
Isobutane	200	46.11	49.04	258.5	261.5	67.11	70.50
	400	68.71	73.18	319.7	326.9	117.36	123.93
Neopentane	200	51.44	56.19	261.8	258.4	82.40	80.54
	400	82.80	95.06	338.3	347.5	146.75	159.98
Butane	200	51.41	56.11	270.3	276.1	66.64	76.82
	400	71.86	77.36	331.4	342.5	115.79	123.22
Pentane	200	64.35	68.87	292.9	307.5	80.34	93.55
	400	88.74	95.14	372.1	389.2	142.15	152.55
Cyclohexane	400	73.3	76.9[42]	329.1	335.5[42]	142.3	149.9[42]

selected for a different purpose. There will be a tendency to overestimate the zero-point energy and underestimate vibrational contributions to thermodynamic function. These errors are more serious than those introduced by erroneous rotational constants.

Thermodynamic functions. We have chosen to compare our calculated values with a fairly recent compilation of correlated data for alkanes.[41] In Table 6 we present excerpts from our comparisons.

For n-butane and n-pentane, the calculated values of Table 6 are average values. Data for individual conformers are weighted according to their equilibrium distributions calculated from computed G values corrected with statistical weights. S values are corrected with the entropy of mixing.

The calculated equilibrium distributions can be compared with data derived from electron diffraction. For n-butane we calculate a ratio A:G = 0.63:0.37 at 300 K; Bradford *et al.*[32] found A:G = 0.54:0.46 with an uncertainty of 0.09; the nozzle temperature was about 30 °C. The derived ΔG(G − A) is (2.08 ± 0.92) kJ mol^{-1}; our calculated value at 300 K is 1.35 kJ mol^{-1}.

Also enthalpy differences may be compared. From Raman intensity data on n-butane in the range 399 − 500 K, Verma *et al.*[43] derived ΔH(G − A) = (4.08 ± 0.18) kJ mol^{-1}; the calculated value at 400 K is 2.80 kJ mol^{-1}. Similarly, for n-pentane Harada *et al.*[44] found ΔH(AG − AA) ≃ 2.5 kJ mol^{-1} for the range 160 − 300 K; the calculated value at 200 K is 2.9 kJ mol^{-1}. (Only less than 5 % GG and virtually no −GG conformers are present.)

Conclusion. We feel justified in claiming that the force field employed here, though not ideal, is sufficiently accurate to account for the main features of the structures and energetics of smaller alkanes, and that the approximations in the statistical-mechanical procedure are valid. We thus have reason to presume that an application to coordination complexes is meaningful.

REFERENCES

1. Lifson, S. and Warshall, A. *J. Chem. Phys. 49* (1968) 5116.
2. Niketic, S. R. and Rasmussen, K. *The Consistent Force Field: A Documentation, Lecture Notes in Chemistry*, Vol. 3, Springer, Berlin-Heidelberg-New York 1977.
3. Niketic, S. R., Rasmussen, K., Woldbye, F. and Lifson, S. *Acta Chem. Scand. A 30* (1976) 485.
4. Niketic, S. R. and Rasmussen, K. *Acta Chem. Scand. A 32* (1978) 391.
5. Hald, N. C. P. and Rasmussen, K. *Acta Chem. Scand. A 32* (1978) 753.
6. Kildeby, K., Melberg, S. and Rasmussen, K. *Acta Chem. Scand. A 31* (1977) 1.
7. Melberg, S. and Rasmussen, K. *Acta Chem. Scand. A 32* (1978) 187.
8. Melberg, S. and Rasmussen, K. *Carbohydr. Res. In press.*
9. Melberg, S. and Rasmussen, K. *Carbohydr. Res. In press.*

10. Sundius, T. and Rasmussen, K. *Commentat. Phys.-Math. Soc. Sci. Fenn. 47* (1977) 91.
11. Bjerrum, J. *Metal Ammine Formation in Aqueous Solution*, Haase & Søn, Copenhagen 1941, reprinted 1957.
12. Bang, O. *M.Sc. Thesis*, Chem. Dep. A, Tech. Univ. Den., Lyngby 1971.
13. Bang, O. *Ph.D. Thesis*, Chem. Dep. A Tech. Univ. Den., Lyngby 1976.
14. Bagger, S., Bang, O. and Woldbye, F. *Acta Chem. Scand. A 30* (1976) 98.
15. Godnew, I. N. *Berechnung thermodynamischer Funktionen aus Molekülдaten*, VEB Deutscher Verlag der Wissenschaften, Berlin 1963.
16. Janz, G. G. *Thermodynamic Properties of Organic Compounds*, Academic, New York 1967.
17. DeHayes, L. J. and Busch, D. H. *Inorg. Chem. 12* (1973) 1505.
18. Berg, R. W. and Rasmussen, K. *Spectrosc. Lett. 5* (1972) 349.
19. Corey, E. J. and Bailar, Jr., J. C. *J. Am. Chem. Soc. 81* (1959) 2620.
20. Gollogly, J. R., Hawkins, C. J. and Beattie, J. K. *Inorg. Chem. 10* (1971) 317.
21. DeHayes, L. J. *Thesis*, Ohio State University, Ohio 1972. *Univ. Microfilms 72-20,952*, p. 172.
22. Sudmeier, J. L., Blackmer, G. L., Bradley, C. H. and Anet, F. A. L. *J. Am. Chem. Soc. 94* (1972) 757.
23. Harnung, S. E., Kallesøe, S., Sargeson, A. M. and Schäffer, C. E. *Acta Chem. Scand. A 28* (1974) 385.
24. Kojima, M., Funaki, H., Yoshikawa, Y. and Yamasaki, K. *Bull. Chem. Soc. Jpn. 48* (1975) 2801.
25. Toftlund, H. and Laier, T. *Acta Chem. Scand. A 31* (1977) 651.
26. Kojima, M., Yoshikawa, Y. and Yamasaki, K. *Bull. Chem. Soc. Jpn. 46* (1973) 1687.
27. Bartell, L. S., Kuchitsu, K. and de Neui, R. J. *J. Chem. Phys. 35* (1961) 1211.
28. Bartell, L. S. and Higginbotham, H. K. *J. Chem. Phys. 42* (1965) 851.
29. Iijima, T. *Bull. Chem. Soc. Jpn. 45* (1972) 1291.
30. Hilderbrandt, R. L. and Wieser, J. D. *J. Mol. Struct. 15* (1973) 27.
31. Beagley, B., Brown, D. P. and Monaghan, J. J. *J. Mol. Struct. 4* (1969) 233.
32. Bradford, W. F., Fitzwater, S. and Bartell, L. S. *J. Mol. Spectrosc. 38* (1977) 185.
33. Bonham, R. A., Bartell, L. S. and Kohl, D. A. *J. Am. Chem. Soc. 81* (1959) 4765.
34. Bastiansen, O., Fernholt, L., Seip, H. H., Kambara, H. and Kuchitsu, K. *J. Mol. Struct. 18* (1973) 163.
35. Thomas, M. A. and Welsh, H. L. *Can. J. Phys. 38* (1960) 1291.
36. Lepard, D. W., Shaw, D. E. and Welsh, H. L. *Can. J. Phys. 44* (1966) 2353.
37. Cole, A. R. H., Lafferty, W. J. and Thiebault, R. J. *J. Mol. Spectrosc. 29* (1969) 365.
38. Lide, Jr., D. R. *J. Chem. Phys. 33* (1960) 1514.
39. Lide, Jr., D. R. and Mann, D. E. *J. Chem. Phys. 29* (1958) 914.
40. Peters, R. A., Walker, W. J. and Weber, A. *J. Raman Spectrosc. 1* (1973) 159.
41. Scott, D. W. *U.S. Dept. of the Interior, Bureau of Mines Bull. 666* (1974).
42. Landolt-Børnstein 6. Aufl. 2. Band 4. Teil p. 461. Springer, Berlin 1961.
43. Verma, A. L., Murphy, W. F. and Bernstein, H. J. *J. Chem. Phys. 60* (1974) 1540.
44. Harada, J., Takeuchi, H., Sakakibara, M., Matsuura, H. and Shimanouchi, T. *Bull. Chem. Soc. Jpn. 50* (1977) 102.

Received May 22, 1978.

Acta Chemica Scandinavica A 32 (1978) 887 – 894

Short Communications

The Ion Pair – Triple Ion Borderland of Sodium Iodide in 1-Butanol at 25 °C

PER BERONIUS

Department of Physical Chemistry, University of Umeå, S-901 87 Umeå, Sweden

The present study of the aggregation of sodium iodide in 1-butanol by means of the conductimetric method constitutes part of a programme the intention of which is to identify aggregates formed by electrolytes in organic solvent media and to establish their structures.

Experimental. The solvent (Merck, *p.a.*) and the salt (Merck, *suprapur*) were pretreated according to Ref. 1. A Daggett-Bair-Kraus type conductivity cell[2] of 1300 ml capacity was used. By means of a calibrated precision buret (Metrohm Herisau, Dosimat E 535) kept in an air thermostat at 25 °C portions of a stock sodium iodide solution were added to the cell initially containing a known quantity of the pure solvent. After each addition the cell resistance at 25.00±0.02 °C was measured as previously outlined.[1]

Results and conclusions. In Table 1 the experimentally established molar conductivity, Λ(exp), is given at different analytical concentrations, c, of the salt.

The FHFP conductance equation[3-5] for associated symmetrical electrolytes,

$$\Lambda = \Lambda_\infty - Sc_i^{1/2} + Ec_i\,{}^{10}\log c_i + J_1 c_i - J_2 c_i^{3/2} - K_A c_i \gamma^2 \Lambda \qquad (1)$$

was fitted[6] by means of a Cyber 172 computer to the four lowest concentration points (Table 1) using $\eta = 0.0246$ P for the viscosity[7] and $\varepsilon = 17.51$ for the relative permittivity[8] of the solvent, and $R = 16$ Å (Bjerrum radius) for the maximum distance[9-11] between centers of charge in the ion pair.

In eqn. (1) Λ is the molar conductivity at the concentration c_i of free ions, Λ_∞ is that at infinite dilution, S and E are defined in Ref. 12, and J_1 and J_2 in Ref. 5, K_A is the ion pair association constant, and γ is the mean molar activity coefficient of free ions which was calculated from the Debye-Hückel equation,[13]

$$^{10}\log \gamma \simeq {}^{10}\log f = -Ac_i^{1/2}/[1 + BRc_i^{1/2}] \qquad (2)$$

where f is the mean rational activity coefficient.

The curve fitting outlined above was repeated upon increasing the concentration range to the five, six, *etc.* lowest concentration points. By this means

Table 1. Data for NaI in 1-butanol at 25 °C.

$c \times 10^4$ M	Λ (exp) $cm^2\,\Omega^{-1}\,mol^{-1}$	ΔΛ $cm^2\,\Omega^{-1}\,mol^{-1}$
3.1860	13.841	0.000
3.2155	13.824	−0.002
5.2622	12.983	0.007
5.3108	12.962	0.003
7.3011	12.340	0.002
7.3688	12.317	−0.002
9.3042	11.831	−0.002
9.3904	11.808	−0.005
11.272	11.415	−0.002
11.377	11.390	−0.006
13.205	11.064	−0.001
13.328	11.039	−0.005
15.105	10.762	0.002
15.246	10.738	−0.001
16.973	10.498	0.006
17.132	10.475	0.005
18.809	10.266	0.013
18.985	10.242	0.010
20.614	10.058	0.019
20.807	10.034	0.017
22.389	9.8710	0.027
22.599	9.8471	0.025
24.135	9.7015	0.035
24.362	9.6778	0.033
25.852	9.5468	0.043
26.095	9.5231	0.042
27.541	9.4046	0.052
27.800	9.3812	0.051
30.838	9.1523	0.070
31.129	9.1293	0.070
34.031	8.9349	0.090
34.354	8.9115	0.089

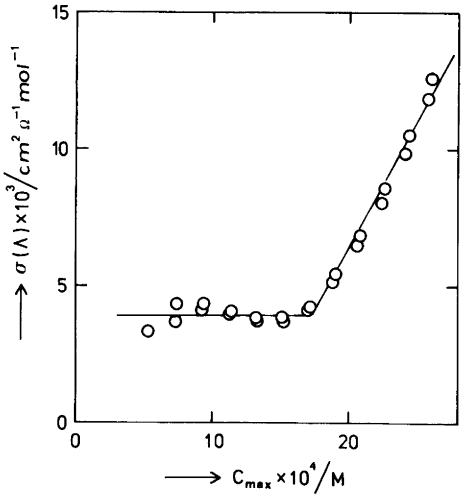

Fig. 1. Dependence of $\sigma(\Lambda)$ on maximum electrolyte concentration for application of the FHFP equation, eqn. (1), to conductivity data of NaI in 1-butanol at 25 °C.

$\sigma(\Lambda)$, *i.e.* the standard deviation between experimental and calculated Λ values, was obtained as a function of the upper limit of the concentration interval studied, see Fig. 1 according to which the fit of eqn. (1) to the experimental points deteriorates markedly at salt concentrations above $c = 17 \times 10^{-4}$ M. This effect may be taken as evidence of the formation of higher aggregates than ion pairs at concentrations above this value.

According to theory[12] the maximum concentration of negligible triple ion formation for 1:1-electrolytes in a solvent of relative permittivity, ε, at 25 °C is,

$$c_{max} = 3.2 \times 10^{-7} \varepsilon^3 \qquad (3)$$

which for the system under investigation yields, $c_{max} = 17.2 \times 10^{-4}$ M. The prediction according to eqn. (3) and the experimentally established concentration limit, *cf.* Fig. 1, are thus in complete agreement.

Application of eqn. (1) to the points within the free ion – ion pair range ($c \leq 17.132 \times 10^{-4}$ M; *cf.* Table 1) yielded: $\Lambda_\infty = 16.739 \pm 0.007$ cm^2 Ω^{-1} mol^{-1}; $S = 82.82$; $E = 648.2$; $J_1 = 3413$; $J_2 = 20\,670$; and $K_A = 602 \pm 1$ (M^{-1}) where the errors quoted are standard deviations. Using these values of the constants eqn. (1) was extrapolated to the higher concentrations investigated ($c \geq 18.809 \times 10^{-4}$ M) to obtain the difference,

$$\Delta\Lambda = \Lambda(\text{exp}) - \Lambda(\text{calc}) \qquad (4)$$

between experimental and calculated Λ values. The results in the last column of Table 1 reveal that for electrolyte concentrations above $c = 17 \times 10^{-4}$ M the difference $\Delta\Lambda$ is positive and increases with increasing concentration. An effect of this kind is to be expected in case of triple ion formation, *cf.* Refs. 13 and 14.

Acknowledgements. The author thanks Mrs. Margareta Ögren for technical assistance and the Swedish Natural Science Research Council for financial support.

1.-Beronius, P. *Acta Chem. Scand. A 32* (1978) 467.
2. Daggett, Jr., H. M., Bair, E. J. and Kraus, C. A. *J. Am. Chem. Soc. 73* (1951) 799.
3. Fuoss, R. M. and Hsia, K.-L. *Proc. Natl. Acad. Sci. U.S.A. 57* (1967) 1550.
4. Fuoss, R. M. and Hsia, K.-L. *Proc. Natl. Acad. Sci. U.S.A. 58* (1968) 1818.
5. Fernández-Prini, R. *Trans. Faraday Soc. 65* (1969) 3311.
6. Beronius, P. *Acta Chem. Scand. A 28* (1974) 77.
7. Janz, G. J. and Tomkins, R. P. T. *Nonaqueous Electrolytes Handbook*, Academic, New York 1972, Vol. I.
8. Riddik, J. A. and Bunger, W. B. *Techniques of Chemistry, Organic Solvents*, 3rd Ed., Wiley-Interscience, New York 1970, Vol. II.
9. Justice, J.-C. *Electrochim. Acta 16* (1971) 701.
10. Beronius, P. *Acta Chem. Scand. A 29* (1975) 289.
11. Beronius, P. *Acta Chem. Scand. A 30* (1976) 115.
12. Fuoss, R. M. and Accascina, F. *Electrolytic Conductance*, Interscience, New York 1959.
13. Robinson, R. A. and Stokes, R. H. *Electrolyte Solutions*, Butterworths, London 1965.
14. Beronius, P. and Lindbäck, T. *Acta Chem. Scand. A 32* (1978) 423.

Received August 31, 1978.

Analysis and Prediction of Angular Deformations in Phenyl Rings

R. NORRESTAM and L. SCHEPPER

Structural Chemistry Group, Chemistry Department B, The Technical University of Denmark, DK-2800 Lyngby, Denmark

The geometry of the benzene ring is known to deviate from the ideal 6/*mmm* symmetry, when one (or more) of its hydrogen atoms is substituted.[1,2] Recently Domenicano, Vaciago and Coulson[3,4] have investigated the angular deformations in mono- and *para*-disubstituted benzenes in more detail. With the notations Δ_1, Δ_2, Δ_3 and Δ_4 for the deviations of the endocyclic bond angles from 120° at the *ipso*, *orto*, *meta* and *para* positions from the substituent, Domenicano *et al.* found that Δ_1 was linearly dependent on the electronegativity of the substituent and that the value of Δ_2 was approximately $-\Delta_1/2$. Furthermore, they concluded that Δ_3 and Δ_4 were scarcely if at all affected (*e.g.* $\Delta_3=\Delta_4=0$) and also that angular deformations induced by one substituent are usually unaffected by a second substituent *para* or *meta* to it.[5] However, in the case of substituents, like $-NH_2$, expected to interact with the π-system of the ring, Domenicano and Vaciago[6] have noted that a more complex pattern of distortions is obtained.

In order to interpret the statistically very significant angular deformations observed in recent accurate studies on multisubstituted benzene rings (*e.g.* Ref. 8), we found the earlier approaches inadequate. Thus, we have developed and tested a more general approach for the description and analysis of angular distortions.

Method. Let us make the following assumptions:

1. Additivity: The angular distortions in a highly substituted ring can be described as a superimposition of the effects from each substituent.

2. Symmetry: The distortion effect from each substituent has two-fold symmetry (two-fold axis through the *ipso* and *para* carbon atoms).

3. The distortions can be treated as independent of possible bond length effects caused by the substituents.

Provided that the ring can be considered planar, these assumptions imply that we need to specify three deformation parameters (*e.g.* Δ_1, Δ_2 and Δ_3) per substituent type since the fourth is given by the condition $\Delta_1+2\Delta_2+2\Delta_3+\Delta_4=0$. Thus, the distortion of an angle can be expressed as a linear combination of the effect from all the substituents.

With observations from several different related molecules a set of linear relations can be derived and solved by conventional least-squares techniques, using individual weights derived from the estimated variances of the angles.

The values of the different Δ's range from a few tenths of a degree up to a few degrees.[7] Thus, it would be advantageous to have observations of angular deformations with accuracies of about 0.2° or better, to test the validity of the present method.

Results. Preliminary deformation parameters for methyl and hydroxyl groups were determined from crystallographic data on five different structures, *viz.* 3,5-dihydroxytoluene,[8] 2,5-dihydroxytoluene,[8] durene,[9] resorcinol[10] and catechol.[11] The experimental data are listed in Table 1. From the altogether 27 observations, the following 6 independent parameters were obtained as the weighted least-squares solution (°):

	Δ_1	Δ_2	Δ_3	(Δ_4)
CH_3-	−1.9(1)	1.0(1)	0.3(1)	−0.7(1)
HO−	0.5(1)	−0.5(1)	0.5(1)	−0.5(1)

Obviously, the distortion effects from methyl are such that $\Delta_2 \approx -\Delta_1/2$, in accordance with the earlier suggestions by Domenicano *et al.*[3] However, the distortion −0.7(1) at the *para* position deviates significantly from 0°. The effects from a hydroxy-group are completely different by yielding a constant but alternating deformation of 0.5° over the whole benzene ring. This difference is probably due to the fact that the hydroxy-group, but not the methyl, is a strong π donor (see, *e.g.*, Refs. 13 and 14).

To test whether the weighted differences between

Table 1. Observed deviations (°) from 120° by the endocyclic bond angles for the five methyl- and hydroxy-substituted benzenes used in the present study.

Compound	Ref.	C-1	C-2	C-3	C-4	C-5	C-6
1-Methyl-2,5-dihydroxybenzene	8	−1.96(15)	1.25(15)	0.01(17)	−0.99(16)	0.69(15)	0.98(16)
1-Methyl-3,5-dihydroxybenzene	8	−0.41(12)	−0.22(11)	1.03(11)	−1.39(11)	1.17(10)	−0.17(12)
1,2,4,5-Tetramethylbenzene	9	−1.44(11)	−1.41(11)	2.86(14)			
1,3-Dihydroxybenzene	10	1.28(20)	−1.08(28)	0.93(20)	−0.98(22)	0.90(29)	−1.06(26)
1,2-Dihydroxybenzene	11	0.14(17)	−0.19(20)	0.07(20)	0.11(17)	−0.25(15)	0.11(15)

the bond angle observations and the least-squares estimates have a normal distribution, a half-normal probability plot[15] was performed. The linearity (correlation coefficient 0.988) of this plot indicates that a normal distribution of differences is not unreasonable. The slope suggests that the e.s.d.'s of either the observed or calculated values are slightly underestimated by a factor of 1.1. A plot of observed *versus* calculated bond angle distortion yields a correlation coefficient of 0.978. The root mean square (r.m.s.) deviation between observed and calculated values was 0.21°.

As another check on the validity of this method of treating angular distortions, a different combination of substituents, *viz.* chloro- and phenyl-substituents have been analyzed. The experimental data used consist of the preliminary but fairly accurate crystal structure determinations[12] of three chloro-substituted biphenyls (2,5,2′,6′-tetra-, 2,5,2′,5′-tetra- and 2,3,4-trichlorobiphenyl). The 6 distortion parameters for chloro- and phenyl-substituents given below were thus determined from 30 observations with e.s.d.'s of 0.2° (°):

	Δ_1	Δ_2	Δ_3	(Δ_4)
Chloro-	1.0(1)	−1.1(1)	0.7(1)	−0.4(1)
Phenyl-	−2.0(1)	0.8(1)	0.5(1)	−0.6(1)

In this case the correlation coefficient for the halfnormal probability plot (slope 1.2) is 0.993 and that for the plot of observed *versus* calculated angle distortions is 0.982. The r.m.s. deviation is 0.29°. According to our results the phenyl distortions were found to be independent of the biphenyl conformation. The distortion effects from the π-donating chloro-substituent show a similar alternating pattern as was obtained for the π-donating hydroxy-substituent. The similarity between the values obtained for the phenyl- and the methyl-groups is very close.

In the analysis of chloro-substituted biphenyls, two sets of data, *viz.* those of 2,4,5,2′,4′,5′-hexachlorobiphenyl[16] and of biphenyl[17] itself were left out of the least-squares determination of the Δ's. Both these structural investigations have yielded e.s.d.'s in the bond angles of about 0.2°. These observations can thus be utilized to illustrate the possibility of reliable predictions of endocyclic bond angles. The bond angles (°) for biphenyl are averaged.

	C-1	C-2	C-3	C-4	C-5	C-6
Hexachlorobiphenyl						
Obs.	117.6	121.8	119.7	119.7	120.0	121.2
Calc.	117.3	122.1	119.2	120.1	120.1	121.2
Biphenyl						
Obs.	117.9	120.9	120.7	118.9		
Calc.	118.0	120.8	120.5	119.4		

In conclusion, the outcome of our analysis indicated that the endocyclic angular distortions of also very highly substituted benzene derivatives can be predicted with an accuracy of about 0.2° by determining three deformation parameters per substituent type. This accuracy is of the same order as that obtained in accurate crystal structural investigations by diffraction methods.

The investigations described here are presently being extended to several other types of substituted phenyl rings. Studies of these effects by molecular orbital calculations are in progress.

1. Bent, H. A. *Chem. Rev. 61* (1961) 275.
2. Carter, O. L., McPhail, A. T. and Sim, G. A. *J. Chem. Soc. A* (1966) 822.
3. Domenicano, A., Vaciago, A. and Coulson, C. A. *Acta Crystallogr. B 31* (1975) 221.
4. Domenicano, A., Vaciago, A. and Coulson, C. A. *Acta Crystallogr. B 31* (1975) 1630.
5. Domenicano, A., Foresti Serantoni, E. and Riva di Sanseverino, L. *Acta Crystallogr. B 33* (1977) 1664.
6. Domenicano, A. and Vaciago, A. *Third European Cryst. Meeting, Zürich* (1976) 274.
7. Bak, B., Christensen, D., Dixon, W. B., Hansen-Nygaard, L. and Rastrup-Andersen, J. *J. Chem. Phys. 37* (1962) 2027.
8. Norrestam, R. and Schepper, L. *Acta Crystallogr. A 34* (1978) S111.
9. Baudour, J. L. and Sanquer, M. *Acta Crystallogr. B 30* (1974) 2371.
10. Bacon, G. E. and Jude, R. J. *Z. Kristallogr. 138* (1973) 19.
11. Wunderlich, H. and Mootz, D. *Acta Crystallogr. B 27* (1971) 1684.
12. Palm, T.-B. *To be published.*
13. Dickens, P. G., Linnett, J. W. and Phil, D. *Q. Rev. Chem. Soc. 11* (1957) 291.
14. Hehre, W. J., Radom, L. and Pople, J. A. *J. Am. Chem. Soc. 94* (1972) 1496.
15. *International Tables for X-Ray Crystallography*, Kynoch Press, Birmingham 1974, Vol. 4, p. 293.
16. Palm, T.-B. and Norrestam, R. *To be published.*
17. Charbonneau, G.-P. and Delugeard, Y. *Acta Crystallogr. B 32* (1976) 1420.

Received August 24, 1978.

A Neutron Powder Diffraction Study of W_2C

ANDERS HÅRSTA, STIG RUNDQVIST and JOHN O. THOMAS

Institute of Chemistry, University of Uppsala, Box 531, S-751 21 Uppsala, Sweden

In connection with studies of $\varkappa$-type transition metal carbides,[1] it became desirable to obtain accurate crystallographic data for W_2C to be used in subsequent structure refinements of $\varkappa$-carbides from multiphase X-ray and neutron diffraction data.[2] The crystal structure of W_2C can be described as a slightly distorted hexagonal close-packing of tungsten atoms, with carbon atoms occupying half of the octahedral interstices. The carbon atoms may be distributed in an ordered manner, the type and degree of ordering depending on temperature.[3,4]

We decided to investigate the W_2C structure by neutron diffraction in samples prepared under the same thermal conditions as those employed for the $\varkappa$-carbide syntheses. The results of a crystal structure refinement, together with some phase-analytical information, are reported in the present communication.

W_2C was synthesized from tungsten powder (H. C. Starck, Berlin, claimed purity 99.95 %) and tungsten monocarbide powder (H. C. Starck, Berlin, claimed purity 99.9 %). Appropriate mixtures of the powders were pressed into pellets, placed in zirconia crucibles and heated in a graphite tube resistance furnace at 1650 °C for 30 – 50 h. The products were examined by X-ray powder diffraction, and the composition was adjusted until a sample was finally obtained for which only very faint traces of WC were discernible on heavily overexposed powder films. The sample was ground to a fine powder in a tungsten carbide ball mill.

Chemical analysis was made as follows. Tungsten was determined by firing samples at 720 °C in air and weighing as WO_3. Carbon was determined as CO_2 in a LECO IR-12 instrument, and oxygen as CO in a Ströhlein Monomat 300 apparatus using standard techniques.

Neutron diffraction data were collected using the same equipment and experimental conditions as described in Ref. 1. The intensities were corrected for absorption using an experimental μR of 0.35. Refinement of the structure was carried out using a local modification NREF[5] of the full-matrix least squares powder profile analysis program of Rietveld.[6]

The neutron diffraction data indicated ordering of the carbon atoms corresponding to an ε-Fe_2N type structure. This is in agreement with results reported by Yvon, Nowotny and Benesovsky[7] for W_2C samples subjected to different heat-treatments between 2400 °C and 2100 °C. They observed that the carbon atoms were only partially ordered in samples quenched from higher temperatures.

The ideal ε-Fe_2N type structure of W_2C can be described in the space group $P\bar{3}1m$ (No. 162), with W in 6*k*: $x \sim 0.33$, $z \sim 0.25$; C(1) in 2*d* and C(2) in 1*a*. Preliminary calculations based on this structure model gave a poor agreement between observed and calculated intensities, indicating disorder and/or vacancies in the carbon atom sublattice. Refinement of the occupancy parameters for the two carbon positions indicated carbon deficiency and led to a substantially improved agreement. Introducing disorder by allowing carbon occupation of the remaining octahedral interstices at 2*c* and 1*b* (and a corresponding number of vacancies at 2*d* and 1*a* to retain the ideal 2/1 tungsten/carbon atomic ratio) also improved the agreement considerably. A model incorporating both types of defect structure simultaneously was therefore used in the final refinement, where the occupation parameters for all four types of octahedral carbon positions were allowed to vary. From the values returned by the program after convergence, the composition of the W_2C phase was calculated to be $W_2C_{0.85}$. To substantiate this result the sample was chemically analyzed. The result obtained: tungsten 96.77 %, carbon 2.83 %, corresponds to a W/C atomic ratio of 2/0.90. Unfortunately, the finely ground powder had been stored unprotected in air for more than a year before the chemical analysis was made. We suspected that some oxidation might have occurred. Analysis revealed an oxygen content of 0.5 %. Since the chemical state of the oxygen present could not easily be determined, the true composition of the W_2C phase remained somewhat uncertain.

A second W_2C sample (containing traces of WC) was synthesized under the same conditions as previously, now taking the necessary precautions to protect the sample as far as possible from air before analysis. Chemical analysis of the new sample gave (including estimated maximum errors): tungsten 97.14 ± 0.04 %, carbon 2.82 ± 0.03 %, oxygen 0.12 ± 0.02 %. Disregarding the impurities, this corresponds to a composition of $W_2C_{0.89 \pm 0.01}$ for the W_2C phase. Even if all oxygen present was dissolved interstitially in W_2C, the tungsten/non-metal atomic ratio would still be much larger than 2/1.

Neutron diffraction data were also recorded for the second sample, with much improved counting statistics following an improvement in the experimental facilities. Structure refinement was carried

Table 1. Structure data for W_2C. Space group $P\bar{3}1m$ (No. 162); $a=5.1852(4)$ Å, $c=4.7232(5)$ Å (24 °C).

Atom	Position	x	y	z	B(Å^2)	Occupancy (%)
W	6*k*	0.335(1)	0	0.2521(5)	0.11(8)	100
C(1)	2*d*	$\frac{1}{3}$	$\frac{2}{3}$	$\frac{1}{2}$	0.19(8)	65(1)
C(2)	1*a*	0	0	0		100
C(3)	2*c*	$\frac{1}{3}$	$\frac{2}{3}$	0		12(1)

out in the same manner as before, and the results agreed within experimental error with those obtained for the first sample. The following parameters were refined (*a*) *profile parameters:* half-width parameters (3), 2θ-zeropoint (1), wavelength (1); (*b*) *structural parameters:* scale factor (1), positional parameters (2), isotropic temperature factors (2), 2*c* and 2*d* occupancies (2). The occupancy for 1*a* tended to increase beyond 100 % and that for 1*b* tended to become negative. In the final refinement cycles these parameters were fixed at 100 and 0 %, respectively. Two isotropic temperature factors were refined, one for tungsten and one for carbon atoms. The scattering lengths used were: $b_W = 0.48 \times 10^{-14}$ m and $b_C = 0.665 \times 10^{-14}$ m.[8] The final R-values (for definitions, see Ref. 1) were: $R_I = 0.058$, $R_P = 0.144$, $R_{wP} = 0.122$. Unit cell dimensions were determined from X-ray powder films recorded in a Philips XDC-700 camera with Cu$K\alpha_1$ radiation and silicon ($a = 5.431065$ Å)[9] as internal calibration standard. The cell dimensions were refined by the least-squares program CELNE.[10]

The structure data are presented in Table 1. Corresponding interatomic distances (Å) are: W – 12 W: 2.90, 2.92 (×2), 2.93, 2.94 (×2), 2.99 (×4), 3.01 (×2); W – 2 C(1): 2.09; W – 2 C(3): 2.09; W – C(2): 2.11.

The phase analysis and the structure refinement consistently show that the W_2C phase is carbon-deficient under the conditions of synthesis employed in the present study. The presence of trace amounts of WC in the samples ensures that the composition of the W_2C phase must lie at the carbon-rich limit of the homogeneity range. It should be stressed, however, that the formula $W_2C_{0.89}$ does not necessarily represent the limiting composition at 1650 °C, since the cooling-rate for samples in the furnace was only moderately large (room temperature attained in about 10 min), while the carbon diffusion rate might initially be quite high during the cooling process.

A third W_2C sample was prepared under the same thermal conditions as before for the purpose of estimating the width of the homogeneity range. X-Ray phase analysis now indicated faint traces of α-W. Chemical analysis gave a composition of $W_2C_{0.86\pm0.01}$. The unit cell dimensions [$a = 5.1833(5)$ Å, $c = 4.7240(6)$ Å] were barely significantly different from those found for the carbon-rich preparations.

Acknowledgements. The work has been supported financially by the Swedish Natural Science Research Council. We are most grateful to Dr. Lilly Gustafsson, Department of Analytical Chemistry, University of Uppsala, for carrying out the tungsten analyses, and to Uddeholm AB, High Speed Steel Division, Söderfors, Sweden through the kind auspices of Dr. Tor Johansson, for the carbon and oxygen analyses.

1. Hårsta, A., Johansson, T., Rundqvist, S. and Thomas, J. O. *Acta Chem. Scand. A 31* (1977) 260.
2. Werner, P.-E., Salomé, S., Malmros, G. and Thomas, J. O. *J. Appl. Crystallogr. In press.*
3. Storms, E. K. *The Refractory Carbides*, Academic, New York and London 1967.
4. Toth, L. E. *Transition Metal Carbides and Nitrides*, Academic, New York and London 1971.
5. Thomas, J. O. Institute of Chemistry, University of Uppsala, Sweden, Publ. No. UUIC-B13-9.
6. Rietveld, H. M. *J. Appl. Crystallogr. 2* (1969) 65.
7. Yvon, K., Nowotny, H. and Benesovsky, F. *Monatsh. Chem. 99* (1968) 726.
8. Bacon, G. E. *Acta Crystallogr. A 28* (1972) 357.
9. Deslattes, R. D. and Henins, A. *Phys. Rev. Lett. 31* (1973) 972.
10. Ersson, N. O. Institute of Chemistry, Uppsala. *Unpublished.*

Received October 16, 1978.

The Conformation and Structure of Nitrosocyclopropane

ANNE SKANCKE * and JAMES E. BOGGS

Department of Chemistry, The University of Texas, Austin, Texas 78712, U.S.A.

For many decades there has been lively interest both among experimentalists and theoreticians in the electronic interaction of cyclopropyl rings with substituents. One observable consequence of such interaction that has aroused recent attention is the asymmetry induced in the ring by the presence of the substituent. In a survey of microwave spectroscopic data, Penn and Boggs [1] pointed out that substituents containing double bonds capable of entering into conjugative interaction with the ring all produce a shortening of the C–C bond opposite the point of attachement. This was expected for theoretical reasons,[2] which also predicted that the adjacent bonds would be lengthened. No direct experimental confirmation of this is available except for cyclopropyl cyanide, for which a complete experimental structure has recently been obtained.[3] The present work provides an additional test of the effect.

We have shown in a series of papers [4-7] that it is possible to obtain accurate structural parameters for cyclopropyl derivatives from *ab initio* calculations within the Hartree-Fock approximation. These papers also provide a discussion of sigma and pi electron transfer between the ring and a variety of substituents. Optimization of geometries is simplified by use of the gradient technique [8,9] using the computer programme TEXAS written by Péter Pulay.[10] In this method, the forces on all atoms are calculated analytically and all internal coordinates are optimized simultaneously, resulting in a great saving of computer time and a significant increase in accuracy.

We now report similar results for nitrosocyclopropane. The computations used a 4-21G basis set with other conditions as in our previous work.[4-7] The results show that nitrosocyclopropane exists in two stable forms, *s-cis* and *s-trans*, with equilibrium geometries as shown in Fig. 1. The C–C bond length in cyclopropane computed with the same basis set is 1.509 Å. It can be seen from the figure that interaction with the nitroso group produces a lengthening of the adjacent bond and a shortening of the opposite bond, in agreement with

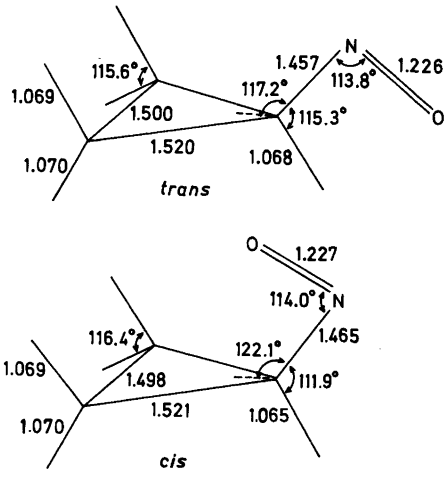

Fig. 1. Computed geometries for *s-cis* and *s-trans* nitrosocyclopropane. Calculated distortions of the methylene groups are: *s-trans* form: rock 0.5° (toward N), wag 1.83° (toward N), twist 0.4° ("upper" hydrogens out). *s-cis* form: rock 1.3° (toward N), wag 2.08° (toward N), twist 0°.

theoretical expectation and with the results obtained in our previous work on vinylcyclopropane and cyclopropyl cyanide.[6] There is no dramatic difference between the structures of the two conformers. The C–N bond is slightly longer in the *s-cis* form, which might be taken as an indication of slightly less conjugation in this form. On the other hand, the almost identical values of the N=O and the ring C–C bond lengths in the two conformers show that such a difference in conjugation must be quite small.

A recent microwave study [11] has identified the *s-trans* conformer of nitrosocyclopropane. No bond lengths could be determined directly from this work, but use of the relationship of Penn and Boggs [1] gave an estimate of 1.490 Å for the C–C bond length opposite the substituent. This value was obtained after correcting the observed planar moment for vibrational effects arising from the torsional motion of the nitroso group. Such a correction was not made for the other molecules discussed by Penn and Boggs, so a more direct comparison would result from using the planar moment coming directly from the observed microwave data without correction. This procedure would yield an observed opposite C–C bond length of 1.496 Å which compares well with the corresponding bond lengths for similar molecules in the compilation by Penn and Boggs. The agree-

* Permanent address: Department of Chemistry, University of Tromsø, N-9000 Tromsø, Norway.

ment between the measured and computed values is well within the combined accuracy of the methods and the difference between the computed r_e value and the measured vibrationally averaged value.

With the exception of vinylcyclopropane, all cyclopropyl compounds with substituents capable of conjugative interaction have been found to exist in *s-cis* and *s-trans* forms. The present computation clearly establishes potential minima corresponding to both forms for nitrosocyclopropane. In agreement with experiments,[11] we find the *s-trans* form to be more stable. With the basis set used, the calculated energy difference between the two conformers, 0.4 kcal/mol, is less reliable than is the geometry. In view of the inability of the microwave workers to identify the spectrum of the *s-cis* form, it must be considered likely that the energy difference is somewhat larger than the calculated value.

As in the cases of vinylcyclopropane and cyclopropyl cyanide,[11] the ring deformations in nitrosocyclopropane are caused by electron donation from the ring to the substituent. The 5a orbital, which is the highest occupied orbital from which electron donation to the pi system of the substituent is possible, is bonding between the adjacent carbon atoms and antibonding between the opposite carbon atoms. Consequently, removal of electron density from this orbital produces the observed structural effects.

Acknowledgement. This research has been supported by a grant from The Robert A. Welch Foundation.

1. Penn, R. E. and Boggs, J. E. *J. Chem. Soc. Chem. Commun.* (1972) 666.
2. Hoffmann, R. *Tetrahedron Lett. 33* (1970) 2907.
3. Pearson, R., Jr., Choplin, A. and Laurie, V. W. *J. Chem. Phys. 62* (1975) 4859.
4. Skancke, A., Flood, E. and Boggs, J. E. *J. Mol. Struct. 40* (1977) 263.
5. Skancke, A. *J. Mol. Struct. 42* (1977) 235.
6. Skancke, A. and Boggs, J. E. *J. Mol. Struct. 50* (1978) 173.
7. Skancke, A. and Boggs, J. E. *J. Mol. Struct. In press.*
8. Pulay, P. *Mol. Phys. 17* (1969) 197.
9. Pulay, P. In Shaefer, H. F., III, Ed., *Modern Theoretical Chemistry*, Plenum, New York 1977, Vol. IV, p. 153.
10. Pulay, P. *To be published.*
11. Corkill, M. J., Cox, A. P. and Norris, J. A. *J. Chem. Soc. Chem. Commun.* (1978) 388.

Received October 6, 1978.

Acta Chemica Scandinavica A 32 (1978) 895–900

Molecular and Electronic Structure in Copper(II) Complexes with Schiff Bases of Formylcamphor and Diamines as Obtained from Absorption and Circular Dichroism Spectroscopy

HANS PETER JENSEN

Chemistry Department A, Building 207, The Technical University of Denmark, DK-2800 Lyngby, Denmark

Absorption and circular dichroism spectra of the internal ligand $\pi^* \leftarrow \pi$ transitions in compounds such as the copper(II) complex of the Schiff base from (*R*,*R*)-1,2-cyclohexanediamine and two molecules of formylcamphor derived from natural $(+)_D$-camphor have been studied. The results have been interpreted by means of exciton theory to give information about stereochemistry.

The Cotton effects in the ligand field range may be understood using simple LCAO–MO theory and the assumption that $d \leftarrow d$ transitions borrow electric transition dipole moments from the nearest allowed transitions: the ligand $\pi^* \leftarrow \pi$.

Absorption and circular dichroism spectra of the internal ligand $\pi^* \leftarrow \pi$ transitions in Schiff bases of acetylacetone and thioacetylacetone with diamines,[1,2] of formylcamphor with amines,[3,4] and of acetylcamphor with amines,[5] have been studied and interpreted by means of exciton theory to give information about stereochemistry. Also copper(II) complexes of the acetylacetone Schiff bases have been studied and the spectra interpreted similarly.[2,6,7] The stereochemical results have been checked by independent means.[2,8] Assignments of ligand field circular dichroism (CD) spectra have been performed using simple LCAO–MO theory and the assumption that the $d \leftarrow d$ transitions borrow electric transition dipole moments from the nearest allowed transitions, the ligand $\pi^* \leftarrow \pi$ transitions,[6] and the assignments have been checked through polarization spectroscopy.[9,10]

For the sake of further investigations of the model, copper(II) complexes of Schiff bases derived from formylcamphor and diamines have been prepared and their absorption and circular dichroism spectra measured.

EXPERIMENTAL

Schiff bases of formylcamphor and diamines were prepared as described earlier,[3,4] and neutral inner-sphere copper(II) complexes thereof according to the procedure of Pfeiffer *et al.*[11] The identity of the compounds have been established through chemical analyses. A Cary 11 spectrophotometer and Roussel-Jouan Dichrographs II & III were used for the measurements of optical spectra. All spectra were recorded in methanol.

Abbreviations. Amines. en = 1,2-ethanediamine, *R*-pn = (*R*)-$(-)_D$-1,2-propanediamine, *S*-pn = (*S*)-$(+)_D$-1,2-propanediamine, *R*-2,3-bn = (*R*,*R*)-$(-)_D$-2,3-butanediamine, *S*-2,3-bn = (*S*,*S*)-$(+)_D$-2,3-butanediamine, *R*,*S*-2,3-bn = *meso*-(*R*,*S*)-2,3-butanediamine, *R*-chxn = *trans*-(*R*,*R*)-$(-)_D$-1,2-cyclohexanediamine, *S*-chxn = *trans*-(*S*,*S*)-$(+)_D$-1,2-cyclohexanediamine, *R*,*S*-chxn = *meso*-(*R*,*S*)-1,2-cyclohexanediamine, ibn = 1,2-diamino-2-methylpropane, tn = 1,3-propanediamine.

Dioxo compounds. acacH = acetylacetone, fmcH = formylcamphor. en(fmcH)$_2$ *etc.* symbolize the Schiff base condensate from 1 mol of diamine and 2 mol of dioxo compound.

THEORETICAL RESULTS

Ligand range. It can be assumed that the β-diketone chromophoric parts in the complexes take on a *syn* (*Z*) conformation and that the two

chromophoric parts linked together through the substituted ethylene bridge are in a *gauche* arrangement. If π bonding to the metal is negligible we may then directly determine the absolute configuration from the envelope of the CD spectrum in the $\pi^* \leftarrow \pi$ transition range in terms of the handedness of a pair of vectors representing the allowed N←O transitions in the conjugated parts of the ligands. Furthermore the angle θ between the two transition moments can be estimated and checked independently through eqns. 3 and 6 of Ref. 1.

Ligand field range. As with Cu *R*-pn(acac)$_2$ orbitals and states will be characterized in terms of irreducible representations belonging to the point group D_2. Further it will be assumed that the relative energies of ligand and metal orbitals are $3\pi \leq 3d < 4\pi$, (xy) being the un-filled $3d$ orbital and (x^2-y^2) the highest filled.[6] With this ordering of the orbitals four electronic transitions in the ligand field range of the Cu(II) d^9-system may be expected namely: $(xy) \leftarrow (x^2-y^2)$, $(xy) \leftarrow (xz)$, $(xy) \leftarrow (yz)$, and $(xy) \leftarrow (z^2)$ of excited state symmetries A, B_2, B_3 and A, respectively. Since the excited state symmetries of the $\pi^* \leftarrow \pi$ transitions are A (out-of-phase) and B_2 (in-phase), three of the ligand-field transitions can gain transition intensity for CD bands through mixing with the π-excited states.

Also transitions from the former non-bonding oxygen σ^n-orbitals to π^*-orbitals ($\pi^* \leftarrow n$) can be expected, and as such transitions have excited state symmetries A and B_2 these may mix with the internal ligand transitions in producing two CD-bands.

In conclusion we expect, in the spectral range 12 000 – 32 000 cm^{-1} of optical active copper(II) complexes of Schiff bases derived from diamines and β-diketones, seven CD-bands, three of mainly $d \leftarrow d$ origin, two of mainly $\pi^* \leftarrow n$ origin and two of mainly $\pi^* \leftarrow \pi$ origin.

RESULTS AND DISCUSSION

It is often valuable in stereochemical work to use compounds of high rigidity, and, *e.g.*, *R*-chxn-(acacH)$_2$ was used when the spectral properties of Schiff bases of acetylacetone were discussed.[1] It would indeed have been desirable to use this particular ligand in a copper complex, however, we were,[6] as was also Schwarzenbach,[12] unable to prepare Cu *R*-chxn(acac)$_2$.

The situation is quite different with the Schiff bases of diamines and formylcamphor as Cu *R*-chxn(fmc)$_2$ and Cu *S*-chxn(fmc)$_2$ are easily prepared by standard procedures.[11] Spectra of these compounds are given in Fig. 1.

It is immediately obvious from Fig. 1 that the two compounds show an overall mirror image relationship. Small deviations can be attributed to the fact that the two ligands are not enantiomeric since the formylcamphor chromophore in both are derived from natural $(+)_D$-camphor.[13]

It is obvious that the predicted seven CD-bands are present: three in the region 12 000 – 18 000 cm^{-1}, two in the region 20 000 – 25 000 cm^{-1} and two in the region 26 000 – 32 000 cm^{-1}.

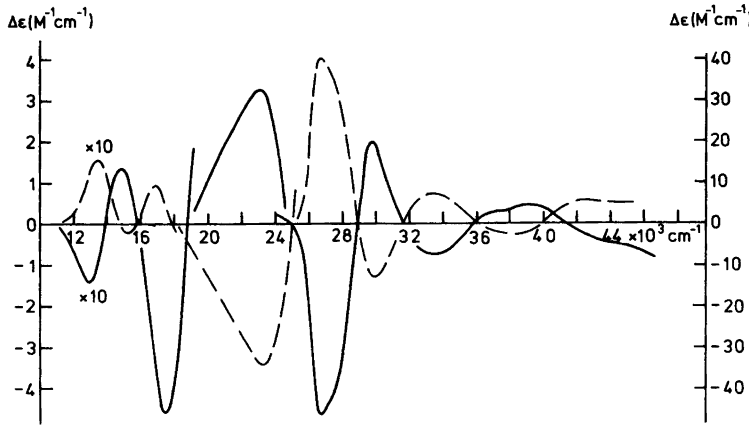

Fig. 1. CD spectra of Cu *R*-chxn(fmc)$_2$ (——) and Cu *S*-chxn(fmc)$_2$ (– – –).

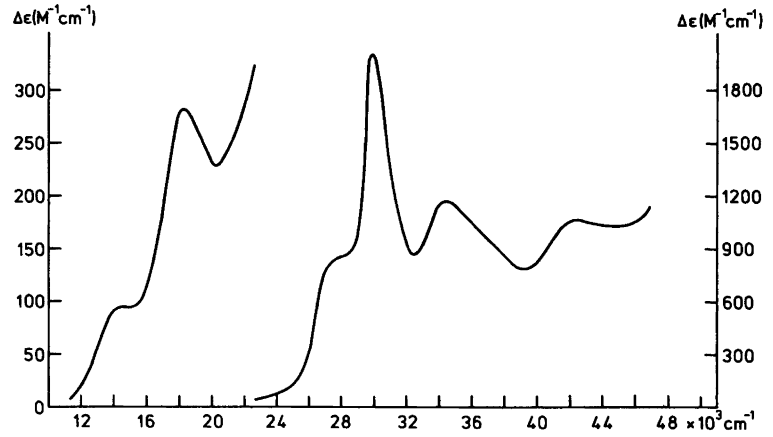

Fig. 2. Absorption spectrum of Cu en(fmc)$_2$ and all other discussed 1,2-diamine Schiff base derivatives of formylcamphor.

Let us first consider the bands in the $\pi^* \leftarrow \pi$ region. It is, with reference to spectra of the free ligands in *syn* conformation,[3,4] striking that the chirality of the pair of vectors, representing the allowed polarized internal ligand transitions, does not change on complexation as is the case with, *e.g.*, *R*-pn(acacH). This means that the absolute configuration of Cu *S*-chxn(fmc)$_2$ is the same as that of Cu *R*-pn(acac)$_2$ (Fig. 2 of Ref. 6).

The spectra in Fig. 1 and Fig. 2 furthermore give indirect information as to the cause of the non-existence of Cu *R*-chxn(acac)$_2$ and Cu *S*-chxn(acac)$_2$. Obviously the two chromophoric parts of the ligands are forced towards a more planar overall configuration during complexation, as may be seen from absorption spectra (Fig. 2 and Fig. 5 of Ref. 4) and through use of eqn. 3 of Ref. 1. This has, due to the cyclohexane ring, to happen through the smallest possible angle, and in the case of acetylacetone this leads to unfavourable interactions between methyl groups and the substituted ethylene bridge with the non-existence of Cu *R*-chxn(acac)$_2$ and Cu *S*-chxn(acec)$_2$ as a consequence. However, as formylcamphor does not have a methyl group at the keto group involved in Schiff base formation, Cu *R*-chxn(fmc)$_2$ and Cu *S*-chxn(fmc)$_2$ exist. The fact that Cu *R,S*-chxn(acac)$_2$ exists[12] may, in combination with the other observations mentioned above and through conformational calculations, give detailed information about nonbonding interactions in this type of complexes.

Focusing now on the three CD-bands in the ligand field range we may first of all stress the agreement between the actual number of bands and the number predicted by the model in use. Secondly, we can assign transitions, and for that purpose note that of the three transitions $(xy) \leftarrow (x^2-y^2)$, $(xy) \leftarrow (xz)$ and $(xy) \leftarrow (z^2)$ the latter is both electric as well as magnetic dipole forbidden, whereas the two former transitions are electric dipole forbidden but magnetic dipole allowed. This means in the present model that a Cotton effect connected to the transition $(xy) \leftarrow (z^2)$ must be small, since both electric and magnetic transition moments are "borrowed".

From earlier investigations of our model we know definitely that the high-energy Cotton effect under $\pi^* \leftarrow \pi$ and the Cotton effect under $(xy) \leftarrow (xz)$ are interrelated in such a way as to have opposite signs, since the phases in the construction of the molecular orbitals are chosen so that the overlap integrals between metal *d* orbitals and ligand π orbitals are positive in a planar or near planar complex.[6]

Thus in Fig. 1 the bands at $\sim$13 000 cm^{-1} are assigned as $(xy) \leftarrow (x^2-y^2)$, the bands at 15 000 cm^{-1} as $(xy) \leftarrow (z^2)$ and the bands at 18 000 cm^{-1} as $(xy) \leftarrow (xz)$.

Since five out of seven transitions have been assigned, the bands around 22 000 cm^{-1} are accordingly assumed to be the $\pi^* \leftarrow n$ transitions.

Carrying the discussion a little further we may consider the CD-spectra of neutral inner-sphere

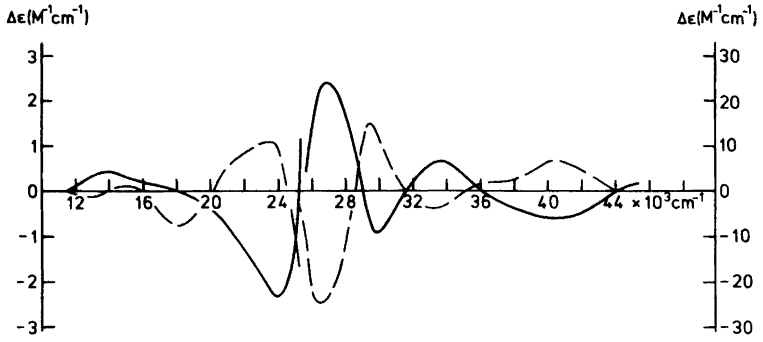

Fig. 3. CD spectra of Cu *R*-pn(fmc)$_2$ (———) and Cu *S*-pn(fmc)$_2$ (– – –).

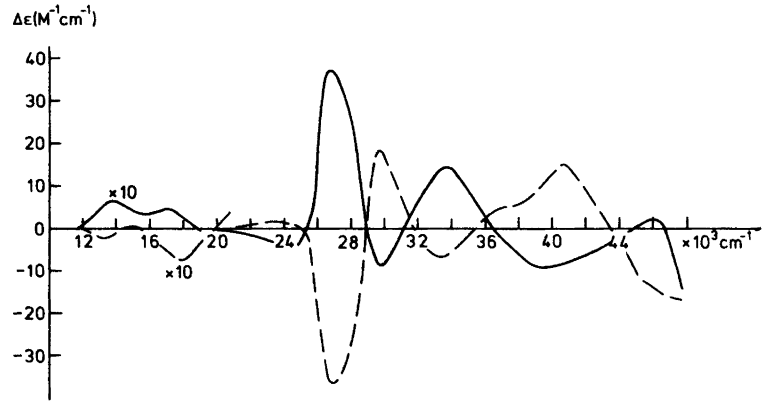

Fig. 4. CD spectra of Cu *R*-2,3-bn(fmc)$_2$ (———) and Cu *S*-2,3-bn(fmc)$_2$ (– – –).

copper(II) complexes of *R*- and *S*-pn(fmcH)$_2$ (Fig. 3) and of *R*- and *S*-2,3-bn(fmcH)$_2$ (Fig. 4), respectively.

Considering the $\pi^* \leftarrow \pi$ transition region of these complexes, it is worth noting that the ligands change chirality on complexation just as it is the case with the acetylacetone analogous,[3,4,6] and this is, of course, possible since the barrier towards rotation around the substituted ethylene bridge in these cases is relatively low. Suggestions as to the cause of this change in chirality as well as to the route of rotation may only be given through a detailed conformational analysis, involving also the information about non-bonding interactions which may be gathered from the experimental evidences about the copper(II) complexes of cyclohexanediamine Schiff base derivatives mentioned above.

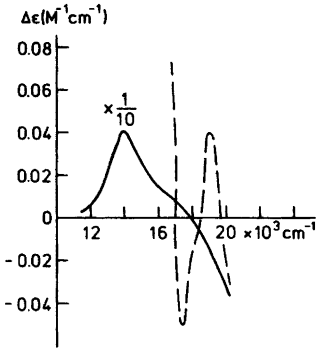

Fig. 5. CD spectra of Cu *R*-pn(fmc)$_2$ in methanol at room temperature (———) and in EPA at −187 °C (– – –).

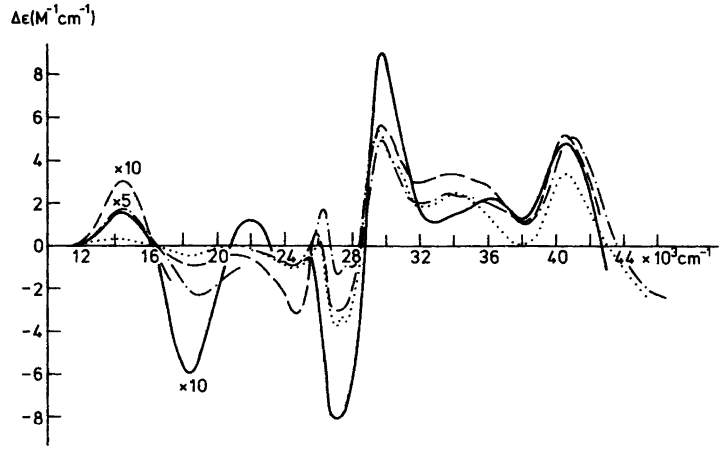

Fig. 6. CD spectra of Cu en(fmc)$_2$ (——) Cu ibn(fmc)$_2$ (– – –) Cu *R,S*-chxn(fmc)$_2$ (– · –) and Cu *R,S*-2,3-bn(fmc)$_2$ (· · ·).

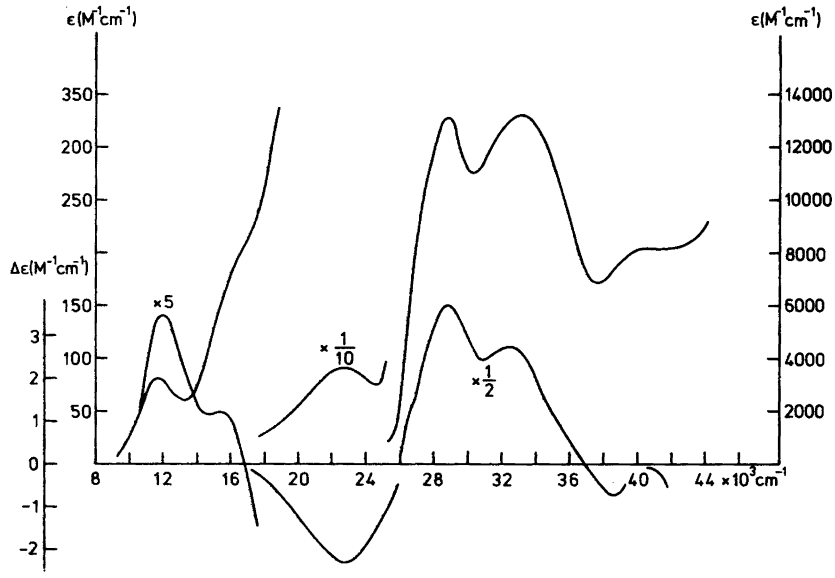

Fig. 7. Absorption and CD spectra of Cu tn(fmc)$_2$.

With this point noted we may from the spectra conclude that Cu *R*-pn(acac)$_2$, Cu *R*-2,3-bn(fmc)$_2$ and Cu *R*-pn(fmc)$_2$ have the same absolute configuration (Λ)[14] and the corresponding compounds of *S* configuration the opposite (Δ).[14]

The ligand field ranges of Figs. 3 and 4 are seen to be in accordance with the assignments given above in the case of cyclohexanediamine derivative complexes, although the three ligand field bands as far as concerns Cu *R*-pn(fmc)$_2$ are only visible on cooling (Fig. 5), and although the $(xy)\leftarrow(z^2)$ band (presumably negative) in the case of Cu *R*-2,3-bn(fmc)$_2$ seems to be cancelled to a major extent by the two visible positive components.

The stereochemical induction from the camphor group itself may also be studied in this type of complexes preparing Schiff bases with optically inactive diamines, examples of which are given in Fig. 6. Obviously the predominating absolute configuration in these compounds are the same (Δ), and it is especially interesting to note that contrary to the case of complexes with optically active diamines we here observe no difference between the chirality of the derivative of cyclohexanediamine and the other substituted ethylenediamine derivatives.

Generally, however, the Cotton effects are rather small and furthermore only four bands are clearly visible in the range 12 000 – 26 000 cm^{-1}. The "missing" band seems to be in the ligand field range, and this is not surprising as we already have argued for the $(xy) \leftarrow (z^2)$ transition to be of small intensity.

It has earlier been demonstrated that the introduction of a three-membered chain between the two chromophoric parts instead of the ethylene bridge changes the spectral properties radically as, *e.g.*, the $\pi^* \leftarrow \pi$ transition region of Cu tn(acac)$_2$ shows the transition moments to be much more co-planar than in, *e.g.*, Cu pn(acac)$_2$.[6]

We may with formylcamphor as chromophoric part investigate this point a little further, since the ligand tn(fmcH)$_2$ is optically active, and spectral properties of the copper(II) complex are shown in Fig. 7.

As is seen, neither the absorption nor the CD-spectra show properties typical of exciton coupling which demonstrates the postulated planarity of the compound.

Acknowledgement. The author wishes to acknowledge the skilful technical assistance of Mrs. L. Penzien.

REFERENCES

1. Larsen, E. *Acta Chem. Scand. 23* (1969) 2158.
2. Jensen, H. P., Kristensen, B. S., Mosbæk, H. and Søtofte, I. *Acta Chem. Scand. A 32* (1978) 141.
3. Jensen, H. P. and Larsen, E. *Acta Chem. Scand. A 29* (1975) 157.
4. Jensen, H. P. and Larsen, E. *Gazz. Chim. Ital. 107* (1977) 143.
5. Jensen, H. P. *Acta Chem. Scand. A 32* (1978) 149.
6. Jensen, H. P. and Larsen, E. *Acta Chem. Scand. 25* (1971) 1439.
7. Jensen, H. P., Davidsson, Å. and Nordén, B. *Inorg. Nucl. Chem. Lett. 11* (1975) 67.
8. Larsen, E., Larsen, S., Røen, S. and Watson, K. J. *Acta Chem. Scand. A 30* (1976) 125.
9. Jensen, H. P. *Acta Chem. Scand. A 30* (1976) 137.
10. Davidsson, Å., Jensen, H. P. and Nordén, B. *Chem. Scr. 11* (1977) 83.
11. Pfeiffer, P., Christeleit, W., Hesse, T., Pfitzner, H. and Thielert, H. *J. Prakt. Chem. N.F. 150* (1938) 261.
12. Honda, M. and Schwarzenbach, G. *Helv. Chim. Acta 40* (1957) 27.
13. Bishop, A. W., Claisen, L. and Sinclair, W. *Justus Liebigs Ann. Chem. 281* (1894) 314.
14. IUPAC, *Inorg. Chem. 9* (1970) 1.

Received May 22, 1978.

Acta Chemica Scandinavica A 32 (1978) 901–907

The Crystal Structure of Phenylbis(selenourea)tellurium(II) Chloride and Refinement of the Crystal Structure of Phenylbis(thiourea)tellurium(II) Chloride

SVERRE HAUGE, ØYVIND JOHANNESEN and OLAV VIKANE

Department of Chemistry, University of Bergen, N-5014 Bergen – Univ., Norway

Phenylbis(selenourea)tellurium(II) chloride, $C_6H_5Te(su)_2Cl$, I, forms triclinic crystals with space group $P\bar{1}$, and phenylbis(thiourea)tellurium(II) chloride, $C_6H_5Te(tu)_2Cl$, II, forms orthorhombic crystals with space group $P2_12_12_1$. The unit cell dimensions for I are: $a=11.2593(8)$ Å, $b=12.1588(4)$ Å, $c=5.9748(4)$ Å, $\alpha=99.029(6)°$, $\beta=93.966(5)°$ $\gamma=62.507(3)°$, and for II: $a=11.9509(5)$ Å, $b=20.7517(7)$ Å, $c=5.7816(3)$ Å.

In I and II each tellurium atom is primarily three-coordinated, being bonded to one phenyl carbon atom and, in directions nearly perpendicular to the Te–C bond, to two selenourea selenium atoms in I, and to two thiourea sulfur atoms in II. The three-centre systems Se–Te–Se and S–Te–S are nearly linear, and the Te–C bond nearly bisects the angle of the three-centre system. The bond lengths and angles involving tellurium are: Te–Se=2.7229(16) Å, 2.8895(17) Å; Te–C=2.129(6) Å; Se–Te–Se=173.09(4)°; Se–Te–C=88.71(15)°, 86.65(16)° in I, and Te–S=2.616(2) Å, 2.766(3) Å; Te–C=2.102(7) Å; S–Te–S=172.37(8)°; S–Te–C=87.9(2)°, 84.6(2)° in II. In II, the fourth position of a square-planar arrangement around tellurium is approached by the chloride ion, which lies 3.578(2) Å from tellurium in a direction which makes an angle of 163.8(2)° with the direction of the Te–C bond.

The crystal structures of several three-coordinated complexes of divalent tellurium have been reported.[1–6] The present paper reports the crystal structure determination of phenylbis(selenourea)-tellurium(II) chloride, and the refinement of the crystal structure of phenylbis(thiourea)tellurium(II) chloride. The crystal structure of the latter compound was reported by Foss and Marøy in 1966.[1] The refinement of the latter structure was undertaken in order to gain more accurate structural parameters. The syntheses and crystal data of the two present compounds are reported earlier.[1,7,8]

EXPERIMENTAL

Methods used for data collections and reductions, and computational procedures are described elsewhere.[3,9] For phenylbis(selenourea)tellurium(II) chloride, $C_6H_5Te(su)_2Cl$, I, the measurements were performed on a crystal with the following dimensions, given as distances from the point of intersection of the crystal faces (001), (010), and ($\bar{1}00$): to (00$\bar{1}$), 0.134 mm; to (0$\bar{1}$0), 0.059 mm; to (100), 0.074 mm; to (11$\bar{1}$), 0.067 mm; to ($\bar{1}\bar{1}$1), 0.037 mm. For phenylbis(thiourea)tellurium(II) chloride, $C_6H_5Te(tu)_2Cl$, II, the crystal used had the following dimensions, given as distances from the point of intersection of the crystal faces (120), ($\bar{1}$10), and (001): to (00$\bar{1}$), 0.253 mm; to (1$\bar{1}$0), 0.061 mm; to ($\bar{1}\bar{1}$0), 0.036 mm. The intensities were corrected for absorption.

The net count of the reference reflections varied within 11 % for I, and within 2.5 % for II. 2641 of 4177 independent reflections within $\theta=30°$ were found to be stronger than the lower limit for I. The corresponding numbers for II are 1417 of 2428.

CRYSTAL DATA

The crystals of $C_6H_5Te(su)_2Cl$, I, are yellow, triclinic prisms with space group $P\bar{1}$ (No. 2). The crystals of $C_6H_5Te(tu)_2Cl$, II, are long orthorhombic prisms, extended along the c-axis. Systematic

Table 1. Positional and thermal parameters. The anisotropic temperature factor is $\exp-[2\pi^2(U11h^2a^{*2}+\cdots+2U12hka^*b^*+\cdots)]$. The isotropic temperature factor is $\exp-[8\pi^2U(\sin^2\theta/\lambda^2]$. The values of the anisotropic temperature factors have been multiplied by 10^3.

$C_6H_5Te(su)_2Cl$

	x	*y*	*z*	*U*11	*U*22	*U*33	*U*12	*U*23	*U*13
Te	0.37686(5)	0.45416(4)	0.74729(7)	47.8(3)	31.1(2)	34.1(2)	-15.5(2)	7.4(2)	7.8(2)
Se(1)	0.64560(7)	0.31850(6)	0.67456(11)	34.3(4)	40.7(4)	36.7(4)	-12.8(3)	15.5(3)	-3.3(3)
Se(2)	0.09158(7)	0.56967(6)	0.82625(11)	36.5(4)	30.6(4)	34.2(4)	-8.2(3)	10.0(3)	-2.3(3)
Cl	0.87985(18)	0.95967(16)	0.2812(3)	62.6(11)	46.4(9)	44.4(10)	-27.2(9)	17.8(8)	-13.5(8)
C(1)	0.3480(6)	0.3254(5)	0.4921(9)	36(3)	34(3)	34(3)	-12(3)	2(3)	-4(3)
C(2)	0.3858(7)	0.2045(6)	0.5353(12)	72(5)	33(4)	62(5)	-20(4)	9(3)	-19(4)
C(3)	0.3607(9)	0.1225(7)	0.3677(14)	85(6)	42(4)	79(6)	-26(4)	2(4)	-21(5)
C(4)	0.3052(7)	0.1607(7)	0.1573(12)	61(5)	55(5)	57(5)	-27(4)	-2(4)	-10(4)
C(5)	0.2677(7)	0.2800(7)	0.1220(11)	41(4)	60(4)	41(4)	-21(4)	1(3)	0(3)
C(6)	0.2879(6)	0.3664(6)	0.2890(9)	37(4)	50(4)	29(3)	-16(3)	5(3)	-3(3)
C(7)	0.6924(6)	0.2021(6)	0.8826(10)	42(4)	42(4)	32(3)	-18(3)	4(3)	-5(3)
C(8)	0.0332(6)	0.6952(6)	0.6351(10)	30(3)	36(3)	43(4)	-11(3)	9(3)	5(3)
N(1)	0.8088(6)	0.1030(6)	0.8555(11)	52(4)	62(4)	85(5)	3(3)	39(4)	9(4)
N(2)	0.6161(6)	0.2175(6)	1.0548(9)	61(4)	66(4)	42(3)	-23(3)	15(3)	8(3)
N(3)	-0.0088(6)	0.6762(5)	0.4298(9)	79(5)	45(3)	39(3)	-22(3)	10(3)	-15(3)
N(4)	0.0390(7)	0.7999(5)	0.7114(11)	93(5)	40(3)	73(4)	-34(4)	13(3)	-14(4)

$C_6H_5Te(tu)_2Cl$

	x	*y*	*z*	*U*11	*U*22	*U*33	*U*12	*U*23	*U*13
Te	0.42660(5)	0.11802(3)	0.36053(12)	43.5(3)	49.4(3)	45.9(3)	10.0(4)	7.3(4)	2.4(4)
S(1)	0.4084(2)	0.00884(11)	0.5836(4)	74.2(18)	42.8(13)	33.0(14)	2.2(14)	6.2(11)	5.7(14)
S(2)	0.47597(19)	0.23250(11)	0.1380(5)	48.9(13)	60.5(15)	50.4(14)	-12.4(12)	17.5(17)	-13.5(17)
Cl	0.14972(19)	0.18005(12)	0.4370(4)	48.3(14)	64.2(16)	35.7(14)	6.5(12)	5.7(12)	2.5(11)
C(1)	0.6010(6)	0.1053(4)	0.3675(18)	36(5)	35(5)	48(5)	2(4)	0(5)	3(5)
C(2)	0.6577(9)	0.0746(5)	0.1919(19)	49(6)	54(6)	57(7)	7(5)	0(6)	-2(6)
C(3)	0.7748(9)	0.0631(6)	0.206(3)	44(7)	70(8)	114(12)	13(6)	28(8)	21(8)
C(4)	0.8316(9)	0.0849(6)	0.398(3)	51(7)	67(8)	97(11)	8(6)	27(8)	-16(9)
C(5)	0.7768(9)	0.1160(7)	0.575(2)	63(7)	76(8)	76(9)	-11(8)	26(9)	-24(7)
C(6)	0.6599(9)	0.1282(5)	0.5650(17)	62(7)	56(7)	48(6)	-8(6)	15(6)	-5(5)
C(7)	0.4040(7)	-0.0498(4)	0.3739(17)	40(5)	52(5)	41(5)	-12(4)	-1(6)	-4(6)
C(8)	0.3778(8)	0.2392(4)	-0.0749(15)	59(6)	28(5)	32(5)	-1(4)	-2(4)	-2(5)
N(1)	0.3922(6)	-0.0367(4)	0.1489(15)	67(5)	74(5)	30(4)	-1(4)	9(5)	8(5)
N(2)	0.4150(9)	-0.1108(4)	0.4397(13)	144(8)	40(4)	53(5)	-19(7)	-2(4)	2(6)
N(3)	0.4085(7)	0.2618(3)	-0.2797(12)	71(6)	49(5)	43(5)	-3(5)	10(4)	-3(5)
N(4)	0.2705(6)	0.2234(5)	-0.0373(15)	33(5)	128(8)	60(6)	-26(5)	23(6)	-10(5)

				U
H(2)	0.611(7)	0.058(4)	0.075(18)	0.08(4)
H(3)	0.849(10)	0.041(5)	0.10(2)	0.15(5)
H(4)	0.938(8)	0.071(4)	0.441(18)	0.11(3)
H(5)	0.819(7)	0.131(5)	0.730(16)	0.07(3)
H(6)	0.587(10)	0.160(6)	0.74(2)	0.22(6)

absences are: $h00$ for h odd, $0k0$ for k odd, $00l$ for l odd. The space group is $P2_12_12_1$ (No. 19).

The unit cell dimensions were determined as described elsewhere.[4] The θ-values (all about 20°) of 21 reflections for I, and 30 reflections for II were measured as described by Maartmann-Moe.[10] The unit cell dimensions are: $a=11.2593(8)$ Å, $b=12.1588(4)$ Å, $c=5.9748(4)$ Å, $\alpha=99.029(6)°$, $\beta=93.966(5)°$, $\gamma=62.507(3)°$. $Z=2$, $D_x=2.28$ g/cm^3, $D_m=2.30$ g/cm^3, $\mu(MoK\alpha)=78.54$ cm^{-1} for I, and: $a=11.9509(5)$ Å, $b=20.7517(7)$ Å, $c=5.7816(3)$ Å, $Z=4$, $D_x=1.81$ g/cm^3, $D_m=1.81$ g/cm^3, $\mu(MoK\alpha)=25.96$ cm^{-1} for II.

STRUCTURE DETERMINATION

The structure of I was solved by Patterson and Fourier methods, and for II the coordinates given by Foss and Marøy[1] were used. Of the hydrogen atoms, only positions of the phenyl hydrogen atoms in II were located. The final full-matrix least-squares refinements, with weighting scheme, $w=1/\sigma^2(F)$, resulted in the R values 0.037 for I and 0.038 for II. Altogether 145 parameters were refined for I and 165 parameters for II.

Observed and calculated structure factors for the two structures are available from the authors. The atomic coordinates and thermal parameters are listed in Table 1.

RESULTS

Bond lengths and angles in phenylbis(selenourea)-tellurium(II) chloride and phenylbis(thiourea)tellurium(II) chloride, based on the atomic coordinates in Table 1, are listed in Tables 2 and 3. The uncertainties in the unit cell dimensions are taken into account in the given standard deviations.

Views of the structure of I and II, as seen normal to the plane through the coordination group, are shown in Figs. 1 and 2. Stereoscopic views of the content of the unit cell of I and II are shown in Figs. 3 and 4.

The structure of phenylbis(thiourea)tellurium(II) chloride has previously been described by Foss and Marøy.[1] In each of the two present structures the tellurium atom is three-coordinated, being bonded to one phenyl carbon atom and, in directions nearly perpendicular to the Te–C bond, to two selenourea selenium atoms in I, and to two thiourea sulfur atoms in II.

The coordination around the tellurium atom is nearly planar in each structure. The largest deviation from a least-squares plane through Te, Se(1), Se(2), and C(1) is 0.07 Å in I. The largest deviation from the corresponding least-squares plane through Te, S(1), S(2), and C(1) is 0.023 Å in II. The least-squares plane through the coordination group passes 0.075 Å from C(4) in I and 0.069 Å from C(4) in II.

Table 2. Bond lengths (Å) and angles (°) in phenylbis(selenourea)tellurium(II) chloride.

Te–Se(1)	2.7229(16)	Se(1)–Te–Se(2)	173.09(4)
Te–Se(2)	2.8895(17)	Se(1)–Te–C(1)	88.71(15)
Te–C(1)	2.129(6)	Se(2)–Te–C(1)	86.65(16)
C(1)–C(2)	1.391(10)	Te–C(1)–C(2)	119.2(4)
C(1)–C(6)	1.394(8)	Te–C(1)–C(6)	118.7(4)
C(2)–C(3)	1.408(12)	C(2)–C(1)–C(6)	122.0(6)
C(3)–C(4)	1.412(11)	C(1)–C(2)–C(3)	118.2(6)
C(4)–C(5)	1.358(12)	C(2)–C(3)–C(4)	120.4(7)
C(5)–C(6)	1.418(10)	C(3)–C(4)–C(5)	119.7(6)
		C(4)–C(5)–C(6)	121.4(6)
		C(5)–C(6)–C(1)	118.1(6)
Se(1)–C(7)	1.897(7)	Te–Se(1)–C(7)	101.1(2)
Se(2)–C(8)	1.893(7)	Te–Se(2)–C(8)	99.8(2)
C(7)–N(1)	1.306(7)	Se(1)–C(7)–N(1)	117.3(5)
C(7)–N(2)	1.321(9)	Se(1)–C(7)–N(2)	123.8(4)
C(8)–N(3)	1.309(8)	N(1)–C(7)–N(2)	118.8(6)
C(8)–N(4)	1.313(10)	Se(2)–C(8)–N(3)	120.5(5)
		Se(2)–C(8)–N(4)	118.4(4)
		N(3)–C(8)–N(4)	121.1(6)

Table 3. Bond lengths (Å) and angles (°) in phenylbis-(thiourea)tellurium(II) chloride.[a]

Te–S(1)	2.616(2)	S(1)–Te–S(2)	172.37(8)
Te–S(2)	2.766(3)	S(1)–Te–C(1)	87.9(2)
Te–C(1)	2.102(7)	S(2)–Te–C(1)	84.6(2)
Te–Cl	3.578(2)	C(1)–Te–Cl	163.8(2)
C(1)–C(2)	1.376(14)	Te–C(1)–C(2)	122.2(6)
C(1)–C(6)	1.423(14)	Te–C(1)–C(6)	117.6(6)
C(2)–C(3)	1.422(15)	C(2)–C(1)–C(6)	120.2(8)
C(3)–C(4)	1.38(2)	C(1)–C(2)–C(3)	121.3(9)
C(4)–C(5)	1.377(19)	C(2)–C(3)–C(4)	118.4(11)
C(5)–C(6)	1.421(15)	C(3)–C(4)–C(5)	121.3(10)
		C(4)–C(5)–C(6)	121.3(9)
		C(5)–C(6)–C(1)	117.4(9)
S(1)–C(7)	1.719(9)	Te–S(1)–C(7)	105.5(3)
S(2)–C(8)	1.706(9)	Te–S(2)–C(8)	105.0(3)
C(7)–N(1)	1.337(10)	S(1)–C(7)–N(1)	123.1(6)
C(7)–N(2)	1.328(12)	S(1)–C(7)–N(2)	118.0(6)
C(8)–N(3)	1.325(11)	N(1)–C(7)–N(2)	118.9(7)
C(8)–N(4)	1.341(12)	S(2)–C(8)–N(3)	118.9(6)
		S(2)–C(8)–N(4)	121.4(6)
		N(3)–C(8)–N(4)	119.7(8)

[a] The C–H bond lengths vary from 0.94(9) Å to 1.18(9) Å, with an average value of 1.07 Å. The C–C–H bond angles vary from 111(5)° to 129(5)° with an average value of 120°.

The three-centre systems Se–Te–Se and S–Te–S are nearly linear, and the Te–C bond nearly bisects the angle of the three-centre system. Small deviations from linearity are also found in the structures of the phenyldithiocyanatotellurate-(II) and the phenyldiselenocyanatotellurate(II) anions.[3]

The Se–Te–Se bonding system in I is slightly asymmetric. The average value of the two Te–Se bond lengths, 2.806 Å is, within the error, equal to the average Te–Se bond length found in the crystals of centrosymmetric square-planar com-

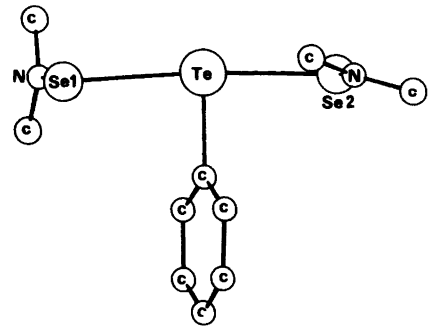

Fig. 1. Phenylbis(selenourea) tellurium(II) cation, as seen normal to the plane through the coordination group.

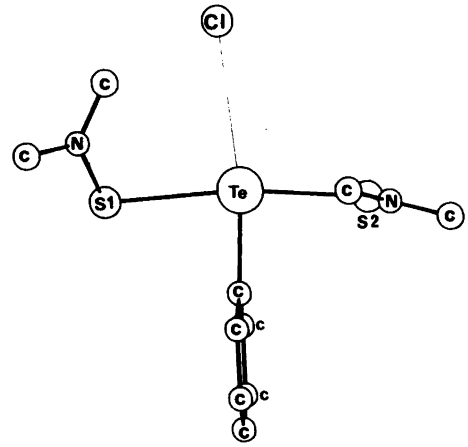

Fig. 2. Phenylbis(thiourea)tellurium(II) chloride, as seen normal to the plane through the coordination group.

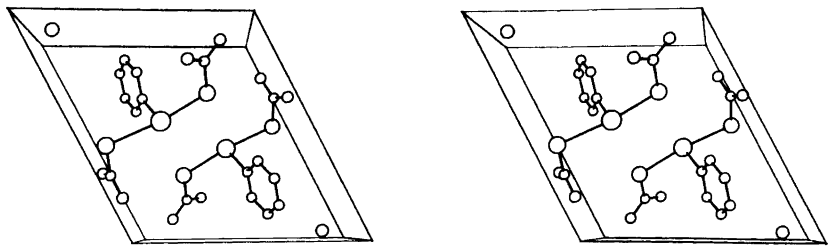

Fig. 3. A stereoscopic view of the content of the unit cell for phenylbis(selenourea)tellurium(II) chloride, as seen along the *c* crystal axis.

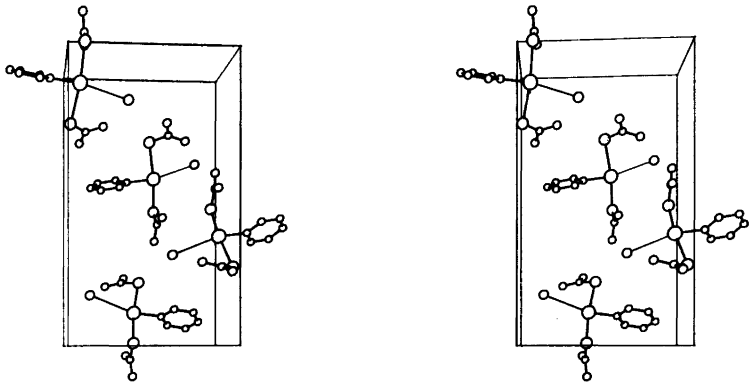

Fig. 4. A stereoscopic view of the content of the unit cell for phenylbis(thiourea)tellurium(II) chloride, as seen along the *c* crystal axis.

plexes of divalent tellurium,[11-13] and about 0.02 Å longer than the average Te–Se bond length found in the structure of the phenyldiselenocyanatotellurate(II) anion.[3]

The two Te–S bond lengths indicate about the same asymmetry in the S–Te–S bonding as in the Se–Te–Se bonding. The average Te–S bond length, 2.691 Å is, within the error, equal to the average Te–S bond length found in the crystals of centrosymmetric square-planar complexes of divalent tellurium,[14,15] and also equal to the average Te–S bond length found in the structure of the phenyldithiocyanatotellurate(II) anion.[3]

The Te–C bond lengths found in the two structures are equal within the accuracy of the structure determinations. The same Te–C bond length has been found in all structures where divalent tellurium is bonded to a phenyl group.[1-6]

As pointed out by Foss *et al.*[1,14,15] the coordination around the tellurium atom in the structure of II may be regarded as based on square-planar coordination, with the fourth position, *trans* to the phenyl group, virtually vacant. In II the chloride ion lies 0.84 Å from the least-squares plane through the coordination group. Thus, although at such a distance as to indicate only very weak bonding interaction, the chloride ion may be regarded as approaching the fourth coordination site of a square-planar arrangement.

In I the chloride ion is placed in a completely different position so that the tellurium atom is strictly three-coordinated. This is similar to what has been found in the structures of the phenyldithiocyanato- and the phenyldiselenocyanatotellurate(II) anions.[3]

The atoms of the phenyltellurium group are nearly co-planar in each structure, the largest deviation from the least-squares plane through the phenyltellurium group is 0.020 Å in I and 0.037 Å in II. The angle between this plane and the least-squares plane through the coordination group is 72.74° in I and 88.45° in II.

The selenourea groups in I and the thiourea groups in II are nearly planar, the largest deviations being 0.019 Å in I and 0.080 Å in II. The angle between the two planes is 75.3° in I and 80.5° in II. The least-squares plane through the coordination group makes an angle of 87.5 and 77.5° with the least-squares plane through each of the two selenourea groups in I. The corresponding angles in II are 89.3 and 45.5°.

The Se–C bond lengths are, within the error, equal to the Se–C bond lengths found in the structures of bromo(ethyleneselenourea)phenyltellurium(II),[5] ethyleneselenourea(iodo)phenyltellurium(II),[6] and tetrakis(selenourea)tellurium(II) dichloride.[12] In II the S–C bond lengths are, within the error, equal to the S–C bond length found in the structures of chloro- and bromo(ethylenethiourea)phenyltellurium(II).[4,5] The Te–S–C bond angles are equal within the error of the structure determination.

Table 4. Nitrogen–chlorine distances (Å) and angles (°) in the structure of phenylbis(selenourea)-tellurium(II) chloride. *x*, *y*, *z* are the coordinates of the chloride ion given in Table 1.

Distance	Length N···Cl	Angle C–N···Cl	Distance from plane
N(1)···Cl($x,y-1,z+1$)	3.158(7)	110.6(5)	0.581
N(1)···Cl($2-x,1-y,1-z$)	3.357(8)	136.4(5)	1.540
N(2)···Cl($x,y-1,z+1$)	3.557(8)	91.1(3)	0.581
N(3)···Cl($x-1,y,z$)	3.326(6)	100.1(4)	−0.425
N(4)···Cl($x-1,y,z$)	3.363(6)	98.3(4)	−0.425
N(4)···Cl($1-x,2-y,1-z$)	3.436(8)	157.9(4)	1.059

Table 5. Nitrogen–chlorine distances (Å) and angles (°) in the structure of phenylbis(thiourea)-tellurium(II) chloride. *x*, *y*, *z* are the coordinates of the chloride ion given in Table 2.

Distance	Length N···Cl	Angle C–N···Cl	Distance from plane
N(1)···Cl($\frac{1}{2}-x,\bar{y},z-\frac{1}{2}$)	3.256(8)	101.3(5)	−0.564
N(2)···Cl($\frac{1}{2}-x,\bar{y},z-\frac{1}{2}$)	3.333(8)	97.9(6)	−0.564
N(2)···Cl($\frac{1}{2}-x,\bar{y},\frac{1}{2}+z$)	3.306(8)	129.8(6)	1.151
N(3)···Cl($\frac{1}{2}+x,\frac{1}{2}-y,\bar{z}$)	3.255(8)	128.8(6)	0.290
N(4)···Cl(x,y,z)	3.227(9)	129.3(5)	0.269
N(4)···Cl($x,y,z-1$)	3.483(9)	108.5(5)	−1.465

HYDROGEN BONDING

Short intermolecular distances, probably involving hydrogen bonds, occur between amino nitrogen atoms and chloride ions. The nitrogen atoms are assumed to have a trigonal-planar bonding system, *i.e.*, the hydrogen atoms lie in or close to the planes through the selenourea groups in I, and the thiourea groups in II. The N···Cl distances, the N–C···Cl angles, and the distances of the chloride ions from the least-squares planes for I and II, are listed in Tables 4 and 5, respectively. The chloride ion, in both structures, takes part in six hydrogen bonds.

Hydrogen bonding to selenium, N–H···Se, has been found in crystals of selenourea[16] and related compounds.[12,17,18] In the crystals of I such hydrogen bonding probably occurs between N(2) (x,y,z) and Se(1)′($x,y,z+1$), and between N(3)(x,y,z) and Se(2)′($x,1-y,1-z$). The N(2)···Se(1)′ distance is 3.721(8) Å, and the N(3)···Se(2)′ distance is 3.614(6) Å. The C(7)–N(2)···Se(1)′ angle is 129.9(4)°, the C(8)–N(3)···Se(1)′ angle is 129.9(4)°, and the C(8)–N(3)···Se(2)′ angle is 145.0(4)°.

Hydrogen bonding to sulfur, N–H···S, has been found in crystals of thiourea.[19] In the crystals of II such hydrogen bonding probably occurs between N(1)(x,y,z) and S(1)′($x,y,z-1$), and between N(3)-(x,y,z) and S(2)′($x,y,z-1$). The N(1)···S(1)′ distance is 3.407(4) Å, and the N(3)···S(2)′ distance is 3.515(7) Å. The C(7)–N(1)···S(1)′ angle is 169.7(5)°, and the C(8)–N(3)···S(2)′ angle is 149.1(5)°.

REFERENCES

1. Foss, O. and Marøy, K. *Acta Chem. Scand. 20* (1966) 123.
2. Foss, O. and Husebye, S. *Acta Chem. Scand. 20* (1966) 132.
3. Hauge, S. and Vikane, O. *Acta Chem. Scand. A 29* (1975) 755.
4. Vikane, O. *Acta Chem. Scand. A 29* (1975) 738.
5. Vikane, O. *Acta Chem. Scand. A 29* (1975) 763.
6. Vikane, O. *Acta Chem. Scand. A 29* (1975) 787.
7. Hauge, S. and Vikane, O. *Acta Chem. Scand. 27* (1973) 3596.
8. Foss, O. and Hauge, S. *Acta Chem. Scand. 13* (1959) 2155.
9. Åse, K. *Acta Chem. Scand. 25* (1971) 838.
10. Maartmann-Moe, K. *Siemens Review XLI* (1974) 54.
11. Åse, K., Bøyum, K., Foss, O. and Marøv, K. *Acta Chem. Scand. 25* (1971) 2457.

12. Hauge, S. and Tysseland, M. *Acta Chem. Scand. 25* (1971) 3072.
13. Åse, K., Foss, O. and Roti, I. *Acta Chem. Scand. 25* (1971) 3808.
14. Foss, O. *Pure Appl. Chem. 24* (1970) 31.
15. Foss, O. In Andersen, P., Bastiansen, O. and Furberg, S., Eds., *Selected Topics in Structure Chemistry*, Universitetsforlaget, Oslo 1967, p. 145.
16. Rutherford, J. S. and Calvo, C. *Z. Z. Kristallogr. 128* (1966) 229.
17. Hope, H. *Acta Crystallogr. 18* (1965) 259.
18. Shefter, E., James, M. N. G. and Mautner, H. G. *J. Pharm. Sci. 55* (1966) 643.
19. Truter, M. R. *Acta Crystallogr. 22* (1967) 556.

Received June 8, 1978.

Acta Chemica Scandinavica A 32 (1978) 909–916

On the Mechanisms of the Zn(II)/Zn(Hg) and Cd(II)/Cd(Hg) Electrode Reactions in DMSO Solutions of the Thiocyanate Ion

STURE FRONÆUS and BIRGER PALM

Inorganic Chemistry 1, Chemical Center, University of Lund, P.O.Box 740, S-220 07 Lund, Sweden

Dedicated to Jannik Bjerrum on the occasion of his 70th birthday

The electrode reactions Zn(II)/Zn(Hg) and Cd(II)/Cd(Hg) in complex thiocyanate solutions with DMSO as solvent have been studied at the equilibrium potentials by the faradaic impedance method and a cyclic current-step method. All the kinetic data refer to 25 °C and the ionic strength 1 M with ammonium perchlorate as supporting electrolyte. Double-layer data have been determined by electrocapillary measurements.

The results for the zinc system indicate that the solvated Zn^{2+} predominates in the electrode reaction, whereas the complexes do not take part noticeably. It is concluded that in DMSO ligand bridging by SCN^- at the electrode is hindered by the larger solvent molecules.

For the cadmium system it has been found that the solvated Cd^{2+} as well as the complexes $CdSCN^+$ and $Cd(SCN)_2$ take part in the rate-controlling charge transfer step Cd(II)/Cd(I). Furthermore the results confirm a suggestion that a decrease in or labilization of the inner sphere solvation of Cd(II) at the formation of a complex is of great importance for its contribution to the exchange current density.

The electrode reaction Zn(II)/Zn(Hg) in complex chloride, bromide, and iodide solutions with dimethyl sulfoxide (DMSO) as solvent was recently studied[1] in this laboratory. It was found that a rate-increasing effect on this electrode reaction by the halide ions, which is well-known for water solutions,[2-4] does not exist for the DMSO solutions. On the contrary, the measurements proved that in DMSO the solvated zinc ion takes part in the electrode reaction, whereas the chloride and bromide complexes do not. However, in the iodide system also the first complex contributes to the exchange current density. This solvent influence was explained with a model involving steric hindrance by the larger DMSO molecules to ligand bridging at the electrode by Cl^- and Br^-. The large and more polarizable I^-, on the other hand, could possibly act also in DMSO as an electron conducting bridge between the coordinated Zn^{2+} and the amalgam.

Then, it seemed interesting to supplement the studies of the halide systems by investigating the zinc thiocyanate system in DMSO, since for water solutions it is known[2] that the acceleration effect of the heavier halide ions and SCN^- on the electrode reaction increases in the order $Br^- < SN^- < I^-$. Furthermore, because of its linear shape[5] also SCN^- could be expected to have a capability of ligand bridging at the electrode in DMSO solutions.

A recent investigation[6] of the electrode reaction Cd(II)/Cd(Hg) in halide solutions in DMSO gave further support to the model given for the zinc systems. Furthermore, the complexes $CdBr_2$ and CdI_2 proved to give large contributions to the exchange current density which can be correlated to a pronounced change in the inner sphere solvation[7] at this step of the complex formation. As there is no indication of such a sudden change in the solvation at the formation of $Cd(SCN)_2$ in DMSO solution, the cadmium thiocyanate system provides a valuable possibility to test the validity of the correlation suggested.

Stability constants relating to the complex formation in the zinc and cadmium thiocyanate systems in DMSO and necessary for the calculations of the

rate constants of the electrode reactions, have recently been determined in this laboratory.[8] To be able to use these stability constants we carried out the present investigation with the same ammonium perchlorate medium.

For the two systems studied the rates of the electrode reactions, *i.e.* values of the exchange current density, i_0, can be conveniently determined by alternating current methods. We used a square-wave method and in some measurements the faradaic impedance method.

As double-layer data for thiocyanate solutions in DMSO do not seem to be available in the literature, electrocapillary measurements have also been performed. In these measurements lithium salts were chosen as the most suitable ones for the ionic media.

EXPERIMENTAL

Chemicals. The hexasolvates $Zn(DMSO)_6(ClO_4)_2$ and $Cd(DMSO)_6(ClO_4)_2$ were the same preparations as used previously.[1,6] They were analyzed with respect to zinc and cadmium by titration with EDTA.

Liquid zinc and cadmium amalgams of 0.3 and 0.1 % by weight, respectively, were also prepared as before[6,9] and were kept in a nitrogen atmosphere. These amalgams were used throughout the kinetic measurements.

Analytical grade ammonium perchlorate and thiocyanate and lithium chloride were dried at 110 °C before use. The lithium perchlorate was dried at 185 °C.

Lithium thiocyanate was prepared by mixing equivalent amounts of lithium perchlorate and potassium thiocyanate in water solution. After cooling the solution it was separated from the crystallized potassium perchlorate and then evaporated at 130 °C. The salt is very hygroscopic. Its thiocyanate content was checked titrimetrically.

Stock solutions of the different salts were prepared with purified[10] DMSO. The ionic strength of the cell solutions in the measurements of the electrode kinetics was 1 M with ammonium perchlorate as supporting electrolyte.

Experimental details. In the kinetic measurements two stationary small amalgam drops (*cf.* Ref. 11) of equal size were used as polarizable electrodes in the cell. By this arrangement the effect of some small dissolution of zinc and especially cadmium from the amalgams could be reduced. The surface area of a single drop was determined according to the drop weight method. Both drops were renewed before every new measurement.

In those measurements where the charge transfer resistance, R_t, was obtained from faradaic impedances the same a.c. bridge and procedure were used as in some earlier investigations (*cf.* Ref. 12).

However, the measurements in the main series were performed according to a cyclic current-step method.[1,13] The bridge and procedure applied in this case for determining R_t were the same as described previously.[1]

In both measurement methods the amplitude of the voltage response of the cell was kept smaller than 10 mV. Very reproducible R_t-values were obtained.

The electrocapillary measurements for determinations of double-layer data were made using the same apparatus and process as before.[1]

All measurements were carried out at 25.0± 0.2 °C. Nitrogen gas that had been freed from oxygen was led through the complex solutions to protect the amalgam from oxidation and to ensure good mixing in the cell.

THE ELECTRODE KINETICS

The zinc thiocyanate system

Investigations[8] of the complex formation have shown that SCN^- gives four mononuclear complexes with Zn^{2+} in DMSO. According to results from IR spectroscopy[14] on water solutions Zn^{2+} coordinates the ligand *via* the N atom, and probably the same is valid for DMSO solutions. We then have to take into account the following set of parallel electrode reactions

$$Zn(NCS)_j^{2-j} + 2e^- \rightleftharpoons Zn(am) + jSCN^- \quad (1)$$

The previous investigation[1] on the chloride system indicated that in DMSO the charge transfer process for the solvated Zn^{2+} is likely to be a simple one-step transfer. If this holds also for the electrode reactions (1) we should have eqn. (2) for the total exchange current density.

$$i_0 = \sum_j k_j [Zn^{2+}]^{\alpha_j} [SCN^-]^j \quad (2)$$

For the composite coefficients k_j the expression (3) holds.

$$k_j = 2Fk_j^{\ominus} \beta_j^{\alpha_j} [Zn(am)]^{1-\alpha_j} \exp\{(j-2\alpha_j)F\phi_2/RT\} \quad (3)$$

Here $k_j^{\ominus}$ denotes the true rate constant and α_j the anodic transfer coefficient of reaction (1). β_j is the stability constant of $Zn(NCS)_j^{2-j}$ and the exponen-

tial factor represents the Frumkin correction for the influence of the ϕ_2-potential. At a constant amalgam concentration k_j should be constant at varying $[SCN^-]$, if a supporting electrolyte in high and constant concentration is used, ensuring that variations in activity coefficients and in the ϕ_2-potential are suppressed.

However, it could also be assumed that the charge transfer proceeds step-wise with Zn(I) as an intermediate. Then, if the step Zn(II)/Zn(I) is rate-controlling and furthermore the disproportionation equilibrium (4) is established at the amalgam,

$$Zn(II) + Zn(am) \rightleftharpoons 2\,Zn(I) \qquad (4)$$

the exponent for $[Zn^{2+}]$ in the equation for i_0 will be changed to $(1+\alpha_{j,2})/2$, where $\alpha_{j,2}$ stands for the anodic transfer coefficient of the electrode reaction $Zn(NCS)_j^{2-j}/Zn(NCS)_j^{1-j}$. This is evident from the corresponding equation applied below for the cadmium system.

In both cases discussed i_0 is calculated in the same way[15] from R_t.

An average of the different exponents for $[Zn^{2+}]$ in the equation for i_0 can be obtained from the quantity $\bar{\alpha}=(\partial \lg i_0/\partial \lg [Zn^{2+}])_{[SCN^-]}$ (*cf.* Ref. 16). It can be stated that if i_0 is controlled by the step Zn(II)/Zn(I) then $\bar{\alpha}$-values between 0.5 and 1.0 should be found.

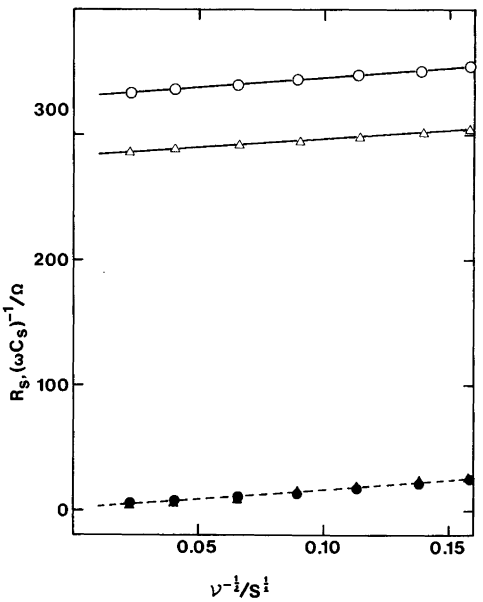

Fig. 1. The resistance R_s(——) and reactance $(\omega C_s)^{-1}$ (– – –) of the faradaic impedance as functions of $\nu^{-1/2}$ in the zinc thiocyanate system at C_{Zn}/mM = 4.00 and C_{SCN}/mM: 0(△▲); 7.90 (○●).

Table 1. Measurements of i_0 in the zinc thiocyanate system. $C_{Zn} = 4.00$ mM.

C_{SCN}/mM, $[SCN^-]$/mM, $[Zn^{2+}]$/mM, i_0/mA cm^{-2};
1.97, 1.78, 3.85, 1.45; 3.95, 3.50, 3.65, 1.35; 5.90, 5.10, 3.45, 1.30; 7.85, 6.55, 3.20, 1.20; 11.7, 9.2, 2.75, 1.05; 15.6, 11.6, 2.30, 0.92; 19.4, 13.9, 1.85, 0.75; 24.1, 16.8, 1.40, 0.62; 28.8, 19.8, 0.98, 0.49; 33.5, 23.0, 0.67, 0.38; 38.0, 26.5, 0.46, 0.30; 42.5, 30.2, 0.32, 0.25; 47.0, 34.0, 0.22, 0.21.

Measurements and calculations. The faradaic impedance, determined at different frequencies ν, proved to be in accordance with the expression $R_t + \text{const}(1-j)\nu^{-1/2}$, where j denotes the imaginary unit vector (Fig. 1). This Randles behaviour indicates that the electrode process is controlled by charge transfer and diffusion. Thus, a possible specific adsorption of charge transferring zinc species on the amalgam must be a rapid step and furthermore be weak. This means that the cyclic current-step method, used in the other kinetic measurements, should give true values of R_t.

In the main series given in Table 1 the total zinc(II) concentration, C_{Zn}, was kept constant while C_{SCN} was increased. Then i_0 decreased monotonically, and in order to obtain reliable R_t-values it was necessary to keep $C_{SCN} < 50$ mM. From the stability constants[8] $\beta_1 = 24\ M^{-1}$, $\beta_2 = 600\ M^{-2}$, $\beta_3 = 1.6 \times 10^5\ M^{-3}$ and $\beta_4 = 7.2 \times 10^6\ M^{-4}$ $[Zn^{2+}]$ and $[SCN^-]$ were calculated as described for the halide systems.[1]

In other series of measurements at selected fixed values of $[SCN^-]$, giving values of $\bar{\alpha}$, the compositions of the solutions to be used and $[Zn^{2+}]$ were also calculated by means of the constants. In these series, which are presented in Fig. 2, C_{Zn} was varied between about 1.5 and 15 mM.

From Fig. 2 it is evident that the $(\lg i_0/\lg [Zn^{2+}])$-data can be represented by a single straight line with the slope $\bar{\alpha} = 0.65 \pm 0.03$, independent of whether C_{Zn} or $[SCN^-]$ is chosen as a parameter. Thus, for all the measurements the very simple expression (5) is valid.

$$i_0/[Zn^{2+}]^{0.65} = 50 \pm 5 \qquad (5)$$
(i_0 in mA cm^{-2}, $[Zn^{2+}]$ in M)

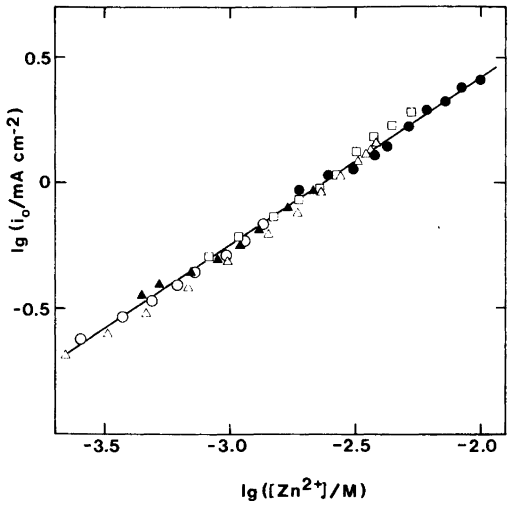

Fig. 2. lg i_0 as a function of lg[Zn^{2+}] in the thiocyanate system at a constant C_{Zn} or [SCN^-]. C_{Zn}/mM = 4.00 (△); [SCN^-]/mM; 2.00 (●); 12.0 (□); 20.0 (▲); 30.0 (○).

A comparison between eqns. (2) and (5) shows that at the [SCN^-] used the solvated Zn^{2+} predominates in the electrode reaction, whereas the thiocyanate complexes do not take part noticeably, though in the bulk of the solution $[Zn^{2+}]/C_{Zn} < 0.1$ at [SCN^-] = 30 mM (Table 1).

The cadmium thiocyanate system

From an investigation[8] of the complex formation in DMSO it is known that SCN^- can give three mononuclear complexes with Cd^{2+}. It can be presumed that in these complexes Cd^{2+}, at least partly, coordinates the ligand *via* the S atom, in conformity with what has been found[14] for water solutions. Then, we should have the following set of parallel electrode reactions

$$Cd(SCN)_j^{2-j} + 2e^- \rightleftharpoons Cd(am) + jSCN^- \quad (6)$$

The studies[6] of the cadmium halide systems in DMSO have shown that the charge transfer reactions most probably proceed step-wise with Cd(I) as an intermediate. Furthermore, there was no indication that any complexes of Cd(I) take part in the charge transfer step Cd(I)/Cd(am). Provided that these results are valid also for the thiocyanate system, the following reaction scheme should be applicable.

$$Cd^+ + e^- \rightleftharpoons Cd(am) \quad (7)$$

$$Cd(SCN)_j^{2-j} + e^- \rightleftharpoons Cd^+ + jSCN^- \quad (8)$$

In addition we have also the disproportionation equilibrium (9) to take into consideration.

$$Cd(II) + Cd(am) \rightleftharpoons 2\,Cd(I) \quad (9)$$

Then the equations[15] for the current densities i_{01} and i_{02} of the reactions (7) and (8) should be of the form

$$i_{01} = k_{0,1}[Cd^{2+}]^{\alpha_{0,1}/2} \quad (10)$$

$$i_{02} = \sum_j k_{j,2}[Cd^{2+}]^{(1+\alpha_{j,2})/2}[SCN^-]^j \quad (11)$$

$k_{0,1}$ and $k_{j,2}$ are composite coefficients,[6] but only the complete expression (12) for $k_{j,2}$ will be of interest in the present study.

$$k_{j,2} = Fk_{j,2}^{\ominus}\beta_j^{\alpha_{j,2}}(K^{\frac{1}{2}}[Cd(am)]^{\frac{1}{2}}[DMSO]^{-j})^{1-\alpha_{j,2}} \exp\{(j-1-\alpha_{j,2})F\phi_2/RT\} \quad (12)$$

Here $k_{j,2}^{\ominus}$ is the true rate constant and $\alpha_{j,2}$ the anodic transfer coefficient of reaction (8). K is the equilibrium constant of (9), applied to the free solvated ions Cd^{2+} and Cd^+. Then, because of the formulation of the step Cd(II)/Cd(I) according to (8), we have found it convenient to separate in eqn. (12) a factor $[DMSO]^{j(\alpha_{j,2}-1)}$ from the rate constant. In this way all the rate constants $k_{j,2}^{\ominus}$ retain the usual dimension length/time. Of course the rate constants can still be functions of [DMSO], since the number of DMSO molecules taking part in reaction (8) is not known.

For $i_0 \sim i_{01}$ and $i_0 \sim i_{02}$ the quantity $\bar{\alpha}$, which is analogous to that defined above for the zinc system, should have values of about 0.25 and 0.75, respectively.

In the investigation of the halide systems[6] it was found that the electrochemically determined i_0 could be represented according to eqn. (13)

$$i_0 = 0.5\,(i_{01} + i_{02}) \quad (13)$$

This means that the disproportionation of Cd(I) is so fast that the two charge transfer steps (7) and (8) are parallel instead of consecutive. It can be

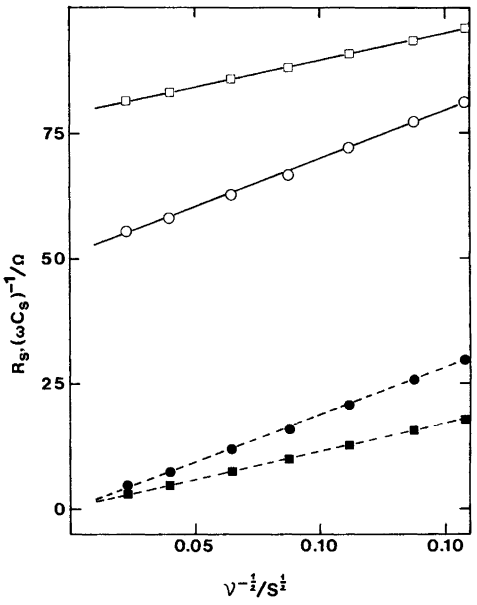

Fig. 3. The series resistance R_s(——) and reactance $(\omega C_s)^{-1}$ (– – –) of the faradaic impedance as functions of $\nu^{-1/2}$ in the cadmium thiocyanate system at different values of C_{Cd} and C_{SCN}. C_{Cd}/mM, C_{SCN}/mM: 2.00, 0(○ ●); 4.00, 100 (□ ■).

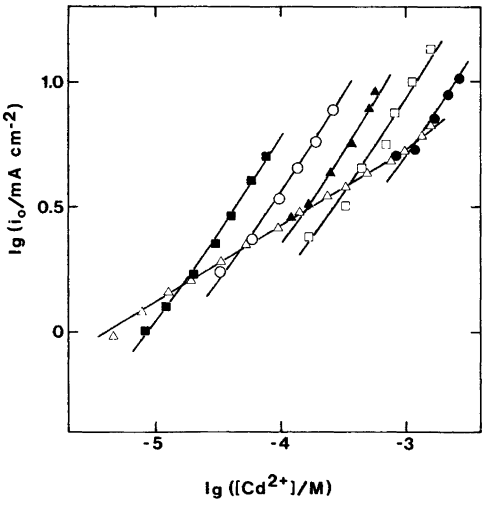

Fig. 4. lg i_0 as a function of lg[Cd^{2+}] in the thiocyanate system at a constant C_{Cd} or [SCN^-]. C_{Cd}/mM = 2.00 (△); [SCN^-]/mM: 10.0 (●); 50.0 (□); 100 (▲); 200 (○); 350 (■). The curves have been calculated from eqn. (14).

presupposed that eqn. (13) is applicable also for the thiocyanate system.

Measurements and calculations. From Fig. 3 it is obvious that the faradaic impedance displays a Randles behaviour, and thus there is no slow adsorption of cadmium species influencing the determination of R_t-values. The main measurement series at a constant C_{Cd} is given in Table 2. Also in this system i_0 decreases on addition of thiocyanate ions. The stability constants[8] used in the calculations of [Cd^{2+}] and [SCN^-] are $\beta_1 = 64$ M^{-1}, $\beta_2 = 520$ M^{-2} and $\beta_3 = 850$ M^{-3}. The other series of measurements, carried out at constant values of [SCN^-] are given in Fig. 4. In these series C_{Cd} was varied between 1.0 and 11 mM.

From the plots in Fig. 4 it is seen that in this case i_0 is not a function of [Cd^{2+}] solely but depends also upon [SCN^-]. From the last-mentioned series $\bar{\alpha} \approx 0.8$ is also found at different [SCN^-]. Thus it can be concluded that in eqn. (13) i_{01} is of minor importance in the whole [Cd^{2+}]-range used. It was presumed that $\alpha_{0,1}$ and $\alpha_{j,2}$ could be put equal to 0.40 and 0.70, respectively, as in the halide systems. Accordingly, $i_0/[Cd^{2+}]^{0.20}$ was plotted *versus* $[Cd^{2+}]^{0.65}$ at the different constant [SCN^-]. Straight lines with an approximate constant intercept, $0.5k_{0,1}$, on the ordinate axis were obtained, indicating that i_{01} can be represented by the single term $k_{0,1}[Cd^{2+}]^{0.20}$ and thus confirming the validity of eqn. (10). Then in the function $(i_0 - 0.5i_{01})/[Cd^{2+}]^{0.85}$, which should be a polynomial in [SCN^-], the coefficients $k_{j,2}$ were adjusted to the best fit with the measurements. From Fig. 4 it is seen that the i_0-function calculated from eqn. (14) represents the measurement data very well.

Table 2. Measurements of i_0 in the cadmium thiocyanate system. $C_{Cd} = 2.00$ mM.

C_{SCN}/mM, [SCN^-]/mM, [Cd^{2+}]/mM, i_0/mA cm^{-2};
3.95, 3.55, 1.60, 6.7; 7.90, 7.20, 1.35, 6.1; 15.7, 14.5, 0.98, 5.3; 23.5, 22.0, 0.75, 4.8; 38.0, 36.5, 0.49, 4.3; 56.5, 54.0, 0.33, 3.8; 73.5, 71.0, 0.235, 3.5; 107, 104, 0.140, 3.0; 137, 134, 0.095, 2.60; 192, 189, 0.053, 2.25; 250, 245, 0.033, 1.90; 330, 325, 0.0190, 1.60; 395, 390, 0.0125, 1.45; 495, 490, 0.0078, 1.20; 620, 615, 0.0046, 0.95.

$$i_0 = 3.5[Cd^{2+}]^{0.20} + [Cd^{2+}]^{0.85}(1.2 \times 10^3 + 3.0 \times 10^4[SCN^-] + 1.5 \times 10^4[SCN^-]^2) \quad (14)$$

(i_0 in mA cm^{-2}, [Cd^{2+}] and [SCN^-] in M)

Only at the lowest C_{Cd} are there in some cases differences that could be ascribed to a small dissolution of cadmium from the amalgam.

The results obtained confirm that no complexes of Cd(I) contribute noticeably to the charge transfer step Cd(I)/Cd(am). For the step Cd(II)/Cd(I), on the other hand, we arrive at the conclusion that the solvated Cd^{2+} as well as the complexes $CdSCN^+$ and $Cd(SCN)_2$ take part.

THE DOUBLE-LAYER AND THE TRUE RATE CONSTANTS

Electrocapillary measurements were performed on pure mercury in contact with 1 M LiSCN in DMSO. From Fig. 5 it is seen that the electrocapillary curve obtained is very similar to that for 1 M LiCl. The charge density, q, on the mercury, the contribution, q^1_{SCN}, from the specifically adsorbed SCN^- to the charge on the solution side and the ϕ_2-potential were determined at the applied potential, E, *versus* a fixed reference electrode (see Fig. 5)

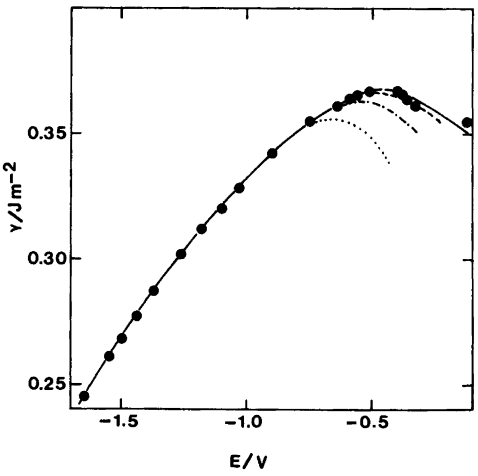

Fig. 5. The electrocapillary curve (●) for mercury and 1 M lithium thiocyanate in DMSO at 25 °C. The potentials are referred to the reference electrode Ag, AgCl in 10 mM LiCl+990 mM $LiClO_4$. The corresponding curves for lithium chloride (– – –), bromide (–·–), and iodide (···) are also given (*cf.* Ref. 1).

as described previously.[1] For the sake of comparison the same potentials, $E=-1175$ and -785 mV, were used as in the studies of the halide systems.[1,6] They are within the ranges of the equilibrium potentials of the zinc and cadmium amalgams, respectively, in the complex thiocyanate solutions. At $E=-1175$ mV the following values were obtained: $q=-12.1$ μC cm^{-2}, $q^1_{SCN}=-1.0$ μC cm^{-2} and $\phi_2=-60$ mV. The q^1_{SCN}-value confirms that in DMSO the specific adsorbability of SCN^- is approximately the same as that of Cl^- (*cf.* Ref. 1). At $E=-785$ mV we got $q=-7.9$ μC cm^{-2} and $\phi_2=-44$ mV. However, in this case it proved more difficult to obtain a reliable value of q^1_{SCN}.

For $\alpha_j=0.65$ and $\phi_2=-60$ mV the Frumkin factor in eqn. (3) has the approximate value $10^{1.3-j}$. From the k_0-value in eqn. (5), [Zn(am)]=0.60 M and the Frumkin factor for $j=0$, the true rate constant $k^\ominus_0=(1.5\pm0.2)\times10^{-5}$ cm s^{-1} of the electrode reaction (1) of the solvated Zn^{2+} is obtained.

The Frumkin factor in eqn. (12), for $\alpha_{j,2}=0.70$ and $\phi_2=-44$ mV, has the value $10^{1.3-0.75j}$. With [DMSO]=14 M and using the values of the coefficients $k_{j,2}$, given by the expression (14), we finally calculated the ratios $k^\ominus_{1,2}/k^\ominus_{0,2}$ and $k^\ominus_{2,2}/k^\ominus_{1,2}$ of the true rate constants relating to the electrode reactions (8). For comparison these ratios have been put together (Table 3) with those of the cadmium halide systems.

DISCUSSION

The exponent $\alpha_0=0.65\pm0.03$ for [Zn^{2+}] in eqn. (5) does not permit a distinction to be made between two possible mechanisms of the charge transfer for the solvated Zn^{2+}, either a one-step or a two-step transfer with Zn(II)/Zn(I) as the rate-

Table 3. Ratios of the rate constants $k^\ominus_{j,2}$ relating to the charge transfer step Cd(II)/Cd(I) in the thiocyanate, bromide and iodide systems, and enthalpy changes, ΔH°_j, in the reactions $CdL_j^{3-j}+L^- \rightleftharpoons CdL_j^{2-j}$. Medium: 1 M NH_4ClO_4 in DMSO.

L^-	$k^\ominus_{1,2}/k^\ominus_{0,2}$	$k^\ominus_{2,2}/k^\ominus_{1,2}$	ΔH°_1/ kJ mol^{-1}	ΔH°_2/ kJ mol^{-1}
SCN^-	17	1.4	−3.0	−2.8
Br^-	7	235	−3.9	17
I^-	180	360	2.4	27
Ref.			7	7

limiting step in the latter case and with the disproportionation equilibrium (4) established. However, the fact that the same $k_0^{\ominus}$-value has been obtained for the thiocyanate and chloride systems gives support to the conclusion that also the mechanism is the same. Now, the exponent $\alpha_0 = 0.50 \pm 0.03$ of the chloride system led to the presumption[1] that in DMSO the electrode reaction for Zn^{2+} is predominantly a one-step transfer, and thus the same should hold for the thiocyanate system. Furthermore, it is very improbable that the presence of SCN^- could change the mechanism, since according to the measurements i_0 is not a function of $[SCN^-]$. On the other hand, the difference found between the α_0-values indicates that the different influences from SCN^- and Cl^- on the electrode double-layer are observable already at concentrations that are low compared with the ionic strength.

At the thiocyanate concentrations used in the kinetic measurements $[ZnNCS^+]/[Zn^{2+}] < 0.85$ and $[Zn(NCS)_2]/[Zn^{2+}] < 0.70$ in the bulk of the solutions. Then, if there is no effect that catalyzes the charge transfer, the calculated Frumkin factor in eqn. (3), which decreases rapidly with increasing values of j, should give the result that the contributions from these complexes to i_0 are not observed. For the anionic complexes similar conclusions can be drawn.

The result that the electrode reaction Zn(II)/Zn(am) in DMSO is not catalyzed by the presence of SCN^- as in water solutions would mean, according to the model given[1] for the solvent influence, that the DMSO molecules make the distance of closest approach of the zinc ion in the complexes to the amalgam surface too large to permit an effective ligand bridging at the electrode by SCN^-. Thus, in this respect SCN^- would be inferior to I^- in DMSO.

This conclusion could seem surprising in view of the linear shape of SCN^-. However, in crystalline AgSCN, containing bridging $-SCN-$ groups,[5] the chains formed are bent at the S atoms with a bond angle Ag–S–C of 104°. From this value and the bond lengths given an Ag–Ag distance of about 6 Å can be calculated. If the ionic radii[17] of the two Ag^+ are subtracted, the resulting "length" of the bridge is found to be not longer than the crystallographic diameter[18] of Br^-. Thus, on the assumption that the bond angle at the S atom is of about the same magnitude for a specifically adsorbed SCN^-, which probably is bonded to the amalgam surface through the S atom, the conclusion about the low ligand bridging ability of SCN^- in DMSO seems reasonable.

The finding in the electrocapillary measurements that in DMSO the specific adsorbability increases in the order $SCN^- < Br^-$, whereas the reverse order[19] is found for water solutions, could to some extent be explained by such a bond angle Hg–S–C. In this case the specifically adsorbed DMSO molecules should be expected to exert an extra large hindrance to adsorption of SCN^-.

For the cadmium thiocyanate system the calculated Frumkin factor in eqn. (12) does not decrease as rapidly at increasing values of j as for the zinc system, which helps to make the participation of $CdSCN^+$ and $Cd(SCN)_2$ in the electrode reaction (8) observable. From the values of $k_{1,2}^{\ominus}/k_{0,2}^{\ominus}$ in Table 3 it is evident that on formation of the first complex CdL^+ the rate enhancing effect of L^- on the charge transfer step Cd(II)/Cd(I) increases in the order $Br^- < SCN^- < I^-$. However, neither for Br^- nor for SCN^- do the values indicate an operative ligand bridging at the electrode, and this conclusion is in agreement with those arrived at for the zinc systems.

From the ratio $k_{2,2}^{\ominus}/k_{1,2}^{\ominus}$ in Table 3 it is seen that the increase in the rate constant at the formation of $Cd(SCN)_2$ is very small compared with the corresponding effect for $CdBr_2$ and CdI_2. The large increase for the last-mentioned complexes has been correlated[6] to the large, positive enthalpy change, ΔH_2°, accompanying their formation in DMSO. These positive ΔH_2°-values indicate a pronounced decrease in the inner sphere solvation[7] or a labilization of the solvation shell of the complex. In both cases a lowering of the energy of activation of the charge transfer step Cd(II)/Cd(I) can be anticipated. Now, for the thiocyanate system the small and negative values of ΔH_1° and ΔH_2° do not indicate a strong change of the solvation in any of the corresponding steps of the complex formation. Accordingly, no large rate enhancement of the electrode reaction should be expected, and the results from the thiocyanate system give good support of the validity of the correlation suggested. Thus, we have a plausible explanation of why in some of the cadmium systems a certain complex can be especially electroactive.

Acknowledgements. The financial support given to this investigation by the Swedish Natural Science Research Council is gratefully acknowledged. The authors wish to thank Dr. C. L.

Johansson for valuable discussions, Mrs C. Oskarsson for her assistance in the measurements and Dr. P. Sellers for revising the English.

REFERENCES

1. Fronæus, S. and Johansson, C. L. *J. Electroanal. Chem. 80* (1977) 283.
2. Randles, J. E. B. and Somerton, K. W. *Trans. Faraday Soc. 48* (1952) 951.
3. Tamamushi, R. and Tanaka, N. *Z. Phys. Chem. (Frankfurt am Main) 39* (1963) 117.
4. Blackledge, J. and Hush, N. S. *J. Electroanal. Chem. 5* (1963) 435.
5. Wells, A. F. *Structural Inorganic Chemistry*, 4th Ed., Clarendon Press, Oxford 1975, p. 746.
6. Fronæus, S., Johansson, C. L. and Palm, B. *J. Electroanal. Chem. 88* (1978) 1.
7. Ahrland, S. and Björk, N. O. *Acta Chem. Scand. A 30* (1976) 257.
8. Ahrland, S. and Björk, N. O. *Acta Chem. Scand. A 30* (1976) 249, 265.
9. Persson, H. *Acta Chem. Scand. 24* (1970) 3739.
10. Ahrland, S. and Björk, N. O. *Acta Chem. Scand. A 28* (1974) 823.
11. Johansson, R. and Östman, C. O. *Acta Chem. Scand. 23* (1969) 2939.
12. Johansson, R. *Acta Chem. Scand. 18* (1964) 1809.
13. Wijnen, M. D. and Smit, W. M. *Recl. Trav. Chim. Pays-Bas 79* (1960) 22, 203.
14. Fronæus, S. and Larsson, R. *Acta Chem. Scand. 16* (1962) 1447.
15. Fronæus, S., Johansson, R. and Östman, C. O. *Chem. Scr. 1* (1971) 52.
16. Fronæus, S. and Johansson, C. L. *J. Electroanal. Chem. 48* (1973) 195.
17. Shannon, R. D. and Prewitt, C. T. *Acta Crystallogr. B 25* (1969) 925.
18. Morris, D. F. C. In *Structure and Bonding*, Springer, Berlin 1968, Vol. 4, p. 63.
19. Grahame, D. C. *Chem. Rev. 41* (1947) 441.

Received June 2, 1978.

Acta Chemica Scandinavica A 32 (1978) 917 – 923

Reaction Rate Studies of the Acid Hydrolysis of Some Chromium(III) Complexes. X. Structure and Reactivity of Ammineaquadichloridochromium(III) Complexes

L. MØNSTED and O. MØNSTED

Department I, Inorganic Chemistry, H. C. Ørsted Institute, University of Copenhagen, Universitetsparken 5, DK-2100 Copenhagen Ø, Denmark

Dedicated to Jannik Bjerrum on the occasion of his 70th birthday

Four compounds with the stoichiometric composition: $[Cr(NH_3)_x(OH_2)_{4-x}Cl_2]Cl$ (x = *mer*-3, *cis*-2, *trans*-2 and 1) have been investigated. They all have been shown to have a *trans* dichlorido configuration. In acid solution both isomerization to *cis* dichlorido isomers with unchanged ammine configuration and also chloride ligand substitution take place. The kinetics of the latter process have been investigated by using a chloride ion sensitive electrode, and data at 50 – 80 °C, 0.25 – 1.00 M H^+ for a 1.00 M (Na,H)ClO_4 medium are reported. In combination with previous data for hydrolysis of the ammineaquachromium(III) isomers, a common pattern has been established for the effect of coordinated water and ammonia in *cis* position to the reacting ligand for the three series of complexes.

Isomerization of *cis*- and *trans*-tetraaquadichloridochromium(III) occurs in acid aqueous solution in addition to the formation of pentaaquachloridochromium(III).[1,2] This contrasts the reported behaviour both of the pair of tetraamminedichloridochromium(III) complexes,[3,4] and of a pair of amminetriaquadichloridochromium(III) complexes.[5] In none of these latter cases was isomerization detected. Dichloridochromium(III) species derived from *mer*-triammine-[6,7] and *cis*-[8] and *trans*-diamminechromium(III)[9] have been prepared, but these compounds have apparently not been investigated kinetically. Information on stereochemical changes of chromium(III) complexes is very limited, and therefore this study was undertaken to find whether these complexes would conform to the picture established for the tetraaqua- or the tetraamminechromium(III) species.

EXPERIMENTAL

Chemicals. *trans*-$[Cr(NH_3)_4Cl_2]Cl.H_2O$,[10] *trans*-$[Cr(NH_3)_4Cl_2]ClO_4$,[10] *cis*-$[Cr(NH_3)_4Cl_2]Cl.H_2O$,[4] *cis*-$[Cr(NH_3)_4Cl_2]ClO_4$,[4] *mer*-$[Cr(NH_3)_3(OH_2)Cl_2]Cl$,[6,7] *cis*-$[Cr(NH_3)_2(OH_2)_2Cl_2]Cl$,[8] and *trans*-$[Cr(NH_3)_2(OH_2)_2Cl_2]Cl$,[9] where all the prefixes relate to the ammine configuration, were prepared by literature methods. Crude $[Cr(NH_3)(OH_2)_3Cl_2]Cl$ was prepared by vacuum evaporation to dryness of a solution of $[Cr(NH_3)(OH_2)_5]^{3+}$ in 4 M hydrochloric acid at 50 °C.[11] The solid substance thus obtained was recrystallized twice by the method described for *trans*-$[Cr(OH_2)_4Cl_2]Cl.2H_2O$.[12] The sources of the other chemicals employed have been described earlier.[13]

Ion exchange separations of this type of complexes,[2] *methods of analyses*[13] and *spectrophotometric measurements*[2] have all been described earlier.

X-Ray powder photographs were taken with Cu$K\alpha$ radiation using a focusing camera of the Guinier type.

Kinetic measurements. All the reactions studied in this paper proceed with the release of coordinated chloride ions. The progress of the reactions could therefore conveniently be followed potentiometrically. The measurements were carried out directly in the reacting solutions using a silver/silver chloride

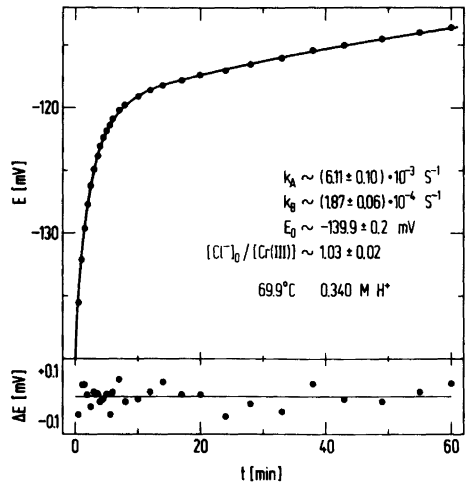

Fig. 1. Kinetic experiment started by dissolving *trans*-$[Cr(NH_3)_4Cl_2]Cl.H_2O$ in 1 M perchlorate solution. Upper part: Experimental (●) and calculated (——) time dependence of the potential. The solid curve is calculated from the parameter values shown on the figure.

Lower part: Differences between experimental and calculated potentials.

electrode, prepared in a way which assured rapid response,[14] in combination with either a Radiometer PHM 52 digital pH-meter or a Varian G-2000 strip-chart recorder. The need to raise the temperature up to 80 °C and the requirement for accurate measurements of small potential differences place severe limitations on usable reference electrodes. Finally a silver/silver chloride electrode in the reaction medium, made ~1 mM in chloride ions, and separated from the reaction solution by a porous glass disc, was employed.

The kinetic experiments were all started by the addition of a suitable amount of the solid chromium(III) compound as the chloride or the perchlorate salt to the thermostated reaction medium. The results of a typical experiment are shown in Fig. 1. To ascertain the validity of the present experimental approach, the first stage of the hydrolysis of *trans*-tetraamminedichloridochromium(III) was reexamined. This process has earlier been investigated spectrophotometrically,[3] and a comparison is given in Table 1. The agreement is satisfactory and supports the use of the direct potentiometric method for the study of the present reactions.

cis-Tetraamminedichloridochromium(III) was also re-examined analogously in order to obtain data for a 1.00 M perchlorate medium. The results for this reaction are given in Table 2. They are slightly different from those obtained earlier by a spectrophotometric method, but this is not unexpected since the reaction medium is changed.

Table 1. Kinetic data for the process: *trans*-$[Cr(NH_3)_4Cl_2]^+ \rightarrow$ *trans*-$[Cr(NH_3)_4(OH_2)Cl]^{2+} + Cl^-$ in 1.00 M (Na,H)ClO_4.

$10^4 k$ (45 °C) $[s^{-1}]$	E $[kJ\ mol^{-1}]$	Ref.
4.8±0.1	90.4±1.3	3 [a]
4.6±0.2	91.4±1.6	[b]

[a] Spectrophotometric data at 45–55 °C, 0.20–1.00 M H^+. [b] This work. Potentiometric data at 50–80 °C, 0.25–1.00 M H^+.

Table 2. Kinetic data for the process: *cis*-$[Cr(NH_3)_4Cl_2]^+ \rightarrow$ *cis*-$[Cr(NH_3)_4(OH_2)Cl]^{2+} + Cl^-$.

$10^5 k$ (25 °C) $[s^{-1}]$	E $[kJ\ mol^{-1}]$	Ref.
33.0±1.5	87.0±2.1	4 [a]
21.2±0.9	92.4±1.1	[b]

[a] Spectrophotometric data at 20–45 °C, 0.01–0.40 M H^+ in 0.40 M (Na,H)NO_3. [b] This work. Potentiometric data at 30–70 °C, 0.33–1.00 M H^+ in 1.00 M (Na,H)-ClO_4.

Method of calculation. When chloride ions are released in a two stage process:

$$A \xrightarrow{k_A} B + Cl^-$$

$$B \xrightarrow{k_B} C + Cl^-$$

and $k_A \neq k_B$, the following expression, for an experiment started without B and C, is valid for the chloride ion concentration at time t:

$$[Cl^-]_t = [Cl^-]_0 + [A]_0\{2 + \frac{2k_B - k_A}{k_A - k_B}\exp(-k_A t) - \frac{k_A}{k_A - k_B}\exp(-k_B t)\}$$

and the potential of a chloride sensitive electrode is given by:

$$E_t = E_0 + \frac{RT}{F}\ln\frac{[Cl^-]_t}{[Cl^-]_0}$$

The experimental points $E(t)$ were approximated by a curve calculated using these expressions from the four parameters: k_A, k_B, E_0 and $[Cl^-]_0/[A]_0$, estimated by minimization of:

$$\sum_t (E(t)-E_t)^2/(\sigma_E^2+\left(\frac{dE}{dt}\right)^2\sigma_t^2)$$

where σ_E^2 and σ_t^2 are the variances of potential and time measurements, respectively. This proceeded without difficulties, *cf.* Fig. 1, and is a convenient way to overcome the difficulties encountered in an analytical estimation of $[Cl^-]_0$. The further calculations to yield activation parameters were carried out essentially as described previously.[2]

RESULTS AND DISCUSSION

Solid dichloridochromium(III) compounds have been prepared with various combinations of ammonia and water ligands at the four remaining coordination positions. Only one of the two possible tetraaquadichloridochromium(III) isomers has been crystallized, and this is known to have the *trans* dichlorido configuration.[15,16] Tetraamminedichloridochromium(III) may be crystallized as salts of various anions,[3,4,10] and although no direct structural investigations have apparently been carried out on any of these compounds the existence and properties of both isomers have allowed unambiguous structural conclusions to be drawn.

Four solid dichlorido derivatives of triammine-, diammine- and monoamminechromium(III) have so far been obtained, but these ammineaquadichloridochromium(III) ions are structurally less well characterized than the dichlorido derivatives of tetraammine- and tetraaquachromium(III). Mercury(II)-accelerated chloride ligand substitution yields usually for this type of complexes products in which the major component has an unchanged ammine configuration. For the dichloridochromium(III) complexes dealt with here mercury(II) generates pure *mer*-triamminetriaquachromium(III) from the dichlorido compound prepared from triaminediperoxochromium(IV)[6,7] and pure *cis*- and *trans*-diamminetetraaquachromium(III) from the two diammines prepared from "Rhodosochromium(III) chloride"[8] and "Reinecke salt",[9] respectively. Structural investigations on the three starting materials show that these also have a *mer*-triammine[17] and a *cis*-[18] and a *trans*-diammine[19] configuration. Therefore, since the three compounds investigated here are both generated from and yield products with identical ammine configurations, these configurations most likely also persist in the solid ammineaquadichloridochromium(III) chlorides.

Information on the configuration of the two chloride ligands is less easily obtained. For the *mer* triammine and *trans* diammine derivatives both a *trans* and a *cis* dichlorido configuration is possible whereas for both the *cis* diammine and the monoammine two *cis* and one *trans* isomer may exist.

The isomeric pairs of both the tetraammine- and the tetraaquadichloridochromium(III) ions can be separated by ion exchange chromatography,[2] and in both cases the *trans* isomer is eluted first. Similar fractionation experiments on freshly prepared solutions of the other four monopositive ammineaquadichlorido ions do not reveal the existence of separable isomers in these solutions, judged from the visible absorption spectra of successive column eluates. The spectral characteristics are given in Table 3.

Solutions of these dichlorido ions aged for 1–2 half-lives with respect to substitution of the first chloride ligand exhibit, however, an elution behaviour, for the band of monopositive species, which is different: For all the four ions in question only the first fractions of the band of monopositive species contain a species with an absorption spectrum identical to that of the freshly prepared

Table 3. Spectral characteristics of solutions of *trans*-dichlorido complexes prepared and purified as described in the text and diluted with perchloric acid to yield a 0.5 M perchloric acid solution.

Complex	λ_1 max [nm]	ε_1 max [l mol^{-1} cm^{-1}]	λ_2 max [nm]	ε_2 max [l mol^{-1} cm^{-1}]	ε_1 max/ε_2 max
mer-$[Cr(NH_3)_3(H_2O)Cl_2]^+$	597	25.9	409	27.1	0.956
cis-$[Cr(NH_3)_2(H_2O)_2Cl_2]^+$	604	33.8	419	24.8	1.363
trans-$[Cr(NH_3)_2(H_2O)_2Cl_2]^+$	583	23.9	421	26.4	0.905
$[Cr(NH_3)(H_2O)_3Cl_2]^+$	612	31.7	434	23.4	1.355

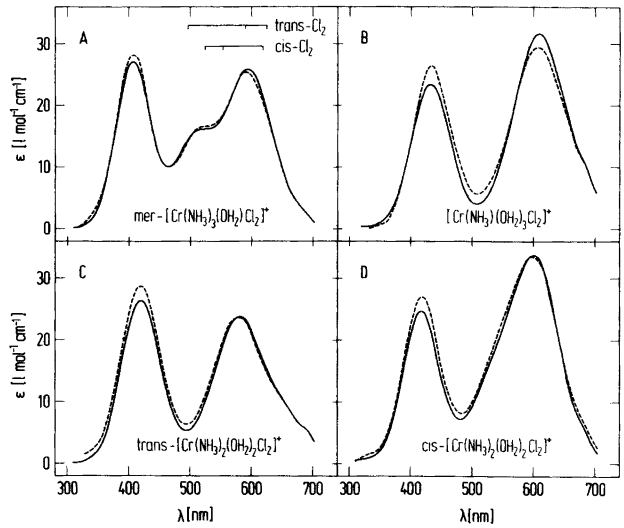

Fig. 2. Visible absorption spectra of ammineaquadichloridochromium(III) complexes. Solid curves: Pure isomers. Broken curves: Last fraction of dichlorido species after ageing in solution (see the text).

solutions. The latter fractions have a different absorption spectrum. This is shown in Fig. 2A – D. Treatment of the eluates with mercury(II) reveal an unchanged ammine configuration, and therefore the observed difference in elution behaviour is caused by a change in the configuration of the remaining ligands. The elution behaviour of these fresh and aged solutions can be compared with that of the isomeric tetraammine- and tetraaquadichloridochromium(III) isomers. This indicates firstly that the four solid ammineaquachromium(III) salts contain *trans* dichlorido isomers, and secondly that these in aqueous solution slowly isomerize to form *cis* dichlorido isomers.

Additional evidence in favour of a *trans* dichlorido configuration of the solid ammineaquadichloridochromium(III) chlorides comes from absorption spectra and X-ray powder diffraction photographs:

Fig. 2A shows calculated band component positions, using the model and the parameters described in Ref. 20, for the *cis* and *trans* dichlorido isomers derived from the *mer* triammine. Comparisons with the observed absorption spectrum clearly support the assignment of a *trans* dichlorido configuration to the cation of solid *mer*-triammineaquadichloridochromium(III) chloride. For the remaining dichlorido complexes this approach yields no additional information, since the calculated band component positions differ too little to be of value in this respect.

Empirically the same pattern of variation of the intensities of the first and second spin-allowed absorption band is observed for all the pairs of dichlorido isomers: The second band shows an increase in intensity and the first a decrease in intensity on the lower wave-length side when going from the assumed pure *trans* dichlorido isomers to the mixtures of *cis* and *trans* isomers. This is similar to the variation observed from *trans*- to *cis*-tetraammine- and -tetraaquadichloridochromium-(III),[3,4,2] and support the assumption that *cis* dichlorido isomers are formed in solution from the *trans* isomers.

Significant similarities exist between the so-called "dichrochloride" and the solid chloride salts of the dichlorido derivatives of the *mer* triammine and the *cis* diammine. This can be seen both from the marked red – blue-green dichroism of all these three substances and also from the very similar X-ray powder diffraction photographs. "Dichrochloride" is known from a crystal structure analysis to be *mer*-triammineaqua-*trans*-dichloridocobalt-(III) chloride,[21] and this again supports the configurational assignments.

Kinetic investigations of the reactions of these dichlorido complexes are obviously complicated by the concurrent isomerization and loss of chloride ligand, in particular since the generated *cis* isomers

Table 4. Rate constants at 70 °C and activation energies for the acid independent reactions of some *trans*-dichloridochromium(III) complexes in aqueous 1.00 M (Na,H)ClO_4 solution.

Complex	$10^3 k$ (70 °C)[a] [s^{-1}]	E^a [kJ mol^{-1}]
mer-$[Cr(NH_3)_3(OH_2)Cl_2]^+$	7.45±0.14	102.3±1.3
cis-$[Cr(NH_3)_2(OH_2)_2Cl_2]^+$	9.9±0.3	96.2±2.1
trans-$[Cr(NH_3)_2(OH_2)_2Cl_2]^+$	4.39±0.05	96.5±1.1
$[Cr(NH_3)(OH_2)_3Cl_2]^+$	7.2±0.3[b]	96.2±2.5[b]

[a] Data based on 15 – 20 experiments for each complex, covering the temperature and hydrogen ion concentration ranges 50 – 80 °C and 0.25 – 1.00 M H^+, respectively. For this range of hydrogen ion concentrations, the reaction rate constants were independent of the hydrogen ion concentration. [b] These data are at variance with an earlier investigation in 1 M perchlorate solution of a complex said to be amminetriaqua-*trans*-dichloridochromium(III).[5] From the data in Ref. 5 it may be calculated that k (70 °C) ~ (4.2±0.3) 10^{-3} s^{-1} and E ~84.5±0.9 kJ mol^{-1}. Two absorption spectra of this species given in Ref. 5 do not agree with each other, nor do they agree with Fig. 2B of this paper, but both may be expressed as a linear combination of this latter spectrum and that of the *cis* isomer in Ref. 5. From the reported $\varepsilon_1/\varepsilon_2$ ratios *trans* isomer contents in the said *trans* isomer of Ref. 5 of about 77 % and 51 % are calculated from Figs. 1 and 2B in Ref. 5, respectively. This explains the discrepancy between the present data and those earlier reported.

have not yet been obtained in a pure state. It has earlier been demonstrated that spectrophotometric measurements are less readily interpreted when components of unknown spectral characteristics are present.[1] Therefore the kinetic investigations in this work were based upon measurements of generated chloride ions. A series of experiments were carried out using a 1.00 M perchlorate medium, over a range of temperature and hydrogen ion concentration of 50 – 80 °C and 0.25 – 1.00 M H^+, respectively. All the results could be interpreted by the simplified reaction scheme:

$$[Cr(NH_3)_x(OH_2)_{4-x}Cl_2]^+ \rightarrow [Cr(NH_3)_x(OH_2)_{5-x}Cl]^{2+} + Cl^-$$

$$[Cr(NH_3)_x(OH_2)_{5-x}Cl]^{2+} \rightarrow [Cr(NH_3)_x(OH_2)_{6-x}]^{3+} + Cl^-$$

which is additional evidence in favour of the presence of only small amounts of *cis* dichlorido isomers. A summary of the data thus obtained for the first step is given in Table 4.

The absence of noticeable amounts of *cis* isomers, indicated by the chromatographic experiments, does not preclude the possibility that these isomers are important for the observed release of coordinated chloride ions. Comparisons with the known reactivities of other chloridochromium(III) complexes, *cf.* Table 5, indicate that provided at least one of the chloride ligands in the generated *cis* dichlorido isomer is in *trans* position to coordinated ammonia this complex is expected to

Table 5. Kinetic parameters for hydrolysis of chloridochromium(III) complexes in 1 M perchlorate solution.

Complex	$10^5 k$ (25 °C)[b] [s^{-1}]	$\Delta H^{\neq}$ [kJ mol^{-1}]	$\Delta S^{\neq}$ [b] [J K^{-1} mol^{-1}]	Ref.
trans-$[Cr(NH_3)_4Cl_2]^+$	4.5±0.3	88.9±1.2	−29±4	3,[a]
cis-$[Cr(NH_3)_4Cl_2]^+$	21.2±0.9	89.7±1.1	−14±3	[a]
trans-$[Cr(OH_2)_4Cl_2]^+$	4.53±0.11	95.7±1.4	−7±4	2
cis-$[Cr(OH_2)_4Cl_2]^+$	1.53±0.15	101±5	+1±17	2
mer-$[Cr(NH_3)_3(OH_2)Cl_2]^+$	3.31±0.21	99.5±1.3	+4±4	[a]
cis-$[Cr(NH_3)_2(OH_2)_2Cl_2]^+$	6.1±0.6	93.4±2.1	−11±6	[a]
trans-$[Cr(NH_3)_2(OH_2)_2Cl_2]^+$	2.65±0.16	93.7±1.1	−17±3	[a]
$[Cr(NH_3)(OH_2)_3Cl_2]^+$	4.5±0.5	93.4±2.5	−14±7	[a]
$[Cr(NH_3)_5Cl]^{2+}$ [c]	0.98±0.03	90.4±1.3	−38±4	22, 23, 24
$[Cr(OH_2)_5Cl]^{2+}$	0.0277	101.7±0.8	−30±2	25

[a] This work. [b] Rate constants and activation entropies are not corrected statistically for the dichlorido complexes (R ln 2 ~ 5.8 J K^{-1} mol^{-1}). [c] 0.1 M perchlorate solution.

hydrolyze so fast that it will not accumulate in significant quantities. In this case the observed rate constant will be a mixture of that for the direct chloride release path and that for the isomerization path which is followed by the rapid chloride ligand release. For the *cis* dichlorido isomers derived from both the *mer* triammine and the *cis* diammine one chloride ligand is always in *trans* position to coordinated ammonia, for the monoammine derivative such a configuration is present in one of the *cis* dichlorido isomers, whereas for the *cis* dichlorido derivative of the *trans* diammine the possibility of a chloride ligand in *trans* position to an ammonia ligand does not exist. Consequently, except for the *trans* diammine derivative, the possibility of significant contributions from an isomerization reaction to the observed rate of chloride ligand release cannot be eliminated.

Both the $\Delta H^{\neq}$ and the $\Delta S^{\neq}$ values of the series of reactions of the *trans* dichlorido isomers increase almost linearly as functions of the number of water ligands in the complex, if the reactivity parameters of the *trans* dichlorido isomer derived from the *mer* triammine are disregarded. For this latter complex positive deviations from the linear correlation of about $+9$ kJ mol^{-1} and $+26$ J K^{-1} mol^{-1}, respectively, are found. The activation parameters for the isomerization reaction of the *trans*-tetraaquadichloridochromium(III) ion are about 18 kJ mol and 57 J K^{-1} mol^{-1} more positive than those for the hydrolysis reaction.[2] The result of a comparison between these two sets of values is therefore a strong indication of a significant contribution from an isomerization path to the observed chloride release for the *mer* triammine derivative, in contrast to the remaining data, which correlate well with those for the tetraammine and the tetraaqua complexes, for which the reported values are those for the direct chloride release path. Therefore the reactivity parameters of the dichlorido derivatives of both the *cis*- and the *trans* diammine and the monoammine do not seem to be influenced significantly by isomerization reactions.

In Table 6 the influences of the systematic variation of the four *cis* ligands from tetraammine to tetraaqua are shown for the three types of reaction where all the possible combinations of water and ammonia ligands are known. In all the three series of reactions the effect of this variation of the *cis* ligands is small, amounting usually to less than a factor of two on the reaction rate constants. Within this range, however, the variation in rate constants as function of the *cis* ligands is rather consistent: If the rate constants are labeled according to the number (1, 2, 3 or 4) and configuration (*cis* or *trans*) of ammonia ligands in the four *cis* positions to the reacting ligand which may be thought of as a square planar complex the following series of inequalities:

$$k_4 < k_3 \sim k_1 < k_{2c}$$
and: $$k_3 \sim k_1 > k_{2t}$$

for the kinetic *cis* effect of water compared to ammonia holds through the three series of complexes. In view of the differences in both leaving ligands and *trans* ligands of the series of reactions upon which this pattern is based, the consistency of the *cis* effect is somewhat surprising and may be taken as evidence in favour of the hypothesis

Table 6. Statistically corrected rate constants for some reactions of the type: $[Cr(cis)_4(trans)X] + H_2O \rightarrow [Cr(cis)_4(trans)(OH_2)] + X$.

$(cis)_4$	$10^6 k$ (70 °C)[a] [s^{-1}]	$10^6 k$ (70 °C)[a] [s^{-1}]	$10^3 k$ (70 °C)[b] [s^{-1}]
$(NH_3)_4$	8.0±0.2	0.0±0.5	2.89±0.06
$(NH_3)_3(OH_2)$	11.8±0.2	1.7±0.3	3.72±0.07
cis-$(NH_3)_2(OH_2)_2$	12.1±0.3	2.53±0.10	4.45±0.14
trans-$(NH_3)_2(OH_2)_2$	11.1±0.2	0.5±0.4	2.19±0.03
$(NH_3)(OH_2)_3$	11.8±0.2	1.69±0.04	3.62±0.13
$(OH_2)_4$	8.75±0.15	1.108±0.011	4.1±0.3
trans	NH_3	OH_2	Cl^-
X	NH_3	NH_3	Cl^-

[a] Ref. 26. [b] This work, Tables 1 and 4, and Ref. 2.

earlier advanced for the interactions between the leaving ligand and the *cis* ligands,[27] namely that these interactions are not very different in the transition state and the ground state for the present type of complexes.

With the work described here and that in the literature the whole series of ammineaqua-*trans*-dichloridochromium(III) complexes has been investigated kinetically. Isomerization reactions are only observed when water is present in the first coordination sphere and this supports the view earlier advanced that configurational changes of such simple chromium(III) complexes occur as the result of solvent exchange.[2,28]

Acknowledgement. The authors wish to thank F. S. Nielsen and M. Olsen who carried out most of the potentiometric measurements.

REFERENCES

1. Salzman, J. D. and King, E. L. *Inorg. Chem. 6* (1967) 426.
2. Mønsted, L. and Mønsted, O. *Acta Chem. Scand. A 32* (1978) 19.
3. Hoppenjans, D. W., Hunt, J. B. and Gregoire, C. R. *Inorg. Chem. 7* (1968) 2506.
4. Jackson, W. G., Vowles, P. D. and Fee, W. W. *Inorg. Chim. Acta 19* (1976) 221.
5. Williams, T. J. and Garner, C. S. *Inorg. Chem. 9* (1970) 52.
6. Schlessinger, G. G. *Inorganic Laboratory Preparations*, New York 1962, p. 249.
7. Caldwell, S. H. and House, D. A. *Inorg. Chem. 8* (1969) 151.
8. Berg, T. and Andersen, P. *To be published.*
9. Werner, A. and Klien, J. *Ber. Dtsch. Chem. Ges. 35* (1902) 277.
10. Glerup, J. and Schäffer, C. E. *Inorg. Chem. 15* (1976) 1408.
11. Ardon, M. and Mayer, B. E. *J. Chem. Soc.* (1962) 2816.
12. Bjerrum, N. *K. Dan. Vidensk. Selsk. Skr. Naturvidensk. Math. Afd. IV. 1* (1907) 8.
13. Mønsted, L. and Mønsted, O. *Acta Chem. Scand. 27* (1973) 2121.
14. Durst, R. A., Ed., Ion-Selective Electrodes, p. 115 ff; *NBS Special Publication No. 314*, Washington 1969, and references therein.
15. Dance, I. G. and Freeman, H. C. *Inorg. Chem. 4* (1965) 1555.
16. Morosin, B. *Acta Crystallogr. 21* (1966) 280.
17. McLaren, E. H. and Helmholz, L. *J. Phys. Chem. 63* (1959) 1279.
18. Bang, E. *Acta Chem. Scand. 22* (1968) 2671.
19. Takéuchi, Y. and Saito, Y. *Bull. Chem. Soc. Jpn. 30* (1957) 319.
20. Glerup, J., Mønsted, O. and Schäffer, C. E. *Inorg. Chem. 15* (1976) 1399.
21. Tanito, Y., Saito, Y. and Kuroya, H. *Bull. Chem. Soc. Jpn. 25* (1952) 328.
22. Levine, M. A., Jones, T. P., Harris, W. E. and Wallace, W. J. *J. Am. Chem. Soc. 83* (1961) 2453, recalculated in Ref. 23.
23. Jones, T. P. and Phillips, J. K. *J. Chem. Soc. A* (1968) 674.
24. Duffy, N. V. and Early, J. E. *J. Am. Chem. Soc. 89* (1967) 272.
25. Swaddle, T. W. and King, E. L. *Inorg. Chem. 4* (1965) 532.
26. Mønsted, L. and Mønsted, O. *Acta Chem. Scand. A 28* (1974) 569.
27. Mønsted, O. *Acta Chem. Scand. A 32* (1978) 297.
28. Mønsted, L. and Mønsted, O. *Acta Chem. Scand. A 29* (1975) 29.

Received June 8, 1978.

Acta Chemica Scandinavica A 32 (1978) 925–928

Ultrasonic Velocity and the Gel/Sol Transition for Differently Irradiated Gelatins

KIRSTEN DELA and JØRGEN RASSING

Royal Danish School of Pharmacy, Department of Chemistry and Pharmaceutical Inorganic and Physical Chemistry. Universitetsparken 2, DK-2100 Copenhagen Ø, Denmark

Dedicated to Jannik Bjerrum on the occasion of his 70th birthday

The ultrasonic technique has been extended in a way that permits melting points and melting intervals for the gel/sol phase transition in diluted gelatin gels to be investigated. The method has been used in the investigation of two different gelatins with the same mechanical properties. The effect of γ-irradiation and accelerator irradiation on the two gelatins has furthermore been studied and a physico-chemical treatment of the data has been carried out with special emphasis on the melting enthalpies for the systems in question.

The effect of high energy radiation on gelatin has been intensively investigated mainly due to the importance of the material in food, film, and the pharmaceutical industry.[1] It is well known that the characteristics of the gelatin and the radiation, the dosage and the experimental conditions, have a vast influence on the obtained results but the mode of this influence is not clearly resolved. This situation is probably responsible for the fact that in the literature the effect of high energy radiation on gelatin appears to be contradictory, some works suggesting cross-linking[2] and other works suggesting degradation.[3] It seems likely, however, that the radiation effect is caused by a highly complex process which involves free radicals that may cause intermolecular cross-linking and peptide bond hydrolysis simultaneously. γ-Irradiation of dry gelatin using a ^{60}Co source does not change the viscosity or the melting point of the gelatin[4] whereas γ-irradiation on gelatin/water mixtures causes a change in those parameters[5] indicating that water molecules play a significant role.

A decrease in the viscosity and in the gel melting point is generally attributed to a decrease in the average molecular weight of the protein molecules. It is important to notice, however, that the melting point of the gel depends strongly on its thermal history. For instance, the melting point of a gel formed by slow cooling of a sol is different from that of a gel formed by quick chilling of the same sol. Consequently, the experimental conditions for the entire working procedure must be carefully specified in order for the obtained melting points to be comparable. Furthermore, it is necessary empirically to define the phase transition temperature. For instance, the melting point may be defined as the temperature at which a specified Neoprene ball inserted under the gel surface reaches the bottom of a tube of a gel that is heated by a certain number of degrees per hour,[6] or as the temperature at which the gel softens sufficiently to allow a drop of coloured Carbon Tetrachloride to sink through.[7] Although the gel melting pont, determined by either of these methods is arbitrary, it provides a useful guide to the changes in the structure that may arise in the gel. Of course, a measurement that gives a single value for the melting point, although a melting interval exists, only provides information about the strength of the last bonds that maintain the network throughout the system. Weaker links are presumably broken at lower temperature and probably even stronger links remain in the aggregates which persist at temperatures slightly above the quoted melting point. An experimental method that makes it possible to monitor very small changes in the gel structure over the entire melting

interval might provide progress in the understanding of the sol/gel transition in gelatin. Although the ultrasonic velocity has proved to be a useful tool for investigating polymer structure[10] it has not yet been used for investigations of the gel/sol transition temperature. This paper presents, for the first time, such an experiment and it is based on the ultrasound velocity at 4 MHz.

A serious problem concerning work on gelatin deals with the characterization of the sample. Modern work is often based on a gelatin specifically prepared in a way that makes the material well defined to the extent possible as far as the molecular weight distribution and composition are concerned. This work deals with two different commercially available gelatins, A and B, with the only basic specifications that they have identical rigidity or mechanical properties (Bloom factors). The work is based on changes in the unknown molecular weight distribution produced by means of controlled irradiation. Different doses of γ-irradiation from a ^{60}Co source are used for this purpose. Furthermore accelerator irradiation is used in order to evaluate possible differences between uncharged and charged irradiation.

EXPERIMENTAL

The sound velocity was measured by means of the sing around technique. In principle the sample is kept in a cylindrical cell, the ends of which are sealed with piezoelectrical quartz crystals. By means of an oscillator the sending crystal is excited by a radio frequency signal of 4 MHz for a duration time of 3 μs. The resulting sound wave produced in the system is detected by the other crystal and the created voltage triggers the oscillator to produce a second frequency signal across the sending crystal and so on. Thus the pulse repetition frequency in the circuit is related to the velocity of the sound wave that travels through the sample. The equipment is a modified NUS – Sonic Solution Monitor. The modification involves an attachment that makes it possible for the oscillator successively to operate two different cells and to print the pulse repetition frequency as well as the temperature inside the cells with convenient time intervals. The change in temperature is controlled by a synchronous motor that drives the contact thermometer of the thermostat. The following additional equipment is used: frequency counter (Philips PM 6630), digital printer (Philips PM 2466) and digital thermometer (Doric).

The powdered gelatin was obtained from Nordisk Gelatine, Slangerup, Denmark with the specifications that gelatin A is prepared from pig skin and bone by acid extraction and gelatin B is prepared from calf skin and bone by basic extraction. The Bloom strength for both gelatins is 225.

The sol was made up from the powdered gelatin by adding cold water and then heating slowly to 60 °C. The pH of all the samples was 5 ± 0.5. The solution was placed in the measuring cell and kept at 55 °C for 4 h. The cooling rate was 17.5 degrees per hour. The system was kept at 10 °C for 7 h and was then heated at the heating rate of 17.5 °C/h. The system was monitored during the heating period only. Experiments involving the cooling period as well show the characteristic hysteresis behaviour resulting in considerably less reproducible values of the gel setting point. Each gelatin probe was investigated in 3 concentrations (2.0, 3.5, and 5.0 % w/w) and each experiment was repeated twice giving rise to the uncertainties given in Table 1.

The γ-irradiation using a ^{60}Co source and the accelerator irradiation were carried out at RISØ, Roskilde, Denmark. Before irradiation the powdered gelatin was equilibrated over saturated $NaNO_2$ solution at 25 °C for 12 h corresponding to an atmosphere with 64 % water content.

THEORY

The sound velocity, u, is given by eqn. (1)

$$u^2 = 1/(\rho\beta) \quad (1)$$

where ρ and β denote the density and the adiabatic compressibility of the system, respectively.

The inflection point of the plot of sound velocity *vs.* temperature may be regarded as the average melting temperature of the gel whereas the further curvature shows a melting interval, indicating structural changes at slightly lower as well as at slightly higher temperatures.

The enthalpy change for the gel/sol transition is related to the dependence of the average melting temperature, T_g, on the concentration of gelatin. The following equation[11] may be derived on the basis of several approximations that are only fulfilled if small concentration variations are involved below about 5 % overall concentration:

$$\mathrm{d}(\ln c)/\mathrm{d}T_g = \Delta H^\circ/(RT_g^2) \quad (2)$$

c and T_g being the concentration of gelatin (w/w) and the temperature in Kelvin degrees, respectively.

The enthalpy change is that of the cross-linking process provided that the links holding the gel together result mainly from a binary association of polymer chains. Thus $\Delta H°$ represents the heat of reaction for the process:

1 mol cross-links → 2 mol cross-linking loci

RESULTS

Fig. 1 shows a typical plot of the sound velocity *vs.* temperature when the matured gel is heated following the above described procedure. The curvature clearly indicates a melting interval. The data obtained from the different gelatins are given in Table 1. Table 2 gives the melting enthalpies for the different gelatins calculated on the basis of eqn. (2). All standard deviations are smaller than 0.1 %.

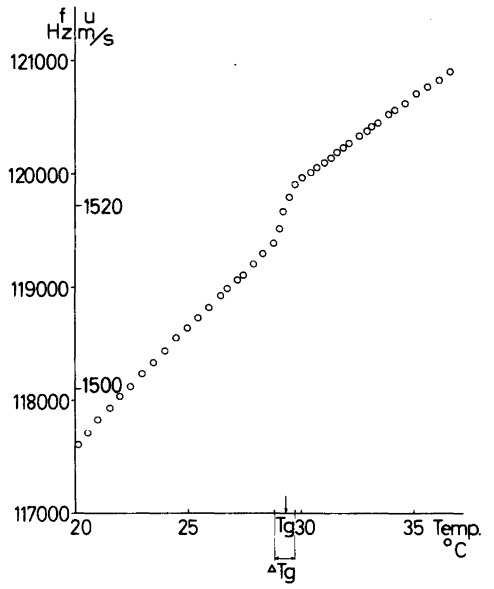

Fig. 1. A typical plot of the sound velocity, u, (and the pulse repetition frequency, f) *vs.* the temperature for 2.5 Mrad accelerator irradiated gelatin B-gel (3.5 % W/W).

DISCUSSION

The irradiation of powdered gelatin A and B in doses from 2.5 to 10 Mrad causes a decrease in the melting point of the diluted gels prepared from the material after irradiation. The effect of the uncharged γ-irradiation differs slightly from that of the charged accelerator irradiation, the latter giving rise to smaller changes in the melting points. This may be related to different efficiencies as far as penetration is concerned. The melting intervals, although these are difficult to obtain with satisfactory reproducibility, show a tendency to increase with increasing irradiation dosage indicating that

Table 1. Melting points (°C) and melting intervals for a typical gelatin gel (gelatin B, 3.5 % w/w). The irradiation has been carried out on the powdered gelatin.

	Non irradiated	γ-Irradiated			Accel. irradiated		
Mrad	–	2.5	5.0	10.0	2.5	5.0	10.0
T_g (±0.15)	30.26	28.77	27.96	26.76	29.61	28.89	27.05
ΔT_g (±0.09)	0.63	0.46	0.67	0.98	0.71	0.75	0.76

Table 2. Melting enthalpies for non irradiated and for differently irradiated gelatin A and gelatin B gels.

	$\Delta H°$ kJ per mol of cross-links						
	Non irradiated	γ-Irradiated			Accel. irradiated		
Mrad	–	2.5	5.0	10.0	2.5	5.0	10.0
Gelatin A	309	309	293	207	256	215	287
Gelantin B	250	370	239	222	333	351	170

irradiation may cause a wider range of bond-strengths that maintain the gel network.

The enthalpy change reflecting the cross-link stability shows a vast variation with irradiation although the actual changes are difficult to correlate with the irradiation doses in a simple manner. A decrease in this enthalpy change and hence a decrease in the bond-strength that maintain the gel network may be attributed to a higher content of covalent links introduced in the dry bulk material by the irradiation. Thus further covalently cross-linked gelatin, when dissolved, may produce weaker gels on cooling because these additional links interfere with the freedom of the polypeptide chains to adopt the conformation necessary for the gel structure to be established. The fact that high irradiation doses cause decreasing enthalpy changes supports this point of view. Thus a decrease in the melting point for a diluted gel made up from irradiated material may also reflect that cross-linking has taken place in the bulk material. The general conclusion being that enthalpy changes rather than changes in melting points should be considered and that cross-linking is the dominating process when powdered gelatin is irradiated with high doses (5–10 Mrad).

It must be noticed that the two different gelatins, although they have the same Bloom strength, *i.e.* the same mechanical property, and about the same melting temperature show distinct differences as far as melting enthalpies are concerned. This clearly illustrates the need for further physico-chemical information in relation to the characterization of commercially available gelatins. The data furthermore indicate that the two gelatins respond differently on irradiation, and that may be important information, in particular if the gelatin is going to be involved in an irradiation procedure for sterilization or other preparation purposes.

Finally, the point may be stressed that although the melting temperatures and the melting intervals are affected only to a very small extent by irradiation, the values of the melting enthalpies of the diluted gels show a drastic dependence on gelatin type and on irradiation, giving preference to that parameter, if additional physico-chemical characterization of gelatin is desired. The ultrasonic method described in this paper may be a very useful tool for obtaining this information.

Acknowledgements. The authors wish to express their appreciation to lic. techn. W. Batsberg Pedersen, RISØ, Denmark, for carrying out the irradiation and to U. Wolther, Roskilde University Center, Denmark for being helpful in connection with the experimental device.

REFERENCES

1. Ward, A. G. and Courts, A., Eds., *The Science and Technology of Gelatine*, Academic, London 1977.
2. Baily, A. J. *Radiation Res. 31* (1967) 206.
3. Cooper, D. R. and Russell, A. E. *Biochem. J. 113* (1969) 263.
4. Tomoda, Y. *Kogyo Kagaku Zasshi 63* (1960) 1436.
5. Tomoda, Y. and Tsuda, M. J. *Polymer Sci. 54* (1961) 321.
6. Bello, J., Bello, H. R. and Vinograd, J. R. *Biochim. Biophys. Acta 57* (1962) 222.
7. Stainsby, G. In Sauvenier, H., Ed., *Scientific Photography*, Pergamon, London 1962, p. 253.
8. Rassing, J. *Acta Chem. Scand. 25* (1971) 1506.
9. Sams, P. J., Rassing, J. and Wyn-Jones, E. *J. Chem. Soc. Faraday 2, 70* (1974) 1247.
10. Wada, Y., Sasabe, H. and Tomono, M. *Biopolymers 5* (1967) 887.
11. Eldrige, J. E. and Ferry, J. D. *J. Phys. Chem. 58* (1954) 992.

Received June 19, 1978.

Acta Chemica Scandinavica A 32 (1978) 929–932

Preparation and Characterization of Tris(thioacethydrazide)-nickel(II) and Cobalt(III) Complexes

J. GABEL and ERIK LARSEN

Chemistry Department I, The H. C. Ørsted Institute, Universitetsparken 5, DK-2100 Copenhagen, Denmark

Dedicated to Jannik Bjerrum on the occasion of his 70th birthday

Tris(thioacethydrazide)nickel(II) salts have been prepared by disproportionation of acidified bis-(thioacethydrazidato)nickel(II). This reaction proves that thioacethydrazide has more stability than formerly believed. Tris(thioacethydrazide)nickel(II) reacts in acidified ethanol with *trans*-dichloridotetrapyridinecobalt(III) ions to produce *fac*-tris(thioacethydrazide)cobalt(III) ions. This complex has been resolved into its catoptric forms and characterized by various spectroscopic means (visible and UV absorption, circular dichroism and ^{1}H NMR). The absolute configuration has been established by considering the exciton coupling of the ligand $\pi \rightarrow \pi^*$ transition. The acidity strengths of *fac*-tris(thioacethydrazide)cobalt(III) and *fac*-tris(thiosemicarbazide)cobalt(III) have been determined and the pronounced difference rationalized.

While thiosemicarbazide has been known since 1895[1] the closely analogous thioacethydrazide is until now only known as a ligand in bis(thioacethydrazidato)nickel(II). This complex precipitates when nickel(II) ions, thioacetamide and hydrazine are all present in an aqueous solution at pH near 4.[2] The ligand has been identified by an X-ray investigation and also complexes of a number of ketone thioacylhydrazones have been characterized structurally.[3–6] It has been inferred that a thiohydrazide derived from an acid having one or more α-hydrogen atoms should be unstable because of a tendency for ring closure reactions.[7,8] In accordance with this, thioacethydrazide has not yet been isolated. However, the molecule must at least be robust enough to survive the transfer from one metal ion to another as this paper will demonstrate, and it can therefore be anticipated that thioacethydrazide, Htah, can be isolated.

EXPERIMENTAL

Tris(thioacethydrazide)nickel(II) chloride. 100 g (0.4 mol) of $[Ni(tah)_2]$[2] was stirred vigorously in 300 ml 6 M hydrochloric acid for 12 h at ambient temperature. After cooling to 5 °C for 1 h the blue precipitate was filtered and washed with 100 ml of a cold 1:1 mixture of 4 M hydrochloric acid and ethanol and then with 3 × 50 ml of ethanol. Yield 104 g (0.25 mol) $[Ni(Htah)_3]Cl_2.H_2O$. The product was purified by dissolving 5 g in 100 ml of hot water. A small amount of unreacted $[Ni(tah)_2]$ was removed by filtration. The volume of the solution was reduced to 20 ml on a rotatory evaporator. 4 g of $[Ni(Htah)_3]Cl_2.H_2O$ was isolated after the addition of 10 ml 12 M hydrochloric acid. Analysis C, H, N, S, Cl, Ni.

The nitrate, sulfate and perchlorate were isolated by analogous procedures.

Tris(thioacethydrazide)cobalt(III) chloride. 4.2 g (10 mmol) of $[Ni(Htah)_3]Cl_2.H_2O$ was dissolved in 50 ml of water. To the solution was added 5 ml 12 M hydrochloric acid and 25 ml of ethanol. This mixture was poured into a solution of 8.9 g (15 mmol) of *trans*-dichloridotetrapyridinecobalt(III) chloride hexahydrate in 200 ml of ethanol. The solution was evaporated to dryness on a rotatory evaporator. From the green crude material the red cobalt complex was obtained either by repeated washing with 50 ml portions of ethanol (up to 1 l) or by ion exchange. For the isolation by ion exchange the crude product was dissolved in 200 ml

of water. After filtration the solution was placed on a 2.5×12 cm^2 column of Dowex 50 W X-2 (200–400 mesh) in hydrogen ion form. The complex was eluted with 10 M hydrochloric acid. 3 g (6.7 mmol) $[Co(Htah)_3]Cl_3.H_2O$ precipitated from the eluate on standing at 5 °C for 2 h. Analysis C, H, N, S, Cl, Co.

Resolution of $[Co(Htah)_3]^{3+}$. Initial experiments involving cation exchange chromatography of 20 mg portions on SP Sephadex C 25 (2×50 cm^2) eluted with 0.02 M sodium antimony(III) $(+)_D$-tartrate showed that the complex could be separated into two bands each containing one catoptric form. On a larger scale the method invariably failed because a precipitate formed on the column and functioned as a cement resulting in a very slow flow. Instead of using chromatography for larger scale resolution the diastereoisomeric salt $(-)_D$-*fac*-tris(thioacethydrazide)cobalt(III) bromocamphor-π-sulfonate dichloride hydrate was precipitated from an aqueous solution made up at 60 °C from 8 g of *fac*-$[Co(Htah)_3]Cl_3.H_2O$ and 8 g of $(+)_D$-ammonium bromocamphor-π-sulfonate (from natural $(+)_D$-camphor). Analysis C, H, N, S.

$(-)_D$-$[Co(Htah)_3]Cl_3$ was obtained from the diastereoisomer by dissolving 1 g in 25 ml H_2O and passing it first through a 0.5×2 cm^2 column of the weak anion exchanger Amberlite CG 4 B as chloride. (From this column the ammonium bromocamphorsulfonate was later isolated by eluting with aqueous ammonia). From the solution passing through the column $(-)_D$-$[Co(Htah)_3]Cl_3$ was isolated by ion exchange on Dowex 50 W. Specific rotations at 25 °C were $[\alpha]_{589}$ −4410; $[\alpha]_{578}$ −3950; $[\alpha]_{546}$ −3320; $[\alpha]_{436}$ 5920; $[\alpha]_{364}$ 7800. The most soluble diastereoisomer was not isolated but $(+)_D$-*fac*-$[Co(Htah)_3]Cl_3.H_2O$ was obtained by ion exchange.

Tris(thiosemicarbazide)cobalt(III) chloride trihydrate. The complex was prepared as described in the literature.[10] Analysis C, H, N, S.

Acid-base titrations. $Co(Htah)_3Cl_3.H_2O$ and $Co(Htsc)_3Cl_3.3H_2O$ were both titrated in a 1 M $(Na)ClO_4$ medium thermostated to 25.0 °C with 0.1 M NaOH (+0.9 M $NaClO_4$). pH was measured with Radiometer glass and calomel electrodes on a Radiometer PHM 64 pH-meter. A least squares minimization program written by O. Mønsted[9] was used to calculate pK_a values.

Apparatus. Absorption spectra were recorded on a Cary 118 spectrophotometer and circular dichroism spectra were obtained with an R-J Dichrograph IIIs interfaced with a Tektronix 4051 minicomputer. Optical rotations were measured with a Perkin Elmer 141 polarimeter.

RESULTS AND DISCUSSION

It has been demonstrated that bis(thioacethydrazidato)nickel(II) disproportionates on treatment with excess acid analogously to the behaviour of the bis(thiosemicarbazidato)nickel(II) complex. The preparative yield is close to 100 % based on $[Ni(tah)_2]$ and this indicates that the reaction

$$3[Ni(tah)_2] + 6H^+ \rightarrow Ni^{2+} + 2[Ni(Htah)_3]^{2+}$$

is not seriously affected by side reactions leading to destruction of the ligand. Some destruction is, however, obvious from the smell of the reaction mixture. The chloride, sulfate, nitrate, and perchlorate salts have been made. These salts were found to have X-ray powder photographs different from their thiosemicarbazide analogs.

$[Ni(Htah)_3]^{2+}$ reacts with base to reform the inner complex quantitatively. Thereby free ligand is liberated and accordingly the mother liquor from the reaction precipitates further $[Ni(tah)_2]$ when a solution of $[Ni(NH_3)_6]^{2+}$ is added. $[Ni(Htah)_3]^{2+}$ has the same colour as $[Ni(Htsc)_3]^{2+}$ and it is labile in solution. This latter point is demonstrated very dramatically in the preparation of $[Co(Htah)_3]^{3+}$ according to the scheme:

$$[Ni(Htah)_3]^{2+} + \textit{trans}[Co(pyridine)_4Cl_2]^+ \rightarrow [Co(Htah)_3]^{3+} + NiCl_2 + 4 \text{ pyridine}$$

The red cobalt complex is shown to be the *facial* isomer by ^{1}H NMR of D_2O and DMSO-d_6 solutions. In both solvents there is observed only one signal due to the three methyl groups giving evidence for the presence of a threefold axis of symmetry. The complex has been resolved into its catoptric forms by precipitation of the salt $(-)_D$-tris(thioacethydrazide)cobalt(III) dichloride $(+)_D$-bromocamphor-π-sulfonate. From the diastereoisomeric salt the cation was isolated as the chloride by ion exchange chromatography. The absorption and circular dichroism spectra shown in Fig. 1 are similar (but CD mirror image) to those reported[10] for $(+)_D$-$[Co(Htsc)_3]^{3+}$. Empirical rules connecting the absolute configurations of cobalt(III) complexes with the circular dichroism components of the first spin-allowed absorption band was used to predict that $(+)_D$-*fac*-$[Co(Htsc)_3]^{3+}$ has the absolute configuration Λ.[10] However, it is possible to obtain a certain assignment of the absolute configuration based on the exciton coupling of the π-

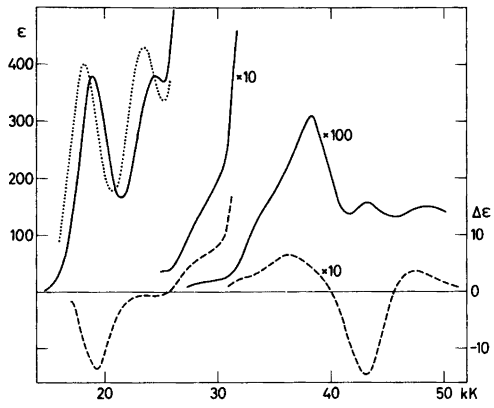

Fig. 1. The absorption (——) and circular dichroism (– – –) spectra for *fac*-$[Co(Htah)_3]Cl_3.H_2O$ in 1 M aqueous perchloric acid (solid lines) and the *vis* absorption of *fac*-$[Co(Htsc)_3]Cl_3.3H_2O$ (· · · ·) also in 1 M $HClO_4$.

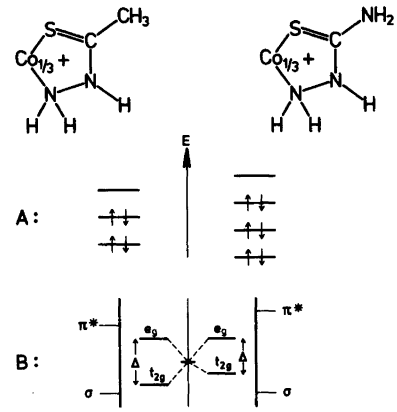

Fig. 2. A: Qualitative MO energies for the π systems of the above given formulas.

B: Schematical demonstration of the interactions between the Co(III) 3*d* orbitals and the antibonding ligand π orbital of thioacethydrazide and thiosemicarbazide.

chromophores. The $\pi \rightarrow \pi^*$ transition in H_2tsc^+ is found at 41 600 cm^{-1} and it is expected to be at nearly the same energy in H_2tah^+. Near these frequencies the two *fac* complexes $(+)_D$-$[Co(Htsc)_3]^{3+}$ [10] and $(+)_D$-$[Co(Htah)_3]^{3+}$ have strong absorption bands and circular dichroism components of the typical shape [11] for exciton coupled transitions of the absolute configuration Λ.

The absorption maximum at lowest energy is found at 19 100 cm^{-1} for *fac*-$[Co(Htah)_3]^{3+}$ and at 18 200 cm^{-1} for *fac*-$[Co(Htsc)_3]^{3+}$. Considering the similarity between the two ligands this difference in excitation energy may seem large. The difference can be rationalized by simple π-MO theory assuming that the σ conditions are identical for the two complexes. The observed excitation is due to the one electron transition $t_{2g} \rightarrow e_g$ (for simplicity expressed as if the symmetry was O_h). Of these two sets of orbitals the filled d_π orbitals, t_{2g}, interact with the empty antibonding ligand π orbital spanned by S=C−N in Htah and by S=C(NH$_2$)−N in Htsc. The latter ligand π^*-orbital must have higher energy than that of Htah and therefore the stabilizing effect on the t_{2g} orbitals is largest in $[Co(Htah)_3]^{3+}$ producing the largest difference in $E(e_g)-E(t_{2g})$ which equals Δ in the schematical illustration of these aspects in Fig. 2.

$[Co(Htah)_3]^{3+}$ is an acid and spectroscopic properties will depend on the pH conditions used. The above spectra were obtained from 1 M perchloric acid solutions. From titration curves of solutions at 25 °C containing 1 M $NaClO_4$ the pK_a values 1.4, 3.17, and 4.63 have been found. The corresponding pK_a values for the analogous tris(thiosemicarbazide)cobalt(III) complex have been determined under the same conditions to 4.77, 6.16, and 7.53. The difference between the two sets of constants demonstrates very clearly the donation of π-electron density from the amide groups of thiosemicarbazide to the chelate rings.

In spite of the above demonstrated differences between *fac*-$[Co(Htah)_3]^{3+}$ and *fac*-$[Co(Htsc)_3]^{3+}$ the two complex ions resemble each other. On base addition both yield first the *fac* isomer of the neutral complex. This isomer is unstable relative to the *mer* isomer which on acid addition will give first the *meridional* 3+ charged complexes:[10]

$$\begin{array}{ccc} fac\ [Co(HL)_3]^{3+} & \xrightarrow{OH^-} & fac\ [CoL_3] \\ \uparrow \text{ time} & & \downarrow \text{ time} \\ mer\ [Co(HL)_3]^{3+} & \xleftarrow{H^+} & mer\ [CoL_3] \end{array}$$

The relative instability of thioacethydrazide compared to thiosemicarbazide may be the reason why the above scheme is to some extent disturbed by decompositions and only the *fac* trication form has been characterized as a pure substance. The very fact that the stabilities vary as shown above is in

accordance with the intuitive description behind the formulas I and II.

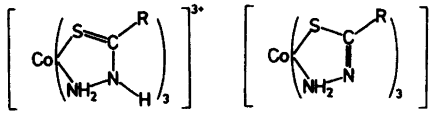

I II

For $[Co(HL)_3]^{3+}$ the *fac* form is most stable mainly because the *mer* isomer has some repulsion between sulfur and the hydrogen on nitrogen. However, in the neutral complexes the sulfur atoms are formally negatively charged and the coulombic repulsion in the *fac* isomer is larger than the S---H repulsion in the *mer* form.

Acknowledgement. The authors are indebted to Dr. O. Mønsted for a computer program computing acidity constants and to Miss Margit Olsen for preparative assistance. E.L. also acknowledges the award of a grant from the Danish Science Research Council (No. 511-6670) enabling the purchase of a dichrograph with computer for data collection.

REFERENCES

1. Freund, M. and Imgart, H. *Ber. Dtsch. Chem. Ges. 28* (1895) 946.
2. Larsen, E., Trinderup, P., Olsen, B. and Watson, K. J. *Acta Chem. Scand. 24* (1970) 261.
3. Larsen, S. *Acta Chem. Scand. A 28* (1974) 779.
4. Gabel, J., Larsen, E. and Trinderup, P. *Acta Chem. Scand. A 31* (1977) 657.
5. Hansen, F. and Larsen, S. *Acta Chem. Scand. A 31* (1977) 825.
6. Gabel, J., Hasemann, V., Henriksen, H., Larsen, E. and Larsen, S. *Inorg. Chem. To be published.*
7. Jensen, K. A. and Pedersen, C. *Acta Chem. Scand. 15* (1961) 1097.
8. King, D. M. and Anson, F. C. *Anal. Chem. 33* (1961) 572.
9. Mønsted, L. and Mønsted, O. *Acta Chem. Scand. A 30* (1976) 203.
10. Sun, K. K. W. and Haines, R. A. *Can. J. Chem. 48* (1970) 2327.
11. Larsen, E., Mason, S. F. and Searle, G. H. *Acta Chem. Scand. 20* (1966) 191.

Received June 8, 1978.

Acta Chemica Scandinavica A 32 (1978) 933–941

Thermodynamics of Complex Formation in Dimethyl Sulfoxide with Ligands Coordinating *via* N, P, As, Sb or Bi. II. Copper(I) and Mercury(II) Complexes

STEN AHRLAND,[a] TORSTEN BERG[b] and PETER BLÄUENSTEIN[a]

[a] Inorganic Chemistry 1, Chemical Center, University of Lund, P.O.B. 740, S-220 07 Lund, Sweden and [b] Chemistry Department 1, Inorganic Chemistry, H. C. Ørsted Institute, University of Copenhagen, DK-2100 Copenhagen Ø, Denmark

Dedicated to Jannik Bjerrum on the occasion of his 70th birthday

The thermodynamics of the complex formation between the metal ions Cu^+ and Hg^{2+} and the ligands Ph_3X (Ph = phenyl; X = N, P, As, Sb, Bi) has been studied in dimethyl sulfoxide (DMSO) at 25 °C, in an ammonium perchlorate medium of ionic strength 0.1 M. Stability constants have been determined potentiometrically, by copper amalgam and mercury electrodes, and enthalpy changes calorimetrically.

For copper(I), the stabilities follow the affinity sequence $N \ll P > As > Sb > Bi$, *i.e.* the same as for silver(I). For mercury(II), measurements are feasible only when X = N, P, As, as the ligands Ph_3Sb and Ph_3Bi are rapidly oxidized. For the systems measured, the same sequence is again found: $N \ll P > As$. As to the first two steps, the affinities of a certain ligand Ph_3X (X = P, As) for the acceptors investigated increase in the order $Cu^+ < Ag^+ < Hg^{2+}$ while the tendency to form a third complex is strongest for Ag^+.

All complexes are strongly enthalpy stabilized. The entropy changes counteract the complex formation, except for the first step in the mercury(II) systems where an entropy stabilization is found. The very negative, and hence strongly destabilizing, entropy changes generally found for the latter steps are no doubt due to the strict conformational demands connected with the formation of these complexes.

Jannik Bjerrum and his school have contributed greatly to our knowledge of the complex-forming properties of ligands coordinating *via* phosphorus by their investigations in aqueous solution of the complexes formed between the water-soluble diphenylphosphinobenzene-*m*-sulfonate, Dpm, and soft metallic centers of various oxidation states and electron configurations. The metallic centers included Pt(II) and Pd(II)[1] (d^8); Cu(I)[2], Au(I)[3] and Hg(II)[4] (d^{10}); and Bi(III)[5] ($d^{10}s^2$), of which Pd(II), Hg(II) and Bi(III) were the aquo metal ions. Disproportionation reactions precluded the use of aquo Cu(I) and Au(I), so that in these cases the complex formation was referred to the chloro and the thiocyanato complexes respectively. At that time the aquo Pt^{2+} had not yet been prepared,[6] so for Pt(II) the diammine complexes (*cis*- and *trans*-) were used. In a related investigation the complexes formed by Ag^+ and $HgCl_2$ with triphenylarsine were studied.[7] This ligand, like the other non-substituted triphenyl compounds of the nitrogen group donor atoms (Ph_3X; X = N, P, As, Sb, Bi) is not soluble in water so that the measurements were performed in a mixed water/methanol solvent.

Jannik Bjerrum has stated[8] that his great interest in these complexes was inspired by the remarkable complex formation observed between Ag^+ and the phosphine ligand Dpm.[9] In marked contrast to the conditions prevailing in most silver(I) systems,[10] the first and the third complex predominate strongly over a large range of ligand concentration, while the second one possesses a

fairly narrow range of existence. In the studies referred to above similar unusual features were found in various degrees also for gold(I)[3] and mercury(II).[4]

It is evidently of interest to investigate the complexes formed by these metallic centers with the analogous arsine, stibine, and bismuthine ligands. Attempts to prepare these have so far been abortive. Sulfonation of triphenylarsine gives a trisulfonate[9] in which arsenic is likely to have donor properties which are markedly different from those found in a monosulfonate. The higher anionic charge presumably also influences the complex formation. The sulfonation of triphenylstibine or triphenylbismuthine has so far not been achieved.

The large influence exerted on the donor properties of the ligand atom by its environment is demonstrated by the complex-forming properties of the aliphatic and uncharged phosphine diethyl-β-hydroxyethylphosphine, Dop.[11] Due to its alcoholic group this ligand is sufficiently water-soluble to be used in aqueous solution. Both the absolute and the relative stabilities of the consecutive complexes differ considerably from those found for Dpm.[8,11] Perhaps most important, the complexes formed by Dop are generally more stable, reflecting the stronger donating properties of phosphorus in the aliphatic environment.

As a consequence of these difficulties the measurements so far performed in aqueous solution have failed to confirm the stability sequence $N \ll P > As > Sb > Bi$ which as early as 1958 was postulated to be generally valid for soft acceptors on the basis of scarce and largely qualitative evidence.[12]

Moreover, even for the sulfonated ligands and their complexes, the solubilities in water are still too low to allow precise calorimetric measurements. Consequently, the complete thermodynamics of the complex formation reactions cannot be determined. This is indeed a serious drawback, as important conclusions about the structure and bonding of the complexes formed can be drawn from the enthalpy and entropy changes involved.[13,14]

In the present series of investigations we have therefore chosen another approach. By changing the solvent from water to dimethyl sulfoxide (DMSO) where the simple triphenyl compounds, Ph_3X, and in most cases also their complexes, are readily soluble, a comparative study of the affinities of all the nitrogen group donor atoms towards various acceptors becomes possible. Moreover the influence on the stabilities of the enthalpy and the entropy terms can be precisely determined.

In the first paper of this series,[15] the thermodynamic functions of the silver(I) complexes formed with all the ligands Ph_3X were determined. As a result the affinity sequence stated above was quantitatively confirmed, seemingly for the first time. The present paper deals with the corresponding copper(I) and mercury(II) complexes. Like silver(I), these acceptors have both d^{10} configurations, but while copper(I) differs from silver(I) only by one electron shell, mercury(II) also possesses one additional ionic charge.

Relative to water, DMSO has the further advantage that not only silver(I) and mercury(II) but also copper(I) can exist in the solution as the solvated ions. This of course much facilitates the comparison between the complex forming properties of the acceptors. The disproportionation constant referring to the reaction

$$2\ Cu^+ \rightleftharpoons Cu^2 + Cu(0) \qquad (1)$$

is so much lower in DMSO than in water[16,17] that copper(I) perchlorate solutions of a concentration as high as $\simeq 15$ mM (which are used in the present investigation) only disproportionate to $\simeq 2\,\%$ in DMSO while the disproportionation would be virtually complete, $\simeq 99\,\%$ in water. This drastic change is connected with the changes of the solvation enthalpies for Cu^+ and Cu^{2+} from water to DMSO, which bring about a very considerable stabilization of Cu^+ relative to Cu^{2+} as the system is transferred from water to DMSO.[18]

Also the relative stabilities of mercury(I) and mercury(II) according to the reaction

$$Hg^{2+} + Hg(0) \rightleftharpoons Hg_2^{2+} \qquad (2)$$

are different in water and in DMSO. In this case, however, the transfer to DMSO favours the divalent oxidation state relative to the monovalent one.[19] The equilibrium change is much smaller than for copper but is nevertheless advantageous for the measurements described below, where mercury electrodes are employed. In DMSO such measurements can be extended to higher concentrations of solvated mercury(II) than would be possible in water.

For both systems the stability constants have been determined potentiometrically, by means of copper amalgam and mercury electrodes, respec-

tively. The enthalpy changes have been determined calorimetrically, applying in the calculations the stability constants already determined. From the changes of free energy and enthalpy thus found, the entropy changes have been calculated.

As in the previous study, the measurements refer to a medium of ionic strength 0.1 M, maintained by ammonium perchlorate, and a temperature of 25 °C.

EXPERIMENTAL

Chemicals. Dimethyl sulfoxide was purified and analyzed for water as described before.[15] Ammonium perchlorate was dried at about 110 °C. Triphenylamine, -phosphine, -stibine and -bismuthine were recrystallized from a mixture of 1:1 ether/ethanol[20,21] and triphenylarsine from ethanol.[22] All ligands were dried *in vacuo* at room temperature. Ligand solutions were not kept longer than two days because of their limited stability. The ligands are oxidized to Ph_3XO with concomitant reduction of DMSO to $(CH_3)_2S$, which is easily detected by its characteristic smell.[23] The solvates $Cu(ClO_4)_2.4DMSO$, $Hg(ClO_4)_2.4DMSO$ and $[Cd(DMSO)_6](ClO_4)_2$ were prepared and analyzed as described previously.[16,24-26] The copper amalgam, and the cadmium amalgam used for the reference electrodes, were prepared according to standard methods.[16,27] Solutions of copper(I) perchlorate in DMSO were prepared by reducing copper(II) perchlorate with copper foil at 60 °C. Because of the disproportionation of copper(I), no solution of copper(I) concentration >0.02 M was prepared.[16]

Potentiometry, copper(I) systems. The potentiometric titrations were performed in a glove box in dry carbon dioxide atmosphere as described in Ref. 16. In addition a stream of purified nitrogen was bubbled through the solution. The emf of the cell in Scheme 1 was measured. Initially the right hand half cell contained only copper(I) perchlorate of a C_M between 3 and 15 mM ($I=0.1$ M). When a stable initial potential had been reached, portions of ligand solutions of a C_L between 100 and 300 mM ($I=0.1$ M) were added. Generally three titrations were performed for every value of C_M and C_L. The emf's could be reproduced within $\simeq 1$ mV. In the phosphine system the reproducibility was not as good for $\bar{n}>2$, *viz.* $\simeq 3$ mV. From the potential difference measured the constants β_j were calculated according to the procedure described before.[15,16]

Generally a slight oxidation of Cu(I) by traces of O_2 could not be avoided, but the products formed were again rapidly reduced by Cu(Hg). The overall result is an increase of C_M. In the phosphine system the decrease of the concentration of free copper(I) ions $[Cu^+]$ at $\bar{n}=1$ and $\bar{n}=2$ was steep enough to allow the calculation of C_M. This was not the case with the arsine and stibine systems, where C_M had to be determined separately by EDTA titration.[16] It was then necessary to extract most of the ligand with ether as the point of equivalence was approached. The precision was $\simeq 1\,\%$. For some samples the final C_M was also measured by atomic absorption spectrophotometry. The results agreed well with those found by EDTA titration, but the precision was lower.

In the phosphine titrations it was observed that the oxidation rate was perceptible when $\bar{n}<1$, *i.e.* when $[Cu^+]$ is relatively high. For $\bar{n}>2$ the solutions were very stable, giving emf's which did not change appreciably overnight. Therefore C_M had only to be corrected in the first part of the titrations. For the arsine and stibine systems the highest values of $\bar{n}$ reached were 1.9 and 1.5, respectively. In these systems where only the initial and final value of C_M were determined it was therefore considered adequate to calculate the intermediate values of C_M by a linear interpolation. If C_M increased $>5\,\%$, the titration was discarded.

Potentiometry, mercury systems. To exclude moisture, the potentiometric measurements were performed in a glove box as described before,[15,16,28] and dry nitrogen was bubbled through the electrode solutions. The emf of cell in Scheme 2 was measured. In the absence of stabilizing ligands, solutions of mercury(II) perchlorate in DMSO are reduced by metallic mercury according to eqn. (2). In the present medium,[19] the reproportionation constant $K_r=[Hg_2^{2+}]/[Hg^{2+}]=35\pm5$. In 1 M NH_4ClO_4, a value of $K_r=24\pm3$ has been determined[19] which is again not very different from $K_r=40$ recently found for another 1 M perchlorate medium.[29] The earlier value determined indirectly in 0.1 M Et_4NClO_4 disagrees very markedly, however.[30]

The value of K_r found for DMSO implies, as

$$-\mathrm{Cd(Hg)}\;\left|\begin{array}{l}0.01\ \mathrm{M\ Cd^{2+}}\\ I=1.0\ \mathrm{M}\\ (\mathrm{NH_4ClO_4})\end{array}\right|\;\begin{array}{l}0.1\ \mathrm{M}\\ \mathrm{NH_4ClO_4}\end{array}\;\left|\begin{array}{l}C_M\ \mathrm{Cu(I)}\\ C_L\ \mathrm{Ph_3X}\\ I=0.1\ \mathrm{M}\\ (\mathrm{NH_4ClO_4})\end{array}\right|\;\mathrm{Cu(Hg)}+$$

Scheme 1.

$$-\mathrm{Cd(Hg)}\,\Big|\begin{array}{l}0.02\ \mathrm{M\ Cd^{2+}}\\ I=0.1\ \mathrm{M}\\ (\mathrm{NH_4ClO_4})\end{array}\Big|\,0.1\ \mathrm{M}\ \mathrm{NH_4ClO_4}\,\Big|\begin{array}{l}C_\mathrm{M}\ \mathrm{Hg(II)}\\ C_\mathrm{L}\ \mathrm{Ph_3X}\\ I=0.1\ \mathrm{M}\\ (\mathrm{NH_4ClO_4})\end{array}\Big|\,\mathrm{Hg}+$$

Scheme 2.

already stated, a stabilization of Hg(II) relative to Hg(I) as compared with aqueous solution. Evidently, this stabilization is not large enough, however, to allow any considerable concentration of Hg^{2+} in equilibrium with the mercury electrode. The titrations were therefore conducted from higher to lower values of $\bar{n}$ and interrupted when reproportionation became perceptible; the initial solution thus contained an excess of ligand. To this solution portions of mercury(II) perchlorate solution of the same concentration C_M were added. Consequently only C_L decreased during the titration, while C_M remained constant. Using this procedure it is necessary to determine independently the emf referring to a non-complex solution containing only free Hg^{2+} of a known concentration. The potential of a standard mercury half-cell 1 M Hg^{2+}/Hg(l) relative to the cadmium reference cell used here has been found to be 1192.65 mV under the present conditions.[19] As the potential of the reference electrode is easily reproducible within 0.5 mV and remains constant for about three days, this procedure is quite adequate.

Two independent reference electrodes were used, and the emf was taken as the average of the values measured between the mercury electrode in the reaction vessel and each of the reference electrodes. The equilibrium emf was normally reached within 20 min and remained constant for more than 5 h. Titration series were generally performed for three values of C_M and each series were made at least three times. In the arsine system, the emf values were readily reproduced within 2 mV. The same reproducibility was found in the phosphine system except for solutions that contained a large excess of ligand or had values of C_L/C_M around 2.

Contrary to this, no reproducible emf values at all were established in the stibine and the bismuthine systems. The values decreased rapidly, signifying a fast decrease of Hg^{2+}. Very likely, this decrease is due to a reduction of Hg(II) by the ligands although another possibility is that Hg(II) catalyzes an oxidation of the ligands by DMSO, resulting in a formation of dimethyl sulfide which would strongly sequester Hg^{2+}.

The least-squares programme EMK was used to calculate the stability constants from the potential measurements.[28]

Calorimetry, copper(I) systems. The calorimeter is described in Ref. 16. To prevent oxidation of Cu(I) a steady stream of CO_2 was bubbled through the solutions. Initially the calorimeter contained pure perchlorate solutions of $C_M \simeq 10$ mM, which were titrated with ligand solutions of a C_L between 100 and 300 mM ($I=0.1$ M). The heats measured were reproduced within $\simeq 0.1$ J. Corrections were introduced for the heats of dilution. These were slightly positive for the ligand solutions and negligible for the copper(I) solutions. At high ligand concentrations traces of copper(II) tended to oxidize the gold vessel. This was prevented by placing a piece of copper wire in the vessel. By weighing the the copper wire before and after the measurement the increase of copper(I) during the experiment could be determined. Assuming that this increase took place during the first part of the phosphine titrations, but continuously in the arsine and stibine ones, the actual values of C_M were calculated (*cf.* potentiometry, copper(I) systems).

The least-squares program KALORI[31,32] was used for the numerical treatment of the experimental data yielding $\Delta H^\circ_{\beta_j}$. The stability constants found in the potentiometric measurements were applied.

Calorimetry, mercury systems. The calorimeter used was the same as described in the first paper of this series.[15,33] In the present measurements, however, the inner gold vessel was oxidized by the mercury(II) as triphenylphosphine was added. Metallic mercury seemingly precipitated, and by analysis it was found, that for each mol of mercury reduced, 2 mol of gold metal had been dissolved, in accordance with

$$\mathrm{Hg(II)} + 2\ \mathrm{Au(0)} \rightarrow \mathrm{Hg(0)} + 2\ \mathrm{Au(I)} \qquad (3)$$

This reaction must be due to a very strong affinity between Au(I) and the phosphine ligand. The complexes formed are evidently so thermodynamically stable that not only did they compete successfully with the Hg(II) complexes, but also the oxidation potential of the couple Au(I)/Au(0) was changed so much that the metallic gold was oxidized. This complication was avoided by coating electrolytically the gold with a 3 μm rhodium layer.

The calorimetric measurements could then be performed in the conventional manner.[34] For each system 6 – 15 titrations were made. In most of these, ligand solutions of $\simeq 100$ mM were titrated into mercury(II) perchlorate solutions of C_M varying from $\simeq 2$ to $\simeq 10$ mM. In other series, mercury(II)

Table 1. Overall stability constants (β_j in M^{-j}) and enthalpy changes ($\Delta H^\circ_{\beta_j}$ in kJ mol^{-1}) calculated for the complexes formed between copper(I) and mercury(II) and the ligands Ph_3X in DMSO at 25 °C and ionic strength $I=0.1$ M (NH_4ClO_4). The errors given (for β_j in the last digit(s)) are three times the standard deviation given by the computer.

	Copper(I) X=P	X=As	X=Sb	Mercury(II) X=P	X=As
$\log\beta_1$	6.57(2)	2.65(2)	1.26(3)	11.06(1)	6.77(2)
$\log\beta_2$	10.43(3)	4.04(2)	1.79(5)	17.62(1)	8.97(3)
$\log\beta_3$	11.83(10)				
$-\Delta H^\circ_{\beta_1}$	46.9(0.7)	22.3(0.4)	10.6(0.8)	56.8(1.2)	34.0(1.3)
$-\Delta H^\circ_{\beta_2}$	87.9(1.0)	56.0(1.2)	35.4(4.1)	107.7(2.0)	61.3(2.0)
$-\Delta H^\circ_{\beta_3}$	112.3(3.7)				

Table 2. Equilibrium constants (K_j in M^{-1}) and thermodynamic functions (ΔH°_j, ΔG°_j in kJ mol^{-1}, ΔS°_j in $JK^{-1}mol^{-1}$) for the stepwise formation of complexes between copper(I), silver(I) and mercury(II) and ligands Ph_3X in DMSO, at 25 °C and $I=0.1$ M (NH_4ClO_4).

	Copper(I) [a]			Silver(I) [b]			Mercury(II) [a]	
	X=P	X=As	X=Sb	X=P	X=As [c]	X=Sb	X=P	X=As
$\log K_1$	6.57	2.65	1.25	6.58	3.56	3.16	11.06	6.77
$\log K_2$	3.87	1.40	0.54	4.15	1.81	1.45	6.55	2.20
$\log K_3$	1.40			2.44	1.31	1.45		
K_1/K_2	510	18	5	269	56	51	32 000	38 000
K_2/K_3	300			52	3.2	1		
$-\Delta G^\circ_1$	37.5	15	7	37.6	20.3	18.1	63.2	38.6
$-\Delta G^\circ_2$	22.0	8	3	23.7	10.4	8.3	37.4	12.5
$-\Delta G^\circ_3$	8			13.9	7.5	8.3		
$-\Delta H^\circ_1$	47	23	11	51.8	34.5	32.1	57	34
$-\Delta H^\circ_2$	41	32	25	38.1	19.4	8.6	51	27
$-\Delta H^\circ_3$	25			36.3	44.5	57.1		
ΔS°_1	−32	−27	−13	−48	−48	−47	20	15
ΔS°_2	−64	−80	−74	−48	−30	−1	−47	−49
ΔS°_3	−57			−75	−124	−164		

[a] This work. [b] Ref. 15. [c] From Table 1, Ref. 15. slightly different values of ΔH°_j are calculated for the arsine system. The present values, taken from Table 2, Ref. 15, are to be preferred, however.

perchlorate solutions of $C_M \simeq 40$ mM were titrated into ligand solutions of $C_L \simeq 60$ mM. Each series was run at least twice with a reproducibility generally better than 0.1 J. The experimental heat changes were corrected for heats of dilution. The calculations were performed as for copper(I).

RESULTS

The measurements yield the overall stability constants β_j and enthalpy changes $\Delta H^\circ_{\beta j}$ listed in Table 1. Complex formation is neither observed between copper(I) and the ligands Ph_3N or Ph_3Bi, nor be-

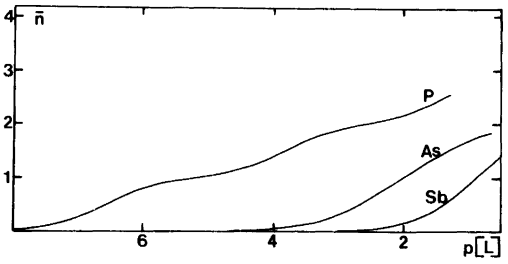

Fig. 1. The complex formation curves of the systems $Cu^+ - Ph_3X$, X=P, As, Sb, in DMSO. Medium 0.1 M NH_4ClO_4; 25 °C.

tween mercury(II) and Ph_3N. The redox reactions discussed above preclude the investigation of the Ph_3Sb and Ph_3Bi complexes of mercury(II).

From the data of Table 1, the values of the stepwise stability constants K_j and thermodynamic functions ΔG_j° ΔH_j° and ΔS_j° are calculated, Table 2.

Within the range of ligand concentrations available (indicated on Figs. 1 and 2), a third complex is formed with certainty only between copper(I) and Ph_3P, Tables 1 and 2. A corresponding complex is presumably formed also by mercury(II), but in this case the results of the potentiometric and calorimetric measurements are difficult to reconcile. Potentiometrically, a value of $K_3 = 1.7 \pm 0.3$ M^{-1} is found. With this value of K_3, the calorimetric data yield the quite improbable value $\Delta H_3^\circ = -240 \pm 75$ kJ mol^{-1}. If, on the other hand, K_3 and ΔH_3° are both calculated from the calorimetric data, $K_3 = 35 \pm 32$ M^{-1} and $\Delta H_3^\circ = -26 \pm 21$ kJ mol^{-1} are found, *i.e.* values which are quite reasonable, but unfortunately very imprecise. Evidently the measurements are not able to provide any reliable values for these quantities.

DISCUSSION

Stabilities of the complexes. Both copper(I) and, within the limits of our measurements, mercury(II) follow the same affinity sequence $N \ll P > As > Sb > Bi$ as found previously for silver(I). This early postulated sequence can thus now be considered as well confirmed by quantitative data for soft acceptors.

For copper(I), the first phosphine complex is as thermodynamically stable as the corresponding silver(I) complex and also the second and the third complexes are comparatively stable, Table 2. The arsine, and even more the stibine complexes are all much weaker for copper(I), however. A third complex is not even formed at the highest ligand concentrations which we are able to attain. As has already been stated ammine and bismuthine complexes do not exist under our conditions. The second complex has a wider range of existence in the copper(I) systems as is evident from those values of K_2/K_3 which can be calculated or estimated. The first complex has a remarkably wide range of existence for the phosphine system only. The ratio K_1/K_2 is even higher than for the corresponding silver(I) system. These features are well illustrated by the complex formation curves of the copper(I) systems, Fig. 1. The phosphine curve is markedly deflected at $\bar{n}=1$ as well as at $\bar{n}=2$, while the arsine curve is only deflected at $\bar{n}=2$.

A still much higher ratio K_1/K_2 has been found for the complex formation between copper(I) and the aliphatic phosphine Dop in aqueous solutions, Table 3. In this system, the ratio K_2/K_3 is moreover quite low implying a narrow range of existence for the second complex. The constants measured for the ligand Dpm refer, as stated, to a chloride solution. Their recalculation to equilibria referred to the hydrated ion cannot be carried out for the first two steps, so the ratios K_1/K_2 and K_2/K_3 remain unknown for this system.

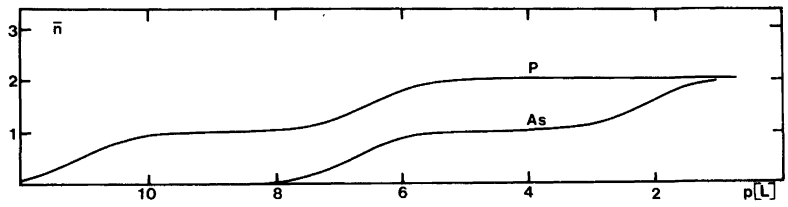

Fig. 2. The complex formation curves of the systems $Hg^{2+} - Ph_3X$; X=P, As, in DMSO. Medium 0.1 M NH_4ClO_4; 25 °C.

Table 3. Stability constants (β_j in M^{-j}) and ratios K_j/K_{j+1} for the complex formation in water between copper(I) and mercury(II) and two substituted phosphines, one aliphatic (Dop[a]) and one aromatic (Dpm[b]).

	Copper(I)			Mercury(II)	
	Dop	Dpm[c]	Dpm[d]	Dop	Dpm[e]
$\log\beta_1$	12.60	5.76			14.3
$\log\beta_2$	20.34	11.20		37.30	24.6
$\log\beta_3$	27.0	16.12	22.0	42.5	29.7
$\log\beta_4$		19.92	25.8		33.0
K_1/K_2	72 400				10 000
K_2/K_3	12				160 000
K_3/K_4					60

[a] Ref. 11. Dop = $Et_2PCH_2CH_2OH$; I = 1 M (KNO_3), 22 °C. [b] Ref. 2 and 4. Dpm = $Ph_2PC_6H_4SO_3^-$ (*m*-); 25 °C. [c] Referred to the actual chloride medium, 1 M LiCl. [d] Referred to the copper(I) aquo ion, Cu^+. [e] Medium 1 M KNO_3.

As has also been found for silver(I),[15] the overall stability of phosphine complexes of copper(I) is much higher in water than in DMSO, Tables 1 and 3. Most probably, this is mainly due to the stronger solvation of these acceptors in DMSO which implies that the ligands have to undergo a stronger competition in this solvent.

For mercury(II), the first phosphine and arsine complexes are considerably stronger than the corresponding copper(I) and silver(I) complexes, Table 2. The same trend, though less marked, also prevails during the formation of the di-ligand complexes. At the third step, however, the trend is reversed. If formed at all, the mercury(II) complexes are considerably weaker. These changes in the relative stability of the consecutive complexes mean that both the first and the second mercury(II) complex have much wider ranges of existence than the corresponding copper(I) or silver(I) complexes. This is expressed by much higher ratios K_1/K_2 and K_2/K_3 and, even more strikingly, by the extended plateaus at $\bar{n}=1$ and 2 characterizing the complex formation curves of these systems, Fig. 2. The ranges of existence of the mono-ligand complexes are even wider than for the mono-Dpm complex formed in aqueous solution, the first mercury(II) complex to display this feature.[4] For the present systems, ratios $K_1/K_2 \simeq 3\times10^4$ are found and can be compared with 10^4 for the Dpm system, Tables 2 and 3. Recently, ratios K_1/K_2 of similar magnitude have also been found for the mercury(II) halide and thiocyanate systems in DMSO.[35]

The overall stabilities of phosphine complexes are for the mercury(II) system considerably higher in water than in DMSO, Tables 2 and 3. The reason is once more that the acceptor is more strongly solvated in DMSO than in water. This applies even more for mercury(II) than for silver(I) (and copper(I)) as is evident from the enthalpies ΔH°_{tr} (W→DMSO) found for the transfer of the acceptors from water to DMSO. These are −54 and −76 kJ mol^{-1} for Ag^+ and Hg^{2+}, respectively.[18]

Thermodynamics of the complex formation. Just as for silver(I), all the complexes are formed in exothermic reactions, Table 2. As already stated, this is a natural consequence of the formation of strong metal to ligand bonds and the weak solvation of the ligands involved.[15] On the other hand, the weak solvation, together with the strict conformational demands imposed upon the ligands as the complexes are formed, generally result in unfavourable entropy terms, Table 2. In several instances, the entropy changes are indeed heavily counteracting the complex formation. Extreme examples are the second step in the copper(I) arsine and stibine systems where the effects of quite large negative enthalpies are almost vitiated by the huge entropy losses. The only favourable entropy terms are found in the first step of the mercury(II) systems. Here the desolvation of the strongly solvated divalent Hg^{2+} brings about a net gain of entropy. This desolvation must be very extensive as even the second steps are characterized by large entropy losses. Relative to the di-Ph_3X complexes, the mono-Ph_3X ones are thus strongly entropy stabilized which causes their remarkably wide range of existence.

In the silver(I) systems, the values of ΔS°_j vary be-

tween different steps in a manner which is highly individual for each ligand, Table 2. From the silver data alone, these variations are indeed very difficult to interpret. Comparison with data pertaining to other suitably chosen acceptors may make this possible, however. In fact, the values of ΔS_j° now determined for the copper(I) and mercury(II) systems seem to present some features that can be utilized in order to rationalize the existing body of entropy data.

In the formation of the mono-Ph_3X complexes, the conformational entropies should be of relatively little importance as the structural requirements are still not very severe. The values of ΔS_1° should thus largely be determined by the desolvation entropies which depend mostly on the solvation of the acceptor. The solvation generally becomes stronger and the desolvation entropies consequently more favourable the smaller the radius and the higher the charge of the acceptor. In accordance with this, the values of ΔS_1° for the smaller copper(I) are less negative *i.e. more favourable* than for the larger silver(I). On the other hand, they are not as favourable as for the larger mercury(II) where the higher charge brings about an even stronger solvation, resulting in $\Delta S_1^\circ > 0$.

As higher complexes are formed, however, the structural requirements become stricter and, consequently, the conformational entropies become very important. These should moreover increase as the size of the acceptor decreases. In accordance with this, the values of ΔS_2° for copper(I) are all more negative, *i.e. less favourable* than for silver(I). In the silver(I) systems, ΔS_2° is moreover less negative than ΔS_1° (or, in the phosphine case, of the same value) which would not be possible should the values of ΔS_2° be determined mainly by the desolvation entropies. The evidence thus strongly indicates that the conformational entropies are indeed of decisive importance from the second step onwards.

The values of ΔS_3° for the silver(I) systems become extremely unfavourable, and increasingly so in the order P < As < Sb. This is indeed to be expected as the conformational demands should be severe when three ligands are to be accommodated, and moreover to an increasing degree as the ligands become larger. For the smaller copper(I), the conformational entropies involved in the coordination of the large arsine and stibine ligands may become even more unfavourable, which is probably the reason why these complexes are in fact not formed in perceptible amounts.

The results now available thus allow rather extensive conclusions about the nature of the complex formation. Quite a few features are still difficult to interpret, however, *e.g.* why the values of ΔS_2° found in the silver(I) systems become more favourable in the order P < As < Sb. Investigations of the thermodynamics of the complex formation between the ligands Ph_3X and further acceptors may hopefully clarify the situation, especially if the thermodynamic data can be combined with structural information.

Acknowledgements. This work has been generously supported by the Swedish Natural Science Research Council. The cooperation between the Copenhagen and Lund Institutes has further been greatly facilitated by the grant of Hovrättsnotarie Gunnar Svenssons Legat to one of us (T.B.).

REFERENCES

1. Chang, J. C. and Bjerrum, J. *Acta Chem. Scand. 26* (1972) 815.
2. George, R. and Bjerrum, J. *Acta Chem. Scand. 22* (1968) 497.
3. Hawkins, C. J., Mønsted, O. and Bjerrum, J. *Acta Chem. Scand. 24* (1970) 1059.
4. Salvesen, B. and Bjerrum, J. *Acta Chem. Scand. 16* (1962) 735.
5. Wright, G. and Bjerrum, J. *Acta Chem. Scand. 16* (1962) 1262.
6. Elding, L. I. *Inorg. Chem. Acta 20* (1976) 65.
7. Olson, D. C. and Bjerrum, J. *Acta Chem. Scand. 20* (1966) 143.
8. Bjerrum, J. and Chang, J. C. *Section Lectures, XIII.I.C.C.C., Cracow-Zakopane, Poland 1970*, Polish Academy of Sciences, Wrocław and Warszawa 1974, p. 229.
9. Ahrland, S., Chatt, J., Davies, N. R. and Williams, A. A. *J. Chem. Soc.* (1958) 276.
10. Sillén, L. G. and Martell, A. E., Eds., *Stability of Metal-Ion Complexes*, Chemical Society, Special Publications Nos. 17 and 25, London 1964, 1971.
11. Meier, M. *Phosphinokomplexe von Metallen*, Diss. No. 3988, Eidgenössische Technische Hochschule, Zürich 1967.
12. Ahrland, S., Chatt, J. and Davies, N. R. *Q. Rev. Chem. Soc. 12* (1958) 265.
13. Schwarzenbach, G. *Pure Appl. Chem. 24* (1970) 307.
14. Ahrland, S. *Struct. Bonding (Berlin) 15* (1973) 167.

15. Ahrland, S., Berg, T. and Trinderup, P. *Acta Chem. Scand. A 31* (1977) 775.
16. Ahrland, S., Bläuenstein, P., Tagesson, B. and Tuhtar, D. *To be published.*
17. Ahrland, S. and Rawsthorne, J. *Acta Chem. Scand. 24* (1970) 157.
18. Ahrland, S. In Lagowski, J. J., Ed., *The Chemistry of Non-Aqueous Solvents*, Academic, London and New York 1978, Vol. 5 A, Chapter 1.
19. Ahrland, S. and Persson, I. *To be published.*
20. Michaelis, A. and v. Soden, H. *Justus Liebigs Ann. Chem. 229* (1885) 295.
21. Michaelis, A. and Reese, A. *Justus Liebigs Ann. Chem. 233* (1886) 39.
22. La Coste, W. and Michaelis, A. *Justus Liebigs Ann. Chem. 201* (1880) 184.
23. Amonoo-Neizer, E. H., Ray, S. K., Shaw, R. A. and Smith, B. C. *J. Chem. Soc.* (1965) 4296.
24. Cotton, F. A. and Francis, R. *J. Am. Chem. Soc. 82* (1960) 2986.
25. Sandström, M., Persson, I. and Ahrland, S. *Acta Chem. Scand. A 32* (1978) 607.
26. Ahrland, S. and Björk, N.-O. *Acta Chem. Scand. A 28* (1974) 823.
27. Persson, H. *Acta Chem. Scand. 24* (1970) 3739.
28. Ahrland, S. and Björk, N.-O. *Acta Chem. Scand. A 30* (1976) 249.
29. Samoilenko, V. M., Lyashenko, V. I. and Polishchuk, N. V. *Russ. J. Inorg. Chem. 19* (1974) 1632.
30. Foll, A., Le Demezet, M. and Courtot-Coupez, J. *Bull. Soc. Chem. Fr.* (1972) 1207.
31. Karlsson, R. and Kullberg, L. *Chem. Scr. 9* (1976) 54.
32. Kullberg, L. *Acta Chem. Scand. A 28* (1974) 829.
33. Ots, H. *Acta Chem. Scand. 26* (1972) 3810.
34. Ahrland, S. and Björk, N.-O. *Acta Chem. Scand. A 30* (1976) 257.
35. Ahrland, S., Persson, I. and Portanova, R. *To be published.*

Received June 12, 1978.

Acta Chemica Scandinavica A 32 (1978) 943–955

The Silver(I) Complexes of Ethylenediamine in Solution

BALAZS MAGYAR and GEROLD SCHWARZENBACH†

Institute of Inorganic Chemistry, Swiss Federal Institute of Technology, ETH-Zentrum, CH-8092 Zürich, Switzerland

Dedicated to Jannik Bjerrum on the occasion of his 70th birthday

The silver(I) complexes of ethylenediamine "en" were investigated in solution. The stability constants of $Ag(Hen)^{2+}$, $Ag(en)^{+}$, $(Ag_2(en)^{2+}$ add $Ag_2(en)_2^{2+}$ have been obtained from potentiometric titrations of H_2en^{2+} with solutions of KOH in the presence of Ag(I). At high concentrations of equimolar mixtures of Ag(I) and "en" the binuclear species $Ag_2(en)_2^{2+}$ becomes the dominant complex. This is unambiguously demonstrated by salt cryoscopy, three-phase vapour tensiometry and solubility measurements. The heat of formation of the complexes $Ag(en)^{+}$, $Ag(en)_2^{2+}$ and $Ag_2(en)_2^{2+}$ were also determined.

Ethylenediamine is the first chelating ligand ever applied and was often used after its introduction in Copenhagen in 1889[1] because of the greater stability of its complexes in comparison to the corresponding ammonia adducts. Half a century later – again in Copenhagen[2] – the impressive stability increase to be achieved with "en" was demonstrated by means of ionic equilibria studies, mainly for the $3d^n$-transition metal(II) cations. These form the series of complexes $[M(en)_n]^{2+}$, and only half as many "en" are bonded as there are ammonia molecules coordinated in the corresponding NH_3-metal system. The stability constants K_1, K_2, K_3 are considerably larger than the quantities β_2, β_4/β_2 and β_6/β_4 of the ammonia complexes.

The silver cation behaves differently, however. With electrodes of metallic silver it was found that although the maximum coordination number of Ag^{+} is $N=2$, in the ammonia system this cation also adds two molecules of bidentate "en" and furthermore that the stability constants β_2 of $[Ag(NH_3)_2]^{+}$ and $[Ag(en)_2]^{+}$ are almost the same.[3] By applying *Bjerrums* pH-method[2] – whereby the cation H_2en^{2+} has to be deprotonated in the presence of Ag^{+} – it is found that the neutralisation function $[H](\bar{p}')$ (see eqn. (1)) cannot be interpreted with the formation of only $Ag(en)^{+}$ and $Ag(en)_2^{+}$. These results are not surprising in view of the prefered linear arrangement N–Ag–N in the diammine-silver cation and the impossibility of spanning the bridge between the opposite atoms with a link of two C-atoms only. A linear arrangement N–Ag–N could only be achieved by adding two "en" molecules as unidentate ligands which explains the stability found for $Ag(en)_2^{+}$. However, when only one N of "en" coordinates, the other amino group must be able to add a proton as well as Ag^{+} again which leads to the adducts $Ag(en)^{+}$, $Ag(Hen)^{2+}$ and $Ag_2(en)^{2+}$ which were identified in the presence of comparatively high concentrations of free Ag^{+}, implying a low concentration [en] of uncomplexed ligand.[4] For the formation of the 1:2-complex on the other hand, [en] must be large, so that the 2:1- and the 1:2-complexes cannot be present simultaneously.

Contrary to expectation, however, it was found[4] that the equilibrated mixtures also contain $Ag_2(en)_2^{2+}$. A certain support for the formation of this 2:2-complex came recently from a new investigation of the system Ag^{+}–en;[5] *Sillen's* method was applied and it was found that the reproduction of the experimental data (pH, pAg) by back-computing was improved when the presence of $Ag_2(en)_2^{2+}$ was postulated. We want to point out that the results obtained 26 years ago were much less vague; the

† Deceased May 20th, 1978.

dimer $(Agen)_2^{2+}$ is strikingly exhibited when H_2en^{2+} is deprotonated in the presence of silver and the concentration of uncomplexed Ag^+ is thereby kept constant.[6] The formation of the dinuclear complex can be demonstrated unambiguously also by Salt Cryoscopy and Three Phase Vapour Tensiometry.[7] Also the solubility of the solid salt $\{Ag(en)ClO_4\}$ in solutions of constant ionic strength containing $NaNO_3$ and $NaClO_4$ can be accounted for quantitatively when it is assumed that the salt dissolves in forming the dinuclear cations mainly, although the units "en" are connected to endless chains by Ag^+ within the solid.[8] Finally we have determined also the heat production in the formation of $Ag(en)^+$, $Ag_2(en)_2^{2+}$ and $Ag(en)_2^+$. These thermodynamic data suggest that the 1:1-complex is a hydrated chelate with some strain within the 5-membered chelate ring, whereas both metal cations are linearly bonded to two nitrogens each in the 2:2-species, very much as in $Ag(NH_3)_2^+$. The atoms of the 2:2-complex present in solution therefore must form a 10-membered ring system which makes it unlikely that higher polymers $Ag_n(en)_n^{n+}$ with $n>2$ will be present as well in the equilibrium mixtures.

RESULTS AND DISCUSSION

Equilibria. The protolytic equilibria have been studied by titrating the diprotonated ligand H_2en^{2+} with alkali hydroxide, keeping the ionic strength constant with alkali nitrate. The procedure was then repeated in the presence of silver and the concentration [Ag] kept constant either by replacing an appreciable amount of the inert electrolyte by $AgNO_3$ ($[Ag] \gg [en]_{tot}$) or by adding an excess of the sparingly soluble $\{AgBrO_3\}$, which remains mainly in suspension, and simultaneously replacing a part of the anion NO_3^- by BrO_3^-, which fixes [Ag] at lower values. When [Ag] remains constant, the protonation of the ligand can be described with function (1) (for the definition of $\bar{p}'$, κ'_n, see eqns. (7') and (9')) as long as only complexes containing a

$$\sum_{n=0}^{n=2} (\bar{p}' - n)\kappa'_n[H]^n = 0, (\kappa_0 = 1) \qquad (1)$$

single molecule of "en" are involved. Deviations from this function are caused by species containing more than a single "en" and the deviations observed can be accounted for quantitatively by postulating the formation of the dimer $Ag_2(en)_2^{2+}$. The apparent protonation constants κ'_1 and κ'_2 furnish the stability constants of the species $Ag(en)^+$, $Ag_2(en)^{2+}$ and $Ag(Hen)^{2+}$. The stability of $Ag(en)_2^+$ is known[9] whereas the stability of $Ag(Hen)_2^{3+}$ can be estimated assuming that the ratio K_1/K_2 of the stability constants of $Ag(Hen)^{2+}$ and $Ag(Hen)_2^{3+}$ is the same under the conditions used in our laboratory ($I = 1.0$ M, KNO_3, 25 °C) and the medium of Ref. 5 ($I = 3$ M, $LiClO_4$, 25 °C). All of these data are collected in Table 1. The data of the first column are from Ref. 4 and those of the second are the results of a new study applying essentially the same procedure at $I = 1$ M and 25 °C. In the last column the results of Ref. 5 are reported.

Fig. 1 illustrates the formation of the various complexes during the alkalimetric titration of H_2en^{2+} at the silver concentrations $[Ag] = 0.1$ and 0.0013 M. When [Ag] is large, the removal of the first proton of H_2en^{2+} furnishes mainly $AgHen^{2+}$, which accumulates to a concentration of about

Table 1. Stability constants of proton and silver complexes of ethylenediamine "en". (Errors are given as confidence limits L_{95} for the 95 % confidence level).

Reaction	Constant	20 °C $I = 0,1$ M $(NaNO_3)$[4]	25 °C $I = 1$ M (KNO_3)	25°C $I = 3$ M $(LiClO_4)$[5]
$H^+ + en = Hen^+$	pK_1	10.03	10.24 ± 0.02	10.65
$H^+ + Hen = H_2en^{2+}$	pK_2	7.22	7.52 ± 0.02	8.04
$Ag^+ + en = Ag(en)^+$	$\log K_{Agen}$	4.7	5.06 ± 0.06	6.13
$Ag(en)^+ + en = Ag(en)_2^+$	$\log K_{Ag(en)_2}$	3.0	(2.6)	–
$Ag^+ + Hen^+ = Ag(Hen)^{2+}$	$\log K_{Ag(Hen)}$	2.35	2.42 ± 0.17	2.91
$Ag(Hen)^{2+} + Hen^+ = Ag(Hen)_2^{3+}$	$\log K_{Ag(Hen)_2}$	–	(2.7)	3.16
$Ag^+ + Ag(en)^+ = Ag_2(en)^{2+}$	$\log K_{Ag_2(en)}$	1.76	1.20 ± 0.45	1.54
$2Ag^+ + 2en = Ag_2(en)_2^{2+}$	$\log K_{Ag_2en_2}$	13.23	13.17 ± 0.25	14.53
$Ag(en)^+ + Ag(en)^+ = Ag_2(en)_2^{2+}$	$\log K_d$	3.83	3.05 ± 0.29	2.27

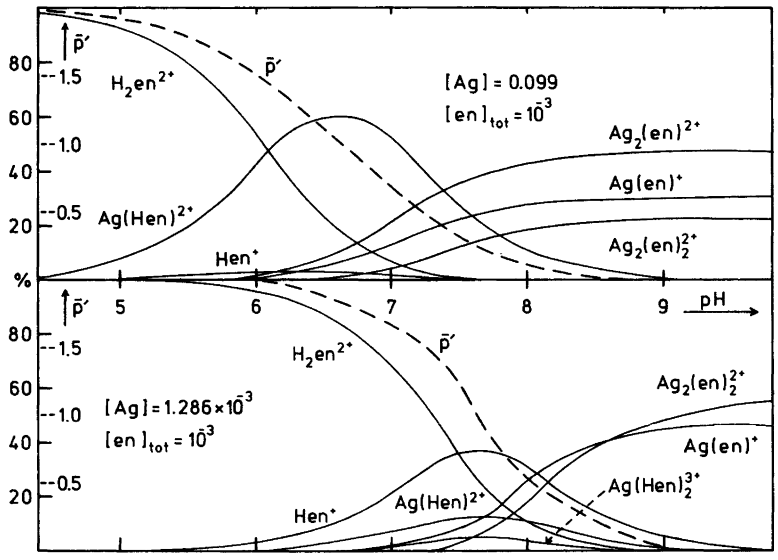

Fig. 1. Fraction [%] of "en" present in a given species and the degree $\bar{p}'$ of protonation of "en" as a function of pH at two different and constant concentrations of the free silver ion Ag(I).

80 % of the total amount of ethylenediamine present at $\bar{p}'=1$ (pH=6). This species is further deprotonated between pH 6 and 9 giving rise to the production of $Ag_2(en)^{2+}$ (47 %), $Ag(en)^+$ (30 %) and $Ag_2(en)_2^{2+}$ (containing 22 % of $[en]_{tot}$). The situation is very different at the lower silver concentration. The main product after removal of one proton of H_2en^{2+} ($\bar{p}'=1$ at about pH 7.6) now is Hen^+ (36 %) accompanied by $Ag(Hen)^{2+}$ (11 %). One quarter of the original H_2en^{2+} is still fully protonated and another quarter is fully deprotonated being present as $Ag(en)^+$ (15 %), $Ag_2(en)_2^{2+}$ (8 %). When the value $\bar{p}'=0$ is reached (pH=10), the solution contains practically only the dimer $Ag_2(en)_2^{2+}$ (with 52 % of $[en]_{tot}$) and the monomer $Ag(en)^+$ (46 %). The various mononuclear 1:2-species are of practically no importance; $Ag(Hen)_2^{3+}$ being the most important of these complexes reaches 2.4 % at large concentrations of uncomplexed silver (pH=6) and reaches 3.3 %, its maximum concentration, in the presence of solid $AgBrO_3$ creating a constant and low [Ag]. The conditions therefore can be chosen such that the main products are $Ag(Hen)^{2+}$ and $Ag_2(en)^{2+}$, or $Ag(en)^+$ and $Ag_2(en)_2^{2+}$.

It is the special advantage of the method used that the concentration of $Ag_2(en)_2^{2+}$ can be obtained as the ratio of two quantities read off directly. A rather reliable value for the stability constant of the dimer is obtained. Although the formation of higher polymers $Ag_n(en)_n^{n+}$ cannot be excluded completely, it can be stated that they are produced in very small quantities at the most.

From the high stability of $Ag(en)^+$, in comparison with the stability of 1:1-complexes of unidentate monoamines (log $K_1 \sim 3.4$), we conclude that $Ag(en)^+$ must be a chelate with both basic nitrogens of "en" coordinated. However, $K_{Ag(en)}$ is not as large by far as the stability constants of 1:2-complexes of monoamines (log $\beta_2 \sim 7.3$) which probably is due to some strain within the chelate ring of $Ag(en)^+$ and the release of that strain may be the driving force for the dimerisation. It is remarkable that $K_{Ag(en)}$ increases considerably with increasing ionic strength whereas simultaneously K_d becomes smaller. It looks as if the strain within $Ag(en)^+$ is lessened with increasing I reducing the tendency for dimerisation. The ratio $q=K_1/K_2$ in the sequence $Ag^+ \rightarrow Ag(en)^+ \rightarrow Ag(en)_2^+$ is very much larger ($q=300$) than for unidentate monoamine complexes ($q=0.3$) which is also explained with the assumption that $Ag(en)^+$ is a chelate. The ratio q on the other hand is only slightly larger than usual in the sequence $Ag^+ \rightarrow Ag(Hen)^{2+} \rightarrow Ag(Hen)_2^{3+}$ ($q=0.5$), which is also reasonable.

Mean nuclearity. Although highly soluble, salts of

the 1:1-complex of silver and ethylenediamine can be obtained crystalline: $[Ag(en)]_2SO_4.H_2O$; $[Ag(en)]ClO_4$; $[Ag(en)]NO_3.H_2O$. According to the data of Table 1, solutions of these salts should contain mainly the dinuclear cation $Ag_2(en)_2^{2+}$ besides the appropriate anion, if they are not too dilute [the dissociation into mononuclear $Ag(en)^+$ and the hydrolysis of the latter $Ag(en)^+ + H_2O \rightarrow Ag^+ + Hen^+ + OH^-$) should amount to less than 3 % at concentrations $[Ag]_{tot}$ above 0.1 M]. It must be possible therefore to demonstrate this cryoscopically.

The cryoscopic and the ebullioscopic methods applied to ionic compounds in a solvent consisting of uncharged molecules have two main disadvantages: 1. Not only the complex ion, the nuclearity of which is to be investigated, but also its counter ion (SO_4^{2-}, NO_3^-, ClO_4^- of the salts mentioned) contribute to ΔT (freezing point depression, elevation of boiling point). 2. The strong deviations from Raoult's law become negligible only at high dilution after ΔT has become so small that it can no longer be determined accurately. Unfortunately ΔT does not change linearly with the salt concentration m (mol salt per kg of solvent) which makes extrapolation difficult. In the case of complexes which are labile and of moderate stability only, such as $Ag_2(en)_2^{2+}$, dilution furthermore would lead to dissociation, so that the measurements have to be carried out at concentrations which are not extremely small. In studying ionic equilibria, the difficulties arising from nonideality due to the interionic forces are overcome by adding an inert electrolyte which keeps the activity coefficients of the ionic equilibrium participants constant. Similarly it is advantageous to carry out cryoscopic and ebullioscopic measurements in the presence of an inert salt which already contains the counter ion of the complex salt to be investigated. The complex $[Ag(en)]_2SO_4$ for instance may be dissolved in molten Glauber's salt (the decahydrate $Na_2SO_4.10H_2O$), which actually is a suspension of the anhydrous sodium sulfate in its saturated solution. The transition:

$$Na_2SO_4.10H_2O\ (solid) \rightarrow Na_2SO_4\ (solid)\ in\ melt$$

is a fixed point according to the phase rule at constant pressure, taking place exactly at 32.384 °C under atmospheric conditions. In the presence of a foreign solute this transition point is lowered, but neither Na^+ nor SO_4^{2-} – being constituents of the medium – are foreign solutes and are therefore cryoscopically active. The anion of the salt $[Ag(en)]_2SO_4$ therefore does not contribute to the lowering of the transition point of Glauber's salt, which makes it easy to distinguish between mononuclear and polynuclear complex cations. The complex sulfate produces the same depression as K_2SO_4 if the complex cation in solution is mononuclear, but the depression is only half as great if dinuclear units $Ag_2(en)_2^{2+}$ are present. This is exactly true only at infinite dilution, but the ratio $\Delta T/m$ changes only little with concentration m and the function is linear, so that extrapolation to $m=0$ does not create any difficulty.

The following values were found on extrapolation:[10]

$$(\Delta T/m)_{m\rightarrow 0} = 6.1\ ^\circ C\ kg\ mol^{-1}\ for\ K_2SO_4$$
$$= 3.1\ ^\circ C\ kg\ mol^{-1}\ for\ [Ag(en)]_2SO_4$$

These data prove that the solution of the silver complex in the melt of Glauber's salt contains the dinuclear species $[Ag_2(en)_2]^{2+}$.

Whereas Glauber's salt has been used as a cryoscopic medium for 80 years,[11] although without recognizing its implications and usefulness, the Three-Phase Vapour Tensiometry (TPVT) analogue to salt-cryoscopy has been developed only recently.[7] In this technique we have a two-phase medium of a crystalline inert salt and its saturated solution and a third phase, the gaseous phase. According to Gibbs phase rule, such a system has a definite vapour pressure just as pure water. Any addition of foreign solute molecules – charged or uncharged – to the two-phase medium causes a lowering of the vapour pressure, and again the ions of the inert salt are inactive. If the inert salt for instance is KNO_3 – the two-phase medium being now solid potassium nitrate and its saturated solution – and dissolved $AgNO_3$, only the cation Ag^+ causes a lowering of the water pressure p above the medium, the anion NO_3^- does not. Nitrate is again inactive when we dissolve the complex $[Ag(en)]NO_3$, but the depression of p amounts now only to half the value obtained with $AgNO_3$ for equimetallic concentrations, if the complex salt produces a dinuclear cation $Ag_2(en)_2^{2+}$.

The isothermic pressure lowering $[\Delta p]_T$ is thermodynamically equivalent to the isobaric temperature enhancement $[\Delta T]_p$, which must be maintained between the two media with and without the foreign solute to get the same vapour pressure above both media.

In order to avoid cumbersome vapour pressure determinations, *Hill's* method[12] has been applied. In this method $[\Delta p]_T$ or $[\Delta T]_p$ are obtained by determination of the stationary temperature difference ΔT_s, ($\Delta T_s \leq [\Delta T]_p$), which sets in between the two media with and without the foreign solute if they are kept in the atmosphere of the pure two-phase medium. ΔT_s was measured using thermistors with a Wheatstone bridge. The signal S of this bridge is proportional to "i_f", the number of foreign species created by the dissolution of $AgNO_3$ or $Ag(en)NO_3$.

$$i_f = \frac{55.51[\Delta p]_T}{p_0 m_{Ag}} = \frac{[\Delta T]_p}{E m_{Ag}} = \frac{\Delta T_s}{k_T m_{Ag}} = \frac{S}{k_S m_{Ag}} \qquad (2)$$

p_0 is the vapour pressure of the pure two-phase medium at the temperature T and E is the three-phase ebullioscopic constant.

The calibration constants k_T and k_S were determined by using KCl as solute with $i_f = 1$. The quantity i_f varies linearly with the concentration of the solute and the slope of the line can be predicted (see Ref. 7 and Fig. 2).

Fig. 3 illustrates the salt-ebullioscopic titration with ethylenediamine of a solution of $AgNO_3$ in the saturated solution of KNO_3 (molality $m_{Ag} = 0.5$ mol per kg of water in the two-phase medium). Before the start of the titration, the number of foreign solute molecules is $i_f = 1$ (the cation Ag^+). The free base "en" which is now added is bonded quantitatively and i_f would not change if the product of the reaction would be mononuclear $Ag(en)^+$ (line 1). However, although a new substance is introduced, i_f is lowered at the beginning of the titration. The slope at the very start is -1 (line 2) because of the formation of $Ag_2(en)^{2+}$. But the 2:1-complex is not very stable (Table 1) and adds "en" very efficiently:

$$Ag_2(en)^{2+} + en \rightarrow Ag_2(en)_2^{2+}$$

The slope changes therefore soon with increasing $[en]_{tot}/[Ag]_{tot}$ to -0.5 (line 3), the dominant reaction becoming:

$$2Ag^+ + 2en \rightarrow Ag_2(en)_2^{2+}$$

When one mol of "en" per silver has been added, almost all the metal and all of the diamine are present in the form of $Ag_2(en)_2^{2+}$ and the number of solute species per metal is only slightly larger than $i_f = \frac{1}{2}$. With further amounts of base introduced, i_f increases again, (line 3'), demonstrating the change of the nuclearity from the value 2 back to 1 again:

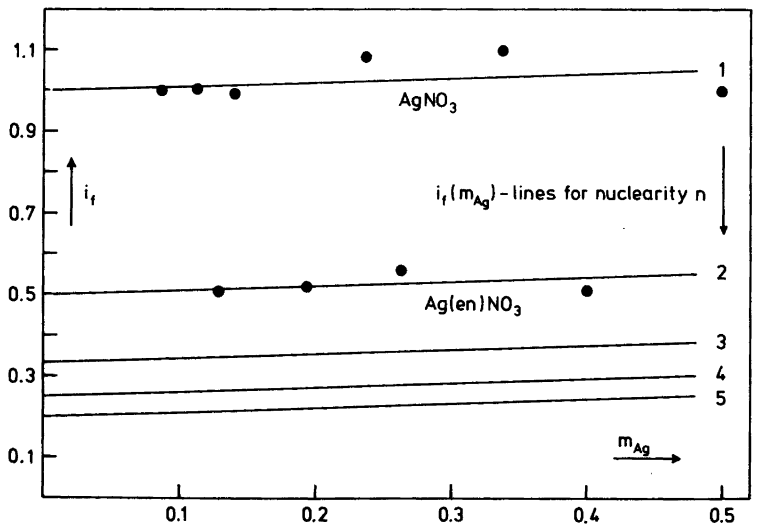

Fig. 2. The dependence of i_f, the apparent number of foreign species per silver atom present after the dissolution of $AgNO_3$ or $[Ag(en)]NO_3$ in the saturated solution of the two-phase medium with the inert salt KNO_3, on the molality m_{Ag} (= the total number of mol Ag per kg of water present in the two-phase medium). Lines 1. 2, 3, 4 and 5 represent the predicted values of i_f for the nuclearity $n = 1, 2, 3, 4$ and 5 of the complex $[AgL \times aq]_n(NO_3)_n$ (L = en or H_2O).

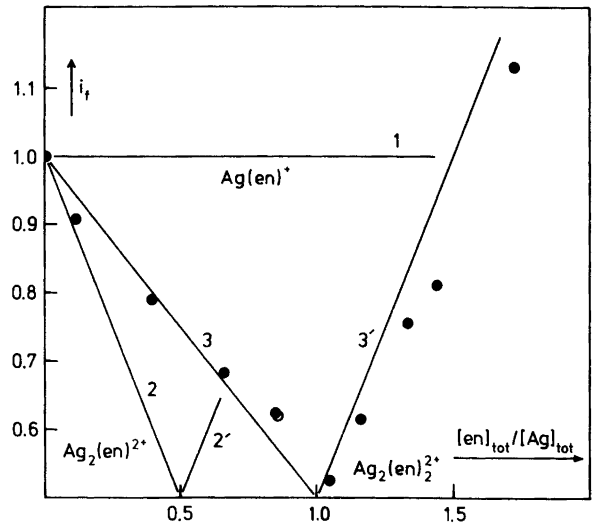

Fig. 3. The TPVT-titration of $AgNO_3$ with "en", both dissolved in the solution of the two-phase medium with KNO_3 at constant m_{Ag} (=0.5 mol/kg). Lines 1, (2,2') and (3,3') are predicted courses of the function i_f ($[en]_{tot}/[Ag]_{tot}$) for the formation of the mononuclear $Ag(en)^+$ only, the dinuclear $Ag_2(en)^{2+}$ only or the dinuclear $Ag_2(en)_2^{2+}$ only.

$$Ag_2(en)_2^{2+} + 2en \rightarrow 2Ag(en)_2^+$$

This titration shows up the dimerisation of $Ag(en)^+$ strikingly.

Solubility of [Ag(en)](ClO$_4$). During TPVT-measurements we found that the perchlorate $[Ag(en)](ClO_4)$ was salted out by ethyltrimethylammonium perchlorate, which we first intended to use as an inert salt. This observation led us to the assumption that the interpretation of solubility curves $[Ag]_{tot}([ClO_4^-])$ could yield additional evidence about the nuclearity of the dominating complex in the saturated solution of $[Ag(en)](ClO_4)$.

As a matter of fact, the solubility curve is described at concentrations $[Ag]_{tot}$ between 123 and 6 mM by eqn. 3 which is easily obtained by the assumption of the presence of only two complexes $Ag(en)^+$ and $Ag_2(en)_2^{2+}$ in the saturated solution of $[Ag(en)](ClO_4)$:

$$-\log [Ag]_{tot} = -\log(K_{sp}/[ClO_4^-] + 2K_{sp}^2 K_d/[ClO_4^-]^2) \quad (3)$$

At low perchlorate ion concentrations the quadratic term of the sum becomes dominant and causes the quasi-linear form of the solubility curve $-\log[Ag]_{tot}$ ($-\log[ClO_4^-]$) (see Fig. 4). The slope calculated from the 12 points at low $[ClO_4^-]$-values differs only by 5 % from the theoretical value of -2. Therefore, higher polymers $[Ag(en)]_n^{n+}$ with $n>2$ are either not present at all or only in small concentration. Nevertheless, a very elegant but risky hypothesis of a "continued polymerisation" of $Ag(en)^+$ was presented[13] recently. In our opinion the calculation of more than one constant from these solubility data is mathematically possible but has no real meaning chemically because the part of the solubility curve at high $[ClO_4^-]$-values cannot be determined accurately for the following reasons: (a) besides the two main complexes $Ag(en)^+$ and $Ag_2(en)_2^{2+}$ there are 4 other complexes present. The distribution of silver (as % Ag in a given complex of the totally dissolved Ag) was calculated for the saturated solution of $[Ag(en)](ClO_4)$ and experimental conditions given in the legend for Fig. 4 using the data of Table 1 for 1 M KNO_3 and the stability constant[5] of [Ag(en)OH]: $Ag(Hen)^+$ (1.24 %), [Ag(en)-OH] (4.02 %), $Ag(en)_2^+$ (4.15 %), $Ag(Hen)_2^{3+}$ (9.07 %), $Ag(en)^+$ (23.65 %) and $Ag_2(en)_2^{2+}$ (53.71 %), (b) the solid $\{[Ag(en)](ClO_4)\}$ is not stable if it is suspended in a solution of 0.01 M $HenClO_4$ and partially decomposes to Ag_2O involving the liberation of Hen^+ and the enhancement of $[Ag]_{tot}$. This enhancement is negligible at high $[Ag]_{tot}$-values but causes

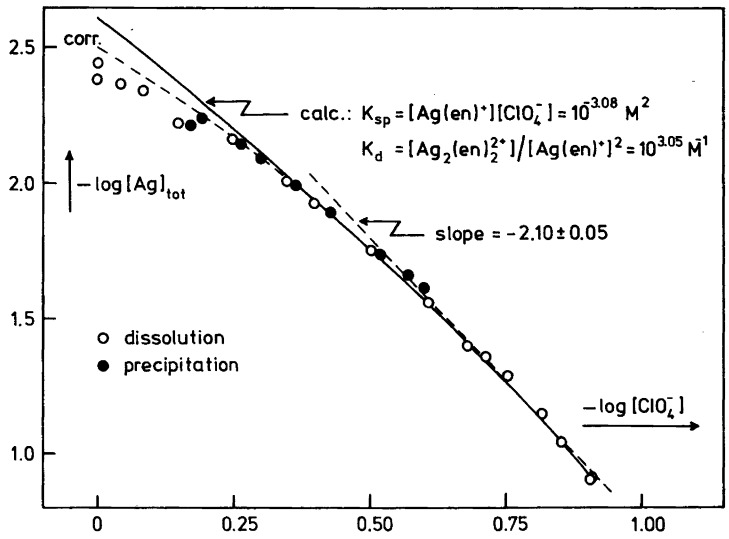

Fig. 4. The solubility of $[Ag(en)]ClO_4$ in water containing 0.01 M $HenNO_3$, $([ClO_4^-] - [Ag]_{tot})$ M $NaClO_4$ and $(0.99 - [ClO_4^-])$ M KNO_3 at 25 °C ($K_{sp} = [Ag(en)^+][ClO_4^-]$).

serious interference at low values of $[Ag]_{tot}$.

For these reasons the seven points at high $-\log[Ag]_{tot}$-values (see Fig. 4) were omitted in the calculation of the solubility product K_{sp}. In this calculation the dimerisation constant K_d of $10^{3.05}$ (see Table 1) was taken and K_{sp} calculated from eqn. 3 using all other points of the solubility curve. The average value of $\log K_{sp}$ was -3.08 ± 0.01 and was used to calculate the solid line in Fig. 4 by means of eqn. 3. If $[Ag]_{tot}^{calc}$ is corrected for the contribution of the first 4 complexes mentioned above, a better representation of the experimental points results (see dotted line "corr" in Fig. 4). For the calculation of a still better "corrected line" the amount of the Hen^+ liberated in the decomposition of $\{[Ag(en)](ClO_4)\}$ should be measured. The use of stability constants determined in the same medium would also improve the fit somewhat.

Table 2. Comparison of thermodynamic data of Ag(I) complexes of ammonia,[14] ethylenediamine "en", 1,3-propandiamine "pn",[15] 1,4-butanediamine "bn",[15] and ethalnolamine "ea".[16] ($\pm$ values are the 95 % confidence limits, L_{95}).

Reaction	ΔG kJ/mol	ΔH kJ/mol	ΔS J/mol K
$Ag^+ + en = Ag(en)^+$	-28.9 ± 0.3	-48.5 ± 1.4	-66 ± 5
$Ag^+ + 2en = Ag(en)_2^+$	-43.7 ± 0.6	-55.2 ± 1.3	-39 ± 5
$2Ag^+ + 2en = Ag_2(en)_2^{2+}$	-75.2 ± 1.4	-107.8 ± 2.7	-109 ± 9
$Ag(en)^+ + Ag(en)^+ = Ag_2(en)_2^{2+}$	-17.4 ± 1.7	-10.8 ± 0.1	$+22 \pm 6$
$Ag^+ + 2NH_3 = Ag(NH_3)^+$	-41.2	-56.1 ± 0.6	-50 ± 2
[a] $Ag^+ + pn = Ag(pn)^+$	-32.9	-61.2 ± 9.7	-95 ± 32
$Ag^+ + bn = Ag(bn)^+$	-31.6	-47.7 ± 3.9	-54 ± 13
$Ag^+ + ea = Ag(ea)^+$	-18.1	-23.0 ± 5.6	-16 ± 19
$Agea^+ + ea = Ag(ea)_2^+$	-20.7	-27.1 ± 7.7	-21 ± 26

[a] All succeeding values were calculated from log K values[15,16] measured at 10, 20, 30 and 40 °C using the constants A, B and the standard deviation σ_B of the corresponding linear regression $\log K = A + B/T$: $\log K_{25} = B/298.15 + A$, $-\Delta G = 5.708 \log K_{25}$, $-\Delta H = 0.019144B$, $L_{95}(\Delta H) = 0.0304\sigma_B$, ΔS, $= 3.354(\Delta H - \Delta G)$ and $L_{95}(\Delta S) = 3.35 L_{95}(\Delta H)$.

Heats of formation. The heat production in the reaction of Ag(I) with "en" at various pH-values and the heat consumption in the dissociation of $Ag_2(en)_2^{2+}$ to 2 $Ag(en)^+$ by dilution with solutions of KNO_3 were measured. Using these data and the stability constants of Table 1 for 1 M KNO_3 the heats and entropies of formation were calculated and compared in Table 2 with corresponding values of Ag(I) complexes of ammonia, and some amines.

The heat of formation of $Ag(en)_2^+$, $Ag(ea)_2^+$, $Ag(pn)^+$ and $Ag(bn)^+$ agree within the 95 % confidence limits. Additionally, the number of Ag–N bonds is certainly two in these complexes. Therefore, we calculated the most probable value ΔH_{Ag-N} for the enthalpy of formation of an Ag–N bond as the half of the weighted average of the ΔH values of the four complexes mentioned above and obtained the value of -27.9 ± 0.3 kJ/mol. Because $\Delta H_{Ag(en)}$ is 1.74 times larger than ΔH_{Ag-N}, the complex $Ag(en)^+$ must be a chelate. The deficit of 7.3 kJ/mol is presumably due to some strain within the chelate ring. We can also assume that a strained chelate ring is more hydrated than linear or large ring complexes. In the dimerisation reaction the ring relaxes and water molecules become free. This enhancement of the total number of particles involved in the dimerisation reaction is demonstrated by the positive entropy change of this reaction. Due to the poor precision of the entropy data no further discussion of entropy effects is possible. Nevertheless, it is very interesting to note that $3(\Delta H_{Ag-N})$ and $4(\Delta H_{Ag-N})$ are -83.7 ± 0.9 and -111.6 ± 1.2 kJ/mol, respectively. As the latter value is almost the same as the enthalpy of formation of $Ag_2(en)_2^{2+}$, the number of the Ag–N bonds in the dimer must be four. Hence a linear arrangement of $Ag_2(en)_2^{2+}$ would provide only three Ag–N bonds, the dissolved complex has most probably the 10-membered ring structure proposed[4] 26 years ago. The relatively small ring stabilization energy of -14 kJ/mol Ag can of course easily be compensated by lattice packing energies. The difference of the crystal structure[8] and the molecular structure of the dominant complex in the saturated solution of $[Agen](ClO_4)$ is therefore not a real contradiction at all.

METHODS AND EXPERIMENTAL

Potentiometric titrations. The calibration of the cell Hg°, Hg_2Cl_2/3.5 M KCl/1 M KNO_3/Glass was carried out by titration of 100 m^3 of a solution containing 0.01 M HNO_3 and 0.99 M KNO_3 with a solution of 0.5 M KOH and 0.5 M KNO_3 at 25 ± 0.2 °C under nitrogen. From the combination $(E^\circ_H - E^\circ_{OH})/59.16$, a $-\log[H][OH]$ value of 13.76 was obtained. Using this cell, 100 cm^3 aliquots of the following 6 solutions were titrated in the same way:

(1) 10^{-3} M $[H_2en](ClO_4)_2$,
(2) 10^{-2} M $[H_2en](ClO_4)_2$,
(3) 10^{-3} M $[H_2en](ClO_4)_2$, 0.2 M $KBrO_4$ and 1 g $AgBrO_3$,
(4) 10^{-3} M $[H_2en](ClO_4)_2$, 5×10^{-2} M $KBrO_3$ and 1 g $AgBrO_3$
(5) 10^{-3} M $[H_2en](ClO_4)_2$ and 0.1 M $AgNO_3$ and
(6) 10^{-2} M $[H_2en](ClO_4)_2$ and 0.2 M $AgNO_3$.

All solutions contained KNO_3 in such a concentration that the ionic strength was 1 M. The concentration of free silver ion in solutions 3 and 4 was obtained from eqn. (4):

$$[Ag] = K^*_{sp}/([KBrO_3] + [Ag]_{tot}) \qquad (4)$$

where K^*_{sp} is the solubility product of $AgBrO_3$. The value of $(2.60\pm0.03)10^{-4}$ M^2 was used, which was obtained by atomic absorptiometric determination of [Ag] in filtrates (0.45 μm membrane filter) of suspensions and precipitations of $AgBrO_3$ in 1 M solutions of KNO_3 containing 10^{-3} M HNO_3.

Because of the presence of silver in excess, the concentration of uncomplexed Hen^+ and en will always remain so small in these solutions that mononuclear 1:2-complexes cannot form in significant amounts. The diprotonated H_2en^{2+} therefore was expected to be in equilibrium with protonated species Hen^+, $Ag(Hen)^{2+}$ and three completely deprotonated species en, $Ag(en)^+$, $Ag_2(en)^{2+}$. Because of the constancy of the concentration [Ag], the following concentration ratios remain constant throughout the process:

$$\frac{[Ag(Hen)]}{[Hen]} = [Ag]K_{AgHen};\ \frac{[Ag(en)]}{[en]} = [Ag]K_{Agen};$$

$$\frac{[Ag_2(en)]}{[en]} = [Ag]^2K_{Agen}K_{Ag_2en} \qquad (5)$$

(the formation constants K_{Agen}, K_{AgHen}, K_{Ag_2en} are defined in Table 1). Now the concentration of acidic hydrogen bonded to the free or complexed ligand, *i.e.* the degree of protonation ($\bar{p}$ when silver is absent or $\bar{p}'$ in the presence of silver) is obtained with eqn. (6); $[H]_{tot}$ being the total concentration of acidic hydrogen ($=2[en]_{tot} - [KOH]$):

$$\bar{p}\ (\text{or } \bar{p}') = \frac{[H]_{tot} - [H] + [OH]}{[en]_{tot}} \qquad (6)$$

The quantities $\bar{p}$ and $\bar{p}'$ can also be expressed by (7) and (7')

$$\bar{p} = \frac{[\mathrm{Hen}]+2[\mathrm{H_2en}]}{[\mathrm{en}]+[\mathrm{Hen}]+[\mathrm{H_2en}]} \tag{7}$$

$$\bar{p}' = \frac{[\mathrm{Hen}]'+2[\mathrm{H_2en}]}{[\mathrm{en}]'+[\mathrm{Hen}]'+[\mathrm{H_2en}]} \tag{7'}$$

with

$$\begin{aligned}[\mathrm{Hen}]' &= [\mathrm{Hen}]+[\mathrm{AgHen}] \\ [\mathrm{en}]' &= [\mathrm{en}]+[\mathrm{Agen}]+[\mathrm{Ag_2en}]\end{aligned} \tag{8}$$

Eqn. (9) defines the usual basicity constants and

$$\begin{aligned}\frac{[\mathrm{Hen}]}{[\mathrm{H}][\mathrm{en}]} &= 10^{\mathrm{p}K_1} = \kappa_1; \\ \frac{[\mathrm{H_2en}]}{[\mathrm{H}][\mathrm{Hen}]} &= 10^{\mathrm{p}K_2} = \kappa_2/\kappa_1\end{aligned} \tag{9}$$

analogous expressions are used for the apparent basicities of en' and Hen' in the presence of silver:

$$\frac{[\mathrm{Hen}]'}{[\mathrm{H}][\mathrm{en}]'} = 10^{\mathrm{p}K'_1} = \kappa'_1;$$

$$\frac{[\mathrm{H_2en}]}{[\mathrm{H}][\mathrm{Hen}]'} = 10^{\mathrm{p}K'_2} = \kappa'_2/\kappa'_1 \tag{9'}$$

Replacement of the concentrations of the metal-containing species in (8) and (9') with the help of (5) leads to the expressions (10) for the apparent basicity constants determined in the presence of silver [eqn. (10)].

$$10^{\mathrm{p}K'_1} = \frac{[\mathrm{Hen}](1+[\mathrm{Ag}]K_{\mathrm{AgHen}})}{[\mathrm{H}][\mathrm{en}](1+[\mathrm{Ag}]K_{\mathrm{Agen}}+[\mathrm{Ag}]^2K_{\mathrm{Agen}}K_{\mathrm{Ag_2en}}} \tag{10}$$

$$10^{\mathrm{p}K'_2} = \frac{[\mathrm{H_2en}]}{[\mathrm{H}][\mathrm{Hen}](1+[\mathrm{Ag}]K_{\mathrm{AgHen}})}$$

According to (10) the dashed pK's (pK'_1 and pK'_2) differ from the (pK)'s determined when silver is absent (eqn. 9) by a term remaining constant because of the constancy [Ag]. The protonation in the presence of silver can therefore be described with a function pH($\bar{p}'$) analogous to that when the metal is absent pH($\bar{p}$). A combination of (7) and (9) furnishes (11) and a combination of (7') and (9') the eqn. (11'):

$$\bar{p}+(\bar{p}-1)10^{(\mathrm{p}K_1-\mathrm{pH})}+(\bar{p}-2)10^{(\mathrm{p}K_1+\mathrm{p}K_2-2\mathrm{pH})} = 0 \tag{11}$$

$$\bar{p}+(\bar{p}'-1)10^{(\mathrm{p}K'_1-\mathrm{pH})}+(\bar{p}'-2)10^{(\mathrm{p}K'_1+\mathrm{p}K'_2-2\mathrm{pH})} = 0 \tag{11'}$$

It is readily recognized that the stability constants of the three complexes assumed to form in the presence of an excess of silver can be calculated from the differences (pK_1 − pK'_1) and (pK_2 − pK'_2). From (10), (11) and (11') we obtain:

$$\begin{aligned}(\mathrm{p}K_2-\mathrm{p}K'_2) &= \log(1+[\mathrm{Ag}]K_{\mathrm{AgHen}}) \\ (\mathrm{p}K_1-\mathrm{p}K'_1)+(\mathrm{p}K_2-\mathrm{p}K'_2) &= \log(1+[\mathrm{Ag}]K_{\mathrm{Agen}} \\ &\quad +[\mathrm{Ag}]^2K_{\mathrm{Agen}}K_{\mathrm{Ag_2en}})\end{aligned} \tag{12}$$

At least three titrations are needed therefore if the three unknown constants K_{AgHen}, K_{Agen} and $K_{\mathrm{Ag_2en}}$ are to be calculated: the deprotonation of H_2en without any silver present gives pK_1 and pK_2 [eqn. (11)] and titrations at two different concentrations [Ag] furnish two pairs pK'_1, pK'_2

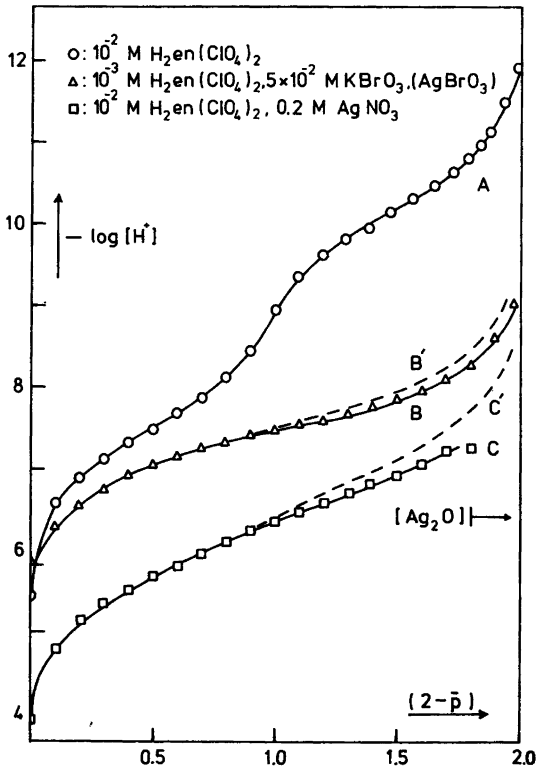

Fig. 5. Deprotonation of H_2en^{2+}: (A) without Ag(I) (pK_1 = 10.21, pK_2 = 7.50), (B) [Ag] = 4.66.10^{-3} M, constant (B' calculated with pK'_1 = 7.74 and pK'_2 = 7.22) and (C) [Ag] = (0.195 ± 0.005) M [C' calculated from the protonation function (11') using pK'_1 = 7.09 and pK'_2 = 5.72].

[eqn. (11')] allowing the calculation of the stability constants with (12).

A set of three protonation curves illustrating the procedure is shown in Fig. 5. When no silver is present (curve A) the buffer regions $en \rightarrow Hen^+$ ($pK_1 \sim 10.2$) and $Hen^+ \rightarrow H_2en^{2+}$ ($pK_2 \sim 7.5$) are well separated. In the presence of silver, however, an uninterrupted flat region of gradually falling pH between $\bar{p}' = 0.1$ and 1.9 is obtained (curves B and C). This phenomenon is caused by the higher stability of $Ag(en)^+$ in comparison to $Ag(Hen)^{2+}$ ($K_{Agen} \gg K_{AgHen}$) making the difference ($pK_1 - pK_1'$) much larger than ($pK_2 - pK_2'$) and consequently ($pK_1 - pK_2$) larger than ($pK_1' - pK_2'$). In the case of curve A pK_1 is obtained from the upper buffer region with the first two terms of eqn. (11), the third term being negligibly small in the range $0 < \bar{p} < 1$; whereas $\bar{p}$ in eqn. (11) may be neglected in the lower buffer region ($1 < \bar{p} < 2$) which is determined practically only by pK_2.

The apparent basicities pK_1' and pK_2' cannot be obtained so simply from the curves B and C, their difference being so small that all the terms of (11') make an appreciable contribution over the entire buffer region $0 < \bar{p}' < 2$, *i.e.* the species containing en', Hen' and H_2en are present simultaneously. Both pK'-values have to be taken into account over the whole region. On the other hand this situation makes it also possible to find both pK'-values from only a part of the extended buffer region. A graphical method proved to be especially suitable, first to find out whether the experimental curves (B and C, Fig. 5) can be reproduced with eqn. (11') and second to obtain the values pK_1' and pK_2'. When eqn. (11') is divided by the factor $10^{(pK_1' - pH)}$ a linear eqn. (13) is obtained of the variables x and y defined as: $x = 10^{-pK_1'}$ and $y = 10^{pK_2'}$. Every point of the experimental protonation curve $\bar{p}'(pH)$ furnishes a straight line in a plot

$$x\bar{p}'/[H] + y(\bar{p}' - 2)[H] + (\bar{p}' - 1) = 0 \qquad (13)$$

$y(x)$ according to (13) and when the eqn. (11') is valid, these straight lines have a common point of intersection at the values:

$$x_0 = 10^{-pK_1'};\ y_0 = 10^{pK_2'}$$

The lines were drawn by connecting the axial intercepts:

$$\text{for } y = 0:\ x = \frac{(1 - \bar{p}')}{\bar{p}'}\,[H]$$

$$\text{for } x = 0:\ y = \frac{(1 - \bar{p}')}{(\bar{p}' - 2)[H]}$$

Applying this criterion it is found that only about half of the experimental curves taken in the presence of silver (B and C, Fig. 1) can be represented by (11'), only the part at lower pH-values, where $\bar{p}' > 1$. Starting the investigation at the acidic end of the curve, the lines [eqn. (13)] from consecutive points with $\bar{p}' = 1.9, 1.8, 1.7$ *etc.* first all cross at the same point, but deviate later more and more from that common point of intersection at higher pH values when $\bar{p}' < 1$. The experimental curves taken at constant [Ag] are as expected only at the beginning of the deprotonation of H_2en^{2+}, but in the later stages of the process the pH-value does not rise as much as it should according to eqn. (11') with descending $\bar{p}'$. This result is illustrated in Fig. 5 with B' and C' which show the expected course of the curves calculated with pK_1' and pK_2' from the common point of intersection at the start of the deprotonation in the region $\bar{p}' \geq 1.4$.

The described deviation from eqn. (11') must be caused by the formation of species containing more than a single molecule of "en". Of the mononuclear 1:2-complexes $Ag(en)_2^+$, $Ag(en)(Hen)^{2+}$ and $Ag(Hen)_2^{3+}$ which might be considered only the last is of some importance,* but even $Ag(Hen)_2^{3+}$ can only be formed, at the most, in amounts of a few percent of $[en]_{tot}$.

This causes hardly any changes in the protonation curve. Furthermore the small deviations from (11') caused by $Ag(Hen)_2^{3+}$ are largest at $\bar{p}' = 1$. Clearly, however, the observed deviations begin only at this position and become more and more pronounced with falling $\bar{p}'$. This fact indicates that the complex causing the deviation contains completely deprotonated "en" and more than a single molecule of it. The mononuclear $Ag(en)_2^+$ can be ruled out, it must be a species containing not only more than a single "en" but more than a single Ag^+ as well and indeed, the experimental curves can be reproduced qualitatively by assuming the formation of $Ag_2(en)_2^{2+}$.

The concentration of this 2:2-complex is obtained immediately from the difference $(\bar{p}')^{obs} - (\bar{p}')^*$ given by the curves B and B' or C and C', respectively.

* The comparatively small constant $[Ag(en)_2]/[Ag(en)][en]$ (~ 500) is obtained from β_2 (Refs. 3 and 9) and $K_{Ag(en)}$. In the presence of an excess of silver the deprotonation of H_2en^{2+} takes place at comparatively low pH values so that [en] becomes extremely small and also the concentration $[Ag(en)_2]$ (order of magnitude 10^{-7} M). The concentration of Hen^+ of course is much larger than [en] in these pH-ranges, but Hen^+ is not as good a ligand as "en" and the concentration of $Ag(en)(Hen)^{2+}$ is not expected to be important. The constant $[Ag(Hen)_2]/[Ag(Hen)][Hen]$ can be guessed from $K_{Ag(Hen)}$ and K_1/K_2-ratios of other amine-complexes of silver. Its order of magnitude is also about 500.

Inspection of eqn. (6) used to find the experimental $(\bar{p}')^{obs}$ and comparison with (7') which is involved when $\bar{p}'$ is calculated with (11') from the constants pK'_1, pK'_2 found in the high acidity range ($\bar{p}' > 1$), gives:

$$[H]_{tot} - [H] + [OH] = [Hen]' + 2[H_2en]$$

and therefore:

$$(\bar{p}')^* ([en]' + [Hen]' + [H_2en]) = (\bar{p}')^{obs}[en]_{tot} \quad (14)$$

The degree of protonation $(\bar{p}')^*$ calculated with (11') and the primed pK's is larger than the observed $(\bar{p}')^{obs}$ (see Fig. 5), but the sum $[en]_{tot}$ is larger than the sum in brackets on the left hand side of the equation [see eqn. (8)] because of the presence of the 2:2-complex:

$$[en]_{tot} = [en]' + [Hen]' + [H_2en] + 2[Ag_2(en)_2], \quad (15)$$

the concentration of which is obtained by combining (14) and (15):

$$[Ag_2(en)_2] = \tfrac{1}{2}[en]_{tot}\left(1 - \frac{(\bar{p}')^{obs}}{(\bar{p}')^*}\right) \quad (16)$$

In order to obtain $K_{Ag_2en_2}$, according to its definition $[Ag_2(en)_2]/[Ag]^2[en]^2$ we need first to calculate [en] the concentration of the free "en". Introducing the constants already obtained at this stage, we get eqn. (17) from (14). In the calculation

$$[en]_{tot}\frac{(\bar{p}')^{obs}}{(\bar{p}')^*} = [en][10^{(pK_1 + pK_2 - 2pH)} + 1 + 10^{(pK_1 - pH)} + [Ag]K_{Ag(Hen)}10^{(pK_1 - pH)} + [Ag]K_{Ag(en)} + [Ag]^2K_{Ag_2en}K_{Ag(en)}] \quad (17)$$

of [en] from (17) the weighted averages of the constants obtained from titrations 3–6 were used (see Table 1).

Finally, $\log K_d$ was obtained from the difference

$$(\log K_{Ag_2en_2} - 2\log K_{Ag(en)}).$$

Three-phase vapour tensiometry (TPVT). The TPVT-measurements were carried out as described earlier.[7] Weighted samples of the solid $[Ag(en)]NO_3.H_2O$ and *ca.* 400 mg KNO_3 were mixed with 1 g water and equilibrated at 30 °C for 20–40 h before introduction into the cell, which was thermostated at 30 °C. The solid was prepared by addition of a mixture of 22 cm³ 1 M "en" and 2 cm³ 1 M HNO_3 to the solution of 20 mmol $AgNO_3$ in a small amount of water. The crystals were washed twice with small quantities of cold water and dried in vacuo (*ca.* 1 Pa) at room temperature (*ca.* 25 °C).

In the PTVT-titration, quantities of 1 g of a 0.5 m (mmol Ag/g H_2O) $AgNO_3$ solution were mixed with various amounts of a solution containing 5 m "en" and 0.25 m HNO_3. After the addition of *ca.* 400 mg KNO_3 the apparent number of foreign species i_f was determined as described above. The addition of HNO_3 was necessary to avoid the precipitation of Ag_2O by mixing of the two solutions. As the contribution of Hen^+ produced by the HNO_3 addition to i_f is limited to 5–10 %, it is comparable with the relative standard deviation of i_f, hence no corrections were made.

Solubility measurements. Solubility data should be independent of crystalline form and method of measurement. Therefore crystals of different size were dissolved (s. empty circles in Fig. 4). Although the dissolution process seems to be rapid, suspensions (100 cm³ saturated solution and 1 g solid) were equilibrated at (25±0.2) °C a relatively long time (15–70 h) in closed vessels under nitrogen. The solvent consisted of 0.01 M $HenNO_3$, (0–0.99) M $NaClO_4$ and (1 – $[NaClO_4]$ – $[Ag]_{tot}$) M $NaNO_3$. At the start of the experiment $[Ag]_{tot}$ was estimated using eqn. 3 with an estimated value of $K_{sp}(10^{-3}\ M^2)$. Aliquots of 2 or 5 cm³ were taken when the solution became clear (10 min after interruption of the magnetic stirrer). The aliquots were immediately filtered on membrane filter of porosity 0.45 μm. Both filtrates were acidified with HNO_3 to *ca.* 0.1 M and analysed using atomic absorption spectrometry (AAS) for the determination of $[Ag]_{tot}$. After sampling 20–50 cm³ of a solution containing 0.01 M $HenNO_3$ and 0.99 M $NaClO_4$ were added to the rest of the equilibrated suspension which was stirred and equilibrated again. The addition of this solution caused the precipitation of $[Ag(en)]ClO_4$, or in other words, the equilibrium was approached from the opposite side (s. filled circles in Fig. 4. Sampling and analysis of the filtrates was carried out as described above).

The preparation of small crystals was carried out by mixing the precooled (~0 °C) solution of 110 mmol "en" in *ca.* 100 cm³ water and 10 cm³ 1 M $HClO_4$ with 100 cm³ precooled 1 M solution of $AgClO_4$. After 1 h in ice water the colorless crystals were filtered off and washed with small quantities of cold water. A part was immediately used for the solubility experiments. Another part was dried as described for $[Ag(en)]NO_3.H_2O$. A third part was recrystalized from a 0.1 M solution of $HenClO_4$; the crystals were dissolved at *ca.* 70 °C and the filtered solution was cooled very slowly. Large, slightly yellowish brown crystals were obtained which, like the small crystals, became darker on drying. Anal. $[Ag(en)]ClO_4$: Ag, "en".

No systematic dependence of the solubility of $[Ag(en)]ClO_4$ on the size of the crystals, performance of the experiment (dissolution or precipitation and time of equilibration), was found. Never-

theless, the deviations of the $-\log[Ag]_{tot}$-values determined at a given, high perchlorate ion concentration, were about 20 times poorer than the 95 % confidence limit of the AAS determinations for the same filtrate [$L_{95}(-\log[Ag]_{tot}^{AAS})=0.0027$ on average].

Because of the high sensitivity and selectivity of the AAS-determinations this low confidence limit remains about the same over the whole concentration range of $[Ag]_{tot}$. The bad reproducibility of $-\log[Ag]_{tot}$ in *ca.* 1 M solutions of $NaClO_4$ (see Fig. 4) is caused by decomposition of $[Ag(en)]ClO_4$ which set in irregulary and enhances the solubility from suspension to suspension by somewhat different amounts.

As the dissolution of one mol Ag is accompanied by the liberation of one mol ClO_4^-, $-\log[ClO_4^-]$ was obtained as $-\log([NaClO_4]+[Ag]_{tot})$.

Calorimetry. The consumption of heat Q in the dissociation reaction $Ag(en)_2^{2+} \rightarrow 2Ag(en)^+$ was determined by measuring the temperature decrease of 80 cm³ of a solution containing

(a) 10^{-3} M $H_2en(ClO_4)_2$, 10^{-3} M KOH and 0.998 M KNO_3
(b) 10^{-3} M "en", 10^{-3} M HNO_3 and 0.999 M KNO_3,

after the addition of 0.2 – 2 cm³ aliquots ($=V_{std}$) of a solution ("std") containing 0.5 M $[Ag(en)]NO_3$ ($=[Ag]_{std}$), 0.1 M $HenNO_3$ and 0.4 M KNO_3. The calorimeter was thereafter calibrated by heat generation of an electrical power of 200 mW during 2 min. Finally, the background heat conversion Q_b was also measured in the same way, whereby 0.2 – 2 cm³ aliquots of a blank solution containing 0.1 M $HenNO_3$ and 0.4 M KNO_3 are added to 80 cm³ of the solutions a and b. The enthalpy of dimerisation was then calculated from eqn. (18), where ΔH_{av} is

$$\tfrac{1}{2}\Delta H_d = -(Q-Q_b)/V_{Ag}[Ag]_{std}(1-f_{Ag_2en_2})-\Delta H_{av}f_{Ag} \qquad (18)$$

an average value of reaction enthalpies of simultaneous formation of Ag(I)-en-complexes in the pH-range of 8.7 – 10.5. A value of -53.4 ± 0.9 was obtained in the experiments described below. f_x is the fraction of silver present in the complex X in question, *e.g.* $f_{Ag_2en_2}=2[Ag_2(en)_2]/[Ag]_{tot}$ and $f_{Ag}=[Ag]/[Ag]_{tot}$.

In the calculation of the f_x values $[Ag]_{tot}$, pH and $[en]''_{tot}$, the total concentration of "en" not bonded to Ag(I) are needed. Because the dissolution of $[Ag(en)]NO_3$ was always accompanied by some decomposition, the solution was filtered off and the quantity of Ag precipitated as Ag_2O was measured by AAS after dissolution of the Ag_2O in a solvent containing 0.1 M NH_3 and 0.01 M KCN. The $[Ag]_{std}$ and $[en]''_{std}$ values computed from the weight in quantities of $[Ag(en)]NO_3$ and "en" were corrected for decrease and increase, respectively, effected by this decomposition (about 1 %) of $[Agen]NO_3$. The pH value was measured with the cell described above, whereby exactly the same dilutions were made as in the calorimeter. [en] was obtained from eqn. (19).

$$[en] = [en]''_{tot}10^{(pH-pK_1)}/[10^{(pK_2-pH)}+1+10^{(pH-pK_1)}] \qquad (19)$$

With the known values of pH and [en] all mol ratios [X]/[Ag] can be calculated. Using the constants of Table 1 for 1 M KNO_3 the following ratios were calculated and inserted in eqn. (20).

$$[Ag]_{tot} = [Ag]\left(1+\frac{[Ag(Hen)]}{[Ag]}+\frac{[Ag(Hen)_2]}{[Ag]}+\frac{[Ag(en)]}{[Ag]}+\frac{[Ag(en)_2]}{[Ag]}\right)+[Ag]^2\left(\frac{2[Ag_2(en)]}{[Ag]^2}+\frac{2[Ag_2(en)_2]}{[Ag]^2}\right) \qquad (20)$$

Eqn. (20) was then solved for [Ag] and the f_X values calculated by multiplication of the corresponding term with $[Ag]/[Ag]_{tot}$ or $[Ag]^2/[Ag]_{tot}$.

The heat production Q in the reaction of $AgNO_3$ with "en" at various pH values was determined by measurement of the increase in temperature of 80 cm³ of a solution containing $(5-20)\times10^{-3}$ M $[en]''_{tot}$, $(0-10^{-2})$ M $Ag(en)NO_3$ and KNO_3 (to keep I at 1 M) by additions of 0.2 – 1 cm³ aliquots of a standard Ag solution containing 0.5 M $AgNO_3$ and 0.5 M KNO_3. The pH value and the background Q_b were determined again by carrying out the separate measurements mentioned above. The reaction enthalpy ΔH_m of formation of a mixture of Ag(I)-en-complexes was obtained from eqn. (21).

$$\Delta H_m = (Q-Q_b)/0.5V_{std}(1-f_{Ag}) \qquad (21)$$

In order to obtain the enthalpies of the main complexes present in the mixtures, two ΔH_m were combined according to eqn. (22).

$$\Delta H_m - \tfrac{1}{2}\Delta H_d f_{Ag_2en_2} - \Delta H_{av}(1-f_{Ag(en)}-f_{Ag(en)_2}-f_{Ag_2en_2}) = \Delta H_{Ag(en)}(f_{Ag(en)}+f_{Ag_2en_2})+\Delta H_{Ag(en)_2}f_{Ag(en)_2} \qquad (22)$$

First estimates of the f_X values were obtained from (20) as described above. Trhereby it was assumed that one mol of Ag(I) would bind one mol "en". The true values $([en]''_{tot})_n$ and f_X were obtained by an iteration, because [Ag] and $[Ag(Hen)_2]$ were not

always diminishingly small and $[Ag(en)_2]$ was relatively large at high pH and $[en]''_{tot}$ values.

The iteration was carried out according to eqn. (23), where n is the number of iteration. No more

$$([en]''_{tot})_n = [en]_{tot} - [Ag]_{tot}(1 + f_{Ag(Hen)_2} + f_{Ag(en)_2} - f_{Ag})_{n-1} \quad (23)$$

than 2 iterations were ever needed. Finally, the iterated f_X and the ΔH_m values from the pH range 9.7–10.5 were used to calculate the enthalpies of formation. The averages and their 95 % confidence limits obtained from 15 combinations according to eqn. 22 are given in Table 2.

REFERENCES

1. Jörgensen, S. M. *J. Prakt. Chem. 147* (1889) 1.
2. Bjerrum, J. *Metal Ammine Formation in Aqueous Solution*, Copenhagen 1941.
3. Job, P. *Ann. Chem. (Paris) 9* (1928) 113.
4. Schwarzenbach, G., Ackermann, H., Maissen, B. and Anderegg, G. *Helv. Chim. Acta 35* (1952) 2337.
5. Ohtaki, H. and Ito, Y. *J. Coord. Chem. 3* (1973) 131.
6. Schwarzenbach, G. *Helv. Chim. Acta 33* (1950) 947.
7. Magyar, B. *Helv. Chim. Acta 51* (1968) 194; *Struct. Bonding (Berlin) 14* (1973) 111.
8. Bang, E. *The Third European Crystallographic Meeting*, Zürich 1976, Collected Abstracts, p. 160.
9. Ref. 3 as well as: Bjerrum, J. Essays in *Coordination Chemistry Experentia Supplementum IX*, Birkhäuser Verlag, Basel 1964; Armenau, V. and Luca, C. *Z. Phys. Chem. (Leipzig) 217* (1961) 389.
10. Schwarzenbach, G. and Parissakis, G. *Helv. Chim. Acta 41* (1958) 2431.
11. Löwenherz, I. *Z. Phys. Chem. (Leipzig) 18* (1895) 71.
12. Hill, A. V. *Proc. R. Soc. London A 127* (1930) 9.
13. Bjerrum, J. *Coord. Chem. Meeting, Lund 1977.*
14. Smith, W. V., Brown, O. L. I. and Pitzer, K. S. *J. Am. Chem. Soc. 59* (1937) 1213.
15. Bertsch, C. R., Fernelius, W. C. and Block, B. P. *J. Phys. Chem. 62* (1958) 444.
16. Lotz, J. R., Block, B. P. and Fernelius, W. C. *J. Phys. Chem. 63* (1959) 541.

Received June 14, 1978.

Acta Chemica Scandinavica A 32 (1978) 957–962

The Influence of Nitrate and Other Anions on the Absorption Spectra of Palladium(II)

CHRISTIAN KLIXBÜLL JØRGENSEN and VANAJA PARTHASARATHY

Département de Chimie minérale, analytique et appliquée, Université de Geneve, CH 1211 Geneva 4, Switzerland

Dedicated to Jannik Bjerrum on the occasion of his 70th birthday

Whereas (at negative pH) *p*-toluenesulfonate and perchlorate only produce marginal "salt effects" on the spectrum of palladium(II) aqua ions, nitrate shows a definite change of the band positions and intensities indicating the first complex to have $K_1 = (1.2 \pm 0.4)\ M^{-1}$ though it is likely that bis- and perhaps higher complexes also occur. Sulfate complexes, and general treatments of data about weak complexes (and their first-order band shift), as well as the stereochemistry of Pd(II) and its behaviour compared to copper(II), are also discussed.

I. INTRODUCTION

Though unidentate nitrate complexes such as $Co(NH_3)_5(ONO_2)^{+2}$ and $Co(NH_3)_3(ONO_2)_3$ were prepared by S. M. Jørgensen, and a large number of crystal structures are known to involve bidentate nitrate, such as anhydrous $Co(O_2NO)_3$ isoelectronic with $Co(O_2CO)_3^{-3}$, icosahedral $Ce(O_2NO)_6^{-3}$, hexagonal-bipyramidic $UO_2(O_2NO)_3^-$, ... most solution chemists consider nitrate almost as non-complexing as perchlorate. This may very well be a specific property of aqueous solutions, since the spectacular intensification of visible bands of cobalt(II) and nickel(II) nitrate in approximately anhydrous ethanol[1] was shown by Katzin[2,3] to be dependent on the presence of one nitrate ligand besides nearly all the other ligands being ethanol. This observation cannot be explained simply as an order of affinity $H_2O > NO_3^- > C_2H_5OH$ since a huge excess of nitrate[1,3] does not modify perceptibly the aqua ion spectrum in 80 vol. % alcohol (5 M H_2O) nor in mixtures containing 50 % CCl_4 having a far lower dielectric constant. Strong aqueous solutions of lithium or calcium nitrate, or to a somewhat larger extent nitric acid, modify the visible spectrum of the aqua ion measurably, and about three times more than comparable concentrations of perchlorates. It is a fundamental difficulty that such "salt effects" always can be interpreted[1] as formation of a weak complex with the formation constant $K_1 = [MX]/[M][X]$ and the molar extinction coefficient ε_1 (as function of the wave-length).

$$\varepsilon_1 = \varepsilon_0 + (\varepsilon_s/K_1) \qquad (1)$$

where the salt effect is linear ($\varepsilon = \varepsilon_0 + \varepsilon_s C_x$) and the amount of complex so small that the total and free concentrations C_x and [X] cannot be distinguished within experimental uncertainty. Such a result is indeterminate insofar as the ratio (ε_s/K_1) cannot be separated in its two terms unless the mass-action law remains approximately valid in concentration units, *and* K_1 is sufficiently large that [X] can be made larger than $(1/K_1)$ (at which point $\bar{n} = 1/2$). It is an additional difficulty that perchlorate and nitrate "salt effects" have ε_s positive and actually roughly proportional to ε_0 (the bands are not shifted much) whereas robust complexes dissolved in mixtures of two solvents do not normally obey eqn. (1) but show a smooth shift of the band positions[4,5] without an isosbestic point (as when ε_s changes its sign) or being expressed as a linear combination of two spectra ε_0 and ε_1.

Table 1. Absorption spectra of 0.01 M palladium(II) solutions (when marked with an asterisk, 0.001 M only). Hts is *p*-toluenesulfonic acid.

No.	Composition	λ_{max} (nm)	ε_{max}	ε_{490}	ε_{520}
1	2 M Hts	382	86	6.6	4.3
2	1 M Hts	380	85	6.3	4.2
3	1 M Hts + 1 M $HClO_4$	381	83	6.5	4.2
4	1 M Hts + 1 M $NaClO_4$	381	84	6.7	4.4
5	1 M Hts + 2 M $NaClO_4$	383	85	6.8	4.3
6	1 M Hts + 0.5 M H_2SO_4	390	106	9.5	5.7
7	0.5 M H_2SO_4	392	120	12.1	7.2
8	0.5 M H_2SO_4 + 0.25 M Na_2SO_4	395	141	14.7	8.6
9	0.5 M H_2SO_4 + 0.5 M Na_2SO_4	396	145	15.5	8.8
10	0.5 M H_2SO_4 + 1 M $NaClO_4$	392	118	11.8	6.7
11	0.5 M H_2SO_4 + 1 M $NaNO_3$	396	127	14.4	9.2
12	1 M Hts + 1 M $NaNO_3$	395	111	14.1	10.4
13	1 M Hts + 1 M HNO_3	396	114	19.3	11.2
14	1 M Hts + 0.1 M HNO_3	382	91	8.4	5.6
15*	1 M Hts + 0.01 M HNO_3	381	83	–	–
16	0.5 M Hts + 0.1 M HNO_3	381	90	7.5	5.0
17	5 M HNO_3	414	143	42.3	23.5
18	1 M HNO_3 + 4 M $NaNO_3$	408	134	34.2	18.8
19	1.1 M HNO_3 + 2 M $NaNO_3$	404	129	27.0	15.0
20	1.1 M HNO_3	395	116	17.2	9.8
21	1.1 M HNO_3 + 4 M $NaClO_4$	402	116	22.4	12.3
22	1.1 M HNO_3 + 1 M $NaClO_4$	395	115	18.0	10.0
23	0.6 M HNO_3 + 1.5 M $NaClO_4$	392	104	13.3	7.7
24*	0.5 M HNO_3 + 1.5 M $NaClO_4$	390	101	–	–
25	0.35 M HNO_3 + 1.75 M $NaClO_4$	388	95	10.4	6.1
26*	0.25 M HNO_3 + 1.75 M $NaClO_4$	386	95	–	–
27	0.1 M HNO_3 + 1 M $HClO_4$ + 1 M $NaClO_4$	382	87	7.4	4.5

II. THE PALLADIUM(II) AQUA ION

It is a condition for studying this yellow species[6] to have pH below 0.5 in order to avoid slow irreversible hydrolysis to dark brown products. Since a positively charged ion cannot be studied without the presence of anions, the first step is to assure that two solutions in different strong acids, say perchloric and *p*-toluenesulfonic, have the same spectrum. The latter acid has the advantage[3] not to esterify alcohols at a detectable rate. In the following, $CH_3C_6H_4SO_3^-$ is called ts^-. From a critical point of view,[7] coincidence of two such spectra does not prove the exclusive presence of the aqua ion, because it may have (though rather unlikely) exactly the same ε values as one of the anion complexes (or both). Fig. 1 and Table 1 show that the spectra are indeed very similar at pH = 0, whereas sulfuric acid shows a small, and nitric acid a marked shift toward longer wave-lengths. Such a shift and intensification in nitrate solutions has been mentioned in a qualitative

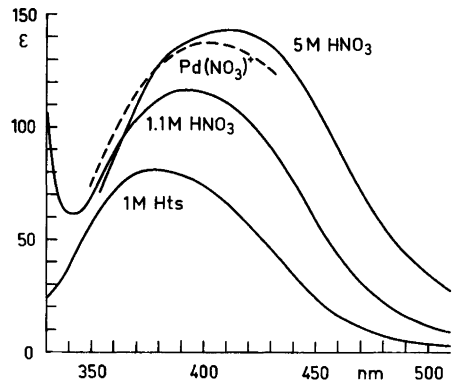

Fig. 1. Absorption spectra of the solutions Nos. 2, 20 and 17 (compositions given in Table 1) and the mono-nitrato complex extrapolated according to eqn. (6).

way[8] though many results in literature are hampered by the brown hydrolysis products occurring when precipitated palladium hydroxide (oxide?) is dissolved in acidic solutions.

Palladium(II) has exceedingly large formation constants with "conventional" ligands. Thus, log $\beta_4 = 12$ for the chloro and 32.8 for the ammonia[6] complexes. It might be argued that in such a situation, nitrate may very well have the much smaller $K_1 = 1$. However, NO_3^- is not normally considered a "soft" ligand in Pearson's sense[7,9] and it would not be expected to compete more successfully with water as a ligand than, say, with Co(II). Arguments of "ligand field stabilization" applicable to octahedral complexes[10] are not as relevant in quadratic complexes. Actually, the absorption spectra are closely similar[7] to copper(II) having roughly half the wave-numbers of Pd(II) with the same ligands, but higher wave-numbers than Ni(II), expressing a certain "tetragonality ratio". It is an experimental fact[6] that most Pd(II) ammine complexes show only one, almost symmetrical absorption band. Seen from the point of the *angular overlap model*[11,12] this suggests almost identical one-electron energies of all four filled 4*d*-like orbitals, showing transitions to the strongly anti-bonding empty (x^2-y^2). One would have expected the filled $(3z^2-r^2)$ to be one-third as anti-bonding. This experiment discrepancy (first noted[13] in $PtCl_4^{-2}$) is most readily explained by a mixture of 4*d* and 5*s* characters. More direct experimental evidence has recently been obtained[14] for such $3d-4s$ mixing in the yellow nickel(II) complex of the strained cyclic aliphatic diamine "daco" where the three almost coinciding transitions (at 22370, 23480 and 24540 cm^{-1}) can be distinguished, using polarized light. Like in the Cu(II) aqua ion,[7] the Pd(II) aqua ion[6] shows a perceptible shoulder at 410 nm (*cf.* Fig. 1) and it has even been suggested[12] that it might be tetragonal-pyramidic $Pd(OH_2)_5^{+2}$ with a loosely bound fifth water molecule destabilizing $(3z^2-r^2)$. Another argument is the marginal increase[6,15] of ε from 200 to 210 for $Pd(NH_3)_4^{+2}$ going from dilute solution to 1 M $NaClO_4$. This may either be a salt effect as discussed above, or due to a five-coordinate $Pd(NH_3)_4(OClO_3)^+$. Many such observations are known, but not fully understood. For instance Harry C. Jones found in 1909 that moderate nitrate concentrations (above 0.5 M) modify the narrow absorption bands of trivalent lanthanides, and the spectroscopic effects[16] of such nitrate complexation can be quite spectacular. This forms a striking contrast with chloro complexes, where spectral changes indicating direct Ln–Cl contacts only occur well above 5 M HCl, though classical physico-chemical techniques (measuring activities) suggest outer-sphere complexes with K_1 close to 1. Anyhow, it is beyond doubt that Pd(II) phenanthroline[17] with two (three in the case of OH^-) residual coordination positions shows a considerable affinity for nitrate, and Schurter[18] prepared complexes of php^-, the deprotonated 2-phenylpyridine (becoming isoelectronic with bidentate 2,2′-dipyridyl) containing either nitrate or even solid Pd(php)-$(OClO_3)(OH_2)$. A recent review[19] of platinum group nitrato complexes notes that low electronegativity of the other ligands enhances the affinity to nitrate, based on preparative methods. A characteristic of the (usually single) Pd(II) absorption band[6,7] is the unusually large ε. It must be noted that multidentate organic ligands[20,21] readily can enhance ε to the region 500 to 1500 again showing a certain similarity with Cu(II). The less pronounced intensification (ε increasing 60 %) by one nitrate ligand is reminiscent of the hypersensitive pseudoquadrupolar transitions.[16]

It is worthwhile to start the discussion with a few remarks about the sulfate complexes. It is seen from Table 1 that 0.25 M Na_2SO_4 added to 0.5 M H_2SO_4 almost doubles the effect of the acid alone. This seems to indicate a weak complex of SO_4^{-2} of which the free concentration is decreased by protonation (pK_2 around 1) as seen from the effect of 1 M Hts. The question of sulfate complexes is important to us, because the preparation of anhydrous and hydrated modifications of $PdSO_4$ described by Kane in 1842 serves[6,17] to make solutions of the aqua ion (say 0.01 M) of which the spectra do not change perceptibly if treated by stoichiometric amounts of $Ba(ClO_4)_2$ or $Ba(ts)_2$ and the $BaSO_4$ is carefully filtered off. Actually, eleven of our solutions were made in parallel experiments either using the sulfate or with the alternative of making 1.5 M Pd(II) from the metal in concentrated nitric acid. However, it is necessary to boil such a solution for several hours in order to avoid subsequent persistent formation of NO_2 presumably due to intermediate nitrosyl or nitrito complexes.

III. NITRIC ACID AND NITRATE SOLUTIONS AND BAND SHIFTS OF WEAK COMPLEXES

Spectral data for 27 solutions are given in Table 1, Nos. 1–13 made from 0.01 M $PdSO_4$ and 14–27 from a stock solution of Pd(II) in 5 M HNO_3 to a final palladium concentration 0.01 M (except 15, 24 and 26 marked with an asterisk, 0.001 M). Five solutions of 0.001 M Pd(II), but otherwise having the compositions of Nos. 17, 18, 29, 21 and 22, were shown to have the same spectra, with ε_{max} not differing more than 1 or 2 %, and λ_{max} within 1 nm. As one would expect, no evidence for oligomeric complexes occurs, and the differences in 24* and 26* are due to differing nitrate concentration originating from the stock solution.

There is a smooth shift of the spectra (in contrast to the marginal salt effects in presence of high concentrations of ts^- and ClO_4^-) as a function of increasing total nitrate concentration C_x. However, a comparison of 17 with 18 shows that 5 M nitric acid, rather than being partly undissociated, actually exhibits an activity higher than 5 M sodium nitrate. It is noted in solution 10 that 1 M $NaClO_4$ rather counteracts the formation of sulfate complexes slightly, whereas the spectrum 11 may be due to mixed nitrate-sulfate coordination. Also solution 21 with 4 M $NaClO_4$ may contain nitrate-perchlorate complexes.

One might imagine that the shift of ε_{max} would be a quadratically unstable function of small $\bar{n}$ values in the case of an aqua ion (ε_0) in equilibrium with a mono-complex (ε_1) showing an apparent

$$\varepsilon = (1-\bar{n})\,\varepsilon_0 + \bar{n}\varepsilon_1 \tag{2}$$

However, this is not true, as seen from the simple model of ε_0 varying as an inverted parabola close to the maximum ε_0^0 at λ_0 (we are here adapting the description by Claus Schäffer of absorption bands as Gaussian error-curves with the wavelength λ as variable) and ε_1 increasing linearly for λ slightly above λ_0:

$$\varepsilon_0 = \varepsilon_0^0 - \tfrac{1}{2}\varepsilon''(\lambda-\lambda_0)^2$$
$$\varepsilon_1 = \varepsilon_1^0 + \varepsilon'(\lambda-\lambda_0)$$

The differential quotient of ε in eqn. (2) is then

$$(\bar{n}-1)\,\varepsilon''\,(\lambda-\lambda_0) + \bar{n}\varepsilon' \tag{4}$$

which is zero for the maximum at

$$(\lambda-\lambda_0) = \frac{\bar{n}\varepsilon'}{(1-\bar{n})\varepsilon''} \tag{5}$$

The aqua ion spectrum seen in Fig. 1 has $\varepsilon''=0.04$ nm^{-2}. If ε' has the plausible value 1 nm^{-1}, eqn. (5) indicates a shift of λ_{max} to the extent 25 nm times the quantity $\bar{n}/(1-\bar{n})$ which is equal to the product K_1C_x. If the solutions in Table 1 having total nitrate concentrations C_x between 0.25 and 0.6 M are considered, λ_{max} is seen to shift (20 nm) C_x. Taken at its face value, this argument gives $K_1=(20/25)=0.8$. However, the extrapolated spectrum of the mono-nitrato complex discussed below (and given as a dashed line in Fig. 1) suggests $\varepsilon'=0.8$ nm^{-1} which has the corollary $K_1=1$. Obviously, this method can only produce the order of magnitude of K_1 but it should be emphasized that the shift of λ_{max} has no direct relation to the actual maximum of ε_1 at λ_1 since small shifts are determined by the ratio $(\varepsilon'/\varepsilon'')$.

If higher complexes are not formed, or if (K_2/K_1) is reasonably small, it is possible to exploit a set of spectra like ours without having the opportunity of evaluating the depletion of $[X]=C_x-\bar{n}C_M$. The most practical technique is to study ε as a function $(1/C_x)$. We know the asymptotic ε_0 from the aqua ion, and the mass-action law for one complex then gives

$$\varepsilon = \varepsilon_1 + \frac{\bar{n}}{K_1C_X}(\varepsilon_0-\varepsilon_1) \tag{6}$$

Thus, the spectra for $(1/C_X)=1.67$, 0.91 and 0.33 M^{-1} allow an extrapolation to 0 M^{-1} giving $\varepsilon_1=137$ at 410 nm and $\varepsilon_1=133$ at 420 nm. In both cases, $\varepsilon=(\varepsilon_0+\varepsilon_1)/2$ indicating $\bar{n}=\frac{1}{2}$ (=102 and 95, respectively) occurs for $(1/C_X)=1.4$ M^{-1} corresponding to $K_1=1.4$.

However, there is no doubt that higher complexes are formed. The maximum for ε_1 derived from eqn. (6) every 10 nm in the interval 360 to 420 nm occurs at 404 ± 2 nm, 10 nm below the observed maximum in 5 M HNO_3. If one had the extreme situation of four complexes, up to $Pd(NO_3)_4^{-2}$, formed statistically, K_1 in eqn. (6) would be the average K_{av} and the real $K_1=4K_{av}$. However, this is entirely improbable in view of the pronounced[6] characteristic coordination number $N_0=2$ for Pd(II). If $K_1=2K_{av}$ and $K_2=\frac{1}{2}K_{av}$ the spectra ε_1 and ε_2 can be determined in a way

compatible with our data, ε_2 having its maximum close to 422 nm. It is not possible without circumspection[6,7] to apply Tsuchida's rule of average environment to quadratic complexes, though the spectrochemical position of nitrate then at first seems almost as low as of chloride.

Table 1 indicates the ε values at 490 and at 520 nm. We measured the spectra of 0.01 M Pd(II) in 4 cm cells in the region below 650 nm in the hope of finding an interval with $\varepsilon_2 \gg \varepsilon_1 > \varepsilon_0$ which might have helped to characterize the bis-complex, much like $CoCl_4^{-2}$ and $CuCl_4^{-2}$ in the visible.[22] However, this did not succeed, insofar ε at several λ varies with the same proportionality factor. This unexpected regularity is connected with the spin-forbidden transitions to excited triplet states in the 500–550 nm region. If these absorption band tails are treated according to eqn. (6), K_1 is close to 1.0. However, this value may be influenced by the bis-complex having $\varepsilon_2 > 2\varepsilon_1$ with resulting admixture of the smaller K_2 during the extrapolation.

IV. CONCLUSION

In aqueous solution, at pH close to zero, palladium(II) forms a mono-nitrato complex with

$$K_1 = (1.2 \pm 0.4)\ \text{l/mol}$$

There is little hope of ameliorating the uncertainty, because of variable activity coefficients. As discussed in the text, several of the techniques for evaluating the spectra tend to weight the contribution from a bis-complex at higher nitrate concentration. On the other hand, *p*-toluenesulfonate and perchlorate at 1 to 2 M only induce marginal "salt effects" which is surprising, since one might expect the stereochemistry of the aqua ion to be rather flexible. It is noteworthy that Pd(II) both forms an ethylenediamine complex[6] of which K_1 is so large that it cannot be determined in solvents remaining essentially aqueous solutions with a few M ions, and a nitrate complex where K_1 is so small that it is difficult to determine in a meaningful way, much like the first chloro complex[22] of copper(II).

V. EXPERIMENTAL

The spectra were measured in 1 cm (or 4 cm) cells on a Unicam SP8-100 spectrophotometer. Palladium sulfate was prepared[6] and found by gravimetric analysis (Pd as dimethylglyoximate, SO_4 as barium sulfate) to be almost anhydrous and stoichiometric: Pd 51.5 %, SO_4 46.5 % and 2 % of water. The solutions were made from Merck *p.a.* 65 % concentrated nitric acid, *p.a.* 96 % sulfuric acid, 70 % perchloric acid, sodium perchlorate monohydrate, sodium nitrate and sodium sulfate and from Fluka *p.a.* *p*-toluenesulfonic acid monohydrate (known to contain H_3O^+ ts^-).

A solution of *palladium nitrate* was made by boiling 5.4 g of palladium powder (Métaux Précieux, Neuchatel) in 34.6 ml of conc. nitric acid, to complete dissolution, followed by prolonged heating for 3 h to destroy an unidentified source of NO_2, and finally diluted to 100 ml with water.

A solution of $Ba(ts)_2$ was obtained by dissolving Merck *p.a.* barium carbonate in 1 M Hts. All the solutions were tested with a drop of silver nitrate solution under conditions[6] particularly sensitive to the presence of Cl^- (or Br^-) forming strongly coloured complexes with palladium.

Acknowledgement. One of us (C.K.J.) is grateful to Professor Jannik Bjerrum for 30 years of fascinating discussions, and during the first third of this period, for his great tolerance toward a collaborator with rather diversified interests.

REFERENCES

1. Jørgensen, C. K. *Acta Chem. Scand. 8* (1954) 175.
2. Katzin, L. I. *Nature 175* (1955) 425.
3. Jørgensen, C. K. and Bjerrum, J. *Nature 175* (1955) 426.
4. Bjerrum, J., Adamson, A. W. and Bostrup, O. *Acta Chem. Scand. 10* (1956) 329.
5. Jørgensen, C. K. *J. Inorg. Nucl. Chem. 24* (1962) 1571.
6. Rasmussen, L. and Jørgensen, C. K. *Acta Chem. Scand. 22* (1968) 2313.
7. Jørgensen, C. K. *Topics in Current Chemistry 56* (1975) 1.
8. Sundaram, A. K. and Sandell, E. B. *J. Am. Chem. Soc. 77* (1955) 855.
9. Bjerrum, J. *Essays on Analytical Chemistry in Memory of Professor Anders Ringbom*, Pergamon, Oxford 1976.
10. Jørgensen, C. K. *Chimia 28* (1974) 6.
11. Schäffer, C. E. *Struct. Bonding (Berlin) 5* (1968) 68; *14* (1973) 69.
12. Jørgensen, C. K. *Modern Aspects of Ligand Field Theory*, North-Holland, Amsterdam 1971.
13. Chatt, J., Gamlen, G. A. and Orgel, L. E. *J. Chem. Soc.* (1958) 486.
14. Hitchman, M. A. and Bremner, J. B. *Inorg. Chim. Acta 27* (1978) L61.

15. Reinhart, R. A. and Coe, J. S. *Inorg. Chim. Acta 3* (1969) 438.
16. Reisfeld, R. and Jørgensen, C. K. *Lasers and Excited States of Rare Earths*, Springer, Berlin 1977.
17. Parthasarathy, V. and Jørgensen, C. K. *Chimia 29* (1975) 210.
18. Schurter, M. F. *Diss. ETH 6077*, Zentralstelle der Studentenschaft, Zürich 1977.
19. Crichlow, P. B. and Robinson, S. D. *Coord. Chem. Rev. 25* (1978) 69.
20. Schmidtke, H. H. and Jørgensen, C. K. *Chem. Phys. Lett. 5* (1970) 202.
21. Anderegg, G. and Malik, S. C. *Helv. Chim. Acta 59* (1976) 1498.
22. Bjerrum, J. and Skibsted, L. H. *Acta Chem. Scand. A 31* (1977) 673.

Received June 8, 1978.

Acta Chemica Scandinavica A 32 (1978) 963–967

The Oxidation of Captive Oxalate by Thallium(III) in Aqueous Solution *

OLE FARVER[a] and GWYNETH NORD[b]

[a] Department of Chemistry AD (Inorganic and Physical Chemistry), Royal Danish School of Pharmacy and [b] Chemical Laboratory I (Inorganic Chemistry), H. C. Ørsted Institute, University of Copenhagen, DK-2100 Copenhagen Ø, Denmark

Dedicated to Jannik Bjerrum on the occasion of his 70th birthday

The rate of the reaction **

$$Cr(L-L)_2C_2O_4^+ + Tl(III)_{aq} \rightarrow Tl^+ + Cr(L-L)_2(H_2O)_2^{3+} + 2CO_2$$

is greater than that for the acid catalyzed aquation of the above chromium complexes. In 1 M nitric acid at 25 °C the respective second-order rate constants for L–L = bipy and phen are: 3.7×10^{-4} M^{-1} s^{-1} and 2.4×10^{-4} M^{-1} s^{-1}. The activation parameters for the same reactions are: $\Delta H^{\neq} = 70$ kJ mol^{-1}, $\Delta S^{\neq} = -75$ J K^{-1} mol^{-1}, and $\Delta H^{\neq} = 69$ kJ mol^{-1}, $\Delta S^{\neq} = -83$ J K^{-1} mol^{-1}. The reaction is inhibited by chloride. $Cr(bipy)_2C_2O_4^+$ also reacts with Fe(III) and Ce(IV) to give the same diaqua product. The rate-determining step involves electron transfer to the oxidizing cation from the oxalate which is bound to both this and to Cr(III) in a bridged intermediate. No aquation was detected when the above metal ions were replaced by Zn^{2+}, Cd^{2+}, Hg^{2+}, a series of rare earth cations, and also the tris(2,2'-bipyridine)iron(III) ion.

In recent years the reduction of aqueous Tl(III) has been much studied. However apart from the Tl(I) – Tl(III) exchange which occurs by two electron transfer,[1] the presence of Tl(II) as an intermediate either has been demonstrated[2,3] or cannot be eliminated. The present work is a continuation of a series in which the oxidation of the two-electron reducing agent $C_2O_4^{2-}$ by Tl(III) has been studied. Thus we have previously found[4] that oxalic acid and Tl(III) form a complex, $TlC_2O_4^+$ and have suggested that the redox reaction accompanies the slow decomposition of this complex. In accordance with this oxalate, like chloride, inhibits the two-electron exchange reaction of Tl(I) with Tl(III).[5] The substitution of bound oxalate by water in the title complexes is acid catalyzed and the mechanism of this has been discussed.[6] In the present paper we have studied the effect of Tl(III) on the aquation rate of these complexes and attempted to elucidate the mechanism firstly, by comparing the rate of the Tl(III) reaction with other metal ions which also are known to form stable oxalato complexes or to be efficient oxidants and secondly, by comparing the activation parameters for the oxidation by Tl(III) of oxalate bound to Cr(III) and for free oxalic acid.

EXPERIMENTAL

Details of the preparation of $[Cr(bipy)_2C_2O_4]Cl.4H_2O$ and $[Cr(phen)_2C_2O_4]CF_3COO.2H_2O$ together with the spectral properties of these compounds are given elsewhere.[7]

Due to the low solubilities of the perchlorate complex salts, nitric acid (Merck *pro analysi*) was used throughout. A Tl(III) nitrate stock solution

* Some of these results were briefly reported at the XIV International Conference on Coordination Chemistry, Toronto 1972.

** The following abbreviations are used in this paper: phen = 1,10-phenanthroline, bipy = 2,2'-bipyridine, and L–L = bipy or phen.

was prepared by anodic oxidation of standardized Tl(I) nitrate in 2 M nitric acid. The latter was prepared by dissolving recrystallized thallous carbonate (B.D.H. Laboratory Reagent) in nitric acid. The concentration of Tl(III) was determined gravimetrically with 8-hydroxyquinoline as described elsewhere.[8]

The complex concentrations were about 5 mM or less, while for all reactions the concentration of Tl(III) was in pseudo first-order excess (at least 15-fold). The ionic strength was adjusted to 1.0 M with sodium or lithium nitrate (Merck *pro analysi*). All other chemicals were of reagent grade purity. Water redistilled twice in an all quartz apparatus was used to make up the solutions.

The reaction solutions were kept in a thermostat (±0.1 °C). Spectra were measured in the range 700 to 200 nm using thermostatted cells and a Zeiss DMR 10 spectrophotometer. The disappearance of the oxalato complex was followed at an absorption maximum of $Cr(L-L)_2C_2O_4^+$ (497 nm for L−L= bipy and 501 nm for L−L=phen), the difference between the spectrum of the oxalato and the diaqua complex rendering it possible to follow the reaction spectrophotometrically. Observed absorbance *vs.* time data from individual runs were collected on punched paper tape and analyzed in a UNIVAC 1110 computer.

The formation of Tl^+ was determined by the following procedure: Aliquots of the reaction solution were added to 10 ml of an 8 M aqueous ammonia solution containing 0.5 M sodium chromate, 1 M sodium cyanide, and 10 % ethanol. This mixture was cooled in ice and centrifuged. The thallous chromate was washed with ice-cold 10 % ethanol, was then redissolved in 10 ml 5 M sulfuric acid, and the amount of Tl^+ was determined from the absorbancy at 208 nm.

RESULTS

a. The effect of Tl(III). The final product has the visible absorption spectrum of the *cis*-diaqua-$(L-L)_2Cr(III)$ complex,[9] and a stoichiometric amount of Tl^+ is formed concomitantly so the overall reaction is (1).

$$Tl^{3+} + Cr(L-L)_2C_2O_4^+ + 2H_2O \rightarrow Tl^+ + Cr(L-L)_2(H_2O)_2^{3+} + 2CO_2 \quad (1)$$

Addition of Tl^+ has no influence on the reaction rate. With excess Tl(III) the absorbance data were treated by standard nonlinear least-squares techniques, minimizing the error square sum

$$s^2 = \sum_n (A_{obs} - A_{calc})^2$$

where n is the number of measurements (always greater than 2000), A_{obs} is the measured, and A_{calc} the absorbancy calculated from

$$A_{calc} = (A_0 - A_\infty)\exp(-k_{obs}t) + A_\infty$$

where k_{obs} is the observed pseudo first-order rate constant, A_0 and A_∞ the absorbancies at $t=0$ and $t=\infty$, respectively. The minimum of s^2 was found allowing k_{obs}, A_0, and A_∞ to be adjustable parameters.

Excellent first-order kinetics were obeyed over at least 3−4 half lives. The reaction was also first order in Tl(III) in the range covered (1×10^{-2} M to 8×10^{-2} M). k_{obs} was found to be independent of $[H^+]$ (0.25 to 1.0 M) within the experimental error (*cf.* Table 4). The acid hydrolysis of the oxalato complexes reported earlier[6] is much slower contributing less than 1 % to the above reaction under the present experimental conditions.

The effect of low concentrations of chloride ions on the rate of reaction is illustrated in Fig. 1 and is therefore consistent with (2)

$$k_{obs} = k_{Tl^{3+}}[Tl^{3+}] + k_{TlCl^{2+}}[TlCl^{2+}] \quad (2)$$

No reaction could be detected with sufficient $[Cl^-]$ to ensure that Tl(III) was predominantly present as $TlCl_2^+$ which is consistent with complete inhibition by this species. This kinetic effect of chloride

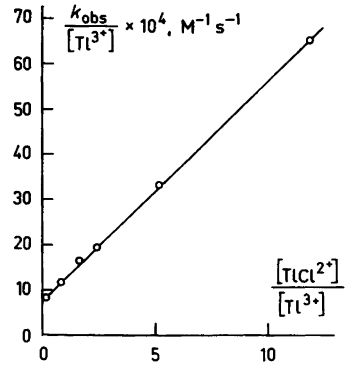

Fig. 1. Chloride ion dependence of k_{obs} for Tl(III) oxidation of $Cr(bipy)_2C_2O_4^+$ at $t=34.7$ °C and unit ionic strength.

Table 1. Second-order rate constants and activation parameters for the oxidation of the chromium complexes by Tl(III).

T K	$k \times 10^4$ $M^{-1} s^{-1}$	$\Delta H^{\neq}$ kJ mol^{-1}	$\Delta S^{\neq}$ J K^{-1} mol^{-1}
$Cr(bipy)_2C_2O_4^+$			
298.2	3.69		
299.0	3.64		
307.9	7.54	70 ± 2	-75 ± 6
313.3	14.0		
318.8	23.9		
327.2	46.5		
$Cr(phen)_2C_2O_4^+$			
298.2	2.36		
307.7	6.56	69 ± 2	-83 ± 6
317.1	12.9		
326.8	30.7		

Table 2. Second-order rate constants and activation parameters for the oxidation of $Cr(bipy)_2C_2O_4^+$ by $TlCl^{2+}$.

T K	$k \times 10^4$ $M^{-1} s^{-1}$	$\Delta H^{\neq}$ kJ mol^{-1}	$\Delta S^{\neq}$ J K^{-1} mol^{-1}
298.2	1.86		
307.9	4.85	74 ± 2	-67 ± 6
318.8	13.1		
326.7	28.2		

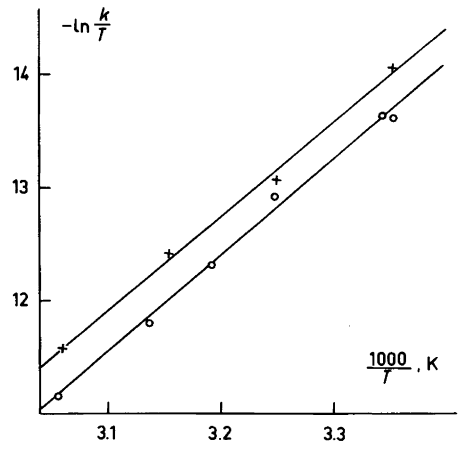

Fig. 2. Eyring plots for oxidation by Tl^{3+} of the $Cr(bipy)_2C_2O_4^+$ (○) and $Cr(phen)_2C_2O_4^+$ (×) complexes.

Table 3. Stability constants of $MC_2O_4^{(n-2)+}$, redox potentials of the $M^{n+}/M^{(n-1)+}$ couple, and second-order rate constants (k) for the metal ion catalyzed aquation of $Cr(bipy)_2C_2O_4^+$. $I = 1.0$ M and $t = 25$ °C. Where nothing else is indicated the stability constants are found in Martell, A. E. and Smith, R. M. *Critical Stability Constants, Vol. 3*, Plenum, New York and London, 1977.

Metal ion	K ($MC_2O_4^{(n-2)+}$) M^{-1}	$E°$ V	k $M^{-1} s^{-1}$
Ce(IV)	$>10^9$ [a]	1.61 [c]	1.1
Tl^{3+}	6.2×10^8 [b]	0.30 [d]	3.7×10^{-4}
$TlCl^{2+}$	–	0.19 [e]	1.9×10^{-4}
Fe^{3+}	4×10^7	0.77 [c]	9.3×10^{-5}
$Fe(bipy)_3^{3+}$	–	1.06 [c]	–
In^{3+}	2×10^5	–	–
Ce^{3+}	3×10^3	–	–
Nd^{3+}	1.6×10^4	–	–
Yb^{3+}	2×10^4	−0.58	–
Zn^{2+}	3×10^3	–	–
Cd^{2+}	6×10^2	–	–
Hg^{2+}	$\sim 10^2$ [a]	–	–
Mn^{2+}	66	–	–

[a] Estimated. K for Ce(IV) from known K values for actinides in oxidation state (IV). [b] Ref. 4, corrected to $I = 1.0$ M. [c] Latimer, W. M. *Oxidation Potentials, 2nd Ed.*, Prentice Hall, 1952. [d] Ref. 3 and references therein. [e] Calculated from data in Schwarz, H. A. and Dodson, R. W. *J. Phys. Chem. 80* (1976) 2543.

is analogous to that known for redox reactions involving Tl(III) as oxidant.

Second-order rate constants, $k = k_{obs}/[Tl(III)]$ are given in Table 1 and 2 together with enthalpies and entropies of activation calculated from Eyring plots shown in Fig. 2.

There was no spectral evidence between 700 and 200 nm for any other complex product than the diaqua species shown in (1) (see Discussion).

b. The effect of other metal ions. Of the other metal ions, all in 1.0 M nitric acid, which are given in Table 3, only Fe(III) and Ce(IV) increased the rate of aquation of $Cr(bipy)_2C_2O_4^+$. (The effect of the same metal ions on the phen complex has not been studied.) These latter reacted according to (3) and (4)

$$Cr(bipy)_2C_2O_4^+ + Fe(III) \rightarrow Cr(bipy)_2(H_2O)_2^{3+} + FeC_2O_4^+ \quad (3)$$

$$Cr(bipy)_2C_2O_4^+ + 2Ce(IV) \rightarrow Cr(bipy)_2(H_2O)_2^{3+} + 2Ce(III) + 2CO_2 \quad (4)$$

For the Ce(IV) reaction additional absorption showed the presence of an intensely red intermediate the formation and decay of which could be followed spectrophotometrically. This has previously been detected during the oxidation of free oxalate by Ce(IV) sulfate, was considered to be a 1:1 complex of Ce(IV) and oxalate, and was shown to decompose to give Ce(III) and the oxalate radical, $C_2O_4^{\cdot -}$.[10]

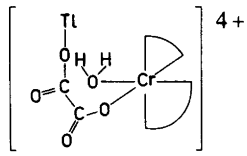

Fig. 3. Suggested intermediate in the oxidation of the oxalato complexes by Tl(III).

DISCUSSION

We calculate that the Tl(III) species present in the reactant solutions are those given in Table 4 which also shows that since the oxidation rate by Tl(III) is within the experimental error independent of $[H^+]$ the major reactant is Tl^{3+}, possibly with a coordinated nitrate.*

The activation parameters for the oxidation of the captive oxalate by Tl(III) are very different from those reported for the oxidation of oxalic acid by Tl(III) ($\Delta H^{\neq} = 102$ kJ mol^{-1}, $\Delta S^{\neq} = +59$ J k^{-1} mol^{-1}).[4] Since the enthalpies of activation found in the present work are about 30 kJ mol^{-1} less than that for the latter reaction then $TlC_2O_4^+$ cannot be an intermediate here.

The ratio between the rates for the bipy and phen oxalato complexes is the same for acid hydrolysis and for Tl(III) oxidation (1.5 at 25 °C). In both cases the higher rate of reaction of the bipy complex is due to the entropy term. We therefore suggest a mechanism through an intermediate which is formally very similar to the one which we proposed for the acid hydrolysis,[6] namely the attack of a water molecule on the Cr(III) centre accompanied by breaking of a Cr–O bond and making of a Tl–O bond giving the intermediate depicted in Fig. 3. We do not know whether an NO_3^- is attached to Tl^{3+} and have therefore neither included this in the figure nor in the following discussion. A bridged transition state could also explain the large negative entropy of activation. This intermediate is, however, not sufficient to explain all the facts because a consideration of the data included in Table 3 for all the metal ions clearly shows that for a metal ion to be an efficient aquating agent towards $(L-L)_2CrC_2O_4^+$ it must satisfy two requirements, *i.e.* not only must it be capable of forming a thermodynamically stable oxalato complex but also it must be oxidizing towards the bridging oxalate. The lack of reactivity of $Fe(bipy)_3^{3+}$, which has a high redox potential, shows that fulfilling only one of the requirements is not sufficient and confirms that the accompanying redox reaction must be of the "inner sphere" type. The lower reactivity of $TlCl^{2+}$ when compared with Tl^{3+} can be attributed both to the decreased affinity for oxalate and also to the fact that the redox potential of the $TlCl^{2+}/TlCl^+$ couple is 110 mV less that of the Tl^{3+}/Tl^{2+} couple.

For the three oxidizing cations studied here the reaction mechanism may be unified if the rate-determining step involves the formation of a precursor complex in which electron transfer can occur and which leads to a reactive intermediate

$$[(L-L)_2\text{—}\underset{\displaystyle OH_2}{\overset{\displaystyle |}{Cr}}\text{—}C_2\dot{O}_4\text{—}M^{(n-1)+}]^{(n+1)+}$$

where $M^{(n-1)+}$ is either Ce(III), Tl(II), or Fe(II) and where a $C_2O_4^{\cdot -}$ radical bridges Cr(III) and $M^{(n-1)+}$. This intermediate differs from that proposed by H. Taube[11,12] for the oxidation by

* Since we found no $[H^+]$ dependence on the rate we have not considered the possible contribution from mixed hydroxo/nitrato complexes.

Table 4. Distribution of Tl(III) among different species in a 1.0 M nitrate solution at different acidities and $t = 25$ °C. K for $TlNO_3^{2+} = 5.0$ M^{-1} at $I = 1.0$ (interpolated) K_d for $TlOH^{2+} = 0.095$ M at $I = 1.0$ (interpolated) $\alpha_{aq} = [Tl^{3+}]/[Tl(III)]$, $\alpha_{OH} = [TlOH^{2+}]/[Tl(III)]$, and $\alpha_{NO_3} = [TlNO_3^{2+}]/[Tl(III)]$. k is the experimentally found second-order rate constant of the $Cr(bipy)_2C_2O_4^+$ reaction.

$[H^+]$ M	α_{aq}	α_{OH}	α_{NO_3}	$k \times 10^4$ M^{-1} s^{-1}
0.25	.157	.060	.784	3.60
0.50	.162	.031	.808	3.65
0.75	.163	.021	.816	3.65
1.00	.164	.016	.820	3.69

Ce(IV) and also by some 2 e oxidants of captive oxalate in $(NH_3)_5Co(III)C_2O_4H^{2+}$, only in that the $C_2O_4^{\cdot -}$ radical is attached both to the metal centre and to the external oxidizing cation, *i.e.* in that the $C_2O_4^{\cdot -}$ radical is bridging.

On breaking of the second Cr–O bond the oxalate radical is required to be a reducing agent towards Tl(II) ($E°$ $(Tl^{2+}/Tl^{+})=2.2$ V) and an oxidizing agent towards Fe(II) ($E°$ $(Fe^{3+}/Fe^{2+})=$ 0.77 V) giving the thermodynamically stable products, Tl(I) and Fe(III),* respectively. These latter reactions may be so fast that the reactants do not diffuse out of the solvent cage. The Cr(III) centre, however, (unlike the Co(III) centre of $(NH_3)_5$-$CoC_2O_4H^{2+}$ of Ref. 11) is unable to accept an electron so that an extra oxidizing cation is required in order to complete the overall Ce(IV) reaction. In agreement with this it is only with Ce(IV) that we have been able to detect an $[M^{(n-1)+}C_2O_4^{\cdot -}]$ complex as a first product.

REFERENCES

1. Schwarz, H. A., Comstock, D., Yandell, J. K. and Dodson, R. W. *J. Phys. Chem. 78* (1974) 488.
2. Ashurst, K. G. and Higginson, W. C. E. *J. Chem. Soc.* (1953) 3044.
3. Nord, G. *Inorg. Chem. 16* (1977) 201.
4. Mønsted, L. B., Mønsted, O. and Nord, G. *Trans. Faraday Soc. 66* (1970) 936.
5. Farver, O. *Acta Chem. Scand. 26* (1972) 534.
6. Farver, O. and Nord, G. *Acta Chem. Scand. A 30* (1976) 121.
7. Hancock, M. P., Josephsen, J. and Schäffer, C. E. *Acta Chem. Scand. A 30* (1976) 79.
8. Jonasson, I. R. and Stranks, D. R. *Electrochim. Acta 13* (1968) 1147.
9. Inskeep, R. G. and Bjerrum, J. *Acta Chem. Scand. 15* (1961) 62.
10. El-Tantawy, Y. A. and Rechnitz, G. A. *Anal. Chem. 36* (1964) 1774.
11. Saffir, P. and Taube, H. *J. Am. Chem. Soc. 82* (1960) 13.
12. Taube, H. *Electron Transfer Reactions of Complex Ions in Solution.* Academic, New York and London 1970, p. 77.

Received June 8, 1978.

* The Fe(III) reaction is thus an example of redox catalyzed substitution.

Acta Chemica Scandinavica A 32 (1978) 969–972

The Phase Diagram $CuCl_2$—LiCl—KCl

SUPREYA SUTAKSHUTO-TRIVIJITKASEM,* BIRGIT JENSSEN HOLM and HARALD A. ØYE

Institutt for uorganisk kjemi, Norges tekniske høgskole, Universitetet i Trondheim, N-7034 Trondheim – NTH, Norway

The systems $CuCl_2$ – LiCl and $CuCl_2$ – LiCl – KCl were studied by DTA. $CuCl_2$ – LiCl is a simple eutectic system, while $CuCl_2$ – LiCl – KCl contains one congruent melting compound, $KCuCl_3$. In a subsequent publication, the ternary phase diagram has been calculated on the basis of the conformal ionic solution theory, and there is good agreement between the experimental and calculated phase diagram.

As part of a phase study of systems of interest as oxychlorination catalysts, the phase diagram $CuCl_2$ – LiCl – KCl was determined. The phase diagram can also be calculated by the use of the conformal ionic solution theory[1-6] and it was possible to extend the calculation to the present charge-asymmetric additive ternary system.[7] This gave a satisfactory description of the phase diagram except in the area where the compound $KCuCl_3$(s) was present, as this compound was not taken into consideration by the model. In a subsequent publication the conformal solution model is expanded to include compound formation.[8]

EXPERIMENTAL

Chemicals. $CuCl_2.2H_2O$ ('Baker Analyzed' REAGENT, min. 99.0 % $CuCl_2.2H_2O$, J. T. Baker, Holland) was dried by heating to 400 °C in a stream of HCl gas, whereupon Cl_2 gas was bubbled through the melt to prevent reduction to CuCl.

LiCl ('Baker Analyzed' REAGENT, min. 99.1 % LiCl, J. T. Baker, Holland) was heated gradually to melting under a stream of HCl gas, and then filtered.

KCl (*p.a.*, E. Merck, Germany) was dried in vacuum at 400 °C, and was afterwards melted in a nitrogen atmosphere. After cooling, clear crystals were picked out and used.

The DTA samples were made by weighing out about 2 g of the chlorides in a dry-box under nitrogen atmosphere, and transferring the mixture to a quartz tube. This was evacuated to 10^{-4} Torr and then filled with Cl_2 gas to *ca.* 350 Torr before it was sealed. All samples were equilibrated at about 500 °C for 12 h and then quenched in water, before DTA.

Al_2O_3 (E. Merck, Germany), the reference material for DTA, was heated to 1200 °C, and was then cooled and filled into a quartz tube. This was evacuated to 10^{-4} Torr and sealed.

DTA equipment. The specimen-holder assembly is shown in Fig. 1. The quartz ampoules containing the sample and reference materials were placed in wells in a copper block, covered by a copper lid. The thermocouples were Pt/Pt10 %Rh with the junctions in the cavities in the bottom of the specimen holders. The temperature was measured at the bottom of the sample holder. The specimen-holder assembly was mounted in a vertical Kanthal A-wired laboratory furnace. The furnace temperature was controlled by an Eurotherm temperature programmer, *via* a chromel-alumel thermocouple. The temperature signal was fed to a recorder *via* a Fluke DC differential voltmeter, which was used as a reference voltage supply. The differential signal was amplified by a Leeds & Northrup microvolt indicating amplifier. The recorder was a Yokogawa dual-channel line recorder. Gas of composition 94 % N_2, 6 % H_2 was passed through the furnace during all runs. Both heating and cooling curves were recorded. Typical heating and cooling rates were 1.6 °C/min. The DTA temperatures were calibrated using the following transition or melting points: KNO_3(128 °C), Sn(232 °C), $KClO_4$(300 °C), Ag_2SO_4 (412 °C), Zn(420 °C) and AgCl(455 °C). The corrections found were $+3 \pm 3$ °C for the heating curves

* Present address: Department of Physics, Faculty of Science and Arts, Kasetsart University, Bangkok, Thailand.

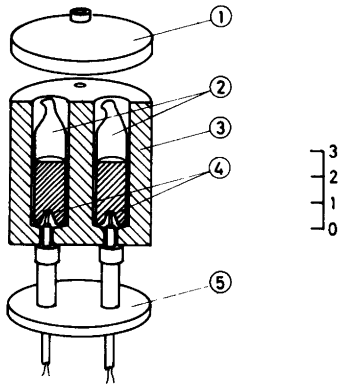

Fig. 1. Cross section of the specimen-holder assembly for DTA. 1. Copper lid. 2. Sample and reference quartz ampoules. 3. Copper block. 4. Pt/Pt 10 % Rh thermocouples. 5. Radiation shield.

and $+7\pm3$ °C for the cooling curves. The main reason for these rather large discrepancies is probably the poor heat conductance through the walls of the quartz ampoules. These walls had a thickness of about 1.2 mm, but at the bottom, where the thermocouple junctions are placed, they were often thicker due to the sealing-off process.

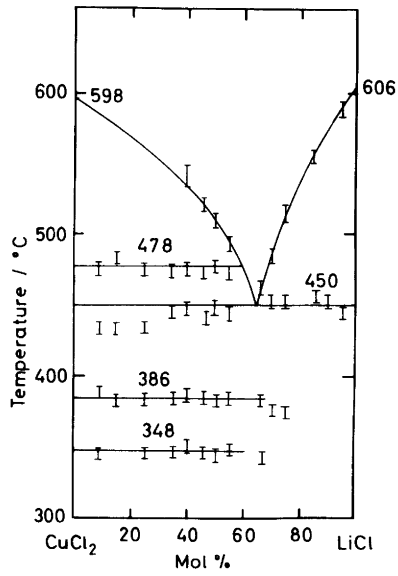

Fig. 2. Experimental phase diagram of the system $CuCl_2-LiCl$.

RESULTS AND DISCUSSION

The experimental phase diagram of the system $CuCl_2-LiCl$ is shown in Fig. 2. This is a simple eutectic system with the eutectic point at 36 mol %

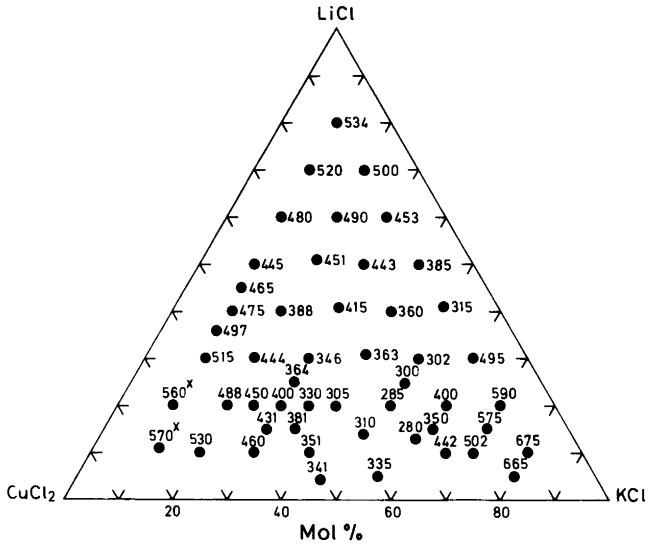

Fig. 3. Experimental liquidus temperatures (in °C) in the system $CuCl_2-LiCl-KCl$. ×, Points found by extrapolation.

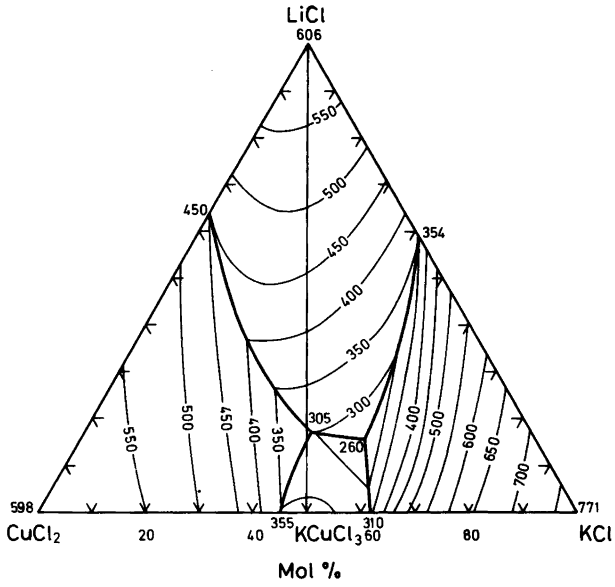

Fig. 4. Phase diagram of the system $CuCl_2-LiCl-KCl$. Temperatures are in °C.

$CuCl_2$, 450 °C. Because the ampoules holding $CuCl_2$-rich samples tended to explode at temperatures above 560 °C, the liquidus temperatures were not recorded in this region. The liquidus line was extrapolated from below 550 °C to the melting point found by Vorobei and Skiba,[9] 598 °C. The melting point of LiCl, 606 °C, was taken from Aukrust *et al.*[10a,b] The reaction at 478 °C is a solid-state transition in $CuCl_2$, as reported previously in other systems.[9] The reactions at 348 °C and 386 °C have not been identified. They are probably reactions in the ternary system $CuCl_2-LiCl-CuCl$, as some CuCl will be formed by the reaction

$$CuCl_2 \rightleftharpoons CuCl + \tfrac{1}{2}Cl_2$$

The ampoules were filled with Cl_2 in order to depress this reaction, but even so it will take place to some extent in the $CuCl_2$-rich region.

The experimental liquidus temperatures of the system $CuCl_2-LiCl-KCl$ are shown in Fig. 3. On the basis of these values and data for the component binary systems $CuCl_2-LiCl$ (present work), $LiCl-KCl$ (Aukrust *et al.*[10a,b]) and $CuCl_2-KCl$ (Vorobei and Skiba[9]) the phase diagram in Fig. 4 was constructed.

There are some inherent uncertainties in these measurements, mainly due to a strong tendency to undercooling in the system, especially in KCl-rich samples. The magnitude of this undercooling was not reproducible; it might vary from a very few to 30–40 degrees. Another source of error is the formation of CuCl. Analysis of $CuCl_2-LiCl-KCl$ samples gave a CuCl content between 1 and 5 mol % CuCl.

The ternary phase diagram was constructed by plotting several quasi-binary sections and smoothing the liquidus curves. By this method the errors due to undercooling were reduced, and the uncertainties in the liquidus temperatures given in Fig. 4 are estimated to be less than ±10 °C.

The phase diagram (Fig. 4) shows a peritectic point ($CuCl_2(s)$ + liq. = $KCuCl_3(s)$ + LiCl(s)) at 40 % $CuCl_2$ – 18 % LiCl – 42 % KCl, 305 °C and a eutectic point at 31 % $CuCl_2$ – 16 % LiCl – 53 % KCl, 260 °C.

As demonstrated by a subsequent publication[8] the present phase diagram lends itself to a satisfactory calculation by use of the conformal ionic solution theory.

REFERENCES

1. Reiss, H., Katz, J. L. and Kleppa, O. J. *J. Chem. Phys. 36* (1962) 144.

2. Blander, M. and Yosim, S. J. *J. Chem. Phys. 39* (1963) 2610.
3. Blander, M. and Topol, L. E. *Inorg. Chem. 5* (1966) 1641.
4. Saboungi, M.-L., Vallet, C. and Doucet, Y. *J. Phys. Chem. 77* (1973) 1699.
5. Saboungi, M.-L. and Cerisier, P. *J. Electrochem. Soc. 121* (1974) 1258.
6. Saboungi, M.-L. and Blander, M. *J. Am. Ceram. Soc. 58* (1974) 1.
7. Sutakshuto, S. *Thesis*, No. 31, Institutt for uorganisk kjemi, Norges tekniske høgskole, Trondheim 1976.
8. Foosnæs, T., Østvold, T. and Øye, H. A. *Acta Chem. Scand. A 32* (1978) 973.
9. Vorobei, M. P. and Skiba, O. V. *Russ. J. Inorg. Chem. 15* (1970) 725.
10. a. Aukrust, E., Bjørge, B., Flood, H. and Førland, T. *Ann. N.Y. Acad. Sci. 79* (1960) 830; b. Aukrust, E. *Diploma Thesis*, Institutt for uorganisk kjemi, Norges tekniske høgskole, Trondheim 1957.

Received June 19, 1978.

Acta Chemica Scandinavica A 32 (1978) 973–987

Calculation of Charge Asymmetric Additive Ternary Phase Diagrams with and without Compound Formation

TRYGVE FOOSNÆS, TERJE ØSTVOLD and HARALD A. ØYE

Institutt for uorganisk kjemi, Norges tekniske høgskole, Universitetet i Trondheim, N-7034 Trondheim – NTH, Norway

Liquidus temperatures have been calculated for fourteen ternary additive charge asymmetric molten salt systems. The second-order terms of the conformal ionic solution theory have been used, replacing mol fractions with equivalent fractions of the ions. The calculations indicate that this simple representation of the excess Gibbs energy of mixing in most cases gives a satisfactory representation of the phase diagrams. A method is shown for calculation of ternary additive phase diagrams where a congruently melting compound is formed in one of the constituting binaries.

I. INTRODUCTION

The conformal ionic solution theory (CIS)[1] has been extended and applied to calculate liquidus temperatures and liquid-liquid miscibility gaps for reciprocal molten salt systems.[2–5] Although the CIS theory has been extended to additive ternary molten salt systems up to fourth-order terms,[6] a representation of the excess Gibbs energy of mixing on the basis of the second-order terms is known to be satisfactory for systems with monovalent ions, where deviations from ideality are small.[7] By use of second-order terms only, it is assumed that the deviation from ideality in the binaries may be described by one parameter, not allowing for asymmetry of the excess Gibbs energy of mixing.

Charge asymmetric ternary systems have been calculated on the basis of a different theoretical approach.[8] For this type of systems, the formation of binary compounds has been taken into account.[9] Calculation of ternary phase diagrams also has been performed in metallic systems.[10]

Expressing the excess Gibbs energy of mixing by the second-order terms derived from CIS theory, with equivalent fractions instead of mol fractions, we will calculate phase diagrams for ternary additive molten mixtures of the salts AX_{q_A}, BX_{q_B} and CX_{q_C}, where q_i represents the absolute value of the charge of the cation. The same approach also is applied in calculations of ternary additive systems where a compound is formed in one of the constituting binaries.

II. THEORY

The basic set of equations needed to express the excess Gibbs energy of mixing is derived from conformal ionic solution theory.[1] When only second-order terms are used, the excess Gibbs energy of mixing per equivalent for the binary systems may be expressed by:

$$\Delta G^{E}(AX_{q_A}-BX_{q_B}) = X'_A X'_B \lambda_{AB}$$

$$\Delta G^{E}(BX_{q_B}-CX_{q_C}) = X'_B X'_C \lambda_{BC} \qquad (1)$$

$$\Delta G^{E}(AX_{q_A}-CX_{q_C}) = X'_A X'_C \lambda_{AC}$$

where $X'_i = q_i X_i / (\sum_j q_j X_j)$

X_i is the ionic fraction, and q_i is the absolute value of the charge of the i'th ion. The summation is over all ions with charges of the same sign.

Eqn. (1) corresponds to a regular solution model. The λ_{ij}'s are the binary interaction parameters, which are determined experimentally for a number of systems with one common ion.

The activity coefficient of AX_{q_A} in a molten mixture of AX_{q_A} and BX_{q_B} is given by:

$$RT\ln\gamma(AX_{q_A}) = \frac{\partial(n_{tot}\Delta G_m^E)}{\partial n(AX_{q_A})} = q_A X'^2_B \lambda_{AB} \quad (2)$$

where ΔG_m^E is the excess Gibbs energy of formation of the mixture from the pure liquid compounds, and n_{tot} is the total number of equivalents in the mixture. $n(AX)_{q_A}$ is the number of mol of AX_{q_A} in the mixture. When the heat of fusion of the salts. ΔH_f, is temperature independent, and the heat capacity difference between liquid and solid at constant pressure is negligible, the activity of AX_{q_A} in the binary mixture may be expressed by:

$$R\ln a(AX_{q_A}) = -\Delta H_f(AX_{q_A})\left[\frac{1}{T} - \frac{1}{T^\circ(AX)_{q_A}}\right]$$
$$= R\ln X_A X_X^{q_A}\gamma(AX_{q_A}) \quad (3)$$

where $T^\circ(AX_{q_A})$ is the melting point of AX_{q_A}. X_X is the ionic fraction of the common ion, hence $X_X = 1$. For simplicity, X_X is omitted from the following equations. Combination of eqns. (2) and (3), applied to each component of the binary, yields:

$$T[\Delta H_f(AX_{q_A})/T^\circ(AX_{q_A}) - R\ln X_A] - \Delta H_f(AX_{q_A}) = q_A X'^2_B \lambda_{AB}$$
$$T[\Delta H_f(BX_{q_B})/T^\circ(BX_{q_B}) - R\ln X_B] - \Delta H_f(BX_{q_B}) = q_B X'^2_A \lambda_{AB} \quad (4)$$

From these equations the binary interaction parameter, λ_{AB}, may be calculated.

The excess Gibbs energy of mixing per equivalent for the ternary system is expressed as:

$$\Delta G_m^E = X'_A X'_B \lambda_{AB} + X'_B X'_C \lambda_{BC} + X'_A X'_C \lambda_{AC} \quad (5)$$

The pure liquid compounds are chosen as standard state for the salts. The activity coefficients of the salts in the ternary mixture are calculated by combining eqn. (2) and eqn. (5).

$$RT\ln\gamma(AX_{q_A}) = q_A(X'_B + X'_C)X'_B\lambda_{AB} - q_A X'_B X'_C \lambda_{BC} + q_A(X'_B + X'_C)X'_C\lambda_{AC}$$

$$RT\ln\gamma(BX_{q_B}) = q_B(X'_A + X'_C)X'_A\lambda_{AB} + + q_B(X'_A + X'_C)X'_C\lambda_{BC} - q_B X'_A X'_C \lambda_{AC} \quad (6)$$

$$RT\ln\gamma(CX_{q_C}) = -q_C X'_A X'_B \lambda_{AB} + q_C(X'_A + X'_B)X'_B\lambda_{BC} + q_C(X'_A + X'_B)X'_A\lambda_{AC}$$

The expressions for the activity coefficients are introduced in eqn. (3), and the set of equations is solved, giving the liquidus temperatures in the primary phase fields of the three components:

$$T(AX_{q_A}) = \{\Delta H_f(AX_{q_A}) + q_A[(X'_B + X'_C)X'_B\lambda_{AB} - - X'_B X'_C\lambda_{BC} + (X'_B + X'_C)X'_C\lambda_{AC}]\}/[\Delta H_f(AX_{q_A})/ T^\circ(AX_{q_A}) - R\ln X_A]$$

$$T(BX_{q_B}) = \{\Delta H_f(BX_{q_B}) + q_B[(X'_A + X'_C)X'_A\lambda_{AB} + (X'_A + X'_C)X'_C\lambda_{BC} - X'_A X'_C\lambda_{AC}]\}/ [\Delta H_f(BX_{q_B})/T^\circ(BX_{q_B}) - R\ln X_B] \quad (7)$$

$$T(CX_{q_C}) = \{\Delta H_f(CX_{q_C}) + q_C[-X'_A X'_B\lambda_{AB} + (X'_A + X'_B)X'_B\lambda_{BC} + (X'_A + X'_B)X'_A\lambda_{AC}]\}/ [\Delta H_f(CX_{q_C})/T^\circ(CX_{q_C}) - R\ln X_C]$$

A congruently melting compound $B_mC_nX_{(mq_B+nq_C)}$*, which dissociates completely on melting, is assumed to be formed in the binary system $BX_{q_B} - CX_{q_C}$. The standard state for the binary compound is chosen to be the melt with the composition corresponding to this compound. The mol fractions of B and C are X_B^0 and X_C^0.

To calculate the activity coefficient of the compound, the excess Gibbs energy of mixing must be related to the standard state for the binary compound. The excess Gibbs energy of mixing for a melt with the composition corresponding to the compound is:

$$\Delta G_m^E(0) = X'^0_B X'^0_C \lambda_{BC}$$

For a melt with any other composition, the excess Gibbs energy of mixing is given by eqn. (1).

When related to the new standard state, the excess Gibbs energy of mixing for the binary system $BX_{q_B} - CX_{q_C}$ will be:

$$\Delta G_m^E = [X'_B X'_C - X'^0_B X'^0_C]\lambda_{BC}$$

When mol fractions are introduced:

$$\Delta G_m^E = [X'_B X'_C - X_B^0 X_C^0 q_B q_C(mq_B + nq_C)/ (q_B X_B^0 + q_C X_C^0)^2]\lambda_{BC} \quad (8)$$

The activity coefficient of B–C–X in the binary system is calculated by partial differentiation of the expression for the total excess Gibbs energy of mixing:

* The compound is denoted B–C–X in the following text and formulas.

$$RT\ln\gamma(\mathrm{B-C-X}) = \frac{\partial(n_{\mathrm{tot}}\,\Delta G_m^{\mathrm{E}})}{\partial n(\mathrm{B-C-X})}$$
$$= m\frac{\partial(n_{\mathrm{tot}}\Delta G_m^{\mathrm{E}})}{\partial n_{\mathrm{B}}} + n\frac{\partial(n_{\mathrm{tot}}\,\Delta G_m^{\mathrm{E}})}{\partial n_{\mathrm{C}}}$$

$$RT\ln\gamma(\mathrm{B-C-X}) = [mq_{\mathrm{B}}X'^{2}_{\mathrm{C}} + nq_{\mathrm{C}}X'^{2}_{\mathrm{B}} - X^{0}_{\mathrm{B}}X^{0}_{\mathrm{C}}q_{\mathrm{B}}q_{\mathrm{C}}(mq_{\mathrm{B}}+nq_{\mathrm{C}})/(q_{\mathrm{B}}X^{0}_{\mathrm{B}}+q_{\mathrm{C}}X^{0}_{\mathrm{C}})^{2}]\lambda_{\mathrm{BC}} \quad (9)$$

The activity of the binary compound is expressed by:

$$a(\mathrm{B-C-X}) = kX^{m}_{\mathrm{B}}X^{n}_{\mathrm{C}}\gamma(\mathrm{B-C-X}) \quad (10)$$

k is a factor which normalizes the activity of the molten compound to unity. Combination of eqns. (9) and (10) with eqn. (3) gives an equation for the liquidus temperatures for the compound in equilibrium with the binary melt:

$$T[\Delta H_{\mathrm{f}}(\mathrm{B-C-X})/T^{\circ}(\mathrm{B-C-X}) - R\ln(kX^{m}_{\mathrm{B}}X^{n}_{\mathrm{C}})] - \Delta H_{\mathrm{f}}(\mathrm{B-C-X}) = [mq_{\mathrm{B}}X'^{2}_{\mathrm{C}} + nq_{\mathrm{C}}X'^{2}_{\mathrm{B}} - X^{0}_{\mathrm{B}}X^{0}_{\mathrm{C}}q_{\mathrm{B}}q_{\mathrm{C}}(mq_{\mathrm{B}}+nq_{\mathrm{C}})/(q_{\mathrm{B}}X^{0}_{\mathrm{B}}+q_{\mathrm{C}}X^{0}_{\mathrm{C}})^{2}]\lambda_{\mathrm{BC}} \quad (11)$$

An equation for the liquidus curve for binary systems with a congruently melting compound also has been derived by methods of statistical mechanics in terms of nearest-neighbour interactions.[11] For a compound with 1:1 composition, the equation may be shown to be identical to eqn. (11).

When a compound is formed in one of the binary systems, the equations for the ternary activity coefficients of AX_{q_A}, BX_{q_B} and CX_{q_C} are unchanged from the previous case where no compound was formed. The equations for the liquidus temperatures in the phase fields of these components are thus the same as before. The excess Gibbs energy of mixing for the ternary system when a binary compound B−C−X is formed, is obtained by combining eqns. (5) and (8):

$$\Delta G_m^{\mathrm{E}} = X'_{\mathrm{A}}X'_{\mathrm{B}}\lambda_{\mathrm{AB}} + [X'_{\mathrm{B}}X'_{\mathrm{C}} - X^{0}_{\mathrm{B}}X^{0}_{\mathrm{C}}q_{\mathrm{B}}q_{\mathrm{C}}(mq_{\mathrm{B}}+nq_{\mathrm{C}})/(q_{\mathrm{B}}X^{0}_{\mathrm{B}}+q_{\mathrm{C}}X^{0}_{\mathrm{C}})^{2}]\lambda_{\mathrm{BC}} + X'_{\mathrm{A}}X'_{\mathrm{C}}\lambda_{\mathrm{AC}} \quad (12)$$

By partial differentiation of eqn. (12) the activity coefficient of B−C−X in the ternary system is found:

$$RT\ln\gamma(\mathrm{B-C-X}) = A = mq_{\mathrm{B}}(X'_{\mathrm{A}}+X'_{\mathrm{C}})[X'_{\mathrm{A}}\lambda_{\mathrm{AB}} + X'_{\mathrm{C}}\lambda_{\mathrm{BC}}] + nq_{\mathrm{C}}(X'_{\mathrm{A}}+X'_{\mathrm{B}})[X'_{\mathrm{A}}\lambda_{\mathrm{AC}} + X'_{\mathrm{B}}\lambda_{\mathrm{BC}}] - X'_{\mathrm{A}}[mq_{\mathrm{B}}X'_{\mathrm{C}}\lambda_{\mathrm{AC}} + nq_{\mathrm{C}}X'_{\mathrm{B}}\lambda_{\mathrm{AB}}] - X^{0}_{\mathrm{B}}X^{0}_{\mathrm{C}}q_{\mathrm{B}}q_{\mathrm{C}}\lambda_{\mathrm{BC}}(mq_{\mathrm{B}}+nq_{\mathrm{C}})/(q_{\mathrm{B}}X^{0}_{\mathrm{B}}+q_{\mathrm{C}}X^{0}_{\mathrm{C}})^{2} \quad (13)$$

The liquidus temperatures in the primary phase field of B−C−X then may be calculated:

$$T(\mathrm{B-C-X}) = [\Delta H_{\mathrm{f}}(\mathrm{B-C-X}) + A]/[\Delta H_{\mathrm{f}}(\mathrm{B-C-X})/T^{\circ}(\mathrm{B-C-X}) - R\ln(kX^{m}_{\mathrm{B}}X^{n}_{\mathrm{C}})] \quad (14)$$

III. CALCULATION OF PHASE DIAGRAMS FOR TERNARY ADDITIVE SYSTEMS

The calculation of the phase diagrams was performed by a UNIVAC 1108 computer. Thermodynamic input data were the heats of fusion and the melting points of the pure salts, and the binary eutectic temperatures.

In the ternary additive systems with no compound formation, the melt composition was used as a variable to calculate both the interaction parameters and the melt compositions in the binary eutectics, according to eqn. (4). In systems with a binary compound, eqn. (11) was used to calculate the interaction parameter. To perform this calculation, the data needed were the temperatures and melt compositions of the two eutectic points, and the heat of fusion and the melting point of the compound.

The isotherms of the ternary system and the phase field boundaries were calculated using eqn. (7), and eqns. (7) and (14) when a congruently melting binary compound was formed. The mol fraction of each component was changed in steps of 0.005 throughout the entire concentration range, and the liquidus temperatures were calculated for each composition. The phase field boundaries were assigned to compositions at which the liquidus temperatures in two phase fields differed by less than ± 0.5 K. The ternary eutectic was assigned to the composition where the three calculated liquidus temperatures agreed within ± 2.5 K.

IV. RESULTS

The enthalpies of fusion and the melting points of the salts are given in Table 1. Structural transitions are not taken into account in the calculations. The eutectic temperatures given by the investigators of the particular ternary system have been used in the calculation, and reported phase diagrams are shown in Figs. 1 – 14.

Table 1. Melting points and enthalpies of fusion for the salts selected in this work.

Salt	M.p. (°C)	ΔH_f kJ/mol	Ref.
LiF	848	27.087	12
NaF	996	32.593	12
KF	858	27.196	12
CaF_2	1418	41.171	38
SrF_2	1400	43.514	39
LiCl	606	19.920	14
NaCl	801	28.158	12
KCl	770	26.531	14
CsCl	645	20.250	16
$CaCl_2$	772	28.543	12
$FeCl_2$	677	43.095	12
$CuCl_2$	598	44.493 [a]	15
$SnCl_2$	247	12.761	13
$LaCl_3$	855	54.392	13
$CeCl_3$	822	53.555	16
$NdCl_3$	760	50.208	17
$KCuCl_3$	365	24.895 [a]	15
$CsCaCl_3$	910	82.467	18
NaBr	747	26.108	12
Na_2CO_3	850	29.665	12
Na_2SO_4	884	23.012	13
$LiNO_3$	254	25.606	16
$NaNO_3$	306	14.602	13
$TlNO_3$	206	8.201	16
$Ca(NO_3)_2$	561	21.338	13
$Cd(NO_3)_2$	300	18.200	13

[a] The ΔH_f-values are calculated from the phase diagram given in Ref. 15.

Reported and calculated eutectic compositions and temperatures for binaries are given in Table 2 and for ternary systems in Table 3.

V. DISCUSSION

V.1. Ternary additive systems without a binary compound

In spite of the simple equations used to describe the binary systems, experimental and calculated values for the eutectic compositions show a reasonable agreement for most systems (Table 2). The interaction parameters calculated from the binaries have the same sign as the reported data,[16,28,29,36] except from the binaries NaF–KF, NaF–NaBr and NaCl–Na_2CO_3. The values, however, may deviate from those reported.

The shape of the calculated isotherms of the ternary systems are compared with that found experimentally in Table 4. The calculated binary interaction parameters also are given. At first, the difference between calculated and reported diagrams might seem considerable. However, the difference between the classifications +, 0 and − is small in most cases. In three of the systems, some of the phase fields are small, and no isotherms were reported or calculated.

The activity of a component along a liquidus isotherm will be constant. When the isotherms in a phase field are convex, as viewed from the corner representing the component AX_{q_A}, *i.e.* they bend

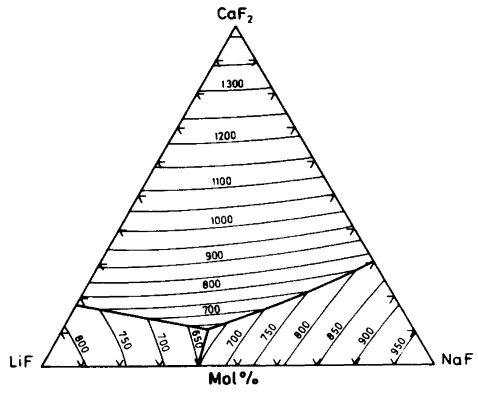

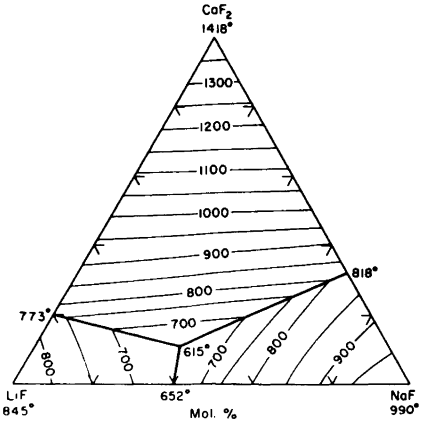

FIG. 1544.—System LiF–NaF–CaF_2.

Fig. 1. Phase diagram of the (Li,Na,Ca)F system. Calc. (left) and measured[31] (right).

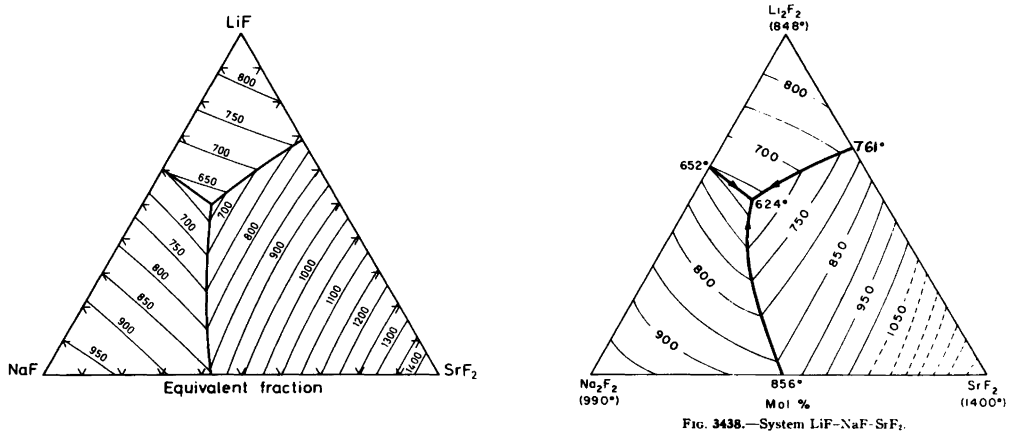

FIG. 3438.—System LiF-NaF-SrF_2.

Fig. 2. Phase diagram of the (Na,Sr,Li)F system. Calc. (left) and measured[21] (right).

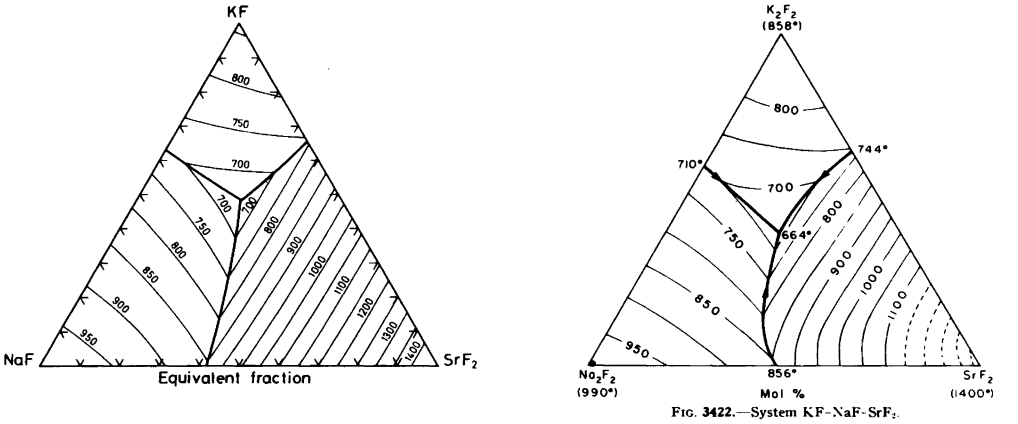

FIG. 3422.—System KF-NaF-SrF_2.

Fig. 3. Phase diagram of the (Na,Sr,K)F system. Calc. (left) and measured[21] (right).

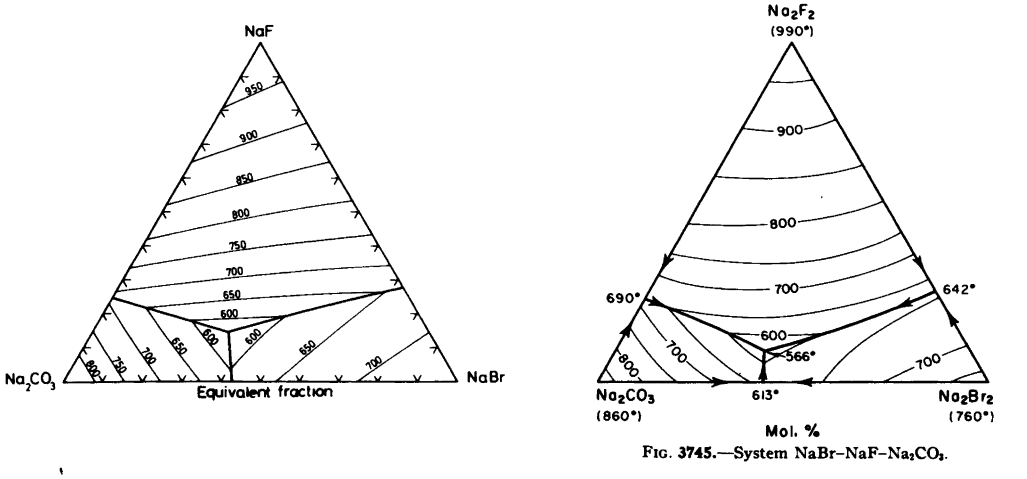

FIG. 3745.—System NaBr-NaF-Na_2CO_3.

Fig. 4. Phase diagram of the $Na(CO_3,Br,F)$ system. Calc. (left) and measured[32] (right).

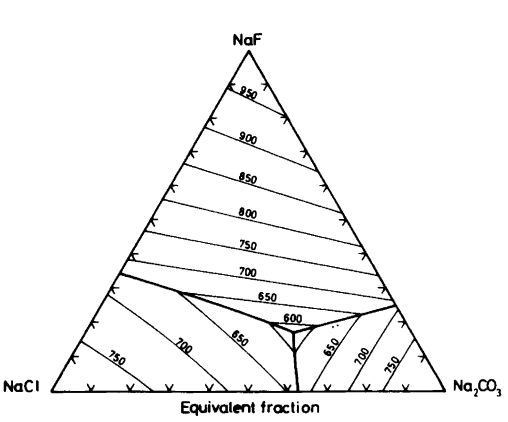

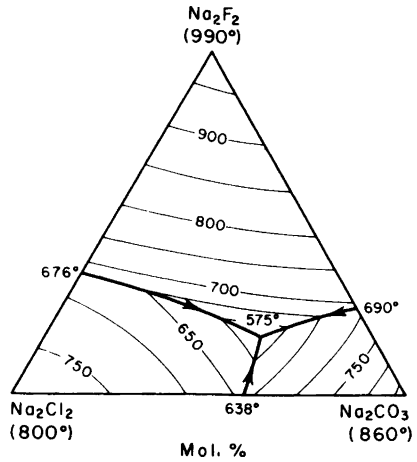

FIG. 3750.—System Na_2Cl_2–Na_2F_2–Na_2CO_3.

Fig. 5. Phase diagram of the Na(Cl,CO_3,F) system. Calc. (left) and measured[19] (right).

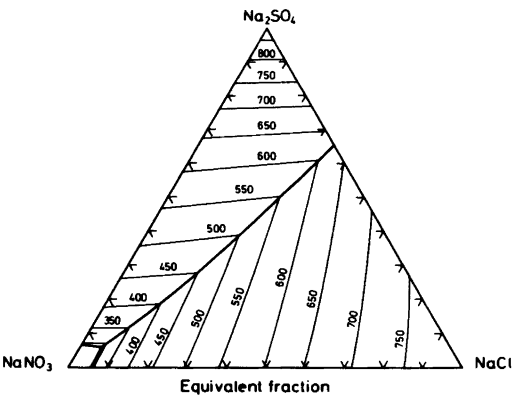

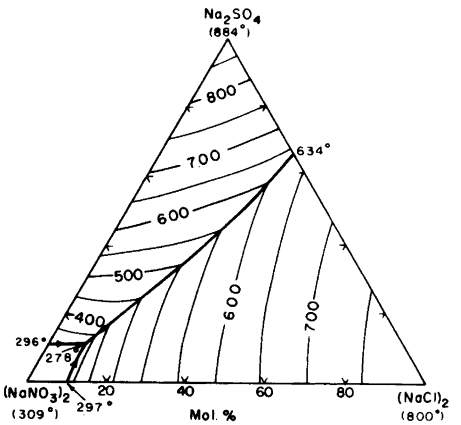

FIG. 3913.—System $(NaCl)_2$–$(NaNO_3)_2$–Na_2SO_4.

Fig. 6. Phase diagram of the Na(NO_3,Cl,SO_4) system. Calc. (left) and measured[19] (right).

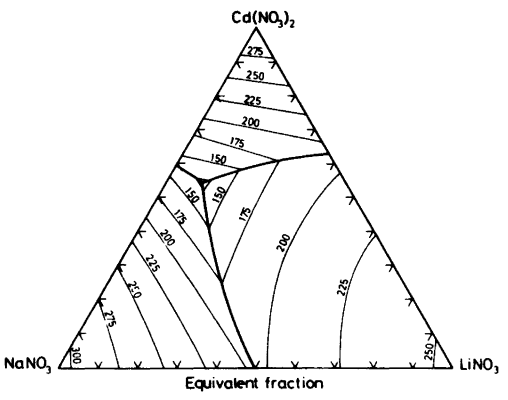

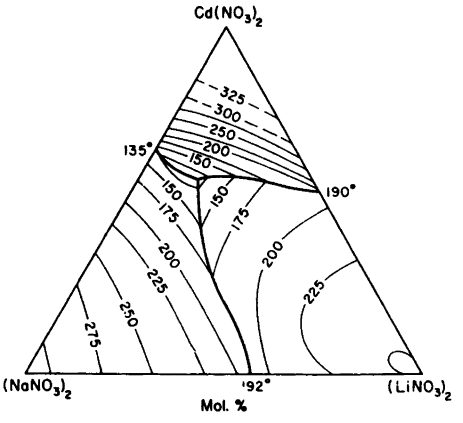

FIG. 1076.—System $LiNO_3$–$NaNO_3$–$Cd(NO_3)_2$.

Fig. 7. Phase diagram of the (Na,Li,Cd)NO_3 system. Calc. (left) and measured[33] (right).

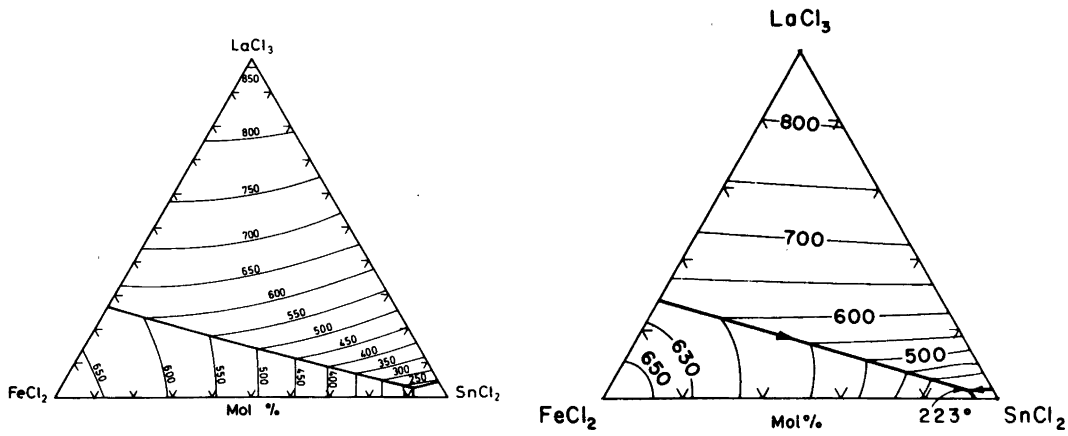

Fig. 8. Phase diagram of the (Fe,Sn,La)Cl system. Calc. (left) and measured[24] (right).

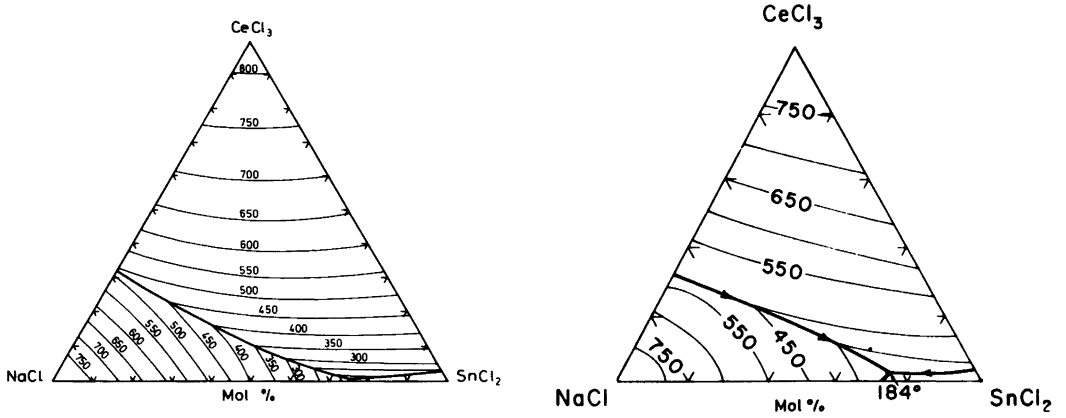

Fig. 9. Phase diagram of the (Na,Sn,Ce)Cl system. Calc. (left) and measured[24] (right).

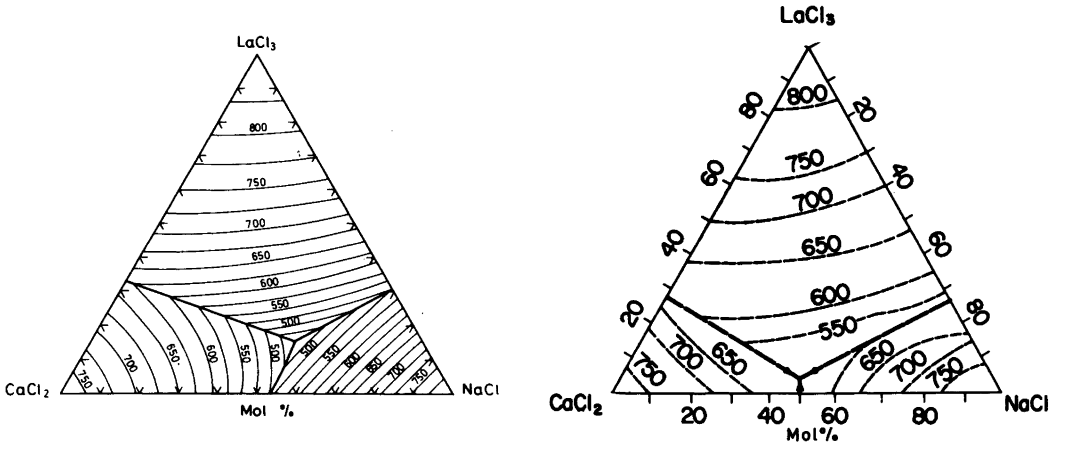

Fig. 10. Phase diagram of the (Ca,Na,La)Cl system. Calc. (left) and measured[19] (right).

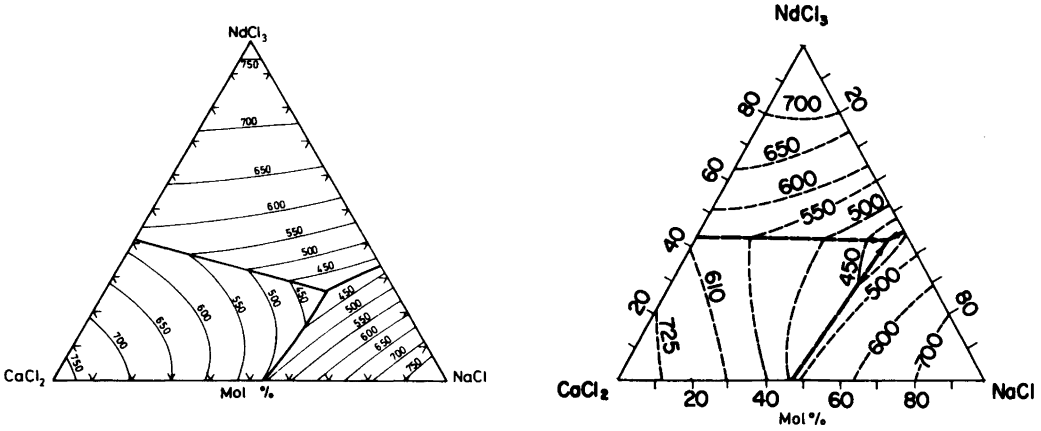

Fig. 11. Phase diagram of the (Ca,Na,Nd)Cl system. Calc. (left) and measured[25] (right).

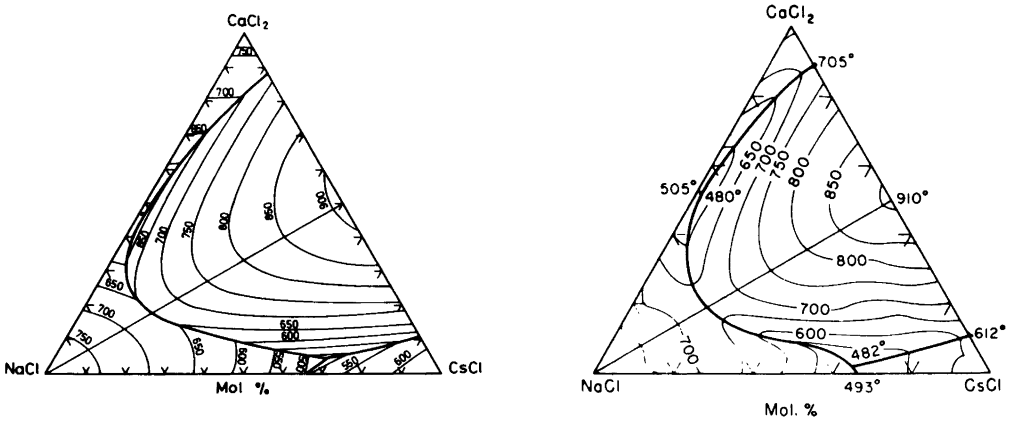

FIG. 1405.—System CsCl–NaCl–$CaCl_2$.

Fig. 12. Phase diagram of the (Na,Cs,Ca)Cl system. Calc. (left) and measured[26] (right).

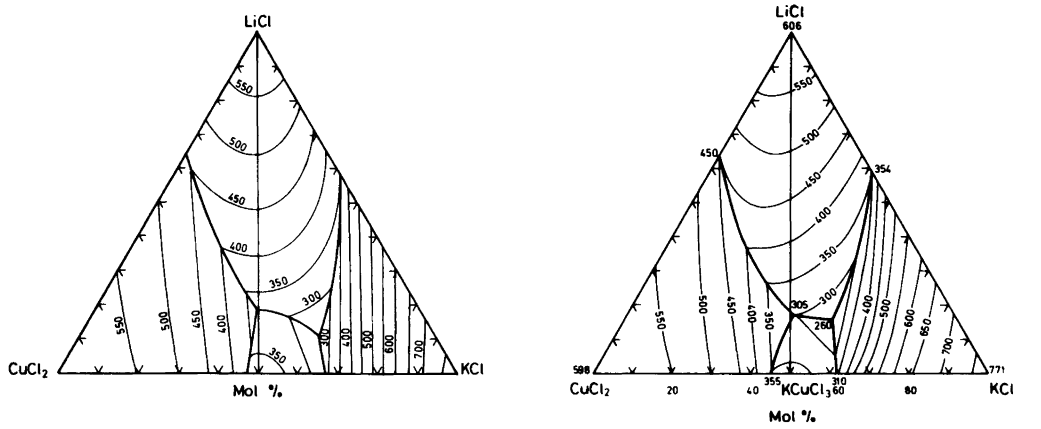

Fig. 13. Phase diagram of the (K,Cu,Li)Cl system. Calc. (left) and measured[27] (right).

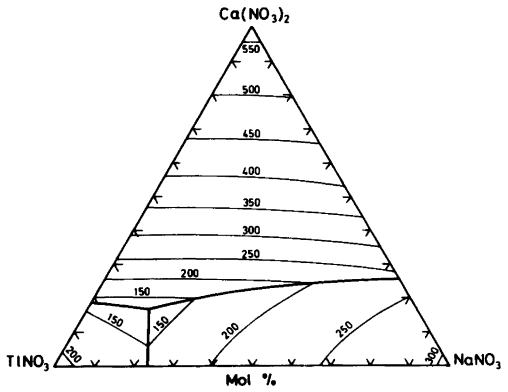

Fig. 14. Calculated phase diagram of the (Tl,Na,Ca)-NO_3 system.

towards the corner, the activity of the component is the same as in the binaries $AX_{q_A}-BX_{q_B}$ and $AX_{q_B}-CX_{q_C}$, but at a higher concentration of AX_{q_A} than in the two binaries. The compound AX_{q_A} exhibits negative deviation from the values in the binaries in this case. When the isotherms of a phase field are concave, the component thus exhibits positive deviations. A ternary additive ideal system will have linear isotherms in all phase fields, as may be seen from eqn. (7).

When the signs of the binary interaction parameters are equal, one can see how the shape of the isotherms will depend on the magnitude of the interaction parameters from eqn. (7). The equation for the liquidus temperatures in the AX_{q_A} phase field reduces to the binary expression, eqn. (4), when X_B or X_C is zero.

When the sign of the interaction parameters is changed, while the magnitude is kept equal, four different cases must be considered.

Case a. In this case all binary interaction parameters are positive. For a constant value of X_A, all calculated liquidus temperatures in the phase field of AX_{q_A} will be lower than calculated at the same composition in the binaries $AX_{q_A}-BX_{q_B}$ and $AX_{q_A}-CX_{q_C}$, eqn. (4). Thus, the isotherms in the phase field will be convex.

Case b. When all binary interaction parameters are negative, the same kind of reasoning leads to the AX_{q_A} phase field isotherms being concave.

Case c. $\lambda(AX_{q_A}-BX_{q_B})$, $\lambda(AX_{q_A}-CX_{q_C})>0$; $\lambda(BX_{q_B}-CX_{q_C})<0$. The isotherms in the phase field will be concave in the AX_{q_A} corner. Their symmetry around the line connecting the AX_{q_A} corner and the composition of $X_B=0.50$ in the binary system $BX_{q_B}-CX_{q_C}$, is dependent on the charges of the cations and the magnitude of the interaction parameters.

Case c. 1. $\lambda(AX_{q_A}-BX_{q_B})$, $\lambda(BX_{q_B}-CX_{q_C})>0$; $\lambda(AX_{q_A}-CX_{q_C})<0$. This case may be obtained from *case c* by a rotation of the diagram. However, if the discussion is restricted to one phase field only, this situation must be considered. For a constant value of X_A, eqn. (7) now gives lower temperatures in the ternary than in the $AX_{q_A}-BX_{q_B}$ binary system, and higher temperatures than in the $AX_{q_A}-CX_{q_C}$ binary. Hence, the isotherms in the phase field of AX_{q_A} are asymmetric around the line connecting the AX_{q_A} corner and the composition of $X_B=0.50$ in the $BX_{q_B}-CX_{q_C}$ binary. At the binary ends of an isotherm, X_A in the $AX_{q_A}-CX_{q_C}$ binary will be higher than the corresponding value in the $AX_{q_A}-BX_{q_B}$ binary.

Case d. $\lambda(AX_{q_A}-BX_{q_B})$, $\lambda(AX_{q_A}-CX_{q_C})<0$: $\lambda(BX_{q_B}-CX_{q_C})>0$. Eqn. (7) now gives lower temperatures in the ternary than in the $AX_{q_A}-BX_{q_B}$ and $AX_{q_A}-CX_{q_C}$ binaries at a constant X_A. The isotherms are convex in the AX_{q_A} corner.

From eqn. (7) it may be seen that when two of the calculated binary interaction parameters have the same sign, the shape of the isotherms in a phase field may be related to the sign of the interaction parameter in the binary, which in the ternary diagram is opposite the phase field in question. This also may be observed in Table 4. If $\lambda(BX_{q_B}-CX_{q_C})$ is negative, the contribution from this term to the liquidus temperature in the AX_{q_A} phase field, eqn. (7), is positive, and *vice versa.* Provided the magnitudes of the binary interaction parameters are not too different, the isotherms in a phase field will be concave when the interaction parameter in the opposite binary is negative and convex when the parameter is positive.

By changing the sign of the interaction parameters cases which are equivalent to *c* and *d* will be obtained.

In the phase diagram calculations by Fellner *et al.*[8] the excess Gibbs energy of mixing is given by a two-parameter equation, which corresponds to the equation given by Saboungi and Blander[6] up to third order. The difference between a one- and two-parameter representation of the excess Gibbs energy of mixing is found to have little effect on the topology of the phase diagram for the system $LiF-NaF-CaF_2$. Both representations reproduce the reported diagram satisfactorily. In the measured

Table 2. Experimental and calculated values for eutectic compositions and interaction parameters.

Binary system	Eutectic temp. (°C)	Eutectic composition		Interaction parameters [a]		Ref.[b]
Comp. 1 – Comp. 2		Rep. ($X_{comp.\ 1}$)	Calc. ($X_{comp.\ 1}$)	Rep. (J/mol)	Calc. (J/mol)	
LiF – NaF	652	0.61	0.603	−5440, −5858	−5322	19, 20
CaF_2 – NaF	818	0.325	0.302	−19665	−6581	19, 38
LiF – CaF_2	773	0.79	0.819	−5440	−874	19, 20, 38
NaF – SrF_2	856	0.734	0.734	−12134	−4481	21, 39
LiF – SrF_2	761	0.802	0.815	−10460	−3485	21, 39
KF – SrF_2	744	0.78	0.789	−23430	−5975	21, 39
NaF – KF	710	0.40	0.370	1046, −377	1586	19, 21
NaF – Na_2CO_3	690	0.39	0.399	−837	−1209	19
NaBr – Na_2CO_3	613	0.62	0.596		1153	19
NaF – NaBr	656	0.28	0.275	−2092	2042	20
NaCl – Na_2CO_3	638	0.55	0.540	−837	1028	19
NaF – NaCl	676	0.34	0.341	0	111	19
NaCl – Na_2SO_4	628	0.52	0.511	0	1133	20
NaCl – $NaNO_3$	296	0.065	0.052	0	153	19
$NaNO_3$ – Na_2SO_4	300	0.95	0.967	0	2644	20
$NaNO_3$ – $Ca(NO_3)_2$	232	0.73	0.745		−3804	22
$NaNO_3$ – $TlNO_3$	162	0.23	0.234		2723	20
$TlNO_3$ – $Ca(NO_3)_2$	137	0.78	0.814		−5429	23
$LiNO_3$ – $Cd(NO_3)_2$	135	0.54	0.540		−1858	19
$NaNO_3$ – $Cd(NO_3)_2$	190	0.53	0.578		−7004	19
$LiNO_3$ – $NaNO_3$	194 [c]		0.495	−2259	−703	20
NaCl – $LaCl_3$	525		0.692		−14724	19
$CaCl_2$ – $LaCl_3$	630		0.672		−2481	19
NaCl – $CaCl_2$	494	0.48	0.536	−9414	−9656	19
NaCl – $SnCl_2$	184	0.28	0.237		−14342	19, 24
NaCl – $CeCl_3$	488	0.675	0.680		−16761	19, 24
$SnCl_2$ – $CeCl_3$	240	0.975	0.966		−4823	19, 24
NaCl – $NdCl_3$	430	0.588	0.660		−21024	25
$CaCl_2$ – $NdCl_3$	585	0.57	0.590		−2984	25
$FeCl_2$ – $LaCl_3$	620	0.723	0.734		−1192	24
$SnCl_2$ – $LaCl_3$	237	0.977	0.956		−6307	24
$FeCl_2$ – $SnCl_2$	228	0.06	0.086		−6201	24
CsCl – $CaCl_2$	612	0.89			−25096	26
	705	0.11				
KCl – $CuCl_2$	310	0.54			−44576	15
	355	0.45				
LiCl – KCl	354	0.58	0.59		−17142	19
LiCl – $CuCl_2$	454	0.64			−2665	27
NaCl – CsCl	493	0.34			−2821	20

[a] Taken from Refs. 16, 28 and 39. The lowest values for the binaries LiF – NaF and NaF – KF are from Ref. 29. [b] References for the binary systems. [c] Several values for the eutectic composition are given in Ref. 20.

Table 3. Experimental and calculated eutectic temperatures and compositions.

Ternary system	Eutectic composition		Eutectic temp.		Ref.
	Rep. (mol fraction)	Calc. (mol fraction)	Rep. (°C)	Calc. (°C)	
LiF NaF CaF_2	0.517; 0.53 0.372; 0.36 0.111; 0.11	0.525 0.370 0.105	615; 607	623.1	31, 30
LiF NaF SrF_2	0.554 0.359 0.087	0.550 0.355 0.095	624	625.3	21
KF NaF SrF_2	0.47 0.36 0.17	0.550 0.295 0.155	664	656.7	21
NaF NaBr Na_2CO_3	0.124 0.532 0.344	0.200 0.460 0.340	566	564.2	32
NaF NaCl Na_2CO_3		0.233 0.409 0.358		578.4	19
NaCl $NaNO_3$ Na_2SO_4		0.058 0.912 0.030	278	288.7	19
$NaNO_3$ $TlNO_3$ $Ca(NO_3)_2$		0.150 0.680 0.170		116.2	33
$NaNO_3$ $LiNO_3$ $Cd(NO_3)_2$	0.560 0.145 0.295	0.500 0.130 0.370		121.3	
$FeCl_2$ $SnCl_2$ $LaCl_3$	0.06 0.92 0.02	0.075 0.900 0.025	223	223.5	24
NaCl $SnCl_2$ $CeCl_3$	0.22 0.76 0.02	0.235 0.755 0.010	184	181.3	24
NaCl $CaCl_2$ $LaCl_3$		0.520 0.325 0.155		449.5	
NaCl $CaCl_2$ $NdCl_3$	0.45 0.50 0.05	0.563 0.177 0.260	428	392	25
NaCl CsCl $CaCl_2$	0.345; 0.462 0.642; 0.017 0.013; 0.521	0.270; 0.515 0.685; 0.015 0.045; 0.470	482; 480	470; 494	26
KCl LiCl $CuCl_2$	0.532; 0.481 [a] 0.200; 0.139 0.268; 0.380	0.600; 0.410 0.105; 0.180 0.295; 0.410	257; 285	236.3; 316.5	27

[a] In the cited work, the composition in the second column corresponds to a peritectic. The calculated phase diagram shows two eutectics.

Table 4. Comparison between calculated and experimentally determined shape of isotherms in the ternary systems.

Ternary system components			Calculated binary interaction parameters (J/mol)			Shape of isotherms [a] Calculated			Reported		
AX_{q_A}	BX_{q_B}	CX_{q_C}	λ_{BC}	λ_{AC}	λ_{AB}	AX_{q_A}	BX_{q_B}	CX_{q_C}	AX_{q_A}	BX_{q_B}	CX_{q_C}
LiF	NaF	CaF_2	−6581	−874	−5322	−	−	−	−	−	0
NaF	SrF_2	LiF	−3485	−5322	−4481	−	−	−	+	+	+
NaF	SrF_2	KF	−5975	1586	−4481	−	+	−	−	−	−
Na_2CO_3	NaBr	NaF	2042	−1209	1153	+	−	+	+	−	−
NaCl	Na_2CO_3	NaF	−1209	111	1028	−	−	0	−	+	−
$NaNO_3$	NaCl	Na_2SO_4	1133	2644	153		+	0		−	−
$TlNO_3$	NaNO	$Ca(NO_3)_2$	−3804	−5429	2723	−	−	+			
$NaNO_3$	$LiNO_3$	$Cd(NO_3)_2$	−1858	−7004	−703	−	−	0	−	−	+
$FeCl_2$	$SnCl_2$	$LaCl_3$	−6307	−1192	−6201	−		−	−		−
NaCl	$SnCl_2$	$CeCl_3$	−4823	−16761	−14342	−		−	−		−
$CaCl_2$	NaCl	$LaCl_3$	−14724	−2481	−9656	−	−	−	+	−	−
$CaCl_2$	NaCl	$NdCl_3$	−21024	−2984	−9656	−	−	−		−	−
NaCl	CsCl	$CaCl_2$	−25096	−9656	−2821	−	−	−	−	−	−
KCl	$CuCl_2$	LiCl	−2665	−17142	−44576	+	+	−	+	+	−

[a] −, Isotherm bends away from the corner (concave); 0, Linear isotherms; +, Isotherm bends towards the corner (convex).

diagram the isotherms in the CaF_2 phase field are straight lines. The calculation of Fellner *et al.*[8] shows a tendency of the isotherms to be convex in the CaF_2 corner, while the present calculation gives isotherms which are weakly concave. Both the experimental and the calculated values of the interaction parameters are negative. Hence, it would be expected that the isotherms are concave in all phase fields in this system.

In addition to the system discussed above, two other fluoride systems were calculated. In the system $LiF-NaF-SrF_2$ all calculated binary interaction parameters are negative, and the isotherms are concave. The experimental interaction parameters also are negative in this system. In the experimental diagram all isotherms are slightly convex. This tendency is weak, however, in the LiF and SrF_2 phase fields.

For the system $KF-NaF-SrF_2$ the calculated interaction parameters are negative for the binaries $KF-SrF_2$ and $NaF-SrF_2$, and positive for the $NaF-KF$ binary, as are the experimental values. The calculated shape of the isotherms gives a reasonable reproduction of those experimentally determined in the NaF and KF phase fields, whereas the calculation shows some deviation from the experimental isotherms in the SrF_2 phase field.

In the calculated phase diagram of the system $NaCl-NaNO_3-Na_2SO_4$, the shapes of the isotherms are slightly different from those of the reported diagram, and the phase field of $NaNO_3$ is calculated to be smaller than reported. No isotherms are reported or calculated for this phase field. In spite of the positive values of the calculated binary interaction parameters, the isotherms in the Na_2SO_4 phase field are straight lines. This is due to the relatively large values of $\lambda_{NO_3-SO_4}$ and λ_{Cl-SO_4}.

The phase diagrams of two nitrate systems were calculated. The system $NaNO_3-TlNO_3-Ca(NO_3)_2$ to our knowledge is not experimentally determined. The calculated ternary eutectic composition for the system $LiNO_3-NaNO_3-Cd(NO_3)_2$ deviates from the reported value.[33] Calculated isotherms and phase field boundaries exhibit the same shape as those reported, but are more regular.

The phase diagrams of two additive ternary systems containing Na_2CO_3 were calculated. In the system $NaF-NaBr-Na_2CO_3$ the calculated isotherms of the Na_2CO_3 and NaBr phase fields have the same shape as in the experimental diagram. The isotherms are concave in the NaBr field, and convex in the Na_2CO_3 phase field. In the NaF field, the calculated isotherms are weakly

convex, whereas the experimental isotherms are concave.

In the system $NaCl-NaF-Na_2CO_3$, the shape of the experimental isotherms in the NaCl phase field is reproduced by the calculated ones. The isotherms in the NaF field are calculated to be straight lines. The experimental isotherms are slightly concave in the same phase field. The calculated shapes of the isotherms in the Na_2CO_3 phase field are the opposite of the experimental.

The phase diagrams of four chloride systems were calculated. For the ternary systems $NaCl-SnCl_2-CeCl_3$ and $FeCl_2-SnCl_2-LaCl_3$ the calculated phase diagrams agree satisfactorily with reported diagrams. Isotherms are neither calculated nor reported for the small phase field of $SnCl_2$ in these systems. For the systems $NaCl-CaCl_2-LaCl_3$ and $NaCl-CaCl_2-NdCl_3$ the isotherms are calculated to have the same shape as in the reported systems, but there are discrepancies between calculated and reported eutectic compositions.

The discussion given here on the shapes of the isotherms is based on eqn. (7) and calculated values of the binary interaction parameters. This might suggest that the shape of the isotherms in a phase field can be predicted from the sign of the experimental interaction parameters, provided the difference in magnitude is small. As seen from the calculations, the curved shape of the isotherms may be difficult to predict in cases where the interaction parameters are small or when the difference in magnitude is substantial.

V.2. Ternary additive systems with one congruently melting compound

Two additive ternary systems, where a congruently melting compound exists in one of the constituting binaries, were calculated. Complete dissociation of this compound was assumed. Fellner *et al.*[9] with good results have calculated parts of the phase diagrams containing cryolite, by splitting the ternary systems into a necessary number of partial ternary systems. The authors also assumed a certain number of species present in the melt.

The interaction parameter for the $CsCl-CaCl_2$ binary was calculated from eqn. (11), using the heat of fusion for $CsCaCl_3$ obtained by Markov *et al.*,[18] while the melting point of $CsCaCl_3$, and the eutectic compositions and temperatures were taken from Plyushchev *et al.*[26] Dergunov and Bergman[20] determined the melting point of $CsCaCl_3$ to be 120 °C higher than reported by Plyushchev *et al.* Two values of the binary interaction parameter were found. In the $CaCl_2$-rich range of the binary $\lambda_{Cs-Ca} = -21\,171$ J/mol, and in the CsCl-rich range $\lambda_{Cs-Ca} = -29\,016$ J/mol. The mean value, $\lambda_{Cs-Ca} = -25\,094$ J/mol, was used in the calculation of the ternary phase diagram.

Different values were obtained for λ_{Cs-Na} when the calculation was based on the NaCl- or CsCl rich side of the $NaCl-CsCl$ binary. This may be due to a large uncertainty, ~25 %, in the reported enthalpy of fusion for CsCl.[12] The value of λ_{Cs-Na} calculated from thermodynamic data for NaCl was used in the calculation of the ternary system.

The topology of the ternary phase diagram is largely reproduced in the calculation. The shifts in the calculated ternary eutectics probably may be related to the crude treatment of λ_{Cs-Ca}, but uncertainties in the heat of fusion and in the melting point of $CsCaCl_3$ also partly may be responsible. The area of the primary phase field of $CsCaCl_3$ in the reported diagram is in accordance with a high value for the enthalpy of fusion for the compound.

The phase diagram of the system $LiCl-KCl-CuCl_2$ was measured by Sutakshuto *et al.*[27] who also determined the binary $LiCl-CuCl_2$. In the binary $KCl-CuCl_2$ the compound $KCuCl_3$ is formed. The heats of fusion of $KCuCl_3$ and $CuCl_2$ were not found in the literature, and it was decided to calculate the necessary data from the binary phase diagrams. From the $LiCl-CuCl_2$ phase diagram the enthalpy of fusion of $CuCl_2$ was calculated to be 44.5 kJ/mol.

The binary interaction parameter for the $KCl-CuCl_2$ system was obtained from the quasi-binary eutectic compositions and temperatures given by Vorobei and Skiba.[15] In the $CuCl_2$-rich range of the binary $\lambda_{K-Cu} = -55\,124$ J/mol, and in the KCl-rich range $\lambda_{K-Cu} = -34\,024$ J/mol.

Eqn. (11) then was used to derive the heat of fusion of $KCuCl_3$. Each of the calculated values of λ_{K-Cu} gave one value for the heat of fusion. λ_{K-Cu} on the $CuCl_2$-rich side of the binary gave $\Delta H_f(KCuCl_3) = 22.9$ kJ/mol, and λ_{K-Cu} on the KCl-rich side gave $\Delta H_f(KCuCl_3) = 26.9$ kJ/mol. The mean value of the calculated interaction parameters and the mean value of the heat of fusion were used in the calculation of the ternary phase diagram.

In the calculated ternary system, the phase field boundaries between KCl and $KCuCl_3$, and $CuCl_2$

and $KCuCl_3$ show some inconsistencies, as the boundaries do not pass through the binary eutectic compositions. These deviations are small, however. The calculated ternary phase diagram shows two eutectic points, whereas the experimental diagram has one eutectic and one peritectic point. However, a lower value for the heat of fusion of $KCuCl_3$ very easily may change the calculated eutectic point at 316 °C into a peritectic point. The calculated ternary eutectic point is shifted towards the $KCl-CuCl_2$ binary, and a temperature lower than experimentally determined, is calculated.

There is reasonable agreement between the calculated and the experimental phase diagram. The marked concavity of the isotherms in the LiCl phase field may be attributed to the large and negative value of the interaction parameter in the $KCl-CuCl_2$ binary.

VI. CONCLUSION

From the present calculation of phase diagrams of ternary systems with binary congruently melting compounds, it appears that such systems may be predicted with a reasonable accuracy even if the predictions are based on relatively crude information on the binaries. A more general way to include compounds in the calculations will probably be to minimize the total Gibbs energy of the system, as proposed in a recent publication by Saboungi and Blander.[37] The number of systems which can be calculated then will be larger, as incongruently melting compounds also may be taken into consideration.

The present calculations indicate that a fairly simple representation of the ternary excess Gibbs energy of mixing is sufficient to calculate, with relatively small errors, additive ternary systems with ions of different charge. The equations also may may be used in the prediction of phase diagrams with congruently melting binary compounds.

Acknowledgement. We wish to thank the American Ceramic Society, Inc. for permission to reproduce figures from "Phase Diagrams for Ceramists".

REFERENCES

1. Reiss, H., Katz, J. L. and Kleppa, O. J. *J. Chem. Phys. 36* (1962) 144.
2. Blander, M. and Yosim, S. J. *J. Chem. Phys. 39* (1963) 2610.
3. Blander, M. and Topol, L. E. *Inorg. Chem. 5* (1966) 1641.
4. Saboungi, M. L. and Blander, M. *J. Am. Ceram. Soc. 58* (1974) 1.
5. Saboungi, M. L., Schnyders, H., Foster, M. S. and Blander, M. *J. Phys. Chem. 78* (1974) 1091.
6. Saboungi, M. L. and Blander, M. *J. Chem. Phys. 63* (1975) 212.
7. Saboungi, M. L. and Cerisier, P. *J. Electrochem. Soc. 121* (1974) 1258.
8. Fellner, P., Chrenková-Paučirová, M. and Matiašovský, K. *Z. Phys. Chem. Neue Folge 102* (1976) 175.
9. Fellner, P., Chrenková-Paučirová, M. and Matiašovský, K. *Chem. Zvesti 30* (1976) 805.
10. Stringfellow, G. B. *J. Phys. Chem. Solids 33* (1972) 665.
11. Korner, V. V., Korenchuk, N. M. and Dutchak, Ya. I. *Russ. J. Phys. Chem. 51* (1977) 9.
12. Stull, D. R. and Prophet, H., Eds., *JANAF Thermochemical Tables, Natl. Stand. Ref. Data Ser., Natl. Bur. Stand. 37* (1971).
13. Barin, I. and Knacke, O. *Thermochemical Properties of Inorganic Substances*, Springer, Berlin 1973.
14. Blander, M. *Molten Salt Chemistry*, Interscience, New York 1964.
15. Vorobei, M. P. and Skiba, O. V. *Russ. J. Inorg. Chem. 15* (1970) 725.
16. Janz, G. J. *Molten Salts Handbook*, Academic, New York 1967.
17. Dworkin, A. S. and Bredig, M. A. *J. Phys. Chem. 67* (1963) 697.
18. Markov, B. F., Tishura, T. A. and Budarina, A. N. *Ukr. Khim. Zh. 40* (1974) 242; *Chem. Abstr. 81* (1974) 17538b.
19. Levin, E. M., Robbins, C. R. and McMurdie, H. F. *Phase Diagrams for Ceramists*, American Ceramic Society, Columbus, Ohio 1964 and 1969.
20. Voskresenskaya, N. K. *Handbook of Solid-Liquid Equilibria in Systems of Anhydrous Inorganic Salts*, Izdatel' stvo Akademii Nauk SSSR, Moskva – Leningrad 1961, Vols. I and II.
21. Berezhnaya, V. T. and Bukhalova, G. A. *Russ. J. Inorg. Chem. 5* (1960) 445.
22. Protsenko, P. I. and Bergman, A. G. *J. Gen. Chem. USSR 20* (1950) 1367.
23. Protsenko, P. I. and Belova, Z. I. *Russ. J. Inorg. Chem. 2* (1957) 220.
24. Ch'ih-fa, L. and Morozov, I. S. *Russ. J. Inorg. Chem. 7* (1962) 1442.
25. Morozov, I. S., Shevtsova, Z. N. and Klyukina, L. V. *Russ. J. Inorg. Chem. 2* (1957) 301.
26. Plyushchev, V. E., Shakno, I. V. and Pozhitkova, S. A., Eds., *Soviet Research in Fused Salts 1949–*

1955, Consultants Bureau, Inc., New York 1959, Vol. 1b.
27. Sutakshuto-Trivijitkasem, S., Holm, B. J. and Øye, H. A. *Acta Chem. Scand. A 32* (1978) 969.
28. Lumsden, J. *Thermodynamics of Molten Salt Mixtures*, Academic, London 1966.
29. Holm, J. L. and Kleppa, O. J. *J. Chem. Phys. 49* (1968) 2425.
30. Bukhalova, G. A., Sulaĭmankulov, K. and Bostandzhiyan, K. A. *Zh. Neorg. Khim. 4* (1959) 1138.
31. Barton, C. J., Bratcher, L. M. and Grimes, W. R. In Thoma, R. E., Ed., *Phase Diagrams of Nuclear Reactor Materials, ORNL – 2548* (1959) 29.
32. Nyankovskaya, R. N., Guseva, A. D., Yaroslavtseva, Y. A., Kalinka, I. F. and Mazilova, N. V. *Russ. J. Inorg. Chem. 8* (1963) 98.
33. Protsenko, P. I. *Zh. Obshch. Khim. 22* (1952) 1307.
34. Flood, H. and Seltveit, A. *Acta Chem. Scand. 12* (1958) 1036.
35. Kleppa, O. J. and McCarthy, F. G. *J. Phys. Chem. 70* (1966) 1249.
36. Holm, J. L. and Kleppa, O. J. *J. Inorg. Chem. 8* (1969) 207.
37. Saboungi, M. L. and Blander, M. *Theoretical Concepts useful in the Calculation or Storage of Phase Diagrams of Ionic Systems*, presented at "Workshop on Application of Phase Diagrams in Metallurgy and Ceramics", National Bureau of Standards, Gaithersburg, Maryland, January 1977.
38. Kleppa, O. J. and Hong, K. C. *J. Phys. Chem. 78* (1974) 1478.
39. Hong, K. C. and Kleppa, O. J. *J. Phys. Chem. In press.*

Received June 19, 1978.

Acta Chemica Scandinavica A 32 (1978) 989 – 1003

New Hydroxo-bridged Polynuclear Ethylenediamine Chromium(III) Complexes

PETER ANDERSEN and TORSTEN BERG*

Chemistry Department I, Inorganic Chemistry, H. C. Ørsted Institute, University of Copenhagen, DK-2100 Copenhagen Ø, Denmark

Dedicated to Jannik Bjerrum on the occasion of his 70th birthday

New polynuclear μ-hydroxo ethylenediamine chromium(III) complexes have been isolated and identified. Together with mononuclear complexes they were found in aqueous ethylenediamine (=en) buffer solutions with $C_{Cr(III)}=0.1$ M, $C_{en.2HCl}=0.3$ M, and pH $\simeq 8$, in which equilibrium between the mononuclear species was established by the catalytic effect of chromium(II)+charcoal at room temperature. The same polynuclear complexes were also found in similar solutions kept at 40 – 50 °C for 3 – 5 days.

Crystalline salts of $en_2Cr(OH)_2Cr\,en(OH)_2Cr\,en_2^{5+}$ and of three tetranuclear complexes with the formula $Cr_4en_6(OH)_6^{6+}$, *viz.* one of unknown structure (b1), the racemic complex $\Delta\{\Delta\Lambda\Lambda\}/\Lambda\{\Lambda\Delta\Delta\}$-$Cr\{(OH)_2Cr\,en_2\}_3^{6+}$ (b2) (*i.e.* the analogue of Werner's brown salt) and the centrosymmetric $\Delta\Lambda\Delta\Lambda$-$lel_6$-$en_2Cr(OH)_2Cr\,en(OH)_2Cr\,en(OH)_2Cr\,en_2^{6+}$ (b3), were isolated. The salts were isolated by ion-exchange chromatography followed by precipitation as iodides and purification by fractional crystallization from water – ethanol mixtures.

The identification was based primarily on the following observations: Hydrolysis of these and other hydroxo-bridged Cr(III)-en complexes with 70 % perchloric acid gave the corresponding mononuclear aquaamines quantitatively as shown by, *e.g.*, ESR spectroscopy. X-Ray diffraction patterns of powders and single crystals of salts of b2 confirmed the proposed structure by their similarity to the patterns for corresponding cobalt salts of known structure, and a single crystal X-ray structure analysis of the bromide dihydrate (tetrahydrate) of b3 provided the structural details for this compound. The latter crystallizes in the monoclinic space group $P2_1/n$ with $a=15.45_0$ Å, $b=16.42_0$ Å, $c=7.95_2$ Å, $\beta=99.3_6°$, and $Z=2$. Final refinement of 3319 diffractometer reflections (Mo$K\alpha$ radiation) led to $R=0.044$ and $R_w=0.048$.

Remarkably few polynuclear chromium(III) complexes have been isolated considering the enormous amount of work that has been devoted to mononuclear species, and considering the fact that the dominant species present in aqueous solutions of chromium(III) under appropriate conditions are polynuclear.

In the case of hydroxo-bridged ethylenediamine (=en) chromium(III) complexes only a few have been isolated. The dinuclear $en_2Cr(OH)_2Cr\,en_2^{4+}$ [1] (often called the diol) and its open form, (H_2O)-$en_2Cr(OH)Cr\,en_2(OH)^{4+}$, are known in the $\Delta\Lambda$ (*meso*) [2] as well as in the $\Delta\Delta/\Lambda\Lambda$ (racemic) [3] form. The rhodoso, $Cr_4en_6(OH)_6^{6+}$,[1] has been shown by X-ray analysis to consist of an eight-membered ring

$$en_2Cr\begin{matrix}\diagup\\\diagdown\end{matrix}\begin{matrix}OH-Cr\,en-OH\\(OH)_2\\OH-Cr\,en-OH\end{matrix}\begin{matrix}\diagdown\\\diagup\end{matrix}Cren_2^{6+}$$

with the two bis(ethylenediamine)chromium(III) moieties having Δ and Λ configuration, respectively.[4] Analogues of the diol and the rhodoso with ammonia are also known.[5-7]

In an investigation of equilibria in aqueous solution between chromium(III) and ethylenediamine[8] we observed several bands containing polynuclear species during ion-exchange chromatography of the equilibrium mixtures. However, it is difficult to

* T. Berg's contribution is specified under "Acknowledgements".

crystallize salts of these usually highly charged molecules when they constitute only a minor fraction of the products in solution, and such difficulties may be partly responsible for the small number of polynuclear chromium(III) complexes which are known. In order to throw more light on the condensation of chromium(III) we decided to investigate some of the ion-exchange bands containing polynuclear complexes in the hope of finding sufficiently few species in these bands to make crystallization feasible.

EXPERIMENTAL

Chromium(III)-en solutions. The basis for the work is the chromium(II)+charcoal catalyzed solutions described elsewhere.[8] For preparative purposes we used solutions with higher C_{Cr} ($\simeq 0.1$ M) and pH $\simeq 8$, and instead of catalysis at room temperature we simply kept the solutions at 40–50 °C for 3–5 days uncatalyzed. This resulted in solutions with almost the same composition of complexes as similar catalyzed ones. The procedure below for the separation and precipitation made use of solutions prepared in the following way:

26 g $[Cren_3]Cl_3.3H_2O$, 20 g en.2HCl, and 1.5 g en (anhydrous) were dissolved in water to 500 ml. This solution with $C_{Cr}=0.13$ M was kept at 40–50 °C for 3–5 days, and then cooled to room temperature and its components were separated in the course of the next few days.

Ion-exchange separation. This and the following sections should be read in conjunction with Table 1, which gives a survey of the contents of the different bands.

50 ml of the chromium solution were diluted ×10 with ice-cold water and passed down a column of Sephadex SP-C25 (2 cm × 7 cm Ø). A part of the mononuclear complexes was removed in this way. The chromium-containing resin was then transferred to the top of another column of Sephadex SP-C25 (15–20 cm × 2.5 cm Ø) and eluted with 0.7 M NaCl. In this way we isolated two bands: (a) A rather well-defined violet band directly following the mononuclear bands, the slowest of which contained the yellow $Cren_3^{3+}$. As this violet a-band left the column it was diluted ×10 with water (0 °C) and concentrated on another column of Sephadex SP-C25 (2 cm × 2.5 cm Ø). (b) The a-band was followed by a red-brown b-band, which was less well separated from the subsequent violet bands. When this b-band reached the bottom of the column the dark violet top of the column was replaced by a 1 cm layer of pure Sephadex SP-C25 and the b-band eluted further with more concentrated eluent (see below).

Precipitation of crude iodides. The columns containing the isolated bands, a and b, were washed with water and then eluted slowly with 2 M NaI. The most concentrated portions of the eluates (15–20 ml) were allowed to stand at room temperature for 1–2 h (some more solid NaI was added when necessary) after which the precipitates formed were washed with a little 2 M NaI and then washed free of NaI with ethanol. Yields: 70 mg iodide from the a-band and 130 mg iodide from the b-band, corresponding to 3 % and 5 %, respectively.

Precipitation of pure salts from the crude iodides. (α) 100 mg of the crude iodide from the a-band were mixed with 1.0 ml 70 % ethanol + 0.40 g $LiNO_3$ and the mixture was allowed to stand overnight at room temperature. The precipitate was washed free of $LiNO_3$ with ethanol. Yield: 65 mg crude nitrate containing iodide. The 65 mg crude nitrate were dissolved in 5.0 ml 70 % ethanol after which 1.0 g $LiNO_3$ was added. After a day at room temperature thin violet crystal plates of *a nitrate* were isolated and washed with ethanol. Yield: 50 mg (74 %). The product contained traces of iodide, which were removed by a further recrystallization by the same procedure, with a loss of 15 %.

Table 1. Summary of the content of the different bands from ion-exchange separation of a typical chromium(III)–en solution, Cr(II)+charcoal catalyzed or heat-treated, with $C_{Cr}=0.1$ M, $C_{en.2HCl}=0.3$ M and pH $\simeq 8$.

Band	Cr [a] (mol %)	Isolated complexes
First	5–10	Mainly mononuclear species such as $Cr\,en_2(OH)_2^+$ and $Cr\,en_3^{3+}$ [8]
a	11–12	a, $en_2Cr(OH)_2Cr\,en(OH)_2Cr\,en_2^{5+}$
b	16–17	b1, $Cr_4en_6(OH)_6^{6+}$ (from fraction bI)
		b2, $Cr\{(OH)_2Cr\,en_2\}_3^{6+}$ (from fractions bI and bII)
		b3, $en_2Cr(OH)_2Cr\,en(OH)_2Cr\,en(OH)_2Cr\,en_2^{6+}$ (from fraction bIII)
Last	63–65	

[a] Cr content in the bands relative to total Cr content.

(β) 200 mg of the crude iodide from the b-band were extracted with 2 ml portions of water at room temperature and reprecipitated with solid NaI to give the following three crystal powder fractions:

bI, 40 mg blue-violet iodide from the first two extracts.

bII, 80 mg violet iodide from the next 2–3 extracts.

bIII, 30 mg blue-violet iodide from the last 1–2 extracts (which were blue in contrast to the previous which were violet).

100 mg of the bI-fraction were extracted with 1 ml portions of 50 % ethanol and each of the first two extracts was treated with *ca.* 100 mg solid $LiNO_3$. Within 0.5 h these two fractions gave violet precipitates which were reprecipitated by dissolving in *ca.* 0.5 ml 50 % ethanol and adding a few crystals of solid $LiNO_3$. The red-violet crystal needles were washed with ethanol to give 5–10 mg *b1 nitrate*. The subsequent 2–3 extracts gave, after addition of $LiNO_3$ to near saturation, *ca.* 20 mg of red-brown thin crystal plates of *b2 nitrate*.

100 mg of the bII-fraction were extracted with 1 ml portions of water and the extracted material was precipitated by addition of an equal volume of ethanol and $LiNO_3$ almost to saturation, giving 40–50 mg *b2 nitrate* after washing with ethanol. The salt was reprecipitated in the same manner.

50 mg of the bIII-fraction were dissolved in 5 ml water at room temperature and solid LiBr was added gradually until precipitation began, the temperature being kept at room temperature. After a couple of hours, when pronounced precipitation had taken place, 5 ml of ethanol were added and the mixture was left overnight. The isolated product was washed with ethanol to give 30 mg of dark violet-blue crystals of *b3 bromide*. The salt was reprecipitated without significant loss by dissolving the 30 mg in 0.5 ml water and adding a little solid LiBr until beginning precipitation. The remaining material in the filtrate from this precipitation could be almost completely precipitated by addition of 0.5 ml ethanol.

(γ) It was possible to prepare salts of a and b1-3 with other anions by metathesis in water/ethanol mixtures with salts such as $LiNO_3$, $Li_2S_2O_6$, $LiClO_4$, LiBr, and NaI. This generally resulted in crystalline powders. In addition to the above-mentioned nitrates of a, b1, and b2, large crystals of b2 dithionate were obtained by dissolving 5–10 mg of the nitrate in 0.5 ml of a saturated aqueous solution of $Li_2S_2O_6$ and subsequently adding 2–3 drops of methanol. The crystals formed at room temperature were washed with water (0 °C) and could be recrystallized from a little water at 30–

Table 2. Chemical analyses of some of the salts of a and b1–b3. The numbers in parentheses are values calculated on the basis of the formulae given.

	Compound	% Cr	% Halogen	% N (total)	% N (from en)	% C	% H
a	$[Cr_3en_5(OH)_4](NO_3)_5.2H_2O$	17.64 (17.93)		24.07 (24.14)	16.27 (16.09)	14.16 (13.79)	5.50 (5.51)
	$[Cr_3en_5(OH)_4]I_5.6H_2O$	12.39 (12.32)	50.28 (50.10)	11.00 (11.05)			
b1	$[Cr_4en_6(OH)_6](NO_3)_6.6H_2O$	18.18 (18.09)		21.78 (21.93)		13.04 (12.52)	5.61 (5.74)
b2	$[Cr_4en_6(OH)_6](NO_3)_6.6H_2O$	18.05 (18.09)		21.90 (21.93)	14.62 (14.62)	12.24 (12.52)	5.62 (5.74)
	$[Cr_4en_6(OH)_6]I_6.6H_2O$	13.60 (13.51)	49.48 (49.45)	10.93 (10.92)			
b3	$[Cr_4en_6(OH)_6](NO_3)_6.3H_2O$	19.11 (18.98)		23.21 (23.01)	15.26 (15.34)		
	$[Cr_4en_6(OH)_6]Br_6.4H_2O$ [a]	17.08 (17.03)	39.29 (39.25)	13.80 (13.76)			

[a] The single crystal X-ray analysis (see later) revealed only two water molecules of crystallization per complex ion (the difference Fourier synthesis did not indicate any major peaks that could be interpreted as corresponding to other oxygen atoms).

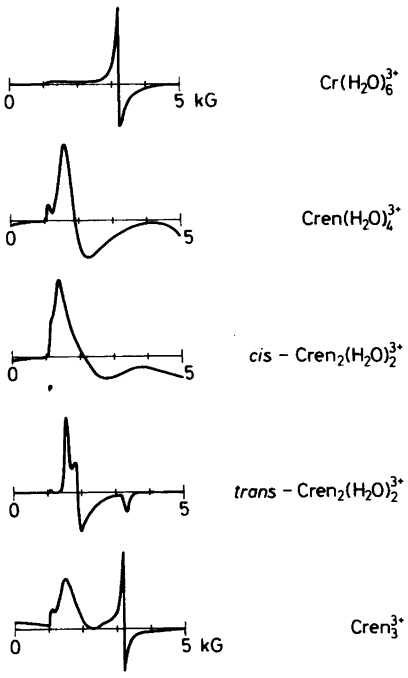

Fig. 1. First derivative ESR spectra at 9.2 GHz of frozen glasses (−130 °C) of 50 % (v/v) glycerol/$HClO_4$ solutions of the 3+-charged aquaamines; $C_{Cr}=0.01-0.1$ M.

Table 3. The amount of Cr en$(H_2O)_4^{3+}$ relative to the sum of those of Cr en$(H_2O)_4^{3+}$ and *cis*-Cr en_2-$(H_2O)_2^{3+}$ in hydrolyzed polynuclear complexes, as derived from *b*/*a* and Fig. 3.

Hydrolyzed compound	*b*/*a*	mol % Cr en$(H_2O)_4^{3+}$
Rhodoso perchlorate	3.0_3	48
b1 Nitrate	3.2_0	52
b3 Nitrate	3.2_6	53
a Nitrate	2.5_5	35
Diol perchlorate	1.8_0	0
b2 Nitrate	1.8_5	0

35 °C. Large violet-blue crystal plates of b3 nitrate were prepared almost quantitatively by dissolving the bromide or the iodide in water at room temperature followed by precipitation with a little $LiNO_3$ and reprecipitation in the same way.

Chemical analysis. The prepared compounds were analysed on a microscale (2 – 5 mg): chromium by atomic absorption spectrophotometry, nitrogen by Kjeldahl, halides by potentiometry, and CHN by usual microtechniques. The results are given in Table 2.

Hydrolysis with 70 % perchloric acid. 5 – 10 mg of the crystalline nitrates or perchlorates of six different polynuclear chromium(III) ethylenediamine complexes were treated for 2 – 5 min at

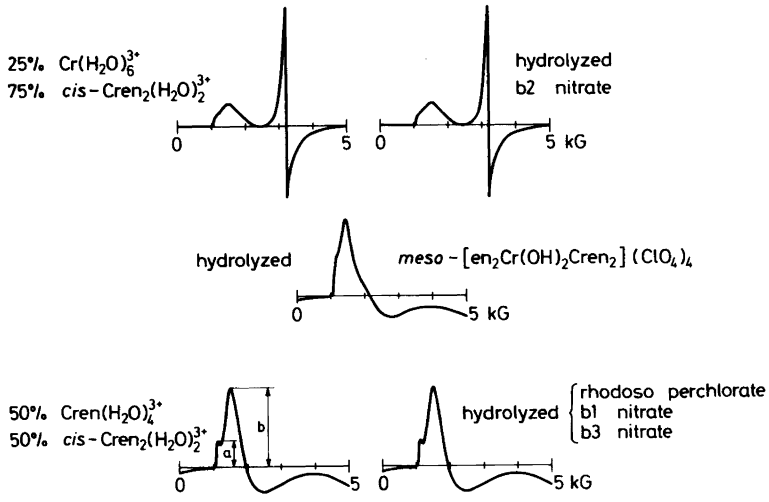

Fig. 2. First derivative ESR spectra (frozen glasses) of mixtures of aquaamines (% = mol %) compared with those of polynuclear salts hydrolyzed at 70 °C for *ca.* 5 min with 70 % perchloric acid. The ratio between the peak heights *b* and *a* was used to determine the relative amount of Cr en$(H_2O)_4^{3+}$ in mixtures of Cr en$(H_2O)_4^{3+}$ and *cis*-Cr $en_2(H_2O)_2^{3+}$ as shown in Fig. 3 and Table 3.

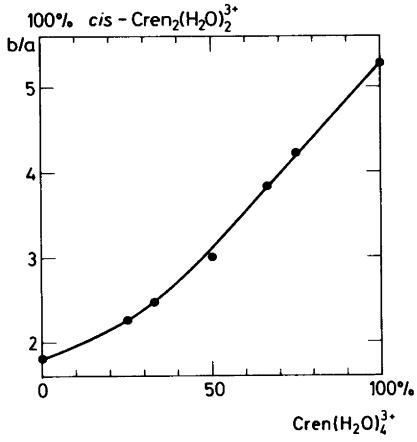

Fig. 3. b/a (see Fig. 2) as a function of 100[Cr en-$(H_2O)_4^{3+}$]/C_{Cr} (C_{Cr} = [Cr en$(H_2O)_4^{3+}$] + [*cis*-Cr en_2-$(H_2O)_2^{3+}$]). Known amounts of Cs[Cr $enCl_4$] and *cis*-[Cr en_2Cl_2](ClO_4) were dissolved in 0.5 ml *ca.* 0.5 M $Hg(ClO_4)_2$, 0.1 M $HClO_4$ to give aquaamine solutions with $C_{Cr} \simeq 0.1$ M. 0.5 ml glycerol was added before freezing to −130 °C.

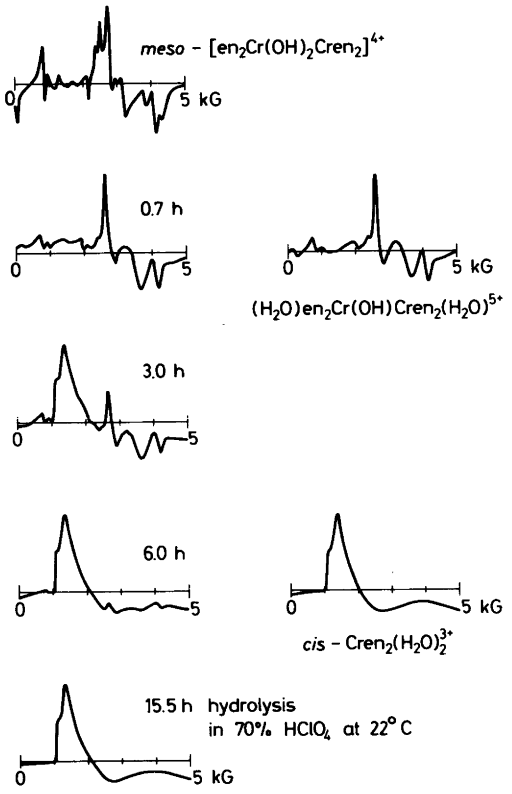

Fig. 4. First derivative ESR spectra (frozen glasses) at different stages of the hydrolysis at room temperature of *meso*-[$en_2Cr(OH)_2Cr\ en_2$]$(ClO_4)_4$ (left) to be compared with those of [(HO)$en_2Cr(OH)Cr\ en_2$-(OH)]$(ClO_4)_3.2H_2O$ and *cis*-[Cr $en_2(H_2O)_2$]Br_3.-$2H_2O$ in 4 M $HClO_4$.

70 °C with 0.5 ml 70 % $HClO_4$ and then cooled in ice. The content of mononuclear complexes after this treatment was determined in two different ways:

(a) The hydrolyzed mixtures were diluted × 1 − 2 with glycerol and cooled to −130 °C within 0.5 − 1 min to give frozen glasses the ESR spectra of which were measured from 0 to 5 kG at 9.2 GHz. The resulting spectra were compared with similar spectra of glycerol/water glasses containing known amounts of $Cr(H_2O)_6^{3+}$, Cr $en(H_2O)_4^{3+}$, *cis*-Cr en_2-$(H_2O)_2^{3+}$, and *trans*-Cr $en_2(H_2O)_2^{3+}$. The concentration ratios of the species in the former glasses could then be calculated provided that other species were only present in minor amounts. We previously used this procedure successfully to determine the ratio of *cis*- to *trans*-Cr $en_2(H_2O)_2^{3+}$ [8] and of *cis*- to *trans*-$Cr(NH_3)_4(H_2O)_2^{3+}$.[9] The results are shown in Figs. 1 − 4 and Table 3.

(b) The hydrolyzed mixtures were diluted × 200 with water (0 °C) and separated on an ion-exchange column of Sephadex SP-C 25 (10 cm × 1 cm Ø) with either 0.5 M $NaClO_4$ or 0.1 M Na_2SO_4. The $NaClO_4$ elution separated 3+-charged complexes from more highly charged species such as CrenenH-$(H_2O)_3^{4+}$ and polynuclear complexes. The Na_2SO_4 elution separated Cren$(H_2O)_4^{3+}$ and *cis*-$Cren_2$-$(H_2O)_2^{3+}$ (the former being eluted faster) provided that the separation was performed with ice-cooled eluent within 0.5 − 1 h. $Cr(H_2O)_6^{3+}$ was separated from *cis*-$Cren_2(H_2O)_2^{3+}$ on a 1 − 2 cm × 1 cm Ø ion-exchange column of Dowex 50 W X8, $Cr(H_2O)_6^{3+}$ being eluted with 1.5 M H_2SO_4 and subsequently *cis*-Cr $en_2(H_2O)_2^{3+}$ with 5 M H_2SO_4. The content of chromium complexes in each chromatographic fraction was determined from visible spectra and chromium analyses. The results are given in Table 4.

Preparation of rhodoso perchlorate and cleavage with 12 M hydrochloric acid. Rhodoso sulfate, $[Cr_4en_6(OH)_6](SO_4)_3.aq$, was prepared by a modification[10] of the method of Pfeiffer *et al.*[1]:

150 g $KCr(SO_4)_2.12H_2O$, 150 ml ethylenediamine, and 250 ml 1-pentanol were heated to 110 °C under stirring for 6 − 15 h and the mixture then left to cool. After filtration and washing with methanol an orange, crude product consisting mainly of [Cr_4en_6-

Table 4. Ion-exchange separations of polynuclear compounds hydrolyzed with 70 % $HClO_4$ at 70 °C for 2 – 5 min.

Hydrolyzed compound	Eluent	% Chromium relative to total chromium content 1st Band	2nd Band
Rhodoso perchlorate on Sephadex SP-C25	0.5 M $NaClO_4$	101 [a]	
	0.1 M Na_2SO_4	54 [c]	47 [d]
b2 Nitrate on Dowex 50 W X8	1.5 M H_2SO_4 then 5 M H_2SO_4	23 [e]	75
b3 Nitrate on Sephadex SP-C25	0.5 M $NaClO_4$	96 [a]	
	0.1 M Na_2SO_4	50 [c]	47 [d]
a Nitrate on Sephadex SP-C25	0.5 M $NaClO_4$	98 [b]	
	0.1 M Na_2SO_4	34 [c]	62 [d]

Same optical spectrum as: [a] a 1:1 mixture of Cr en$(H_2O)_4^{3+}$ and *cis*-Cr $en_2(H_2O)_2^{3+}$; [b] 1:2 mixture of Cr en$(H_2O)_4^{3+}$ and *cis*-Cr $en_2(H_2O)_2^{3+}$; [c] Cr en$(H_2O)_4^{3+}$ treated similarly with Na_2SO_4; [d] *cis*-Cr $en_2(H_2O)_2^{3+}$ treated similarly with Na_2SO_4; [e] $Cr(H_2O)_6^{3+}$ treated similarly with H_2SO_4.

$(OH)_6](SO_4)_3$.aq and $[Cr\,en_3]_2(SO_4)_3$ was obtained. This product was stirred for a few minutes in 1 l of water to remove $[Cr\,en_3]_2(SO_4)_3$. Filtration yielded 25 g of crude $[Cr_4en_6(OH)_6](SO_4)_3$.aq (32 %).

After addition of 100 ml 12 M HCl to the above filtrate, 55 g of $[Cr\,en_3]Cl_3$.aq containing a little sulfate could be isolated.

4.5 g of finely powdered crude rhodoso sulfate were dissolved in 30 ml ice-cooled 1 M HCl and the solution filtered. 20 g of $NaClO_4$ were added to the filtrate under stirring and after 30 min the precipitate was filtered off, washed with a little ice-cooled 1 M $HClO_4$, then with a 1:1 mixture of 1 M $HClO_4$ and ethanol, and finally with ethanol and ether. Yield: 4.5 g of $[Cr_4en_6(OH)_6](ClO_4)_6.3H_2O$ (80 % from the crude sulfate). The product can be reprecipitated almost quantitatively with $NaClO_4$ from an ice-cooled aqueous solution.

For the cleavage 4.50 g of $[Cr_4en_6(OH)_6](ClO_4)_3.3H_2O$ were treated with 5 ml of 12 M HCl for a few min at room temperature, after which the solution, now containing mononuclear complexes, was cooled to 0 °C and saturated with gaseous HCl at this temperature. 5 ml of ice-cooled 70 % $HClO_4$ were added and the solution was resaturated with gaseous HCl at 0 °C. After 3 days at 5 °C the precipitate was filtered off, washed with a few drops of ice-cooled 12 M HCl which were afterwards added to the filtrate, then with ice-cooled 4 M $HClO_4$ and ethanol. Yield: 2.25 g of *cis*-$[Cr\,en_2Cl_2]ClO_4$ (48 %).

9.5 g of NH_4Cl were added to the filtrate, and after keeping it overnight at 5 °C the NH_4ClO_4 was filtered off and 7.7 g of CsCl were added. The filtrate was then resaturated with gaseous HCl at 0 °C and after 6 days at 5 °C the precipitate was filtered off, washed with a 3:1 mixture of methanol and ethanol, and then with ethanol and ether. Yield: 2.1 g of $Cs[Cr\,enCl_4]$ (40 %). For purification 6 g of this product were dissolved in 70 ml 12 M HCl; after filtration 10 g of CsCl were added to the filtrate, which was then saturated with gaseous HCl at 0 °C. After a few days at 5 °C 5 g of $Cs[Cr\,enCl_4]$ could be isolated as described above.

Chemicals and apparatus. All chemicals used were reagent grade or were analysed by us. $Cs[Cr\,enCl_4]$ (see above), *cis*-$[Cr\,en_2Cl_2](ClO_4)$ (see above), *cis*-$[Cr\,en_2(H_2O)_2]Br_3.2H_2O$,[11] *trans*-$[Cr\,en_2Cl_2]Cl.H_2O$,[12] *trans*-$[Cr\,en_2(OH)(H_2O)]Br_2.H_2O$,[12] $[Cr\,en_3]Cl_3.3H_2O$,[13] *meso*-$[en_2Cr(OH)_2Cr\,en_2](ClO_4)_4$,[11] $[(OH)en_2Cr(OH)Cr\,en_2(OH)](ClO_4)_3.2H_2O$,[2] $[Cr_4en_6(OH)_6](ClO_4)_6.3H_2O$/rhodoso (see above), and $[Co\{(OH)_2Co\,en_2\}_3](NO_3)_6$.aq[14] were prepared according to, or analogously to, the literature methods and were analysed for Cr(Co), N, and halogen. All analyses agreed within 1 – 2 % (relative) with the formulae given.

Visible spectra were measured on a Cary 118 spectrophotometer and ESR spectra on a Jeol JES-ME-1X instrument. A Perkin-Elmer 403 apparatus was used for atomic absorption spectrophotometry. The X-ray equipment is referred to in the next section.

X-Ray diffraction. X-Ray powder photographs of most of the crystalline compounds were taken using a Guinier camera with Cu$K\alpha$ radiation and with silicon as internal standard. Single crystal Weissenberg photographs with Cu$K\alpha$ radiation were taken for preliminary purposes, space group determinations *etc.* Some results for salts of b2 and the analogous cobalt(III) compounds are given in Table 5.

Structure determination of b3 bromide by single crystal X-ray diffraction. (a) Crystal data. Some of the crystal data are given in Table 6. The unit cell dimensions were determined on a Picker FACS-1 diffractometer using Mo$K\alpha$ radiation from 24 high-angle reflections by least-squares refinement and were in agreement with those determined from powder photographs. The density of the crystals was determined by flotation in mixtures of 1-bromonaphthalene and 1,2-dibromoethane.

(b) Data collection. The diffraction data were collected at 22 °C with a Picker FACS-1 diffrac-

Table 5. X-Ray diffraction data for salts of $Cr\{(OH)_2Cr\,en_2\}_3^{6+}$ compared with those for the corresponding Werner's brown salts.

(a) Guinier powder photographs (Cu$K\alpha$)

$[Cr\{(OH)_2Cren_2\}_3](NO_3)_6.6H_2O$				$[Co\{(OH)_2Coen_2\}_3](NO_3)_6.aq$		
hkl	Int.	d_{obs} (Å)	d_{calc} (Å)	Int.	d_{obs} (Å)	d_{calc} (Å)
020	w	12.71	12.72	w	12.60	12.57
120	mw	10.60	10.62	w	10.47	10.45
200	w	9.67	9.67	vw	9.40	9.40
$\bar{1}01$	mw	8.49	8.50	w	8.46	8.45
$\bar{1}11$	mw	8.07	8.06	vw	8.00	8.01
111 } 220 }	mw(br.)	7.69	7.67 7.70	w(br.)	7.58	7.56 7.53
021	w	7.42	7.42	vw	7.37	7.36
$\bar{1}21$	vvw	7.07	7.06	vvw	7.01	7.01
040	vvw	6.33	6.36	vw	6.28	6.28
221 } 320 }	vw	5.741	5.733 5.751	vvw	5.606	5.618 5.606
$\bar{1}41$	mw	5.093	5.090			
012	m(br.)	4.499	4.499	mw	4.469	4.470
420			4.521	vvw	4.398	4.401

Indexing based on:

$a = 19.3_9$ Å $\quad \alpha = \gamma = 90.00°$
$b = 25.4_2$ Å $\quad \beta = 94._0°$
$c = 9.1_6$ Å

$a = 18.8_5$ Å $\quad a = \gamma = 90.00°$
$b = 25.1_4$ Å $\quad \beta = 94._7°$
$c = 9.1_1$ Å

(b) $[Co\{(OH)_2Co\,en_2\}_3](S_2O_6)_3.8H_2O$ (Thewalt[27]):
Sp.gr.: $P2_1/n$
$a = 9.46_4$ Å, $\quad b = 22.35_5$ Å, $\quad c = 22.72_5$ Å, $\quad \beta = 94.3_3°$

Data from Weissenberg photographs (Cu$K\alpha$)
$[Cr\{(OH)_2Cr\,en_2\}_3](S_2O_6)_3.aq$: Space group: $P2_1/n$
$a = 9._5$ Å, $\quad b = 22._4$ Å, $\quad c = 23._0$ Å, $\quad \beta = 94._6°$

tometer from a single crystal, $0.19 \times 0.10 \times 0.27$ mm^3 in the *a*-, *b*-, and *c*-direction, respectively, using graphite monochromated Mo$K\alpha$ radiation. A $\theta - 2\theta$ scan mode was used with a rate in 2θ of 1° min^{-1}. The scan range was from $2\theta_0 - (1.5° + 0.346° \tan\theta)$ to $2\theta_0 + (1.7° + 0.346° \tan\theta)$. Background counts were made for 20 s at each end of the scan range. The intensities of five standard reflections were measured after each 40 reflections and these measurements showed that no deterioration or misalignment of the crystal occurred during the data collections.

Intensity data were collected for two symmetry-related sets of reflections, $5.5° < 2\theta \leq 54°$:

Set 1: octants *hkl* and *hkl̄*.
Set 2: octants *hk̄l* and *hk̄l̄*.

The graphite crystal in the monochromator had to be renewed between the measurements of set 1 and set 2.

The two sets were corrected for Lorentz and polarization effects, and a Gaussian numerical integration procedure[15] was used for absorption correction (grid: $8 \times 6 \times 6$ sampling points; the transmission factors varied between 0.39 and 0.56). The two sets were then averaged after the application of a scale factor to one of the sets. The R_s value between symmetry related reflections were 0.056 ($R_s = \sum_{hkl}\sum_i \| |F_s|^2 - |F_i|^2 | / \sum_{hkl}\sum_i |F_i|^2$, where F_s designates the averaged structure amplitude and F_i the amplitudes for the individual measurements. This resulted in 4469 independent reflections which were reduced to 3319 observed reflections using the

Table 6. Crystal data for $[en_2Cr(OH)_2Cr\,en(OH)_2Cr\,en(OH)_2Cr\,en_2]Br_6.2H_2O$.

Molecular weight for $Cr_4C_{12}H_{58}N_{12}O_8Br_6$: 1186.1

Monoclinic: $a = 15.470(4)$ Å, $b = 16.420(4)$ Å, $c = 7.952(3)$ Å, $\beta = 99.364(18)°$; $V = 1993.0$ Å^3.

Density: $d_{obs} = 2.00_3$ g/cm^3, $d_{calc} = 1.976$ g/cm^3 for $Z = 2$.

$\mu(MoK\alpha) = 70.6$ cm^{-1}, $F(000) = 1168$.

Systematically absent reflections: $h0l$: $h + l \neq 2n$; $0k0$: $k \neq 2n$

Space group: $P2_1/n$

General equivalent positions: x,y,z $\frac{1}{2}+x,\frac{1}{2}-y,\frac{1}{2}+z$; $\bar{x},\bar{y},\bar{z}$ $\frac{1}{2}-x,\frac{1}{2}+y,\frac{1}{2}-z$

Developed faces: {110}, {011}, and {010}

criterion $I > 2\sigma(I)$, where $\sigma(I)$ is the standard deviation calculated by counting statistics.

The following programs were used for computation: The Vanderbilt System[16] for diffractometer operations, an absorption correction program and a data reduction program both of local origin, ORTEP II for the illustrations,[17] the X-Ray System[18] for the crystal structure analysis, and Simplex[19] for the weighting analysis.

The atomic scattering factors used were those reported by Cromer and Mann[20] for the uncharged atoms; for hydrogen the factor calculated by Stewart *et al.*[21] was used. The anomalous dispersion corrections for chromium and bromine were taken from Cromer and Liberman.[22]

(c) Structure determination and refinement. The three-dimensional Patterson function calculated from 2300 independent reflections from the first data set showed the octahedral ligand arrangement around the chromium atoms, and a Fourier synthesis based on a centrosymmetric tetranuclear chromium skeleton including oxygen and nitrogen ligands revealed the positions of the bromine atoms. Another approach to the solution was a Harker section analysis of the Patterson function, which revealed the positions of the bromine and chromium atoms, and Fourier syntheses based on these gave the positions of the nitrogen and oxygen ligand atoms, which, when included, showed the positions of the carbon atoms and one oxygen from water of crystallization (O4).

The final analysis was based on the 3319 independent reflections considered observed from the two data sets. Hamilton R-ratio tests were used as an aid to select the simplest model compatible with the data. Full-matrix least-squares refinement minimiz-

Table 7. b3 Bromide. Final fractional coordinates with e.s.d. The labelling is explained in Fig. 7. Parameters for hydrogen atoms are given in Table 9.

Atom	x	y	z
Br 1	0.17945(6)	0.11369(5)	0.00796(8)
Br 2	0.79243(4)	0.20916(4)	0.11472(9)
Br 3	0.47245(5)	0.13791(5)	0.35077(12)
Cr 1	0.26100(5)	−0.01301(5)	0.56393(10)
Cr 2	0.07722(5)	0.05486(5)	0.48991(10)
O 1	0.1839(2)	0.0472(3)	0.3908(6)
O 2	0.1579(2)	−0.0004(2)	0.6745(5)
O 3	−0.0277(3)	0.0499(3)	0.5976(6)
O 4	0.4300(4)	0.3432(5)	0.3551(9)
N 1	0.2165(3)	−0.1266(3)	0.4740(6)
N 2	0.3530(3)	−0.0350(3)	0.4048(7)
N 3	0.3380(3)	−0.0663(3)	0.7730(6)
N 4	0.3266(3)	0.0902(3)	0.6710(7)
N 5	0.1029(4)	0.1723(3)	0.5851(7)
N 6	0.0105(3)	0.1190(3)	0.2830(6)
C 1	0.2793(4)	−0.1652(4)	0.3767(8)
C 2	0.3179(5)	−0.0986(4)	0.2798(8)
C 3	0.3758(4)	−0.0034(4)	0.8969(8)
C 4	0.4035(4)	0.0680(4)	0.7992(9)
C 5	0.0403(4)	0.2297(4)	0.4855(8)
C 6	0.0324(5)	0.2067(4)	0.3002(8)

Table 8. b3 Bromide. Final thermal parameters, $u_{ij} \times 100(\text{Å}^2)$, with e.s.d. The expression for the temperature factors is $\exp\{-2\pi^2(u_{11}h^2a^{*2}+u_{22}k^2b^{*2}+u_{33}l^2c^{*2}+2u_{12}hka^*b^*+2u_{13}hla^*c^*+2u_{23}klb^*c^*)\}$. Parameters for hydrogen atoms are given in Table 9.

Atom	u_{11}	u_{22}	u_{33}	u_{12}	u_{13}	u_{23}
Br 1	9.36(6)	6.61(5)	2.92(3)	1.79(4)	1.47(3)	−0.15(3)
Br 2	4.07(3)	2.95(3)	5.29(3)	−0.06(2)	1.47(3)	0.48(3)
Br 3	3.77(3)	5.50(4)	8.88(6)	0.71(3)	2.27(4)	1.75(4)
Cr 1	1.91(4)	2.17(4)	2.68(4)	0.06(3)	0.27(3)	0.35(3)
Cr 2	1.74(4)	2.06(4)	2.23(4)	−0.04(3)	0.13(3)	0.14(3)
O 1	2.55(19)	4.0(2)	2.8(2)	0.32(16)	0.74(17)	1.11(19)
O 2	2.48(18)	2.9(2)	2.7(2)	0.16(15)	0.24(15)	0.26(17)
O 3	2.8(2)	3.1(2)	2.6(2)	−0.20(16)	0.48(17)	−0.89(19)
O 4	7.8(4)	12.6(6)	9.1(5)	0.3(4)	2.5(4)	5.4(5)
N 1	3.1(3)	3.4(3)	3.5(3)	−0.4(2)	0.8(2)	0.2(2)
N 2	3.4(3)	3.8(3)	5.0(3)	0.4(2)	1.4(2)	0.9(2)
N 3	2.5(2)	3.4(3)	3.8(3)	0.17(19)	0.50(19)	0.8(2)
N 4	3.8(3)	3.0(3)	5.3(3)	−0.5(2)	−0.7(2)	0.6(2)
N 5	3.2(3)	2.9(2)	3.3(3)	−0.5(2)	0.0(2)	0.1(2)
N 6	2.5(2)	3.3(3)	3.1(3)	0.5(2)	0.1(2)	0.2(2)
C 1	5.3(4)	3.6(3)	4.2(3)	0.7(3)	1.1(3)	−0.7(3)
C 2	5.5(4)	4.7(4)	4.1(3)	0.6(3)	1.9(3)	−0.2(3)
C 3	3.6(3)	5.2(4)	3.2(3)	−0.4(3)	−0.6(2)	−0.1(3)
C 4	3.3(3)	4.0(3)	5.5(4)	−0.5(3)	−1.1(3)	0.2(3)
C 5	4.0(3)	3.2(3)	4.4(4)	0.9(3)	0.0(3)	−0.4(3)
C 6	4.5(4)	3.5(3)	3.8(3)	0.2(3)	0.3(3)	1.1(3)

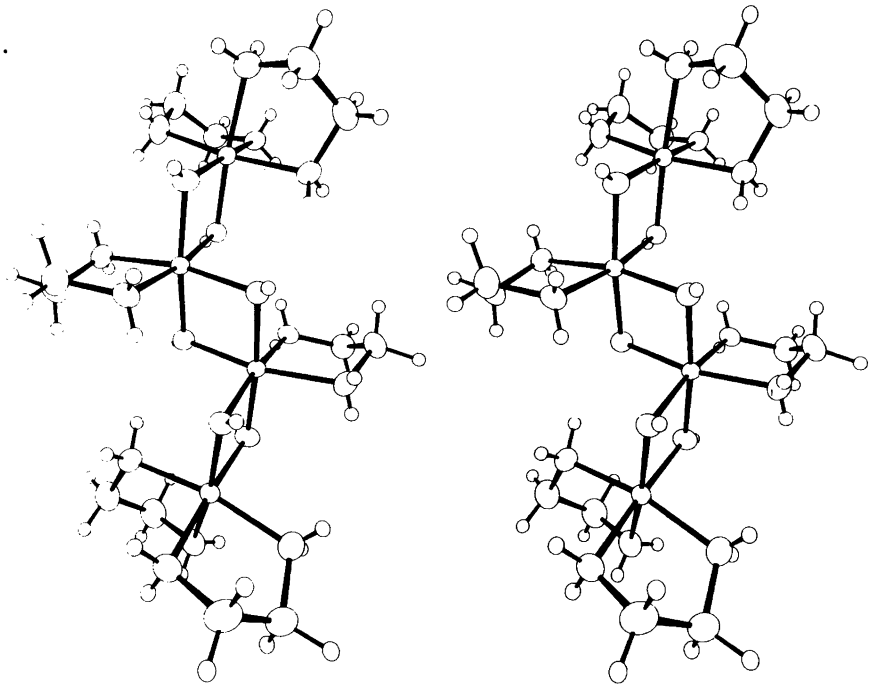

Fig. 5. Stereoscopic drawing of the b3 complex ion. The thermal ellipsoids enclose 50 % probability with the exception of hydrogen atoms, which are shown as spheres with 0.1 Å radius. The four chromium atoms in the molecule are surrounded octahedrally by ethylenediamine and di-μ-hydroxo groups.

Table 9. b3 Bromide. Final hydrogen atom parameters with e.s.d. The labelling is explained in Fig. 7. The temperature factors are $\exp(-8\pi^2 U \sin^2\theta/\lambda)$.

Atom	x	y	z	$U \times 100(\text{Å}^2)$
H 1	0.185(5)	0.061(5)	0.317(9)	4(3)
H 2	0.155(6)	0.015(5)	0.754(11)	7(3)
H 3	−0.027(4)	0.060(4)	0.665(8)	2(2)
H 4	0.160(4)	−0.119(4)	0.417(8)	3.5(17)
H 5	0.205(4)	−0.154(4)	0.546(7)	3.1(15)
H 6	0.324(3)	−0.192(3)	0.458(6)	1.7(12)
H 7	0.254(4)	−0.200(4)	0.297(8)	4.5(18)
H 8	0.363(5)	−0.120(5)	0.239(10)	8(3)
H 9	0.266(4)	−0.073(4)	0.185(8)	5.0(19)
H 10	0.396(3)	−0.052(3)	0.459(6)	2.0(13)
H 11	0.360(4)	0.006(4)	0.349(8)	4.2(17)
H 12	0.375(4)	−0.090(3)	0.740(7)	2.7(15)
H 13	0.307(5)	−0.104(5)	0.810(9)	6(2)
H 14	0.332(5)	0.016(5)	0.959(9)	6(2)
H 15	0.421(5)	−0.022(4)	0.968(9)	5(2)
H 16	0.425(6)	0.117(5)	0.873(11)	8(3)
H 17	0.446(5)	0.055(5)	0.736(10)	8(3)
H 18	0.297(7)	0.125(6)	0.728(14)	12(4)
H 19	0.338(4)	0.109(4)	0.611(7)	2.9(16)
H 20	0.147(4)	0.183(4)	0.571(7)	1.7(15)
H 21	0.097(5)	0.169(4)	0.689(10)	5(2)
H 22	−0.017(6)	0.229(5)	0.517(11)	7(3)
H 23	0.064(5)	0.291(5)	0.508(9)	6(2)
H 24	−0.003(6)	0.233(5)	0.231(11)	8(3)
H 25	0.091(4)	0.223(4)	0.272(8)	3.4(16)
H 26	−0.042(4)	0.108(3)	0.271(7)	2.1(14)
H 27	0.023(5)	0.105(4)	0.186(9)	5(2)

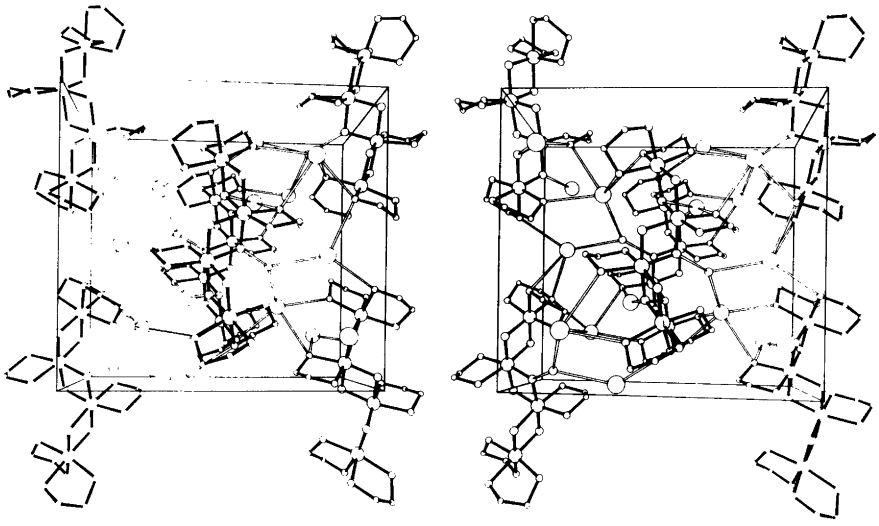

Fig. 6. Stereoscopic drawing of the unit cell content of b3 bromide. The radii of the spheres symbolizing Br, Cr, O, N, and C are 0.30, 0.25, 0.15, 0.125, and 0.10 Å, respectively. The view is along the negative c-axis, having the a-axis going down and the b-axis right.

Table 10. b3 Bromide. Bond lengths and contact distances (Å) with e.s.d.

Cr 1 – O 1	1.939(4)	N 1 – C 1	1.480(9)
Cr 1 – O 2	1.954(4)	N 2 – C 2	1.483(8)
Cr 2 – O 1	1.945(4)	N 3 – C 3	1.480(8)
Cr 2 – O 2	1.984(4)	N 4 – C 4	1.480(8)
Cr 2 – O 3	1.956(5)	N 5 – C 5	1.485(8)
Cr 2 – O 3′	1.964(4)	N 6 – C 6	1.480(8)
Cr 1 – N 1	2.075(5)	C 1 – C 2	1.515(10)
Cr 1 – N 2	2.084(6)	C 3 – C 4	1.506(10)
Cr 1 – N 3	2.074(5)	C 5 – C 6	1.507(9)
Cr 1 – N 4	2.084(5)		
Cr 2 – N 5	2.086(5)	O 1 – H 1	0.63(7)
Cr 2 – N 6	2.081(5)	O 2 – H 2	0.69(9)
		O 3 – H 3	0.56(6)

N – H: 0.7 – 0.9; average 0.81(7)
C – H: 0.9 – 1.1; average 0.96(7)

O3(in(.9723, .0499, .5976)) – O4(in(.9300, .1568, .8551)): 2.853(9)

Contact distances Br---O and Br---N: 3.2 – 3.5

ing $R = \sum w(|F_o| - K|F_c|)^2$ with the positional parameters and anisotropic temperature factors of the 3 Br, 2 Cr, 4 O, 6 N, and 6 C atoms led to an *R*-value of 0.052. A difference Fourier analysis showed the positions of all hydrogen atoms except those in the water molecule, and further refinement with two blocks including positions and isotropic temperature factors of hydrogen atoms and with application of a weighting scheme, $1/w = 3.59 + 2.11\sigma^2(F) + 0.036|F| + 0.00029|F|^2 - 5.75 \sin\theta/\lambda$ (the coefficients were obtained as described by Nielsen[19]), gave a final *R*-value of 0.044 and $R_w = 0.048$ (average shift/error 0.03, max. 0.3). The final results of this structure analysis are given in Tables 6 – 11 and Figs. 5 – 7. A list of observed and calculated structure amplitudes is available from the authors upon request.

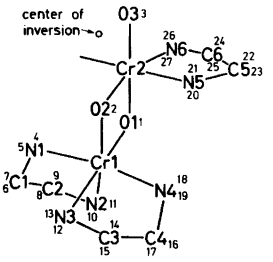

Fig. 7. Labelling of the atoms in the b3 complex molecule. Small numbers symbolize hydrogen atoms. The atoms in the other half of the molecule, symmetrically connected through the centre of inversion, are in Tables 10 and 11 labelled with primes: Cr2′, O3′ *etc.*

RESULTS AND DISCUSSION

The polynuclear complexes involved in this investigation are, in order of increasing charge (see Table 1):

en$_2$*Cr(OH)*$_2$*Cr en*$_2^{4+}$. This di-μ-hydroxo-bis[bis-(ethylenediamine)chromium(III)] ion, often called the diol, exists in racemic (ΔΔ/ΛΛ)[3] and *meso* (ΔΛ)[2] forms, and the latter has been established by X-ray diffraction.[23,24] The *meso*-form was identified as a major part of the first polynuclear chromatographic band from separations of Cr(II) + charcoal catalyzed equilibrium solutions with $C_{Cr} \simeq 0.01$ M.[8] In basic solution the cation of the *meso*-form is eluted at almost the same rate as Cr en$_3^{3+}$, but in acidic solution somewhat slower. It was isolated as the iodide and identified by means of X-ray powder diffraction and ESR. The *meso*-diol perchlorate[11] was used as a model compound to follow the hydrolysis with 70 % perchloric acid using ESR spectroscopy. Fig. 4 shows that the hydrolysis product after 10 – 15 h at room temperature is pure *cis*-Cr en$_2$(H$_2$O)$_2^{3+}$, and that the reaction proceeds *via* a species with an ESR spectrum similar to that of [(OH)en$_2$Cr(OH)Cr en$_2$(OH)](ClO$_4$)$_3$·2H$_2$O in 4 M HClO$_4$, presumably (H$_2$O)en$_2$Cr(OH)Cr en$_2$(H$_2$O)$^{5+}$.[2] We found hydrolysis at room temperature (at the end increased to 70 °C) with 1 M HClO$_4$ to be much slower than with 12 M HClO$_4$, and ESR spectra showed that the products are a mixture of polynuclear species, *cis*-Cr en$_2$(H$_2$O)$_2^{3+}$, and apparently mononuclear species with less than four nitrogen coordinated per chromium atom (*cf.* Mønsted's investigation of the acid hydrolysis of chromium(III) amines[25]).

en$_2$*Cr(OH)*$_2$*Cr en(OH)*$_2$*Cr en*$_2^{5+}$. This μ-{mono-(ethylenediamine)bis(dihydroxo)chromium(III)}-bis-[bis(ethylenediamine)chromium(III)] ion, a, constitutes a major part of the a-band from the chromatographic separation. This new complex has so far only been isolated in satisfactorily crystalline form as the nitrate. The identification was based on chemical analysis (Table 2) and on analysis of the products obtained on hydrolysis in 70 % perchloric acid; the two methods applied both showed the

Table 11. b3 Bromide. Selected bond angles (°) with e.s.d.

O 1 – Cr 1 – O 2	79.2(2)	Cr 1 – O 1 – Cr 2	102.1(2)
O 1 – Cr 2 – O 2	78.3(2)	Cr 1 – O 2 – Cr 2	100.2(2)
O 3 – Cr 2 – O 3′	79.3(2)	Cr 2 – O 3 – Cr 2′	100.7(2)
N 1 – Cr 1 – N 2	81.7(2)	Cr 1 – N 1 – C 1	110.8(4)
N 3 – Cr 1 – N 4	80.7(2)	Cr 1 – N 2 – C 2	108.5(4)
N 5 – Cr 2 – N 6	81.9(2)	Cr 1 – N 3 – C 3	110.6(4)
		Cr 1 – N 4 – C 4	111.4(4)
O 1 – Cr 2 – O 3′	96.2(2)	Cr 2 – N 5 – C 5	108.9(4)
O 2 – Cr 2 – O 3	97.1(2)	Cr 2 – N 6 – C 6	110.0(4)
O 2 – Cr 2 – O 3′	91.4(2)		
		N 1 – C 1 – C 2	107.7(5)
O 1 – Cr 1 – N 1	94.7(2)	N 2 – C 2 – C 1	107.4(5)
O 1 – Cr 1 – N 2	93.4(2)	N 3 – C 3 – C 4	108.3(5)
O 1 – Cr 1 – N 4	94.5(2)	N 4 – C 4 – C 3	106.4(5)
O 2 – Cr 1 – N 1	90.1(2)	N 5 – C 5 – C 6	107.7(5)
O 2 – Cr 1 – N 3	95.1(2)	N 6 – C 6 – C 5	108.4(5)
O 2 – Cr 1 – N 4	96.2(2)		
O 1 – Cr 2 – N 5	94.8(2)	Other tetrahedral angles	
O 1 – Cr 2 – N 6	93.3(2)	involving H: ~102 – 117(5)	
O 2 – Cr 2 – N 5	95.4(2)		
O 3 – Cr 2 – N 5	90.1(2)	H 1 – O 1 – Cr 1	137(7)
O 3 – Cr 2 – N 6	91.6(2)	H 1 – O 1 – Cr 2	120(7)
O 3′ – Cr 2 – N 6	92.8(2)	H 2 – O 2 – Cr 1	129(7)
		H 2 – O 2 – Cr 2	112(7)
N 1 – Cr 1 – N 3	90.7(2)	H 3 – O 3 – Cr 2	121(7)
N 2 – Cr 1 – N 3	93.1(2)	H 3 – O 3 – Cr 2′	122(7)
N 2 – Cr 1 – N 4	93.1(2)		

Dihedral angles:	N 1 – C 1 – C 2 – N 2	53.4(6)
	N 3 – C 3 – C 4 – N 4	51.9(6)
	N 5 – C 5 – C 6 – N 6	52.9(7)

latter products to be *cis*-Cr en$_2$(H$_2$O)$_2^{3+}$ and Cr en(H$_2$O)$_4^{3+}$ in 2:1 ratio (see Tables 3 and 4).

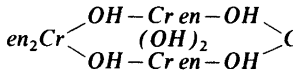

$en_2Cr\begin{matrix}OH-Cren-OH\\(OH)_2\\OH-Cren-OH\end{matrix}Cren_2^{6+}$. This μ-{di-μ-hydroxo-bis[mono(ethylenediamine)*trans*-dihydroxochromium(III)]}-bis[bis(ethylenediamine)-chromium(III)] ion, the rhodoso, was first isolated by Pfeiffer[1] and later shown by X-ray diffraction to have the indicated structure in the *meso*-form.[4] It is eluted at the same rate as the b-band but was not found in this band. In this work rhodoso served as a model compound for the hydrolysis in 70 % perchloric acid and is in this medium hydrolyzed to give *cis*-Cr en$_2$(H$_2$O)$_2^{3+}$ and Cren(H$_2$O)$_4^{3+}$ in 1:1 ratio (see Tables 3 and 4, and Fig. 2). After hydrolysis with 12 M hydrochloric acid 48 % of the chromium was isolated as *cis*-[Cr en$_2$Cl$_2$](ClO$_4$) and 40 % as Cs[Cr enCl$_4$] (see experimental section).

$Cr\{(OH)_2Cren_2\}_3^{6+}$. This tris[di-$\mu$-hydroxo-bis(ethylenediamine)chromium(III)]chromium(III) ion was the first new polynuclear complex to be isolated from the Cr(II)+charcoal catalyzed equilibrium solutions,[8,26] and constitutes a major part, b2, of the b-band from the chromatographic separations. It is the chromium analogue of the cobalt(III) complex often referred to as Werner's brown salt.[14] The structure of the dithionate of the cobalt species has been established by X-ray diffraction,[27] and comparison of Weissenberg films of this compound (kindly placed at our disposal by U. Thewalt) with those of the chromium dithionate unambiguously demonstrated the isomorphism. The chromium dithionate was prepared nearly quantitatively by metathesis from the nitrate, and one may assume the configurations around the four chromium atoms to be $\Delta\{\Delta\Lambda\Lambda\}/\Delta\{\Lambda\Delta\Delta\}$ as in the cobalt dithionate. X-Ray powder photographs of the nitrates of the

cobalt and chromium complexes likewise showed isomorphism. Some of the X-ray data are given in Table 5.

Analysis of the products of hydrolysis of the b2 nitrate with 70 % perchloric acid showed them to consist of *cis*-Cr en$_2$(H$_2$O)$_2^{3+}$ and Cr(H$_2$O)$_6^{3+}$ in 3:1 ratio (Fig. 2 and Tables 3 and 4).

ΔΛΔΛ-*en*$_2$*Cr(OH)*$_2$*Cr en(OH)*$_2$*Cr en(OH)*$_2$*Cr-en*$_2^{6+}$. This μ-{di-μ-hydroxo-bis[mono(ethylenediamine)*cis*-dihydroxochromium(III)]}-bis[bis(ethylenediamine)chromium(III)] ion was found as a minor constituent, b3, in the b-band. This new complex readily forms nice crystals of, *e.g.*, the bromide and the nitrate. Hydrolysis of the nitrate with 70 % perchloric acid gave *cis*-Cr en$_2$(H$_2$O)$_2^{3+}$ and Cr en(H$_2$O)$_4^{3+}$ in 1:1 ratio (Fig. 2 and Tables 3 and 4).

The X-ray structure analysis (see the experimental section) of the bromide showed that the complex ions all lie on centres of inversion, that the configuration of this centrosymmetric *meso* form is ΔΛΔΛ, and that the ring conformations are lel$_6$, *i.e.* all the C–C bonds are parallel to the pseudo threefold axis of the metal atoms. Bond distances and angles in the complex are in excellent agreement with those found for similar structures, *cf.*, *e.g.*, that of *meso*-[en$_2$Cr(OH)$_2$Cr en$_2$](ClO$_4$)$_2$Cl$_2$·2H$_2$O.[23]

Cr$_4$*en*$_6$*(OH)*$_6^{6+}$. This b1 compound was isolated in low yield from the b-band as a crystalline red-violet nitrate. Hydrolysis of this nitrate with 70 % perchloric acid produced *cis*-Cr en$_2$(H$_2$O)$_2^{3+}$ and Cr en(H$_2$O)$_4^{3+}$ in 1:1 ratio. The formula Cr$_4$en$_6$(OH)$_6^{6+}$ embraces all the 6+-charged complexes mentioned above, but the b1 nitrate differs in many respects from the others, *e.g.* in solubility and optical spectrum (which is very closely similar to that of the a nitrate, see Fig. 8), and no isomorphism could be demonstrated by X-ray powder diffraction. We intend to try to grow larger crystals for single crystal X-ray analysis.

The above argument for ascribing the structure en$_2$Cr(OH)$_2$Cr en(OH)$_2$Cr en$_2^{5+}$ to a rested, apart from elemental microanalysis, solely on analysis of the hydrolysis products. However, in the better established cases (diol, rhodoso, b2, and b3) this hydrolysis produced the mononuclear aquaamines with full retention of configuration. It is also noteworthy that only one charge type has been found so far within each band from the ion-exchange separations on Sephadex SP-C25, the rate of elution decreasing with increasing charge. The assignment of a charge of 5+ to a is then consistent with this "rule". Furthermore it is characteristic that apart from the diol all of these polynuclear complexes exhibited very small changes in their visible spectra on going from acidic to basic medium (< 1 – 2 nm for the first spin-allowed absorption band). This is as would be expected for chromium(III) amine complexes lacking H$_2$O or terminal OH$^-$ ligands. The ESR spectra showed the same pH-independency (3 < pH < 9), with the exception

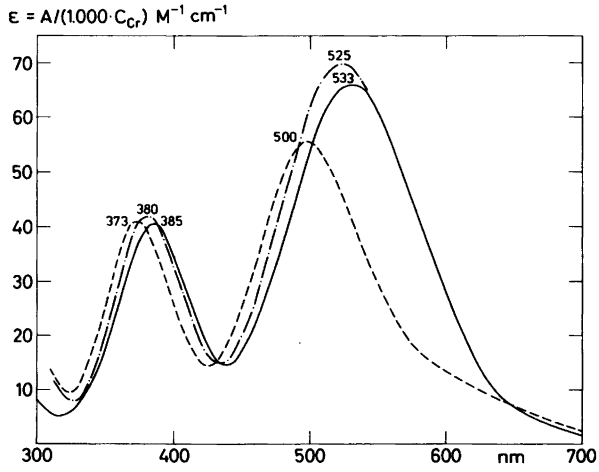

Fig. 8. Optical spectra of: a nitrate (– · –), b2 nitrate (– – –), and b3 bromide (———) in water. The spectra showed no changes after 5 – 10 min.

of that for the diol, which under these conditions (aqueous solutions at room temperature) undergoes opening of one of the OH – bridges [2] (see later).

This same sort of argumentation leads to the formula for b1, namely $Cr_4en_6(OH)_6^{6+}$, consisting of 2 *cis*-Cr en_2 – and 2 Cr en-moieties connected by OH – bridges.

It seems to be characteristic that most of the above-mentioned complexes remain unchanged for hours in acidic (concentrated mineral acids excepted) and neutral solution. However, as mentioned above, the diol opens one of the OH – bridges,[2,3] but similar phenomena have yet to be examined further for the other complexes containing di-μ-hydroxo groups.

Chromium(III) in these amine buffers seems to prefer condensation *via* di-μ-hydroxo bridge formation. Fig. 9 shows the 4+- to 6+-charged skeletons of such edge-sharing octahedra with the free edges imagined occupied by chelating ethylenediamine. Except for II and III they all have the chromium atoms in the same plane. The number of configurational isomers is of course much higher than the number of skeletons, and if one includes the different combinations of ring conformations the number of isomers is enormous (208 for the brown salt [28]). In Fig. 9 the configurational Δ and Λ designations are quoted where determined by the

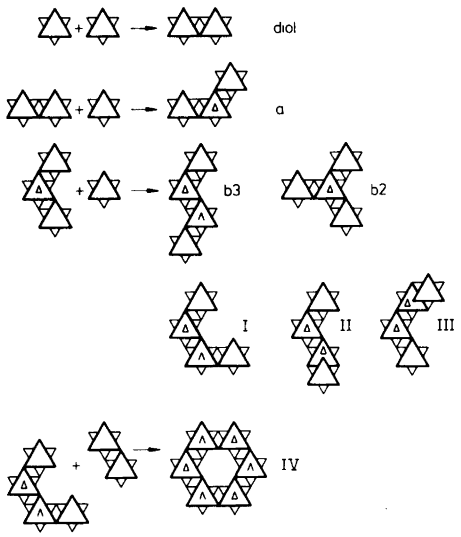

Fig. 9. The 4+- to 6+-charged skeletons of edge-sharing octahedra with the free edges occupied by chelating ethylenediamine.

di-μ-hydroxo groups. The chromium atoms without this designation may have either Δ or Λ configuration. Thus the skeleton b3 gives two *meso*-forms, namely the $\Delta\Lambda\Delta\Lambda$ found in the b3 bromide and a $\Lambda\Lambda\Delta\Delta$-form, both with a centre of inversion. Likewise the skeleton I has two *meso*-forms, $\Delta\Lambda\Delta\Lambda$ and $\Lambda\Lambda\Delta\Delta$, both with a symmetry plane. In addition b3 as well as I have a racemic form, $\Delta\Lambda\Delta\Delta/\Lambda\Delta\Lambda\Lambda$.

After having established equilibrium among the mononuclear species in the chromium(III) ethylenediamine system we observed [8] that, when the catalyst was removed, the solutions had a tendency to form more of the polynuclear species at the expense of the mononuclear ones during the next months. This phenomenon was more pronounced at lower pH, and was observed even more markedly in similar investigations in ammonia buffers.[9] The concentration ratios for the various mononuclear complexes were, however, maintained. Thus, whereas equilibrium involving only mononuclear chromium(III) amines could be demonstrated, this was not so for reactions involving polynuclear complexes. Chromium(III) ethylenediamine buffers kept at 40 – 50 °C for 3 – 5 days did not differ much in composition from the chromium(II) + charcoal catalyzed ones (room temperature), and likewise we observed the same final distribution of species when starting with another chromium(III) compound than Cr en_3^{3+} (rhodoso was tried). A common feature was that the amount of polynuclear species increased with increasing chromium concentration and decreasing pH in the investigated pH interval. This is in accordance with what would be expected from pure equilibrium considerations for the formation of polynuclear amine complexes containing oxygen solely in the form of OH-bridges, *e.g.*

$$2Cr\,en_2(OH)_2^+ + 2H^+ \rightleftharpoons en_2Cr(OH)_2Cr\,en_2^{4+} + 2H_2O$$

In still more acidic media mononuclear species should again be favoured:

$$en_2Cr(OH)_2Cr\,en_2^{4+} + 2H^+ + 2H_2O \rightleftharpoons 2Cr\,en_2(H_2O)_2^{3+}$$

The present difficulties in isolating the polynuclear complexes quantitatively make it impossible to tell exactly how much of the involved species are present in the ethylenediamine system. There is no doubt that other isomers are there, some of which are suggested in connection with Fig. 9. On the

other hand, most of the chromium species with charges up to +6 have been accounted for, and there is little doubt that the fractions which are eluted more slowly on Sephadex SP-C 25 than the b-band contain polynuclear complexes of higher charge and with more than four chromium atoms per molecule. Some of them will probably prove to belong to the many isomers obtained by adding an extra di-μ-hydroxo bridged chromium to the tetranuclear complexes shown in Fig. 9.

Acknowledgements. T. Berg's contribution to the present work was in the preparation and hydrolysis of rhodoso and in the isolation and identification of the chromium analogue of Werner's brown salt. The authors are grateful to J. Bjerrum and C. E. Schäffer for valuable discussions, to S. Larsen and A. Hammershøi for help with the X-ray work, and to K. M. Nielsen and K. Jørgensen for their contributions to the analytical and synthetic work.

REFERENCES

1. Pfeiffer, P., Vorster, W. and Stern, R. *Z. Anorg. Allg. Chem. 58* (1908) 272.
2. Springborg, J. and Toftlund, H. *Acta Chem. Scand. A 30* (1976) 171.
3. Toftlund, H. and Springborg, J. *Chem. Commun.* (1976) 1017.
4. Flood, M. T., Marsh, R. E. and Gray, H. B. *J. Am. Chem. Soc. 91* (1969) 193.
5. Dubsky, J. V. *J. Prakt. Chem. 90* (1914) 61.
6. Jørgensen, S. M. *J. Prakt. Chem. 45* (1892) 260.
7. Bang, E. *Acta Chem. Scand. 22* (1968) 2671.
8. Andersen, P., Berg, T. and Jacobsen, J. *Acta Chem. Scand. A 29* (1975) 381.
9. Andersen, P., Berg, T. and Jacobsen, J. *Acta Chem. Scand. A 29* (1975) 599.
10. Schäffer, C. E. *Private communication.*
11. Springborg, J. and Schäffer, C. E. *Inorg. Synth. 18* (1978) 75.
12. Glerup, J., Josephsen, J., Michelsen, K., Pedersen, E. and Schäffer, C. E. *Acta Chem. Scand. 24* (1970) 247.
13. Pedersen, E. *Acta Chem. Scand. 24* (1970) 3362.
14. Werner, A. *Ber. Dtsch. Chem. Ges. 40* (1907) 2103.
15. Coppens, P., Leiserowitz, L. and Rabinovich, D. *Acta Crystallogr. 18* (1965) 1035.
16. Lehnert, P. G. *J. Appl. Crystallogr. 8* (1975) 568.
17. Johnson, C. K. ORTEP: *A Fortran Ellipsoid Plot Program for Crystal Structure Illustrations*, Report ORNL-3794, Second Rev., Oak Ridge National Laboratory, Oak Ridge 1970.
18. Stewart, J. M. *et al. The X-Ray System 1972*, Technical Report Tr-192, Computer Science Center, University of Maryland, College Park 1972.
19. Nielsen, K. *Acta Crystallogr. A 33* (1977) 1009.
20. Cromer, D. T. and Mann, J. B. *Acta Crystallogr. A 24* (1968) 321.
21. Stewart, R. F., Davidson, E. R. and Simpson, W. T. *J. Chem. Phys. 42* (1965) 3175.
22. Cromer, D. T. and Liberman, D. *J. Chem. Phys. 53* (1970) 1891.
23. Kaas, K. *Acta Crystallogr. B 32* (1976) 2021.
24. Cline, S. J., Scaringe, R. P., Hatfield, W. E. and Hodgson, D. J. *J. Chem. Soc. Dalton Trans.* (1977) 1662.
25. Mønsted, L. and Mønsted, O. *Acta Chem. Scand. A 29* (1975) 29.
26. Andersen, P. and Berg, T. *Chem. Commun.* (1974) 600.
27. Thewalt, U. *Chem. Ber. 104* (1971) 2657.
28. Thewalt, U. and Ernst, J. *Z. Naturforsch. Teil B 30* (1975) 818.

Received June 14, 1978.

Acta Chemica Scandinavica A 32 (1978) 1005 – 1016

The Molecular Structure of Gaseous 1,3,4-Oxathiazol-2-one

BØRGE BAK,[a] OLE NIELSEN,[a] HENRIK SVANHOLT,[a] ARNE ALMENNINGEN,[b] OTTO BASTIANSEN,[b] LIV FERNHOLT,[b] GRETE GUNDERSEN,[b] CLAUS J. NIELSEN,[b] BJØRG N. CYVIN,[c] and SVEN J. CYVIN[c]

[a] Chemical Laboratory V, The H. C. Ørsted Institute, University of Copenhagen, DK-2100 Copenhagen, Denmark, [b] Department of Chemistry, University of Oslo, Oslo 3, Norway and [c] Division of Physical Chemistry, University of Trondheim, N-7034 Trondheim-NTH, Norway

1,3,4-Oxathiazol-2-one has been studied by microwave, infrared and Raman spectroscopy and by electron diffraction from the vapour. The analysis of the spectroscopic data established a coplanar molecular structure. The rotational constants were $A_0 = 5587.411(11)$, $B_0 = 3645.8735(89)$ and $C_0 = 2205.4635(89)$ MHz and the inertial defect was $\Delta = 0.08236(57)$ μÅ^2. The structural refinements based upon the electron-diffraction data led to three very similar sets of geometrical parameters for three different sets of fixed u-values which were derived from: I, analogy to similar molecules; II, an estimated force field; and III, from a normal coordinate analysis based upon the spectroscopic data. The electron-diffraction work also demonstrated an essentially planar molecule and produced bond distances and angles in agreement with the experimental spectroscopic rotational constants. The final refinement of a planar molecular model was carried out based upon electron-diffraction data in combination with the measured rotational constants (corrected to A_z, B_z and C_z). An r_α°-model was used to account for shrinkage effects, and the u-values and the various correction terms needed were as obtained from the normal coordinate analysis. The bond distances (r_a) and independent valence angles thus obtained are: $r(C-H) = 1.102(19)$ Å, $r(C=O) = 1.192(2)$ Å, $r(N=C) = 1.286(2)$ Å, $r(O-C(H)) = 1.356(3)$ Å, $r(O-C(=O)) = 1.402(3)$ Å, $r(S-N) = 1.690(2)$ Å, $r(S-C) = 1.767(2)$ Å, $\angle OCH = 114.5(31)°$, $\angle OCO = 122.6(3)°$, $\angle COC = 110.8(2)°$, $\angle CSN = 93.8(1)°$. The parenthesized values are the estimated standard deviations including effects of correlation among the electron-diffraction data.

Knowledge of the structure of 1,3,4-oxathiazol-2-one HC=N–S–CO–O, is necessary for a future theoretical treatment of its interesting pyrolysis.[1,2] Dependent upon the extent of electron delocalization the molecule is a planar or a non-planar unsubstituted 5-membered ring compound.

In this paper the results of a combined spectroscopic and electron-diffraction investigation of 1,3,4-oxathiazol-2-one will be presented. By the electron-diffraction method on gaseous molecules a three dimensional structure is determined from a one dimensional intensity curve. The Fourier inverse of the molecular intensity curve is a one dimensional radial distribution curve, the resolution of which is limited due to the widths of individual peaks. The widths of the individual peaks, depending upon the molecular vibrations, are of the order of magnitude from about 0.08 to 0.2 Å. In a molecule like 1,3,4-oxathiazol-2-one there exist altogether 21 different internuclear distances in the distance range from about 1.0 to 4.5 Å. Even if the molecule is assumed to be planar, there exist 11 independent geometrical parameters. If the vibrational parameters are included, 32 structure parameters have in the general case to be determined. Experience shows that rigid molecules of this kind give good quality electron-diffraction intensity data. The idea of the approach chosen was to try to estimate how well the electron-diffraction method could solve the geometry of a many parameter molecule with complex distance overlaps if the vibrational parameters were obtained from other approaches, and to attempt a structure refinement based upon electron-diffraction data in combination with information obtained from rotational and vibrational spectroscopy.

EXPERIMENTAL

(a) Sample. 1,3,4-Oxathiazol-2-one was prepared in analogy to its methyl derivative, $CH_3-C=N-S-CO-O$,[3] by Arne Holm, the H. C. Ørsted Institute, and purified by distillation *in vacuo* (12 Torr) at 47–48 °C. None of the recorded microwave, infrared and Raman spectra indicated the presence of impurities.

(b) Microwave. Microwave spectra were recorded at 50–100 mTorr and at room temperature in the 12.5–18 and 26.5–40 GHz regions using a Hewlett-Packard 8460 A MRR instrument. Stark voltages in the range 400–1600 V/cm were applied.

(c) Infrared and Raman. Infrared spectra were recorded of the vapour, the CCl_4 solution, the pure liquid and of the unannealed and annealed solid at liquid nitrogen temperature on a Perkin-Elmer Model 225 spectrometer. Far infrared spectra of a cyclohexane solution were obtained with a fast scan Bruker Model 114C Fourier transform spectrometer over the range 400–50 cm^{-1}.

Raman spectra were obtained on a modified[4] Cary Model 81 Raman spectrometer using the 5145 Å line from an argon ion laser for excitation. The liquid sample was studied in a sealed glass tube and polarization data were obtained.

(d) Electron diffraction. The electron-diffraction data were recorded in the Oslo Apparatus[5] for nozzle-to-plate distances of 480.32, 200.32 and 128.27 mm, using Kodac Electron Image plates and a nozzle-tip temperature of 56 °C. The electron wavelength was 0.06465 Å as calibrated against diffraction patterns of gaseous benzene using $r_a(C-C)=1.3975$ Å as a standard. The estimated standard deviation in the determination of the electron wavelength is 0.1 %.

The scattering patterns were transferred to intensity data in intervals of 0.25 mm while oscillating the plates on an integrating densitometer constructed by A. Almenningen and P. Molin. In order to avoid problems due to uncertainties of blackness correction for the darker regions, plates with optical densities less than 1.35 were selected for the structure analysis. The data were processed the usual way[6] to yield for each of the three camera distances averaged modified molecular intensity curves based upon four plates for the long and intermediate camera distances and three plates for the shorter one. The modification function used was $s/|f'_s||f'_c|$. The scattering amplitudes and phases[6] were calculated using the partial-wave method[7] based upon the analytical HF potentials for the C-, N-, O-, and S-atoms[8] and the best electron density of bonded hydrogen for the H-atom.[9] The inelastic scattering factors used were those of Tavard *et al.*[10]

ANALYSIS OF MICROWAVE DATA

Approximate rotational constants, A'_0, B'_0, C'_0, were calculated from a preliminary unrefined structure of 1,3,4-oxathiazol-2-one provided by electron-diffraction ($A'_0=5625$; $B'_0=3628$; $C'_0=2205$ MHz. Asymmetry parameter, $\kappa=-0.1678$). Then, a number of low-J transitions were identified within 5–60 MHz of their precalculated positions by their Stark patterns and their relative intensities. A revised set of rotational constants then allowed the precalculation and identification of higher-J transitions. Number and types of measured transitions are summarized in Table 1 (93 transition frequencies available on request). Table 2 summarizes the final analysis in terms of ground-state rotational and distortion constants. As seen, the inertial defect $I_c-I_b-I_a=0.08236(57)$ $\mu Å^2$ is in accordance with inertial defects for other planar, 5-membered ring molecules.[12]

VIBRATIONAL SPECTRA

The planarity of 1,3,4-oxathiazol-2-one in the vapour phase is well established from the micro-

Table 1. Number and type of observed transitions (12.5–18 and 26.5–40 GHz). J_{max} = maximum rotational quantum number. R, Q, μ_a and μ_b in conventional sense.

R type		Q type		ROTFIT r.m.s.[a]
μ_a	μ_b	μ_a	μ_b	
28	2	10	53	0.1672 MHz
8[b]	7[b]	27[b]	30[b]	

[a] By G. O. Sørensen, the H. C. Ørsted Institute. [b] J_{max}.

Table 2. Rotational ground state constants A_0, B_0, C_0 in MHz of 1,3,4-oxathiazol-2-one. Quartic distortion constants in kHz.[a] Asymmetry parameter κ. Intertial defect $\Delta=I_c-I_b-I_a$ in $\mu Å^2$.

$A_0=5587.411$ (11)
$B_0=3645.8735$ (89)
$C_0=2205.4635$ (89)

$T_1=-0.061(20)$; $T_2=0.099(17)$; $T_3=-0.749(95)$
$T_4=1.186(22)$; $T_5=-0.05(10)$
$\kappa=-0.1481772(13)$; $\Delta=0.08236(57)$

[a] As defined in Ref. 11.

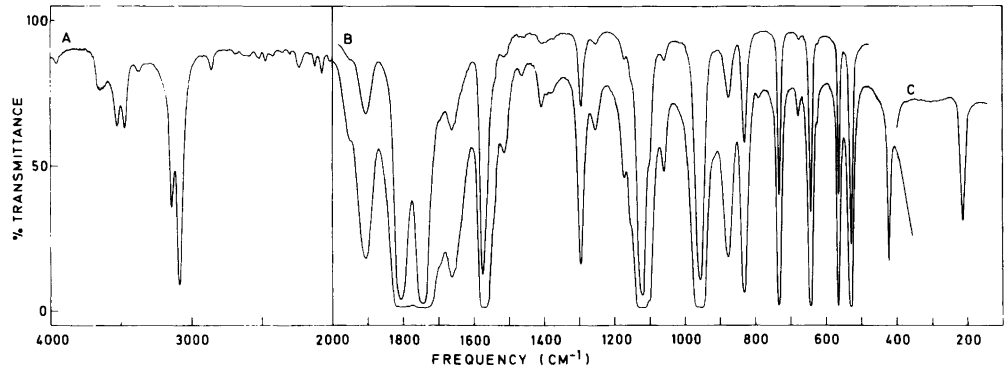

Fig. 1. Infrared spectrum of 1,3,4-oxathiazol-2-one in the liquid phase, (A) 0.025 mm cell and (B) thin film and in cyclohexane-solution (C).

wave investigation. Accordingly, the vibrational spectra can be interpreted in terms of C_s symmetry. The 15 fundamental vibrations divide into: $12A'+3A''$ with all modes active in both IR and Raman, the A' modes being polarized and having A/B hybrid contours, the A'' modes C-type contours. From the rotational constants determined by microwave spectroscopy the PR separations were calculated[13] to be 16, 13 and 25 cm^{-1} for the A, B and C bands, respectively.

The infrared and Raman spectra of the liquid are shown in Figs. 1 and 2, respectively, while the wavenumbers of the observed IR and Raman bands are listed in Table 3. As apparent from these data, the assignment is a straightforward matter with the exception of the intense doublet in the carbonyl stretching region. The relative intensities of these two bands are sensitive to changes in the polarity of the solvent. In the liquid phase the lower band is the most intense, but in a CCl_4 solution the intensities become almost equal. This shift is most pronounced in the Raman spectra. Further, in the CCl_4 solution the bands at about 1800 cm^{-1} split into two close components in both IR and Raman. We have no ready explanation for this effect. In the vapour phase the ratio of extinction between the bands at 1826 and 1745 cm^{-1} is drastically reversed: $\varepsilon_{1826}/\varepsilon_{1745} \sim 4.5$.

Similar effects occur in a large number of carbonyl compounds, such as unsaturated γ-lactones,[14] and

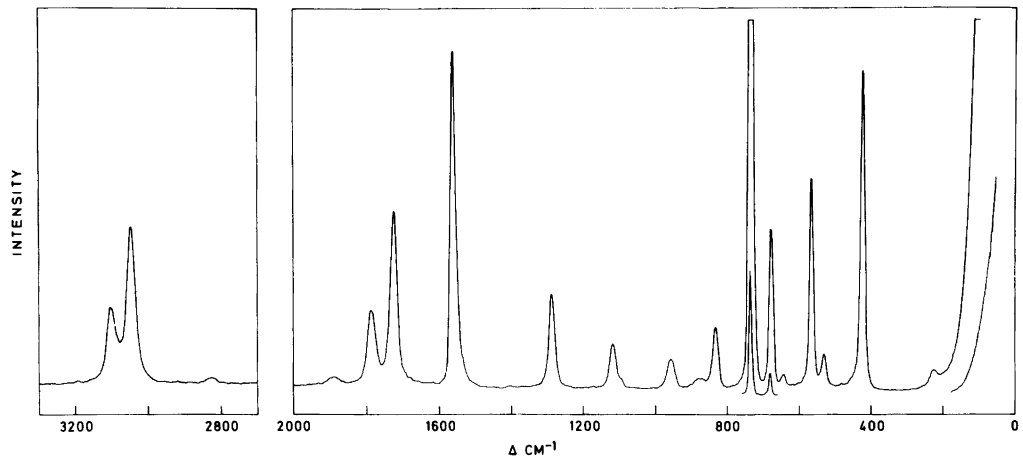

Fig. 2. Raman spectrum of 1,3,4-oxathiazol-2-one in the liquid phase.

Table 3. Infrared and Raman spectral data for 1,3,4-oxathiazol-2-one.

Infrared[a]				Raman[a]		Assignment	
CCl_4 solution	Vapour	Liquid	Amorphous solid-180°	CCl_4 solution	Liquid		
		3950 w[b]				$\nu_1+\nu_{12}$	
		3650 w				$\nu_1+\nu_{10}$	
3610		3610 w				$\nu_1+\nu_{14}$	
3535		3528 w				$2\times\nu_2$	FR
3470		3475 w				$\nu_2+\nu_6+\nu_7$	FR
		3370 w				$\nu_2+\nu_3$	
3146		3143 m	3143	3145	3144 m P	$2\times\nu_3$	
3089		3086 s	3073	3088	3088 s P	ν_1	
1956		1955 w sh				comb.	
	1896						
1889	1889 A/B	1908 m	1923		1904 vw	$2\times\nu_6$	
	1880						
	1833						
1810	1826 A/B	1809 vs	1812	1807	1806 m P	ν_2	FR
1803	1817			1801			
	1751						
1745	1745 A/B	1747 vs	1743	1746	1740 s P	$\nu_6+\nu_7$	FR
	1735						
		1663 m	1680			comb.	
	1587						
1577	1581 A/B	1576 vs	1573	1578	1573 s P	ν_3	
	1574						
		1540 w sh				comb.	
		1516 w				comb.	
		1464 w				comb.	
		1409 w				$\nu_8+\nu_9$	
		1380 w				comb.	
	1303						
1293	1294 A/B	1297 m	1298	1295	1297 m P	ν_4	
	1287						
		1256 w				comb.	
1173		1175 w	1180			comb.	
1157		1157 w sh	1163			comb.	
	1144						
1128	1136 A/B	1124 vs	1123	1127	1124 w P	ν_5	
	1127						
1096		1101 w sh	1108		1102 vw	comb.	
1059		1061 w	1070			$\nu_{11}+\nu_{13}$	
	952						
948	946 A/B	958 vs	966	955	959 w P	ν_6	
	939						
	878						
868	867 C	879 m	888		878 vw D	ν_{12}	
	852						
	824						
823	812	833 s	840	827	835 w P	ν_7	
		792 w				impurity	
	741						
	734 A/B	734	736	735	737 vs P	ν_8	
	726						
677		680 w	686	679	681 s P	ν_9	

Table 3. Continued.

643	656 643 632 C	643	645		646 vw D	ν_{13}
		626 w sh	627			$\nu_{11}+\nu_{15}$
565	569 562 556 A/B	566 s	568	567	570 s P	ν_{10}
531	544 529 516 C	529 s	532	534	532 w D	ν_{14}
421		422 m	425	424	426 s P	ν_{11}
214		212[c] m	232		223 vw D	ν_{15}

[a] The weak infrared and Raman bands in the regions 5000 – 4000 and 3000 – 2000 cm^{-1} are omitted. [b] w, weak; m, medium; s, strong; v, very; sh, shoulder; P, polarized; D, depolarized; FR, Fermi resonance. [c] In cyclohexane solution.

it is assumed that this behaviour is caused by Fermi resonance between ν_2 and the combination band $\nu_6+\nu_7$. It may be noticed that the same changes in intensities are observed with the overtone bands at 3528 and 3475 cm^{-1}.

STRUCTURE DETERMINATION AND RESULTS

The molecular electron-diffraction intensities for each of the three camera distances are shown in Fig. 3, and the data ranges and the weight schemes

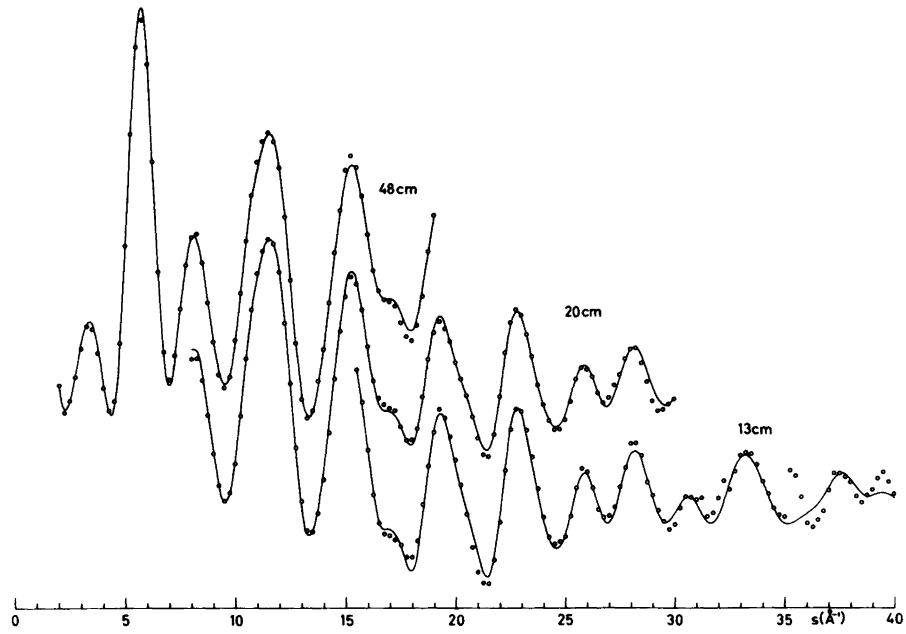

Fig. 3. Observed molecular intensity data (o) for 1,3,4-oxathiazol-2-one obtained from electron-diffraction experiments at three camera distances, compared to calculated intensities (full line) from parameter values given in Table 6*a*, IIIB.

Table 4. Ranges and weighting of the electron-diffraction data used in the structure refinements.

Curve	Data range		Data interval	Constants of the weighting schemes[a]						
(camera dist.)	s_{min}	s_{max}	Δs	s_1	s_2	w_1	w_2	p_2	p_3	W
48 cm	2.00	19.00	0.125	2.25	19.00	0.1	0.1	−0.64	0.146	1.0
20 cm	8.00	30.00	0.250	8.00	29.00	0.1	0.1	−0.60	0.125	1.0
13 cm	15.50	45.00	0.250	15.50	35.00	0.1	0.1	−0.57	0.100	1.0

[a] See Refs. 6 and 15 for the meaning of the symbols. For diagonal weight matrcices $p_2 = p_3 = 0$.

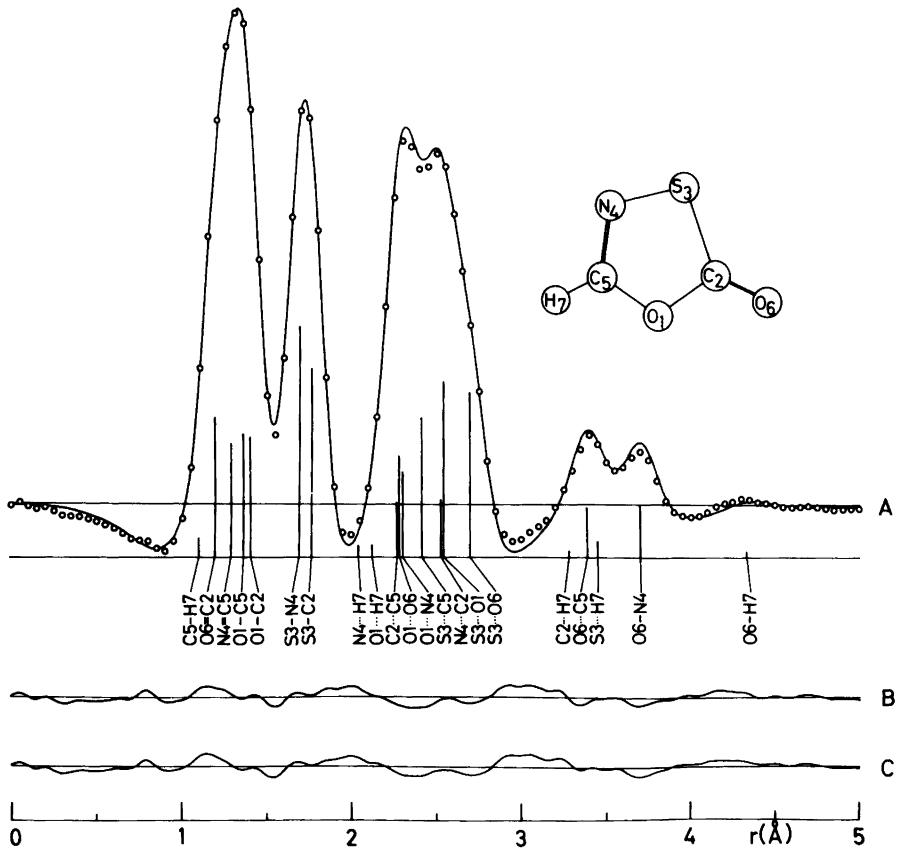

Fig. 4. (A) Experimental radial distribution curve (o) for 1,3,4-oxathiazol-2-one calculated from the intensity data given in Fig. 3 using an artificial damping constant of $k = 0.0020$ Å^2, and the calculated counterpart (full line) based on the parameter values of Table 6*a*, IIIB; (B) the corresponding difference curve; and (C) the difference curve using parameter values of Table 6*a*, IIIC.

A molecular model with numbering of the atoms is shown and the vertical lines indicate the positions of the interatomic distances.

used in the structure analysis are summarized in Table 4.

From the experimental modified molecular intensity curves shown in Fig. 3 a composite curve was computed by scaling and averaging intensity values in the overlap regions. In Fig. 4 the radial distribution curve calculated from this connected curve is presented together with a molecular model. The line diagram under the curve gives the positions and the relative weights of the 21 different interatomic distances of the molecule according to one of the final models. The line diagram demonstrates the high degree of distance overlap and also the discouraging expectation of a conventional approach refining all the 32 geometrical and vibrational parameters together. An attempt to refine a few of the u-values together with the geometrical parameters demonstrated this quite clearly. On the other hand the geometric parameters refined normally in a few cycles if assumed u-values were kept constant.

In order to determine the geometrical parameters with confidence, it is of course important to obtain as reliable u-values as possible. Further, in order to test the influence of the chosen set of u-values on the geometrical parameters it was judged useful to try several independently obtained sets. Three such sets were used as given in Table 5. The first set (I) is composed of values simply assumed by one of us (L.F.) based upon many years of experience and analogy to other compounds with similar structure features. The second set (II) was computed from an estimated force field with a diagonal F matrix in terms of valence coordinates including redundancies. Force constant values were estimated with the aid of previous normal coordinate analyses of related molecules: maleic anhydride,[16,17] furan[18] and different diazoles.[18] The third set of u-values (III) was obtained together with the perpendicular amplitude correction coefficients (K-values) from a force field adjusted so as to give a fair fit to the observed fundamental frequencies and reproduce sign and magnitude of the centrifugal distortion constants and the inertial defect.

Several preliminary refinement approaches were tried including the assumption of unplanarity and

Table 5. Vibrational amplitude quantities in Å for 1,3,4-oxathiazol-2-one. I, II and III refer, respectively, to assumed values, values computed from an assumed force field and values calculated from a force field adjusted to fit the observed fundamental frequencies as described in the text. The subscripts T and 0 refer to the temperatures 328 K and 0 K, respectively.

	I	II	III			
	u	u_T	u_T	K_T	u_0	K_0
O1–C2	0.045	0.045	0.0471	0.00246	0.0461	0.00211
O1–C5	0.045	0.045	0.0473	0.00433	0.0465	0.00269
S3–C2	0.050	0.043	0.0502	0.00136	0.0471	0.00117
S3–N4	0.050	0.044	0.0541	0.00275	0.0505	0.00169
N4=C5	0.040	0.045	0.0417	0.00250	0.0416	0.00219
O6=C2	0.039	0.039	0.0377	0.00641	0.0375	0.00387
C5–H7	0.074	0.077	0.0767	0.02522	0.0767	0.02099
S3···O1	0.056	0.046	0.0561	0.00078	0.0513	0.00053
N4···C2	0.056	0.051	0.0606	0.00236	0.0564	0.00145
S3···C5	0.050	0.048	0.0564	0.00115	0.0520	0.00078
O1···N4	0.050	0.049	0.0532	0.00335	0.0515	0.00180
C2···C5	0.055	0.051	0.0576	0.00198	0.0545	0.00141
O1···O6	0.057	0.057	0.0582	0.00400	0.0541	0.00204
S3···O6	0.058	0.055	0.0612	0.00176	0.0540	0.00093
O1···H7	0.099	0.101	0.0999	0.01715	0.0992	0.01226
N4···H7	0.077	0.101	0.0972	0.01452	0.0968	0.01186
O6···N4	0.080	0.055	0.0638	0.00044	0.0584	0.00036
O6···C5	0.066	0.057	0.0615	0.00070	0.0571	0.00052
S3···H7	0.090	0.090	0.0940	0.00871	0.0912	0.00662
C2···H7	0.090	0.093	0.0957	0.00996	0.0939	0.00750
O6···H7	0.090	0.102	0.1031	0.00580	0.0999	0.00482

Table 6a. Bond distances (r_a-values in Å) and valence angles (in degrees) for 1,3,4-oxathiazol-2-one obtained in structural refinement of planar models by the method of least squares based upon electron-diffraction data alone (ED) or combined with data from microwave spectroscopy (ED&MW). The *R*-values express the quality of fit for the electron-diffraction data ($R = \Sigma w_i(I_{obs} - I_{calc})^2/\Sigma w_i I_{obs}^2$). I, II and III refer to the set of values for the vibrational parameters used (See Table 3). The meaning of r_a, r_x, r_x° and r_z is described in the text.

	I(ED) r_a-model	II(ED) r_a-model	IIIA(ED) r_a-model	IIIB(ED) r_x-model	IIIC(ED&MW) r_x°-model
r(O1 – C2)	1.398(3)	1.395(4)	1.398(4)	1.399(4)	1.402(3)
r(O1 – C5)	1.356(3)	1.355(4)	1.356(3)	1.356(3)	1.356(3)
r(S3 – C2)	1.769(2)	1.772(2)	1.765(2)	1.766(2)	1.767(2)
r(S3 – N4)	1.690(2)	1.687(1)	1.690(2)	1.690(2)	1.690(2)
r(N4 = C5)	1.280(3)	1.280(3)	1.283(3)	1.284(3)	1.286(2)
r(O6 = C2)	1.189(2)	1.192(2)	1.191(2)	1.191(2)	1.192(2)
r(C5 – H7)	1.095 –	1.095 –	1.095 –	1.095 –	1.102(19)
∠C5O1C2	110.7(2)	110.7(2)	110.8(2)	110.9(2)	110.8(2)
∠O1C2O6	122.9(3)	123.5(3)	122.7(3)	122.7(3)	122.6(3)
∠C2S3N4	93.6(1)	93.5(1)	93.8(1)	93.8(1)	93.8(1)
∠O1C5H7	120.0 –	120.0 –	120.0 –	120.0 –	114.5(31)
∠O1C2S3, dep.	106.4	106.4	106.4	106.2	106.3
∠O1C5N4, dep.	121.2	121.2	121.1	121.3	121.1
∠C5N4S3, dep.	108.0	108.0	107.9	107.9	107.9
R (%)	9.86	9.58	9.92	9.94	9.91

Table 6b. Rotational constants (*A*, *B*, *C* in MHz) calculated from models given above, and in square brackets the values obtained from the microwave study expressed in terms of the operational parameter r_0.

	I(r_a)	II(r_a)	IIIA(r_a)	IIIB(r_x)	IIIC(r_x°)
A_0[5587.411(11)]	5594.8(174)	5595.0(163)	5603.0(178)	5613.7(177)	5582.6(13)
B_0[3645.873(9)]	3638.6(41)	3639.6(37)	3636.7(41)	3643.7(41)	3643.8(4)
C_0[2205.464(9)]	2204.7(25)	2205.1(25)	2205.3(26)	2209.6(26)	2204.7(2)

Table 6c. Rotational constants corresponding to distances between mean positions of atoms in ground vibrational state, *i.e.* the comparable quantities r_x° for electron-diffraction and r_z for microwave results.

	I	II	IIIA	IIIB	IIIC
A_z[5582.0(16)]	5604.8(174)	5605.2(163)	5613.2(178)	5611.2(177)	5582.6(13)
B_z[3643.5(7)]	3646.8(41)	3647.9(37)	3645.1(41)	3639.7(41)	3643.8(4)
C_z[2204.8(2)]	2209.3(25)	2209.8(25)	2210.0(26)	2207.7(26)	2204.7(2)

the assumption that the two ring C – O distances were equal. The first assumption led to the conclusion that a possible deviation from planarity had to be very small, in accordance with the microwave data unambiguously demonstrating the planarity. The second assumption seemed not necessary since the $O_1 - C_2$ distance repeatedly refined to be about 0.05 Å larger than the $O_1 - C_5$ distance, even for refinements where the distances had the reverse relative magnitude for the start

model. In attempts to refine r(C–H) and ∠O1C5H7 rather large oscillations were encountered and the position of the hydrogen atom was therefore kept constant. The results of three refinements (I, II and III A) using the corresponding three sets of u-values given in Table 5, are presented in Table 6*a*. Only the independent distance parameters are given while both independent and dependent angle values are listed. In these refinements shrinkage effects were neglected. In refinement III B (see Table 6*a*) shrinkage effects were accounted for using the u_T- and K_T-values of Table 5 (III) and the relation [19,20]

$$r_a = r_z - u_T^2/r_a + K_T \quad (1)$$

to obtain the geometrically inconsistent set of r_a values from the geometrically consistent set of r_z-values (*i.e.* r_z-model). In each of the four refinements the rotational constants were computed from the distance and angle parameters describing the geometry of the molecule, *i.e.* based on r_a-values for refinements I, II and III A and on r_z-values for refinement III B. The results are compared with the values based upon r_0-parameters obtained from the microwave study in Table 6*b*. The refinements were carried out both using diagonal and non-diagonal weight matrices (see Table 4). The actual parameter values given are obtained using diagonal weight matrices, while the standard deviations given in parentheses are obtained with non-diagonal weight matrices. Comparisons of the standard deviations obtained for the two types of weight matrices showed that correlation among the data could be accounted for by applying factors of 1.5–2.0 to the standard deviations obtained in refinements with diagonal weight matrices. The standard deviations given in Tables 6*a*–*c* do not include estimates of the uncertainty in the s-scale (0.1 % in the electron wavelength) which corresponds to 0.1 % for the distance parameters and about 0.2 % for the rotational constants.

The good correspondence between the values of the refinements I to III A given in Table 6 may be interpreted as a demonstration of the insensitivity of the geometrical parameters to the choice of u-values. However, other less carefully chosen sets of u-values were also tried with considerably less success. Comparisons of the results of refinements III A and III B show that the effect of neglecting shrinkage effects is small. However, the relatively large differences in the computed rotational constants for these two refinements as compared to the small shifts in the parameter values for the bond distances and valence angles, reflect the fact that the calculations are based upon two different types of distance parameters, namely r_a and r_z for refinements IIIA and IIIB, respectively. The rotational constants originating from the electron-diffraction data are not significantly different from the microwave values even in comparisons on the r_a to r_0 and r_z to r_0 level, and the results of the two investigations seem to be consistent. The results appear to indicate that the error introduced by such comparisons is small since both the r_a and r_z distances should be longer than r_0 resulting in systematically lower values for the corresponding rotational constants, whereas the rotational constants from the two methods (Table 6*b*) do not show such systematic discrepancies. For the same reason scale problems appear to be ruled out. However, one should note the effect of the fixed hydrogen position. The rotational constants obtained in a refinement corresponding to III B for ∠O1C5H7 = 115° were, for example, all found to be larger than the corresponding microwave values. This change also caused an improved least-squares fit to the electron-diffraction data (R = 9.79 %).

To provide a better basis for comparisons of the results and to attempt conjoint refinements based on information from both methods, the rotational constants were corrected so as to be expressed in terms of distances corresponding to the mean positions of the atoms in the ground vibrational state, which are denoted r_z and r_z^0 when derived from microwave and electron-diffraction data, respectively. The necessary correction terms were computed from the force field used to calculate u-value set III. For the microwave rotational constants centrifugal corrections and electronic contributions were neglected giving $B_z - B_0 \approx \partial B_{vib}$ where the vibrational corrections, ∂B_{vib}, require only harmonic force constants.[19,20] The corrected values are given in Table 6*c*, and the estimated standard deviations (σ_z) are taken to be 30 % of the δB_{vib} correction terms. For the electron-diffraction rotational constants the following relation was used in addition to Eqn. 1,[19,20]

$$r_z^0 = r_z + (K_T - K_0) - \frac{3}{2} a_3 (u_T^2 - u_0^2) \quad (2)$$

where K_0 and u_0 refer to 0 K (See Table 5). a_3 is an anharmonicity constant assumed to be 0 and 2 Å^{-1}

for nonbonded interactions and for bond distances, respectively.[20] The rotational constants expressed by r_α^0 parameters calculated from the r_a-values of Table 6*a* are given in Table 6*c* for the four refinements, I, II, III A and III B. The standard deviations do not include uncertainties in the applied correction terms.

A structure based on r_α^0-parameters is, like the r_α-model, corrected for shrinkage. In comparative refinements based on r_α and r_α^0-models, the respective angle parameters[21] were found to be nearly equal, the largest difference between $\angle_\alpha$ and $\angle_\alpha^0$ being 0.09°. In the r_α^0-refinement the rotational constants were directly calculated from r_α^0-parameters, and the rotational constants A_z, B_z and C_z could be included together with the electron-diffraction data in the least-squares refinement of the structure.[20] The observed rotational constants were given relative weights according to their estimated standard deviations (σ_z^{-2}), and the data originating from the two methods were weighted so as to give standard deviations for the r_α^0 rotational constants within the values for the corresponding σ_z-estimates. Using the model with fixed hydrogen position, such requirements were obtained for a model which gave a least-squares fit to the electron-diffraction data of $R = 10.06\,\%$. In the combined analysis including variation of the hydrogen position convergence was obtained also for r(C5–H7) and $\angle$O1C5H7. For fixed C–H distance (1.095 Å) the hydrogen angle parameter refined to 114.8(3.1)°. The final result of the combined refinement of the structure is given in Table 6 *a* (III C). The refinement of the hydrogen position did not significantly affect the determination of the other geometrical parameters. The larger elements of the correlation matrix ($|\rho| > 0.6$) are $\rho(r(\text{O1C2}), r(\text{O1C5})) = -0.73$ and $\rho(\angle\text{C2S3N4}, \angle\text{O1C5H7}) = -0.72$. The standard deviations given are obtained using diagonal weight matrices and factors to account for correlation among the electron-diffraction data as established by previous refinements.

The molecular intensities and radial distributions calculated from the parameter values of III B, Table 5, are shown in Figs. 3 and 4, respectively, together with the experimental counterparts. The differences between experimental and calculated radial distribution curves are included in Fig. 4 for parameter set III B as well as for III C.

DISCUSSION

The consistency in the geometrical parameters obtained using three different sets of fixed u-values (see Table 6*a*, refinements I, II, and IIIA) is satisfactory. Provided the existence of data from which reasonable estimates of u-values or force constants may be made, this demonstrates that electron-diffraction results for molecules with complex distance overlaps may not be as dubious as one could fear. In the present case the electron-diffraction results could also be controlled against the experimental spectroscopic rotational constants and the comparison was gratifying for all three sets of parameter values (Table 6*b*). The vibrational spectroscopic results provided data for a normal coordinate analysis which gave the u-value set III and various correction terms needed for comparison on a higher level of confidence (Table 6*c*) and the final structure determination could be based on the electron-diffraction intensity data in combination with the experimental spectroscopic rotational constants. The results of such a refinement (IIIC of Table 6) represent our final structural parameters. It is seen that this combined approach led to determination of the hydrogen position which had to be assumed in the previous refinements. The difference curves of Fig. 4 and the obtained R-factors show the good correspondence with the microwave data since no significant loss in the agreement between experimental and calculated curves was encountered when the parameters were adjusted so as to give a good fit to the microwave rotational constants.

The established planarity of the molecule is naturally related to π-electron delocalization. However, 1,3,4-oxathiazol-2-one pyrolyzes fast at 500 °C, furan slowly at 1000 °C, while benzene is stable even at 1150 °C, all on a quartz surface under low-pressure conditions (20–30 mTorr).[21] It is therefore tentatively suggested that π-type orbitals of 1,3,4-oxathiazol-2-one are of less importance for maintaining molecular planarity than corresponding orbitals in furan. Comparisons of bond lengths should also yield some information about the degree of delocalization, although effects due to variations in hybridization of the atoms involved and differences in adjacent atoms may obscure the conclusions from such comparisons. Fig. 5 shows the bond lengths of 1,3,4-oxathiazol-2-one and of some related five-membered ring compounds *1* – *6*. Within the experimental error, these are all found to be planar in gas phase.[22–27] Varying numbers and

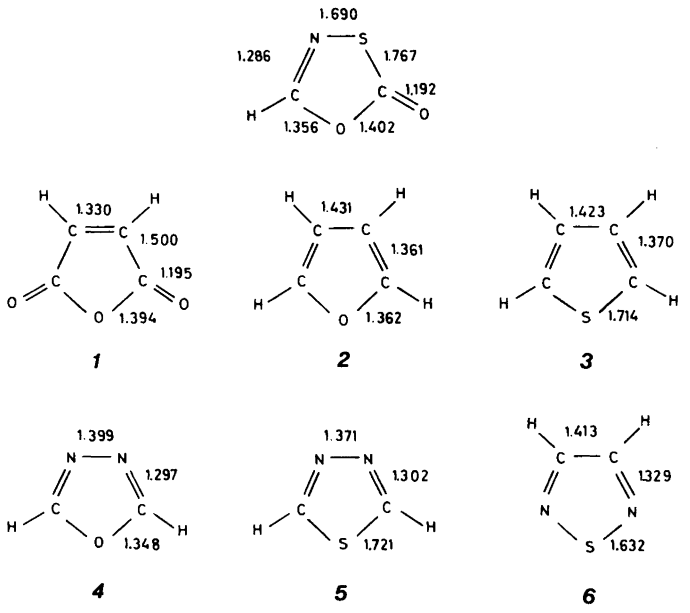

Fig. 5. Bond lengths (in Å) for 1,3,4-oxathiazol-2-one (r_a-values) and of some related compounds as obtained in electron-diffraction (r_g-values) and microwave (r_s-values) investigations: *1* maleic anhydride[22] (r_g), *2* furan[23] (r_s), *3* thiophene[24] (r_s), *4* 1,3,4-oxadiazole[25] (r_s), *5* 1,3,4-thiadiazole[26] (r_s) and *6* 1,2,5-thiadiazole[27] (r_g).

types of heteroatoms have caused variations in the angle deformations needed for ring closure throughout this series. In 1,3,4-oxathiazol-2-one the C–H and C=O bonds are tilted approximately the same amount towards the oxygen atom from the bisectors of the corresponding ring angles, as the corresponding bonds in *1* and *4*. The difference in lengths of the two types of O–C(sp^2) bonds, r(O–C(=O)) = 1.402 Å and r(O–C(=N)) = 1.356 Å, may be seen as a consequence of the difference in electronegativity of the neighbouring oxygen and nitrogen atoms, and the result is consistent with the values of 1.394 and 1.348 Å, respectively, for the corresponding bonds in *1* and *4*. The length of the C=O bond (1.192 Å) suggests, as for *1*, that the carbonyl π-electrons do not participate in delocalization of the π-electron system. As compared to the N=C bonds of *4*–*6* the N=C bond of 1.286 Å in 1,3,4-oxathiazol-2-one is short, and it approaches the value of 1.277(2) Å in formaldazine[28] ($H_2C=N-N=CH_2$) for which the antiperiplanar conformer is the more stable, and the N–N bond of 1.418(3) Å is longer than the corresponding bonds of *4* and *5*. The described shortening of the N=C bond is consistent with the lengthening of the two adjacent bonds C–O and N–S as compared to the C–O bond in *4* and the N–S bond in *6*. Also the S–C(sp^2) bond of 1.767 Å is long compared to the corresponding bonds of 1.714 Å in *3* and 1.721 Å in *5*, and it is found to be closer to the values of 1.747(3) Å and 1.777(4) Å of methylvinylsulfide[29] ($H_2C=CHSCH_3$) and dimethyldithiocarbonate[30] ($O=C(SCH_3)_2$), respectively. The neighbouring strongly electronegative oxygen may be responsible for part of the described lengthening of the S–C(sp^2) bond as it was suggested for the O–C(sp^2) bond of 1.402 Å. Assuming that the σ bond lengths are more or less the same for corresponding atom pairs in the different compounds, this qualitative discussion of the structural results for 1,3,4-oxathiazol-2-one suggests that π-electron delocalization is less pronounced in this compound than in compounds *2*–*6*, which supports the tentative conclusion from the pyrolysis experiments.[21]

REFERENCES

1. Bak, B., Christiansen, J. J., Nielsen, O. J. and Svanholt, H. *Acta Chem. Scand. A 31* (1977) 666.
2. Troe, J. *J. Chem. Phys. 66* (1977) 4745, 4758.
3. *British Pat.* 1079 348 (1967); *Chem. Abstr. 68* (1968) 69000w.
4. Gilbert, B. and Duyckaerts, G. *Spectrochim. Acta A 26* (1970) 2197.
5. Bastiansen, O., Hassel, O. and Risberg, E. *Acta Chem. Scand. 9* (1955) 232.
6. Andersen, B., Seip, H. M., Strand, T. G. and Stølevik, R. *Acta Chem. Scand. 23* (1969) 3224.
7. Yates, A. C. *Comput. Phys. Commun. 2* (1971) 175.
8. Strand, T. G. and Bonham, R. A. *J. Chem. Phys. 40* (1964) 1686.
9. Stewart, R. F., Davidson, E. R. and Simpson, W. T. *J. Chem. Phys. 42* (1965) 3175.
10. Tavard, C., Nicolas, D. and Rouault, M. *J. Chem. Phys. 64* (1967) 540.
11. Casado, J., Nygaard, L. and Sørensen, G. O. *J. Mol. Struct. 8* (1971) 211.
12. Herschbach, D. R. and Laurie, V. W. *J. Chem. Phys. 40* (1964) 3142.
13. Seth-Paul, W. A. and Demeyer, H. *J. Mol. Struct. 3* (1969) 403.
14. Jones, R. N., Angell, C. L., Ito, T. and Smith, R. J. D. *Can. J. Chem. 37* (1959) 2007.
15. Seip, H. M., Strand, T. G. and Stølevik, R. *Chem. Phys. Lett. 3* (1969) 617.
16. di Lauro, C., Califano, S. and Adembri, G. *J. Mol. Struct. 2* (1968) 173.
17. Rogstad, A., Klæboe, P., Baranska, H., Bjarnov, E., Christensen, D. H., Nicolaisen, F., Nielsen, O. F., Cyvin, B. N. and Cyvin, S. J. *J. Mol. Struct. 20* (1974) 403.
18. Cyvin, B. N. and Cyvin, S. J. *Acta Chem. Scand. 23* (1969) 3139.
19. Kuchitsu, K. and Cyvin, S. J. In Cyvin, S. J., Ed., *Molecular Structures and Vibrations*, Elsevier, Amsterdam 1972, Chapter 12, and references therein.
20. Kuchitsu, K., Fukuyama, T. and Morino, Y. *J. Mol. Struct. 1* (1967–68) 463.
21. Bak, B., Nielsen, O. and Svanholt, H. *Unpublished results.* Details on request.
22. Hilderbrandt, R. L. and Peixoto, E. M. A. *J. Mol. Struct. 12* (1972) 31.
23. Bak, B., Christensen, D., Dixon, W. B., Hansen-Nygaard, L., Rastrup-Andersen, J. and Schottländer, M. *J. Mol. Spectrosc. 9* (1962) 124.
24. Bak, B., Christensen, D., Hansen-Nygaard, L. and Rastrup-Andersen, J. *J. Mol. Spectrosc. 7* (1961) 58.
25. Nygaard, L., Lykke-Hansen, R., Nielsen, J. T., Rastrup-Andersen, J., Sørensen, G. O. and Steiner, P. A. *J. Mol. Struct. 12* (1972) 59.
26. Nygaard, L., Lykke-Hansen, R. and Sørensen, G. O. *J. Mol. Struct. 9* (1971) 163.
27. Momany, F. A. and Bonham, R. A. *J. Am. Chem. Soc. 86* (1964) 162.
28. Hagen, K., Bondybey, V. and Hedberg, K. *J. Am. Chem. Soc. 99* (1977) 1365.
29. Samdal, S. and Seip, H. M. *J. Mol. Struct. 28* (1975) 193.
30. Almenningen, A., Auberg, E., Samdal, S. and Seip, H. M. *Unpublished results.*

Received May 10, 1978.

Acta Chemica Scandinavica A 32 (1978) 1017 – 1020

Short Communications

Human Spectrin. IV. A Preliminary X-Ray Study

ARNE MIKKELSEN and
ARNLJOT ELGSAETER

Institute of Biophysics, The Norwegian Institute of Technology, N-7034 Trondheim-NTH, Norway

In an earlier study we found that spectrin plays an important role in controlling the lateral mobility of the human erythrocyte intramembrane particles.[1,2] This can most easily be understood in terms of spectrin being long molecules and forming a molecular meshwork on the cytoplasmic side of the erythrocyte membrane. The reported lengths of spectrin vary from 28 nm to 210 nm.[3,4] We have recently obtained data indicating that spectrin heterodimers are flexible and highly elongated molecules.[5,6] X-Ray fibre analysis has proved to be a very powerful technique for the study of such molecules, and we here report on the first X-ray study of spectrin.

Experimental. Spectrin heterodimers were prepared as described earlier (procedure A)[5] except that recently outdated human blood was used instead of fresh blood. The spectrin heterodimer solutions were dialyzed for 40 h at 0 – 4 °C against 2 × 1 l distilled water pH 7 before the spectrin solution was concentrated. The concentration was either done by ultrafiltration through a Diaflo PM30 membrane or by employing Aquacide II-A. In the latter case the spectrin solutions were placed inside two dialysis bags, one inside the other.

Spectrin films were made by allowing the concentrated spectrin solutions to dry out on sheets of polytetrafluoroethylene. The spectrin films were then cut into 2 – 3 mm wide strips and stretched as described by Atkins and coworkers.[7,8]

The X-ray diffraction photographs were recorded on flat film using a camera with pinhole collimation (0.5 mm diameter) and Ni-filtered Cu$K\alpha$ radiation. The atmosphere in the camera was maintained at the desired relative humidity by placing an appropriate saturated salt solution in the camera. The total pressure in the camera was kept at 20 – 25 Torr (2.6 – 3.3 kPa).

The X-ray diffraction photographs were scanned employing a Joyce MK III CS microdensitometer.

Results and discussion. X-Ray diffraction photographs of strips of unstretched spectrin film exhibited two diffuse concentric rings having maxima at the reciprocal distances 1.0 and 2.2 nm^{-1}, respectively.

Bundles consisting of 6 – 7 spectrin film strips were elongated at 25 °C by loading the bundles with 13 gram and stepwise increasing the relative humidity from 75 to 98 – 100 %. The relative humidity at which the elongation of the bundle of film strips started varied from 88 to 98 % depending on the spectrin concentration procedure used. When the elongation had started it would continue without any further increase of the relative humidity. During the first 1 – 2 h after the onset of the elongation the bundles of spectrin film strips would approximately double their lengths. After that the elongation slowed down and a further increase of the relative humidity to 90 – 100 % was needed to make the

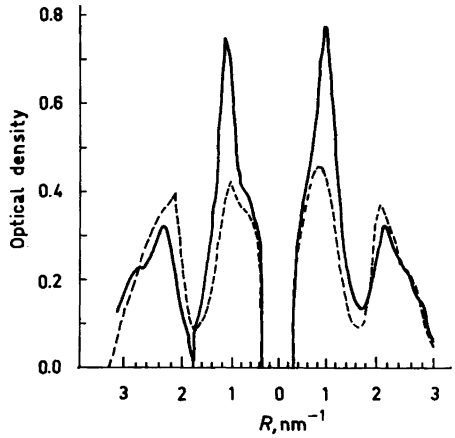

Fig. 1. Densitometer scan of X-ray diffraction photograph of strips of spectrin film elongated at 88 – 95 % relative humidity to 16 times their original lengths. The X-ray diffraction photograph was obtained with the incident X-ray beam at 90° to the long axis of the elongated spectrin fibre and the sample kept at 72 % relative humidity. The X-ray diffraction photograph optical density along the equator (–) and along the meridian (– – –).

bundles elongate to 10–15 times their original lengths. At the end of the elongation the bundle of of spectrin film strips exhibited a fibre-like appearance.

X-Ray diffraction photographs of the elongated spectrin fibres showed two strong reflections on the equator indicating that the elongation of the spectrin fibres resulted in some ordering of the spectrin molecules. The X-ray diffraction photographs of the elongated spectrin fibres are very similar to the X-ray photographs of keratin, myosin and fibrinogen (the kmf-group).[9] A densitomter scan of an X-ray diffraction photograph of an elongated spectrin fibre is shown in Fig. 1. We have not been able to find any spectrin fibre preparation procedure which yields X-ray diffraction photographs containing layer lines.

The observation that X-ray diffraction photographs of elongated spectrin fibres belong to the kmf-group indicates that the spectrin secondary structure to a considerable extent consists of α-helices.[10] This is consistent with circular dichroism measurements of spectrin indicating that spectrin consists of 35–65 % α-helix.[11-14] The ordering resulting from elongation of the spectrin fibres further indicates that the spectrin molecules are highly asymmetric or flexible worm-like/coil-like molecules. This is in agreement with our earlier observations.[5,6,15]

Acknowledgements. We gratefully acknowledge the advice of Dr. E. Atkins, H. H. Wills Physics Laboratory, Bristol, England on building the X-ray fibre camera. We thank Trondheim Regional Hospital Blood Bank for supplying outdated human blood and Ms. Mildrid Engen for technical assistance. This work has in part been supported by a grant from "Norges Tekniske Høgskoles Fond" to A.E.

1. Elgsaeter, A. and Branton, D. *J. Cell. Biol. 63* (1974) 1018.
2. Elgsaeter, A., Shotton, D. M. and Branton, D. *Biochim. Biophys. Acta 426* (1976) 101.
3. Kam, Z., Josephs, R., Eisenberg, H. and Gratzer, W. B. *Biochemistry 16* (1977) 5568.
4. Clarke, M. and Griffith, J. *Fed. Proc. Fed. Am. Soc. Exp. Biol. 31* (1972) 412.
5. Elgsaeter, A. *Biochim. Biophys. Acta 536* (1978) 235.
6. Mikkelsen, A. and Elgsaeter, A. *Biochim. Biophys. Acta 536* (1978) 245.
7. Atkins, E. D. T., Phelps, C. F. and Sheehan, J. K. *Biochem. J. 128* (1972) 1255.
8. Atkins, E. D. T. and Mackie, W. *Biopolymers 11* (1972) 1685.
9. Astbury, W. T. *Proc. R. Soc. London Ser. B 134* (1974) 303.
10. Pauling, L. and Corey, R. B. *Proc. R. Soc. London Ser. B 141* (1953) 21.
11. Clarke, M. B. *Ph.D. Diss.*, University of California, Berkeley, USA 1971.
12. Gratzer, W. B. and Beaven, G. H. *Eur. J. Biochem. 58* (1975) 403.
13. Erickson, L. M. *Ph.D. Diss.*, University of Massachusetts, USA 1976.
14. Ralston, G. B. *Aust. Biochem. Soc. Proc. 9* (1976) 15.
15. Bøe, A., Elgsaeter, A., Oftedal, G. and Strand, K. A. *Acta Chem. Scand. A 33* (1979). *In press.*

Received September 4, 1978.

On the Molecular Structure of VO^{2+} and Ni^{2+} Complexes with Schiff Bases of Formylcamphor and Diamines

HANS PETER JENSEN

Chemistry Department A, Building 207,
The Technical University of Denmark,
DK-2800 Lyngby, Denmark

Proviously a rather simple model, usable on transition metal complexes for the explanation of intensity in circular dichroism (CD) spectra under absorptions which may be described mainly by *d*-orbitals, has been proposed.[1] Although the model is not general it may well be dominating for complexes with ligands having internal transitions which in energy are not very much separated from the ligand field transitions.

Certainly the model has proven operative for complexes of Cu^{2+} with Schiff bases derived from acetylacetone[1,2] and formylcamphor (prepared from natural $(+)_D$-camphor)[3] as well as for VO^{2+} and Ni^{2+} complexes of the former type of ligand.[1]

Obviously it is important to verify as firmly as possible the suggested model. Consequently, to extend the experimental basis, various neutral inner-sphere complexes of VO^{2+} and Ni^{2+} with formylcamphor Schiff bases of 1,2-diamines have been prepared and spectroscopically investigated.

The proposed model operates in two stages which are, however, intimately related. Firstly, the absolute configuration of a given chiral complex is determined in terms of handedness of a pair of vectors representing the allowed, polarized internal ligand $\pi^* \leftarrow \pi$ transitions. Secondly, the ligand field CD-spectrum may be interpreted using simple LCAO–MO theory and the assumption that the $d \leftarrow d$ transitions borrow electric transition dipole moments for production of rotatory strength from the internal ligand transitions used in the structural assignment.

Studying complexation of formylcamphor Schiff bases it is, however, necessary to be aware of some complicating experimental facts which influence the otherwise obvious comparisons with analogous Schiff bases of acetylacetone.

The condensation products between diamines and formylcamphor show a configuration of the ketoenamine groups which is strongly dependent on the choice of solvent. *I.e.*, in chloroform these chromophores have dominantly a *syn* (*Z*) structure with intramolecular hydrogen bonding, whereas in methanol solutions an *anti* (*E*) structure is the most abundant.[4,5]

In preparing Cu^{2+} complexes of such ligands from methanol–water mixtures, complexation occurs with the *syn* isomer since spectra of the formylcamphor Schiff base complexes are similar to those of the corresponding acetylacetone complexes. Furthermore, with respect to 1,2-diamines with low barrier towards rotation around the substituted ethylene bridge, the Schiff bases change configuration (handedness of the set of $\pi^* \leftarrow \pi$ transition moments) on complexation,[3] just as do the acetylacetone analogues.[6,1]

These facts mean that the envelope of the CD spectrum in the $\pi^* \leftarrow \pi$ transition region (representing exciton coupling) of the Schiff base between *trans*-(*R*,*R*)-$(-)_D$-1,2-cyclohexanediamine and formylcamphor [*R*-chxn(fmcH)$_2$] in methanol (298 nm $\Delta\varepsilon = -52$, 333 nm $\Delta\varepsilon = 61$)[4] reverses in chloroform (300 nm $\Delta\varepsilon = 45$, 340 nm $\Delta\varepsilon = -47$)[4] and on complexation with Cu^{2+} [Cu *R*-chnx(fmc)$_2$] (333 nm $\Delta\varepsilon = 21$, 371 nm $\Delta\varepsilon = -48$),[3] whereas the envelope of the Schiff base between *R*-$(-)_D$-1,2-propanediamine and formylcamphor [*R*-pn(fmcH)$_2$] in methanol (295 nm $\Delta\varepsilon = -24$, 333 nm $\Delta\varepsilon = 36$)[4] reverses in chloroform (296 nm $\Delta\varepsilon = 23$, 333 nm $\Delta\varepsilon = -30$)[4] and reverts again on complexation with Cu^{2+} [Cu *R*-pn(fmc)$_2$] (333 nm $\Delta\varepsilon = -10$, 371 nm $\Delta\varepsilon = 26$).[4]

With these points noted, we may consider ligand range CD spectra of VO^{2+} complexes of formylcamphor Schiff bases prepared according to standard procedure[7,8] and identified through chemical analysis.

The CD envelope of VO *R*-chxn(fmc)$_2$ is characteristic by being similar to that of the free ligand in methanol (297 nm $\Delta\varepsilon = -42$, 331 nm $\Delta\varepsilon = 54$) which is opposite to the case of the corresponding Cu^{2+} complex, and since cyclohexanediamine does not allow rotation around the substituted ethylene-bridge in *R*-chxn(fmcH)$_2$ it is concluded that the chromophoric parts of the ligand in VO *R*-chxn(fmc)$_2$ take on the *anti* configuration.

As far as concerns VO *R*-pn(fmc)$_2$, the ligand part of the CD spectrum has low intensity and is furthermore uncharacteristic in shape with respect to exciton coupling as it contains only one extremum ($\Delta\varepsilon_{max} = 6$ at 330 nm). With the result presented above for VO *R*-chxn(fmc)$_2$ also taken into consideration, it may tentatively be concluded that VO *R*-pn(fmc)$_2$ exhibits an almost planar coordination of the quadridentate ligand having the chromophoric parts in *anti* configuration.

What has been said about spectra of VO^{2+} complexes of formylcamphor Schiff bases is also true for the corresponding Ni^{2+} complexes; thus Ni *R*-chxn(fmc)$_2$ exhibits a CD spectrum characteristic of having the chromophoric parts in *anti* configuration, and Ni *R*-pn(fmc)$_2$ a CD spectrum of low intensity and uncharacteristic shape.

It thus materializes that it is impossible to present a discussion concerning the electronic transitions in the ligand field range of these complexes within the model mentioned above,[1] as the molecular geometry of the ligand parts is quite different from that of acetylacetone, *i.e.* the relative position of the exciton coupled $\pi^* \leftarrow \pi$ transitions to the substituted ethylene bridge between the two chromophoric parts is ill-defined.

A study of acetylcamphor Schiff base complexes, however, would be worthwhile, as these ligands are known to behave spectroscopically similar to acetylacetone Schiff bases.[9]

Acknowledgement. The author wishes to thank Mrs. L. Penzien for valuable technical assistance.

1. Jensen, H. P. and Larsen, E. *Acta Chem. Scand. 25* (1971) 1439.
2. Jensen, H. P., Kristensen, B. S., Mosbæk, H. and Søtofte, I. *Acta Chem. Scand. A 32* (1978) 141.
3. Jensen, H. P. *Acta Chem. Scand. A 32* (1978) 895.
4. Jensen, H. P. and Larsen, E. *Acta Chem. Scand. A 29* (1975) 157.
5. Jensen, H. P. and Larsen, E. *Gazz. Chim. Ital. 107* (1977) 143.
6. Larsen, E. *Acta Chem. Scand. 23* (1969) 2158.
7. Ramaiah, K., Anderson, F. E. and Martin, D. F. *Inorg. Chem. 3* (1964) 296.
8. Jones, K. M. and Larsen, E. *Acta Chem. Scand. 19* (1965) 1210.
9. Jensen, H. P. *Acta Chem. Scand. A 32* (1978) 149.

Received September 29, 1978.